

Bibliography of Lewis Research Center Technical Publications Announced in 1993



National Aeronautics and
Space Administration

Office of Management

Scientific and Technical
Information Program

1994

PREFACE

Making the results of our research available to others has always been a vital part of Lewis' mission. In 1993, Lewis Research Center's 1850 research authors (1373 civil servants and 477 on-site contractor and university staff) published 733 technical publications that were announced to and reached the worldwide scientific community. Included in this total are 166 high-numbered Technical Memorandums and 378 society presentations—the most published in a single year. In addition to this total, 283 contractor-authored research reports were produced at NASA Lewis in 1993.

In 1993, Lewis authors published approximately 57 percent of their research contributions in outside publications and the remainder as NASA research reports. Although our research authors wrote technical papers for 73 societies and associations, eighty percent of Lewis-authored society presentations and journal articles were addressed to members of the following 10 organizations—the American Institute of Aeronautics and Astronautics (AIAA), the American Society of Mechanical Engineers (ASME), the Society of Automotive Engineering (SAE), the Combustion Institute, the American Society of Engineering Education (ASEE), the Institute of Electrical and Electronic Engineers (IEEE), the American Nuclear Society (ANS), the Society of Photo-Optical Instrumentation Engineers (SPIE), the American Chemical Society (ACS), and Pergamon Press.

This year, the staff of the Solar Dynamic Power System Branch Staff wrote a reference manual about the "Solar Dynamic Power System Development for Space Station Freedom" (NASA RP-1310). In addition, Lewis hosted or sponsored fourteen research conferences and workshops in 1993. Eight of these resulted in the following NASA Conference Publications:

- NASA CP-10129, Vision-21: Interdisciplinary Science and Engineering in the Era of Cyberspace, March 30-31
- NASA CP-3228, Space Electrochemical Research and Technology, April 14-15
- NASA CP-3239, Rotordynamic Instability Problems in High-Performance Turbomachinery—1993, May 10-12
- NASA CP-10122, Fifth Annual Thermal and Fluids Analysis Workshop, August 16-20
- NASA CP-10130, Workshop on Computational Turbulence Modeling, September 15-16
- NASA CP-3244, Second NASA Workshop on Wiring for Space Applications, October 6-7
- NASA CP-19117, HITEMP Review—1993: Advanced High Temperature Engine Materials Technology Program, October 25-27
- NASA CP-10136, Seals Flow Code Development—93, November 3-4

Other conferences and workshops hosted or sponsored by Lewis in 1993 included

- Enabling Propulsion Materials Review, April 27-28
- HSR Propulsion System Review, May 5-6
- Neural Net Workshop, June 14-15
- The Lewis Turbomachinery Forced Vibration Response Workshop, August 11
- Seals Workshop, August 17-19
- MMIC Space Quality Workshop, August 31—September 1

In 1993, 29 patents were applied for and 15 patents were issued. Items patented include a "method of applying a thermal barrier coating system to a substrate," a "multi-heat addition turbine engine," a "spectroscopic wear detector," and "ceramic fiber reinforced glass-ceramic matrix composite."

Several Lewis researchers received awards for their publications. The 1993 Lewis Distinguished Publication Award was presented to Pilar Herrera-Fierro, William R. Jones, Jr., and Stephen V. Pepper for their paper entitled "Interfacial Chemistry of a Perfluoropolyether Lubricant Studied by X-Ray Photoelectron Spectroscopy and Temperature Desorption Spectroscopy."

For his paper "Temperature Dependence of Tensile Properties of 2.21Cr-1Mo Steel Base, Welds, Weldments, and Simulated Heat Affected Zone Structures," K. Bhanu Sankara Rao, a National Research Council Associate at Lewis, received the 1993 D & H Scheron Award, presented by the Indian Institute of Welding for the best design-oriented research paper of the year in welding research conducted in India. Richard T. Barrett received the Federal Laboratory Consortium (FLC) Award of Excellence in Technology Transfer for 1993 for his preparation of the first comprehensive fastener design manual. This manual helps design engineers in the aerospace and construction industries select the proper fasteners for each application.

This year, NASA Lewis and Peachtree Scientific, Inc. were joint winners of Research and Development Magazine's R&D 100 award. Their winning entry, "Pioneer II Melt Modulation Fiber Growth System," is a new apparatus for growing single-crystal reinforcing fibers for high-temperature composites. It enables researchers to experiment with a much wider variety of fiber materials. Lewis has won 63 of the R&D awards since they were established by Research and Development Magazine in 1962.

A few of the other awards received by Lewis scientists and engineers in 1993 follow. For their contributions to astronaut safety in the manned flight program, astronaut Carl Walz presented Silver Snoopy awards, the highest honor that can be bestowed by a U.S. astronaut, to six Lewis researchers. This year's recipients were Glen Horvat, Thomas Jacobson, Michael Lewis, Alexander Pline, Kurt Sacksteder, and Mark Weislogel. Also this year, Alex Vary received the Lester Honor Award presented by the American Society for Nondestructive Testing (ASNT). The award recognized his "major contributions to the field of nondestructive testing...." Bonnie McBride and Sanford Gordon received a Space Act Monetary Award for their development of the CET89 code, one of the most important and widely used computer programs in the aerospace industry. Robert Siegel received the American Institute of Aeronautics and Astronautics (AIAA) Thermophysics Award for 1993 for his "outstanding contributions to thermophysics...." and Nancy McNelis received a Gene Zara Memorial Award for her dedication to advancing technology for the National Aerospace Plane. Jacques C. Richard received the Dr. A.T. Weathers Award from the National Technical Association (NTA) for his work in unsteady, inviscid, and compressible flow codes in support of propulsion system dynamic analyses; and Harold Sliney received the Society of Tribologists and Lubrication Engineers' (STLE) highest award, the National Award, for his research on high-temperature lubrication.

All of the publications in this collection were announced in the 1993 issues of STAR (Scientific and Technical Aerospace Reports) and IAA (International Aerospace Abstracts). Some 1993 publications will be announced in the 1994 issues of STAR and IAA and will thus appear in the 1994 Lewis Bibliography. However, a few Lewis-authored publications are not included in this compilation because of FEDD (For Early Domestic Dissemination) and ITAR (International Traffic in Arms Regulations) considerations which limit their announcement and distribution.

The arrangement of the material is by NASA subject category, as noted in the Contents. In addition, the various indexes will help locate specific publications by subject, author, contractor organization, contract number, and report number.

The Publishing Services Team

TABLE OF CONTENTS

AERONAUTICS	For related information see also <i>Astronautics</i> .	
01 AERONAUTICS (GENERAL)		1
02 AERODYNAMICS	Includes aerodynamics of bodies, combinations, wings, rotors, and control surfaces; and internal flow in ducts and turbomachinery. For related information see also <i>34 Fluid Mechanics and Heat Transfer</i> .	2
03 AIR TRANSPORTATION AND SAFETY	Includes passenger and cargo air transport operations; and aircraft accidents. For related information see also <i>16 Space Transportation</i> and <i>85 Urban Technology and Transportation</i> .	18
04 AIRCRAFT COMMUNICATIONS AND NAVIGATION	Includes digital and voice communication with aircraft; air navigation systems (satellite and ground based); and air traffic control. For related information see also <i>17 Space Communications, Spacecraft Communications, Command and Tracking</i> and <i>32 Communications and Radar</i> .	N.A.
05 AIRCRAFT DESIGN, TESTING AND PERFORMANCE	Includes aircraft simulation technology. For related information see also <i>18 Spacecraft Design, Testing and Performance</i> and <i>39 Structural Mechanics</i> . For land transportation vehicles see <i>85 Urban Technology and Transportation</i> .	20
06 AIRCRAFT INSTRUMENTATION	Includes cockpit and cabin display devices; and flight instruments. For related information see also <i>19 Spacecraft Instrumentation</i> and <i>35 Instrumentation and Photography</i> .	21
07 AIRCRAFT PROPULSION AND POWER	Includes prime propulsion systems and systems components, e.g., gas turbine engines and compressors; and onboard auxiliary power plants for aircraft. For related information see also <i>20 Spacecraft Propulsion and Power</i> , <i>28 Propellants and Fuels</i> , and <i>44 Energy Production and Conversion</i> .	22
08 AIRCRAFT STABILITY AND CONTROL	Includes aircraft handling qualities; piloting; flight controls; and autopilots. For related information see also <i>05 Aircraft Design, Testing and Performance</i> .	40
09 RESEARCH AND SUPPORT FACILITIES (AIR)	Includes airports, hangars and runways; aircraft repair and overhaul facilities; wind tunnels; shock tubes; and aircraft engine test stands. For related information see also <i>14 Ground Support Systems and Facilities (Space)</i> .	42
ASTRONAUTICS	For related information see also <i>Aeronautics</i> .	
12 ASTRONAUTICS (GENERAL)	For extraterrestrial exploration see <i>91 Lunar and Planetary Exploration</i> .	43
13 ASTRODYNAMICS	Includes powered and free-flight trajectories; and orbital and launching dynamics.	45
14 GROUND SUPPORT SYSTEMS AND FACILITIES (SPACE)	Includes launch complexes, research and production facilities; ground support equipment, e.g., mobile transporters; and simulators. For related information see also <i>09 Research and Support Facilities (Air)</i> .	45
15 LAUNCH VEHICLES AND SPACE VEHICLES	Includes boosters; operating problems of launch/space vehicle systems; and reusable vehicles. For related information see also <i>20 Spacecraft Propulsion and Power</i> .	50
16 SPACE TRANSPORTATION	Includes passenger and cargo space transportation, e.g., shuttle operations; and space rescue techniques. For related information see also <i>03 Air Transportation and Safety</i> and <i>18 Spacecraft Design, Testing and Performance</i> . For space suits see <i>54 Man/System Technology and Life Support</i> .	51
17 SPACE COMMUNICATIONS, SPACECRAFT COMMUNICATIONS, COMMAND AND TRACKING	Includes telemetry; space communications networks; astronavigation and guidance; and radio blackout. For related information see also <i>04 Aircraft Communications and Navigation</i> and <i>32 Communications and Radar</i> .	52

N.A.—No abstracts were assigned to this category for this issue.

18 SPACECRAFT DESIGN, TESTING AND PERFORMANCE 54
Includes satellites; space platforms; space stations; spacecraft systems and components such as thermal and environmental controls; and attitude controls. For life support systems see *54 Man/System Technology and Life Support*. For related information see also *05 Aircraft Design, Testing and Performance*, *39 Structural Mechanics*, and *16 Space Transportation*.

19 SPACECRAFT INSTRUMENTATION 63
For related information see also *06 Aircraft Instrumentation* and *35 Instrumentation and Photography*.

20 SPACECRAFT PROPULSION AND POWER 64
Includes main propulsion systems and components, e.g., rocket engines; and spacecraft auxiliary power sources. For related information see also *07 Aircraft Propulsion and Power*, *28 Propellants and Fuels*, *44 Energy Production and Conversion*, and *15 Launch Vehicles and Space Vehicles*.

CHEMISTRY AND MATERIALS

23 CHEMISTRY AND MATERIALS (GENERAL) 93

24 COMPOSITE MATERIALS 97
Includes physical, chemical, and mechanical properties of laminates and other composite materials. For ceramic materials see *27 Nonmetallic Materials*.

25 INORGANIC AND PHYSICAL CHEMISTRY 112
Includes chemical analysis, e.g., chromatography; combustion theory; electrochemistry; and photochemistry. For related information see also *77 Thermodynamics and Statistical Physics*.

26 METALLIC MATERIALS 122
Includes physical, chemical, and mechanical properties of metals, e.g., corrosion; and metallurgy.

27 NONMETALLIC MATERIALS 130
Includes physical, chemical, and mechanical properties of plastics, elastomers, lubricants, polymers, textiles, adhesives, and ceramic materials. For composite materials see *24 Composite Materials*.

28 PROPELLANTS AND FUELS 139
Includes rocket propellants, igniters and oxidizers; their storage and handling procedures; and aircraft fuels. For related information see also *07 Aircraft Propulsion and Power*, *20 Spacecraft Propulsion and Power*, and *44 Energy Production and Conversion*.

29 MATERIALS PROCESSING 142
Includes space-based development of products and processes for commercial application. For biological materials see *55 Space Biology*.

ENGINEERING For related information see also *Physics*.

31 ENGINEERING (GENERAL) 146
Includes vacuum technology; control engineering; display engineering; cryogenics; and fire prevention.

32 COMMUNICATIONS AND RADAR 147
Includes radar; land and global communications; communications theory; and optical communications. For related information see also *04 Aircraft Communications and Navigation* and *17 Space Communications, Spacecraft Communications, Command and Tracking*. For search and rescue see *03 Air Transportation and Safety*, and *16 Space Transportation*.

33 ELECTRONICS AND ELECTRICAL ENGINEERING 150
Includes test equipment and maintainability; components, e.g., tunnel diodes and transistors; microminiaturization; and integrated circuitry. For related information see also *60 Computer Operations and Hardware* and *76 Solid-State Physics*.

34 FLUID MECHANICS AND HEAT TRANSFER 162
Includes boundary layers; hydrodynamics; fluidics; mass transfer and ablation cooling. For related information see also *02 Aerodynamics* and *77 Thermodynamics and Statistical Physics*.

35 INSTRUMENTATION AND PHOTOGRAPHY 204
Includes remote sensors; measuring instruments and gauges; detectors; cameras and photographic supplies; and holography. For aerial photography see *43 Earth Resources and Remote Sensing*. For related information see also *06 Aircraft Instrumentation* and *19 Spacecraft Instrumentation*.

36 LASERS AND MASERS 217
Includes parametric amplifiers. For related information see also *76 Solid-State Physics*.

37 MECHANICAL ENGINEERING	218
Includes auxiliary systems (nonpower); machine elements and processes; and mechanical equipment.	
38 QUALITY ASSURANCE AND RELIABILITY	231
Includes product sampling procedures and techniques; and quality control.	
39 STRUCTURAL MECHANICS	233
Includes structural element design and weight analysis; fatigue; and thermal stress. For applications see <i>05 Aircraft Design, Testing and Performance</i> and <i>18 Spacecraft Design, Testing and Performance</i> .	
GEOSCIENCES For related information see also <i>Space Sciences</i> .	
42 GEOSCIENCES (GENERAL)	N.A.
43 EARTH RESOURCES AND REMOTE SENSING	N.A.
Includes remote sensing of earth resources by aircraft and spacecraft; photogrammetry; and aerial photography. For instrumentation see <i>35 Instrumentation and Photography</i> .	
44 ENERGY PRODUCTION AND CONVERSION	252
Includes specific energy conversion systems, e.g., fuel cells; global sources of energy; geophysical conversion; and windpower. For related information see also <i>07 Aircraft Propulsion and Power</i> , <i>20 Spacecraft Propulsion and Power</i> , and <i>28 Propellants and Fuels</i> .	
45 ENVIRONMENT POLLUTION	257
Includes atmospheric, noise, thermal, and water pollution.	
46 GEOPHYSICS	257
Includes aeronomy; upper and lower atmosphere studies; ionospheric and magnetospheric physics; and geomagnetism. For space radiation see <i>93 Space Radiation</i> .	
47 METEOROLOGY AND CLIMATOLOGY	N.A.
Includes weather forecasting and modification.	
48 OCEANOGRAPHY	N.A.
Includes biological, dynamic, and physical oceanography; and marine resources. For related information see also <i>43 Earth Resources and Remote Sensing</i> .	
LIFE SCIENCES	
51 LIFE SCIENCES (GENERAL)	N.A.
52 AEROSPACE MEDICINE	257
Includes physiological factors; biological effects of radiation; and effects of weightlessness on man and animals.	
53 BEHAVIORAL SCIENCES	N.A.
Includes psychological factors; individual and group behavior; crew training and evaluation; and psychiatric research.	
54 MAN/SYSTEM TECHNOLOGY AND LIFE SUPPORT	258
Includes human engineering; biotechnology; and space suits and protective clothing. For related information see also <i>16 Space Transportation</i> .	
55 SPACE BIOLOGY	N.A.
Includes exobiology; planetary biology; and extraterrestrial life.	
MATHEMATICAL AND COMPUTER SCIENCES	
59 MATHEMATICAL AND COMPUTER SCIENCES (GENERAL)	258
60 COMPUTER OPERATIONS AND HARDWARE	N.A.
Includes hardware for computer graphics, firmware, and data processing. For components see <i>33 Electronics and Electrical Engineering</i> .	
61 COMPUTER PROGRAMMING AND SOFTWARE	258
Includes computer programs, routines, algorithms, and specific applications, e.g., CAD/CAM.	
62 COMPUTER SYSTEMS	261
Includes computer networks and special application computer systems.	

63 CYBERNETICS	263
Includes feedback and control theory, artificial intelligence, robotics and expert systems. For related information see also <i>54 Man/System Technology and Life Support</i> .	
64 NUMERICAL ANALYSIS	266
Includes iteration, difference equations, and numerical approximation.	
65 STATISTICS AND PROBABILITY	270
Includes data sampling and smoothing; Monte Carlo method; and stochastic processes.	
66 SYSTEMS ANALYSIS	270
Includes mathematical modeling; network analysis; and operations research.	
67 THEORETICAL MATHEMATICS	N.A.
Includes topology and number theory.	
 PHYSICS For related information see also <i>Engineering</i> .	
70 PHYSICS (GENERAL)	271
For precision time and time interval (PTI) see <i>35 Instrumentation and Photography</i> , for geophysics, astrophysics or solar physics see <i>46 Geophysics</i> , <i>90 Astrophysics</i> , or <i>92 Solar Physics</i> .	
71 ACOUSTICS	271
Includes sound generation, transmission, and attenuation. For noise pollution see <i>45 Environment Pollution</i> .	
72 ATOMIC AND MOLECULAR PHYSICS	276
Includes atomic structure, electron properties, and molecular spectra.	
73 NUCLEAR AND HIGH-ENERGY PHYSICS	276
Includes elementary and nuclear particles; and reactor theory. For space radiation see <i>93 Space Radiation</i> .	
74 OPTICS	277
Includes light phenomena and optical devices. For lasers see <i>36 Lasers and Masers</i> .	
75 PLASMA PHYSICS	278
Includes magnetohydrodynamics and plasma fusion. For ionospheric plasmas see <i>46 Geophysics</i> . For space plasmas see <i>90 Astrophysics</i> .	
76 SOLID-STATE PHYSICS	279
Includes superconductivity. For related information see also <i>33 Electronics and Electrical Engineering</i> and <i>36 Lasers and Masers</i> .	
77 THERMODYNAMICS AND STATISTICAL PHYSICS	284
Includes quantum mechanics; theoretical physics; and Bose and Fermi statistics. For related information see also <i>25 Inorganic and Physical Chemistry</i> and <i>34 Fluid Mechanics and Heat Transfer</i> .	
 SOCIAL SCIENCES	
80 SOCIAL SCIENCES (GENERAL)	N.A.
Includes educational matters.	
81 ADMINISTRATION AND MANAGEMENT	286
Includes management planning and research.	
82 DOCUMENTATION AND INFORMATION SCIENCE	287
Includes information management; information storage and retrieval technology; technical writing; graphic arts; and micrography. For computer documentation see <i>61 Computer Programming and Software</i> .	
83 ECONOMICS AND COST ANALYSIS	287
Includes cost effectiveness studies.	
84 LAW, POLITICAL SCIENCE AND SPACE POLICY	N.A.
Includes NASA appropriation hearings; aviation law; space law and policy; international law; international cooperation; and patent policy.	
85 URBAN TECHNOLOGY AND TRANSPORTATION	287
Includes applications of space technology to urban problems; technology transfer; technology assessment; and surface and mass transportation. For related information see <i>03 Air Transportation and Safety</i> , <i>16 Space Transportation</i> , and <i>44 Energy Production and Conversion</i> .	

SPACE SCIENCES For related information see also *Geosciences*.

88 SPACE SCIENCES (GENERAL) N.A.

89 ASTRONOMY N.A.
Includes radio, gamma-ray, and infrared astronomy; and astrometry.

90 ASTROPHYSICS 288
Includes cosmology; celestial mechanics; space plasmas; and interstellar and interplanetary gases and dust.
For related information see also *75 Plasma Physics*.

91 LUNAR AND PLANETARY EXPLORATION 293
Includes planetology; and manned and unmanned flights. For spacecraft design or space stations see *18 Spacecraft Design, Testing and Performance*.

92 SOLAR PHYSICS 293
Includes solar activity, solar flares, solar radiation and sunspots. For related information see also *93 Space Radiation*.

93 SPACE RADIATION 294
Includes cosmic radiation; and inner and outer earth's radiation belts. For biological effects of radiation see *52 Aerospace Medicine*. For theory see *73 Nuclear and High-Energy Physics*.

GENERAL

Includes aeronautical, astronautical, and space science related histories, biographies, and pertinent reports too broad for categorization; histories or broad overviews of NASA programs.

99 GENERAL N.A.

SUBJECT INDEX A-1

PERSONAL AUTHOR INDEX B-1

CORPORATE SOURCE INDEX C-1

CONTRACT NUMBER INDEX D-1

REPORT/ACCESSION NUMBER INDEX E-1

Bibliography of Lewis Research Center Technical Publications Announced in 1993

01

AERONAUTICS (GENERAL)

N93-14102*# National Aeronautics and Space Administration.
Lewis Research Center, Cleveland, OH.

AN ALGEBRAIC TURBULENCE MODEL FOR THREE-DIMENSIONAL VISCOUS FLOWS

R. V. CHIMA, P. W. GIEL (Sverdrup Technology, Inc., Brook Park, OH.), and R. J. BOYLE Jan. 1993 11 p Proposed for presentation at the 31st Aerospace Sciences Meeting and Exhibit, Reno, NV, 11-14 Jan. 1993; sponsored by AIAA (Contract RTOP 535-05-10) (NASA-TM-105931; E-7442; NAS 1.15:105931) Copyright Avail: CASI HC A03/MF A01

An algebraic turbulence model is proposed for use with three-dimensional Navier-Stokes analyses. It incorporates features of both the Baldwin-Lomax and Cebeci-Smith models. The Baldwin-Lomax model uses the maximum of a function $f(y)$ to determine length and velocity scales. An analysis of the Baldwin-Lomax model shows that $f(y)$ can have a spurious maximum close to the wall, causing numerical problems and non-physical results. The proposed model uses integral relations to determine $\Delta^+ u_{sub e}$ and Δ^+ used in the Cebeci-Smith mode. It eliminates a constant in the Baldwin-Lomax model and determines the two remaining constants by comparison to the Cebeci-Smith formulation. Pressure gradient effects, a new wake model, and the implementation of these features in a three-dimensional Navier-Stokes code are also described. Results are shown for a flat plate boundary layer, an annular turbine cascade, and endwall heat transfer in a linear turbine cascade. The heat transfer results agree well with experimental data which shows large variations in endwall Stanton number contours with Reynolds number. Author

N93-15573*# National Aeronautics and Space Administration.
Lewis Research Center, Cleveland, OH.

VIBRATION ISOLATION TECHNOLOGY: AN EXECUTIVE SUMMARY OF SYSTEMS DEVELOPMENT AND DEMONSTRATION

CARLOS M. GRODSINSKY, KIRK A. LOGSDON, and JOSEPH F. LUBOMSKI Jan. 1993 7 p Presented at the 31st Aerospace Sciences Meeting, Reno, NV, 11-14 Jan. 1993; sponsored by American Association of Aeronautics and Astronautics (Contract RTOP 694-03-0C) (NASA-TM-105937; E-7454; NAS 1.15:105937) Avail: CASI HC A02/MF A01

A program was organized to develop the enabling technologies needed for the use of Space Station Freedom as a viable microgravity experimental platform. One of these development programs was the Vibration Isolation Technology (VIT). This technology development program grew because of increased awareness that the acceleration disturbances present on the Space Transportation System (STS) orbiter can and are detrimental to many microgravity experiments proposed for STS, and in the future, Space Station Freedom (SSF). Overall technological organization

are covered of the VIT program. Emphasis is given to the results from development and demonstration of enabling technologies to achieve the acceleration requirements perceived as those most likely needed for a variety of microgravity science experiments. In so doing, a brief summary of general theoretical approaches to controlling the acceleration environment of an isolated space based payload and the design and/or performance of two prototype six degree of freedom active magnetic isolation systems is presented. Author

N93-20902*# National Aeronautics and Space Administration.
Lewis Research Center, Cleveland, OH.

THE 1992 RESEARCH/TECHNOLOGY REPORT

1992 172 p
(NASA-TM-105924; E-7425; NAS 1.15:105924) Avail: CASI HC A08/MF A02

The 1992 Research & Technology report is organized so that a broad cross section of the community can readily use it. A short introductory paragraph begins each article and will prove to be an invaluable reference tool for the layperson. The approximately 200 articles summarize the progress made during the year in various technical areas and portray the technical and administrative support associated with Lewis technology programs. Author (revised)

N93-26136*# National Aeronautics and Space Administration.
Lewis Research Center, Cleveland, OH.

BIBLIOGRAPHY ON PROPULSION AIRFRAME INTEGRATION TECHNOLOGIES FOR HIGH-SPEED CIVIL TRANSPORT APPLICATIONS, 1980-1991

DAVID J. ANDERSON and MASASHI MIZUKAMI Mar. 1993 343 p
(Contract RTOP 537-02-23)
(NASA-TM-105602; E-6938; NAS 1.15:105602) Avail: CASI HC A15/MF A03

NASA has initiated the High Speed Research (HSR) program with the goal to develop technologies for a new generation, economically viable, environmentally acceptable, supersonic transport (SST) called the High Speed Civil Transport (HSCT). A significant part of this effort is expected to be in multidisciplinary systems integration, such as in propulsion airframe integration (PAI). In order to assimilate the knowledge database on PAI for SST type aircraft, a bibliography on this subject was compiled. The bibliography with over 1200 entries, full abstracts, and indexes. Related topics are also covered, such as the following: engine inlets, engine cycles, nozzles, existing supersonic cruise aircraft, noise issues, computational fluid dynamics, aerodynamics, and external interference. All identified documents from 1980 through early 1991 are included; this covers the latter part of the NASA Supersonic Cruise Research (SCR) program and the beginnings of the HSR program. In addition, some pre-1980 documents of significant merit or reference value are also included. The references were retrieved via a computerized literature search using the NASA RECON database system. Author (revised)

N93-72738*# National Aeronautics and Space Administration.
Lewis Research Center, Cleveland, OH.

FOUR GIANTS OF THE LEWIS RESEARCH CENTER

ROBERT W. GRAHAM May 1984 12 p
(NASA-TM-83642; E-2087; NAS 1.15:83642) Avail: CASI HC A03/MF A01

During its 42-year history, the Lewis Research Center (LeRC) has been guided by a number of outstanding leaders. In this article, four of these leaders, Dr. George W. Lewis, Dr. Hugh L. Dryden, Dr. Edward R. Sharp, and Dr. Abe Silverstein, are singled out for their contributions to LeRC and to the advance of the aerospace field. Some of their backgrounds and some personal anecdotes about their influence on LeRC are shared. It will be evident that they have influenced the history of this local region as well as that of LeRC. Author (revised)

02

AERODYNAMICS

Includes aerodynamics of bodies, combinations, wings, rotors, and control surfaces; and internal flow in ducts and turbomachinery.

A93-14118# National Aeronautics and Space Administration. Lewis Research Center, Cleveland, OH.

EVALUATION AND APPLICATION OF THE BALDWIN-LOMAX TURBULENCE MODEL IN TWO-DIMENSIONAL, UNSTEADY, COMPRESSIBLE BOUNDARY LAYERS WITH AND WITHOUT SEPARATION IN ENGINE INLETS

BARBARA SAKOWSKI, DOUGLAS DARLING (NASA, Lewis Research Center, Cleveland, OH), ROBERT L. ROACH (Georgia Inst. of Technology, Atlanta), and ALLAN VAN DE WALL (Case Western Reserve Univ., Cleveland, OH) Jul. 1992 10 p. AIAA, SAE, ASME, and ASEE, Joint Propulsion Conference and Exhibit, 28th, Nashville, TN, July 6-8, 1992 Previously announced in STAR as N93-10087 refs (Contract RTOP 505-62-20) (AIAA PAPER 92-3676) Copyright

The Baldwin-Lomax model is used in many CFD codes because it is quick and easy to implement. In this paper, we discuss implementing the Baldwin-Lomax turbulence model for both steady and unsteady compressible flows. In addition, these flows may be either separated or attached. In order to apply this turbulence model to flows which may be subjected to these conditions, certain modifications should be made to the original Baldwin-Lomax model. We discuss these modifications and determine whether the Baldwin-Lomax model is a viable turbulence model that produces reasonably accurate results for high speed flows that can be found in engine inlets. Author

A93-14169 National Aeronautics and Space Administration. Ames Research Center, Moffett Field, CA.

THE NEW CHALLENGE OF COMPUTATIONAL AEROSCIENCE

F. R. BAILEY (NASA, Ames Research Center, Moffett Field, CA), DOUGLAS L. DWOYER (NASA, Langley Research Center, Hampton, VA), and LESTER D. NICHOLS (NASA, Lewis Research Center, Cleveland, OH) In ICAS, Congress, 18th, Beijing, China, Sept. 20-25, 1992, Proceedings. Vol. 1 Washington American Institute of Aeronautics and Astronautics, Inc. 1992 p. 83-96. refs

This paper discusses NASA's Computational Aerosciences (CAS) Project of the High Performance Computing and Communications Program (HPCCP). The project is aimed at developing advanced, multidisciplinary simulation capabilities for aerospace vehicle and propulsion system design. It is also aimed at overcoming computational performance barriers by accelerating the development of parallel computer technology. The goals and approach of the CAS Project are described and the challenges to its implementation are addressed. Specific vehicle class simulations to be demonstrated and the principal multidisciplinary modeling approaches to be emphasized are described. The computational speed and memory requirements for representative multidisciplinary applications are estimated. Finally, the state of parallel computer technology including programming issues and the results of performance measurements are explored. Author

A93-14520* National Aeronautics and Space Administration. Lewis Research Center, Cleveland, OH.

STUDY ON VORTEX FLOW CONTROL OF INLET DISTORTION

BERNHARD H. ANDERSON (NASA, Lewis Research Center, Cleveland, OH), PAO S. HUANG, WILLIAM A. PASCHAL, and ENRICO CAVATORTA (Dee Howard Co., San Antonio, TX) Journal of Propulsion and Power (ISSN 0748-4658) vol. 8, no. 6 Nov.-Dec. 1992 p. 1266-1272. Previously cited in issue 08, p. 1167, Accession no. A92-23767 AIAA, Aerospace Sciences Meeting and Exhibit, 30th, Reno, NV, Jan. 6-9, 1992, AIAA Paper 92-0152 refs Copyright

A93-19151* National Aeronautics and Space Administration. Lewis Research Center, Cleveland, OH.

DISPERSION-RELATION-PRESERVING SCHEMES FOR COMPUTATIONAL AEROACOUSTICS

CHRISTOPHER K. W. TAM and JAY C. WEBB (Florida State Univ., Tallahassee) In DGLR/AIAA Aeroacoustics Conference, 14th, Aachen, Germany, May 11-14, 1992, Proceedings. Vol. 1 Bonn Deutsche Gesellschaft fuer Luft- und Raumfahrt 1992 p. 214-222. refs (Contract NAG3-1267; N00014-89-J-1836)

Finite difference schemes that have the same dispersion relations as the original partial differential equations are referred to as dispersion-relation-preserving (DRP) schemes. A method to construct time marching DRP schemes by optimizing the finite difference approximations of the space and time derivatives in the wave number and frequency space is presented. A sequence of numerical simulations is then performed. R.E.P.

A93-19221* National Aeronautics and Space Administration. Lewis Research Center, Cleveland, OH.

FORWARD ROTOR VORTEX EFFECTS ON COUNTER ROTATING PROPELLER NOISE

MICHELE LAUR, BECKY SQUIRES, and ROBERT T. NAGEL (North Carolina State Univ., Raleigh) In DGLR/AIAA Aeroacoustics Conference, 14th, Aachen, Germany, May 11-14, 1992, Proceedings. Vol. 2 Bonn Deutsche Gesellschaft fuer Luft- und Raumfahrt 1992 p. 890-897. Research supported by McDonnell Douglas Corp. and General Electric Co. refs (Contract NAG3-855)

Three configurations of a model counter rotating propeller manipulate the blade tip flow by: placing the CRP at angle of attack, installing shrouds, and turning the upstream blades to provide forward sweep. Flow visualization and flow measurements with thermal anemometry show no evidence of a tip vortex; however, a leading edge vortex was detected on aft swept blades. The modifications served to alter the strength and/or path of the leading edge vortex. The vortical flow is eliminated by forward sweep on the upstream propeller blades. Far field acoustic data from each test indicate only small influences on the level and directivity of the BPFs. The interaction tone at the sum of the two BPF's was significantly altered in a consistent manner. As the vortex system varied, the interaction tone was affected: far field noise levels in the forward quadrant increased and the characteristic noise minimum near the plane of rotation became less pronounced and in some cases were eliminated. If the forward propeller leading edge vortex system does not impact the rear propeller in the standard manner, a net increase in the primary interaction tone occurs for the model tested. If the leading edge vortex is removed, the interaction tone increases. Author

A93-19322* National Aeronautics and Space Administration. Lewis Research Center, Cleveland, OH.

AEROLOADS AND SECONDARY FLOWS IN A TRANSONIC MIXED FLOW TURBINE STAGE

K. R. KIRTLEY, T. A. BEACH (Sverdrup Technology, Inc.; NASA, Lewis Research Center, Cleveland, OH), and CASS ROGO (Teledyne CAE, Toledo, OH) Jun. 1992 13 p. ASME, International Gas Turbine and Aeroengine Congress and Exposition, 37th, Cologne, Germany, June 1-4, 1992 refs

(Contract NAS3-25266)
(ASME PAPER 92-GT-72)

A numerical simulation of a transonic mixed flow turbine stage has been carried out using an average passage Navier-Stokes analysis. The mixed flow turbine stage considered here consists of a transonic nozzle vane and a highly loaded rotor. The simulation was run at the design pressure ratio and is assessed by comparing results with those of an established throughflow design system. The three-dimensional aerodynamic loads are studied as well as the development and migration of secondary flows and their contribution to the total pressure loss. The numerical results indicate that strong passage vortices develop in the nozzle vane, mix out quickly, and have little impact on the rotor flow. The rotor is highly loaded near the leading edge. Within the rotor passage, strong spanwise flows and other secondary flows exist along with the tip leakage vortex. The rotor exit loss distribution is similar in character to that found in radial inflow turbines. The secondary flows and non-uniform work extraction also tend to significantly redistribute a non-uniform inlet total temperature profile by the exit of the stage.

Author

A93-19324* National Aeronautics and Space Administration. Lewis Research Center, Cleveland, OH.

AERODYNAMIC DESIGN OF TURBOMACHINERY BLADING IN THREE-DIMENSIONAL FLOW - AN APPLICATION TO RADIAL INFLOW TURBINES

Y. L. YANG, C. S. TAN, and W. R. HAWTHORNE (MIT, Cambridge, MA) Jun. 1992 13 p. ASME, International Gas Turbine and Aeroengine Congress and Exposition, 37th, Cologne, Germany, June 1-4, 1992 Research supported by U.S. Army refs (Contract NAG3-772)
(ASME PAPER 92-GT-74)

A computational method, based on a theory for turbomachinery blading design in three-dimensional inviscid flow, is applied to a parametric design study of a radial inflow turbine wheel. As the method requires the specification of swirl distribution, a technique for its smooth generation within the blade region is proposed. Excellent agreements have been obtained between the computed results from this design method and those from direct Euler computations, demonstrating the correspondence and consistency between the two. The computed results indicate the sensitivity of the pressure distribution to a lean in the stacking axis and a minor alteration in the hub/shroud profiles. Analysis based on Navier-Stokes solver shows no breakdown of flow within the designed blade passage and agreement with that from design calculation; thus the flow in the designed turbine rotor closely approximates that of an inviscid one. These calculations illustrate the use of a design method coupled to an analysis tool for establishing guidelines and criteria for designing turbomachinery blading.

Author

A93-19395* National Aeronautics and Space Administration. Lewis Research Center, Cleveland, OH.

THREE-DIMENSIONAL FLOW PHENOMENA IN A TRANSONIC, HIGH-THROUGH-FLOW, AXIAL-FLOW COMPRESSOR STAGE
WILLIAM W. COPENHAVER (USAF, Wright Lab., Wright-Patterson AFB, OH), CHUNILL HAH (NASA, Lewis Research Center, Cleveland, OH), and STEVEN L. PUTERBAUGH (USAF, Wright Lab., Wright-Patterson AFB, OH) Jun. 1992 10 p. ASME, International Gas Turbine and Aeroengine Congress and Exposition, 37th, Cologne, Germany, June 1-4, 1992 Research supported by USAF refs
(ASME PAPER 92-GT-169)

A detailed aerodynamic study of a transonic, high-through-flow, single stage compressor is presented. The compressor stage was comprised of a low-aspect-ratio rotor combined alternately with two different stator designs. Both experimental and numerical studies are conducted to understand the details of the complex flow field present in this stage. Aerodynamic measurements using high-frequency, Kulite pressure transducers and conventional probes are compared with results from a three-dimensional viscous flow analysis. A steady multiple blade row approach is used in the numerical technique to examine the detailed flow structure

inside the rotor and the stator passages. The comparisons indicate that many flow field features are correctly captured by viscous flow analysis, and therefore unmeasured phenomena can be studied with some level of confidence.

Author

A93-19399* National Aeronautics and Space Administration. Lewis Research Center, Cleveland, OH.

NUMERICAL SOLUTIONS FOR UNSTEADY SUBSONIC VORTICAL FLOWS AROUND LOADED CASCADES

J. FANG and H. M. ATASSI (Notre Dame Univ., IN) Jun. 1992 8 p. ASME, International Gas Turbine and Aeroengine Congress and Exposition, 37th, Cologne, Germany, June 1-4, 1992 refs (Contract NAG3-732)
(ASME PAPER 92-GT-173)

A frequency domain linearized unsteady aerodynamic analysis is presented for three-dimensional unsteady vortical flows around a cascade of loaded airfoils. The analysis fully accounts for the distortion of the impinging vortical disturbances by the mean flow. The entire unsteady flow field is calculated in response to upstream three-dimensional harmonic disturbances. Numerical results are presented for two standard cascade configurations representing turbine and compressor bladings for a reduced frequency range from 0.1 to 5. Results show that the upstream gust conditions and blade sweep strongly affect the unsteady blade response.

Author

A93-19400* National Aeronautics and Space Administration. Lewis Research Center, Cleveland, OH.

FORCING FUNCTION EFFECTS ON UNSTEADY AERODYNAMIC GUST RESPONSE. I - FORCING FUNCTIONS

GREGORY H. HENDERSON and SANFORD FLEETER (Purdue Univ., West Lafayette, IN) Jun. 1992 11 p. ASME, International Gas Turbine and Aeroengine Congress and Exposition, 37th, Cologne, Germany, June 1-4, 1992 Research sponsored by NASA refs
(ASME PAPER 92-GT-174)

The paper investigates the fundamental gust modeling assumption on the basis of a series of experiments performed in the Purdue Annular Cascade Research Facility. The measured unsteady flow fields are compared to linear-theory gust requirements. The perforated plate forcing functions closely resemble linear-theory forcing functions, with the static pressure fluctuations small and the periodic velocity vectors parallel to the downstream mean-relative flow angle over the entire periodic cycle. The airfoil forcing functions exhibit characteristics far from linear-theory gusts, with the alignment of the velocity vectors and the static pressure fluctuation amplitudes dependent on the rotor-loading condition, rotor solidity, and the inlet mean-relative flow angle. It is shown that airfoil wakes, both compressor and turbine, cannot be modeled with the boundary conditions of current state-of-the-art linear unsteady aerodynamic theory.

P.D.

A93-19401* National Aeronautics and Space Administration. Lewis Research Center, Cleveland, OH.

FORCING FUNCTION EFFECTS ON UNSTEADY AERODYNAMIC GUST RESPONSE. II - LOW SOLIDITY AIRFOIL ROW RESPONSE

GREGORY H. HENDERSON and SANFORD FLEETER (Purdue Univ., West Lafayette, IN) Jun. 1992 10 p. ASME, International Gas Turbine and Aeroengine Congress and Exposition, 37th, Cologne, Germany, June 1-4, 1992 Research sponsored by NASA refs
(ASME PAPER 92-GT-175)

The paper investigates the fundamental gust modeling assumption on the basis of a series of experiments performed in the Purdue Annular Cascade Research Facility. The unsteady period flow field is generated by rotating flows of perforated plates and airfoil cascades, with the resulting unsteady periodic chordwise pressure response of a downstream low solidity stator row determined by miniature pressure transducers embedded within selected airfoils. When the forcing function exhibited the characteristics of a linear-theory gust, the resulting response on the downstream stator airfoils was in excellent agreement with

the linear-theory models. When the forcing function did not exhibit linear-theory gust characteristics, the resulting unsteady aerodynamic response of the downstream stators was much more complex and correlated poorly with the linear-theory gust predictions. It is shown that the forcing function generator significantly affects the resulting gust response, with the complexity of the response characteristics increasing from the perforated-plate to the airfoil-cascade forcing functions. P.D.

A93-19436* National Aeronautics and Space Administration. Lewis Research Center, Cleveland, OH.
EXPERIMENTAL AND COMPUTATIONAL INVESTIGATION OF THE NASA LOW-SPEED CENTRIFUGAL COMPRESSOR FLOW FIELD

M. D. HATHAWAY (U.S. Army, Combat and Material Research Labs., Cleveland, OH), R. M. CHRISS, J. R. WOOD, and A. J. STRAZISAR (NASA, Lewis Research Center, Cleveland, OH) Jun. 1992 17 p. ASME, International Gas Turbine and Aeroengine Congress and Exposition, 37th, Cologne, Germany, June 1-4, 1992 refs (ASME PAPER 92-GT-213)

An experimental and computational investigation of the NASA Low-Speed Centrifugal Compressor (LSCC) flow field has been conducted using laser anemometry and Dawes' 3D viscous code. The experimental configuration consists of a backswep impeller followed by a vaneless diffuser. Measurements of the three-dimensional velocity field were acquired at several measurement planes through the compressor. The measurements describe both the throughflow and secondary velocity field along each measurement plane. In several cases the measurements provide details of the flow within the blade boundary layers. Insight into the complex flow physics within centrifugal compressors is provided by the computational analysis, and assessment of the CFD predictions is provided by comparison with the measurements. Five-hole probe and hot-wire surveys at the inlet and exit to the rotor as well as surface flow visualization along the impeller blade surfaces provide independent confirmation of the laser measurement technique. Author

A93-19490* National Aeronautics and Space Administration. Lewis Research Center, Cleveland, OH.
NUMERICAL SIMULATION OF COMPRESSOR ENDWALL AND CASING TREATMENT FLOW PHENOMENA

A. J. CROOK (General Motors Corp., Allison Gas Turbine Div., Indianapolis, IN), E. M. GREITZER, C. S. TAN (MIT, Cambridge, MA), and J. J. ADAMCZYK (NASA, Lewis Research Center, Cleveland, OH) Jun. 1992 12 p. ASME, International Gas Turbine and Aeroengine Congress and Exposition, 37th, Cologne, Germany, June 1-4, 1992 Research supported by General Motors Corp refs (ASME PAPER 92-GT-300)

A numerical study is presented of the flow in the endwall region of a compressor blade row, in conditions of operation with both smooth and grooved endwalls. The computations are first compared to velocity field measurements in a cantilevered stator/rotating hub configuration to confirm that the salient features are captured. Computations are then interrogated to examine the tip leakage flow structure since this is a dominant feature of the endwall region. In particular, the high blockage that can exist near the endwalls at the rear of a compressor blade passage appears to be directly linked to low total pressure fluid associated with the leakage flow. The fluid dynamic action of the grooved endwall, representative of the casing treatments that have been most successful in suppressing stall, is then simulated computationally and two principal effects are identified. One is suction of the low total pressure, high blockage fluid at the rear of the passage. The second is energizing of the tip leakage flow, most notably in the core of the leakage vortex, thereby suppressing the blockage at its source. Author

A93-20144* National Aeronautics and Space Administration. Lewis Research Center, Cleveland, OH.
EFFECTS OF ICING ON THE AERODYNAMIC PERFORMANCE OF HIGH LIFT AIRFOILS

L. N. SANKAR, N. PHAENGSOOK, and A. BANGALORE (Georgia Inst. of Technology, Atlanta) Jan. 1993 10 p. AIAA, Aerospace Sciences Meeting and Exhibit, 31st, Reno, NV, Jan. 11-14, 1993 refs

(Contract NAG3-768)
 (AIAA PAPER 93-0026) Copyright

A 2D compressible Navier-Stokes solver capable of analyzing multi-element airfoils is described. The flow field is divided into multiple zones. In each zone, the governing equations are solved using an implicit finite difference scheme. The flow solver is validated through a study of the aerodynamic characteristics of a GA(W)-1 configuration, for which good quality measured surface pressure data and load data are available. The solver is next applied to a study of the effects of icing on an iced 5-element airfoil configuration, experimentally studied at NASA Lewis Research Center. It is demonstrated that the formation of ice over the leading edge slat and the main airfoil can lead to significant flow separation, and a significant loss in lift, compared to clean configurations. Author

A93-22552* National Aeronautics and Space Administration. Lewis Research Center, Cleveland, OH.
AN ALGEBRAIC TURBULENCE MODEL FOR THREE-DIMENSIONAL VISCOUS FLOWS

R. V. CHIMA (NASA, Lewis Research Center, Cleveland, OH), P. W. GIEL (Sverdrup Technology, Inc., Brook Park, OH), and R. J. BOYLE (NASA, Lewis Research Center, Cleveland, OH) Jan. 1993 10 p. AIAA, Aerospace Sciences Meeting and Exhibit, 31st, Reno, NV, Jan. 11-14, 1993 Previously announced in STAR as N93-14102 refs (AIAA PAPER 93-0083) Copyright

An algebraic turbulence model is proposed for use with three-dimensional Navier-Stokes analyses. It incorporates features of both the Baldwin-Lomax and Cebeci-Smith models. The Baldwin-Lomax model uses the maximum of a function $f(v)$ to determine length and velocity scales. An analysis of the Baldwin-Lomax model shows that $f(v)$ can have a spurious maximum close to the wall, causing numerical problems and non-physical results. The proposed model uses integral relations to determine $\delta^+ u_{sub e}$ and δ^+ used in the Cebeci-Smith mode. It eliminates a constant in the Baldwin-Lomax model and determines the two remaining constants by comparison to the Cebeci-Smith formulation. Pressure gradient effects, a new wake model, and the implementation of these features in a three-dimensional Navier-Stokes code are also described. Results are shown for a flat plate boundary layer, an annular turbine cascade, and endwall heat transfer in a linear turbine cascade. The heat transfer results agree well with experimental data which shows large variations in endwall Stanton number contours with Reynolds number. Author

A93-22591* National Aeronautics and Space Administration. Lewis Research Center, Cleveland, OH.
PREDICTION OF ACTIVE CONTROL OF SUBSONIC CENTRIFUGAL COMPRESSOR ROTATING STALL

PATRICK B. LAWLESS and SANFORD FLEETER (Purdue Univ., West Lafayette, IN) Jan. 1993 14 p. AIAA, Aerospace Sciences Meeting and Exhibit, 31st, Reno, NV, Jan. 11-14, 1993 Research supported by U.S. Army and NASA refs (AIAA PAPER 93-0153) Copyright

A mathematical model is developed to predict the suppression of rotating stall in a centrifugal compressor with a vaned diffuser. This model is based on the employment of a control vortical waveform generated upstream of the impeller inlet to damp weak potential disturbances that are the early stages of rotating stall. The control system is analyzed by matching the perturbation pressure in the compressor inlet and exit flow fields with a model for the unsteady behavior of the compressor. The model was effective at predicting the stalling behavior of the Purdue Low

02 AERODYNAMICS

measurements. Computationally, the estimated lift variations are compared with the corresponding variation obtained from the surface pressure distribution. Four analytical formulations for the lift estimation from wake surveys are considered and relative successes of the four are discussed. Author

A93-23387*# National Aeronautics and Space Administration. Lewis Research Center, Cleveland, OH.

HIGH ACCURACY COMPUTATION OF FLUID-STRUCTURE INTERACTION IN TRANSONIC CASCADES

ALEXANDER BOSCHITSCH and TODD QUACKENBUSH (Continuum Dynamics, Inc., Princeton, NJ) Jan. 1993 15 p. AIAA, Aerospace Sciences Meeting and Exhibit, 31st, Reno, NV, Jan. 11-14, 1993 refs (Contract NAS3-26064) (AIAA PAPER 93-0485) Copyright

A coupling strategy for simulating fluid-structure interaction phenomena is formulated and applied to the prediction of flutter in transonic cascades. The flow is governed by the Euler equations and discretized using a finite volume flux-splitting scheme. The structure is modeled using an isoparametric finite element formulation. The coupling strategy successfully reconciles these two formulations at the fluid-structure interface by enforcing both kinematic and kinetic boundary conditions. In particular, the conservation laws applicable to the combined fluid-structure system are preserved across the interface. Since the primary mechanism driving aeroelastic phenomena involves energy exchange occurring at the interface, this highly accurate coupling mechanism is believed to improve the predictive capability of the scheme. The coupled equations are advanced simultaneously in time using an implicit time integration method. Results obtained using the coupling method are presented for cascade geometries operating in transonic flow. Author

A93-24233*# National Aeronautics and Space Administration. Lewis Research Center, Cleveland, OH.

THREE-DIMENSIONAL UNSTRUCTURED GRID EULER METHOD APPLIED TO TURBINE BLADES

OH J. KWON (Sverdrup Technology, Inc., Brook Park, OH) and CHUNILL HAH (NASA, Lewis Research Center, Cleveland, OH) Jan. 1993 11 p. AIAA, Aerospace Sciences Meeting and Exhibit, 31st, Reno, NV, Jan. 11-14, 1993 refs (AIAA PAPER 93-0196)

Flow through a turbine annular cascade is calculated using a three-dimensional Euler method based on unstructured tetrahedral meshes. The equations are integrated in time using an explicit Runge-Kutta time-stepping scheme. The inviscid flux terms are discretized using a cell-centered finite-volume formulation with upwind flux-difference splitting. The tetrahedral meshes around the turbine blade are generated using an advancing-front technique with forced geometric periodicity between the blades. Good agreement is obtained between the present calculation and the experiment for both surface pressure distribution and flow behavior in the passage between the blades, demonstrating the capability of the present methodology for turbomachinery flow applications. Author

A93-24238*# National Aeronautics and Space Administration. Lewis Research Center, Cleveland, OH.

DRIVEN CAVITY SIMULATION OF TURBOMACHINE BLADE FLOWS WITH VORTEX CONTROL

M. M. ATHAVALE, A. J. PRZEKOWAS (CFD Research Corp., Huntsville, AL), and R. C. HENDRICKS (NASA, Lewis Research Center, Cleveland, OH) Jan. 1993 12 p. AIAA, Aerospace Sciences Meeting and Exhibit, 31st, Reno, NV, Jan. 11-14, 1993 refs (AIAA PAPER 93-0390) Copyright

This paper presents a computational study of the three-dimensional flows in a rotating cavity with clearance between cavity walls and lid wall. The objectives of this study is to understand the interaction mechanism between tip leakage and blade passage flows and to assess the means to control the flow pattern and pressure losses. The classes of problems addressed include:

passage geometry, passage loading including lid velocity and anti-vortex strength, and placement necessary to provide flow control. The computational model is first validated on generic flow problems and then applied to a specific blade passage configuration. Results of parametric studies for secondary flow pattern control are analyzed, and practical means of vortex control are discussed. Author

A93-24240*# National Aeronautics and Space Administration. Lewis Research Center, Cleveland, OH.

THREE-DIMENSIONAL NAVIER-STOKES CALCULATIONS USING SOLUTION-ADAPTED GRIDS

T. L. HENDERSON, W. HUANG, K. D. LEE (Illinois Univ., Urbana), and Y. K. CHOO (NASA, Lewis Research Center, Cleveland, OH) Jan. 1993 14 p. AIAA, Aerospace Sciences Meeting and Exhibit, 31st, Reno, NV, Jan. 11-14, 1993 refs (AIAA PAPER 93-0431) Copyright

A three-dimensional solution-adaptive grid generation technique is presented. The adaptation technique redistributes grid points to improve the accuracy of a flow solution without increasing the number of grid points. It is applicable to structured grids with a multiblock topology. The method uses a numerical mapping and potential theory to modify the initial grid distribution based on the properties of the flow solution on the initial grid. The technique is demonstrated with two examples - a transonic finite wing and a supersonic blunt fin. The advantages are shown by comparing flow solutions on the adapted grids with those on the initial grids. Author

A93-24786*# National Aeronautics and Space Administration. Lewis Research Center, Cleveland, OH.

NAVIER-STOKES CALCULATIONS FOR THE UNSTEADY FLOWFIELD OF TURBOMACHINERY

JEN P. CHEN and DAVID L. WHITFIELD (Mississippi State Univ., Mississippi State) Jan. 1993 15 p. AIAA, Aerospace Sciences Meeting and Exhibit, 31st, Reno, NV, Jan. 11-14, 1993 refs (Contract NAG3-869) (AIAA PAPER 93-0676) Copyright

The Multistage Unsteady Turbomachinery Code is presently used to numerically simulate the flowfield generated by rotating machinery. The code, which simplifies the Reynolds-averaged Navier-Stokes equations via the thin-layer approximation, is an implicit finite-volume scheme with flux Jacobians that are evaluated by flux-vector splitting, while residual fluxes are evaluated by flux-difference splitting. Attention is given to the computational results this obtained for three engineering problems, involving propfan, rotating blade, and both rotating and static blade flows. O.C.

A93-24951*# National Aeronautics and Space Administration. Lewis Research Center, Cleveland, OH.

COMPUTING 3-D STEADY SUPERSONIC FLOW VIA A NEW LAGRANGIAN APPROACH

C. Y. LOH and M.-S. LIOU (NASA, Lewis Research Center, Cleveland, OH) Jan. 1993 12 p. AIAA, Aerospace Sciences Meeting and Exhibit, 31st, Reno, NV, Jan. 11-14, 1993 refs (AIAA PAPER 93-0891)

The new Lagrangian method introduced by Loh and Hui (1990) is extended for 3-D steady supersonic flow computation. Details of the conservation form, the implementation of the local Riemann solver, and the Godunov and the high resolution TVD schemes are presented. The new approach is robust yet accurate, capable of handling complicated geometry and reactions between discontinuous waves. It keeps all the advantages claimed in the 2-D method of Loh and Hui, e.g., crisp resolution for a slip surface (contact discontinuity) and automatic grid generation along the stream. Author

A93-24978# National Aeronautics and Space Administration. Lewis Research Center, Cleveland, OH.

EFFECT OF A ROTATING PROPELLER ON THE SEPARATION ANGLE OF ATTACK

D. R. BOLDMAN, C. IEK, D. P. HWANG (NASA, Lewis Research

Speed Centrifugal Compressor for two distinctly different stall patterns. Predictions made for the effect of a controlled inlet vorticity wave on the stability of the compressor show that for minimum control wave magnitudes, on the order of the total inlet disturbance magnitude, significant damping of the instability can be achieved. For control waves of sufficient amplitude, the control phase angle appears to be the most important factor in maintaining a stable condition in the compressor. Author

A93-22601*# National Aeronautics and Space Administration. Lewis Research Center, Cleveland, OH.

CFD ZONAL MODELING OF LEADING-EDGE ICE EFFECTS FOR A COMPLETE AIRCRAFT

J. M. SUMMA, D. J. STRASH, and D. A. LEDNICER (Analytical Methods, Inc., Redmond, WA) Jan. 1993 8 p. AIAA, Aerospace Sciences Meeting and Exhibit, 31st, Reno, NV, Jan. 11-14, 1993 refs

(Contract NAS3-26310)

(AIAA PAPER 93-0167) Copyright

A simplified, uncoupled zonal procedure was utilized to assess the capability of numerically simulating icing effects on a Boeing 727-200 aircraft. The computational approach combines potential flow, plus boundary layer simulations by VSAERO for the un-iced aircraft forces and moments, with Navier-Stokes simulations by ARC3D for the incremental forces and moments due to iced components. These are compared with wind tunnel longitudinal force and moment data. Although the computational results compared favorably with the test data in the linear angle of attack range, it is clear that for general aircraft icing calculations, a multiblock Navier-Stokes code will be required for the viscous component of this zonal method. Author

A93-22694*# National Aeronautics and Space Administration. Lewis Research Center, Cleveland, OH.

A PARAMETRIC STUDY OF BLEED IN SHOCK BOUNDARY LAYER INTERACTIONS

A. HAMED, S. H. SHIH, and J. J. YEUN (Cincinnati Univ., OH) Jan. 1993 10 p. AIAA, Aerospace Sciences Meeting and Exhibit, 31st, Reno, NV, Jan. 11-14, 1993 refs

(Contract AF-AFOSR-91-0101; NAG3-1213)

(AIAA PAPER 93-0294) Copyright

A numerical investigation was conducted to study the effect of bleed configuration on oblique-shock wave/turbulent boundary-layer interactions. Bleed is applied through a normal slot across the shock impingement location. The numerical solution to the compressible Navier-Stokes equations is obtained for the turbulent flow throughout the interaction zone and inside the bleed slot for bleed mass flow rates up to 57 percent of the boundary layer mass flow upstream of the interaction. The results indicate that the bleed slot performance improves as the slot width decreases and the length to width ratio increases. This is reflected as an increase in the bleed discharge coefficient and total pressure, and a reduction in the boundary layer momentum and displacement thickness downstream. Author

A93-23001*# National Aeronautics and Space Administration. Lewis Research Center, Cleveland, OH.

LDV FLOWFIELD MEASUREMENTS ON A STRAIGHT AND SWEEPED WING WITH A SIMULATED ICE ACCRETION

M. B. BRAGG, M. F. KERHO, and A. KHODADOUST (Illinois Univ., Urbana) Jan. 1993 20 p. AIAA, Aerospace Sciences Meeting and Exhibit, 31st, Reno, NV, Jan. 11-14, 1993 refs

(Contract NAG3-1134)

(AIAA PAPER 93-0300) Copyright

Simulated glaze ice accretion effects on a flowfield are presently studied for the case of a 3D semispan wing with NACA 0012 airfoil section on a rectangular untwisted planform. The model was tested at both zero-sweep and 30-deg sweep setting with four-beam/two-color LDV flowfield mapping. The comparison of LDV-measured velocity profiles with 3D Navier-Stokes predictions revealed correct trends, but with several differences that are attributable to the turbulence models and grid resolution used in the computations. O.C.

A93-23240# National Aeronautics and Space Administration. Lewis Research Center, Cleveland, OH.

SURFACE ROUGHNESS DUE TO RESIDUAL ICE IN THE USE OF LOW POWER DEICING SYSTEMS

JAIWON SHIN and THOMAS H. BOND (NASA, Lewis Research Center, Cleveland, OH) Jan. 1993 15 p. AIAA, Aerospace Sciences Meeting and Exhibit, 31st, Reno, NV, Jan. 11-14, 1993 Previously announced in STAR as N93-15338 refs

(Contract RTOP 505-68-10)

(AIAA PAPER 93-0031) Copyright

Thicknesses of residual ice are presented to provide information on surface contamination and associated roughness during deicing events. Data was obtained from low power ice protection systems tests conducted in the Icing Research Tunnel at NASA Lewis Research Center (LeRC) with nine different deicing systems. Results show that roughness associated with residual ice is not characterized by uniformly distributed roughness. Results also show that deicing systems require a critical mass of ice to generate a sufficient expelling force to remove the ice. Author

A93-23247*# National Aeronautics and Space Administration. Lewis Research Center, Cleveland, OH.

AN OVERVIEW OF SHED ICE IMPACT STUDIES IN THE NASA LEWIS ICING RESEARCH TUNNEL

RANDALL K. BRITTON (Sverdrup Technology, Inc., Brook Park, OH) and THOMAS H. BOND (NASA, Lewis Research Center, Cleveland, OH) Jan. 1993 13 p. AIAA, Aerospace Sciences Meeting and Exhibit, 31st, Reno, NV, Jan. 11-14, 1993 Previously announced in STAR as N93-15404 refs

(AIAA PAPER 93-0301) Copyright

One of the areas of active research in commercial and military rotorcraft is directed toward developing the capability of sustained flight in icing conditions. The emphasis to date has been on the accretion and subsequent shedding of ice in an icing environment, where the shedding may be natural or induced. Historically, shed-ice particles have been a problem for aircraft, particularly rotorcraft. Because of the high particle velocities involved, damage to a fuselage or other airframe component from a shed-ice impact can be significant. Design rules for damage tolerance from shed-ice impact are not well developed because of a lack of experimental data. Thus, NASA Lewis (LeRC) has begun an effort to develop a database of impact force and energy resulting from shed ice. This effort consisted of a test of NASA LeRC's Model Rotor Test Rig (MRTR) in the Icing Research Tunnel (IRT). Both natural shedding and forced shedding were investigated. Forced shedding was achieved by fitting the rotor blades with Small Tube Pneumatic (STP) deicer boots manufactured by BF Goodrich. A detailed description of the test is given as well as the design of a new impact sensor which measures the force-time history of an impacting ice fragment. A brief discussion of the procedure to infer impact energy from a force-time trace are required for the impact-energy calculations. Recommendations and future plans for this research area are also provided. Author

A93-23351# National Aeronautics and Space Administration. Lewis Research Center, Cleveland, OH.

ESTIMATION OF UNSTEADY LIFT ON A PITCHING AIRFOIL FROM WAKE VELOCITY SURVEYS

K. B. M. Q. ZAMAN, J. PANDA (NASA, Lewis Research Center, Cleveland, OH), and C. L. RUMSEY (NASA, Langley Research Center, Hampton, VA) Jan. 1993 15 p. AIAA, Aerospace Sciences Meeting and Exhibit, 31st, Reno, NV, Jan. 11-14, 1993

Previously announced in STAR as N93-14791 refs

(Contract RTOP 505-52-62)

(AIAA PAPER 93-0437) Copyright

The results of a joint experimental and computational study on the flowfield over a periodically pitched NACA0012 airfoil, and the resultant lift variation, are reported in this paper. The lift variation over a cycle of oscillation, and hence the lift hysteresis loop, is estimated from the velocity distribution in the wake measured or computed for successive phases of the cycle. Experimentally, the estimated lift hysteresis loops are compared with available data from the literature as well as with limited force balance

Center, Cleveland, OH), M. LARKIN, and P. SCHWEIGER (Pratt & Whitney Group, East Hartford, CT) Jan. 1993 15 p. AIAA, Aerospace Sciences Meeting and Exhibit, 31st, Reno, NV, Jan. 11-14, 1993 Previously announced in STAR as N93-16625 refs

(Contract RTOP 505-03-10)

(AIAA PAPER 93-0017) Copyright

The present study represents an extension of an earlier wind tunnel experiment performed with the P&W 17-in. Advanced Ducted Propeller (ADP) Simulator operating at Mach 0.2. In order to study the effects of a rotating propeller on the inlet flow, data were obtained in the UTRC 10- by 15-Foot Large Subsonic Wind Tunnel with the same hardware and instrumentation, but with the propeller removed. These new tests were performed over a range of flow rates which duplicated flow rates in the powered simulator program. The flow through the inlet was provided by a remotely located vacuum source. A comparison of the results of this flow-through study with the previous data from the powered simulator indicated that in the conventional inlet the propeller produced an increase in the separation angle of attack between 4.0 deg at a specific flow of 22.4 lb/sec-sq ft to 2.7 deg at a higher specific flow of 33.8 lb/sec-sq ft. A similar effect on separation angle of attack was obtained by using stationary blockage rather than a propeller.

Author

A93-25553* National Aeronautics and Space Administration. Lewis Research Center, Cleveland, OH.

NONREFLECTING BOUNDARY CONDITIONS FOR LINEARIZED UNSTEADY AERODYNAMIC CALCULATIONS

KENNETH C. HALL, CHRISTOPHER B. LORENCE, and WILLIAM S. CLARK (Duke Univ., Durham, NC) Jan. 1993 16 p. AIAA, Aerospace Sciences Meeting and Exhibit, 31st, Reno, NV, Jan. 11-14, 1993 Research supported by NSF and GE Aircraft Engines refs

(Contract NAG3-1192)

(AIAA PAPER 93-0882) Copyright

The present method for the implementation of nonreflecting boundary conditions in 2D and 3D linearized unsteady flow computations is applied to cases of unsteady flows in turbomachine blade rows. The eigenmodes of a discrete representation of the governing equations are computed and used to construct nonreflecting boundary conditions. In 3D, a mixed numerical method is used; in 2D, the discrete representation of the governing equations is obtained from the discretized equations used by the flow solver itself. Wavenumbers and radial mode shapes are computed.

O.C.

A93-29318* National Aeronautics and Space Administration. Lewis Research Center, Cleveland, OH.

LINEARIZED EULER PREDICTIONS OF UNSTEADY AERODYNAMIC LOADS IN CASCADES

KENNETH C. HALL and WILLIAM S. CLARK (Duke Univ., Durham, NC) AIAA Journal (ISSN 0001-1452) vol. 31, no. 3 March 1993 p. 540-550. Previously cited in issue 18, p. 3062, Accession no. A91-44318 AIAA, SAE, ASME, and ASEE, Joint Propulsion Conference, 27th, Sacramento, CA, June 24-26, 1991, AIAA Paper 91-3378 refs

(Contract NAG3-1192)

Copyright

A93-31494* National Aeronautics and Space Administration. Lewis Research Center, Cleveland, OH.

SEMI-EMPIRICAL MODEL FOR PREDICTION OF UNSTEADY FORCES ON AN AIRFOIL WITH APPLICATION TO FLUTTER

A. J. MAHAJAN, K. R. V. KAZA (NASA, Lewis Research Center, Cleveland, OH), and E. H. DOWELL (Duke Univ., Durham, NC) Journal of Fluids and Structures (ISSN 0889-9746) vol. 7, no. 1 Jan. 1993 p. 87-103. Previously announced in STAR as N92-18760 refs

(Contract NAG3-724)

Copyright

A semi-empirical model is described for predicting unsteady aerodynamic forces on arbitrary airfoils under mildly stalled and

unstalled conditions. Aerodynamic forces are modeled using second order ordinary differential equations for lift and moment with airfoil motion as the input. This model is simultaneously integrated with structural dynamics equations to determine flutter characteristics for a two degrees-of-freedom system. Results for a number of cases are presented to demonstrate the suitability of this model to predict flutter. Comparison is made to the flutter characteristics determined by a Navier-Stokes solver and also the classical incompressible potential flow theory.

Author

A93-34483* National Aeronautics and Space Administration. Lewis Research Center, Cleveland, OH.

EFFICIENT HYBRID SCHEME FOR THE ANALYSIS OF COUNTER-ROTATING PROPELLERS

R. SRIVASTAVA (NASA, Lewis Research Center, Cleveland, OH) and LAKSHMI N. SANKAR (Georgia Inst. of Technology, Atlanta) Journal of Propulsion and Power (ISSN 0748-4658) vol. 9, no. 3 May-June 1993 p. 382-388. AIAA, Aerospace Sciences Meeting, 29th, Reno, NV, Jan. 7-10, 1991, AIAA Paper 91-0703. Previously cited in issue 06, p. 802, Accession no. A91-19422 refs

(Contract NAG3-730)

Copyright

A93-34488* National Aeronautics and Space Administration. Lewis Research Center, Cleveland, OH.

STUDY ON VORTEX GENERATOR FLOW CONTROL FOR THE MANAGEMENT OF INLET DISTORTION

BERNHARD H. ANDERSON (NASA, Lewis Research Center, Cleveland, OH) and JAMES GIBB (Defence Research Agency, Bedford, United Kingdom) Journal of Propulsion and Power (ISSN 0748-4658) vol. 9, no. 3 May-June 1993 p. 422-430. AIAA, SAE, ASME, and ASEE, Joint Propulsion Conference and Exhibit, 28th, Nashville, TN, July 6-8, 1992, AIAA Paper 92-3177. Previously cited in issue 23, p. 4052, Accession no. A92-54013 refs

Copyright

A93-34490* National Aeronautics and Space Administration. Lewis Research Center, Cleveland, OH.

COMPUTATIONAL STUDY OF ADVANCED EXHAUST SYSTEM TRANSITION DUCTS WITH EXPERIMENTAL VALIDATION

C. WU, S. FAROKHI, and R. TAGHAVI (Kansas Univ., Lawrence) Journal of Propulsion and Power (ISSN 0748-4658) vol. 9, no. 3 May-June 1993 p. 437-442. AIAA, SAE, ASME, and ASEE, Joint Propulsion Conference and Exhibit, 28th, Nashville, TN, July 6-8, 1992, AIAA Paper 92-3794. Previously cited in issue 20, p. 3554, Accession no. A92-49126 Research supported by GE Aircraft Engines refs

(Contract NAG3-841)

Copyright

A93-37374* National Aeronautics and Space Administration. Lewis Research Center, Cleveland, OH.

PNS PREDICTIONS FOR SUPERSONIC/HYPERSONIC FLOWS OVER FINNED MISSILE CONFIGURATIONS

BILAL A. BHUTTA and CLARK H. LEWIS (VRA, Inc., Blacksburg, VA) Jun. 1992 16 p. AIAA, Applied Aerodynamics Conference, 10th, Palo Alto, CA, June 22-24, 1992 refs

(Contract NAS3-25450)

(AIAA PAPER 92-2695) Copyright

Finned missile design entails accurate and computationally fast numerical techniques for predicting viscous flows over complex lifting configurations at small to moderate angles of attack and over Mach 3 to 15; these flows are often characterized by strong embedded shocks, so that numerical algorithms are also required to capture embedded shocks. The recent real-gas Flux Vector Splitting technique is here extended to investigate the Mach 3 flow over a typical finned missile configuration with/without side fin deflections. Elliptic grid-generation techniques for Mach 15 flows are shown to be inadequate for Mach 3 flows over finned configurations and need to be modified. Fin-deflection studies indicate that even small amounts of missile fin deflection can substantially modify vehicle aerodynamics. This 3D parabolized

02 AERODYNAMICS

Navier-Stokes scheme is also extended into an efficient embedded algorithm for studying small axially separated flow regions due to strong fin and control surface deflections. Author (revised)

A93-38695* National Aeronautics and Space Administration. Lewis Research Center, Cleveland, OH.

CHARACTERISTICS OF THREE-DIMENSIONAL TURBULENT JETS IN CROSSFLOW

A. O. DEMUREN (NASA, Lewis Research Center, Cleveland, OH) International Journal of Engineering Science (ISSN 0020-7225) vol. 31, no. 6 June 1993 p. 899-913. Previously announced in STAR as N91-22536 refs
(Contract NASA ORDER C-99066-G)
Copyright

Three-dimensional turbulent jets in crossflow at low to medium jet-to-crossflow velocity ratios are computed with a finite volume numerical procedure which utilizes a second-moment closure model to approximate the Reynolds stresses. A multigrid method is used to accelerate the convergence rate of the procedure. Comparison of the computations to measured data show good qualitative agreement. All trends are correctly predicted, though there is some uncertainty on the height of penetration of the jet. The evolution of the vorticity field is used to explore the jet-crossflow interaction. Author

A93-39409* National Aeronautics and Space Administration. Lewis Research Center, Cleveland, OH.

FLIP-FLOP JET NOZZLE EXTENDED TO SUPERSONIC FLOWS

GANESH RAMAN (Sverdrup Technology, Inc., Brook Park, OH), MICHAEL HAILYE (Michigan Univ., Ann Arbor), and EDWARD J. RICE (NASA, Lewis Research Center, Cleveland, OH) AIAA Journal (ISSN 0001-1452) vol. 31, no. 6 June 1993 p. 1028-1035. AIAA Applied Aerodynamics Conference, 10th, Palo Alto, CA, June 22-24, 1992, Technical Papers. Pt. 2, p. 928-951. Previously cited in issue 19, p. 3252, Accession no. A92-45561 refs
Copyright

A93-39412 National Aeronautics and Space Administration. Ames Research Center, Moffett Field, CA.

UNSTEADY TRANSONIC TWO-DIMENSIONAL EULER SOLUTIONS USING FINITE ELEMENTS

GARY A. DAVIS and ODDVAR O. BENDIKSEN (California Univ., Los Angeles) AIAA Journal (ISSN 0001-1452) vol. 31, no. 6 June 1993 p. 1051-1059. AIAA/ASME/ASCE/AHS/ASC Structures, Structural Dynamics and Materials Conference, 33rd, Dallas, TX, Apr. 13-15, 1992, Technical Papers. Pt. 4, p. 2203-2213. Previously cited in issue 13, p. 2089, Accession no. A92-34499 refs
(Contract NCC2-374; NAS3-26064)
Copyright

A93-42579* National Aeronautics and Space Administration. Lewis Research Center, Cleveland, OH.

HYPERSONIC STABILITY AND TRANSITION

ELI RESHOTKO (Case Western Reserve Univ., Cleveland, OH) In Hypersonic flows for reentry problems. Vol. 1 Berlin and New York Springer-Verlag 1991 p. 18-34. refs
(Contract NCC3-124)
Copyright

An evaluation is conducted of the development status of growing normal modes in the computation of flow fields over hypersonic vehicles, giving attention to the effects of surface cooling, pressure gradients, and suction on the growth rates of the normal modes. Also noted are the effects of bluntness on the stability properties of hypersonic vehicles, and the efficacy of the $e^{exp N}$ method of transition estimation at supersonic and hypersonic speeds. A survey is made of the precautions that must be taken to ensure the effectiveness of experimental and computational studies of hypersonic flow phenomena. AIAA

A93-42585* National Aeronautics and Space Administration. Lewis Research Center, Cleveland, OH.

CFD FOR HYPERSONIC PROPULSION

LOUIS A. POVINELLI (NASA, Lewis Research Center, Cleveland, OH) In Hypersonic flows for reentry problems. Vol. 1 Berlin and New York Springer-Verlag 1991 p. 170-186. Previously announced in STAR as N91-21447 refs
Copyright

An overview is given of research activity on the application of computational fluid dynamics (CFD) for hypersonic propulsion systems. After the initial consideration of the highly integrated nature of air-breathing hypersonic engines and airframe, attention is directed toward computations carried out for the components of the engine. A generic inlet configuration is considered in order to demonstrate the highly three dimensional viscous flow behavior occurring within rectangular inlets. Reacting flow computations for simple jet injection as well as for more complex combustion chambers are then discussed in order to show the capability of viscous finite rate chemical reaction computer simulations. Finally, the nozzle flow fields are demonstrated, showing the existence of complex shear layers and shock structure in the exhaust plume. The general issues associated with code validation as well as the specific issue associated with the use of CFD for design are discussed. A prognosis for the success of CFD in the design of future propulsion systems is offered. Author

A93-42889* National Aeronautics and Space Administration. Lewis Research Center, Cleveland, OH.

MULTIGRID CALCULATION OF THREE-DIMENSIONAL VISCOUS CASCADE FLOWS

A. ARNONE (Florence Univ., Italy), M.-S. LIOU, and L. A. POVINELLI (NASA, Lewis Research Center, Cleveland, OH) Journal of Propulsion and Power (ISSN 0748-4658) vol. 9, no. 4 July-Aug. 1993 p. 605-614. AIAA Applied Aerodynamics Conference, 9th, Baltimore, MD, Sept. 23-25, 1991, Technical Papers. Vol. 1, p. 297-311. Previously cited in issue 23, p. 4000, Accession no. A91-53754 refs
Copyright

A93-45000* National Aeronautics and Space Administration. Lewis Research Center, Cleveland, OH.

FIELD BY FIELD HYBRID UPWIND SPLITTING METHODS

FREDERIC COQUEL (ONERA, Chatillon, France) and MENG-SING LIOU (NASA, Lewis Research Center, Cleveland, OH) In AIAA Computational Fluid Dynamics Conference, 11th, Orlando, FL, July 6-9, 1993, Technical Papers. Pt. 1 Washington American Institute of Aeronautics and Astronautics 1993 p. 51-61. refs
(AIAA PAPER 93-3302) Copyright

A new and general approach to upwind splitting is presented. The design principle combines the robustness of flux vector splitting schemes in the capture of nonlinear waves and the accuracy of some flux difference splitting schemes in the resolution of linear waves. The new schemes are derived following a general hybridization technique performed directly at the basic level of the field by field decomposition involved in FDS methods. The scheme does not use a spatial switch to be tuned up according to the local smoothness of the approximate solution. AIAA

A93-45003* National Aeronautics and Space Administration. Lewis Research Center, Cleveland, OH.

AN EXTENDED LAGRANGIAN METHOD

MENG-SING LIOU (NASA, Lewis Research Center, Cleveland, OH) In AIAA Computational Fluid Dynamics Conference, 11th, Orlando, FL, July 6-9, 1993, Technical Papers. Pt. 1 Washington American Institute of Aeronautics and Astronautics 1993 p. 92-105. refs
(AIAA PAPER 93-3305)

A unique formulation of describing fluid motion is presented. The method, referred to as 'extended Lagrangian method', is interesting from both theoretical and numerical points of view. The formulation offers accuracy in numerical solution by avoiding numerical diffusion resulting from mixing of fluxes in the Eulerian description. Meanwhile, it also avoids the inaccuracy incurred due

to geometry and variable interpolations used by the previous Lagrangian methods. The present method is general and capable of treating subsonic flows as well as supersonic flows. The method proposed in this paper is robust and stable. It automatically adapts to flow features without resorting to clustering, thereby maintaining rather uniform grid spacing throughout and large time step. Moreover, the method is shown to resolve multidimensional discontinuities with a high level of accuracy, similar to that found in 1D problems. Author (revised)

A93-45014* # National Aeronautics and Space Administration. Lewis Research Center, Cleveland, OH.

TWO-DIMENSIONAL CFD MODELING OF WAVE ROTOR FLOW DYNAMICS

GERARD E. WELCH and RODRICK V. CHIMA (NASA, Lewis Research Center, Cleveland, OH) / In AIAA Computational Fluid Dynamics Conference, 11th, Orlando, FL, July 6-9, 1993, Technical Papers. Pt. 1 Washington American Institute of Aeronautics and Astronautics 1993 p. 234-247. refs (AIAA PAPER 93-3318) Copyright

A two-dimensional Navier-Stokes solver developed for detailed study of wave rotor flow dynamics is described. The CFD model is helping characterize important loss mechanisms within the wave rotor. The wave rotor stationary ports and the moving rotor passages are resolved on multiple computational grid blocks. The finite-volume form of the thin-layer Navier-Stokes equations with laminar viscosity are integrated in time using a four-stage Runge-Kutta scheme. The Roe approximate Riemann solution scheme or the computationally less expensive Advection Upstream Splitting Method (AUSM) flux-splitting scheme are used to effect upwind-differencing of the inviscid flux terms, using cell interface primitive variables set by MUSCL-type interpolation. The diffusion terms are central-differenced. The solver is validated using a steady shock/laminar boundary layer interaction problem and an unsteady, inviscid wave rotor passage gradual opening problem. A model inlet port/passage charging problem is simulated and key features of the unsteady wave rotor flow field are identified. Lastly, the medium pressure inlet port and high pressure outlet port portion of the NASA Lewis Research Center experimental divider cycle is simulated and computed results are compared with experimental measurements. The model accurately predicts the wave timing within the rotor passage and the distribution of flow variables in the stationary inlet port region. Author

A93-45029* # National Aeronautics and Space Administration. Lewis Research Center, Cleveland, OH.

AN ACCURACY ASSESSMENT OF CARTESIAN-MESH APPROACHES FOR THE EULER EQUATIONS

WILLIAM J. COIRIER (NASA, Lewis Research Center, Cleveland, OH) and KENNETH G. POWELL (Michigan Univ., Ann Arbor) / In AIAA Computational Fluid Dynamics Conference, 11th, Orlando, FL, July 6-9, 1993, Technical Papers. Pt. 1 Washington American Institute of Aeronautics and Astronautics 1993 p. 423-437. refs

(AIAA PAPER 93-3335) Copyright

A critical assessment of the accuracy of Cartesian-mesh approaches for solving the Euler equations is made. An exact solution of the Euler equations (Ringleb's flow) is used not only to infer the order of error of the Cartesian mesh approaches, but also to compare the magnitude of the error directly to that obtained with a structured mesh approach. The effect of cell merging is investigated as well as the use of two different K-exact reconstruction procedures. The solution methodology of the schemes is explained and tabulated results are presented to compare the solution accuracies. Adaptive and uniform mesh refinement is evaluated for Ringleb's flow and the supersonic flow through an axisymmetric inlet. Author

A93-45146* National Aeronautics and Space Administration. Lewis Research Center, Cleveland, OH.

NAVIER-STOKES ANALYSIS OF THREE-DIMENSIONAL S-DUCTS

G. J. HARLOFF, C. F. SMITH, J. E. BRUNS, and J. R. DEBONIS

(Sverdrup Technology, Inc., Brook Park, OH) Journal of Aircraft (ISSN 0021-8669) vol. 30, no. 4 July-Aug. 1993 p. 526-533. refs

(Contract NAS3-25266)

Copyright

Full 3D Navier-Stokes computational results are presented for compressible flows within nondiffusing and diffusing S-ducts. The present study provides an understanding of the performance characteristics of typical S-ducts with attached and separated flows and provides a frame of reference for future computational fluid dynamic studies of internal flows with strong secondary flows. The predicted results, which were obtained using both H- and O-grids, are compared with the experimental wall pressures, static and total pressure fields, and velocity vectors. In addition, computed boundary-layer thickness, velocity profiles in wall coordinates and skin friction values are presented. The inviscid contributions to the secondary flows are quantified. The S-duct entrance Mach number was 0.6, and the Reynolds number was 1.76×10^6 based on the upstream duct diameter. Author (revised)

A93-46823* National Aeronautics and Space Administration. Lewis Research Center, Cleveland, OH.

COMPARATIVE WIND TUNNEL TESTS AT HIGH REYNOLDS NUMBERS OF NACA 64 621 AIRFOILS WITH TWO AILERON CONFIGURATIONS

G. M. GREGOREK (Ohio State Univ., Columbus) May 1984 14 p. Horizontal-Axis Wind Turbine Technology Workshop, Cleveland, OH, May 8-10, 1984, Paper (Contract NAG3-330)

An experimental program to measure the aerodynamic characteristics of the NACA 64-621 airfoil when equipped with plain ailerons of 0.38 chord and 0.30 chord and with 0.38 chord balanced aileron has been conducted in a pressurized 6 x 12-inch High Reynolds Number Wind Tunnel. Surface pressures were measured and integrated to yield lift and pressure drag coefficients for angles of attack from -3 deg to +42 deg, and for selected aileron deflections from 0 to -90 deg at nominal Mach and Reynolds numbers of 0.25 and 5×10^6 , respectively. When resolved into thrust coefficient for wind turbine aerodynamic control applications, the data indicated the anticipated decrease in thrust coefficient with negative aileron deflection at low angles of attack; however, as angle of attack increased, thrust coefficients eventually became positive. All aileron configurations, even at -90 deg deflections, showed this trend. Hinge moments for each configuration complete the data set. Author (revised)

A93-47189 National Aeronautics and Space Administration. Lewis Research Center, Cleveland, OH.

A NEW FLUX SPLITTING SCHEME

MENG-SING LIOU and CHRISTOPHER J. STEFFEN, JR. (NASA, Lewis Research Center, Cleveland, OH) Journal of Computational Physics (ISSN 0021-9991) vol. 107, no. 1 July 1993 p. 23-39. Previously announced in STAR as N91-22814 refs (Contract RTOP 505-61-52)

Copyright

A new flux splitting scheme is proposed. The scheme is remarkably simple and yet its accuracy rivals and in some cases surpasses that of Roe's solver in the Euler and Navier-Stokes solutions performed in this study. The scheme is robust and converges as fast as the Roe splitting. An approximately defined cell-face advection Mach number is proposed using values from the two straddling cells via associated characteristic speeds. This interface Mach number is then used to determine the upwind extrapolation for the convective quantities. Accordingly, the name of the scheme is coined as Advection Upstream Splitting Method (AUSM). A new pressure splitting is introduced which is shown to behave successfully, yielding much smoother results than other existing pressure splittings. Of particular interest is the supersonic blunt body problem in which the Roe scheme gives anomalous solutions. The AUSM produces correct solutions without difficulty for a wide range of flow conditions as well as grids.

A93-47202*# National Aeronautics and Space Administration. Lewis Research Center, Cleveland, OH.

ADAPTIVE COMPUTATIONS OF FLOW AROUND A DELTA WING WITH VORTEX BREAKDOWN

DAVID L. MODIANO (MIT, Cambridge, MA; NASA, Lewis Research Center, Cleveland, OH) and EARLL M. MURMAN (MIT, Cambridge, MA) *In* AIAA Applied Aerodynamics Conference, 11th, Monterey, CA, Aug. 9-11, 1993, Technical Papers. Pt. 1 Washington American Institute of Aeronautics and Astronautics 1993 p. 1-9. Research supported by McDonnell Aircraft Co. refs (Contract AF-AFOSR-89-0395A) (AIAA PAPER 93-3400) Copyright

An adaptive unstructured mesh solution method for the three-dimensional Euler equations was used to simulate the flow around a sharp edged delta wing. Emphasis was on the breakdown of the leading edge vortex at high angle of attack. Large values of entropy, which indicate vortical regions of the flow, specified the region in which adaptation was performed. The aerodynamic normal force coefficients show excellent agreement with wind tunnel data measured by Jarrah, and demonstrate the importance of adaptation in obtaining an accurate solution. The pitching moment coefficient and the location of vortex breakdown are compared with experimental data measured by Hummel and Srinivasan, showing good agreement in cases in which vortex breakdown is located over the wing.

A93-47213*# National Aeronautics and Space Administration. Lewis Research Center, Cleveland, OH.

AN IMPROVED FAR FIELD DRAG CALCULATION METHOD FOR NONLINEAR CFD CODES

JAMES R. SIRBAUGH (Sverdrup Technology, Inc., Brook Park, OH) *In* AIAA Applied Aerodynamics Conference, 11th, Monterey, CA, Aug. 9-11, 1993, Technical Papers. Pt. 1 Washington American Institute of Aeronautics and Astronautics 1993 p. 154-161. refs (Contract NAS3-25266) (AIAA PAPER 93-3417)

An improved method to calculate drag based on far field conditions is presented and demonstrated. The method is illustrated using two CFD codes, PARC and CFL3D, and examining their ability to preserve lift and drag coefficients along grid line defined integration paths. The flow fields were generated by solving the Euler equations for a NACA 0012 airfoil at a free stream Mach number of 0.8 and angle of attack of 1.25 degrees. In comparison to force coefficients obtained by surface pressure integration, neither code acceptably preserved both force coefficients throughout the near and far fields. An investigation into the relationship between numerical prediction error and calculated force coefficients revealed a direct connection between solution mass conservation error and force coefficients error. A method to correct the predicted force coefficients based on integrated mass conservation error is described and demonstrated. The corrected force coefficients for both codes are shown to be more accurate than the uncorrected values. The correction method is applicable to both two and three dimensions and is independent of the algorithm used to generate the flow field.

A93-48128*# National Aeronautics and Space Administration. Lewis Research Center, Cleveland, OH.

A NUMERICAL INVESTIGATION OF SUPERSONIC STRUT/ENDWALL INTERACTIONS IN ANNULAR FLOW WITH VARYING STRUT THICKNESS

K. E. WILLIAMS (Washington Univ., Seattle), G. J. HARLOFF (Sverdrup Technology, Inc., Brook Park, OH), and F. B. GESSNER (Washington Univ., Seattle) Jul. 1993 12 p. AIAA, Fluid Dynamics Conference, 24th, Orlando, FL, July 6-9, 1993 refs (Contract NAG3-376; NAS3-25266) (AIAA PAPER 93-2927) Copyright

A full 3D Navier-Stokes numerical investigation has been conducted of the shock-wave/boundary-layer flow interactions caused by four diamond-shaped struts, of varying thickness, in an annular duct with Mach 3 core flow and turbulent boundary-layers on both walls. Secondary flows caused by weak-to-strong

interactions are examined in the vicinity of a strut which is bounded by curved endwalls. The duct endwall boundary-layer separated for the strongest interaction. The struts studied had maximum thickness-to-chord ratios of 0.125, 0.188, 0.250, and 0.500. The duct gap height is 0.7 strut chords, the duct inner-to-outer wall radius ratio is 0.7, and the Reynolds number is 3×10^5 based on the strut chord length which was held constant for all interactions considered. The effects of strut thickness on the secondary flows are discussed, including: trajectories for the leading and trailing edge horseshoe vortices, strut/endwall corner vortices, and boundary-layer separation. The line of coalescence discussed in the literature, previously ascribed to boundary-layer separation, is shown to be caused by the leading edge horseshoe vortex convecting along the shock front. Author (revised)

A93-48158*# National Aeronautics and Space Administration. Lewis Research Center, Cleveland, OH.

SOME PRACTICAL TURBULENCE MODELING OPTIONS FOR REYNOLDS-AVERAGED FULL NAVIER-STOKES CALCULATIONS OF THREE-DIMENSIONAL FLOWS

TRONG T. BUI (NASA, Lewis Research Center, Cleveland, OH) Jul. 1993 37 p. AIAA, Fluid Dynamics Conference, 24th, Orlando, FL, July 6-9, 1993 refs (AIAA PAPER 93-2964) Copyright

New turbulence modeling options recently implemented for the 3D version of Proteus, a Reynolds-averaged compressible Navier-Stokes code, are described. The implemented turbulence models include: the Baldwin-Lomax algebraic model, the Baldwin-Barth one-equation model, the Chien k-epsilon model, and the Launder-Sharma k-epsilon model. Features of this turbulence modeling package include: well documented and easy to use turbulence modeling options, uniform integration of turbulence models from different classes, automatic initialization of turbulence variables for calculations using one- or two-equation turbulence models, multiple solid boundaries treatment, and fully vectorized L-U solver for one- and two-equation models. Good agreements are obtained between the computational results and experimental data. Sensitivity of the compressible turbulent solutions with the method of y^+ computation, the turbulent length scale correction, and some compressibility corrections are examined in detail. Test cases show that the highly optimized one- and two-equation turbulence models can be used in routine 3D Navier-Stokes computations with no significant increase in CPU time as compared with the Baldwin-Lomax algebraic model. Author (revised)

A93-48181*# National Aeronautics and Space Administration. Lewis Research Center, Cleveland, OH.

A LAG MODEL FOR TURBULENT BOUNDARY LAYERS DEVELOPING OVER ROUGH BLEED SURFACES

J. LEE, M. L. SLOAN, and G. C. PAYNTER (Boeing Commercial Airplane Group, Seattle, WA) Jul. 1993 10 p. AIAA, Fluid Dynamics Conference, 24th, Orlando, FL, July 6-9, 1993 refs (Contract NAS3-25963) (AIAA PAPER 93-2988) Copyright

Boundary layer mass removal (bleed) through spanwise bands of holes on a surface is used to prevent or control separation and to stabilize the normal shock in supersonic inlets. The addition of a transport equation lag relationship for eddy viscosity to the rough wall algebraic turbulence model of Cebeci and Chang was found to improve agreement between predicted and measured mean velocity distributions downstream of a bleed band. The model was demonstrated for a range of bleed configurations, bleed rates, and local free stream Mach numbers. In addition, the model was applied to the boundary layer development over acoustic lining materials for the inlets and nozzles of commercial aircraft. The model was found to yield accurate results for integral boundary layer properties unless there was a strong adverse pressure gradient.

A93-48184*# National Aeronautics and Space Administration. Lewis Research Center, Cleveland, OH.

AN INVESTIGATION OF SHOCK WAVE TURBULENT BOUNDARY LAYER INTERACTION WITH BLEED THROUGH SLANTED SLOTS

A. HAMED, J. J. YEUN, and S. H. SHIH (Cincinnati Univ., OH) Jul. 1993 10 p. AIAA, Fluid Dynamics Conference, 24th, Orlando, FL, July 6-9, 1993 Research supported by NASA refs (AIAA PAPER 93-2992) Copyright

Flow-field characteristics are simulated numerically in an oblique shock wave/turbulent boundary layer interactions with six different bleed slot configurations. The strong conservation-law form of the 2D compressible Navier-Stokes equations and the k-epsilon equations are solved throughout the interaction region and inside the bleed slot. The computed results are presented for a normal and 20-deg slanted bleed slots at three different locations, upstream, across and downstream of the impingement point of an oblique shock of sufficient strength to cause boundary layer separation without bleed. The detailed flow characteristics in the interaction zone and inside the bleed slot are compared for the different bleed slot configurations. The resulting surface pressure and shear stress distributions as well as the boundary layer characteristics downstream of the interaction region are also presented for the mix bleed configurations at different bleed mass flows up to choking. Author (revised)

A93-48239*# National Aeronautics and Space Administration. Lewis Research Center, Cleveland, OH.

A THREE-DIMENSIONAL PRESSURE FLUX-SPLIT RNS APPLICATION TO SUB/SUPERSONIC FLOW IN INLETS AND DUCTS

P. K. KHOSLA, H. S. PORDAL, and S. G. RUBIN (Cincinnati Univ., OH) Jul. 1993 11 p. AIAA, Fluid Dynamics Conference, 24th, Orlando, FL, July 6-9, 1993 refs (Contract NAG3-1178) (AIAA PAPER 93-3063) Copyright

The reduced Navier-Stokes (RNS) formulation is combined with a pressure based flux split procedure for the computational analysis of three dimensional flow. Only lowest order diffusion, that is required to satisfy the no-slip boundary condition is retained in this approximation. The governing equations are appropriately differenced such that the physical boundary conditions are closely coupled and combined to form a closed discrete system. No numerical or characteristic type boundary conditions are required. A global pressure relaxation procedure, i.e. multi-sweep PNS, is considered. A sparse matrix direct solver is applied to the crossplane solution. At the outflow boundary only the pressure or pressure gradient is prescribed. The resulting formulation has been applied to the solution of three-dimensional subsonic/supersonic internal flows in inlets and ducts.

A93-48241*# National Aeronautics and Space Administration. Lewis Research Center, Cleveland, OH.

AVERAGING TECHNIQUES FOR STEADY AND UNSTEADY CALCULATIONS OF A TRANSONIC FAN STAGE

M. L. WYSS (Cincinnati Univ., OH), R. V. CHIMA, and D. L. TWEEDT (NASA, Lewis Research Center, Cleveland, OH) Jul. 1993 11 p. AIAA, Fluid Dynamics Conference, 24th, Orlando, FL, July 6-9, 1993 refs (AIAA PAPER 93-3065) Copyright

It is often desirable to characterize a turbomachinery flow field with a few lumped parameters such as total pressure ratio or stage efficiency. Various averaging schemes may be used to compute these parameters. Here three averaging schemes, the momentum, energy, and area averaging schemes, are described and compared for two computed solutions of the midspan section of a transonic fan stage: a steady averaging-plane solution in which average rotor outflow conditions were used as stator inflow conditions and an unsteady rotor-stator interaction solution. The unsteady solution is described, some unsteady flow phenomena are discussed and the steady pressure distributions are compared. Despite large unsteady pressure fluctuations on the stator surface, the steady pressure distribution matched the average unsteady

distribution almost exactly. Stator wake profiles, stator loss coefficient, and stage efficiency were computed for the two solutions with the three averaging schemes and are compared. In general the energy averaging scheme gave good agreement between the averaging-plane solution and the time-averaged unsteady solution, even though certain phenomena due to unsteady wake migration were neglected. Author (revised)

A93-48291*# National Aeronautics and Space Administration. Lewis Research Center, Cleveland, OH.

EXPERIMENTAL AND NUMERICAL INVESTIGATION OF SUPERSONIC TURBULENT FLOW IN AN ANNULAR DUCT

K. E. WILLIAMS, F. B. GESSNER (Washington Univ., Seattle), and G. J. HARLOFF (Sverdrup Technology, Inc., Brook Park, OH) Jul. 1993 8 p. AIAA, Fluid Dynamics Conference, 24th, Orlando, FL, July 6-9, 1993 refs (Contract NAG3-376; NAS3-25266) (AIAA PAPER 93-3123) Copyright

Experimental and numerical results are presented for developing supersonic turbulent flow in an annular duct formed by a circular centerbody and outer shroud. The experimental results are based on data taken in a new flow facility that was designed to generate a shock-free, supersonic annular flow. Numerical computations were performed using the Baldwin-Lomax turbulence model for comparison with experimentally measured profiles. The results demonstrate that computed and measured profiles are in excellent agreement, so that studies can now be conducted of shock wave/boundary layer interaction phenomena within the duct, such as those induced by changes in downstream duct geometry or by the placement of struts between the duct walls.

A93-48293*# National Aeronautics and Space Administration. Lewis Research Center, Cleveland, OH.

NUMERICAL SIMULATION OF A SHOCK WAVE/TURBULENT BOUNDARY LAYER INTERACTION IN A DUCT

WEI-LI YANG and ISAAC GREBER (Case Western Reserve Univ., Cleveland, OH) Jul. 1993 11 p. AIAA, Fluid Dynamics Conference, 24th, Orlando, FL, July 6-9, 1993 refs (Contract NAG3-725) (AIAA PAPER 93-3127) Copyright

A numerical investigation of the interaction of an incident oblique shock wave with a turbulent duct flow is presented. The investigation consists of solving the three-dimensional, unsteady, compressible, mass averaged Navier-Stokes equations, using an implicit finite volume, lower-upper time marching code and incorporates the three-dimensional Baldwin-Lomax turbulence model. Computed results are obtained Mach number 2.9 for a turning angle of 13 degrees and Reynolds number based on duct width of 1.36×10^7 . Under various inlet conditions, the results clearly depict the flow characteristics, including the shock geometry, the separated flow region, the wall pressure distribution, and the skin friction distribution. The findings provide a physical understanding of the three-dimensional vortex structure of the flow in a duct in which a shock wave interacts with a turbulent boundary layer. The results show that the ratio of the boundary layer thickness to the duct width is the critical parameter in determining the separation structure. Author (revised)

A93-48298*# National Aeronautics and Space Administration. Lewis Research Center, Cleveland, OH.

FLOWFIELD DYNAMICS IN BLUNT FIN-INDUCED SHOCK WAVE/TURBULENT BOUNDARY LAYER INTERACTIONS

L. BRUSNIAK and D. S. DOLLING (Texas Univ., Austin) Jul. 1993 30 p. AIAA, Fluid Dynamics Conference, 24th, Orlando, FL, July 6-9, 1993 refs (Contract NAG3-1023) (AIAA PAPER 93-3133) Copyright

Fluctuating wall pressure measurements were made on centerline upstream of a blunt fin in a Mach 5 turbulent boundary layer. By examining the ensemble average wall pressure distributions for different fixed shock foot positions, it was shown that local fluctuating wall pressure measurements are due to a distinct pressure distribution, $P(i)$, which undergoes a stretching

and flattening effect as its upstream boundary translates aperiodically between the upstream influence and separation lines. The locations of the maxima and minima in the centerline wall standard deviation distribution can be accurately predicted using this distribution, providing quantitative confirmation of the model. This model also explains the observed cross-correlations and ensemble average measurements within the interaction. Using the P(i) model, wall pressure signals from under the separated flow region were able to reproduce the position-time history of the separation shock foot. The negative time delay peak in the cross-correlation between the predicted and actual shock foot histories shows that the separated region fluctuations precede shock foot motion. Author (revised)

A93-49695* # National Aeronautics and Space Administration. Lewis Research Center, Cleveland, OH.
INSTALLED F/A-18 INLET FLOW CALCULATIONS AT 60 DEG ANGLE-OF-ATTACK AND 10 DEG SIDE SLIP
 S. D. PODLESKI (Sverdrup Technology, Inc., Brook Park, OH) Jun. 1993 21 p. AIAA, SAE, ASME, and ASEE, Joint Propulsion Conference and Exhibit, 29th, Monterey, CA, June 28-30, 1993 refs
 (Contract NAS3-25266)
 (AIAA PAPER 93-1806)

This paper presents the results of PARC3D numerical calculations on a 19.78 percent scale forebody/inlet model of the F/A-18 at a Mach number of 0.20, an angle-of-attack of 60 deg, and a side-slip angle of 10 deg. The main purpose of these calculations is to support an upcoming wind-tunnel test program in the prediction of engine inlet compressor face total pressure recovery and flow distortion. The GRIDGEN system was used to generate a grid which includes the inlet and lip, and other aircraft components which are considered to be important to inlet performance, such as the ramp/splitter plate, the diverter and slot, and the deflected leading edge flap. PARC3D shows complex flow patterns on the fuselage surfaces below the leading edge extensions, on the ramp/splitter plate, inlet lip, and inside the inlet. PARC3D tends to underpredict total pressure recovery and overpredict the flow distortion at the inlet compressor face. Author (revised)

A93-49720* # National Aeronautics and Space Administration. Lewis Research Center, Cleveland, OH.
CALCULATION OF SCRAMJET INLET WITH THICK BOUNDARY-LAYER INGESTION
 H. T. LAI, S. C. KIM (Sverdrup Technology, Inc., Brook Park, OH), and H. T. NAGAMATSU (Rensselaer Polytechnic Inst., Troy, NY) Jun. 1993 15 p. AIAA, SAE, ASME, and ASEE, Joint Propulsion Conference and Exhibit, 29th, Monterey, CA, June 28-30, 1993 refs
 (Contract NAS3-24105; NAS3-25266)
 (AIAA PAPER 93-1836)

Numerical flowfields around a scramjet inlet model are simulated and analyzed. The present inlet flowfield is characterized by thick boundary-layer ingestion and strong viscous/inviscid interaction because of a combined effect of high hypersonic freestream Mach and low Reynolds numbers. Shock-induced separation further enlarges regions of viscous flows which occupy most of the inlet flowfield. Results obtained from the computations with the PARC code developed for ideal gas are presented for several 2D cases at various hypersonic Mach numbers ranging from 10 to 25, and two 3D simulations at Mach numbers of 12 and 19 are also discussed. Comparison between computation and experiment is made in terms of pressure distributions at the wall center line. Large discrepancy is observed and may be partially attributed to the lack of real gas and/or 3D effects in the simulation as well as to the uncertainty of the experiment.

A93-49728* # National Aeronautics and Space Administration. Lewis Research Center, Cleveland, OH.
3-D VISCOUS FLOW CFD ANALYSIS OF THE PROPELLER EFFECT ON AN ADVANCED DUCTED PROPELLER SUBSONIC INLET

CHANTHY IEK, DONALD R. BOLDMAN (NASA, Lewis Research Center, Cleveland, OH), and MOUNIR IBRAHIM (Cleveland State Univ., OH) Jun. 1993 40 p. AIAA, SAE, ASME, and ASEE, Joint Propulsion Conference and Exhibit, 29th, Monterey, CA, June 28-30, 1993 Previously announced in STAR as N93-29162 refs
 (AIAA PAPER 93-1847) Copyright

The time-marching Navier-Stokes code PARC3D was used to study the 3D viscous flow associated with an advanced ducted propeller subsonic inlet at take-off operating conditions. At a free stream Mach number of 0.2, experimental data for the inlet-with-propeller test model indicated that the airflow was attached on the cowl windward lip at an angle of attack of 25 deg became unstable at 29 deg, and separated at 30 deg. An experimental study with a similar inlet and without propeller (through-flow) indicated that flow separation occurred at an angle of attack a few degrees below the value observed when the inlet was tested with the propeller, indicating the propeller's favorable effect on inlet performance. In the present numerical study, flow blockage analogous to the propeller was modeled via a PARC3D computational boundary condition (BC), the 'screen BC', based on 1-1/2 dimension actuator disk theory. The application of the screen BC in this numerical study provided results similar to those of past experimental efforts in which either the blockage device or the propeller was used. Author (revised)

A93-49743* # National Aeronautics and Space Administration. Lewis Research Center, Cleveland, OH.
UNSTEADY AERODYNAMIC FLOW PHENOMENA IN A TRANSONIC COMPRESSOR STAGE
 C. HAH (NASA, Lewis Research Center, Cleveland, OH), S. L. PUTERBAUGH, and W. W. COPENHAVER (USAF, Wright Lab., Wright-Patterson AFB, OH) Jun. 1993 12 p. AIAA, SAE, ASME, and ASEE, Joint Propulsion Conference and Exhibit, 29th, Monterey, CA, June 28-30, 1993 refs
 (AIAA PAPER 93-1868)

A three-dimensional unsteady, viscous aerodynamic analysis has been developed for the flow inside a transonic, high-through-flow, single stage compressor. The compressor stage is comprised of a low-aspect-ratio rotor and a closely coupled stator. The analysis is based on a numerical method for solving the three-dimensional Navier-Stokes equation for unsteady viscous flow through multiple turbomachinery blade rows. The method solves the fully three-dimensional Navier-Stokes equation with an implicit scheme. A two-equation turbulence model with a low-Reynolds-number modification is applied for the turbulence closure. A third-order accurate upwinding scheme is used to approximate convection terms while a second-order accurate central difference scheme is used for the discretization of the viscous terms. A second-order accurate scheme is employed for the temporal discretization. The numerical method is applied to study the unsteady flow field inside a transonic, high-through-flow, axial compressor stage. The numerical results are compared with available experimental data.

A93-49791* # National Aeronautics and Space Administration. Lewis Research Center, Cleveland, OH.
INVESTIGATION OF A STRUT-ENDWALL INTERACTION IN SUPERSONIC ANNULAR FLOW
 K. E. WILLIAMS (Washington Univ., Seattle), G. J. HARLOFF (Sverdrup Technology, Inc., NASA Lewis Research Center Group, Brook Park, OH), and F. B. GESSNER (Washington Univ., Seattle) Jun. 1993 15 p. AIAA, SAE, ASME, and ASEE, Joint Propulsion Conference and Exhibit, 29th, Monterey, CA, June 28-30, 1993 Research supported by NASA refs
 (Contract NAG3-376; NAS3-25266)
 (AIAA PAPER 93-1925) Copyright

A combined experimental and numerical investigation of strut/endwall interactions within an annular duct having a supersonic core flow has been conducted. Four diamond-shaped struts with a 7 deg half angle were positioned circumferentially equidistant within an annular duct having a gap height of 0.7 strut chords, and an inner-to-outer wall radius ratio of 0.7. Turbulent

boundary layers exist on both inner and outer walls of the duct, but have not merged. The core flow upstream of the struts is uniform at a nominal Mach number of 3.0 and a Reynolds number of 3×10^5 based on the strut chord length. Experimental results, which include Pitot pressure distributions within the flow field, static pressure distributions on the inner and outer walls of the duct, and oil flow visualization on the centerbody and strut, are presented and compared with CFD predictions. Secondary flows associated with the interactions are examined including the trajectories of the horseshoe vortices formed at the leading and trailing edges of the strut and the trajectories of the vortices formed in the corner of the strut/endwall intersection. Author (revised)

A93-49913* # National Aeronautics and Space Administration. Lewis Research Center, Cleveland, OH.

UNSTEADY AERODYNAMICS AND FLUTTER BASED ON THE POTENTIAL EQUATION

MILIND A. BAKHLE, THEO G. KEITH, JR. (Toledo Univ., OH), and MARC H. WILLIAMS (Purdue Univ., West Lafayette, IN) Jun. 1993 13 p. AIAA, SAE, ASME, and ASEE, Joint Propulsion Conference and Exhibit, 29th, Monterey, CA, June 28-30, 1993 refs

(Contract NAG3-1234)

(AIAA PAPER 93-2086) Copyright

A time-domain three-dimensional full-potential solver is coupled with a linear structural dynamics model to investigate the unsteady aerodynamics and aeroelasticity of propfans. The solver allows calculations in multiple blade passages with independent blade motions. Aeroelastic calculations are performed in both frequency and time domains. Results are presented for two propfan configurations. Good agreement is seen between the full-potential results and results from linear theory since the flow is subsonic and the thickness of the propfan blades is small; the agreement is not as good for the cases in which the angle of attack is high. Some difficulty is encountered due to wave reflections from outer computational boundaries; however, this does not affect the results in the range of frequencies of interest.

A93-49970* # National Aeronautics and Space Administration. Lewis Research Center, Cleveland, OH.

A COMPARATIVE STUDY OF FULL NAVIER-STOKES AND REDUCED NAVIER-STOKES ANALYSES FOR SEPARATING FLOWS WITHIN A DIFFUSING INLET S-DUCT

B. H. ANDERSON, D. R. REDDY, and K. KAPOOR (NASA, Lewis Research Center, Cleveland, OH) Jun. 1993 8 p. AIAA, SAE, ASME, and ASEE, Joint Propulsion Conference and Exhibit, 29th, Monterey, CA, June 28-30, 1993 refs

(AIAA PAPER 93-2154) Copyright

A three-dimensional implicit Full Navier-Stokes (FNS) analysis and a 3D Reduced Navier Stokes (RNS) initial value space marching solution technique has been applied to a class of separated flow problems within a diffusing S-duct configuration characterized by vortex-lift-off. Both the FNS and the RNS solution technique were able to capture the overall flow physics of vortex lift-off, and gave remarkably similar results which agreed reasonably well with the experimental measured averaged performance parameters of engine face total pressure recovery and distortion. However, the Full Navier-Stokes and Reduced Navier-Stokes also consistently predicted separation further downstream in the M2129 inlet S-duct than was indicated by experimental data, thus compensating errors were present in the two Navier-Stokes analyses. The difficulties encountered in the Navier-Stokes separations analyses of the M2129 inlet S-duct center primarily on turbulence model issues, and these focused on two distinct but different phenomena, namely, (1) characterization of low skin friction adverse pressure gradient flows, and (2) description of the near wall behavior of flows characterized by vortex lift-off.

A93-50039* # National Aeronautics and Space Administration. Lewis Research Center, Cleveland, OH.

A MODEL FOR THE SELECTIVE AMPLIFICATION OF SPATIALLY COHERENT WAVES IN A CENTRIFUGAL COMPRESSOR ON THE VERGE OF ROTATING STALL

PATRICK B. LAWLESS and SANFORD FLEETER (Purdue Univ., West Lafayette, IN) Jun. 1993 14 p. AIAA, SAE, ASME, and ASEE, Joint Propulsion Conference and Exhibit, 29th, Monterey, CA, June 28-30, 1993 Research supported by U.S. Army and NASA refs

(AIAA PAPER 93-2236) Copyright

A simple model for the stability zones of a low speed centrifugal compressor is developed, with the goal of understanding the driving mechanism for the changes in stalling behavior predicted for, and observed in, the Purdue Low Speed Centrifugal Research Compressor Facility. To this end, earlier analyses of rotating stall suppression in centrifugal compressors are presented in a reduced form that preserves the essential parameters of the model that affect the stalling behavior of the compressor. The model is then used to illuminate the relationship between compressor geometry, expected mode shape, and regions of amplification for weak waves which are indicative of the susceptibility of the system to rotating stall. The results demonstrate that increasing the stagger angle of the diffuser vanes, and consequently the diffusion path length, results in the compressor moving towards a condition where higher-order spatial modes are excited during stall initiation. Similarly, flow acceleration in the diffuser section caused by an increase in the number of diffuser vanes also results in the excitation of higher modes. Author (revised)

A93-50278* # National Aeronautics and Space Administration. Lewis Research Center, Cleveland, OH.

THREE-DIMENSIONAL FLOW FIELD IN A TURBINE NOZZLE PASSAGE

M. ZACCARIA, D. RISTIC, and B. LAKSHMINARAYANA (Pennsylvania State Univ., University Park) Jun. 1993 19 p. AIAA, SAE, ASME, and ASEE, Joint Propulsion Conference and Exhibit, 29th, Monterey, CA, June 28-30, 1993 refs

(Contract NSG-3555)

(AIAA PAPER 93-2556) Copyright

Detailed measurements were taken in the nozzle of a low speed single stage axial flow turbine at two axial planes inside the nozzle and on the nozzle and endwall surfaces. Velocity, turbulence and angle measurements were taken at midchord with an LDV while a five hole probe was used to measure the pressure, velocities and angles just upstream of the trailing edge. Nozzle surface and endwall static pressures were also measured. These measurements were compared to measurements previously completed at two axial planes downstream of the nozzle. The results show that at midchord, the secondary flow seems to be weak and it is in the early stages of development. Just upstream of the trailing edge, the secondary flow is clearly visible. The radially inward flow near the suction surface augments the casing passage vortex, while counteracting the hub passage vortex. Traveling downstream, the casing passage vortex remains strong while at the hub, the radially inward flow of the suction surface boundary layer has reversed direction due to the rotating hub. The blade static pressures and the passage averaged velocities compare well with Katsanis' quasi-three-dimensional code. These and other data are presented, interpreted and synthesized to understand the nozzle flow field.

A93-52006 National Aeronautics and Space Administration. Lewis Research Center, Cleveland, OH.

A TIME-ACCURATE HIGH-RESOLUTION TVD SCHEME FOR SOLVING THE NAVIER-STOKES EQUATIONS

HYUN D. KIM and NAN-SUEY LIU (NASA, Lewis Research Center, Cleveland, OH) Computers & Fluids (ISSN 0045-7930) vol. 22, no. 4-5 July-Sept. 1993 p. 517-528. Previously announced in STAR as N93-22664 refs

(Contract RTOP 505-62-52)

Copyright

A total variation diminishing (TVD) scheme has been developed and incorporated into an existing time-accurate high-resolution Navier-Stokes code. The accuracy and the robustness of the resulting solution procedure have been assessed by performing many calculations in four different areas: shock tube flows, regular

shock reflection, supersonic boundary layer, and shock boundary layer interactions. These numerical results compare well with corresponding exact solutions or experimental data.

A93-52436* National Aeronautics and Space Administration. Lewis Research Center, Cleveland, OH.

UNSTEADY WING SURFACE PRESSURES IN THE WAKE OF A PROPELLER

R. T. JOHNSTON and J. P. SULLIVAN (Purdue Univ., West Lafayette, IN) *Journal of Aircraft* (ISSN 0021-8669) vol. 30, no. 5 Sept.-Oct. 1993 p. 644-651. AIAA, Aerospace Sciences Meeting and Exhibit, 30th, Reno, NV, Jan. 6-9, 1992, AIAA Paper 92-0277. Previously cited in issue 09, p. 1348, Accession no. A92-25731 Research supported by NSERC and NASA refs Copyright

A93-53208* National Aeronautics and Space Administration. Lewis Research Center, Cleveland, OH.

LOW-REYNOLDS-NUMBER K-EPSILON MODEL FOR UNSTEADY TURBULENT BOUNDARY-LAYER FLOWS

SIXIN FAN, BUDUGUR LAKSHMINARAYANA (Pennsylvania State Univ., University Park), and MARK BARNETT (United Technologies Research Center, East Hartford, CT) *AIAA Journal* (ISSN 0001-1452) vol. 31, no. 10 Oct. 1993 p. 1777-1784. refs (Contract NAG3-1168) Copyright

An assessment of the near-wall and low-Reynolds-number functions used in low-Reynolds-number k-epsilon models suggests that they are not suitable for the near-wall region of unsteady turbulent boundary layers, where the flow is characterized by rapid changes in phase. An improved low-Reynolds-number k-epsilon model is developed in this paper. The near-wall and low-Reynolds-number functions in this model are formulated as functions of the local turbulent Reynolds numbers instead of the inner variable y^+ . The present model also has the correct asymptotic behavior in the near-wall region. The turbulence model has been incorporated in an unsteady boundary-layer code and validated for unsteady turbulent boundary layers with and without adverse pressure gradients. The predictions agree well with the experimental data and the theoretical analysis. For the cases tested, the present model correctly predicts the unsteady near-wall flow and the unsteady skin friction at various frequencies.

Author (revised)

A93-53591*# National Aeronautics and Space Administration. Lewis Research Center, Cleveland, OH.

LASER VELOCIMETER MEASUREMENTS OF THE FLOW FIELD GENERATED BY A FORWARD-SWEPT PROPPAN DURING FLUTTER

GARY G. PODBOY and MARTIN J. KRUPAR (NASA, Lewis Research Center, Cleveland, OH) Jul. 1993 50 p. AIAA, Fluid Dynamics Conference, 24th, Orlando, FL, July 6-9, 1993 refs (AIAA PAPER 93-2919) Copyright

Results are presented from an investigation to measure the flow field generated by a forward-swept propfan operating in flutter at a low forward velocity. For comparison to the flutter condition, flow field data are also presented for a slightly reduced rotational speed just below flutter. The forward-swept propfan was tested as the front rotor of a counterrotating pusher propeller. A laser Doppler velocimeter (LDV) was used to measure the velocity field in planes normal to the model centerline downstream of the rotor and in planes of constant radius within the blade passages at each operating condition. The mean time-averaged flow about the blades did not change drastically as the propfan rotational speed was increased from the stable operating point to the flutter condition. No regions of flow separation could be identified in the data plots of the mean intrablade flow field. The relative flow about the blades remained subsonic during flutter operation. The blades were found to have a higher than expected tip loading at both operating conditions. This is thought to have been caused by the outer blade sections twisting under load to higher than expected effective blade angles. This high tip loading resulted in

strong vortices and a very nonuniform flow downstream of the tips of the forward-swept blades. This high tip loading may also have caused the blade flutter.

Author (revised)

A93-53592*# National Aeronautics and Space Administration. Lewis Research Center, Cleveland, OH.

STREAMWISE VORTICITY GENERATION AND MIXING ENHANCEMENT IN FREE JETS BY 'DELTA-TABS'

K. B. M. Q. ZAMAN (NASA, Lewis Research Center, Cleveland, OH) Jul. 1993 14 p. AIAA, Shear Flow Conference, Orlando, FL, July 6-9, 1993 Previously announced in STAR as N93-31648 refs (AIAA PAPER 93-3253) Copyright

The effect of triangular tabs, placed at the nozzle exit, on the evolution of free jets is investigated. The effect, a large distortion of the jet cross section and a resultant increase in mixing downstream, has been inferred before to be due to a pair of streamwise vortices originating from each tab. In this paper, the generation mechanism of the streamwise vorticity ($\omega_{\text{sub } x}$) is considered first. Two sources are postulated. One is the upstream 'pressure hill', produced by the tab, which appears to be the dominant source. Another is due to vortex filaments shed from the sides of the tab and reoriented downstream by the mean shear of the mixing layer. In the case of a 'delta-tab', a triangular tab with its apex leaning downstream, vorticity from the two sources explain the stronger effect in that configuration. Data on the vorticity evolution for the effect of two delta-tabs are presented, up to twelve jet diameters from the exit, which show that the streamwise vortices persist even at the farthest measurement station. The magnitude of $\omega_{\text{sub } x}$ -maximum decays continually with distance from the nozzle, its ratio to azimuthal vorticity maximum is found to be about 1/5 everywhere. The relative effect of a delta-tab on jets from an axisymmetric nozzle and a 8:1 rectangular nozzle is also studied. The mixing layer distortion is found to be less pronounced in the rectangular case. The jet mixing, as manifested by the mass flux measured at a downstream station, is increased in the axisymmetric jet but it is decreased in the rectangular jet under consideration by the delta-tab.

A93-54062* National Aeronautics and Space Administration. Lewis Research Center, Cleveland, OH.

AERODYNAMIC INVERSE DESIGN AND ANALYSIS FOR A FULL ENGINE

JOSE M. SANZ (NASA, Lewis Research Center, Cleveland, OH) *In* ISABE - International Symposium on Air Breathing Engines, 11th, Tokyo, Japan, Sept. 20-24, 1993, Proceedings. Vol. 2 Washington American Institute of Aeronautics and Astronautics 1993 p. 895-902. (ISABE 93-7086) Copyright

A numerical design methodology for multistage turbomachinery is being developed that minimizes the use of experimental data required in the design process. This approach is resulting in an efficient method of enlarging the design database for turbomachinery blading. This capability has been demonstrated for blade sections, and the goal is to extend it to fully three dimensional, multistage configurations.

A93-54071* National Aeronautics and Space Administration. Lewis Research Center, Cleveland, OH.

THREE-DIMENSIONAL FLOW ANALYSIS INSIDE TURBOMACHINERY STAGES WITH STEADY AND UNSTEADY NAVIER-STOKES METHOD

W. W. COPENHAVER, S. L. PUTERBAUCH (USAF, Aeropropulsion Lab., Wright-Patterson AFB, OH), and C. HAH (NASA, Lewis Research Center, Cleveland, OH) *In* ISABE - International Symposium on Air Breathing Engines, 11th, Tokyo, Japan, Sept. 20-24, 1993, Proceedings. Vol. 2 Washington American Institute of Aeronautics and Astronautics 1993 p. 974-983. refs (ISABE 93-7095) Copyright

This study presents a numerical method for solving the three-dimensional, Navier-Stokes equations for unsteady, viscous flow through multiple turbomachinery blade rows. The method solves the fully three-dimensional Navier-Stokes equations with

an implicit scheme which is based on a control volume approach. A two-equation turbulence model with a low Reynolds number modification is employed in the present study. A third-order accurate upwinding scheme is used to approximate convection terms while a second order accurate central difference scheme is used for the discretization of viscous terms. A second-order accurate scheme is employed for the temporal discretization. The numerical method is applied to study the unsteady flow field of a subsonic turbine stage and the unsteady flow field inside a transonic, high-through-flow, axial compressor stage. The stage calculation is performed by coupling the stator and the rotor flow fields at each time step through an over-laid grid.

A93-54324* National Aeronautics and Space Administration. Lewis Research Center, Cleveland, OH.

MIXING OF MULTIPLE JETS WITH A CONFINED SUBSONIC CROSSFLOW

JAMES D. HOLDEMAN (NASA, Lewis Research Center, Cleveland, OH) Progress in Energy and Combustion Science (ISSN 0360-1285) vol. 19, no. 1 Feb. 1993 p. 31-70. refs
Copyright

An account is given of experimental and computational results on the mixing of single, double, and opposed rows of jets characterized by an either isothermal or variable temperature mainstream in a confined subsonic crossflow; these flow configurations are typical of gas turbine combustor dilution chambers. It is established that the momentum-flux ratio is the most significant flow variable. Combinations of flow and geometry yielding optimum mixing were identified from experimental and computational results. The orifice spacing and momentum-flux relationships affected jet structure, which was significantly different between jets injected from the inner wall of a turn and those injected from the outer wall. AIAA

A93-55351* National Aeronautics and Space Administration. Lewis Research Center, Cleveland, OH.

ANALYSIS OF HIGH REYNOLDS NUMBER INVISCID/VISCID INTERACTIONS IN CASCADES

M. BARNETT, J. M. VERDON, and T. C. AYER (United Technologies Research Center, East Hartford, CT) AIAA Journal (ISSN 0001-1452) vol. 31, no. 11 Nov. 1993 p. 1969-1976. AIAA, SAE, ASME, and ASEE, Joint Propulsion Conference and Exhibit, 28th, Nashville, TN, July 6-8, 1992, AIAA Paper 92-3073. Previously cited in issue 20, p. 3471, Accession no. A92-48723 refs
(Contract NAS3-25425)
Copyright

N93-11223* National Aeronautics and Space Administration. Lewis Research Center, Cleveland, OH.

THE ENGINE DESIGN ENGINE. A CLUSTERED COMPUTER PLATFORM FOR THE AERODYNAMIC INVERSE DESIGN AND ANALYSIS OF A FULL ENGINE

J. SANZ, K. PISCHEL, and D. HUBLER 1992 10 p Presented at the Grand Challenges, Washington, DC, 20-22 Sep. 1992, sponsored by NRL
(Contract RTOP 505-62-52)
(NASA-TM-105838; E-7278; NAS 1.15:105838) Avail: CASI HC A02/MF A01

An application for parallel computation on a combined cluster of powerful workstations and supercomputers was developed. A Parallel Virtual Machine (PVM) is used as message passage language on a macro-tasking parallelization of the Aerodynamic Inverse Design and Analysis for a Full Engine computer code. The heterogeneous nature of the cluster is perfectly handled by the controlling host machine. Communication is established via Ethernet with the TCP/IP protocol over an open network. A reasonable overhead is imposed for internode communication, rendering an efficient utilization of the engaged processors. Perhaps one of the most interesting features of the system is its versatile nature, that permits the usage of the computational resources available that are experiencing less use at a given point in time.

Author

N93-13292* National Aeronautics and Space Administration. Lewis Research Center, Cleveland, OH.

RADIAL TURBINE COOLING

RICHARD J. ROELKE Apr. 1992 42 p Presented at the Lecture Series on Radial Turbines at the von Karman Inst. for Fluid Dynamics, Brussels, Belgium, 6-10 Apr. 1992 Original contains color illustrations
(Contract RTOP 535-05-10)
(NASA-TM-105658; E-7022; NAS 1.15:105658) Avail: CASI HC A03/MF A01; 2 functional color pages

Radial turbines have been used extensively in many applications including small ground based electrical power generators, automotive engine turbochargers and aircraft auxiliary power units. In all of these applications the turbine inlet temperature is limited to a value commensurate with the material strength limitations and life requirements of uncooled metal rotors. To take advantage of all the benefits that higher temperatures offer, such as increased turbine specific power output or higher cycle thermal efficiency, requires improved high temperature materials and/or blade cooling. Extensive research is on-going to advance the material properties of high temperature superalloys as well as composite materials including ceramics. The use of ceramics with their high temperature potential and low cost is particularly appealing for radial turbines. However until these programs reach fruition the only way to make significant step increases beyond the present material temperature barriers is to cool the radial blading. Author

N93-14791* National Aeronautics and Space Administration. Lewis Research Center, Cleveland, OH.

ESTIMATION OF UNSTEADY LIFT ON A PITCHING AIRFOIL FROM WAKE VELOCITY SURVEYS

K. B. M. Q. ZAMAN, J. PANDA, and C. L. RUMSEY (National Aeronautics and Space Administration, Langley Research Center, Hampton, VA.) Jan. 1993 16 p Presented at the 31st Aerospace Sciences Meeting and Exhibit, Reno, NV, 11-14 Jan. 1993
(Contract RTOP 505-52-62)
(NASA-TM-105947; E-7465; NAS 1.15:105947) Avail: CASI HC A03/MF A01

The results of a joint experimental and computational study on the flowfield over a periodically pitched NACA0012 airfoil, and the resultant lift variation, are reported in this paper. The lift variation over a cycle of oscillation, and hence the lift hysteresis loop, is estimated from the velocity distribution in the wake measured or computed for successive phases of the cycle. Experimentally, the estimated lift hysteresis loops are compared with available data from the literature as well as with limited force balance measurements. Computationally, the estimated lift variations are compared with the corresponding variation obtained from the surface pressure distribution. Four analytical formulations for the lift estimation from wake surveys are considered and relative successes of the four are discussed. Author

N93-14911* National Aeronautics and Space Administration. Lewis Research Center, Cleveland, OH.

RESULTS OF LOW POWER DEICER TESTS ON A SWEEP INLET COMPONENT IN THE NASA LEWIS ICING RESEARCH TUNNEL

THOMAS H. BOND and JAIWON SHIN Jan. 1993 21 p Presented at the 31st Aerospace Sciences Meeting and Exhibit, Reno, NV, 11-14 Jan. 1993; sponsored by AIAA
(Contract RTOP 505-68-10)
(NASA-TM-105968; E-7495; NAS 1.15:105968; AIAA PAPER 93-0032) Avail: CASI HC A03/MF A01

Tests were conducted under a USAF/NASA Low Power Deicer program on two expulsive technologies to examine system performance on hardware representative of a modern aircraft part. The BF Goodrich Electro-Expulsive Deicing System and Pneumatic Impulse Ice Protection System were installed on a swept, compound curve, engine inlet component with varying leading edge radius, and tested through a range of icing and system operating conditions in the NASA Lewis Icing Research Tunnel. A description of the experimental procedure and results, including residual ice thickness,

02 AERODYNAMICS

shed ice particle size, and changes in system energy/pressure characteristics are presented. Author

N93-15338* National Aeronautics and Space Administration. Lewis Research Center, Cleveland, OH.

SURFACE ROUGHNESS DUE TO RESIDUAL ICE IN THE USE OF LOW POWER DEICING SYSTEMS

JAIWON SHIN and THOMAS H. BOND Jan. 1993 16 p
Presented at the 31st Aerospace Sciences Meeting and Exhibit, Reno, NV, 11-14 Jan. 1993; sponsored by AIAA
(Contract RTOP 505-68-10)

(NASA-TM-105971; E-7494; NAS 1.15:105971; AIAA PAPER 93-0031) Avail: CASI HC A03/MF A01

Thicknesses of residual ice are presented to provide information on surface contamination and associated roughness during deicing events. Data was obtained from low power ice protection systems tests conducted in the Icing Research Tunnel at NASA Lewis Research Center (LeRC) with nine different deicing systems. Results show that roughness associated with residual ice is not characterized by uniformly distributed roughness. Results also show that deicing systems require a critical mass of ice to generate a sufficient expelling force to remove the ice. Author

N93-15404* National Aeronautics and Space Administration. Lewis Research Center, Cleveland, OH.

AN OVERVIEW OF SHED ICE IMPACT IN THE NASA LEWIS ICING RESEARCH TUNNEL

THOMAS H. BOND and RANDALL K. BRITTON (Sverdrup Technology, Inc., Brook Park, OH.) 14 Jan. 1993 14 p
(NASA-TM-105969; E-7492; NAS 1.15:105969; AIAA PAPER 93-0301) Avail: CASI HC A03/MF A01

One of the areas of active research in commercial and military rotorcraft is directed toward developing the capability of sustained flight in icing conditions. The emphasis to date has been on the accretion and subsequent shedding of ice in an icing environment, where the shedding may be natural or induced. Historically, shed-ice particles have been a problem for aircraft, particularly rotorcraft. Because of the high particle velocities involved, damage to a fuselage or other airframe component from a shed-ice impact can be significant. Design rules for damage tolerance from shed-ice impact are not well developed because of a lack of experimental data. Thus, NASA Lewis (LeRC) has begun an effort to develop a database of impact force and energy resulting from shed ice. This effort consisted of a test of NASA LeRC's Model Rotor Test Rig (MRTR) in the Icing Research Tunnel (IRT). Both natural shedding and forced shedding were investigated. Forced shedding was achieved by fitting the rotor blades with Small Tube Pneumatic (STP) deicer boots manufactured by BF Goodrich. A detailed description of the test is given as well as the design of a new impact sensor which measures the force-time history of an impacting ice fragment. A brief discussion of the procedure to infer impact energy from a force-time trace are required for the impact-energy calculations. Recommendations and future plans for this research area are also provided. Author

N93-16596* National Aeronautics and Space Administration. Lewis Research Center, Cleveland, OH.

A REALIZABLE REYNOLDS STRESS ALGEBRAIC EQUATION MODEL

TSAN-HSING SHIH, JIANG ZHU, and JOHN L. LUMLEY (Cornell Univ., Ithaca, NY.) Jan. 1993 36 p Presented at the Ninth Symposium on Turbulence Shear Flows, Kyoto, Japan, 10-18 Aug. 1993

(Contract NASA ORDER C-99066-G; RTOP 505-62-21)
(NASA-TM-105993; ICOMP-92-27; E-7525; NAS 1.15:105993; CMOTT-92-14) Avail: CASI HC A03/MF A01

The invariance theory in continuum mechanics is applied to analyze Reynolds stresses in high Reynolds number turbulent flows. The analysis leads to a turbulent constitutive relation that relates the Reynolds stresses to the mean velocity gradients in a more general form in which the classical isotropic eddy viscosity model is just the linear approximation of the general form. On the basis of realizability analysis, a set of model coefficients are obtained

which are functions of the time scale ratios of the turbulence to the mean strain rate and the mean rotation rate. The coefficients will ensure the positivity of each component of the mean rotation rate. These coefficients will ensure the positivity of each component of the turbulent kinetic energy - realizability that most existing turbulence models fail to satisfy. Separated flows over backward-facing step configurations are taken as applications. The calculations are performed with a conservative finite-volume method. Grid-independent and numerical diffusion-free solutions are obtained by using differencing schemes of second-order accuracy on sufficiently fine grids. The calculated results are compared in detail with the experimental data for both mean and turbulent quantities. The comparison shows that the present proposal significantly improves the predictive capability of K-epsilon based two equation models. In addition, the proposed model is able to simulate rotational homogeneous shear flows with large rotation rates which all conventional eddy viscosity models fail to simulate. Author

N93-16625* National Aeronautics and Space Administration. Lewis Research Center, Cleveland, OH.

EFFECT OF A ROTATING PROPELLER ON THE SEPARATION ANGLE OF ATTACK AND DISTORTION IN DUCTED PROPELLER INLETS

D. R. BOLDMAN, C. IEK, D. P. HWANG, M. LARKIN (Pratt and Whitney Aircraft, East Hartford, CT.), and P. SCHWEIGER (Pratt and Whitney Aircraft, East Hartford, CT.) Jan. 1993 16 p
Presented at the 31st Aerospace Sciences Meeting and Exhibit, Reno, NV, 11-14 Jan. 1993; Sponsored by AIAA
(Contract RTOP 505-03-10)

(NASA-TM-105935; E-7451; NAS 1.15:105935; AIAA PAPER 93-0017) Avail: CASI HC A03/MF A01

The present study represents an extension of an earlier wind tunnel experiment performed with the P&W 17-in. Advanced Ducted Propeller (ADP) Simulator operating at Mach 0.2. In order to study the effects of a rotating propeller on the inlet flow, data were obtained in the UTRC 10- by 15-Foot Large Subsonic Wind Tunnel with the same hardware and instrumentation, but with the propeller removed. These new tests were performed over a range of flow rates which duplicated flow rates in the powered simulator program. The flow through the inlet was provided by a remotely located vacuum source. A comparison of the results of this flow-through study with the previous data from the powered simulator indicated that in the conventional inlet the propeller produced an increase in the separation angle of attack between 4.0 deg at a specific flow of 22.4 lb/sec-sq ft to 2.7 deg at a higher specific flow of 33.8 lb/sec-sq ft. A similar effect on separation angle of attack was obtained by using stationary blockage rather than a propeller. Author

N93-16704* National Aeronautics and Space Administration. Lewis Research Center, Cleveland, OH.

EXPERIMENTAL INVESTIGATION OF AN EJECTOR-POWERED FREE-JET FACILITY

MARY JO LONG Jul. 1992 15 p Presented at the 28th Joint Propulsion Conference, Nashville, TN, 6-8 Jul. 1992; sponsored by AIAA, ASME, SAE, and ASEE Previously announced in IAA as A92-54058

(Contract RTOP 537-02-23)

(NASA-TM-105868; E-7331; NAS 1.15:105868; AIAA PAPER 92-3569) Avail: CASI HC A03/MF A01

NASA Lewis Research Center's (LeRC) newly developed Nozzle Acoustic Test Rig (NATR) is a large free-jet test facility powered by an ejector system. In order to assess the pumping performance of this ejector concept and determine its sensitivity to various design parameters, a 1/5-scale model of the NATR was built and tested prior to the operation of the actual facility. This paper discusses the results of the 1/5-scale model tests and compares them with the findings from the full-scale tests. Author

N93-19968* National Aeronautics and Space Administration. Lewis Research Center, Cleveland, OH.

AN EXPERIMENTAL INVESTIGATION OF S-DUCT FLOW CONTROL USING ARRAYS OF LOW-PROFILE VORTEX GENERATORS

BRUCE A. REICHERT and BRUCE J. WENDT Feb. 1993 14 p Presented at the 31st Aerospace Sciences Meeting and Exhibit, Reno, NV, 11-14 Jan. 1993; sponsored by AIAA (Contract RTOP 505-62-52) (NASA-TM-106030; E-7595; NAS 1.15:106030) Copyright Avail: CASI HC A03/MF A01

An experimental investigation was undertaken to measure the effect of various configurations of low-profile vortex generator arrays on the flow in a diffusing S-duct. Three parameters that characterize the vortex generator array were systematically varied to determine their effect: (1) the vortex generator height; (2) the streamwise location of the vortex generator array; and (3) the vortex generator spacing. Detailed measurements of total pressure at the duct exit, surface static pressure, and surface flow visualization were gathered for each vortex generator configuration. These results are reported here along with total pressure recovery and distortion coefficients determined from the experimental data. Each array of vortex generators tested improved total pressure recovery. The configuration employing the largest vortex generators was the most effective in reducing total pressure recovery. No configuration of vortex generators completely eliminated the flow separation that naturally occurs in the S-duct, however the extent of the separated flow region was reduced. Author (revised)

N93-24118* National Aeronautics and Space Administration. Lewis Research Center, Cleveland, OH.

ANALYTICAL AND EXPERIMENTAL STUDIES OF A SHORT COMPACT SUBSONIC DIFFUSER FOR A TWO-DIMENSIONAL SUPERSONIC INLET

CHANATHY IEK, RICHARD R. BURLEY, and ALBERT L. JOHNS Mar. 1993 65 p (Contract RTOP 505-62-71) (NASA-TP-3247; E-7111; NAS 1.60:3247) Avail: CASI HC A04/MF A01

An experimental study of a two-dimensional supersonic inlet with a short compact subsonic diffuser, length to exit diameter (dl/d) ratio of 1.25, was conducted to investigate the impact of the short diffuser on inlet performance at low speeds and to assess the diffuser subsonic performance for a simulated diffuser flow corresponding to high-speed inlet conditions near the design flight Mach number of 2.2. For the low-speed testing, a drooped lip was employed to improve the inlet performance at a high angle of attack. For the simulated high-speed testing, air was blown through slots or discrete nozzles as an active boundary-layer control. The results from the low-speed performance test were compared with the results from a previous test program on the same inlet with a long subsonic diffuser (dl/d = 4.5). The comparison indicates that inlet recovery was not affected by the use of the short diffuser for either the baseline (no droop) or the drooped cowl lip configuration. However, the inlet baseline distortion for the short diffuser configuration was substantially higher than for the long diffuser. A comparison of the two configurations with a 70 deg drooped lip showed no significant difference in distortion. For the portion of the experimental program in which diffuser conditions for high-speed flight were simulated, diffuser-induced flow separation occurred. This separation was predicted from an analytical study that used the Hess potential flow panel method and the Herring two-dimensional boundary-layer analysis computer codes. The flow separated mainly on the diffuser ramp. Subsequent tests in which boundary-control systems were utilized showed that blowing with either slots or discrete nozzles could suppress the flow separation in the short subsonic diffuser, thereby substantially improving the diffuser performance. Author (revised)

N93-24911* National Aeronautics and Space Administration. Lewis Research Center, Cleveland, OH.

SURFACE AND FLOW FIELD MEASUREMENTS IN A SYMMETRIC CROSSING SHOCK WAVE/TURBULENT BOUNDARY-LAYER INTERACTION

D. O. DAVIS and W. R. HINGST Jun. 1992 20 p Presented at the 10th AIAA Applied Aerodynamics Conference, Palo Alto, CA, 22-24 Jun. 1992; sponsored by AIAA Previously announced in IAA as A92-45574 (Contract RTOP 505-62-52) (NASA-TM-106086; E-7716; NAS 1.15:106086; AIAA PAPER 92-2634) Avail: CASI HC A03/MF A01

Results of an experimental investigation of a symmetric crossing shock/turbulent boundary layer interaction are presented for a Mach number of 3.44 and deflection angles of 2, 6, 8, and 9 degrees. The interaction strengths vary from weak to strong enough to cause a large region of separated flow. Measured quantities include surface static pressure (both steady and unsteady) and flowfield Pitot pressures. Pitot profiles in the plane of symmetry through the interaction region are shown for various deflection angles. Oil flow visualization and the results of a trace gas streamline tracking technique are also presented. Author

N93-27440* National Aeronautics and Space Administration. Lewis Research Center, Cleveland, OH.

EXPERIMENTAL AND COMPUTATIONAL ICE SHAPES AND RESULTING DRAG INCREASE FOR A NACA 0012 AIRFOIL

JAIWON SHIN and THOMAS H. BOND In California State Univ., The Fifth Symposium on Numerical and Physical Aspects of Aerodynamic Flows 10 p 1992 Previously announced as N92-28674 Avail: CASI HC A02/MF A04

Tests were conducted in the Icing Research Tunnel (IRT) at the NASA Lewis Research Center to document the repeatability of the ice shape over the range of temperatures varying from -15 F to 28 F. Measurements of drag increase due to the ice accretion were also made. The ice shape and drag coefficient data, with varying total temperatures at two different airspeeds, were compared with the computational predictions. The calculations were made with the 2D LEWICE/IBL code which is a combined code of LEWICE and the interactive boundary layer method developed for iced airfoils. Comparisons show good agreement with the experimental data in ice shapes. The calculations show the ability of the code to predict drag increases as the ice shape changes from a rime shape to a glaze shape. Author

N93-31648* National Aeronautics and Space Administration. Lewis Research Center, Cleveland, OH.

STREAMWISE VORTICITY GENERATION AND MIXING ENHANCEMENT IN FREE JETS BY DELTA-TABS

K. B. M. Q. ZAMAN Jun. 1993 15 p Presented at the AIAA Shear Flow Conference, Orlando, FL, 6-9 Jul. 1993; sponsored by AIAA (Contract RTOP 505-62-52) (NASA-TM-106235; E-7955; NAS 1.15:106235; AIAA PAPER 93-3253) Avail: CASI HC A03/MF A01

The effect of triangular tabs, placed at the nozzle exit, on the evolution of free jets is investigated. The effect, a large distortion of the jet cross section and a resultant increase in mixing downstream, has been inferred before to be due to a pair of streamwise vortices originating from each tab. In this paper, the generation mechanism of the streamwise vorticity ($\omega_{\text{sub } x}$) is considered first. Two sources are postulated. One is the upstream 'pressure hill', produced by the tab, which appears to be the dominant source. Another is due to vortex filaments shed from the sides of the tab and reoriented downstream by the mean shear of the mixing layer. In the case of a 'delta-tab', a triangular tab with its apex leaning downstream, vorticity from the two sources explain the stronger effect in that configuration. Data on the vorticity evolution for the effect of two delta-tabs are presented, up to twelve jet diameters from the exit, which show that the streamwise vortices persist even at the farthest measurement station. The magnitude of $\omega_{\text{sub } x}$ -maximum decays continually with

distance from the nozzle, its ratio to azimuthal vorticity maximum is found to be about 1/5 everywhere. The relative effect of a delta-tab on jets from an axisymmetric nozzle and a 8:1 rectangular nozzle is also studied. The mixing layer distortion is found to be less pronounced in the rectangular case. The jet mixing, as manifested by the mass flux measured at a downstream station, is increased in the axisymmetric jet but it is decreased in the rectangular jet under consideration by the delta-tab.

Author (revised)

N93-31672*# National Aeronautics and Space Administration. Lewis Research Center, Cleveland, OH.

ENHANCED MIXING OF A RECTANGULAR SUPERSONIC JET BY NATURAL AND INDUCED SCREECH

EDWARD J. RICE and GANESH RAMAN (Sverdrup Technology, Inc., Brook Park, OH.) Jul. 1993 14 p Presented at the AIAA Shear Flow Conference, Orlando, FL, 6-9 Jul. 1993; sponsored by AIAA

(Contract RTOP 505-62-52)

(NASA-TM-106245; E-7964; NAS 1.15:106245; AIAA PAPER 93-3263) Avail: CASI HC A03/MF A01

The influence of shear layer excitation on the mixing of supersonic rectangular jets was studied experimentally. Two methods of excitation were used to control the jet mixing. The first used the natural screech of an underexpanded supersonic jet from a converging nozzle. The level of the screech excitation was controlled by the use of a pair of baffles located to block the acoustic feedback path between the downstream shock structure and the nozzle lip. A screech level variation of over 30 decibels was achieved and the mixing was completely determined by the level of screech attained at the nozzle lip. The second form of self-excitation used the induced screech caused by obstacles or paddles located in the shear layers on either long side of the rectangular jet. With sufficient immersion of the paddles intense jet mixing occurred and large flapping wave motion was observed using a strobed focused Schlieren system. Each paddle was instrumented with a total pressure tap and strain gages to determine the pressure and drag force on the square cross-section paddle. Considerable drag was observed in this initial exploratory study. Future studies using alternate paddle geometries will be conducted to maximize jet mixing with minimum drag.

Author

N93-31839*# National Aeronautics and Space Administration. Lewis Research Center, Cleveland, OH.

TURBULENCE MEASUREMENT IN A REACTING AND NON-REACTING SHEAR LAYER AT A HIGH SUBSONIC MACH NUMBER

C. T. CHANG, C. J. MAREK, C. WEY (Sverdrup Technology, Inc., Brook Park, OH.), R. A. JONES (Rensselaer Polytechnic Inst., Troy, NY.), and M. J. SMITH (Purdue Univ., West Lafayette, IN.) Jun. 1993 8 p Prepared for presentation at the Ninth Symposium on Turbulent Shear Flows, Kyoto, Japan, 16-18 Aug. 1993

(Contract RTOP 505-62-52)

(NASA-TM-106186; E-7891; NAS 1.15:106186) Avail: CASI HC A02/MF A01

The results of two component velocity and turbulence measurements are presented which were obtained on a planar reacting shear layer burning hydrogen. Quantitative LDV and temperature measurements are presented with and without chemical reaction within the shear layer at a velocity ratio of 0.34 and a high speed Mach number of 0.7. The comparison showed that the reacting shear layer grew faster than that without reaction. Using a reduced width coordinate, the reacting and non-reacting profiles were very similar. The peak turbulence for both cases was 20 percent.

Author

AIR TRANSPORTATION AND SAFETY

Includes passenger and cargo air transport operations; and aircraft accidents.

A93-23239# National Aeronautics and Space Administration. Lewis Research Center, Cleveland, OH.

CLOSE-UP ANALYSIS OF AIRCRAFT ICE ACCRETION

R. J. HANSMAN, JR., KENNETH S. BREUER, DIDIER HAZAN (MIT, Cambridge, MA), ANDREW REEHORST, and MARIO VARGAS (NASA, Lewis Research Center, Cleveland, OH) Jan. 1993 14 p. AIAA, Aerospace Sciences Meeting and Exhibit, 31st, Reno, NV, Jan. 11-14, 1993 Previously announced in STAR as N93-15360 refs

(Contract NAG3-666; NGL-22-069-640; RTOP 505-68-10)

(AIAA PAPER 93-0029) Copyright

Various types of ice formation have been studied by analysis of high magnification video observations. All testing was conducted in the NASA Lewis Icing Research Tunnel (IRT). A faired 8.9 cm (3.5 in.) diameter metal-clad cylinder and a 5.1 (2 in.) aluminum cylinder were observed by close-up and overview video cameras for several wind tunnel conditions. These included close-up grazing angle, close-up side view, as well as overhead and side overview cameras. Still photographs were taken at the end of each spray along with tracings of the subsequent ice shape. While in earlier tests only the stagnation region was observed, the entire area from the stagnation line to the horn region of glaze ice shapes was observed in this test. The modes or horn formation have been identified within the range of conditions observed. In the horn region, Horn Type A ice is formed by 'dry' feather growth into the flow direction and Horn Type B is formed by a 'wet' growth normal to the surface. The feather growth occurs when the freezing fraction is near unity and roughness elements exists to provide an initial growth site.

Author

A93-23243# National Aeronautics and Space Administration. Lewis Research Center, Cleveland, OH.

ADVANCEMENTS IN THE LEWICE ICE ACCRETION MODEL

WILLIAM B. WRIGHT (Sverdrup Technology, Inc., Brook Park, OH) Jan. 1993 18 p. AIAA, Aerospace Sciences Meeting and Exhibit, 31st, Reno, NV, Jan. 11-14, 1993 Previously announced in STAR as N93-15402 refs

(Contract NAS3-25266; RTOP 505-68-10)

(AIAA PAPER 93-0171)

Recent evidence has shown that the NASA/Lewis Ice Accretion Model, LEWICE, does not predict accurate ice shapes for certain glaze ice conditions. This paper will present the methodology used to make a first attempt at improving the ice accretion prediction in these regimes. Importance is given to the correlations for heat transfer coefficient and ice density, as well as runback flow, selection of the transition point, flow field resolution, and droplet trajectory models. Further improvements and refinement of these modules will be performed once tests in NASA's Icing Research Tunnel, scheduled for 1993, are completed.

Author

A93-23244# National Aeronautics and Space Administration. Lewis Research Center, Cleveland, OH.

ICE ACCRETION AND PERFORMANCE DEGRADATION CALCULATIONS WITH LEWICE/NS

MARK G. POTAPCZUK (NASA, Lewis Research Center, Cleveland, OH), KAMEL M. AL-KHALIL (National Research Council, Washington), and MATTHEW T. VELAZQUEZ (MIT, Cambridge, MA) Jan. 1993 21 p. AIAA, Aerospace Sciences Meeting and Exhibit, 31st, Reno, NV, Jan. 11-14, 1993 Previously announced in STAR as N93-15354 refs

(Contract RTOP 505-68-10)

(AIAA PAPER 93-0173) Copyright

The LEWICE ice accretion computer code has been extended to include the solution of the two-dimensional Navier-Stokes

equations. The code is modular and contains separate stand-alone program elements that create a grid, calculate the flow field parameters, calculate the droplet trajectory paths, determine the amount of ice growth, calculate aeroperformance changes, and plot results. The new elements of the code are described. Calculated results are compared to experiment for several cases, including both ice shape and drag rise. Author

A93-23245# National Aeronautics and Space Administration. Lewis Research Center, Cleveland, OH.

ICE ACCRETION PREDICTION FOR A TYPICAL COMMERCIAL TRANSPORT AIRCRAFT

C. S. BIDWELL (NASA, Lewis Research Center, Cleveland, OH) Jan. 1993 22 p. AIAA, Aerospace Sciences Meeting and Exhibit, 31st, Reno, NV, Jan. 11-14, 1993 Previously announced in STAR as N93-15522 refs

(Contract RTOP 505-68-10)

(AIAA PAPER 93-0174) Copyright

Ice accretion calculations were made for a modern commercial transport using the NASA Lewis LEWICE3D ice accretion code. The ice accretion calculations were made for the wing and horizontal tail using both isolated flow models and flow models incorporating the entire airplane. The isolated flow model calculations were made to assess the validity of using these simplified models in lieu of the entire model in the ice accretion analysis for full aircraft. Ice shapes typifying a rime and a mixed ice shape were generated for a 30 minute hold condition. In general, the calculated ice shapes looked reasonable and appeared representative of a rime and a mixed ice conditions. The isolated flow model simplification was good for the main wing except at the root where it overpredicted the amount of accreted ice relative to the full aircraft flow model. For the horizontal tail the size and amount of predicted ice compared well for the two flow models, but the position of the accretions were more towards the upper surface for the aircraft flow model relative to the isolated flow model. This was attributed to downwash from the main wing which resulted in a lower effective angle of attack for the aircraft tail. Author

A93-24239# National Aeronautics and Space Administration. Lewis Research Center, Cleveland, OH.

AIRCRAFT ICING PROBLEMS - AFTER 50 YEARS

PORTER J. PERKINS (Sverdrup Technology, Inc., Brook Park, OH) and WILLIAM J. RIEKE (NASA, Lewis Research Center, Cleveland, OH) Jan. 1993 10 p. AIAA, Aerospace Sciences Meeting and Exhibit, 31st, Reno, NV, Jan. 11-14, 1993 refs (AIAA PAPER 93-0392) Copyright

With the possible exception of tailplane-ice hazards, understanding of aircraft icing processes and their performance penalties and hazards has not changed fundamentally in 40-50 years. A survey is presently conducted of the aircraft design criteria, ice-detection and deicing hardware, and flight procedures, that have been developed to cope with icing phenomena. Attention is given to pilot icing conditions flight-training requirements, which are essential for the recognition of icing situations requiring corrective action. O.C.

A93-31929* National Aeronautics and Space Administration. Lewis Research Center, Cleveland, OH.

AERODYNAMIC EFFECTS OF DEICING AND ANTI-ICING FLUIDS

JOHN J. REINMANN (NASA, Lewis Research Center, Cleveland, OH) and DICK ADAMS Journal of Aircraft (ISSN 0021-8669) vol. 30, no. 1 Jan.-Feb. 1993 p. 8, 9. Copyright

A special session in this issue of the Journal of Aircraft devoted to ground deicing and antiicing fluids is briefly reviewed. This section concentrates on the development of ground deicing and antiicing fluids and the measurement of their effects on takeoff aerodynamics. AIAA

N93-15345*# National Aeronautics and Space Administration. Lewis Research Center, Cleveland, OH.

NUMERICAL MODELING OF ANTI-ICING SYSTEMS AND

COMPARISON TO TEST RESULTS ON A NASA 0012 AIRFOIL

KAMEL M. AL-KHALIL and MARK G. POTAPCZUK Jan. 1993 14 p Presented at the 31st Aerospace Sciences Meeting and Exhibit, Reno, NV, 11-14 Jan. 1993; sponsored by AIAA

(Contract RTOP 505-68-10)

(NASA-TM-105975; E-7498; NAS 1.15:105975; AIAA PAPER 93-0170) Avail: CASI HC A03/MF A01

A series of experimental tests were conducted in the NASA Lewis IRT on an electro-thermally heated NACA 0012 airfoil. Quantitative comparisons between the experimental results and those predicted by a computer simulation code were made to assess the validity of a recently developed anti-icing model. An infrared camera was utilized to scan the instantaneous temperature contours of the skin surface. Despite some experimental difficulties, good agreement between the numerical predictions and the experiment results were generally obtained for the surface temperature and the possibility for each runback to freeze. Some recommendations were given for an efficient operation of a thermal anti-icing system. Author

N93-15354*# National Aeronautics and Space Administration. Lewis Research Center, Cleveland, OH.

ICE ACCRETION AND PERFORMANCE DEGRADATION CALCULATIONS WITH LEWICE/NS

MARK G. POTAPCZUK, KAMEL M. AL-KHALIL (National Academy of Sciences - National Research Council, Washington, DC.), and MATTHEW T. VELAZQUEZ (Massachusetts Inst. of Tech., Cambridge.) Jan. 1993 22 p Presented at the 31st Aerospace Sciences Meeting and Exhibit, Reno, NV, 11-14 Jan. 1993; sponsored by AIAA

(Contract RTOP 505-68-10)

(NASA-TM-105972; E-7497; NAS 1.15:105972; AIAA PAPER 93-0173) Avail: CASI HC A03/MF A01

The LEWICE ice accretion computer code has been extended to include the solution of the two-dimensional Navier-Stokes equations. The code is modular and contains separate stand-alone program elements that create a grid, calculate the flow field parameters, calculate the droplet trajectory paths, determine the amount of ice growth, calculate aeroperformance changes, and plot results. The new elements of the code are described. Calculated results are compared to experiment for several cases, including both ice shape and drag rise. Author

N93-15360*# National Aeronautics and Space Administration. Lewis Research Center, Cleveland, OH.

CLOSE-UP ANALYSIS OF AIRCRAFT ICE ACCRETION

R. JOHN HANSMAN (Massachusetts Inst. of Tech., Cambridge.), KENNETH S. BREUER (Massachusetts Inst. of Tech., Cambridge.), DIDIER HAZAN (Massachusetts Inst. of Tech., Cambridge.), ANDREW REEHORST, and MARIO VARGAS Jan. 1993 15 p Presented at the 31st Aerospace Sciences Meeting and Exhibit, Reno, NV, 11-14 Jan. 1993; sponsored by AIAA

(Contract NAG3-666; NGL-22-0069-640; RTOP 505-68-10)

(NASA-TM-105952; E-7473; NAS 1.15:105952; AIAA PAPER 93-0029) Avail: CASI HC A03/MF A01

Various types of ice formation have been studied by analysis of high magnification video observations. All testing was conducted in the NASA Lewis Icing Research Tunnel (IRT). A faired 8.9 cm (3.5 in.) diameter metal-clad cylinder and a 5.1 (2 in.) aluminum cylinder were observed by close-up and overview video cameras for several wind tunnel conditions. These included close-up grazing angle, close-up side view, as well as overhead and side overview cameras. Still photographs were taken at the end of each spray along with tracings of the subsequent ice shape. While in earlier tests only the stagnation region was observed, the entire area from the stagnation line to the horn region of glaze ice shapes was observed in this test. The modes or horn formation have been identified within the range of conditions observed. In the horn region, Horn Type A ice is formed by 'dry' feather growth into the flow direction and Horn Type B is formed by a 'wet'

03 AIR TRANSPORTATION AND SAFETY

growth normal to the surface. The feather growth occurs when the freezing fraction is near unity and roughness elements exist to provide an initial growth site. Author

A93-15522*# National Aeronautics and Space Administration. Lewis Research Center, Cleveland, OH.

ICE ACCRETION PREDICTION FOR A TYPICAL COMMERCIAL TRANSPORT AIRCRAFT

C. S. BIDWELL Jan. 1993 23 p Presented at the 31st Aerospace Sciences Meeting and Exhibit, Reno, NV, 11-14 Jan. 1993; sponsored by AIAA (Contract RTOP 505-68-10) (NASA-TM-105976; E-7499; NAS 1.15:105976; AIAA PAPER 93-0174) Avail: CASI HC A03/MF A01

Ice accretion calculations were made for a modern commercial transport using the NASA Lewis LEWICE3D ice accretion code. The ice accretion calculations were made for the wing and horizontal tail using both isolated flow models and flow models incorporating the entire airplane. The isolated flow model calculations were made to assess the validity of using these simplified models in lieu of the entire model in the ice accretion analysis of full aircraft. Ice shapes typifying a rime and a mixed ice shape were generated for a 30 minute hold condition. In general, the calculated ice shapes looked reasonable and appeared representative of a rime and a mixed ice conditions. The isolated flow model simplification was good for the main wing except at the root where it overpredicted the amount of accreted ice relative to the full aircraft flow model. For the horizontal tail the size and amount of predicted ice compared well for the two flow models, but the position of the accretions were more towards the upper surface for the aircraft flow model relative to the isolated flow model. This was attributed to downwash from the main wing which resulted in a lower effective angle of attack for the aircraft tail.

Author

05

AIRCRAFT DESIGN, TESTING AND PERFORMANCE

Includes aircraft simulation technology.

A93-20281# National Aeronautics and Space Administration. Lewis Research Center, Cleveland, OH.

CONCURRENT OPTIMIZATION OF AIRFRAME AND ENGINE DESIGN PARAMETERS

THOMAS M. LAVELLE, ROBERT M. PLENCNER, and JONATHAN A. SEIDEL (NASA, Lewis Research Center, Cleveland, OH) Sep. 1992 16 p. AIAA, USAF, NASA, and OAI, Symposium on Multidisciplinary Analysis and Optimization, 4th, Cleveland, OH, Sept. 21-23, 1992 Previously announced in STAR as N93-12402 refs (Contract RTOP 505-69-50) (AIAA PAPER 92-4713) Copyright

An integrated system for the multidisciplinary analysis and optimization of airframe and propulsion design parameters is being developed. This system is known as IPAS, the Integrated Propulsion/Airframe Analysis System. The traditional method of analysis is one in which the propulsion system analysis is loosely coupled to the overall mission performance analysis. This results in a time consuming iterative process. First, the engine is designed and analyzed. Then, the results from this analysis are used in a mission analysis to determine the overall aircraft performance. The results from the mission analysis are used as a guide as the engine redesigned and the entire process repeated. In IPAS, the propulsion system, airframe, and mission are closely coupled. The propulsion system analysis code is directly integrated into the mission analysis code. This allows the propulsion design parameters to be optimized along with the airframe and mission

design parameters, significantly reducing the time required to obtain an optimized solution. Author

A93-20324*# National Aeronautics and Space Administration. Lewis Research Center, Cleveland, OH.

STRUCTURAL TAILORING/ANALYSIS FOR HYPERSONIC COMPONENTS - A COMPUTATIONAL SIMULATION

G. V. NARAYANAN, E. S. REDDY, G. ABUMERI (Sverdrup Technology, Inc., Brook Park, OH), DALE A. HOPKINS, and CHRISTOS C. CHAMIS (NASA, Lewis Research Center, Cleveland, OH) In AIAA/USAF/NASA/OAI Symposium on Multidisciplinary Analysis and Optimization, 4th, Cleveland, OH, Sept. 21-23, 1992, Technical Papers. Pt. 1 Washington American Institute of Aeronautics and Astronautics 1992 p. 251-262. refs (Contract NAS3-25266) (AIAA PAPER 92-4722) Copyright

The development of STAHYC (Structural Tailoring/Analysis for Hypersonic Components), a numerical tool for the optimum design of an engine inlet wall panel for hypersonic aerospace vehicles, is described. STAHYC integrates FORTRAN modules of different disciplines, including fluid dynamics, heat transfer, structural analysis, and optimization. The discussion covers the system design concept, system components, system automation, system testing, established links, and data transfer between different computational modules. The various algorithms used in STAHYC are also discussed. V.L.

A93-22551*# National Aeronautics and Space Administration. Lewis Research Center, Cleveland, OH.

RESULTS OF LOW POWER DEICER TESTS ON A SWEEPED INLET COMPONENT IN THE NASA LEWIS ICING RESEARCH TUNNEL

THOMAS H. BOND and JAIWON SHIN (NASA, Lewis Research Center, Cleveland, OH) Jan. 1993 20 p. AIAA, Aerospace Sciences Meeting and Exhibit, 31st, Reno, NV, Jan. 11-14, 1993 Previously announced in STAR as N93-14911 refs (AIAA PAPER 93-0032) Copyright

Tests were conducted under a USAF/NASA Low Power Deicer program on two expulsive technologies to examine system performance on hardware representative of a modern aircraft part. The BF Goodrich Electro-Expulsive Deicing System and Pneumatic Impulse Ice Protection system were installed on a swept, compound curve, engine inlet component with varying leading edge radius, and tested through a range of icing and system operating conditions in the NASA Lewis Icing Research Tunnel. A description of the experimental procedure and results, including residual ice thickness, shed ice particle size, and changes in system energy/pressure characteristics are presented. Author

A93-22696*# National Aeronautics and Space Administration. Lewis Research Center, Cleveland, OH.

MODELING AND STRAIN GAUGING OF EDDY CURRENT REPULSION DEICING SYSTEMS

SAMUEL O. SMITH (Electroimpact, Inc., Seattle, WA) Jan. 1993 11 p. AIAA, Aerospace Sciences Meeting and Exhibit, 31st, Reno, NV, Jan. 11-14, 1993 refs (Contract NAS3-26252) (AIAA PAPER 93-0296) Copyright

Work described in this paper confirms and extends work done by Zumwalt, et al., on a variety of in-flight deicing systems that use eddy current repulsion for repelling ice. Two such systems are known as electro-impulse deicing (EIDI) and the eddy current repulsion deicing strip (EDS). Mathematical models for these systems are discussed for their capabilities and limitations. The author duplicates a particular model of the EDS. Theoretical voltage, current, and force results are compared directly to experimental results. Dynamic strain measurements results are presented for the EDS system. Dynamic strain measurements near EDS or EIDI coils are complicated by the high magnetic fields in the vicinity of the coils. High magnetic fields induce false voltage signals out of the gauges. Author

A93-23242# National Aeronautics and Space Administration. Lewis Research Center, Cleveland, OH.

NUMERICAL MODELING OF ANTI-ICING SYSTEMS AND COMPARISON TO TEST RESULTS ON A NACA 0012 AIRFOIL
KAMEL M. AL-KHALIL and MARK G. POTAPCZUK (NASA, Lewis Research Center, Cleveland, OH) Jan. 1993 13 p. AIAA, Aerospace Sciences Meeting and Exhibit, 31st, Reno, NV, Jan. 11-14, 1993 Previously announced in STAR as N93-15345 Research supported by National Research Council refs (Contract RTOP 505-68-10)

(AIAA PAPER 93-0170) Copyright

A series of experimental tests were conducted in the NASA Lewis IRT on an electro-thermally heated NACA 0012 airfoil. Quantitative comparisons between the experimental results and those predicted by a computer simulation code were made to assess the validity of a recently developed anti-icing model. An infrared camera was utilized to scan the instantaneous temperature contours of the skin surface. Despite some experimental difficulties, good agreement between the numerical predictions and the experimental results were generally obtained for the surface temperature and the possibility for the runback to freeze. Some recommendations were given for an efficient operation of a thermal anti-icing system.

Author

A93-35932* National Aeronautics and Space Administration. Lewis Research Center, Cleveland, OH.

RESULTS OF A LOW POWER ICE PROTECTION SYSTEM TEST AND A NEW METHOD OF IMAGING DATA ANALYSIS
JAIWON SHIN, THOMAS H. BOND (NASA, Lewis Research Center, Cleveland, OH), and GEERT A. MESANDER (USAF, Air Logistics Center, Tinker AFB, OK) In AHS, Annual Forum, 48th, Washington, June 3-5, 1992, Proceedings. Vol. 1 Alexandria, VA American Helicopter Society 1992 p. 375-390. Previously announced in STAR as N92-28696 refs

Copyright

Tests were conducted on a BF Goodrich De-Icing System's Pneumatic Impulse Ice Protection (PIIP) system in the NASA Lewis Icing Research Tunnel (IRT). Characterization studies were done on shed ice particle size by changing the input pressure and cycling time of the PIIP de-icer. The shed ice particle size was quantified using a newly developed image software package. The tests were conducted on a 1.83 m (6 ft) span, 0.53 m (221 in) chord NACA 0012 airfoil operated at a 4 degree angle of attack. The IRT test conditions were a -6.7 C (20 F) glaze ice, and a -20 C (-4 F) rime ice. The ice shedding events were recorded with a high speed video system. A detailed description of the image processing package and the results generated from this analytical tool are presented.

Author

A93-51401*# National Aeronautics and Space Administration. Lewis Research Center, Cleveland, OH.

A COMPARATIVE STUDY OF MULTIVARIABLE ROBUSTNESS ANALYSIS METHODS AS APPLIED TO INTEGRATED FLIGHT AND PROPULSION CONTROL

JOHN D. SCHIERMAN, T. A. LOVELL, and DAVID K. SCHMIDT (Arizona State Univ., Tempe) In AIAA Guidance, Navigation and Control Conference, Monterey, CA, Aug. 9-11, 1993, Technical Papers. Pt. 2 Washington American Institute of Aeronautics and Astronautics 1993 p. 984-994. refs (Contract NAG3-998)

(AIAA PAPER 93-3809) Copyright

Three multivariable robustness analysis methods are compared and contrasted. The focus of the analysis is on system stability and performance robustness to uncertainty in the coupling dynamics between two interacting subsystems. Of particular interest is interacting airframe and engine subsystems, and an example airframe/engine vehicle configuration is utilized in the demonstration of these approaches. The singular value (SV) and structured singular value (SSV) analysis methods are compared to a method especially well suited for analysis of robustness to uncertainties in subsystem interactions. This approach is referred to here as the interacting subsystem (IS) analysis method. This method has been used previously to analyze airframe/engine

systems, emphasizing the study of stability robustness. However, performance robustness is also investigated here, and a new measure of allowable uncertainty for acceptable performance robustness is introduced. The IS methodology does not require plant uncertainty models to measure the robustness of the system, and is shown to yield valuable information regarding the effects of subsystem interactions. In contrast, the SV and SSV methods allow for the evaluation of the robustness of the system to particular models of uncertainty, and do not directly indicate how the airframe (engine) subsystem interacts with the engine (airframe) subsystem.

Author (revised)

A93-52443* National Aeronautics and Space Administration. Lewis Research Center, Cleveland, OH.

EFFICIENT FINITE ELEMENT METHOD FOR AIRCRAFT DEICING PROBLEMS

J. R. HUANG, THEO G. KEITH, JR., and KENNETH J. DE WITT (Toledo Univ., OH) Journal of Aircraft (ISSN 0021-8669) vol. 30, no. 5 Sept.-Oct. 1993 p. 695-704. AIAA, Aerospace Sciences Meeting and Exhibit, 30th, Reno, NV, Jan. 6-9, 1992, AIAA Paper 92-0532. Previously cited in issue 12, p. 1905, Accession no. A92-31670 Research supported by NASA refs Copyright

N93-22588*# National Aeronautics and Space Administration. Lewis Research Center, Cleveland, OH.

JET ENGINE HOT PARTS IR ANALYSIS PROCEDURE (J-EIRP)
JOSEPH F. BAUMEISTER Feb. 1993 20 p (Contract RTOP 505-62-00) (NASA-TM-105914; E-7605; NAS 1.15:105914) Avail: CASI HC A03/MF A01

A thermal radiation analysis method called Jet Engine IR Analysis Procedure (J-EIRP) was developed to evaluate jet engine cavity hot parts source radiation. The objectives behind J-EIRP were to achieve the greatest accuracy in model representation and solution, while minimizing computer resources and computational time. The computer programs that comprise J-EIRP were selected on the basis of their performance, accuracy, and flexibility to solve both simple and complex problems. These programs were intended for use on a personal computer, but include the ability to solve large problems on a mainframe or supercomputer. J-EIRP also provides the user with a tool for developing thermal design experience and engineering judgment through analysis experimentation, while using minimal computer resources. A sample jet engine cavity analysis demonstrates the procedure and capabilities within J-EIRP, and is compared to a simplified method for approximating cavity radiation. The goal is to introduce the terminology and solution process used in J-EIRP and to provide insight into the radiation heat transfer principles used in this procedure.

Author (revised)

06

AIRCRAFT INSTRUMENTATION

Includes cockpit and cabin display devices; and flight instruments.

A93-32916* National Aeronautics and Space Administration. Lewis Research Center, Cleveland, OH.

REVIEW OF THE FOCSI (FIBER OPTIC CONTROL SYSTEM INTEGRATION) PROGRAM

ROBERT BAUMBICK (NASA, Lewis Research Center, Cleveland, OH) In Specialty fiber optic systems for mobile platforms; Proceedings of the Meeting, Boston, MA, Sept. 5, 1991 Bellingham, WA Society of Photo-Optical Instrumentation Engineers 1991 p. 12-19. Copyright

A joint NASA/NAVY program, called FOCSI, is reviewed which is aimed at designing optical sensor systems to fit the installation and environmentally test passive optical sensors and electrooptic

06 AIRCRAFT INSTRUMENTATION

architectures. These optical sensor systems will be flown on an F18 aircraft to collect data on the operability and maintainability of these systems in a flight environment. The NASA F-18 aircraft will be equipped with a 1773 optical databus to transfer the optical sensor information to the aircraft data collection location. AIAA

A93-49476 National Aeronautics and Space Administration. Lewis Research Center, Cleveland, OH.

FLIGHT TESTING OF A FIBER OPTIC TEMPERATURE SENSOR

M. J. FINNEY, G. W. TREGAY, and P. R. CALABRESE (Conax Buffalo Corp., NY) *In* Specialty fiber optic systems for mobile platforms and plastic optical fibers; Proceedings of the Meeting, Boston, MA, Sept. 9-11, 1992 Bellingham, WA Society of Photo-Optical Instrumentation Engineers 1993 p. 194-203. Research supported by NASA, Conax Buffalo Corp., and Simmonds Precision Engine Systems refs Copyright

A fiber optic temperature sensor (FOTS) system consisting of an optical probe, a flexible fiber optic cable, and an electro-optic signal processor was fabricated to measure the gas temperature in a turbine engine. The optical probe contained an emissive source embedded in a sapphire lightguide coupled to a fiber-optic jumper cable and was retrofitted into an existing thermocouple probe housing. The flexible fiber optic cable was constructed with 200 micron core, polyimide-coated fiber and was ruggedized for an aircraft environment. The electro-optic signal processing unit was used to ratio the intensities of two wavelength intervals and provided an analog output value of the indicated temperature. Subsequently, this optical sensor system was installed on a NASA Dryden F-15 Highly Integrated Digital Electronic Control (HIDEC) Aircraft Engine and several flight tests were conducted. Over the course of flight testing, the FOTS system's response was proportional to the average of the existing thermocouples sensing the changes in turbine engine thermal conditions.

07

AIRCRAFT PROPULSION AND POWER

Includes prime propulsion systems and systems components, e.g., gas turbine engines and compressors; and onboard auxiliary power plants for aircraft.

A93-13333* National Aeronautics and Space Administration. Lewis Research Center, Cleveland, OH.

DYNAMIC ANALYSIS OF A PRE-AND-POST ICE IMPACTED BLADE

G. H. ABUMERI, E. S. REDDY (Sverdrup Technology, Inc., Brook Park; NASA, Lewis Research Center, Cleveland, OH), P. L. N. MURTHY, and C. C. CHAMIS (NASA, Lewis Research Center, Cleveland, OH) Aug. 1992 9 p. AIAA, Aircraft Design Systems Meeting, Hilton Head Island, SC, Aug. 24-26, 1992 refs (AIAA PAPER 92-4273) Copyright

The dynamic characteristics of an engine blade are evaluated under pre-and-post ice impact conditions using the NASA in-house computer code BLASIM. The ice impacts the leading edge of the blade causing severe local damage. The local structural response of the blade due to the ice impact is predicted via a transient response analysis by modeling only a local patch around the impact region. After ice impact, the global geometry of the blade is updated using deformations of the local patch and a free vibration analysis is performed. The effects of ice impact location, ice size and ice velocity on the blade mode shapes and natural frequencies are investigated. The results indicate that basic nature of the mode shapes remains unchanged after impact and that the maximum variation in natural frequencies occurs for the twisting mode of the blade. Author

A93-13334* National Aeronautics and Space Administration. Lewis Research Center, Cleveland, OH.

THE MULTI-HEAT ADDITION TURBINE ENGINE

LEO C. FRANCISCUS (NASA, Lewis Research Center, Cleveland, OH) Aug. 1992 15 p. AIAA, Aircraft Design Systems Meeting, Hilton Head Island, SC, Aug. 24-26, 1992 refs (AIAA PAPER 92-4272) Copyright

A study was made of multiheat addition turbine engines (MHATE) which incorporate multiple burners and turbines. The types of engines studied were a MHATE two-spool duct burning turbofan and a single-spool turbojet. A conventional duct burning turbofan and a TBE turbojet were studied for comparison. Comparisons of the thrust and specific fuel consumption of the engines were made for maximum burner temperatures of 2400 F and 2900 F. The results of the study show that the MHATE engines with maximum burner temperatures of 2400 F obtain the same thrust and specific fuel consumption as the conventional engines having maximum burner temperatures of 2900 F. This would have the potential for significant reductions in harmful emissions of NO(x). When the MHATE and conventional engines have the same maximum burner temperatures, the MHATE engines achieve 15 to 50 percent more thrust. Author

A93-13383# National Aeronautics and Space Administration. Lewis Research Center, Cleveland, OH.

EFFECTS OF TURBINE COOLING ASSUMPTIONS ON PERFORMANCE AND SIZING OF HIGH-SPEED CIVIL TRANSPORT

PAUL F. SENICK (NASA, Lewis Research Center, Cleveland, OH) Aug. 1992 8 p. AIAA, Aircraft Design Systems Meeting, Hilton Head Island, SC, Aug. 24-26, 1992 Previously announced in STAR as N92-23537 refs (Contract RTOP 537-01-22) (AIAA PAPER 92-4217) Copyright

The analytical study presented examines the effects of varying turbine cooling assumptions on the performance of a high speed civil transport propulsion system as well as the sizing sensitivity of this aircraft to these performance variations. The propulsion concept employed in this study was a two spool, variable cycle engine with a sea level thrust of 55,000 lbf. The aircraft used for this study was a 250 passenger vehicle with a cruise Mach number of 2.4 and 500 nautical mile range. The differences in turbine cooling assumptions were represented by varying amount of high pressure compressor bleed air used to cool the turbines. It was found that as this cooling amount increased, engine size and weight increased, but specific fuel consumption (SFC) decreased at takeoff and climb only. Because most time is spent at cruise, the SFC advantage of the higher bleed engines seen during subsonic flight was minimized and the lower bleed, lighter engines led to the lowest takeoff gross weight vehicles. Finally, the change in aircraft takeoff gross weight versus turbine cooling level is presented. Author

A93-14077* National Aeronautics and Space Administration. Lewis Research Center, Cleveland, OH.

NUMERICAL SIMULATION OF A LOW-EMISSION GAS TURBINE COMBUSTOR USING KIVA-II

S. L. YANG, R. CHEN (Michigan Technological Univ., Houghton), M. C. CLINE (Los Alamos National Lab., NM), H. L. NGUYEN (NASA, Lewis Research Center, Cleveland, OH), and G. J. MICKLOW (Florida Univ., Gainesville) International Journal for Numerical Methods in Fluids (ISSN 0271-2091) vol. 15, no. 8 Oct. 30, 1992 p. 865-881. refs (Contract NAG3-1109; NAG3-1113; NASA ORDER C-30050-R) Copyright

A modified version of the KIVA-II code was used to obtain a multidimensional numerical solution for the turbulent two-phase chemically reacting flows inside a staged turbine combustor (STC). The STC under consideration is equipped with an advanced airblast fuel nozzle and encompasses a fuel nozzle (FN), a rich-burn (RB) zone, a converging connecting pipe, a quick-quench (QQ) zone, a diverging connecting pipe, and a lean-combustion (LC) zone. The STC was divided into two subsystems, namely, FN/RB zone and

QQ/LC zones, and the numerical solutions were obtained separately for each subsystem. Preliminary data characterize the major features of the flow and temperature fields inside the STC. Information on velocity, temperature, and some critical species in the FN/RB zone is presented. In the QQ/LC zones, formation of the co- and counter-rotating bulk flow and the sandwiched-ring-shaped temperature field can be clearly seen. The calculations of the mass-weighted standard deviation and the pattern factor of temperature indicated that the mixing performance of the STC is very promising. O.G.

A93-14624* National Aeronautics and Space Administration. Lewis Research Center, Cleveland, OH.

CONCURRENT PROCESSING ADAPTATION OF AEROELASTIC ANALYSIS OF PROPFANS

D. V. MURTHY and D. C. JANETZKE (NASA, Lewis Research Center, Cleveland, OH) Computers & Structures (ISSN 0045-7949) vol. 45, no. 2 Oct. 3, 1992 p. 397-404. Previously announced in STAR as N90-14656 refs

Copyright

Discussed here is a study involving the adaptation of an advanced aeroelastic analysis program to run concurrently on a shared memory multiple processor computer. The program uses a three-dimensional compressible unsteady aerodynamic model and blade normal modes to calculate aeroelastic stability and response of propfan blades. The identification of the computational parallelism within the sequential code and the scheduling of the concurrent subtasks to minimize processor idle time are discussed. Processor idle time in the calculation of the unsteady aerodynamic coefficients was reduced by the simple strategy of appropriately ordering the computations. Speedup and efficiency results are presented for the calculation of the matched flutter point of an experimental propfan model. The results show that efficiencies above 70 percent can be obtained using the present implementation with 7 processors. The parallel computational strategy described here is also applicable to other aeroelastic analysis procedures based on panel methods. Author

A93-19279* National Aeronautics and Space Administration. Lewis Research Center, Cleveland, OH.

COUPLED MULTI-DISCIPLINARY SIMULATION OF COMPOSITE ENGINE STRUCTURES IN PROPULSION ENVIRONMENT

CHRISTOS C. CHAMIS (NASA, Lewis Research Center, Cleveland, OH) and SURENDRA N. SINGHAL (Sverdrup Technology, Inc., Cleveland, OH) Jun. 1992 11 p. ASME, International Gas Turbine and Aeroengine Congress and Exposition, 37th, Cologne, Germany, June 1-4, 1992 Previously announced in STAR as N92-23267 refs

(ASME PAPER 92-GT-6)

A computational simulation procedure is described for the coupled response of multi-layered multi-material composite engine structural components which are subjected to simultaneous multi-disciplinary thermal, structural, vibration, and acoustic loadings including the effect of hostile environments. The simulation is based on a three dimensional finite element analysis technique in conjunction with structural mechanics codes and with acoustic analysis methods. The composite material behavior is assessed at the various composite scales, i.e., the laminate/ply/constituents (fiber/matrix), via nonlinear material characterization model. Sample cases exhibiting nonlinear geometrical, material, loading, and environmental behavior of aircraft engine fan blades, are presented. Results for deformed shape, vibration frequency mode shapes, and acoustic noise emitted from the fan blade, are discussed for their coupled effect in hot and humid environments. Results such as acoustic noise for coupled composite-mechanics/heat transfer/structural/vibration/acoustic analyses demonstrate the effectiveness of coupled multi-disciplinary computational simulation the various advantages of composite materials compared to metals. Author

A93-19307* National Aeronautics and Space Administration. Lewis Research Center, Cleveland, OH.

STABILITY OF FULLY DEVELOPED ROTATING STALL

F. E. MCCAUGHAN and HONG X. XUE (Case Western Reserve Univ., Cleveland, OH) Jun. 1992 8 p. ASME, International Gas Turbine and Aeroengine Congress and Exposition, 37th, Cologne, Germany, June 1-4, 1992 refs

(Contract NAG3-1179)

(ASME PAPER 92-GT-57)

In McCaughan (1989b) it was observed that the slopes of both the axisymmetric and rotating stall characteristics play a major role in determining the mode of instability of the engine and the recovery point. That analysis was carried out for the grossly simplified model where the stall cell was considered as a traveling sine wave. That work has been extended to the more reasonable situation where the stall cell is represented by forty Fourier modes. The results from the simple model of three ordinary differential equations are discussed in the light of the more realistic calculations. In particular we discuss the effects of two parameters: the steepness of the axisymmetric characteristic and the shutoff head. Author

A93-20280*# National Aeronautics and Space Administration. Lewis Research Center, Cleveland, OH.

AN EFFICIENT CONSTRAINT TO ACCOUNT FOR MISTUNING EFFECTS IN THE OPTIMAL DESIGN OF ENGINE ROTORS

DURBHA V. MURTHY (Toledo Univ.; NASA, Lewis Research Center, Cleveland, OH), CHRISTOPHE PIERRE, and GISLI OTTARSSON (Michigan Univ., Ann Arbor) Sep. 1992 7 p. AIAA, USAF, NASA, and OAI, Symposium on Multidisciplinary Analysis and Optimization, 4th, Cleveland, OH, Sept. 21-23, 1992 refs

(AIAA PAPER 92-4711) Copyright

Blade-to-blade differences in structural properties, unavoidable in practice due to manufacturing tolerances, can have significant influence on the vibratory response of engine rotor blade. Accounting for these differences, also known as mistuning, in design and in optimization procedures is generally not possible. This note presents an easily calculated constraint that can be used in design and optimization procedures to control the sensitivity of final designs to mistuning. Author

A93-20319*# National Aeronautics and Space Administration. Lewis Research Center, Cleveland, OH.

STRUCTURAL TAILORING OF AIRCRAFT ENGINE BLADE SUBJECT TO ICE IMPACT CONSTRAINTS

E. S. REDDY, G. H. ABUMERI (Sverdrup Technology, Inc., Brook Park, OH), P. L. N. MURTHY, and C. C. CHAMIS (NASA, Lewis Research Center, Cleveland, OH) In AIAA/USAF/NASA/OAI Symposium on Multidisciplinary Analysis and Optimization, 4th, Cleveland, OH, Sept. 21-23, 1992, Technical Papers. Pt. 1 Washington American Institute of Aeronautics and Astronautics 1992 p. 197-206. refs

(AIAA PAPER 92-4710) Copyright

In this paper, results are presented for the minimum weight design of SR2 unswept blade made of (Titanium/Graphite-Epoxy/Titanium)s fiber composite. The blade which is rotating at high RPM is subject to ice impact. The root chord length, blade thicknesses at five stations, and graphite-epoxy ply orientation are chosen as design variables. The design constraints are placed on the behavior variables: leading edge strain and root damage parameter due to ice impact, maximum post-impact bending stress at the root due to rotation, first three natural frequencies and resonance margin after impact. The method of feasible directions is employed to solve the inequality constrained minimization problem. The effect of ice speed and the ice impact location on the final design are discussed. Author

A93-20320* National Aeronautics and Space Administration. Lewis Research Center, Cleveland, OH.

APPLE - AN AEROELASTIC ANALYSIS SYSTEM FOR TURBOMACHINES AND PROPFANS

T. S. R. REDDY, MILIND A. BAKHLE, R. SRIVASTAVA (Toledo

Univ., OH), and ORAL MEHMED (NASA, Lewis Research Center, Cleveland, OH) /in AIAA/USAF/NASA/OAI Symposium on Multidisciplinary Analysis and Optimization, 4th, Cleveland, OH, Sept. 21-23, 1992, Technical Papers. Pt. 1 Washington American Institute of Aeronautics and Astronautics 1992 p. 207-225. refs

(Contract NAG3-1137; NAG3-1234; NAG3-1230)

(AIAA PAPER 92-4712) Copyright

This paper reviews aeroelastic analysis methods for propulsion elements (advanced propellers, compressors and turbines) being developed and used at NASA Lewis Research Center. These aeroelastic models include both structural and aerodynamic components. The structural models include the typical section model, the beam model with and without disk flexibility, and the finite element blade model with plate bending elements. The aerodynamic models are based on the solution of equations ranging from the two-dimensional linear potential equation for a cascade to the three-dimensional Euler equations for multi-blade configurations. Typical results are presented for each aeroelastic model. Suggestions for further research are indicated. All the available aeroelastic models and analysis methods are being incorporated into a unified computer program named APPLE (Aeroelasticity Program for Propulsion at LEWIS). Author

A93-23246# National Aeronautics and Space Administration. Lewis Research Center, Cleveland, OH.

OPTIMIZATION OF CIRCULAR ORIFICE JETS MIXING INTO A HEATED CROSSFLOW IN A CYLINDRICAL DUCT

J. T. KROLL, W. A. SOWA, G. S. SAMUELSEN (California Univ., Irvine), and J. D. HOLDEMAN (NASA, Lewis Research Center, Cleveland, OH) Jan. 1993 18 p. AIAA, Aerospace Sciences Meeting and Exhibit, 31st, Reno, NV, Jan. 11-14, 1993 Previously announced in STAR as N93-15359 refs

(Contract NAG3-1110; RTOP 505-68-10)

(AIAA PAPER 93-0249) Copyright

To examine the mixing characteristics of circular jets in an axisymmetric can geometry, temperature measurements were obtained downstream of a row of cold jet injected into a heated cross stream. The objective was to obtain uniform mixing within one duct radius downstream of the leading edge of the jet orifices. An area weighted standard deviation of the mixture fraction was used to help quantify the degree of mixedness at a given plane. Non-reacting experiments were conducted to determine the influence of the number of jets on the mixedness in a cylindrical configuration. Results show that the number of orifices significantly impacts the mixing characteristics of jets injected from round hole orifices in a can geometry. Optimum mixing occurs when the mean jet trajectory aligns with the radius which divides the cross sectional area of the can into two equal parts at one mixer radius downstream of the leading edge of the orifice. The optimum number of holes at momentum-flux ratios of 25 and 52 is 10 and 15 respectively.

Author

A93-23324# National Aeronautics and Space Administration. Lewis Research Center, Cleveland, OH.

ACOUSTIC MODE MEASUREMENTS IN THE INLET OF A MODEL TURBOFAN USING A CONTINUOUSLY ROTATING RAKE - DATA COLLECTION/ANALYSIS TECHNIQUES

DAVID G. HALL (Sverdrup Technology, Inc., Brook Park; NASA, Lewis Research Center, Cleveland, OH), LAURENCE HEIDELBERG, and KEVIN KONNO (NASA, Lewis Research Center, Cleveland, OH) Jan. 1993 14 p. AIAA, Aerospace Sciences Meeting and Exhibit, 31st, Reno, NV, Jan. 11-14, 1993 Previously announced in STAR as N93-15403 refs

(Contract RTOP 535-03-10)

(AIAA PAPER 93-0599) Copyright

The rotating microphone measurement technique and data analysis procedures are documented which are used to determine circumferential and radial acoustic mode content in the inlet of the Advanced Ducted Propeller (ADP) model. Circumferential acoustic mode levels were measured at a series of radial locations using the Doppler frequency shift produced by a rotating inlet microphone probe. Radial mode content was then computed using

a least squares curve fit with the measured radial distribution for each circumferential mode. The rotating microphone technique is superior to fixed-probe techniques because it results in minimal interference with the acoustic modes generated by rotor-stator interaction. This effort represents the first experimental implementation of a measuring technique developed by T. G. Sofrin. Testing was performed in the NASA Lewis Low Speed Anechoic Wind Tunnel at a simulated takeoff condition of Mach 0.2. The design is included of the data analysis software and the performance of the rotating rake apparatus. The effect of experiment errors is also discussed. Author

A93-23384# National Aeronautics and Space Administration. Lewis Research Center, Cleveland, OH.

AN IMPROVED NUMERICAL MODEL FOR WAVE ROTOR DESIGN AND ANALYSIS

DANIEL E. PAXSON (NASA, Lewis Research Center, Cleveland, OH) and JACK WILSON (Sverdrup Technology, Inc., Cleveland, OH) Jan. 1993 11 p. AIAA, Aerospace Sciences Meeting and Exhibit, 31st, Reno, NV, Jan. 11-14, 1993 Previously announced in STAR as N93-12418 refs

(Contract RTOP 505-62-10)

(AIAA PAPER 93-0482) Copyright

A numerical model has been developed which can predict both the unsteady flows within a wave rotor and the steady averaged flows in the ports. The model is based on the assumptions of one-dimensional, unsteady, and perfect gas flow. Besides the dominant wave behavior, it is also capable of predicting the effects of finite tube opening time, leakage from the tube ends, and viscosity. The relative simplicity of the model makes it useful for design, optimization, and analysis of wave rotor cycles for any application. This paper discusses some details of the model and presents comparisons between the model and two laboratory wave rotor experiments. Author

A93-24782*# National Aeronautics and Space Administration. Lewis Research Center, Cleveland, OH.

TAKEOFF/APPROACH NOISE FOR A MODEL COUNTERROTATION PROPELLER WITH A FORWARD-SWEPT UPSTREAM ROTOR

RICHARD P. WOODWARD (NASA, Lewis Research Center, Cleveland, OH), DAVID G. HALL (Sverdrup Technology, Inc., Brook Park, OH), GARY G. PODBOY, and ROBERT J. JERACKI (NASA, Lewis Research Center, Cleveland, OH) Jan. 1993 22 p. AIAA, Aerospace Sciences Meeting and Exhibit, 31st, Reno, NV, Jan. 11-14, 1993 Previously announced in STAR as N93-16715 refs

(AIAA PAPER 93-0596) Copyright

A scale model of a counterrotating propeller with forward-swept blades in the forward rotor and aft-swept blades in the aft rotor (designated F39/A31) has been tested in the NASA Lewis 9- by 15-Foot Anechoic Wind Tunnel. This paper presents aeroacoustic results at a takeoff/approach condition of Mach 0.20. Laser Doppler Velocimeter results taken in a plane between the two rotors are also included to quantify the interaction flow field. The intention of the forward-swept design is to reduce the magnitude of the forward rotor tip vortex and/or wakes which impinge on the aft rotor, thus lowering the interaction tone levels. Author

A93-25997 National Aeronautics and Space Administration. Lewis Research Center, Cleveland, OH.

COMPARISON OF ALL-ELECTRIC SECONDARY POWER SYSTEMS FOR CIVIL TRANSPORT

DAVID D. RENZ (NASA, Lewis Research Center, Cleveland, OH) /in IECEC '92; Proceedings of the 27th Intersociety Energy Conversion Engineering Conference, San Diego, CA, Aug. 3-7, 1992. Vol. 2 Warrendale, PA Society of Automotive Engineers, Inc. 1992 p. 2.451-2.454. Previously announced in STAR as N93-10456 refs

(Contract RTOP 538-01-10)

Copyright

Three separate studies have shown operational, weight, and cost advantages for commercial subsonic transport aircraft using

an all-electric secondary power system. The first study in 1982 showed that all-electric secondary power systems produced the second largest benefit compared to four other technology upgrades. The second study in 1985 showed a 10 percent weight and fuel savings using an all-electric high frequency (20 kHz) secondary power system. The last study in 1991 showed a 2 percent weight savings using today's technology (400 Hz) in an all-electric secondary power system. This paper will compare the 20 kHz and 400 Hz studies, analyze the 2 to 10 percent difference in weight savings and comment on the common benefits of the all-electric secondary power system. Author

A93-27801# National Aeronautics and Space Administration. Lewis Research Center, Cleveland, OH.

A NUMERICAL STUDY OF MIXING IN SUPERSONIC COMBUSTORS WITH HYPERMIXING INJECTORS

J. LEE (Sverdrup Technology, Inc., Lewis Research Center Group, Brook Park, OH) Jan. 1993 26 p. AIAA, Aerospace Sciences Meeting and Exhibit, 31st, Reno, NV, Jan. 11-14, 1993 Previously announced in STAR as N93-17884 refs (Contract NAS3-25266; RTOP 505-62-40) (AIAA PAPER 93-0215) Copyright

A numerical study was conducted to evaluate the performance of wall mounted fuel-injectors designed for potential Supersonic Combustion Ramjet (SCRAM-jet) engine applications. The focus of this investigation was to numerically simulate existing combustor designs for the purpose of validating the numerical technique and the physical models developed. Three different injector designs of varying complexity were studied to fully understand the computational implications involved in accurate predictions. A dual transverse injection system and two streamwise injector designs were studied. The streamwise injectors were designed with swept ramps to enhance fuel-air mixing and combustion characteristics at supersonic speeds without the large flow blockage and drag contribution of the transverse injection system. For this study, the Mass-Average Navier-Stokes equations and the chemical species continuity equations were solved. The computations were performed using a finite-volume implicit numerical technique and multiple block structured grid system. The interfaces of the multiple block structured grid systems were numerically resolved using the flux-conservative technique. Detailed comparisons between the computations and existing experimental data are presented. These comparisons show that numerical predictions are in agreement with the experimental data. These comparisons also show that a number of turbulence model improvements are needed for accurate combustor flowfield predictions. Author

A93-30833* National Aeronautics and Space Administration. Lewis Research Center, Cleveland, OH.

EFFECT OF TABS ON THE FLOW AND NOISE FIELD OF AN AXISYMMETRIC JET

M. SAMIMY (Ohio State Univ., Columbus), K. B. M. Q. ZAMAN (NASA, Lewis Research Center, Cleveland, OH), and M. F. REEDER (Ohio State Univ., Columbus) AIAA Journal (ISSN 0001-1452) vol. 31, no. 4 April 1993 p. 609-619. Research supported by Ohio Aerospace Inst refs Copyright

The effect of vortex generators, in the form of small tabs projecting normally into the flow at the nozzle exit, on the characteristics of an axisymmetric jet is investigated experimentally over the jet Mach number range of 0.3-1.81. The tabs eliminate screech noise from supersonic jets and alter the shock structure drastically. They distort the jet cross section and increase the jet spread rate significantly. The distortion produced is essentially the same at subsonic and underexpanded supersonic conditions. Thus, the underlying mechanism must be independent of compressibility effects. A tab with a height as small as 2 percent of the jet diameter, but larger than the efflux boundary-layer thickness, is found to produce a significant effect. Flow visualization reveals that each tab introduces an 'indentation' into the high speed side of the shear layer via the action of streamwise vortices. These vortices are inferred to be of the 'trailing vortex' type rather than of the 'necklace vortex' type. It is apparent that a substantial

pressure differential must exist between the upstream and the downstream sides of the tab to effectively produce these trailing vortices. This explains why the tabs are ineffective in the overexpanded flow, as in that case an adverse pressure gradient exists near the nozzle exit which reduces the pressure differential produced by the tab. Author

A93-34159*# National Aeronautics and Space Administration. Lewis Research Center, Cleveland, OH.

AN EFFICIENT PROCEDURE FOR CASCADE AEROELASTIC STABILITY DETERMINATION USING NONLINEAR, TIME-MARCHING AERODYNAMIC SOLVERS

APARAJIT J. MAHAJAN, MILIND A. BAKHLE (Toledo Univ.; NASA, Lewis Research Center, Cleveland, OH), and EARL H. DOWELL (Duke Univ., Durham, NC) In AIAA/ASME/ASCE/AHS/ASC Structures, Structural Dynamics, and Materials Conference, 34th and AIAA/ASME Adaptive Structures Forum, La Jolla, CA, Apr. 19-22, 1993, Technical Papers. Pt. 5 Washington American Institute of Aeronautics and Astronautics 1993 p. 2856-2866. refs

(Contract NAG3-724; NAG3-1068; NAG3-1234) (AIAA PAPER 93-1631) Copyright

A numerical eigenvalue problem formulation and a practical calculation procedure for exact eigenvalues and corresponding eigenvectors are developed and applied to a nonlinear, two-dimensional, time-marching full potential solver for cascade aeroelastic stability analysis. This procedure is based on the Lanczos recursive method and it directly calculates stability information about a nonlinear steady state. It is compared to conventional approaches in the frequency and time domains developed earlier and is found to be 100-10,000 times more computationally efficient. Eigenvalue constellations and the flutter results for flow through a cascade SR5 propfan airfoil are presented. Author

A93-34160*# National Aeronautics and Space Administration. Lewis Research Center, Cleveland, OH.

EXPERIMENTAL INVESTIGATION OF COUNTER-ROTATING PROPFAN FLUTTER AT CRUISE CONDITIONS

ORAL MEHMET and ANATOLE P. KURKOV (NASA, Lewis Research Center, Cleveland, OH) In AIAA/ASME/ASCE/AHS/ASC Structures, Structural Dynamics, and Materials Conference, 34th and AIAA/ASME Adaptive Structures Forum, La Jolla, CA, Apr. 19-22, 1993, Technical Papers. Pt. 5 Washington American Institute of Aeronautics and Astronautics 1993 p. 2867-2875. refs (AIAA PAPER 93-1632) Copyright

The paper presents wind tunnel experimental flutter results, at transonic relative flows, for a 0.62-m diameter composite propfan model. A blade row that fluttered was tested alone, and with a stable aft counter-rotating blade row. The major objectives of the experiment were to study the effect of the second blade row on the row in flutter, and to investigate the flutter. Results show that the second row had a stabilizing effect. Two distinct flutter modes were found. For both flutter modes: flutter boundary, frequency, nodal diameter, and blade displacement data are given. The blade displacement data, obtained with an optical method, gives an indication of the flutter mode shape at a span near the blade tip. Author

A93-34161*# National Aeronautics and Space Administration. Lewis Research Center, Cleveland, OH.

UNSTEADY AERODYNAMICS AND FLUTTER OF PROPFANS USING A THREE-DIMENSIONAL FULL-POTENTIAL SOLVER

MILIND A. BAKHLE and T. S. R. REDDY (Toledo Univ., OH) In AIAA/ASME/ASCE/AHS/ASC Structures, Structural Dynamics, and Materials Conference, 34th and AIAA/ASME Adaptive Structures Forum, La Jolla, CA, Apr. 19-22, 1993, Technical Papers. Pt. 5 Washington American Institute of Aeronautics and Astronautics 1993 p. 2876-2886. refs

(Contract NAG3-1234) (AIAA PAPER 93-1633) Copyright

A full-potential solver coupled with a linear structural dynamics

model is used to calculate the unsteady aerodynamics and aeroelasticity of propfans. The solver allows calculations for arbitrary interblade phase angles. Results are presented for two propfan configurations. Good agreement is seen between the full-potential results and results from linear theory since the flow is subsonic and the thickness of the propfan blades is small. Some difficulty is encountered due to wave reflections from outer computational boundaries; however, this does not affect the results in the range of frequencies of aeroelastic interest. Author

A93-34162* National Aeronautics and Space Administration. Lewis Research Center, Cleveland, OH.

ON THE STATIC STABILITY OF FORWARD SWEEPED PROPFANS

R. SRIVASTAVA (Toledo Univ., OH) and O. MEHMED (NASA, Lewis Research Center, Cleveland, OH) In AIAA/ASME/ASCE/AHS/ASC Structures, Structural Dynamics, and Materials Conference, 34th and AIAA/ASME Adaptive Structures Forum, La Jolla, CA, Apr. 19-22, 1993, Technical Papers. Pt. 5 Washington American Institute of Aeronautics and Astronautics 1993 p. 2887-2892. refs (AIAA PAPER 93-1634)

An hybrid Euler solver coupled with a NASTRAN structural analysis is used to investigate the static stability characteristics of two forward swept propfan blades. The designs, having same geometry but different structural properties - one being statically stable and the other unstable, are analyzed. The stable design takes more iterations to converge than previously designed aft swept blades. The unstable design diverges to an unrealistic shape within five iterations. Author

A93-34165* National Aeronautics and Space Administration. Lewis Research Center, Cleveland, OH.

BLASIM - A COMPUTATIONAL TOOL TO ASSESS ICE IMPACT DAMAGE ON ENGINE BLADES

E. S. REDDY, G. H. ABUMERI (Sverdrup Technology, Inc., Brook Park, OH), and C. C. CHAMIS (NASA, Lewis Research Center, Cleveland, OH) In AIAA/ASME/ASCE/AHS/ASC Structures, Structural Dynamics, and Materials Conference, 34th and AIAA/ASME Adaptive Structures Forum, La Jolla, CA, Apr. 19-22, 1993, Technical Papers. Pt. 5 Washington American Institute of Aeronautics and Astronautics 1993 p. 2912-2918. refs (AIAA PAPER 93-1638) Copyright

A portable computer code called BLASIM is developed at NASA LeRC to assess the ice impact damage on aircraft engine blades. In addition to the ice impact analyses, the code is also capable of carrying out static, dynamic, resonance margin and flutter analyses. The blade can be solid, hollow, superhybrid or composite material. An optional preprocessor (input generator) is also developed to generate input to the code through interactive process. The blade geometry can be defined either by a series of airfoils at discrete input stations or by a finite element grid. The code employs a coarse fixed finite element mesh with triangular plate finite elements and has quick turnaround time. The ice piece is modeled as an equivalent spherical object and has the velocity opposite to that of the aircraft with direction parallel to the engine axis. For the local impact damage assessment, the impact force is considered as a distributed load acting over a region around the impact point and the average radial strain of the finite elements along the leading edge is taken as a measure of the local damage. To estimate the damage at the blade root, the impact is considered to be an impulse and a combined stress failure criteria is employed. Parametric studies for local and root ice impact damage, and post-impact dynamics are discussed for solid and composite blades. Author

A93-35934* National Aeronautics and Space Administration. Lewis Research Center, Cleveland, OH.

IDENTIFICATION OF THE OPEN LOOP DYNAMICS OF THE T700 TURBOSHAFT ENGINE

AHMET DUYAR, ZHEN GU (Florida Atlantic Univ., Boca Raton), and JONATHAN S. LITT (U.S. Army, Aviation Systems Command; NASA, Lewis Research Center, Cleveland, OH) In AHS, Annual

Forum, 48th, Washington, June 3-5, 1992, Proceedings. Vol. 1 Alexandria, VA American Helicopter Society 1992 p. 399-416. refs (Contract NAG3-1198) Copyright

A simplified model of the T700 turboshaft engine open loop dynamics valid within the normal operating range of the engine is developed. This model is obtained by linking the linearized point models obtained at five different operating conditions of the engine. The simplified model may be used with a model-based real time diagnostic scheme for fault detection and diagnostics, as well as for open loop engine dynamics studies and closed loop control analysis utilizing a user generated control law. Author

A93-37389* National Aeronautics and Space Administration. Lewis Research Center, Cleveland, OH.

UNSTEADY BLADE PRESSURES ON A PROPFAN AT TAKEOFF - EULER ANALYSIS AND FLIGHT DATA

M. NALLASAMY (Sverdrup Technology, Inc., Brook Park; NASA, Lewis Research Center, Cleveland, OH) Journal of Aircraft (ISSN 0021-8669) vol. 30, no. 3 May-June 1993 p. 372-376. AIAA, Aerospace Sciences Meeting and Exhibit, 30th, Reno, NV, Jan. 6-9, 1992, AIAA Paper 92-0376. Previously cited in issue 09, p. 1361, Accession no. A92-26234 refs (Contract NAS3-25266)

A93-37446* National Aeronautics and Space Administration. Lewis Research Center, Cleveland, OH.

AEROELASTIC DYNAMICS OF MISTUNED BLADE ASSEMBLIES WITH CLOSELY SPACED BLADE MODES

CHRISTOPHE PIERRE (Michigan Univ., Ann Arbor) and DURBHA V. MURTHY (NASA, Lewis Research Center, Cleveland; Toledo Univ., OH) Apr. 1993 13 p. AIAA, ASME, ASCE, AHS, and ASC, Structures, Structural Dynamics and Materials Conference, 34th and AIAA and ASME, Adaptive Structures Forum, La Jolla, CA, Apr. 19-22, 1993 refs (Contract NAG3-1163) (AIAA PAPER 93-1628) Copyright

The aeroelastic characteristics of tuned and randomly mistuned blade assemblies which possess two blade-alone natural modes with close frequencies are studied. Modal interactions among the two blade modes are shown to be come extremely significant for small frequency separation. The two distinct loci of the aeroelastic eigenvalues, which characterize an assembly with well separated modes, fully merge into a single root locus as the blade-mode frequency separation vanishes. Also, while in the case of well separated blade modes the introduction of random mistuning into one blade mode affects only the assembly modes which are predominantly of that blade-mode type, mistuning results in the localization of all the assembly modes when the blade-alone natural frequencies are close. Results indicate that in the case of closely-spaced blade modes a single-degree of freedom blade model yields qualitatively erroneous results and that an N-blade assembly with two close blade modes behaves like an equivalent 2Nb-blade assembly with a single blade mode. Author

A93-49329# National Aeronautics and Space Administration. Lewis Research Center, Cleveland, OH.

SCREENING STUDIES OF ADVANCED CONTROL CONCEPTS FOR AIRBREATHING ENGINES

PETER J. OUZTS, CARL F. LORENZO, and WALTER C. MERRILL (NASA, Lewis Research Center, Cleveland, OH) Jul. 1992 21 p. AIAA, SAE, ASME, and ASCE, Joint Propulsion Conference and Exhibit, 28th, Nashville, TN, July 6-8, 1992 Previously announced in STAR as N93-25079 refs (Contract RTOP 505-62-50) (AIAA PAPER 92-3320)

The application of advanced control concepts to airbreathing engines may yield significant improvements in aircraft/engine performance and operability. Accordingly, the NASA Lewis Research Center has conducted screening studies of advanced control concepts for airbreathing engines to determine their potential impact on turbine engine performance and operability.

The purpose of the studies was to identify concepts which offered high potential yet may incur high research and development risk. A target suite of proposed concepts was formulated by NASA and industry. These concepts were evaluated in a two phase study to quantify each concept's impact on desired engine characteristics. To aid in the evaluation, three target aircraft/engine combinations were considered: a military high performance fighter mission, a high speed civil transport mission, and a civil tiltrotor mission. Each of the advanced control concepts considered in the study were defined and described. The concept's potential impact on engine performance was determined. Relevant figures of merit on which to evaluate the concepts were also determined. Finally, the concepts were ranked with respect to the target aircraft/engine missions.

A93-49508* National Aeronautics and Space Administration. Lewis Research Center, Cleveland, OH.

A REVIEW OF CHEMICALLY REACTIVE TURBULENT FLOW MIXING MECHANISMS AND A NEW DESIGN FOR A LOW NO(X) COMBUSTOR

GIORGIO MCBEATH, BAHMAN GHORASHI (Cleveland State Univ., OH), and KUE CHUN (NASA, Lewis Research Center, Cleveland, OH) *In* Heat Transfer and Fluid Mechanics Institute, 33rd, California State Univ., Sacramento, June 3, 4, 1993, Proceedings Sacramento, CA California State University 1993 p. 55-67. refs

Copyright

A review of chemically reactive flow analysis is presented. Key studies are reviewed. The approaches to modeling chemically reactive flows that are discussed are PDF, conserved PDF, conserved scalar, stochastic, and mixing length. Turbulent mixing mechanisms are also discussed and a model is formulated that could be used for optimizing non-premixed gas reacting systems. Consequently, a re-examination of the NO(x) reduction concepts for nonpremixed reactants are suggested together with two new designs for low NO(x) subsonic combustor research.

A93-49612* National Aeronautics and Space Administration. Lewis Research Center, Cleveland, OH.

MIXING IN THE DOME REGION OF A STAGED GAS TURBINE COMBUSTOR

W. A. SOWA, R. A. BRADY, and G. S. SAMUELSEN (California Univ., Irvine) *Journal of Propulsion and Power* (ISSN 0748-4658) vol. 9, no. 5 Sept.-Oct. 1993 p. 702-707. AIAA, SAE, ASME, and ASEE, Joint Propulsion Conference and Exhibit, 28th, Nashville, TN, July 6-8, 1992, AIAA Paper 92-3089. Previously cited in issue 20, p. 3549, Accession no. A92-48734 refs

(Contract NAG3-1124)
Copyright

A93-49660*# National Aeronautics and Space Administration. Lewis Research Center, Cleveland, OH.

AN EFFICIENT LINER COOLING SCHEME FOR ADVANCED SMALL GAS TURBINE COMBUSTORS

MARC D. PASKIN, HUKAM C. MONGIA (General Motors Corp., Allison Gas Turbine Div., Indianapolis, IN), and WALDO A. ACOSTA (U.S. Army, Vehicle Propulsion Directorate; NASA, Lewis Research Center, Cleveland, OH) Jun. 1993 14 p. AIAA, SAE, ASME, and ASEE, Joint Propulsion Conference and Exhibit, 29th, Monterey, CA, June 28-30, 1993 Research supported by U.S. Army refs

(AIAA PAPER 93-1763) Copyright

A joint Army/NASA program was conducted to design, fabricate, and test an advanced, small gas turbine, reverse-flow combustor utilizing a compliant metal/ceramic (CMC) wall cooling concept. The objectives of this effort were to develop a design method (basic design data base and analysis) for the CMC cooling technique and then demonstrate its application to an advanced cycle, small, reverse-flow combustor with 3000 F burner outlet temperature. The CMC concept offers significant improvements in wall cooling effectiveness resulting in a large reduction in cooling air requirements. Therefore, more air is available for control of burner outlet temperature pattern in addition to the benefits of

improved efficiency, reduced emissions, and lower smoke levels. The program was divided into four tasks. Task 1 defined component materials and localized design of the composite wall structure in conjunction with development of basic design models for the analysis of flow and heat transfer through the wall. Task 2 included implementation of the selected materials and validated design models during combustor preliminary design. Detail design of the selected combustor concept and its refinement with 3D aerothermal analysis were completed in Task 3. Task 4 covered detail drawings, process development and fabrication, and a series of burner rig tests. The purpose of this paper is to provide details of the investigation into the fundamental flow and heat transfer characteristics of the CMC wall structure as well as implementation of the fundamental analysis method for full-scale combustor design.

Author (revised)

A93-49685*# National Aeronautics and Space Administration. Lewis Research Center, Cleveland, OH.

EXPERIMENTAL EVALUATION OF A COOLED RADIAL-INFLOW TURBINE

LIZET TIRRES (Sverdrup Technology, Inc., Brook Park, OH), L. D. DICICCO, and BRENT C. NOWLIN (NASA, Lewis Research Center, Cleveland, OH) Jun. 1993 18 p. AIAA, SAE, ASME, and ASEE, Joint Propulsion Conference and Exhibit, 29th, Monterey, CA, June 28-30, 1993 Previously announced in STAR as N93-28697 refs

(AIAA PAPER 93-1795)

Two 14.4 inch tip diameter rotors were installed and tested in the Small Engines Component Turbine Facility (SECTF) at NASA Lewis Research Center. The rotors, a solid and a cooled version of a radial-inflow turbine, were tested with a 15 vane stat or over a set of rotational speeds ranging from 80 to 120 percent design speed (17,500 to 21,500 rpm). The total-to-total stage pressure ratios ranged from 2.5 to 5.5. The data obtained at the equivalent conditions using the solid version of the rotor are presented with the cooled rotor data. A Reynolds number of 381,000 was maintained for both rotors, whose stages had a design mass flow of 4.0 lbm/sec, a design work level of 59.61 Btu/lbm, and a design efficiency of 87 percent. The results include mass flow data, turbine torque, turbine exit flow angles, stage efficiency, and rotor inlet and exit surveys.

A93-49876*# National Aeronautics and Space Administration. Lewis Research Center, Cleveland, OH.

AN ANALYTICAL STUDY OF DILUTION JET MIXING IN A CYLINDRICAL DUCT

V. L. OECHSLE, H. C. MONGIA (General Motors Corp., Allison Gas Turbine Div., Indianapolis, IN), and J. D. HOLDEMAN (NASA, Lewis Research Center, Cleveland, OH) Jun. 1993 40 p. AIAA, SAE, ASME, and ASEE, Joint Propulsion Conference and Exhibit, 29th, Monterey, CA, June 28-30, 1993 Previously announced in STAR as N93-27160 refs

(Contract NAS3-25950)

(AIAA PAPER 93-2043) Copyright

The mixing performance in a mixing section of a rich burn/quick mix/lean burn (RQL) combustor was calculated using a 3-D numerical model in a non-reacting environment. The numerically calculated results were compared with the measured data reported by Hatch, Sowa, Samuelson, and Holdeman, 1992. The numerical 3-D temperature fields qualitatively agree with the experimental data. Also, the development of the mixing flow and temperature non-uniformity trends throughout the mixing section for the numerically calculated results quantitatively agree with the measured data. The numerical model predicts less mixing and enhances the temperature gradients as compared to the measured data for the cases reported by Hatch et al. (1992) which include circular and slot orifice shapes (with different slant angles and aspect ratios). The predicted and measured results generally agree in the selection of the slanted slot orifice configuration yielding the best overall mixing performance (based on temperature uniformity) of all the configurations analyzed.

A93-49903* National Aeronautics and Space Administration. Lewis Research Center, Cleveland, OH.

COMPUTATION OF THE FLOW FIELD IN AN ANNULAR GAS TURBINE COMBUSTOR

MICHAEL C. CLINE (Los Alamos National Lab., NM), JOHN M. DEUR (Sverdrup Technology, Inc., Brook Park, OH), GERALD J. MICKLOW, MICHAEL R. HARPER (Florida Univ., Gainesville), and KRISHNA P. KUNDU (NASA, Lewis Research Center, Cleveland, OH) Jun. 1993 13 p. AIAA, SAE, ASME, and ASEE, Joint Propulsion Conference and Exhibit, 29th, Monterey, CA, June 28-30, 1993 refs
(Contract NASA ORDER C-30050-R; NAG3-1113)
(AIAA PAPER 93-2074)

The KIVA-II code was modified to calculate the 3D flow field in a typical annular gas turbine combustor. The airblast fuel nozzle, cooling baffle, cooling slots, primary and dilution jets, and effusion cooling (bleed) pads were accounted for in this calculation. The turbulence and combustion were modeled using the k-epsilon model and laminar Arrhenius kinetics, respectively. The fuel was modeled as an evaporating liquid spray. The results illustrate the complicated flow fields present in such combustors. From the results obtained to date it appears that the modified KIVA-II code can be used to study the effects of different annular combustor designs and operating conditions. Author (revised)

A93-49911* National Aeronautics and Space Administration. Lewis Research Center, Cleveland, OH.

BLADE ROW INTERACTION EFFECTS ON FLUTTER AND FORCED RESPONSE

DANIEL H. BUFFUM (NASA, Lewis Research Center, Cleveland, OH) Jun. 1993 18 p. AIAA, SAE, ASME, and ASEE, Joint Propulsion Conference and Exhibit, 29th, Monterey, CA, June 28-30, 1993 refs
(AIAA PAPER 93-2084) Copyright

In the flutter or forced response analysis of a turbomachine blade row, the blade row in question is commonly treated as if it is isolated from the neighboring blade rows. Disturbances created by vibrating blades are then free to propagate away from this blade row without being disturbed. In reality, neighboring blade rows will reflect some portion of this wave energy back toward the vibrating blades, causing additional unsteady forces on them. It is of fundamental importance to determine whether or not these reflected waves can have a significant effect on the aeroelastic stability or forced response of a blade row. Therefore, a procedure to calculate intra-blade-row unsteady aerodynamic interactions has been developed which relies upon results available from isolated blade row unsteady aerodynamic analyses. In addition, an unsteady aerodynamic influence coefficient technique is used to obtain a model for the vibratory response in which the neighboring blade rows are also flexible. The flutter analysis shows that interaction effects can be destabilizing, and the forced response analysis shows that interaction effects can result in a significant increase in the resonant response of a blade row.

A93-49912* National Aeronautics and Space Administration. Lewis Research Center, Cleveland, OH.

AN ITERATIVE MULTIDISCIPLINARY ANALYSIS FOR ROTOR BLADE SHAPE DETERMINATION

APARAJIT J. MAHAJAN and GEORGE L. STEFKO (NASA, Lewis Research Center, Cleveland, OH) Jun. 1993 12 p. AIAA, SAE, ASME, and ASEE, Joint Propulsion Conference and Exhibit, 29th, Monterey, CA, June 28-30, 1993 refs
(Contract NAG3-1068)
(AIAA PAPER 93-2085) Copyright

A CFD solver called ADPAC-APES is coupled with a NASTRAN structural analysis and a MARC thermal/heat transfer analysis to determine rotor blade shape. Nonlinear blade displacements due to centrifugal loads, aerodynamic pressures, and nonuniform temperature distribution are determined simultaneously. The effect of blade displacements on aerodynamic pressures and temperatures is then analyzed. These calculations are iterated till a steady state is reached across all the disciplines. This iterative procedure is applied to a ducted fan rotor blade and the

manufactured shape is determined from a given operating shape. Effect of a part-span shroud on blade deflections is also analyzed. Author (revised)

A93-50008* National Aeronautics and Space Administration. Lewis Research Center, Cleveland, OH.

INTEGRATED CFD MODELING OF GAS TURBINE COMBUSTORS

E. J. FULLER and C. E. SMITH (CFD Research Corp., Huntsville, AL) Jun. 1993 22 p. AIAA, SAE, ASME, and ASEE, Joint Propulsion Conference and Exhibit, 29th, Monterey, CA, June 28-30, 1993 refs
(Contract NAS3-26616)
(AIAA PAPER 93-2196) Copyright

3D, curvilinear, multi-domain CFD analysis is becoming a valuable tool in gas turbine combustor design. Used as a supplement to experimental testing, CFD analysis can provide improved understanding of combustor aerodynamics and used to qualitatively assess new combustor designs. This paper discusses recent advancements in CFD combustor methodology, including the timely integration of the design (i.e. CAD) and analysis (i.e. CFD) processes. Allied Signal's F124 combustor was analyzed at maximum power conditions. The assumption of turbulence levels at the nozzle/swirler inlet was shown to be very important in the prediction of combustor exit temperatures. Predicted exit temperatures were compared to experimental rake data, and good overall agreement was seen. Exit radial temperature profiles were well predicted, while the predicted pattern factor was 25 percent higher than the harmonic-averaged experimental pattern factor.

A93-50052* National Aeronautics and Space Administration. Lewis Research Center, Cleveland, OH.

OPTIMIZATION OF BLADE ARRANGEMENT IN A RANDOMLY MISTUNED CASCADE USING SIMULATED ANNEALING

EDWARD A. THOMPSON and GEORGES A. BECUS (Cincinnati Univ., OH) Jun. 1993 8 p. AIAA, SAE, ASME, and ASEE, Joint Propulsion Conference and Exhibit, 29th, Monterey, CA, June 28-30, 1993 refs
(Contract NAG3-1173)
(AIAA PAPER 93-2254) Copyright

This paper presents preliminary results of an investigation on mistuning of bladed-disk assemblies aimed at capturing the benefits of mistuning on stability, while at the same time, minimizing the adverse effects on response by solving the following problem: given a set of N turbine blades, each being a small random perturbation of the same nominal blade, determine the best arrangement of the N blades in a mistuned cascade with regard to aeroelastic response. In the studies reported here, mistuning of the blades is restricted to small differences in torsional stiffness. The large combinatorial optimization problem of seeking the best arrangement by blade exchanges is solved using a simulated annealing algorithm.

A93-50104* National Aeronautics and Space Administration. Lewis Research Center, Cleveland, OH.

IN-STREAM MEASUREMENTS OF COMBUSTION DURING MACH 5 TO 7 TESTS OF THE HYPERSONIC RESEARCH ENGINE (HRE)

ERWIN A. LEZBERG, ALLEN J. METZLER, and WILLIAM D. PACK (NASA, Lewis Research Center, Cleveland, OH) Jun. 1993 21 p. AIAA, SAE, ASME, and ASEE, Joint Propulsion Conference and Exhibit, 29th, Monterey, CA, June 28-30, 1993 refs
(AIAA PAPER 93-2324) Copyright

Results of in-stream combustion measurements taken during Mach 5 to 7 true simulation testing of the Hypersonic Research Engine/Aerothermodynamic Integration Model (HRE/AIM) are presented. These results, the instrumentation techniques, and configuration changes to the engine installation that were required to test this model are described. In test runs at facility Mach numbers of 5 to 7, an exhaust instrumentation ring which formed an extension of the engine exhaust nozzle shroud provided diagnostic measurements at 10 circumferential locations in the HRE combustor exit plane. The measurements included static and

pitot pressures using conventional conical probes, combustion gas temperatures from cooled-gas pyrometer probes, and species concentration from analysis of combustion gas samples. Results showed considerable circumferential variation, indicating that efficiency losses were due to nonuniform fuel distribution or incomplete mixing. Results using the Mach 7 facility nozzle but with Mach 6 temperature simulation, 1590 to 1670 K, showed indications of incomplete combustion. Nitric oxide measurements at the combustor exit peaked at 2000 ppmv for stoichiometric combustion at Mach 6.

Author (revised)

A93-50189*# National Aeronautics and Space Administration. Lewis Research Center, Cleveland, OH.

PERFORMANCE CHARACTERISTICS OF A VARIABLE-AREA VANE NOZZLE FOR VECTORING AN ASTOVL EXHAUST JET UP TO 45 DEG

JACK G. MCARDLE and BARBARA S. ESKER (NASA, Lewis Research Center, Cleveland, OH) Jun. 1993 33 p. AIAA, SAE, ASME, and ASEE, Joint Propulsion Conference and Exhibit, 29th, Monterey, CA, June 28-30, 1993 Previously announced in STAR as N93-27131 refs (AIAA PAPER 93-2437) Copyright

Many conceptual designs for advanced short-takeoff, vertical landing (ASTOVL) aircraft need exhaust nozzles that can vector the jet to provide forces and moments for controlling the aircraft's movement or attitude in flight near the ground. A type of nozzle that can both vector the jet and vary the jet flow area is called a vane nozzle. Basically, the nozzle consists of parallel, spaced-apart flow passages formed by pairs of vanes (vanesets) that can be rotated on axes perpendicular to the flow. Two important features of this type of nozzle are the abilities to vector the jet rearward up to 45 degrees and to produce less harsh pressure and velocity footprints during vertical landing than does an equivalent single jet. A one-third-scale model of a generic vane nozzle was tested with unheated air at the NASA Lewis Research Center's Powered Lift Facility. The model had three parallel flow passages. Each passage was formed by a vaneset consisting of a long and a short vane. The longer vanes controlled the jet vector angle, and the shorter controlled the flow area. Nozzle performance for three nominal flow areas (basic and plus or minus 21 percent of basic area), each at nominal jet vector angles from -20 deg (forward of vertical) to +45 deg (rearward of vertical) are presented. The tests were made with the nozzle mounted on a model tailpipe with a blind flange on the end to simulate a closed cruise nozzle, at tailpipe-to-ambient pressure ratios from 1.8 to 4.0. Also included are jet wake data, single-vaneset vector performance for long/short and equal-length vane designs, and pumping capability. The pumping capability arises from the subambient pressure developed in the cavities between the vanesets, which could be used to aspirate flow from a source such as the engine compartment. Some of the performance characteristics are compared with characteristics of a single-jet nozzle previously reported.

A93-50190*# National Aeronautics and Space Administration. Lewis Research Center, Cleveland, OH.

EFFECTS OF FLOW-PATH VARIATIONS ON INTERNAL REVERSING FLOW IN A TAILPIPE OFFTAKE CONFIGURATION FOR ASTOVL AIRCRAFT

JACK G. MCARDLE and BARBARA S. ESKER (NASA, Lewis Research Center, Cleveland, OH) Jun. 1993 22 p. AIAA, SAE, ASME, and ASEE, Joint Propulsion Conference and Exhibit, 29th, Monterey, CA, June 28-30, 1993 Previously announced in STAR as N93-29065 refs (AIAA PAPER 93-2438) Copyright

A one-third-scale model of a generic tailpipe offtake system for an advanced short takeoff, vertical landing (ASTOVL) aircraft was tested at the NASA Lewis Research Center Powered Lift Facility. The basic model consisted of a tailpipe with a center body to form an annulus simulating turbine outflow with no swirl; twin offtake ducts with elbows at the ends to turn the flow to a downward direction; flow control nozzles at the ends of the elbows; and a blind flange at the end of the tailpipe to simulate a closed cruise nozzle. The offtake duct-to-tailpipe diameter ratio was 0.74.

Modifications of a generic nature were then made to this basic configuration to measure the effects of flow-path changes on the flow and pressure-loss characteristics. The modifications included adding rounded entrances at the forward edges of the offtake openings, blocking the tailpipe just aft the openings instead of at the cruise nozzle, changing the location of the openings along the tailpipe, removing the center body, and varying the Mach number (flow rate) over a wide range in the tailpipe ahead of the openings by changing the size of the flow control nozzles. The tests were made with unheated air at tailpipe-to-ambient pressure ratios from 1.4 to 5. Results are presented and compared with performance graphs, total-pressure contour plots, paint streak flow visualization photographs, and a flow-angle probe traverse at the offtake entrance.

A93-50192*# National Aeronautics and Space Administration. Lewis Research Center, Cleveland, OH.

INITIAL DEVELOPMENT OF THE TWO-DIMENSIONAL EJECTOR SHEAR LAYER - EXPERIMENTAL RESULTS

M. A. BENJAMIN, M. DUFFLOCQ, and V. P. ROAN (Florida Univ., Gainesville) Jun. 1993 11 p. AIAA, SAE, ASME, and ASEE, Joint Propulsion Conference and Exhibit, 29th, Monterey, CA, June 28-30, 1993 refs (Contract NAG3-1187)

(AIAA PAPER 93-2440) Copyright

An experimental investigation designed to study the development of shear layers in a two-dimensional single-nozzle ejector has been completed. In this study, combinations of air/air, argon/air, helium/air, and air/helium were used as the supersonic primary and subsonic secondary, respectively. Mixing of the gases occurred in a constant-area tube 39.1 mm high by 25.4 mm wide, where the inlet static pressure was maintained at 35 kPa. The cases studied resulted in convective Mach numbers between 0.058 and 1.64, density ratios between 0.102 and 3.49, and velocity ratios between 0.065 and 0.811. The resulting data shows the differences in the shear-layer development for the various combinations of independent variables utilized in the investigation. The normalized growth-rates in the near-field were found to be similar to two-dimensional mixing layers. These results have enhanced the ability to analyze and design ejector systems as well as providing a better understanding of the physics.

A93-50193*# National Aeronautics and Space Administration. Lewis Research Center, Cleveland, OH.

COMPARISON OF THE INITIAL DEVELOPMENT OF SHEAR LAYERS IN TWO-DIMENSIONAL AND AXISYMMETRIC EJECTOR CONFIGURATIONS

M. DUFFLOCQ, M. A. BENJAMIN, and V. P. ROAN (Florida Univ., Gainesville) Jun. 1993 10 p. AIAA, SAE, ASME, and ASEE, Joint Propulsion Conference and Exhibit, 29th, Monterey, CA, June 28-30, 1993 refs (Contract NAG3-1187)

(AIAA PAPER 93-2441) Copyright

A two-phase experimental investigation designed to study the development of shear layers in axisymmetric and two-dimensional single-nozzle ejectors has been completed. In this study, combinations of similar and dissimilar gases were used as the supersonic primary and subsonic secondary. Test cases included combinations of air/air, argon/air and helium/air as the supersonic primary and subsonic secondary, respectively. Similar flow conditions were studied for each ejector configuration. Mixing of the gases occurred in a constant-area tube, where the inlet pressure was maintained at 34.5 kPa. The cases studied resulted in convective Mach numbers that range between 0.06 and 1.9. The data gathered shows differences between the initial shear-layer development for the two ejector geometries, and also between the different test cases studied for each ejector configuration. The measured growth rates for the axisymmetric ejector are more than twice those measured for the two-dimensional ejector. However, in both cases the results show that compressibility has a reducing effect on the growth rate. Further, in the region immediately after the inlet to the mixing tube, compressibility seems to affect the

07 AIRCRAFT PROPULSION AND POWER

ejector shear layers in a manner similar to that of two-stream two-dimensional mixing layers.

A93-50252*# National Aeronautics and Space Administration. Lewis Research Center, Cleveland, OH.

A COMPARISON BETWEEN NUMERICALLY MODELLED AND EXPERIMENTALLY MEASURED LOSS MECHANISMS IN WAVE ROTORS

DANIEL E. PAXSON (NASA, Lewis Research Center, Cleveland, OH) Jun. 1993 12 p. AIAA, SAE, ASME, and ASEE, Joint Propulsion Conference and Exhibit, 29th, Monterey, CA, June 28-30, 1993 refs

(AIAA PAPER 93-2522) Copyright

A numerical model has been developed which is capable of predicting the performance of a wave rotor (pressure exchanger) of specified geometry over a wide range of operating conditions. The model can account for the major loss mechanisms of leakage from the tube ends, fluid viscosity, heat transfer to the tube walls, finite tube opening time, shock waves, and non-uniform port flows. It is a one dimensional flow model which follows a single tube as it rotates past the various stationary ports. Since the model is relatively simple (i.e., one dimensional) it uses little computer time. This makes it suitable for design as well as analytical purposes. This paper will present a brief description of the model then discuss a comparison between the model predictions and several wave rotor experiments.

A93-50253*# National Aeronautics and Space Administration. Lewis Research Center, Cleveland, OH.

ANALYTIC METHODS FOR DESIGN OF WAVE CYCLES FOR WAVE ROTOR CORE ENGINES

EDWIN L. RESLER, JR., JEFFREY C. MOCSARI, and M. R. NALIM (Cornell Univ., Ithaca, NY) Jun. 1993 13 p. AIAA, SAE, ASME, and ASEE, Joint Propulsion Conference and Exhibit, 29th, Monterey, CA, June 28-30, 1993 Research supported by NASA refs

(AIAA PAPER 93-2523) Copyright

A procedure to design a preliminary wave rotor cycle for any application is presented. To complete a cycle with heat addition there are two separate but related design steps that must be followed. The 'wave' boundary conditions determine the allowable amount of heat added in any case and the ensuing wave pattern requires certain pressure discharge conditions to allow the process to be made cyclic. This procedure, when applied, gives a first estimate of the cycle performance and the necessary information for the next step in the design process, namely the application of a characteristic based or other appropriate detailed one dimensional wave calculation that locates the proper porting around the periphery of the wave rotor. Four examples of the design procedure are given to demonstrate its utility and generality. These examples also illustrate the large gains in performance that could be realized with the use of wave rotor enhanced propulsion cycles.

A93-50277*# National Aeronautics and Space Administration. Lewis Research Center, Cleveland, OH.

NAVIER-STOKES ANALYSIS OF RADIAL TURBINE ROTOR PERFORMANCE

L. M. LAROSILIERE (Ohio Aerospace Inst., Brook Park) Jun. 1993 19 p. AIAA, SAE, ASME, and ASEE, Joint Propulsion Conference and Exhibit, 29th, Monterey, CA, June 28-30, 1993 Previously announced in STAR as N93-28609 Research sponsored by NASA refs

(AIAA PAPER 93-2555) Copyright

An analysis of flow through a radial turbine rotor using the three-dimensional, thin-layer Navier-Stokes code RVC3D is described. The rotor is a solid version of an air-cooled metallic radial turbine having thick trailing edges, shroud clearance, and scalloped-backface clearance. Results are presented at the nominal operating condition using both a zero-clearance model and a model simulating the effects of the shroud and scalloped-backface clearance flows. A comparison with the available test data is made and details of the internal flow physics are discussed, allowing a

better understanding of the complex flow distribution within the rotor.

A93-50294*# National Aeronautics and Space Administration. Lewis Research Center, Cleveland, OH.

NONLINEAR DYNAMIC SIMULATION OF SINGLE- AND MULTI-SPOOL CORE ENGINES

T. SCHOBELI, C. LIPPKE, and M. ABOUELKHEIR (Texas A & M Univ., College Station) Jun. 1993 15 p. AIAA, SAE, ASME, and ASEE, Joint Propulsion Conference and Exhibit, 29th, Monterey, CA, June 28-30, 1993 Research supported by NASA refs

(AIAA PAPER 93-2580) Copyright

In this paper a new computational method for accurate simulation of the nonlinear dynamic behavior of single- and multi-spool core engines, turbofan engines, and power generation gas turbine engines is presented. In order to perform the simulation, a modularly structured computer code has been developed which includes individual mathematical modules representing various engine components. The generic structure of the code enables the dynamic simulation of arbitrary engine configurations ranging from single-spool thrust generation to multi-spool thrust/power generation engines under adverse dynamic operating conditions. For precise simulation of turbine and compressor components, row-by-row calculation procedures were implemented that account for the specific turbine and compressor cascade and blade geometry and characteristics. The dynamic behavior of the subject engine is calculated by solving a number of systems of partial differential equations, which describe the unsteady behavior of the individual components. In order to ensure the capability, accuracy, robustness, and reliability of the code, comprehensive critical performance assessment and validation tests were performed. As representatives, three different transient cases with single- and multi-spool thrust and power generation engines were simulated. The transient cases range from operating with a prescribed fuel schedule, to extreme load changes, to generator and turbine shut down.

A93-51403*# National Aeronautics and Space Administration. Lewis Research Center, Cleveland, OH.

ANTIWINDUP ANALYSIS AND DESIGN APPROACHES FOR MIMO SYSTEMS

VINCENT R. MARCOPOLI and STEPHEN M. PHILLIPS (Case Western Reserve Univ., Cleveland, OH) In AIAA Guidance, Navigation and Control Conference, Monterey, CA, Aug. 9-11, 1993, Technical Papers. Pt. 2 Washington American Institute of Aeronautics and Astronautics 1993 p. 1006-1011. refs

(Contract NAG3-1232)

(AIAA PAPER 93-3811) Copyright

Performance degradation of multiple-input multiple-output (MIMO) control systems having limited actuators is often handled by augmenting the controller with an antiwindup mechanism, which attempts to maintain system performance when limits are encountered. The goals of this paper are: 1) to develop a method to analyze antiwindup systems to determine precisely what stability and performance degradation is incurred under limited conditions. It is shown that by reformulating limited actuator commands as resulting from multiplicative perturbations to the corresponding controller requests, mu-analysis tools can be utilized to obtain quantitative measures of stability and performance degradation. 2) To propose a linear, time invariant (LTI) criterion on which to base the antiwindup design. These analysis and design methods are illustrated through the evaluation of two competing antiwindup schemes augmenting the controller of a Short Take-Off and Vertical Landing (STOVL) aircraft in transition flight.

A93-53589*# National Aeronautics and Space Administration. Lewis Research Center, Cleveland, OH.

INITIAL RESULTS FROM THE NASA LEWIS WAVE ROTOR EXPERIMENT

JACK WILSON (Sverdrup Technology, Inc., Lewis Research Center Group, Brook Park, OH) and DENNIS FRONEK (NASA, Lewis Research Center, Cleveland, OH) Jun. 1993 10 p. AIAA,

SAE, ASME, and ASEE, Joint Propulsion Conference and Exhibit, 29th, Monterey, CA, June 28-30, 1993 Previously announced in STAR as N93-32368 refs (AIAA PAPER 93-2521) Copyright

Wave rotors may play a role as topping cycles for jet engines, since by their use, the combustion temperature can be raised without increasing the turbine inlet temperature. In order to design a wave rotor for this, or any other application, knowledge of the loss mechanisms is required, and also how the design parameters affect those losses. At NASA LeRC, a 3-port wave rotor experiment operating on the flow-divider cycle, has been started with the objective of determining the losses. The experimental scheme is a three factor Box-Behnken design, with passage opening time, friction factor, and leakage gap as the factors. Variation of these factors is provided by using two rotors, of different length, two different passage widths for each rotor, and adjustable leakage gap. In the experiment, pressure transducers are mounted on the rotor, and give pressure traces as a function of rotational angle at the entrance and exit of a rotor passage. In addition, pitot rakes monitor the stagnation pressures for each port, and orifice meters measure the mass flows. The results show that leakage losses are very significant in the present experiment, but can be reduced considerably by decreasing the rotor to wall clearance spacing.

A93-53980 National Aeronautics and Space Administration. Lewis Research Center, Cleveland, OH.

PROPULSION TECHNOLOGY CHALLENGES FOR TURN-OF-THE-CENTURY COMMERCIAL AIRCRAFT

JOSEPH A. ZIEMIANSKI and CALVIN L. BALL (NASA, Lewis Research Center, Cleveland, OH) /n ISABE - International Symposium on Air Breathing Engines, 11th, Tokyo, Japan, Sept. 20-24, 1993, Proceedings. Vol. 1 Washington American Institute of Aeronautics and Astronautics 1993 p. 26-37. Previously announced in STAR as N93-32351 refs (Contract RTOP 505-62-10) (ISABE 93-7003) Copyright

This paper highlights the efforts being performed or sponsored by NASA, in cooperation with the U.S. civil aviation industry, to address the propulsion system technological challenges that must be met in order to ensure a viable future for the industry. Both the subsonic and supersonic aeropropulsion programs are considered. Subsonic transport propulsion program elements, including ultra-high-bypass-ratio turbofans with attendant noise reduction efforts, high-efficiency cores, and combustor emissions reductions are discussed in terms of goals, technical issues, and problem solutions. Similarly, the high-speed research propulsion efforts addressing a high-speed commercial transport are reviewed in terms of environmental barrier issues, such as oxides of nitrogen and noise reduction, and the related economic issues.

A93-53999* National Aeronautics and Space Administration. Lewis Research Center, Cleveland, OH.

EMISSION CHARACTERISTICS OF A MODEL GAS TURBINE COMBUSTOR AT PRACTICAL CONDITIONS

S. A. DRENNAN, W. A. SOWA, and G. S. SAMUELSEN (California Univ., Irvine) /n ISABE - International Symposium on Air Breathing Engines, 11th, Tokyo, Japan, Sept. 20-24, 1993, Proceedings. Vol. 1 Washington American Institute of Aeronautics and Astronautics 1993 p. 244-253. Research supported by Northrop Corp. refs (Contract F08635-90-C-0100; NAG3-1124) (ISABE 93-7023)

This paper reports on in situ and exit plane emissions measurements from a model gas turbine combustor at practical air preheat temperatures and pressures for a range of operating conditions. The model combustor chosen for the study features two rows of jets (primary and dilution) with four jets per row, and utilizes effusive air cooling holes on the liner wall. The combustor dome is equipped with a flat-vaned swirler with a vane angle of 60 deg. Data are obtained at combustor pressures ranging from 2 to 10 atmospheres, air preheat temperatures from 204 C to 427 C, and combustor reference velocities from 10.0 to 20.0 m/s. An overall equivalence ratio of 0.3 was constant for all conditions.

Exit plane and in situ measurements are presented for HC, O₂, CO₂, CO, and NO(x). The results from exit plane NO(x) measurements illustrate that the model combustor is representative of current gas turbine combustors. The in situ data reveal effects of fuel/air and wall jet mixing on emission performance.

Author (revised)

A93-54003* National Aeronautics and Space Administration. Lewis Research Center, Cleveland, OH.

FORCING FUNCTION MODELING FOR FLOW INDUCED VIBRATION

SANFORD FLEETER (Purdue Univ., West Lafayette, IN) /n ISABE - International Symposium on Air Breathing Engines, 11th, Tokyo, Japan, Sept. 20-24, 1993, Proceedings. Vol. 1 Washington American Institute of Aeronautics and Astronautics 1993 p. 305-318. Research sponsored by NASA refs (ISABE 93-7027) Copyright

The fundamental forcing function unsteady aerodynamics for application to turbomachine blade row forced response are considered, accomplished through a series of experiments performed in a rotating annular cascade and a research axial flow turbine. In particular, the unsteady periodic flowfields downstream of rotating rows of perforated plates, airfoils and turbine blade rows are measured with a cross hot-wire and an unsteady total pressure probe. The unsteady velocity and static pressure fields were then analyzed harmonically and split into vortical and potential gusts, accomplished by developing a gust splitting analysis which includes both gust unsteady static pressure and velocity data. The perforated plate gusts closely were found to be linear theory vortical gusts, satisfying the vortical gust constraints. The airfoil and turbine blade row generated velocity perturbations did not satisfy the vortical gust constraints. However, the decomposition of the unsteady flow field separated the data into a propagating vortical component which satisfied these vortical gust constraints and a decaying potential component.

A93-54040 National Aeronautics and Space Administration. Lewis Research Center, Cleveland, OH.

ENGINE TECHNOLOGY CHALLENGES FOR A 21ST CENTURY HIGH-SPEED CIVIL TRANSPORT

ROBERT J. SHAW (NASA, Lewis Research Center, Cleveland, OH), SAMUEL GILKEY (GE Aircraft Engines, Evendale, OH), and RICHARD HINES (Pratt & Whitney Group, Hartford, CT) /n ISABE - International Symposium on Air Breathing Engines, 11th, Tokyo, Japan, Sept. 20-24, 1993, Proceedings. Vol. 1 Washington American Institute of Aeronautics and Astronautics 1993 p. 673-683. Previously announced in STAR as N93-31671 refs (Contract RTOP 537-02-00) (ISABE 93-7064) Copyright

Ongoing NASA-funded studies by Boeing, McDonnell-Douglas, General Electric, and Pratt & Whitney indicate that an opportunity exists for a 21st Century High-Speed Civil Transport (HSCT) to become a major part of the international air transportation system. However, before industry will consider an HSCT product launch and an investment estimated to be over \$15 billion for design and certification, major technology advances must be made. An overview of the propulsion-specific technology advances that must be in hand before an HSCT product launch could be considered is presented.

A93-54043* National Aeronautics and Space Administration. Lewis Research Center, Cleveland, OH.

MATERIAL REQUIREMENTS FOR THE HIGH SPEED CIVIL TRANSPORT

JOSEPH R. STEPHENS (NASA, Lewis Research Center, Cleveland, OH), RALPH J. HECHT (Pratt & Whitney Group, West Palm Beach, FL), and ANDREW M. JOHNSON (GE Aircraft Engines, Cincinnati, OH) /n ISABE - International Symposium on Air Breathing Engines, 11th, Tokyo, Japan, Sept. 20-24, 1993, Proceedings. Vol. 1 Washington American Institute of Aeronautics and Astronautics 1993 p. 701-710. refs (ISABE 93-7067) Copyright

Under NASA-sponsored High Speed Research (HSR) programs,

07 AIRCRAFT PROPULSION AND POWER

the materials and processing requirements have been identified for overcoming the environmental and economic barriers of the next generation High Speed Civil Transport (HSCT) propulsion system. The long (2 to 5 hours) supersonic cruise portion of the HSCT cycle will place additional durability requirements on all hot section engine components. Low emissions combustor designs will require high temperature ceramic matrix composite liners to meet an emission goal of less than 5g NO(x) per Kg fuel burned. Large axisymmetric and two-dimensional exhaust nozzle designs are now under development to meet or exceed FAR 36 Stage III noise requirements, and will require lightweight, high temperature metallic, intermetallic, and ceramic matrix composites to reduce nozzle weight and meet structural and acoustic component performance goals. This paper describes and discusses the turbomachinery, combustor, and exhaust nozzle requirements of the High Speed Civil Transport propulsion system.

N93-10456* # National Aeronautics and Space Administration. Lewis Research Center, Cleveland, OH.

COMPARISON OF ALL-ELECTRIC SECONDARY POWER SYSTEMS FOR CIVIL SUBSONIC TRANSPORTS

DAVID D. RENZ 1992 6 p Presented at the 27th Intersociety Energy Conversion Engineering Conference, San Diego, CA, 3-7 Aug. 1992; sponsored by SAE, ACS, AIAA, ASME, IEEE, AIChE, and ANS

(Contract RTOP 538-01-10)

(NASA-TM-105852; E-7300; NAS 1.15:105852) Avail: CASI HC A02/MF A01

Three separate studies have shown operational, weight, and cost advantages for commercial subsonic transport aircraft using an all-electric secondary power system. The first study in 1982 showed that all-electric secondary power systems produced the second largest benefit compared to four other technology upgrades. The second study in 1985 showed a 10 percent weight and fuel savings using an all-electric high frequency (20 kHz) secondary power system. The last study in 1991 showed a 2 percent weight savings using today's technology (400 Hz) in an all-electric secondary power system. This paper will compare the 20 kHz and 400 Hz studies, analyze the 2 to 10 percent difference in weight savings and comment on the common benefits of the all-electric secondary power system. Author

N93-10983* # National Aeronautics and Space Administration. Lewis Research Center, Cleveland, OH.

AN INTERACTIVE PREPROCESSOR FOR THE NASA ENGINE PERFORMANCE PROGRAM

JEFFREY J. BERTON and ROBERT M. PLENCNER Aug. 1992 28 p

(Contract RTOP 505-69-50)

(NASA-TM-105786; E-7216; NAS 1.15:105786) Avail: CASI HC A03/MF A01

The Simplified NEPP Automated Preprocessor (SNAP), which is written to aid in the preparation of input data files for the NASA Engine Performance Program (NEPP), is described. Specifically, SNAP is a software package on the Virtual Machine operating system that prompts the NEPP user for input information via a series of menus. The data collected from these menus are assimilated into an input file suitable for the running of NEPP. SNAP acts as a user-friendly preprocessing interface for NEPP. This serves as an introduction to the SNAP software, a user's manual, a description of the program logic, and a maintenance manual for future modifications to the software. Author

N93-11530* # National Aeronautics and Space Administration. Lewis Research Center, Cleveland, OH.

OVERVIEW OF HIGH PERFORMANCE AIRCRAFT PROPULSION RESEARCH

THOMAS J. BIESIADNY Oct. 1992 17 p Presented at the Aerotech 1992 Conference, Anaheim, CA, 5-8 Oct. 1992

(Contract RTOP 505-68-32)

(NASA-TM-105839; E-7280; NAS 1.15:105839) Avail: CASI HC A03/MF A01

The overall scope of the NASA Lewis High Performance Aircraft

Propulsion Research Program is presented. High performance fighter aircraft of interest include supersonic flights with such capabilities as short take off and vertical landing (STOVL) and/or high maneuverability. The NASA Lewis effort involving STOVL propulsion systems is focused primarily on component-level experimental and analytical research. The high-maneuverability portion of this effort, called the High Alpha Technology Program (HATP), is part of a cooperative program among NASA's Lewis, Langley, Ames, and Dryden facilities. The overall objective of the NASA Inlet Experiments portion of the HATP, which NASA Lewis leads, is to develop and enhance inlet technology that will ensure high performance and stability of the propulsion system during aircraft maneuvers at high angles of attack. To accomplish this objective, both wind-tunnel and flight experiments are used to obtain steady-state and dynamic data, and computational fluid dynamics (CFD) codes are used for analyses. This overview of the High Performance Aircraft Propulsion Research Program includes a sampling of the results obtained thus far and plans for the future. Author

N93-12077* # National Aeronautics and Space Administration. Lewis Research Center, Cleveland, OH.

AN EXPERIMENTAL INVESTIGATION OF THE FLOW IN A DIFFUSING S-DUCT

STEVEN R. WELLBORN (Iowa State Univ. of Science and Technology, Ames.), BRUCE A. REICHERT, and THEODORE H. OKIISHI (Iowa State Univ. of Science and Technology, Ames.) Aug. 1992 13 p Presented at the 28th Joint Propulsion Conference and Exhibit, Nashville, TN, 6-8 Jul. 1992; sponsored by AIAA, SAE, ASME, and ASEE Previously announced in IAA as A92-54090

(Contract RTOP 505-62-52)

(NASA-TM-105809; E-7240; NAS 1.15:105809; AIAA PAPER 92-3622) Copyright Avail: CASI HC A03/MF A01

Compressible, subsonic flow through a diffusing S-duct has been experimentally investigated. Benchmark aerodynamic data are presented for flow through a representative S-duct configuration. The collected data would be beneficial to aircraft inlet designers and is suitable for the validation of computational codes. Measurements of the 3D velocity field and total and static pressures were obtained at five cross-sectional planes. Surface static pressures and flow visualization also helped to reveal flow field characteristics. All reported tests were conducted with an inlet centerline Mach number of 0.6 and a Reynolds number, based on the inlet centerline velocity and duct inlet diameter, of 2.6×10^6 (exp 6). The results show that a larger region of streamwise flow separation occurred within the duct. Details about the separated flow region, including mechanisms which drive this complicated flow phenomenon, are discussed. Transverse velocity components indicate that the duct curvature induces strong pressure driven secondary flows, which evolve into a large pair of counter-rotating vortices. These vortices convect the low momentum fluid of the boundary layer towards the center of the duct, degrading both the uniformity and magnitude of the total pressure profile. Author

N93-12402* # National Aeronautics and Space Administration. Lewis Research Center, Cleveland, OH.

CONCURRENT OPTIMIZATION OF AIRFRAME AND ENGINE DESIGN PARAMETERS

THOMAS M. LAVELLE, ROBERT M. PLENCNER, and JONATHAN A. SEIDEL Oct. 1991 17 p Presented at the Fourth Symposium on Multidisciplinary Analysis and Optimization, Cleveland, OH, 21-23 Sep. 1992; sponsored by AIAA, USAF, and OAI

(Contract RTOP 505-69-50)

(NASA-TM-105908; E-7382; NAS 1.15:105908; AIAA PAPER 92-4713) Avail: CASI HC A03/MF A01

An integrated system for the multidisciplinary analysis and optimization of airframe and propulsion design parameters is being developed. This system is known as IPAS, the Integrated Propulsion/Airframe Analysis System. The traditional method of analysis is one in which the propulsion system analysis is loosely coupled to the overall mission performance analysis. This results

in a time consuming iterative process. First, the engine is designed and analyzed. Then, the results from this analysis are used in a mission analysis to determine the overall aircraft performance. The results from the mission analysis are used as a guide as the engine is redesigned and the entire process repeated. In IPAS, the propulsion system, airframe, and mission are closely coupled. The propulsion system analysis code is directly integrated into the mission analysis code. This allows the propulsion design parameters to be optimized along with the airframe and mission design parameters, significantly reducing the time required to obtain an optimized solution.

Author

N93-12418*# National Aeronautics and Space Administration. Lewis Research Center, Cleveland, OH.

AN IMPROVED NUMERICAL MODEL FOR WAVE ROTOR DESIGN AND ANALYSIS

DANIEL E. PAXSON and JACK WILSON (Sverdrup Technology, Inc., Brook Park, OH.) Oct. 1992 12 p Proposed for presentation at the 31st Aerospace Sciences Meeting, Reno, NV, 11-14 Jan. 1993; sponsored by AIAA (Contract RTOP 505-62-10) (NASA-TM-105915; E-7398; NAS 1.15:105915; AIAA PAPER 93-0482) Avail: CASI HC A03/MF A01

A numerical model has been developed which can predict both the unsteady flows within a wave rotor and the steady averaged flows in the ports. The model is based on the assumptions of one-dimensional, unsteady, and perfect gas flow. Besides the dominant wave behavior, it is also capable of predicting the effects of finite tube opening time, leakage from the tube ends, and viscosity. The relative simplicity of the model makes it useful for design, optimization, and analysis of wave rotor cycles for any application. This paper discusses some details of the model and presents comparisons between the model and two laboratory wave rotor experiments.

Author

N93-15342*# National Aeronautics and Space Administration. Lewis Research Center, Cleveland, OH.

SUPERSONIC INVESTIGATION OF TWO DIMENSIONAL HYPERSONIC EXHAUST NOZZLES

JEANNE D. CARBONI, RICKEY J. SHYNE, LAURENCE D. LEAVITT (National Aeronautics and Space Administration. Langley Research Center, Hampton, VA.), JOHN G. TAYLOR (National Aeronautics and Space Administration. Langley Research Center, Hampton, VA.), and MILTON LAMB (National Aeronautics and Space Administration. Langley Research Center, Hampton, VA.) Oct. 1992 46 p (Contract RTOP 763-01-21) (NASA-TM-105687; E-7067; NAS 1.15:105687) Avail: CASI HC A03/MF A01

An experimental investigation was conducted in the NASA Lewis 10 x 10 ft supersonic Wind Tunnel to determine the performance characteristics of 2D hypersonic exhaust nozzles/afterbodies at low supersonic conditions. Generally, this type of application requires a single expansion ramp nozzle (SERN) that is highly integrated with the airframe of the hypersonic vehicle. At design conditions (hypersonic speeds), the nozzle generally exhibits acceptable performance. At off-design conditions (transonic to mid-supersonic speeds), nozzle performance of a fixed geometry configuration is generally poor. Various 2-D nozzle configurations were tested at off-design conditions from Mach 2.0 to 3.5. Performance data is presented at nozzle pressure ratios from 1 to 35. Jet exhaust was simulated with high-pressure air. To study performance of different geometries, nozzle configurations were varied by interchanging the following model parts: internal upstream contour, expansion ramp, sidewalls, and cowl.

Author

N93-15359*# National Aeronautics and Space Administration. Lewis Research Center, Cleveland, OH.

OPTIMIZATION OF CIRCULAR ORIFICE JETS MIXING INTO A HEATED CROSS FLOW IN A CYLINDRICAL DUCT

J. T. KROLL (California Univ., Irvine.), W. A. SOWA (California Univ., Irvine.), G. S. SAMUELSEN (California Univ., Irvine.), and J. D. HOLDEMAN Dec. 1992 19 p Presented at the 31st

Aerospace Sciences Meeting and Exhibit, Reno, NV, 11-14 Jan. 1993; sponsored by AIAA

(Contract NAG3-1110; RTOP 537-02-20)

(NASA-TM-105984; E-7508; NAS 1.15:105984; AIAA PAPER 93-0249) Avail: CASI HC A03/MF A01; 2 functional color pages

To examine the mixing characteristics of circular jets in an axisymmetric can geometry, temperature measurements were obtained downstream of a row of cold jet injected into a heated cross stream. The objective was to obtain uniform mixing within one duct radius downstream of the leading edge of the jet orifices. An area weighted standard deviation of the mixture fraction was used to help quantify the degree of mixedness at a given plane. Non-reacting experiments were conducted to determine the influence of the number of jets on the mixedness in a cylindrical configuration. Results show that the number of orifices significantly impacts the mixing characteristics of jets injected from round hole orifices in a can geometry. Optimum mixing occurs when the mean jet trajectory aligns with the radius which divides the cross sectional area of the can into two equal parts at one mixer radius downstream of the leading edge of the orifice. The optimum number of holes at momentum-flux ratios of 25 and 52 is 10 and 15 respectively.

Author

N93-15403*# National Aeronautics and Space Administration. Lewis Research Center, Cleveland, OH.

ACOUSTIC MODE MEASUREMENTS IN THE INLET OF A MODEL TURBOFAN USING A CONTINUOUSLY ROTATING RAKE: DATA COLLECTION/ANALYSIS TECHNIQUES

DAVID G. HALL (Sverdrup Technology, Inc., Brook Park, OH.), LAURENCE HEIDELBERG, and KEVIN KONNO Jan. 1993 14 p Presented at the 31st Aerospace Sciences Meeting, Reno, NV, 11-14 Jan. 1993; Sponsored by AIAA (Contract RTOP 535-03-10)

(NASA-TM-105936; E-7452; NAS 1.15:105936; AIAA PAPER 93-0599) Avail: CASI HC A03/MF A01

The rotating microphone measurement technique and data analysis procedures are documented which are used to determine circumferential and radial acoustic mode content in the inlet of the Advanced Ducted Propeller (ADP) model. Circumferential acoustic mode levels were measured at a series of radial locations using the Doppler frequency shift produced by a rotating inlet microphone probe. Radial mode content was then computed using a least squares curve fit with the measured radial distribution for each circumferential mode. The rotating microphone technique is superior to fixed-probe techniques because it results in minimal interference with the acoustic modes generated by rotor-stator interaction. This effort represents the first experimental implementation of a measuring technique developed by T. G. Sofrin. Testing was performed in the NASA Lewis Low Speed Anechoic Wind Tunnel at a simulated takeoff condition of Mach 0.2. The design is included of the data analysis software and the performance of the rotating rake apparatus. The effect of experiment errors is also discussed.

Author

N93-15521*# National Aeronautics and Space Administration. Lewis Research Center, Cleveland, OH.

AN INTEGRAL EQUATION SOLUTION FOR MULTISTAGE TURBOMACHINERY DESIGN CALCULATIONS

ERIC R. MCFARLAND 1993 12 p Proposed for presentation at the 38th International Gas Turbine and Aeroengine Congress and Exposition, Cincinnati, OH, 24-27 May 1993; sponsored by ASME

(Contract RTOP 505-62-52)

(NASA-TM-105970; E-7493; NAS 1.15:105970) Avail: CASI HC A03/MF A01

A method was developed to calculate flows in multi-stage turbomachinery. The method is an extension of quasi-three-dimensional blade-to-blade solution methods. Governing equations for steady compressible inviscid flow are linearized by introducing approximations. The linearized flow equations are solved using integral equation techniques. The flows through both stationary and rotating blade rows are determined in

07 AIRCRAFT PROPULSION AND POWER

a single calculation. Multiple bodies can be modelled for each blade row, so that arbitrary blade counts can be analyzed. The method's benefits are its speed and versatility. Author

N93-15525*# National Aeronautics and Space Administration. Lewis Research Center, Cleveland, OH.

PROPULSION SYSTEM PERFORMANCE RESULTING FROM AN INTEGRATED FLIGHT/PROPULSION CONTROL DESIGN

DUANE MATTERN (Sverdrup Technology, Inc., Brook Park, OH.) and SANJAY GARG Oct. 1992 22 p Presented at the AIAA Guidance, Navigation, and Control Conference, Hilton Head, SC, 10-12 Aug. 1992; sponsored by AIAA Previously announced in IAA as A92-55281

(Contract RTOP 505-62-50)

(NASA-TM-105874; E-7339; NAS 1.15:105874) Avail: CASI HC A03/MF A01

Propulsion-system-specific results are presented from the application of the integrated methodology for propulsion and airframe control (IMPAC) design approach to integrated flight/propulsion control design for a 'short takeoff and vertical landing' (STOVL) aircraft in transition flight. The IMPAC method is briefly discussed and the propulsion system specifications for the integrated control design are examined. The structure of a linear engine controller that results from partitioning a linear centralized controller is discussed. The details of a nonlinear propulsion control system are presented, including a scheme to protect the engine operational limits: the fan surge margin and the acceleration/deceleration schedule that limits the fuel flow. Also, a simple but effective multivariable integrator windup protection scheme is examined. Nonlinear closed-loop simulation results are presented for two typical pilot commands for transition flight: acceleration while maintaining flightpath angle and a change in flightpath angle while maintaining airspeed. The simulation nonlinearities include the airframe/engine coupling, the actuator and sensor dynamics and limits, the protection scheme for the engine operational limits, and the integrator windup protection. Satisfactory performance of the total airframe plus engine system for transition flight, as defined by the specifications, was maintained during the limit operation of the closed-loop engine subsystem.

Author

N93-16705*# National Aeronautics and Space Administration. Lewis Research Center, Cleveland, OH.

ACOUSTIC MODE MEASUREMENTS IN THE INLET OF A MODEL TURBOFAN USING A CONTINUOUSLY ROTATING RAKE

LAURENCE J. HEIDELBERG and DAVID G. HALL (Sverdrup Technology, Inc., Brook Park, OH.) Dec. 1992 31 p Presented at the 31st Aerospace Sciences Meeting, Reno, NV, 11-14 Jan. 1993; sponsored by AIAA

(Contract RTOP 535-03-10)

(NASA-TM-105989; E-7476; NAS 1.15:105989; AIAA PAPER 93-0598) Avail: CASI HC A03/MF A01

Comprehensive measurements of the spinning acoustic mode structure in the inlet of the Advanced Ducted Propeller (ADP) have been completed. These measurements were taken using a unique and previously untried method which was first proposed by T.G. Sofrin. A continuously rotating microphone system was employed. The ADP model was designed and built by Pratt & Whitney and tested in the NASA Lewis 9- by 15-foot Anechoic Wind Tunnel. Three inlet configurations were tested with cut-on and cutoff stator vane sets. The cutoff stator was designed to suppress all modes at the blade passing frequency. Rotating rake measurements indicate that several extraneous circumferential modes were active. The mode orders suggest that their source was an interaction between the rotor and small interruptions in the casing tip treatment. The cut-on stator produced the expected circumferential modes plus higher levels of the unexpected modes seen with the cutoff stator. Author

N93-16715*# National Aeronautics and Space Administration. Lewis Research Center, Cleveland, OH.

TAKEOFF/APPROACH NOISE FOR A MODEL COUNTERROTATION PROPELLER WITH A FORWARD-SWEPT UPSTREAM ROTOR

RICHARD P. WOODWARD, DAVID G. HALL (Sverdrup Technology, Inc., Brook Park, OH.), GARY G. PODBOY, and ROBERT J. JERACKI Jan. 1993 23 p Presented at the 31st AIAA Aerospace Sciences Meeting and Exhibit, Reno, NV, 11-14 Jan. 1993; sponsored by AIAA

(Contract RTOP 535-03-10)

(NASA-TM-105979; E-7479; NAS 1.15:105979; AIAA PAPER 93-0596) Avail: CASI HC A03/MF A01

A scale model of a counterrotating propeller with forward-swept blades in the forward rotor and aft-swept blades in the aft rotor (designated F39/A31) has been tested in the NASA Lewis 9- by 15-Foot Anechoic Wind Tunnel. This paper presents aeroacoustic results at a takeoff/approach condition of Mach 0.20. Laser Doppler velocimeter results taken in a plane between the two rotors are also included to quantify the interaction flow field. The intention of the forward-swept design is to reduce the magnitude of the forward rotor tip vortex and/or wakes which impinge on the aft rotor, thus lowering the interaction tone levels. A reference model propeller (designated F31/A31), having aft-swept blades in both rotors, was also tested. Aeroelastic performance of the F39/A31 propeller was disappointing. The forward rotor tip region tended to untwist toward higher effective blade angles under load. The forward rotor also exhibited steady state blade flutter at speeds and loadings well below the design condition. The noise results, based on sideline acoustic data, show that the interaction tone levels were up to 8 dB higher with the forward-swept design compared to those for the reference propeller at similar operating conditions, with these tone level differences extending down to lower propeller speeds where flutter did not occur. These acoustic results are for a poorly-performing forward-swept propeller. It is quite possible that a properly-designed forward-swept propeller would exhibit substantial interaction tone level reductions.

Author

N93-16941*# National Aeronautics and Space Administration. Lewis Research Center, Cleveland, OH.

A CRITICAL ANALYSIS OF THE ACCURACY OF SEVERAL NUMERICAL TECHNIQUES FOR COMBUSTION KINETIC RATE EQUATIONS

KRISHNAN RADHADRISHNAN Jan. 1993 62 p

(Contract RTOP 505-31-42)

(NASA-TP-3315; E-5861; NAS 1.60:3315) Avail: CASI HC A04/MF A01

A detailed analysis of the accuracy of several techniques recently developed for integrating stiff ordinary differential equations is presented. The techniques include two general-purpose codes EPISODE and LSODE developed for an arbitrary system of ordinary differential equations, and three specialized codes CHEMEQ, CREK1D, and GCKP4 developed specifically to solve chemical kinetic rate equations. The accuracy study is made by application of these codes to two practical combustion kinetics problems. Both problems describe adiabatic, homogeneous, gas-phase chemical reactions at constant pressure, and include all three combustion regimes: induction, heat release, and equilibration. To illustrate the error variation in the different combustion regimes the species are divided into three types (reactants, intermediates, and products), and error versus time plots are presented for each species type and the temperature. These plots show that CHEMEQ is the most accurate code during induction and early heat release. During late heat release and equilibration, however, the other codes are more accurate. A single global quantity, a mean integrated root-mean-square error, that measures the average error incurred in solving the complete problem is used to compare the accuracy of the codes. Among the codes examined, LSODE is the most accurate for solving chemical kinetics problems. It is also the most efficient code, in the sense that it requires the least computational work to attain a specified accuracy level. An important finding is that use of the algebraic enthalpy conservation

equation to compute the temperature can be more accurate and efficient than integrating the temperature differential equation.

Author

N93-20109* National Aeronautics and Space Administration. Lewis Research Center, Cleveland, OH.

IDENTIFICATION OF PROPULSION SYSTEMS

WALTER MERRILL, TEN-HUEI GUO, and AHMET DUYAR (Florida Atlantic Univ., Boca Raton.) Aug. 1991 32 p Workshop held in Cleveland, OH, 9 Aug. 1991; sponsored by the Ohio Aerospace Institute

(Contract RTOP 506-42-72)

(NASA-TM-106007; E-7171; NAS 1.15:106007) Avail: CASI HC A03/MF A01

This paper presents a tutorial on the use of model identification techniques for the identification of propulsion system models. These models are important for control design, simulation, parameter estimation, and fault detection. Propulsion system identification is defined in the context of the classical description of identification as a four step process that is unique because of special considerations of data and error sources. Propulsion system models are described along with the dependence of system operation on the environment. Propulsion system simulation approaches are discussed as well as approaches to propulsion system identification with examples for both air breathing and rocket systems. Author

N93-22034* National Aeronautics and Space Administration. Lewis Research Center, Cleveland, OH.

MULTI-HEAT ADDITION TURBINE ENGINE Patent

LEO C. FRANCISCUS, inventor (to NASA) and THEODORE A. BRABBS, inventor (to NASA) 9 Feb. 1993 7 p Filed 30 Jan. 1991 Supersedes N91-23180 (29 - 15, p 2381)

(NASA-CASE-LEW-15094-1; US-PATENT-5,184,460;

US-PATENT-APPL-SN-647902; US-PATENT-CLASS-60-226.1;

US-PATENT-CLASS-60-39.17; INT-PATENT-CLASS-F02K-3/04;

INT-PATENT-CLASS-F02K-3/08) Avail: US Patent and Trademark Office

A multi-heat addition turbine engine (MHATE) incorporates a plurality of heat addition devices to transfer energy to air and a plurality of turbines to extract energy from the air while converting it to work. The MHATE provides dry power and lower fuel consumption or lower combustor exit temperatures.

Official Gazette of the U.S. Patent and Trademark Office

N93-22480* National Aeronautics and Space Administration. Lewis Research Center, Cleveland, OH.

A FULL-SCALE STOVL EJECTOR EXPERIMENT

WENDY S. BARANKIEWICZ Feb. 1993 134 p

(Contract RTOP 505-68-32)

(NASA-TM-106019; E-7433-1; NAS 1.15:106019) Avail: CASI HC A07/MF A02

The design and development of thrust augmenting short take-off and vertical landing (STOVL) ejectors has typically been an iterative process. In this investigation, static performance tests of a full-scale vertical lift ejector were performed at primary flow temperatures up to 1560 R (1100 F). Flow visualization (smoke generators, yarn tufts and paint dots) was used to assess inlet flowfield characteristics, especially around the primary nozzle and end plates. Performance calculations are presented for ambient temperatures close to 480 R (20 F) and 535 R (75 F) which simulate 'seasonal' aircraft operating conditions. Resulting thrust augmentation ratios are presented as functions of nozzle pressure ratio and temperature. Full-scale experimental tests such as this are expensive, and difficult to implement at engine exhaust temperatures. For this reason the utility of using similarity principles -- in particular, the Munk and Prim similarity principle for isentropic flow -- was explored. At different primary temperatures, exit pressure contours are compared for similarity. A nondimensional flow parameter is then shown to eliminate primary nozzle temperature dependence and verify similarity between the hot and cold flow experiments. Under the assumption that an appropriate similarity principle can be established, then properly chosen

performance parameters should be similar for both hot flow and cold flow model tests.

Author (revised)

N93-22599* National Aeronautics and Space Administration. Lewis Research Center, Cleveland, OH.

MATHEMATICAL RELATIONSHIP BETWEEN TWO SETS OF LASER ANEMOMETER MEASUREMENTS FOR RESOLVING THE TOTAL VELOCITY VECTOR

ALBERT K. OWEN Mar. 1993 20 p

(Contract DA PROJ. 1L1-61102-AH-45)

(NASA-TM-105986; E-7511; NAS 1.15:105986;

AVSCOM-TR-92-C-038) Avail: CASI HC A03/MF A01

The mathematical relations between the measured velocity fields for the same compressor rotor flow field resolved by two fringe type laser anemometers at different observational locations are developed in this report. The relations allow the two sets of velocity measurements to be combined to produce a total velocity vector field for the compressor rotor. This report presents the derivation of the mathematical relations, beginning with the specification of the coordinate systems and the velocity projections in those coordinate systems. The vector projections are then transformed into a common coordinate system. The transformed vector coordinates are then combined to determine the total velocity vector. A numerical example showing the solution procedure is included.

Author

N93-23013* National Aeronautics and Space Administration. Lewis Research Center, Cleveland, OH.

STUDY OF THE CAPACITANCE TECHNIQUE FOR MEASURING HIGH-TEMPERATURE BLADE TIP CLEARANCE ON CERAMIC ROTORS

JOHN P. BARRANGER Mar. 1993 17 p

(Contract RTOP 510-01-50)

(NASA-TM-105978; E-7502; NAS 1.15:105978) Avail: CASI HC A03/MF A01

Higher operating temperatures required for increased engine efficiency can be achieved by using ceramic materials for engine components. Ceramic turbine rotors are subject to the same limitations with regard to gas path efficiency as their superalloy predecessors. In this study, a modified frequency-modulation system is proposed for the measurement of blade tip clearance on ceramic rotors. It is expected to operate up to 1370 C (2500 F), the working temperature of present engines with ceramic turbine rotors. The design of the system addresses two special problems associated with nonmetallic blades: the capacitance is less than that of a metal blade and the effects of temperature may introduce uncertainty with regard to the blade tip material composition. To increase capacitance and stabilize the measurement, a small portion of the rotor is modified by the application of 5-micron-thick platinum films. The platinum surfaces on the probe electrodes and rotor that are exposed to the high-velocity gas stream are coated with an additional 10-micron-thick protective ceramic topcoat. A finite-element method is applied to calculate the capacitance as a function of clearance.

Author

N93-24754* National Aeronautics and Space Administration. Lewis Research Center, Cleveland, OH.

FUEL INJECTOR: AIR SWIRL CHARACTERIZATION

AEROTHERMAL MODELING, PHASE 2, VOLUME 1 Final Report

M. NIKJOOY (General Motors Corp., Indianapolis, IN.), H. C. MONGIA (General Motors Corp., Indianapolis, IN.), V. G. MCDONELL (California Univ., Irvine.), and G. S. SAMUELSEN (California Univ., Irvine.) Mar. 1993 407 p

(Contract NAS3-24350; RTOP 505-62-52)

(NASA-CR-189193-VOL-1; E-7593-VOL-1; NAS

1.26:189193-VOL-1) Avail: CASI HC A18/MF A04

A well integrated experimental/analytical investigation was conducted to provide benchmark quality relevant to a preflaming type airblast fuel nozzle and its interaction with the combustor dome air swirler. The experimental investigation included a systematic study of both single-phase flows that involved single and twin co-axial jets with and without swirl. A two-component

07 AIRCRAFT PROPULSION AND POWER

Phase Doppler Particle Analyzer (PDPA) was used to document the interaction of single and co-axial air jets with glass beads that simulate nonevaporating spray and simultaneously avoid the complexities associated with fuel atomization processes and attendant issues about the specification of relevant boundary conditions. The interaction of jets with methanol spray produced by practical airblast nozzle was also documented in the spatial domain of practical interest. Model assessment activities included the use of three turbulence models (k-epsilon, algebraic second moment (ASM), and differential second moment (DSM)) for the carrier phase, deterministic or stochastic Lagrangian treatment of the dispersed phase, and advanced numerical schemes. Although qualitatively good comparison with data was obtained for most of the cases investigated, the model deficiencies in regard to modeled dissipation rate transport equation, single length scale, pressure-strain correlation, and other critical closure issues need to be resolved before one can achieve the degree of accuracy required to analytically design combustion systems.

Author (revised)

N93-25079*# National Aeronautics and Space Administration. Lewis Research Center, Cleveland, OH.

SCREENING STUDIES OF ADVANCED CONTROL CONCEPTS FOR AIRBREATHING ENGINES

PETER J. OUZTS, CARL F. LORENZO, and WALTER C. MERRILL Mar. 1993 22 p Presented at the 28th Joint Propulsion Conference and Exhibit, Nashville, TN, 6-8 Jul. 1992; sponsored by AIAA, SAE, ASME, and ASEE (Contract RTOP 505-62-50) (NASA-TM-106042; E-7620; NAS 1.15:106042) Avail: CASI HC A03/MF A01

The application of advanced control concepts to airbreathing engines may yield significant improvements in aircraft/engine performance and operability. Accordingly, the NASA Lewis Research Center has conducted screening studies of advanced control concepts for airbreathing engines to determine their potential impact on turbine engine performance and operability. The purpose of the studies was to identify concepts which offered high potential yet may incur high research and development risk. A target suite of proposed concepts was formulated by NASA and industry. These concepts were evaluated in a two phase study to quantify each concept's impact on desired engine characteristics. To aid in the evaluation, three target aircraft/engine combinations were considered: a military high performance fighter mission, a high speed civil transport mission, and a civil tiltrotor mission. Each of the advanced control concepts considered in the study were defined and described. The concept's potential impact on engine performance was determined. Relevant figures of merit on which to evaluate the concepts were also determined. Finally, the concepts were ranked with respect to the target aircraft/engine missions.

Author

N93-25129*# National Aeronautics and Space Administration. Lewis Research Center, Cleveland, OH.

EXPERIMENTAL PERFORMANCE OF A VENTRAL NOZZLE WITH PITCH AND YAW VECTORING CAPABILITY FOR SSTOVL AIRCRAFT

BARBARA S. ESKER and JACK G. MCARDLE Apr. 1993 12 p Presented at the Aerospace Atlantic Conference, Dayton, OH, 20-23 Apr. 1993; sponsored by SAE (Contract RTOP 505-68-32) (NASA-TM-106054; E-7648; NAS 1.15:106054) Avail: CASI HC A03/MF A01

Aircraft with supersonic, short takeoff, and vertical landing capability were proposed to replace some of the current high-performance aircraft. Several of these configurations use a ventral nozzle in the lower fuselage, aft of the center of gravity, for lift or pitch control. Internal vanes canted at 20 deg were added to a swivel-type ventral nozzle and tested at tailpipe-to-ambient pressure ratios up to 5.0 on the Powered Lift Facility at NASA LeRC. The addition of sets of four and seven vanes decreased the discharge coefficient by at least 6 percent and did not affect the thrust coefficient. Side force produced by

the nozzle with vanes was 14 percent or more of the vertical force. In addition, this side force caused only a small loss in vertical force in comparison to the nozzle without vanes. The net thrust force was 8 deg from the vertical for four vanes and 10.5 deg for seven.

Author (revised)

N93-25673*# National Aeronautics and Space Administration. Lewis Research Center, Cleveland, OH.

GAS TURBINE SYSTEM SIMULATION: AN OBJECT-ORIENTED APPROACH

COLIN K. DRUMMOND, GREGORY J. FOLLEN, and CHARLES W. PUTT Apr. 1993 14 p Presented at the 23rd Annual Pittsburgh Conference on Modeling and Simulation, Pittsburgh, PA, 30 Apr. - 1 May 1992; sponsored by the Univ. of Pittsburgh, IEEE, ISA, and SCS (Contract RTOP 505-62-51) (NASA-TM-106044; E-7632; NAS 1.15:106044) Avail: CASI HC A03/MF A01

A prototype gas turbine engine simulation has been developed that offers a generalized framework for the simulation of engines subject to steady-state and transient operating conditions. The prototype is in preliminary form, but it successfully demonstrates the viability of an object-oriented approach for generalized simulation applications. Although object oriented programming languages are relative to FORTRAN-somewhat austere, it is proposed that gas turbine simulations of an interdisciplinary nature will benefit significantly in terms of code reliability, maintainability, and manageability. This report elucidates specific gas turbine simulation obstacles that an object-oriented framework can overcome and describes the opportunity for interdisciplinary simulation that the approach offers.

Author

N93-26161*# National Aeronautics and Space Administration. Lewis Research Center, Cleveland, OH.

ROTATING RAKE DESIGN FOR UNIQUE MEASUREMENT OF FAN-GENERATED SPINNING ACOUSTIC MODES

KEVIN E. KONNO and CLIFFORD R. HAUSMANN Apr. 1993 23 p (Contract RTOP 535-03-01) (NASA-TM-105946; E-7814; NAS 1.15:105946) Avail: CASI HC A03/MF A01

In light of the current emphasis on noise reduction in subsonic aircraft design, NASA has been actively studying the source of and propagation of noise generated by subsonic fan engines. NASA/LeRC has developed and tested a unique method of accurately measuring these spinning acoustic modes generated by an experimental fan. This mode measuring method is based on the use of a rotating microphone rake. Testing was conducted in the 9 x 15 Low-speed Wind Tunnel. The rotating rake was tested with the Advanced Ducted Propeller (ADP) model. This memorandum discusses the design and performance of the motor/drive system for the fan-synchronized rotating acoustic rake. This novel motor/drive design approach is now being adapted for additional acoustic mode studies in new test rigs as baseline data for the future design of active noise control for subsonic fan engines. Included in this memorandum are the research requirements, motor/drive specifications, test performance results, and a description of the controls and software involved.

Author (revised)

N93-27026*# National Aeronautics and Space Administration. Lewis Research Center, Cleveland, OH.

EXPERIMENTAL INVESTIGATION OF CROSSFLOW JET MIXING IN A RECTANGULAR DUCT

D. S. LISCINSKY (United Technologies Research Center, East Hartford, CT.), B. TRUE (United Technologies Research Center, East Hartford, CT.), and J. D. HOLDEMAN Jun. 1993 10 p Proposed for presentation at the 29th Joint Propulsion Conference and Exhibit, Monterey, CA, 28-30 Jun. 1993; sponsored by AIAA, SAE, ASME, and ASEE Original contains color illustrations (Contract RTOP 537-02-21) (NASA-TM-106152; E-7834; NAS 1.15:106152; AIAA PAPER 93-2037) Avail: CASI HC A02/MF A01; 2 functional color pages

An experimental investigation of the mixing of nonreacting opposed rows of jets injected normal to a confined rectangular crossflow has been conducted. Planar Mie-scattering was used to measure the time-average concentration distribution of the jet fluid in planes perpendicular to the duct axis. The mixing effectiveness of round orifice injectors was measured as a function of orifice spacing and orifice diameter. Mixing effectiveness was determined using a spatial unmixedness parameter based on the variance of mean jet concentration distributions. Optimum mixing was obtained when the spacing-to-duct height ratio was inversely proportional to the square root of the jet-to-mainstream momentum-flux ratio. For opposed rows of round holes with centerlines inline, mixing was similar for blockages up to 75 percent. Lower levels of unmixedness were obtained as a function of downstream location when axial injection length was minimized. Mixing may be enhanced if orifice centerlines of opposed rows are staggered, but note that blockage must be less than 50 percent for this configuration.

Author

N93-27128* National Aeronautics and Space Administration. Lewis Research Center, Cleveland, OH.

CFD MIXING ANALYSIS OF AXIALLY OPPOSED ROWS OF JETS INJECTED INTO CONFINED CROSSFLOW

D. B. BAIN (CFD Research Corp., Huntsville, AL.), C. E. SMITH (CFD Research Corp., Huntsville, AL.), and J. D. HOLDEMAN May 1993 29 p Prepared for presentation at the 28th Joint Propulsion Conference and Exhibit, Monterey, CA, 28-30 Jun. 1993; sponsored by AIAA, SAE, ASME, and ASEE Original contains color illustrations

(Contract RTOP 537-02-21)

(NASA-TM-106179; E-7884; NAS 1.15:106179; AIAA PAPER 93-2044) Avail: CASI HC A03/MF A01; 12 functional color pages

A computational fluid dynamics (CFD) parametric study was performed to analyze axially opposed rows of jets mixing with crossflow in a rectangular duct. Isothermal analysis was conducted to determine the influence of lateral geometric arrangement on mixing. Two lateral arrangements were analyzed: (1) inline (jets' centerlines aligned with each other on top and bottom walls), and (2) staggered (jets' centerlines offset with each other on top and bottom walls). For a jet-to-mainstream mass flow ratio (MR) of 2.0, design parameters were systematically varied for jet-to-mainstream momentum-flux ratios (J) between 16 and 64 and orifice spacing-to-duct height ratios (S/H) between 0.125 and 1.5. Comparisons were made between geometries optimized for S/H at a specified J. Inline configurations had a unique spacing for best mixing at a specified J. In contrast, staggered configurations had two 'good mixing' spacings for each J, one corresponding to optimum inline spacing and the other corresponding to optimum non-impinging jet spacing. The inline configurations, due to their smaller orifice size at optimum S/H, produced better initial mixing characteristics. At downstream locations (e.g. x/H of 1.5), the optimum non-impinging staggered configuration produced better mixing than the optimum inline configuration for J of 64; the opposite results were observed for J of 16. Increasing J resulted in better mixing characteristics if each configuration was optimized with respect to orifice spacing. Mixing performance was shown to be similar to results from previous dilution jet mixing investigations (MR less than 0.5).

Author (revised)

N93-27130* National Aeronautics and Space Administration. Lewis Research Center, Cleveland, OH.

VELOCITY AND DROP SIZE MEASUREMENTS IN A SWIRL-STABILIZED, COMBUSTING SPRAY

DANIEL L. BULZAN Jan. 1993 12 p Presented at the Laser Applications in Combustion and Combustion Diagnostics Meeting, Los Angeles, CA, 16-23 Jan. 1993; sponsored by Society of Photo-Optical Instrumentation Engineers

(Contract RTOP 505-62-52)

(NASA-TM-106130; E-7799; NAS 1.15:106130) Avail: CASI HC A03/MF A01

Velocity and drop size measurements are reported for a swirl-stabilized, combustive spray. For the gas phase, three

components of mean and fluctuating velocity are reported. For the droplets, three components of mean and fluctuating velocity, diameter, and number flux are reported. The liquid fuel utilized for all the tests was heptane. The fuel was injected using an air-assist atomizer. The combustor configuration consisted of a center-mounted, air-assist atomizer surrounded by a coflowing air stream. Both the coflow and the atomizing air streams were passed through 45 degree swirlers. The swirl was imparted to both streams in the same direction. The combustion occurred unconfined in stagnant surroundings. The nonintrusive measurements were obtained using a two-component phase/Doppler particle analyzer. The laser-based instrument measured two components of velocity as well as droplet size at a particular point. Gas phase measurements were obtained by seeding the air streams with nominal 1 micron size aluminum-oxide particles and using the measured velocity from that size to represent the gas phase velocity. The atomizing air, coflow air, and ambient surroundings were all seeded with the aluminum-oxide particles to prevent biasing. Measurements are reported at an axial distance of 5 mm from the nozzle. Isothermal single-phase gas velocities are also reported for comparison with the combustive case.

Author

N93-27131* National Aeronautics and Space Administration. Lewis Research Center, Cleveland, OH.

PERFORMANCE CHARACTERISTICS OF A VARIABLE-AREA VANE NOZZLE FOR VECTORING AN ASTOVL EXHAUST JET UP TO 45 DEG

JACK G. MCARDLE and BARBARA S. ESKER Jun. 1993 34 p Presented at the 29th AIAA Joint Propulsion Conference, Monterey, CA, 28-30 Jun. 1993; sponsored by AIAA, SAE, ASME, and ASEE

(Contract RTOP 505-68-32)

(NASA-TM-106114; E-7768; NAS 1.15:106114; AIAA PAPER 93-2437) Avail: CASI HC A03/MF A01

Many conceptual designs for advanced short-takeoff, vertical landing (ASTOVL) aircraft need exhaust nozzles that can vector the jet to provide forces and moments for controlling the aircraft's movement or attitude in flight near the ground. A type of nozzle that can both vector the jet and vary the jet flow area is called a vane nozzle. Basically, the nozzle consists of parallel, spaced-apart flow passages formed by pairs of vanes (vanesets) that can be rotated on axes perpendicular to the flow. Two important features of this type of nozzle are the abilities to vector the jet rearward up to 45 degrees and to produce less harsh pressure and velocity footprints during vertical landing than does an equivalent single jet. A one-third-scale model of a generic vane nozzle was tested with unheated air at the NASA Lewis Research Center's Powered Lift Facility. The model had three parallel flow passages. Each passage was formed by a vaneset consisting of a long and a short vane. The longer vanes controlled the jet vector angle, and the shorter controlled the flow area. Nozzle performance for three nominal flow areas (basic and plus or minus 21 percent of basic area), each at nominal jet vector angles from -20 deg (forward of vertical) to +45 deg (rearward of vertical) are presented. The tests were made with the nozzle mounted on a model tailpipe with a blind flange on the end to simulate a closed cruise nozzle, at tailpipe-to-ambient pressure ratios from 1.8 to 4.0. Also included are jet wake data, single-vaneset vector performance for long/short and equal-length vane designs, and pumping capability. The pumping capability arises from the subambient pressure developed in the cavities between the vanesets, which could be used to aspirate flow from a source such as the engine compartment. Some of the performance characteristics are compared with characteristics of a single-jet nozzle previously reported.

Author (revised)

N93-27160* National Aeronautics and Space Administration. Lewis Research Center, Cleveland, OH.

AN ANALYTICAL STUDY OF DILUTION JET MIXING IN A CYLINDRICAL DUCT

V. L. OECHSLE (General Motors Corp., Indianapolis, IN.), H. C. MONGIA (General Motors Corp., Indianapolis, IN.), and J. D. HOLDEMAN May 1993 41 p Proposed for presentation at

07 AIRCRAFT PROPULSION AND POWER

the 29th Joint Propulsion Conference and Exhibit, Monterey, CA, 28-30 Jun. 1993; sponsored by AIAA, SAE, ASME, and ASEE Limited Reproducibility: More than 20% of this document may be affected by color photographs Original contains color illustrations (Contract RTOP 537-02-21)
(NASA-TM-106181; E-7887; NAS 1.15:106181; AIAA PAPER 93-2043) Copyright Avail: CASI HC A03/MF A01; 17 functional color pages

The mixing performance in a mixing section of a rich burn/quick mix/lean burn (RQL) combustor was calculated using a 3-D numerical model in a non-reacting environment. The numerically calculated results were compared with the measured data reported by Hatch, Sowa, Samuelsen, and Holdeman, 1992. The numerical 3-D temperature fields qualitatively agree with the experimental data. Also, the development of the mixing flow and temperature non-uniformity trends throughout the mixing section for the numerically calculated results quantitatively agree with the measured data. The numerical model predicts less mixing and enhances the temperature gradients as compared to the measured data for the cases reported by Hatch et al. (1992) which include circular and slot orifice shapes (with different slant angles and aspect ratios). The predicted and measured results generally agree in the selection of the slanted slot orifice configuration yielding the best overall mixing performance (based on temperature uniformity) of all the configurations analyzed. Author (revised)

N93-27610* # National Aeronautics and Space Administration. Lewis Research Center, Cleveland, OH.

COMPARISON OF REACTING AND NON-REACTING SHEAR LAYERS AT A HIGH SUBSONIC MACH NUMBER

C. T. CHANG, C. J. MAREK, C. WEY (Sverdrup Technology, Inc., Brook Park, OH.), R. A. JONES (Rensselaer Polytechnic Inst., Troy, NY.), and M. J. SMITH (Purdue Univ., West Lafayette, IN.) Jun. 1993 13 p Presented at the 29th Joint Propulsion Conference and Exhibit, Monterey, CA, 28-30 Jun. 1993; cosponsored by AIAA, SAE, ASME, and ASEE (Contract RTOP 505-62-52)
(NASA-TM-106198; E-7905; NAS 1.15:106198; AIAA PAPER 93-2381) Avail: CASI HC A03/MF A01

The flow field in a hydrogen-fueled planar reacting shear layer was measured with an LDV system and is compared with a similar air to air case without combustion. Measurements were made with a speed ratio of 0.34 with the highspeed stream at Mach 0.71. They show that the shear layer with reaction grows faster than one without, and both cases are within the range of data scatter presented by the established database. The coupling between the streamwise and the cross-stream turbulence components inside the shear layer is slow, and reaction only increased it slightly. However, a more organized pattern of the Reynolds stress is present in the reacting shear layer, possibly as a result of larger scale structure formation in the layer associated with heat release. Author

N93-27640* # National Aeronautics and Space Administration. Lewis Research Center, Cleveland, OH.

NDE OF PWA 1480 SINGLE CRYSTAL TURBINE BLADE MATERIAL

STANLEY J. KLIMA, THOMAS W. ORANGE, and ROBERT L. DRESHFIELD Apr. 1993 11 p Presented at the SAE Aerospace Atlantic Conference, Dayton, OH, 20-23 Apr. 1993 (Contract RTOP 323-51-60)
(NASA-TM-106140; E-7351; NAS 1.15:106140) Avail: CASI HC A03/MF A01

Cantilever bending fatigue specimens were examined by fluorescent liquid penetrant and radioactive gas penetrant (Krypton) non-destructive evaluation (NDE) methods and tested. Specimens with cast, ground, or polished surface were evaluated to study the effect of surface condition on NDE and fatigue crack initiation. Fractographic and metallurgical analyses were performed to determine the nature of crack precursors. Preliminary results show that fatigue strength was lower for specimens with cast surfaces than for specimens with machined surfaces. The liquid penetrant and gas penetrant techniques both provided indications of a large

population of defects on the cast surfaces. On ground or polished specimen surfaces, the gas penetrant appeared to estimate the actual number of voids more accurately than the liquid penetrant. Author (revised)

N93-28697* # National Aeronautics and Space Administration. Lewis Research Center, Cleveland, OH.

EXPERIMENTAL EVALUATION OF A COOLED RADIAL-INFLOW TURBINE

LIZET TIRRES (Sverdrup Technology, Inc., Brook Park, OH.), L. DANIELLE DICICCO, and BRENT C. NOWLIN Jun. 1993 18 p Presented at the 29th AIAA Joint Propulsion Conference and Exhibit, Monterey, CA, 28-30 Jun. 1993; cosponsored by SAE, ASME, and ASEE (Contract RTOP 535-05-10)
(NASA-TM-106230; E-7948; NAS 1.15:106230; AIAA PAPER 93-1795) Avail: CASI HC A03/MF A01

Two 14.4 inch tip diameter rotors were installed and tested in the Small Engines Component Turbine Facility (SECTF) at NASA Lewis Research Center. The rotors, a solid and a cooled version of a radial-inflow turbine, were tested with a 15 vane stat or over a set of rotational speeds ranging from 80 to 120 percent design speed (17,500 to 21,500 rpm). The total-to-total stage pressure ratios ranged from 2.5 to 5.5. The data obtained at the equivalent conditions using the solid version of the rotor are presented with the cooled rotor data. A Reynolds number of 381,000 was maintained for both rotors, whose stages had a design mass flow of 4.0 lbm/sec, a design work level of 59.61 Btu/lbm, and a design efficiency of 87 percent. The results include mass flow data, turbine torque, turbine exit flow angles, stage efficiency, and rotor inlet and exit surveys. Author

N93-29065* # National Aeronautics and Space Administration. Lewis Research Center, Cleveland, OH.

EFFECTS OF FLOW-PATH VARIATIONS ON INTERNAL REVERSING FLOW IN A TAILPIPE OFFTAKE CONFIGURATION FOR ASTOVL AIRCRAFT

JACK G. MCARDLE and BARBARA S. ESKER Jun. 1993 23 p Presented at the 29th Joint Propulsion Conference and Exhibit, Monterey, CA, 28-30 Jun. 1993; cosponsored by AIAA, SAE, ASME, and ASEE (Contract RTOP 505-68-32)
(NASA-TM-106149; E-7643; NAS 1.15:106149; AIAA PAPER 93-2438) Avail: CASI HC A03/MF A01

A one-third-scale model of a generic tailpipe offtake system for an advanced short takeoff, vertical landing (ASTOVL) aircraft was tested at the NASA Lewis Research Center Powered Lift Facility. The basic model consisted of a tailpipe with a center body to form an annulus simulating turbine outflow with no swirl; twin offtake ducts with elbows at the ends to turn the flow to a downward direction; flow control nozzles at the ends of the elbows; and a blind flange at the end of the tailpipe to simulate a closed cruise nozzle. The offtake duct-to-tailpipe diameter ratio was 0.74. Modifications of a generic nature were then made to this basic configuration to measure the effects of flow-path changes on the flow and pressure-loss characteristics. The modifications included adding rounded entrances at the forward edges of the offtake openings, blocking the tailpipe just aft the openings instead of at the cruise nozzle, changing the location of the openings along the tailpipe, removing the center body, and varying the Mach number (flow rate) over a wide range in the tailpipe ahead of the openings by changing the size of the flow control nozzles. The tests were made with unheated air at tailpipe-to-ambient pressure ratios from 1.4 to 5. Results are presented and compared with performance graphs, total-pressure contour plots, paint streak flow visualization photographs, and a flow-angle probe traverse at the offtake entrance. Derived from text

N93-29162* # National Aeronautics and Space Administration. Lewis Research Center, Cleveland, OH.

THE 3-D VISCOUS FLOW CFD ANALYSIS OF THE PROPELLER EFFECT ON AN ADVANCED DUCTED PROPELLER SUBSONIC INLET

CHANTHY IEK, DONALD R. BOLDMAN, and MOUNIR IBRAHIM (Cleveland State Univ., OH.) Jun. 1993 41 p Presented at the 29th Joint Propulsion Conference and Exhibit, Monterey, CA, 28-30 Jun. 1993; sponsored by AIAA, SAE, ASME, and ASEE Original contains color illustrations (Contract RTOP 505-03-10) (NASA-TM-106240; E-7958; NAS 1.15:106240; AIAA PAPER 93-1847) Avail: CASI HC A03/MF A01; 14 functional color pages

A time marching Navier-Stokes code called PARC3D was used to study the 3-D viscous flow associated with an advanced ducted propeller (ADP) subsonic inlet at take-off operating conditions. At a free stream Mach number of 0.2, experimental data for the inlet-with-propeller test model indicated that the airflow was attached on the cowl windward lip at an angle of attack of 25 degrees became unstable at 29 degrees, and separated at 30 degrees. An experimental study with a similar inlet and with no propeller (through-flow) indicated that flow separation occurred at an angle of attack a few degrees below the value observed when the inlet was tested with the propeller. This tends to indicate that the propeller exerts a favorable effect on the inlet performance. During the through-flow experiment a stationary blockage device was used to successfully simulate the propeller effect on the inlet flow field at angles of attack. In the present numerical study, this flow blockage was modeled via a PARC3D computational boundary condition (BC) called the screen BC. The principle formulation of this BC was based on the one-and-half dimension actuator disk theory. This screen BC was applied at the inlet propeller face station of the computational grid. Numerical results were obtained with and without the screen BC. The application of the screen BC in this numerical study provided results which are similar to the results of past experimental efforts in which either the blockage device or the propeller was used. Author (revised)

N93-29963* # National Aeronautics and Space Administration. Lewis Research Center, Cleveland, OH.

NAVIER-STOKES ANALYSIS OF THREE-DIMENSIONAL FLOW AND HEAT TRANSFER INSIDE TURBINE BLADE ROWS

C. HAH /in AGARD, Heat Transfer and Cooling in Gas Turbines 11 p Feb. 1993

Copyright Avail: CASI HC A03/MF A04

A numerical method for solving the three-dimensional, Navier-Stokes equations for unsteady, viscous flow and heat transfer through multiple turbomachinery blade rows is presented. The method solves the fully three-dimensional Navier-Stokes equations with an implicit scheme which is based on a control volume approach. A two-equation turbulence model with a low Reynolds number modification is employed. A third-order accurate upwinding scheme is used to approximate convection terms while a second order accurate central difference scheme is used for the discretization of viscous terms. A second-order accurate scheme is employed for the temporal discretization. The numerical method is applied to study the unsteady flow and heat transfer field of the High Pressure Fuel side Turbo-Pump (HPFTP) of the Space Shuttle Main Engine (SSME). The stage calculation is performed by coupling the stator and the rotor flow fields at each time step through an over-laid grid. Numerical results for the complete geometry with the vane trailing edge cutback are presented and compared with the available experimental data.

Author (revised)

N93-31671* # National Aeronautics and Space Administration. Lewis Research Center, Cleveland, OH.

ENGINE TECHNOLOGY CHALLENGES FOR A 21ST CENTURY HIGH-SPEED CIVIL TRANSPORT

ROBERT J. SHAW, SAMUEL GILKEY (General Electric Co., Evendale, OH.), and RICHARD HINES (Pratt & Whitney Aircraft, East Hartford, CT.) Sep. 1993 13 p Proposed for presentation at the International Symposium on Air Breathing Engines, Tokyo, Japan, 20-24 Sep. 1993 Original contains color illustrations (Contract RTOP 537-02-00)

(NASA-TM-106216; E-7925; NAS 1.15:106216) Avail: CASI HC A03/MF A01; 3 functional color pages

Ongoing NASA-funded studies by Boeing, McDonnell-Douglas, General Electric, and Pratt & Whitney indicate that an opportunity exists for a 21st Century High-Speed Civil Transport (HSCT) to become a major part of the international air transportation system. However, before industry will consider an HSCT product launch and an investment estimated to be over \$15 billion for design and certification, major technology advances must be made. An overview of the propulsion-specific technology advances that must be in hand before an HSCT product launch could be considered is presented. Author (revised)

N93-32351* # National Aeronautics and Space Administration. Lewis Research Center, Cleveland, OH.

PROPULSION TECHNOLOGY CHALLENGES FOR TURN-OF-THE-CENTURY COMMERCIAL AIRCRAFT

JOSEPH A. ZIEMIANSKI and CALVIN L. BALL Jun. 1993 14 p Prepared for presentation at the 11th ISABE Conference, Tokyo, Japan, 20-24 Sep. 1993

(Contract RTOP 505-62-10)

(NASA-TM-106192; E-7898; NAS 1.15:106192) Avail: CASI HC A03/MF A01

This paper highlights the efforts being performed or sponsored by NASA, in cooperation with the U.S. civil aviation industry, to address the propulsion system technological challenges that must be met in order to ensure a viable future for the industry. Both the subsonic and supersonic aeropropulsion programs are considered. Subsonic transport propulsion program elements, including ultra-high-bypass-ratio turbofans with attendant noise reduction efforts, high-efficiency cores, and combustor emissions reductions are discussed in terms of goals, technical issues, and problem solutions. Similarly, the high-speed research propulsion efforts addressing a high-speed commercial transport are reviewed in terms of environmental barrier issues, such as oxides of nitrogen and noise reduction, and the related economic issues.

Author (revised)

N93-32368* # National Aeronautics and Space Administration. Lewis Research Center, Cleveland, OH.

INITIAL RESULTS FROM THE NASA-LEWIS WAVE ROTOR EXPERIMENT

JACK WILSON (Sverdrup Technology, Inc., Brook Park, OH.) and DENNIS FRONEK May 1993 11 p Presented at the AIAA, SAE, ASME, and ASEE 29th Joint Propulsion Conference and Exhibit, Monterey, CA, 28 Jun. - 1 Jul. 1993; sponsored by AIAA (Contract RTOP 505-62-10)

(NASA-TM-106148; E-7831; NAS 1.15:106148; AIAA PAPER 93-2521) Avail: CASI HC A03/MF A01

Wave rotors may play a role as topping cycles for jet engines, since by their use, the combustion temperature can be raised without increasing the turbine inlet temperature. In order to design a wave rotor for this, or any other application, knowledge of the loss mechanisms is required, and also how the design parameters affect those losses. At NASA LeRC, a 3-port wave rotor experiment operating on the flow-divider cycle, has been started with the objective of determining the losses. The experimental scheme is a three factor Box-Behnken design, with passage opening time, friction factor, and leakage gap as the factors. Variation of these factors is provided by using two rotors, of different length, two different passage widths for each rotor, and adjustable leakage gap. In the experiment, pressure transducers are mounted on the rotor, and give pressure traces as a function of rotational angle at the entrance and exit of a rotor passage. In addition, pitot rakes monitor the stagnation pressures for each port, and orifice meters measure the mass flows. The results show that leakage losses are very significant in the present experiment, but can be reduced considerably by decreasing the rotor to wall clearance spacing.

Author (revised)

AIRCRAFT STABILITY AND CONTROL

Includes aircraft handling qualities; piloting; flight controls; and autopilots.

A93-14596* National Aeronautics and Space Administration. Lewis Research Center, Cleveland, OH.

ANALYSIS OF AIRFRAME AND ENGINE CONTROL INTERACTIONS AND INTEGRATED FLIGHT/PROPULSION CONTROL

JOHN D. SCHIERMAN and DAVID K. SCHMIDT (Arizona State Univ., Tempe) Journal of Guidance, Control, and Dynamics (ISSN 0731-5090) vol. 15, no. 6 Nov.-Dec. 1992 p. 1388-1396. Previously cited in issue 17, p. 2653, Accession no. A90-40557 AIAA, SAE, ASME, and ASEE, Joint Propulsion Conference, 26th, Orlando, FL, July 16-18, 1990, AIAA Paper 90-1918 refs (Contract NAG3-998) Copyright

A93-23073*# National Aeronautics and Space Administration. Lewis Research Center, Cleveland, OH.

ICING EFFECTS ON AIRCRAFT STABILITY AND CONTROL DETERMINED FROM FLIGHT DATA - PRELIMINARY RESULTS

T. P. RATVASKY and R. J. RANAUDO (NASA, Lewis Research Center, Cleveland, OH) Jan. 1993 27 p. AIAA, Aerospace Sciences Meeting and Exhibit, 31st, Reno, NV, Jan. 11-14, 1993 Previously announced in STAR as N93-14831 refs (AIAA PAPER 93-0398) Copyright

The effects of airframe icing on the stability and control characteristics of the NASA DH-6 Twin Otter icing research aircraft were investigated by flight test. The flight program was developed to obtain stability and control parameters of the DH-6 in a baseline ('uniced') configuration and an 'artificially iced' configuration for specified thrust conditions. Stability and control parameter identification maneuvers were performed over a wide range of angles of attack for wing flaps retracted (0 deg) and wing flaps partially deflected (10 deg). Engine power was adjusted to hold thrust constant at one of three thrust coefficients ($C_{sub T} = 0.14$, $C_{sub T} = 0.07$, $C_{sub T} = 0.00$). This paper presents only the pitching- and yawing-moment results from the flight test program. Stability and control parameters were estimated for the uniced and artificially iced configurations using a modified stepwise regression algorithm. Comparisons of the uniced and iced stability and control parameters are presented for the majority of the flight envelope. The artificial ice reduced the elevator and rudder control effectiveness by 12 percent and 8 percent respectively for the 0 deg flap setting. The longitudinal static stability was also decreased substantially (approximately 10 percent) because of the tail ice. Further discussion is provided to explain some of the effects of ice on the stability and control parameters. Author

A93-26432* National Aeronautics and Space Administration. Lewis Research Center, Cleveland, OH.

ROBUST INTEGRATED FLIGHT/PROPULSION CONTROL DESIGN FOR A STOVL AIRCRAFT USING H-INFINITY CONTROL DESIGN TECHNIQUES

SANJAY GARG (NASA, Lewis Research Center, Cleveland, OH) Automatica (ISSN 0005-1098) vol. 29, no. 1 Jan. 1993 p. 129-145. refs Copyright

Results are presented from an application of H-infinity control design methodology to a centralized integrated flight/propulsion control (IFPC) system design for a supersonic STOVL fighter aircraft in transition flight. The emphasis is on formulating the H-infinity optimal control synthesis problem such that the critical requirements for the flight and propulsion systems are adequately reflected within the linear, centralized control problem formulation and the resulting controller provides robustness to modeling uncertainties and model parameter variations with flight condition. Detailed evaluation results

are presented for a reduced order controller obtained from the improved H-infinity control design showing that the control design meets the specified nominal performance objective as well as provides stability robustness for variations in plant system dynamics with changes in aircraft trim speed within the transition flight envelope. Author

A93-37004 National Aeronautics and Space Administration. Lewis Research Center, Cleveland, OH.

DESIGN AND EVALUATION OF A ROBUST DYNAMIC NEUROCONTROLLER FOR A MULTIVARIABLE AIRCRAFT CONTROL PROBLEM

T. TROUDET, S. GARG, and W. MERRILL (NASA, Lewis Research Center, Cleveland, OH) In IJCNN - International Joint Conference on Neural Networks, Baltimore, MD, June 7-11, 1992, Proceedings. Vol. 1 New York Institute of Electrical and Electronics Engineers, Inc. 1992 p. I-308 to I-314. Previously announced in STAR as N92-20586 refs (Contract RTOP 505-62-50) Copyright

The design of a dynamic neurocontroller with good robustness properties is presented for a multivariable aircraft control problem. The internal dynamics of the neurocontroller are synthesized by a state estimator feedback loop. The neurocontrol is generated by a multilayer feedforward neural network which is trained through backpropagation to minimize an objective function that is a weighted sum of tracking errors, and control input commands and rates. The neurocontroller exhibits good robustness through stability margins in phase and vehicle output gains. By maintaining performance and stability in the presence of sensor failures in the error loops, the structure of the neurocontroller is also consistent with the classical approach of flight control design. Author

A93-41894* National Aeronautics and Space Administration. Lewis Research Center, Cleveland, OH.

NEUROCONTROL DESIGN AND ANALYSIS FOR A MULTIVARIABLE AIRCRAFT CONTROL PROBLEM

TERRY TROUDET (Sverdrup Technology, Inc., Brook Park, OH), SANJAY GARG, and WALTER MERRILL (NASA, Lewis Research Center, Cleveland, OH) Journal of Guidance, Control, and Dynamics (ISSN 0731-5090) vol. 16, no. 4 July-Aug. 1993 p. 738-747. AIAA Guidance, Navigation and Control Conference, New Orleans, LA, Aug. 12-14, 1991, Technical Papers. Vol. 2, p. 993-1009. Previously cited in issue 21, p. 3600, Accession no. A91-49676 refs Copyright

A93-51361*# National Aeronautics and Space Administration. Lewis Research Center, Cleveland, OH.

APPLICATION OF CONTROLLER PARTITIONING OPTIMIZATION PROCEDURE TO INTEGRATED FLIGHT/PROPULSION CONTROL DESIGN FOR A STOVL AIRCRAFT

SANJAY GARG (NASA, Lewis Research Center, Cleveland, OH) and PHILLIP H. SCHMIDT (Akron Univ., OH) In AIAA Guidance, Navigation and Control Conference, Monterey, CA, Aug. 9-11, 1993, Technical Papers. Pt. 2 Washington American Institute of Aeronautics and Astronautics 1993 p. 610-618. refs (AIAA PAPER 93-3766) Copyright

A parameter optimization framework has earlier been developed to solve the problem of partitioning a centralized controller into a decentralized, hierarchical structure suitable for integrated flight/propulsion control implementation. This paper presents results from the application of the controller partitioning optimization procedure to IFPC design for a Short Take-Off and Vertical Landing (STOVL) aircraft in transition flight. The controller partitioning problem and the parameter optimization algorithm are briefly described. Insight is provided into choosing various 'user' selected parameters in the optimization cost function such that the resulting optimized subcontrollers will meet the characteristics of the centralized controller that are crucial to achieving the desired closed-loop performance and robustness, while maintaining the desired subcontroller structure constraints that are crucial for IFPC

implementation. The optimization procedure is shown to improve upon the initial partitioned subcontrollers and lead to performance comparable to that achieved with the centralized controller. This application also provides insight into the issues that should be addressed at the centralized control design level in order to obtain implementable partitioned subcontrollers.

A93-51400*# National Aeronautics and Space Administration. Lewis Research Center, Cleveland, OH.

INTEGRATED FLIGHT/PROPULSION CONTROL - SUBSYSTEM SPECIFICATIONS FOR PERFORMANCE

W. K. NEIGHBORS and STEPHEN M. ROCK (Stanford Univ., CA) In AIAA Guidance, Navigation and Control Conference, Monterey, CA, Aug. 9-11, 1993, Technical Papers. Pt. 2 Washington American Institute of Aeronautics and Astronautics 1993 p. 975-983. refs

(Contract NAG3-1177)

(AIAA PAPER 93-3808) Copyright

A procedure is presented for calculating multiple subsystem specifications given a number of performance requirements on the integrated system. This procedure applies to problems where the control design must be performed in a partitioned manner. It is based on a structured singular value analysis, and generates specifications as magnitude bounds on subsystem uncertainties. The performance requirements should be provided in the form of bounds on transfer functions of the integrated system. This form allows the expression of model following, command tracking, and disturbance rejection requirements. The procedure is demonstrated on a STOVL aircraft design.

A93-54268 National Aeronautics and Space Administration. Lewis Research Center, Cleveland, OH.

A PARAMETER OPTIMIZATION APPROACH TO CONTROLLER PARTITIONING FOR INTEGRATED FLIGHT/PROPULSION CONTROL APPLICATION

PHILLIP H. SCHMIDT (Akron Univ., OH), SANJAY GARG (NASA, Lewis Research Center, Cleveland, OH), and BRIAN R. HOLOWECKY (Akron Univ., OH) IEEE Transactions on Control Systems Technology (ISSN 1063-6536) vol. 1, no. 1 March 1993 p. 21-36. refs

(Contract NAG3-1146; RTOP 505-62-50)

Copyright

A parameter optimization framework is presented to solve the problem of partitioning a centralized controller into a decentralized hierarchical structure suitable for integrated flight/propulsion control implementation. The controller partitioning problem is briefly discussed and a cost function to be minimized is formulated, such that the resulting 'optimal' partitioned subsystem controllers will closely match the performance (including robustness) properties of the closed-loop system with the centralized controller while maintaining the desired controller partitioning structure. The cost function is written in terms of parameters in a state-space representation of the partitioned sub-controllers. Analytical expressions are obtained for the gradient of this cost function with respect to parameters, and an optimization algorithm is developed using modern computer-aided control design and analysis software. The capabilities of the algorithm are demonstrated by application to partitioned integrated flight/propulsion control design for a modern fighter aircraft in the short approach to landing task. The partitioning optimization is shown to lead to reduced-order subcontrollers that match the closed-loop command tracking and decoupling performance achieved by a high-order centralized controller.

N93-12305*# National Aeronautics and Space Administration. Lewis Research Center, Cleveland, OH.

ANALYSIS OF FAULT-TOLERANT NEUROCONTROL ARCHITECTURES

T. TROUDET (Sverdrup Technology, Inc., Brook Park, OH.) and W. MERRILL 1992 12 p Proposed for presentation at the 31st Conference on Decision and Control, Tucson, AZ, 16-18 Dec. 1992; sponsored by IEEE

(Contract RTOP 505-62-50)

(NASA-TM-105898; E-7210; NAS 1.15:105898) Avail: CASI HC A03/MF A01

The fault-tolerance of analog parallel distributed implementations of a multivariable aircraft neurocontroller is analyzed by simulating weight and neuron failures in a simplified scheme of analog processing based on the functional architecture of the ETANN chip (Electrically Trainable Artificial Neural Network). The neural information processing is found to be only partially distributed throughout the set of weights of the neurocontroller synthesized with the backpropagation algorithm. Although the degree of distribution of the neural processing, and consequently the fault-tolerance of the neurocontroller, could be enhanced using Locally Distributed Weight and Neuron Approaches, a satisfactory level of fault-tolerance could only be obtained by retraining the degraded VLSI neurocontroller. The possibility of maintaining neurocontrol performance and stability in the presence of single weight of neuron failures was demonstrated through an automated retraining procedure of the neurocontroller based on a pre-programmed choice and sequence of the training parameters.

Author

N93-14831*# National Aeronautics and Space Administration. Lewis Research Center, Cleveland, OH.

ICING EFFECTS ON AIRCRAFT STABILITY AND CONTROL DETERMINED FROM FLIGHT DATA: PRELIMINARY RESULTS

T. P. RATVASKY and R. J. RANAUDO Jan. 1993 28 p Presented at the 31st Aerospace Sciences Meeting and Exhibit, Reno, NV, 11-14 Jan. 1993

(Contract RTOP 505-68-10)

(NASA-TM-105977; E-7500; NAS 1.15:105977; AIAA PAPER 93-0398) Avail: CASI HC A03/MF A01

The effects of airframe icing on the stability and control characteristics of the NASA DH-6 Twin Otter icing research aircraft were investigated by flight test. The flight program was developed to obtain the stability and control parameters of the DH-6 in a baseline ('uniced') configuration and an 'artificially iced' configuration for specified thrust conditions. Stability and control parameter identification maneuvers were performed over a wide range of angles of attack for wing flaps retracted (0 deg) and wing flaps partially deflected (10 deg). Engine power was adjusted to hold thrust constant at one of three thrust coefficients ($C_{sub T} = 0.14$, $C_{sub T} = 0.07$, $C_{sub T} = 0.00$). This paper presents only the pitching- and yawing-moment results from the flight test program. Stability and control parameters were estimated for the uniced and artificially iced configurations using a modified stepwise regression algorithm. Comparisons of the uniced and iced stability and control parameters are presented for the majority of the flight envelope. The artificial ice reduced the elevator and rudder control effectiveness by 12 percent and 8 percent respectively for the 0 deg flap setting. The longitudinal static stability was also decreased substantially (approximately 10 percent) because of the tail ice. Further discussion is provided to explain some of the effects of ice on the stability and control parameters.

Author

N93-21197*# National Aeronautics and Space Administration. Lewis Research Center, Cleveland, OH.

CONTROLLER PARTITIONING FOR INTEGRATED FLIGHT/PROPULSION CONTROL IMPLEMENTATION

SANJAY GARG Feb. 1993 28 p Presented at the American Control Conference, Chicago, IL, 24-26 Jun. 1992; sponsored by the AACC

(Contract RTOP 505-62-50)

(NASA-TM-105804; E-7234; NAS 1.15:105804) Avail: CASI HC A03/MF A01

The notion of partitioning a centralized controller into a decentralized, hierarchical structure suitable for integrated flight/propulsion control (IFPC) implementation is discussed. A systematic procedure is developed for determining partitioned airframe and engine subsystem controllers (subcontrollers), with the desired interconnection structure, that approximate the closed-loop performance and robustness characteristics of a given centralized controller. The procedure is demonstrated by application

08 AIRCRAFT STABILITY AND CONTROL

to IFPC design for a Short Take-Off and Vertical Landing (STOVL) aircraft in the landing approach to hover transition flight phase.

Author

N93-26907*# National Aeronautics and Space Administration. Lewis Research Center, Cleveland, OH.

ROBUSTNESS ENHANCEMENT OF NEUROCONTROLLER AND STATE ESTIMATOR

TERRY TROUDET (Sverdrup Technology, Inc., Brook Park, OH.) Feb. 1993 7 p Proposed for presentation at the World Congress on Neural Networks (WCNN), Portland, OR, 11-15 Jul. 1993; sponsored by International Neural Network Society (Contract RTOP 505-62-50) (NASA-TM-106028; E-7590; NAS 1.15:106028) Avail: CASI HC A02/MF A01

The feasibility of enhancing neurocontrol robustness, through training of the neurocontroller and state estimator in the presence of system uncertainties, is investigated on the example of a multivariable aircraft control problem. The performance and robustness of the newly trained neurocontroller are compared to those for an existing neurocontrol design scheme. The newly designed dynamic neurocontroller exhibits a better trade-off between phase and gain stability margins, and it is significantly more robust to degradations of the plant dynamics.

Author

09

RESEARCH AND SUPPORT FACILITIES (AIR)

Includes airports, hangars and runways; aircraft repair and overhaul facilities; wind tunnels; shock tubes; and aircraft engine test stands.

A93-23698*# National Aeronautics and Space Administration. Lewis Research Center, Cleveland, OH.

LIQUID WATER CONTENT MEASUREMENTS USING THE PHASE DOPPLER PARTICLE ANALYZER IN THE NASA LEWIS ICING RESEARCH TUNNEL

R. C. RUDOFF, E. J. BACHALO, W. D. BACHALO (Aerometrics, Inc., Sunnyvale, CA), and J. R. OLDENBURG (NASA, Lewis Research Center, Cleveland, OH) Jan. 1993 17 p. AIAA, Aerospace Sciences Meeting and Exhibit, 31st, Reno, NV, Jan. 11-14, 1993 refs (Contract NAS3-25653) (AIAA PAPER 93-0298) Copyright

The performance of a Phase Doppler Particle Analyzer (PDPA) based icing probe suitable for use in icing tunnels and airborne applications is assessed. The instrument is shown to accurately and repeatably measure liquid water content (LWC) to within better than 20 percent of the nominal expected value in the NASA Lewis IRT. This was seen to be true over a wide range of tunnel operating conditions. The principles used by the PDPA for MVD and LWC determination are discussed. Calibration curves for the IRT median volume diameter are also determined and compared to the existing calibration determined via the PMS instruments. As has been shown in previous work, the PDPA is quite repeatable. The results are typically 3 to 5 microns smaller than the existing calibrations for a given run condition. Reasons for these differences are also discussed.

Author

A93-49988*# National Aeronautics and Space Administration. Lewis Research Center, Cleveland, OH.

DEVELOPMENT AND USE OF HYDROGEN-AIR TORCHES IN AN ALTITUDE FACILITY

ROY A. LOTTIG (NASA, Lewis Research Center, Cleveland, OH) and GARY T. HUBER (Sverdrup Technology, Inc., Brook Park, OH) Jun. 1993 14 p. AIAA, SAE, ASME, and ASEE, Joint Propulsion Conference and Exhibit, 29th, Monterey, CA, June 28-30, 1993 Previously announced in STAR as N93-26214 refs (AIAA PAPER 93-2176) Copyright

A hydrogen-air ignition torch concept that had been used successfully in two rocket engine test facilities to consume excess hydrogen in their exhausters at atmospheric conditions was experimentally evaluated and developed in an altitude test facility at NASA Lewis Research Center. The idea was to use several of these torches in conjunction with hydrogen detectors and dilution air to prevent excess accumulation of unburned hydrogen or mixtures of hydrogen and air exceeding the sea-level lower flammability limit in the altitude facility exhaust system during hydrogen-fueled propulsion system tests. The torches were evaluated for a range of fuel-to-air ratios from 0.09 to 0.39 and for a range of exit diameters from 19/64 to 49/64 in. From the results of these tests a torch geometry and a fuel-to-air ratio were selected that produced a reasonably sized torch exhaust flame for consumption of unburned hydrogen at altitude pressures from sea level to 4 psia.

N93-12016*# National Aeronautics and Space Administration. Lewis Research Center, Cleveland, OH.

ACOUSTICAL EVALUATION OF THE NASA LEWIS 9 BY 15 FOOT LOW SPEED WIND TUNNEL

MILO D. DAHL and RICHARD P. WOODWARD Nov. 1992 64 p

(Contract RTOP 505-62-21) (NASA-TP-3274; E-6137; NAS 1.60:3274) Avail: CASI HC A04/MF A01

The test section of the NASA Lewis 9- by 15-Foot Low Speed Wind Tunnel was acoustically treated to allow the measurement of acoustic sources located within the tunnel test section under simulated free field conditions. The treatment was designed for high sound absorption at frequencies above 250 Hz and to withstand tunnel airflow velocities up to 0.2 Mach. Evaluation tests with no tunnel airflow were conducted in the test section to assess the performance of the installed treatment. This performance would not be significantly affected by low speed airflow. Time delay spectrometry tests showed that interference ripples in the incident signal resulting from reflections occurring within the test section average from 1.7 dB to 3.2 dB wide over a 500 to 5150 Hz frequency range. Late reflections, from upstream and downstream of the test section, were found to be insignificant at the microphone measuring points. For acoustic sources with low directivity characteristics, decay with distance measurements in the test section showed that incident free field behavior can be measured on average with an accuracy of +/- 1.5 dB or better at source frequencies from 400 Hz to 10 kHz. The free field variations are typically much smaller with an omnidirectional source.

Author

N93-15498*# National Aeronautics and Space Administration. Lewis Research Center, Cleveland, OH.

USER MANUAL FOR NASA LEWIS 10 BY 10 FOOT SUPERSONIC WIND TUNNEL

RONALD H. SOEDER 1992 54 p

(Contract RTOP 505-62-84) (NASA-TM-105626; E-6967; NAS 1.15:105626) Avail: CASI HC A04/MF A01

This manual describes the 10- by 10-Foot Supersonic Wind Tunnel at the NASA Lewis Research Center and provides information for users who wish to conduct experiments in this facility. Tunnel performance operating envelopes of altitude, dynamic pressure, Reynolds number, total pressure, and total temperature as a function of test section Mach number are presented. Operating envelopes are shown for both the aerodynamic (closed) cycle and the propulsion (open) cycle. The tunnel test section Mach number range is 2.0 to 3.5. General support systems, such as air systems, hydraulic system, hydrogen system, fuel system, and Schlieren system, are described. Instrumentation and data processing and acquisition systems are also described. Pretest meeting formats and schedules are outlined. Tunnel user responsibility and personnel safety are also discussed.

Author

N93-25080*# National Aeronautics and Space Administration. Lewis Research Center, Cleveland, OH.

NASA LEWIS 8- BY 6-FOOT SUPERSONIC WIND TUNNEL USER MANUAL

RONALD H. SOEDER Feb. 1993 55 p

(Contract RTOP 505-62-84)

(NASA-TM-105771; E-7196; NAS 1.15:105771) Avail: CASI HC A04/MF A01

The 8- by 6-Foot Supersonic Wind Tunnel (SWT) at Lewis Research Center is available for use by qualified researchers. This manual contains tunnel performance maps which show the range of total temperature, total pressure, static pressure, dynamic pressure, altitude, Reynolds number, and mass flow as a function of test section Mach number. These maps are applicable for both the aerodynamic and propulsion cycle. The 8- by 6-Foot Supersonic Wind Tunnel is an atmospheric facility with a test section Mach number range from 0.36 to 2.0. General support systems (air systems, hydraulic system, hydrogen system, infrared system, laser system, laser sheet system, and schlieren system) are also described as are instrumentation and data processing and acquisition systems. Pretest meeting formats are outlined. Tunnel user responsibility and personal safety requirements are also stated.

Author

N93-26214*# National Aeronautics and Space Administration. Lewis Research Center, Cleveland, OH.

DEVELOPMENT AND USE OF HYDROGEN-AIR TORCHES IN AN ALTITUDE FACILITY

ROY A. LOTTIG and GARY T. HUBER (Sverdrup Technology, Inc., Brook Park, OH.) Jun. 1993 15 p Prepared for presentation at the 29th Joint Propulsion Conference and Exhibit, Monterey, CA, 28-30 Jun. 1993; sponsored by AIAA, SAE, ASME, and ASEE

(Contract RTOP 505-62-84)

(NASA-TM-106047; E-7633; NAS 1.15:106047; AIAA PAPER 93-2176) Avail: CASI HC A03/MF A01

A hydrogen-air ignition torch concept that had been used successfully in two rocket engine test facilities to consume excess hydrogen in their exhausters at atmospheric conditions was experimentally evaluated and developed in an altitude test facility at NASA Lewis Research Center. The idea was to use several of these torches in conjunction with hydrogen detectors and dilution air to prevent excess accumulation of unburned hydrogen or mixtures of hydrogen and air exceeding the sea-level lower flammability limit in the altitude facility exhaust system during hydrogen-fueled propulsion system tests. The torches were evaluated for a range of fuel-to-air ratios from 0.09 to 0.39 and for a range of exit diameters from 19/64 to 49/64 in. From the results of these tests a torch geometry and a fuel-to-air ratio were selected that produced a reasonably sized torch exhaust flame for consumption of unburned hydrogen at altitude pressures from sea level to 4 psia.

Author

12

ASTRONAUTICS (GENERAL)

A93-13752 National Aeronautics and Space Administration, Washington, DC.

PLANNING FOR THE SPACE EXPLORATION INITIATIVE - THE NUCLEAR PROPULSION OPTION

GARY L. BENNETT (NASA, Washington) and THOMAS J. MILLER (NASA, Lewis Research Center, Cleveland, OH) In Space nuclear power systems; Proceedings of the 8th Symposium, Albuquerque, NM, Jan. 6-10, 1991. Pt. 1 New York American Institute of Physics 1991 p. 1-4. refs

Copyright

The Space Exploration Initiative includes both lunar and Mars

program elements as well as robotic science missions. Space transportation is a primary part of all planning for exploration. The high performance propulsion capabilities of nuclear propulsion offer the potential to reduce substantially the flight times to and from Mars and to reduce the mass launched into low earth orbit.

Author

A93-23700# National Aeronautics and Space Administration. Lewis Research Center, Cleveland, OH.

A REVIEW OF DESIGN CONCEPTS FOR THE ADVANCED FLUIDS MODULE (AFM) PROJECT

MYRON E. HILL and PETER S. TSCHEN (NASA, Lewis Research Center, Cleveland, OH) Jan. 1993 15 p. AIAA, Aerospace Sciences Meeting and Exhibit, 31st, Reno, NV, Jan. 11-14, 1993 Research supported by NASA refs

(AIAA PAPER 93-0258) Copyright

This paper reviews preliminary fluid module design concepts for the Advanced Fluids Module (AFM) project. The objective of this effort is to provide a facility that can handle a wide variety of fluids experiments. Sample science requirements were written and conceptual designs were subsequently generated during the last year. Experiments from the following fluid physics subject areas were used as conceptual design drivers: static and dynamic interfacial phenomena; bubble/droplet thermocapillary migration; surface tension convection and instabilities; thermal/solutal convection; pool boiling; and multiphase flow. After the conceptual designs were completed, the next phase attempted to combine experiments capabilities into a multipurpose, multiuser apparatus configured for the Space Station Freedom. It was found that all the fluid subject areas considered could be accommodated by three basic types of fluids modules. These modules are the Static Fluid Cell Module, the Dynamic Fluid Cell Module, and the Multiphase Flow Module. Descriptions of these preliminary modules designs and their particular sub-systems (e.g., fluid and thermal systems) are discussed. These designs will be refined as the nature of the flight program becomes clearer over the next six to twelve months.

Author

A93-24245*# National Aeronautics and Space Administration. Lewis Research Center, Cleveland, OH.

MICROGRAVITY RESEARCH ON THE NASA LEWIS LEARJET TEST FACILITY

E. O. BOYER, W. J. RIEKE, and C. M. GRODSINSKY (NASA, Lewis Research Center, Cleveland, OH) Jan. 1993 16 p. AIAA, Aerospace Sciences Meeting and Exhibit, 31st, Reno, NV, Jan. 11-14, 1993 refs

(AIAA PAPER 93-0573) Copyright

Results from preliminary performance tests conducted in an aircraft low-G testbed for nonfree-floating experimental packages have identified several operational variables that directly influence the duration and quality of each trajectory. Flight test measurements were made to identify and quantify the presence of higher-frequency airborne and structureborne noise that may affect the correlation of research data with acceleration levels recorded on trajectory traces.

O.C.

A93-25854 Jet Propulsion Lab., California Inst. of Tech., Pasadena.

ROBOTIC PLANETARY MISSION BENEFITS FROM NUCLEAR ELECTRIC PROPULSION

JAMES H. KELLEY and CHEN-WAN YEN (JPL, Pasadena, CA) In IECEC '92; Proceedings of the 27th Intersociety Energy Conversion Engineering Conference, San Diego, CA, Aug. 3-7, 1992. Vol. 1 Warrendale, PA Society of Automotive Engineers, Inc. 1992 p. 1.9-1.19. Research sponsored by DOE and NASA refs

Copyright

Several interesting planetary missions are either enabled or significantly enhanced by nuclear electric propulsion (NEP) in the 50 to 100 kW power range. These missions include a Pluto Orbiter/Probe with an 11-year flight time and several years of operational life in orbit versus a ballistic very fast (13 km/s) flyby which would take longer to get to Pluto and would have a very

12 ASTRONAUTICS (GENERAL)

short time to observe the planet. (A ballistic orbiter would take about 40 years to get to Pluto). Other missions include a Neptune Orbiter/Probe, a Jupiter Grand Tour orbiting each of the major moons in order, an Uranus Orbiter/Probe, a Multiple Mainbelt Asteroid Rendezvous orbiting six selected asteroids, and a Comet Nucleus Sample Return. This paper discusses potential missions and compares the nuclear electric propulsion option to the conventional ballistic approach on a parametric basis. Author

A93-30937* # National Aeronautics and Space Administration. Lewis Research Center, Cleveland, OH.

AN APPROACH TO STUDYING THE RELIABILITY OF MICROGRAVITY EXPERIMENTS

MICHAEL THAGGARD (Science Applications International Corp., Brook Park, OH) and DANIEL P. MORILAK (NASA, Lewis Research Center, Cleveland, OH) Feb. 1993 11 p. AIAA, AHS, and ASEE, Aerospace Design Conference, Irvine, CA, Feb. 16-19, 1993 refs
(AIAA PAPER 93-1024) Copyright

The identification of key factors that influence the non-success of experiments conducted under microgravity conditions will aid in the planning, design and implementation of future space shuttle experiments, as well as other microgravity experiments (i.e., experiments conducted on the Space Station). Similarly, knowledge of the experiments' reliability will assist in forecasting the success of forthcoming experiments. Since a relatively large number of Space Shuttle experiments have been conducted to date, a substantial pool of data exists for assessing the possible causes or factors which influence experiment non-successes. This report details the task being undertaken at NASA Lewis Research Center (LeRC) to measure the Space Shuttle experiments non-success trends and identify causes that significantly affect their performance. It addresses the activities associated with correlating experiment macro-factors with experiment non-successes. The development and implementation of a microgravity database to be used for tracking and correlating experiment non-success factors, as well as the criteria for measuring experiment success and non-success is also discussed. Author

A93-32293* National Aeronautics and Space Administration. Lewis Research Center, Cleveland, OH.

LOW EARTH SIMULATION AND MATERIALS CHARACTERIZATION

R. A. SYNOWICKI, JEFFREY S. HALE, and JOHN A. WOOLLAM (Nebraska Univ., Lincoln) Journal of Spacecraft and Rockets (ISSN 0022-4650) vol. 30, no. 1 Jan.-Feb. 1993 p. 116-119. refs
(Contract NAG3-95)
Copyright

Oxygen plasma ashers and an electron cyclotron resonance (ECR) sources are currently being used for low Earth orbit (LEO) simulation. The suitability of each of these simulation techniques is considered. Thin film coatings are characterized by optical techniques, including variable-angle spectroscopic ellipsometry, optical spectrophotometry, and laser light scatterometry. Atomic force microscopy (AFM) has been used to characterize the surface morphology of thin aluminum films as a function of substrate temperature during deposition. Results on diamondlike carbon (DLC) films show that DLC degrades with simulated atomic oxygen (AO) exposure at a rate comparable to Kapton polyimide. Since DLC is not as susceptible as Kapton to environmental factors such as moisture absorption, it could potentially provide more accurate measurements of AO fluence on short space flights. Author

A93-49804* # National Aeronautics and Space Administration. Lewis Research Center, Cleveland, OH.

SPACE VEHICLE DESIGN AND OPERATION FOR EFFICIENT USE OF NUCLEAR THERMAL PROPULSION

MIKE L. STANCATI (Science Applications International Corp., Schaumburg, IL), JOHN R. HODGE (Martin Marietta Astronautics Group, Denver, CO), and STANLEY K. BOROWSKI (NASA, Lewis Research Center, Cleveland, OH) Jun. 1993 14 p. AIAA,

SAE, ASME, and ASEE, Joint Propulsion Conference and Exhibit, 29th, Monterey, CA, June 28-30, 1993 refs
(AIAA PAPER 93-1946) Copyright

Nuclear Thermal Propulsion (NTP) is a high-leverage, and possibly enabling, propulsion choice for sending humans to Mars. Important performance gains are expected for NTP Mars transfer vehicle over their counterparts, the conventional chemical systems. These gains come in spite of vehicle unique requirements for NTP engine development and operations: expected higher development costs, prelaunch and in-space handling safeguards, extra propellant for reactor cool-down after engine burns, and safe, managed disposal of spent NTP engines. Prior studies have also shown that these NTP engines and stages, sized for Mars missions, could increase delivered payloads for some piloted lunar mission as well.

A93-50057* # National Aeronautics and Space Administration. Lewis Research Center, Cleveland, OH.

A COMPARISON OF NUCLEAR THERMAL ROCKET DEVELOPMENT COST AND SCHEDULE FOR PILOTED MISSIONS TO MARS

JOHN S. CLARK, STANLEY K. BOROWSKI, ROBERT J. SEFCIK, and THOMAS J. MILLER (NASA, Lewis Research Center, Cleveland, OH) Jun. 1993 14 p. AIAA, SAE, ASME, and ASEE, Joint Propulsion Conference and Exhibit, 29th, Monterey, CA, June 28-30, 1993 refs
(AIAA PAPER 93-2263) Copyright

In Fiscal Year 1992, NASA led a team, including DOE, universities, and industry, that evaluated various schedule and cost scenarios for development of nuclear thermal rocket propulsion systems for piloted Mars exploration. This paper summarizes the results of two of these studies: (1) a so-called 'Fast Track' approach, that would result in technology readiness level 6 (TRL-6-system ground testing complete) by the year 2000, and (2) a slower program that results in TRL-6 by 2006. Both scenarios included a concurrent engineering approach. Costs and schedules for the two scenarios are compared. In addition to the six-year schedule delay, the TRL-6 in 2006 scenario is estimated to increase the cost of the program from \$4.7 billion to \$5.8 billion (in real-year dollars). On the positive side, the technical program should be better, since nuclear testing of fuel elements may be possible prior to concept down-select, resulting in a more informed decision. Author (revised)

A93-50125# National Aeronautics and Space Administration, Washington, DC.

PROGRESS REPORT ON NUCLEAR PROPULSION FOR SPACE EXPLORATION AND SCIENCE

GARY L. BENNETT (NASA, Washington) and THOMAS J. MILLER (NASA, Lewis Research Center, Cleveland, OH) Jun. 1993 12 p. AIAA, SAE, ASME, and ASEE, Joint Propulsion Conference and Exhibit, 29th, Monterey, CA, June 28-30, 1993 refs
(AIAA PAPER 93-2352) Copyright

NASA is continuing its work in cooperation with the Department of Energy (DOE) on nuclear propulsion - both nuclear thermal propulsion (NTP) and nuclear electric propulsion (NEP). The focus of the NTP studies remains on piloted and cargo missions to Mars (with precursor missions to the moon) although studies are under way to examine the potential uses of NTP for science missions. The focus of the NEP studies has shifted to space science missions with consideration of combining a science mission with an earlier demonstration of NEP using the SP-100 space nuclear reactor power system. Both NTP and NEP efforts are continuing in 1993 to provide a good foundation for science and exploration planners. Both NTP and NEP provide a very important transportation resource and in a number of cases enable missions that could not otherwise be accomplished.

A93-53588# National Aeronautics and Space Administration. Lewis Research Center, Cleveland, OH.

SPACE TRANSPORTATION ALTERNATIVES FOR LARGE SPACE PROGRAMS - THE INTERNATIONAL SPACE UNIVERSITY SUMMER SESSION - 1992

14 GROUND SUPPORT SYSTEMS AND FACILITIES (SPACE)

BRYAN PALASZEWSKI (NASA, Lewis Research Center, Cleveland, OH) Jun. 1993 24 p. AIAA, SAE, ASME, and ASEE, Joint Propulsion Conference and Exhibit, 29th, Monterey, CA, June 28-30, 1993 Research supported by NASA refs (AIAA PAPER 93-2278) Copyright

The issues discussed in this paper are the result of a 10-week study by the Space Solar Power Program design project members and the Space Transportation Group at the International Space University (ISU) summer session of 1992 to investigate new paradigms in space propulsion and how those paradigms might reduce the costs for large space programs. The program plan was to place a series of power satellites in Earth orbit. Several designs were studied where many kW, MW or GW of power would be transmitted to Earth or to other spacecraft in orbit. During the summer session, a space solar power system was also detailed and analyzed. At ISU, the focus of the study was to foster and develop some of the new paradigms that may eliminate the barriers to low cost for space exploration and exploitation. Many international and technical aspects of a large multinational program were studied. Environmental safety, space construction and maintenance, legal and policy issues of frequency allocation, technology transfer and control and many other areas were addressed.

Author (revised)

N93-28734*# National Aeronautics and Space Administration. Lewis Research Center, Cleveland, OH.

TRANSFER ORBIT PLASMA INTERACTION EXPERIMENT (TROPIX)

MARK HICKMAN In NASA, Washington, NASA/DOD Flight Experiments Technical Interchange Meeting Proceedings 12 p 1992

Avail: CASI HC A03/MF A10

Viewgraphs on the Transfer Orbit Plasma Interaction Experiment (TROPIX) are presented. Objectives of this research are (1) to map the charged particles in Earth's magnetosphere from LEO to GEO at high inclinations; (2) to measure plasma current collection and resulting shifts in vehicle electrical potential from LEO to GEO across range of orbital inclinations; (3) to study spacecraft interaction with plasma environment using solar electric propulsion (SEP) thrusters as plasma contactors; (4) to measure array degradation over mission duration; (5) to evaluate the potential of various microelectronics, spacecraft components, and instruments for future space missions; and (6) to demonstrate SEP technology applied to a flight vehicle. An overview of TROPIX is presented.

CASI

13

ASTRODYNAMICS

Includes powered and free-flight trajectories; and orbital and launching dynamics.

A93-31532* National Aeronautics and Space Administration. Lewis Research Center, Cleveland, OH.

MINIMUM-FUEL, POWER-LIMITED TRANSFERS BETWEEN COPLANAR ELLIPTICAL ORBITS

CHRISTINE M. HAISSIG, KENNETH D. MEASE (Princeton Univ., NJ), and NGUYEN X. VINH (Michigan Univ., Ann Arbor) Acta Astronautica (ISSN 0094-5765) vol. 29, no. 1 Jan. 1993 p. 1-15. Previously cited in issue 03, p. 326, Accession no. A92-14752 IAF, International Astronautical Congress, 42nd, Montreal, Canada, Oct. 5-11, 1991, IAF Paper 91-346 Research sponsored by DOD refs

(Contract NAG3-915)
Copyright

A93-34521 National Aeronautics and Space Administration. Lyndon B. Johnson Space Center, Houston, TX.

OPTIMAL IMPULSIVE INTERCEPT WITH LOW-THRUST RENDEZVOUS RETURN

CATHERINE A. LEMBECK (NASA, Johnson Space Center, Houston, TX) and JOHN E. PRUSSING (Illinois Univ., Urbana) Journal of Guidance, Control, and Dynamics (ISSN 0731-5090) vol. 16, no. 3 May-June 1993 p. 426-433. Astrodynamics 1989; Proceedings of the AAS/AIAA Astrodynamics Conference, Stowe, VT, Aug. 7-10, 1989. Pt. 1, p. 513-532. Previously cited in issue 21, p. 3320, Accession no. A90-46786 refs

(Contract NAG3-805)
Copyright

14

GROUND SUPPORT SYSTEMS AND FACILITIES (SPACE)

Includes launch complexes, research and production facilities; ground support equipment, e.g., mobile transporters; and simulators.

A93-13783* National Aeronautics and Space Administration. Lewis Research Center, Cleveland, OH.

ESTIMATES OF POWER REQUIREMENTS FOR A MANNED MARS ROVER POWERED BY A NUCLEAR REACTOR

NICHOLAS J. MORLEY, MOHAMED S. EL-GENK (New Mexico Univ., Albuquerque), ROBERT CATALDO, and HARVEY BLOOMFIELD (NASA, Lewis Research Center, Cleveland, OH) In Space nuclear power systems; Proceedings of the 8th Symposium, Albuquerque, NM, Jan. 6-10, 1991. Pt. 1 New York American Institute of Physics 1991 p. 245-252. refs

(Contract NAG3-992)

Copyright

This paper assesses the power requirement for a Manned Mars Rover vehicle. Auxiliary power needs are fulfilled using a hybrid solar photovoltaic/regenerative fuel cell system, while the primary power needs are met using an SP-100 type reactor. The primary electric power needs, which include 30-kW(e) net user power, depend on the reactor thermal power and the efficiency of the power conversion system. Results show that an SP-100 type reactor coupled to a Free Piston Stirling Engine yields the lowest total vehicle mass and lowest specific mass for the power system. The second lowest mass was for a SP-100 reactor coupled to a Closed Brayton Cycle using He/Xe as the working fluid. The specific mass of the nuclear reactor power system, including a man-rated radiation shield, ranged from 150-kg/kW(e) to 190-kg/KW(e) and the total mass of the Rover vehicle varied depend upon the cruising speed.

Author

A93-13793* National Aeronautics and Space Administration. Lewis Research Center, Cleveland, OH.

SHIELDING ANALYSIS FOR A MANNED MARS ROVER POWERED BY AN SP-100 TYPE REACTOR

NICHOLAS J. MORLEY and MOHAMED S. EL-GENK (New Mexico Univ., Albuquerque) In Space nuclear power systems; Proceedings of the 8th Symposium, Albuquerque, NM, Jan. 6-10, 1991. Pt. 1 New York American Institute of Physics 1991 p. 347-354. Research supported by Univ. of New Mexico refs

(Contract NAG3-992)

Copyright

Shield design is one of the most crucial tasks in the integration of a nuclear reactor power system to a manned Mars rover. A multilayered W and LiH shield is found to minimize the shield mass and satisfy the dose rate limit of 30 rem/y to the rover crew. The effect on dose rate of tungsten layers thicknesses and position within the lithium hydride shields is investigated. Due to the large cross section for the W (n,gamma) reaction, secondary gammas become a significant radiation source. The man-rated

14 GROUND SUPPORT SYSTEMS AND FACILITIES (SPACE)

shield mass for the Mars rover vehicle is correlated to the reactor thermal power. The correlation fits to within 9 percent of the calculated shield mass and results in an uncertainty of below 4 percent in the overall rover mass. The shield mass varied from 8600 kg to 20580 kg for a reactor thermal power of 100 to 1000 kW(t), respectively. Author

A93-13819* National Aeronautics and Space Administration. Lewis Research Center, Cleveland, OH.

VERSATILE DYNAMIC ISOTOPE POWER SYSTEMS FOR THE EXPLORATION OF SPACE

RICHARD A. JOHNSON, ANDREW G. STADNIK (Rockwell International Corp., Rocketdyne Div., Canoga Park, CA), ROBERT CATALDO (NASA, Lewis Research Center, Cleveland, OH), and REX WILLIAMS (DOE, Germantown, MD) *In* Space nuclear power systems; Proceedings of the 8th Symposium, Albuquerque, NM, Jan. 6-10, 1991. Pt. 2 New York American Institute of Physics 1991 p. 544-550. (Contract DE-AC03-88NE-32129)

Copyright

Dynamic, isotope-heated power systems are needed to carry out the exploration of space and are major elements identified by NASA for the Space Exploration Initiative (SEI). The Dynamic Isotope Power System (DIPS) Demonstration Program is aimed at establishing the advanced technology as well as the system designs and hardware for the SEI and other exploratory missions. Several conceptual designs of DIPS systems have been developed to provide compact, reliable, and long-lived power systems. Author

A93-13822 National Aeronautics and Space Administration. Lewis Research Center, Cleveland, OH.

SPACE REACTOR/STIRLING CYCLE SYSTEMS FOR HIGH POWER LUNAR APPLICATIONS

PAUL C. SCHMITZ (Sverdrup Technology, Inc., Cleveland, OH) and LEE S. MASON (NASA, Lewis Research Center, Cleveland, OH) *In* Space nuclear power systems; Proceedings of the 8th Symposium, Albuquerque, NM, Jan. 6-10, 1991. Pt. 2 New York American Institute of Physics 1991 p. 567-574. Previously announced in STAR as N91-19112 refs (Contract RTOP 590-13-11)

Copyright

An analysis is performed to mathematically model a 550 kW lunar base power supply which uses a SP-100 reactor coupled with Stirling converters. The reactor is placed in an excavation to keep activated coolant in the hole and to allow maintenance of the components outside the hole. Two technology levels are considered. They are 1050 and 1300 K heater head Stirling converters. It is found that for a 1050 K converter the total mass which provided 1000 volts dc at 250 m is 14,366 kg while the 1300 K system mass is 12,104 kg. The radiation area of the 1050 and 1300 K systems are 641 and 356 sq m respectively. Comparisons are made with Brayton and thermionic systems with both near term and advanced technology considered. Author

A93-13825 National Aeronautics and Space Administration. Lewis Research Center, Cleveland, OH.

COMPARISON OF DYNAMIC ISOTOPE POWER SYSTEMS FOR DISTRIBUTED PLANETARY SURFACE APPLICATIONS

DAVID J. BENTS, BARBARA I. MCKISSOCK, COLLEEN A. WITHROW (NASA, Lewis Research Center, Cleveland, OH), JAMES C. HANLON, and PAUL C. SCHMITZ (Sverdrup Technology, Inc., Brook Park; NASA, Lewis Research Center, Cleveland, OH) *In* Space nuclear power systems; Proceedings of the 8th Symposium, Albuquerque, NM, Jan. 6-10, 1991. Pt. 2 New York American Institute of Physics 1991 p. 586-597. Previously announced in STAR as N91-28278 refs (Contract RTOP 326-81-10)

Copyright

Dynamic isotope power system (DIPS) alternatives were investigated and characterized for the surface mission elements associated with a lunar base and subsequent manned Mars expedition. System designs based on two converter types were studied. These systems were characterized parametrically and

compared over the steady-state electrical output power range 0.2 to 20 kWe. Three methods of thermally integrating the heat source and the Stirling heater head were considered, depending on unit size. Figures of merit were derived from the characterizations and compared over the parametric range. Design impacts of mission environmental factors are discussed and quantitatively assessed. Author

A93-13836* National Aeronautics and Space Administration. Lewis Research Center, Cleveland, OH.

LUNAR IN-CORE THERMIONIC NUCLEAR REACTOR POWER SYSTEM CONCEPTUAL DESIGN

LEE S. MASON (NASA, Lewis Research Center, Cleveland, OH), PAUL C. SCHMITZ (Sverdrup Technology, Inc., Brook Park, OH), and DONALD R. GALLUP (Sandia National Labs., Albuquerque, NM) *In* Space nuclear power systems; Proceedings of the 8th Symposium, Albuquerque, NM, Jan. 6-10, 1991. Pt. 2 New York American Institute of Physics 1991 p. 651-656. refs

Copyright

This paper presents a conceptual design of a lunar in-core thermionic reactor power system. The concept consists of a thermionic reactor located in a lunar excavation with surface mounted waste heat radiators. The system was integrated with a proposed lunar base concept representative of recent NASA Space Exploration Initiative studies. The reference mission is a permanently-inhabited lunar base requiring a 550 kWe, 7 year life central power station. Performance parameters and assumptions were based on the Thermionic Fuel Element (TFE) Verification Program. Five design cases were analyzed ranging from conservative to advanced. The cases were selected to provide sensitivity effects on the achievement of TFE program goals. Author

A93-13901* National Aeronautics and Space Administration. Lewis Research Center, Cleveland, OH.

A STUDY OF ELECTRIC POWER TRANSMISSION LINES FOR USE ON THE LUNAR SURFACE

LLOYD B. GORDON and KRISTA L. GAUSTAD (Auburn Univ., AL) *In* Space nuclear power systems; Proceedings of the 8th Symposium, Albuquerque, NM, Jan. 6-10, 1991. Pt. 3 New York American Institute of Physics 1991 p. 1119-1125. refs (Contract NAG3-1055)

Copyright

Analytical models have been developed to study the operating characteristics of electrical transmission lines for use on the lunar surface. Important design considerations for a transmission line operating on the lunar surface are mass, temperature, and efficiency. Transmission line parameters which impact these considerations include voltage, power loss, and waveform. The electrical and thermal models developed are used to calculate transmission line mass, size, and temperature as a function of voltage, geometry, waveform, location, and efficiency. The analyses include ac and dc for above and below ground operation. Geometries studied include a vacuum-insulated, two-wire transmission line and a solid-dielectric insulated, coaxial transmission line. A brief discussion of design considerations and the models developed is followed by results for parameter studies for both dc and ac transmission lines. Author

A93-13908* National Aeronautics and Space Administration. Lewis Research Center, Cleveland, OH.

DESIGN AND EMPLACEMENT OF AN INTEGRATED LUNAR POWER SYSTEM - ISSUES AND CONCERNS

KENNETH M. SPROUSE, JAMES E. ROBIN, KENNETH J. METCALF (Rockwell International Corp., Rocketdyne Div., Canoga Park, CA), and ROBERT CATALDO (NASA, Lewis Research Center, Cleveland, OH) *In* Space nuclear power systems; Proceedings of the 8th Symposium, Albuquerque, NM, Jan. 6-10, 1991. Pt. 3 New York American Institute of Physics 1991 p. 1169-1174. refs (Contract NAS3-25808)

Copyright

Issues regarding the construction and operation of a stationary

lunar surface power system that must be resolved in order to create a permanent manned presence on the moon are addressed. The issues considered include: (1) the centralization or decentralization of the electrical power system; (2) whether power transmission should be ac or dc; (3) what mix of power generating technology should be used; and (4) the physical interface requirements between the power-system hardware and the construction equipment to be used in placing the hardware on the lunar surface. C.D.

A93-16413* National Aeronautics and Space Administration. Lewis Research Center, Cleveland, OH.

IMPLEMENTATION OF A MODEL BASED FAULT DETECTION AND DIAGNOSIS TECHNIQUE FOR ACTUATION FAULTS OF THE SSME

A. DUYAR (Florida Atlantic Univ., Boca Raton), T.-H. GUO, W. MERRILL, and J. MUSGRAVE (NASA, Lewis Research Center, Cleveland, OH) *In* Annual Health Monitoring Conference for Space Propulsion Systems, 3rd, Cincinnati, OH, Nov. 13, 14, 1991, Proceedings Cincinnati, OH University of Cincinnati 1991 p. 248-264. Previously announced in STAR as N93-11401 refs

In a previous study, Guo, Merrill and Duyar, 1990, reported a conceptual development of a fault detection and diagnosis system for actuation faults of the Space Shuttle main engine. This study, which is a continuation of the previous work, implements the developed fault detection and diagnosis scheme for the real time actuation fault diagnosis of the Space Shuttle Main Engine. The scheme will be used as an integral part of an intelligent control system demonstration experiment at NASA Lewis. The diagnosis system utilizes a model based method with real time identification and hypothesis testing for actuation, sensor, and performance degradation faults. Author

A93-20761* National Aeronautics and Space Administration. Lewis Research Center, Cleveland, OH.

ELECTROMAGNETIC POWERED VEHICLES (EMPV) FOR MARS EXPLORATION

JOSE L. CHRISTIAN, JR., IRA T. MYERS, and RONALD C. CULL (NASA, Lewis Research Center, Cleveland, OH) *In* Space nuclear power systems 1989; Proceedings of the 6th Symposium, Albuquerque, NM, Jan. 8-12, 1989. Vol. 1 Malabar, FL Orbit Book Co., Inc. 1992 p. 77-83. refs

Copyright
Microwave power beamed down from a Mars synchronous nuclear reactor power source to a rectifying antenna on a Mars rover is examined and compared to isotope, reactor, or photovoltaic systems as a power source to move a rover. Large ranges and higher power levels are possible with this microwave powered concept. The advantage of using higher frequencies, in the range of 500 to 1000 GHz, is examined and found to be substantial. Author

A93-25866 National Aeronautics and Space Administration. Lewis Research Center, Cleveland, OH.

OPTIMIZATION OF ARMORED SPHERICAL TANKS FOR STORAGE ON THE LUNAR SURFACE

D. J. BENTS and D. A. KNIGHT (NASA, Lewis Research Center, Cleveland, OH) *In* IECEC '92; Proceedings of the 27th Intersociety Energy Conversion Engineering Conference, San Diego, CA, Aug. 3-7, 1992. Vol. 1 Warrendale, PA Society of Automotive Engineers, Inc. 1992 p. 1.89-1.94. Previously announced in STAR as N92-30187 refs

(Contract RTOP 326-81-10)
Copyright

A redundancy strategy for reducing micrometeoroid armoring mass is investigated, with application to cryogenic reactant storage for a regenerative fuel cell (RFC) on the lunar surface. In that micrometeoroid environment, the cryogenic fuel must be protected from loss due to tank puncture. The tankage must have a sufficiently high probability of survival over the length of the mission so that the probability of system failure due to tank puncture is low compared to the other mission risk factors. Assuming that a single meteoroid penetration can cause a storage tank to lose its contents,

two means are available to raise the probability of surviving micrometeoroid attack to the desired level. One can armor the tanks to a thickness sufficient to reduce probability of penetration of any tank to the desired level or add extra capacity in the form of space tanks that results in survival of a given number out of the ensemble at the desired level. A combination of these strategies (armor and redundancy) is investigated. Author

A93-26099 National Aeronautics and Space Administration. Lewis Research Center, Cleveland, OH.

OVERVIEW AND EVOLUTION OF THE LERC PMAD DC TEST BED

JAMES F. SOEDER and ROBERT J. FRYE (NASA, Lewis Research Center, Cleveland, OH) *In* IECEC '92; Proceedings of the 27th Intersociety Energy Conversion Engineering Conference, San Diego, CA, Aug. 3-7, 1992. Vol. 6 Warrendale, PA Society of Automotive Engineers, Inc. 1992 p. 6.43-6.48. Previously announced in STAR as N92-32867 refs

(Contract RTOP 474-42-10)

Copyright

Since the beginning of the Space Station Freedom Program (SSFP), the Lewis Research Center (LeRC) has been developed electrical power system test beds to support the overall design effort. Through this time, the SSFP has changed the design baseline numerous times, however, the test bed effort has endeavored to track these changes. Beginning in August 1989 with the baseline and an all DC system, a test bed was developed to support the design baseline. The LeRC power measurement and distribution (PMAD) DC test bed and the changes in the restructure are described. The changes included the size reduction of primary power channel and various power processing elements. A substantial reduction was also made in the amount of flight software with the subsequent migration of these functions to ground control centers. The impact of these changes on the design of the power hardware, the controller algorithms, the control software, and a description of their current status is presented. An overview of the testing using the test bed is described, which includes investigation of stability and source impedance, primary and secondary fault protection, and performance of a rotary utility transfer device. Finally, information is presented on the evolution of the test bed to support the verification and operational phases of the SSFP in light of these restructure scrubs. Author

A93-26102* National Aeronautics and Space Administration. Lewis Research Center, Cleveland, OH.

DESCRIPTION OF THE PMAD SYSTEMS TEST BED FACILITY AND DATA SYSTEM

LARRY TRASE, DON FONG, VICKI ADKINS, and ARTHUR BIRCHENOUGH (NASA, Lewis Research Center, Cleveland, OH) *In* IECEC '92; Proceedings of the 27th Intersociety Energy Conversion Engineering Conference, San Diego, CA, Aug. 3-7, 1992. Vol. 6 Warrendale, PA Society of Automotive Engineers, Inc. 1992 p. 6.61-6.65. refs

Copyright

The power management and distribution (PMAD) systems test bed facility, including the power sources and loads available, is discussed, and the PMAD data system (PDS) is described. The PDS controls the test-bed facility hardware, and monitors and records the electric power system control data bus and external data. The PDS architecture is discussed, and each of the subsystems is described. C.A.B.

A93-26103* National Aeronautics and Space Administration. Lewis Research Center, Cleveland, OH.

DESCRIPTION OF THE SSF PMAD DC TESTBED CONTROL SYSTEM DATA ACQUISITION FUNCTION

ANASTACIO N. BAEZ, MICHAEL MACKIN, and THEODORE WRIGHT (NASA, Lewis Research Center, Cleveland, OH) *In* IECEC '92; Proceedings of the 27th Intersociety Energy Conversion Engineering Conference, San Diego, CA, Aug. 3-7, 1992. Vol. 6 Warrendale, PA Society of Automotive Engineers, Inc. 1992 p. 6.67-6.71. Previously announced in STAR as N93-11005

14 GROUND SUPPORT SYSTEMS AND FACILITIES (SPACE)

refs

Copyright

A functional description of the various levels of the SSF power management and distribution dc test-bed control system architecture is presented, and the data acquisition function and the status of its implementation are described. The data requirements for the test-bed control system are dictated by the functionality being implemented at each level of the architecture. The test-bed control system hierarchy data acquisition function is distributed among its various levels. Fast-acting control functions that require time critical data are implemented at the lowest level. These functions require periodic data sampling to assure safe system operation and performance. Slower response control functions are implemented at the higher levels and require data to be reported at least every second. The present data acquisition function meets the requirements for a hierarchical and distributed power management and control system. C.A.B.

A93-34482* National Aeronautics and Space Administration. Lewis Research Center, Cleveland, OH.

SIMULATING A 1-KW ARCJET THRUSTER USING A NONLINEAR ACTIVE LOAD

GENE P. ALTENBURGER (Devilbiss-Ransburg Industrial Liquid Systems, Toledo, OH) and ROGER J. KING (Toledo Univ., OH) *Journal of Propulsion and Power* (ISSN 0748-4658) vol. 9, no. 3 May-June 1993 p. 377-381. AIAA, SAE, ASME, and ASEE, Joint Propulsion Conference and Exhibit, 28th, Nashville, TN, July 6-8, 1992, AIAA Paper 92-3528. Previously cited in issue 20, p. 3490, Accession no. A92-49052 refs (Contract NAG3-1102) Copyright

A93-49711* National Aeronautics and Space Administration. Lewis Research Center, Cleveland, OH.

A LABORATORY MODEL OF A HYDROGEN/OXYGEN ENGINE FOR COMBUSTION AND NOZZLE STUDIES

SYBIL H. MORREN (NASA, Lewis Research Center, Cleveland, OH), ROGER M. MYERS (Sverdrup Technology, Inc., Brook Park, OH), STEPHEN E. BENKO (NASA, Lewis Research Center, Cleveland, OH), LYNN A. ARRINGTON (Sverdrup Technology, Inc., Brook Park, OH), and BRIAN D. REED (NASA, Lewis Research Center, Cleveland, OH) Jun. 1993 33 p. AIAA, SAE, ASME, and ASEE, Joint Propulsion Conference and Exhibit, 29th, Monterey, CA, June 28-30, 1993 refs (AIAA PAPER 93-1825) Copyright

A small laboratory diagnostic thruster was developed in order to evaluate approaches for the use of temperature and pressure sensors for the investigation of low thrust rocket flowfields. Tests were performed at chamber pressures of about 255 kPa, 370 kPa, and 500 kPa with oxidizer/fuel mixture ratios between 4.0 and 8.0. Two gaseous hydrogen/gaseous oxygen injector designs were tested with 60 and 75 fuel film cooling. The results of hot-wire tests showed the thruster and instrumentation designs to be effective. Azimuthal temperature distributions were found to be a function of operating conditions and hardware configuration. Results indicated that small differences in injector design can result in dramatically different thruster performance and wall temperature behavior. However, the importance of these injector effects may be decreased by operating at a high fuel film cooling rate. AIAA

A93-49737* National Aeronautics and Space Administration. Lewis Research Center, Cleveland, OH.

A NEW FACILITY FOR ADVANCED ROCKET PROPULSION RESEARCH

JOSEPH G. ZOECKLER (NASA, Lewis Research Center, Cleveland, OH), JAMES M. GREEN (Sverdrup Technology, Inc., Brook Park, OH), and PAUL RAITANO (NASA, Lewis Research Center, Cleveland, OH) Jun. 1993 9 p. AIAA, SAE, ASME, and ASEE, Joint Propulsion Conference and Exhibit, 29th, Monterey, CA, June 28-30, 1993 Previously announced in STAR as N93-28696 (AIAA PAPER 93-1859) Copyright

A new test facility was constructed at the NASA Lewis Research

Center Rocket Laboratory for the purpose of conducting rocket propulsion research at up to 8.9 kN (2000 lbf) thrust, using liquid oxygen and gaseous hydrogen propellants. A laser room adjacent to the test cell provides access to the rocket engine for advanced laser diagnostic systems. The size and location of the test cell provide the ability to conduct large amounts of testing in short time periods, with rapid turnover between programs. These capabilities make the new test facility an important asset for basic and applied rocket propulsion research.

A93-49952* National Aeronautics and Space Administration. Lewis Research Center, Cleveland, OH.

DESIGN OF AN ADVANCED EXPANDER TEST BED

JOHN C. MITCHELL (Pratt & Whitney Group, West Palm Beach, FL) and WILLIAM K. TABATA (NASA, Lewis Research Center, Cleveland, OH) Jun. 1993 10 p. AIAA, SAE, ASME, and ASEE, Joint Propulsion Conference and Exhibit, 29th, Monterey, CA, June 28-30, 1993 refs (AIAA PAPER 93-2133) Copyright

The final design of the Advanced Expander Test Bed (AETB) is discussed. The AETB is a cryogenic rocket ground test unit being designed and built for NASA to enable validation of mission-focused technologies for advanced space engines. Based on the split expander cycle, it will operate at a nominal thrust of 20,000 lbf, a chamber pressure of 1200 psia, and may be operated off-design over a wide range of throttling conditions and mixture ratios. The design approach and configuration of the major components are described.

A93-49955* National Aeronautics and Space Administration. Lewis Research Center, Cleveland, OH.

DESIGN OF AN OXYGEN TURBOPUMP FOR USE IN AN ADVANCED EXPANDER TEST BED ENGINE

WILLIAM W. PATTISON, CHRISTINE B. COOLEY (Pratt & Whitney Group, West Palm Beach, FL), and JERRY CAREK (NASA, Lewis Research Center, Cleveland, OH) Jun. 1993 8 p. AIAA, SAE, ASME, and ASEE, Joint Propulsion Conference and Exhibit, 29th, Monterey, CA, June 28-30, 1993 (AIAA PAPER 93-2137) Copyright

A liquid oxygen (LOX) turbopump with a gaseous hydrogen turbine drive was designed for the Advanced Expander Test Bed (AETB), which is a technology test bed to develop future space engines. This turbopump features a single stage, full admission, high reaction turbine: a three-bladed axial flow inducer, a high efficiency single stage centrifugal pump with an integrally shrouded impeller; an interpropellant seal package with an oxygen vaporizer; and a subcritical rotor with two ball bearings for axial loads and one roller bearing for turbine radial loads. Material selections were based on compatibility with operating fluids and temperatures. The pump was designed to operate over a 20:1 power range with a maximum performance point of 283.0 GPM of liquid oxygen at a pump discharge pressure of 2198 psia, and a shaft speed of 47,914 rpm. The split expander cycle engine and the performance it requires of the LOX turbopump is discussed as well as the design of the turbopump components. Author (revised)

N93-11398* National Aeronautics and Space Administration. Lewis Research Center, Cleveland, OH.

THE NASA CSTI HIGH CAPACITY POWER PROJECT

J. WINTER, J. DUDENHOEFER, A. JUHASZ, G. SCHWARZE, R. PATTERSON, D. FERGUSON, R. TITRAN, P. SCHMITZ (Sverdrup Technology, Inc., Brook Park, OH.), and J. VANDERSANDE (Jet Propulsion Lab., California Inst. of Tech., Pasadena.) Aug. 1992 9 p. Presented at the 27th Intersociety Energy Conversion Engineering Conference, San Diego, CA, 3-7 Aug. 1992; sponsored by SAE, ACS, AIAA, ASME, IEEE, AIChE, and ANS (Contract RTOP 590-13-00) (NASA-TM-105813; E-7244; NAS 1.15:105813) Avail: CASI HC A02/MF A01

The SP-100 Space Nuclear Power Program was established in 1983 by DOD, DOE, and NASA as a joint program to develop technology for military and civil applications. Starting in 1986, NASA has funded a technology program to maintain the momentum of

promising aerospace technology advancement started during Phase 1 of SP-100 and to strengthen, in key areas, the chances for successful development and growth capability of space nuclear reactor power systems for a wide range of future space applications. The elements of the Civilian Space Technology Initiative (CSTI) High Capacity Power Project include Systems Analysis, Stirling Power Conversion, Thermoelectric Power Conversion, Thermal Management, Power Management, Systems Diagnostics, Environmental Interactions, and Material/Structural Development. Technology advancement in all elements is required to provide the growth capability, high reliability and 7 to 10 year lifetime demanded for future space nuclear power systems. The overall project will develop and demonstrate the technology base required to provide a wide range of modular power systems compatible with the SP-100 reactor which facilitates operation during lunar and planetary day/night cycles as well as allowing spacecraft operation at any attitude or distance from the sun. Significant accomplishments in all of the project elements will be presented, along with revised goals and project timelines recently developed. Author

N93-11401*# National Aeronautics and Space Administration. Lewis Research Center, Cleveland, OH.

IMPLEMENTATION OF A MODEL BASED FAULT DETECTION AND DIAGNOSIS FOR ACTUATION FAULTS OF THE SPACE SHUTTLE MAIN ENGINE

A. DUYAR (Florida Atlantic Univ., Boca Raton.), T.-H. GUO, W. MERRILL, and J. MUSGRAVE Jul. 1992 15 p Presented at the Third Annual Conference on Health Monitoring for Space Propulsion Systems, Cincinnati, OH, 13-14 Nov. 1991; sponsored by Cincinnati Univ. (Contract RTOP 582-01-41) (NASA-TM-105781; E-7208; NAS 1.15:105781) Avail: CASI HC A03/MF A01

In a previous study, Guo, Merrill and Duyar, 1990, reported a conceptual development of a fault detection and diagnosis system for actuation faults of the space shuttle main engine. This study, which is a continuation of the previous work, implements the developed fault detection and diagnosis scheme for the real time actuation fault diagnosis of the space shuttle main engine. The scheme will be used as an integral part of an intelligent control system demonstration experiment at NASA Lewis. The diagnosis system utilizes a model based method with real time identification and hypothesis testing for actuation, sensor, and performance degradation faults. Author

N93-20184*# National Aeronautics and Space Administration. Lewis Research Center, Cleveland, OH.

CAPABILITIES AND CONSTRAINTS OF NASA'S GROUND-BASED REDUCED GRAVITY FACILITIES

JACK LEKAN, ERIC S. NEUMANN, and RAYMOND G. SOTOS *In its* The Second International Microgravity Combustion Workshop p 45-60 Feb. 1993 Avail: CASI HC A03/MF A03; 11 functional color pages

The ground-based reduced gravity facilities of NASA have been utilized to support numerous investigations addressing various processes and phenomena in several disciplines for the past 30 years. These facilities, which include drop towers, drop tubes, aircraft, and sounding rockets are able to provide a low gravity environment (gravitational levels that range from 10(exp -2)g to 10(exp -6)g) by creating a free fall or semi-free fall condition where the force of gravity on an experiment is offset by its linear acceleration during the 'fall' (drop or parabola). The low gravity condition obtained on the ground is the same as that of an orbiting spacecraft which is in a state of perpetual free fall. The gravitational levels and associated duration times associated with the full spectrum of reduced gravity facilities including spaced-based facilities are summarized. Even though ground-based facilities offer a relatively short experiment time, this available test time has been found to be sufficient to advance the scientific understanding of many phenomena and to provide meaningful hardware tests during the flight experiment development process. Also, since experiments can be quickly repeated in these facilities, multistep

phenomena that have longer characteristic times associated with them can sometimes be examined in a step-by-step process. There is a large body of literature which has reported the study results achieved through using reduced-gravity data obtained from the facilities. Author

N93-26963*# National Aeronautics and Space Administration. Lewis Research Center, Cleveland, OH.

FACILITIES

In its Nuclear Propulsion Technical Interchange Meeting, Volume 2 p 741-742 1993

Avail: CASI HC A01/MF A06

The topics are presented in viewgraph form and include the following: nuclear propulsion facility requirements; LeRC candidate facilities; and the Interagency Facility Panel (NASA, DOE, and DOD) Derived from text

N93-26964*# National Aeronautics and Space Administration. Lewis Research Center, Cleveland, OH.

PLUM BROOK FACILITIES

ROBERT KOZAR *In its* Nuclear Propulsion Technical Interchange Meeting, Volume 2 p 743-745 1993

Avail: CASI HC A01/MF A06

The topics are presented in viewgraph form and include the following: the Spacecraft Propulsion Research Facility (B-2); the Hydrogen Heat Transfer Facility (HHTF); the Rocket Dynamics and Control Facility (B-3); the Cryogenic Propellant Tank Site (K-Site); and the Space Power Facility (SPF).

Derived from text

N93-26965*# National Aeronautics and Space Administration. Lewis Research Center, Cleveland, OH.

NEP FACILITIES (LERC)

ROBERT H. VETRONE *In its* Nuclear Propulsion Technical Interchange Meeting, Volume 2 p 746-751 1993

Avail: CASI HC A02/MF A06

The topics are presented in viewgraph form and include the following: the Electric Propulsion Research Building (no. 16) the Electric Power Laboratory (BLDG. 301); the Tank 6 Vacuum Facility; and test facilities for electric propulsion and LeRC.

Derived from text

N93-26970*# National Aeronautics and Space Administration. Lewis Research Center, Cleveland, OH.

NUCLEAR ELECTRIC PROPULSION SYSTEMS OVERVIEW

MICHAEL P. DOHERTY *In its* Nuclear Propulsion Technical Interchange Meeting, Volume 2 p 790-797 1993

Avail: CASI HC A02/MF S06

The topics are presented in viewgraph form and include the following: nuclear propulsion background; schedule for the nuclear electric propulsion (NEP) project; NEP for the Space Exploration Initiative; NEP on-going systems tasks; 20KWe mission/system study; and agenda. CASI

N93-28696*# National Aeronautics and Space Administration. Lewis Research Center, Cleveland, OH.

A NEW FACILITY FOR ADVANCED ROCKET PROPULSION RESEARCH

JOSEPH G. ZOECKLER, JAMES M. GREEN (Sverdrup Technology, Inc., Brook Park, OH.), and PAUL RAITANO Jun. 1993 10 p Presented at the 29th Joint Propulsion Conference and Exhibit, Monterey, CA, 28-30 Jun. 1993; cosponsored by AIAA, SAE, ASME, and ASEE

(Contract RTOP 506-42-72)

(NASA-TM-106193; E-7899; NAS 1.15:106193; AIAA PAPER 93-1859) Avail: CASI HC A02/MF A01

A new test facility was constructed at the NASA Lewis Research Center Rocket Laboratory for the purpose of conducting rocket propulsion research at up to 8.9 kN (2000 lbf) thrust, using liquid oxygen and gaseous hydrogen propellants. A laser room adjacent to the test cell provides access to the rocket engine for advanced laser diagnostic systems. The size and location of the test cell provide the ability to conduct large amounts of testing in short

15 LAUNCH VEHICLES AND SPACE VEHICLES

time periods, with rapid turnover between programs. These capabilities make the new test facility an important asset for basic and applied rocket propulsion research. Author (revised)

15

LAUNCH VEHICLES AND SPACE VEHICLES

Includes boosters; operating problems of launch/space vehicle systems; and reusable vehicles.

A93-12072 National Aeronautics and Space Administration. Marshall Space Flight Center, Huntsville, AL.

ESTABLISHING THE INFRASTRUCTURE - AN INTEGRATED SPACE TRANSPORTATION SYSTEM

W. G. HUBER and J. P. SUMRALL (NASA, Marshall Space Flight Center, Huntsville, AL) *In* Mars: Past, present, and future; Proceedings of the Conference, Williamsburg, VA, July 16-19, 1991. Washington American Institute of Aeronautics and Astronautics 1992 p. 195-211. Research supported by Boeing Co. and NASA

Copyright

A discussion is presented concerning the various transfer vehicle/propulsion systems that are currently under consideration within theegis of the NASA Space Exploration Initiative for the establishment of an infrastructure for lunar base construction and Mars exploration. Cryogenically fueled and nuclear propulsion alternatives are considered, as well as such advanced concepts as that employing nuclear-electric propulsion and artificial gravity and a solar-electric propulsion zero-gravity concept. Mars lander and earth-to-LEO launcher concepts are also noted. O.C.

A93-13332*# National Aeronautics and Space Administration. Lewis Research Center, Cleveland, OH.

PROPULSION AND AERODYNAMIC ANALYSIS OF THE BETA II TWO-STAGE-TO-ORBIT VEHICLE

JAMES R. DAVIC and ANTHONY C. MIDEA (Sverdrup Technology, Inc., Brook Park; NASA, Lewis Research Center, Cleveland, OH) Aug. 1992 13 p. AIAA, Aircraft Design Systems Meeting, Hilton Head Island, SC, Aug. 24-26, 1992 refs (Contract NAS3-25266) (AIAA PAPER 92-4245)

A study of a revised version of the Beta II two-stage-to-orbit vehicle has been undertaken. The goal of the study was to modify and refine critical components of the NASA/Boeing/Wright Laboratory Beta II booster design to better define a successful baseline vehicle that can provide routine access to space. The vehicle geometry was modified and corresponding aerodynamics were predicted. The propulsion system was improved by refining the nacelle design which included incorporating a variable capture area inlet, replacing the five High Speed Civil Transport derived turbine bypass turbojet engines with four variable cycle turbofan engines per nacelle, and removing the bypass duct system. The ramjet performance was adjusted for the change in airflow due to the variable capture area inlet. The second stage wing-body orbiter design was not modified for this study. The total Beta II takeoff weight which resulted was approximately 1.0 million pounds.

Author

A93-22350*# National Aeronautics and Space Administration. Lewis Research Center, Cleveland, OH.

THE DESIGN AND EVOLUTION OF THE BETA TWO-STAGE-TO-ORBIT HORIZONTAL TAKEOFF AND LANDING LAUNCH SYSTEM

LEO BURKARDT (NASA, Lewis Research Center, Cleveland, OH) and RICK NORRIS (USAF, Wright Lab., Wright-Patterson AFB, OH) Dec. 1992 17 p. AIAA, International Aerospace Planes Conference, 4th, Orlando, FL, Dec. 1-4, 1992 refs (AIAA PAPER 92-5080) Copyright

The paper describes the design guidelines and operational

characteristics of a two-stage-to-orbit (TSTO) horizontal takeoff and landing launch vehicle termed Beta, designed for low-cost aircraftlike operations. It can take off and land from standard Strategic Air Command runways and is fully recoverable and reusable. The original Beta I has a payload capability of 50,000, while the newer downsized Beta II will deploy payloads of about 10,000 lbs to low polar orbit. The last Beta vehicle, Beta III which is in early stages of design, has increased operational efficiency. Design diagrams are presented illustrating Beta I and Beta II booster, nacelle, and orbiter concepts. I.S.

A93-25891 National Aeronautics and Space Administration. Lewis Research Center, Cleveland, OH.

AN ELECTROMECHANICAL ACTUATION SYSTEM FOR AN EXPENDABLE LAUNCH VEHICLE

LINDA M. BURROWS and MARY E. ROTH (NASA, Lewis Research Center, Cleveland, OH) *In* IECEC '92; Proceedings of the 27th Intersociety Energy Conversion Engineering Conference, San Diego, CA, Aug. 3-7, 1992. Vol. 1 Warrendale, PA Society of Automotive Engineers, Inc. 1992 p. 1.251-1.255. Previously announced in STAR as N92-30310 refs (Contract RTOP 506-41-41)

Copyright

A major effort at NASA-Lewis in recent years has been to develop electro-mechanical actuators (EMA's) to replace the hydraulic systems used for thrust vector control (TVC) on launch vehicles. This is an attempt to overcome the inherent inefficiencies and costs associated with the existing hydraulic structures. General Dynamics Space Systems Division, under contract to NASA Lewis, is developing 18.6 kW (25 hp), 29.8 kW (40 hp), and 52.2 kW (70 hp) peak EMA systems to meet the power demands for TVC on a family of vehicles developed for the National Launch System. These systems utilize a pulse population modulated converter and field-oriented control scheme to obtain independent control of both the voltage and frequency. These techniques allow an induction motor to be operated at its maximum torque at all times. Author

A93-51473*# National Aeronautics and Space Administration. Lewis Research Center, Cleveland, OH.

MONTE CARLO ANALYSIS OF THE TITAN III/TRANSFER ORBIT STAGE GUIDANCE SYSTEM FOR THE MARS OBSERVER MISSION

STEPHEN C. BELL, MARC A. GINSBURG, and PRABHAKARA P. RAO (Martin Marietta Corp., Denver, CO) *In* AIAA Guidance, Navigation and Control Conference, Monterey, CA, Aug. 9-11, 1993, Technical Papers. Pt. 3 Washington American Institute of Aeronautics and Astronautics 1993 p. 1692-1706. refs (Contract NAS3-25807) (AIAA PAPER 93-3889) Copyright

An important part of space launch vehicle mission planning for a planetary mission is the integrated analysis of guidance and performance dispersions for both booster and upper stage vehicles. For the Mars Observer mission, an integrated trajectory analysis was used to maximize the scientific payload and to minimize injection errors by optimizing the energy management of both vehicles. This was accomplished by designing the Titan III booster vehicle to inject into a hyperbolic departure plane, and the Transfer Orbit Stage (TOS) to correct any booster dispersions. An integrated Monte Carlo analysis of the performance and guidance dispersions of both vehicles provided sensitivities, an evaluation of their guidance schemes and an injection error covariance matrix. The polynomial guidance schemes used for the Titan III variable flight azimuth computations and the TOS solid rocket motor ignition time and burn direction derivations accounted for a wide variation of launch times, performance dispersions, and target conditions. The Mars Observer spacecraft was launched on 25 September 1992 on the Titan III/TOS vehicle. The post flight analysis indicated that a near perfect park orbit injection was achieved, followed by a trans-Mars injection with less than 2sigma errors.

A93-53747* National Aeronautics and Space Administration. Lewis Research Center, Cleveland, OH.

TITAN III FEASIBILITY FOR HL-20 PROTOTYPE MISSIONS

SCOTT W. BENSON (NASA, Lewis Research Center, Cleveland, OH), BRIAN A. BEAVER (Analex Corp., Brook Park, OH), AMY L. EDELMAN (NASA, Lewis Research Center, Cleveland, OH), and ELIZABETH H. SHOLES (Martin Marietta Astronautics Group, Denver, CO) *Journal of Spacecraft and Rockets* (ISSN 0022-4650) vol. 30, no. 5 Sept.-Oct. 1993 p. 615-621. refs Copyright

A set of studies was performed to investigate the feasibility of using the Titan III launch vehicle to launch an unmanned prototype HL-20 personnel launch system and, potentially, operational HL-20 missions. The launch of an HL-20 spacecraft on a Titan III poses a unique set of concerns, primarily because the lifting body vehicle is carried on top of the Titan vehicle without a fairing. The Titan III/HL-20 feasibility study addressed the primary vehicle issues of performance, aerodynamics, loads, control and stability, launch availability, and vehicle configuration for the launch of an unmanned HL-20 prototype vehicle. Titan launch operations, launch site systems, and facilities were assessed to determine HL-20 operations compatibility. Additional studies determined the potential launch opportunity and window capabilities of the Titan III for the operational HL-20 mission and the existing Titan III's reliability. The feasibility study determined that the Titan III system, with minor changes, is compatible with the HL-20 vehicle and mission. It could provide nearly daily launch windows for a rendezvous with Space Station Freedom. Titan III reliability, when combined with the HL-20 launch escape system, provides a sufficiently high probability of crew survival to support its consideration as the primary vehicle for HL-20 operational missions.

N93-27018* National Aeronautics and Space Administration. Lewis Research Center, Cleveland, OH.

THE DESIGN AND EVOLUTION OF THE BETA TWO-STAGE-TO-ORBIT HORIZONTAL TAKEOFF AND LANDING LAUNCH SYSTEM

LEO A. BURKARDT and RICK B. NORRIS (Wright Lab., Wright-Patterson AFB, OH.) Dec. 1992 18 p Presented at the Fourth International Aerospace Planes Conference, Orlando, FL, 1-4 Dec. 1992; sponsored by AIAA Previously announced in IAA as A93-22350

(Contract RTOP 505-69-40)

(NASA-TM-106118; E-7776; NAS 1.15:106118; AIAA PAPER 92-25080) Avail: CASI HC A03/MF A01

The Beta launch system was originally conceived in 1986 as a horizontal takeoff and landing, fully reusable, two-stage-to-orbit, manned launch vehicle to replace the Shuttle. It was to be capable of delivering a 50,000 lb. payload to low polar orbit. The booster propulsion system consisted of JP fueled turbojets and LH fueled ramjets mounted in pods in an over/under arrangement, and a single LOX/LH fueled SSME rocket. The second stage orbiter, which staged at Mach 8, was powered by an SSME rocket. A major goal was to develop a vehicle design consistent with near term technology. The vehicle design was completed with a GLOW of approximately 2,000,000 lbs. All design goals were met. Since then, interest has shifted to the 10,000 lbs. to low polar orbit payload class. The original Beta was down-sized to meet this payload class. The GLOW of the down-sized vehicle was approximately 1,000,000 lbs. The booster was converted to exclusively air-breathing operation. Because the booster depends on conventional air-breathing propulsion only, the staging Mach number was reduced to 5.5. The orbiter remains an SSME rocket-powered stage.

Author

N93-28052* National Aeronautics and Space Administration. Lewis Research Center, Cleveland, OH.

QUALITATIVE MODEL-BASED DIAGNOSTICS FOR ROCKET SYSTEMS

WILLIAM MAUL (Sverdrup Technology, Inc., Brook Park, OH.), CLAUDIA MEYER (Sverdrup Technology, Inc., Brook Park, OH.), AMY JANKOVSKY, and CHRISTOPHER FULTON (Analex Corp., Brook Park, OH.) Jun. 1993 13 p Presented at the 29th Joint Propulsion Conference and Exhibit, Monterey, CA, 28-30 Jun. 1993; sponsored by AIAA, SAE, ASME, and ASEE

(Contract RTOP 584-03-11)

(NASA-TM-106234; E-7954; NAS 1.15:106234; AIAA PAPER 93-1779) Avail: CASI HC A03/MF A01

A diagnostic software package is currently being developed at NASA LeRC that utilizes qualitative model-based reasoning techniques. These techniques can provide diagnostic information about the operational condition of the modeled rocket engine system or subsystem. The diagnostic package combines a qualitative model solver with a constraint suspension algorithm. The constraint suspension algorithm directs the solver's operation to provide valuable fault isolation information about the modeled system. A qualitative model of the Space Shuttle Main Engine's oxidizer supply components was generated. A diagnostic application based on this qualitative model was constructed to process four test cases: three numerical simulations and one actual test firing. The diagnostic tool's fault isolation output compared favorably with the input fault condition.

Author (revised)

N93-31670* National Aeronautics and Space Administration. Lewis Research Center, Cleveland, OH.

LUBRICATION OF AN 85-MM BALL BEARING WITH RP-1

HAROLD E. ADDY, JR. and FREDERICK T. SCHULLER (Sverdrup Technology, Inc., Brook Park, OH.) Jun. 1993 11 p Presented at the 29th AIAA Joint Propulsion Conference and Exhibit, Monterey, CA, 28-30 Jun. 1993; sponsored by AIAA, SAE, ASME, and ASEE

(Contract RTOP 584-03-11)

(NASA-TM-106254; E-7978; NAS 1.15:106254; AIAA PAPER 93-2538) Avail: CASI HC A03/MF A01

A parametric experimental investigation of an 85 millimeter bore angular contact ball bearing running in RP-1 fuel was performed at speeds of 10000 to 24000 RPM. Thrust loads were varied from 4450 to 17800 Newtons (1000 to 4000 lbs.). Radial loads were varied from 1335 to 13350 Newtons (300 to 3000 lbs.). RP-1 lubrication for the bearing was provided through a stationary jet ring located adjacent to the test bearing outer ring. Increases in both the thrust and radial loads resulted in increased bearing temperature, while increases in shaft speed resulted in much more dramatic increases in bearing temperature. These trends are typical for ball bearings operating under these types of conditions. Results are given for outer ring temperatures of the test bearing at the various test conditions employed. In addition, the heat energy removed from the bearing by the RP-1 was determined by measuring the increase in temperature as the RP-1 passed through the bearing. Results showed that the amount of heat energy removed by the RP-1 increased with both shaft speed and RP-1 flow rate to the bearing.

Author

16

SPACE TRANSPORTATION

Includes passenger and cargo space transportation, e.g., shuttle operations; and space rescue techniques.

A93-24902* National Aeronautics and Space Administration. Marshall Space Flight Center, Huntsville, AL.

REVIEW OF THE SHUTTLE VIBRATION ENVIRONMENT

CHARLES R. BAUGHER (NASA, Marshall Space Flight Center, Huntsville, AL), GARY L. MARTIN (NASA, Washington), and RICHARD DELOMBARD (NASA, Lewis Research Center, Cleveland, OH) Jan. 1993 10 p AIAA, Aerospace Sciences Meeting and Exhibit, 31st, Reno, NV, Jan. 11-14, 1993 refs (AIAA PAPER 93-0832) Copyright

This paper will review the Microgravity Science and Applications Division's (MSAD) program to record and analyze the Shuttle's vibration environment. This program provides microgravity experimenters with time histories of the acceleration environment during their experiments and provides information for future investigators on the expected Shuttle vibration environment. The

17 SPACE COMMUNICATIONS, SPACECRAFT COMMUNICATIONS, COMMAND AND TRACKING

two major elements of the program will be discussed, the Space Acceleration Measurement System (SAMS) and the Acceleration Characterization and Analysis Project (ACAP). A comparison of the acceleration measurements from five Spacelab missions will be reviewed. Author

17

SPACE COMMUNICATIONS, SPACECRAFT COMMUNICATIONS, COMMAND AND TRACKING

Includes telemetry; space communications networks; astronavigation and guidance; and radio blackout.

A93-17329* National Aeronautics and Space Administration. Lewis Research Center, Cleveland, OH.

HIGH DATA RATE APPLICATIONS OF ACTS TECHNOLOGY
THOMAS VONDEAK (NASA, Lewis Research Center, Cleveland, OH) IEEE Aerospace and Electronic Systems Magazine (ISSN 0885-8985) vol. 7, no. 10 Oct. 1992 p. 38-42. refs

Consideration is given to the existing Broadband Integrated Services Digital Network (BISDN), a delivery method as defined by the International Consultative Committee for Telephone and Telegraph, satellites' role in providing these services, and the NASA high data rate ACTS experiments. It is concluded that satellites have the capability to extend BISDN services beyond the range of the terrestrial BISDN and will provide certain BISDN services more cost effectively in a direct competitive or hybrid satellite-fiber implementation. O.G.

A93-18966 National Aeronautics and Space Administration. Goddard Space Flight Center, Greenbelt, MD.

GSFC CONCEPTUAL DESIGN STUDY FOR AN INTER-SATELLITE OPTICAL MULTIPLE ACCESS COMMUNICATION SYSTEM

NEIL FOX (Stanford Telecommunications, Inc., Reston, VA), WILL MAYNARD (NASA, Goddard Space Flight Center, Greenbelt, MD), ERNEST CLARKE (Laser Data Technology, Inc., Saint Louis, MO), and RONALD BRUNO (Stanford Telecommunications, Inc., Reston, VA) In Free-space laser communication technologies III; Proceedings of the Meeting, Los Angeles, CA, Jan. 21, 22, 1991 Bellingham, WA Society of Photo-Optical Instrumentation Engineers 1991 p. 452-463. refs
(Contract NAS5-31170; NAS3-25091)
Copyright

System and terminal level specifications for an inter-satellite Optical Multiple Access (OMA) communication system are presented, as well as the resulting hardware designs for both OMA relay and OMA user terminals. The OMA relay terminal design uses a mechanical innovation which moves multiple fiber optic pickups in the focal plane, thereby providing simultaneous links with multiple OMA user terminals via a single telescope. Thus, with such a terminal on a relay satellite, multiple access service can be provided with a minimum of impact on the relay satellite. Author

A93-24456* National Aeronautics and Space Administration. Lewis Research Center, Cleveland, OH.

ADVANCED COMMUNICATIONS TECHNOLOGY SATELLITE (ACTS)

RICHARD T. GEDNEY, DAVID L. WRIGHT, JOSEPH L. BALOMBIN, PHILIP Y. SOHN (NASA, Lewis Research Center, Cleveland, OH), WILLIAM F. CASHMAN, and ALAN L. STERN (General Electric Co., Astro-Space Div., Princeton, NJ) Acta Astronautica (ISSN 0094-5765) vol. 26, no. 11 Nov. 1992 p. 813-825. Previously cited in issue 03, p. 302, Accession no. A91-14056 IAF, International Astronautical Congress, 41st, Dresden, Germany, Oct. 6-12, 1990, IAF Paper 90-481 refs
Copyright

A93-32820* National Aeronautics and Space Administration. Lewis Research Center, Cleveland, OH.

ANALYSIS OF REFLECTOR ANTENNA SYSTEM INCLUDING FREQUENCY SELECTIVE SURFACES

M. L. ZIMMERMAN (Analex Corp., Cleveland, OH), S. W. LEE (Illinois Univ., Urbana), and G. FUJIKAWA (NASA, Lewis Research Center, Cleveland, OH) IEEE Transactions on Antennas and Propagation (ISSN 0018-926X) vol. 40, no. 10 Oct. 1992 p. 1264-1266. refs

Copyright

Frequency selective surfaces (FSS's) are often used in spaceborne applications of reflector antennas due to their ability to allow multiple feeds to utilize the same reflector dish. The problems inherent in evaluating the FSS separately from the reflector system are discussed. A method of integrating the FSS effects into the reflector system analysis is presented. An example is given for the proposed Advanced Tracking and Delay Relay Satellite System (ATDRSS) single-access triband reflector antenna. Author

N93-11430*# National Aeronautics and Space Administration. Lewis Research Center, Cleveland, OH.

DIRECT BROADCAST SATELLITE: RADIO PROGRAM

JAMES E. HOLLANSWORTH Oct. 1992 11 p
(Contract RTOP 144-10-2A)
(NASA-TM-105910; E-7355; NAS 1.15:105910) Avail: CASI HC A03/MF A01

NASA is committed to providing technology development that leads to the introduction of new commercial applications for communications satellites. The Direct Broadcast Satellite-Radio (DBS-R) Program is a joint effort between The National Aeronautics and Space Administration (NASA) and The United States Information Agency/Voice of America (USIA/VOA) directed at this objective. The purpose of this program is to define the service and develop the technology for a direct-to-listener satellite sound broadcasting system. The DBS-R Program, as structured by NASA and VOA, is now a three-phase program designed to help the U.S. commercial communications satellite and receiver industry bring about this new communications service. Major efforts are being directed towards frequency planning hardware and service development, service demonstration, and experimentation with new satellite and receiver technology. Author

N93-18854*# National Aeronautics and Space Administration. Lewis Research Center, Cleveland, OH.

OPTICAL COMMUNICATIONS AND A COMPARISON OF OPTICAL TECHNOLOGIES FOR A HIGH DATA RATE RETURN LINK FROM MARS

RODNEY L. SPENCE Washington Jan. 1993 61 p
(Contract RTOP 316-30-19)
(NASA-TP-3180; E-6030; NAS 1.60:3180) Avail: CASI HC A04/MF A01

The important principles of direct- and heterodyne-detection optical free-space communications are reviewed. Signal-to-noise-ratio (SNR) and bit-error-rate (BER) expressions are derived for both the direct-detection and heterodyne-detection optical receivers. For the heterodyne system, performance degradation resulting from received-signal and local oscillator-beam misalignment and laser phase noise is analyzed. Determination of interfering background power from local and extended background sources is discussed. The BER performance of direct- and heterodyne-detection optical links in the presence of Rayleigh-distributed random pointing and tracking errors is described. Finally, several optical systems employing Nd:YAG, GaAs, and CO₂ laser sources are evaluated and compared to assess their feasibility in providing high-data-rate (10- to 1000-Mbps) Mars-to-Earth communications. It is shown that the root mean square (rms) pointing and tracking accuracy is a critical factor in defining the system transmitting laser-power requirements and telescope size and that, for a given rms error, there is an optimum telescope aperture size that minimizes the required power. The results of the analysis conducted indicate that, barring the achievement of extremely small rms pointing and tracking errors

17 SPACE COMMUNICATIONS, SPACECRAFT COMMUNICATIONS, COMMAND AND TRACKING

(less than 0.2 microrad), the two most promising types of optical systems are those that use an Nd:YAG laser ($\lambda = 1.064$ microns) and high-order pulse position modulator (PPM) and direct detection, and those that use a CO₂ laser ($\lambda = 10.6$ microns) and phase shifting keying homodyne modulation and coherent detection. For example, for a PPM order of $M = 64$ and an rms pointing accuracy of 0.4 microrad, an Nd:YAG system can be used to implement a 100-Mbps Mars link with a 40-cm transmitting telescope, a 20-W laser, and a 10-m receiving photon bucket. Under the same conditions, a CO₂ system would require 3-m transmitting and receiving telescopes and a 32-W laser to implement such a link. Other types of optical systems, such as a semiconductor laser systems, are impractical in the presence of large rms pointing errors because of the high power requirements of the 100-Mbps Mars link, even when optimal-size telescopes are used.

Author

N93-22589*# National Aeronautics and Space Administration. Lewis Research Center, Cleveland, OH.

ANALYSIS OF MMIC ARRAYS FOR USE IN THE ACTS AERO EXPERIMENT

M. ZIMMERMAN (Analex Corp., Brook Park, OH.), R. LEE, E. RHO, and Z. ZAMAN Mar. 1993 29 p

(Contract RTOP 506-72-1C)

(NASA-TM-106073; E-7682; NAS 1.15:106073) Avail: CASI HC A03/MF A01

The Aero Experiment is designed to demonstrate communication from an aircraft to an Earth terminal via the ACTS. This paper describes the link budget and antenna requirements for a 4.8 kbps full-duplex voice link at Ka-Band frequencies. Three arrays, one transmit array developed by TI and two receive arrays developed by GE and Boeing, were analyzed. The predicted performance characteristics of these arrays are presented and discussed in the paper.

Author

N93-26895*# National Aeronautics and Space Administration. Lewis Research Center, Cleveland, OH.

FAULT-TOLERANT ONBOARD DIGITAL INFORMATION SWITCHING AND ROUTING FOR COMMUNICATIONS SATELLITES

MARY JO SHALKHAUSER, JORGE A. QUINTANA, NITIN J. SONI, and HEECHUL KIM Washington Apr. 1993 11 p

(Contract RTOP 506-72-21)

(NASA-TM-4471; E-7332; NAS 1.15:4471) Avail: CASI HC A03/MF A01

The NASA Lewis Research Center is developing an information-switching processor for future meshed very-small-aperture terminal (VSAT) communications satellites. The information-switching processor will switch and route baseband user data onboard the VSAT satellite to connect thousands of Earth terminals. Fault tolerance is a critical issue in developing information-switching processor circuitry that will provide and maintain reliable communications services. In parallel with the conceptual development of the meshed VSAT satellite network architecture, NASA designed and built a simple test bed for developing and demonstrating baseband switch architectures and fault-tolerance techniques. The meshed VSAT architecture and the switching demonstration test bed are described, and the initial switching architecture and the fault-tolerance techniques that were developed and tested are discussed.

Author (revised)

N93-27064*# National Aeronautics and Space Administration. Lewis Research Center, Cleveland, OH.

UTILIZING A TDRS SATELLITE FOR DIRECT BROADCAST SATELLITE-RADIO PROPAGATION EXPERIMENTS AND DEMONSTRATIONS

JAMES E. HOLLANSWORTH Jun. 1993 16 p Presented at the Third International Mobile Satellite Conference and Exhibition, Pasadena, CA, 16-18 Jun. 1993

(Contract RTOP 106-70-00)

(NASA-TM-106172; E-7872; NAS 1.15:106172) Avail: CASI HC A03/MF A01

The NASA/VOA Direct Broadcast Satellite-Radio (DBS-R)

Program will be using a NASA Tracking Data Relay Satellite (TDRS) satellite at 62 deg. West longitude to conduct live satellite S-band propagation experiments and demonstrations of satellite sound broadcasting over the next two years (1993-1994). The NASA/VOA DBS-R program has applied intensive effort to garner domestic and international support for the DBS-R concept. An S-band DBS-R allocation was achieved for Region 2 at WARC-92 held in Spain. With this allocation, the DBS-R program now needs to conduct S-band propagation experiments and systems demonstrations that will assist in the development of planning approaches for the use of Broadcast Satellite Service (Sound) frequency bands prior to the planning conference called for by WARC-92. These activities will also support receiver concept development applied to qualities ranging from AM to Monophonic FM, Stereophonic FM, Monophonic CD, and Stereophonic CD quality.

Author

N93-29195*# National Aeronautics and Space Administration. Lewis Research Center, Cleveland, OH.

SYSTEM OVERVIEW ON ELECTROMAGNETIC COMPENSATION FOR REFLECTOR ANTENNA SURFACE DISTORTION

R. J. ACOSTA, A. J. ZAMAN, and J. D. TERRY Jun. 1993 10 p Presented at the 1993 IEEE AP-S International Symposium, Ann Arbor, MI, 27 Jun. - 2 Jul. 1993

(Contract RTOP 579-50-00)

(NASA-TM-106217; E-7928; NAS 1.15:106217) Avail: CASI HC A02/MF A01

The system requirements and hardware implementation for electromagnetic compensation of antenna performance degradations due to thermal effects was investigated. Future commercial space communication antenna systems will utilize the 20/30 GHz frequency spectrum and support very narrow multiple beams (0.3 deg) over wide angle field of view (15-20 beamwidth). On the ground, portable and inexpensive very small aperture terminals (VSAT) for transmitting and receiving video, facsimile and data will be employed. These types of communication system puts a very stringent requirement on spacecraft antenna beam pointing stability (less than .01 deg), high gain (greater than 50 dB) and very low side lobes (less than -25 dB). Thermal analysis performed on the advanced communication technology satellite (ACTS) has shown that the reflector surfaces, the mechanical supporting structures and metallic surfaces on the spacecraft body will distort due to thermal effects from a varying solar flux. The antenna performance characteristics (e.g., pointing stability, gain, side lobe, etc.) will degrade due to thermal distortion in the reflector surface and supporting structures. Specifically, antenna RF radiation analysis has shown that pointing error is the most sensitive antenna performance parameter to thermal distortions. Other antenna parameters like peak gain, cross polarization level (beam isolation), and side lobe level will also degrade with thermal distortions. In order to restore pointing stability and in general antenna performance several compensation methods were proposed. In general these compensation methods can be classified as being either of mechanical or electromagnetic type. This paper will address only the later one. In this approach an adaptive phased array antenna feed is used to compensate for the antenna performance degradation. Extensive work has been devoted to demonstrate the feasibility of adaptive feed compensation on space communication antenna systems. This paper addresses the system requirements for such a system and identify candidate technologies (analog and digital) for possible hardware implementation.

Author (revised)

SPACECRAFT DESIGN, TESTING AND PERFORMANCE

Includes satellites; space platforms; space stations; spacecraft systems and components such as thermal and environmental controls; and attitude controls.

A93-12144* National Aeronautics and Space Administration. Lewis Research Center, Cleveland, OH.

GROUNDING OF SPACE STRUCTURES

P. A. BOSELA (Cleveland State Univ., OH), D. G. FERTIS (Akron Univ., OH), and F. J. SHAKER (NASA, Lewis Research Center, Cleveland, OH) *Computers & Structures* (ISSN 0045-7949) vol. 45, no. 1 Sept. 17, 1992 p. 143-153. refs

Copyright

Space structures, such as the Space Station solar arrays, must be extremely light-weight, flexible structures. Accurate prediction of the natural frequencies and mode shapes is essential for determining the structural adequacy of components, and designing a controls system. The tension pre-load in the 'blanket' of photovoltaic solar collectors, and the free/free boundary conditions of a structure in space, causes serious reservations on the use of standard finite element techniques of solution. In particular, a phenomenon known as 'grounding', or false stiffening, of the stiffness matrix occurs during rigid body rotation. This paper examines the grounding phenomenon in detail. Numerous stiffness matrices developed by others are examined for rigid body rotation capability, and found lacking. A force imbalance inherent in the formulations examined is the likely cause of the grounding problem, suggesting the need for a directed force formulation. Author

A93-12145* National Aeronautics and Space Administration. Lewis Research Center, Cleveland, OH.

A NEW PRE-LOADED BEAM GEOMETRIC STIFFNESS MATRIX WITH FULL RIGID BODY CAPABILITIES

P. A. BOSELA (Cleveland State Univ., OH), D. G. FERTIS (Akron Univ., OH), and F. J. SHAKER (NASA, Lewis Research Center, Cleveland, OH) *Computers & Structures* (ISSN 0045-7949) vol. 45, no. 1 Sept. 17, 1992 p. 155-163. refs

Copyright

Space structures, such as the Space Station solar arrays, must be extremely light-weight, flexible structures. Accurate prediction of the natural frequencies and mode shapes is essential for determining the structural adequacy of components, and designing a controls system. The tension pre-load in the 'blanket' of photovoltaic solar collectors, and the free/free boundary conditions of a structure in space, causes serious reservations on the use of standard finite element techniques of solution. In particular, a phenomenon known as 'grounding', or false stiffening, of the stiffness matrix occurs during rigid body rotation. The authors have previously shown that the grounding phenomenon is caused by a lack of rigid body rotational capability, and is typical in beam geometric stiffness matrices formulated by others, including those which contain higher order effects. The cause of the problem was identified as the force imbalance inherent in the formulations. In this paper, the authors develop a beam geometric stiffness matrix for a directed force problem, and show that the resultant global stiffness matrix contains complete rigid body mode capabilities, and performs very well in the diagonalization methodology customarily used in dynamic analysis. Author

A93-13132* National Aeronautics and Space Administration. Lewis Research Center, Cleveland, OH.

CONTROL-STRUCTURE INTERACTION STUDY FOR THE SPACE STATION SOLAR DYNAMIC POWER MODULE

J. CHENG, G. IANCULESCU, J. LY (Rockwell International Corp., Rocketdyne Div., Canoga Park, CA), and M. KIM (Rockwell International Corp., Space Systems Div., Downey, CA) *In IEEE Conference on Decision and Control*, 30th, Brighton, United

Kingdom, Dec. 11-13, 1991, Proceedings. Vol. 3 New York Institute of Electrical and Electronics Engineers, Inc. 1991 p. 2219-2223. refs

(Contract NAS3-25082)

Copyright

The authors investigate the feasibility of using a conventional PID (proportional plus integral plus derivative) controller design to perform the pointing and tracking functions for the Space Station Freedom solar dynamic power module. Using this simple controller design, the control/structure interaction effects were also studied without assuming frequency bandwidth separation. From the results, the feasibility of a simple solar dynamic control solution with a reduced-order model, which satisfies the basic system pointing and stability requirements, is suggested. However, the conventional control design approach is shown to be very much influenced by the order of reduction of the plant model, i.e., the number of the retained elastic modes from the full-order model. This suggests that, for complex large space structures, such as the Space Station Freedom solar dynamic, the conventional control system design methods may not be adequate. I.E.

A93-13133* National Aeronautics and Space Administration. Lewis Research Center, Cleveland, OH.

OPTIMAL CONTROL STUDY FOR THE SPACE STATION SOLAR DYNAMIC POWER MODULE

P. M. PAPADOPOULOS, A. J. LAUB, C. S. KENNEY, P. PANDEY (California Univ., Santa Barbara), G. IANCULESCU, and J. LY (Rockwell International Corp., Rocketdyne Div., Canoga Park, CA) *In IEEE Conference on Decision and Control*, 30th, Brighton, United Kingdom, Dec. 11-13, 1991, Proceedings. Vol. 3 New York Institute of Electrical and Electronics Engineers, Inc. 1991 p. 2224-2229. refs

(Contract NSF ECS-87-18897; AF-AFOSR-91-0240; NAS3-25082)

Copyright

The authors present the design of an optimal control system for the Space Station Freedom's Solar Dynamic Fine Pointing and Tracking (SDFPT) module. A very large state model of six rigid body modes and 272 flexible modes is used in conjunction with classical LQG optimal control to produce a full-order controller which satisfies the requirements. The results obtained are compared with those of a classically designed PID (proportional plus integral plus derivative) controller that was implemented for a six-rigid-body-mode forty-flexible-mode model. A major difficulty with designing LQG controllers for large models is solving the Riccati equation that arises from the optimal formulation. A Riccati solver based on a Pade approximation to the matrix sign function is used. A symmetric version of this algorithm is derived for the special class of Hamiltonian matrices, thereby yielding, for large problems, a nearly twofold speed increase over a previous algorithm. I.E.

A93-14687* National Aeronautics and Space Administration. Lewis Research Center, Cleveland, OH.

CONTROL-STRUCTURE INTERACTION

JOSEPH K. CHENG, GEORGE D. IANCULESCU (Rockwell International Corp., Rocketdyne Div., Canoga Park, CA), CHARLES S. KENNEY, ALAN J. LAUB (California Univ., Santa Barbara), JASON H. Q. LY (Rockwell International Corp., Rocketdyne Div., Canoga Park, CA), and PHILIP M. PAPADOPOULOS (California Univ., Santa Barbara) *IEEE Control Systems Magazine* (ISSN 0272-1708) vol. 12, no. 5 Oct. 1992 p. 4-13. refs

(Contract AF-AFOSR-91-0240; NAS3-25082)

Copyright

The feasibility of using conventional proportional-integral-derivative (PID) control and an alternative optimal control to perform the pointing and tracking functions of the Space Station solar dynamic power module is investigated. A very large state model of 6 rigid body modes and 272 flexible modes is used in conjunction with classical linear-quadratic-Gaussian (LQG) optimal control to produce a full-order controller that satisfies the requirements. The results are compared with a classically designed PID controller that was implemented for a much smaller (6 rigid body, 40 flexible modes)

model. The conventional control design approach is shown to be very much influenced by the order reduction of the plant model, i.e., the number of retained elastic modes from the full-order model, suggesting that for a complex, large space structure, such as the Space Station Freedom solar dynamic module, application of conventional control system design methods may not be adequate. The use of LQG control is recommended, and method for solving the large matrix Riccati equation that arises from the optimal formulation is provided. I.E.

A93-20330# National Aeronautics and Space Administration. Lewis Research Center, Cleveland, OH.

MODAL TEST/ANALYSIS CORRELATION OF SPACE STATION STRUCTURES USING NONLINEAR SENSITIVITY

VINEY K. GUPTA, JAMES F. NEWELL (Rockwell International Corp., Rocketdyne Div., Canoga Park, CA), LASZLO BERKE, and SASAN ARMAND (NASA, Lewis Research Center, Cleveland, OH) In AIAA/USAF/NASA/OAI Symposium on Multidisciplinary Analysis and Optimization, 4th, Cleveland, OH, Sept. 21-23, 1992, Technical Papers. Pt. 1 Washington American Institute of Aeronautics and Astronautics 1992 p. 332-339. Previously announced in STAR as N92-34221 refs (Contract RTOP 474-46-10)

(AIAA PAPER 92-4731) Copyright

The modal correlation problem is formulated as a constrained optimization problem for validation of finite element models (FEM's). For large-scale structural applications, a pragmatic procedure for substructuring, model verification, and system integration is described to achieve effective modal correlations. The space station substructure FEM's are reduced using Lanczos vectors and integrated into a system FEM using Craig-Bampton component modal synthesis. The optimization code is interfaced with MSC/NASTRAN to solve the problem of modal test/analysis correlation; that is, the problem of validating FEM's for launch and on-orbit coupled loads analysis against experimentally observed frequencies and mode shapes. An iterative perturbation algorithm is derived and implemented to update nonlinear sensitivity (derivatives of eigenvalues and eigenvectors) during optimizer iterations, which reduced the number of finite element analyses.

Author

A93-21108# National Aeronautics and Space Administration. Langley Research Center, Hampton, VA.

DESIGN OF A HYPERSONIC WAVERIDER-DERIVED AIRPLANE

ROBERT J. PEGG, JAMES L. HUNT, DENNIS H. PETLEY (NASA, Langley Research Center, Hampton, VA), LEO BURKHARDT (NASA, Lewis Research Center, Cleveland, OH), DANIEL R. STEVENS, PAUL L. MOSES, S. Z. PINCKNEY, HANEE Z. KABIS, KEVIN A. SPOTH, WILLIAM M. DZIEDZIC (Lockheed Engineering and Sciences Co., Hampton, VA) et al. Jan. 1993 28 p. AIAA, Aerospace Sciences Meeting and Exhibit, 31st, Reno, NV, Jan. 11-14, 1993 refs

(AIAA PAPER 93-0401) Copyright

The paper describes the first assessment study of a waverider-derived Mach 5 aircraft design using fuselage integrated-underslung over/under turboramjets with endothermic fuel. The study is based on a tanker-to-tanker mission, which begins at Mach 0.8 and 30,000 feet, with the vehicle accelerating to Mach 12 at constant altitude and then to Mach 5 while climbing to about 90,000 feet. The paper describes the vehicle, the aerodynamic analysis, and the propulsion system and its installed performance, structure design, and analysis. The mission simulation was run using the CSOTAV code developed by the NASA Langley Research Center. I.S.

A93-24243*# National Aeronautics and Space Administration. Lewis Research Center, Cleveland, OH.

PLASMA SHEATH EFFECTS ON ION COLLECTION BY A PINHOLE

JOEL L. HERR (Sverdrup Technology, Inc., Cleveland, OH) and DAVID B. SNYDER (NASA, Lewis Research Center, Cleveland, OH) Jan. 1993 11 p. AIAA, Aerospace Sciences Meeting

and Exhibit, 31st, Reno, NV, Jan. 11-14, 1993 refs (Contract NAS3-25266) (AIAA PAPER 93-0567)

The data tabulations presented, which express the results of particle-track trajectories through a simplified plasma-sheath electric field, should prove useful in the assessment of spacecraft 'pinhole-collection' effects. Attention is given to a method accounting for plasma-sheath effects in the application of these results. In addition, scaling rules are given for the application of these calculations to specific cases. A comparison is made between the present model's results and those of recent ion current measurements. Good agreement is obtained. O.C.

A93-24801*# National Aeronautics and Space Administration. Lewis Research Center, Cleveland, OH.

INTERACTIONS BETWEEN SPACECRAFT AND THEIR ENVIRONMENTS

DALE C. FERGUSON (NASA, Lewis Research Center, Cleveland, OH) Jan. 1993 11 p. AIAA, Aerospace Sciences Meeting and Exhibit, 31st, Reno, NV, Jan. 11-14, 1993 refs (AIAA PAPER 93-0705) Copyright

Interactions between spacecraft and their environments are discussed using the SSF and the SP-100 power system. It is recommended that discontinuous structure potentials of more than 100 V on a spacecraft must be connected with an insulating material of sufficient thickness to stand off the potential difference. Particular attention must be paid to conductors with a plasma arcing threshold higher than the conductor potential relative to the surrounding plasma. To avoid arcing, spacecraft surfaces should avoid exposed conductors, or at least exposed conductor-insulator junctions for LEO missions. To avoid differential charging, fully conductive surfaces should be used every where for GEO missions. O.G.

A93-24904# National Aeronautics and Space Administration. Lewis Research Center, Cleveland, OH.

VIBRATION ISOLATION TECHNOLOGY - AN EXECUTIVE SUMMARY OF SYSTEMS DEVELOPMENT AND DEMONSTRATION

C. M. GRODSINSKY, K. A. LOGSDON, and J. F. LUBOMSKI (NASA, Lewis Research Center, Cleveland, OH) Jan. 1993 6 p. AIAA, Aerospace Sciences Meeting and Exhibit, 31st, Reno, NV, Jan. 11-14, 1993 Previously announced in STAR as N93-15573 refs

(Contract RTOP 694-03-0C)

(AIAA PAPER 93-0834) Copyright

A program was organized to develop the enabling technologies needed for the use of Space Station Freedom as a viable microgravity experimental platform. One of these development programs was the Vibration Isolation Technology (VIT). This technology development program grew because of increased awareness that the acceleration disturbances present on the Space Transportation System (STS) orbiter can and are detrimental to many microgravity experiments proposed for STS, and in the future, Space Station Freedom (SSF). Overall technological organization are covered of the VIT program. Emphasis is given to the results from development and demonstration of enabling technologies to achieve the acceleration requirements perceived as those most likely needed for a variety of microgravity science experiments. In so doing, a brief summary of general theoretical approaches to controlling the acceleration environment of an isolated space based payload and the design and/or performance of two prototype six degree of freedom active magnetic isolation systems is presented. Author

A93-24905# National Aeronautics and Space Administration. Lewis Research Center, Cleveland, OH.

EVALUATION OF PASSIVE AND ACTIVE VIBRATION CONTROL MECHANISMS IN A MICROGRAVITY ENVIRONMENT

J. ELLISON, G. AHMADI (Clarkson Univ., Potsdam, NY), and C. GRODSINSKY (NASA, Lewis Research Center, Cleveland, OH) Jan. 1993 8 p. AIAA, Aerospace Sciences Meeting and Exhibit,

31st, Reno, NV, Jan. 11-14, 1993 refs
(Contract NGT-50825)

(AIAA PAPER 93-0838) Copyright

The behavior of equipment and their light secondary attachments in large space structures under orbital excitation is studied. The equipment is modeled as a shear beam and its secondary attachment is treated as a single-degree-of-freedom lumped mass system. Peak responses of the equipment and its secondary system for a variety of vibration control mechanisms are evaluated. A novel active friction control mechanism, by varying the normal force, is suggested. The device uses a magnetic field control to minimize the stick condition, thereby reducing the overall structural response. The results show that the use of the passive vibration control devices could reduce the peak equipment responses to a certain extent. However, major reduction of vibration levels could be achieved only by the use of active devices. Using active control of the interface normal force, the peak responses of the equipment and its attachment are reduced by a factor of 10 over the fixed-base equipment response. Author

A93-26101* National Aeronautics and Space Administration. Lewis Research Center, Cleveland, OH.

ELECTRICAL CHARACTERIZATION OF A SPACE STATION FREEDOM ALPHA UTILITY TRANSFER ASSEMBLY

EDWARD J. YENNI (Rockwell International Corp., Cleveland, OH) In IECEC '92; Proceedings of the 27th Intersociety Energy Conversion Engineering Conference, San Diego, CA, Aug. 3-7, 1992. Vol. 6 Warrendale, PA Society of Automotive Engineers, Inc. 1992 p. 6.55-6.59. refs
(Contract NAS3-25711) Copyright

Electrical testing of a utility transfer assembly (UTA) developmental unit performed from January 22 through February 25, 1992 at the NASA Lewis Research Center using the power management and distribution dc test bed. The dc resistance and steady state temperatures recorded are evidence of the UTA's high electrical transfer efficiency. The impedance test results suggest the total inductance of a UTA crossing pair is substantially higher than originally specified in the Space Station Electrical Power System Architectural Control Document. C.A.B.

A93-29156 Jet Propulsion Lab., California Inst. of Tech., Pasadena.

ELECTRODYNAMIC INTERACTIONS BETWEEN A SPACE STATION AND THE IONOSPHERIC PLASMA ENVIRONMENT

J. WANG (MIT, Cambridge, MA; JPL, Pasadena, CA), D. E. HASTINGS, and M. MARTINEZ-SANCHEZ (MIT, Cambridge, MA) Journal of Spacecraft and Rockets (ISSN 0022-4650) vol. 30, no. 2 Mar.-Apr. 1993 p. 176-188. Previously cited in issue 06, p. 817, Accession no. A91-19143 AIAA, Aerospace Sciences Meeting, 29th, Reno, NV, Jan. 7-10, 1991, AIAA Paper 91-0114 refs
(Contract NAG3-695) Copyright

A93-30899* National Aeronautics and Space Administration. Lewis Research Center, Cleveland, OH.

DESIGN OF DEPLOYABLE-TRUSS MASTS FOR SPACE STATION

MARY BOWDEN and MAX BENTON (Able Engineering Co., Goleta, CA) Feb. 1993 11 p. AIAA, AHS, and ASEE, Aerospace Design Conference, Irvine, CA, Feb. 16-19, 1993 Research supported by Lockheed Missiles & Space Co., Inc., Rockwell International, and NASA
(AIAA PAPER 93-0975) Copyright

This paper presents an overview of three deployable-truss designs that were considered for use on Space Station Freedom to deploy the solar array wings. The first design chosen early in the program was a nut-deployed coilable longeron mast which has the advantage of being lightweight and reliable, with considerable flight history. Subsequently, because of the restructure of Space Station, a second design was chosen: a lanyard-deployed FASTMast (Folding Articulated Square Truss Mast), which has

improved strength and redundancy characteristics for a given stowed volume. After further definition of the load requirements during deployment, however, it became necessary to modify the deployment system, resulting in the third mast design for space station solar arrays: a nut-deployed FASTMast, which was ultimately selected to provide increased stiffness and strength during deployment. This paper presents a brief review of these mast designs and their associated deployment systems, emphasizing the trade-offs involved in selecting between them. In addition, some innovative features of the FASTMast design as it stands currently for Space Station are described, and a brief review of the test program that is underway to qualify this design for flight is included. Author

A93-31028* National Aeronautics and Space Administration. Lewis Research Center, Cleveland, OH.

CONTRIBUTIONS OF MICROGRAVITY TEST RESULTS TO THE DESIGN OF SPACECRAFT FIRE-SAFETY SYSTEMS

ROBERT FRIEDMAN (NASA, Lewis Research Center, Cleveland, OH) and DAVID L. URBAN (Sverdrup Technology, Inc., Brook Park, OH) Feb. 1993 12 p. AIAA, AHS, and ASEE, Aerospace Design Conference, Irvine, CA, Feb. 16-19, 1993 refs
(AIAA PAPER 93-1152) Copyright

Experiments conducted in spacecraft and drop towers show that thin-sheet materials have reduced flammability ranges and flame-spread rates under quiescent low-gravity environments (microgravity) compared to normal gravity. Furthermore, low-gravity flames may be suppressed more easily by atmospheric dilution or decreasing atmospheric total pressure than their normal-gravity counterparts. The addition of a ventilating air flow to the low-gravity flame zone, however, can greatly enhance the flammability range and flame spread. These results, along with observations of flame and smoke characteristics useful for microgravity fire-detection 'signatures', promise to be of considerable value to spacecraft fire-safety designs. The paper summarizes the fire detection and suppression techniques proposed for the Space Station Freedom and discusses both the application of low-gravity combustion knowledge to improve fire protection and the critical needs for further research. Author

A93-33908* National Aeronautics and Space Administration. Lewis Research Center, Cleveland, OH.

THE APPLICATION OF STRUCTURAL RELIABILITY TECHNIQUES TO PLUME IMPINGEMENT LOADING OF THE SPACE STATION FREEDOM PHOTOVOLTAIC ARRAY

ISAM S. YUNIS and KELLY S. CARNEY (NASA, Lewis Research Center, Cleveland, OH) In AIAA/ASME/ASCE/AHS/ASC Structures, Structural Dynamics, and Materials Conference, 34th and AIAA/ASME Adaptive Structures Forum, La Jolla, CA, Apr. 19-22, 1993, Technical Papers. Pt. 1 Washington American Institute of Aeronautics and Astronautics 1993 p. 361-377. Previously announced in STAR as N93-17988 refs
(AIAA PAPER 93-1338) Copyright

A new aerospace application of structural reliability techniques is presented, where the applied forces depend on many probabilistic variables. This application is the plume impingement loading of the Space Station Freedom Photovoltaic Arrays. When the space shuttle berths with Space Station Freedom it must brake and maneuver towards the berthing point using its primary jets. The jet exhaust, or plume, may cause high loads on the photovoltaic arrays. The many parameters governing this problem are highly uncertain and random. An approach, using techniques from structural reliability, as opposed to the accepted deterministic methods, is presented which assesses the probability of failure of the array mast due to plume impingement loading. A Monte Carlo simulation of the berthing approach is used to determine the probability distribution of the loading. A probability distribution is also determined for the strength of the array. Structural reliability techniques are then used to assess the array mast design. These techniques are found to be superior to the standard deterministic dynamic transient analysis, for this class of problem. The results show that the probability of failure of the current array mast design, during its 15 year life, is minute. Author

A93-33955* National Aeronautics and Space Administration. Lewis Research Center, Cleveland, OH.

DESIGN OF STRUCTURES FOR NUCLEAR ELECTRIC PROPULSION VEHICLES

JOHN M. HEDGEPEETH (Digisim Corp., Santa Barbara, CA) and CHARLES LAWRENCE (NASA, Lewis Research Center, Cleveland, OH) In AIAA/ASME/ASCE/AHS/ASC Structures, Structural Dynamics, and Materials Conference, 34th and AIAA/ASME Adaptive Structures Forum, La Jolla, CA, Apr. 19-22, 1993, Technical Papers. Pt. 2 Washington American Institute of Aeronautics and Astronautics 1993 p. 810-818. refs (Contract NAS3-25266)

(AIAA PAPER 93-1393) Copyright

This paper reports a study of efficient structures for connecting various elements of Nuclear Electric Propulsion (NEP) vehicles. The design requirements for the structure are discussed and a truss beam is selected for the application. Evaluation of stiffness and weight indicate that the required structure is less than 5 percent of the dry weight of the vehicle.

Author

A93-35050* National Aeronautics and Space Administration. Lewis Research Center, Cleveland, OH.

THE EFFECTS OF 1 KW CLASS ARCJET THRUSTER PLUMES ON SPACECRAFT CHARGING AND SPACECRAFT THERMAL CONTROL MATERIALS

A. BOGORAD, D. A. LIGHTIN, C. BOWMAN, J. ARMENTI (General Electric Co., Astro-Space Div., Princeton, NJ), E. PENCIL, and C. SARMIENTO (NASA, Lewis Research Center, Cleveland, OH) IEEE Transactions on Nuclear Science (ISSN 0018-9499) vol. 39, no. 6, pt. 1 Dec. 1992 p. 1783-1789. 1992 IEEE Annual Conference on Nuclear and Space Radiation Effects, 29th, New Orleans, LA, July 13-17, 1992, Proceedings. A93-35026 13-33 Research sponsored by General Electric Co. refs

Copyright

Arcjet thrusters are soon to be used for north/south stationkeeping on commercial communications satellites. A series of tests was performed to evaluate the possible effects of these thrusters on spacecraft charging and the degradation of thermal control material. During the tests the interaction between arcjet plumes and both charged and uncharged surfaces did not cause any significant material degradation. In addition, firing an arcjet thruster benignly reduced the potential of charged surfaces to near zero.

Author

A93-39265* National Aeronautics and Space Administration. Lewis Research Center, Cleveland, OH.

SPACE STATION FREEDOM STRUCTURE FLOATING POTENTIAL AND THE PROBABILITY OF ARCING

DANIEL E. HASTINGS, MENGU CHO, and JIONG WANG (MIT, Cambridge, MA) Journal of Spacecraft and Rockets (ISSN 0022-4650) vol. 29, no. 6 Nov.-Dec. 1992 p. 830-834. refs (Contract NAG3-695)

Copyright

The interaction between a space system and the space environment has been one of the driving questions for the design of spacecraft since the dawn of the space age. The Space Station Freedom will represent a significant increase in spacecraft size, power, and activity relative to spacecraft that are currently in orbit. The structure floating potential on Space Station Freedom is studied with simple analytical models of the current collection. The probability of arcing due to dielectric breakdown is assessed.

Author

A93-41305* National Aeronautics and Space Administration. Lewis Research Center, Cleveland, OH.

THERMAL CONTROL SYSTEM FOR SPACE STATION FREEDOM PHOTOVOLTAIC POWER MODULE

THOMAS H. HACHA (NASA, Lewis Research Center, Cleveland, OH) and LAURA S. HOWARD (Rockwell International Corp., El Segundo, CA) Jul. 1992 13 p. SAE, International Conference on Environmental Systems, 22nd, Seattle, WA, July 13-16, 1992 (SAE PAPER 921110) Copyright

The electric power for Space Station Freedom (SSF) is

generated by the solar arrays of the photovoltaic power modules (PVM's) and conditioned, controlled, and distributed by a power management and distribution system. The PVM's are located outboard of the alpha gimbals of SSF. A single-phase thermal control system is being developed to provide thermal control of PVM electrical equipment and energy storage batteries. This system uses ammonia as the coolant and a direct-flow deployable radiator. This paper presents the description and development status of the PVM thermal control system.

Author

A93-41878* National Aeronautics and Space Administration. Lewis Research Center, Cleveland, OH.

CONTROL/STRUCTURE INTERACTIONS OF SPACE STATION SOLAR DYNAMIC MODULES

ROGER D. QUINN (Case Western Reserve Univ., Cleveland, OH) and ISAM S. YUNIS (NASA, Lewis Research Center, Cleveland, OH) Journal of Guidance, Control, and Dynamics (ISSN 0731-5090) vol. 16, no. 4 July-Aug. 1993 p. 623-629. AIAA Guidance, Navigation and Control Conference, Portland, OR, Aug. 20-22, 1990, Technical Papers. Pt. 1, p. 79-88. Previously cited in issue 21, p. 3330, Accession no. A90-47585 refs (Contract NAG3-1099)

Copyright

A93-50034* National Aeronautics and Space Administration. Lewis Research Center, Cleveland, OH.

PLASMA CONTACTOR TECHNOLOGY FOR SPACE STATION FREEDOM

MICHAEL J. PATTERSON, JOHN A. HAMLEY (NASA, Lewis Research Center, Cleveland, OH), TIMOTHY SARVER-VERHEY, GEORGE C. SOULAS, JAMES PARKES (Sverdrup Technology, Inc., Brook Park, OH), WAYNE L. OHLINGER (Georgia Inst. of Technology, Atlanta), MICHAEL S. SCHAFFNER (Cleveland State Univ., OH), and AMY NELSON (Purdue Univ., West Lafayette, IN) Jun. 1993 21 p. AIAA, SAE, ASME, and ASEE, Joint Propulsion Conference and Exhibit, 29th, Monterey, CA, June 28-30, 1993 refs

(AIAA PAPER 93-2228) Copyright

Hollow cathode plasma contactors have been baselined for Space Station Freedom to control the electrical potentials of surfaces to eliminate/mitigate damaging interactions with the space environment. The system represents a dual-use technology which is a direct outgrowth of the NASA electric propulsion program and in particular the technology development effort on ion thruster systems. Specific efforts include optimizing the design and configuration of the contactor, validating its required lifetime, and characterizing the contactor plume and electromagnetic interference. The plasma contactor subsystems include the plasma contactor unit, a power electronics unit, and an expellant management unit. Under this program these will all be brought to breadboard and engineering model development status. New test facilities have been developed, and existing facilities have been augmented, to support characterizations and life testing of contactor components and systems. This paper discusses the magnitude, scope, and status of the plasma contactor hardware development program now under way and preliminary test results on system components.

Author (revised)

N93-10841* National Aeronautics and Space Administration. Lewis Research Center, Cleveland, OH.

ACCEPTANCE TESTING OF THE PROTOTYPE ELECTROMETER FOR THE SAMPIE FLIGHT EXPERIMENT

G. BARRY HILLARD Sep. 1992 24 p (Contract RTOP 589-01-1B) (NASA-TM-105880; E-7343; NAS 1.15:105880) Avail: CASI HC A03/MF A01

The Solar Array Module Plasma Interaction Experiment (SAMPIE) has two key instruments at the heart of its data acquisition capability. One of these, the electrometer, is designed to measure both ion and electron current from most of the samples included in the experiment. The accuracy requirement, specified by the project's Principal Investigator, is for agreement within 10 percent with a calibrated laboratory instrument. Plasma chamber

18 SPACECRAFT DESIGN, TESTING AND PERFORMANCE

testing was performed to assess the capabilities of the prototype design. Agreement was determined to be within 2 percent for electron collection and within 3 percent for ion collection. Author

N93-11001*# National Aeronautics and Space Administration. Lewis Research Center, Cleveland, OH.

SITE PROJECT. PHASE 1: CONTINUOUS DATA

BIT-ERROR-RATE TESTING Final Report

GENE FUJIKAWA and ROBERT J. KERCZEWSKI Sep. 1992

90 p

(Contract RTOP 650-60-23)

(NASA-TP-3279; E-6513; NAS 1.60:3279) Avail: CASI HC

A05/MF A01

The Systems Integration, Test, and Evaluation (SITE) Project at NASA LeRC encompasses a number of research and technology areas of satellite communications systems. Phase 1 of this project established a complete satellite link simulator system. The evaluation of proof-of-concept microwave devices, radiofrequency (RF) and bit-error-rate (BER) testing of hardware, testing of remote airlinks, and other tests were performed as part of this first testing phase. This final report covers the test results produced in phase 1 of the SITE Project. The data presented include 20-GHz high-power-amplifier testing, 30-GHz low-noise-receiver testing, amplitude equalization, transponder baseline testing, switch matrix tests, and continuous-wave and modulated interference tests. The report also presents the methods used to measure the RF and BER performance of the complete system. Correlations of the RF and BER data are summarized to note the effects of the RF responses on the BER. Author

N93-12772*# National Aeronautics and Space Administration. Lewis Research Center, Cleveland, OH.

LDEF YAW AND PITCH ANGLE ESTIMATES

BRUCE A. BANKS and LINDA GEBAUER (Cleveland State Univ., OH.) In NASA. Langley Research Center, LDEF Materials Workshop 1991, Part 1 p 71-92 Sep. 1992

Avail: CASI HC A03/MF A04

Quantification of the LDEF yaw and pitch misorientations is crucial to the knowledge of atomic oxygen exposure of samples placed on LDEF. Video camera documentation of the LDEF spacecraft prior to grapple attachment, atomic oxygen shadows on experiment trays and longerons, and a pinhole atomic oxygen camera placed on LDEF provided sources of documentation of the yaw and pitch misorientation. Based on uncertainty-weighted averaging of data, the LDEF yaw offset was found to be 8.1 plus or minus 0.6 degrees, allowing higher atomic oxygen exposure of row 12 than initially anticipated. The LDEF pitch angle offset was found to be 0.8 plus or minus 0.4 degrees, such that the space end was tipped forward toward the direction of travel. The resulting consequences of the yaw and pitch misorientation of LDEF on the atomic oxygen fluence is a factor of 2.16 increase for samples located on row 12, and a factor of 1.18 increase for samples located on the space end compared to that which would be expected for perfect orientation. Author

N93-15594*# National Aeronautics and Space Administration. Lewis Research Center, Cleveland, OH.

LOW EARTH ORBIT ATOMIC OXYGEN SIMULATION FOR DURABILITY EVALUATION OF SOLAR REFLECTOR SURFACES

KIM K. DEGROH and BRUCE A. BANKS In NASA. Goddard Space Flight Center, The Seventeenth Space Simulation Conference. Terrestrial Test for Space Success p 1-17 Nov. 1992

Avail: CASI HC A03/MF A03

To evaluate the performance and durability of solar reflector surfaces in the atomic oxygen environment typical of low Earth orbit (LEO), one must expose the reflector surface either directly to LEO or to ground-laboratory atomic oxygen environments. Although actual LEO exposures are most desired, such opportunities are typically scarce, expensive, and of limited duration. As a result, ground-laboratory exposures must be relied upon as the most practical long-term durability evaluation technique. Plasma

ashers are widely used as LEO simulation facilities by producing atomic oxygen environments for durability evaluation of potential spacecraft materials. Atomic oxygen arrival differs between ground and space exposure in that plasma asher exposure produces isotropic arrival and space solar tracking produces sweeping arrival. Differences in initial impact reaction probability occur, dependent upon the energy and species existing in these environments. Due to the variations in ground-laboratory and space atomic oxygen, quantification of in-space performance based on plasma asher testing is not straightforward. The various atomic oxygen interactions that can occur with reflector surfaces, such as undercutting in organic substrates at protective coating defect sites, ground-laboratory techniques recommended for evaluating the atomic oxygen durability of reflectors based on asher exposures, and computational techniques which make use of ground-laboratory atomic oxygen exposure to predict in-space LEO durability are addressed. Author

N93-15595*# National Aeronautics and Space Administration. Lewis Research Center, Cleveland, OH.

SIMULATION OF THE SYNERGISTIC LOW EARTH ORBIT EFFECTS OF VACUUM THERMAL CYCLING, VACUUM UV RADIATION, AND ATOMIC OXYGEN

JOYCE A. DEVER, KIM K. DEGROH, CURTIS R. STIDHAM (Sverdrup Technology, Inc., Brook Park, OH.), THOMAS J. STUEBER (Sverdrup Technology, Inc., Brook Park, OH.), THERESE M. DEVER (Cleveland State Univ., OH.), ELVIN RODRIGUEZ (Cleveland State Univ., OH.), and JUDITH A. TERLEP (Case Western Reserve Univ., Cleveland, OH.) In NASA. Goddard Space Flight Center, The Seventeenth Space Simulation Conference. Terrestrial Test for Space Success p 19-36 Nov. 1992

Avail: CASI HC A03/MF A03

In order to assess the low Earth orbit (LEO) durability of candidate space materials, it is necessary to use ground laboratory facilities which provide LEO environmental effects. A facility combining vacuum thermal cycling and vacuum ultraviolet (VUV) radiation has been designed and constructed at NASA Lewis Research Center for this purpose. This facility can also be operated without the VUV lamps. An additional facility can be used to provide VUV exposure only. By utilizing these facilities, followed by atomic oxygen exposure in an RF plasma asher, the effects of the individual vacuum thermal cycling and VUV environments can be compared to the effect of the combined vacuum thermal cycling/VUV environment on the atomic oxygen durability of materials. The synergistic effects of simulated LEO environmental conditions on materials were evaluated by first exposing materials to vacuum thermal cycling, VUV, and vacuum thermal cycling/VUV environments followed by exposure to atomic oxygen in an RF plasma asher. Candidate space power materials such as atomic oxygen protected polyimides and solar concentrator mirrors were evaluated using these facilities. Characteristics of the Vacuum Thermal Cycling/VUV Exposure Facility which simulates the temperature sequences and solar ultraviolet radiation exposure that would be experienced by a spacecraft surface in LEO are discussed. Results of durability evaluations of some candidate space power materials to the simulated LEO environmental conditions will also be discussed. Such results have indicated that for some materials, atomic oxygen durability is affected by previous exposure to thermal cycling and/or VUV exposure. Author

N93-15596*# National Aeronautics and Space Administration. Lewis Research Center, Cleveland, OH.

THE USE OF PLASMA ASHERS AND MONTE CARLO MODELING FOR THE PROJECTION OF ATOMIC OXYGEN DURABILITY OF PROTECTED POLYMERS IN LOW EARTH ORBIT

BRUCE A. BANKS, BRUCE M. AUER, SHARON K. RUTLEDGE, KIM K. DEGROH, and LINDA GEBAUER (Cleveland State Univ., OH.) In NASA. Goddard Space Flight Center, The Seventeenth Space Simulation Conference. Terrestrial Test for Space Success p 37-48 Nov. 1992

Avail: CASI HC A03/MF A03

The results of ground laboratory and in-space exposure of

polymeric materials to atomic oxygen has enabled the development of a Monte Carlo computational model which simulates the oxidation processes of both environments. The cost effective projection of long-term low-Earth-orbital durability of protected polymeric materials such as SiO(x)-coated polyimide Kapton photovoltaic array blankets will require ground-based testing to assure power system reliability. Although silicon dioxide thin film protective coatings can greatly extend the useful life of polymeric materials in ground-based testing, the projection of in-space durability based on these results can be made more reliable through the use of modeling which simulates the mechanistic properties of atomic oxygen interaction, and replicates test results in both environments. Techniques to project long-term performance of protected materials, such as the Space Station Freedom solar array blankets, are developed based on ground laboratory experiments, in-space experiments, and computational modeling.

Author

N93-15597* National Aeronautics and Space Administration, Lewis Research Center, Cleveland, OH.

LEVELING COATINGS FOR REDUCING THE ATOMIC OXYGEN DEFECT DENSITY IN PROTECTED GRAPHITE FIBER EPOXY COMPOSITES

D. A. JAWORSKE, KIM K. DEGROH, G. PODOJIL (Cleveland State Univ., OH.), T. MCCOLLUM (Cleveland State Univ., OH.), and J. ANZIC (Cleveland State Univ., OH.) In NASA. Goddard Space Flight Center, The Seventeenth Space Simulation Conference. Terrestrial Test for Space Success p 49-58 Nov. 1992
Avail: CASI HC A02/MF A03

Pinholes or other defect sites in a protective oxide coating provide pathways for atomic oxygen in low Earth orbit to reach underlying material. One concept of enhancing the lifetime of materials in low Earth orbit is to apply a leveling coating to the material prior to applying any reflective and protective coatings. Using a surface tension leveling coating concept, a low viscosity epoxy was applied to the surface of several composite coupons. A protective layer of 1000 Å of SiO₂ was deposited on top of the leveling coating, and the coupons were exposed to an atomic oxygen environment in a plasma asher. Pinhole populations per unit area were estimated by counting the number of undercut sites observed by scanning electron microscopy. Defect density values of 180,000 defects/sq cm were reduced to about 1000 defects/sq cm as a result of the applied leveling coating. These improvements occur at a mass penalty of about 2.5 mg/sq cm.

Author

N93-15616* National Aeronautics and Space Administration, Lewis Research Center, Cleveland, OH.

DEGRADATION OF RADIATOR PERFORMANCE ON MARS DUE TO DUST

JAMES R. GAIER, MARLA E. PEREZ-DAVIS, SHARON K. RUTLEDGE, and MARK FORKAPA (Cleveland State Univ., OH.) In NASA. Goddard Space Flight Center, The Seventeenth Space Simulation Conference. Terrestrial Test for Space Success p 275-288 Nov. 1992
Avail: CASI HC A03/MF A03

An artificial mineral of the approximate elemental composition of Martian soil was manufactured, crushed, and sorted into four different size ranges. Dust particles from three of these size ranges were applied to arc-textured Nb-1 percent Zr and Cu radiator surfaces to assess their effect on radiator performance. Particles larger than 75 microns did not have sufficient adhesive forces to adhere to the samples at angles greater than about 27 deg. Pre-deposited dust layers were largely removed by clear wind velocities greater than 40 m/s, or by dust-laden wind velocities as low as 25 m/s. Smaller dust grains were more difficult to remove. Abrasion was found to be significant only in high velocity winds (89 m/s or greater). Dust-laden winds were found to be more abrasive than clear wind. Initially dusted samples abraded less than initially clear samples in dust laden wind. Smaller dust particles of the simulant proved to be more abrasive than large. This probably indicates that the larger particles were in fact agglomerates.

Author

N93-17988* National Aeronautics and Space Administration, Lewis Research Center, Cleveland, OH.

THE APPLICATION OF STRUCTURAL RELIABILITY TECHNIQUES TO PLUME IMPINGEMENT LOADING OF THE SPACE STATION FREEDOM PHOTOVOLTAIC ARRAY

ISAM S. YUNIS and KELLY S. CARNEY 19 Apr. 1993 19 p
Prepared for the 34th Structures, Structural Dynamics and Materials Conference, La Jolla, CA, 19-21 Apr. 1993; Cosponsored by the AIAA, ASME, ASCE, AHS, and ASC
(NASA-TM-105949; E-7468; NAS 1.15:105949; AIAA PAPER 93-1338) Avail: CASI HC A03/MF A01

A new aerospace application of structural reliability techniques is presented, where the applied forces depend on many probabilistic variables. This application is the plume impingement loading of the Space Station Freedom Photovoltaic Arrays. When the space shuttle berths with Space Station Freedom it must brake and maneuver towards the berthing point using its primary jets. The jet exhaust, or plume, may cause high loads on the photovoltaic arrays. The many parameters governing this problem are highly uncertain and random. An approach, using techniques from structural reliability, as opposed to the accepted deterministic methods, is presented which assesses the probability of failure of the array mast due to plume impingement loading. A Monte Carlo simulation of the berthing approach is used to determine the probability distribution of the loading. A probability distribution is also determined for the strength of the array. Structural reliability techniques are then used to assess the array mast design. These techniques are found to be superior to the standard deterministic dynamic transient analysis, for this class of problem. The results show that the probability of failure of the current array mast design, during its 15 year life, is minute.

Author

N93-19988* National Aeronautics and Space Administration, Lewis Research Center, Cleveland, OH.

COLD-SAT DYNAMIC MODEL

NEIL S. ADAMS (Analex Corp., Brook Park, OH.) and GARY BOLLENBACHER Dec. 1992 108 p
(Contract RTOP 506-42-73)
(NASA-TM-105185; E-6483; NAS 1.15:105185) Avail: CASI HC A06/MF A02

This report discusses the development and underlying mathematics of a rigid-body computer model of a proposed cryogenic on-orbit liquid depot storage, acquisition, and transfer spacecraft (COLD-SAT). This model, referred to in this report as the COLD-SAT dynamic model, consists of both a trajectory model and an attitudinal model. All disturbance forces and torques expected to be significant for the actual COLD-SAT spacecraft are modeled to the required degree of accuracy. Control and experimental thrusters are modeled, as well as fluid slosh. The model also computes microgravity disturbance accelerations at any specified point in the spacecraft. The model was developed by using the Boeing EASY5 dynamic analysis package and will run on Apollo, Cray, and other computing platforms.

Author

N93-20204* National Aeronautics and Space Administration, Lewis Research Center, Cleveland, OH.

FIRE SAFETY PRACTICES IN THE SHUTTLE AND THE SPACE STATION FREEDOM

ROBERT FRIEDMAN In its The Second International Microgravity Combustion Workshop p 213-225 Feb. 1993
Avail: CASI HC A03/MF A03; 11 functional color pages

The Shuttle reinforces its policy of fire-preventive measures with onboard smoke detectors and Halon 1301 fire extinguishers. The forthcoming Space Station Freedom will have expanded fire protection with photoelectric smoke detectors, radiation flame detectors, and both fixed and portable carbon dioxide fire extinguishers. Many design and operational issues remain to be resolved for Freedom. In particular, the fire-suppression designs must consider the problems of gas leakage in toxic concentrations, alternative systems for single-failure redundancy, and commonality with the corresponding systems of the Freedom international partners. While physical and engineering requirements remain the primary driving forces for spacecraft fire-safety technology, there

18 SPACECRAFT DESIGN, TESTING AND PERFORMANCE

are, nevertheless, needs and opportunities for the application of microgravity combustion knowledge to improve and optimize the fire-protective systems. Author

N93-22551* National Aeronautics and Space Administration. Lewis Research Center, Cleveland, OH.

SPACE STATION FREEDOM BETA GIMBAL CONTROL VIA SENSITIVITY MODELS

DAVID A. SCHOENWALD (Martin Marietta Energy Systems, Inc., Oak Ridge, TN.), UMIT OZGUNER (Ohio State Univ., Columbus.), and RONALD E. GRAHAM Jan. 1993 10 p (NASA-TM-106000; E-7543; NAS 1.15:106000) Avail: CASI HC A02/MF A01

Tracking control of the Space Station Freedom solar array beta gimbals is investigated. Of particular interest is the issue of control in the presence of uncertainty in gimbal friction parameters. Sensitivity functions are incorporated into the feedback loop to desensitize the gimbal control law to parameter variations. Simulation results indicated that one such sensitivity function improves the closed-loop performance of the gimbals in the presence of unexpected friction parameter dispersions. Author

N93-22636* National Aeronautics and Space Administration. Lewis Research Center, Cleveland, OH.

SELECTED OAST/OSSA SPACE EXPERIMENT ACTIVITIES IN SUPPORT OF SPACE STATION FREEDOM

RICHARD DELOMBARD In NASA, Washington, Space Station Freedom Utilization Conference p 363-371 1992 Avail: CASI HC A02/MF A04

The Space Experiments Division at NASA Lewis Research Center is developing technology and science space experiments for the Office of Aeronautics and Space Technology (OAST) and the Office of Space Sciences and Applications (OSSA). Selected precursor experiments and technology development activities supporting the Space Station Freedom (SSF) are presented. The Tank Pressure Control Experiment (TPCE) is an OAST-funded cryogenic fluid dynamics experiment, the objective of which is to determine the effectiveness of jet mixing as a means of equilibrating fluid temperatures and controlling tank pressures, thereby permitting the design of lighter cryogenic tanks. The information from experiments such as this will be utilized in the design and operation of on board cryogenic storage for programs such as SSF. The Thermal Energy Storage Flight Project (TES) is an OAST-funded thermal management experiment involving phase change materials for thermal energy storage. The objective of this project is to develop and fly in-space experiments to characterize void shape and location in phase change materials used in a thermal energy storage configuration representative of an advanced solar dynamic system design. The information from experiments such as this will be utilized in the design of future solar dynamic power systems. The Solar Array Module Plasma Interaction Experiment (SAMPIE) is an OAST-funded experiment to determine the environmental effects of the low earth orbit (LEO) space plasma environment on state-of-the-art solar cell modules biased to high potentials relative to the plasma. Future spacecraft designs and structures will push the operating limits of solar cell arrays and other high voltage systems. SAMPIE will provide key information necessary for optimum module design and construction. The Vibration Isolation Technology (VIT) Advanced Technology Development effort is funded by OSSA to provide technology necessary to maintain a stable microgravity environment for sensitive payloads on board spacecraft. The proof of concept will be demonstrated by laboratory tests and in low-gravity aircraft flights. VIT is expected to be utilized by many SSF microgravity science payloads. The Space Acceleration Measurement System (SAMS) is an OSSA-funded instrument to measure the microgravity acceleration environment for OSSA payloads on the shuttle and SSF. Author

N93-23742* National Aeronautics and Space Administration. Lewis Research Center, Cleveland, OH.

PLASMA CHAMBER TESTING OF APSA COUPONS FOR THE SAMPIE FLIGHT EXPERIMENT

G. BARRY HILLARD Jan. 1993 9 p Presented at the 31st Aerospace Sciences Meeting and Exhibit, Reno, NV, 11-14 Jan. 1993; sponsored by the AIAA Previously announced in IAA as A93-24244

(Contract RTOP 589-01-1B)

(NASA-TM-106084; E-7707; NAS 1.15:106084; AIAA PAPER 93-0568) Avail: CASI HC A02/MF A01

Among the solar cell technologies to be tested in space as part of the Solar Array Module Plasma Interactions Experiment (SAMPIE) will be the Advanced Photovoltaic Solar Array (APSA). Several prototype twelve cell coupons were built for NASA using different blanket materials and mounting techniques. The first conforms to the baseline design for APSA which calls for the cells to be mounted on a carbon loaded Kapton blanket to control charging in GEO. When deployed, this design has a flexible blanket supported around the edges. A second coupon was built with the cells mounted on Kapton-H, which was in turn cemented to a solid aluminum substrate. A final coupon was identical to the latter but used germanium coated Kapton to control atomic oxygen attack in LEO. Ground testing of these coupons in a plasma chamber showed considerable differences in plasma current collection. The Kapton-H coupon demonstrated current collection consistent with exposed interconnects and some degree of cell snapover. The other two coupons experienced anomalously large collection currents. This behavior is believed to be a consequence of enhanced plasma sheaths supported by the weakly conducting carbon and germanium used in these coupons. The results reported here are the first experimental evidence that the use of such materials can result in power losses to high voltage space power systems. Author

N93-24755* National Aeronautics and Space Administration. Lewis Research Center, Cleveland, OH.

CONTRIBUTIONS OF MICROGRAVITY TEST RESULTS TO THE DESIGN OF SPACECRAFT FIRE SAFETY SYSTEMS

ROBERT FRIEDMAN and DAVID L. URBAN (Sverdrup Technology, Inc., Brook Park, OH.) Mar. 1993 13 p Presented at the AHS/ASEE Second Aerospace Design Conference, Irvine, CA, 16-19 Feb. 1993; sponsored by AIAA

(Contract RTOP 323-53-62)

(NASA-TM-106093; E-7445; NAS 1.15:106093; AIAA PAPER 93-1152) Copyright Avail: CASI HC A03/MF A01

Experiments conducted in spacecraft and drop towers show that thin-sheet materials have reduced flammability ranges and flame-spread rates under quiescent low-gravity environments (microgravity) as compared to normal gravity. Furthermore, low-gravity flames may be suppressed more easily by atmospheric dilution or decreasing atmospheric total pressure than their normal-gravity counterparts. The addition of a ventilating air flow to the low-gravity flame zone, however, can greatly enhance the flammability range and flame spread. These results, along with observations of flame and smoke characteristics useful for microgravity fire-detection 'signatures', promise to be of considerable value to spacecraft fire-safety designs. The paper summarizes the fire detection and suppression techniques proposed for the Space Station Freedom and discusses both the application of low-gravity combustion knowledge to improve fire protection and the critical needs for further research. Author (revised)

N93-25090* National Aeronautics and Space Administration. Lewis Research Center, Cleveland, OH.

PLASMA SHEATH EFFECTS ON ION COLLECTION BY A PINHOLE

JOEL L. HERR (Sverdrup Technology, Inc., Brook Park, OH.) and DAVID B. SNYDER Apr. 1993 12 p Presented at the 31st AIAA Aerospace Sciences Meeting and Exhibit, Reno, NV, 11-14 Jan. 1993; sponsored by AIAA Previously announced in IAA as A93-24243

(Contract RTOP 506-41-41)

(NASA-TM-106098; E-7740; NAS 1.15:106098) Avail: CASI HC A03/MF A01

This work presents tables to assist in the evaluation of pinhole

collection effects on spacecraft. These tables summarize results of a computer model which tracks particle trajectories through a simplified electric field in the plasma sheath. A technique is proposed to account for plasma sheath effects in the application of these results and scaling rules are proposed to apply the calculations to specific situations. This model is compared to ion current measurements obtained by another worker, and the agreement is very good. Author

N93-26148*# National Aeronautics and Space Administration. Lewis Research Center, Cleveland, OH.

THE INTERACTION OF HIGH VOLTAGE SYSTEMS WITH THE ENVIRONMENTS OF THE MOON AND MARS

G. BARRY HILLARD and JOSEPH C. KOLECKI Jan. 1993 6 p Presented at the 31st Aerospace Sciences Meeting and Exhibit, Reno, NV, 11-14 Jan. 1993; sponsored by AIAA Previously announced in IAA as A93-24800 (Contract RTOP 506-41-41) (NASA-TM-106107; E-7756; NAS 1.15:106107; AIAA PAPER 93-0704) Avail: CASI HC A02/MF A01

High voltage systems designed for use on the lunar and Martian surfaces or in orbit will interact with environmental components such as electrically charged dust, low pressure atmospheres, ionospheric plasmas and neutrals, and chemically reactive species. As the Space Exploration Initiative (SEI) advances from the realm of feasibility study to that of conceptual design, guidelines will be required to ensure that these effects are properly accounted for. A first step in providing such guidelines is the prioritization of interactions for each of the space or surface environments that will be encountered. For those issues that are identified as high priority, the state of environmental knowledge, emphasizing essential data, must be determined. This report describes possible means of obtaining such information, including ground tests, modeling and analysis, and flight experiments. The development of computational tools which will enable engineers to simulate and thereby quantify the interactions will be especially considered. Our analysis is drawn from various study and workshop activities undertaken within the last two years. Author

N93-26209*# National Aeronautics and Space Administration. Lewis Research Center, Cleveland, OH.

CONCEPTUAL DESIGN FOR THE SPACE STATION FREEDOM FLUID PHYSICS/DYNAMICS FACILITY

ROBERT L. THOMPSON, RONALD J. CHUCKSA, TERENCE F. OMALLEY, and RICHARD C. OEFTERING Apr. 1993 83 p Workshop held in Cleveland, OH, 24-25 Jan. 1990; sponsored by NASA Headquarters OSSA/MSAD Code SN (Contract RTOP 694-03-03) (NASA-TM-103663; E-5868; NAS 1.15:103663) Avail: CASI HC A05/MF A01

A study team at NASA's Lewis Research Center has been working on a definition study and conceptual design for a fluid physics and dynamics science facility that will be located in the Space Station Freedom's baseline U.S. Laboratory module. This modular, user-friendly facility, called the Fluid Physics/Dynamics Facility, will be available for use by industry, academic, and government research communities in the late 1990's. The Facility will support research experiments dealing with the study of fluid physics and dynamics phenomena. Because of the lack of gravity-induced convection, research into the mechanisms of fluids in the absence of gravity will help to provide a better understanding of the fundamentals of fluid processes. This document has been prepared as a final version of the handout for reviewers at the Fluid Physics/Dynamics Facility Assessment Workshop held at Lewis on January 24 and 25, 1990. It covers the background, current status, and future activities of the Lewis Project Study Team effort. It is a revised and updated version of a document entitled 'Status Report on the Conceptual Design for the Space Station Fluid Physics/Dynamics Facility', dated January 1990. Author

N93-26215*# National Aeronautics and Space Administration. Lewis Research Center, Cleveland, OH.

PLASMA CURRENT COLLECTION OF Z-93 THERMAL CONTROL PAINT AS MEASURED IN THE LEWIS RESEARCH CENTER'S PLASMA INTERACTION FACILITY

G. BARRY HILLARD Apr. 1993 14 p (Contract RTOP 506-41-41) (NASA-TM-106132; E-7804; NAS 1.15:106132) Avail: CASI HC A03/MF A01

A sample of Z-93 thermal control paint was exposed to a simulated space environment in a plasma chamber. The sample was biased through a series of voltages ranging from -100 volts to +300 volts and electron and ion currents were measured. Currents were found to be in the micro-ampere range indicating that the material remains a reasonably good insulator under plasma conditions. As a second step, the sample was left in the chamber for six days and retested. Collected currents were reduced by from two to five times from the previous values indicating a substantial loss of conductivity. As a final test, the sample was removed, exposed to room conditions for two days, and returned to the chamber. Current measurements showed that the sample had partially recovered the lost conductivity. In addition to presenting these results, this report documents all of the experimental data as well as the statistical analyses performed. Author

N93-27019*# National Aeronautics and Space Administration. Lewis Research Center, Cleveland, OH.

THE EFFECTS OF SIMULATED LOW EARTH ORBIT ENVIRONMENTS ON SPACECRAFT THERMAL CONTROL COATINGS

JOYCE A. DEVER, SHARON K. RUTLEDGE, ERIC J. BRUCKNER (Cleveland State Univ., OH.), CURTIS R. STIDHAM (Sverdrup Technology, Inc., Brook Park, OH.), THOMAS J. STUEBER (Sverdrup Technology, Inc., Brook Park, OH.), and ROY E. BOOTH (Vought Corp., Dallas, TX.) May 1993 18 p Presented at the 38th International SAMPE Symposium and Exhibition, Anaheim, CA, 10-13 May 1993; sponsored by the Society for the Advancement of Materials and Process Engineering (Contract RTOP 474-46-10) (NASA-TM-106146; E-7829; NAS 1.15:106146) Avail: CASI HC A03/MF A01

Candidate Space Station Freedom radiator coatings including Z-93, YB-71, anodized aluminum and SiO(x) coated silvered Teflon have been characterized for optical properties degradation upon exposure to environments containing atomic oxygen, vacuum ultraviolet (VUV) radiation, and/or silicone contamination. YB-71 coating showed a blue-gray discoloration, which has not been observed in space, upon exposure in atomic oxygen facilities which also provide exaggerated VUV radiation. This is evidence that damage mechanisms occur in these ground laboratory facilities which are different from those which occur in space. Radiator coatings exposed to an electron cyclotron resonance (ECR) atomic oxygen source in the presence of silicone-containing samples showed severe darkening from the intense VUV radiation provided by the ECR and from silicone contamination. Samples exposed to atomic oxygen from the ECR source and to VUV lamps, simultaneously, with in situ reflectance measurement, showed that significantly greater degradation occurred when samples received line-of-site ECR beam exposure than when samples were exposed to atomic oxygen scattered off of quartz surfaces without line-of-site view of the ECR beam. For white paints, exposure to air following atomic oxygen/VUV exposure reversed the darkening due to VUV damage. This illustrates the importance of in situ reflectance measurement. Author

N93-27038*# National Aeronautics and Space Administration. Lewis Research Center, Cleveland, OH.

BATTERY SELECTION FOR SPACE SHUTTLE EXPERIMENTS

DAVID R. FRANCISCO Apr. 1993 14 p (Contract RTOP 694-03-03) (NASA-TM-106142; E-7822; NAS 1.15:106142) Avail: CASI HC A03/MF A01

18 SPACECRAFT DESIGN, TESTING AND PERFORMANCE

This paper will delineate the criteria required for the selection of batteries as a power source for space experiments. Four basic types of batteries will be explored, lead acid, silver zinc, alkaline manganese, and nickel cadmium. A detailed description of the lead acid and silver zinc cells and a brief exploration of the alkaline manganese and nickel cadmium will be given. The factors involved in battery selection such as packaging, energy density, discharge voltage regulation, and cost will be thoroughly examined. The pros and cons of each battery type will be explored. Actual laboratory test data acquired for the lead acid and silver zinc cell will be discussed. This data will include discharging under various temperature conditions, after three months of storage, and with different types of loads. The lifetime and number of charge/discharge cycles will also be discussed. A description of the required maintenance for each type of battery will be investigated. Author (revised)

N93-27081*# National Aeronautics and Space Administration. Lewis Research Center, Cleveland, OH.

ENHANCED PLASMA CURRENT COLLECTION FROM WEAKLY CONDUCTING SOLAR ARRAY BLANKETS

G. BARRY HILLARD May 1993 23 p
(Contract RTOP 506-48-2B)
(NASA-TM-106168; E-7860; NAS 1.15:106168) Avail: CASI HC A03/MF A01

Among the solar cell technologies to be tested in space as part of the Solar Array Module Plasma Interactions Experiment (SAMPIE) will be the Advanced Photovoltaic Solar Array (APSA). Several prototype twelve cell coupons were built for NASA using different blanket materials and mounting techniques. The first conforms to the baseline design for APSA which calls for the cells to be mounted on a carbon loaded Kapton blanket to control charging in GEO. When deployed, this design has a flexible blanket supported around the edges. A second coupon was built with the cells mounted on Kapton-H, which was in turn cemented to a solid aluminum substrate. A final coupon was identical to the latter but used germanium coated Kapton to control atomic oxygen attack in LEO. Ground testing of these coupons in a plasma chamber showed considerable differences in plasma current collection. The Kapton-H coupon demonstrated current collection consistent with exposed interconnects and some degree of cell snapover. The other two coupons experienced anomalously large collection currents. This behavior is believed to be a consequence of enhanced plasma sheaths supported by the weakly conducting carbon and germanium used in these coupons. The results reported here are the first experimental evidence that the use of such materials can result in power losses to high voltage space power systems. Author

N93-27260*# National Aeronautics and Space Administration. Lewis Research Center, Cleveland, OH.

ELECTRICAL DESIGN OF SPACE SHUTTLE PAYLOAD G-534: THE POOL BOILING EXPERIMENT

DAVID R. FRANCISCO May 1993 15 p
(Contract RTOP 694-03-03)
(NASA-TM-106143; E-7824; NAS 1.15:106143) Avail: CASI HC A03/MF A01

Payload G-534, the Pool Boiling Experiment (PBE), is a Get Away Special (GAS) payload that flew on the Space Shuttle Spacelab Mission J (STS 47) on September 19-21, 1992. This paper will give a brief overall description of the experiment with the main discussion being the electrical design with a detailed description of the power system and interface to the GAS electronics. The batteries used and their interface to the experiment Power Control Unit (PCU) and GAS electronics will be examined. The design philosophy for the PCU will be discussed in detail. The criteria for selection of fuses, relays, power semiconductors, and other electrical components along with grounding and shielding policy for the entire experiment are presented. The intent of this paper is to discuss the use of military tested parts and basic design guidelines to build a quality experiment for minimal additional cost. Author (revised)

N93-27801*# National Aeronautics and Space Administration. Lewis Research Center, Cleveland, OH.

ORBITAL STORAGE AND SUPPLY OF SUBCRITICAL LIQUID NITROGEN

JOHN C. AYDELOTT In NASA, Washington, Technology for Space Station Evolution. Volume 3: EVA/Manned Systems/Fluid Management System p 307-321 1990

Avail: CASI HC A03/MF A03; 1 functional color page

Subcritical cryogenic fluid management has long been recognized as an enabling technology for key propulsion applications, such as space transfer vehicles (STV) and the on-orbit cryogenic fuel depots which will provide STV servicing capability. The LeRC Cryogenic Fluids Technology Office (CFTO), under the sponsorship of OAST, has the responsibility of developing the required technology via a balanced program involving analytical modeling, ground based testing, and in-space experimentation. Topics covered in viewgraph form include: cryogenic management technologies; nitrogen storage and supply; cryogenic nitrogen cooling capability; and LN2 system demonstration technical objectives. CASI

N93-27861*# National Aeronautics and Space Administration. Lewis Research Center, Cleveland, OH.

FLUID MANAGEMENT SYSTEM TECHNOLOGY DISCIPLINE

E. PATRICK SYMONS In NASA, Washington, Technology for Space Station Evolution. Executive Summary and Overview p 141-156 1990

Avail: CASI HC A03/MF A03; 1 functional color page

Viewgraphs on fluid management system technology discipline for Space Station Freedom are presented. Topics covered include: subcritical cryogenic storage and transfer; fluid handling; and components and instrumentation. CASI

N93-27862*# National Aeronautics and Space Administration. Lewis Research Center, Cleveland, OH.

POWER SYSTEM TECHNOLOGY DISCIPLINE

HENRY BRANDHORST In NASA, Washington, Technology for Space Station Evolution. Executive Summary and Overview p 157-178 1990

Avail: CASI HC A03/MF A03; 1 functional color page

Viewgraphs on power system technology discipline for Space Station Freedom are presented. Topics covered include: power generation subsystem; energy storage subsystem; and power distribution. CASI

N93-28716*# National Aeronautics and Space Administration. Lewis Research Center, Cleveland, OH.

SOLAR ARRAY MODULE PLASMA INTERACTION EXPERIMENT (SAMPIE)

DALE C. FERGUSON In NASA, Washington, NASA/DOD Flight Experiments Technical Interchange Meeting Proceedings 23 p 1992

Avail: CASI HC A03/MF A10

The objective of the Solar Array Module Plasma Interaction Experiment (SAMPIE) is to investigate, by means of a shuttle-based flight experiment and relevant ground-based testing, the arcing and current collection behavior of materials and geometries likely to be exposed to the LEO plasma on high-voltage space power systems, in order to minimize adverse environmental interactions. An overview of the SAMPIE program is presented in outline and graphical form. CASI

N93-29363*# National Aeronautics and Space Administration. Lewis Research Center, Cleveland, OH.

CHARACTERISTICS OF HYPERVELOCITY IMPACT CRATERS ON LDEF EXPERIMENT S1003 AND IMPLICATIONS OF SMALL PARTICLE IMPACTS ON REFLECTIVE SURFACES

MICHAEL J. MIRTICH, SHARON K. RUTLEDGE, BRUCE A. BANKS, CHRISTOPHER DEVRIES (Cornell Univ., Ithaca, NY.), and JAMES E. MERROW (Cleveland State Univ., OH.) In NASA. Langley Research Center, LDEF: 69 Months in Space. Second Post-Retrieval Symposium, Part 2 p 431-451 Apr. 1993

Avail: CASI HC A03/MF A04

The Ion Beam textured and coated surfaces EXperiment (IBEX), designated S1003, was flown on LDEF at a location 98 deg in a north facing direction relative to the ram direction. Thirty-six diverse materials were exposed to the micrometeoroid (and some debris) environment for 5.8 years. Optical property measurements indicated no changes for almost all of the materials except S-13G, Kapton, and Kapton-coated surfaces, and these changes can be explained by other environmental effects. From the predicted micrometeoroid flux of NASA SP-8013, no significant changes in optical properties of the surfaces due to micrometeoroids were expected. There were hypervelocity impacts on the various diverse materials flown on IBEX, and the characteristics of these craters were documented using scanning electron microscopy (SEM). The S1003 aluminized-coated aluminum cover tray was sectioned into 2 cm x 2 cm pieces for crater documentation. The flux curve generated from this crater data fits well between the 1969 micrometeoroid model and the Kessler debris model for particles less than 10(exp -9) gm which were corrected for the S1003 positions (98 deg to ram). As the particle mass increases, the S1003 impact data is greater than that predicted by even the debris model. This, however, is consistent with data taken on intercostal F07 by the Micrometeoroid/Debris Special Investigating Group (M/D SIG). The mirrored surface micrometeoroid detector flown on IBEX showed no change in solar reflectance and corroborated the S1003 flux curve, as well as results of this surface flown on SERT 2 and OSO 3 for as long as 21 years.

Author (revised)

19

SPACECRAFT INSTRUMENTATION

A93-50242*# National Aeronautics and Space Administration. Lewis Research Center, Cleveland, OH.

A PLUME SPECTROSCOPY SYSTEM FOR FLIGHT APPLICATIONS

D. B. MAKEL, T. V. PETERSEN (Aerojet, Propulsion Div., Sacramento, CA), D. B. DUNCAN (Duncan Technologies, Auburn, CA), and G. C. MADZSAR (NASA, Lewis Research Center, Cleveland, OH) Jun. 1993 10 p. AIAA, SAE, ASME, and ASEE, Joint Propulsion Conference and Exhibit, 29th, Monterey, CA, June 28-30, 1993 Research supported by Duncan Technologies refs

(Contract NAS3-25624)

(AIAA PAPER 93-2511) Copyright

An operational plume spectroscopy system will be an important element of any rocket engine health management system (HMS). The flight capable FPI spectrometer will enable prognosis and response to incipient rocket engine failures as well as diagnosis of wear and degradation for on-condition maintenance. Spectrometer application to development programs, such as the Space Lifter, NASP, and SSTO, will reduce program risks, allow better adherence to schedules and save money by reducing or eliminating redesign and test costs. The diagnostic capability of a proven, calibrated spectrometer will enhance post-burn certification of high value, reusable engines, such as the Space Shuttle Main Engine (SSME), where life and reliability are key cost drivers. This paper describes a prototype FPI spectrometer for demonstration and validation testing on NASA's Technology Test Bed Engine (TTBE) at Marshall Space Flight Center. The TTBE test unit is designed with flight prototype optics and a commercial off-the-shelf data processing system.

A93-54401 National Aeronautics and Space Administration. Lewis Research Center, Cleveland, OH.

PROPOSED GROUND-BASED CONTROL OF ACCELEROMETER ON SPACE STATION FREEDOM

RICHARD DELOMBARD (NASA, Lewis Research Center, Cleveland, OH) In International Instrumentation Symposium,

39th, Albuquerque, NM, May 2-6, 1993, Proceedings Research Triangle Park, NC Instrument Society of America 1993 p. 949-959. Previously announced in STAR as N93-23738 refs (Contract RTOP 694-03-OH) Copyright

This paper describes the innovative control of an accelerometer to support the needs of the scientists operating science experiments that are on-board Space Station Freedom (SSF). Accelerometers in support of science experiments on the shuttle have typically been passive, record-only devices that present data only after the mission or that present limited data to the crew or ground operators during the mission. With the advent of science experiment operations on SSF, the principal investigators will need microgravity acceleration data during, as well as after, experiment operations. Because their data requirements may change during the experiment operations, the principal investigators will be allocated some control of accelerometer parameters. This paper summarizes the general-purpose Space Acceleration Measurement System (SAMS) operation that supports experiments on the shuttle and describes the control of the SAMS for Space Station Freedom. Emphasis is placed on the proposed ground-based control of the accelerometer by the principal investigators.

N93-23738*# National Aeronautics and Space Administration. Lewis Research Center, Cleveland, OH.

PROPOSED GROUND-BASED CONTROL OF ACCELEROMETER ON SPACE STATION FREEDOM

RICHARD DELOMBARD May 1993 15 p Proposed for presentation at the 39th International Instrumentation Symposium, Albuquerque, NM, 2-6 May 1993; sponsored by the Instrument Society of America Original contains color illustrations (Contract RTOP 694-03-OH)

(NASA-TM-105960; E-7478; NAS 1.15:105960) Avail: CASI HC A03/MF A01; 1 functional color page

This paper describes the innovative control of an accelerometer to support the needs of the scientists operating science experiments that are on-board Space Station Freedom (SSF). Accelerometers in support of science experiments on the shuttle have typically been passive, record-only devices that present data only after the mission or that present limited data to the crew or ground operators during the mission. With the advent of science experiment operations on SSF, the principal investigators will need microgravity acceleration data during, as well as after, experiment operations. Because their data requirements may change during the experiment operations, the principal investigators will be allocated some control of accelerometer parameters. This paper summarizes the general-purpose Space Acceleration Measurement System (SAMS) operation that supports experiments on the shuttle and describes the control of the SAMS for Space Station Freedom. Emphasis is placed on the proposed ground-based control of the accelerometer by the principal investigators.

Author

N93-28554*# National Aeronautics and Space Administration. Lewis Research Center, Cleveland, OH.

LOW-FREQUENCY VIBRATION ENVIRONMENT FOR FIVE SHUTTLE MISSIONS

GEORGE R. BAUGHER (National Aeronautics and Space Administration, Marshall Space Flight Center, Huntsville, AL.), GARY L. MARTIN (National Aeronautics and Space Administration, Washington, DC.), and RICHARD DELOMBARD Mar. 1993 13 p Presented at the 31st Aerospace Sciences Meeting, Reno, NV, 11-14 Jan. 1993; sponsored by AIAA (Contract RTOP 694-03-OH)

(NASA-TM-106059; E-7661; NAS 1.15:106059) Avail: CASI HC A03/MF A01

The Microgravity Science and Applications Division's (MSAD) program to record and analyze the Shuttle's vibration environment is reviewed. This program provides microgravity science investigators with time and frequency analyses of the acceleration environment during their experiments' operation. Information is also provided for future investigators on the expected Shuttle vibration environment. As background, the two major elements of the program are discussed, the Space Acceleration Measurement

20 SPACECRAFT PROPULSION AND POWER

System (SAMS) and the Acceleration Characterization and Analysis Project (ACAP). A comparison of the acceleration measurements from five Shuttle missions is discussed. Author (revised)

20

SPACECRAFT PROPULSION AND POWER

Includes main propulsion systems and components, e.g., rocket engines; and spacecraft auxiliary power sources.

A93-12074* National Aeronautics and Space Administration. Lewis Research Center, Cleveland, OH.

NUCLEAR PROPULSION TECHNOLOGY DEVELOPMENT - A JOINT NASA/DEPARTMENT OF ENERGY PROJECT

JOHN S. CLARK (NASA, Lewis Research Center, Cleveland, OH) *In Mars: Past, present, and future; Proceedings of the Conference, Williamsburg, VA, July 16-19, 1991* Washington American Institute of Aeronautics and Astronautics 1992 p. 225-237. refs

Copyright

NASA-Lewis has undertaken the conceptual development of spacecraft nuclear propulsion systems with DOE support, in order to establish the bases for Space Exploration Initiative lunar and Mars missions. This conceptual evolution project encompasses nuclear thermal propulsion (NTP) and nuclear electric propulsion (NEP) systems. A technology base exists for NTP in the NERVA program files; more fundamental development efforts are entailed in the case of NEP, but this option is noted to offer greater advantages in the long term. O.C.

A93-13696# National Aeronautics and Space Administration. Lewis Research Center, Cleveland, OH.

LOW-ISP DERATED ION THRUSTER OPERATION

MICHAEL J. PATTERSON (NASA, Lewis Research Center, Cleveland, OH) Jul. 1992 17 p. AIAA, SAE, ASME, and ASEE, Joint Propulsion Conference and Exhibit, 28th, Nashville, TN, July 6-8, 1992 Previously announced in STAR as N92-32237 refs

(Contract RTOP 506-42-31)

(AIAA PAPER 92-3203) Copyright

The performance and lifetime expectations of 30 cm xenon ion thruster technology at low values of specific impulse were evaluated, with emphasis on 1000-2500 s operation. Power levels of up to 2.0 kW, appropriate for auxiliary and orbit maneuvering propulsion, were processed at thrust-to-power ratios up to 57 mN/kW. These tests were conducted using a derated 30 cm ion thruster with high-perveance design two-grid ion optics with xenon propellant. Lifetime projections were made based on a simple analysis of critical component erosion rates, and it was found that a strong correlation exists with the ratio of the specific impulse-to-input power. Under all operating conditions for which the projected thruster lifetime is less than 10,000 hrs, the life-limiting component of this technology is erosion of the accelerator grid due to charge-exchange ions. The use of alternative grid materials such as carbon is estimated to increase useful thruster lifetimes by as much as an order of magnitude and may enable long-life high thrust-density, sub-2500 s lsp operation. The performance and life of the derated thruster appears similar to that of the Russian SPT-100 thruster in the 1.0-2.0 kW, 1600-2000 s operational envelope. Author

A93-13698* National Aeronautics and Space Administration. Lewis Research Center, Cleveland, OH.

SMALL EXPERIMENTS FOR THE MATURATION OF ORBITAL CRYOGENIC TRANSFER TECHNOLOGIES

DAVID J. CHATO and WILLIAM J. TAYLOR (NASA, Lewis Research Center, Cleveland, OH) Aug. 1992 10 p. IAF, International Astronautical Congress, 43rd, Washington, Aug.

28-Sept. 5, 1992 refs

(IAF PAPER 92-0777)

The no-vent fill method is a promising approach to handle the problems of low-g venting during propellant transfer. A receiver tank is first cooled to remove thermal energy from the tank wall and the resultant vapor vented overboard. Then nozzles mix the incoming liquid and residual vapor in the tank maintaining a thermodynamic state which allows the tank to fill with liquid without venting. Ground based testing at NASA Lewis Research Center (LeRC) has demonstrated the no-vent fill process and attempted to bound its low-gravity performance. But, low-gravity testing is required to validate the method. As an alternative to using a dedicated spacecraft for validation the authors have formulated several small scale experiments to study no-vent fill in low-g. Cost goals quickly limited the search to two possibilities: a secondary payload on the Space Shuttle, or a small scale sounding rocket experiment. This paper will discuss the key issues of small scale experimentation and present a conceptual design of a sounding rocket experiment with liquid hydrogen for studying the fill process. Author

A93-13751 National Aeronautics and Space Administration, Washington, DC.

SPACE NUCLEAR POWER SYSTEMS; PROCEEDINGS OF THE 8TH SYMPOSIUM, ALBUQUERQUE, NM, JAN. 6-10, 1991. PTS. 1-3

MOHAMED S. EL-GENK, ED. (New Mexico Univ., Albuquerque) and MARK D. HOOVER, ED. (Lovelace Inhalation Toxicology Research Inst., Albuquerque, NM) New York American Institute of Physics (AIP Conference Proceedings, No. 217) 1991 p. Pt. 1, 518 p.; pt. 2, 508 p.; pt. 3, 466 p. (ISBN 0-88318-838-4) Copyright

The present conference discusses NASA mission planning for space nuclear power, lunar mission design based on nuclear thermal rockets, inertial-electrostatic confinement fusion for space power, nuclear risk analysis of the Ulysses mission, the role of the interface in refractory metal alloy composites, an advanced thermionic reactor systems design code, and space high power nuclear-pumped lasers. Also discussed are exploration mission enhancements with power-beaming, power requirement estimates for a nuclear-powered manned Mars rover, SP-100 reactor design, safety, and testing, materials compatibility issues for fabric composite radiators, application of the enabler to nuclear electric propulsion, orbit-transfer with TOPAZ-type power sources, the thermoelectric properties of alloys, ruthenium silicide as a promising thermoelectric material, and innovative space-saving device for high-temperature piping systems. The second volume of this conference discusses engine concepts for nuclear electric propulsion, nuclear technologies for human exploration of the solar system, dynamic energy conversion, direct nuclear propulsion, thermionic conversion technology, reactor and power system control, thermal management, thermionic research, effects of radiation on electronics, heat-pipe technology, radioisotope power systems, and nuclear fuels for power reactors. The third volume discusses space power electronics, space nuclear fuels for propulsion reactors, power systems concepts, space power electronics systems, the use of artificial intelligence in space, flight qualifications and testing, microgravity two-phase flow, reactor manufacturing and processing, and space and environmental effects. (For individual items see A93-13752 to A93-13937) O.C.

A93-13765 National Aeronautics and Space Administration. Lewis Research Center, Cleveland, OH.

NUCLEAR PROPULSION PROJECT WORKSHOP SUMMARY

THOMAS J. MILLER, JOHN S. CLARK (NASA, Lewis Research Center, Cleveland, OH), and JOHN W. BARNETT (JPL, Pasadena, CA) *In Space nuclear power systems; Proceedings of the 8th Symposium, Albuquerque, NM, Jan. 6-10, 1991. Pt. 1* New York American Institute of Physics 1991 p. 84-91. refs

Copyright

NASA-Lewis has undertaken the planning and coordination of a joint NASA/DOE/DOD Nuclear Propulsion Project which will investigate both nuclear electric and nuclear thermal concepts.

The three-agency team has been tasked with the development of an Interagency Agreement and Memorandum of Understanding, as well as the drafting of a statement as to astronaut crew guidelines and values, the assessment of human-rating requirements, the development of an interagency safety and environmental assessment plan, and the development of test facility requirements. Attention is to be given to the role of SP-100 for nuclear-electric propulsion applications. O.C.

A93-13767* National Aeronautics and Space Administration. Lewis Research Center, Cleveland, OH.

LUNAR MISSION DESIGN USING NUCLEAR THERMAL ROCKETS

MICHAEL L. STANCATI, JOHN T. COLLINS (Science Applications International Corp., Schaumburg, IL), and STANLEY K. BOROWSKI (NASA, Lewis Research Center, Cleveland, OH) *In* Space nuclear power systems; Proceedings of the 8th Symposium, Albuquerque, NM, Jan. 6-10, 1991. Pt. 1 New York American Institute of Physics 1991 p. 100-105. refs
(Contract NAS3-25809)
Copyright

The NERVA-class Nuclear Thermal Rocket (NTR), with performance nearly double that of advanced chemical engines, has long been considered an enabling technology for human missions to Mars. NTR engines address the demanding trip time and payload delivery needs of both cargo-only and piloted flights. But NTR can also reduce the Earth launch requirements for manned lunar missions. First use of NTR for the Moon would be less demanding and would provide a test-bed for early operations experience with this powerful technology. Study of application and design options indicates that NTR propulsion can be integrated with the Space Exploration Initiative scenarios to deliver performance gains while managing controlled, long-term disposal of spent reactors to highly stable orbits. Author

A93-13797* National Aeronautics and Space Administration. Lewis Research Center, Cleveland, OH.

MULTIMEGAWATT POTASSIUM RANKINE POWER FOR NUCLEAR ELECTRIC POWER

RICHARD D. ROVANG, JOSEPH C. MILLS, and ERNIE B. BAUMEISTER (Rockwell International Corp., Rocketdyne Div., Canoga Park, CA) *In* Space nuclear power systems; Proceedings of the 8th Symposium, Albuquerque, NM, Jan. 6-10, 1991. Pt. 1 New York American Institute of Physics 1991 p. 373-378.
(Contract NAS3-25808; DE-AC07-88ID-12749)
Copyright

A cermet fueled potassium rankine power system concept has been developed for various power ranges and operating lifetimes. This concept utilizes a single primary lithium loop to transport thermal energy from the reactor to the boiler. Multiple, independent potassium loops are employed to achieve the required reliability of 99 percent. The potassium loops are two phase systems which expand heated potassium vapor through multistage turboalternators to produce a 10-kV dc electrical output. Condensation occurs by-way-of a shear-flow condenser, producing a 100 percent liquid potassium stream which is pumped back to the boiler. Waste heat is rejected by an advanced carbon-carbon radiator at approximately 1000 K. Overall system efficiencies of 19.3 percent to 20.5 percent were calculated depending on mission life and power level. Author

A93-13824 National Aeronautics and Space Administration. Lewis Research Center, Cleveland, OH.

STIRLING ENGINE - AVAILABLE TOOLS FOR LONG-LIFE ASSESSMENT

GARY R. HALFORD and PAUL A. BARTOLOTTA (NASA, Lewis Research Center, Cleveland, OH) *In* Space nuclear power systems; Proceedings of the 8th Symposium, Albuquerque, NM, Jan. 6-10, 1991. Pt. 2 New York American Institute of Physics 1991 p. 581-585. Previously announced in STAR as N91-12980 refs
(Contract RTOP 590-13-11)
Copyright

A review is presented for the durability approaches applicable to long-time life assessment of Stirling engine hot-section components. The crucial elements are experimental techniques for generating long-time materials property data (both monotonic and cyclic flow and failure properties); analytic representations of slow strain rate material stress-strain response characteristics (monotonic and cyclic constitutive relations) at high temperatures and low stresses and strains; analytic creep-fatigue-environmental interaction life prediction methods applicable to long lifetimes at high temperatures and small stresses and strains; and experimental verification of life predictions. Long-lifetime design criteria for materials of interest are woefully lacking. Designing against failures due to creep, creep-rupture, fatigue, environmental attack, and creep-failure-environmental interaction will require considerable extrapolation. Viscoplastic constitutive models and time-temperature parameters will have to be calibrated for the hot-section materials of interest. Analysis combined with limited verification testing in a short-time regime will be required to build confidence in long-lifetime durability models. Author

A93-13850* National Aeronautics and Space Administration. Lewis Research Center, Cleveland, OH.

A COMPARISON OF NUCLEAR THERMAL PROPULSION CONCEPTS - RESULTS OF A WORKSHOP

JOHN S. CLARK (NASA, Lewis Research Center, Cleveland, OH) *In* Space nuclear power systems; Proceedings of the 8th Symposium, Albuquerque, NM, Jan. 6-10, 1991. Pt. 2 New York American Institute of Physics 1991 p. 740-747. refs
Copyright

A Nuclear Thermal Propulsion Workshop, co-sponsored by NASA, DOE and DOD, was held in Cleveland, Ohio on July 10-12, 1990. The workshop was to provide a database of nuclear propulsion concepts and technologies to assist in planning a nuclear propulsion project, identify high priority activities to be initiated early, and to provide cost and schedule estimates for development of concepts to technology readiness level 6 - full system verification in a simulated environment. Sixteen concepts were presented to Technology Review Panels (TRP), and discussed. Each concept was compared to a baseline manned Mars mission. A preliminary comparison of ratings made by the TRP's is presented herein for mission benefit, safety, technical risk, and development cost. Author

A93-13877* National Aeronautics and Space Administration. Lewis Research Center, Cleveland, OH.

AN ISOTOPE-POWERED THERMAL STORAGE UNIT FOR SPACE APPLICATIONS

MICHAEL E. LISANO and M. F. ROSE (Auburn Univ., AL) *In* Space nuclear power systems; Proceedings of the 8th Symposium, Albuquerque, NM, Jan. 6-10, 1991. Pt. 2 New York American Institute of Physics 1991 p. 928-933. Research supported by Auburn Univ., SDIO, and NASA refs
Copyright

An Isotope-Powered Thermal Storage Unit (ITSU), that would store and utilize heat energy in a 'pulsed' fashion in space operations, is described. Properties of various radioisotopes are considered in conjunction with characteristics of thermal energy storage materials, to evaluate possible implementation of such a device. The utility of the unit is discussed in light of various space applications, including rocket propulsion, power generation, and spacecraft thermal management. Author

A93-13905 National Aeronautics and Space Administration. Lewis Research Center, Cleveland, OH.

KEY ISSUES IN SPACE NUCLEAR POWER CHALLENGES FOR THE FUTURE

HENRY W. BRANDHORST, JR. (NASA, Lewis Research Center, Cleveland, OH) *In* Space nuclear power systems; Proceedings of the 8th Symposium, Albuquerque, NM, Jan. 6-10, 1991. Pt. 3 New York American Institute of Physics 1991 p. 1153-1158a. Previously announced in STAR as N91-19179 refs
(Contract RTOP 590-13-11)
Copyright

The future appears rich in missions that will extend the frontiers of knowledge, human presence in space, and opportunities for profitable commerce. Key to the success of these ventures is the availability of plentiful, cost effective electric power and assured, low cost access to space. While forecasts of space power needs are problematic, an assessment of future needs based on terrestrial experience has been made. These needs fall into three broad categories: survival, self sufficiency, and industrialization. The cost of delivering payloads to orbital locations from LEO to Mars has been determined and future launch cost reductions projected. From these factors, then, projections of the performance necessary for future solar and nuclear space power options has been made. These goals are largely dependent upon orbital location and energy storage needs. Finally the cost of present space power systems has been determined and projections made for future systems.

Author

A93-14509* National Aeronautics and Space Administration. Lewis Research Center, Cleveland, OH.

METALLIZED PROPELLANTS FOR THE HUMAN EXPLORATION OF MARS

BRYAN PALASZEWSKI (NASA, Lewis Research Center, Cleveland, OH) *Journal of Propulsion and Power* (ISSN 0748-4658) vol. 8, no. 6 Nov.-Dec. 1992 p. 1192-1199. refs
Copyright

An evaluation is conducted of the use of novel, metallized-propellant propulsion systems to reduce launch masses for manned Mars missions on the basis of density and I(sp) enhancements. The use of metallized propellants leads to a 3.3 percent LEO mass saving which represents 38,000 kg less than O₂/H₂ propulsion. Attention is given to the possibility of using space-storable propellants for the Mars excursion vehicle, as an alternative to the storing of cryogenic H₂ on Mars, albeit at the cost of lower I(sp).

O.C.

A93-14654 National Aeronautics and Space Administration. Lewis Research Center, Cleveland, OH.

INTEGRATED HEALTH MONITORING AND CONTROLS FOR ROCKET ENGINES

W. C. MERRILL, J. L. MUSGRAVE, and T. H. GUO (NASA, Lewis Research Center, Cleveland, OH) Apr. 1992 7 p. SAE, Aerospace Atlantic Conference, Dayton, OH, Apr. 7-10, 1992 Previously announced in STAR as N92-28693 refs
(Contract RTOP 506-42-72)
(SAE PAPER 921031) Copyright

Current research in intelligent control systems at the Lewis Research Center is described in the context of a functional framework. The framework is applicable to a variety of reusable space propulsion systems for existing and future launch vehicles. It provides a 'road map' technology development to enable enhanced engine performance with increased reliability, durability, and maintainability. The framework hierarchy consists of a mission coordination level, a propulsion system coordination level, and an engine control level. Each level is described in the context of the Space Shuttle Main Engine. The concept of integrating diagnostics with control is discussed within the context of the functional framework. A distributed real time simulation testbed is used to realize and evaluate the functionalities in closed loop.

Author

A93-16415* National Aeronautics and Space Administration. Lewis Research Center, Cleveland, OH.

AN SSME HIGH PRESSURE OXIDIZER TURBOPUMP DIAGNOSTIC SYSTEM USING G2 REAL-TIME EXPERT SYSTEM

TEN-HUEI GUO (NASA, Lewis Research Center, Cleveland, OH) *In Annual Health Monitoring Conference for Space Propulsion Systems*, 3rd, Cincinnati, OH, Nov. 13, 14, 1991, Proceedings Cincinnati, OH University of Cincinnati 1991 p. 296-307. refs

An expert system which diagnoses various seal leakage faults in the High Pressure Oxidizer Turbopump of the SSME was developed using G2 real-time expert system. Three major functions of the software were implemented: model-based data generation,

real-time expert system reasoning, and real-time input/output communication. This system is proposed as one module of a complete diagnostic system for the SSME. Diagnosis of a fault is defined as the determination of its type, severity, and likelihood. Since fault diagnosis is often accomplished through the use of heuristic human knowledge, an expert system based approach has been adopted as a paradigm to develop this diagnostic system. To implement this approach, a software shell which can be easily programmed to emulate the human decision process, the G2 Real-Time Expert System, was selected. Lessons learned from this implementation are discussed.

Author

A93-20752* National Aeronautics and Space Administration. Lewis Research Center, Cleveland, OH.

SPACE NUCLEAR POWER SYSTEMS 1989; PROCEEDINGS OF THE 6TH SYMPOSIUM, ALBUQUERQUE, NM, JAN. 8-12, 1989. VOLS. 1 & 2

MOHAMED S. EL-GENK, ED. (New Mexico Univ., Albuquerque) and MARK D. HOOVER, ED. (Inhalation Toxicology Research Inst., Albuquerque, NM) Malabar, FL Orbit Book Co., Inc. (Space Nuclear Power Systems. Vol. 10) 1992 p. Vol. 1, 315 p.; vol. 2, 229 p.
(ISBN 0-89464-030-5) Copyright

The present conference discusses such space nuclear power (SNP) issues as current design trends for SDI applications, ultrahigh heat-flux systems with curved surface subcooled nucleate boiling, design and manufacturing alternatives for low cost production of SNPs, a lightweight radioisotope heater for the Galileo mission, compatible materials for uranium fluoride-based gas core SNPs, Johnson noise thermometry for SNPs, and uranium nitride/rhenium compatibility studies for the SP-100 SNP. Also discussed are system issues in antimatter energy conversion, the thermal design of a heat source for a Brayton cycle radioisotope power system, structural and thermal analyses of an isotope heat source, a novel plant protection strategy for transient reactors, and beryllium toxicity. (For individual items see A93-20753 to A93-20801) O.C.

A93-21663* National Aeronautics and Space Administration. Lewis Research Center, Cleveland, OH.

ULTRAHIGH TEMPERATURE VAPOR-CORE REACTOR - MAGNETOHYDRODYNAMIC SYSTEM FOR SPACE NUCLEAR ELECTRIC POWER

ISAAC MAYA, SAMIM ANGHAE, NILS J. DIAZ, and EDWARD T. DUGAN (Florida Univ., Gainesville) *Journal of Propulsion and Power* (ISSN 0748-4658) vol. 9, no. 1 Jan.-Feb. 1993 p. 98-104. Previously cited in issue 23, p. 4034, Accession no. A91-54799 AIAA, NASA, and OAI, Conference on Advanced SEI Technologies, Cleveland, OH, Sept. 4-6, 1991, AIAA Paper 91-3632 Research supported by Univ. of Florida, NSF, and San Diego Supercomputer Center refs
(Contract NAS3-26314)
Copyright

A93-21664* National Aeronautics and Space Administration. Lewis Research Center, Cleveland, OH.

PHOTOVOLTAIC RECEIVERS FOR LASER BEAMED POWER IN SPACE

GEOFFREY A. LANDIS (Sverdrup Technology, Inc.; NASA, Lewis Research Center, Cleveland, OH) *Journal of Propulsion and Power* (ISSN 0748-4658) vol. 9, no. 1 Jan.-Feb. 1993 p. 105-112. Previously cited in issue 22, p. 3904, Accession no. A92-53201 IEEE Photovoltaic Specialists Conference, 22nd, Las Vegas, NV, Oct. 7-11, 1991, Conference Record. Vol. 2, p. 1494-1502 refs
(Contract NAS3-25266)
Copyright

A93-22649# National Aeronautics and Space Administration. Lewis Research Center, Cleveland, OH.

PREDICTION OF ENGINE AND NEAR-FIELD PLUME REACTING FLOWS IN LOW-THRUST CHEMICAL ROCKETS

JONATHAN M. WEISS and CHARLES L. MERKLE (Pennsylvania State Univ., University Park) Jan. 1993 14 p. AIAA, Aerospace

Sciences Meeting and Exhibit, 31st, Reno, NV, Jan. 11-14, 1993 refs

(Contract NAG3-1020; NAGW-1356)

(AIAA PAPER 93-0237) Copyright

A computational model is employed to study the reacting flow within the engine and near-field plumes of several small gaseous hydrogen-oxygen thrusters. The model solves the full Navier-Stokes equations coupled with species diffusion equations for a hydrogen-oxygen reaction kinetics system and includes a two-equation q - ω model for turbulence. Predictions of global performance parameters and localized flowfield variables are compared with experimental data in order to assess the accuracy with which these flowfields are modeled and to identify aspects of the model which require improvement. Predicted axial and radial velocities 3 mm downstream of the exit plane show reasonable agreement with the measurements. The predicted peak in axial velocity in the hydrogen film coolant along the nozzle wall shows the best agreement; however, predictions within the core region are roughly 15 percent below measured values, indicating an underprediction of the extent to which the hydrogen diffuses and mixes with the core flow. There is evidence that this is due to three-dimensional mixing processes which are not included in the axisymmetric model.

Author

A93-24244* National Aeronautics and Space Administration. Lewis Research Center, Cleveland, OH.

PLASMA CHAMBER TESTING OF APSA COUPONS FOR THE SAMPE FLIGHT EXPERIMENT

G. B. HILLARD (NASA, Lewis Research Center, Cleveland, OH) Jan. 1993 8 p. AIAA, Aerospace Sciences Meeting and Exhibit, 31st, Reno, NV, Jan. 11-14, 1993 refs

(AIAA PAPER 93-0568) Copyright

Different blanket materials and mounting techniques have been used to build 12 Advanced Photovoltaic Solar Array cell coupons for NASA's Solar Array Module Plasma Interactions Experiment. Ground testing of these coupons in a plasma chamber revealed significant differences among them in plasma current collection; while the Kapton-H coupon exhibited current collection consistent with the exposed interconnects, the other two coupon types tested experienced anomalously large collection currents. This may be due to enhanced plasma sheaths supported by the weakly conducting C and Ge employed in these coupons.

O.C.

A93-24800* National Aeronautics and Space Administration. Lewis Research Center, Cleveland, OH.

THE INTERACTION OF HIGH VOLTAGE SYSTEMS WITH THE ENVIRONMENTS OF THE MOON AND MARS

G. B. HILLARD and JOSEPH C. KOLECKI (NASA, Lewis Research Center, Cleveland, OH) Jan. 1993 5 p. AIAA, Aerospace Sciences Meeting and Exhibit, 31st, Reno, NV, Jan. 11-14, 1993 refs

(AIAA PAPER 93-0704) Copyright

An evaluation is made of the consequences of the interaction of high-voltage spacecraft systems designed for use in orbit or on the lunar and Martian surfaces with such environmental components as electrically charged dust, low pressure atmospheres, ionospheric plasmas and neutral gas species, and chemically reactive species. An account is given of plausible means for obtaining the requisite data and developing priorities for the study of each of the identified interactions. Attention is given to the computational tools whose development is required for the simulation and quantification of risk factors for the various likely interactions.

O.C.

A93-24891* National Aeronautics and Space Administration. Lewis Research Center, Cleveland, OH.

A COMPARISON OF ARCJET PLUME PROPERTIES TO MODEL PREDICTIONS

M. A. CAPPELLI, J. G. LIEBESKIND, R. K. HANSON (Stanford Univ., CA), G. W. BUTLER, and D. Q. KING (Olin Rocket Research Co., Redmond, WA) Jan. 1993 13 p. AIAA, Aerospace Sciences Meeting and Exhibit, 31st, Reno, NV, Jan. 11-14, 1993

Research supported by NASA, USAF, and Rocket Research Co refs

(AIAA PAPER 93-0820) Copyright

This paper describes an experimental study of the plasma plume properties of a 1 kW class hydrogen arcjet thruster and the comparison of measured temperature and velocity field to model predictions. The experiments are based on laser-induced fluorescence excitation of the Balmer-alpha transition. The model is based on a single-fluid magnetohydrodynamic description of the flow originally developed to predict arcjet thruster performance. Excellent agreement between model predictions and experimental velocity is found, despite the complex nature of the flow. Measured and predicted exit plane temperatures are in disagreement by as much as 2000K over a range of operating conditions. The possible sources for this discrepancy are discussed.

Author

A93-24948* National Aeronautics and Space Administration. Lewis Research Center, Cleveland, OH.

CALCULATIONS OF LOW REYNOLDS NUMBER ROCKET NOZZLES

SUK C. KIM (Sverdrup Technology Corp., Brook Park; NASA, Lewis Research Center, Cleveland, OH) Jan. 1993 11 p. AIAA, Aerospace Sciences Meeting and Exhibit, 31st, Reno, NV, Jan. 11-14, 1993 refs

(Contract NAS3-25266)

(AIAA PAPER 93-0888)

The performance of low-thrust rocket nozzles was studied with a full Navier-Stokes code. The effect of the reduction of the nozzle length on the viscous loss and on the two-dimensional loss due to the increase in the nozzle exit angle was examined by calculating the flowfield and performance values of hydrogen resistojet nozzle with various lengths and shapes (such as 20-deg or 30-deg conical nozzles and a nozzle whose wall contour is given by the Rao nozzle optimization code). It was found that the vacuum specific impulse value of the 30-deg conical nozzle was the highest and that of the contoured nozzle was the lowest among the three nozzles, whose throat Reynolds number and area ratio were 1150 and 82, respectively.

I.S.

A93-25303* National Aeronautics and Space Administration. Lewis Research Center, Cleveland, OH.

ON-ORBIT CHARACTERIZATION OF ELECTRIC PROPULSION ON LEO SATELLITES

D. BARNHART (USAF, Phillips Lab., Edwards AFB, CA) and J. SANKOVIC (NASA, Lewis Research Center, Cleveland, OH) In Space Congress, 29th, Cocoa Beach, FL, Apr. 21-24, 1992, Proceedings Cape Canaveral, FL Canaveral Council of Technical Societies 1992 p. 7-7 to 7-17. refs

Copyright

Utilizing commercial or military satellites as testbeds for subsystems is a potential platform for small devices. Electric propulsion is a viable and upcoming subsystem that is of high interest to planetary mission engineers as well as commercial satellite developers. It is proposed that by incorporating small lightweight electric propulsion devices onto small satellites as external or 'bolt-on' experiments, an increase in the number of flight opportunities can occur. Specific problems are spacecraft body interaction, contamination effects, thermal interface problems, power conditioning control electronics, and propulsion feed system interfaces.

Author

A93-25856* National Aeronautics and Space Administration. Lewis Research Center, Cleveland, OH.

100-KWE LUNAR/MARS SURFACE POWER UTILIZING THE SP-100 REACTOR WITH DYNAMIC CONVERSION

RICHARD B. HARTY (Rockwell International Corp., Canoga Park, CA) and LEE S. MASON (NASA, Lewis Research Center, Cleveland, OH) In IECEC '92; Proceedings of the 27th Intersociety Energy Conversion Engineering Conference, San Diego, CA, Aug. 3-7, 1992. Vol. 1 Warrendale, PA Society of Automotive Engineers, Inc. 1992 p. 1.33-1.39. refs

Copyright

Results are presented from a study of the coupling of an SP-100

20 SPACECRAFT PROPULSION AND POWER

nuclear reactor with either a Stirling or Brayton power system, at the 100 kWe level, for a power generating system suitable for operation in the lunar and Martian surface environments. In the lunar environment, the reactor and primary coolant loop would be contained in a guard vessel to protect from a loss of primary loop containment. For Mars, all refractory components, including the reactor, coolant, and power conversion components will be contained in a vacuum vessel for protection against the CO₂ environment. O.C.

A93-25859* National Aeronautics and Space Administration. Lewis Research Center, Cleveland, OH.

OPTIMIZATION OF CLOSED BRAYTON CYCLES FOR SPACE POWER GENERATION

JAMES C. HANLON (Sverdrup Technology, Inc., Brook Park, OH) *In* IECEC '92; Proceedings of the 27th Intersociety Energy Conversion Engineering Conference, San Diego, CA, Aug. 3-7, 1992. Vol. 1 Warrendale, PA Society of Automotive Engineers, Inc. 1992 p. 1.51-1.55. refs
(Contract NAS3-25266)

A development status evaluation is presented for methods that allow accurate preliminary design and optimization of closed Brayton cycle engines for space electrical power generation. The basis for such work is the Closed Cycle Engine Performance simulation code, in conjunction with the optimization code COPES/ADS; the joining of the two codes has greatly expedited the optimization process. Attention is given to a variety of other model-versatility enhancers. O.C.

A93-25879* National Aeronautics and Space Administration. Lewis Research Center, Cleveland, OH.

LESSONS LEARNED FROM THE AUTONOMOUS POWER SYSTEM

MARK J. RINGER, TODD M. QUINN, and ANTHONY MEROLLA (Sverdrup Technology, Inc., Brook Park, OH) *In* IECEC '92; Proceedings of the 27th Intersociety Energy Conversion Engineering Conference, San Diego, CA, Aug. 3-7, 1992. Vol. 1 Warrendale, PA Society of Automotive Engineers, Inc. 1992 p. 1.171-1.176. refs
(Contract NAS3-25266)
Copyright

The Autonomous Power System (APS) project at the NASA Lewis Research Center is designed to demonstrate the applications of integrated intelligent diagnosis, control and scheduling techniques to space power distribution systems. The project consists of three elements: the Autonomous Power Expert System (APEX) for Fault Diagnosis, Isolation, and Recovery (FDIR); the Autonomous Intelligent Power Scheduler (AIPS) to efficiently assign activities start times and resources; and power hardware (Brassboard) to emulate a space-based power system. The APS project had been through one design iteration. Each of the three elements of the APS project has been designed, tested, and integrated into a complete working system. After these three portions were completed, an evaluation period was initiated. Each piece of the system was critiqued based on individual performance as well as the ability to interact with the other portions of the APS project. These critiques were then used to determine guidelines for new and improved components of the APS system. Author

A93-25898* National Aeronautics and Space Administration. Lewis Research Center, Cleveland, OH.

PHOTOVOLTAIC ARRAY SPACE POWER FLIGHT EXPERIMENT PLUS DIAGNOSTICS (PASP+) MODULES

WILLIAM T. COOLEY, STEVEN F. ADAMS, KITT C. REINHARDT (USAF, Wright Lab., Wright-Patterson AFB, OH), and MICHAEL F. PISZCZOR (NASA, Lewis Research Center, Cleveland, OH) *In* IECEC '92; Proceedings of the 27th Intersociety Energy Conversion Engineering Conference, San Diego, CA, Aug. 3-7, 1992. Vol. 1 Warrendale, PA Society of Automotive Engineers, Inc. 1992 p. 1.295-1.301. refs
Copyright

The Photovoltaic Array Space Power Plus Diagnostics flight

experiment (PASP+) subsumes twelve solar array modules which represent the state of the art in the space photovoltaic array industry. Each of the twelve modules individually feature specific photovoltaic technologies such as advanced semiconductor materials, multi-bandgap structures, lightweight array designs, advanced interconnect technologies, or concentrator array designs. This paper will describe each module in detail including the configuration, components, materials, anticipated on orbit performance, and some of the aspects of each array technology. The layout of each module and the photovoltaic cells or array cross section will be presented graphically. A discussion on the environmental constraints and materials selection will be included as well as a delineation of the differences between the modules and the baseline array configuration in its intended application. Author

A93-25918* National Aeronautics and Space Administration. Lewis Research Center, Cleveland, OH.

THE GROUND TESTING OF A 2 KWE SOLAR DYNAMIC SPACE POWER SYSTEM

JAMES E. CALOGERAS (NASA, Lewis Research Center, Cleveland, OH) and MILES O. DUSTIN (Sverdrup Technology, Inc., Cleveland, OH) *In* IECEC '92; Proceedings of the 27th Intersociety Energy Conversion Engineering Conference, San Diego, CA, Aug. 3-7, 1992. Vol. 1 Warrendale, PA Society of Automotive Engineers, Inc. 1992 p. 1.455-1.459.
Copyright

The solar dynamic power system chosen by NASA for Space Station Freedom SSF requires validation in the vacuum/microgravity environment. The planned ground tests of a proof-of-concept 2 kWe solar dynamic system with address subsystem integration issues involving such major system components as the behavior of thermal energy storage materials. This test scheme will be scalable to 25 kWe, and will be flight-configured to incorporate features of the SSF's power module design. O.C.

A93-25958 National Aeronautics and Space Administration. Lewis Research Center, Cleveland, OH.

ENERGY LOSS ANALYSIS OF AN INTEGRATED SPACE POWER DISTRIBUTION SYSTEM

M. D. KANKAM (NASA, Lewis Research Center, Cleveland, OH) and P. F. RIBEIRO (Dordt College, Sioux Center, IA) *In* IECEC '92; Proceedings of the 27th Intersociety Energy Conversion Engineering Conference, San Diego, CA, Aug. 3-7, 1992. Vol. 2 Warrendale, PA Society of Automotive Engineers, Inc. 1992 p. 2.189-2.194. Previously announced in STAR as N93-14834 refs
(Contract RTOP 506-41-41)
Copyright

The results of studies related to conceptual topologies of an integrated utility-like space power system are described. The system topologies are comparatively analyzed by considering their transmission energy losses as functions of mainly distribution voltage level and load composition. The analysis is expedited by use of a Distribution System Analysis and Simulation (DSAS) software. This recently developed computer program by the Electric Power Research Institute (EPRI) uses improved load models to solve the power flow within the system. However, present shortcomings of the software with regard to space applications, and incompletely defined characteristics of a space power system make the results applicable to only the fundamental trends of energy losses of the topologies studied. Accountability, such as included, for the effects of the various parameters on the system performance can constitute part of a planning tool for a space power distribution system. Author

A93-25964* National Aeronautics and Space Administration. Lewis Research Center, Cleveland, OH.

FREE-PISTON STIRLING COMPONENT TEST POWER CONVERTER TEST RESULTS AND POTENTIAL STIRLING APPLICATIONS

G. R. DOCHAT (Mechanical Technology, Inc., Latham, NY) *In*

IECEC '92; Proceedings of the 27th Intersociety Energy Conversion Engineering Conference, San Diego, CA, Aug. 3-7, 1992. Vol. 2 Warrendale, PA Society of Automotive Engineers, Inc. 1992 p. 2.225-2.231. Research supported by NASA refs Copyright

As the principal contractor to NASA-Lewis Research Center, Mechanical Technology Incorporated is under contract to develop free-piston Stirling power converters in the context of the competitive multiyear Space Stirling Technology Program. The first generation Stirling power converter, the component test power converter (CTPC) initiated cold end testing in 1991, with hot testing scheduled for summer of 1992. This paper reviews the test progress of the CTPC and discusses the potential of Stirling technology for various potential missions at given point designs of 250 watts, 2500 watts, and 25,000 watts. C.D.

A93-25965* National Aeronautics and Space Administration. Lewis Research Center, Cleveland, OH.

BIPS TURBOALTERNATOR-COMPRESSOR CHARACTERISTICS AND APPLICATION TO THE NASA SOLAR DYNAMIC GROUND DEMONSTRATION PROGRAM

PETER C. AMUNDSEN and WILLIAM B. HARPER, JR. (Allied-Signal Aerospace Co., Tempe, AZ) In IECEC '92; Proceedings of the 27th Intersociety Energy Conversion Engineering Conference, San Diego, CA, Aug. 3-7, 1992. Vol. 2 Warrendale, PA Society of Automotive Engineers, Inc. 1992 p. 2.239-2.244. Research supported by NASA refs Copyright

The NASA-sponsored 2kW(e) Solar Dynamic Space Power System Ground Test Demonstration Program requires the physical and the thermodynamic integration of the Brayton Isotope Power System (BIPS) Turboalternator-Compressor (TAC) and recuperator with a heat receiver, solar concentrator, and radiator based on Space Station Freedom designs. The aim of the designs is to provide a cost-effective, minimal-risk, viable ground test system. This paper describes the BIPS TAC configuration and performance characteristics along with the cycle analysis of BIPS TAC. C.D.

A93-26105 National Aeronautics and Space Administration. Lewis Research Center, Cleveland, OH.

THE NASA CSTI HIGH CAPACITY POWER PROJECT

J. WINTER, J. DUDENHOEFER, A. JUHASZ, G. SCHWARZE, R. PATTERSON, D. FERGUSON (NASA, Lewis Research Center, Cleveland, OH), P. SCHMITZ (Sverdrup Technology, Inc., Cleveland, OH), and J. VANDERSANDE (JPL, Pasadena, CA) In IECEC '92; Proceedings of the 27th Intersociety Energy Conversion Engineering Conference, San Diego, CA, Aug. 3-7, 1992. Vol. 6 Warrendale, PA Society of Automotive Engineers, Inc. 1992 p. 6.79-6.85. Previously announced in STAR as N93-11398 refs

(Contract RTOP 590-13-00)

Copyright

The elements of the Civilian Space Technology Initiative (CSTI) High Capacity Power Project include Systems Analysis, Stirling Power Conversion, Thermoelectric Power Conversion, Thermal Management, Power Management, Systems Diagnostics, Environmental Interactions, and Material/Structural Development. The overall project will develop and demonstrate the technology base required to provide a wide range of modular power systems compatible with the SP-100 reactor which facilitates operation during lunar and planetary day/night cycles as well as allowing spacecraft operation at any attitude or distance from the sun. Significant accomplishments in all of the project elements are presented, along with revised goals and project timelines recently developed. Author

A93-26109 National Aeronautics and Space Administration. Lewis Research Center, Cleveland, OH.

POWER SYSTEM MONITORING AND SOURCE CONTROL OF THE SPACE STATION FREEDOM DC-POWER SYSTEM TESTBED

GREG L. KIMNACH and ANASTACIO N. BAEZ (NASA, Lewis Research Center, Cleveland, OH) In IECEC '92; Proceedings of

the 27th Intersociety Energy Conversion Engineering Conference, San Diego, CA, Aug. 3-7, 1992. Vol. 6 Warrendale, PA Society of Automotive Engineers, Inc. 1992 p. 6.105-6.110. Previously announced in STAR as N93-10734 refs

(Contract RTOP 474-42-10)

Copyright

Unlike a terrestrial electric utility which can purchase power from a neighboring utility, the Space Station Freedom (SSF) has strictly limited energy resources; as a result, source control, system monitoring, system protection, and load management are essential to the safe and efficient operation of the SSF Electric Power System (EPS). These functions are being evaluated in the dc Power Management and Distribution (PMAD) Testbed which NASA LeRC has developed at the Power System Facility (PSF) located in Cleveland, Ohio. The testbed is an ideal platform to develop, integrate, and verify power system monitoring and control algorithms. State Estimation (SE) is a monitoring tool used extensively in terrestrial electric utilities to ensure safe power system operation. It uses redundant system information to calculate the actual state of the EPS, to isolate faulty sensors, to determine source operating points, to verify faults detected by subsidiary controllers, and to identify high impedance faults. Source control and monitoring safeguard the power generation and storage subsystems and ensure that the power system operates within safe limits while satisfying user demands with minimal interruptions. System monitoring functions, in coordination with hardware implemented schemes, provide for a complete fault protection system. The objective of this paper is to overview the development and integration of the state estimator and the source control algorithms. Author

A93-30956*# National Aeronautics and Space Administration. Lewis Research Center, Cleveland, OH.

SOLAR ARRAY ELECTRICAL PERFORMANCE ASSESSMENT FOR SPACE STATION FREEDOM

BRYAN K. SMITH (NASA, Lewis Research Center, Cleveland, OH) and HOLLY BRISCO (Lockheed Missiles and Space Co., Inc., Sunnyvale, CA) Feb. 1993 12 p. AIAA, AHS, and ASEE, Aerospace Design Conference, Irvine, CA, Feb. 16-19, 1993 refs

(AIAA PAPER 93-1052) Copyright

Electrical power for Space Station Freedom will be generated by large photovoltaic arrays with a beginning of life power requirement of 30.8 kW per array. The solar arrays will operate in a Low Earth Orbit (LEO) over a design life of fifteen years. This paper provides an analysis of the predicted solar array electrical performance over the design life and presents a summary of supporting analysis and test data for the assigned model parameters and performance loss factors. Each model parameter and loss factor is assessed based upon program requirements, component analysis and test data to date. A description of the LMSC performance model future test plans and predicted performance ranges are also given. Author

A93-30975*# National Aeronautics and Space Administration. Lewis Research Center, Cleveland, OH.

ELECTROMAGNETIC PROPULSION FOR SPACECRAFT

ROGER M. MYERS (Sverdrup Technology, Inc., Brook Park; NASA, Lewis Research Center, Cleveland, OH) Feb. 1993 31 p. AIAA, AHS, and ASEE, Aerospace Design Conference, Irvine, CA, Feb. 16-19, 1993 refs

(AIAA PAPER 93-1086) Copyright

Three electromagnetic propulsion technologies, solid propellant pulsed plasma thrusters (PPT), magnetoplasmadynamic (MPD) thrusters, and pulsed inductive thrusters (PIT) have been developed for application to auxiliary and primary spacecraft propulsion. Both the PPT and MPD thrusters have been flown in space, though only PPTs have been used on operational satellites. The performance of operational PPTs is quite poor, providing only about 8 percent efficiency at about 1000 sec specific impulse. Laboratory PPTs yielding 34 percent efficiency at 5170 sec specific impulse have been demonstrated. Laboratory MPD thrusters have been demonstrated with up to 70 percent efficiency and 7000 sec specific

20 SPACECRAFT PROPULSION AND POWER

impulse. Recent PIT performance measurements using ammonia and hydrazine propellants are extremely encouraging, reaching 50 percent efficiency for specific impulses between 4000 and 8000 sec. Author

A93-31968* National Aeronautics and Space Administration. Lewis Research Center, Cleveland, OH.

EVALUATION OF THE MUNICH METHOD FOR MODELING ROCKET ENGINE PERFORMANCE

FRANK J. ZELEZNIK (NASA, Lewis Research Center, Cleveland, OH) Journal of Propulsion and Power (ISSN 0748-4658) vol. 9, no. 2 Mar.-Apr. 1993 p. 191-196. refs Copyright

A new procedure, dubbed the Munich Method, has been proposed recently for the modeling of rocket engine performance. The author of the Munich Method claims it to be an extension and improvement of the thermodynamic procedures used to model rocket engines in the NASA-Lewis chemical equilibrium program. An examination of the Munich Method shows that it contains several flaws. If these defects are corrected then the Munich Method will produce results identical to those generated by the NASA-Lewis Code. Author

A93-32554* National Aeronautics and Space Administration. Lewis Research Center, Cleveland, OH.

EXTENDED LIFE AND PERFORMANCE TEST OF A LOW-POWER ARCJET

FRANCIS M. CURRAN and THOMAS W. HAAG (NASA, Lewis Research Center, Cleveland, OH) Journal of Spacecraft and Rockets (ISSN 0022-4650) vol. 29, no. 4 July-Aug. 1992 p. 444-452. AIAA, ASME, SAE, and ASEE, Joint Propulsion Conference, 24th, Boston, MA, July 11-13, 1988, AIAA Paper 88-3106. Previously cited in issue 20, p. 3357, Accession no. A88-48756 refs Copyright

A93-32567* National Aeronautics and Space Administration. Lewis Research Center, Cleveland, OH.

ARCING RATES FOR HIGH VOLTAGE SOLAR ARRAYS - THEORY, EXPERIMENT, AND PREDICTIONS

DANIEL E. HASTINGS, MENGU CHO (MIT, Cambridge, MA), and HITOSHI KUNINAKA (Inst. of Space and Astronautical Science, Sagami-hara, Japan) Journal of Spacecraft and Rockets (ISSN 0022-4650) vol. 29, no. 4 July-Aug. 1992 p. 538-554. Research supported by NASA, NSF, USAF, and Japan Society for the Promotion of Science refs Copyright

All solar arrays have biased surfaces that can be exposed to the space environment. It has been observed that when the array bias is less than a few hundred volts negative, then the exposed conductive surfaces may undergo arcing in the space plasma. A theory for arcing is developed on these high voltage solar arrays that ascribes the arcing to electric field runaway at the interface of the plasma, conductor, and solar cell dielectric. Experiments were conducted in the laboratory for the High Voltage Solar Array experiment that will fly on the Japanese Space Flyer Unit (SFU) in 1994. The theory was compared in detail with the experiment and shown to give a reasonable explanation for the data. The combined theory and ground experiments were then used to develop predictions for the SFU flight. Author

A93-34481* National Aeronautics and Space Administration. Lewis Research Center, Cleveland, OH.

EROSION RATE DIAGNOSTICS IN ION THRUSTERS USING LASER-INDUCED FLUORESCENCE

C. J. GAETA, J. N. MATOSSIAN, R. S. TURLEY, J. R. BEATTIE, J. D. WILLIAMS, and W. S. WILLIAMSON (Hughes Research Labs., Malibu, CA) Journal of Propulsion and Power (ISSN 0748-4658) vol. 9, no. 3 May-June 1993 p. 369-376. refs (Contract NAS3-25553) Copyright

We have used laser-induced fluorescence (LIF) to monitor the charge-exchange ion erosion of the molybdenum accelerator

electrode in ion thrusters. This real-time, nonintrusive method was implemented by operating a 30cm-diam ring-cusp thruster using xenon propellant. With the thruster operating at a total power of 5 kW, laser radiation at a wavelength of 390 nm (corresponding to a ground state atomic transition of molybdenum) was directed through the extracted ion beam adjacent to the downstream surface of the molybdenum accelerator electrode. Molybdenum atoms, sputtered from this surface as a result of charge-exchange ion erosion, were excited by the laser radiation. The intensity of the laser-induced fluorescence radiation, which is proportional to the sputter rate of the molybdenum atoms, was measured and correlated with variations in thruster operating conditions such as accelerator electrode voltage, accelerator electrode current, and test facility background pressure. We also demonstrated that the LIF technique has sufficient sensitivity and spatial resolution to evaluate accelerator electrode lifetime in ground-based test facilities. Author

A93-34492* National Aeronautics and Space Administration. Lewis Research Center, Cleveland, OH.

EVOLVING SP-100 POWERPLANTS VIA ELECTRIC PROPULSION TO GEO AND LUNAR ORBIT

ROBERT E. ENGLISH (NASA, Lewis Research Center, Cleveland, OH) Journal of Propulsion and Power (ISSN 0748-4658) vol. 9, no. 3 May-June 1993 p. 449-455. AIAA, NASA, and OAI, Conference on Advanced SEI Technologies, Cleveland, OH, Sept. 4-6, 1991, AIAA Paper 91-3562. Previously cited in issue 23, p. 4033, Accession no. A91-53712 refs Copyright

A93-36197 National Aeronautics and Space Administration. Lewis Research Center, Cleveland, OH.

ON PROTECTION OF FREEDOM'S SOLAR DYNAMIC RADIATOR FROM THE ORBITAL DEBRIS ENVIRONMENT. I - PRELIMINARY ANALYSIS AND TESTING

JENNIFER L. RHATIGAN (NASA, Lewis Research Center, Cleveland, OH), ERIC L. CHRISTIANSEN (NASA, Johnson Space Center, Houston, TX), and MICHAEL L. FLEMING (LTV Missiles & Electronics Group, Dallas, TX) ASME, Transactions, Journal of Solar Energy Engineering (ISSN 0199-6231) vol. 114 Aug. 1992 p. 135-141. Previously announced in STAR as N90-14285 refs Copyright

A great deal of experimentation and analysis was performed to quantify penetration thresholds of components which will experience orbital debris impacts. Penetration was found to depend upon mission specific parameters such as orbital altitude, inclination, and orientation of the component; and upon component specific parameters such as material, density and the geometry particular to its shielding. Experimental results are highly dependent upon shield configuration and cannot be extrapolated with confidence to alternate shield configurations. Also, current experimental capabilities are limited to velocities which only approach the lower limit of predicted orbital debris velocities. Therefore, prediction of the penetrating particle size for a particular component having a complex geometry remains highly uncertain. An approach is described which was developed to assess on-orbit survivability of the solar dynamic radiator due to micrometeoroid and space debris impacts. Preliminary analyses are presented to quantify the solar dynamic radiator survivability, and include the type of particle and particle population expected to defeat the radiator bumpering (i.e., penetrate a fluid flow tube). Results of preliminary hypervelocity impact testing performed on radiator panel samples (in the 6 to 7 km/sec velocity range) are also presented. Author (revised)

A93-36589 National Aeronautics and Space Administration. Lewis Research Center, Cleveland, OH.

ON PROTECTION OF FREEDOM'S SOLAR DYNAMIC RADIATOR FROM THE ORBITAL DEBRIS ENVIRONMENT. II - FURTHER TESTING AND ANALYSES

JENNIFER L. RHATIGAN (NASA, Lewis Research Center, Cleveland, OH), ERIC L. CHRISTIANSEN (NASA, Johnson Space

Center, Houston, TX), and MICHAEL L. FLEMING (LTV Missiles & Electronics Group, Dallas, TX) ASME, Transactions, Journal of Solar Energy Engineering (ISSN 0199-6231) vol. 114 Aug. 1992 p. 142-149. Previously announced in STAR as N91-30265 refs Copyright

Presented here are results of a test program undertaken to further define the response of the solar dynamic radiator to hypervelocity impact (HVI). Tests were conducted on representative radiator panels (under ambient, nonoperating conditions) over a range of velocity. Target parameters are also varied. Data indicate that analytical penetration predictions are conservative (i.e., pessimistic) for the specific configuration of the solar dynamic radiator. Test results are used to define the solar dynamic radiator reliability with respect to HVI more rigorously than previous studies. Test data, reliability, and survivability results are presented.

Author

A93-38976* National Aeronautics and Space Administration. Lewis Research Center, Cleveland, OH.

DEVELOPMENT AND FLIGHT HISTORY OF THE SERT II SPACECRAFT

WILLIAM R. KERSLAKE and LOUIS R. IGNACZAK (NASA, Lewis Research Center, Cleveland, OH) Journal of Spacecraft and Rockets (ISSN 0022-4650) vol. 30, no. 3 May-June 1993 p. 258-290. AIAA, SAE, ASME, and ASEE, Joint Propulsion Conference and Exhibit, 28th, Nashville, TN, July 6-8, 1992, AIAA Paper 92-3516. Previously cited in issue 23, p. 4100, Accession no. A92-54038 refs Copyright

A93-42895* National Aeronautics and Space Administration. Lewis Research Center, Cleveland, OH.

MEASUREMENT AND ANALYSIS OF A SMALL NOZZLE PLUME IN VACUUM

P. F. PENKO (NASA, Lewis Research Center, Cleveland, OH), I. D. BOYD (Cornell Univ., Ithaca, NY), D. L. MEISSNER, and K. J. DEWITT (Toledo Univ., OH) Journal of Propulsion and Power (ISSN 0748-4658) vol. 9, no. 4 July-Aug. 1993 p. 646-648. Abridged. AIAA, SAE, ASME, and ASEE, Joint Propulsion Conference, 28th, Nashville, TN, July 6-8, 1992, AIAA Paper 92-3108. Previously cited in issue 20, p. 3498, Accession no. A92-48748 refs Copyright

A93-46418* National Aeronautics and Space Administration. Lewis Research Center, Cleveland, OH.

SOLAR ARRAY MODULE PLASMA INTERACTIONS EXPERIMENT (SAMPIE) - SCIENCE AND TECHNOLOGY OBJECTIVES

G. B. HILLARD and DALE C. FERGUSON (NASA, Lewis Research Center, Cleveland, OH) Journal of Spacecraft and Rockets (ISSN 0022-4650) vol. 30, no. 4 July-Aug. 1993 p. 488-494. refs Copyright

The solar array module plasma interactions experiment (SAMPIE) is an approved NASA flight experiment manifested for Shuttle deployment in early 1994. The SAMPIE experiment is designed to investigate the interaction of high voltage space power systems with ionospheric plasma. To study the behavior of solar cells, a number of solar cell coupons (representing design technologies of current interest) will be biased to high voltages to measure both arcing and current collection. Various theories of arc suppression will be tested by including several specially modified cell coupons. Finally, SAMPIE will include experiments to study the basic nature of arcing and current collection. This paper describes the rationale for a space flight experiment, the measurements to be made, and the significance of the expected results. A future paper will present a detailed discussion of the engineering design.

A93-48648* National Aeronautics and Space Administration. Lewis Research Center, Cleveland, OH.

AUTOGENOUS PRESSURIZATION OF CRYOGENIC VESSELS USING SUBMERGED VAPOR INJECTION

ROBERT J. STOCHL, NEIL T. VAN DRESAR, and RAYMOND F. LACOVIC (NASA, Lewis Research Center, Cleveland, OH) In Advances in cryogenic engineering. Vol. 37B - Proceedings of the 1991 Cryogenic Engineering Conference, Univ. of Alabama, Huntsville, June 11-14, 1991 New York Plenum Press 1991 p. 1273-1280. refs Copyright

Experimental results are reported for submerged injection pressurization and expulsion tests of a 4.89 cu m liquid hydrogen tank. The pressurant injector was positioned near the bottom of the test vessel to simulate liquid engulfment of the pressurant gas inlet, a condition that may occur in low-gravity conditions. Results indicate a substantial reduction in pressurization efficiency with pressurant gas requirements approximately five times greater than ideal amounts. Consequently, submerged vapor injection should be avoided as a low-gravity autogenous pressurization method whenever possible. The work presented herein validates that pressurant requirements are accurately predicted by a homogeneous thermodynamic model when the submerged injection technique is employed.

Author (revised)

A93-49334* National Aeronautics and Space Administration. Lewis Research Center, Cleveland, OH.

U.S./CIS JOINT NUCLEAR ROCKET VENTURE

JOHN S. CLARK (NASA, Lewis Research Center, Cleveland, OH), MELVIN C. MCILWAIN (Aerojet, Rancho Cordova, CA), VLADIMIR SMETANIKOV (Research and Development Inst. of Power Engineering, Moscow, Russia), EVGENIJ K. D'YAKOV (NPO Luch, Podolsk, Russia), and VLADIMIR A. PAVSHUK (Inst. of Atomic Energy, Moscow, Russia) Aerospace America (ISSN 0740-722X) vol. 31, no. 7 July 1993 p. 28-30, 35. Copyright

An account is given of the significance for U.S. spacecraft development of a nuclear thermal rocket (NTR) reactor concept that has been developed in the (formerly Soviet) Commonwealth of Independent States (CIS). The CIS NTR reactor employs a hydrogen-cooled zirconium hydride moderator and ternary carbide fuels; the comparatively cool operating temperatures associated with this design promise overall robustness.

AIAA

A93-49657*# National Aeronautics and Space Administration. Lewis Research Center, Cleveland, OH.

FLOW INSTABILITY IN PARTICLE-BED NUCLEAR REACTORS

J. L. KERREBROCK and J. KALAMAS (MIT, Cambridge, MA) Jun. 1993 15 p. AIAA, SAE, ASME, and ASEE, Joint Propulsion Conference and Exhibit, 29th, Monterey, CA, June 28-30, 1993 Research supported by NASA refs (AIAA PAPER 93-1758) Copyright

A three-dimensional model of the stability of the particle-bed reactor is presented, in which the fluid, has mobility in three dimensions. The model accurately represents the stability at low Re numbers as well as the effects of the cold and hot frits and of the heat conduction and radiation in the particle bed. The model can be easily extended to apply to the cylindrical geometry of particle-bed reactors. Exemplary calculations are carried out, showing that a particle bed without a cold frit would be subject to instability if operated at the high-temperature ratios used for nuclear rockets and at power densities below about 4 MW/l; since the desired power density for such a reactor is about 40 MW/l, the operation at design exit temperature but at reduced power could be hazardous. Calculations show however that it might be possible to remove the instability problem by appropriate combinations of cold and hot frits.

AIAA

A93-49671*# National Aeronautics and Space Administration. Lewis Research Center, Cleveland, OH.

A FUNCTION APPROXIMATION APPROACH TO ANOMALY DETECTION IN PROPULSION SYSTEM TEST DATA

BRUCE A. WHITEHEAD (Tennessee Univ., Tullahoma) and W. A.

20 SPACECRAFT PROPULSION AND POWER

HOYT (ERC, Inc., Tullahoma, TN) Jun. 1993 14 p. AIAA, SAE, ASME, and ASEE, Joint Propulsion Conference and Exhibit, 29th, Monterey, CA, June 28-30, 1993 refs (Contract NAS3-39184) (AIAA PAPER 93-1776) Copyright

Ground test data from propulsion systems such as the Space Shuttle Main Engine (SSME) can be automatically screened for anomalies by a neural network. The neural network screens data after being trained with nominal data only. Given the values of 14 measurements reflecting external influences on the SSME at a given time, the neural network predicts the expected nominal value of a desired engine parameter at that time. We compared the ability of three different function-approximation techniques to perform this nominal value prediction: a novel neural network architecture based on Gaussian basis functions, a conventional back propagation neural network, and linear regression. These three techniques were tested with real data from six SSME ground tests containing two anomalies. The basis function network trained more rapidly than back propagation. It yielded nominal predictions with a tight enough confidence interval to distinguish anomalous deviations from the nominal fluctuations in an engine parameter. Since the function-approximation approach requires nominal training data only, it is capable of detecting unknown classes of anomalies for which training data is not available.

A93-49674*# National Aeronautics and Space Administration. Lewis Research Center, Cleveland, OH.

QUALITATIVE MODEL-BASED DIAGNOSTICS FOR ROCKET SYSTEMS

WILLIAM MAUL, CLAUDIA MEYER (Sverdrup Technology, Inc., Brook Park, OH), AMY JANKOVSKY (NASA, Lewis Research Center, Cleveland, OH), and CHRISTOPHER FULTON (Analex Corp., Brook Park, OH) Jun. 1993 12 p. AIAA, SAE, ASME, and ASEE, Joint Propulsion Conference and Exhibit, 29th, Monterey, CA, June 28-30, 1993 Previously announced in STAR as N93-28052 refs (Contract NAS3-25266) (AIAA PAPER 93-1779) Copyright

A diagnostic software package is currently being developed at NASA LeRC that utilizes qualitative model-based reasoning techniques. These techniques can provide diagnostic information about the operational condition of the modeled rocket engine system or subsystem. The diagnostic package combines a qualitative model solver with a constraint suspension algorithm. The constraint suspension algorithm directs the solver's operation to provide valuable fault isolation information about the modeled system. A qualitative model of the Space Shuttle Main Engine's oxidizer supply components was generated. A diagnostic application based on this qualitative model was constructed to process four test cases: three numerical simulations and one actual test firing. The diagnostic tool's fault isolation output compared favorably with the input fault condition.

A93-49759*# National Aeronautics and Space Administration. Lewis Research Center, Cleveland, OH.

RELIABILITY STUDIES OF INTEGRATED MODULAR ENGINE SYSTEM DESIGNS

TERRY L. HARDY (NASA, Lewis Research Center, Cleveland, OH) and DOUGLAS C. RAPP (Sverdrup Technology, Inc., Brook Park, OH) Jun. 1993 18 p. AIAA, SAE, ASME, and ASEE, Joint Propulsion Conference and Exhibit, 29th, Monterey, CA, June 28-30, 1993 Previously announced in STAR as N93-27022 refs (AIAA PAPER 93-1886) Copyright

A study was performed to evaluate the reliability of Integrated Modular Engine (IME) concepts. Comparisons were made between networked IME systems and non-networked discrete systems using expander cycle configurations. Both redundant and non-redundant systems were analyzed. Binomial approximation and Markov analysis techniques were employed to evaluate total system reliability. In addition, Failure Modes and Effects Analyses (FMEA), Preliminary Hazard Analyses (PHA), and Fault Tree Analysis (FTA)

were performed to allow detailed evaluation of the IME concept. A discussion of these system reliability concepts is also presented.

A93-49760*# National Aeronautics and Space Administration. Lewis Research Center, Cleveland, OH.

FLUID DESIGN STUDIES OF INTEGRATED MODULAR ENGINE SYSTEM

BRUCE FRANKENFIELD and JERRY CAREK (NASA, Lewis Research Center, Cleveland, OH) Jun. 1993 12 p. AIAA, SAE, ASME, and ASEE, Joint Propulsion Conference and Exhibit, 29th, Monterey, CA, June 28-30, 1993 refs (AIAA PAPER 93-1887) Copyright

A study was performed to develop a fluid system design and show the feasibility of constructing an integrated modular engine (IME) configuration, using an expander cycle engine. The primary design goal of the IME configuration was to improve the propulsion system reliability. The IME fluid system was designed as a single fault tolerant system, while minimizing the required fluid components. This study addresses the design of the high pressure manifolds, turbopumps and thrust chambers for the IME configuration. A physical layout drawing was made, which located each of the fluid system components, manifolds and thrust chambers. Finally, a comparison was made between the fluid system designs of an IME system and a non-network (clustered) engine system.

A93-49761*# National Aeronautics and Space Administration. Lewis Research Center, Cleveland, OH.

PREDICTED PERFORMANCE OF AN INTEGRATED MODULAR ENGINE SYSTEM

MICHAEL BINDER and JAMES L. FELDER (Sverdrup Technology, Inc., Lewis Research Center Group, Brook Park, OH) Jun. 1993 17 p. AIAA, SAE, ASME, and ASEE, Joint Propulsion Conference and Exhibit, 29th, Monterey, CA, June 28-30, 1993 refs (Contract NAS3-25266; NAS3-25960) (AIAA PAPER 93-1888) Copyright

Space vehicle propulsion systems are traditionally comprised of a cluster of discrete engines, each with its own set of turbopumps, valves, and a thrust chamber. The Integrated Modular Engine (IME) concept proposes a vehicle propulsion system comprised of multiple turbopumps, valves, and thrust chambers which are all interconnected. The IME concept has potential advantages in fault-tolerance, weight, and operational efficiency compared with the traditional clustered engine configuration. The purpose of this study is to examine the steady-state performance of an IME system with various components removed to simulate fault conditions. An IME configuration for a hydrogen/oxygen expander cycle propulsion system with four sets of turbopumps and eight thrust chambers has been modeled using the Rocket Engine Transient Simulator program. The nominal steady-state performance is simulated, as well as turbopump, thrust chamber, and duct failures. The impact of component failures on system performance is discussed in the context of the system's fault tolerant capabilities. Author (revised)

A93-49768*# National Aeronautics and Space Administration. Lewis Research Center, Cleveland, OH.

PERFORMANCE OF A LOW-POWER SUBSONIC-ARC-ATTACHMENT ARCJET THRUSTER

JOHN M. SANKOVIC (NASA, Lewis Research Center, Cleveland, OH) and DARREN H. BERNIS (Minnesota Univ., Minneapolis) Jun. 1993 28 p. AIAA, SAE, ASME, and ASEE, Joint Propulsion Conference and Exhibit, 29th, Monterey, CA, June 28-30, 1993 refs (AIAA PAPER 93-1898) Copyright

A subsonic-arc-attachment thruster design was scaled from a 30 kW 1960's vintage thruster to operate at nominally 3 kW. Performance measurements were obtained over a 1-4 kW power range using hydrogen as the propellant. Several modes of operation were identified and were characterized by varying degrees of voltage instability. A stability map was developed showing that the voltage oscillations were brought upon by elevated current or

propellant levels. At a given specific energy level the specific impulse increased asymptotically with increased flow rates. Comparisons of performance were made between radial and tangential propellant injection. When the vortex flow was eliminated using radial injection, the operating voltages were lower at a given current, and the specific impulse and efficiency decreased. Tests were also conducted to determine the effects of background pressure on operation. Performance data were obtained at pressures of 0.047 Pa and 18 Pa. For a given specific energy level, the performance increased with a decrease in facility background pressure. Lowering the background pressure also caused a dramatic change in the voltage-current characteristic and the voltage stability, a phenomenon not previously reported with conventional supersonic-arc-attachment thrusters.

A93-49769* # National Aeronautics and Space Administration. Lewis Research Center, Cleveland, OH.

INVESTIGATION OF A SUBSONIC-ARC-ATTACHMENT THRUSTER USING SEGMENTED ANODES

DARREN H. BERNIS (Minnesota Univ., Minneapolis), JOHN M. SANKOVIC, and CHARLES J. SARMIENTO (NASA, Lewis Research Center, Cleveland, OH) Jun. 1993 25 p. AIAA, SAE, ASME, and ASEE, Joint Propulsion Conference and Exhibit, 29th, Monterey, CA, June 28-30, 1993 refs (AIAA PAPER 93-1899) Copyright

To investigate high frequency arc instabilities observed in subsonic-arc-attachment thrusters, a 3 kW, segmented-anode arcjet was designed and tested using hydrogen as the propellant. The thruster nozzle geometry was scaled from a 30 kW design previously tested in the 1960's. By observing the current to each segment and the arc voltage, it was determined that the 75-200 kHz instabilities were results of axial movements of the arc anode attachment point. The arc attachment point was fully contained in the subsonic portion of the nozzle for nearly all flow rates. The effects of isolating selected segments were investigated. In some cases, forcing the arc downstream caused the restrike to cease. Finally, decreasing the background pressure from 18 Pa to 0.05 Pa affected the pressure distribution in the nozzle, including the pressure in the subsonic arc chamber.

A93-49772* # National Aeronautics and Space Administration. Lewis Research Center, Cleveland, OH.

RECENT TESTING OF 30 KW HYDROGEN ARCJET THRUSTERS

THOMAS W. HAAG (NASA, Lewis Research Center, Cleveland, OH) Jun. 1993 18 p. AIAA, SAE, ASME, and ASEE, Joint Propulsion Conference and Exhibit, 29th, Monterey, CA, June 28-30, 1993 refs (AIAA PAPER 93-1902) Copyright

NASA is conducting efforts to evaluate high-power hydrogen arcjets for orbit transfer propulsion applications. As part of this program, an attempt was made to reexamine both radiatively- and regeneratively-cooled, 30 kW thrusters first demonstrated by the Giannini Scientific Corp. in 1963. The arcjets were configured to force arc attachment upstream of the throat in a subsonic chamber region. While thruster currents were steady, the voltage traces exhibited sawtooth waveforms at frequencies on the order of 20 kHz. Voltage variations per cycle were typically between 100 and 310 volts, indicating major changes in the position of the arc attachment with time. When operated at their respective design points, the performance of both thrusters fell below the values listed in the 1960's development reports. The reason for the discrepancies is not currently understood and further investigations are in progress. However, the recently measured efficiencies were high compared to those obtained with constricted-arc designs at similar conditions, and further arcjet performance optimizations may be possible.

A93-49797* # National Aeronautics and Space Administration. Lewis Research Center, Cleveland, OH.

THE NASA ELECTRIC PROPULSION PROGRAM

FRANCIS M. CURRAN (NASA, Lewis Research Center, Cleveland, OH), JOHN R. BROPHY (JPL, Pasadena, CA), and GARY L.

BENNETT (NASA, Office of Advanced Concepts and Technology, Washington) Jun. 1993 25 p. AIAA, SAE, ASME, and ASEE, Joint Propulsion Conference and Exhibit, 29th, Monterey, CA, June 28-30, 1993 refs

(AIAA PAPER 93-1935) Copyright

NASA has defined and undertaken an evolutionary technology program for high performance electric propulsion systems, which could greatly affect the logistics weight requirements for such large space structures as Space Station Freedom. Attention is presently given to the development status of hydrazine and high power arcjets, resistojets, the characterization of rocket flows and plumes, electrostatic and electromagnetic propulsion systems, and development programs aimed at the determination of opportune technology-insertion activities.

AIAA

A93-49814* # National Aeronautics and Space Administration. Lewis Research Center, Cleveland, OH.

PRESSURIZATION AND EXPULSION OF A FLIGHTWEIGHT LIQUID HYDROGEN TANK

N. T. VAN DRESAR and R. J. STOCHL (NASA, Lewis Research Center, Cleveland, OH) Jun. 1993 10 p. AIAA, SAE, ASME, and ASEE, Joint Propulsion Conference and Exhibit, 29th, Monterey, CA, June 28-30, 1993 refs (AIAA PAPER 93-1966) Copyright

Experimental results are presented for pressurization and expulsion of a flightweight 4.89 cu m liquid hydrogen storage tank under normal gravity conditions. Pressurization and expulsion times were parametrically varied to study the effects of longer transfer times expected in future space flight applications. It was found that the increase in pressurant consumption with increased operational time is significant at shorter pressurization or expulsion durations and diminishes as the duration lengthens. Gas-to-wall heat transfer in the ullage was the dominant mode of energy exchange, with more than 50 percent of the pressurant energy being lost to tank wall heating in expulsions and the long duration pressurizations. Advanced data analysis will require a multidimensional approach combined with improved measurement capabilities of liquid-vapor interfacial transport phenomena.

A93-49815* # National Aeronautics and Space Administration. Lewis Research Center, Cleveland, OH.

GROUND TESTING FOR THE NO-VENT FILL OF CRYOGENIC TANKS - RESULTS OF TESTS FOR A 71 CUBIC FOOT TANK

DAVID J. CHATO (NASA, Lewis Research Center, Cleveland, OH) Jun. 1993 16 p. AIAA, SAE, ASME, and ASEE, Joint Propulsion Conference and Exhibit, 29th, Monterey, CA, June 28-30, 1993 refs

(AIAA PAPER 93-1967) Copyright

NASA Lewis Research has been investigating the no-vent till method, since it is a promising approach to transfer liquid while handling the problems of low-g venting. This paper reports the results of a test series for filling a 71 cu ft tank with liquid hydrogen without venting. Twenty two tests were conducted, ten with a bottom orifice as the inlet and 12 with a spray bar. Parameters investigated included inlet saturation pressures of approximately 5, 15, and 25 psia; transfer pressures of 20, 30, and 45 psia; and various starting wall temperatures. Of the tests, only the one run at the highest wall temperature (238 R) failed to fill the tank. Test results are compared to a thermodynamic equilibrium model. Overall model-data agreement was good except for the tendency of the model to overshoot during the initial wall cool-down of the higher starting wall temperature fills.

Author (revised)

A93-49845* # National Aeronautics and Space Administration. Lewis Research Center, Cleveland, OH.

THE QED ENGINE SPECTRUM - FUSION-ELECTRIC PROPULSION FOR AIR-BREATHING TO INTERSTELLAR FLIGHT

ROBERT W. BUSSARD and LORIN W. JAMESON (Energy/Matter Conversion Corp., Manassas, VA) Jun. 1993 11 p. AIAA, SAE, ASME, and ASEE, Joint Propulsion Conference and Exhibit, 29th, Monterey, CA, June 28-30, 1993 Research supported by

20 SPACECRAFT PROPULSION AND POWER

SDIO and Energy/Matter Conversion Corp. refs
(Contract NAS3-26711)
(AIAA PAPER 93-2006) Copyright

A new inertial-electrostatic-fusion direct electric power source can be used to drive a relativistic e-beam to heat propellant. The resulting system is shown to yield specific impulse and thrust/mass ratio 2-3 orders of magnitude larger than from other advanced propulsion concepts. This QED system can be applied to aerospace vehicles from air-breathing to near-interstellar flight. Examples are given for Earth/Mars flight missions, that show transit times of 40 d with 20 percent payload in single-stage vehicles.

Author (revised)

A93-49861* National Aeronautics and Space Administration. Lewis Research Center, Cleveland, OH.

PROSPECTS FOR UTILIZATION OF AIR LIQUEFACTION AND ENRICHMENT SYSTEM (ALES) PROPULSION IN FULLY REUSABLE LAUNCH VEHICLES

W. H. BOND and A. C. YI (Rockwell International Corp., Space Systems Div., Downey, CA) Jun. 1993 15 p. AIAA, SAE, ASME, and ASEE, Joint Propulsion Conference and Exhibit, 29th, Monterey, CA, June 28-30, 1993 Research sponsored by NASA and USAF refs
(AIAA PAPER 93-2025) Copyright

A concept is shown for a fully reusable, earth to orbit launch vehicle with horizontal takeoff and landing, employing an air-turbo-rocket for low speed and a rocket for high speed acceleration, both using LH2 fuel. The turbo-rocket employs a modified liquid air cycle to supply the oxidizer. The rocket uses 90 percent pure LOX that is collected from the atmosphere, separated, and stored during operation of the turbo-rocket from about Mach 2 to Mach 5 or 6. The takeoff weight and the thrust required at takeoff are markedly reduced by collecting the rocket oxidizer in-flight. The paper shows an approach and the corresponding technology needs for using ALES propulsion in a SSTO vehicle. Reducing the trajectory altitude at the end of collection reduces the wing area and increases payload. The use of state-of-the-art materials, such as graphite polyimide, is critical to meet the structure weight objective for SSTO. Configurations that utilize 'waverider' aerodynamics show great promise to reduce the vehicle weight.

Author (revised)

A93-49907* National Aeronautics and Space Administration. Lewis Research Center, Cleveland, OH.

DAMAGE-MITIGATING CONTROL OF SPACE PROPULSION SYSTEMS FOR HIGH PERFORMANCE AND EXTENDED LIFE

ASOK RAY, MIN-KUANG WU, XIAOWEN DAI, MARC CARPINO (Pennsylvania State Univ., University Park), and CARL F. LORENZO (NASA, Lewis Research Center, Cleveland, OH) Jun. 1993 21 p. AIAA, SAE, ASME, and ASEE, Joint Propulsion Conference and Exhibit, 29th, Monterey, CA, June 28-30, 1993 refs
(Contract NAG3-1240; NSF ECS-92-16386)
(AIAA PAPER 93-2080) Copyright

Calculations are presented showing that a substantial improvement in service life of a reusable rocket engine can be achieved by an insignificant reduction in the system dynamic performance. The paper introduces the concept of damage mitigation and formulates a continuous-time model of fatigue damage dynamics. For control of complex mechanical systems, damage prediction and damage mitigation are carried out based on the available sensory and operational information such that the plant can be inexpensively maintained and safely and efficiently steered under diverse operating conditions. The results of simulation experiments are presented for transient operations of a reusable rocket engine.

AIAA

A93-49928* National Aeronautics and Space Administration. Lewis Research Center, Cleveland, OH.

PRELIMINARY INVESTIGATION OF HIGH POWER MICROWAVE PLASMAS FOR ELECTROTHERMAL THRUSTER USE

JOHN L. POWER and DANIEL J. SULLIVAN (NASA, Lewis Research Center, Cleveland, OH) Jun. 1993 18 p. AIAA,

SAE, ASME, and ASEE, Joint Propulsion Conference and Exhibit, 29th, Monterey, CA, June 28-30, 1993 Previously announced in STAR as N93-29158 refs
(AIAA PAPER 93-2106) Copyright

Results are reported from preliminary tests to evaluate the high power microwave electrothermal thruster concept, which employs a free-floating plasma discharge maintained by applied CW microwave power to heat a propellant gas flow. Stable plasmas have been created and maintained in He, N2, and H2 as propellants in both the TM(sub 011) and TM(sub 012) modes at discharge pressures from 10 Pa to 69 kPa. Vortical inflow of the propellant gas was observed to cause the formation of on-axis 'spike' plasmas. Operation in the spike plasma condition yields maximum power absorption with minimum wall heating and maximum propellant-heating efficiency; plasmas of the three propellant gases were investigated in the spike condition in an open channel to a maximum applied power level of 11.2 kW (in N2). Microwave power coupling efficiencies of over 90 percent were routinely obtained at absorbed power levels up to 2 kW. Magnetic nozzle effects were investigated with a superconducting solenoid Al magnet applying a high magnetic field to the plasmas in, and exiting from, the discharge tube.

Author (revised)

A93-49949* National Aeronautics and Space Administration. Lewis Research Center, Cleveland, OH.

DURABILITY TESTING OF THE AJ10-221 490 N HIGH PERFORMANCE (321 SEC ISP) ENGINE

D. M. JASSOWSKI, S. D. ROSENBERG, and L. SCHOENMAN (Aerojet, Propulsion Div., Sacramento, CA) Jun. 1993 11 p. AIAA, SAE, ASME, and ASEE, Joint Propulsion Conference and Exhibit, 29th, Monterey, CA, June 28-30, 1993 Research supported by NASA refs
(AIAA PAPER 93-2130) Copyright

The durability of the 490 N AJ10-221 engine is characterized on the basis of data from 93 tests and a total firing life of 6.3 hr. For the three Ir/Re chambers tested, no limiting conditions were encountered in the 43,379 sec and 229 test thermal cycles. A wide range of off nominal operating conditions was successfully demonstrated.

AIAA

A93-49951* National Aeronautics and Space Administration. Lewis Research Center, Cleveland, OH.

DESIGN AND FABRICATION OF A HYDROGEN/OXYGEN THRUST CHAMBER ASSEMBLY

THOMAS R. HERNACKI (Pratt & Whitney Group, West Palm Beach, FL) and TIMOTHY D. SMITH (NASA, Lewis Research Center, Cleveland, OH) Jun. 1993 9 p. AIAA, SAE, ASME, and ASEE, Joint Propulsion Conference and Exhibit, 29th, Monterey, CA, June 28-30, 1993 Research supported by Pratt & Whitney Group refs
(AIAA PAPER 93-2132) Copyright

The combustion system for the Advance Expander Test Bed engine consists of a thrust mount, an injector with a H2-O2 torch igniter, a combustion chamber, and a conical nozzle extension. These components constitute the thrust chamber assembly. The design, fabrication, and testing of these components are described in detail.

AIAA

A93-49954* National Aeronautics and Space Administration. Lewis Research Center, Cleveland, OH.

DESIGN AND TEST OF A SMALL TWO STAGE COUNTER-ROTATING TURBINE FOR ROCKET ENGINE APPLICATION

F. W. HUBER, B. R. BRANSTROM, A. K. FINKE, P. D. JOHNSON, R. J. ROWEY (Pratt & Whitney Group, Government Engines and Space Propulsion Div., West Palm Beach, FL), and J. P. VERES (NASA, Lewis Research Center, Cleveland, OH) Jun. 1993 13 p. AIAA, SAE, ASME, and ASEE, Joint Propulsion Conference and Exhibit, 29th, Monterey, CA, June 28-30, 1993 refs
(AIAA PAPER 93-2136) Copyright

The aerodynamic design and rig test evaluation of a small counter-rotating turbine system is described. The technology represented by this turbine is being developed for application in

an advanced upper stage rocket engine turbopump. This engine will employ an oxygen/hydrogen expander cycle and achieve high performance through efficient combustion, high combustion pressure, and high area ratio exhaust nozzle expansion. Engine performance goals require that the turbopump drive turbines achieve high efficiency at low gas flow rates. The low flow rates result in very small airfoil diameter, height and chord. The high efficiency and small size requirements present a challenging turbine design problem. The unconventional approach employed to meet this challenge is described, along with the detailed design process and resulting airfoil configurations. The method and results of full scale aerodynamic performance evaluation testing of both one and two stage configurations, as well as operation without the secondary stage stator are presented. The overall results of this effort illustrate that advanced aerodynamic design tools and hardware fabrication techniques have provided improved capability to produce small high performance turbines for advanced rocket engines.

A93-49978* National Aeronautics and Space Administration. Lewis Research Center, Cleveland, OH.

RELIABILITY ASSESSMENT OF THRUST CHAMBER COOLING CONCEPTS USING PROBABILISTIC ANALYSIS TECHNIQUES

DOUGLAS C. RAPP (Sverdrup Technology, Inc., Brook Park, OH) Jun. 1993 19 p. AIAA, SAE, ASME, and ASEE, Joint Propulsion Conference and Exhibit, 29th, Monterey, CA, June 28-30, 1993 Previously announced in STAR as N93-29068 refs (Contract NAS3-25266)

(AIAA PAPER 93-2163) Copyright

The reliability of OFHC (Oxygen Free High Conductivity) copper and NARloy-Z thrust chambers is assessed by applying probabilistic structural analysis techniques to incorporate design parameter variability and uncertainty. Thrust chambers specifically evaluated are the cylindrical test fixtures employed in a plug-nozzle configuration at the NASA Lewis Research Center. Direct sampling Monte Carlo simulations based on a simplified life prediction methodology established probability densities of firing cycles to structural failure. Simulated cyclic lives demonstrated modest agreement to experiment. Similarly, regions of high structural failure probability were determined using a limit state approach employing calculated cumulative distribution functions for effective stress response and an assumed material strength distribution. A probability of failure of 0.012 was calculated at the center of the coolant channel hot-gas-side wall for an OFHC milled channel. Structural response was found to be sensitive to the uncertainties in the thrust chamber thermal environment and the material's thermal expansion coefficient.

A93-50023* National Aeronautics and Space Administration. Lewis Research Center, Cleveland, OH.

CHARACTERIZATION OF IN-FLIGHT PERFORMANCE OF ION PROPULSION SYSTEMS

JAMES S. SOVEY and VINCENT K. RAWLIN (NASA, Lewis Research Center, Cleveland, OH) Jun. 1993 15 p. AIAA, SAE, ASME, and ASEE, Joint Propulsion Conference and Exhibit, 29th, Monterey, CA, June 28-30, 1993 refs (AIAA PAPER 93-2217) Copyright

In-flight measurements of ion propulsion performance, ground test calibrations, and diagnostic performance measurements were reviewed. It was found that accelerometers provided the most accurate in-flight thrust measurements compared with four other methods that were surveyed. An experiment has also demonstrated that pre-flight alignment of the thrust vector was sufficiently accurate so that gimbal adjustments and use of attitude control thrusters were not required to counter disturbance torques caused by thrust vector misalignment. The effects of facility background pressure, facility enhanced charge-exchange reactions, and contamination on ground-based performance measurements are also discussed. Vacuum facility pressures for inert-gas ion thruster life tests and flight qualification tests will have to be less than 2 mPa to ensure accurate performance measurements.

A93-50031* National Aeronautics and Space Administration. Lewis Research Center, Cleveland, OH.

DERATED ION THRUSTER DEVELOPMENT STATUS

MICHAEL J. PATTERSON, THOMAS W. HAAG (NASA, Lewis Research Center, Cleveland, OH), and GEORGE J. WILLIAMS, JR. (Princeton Univ., NJ) Jun. 1993 15 p. AIAA, SAE, ASME, and ASEE, Joint Propulsion Conference and Exhibit, 29th, Monterey, CA, June 28-30, 1993 refs (AIAA PAPER 93-2225) Copyright

A 30 cm diameter xenon ion thruster is under development at NASA to provide an ion propulsion option for auxiliary and primary propulsion on missions of national interest. Specific efforts include thruster design optimizations, component life testing and validation, vibration testing, and performance characterizations. Under this program, the ion thruster will be brought to engineering model development status. This paper discusses the activities and preliminary test results to develop a 30 cm engineering model thruster.

A93-50056* National Aeronautics and Space Administration. Lewis Research Center, Cleveland, OH.

ADVANCES IN NASA'S NUCLEAR THERMAL PROPULSION TECHNOLOGY PROJECT

KEITH M. PEECOCK and JAMES R. STONE (NASA, Lewis Research Center, Cleveland, OH) Jun. 1993 9 p. AIAA, SAE, ASME, and ASEE, Joint Propulsion Conference and Exhibit, 29th, Monterey, CA, June 28-30, 1993 refs (AIAA PAPER 93-2258) Copyright

The status of the Nuclear Thermal Propulsion (NTP) project for space exploration and the future plans for NTP technology are discussed. Current activities in the framework of the NTP project deal with nonnuclear material tests; instrumentation, controls, and health management; turbopumps; nozzles and nozzle extension; and an exhaust plume.

AIAA

A93-50126* National Aeronautics and Space Administration. Lewis Research Center, Cleveland, OH.

CRYOGENIC PROPELLANT THERMAL CONTROL SYSTEM DESIGN CONSIDERATIONS, ANALYSES, AND CONCEPTS APPLIED TO A MARS HUMAN EXPLORATION MISSION

DAVID W. PLACHTA (NASA, Lewis Research Center, Cleveland, OH), STEPHEN TUCKER (NASA, Marshall Space Flight Center, Huntsville, AL), and DAVID J. HOFFMAN (NASA, Lewis Research Center, Cleveland, OH) Jun. 1993 17 p. AIAA, SAE, ASME, and ASEE, Joint Propulsion Conference and Exhibit, 29th, Monterey, CA, June 28-30, 1993 refs (AIAA PAPER 93-2353) Copyright

This paper analyzes, defines, and sizes cryogenic storage thermal control systems that meet the requirements of future NASA Mars human exploration missions. The design issues of this system include the projection of the existing Multilayer Insulation data base for cryogenic storage to much thicker (10 cm or more) insulation systems, the unknown heat leak from mechanical interfaces, and the thermal and structural performance effects of the large tank sizes required for a Mars mission. Acknowledging these unknown effects, heat loss projections are made based on extrapolation of the existing data base. The results indicate that hydrogen, methane, and oxygen are feasible propellants, and that the best suited thermal control systems are 'thick' MLI, thermodynamic vent systems, cryocoolers, and vacuum jackets.

AIAA

A93-50129* National Aeronautics and Space Administration. Lewis Research Center, Cleveland, OH.

AN RL10A-3-3A ROCKET ENGINE MODEL USING THE ROCKET ENGINE TRANSIENT SIMULATOR (ROCETS) SOFTWARE

MICHAEL BINDER (Sverdrup Technology, Inc., Brook Park, OH) Jun. 1993 12 p. AIAA, SAE, ASME, and ASEE, Joint Propulsion Conference and Exhibit, 29th, Monterey, CA, June 28-30, 1993 refs

(Contract NAS3-25266)

(AIAA PAPER 93-2357) Copyright

20 SPACECRAFT PROPULSION AND POWER

The RL10 engine is a critical component of past, present, and future space missions. The paper discusses the RL10A-3-3A engine system and its model created using the ROCETS computer code. The simulation model will give NASA an in-house capability to simulate the performance of the engine under various operating conditions and mission profiles. A comparison of steady-state model predictions with test-stand data is presented together with a comparison of predicted start transient behavior with flight data.

AIAA

A93-50138* National Aeronautics and Space Administration. Lewis Research Center, Cleveland, OH.

US/CIS INTEGRATED NTRE

M. J. BULMAN, D. W. CULVER, M. C. MCILWAIN (Aerojet, Propulsion Div., Sacramento, CA), RICHARD ROCHOW (Babcock & Wilcox Space and Nuclear Systems, Lynchburg, VA), E. K. D'YAKOV, and V. P. SMETANNIKOV Jun. 1993 6 p. AIAA, SAE, ASME, and ASEE, Joint Propulsion Conference and Exhibit, 29th, Monterey, CA, June 28-30, 1993 Research supported by NASA

(AIAA PAPER 93-2367) Copyright

The paper describes the Nuclear Thermal Energy (NTRE) engine, developed by taking advantage of mature fuel technology developed in the former Soviet Union, thus shortening the development schedule of this engine for moon and Mars explorations. The near-term NTRE engine has a number of features that provide safety, mission performance, cost, and risk benefits. These include: (1) high-temperature long-life CIS fuel, (2) high-pressure recuperated expander cycle, (3) assured restart, (4) long-life cooled nozzle with thin inner wall, (5) long-life turbopumps, (6) heat radiation and electrical power generation, and (7) component integration synergy. Diagrams of the reactor core, the recuperated bottoming cycle flow schematic, and the recuperated bottoming cycle engine schematic are presented.

AIAA

A93-50156* National Aeronautics and Space Administration. Lewis Research Center, Cleveland, OH.

LOW POWER PULSED MPD THRUSTER SYSTEM ANALYSIS AND APPLICATIONS

ROGER M. MYERS (Sverdrup Technology, Inc.; NASA, Lewis Research Center, Cleveland, OH), MATTHEW DOMONKOS (New Mexico Univ., Albuquerque), and JAMES H. GILLAND (Sverdrup Technology, Inc.; NASA, Lewis Research Center, Cleveland, OH) Jun. 1993 27 p. AIAA, SAE, ASME, and ASEE, Joint Propulsion Conference and Exhibit, 29th, Monterey, CA, June 28-30, 1993 refs

(AIAA PAPER 93-2391)

Pulsed MPD thruster systems were analyzed for application to solar-electric orbit transfer vehicles at power levels ranging from 10 to 40 kW. Potential system level benefits of pulsed propulsion technology include ease of power scaling without thruster performance changes, improved transportability from low power flight experiments to operational systems, and reduced ground qualification costs. Required pulsed propulsion system components include a pulsed applied-field MPD thruster, a pulse-forming network, a charge control unit, a cathode heater supply, and high speed valves. Mass estimates were obtained for each propulsion subsystem and spacecraft component. Results indicate that for payloads of 1000 and 2000 kg, pulsed MPD thrusters can reduce launch mass by between 1000 and 2500 kg relative to hydrogen arcjets, reducing launch vehicle class and launch cost. While the achievable mass savings depends on the trip time allowed for the mission, cases are shown in which the launch vehicle required for a mission is decreased from an Atlas IIAS to an Atlas I or Delta 7920.

Author (revised)

A93-50157* National Aeronautics and Space Administration. Lewis Research Center, Cleveland, OH.

LOW POWER ARCJET SYSTEM SPACECRAFT IMPACTS

ERIC J. PENCIL, CHARLES J. SARMIENTO (NASA, Lewis Research Center, Cleveland, OH), D. A. LICHTIN, J. W. PALCHEFSKY, and A. L. BOGORAD (Martin Marietta Astro Space, Princeton, NJ) Jun. 1993 32 p. AIAA, SAE, ASME, and

ASEE, Joint Propulsion Conference and Exhibit, 29th, Monterey, CA, June 28-30, 1993 Research sponsored by Martin Marietta Astro Space and NASA refs
(AIAA PAPER 93-2392) Copyright

Potential plume contamination of spacecraft surfaces was investigated by positioning spacecraft material samples relative to an arcjet thruster. Samples in the simulated solar array region were exposed to the cold gas arcjet plume for 40 hrs to address concerns about contamination by backstreaming diffusion pump oil. Except for one sample, no significant changes were measured in absorbance and emittance within experimental error. Concerns about surface property degradation due to electrostatic discharges led to the investigation of the discharge phenomenon of charged samples during arcjet ignition. Short duration exposure of charged samples demonstrated that potential differences are consistently and completely eliminated within the first second of exposure to a weakly ionized plume. The spark discharge mechanism was not the discharge phenomenon. The results suggest that the arcjet could act as a charge control device on spacecraft.

AIAA

A93-50161* National Aeronautics and Space Administration. Lewis Research Center, Cleveland, OH.

A SOFT-START CIRCUIT FOR ARCJET IGNITION

JOHN A. HAMLEY and JOHN M. SANKOVIC (NASA, Lewis Research Center, Cleveland, OH) Jun. 1993 23 p. AIAA, SAE, ASME, and ASEE, Joint Propulsion Conference and Exhibit, 29th, Monterey, CA, June 28-30, 1993 refs
(AIAA PAPER 93-2396) Copyright

The reduced propellant flow rates associated with high performance arcjets have placed new emphasis on electrode erosion, especially at startup. A soft-start current profile was defined which limited current overshoot during the initial 30 to 50 ms of operation, and maintained significantly lower than the nominal arc current for the first eight seconds of operation. A 2.5 kW arcjet PPU was modified to provide this current profile, and a 500 cycle test using simulated fully decomposed hydrazine was conducted to determine the electrode erosion during startup. Electrode geometry and mass flow rates were selected based on requirements for a 600 sec specific impulse (mission average) arcjet system. The flow rate was varied throughout the test to simulate the blow down of a flight propellant system. Electrode damage was negligible at flow rates above 33 mg/s, and minor chamfering of the constrictor occurred at flow rates of 33 to 30 mg/s, corresponding to flow rates expected in the last 40 percent of the mission. The soft-start current profile significantly reduced electrode damage when compared to state-of-the-art starting techniques.

Author (revised)

A93-50162* National Aeronautics and Space Administration. Lewis Research Center, Cleveland, OH.

SIMPLIFIED POWER PROCESSING FOR INERT GAS ION THRUSTERS

V. K. RAWLIN, L. R. PINERO, and J. A. HAMLEY (NASA, Lewis Research Center, Cleveland, OH) Jun. 1993 23 p. AIAA, SAE, ASME, and ASEE, Joint Propulsion Conference and Exhibit, 29th, Monterey, CA, June 28-30, 1993 refs
(AIAA PAPER 93-2397) Copyright

Significant simplifications to power processors for inert gas ion thrusters in the 1 to 5 kW range have been identified. They include elimination of all but three power supplies - one each for the neutralizer, main discharge, and beam. The neutralizer and discharge power supplies would provide both cathode heating and plasma generating functions. This dual-use power supply concept was validated via integration tests with a 30 cm diameter xenon ion thruster. The beam/accelerator power supply would have positive and negative outputs to allow a single power supply to provide both functions. The discharge and beam power supplies would incorporate full-bridge inverters similar to those proven for flight-ready arcjet propulsion systems. Operation of this simplified power processing scheme at an inverter frequency of 50 kHz results in a projected power processor design with low mass and high efficiency. A 2 kW reference point design has estimated values of specific mass of 5.4 kg/kW and an efficiency of 93 percent.

A93-50164*# National Aeronautics and Space Administration. Lewis Research Center, Cleveland, OH.

EOTV PROPELLANT TANK PRESSURE CONTROL AND LIQUID DYNAMICS

J. R. PIETRZYK, J. R. SCHUSTER (General Dynamics Corp., Space Systems Div., San Diego, CA), and E. W. KROEGER (NASA, Lewis Research Center, Cleveland, OH) Jun. 1993 13 p. AIAA, SAE, ASME, and ASEE, Joint Propulsion Conference and Exhibit, 29th, Monterey, CA, June 28-30, 1993 refs

(Contract NAS3-25972)

(AIAA PAPER 93-2399) Copyright

The solar-powered Electric Orbit Transfer Vehicle (EOTV) will transfer payloads from LEO to higher orbits, using hydrogen propellant and low-thrust arcjet propulsion to provide specific impulse in the range to 1,200 to 1,400 seconds. All the boiloff from the tank provides the vaporized propellant for the arcjet thrusters, with no boiloff being vented to space. The system consists of an insulated lightweight tank where the cryogenic hydrogen is stored subcritically at low pressure, a compressor to raise the pressure of the hydrogen vapor flow for the arcjets to the proper level, an accumulator, and mass flow controllers. The results of studies of the management of the tank pressure and liquid dynamics are presented.

AIAA

A93-50231*# National Aeronautics and Space Administration. Lewis Research Center, Cleveland, OH.

ANALYSIS OF PLUME BACKFLOW AROUND A NOZZLE LIP IN A NUCLEAR ROCKET

CHAN H. CHUNG, SUK C. KIM, ROBERT M. STUBBS (NASA, Lewis Research Center, Cleveland, OH), and KENNETH J. DE WITT (Toledo Univ., OH) Jun. 1993 10 p. AIAA, SAE, ASME, and ASEE, Joint Propulsion Conference and Exhibit, 29th, Monterey, CA, June 28-30, 1993 refs

(Contract NCC3-171; NAS3-25266)

(AIAA PAPER 93-2497)

The structure of the flow around a nuclear thermal rocket nozzle lip has been investigated using the direct simulation Monte Carlo method. Special attention has been paid to the behavior of a small amount of harmful particles that may be present in the rocket exhaust gas. The harmful fission product particles are modeled by four inert gases whose molecular weights are in a range of 4 to 131. Atomic hydrogen, which exists in the flow due to the extremely high nuclear fuel temperature in the reactor, is also included. It is shown that the plume backflow is primarily determined by the thin subsonic fluid layer adjacent to the surface of the nozzle lip, and that the inflow boundary in the plume region has negligible effect on the backflow. It is also shown that a relatively large amount of the lighter species is scattered into the backflow region while the amount of the heavier species becomes negligible in this region due to extreme separation between the species. Results indicate that the backscattered molecules are very energetic and are fast-moving along the surface in the backflow region near the nozzle lip.

A93-50232*# National Aeronautics and Space Administration. Lewis Research Center, Cleveland, OH.

NUMERICAL STUDY OF NOZZLE WALL COOLING FOR NUCLEAR THERMAL ROCKETS

SUK C. KIM (Sverdrup Technology, Inc., Lewis Research Center Group, Brook Park, OH) and ROBERT M. STUBBS (NASA, Lewis Research Center, Cleveland, OH) Jun. 1993 12 p. AIAA, SAE, ASME, and ASEE, Joint Propulsion Conference and Exhibit, 29th, Monterey, CA, June 28-30, 1993 refs

(Contract NAS3-25266)

(AIAA PAPER 93-2498)

The flowfields and performance of nuclear thermal rockets, which utilize radiation and film-cooling to cool the nozzle extension, are studied by solving the Navier-Stokes equations and species equations. The thrust level of the rocket for the present study is about 75,000 lb(f) for a chamber pressure of 68 atm(1,000 psi) and a chamber temperature of 2700 K. The throat radius of the nozzle is 0.0936 m and the area ratios of the nozzles are 300 and 500. It is assumed that the flow is chemically frozen and the

turbulence is simulated by the modified Baldwin-Lomax turbulence model. The calculated results for various area ratios and film mass-flow rates are presented as Mach number contours, variations of nozzle wall temperature, exit profiles, and vacuum specific impulses. The present study shows that by selecting the flow rate of the film-cooling hydrogen and area ratio of the nozzle correctly, high area ratio nozzle extensions can be cooled effectively with radiation and film-cooling without significant penalty in performance.

Author (revised)

A93-50256*# National Aeronautics and Space Administration. Lewis Research Center, Cleveland, OH.

ASSESSMENT OF THREE NUMERICAL METHODS FOR THE COMPUTATION OF A LOW-DENSITY PLUME FLOW

PAUL F. PENKO (NASA, Lewis Research Center, Cleveland, OH), BEN R. RILEY (Evansville Univ., IN), and IAIN D. BOYD (Cornell Univ., Ithaca, NY) Jun. 1993 16 p. AIAA, SAE, ASME, and ASEE, Joint Propulsion Conference and Exhibit, 29th, Monterey, CA, June 28-30, 1993 refs

(Contract NAG3-1451; NAG3-746)

(AIAA PAPER 93-2528) Copyright

Results from three numerical methods including one based on the Navier-Stokes equations, one based on kinetic theory using the DSMC method, and one based on the Boltzmann equation with a Krook-type collision term are compared to each other and to experimental data for a model problem of heated nitrogen flow in a conical nozzle expanding into a vacuum. The problem simulates flow in a resistojet, a low-thrust, electrothermal rocket. The continuum method is applied to both the internal flow and near-field plume. The DSMC and Boltzmann methods are applied primarily to the plume. Experimental measurements of Pitot pressure and flow angle, taken with an apparatus that duplicates the model nozzle flow, are used in the comparisons.

A93-50257*# National Aeronautics and Space Administration. Lewis Research Center, Cleveland, OH.

MONTE CARLO AND EXPERIMENTAL STUDIES OF NOZZLE FLOW IN A LOW-POWER HYDROGEN ARCJET

IAIN D. BOYD (Cornell Univ., Ithaca, NY), MARK A. CAPPELLI, and DOUG R. BEATTIE (Stanford Univ., CA) Jun. 1993 14 p. AIAA, SAE, ASME, and ASEE, Joint Propulsion Conference and Exhibit, 29th, Monterey, CA, June 28-30, 1993 Research supported by Norton Co. refs

(Contract NAG3-1451; NAG3-1040)

(AIAA PAPER 93-2529) Copyright

The flow in the nozzle of a small hydrogen arcjet intended for low-thrust propulsion is studied without arc ignition using numerical and experimental techniques. The flow conditions in the thruster indicate that low-density nonequilibrium effects will significantly influence the flow. Therefore, the numerical analysis is undertaken using a Monte Carlo approach. The experimental studies employ laser Raman scattering. Comparisons of the measured and computed results are made for total number density, rotational temperature, and for the number density of the first rotational level. The numerical results are found to be quite sensitive to the rotational relaxation rate, and a strong degree of thermal nonequilibrium is observed at the exit plane of the nozzle. Successful comparisons between experiment and analysis permit estimation of the rotational relaxation rate for hydrogen.

A93-50258*# National Aeronautics and Space Administration. Lewis Research Center, Cleveland, OH.

PLUME CHARACTERISTICS OF AN ARCJET THRUSTER

JOHN G. LIEBESKIND, RONALD K. HANSON, and MARK A. CAPPELLI (Stanford Univ., CA) Jun. 1993 11 p. AIAA, SAE, ASME, and ASEE, Joint Propulsion Conference and Exhibit, 29th, Monterey, CA, June 28-30, 1993 Research supported by NASA and SDIO refs

(AIAA PAPER 93-2530) Copyright

An experimental investigation is conducted of the plume of a 1.5 kW hydrogen-fueled arcjet thruster. The velocity and translational temperature are measured by laser induced fluorescence of excited-state atomic hydrogen at a variety of

20 SPACECRAFT PROPULSION AND POWER

locations and operating conditions. The peak velocity and temperature at the center of the exit plane of 14.7 km/s and 5000 K lead to a Mach number of 1.9. Evidence is presented which demonstrates the extent to which viscous forces dominate the flow, such as the exit plane Reynolds number of 18. Data taken in the plume suggest a transition from supersonic to subsonic flow via viscous dissipation. In addition, the results suggest that high tank pressures (0.4 to 1.5 Torr) limit the ability to simulate space environments for different portions of the plume.

A93-50322# National Aeronautics and Space Administration. Lewis Research Center, Cleveland, OH.

BMDO ELECTRIC SPACE-PROPULSION PROGRAM

LEONARD H. CAVENY (Ballistic Missile Defense Organization, Washington), FRANCIS M. CURRAN (NASA, Lewis Research Center, Cleveland, OH), and JOHN R. BROPHY (JPL, Pasadena, CA) Jun. 1993 13 p. AIAA, SAE, ASME, and ASEE, Joint Propulsion Conference and Exhibit, 29th, Monterey, CA, June 28-30, 1993 refs

(AIAA PAPER 93-1934) Copyright

Electric propulsion (EP) applications being considered include: orbit insertion, orbit repositioning, station keeping, and elusive maneuvering. Typically, 1 to 5 kW are available for EP. A class of thrusters, the Hall-effect thrusters, is extensively researched, developed and flown by Russia. These thrusters, using xenon propellant, perform reliably, e.g., at 1.35 kW, 600 s specific impulse, 50 percent efficiency and greater than 2000 hr life. This specific impulse and efficiency combination is superior to the present arcjets for several Ballistic Missile Defense Organization (BMDO) applications. Three versions of the Hall thrusters are part of the experimental evaluation. Since today's goals are within reach of available thrusters and power sources, emphasis is being placed on such topics as: thruster lifetime, spacecraft interactions, electromagnetic interference, and erosion product deposition. Facilities in U.S. laboratories are being specially configured to achieve these goals. Author (revised)

A93-50822 National Aeronautics and Space Administration. Lewis Research Center, Cleveland, OH.

VALIDATION TEST OF 125 AH ADVANCED DESIGN IPV NICKEL-HYDROGEN FLIGHT CELLS

JOHN J. SMITHRICK (NASA, Lewis Research Center, Cleveland, OH) and STEPHEN W. HALL (U.S. Navy, Naval Weapons Support Center, Crane, IN) IEEE Aerospace and Electronic Systems Magazine (ISSN 0885-8985) vol. 8, no. 5 May 1993 p. 11-15. Previously announced in STAR as N93-14079 refs

(Contract RTOP 506-41-21)

Copyright

An update of validation test results confirming the advanced design nickel-hydrogen cell is presented. An advanced 125 Ah individual pressure vessel Ni-H cell was designed. The primary function of the advanced cell is to store and deliver energy for long-term LEO spacecraft missions. The new features of this design are: (1) use of 26 percent rather than 31 percent KOH electrolyte; (2) use of a patented catalyzed wall wick; (3) use of serrated-edge separators to facilitate gaseous O and H flow within the cell, while maintaining physical contact with the wall wick for electrolyte management; and (4) use of a floating rather than a fixed stack to accommodate Ni electrode expansion due to charge/discharge cycling. The significant improvements resulting from these innovations are extended cycle life; enhanced thermal, electrolyte, and oxygen management; and accommodation of Ni electrode expansion. Six 125 Ah flight cells based on this design were fabricated; the catalyzed wall wick cells have been cycled for over 19,000 cycles with no cell failures in the continuing test. Two of the noncatalyzed wall wick cells failed (cycles 9588 and 13,900). Author (revised)

A93-53587# National Aeronautics and Space Administration. Lewis Research Center, Cleveland, OH.

NASA'S PROGRESS IN NUCLEAR ELECTRIC PROPULSION TECHNOLOGY

JAMES R. STONE, MICHAEL P. DOHERTY, and KEITH M.

PEECOOK (NASA, Lewis Research Center, Cleveland, OH) Jun. 1993 17 p. AIAA, SAE, ASME, and ASEE, Joint Propulsion Conference and Exhibit, 29th, Monterey, CA, June 28-30, 1993 Previously announced in STAR as N93-31858 refs

(AIAA PAPER 93-1936) Copyright

The National Aeronautics and Space Administration (NASA) has established a requirement for Nuclear Electric Propulsion (NEP) technology for robotic planetary science mission applications with potential future evolution to systems for piloted Mars vehicles. To advance the readiness of NEP for these challenging missions, a near-term flight demonstration on a meaningful robotic science mission is very desirable. The requirements for both near-term and outer planet science missions are briefly reviewed, and the near-term baseline system established under a recent study jointly conducted by the Lewis Research Center (LeRC) and the Jet Propulsion Laboratory (JPL) is described. Technology issues are identified where work is needed to establish the technology for the baseline system, and technology opportunities which could provide improvement beyond baseline capabilities are discussed. Finally, the plan to develop this promising technology is presented and discussed.

A93-56168* National Aeronautics and Space Administration. Lewis Research Center, Cleveland, OH.

ELECTRIC PROPULSION - AN EVOLUTIONARY TECHNOLOGY

FRANCIS M. CURRAN, JAMES S. SOVEY (NASA, Lewis Research Center, Cleveland, OH), and ROGER M. MYERS (Sverdrup Technology, Inc., Brook Park, OH) Acta Astronautica (ISSN 0094-5765) vol. 29, no. 9 Sept. 1993 p. 651-665. IAF, International Astronautical Congress, 42nd, Montreal, Canada, Oct. 5-11, 1991, IAF Paper 91-241. Previously cited in issue 02, p. 171, Accession no. A92-13158 refs

Copyright

N93-10016* National Aeronautics and Space Administration. Lewis Research Center, Cleveland, OH.

COMBUSTION-WAVE IGNITION FOR ROCKET ENGINES

LARRY C. LIOU In JHU, The 1992 JANNAF Propulsion Meeting, Volume 1 p 295-311 Feb. 1992 Previously announced as N92-20043

Avail: CPIA, 10630 Little Patuxent Pkwy., Suite 202, Columbia, MD, 21044-3200 HC

The combustion wave ignition concept was experimentally studied in order to verify its suitability for application in baffled sections of a large booster engine combustion chamber. Gaseous oxygen/gaseous methane (GOX/GH4) and gaseous oxygen/gaseous hydrogen (GOX/GH2) propellant combinations were evaluated in a subscale combustion wave ignition system. The system included four element tubes capable of carrying ignition energy simultaneously to four locations, simulating four baffled sections. Also, direct ignition of a simulated Main Combustion Chamber (MCC) was performed. Tests were conducted over a range of mixture ratios and tube geometries. Ignition was consistently attained over a wide range of mixture ratios. At every ignition, the flame propagated through all four element tubes. For GOX/GH4, the ignition system ignited the MCC flow at mixture ratios from 2 to 10 and for GOX/GH2 the ratios is from 2 to 13. The ignition timing was found to be rapid and uniform. The total ignition delay when using the MCC was under 11 ms, with the tube-to-tube, as well as the run-to-run, variation under 1 ms. Tube geometries were found to have negligible effect on the ignition outcome and timing. Author

N93-10019* National Aeronautics and Space Administration. Lewis Research Center, Cleveland, OH.

THERMAL STRATIFICATION POTENTIAL IN ROCKET ENGINE COOLANT CHANNELS

KENNETH J. KACYNSKI In JHU, The 1992 JANNAF Propulsion Meeting, Volume 1 p 329-338 Feb. 1992 Previously announced as N92-25616

Avail: CPIA, 10630 Little Patuxent Pkwy., Suite 202, Columbia, MD, 21044-3200 HC

The potential for rocket engine coolant channel flow stratification was computationally studied. A conjugate, 3-D, conduction/advection analysis code (SINDA/FLUINT) was used. Core fluid temperatures were predicted to vary by over 360 K across the coolant channel, at the throat section, indicating that the conventional assumption of a fully mixed fluid may be extremely inaccurate. Because of the thermal stratification of the fluid, the walls exposed to the rocket engine exhaust gases will be hotter than an assumption of full mixing would imply. In this analysis, wall temperatures were 160 K hotter in the turbulent mixing case than in the full mixing case. The discrepancy between the full mixing and turbulent mixing analyses increased with increasing heat transfer. Both analysis methods predicted identical channel resistances at the coolant inlet, but in the stratified analysis the thermal resistance was negligible. The implications are significant. Neglect of thermal stratification could lead to underpredictions in nozzle wall temperatures. Even worse, testing at subscale conditions may be inadequate for modeling conditions that would exist in a full scale engine.

Author

N93-10020* National Aeronautics and Space Administration. Lewis Research Center, Cleveland, OH.

HOT FIRE TEST RESULTS OF SUBSCALE TUBULAR COMBUSTION CHAMBERS

JOHN M. KAZAROFF, ROBERT S. JANKOVSKY, and ALBERT J. PAVLI (Sverdrup Technology, Inc., Brook Park, OH.) *In* JHU, The 1992 JANNAF Propulsion Meeting, Volume 1 p 339-352 Feb. 1992

Avail: CPIA, 10630 Little Patuxent Pkwy., Suite 202, Columbia, MD, 21044-3200 HC

Advanced subscale tubular combustion chambers have been built and test fired with Hydrogen-Oxygen propellants to assess the increase in fatigue life that can be obtained with this type of construction. Two chambers were tested; one ran for 637 cycles without failing compared to a predicted life of 200 cycles for a comparable smooth-wall milled-channel liner configuration. The other chamber failed at 256 cycles, compared to a predicted life of 118 cycles for a comparable smooth-wall milled-channel liner configuration. Post-test metallographic analysis determined that the strain relieving design (structural compliance) of the tubular configuration was the cause of this increase in life.

Author

N93-10033* National Aeronautics and Space Administration. Lewis Research Center, Cleveland, OH.

10 KW POWER ELECTRONICS FOR HYDROGEN ARCJETS

JOHN A. HAMLEY, LUIS R. PINERO, and GERALD M. HILL *In* JHU, The 1992 JANNAF Propulsion Meeting, Volume 1 p 539-553 Feb. 1992

Avail: CPIA, 10630 Little Patuxent Pkwy., Suite 202, Columbia, MD, 21044-3200 HC

A combination of emerging mission considerations such as launch on schedule, resource limitations, and the development of higher power spacecraft buses has resulted in renewed interest in high power hydrogen arcjet systems with specific impulses greater than 1000 s for Earth-space orbit transfer and maneuver applications. Solar electric propulsion systems with about 10 kW appear to offer payload benefits at acceptable trip times. The design and development of 10 kW hydrogen arcjet power electronics and the results of arcjet integration testing are discussed. The power electronics incorporated a full bridge switching topology similar to that employed in state of the art 5 kW power electronics, and the output filter included an output current averaging inductor with an integral pulse generation winding for arcjet ignition. Phase shifted, pulse width modulation with current mode control was used to regulate the current delivered to the arcjet; a low inductance power stage minimized switching transients. Hybrid power MOSFET's were used to minimize conduction losses. Switching losses were minimized using a fast response, optically isolated, totem-pole gate drive circuit. The input bus voltage for the unit was 150 V, with a maximum output voltage of 225 V. The switching frequency of 20 kHz was a compromise between mass savings and higher efficiency. Power conversion efficiencies in excess of 0.94 were demonstrated, along with steady state load current

regulation of 1 percent. The power electronics were successfully integrated with a 10 kW laboratory hydrogen arcjet, and reliable, non-destructive starts, and transitions to steady state operation were demonstrated. The estimated specific mass for a flight packaged unit was 2 kg/kW.

Author

N93-10038* National Aeronautics and Space Administration. Lewis Research Center, Cleveland, OH.

HOT FIRE FATIGUE TESTING RESULTS FOR THE COMPLIANT COMBUSTION CHAMBER

AL J. PAVLI (Sverdrup Technology, Inc., Brook Park, OH.), JOHN M. KAZAROFF, and ROBERT S. JANKOVSKY *In* JHU, The 1992 JANNAF Propulsion Meeting, Volume 1 p 605-614 Feb. 1992

Avail: CPIA, 10630 Little Patuxent Pkwy., Suite 202, Columbia, MD, 21044-3200 HC

A hydrogen-oxygen subscale rocket combustion chamber was designed incorporating an advanced design concept to reduce strain and increase life. The design permits unrestrained thermal expansion in a circumferential direction and, thereby, provides structural compliance during the thermal cycling of hot-fire testing. The chamber was built and test fired at a chamber pressure of 4137kn/sq m (600 psia) and a mixture ratio of 6.0. Compared to a conventional milled-channel configuration, the new structurally compliant chamber had a 134 or 287 percent increase in fatigue life depending on the life predicted for the conventional configuration.

Author

N93-10044* National Aeronautics and Space Administration. Lewis Research Center, Cleveland, OH.

EFFECTS OF ANODE MATERIAL ON ARCJET PERFORMANCE

JOHN M. SANKOVIC, F. M. CURRAN, and C. A. LARSON (Air Force Academy, CO.) *In* JHU, The 1992 JANNAF Propulsion Meeting, Volume 1 p 679-691 Feb. 1992

Avail: CPIA, 10630 Little Patuxent Pkwy., Suite 202, Columbia, MD, 21044-3200 HC

Anodes fabricated from four different materials were tested in a modular arcjet thruster at the 1 kW power level on nitrogen/hydrogen mixtures. A two-percent thoriated tungsten anode served as the control. Graphite was chosen for its ease in fabrication, but experienced severe erosion in the constrictor and diverging side. Hafnium carbide and lanthanum hexaboride were chosen for their low work functions but failed due to thermal stress and reacted with the propellant. When compared to the thoriated tungsten nozzle, thruster performance was significantly lower for the lanthanum hexaboride insert and the graphite nozzle, but was slightly higher for the hafnium carbide nozzle. Both the lanthanum hexaboride and hafnium carbide nozzle operated at higher voltages. An attempt was made to duplicate higher performance hafnium carbide results, but repeated attempts at machining a second anode insert were unsuccessful. Graphite, hafnium carbide, and lanthanum hexaboride do not appear viable anode materials for low power arcjet thrusters.

Author

N93-10197*# National Aeronautics and Space Administration. Lewis Research Center, Cleveland, OH.

EFFECTS OF ANODE MATERIAL ON ARCJET PERFORMANCE

JOHN M. SANKOVIC, FRANK M. CURRAN, and C. A. LARSON (Air Force Academy, CO.) 1992 15 p Presented at the 1992 JANNAF Propulsion Meeting, Indianapolis, IN, 24-28 Feb. 1992 (Contract RTOP 506-42-31)

(NASA-TM-105799; E-6873; NAS 1.15:105799) Avail: CASI HC A03/MF A01

Anodes fabricated from four different materials were tested in a modular arcjet thruster at 1 kW power level on nitrogen/hydrogen mixtures. A two-percent thoriated tungsten anode served as the control. Graphite was chosen for its ease in fabrication, but experienced severe erosion in the constrictor and diverging side. Hafnium carbide and lanthanum hexaboride were chosen for their low work functions but failed due to thermal stress and reacted with the propellant. When compared to the thoriated tungsten nozzle, thruster performance was significantly lower for the lanthanum hexaboride insert and the graphite nozzle, but was

20 SPACECRAFT PROPULSION AND POWER

slightly higher for the hafnium carbide nozzle. Both the lanthanum hexaboride and hafnium carbide nozzle operated at higher voltages. An attempt was made to duplicate higher performance hafnium carbide results, but repeated attempts at machining a second anode insert were unsuccessful. Graphite, hafnium carbide, and lanthanum hexaboride do not appear viable anode materials for low power arcjet thrusters. Author

N93-10457* # National Aeronautics and Space Administration. Lewis Research Center, Cleveland, OH.

SYSTEM MODEL DEVELOPMENT FOR NUCLEAR THERMAL PROPULSION

JAMES T. WALTON, NELSON A. HANNAN (Argonne National Lab., IL.), KEN R. PERKINS (Brookhaven National Lab., Upton, NY.), JOHN H. BUKSA (Los Alamos National Lab., NM.), BRIAN A. WORLEY (Oak Ridge National Lab., TN.), and DEAN DOBRANICH (Sandia National Labs., Albuquerque, NM.) Aug. 1992 15 p Presented at the World Space Congress, Washington, DC, 2-5 Sep. 1992; sponsored by AIAA (Contract RTOP 593-71-00) (NASA-TM-105761; E-7178; NAS 1.15:105761) Avail: CASI HC A03/MF A01

A critical enabling technology in the evolutionary development of nuclear thermal propulsion (NTP) is the ability to predict the system performance under a variety of operating conditions. This is crucial for mission analysis and for control subsystem testing as well as for the modeling of various failure modes. Performance must be accurately predicted during steady-state and transient operation, including startup, shutdown, and post operation cooling. The development and application of verified and validated system models has the potential to reduce the design, testing, and cost and time required for the technology to reach flight-ready status. Since Oct. 1991, the U.S. Department of Energy (DOE), Department of Defense (DOD), and NASA have initiated critical technology development efforts for NTP systems to be used on Space Exploration Initiative (SEI) missions to the Moon and Mars. This paper presents the strategy and progress of an interagency NASA/DOE/DOD team for NTP system modeling. It is the intent of the interagency team to develop several levels of computer programs to simulate various NTP systems. The first level will provide rapid, parameterized calculations of overall system performance. Succeeding computer programs will provide analysis of each component in sufficient detail to guide the design teams and experimental efforts. The computer programs will allow simulation of the entire system to allow prediction of the integrated performance. An interagency team was formed for this task to use the best capabilities available and to assure appropriate peer review. Author

N93-10734* # National Aeronautics and Space Administration. Lewis Research Center, Cleveland, OH.

POWER SYSTEM MONITORING AND SOURCE CONTROL OF THE SPACE STATION FREEDOM DC POWER SYSTEM TESTBED

GREG L. KIMNACH and ANASTACIO N. BAEZ Aug. 1992 9 p Presented at the 27th Intersociety Energy Conversion Engineering Conference, San Diego, CA, 3-7 Aug. 1992; cosponsored by SAE, ACS, AIAA, ASME, IEEE, AIChE, and ANS (Contract RTOP 474-42-10) (NASA-TM-105841; E-7284; NAS 1.15:105841) Avail: CASI HC A02/MF A01

Unlike a terrestrial electric utility which can purchase power from a neighboring utility, the Space Station Freedom (SSF) has strictly limited energy resources; as a result, source control, system monitoring, system protection, and load management are essential to the safe and efficient operation of the SSF Electric Power System (EPS). These functions are being evaluated in the DC Power Management and Distribution (PMAD) Testbed which NASA LeRC has developed at the Power System Facility (PSF) located in Cleveland, Ohio. The testbed is an ideal platform to develop, integrate, and verify power system monitoring and control algorithms. State Estimation (SE) is a monitoring tool used extensively in terrestrial electric utilities to ensure safe power

system operation. It uses redundant system information to calculate the actual state of the EPS, to isolate faulty sensors, to determine source operating points, to verify faults detected by subsidiary controllers, and to identify high impedance faults. Source control and monitoring safeguard the power generation and storage subsystems and ensure that the power system operates within safe limits while satisfying user demands with minimal interruptions. System monitoring functions, in coordination with hardware implemented schemes, provide for a complete fault protection system. The objective of this paper is to overview the development and integration of the state estimator and the source control algorithms. Author

N93-10743* # National Aeronautics and Space Administration. Lewis Research Center, Cleveland, OH.

HOT FIRE FATIGUE TESTING RESULTS FOR THE COMPLIANT COMBUSTION CHAMBER

ALBERT J. PAVLI (Sverdrup Technology, Inc., Brook Park, OH.), JOHN M. KAZAROFF, and ROBERT S. JANKOVSKY Sep. 1992 12 p (Contract RTOP 593-12-21) (NASA-TP-3223; E-6850; NAS 1.60:3223) Avail: CASI HC A03/MF A01

A hydrogen-oxygen subscale rocket combustion chamber was designed incorporating an advanced design concept to reduce strain and increase life. The design permits unrestrained thermal expansion of a circumferential direction and, thereby, provides structural compliance during the thermal cycling of hot-fire testing. The chamber was built and test fired at a chamber pressure of 4137 kN/sq m (600 psia) and a hydrogen-oxygen mixture ratio of 6.0. Compared with a conventional milled-channel configuration, the new structurally compliant chamber had a 134 or 287 percent increase in fatigue life, depending on the life predicted for the conventional configuration. Author

N93-10965* # National Aeronautics and Space Administration. Lewis Research Center, Cleveland, OH.

LUNAR AND MARTIAN ENVIRONMENTAL INTERACTIONS WITH NUCLEAR POWER SYSTEM RADIATORS

MARLA E. PEREZ-DAVIS, JAMES R. GAIER, and CYNTHIA M. KATZAN (Sverdrup Technology, Inc., Brook Park, OH.) Aug. 1992 10 p Presented at the Nuclear Technologies Space Exploration, Jackson Hole, WY, 16-19 Aug. 1992; sponsored by ANS (Contract RTOP 506-41-41) (NASA-TM-105747; E-7045-1; NAS 1.15:105747) Avail: CASI HC A02/MF A01

Future NASA space missions include a permanent manned presence on the moon and an expedition to the planet Mars. Such steps will require careful consideration of environmental interactions in the selection and design of required power systems. Several environmental constituents may be hazardous to performance integrity. Potential threats common to both the moon and Mars are low ambient temperatures, wide daily temperature swings, solar flux, and large quantities of dust. The surface of Mars provides the additional challenges of dust storms, winds, and a carbon dioxide atmosphere. In this review, the anticipated environmental interactions with surface power system radiators are described, as well as the impacts of these interactions on radiator durability, which were identified at NASA Lewis Research Center. Author

N93-11402* # National Aeronautics and Space Administration. Lewis Research Center, Cleveland, OH.

PRELIMINARY CHARACTERIZATION OF A WATER VAPORIZER FOR RESISTOJET APPLICATIONS

W. EARL MORREN Sep. 1992 17 p Presented at the 28th Joint Propulsion Conference and Exhibit, Nashville, TN, 6-8 Jul. 1992; sponsored by AIAA, SAE, ASME, and ASEE Previously announced in IAA as A92-54041 (Contract RTOP 506-42-31) (NASA-TM-105877; E-7342; NAS 1.15:105877; AIAA PAPER 92-3533) Avail: CASI HC A03/MF A01

A series of tests was conducted to explore the characteristics of a water vaporizer intended for application to resistojet propulsion systems. The objectives of these tests were to (1) observe the effect of orientation with respect to gravity on vaporizer stability, (2) characterize vaporizer efficiency and outlet conditions over a range of flow rates, and (3) measure the thrust performance of a vaporizer/resistojet thruster assembly. A laboratory model of a forced-flow, once-through water vaporizer employing a porous heat exchange medium was built and characterized over a range of flow rates and power levels of interest for application to water resistojets. In a test during which the vaporizer was rotated about a horizontal axis normal to its own axis, the outlet temperature and mass flow rate through the vaporizer remained steady. Throttling to 30 percent of the maximum flow rate tested was demonstrated. The measured thermal efficiency of the vaporizer was near 0.9 for all tests. The water vaporizer was integrated with an engineering model multipropellant resistojet. Performance of the vaporizer/thruster assembly was measured over a narrow range of operating conditions. The maximum specific impulse measured was 234 s at a mass flow rate and specific power level (vaporizer and thruster combined) of $154 \times 10(\text{exp-6})\text{kg/s}$ and 6.8 MJ/kg, respectively. Author

N93-11614*# National Aeronautics and Space Administration. Lewis Research Center, Cleveland, OH.

HOT FIRE TEST RESULTS OF SUBSCALE TUBULAR COMBUSTION CHAMBERS

JOHN M. KAZAROFF, ROBERT S. JANKOVSKY, and ALBERT J. PAVLI (Sverdrup Technology, Inc., Brook Park, OH.) Nov. 1992 12 p Previously announced as N93-10020 (Contract RTOP 593-12-21) (NASA-TP-3222; E-6849; NAS 1.60:3222) Avail: CASI HC A03/MF A01

Advanced, subscale, tubular combustion chambers were built and test fired with hydrogen-oxygen propellants to assess the increase in fatigue life that can be obtained with this type of construction. Two chambers were tested: one ran for 637 cycles without failing, compared to a predicted life of 200 cycles for a comparable smooth-wall milled-channel liner configuration. The other chamber failed at 256 cycles, compared to a predicted life of 118 cycles for a comparable smooth-wall milled-channel liner configuration. Posttest metallographic analysis determined that the strain-relieving design (structural compliance) of the tubular configuration was the cause of this increase in life. Author

N93-12363*# National Aeronautics and Space Administration. Lewis Research Center, Cleveland, OH.

NUCLEAR THERMAL PROPULSION TRANSPORTATION SYSTEMS FOR LUNAR/MARS EXPLORATION

JOHN S. CLARK, STANLEY K. BOROWSKI, MELVIN C. MCILWAIN (GenCorp Aerojet, Sacramento, CA.), and DENNIS G. PELLACCIO (Science Applications International Corp., Albuquerque, NM.) Sep. 1992 13 p Presented at the Nuclear Power Engineering in Space Nuclear Rocket Engines Conference, Kazakhstan, Russia, 22-26 Sep. 1992; sponsored by the Research and Production Association LUCH Semipalatinsk (Contract RTOP 593-71-00) (NASA-TM-105870; E-7334; NAS 1.15:105870) Avail: CASI HC A03/MF A01

Nuclear thermal propulsion technology development is underway at NASA and DoE for Space Exploration Initiative (SEI) missions to Mars, with initial near-earth flights to validate flight readiness. Several reactor concepts are being considered for these missions, and important selection criteria will be evaluated before final selection of a system. These criteria include: safety and reliability, technical risk, cost, and performance, in that order. Of the concepts evaluated to date, the Nuclear Engine for Rocket Vehicle Applications (NERVA) derivative (NDR) is the only concept that has demonstrated full power, life, and performance in actual reactor tests. Other concepts will require significant design work and must demonstrate proof-of-concept. Technical risk, and hence, development cost should therefore be lowest for the concept, and the NDR concept is currently being considered for the initial

SEI missions. As lighter weight, higher performance systems are developed and validated, including appropriate safety and astronaut-rating requirements, they will be considered to support future SEI application. A space transportation system using a modular nuclear thermal rocket (NTR) system for lunar and Mars missions is expected to result in significant life cycle cost savings. Finally, several key issues remain for NTR's, including public acceptance and operational issues. Nonetheless, NTR's are believed to be the 'next generation' of space propulsion systems - the key to space exploration. Author

N93-12484*# National Aeronautics and Space Administration. Lewis Research Center, Cleveland, OH.

THE 10 KW POWER ELECTRONICS FOR HYDROGEN ARCJETS

JOHN A. HAMLEY, LUIS R. PINERO, and GERALD M. HILL 1992 22 p Presented at the 1992 JANNAF Propulsion Meeting, Indianapolis, IN, 24-28 Feb. 1992 Previously announced as N93-10033 (Contract RTOP 506-42-31) (NASA-TM-105614; E-6951; NAS 1.15:105614) Avail: CASI HC A03/MF A01

A combination of emerging mission considerations such as 'launch on schedule', resource limitations, and the development of higher power spacecraft busses has resulted in renewed interest in high power hydrogen arcjet systems with specific impulses greater than 1000 s for Earth-space orbit transfer and maneuver applications. Solar electric propulsion systems with about 10 kW of power appear to offer payload benefits at acceptable trip times. This work outlines the design and development of 10 kW hydrogen arcjet power electronics and results of arcjet integration testing. The power electronics incorporated a full bridge switching topology similar to that employed in state of the art 5 kW power electronics, and the output filter included an output current averaging inductor with an integral pulse generation winding for arcjet ignition. Phase shifted, pulse width modulation with current mode control was used to regulate the current delivered to arcjet, and a low inductance power stage minimized switching transients. Hybrid power Metal Oxide Semiconductor Field Effect Transistors were used to minimize conduction losses. Switching losses were minimized using a fast response, optically isolated, totem-pole gate drive circuit. The input bus voltage for the unit was 150 V, with a maximum output voltage of 225 V. The switching frequency of 20 kHz was a compromise between mass savings and higher efficiency. Power conversion efficiencies in excess of 0.94 were demonstrated, along with steady state load current regulation of 1 percent. The power electronics were successfully integrated with a 10 kW laboratory hydrogen arcjet, and reliable, nondestructive starts and transitions to steady state operation were demonstrated. The estimated specific mass for a flight packaged unit was 2 kg/kW. Author

N93-14079*# National Aeronautics and Space Administration. Lewis Research Center, Cleveland, OH.

VALIDATION TEST OF 125 AH ADVANCED DESIGN IPV NICKEL-HYDROGEN FLIGHT CELLS

JOHN J. SMITHRICK and STEPHEN W. HALL (Naval Weapons Support Center, Crane, IN.) Jan. 1993 12 p Proposed for presentation at the Eighth Annual Battery Conference on Applications and Advances, Long Beach, CA, 12-14 Jan. 1993; sponsored by California State Univ. (Contract RTOP 506-41-21) (NASA-TM-105912; E-7393; NAS 1.15:105912) Avail: CASI HC A03/MF A01

An update of validation test results confirming the advanced design nickel-hydrogen cell is presented. An advanced 125 Ah individual pressure vessel (IPV) nickel-hydrogen cell was designed. The primary function of the advanced cell is to store and deliver energy for long-term, Low-Earth-Orbit (LEO) spacecraft missions. The new features of this design, which are not incorporated in state-of-the-art design cells, are: (1) use of 26 percent rather than 31 percent potassium hydroxide (KOH) electrolyte; (2) use of a patented catalyzed wall wick; (3) use of serrated-edge separators

20 SPACECRAFT PROPULSION AND POWER

to facilitate gaseous oxygen and hydrogen flow within the cell, while still maintaining physical contact with the wall wick for electrolyte management; and (4) use of a floating rather than a fixed stack (state-of-the-art) to accommodate nickel electrode expansion due to charge/discharge cycling. The significant improvements resulting from these innovations are extended cycle life; enhanced thermal, electrolyte, and oxygen management; and accommodation of nickel electrode expansion. Six 125 Ah flight cells based on this design were fabricated by Eagle-Picher. Three of the cells contain all of the advanced features (test cells) and three are the same as the test cells except they do not have catalyst on the wall wick (control cells). All six cells are in the process of being evaluated in a LEO cycle life test at the Naval Weapons Support Center, Crane, IN, under a NASA Lewis Research Center contract. The catalyzed wall wick cells have been cycled for over 19000 cycles with no cell failures in the continuing test. Two of the noncatalyzed wall wick cells failed (cycles 9588 and 13,900). Author

N93-14482*# National Aeronautics and Space Administration. Lewis Research Center, Cleveland, OH.

CLOSED BRAYTON CYCLE POWER SYSTEM WITH A HIGH TEMPERATURE PELLET BED REACTOR HEAT SOURCE FOR NEP APPLICATIONS

ALBERT J. JUHASZ, MOHAMED S. EL-GENK (New Mexico Univ., Albuquerque.), and WILLIAM B. HARPER, JR. (Allied-Signal Aerospace Co., Tempe, AZ.) Oct. 1992 12 p Presented at the 10th Symposium on Space Nuclear Power and Propulsion, Albuquerque, NM, 10-14 Jan. 1993 (Contract RTOP 590-13-11) (NASA-TM-105933; E-7446; NAS 1.15:105933) Avail: CASI HC A03/MF A01

Capitalizing on past and future development of high temperature gas reactor (HTGR) technology, a low mass 15 MWe closed gas turbine cycle power system using a pellet bed reactor heating helium working fluid is proposed for Nuclear Electric Propulsion (NEP) applications. Although the design of this directly coupled system architecture, comprising the reactor/power system/space radiator subsystems, is presented in conceptual form, sufficient detail is included to permit an assessment of overall system performance and mass. Furthermore, an attempt is made to show how tailoring of the main subsystem design characteristics can be utilized to achieve synergistic system level advantages that can lead to improved reliability and enhanced system life while reducing the number of parasitic load driven peripheral subsystems. Author

N93-15428*# National Aeronautics and Space Administration. Lewis Research Center, Cleveland, OH.

DEVELOPMENT OF NASA/DOE NTP SYSTEM PERFORMANCE MODELS

JAMES T. WALTON Dec. 1992 15 p Presented at the 10th Space Nuclear Power Symposium, Albuquerque, NM, 10-14 Jan. 1993; Sponsored by Univ. of New Mexico Inst. for Space Nuclear Power (Contract RTOP 593-00-71) (NASA-TM-105982; E-7506; NAS 1.15:105982) Avail: CASI HC A03/MF A01

A critical enabling technology in the evolutionary development of Nuclear Thermal Propulsion (NTP) is the ability to predict the system performance under a variety of operating conditions. The ability to predict the system performance is critical for mission analysis and for control subsystem testing, as well as for the modeling of various failure modes. Performance must be accurately predicted during steady-state and transient operation, such as start-up, shut-down and after-cooling. The development and application of verified and validated system models has the potential to reduce testing, cost and time required for the technology to again reach flight-ready status. An integrated NASA/DOE team was formed in late 1991 to develop and implement a strategy for modeling NTP systems. It is the intent of the interagency team to develop several levels of computer programs, which vary in detail, to simulate NTP systems based

on either prismatic, particle or advanced fuel forms. This paper presents an overview of the models under development by the interagency team. In addition, the status of the development and validation efforts for the Level 1 steady-state parametric model is discussed. Author

N93-15429*# National Aeronautics and Space Administration. Lewis Research Center, Cleveland, OH.

ION THRUSTER DEVELOPMENT AT NASA LEWIS RESEARCH CENTER

JAMES S. SOVEY, JOHN A. HAMLEY, MICHAEL J. PATTERSON, VINCENT K. RAWLIN, and TIMOTHY R. SARVER-VERHEY (Sverdrup Technology, Inc., Brook Park, OH.) Dec. 1992 10 p Presented at the 10th Symposium on Space Nuclear Power and Propulsion, Albuquerque, NM, 10-14 Jan. 1993; Sponsored by the Univ. of New Mexico Inst. for Space Nuclear Power (Contract RTOP 506-42-31) (NASA-TM-105983; E-7507; NAS 1.15:105983) Avail: CASI HC A02/MF A01

Recent ion propulsion technology efforts at NASA's Lewis Research Center including development of kW-class xenon ion thrusters, high power xenon and krypton ion thrusters, and power processors are reviewed. Thruster physical characteristics, performance data, life projections, and power processor component technology are summarized. The ion propulsion technology program is structured to address a broad set of mission applications from satellite stationkeeping and repositioning to primary propulsion using solar or nuclear power systems. Author

N93-15526*# National Aeronautics and Space Administration. Lewis Research Center, Cleveland, OH.

SUMMARY OF THE NASA LEWIS COMPONENT TECHNOLOGY PROGRAM FOR STIRLING POWER CONVERTERS

LANNY G. THIEME and DIANE M. SWEC Oct. 1992 23 p Presented at the 27th Intersociety Energy Conversion Engineering Conference, San Diego, CA, 3-7 Aug. 1992; sponsored by the Society of Automotive Engineers (Contract RTOP 590-13-11) (NASA-TM-105640; E-7070-1; NAS 1.15:105640) Avail: CASI HC A03/MF A01

An update is presented on the NASA Lewis Stirling component technology program. The component technology program has been organized as part of the NASA Lewis effort to develop Stirling converter technology for space power applications. The Stirling converter technology project is part of the High Capacity Power element of the NASA Civil Space Technology Initiative (CSTI). Lewis is also providing technical management of a DOE funded project to develop Stirling converter systems for distributed dish solar terrestrial power applications. The primary contractors for the space power and solar terrestrial projects develop component technologies directly related to their project goals. This Lewis component technology program, while coordinated with these main projects, is aimed at longer term issues, advanced technologies, and independent assessments. Topics to be discussed include bearings, linear alternators, controls and load interaction, materials/life assessment, and heat exchangers. Author

N93-15528*# National Aeronautics and Space Administration. Lewis Research Center, Cleveland, OH.

AEROTHERMODYNAMIC FLOW PHENOMENA OF THE AIRFRAME-INTEGRATED SUPERSONIC COMBUSTION RAMJET

JAMES T. WALTON Nov. 1992 24 p (NASA-TM-4376; E-6751; NAS 1.15:4376) Avail: CASI HC A03/MF A01

The unique component flow phenomena is discussed of the airframe-integrated supersonic combustion ramjet (scramjet) in a format geared towards new players in the arena of hypersonic propulsion. After giving an overview of the scramjet aerothermodynamic cycle, the characteristics are then covered individually of the vehicle forebody, inlet, combustor, and vehicle

afterbody/nozzle. Attention is given to phenomena such as inlet speeding, inlet starting, inlet spillage, fuel injection, thermal choking, and combustor-inlet interaction. Author

N93-15571* National Aeronautics and Space Administration. Lewis Research Center, Cleveland, OH.

NUCLEAR THERMAL ROCKET NOZZLE TESTING AND EVALUATION PROGRAM

KENNETH O. DAVIDIAN and KENNETH J. KACYNSKI Jan. 1993 8 p Presented at the 10th Symposium on Space Nuclear Power and Propulsion, Albuquerque, NM, 10-13 Jan. 1993; sponsored by the Inst. for Space Nuclear Power Studies (Contract RTOP 506-42-72) (NASA-TM-105962; E-7482; NAS 1.15:105962) Avail: CASI HC A02/MF A01

Performance characteristics of the Nuclear Thermal Rocket can be enhanced through the use of unconventional nozzles as part of the propulsion system. The Nuclear Thermal Rocket nozzle testing and evaluation program being conducted at the NASA Lewis is outlined and the advantages of a plug nozzle are described. A facility description, experimental designs and schematics are given. Results of pretest performance analyses show that high nozzle performance can be attained despite substantial nozzle length reduction through the use of plug nozzles as compared to a convergent-divergent nozzle. Pretest measurement uncertainty analyses indicate that specific impulse values are expected to be within + or - 1.17 pct. Author

N93-15572* National Aeronautics and Space Administration. Lewis Research Center, Cleveland, OH.

LOW THRUST CHEMICAL ROCKET TECHNOLOGY

STEVEN J. SCHNEIDER Nov. 1992 32 p Presented at the 43rd Congress of the International Astronautical Federation, Washington, DC, 28 Aug. - 5 Sep. 1992 (Contract RTOP 506-42-31) (NASA-TM-105927; E-7434; NAS 1.15:105927; IAF-92-0669) Avail: CASI HC A03/MF A01

An on-going technology program to improve the performance of low thrust chemical rockets for spacecraft on-board propulsion applications is reviewed. Improved performance and lifetime is sought by the development of new predictive tools to understand the combustion and flow physics, introduction of high temperature materials and improved component designs to optimize performance, and use of higher performance propellants. Improved predictive technology is sought through the comparison of both local and global predictions with experimental data. Predictions are based on both the RPLUS Navier-Stokes code with finite rate kinetics and the JANNAF methodology. Data were obtained with laser-based diagnostics along with global performance measurements. Results indicate that the modeling of the injector and the combustion process needs improvement in these codes and flow visualization with a technique such as 2-D laser induced fluorescence (LIF) would aid in resolving issues of flow symmetry and shear layer combustion processes. High temperature material fabrication processes are under development and small rockets are being designed, fabricated, and tested using these new materials. Rhenium coated with iridium for oxidation protection was produced by the Chemical Vapor Deposition (CVD) process and enabled an 800 K increase in rocket operating temperature. Performance gains with this material in rockets using Earth storable propellants (nitrogen tetroxide and monomethylhydrazine or hydrazine) were obtained through component redesign to eliminate fuel film cooling and its associated combustion inefficiency while managing head end thermal soakback. Material interdiffusion and oxidation characteristics indicated that the requisite lifetimes of tens of hours were available for thruster applications. Rockets were designed, fabricated, and tested with thrusts of 22, 62, 440 and 550 N. Performance improvements of 10 to 20 seconds specific impulse were demonstrated. Higher performance propellants were evaluated: Space storable propellants, including liquid oxygen (LOX) as the oxidizer with nitrogen hydrides or hydrocarbon as fuels. Specifically, a LOX/hydrazine engine was designed, fabricated, and shown to have a 95 pct theoretical c-star which translates

into a projected vacuum specific impulse of 345 seconds at an area ratio of 204:1. Further performance improvement can be obtained by the use of LOX/hydrogen propellants, especially for manned spacecraft applications, and specific designs must be developed and advanced through flight qualification. Author

N93-16714* National Aeronautics and Space Administration. Lewis Research Center, Cleveland, OH.

PERFORMANCE COMPARISON OF AXISYMMETRIC AND THREE-DIMENSIONAL HYDROGEN FILM COOLANT INJECTION IN A 110N HYDROGEN/OXYGEN ROCKET

LYNN A. ARRINGTON (Sverdrup Technology, Inc., Brook Park, OH.) and BRIAN D. REED Dec. 1992 22 p Presented at the 28th Joint Propulsion Conference and Exhibit, Nashville, TN, 6-8 Jul. 1992; sponsored by AIAA, SAE, ASME, and ASEE Previously announced in IAA as A92-54027 (Contract RTOP 506-42-31) (NASA-TM-105967; E-7490; NAS 1.15:105967; AIAA PAPER 92-3390) Avail: CASI HC A03/MF A01

An experimental performance comparison of two geometrically different fuel film coolant injection sleeves was conducted on a 110 N gaseous hydrogen/oxygen rocket. One sleeve had slots milled axially down the walls and the other had a smooth surface to give axisymmetric flow. The comparison was made to investigate a conclusion in an earlier study that attributed a performance underprediction to a simplifying modeling assumption of axisymmetric fuel film flow. The smooth sleeve had higher overall performance at one film coolant percentage and approximately the same or slightly better at another. The study showed that the lack of modeling of three-dimensional effects was not the cause of the performance underprediction as speculated in earlier analytical studies. Author

N93-17995* National Aeronautics and Space Administration. Lewis Research Center, Cleveland, OH.

LASER RAYLEIGH AND RAMAN DIAGNOSTICS FOR SMALL HYDROGEN/OXYGEN ROCKETS

WILHELMUS A. DEGROOT and FRANK J. ZUPANC (Sverdrup Technology, Inc., Brook Park, OH.) 16 Jan. 1993 17 p Prepared for the SPIE International Symposium on Lasers, Sensors, and Applications, Los Angeles, CA, 16-23 Jan. 1993; Sponsored by the Society of Photo-Optical Instrumentation Engineers (Contract RTOP 506-42-31) (NASA-TM-105999; E-7540; NAS 1.15:105999) Avail: CASI HC A03/MF A01

Localized velocity, temperature, and species concentration measurements in rocket flow fields are needed to evaluate predictive computational fluid dynamics (CFD) codes and identify causes of poor rocket performance. Velocity, temperature, and total number density information have been successfully extracted from spectrally resolved Rayleigh scattering in the plume of small hydrogen/oxygen rockets. Light from a narrow band laser is scattered from the moving molecules with a Doppler shifted frequency. Two components of the velocity can be extracted by observing the scattered light from two directions. Thermal broadening of the scattered light provides a measure of the temperature, while the integrated scattering intensity is proportional to the number density. Spontaneous Raman scattering has been used to measure temperature and species concentration in similar plumes. Light from a dye laser is scattered by molecules in the rocket plume. Raman spectra scattered from major species are resolved by observing the inelastically scattered light with linear array mounted to a spectrometer. Temperature and oxygen concentrations have been extracted by fitting a model function to the measured Raman spectrum. Results of measurements on small rockets mounted inside a high altitude chamber using both diagnostic techniques are reported. Author

N93-18856* National Aeronautics and Space Administration. Lewis Research Center, Cleveland, OH.

SPECTROSCOPIC WEAR DETECTOR Patent

GEORGE C. MADZSAR, inventor (to NASA) 16 Feb. 1993 7 p Filed 27 Jun. 1991 Supersedes N91-32167 (29 - 24, p 3968)

20 SPACECRAFT PROPULSION AND POWER

(NASA-CASE-LEW-15200-1; US-PATENT-5,187,542;
US-PATENT-APPL-SN-722446; US-PATENT-CLASS-356-300;
US-PATENT-CLASS-73-86; US-PATENT-CLASS-60-223;
US-PATENT-CLASS-356-311; US-PATENT-CLASS-356-36;
INT-PATENT-CLASS-G01J-3/00;
INT-PATENT-CLASS-G01N-21/00) Avail: US Patent and
Trademark Office

The elemental composition of a material exposed to hot gases and subjected to wear is determined. Atoms of an elemental species not appearing in this material are implanted in a surface at a depth based on the maximum allowable wear. The exhaust gases are spectroscopically monitored to determine the exposure of these atoms when the maximum allowable wear is reached.

Official Gazette of the U.S. Patent and Trademark Office

N93-18877*# National Aeronautics and Space Administration.
Lewis Research Center, Cleveland, OH.

ENVIRONMENTAL INTERACTIONS AND THE SP-100 POWER SYSTEM

DALE C. FERGUSON Jan. 1993 14 p

(Contract RTOP 590-13-51)

(NASA-TM-105866; E-7328; NAS 1.15:105866) Avail: CASI HC
A03/MF A01

Interactions of the SP-100 power system with its expected ambient environments are defined. SP-100 payloads will float 100 V negative of the low Earth orbit (LEO) plasma. Choice of proper geometries and materials will prevent arcing at conductor-insulator junctions in LEO. Care in selecting surface coatings will prevent dielectric breakdown. Sputtering is a concern for long-duration LEO missions. Atomic oxygen durability of SP-100 materials will be tested in ground and flight tests. Evaluation of SP-100 in lunar and planetary environments has begun. The report of a recent workshop on Chemical and Electrical Interactions on Mars identified many of the primary interactions. Author

N93-18878*# National Aeronautics and Space Administration.
Lewis Research Center, Cleveland, OH.

PERFORMANCE AND HEAT TRANSFER CHARACTERISTICS OF A CARBON MONOXIDE/OXYGEN ROCKET ENGINE

DIANE L. LINNE Feb. 1993 13 p

(Contract RTOP 506-42-72)

(NASA-TM-105897; E-7521; NAS 1.15:105897) Avail: CASI HC
A03/MF A01

The combustion and heat transfer characteristics of a carbon monoxide and oxygen rocket engine were evaluated. The test hardware consisted of a calorimeter combustion chamber with a heat sink nozzle and an eighteen element concentric tube injector. Experimental results are given at chamber pressures of 1070 and 3070 kPa, and over a mixture ratio range of 0.3 to 1.0. Experimental C efficiency was between 95 and 96.5 percent. Heat transfer results are discussed both as a function of mixture ratio and axial distance in the chamber. They are also compared to a Nusselt number correlation for fully developed turbulent flow. Author

N93-19106*# National Aeronautics and Space Administration.
Lewis Research Center, Cleveland, OH.

PROGRAM ELM: A TOOL FOR RAPID THERMAL-HYDRAULIC ANALYSIS OF SOLID-CORE NUCLEAR ROCKET FUEL ELEMENTS

JAMES T. WALTON Nov. 1992 50 p

(Contract RTOP 593-71-00)

(NASA-TM-105867; E-7330; NAS 1.15:105867) Avail: CASI HC
A03/MF A01

This report reviews the state of the art of thermal-hydraulic analysis codes and presents a new code, Program ELM, for analysis of fuel elements. ELM is a concise computational tool for modeling the steady-state thermal-hydraulics of propellant flow through fuel element coolant channels in a nuclear thermal rocket reactor with axial coolant passages. The program was developed as a tool to swiftly evaluate various heat transfer coefficient and friction factor correlations generated for turbulent pipe flow with heat addition which have been used in previous programs. Thus, a consistent comparison of these correlations was performed, as well as a

comparison with data from the NRX reactor experiments from the Nuclear Engine for Rocket Vehicle Applications (NERVA) project. This report describes the ELM Program algorithm, input/output, and validation efforts and provides a listing of the code. Author

N93-20614*# National Aeronautics and Space Administration.
Lewis Research Center, Cleveland, OH.

ATOMIC HYDROGEN PROPELLANTS: HISTORICAL PERSPECTIVES AND FUTURE POSSIBILITIES

BRYAN PALASZEWSKI Feb. 1993 25 p Presented at the
Aerospace Sciences Meeting and Exhibit, Reno, NV, 11-14 Jan.
1993; sponsored by AIAA Previously announced in IAA as
A93-24234

(Contract RTOP 506-42-00)

(NASA-TM-106053; E-7646; NAS 1.15:106053) Avail: CASI HC
A03/MF A01

Atomic hydrogen, a very high density free-radical propellant, is anticipated to generate a specific impulse of 600-1500 lb-f sec/lb-mass performance; this may facilitate the development of unique launch vehicles. A development status evaluation is presently given for atomic hydrogen investigations. It is noted that breakthroughs are required in the production, storage, and transfer of atomic hydrogen, before this fuel can become a viable rocket propellant. Author

N93-20615*# National Aeronautics and Space Administration.
Lewis Research Center, Cleveland, OH.

SPACE TRANSFER WITH GROUND-BASED LASER/ELECTRIC PROPULSION

GEOFFREY A. LANDIS (Sverdrup Technology, Inc., Brook Park, OH.), MARK STAVNES (Sverdrup Technology, Inc., Brook Park, OH.), STEVE OLESON (Sverdrup Technology, Inc., Brook Park, OH.), and JOHN BOZEK Jul. 1993 20 p Prepared for
presentation at the 28th Joint Propulsion Conference and Exhibit,
Monterey, CA, 28-30 Jun. 1993; sponsored by AIAA, SAE, ASME,
and ASEE

(Contract RTOP 506-46-11)

(NASA-TM-106060; E-7663; NAS 1.15:106060; AIAA PAPER
92-3213) Avail: CASI HC A03/MF A01

A new method of providing power to space vehicles consists of using ground-based lasers to beam power to photovoltaic receivers in space. This can be used as a power source for electrically propelled orbital transfer vehicles. Author

N93-22092*# National Aeronautics and Space Administration.
Lewis Research Center, Cleveland, OH.

SPACE PROPULSION

JOHN M. KAZAROFF /in NASA Langley Research Center, Space
Transportation Materials and Structures Technology Workshop.
Volume 2: Proceedings p 138-142 Feb. 1993

Avail: CASI HC A01/MF A04

Lewis Research Center is developing broad-based new technologies for space chemical engines to satisfy long-term needs of ETO launch vehicles and other vehicles operating in and beyond Earth orbit. Specific objectives are focused on high performance LO2/LH2 engines providing moderate thrusts of 7.5-200 klb. This effort encompasses research related to design analysis and manufacturing processes needed to apply advanced materials to subcomponents, components, and subsystems of space-based systems and related ground-support equipment. High-performance space-based chemical engines face a number of technical challenges. Liquid hydrogen turbopump impellers are often so large that they cannot be machined from a single piece, yet high stress at the vane/shroud interface makes bonding extremely difficult. Tolerances on fillets are critical on large impellers. Advanced materials and fabricating techniques are needed to address these and other issues of interest. Turbopump bearings are needed which can provide reliable, long life operation at high speed and high load with low friction losses. Hydrostatic bearings provide good performance, but transients during pump starts and stops may be an issue because no pressurized fluid is available unless a separate bearing pressurization system is included. Durable materials and/or coatings are needed that can demonstrate low wear in the harsh

LO2/LH2 environment. Advanced materials are also needed to improve the lifetime, reliability and performance of other propulsion system elements such as seals and chambers. Author

N93-22093* # National Aeronautics and Space Administration. Lewis Research Center, Cleveland, OH.

NUCLEAR CONCEPTS/PROPULSION

THOMAS J. MILLER /in NASA. Langley Research Center, Space Transportation Materials and Structures Technology Workshop. Volume 2: Proceedings p 143-147 Feb. 1993
Avail: CASI HC A01/MF A04

Nuclear thermal and nuclear electric propulsion systems will enable and/or enhance important space exploration missions to the moon and Mars. Current efforts are addressing certain research areas, although NASA and DOE still have much work yet to do. Relative to chemical systems, nuclear thermal propulsion offers the potential of reduced vehicle weight, wider launch windows, and shorter transit times, even without aerobrakes. This would improve crew safety by reducing their exposure to cosmic radiation. Advanced materials and structures will be an important resource in responding to the challenges posed by safety and test facility requirements, environmental concerns, high temperature fuels and the high radiation, hot hydrogen environment within nuclear thermal propulsion systems. Nuclear electric propulsion (NEP) has its own distinct set of advantages relative to chemical systems. These include low resupply mass, the availability of large amounts of onboard electric power for other uses besides propulsion, improved launch windows, and the ability to share technology with surface power systems. Development efforts for NEP reactors will emphasize long life operation of compact designs. This will require designs that provide high fuel burnup and high temperature operation along with personnel and environmental safety. Author

N93-22482* # National Aeronautics and Space Administration. Lewis Research Center, Cleveland, OH.

100-KW CLASS APPLIED-FIELD MPD THRUSTER COMPONENT WEAR

MARIS A. MANTENIEKS and ROGER M. MYERS (Sverdrup Technology, Inc., Brook Park, OH.) Jan. 1993 12 p Presented at the 10th Symposium on Space Nuclear Power and Propulsion, Albuquerque, NM, 10-14 Jan. 1993; sponsored by the University of New Mexico
(Contract RTOP 506-42-31)
(NASA-TM-106023; E-7586; NAS 1.15:106023) Avail: CASI HC A03/MF A01

Component erosion and material deposition sites were identified and analyzed during tests of various configurations of 100 kW class, applied-field, water-cooled magnetoplasmadynamic (MPD) thrusters. Severe erosion of the cathode and the boron nitride insulator was observed for the first series of tests, which was significantly decreased by reducing the levels of propellant contamination. Severe erosion of the copper anode resulting from sputtering by the propellant was also observed. This is the first observation of this phenomenon in MPD thrusters. The anode erosion indicates that development of long life MPD thrusters requires the use of light gas propellants such as hydrogen, deuterium, or lithium. Author

N93-23017* # National Aeronautics and Space Administration. Lewis Research Center, Cleveland, OH.

SOLAR CONCENTRATORS FOR ADVANCED

SOLAR-DYNAMIC POWER SYSTEMS IN SPACE Final Report

RICHARD ROCKWELL (Hughes Danbury Optical Systems, Inc., CT.) Mar. 1993 50 p
(Contract NAS3-25280; RTOP 506-41-31)
(NASA-CR-187148; E-7712; NAS 1.26:187148) Avail: CASI HC A03/MF A01

This report summarizes the results of a study performed by Hughes Danbury Optical Systems, HDOS, (formerly Perkin-Elmer) to design, fabricate, and test a lightweight (2 kg/sq M), self supporting, and highly reflective sub-scale concentrating mirror panel suitable for use in space. The HDOS panel design utilizes Corning's 'micro sheet' glass as the top layer of a composite

honeycomb sandwich. This approach, whose manufacturability was previously demonstrated under an earlier NASA contract, provides a smooth (specular) reflective surface without the weight of a conventional glass panel. The primary result of this study is a point design and its performance assessment. Author

N93-23405* # National Aeronautics and Space Administration. Lewis Research Center, Cleveland, OH.

SPACE CHEMICAL PROPULSION TEST FACILITIES AT NASA LEWIS RESEARCH CENTER

DONALD C. URASEK and FREDERICK D. CALFO Apr. 1993 13 p Proposed for presentation at the Aerospace Atlantic Conference, Dayton, OH, 20-23 Apr. 1993; sponsored by SAE (Contract RTOP 584-03-11)
(NASA-TM-106050; E-7640; NAS 1.15:106050) Avail: CASI HC A03/MF A01

The NASA Lewis Research Center, located in Cleveland, Ohio, has a number of space chemical propulsion test facilities which constitute a significant national space testing resource. The purpose of this paper is to make more users aware of these test facilities and to encourage their use through cooperative agreements between the government, industry, and universities. Research which is of interest to the government is especially encouraged and often can be done in a cooperative manner that best uses the resources of all parties. An overview of the Lewis test facilities is presented. Author (revised)

N93-23747* # National Aeronautics and Space Administration. Lewis Research Center, Cleveland, OH.

DEVELOPMENT OF ARCJET AND ION PROPULSION FOR SPACECRAFT STATIONKEEPING

JAMES S. SOVEY, FRANCIS M. CURRAN, THOMAS W. HAAG, MICHAEL J. PATTERSON, ERIC J. PENCIL, VINCENT K. RAWLIN, and JOHN M. SANKOVIC Aug. 1992 17 p Presented at the 43rd Congress of the International Astronautical Federation, Washington, DC, 28 Aug. - 5 Sep. 1992; sponsored by COSPAR, IAF, and AIAA Previously announced in IAA as A92-57058
(Contract RTOP 506-42-31)
(NASA-TM-106102; E-7722; NAS 1.15:106102; IAF-92-0607)
Avail: CASI HC A03/MF A01

Near term flight applications of arc jet and ion thruster satellite station-keeping systems as well as development activities in Europe, Japan, and the United States are reviewed. At least two arc jet and three ion propulsion flights are scheduled during the 1992-1995 period. Ground demonstration technology programs are focusing on the development of kW-class hydrazine and ammonia arc jets and xenon ion thrusters. Recent work at NASA LeRC on electric thruster and system integration technologies relating to satellite station keeping and repositioning will also be summarized. Author (revised)

N93-23875* # National Aeronautics and Space Administration. Lewis Research Center, Cleveland, OH.

NUCLEAR ENGINE SYSTEM SIMULATION (NESS). VERSION 2.0: PROGRAM USER'S GUIDE Final Report

DENNIS G. PELACCIO (Science Applications International Corp., Torrance, CA.), CHRISTINE M. SCHEIL (Science Applications International Corp., Torrance, CA.), and LYMAN PETROSKY (Science Applications International Corp., Torrance, CA.) Mar. 1993 312 p
(Contract NAS3-25809; RTOP 593-71-00)
(NASA-CR-191081; E-7623; NAS 1.26:191081) Avail: CASI HC A14/MF A03

This Program User's Guide discusses the Nuclear Thermal Propulsion (NTP) engine system design features and capabilities modeled in the Nuclear Engine System Simulation (NESS): Version 2.0 program (referred to as NESS throughout the remainder of this document), as well as its operation. NESS was upgraded to include many new modeling capabilities not available in the original version delivered to NASA LeRC in Dec. 1991. NESS's new features include the following: (1) an improved input format; (2) an advanced solid-core NERVA-type reactor system model (ENABLER 2); (3) a bleed-cycle engine system option; (4) an

20 SPACECRAFT PROPULSION AND POWER

axial-turbopump design option; (5) an automated pump-out turbopump assembly sizing option; (6) an off-design gas generator engine cycle design option; (7) updated hydrogen properties; (8) an improved output format; and (9) personal computer operation capability. Sample design cases are presented in the user's guide that demonstrate many of the new features associated with this upgraded version of NESS, as well as design modeling features associated with the original version of NESS. Author (revised)

N93-23876*# National Aeronautics and Space Administration. Lewis Research Center, Cleveland, OH.

NUCLEAR ENGINE SYSTEM SIMULATION (NESS). VOLUME 1: PROGRAM USER'S GUIDE Final Report

DENNIS G. PELACCIO (Science Applications International Corp., Torrance, CA.), CHRISTINE M. SCHEIL (Science Applications International Corp., Torrance, CA.), and LYMAN J. PETROSKY (Science Applications International Corp., Torrance, CA.) Mar. 1993 125 p

(Contract NAS3-25809; RTOP 593-71-00)

(NASA-CR-191080; E-7622; NAS 1.26:191080) Avail: CASI HC A06/MF A02

A Nuclear Thermal Propulsion (NTP) engine system design analysis tool is required to support current and future Space Exploration Initiative (SEI) propulsion and vehicle design studies. Currently available NTP engine design models are those developed during the NERVA program in the 1960's and early 1970's and are highly unique to that design or are modifications of current liquid propulsion system design models. To date, NTP engine-based liquid design models lack integrated design of key NTP engine design features in the areas of reactor, shielding, multi-propellant capability, and multi-redundant pump feed fuel systems. Additionally, since the SEI effort is in the initial development stage, a robust, verified NTP analysis design tool could be of great use to the community. This effort developed an NTP engine system design analysis program (tool), known as the Nuclear Engine System Simulation (NESS) program, to support ongoing and future engine system and stage design study efforts. In this effort, Science Applications International Corporation's (SAIC) NTP version of the Expanded Liquid Engine Simulation (ELES) program was modified extensively to include Westinghouse Electric Corporation's near-term solid-core reactor design model. The ELES program has extensive capability to conduct preliminary system design analysis of liquid rocket systems and vehicles. The program is modular in nature and is versatile in terms of modeling state-of-the-art component and system options as discussed. The Westinghouse reactor design model, which was integrated in the NESS program, is based on the near-term solid-core ENABLER NTP reactor design concept. This program is now capable of accurately modeling (characterizing) a complete near-term solid-core NTP engine system in great detail, for a number of design options, in an efficient manner. The following discussion summarizes the overall analysis methodology, key assumptions, and capabilities associated with the NESS presents an example problem, and compares the results to related NTP engine system designs. Initial installation instructions and program disks are in Volume 2 of the NESS Program User's Guide. Author

N93-24740*# National Aeronautics and Space Administration. Lewis Research Center, Cleveland, OH.

NUCLEAR THERMAL PROPULSION TECHNOLOGY: RESULTS OF AN INTERAGENCY PANEL IN FY 1991

JOHN S. CLARK, PATRICK MCDANIEL (Phillips Lab., Kirtland AFB, NM.), STEVEN HOWE (Los Alamos National Lab., NM.), IRA HELMS (Nuclear Utility Services, Inc., Damascus, MD.), and MARLAND STANLEY (EI International, Inc., Idaho Falls, ID.) Apr. 1993 137 p

(Contract RTOP 593-71-00)

(NASA-TM-105711; E-7099; NAS 1.15:105711) Avail: CASI HC A07/MF A02

NASA LeRC was selected to lead nuclear propulsion technology development for NASA. Also participating in the project are NASA MSFC and JPL. The U.S. Department of Energy will develop nuclear technology and will conduct nuclear component,

subsystem, and system testing at appropriate DOE test facilities. NASA program management is the responsibility of NASA/RP. The project includes both nuclear electric propulsion (NEP) and nuclear thermal propulsion (NTP) technology development. This report summarizes the efforts of an interagency panel that evaluated NTP technology in 1991. Other panels were also at work in 1991 on other aspects of nuclear propulsion, and the six panels worked closely together. The charters for the other panels and some of their results are also discussed. Important collaborative efforts with other panels are highlighted. The interagency (NASA/DOE/DOD) NTP Technology Panel worked in 1991 to evaluate nuclear thermal propulsion concepts on a consistent basis. Additionally, the panel worked to continue technology development project planning for a joint project in nuclear propulsion for the Space Exploration Initiative (SEI). Five meetings of the panel were held in 1991 to continue the planning for technology development of nuclear thermal propulsion systems. The state-of-the-art of the NTP technologies was reviewed in some detail. The major technologies identified were as follows: fuels, coatings, and other reactor technologies; materials; instrumentation, controls, health monitoring and management, and associated technologies; nozzles; and feed system technology, including turbopump assemblies. Author (revised)

N93-24744*# National Aeronautics and Space Administration. Lewis Research Center, Cleveland, OH.

SUMMARY AND RECOMMENDATIONS ON NUCLEAR ELECTRIC PROPULSION TECHNOLOGY FOR THE SPACE EXPLORATION INITIATIVE

MICHAEL P. DOHERTY and ROBERT S. HOLCOMB (Oak Ridge National Lab., TN.) Apr. 1993 120 p

(Contract RTOP 593-72-00)

(NASA-TM-105707; E-7783; NAS 1.15:105707) Avail: CASI HC A06/MF A02

A project in Nuclear Electric Propulsion (NEP) technology is being established to develop the NEP technologies needed for advanced propulsion systems. A paced approach has been suggested which calls for progressive development of NEP component and subsystem level technologies. This approach will lead to major facility testing to achieve TRL-5 for megawatt NEP for SEI mission applications. This approach is designed to validate NEP power and propulsion technologies from kilowatt class to megawatt class ratings. Such a paced approach would have the benefit of achieving the development, testing, and flight of NEP systems in an evolutionary manner. This approach may also have the additional benefit of synergistic application with SEI extraterrestrial surface nuclear power applications. Author (revised)

N93-24753*# National Aeronautics and Space Administration. Lewis Research Center, Cleveland, OH.

SPACE EXPLORATION INITIATIVE CANDIDATE NUCLEAR PROPULSION TEST FACILITIES

DARRELL BALDWIN (Sverdrup Technology, Inc., Brook Park, OH.) and JOHN S. CLARK Apr. 1993 259 p

(Contract RTOP 593-71-00)

(NASA-TM-105710; E-7759; NAS 1.15:105710) Avail: CASI HC A12/MF A03

One-page descriptions for approximately 200 existing government, university, and industry facilities which may be available in the future to support SEI nuclear propulsion technology development and test program requirements are provided. To facilitate use of the information, the candidate facilities are listed both by location (Index L) and by Facility Type (Index FT). The included one-page descriptions provide a brief narrative description of facility capability, suggest potential uses for each facility, and designate a point of contact for additional information that may be needed in the future. The Nuclear Propulsion Office at NASA Lewis presently plans to maintain, expand, and update this information periodically for use by NASA, DOE, and DOD personnel involved in planning various phases of the SEI Nuclear Propulsion Project. Author (revised)

N93-24758*# National Aeronautics and Space Administration. Lewis Research Center, Cleveland, OH.

EXPERIMENTATION IN THE LOW-DENSITY PLUME OF A SIMULATED ELECTROTHERMAL THRUSTER FOR COMPUTER CODE VALIDATION Final Report

DANA L. MEISSNER (Toledo Univ., OH.) Apr. 1993 86 p

(Contract NAG3-577; RTOP 506-42-31)

(NASA-CR-191112; E-7728; NAS 1.26:191112) Avail: CASI HC A05/MF A01

Pressures and flow angles are measured in the plume of a 20 deg half-angle, conical nozzle in vacuum with Pitot tubes and conical probes. The area of measurement in the plume ranges from the nozzle exit plane to 480 mm axially downstream and from the plume centerline to 60 mm radially. The nozzle has an exit-to-throat area ratio of 100:1 and a throat diameter of 3.2 mm. The nozzle flow exhausts to a vacuum of order $10(\text{exp } -2)$ Pa to simulate a resistojet (an electrothermal rocket of less than 1 N of thrust) operating in space. Experimental data are given for flows of nitrogen at 55 and 68 mg/s, stagnation temperatures between 695 and 921 K, and stagnation pressures ranging from 5600 to 7100 Pa. Data are also given for argon at a rate of 68 mg/s, a stagnation temperature of 648 K, and stagnation pressures of 4500, 4750, and 4770 Pa. Measurements in the nitrogen plume are compared with computational results from a direct-simulation Monte Carlo method. Author (revised)

N93-25089*# National Aeronautics and Space Administration. Lewis Research Center, Cleveland, OH.

A NEURAL NETWORK-BASED ESTIMATOR FOR THE MIXTURE RATIO OF THE SPACE SHUTTLE MAIN ENGINE

T. H. GUO and J. MUSGRAVE Nov. 1992 12 p Presented at the Fourth Annual Health Monitoring Conference for Space Propulsion Systems, Cincinnati, OH, 17-18 Nov. 1992; sponsored by Univ. of Cincinnati

(Contract RTOP 582-01-11)

(NASA-TM-106070; E-7675; NAS 1.15:106070) Avail: CASI HC A03/MF A01

In order to properly utilize the available fuel and oxidizer of a liquid propellant rocket engine, the mixture ratio is closed loop controlled during main stage (65 percent - 109 percent power) operation. However, because of the lack of flight-capable instrumentation for measuring mixture ratio, the value of mixture ratio in the control loop is estimated using available sensor measurements such as the combustion chamber pressure and the volumetric flow, and the temperature and pressure at the exit duct on the low pressure fuel pump. This estimation scheme has two limitations. First, the estimation formula is based on an empirical curve fitting which is accurate only within a narrow operating range. Second, the mixture ratio estimate relies on a few sensor measurements and loss of any of these measurements will make the estimate invalid. In this paper, we propose a neural network-based estimator for the mixture ratio of the Space Shuttle Main Engine. The estimator is an extension of a previously developed neural network based sensor failure detection and recovery algorithm (sensor validation). This neural network uses an auto associative structure which utilizes the redundant information of dissimilar sensors to detect inconsistent measurements. Two approaches have been identified for synthesizing mixture ratio from measurement data using a neural network. The first approach uses an auto associative neural network for sensor validation which is modified to include the mixture ratio as an additional output. The second uses a new network for the mixture ratio estimation in addition to the sensor validation network. Although mixture ratio is not directly measured in flight, it is generally available in simulation and in test bed firing data from facility measurements of fuel and oxidizer volumetric flows. The pros and cons of these two approaches will be discussed in terms of robustness to sensor failures and accuracy of the estimate during typical transients using simulation data. Author (revised)

N93-25105*# National Aeronautics and Space Administration. Lewis Research Center, Cleveland, OH.

SPACE NUCLEAR THERMAL PROPULSION TEST FACILITIES SUBPANEL Final Report

GEORGE C. ALLEN (Sandia National Labs., Albuquerque, NM.), JOHN W. WARREN (Department of Energy, Washington, DC.), JOHN MARTINELL (Idaho National Engineering Lab., Idaho Falls.), JOHN S. CLARK, and DAVID PERKINS (Phillips Lab., Edwards AFB, CA.) Apr. 1993 178 p

(Contract RTOP 593-71-00)

(NASA-TM-105708; E-7781; NAS 1.15:105708) Avail: CASI HC A09/MF A02

On 20 Jul. 1989, in commemoration of the 20th anniversary of the Apollo 11 lunar landing, President George Bush proclaimed his vision for manned space exploration. He stated, 'First for the coming decade, for the 1990's, Space Station Freedom, the next critical step in our space endeavors. And next, for the new century, back to the Moon. Back to the future. And this time, back to stay. And then, a journey into tomorrow, a journey to another planet, a manned mission to Mars.' On 2 Nov. 1989, the President approved a national space policy reaffirming the long range goal of the civil space program: to 'expand human presence and activity beyond Earth orbit into the solar system.' And on 11 May 1990, he specified the goal of landing Astronauts on Mars by 2019, the 50th anniversary of man's first steps on the Moon. To safely and ever permanently venture beyond near Earth environment as charged by the President, mankind must bring to bear extensive new technologies. These include heavy lift launch capability from Earth to low-Earth orbit, automated space rendezvous and docking of large masses, zero gravity countermeasures, and closed loop life support systems. One technology enhancing, and perhaps enabling, the piloted Mars missions is nuclear propulsion, with great benefits over chemical propulsion. Asserting the potential benefits of nuclear propulsion, NASA has sponsored workshops in Nuclear Electric Propulsion and Nuclear Thermal Propulsion and has initiated a tri-agency planning process to ensure that appropriate resources are engaged to meet this exciting technical challenge. At the core of this planning process, NASA, DOE, and DOD established six Nuclear Propulsion Technical Panels in 1991 to provide groundwork for a possible tri-agency Nuclear Propulsion Program and to address the President's vision by advocating an aggressive program in nuclear propulsion. To this end the Nuclear Electric Propulsion Technology Panel has focused its energies; this final report summarizes its endeavor and conclusions. Author (revised)

N93-25236*# National Aeronautics and Space Administration. Lewis Research Center, Cleveland, OH.

CALCULATIONS OF COMBUSTION RESPONSE PROFILES AND OSCILLATIONS

RICHARD J. PRIEM (Priem Consultants, Inc., Cleveland, OH.) and KEVIN J. BREISACHER Apr. 1993 28 p Presented at the 1st International Symposium on Liquid Rocket Combustion Instability, University Park, PA, 18-20 Jan. 1993; sponsored by Pennsylvania State Univ. Original contains color illustrations

(Contract RTOP 590-21-11)

(NASA-TM-106135; E-7775; NAS 1.15:106135) Avail: CASI HC A03/MF A01; 1 functional color page

The theory and procedures for determining the characteristics of pressure oscillations in rocket engines with prescribed burning rate oscillations are presented. Pressure and velocity oscillations calculated using this procedure are presented for the Space Shuttle Main Engine (SSME) to show the influence of baffles and absorbers on the burning rate oscillations required to achieve neutral stability. Results of calculations to determine local combustion responses using detailed physical models for injection, atomization, and vaporization with gas phase oscillations in baffled and unbaffled SSME combustors are presented. The contributions of the various physical phenomena occurring in a combustor to oscillations in combustion response were determined. Author

20 SPACECRAFT PROPULSION AND POWER

N93-26149*# National Aeronautics and Space Administration. Lewis Research Center, Cleveland, OH.
PULSED LASER RAYLEIGH SCATTERING DIAGNOSTIC FOR HYDROGEN/OXYGEN ROCKET EXIT PLANE FLOWFIELD VELOCIMETRY

FRANK J. ZUPANC Jan. 1993 11 p Presented at the 31st Aerospace Sciences Meeting and Exhibit, Reno, NV, 11-14 Jan. 1993; sponsored by AIAA Previously announced in IAA as A93-25552
 (Contract RTOP 506-42-31)
 (NASA-TM-106213; E-7739; NAS 1.15:106213; AIAA PAPER 93-0805) Avail: CASI HC A03/MF A01

A Doppler-resolved, pulsed laser Rayleigh scattering diagnostic has been developed to obtain local flowfield velocity measurements at the exit plane of a low thrust hydrogen/oxygen rocket engine operating in a high-altitude test facility. Fiber optic signal collection was employed to obtain the forescatter and backscatter Doppler shifts necessary to resolve the axial and radial velocity components. A radial profile was obtained by traversing the collection probes along the beam path at the nozzle exit. The results are compared with theoretical predictions from a full Navier Stokes model (RK/RPLUS). Significant discrepancies between the measured and predicted axial velocity profiles are observed, in terms of both magnitude and character. Radial velocity measurements exhibit excellent agreement with predictions near the centerline but show some departure off-axis. The discrepancies between theory and experiment are potentially the result of enhanced mixing between the core and fuel-film region beyond that predicted, and/or flow stratification between the hydrogen and oxygen injected into the central core region. Author

N93-26200*# National Aeronautics and Space Administration. Lewis Research Center, Cleveland, OH.
NUCLEAR SAFETY POLICY WORKING GROUP RECOMMENDATIONS ON NUCLEAR PROPULSION SAFETY FOR THE SPACE EXPLORATION INITIATIVE

ALBERT C. MARSHALL (Sandia National Labs., Albuquerque, NM.), JAMES H. LEE (Sandia National Labs., Albuquerque, NM.), WILLIAM H. MCCULLOCH (Sandia National Labs., Albuquerque, NM.), J. CHARLES SAWYER, JR., ROBERT A. BARI (Brookhaven National Lab., Upton, NY.), HATICE S. CULLINGFORD (National Aeronautics and Space Administration. John F. Kennedy Space Center, Cocoa Beach, FL.), ALVA C. HARDY (National Aeronautics and Space Administration. John F. Kennedy Space Center, Cocoa Beach, FL.), GEORGE F. NIEDERAUER (Los Alamos National Lab., NM.), KERRY REMP, JOHN W. RICE (Idaho National Engineering Lab., Idaho Falls.) et al. Apr. 1993 63 p
 (Contract RTOP 593-71-00)
 (NASA-TM-105705; E-7782; NAS 1.15:105705) Avail: CASI HC A04/MF A01

An interagency Nuclear Safety Working Group (NSPWG) was chartered to recommend nuclear safety policy, requirements, and guidelines for the Space Exploration Initiative (SEI) nuclear propulsion program. These recommendations, which are contained in this report, should facilitate the implementation of mission planning and conceptual design studies. The NSPWG has recommended a top-level policy to provide the guiding principles for the development and implementation of the SEI nuclear propulsion safety program. In addition, the NSPWG has reviewed safety issues for nuclear propulsion and recommended top-level safety requirements and guidelines to address these issues. These recommendations should be useful for the development of the program's top-level requirements for safety functions (referred to as Safety Functional Requirements). The safety requirements and guidelines address the following topics: reactor start-up, inadvertent criticality, radiological release and exposure, disposal, entry, safeguards, risk/reliability, operational safety, ground testing, and other considerations. Author

N93-26210*# National Aeronautics and Space Administration. Lewis Research Center, Cleveland, OH.
NUCLEAR ELECTRIC PROPULSION FOR PLANETARY SCIENCE MISSIONS: NASA TECHNOLOGY PROGRAM PLANNING

MICHAEL P. DOHERTY May 1993 8 p Presented at the Tenth Symposium on Space Nuclear Power and Propulsion, Albuquerque, NM, 10-14 Jan. 1993; sponsored by the Univ. of New Mexico and the American Inst. of Physics
 (Contract RTOP 593-72-00)
 (NASA-TM-106139; E-7820; NAS 1.15:106139) Avail: CASI HC A02/MF A01

This paper presents the status of technology program planning to develop those Nuclear Electric Propulsion technologies needed to meet the advanced propulsion system requirements for planetary science missions in the next century. The technology program planning is based upon technologies with significant development heritage: ion electric propulsion and the SP-100 space nuclear power technologies. Detailed plans are presented for the required ion electric propulsion technology development and demonstration. Closer coordination between space nuclear power and space electric propulsion technology programs is a necessity as technology plans are being further refined in light of NEP concept definition and possible early NEP flight activities. Author

N93-26211*# National Aeronautics and Space Administration. Lewis Research Center, Cleveland, OH.

ON-LINE IMPLEMENTATION OF NONLINEAR PARAMETER ESTIMATION FOR THE SPACE SHUTTLE MAIN ENGINE

JULIA H. BUCKLAND (Cincinnati Univ., OH.), JEFFREY L. MUSGRAVE, and BRUCE K. WALKER (Cincinnati Univ., OH.) Nov. 1992 14 p Presented at the Fourth Annual Health Monitoring Conference for Space Propulsion Systems, Cincinnati, OH, 17-18 Nov. 1992; sponsored by the Space Engineering Center for Health Management Technology
 (Contract RTOP 584-03-11)
 (NASA-TM-106097; E-7738; NAS 1.15:106097) Avail: CASI HC A03/MF A01

We investigate the performance of a nonlinear estimation scheme applied to the estimation of several parameters in a performance model of the Space Shuttle Main Engine. The nonlinear estimator is based upon the extended Kalman filter which has been augmented to provide estimates of several key performance variables. The estimated parameters are directly related to the efficiency of both the low pressure and high pressure fuel turbopumps. Decreases in the parameter estimates may be interpreted as degradations in turbine and/or pump efficiencies which can be useful measures for an online health monitoring algorithm. This paper extends previous work which has focused on off-line parameter estimation by investigating the filter's on-line potential from a computational standpoint. In addition, we examine the robustness of the algorithm to unmodeled dynamics. The filter uses a reduced-order model of the engine that includes only fuel-side dynamics. The on-line results produced during this study are comparable to off-line results generated previously. The results show that the parameter estimates are sensitive to dynamics not included in the filter model. Off-line results using an extended Kalman filter with a full order engine model to address the robustness problems of the reduced-order model are also presented. Author

N93-26561*# National Aeronautics and Space Administration. Lewis Research Center, Cleveland, OH.

MEASUREMENT AND ANALYSIS OF A SMALL NOZZLE PLUME IN VACUUM

P. F. PENKO, I. D. BOYD (Eloret Corp., Moffett Field, CA.), D. L. MEISSNER (Toledo Univ., OH.), and K. J. DEWITT (Toledo Univ., OH.) Apr. 1993 18 p Presented at the 28th Joint Propulsion Conference and Exhibit, Nashville, TN, 6-8 Jul. 1992; sponsored by AIAA, SAE, ASME, and ASEE Previously announced in IAA as A92-48748
 (Contract RTOP 506-42-31)

C-2

(NASA-TM-106066; E-7383; NAS 1.26:106066; AIAA PAPER 92-3108) Avail: CASI HC A03/MF A01

Pitot pressures and flow angles are measured in the plume of a nozzle flowing nitrogen and exhausting to a vacuum. Total pressures are measured with Pitot tubes sized for specific regions of the plume and flow angles measured with a conical probe. The measurement area for total pressure extends 480 mm (16 exit diameters) downstream of the nozzle exit plane and radially to 60 mm (1.9 exit diameters) off the plume axis. The measurement area for flow angle extends to 160 mm (5 exit diameters) downstream and radially to 60 mm. The measurements are compared to results from a numerical simulation of the flow that is based on kinetic theory and uses the direct-simulation Monte Carlo (DSMC) method. Comparisons of computed results from the DSMC method with measurements of flow angle display good agreement in the far-field of the plume and improve with increasing distance from the exit plane. Pitot pressures computed from the DSMC method are in reasonably good agreement with experimental results over the entire measurement area. Author

N93-26908* # National Aeronautics and Space Administration. Lewis Research Center, Cleveland, OH.

NUCLEAR PROPULSION TECHNICAL INTERCHANGE MEETING, VOLUME 1

1993 567 p Meeting held in Sandusky, OH, 20-23 Oct. 1992 (Contract RTOP 506-49-00)

(NASA-CP-10116-VOL-1; E-7638-VOL-1; NAS 1.55:10116-VOL-1) Avail: CASI HC A24/MF A04

The Nuclear Propulsion Technical Interchange Meeting (NP-TIM-92) was sponsored and hosted by the Nuclear Propulsion Office at the NASA Lewis Research Center. The purpose of the meeting was to review the work performed in fiscal year 1992 in the areas of nuclear thermal and nuclear electric propulsion technology development. These proceedings are a compilation of the presentations given at the meeting (many of the papers are presented in outline or viewgraph form). Volume 1 covers the introductory presentations and the system concepts and technology developments related to nuclear thermal propulsion.

N93-26912* # National Aeronautics and Space Administration. Lewis Research Center, Cleveland, OH.

FOCUSED TECHNOLOGY: NUCLEAR PROPULSION

THOMAS J. MILLER *In its* Nuclear Propulsion Technical Interchange Meeting, Volume 1 p 21-23 1993

Avail: CASI HC A01/MF A04

Five viewgraphs are presented that outline the objectives and elements of the Nuclear Propulsion Program, mission considerations, propulsion technologies, and the logic flow path for nuclear propulsion development. CASI

N93-26915* # National Aeronautics and Space Administration. Lewis Research Center, Cleveland, OH.

SYSTEMS OVERVIEW

ROBERT CORBAN *In its* Nuclear Propulsion Technical Interchange Meeting, Volume 1 p 42-47 1993

Avail: CASI HC A02/MF A04

Charts and accompanying text are presented that provide a brief synopsis of the contracted efforts for FY-92 in assessing nuclear thermal propulsion requirements, concepts, and associated issues. The objective of the effort is to provide NASA LeRC with assistance in space nuclear propulsion system requirements management and public acceptance planning. CASI

N93-26926* # National Aeronautics and Space Administration. Lewis Research Center, Cleveland, OH.

NTP COMPARISON PROCESS

ROBERT CORBAN *In its* Nuclear Propulsion Technical Interchange Meeting, Volume 1 p 430-437 1993

Avail: CASI HC A02/MF A04

The systems engineering process for the concept definition phase of the program involves requirements definition, system definition, and consistent concept definition. The requirements definition process involves obtaining a complete understanding of

the system requirements based on customer needs, mission scenarios, and nuclear thermal propulsion (NTP) operating characteristics. A system functional analysis is performed to provide a comprehensive traceability and verification of top-level requirements down to detailed system specifications and provides significant insight into the measures of system effectiveness to be utilized in system evaluation. The second key element in the process is the definition of system concepts to meet the requirements. This part of the process involves engine system and reactor contractor teams to develop alternative NTP system concepts that can be evaluated against specific attributes, as well as a reference configuration against which to compare system benefits and merits. Quality function deployment (QFD), as an excellent tool within Total Quality Management (TQM) techniques, can provide the required structure and provide a link to the voice of the customer in establishing critical system qualities and their relationships. The third element of the process is the consistent performance comparison. The comparison process involves validating developed concept data and quantifying system merits through analysis, computer modeling, simulation, and rapid prototyping of the proposed high risk NTP subsystems. The maximum amount possible of quantitative data will be developed and/or validated to be utilized in the QFD evaluation matrix. If upon evaluation of a new concept or its associated subsystems determine to have substantial merit, those features will be incorporated into the reference configuration for subsequent system definition and comparison efforts. Derived from text

N93-26927* # National Aeronautics and Space Administration. Lewis Research Center, Cleveland, OH.

NUCLEAR THERMAL PROPULSION TECHNOLOGY OVERVIEW

JAMES R. STONE *In its* Nuclear Propulsion Technical Interchange Meeting, Volume 1 p 439-444 1993

Avail: CASI HC A02/MF A04

Viewgraphs on nuclear thermal propulsion technology overview are presented. Topics covered include non-nuclear material; instrumentation, controls, and health monitoring; turbopumps; nozzle and extension; and exhaust plume characteristics. CASI

N93-26951* # National Aeronautics and Space Administration. Lewis Research Center, Cleveland, OH.

NUCLEAR PROPULSION TECHNICAL INTERCHANGE MEETING, VOLUME 2

1993 581 p Meeting held in Sandusky, OH, 20-23 Oct. 1992 (Contract RTOP 506-49-00)

(NASA-CP-10116-VOL-2; E-7638-VOL-2; NAS 1.55:10116-VOL-2) Avail: CASI HC A25/MF A06

The purpose of the meeting was to review the work performed in fiscal year 1992 in the areas of nuclear thermal and nuclear electric propulsion technology development. These proceedings are an accumulation of the presentations provided at the meeting along with annotations provided by authors. The proceedings cover system concepts, technology development, and system modeling for nuclear thermal propulsion (NTP) and nuclear electric propulsion (NEP). The test facilities required for the development of the nuclear propulsion systems are also discussed.

N93-26952* # National Aeronautics and Space Administration. Lewis Research Center, Cleveland, OH.

OVERVIEW OF NASA/DOE/DOD INTERAGENCY MODELING TEAM AND ACTIVITIES

JAMES T. WALTON *In its* Nuclear Propulsion Technical Interchange Meeting, Volume 2 p 562-572 1993

Avail: CASI HC A25/MF A06

The topics are presented in viewgraph form and include the following: background, team mission, team objective, future direction, and concluding remarks. Derived from text

N93-26962* # National Aeronautics and Space Administration. Lewis Research Center, Cleveland, OH.

ROCKET ENGINE NUMERICAL SIMULATOR

20 SPACECRAFT PROPULSION AND POWER

KEN DAVIDIAN *In its* Nuclear Propulsion Technical Interchange Meeting, Volume 2 p 732-739 1993
Avail: CASI HC A02/MF A06

The topics are presented in viewgraph form and include the following: a rocket engine numerical simulator (RENS) definition; objectives; justification; approach; potential applications; potential users; RENS work flowchart; RENS prototype; and conclusion.
Derived from text

N93-26971*# National Aeronautics and Space Administration. Lewis Research Center, Cleveland, OH.

THE 20 KWE NEP SYSTEM STUDIES

JEFFREY A. GEORGE *In its* Nuclear Propulsion Technical Interchange Meeting, Volume 2 p 798-806 1993
Avail: CASI HC A02/MF A06

The topics are presented in viewgraph form and include the following: initial study groundrules; power system groundrules/assumptions; power technologies assessment; prototype SP-100 system specific mass; custom SP-100 system specific mass; radiator packaging limits; Brayton system specific mass and radiator area; thermoelectric specific mass and radiator area; specific mass for prototype vs. custom SP-100-based systems; system packaging limits on power level (kWe); and a conceptual nuclear electric propulsion (NEP) science mission spacecraft design.
CASI

N93-26977*# National Aeronautics and Space Administration. Lewis Research Center, Cleveland, OH.

NEP TECHNOLOGY: FY 1992 MILESTONES (NASA LERC)

JIM SOVEY *In its* Nuclear Propulsion Technical Interchange Meeting, Volume 2 p 992-999 1993
Avail: CASI HC A02/MF A06

A discussion of Nuclear Electric Propulsion (NEP) thrusters and facilities is presented in vugraph form. The NEP thrusters are discussed in the context of the following three items: (1) establishing a 100 H test capability for 100-kW magnetoplasmadynamic (MPD) thrusters; (2) demonstrating a lightweight 20-kW krypton ion thruster; and (3) the optimization of the design of low-mass power processor transformers. The primary accomplishment at NEP facilities was the completion of the Electric Propulsion Laboratory's (EPL's) tank 5 cryopump upgrade.
CASI

N93-26978*# National Aeronautics and Space Administration. Lewis Research Center, Cleveland, OH.

POWER MANAGEMENT AND DISTRIBUTION TECHNOLOGY

JOHN ELLIS DICKMAN *In its* Nuclear Propulsion Technical Interchange Meeting, Volume 2 p 1000-1008 1993
Avail: CASI HC A02/MF A06

Power management and distribution (PMAD) technology is discussed in the context of developing working systems for a piloted Mars nuclear electric propulsion (NEP) vehicle. The discussion is presented in vugraph form. The following topics are covered: applications and systems definitions; high performance components; the Civilian Space Technology Initiative (CSTI) high capacity power program; fiber optic sensors for power diagnostics; high temperature power electronics; 200 C baseplate electronics; high temperature component characterization; a high temperature coaxial transformer; and a silicon carbide mostet.
CASI

N93-26979*# National Aeronautics and Space Administration. Lewis Research Center, Cleveland, OH.

RADIATOR TECHNOLOGY

ALBERT J. JUHASZ *In its* Nuclear Propulsion Technical Interchange Meeting, Volume 2 p 1009-1026 1993
Avail: CASI HC A03/MF A06

Radiator technology is discussed in the context of the Civilian Space Technology Initiative's (CSTI's) high capacity power-thermal management project. The CSTI project is a subset of a project to develop a piloted Mars nuclear electric propulsion (NEP) vehicle. The following topics are presented in vugraph form: advanced radiator concepts; heat pipe codes and testing; composite materials; radiator design and integration; and surface morphology.
CASI

N93-26983*# National Aeronautics and Space Administration. Lewis Research Center, Cleveland, OH.

THE 20 KWE NEP FLIGHT SYSTEM

JIM GILLAND *In its* Nuclear Propulsion Technical Interchange Meeting, Volume 2 p 1063-1077 1993 Prepared in cooperation with Sverdrup Technology, Inc., Brook Park, OH
Avail: CASI HC A03/MF A06

A low-power, near-term nuclear electric propulsion (NEP) system was proposed as a useful interim system for near-term space exploration. Although the ultimate goal of a 100 kWe class, low specific mass for planetary exploration remains, application of the technologies that are currently mature to earlier missions of interest has grown at the higher levels of NASA. In response to this interest, a study of low-power system and mission options was initiated, with the Nuclear Propulsion Office serving to coordinate system activities. A nominal 20 kWe system using Brayton power conversion was selected by the joint NASA/DOE Space Nuclear Power and Propulsion team; however, other power levels and system options will be considered. NASA's Office of Space Science and Applications has expressed interest in exploiting NEP's mission capabilities, both in the near-term and for more difficult, later missions. Technologies considered mature for this type of system are the SP-100 reactor, Brayton dynamic power conversion, and 30 cm ion thrusters, all of which have extensive ground demonstration backgrounds.
Author (revised)

N93-26984*# National Aeronautics and Space Administration. Lewis Research Center, Cleveland, OH.

THE 100-500 KWE NEP SYSTEMS

JEFFREY A. GEORGE *In its* Nuclear Propulsion Technical Interchange Meeting, Volume 2 p 1078-1084 1993
Avail: CASI HC A02/MF A06

Systems technology for nuclear electric propulsion (NEP) vehicles is discussed. The following topics are discussed: the SP-100 reactor; dynamic power conversion; heat rejection; and krypton ion thrusters. The discussion is presented in vugraph form.
CASI

N93-26985*# National Aeronautics and Space Administration. Lewis Research Center, Cleveland, OH.

NUCLEAR ELECTRIC PROPULSION OPTIONS FOR PILOTED MARS MISSIONS

JEFFREY A. GEORGE *In its* Nuclear Propulsion Technical Interchange Meeting, Volume 2 p 1085-1094 1993
Avail: CASI HC A02/MF A06

Three nuclear electric propulsion (NEP) systems are discussed. The three systems are as follows: a system based on current SP-100 technology; a potassium Rankine-cycle based power conversion system, and an argon ion thruster system. The system will be researched for implementation in several possible vehicle configurations. The following are among the possible Mars vehicle configurations: a piloted 15 MWe multi-reactor vehicle; a piloted 10 MWe vehicle with ECCV; a piloted 10 MWe modular vehicle; piloted 10 and 15 MWe vehicles with ECCV and MEV; a piloted 5 MWe vehicle with ECCV; a 5 MWe cargo vehicle with 2 MEV's; and a 2.5 MWe vehicle with MEV.
CASI

N93-26986*# National Aeronautics and Space Administration. Lewis Research Center, Cleveland, OH.

NEP SYSTEMS MODEL

JIM GILLAND and JEFFREY A. GEORGE *In its* Nuclear Propulsion Technical Interchange Meeting, Volume 2 p 1095-1098 1993 Prepared in cooperation with Sverdrup Technology, Inc., Brook Park, OH
Avail: CASI HC A01/MF A06

Various aspects of nuclear electric propulsion (NEP) systems analysis and modeling are discussed. The following specific topics are covered: (1) systems analysis challenges; (2) goals for NEP systems analysis; (3) the Nuclear Propulsion Office approach; and (4) NEP subsystem model development. The discussion is presented in vugraph form.
CASI

N93-26987*# National Aeronautics and Space Administration. Lewis Research Center, Cleveland, OH.

NEP SYSTEMS MODEL

JEFFREY A. GEORGE *In its Nuclear Propulsion Technical Interchange Meeting, Volume 2 p 1098-1102 1993*
 Avail: CASI HC A01/MF A06

A new nuclear electric propulsion (NEP) systems analysis code is discussed. The new code is modular and consists of a driver code and various subsystem models. The code models five different subsystems: (1) reactor/shield; (2) power conversion; (3) heat rejection; (4) power management and distribution (PMAD); and (5) thrusters. The code optimizes for the following design criteria: minimum mass; minimum radiator area; and low mass/low area. The code also optimizes the following parameters: separation distance; temperature ratio; pressure ratio; and transmission frequency. The discussion is presented in vugraph form. CASI

N93-26988*# National Aeronautics and Space Administration. Lewis Research Center, Cleveland, OH.

THRUSTER MODELS FOR NEP SYSTEM ANALYSIS

JIM GILLAND *In its Nuclear Propulsion Technical Interchange Meeting, Volume 2 p 1103-1118 1993* Prepared in cooperation with Sverdrup Technology, Inc., Brook Park, OH
 Avail: CASI HC A03/MF A06

There are currently no thruster modeling codes that can be integrated with power system codes for full propulsion system modeling. Most existing thruster models were written from a 'stand alone' viewpoint, assuming the user is performing analyses on thruster performance alone. The goal of the present modeling effort is to develop thruster codes that model performance and scaling as a function of mission and system inputs, rather than in terms of more elemental physical parameters. System level parameters of interest are as follows: performance, such as specific impulse and efficiency; terminal characteristics, such as voltage or current; and mass. Specific impulse and efficiency couple with mission analyses, while terminal characteristics allow integration with power systems. Additional information on lifetime and operation may be required for detailed designs. Author (revised)

N93-27022*# National Aeronautics and Space Administration. Lewis Research Center, Cleveland, OH.

RELIABILITY STUDIES OF INTEGRATED MODULAR ENGINE SYSTEM DESIGNS

TERRY L. HARDY and DOUGLAS C. RAPP (Sverdrup Technology, Inc., Cleveland, OH.) Jun. 1993 19 p Proposed for presentation at the 29th Joint Propulsion Conference and Exhibit, Monterey, CA, 28-30 Jun. 1992; sponsored by AIAA, SAE, ASME, and ASEE
 (Contract RTOP 468-02-11)

(NASA-TM-106178; E-7774; NAS 1.15:106178; AIAA PAPER 93-1886) Avail: CASI HC A03/MF A01

A study was performed to evaluate the reliability of Integrated Modular Engine (IME) concepts. Comparisons were made between networked IME systems and non-networked discrete systems using expander cycle configurations. Both redundant and non-redundant systems were analyzed. Binomial approximation and Markov analysis techniques were employed to evaluate total system reliability. In addition, Failure Modes and Effects Analyses (FMEA), Preliminary Hazard Analyses (PHA), and Fault Tree Analysis (FTA) were performed to allow detailed evaluation of the IME concept. A discussion of these system reliability concepts is also presented. Author

N93-27039*# National Aeronautics and Space Administration. Lewis Research Center, Cleveland, OH.

SOLAR ARRAY ELECTRICAL PERFORMANCE ASSESSMENT FOR SPACE STATION FREEDOM

BRYAN K. SMITH and HOLLY BRISCO (Lockheed Missiles and Space Co., Sunnyvale, CA.) May 1993 13 p Presented at the Aerospace Design Conference, Irvine, CA, 16-19 Feb. 1993; cosponsored by AIAA, AHS, and ASEE Previously announced in IAA as A93-30956

(Contract RTOP 474-46-10)

(NASA-TM-106161; E-7748; NAS 1.15:106161) Avail: CASI HC A03/MF A01

Electrical power for Space Station Freedom will be generated by large Photovoltaic arrays with a beginning of life power requirement of 30.8 kW per array. The solar arrays will operate in a Low Earth Orbit (LEO) over a design life of fifteen years. This paper provides an analysis of the predicted solar array electrical performance over the design life and presents a summary of supporting analysis and test data for the assigned model parameters and performance loss factors. Each model parameter and loss factor is assessed based upon program requirements, component analysis, and test data to date. A description of the LMSC performance model, future test plans, and predicted performance ranges are also given. Author (revised)

N93-27963*# National Aeronautics and Space Administration. Lewis Research Center, Cleveland, OH.

AN EVOLUTION STRATEGY FOR LUNAR NUCLEAR SURFACE POWER

LEE S. MASON *In Arizona Univ., Proceedings of the Lunar Materials Technology Symposium 14 p Feb. 1992*
 Avail: CASI HC A03/MF A03

The production and transmission of electric power for a permanently inhabited lunar base poses a significant challenge which can best be met through an evolution strategy. Nuclear systems offer the best opportunity for evolution in terms of both life and performance. Applicable nuclear power technology options include isotope systems (either radioisotope thermoelectric generators or dynamic isotope power systems) and reactor systems with either static (thermoelectric or thermionic) or dynamic (Brayton, Stirling, Rankine) conversion. A power system integration approach that takes evolution into account would benefit by reduced development and operations cost, progressive flight experience, and simplified logistics, and would permit unrestrained base expansion. For the purposes of defining a nuclear power system evolution strategy, the lunar base development shall consist of four phases: precursor, emplacement, consolidation, and operations. Author (revised)

N93-28619*# National Aeronautics and Space Administration. Lewis Research Center, Cleveland, OH.

SMALL HYDROGEN/OXYGEN ROCKET FLOWFIELD BEHAVIOR FROM HEAT FLUX MEASUREMENTS

BRIAN D. REED Jun. 1993 30 p Presented at the 29th Joint Propulsion Conference and Exhibit, Monterey, CA, 28-30 Jun. 1993; sponsored by AIAA, SAE, ASME, and ASEE
 (Contract RTOP 506-42-31)

(NASA-TM-106233; E-7953; NAS 1.15:106233; AIAA PAPER 93-2162) Avail: CASI HC A03/MF A01

The mixing and heat transfer phenomena in small rocket flow fields with fuel film cooling is not well understood. An instrumented, water-cooled chamber with a gaseous hydrogen/gaseous oxygen injector was used to gather steady-state inner and outer wall temperature profiles. The chamber was tested at 414 kPa (60 psia) chamber pressure, from mixture ratios of 3.41 to 8.36. Sixty percent of the fuel was used for film cooling. These temperature profiles were used as boundary conditions in a finite element analysis program, MSC/NASTRAN, to calculate the local radial and axial heat fluxes in the chamber wall. The normal heat fluxes were then calculated and used as a diagnostic of the rocket's flow field behavior. The normal heat fluxes determined were on the order of 1.0 to 3.0 MW/meters squared (0.6 to 1.8 Btu/sec-inches squared). In the cases where mixture ratio was 5 or above, there was a sharp local heat flux maximum in the barrel section of the chamber. This local maximum seems to indicate a reduction or breakdown of the fuel film cooling layer, possibly due to increased mixing in the shear layer between the film and core flows. However, the flow was thought to be completely laminar, as the throat Reynolds numbers were below 50,000 for all the cases. The increased mixing in the shear layer in the higher mixture ratio cases appeared not to be due to the transition of the flow

20 SPACECRAFT PROPULSION AND POWER

from laminar to turbulent, but rather due to increased reactions between the hydrogen film and oxidizer-rich core flows.

Author (revised)

N93-28686*# National Aeronautics and Space Administration. Lewis Research Center, Cleveland, OH.

SMALL STIRLING DYNAMIC ISOTOPE POWER SYSTEM FOR ROBOTIC SPACE MISSIONS

D. J. BENTS Aug. 1992 18 p Presented at the Nuclear Technologies for Space Exploration, Jackson Hole, WY, 16-19 Aug. 1992; sponsored by American Nuclear Society (Contract RTOP 596-13-11) (NASA-TM-105785; E-7215; NAS 1.15:105785) Avail: CASI HC A03/MF A01

The design of a multihundred-watt Dynamic Isotope Power System (DIPS), based on the U.S. Department of Energy (DOE) General Purpose Heat Source (GPHS) and small (multihundred-watt) free-piston Stirling engine (FPSE), is being pursued as a potential lower cost alternative to radioisotope thermoelectric generators (RTG's). The design is targeted at the power needs of future unmanned deep space and planetary surface exploration missions ranging from scientific probes to Space Exploration Initiative precursor missions. Power level for these missions is less than a kilowatt. The incentive for any dynamic system is that it can save fuel and reduce costs and radiological hazard. Unlike DIPS based on turbomachinery conversion (e.g. Brayton), this small Stirling DIPS can be advantageously scaled to multihundred-watt unit size while preserving size and mass competitiveness with RTG's. Stirling conversion extends the competitive range for dynamic systems down to a few hundred watts--a power level not previously considered for dynamic systems. The challenge for Stirling conversion will be to demonstrate reliability and life similar to RTG experience. Since the competitive potential of FPSE as an isotope converter was first identified, work has focused on feasibility of directly integrating GPHS with the Stirling heater head. Thermal modeling of various radiatively coupled heat source/heater head geometries has been performed using data furnished by the developers of FPSE and GPHS. The analysis indicates that, for the 1050 K heater head configurations considered, GPHS fuel clad temperatures remain within acceptable operating limits. Based on these results, preliminary characterizations of multihundred-watt units have been established.

Author (revised)

N93-28694*# National Aeronautics and Space Administration. Lewis Research Center, Cleveland, OH.

PRELIMINARY ENDURANCE TESTS OF WATER VAPORIZERS FOR RESISTOJET APPLICATIONS

W. EARL MORREN and GREGORY S. MACRAE Jun. 1993 27 p Presented at the 29th Joint Propulsion Conference and Exhibit, Monterey, CA, 28-30 Jun. 1993; cosponsored by AIAA, SAE, ASME, and ASEE (Contract RTOP 506-42-31) (NASA-TM-106222; E-7871; NAS 1.15:106222; AIAA PAPER 93-2403) Avail: CASI HC A03/MF A01

Three water vaporizers designed for resistojets applications were built and tested for periods up to 500 h and 250 thermal cycles. Two of the vaporizers were not sensitive to orientation with respect to gravity, an indication of likely compatibility with low-gravity environments. Some temperatures and pressures in the third were impacted by orientation, although operation was always stable. The pressure drop across the sand-filled version increased by 147 percent in 38 h and 19 thermal cycles. Bonding of the sand granules in the downstream end of the heat exchanger was the suspected cause of failure of this vaporizer. Pressure drops across the two sintered stainless steel-filled versions were more gradual. One, with a pore size of 60 microns, showed an 80 percent increase in 500 h and 250 thermal cycles and another, with a 10 microns poresize, showed a 29 percent increase in 350 h and 175 thermal cycles. Testing of the latter metal-filled vaporizer was ongoing as of this writing. Oxidation of the porous metal packing materials in these vaporizers, with subsequent deposition

of oxide particles within the pores, was believed to have caused the observed increases in pressure drops.

Author (revised)

N93-28713*# National Aeronautics and Space Administration. Lewis Research Center, Cleveland, OH.

TANK PRESSURE CONTROL EXPERIMENT/THERMAL PHENOMENA (TPCE/TP)

M. M. HASAN and R. H. KNOLL In NASA, Washington, NASA/DOD Flight Experiments Technical Interchange Meeting Proceedings 18 p 1992

Avail: CASI HC A03/MF A10

The 'Tank Pressure Control Experiment/Thermal Phenomena (TPCE/TP)' is a reflight of the tank pressure control experiment (TPCE), flown on STS-43 in a standard Get-Away Special (GAS) container in August 1991. The TPCE obtained extensive video and digital data of the jet induced mixing process in a partially filled tank in low gravity environments. It also provided limited data on the thermal processes involved. The primary objective of the reflight of TPCE is to investigate experimentally the phenomena of liquid superheating and pool nucleate boiling at very low heat fluxes in a long duration low gravity environment. The findings of this experiment will be of direct relevance to space based subcritical cryogenic fluid system design and operation. Experiment hardware and results from the first TPCE are described in outline and graphic form.

Author (revised)

N93-29158*# National Aeronautics and Space Administration. Lewis Research Center, Cleveland, OH.

PRELIMINARY INVESTIGATION OF HIGH POWER MICROWAVE PLASMAS FOR ELECTROTHERMAL THRUSTER USE

JOHN L. POWER and DANIEL J. SULLIVAN Jun. 1993 18 p Presented at the 29th Joint Propulsion Conference and Exhibit, Monterey, CA, 28-30 Jun. 1993; sponsored by AIAA, SAE, ASME, and ASEE Original contains color illustrations (Contract RTOP 506-42-31) (NASA-TM-106207; E-7917; NAS 1.15:106207; AIAA PAPER 93-2106) Avail: CASI HC A03/MF A01; 1 functional color page

Results are reported from preliminary tests to evaluate the high power microwave electrothermal thruster (MET) concept, which employs a free-floating plasma discharge maintained by applied CW microwave power to heat a propellant gas flow. Stable plasmas have been created and maintained in helium (He), nitrogen (N₂), and hydrogen (H₂) as propellants in both the TM(sub 011) and TM(sub 012) modes at discharge pressures from 10 Pa to 69 kPa. Reproducible starting conditions of pressure and power have been documented for all the plasmas. Vortical inflow of the propellant gas was observed to cause the formation of on-axis 'spike' plasmas. The formation and unformation conditions of these plasmas were studied. Operation in the spike plasma condition enables maximum power absorption with minimum wall heating and offers maximum efficiency in heating the propellant gas. In the spike condition, plasmas of the three propellant gases were investigated in an open channel configuration to a maximum applied power level of 11.2 kW (in N₂). Microwave power coupling efficiencies of over 90 percent were routinely obtained at absorbed power levels up to 2 kW. Magnetic nozzle effects were investigated with a superconducting solenoid Al magnet applying a high magnetic field to the plasmas in and exiting from the discharge tube.

Author (revised)

N93-29194*# National Aeronautics and Space Administration. Lewis Research Center, Cleveland, OH.

GRAVITY SENSITIVITY OF A RESISTOJET WATER VAPORIZER

W. EARL MORREN Jun. 1993 24 p Presented at the 29th Joint Propulsion Conference and Exhibit, Monterey, CA, 28-30 Jun. 1993; cosponsored by AIAA, SAE, ASME, ASEE (Contract RTOP 506-42-31)

(NASA-TM-106220; E-7870; NAS 1.15:106220; AIAA PAPER 93-2402) Avail: CASI HC A03/MF A01

A laboratory model of a water vaporizer for resistojets applications was designed, fabricated, and steady and transient

characteristics were measured. Vaporizer operation was not impacted by rotation about a horizontal axis normal to its own. The vaporizer was operated under low and high accelerations aboard a jet aircraft for periods up to 25 s at flow rates ranging from 159(10)(exp -6) to 230(10)(exp -6) kg/s. Slight changes in inlet and outlet pressures and some heat exchanger temperatures were observed during the low-gravity tests. However, the results of these tests indicated probable compatibility of the vaporizer design tested with a low-gravity environment. Author (revised)

N93-31552*# National Aeronautics and Space Administration. Lewis Research Center, Cleveland, OH.

STRUCTURAL INTEGRITY AND DURABILITY OF REUSABLE SPACE PROPULSION SYSTEMS

May 1991 288 p Conference held in Cleveland, OH, 14-15 May 1991

(Contract RTOP 553-13-00)

(NASA-CP-10064; E-6068; NAS 1.55:10064) Avail: CASI HC A13/MF A03

A two-day conference on the structural integrity and durability of reusable space propulsion systems was held on 14 to 15 May 1991 at the NASA Lewis Research Center. Presentations were made by industry, university, and government researchers organized into four sessions: (1) aerothermodynamic loads; (2) instrumentation; (3) fatigue, fracture, and constitutive modeling; and (4) structural dynamics. The principle objectives were to disseminate research results and future plans in each of four areas. This publication contains extended abstracts and the visual material presented during the conference. Particular emphasis is placed on the Space Shuttle Main Engine (SSME) and the SSME turbopump.

N93-31581*# National Aeronautics and Space Administration. Lewis Research Center, Cleveland, OH.

LIFE EXTENDING CONTROL: AN INTERDISCIPLINARY ENGINEERING THRUST

CARL F. LORENZO and WALTER C. MERRILL *In its* Structural Integrity and Durability of Reusable Space Propulsion Systems p 229-237 May 1991

Avail: CASI HC A02/MF A03

The concept of Life Extending Control (LEC) is introduced. Possible extensions to the cyclic damage prediction approach are presented based on the identification of a model from elementary forms. Several candidate elementary forms are presented. These extensions will result in a continuous or differential form of the damage prediction model. Two possible approaches to the LEC based on the existing cyclic damage prediction method, the measured variables LEC and the estimated variables LEC, are defined. Here, damage estimates or measurements would be used directly in the LEC. A simple hydraulic actuator driven position control system example is used to illustrate the main ideas behind LEC. Results from a simple hydraulic actuator example demonstrate that overall system performance (dynamic plus life) can be maximized by accounting for component damage in the control design. Derived from text

N93-31583*# National Aeronautics and Space Administration. Lewis Research Center, Cleveland, OH.

OVERVIEW OF AEROTHERMODYNAMIC LOADS DEFINITION STUDY

RAYMOND E. GAUGLER *In its* Structural Integrity and Durability of Reusable Space Propulsion Systems p 247-254 May 1991

Avail: CASI HC A02/MF A03

The objective of the Aerothermodynamic Loads Definition Study is to develop methods of accurately predicting the operating environment in advanced Earth-to-Orbit (ETO) propulsion systems, such as the Space Shuttle Main Engine (SSME) powerhead. Development of time averaged and time dependent three dimensional viscous computer codes as well as experimental verification and engine diagnostic testing are considered to be essential in achieving that objective. Time-averaged, nonsteady, and transient operating loads must all be well defined in order to accurately predict powerhead life. Described here is work in

unsteady heat flow analysis, improved modeling of preburner flow, turbulence modeling for turbomachinery, computation of three dimensional flow with heat transfer, and unsteady viscous multi-blade row turbine analysis. Derived from text

N93-31585*# National Aeronautics and Space Administration. Lewis Research Center, Cleveland, OH.

THREE-DIMENSIONAL FLOW CALCULATIONS INSIDE SSME GGGT FIRST STAGE BLADE ROWS

CHUNILL HAH, STEVEN NASH (Sverdrup Technology, Inc., Brook Park, OH.), and GREGORY SWARTWOUT *In its* Structural Integrity and Durability of Reusable Space Propulsion Systems p 263-271 May 1991

Avail: CASI HC A02/MF A03

A numerical analysis of the first stage of the Space Shuttle Main Engine (SSME) GGGT was conducted using a 3-D Reynolds averaged Navier-Stokes flow solver. This turbine stage was designed to improve both aerodynamic efficiency and durability. The blade has an unconventional shape with a large blade thickness. No experimental data is available to verify the computational results. The objective of the current study is to analyze this turbine blade stage with a well established Navier-Stokes computational method in order to determine if the turbine is operating in the subsonic flow regime and if there are any significant separated flow regions. The stage was analyzed in a steady state flow condition. The inlet vane was analyzed with the flow conditions from the axisymmetric entire stage solution. The viscous flow solution of the first vane is used as the inlet flow condition for the rotor. Derived from text

N93-31858*# National Aeronautics and Space Administration. Lewis Research Center, Cleveland, OH.

NASA'S PROGRESS IN NUCLEAR ELECTRIC PROPULSION TECHNOLOGY

JAMES R. STONE, MICHAEL P. DOHERTY, and KEITH M. PEECOCK Jun. 1993 18 p Presented at the AIAA 29th Joint Propulsion Conference and Exhibit, Monterey, CA, 28-30 Jun. 1993; sponsored by AIAA, SAE, ASME, and ASEE

(Contract RTOP 584-04-21)

(NASA-TM-106272; E-8000; AIAA PAPER 93-1936; NAS 1.15:106272) Avail: CASI HC A03/MF A01

The National Aeronautics and Space Administration (NASA) has established a requirement for Nuclear Electric Propulsion (NEP) technology for robotic planetary science mission applications with potential future evolution to systems for piloted Mars vehicles. To advance the readiness of NEP for these challenging missions, a near-term flight demonstration on a meaningful robotic science mission is very desirable. The requirements for both near-term and outer planet science missions are briefly reviewed, and the near-term baseline system established under a recent study jointly conducted by the Lewis Research Center (LeRC) and the Jet Propulsion Laboratory (JPL) is described. Technology issues are identified where work is needed to establish the technology for the baseline system, and technology opportunities which could provide improvement beyond baseline capabilities are discussed. Finally, the plan to develop this promising technology is presented and discussed. Author

A93-13505 National Aeronautics and Space Administration. Lewis Research Center, Cleveland, OH.

TRIBOLOGICAL AND MICROSTRUCTURAL COMPARISON OF HIPPED PM212 AND PM212/AU SELF-LUBRICATING COMPOSITES

MICHAEL S. BOGDANSKI (Case Western Reserve Univ.,

23 CHEMISTRY AND MATERIALS (GENERAL)

Cleveland, OH), HAROLD E. SLINEY, and CHRISTOPHER DELLACORTE (NASA, Lewis Research Center, Cleveland, OH) *Lubrication Engineering* (ISSN 0024-7154) vol. 48, no. 11 Nov. 1992 p. 849-856. Previously announced in STAR as N92-26142 ASME and STLE, Joint Tribology Conference, San Diego, CA, Oct. 19-21, 1992 refs
(Contract RTOP 505-63-5A; DE-AI01-91CR-50306)
Copyright

The feasibility of replacing the silver with the volumetric equivalent of gold in the chromium carbide-based self-lubricating composite PM212 (70 wt percent NiCo-Cr₃C₂, 15 percent BaF₂/CaF₂ eutectic) was studied. The new composite, PM212/Au has the following composition: 62 wt percent NiCo-Cr₃C₂, 25 percent Au, 13 percent BaF₂/CaF₂ eutectic. The silver was replaced with gold to minimize the potential reactivity of the composite with possible environmental contaminants such as sulfur. The composites were fabricated by hot isostatic pressing (HIPping) and machined into pin specimens. The pins were slid against nickel-based superalloy disks. Sliding velocities ranged from 0.27 to 10.0 m/s and temperatures from 25 to 900 C. Frictions coefficients ranged from 0.25 to 0.40 and wear factors for the pin and disk were typically low 10(exp -5) cu mm/N-m. HIPped PM212 measured fully dense, whereas PM212/Au had 15 percent residual porosity. Examination of the microstructures with optical and scanning electron microscopy revealed the presence of pores in PM212/Au that were not present in PM212. Though the exact reason for the residual porosity PM212/Au was not determined, it may be due to practice morphology differences between the gold and silver and their effect on powder metallurgy processing.

Author

A93-13506 National Aeronautics and Space Administration. Lewis Research Center, Cleveland, OH.

TRIBOLOGICAL AND MECHANICAL COMPARISON OF SINTERED AND HIPPED PM212 - HIGH TEMPERATURE SELF-LUBRICATING COMPOSITES

CHRISTOPHER DELLACORTE, HAROLD E. SLINEY (NASA, Lewis Research Center, Cleveland, OH), and MICHAEL S. BOGDANSKI (Case Western Reserve Univ., Cleveland, OH) *Lubrication Engineering* (ISSN 0024-7154) vol. 48, no. 11 Nov. 1992 p. 877-885. Previously announced in STAR as N92-15128 STLE, Annual Meeting, 47th, Philadelphia, PA, May 4-7, 1992 refs
(Contract RTOP 505-63-1A)
Copyright

Selected tribological, mechanical and thermophysical properties of two versions of PM212 (sintered and hot isostatically pressed, HIPped) are compared. PM212, a high temperature self-lubricating composite, contains 70 wt percent metal bonded chromium carbide, 15 wt percent CaF₂/BaF₂ eutectic and 15 wt percent silver. PM212 in the sintered form is about 80 percent dense and has previously been shown to have good tribological properties from room temperature to 850 C. Tribological results of a fully densified, HIPped version of PM212 are given. They are compared to sintered PM212. In addition, selected mechanical and thermophysical properties of both types of PM212 are discussed and related to the tribological similarities and differences between the two PM212 composites. In general, both composites display similar friction and wear properties. However, the fully dense PM212 HIPped composite exhibits slight lower friction and wear than sintered PM212. This may be attributed to its generally higher strength properties. The sintered version displays stable wear properties over a wide load range indicating its promise for use in a variety of applications. Based upon their properties, both the sintered and HIPped PM212 have potential as bearing and seal materials for advanced high temperature applications.

Author

A93-35700 National Aeronautics and Space Administration. Lewis Research Center, Cleveland, OH.

BENZONORBORNADIENE END CAPS FOR PMR RESINS

MICHAEL J. PANIGOT (Case Western Reserve Univ., Cleveland, OH), JOHN F. WATERS (Case Western Reserve Univ.; NASA, Lewis Research Center, Cleveland, OH), UDAY VARDE (Case Western Reserve Univ., Cleveland, OH), JAMES K. SUTTER

(NASA, Lewis Research Center, Cleveland, OH), and CHAIM N. SUKENIK (Case Western Reserve Univ., Cleveland, OH) *Macromolecules* (ISSN 0024-9297) vol. 25 Jan. 20, 1992 p. 530-534. Research supported by NASA refs
Copyright

Several ortho-disubstituted benzonorbornadiene derivatives are described. These molecules contain acid, ester, or anhydride functionality permitting their use as end caps in PMR (polymerization of monomer reactants) polyimide systems. The replacement of the currently used norbornenyl end caps with benzonorbornadienyl end caps affords resins of increased aromatic content. It also allows evaluation of some mechanistic aspects of PMR cross-linking. Initial testing of N-phenylimide model compounds and of actual resin formulations using the benzonorbornadienyl end cap reveals that they undergo efficient thermal crosslinking to give oligomers with physical properties and thermal stability comparable to commercial norbornene-end-capped PMR systems.

Author

A93-40618* National Aeronautics and Space Administration. Lewis Research Center, Cleveland, OH.

COMPUTER MODELING OF A HOT FILAMENT DIAMOND DEPOSITION REACTOR

MARIA A. KUCZMARSKI (NASA, Lewis Research Center, Cleveland, OH), PAUL A. WASHLOCK, and JOHN C. ANGUS (Case Western Reserve Univ., Cleveland, OH) *In Applications of diamond films and related materials; Proceedings of the 1st International Conference, Auburn, AL, Aug. 17-22, 1991 Amsterdam Elsevier 1991 p. 591-596. Research supported by Creare, Inc. and DARPA refs*
Copyright

A commercial fluid mechanics program, FLUENT, has been applied to the modeling of a hot-filament diamond deposition reactor. Streamlines and contours of constant temperature and species concentrations are obtained for practical reactor geometries and conditions. The modeling is presently restricted to two-dimensional simulations and to a chemical mechanism of ten independent homogeneous and surface reactions. Comparisons are made between predicted power consumption, substrate temperature, and concentrations of atomic hydrogen and methyl-radical with values taken from the literature. The results to date indicate that the modeling can aid in the rational design and analysis of practical reactor configurations.

Author

A93-53392* National Aeronautics and Space Administration. Lewis Research Center, Cleveland, OH.

THE EVOLUTION OF PROCUREMENT AND ASSURANCE METHODS USED TO PROOF AN ADVANCED SPACE MATERIAL

MARJORIE BERENDT and LEONARD G. RADO (Sheldahl, Inc., Northfield, MN) *In International SAMPE Technical Conference, 24th and International SAMPE Metals and Metals Processing Conference, 3rd, Toronto, Canada, Oct. 20-22, 1992, Proceedings. Vol. 24 Covina, CA Society for the Advancement of Material and Process Engineering 1992 p. T201-T211. Research supported by Rockwell International Corp. refs*
(Contract NAS3-25082)
Copyright

A development history and current performance evaluation is presented for a Kapton polyimide for the Space Station Freedom. Analyses of results obtained for this class of materials by the Long Duration Exposure Facility led to major revisions of procurement specifications and test requirements for this material. Attention is given to the use of oxygen plasma etching and blocking, as well as the evolution of test methodologies due to preproduction test data evaluations and the relationship between tests and product-improvement cycles.

AIAA

A93-53453* National Aeronautics and Space Administration. Lewis Research Center, Cleveland, OH.

OVERVIEW OF NASA'S ADVANCED HIGH TEMPERATURE ENGINE MATERIALS TECHNOLOGY PROGRAM

CAROL A. GINTY and HUGH R. GRAY (NASA, Lewis Research

Center, Cleveland, OH) /in International SAMPE Technical Conference, 24th and International SAMPE Metals and Metals Processing Conference, 3rd, Toronto, Canada, Oct. 20-22, 1992, Proceedings. Vol. 24 Covina, CA Society for the Advancement of Material and Process Engineering 1992 p. T1029-T1043. refs

NASA's 'HITEMP' program has been charged with development of propulsion systems technologies for next-generation civil and military aircraft, stressing high-temperature/low-density composites. These encompass polymer-matrix composites for fans, ducts, and compressor cases, and intermetallic and metallic alloy matrix composites for applications in turbine disks, blades, and vanes, and ceramic matrix composites for combustors and turbines. An overview is presented of program concerns and achievements to date.

AIAA

N93-10978*# National Aeronautics and Space Administration. Lewis Research Center, Cleveland, OH.

RELATIVE SLIDING DURABILITY OF CANDIDATE HIGH TEMPERATURE FIBER SEAL MATERIALS

CHRISTOPHER DELLACORTE and BRUCE M. STEINETZ Aug. 1992 21 p

(Contract RTOP 505-63-1A; RTOP 763-22-28)

(NASA-TM-105806; E-7236; NAS 1.15:105806) Avail: CASI HC A03/MF A01

The relative sliding durability behavior of six candidate ceramic fibers for high temperature sliding seal applications is reviewed and compared. Pin on disk tests were used to evaluate potential seal materials by sliding a tow or bundle of the candidate ceramic fiber against a superalloy test disk. Tests were conducted in air under a 2.65 N load, at a sliding velocity of 0.025 m/sec and at temperatures from 25 to 900 C. Friction was measured during the tests and fiber wear, indicated by the extent of fibers broken in the tow or bundle, was measured at the end of each test. For most of the fibers, friction and wear increase with test temperature. The relative fiber durability ranking correlates with tensile strength, indicating that tensile data, which is more readily available than sliding durability data, may be useful in predicting fiber wear behavior under various conditions. A dimensional analysis of the wear data shows that the fiber durability is related to a dimensionless durability ratio which represents the ratio of the fiber strength to the fiber stresses imposed by sliding. The analysis is applicable to fibers with similar diameters and elastic moduli. Based upon the results of the research program, three fiber candidates are recommended for further study as potential seal materials. They are a silicon based complex carbide-oxide fiber, an alumina-boria-silica and an aluminosilicate fiber.

Author

N93-15576*# National Aeronautics and Space Administration. Lewis Research Center, Cleveland, OH.

THE EFFECT OF PROCESSING AND COMPOSITIONAL CHANGES ON THE TRIBOLOGY OF PM212 IN AIR

MICHAEL S. BOGDANSKI (Case Western Reserve Univ., Cleveland, OH.), HAROLD E. SLINNEY, and CHRISTOPHER DELLACORTE 1993 16 p Preposed for presentation at the 1993 STLE Annual Meeting, Calgary, Alberta, 17-20 May 1993; sponsored by the Society of Tribologists and Lubrication Engineers

(Contract RTOP 505-63-5A)

(NASA-TM-105945; E-7462; NAS 1.15:105945) Avail: CASI HC A03/MF A01

The effects of processing and compositional variations on the tribological performance of PM212 were studied. PM212 is a self lubricating powder metallurgy composite, comprised of a wear resistant metal bonded chromium carbide matrix, containing the solid lubricants barium fluoride/calcium fluoride eutectic and silver. Several composites were formulated which had lubricant, matrix, and processing variations. Processing variations included sintering and hot isostatic pressing. Pins fabricated from the composites were slid against superalloys disks in a pin-on-disk tribometer to study the tribological properties. Several composites exhibited low friction and wear in sliding against a nickel based superalloy. The

tribological performance by several different composites showed that the composition of PM212 can be altered without dramatically affecting performance.

Author

N93-17412*# National Aeronautics and Space Administration. Lewis Research Center, Cleveland, OH.

SUBSTITUTED 1,1,1-TRIARYL 2,2,2-TRIFLUOROETHANES

AND PROCESSES FOR THEIR SYNTHESIS Patent Application WILLIAM B. ALSTON, inventor (to NASA) and ROY F. GRATZ, inventor (to NASA) 27 Nov. 1992 23 p

(NASA-CASE-LEW-14345-7; NAS 1.71:LEW-14345-7;

US-PATENT-APPL-SN-982350) Avail: CASI HC A03/MF A01

Synthetic procedures to tetraalkyls, tetraacids, and dianhydrides substituted 1,1,1-triaryl 2,2,2-trifluoroethanes, which comprises: (1) 1,1-bis(dialkylaryl) 1-aryl-2,2,2-trifluoroethane, (2) 1,1-bis(dicarboxyaryl) 1-aryl-2,2,2-trifluoroethane, or (3) cyclic dianhydride or diamine of 1,1-bis(dialkylaryl) 1-aryl-2,2,2-trifluoroethanes. The synthesis of (1) is accomplished by the condensation reaction of an aryltrifluoromethyl ketone with a dialkylaryl compound. The synthesis of (2) is accomplished by oxidation of (1). The synthesis dianhydride of (3) is accomplished by the conversion of (2) to its corresponding cyclic dianhydride. The synthesis of the diamine is accomplished by the similar reaction of an aryltrifluoromethyl ketone with aniline or alkyl substituted or disubstituted anilines. Also, other derivatives of the above are formed by nucleophilic displacement reactions.

NASA

N93-22586*# National Aeronautics and Space Administration. Lewis Research Center, Cleveland, OH.

OPTICAL AND SCRATCH RESISTANT PROPERTIES OF DIAMONDLIKE CARBON FILMS DEPOSITED WITH SINGLE AND DUAL ION BEAMS

MICHAEL T. KUSSMAUL (Sverdrup Technology, Inc., Brook Park, OH.), MICHAEL S. BOGDANSKI (Case Western Reserve Univ., Cleveland, OH.), BRUCE A. BANKS, and MICHAEL J. MIRTICH Jan. 1993 11 p Presented at the Technology 2002 Conference, Baltimore, MD, 1-3 Dec. 1992; sponsored by Technology Utilization

(Contract RTOP 141-20-0J)

(NASA-TM-105943; E-7571; NAS 1.15:105943) Avail: CASI HC A03/MF A01

Amorphous diamondlike carbon (DLC) films were deposited using both single and dual ion beam techniques utilizing filament and hollow cathode ion sources. Continuous DLC films up to 3000 A thick were deposited on fused quartz plates. Ion beam process parameters were varied in an effort to create hard, clear films. Total DLC film absorption over visible wavelengths was obtained using a Perkin-Elmer spectrophotometer. An ellipsometer, with an Ar-He laser (wavelength 6328 A) was used to determine index of refraction for the DLC films. Scratch resistance and frictional and adherence properties were determined for select films. Applications for these films range from military to the ophthalmic industries.

Author

N93-22590*# National Aeronautics and Space Administration. Lewis Research Center, Cleveland, OH.

SLIDING DURABILITY OF CANDIDATE SEAL FIBER MATERIALS IN HYDROGEN FROM 25 TO 900 C

CHRISTOPHER DELLACORTE and BRUCE M. STEINETZ 1992 18 p Prepared for presentation at the 5th NASA/NASP Hydrogen-Material Interactions Workshop, Scottsdale, AZ, 23-25 Sep. 1993

(Contract RTOP 505-63-1A)

(NASA-TM-105939; E-7456; NAS 1.15:105939) Avail: CASI HC A03/MF A01

Sliding durability studies of candidate ceramic fibers were conducted in hydrogen to support the high temperature seal development program at NASA LeRC. Pin-on-disk tests were used to measure the friction and durability of a tow or bundle of ceramic fibers in sliding against a superalloy disk. This procedure was used previously to test candidate fibers in an air environment. The fibers based upon mullite (Al₂O₃-SiO₂) chemistry (Nextel 550, 440, and 312) exhibited better durability in hydrogen than in air.

23 CHEMISTRY AND MATERIALS (GENERAL)

HPZ, a complex silicon carboxynitride fiber which showed good durability in air, however, showed a significant loss of durability in hot hydrogen. These results are consistent with recent thermodynamic and experimental studies of ceramic compatibility with hydrogen at elevated temperatures. These research results indicate that only oxide fibers display good durability in both air and hydrogen environments. Also, simple, low cost testing in air can provide an adequate data base for initial seal material screening and selection, especially for oxide fiber candidates. The findings of this research provide critical input to the seal design team.

Author (revised)

N93-22605* # National Aeronautics and Space Administration. Lewis Research Center, Cleveland, OH.

DETERMINATION OF ATOMIC OXYGEN FLUENCE USING SPECTROPHOTOMETRIC ANALYSIS OF INFRARED TRANSPARENT WITNESS COUPONS FOR LONG DURATION EXPOSURE TESTS

GREGG M. PODOJIL (Cleveland State Univ., OH.) and DONALD A. JAWORSKE Feb. 1993 14 p
(Contract RTOP 506-41-41)
(NASA-TM-106021; E-7582; NAS 1.15:106021) Avail: CASI HC A03/MF A01

Atomic oxygen degradation is one of several major threats to the durability of spaceborne systems in low Earth orbit. Ground-based simulations are conducted to learn how to minimize the adverse effects of atomic oxygen exposure. Assessing the fluence of atomic oxygen in test chambers such as a plasma asher over long periods of time is necessary for accurate determination of atomic oxygen exposure. Currently, an atomic oxygen susceptible organic material such as Kapton is placed next to samples as a witness coupon and its mass loss is monitored and used to determine the effective atomic oxygen fluence. However, degradation of the Kapton witness coupons occurs so rapidly in plasma ashers that for any long term test many witness coupons must be used sequentially in order to keep track of the fluence. This necessitates opening vacuum to substitute fresh coupons. A passive dosimetry technique was sought to monitor atomic oxygen exposure over longer periods without the need to open the plasma asher to the atmosphere. This paper investigates the use of spectrophotometric analysis of durable IR transparent witness coupons to measure atomic oxygen exposure for longer duration testing. The method considered would be conducive to making in situ measurements of atomic oxygen fluence. Author

N93-23014* # National Aeronautics and Space Administration. Lewis Research Center, Cleveland, OH.

AN ALTERNATIVE MODEL FOR ESTIMATING LIQUID DIFFUSION COEFFICIENTS REQUIRING NO VISCOSITY DATA

WILFREDO MORALES Mar. 1993 22 p
(Contract RTOP 505-63-5A)
(NASA-TM-106079; E-7695; NAS 1.15:106079) Avail: CASI HC A03/MF A01

An equation, based on the free volume of a liquid solvent, was derived via dimensional analysis, to predict binary diffusion coefficients. The equation assumed that interaction between the solute and liquid solvent molecules followed a Lennard-Jones potential. The equation was compared to other diffusivity equations and was found to give good results over the temperature range examined. Author

N93-26204* # National Aeronautics and Space Administration. Lewis Research Center, Cleveland, OH.

VICKERS INDENTATION HARDNESS OF STOICHIOMETRIC AND REDUCED SINGLE CRYSTAL TiO₂ (RUTILE) FROM 25 TO 800 C

CHRISTOPHER DELLACORTE and DANIEL L. DEADMORE Apr. 1993 10 p
(Contract RTOP 505-63-1A)
(NASA-TM-105959; E-7464; NAS 1.15:105959) Avail: CASI HC A02/MF A01

The indentation microhardness of stoichiometric and reduced single crystal rutile (TiO₂) from 25 to 800 C is presented in this

paper. The results serve two main purposes. One is to assess the effect of rutile's stoichiometry on its hardness. The other is to test recently suggested theory on solid lubrication with sub stoichiometric rutile in an effort to better understand shear controlled phenomenon. Microhardness was measured using a Vickers diamond indenter on both vacuum and hydrogen reduced single crystal rutile from 25 to 800 C. The results indicate that stoichiometry and temperature have a pronounced effect on rutile's hardness. The measured effects lend support to theory on solid lubrication by enhanced crystallographic slip and suggest that solid lubricant materials may be produced by careful atomic level tailoring (stoichiometry control). Author

N93-27003* # National Aeronautics and Space Administration. Lewis Research Center, Cleveland, OH.

A KINETIC AND EQUILIBRIUM ANALYSIS OF SILICON CARBIDE CHEMICAL VAPOR DEPOSITION ON MONOFILAMENTS

S. A. GOKOGLU and M. A. KUCZMARSKI May 1993 10 p
Presented at the 12th International Conference on Chemical Vapor Deposition (CVD 12), Honolulu, HI, 16-21 May 1993; sponsored by Electrochemical Society
(Contract RTOP 505-63-5A)
(NASA-TM-106137; E-7818; NAS 1.15:106137) Avail: CASI HC A02/MF A01

Chemical kinetics of atmospheric pressure silicon carbide (SiC) chemical vapor deposition (CVD) from dilute silane and propane source gases in hydrogen is numerically analyzed in a cylindrical upflow reactor designed for CVD on monofilaments. The chemical composition of the SiC deposit is assessed both from the calculated total fluxes of carbon and silicon and from chemical equilibrium considerations for the prevailing temperatures and species concentrations at and along the filament surface. The effects of gas and surface chemistry on the evolution of major gas phase species are considered in the analysis. Author (revised)

N93-27266* # National Aeronautics and Space Administration. Lewis Research Center, Cleveland, OH.

LOW EARTH ORBITAL ATOMIC OXYGEN ENVIRONMENTAL SIMULATION FACILITY FOR SPACE MATERIALS EVALUATION

CURTIS R. STIDHAM (Sverdrup Technology, Inc., Brook Park, OH.), BRUCE A. BANKS, THOMAS J. STUEBER (Sverdrup Technology, Inc., Brook Park, OH.), JOYCE A. DEVER, SHARON K. RUTLEDGE, and ERIC J. BRUCKNER (Cleveland State Univ., OH.) May 1993 15 p
Presented at the 38th International SAMPE Symposium and Exhibition, Anaheim, CA, 10-13 May 1993; sponsored by the Society for the Advancement of Material and Process Engineering
(Contract RTOP 474-46-10)
(NASA-TM-106128; E-7797; NAS 1.15:106128) Avail: CASI HC A03/MF A01

Simulation of low Earth orbit atomic oxygen for accelerated exposure in ground-based facilities is necessary for the durability evaluation of space power system component materials for Space Station Freedom (SSF) and future missions. A facility developed at the National Aeronautics and Space Administration's (NASA) Lewis Research Center provides accelerated rates of exposure to a directed or scattered oxygen beam, vacuum ultraviolet (VUV) radiation, and offers in-situ optical characterization. The facility utilizes an electron-cyclotron resonance (ECR) plasma source to generate a low energy oxygen beam. Total hemispherical spectral reflectance of samples can be measured in situ over the wavelength range of 250 to 2500 nm. Deuterium lamps provide VUV radiation intensity levels in the 115 to 200 nm range of three to five equivalent suns. Retarding potential analyses show distributed ion energies below 30 electron volts (eV) for the operating conditions most suited for high flux, low energy testing. Peak ion energies are below the sputter threshold energy (approximately 30 eV) of the protective coatings on polymers that are evaluated in the facility, thus allowing long duration exposure without sputter erosion. Neutral species are expected to be at thermal energies of approximately .04 eV to .1 eV. The maximum effective flux level

based on polyimide Kapton mass loss is $4.4 \times 10 \exp 6$ atoms/((sq. cm)*s), thus providing a highly accelerated testing capability.

Author (revised)

24

COMPOSITE MATERIALS

Includes physical, chemical, and mechanical properties of laminates and other composite materials.

A93-11422* National Aeronautics and Space Administration. Lewis Research Center, Cleveland, OH.

ELEVATED TEMPERATURE COMPRESSIVE PROPERTIES OF REACTION MILLED NIAL-ALN AND ZR-DOPED NIAL-ALN COMPOSITES

J. D. WHITTENBERGER (NASA, Lewis Research Center, Cleveland, OH) and MICHAEL J. LUTON (Exxon Research and Engineering Co., Annandale, NJ) *Journal of Materials Research* (ISSN 0884-2914) vol. 7, no. 10 Oct. 1992 p. 2724-2732. refs

Copyright

Previous studies of a single lot of NiAl powder which had been ground under high intensity conditions in liquid nitrogen (cryomilling) indicated that this processing leads to a high strength, elevated temperature NiAl-AlN composite. Because this was the first known example of the use of the reaction milling process to produce a high temperature composite, the reproducibility of this technique was unknown. Two additional lots of NiAl powder and a lot of a Zr-doped NiAl powder have been cryomilled, and analyses indicate that AlN was formed within a NiAl matrix in all three cases. Compression testing between 1200 K and 1400 K has shown that the deformation resistance of these heats is similar to that of the first lot of NiAl-AlN; thus cryomilling can improve the creep resistance of NiAl by a factor of six. Based on this work, it is concluded that cryomilling of NiAl powder to form high temperature, high strength NiAl-AlN composites is a reproducible process.

Author

A93-11459* National Aeronautics and Space Administration. Lewis Research Center, Cleveland, OH.

APPLICATION OF COMPOSITE MATERIALS TO IMPACT-INSENSITIVE MUNITIONS

VINCENT F. NERADKA, YALE CHANG (Johns Hopkins Univ., Laurel, MD), JOSEPH E. GRADY (NASA, Lewis Research Center, Cleveland, OH), and DANIEL A. TROWBRIDGE (Johns Hopkins Univ., Laurel, MD) *Johns Hopkins APL Technical Digest* (ISSN 0270-5214) vol. 13, no. 3 July-Sept. 1992 p. 418-425. refs (Contract N00039-89-C-0001)

Copyright

An approach is outlined for developing bullet-impact-insensitive munitions based on composite materials that provide rapid venting of the rocket-motor case. Impact experiments are conducted with test specimens of hybrid laminates of graphite/epoxy and epoxy reinforcing with woven glass fibers. The dynamic strain response and initial impact force are measured with strain gauges, and perforation damage is examined in the plates. The results show that impact damage can be designed by means of parametric variations of the fiber, matrix, and ply orientations. It is suggested that rocket-motor cases can be designed with composite materials to provide rapid venting during the failure mode. The experimental ballistic testing performed provides data that can be used comparatively with analytical data on composite materials.

C.C.S.

A93-12356* National Aeronautics and Space Administration. Lewis Research Center, Cleveland, OH.

OBSERVATIONS ON INFILTRATION OF SILICON CARBIDE COMPACTS WITH AN ALUMINIUM ALLOY

R. ASTHANA (Cleveland State Univ.; NASA, Lewis Research

Center, OH) and P. K. ROHATGI (Wisconsin Univ., Milwaukee) *Journal of Materials Science Letters* (ISSN 0261-8028) vol. 11, no. 19 Oct. 1, 1992 p. 1278-1281. refs

Copyright

The melt infiltration of ceramic particulates permits an opportunity to observe such fundamental materials phenomena as nucleation, dynamic wetting and growth in constrained environments. Experimental observations are presented on the infiltration behavior and matrix microstructures that form when porous compacts of platelet-shaped single crystals of alpha-(hexagonal) silicon carbide are infiltrated with a liquid 2014 Al alloy. The infiltration process involved counter gravity infiltration of suitably tamped and preheated compacts of silicon carbide platelets under an external pressure in a special pressure chamber for a set period, then by solidification of the infiltrant metal in the interstices of the bed at atmospheric pressure.

R.E.P.

A93-13760 National Aeronautics and Space Administration. Lewis Research Center, Cleveland, OH.

VOID CONTROL IN THE CRYSTALLIZATION OF LITHIUM FLUORIDE

DONALD A. JAWORSKE (NASA, Lewis Research Center, Cleveland, OH) and WILLIAM D. PERRY (Auburn Univ., AL) *In Space nuclear power systems; Proceedings of the 8th Symposium, Albuquerque, NM, Jan. 6-10, 1991. Pt. 1* New York American Institute of Physics 1991 p. 49-54. Research supported by NASA refs

Copyright

The effect of tungsten-coated graphite fibers on the radiant heat transfer characteristics of salt-fiber composites was studied by measuring the onset of melting as a function of applied furnace power. As the fiber concentration was increased from 0 to 5.40 percent fiber by weight, the furnace temperature required to melt the lithium fluoride also increased. Upon cooling, each of the crystalline salt-fiber composites were cut open with a diamond saw to expose the void. Optical photographs of the voids revealed a trend in void location and size, with the largest void, and the least change in the outer dimension of the boule upon cooling, occurring in the sample with the most fiber.

Author

A93-13777* National Aeronautics and Space Administration. Lewis Research Center, Cleveland, OH.

THE ROLE OF THE INTERFACE IN REFRACTORY METAL ALLOY COMPOSITES

TONI GROBSTEIN (NASA, Lewis Research Center, Cleveland, OH) and HEE M. YUN (Cleveland State Univ.; NASA, Lewis Research Center, Cleveland, OH) *In Space nuclear power systems; Proceedings of the 8th Symposium, Albuquerque, NM, Jan. 6-10, 1991. Pt. 1* New York American Institute of Physics 1991 p. 186-192. refs

Copyright

Creep-rupture and tensile tests have been used to evaluate thoriated W-wire reinforced Nb-1 percent Zr alloy matrix composites fabricated via arc-spray monotape technique. A significant creep strength enhancement was observed over the unreinforced matrix alloy while matrix integrity was maintained; the fiber/matrix interface phase is noted to be a strong and ductile W/Nb alloy, which is formed due to the mutual solubility of the constituent metals. High strength, toughness, and thermal stability are demonstrated by this material system, which is also resistant to liquid alkali metal corrosion.

O.C.

A93-14840 National Aeronautics and Space Administration. Lewis Research Center, Cleveland, OH.

TENSILE STRAIN-RATE SENSITIVITY OF TUNGSTEN/NIOBIUM COMPOSITES AT 1300 TO 1600 K

H. M. YUN (NASA, Lewis Research Center; Cleveland State Univ., OH) and R. H. TITRAN (NASA, Lewis Research Center, Cleveland, OH) *Metallurgical Transactions A - Physical Metallurgy and Materials Science* (ISSN 0360-2133) vol. 23A, no. 11 Nov. 1992 p. 3121-3133. Previously announced in STAR as N91-16128 refs

(Contract RTOP 590-13-11)

The tensile behavior of continuous tungsten fiber reinforced niobium composites (W/Nb), fabricated by an arc-spray process, was studied in the 1300 to 1600 K temperature range. The tensile properties of the fiber and matrix components as well as of the composites were measured and were compared to rule of mixtures (ROM) predictions. The deviation from the ROM was found to depend upon the chemistry of the tungsten alloy fibers, with positive deviations for ST300/Nb (i.e., stronger composite strength than the ROM) and negative or zero deviations for 218/Nb. Author

A93-15729* National Aeronautics and Space Administration. Lewis Research Center, Cleveland, OH.

THREE-DIMENSIONAL FINITE ELEMENT SIMULATION OF INTERMINGLED-FIBER HYBRID COMPOSITE BEHAVIOR

SUBODH K. MITAL (Toledo Univ., OH) and CHRISTOS C. CHAMIS (NASA, Lewis Research Center, Cleveland, OH) / In International SAMPE Symposium and Exhibition, 37th, Anaheim, CA, Mar. 9-12, 1992, Proceedings Covina, CA Society for the Advancement of Material and Process Engineering 1992 p. 88-99.

Three-dimensional finite element methods and the intraply hybrid micromechanics equations are used to predict composite properties for a unidirectional graphite-epoxy primary composite with S-glass fibers used as hybridizing fibers. The micromechanics equations are embedded in a computer code ICAN (Integrated Composites Analyzer). The three-dimensional finite element model consists of three-by-three unit cell array, with a total fiber volume ratio of 0.54. There is a good agreement between the composite properties and microstresses obtained from both methods. The results indicate that the finite element methods and micromechanics equations can be used to obtain the properties of intermingled hybrid composites needed for analysis/design of hybrid composite structures. Author

A93-15752* National Aeronautics and Space Administration. Lewis Research Center, Cleveland, OH.

FIBER SHAPE EFFECTS ON METAL MATRIX COMPOSITE BEHAVIOR

H. C. BROWN (Sverdrup Technology, Inc., Brook Park; NASA, Lewis Research Center, Cleveland, OH) and H.-J. LEE (NASA, Lewis Research Center, Cleveland, OH) / In International SAMPE Symposium and Exhibition, 37th, Anaheim, CA, Mar. 9-12, 1992, Proceedings Covina, CA Society for the Advancement of Material and Process Engineering 1992 p. 378-389. refs

The effects of different fiber shapes on the behavior of metal matrix composites is computationally simulated. A three-dimensional finite element model consisting of a group of nine unidirectional fibers in a three by three unit cell array of a SiC/Ti-15-3 metal matrix composite is used in the analysis. The model is employed to represent five fiber shapes that include a circle, an ellipse, a kidney, and two different cross shapes. The distribution of stresses and the composite material properties, such as moduli, coefficients of thermal expansion, and Poisson's ratios, are obtained from the finite element analysis using the various fiber shapes. Comparisons of these results are used to determine the sensitivity of the composite behavior to the different fiber shapes. In general, fiber dominated properties are not affected by fiber geometry and matrix dominated properties are only moderately affected. Author

A93-15753 National Aeronautics and Space Administration. Lewis Research Center, Cleveland, OH.

TAILORED METAL MATRIX LAMINATES FOR HIGH-TEMPERATURE PERFORMANCE

MICHAEL R. MOREI, DIMITRIS A. SARAVANOS, and C. C. CHAMIS (NASA, Lewis Research Center, Cleveland, OH) / In International SAMPE Symposium and Exhibition, 37th, Anaheim, CA, Mar. 9-12, 1992, Proceedings Covina, CA Society for the Advancement of Material and Process Engineering 1992 p. 390-402. Previously announced in STAR as N92-31854 refs (Contract RTOP 510-01-08)

A multi-objective tailoring methodology is presented to maximize stiffness and load carrying capacity of a metal matrix cross-ply laminated at elevated temperatures. The fabrication process and

fiber volume ratio are used as the design variables. A unique feature is the concurrent effects from fabrication, residual stresses, material nonlinearity, and thermo-mechanical loading on the laminate properties at the post-fabrication phase. For a (0.90) (sub s) graphite/copper laminate, strong coupling was observed between the fabrication process, laminate characteristics, and thermo-mechanical loading. The multi-objective tailoring was found to be more effective than single objective tailoring. Results indicate the potential to increase laminate stiffness and load carrying capacity by controlling the critical parameters of the fabrication process and the laminate. Author

A93-15822 National Aeronautics and Space Administration. Lewis Research Center, Cleveland, OH.

COMPUTATIONAL SIMULATION OF SURFACE WAVINESS IN GRAPHITE/EPOXY WOVEN COMPOSITES DUE TO INITIAL CURING

JOSE G. SANFELIZ, PAPPU L. N. MURTHY, and CHRISTOS C. CHAMIS (NASA, Lewis Research Center, Cleveland, OH) / In International SAMPE Symposium and Exhibition, 37th, Anaheim, CA, Mar. 9-12, 1992, Proceedings Covina, CA Society for the Advancement of Material and Process Engineering 1992 p. 1325-1338. Previously announced in STAR as N92-14118 refs (Contract RTOP 505-63-5B)

Several models simulating plain weave, graphite/epoxy woven composites are presented, along with the effects that the simultaneous application of pressure and thermal loads have on their surfaces. The surface effects created by moisture absorption are also examined. The computational simulation consisted of using a two-dimensional finite element model for the composite. The properties of the finite element (FE) model are calculated by using the in-house composite mechanics computer code ICAN (Integrated Composite Analyzer). MSC/NASTRAN is used for the FE analysis which yields the composite's top surface normalized displacements. These results demonstrate the importance of parameters such as the cure temperature ($T_{sub o}$) and the resin content in the curing process of polymer-matrix composites. The modification of these parameters will help tailor the composite system to the desired requirements and applications. Author

A93-17675 National Aeronautics and Space Administration. Lewis Research Center, Cleveland, OH.

PROPERTIES OF HYBRID CVD/PAN GRAPHITE FIBERS AND THEIR BROMINE INTERCALATION COMPOUNDS

JAMES R. GAIER (NASA, Lewis Research Center, Cleveland, OH), MAX L. LAKE (Applied Sciences, Inc., Yellow Springs, OH), ALIA MOINUDDIN, and MARK MARABITO (Cleveland State Univ., OH) Carbon (ISSN 0008-6223) vol. 30, no. 3 1992 p. 345-349. Previously announced in STAR as N92-14170 refs (Contract RTOP 506-41-41) Copyright

A hybrid fiber with a PAN core surrounded by a vapor grown carbon fiber (VGCF) sheath was fabricated using a proprietary process. The density, ultimate tensile strength, Young's modulus, and resistivity of pristine and bromine intercalated fibers made by this technique having diameters varying from 5 to 50 microns were compared with the values predicted from the rule of mixtures model. For both the pristine and intercalated fibers, the density, ultimate tensile strength, and Young's modulus of the fibers were lower than predicted, but the resistivity was measured to be consistent with predictions. The lower than theoretical mechanical properties may be evidence of a low density disordered interface between the core and the sheath which would lower the density and degrade the mechanical properties, but would leave the resistivity nearly unaffected. Intercalation had little if any effect on the ultimate tensile strength and Young's modulus, but raised the density by about 11 pct., and lowered the resistivity by an order of magnitude. The diameter dependence of the resistivity showed evidence of a depletion layer of the type found in VGCF. Author

A93-18709* National Aeronautics and Space Administration. Lewis Research Center, Cleveland, OH.

FRACTURE TOUGHNESS TESTING OF POLYMER MATRIX COMPOSITES

JOSEPH E. GRADY (NASA, Lewis Research Center, Cleveland, OH) *In* Handbook of ceramics and composites. Vol. 2 - Mechanical properties and specialty applications New York Marcel Dekker, Inc. 1992 p. 1-50. refs

Copyright

The experimental techniques and associated data analysis methods used to measure the resistance to interlaminar fracture, or 'fracture toughness', of polymer matrix composite materials are described. A review in the use of energy techniques to characterize fracture behavior in elastic solids is given. An overview is presented of the types of approaches employed in the design of delamination-resistant composite materials. R.E.P.

A93-18990* National Aeronautics and Space Administration. Lewis Research Center, Cleveland, OH.

COMBINED MICROMECHANICAL AND FABRICATION PROCESS OPTIMIZATION FOR METAL-MATRIX COMPOSITES

M. MOREL (Sverdrup Technology, Inc., Cleveland, OH), D. A. SARAVANOS (Case Western Reserve Univ., Cleveland, OH), and C. C. CHAMIS (NASA, Lewis Research Center, Cleveland, OH) *In* Struceng & Femcad - Structural engineering and optimization Gournay-sur-Marne, France Institute for Industrial Technology Transfer-International 1991 p. 247-254. Previously announced in STAR as N91-19237 refs

A method is presented to minimize the residual matrix stresses in metal matrix composites. Fabrication parameters such as temperature and consolidation pressure are optimized concurrently with the characteristics (i.e., modulus, coefficient of thermal expansion, strength, and interphase thickness) of a fiber-matrix interphase. By including the interphase properties in the fabrication process, lower residual stresses are achievable. Results for an ultra-high modulus graphite (P100)/copper composite show a reduction of 21 percent for the maximum matrix microstress when optimizing the fabrication process alone. Concurrent optimization of the fabrication process and interphase properties show a 41 percent decrease in the maximum microstress. Therefore, this optimization method demonstrates the capability of reducing residual microstresses by altering the temperature and consolidation pressure histories and tailoring the interphase properties for an improved composite material. In addition, the results indicate that the consolidation pressures are the most important fabrication parameters, and the coefficient of thermal expansion is the most critical interphase property. Author

A93-19123* National Aeronautics and Space Administration. Lewis Research Center, Cleveland, OH.

SEGMENTED MULTIGRID DOMAIN DECOMPOSITION PROCEDURE FOR INCOMPRESSIBLE VISCOUS FLOWS

KUMAR SRINIVASAN and STANLEY G. RUBIN (Cincinnati Univ., OH) *International Journal for Numerical Methods in Fluids* (ISSN 0271-2091) vol. 15, no. 11 Dec. 15, 1992 p. 1333-1355. refs

(Contract NAG3-397; AF-AFOSR-90-0096)

Copyright

In this paper, the Navier-Stokes (NS) equations are approximated with a reduced NS system, that represents the lowest-order terms in an asymptotic Re expansion. This system allows for simplified boundary conditions, more generality in the location of the outflow boundary, and insures mass conservation in all subdomain grid interfaces, and also at the outflow boundary. The higher-order NS diffusion terms are included through a deferred corrector, in chosen subdomains, when required. R.E.P.

A93-19502* National Aeronautics and Space Administration. Lewis Research Center, Cleveland, OH.

CERAMIC MATRIX COMPOSITE APPLICATIONS IN ADVANCED LIQUID FUEL ROCKET ENGINE TURBOMACHINERY

JERRY W. BROCKMEYER (Rockwell International Corp.,

Rocketdyne Div., Canoga Park, CA) Jun. 1992 8 p. ASME, International Gas Turbine and Aeroengine Congress and Exposition, 37th, Cologne, Germany, June 1-4, 1992 Research supported by SEP, Du Pont de Nemours & Co., NASA, et al refs (ASME PAPER 92-GT-316)

Fiber-reinforced ceramic matrix composites have been identified with properties suitable for near term applications. Conceptual design studies indicate the feasibility of applying C/SiC, and subelements were manufactured that verify selected fabrication features and key material properties. Tests and inspection of these subelements confirmed their capabilities. R.E.P.

A93-19547* National Aeronautics and Space Administration. Lewis Research Center, Cleveland, OH.

CERAMIC MATRIX COMPOSITES FOR ROCKET ENGINE TURBINE APPLICATIONS

THOMAS P. HERBELL and ANDREW J. ECKEL (NASA, Lewis Research Center, Cleveland, OH) Jun. 1992 7 p. ASME, International Gas Turbine and Aeroengine Congress and Exposition, 37th, Cologne, Germany, June 1-4, 1992 refs (ASME PAPER 92-GT-394)

A program to establish the potential for introducing fiber reinforced ceramic matrix composites (FRCMC) in future rocket engine turbopumps was instituted in 1987. A brief summary of the overall program (both contract and in-house research) is presented. Tests at NASA Lewis include thermal upshocks in a hydrogen/oxygen test rig capable of generating heating rates up to 2500 C/sec. Post thermal upshock exposure evaluation includes the measurement of residual strength and failure analysis. Test results for monolithic ceramics and several FRCMC are presented. Hydrogen compatibility was assessed by isothermal exposure of monolithic ceramics in high temperature gaseous hydrogen plus water vapor. Author

A93-19624* National Aeronautics and Space Administration. Lewis Research Center, Cleveland, OH.

ULTRASONIC AND MICROMECHANICAL STUDY OF DAMAGE AND ELASTIC PROPERTIES OF SiC/RBSN CERAMIC COMPOSITES

Y. C. CHU, M. HEFETZ, S. I. ROKHLIN (Ohio State Univ., Columbus), and G. Y. BAAKLINI (NASA, Lewis Research Center, Cleveland, OH) *In* Review of progress in quantitative nondestructive evaluation. Vol. 11B; Proceedings of the 18th Annual Review, Brunswick, ME, July 28-Aug. 2, 1991 New York Plenum Press 1992 p. 1531-1538. refs (Contract NAG3-1220)

Copyright

Ultrasonic techniques are employed to develop methods for nondestructive evaluation of elastic properties and damage in SiC/RBSN composites. To incorporate imperfect boundary conditions between fibers and matrix into a micromechanical model, a model of fibers having effective anisotropic properties is introduced. By inverting Hashin's (1979) microstructural model for a composite material with microscopic constituents the effective fiber properties were found from ultrasonic measurements. Ultrasonic measurements indicate that damage due to thermal shock is located near the surface, so the surface wave is most appropriate for estimation of the ultimate strength reduction and critical temperature of thermal shock. It is concluded that bonding between laminates of SiC/RBSN composites is severely weakened by thermal oxidation. Generally, nondestructive evaluation of thermal oxidation effects and thermal shock shows good correlation with measurements previously performed by destructive methods. P.D.

A93-20758 National Aeronautics and Space Administration. Lewis Research Center, Cleveland, OH.

CREEP BEHAVIOR OF TUNGSTEN FIBER REINFORCED NIOBIUM METAL MATRIX COMPOSITES

TONI L. GROBSTEIN (NASA, Lewis Research Center, Cleveland, OH) *In* Space nuclear power systems 1989; Proceedings of the 6th Symposium, Albuquerque, NM, Jan. 8-12, 1989. Vol. 1 Malabar, FL Orbit Book Co., Inc. 1992 p. 53-60. Previously announced

24 COMPOSITE MATERIALS

in STAR as N89-29522 refs
(Contract DE-AI03-86SF-16310; RTOP 586-01-11)
Copyright

Tungsten fiber reinforced niobium metal matrix composites were evaluated for use in space nuclear power conversion systems. The composite panels were fabricated using the arc-spray monotape technique at the NASA Lewis Research Center. The creep behavior of W/Nb composite material was determined at 1400 and 1500 K in vacuum over a wide range of applied loads. The time to reach 1 percent strain, the time to rupture, and the minimum creep rate were measured. The W/Nb composites exceeded the properties of monolithic niobium alloys significantly even when compared creep strength also was evaluated. Kirkendall void formation was observed at the fiber/matrix interface; the void distribution differed depending the fiber orientation relative to the stress axis. A relationship was found between the fiber orientation and the creep strength. Author

A93-24514 National Aeronautics and Space Administration. Lewis Research Center, Cleveland, OH.

TRANSVERSE FLEXURAL TESTS AS A TOOL FOR ASSESSING DAMAGE TO PMR-15 COMPOSITES FROM ISOTHERMAL AGING IN AIR AT ELEVATED TEMPERATURES

KENNETH J. BOWLES (NASA, Lewis Research Center, Cleveland, OH) SAMPE Quarterly (ISSN 0036-0821) vol. 24, no. 2 Jan. 1993 p. 49-53. Previously announced in STAR as N93-12737 refs
(Contract RTOP 510-01-50)
Copyright

To date, the effect of thermo-oxidative aging on unidirectional composite mechanical properties has been monitored by the measurement of interlaminar shear strength (ILSS) and either three or four point longitudinal flexural strength (LFS) of the composites being tested. Both results are affected by the fiber-to-matrix bonding, the former being dependent on the shear resistance of the interface and the latter on the degree of load sharing by the fibers through the fiber/matrix interface. Recently, fiber/matrix interfacial bond strengths have been monitored using a transverse flexural strength (TFS) test method. This test method was used to evaluate the effect of fiber surface treatment on the fiber/matrix. Author

A93-25104 National Aeronautics and Space Administration. Lewis Research Center, Cleveland, OH.

THERMAL CONDUCTIVITY AND THERMAL EXPANSION OF GRAPHITE FIBER-REINFORCED COPPER MATRIX COMPOSITES

DAVID L. ELLIS (Case Western Reserve Univ.; NASA, Lewis Research Center, Cleveland, OH) and DAVID L. MCDANIELS (NASA, Lewis Research Center, Cleveland, OH) Metallurgical Transactions A - Physical Metallurgy and Materials Science (ISSN 0360-2133) vol. 24A, no. 1 Jan. 1993 p. 43-52. Previously announced in STAR as N92-14120 refs
(Contract NCC3-94; RTOP 590-13-11)
Copyright

The high specific conductivity of graphite fiber/copper matrix (Gr/Cu) composites offers great potential for high heat flux structures operating at elevated temperatures. To determine the feasibility of applying Gr/Cu composites to high heat flux structures, composite plates were fabricated using unidirectional and cross-ply pitch-based P100 graphite fibers in a pure copper matrix. Thermal conductivity of the composites was measured from room temperature to 1073 K, and thermal expansion was measured from room temperature to 1050 K. The longitudinal thermal conductivity, parallel to the fiber direction, was comparable to pure copper. The transverse thermal conductivity, normal to the fiber direction, was less than that of pure copper and decreased with increasing fiber content. The longitudinal thermal expansion decreased with increasing fiber content. The transverse thermal expansion was greater than pure copper and nearly independent of fiber content. Author

A93-25105 National Aeronautics and Space Administration. Lewis Research Center, Cleveland, OH.

REACTION LAYER FORMATION AT THE GRAPHITE/COPPER-CHROMIUM ALLOY INTERFACE

SANDRA M. DEVINCENT and GARY M. MICHAL (Case Western Reserve Univ., Cleveland, OH) Metallurgical Transactions A - Physical Metallurgy and Materials Science (ISSN 0360-2133) vol. 24A, no. 1 Jan. 1993 p. 53-60. Previously announced in STAR as N92-23436 Research supported by DARPA refs
(Contract NCC3-94; RTOP 505-63-40)
Copyright

Sessile drop tests were used to obtain information about copper chromium alloys that suitably wet graphite. Characterization of graphite/copper-chromium alloy interfaces subjected to elevated temperatures were conducted using scanning electron micrography, energy dispersive spectroscopy, Auger electron spectroscopy, and X-ray diffraction analyses. These analyses indicate that during sessile drop tests conducted at 1130 C for one hour, copper alloys containing greater than 0.98 percent chromium form continuous reaction layers of approximately 10 micron thickness. The reaction layers adhere to the graphite surface. The copper wets the reaction layer to form a contact angle of 60 degrees or less. X-ray diffraction results indicate that the reaction layer is chromium carbide. The kinetics of reaction layer formation were modelled in terms of bulk diffusion mechanisms. Reaction layer thickness is controlled initially by the diffusion of Cr out of Cu alloy and later by the diffusion of C through chromium carbide. Author

A93-26275* National Aeronautics and Space Administration. Lewis Research Center, Cleveland, OH.

FATIGUE-ENVIRONMENT INTERACTIONS IN A SiC/Ti-15-3 COMPOSITE

J. GAYDA, T. P. GABB, and B. A. LERCH (NASA, Lewis Research Center, Cleveland, OH) International Journal of Fatigue (ISSN 0142-1123) vol. 15, no. 1 Jan. 1993 p. 41-45. refs
Copyright

Load-controlled isothermal and nonisothermal fatigue lives of a (0-deg) SiC/Ti-15-3 were evaluated at temperatures between 150 and 550 C and a target strain range of about 0.45 percent. In nonisothermal fatigue tests, load was first cycled at minimum temperature and then temperature was cycled at zero load. For fatigue tests with peak temperatures at or above 300 C, fatigue life was dramatically reduced compared to that at 150 C. The shortest life was produced by the nonisothermal test with the greatest temperature range ($\Delta T = 400$ C) and highest peak temperature ($T(\max) = 550$ C). Vacuum testing showed that much of the life reduction under isothermal and nonisothermal conditions was related to environmental effects, although the nature of the fatigue-environment interaction was decidedly different for the isothermal and nonisothermal test cycles which were studied. Author

A93-26674* National Aeronautics and Space Administration. Lewis Research Center, Cleveland, OH.

EFFECT OF HIPING ON THE EFFECTIVE THERMAL CONDUCTIVITY/DIFFUSIVITY AND THE INTERFACIAL THERMAL CONDUCTANCE OF UNIAXIAL SiC FIBRE-REINFORCED RBSN

H. BHATT, K. Y. DONALDSON, D. P. H. HASSELMAN (Virginia Polytechnic Inst. and State Univ., Blacksburg), and R. T. BHATT (NASA, Lewis Research Center, Cleveland, OH) Journal of Materials Science (ISSN 0022-2461) vol. 27, no. 24 Dec. 15, 1992 p. 6653-6661. refs
Copyright

Hot isostatic pressing (HIPing) was found to increase the thermal diffusivity/conductivity of uniaxial silicon carbide fiber-reinforced reaction-bonded silicon nitride (RBSN) matrix composites, as the result of the densification of the matrix, the increase in the grain size of the silicon carbide and the improved thermal contact between the fibers and the matrix. Transverse to the fiber direction the thermal diffusivity/conductivity was found to be a function of the surrounding gaseous atmosphere due to the access of the

gas phase to the fiber-matrix interface, which was facilitated by the existence of an interfacial gap due to the thermal expansion mismatch between the fibers and the matrix. The interfacial conductance was found to exhibit a strong positive temperature dependence as the result of the closure of the interfacial gap with increasing temperature. Author

A93-27494* National Aeronautics and Space Administration. Lewis Research Center, Cleveland, OH.

MELT INFILTRATION OF SILICON CARBIDE COMPACTS. I - STUDY OF INFILTRATION DYNAMICS

RAJIV ASTHANA (Cleveland State Univ.; NASA, Lewis Research Center, OH) and PRADEEP K. ROHATGI (Wisconsin Univ., Milwaukee) Zeitschrift fuer Metallkunde (ISSN 0044-3093) vol. 83, no. 12 Dec. 1992 p. 887-892. Research supported by EPRI, U.S. Navy, Wisconsin Applied Research Grant, et al refs Copyright

Countergravity, pressure-assisted infiltration with a 2014 Al alloy of suitably tamped porous compacts of platelet shaped single crystals of alpha (hexagonal) silicon carbide was used to measure particulate wettability and infiltration kinetics under dynamic conditions relevant to pressure casting of composites. A threshold pressure P_{th} for ingress of the infiltrant was identified based on the experimental penetration length versus pressure profiles for a range of experimental variables which included infiltration pressure, infiltration time, SiC size and SiC surface chemistry. The results showed that P_{th} decreased whereas the penetration length increased with increasing SiC size and infiltration time. Cu-coated SiC led to lower P_{th} and larger penetration lengths compared to uncoated SiC under identical conditions. These observations have been discussed in the light of theoretical models of infiltration and the kinetics of wetting. Author

A93-28283* National Aeronautics and Space Administration. Lewis Research Center, Cleveland, OH.

MELT INFILTRATION OF SILICON CARBIDE COMPACTS. II - EVALUATION OF SOLIDIFICATION MICROSTRUCTURES

RAJIV ASTHANA (Cleveland State Univ.; NASA, Lewis Research Center, OH) and PRADEEP K. ROHATGI (Wisconsin Univ., Milwaukee) Zeitschrift fuer Metallkunde (ISSN 0044-3093) vol. 84, no. 1 Jan. 1993 p. 44-47. Research supported by EPRI, U.S. Navy, Wisconsin Applied Research Grant, et al refs Copyright

Microstructural aspects of alloy solidification within the interstices of porous compacts of platelet-shaped single crystals of alpha-SiC, when the latter are infiltrated with a hot metal under pressure, have been described. Microstructural evidence is presented of selective reorientation of platelets and nonhomogeneous solute distribution under shear of pressurized melt, of constrained growth of primary solid within finite width zones, and of the modulation of coring due to microsegregation as a result of variations in the pore size of compacts. Author

A93-29948* National Aeronautics and Space Administration. Lewis Research Center, Cleveland, OH.

SLIDING WEAR OF SELF-MATED AL₂O₃-SiC

WHISKER-REINFORCED COMPOSITES AT 23-1200 C

S. C. FARMER, C. DELLACORTE (NASA, Lewis Research Center, Cleveland, OH), and P. O. BOOK (Cleveland State Univ.; NASA, Lewis Research Center, OH) Journal of Materials Science (ISSN 0022-2461) vol. 28, no. 5 March 1, 1993 p. 1147-1154. refs Copyright

Microstructural changes occurring during sliding wear of self-mated Al₂O₃ SiC whisker-reinforced composites were studied using optical, scanning electron microscopy and transmission electron microscopy. Pin-on-disc specimens were slid in air at 2.7 m/s sliding velocity under a 26.5 N load for 1 h. Wear tests were conducted at 23, 600, 800 and 1200 C. Mild wear with a wear factor of 2.4×10^{-7} to 1.5×10^{-6} cu mm /N per m was experienced at all test temperatures. The composite showed evidence of wear by fatigue mechanisms at 800 C and below. Tribochemical reaction (SiC oxidation and reaction of SiO₂ and

Al₂O₃) leads to intergranular failure at 1200 C. Distinct microstructural differences existing at each test temperature are reported. Author

A93-31355* National Aeronautics and Space Administration. Lewis Research Center, Cleveland, OH.

TRANSVERSE DUCTILITY OF METAL MATRIX COMPOSITES

S. R. GUNAWARDENA, S. JANSSON, and F. A. LECKIE (California Univ., Santa Barbara) In Failure mechanisms in high temperature composite materials; Proceedings of the Symposium, 112th ASME Winter Annual Meeting, Atlanta, GA, Dec. 1-6, 1991 New York American Society of Mechanical Engineers 1991 p. 23-30. Research supported by NASA refs Copyright

The role of the fiber matrix interface bond on the transverse ductility of continuous fiber reinforced composites has been investigated. Two specific systems have been considered: an Aluminum alloy matrix reinforced by Alumina fibers, characterized by a strong interface and a Titanium alloy reinforced by coated Silicon Carbide fibers, characterized by a weak interface. A micro-mechanical study indicates that the bond condition has a significant effect on the state of stress in the matrix which in turn dictates the available matrix ductility. The micro-mechanical predictions are in good agreement with the experimental results for the two systems. Author

A93-31356 National Aeronautics and Space Administration. Lewis Research Center, Cleveland, OH.

MICROFRACTURE IN HIGH TEMPERATURE METAL MATRIX CROSSPLY LAMINATES

SUBODH K. MITAL and CHRISTOS C. CHAMIS (NASA, Lewis Research Center, Cleveland, OH) In Failure mechanisms in high temperature composite materials; Proceedings of the Symposium, 112th ASME Winter Annual Meeting, Atlanta, GA, Dec. 1-6, 1991 New York American Society of Mechanical Engineers 1991 p. 31-36. Previously announced in STAR as N91-25198 refs

(Contract NASA ORDER C-99066-G; RTOP 510-10-50)

Copyright

Microfracture (fiber/matrix fracture, interphase debonding and inter-ply delamination) in high temperature metal matrix composites (HTMMC), subjected to both mechanical and thermal loading, is computationally simulated. A crossply 0.3 fiber volume ratio SiC/Ti15 composite with 0/90/0 layup is evaluated for microfracture using a multicell finite element model. A computational simulation procedure based on strain energy release rates is used to predict the fracture process and establish the hierarchy of fracture modes. Microfracture results for various loading cases are presented and discussed. Author

A93-31358 National Aeronautics and Space Administration. Lewis Research Center, Cleveland, OH.

FATIGUE LIFE PREDICTION OF AN INTERMETALLIC MATRIX COMPOSITE AT ELEVATED TEMPERATURES

P. A. BARTOLOTTA (NASA, Lewis Research Center, Cleveland, OH) In Failure mechanisms in high temperature composite materials; Proceedings of the Symposium, 112th ASME Winter Annual Meeting, Atlanta, GA, Dec. 1-6, 1991 New York American Society of Mechanical Engineers 1991 p. 45-54. Previously announced in STAR as N91-25442 refs

(Contract RTOP 510-01-50)

Copyright

A strain-based fatigue life prediction method is proposed for an intermetallic matrix composite (IMC) under tensile cyclic loadings at elevated temperatures. Styled after the 'Universal Slopes' method, the model utilizes the composite's tensile properties to estimate fatigue life. Factors such as fiber volume ratio (V_f), number of plies and temperature dependence are implicitly incorporated into the model through these properties. The model constants are determined by using unidirectional fatigue data at temperatures of 425 and 815 C. Fatigue lives from two independent sources are used to verify the model at temperatures of 650 and 760 C.

24 COMPOSITE MATERIALS

Cross-ply lives at 760 C are also predicted. It is demonstrated that the correlation between experimental and predicted lives is within a factor of two. Author

A93-31359* National Aeronautics and Space Administration. Lewis Research Center, Cleveland, OH.

DEFORMATION AND FAILURE MECHANISMS IN METAL MATRIX COMPOSITES

G. NEWAZ and B. S. MAJUMDAR (Battelle, Columbus, OH) /n Failure mechanisms in high temperature composite materials; Proceedings of the Symposium, 112th ASME Winter Annual Meeting, Atlanta, GA, Dec. 1-6, 1991 New York American Society of Mechanical Engineers 1991 p. 55-65. refs (Contract NAS3-26053) Copyright

An investigation was undertaken to determine the key deformation mechanisms and their interaction leading to failure of both 0 degree and 90 degree Ti 15-3/SCS-6 laminae under monotonic loading. The experimental results suggest that inelastic deformation in the 0-degree lamina is dominated by plastic deformation and that in the 90-degree lamina is dominated by both fiber-matrix debonding and plasticity. The loading-unloading response, monitoring of Poisson's ratio and microscopy were utilized to identify the key deformation mechanisms. The sequence of deformation mechanisms leading to failure are identified for both the 0 and the 90-degree specimens. The threshold strains for plasticity or damage which are referred to as 'microdeformation' in the 0 deg and 90 deg laminae are approximately 0.004 and 0.002, respectively, at room temperature. These strain levels may be considered critical in initiation based structural design with these composites. Author

A93-32461* National Aeronautics and Space Administration. Lewis Research Center, Cleveland, OH.

COMPUTATIONAL CHARACTERIZATION OF HIGH TEMPERATURE COMPOSITES VIA METCAN

H. C. BROWN (Sverdrup Technology Corp., Brook Park, OH) and CHRISTOS C. CHAMIS (NASA, Lewis Research Center, Cleveland, OH) /n Mechanics of composites at elevated and cryogenic temperatures; Proceedings of the Symposium, ASME Applied Mechanics Conference, Columbus, OH, June 16-19, 1991 New York American Society of Mechanical Engineers 1991 p. 133-143. refs Copyright

The computer code 'METCAN' (METal matrix Composite ANalyzer) developed at NASA Lewis Research Center can be used to predict the high temperature behavior of metal matrix composites using the room temperature constituent properties. A reference manual that characterizes some common composites is being developed from METCAN generated data. Typical plots found in the manual are shown for graphite/copper. These include plots of stress-strain, elastic and shear moduli, Poisson's ratio, thermal expansion, and thermal conductivity. This manual can be used in the preliminary design of structures and as a guideline for the behavior of other composite systems. Author

A93-32466* National Aeronautics and Space Administration. Lewis Research Center, Cleveland, OH.

MECHANICS OF INTERFACES IN FIBER REINFORCED SIC/RBSN CERAMIC MATRIX COMPOSITES

ABHISAK CHULYA (Cleveland State Univ., OH) and JOHN P. GYEKENYESI (NASA, Lewis Research Center, Cleveland, OH) /n Mechanics of composites at elevated and cryogenic temperatures; Proceedings of the Symposium, ASME Applied Mechanics Conference, Columbus, OH, June 16-19, 1991 New York American Society of Mechanical Engineers 1991 p. 217-229. refs Copyright

The mechanical behavior of continuous fiber reinforced SiC/RBSN composites with strong and weak interface characteristics is evaluated. Both catastrophic and noncatastrophic failures are observed in tensile specimens. Effects of fiber/matrix interface debonding (splitting) parallel to the fibers are discussed.

Micromechanical models incorporating residual stresses to calculate the critical matrix cracking strength, ultimate strength and work of pull-out are reviewed and used to predict composite response. Experimental results are compared to analytical predictions. Author

A93-32471* National Aeronautics and Space Administration. Lewis Research Center, Cleveland, OH.

DUCTILITY OF A CONTINUOUS FIBER REINFORCED ALUMINUM MATRIX COMPOSITE

S. JANSSON and FREDERICK A. LECKIE (California Univ., Santa Barbara) /n Mechanics of composites at elevated and cryogenic temperatures; Proceedings of the Symposium, ASME Applied Mechanics Conference, Columbus, OH, June 16-19, 1991 New York American Society of Mechanical Engineers 1991 p. 267-275. Research supported by NASA refs Copyright

The transverse properties of an aluminum alloy metal matrix composite reinforced by continuous alumina fibers have been investigated. The composite is subjected to both mechanical and cyclic thermal loading. The ductility can vary by an order of magnitude according to the operating conditions. For high mechanical and low thermal loading the ductility is small, for low mechanical and high thermal loading the ductility is an order of magnitude higher. Experiments on a beam in bending confirm that the ductility is strongly dependent on the loading conditions. The observations suggest a means of utilizing the inherent ductility of the matrix. Author

A93-33016* National Aeronautics and Space Administration. Lewis Research Center, Cleveland, OH.

NONDESTRUCTIVE EVALUATION OF A CERAMIC MATRIX COMPOSITE MATERIAL

PAUL P. GROSSKOPF (Michelin Americas R&D Corp., Greenville, SC) and JOHN C. DUKE, JR. (Virginia Polytechnic Inst. and State Univ., Blacksburg) /n Cyclic deformation, fracture, and nondestructive evaluation of advanced materials Philadelphia, PA American Society for Testing and Materials 1992 p. 278-292. Research supported by NASA refs Copyright

Monolithic ceramic materials have proven their usefulness in many applications, yet, their potential for critical structural applications is limited because of their sensitivity to small imperfections. To overcome this extreme sensitivity to small imperfections, ceramic matrix composite materials have been developed that have the ability to withstand some distributed damage. A borosilicate glass reinforced with several layers of silicon-carbide fiber mat has been studied. Four-point flexure and tension tests were performed not only to determine some of the material properties, but also to initiate a controlled amount of damage within each specimen. Acousto-ultrasonic (AU) measurements were performed periodically during mechanical testing. This paper will compare the AU results to the mechanical test results and data from other nondestructive methods including acoustic emission monitoring and X-ray radiography. It was found that the AU measurements were sensitive to the damage that had developed within the material. Author

A93-33989*# National Aeronautics and Space Administration. Lewis Research Center, Cleveland, OH.

QUANTIFICATION OF UNCERTAINTIES IN COMPOSITES

D. G. LIAW, S. N. SINGHAL (Sverdrup Technology, Inc., Brook Park, OH), P. L. N. MURTHY, and CHRISTOS C. CHAMIS (NASA, Lewis Research Center, Cleveland, OH) /n AIAA/ASME/ASCE/AHS/ASC Structures, Structural Dynamics, and Materials Conference, 34th and AIAA/ASME Adaptive Structures Forum, La Jolla, CA, Apr. 19-22, 1993, Technical Papers. Pt. 2 Washington American Institute of Aeronautics and Astronautics 1993 p. 1163-1173. refs (AIAA PAPER 93-1440) Copyright

An integrated methodology is developed for computationally simulating the probabilistic composite material properties at all composite scales. The simulation requires minimum input consisting

of the description of uncertainties at the lowest scale (fiber and matrix constituents) of the composite and in the fabrication process variables. The methodology allows the determination of the sensitivity of the composite material behavior to all the relevant primitive variables. This information is crucial for reducing the undesirable scatter in composite behavior at its macro scale by reducing the uncertainties in the most influential primitive variables at the micro scale. The methodology is computationally efficient. The computational time required by the methodology described herein is an order of magnitude less than that for Monte Carlo Simulation. The methodology has been implemented into the computer code PICAN (Probabilistic Integrated Composite ANalyzer). The accuracy and efficiency of the methodology/code are demonstrated by simulating the uncertainties in the heat-transfer, thermal, and mechanical properties of a typical laminate and comparing the results with the Monte Carlo simulation method and experimental data. The important observation is that the computational simulation for probabilistic composite mechanics has sufficient flexibility to capture the observed scatter in composite properties.

Author

A93-33991* National Aeronautics and Space Administration. Lewis Research Center, Cleveland, OH.

PROBABILISTIC SIMULATION OF STRESS CONCENTRATION IN COMPOSITE LAMINATES

C. C. CHAMIS, P. L. N. MURTHY (NASA, Lewis Research Center, Cleveland, OH), and L. LIAW (Sverdrup Technology, Inc., Brook Park, OH) *In* AIAA/ASME/ASCE/AHS/ASC Structures, Structural Dynamics, and Materials Conference, 34th and AIAA/ASME Adaptive Structures Forum, La Jolla, CA, Apr. 19-22, 1993, Technical Papers. Pt. 2 Washington American Institute of Aeronautics and Astronautics 1993 p. 1187-1197. refs (AIAA PAPER 93-1442) Copyright

A computational methodology is described to probabilistically simulate the stress concentration factors in composite laminates. This new approach consists of coupling probabilistic composite mechanics with probabilistic finite element structural analysis. The probabilistic composite mechanics is used to probabilistically describe all the uncertainties inherent in composite material properties while probabilistic finite element is used to probabilistically describe the uncertainties associated with methods to experimentally evaluate stress concentration factors such as loads, geometry, and supports. The effectiveness of the methodology is demonstrated by using it to simulate the stress concentration factors in composite laminates made from three different composite systems. Simulated results match experimental data for probability density and for cumulative distribution functions. The sensitivity factors indicate that the stress concentration factors are influenced by local stiffness variables, by load eccentricities and by initial stress fields.

Author

A93-34045# National Aeronautics and Space Administration. Lewis Research Center, Cleveland, OH.

GLOBAL/LOCAL FINITE ELEMENT ANALYSIS FOR TEXTILE COMPOSITES

KYEONGSIK WOO and JOHN WHITCOMB (Texas A & M Univ., College Station) *In* AIAA/ASME/ASCE/AHS/ASC Structures, Structural Dynamics, and Materials Conference, 34th and AIAA/ASME Adaptive Structures Forum, La Jolla, CA, Apr. 19-22, 1993, Technical Papers. Pt. 3 Washington American Institute of Aeronautics and Astronautics 1993 p. 1721-1731. refs (Contract NAG3-1270; NAG1-1324) (AIAA PAPER 93-1506) Copyright

Conventional analysis of textile composites is impractical because of the complex microstructure. Global/local methodology combined with special macro elements is proposed herein as a practical alternative. Initial tests showed dramatic reductions in the computational effort with only small loss in accuracy. Author

A93-35882* National Aeronautics and Space Administration. Lewis Research Center, Cleveland, OH.

EFFECT OF THERMAL CYCLING ON INTERFACE BONDING REQUIREMENTS IN AL2O3 FIBER-REINFORCED SUPERALLOY COMPOSITES

AJAY K. MISRA (Sverdrup Technology, Inc.; NASA, Lewis Research Center, Cleveland, OH) *Scripta Metallurgica et Materialia* (ISSN 0956-716X) vol. 28, no. 10 May 15, 1993 p. 1189-1194. refs

Copyright

CTE (coefficient of thermal expansion) mismatch-induced stresses as they affect the fiber-matrix bond integrity of Al₂O₃ fiber-reinforced superalloy composites are examined. Of the three individual stress components, only the radial stress directly affects the integrity of the fiber-matrix interface. It is noted that a compressive radial stress leads to a clamping action on the fiber and is therefore beneficial to the integrity of the fiber-matrix bond. A radial tensile stress, on the other hand, can cause debonding of the fiber from the matrix for a weak fiber-matrix bond. AIAA

A93-38895* National Aeronautics and Space Administration. Lewis Research Center, Cleveland, OH.

A GENERIC MODEL FOR CREEP RUPTURE LIFETIME ESTIMATION ON FIBROUS CERAMIC COMPOSITES

TZE-JER CHUANG (NIST, Ceramics Div., Gaithersburg, MD) *In* Fracture mechanics of ceramics. Vol. 10 - Fracture fundamentals, high-temperature deformation, damage, and design; Proceedings of the 5th International Symposium, Nagoya, Japan, July 15-17, 1991 New York Plenum Press 1992 p. 441-457. refs (Contract NASA ORDER C-82000-R)

Copyright

Because of their high strength and toughness at elevated temperatures, fiber reinforced ceramic composites such as SiC(f)/SiC and SiC(f)/Si₃N₄ have become candidates for next-generation turbine engine materials. A generic model is proposed for assessing the lifetime of this class of materials when subjected to long-term creep rupture conditions. This 2D model consists of interfacial cracks growing between square grains and rectangular fibers in the direction normal to the principal tensile stress axis. Neglecting transient effects, the total lifetime is derived based on the criterion that rupture is due to coalescence of adjacent cracks. Lifetime is inversely proportional to crack growth rate, volume fraction, and aspect ratio of the fibers; but extremely sensitive to the applied stress, due to the high power of the V-K(I) law. This lifetime estimation seems to be in fair agreement with the creep rupture data of SiC(w)/Si₃N₄ composite with 0 and 30 vol percent reinforcement tested at 1250 C in air. TEM performed on the postcrept specimens revealed that creep damage is predominantly in the form of microcracks at matrix/matrix as well as fiber/matrix interfaces, approximately in accord with the model simulation.

Author (revised)

A93-39580* National Aeronautics and Space Administration. Lewis Research Center, Cleveland, OH.

RESIDUAL STRAIN GRADIENT DETERMINATION IN METAL MATRIX COMPOSITES BY SYNCHROTRON X-RAY ENERGY DISPERSIVE DIFFRACTION

TODD A. KUNTZ (Aptech Engineering Services, Inc., Sunnyvale, CA), HAYDN N. G. WADLEY (Virginia Univ., Charlottesville), and DAVID R. BLACK (NIST, Gaithersburg, MD) *Metallurgical Transactions A - Physical Metallurgy and Materials Science* (ISSN 0360-2133) vol. 24A, no. 5 May 1993 p. 1117-1124. Research supported by GE Aircraft Engines and Univ. of Virginia refs (Contract NAS3-25790)

An X-ray technique for the measurement of internal residual strain gradients near the continuous reinforcements of metal matrix composites has been investigated. The technique utilizes high intensity white X-ray radiation from a synchrotron radiation source to obtain energy spectra from small (0.001 cu mm) volumes deep within composite samples. The viability of the technique was tested using a model system with 800 micron Al₂O₃ fibers and a commercial purity titanium matrix. Good agreement was observed between the measured residual radial and hoop strain gradients

24 COMPOSITE MATERIALS

and those estimated from a simple elastic concentric cylinders model. The technique was then used to assess the strains near (SCS-6) silicon carbide fibers in a Ti-14Al-21Nb matrix after consolidation processing. Reasonable agreement between measured and calculated strains was seen provided the probe volume was located 50 microns or more from the fiber/matrix interface. Author (revised)

A93-40290* National Aeronautics and Space Administration. Lewis Research Center, Cleveland, OH.

TENSILE CREEP AND CREEP-RECOVERY BEHAVIOR OF A SIC-FIBER-Si3N4-MATRIX COMPOSITE

JOHN W. HOLMES, YONG H. PARK, and J. W. JONES (Michigan Univ., Ann Arbor) American Ceramic Society, Journal (ISSN 0002-7820) vol. 76, no. 5 May 1993 p. 1281-1293. Research supported by Univ. of Michigan and NASA refs Copyright

The tensile creep and creep-recovery behavior of a hot-pressed unidirectional SiC-fiber/Si3N4-matrix composite was investigated at 1200 C in air, in order to determine how various sustained and cyclic creep loading histories would influence the creep rate, accumulated creep strain, and the amount of strain recovered upon specimen unloading. The data accumulated indicate that the fundamental damage mode for sustained tensile creep at stresses of 200 and 250 MPa was periodic fiber fracture and that the creep life and the failure mode at 250 MPa were strongly influenced by the rate at which the initial creep stress was applied. Cyclic loading significantly lowered the duration of primary creep and the overall creep-strain accumulation. The implications of the results for microstructural and component design are discussed. AIAA

A93-40888* National Aeronautics and Space Administration. Lewis Research Center, Cleveland, OH.

MODEL OF BRITTLE MATRIX COMPOSITE TOUGHENING BASED ON DISCRETE FIBER REINFORCEMENT

ASHER A. RUBINSTEIN (Tulane Univ., New Orleans, LA) *In* Mechanical behaviour of materials - VI; Proceedings of the 6th International Conference, Kyoto, Japan, July 29-Aug. 2, 1991. Vol. 3 Oxford and New York Pergamon Press 1992 p. 465-470. refs (Contract NAG3-967) Copyright

An analytical approach for the analysis of the effectiveness of fiber reinforcement in brittle matrix composites is presented. The analytical method allows consideration of discrete fiber distribution and examination of the development of crack growth parameters on microscale. The problem associated with the bridging zone development is addressed here; therefore, the bridging zone is considered to be smaller than the main preexisting crack, and the small scale approach is used. The mechanics of the reinforcement is accurately accounted for in the process zone of a growing crack. Closed form solutions characterizing the initial failure process are presented for linear and nonlinear force - fiber pullout displacement relationships. The implicit exact solution for the extended bridging zone is presented as well. Author

A93-41573* National Aeronautics and Space Administration. Lewis Research Center, Cleveland, OH.

INTERCALATED GRAPHITE FIBER COMPOSITES AS EMI SHIELDS IN AEROSPACE STRUCTURES

JAMES R. GAIER (NASA, Lewis Research Center, Cleveland, OH) IEEE Transactions on Electromagnetic Compatibility (ISSN 0018-9375) vol. 34, no. 3, pt. 2 Aug. 1992 p. 351-356. refs Copyright

The requirements for electromagnetic interference (EMI) shielding in aerospace structures are more complicated than those for ground structures because of their weight limitations. As a result, the best EMI shielding materials must combine low density, high strength, and high elastic modulus with high shielding ability. EMI shielding characteristics were calculated for shields formed from pristine and intercalated graphite fiber/epoxy composites and compare to preliminary experimental results for these materials and to the characteristics of shields made from aluminum.

Calculations indicate that effective EMI shields could be fabricated from intercalated graphite composites which would have less than 12 percent of the mass of conventional aluminum shields, based on mechanical properties and shielding characteristics alone. Author

A93-42085* National Aeronautics and Space Administration. Lewis Research Center, Cleveland, OH.

THE EFFECT OF MULTIPLE COMPLIANT LAYERS AT THE FIBER-MATRIX INTERFACE ON RESIDUAL THERMAL STRESSES IN METAL MATRIX COMPOSITES

MAREK-JERZY PINDERA (Virginia Univ., Charlottesville) and ALAN D. FREED (NASA, Lewis Research Center, Cleveland, OH) *In* Engineering, construction, and operations in space III: Space '92; Proceedings of the 3rd International Conference, Denver, CO, May 31-June 4, 1992. Vol. 2 New York American Society of Civil Engineers 1992 p. 1262-1272. refs Copyright

The large mismatch in thermoelastic properties of the fiber and matrix phases in advanced metal matrix composites, coupled with high consolidation temperatures, produces severe residual stresses that can be large enough to initiate microcracks in the matrix phase adjacent to the fiber/matrix interface. Previous investigations have demonstrated that the use of a compliant interfacial layer between fiber and matrix phases has the potential for reducing these residual stresses. In this paper, the influence of multiple compliant layers in reducing residual thermal stresses is investigated. Author

A93-48498* National Aeronautics and Space Administration. Lewis Research Center, Cleveland, OH.

EVOLUTION OF DAMAGE AND PLASTICITY IN TITANIUM-BASED, FIBER-REINFORCED COMPOSITES

B. S. MAJUMDAR (Universal Energy Systems, Inc., Dayton, OH), G. M. NEWAZ (Battelle Memorial Inst., Columbus, OH), and J. R. ELLIS (NASA, Lewis Research Center, Cleveland, OH) Metallurgical Transactions A - Physical Metallurgy and Materials Science (ISSN 0360-2133) vol. 24A, no. 7 July 1993 p. 1597-1610. refs Copyright

The inelastic deformation mechanisms were evaluated for a model titanium-based, fiber-reinforced composite: a beta titanium alloy (Ti-15V-3Al-3Cr-3Sn) reinforced with SiC (SCS-6) fibers. The primary emphasis of this article is to illustrate the sequence in which damage and plasticity evolved for this system. The mechanical responses and the results of detailed microstructural evaluations for the 0(8), 90(8), and +/- 45(2s) line oriented laminates are provided. It is shown that the characteristics of the reaction zone around the fiber play a very important role in the way damage and plasticity evolve, particularly in the microyield regime of deformation, and must be included in any realistic constitutive model. Fiber-matrix debonding was a major damage mode for the off-axis systems. The tension test results are also compared with the predictions of a few constitutive models. Author (revised)

A93-49253* National Aeronautics and Space Administration. Lewis Research Center, Cleveland, OH.

AN ANALYSIS OF THE WEAR BEHAVIOR OF SIC WHISKER-REINFORCED ALUMINA FROM 25 TO 1200 C

CHRISTOPHER DELLACORTE (NASA, Lewis Research Center, Cleveland, OH) STLE Tribology Transactions (ISSN 0569-8197) vol. 36, no. 3 July 1993 p. 452-460. ASME and STLE, Tribology Conference, San Diego, CA, Oct. 19-21, 1992. Previously announced in STAR as N91-29235 refs Copyright

A model is described for predicting the wear behavior of whisker reinforced ceramics. The model was successfully applied to a silicon carbide whisker reinforced alumina ceramic composite subjected to sliding contact. The model compares the friction forces on the whiskers due to sliding, which act to pull or push them out of the matrix, to the clamping or compressive forces on the whiskers due to the matrix, which act to hold the whiskers in the composite.

At low temperatures, the whiskers are held strongly in the matrix and are fractured into pieces during the wear process along with the matrix. At elevated temperatures differential thermal expansion between the whiskers and matrix can cause loosening of the whiskers and lead to pullout during the wear process and to higher wear. The model, which represents the combination of elastic stress analysis and a friction heating analysis, predicts a transition temperature at which the strength of the whiskers equals the clamping force holding them in the matrix. Above the transition the whiskers are pulled out of the matrix during sliding, and below the transition the whiskers are simply fractured. The existence of the transition gives rise to a dual wear mode or mechanism behavior for this material which was observed in laboratory experiments. The results from this model correlate well with experimentally observed behavior indicating that the model may be useful in obtaining a better understanding of material behavior and in making material improvements.

A93-52473* National Aeronautics and Space Administration, Lewis Research Center, Cleveland, OH.

CHEMICAL STABILITY OF TITANIUM DIBORIDE REINFORCEMENT IN NICKEL ALUMINIDE MATRICES

J. D. RIGNEY and J. J. LEWANDOWSKI (Case Western Reserve Univ., Cleveland, OH) *Journal of Materials Science* (ISSN 0022-2461) vol. 28, no. 14 July 15, 1993 p. 3911-3922. Research supported by NASA and MTS Systems Corp. refs (Contract AF-AFOSR-89-0508) Copyright

Chemical stability of TiB₂ reinforcement in NiAl (45 at percent Al) and Ni₃Al (24 at percent Al) matrices has been theoretically and experimentally investigated. Calculations were made using thermodynamic properties of the systems to predict behavior at temperatures between 1173 and 1573 K. Experimental investigation of hot-press consolidated TiB₂ particulate/prealloyed matrix powder blends were conducted using energy dispersive X-ray analysis, XRD, AES, and TEM. The theoretical and experimental analyses suggest that TiB₂ is chemically stable in both matrices up to 1573 K; however, TiB₂ was found to be less active in NiAl than in Ni₃Al due to lower nickel activity in NiAl. Author (revised)

A93-52919* National Aeronautics and Space Administration, Lewis Research Center, Cleveland, OH.

ULTRASONIC ASSESSMENT OF INTERFACIAL OXIDATION DAMAGE IN CERAMIC MATRIX COMPOSITES

Y. C. CHU, S. I. ROKHLIN (Ohio State Univ., Columbus), and G. Y. BAAKLINI (NASA, Lewis Research Center, Cleveland, OH) *ASME, Transactions, Journal of Engineering Materials and Technology* (ISSN 0094-4289) vol. 115, no. 3 July 1993 p. 237-243. ASME, Winter Annual Meeting, Symposium on Micromechanics of Ceramics and Ceramic Composites, Anaheim, CA, Nov. 8-13, 1992 refs (Contract NAG3-1220) Copyright

A new approach to characterizing oxidation damage in ceramic matrix composites using ultrasonic techniques is proposed. In this approach, the elastic constants of the composite are determined nondestructively by measuring the angular dependence of both longitudinal and transverse wave velocities. A micromechanical model for composites with anisotropic constituents is used to find the anisotropic properties of an effective fiber, which is a combination of the fiber and the interface. Interfacial properties are extracted from the properties of this effective fiber by analyzing the difference between effective and actual fiber properties. Unidirectional /0/28 SiC/Si₃N₄ composites with 30 percent fiber volume fraction and 30 percent matrix porosity are used. The samples are exposed in a flowing oxygen environment at elevated temperatures, up to 1400 C, for 100 hours and then measured by ultrasonic methods at room temperature. The Young's modulus in the fiber direction of the sample oxidized at 600 C decreased significantly but it was unchanged for samples oxidized at temperatures above 1200 C. The transverse moduli obtained from ultrasonic measurements decrease continuously up to 1200 C. The shear stiffnesses show behavior similar to the transverse

moduli. The effective elastic moduli of the interfacial carbon coating are determined from the experimental data, and their change due to thermal oxidation is discussed. Author (revised)

A93-53446 National Aeronautics and Space Administration, Lewis Research Center, Cleveland, OH.

APPROACHES TO POLYMER-DERIVED CMC MATRICES

FRANCES I. HURWITZ (NASA, Lewis Research Center, Cleveland, OH) *In* International SAMPE Technical Conference, 24th and International SAMPE Metals and Metals Processing Conference, 3rd, Toronto, Canada, Oct. 20-22, 1992, Proceedings. Vol. 24 Covina, CA Society for the Advancement of Material and Process Engineering 1992 p. T950-T961. Previously announced in STAR as N92-29660 refs (Contract RTOP 505-63-40)

The use of polymeric precursors to ceramics permits the fabrication of large, complex-shaped ceramic matrix composites (CMC's) at temperatures which do not degrade the fiber. Processing equipment and techniques readily available in the resin matrix composite industry can be adapted for CMC fabrication using this approach. Criteria which influence the choice of candidate precursor polymers, the use of fillers, and the role of fiber architecture and ply layup are discussed. Three polymer systems, polycarbosilanes, polysilazanes, and polysilsesquioxanes, are compared as candidate ceramic matrix precursors.

A93-53455* National Aeronautics and Space Administration, Lewis Research Center, Cleveland, OH.

THERMAL EMITTANCE ENHANCEMENT OF GRAPHITE-ALUMINUM AND GRAPHITE-COPPER COMPOSITE RADIATOR SURFACES FOR SPACE POWER APPLICATIONS

SHARON K. RUTLEDGE (NASA, Lewis Research Center, Cleveland, OH) and MARK J. FORKAPA (Cleveland State Univ., OH) *In* International SAMPE Technical Conference, 24th and International SAMPE Metals and Metals Processing Conference, 3rd, Toronto, Canada, Oct. 20-22, 1992, Proceedings. Vol. 24 Covina, CA Society for the Advancement of Material and Process Engineering 1992 p. T1055-T1066. refs Copyright

A93-54116* National Aeronautics and Space Administration, Lewis Research Center, Cleveland, OH.

FABRICATION AND PROPERTIES OF FUNCTIONALLY GRADED NIAL/AL₂O₃ COMPOSITES

D. P. MILLER, J. J. LANNUTTI (Ohio State Univ., Columbus), and R. D. NOEBE (NASA, Lewis Research Center, Cleveland, OH) *Journal of Materials Research* (ISSN 0884-2914) vol. 8, no. 8 Aug. 1993 p. 2004-2013. refs Copyright

A modified sedimentation process was used in the production of a functionally gradient material (FGM), NiAl/Al₂O₃. A simple finite element model was used to guide our design and fabrication efforts by estimating residual stress states as a function of composite structure. This approach could lead to tailored designs that enhance or avoid specific residual stress states. Thermal cycling tests were factored into the model to predict time dependent or steady-state internal temperature and stress profiles. Four-point bend tests were conducted to establish the mechanical load-displacement behavior of a single interlayer FGM at room temperature, 800 and 1000 K. Room temperature bend strength of the FGM was 3-4 times that of the base NiAl. At elevated temperatures, composite fracture occurred in a gradual, noncatastrophic mode involving NiAl retardation of a succession of cracks originating in the alumina face. Author (revised)

A93-54705* National Aeronautics and Space Administration, Lewis Research Center, Cleveland, OH.

PROBABILISTIC MICROMECHANICS AND MACROMECHANICS OF POLYMER MATRIX COMPOSITES

G. T. MASE (GMI Engineering and Management Inst., Flint, MI), P. L. N. MURTHY, and C. C. CHAMIS (NASA, Lewis Research Center, Cleveland, OH) *In* Composite material technology - 1991; Proceedings of the Symposium, 14th Annual Energy-sources

Technology Conference and Exhibition, Houston, TX, Jan. 20-23, 1991 New York American Society of Mechanical Engineers 1991 p. 285-291. Previously announced in STAR as N91-19236 refs

Copyright

A probabilistic evaluation of an eight ply graphite-epoxy quasi-isotropic laminate was completed using the Integrated Composite Analyzer (ICAN) in conjunction with Monte Carlo simulation and Fast Probability Integration (FPI) techniques. Probabilistic input included fiber and matrix properties, fiber misalignment, fiber volume ratio, void volume ratio, ply thickness and ply layup angle. Cumulative distribution functions (CDFs) for select laminate properties are given. To reduce the number of simulations, a Fast Probability Integration (FPI) technique was used to generate CDFs for the select properties in the absence of fiber misalignment. These CDFs were compared to a second Monte Carlo simulation done without fiber misalignment effects. It was found that FPI requires fewer simulations to obtain the cumulative distribution functions as opposed to Monte Carlo simulation techniques. Furthermore, FPI provides valuable information regarding the sensitivities of composite properties to the constituent properties, fiber volume ratio and void volume ratio.

A93-54771* National Aeronautics and Space Administration. Lewis Research Center, Cleveland, OH.

THE EFFECT OF FIBER MICROSTRUCTURE ON EVOLUTION OF RESIDUAL STRESSES IN SILICON CARBIDE/TITANIUM ALUMINIDE COMPOSITES

MAREK-JERZY PINDER (Virginia Univ., Charlottesville) and ALAN D. FREED (NASA, Lewis Research Center, Cleveland, OH) In Topics in composite materials and structures; Proceedings of the Sessions, ASME Summer Mechanics and Materials Conference, Tempe, AZ, Apr. 28-May 1, 1992 New York American Society of Mechanical Engineers 1992 p. 21-26. refs

Copyright

This paper examines the effect of the morphology of the SiC/SiC silicon carbide fiber on the evolution of residual stresses in SiC/Ti composites. A micromechanics model based on the concentric cylinder concept is presented which is used to calculate residual stresses in a SiC/Ti composite during axisymmetric cooling by a spatially uniform temperature change. The silicon carbide fiber is modeled as a layered material with five distinct transversely isotropic and orthotropic, elastic layers, whereas the titanium matrix is taken to be isotropic, with temperature-dependent elastoplastic properties. The results are compared with those obtained based on the assumption that the silicon carbide fiber is isotropic and homogeneous.

A93-55685* National Aeronautics and Space Administration. Lewis Research Center, Cleveland, OH.

INTERFACIAL SHEAR STRENGTH OF CAST AND DIRECTIONALLY SOLIDIFIED NIAL-SAPPHIRE FIBER COMPOSITES

S. N. TEWARI, R. ASTHANA (Cleveland State Univ., OH), and R. D. NOEBE (NASA, Lewis Research Center, Cleveland, OH) Metallurgical Transactions A - Physical Metallurgy and Materials Science (ISSN 0360-2133) vol. 24A, no. 9 Sept. 1993 p. 2119-2125. refs

(Contract NCC3-287)

The feasibility of fabricating intermetallic NiAl-sapphire fiber composites by casting and zone directional solidification has been examined. The fiber-matrix interfacial shear strengths measured using a fiber push-out technique in both cast and directionally solidified composites are greater than the strengths reported for composites fabricated by powder cloth process using organic binders. Microscopic examination of fibers extracted from cast, directionally solidified (DS), and thermally cycled composites, and the high values of interfacial shear strengths suggest that the fiber-matrix interface does not degrade due to casting and directional solidification. Sapphire fibers do not pin grain boundaries during directional solidification, suggesting that this technique can be used to fabricate sapphire fiber reinforced NiAl composites with single crystal matrices.

A93-56351* National Aeronautics and Space Administration. Lewis Research Center, Cleveland, OH.

INTERFACIAL AND CAPILLARY PHENOMENA IN SOLIDIFICATION PROCESSING OF METAL-MATRIX COMPOSITES

R. ASTHANA (Cleveland State Univ.; NASA, Lewis Research Center, OH) and S. N. TEWARI (Cleveland State Univ., OH) Composites Manufacturing (ISSN 0956-7143) vol. 4, no. 1 March 1993 p. 3-25. refs

Copyright

Chemical and hydrodynamic aspects of wetting and interfacial phenomena during the solidification processing of metal-matrix composites are reviewed. Significant experimental results on fiber-matrix interactions and wetting under equilibrium and non-equilibrium conditions in composites of engineering interest have been compiled, based on a survey of the recent literature. Finally, certain aspects of wetting relevant to stir-casting and infiltration processing of composites are discussed.

N93-11399*# National Aeronautics and Space Administration. Lewis Research Center, Cleveland, OH.

THERMOMECHANICAL FATIGUE BEHAVIOR OF SIC/TI-24AL-11NB IN AIR AND ARGON ENVIRONMENTS

PAUL A. BARTOLOTTA and MICHAEL J. VERRILLI Aug. 1992 16 p Presented at the 11th Symposium on Composite Materials: Testing and Design, Pittsburgh, PA, 4-5 May 1992; sponsored by the American Society for Testing and Materials (Contract RTOP 510-01-50)

(NASA-TM-105723; E-7122; NAS 1.15:105723) Avail: CASI HC A03/MF A01

A series of tension-tension, load-controlled thermomechanical fatigue (TMF) tests were conducted on a titanium aluminide composite in both laboratory air and a flowing argon environment. Results from these tests show that the environment plays an increasingly important role as applied stress levels are decreased. Differences in damage mechanisms between the two environments were observed which corresponds to observed variations in TMF lives.

Author

N93-11543*# National Aeronautics and Space Administration. Lewis Research Center, Cleveland, OH.

SILICON CARBIDE FIBER REINFORCED STRONTIUM ALUMINOSILICATE GLASS-CERAMIC MATRIX COMPOSITE Patent Application

NAROTTAM BANSAL, inventor (to NASA) 4 Jun. 1992 7 p (NASA-CASE-LEW-15263-1; NAS 1.71:LEW-15263-1; US-PATENT-APPL-SN-892054) Avail: CASI HC A02/MF A01

A SrO-Al₂O₃ - 2SrO₂ (SAS) glass ceramic matrix is reinforced with CVD SiC continuous fibers. This material is prepared by casting a slurry of SAS glass powder into tapes. Mats of continuous CVD-SiC fibers are alternately stacked with the matrix tapes. This tape-mat stack is warm-pressed to produce a 'green' composite. Organic constituents are burned out of the 'green' composite, and the remaining interim material is hot pressed.

NASA

N93-12015*# National Aeronautics and Space Administration. Lewis Research Center, Cleveland, OH.

ICAN/DAMP-INTEGRATED COMPOSITE ANALYZER WITH DAMPING ANALYSIS CAPABILITIES: USER'S MANUAL

DIMITRIOS A. SARAVANOS (Ohio Aerospace Inst., Brook Park.) and JOSE G. SANFELIZ Nov. 1992 39 p (Contract RTOP 505-63-53)

(NASA-TP-3292; E-6898; NAS 1.60:3292) Avail: CASI HC A03/MF A01

This manual describes the use of the computer code ICAN/DAMP (Integrated Composite Analyzer with Damping Analysis Capabilities) for the prediction of damping in polymer-matrix composites. The code is written in FORTRAN 77 and is a version of the ICAN (Integrated Composite Analyzer) computer program. The code incorporates a new module for synthesizing the material damping from micromechanics to laminate level. Explicit micromechanics equations based on hysteretic damping are programmed relating the on-axis damping capacities

to the fiber and matrix properties and fiber volume ratio. The damping capacities of unidirectional composites subjected to off-axis loading are synthesized from on-axis damping values. The hygrothermal effect on the damping performance of unidirectional composites caused by temperature and moisture variation is modeled along with the damping contributions from interfacial friction between broken fibers and matrix. The temperature rise is continuously vibrating composite plies and composite laminates is also estimated. The ICAN/DAMP user's manual provides descriptions of the damping analysis module's functions, structure, input requirements, output interpretation, and execution requirements. It only addresses the changes required to conduct the damping analysis and is used in conjunction with the 'Second Generation Integrated Composite Analyzer (ICAN) Computer Code' user's manual (NASA TP-3290). Author

N93-12076*# National Aeronautics and Space Administration, Lewis Research Center, Cleveland, OH.

THE EFFECT OF CONTACT STRESSES IN FOUR-POINT BEND TESTING OF GRAPHITE/EPOXY AND GRAPHITE/PMR-15 COMPOSITE BEAMS

WIESLAW K. BINIENDA (Akron Univ., OH.), GARY D. ROBERTS, and DEMETRIOS S. PAPADOPOULOS (Case Western Reserve Univ., Cleveland, OH.) Oct. 1992 24 p Previously announced in IAA as A92-33589 (Contract RTOP 505-63-5A) (NASA-TM-105891; E-7358; NAS 1.15:105891) Avail: CASI HC A03/MF A01

The results of in-plane four-point bend experiments on unidirectionally reinforced composite beams are presented for graphite/epoxy (T300/934) and graphite/polyimide (G30-500/PMR-15) composites. The maximum load and the location of cracks formed during failure were measured for testpieces with fibers oriented at various angles to the beam axis. Since most of the beams failed near one or more of the load points, the strength of the beams was evaluated in terms of a proposed model, for the local stress distribution. In this model, an exact solution to the problem of a localized contact force acting on a unidirectionally reinforced half plane is used to describe the local stress field. The stress singularity at the load points is treated in a manner similar to the stress singularity at a crack tip in fracture mechanisms problems. Using this approach, the effect of fiber angle and elastic material properties on the strength of the beam is described in terms of a load intensity factor. For fiber angles less than 45 deg from the beam axis, a single crack is initiated near one of the load points at a critical value of the load intensity factor. The critical load intensity factor decreases with the increasing fiber angle. For larger fiber angles, multiple cracks occur at locations both near and away from the load points, and the load intensity factor at failure increases sharply with increasing fiber angle. Author

N93-12078*# National Aeronautics and Space Administration, Lewis Research Center, Cleveland, OH.

THERMOSTRUCTURAL TAILORING OF FIBER COMPOSITE STRUCTURES

THOMAS H. ACQUAVIVA Oct. 1992 116 p (Contract RTOP 505-90-52) (NASA-TM-105882; E-7349; NAS 1.15:105882) Avail: CASI HC A06/MF A02

A significant area of interest in design of complex structures involves the study of multidisciplinary problems. The coordination of several different intricate areas of study to obtain a particular design of a structure is a new and pressing area of research. In the past, each discipline would perform its task consecutively using the appropriate inputs from the other disciplines. This process usually required several time-consuming iterations to obtain a satisfactory design. The alternative pursued here is combining various participating disciplines and specified design requirements into a formal structural computer code. The main focus of this research is to develop a multidiscipline structural tailoring method for select composite structures and to demonstrate its application to specific areas. The development of an integrated computer

program involves the coupling of three independent computer programs using an executive module. This module will be the foundation for integrating a structural optimizer, a composites analyzer and a thermal analyzer. With the completion of the executive module, the first step was taken toward the evolution of multidiscipline software in the field of composite mechanics. Through the use of an array of cases involving a variety of objective functions/constraints and thermal-mechanical load conditions, it became evident that simple composite structures can be designed to a combined loads environment. Author

N93-12302*# National Aeronautics and Space Administration, Lewis Research Center, Cleveland, OH.

FRACTURE TOUGHNESS TESTING OF POLYMER MATRIX COMPOSITES

JOSEPH E. GRADY Nov. 1992 39 p (Contract RTOP 505-63-1B) (NASA-TP-3199; E-6455; NAS 1.60:3199) Avail: CASI HC A03/MF A01

A review of the interlaminar fracture indicates that a standard specimen geometry is needed to obtain consistent fracture toughness measurements in polymer matrix composites. In general, the variability of measured toughness values increases as the toughness of the material increases. This variability could be caused by incorrect sizing of test specimens and/or inconsistent data reduction procedures. A standard data reduction procedure is therefore needed as well, particularly for the tougher materials. Little work has been reported on the effects of fiber orientation, fiber architecture, fiber surface treatment or interlaminar fracture toughness, and the mechanisms by which the fibers increase fracture toughness are not well understood. The little data that is available indicates that woven fiber reinforcement and fiber sizings can significantly increase interlaminar fracture toughness. Author

N93-12737*# National Aeronautics and Space Administration, Lewis Research Center, Cleveland, OH.

TRANSVERSE FLEXURAL TESTS AS A TOOL FOR ASSESSING DAMAGE TO PMR-15 COMPOSITES FROM ISOTHERMAL AGING IN AIR AT ELEVATED TEMPERATURES

KENNETH J. BOWLES Oct. 1992 15 p (Contract RTOP 510-01-50) (NASA-TM-105848; E-7293; NAS 1.15:105848) Avail: CASI HC A03/MF A01

To date, the effect of thermo-oxidative aging on unidirectional composite mechanical properties has been monitored by the measurement of interlaminar shear strength (ILSS) and either three or four point longitudinal flexural strength (LFS) of the composites being tested. Both results are affected by the fiber-to-matrix bonding, the former being dependent on the shear resistance of the interface and the latter on the degree of load sharing by the fibers through the fiber/matrix interface. Recently, fiber/matrix interfacial bond strengths have been monitored using a transverse flexural strength (TFS) test method. This test method was used to evaluate the effect of fiber surface treatment on the fiber/matrix bond. The interface bonding was varied in these tests using Hercules A-fibers with three-types of surfaces that produce bonds of poor, better, and good quality. The TFS was found not only to be sensitive to the bonding, but also to the aging time of unidirectional A-fiber/PMR-15 composites. This relationship reflects the mechanism by which the PMR-15 degrades during thermal aging. Author

N93-14706* National Aeronautics and Space Administration, Lewis Research Center, Cleveland, OH.

METHOD OF APPLYING A THERMAL BARRIER COATING SYSTEM TO A SUBSTRATE Patent

ROBERT A. MILLER, inventor (to NASA) 8 Dec. 1992 5 p Filed 23 May 1991 Supersedes N91-25202 (29 - 17, p 2747) Division of abandoned US-Patent-Appl-SN-601957, filed 23 Oct. 1990 (NASA-CASE-LEW-15020-2; US-PATENT-5,169,674; US-PATENT-APPL-SN-708255; US-PATENT-APPL-SN-601957; US-PATENT-CLASS-427-456; US-PATENT-CLASS-427-367;

24 COMPOSITE MATERIALS

US-PATENT-CLASS-427-404; US-PATENT-CLASS-427-419.2;
INT-PATENT-CLASS-B05D-1/02;
INT-PATENT-CLASS-B05D-3/12) Avail: US Patent and
Trademark Office

A metallic close-out layer is applied to the surface of a thermal barrier coating system to seal the ceramic material in the coating. The close-out layer is glass-bead preened to densify the surface.

Official Gazette of the U.S. Patent and Trademark Office

N93-18139*# National Aeronautics and Space Administration. Lewis Research Center, Cleveland, OH.

SECOND GENERATION INTEGRATED COMPOSITE

ANALYZER (ICAN) COMPUTER CODE

PAPPU L. N. MURTHY, CAROL A. GINTY, and JOSE G. SANFELIZ Jan. 1993 93 p

(Contract RTOP 505-63-5B)

(NASA-TP-3290; E-6831; NAS 1.60:3290) Avail: CASI HC A05/MF A01

This manual updates the original 1986 NASA TP-2515, Integrated Composite Analyzer (ICAN) Users and Programmers Manual. The various enhancements and newly added features are described to enable the user to prepare the appropriate input data to run this updated version of the ICAN code. For reference, the micromechanics equations are provided in an appendix and should be compared to those in the original manual for modifications. A complete output for a sample case is also provided in a separate appendix. The input to the code includes constituent material properties, factors reflecting the fabrication process, and laminate configuration. The code performs micromechanics, macromechanics, and laminate analyses, including the hygrothermal response of polymer-matrix-based fiber composites. The output includes the various ply and composite properties, the composite structural response, and the composite stress analysis results with details on failure. The code is written in FORTRAN 77 and can be used efficiently as a self-contained package (or as a module) in complex structural analysis programs. The input-output format has changed considerably from the original version of ICAN and is described extensively through the use of a sample problem.

Author

N93-20040*# National Aeronautics and Space Administration. Lewis Research Center, Cleveland, OH.

FIBER-REINFORCED MONOCLINIC CELSIAN MATRIX

COMPOSITE MATERIAL Patent Application

N. P. BANSAL, inventor (to NASA) and J. A. DICARLO, inventor (to NASA) 7 Dec. 1992 5 p

(NASA-CASE-LEW-15269-1; NAS 1.71:LEW-15269-1;

US-PATENT-APPL-SN-986399) Avail: CASI HC A01/MF A01

A hydriopolysilazane-derived ceramic fiber reinforced monoclinic celsian phase barium aluminum silicate glass-ceramic matrix composite material is prepared by ball-milling an aqueous slurry of BAS glass powder and fine monoclinic celsian seeds. The fibers improve the mechanical strength and fracture toughness. These fibers further provide superior dielectric properties.

NASA

N93-20317*# National Aeronautics and Space Administration. Lewis Research Center, Cleveland, OH.

EFFECTS OF THERMAL AND MECHANICAL FATIGUE ON THE FLEXURAL STRENGTH OF G40-600/PMR-15 CROSS-PLY LAMINATES

GARY D. ROBERTS, BARRY PING HSIAO HO (Case Western Reserve Univ., Cleveland, OH.), and JOHN F. WALLACE (Case Western Reserve Univ., Cleveland, OH.) Feb. 1993 24 p

(Contract RTOP 505-63-5A)

(NASA-TM-106016; E-7573; NAS 1.15:106016) Avail: CASI HC A03/MF A01

The effects of thermal and mechanical fatigue on the flexural strength of G40-600/PMR-15 cross-ply laminates with ply orientation of (0(2),90(2))₂S and (90(2),0(2))₂S are examined. The relative importance of shear and tensile stresses is examined by varying the span-to-depth ratios of flexural test specimens from 8 to 45. Acoustic emission signals are measured during the flexural tests in order to monitor the initiation and growth of damage.

Optical microscopy is used to examine specimens for resin cracking, delamination, and fiber breaks after testing. Transverse matrix cracks and delaminations occur in all specimens, regardless of ply orientation, span-to-depth ratio, or previous exposure of specimens to thermal and mechanical fatigue. A small amount of fiber tensile fracture occurs in the outer 0 deg ply of specimens with high span-to-depth ratios. Because of the complex failure modes, the flexural test results represent the 'apparent' strengths rather than the true flexural or shear strengths for these cross-ply laminates. Thermal cycling of specimens prior to flexural testing does not reduce the apparent flexural strength or change the mode of failure. However, fewer acoustic events are recorded at all strains during flexural testing of specimens exposed to prior thermal cycling. High temperature thermal cycling (32 to 260 C, 100 cycles) causes a greater reduction in acoustic events than low temperature thermal cycling (-85 to +85 C, 500 cycles). Mechanical cycling (0 to 50 percent of the flexural strength, 100 cycles) has a similar effect, except that acoustic events are reduced only at strains less than the maximum strain applied during flexural fatigue.

Author

N93-20568*# National Aeronautics and Space Administration. Lewis Research Center, Cleveland, OH.

HEAT TRANSFER DEVICE Patent Application

BRUCE A. BANKS, inventor (to NASA) and J. R. GAIER, inventor (to NASA) 10 Feb. 1993 11 p

(NASA-CASE-LEW-14162-4; NAS 1.71:LEW-14162-4;

US-PATENT-APPL-SN-017402) Avail: CASI HC A03/MF A01

Gas derived graphite fibers generated by the decomposition of an organic gas are joined with a suitable binder. This produces a high thermal conductivity composite material which passively conducts heat from a source, such as a semiconductor, to a heat sink. The fibers may be intercalated. The intercalate can be halogen or halide salt, alkaline metal, or any other species which contributes to the electrical conductivity improvement of the graphite fiber. The fibers are bundled and joined with a suitable binder to form a high thermal conductivity composite material device. The heat transfer device may also be made of intercalated highly oriented pyrolytic graphite and machined, rather than made of fibers.

NASA

N93-21515*# National Aeronautics and Space Administration. Lewis Research Center, Cleveland, OH.

PROGRESSIVE DELAMINATION IN POLYMER MATRIX

COMPOSITE LAMINATES: A NEW APPROACH

C. C. CHAMIS, P. L. N. MURTHY, and L. MINNETYAN (Clarkson Univ., Potsdam, NY.) In AGARD, Debonding/Delamination of Composites 9 p Dec. 1992

Copyright Avail: CASI HC A02/MF A03

A new approach independent of stress intensity factors and fracture toughness parameters has been developed and is described for the computational simulation of progressive delamination in polymer matrix composite laminates. The damage stages are quantified based on physics via composite mechanics while the degradation of the laminate behavior is quantified via the finite element method. The approach accounts for all types of composite behavior, laminate configuration, load conditions, and delamination processes starting from damage initiation, to unstable propagation, and to laminate fracture. Results of laminate fracture in composite beams, panels, plates, and shells are presented to demonstrate the effectiveness and versatility of this new approach.

Author

N93-25071*# National Aeronautics and Space Administration. Lewis Research Center, Cleveland, OH.

STRESS DISTRIBUTION IN COMPOSITE FLATWISE TENSION TEST SPECIMENS

CURTIS A. SCOTT (Ohio Aerospace Inst., Brook Park.) and J. MICHAEL PEREIRA Mar. 1993 12 p

(Contract RTOP 505-63-1B)

(NASA-TM-106074; E-7683; NAS 1.15:106074) Avail: CASI HC A03/MF A01

A finite element analysis was conducted to determine the

stress distribution in typical graphite/epoxy composite flat wise tension (FWT) specimens under normal loading conditions. The purpose of the analysis was to determine the relationship between the applied load and the stress in the sample to evaluate the validity of the test as a means of measuring the out-of-plane strength of a composite laminate. Three different test geometries and three different material lay ups were modeled. In all cases, the out-of-plane component of stress in the test section was found to be uniform, with no stress concentrations, and very close to the nominal applied stress. The stress in the sample was found to be three-dimensional, and the magnitude of in-plane normal and shear stresses varied with the anisotropy of the test specimen. However, in the cases considered here, these components of stress were much smaller than the out-of-plane normal stress. The geometry of the test specimen had little influence on the results. It was concluded that the flat wise tension test provides a good measure of the out-of-plane strength for the representative materials that were studied.

Author

N93-25587*# National Aeronautics and Space Administration. Lewis Research Center, Cleveland, OH.

GRAPHITE/EPOXY COMPOSITE LAMINATES WITH CO-CURED INTERLAMINAR DAMPING LAYERS

J. MICHAEL PEREIRA / In NASA, Washington, Technology 2002: The Third National Technology Transfer Conference and Exposition, Volume 1 p 250-255 Feb. 1993
 Avail: CASI HC A02/MF A04

Damped composite laminates were fabricated by co-curing viscoelastic damping film with graphite/epoxy prepreg plies. The dynamic response of the damped plates was measured using an impulse response technique and compared with the response of similar undamped laminates. Modal damping was computed from the frequency response data. Micrographs of the damped laminates showed that the damping layers retained their integrity during the fabrication process. The layers significantly increased the damping in the composite laminates. The use of the constrained viscoelastic film as an integral part of composite structures appears to be a feasible approach to passive vibration control. Composite plates manufactured with co-cured damping layers may have commercial applications in cases where light weight, strength, and vibration and noise reduction are important considerations.

Author (revised)

N93-26100* National Aeronautics and Space Administration. Lewis Research Center, Cleveland, OH.

CERAMIC FIBER REINFORCED GLASS-CERAMIC MATRIX COMPOSITE Patent

NAROTTAM P. BANSAL, inventor (to NASA) 25 May 1993
 4 p Filed 4 Jun. 1992

(NASA-CASE-LEW-15262-1; US-PATENT-5,214,004;
 US-PATENT-APPL-SN-892055; US-PATENT-CLASS-501-8;
 US-PATENT-CLASS-501-32; US-PATENT-CLASS-501-89;
 US-PATENT-CLASS-501-95; US-PATENT-CLASS-428-428;
 US-PATENT-CLASS-428-698; US-PATENT-CLASS-264-58)

Avail: US Patent and Trademark Office

A slurry of BSAS glass powders is cast into tapes which are cut to predetermined sizes. Mats of continuous chemical vapor deposition (CVD)-SiC fibers are alternately stacked with these matrix tapes. This tape-mat stack is warm-pressed to produce a 'green' composite which is heated to burn out organic constituents. The remaining interim material is then hot-pressed to form a BSAS glass-ceramic fiber-reinforced composite.

Official Gazette of the U.S. Patent and Trademark Office

N93-26552*# National Aeronautics and Space Administration. Lewis Research Center, Cleveland, OH.

METAL MATRIX COMPOSITE ANALYZER (METCAN): THEORETICAL MANUAL

P. L. N. MURTHY and C. C. CHAMIS Feb. 1993 36 p
 (Contract RTOP 510-01-50)

(NASA-TM-106025; E-7588; NAS 1.15:106025) Avail: CASI HC A03/MF A01

This manuscript is intended to be a companion volume to the

'METCAN User's Manual' and the 'METAN Demonstration Manual.' The primary purpose of the manual is to give details pertaining to micromechanics and macromechanics equations of high temperature metal matrix composites that are programmed in the METCAN computer code. The subroutines which contain the programmed equations are also mentioned in order to facilitate any future changes or modifications that the user may intend to incorporate in the code. Assumptions and derivations leading to the micromechanics equations are briefly mentioned.

Author (revised)

N93-26702*# National Aeronautics and Space Administration. Lewis Research Center, Cleveland, OH.

AN OVERVIEW OF ELEVATED TEMPERATURE DAMAGE MECHANISMS AND FATIGUE BEHAVIOR OF A UNIDIRECTIONAL SCS-6/TI-15-3 COMPOSITE

MICHAEL G. CASTELLI (Sverdrup Technology, Inc., Brook Park, OH.) and JOHN GAYDA Apr. 1993 16 p Proposed for presentation at the Tenth Biennial Conference on Reliability, Stress Analysis and Failure Prevention, Albuquerque, NM, 19-22 Sep. 1993; sponsored by ASME
 (Contract RTOP 510-06-50)
 (NASA-TM-106131; E-7729; NAS 1.15:106131) Avail: CASI HC A03/MF A01

The fatigue behavior of a unidirectionally reinforced titanium matrix composite (TMC), SiC/Ti-15-3, was thoroughly characterized to support life prediction modeling of advanced TMC disks designed for gas turbine engine applications. The results of this coupon-level experimental investigation are reviewed. On a stress basis, the isothermal fatigue behavior of the (0 deg) TMC revealed significant improvements over the unreinforced matrix. In contrast, the (90 deg) TMC exhibited degraded properties and lives for similar comparisons. This was attributed to the weak fiber/matrix interfacial bond. Encasing the (0 deg) TMC with a Ti-15-3 case did not affect isothermal fatigue lives at higher strain levels. However, at lower strain levels, rapid initiation and propagation of large fatigue cracks in the case degraded the fatigue lives. Thermomechanical fatigue (TMF) lives were significantly reduced for the (0 deg) TMC when compared to isothermal lives. At high strains, in-phase TMF produced extremely short lives. This degradation was attributed to fiber overload failures brought about by stress relaxation in the matrix. At low strains, out-of-phase TMF conditions became life limiting. Environment-assisted surface cracking was found to accelerate fatigue failure. This produced extensive matrix damage with minimal fiber damage. For the (90 deg) TMC, TMF conditions did not promote an additional degradation in cyclic life beyond that observed under isothermal conditions.

Author (revised)

N93-26704*# National Aeronautics and Space Administration. Lewis Research Center, Cleveland, OH.

FIBER SHAPE EFFECTS ON METAL MATRIX COMPOSITE BEHAVIOR

H. C. BROWN (Sverdrup Technology, Inc., Brook Park, OH.), H.-J. LEE, and C. C. CHAMIS Mar. 1992 33 p Presented at the 37th International SAMPE Symposium and Exhibition, Anaheim, CA, 9-12 Mar. 1992; sponsored by the Society for the Advancement of Materials and Process Engineering
 (Contract RTOP 510-01-50)
 (NASA-TM-106067; E-7672; NAS 1.15:106067) Avail: CASI HC A03/MF A01

The effects of different fiber shapes on the behavior of a SiC/Ti-15 metal matrix composite is computationally simulated. A three-dimensional finite element model consisting of a group of nine unidirectional fibers is used in the analysis. The model is employed to represent five different fiber shapes: a circle, an ellipse, a kidney, and two different cross shapes. The distribution of microstresses and the composite material properties, such as moduli, coefficients of thermal expansion, and Poisson's ratios, are obtained from the finite element analysis for the various fiber shapes. Comparisons of these results are used to determine the sensitivity of the composite behavior to the different fiber shapes and assess their potential benefits. No clear benefits result from

24 COMPOSITE MATERIALS

different fiber shapes though there are some increases/decreases in isolated properties. Author

N93-26705*# National Aeronautics and Space Administration. Lewis Research Center, Cleveland, OH.
DYNAMIC CHARACTERISTICS OF SPECIALTY COMPOSITE STRUCTURES WITH EMBEDDED DAMPING LAYERS
D. A. SARAVANOS (Ohio Aerospace Inst., Brook Park.) and C. C. CHAMIS May 1993 32 p Presented at the Symposium on Vibroacoustic Characterization of Materials and Structures, Anaheim, CA, 8-12 Nov. 1992; sponsored by ASME (Contract NCC3-208/4; RTOP 510-02-12) (NASA-TM-106165; E-7863; NAS 1.15:106165) Avail: CASI HC A03/MF A01

Damping mechanics for simulating the damped dynamic characteristics in specialty composite structures with compliant interlaminar damping layers are presented. Finite-element based mechanics incorporating a discrete layer (or layer-wise) laminate damping theory are utilized to represent general laminate configurations in terms of lay-up and fiber orientation angles, cross-sectional thickness, shape, and boundary conditions. Evaluations of the method with exact solutions and experimental data illustrate the accuracy of the method. Additional applications investigate the potential for significant damping enhancement in angle-ply composite laminates with cocured interlaminar damping layers. Author

N93-27082*# National Aeronautics and Space Administration. Lewis Research Center, Cleveland, OH.
PROBABILISTIC SIZING OF LAMINATES WITH UNCERTAINTIES
A. R. SHAH (Sverdrup Technology, Inc., Brook Park, OH.), D. G. LIAW (Sverdrup Technology, Inc., Brook Park, OH.), and C. C. CHAMIS May 1993 19 p Presented at the 24th International SAMPE Technical Conference, Toronto, Ontario, 20-22 Oct. 1992; sponsored by Society for the Advancement of Materials and Process Engineering (Contract RTOP 510-02-12) (NASA-TM-106145; E-7826; NAS 1.15:106145) Avail: CASI HC A03/MF A01

A reliability based design methodology for laminate sizing and configuration for a special case of composite structures is described. The methodology combines probabilistic composite mechanics with probabilistic structural analysis. The uncertainties of constituent materials (fiber and matrix) to predict macroscopic behavior are simulated using probabilistic theory. Uncertainties in the degradation of composite material properties are included in this design methodology. A multi-factor interaction equation is used to evaluate load and environment dependent degradation of the composite material properties at the micromechanics level. The methodology is integrated into a computer code IPACS (Integrated Probabilistic Assessment of Composite Structures). Versatility of this design approach is demonstrated by performing a multi-level probabilistic analysis to size the laminates for design structural reliability of random type structures. The results show that laminate configurations can be selected to improve the structural reliability from three failures in 1000, to no failures in one million. Results also show that the laminates with the highest reliability are the least sensitive to the loading conditions. Author

N93-27092*# National Aeronautics and Space Administration. Lewis Research Center, Cleveland, OH.
PROBABILISTIC ASSESSMENT OF COMPOSITE STRUCTURES
C. C. CHAMIS and MICHAEL C. SHIAO (Sverdrup Technology, Inc., Brook Park, OH.) Feb. 1993 20 p (Contract RTOP 510-02-12) (NASA-TM-106024; E-7587; NAS 1.15:106024) Avail: CASI HC A03/MF A01

A methodology and attendant computer code were developed and are used to computationally simulate the uncertain behavior of composite structures. The uncertain behavior includes buckling loads, stress concentration factors, displacements, stress/strain, etc., which are the consequences of the inherent uncertainties

(scatter) in the primitive (independent random) variables (constituent, ply, laminate, and structural) that describe the composite structures. The computer code is IPACS (Integrated Probabilistic Assessment of Composite Structures). IPACS can simulate both composite mechanics and composite structural behavior. Application to probabilistic composite mechanics is illustrated by its use to evaluate the uncertainties in the major Poisson's ratio and in laminate stiffness and strength. IPACS' application to probabilistic structural analysis is illustrated by its use to evaluate the uncertainties in the buckling of a composite plate, the stress concentration factor in a composite panel, and the vertical displacement and ply stress in a composite aircraft wing segment. IPACS' application to probabilistic design is illustrated by its use to assess the thin composite shell (pipe). Author (revised)

N93-27129*# National Aeronautics and Space Administration. Lewis Research Center, Cleveland, OH.
RADIAL BASIS FUNCTION NETWORK LEARNS CERAMIC PROCESSING AND PREDICTS RELATED STRENGTH AND DENSITY
KRZYSZTOF J. CIOS (Toledo Univ., OH.), GEORGE Y. BAAKLINI, ALEX VARY, and ROBERT E. TJIA (Toledo Univ., OH.) May 1993 20 p (Contract RTOP 505-63-1M) (NASA-TM-106048; E-7795; NAS 1.15:106048) Avail: CASI HC A03/MF A01

Radial basis function (RBF) neural networks were trained using the data from 273 Si₃N₄ modulus of rupture (MOR) bars which were tested at room temperature and 135 MOR bars which were tested at 1370 C. Milling time, sintering time, and sintering gas pressure were the processing parameters used as the input features. Flexural strength and density were the outputs by which the RBF networks were assessed. The 'nodes-at-data-points' method was used to set the hidden layer centers and output layer training used the gradient descent method. The RBF network predicted strength with an average error of less than 12 percent and density with an average error of less than 2 percent. Further, the RBF network demonstrated a potential for optimizing and accelerating the development and processing of ceramic materials. Author (revised)

N93-27270*# National Aeronautics and Space Administration. Lewis Research Center, Cleveland, OH.
FUZZY SETS PREDICT FLEXURAL STRENGTH AND DENSITY OF SILICON NITRIDE CERAMICS
KRZYSZTOF J. CIOS (Toledo Univ., OH.), LESZEK M. SZTANDERA (Toledo Univ., OH.), GEORGE Y. BAAKLINI, and ALEX VARY May 1993 23 p (Contract RTOP 506-01-50) (NASA-TM-106049; E-7794; NAS 1.15:106049) Avail: CASI HC A03/MF A01

In this work, we utilize fuzzy sets theory to evaluate and make predictions of flexural strength and density of NASA 6Y silicon nitride ceramic. Processing variables of milling time, sintering time, and sintering nitrogen pressure are used as an input to the fuzzy system. Flexural strength and density are the output parameters of the system. Data from 273 Si₃N₄ modulus of rupture bars tested at room temperature and 135 bars tested at 1370 C are used in this study. Generalized mean operator and Hamming distance are utilized to build the fuzzy predictive model. The maximum test error for density does not exceed 3.3 percent, and for flexural strength 7.1 percent, as compared with the errors of 1.72 percent and 11.34 percent obtained by using neural networks, respectively. These results demonstrate that fuzzy sets theory can be incorporated into the process of designing materials, such as ceramics, especially for assessing more complex relationships between the processing variables and parameters, like strength, which are governed by randomness of manufacturing processes. Author (revised)

N93-28624*# National Aeronautics and Space Administration. Lewis Research Center, Cleveland, OH.

SOFT COMPUTING IN DESIGN AND MANUFACTURING OF ADVANCED MATERIALS

GEORGE Y. BAAKLINI, ALEX VARY, and KRZYSZTOF J. CIOŚ (Toledo Univ., OH.) Apr. 1993 8 p Presented at the ASME Conference, Cincinnati, OH, 24-27 May 1993; sponsored by IGTI and ASME

(Contract RTOP 510-01-50)

(NASA-TM-106032; E-7597; NAS 1.15:106032) Avail: CASI HC A02/MF A01

The potential of fuzzy sets and neural networks, often referred to as soft computing, for aiding in all aspects of manufacturing of advanced materials like ceramics is addressed. In design and manufacturing of advanced materials, it is desirable to find which of the many processing variables contribute most to the desired properties of the material. There is also interest in real time quality control of parameters that govern material properties during processing stages. The concepts of fuzzy sets and neural networks are briefly introduced and it is shown how they can be used in the design and manufacturing processes. These two computational methods are alternatives to other methods such as the Taguchi method. The two methods are demonstrated by using data collected at NASA Lewis Research Center. Future research directions are also discussed.

Author (revised)

N93-28681*# National Aeronautics and Space Administration. Lewis Research Center, Cleveland, OH.

METAL MATRIX LAMINATE TAILORING (MMLT) CODE: USER'S MANUAL

P. L. N. MURTHY, M. R. MOREL (Sverdrup Technology, Inc., Brook Park, OH.), and D. A. SARAVANOS (Ohio Aerospace Inst., Brook Park.) May 1993 132 p

(Contract RTOP 510-01-50)

(NASA-TM-106052; E-7644; NAS 1.15:106052) Avail: CASI HC A07/MF A02

The User's Manual for the Metal Matrix Laminate Tailoring (MMLT) program is presented. The code is capable of tailoring the fabrication process, constituent characteristics, and laminate parameters (individually or concurrently) for a wide variety of metal matrix composite (MMC) materials, to improve the performance and identify trends or behavior of MMC's under different thermo-mechanical loading conditions. This document is meant to serve as a guide in the use of the MMLT code. Detailed explanations of the composite mechanics and tailoring analysis are beyond the scope of this document, and may be found in the references. MMLT was developed by the Structural Mechanics Branch at NASA Lewis Research Center (LeRC).

Author (revised)

N93-29071*# National Aeronautics and Space Administration. Lewis Research Center, Cleveland, OH.

CERAMIC MATRIX COMPOSITES PROPERTIES/MICROSTRESSES WITH COMPLETE AND PARTIAL INTERPHASE BOND

SUBODH K. MITAL (Toledo Univ., OH.), PAPPU L. N. MURTHY, and CHRISTOS C. CHAMIS May 1993 13 p Presented at the 38th International SAMPE Symposium/Exhibition, Anaheim, CA, 10-13 May 1993

(Contract RTOP 510-01-50)

(NASA-TM-106136; E-7816; NAS 1.15:106136) Avail: CASI HC A03/MF A01

A multilevel substructuring technique which includes a unique fiber substructuring concept is used for the analysis of continuous fiber reinforced ceramic matrix composites. This technique has four levels of substructuring--from laminate to ply, to supply, and then to fiber. A stand-alone computer code CEMCAN (Ceramic Matrix Composites Analyzer), incorporating this technique and specifically for the simulation of ceramic matrix composites behavior, is currently under development at NASA Lewis Research Center in Cleveland, Ohio. The thermal and mechanical properties, along with the microstresses, for a SiC/RBSN (silicon carbide fiber and reaction bonded silicon nitride matrix) composite at

different fiber volume ratios and varying degrees of interfacial bond around the fiber circumference are computed. Values predicted by CEMCAN computer code are shown to bound the experimentally measured values. Results also show that transverse tensile strength test can be a sensitive test method to assess interfacial conditions.

Author (revised)

N93-29074*# National Aeronautics and Space Administration. Lewis Research Center, Cleveland, OH.

THERMOVISCOPLASTIC ANALYSIS OF FIBROUS PERIODIC COMPOSITES USING TRIANGULAR SUBVOLUMES

KEVIN P. WALKER (Engineering Science Software, Inc., Smithfield, RI.), ALAN D. FREED, and ERIC H. JORDAN (Connecticut Univ., Storrs.) Mar. 1993 28 p

(Contract RTOP 505-63-5A)

(NASA-TM-106076; E-7686; NAS 1.15:106076) Avail: CASI HC A03/MF A01

The nonlinear viscoplastic behavior of fibrous periodic composites is analyzed by discretizing the unit cell into triangular subvolumes. A set of these subvolumes can be configured by the analyst to construct a representation for the unit cell of a periodic composite. In each step of the loading history, the total strain increment at any point is governed by an integral equation which applies to the entire composite. A Fourier series approximation allows the incremental stresses and strains to be determined within a unit cell of the periodic lattice. The nonlinearity arising from the viscoplastic behavior of the constituent materials comprising the composite is treated as fictitious body force in the governing integral equation. Specific numerical examples showing the stress distributions in the unit cell of a fibrous tungsten/copper metal matrix composite under viscoplastic loading conditions are given. The stress distribution resulting in the unit cell when the composite material is subjected to an overall transverse stress loading history perpendicular to the fibers is found to be highly heterogeneous, and typical homogenization techniques based on treating the stress and strain distributions within the constituent phases as homogeneous result in large errors under inelastic loading conditions.

Author (revised)

N93-29609* National Aeronautics and Space Administration. Lewis Research Center, Cleveland, OH.

APPARATUS FOR INTERCALATING LARGE QUANTITIES OF FIBROUS STRUCTURES Patent

JAMES R. GAIER, inventor (to NASA) 6 Jul. 1993 7 p Filed 24 Jul. 1991 Supersedes N91-28289 (29 - 20, p 3304) Division of US-Patent-Appl-SN-608493, filed 2 Nov. 1990

(NASA-CASE-LEW-15077-2; US-PATENT-5,225,171;

US-PATENT-APPL-SN-735548; US-PATENT-APPL-SN-608493;

US-PATENT-CLASS-422-209; US-PATENT-CLASS-422-136;

INT-PATENT-CLASS-B01J-19/28) Avail: US Patent and

Trademark Office

Apparatus for intercalating large quantities of fibrous structures uses a rotatable reaction chamber containing a liquid phase intercalate. The intercalate liquid phase is controlled by appropriately heating, cooling or pressurizing the reaction. Rotation of the chamber containing the fiber sample ensures total submergence of the fiber during intercalation. Intercalated graphite fibers having metal-like resistivities are produced and are conceivably useful as electrical conductors.

Official Gazette of the U.S. Patent and Trademark Office

N93-29614* National Aeronautics and Space Administration. Lewis Research Center, Cleveland, OH.

SEMICONDUCTOR COOLING APPARATUS Patent

BRUCE A. BANKS, inventor (to NASA) and JAMES R. GAIER, inventor (to NASA) 29 Jun. 1993 7 p Filed 11 May 1992

Supersedes N92-34208 (30 - 24, p 4148) Continuation-in-part of abandoned US-Patent-Appl-SN-657238, filed 19 Feb. 1991, which is a continuation-in-part of abandoned US-Patent-Appl-SN-501893, filed 30 Mar. 1990

(NASA-CASE-LEW-14162-3; US-PATENT-5,224,030;

US-PATENT-APPL-SN-880851; US-PATENT-APPL-SN-657238;

US-PATENT-APPL-SN-501893; US-PATENT-CLASS-361-386;

24 COMPOSITE MATERIALS

US-PATENT-CLASS-165-185; US-PATENT-CLASS-174-16.3;
US-PATENT-CLASS-428-614; INT-PATENT-CLASS-H05K-7/20)
Avail: US Patent and Trademark Office

Gas derived graphite fibers generated by the decomposition of an organic gas are joined with a suitable binder. This produces a high thermal conductivity composite material which passively conducts heat from a source, such as a semiconductor, to a heat sink. The fibers may be intercalated. The intercalate can be halogen or halide salt, alkaline metal, or any other species which contributes to the electrical conductivity improvement of the graphite fiber. The fibers are bundled and joined with a suitable binder to form a high thermal conductivity composite material device. The heat transfer device may also be made of intercalated highly oriented pyrolytic graphite and machined, rather than made of fibers.

Official Gazette of the U.S. Patent and Trademark Office

N93-30868*# National Aeronautics and Space Administration.
Lewis Research Center, Cleveland, OH.

PROBABILISTIC COMPOSITE ANALYSIS

C. C. CHAMIS and P. L. N. MURTHY *In* NASA. Langley Research Center, First NASA Advanced Composites Technology Conference, Part 2 p 891-900 Jan. 1991
Avail: CASI HC A02/MF A06

Formal procedures are described which are used to computationally simulate the probabilistic behavior of composite structures. The computational simulation starts with the uncertainties associated with all aspects of a composite structure (constituents, fabrication, assembling, etc.) and encompasses all aspects of composite behavior (micromechanics, macromechanics, combined stress failure, laminate theory, structural response, and tailoring) optimization. Typical cases are included to illustrate the formal procedure for computational simulation. The collective results of the sample cases demonstrate that uncertainties in composite behavior and structural response can be probabilistically quantified.

Author

N93-31293*# National Aeronautics and Space Administration.
Lewis Research Center, Cleveland, OH.

SIC FIBER-REINFORCED CELSIAN GLASS-CERAMIC MATRIX COMPOSITE Patent Application

NAROTTAM P. BANSAL, inventor (to NASA) 16 Apr. 1992 7 p
(NASA-CASE-LEW-15264-1; NAS 1.71:LEW-15264-1;
US-PATENT-APPL-SN-872262) Avail: CASI HC A02/MF A01

A fiber-reinforced composite composed of a BaO-Al₂O₃-2SiO₂ (BAS) glass ceramic matrix is reinforced with CVD silicon carbide continuous fibers. A slurry of BAS glass powders is cast into tapes which are cut to the proper size. Continuous CVD-SiC fibers are formed into mats of the desired size. The matrix tapes and the fiber mats are alternately stacked in the proper orientation. This tape-mat stack is warm pressed to produce a 'green' composite. The 'green' composite is then heated to an elevated temperature to burn out organic constituents. The remaining interim material is then hot pressed to form a silicon carbide fiber-reinforced celsian (BAS) glass-ceramic matrix composite which may be machined to size.

NASA

N93-31296*# National Aeronautics and Space Administration.
Lewis Research Center, Cleveland, OH.

METHOD FOR PRODUCING HYBRID GRAPHITE COMPOSITE Patent Application

JAMES R. GAIER, inventor (to NASA) 22 Jul. 1993 13 p
(NASA-CASE-LEW-15241-2; NAS 1.71:LEW-15241-2;
US-PATENT-APPL-SN-094732) Avail: CASI HC A03/MF A01

Highly conducting lightweight hybrid materials are obtained by weaving strands of carbon or graphite fibers into a 2-dimensional fabric-like structure, depositing a layer of carbon onto the fibers of the fabric-like structure, heating the fabric-like structure to graphitize the carbon layer and intercalating the graphitized carbon layer. Composite materials for use in lightning strike protection are composed of at least one layer of the highly conducting lightweight hybrid material and at least one layer of traditional composite materials.

NASA

N93-31299*# National Aeronautics and Space Administration.
Lewis Research Center, Cleveland, OH.

METHOD OF PRODUCING A CERAMIC FIBER-REINFORCED GLASS-CERAMIC MATRIX COMPOSITE Patent Application

N. P. BANSAL, inventor (to NASA) 30 Jun. 1993 8 p
(NASA-CASE-LEW-15264-2; NAS 1.71:LEW-15264-2;
US-PATENT-APPL-SN-084058) Avail: CASI HC A02/MF A01

A fiber-reinforced composite composed of a BaO-Al₂O₃-2SiO₂ (BAS) glass ceramic matrix is reinforced with CVD silicon carbide continuous fibers. A slurry of BAS glass powders is prepared and celsian seeds are added during ball melting. The slurry is cast into tapes which are cut to the proper size. Continuous CVD-SiC fibers are formed into mats of the desired size. The matrix tapes and the fiber mats are alternately stacked in the proper orientation. This tape-mat stack is warm pressed to produce a 'green' composite. The 'green' composite is then heated to an elevated temperature to burn out organic constituents. The remaining interim material is then hot pressed to form a silicon carbide fiber-reinforced celsian (BAS) glass-ceramic matrix composite which may be machined to size.

NASA

N93-31579*# National Aeronautics and Space Administration.
Lewis Research Center, Cleveland, OH.

A MODEL FOR PREDICTING HIGH-TEMPERATURE FATIGUE FAILURE OF A W/CU COMPOSITE

M. J. VERRILLI, Y.-S. KIM (National Academy of Sciences - National Research Council, Washington, DC.), and T. P. GABB *In its* Structural Integrity and Durability of Reusable Space Propulsion Systems p 207-218 May 1991
Avail: CASI HC A03/MF A03

The material studied, a tungsten-fiber-reinforced, copper-matrix composite, is a candidate material for rocket nozzle liner applications. It was shown that at high temperatures, fatigue cracks initiate and propagate inside the copper matrix through a process of initiation, growth, and coalescence of grain boundary cavities. The ductile tungsten fibers neck and rupture locally after the surrounding matrix fails, and complete failure of the composite then ensues. A simple fatigue life prediction model is presented for the tungsten/copper composite system.

Derived from text

25

INORGANIC AND PHYSICAL CHEMISTRY

Includes chemical analysis, e.g., chromatography; combustion theory; electrochemistry; and photochemistry.

A93-11450 National Aeronautics and Space Administration.
Lyndon B. Johnson Space Center, Houston, TX.

PRESSURE DEPENDENCE OF THE OXYGEN REDUCTION REACTION AT THE PLATINUM MICROELECTRODE/NAFION INTERFACE - ELECTRODE KINETICS AND MASS TRANSPORT

ARVIND PARTHASARATHY, SUPRAMANIAM SRINIVASAN, A. J. APPLEBY (Texas A & M Univ., College Station), and CHARLES R. MARTIN (Colorado State Univ., Fort Collins) *Electrochemical Society, Journal* (ISSN 0013-4651) vol. 139, no. 10 Oct. 1992 p. 2856-2862. refs
(Contract NAG9-342; NAG3-1255)
Copyright

The investigation of oxygen reduction kinetics at the platinum/Nafion interface is of great importance in the advancement of proton-exchange-membrane (PEM) fuel-cell technology. This study focuses on the dependence of the oxygen reduction kinetics on oxygen pressure. Conventional Tafel analysis of the data shows that the reaction order with respect to oxygen is unity at both high and low current densities. Chronoamperometric measurements of the transport parameters for oxygen in Nafion show that oxygen dissolution follows Henry's isotherm. The diffusion coefficient of oxygen is invariant with pressure; however,

the diffusion coefficient for oxygen is lower when air is used as the equilibrating gas as compared to when oxygen is used for equilibration. These results are of value in understanding the influence of O₂ partial pressure on the performance of PEM fuel cells and also in elucidating the mechanism of oxygen reduction at the platinum/Nafion interface. Author

A93-13323* National Aeronautics and Space Administration. Lewis Research Center, Cleveland, OH.

ASYMPTOTIC ANALYSIS WITH REDUCED CHEMISTRY FOR THE BURNING OF N-HEPTANE DROPLETS

J. M. CARD and F. A. WILLIAMS (California Univ., La Jolla) Combustion and Flame (ISSN 0010-2180) vol. 91, no. 2 Nov. 1992 p. 187-199. refs
(Contract NAG3-1081; NSF CTS-89-18527)
Copyright

The method of rate-ratio asymptotics is used with reduced chemistry to analyze the flame structure and extinction of an isolated n-heptane droplet burning under quasisteady, spherically symmetrical conditions. The outer transport zones are described by the classical Burke-Schumann solution. The inner reaction zone consists of a thin layer, on the rich side of the flame, where the fuel is consumed, and on the lean side, a broader but still asymptotically thin oxidation layer, where H₂ and CO are consumed. Special attention is given to differences in predictions of extinction conditions, caused by different chemical-kinetic approximations in the reduced chemistry, including fuel-chemistry effects through molecules containing more than one carbon atom. From the analysis, extinction diameters for n-heptane droplets are estimated for different pressures and ambient oxygen concentrations. The results show that extinction diameters are extremely sensitive to the number of radicals consumed in breaking down each fuel molecule. Author

A93-17198* National Aeronautics and Space Administration. Lewis Research Center, Cleveland, OH.

PREDICTION OF CHEMICAL VAPOR DEPOSITION RATES ON MONOFILAMENTS AND ITS IMPLICATIONS FOR FIBER PROPERTIES

S. A. GOKOGLU, M. KUCZMARSKI, and L. C. VEITCH (NASA, Lewis Research Center, Cleveland, OH) Journal of Materials Research (ISSN 0884-2914) vol. 7, no. 11 Nov. 1992 p. 3023-3031. refs
Copyright

Deposition rates are predicted in a cylindrical upflow reactor designed for chemical vapor deposition (CVD) on monofilaments. Deposition of silicon from silane in a hydrogen carrier gas is chosen as a relevant example. The effects of gas and surface chemistry are studied in a two-dimensional axisymmetric flow field for this chemically well-studied system. Model predictions are compared to experimental CVD rate measurements. The differences in some physical and chemical phenomena between such small diameter (about 150 microns) fiber substrates and other typical CVD substrates are highlighted. The influence of the Soret mass transport mechanism is determined to be extraordinarily significant. The difficulties associated with the accurate measurement and control of the fiber temperature are discussed. Model prediction sensitivities are investigated with respect to fiber temperatures, fiber radii, Soret transport, and chemical kinetic parameters. The implications of the predicted instantaneous rates are discussed relative to the desired fiber properties for both the batch and the continuous processes. Author

A93-22030* National Aeronautics and Space Administration. Lewis Research Center, Cleveland, OH.

IGNITION AND COMBUSTION OF ALUMINUM/MAGNESIUM ALLOY PARTICLES IN O₂ AT HIGH PRESSURES

TED A. ROBERTS, RODNEY L. BURTON, and HERMAN KRIER (Illinois Univ., Urbana) Combustion and Flame (ISSN 0010-2180) vol. 92, no. 1-2 Jan. 1993 p. 125-143. Research supported by Univ. of Illinois refs
(Contract NAG3-1184)
Copyright

The ignition and combustion of Al, Mg, and Al/Mg alloy particles in 99 percent O₂/1 percent N₂ mixtures is investigated at high temperatures and pressures for rocket engine applications. The 20-micron particles contain 0, 5, 10, 20, 40, 60, 80, and 100 wt pct Mg alloyed with Al, and are ignited in oxygen using the reflected shock in a single-pulse shock tube near the endwall. Using this technique, the ignition delay and combustion times of the particles are measured at temperatures up to 3250 K as a function of Mg content for oxygen pressures of 8.5, 17, and 34 atm. An ignition model is developed that employs a simple lumped capacitance energy equation and temperature and pressure dependent particle and gas properties. Good agreement is achieved between the measured and predicted trends in the ignition delay times. Author

A93-22648* National Aeronautics and Space Administration. Lewis Research Center, Cleveland, OH.

MULTIGRID METHODS FOR NUMERICAL SIMULATION OF LAMINAR DIFFUSION FLAMES

C. LIU, Z. LIU, and S. MCCORMICK (Colorado Univ., Denver) Jan. 1993 12 p. AIAA, Aerospace Sciences Meeting and Exhibit, 31st, Reno, NV, Jan. 11-14, 1993 refs
(Contract NAS3-26328)
(AIAA PAPER 93-0236) Copyright

This paper documents the result of a computational study of multigrid methods for numerical simulation of 2D diffusion flames. The focus is on a simplified combustion model, which is assumed to be a single step, infinitely fast and irreversible chemical reaction with five species (C₃H₈, O₂, N₂, CO₂ and H₂O). A fully-implicit second-order hybrid scheme is developed on a staggered grid, which is stretched in the streamwise coordinate direction. A full approximation multigrid scheme (FAS) based on line distributive relaxation is developed as a fast solver for the algebraic equations arising at each time step. Convergence of the process for the simplified model problem is more than two-orders of magnitude faster than other iterative methods, and the computational results show good grid convergence, with second-order accuracy, as well as qualitatively agreement with the results of other researchers. Author

A93-22652* National Aeronautics and Space Administration. Lewis Research Center, Cleveland, OH.

TWO AND THREE-DIMENSIONAL PREFDIFFUSER COMBUSTOR STUDIES WITH AIR-WATER MIXTURE

PETER LAING, C. M. EHRESMAN, and S. N. B. MURTHY (Purdue Univ., West Lafayette, IN) Jan. 1993 19 p. AIAA, Aerospace Sciences Meeting and Exhibit, 31st, Reno, NV, Jan. 11-14, 1993 Research supported by GE Aircraft Engines refs
(Contract NAG3-481; DTFA03-83-A-00328)
(AIAA PAPER 93-0240) Copyright

Two- and three-dimensional gas turbine prediffuser-combustor sectors were experimentally studied under a number of mixture and flow conditions in a tunnel operating with a two-phase, air-liquid film-droplet mixture. It is concluded that water vaporization in the combustor causes changes in both local gas temperature and state of vitiation and reduces reaction rates. Substantial accumulation of water and water vapor takes place in pocket over the combustor volume, even when the air-water mixture is steady in time. The accuracy of determining combustor performance changes increases with a better knowledge of the state of the air-water mixture in the primary zone. To establish flame-out conditions it is considered to be necessary to combine the prediction of detailed flowfield and chemical activity with that of flame stability and motion characteristics. O.G.

A93-23238# National Aeronautics and Space Administration. Lewis Research Center, Cleveland, OH.

SIMPLIFIED JET FUEL REACTION MECHANISM FOR LEAN BURN COMBUSTION APPLICATION

CHI-MING LEE, KRISHNA KUNDU (NASA, Lewis Research Center, Cleveland, OH), and BAHMAN GHORASHI (Cleveland State Univ., OH) Jan. 1993 10 p. AIAA, Aerospace Sciences Meeting and Exhibit, 31st, Reno, NV, Jan. 11-14, 1993 Previously

announced in STAR as N93-15504 refs
(Contract RTOP 537-01-11)
(AIAA PAPER 93-0021) Copyright

Successful modeling of combustion and emissions in gas turbine engine combustors requires an adequate description of the reaction mechanism. Detailed mechanisms contain a large number of chemical species participating simultaneously in many elementary kinetic steps. Current computational fluid dynamic models must include fuel vaporization, fuel-air mixing, chemical reactions, and complicated boundary geometries. A five-step Jet-A fuel mechanism which involves pyrolysis and subsequent oxidation of paraffin and aromatic compounds is presented. This mechanism is verified by comparing with Jet-A fuel ignition delay time experimental data, and species concentrations obtained from flametube experiments. This five-step mechanism appears to be better than the current one- and two-step mechanisms. Author

A93-23358* National Aeronautics and Space Administration. Lewis Research Center, Cleveland, OH.

PDF PREDICTION OF SUPERSONIC HYDROGEN FLAMES

P. EIFLER and W. KOLLMANN (California Univ., Davis) Jan. 1993 18 p. AIAA, Aerospace Sciences Meeting and Exhibit, 31st, Reno, NV, Jan. 11-14, 1993 Research supported by DAAD refs
(Contract NAG3-836)

(AIAA PAPER 93-0448) Copyright

A hybrid method for the prediction of supersonic turbulent flows with combustion is developed consisting of a second order closure for the velocity field and a multi-scalar pdf method for the local thermodynamic state. It is shown that for non-premixed flames and chemical equilibrium mixture fraction, the logarithm of the (dimensionless) density, internal energy per unit mass and the divergence of the velocity have several advantages over other sets of scalars. The closure model is applied to a supersonic non-premixed flame burning hydrogen with air supplied by a supersonic coflow and the results are compared with a limited set of experimental data. Author

A93-24803# National Aeronautics and Space Administration. Lewis Research Center, Cleveland, OH.

COMPARISON OF NUMERICAL MODEL RESULTS WITH DIFFUSION FLAMES IN MICROGRAVITY

PAUL V. HYER (Lockheed Engineering & Sciences Co., Hampton, VA), DENNIS P. STOCKER (NASA, Lewis Research Center, Cleveland, OH), and IVAN O. CLARK (NASA, Langley Research Center, Hampton, VA) Jan. 1993 10 p. AIAA, Aerospace Sciences Meeting and Exhibit, 31st, Reno, NV, Jan. 11-14, 1993 Research supported by NASA refs
(AIAA PAPER 93-0707) Copyright

The effects of gravity on methane diffusion flames were studied using a finite difference numerical model. Variables under consideration included velocity, pressure, temperature, enthalpy, reactive species, and inert carrier gas. Results obtained showed that flames in zero gravity were wider and taller than those in normal gravity. The use of a six reaction scheme produced similar predictions of flame width and height compared to those of the single reaction case. The numerical models predicted a considerable difference in the flame base region between normal gravity and low gravity. This region is considered to be beyond the boundaries of current analytical models. O.G.

A93-24804* National Aeronautics and Space Administration. Lewis Research Center, Cleveland, OH.

STRUCTURE OF SOOT-CONTAINING LAMINAR JET DIFFUSION FLAMES

S. MORTAZAVI, P. B. SUNDERLAND, J. JURNG, U. O. KOYLU, and G. M. FAETH (Michigan Univ., Ann Arbor) Jan. 1993 12 p. AIAA, Aerospace Sciences Meeting and Exhibit, 31st, Reno, NV, Jan. 11-14, 1993 refs
(Contract NAG3-1245)
(AIAA PAPER 93-0708) Copyright

The structure and soot properties of nonbuoyant and weakly-buoyant round jet diffusion flames were studied, considering

ethylene, propane and acetylene burning in air at pressures of 0.125-2.0 atm. Measurements of flame structure included radiative heat loss fractions, flame shape and temperature distributions in the fuel-lean (overfire) region. These measurements were used to evaluate flame structure predictions based on the conserved-scalar formalism in conjunction with the laminar flamelet concept, finding good agreement between predictions and measurements. Soot property measurements included laminar smoke points, soot volume function distributions using laser extinction, and soot structure using thermophoretic sampling and analysis by transmission electron microscopy. Nonbuoyant flames were found to exhibit laminar smoke points like buoyant flames but their properties are very different; in particular, nonbuoyant flames have laminar smoke point flame lengths and residence times that are shorter and longer, respectively, than buoyant flames. Author

A93-24805* National Aeronautics and Space Administration. Lewis Research Center, Cleveland, OH.

EFFECTS OF GRAVITY ON THE TRANSITION TO TURBULENCE OF GAS JET DIFFUSION FLAMES

M. Y. BAHADORI (Science Applications International Corp., Torrance, CA), U. HEGDE (Sverdrup Technology, Inc., Brook Park; NASA, Lewis Research Center, Cleveland, OH), L. ZHOU (California Univ., Berkeley), and D. P. STOCKER (NASA, Lewis Research Center, Cleveland, OH) Jan. 1993 8 p. AIAA, Aerospace Sciences Meeting and Exhibit, 31st, Reno, NV, Jan. 11-14, 1993 refs
(Contract NAS3-25982; NAS3-25266; NCC3-239)

(AIAA PAPER 93-0710)

An ongoing study of the transition to turbulence of gas jet diffusion flames conducted in a reduced microgravity environment at the NASA Lewis 2.2 second drop tower is described. The experiments were based on propane injected into quiescent air. Several differences with the corresponding normal gravity process were observed. In particular, large scale structures appeared intermittently in microgravity which are manifested at the flame base and convected down stream. As the Reynolds number increased, a continuous train of structures was observed along the flame front. These observations are explained by instability of the shear layer associated with injection of flow into quiescent surroundings. O.G.

A93-24806* National Aeronautics and Space Administration. Lewis Research Center, Cleveland, OH.

EFFECTS OF PARTICULATE RADIATION ON PREMIXED GAS FLAMES

ANGEL ABBUD-MADRID and PAUL D. RONNEY (Princeton Univ., NJ) Jan. 1993 7 p. AIAA, Aerospace Sciences Meeting and Exhibit, 31st, Reno, NV, Jan. 11-14, 1993 refs
(Contract NAG3-1242)
(AIAA PAPER 93-0711) Copyright

Observations of the effect of the addition of fine solid particles to weakly combustible methane-air mixtures are reported. Burning rates, pressure rise, and thermal characteristics are found to exhibit nonmonotonic trends with increasing particle loading. These results are interpreted in terms of the effects of augmentation of radiant loss at small particle loadings and re-absorption of emitted radiation at larger loadings. It is suggested that in sufficiently large systems, flammability limits might not exist because of this reabsorption effect. Author

A93-24807* National Aeronautics and Space Administration. Lewis Research Center, Cleveland, OH.

FLAME BALLS - PAST, PRESENT AND FUTURE

J. BUCKMASTER (Illinois Univ., Urbana), P. RONNEY (Princeton Univ., NJ), and M. SMOOKE (Yale Univ., New Haven, CT) Jan. 1993 12 p. AIAA, Aerospace Sciences Meeting and Exhibit, 31st, Reno, NV, Jan. 11-14, 1993 Research supported by USAF, NASA, and U.S. Navy refs
(AIAA PAPER 93-0712) Copyright

This paper discusses analytical and numerical work that has been carried out in order to understand flame-balls and related phenomena that have been observed in microgravity experiments.

The importance of heat losses is identified, whether from conduction, convection, or radiation. Accurate numerical simulations for hydrogen-air mixtures with radiation losses reveal a flammability limit of 3.5 percent of hydrogen by volume, a value close to the experimental one. The important role of stability analyses is emphasized, with particular attention to the role of three-dimensional instabilities in explaining unsteady spheroidal flames and flame-strings, objects that are observed in the experiments. We speculate that the dynamics of flame-strings is affected by in-depth radiation absorption for mixtures containing SF₆, and report on some preliminary calculations in which this phenomenon is accounted for. Author

A93-24808*# National Aeronautics and Space Administration. Lewis Research Center, Cleveland, OH.

PREMIXED FLAME PROPAGATION IN COMBUSTIBLE PARTICLE CLOUD MIXTURES

K. SESHADRI and B. YANG (California Univ., La Jolla) Jan. 1993 8 p. AIAA, Aerospace Sciences Meeting and Exhibit, 31st, Reno, NV, Jan. 11-14, 1993 (Contract NAG3-1297) (AIAA PAPER 93-0713)

The structures of premixed flames propagating in combustible systems, containing uniformly distributed volatile fuel particles, in an oxidizing gas mixtures is analyzed. The experimental results show that steady flame propagation occurs even if the initial equivalence ratio of the combustible mixture based on the gaseous fuel available in the particles, $\phi(u)$ is substantially larger than unity. A model is developed to explain these experimental observations. In the model it is presumed that the fuel particles vaporize first to yield a gaseous fuel of known chemical composition which then reacts with oxygen in a one-step overall process. It is shown that the interplay of vaporization kinetics and oxidation process, can result in steady flame propagation in combustible mixtures where the value of $\phi(u)$ is substantially larger than unity. This prediction is in agreement with experimental observations. Author

A93-24885# National Aeronautics and Space Administration. Lewis Research Center, Cleveland, OH.

SUPERCRITICAL DROPLET COMBUSTION AND RELATED TRANSPORT PHENOMENA

VIGOR YANG (Pennsylvania State Univ., University Park), K. C. HSIEH, and J. S. SHUEN (Sverdrup Technology, Inc.; NASA, Lewis Research Center, Cleveland, OH) Jan. 1993 16 p. AIAA, Aerospace Sciences Meeting and Exhibit, 31st, Reno, NV, Jan. 11-14, 1993 Research supported by NASA and Pennsylvania State Univ refs (AIAA PAPER 93-0812) Copyright

An overview of recent advances in theoretical analyses of supercritical droplet vaporization and combustion is conducted. Both hydrocarbon and cryogenic liquid droplets over a wide range of thermodynamic states are considered. Various important high-pressure effects on droplet behavior, such as thermodynamic non-ideality, transport anomaly, and property variation, are reviewed. Results indicate that the ambient gas pressure exerts significant control of droplet gasification and burning processes through its influence on fluid transport, gas-liquid interfacial thermodynamics, and chemical reactions. The droplet gasification rate increases progressively with pressure. However, the data for the overall burnout time exhibit a considerable change in the combustion mechanism at the critical pressure, mainly as a result of reduced mass diffusivity and latent heat of vaporization with increased pressure. The influence of droplet size on the burning characteristics is also noted. Author

A93-24893*# National Aeronautics and Space Administration. Lewis Research Center, Cleveland, OH.

SOOT AGGLOMERATION IN ISOLATED, FREE DROPLET COMBUSTION

M. Y. CHOI, F. L. DRYER (Princeton Univ., NJ), G. J. GREEN (Mobil Research and Development Corp., Central Research Lab., Princeton, NJ), and J. J. SANGIOVANNI (United Technologies

Research Center, East Hartford, CT) Jan. 1993 20 p. AIAA, Aerospace Sciences Meeting and Exhibit, 31st, Reno, NV, Jan. 11-14, 1993 refs

(Contract NAS3-1231)

(AIAA PAPER 93-0823) Copyright

Under the conditions of an isolated, free droplet experiment, hollow, carbonaceous structures, called soot spheres, were observed to form during the atmospheric pressure, low Reynolds number combustion of 1-methylnaphthalene. These structures which are agglomerates composed of smaller spheroidal units result from both thermophoretic effects induced by the envelope flame surrounding each drop and aerodynamic effects caused by changes in the relative gas/drop velocities. A chemically reacting flow model was used to analyze the process of sootshell formation during microgravity droplet combustion. The time-dependent temperature and gas property field surrounding the droplet was determined, and the soot cloud location for microgravity combustion of n-heptane droplets was predicted. Experiments showed that the sooting propensity of n-alkane fuel droplets can be varied through diluent substitution, oxygen-index variations, and ambient pressure reductions. O.G.

A93-24895*# National Aeronautics and Space Administration. Lewis Research Center, Cleveland, OH.

COMPUTATIONAL PREDICTIONS OF FLAME SPREAD OVER ALCOHOL POOLS

D. N. SCHILLER, H. D. ROSS, and W. A. SIRIGNANO (California Univ., Irvine) Jan. 1993 16 p. AIAA, Aerospace Sciences Meeting and Exhibit, 31st, Reno, NV, Jan. 11-14, 1993 refs (Contract NAG3-627)

(AIAA PAPER 93-0825) Copyright

The effects of buoyancy and thermocapillarity on pulsating and uniform flame spread above n-propanol fuel pools have been studied using a numerical model. Data obtained indicate that the existence of pulsating flame spread is dependent upon the formation of a gas-phase recirculation cell which entrains evaporating fuel vapor in front of the leading edge of the flame. The size of the recirculation cell which is affected by the extent of liquid motion ahead of the flame, is shown to dictate whether flame spread is uniform or pulsating. The amplitude and period of the flame pulsations are found to be proportional to the maximum extent of the flow head. Under conditions considered, liquid motion was not affected appreciably by buoyancy. Horizontal convection in the liquid is the dominant mechanism for transporting heat ahead of the flame for both the pulsating and uniform regimes. O.G.

A93-24897*# National Aeronautics and Space Administration. Lewis Research Center, Cleveland, OH.

NUMERICAL COMPUTATION OF LOW-SPEED CONCURRENT FLOW FLAME SPREAD IN MIXED BUOYANT AND FORCED FLOW

PAUL V. FERKUL (NASA, Lewis Research Center, Cleveland, OH) and JAMES S. TIEN (Case Western Reserve Univ., Cleveland, OH) Jan. 1993 8 p. AIAA, Aerospace Sciences Meeting and Exhibit, 31st, Reno, NV, Jan. 11-14, 1993 refs (Contract NAG3-1046)

(AIAA PAPER 93-0827) Copyright

The effect of low-speed mixed convection (forced plus buoyant) on concurrent flow flame spread over a thin solid is examined. Computations are carried out using an existing model. Results indicate that seemingly small levels of gravity can significantly alter flame spread rates. Starting with a purely forced flow condition, as gravity is added, the entrainment due to buoyancy lengthens the flame and increases the spread rate significantly. Buoyancy has an influence on the extinction limits. At low speed, the presence of a small gravity level widens the flammability limit. Author

A93-24898*# National Aeronautics and Space Administration. Lewis Research Center, Cleveland, OH.

DOWNWARD DIFFUSION FLAME SPREAD AND EXTINCTION IN VARIABLE GRAVITATIONAL FIELDS - LUNAR AND MARTIAN SIMULATIONS

KURT R. SACKSTEDER (NASA, Lewis Research Center,

Cleveland, OH) and JAMES S. TIEN (Case Western Reserve Univ., Cleveland, OH) Jan. 1993 8 p. AIAA, Aerospace Sciences Meeting and Exhibit, 31st, Reno, NV, Jan. 11-14, 1993 refs (Contract NAG3-1046) (AIAA PAPER 93-0828)

This paper describes experimental observations of downward, opposed-flow flame spreading made under partial-gravity conditions aboard NASA research aircraft. Flame spreading and flammability limit behavior of a thin cellulosic fuel tested at normal pressure in oxygen/nitrogen mixtures of 21 percent oxygen, by volume, and below are described over effective acceleration levels ranging from 0.05 to 0.6 times normal earth gravity. Downward burning flammability and flame spread rates are shown to be enhanced by reductions in gravitational acceleration. These data have fire safety implications for the planning of lunar and Martian outposts. Author

A93-24899* National Aeronautics and Space Administration. Lewis Research Center, Cleveland, OH.

EXPERIMENTAL OBSERVATIONS OF THE EFFECT OF GRAVITY CHANGES ON SMOLDERING COMBUSTION

J. L. TORERO, A. C. FERNANDEZ-PELLO (California Univ., Berkeley), and D. URBAN (Sverdrup Technology, Inc., Brook Park, OH) Jan. 1993 8 p. AIAA, Aerospace Sciences Meeting and Exhibit, 31st, Reno, NV, Jan. 11-14, 1993 refs (Contract NAG3-443) (AIAA PAPER 93-0829) Copyright

The effects of gravity changes on the natural convection smolder characteristics of flexible polyurethane foam were determined in order to provide information on the potential onset of a smolder-initiated fire in a space-based facility. Experiments were conducted in an aircraft following parabolic trajectories providing up to 25 seconds of low gravity. Temperature histories of polyurethane foam were measured at several locations along the fuel sample interior. Results are presented and discussed for both upward and downward smoldering. Results indicate that gravity significantly affects the competition between supply of oxidizer to, and the transfer of heat to and from the reaction zone. This competition determines the characteristics of the smolder reaction. Within the reaction zone the reduction in oxygen supply in low gravity is dominant and the reaction weakens. Away from the reaction zone the reduction in convective cooling at low gravity tends to increase the material temperature. The opposite was observed at high gravity. A.O.

A93-28253* National Aeronautics and Space Administration. Lewis Research Center, Cleveland, OH.

LASER-INDUCED FLUORESCENCE MEASUREMENTS OF NITRIC OXIDE IN LAMINAR C₂H₆/O₂/N₂ FLAMES AT HIGH PRESSURE

JOHN R. REISEL, CAMPBELL D. CARTER, and NORMAND M. LAURENDEAU (Purdue Univ., West Lafayette, IN) Combustion and Flame (ISSN 0010-2180) vol. 92, no. 4 March 1993 p. 485-489. Research supported by NASA refs Copyright

Quantitative measurements of nitric oxide in C₂H₆/O₂/N₂ flames at 1-9 atm were successfully carried out using laser-induced fluorescence. The location of maximum NO concentration is found to shift towards leaner equivalence ratios with increasing pressure. Details of the experimental apparatus and measurement procedure are described. V.L.

A93-34247* National Aeronautics and Space Administration. Lewis Research Center, Cleveland, OH.

HYDRODYNAMIC BEHAVIOR AND ELECTROCHEMICAL IMPEDANCE OF THE HANGING MENISCUS ROTATING DISK (HMRD) ELECTRODE. I - MENISCUS SHAPE UNDER ROTATION. II - I-BIEM CALCULATIONS OF FREQUENCY DISPERSION AND MINIMIZATION

BORIS D. CAHAN (Case Western Reserve Univ., Cleveland, OH) In Modeling of batteries and fuel cells; Proceedings of the Symposium, Phoenix, AZ, Oct. 13-19, 1991 Pennington, NJ

Electrochemical Society, Inc. 1991 p. 351-387. Research supported by NASA and Ohio Aerospace Inst refs Copyright

The shape equations for an HMRD in static and rotating configurations are developed and solved numerically. A rationale for the applicability of the standard Levich equations to the rotating case is given. The region of stability of the HMRD is examined, and the observed small negative intercept for a Levich plot is explained. The iterative boundary integral equation method is applied to the problem of frequency dispersion at an HMRD electrode. It is shown that a range of disk sizes and heights can be chosen to give almost uniform primary and secondary current distribution and minimal frequency dispersion. AIAA

A93-36584* National Aeronautics and Space Administration. Lewis Research Center, Cleveland, OH.

METAL-ORGANIC CHEMICAL VAPOUR DEPOSITION OF POLYCRYSTALLINE TETRAGONAL INDIUM SULPHIDE (INS) THIN FILMS

ANDREW N. MACINNES, WILLIAM M. CLEAVER, ANDREW R. BARRON (Harvard Univ., Cambridge, MA), MICHAEL B. POWER, and ALOYSIUS F. HEPP (NASA, Lewis Research Center, Cleveland, OH) Advanced Materials for Optics and Electronics (ISSN 1057-9257) vol. 1 1992 p. 229-233. Research supported by National Research Council refs

The dimeric indium thiolate $(t\text{-Bu})_2\text{In}(\mu\text{-S})_2$ has been used as a single-source precursor for the MOCVD of InS thin films. The dimeric In₂S₂ core is proposed to account for the formation of the nonequilibrium high-pressure tetragonal phase in the deposited films. Analysis of the deposited films has been obtained by TEM, with associated energy-dispersive X-ray analysis and X-ray photoelectron spectroscopy. Author (revised)

A93-39503 National Aeronautics and Space Administration. Lewis Research Center, Cleveland, OH.

CHEMICAL VAPOR DEPOSITION MODELING FOR HIGH TEMPERATURE MATERIALS

SULEYMAN A. GOKOGLU (NASA, Lewis Research Center, Cleveland, OH) In Chemical vapor deposition of refractory metals and ceramics II; Proceedings of the Symposium, Boston, MA, Dec. 4-6, 1991 Pittsburgh, PA Materials Research Society 1992 p. 17-28. Previously announced in STAR as N92-18457 refs (Contract RTOP 510-01-50) Copyright

The formalism for the accurate modeling of chemical vapor deposition (CVD) processes has matured based on the well established principles of transport phenomena and chemical kinetics in the gas phase and on surfaces. The utility and limitations of such models are discussed in practical applications for high temperature structural materials. Attention is drawn to the complexities and uncertainties in chemical kinetics. Traditional approaches based on only equilibrium thermochemistry and/or transport phenomena are defended as useful tools, within their validity, for engineering purposes. The role of modeling is discussed within the context of establishing the link between CVD process parameters and material microstructures/properties. It is argued that CVD modeling is an essential part of designing CVD equipment and controlling/optimizing CVD processes for the production and/or coating of high performance structural materials. Author

A93-39508 National Aeronautics and Space Administration, Washington, DC.

ONSET CONDITIONS FOR GAS PHASE REACTION AND NUCLEATION IN THE CVD OF TRANSITION METAL OXIDES

J. COLLINS, D. E. ROSNER (Yale Univ., New Haven, CT), and J. CASTILLO (Univ. Nacional de Educacion a Distancia, Madrid, Spain) In Chemical vapor deposition of refractory metals and ceramics II; Proceedings of the Symposium, Boston, MA, Dec. 4-6, 1991 Pittsburgh, PA Materials Research Society 1992 p. 53-58. Research supported by Yale HTRC Lab. refs (Contract NGT-5037; NAG3-884; AF-AFOSR-89-0223) Copyright

A combined experimental/theoretical study is presented of the

onset conditions for gas phase reaction and particle nucleation in hot substrate/cold gas CVD of transition metal oxides. Homogeneous reaction onset conditions are predicted using a simple high activation energy reacting gas film theory. Experimental tests of the basic theory are underway using an axisymmetric impinging jet CVD reactor. No vapor phase ignition has yet been observed in the TiCl_4/O_2 system under accessible operating conditions (below substrate temperature $T_w = 1700$ K). The goal of this research is to provide CVD reactor design and operation guidelines for achieving acceptable deposit microstructures at the maximum deposition rate while simultaneously avoiding homogeneous reaction/nucleation and diffusional limitations.

Author (revised)

A93-39521 National Aeronautics and Space Administration. Lewis Research Center, Cleveland, OH.

CVD OF SILICON CARBIDE ON STRUCTURAL FIBERS - MICROSTRUCTURE AND COMPOSITION

LISA C. VEITCH, FRANCIS M. TEREPA, and SULEYMAN A. GOKOGLU (NASA, Lewis Research Center Cleveland, OH) *In* Chemical vapor deposition of refractory metals and ceramics II; Proceedings of the Symposium, Boston, MA, Dec. 4-6, 1991 Pittsburgh, PA Materials Research Society 1992 p. 251-256. Previously announced in STAR as N92-18439 refs (Contract RTOP 510-01-01)

Copyright

Structural fibers are currently being considered as reinforcements for intermetallic and ceramic materials. Some of these fibers, however, are easily degraded in a high temperature oxidative environment. Therefore, coatings are needed to protect the fibers from environmental attack. Silicon carbide (SiC) was chemically vapor deposited (CVD) on Textron's SCS6 fibers. Fiber temperatures ranging from 1350 to 1500 C were studied. Silane (SiH_4) and propane (C_2H_6) were used for the source gases and different concentrations of these source gases were studied. Deposition rates were determined for each group of fibers at different temperatures. Less variation in deposition rates were observed for the dilute source gas experiments than the concentrated source gas experiments. A careful analysis was performed on the stoichiometry of the CVD SiC coating using electron microprobe. Microstructures for the different conditions were compared. At 1350 C, the microstructures were similar; however, at higher temperatures, the microstructure for the more concentrated source gas group were porous and columnar in comparison to the cross sections taken from the same area for the dilute source gas group.

Author

A93-39525* National Aeronautics and Space Administration. Lewis Research Center, Cleveland, OH.

CVD OF SiC AND ALN USING CYCLIC ORGANOMETALLIC PRECURSORS

L. V. INTERRANTE (Rensselaer Polytechnic Inst., Troy, NY), D. J. LARKIN (NASA, Lewis Research Center, Cleveland, OH), and C. AMATO (Rensselaer Polytechnic Inst., Troy, NY) *In* Chemical vapor deposition of refractory metals and ceramics II; Proceedings of the Symposium, Boston, MA, Dec. 4-6, 1991 Pittsburgh, PA Materials Research Society 1992 p. 283-290. Previously announced in STAR as N93-11413 refs (Contract N00014-91-J-1917)

Copyright

The use of cyclic organometallic molecules as single-source MOCVD precursors is illustrated by means of examples taken from our recent work on AlN and SiC deposition, with particular focus on SiC. Molecules containing $(\text{AlN})_3$ and $(\text{SiC})_2$ rings as the 'core structure' were employed as the source materials for these studies. The organoaluminum amide, $(\text{Me}_2\text{AlNH}_2)_3$, was used as the AlN source and has been studied in a molecular beam sampling apparatus in order to determine the gas phase species present in a hot-wall CVD reactor environment. In the case of SiC CVD, a series of disilacyclobutanes $(\text{Si}(\text{X})\text{CH}_2)_2$ (with $\text{X} = \text{H}$, CH_3 , and $\text{CH}_2\text{SiH}_2\text{CH}_3$), were examined in a cold-wall, hot-stage CVD reactor in order to compare their relative reactivities and prospective utility as single-source CVD precursors. The parent

compound, disilacyclobutane, $(\text{SiH}_2\text{CH}_2)_2$, was found to exhibit the lowest deposition temperature (ca. 670 C) and to yield the highest purity SiC films. This precursor gave a highly textured, polycrystalline film on the $\text{Si}(100)$ substrates.

Author

A93-41711 National Aeronautics and Space Administration. Lewis Research Center, Cleveland, OH.

COMPUTATIONAL/EXPERIMENTAL BASIS FOR CONDUCTING ALKANE DROPLET COMBUSTION EXPERIMENTS ON SPACE-BASED-PLATFORMS

MUN Y. CHOI, SEOG Y. CHO, FREDERICK L. DRYER (Princeton Univ., NJ), and JOHN B. HAGGARD, JR. (NASA, Lewis Research Center, Cleveland, OH) *In* Microgravity fluid mechanics; Proceedings of the IUTAM Symposium, Bremen, Germany, Sept. 2-6, 1991 Berlin and New York Springer-Verlag 1992 p. 337-353. Research supported by NASA refs (Contract NAS3-24640)

Copyright

An analysis is conducted of the requirement for the conduct of spherically symmetric droplet-combustion experiments on space platforms, on the basis of a novel time-dependent computational droplet combustion model that allows the time- and temperature-dependent transport characteristics to be incorporated. While at low oxygen indices the droplet burning extinction becomes a strong function of oxygen index, it becomes a weaker function at higher oxygen index values. The oxygen index that separates these two ranges are dependent on the diluent, being higher for He and lower for N.

AIAA

A93-41952* National Aeronautics and Space Administration. Lewis Research Center, Cleveland, OH.

ASYMPTOTIC ANALYSIS FOR THE BURNING OF N-HEPTANE DROPLETS USING A FOUR-STEP REDUCED MECHANISM

J. M. CARD (California Univ., La Jolla) Combustion and Flame (ISSN 0010-2180) vol. 93, no. 4 June 1993 p. 375-390.

refs

(Contract NAG3-1081)

Copyright

A four-step reduced mechanism is obtained from a minimal chemical-kinetic description, where the effects of the elementary rates are treated as parameters in the expressions for the global rates. This mechanism is used to analyze the extinction characteristics of a single n-heptane droplet burning under quasi-steady, spherically symmetrical conditions. The reaction layer consists of a merged inner zone, on the fuel-rich side of the flame, where fuel and H atoms are consumed thereby producing H_2 and CO along with H_2O and CO_2 , and an oxygen-consumption zone, on the fuel-lean side, where H_2 and CO are oxidized to produce additional H_2O and CO_2 along with H radicals. For the inner zone, a parameter μ is identified which describes the ratio of the thickness of a fuel-consumption layer to that of an H-recombination layer. Analytical solutions for the rate of scalar dissipation at extinction are obtained in the limiting cases of μ tending to 0 and μ tending to infinity. From the results of the analysis, extinction diameters for n-heptane droplets are estimated for different pressures and ambient oxygen concentrations.

Author (revised)

A93-41954* National Aeronautics and Space Administration. Lewis Research Center, Cleveland, OH.

A COMPARISON OF NUMERICAL AND ANALYTICAL SOLUTION OF THE CREEPING FLAME SPREAD OVER THERMALLY THIN MATERIAL

SUBRATA BHATTACHARJEE (San Diego State Univ., CA) Combustion and Flame (ISSN 0010-2180) vol. 93, no. 4 June 1993 p. 434-444.

refs (Contract NCC3-221)

Copyright

The present numerical solution for the de Ris (1969) problem of flame-spread over thin condensed fuel in an opposed-flow environment is obtained by reformulating the problem in terms of four nondimensional parameters, while retaining all assumptions of the original theory. While the de Ris theory sees the location

of the leading edge and the eigenlocation of the onset of evaporation as identical, this analysis treats the leading edge as part of the solution; the location of the flame leading edge is in this way established to be upstream of the eigenlocation, with significant consequences for the spread rate formula. AIAA

A93-46009* National Aeronautics and Space Administration. Lewis Research Center, Cleveland, OH.

ANALYTICAL AND NUMERICAL MODELING OF FLAME-BALLS IN HYDROGEN-AIR MIXTURES

J. BUCKMASTER (Illinois Univ., Urbana), M. SMOOKE (Yale Univ., New Haven, CT), and V. GIOVANGIGLI (CNRS; Ecole Polytechnique, Palaiseau, France) Combustion and Flame (ISSN 0010-2180) vol. 94, no. 1-2 July 1993 p. 113-124. Research supported by USAF, U.S. Navy, and NASA refs Copyright

Flame-balls are stationary spherical premixed flames observed in certain near-limit mixtures. It is believed that radiative heat losses are an important stabilizing influence. Numerical solutions of flame balls are constructed for hydrogen-air mixtures using an accurate description of the chemical kinetics, diffusive transport, and radiation losses. A lean limit equivalence ratio of 0.0866 is predicted and a rich limit of 2.828. For any equivalence ratio between the two limits there are two solutions. One is characterized by a small flame, incomplete reactant consumption, and negligible radiation losses. The other by a large flame, complete consumption of one of the reactants, and significant radiation losses. The maximum temperature varies between 1200 and 900 K as the two solution branches are traversed. Much of our discussion is a reprise and modification of previously published analytical results, for these provide physical insight into the nature of the solutions, and suggest that a portion of the large flame branch near the lean limit is stable and so corresponds to observable flames.

A93-49867*# National Aeronautics and Space Administration. Lewis Research Center, Cleveland, OH.

NONINTRUSIVE, MULTIPOINT VELOCITY MEASUREMENTS IN HIGH-PRESSURE COMBUSTION FLOWS

M. ALLEN, S. DAVIS, W. KESSLER, H. LEGNER, K. MCMANUS, P. MULHALL, T. PARKER, and D. SONNENFROH (Physical Sciences, Inc., Andover, MA) Jun. 1993 14 p. AIAA, SAE, ASME, and ASEE, Joint Propulsion Conference and Exhibit, 29th, Monterey, CA, June 28-30, 1993 Research sponsored by NASA and USAF refs (AIAA PAPER 93-2032) Copyright

A combined experimental and analytical effort was conducted to demonstrate the applicability of OH Doppler-shifted fluorescence imaging of velocity distributions in supersonic combustion gases. The experiments were conducted in the underexpanded exhaust flow from a 6.8 atm, 2400 K, H₂-O₂-N₂ burner exhausting into the atmosphere. In order to quantify the effects of in-plane variations of the gas thermodynamic properties on the measurement accuracy, a set of detailed measurements of the OH (1,0) band collisional broadening and shifting in H₂-air gases was produced. The effect of pulse-to-pulse variations in the dye laser bandshape was also examined in detail and a modification was developed which increased in the single pulse bandwidth, thereby increasing the intramatrix velocity dynamic range as well as reducing the sensitivity of the velocity measurement to the gas property variations. Single point and imaging measurements of the velocity field in the exhaust flowfield were compared with 2D, finite-rate kinetics simulations of the flowfield. Relative velocity accuracies of +/- 50 m/s out of 1600 m/s were achieved in time-averaged imaging measurements of the flow over an order of magnitude variation in pressure and a factor of two variation in temperature. Author (revised)

A93-50001*# National Aeronautics and Space Administration. Lewis Research Center, Cleveland, OH.

THE PROMISING CHEMICAL KINETICS FOR THE SIMULATION OF PROPANE-AIR COMBUSTION WITH KIVA-II CODE

S. J. YING (South Florida Univ., Tampa, FL), RAMA S. R. GORLA

(Cleveland State Univ., OH), and KRISHNA P. KUNDU (NASA, Lewis Research Center, Cleveland, OH) Jun. 1993 7 p. AIAA, SAE, ASME, and ASEE, Joint Propulsion Conference and Exhibit, 29th, Monterey, CA, June 28-30, 1993 refs (AIAA PAPER 93-2189) Copyright

The development of chemical kinetics for the simulation of propane-air combustion with the use of computer code KIVA-II since 1989 is summarized here. In order to let readers understand the general feature well, a brief description of the KIVA-II code, specially related with the chemical reactions is also given. Then the results of recent work with 20 reaction mechanism is presented. It is also compared with the 5 reaction mechanism. It may be expected that the numerical stability of the 20 reaction mechanism is better as compared to that of 5 reaction mechanism, but the CPU time of the CRAY computer is much longer. Details are presented in the paper.

A93-50110*# National Aeronautics and Space Administration. Lewis Research Center, Cleveland, OH.

SECONDARY ATOMIZATION IN THE COMBUSTION OF ELECTROSTATIC SPRAYS

ALESSANDRO GOMEZ and GUNG CHEN (Yale Univ., New Haven, CT) Jun. 1993 10 p. AIAA, SAE, ASME, and ASEE, Joint Propulsion Conference and Exhibit, 29th, Monterey, CA, June 28-30, 1993 Research supported by NSF refs (Contract NAG3-1259) (AIAA PAPER 93-2332) Copyright

The combustion of electrosprays in a laminar counterflow diffusion flame has been experimentally studied by measuring droplet size and velocity distributions and gas-phase temperature. Detailed examination of the evolution of droplet size distribution as droplets approach the flame shows that, if substantial evaporation occurs before droplets 'interact' with the flame, the size distribution becomes bimodal. A secondary, sharp peak, in fact, develops in correspondence of diameters about one order of magnitude smaller than the mean. No evaporation mechanism can account for the development of such bimodality, that can be explained only in terms of a disintegration of droplets into finer fragments of size much smaller than the parent ones. This fission is of electric nature and it occurs when the repulsion of electric charges overcomes the surface tension cohesive force ultimately leading to a disintegration into finer fragments at or about the so-called Rayleigh limit. We here report on the first observation in combustion environments of such 'explosions'. If, on the other hand, droplets enter the very high temperature region before exploding, there appears to be no evidence of bimodality in their size distribution. In this case, in fact, flame chemi-ions may neutralize the charge on the droplets and thus prevent disruption.

A93-50116*# National Aeronautics and Space Administration. Lewis Research Center, Cleveland, OH.

A SIMPLIFIED REACTION MECHANISM FOR CALCULATION OF EMISSIONS IN HYDROCARBON (JET-A) COMBUSTION

K. P. KUNDU (NASA, Lewis Research Center, Cleveland, OH) and J. M. DEUR (Sverdrup Technology, Inc., Brook Park, OH) Jun. 1993 12 p. AIAA, SAE, ASME, and ASEE, Joint Propulsion Conference and Exhibit, 29th, Monterey, CA, June 28-30, 1993 refs (AIAA PAPER 93-2341) Copyright

The paper presents a simplified reaction mechanism developed for use in calculations of NO(x) emissions in Jet-A combustion. The rate for the N₂ + O₂ reaction was selected to match available experimental results, and the reaction rates for other global reactions in the Jet-A are empirical reaction rates adjusted to match species concentrations using the detailed mechanism of Miller and Bowman (1989). The mechanism was validated by comparing the emission of NO(x) calculated using propane as fuel. AIAA

A93-50147* National Aeronautics and Space Administration. Lewis Research Center, Cleveland, OH.

A THERMAL NO(X) PREDICTION MODEL - SCALAR COMPUTATION MODULE FOR CFD CODES WITH FLUID AND KINETIC EFFECTS

GIORGIO MCBEATH, BAHMAN GHORASHI (Cleveland State Univ., OH), and KUE CHUN (NASA, Lewis Research Center, Cleveland, OH) Jun. 1993 11 p. AIAA, SAE, ASME, and ASEE, Joint Propulsion Conference and Exhibit, 29th, Monterey, CA, June 28-30, 1993 refs (AIAA PAPER 93-2378) Copyright

A thermal NO(x) prediction model is developed to interface with a CFD, k-epsilon based code. A converged solution from the CFD code is the input to the postprocessing model for prediction of thermal NO(x). The model uses a decoupled analysis to estimate the equilibrium level of (NO(x))_e which is the constant rate limit. This value is used to estimate the flame (NO(x)) and in turn predict the rate of formation at each node using a two-step Zeldovich mechanism. The rate is fixed on the NO(x) production rate plot by estimating the time to reach equilibrium by a differential analysis based on the reaction: $O + N_2 = NO + N$. The rate is integrated in the nonequilibrium time space based on the residence time at each node in the computational domain. The sum of all nodal predictions yields the total NO(x) level. Author (revised)

A93-51641* National Aeronautics and Space Administration. Lewis Research Center, Cleveland, OH.

CATALYTIC IGNITION MODEL IN MONOLITHIC REACTOR WITH IN-DEPTH REACTION

TA-CHING TIEN and JAMES S. T'IENT (Case Western Reserve Univ., Cleveland, OH) In Aerothermodynamics in combustors; IUTAM Symposium, National Taiwan Univ., Taipei, June 3-5, 1991, Selected Papers Berlin and New York Springer-Verlag 1992 p. 231-244. refs (Contract NAG3-809) Copyright

A transient model has been developed to study ignition in a monolithic catalytic reactor. Special features are the inclusion of thermal and species structures in the porous catalytic layer and the resolution of small-time-scale events. Catalyst loading is used as a parameter to study these structure variations before and after ignition. Regions where the catalytic reaction is kinetically controlled and regions where the reaction is diffusionally controlled are identified in both steady and transient states. Author (revised)

A93-52423* National Aeronautics and Space Administration. Lewis Research Center, Cleveland, OH.

LASER-INDUCED FLUORESCENCE DETECTION STRATEGIES FOR SODIUM ATOMS AND COMPOUNDS IN HIGH-PRESSURE COMBUSTORS

KAREN J. R. WEILAND (SRI International, Molecular Physics Lab., Menlo Park, CA; NASA, Lewis Research Center, Cleveland, OH), MICHAEL L. WISE (SRI International, Molecular Physics Lab., Menlo Park, CA; Colorado Univ., Boulder), and GREGORY P. SMITH (SRI International, Molecular Physics Lab., Menlo Park, CA) Applied Optics (ISSN 0003-6935) vol. 32, no. 21 July 20, 1993 p. 4066-4073. refs (Contract DE-AC21-87MC-24012) Copyright

A variety of laser-induced fluorescence schemes were examined experimentally in atmospheric pressure flames to determine their use for sodium atom and salt detection in high-pressure, optically thick environments. Collisional energy transfer plays a large role in fluorescence detection. Optimum sensitivity, at the parts in 10 exp 9 level for a single laser pulse, was obtained with the excitation of the 4p-3s transition at 330 nm and the detection of the 3d-3p fluorescence at 818 nm. Fluorescence loss processes, such as ionization and amplified spontaneous emission, were examined. A new laser-induced atomization/laser-induced fluorescence detection technique was demonstrated for NaOH and NaCl. A 248-nm excimer laser photodissociates the salt molecules present

in the seeded flames prior to atom detection by laser-induced fluorescence. Author (revised)

A93-52872* National Aeronautics and Space Administration. Lewis Research Center, Cleveland, OH.

MULTILAYER RELAXATION AND SURFACE ENERGIES OF FCC AND BCC METALS USING EQUIVALENT CRYSTAL THEORY

AGUSTIN M. RODRIGUEZ (La Plata, Univ. Nacional, Argentina), GUILLERMO BOZZOLO (Analex Corp., Brook Park; NASA, Lewis Research Center, Cleveland, OH), and JOHN FERRANTE (NASA, Lewis Research Center, Cleveland, OH) Surface Science (ISSN 0039-6028) vol. 289 1993 p. 100-126. Research supported by NASA refs Copyright

The multilayer relaxation of fcc and bcc metal surfaces is calculated using equivalent crystal theory. The results for changes in interplanar spacings of planes close to the surface and the ensuing surface energies are discussed in reference to other theoretical results and compared to available experimental data. The calculation includes high-index surfaces for which no other theoretical results are known.

A93-52873* National Aeronautics and Space Administration. Lewis Research Center, Cleveland, OH.

HEAT OF SEGREGATION OF SINGLE SUBSTITUTIONAL IMPURITIES

GUILLERMO BOZZOLO (Analex Corp., Brook Park; NASA, Lewis Research Center, Cleveland, OH), BRIAN GOOD, and JOHN FERRANTE (NASA, Lewis Research Center, Cleveland, OH) Surface Science (ISSN 0039-6028) vol. 289 1993 p. 169-179. refs Copyright

The method of Bozzolo, Ferrante and Smith (BFS) is applied for the calculation of the heat of segregation of single substitutional impurities in fcc metals. A simple equation for predicting the heat of segregation is derived for the rigid case (no atomic relaxations). The results of including atomic relaxation using a Monte Carlo method are also presented and the results compared with a number of experimental and theoretical results.

A93-53733* National Aeronautics and Space Administration. Lewis Research Center, Cleveland, OH.

CHEMICAL REACTIONS IN THE PROCESSING OF MOSI2 + CARBON COMPACTS

NATHAN S. JACOBSON, KANG N. LEE (NASA, Lewis Research Center, Cleveland, OH), STUART A. MALOY, and ARTHUR H. HEUER (Case Western Reserve Univ., Cleveland, OH) American Ceramic Society, Communications (ISSN 0002-7820) vol. 76, no. 8 Aug. 1993 p. 2005-2009. Research supported by DARPA refs (Contract N00014-86-K-0773) Copyright

Hot-pressing of MoSi₂ powders with carbon at high temperatures reduces the siliceous grain boundary phase in the resultant compact. The chemical reactions in this process were examined using the Knudsen cell technique. A 2.3 wt pct oxygen MoSi₂ powder and a 0.59 wt pct oxygen MoSi₂ powder, both with additions of 2 wt pct carbon, were examined. The reduction of the siliceous grain boundary phase was examined at 1350 K and the resultant P(SiO)/P(CO) ratios interpreted in terms of the SiO(g) and CO(g) isobars on the Si-C-O predominance diagram. The MoSi₂ + carbon mixtures were then heated at the hot-pressing temperature of 2100 K. Large weight losses were observed and could be correlated with the formation of a low-melting eutectic and the formation and vaporization of SiC. Author (revised)

A93-55381* National Aeronautics and Space Administration. Lewis Research Center, Cleveland, OH.

PREMIXED FLAME PROPAGATION IN AN OPTICALLY THICK GAS

ANGEL ABBUD-MADRID and PAUL D. RONNEY (Princeton Univ., NJ) AIAA Journal (ISSN 0001-1452) vol. 31, no. 11 Nov.

1993 p. 2179-2181. refs
(Contract NAG3-1242)
Copyright

Flame propagation in both the optically thin and the optically thick regime of radiative transport was studied experimentally using particle-laden gas mixtures. Data on flame shapes, propagation rates, peak pressure, maximum rate of pressure rise, and thermal decay in the burned gases are consistent with the hypothesis that, at low particle loadings, the particles act to increase the radiative loss from the gases, whereas at higher loadings, reabsorption of emitted radiation becomes significant. The reabsorption acts to decrease the net radiative loss and augment conductive heat transport. It is speculated that, in sufficiently large systems, in which the absorption length is much smaller than the system size, flammability limits might not exist at microgravity conditions because emitted radiation would not constitute a loss mechanism. AIAA

N93-11450*# National Aeronautics and Space Administration. Lewis Research Center, Cleveland, OH.

TEST PROGRAM TO PROVIDE VALIDATION DATA FOR THE ROCKET COMBUSTOR INTERACTIVE DESIGN (ROCCID) CODE

THONG V. NGUYEN (Aerojet-General Corp., Sacramento, CA.), R. E. WALKER (Aerojet-General Corp., Sacramento, CA.), and MARK D. KLEM /in JHU, The 28th JANNAF Combustion Subcommittee Meeting, Volume 2 p 31-50 Oct. 1991 (Contract NAS3-25556)
Avail: CPIA, 10630 Little Patuxent Pkwy., Suite 202, Columbia, MD 21044-3200 HC

A description of the hardware design and test philosophy leading to the successful testing of a LOX/RP-1 engine designed using the ROCCID interactive methodology is provided. The specific test logic that guided this test program as well as the results containing both performance and stability data are provided. All testing was conducted with a single chamber design (diameter = 19.5 cm, contraction ratio = 2.0, length = 35.6 cm) and one 105 element O-F-O injector. The mixture ratio, O/F, was varied from 1.13 to 6.74:1 and chamber pressure ranged from 800 to 1750 psia, exclusive of chug stability tests which were conducted with chamber pressures as low as 250 psia. The testing, which was performed with and without acoustic cavities, included both stable and high frequency combustion instability results. All combustion instabilities were spontaneous. Although combustion perturbation bombs were used and generated over-pressures in the range of approximately 5 to 62 percent of the mean chamber pressure, no tests were driven unstable by the bombs. A comparison between the predicted and actual performance and stability is also provided. The measured performance was lower than the predicted values by approximately 5 percent, probably the result of poorer than predicted propellant mixing. The agreement of the predicted stability trends with the measured trends is reasonable; however, improvements to the component models are needed to increase the accuracy of the methodology. Author

N93-11452*# National Aeronautics and Space Administration. Lewis Research Center, Cleveland, OH.

COAXIAL INJECTOR SPRAY CHARACTERIZATION USING WATER/AIR AS SIMULANTS

MICHELLE M. ZALLER (Sverdrup Technology, Inc., Brook Park, OH.) and MARK D. KLEM /in JHU, The 28th JANNAF Combustion Subcommittee Meeting, Volume 2 p 151-160 Oct. 1991
Previously announced as N92-14112
(Contract NAS3-25266)
Avail: CPIA, 10630 Little Patuxent Pkwy., Suite 202, Columbia, MD 21044-3200 HC

Quantitative information about the atomization of injector sprays is required to improve the accuracy of computational models that predict the performance and stability of liquid propellant rocket engines. An experimental program is being conducted at NASA-Lewis to measure the drop size and velocity distributions in shear coaxial injector sprays. A phase/Doppler interferometer is used to obtain drop size data in water air shear coaxial injector

sprays. Droplet sizes and axial component of droplet velocities are measured at different radii for various combinations of water flow rate, air flow rate, injector liquid jet diameter, injector annular gap, and liquid post recess. Sauter mean diameters measured in the spray center 52 mm downstream of the liquid post tip range from 28 to 68 microns, and mean axial drop velocities at the same location range from 37 to 120 m/s. The shear coaxial injector sprays show a high degree of symmetry; the mean drop size and velocity profiles vary with liquid flow rate, post recess, and distance from the injector face. The drop size data can be used to estimate liquid oxygen/hydrogen spray drop sizes by correcting property differences between water-air and liquid oxygen/hydrogen. Author

N93-11545*# National Aeronautics and Space Administration. Lewis Research Center, Cleveland, OH.

CHRONOPOTENTIOMETRY OF REFRACTORY METALS, ACTINIDES AND OXYANIONS IN MOLTEN SALTS: A REVIEW

NAROTTAM P. BANSAL Sep. 1992 41 p
(Contract RTOP 505-01-50)
(NASA-TM-105862; E-7322; NAS 1.15:105862) Avail: CASI HC A03/MF A01

The applications of chronopotentiometry to the study of electrochemical behavior of three technologically important areas of refractory metals, actinides, and oxyanions in molten salts are critically reviewed. Chronopotentiometry is a very versatile diagnostic tool to understand the reaction mechanism of the electrode processes for the electrochemical reduction/oxidation of these electroactive species in molten salt solutions. Well adherent, compact, and uniformly thick coatings of refractory metals may be electrodeposited from their solutions in molten salts. Author

N93-15504*# National Aeronautics and Space Administration. Lewis Research Center, Cleveland, OH.

SIMPLIFIED JET-A KINETIC MECHANISM FOR COMBUSTOR APPLICATION

CHI-MING LEE, KRISHNA KUNDU, and BAHMAN GHORASHI (Cleveland State Univ., OH.) Jan. 1993 11 p Presented at the 31st Aerospace Sciences Meeting, Reno, NV, 11-14 Jan. 1993; sponsored by AIAA Original contains color illustrations (Contract RTOP 537-01-11)
(NASA-TM-105940; E-7457; NAS 1.15:105940; AIAA PAPER 93-0021) Avail: CASI HC A03/MF A01; 1 functional color page

Successful modeling of combustion and emissions in gas turbine engine combustors requires an adequate description of the reaction mechanism. For hydrocarbon oxidation, detailed mechanisms are only available for the simplest types of hydrocarbons such as methane, ethane, acetylene, and propane. These detailed mechanisms contain a large number of chemical species participating simultaneously in many elementary kinetic steps. Current computational fluid dynamic (CFD) models must include fuel vaporization, fuel-air mixing, chemical reactions, and complicated boundary geometries. To simulate these conditions a very sophisticated computer model is required, which requires large computer memory capacity and long run times. Therefore, gas turbine combustion modeling has frequently been simplified by using global reaction mechanisms, which can predict only the quantities of interest: heat release rates, flame temperature, and emissions. Jet fuels are wide-boiling-range hydrocarbons with ranges extending through those of gasoline and kerosene. These fuels are chemically complex, often containing more than 300 components. Jet fuel typically can be characterized as containing 70 vol pct paraffin compounds and 25 vol pct aromatic compounds. A five-step Jet-A fuel mechanism which involves pyrolysis and subsequent oxidation of paraffin and aromatic compounds is presented here. This mechanism is verified by comparing with Jet-A fuel ignition delay time experimental data, and species concentrations obtained from flametube experiments. This five-step mechanism appears to be better than the current one- and two-step mechanisms. Author

N93-16614*# National Aeronautics and Space Administration. Lewis Research Center, Cleveland, OH.

LSENS, A GENERAL CHEMICAL KINETICS AND SENSITIVITY ANALYSIS CODE FOR GAS-PHASE REACTIONS: USER'S GUIDE

KRISHNAN RADHAKRISHNAN (Sverdrup Technology, Inc., Brook Park, OH.) and DAVID A. BITTKER Jan. 1993 210 p (Contract RTOP 505-62-21)
(NASA-TM-105851; E-7299; NAS 1.15:105851) Avail: CASI HC A10/MF A03

A general chemical kinetics and sensitivity analysis code for complex, homogeneous, gas-phase reactions is described. The main features of the code, LSENS, are its flexibility, efficiency and convenience in treating many different chemical reaction models. The models include static system, steady, one-dimensional, inviscid flow, shock initiated reaction, and a perfectly stirred reactor. In addition, equilibrium computations can be performed for several assigned states. An implicit numerical integration method, which works efficiently for the extremes of very fast and very slow reaction, is used for solving the 'stiff' differential equation systems that arise in chemical kinetics. For static reactions, sensitivity coefficients of all dependent variables and their temporal derivatives with respect to the initial values of dependent variables and/or the rate coefficient parameters can be computed. This paper presents descriptions of the code and its usage, and includes several illustrative example problems. Author

N93-20189*# National Aeronautics and Space Administration. Lewis Research Center, Cleveland, OH.

EFFECTS OF BUOYANCY ON LAMINAR, TRANSITIONAL, AND TURBULENT GAS JET DIFFUSION FLAMES

M. YOUSEF BAHADORI (Science Applications International Corp., Torrance, CA.), DENNIS P. STOCKER, DAVID F. VAUGHAN (Baldwin-Wallace Coll., Berea, OH.), LIMING ZHOU (California Univ., Berkeley.), and RAYMOND B. EDELMAN (Rockwell International Corp., Canoga Park, CA.) *In its* The Second International Microgravity Combustion Workshop p 91-105 Feb. 1993

(Contract NAS3-22822; NAS3-25982)

Avail: CASI HC A03/MF A03; 11 functional color pages

Gas jet diffusion flames have been a subject of research for many years. However, a better understanding of the physical and chemical phenomena occurring in these flames is still needed, and, while the effects of gravity on the burning process have been observed, the basic mechanisms responsible for these changes have yet to be determined. The fundamental mechanisms that control the combustion process are in general coupled and quite complicated. These include mixing, radiation, kinetics, soot formation and disposition, inertia, diffusion, and viscous effects. In order to understand the mechanisms controlling a fire, laboratory-scale laminar and turbulent gas-jet diffusion flames have been extensively studied, which have provided important information in relation to the physico-chemical processes occurring in flames. However, turbulent flames are not fully understood and their understanding requires more fundamental studies of laminar diffusion flames in which the interplay of transport phenomena and chemical kinetics is more tractable. But even this basic, relatively simple flame is not completely characterized in relation to soot formation, radiation, diffusion, and kinetics. Therefore, gaining an understanding of laminar flames is essential to the understanding of turbulent flames, and particularly fires, in which the same basic phenomena occur. In order to improve and verify the theoretical models essential to the interpretation of data, the complexity and degree of coupling of the controlling mechanisms must be reduced. If gravity is isolated, the complication of buoyancy-induced convection would be removed from the problem. In addition, buoyant convection in normal gravity masks the effects of other controlling parameters on the flame. Therefore, the combination of normal-gravity and microgravity data would provide the information, both theoretical and experimental, to improve our understanding of diffusion flames in general, and the effects of gravity on the burning process in particular. Author (revised)

N93-20192*# National Aeronautics and Space Administration. Lewis Research Center, Cleveland, OH.

SOOT FORMATION AND RADIATION IN TURBULENT JET DIFFUSION FLAMES UNDER NORMAL AND REDUCED GRAVITY CONDITIONS

JERRY C. KU (Wayne State Univ., Detroit, MI.), LI TONG (Wayne State Univ., Detroit, MI.), JUN SUN (Wayne State Univ., Detroit, MI.), PAUL S. GREENBERG, and DEVON W. GRIFFIN (Sverdrup Technology, Inc., Brook Park, OH.) *In its* The Second International Microgravity Combustion Workshop p 121-133 Feb. 1993

Avail: CASI HC A03/MF A03; 11 functional color pages

Most practical combustion processes, as well as fires and explosions, exhibit some characteristics of turbulent diffusion flames. For hydrocarbon fuels, the presence of soot particles significantly increases the level of radiative heat transfer from flames. In some cases, flame radiation can reach up to 75 percent of the heat release by combustion. Laminar diffusion flame results show that radiation becomes stronger under reduced gravity conditions. Therefore, detailed soot formation and radiation must be included in the flame structure analysis. A study of sooting turbulent diffusion flames under reduced-gravity conditions will not only provide necessary information for such practical issues as spacecraft fire safety, but also develop better understanding of fundamentals for diffusion combustion. In this paper, a summary of the work to date and of future plans is reported. Author

N93-20193*# National Aeronautics and Space Administration. Lewis Research Center, Cleveland, OH.

VISUALIZATION AND IMAGING METHODS FOR FLAMES IN MICROGRAVITY

KAREN J. WEILAND *In its* The Second International Microgravity Combustion Workshop p 135-140 Feb. 1993

Avail: CASI HC A02/MF A03; 11 functional color pages

The visualization and imaging of flames has long been acknowledged as the starting point for learning about and understanding combustion phenomena. It provides an essential overall picture of the time and length scales of processes and guides the application of other diagnostics. It is perhaps even more important in microgravity combustion studies, where it is often the only non-intrusive diagnostic measurement easily implemented. Imaging also aids in the interpretation of single-point measurements, such as temperature, provided by thermocouples, and velocity, by hot-wire anemometers. This paper outlines the efforts of the Microgravity Combustion Diagnostics staff at NASA Lewis Research Center in the area of visualization and imaging of flames, concentrating on methods applicable for reduced-gravity experimentation. Several techniques are under development: intensified array camera imaging, and two-dimensional temperature and species concentrations measurements. A brief summary of results in these areas is presented and future plans mentioned. Author

N93-20194*# National Aeronautics and Space Administration. Lewis Research Center, Cleveland, OH.

SELECTED MICROGRAVITY COMBUSTION DIAGNOSTIC TECHNIQUES

DEVON W. GRIFFIN (Sverdrup Technology, Inc., Brook Park, OH.) and PAUL S. GREENBERG *In its* The Second International Microgravity Combustion Workshop p 141-147 Feb. 1993

Avail: CASI HC A02/MF A03; 11 functional color pages

During FY 1989-1992, several diagnostic techniques for studying microgravity combustion have moved from the laboratory to use in reduced-gravity facilities. This paper discusses current instrumentation for rainbow schlieren deflectometry and thermophoretic sampling of soot from gas jet diffusion flames. Author

N93-20206*# National Aeronautics and Space Administration. Lewis Research Center, Cleveland, OH.

OPPOSED-FLOW FLAME SPREADING IN REDUCED GRAVITY

ROBERT A. ALTENKIRCH (Mississippi State Univ., Mississippi State.), SUBRATA BHATTACHARJEE (San Diego State Univ., CA.), SANDRA L. OLSON, and KURT R. SACKSTEDER *In its* The

Second International Microgravity Combustion Workshop p 237-243
Feb. 1993

(Contract NAS3-23901; NCC3-221)

Avail: CASI HC A02/MF A03; 11 functional color pages

Experimental results obtained in drop towers and in Space Shuttle based experiments coupled with modelling efforts are beginning to provide information that is allowing an understanding to be developed of the physics of opposed-flow flame spread at reduced gravity where the spread rate and flow velocity are comparable and of the role played by radiative and diffusive processes in flame spreading in microgravity. Here we describe one Space Shuttle based experiment on flame spreading in a quiescent environment, the Solid Surface Combustion Experiment, SSCE, one planned microgravity experiment on flame spreading in a radiatively-controlled, forced opposing flow environment, the Diffusive and Radiative Transport in Fires Experiment, DARTFire, modelling efforts to support these experiments, and some results obtained to date. Author

N93-20207*# National Aeronautics and Space Administration.
Lewis Research Center, Cleveland, OH.

COMBUSTION OF SOLID FUEL IN VERY LOW SPEED OXYGEN STREAMS

JAMES S. TIEN (Case Western Reserve Univ., Cleveland, OH.), KURT R. SACKSTEDER, PAUL V. FERKUL (Case Western Reserve Univ., Cleveland, OH.), and GARY D. GRAYSON (Case Western Reserve Univ., Cleveland, OH.) *In its* The Second International Microgravity Combustion Workshop p 245-250 Feb. 1993

Avail: CASI HC A02/MF A03; 11 functional color pages

In reduced gravity, the combustion of solid fuel in low-speed flow can be studied. The flame behavior in this low-speed regime will fill a void in our understanding of the flow effect on combustion. In addition, it is important for spacecraft fire safety considerations. In this work, modeling and experimental work on low-speed forced-concurrent-flow flame spread are carried out. In addition, experiments on reduced-gravity buoyant-flow flame spread are performed. Author

N93-20209*# National Aeronautics and Space Administration.
Lewis Research Center, Cleveland, OH.

FLAME SPREAD ACROSS LIQUID POOLS

HOWARD ROSS, FLETCHER MILLER (Case Western Reserve Univ., Cleveland, OH.), DAVID SCHILLER (California Univ., Irvine.), and WILLIAM A. SIRIGNANO (California Univ., Irvine.) *In its* The Second International Microgravity Combustion Workshop p 257-264 Feb. 1993

Avail: CASI HC A02/MF A03; 11 functional color pages

For flame spread over liquid fuel pools, the existing literature suggests three gravitational influences: (1) liquid phase buoyant convection, delaying ignition and assisting flame spread; (2) hydrostatic pressure variation, due to variation in the liquid pool height caused by thermocapillary-induced convection; and (3) gas-phase buoyant convection in the opposite direction to the liquid phase motion. No current model accounts for all three influences. In fact, prior to this work, there was no ability to determine whether ignition delay times and flame spread rates would be greater or lesser in low gravity. Flame spread over liquid fuel pools is most commonly characterized by the relationship of the initial pool temperature to the fuel's idealized flash point temperature, with four or five separate characteristic regimes having been identified. In the uniform spread regime, control has been attributed to: (1) gas-phase conduction and radiation; (2) gas-phase conduction only; (3) gas-phase convection and liquid conduction, and most recently (4) liquid convection ahead of the flame. Suggestions were made that the liquid convection was owed to both buoyancy and thermocapillarity. Of special interest to this work is the determination of whether, and under what conditions, pulsating spread can and will occur in microgravity in the absence of buoyant flows in both phases. The approach we have taken to resolving the importance of buoyancy for these flames is: (1) normal gravity experiments and advanced diagnostics; (2) microgravity experiments; and (3) numerical modelling at arbitrary gravitational level. Derived from text

N93-20217*# National Aeronautics and Space Administration.
Lewis Research Center, Cleveland, OH.

COMBUSTION OF INTERACTING DROPLET ARRAYS IN A MICROGRAVITY ENVIRONMENT

DANIEL L. DIETRICH (Sverdrup Technology, Inc., Cleveland, OH.) and JOHN B. HAGGARD *In its* The Second International Microgravity Combustion Workshop p 317-323 Feb. 1993

Avail: CASI HC A02/MF A03; 11 functional color pages

This research program involves the study of one and two dimensional arrays of droplets in a buoyant-free environment. The purpose of the work is to extend the database and theories that exist for single droplets into the regime where droplet interactions are important. The eventual goal being to use the results of this work as inputs to models on spray combustion where droplets seldom burn individually; instead the combustion history of a droplet is strongly influenced by the presence of the neighboring droplets. The emphasis of the present investigation is experimental, although comparison will be made to existing theoretical and numerical treatments when appropriate. Both normal gravity and low gravity testing will be employed, and the results compared. The work to date will be summarized in the next section, followed by a section detailing the future plans. Author

26

METALLIC MATERIALS

Includes physical, chemical, and mechanical properties of metals, e.g., corrosion; and metallurgy.

A93-12130* National Aeronautics and Space Administration.
Lewis Research Center, Cleveland, OH.

ROOM TEMPERATURE CYCLIC DEFORMATION BEHAVIOR OF CAST AND EXTRUDED NIAL

R. D. NOEBE and B. A. LERCH (NASA, Lewis Research Center, Cleveland, OH) *Scripta Metallurgica et Materialia* (ISSN 0956-716X) vol. 27, no. 9 Nov. 1, 1992 p. 1161-1166. refs Copyright

The fully reversed, strain controlled fatigue behavior of cast and extruded NiAl was evaluated at room temperature for plastic strain ranges of 0.0006 to 0.0002 to provide baseline data on the fatigue life of NiAl and to investigate whether the low ductility of NiAl would result in poor low-cycle fatigue behavior. Except at the smallest plastic strain range investigated, NiAl work hardened continuously until failure with a final fracture stress under cyclic conditions which was at least 60 percent greater than the monotonic fracture strength of NiAl. Fatigue fracture initiation occurred at large internal tear-shaped pores, and fatigue life was controlled or limited by the presence of these processing-related defects. Even with the processing defects present in this material and the limited ductility of NiAl in general, cast and extruded NiAl exhibited much greater fatigue life at room temperature than comparable B2 ordered compounds when compared on a strain range basis. P.D.

A93-13776 National Aeronautics and Space Administration. Lewis Research Center, Cleveland, OH.

THERMAL STABILITY OF THE MICROSTRUCTURE OF AN AGED NB-ZR-C ALLOY

MEHMET UZ (Lafayette College, Easton, PA) and ROBERT H. TITRAN (NASA, Lewis Research Center, Cleveland, OH) *In Space nuclear power systems; Proceedings of the 8th Symposium, Albuquerque, NM, Jan. 6-10, 1991. Pt. 1* New York American Institute of Physics 1991 p. 172-185. Previously announced in STAR as N91-14454 Research supported by NASA refs (Contract DE-A103-86SF-16310)

Copyright

The effects of thermal aging with and without an applied stress on the microstructure of a Nb-Zr-C alloy containing 0.9 wt percent Zr and 0.06 percent C were studied. Chemical analysis,

metallographic examination, energy dispersive X-ray spectra of the bulk material, and chemical and X-ray analyses of the phase-extracted residue were used to characterize the microstructure. The samples examined were from a creep strength study involving hot and cold working, and various combinations of exposure to temperatures ranging from 1350 to 1755 K with and without applied load times as long as 34,000 plus hours. The results showed that the initial microstructure consisted primarily of orthorhombic precipitates of Nb sub C which were partially or completely transformed to face-centered cubic carbides of Nb and Zr, (Zr, Nb)C, upon prolonged exposure to elevated temperatures. Furthermore, it was found that the microstructure of the alloy is extremely stable owing to the very finely distributed precipitates throughout its matrix and along the grain boundaries. The lattice parameters of the cubic carbides were determined to vary from 0.458 to 0.465 nm as the Zr/Nb ratio varied from 38/62 to 75/25.

Author

A93-13882* National Aeronautics and Space Administration. Lewis Research Center, Cleveland, OH.

COMPARISON OF HIGH FREQUENCY, HIGH TEMPERATURE CORE LOSS AND B-H LOOP CHARACTERISTICS OF AN 80 NI-FE CRYSTALLINE ALLOY AND TWO IRON-BASED AMORPHOUS ALLOYS

WILLIAM R. WIESERMAN (Pittsburgh Univ., Johnstown, PA), GENE E. SCHWARZE (NASA, Lewis Research Center, Cleveland, OH), and JANIS M. NIEDRA (Sverdrup Technology Inc.; NASA, Lewis Research Center, Cleveland, OH) *In* Space nuclear power systems; Proceedings of the 8th Symposium, Albuquerque, NM, Jan. 6-10, 1991. Pt. 3 New York American Institute of Physics 1991 p. 974-981. refs

Copyright

Limited experimental data exists for the specific core loss and dynamic B-H loops for soft magnetic materials for the combined conditions of high frequency and high temperature. This experimental study investigates the specific core loss and dynamic B-H characteristics of a nickel-iron crystalline magnetic alloy (Supermalloy) and two iron-based amorphous magnetic materials (Metglas 2605S-3A and Metglas 2605SC) over the frequency range of 1-50 kHz and temperature range of 23-300 C under sinusoidal voltage excitation. The effects of maximum magnetic flux density, frequency, and temperature on the specific core loss and on the size and shape of the B-H loops are examined. The Supermalloy and Metglass 2605S-3A and 2605SC data are used to compare the core loss of transformers with identical kVA and voltage ratings.

Author

A93-13937 National Aeronautics and Space Administration. Lewis Research Center, Cleveland, OH.

EFFECTS OF DUST ACCUMULATION AND REMOVAL ON RADIATOR SURFACES ON MARS

JAMES R. GAIER, MARLA E. PEREZ-DAVIS, SHARON K. RUTLEDGE (NASA, Lewis Research Center, Cleveland, OH), DEBORAH HOTES, and RAYMOND OLLE (Cleveland State Univ., OH) *In* Space nuclear power systems; Proceedings of the 8th Symposium, Albuquerque, NM, Jan. 6-10, 1991. Pt. 3 New York American Institute of Physics 1991 p. 1378-1383. Previously announced in STAR as N91-20204 refs

(Contract NCC3-19; RTOP 591-14-41)

Copyright

Tests were carried out to assess the impact of wind blown dust accumulation and abrasion on radiator surfaces on Mars. High emittance arc-textured copper and niobium-1 percent-zirconium samples were subjected to basaltic dust laden wind at Martian pressure (1000 Pa) at speeds varying from 19 to 97 m/s in the Martian Surface Wind Tunnel. The effect of accumulated dust was also observed by pre-dusting some of the samples before the test. Radiator degradation was determined by measuring the change in the emittance after dust was deposited and/or removed. The principle mode of degradation was abrasion. Arc textured Nb-1 percent-Zr proved to be more susceptible to degradation than Cu, and pre-dusting appeared to have lessened the abrasion.

Author

A93-17516* National Aeronautics and Space Administration. Lewis Research Center, Cleveland, OH.

THE EFFECT OF MICROALLOYING ADDITIONS ON THE TENSILE PROPERTIES OF POLYCRYSTALLINE NIAL

R. D. NOEBE and M. K. BEHBEHANI (NASA, Lewis Research Center, Cleveland, OH) *Scripta Metallurgica et Materialia* (ISSN 0956-716X) vol. 27, no. 12 Dec. 15, 1992 p. 1795-1800. refs

Copyright

The presently evaluated 0.1 at. pct Fe and Ga additions to NiAl, while beneficial in the case of monocrystalline NiAl ductility, does not improve ductility in the polycrystalline case; it also has little effect on tensile properties. A similar microalloying addition of Zr, by contrast, significantly depressed the tensile ductility of NiAl, and nearly doubled the brittle-to-ductile transition temperature (BDTT). The dependence of tensile properties on temperature was in all cases similar; tensile elongations remained low and constant until the BDTT was reached, and then dramatically increased.

O.C.

A93-17609 National Aeronautics and Space Administration. Lewis Research Center, Cleveland, OH.

HEATS OF FORMATION OF BCC BINARY ALLOYS

GUILLERMO BOZZOLO (Analex Corp., Brook Park; NASA, Lewis Research Center, Cleveland, OH) and JOHN FERRANTE (NASA, Lewis Research Center, Cleveland, OH) *Physical Review B - Condensed Matter, 3rd Series* (ISSN 0163-1829) vol. 45, no. 21 June 1, 1992 p. 12,191-12,197. Previously announced in STAR as N92-16086 refs

(Contract RTOP 505-90-52)

Copyright

The method of Bozzolo, Ferrante and Smith is applied for the calculation of alloy energies for bcc elements. The heat of formation of several alloys is computed with the help of the Connolly-Williams method within the tetrahedron approximation. The dependence of the results on the choice of different sets of ordered structures is discussed.

Author

A93-17674* National Aeronautics and Space Administration. Lewis Research Center, Cleveland, OH.

INFLUENCE OF GRAIN SIZE ON THE CREEP BEHAVIOR OF HfC-DISPERSED NIAL

J. D. WHITTENBERGER (NASA, Lewis Research Center, Cleveland, OH), RANJAN RAY (Marko Materials, Inc., North Billerica, MA), and SUNIL C. JHA (Texas Instruments, Inc., Attleboro, MA) *Materials Science and Engineering, Part A - Structural Materials: Properties, Microstructure and Processing* (ISSN 0921-5093) vol. A151 1992 p. 137-146. refs

Copyright

Rapid solidification technology has been utilized to produce a NiAl-4(wt pct)HfC composite containing about 0.3 vol pct HfC as dispersed 50 nm particles. Study of the 1300 K compressive creep properties demonstrated that the initial, small grain size microstructure was unstable under slow strain rate deformation conditions. The grain growth which occurred during testing led to considerable strengthening. Subsequent measurements of the creep properties of the coarse grained specimens revealed that this strength was achieved by a large increase in the activation energy for deformation without any change in the stress exponent. Based on this work, it is concluded that large grain microstructures will be required for optimum elevated temperature creep properties in dispersed NiAl.

Author

A93-18075* National Aeronautics and Space Administration. Lewis Research Center, Cleveland, OH.

PROPERTIES OF PURE NICKEL AFTER LONG TERM EXPOSURES TO LIOH AND VACUUM AT 775 K

J. D. WHITTENBERGER (NASA, Lewis Research Center, Cleveland, OH) *Journal of Materials Engineering* (ISSN 0931-7058) vol. 13, no. 4 1991 p. 257-271. Previously announced in STAR as N90-20181 refs

Copyright

The solid to liquid phase transformation of LiOH at 744.3 K is

considered to be an ideal candidate thermal energy storage (TES) mechanism for a Rankine heat engine based solar dynamic system operating at approximately 682 K. While pure nickel is thought to be a suitable containment material for LiOH, long term containment is of concern because molten hydroxides are usually corrosive. Two commercially pure nickel alloys, Ni-200 and Ni-201, were exposed to molten LiOH, its vapor, and vacuum at 775 K for periods ranging from 50 to 5000 h, and simple mechanical property measurements (77 to 900 K tensile and 750 K creep rupture) of exposed alloys were undertaken. The mechanical property test procedures are described and tabular lists of the test data are presented. Author

A93-20556* National Aeronautics and Space Administration. Lewis Research Center, Cleveland, OH.

CREEP-RUPTURE STRENGTH OF A NI-BASE SUPERALLOY AT 1400 K

J. D. WHITTENBERGER, MICHAEL V. NATHAL (NASA, Lewis Research Center, Cleveland, OH), and PATRICIA O. BOOK (Cleveland State Univ., OH) Scripta Metallurgica et Materialia (ISSN 0956-716X) vol. 28, no. 1 Jan. 1, 1993 p. 53-58. refs Copyright

While NASAIR 100 is not the strongest of elevated-temperature single-crystal alloys, its higher-temperature properties are indicative of this technology's behavior. Attention is presently given to test results for this alloy which illuminate its 1400 K creep failure properties in air, and furnish a benchmark for the comparison of advanced materials to existing technology. The creep rupture behavior resembles that found after 1273 K testing, and is indicative of gamma-prime strengthening. O.C.

A93-20667* National Aeronautics and Space Administration. Lewis Research Center, Cleveland, OH.

EFFECT OF OXIDATION ON THE MECHANICAL PROPERTIES OF A NBAL3 ALLOY AT INTERMEDIATE TEMPERATURES

S. V. RAJ (NASA, Lewis Research Center, Cleveland, OH), M. HEBSUR (Sverdrup Technology, Inc., Cleveland, OH), I. E. LOCCI, and J. DOYCHAK (NASA, Lewis Research Center, Cleveland, OH) Journal of Materials Research (ISSN 0884-2914) vol. 7, no. 12 Dec. 1992 p. 3219-3234. refs Copyright

The effect of environment on the mechanical properties of an Nb-67Al-7Cr-0.25W-0.5Y alloy was investigated experimentally in the temperature range 800-1200 K. It is found that the severity of environmental attack in the alloy is determined by both matrix plasticity and oxidation kinetics. The former determines the ability of the matrix to accommodate the localized stresses generated during deformation and oxidation, while the latter governs the rate of formation of a protective oxide scale. The environmental degradation of the alloy can thus be reduced or eliminated by increasing atomic mobility. V.L.

A93-21958* National Aeronautics and Space Administration. Lewis Research Center, Cleveland, OH.

CRITICAL EXPERIMENTS OF THE SELF-CONSISTENT MODEL FOR POLYCRYSTALLINE HASTELLOY-X

SHIXIANG SHI (Connecticut Univ., Storrs), KEVIN P. WALKER (Engineering Science Software, Inc., Smithfield, RI), and ERIC H. JORDAN (Connecticut Univ., Storrs) In Modeling the deformation of crystalline solids; Proceedings of the Symposium, Annual Meeting of the Minerals, Metals & Materials Society, New Orleans, LA, Feb. 17-21, 1991 Warrendale, PA Minerals, Metals & Materials Society 1991 p. 601-612. refs (Contract DE-FG02-88ER-13894; NAG3-512) Copyright

A viscoplastic constitutive model is presented for the estimation of the overall mechanical response of Hastelloy-X polycrystalline metals from a knowledge of single crystal behavior. The behavior of polycrystal is derived from that of single crystals using a self-consistent formulation. The single crystal behavior which has been used was developed by summing postulated slip on crystallographic slip systems. The plasticity and creep are treated coupledly using unified viscoplastic model which includes the

interaction effects between rapid and slow deformation at elevated temperature. The validity of the model is directly tested by experiments on Hastelloy-X in both single crystal and polycrystalline versions. Author

A93-21959* National Aeronautics and Space Administration. Lewis Research Center, Cleveland, OH.

A CONSTITUTIVE MODEL FOR THE HIGH TEMPERATURE INELASTIC RESPONSE OF NICKEL BASE SUPERALLOYS

D. C. STOUFFER (Cincinnati Univ., OH) In Modeling the deformation of crystalline solids; Proceedings of the Symposium, Annual Meeting of the Minerals, Metals & Materials Society, New Orleans, LA, Feb. 17-21, 1991 Warrendale, PA Minerals, Metals & Materials Society 1991 p. 629-646. Research supported by NASA and GE Aircraft Engines refs Copyright

The objective of this research is to develop a constitutive equation for the uniaxial and multiaxial fatigue response of Rene 80 between the temperatures of 538 C and 982 C. The constitutive equation is accompanied by an experimental program for the evaluation of the material constants and extensive verification through the successful prediction of mechanical cycling experiments. These results include the prediction of the high temperature multiaxial response of Rene 80 that includes torsion and proportional and non-proportional loading histories. Author

A93-24066* National Aeronautics and Space Administration. Lewis Research Center, Cleveland, OH.

EVALUATION OF THE FRACTURE TOUGHNESS OF NB-40AL-8CR-1W-1Y-0.05B INTERMETALLIC MATERIAL BY INDENTATION TECHNIQUES

S. R. CHOI, J. A. SALEM (NASA, Lewis Research Center, Cleveland, OH), and M. G. HEBSUR (Sverdrup Technology, Inc., Brook Park, OH) Journal of Materials Science (ISSN 0022-2461) vol. 28, no. 1 Jan. 1, 1993 p. 155-160. refs Copyright

The fracture toughness of an Nb-40Al-8Cr - 1W-1Y-0.05B intermetallic material was evaluated by indentation techniques at room temperature. Two widely used indentation methods, crack size measurement and indent strength, yielded excellent agreement with a conventional fracture toughness technique using straight-through precracked specimens, despite the occasional formation of poorly configured cracks. However, the modified indentation technique, using dummy indent flaws, resulted in a low fracture toughness compared to that evaluated by the other methods. The material did not exhibit rising R-curve behavior, as evaluated from the indentation strength data. These results indicate that indentation fracture principles are applicable to this brittle intermetallic material without modification of the residual contact stress term originally calibrated for ceramic materials. Author

A93-25108* National Aeronautics and Space Administration. Lewis Research Center, Cleveland, OH.

TRANSFORMATION TO NISAL3 IN A 63.0 AT. PCT NI-AL ALLOY

P. S. KHADKIKAR (Therm-O-Disc, Inc., Mansfield, OH), I. E. LOCCI (Case Western Reserve Univ.; NASA, Lewis Research Center, Cleveland, OH), K. VEDULA (Iowa State Univ. of Science and Technology, Ames), and G. M. MICHAL (Case Western Reserve Univ., Cleveland, OH) Metallurgical Transactions A - Physical Metallurgy and Materials Science (ISSN 0360-2133) vol. 24A, no. 1 Jan. 1993 p. 83-94. refs Copyright

Microstructures of 63 at. pct P/M Ni-Al alloys with a composition close to the stoichiometry of the Ni5Al3 phase were investigated using homogenized and quenched specimens aged at low temperatures for various times. Results of analyses of XRD data and electron microscopy observations were used for quantitative phase analysis, performed to calculate the (NiAl + Ni5Al3)/Ni5Al3 phase boundary locations. The measured lattice parameters of Ni5Al3 phase formed at 823, 873, and 923 K indicated an increase in tetragonality of the phase with increasing nickel content. I.S.

A93-25119* National Aeronautics and Space Administration. Lewis Research Center, Cleveland, OH.

PRELIMINARY EVALUATION OF TENSILE AND STRESS-RUPTURE BEHAVIOR OF W + 24 AT. PCT RE + 0.4 AT. PCT HfC WIRE

H. M. YUN (NASA, Lewis Research Center, Cleveland, OH) Metallurgical Transactions A - Physical Metallurgy and Materials Science (ISSN 0360-2133) vol. 24A, no. 1 Jan. 1993 p. 209-214. refs

Copyright

Results are presented of an evaluation of tensile properties and stress-rupture behavior of a small-diameter W24ReHfC (W-24Re-0.4(HfC)) wire, which is considered to be an excellent reinforcing fiber candidate for a variety of metal-matrix composites. The results were compared to data of Petrusek (1972) on W4ReHfC (W-4Re-0.4(HfC)) wire. It was found that the room-temperature (RT) tensile strength of the W24ReHfC wire was about 3250 MPa, higher than that of the W4ReHfC (3160 MPa) and WHfC (2250 MPa) wires. Above 1366 K, the W4ReHfC wire had both a greater tensile strength and the stress rupture strength than the W24ReHfC wire. I.S.

A93-27486* National Aeronautics and Space Administration. Lewis Research Center, Cleveland, OH.

THE VISCOPLASTIC BEHAVIOR OF HASTELLOY-X SINGLE CRYSTAL

ERIC H. JORDAN, SHIXIANG SHI (Connecticut Univ., Storrs), and KEVIN P. WALKER (Engineering Science Software, Inc., Smithfield, RI) International Journal of Plasticity (ISSN 0749-6419) vol. 9, no. 1 1993 p. 119-139. refs

(Contract NAG3-512; DE-FG02-88ER-13894; DE-AC02-88ER-13895)

Copyright

A viscoplastic constitutive model for simulating the behavior of Hastelloy-X single crystal material was derived based on crystallographic slip theory. To determine the appropriate constitutive model constants and to test the predictions of the model, tests on Hastelloy-X crystals were carried out, including the rate sensitivity, cyclic hardening, nonproportional hardening, relaxation, and strain rate dip tests. It was found necessary to include cube slip in the model in order to correlate the uniaxial behavior of the single crystal, to incorporate the interaction effects in both the hardening and the dynamic recovery evolution equations for the drag stress, and to successfully capture correct strain rate sensitivity under biaxial tension-torsion loading conditions. I.S.

A93-29534* National Aeronautics and Space Administration. Lewis Research Center, Cleveland, OH.

THE KINETICS OF COMPOSITE PARTICLE FORMATION DURING MECHANICAL ALLOYING

B. J. M. AIKIN (Case Western Reserve Univ.; NASA, Lewis Research Center, Cleveland, OH) and T. H. COURTNEY (Michigan Technological Univ., Houghton) Metallurgical Transactions A - Physical Metallurgy and Materials Science (ISSN 0360-2133) vol. 24A, no. 3 March 1993 p. 647-657. Research supported by U.S. Army refs

Copyright

The kinetics of composite particle formation during attritor milling of insoluble binary elemental powders have been examined. The effects of processing conditions (i.e., mill power, temperature, and charge ratio) on these kinetics were studied. Particle size distributions and fractions of elemental and composite particles were determined as functions of milling time and processing conditions. This allowed the deduction of phenomenological rate constants describing the propensity for fracture and welding during processing. For the mill-operating conditions investigated, the number of particles in the mill generally decreased with milling time, indicating a greater tendency for particle welding than fracture. Moreover, a bimodal size distribution is often obtained as a result of preferential welding. Copper and chromium 'alloy' primarily by encapsulation of Cr particles within Cu. This form of alloying also occurs in Cu-Nb alloys processed at low mill power and/or for short milling times. For other conditions, however, Cu-Nb alloys

develop a lamellar morphology characteristic of mechanically alloyed two-phase ductile metals. Increasing mill power or charge (ball-to-powder weight) ratio (CR) increases the rate of composite particle formation.

Author

A93-29570* National Aeronautics and Space Administration. Lewis Research Center, Cleveland, OH.

GRAIN BOUNDARY RESISTANCE TO FATIGUE CRACK GROWTH

QI CHEN and H. W. LIU (Syracuse Univ., NY) Scripta Metallurgica et Materialia (ISSN 0956-716X) vol. 28, no. 7 April 1, 1993 p. 849-852. refs

(Contract NAG3-837)

Copyright

Results of an experimental study tracing the grain boundary effect on the fatigue crack growth rate are reported. Direct experimental evidence for the grain boundary blockage mechanism is presented. The orientation difference between two neighboring grains directly contributed to the extent of crack growth retardation. P.D.

A93-32925* National Aeronautics and Space Administration. Lewis Research Center, Cleveland, OH.

VISCOPLASTICITY WITH CREEP AND PLASTICITY BOUNDS

ALAN D. FREED (NASA, Lewis Research Center, Cleveland, OH) and KEVIN P. WALKER (Engineering Science Software, Inc., Smithfield, RI) International Journal of Plasticity (ISSN 0749-6419) vol. 9, no. 2 1993 p. 213-242. refs

Copyright

A viscoplastic theory is developed that reduces analytically to creep theory under steady-state conditions and becomes plasticity theory at its rate-independent bound. A viscoplastic model is then constructed by defining material functions that have close ties to the physics of inelasticity. As a consequence, this model is characterized easily - only steady-state creep data, saturated hysteresis loops, and monotonic stress/strain curves are required. The general applicability of the model is demonstrated by the characterization of three f.c.c. metals. A variety of validation experiments is also provided.

Author

A93-32934* National Aeronautics and Space Administration. Lewis Research Center, Cleveland, OH.

THE MICROSTRUCTURAL EVOLUTION, CRYSTALLOGRAPHY, AND THERMAL PROCESSING OF ULTRAHIGH CARBON FE-1.85 PCT C MELT-SPUN RIBBON

G. SPANOS, J. D. AYERS, C. L. VOLD (U.S. Navy, Naval Research Lab., Washington), and I. E. LOCCI (NASA, Lewis Research Center, Cleveland, OH) Metallurgical Transactions A - Physical Metallurgy and Materials Science (ISSN 0360-2133) vol. 24A, no. 4 April 1993 p. 809-818. Research supported by U.S. Navy refs

A study is presented to determine if fine microstructures could be achieved using rapid solidification to produce a fine-grained fully austenitic starting structure and then using thermal processing cycles to produce an even finer ferrite-cementite structure. The evolution, mechanisms of grain refinement, and crystallography of the resultant microstructures were examined by TEM. A thermal processing cycle consisted of quenching the ribbon in liquid nitrogen, tempering at 600 C for 10 sec, 'upquenching' to 750 C for 10 sec, and subsequently quenching again in liquid nitrogen. The heat-treatment resulted in martensite grains with sizes of about 1 micron or less in both length and thickness and cementite particles of 0.4 micron or less. It is concluded that these microstructures could be used for producing fine-grained ultrahigh carbon steels of very high strength without the brittleness associated with the formation of coarse carbide particles of the loss of strength due to graphite formation.

AI/A

A93-33011 National Aeronautics and Space Administration. Lewis Research Center, Cleveland, OH.

EFFECT OF TENSILE MEAN STRESS ON FATIGUE BEHAVIOR OF SINGLE-CRYSTAL AND DIRECTIONALLY SOLIDIFIED SUPERALLOYS

SREERAMESH KALLURI (Sverdrup Technology, Inc., Cleveland,

OH) and MICHAEL A. MCGAW (NASA, Lewis Research Center, Cleveland, OH) *In* Cyclic deformation, fracture, and nondestructive evaluation of advanced materials Philadelphia, PA American Society for Testing and Materials 1992 p. 136-150. Previously announced in STAR as N91-18452 refs (Contract RTOP 553-13-00) Copyright

Two nickel base superalloys, single crystal PWA 1480 and directionally solidified MAR-M 246 + Hf, were studied in view of the potential usage of the former and usage of the latter as blade materials for the turbomachinery of the Space Shuttle main engine. The baseline zero mean stress (ZMS) fatigue life (FL) behavior of these superalloys was established, and then the effect of tensile mean stress (TMS) on their FL behavior was characterized. A stress range based FL prediction approach was used to characterize both the ZMS and TMS fatigue data. In the past, several researchers have developed methods to account for the detrimental effect of tensile mean stress on the FL for polycrystalline engineering alloys. These methods were applied to characterize the TMS fatigue data of single crystal PWA 1480 and directionally solidified MAR-M 246 + Hf and were found to be unsatisfactory. Therefore, a method of accounting for the TMS effect on FL, that is based on a technique proposed by Heidmann and Manson was developed to characterize the TMS fatigue data of these superalloys. Details of this method and its relationship to the conventionally used mean stress methods in FL prediction are discussed. Author

A93-36586* National Aeronautics and Space Administration. Lewis Research Center, Cleveland, OH.

MECHANICAL PROPERTIES OF HAYNES ALLOY 188 AFTER EXPOSURE TO LiF-22CAF₂, AIR, AND VACUUM AT 1093 K FOR PERIODS UP TO 10,000 HOURS

J. D. WHITTENBERGER (NASA, Lewis Research Center, Cleveland, OH) Journal of Materials Engineering and Performance vol. 1, no. 4 Aug. 1992 p. 469-482. refs Copyright

As part of a program to provide reassurance that the cobalt-base superalloy Haynes Alloy 188 can adequately contain a LiF-CaF₂ eutectic thermal energy storage salt, 4900- and 10,000-hr exposures of Haynes Alloy 188 to LiF-22CaF₂, its vapor, vacuum, and air at 1093 K have been undertaken. Following such exposures, the microstructure has been characterized and the 77 to 1200 K tensile properties measured. In addition, 1050 K vacuum creep-rupture testing of as-received and molten salt- and vacuum-exposed samples has been undertaken. Although slight degradation of the mechanical properties of Haynes Alloy 188 due to prior exposure was observed, basically none of the losses could be ascribed to a particular environment. Hence, observed decreases in properties are due to thermal aging effects, not corrosive attack. In view of these findings, Haynes Alloy 188 is still deemed to be suitable for containment of the eutectic LiF-CaF₂ thermal energy storage media. Author (revised)

A93-37899* National Aeronautics and Space Administration. Lewis Research Center, Cleveland, OH.

CHROMIUM AND REACTIVE ELEMENT MODIFIED ALUMINIDE DIFFUSION COATINGS ON SUPERALLOYS - ENVIRONMENTAL TESTING

ROBERT BIANCO, ROBERT A. RAPP (Ohio State Univ., Columbus), and JAMES L. SMIALEK (NASA, Lewis Research Center, Cleveland, OH) Electrochemical Society, Journal (ISSN 0013-4651) vol. 140, no. 4 April 1993 p. 1191-1203. refs (Contract N00014-87-K-0030; N00014-90-J-1765) Copyright

The high temperature performance of reactive element (RE)-doped and Cr/RE-modified aluminide diffusion coatings on commercial Ni-base alloy substrates was determined. In isothermal oxidation at 1100 C in air, RE-doped aluminide coatings on IN 713LC substrates formed a continuous slow-growing n-Al₂O₃ scale after 44 hrs of exposure. The coatings were protected by either an outer ridge Al₂O₃ scale with an inner compact Al₂O₃ scale rich in RE or by a continuous compact scale without any noticeable

cracks or flaws. The cyclic oxidation behavior of Cr/RE-modified aluminide coatings on Rene 80 and IN 713LC alloys and of RE-doped aluminide coatings on IN 713LC alloys at 1100 C in static air was determined. Pack powder entrapment from the powder contacting (PC) process detracted significantly from the overall cyclic oxidation performance. Type I hot corrosion behavior of Cr/RE-modified aluminide coatings on Rene 80 and Mar-M247 alloy substrates at 900 C in a catalyzed 0.1 percent SO₃/O₃ gas mixture was determined. The modified coatings produced from the PC arrangement provided significantly better resistance to hot corrosion attack than commercial low-activity aluminide coatings produced by the above pack arrangement. AIAA

A93-39796 National Aeronautics and Space Administration. Lewis Research Center, Cleveland, OH.

DETERMINATION OF PARAMETERS OF A METHOD FOR PREDICTING ALLOY PROPERTIES

GUILLERMO BOZZOLO (Analex Corp., Brook Park; NASA, Lewis Research Center, Cleveland, OH) and JOHN FERRANTE (NASA, Lewis Research Center, Cleveland, OH) Physical Review B - Condensed Matter, 3rd Series (ISSN 0163-1829) vol. 46, no. 13 Oct. 1, 1992 p. 8600-8602. Previously announced in STAR as N93-11609 refs (Contract RTOP 505-90-53) Copyright

A93-44887* National Aeronautics and Space Administration. Lewis Research Center, Cleveland, OH.

CREEP DEFORMATION OF B2 ALUMINIDES

M. V. NATHAL (NASA, Lewis Research Center, Cleveland, OH) *In* Ordered intermetallics - Physical metallurgy and mechanical behaviour Dordrecht, Netherlands Kluwer Academic Publishers 1992 p. 541-563. refs Copyright

The creep resistance and elevated temperature deformation mechanisms in CoAl, FeAl, and NiAl are reviewed. The stress and temperature dependencies of the steady state creep rate, the primary creep behavior, the dislocation substructure, and the response during transient tests are used as the main indicators of the deformation processes. In single phase intermetallics, the influence of grain size, stoichiometry, and solid solution hardening have been examined. In addition, the effect of adding dispersoids, precipitates, and other types of reinforcements to improve creep strength are compared. Author

A93-50370* National Aeronautics and Space Administration. Lewis Research Center, Cleveland, OH.

DIFFUSIONAL TRANSPORT AND PREDICTING OXIDATIVE FAILURE DURING CYCLIC OXIDATION OF BETA-NIAL ALLOYS

J. A. NESBITT, E. J. VINARCIK, C. A. BARRETT, and J. DOYCHAK (NASA, Lewis Research Center, Cleveland, OH) Materials Science and Engineering, Part A -Structural Materials: Properties, Microstructure, Microstructure and Processing (ISSN 0921-5093) vol. A153 1992 p. 561-566. refs Copyright

Nickel aluminides (NiAl) containing 40-50 at. percent Al and up to 0.1 at. percent Zr have been studied following cyclic oxidation at 1200, 1300, 1350 and 1400 C. The selective oxidation of aluminum resulted in the formation of protective Al₂O₃ scales on each alloy composition at each temperature. However, repeated cycling eventually resulted in the gradual formation of less protective NiAl₂O₄. The appearance of the NiAl₂O₄, signaling the end of the protective scale-forming capability of the alloy, was related to the presence of gamma-prime-(Ni₃Al) which formed as a result of the loss of aluminum from the sample. A simple methodology is presented to predict the protective life of beta-NiAl alloys. This method predicts the oxidative lifetime due to aluminum depletion when the aluminum concentration decreases to a critical concentration. The time interval preceding NiAl₂O₄ formation (i.e., the lifetime based on protective Al₂O₃ formation) and predicted lifetimes are compared and discussed. Use of the method to predict

the maximum use temperature for NiAl-Zr alloys is also discussed.
Author (revised)

A93-52870* National Aeronautics and Space Administration. Lewis Research Center, Cleveland, OH.

STRESS RELAXATION OF LOW PRESSURE

PLASMA-SPRAYED NICRALY ALLOYS

W. J. BRINDLEY and J. D. WHITTENBERGER (NASA, Lewis Research Center, Cleveland, OH) *Materials Science and Engineering, Part A - Structural Materials: Properties, Microstructures and Processing* (ISSN 0921-5093) vol. A163 1993 p. 33-41. refs

Copyright

The stress relaxation behavior of three NiCrAlY alloys that are commonly used as bond coats for thermal barrier coatings (TBCs) has been directly measured. The relaxation study was conducted at temperatures of 800-1000 C and over a wide range of stresses. It was established that all three bond coat alloys relaxed quite rapidly at temperatures of 900 C and above. Since the upper use temperatures for bond coats in gas turbine engines are between 900 and 1000 C, bond coat relaxation is expected to occur in service. Therefore, relaxation of the bond coat has the potential to affect TBC life. Furthermore, the relaxation differences observed between the three alloys offers a possible explanation for the differences in TBC life observed for these bond coats. While bond coat relaxation is expected to occur for a TBC in service, the mechanism for a relaxation effect on TBC life, if it exists, is yet to be determined.

Author (revised)

A93-52879* National Aeronautics and Space Administration. Lewis Research Center, Cleveland, OH.

THERMODYNAMICS OF IRON-ALUMINUM ALLOYS AT 1573 K

NATHAN S. JACOBSON (NASA, Lewis Research Center, Cleveland, OH) and GOPAL M. MEHROTRA (Wright State Univ., Dayton, OH) *Metallurgical Transactions B - Process Metallurgy* vol. 24B June 1993 p. 481-486. refs

The activities of iron and aluminum were measured in Fe-Al alloys at 1573 K, using the ion-current-ratio technique in a high-temperature Knudsen cell mass spectrometer. The Fe-Al solutions exhibited negative deviations from ideality over the entire composition range. The activity coefficients γ_{Fe} and γ_{Al} are given by six following equations as a function of mole fraction, $X(\text{Fe})$, $X(\text{Al})$. The results show good agreement with those obtained from previous investigations at other temperatures by extrapolation of the activity data to 1573 K.

Author (revised)

A93-53469* National Aeronautics and Space Administration. Lewis Research Center, Cleveland, OH.

SIMS STUDIES OF OXIDE GROWTH ON BETA-NIAL

D. F. MITCHELL, R. PRESCOTT, M. J. GRAHAM (National Research Council of Canada, Inst. for Microstructural Sciences, Ottawa), and J. DOYCHAK (NASA, Lewis Research Center, Cleveland, OH) *In International SAMPE Technical Conference, 24th and International SAMPE Metals and Metals Processing Conference, 3rd, Toronto, Canada, Oct. 20-22, 1992, Proceedings. Vol. 3 Covina, CA Society for the Advancement of Material and Process Engineering* 1992 p. M78-M91. refs

Copyright

This paper reports on a study of the growth of aluminum oxide on beta-NiAl at temperatures up to 1200 C. The scales have been formed in two-stage experiments using O₂-16 and O₂-18 gases, and the various isotopic species have been located by direct imaging using SIMS. Supplementary information on oxide morphologies and structures has been obtained by SEM. SIMS images and depth profiles indicate where oxidation has taken place predominantly by cation or anion diffusion at different stages of the growth process. The way in which the presence of small amounts of reactive elements can affect scale growth is also considered. These results help to provide an improved understanding of the mechanism of alumina scale formation, which is of benefit in the development of oxidation-resistant alloys and intermetallics for service at high temperatures.

Author (revised)

A93-53939* National Aeronautics and Space Administration. Lewis Research Center, Cleveland, OH.

PREDICTING THE OXIDATIVE LIFETIME OF BETA NIAL-ZR ALLOYS

J. A. NESBITT and E. J. VINARCIK (NASA, Lewis Research Center, Cleveland, OH) *In Damage and oxidation protection in high temperature composites. Vol. 1; Proceedings of the Symposium, 112th ASME Winter Annual Meeting, Atlanta, GA, Dec. 1-6, 1991 New York American Society of Mechanical Engineers* 1991 p. 9-22. refs

Copyright

Nickel aluminides containing 40 to 50 at. pct Al and 0.1 at. pct Zr were studied following cyclic oxidation at 1400 C. The selective oxidation of Al resulted in the formation of protective Al₂O₃ scales on each alloy composition. However, repeated cycling eventually resulted in the gradual formation of less-protective NiAl₂O₄, first appearing on the 40Al alloys followed at longer times on the 45Al alloys. The appearance of the NiAl₂O₄, signaling the end of the protective scale-forming capability of the alloy, was related to the presence of gamma-prime (Ni₃Al) which formed as a result of the loss of Al from the sample. A diffusion model, based on finite-difference techniques, was developed to predict the protective life of beta Ni-Al alloys. This model predicts Ni and Al concentration profiles after various oxidation exposures. The model can predict the oxidative lifetime due to Al depletion when the Al concentration decreases to a critical concentration. Measured Al concentration profiles on two alloys after various oxidation exposures are compared to those predicted by the diffusion model. The time to the appearance of the NiAl₂O₄ and that predicted by the diffusion model are compared and discussed.

Author (revised)

N93-11609*# National Aeronautics and Space Administration. Lewis Research Center, Cleveland, OH.

DETERMINATION OF PARAMETERS OF A NEW METHOD FOR PREDICTING ALLOY PROPERTIES

GUILLERMO BOZZOLO (Analex Corp., Brook Park, OH.) and JOHN FERRANTE Oct. 1992 11 p
(Contract RTOP 505-90-53)
(NASA-TM-105895; E-7361; NAS 1.15:105895) Avail: CASI HC A03/MF A01

Recently, a semiempirical method for alloys based on equivalent crystal theory was introduced. The method successfully predicts the concentration dependence of the heat of formation and lattice parameter of binary alloys. A study of the parameters of the method is presented, along with new results for (gamma)Fe-Pd and (gamma)Fe-Ni alloys.

Author

N93-11635*# National Aeronautics and Space Administration. Lewis Research Center, Cleveland, OH.

REVIEW OF THE PHYSICAL AND MECHANICAL PROPERTIES AND POTENTIAL APPLICATIONS OF THE B2 COMPOUND NIAL: UNABRIDGED VERSION OF A PAPER PUBLISHED IN INTERNATIONAL MATERIALS REVIEW

RONALD D. NOEBE, RANDY R. BOWMAN, and MICHAEL V. NATHAL Apr. 1992 124 p
(Contract RTOP 505-63-5A)
(NASA-TM-105598; E-6925; NAS 1.15:105598) Avail: CASI HC A06/MF A02

Considerable work has been performed on NiAl over the last three decades, with an extremely rapid growth in research on this intermetallic occurring in the last few years due to recent interest in this material for electronic and high temperature structural applications. However, many physical properties and the controlling fracture and deformation mechanisms over certain temperature regimes are still in question. Part of this problem lies in the incomplete characterization of many of the alloys previously investigated. Fragmentary data on processing conditions, chemistry, microstructure and the apparent difficulty in accurately measuring composition has made direct comparison between individual studies sometimes tenuous. Therefore, the purpose of this review is to summarize all available mechanical and pertinent physical

26 METALLIC MATERIALS

properties on NiAl, stressing the most recent investigations, in an attempt to understand the behavior of NiAl and its alloys over a broad temperature range. Author

N93-15524*# National Aeronautics and Space Administration. Lewis Research Center, Cleveland, OH.

PROCESSING AND MICROSTRUCTURE OF Nb-1 PERCENT Zr-0.1 PERCENT C ALLOY SHEET

MEHMET UZ (Lafayette Coll., Easton, PA.) and ROBERT H. TITRAN Oct. 1992 17 p Presented at the Tenth Symposium on Space Nuclear Power and Propulsion, Albuquerque, NM, 10-14 Jan. 1993; sponsored by the Inst. for Space Nuclear Power Studies

(Contract DE-AI03-86SF-16310; RTOP 590-13-11)

(NASA-TM-105921; E-7414; NAS 1.15:105921) Avail: CASI HC A03/MF A01

A systematic study was carried out to evaluate the effects of processing on the microstructure of Nb-1 wt. pct. Zr-0.1 wt. pct. C alloy sheet. The samples were fabricated by cold rolling different sheet bars that were single-, double- or triple-extruded at 1900 K. Heat treatment consisted on one- or two-step annealing of different samples at temperatures ranging from 1350 to 1850 K. The assessment of the effects of processing on microstructure involved characterization of the precipitates including the type, crystal structure, chemistry and distribution within the material as well as an examination of the grain structure. A combination of various analytical and metallographic techniques were used on both the sheet samples and the residue extracted from them. The results show that the relatively coarse orthorhombic Nb₂C carbides in the as-rolled samples transformed to rather fine cubic monocarbides of Nb and Zr with varying Zr/Nb ratios upon subsequent heat treatment. The relative amount of the cubic carbides and the Zr/Nb ratio increased with increasing number of extrusions prior to cold rolling. Furthermore, the size and the aspect ratio of the grains appear to be strong functions of the processing history of the material. These and other results obtained will be presented with the emphasis on a possible relationship between processing and microstructure. Author

N93-15586*# National Aeronautics and Space Administration. Lewis Research Center, Cleveland, OH.

PROGRESS TOWARD A TUNGSTEN ALLOY WIRE/HIGH TEMPERATURE ALLOY COMPOSITE TURBINE BLADE

F. J. RITZERT and R. L. DRESHFIELD Nov. 1992 10 p Presented at the International Conference on Tungsten and Tungsten Alloys, Washington, DC, 16-18 Nov. 1992; sponsored by the Metal Powder Industries Federation

(Contract RTOP 590-21-11)

(NASA-TM-105901; E-7368; NAS 1.15:105901) Avail: CASI HC A02/MF A01

A tungsten alloy wire reinforced high temperature alloy composite is being developed for potential application as a hollow turbine blade for advanced rocket engine turbopumps. The W-24Re-HfC alloy wire used for these composite blades provides an excellent balance of strength and wire ductility. Preliminary fabrication, specimen design, and characterization studies were conducted by using commercially available W218 tungsten wire in place of the W-24Re-HfC wire. Subsequently, two-ply, 50 vol pct composite panels using the W-24Re-HfC wire were fabricated. Tensile tests and metallographic studies were performed to determine the material viability. Tensile strengths of a Waspaloy matrix composite at 870 C were 90 pct of the value expected from rule-of-mixtures calculations. During processing of this Waspaloy matrix composite, a brittle phase was formed at the wire/matrix interface. Circumferential wire cracks were found in this phase. Wire coating and process evaluation efforts were performed in an attempt to solve the reaction problem. Although problems were encountered in this study, wire reinforced high temperature alloy composites continue to show promise for turbopump turbine blade material improvement. Author

N93-18069*# National Aeronautics and Space Administration. Lewis Research Center, Cleveland, OH.

A STATISTICAL ANALYSIS OF ELEVATED TEMPERATURE GRAVIMETRIC CYCLIC OXIDATION DATA OF 36 NI- AND CO-BASE SUPERALLOYS BASED ON AN OXIDATION ATTACK PARAMETER

CHARLES A. BARRETT Dec. 1992 49 p

(Contract RTOP 505-63-5A)

(NASA-TM-105934; E-6372; NAS 1.15:105934) Avail: CASI HC A03/MF A01

A large body of high temperature cyclic oxidation data generated from tests at NASA Lewis Research Center involving gravimetric/time values for 36 Ni- and Co-base superalloys was reduced to a single attack parameter, $K(\text{sub } a)$, for each run. This $K(\text{sub } a)$ value was used to rank the cyclic oxidation resistance of each alloy at 1000, 1100, and 1150 C. These $K(\text{sub } a)$ values were also used to derive an estimating equation using multiple linear regression involving $\log(\text{sub } 10)K(\text{sub } a)$ as a function of alloy chemistry and test temperature. This estimating equation has a high degree of fit and could be used to predict cyclic oxidation behavior for similar alloys and to design an optimum high strength Ni-base superalloy with maximum high temperature cyclic oxidation resistance. The critical alloy elements found to be beneficial were Al, Cr, and Ta. Author

N93-19974*# National Aeronautics and Space Administration. Lewis Research Center, Cleveland, OH.

ON THE DRAG OF MODEL DENDRITE FRAGMENTS AT LOW REYNOLDS NUMBER

R. ZAKHEM (Colorado Univ., Boulder.), P. D. WEIDMAN (Colorado Univ., Boulder.), and H. C. DEGROH, III Feb. 1993 36 p Previously announced in IAA as A92-50868

(Contract RTOP 674-27-05)

(NASA-TM-105916; E-7583; NAS 1.15:105916) Avail: CASI HC A03/MF A01

An experimental study of low Reynolds number drag on laboratory models of dendrite fragments has been conducted. The terminal velocities of the dendrites undergoing free fall along their axis of symmetry were measured in a large Stokes flow facility. Corrections for wall interference give nearly linear drag vs Reynolds number curves. Corrections for both wall interference and inertia effects show that the dendrite Stokes settling velocities are always less than that of a sphere of equal mass and volume. In the Stokes limit, the settling speed ratio is found to correlate well with primary dendrite arm aspect ratio and a second dimensionless shape parameter which serves as a measure of the fractal-like nature of the dendrite models. These results can be used to estimate equiaxed grain velocities and distance of travel in metal castings. The drag measurements may be used in numerical codes to calculate the movement of grains in a convecting melt in an effort to determine macrosegregation patterns caused by the sink/float mechanism. Author

N93-22556*# National Aeronautics and Space Administration. Lewis Research Center, Cleveland, OH.

CHARACTERIZATION AND DURABILITY TESTING OF PLASMA-SPRAYED ZIRCONIA-YTRIA AND HAFNIA-YTRIA THERMAL BARRIER COATINGS. PART 1: EFFECT OF SPRAY PARAMETERS ON THE PERFORMANCE OF SEVERAL LOTS OF PARTIALLY STABILIZED ZIRCONIA-YTRIA POWDER

ROBERT A. MILLER, GEORGE W. LEISSLER (Sverdrup Technology, Inc., Brook Park, OH.), and J. MARCUS JOBE (Miami Univ., Oxford, OH.) Feb. 1993 34 p

(Contract NAS3-25266; RTOP 505-63-5A)

(NASA-TP-3295; E-7151; NAS 1.60:3295) Avail: CASI HC A03/MF A01

Initial experiments conducted on thermal barrier coatings prepared in the newly upgraded research plasma spray facility and the burner rig test facilities are discussed. Part 1 discusses experiments which establish the spray parameters for three baseline zirconia-ytria coatings. The quality of five similar coating lots was judged primarily by their response to burner rig exposure supplemented by data from other sources such as specimen

characterizations and thermal diffusivity measurements. After allowing for burner rig variability, although there appears to be an optimum density (i.e., optimum microstructure) for maximum burner rig life, the distribution tends to be rather broad about the maximum. In Part 2, new hafnia-yttria-based coatings were evaluated against both baseline and alternate zirconia-yttria coatings. The hafnia-yttria coatings and the zirconia-yttria coatings that were prepared by an alternate powder vendor were very sensitive to plasma spray parameters, in that high-quality coatings were only obtained when certain parameters were employed. The reasons for this important observation are not understood. Also not understood is that the first of two replicate specimens sprayed for Part 1 consistently performed better than the second specimen. Subsequent experiments did not display this spray order affect, possibly because a chiller was installed in the torch cooling water circuit. Also, large changes in coating density were observed after switching to a new lot of electrodes. Analyses of these findings were made possible, in part, because of the development of a sensitive density measurement technique described herein in detail. The measured thermal diffusivities did not display the expected strong relationship with porosity. This surprising result was believed to have been caused by increased microcracking of the denser coatings on the stainless steel substrates. Author

N93-23418* National Aeronautics and Space Administration. Lewis Research Center, Cleveland, OH.

AUGER ELECTRON SPECTROSCOPY STUDY OF OXIDATION OF A PDCR ALLOY USED FOR HIGH-TEMPERATURE SENSORS

DARWIN L. BOYD (Kent State Univ., OH.), MARY V. ZELLER, and CARLOS VARGAS-ABURTO (Kent State Univ., OH.) Mar. 1993 34 p

(Contract RTOP 763-22-51)

(NASA-TM-106212; E-7538; NAS 1.15:106212) Avail: CASI HC A03/MF A01

A Pd-13 wt. percent Cr solid solution is a promising high-temperature strain gage alloy. In bulk form it has a number of properties that are desirable in a resistance strain gage material, such as a linear electrical resistance versus temperature curve to 1000 C and stable electrical resistance in air at 1000 C. However, unprotected fine wire gages fabricated from this alloy perform well only to 600 C. At higher temperatures severe oxidation degrades their electrical performance. In this work Auger electron spectroscopy was used to study the oxidation chemistry of the alloy wires and ribbons. Results indicate that the oxidation is caused by a complex mechanism that is not yet fully understood. As expected, during oxidation, a layer of chromium oxide is formed. This layer, however, forms beneath a layer of metallic palladium. The results of this study have increased the understanding of the oxidation mechanism of Pd-13 wt. percent Cr. Author (revised)

N93-26201* National Aeronautics and Space Administration. Lewis Research Center, Cleveland, OH.

EXTERNAL STRESS-CORROSION CRACKING OF A 1.22-M-DIAMETER TYPE 316 STAINLESS STEEL AIR VALVE

THOMAS J. MOORE, JACK TELESMA, ALLAN S. MOORE, DERECK F. JOHNSON, and DAVID E. KUIVINEN Washington Mar. 1993 21 p Original contains color illustrations

(Contract RTOP 505-62-84)

(NASA-TP-3190; E-6810; NAS 1.60:3190) Avail: CASI HC A03/MF A01; 7 functional color pages

An investigation was conducted to determine the cause of the failure of a massive AISI Type 316 stainless steel valve which controlled combustion air to a jet engine test facility. Several through-the-wall cracks were present near welded joints in the valve skirt. The valve had been in outdoor service for 18 years. Samples were taken in the cracked regions for metallographic and chemical analyses. Insulating material and sources of water mist in the vicinity of the failed valve were analyzed for chlorides. A scanning electron microscope was used to determine whether foreign elements were present in a crack. On the basis of the information generated, the failure was characterized as external

stress-corrosion cracking. The cracking resulted from a combination of residual tensile stress from welding and the presence of aqueous chlorides. Recommended countermeasures are included. Author

N93-26898* National Aeronautics and Space Administration. Lewis Research Center, Cleveland, OH.

LOW CYCLE FATIGUE BEHAVIOR OF POLYCRYSTALLINE NIAL AT 300 AND 1000 K

BRADLEY A. LERCH and RONALD D. NOEBE Apr. 1993 48 p

(Contract RTOP 510-01-50)

(NASA-TM-105987; E-7566; NAS 1.15:105987) Avail: CASI HC A03/MF A01

The low cycle fatigue behavior of polycrystalline NiAl was determined at 300 and 1000 K - temperatures below and above the brittle-to-ductile transition temperature (BDTT). Fully reversed, plastic strain-controlled fatigue tests were conducted on two differently fabricated alloy samples: hot isostatically pressed (HIP'ed) prealloyed powder and hot extruded castings. HIP'ed powder (HP) samples were tested only at 1000 K, whereas the more ductile cast-and-extruded (C+E) NiAl samples were tested at both 1000 and 300 K. Plastic strain ranges of 0.06 to 0.2 percent were used. The C+E NiAl cyclically hardened until fracture, reaching stress levels approximately 60 percent greater than the ultimate tensile strength of the alloy. Compared on a strain basis, NiAl had a much longer fatigue life than other B2 ordered compounds in which fracture initiated at processing-related defects. These defects controlled fatigue life at 300 K, with fracture occurring rapidly once a critical stress level was reached. At 1000 K, above the BDTT, both the C+E and HP samples cyclically softened during most of the fatigue tests in air and were insensitive to processing defects. The processing method did not have a major effect on fatigue life; the lives of the HP samples were about a factor of three shorter than the C+E NiAl, but this was attributed to the lower stress response of the C+E material. The C+E NiAl underwent dynamic grain growth, whereas the HP material maintained a constant grain size during testing. In both materials, fatigue life was controlled by intergranular cavitation and creep processes, which led to fatigue crack growth that was primarily intergranular in nature. Final fracture by overload was transgranular in nature. Also, HP samples tested in vacuum had a life three times longer than their counterparts tested in air and, in contrast to those tested in air, hardened continuously over half of the sample life, thereby indicating an environmentally assisted fatigue damage mechanism. The C+E samples were tested only in air. At 1000 K, NiAl exhibited a superior fatigue life when compared to most superalloys on a plastic strain basis, but was inferior to most superalloys on a stress basis. Author

N93-28618* National Aeronautics and Space Administration. Lewis Research Center, Cleveland, OH.

TEXTURING OF INP SURFACES FOR DEVICE APPLICATIONS

SHEILA G. BAILEY, NAVID S. FATEMI (Sverdrup Technology, Inc., Brook Park, OH.), and GEOFFREY A. LANDIS (Sverdrup Technology, Inc., Brook Park, OH.) Apr. 1992 9 p Presented at the Materials Research Society Spring Meeting, San Francisco, CA, 27 Apr. - 1 May 1992; sponsored by the Materials Research Society

(Contract RTOP 506-41-11)

(NASA-TM-106061; E-7664; NAS 1.15:106061) Avail: CASI HC A02/MF A01

A unique process for texturing InP (100) wafers by anisotropic etching was developed. The process produces irregular V-grooves on the surface, which reduce the surface reflectivity. The process does not require photolithography or masking. The etching characteristics depend on doping, with etching tending to proceed more rapidly on the more heavily doped samples. Reduced reflectivity surfaces formed using this process can be applied to solar cells, photodetectors, and other optoelectronic devices.

Author

26 METALLIC MATERIALS

N93-29172*# National Aeronautics and Space Administration. Lewis Research Center, Cleveland, OH.

HIGH TEMPERATURE CREEP AND OXIDATION RESISTANT CHROMIUM SILICIDE MATRIX ALLOY CONTAINING MOLYBDENUM Patent Application

SAI V. RAJ, inventor (to NASA) 26 May 1993 14 p
(NASA-CASE-LEW-15697-1; NAS 1.71:LEW-15697-1;
US-PATENT-APPL-SN-067184) Avail: CASI HC A03/MF A01

Cr₃Si is alloyed with molybdenum which produces a two-phase micro structure of (Cr,Mo)₃Si and (Cr,Mo)₅Si₃. The alloy forms two protective oxides over a wide range of temperatures. Chromium and molybdenum oxide volatilize under flowing air at high temperatures above 1200 C which facilitates the formation of SiO₂ on the surface. Below 1200 C Cr₂O₃ is formed. The new alloy has excellent high temperature strength and creep properties.

NASA

N93-31294*# National Aeronautics and Space Administration. Lewis Research Center, Cleveland, OH.

PLASMA SPRAYED CERAMIC THERMAL BARRIER COATING FOR NIAL-BASED INTERMETALLIC ALLOYS Patent Application

R. A. MILLER, inventor (to NASA) and J. DOYCHAK, inventor (to NASA) 26 Oct. 1992 10 p
(NASA-CASE-LEW-15535-1; NAS 1.71:LEW-15535-1;
US-PATENT-APPL-SN-970669) Avail: CASI HC A02/MF A01

A thermal barrier coating system consists of two layers of a zirconia-yttria ceramic. The first layer is applied by low pressure plasma spraying. The second layer is applied by conventional atmospheric pressure plasma spraying. This facilitates the attachment of a durable thermally insulating ceramic coating directly to the surface of a highly oxidation resistant NiAl-based intermetallic alloy after the alloy has been preoxidized to promote the formation of a desirable Al₂O₃ scale.

NASA

N93-31576*# National Aeronautics and Space Administration. Lewis Research Center, Cleveland, OH.

THE EFFECT OF POROSITY AND GAMMA-GAMMA' EUTECTIC CONTENT ON THE LOW CYCLE FATIGUE BEHAVIOR OF HYDROGEN-CHARGED PWA-1480

JOHN GAYDA, ROBERT L. DRESHFIELD, and TIMOTHY P. GABB *In its* Structural Integrity and Durability of Reusable Space Propulsion Systems p 179-185 May 1991
Avail: CASI HC A02/MF A03

Single crystal superalloys such as PWA 1480 are considered for turbopump blades in the main engines of the space shuttle. As fatigue resistance in a hydrogen environment is a key issue in this application, a study of the effect of porosity and gamma-gamma' eutectic content on the fatigue life of a hydrogen-charged PWA 1480 was performed. Porosity and eutectic were linked to fatigue initiation, and therefore reduction of either of both may be one means to improve fatigue life of PWA 1480 when hydrogen is present.

Derived from text

N93-31578*# National Aeronautics and Space Administration. Lewis Research Center, Cleveland, OH.

SECONDARY ORIENTATION EFFECTS IN A SINGLE CRYSTAL SUPERALLOY UNDER MECHANICAL AND THERMAL LOADS

SREERAMESH KALLURI (Sverdrup Technology, Inc., Brook Park, OH.), ALI ABDUL-AZIZ (Sverdrup Technology, Inc., Brook Park, OH.), and MICHAEL A. MCGAW *In its* Structural Integrity and Durability of Reusable Space Propulsion Systems p 197-206 May 1991
Avail: CASI HC A02/MF A03

The nickel-base single crystal superalloy PWA 1480 is a candidate blading material for the advanced turbopump development program of the SSME. In order to improve thermal fatigue resistance of the turbine blades, the single crystal superalloy PWA 1480 is grown along the low modulus zone axes (001) crystal orientation by a directional solidification process. Since cubic single crystal materials such as PWA 1480 exhibit anisotropic elastic behavior, the stresses developed within the single crystal superalloy

due to mechanical and thermal loads are likely to be affected by the exact orientation of the secondary crystallographic direction with respect to the geometry of the turbine blade. The effects of secondary crystal orientation on the elastic response of single crystal PWA 1480 superalloy were investigated.

Derived from text

27

NONMETALLIC MATERIALS

Includes physical, chemical, and mechanical properties of plastics, elastomers, lubricants, polymers, textiles, adhesives, and ceramic materials.

A93-13613 National Aeronautics and Space Administration. Lewis Research Center, Cleveland, OH.

EFFECT OF HYDROGEN ON THE STRENGTH AND MICROSTRUCTURE OF SELECTED CERAMICS

THOMAS P. HERBELL, ANDREW J. ECKEL, DAVID R. HULL (NASA, Lewis Research Center, Cleveland, OH), and AJAY K. MISRA (Sverdrup Technology, Inc., Brook Park, OH) *In* Environmental effects on advanced materials Warrendale, PA Minerals, Metals & Materials Society 1991 p.159-172. Previously announced in STAR as N91-14482 refs
(Contract RTOP 582-01-11)

Copyright

Ceramics in monolithic form and as composite constituents in the form of fibers, matrices, and coatings are currently being considered for a variety of high-temperature applications in aeronautics and space. Many of these applications involve exposure to a hydrogen-containing environment. The compatibility of selected ceramics in gaseous high-temperature hydrogen is assessed. Environmental stability regimes for the long term use of ceramic materials are defined by the parameters of temperature, pressure, and moisture content. Thermodynamically predicted reactions between hydrogen and several monolithic ceramics are compared with actual performance in a controlled environment. Morphology of hydrogen attack and the corresponding strength degradation is reported for silicon carbide, silicon nitride, alumina, magnesia, and mullite.

Author

A93-15994* National Aeronautics and Space Administration. Lewis Research Center, Cleveland, OH.

INDENTATION FLAW FORMATION AND STRENGTH RESPONSE OF SILICON NITRIDE CERAMICS AT LOW INDENTATION LOADS

SUNG R. CHOI (NASA, Lewis Research Center, Cleveland State Univ., OH) and JONATHAN A. SALEM (NASA, Lewis Research Center, Cleveland, OH) *Journal of Materials Science Letters* (ISSN 0261-8028) vol. 11, no. 21 Nov. 1, 1992 p. 1398-1400. refs
(Contract DE-AI05-87OR-21749)

Copyright

The configuration and the strength response of indentation flaws in silicon nitrides are described as a function of indentation loads primarily near the threshold level. Test materials under consideration include 30 vol percent SiC whisker-reinforced composite silicon nitride and similar monolithic silicon nitride. The results of strength testing show that, at indentation loads less than or equal to 1.96, a number of the specimens fail from the intrinsic flaws of the materials rather than from the indent sites, causing a distinct trend to reach a plateau, at a level corresponding to the as-received strength of the material. The ratio of the mirror constant to the fracture toughness for the composite and monolithic materials is found to be 1.44 and 1.51, respectively.

O.G.

A93-16520 National Aeronautics and Space Administration. Lewis Research Center, Cleveland, OH.

ROLE OF Si₂N₂O IN THE PASSIVE OXIDATION OF CHEMICALLY-VAPOR-DEPOSITED Si₃N₄

LINUS U. J. T. OGBUJI (NASA, Lewis Research Center, Cleveland, OH) American Ceramic Society, Journal (ISSN 0002-7820) vol. 75, no. 11 Nov. 1992 p. 2995-3000. ACS, Annual Meeting, 93rd, Cincinnati, OH, Apr. 30, 1991 Research supported by National Research Council and NASA refs Copyright

The results of two-step oxidation experiments on chemically-vapor-deposited Si₃N₄ and SiC at 1350 C show that a correlation exists between the presence of a Si₂N₂O interphase and the strong oxidation resistance of Si₃N₄. During normal oxidation, $k_{\text{sub p}}$ for SiC was 15 times higher than that for Si₃N₄, and the oxide scale on Si₃N₄ was found by SEM and TEM to contain a prominent Si₂N₂O inner layer. However, when oxidized samples are annealed in Ar for 1.5 h at 1500 C and reoxidized at 1350 C as before, three things happen: the oxidation $k_{\text{sub p}}$ increases over 55-fold for Si₃N₄, and 3.5-fold for SiC; the Si₃N₄ and SiC oxidize with nearly equal $k_{\text{sub p}}$'s; and, most significantly, the oxide scale on Si₃N₄ is found to be lacking an inner Si₂N₂O layer. The implications of this correlation for the competing models of Si₃N₄ oxidation are discussed. Author

A93-16645* National Aeronautics and Space Administration. Lewis Research Center, Cleveland, OH.

EFFECTS OF PRECRACKING METHODS ON THE FRACTURE PROPERTIES OF ALUMINA

JONATHAN A. SALEM, JOHN L. SHANNON, JR. (NASA, Lewis Research Center, Cleveland, OH), MICHAEL G. JENKINS, and MATTISON K. FERBER (Oak Ridge National Lab., TN) In 1991 SEM Spring Conference on Experimental Mechanics, Milwaukee, WI, June 10-13, 1991, Proceedings Bethel, CT Society for Experimental Mechanics, Inc. 1991 p. 762-769. refs Copyright

Fracture toughness values were compared for quasi-statically cracked, rapidly precracked, and fatigue precracked specimens of the same 96 percent alumina. The quasi-statically cracked specimens exhibited a rising R-curve and crack length dependent fracture toughness values. The rising R-curve resulted from grain bridging in the crack wake. Tension and compression fatigue precracked specimens did not exhibit crack length dependence, but did produce consistent fracture toughness values from fast fracture tests. Specimens that were rapidly precracked with the bridge indentation method also did not exhibit crack length dependence. These results imply that the measured fracture toughness and observed crack growth resistance of some brittle ceramics are dependent on loading history, crack extension and environment. Author

A93-20464 National Aeronautics and Space Administration. Lewis Research Center, Cleveland, OH.

GLASS FORMATION, PROPERTIES AND STRUCTURE OF SODA-YTTRIA-SILICA GLASSES

PAUL W. ANGEL and RAIFORD E. HANN (NASA, Lewis Research Center, Cleveland, OH) American Ceramic Society, Journal (ISSN 0002-7820) vol. 75, no. 12 Dec. 1992 p. 3278-3282. Previously announced in STAR as N92-11202 refs (Contract RTOP 505-62-00) Copyright

The glass formation region of the soda yttria silicate system was determined. The glasses within this region were measured to have a density of 2.4 to 3.1 g/cu cm, a refractive index of 1.50 to 1.60, a coefficient of thermal expansion of $7 \times 10^{-6}/^{\circ}\text{C}$, softening temperatures between 500 and 780 C, and Vickers hardness values of 3.7 to 5.8 GPa. Aqueous chemical durability measurements were made on select glass compositions while infrared transmission spectra were used to study the glass structure and its effect on glass properties. A compositional region was identified which exhibited high thermal expansion, high softening temperatures, and good chemical durability. Author

A93-20468* National Aeronautics and Space Administration. Lewis Research Center, Cleveland, OH.

HIGH-TEMPERATURE DEFORMATION AND MICROSTRUCTURAL ANALYSIS FOR SILICON NITRIDE-SCANDIUM(III) OXIDE

DEOCK-SOO CHEONG and WILLIAM A. SANDERS (NASA, Lewis Research Center, Cleveland, OH) American Ceramic Society, Journal (ISSN 0002-7820) vol. 75, no. 12 Dec. 1992 p. 3331-3336. Previously announced in STAR as N90-28740 refs Copyright

It was indicated that Si₃N₄ doped with Sc₂O₃ may exhibit high temperature mechanical properties superior to Si₃N₄ systems with various other oxide sintered additives. High temperature deformation of samples was studied by characterizing the microstructures before and after deformation. It was found that elements of the additive, such as Sc and O, exist in small amounts at very thin grain boundary layers and most of them stay in secondary phases at tripple and multiple grain boundary junctions. These secondary phases are devitrified as crystalline Sc₂Si₂O₇. Deformation of the samples was dominated by cavitation processes rather than movements of dislocations. Thus the excellent deformation resistance of the samples at high temperature can be attributed to the very small thickness of the grain boundary layers and the crystalline secondary phase. Author

A93-20842* National Aeronautics and Space Administration. Lewis Research Center, Cleveland, OH.

FRACTURE TOUGHNESS OF ADVANCED CERAMICS AT ROOM TEMPERATURE

GEORGE D. QUINN (NIST, Gaithersburg, MD), JONATHAN SALEM (NASA, Lewis Research Center, Cleveland, OH), ISA BAR-ON, KYU CHO (Worcester Polytechnic Inst., MA), MICHAEL FOLEY (Norton Industrial Ceramics Corp., Northboro, MA), and HO FANG (Allied-Signal Aerospace Co., Garrett Auxiliary Power Div., Phoenix, AZ) National Institute of Standards and Technology, Journal of Research (ISSN 1044-677X) vol. 97, no. 5 Sept.-Oct. 1992 p. 579-607. refs (Contract DE-AC05-84OR-21400)

Results of round-robin fracture toughness tests on advanced ceramics are reported. A gas-pressure silicon nitride and a zirconia-toughened alumina were tested using three test methods: indentation fracture, indentation strength, and single-edge precracked beam. The latter two methods have produced consistent results. The interpretation of fracture toughness test results for the zirconia alumina composite is shown to be complicated by R-curve and environmentally assisted crack growth phenomena. V.L.

A93-22984* National Aeronautics and Space Administration. Lewis Research Center, Cleveland, OH.

CORROSION OF SILICON-BASED CERAMICS IN COMBUSTION ENVIRONMENTS

NATHAN S. JACOBSON (NASA, Lewis Research Center, Cleveland, OH) American Ceramic Society, Journal (ISSN 0002-7820) vol. 76, no. 1 Jan. 1993 p. 3-28. refs Copyright

The processes of passive oxidation, deposit-induced corrosion, active oxidation, scale/substance interactions, and scale volatility are presently studied in the case of high-purity SiC and Si₃N₄ in pure oxygen, giving attention to such secondary elements in the ceramics as water and CO₂ oxidants, combustion environment impurities, and thermal cycling. Deposit-induced corrosion is discussed for the cases of Na₂SO₄ as well as vanadate and oxide-slag deposits; issues associated with the active-to-passive oxidation transition are noted. O.C.

A93-24508 National Aeronautics and Space Administration. Lewis Research Center, Cleveland, OH.

ISOTHERMAL AGING EFFECTS ON PMR-15 RESIN

KENNETH J. BOWLES (NASA, Lewis Research Center, Cleveland, OH), DOUGLAS JAYNE (Case Western Reserve Univ., Cleveland, OH), and TODD A. LEONHARDT (Sverdrup Technology, Inc., Brook Park, OH) SAMPE Quarterly (ISSN 0036-0821) vol. 24, no. 2

27 NONMETALLIC MATERIALS

Jan. 1993 p. 2-9. Previously announced in STAR as N92-30986 refs
(Contract RTOP 510-01-50)
Copyright

Specimens of PMR-15 polyimide neat resin were aged in air at temperatures of 288, 316, and 343 C. Weight losses and dimensional changes were monitored during the course of the exposure time. Physical changes were also observed by optical and electron microscopy. It was found that polyimide polymer degradation occurred within a thin surface layer that developed and grew during thermal aging. The cores of the polymer specimens were protected from oxidative degradation, and they were relatively unchanged by the thermal treatment. Surface cracking was observed at 343 C and was probably due to an interaction between voids and stresses that developed in the surface layer. Author

A93-27115* National Aeronautics and Space Administration. Lewis Research Center, Cleveland, OH.

INTERACTION OF CRACKS BETWEEN TWO ADJACENT INDENTS IN GLASS

S. R. CHOI (Cleveland State Univ.; NASA, Lewis Research Center, OH) and J. A. SALEM (NASA, Lewis Research Center, Cleveland, OH) Journal of Materials Science (ISSN 0022-2461) vol. 28, no. 2 Jan. 15, 1993 p. 501-505. refs
Copyright

Experimental observations of the interaction behavior of cracks between two adjacent indents were made using an indentation technique in soda-lime glass. It was specifically demonstrated how one indent crack initiates and propagates in the vicinity of another indent crack. Several types of crack interactions were examined by changing the orientation and distance of one indent relative to the other. It was found that the residual stress field produced by elastic/plastic indentation has a significant influence on controlling the mode of crack interaction. The interaction of an indent crack with a free surface was also investigated for glass and ceramic specimens. Author

A93-27917 National Aeronautics and Space Administration. Lewis Research Center, Cleveland, OH.

THE EFFECT OF ION-PLATED SILVER AND SLIDING FRICTION ON TENSILE STRESS-INDUCED CRACKING IN ALUMINUM OXIDE

HAROLD E. SLINEY and TALIVALDIS SPALVINS (NASA, Lewis Research Center, Cleveland, OH) Lubrication Engineering (ISSN 0024-7154) vol. 49, no. 2 Feb. 1993 p. 153-159. Previously announced in STAR as N92-19450 STLE, Annual Meeting, 47th, Philadelphia, PA, May 4-7, 1992 refs
(Contract RTOP 505-63-5A)
Copyright

A Hertzian analysis of the effect of sliding friction on contact stresses in alumina is used to predict the critical load for crack generation. The results for uncoated alumina and alumina coated with ion plated silver are compared. Friction coefficient inputs to the analysis are determined experimentally with a scratch test instrument employing an 0.2 mm radius diamond stylus. A series of scratches were made at constant load increments on coated and uncoated flat alumina surfaces. Critical loads for cracking are detected by microscopic examination of cross sections of scratches made at various loads and friction coefficients. Acoustic emission (AE) and friction trends were also evaluated as experimental techniques for determining critical loads for cracking. Analytical predictions correlate well with micrographic evidence and with the lowest load at which AE is detected in multiple scratch tests. Friction/load trends are not good indicators of early crack formation. Lubrication with silver films reduced friction and thereby increased the critical load for crack initiation in agreement with analytical predictions. Author

A93-31354* National Aeronautics and Space Administration. Lewis Research Center, Cleveland, OH.

CREEP AND STRESS RELAXATION MODELING OF POLYCRYSTALLINE CERAMIC FIBERS

JAMES A. DICARLO (NASA, Lewis Research Center, Cleveland,

OH) and GREGORY N. MORSCHER (Case Western Reserve Univ., Cleveland, OH) In Failure mechanisms in high temperature composite materials; Proceedings of the Symposium, 112th ASME Winter Annual Meeting, Atlanta, GA, Dec. 1-6, 1991 New York American Society of Mechanical Engineers 1991 p. 15-22. refs

Copyright

A variety of high performance polycrystalline ceramic fibers are currently being considered as reinforcement for high temperature ceramic matrix composites. However, under mechanical loading above 800 C, these fibers display creep-related instabilities which can result in detrimental changes in composite dimensions, strength, and internal stress distributions. As a first step toward understanding these effects, this study examines the validity of mechanistic-based empirical model which describes primary stage tensile creep and stress relaxation of polycrystalline ceramic fibers as independent functions of time, temperature, and applied stress or strain. To verify these functional dependencies, a simple bend test is used to measure stress relaxation for four types of commercial ceramic fibers for which direct tensile creep data are available. These fibers include both nonoxide (SCS-6, Nicalon) and oxide (PRD-166, FP) compositions. The results of the bend stress relaxation (BSR) test not only confirm the stress, time, and temperature dependencies predicted by the model but also allow measurement of model empirical parameters for the four fiber types. In addition, comparison of model predictions and BSR test results with the literature tensile creep data show good agreement, supporting both the predictive capability of the model and the use of the BSR test as a simple method for parameter determination for other fibers. Author

A93-31983* National Aeronautics and Space Administration. Lewis Research Center, Cleveland, OH.

RELATIVE SLIDING DURABILITY OF TWO CANDIDATE HIGH-TEMPERATURE OXIDE FIBER SEAL MATERIALS

CHRISTOPHER DELLACORTE and BRUCE M. STEINETZ (NASA, Lewis Research Center, Cleveland, OH) Journal of Propulsion and Power (ISSN 0748-4658) vol. 9, no. 2 Mar.-Apr. 1993 p. 307-312. AIAA, SAE, ASME, and ASCE, Joint Propulsion Conference and Exhibit, 28th, Nashville, TN, July 6-8, 1992, AIAA Paper 92-3713. Previously cited in issue 20, p. 3524, Accession no. A92-49095 refs
Copyright

A93-32299* National Aeronautics and Space Administration. Lewis Research Center, Cleveland, OH.

MECHANISM OF INCIPIENT OXIDATION OF BULK CHEMICAL VAPOR DEPOSITED Si3N4

L. U. T. OGBUJI (NASA, Lewis Research Center; Sverdrup Technology, Inc., Cleveland, OH) and D. T. JAYNE (NASA, Lewis Research Center; Case Western Reserve Univ., Cleveland, OH) Electrochemical Society, Journal (ISSN 0013-4651) vol. 140, no. 3 March 1993 p. 759-766. Research supported by National Research Council refs
Copyright

X-ray photoelectron spectroscopy was employed, in conjunction with ion bombardment, to analyze the chemical composition profile across thin (less than 50 nm) oxide films on chemically vapor deposited Si3N4. The thermal oxides were grown in dry oxygen at 1100 C on samples with or without native oxide film (formed in room air). The results show that the thermal oxidation product was silicon oxynitride of graded N:O ratio, and that the presence of a native oxide film promotes the formation of a SiO2 crust over the oxynitride. It is proposed that the fundamental mechanism of Si3N4 oxidation is progressive O-for-N substitution in the silicon oxynitride unit tetrahedron, which is best designated SiN(2-x)O(2+x), where x is also an index of depth. The corresponding equation for nonstoichiometric oxidation of Si3N4 describes a bulk (rather than an interface) reaction process, with significant implications for O2 and N2 fluxes and diffusivities. Author (revised)

A93-38473* National Aeronautics and Space Administration. Lewis Research Center, Cleveland, OH.

INTERFACIAL CHEMISTRY OF A PERFLUOROPOLYETHER LUBRICANT STUDIED BY X-RAY PHOTOELECTRON SPECTROSCOPY AND TEMPERATURE DESORPTION SPECTROSCOPY

PILAR HERRERA-FIERRO, WILLIAM R. JONES, JR., and STEPHEN V. PEPPER (NASA, Lewis Research Center, Cleveland, OH) *Journal of Vacuum Science and Technology A* (ISSN 0734-2101) vol. 11, no. 2 Mar.-Apr. 1993 p. 354-367. Previously announced in STAR as N93-22560 refs Copyright

The interfacial chemistry of Fomblin Z25, a commercial perfluoropolyether used as lubricant for space applications was studied with different metallic surfaces: 440C steel, gold, and aluminum. Thin layers of Fomblin Z25 were evaporated onto the oxide-free substrates, and the interfacial chemistry was studied using XPS and TDS. The reactions were induced by heating the substrate and by rubbing the substrate with a steel ball. Gold was found to be completely unreactive towards Fomblin at any temperature. Reaction at room temperature was observed only in the case of the aluminum substrate, the most reactive towards Fomblin Z25 of the substrates studied. It was necessary to heat the 440C steel substrate to 190 C to induce decomposition of the fluid. The degradation of the fluid was indicated by the formation of a debris layer at the interface. This debris layer, composed of inorganic and organic reaction products, when completely formed, passivated the surface from further attack to the Fomblin on top. The tribologically induced reactions on 440C steel formed a debris layer of similar chemical characteristics to the thermally induced layer. In all cases, the degradation reaction resulted in preferential consumption of the difluoroformyl carbon (-OCF₂O-).

Author (revised)

A93-38887 National Aeronautics and Space Administration. Lewis Research Center, Cleveland, OH.

ANALYSIS OF PRECRACKING PARAMETERS FOR CERAMIC SINGLE-EDGE-PRECRACKED-BEAM SPECIMENS

SUNG R. CHOI, ABHISAK CHULYA (Cleveland State Univ.; NASA, Lewis Research Center, OH), and JONATHAN A. SALEM (NASA, Lewis Research Center, Cleveland, OH) *In* Fracture mechanics of ceramics. Vol. 10 - Fracture fundamentals, high-temperature deformation, damage, and design; Proceedings of the 5th International Symposium, Nagoya, Japan, July 15-17, 1991 New York Plenum Press 1992 p. 73-88. Previously announced in STAR as N93-10962 refs (Contract RTOP 505-63-M; DE-AI05-87OR-21749) Copyright

The single-edge-precracked-beam (SEPB) method involves creation of a straight-through crack from an indentation crack. The straight-through crack is developed by applying a controlled bending load to a specimen via a precracking fixture. The fixture induces the following sequence: (1) stable growth of the indentation crack; (2) pop-in; and finally, (3) arrest - thereby forming a straight-through precrack. The effects of indentation load on precracking load as well as precrack size were studied for experimental variables such as specimen width, fixture span, and material. Finite element analysis was used to obtain the stress distribution and stress intensity factor, thus providing a quantitative prediction of the precracking load and precrack size for silicon nitride, alumina, silicon carbide, and two SiC whisker-reinforced silicon nitrides. Fracture toughness values obtained from the SEPB method were compared with those obtained from other methods.

Author

A93-38888* National Aeronautics and Space Administration. Lewis Research Center, Cleveland, OH.

ELEVATED-TEMPERATURE FRACTURE RESISTANCES OF MONOLITHIC AND COMPOSITE CERAMICS USING CHEVRON-NOTCHED BEND TESTS

ASISH GHOSH (Philips Display Components Co., Ann Arbor, MI), MICHAEL G. JENKINS, MATTISON K. FERBER (Oak Ridge National Lab., TN), JOUKO PEUSSA (Federation of Finnish Metal,

Engineering, and Electronic Technology Industries, Helsinki, Finland), and JONATHAN A. SALEM (NASA, Lewis Research Center, Cleveland, OH) *In* Fracture mechanics of ceramics. Vol. 10 - Fracture fundamentals, high-temperature deformation, damage, and design; Proceedings of the 5th International Symposium, Nagoya, Japan, July 15-17, 1991 New York Plenum Press 1992 p. 89-107. Previously announced in STAR as N91-28418 refs

(Contract DE-AC05-84OR-21400)

Copyright

The quasi-static fracture behaviors of monolithic ceramics (SiC, Si₃N₄, MgAl₂O₄), self-reinforced monoliths (acicular grained Si₃N₄, acicular grained mullite), and ceramic matrix composites (SiC whisker/Al₂O₃ matrix, TiB₂ particulate/SiC matrix, SiC fiber/CVI SiC matrix, Al₂O₃ fiber/CVI SiC matrix) were measured over the temperature range of 20 to 1400 C. The chevron notched, bend bar test geometry was essential for characterizing the elevated temperature fracture resistances of this wide range of quasi-brittle materials during stable crack growth. Fractography revealed the differences in the fracture behavior of the different materials at the various temperatures. The fracture resistances of the self-reinforced monoliths were comparable to those of the composites and the fracture mechanisms were found to be similar at room temperature. However at elevated temperatures the differences of the fracture behavior became apparent where the superior fracture resistance of the self-reinforced monoliths were attributed to the minor amounts of glassy, intergranular phases which were often more abundant in the composites and affected the fracture behavior when softened by elevated temperatures.

Author

A93-39513* National Aeronautics and Space Administration. Lewis Research Center, Cleveland, OH.

EFFECT OF HIGH TEMPERATURE ANNEALING ON THE MICROSTRUCTURE OF SCS-6 SiC FIBERS

X. J. NING, P. PIROUZ (Case Western Reserve Univ., Cleveland, OH), and R. T. BHATT (NASA, Lewis Research Center, Cleveland, OH) *In* Chemical vapor deposition of refractory metals and ceramics II; Proceedings of the Symposium, Boston, MA, Dec. 4-6, 1991 Pittsburgh, PA Materials Research Society 1992 p. 187-192. refs

(Contract NCC3-73)

Copyright

The effect of annealing the SCS-6 SiC fiber for one hour at 2000 C in an argon atmosphere is reported. The SiC grains in the fiber coarsen appreciably and the intergranular carbon films segregate to the grain junctions. It would appear that grain growth in the outer part of the fiber is primarily responsible for the loss in fiber strength and improvement in fiber creep resistance. Author

A93-39584* National Aeronautics and Space Administration. Lewis Research Center, Cleveland, OH.

THERMODYNAMICS OF Si-C-O SYSTEM

N. S. JACOBSON (NASA, Lewis Research Center, Cleveland, OH) and E. J. OPILA (NASA, Lewis Research Center; Cleveland State Univ., OH) *Metallurgical Transactions A - Physical Metallurgy and Materials Science* (ISSN 0360-2133) vol. 24A, no. 5 May 1993 p. 1212-1214. refs

The Si-C-O predominance diagram, in conjunction with a free-energy minimum of the gas phase, has been used to explain several observations in the reactions of SiC and/or carbon with SiO₂. In the predominance diagram, the axes are chosen as the primary activity units for carbon and oxygen. The predominance diagram shows only the stable condensed phases SiO₂, SiC, carbon, and silicon. It also shows the isobars for SiO(g) and CO(g), which are the primary gas-phase species. Only the thermodynamics of the system is considered. The observations explained include the general adjustment of carbon-rich SiC to a free-energy minimum on the SiC/SiO₂ coexistence line and the inability to form free silicon from SiO₂ and carbon, except at very high temperatures.

AIAA

A93-40293 National Aeronautics and Space Administration. Lewis Research Center, Cleveland, OH.

KINETICS OF HEXACELSIAN-TO-CELSIAN PHASE TRANSFORMATION IN $\text{SrAl}_2\text{Si}_2\text{O}_8$

NAROTTAM P. BANSAL (NASA, Lewis Research Center, Cleveland, OH) and CHARLES H. DRUMMOND, III (Ohio State Univ., Columbus) American Ceramic Society, Journal (ISSN 0002-7820) vol. 76, no. 5 May 1993 p. 1321-1324. ACS, Annual Meeting, 94th, Minneapolis, MN, Apr. 13, 1992. Previously announced in STAR as N93-16372 refs (Contract RTOP 510-01-50)

Copyright

The kinetics of hexacelsian to celsian phase transformation in $\text{SrAl}_2\text{Si}_2\text{O}_8$ have been investigated. Phase pure hexacelsian was prepared by heat treatment of glass flakes at 990 C for 10 h. Bulk hexacelsian was isothermally heat treated at 1026, 1050, 1100, 1152, and 1200 C for various times. The amounts of monoclinic celsian formed were determined using quantitative X-ray diffraction. Values of reaction rate constant, k , at various temperatures were evaluated from the Avrami equation. The Avrami parameter was determined to be 1.1, suggesting a diffusionless, one-dimensional transformation mechanism. From the temperature dependence of k , the activation energy for this reaction was evaluated to be 527 plus or minus 50 kJ/mole (126 plus or minus 12 kcal/mole). This value is consistent with a mechanism involving the transformation of the layered hexacelsian structure to a three-dimensional network celsian structure which necessitates breaking of the strongest bonds, the Si-O bonds. Author

A93-40630* National Aeronautics and Space Administration. Lewis Research Center, Cleveland, OH.

TRIBOLOGICAL STUDIES OF AMORPHOUS HYDROGENATED CARBON FILMS IN A VACUUM, SPACELIKE ENVIRONMENT

KAZUHISA MIYOSHI (NASA, Lewis Research Center, Cleveland, OH) In Applications of diamond films and related materials; Proceedings of the 1st International Conference, Auburn, AL, Aug. 17-22, 1991 Amsterdam Elsevier 1991 p. 699-702. refs Copyright

Recent work on the adhesion and friction properties of plasma-deposited amorphous hydrogenated carbon films and their dependence on preparation conditions are reviewed. The results of the study indicate that plasma deposition enables one to deposit a variety of amorphous hydrogenated carbon (a-C:H) exhibiting diamondlike friction behavior. The plasma-deposited a-C:H films can be effectively used as hard lubricating films on ceramic materials such as silicon nitride in vacuum. Author

A93-44526* National Aeronautics and Space Administration. Lewis Research Center, Cleveland, OH.

LOWER TEMPERATURE CURING THERMOSET POLYIMIDES UTILIZING A SUBSTITUTED NORBORNENE ENDCAP

JOHN F. WATERS, CHAIM N. SUKENIK, VANCE O. KENNEDY, MORDECHAI LIVNEH, WILEY J. YOUNGS (Case Western Reserve Univ., Cleveland, OH), JAMES K. SUTTER, MARY A. B. MEADOR (NASA, Lewis Research Center, Cleveland, OH), LUKE A. BURKE (Rutgers Univ., Camden, NJ), and MYONG K. AHN (Indiana State Univ., Terre Haute) Macromolecules (ISSN 0024-9297) vol. 25, no. 15 1992 p. 3868-3873. refs

Copyright

Methoxycarbonyl bridgehead substituted nadic diacid monomethyl ester, when used as an endcapping monomer, lowered the cure temperature of thermoset PMR polyimides without seriously affecting other desirable properties, such as glass transition temperature and thermal oxidative stability. The C-13 CP/MAS NMR of model compounds was used to follow the cure of resin systems using both the unmodified nadic endcap and the methoxycarbonyl-substituted endcap. Rheological analysis and differential scanning calorimetry DSC also provided evidence for the lower curing nature of the substituted endcap. Two regioisomers of the bridgehead-substituted endcap were isolated, and their chemical structures were elucidated by X-ray crystallography. The model compound and molecular modeling studies conducted ruled

out the possibility of regioisomeric imide formation in the substituted endcaps. Author (revised)

A93-44883* National Aeronautics and Space Administration. Lewis Research Center, Cleveland, OH.

X-RAY PHOTOELECTRON SPECTROSCOPY STUDY OF THE STABILITY OF FOMBLIN Z25 ON THE NATIVE OXIDE OF ALUMINUM

PILAR HERRERA-FIERRO, STEPHEN V. PEPPER, and WILLIAM R. JONES (NASA, Lewis Research Center, Cleveland, OH) Journal of Vacuum Science and Technology A (ISSN 0734-2101) vol. 10, no. 4 July-Aug. 1992 p. 2746-2751. refs Copyright

Thin films of Fomblin Z25, a perfluoropolyalkylether lubricant, were vapor deposited onto clean, oxidized aluminum, and onto sapphire surfaces, and their behavior at different temperatures was studied using X-ray photoelectron spectroscopy and temperature desorption spectroscopy (TDS). The interfacial fluid molecules decompose on the native oxide at room temperature, and continue to decompose at elevated temperatures, as previous studies had shown to occur on the clean metal. TDS indicated that different degradation mechanisms were operative for clean and oxidized aluminum. On sapphire substrates, no reaction was observed at room temperature. The native oxide of aluminum is neither passive nor protective towards Fomblin Z25. At higher temperatures (150 C), degradation of the polymer on sapphire produced a debris layer at the interface with a chemical composition similar to the one formed on aluminum oxide. Rubbing a Fomblin film on a single crystal sapphire also induced the decomposition of the lubricant in contact with the interface and the formation of a debris layer. Author (revised)

A93-44955* National Aeronautics and Space Administration. Lewis Research Center, Cleveland, OH.

EFFECT OF ENVIRONMENT ON FRACTURE TOUGHNESS OF 96 WT PCT ALUMINA

SUNG R. CHOI (Cleveland State Univ.; NASA, Lewis Research Center, OH), VEENA TIKARE, and JONATHAN A. SALEM (NASA, Lewis Research Center, Cleveland, OH) Scripta Metallurgica et Materialia (ISSN 0956-716X) vol. 29, no. 2 July 15, 1993 p. 189-192. refs

Copyright

An effort is made to deepen understanding of environmental effects on the fracture toughness of an alumina composition that contains a residual glassy phase, by ascertaining the fracture toughness under atmospheric conditions in such varied environments as air distilled water, silicone oil, and liquid nitrogen. Fracture toughness was determined via the single-edge-precracked beam technique. Weibull strength parameters are compared for polished specimens tested both in air and silicone environments. AIAA

A93-52151* National Aeronautics and Space Administration. Lewis Research Center, Cleveland, OH.

SUBCRITICAL CRACK GROWTH IN SODA-LIME GLASS IN COMBINED MODE I AND MODE II LOADING

DILEEP SINGH and DINESH K. SHETTY (Utah Univ., Salt Lake City) American Ceramic Society, Journal (ISSN 0002-7820) vol. 73, no. 12 Dec. 1990 p. 3597-3606. refs (Contract NAG3-789)

Copyright

Subcritical crack growth under mixed-mode loading was studied in soda-lime glass. Pure mode I, combined mode I and mode II, and pure mode II loadings were achieved in precracked disk specimens by loading in diametral compression at selected angles with respect to the symmetric radial crack. Crack growth was monitored by measuring the resistance changes in a microcircuit grid consisting of parallel, electrically conducting grid lines deposited on the surface of the disk specimens by photolithography. Subcritical crack growth rates in pure mode I, pure mode II, and combined mode I and mode II loading could be described by an exponential relationship between crack growth rate and an effective crack driving force derived from a mode I-mode II fracture

27 NONMETALLIC MATERIALS

experimental variables such as specimen width, fixture span, and material. Finite element analysis was used to obtain the stress distribution and stress intensity factor, thus providing a quantitative prediction of the precracking load and precrack size for silicon nitride, alumina, silicon carbide, and two SiC whisker-reinforced silicon nitrides. Fracture toughness values obtained from the SEPB method were compared with those obtained from other methods.

Author

N93-12398*# National Aeronautics and Space Administration. Lewis Research Center, Cleveland, OH.

STUDIES ON THE REACTIVE MELT INFILTRATION OF SILICON AND SILICON-MOLYBDENUM ALLOYS IN POROUS CARBON

M. SINGH and D. R. BEHRENDT Sep. 1992 11 p Presented at the 94th Annual Meeting of the American Ceramic Society, Minneapolis, MN, 12-16 Apr. 1992

(Contract RTOP 537-04-10)

(NASA-TM-105860; E-7320; NAS 1.15:105860) Avail: CASI HC A03/MF A01

Investigations on the reactive melt infiltration of silicon and silicon-1.7 and 3.2 at percent molybdenum alloys into porous carbon preforms have been carried out by process modeling, differential thermal analysis (DTA) and melt infiltration experiments. These results indicate that the initial pore volume fraction of the porous carbon preform is a critical parameter in determining the final composition of the reaction-formed silicon carbide and other residual phases. The pore size of the carbon preform is very detrimental to the exotherm temperatures due to liquid silicon-carbon reactions encountered during the reactive melt infiltration process. A possible mechanism for the liquid silicon-porous (glassy) carbon reaction has been proposed. The composition and microstructure of the reaction-formed silicon carbide has been discussed in terms of carbon preform microstructures, infiltration materials, and temperatures.

Author

N93-14886*# National Aeronautics and Space Administration. Lewis Research Center, Cleveland, OH.

COMMENTS ON 'KINETIC STUDY ON THE HEXACELSIAN-CELSIAN PHASE TRANSFORMATION'

NAROTTAM P. BANSAL and CHARLES H. DRUMMOND, III (Ohio State Univ., Columbus.) Nov. 1992 9 p

(Contract RTOP 510-01-50)

(NASA-TM-105917; E-7408; NAS 1.15:105917) Avail: CASI HC A02/MF A01

A value of 20.1 \pm 4 kcal/mole for the activation energy (E) for the hexacelsian to celsian phase transformation in BaAl₂Si₂O₈ was reported in an earlier work. In the present work, the earlier experimental data were reanalyzed and a much higher value of E was obtained. This revised E value is consistent with the transformation mechanism of a layered hexacelsian structure into a three-dimensional feldspar structure of celsian which would necessitate the breaking of the Si-O and/or the Al-O bonds.

Author

N93-15344*# National Aeronautics and Space Administration. Lewis Research Center, Cleveland, OH.

LEVELING COATINGS FOR REDUCING THE ATOMIC OXYGEN DEFECT DENSITY IN PROTECTED GRAPHITE FIBER EPOXY COMPOSITES

D. A. JAWORSKE, K. K. DEGROH, G. PODOJIL (Cleveland State Univ., OH.), T. MCCOLLUM (Cleveland State Univ., OH.), and J. ANZIC (Cleveland State Univ., OH.) Nov. 1992 12 p Presented at the 17th Space Simulation Conference, Baltimore, MD, 9-12 Nov. 1992; sponsored by the Inst. of Environmental Sciences

(Contract RTOP 506-41-41)

(NASA-TM-105732; E-7136; NAS 1.15:105732) Avail: CASI HC A03/MF A01

Pinholes or other defect sites in a protective oxide coating provide pathways for atomic oxygen in low Earth orbit to reach underlying material. One concept for enhancing the lifetime of materials in low Earth orbits is to apply a leveling coating to the material prior to applying any reflective and protective coatings.

Using a surface tension leveling coating concept, a low viscosity epoxy was applied to the surface of several composite coupons. A protective layer of 1000 Å of SiO₂ was deposited on top of the leveling coating, and the coupons were exposed to an atomic oxygen environment in a plasma asher. Pinhole populations per unit area were estimated by counting the number of undercut sites observed by scanning electron microscopy. Defect density values of 180,000 defects/sq cm were reduced to about 1000 defects/sq cm as a result of the applied leveling coating. These improvements occur at a mass penalty of about 2.5 mg/sq cm.

Author

N93-16372*# National Aeronautics and Space Administration. Lewis Research Center, Cleveland, OH.

KINETICS OF HEXACELSIAN TO CELSIAN PHASE TRANSFORMATION IN SrAl₂Si₂O₈

NAROTTAM P. BANSAL and CHARLES H. DRUMMOND, III (Ohio State Univ., Columbus.) Nov. 1992 18 p Presented at the 94th Annual Meeting of the American Ceramic Society, Minneapolis, MN, 12-16 Apr. 1992; sponsored by the American Ceramic Society

(Contract RTOP 510-01-50)

(NASA-TM-105913; E-7397; NAS 1.15:105913) Avail: CASI HC A03/MF A01

The kinetics of hexacelsian to celsian phase transformation in SrAl₂Si₂O₈ have been investigated. Phase pure hexacelsian was prepared by heat treatment of glass flakes at 990 °C for 10 h. Bulk hexacelsian was isothermally heat treated at 1026, 1050, 1100, 1152, and 1200 °C for various times. The amounts of monoclinic celsian formed were determined using quantitative X-ray diffraction. Values of reaction rate constant, k, at various temperatures were evaluated from the Avrami equation. The Avrami parameter was determined to be 1.1, suggesting a diffusionless, one-dimensional transformation mechanism. From the temperature dependence of k, the activation energy for this reaction was evaluated to be 527 plus or minus 50 kJ/mole (126 plus or minus 12 kcal/mole). This value is consistent with a mechanism involving the transformation of the layered hexacelsian structure to a three-dimensional network celsian structure which necessitates breaking of the strongest bonds, the Si-O bonds.

Author

N93-19035*# National Aeronautics and Space Administration. Lewis Research Center, Cleveland, OH.

FRICTION AND WEAR OF PLASMA-DEPOSITED DIAMOND FILMS

KAZUHISA MIYOSHI, RICHARD L. C. WU (Universal Energy Systems, Inc., Dayton, OH.), ALAN GARSCADDEN (Wright Lab., Wright-Patterson AFB, OH.), PAUL N. BARNES (Wright Lab., Wright-Patterson AFB, OH.), and HOWARD E. JACKSON (Cincinnati Univ., OH.) Jan. 1993 24 p Proposed for presentation at the International Conference on Metallurgical Coatings and Thin Films, San Diego, CA, 19-23 Apr. 1993; sponsored by the American Vacuum Society

(Contract RTOP 506-43-11)

(NASA-TM-105926; E-7431; NAS 1.15:105926) Avail: CASI HC A03/MF A01

Reciprocating sliding friction experiments in humid air and in dry nitrogen and unidirectional sliding friction experiments in ultrahigh vacuum were conducted with a natural diamond pin in contact with microwave-plasma-deposited diamond films. Diamond films with a surface roughness (R_{rms}) ranging from 15 to 160 nm were produced by microwave-plasma-assisted chemical vapor deposition. In humid air and in dry nitrogen, abrasion occurred when the diamond pin made grooves in the surfaces of diamond films, and thus the initial coefficients of friction increased with increasing initial surface roughness. The equilibrium coefficients of friction were independent of the initial surface roughness of the diamond films. In vacuum the friction for diamond films contacting a diamond pin arose primarily from adhesion between the sliding surfaces. In these cases, the initial and equilibrium coefficients of friction were independent of the initial surface roughness of the diamond films. The equilibrium coefficients of friction were 0.02 to 0.04 in humid air and in dry nitrogen, but 1.5

toughness envelope. The effective crack driving force was based on an empirical representation of the noncoplanar strain energy release rate. Stress intensities for kinked cracks were assessed using the method of caustics and an initial decrease and a subsequent increase in the subcritical crack growth rates of kinked cracks were shown to correlate with the variations of the mode I and the mode II stress intensities.

A93-52181* National Aeronautics and Space Administration. Lewis Research Center, Cleveland, OH.

FRICTION AND WEAR OF PLASMA-DEPOSITED AMORPHOUS HYDROGENATED FILMS ON SILICON NITRIDE

KAZUHISA MIYOSHI (NASA, Lewis Research Center, Cleveland, OH) *In* Advances in Information Storage Systems. Vol. 3 New York American Society of Mechanical Engineers 1991 p. 147-160. refs

Copyright

An investigation was conducted to examine the friction and wear behavior of amorphous hydrogenated carbon (a-C:H) films in sliding contact with silicon nitride pins in both dry nitrogen and humid air environments. Amorphous hydrogenated carbon films approximately 0.06 micron thick were deposited on silicon nitride flat substrates by using the 30 kHz ac glow discharge of a planar plasma reactor. The results indicate that an increase in plasma deposition power gives an increase in film density and hardness. The high-density a-C:H films deposited behaved tribologically much like bulk diamond. In the dry nitrogen environment, a tribochemical reaction produced a substance, probably a hydrocarbon-rich layer, that decreased the coefficient of friction. In the humid air environment, tribochemical interactions drastically reduced the wear life of a-C:H films and water vapor greatly increased the friction. Even in humid air, effective lubrication is possible with vacuum-annealed a-C:H films. The vacuum-annealed high-density a-C:H film formed an outermost superficial graphitic layer, which behaved like graphite, on the bulk a-C:H film. Like graphite, the annealed a-C:H film with the superficial graphitic layer showed low friction when adsorbed water vapor was present.

Author (revised)

A93-52896* National Aeronautics and Space Administration. Lewis Research Center, Cleveland, OH.

TRIBOLOGICAL EVALUATION AND ANALYSIS OF COATING MATERIALS

KAZUHISA MIYOSHI (NASA, Lewis Research Center, Cleveland, OH) *In* Surface science investigations in tribology - Experimental approaches; Proceedings of the Symposium, 201st AChS National Meeting, Atlanta, GA, Apr. 14-19, 1991 Washington American Chemical Society (ACS Symposium Series, No. 485) 1992 p. 58-71. refs

A physical characterization of coating materials by analytical techniques such as XPS, AES, ellipsometry, and nuclear reaction analysis can contribute to the understanding of adhesion and friction of the coatings and can partially predict the tribological properties of the coatings. This two-part paper describes the tribological properties and physical characteristics of (1) diamondlike carbon (DLC) films and (2) silicon nitride (SiN(x)) films. Emphasis is to relate plasma deposition conditions to the film chemistry and composition and to the adhesion and friction of the films. With the DLC films, the higher the plasma deposition power, the less the hydrogen concentration and the greater the film density and the hardness. The friction behavior of DLC films deposited at higher deposition powers (200 to 300 W) is similar to that of bulk diamond. Even in a vacuum, the DLC films effectively lubricate ceramic surfaces (Si₃N₄) at temperatures to 500 C. With SiN(x) films, the silicon to nitrogen ratios and the amount of amorphous silicon depend on deposition frequency. The presence of rich amorphous silicon in the high-frequency plasma-deposited SiN(x) films increases their adhesion and friction above 500 C in vacuum.

Author (revised)

A93-53734* National Aeronautics and Space Administration. Lewis Research Center, Cleveland, OH.

MICROCHEMICAL ANALYSIS OF THE SCS-6 SILICON CARBIDE FIBER

XIAN-JIE NING, PIROUZ PIROUZ (Case Western Reserve Univ., Cleveland, OH), and SERENE C. FARMER (NASA, Lewis Research Center, Cleveland, OH) *American Ceramic Society, Communications* (ISSN 0002-7820) vol. 76, no. 8 Aug. 1993 p. 2033-2041. refs

(Contract NCC3-73)

Copyright

A detailed quantitative study of the microstructural variation of chemical composition of chemically vapor-deposited commercial SiC SCS-6 fiber is presented. Chemical etching and various electron-optical techniques including SEM, TEM, scanning Auger microscopy, AES, and parallel electron energy loss spectroscopy are used to analyze the chemical composition of the as-received fiber. In addition, some results on stereology of the high-temperature annealed fiber are presented. The results show that the carbon-to-silicon atom ratio in the SiC layers decreases in a stepwise fashion from about 3:2 to about 1:1 in going from the innermost layer to the outermost layer.

Author (revised)

A93-55471 National Aeronautics and Space Administration. Lewis Research Center, Cleveland, OH.

SOLID LUBRICANTS

HAROLD E. SLINEY (NASA, Lewis Research Center, Cleveland, OH) *In* Metals handbook. Vol. 18 - Friction, lubrication, and wear technology Materials Park, OH ASM International 1993 p. 113-122. Previously announced in STAR as N91-22396 refs

(Contract RTOP 505-63-5A)

Copyright

The state of knowledge of solid lubricants is reviewed. The results of research on solid lubricants from the 1940's to the present are presented from a historical perspective. Emphasis is placed largely, but not exclusively, on work performed at NASA Lewis Research Center with a natural focus on aerospace applications. However, because of the generic nature of the research, the information presented in this review is applicable to most areas where solid lubricant technology is useful.

A93-55472* National Aeronautics and Space Administration. Lewis Research Center, Cleveland, OH.

AEROSPACE APPLICATIONS

STANLEY R. LEVINE and THOMAS P. HERBELL (NASA, Lewis Research Center, Cleveland, OH) *In* Engineered materials handbook. Vol. 4 - Ceramics and glasses Materials Park, OH ASM International 1992 p. 1003-1006. refs

Copyright

Aerospace applications of ceramics and ceramic composites are discussed. The use of these materials in space propulsion, space power, aerospace vehicles, and space structures is examined.

AIAA

N93-10962*# National Aeronautics and Space Administration. Lewis Research Center, Cleveland, OH.

ANALYSIS OF PRECRACKING PARAMETERS AND FRACTURE TOUGHNESS FOR CERAMIC SINGLE-EDGE-PRECRACKED-BEAM SPECIMENS

SUNG R. CHOI (Cleveland State Univ., OH.), ABHISAK CHULYA (Cleveland State Univ., OH.), and JONATHAN A. SALEM Aug. 1992 25 p

(Contract DE-AI05-87OR-21749; RTOP 505-63-1M)

(NASA-TM-105568; E-6893; NAS 1.15:105568) Avail: CASI HC A03/MF A01

The single-edge-precracked-beam (SEPB) method involves creation of a straight-through crack from an indentation crack. The straight-through crack is developed by applying a controlled bending load to a specimen via a precracking fixture. The fixture induces the following sequence: (1) stable growth of the indentation crack; (2) pop-in; and finally, (3) arrest-thereby forming a straight-through precrack. The effects of indentation load on precracking load as well as precrack size were studied for

to 1.8 in vacuum. The wear factor of the diamond films depended on the initial surface roughness, regardless of environment; it increased with increasing initial surface roughness. The wear factors were considerably higher in vacuum than in humid air and in dry nitrogen.

Author

N93-19332*# National Aeronautics and Space Administration. Lewis Research Center, Cleveland, OH.

OXIDATION RESISTANT OVERLAY COATINGS FOR LOW EXPANSION SUBSTRATES Patent Application

W. J. BRINDLEY, inventor (to NASA), R. A. MILLER, inventor (to NASA), J. L. SMIALEK, inventor (to NASA), and C. J. ROUGE, inventor (to NASA) 16 Dec. 1992 18 p
(NASA-CASE-LEW-15154-1; NAS 1.71:LEW-15154-1;
US-PATENT-APPL-SN-993743) Avail: CASI HC A03/MF A01

A low thermal expansion oxidation resistant coating utilizes an oxidation resistant alloy and an inert low thermal expansion phase which act to reduce overall thermal expansion. This coating is applied to a low thermal expansion substrate.

NASA

N93-20566*# National Aeronautics and Space Administration. Lewis Research Center, Cleveland, OH.

ATOMIC OXYGEN PROTECTIVE COATING WITH RESISTANCE TO UNDERCUTTING AT DEFECT SITES Patent Application

BRUCE A. BANKS, inventor (to NASA) and SHARON K. RUTLEDGE, inventor (to NASA) 6 Jul. 1992 15 p
(NASA-CASE-LEW-15306-1; NAS 1.71:LEW-15306-1;
US-PATENT-APPL-SN-909345) Avail: CASI HC A03/MF A01

Structures composed of at least partially of an organic substrate may be protected from oxidation by applying a catalyst onto said substrate for promoting the combination of atomic oxygen to molecular oxygen. The structure may also be protected by applying both a catalyst and an atomic oxygen shielding layer onto the substrate. The structures to be protected include spacecraft surfaces.

NASA

N93-20813*# National Aeronautics and Space Administration. Lewis Research Center, Cleveland, OH.

ISSUES/CONSIDERATIONS AND PERFORMANCE PREDICTION OF LEO PROTECTIVE COATINGS

BRUCE A. BANKS *In* Canadian Space Agency, Protection of Materials and Surface Finishes from the Low Earth Orbit Space Environment 83 p 1992
Avail: Canadian Space Agency, P.O. Box 7275, Ottawa, ON, Canada K1L 8E3, HC

Organic materials can be used in low earth orbit for long periods only if they are made to be durable to atomic oxygen in addition to the threats of ultraviolet radiation, micrometeoroid and debris impact, thermal cycling, and charged particle radiation. In many materials applications, it is more cost-effective to utilize atomic oxygen protective coatings over materials which are vulnerable to attack by atomic oxygen rather than developing alternative materials which are inherently durable. Many metal and metal oxide coatings have been shown to be potentially suitable for long term protection of organic polymers in low earth orbit. The protection afforded by thin film coatings on polymeric substrates is highly dependent on the completeness of coverage of the coating. Thus, the prime indicator of durability is the size and abundance of pin windows and scratches in the protective coating. Such defects depend on the deposition technique, smoothness of the surface to be protected, and presence of particulate contaminants. Issues and considerations relevant to substrate preparation, deposition of protective coatings, ground laboratory simulation and evaluation of threats in low earth orbit to protective materials, results of in-space tests, and the use of Monte Carlo modeling techniques to predict in-space durability are presented in graphic form.

Author (CISTI)

N93-22560*# National Aeronautics and Space Administration. Lewis Research Center, Cleveland, OH.

INTERFACIAL CHEMISTRY OF A PERFLUOROPOLYETHER LUBRICANT STUDIED BY XPS AND TDS

PILAR C. HERRERA-FIERRO, WILLIAM R. JONES, JR., and STEPHEN V. PEPPER Apr. 1992 39 p
(Contract RTOP 505-63-5A)
(NASA-TM-106014; E-6889-1; NAS 1.15:106014) Avail: CASI HC A03/MF A01

The interfacial chemistry of Fomblin Z25, a commercial perfluoropolyether used as lubricant for space applications, with different metallic surfaces: 440C steel, gold and aluminum was studied. Thin layers of Fomblin Z25 were evaporated onto the oxide-free substrates and the interfacial chemistry studied using XPS and TDS. The reactions were induced by heating the substrate and by rubbing the substrate with a steel ball. Gold was found to be completely unreactive towards Fomblin at any temperature. Reaction at room temperature was observed only in the case of the aluminum substrate, the most reactive towards Fomblin Z25 of the substrates studied. It was necessary to heat the 440C steel substrate to 190 degree C to induce decomposition of the fluid. The degradation of the fluid was indicated by the formation of a debris layer at the interface. This debris layer, composed of inorganic and organic reaction products, when completely formed, passivated the surface from further attack to the Fomblin on top. The tribologically induced reactions on 440C steel formed a debris layer of similar chemical characteristics to the thermally induced layer. In all cases, the degradation reaction resulted in preferential consumption of the difluoroformyl carbon (-OCF₂O-).

Author (revised)

N93-25093*# National Aeronautics and Space Administration. Lewis Research Center, Cleveland, OH.

DETERMINATION OF THE THERMAL STABILITY OF PERFLUOROPOLYALKYL ETHERS BY TENSIMETRY

LARRY A. HELMICK (Cedarville Coll., OH.) and WILLIAM R. JONES, JR. May 1992 32 p Presented at the Society of Tribologists and Lubrication Engineers Annual Meeting, Philadelphia, PA, 4-7 May 1992; sponsored by the Society of Tribologists and Lubrication Engineers
(Contract RTOP 505-53-1A)
(NASA-TM-106081; E-7699; NAS 1.15:106081) Avail: CASI HC A01/MF A01

The thermal decomposition temperatures of several perfluoropolyalkyl ether fluids were determined with a computerized tensimeter. In general, the decomposition temperatures of the commercial fluids were all similar and significantly higher than those for noncommercial fluids. Correlation of the decomposition temperatures with the molecular structures of the primary components of the commercial fluids revealed that the stability of the fluids was not affected by carbon chain length, branching, or adjacent difluoroformal groups. Instead, stability was limited by the presence of small quantities of thermally unstable material and/or chlorine-containing material arising from the use of chlorine containing solvents during synthesis. Finally, correlation of decomposition temperatures with molecular weights for two fluids supports a chain cleavage reaction mechanism for one and an unzipping reaction mechanism for the other.

Author

N93-25564*# National Aeronautics and Space Administration. Lewis Research Center, Cleveland, OH.

OPTICAL AND SCRATCH RESISTANT PROPERTIES OF DIAMONDLIKE CARBON FILMS DEPOSITED WITH SINGLE AND DUAL ION BEAMS

MICHAEL T. KUSSMAUL (Sverdrup Technology, Inc., Brook Park, OH.), MICHAEL S. BOGDANSKI (Case Western Reserve Univ., Cleveland, OH.), BRUCE A. BANKS, and MICHAEL J. MIRTICH *In* NASA, Washington, Technology 2002: The Third National Technology Transfer Conference and Exposition, Volume 1 p 30-40 Feb. 1993

Avail: CASI HC A03/MF A04

Amorphous diamond-like carbon (DLC) films were deposited using both single and dual ion beam techniques utilizing filament and hollow cathode ion sources. Continuous DLC films up to 3000 Å thick were deposited on fused quartz plates. Ion beam process parameters were varied in an effort to create hard, clear films. Total DLC film absorption over visible wavelengths was obtained

27 NONMETALLIC MATERIALS

using a Perkin-Elmer spectrophotometer. An ellipsometer, with an Ar-He laser (wavelength 6328 Å) was used to determine index of refraction for the DLC films. Scratch resistance, frictional, and adherence properties were determined for select films. Applications for these films range from military to the ophthalmic industries.

Author

N93-25565*# National Aeronautics and Space Administration. Lewis Research Center, Cleveland, OH.

PROPERTIES OF EXTRUDED PS-212 TYPE SELF-LUBRICATING MATERIALS

W. J. WATERS (Sverdrup Technology, Inc., Cleveland, OH.), H. E. SLINEY, and R. F. SOLTIS (Cortez 3 Services Corp., Brook Park, OH.) In NASA, Washington, Technology 2002: The Third National Technology Transfer Conference and Exposition, Volume 1 p 41-55 Feb. 1993

Avail: CASI HC A03/MF A04

Research has been underway at the NASA Lewis Research Center since the 1960's to develop high temperature, self-lubricating materials. The bulk of the research has been done in-house by a team of researchers from the Materials Division. A series of self-lubricating solid material systems has been developed over the years. One of the most promising is the composite material system referred to as PS-212 or PM-212. This material is a powder metallurgy product composed of metal bonded chromium carbide and two solid lubricating materials known to be self-lubricating over a wide temperature range. NASA feels this material has a wide potential in industrial applications. Simplified processing of this material would enhance its commercial potential. Processing changes have the potential to reduce processing costs, but tribological and physical properties must not be adversely affected. Extrusion processing has been employed in this investigation as a consolidation process for PM-212/PS-212. It has been successful in that high density bars of EX-212 (extruded PM-212) can readily be fabricated. Friction and strength data indicate these properties have been maintained or improved over the P.M. version. A range of extrusion temperatures have been investigated and tensile, friction, wear, and microstructural data have been obtained. Results indicate extrusion temperatures are not critical from a densification standpoint, but other properties are temperature dependent.

Author

N93-28282*# National Aeronautics and Space Administration. Lewis Research Center, Cleveland, OH.

MONTE CARLO MODELING OF ATOMIC OXYGEN ATTACK OF POLYMERS WITH PROTECTIVE COATINGS ON LDEF

BRUCE A. BANKS, KIM K. DEGROH, BRUCE M. AUER, LINDA GEBAUER (Cleveland State Univ., OH.), and JONATHAN L. EDWARDS (Cleveland State Univ., OH.) In NASA. Langley Research Center, LDEF: 69 Months in Space. Part 3: Second Post-Retrieval Symposium p 1137-1150 Apr. 1993

Avail: CASI HC A03/MF A04; 2 functional color pages

Characterization of the behavior of atomic oxygen interaction with materials on the Long Duration Exposure Facility (LDEF) assists in understanding of the mechanisms involved. Thus the reliability of predicting in-space durability of materials based on ground laboratory testing should be improved. A computational model which simulates atomic oxygen interaction with protected polymers was developed using Monte Carlo techniques. Through the use of an assumed mechanistic behavior of atomic oxygen interaction based on in-space atomic oxygen erosion of unprotected polymers and ground laboratory atomic oxygen interaction with protected polymers, prediction of atomic oxygen interaction with protected polymers on LDEF was accomplished. However, the results of these predictions are not consistent with the observed LDEF results at defect sites in protected polymers. Improved agreement between observed LDEF results and predicted Monte Carlo modeling can be achieved by modifying of the atomic oxygen interactive assumptions used in the model. LDEF atomic oxygen undercutting results, modeling assumptions, and implications are presented.

Author

N93-28423*# National Aeronautics and Space Administration. Lewis Research Center, Cleveland, OH.

GUANIDINE BASED VEHICLE/BINDERS FOR USE WITH OXIDES, METALS, AND CERAMICS Patent Application

WARREN H. PHILIPP, inventor (to NASA), LISA C. VEITCH, inventor (to NASA), and MARTHA H. JASKOWIAK, inventor (to NASA) 25 Jun. 1993 14 p

(NASA-CASE-LEW-15314-2; NAS 1.71:LEW-15314-2;

US-PATENT-APPL-SN-081180) Avail: CASI HC A03/MF A01

The use of guanidine salts of organic fatty acids (guanidine soaps) as vehicles and binders for coating substrate surfaces is disclosed. Being completely organic, the guanidine soaps can be burned off leaving no undesirable residue. Of special interest is the use of guanidine 2-ethyl hexanoate as the vehicle and binder for coating problematic surfaces such as in coating alumina fibers with platinum or zirconia. For this application the guanidine soap is used as a melt. For other applications the guanidine soap may be used in a solution with a variety of solvents, the solution containing chlorometalates or powdered metals, refractories or ceramics.

NASA

N93-28425*# National Aeronautics and Space Administration. Lewis Research Center, Cleveland, OH.

METHOD FOR RETARDING OXIDATION OF AN ORGANIC SUBSTRATE Patent Application

BRUCE A. BANKS, inventor (to NASA) and SHARON K. RUTLEDGE, inventor (to NASA) 24 May 1993 15 p

(NASA-CASE-LEW-15306-2; NAS 1.71:LEW-15306-2;

US-PATENT-APPL-SN-065794) Avail: CASI HC A03/MF A01

Structures composed at least partially of an organic substrate are protected from oxidation by applying a catalyst onto said substrate for promoting the combination of atomic oxygen to molecular oxygen. The structure may also be protected by applying both a catalyst and an atomic oxygen shielding layer onto the substrate. The invention is useful for enhancing the protection of polymeric blankets, solar arrays, and spacecraft surfaces in low earth orbit from cavities produced by atomic oxygen.

NASA

N93-30938*# National Aeronautics and Space Administration. Lewis Research Center, Cleveland, OH.

TENSILE CREEP BEHAVIOR OF POLYCRYSTALLINE ALUMINA FIBERS

H. M. YUN and J. C. GOLDSBY Jul. 1993 11 p

(Contract RTOP 537-04-21)

(NASA-TM-106269; E-7995; NAS 1.15:106269) Avail: CASI HC A03/MF A01

Tensile creep studies were conducted on polycrystalline Nextel 610 and Fiber FP alumina fibers with grain sizes of 100 and 300 nm, respectively. Test conditions were temperatures from 800 to 1050 C and stresses from 60 to 1000 MPa. For both fibers, only a small primary creep portion occurred followed by steady-state creep. The stress exponents for steady-state creep of Nextel 610 and Fiber FP were found to be about 3 and 1, respectively. At lower temperatures, below 1000 C, the finer grained Nextel 610 had a much higher 0.2 percent creep strength for 100 hr than the Fiber FP; while at higher temperatures, Nextel 610 had a comparable creep strength to the Fiber FP. The stress and grain size dependencies suggest Nextel 610 and Fiber FP creep rates are due to grain boundary sliding controlled by interface reaction and Nabarro-Herring mechanisms, respectively. Author (revised)

N93-31300*# National Aeronautics and Space Administration. Lewis Research Center, Cleveland, OH.

OXIDATION RESISTANT OVERLAY COATINGS FOR LOW EXPANSION SUBSTRATES Patent Application

W. J. BRINDLEY, inventor (to NASA), R. A. MILLER, inventor (to NASA), J. L. SMIALEK, inventor (to NASA), and C. J. ROUGE, inventor (to NASA) 29 Jun. 1993 18 p

(NASA-CASE-LEW-15154-2; NAS 1.71:LEW-15154-2;

US-PATENT-APPL-SN-083246) Avail: CASI HC A03/MF A01

A low thermal expansion oxidation resistant coating utilizes an oxidation resistant alloy and an inert low thermal expansion phase which act to reduce overall thermal expansion. This coating is

prepared by mixing powders of an MCrAlX material with a sufficient quantity of powders of an inert low thermal expansion phase ceramic material to reduce the aggregate coefficient of thermal expansion of the resulting mixture to about that of the substrate. The coating is applied by a powder based coating process.

NASA

N93-31316*# National Aeronautics and Space Administration. Lewis Research Center, Cleveland, OH.

ION EXCHANGE POLYMERS AND METHOD FOR MAKING Patent Application

WARREN H. PHILIPP, inventor (to NASA) and KENNETH W. STREET, JR., inventor (to NASA) 21 Jun. 1993 13 p (NASA-CASE-LEW-15576-1; NAS 1.71:LEW-15576-1; US-PATENT-APPL-SN-081910) Avail: CASI HC A03/MF A01

An ion exchange polymer comprised of an alkali metal or alkaline earth metal salt of a poly(carboxylic acid) in a poly(vinyl acetal) matrix is described. The polymer is made by treating a mixture made of poly(vinyl alcohol) and poly(acrylic acid) with a suitable aldehyde and an acid catalyst to cause acetalization with some cross-linking. The material is then subjected to an alkaline aqueous solution of an alkali metal salt or an alkali earth metal salt. All of the film forming and cross-linking steps can be carried out simultaneously, if desired.

NASA

N93-32352*# National Aeronautics and Space Administration. Lewis Research Center, Cleveland, OH.

TRIBOLOGICAL CHARACTERISTICS OF PERFLUOROPOLYETHER LIQUID LUBRICANTS UNDER SLIDING CONDITIONS IN HIGH VACUUM

MASABUMI MASUKO (Tokyo Inst. of Tech., Japan.), WILLIAM R. JONES, JR., and LARRY S. HELMICK Jul. 1993 7 p Prepared for presentation at Eurotrib 1993 Conference, Budapest, Hungary, 30 Aug. - 2 Sep. 1993; sponsored by the Hungarian Society of Mechanical Engineers

(Contract RTOP 505-63-5A)

(NASA-TM-106257; E-7980; NAS 1.15:106257) Avail: CASI HC A02/MF A01

Tribological characteristics of three PFPE's (Fomblin Z, Demnum, and Krytox) were studied under high vacuum using a four-ball apparatus with 440C steel specimens. Fomblin Z and Demnum exhibited initial scuffing-like high friction whereas Krytox did not. Steady state friction with Fomblin Z was the lowest among the three oils. Frictional values for Demnum and Krytox were almost the same. The lowest wear rate in air was provided by Krytox regardless of load, and low wear rates in vacuum at high load were achieved with Krytox and Demnum. Results are explained by reactivity and pressure-viscosity characteristics of the oils.

Author (revised)

N93-32367*# National Aeronautics and Space Administration. Lewis Research Center, Cleveland, OH.

DETERMINATION OF THE OXIDATIVE STABILITY OF PERFLUOROPOLYALKYL ETHERS AND CORRELATION WITH CHEMICAL STRUCTURE

LARRY S. HELMICK (Cedarville Coll., OH.) and WILLIAM R. JONES, JR. May 1992 14 p Presented at the Annual Meeting of the Society of Tribologists and Lubrication Engineers, Philadelphia, PA, 4-7 May 1992; sponsored by the Society of Tribologists and Lubrication Engineers

(Contract RTOP 505-53-1A)

(NASA-TM-106223; E-7940; NAS 1.15:106223) Avail: CASI HC A03/MF A01

The oxidative stabilities of several perfluoropolyalkyl ethers (PFPAE) with related chemical structures were determined by thermal gravimetric analysis and correlated with their chemical structures. These results show that oxidative stability increases as the number of difluoroformal groups decreases and as trifluoromethyl substituents are added. They are also consistent with a recently proposed intramolecular disproportionation reaction mechanism involving coordination of successive ether oxygens to a Lewis acid. Since polytetrafluoroethylene contains no oxygen, it provides an indication of the upper limit to oxidative stability of

PFPAE fluids. These results also show that oxidative decomposition of PFPAE fluids requires the presence of an active metal as well as air. Consequently, it may be possible to minimize decomposition and thus improve oxidative stability by passivating reactive metal surfaces.

Author (revised)

N93-32382*# National Aeronautics and Space Administration. Lewis Research Center, Cleveland, OH.

STRESS-RUPTURE BEHAVIOR OF SMALL DIAMETER POLYCRYSTALLINE ALUMINA FIBERS

HEE MANN YUN (Cleveland State Univ., OH.), JON C. GOLDSBY, and JAMES A. DICARLO Apr. 1993 14 p Presented at the 95th Annual Meeting and Exposition of the American Ceramic Society, Cincinnati, OH, 18-23 Apr. 1993

(Contract RTOP 510-01-50)

(NASA-TM-106256; E-7979; NAS 1.15:106256) Avail: CASI HC A03/MF A01

Continuous length polycrystalline alumina fibers are candidates as reinforcement in high temperature composite materials. Interest therefore exists in characterizing the thermomechanical behavior of these materials, obtaining possible insights into underlying mechanisms, and understanding fiber performance under long term use. Results are reported on the time-temperature dependent strength behavior of Nextel 610 and Fiber FP alumina fibers with grain sizes of 100 and 300 nm, respectively. Below 1000 C and 100 hours, Nextel 610 with the smaller grain size had a greater fast fracture and rupture strength than Fiber FP. The time exponents for stress-rupture of these fibers were found to decrease from approximately 13 at 900 C to below 3 near 1050 C, suggesting a transition from slow crack growth to creep rupture as the controlling fracture mechanism. For both fiber types, an effective activation energy of 690 kJ/mol was measured for rupture. This allowed stress-rupture predictions to be made for extended times at use temperatures below 1000 C.

Author (revised)

28

PROPELLANTS AND FUELS

Includes rocket propellants, igniters, and oxidizers; their storage and handling procedures; and aircraft fuels.

A93-14510* National Aeronautics and Space Administration. Lewis Research Center, Cleveland, OH.

HYDROCARBON-FUEL/COPPER COMBUSTION CHAMBER LINER COMPATIBILITY, CORROSION PREVENTION, AND REFURBISHMENT

S. D. ROSENBERG, M. L. GAGE, G. D. HOMER, and J. E. FRANKLIN (Aerojet, Propulsion Div., Sacramento, CA) Journal of Propulsion and Power (ISSN 0748-4658) vol. 8, no. 6 Nov.-Dec. 1992 p. 1200-1207. Previously cited in issue 17, p. 2899, Accession no. A91-41729 AIAA, SAE, ASME, and ASEE, Joint Propulsion Conference, 27th, Sacramento, CA, June 24-26, 1991, AIAA Paper 91-2213 refs

(Contract NAS3-25070)

Copyright

A93-22577*# National Aeronautics and Space Administration. Lewis Research Center, Cleveland, OH.

EXPERIMENTS ON THE EFFECT OF INITIAL DIAMETER IN SPHERICALLY SYMMETRIC DROPLET COMBUSTION OF SOOTING FUELS

G. S. JACKSON and C. T. AVEDISIAN (Cornell Univ., Ithaca, NY) Jan. 1993 19 p. AIAA, Aerospace Sciences Meeting and Exhibit, 31st, Reno, NV, Jan. 11-14, 1993 Research supported by New York State Center for Hazardous Waste Management refs

(Contract NAG3-987)

(AIAA PAPER 93-0130) Copyright

The effect of initial droplet diameter on the burning rate of

sooting fuels (n-heptane and 1-chloro-octane) is studied experimentally at low gravity. A 1.2 s drop tower provided a low gravity environment to minimize buoyancy and achieve spherically symmetric flames for stationary droplets. Free-floating and fiber supported droplets were burned, and both methods gave matching results for droplets of similar initial diameter. R.E.P.

A93-24234* National Aeronautics and Space Administration. Lewis Research Center, Cleveland, OH.

ATOMIC HYDROGEN PROPELLANTS - HISTORICAL PERSPECTIVES AND FUTURE POSSIBILITIES

BRYAN PALASZEWSKI (NASA, Lewis Research Center, Cleveland, OH) Jan. 1993 24 p. AIAA, Aerospace Sciences Meeting and Exhibit, 31st, Reno, NV, Jan. 11-14, 1993 refs (AIAA PAPER 93-0244) Copyright

Atomic hydrogen, a very high density free-radical propellant, is anticipated to generate a specific impulse of 600-1500 lb-f sec/lb-mass performance; this may facilitate the development of unique launch vehicles. A development status evaluation is presently given for atomic hydrogen investigations. It is noted that breakthroughs are required in the production, storage, and transfer of atomic hydrogen, before this fuel can become a viable rocket propellant. O.C.

A93-34478 National Aeronautics and Space Administration. Lewis Research Center, Cleveland, OH.

SOME ASPECTS OF SECONDARY ATOMIZATION OF ALUMINUM/HYDROCARBON SLURRY PROPELLANTS

DONN C. MUELLER and STEPHEN R. TURNS (Pennsylvania State Univ., University Park) Journal of Propulsion and Power (ISSN 0748-4658) vol. 9, no. 3 May-June 1993 p. 345-352. AIAA, NASA, and OAI, Conference on Advanced SEI Technologies, Cleveland, OH, Sept. 4-6, 1991, AIAA Paper 91-3625. Previously cited in issue 22, p. 3864, Accession no. A91-52489 refs (Contract NAG3-1044; NAGW-1356) Copyright

A93-49752* National Aeronautics and Space Administration. Lewis Research Center, Cleveland, OH.

TECHNOLOGY FOR GELLED LIQUID CRYOGENIC PROPELLANTS - METALLIZED HYDROGEN/ALUMINUM

JOHN STARKOVICH (TRW, Inc., Redondo Beach, CA) and BRYAN PALASZEWSKI (NASA, Lewis Research Center, Cleveland, OH) Jun. 1993 18 p. AIAA, SAE, ASME, and ASEE, Joint Propulsion Conference and Exhibit, 29th, Monterey, CA, June 28-30, 1993 refs (AIAA PAPER 93-1878) Copyright

The theoretical basis for solid-loaded or densified liquid hydrogen propellants for advanced space applications is outlined. Metallized propellants make it possible to increase the safety of propulsion systems as well as the payloads of future vehicles. Nanogellant formulated liquid hydrogen gels and other fuel gels are characterized by excellent settling stability, low yield point, and a high shear thinning index which makes them attractive for propulsion applications. AIAA

A93-50046* National Aeronautics and Space Administration. Lewis Research Center, Cleveland, OH.

BENEFITS OF IN SITU PROPELLANT UTILIZATION FOR A MARS SAMPLE RETURN MISSION

MARY F. WADEL (NASA, Lewis Research Center, Cleveland, OH) Jun. 1993 12 p. AIAA, SAE, ASME, and ASEE, Joint Propulsion Conference and Exhibit, 29th, Monterey, CA, June 28-30, 1993 Previously announced in STAR as N93-28695 refs (AIAA PAPER 93-2244) Copyright

Previous Mars rover sample return mission studies have shown a requirement for Titan 4 or STS Space Shuttle launch vehicles to complete a sample return from a single Mars site. These studies have either used terrestrial propellants or considered in situ production of methane and oxygen for the return portion of the mission. Using in situ propellants for the return vehicles reduces the Earth launch mass and allows for a smaller Earth launch vehicle, since the return propellant is not carried from Earth. Carbon

monoxide and oxygen (CO/O₂) and methane and oxygen (CH₄/O₂) were investigated as in situ propellants for a Mars sample return mission and the results were compared to a baseline study performed by the Jet Propulsion Laboratory using terrestrial propellants. Capability for increased sample return mass, use of an alternate launch vehicle, and an additional mini-rover as payload were included. CO/O₂ and CH₄/O₂ were found to decrease the baseline Earth launch mass by 13.6 and 9.2 percent, respectively. This resulted in higher payload mass margins for the baseline Atlas 2AS launch vehicle. CO/O₂ had the highest mass margin. And because of this, it was not only possible to increase the sample return mass and carry an additional mini-rover, but was also possible to use the smaller Atlas 2A launch vehicle.

A93-50368* National Aeronautics and Space Administration. Lewis Research Center, Cleveland, OH.

MECHANISMS OF MICROGRAVITY FLAME SPREAD OVER A THIN SOLID FUEL - OXYGEN AND OPPOSED FLOW EFFECTS

S. L. OLSON (NASA, Lewis Research Center, Cleveland, OH) Combustion Science and Technology (ISSN 0010-2202) vol. 76 1991 p. 233-249. refs Copyright

Microgravity tests varying oxygen concentration and forced flow velocity have examined the importance of transport processes on flame spread over very thin solid fuels. Flame spread rates, solid phase temperature profiles and flame appearance for these tests are measured. A flame spread map is presented which indicates three distinct regions where different mechanisms control the flame spread process. In the near-quenching region (very low characteristic relative velocities) a new controlling mechanism for flame spread - oxidizer transport-limited chemical reaction - is proposed. In the near-limit, blowoff region, high opposed flow velocities impose residence time limitations on the flame spread process. A critical characteristic relative velocity line between the two near-limit regions defines conditions which result in maximum flammability both in terms of a peak flame spread rate and minimum oxygen concentration for steady burning. In the third region, away from both near-limit regions, the flame spread behavior, which can accurately be described by a thermal theory, is controlled by gas-phase conduction.

N93-10045* National Aeronautics and Space Administration. Lewis Research Center, Cleveland, OH.

TANK CHILLDOWN ANALYSIS AND VERIFICATION WITH A FLIGHTWEIGHT, 175 CU FT TANK UNDER NORMAL GRAVITY WITH LIQUID HYDROGEN

NASEEM H. SAIYED In JHU, The 1992 JANNAF Propulsion Meeting, Volume 1 p 693-702 Feb. 1992 Avail: CPIA, 10630 Little Patuxent Pkwy., Suite 202, Columbia, MD, 21044-3200 HC

In a typical No-Vent Fill (NVF) process the receiver tank wall is cooled to a target temperature before filling proceeds. One way to cool the tank wall is to use the Charge-Hold-Vent (CHV) approach. The three phases of the CHV process--Charge, Hold, and Vent--influence the tank chilldown in very different ways. The enthalpy inflow and the evaporation of the liquid dominate the Charge phase. Direct tank wall to vapor heat transfer, free convection on earth, and mostly conduction in low-g, determines the Hold phase. In the Vent phase the enthalpy outflow and forced convection are the dominant factors. An analysis that encompasses all phases of the CHV approach is developed. The resulting equations are easily programmable. Transient modeling of the CHV process is achieved by evaluating the equations at discrete time intervals. The analysis is compared with data from a CHV demonstration. The trends in the calculated profiles for the tank wall temperature, vapor temperature, and tank pressure match those from the data; however, the calculated profiles are offset from the data. The demonstration does not have sufficient information for properly modeling the parameters that influence the heat transfer processes to reduce the offset. Further research is recommended concerning heat transfer during Charge and Vent phases to improve the analysis. Author

N93-12085*# National Aeronautics and Space Administration. Lewis Research Center, Cleveland, OH.

DESIGN OF SMALL STIRLING DYNAMIC ISOTOPE POWER SYSTEM FOR ROBOTIC SPACE MISSIONS

D. J. BENTS, J. G. SCHREIBER, C. A. WITHROW, B. I. MCKISSOCK, and P. C. SCHMITZ (Sverdrup Technology, Inc., Brook Park, OH.) Oct. 1992 11 p Presented at the Tenth Symposium on Space Nuclear Power and Propulsion, Albuquerque, NM, 10-14 Jan. 1992; sponsored by Inst. for Space Nuclear Power Studies

(Contract RTOP 590-13-11)

(NASA-TM-105919; E-7395; NAS 1.15:105919) Avail: CASI HC A03/MF A01

Design of a multihundred-watt Dynamic Isotope Power System (DIPS) based on the U.S. Department of Energy (DOE) General Purpose Heat Source (GPHS) and small (multihundred-watt) free-piston Stirling engine (FPSE) technology is being pursued as a potential lower cost alternative to radioisotope thermoelectric generators (RTG's). The design is targeted at the power needs of future unmanned deep space and planetary surface exploration missions ranging from scientific probes to Space Exploration Initiative precursor missions. Power level for these missions is less than a kilowatt. Unlike previous DIPS designs which were based on turbomachinery conversion (e.g. Brayton), this small Stirling DIPS can be advantageously scaled down to multihundred-watt unit size while preserving size and mass competitiveness with RTG's. Preliminary characterization of units in the output power ranges 200-600 W indicate that on an electrical watt basis the GPHS/small Stirling DIPS will be roughly equivalent to an advanced RTG in size and mass but require less than a third of the isotope inventory.

Author

N93-14834*# National Aeronautics and Space Administration. Lewis Research Center, Cleveland, OH.

ENERGY LOSS ANALYSIS OF AN INTEGRATED SPACE POWER DISTRIBUTION SYSTEM

M. DAVID KANKAM and P. F. RIBEIRO (Dordt Coll., Sioux Center, IA.) Aug. 1992 8 p Presented at the 27th Intersociety Energy Conversion Engineering Conference, San Diego, CA, 3-7 Aug., 1992; cosponsored by ANS, SAE, ASC, AIAA, IEEE, and AIChE (Contract RTOP 506-41-41)

(NASA-TM-105772; E-7055; NAS 1.15:105772) Avail: CASI HC A02/MF A01

The results of studies related to conceptual topologies of an integrated utility-like space power system are described. The system topologies are comparatively analyzed by considering their transmission energy losses as functions of mainly distribution voltage level and load composition. The analysis is expedited by use of a Distribution System Analysis and Simulation (DSAS) software. This recently developed computer program by the Electric Power Research Institute (EPRI) uses improved load models to solve the power flow within the system. However, present shortcomings of the software with regard to space applications, and incompletely defined characteristics of a space power system make the results applicable to only the fundamental trends of energy losses of the topologies studied. Accountability, such as included, for the effects of the various parameters on the system performance can constitute part of a planning tool for a space power distribution system.

Author

N93-16384*# National Aeronautics and Space Administration. Lewis Research Center, Cleveland, OH.

EXPERIMENTS ON A ROUND TURBULENT BUOYANT PLUME

AAMIR SHABBIR and WILLIAM K. GEORGE (State Univ. of New York, Buffalo.) Dec. 1992 70 p (Contract NSF ATM-80-23699; NSF MSM-83-16833; RTOP 505-62-21)

(NASA-TM-105955; ICOMP-92-25; E-7475; NAS 1.15:105955; CMOTT-92-13) Avail: CASI HC A04/MF A01

This paper reports a comprehensive set of hot-wire measurements of a round buoyant plume which was generated by forcing a jet of hot air vertically up into quiescent environment. The boundary conditions of the experiment were measured, and

are documented in the present paper in an attempt to sort out the contradictory mean flow results from the earlier studies. The ambient temperature was monitored to insure that the facility was not stratified and that the experiment was conducted in a neutral environment. The axisymmetry of the flow was checked by using a planar array of sixteen thermocouples and the mean temperature measurements from these are used to supplement the hot-wire measurements. The source flow conditions were measured so as to ascertain the rate at which the buoyancy was added to the flow. The measurements conserve buoyancy within 10 percent. The results are used to carry out the balances of the mean energy and momentum differential equations. In the mean energy equation it is found that the vertical advection of the energy is primarily balanced by the radial turbulent transport. In the mean momentum equation the vertical advection of momentum and the buoyancy force balance the radial turbulent transport. The buoyancy force is the second largest term in this balance and is responsible for the wider (and higher) velocity profiles in plumes as compared to jets. Budgets of the temperature variance and turbulence kinetic energy are also carried out in which thermal and mechanical dissipation rates are obtained as the closing terms. Similarities and differences between the two balances are discussed. It is found that even though the direct affect of buoyancy on turbulence, as evidenced by the buoyancy production term, is substantial, most of the turbulence is produced by shear. This is in contrast to the mean velocity field where the affect of buoyancy force is quite strong. Therefore, it is concluded that in a buoyant plume the primary affect of buoyancy on turbulence is indirect, and enters through the mean velocity field (giving larger shear production).

Author

N93-20136*# National Aeronautics and Space Administration. Lewis Research Center, Cleveland, OH.

PYROTECHNICALLY ACTUATED SYSTEMS DATABASE AND APPLICATIONS CATALOG

PAUL STEFFES (Analex Corp., Cleveland, OH.) /in NASA. Stennis Space Center, The First NASA Aerospace Pyrotechnic Systems Workshop p 83-92 Jan. 1993

Avail: CASI HC A02/MF A04

The topics are presented in viewgraph form and include the following: the purpose of the database and catalog; implementation ground rules; database menu format; and deliverables.

Derived from text

N93-28695*# National Aeronautics and Space Administration. Lewis Research Center, Cleveland, OH.

BENEFITS OF IN SITU PROPELLANT UTILIZATION FOR A MARS SAMPLE RETURN MISSION

MARY F. WADEL Jun. 1993 13 p Presented at the 29th Joint Propulsion Conference and Exhibit, Monterey, CA, 28-30 Jun. 1993; cosponsored by AIAA, SAE, ASME, ASEE

(Contract RTOP 506-42-72)

(NASA-TM-106243; E-7926; NAS 1.15:106243; AIAA PAPER 93-2244) Avail: CASI HC A03/MF A01

Previous Mars rover sample return mission studies have shown a requirement for Titan 4 or STS Space Shuttle launch vehicles to complete a sample return from a single Mars site. These studies have either used terrestrial propellants or considered in situ production of methane and oxygen for the return portion of the mission. Using in situ propellants for the return vehicles reduces the Earth launch mass and allows for a smaller Earth launch vehicle, since the return propellant is not carried from Earth. Carbon monoxide and oxygen (CO/O₂) and methane and oxygen (CH₄/O₂) were investigated as in situ propellants for a Mars sample return mission and the results were compared to a baseline study performed by the Jet Propulsion Laboratory using terrestrial propellants. Capability for increased sample return mass, use of an alternate launch vehicle, and an additional mini-rover as payload were included. CO/O₂ and CH₄/O₂ were found to decrease the baseline Earth launch mass by 13.6 and 9.2 percent, respectively. This resulted in higher payload mass margins for the baseline Atlas 2AS launch vehicle. CO/O₂ had the highest mass margin. And because of this, it was not only possible to increase the

28 PROPELLANTS AND FUELS

sample return mass and carry an additional mini-rover, but was also possible to use the smaller Atlas 2A launch vehicle.

Author (revised)

N93-32330* National Aeronautics and Space Administration. Lewis Research Center, Cleveland, OH.

NON-CONTACT HEAT FLUX MEASUREMENT USING A TRANSPARENT SENSOR

DANIEL NG and CHARLES M. SPUCKLER Jul. 1993 13 p
(Contract RTOP 303-50-00)
(NASA-TM-106252; E-7974; NAS 1.15:106252) Avail: CASI HC A03/MF A01

A working non-contact heat flux sensor was demonstrated using a transparent material (sapphire) and a multiwavelength pyrometer. The pyrometer is used to measure the temperatures of the two surfaces of the sensor from the spectrum of radiation originating from them. The heat conducted through the material is determined from the temperature difference of the two surfaces and the thermal conductivity of the material. The measured heat flux is equal to the incident heat flux within experimental error indicating that no calibration would be necessary. A steady state heat flux of 100 kW/sq m was easily achieved.

Author (revised)

29

MATERIALS PROCESSING

Includes space-based development of products and processes for commercial applications.

A93-12013* National Aeronautics and Space Administration. Lewis Research Center, Cleveland, OH.

INITIAL STUDY OF VOID FORMATION DURING ALUMINUM SOLIDIFICATION IN REDUCED GRAVITY

FRANCIS P. CHIARAMONTE, GEORGE FOERSTER, DANIEL J. GOTTI, ERIC S. NEUMANN, J. C. JOHNSTON (NASA, Lewis Research Center, Cleveland, OH), and KENNETH J. DE WITT (Toledo Univ., OH) Journal of Spacecraft and Rockets (ISSN 0022-4650) vol. 29, no. 5 Sept.-Oct. 1992 p. 704-708. Previously cited in issue 11, p. 1754, Accession no. A92-29611 AIAA, Aerospace Sciences Meeting and Exhibit, 30th, Reno, NV, Jan. 6-9, 1992, AIAA Paper 92-0845 refs Copyright

A93-22668* National Aeronautics and Space Administration. Lewis Research Center, Cleveland, OH.

THERMOSOLUTAL CONVECTION DURING CELLULAR ARRAYED GROWTH OF PB-SN ALLOYS

S. N. TEWARI, RAJESH SHAH (Cleveland State Univ., OH), and M. A. CHOPRA (NASA, Lewis Research Center, Cleveland, OH; IBM Corp., Austin, TX) Jan. 1993 6 p. AIAA, Aerospace Sciences Meeting and Exhibit, 31st, Reno, NV, Jan. 11-14, 1993 refs
(AIAA PAPER 93-0262) Copyright

Thermosolutal convection caused by the solute build up ahead of the growing arrays of cells and dendrites results in macrosegregation along the length of the Pb-Sn alloy (10 to 58 wt pct Sn) specimens when they are directionally solidified in a positive thermal gradient (melt on top, solid below, and gravity pointing down). At a constant thermal gradient, the extent of macrosegregation increases with decreasing growth speed as the microstructure changes from dendritic, to cellular and to planar. An empirical parameter, effective partition coefficient, obtained from the dependence of the longitudinal macrosegregation on fraction distance solidified can be used to represent the extent of macrosegregation.

Author

A93-23371# National Aeronautics and Space Administration. Lewis Research Center, Cleveland, OH.

NUCLEATE POOL BOILING IN THE LONG DURATION LOW GRAVITY ENVIRONMENT OF THE SPACE SHUTTLE

M. M. HASAN, C. S. LIN, R. H. KNOLL (NASA, Lewis Research Center, Cleveland, OH), M. D. BENTZ, and J. S. MESEROLE (Boeing Defense and Space Group, Seattle, WA) Jan. 1993 10 p. AIAA, Aerospace Sciences Meeting and Exhibit, 31st, Reno, NV, Jan. 11-14, 1993 Previously announced in STAR as N93-15420 refs
(Contract RTOP 589-10-2C)
(AIAA PAPER 93-0465) Copyright

The results are presented of an experimental study of nucleate pool boiling performed in the low gravity environment of the space shuttle. Photographic observations of pool boiling in Freon 113 were obtained during the 'Tank Pressure Control Experiment', flown on the Space Transportation System STS-43 in August 1991. Nucleate boiling data from large (relative to bubble size) flat heating surfaces (0.1046 by 0.0742 m) was obtained at very low heat fluxes (0.22 to 1.19 kw/so m). The system pressure and the bulk liquid subcooling varied in the range of 40 to 60 kPa and 3 to 5 C respectively. Thirty-eight boiling tests, each of 10 min duration for a given heat flux, were conducted. Measurements included the heater power, heater surface temperature, the liquid temperature and the system pressure as functions of heating time. Video data of the first 2 min of heating was recorded for each test. In some tests the video clearly shows the inception of boiling and the growth and departure of bubbles from the surface during the first 2 min of heating. In the absence of video data, the heater temperature variation during heating shows the inception of boiling and stable nucleate boiling. During the stable nucleate boiling, the wall superheat varied between 2.8 to 3.8 C for heat fluxes in the range of 0.95 to 1.19 kw/so m. The wall superheat at the inception of boiling varied between 2 to 13 C.

Author

A93-24242# National Aeronautics and Space Administration. Lewis Research Center, Cleveland, OH.

NUMERICAL MODEL FOR THE PROGRAMMABLE MULTIROLE FURNACE (PMZF)

M. KASSEMI, C. H. PANZARELLA, K. E. DESTRO-SIDIK, C. R. KROLIKOWSKI, and B. W. LICHT (NASA, Lewis Research Center, Cleveland, OH) Jan. 1993 11 p. AIAA, Aerospace Sciences Meeting and Exhibit, 31st, Reno, NV, Jan. 11-14, 1993 Research supported by NASA refs
(AIAA PAPER 93-0471) Copyright

The present account of the Programmable Multizone Furnace numerical model uses various examples to illustrate the ways in which the model serves as an optimization, test, prediction, and visualization tool; a numerical PID-control algorithm obtains the desired sample temperature distributions and allows the model to solve an inverse heat transfer problem where the desired sample temperature profile is the input and the required heater power distribution is the output of numerical simulations. Parametric studies show how the total power consumption of the furnace is affected by such design variables as the conductivity.

O.C.

A93-24903# National Aeronautics and Space Administration. Marshall Space Flight Center, Huntsville, AL.

LOW GRAVITY ENVIRONMENT ON-BOARD COLUMBIA DURING STS-40

M. J. B. ROGERS (Alabama Univ., Huntsville), C. R. BAUGHER (NASA, Marshall Space Flight Center, Huntsville, AL), R. C. BLANCHARD (NASA, Langley Research Center, Hampton, VA), R. DELOMBARD (NASA, Lewis Research Center, Cleveland, OH), W. W. DURING (Worcester Polytechnic Inst., MA), D. H. MATTHIESEN (Case Western Reserve Univ.; NASA, Lewis Research Center, Cleveland, OH), W. NEUPERT (NASA, Goddard Space Flight Center, Greenbelt, MD), and P. ROUSSEL (ESA, Noordwijk, Netherlands) Jan. 1993 9 p. AIAA, Aerospace Sciences Meeting and Exhibit, 31st, Reno, NV, Jan. 11-14, 1993 Research supported by NASA refs
(AIAA PAPER 93-0833) Copyright

The first NASA Spacelab Life Sciences mission (SLS-I) flew 5

June to 14 June 1991 on the orbiter Columbia (STS-40). The purpose of the mission was to investigate the human body's adaptation to the low gravity conditions of space flight and the body's readjustment after the mission to the 1 g environment of earth. In addition to the life sciences experiments manifested for the Spacelab module, a variety of experiments in other scientific disciplines flew in the Spacelab and in Get Away Special (GAS) Canisters on the GAS Bridge Assembly. Several principal investigators designed and flew specialized accelerometer systems to characterize the low gravity environment. This was done to better assess the results of theft experiments. This was also the first flight of the NASA Microgravity Science and Applications Division (MSAD) sponsored Space Acceleration Measurement System (SAMS) and the first flight of the NASA Orbiter Experiments Office (OEX) sponsored Orbital Acceleration Research Experiment accelerometer (OARE). We present a brief introduction to seven STS-40 accelerometer systems and discuss and compare the resulting data.

Author

A93-25515* National Aeronautics and Space Administration. Lewis Research Center, Cleveland, OH.

IDGE - A TEST OF DENDRITIC GROWTH THEORY USING SPACE FLIGHT

M. E. GLICKSMAN, M. B. KOSS, R. C. HAHN, B. A. HERBACH (Rensselaer Polytechnic Inst., Troy, NY), and E. A. WINSA (NASA, Lewis Research Center, Cleveland, OH) Jan. 1993 6 p. AIAA, Aerospace Sciences Meeting and Exhibit, 31st, Reno, NV, Jan. 11-14, 1993

(AIAA PAPER 93-0260) Copyright

The isothermal Dendritic Growth Experiment (IDGE), to be performed on three of the United States Microgravity Payload (USMP) flights, starting with USMP-2, is designed to provide microgravity data on dendritic growth for a critical test of theory. Ground based test data using succinonitrile (SCN), from both a flight growth chamber and a laboratory growth chamber, are compared to theoretical calculations of dendritic tip velocities and radii. The comparison shows that the data from the flight chamber are consistent with the historical data and that dendritic growth in a microgravity environment should exhibit significant differences from the dendritic growth of SCN at g sub 0.

Author

A93-30858* National Aeronautics and Space Administration. Lewis Research Center, Cleveland, OH.

INTENSIFIED ARRAY CAMERA IMAGING OF SOLID SURFACE COMBUSTION ABOARD THE NASA LEARJET

KAREN J. WEILAND (NASA, Lewis Research Center, Cleveland, OH) AIAA Journal (ISSN 0001-1452) vol. 31, no. 4 April 1993 p. 786-788. Abridged. Previously cited in issue 09, p. 1390, Accession no. A92-25702 AIAA, Aerospace Sciences Meeting and Exhibit, 30th, Reno, NV, Jan. 6-9, 1992, AIAA Paper 92-0240 refs

Copyright

A93-32069* National Aeronautics and Space Administration. Lewis Research Center, Cleveland, OH.

ON THE SHEAR STABILIZATION OF CAPILLARY BREAK-UP OF FINITE LIQUID BRIDGES

HENK A. DIJKSTRA (Utrecht Univ., Netherlands) Microgravity - Science and Technology (ISSN 0938-0108) vol. 6, no. 1 March 1993 p. 13-27. refs

(Contract NAG3-801)

Copyright

In this paper we consider an isothermal finite liquid bridge under zero-gravity. A sinusoidal interfacial shear stress drives a nonparallel flow in the bridge. The linear stability of this flow to three-dimensional disturbances (which may deform the cylindrical gas-liquid interface) is determined numerically by solving an elliptic eigenvalue problem. Previous results on shear stabilization of capillary break-up of axially unbounded cylindrical interfaces containing a parallel flow are hereby extended to a nonparallel flow. The turning flow regions influence the stability significantly. However, for the particular cases considered, a small area in parameter space remains where the capillary instability is

suppressed through interfacial shear. Second, non-axisymmetric oscillatory instabilities are found which originate from an interaction of the interface deformation and the basic flow. These instabilities may be the isothermal limit of the oscillatory instabilities observed in float-zone crystal growth.

Author

A93-33075 National Aeronautics and Space Administration. Lewis Research Center, Cleveland, OH.

GROUND-BASED PIV AND NUMERICAL FLOW VISUALIZATION RESULTS FROM THE SURFACE TENSION DRIVEN CONVECTION EXPERIMENT

ALEXANDER D. PLINE, MARK P. WERNER (NASA, Lewis Research Center, Cleveland, OH), and KWANG-CHUNG HSIEH (Sverdrup Technology, Inc., Brook Park, OH) In Crystal growth in space and related optical diagnostics; Proceedings of the Meeting, San Diego, CA, July 22, 23, 1991 Bellingham, WA Society of Photo-Optical Instrumentation Engineers 1991 p. 222-234. Previously announced in STAR as N91-30491 refs (Contract NAS3-25266; RTOP 694-03-00)

Copyright

The Surface Tension Driven Convection Experiment (STDCE) is a Space Transportation System flight experiment to study both transient and steady thermocapillary fluid flows aboard the United States Microgravity Laboratory-1 (USML-1) Spacelab mission planned for June, 1992. One of the components of data collected during the experiment is a video record of the flow field. This qualitative data is then quantified using an all electric, two dimensional Particle Image Velocimetry (PIV) technique called Particle Displacement Tracking (PDT), which uses a simple space domain particle tracking algorithm. Results using the ground based STDCE hardware, with a radiant flux heating mode, and the PDT system are compared to numerical solutions obtained by solving the axisymmetric Navier Stokes equations with a deformable free surface. The PDT technique is successful in producing a velocity vector field and corresponding stream function from the raw video data which satisfactorily represents the physical flow. A numerical program is used to compute the velocity field and corresponding stream function under identical conditions. Both the PDT system and numerical results were compared to a streak photograph, used as a benchmark, with good correlation.

Author

A93-41678* National Aeronautics and Space Administration. Lewis Research Center, Cleveland, OH.

ON ACCURATE DETERMINATION OF CONTACT ANGLE

P. CONCUS (Lawrence Berkeley Lab.; California Univ., Berkeley) and R. FINN (Stanford Univ., CA) In Microgravity fluid mechanics; Proceedings of the IUTAM Symposium, Bremen, Germany, Sept. 2-6, 1991 Berlin and New York Springer-Verlag 1992 p. 19-28. Previously announced in STAR as N91-28450 refs (Contract DE-AC03-76SF-00098; NAG3-1143; NSF DMS-89-02831)

Copyright

Methods are proposed that exploit a microgravity environment to obtain highly accurate measurement of contact angle. These methods, which are based on our earlier mathematical results, do not require detailed measurement of a liquid free-surface, as they incorporate discontinuous or nearly-discontinuous behavior of the liquid bulk in certain container geometries. Physical testing is planned in the forthcoming IML-2 space flight and in related preparatory ground-based experiments.

Author

A93-50455* National Aeronautics and Space Administration. Lewis Research Center, Cleveland, OH.

SCIENTIFIC BASIS FOR THE ISOTHERMAL DENDRITIC GROWTH EXPERIMENT - A USMP-2 SPACE FLIGHT EXPERIMENT

M. E. GLICKSMAN, M. B. KOSS, R. C. HAHN, A. VELOSA, A. ROJAS (Rensselaer Polytechnic Inst., Troy, NY), and E. WINSA (NASA, Lewis Research Center, Cleveland, OH) Materials Science Forum (ISSN 0255-5476) vol. 77 1991 p. 51-59. Solidification and microgravity; Proceedings of the International Conference, Miskolc, Hungary, Apr. 23-25, 1991. A93-50451 21-29 refs

29 MATERIALS PROCESSING

(Contract NAS3-25368)

Copyright

NASA has planned three flight experiments, designated as the Isothermal Dendritic Growth Experiment (IDGE), to be performed on three of the United States Microgravity Payload (USMP) flights. IDGE is designed to provide microgravity data on dendritic growth for a critical test of theory. Terrestrial gravity, g sub 0, and the associated phenomenon of buoyancy driven convection, prevent a truly quantitative test of pure, diffusocapillary dendritic growth theory. However, recent theoretical analysis provides a fluid mechanics framework for estimating the effects of reduced gravity on the dendritic solidification of pure succinonitrile (SCN), the model material selected for the first IDGE flight. The results (dendritic tip radii and velocities) of the recent fully integrated ground-based tests on the IDGE prototype engineering hardware is in general agreement with the 'historical' ground based data for SCN. At undercoolings of 0.5 K or less, a microgravity environment of approximately $10 \exp -3 g$ sub 0 or lower would have a significant difference from the g sub 0 dendritic growth of SCN. Author (revised)

A93-52183* National Aeronautics and Space Administration. Lewis Research Center, Cleveland, OH.

CONTAINERLESS AUTOMATED PROCESSING OF INTERMETALLIC COMPOUNDS AND COMPOSITES

D. R. JOHNSON, S. M. JOSLIN, R. D. REVIERE, B. F. OLIVER (Tennessee Univ., Knoxville), and R. D. NOEBE (NASA, Lewis Research Center, Cleveland, OH) *In* Processing and fabrication of advanced materials for high temperature applications II Warrendale, PA Minerals, Metals & Materials Society 1993 p. 77-90. refs

(Contract NAG3-876)

Copyright

An automated containerless processing system has been developed to directionally solidify high temperature materials, intermetallic compounds, and intermetallic/metallic composites. The system incorporates a wide range of ultra-high purity chemical processing conditions. The utilization of image processing for automated control negates the need for temperature measurements for process control. The list of recent systems that have been processed includes Cr, Mo, Mn, Nb, Ni, Ti, V, and Zr containing aluminides. Possible uses of the system, process control approaches, and properties and structures of recently processed intermetallics are reviewed.

A93-54460* National Aeronautics and Space Administration. Lewis Research Center, Cleveland, OH.

RADIATION AND PHASE CHANGE OF LITHIUM FLUORIDE IN AN ANNULUS

KURT O. LUND (California Univ., La Jolla) *Journal of Thermophysics and Heat Transfer* (ISSN 0887-8722) vol. 7, no. 4 Oct-Dec. 1993 p. 600-607. refs

(Contract NAG3-1106)

Copyright

A one-dimensional thermal model is developed to evaluate the effect of radiation on the phase change of lithium-fluoride (LiF) in an annular canister under gravitational and microgravitational conditions. Specified heat flux at the outer wall of the canister models focused solar flux; adiabatic and convective conditions are considered for the inner wall. A two-band radiation model is used for the combined-mode heat transfer within the canister, and LiF optical properties relate metal surface properties in vacuum to those in LiF. For axial gravitational conditions, the liquid LiF remains in contact with the two bounding walls, whereas a void gap is used at the outer wall to model possible microgravitational conditions. For the adiabatic cases, exact integrals are obtained for the time required for complete melting of the LiF. Melting was found to occur primarily from the outer wall in the 1-g model, whereas it occurred primarily from the inner wall in the μ -g model. For the convective cases, partially melted steady-state conditions and fully melted conditions are determined to depend on the source flux level, with radiation extending the melting times. Author (revised)

N93-12197* National Aeronautics and Space Administration. Lewis Research Center, Cleveland, OH.

DYNAMIC ANALYSIS OF A PRE-AND-POST ICE IMPACTED BLADE

G. H. ABUMERI (Sverdrup Technology, Inc., Brook Park, OH.), E. S. REDDY (Sverdrup Technology, Inc., Brook Park, OH.), P. L. N. MURTHY, and C. C. CHAMIS Oct. 1992 20 p Presented at the Aircraft Design Systems Meeting, Hilton Head, SC, 24-26 Aug. 1992; sponsored by AIAA

(Contract RTOP 505-68-1C)

(NASA-TM-105829; E-7264; NAS 1.15:105829) Avail: CASI HC A03/MF A01

The dynamic characteristics of an engine blade are evaluated under pre-and-post ice impact conditions using the NASA in-house computer code BLASIM. The ice impacts the leading edge of the blade causing severe local damage. The local structural response of the blade due to the ice impact is predicted via a transient response analysis by modeling only a local patch around the impact region. After ice impact, the global geometry of the blade is updated using deformations of the local patch and a free vibration analysis is performed. The effects of ice impact location, size and ice velocity on the blade mode shapes and natural frequencies are investigated. The results indicate that basic nature of the mode shapes remains unchanged after impact and that the maximum variation in natural frequencies occurs for the twisting mode of the blade. Author

N93-13170* National Aeronautics and Space Administration. Lewis Research Center, Cleveland, OH.

ELECTRICAL DESIGN OF PAYLOAD G-534: THE POOL BOILING EXPERIMENT

DAVID R. FRANCISCO *In* NASA. Goddard Space Flight Center, The 1992 Shuttle Small Payloads Symposium p 115-124 Oct. 1992

Avail: CASI HC A02/MF A03

Payload G-534, the Pool Boiling Experiment (PBE), is a Get Away Special that is scheduled to fly on the shuttle in 1992. This paper will give a brief overall description of the experiment with the main discussion being the electrical design with a detailed description of the power system and interface to the GAS electronics. The batteries used and their interface to the experiment Power Control Unit (PCU) and GAS electronics will be examined. The design philosophy for the PCU will be discussed in detail. The criteria for selection of fuses, relays, power semiconductors and other electrical components along with grounding and shielding policy for the entire experiment will be presented. The intent of this paper is to discuss the use of military tested parts and basic design guidelines to build a quality experiment for minimal additional cost. Author

N93-15420* National Aeronautics and Space Administration. Lewis Research Center, Cleveland, OH.

NUCLEATE POOL BOILING IN THE LONG DURATION LOW GRAVITY ENVIRONMENT OF THE SPACE SHUTTLE

M. M. HASAN, C. S. LIN, R. H. KNOLL, M. D. BENTZ (Boeing Co., Seattle, WA.), and J. S. MESEROLE (Boeing Co., Seattle, WA.) Jan. 1993 11 p Presented at the 31st Aerospace Sciences Meeting and Exhibit, Reno, NV, 11-14 Jan. 1993; Sponsored by AIAA

(Contract RTOP 589-01-2C)

(NASA-TM-105973; E-7485; NAS 1.15:105973; AIAA PAPER 93-0465) Avail: CASI HC A03/MF A01

The results are presented of an experimental study of nucleate pool boiling performed in the low gravity environment of the space shuttle. Photographic observations of pool boiling in Freon 113 were obtained during the 'Tank Pressure Control Experiment,' flown on the Space Transportation System, STS-43 in August 1991. Nucleate boiling data from large (relative to bubble size) flat heating surfaces (0.1046 by 0.0742 m) was obtained at very low heat fluxes (0.22 to 1.19 kW/sq m). The system pressure and the bulk liquid subcooling varied in the range of 40 to 60 kPa and 3 to 5 C respectively. Thirty-eight boiling tests, each of 10-min duration for a given heat flux, were conducted. Measurements included

the heater power, heater surface temperature, the liquid temperature and the system pressure as functions of heating time. Video data of the first 2 min of heating was recorded for each test. In some tests the video clearly shows the inception of boiling and the growth and departure of bubbles from the surface during the first 2 min of heating. In the absence of video data, the heater temperature variation during heating shows the inception of boiling and stable nucleate boiling. During the stable nucleate boiling, the wall superheat varied between 2.8 to 3.8 C for heat fluxes in the range of 0.95 to 1.19 kW/sq m. The wall superheat at the inception of boiling varied between 2 to 13 C. Author

N93-20178*# National Aeronautics and Space Administration. Lewis Research Center, Cleveland, OH.

THE SECOND INTERNATIONAL MICROGRAVITY COMBUSTION WORKSHOP

Feb. 1993 347 p Workshop held in Cleveland, OH, 15-17 Sep. 1992 Original contains color illustrations (Contract RTOP 674-22-05) (NASA-CP-10113; E-7309; NAS 1.55:10113) Avail: CASI HC A15/MF A03; 11 functional color pages

This CP contains 40 papers presented at the Second International Microgravity Combustion Workshop held in Cleveland, OH, from September 15 to 17, 1992. The purpose of the workshop was twofold: to exchange information about the progress and promise of combustion science in microgravity and to provide a forum to discuss which areas in microgravity combustion science need to be expanded profitably and which should be included in upcoming NASA Research Announcements (NRA).

N93-20180*# National Aeronautics and Space Administration. Lewis Research Center, Cleveland, OH.

OVERVIEW OF NASA'S MICROGRAVITY COMBUSTION SCIENCE AND FIRE SAFETY PROGRAM

HOWARD D. ROSS *In its* The Second International Microgravity Combustion Workshop p 9-19 Feb. 1993 Avail: CASI HC A02/MF A03; 11 functional color pages

The study of fundamental combustion processes in a microgravity environment is a relatively new scientific endeavor. A few simple, precursor experiments were conducted in the early 1970's. Today the advent of the U.S. space shuttle and the anticipation of the Space Station Freedom provide for scientists and engineers a special opportunity -- in the form of long duration microgravity laboratories -- and need -- in the form of spacecraft fire safety and a variety of terrestrial applications -- to pursue fresh insight into the basic physics of combustion. Through microgravity, a new range of experiments can be performed since: (1) Buoyancy-induced flows are nearly eliminated; (2) Normally obscured forces and flows may be isolated; (3) Gravitational settling or sedimentation is nearly eliminated; and (4) Larger time or length scales in experiments become permissible. Derived from text

N93-20183*# National Aeronautics and Space Administration. Lewis Research Center, Cleveland, OH.

CAPABILITIES AND CONSTRAINTS OF TYPICAL SPACE FLIGHT HARDWARE

JOHN M. KOUELKA *In its* The Second International Microgravity Combustion Workshop p 35-43 Feb. 1993 Avail: CASI HC A02/MF A03; 11 functional color pages

The Space Experiments Division is in the business of performing ground based low gravity testing and designing experiment hardware for space flight on the Space Shuttle and in the future, Space Station Freedom. As witnessed in combustion work, the reduction of gravity brings forward previously negligible processes and parameters. In a similar manner, the design of experiments for microgravity operation aboard the Space Shuttle must consider parameters that are often not factors for laboratory hardware. Author

N93-20185*# National Aeronautics and Space Administration. Lewis Research Center, Cleveland, OH.

CAPABILITIES AND CONSTRAINTS OF COMBUSTION DIAGNOSTICS IN MICROGRAVITY

PAUL S. GREENBERG *In its* The Second International Microgravity Combustion Workshop p 61-66 Feb. 1993 Avail: CASI HC A02/MF A03; 11 functional color pages

A significant scientific return from both existing and proposed microgravity combustion science experiments is substantially dependent on the availability of diagnostic systems for the collection of the required scientific data. To date, the available diagnostic instrumentation has consisted primarily of conventional photographic media and intrusive temperature and velocity probes, such as thermocouples and hot wire anemometers. This situation has arisen primarily due to the unique and severe operational constraints inherent in reduced gravity experimentation. Each of the various reduced gravity facilities is accompanied by its own peculiar envelope of capabilities and constraints. Drop towers, for example, pose strict limitations on available working volume and power, as well as autonomy of operation. In contrast, hardware developed for space flight applications can be somewhat less constrained in regards to the aforementioned quantities, but is additionally concerned with numerous issues involving safety and reliability. Author

N93-25337*# National Aeronautics and Space Administration. Lewis Research Center, Cleveland, OH.

LASER IGNITION APPLICATION IN A SPACE EXPERIMENT

LARRY C. LIQU and DENNIS E. CULLEY Apr. 1993 15 p Presented at the OE/LASE'93 Conference, Los Angeles, CA, 19-20 Jan. 1993; sponsored by the Society of Photo-Optical Instrumentation Engineers (Contract RTOP 694-03-08) (NASA-TM-106133; E-7805; NAS 1.15:106133) Avail: CASI HC A03/MF A01

A laser ignition system is proposed for the Combustion Experiment Module on an orbiting spacecraft. The results of a design study are given using the scheduled 'Flame Ball Experiment' as the design guidelines. Three laser ignition mechanisms and wavelengths are evaluated. A prototype laser is chosen and its specifications are given, followed by consideration of the beam optical arrangement, the ignition power requirement, the laser ignition system weight, size, reliability, and laser cooling and power consumption. Electromagnetic interference to the onboard electronics caused by the laser ignition process is discussed. Finally, ground tests are suggested. Author (revised)

N93-27011*# National Aeronautics and Space Administration. Lewis Research Center, Cleveland, OH.

A MULTI-ZONE MUFFLE FURNACE DESIGN

NEIL D. ROWE and MARTIN KISEL (Analex Corp., Brook Park, OH.) May 1993 20 p (Contract RTOP 694-03-0C) (NASA-TM-106153; E-7837; NAS 1.15:106153) Avail: CASI HC A03/MF A01

A Multi-Zone Muffle-Tube Furnace was designed, built, and tested for the purpose of providing an in-house experience base with tubular furnaces for materials processing in microgravity. As such, it must not only provide the desired temperatures and controlled thermal gradients at several discrete zones along its length but must also be capable of sustaining the rigors of a Space Shuttle launch. The furnace is insulated to minimize radial and axial heat losses. It is contained in a water-cooled enclosure for purposes of dissipating unwanted residual heat, keeping the outer surfaces of the furnace at a 'touch-safe' temperature, and providing a rugged housing. This report describes the salient features of the furnace, testing procedures and results, and concluding remarks evaluating the overall design. Author

N93-30939*# National Aeronautics and Space Administration. Lewis Research Center, Cleveland, OH.

PREDICTION OF GAS-LIQUID TWO-PHASE FLOW REGIME IN MICROGRAVITY

JINHO LEE (National Academy of Sciences - National Research Council, Washington, DC.) and JONATHAN A. PLATT Jul. 1993 41 p

29 MATERIALS PROCESSING

(Contract RTOP 694-03-0A)
(NASA-TM-106274; E-7079; NAS 1.15:106274) Avail: CASI HC
A03/MF A01

An attempt is made to predict gas-liquid two-phase flow regime in a pipe in a microgravity environment through scaling analysis based on dominant physical mechanisms. Simple inlet geometry is adopted in the analysis to see the effect of inlet configuration on flow regime transitions. Comparison of the prediction with the existing experimental data shows good agreement, though more work is required to better define some physical parameters. The analysis clarifies much of the physics involved in this problem and can be applied to other configurations. Author

N93-70290* National Aeronautics and Space Administration.
Lewis Research Center, Cleveland, OH.

SMOLDERING COMBUSTION IN MICROGRAVITY. USML-1 GLOVEBOX EXPERIMENT NO. 6

Jun. 1992 6 p
(NASA-TM-105012; NAS 1.15:105012) Avail: CASI HC A02/MF
A01

The objective of the Smoldering Combustion in Microgravity (SCM) experiment is to investigate the ignition and propagation of the smoldering combustion in microgravity, in both quiescent and convective environments. Smoldering combustion is a nonflaming reaction that spreads through the interior of porous combustible materials. A burning cigarette is an excellent everyday example of smoldering combustion. Smoldering combustion represents a serious fire risk, both on earth and in spacecraft. Smoldering fires are considered to be more dangerous than flaming fires, due to the insidious nature. The smolder reaction can progress undetected for long periods of time, producing toxic gases, and then suddenly change to flaming. This is the initiation process for many fires on earth. This experiment will give us a preliminary assessment of the potential hazard for smoldering fires in spacecraft. The results of the experiment may also suggest improved techniques for the prevention and detection of smoldering conditions on spacecraft, and perhaps on Earth. Author

31

ENGINEERING (GENERAL)

Includes vacuum technology; control engineering; display engineering; cryogenics; and fire prevention.

A93-26077 National Aeronautics and Space Administration. Lewis Research Center, Cleveland, OH.

A FREE-PISTON STIRLING ENGINE/LINEAR ALTERNATOR CONTROLS AND LOAD INTERACTION TEST FACILITY

JEFFREY S. RAUCH (Sverdrup Technology, Inc., Brook Park, OH), M. D. KANKAM, WALTER SANTIAGO (NASA, Lewis Research Center, Cleveland, OH), and FRANK J. MADI (Sverdrup Technology, Inc., Brook Park, OH) In IECEC '92; Proceedings of the 27th Intersociety Energy Conversion Engineering Conference, San Diego, CA, Aug. 3-7, 1992. Vol. 5 Warrendale, PA Society of Automotive Engineers, Inc. 1992 p. 5.309-5.314. Previously announced in STAR as N92-31262 refs
(Contract NAS3-25266; RTOP 590-13-11)
Copyright

A test facility at LeRC was assembled for evaluating free-piston Stirling engine/linear alternator control options, and interaction with various electrical loads. This facility is based on a 'SPIKE' engine/alternator. The engine/alternator, a multi-purpose load system, a digital computer based load and facility control, and a data acquisition system with both steady-periodic and transient capability are described. Preliminary steady-periodic results are included for several operating modes of a digital AC parasitic load control. Preliminary results on the transient response to switching a resistive AC user load are discussed. Author

A93-48589* National Aeronautics and Space Administration.
Lewis Research Center, Cleveland, OH.

DAMPING OF THERMAL ACOUSTIC OSCILLATIONS IN HYDROGEN SYSTEMS

YOUFAN GU and KLAUS D. TIMMERHAUS (Colorado Univ., Boulder) In Advances in cryogenic engineering. Vol. 37A - Proceedings of the 1991 Cryogenic Engineering Conference, Univ. of Alabama, Huntsville, June 11-14, 1991 New York Plenum Press 1991 p. 265-273. refs
(Contract NAG3-1018)
Copyright

Acoustic waves initiated by a large temperature gradient along a tube are defined as thermal acoustic oscillations (TAOs). These oscillations have been damped by introducing such sound absorbing techniques as acoustic filters, resonators, etc.. These devices serve as an acoustic sink that is used to absorb or dissipate the acoustic energy thereby eliminating or damping such oscillations. Several empirical damping techniques, such as attaching a resonator as a side branch or inserting a wire in the tube, have been developed in the past and have provided reasonable success. However, the effect of connecting tube radius, length, and resonator volume on the damping of thermal acoustic oscillations has not been evaluated quantitatively. Further, these methods have not been effective when the oscillating tube radius was relatively large. Detailed theoretical analyses of these techniques including a newly developed method for damping oscillations in a tube of relatively large radius are provided in this presentation.

A93-48637* National Aeronautics and Space Administration.
Lewis Research Center, Cleveland, OH.

THE CONE PROGRAM - AN OVERVIEW

WILLIAM J. BAILEY (Martin Marietta Astronautics Group, Denver, CO) and HUGH ARIF (NASA, Lewis Research Center, Cleveland, OH) In Advances in cryogenic engineering. Vol. 37B - Proceedings of the 1991 Cryogenic Engineering Conference, Univ. of Alabama, Huntsville, June 11-14, 1991 New York Plenum Press 1991 p. 1173-1182.

(Contract NAS3-25063)

Copyright

The Cryogenic Orbital Nitrogen Experiment (CONE) is a liquid nitrogen cryogenic storage and supply system demonstration placed in orbit by the National Space Transportation System (NSTS) Orbiter and operated as an in-bay payload whose objective is to demonstrate needed critical components and technologies. A conceptual approach has been developed and an overview of the CONE program is described which includes the following: (1) a definition of the background and scope of the technology objectives being investigated, (2) a description of the payload design and operation, major features and rationale for the experiments being conducted, and (3) the justification for CONE relating to potential near-term benefits and risk mitigation for future systems. Author (revised)

A93-49245* National Aeronautics and Space Administration.
Lewis Research Center, Cleveland, OH.

A VACUUM (10 EXP -9 TORR) FRICTION APPARATUS FOR DETERMINING FRICTION AND ENDURANCE LIFE OF MOS(X) FILMS

KAZUHIISA MIYOSHI, FRANK S. HONEYC, PHILLIP B. ABEL, STEPHEN V. PEPPER, TALIVALDIS SPALVINS, and DONALD R. WHEELER (NASA, Lewis Research Center, Cleveland, OH) STLE Tribology Transactions (ISSN 0569-8197) vol. 36, no. 3 July 1993 p. 351-358. STLE, Annual Meeting, 47th, Philadelphia, PA, May 4-7, 1992 refs
Copyright

An ultrahigh-vacuum tribometer for use in a ball-on-disk configuration was specially designed for measuring the friction and endurance life of magnetron-sputtered solid lubricating MoS(x) films deposited on sputter-cleaned 400 C stainless-steel disks, when slid against a 6-mm-diameter 440 C stainless-steel ball. The results of tests showed that the tribometer performs satisfactorily in unidirectional rotation in vacuum at a pressure of 10 exp -7 Pa,

10 exp -9 torr. Similarities are observed in the life cycle friction behavior and the coefficient of friction as a function of the number of disk revolutions, for MoS(x) films at average Hertzian contact from 0.33 to 0.69 GPa. AIAA

N93-25177*# National Aeronautics and Space Administration. Lewis Research Center, Cleveland, OH.

HEAT TRANSFER IN ROTATING SERPENTINE PASSAGES WITH SELECTED MODEL ORIENTATION FOR SMOOTH OR SKEWED TRIP WALLS

B. V. JOHNSON (United Technologies Research Center, East Hartford, CT.), J. H. WAGNER (United Technologies Research Center, East Hartford, CT.), G. D. STEUBER (Pratt and Whitney Aircraft, East Hartford, CT.), and F. C. YEH Apr. 1993 10 p Prepared for presentation at the 38th International Gas Turbine and Aeroengine Congress and Exposition, Cincinnati, OH, 24-27 May 1993; sponsored by ASME (Contract RTOP 505-62-52) (NASA-TM-106126; E-7793; NAS 1.15:106126) Avail: CASI HC A02/MF A01

Experiments were conducted to determine the effects of model orientation as well as buoyancy and Coriolis forces on heat transfer in turbine blade internal coolant passages. Turbine blades have internal coolant passage surfaces at the leading and trailing edges of the airfoil with surfaces at angles which are as large as +/- 50 to 60 degrees to the axis of rotation. Most of the previously-presented, multiple-passage, rotating heat transfer experiments have focused on radial passages aligned with the axis of rotation. Results from serpentine passages with orientations 0 and 45 degrees to the axis of rotation which simulate the coolant passages for the mid chord and trailing edge regions of the rotating airfoil are compared. The experiments were conducted with rotation in both directions to simulate serpentine coolant passages with the rearward flow of coolant or with the forward flow of coolant. The experiments were conducted for passages with smooth surfaces and with 45 degree trips adjacent to airfoil surfaces for the radial portion of the serpentine passages. At a typical flow condition, the heat transfer on the leading surfaces for flow outward in the first passage with smooth walls was twice as much for the model at 45 degrees compared to the model at 0 degrees. However, the differences for the other passages and with trips were less. In addition, the effects of buoyancy and Coriolis forces on heat transfer in the rotating passage were decreased with the model at 45 degrees, compared to the results at 0 degrees. The heat transfer in the turn regions and immediately downstream of the turns in the second passage with flow inward and in the third passage with flow outward was also a function of model orientation with differences as large as 40 to 50 percent occurring between the model orientations with forward flow and rearward flow of coolant.

Author

N93-70966*# National Aeronautics and Space Administration. Lewis Research Center, Cleveland, OH.

LEWIS SAFETY MANUAL

KENNETH OCONNOR, ed. and ROBERT W. GRAHAM, ed. (Analex Corp., Brook Park, OH.) Nov. 1992 425 p (Contract NAS3-25776) (NASA-TM-104438; E-6277; NAS 1.15:104438) Avail: CASI HC A18/MF A04

It is the overall safety policy of the NASA-Lewis to manage and conduct its research and development operations in such a manner as to eliminate or minimize potential hazards and to avoid accidents involving personnel or property. In addition, every effort will be made to protect the environment and to avoid exposure to hazardous materials. This Safety Manual has been prepared to update previous compilations of policies and recommended practices and as a guide to implementing the overall safety policy. The Manual describes the safety organizations of the center and outlines the procedures to be followed in safety practices. The Manual is organized into chapters dealing with major topics. Each chapter is further subdivided into subtopics, as indicated by its table of Contents. A comprehensive listing of important references

is included with each chapter. The Lewis Safety Manual applies to the Cleveland and Plum Brook facilities and will be modified or amended when deemed necessary. Author

COMMUNICATIONS AND RADAR

Includes radar; land and global communications; communications theory; and optical communications.

A93-10929* National Aeronautics and Space Administration. Lewis Research Center, Cleveland, OH.

THE PERFORMANCE EVALUATION OF A NEW NEURAL NETWORK BASED TRAFFIC MANAGEMENT SCHEME FOR A SATELLITE COMMUNICATION NETWORK

NIRWAN ANSARI and DEQUAN LIU (New Jersey Inst. of Technology, Newark) In GLOBECOM '91 - IEEE Global Telecommunications Conference, Phoenix, AZ, Dec. 2-5, 1991, Conference Record. Vol. 1 New York Institute of Electrical and Electronics Engineers, Inc. 1991 p. 110-114. refs (Contract NAG3-1244) Copyright

A neural-network-based traffic management scheme for a satellite communication network is described. The scheme consists of two levels of management. The front end of the scheme is a derivation of Kohonen's self-organization model to configure maps for the satellite communication network dynamically. The model consists of three stages. The first stage is the pattern recognition task, in which an exemplar map that best meets the current network requirements is selected. The second stage is the analysis of the discrepancy between the chosen exemplar map and the state of the network, and the adaptive modification of the chosen exemplar map to conform closely to the network requirement (input data pattern) by means of Kohonen's self-organization. On the basis of certain performance criteria, whether a new map is generated to replace the original chosen map is decided in the third stage. A state-dependent routing algorithm, which arranges the incoming call to some proper path, is used to make the network more efficient and to lower the call block rate. Simulation results demonstrate that the scheme, which combines self-organization and the state-dependent routing mechanism, provides better performance in terms of call block rate than schemes that only have either the self-organization mechanism or the routing mechanism. I.E.

A93-10958* National Aeronautics and Space Administration. Lewis Research Center, Cleveland, OH.

PERFORMANCE EVALUATION OF LAND MOBILE SATELLITE SYSTEM UNDER FADING AND INTERFERENCE USING MULTIPLE TCM BY MONTE-CARLO SIMULATION

S. C. KWA, MARK J. VANDERAAR, JUNGHWAN KIM (Toledo Univ., OH), and GRADY H. STEVENS (NASA, Lewis Research Center, Cleveland, OH) In GLOBECOM '91 - IEEE Global Telecommunications Conference, Phoenix, AZ, Dec. 2-5, 1991, Conference Record. Vol. 3 New York Institute of Electrical and Electronics Engineers, Inc. 1991 p. 1564-1568. refs (Contract NAG3-157) Copyright

The performance of the land mobile satellite system (LMSS) was evaluated by using two trellis coded modulation (TCM) schemes under multipath fading and interference. The results were also compared with uncoded QPSK. The trellis coding formats included a trellis code designed for optimum performance on the fading channel that typifies satellite to mobile communications, as well as one designed for optimum performance in the additive white Gaussian noise (AWGN) channel. The results show that, in Rayleigh fading, the TCM code designed for optimum performance in such an environment performs 4 dB better than the TCM code designed for optimum performance in AWGN, and 10 dB better

than the uncoded format, at a bit error rate (BER) of $10 \exp^{-4}$. Additional results on the performance degradation due to the nonlinearities in the satellite transponder and the adjacent and cochannel interference show that the TCM system is more sensitive than the uncoded system to the phase distortion caused by these impairments. I.E.

A93-26237 National Aeronautics and Space Administration. Lewis Research Center, Cleveland, OH.

MULTIPLE-ACCESS PHASED ARRAY ANTENNA SIMULATOR FOR A DIGITAL BEAM-FORMING SYSTEM INVESTIGATION
ROBERT J. KERCZEWSKI, JOHN YU, JOANNE C. WALTON, THOMAS D. PERL, MONTY ANDRO, and ROBERT E. ALEXOVICH (NASA, Lewis Research Center, Cleveland, OH) International Journal of Satellite Communications (ISSN 0737-2884) vol. 10, no. 5 Sept.-Oct. 1992 p. 293-297. Previously announced in STAR as N92-17062 ICDSC-9 - International Conference on Digital Satellite Communications, Copenhagen, Denmark, May 18-22, 1992, Selected Papers. A93-26226 09-32 refs (Contract RTOP 650-60-23)

Future versions of data relay satellite systems are currently being planned by NASA. Being given consideration for implementation are on-board digital beamforming techniques which will allow multiple users to simultaneously access a single S-band phased array antenna system. To investigate the potential performance of such a system, a laboratory simulator has been developed at NASA's Lewis Research Center. This paper describes the system simulator, and in particular, the requirements, design and performance of a key subsystem, the phased array antenna simulator, which provides realistic inputs to the digital processor including multiple signals, noise, and nonlinearities. Author

A93-32561* National Aeronautics and Space Administration. Lewis Research Center, Cleveland, OH.

EFFICIENT DEMULTIPLEXING ALGORITHM FOR NONCONTIGUOUS CARRIERS

A. A. THANAWALA, S. C. KWATRA, M. M. JAMALI (Toledo Univ., OH), and J. BUDINGER (NASA, Lewis Research Center, Cleveland, OH) Journal of Spacecraft and Rockets (ISSN 0022-4650) vol. 29, no. 4 July-Aug. 1992 p. 498-501. refs (Contract NAG3-799) Copyright

A channel separation algorithm for the frequency division multiple access/time division multiplexing (FDMA/TDM) scheme is presented. It is shown that implementation using this algorithm can be more effective than the fast Fourier transform (FFT) algorithm when only a small number of carriers need to be selected from many, such as satellite Earth terminals. The algorithm is based on polyphase filtering followed by application of a generalized Walsh-Hadamard transform (GWHT). Comparison of the transform technique used in this algorithm with discrete Fourier transform (DFT) and FFT is given. Estimates of the computational rates and power requirements to implement this system are also given. Author

A93-35016* National Aeronautics and Space Administration. Lewis Research Center, Cleveland, OH.

SPECTRAL-DOMAIN MOMENT-METHOD ANALYSIS OF COPLANAR MICROSTRIP PARASITIC SUBARRAYS

WEI CHEN, KAI-FONG LEE (Toledo Univ., OH), and R. Q. LEE (NASA, Lewis Research Center, Cleveland, OH) Microwave and Optical Technology Letters (ISSN 0895-2477) vol. 6, no. 3 March 5, 1993 p. 157-163. Research supported by Ohio Supercomputing Center refs Copyright

Basic characteristics of several configurations of coplanar microstrip parasitic subarrays consisting of one fed patch and two or more parasitic patches were investigated by means of a spectral-domain full-wave analysis and the moment method analysis. Results are presented for radiating- and nonradiating edge-coupled three-element linear subarrays and for a five-patch cross. A comparison of the theoretical input impedance results

obtained by the analysis of a three-element linear array showed a reasonable agreement between computed and measured R and X values. AIAA

A93-36991* National Aeronautics and Space Administration. Lewis Research Center, Cleveland, OH.

DIRECTIVITY VERSUS ELEMENT SPACING FOR A SCANNING ARRAY

M. ZIMMERMAN (Analex Corp., Cleveland, OH) and R. Q. LEE (NASA, Lewis Research Center, Cleveland, OH) Microwave and Optical Technology Letters (ISSN 0895-2477) vol. 6, no. 6 May 1993 p. 361-363. refs Copyright

The results of the present examination of the relationship of directivity with element spacings of linear, rectangular, and hexagonal arrays indicate that element spacings for optimal directivity vary with scan angles; this is especially true in the case of changes in aperture sizes and the appearance of grating lobes in the visible space. Grating lobe effects are more pronounced for isotropic than for directive element arrays. Directivity decreases as the beam scans off from boresight, and rapidly diminishes for scans over 30 deg. The hexagonal array has higher directivity for scans of less than 20 deg, and the linear array for those over 30 deg. AIAA

A93-37038* National Aeronautics and Space Administration. Lewis Research Center, Cleveland, OH.

AN ALL DIGITAL IMPLEMENTATION OF A MODIFIED HAMMING NET FOR VIDEO COMPRESSION WITH PREDICTION AND QUANTIZATION CIRCUITS

RICHARD KAUL, KENNETH ADKINS, and STEVEN BIBYK (Ohio State Univ., Columbus) In IEEE International Conference on Systems Engineering, Dayton, OH, Aug. 1-3, 1991, Proceedings New York Institute of Electrical and Electronics Engineers, Inc. 1991 p. 214-217. refs (Contract NAG3-1082) Copyright

The hardware and algorithms used to vector quantize (VQ) predicted pixel intensity differences for real-time video compression are described. The hardware is designed for rapid vector quantization performance, which entails the development of application-specific associative memory circuits. A modified DPCM algorithm is originally examined to determine how neural circuitry could enhance its operation. It was determined that quantization and encoding could be improved by consolidating these two functions into one, and by increasing the amount of information (i.e. number of pixels) quantized at a time. The result is a predictive scheme that vector quantizes differential values. Some of the disadvantages of VQ algorithms are solved using associative memories. The video compression algorithm and the associative memory design are described. Author

A93-38221* National Aeronautics and Space Administration. Lewis Research Center, Cleveland, OH.

MODIFYING REAL CONVOLUTIONAL CODES FOR PROTECTING DIGITAL FILTERING SYSTEMS

G. R. REDINBO (California Univ., Davis) and BERNHARD ZAGAR (Graz Technical Univ., Austria) IEEE Transactions on Information Theory (ISSN 0018-9448) vol. 39, no. 2 March 1993 p. 553-564. refs (Contract NSF MIP-90-02664; NAG3-1166) Copyright

A novel method is proposed for protecting digital filters from temporary and permanent failures that are not easily detected by conventional fault-tolerant computer design principles, on the basis of the error-detecting properties of real convolutional codes. Erroneous behavior is detected by externally comparing the calculated and regenerated parity samples. Great simplifications are obtainable by modifying the code structure to yield simplified parity channels with finite impulse response structures. A matrix equation involving the original parity values of the code and the polynomial of the digital filter's transfer function is formed, and row manipulations separate this equation into a set of

homogeneous equations constraining the modifying scaling coefficients and another set which defines the code parity values' implementation. AIAA

A93-52237* National Aeronautics and Space Administration. Lewis Research Center, Cleveland, OH.

A RECIPROCITY FORMULATION FOR THE EM SCATTERING BY AN OBSTACLE WITHIN A LARGE OPEN CAVITY

PRABHAKAR H. PATHAK and ROBERT J. BURKHOLDER (Ohio State Univ., Columbus) IEEE Transactions on Microwave Theory and Techniques (ISSN 0018-9480) vol. 41, no. 4 April 1993 p. 702-707. Research supported by JSEP refs (Contract NAG3-476; N00014-89-J-1007) Copyright

A formulation based on a generalized reciprocity theorem is developed for analyzing the external high frequency EM scattering by a complex obstacle inside a relatively arbitrary open-ended waveguide cavity when it is illuminated by an external source. This formulation is also extended to include EM fields whose time dependence may be nonperiodic. A significant advantage of this formulation is that it allows one to break up the analysis into two independent parts; one deals with the waveguide cavity shape alone and the other with the obstacle alone. The external scattered field produced by the obstacle (in the presence of the waveguide cavity structure) is given in terms of a generalized reciprocity integral over a surface $S(T)$ corresponding to the interior waveguide cavity cross section located conveniently but sufficiently close to the obstacle. Furthermore, the fields coupled into the cavity from the source in the exterior region generally need to propagate only one-way via the open front end (which is directly illuminated) to the interior surface $S(T)$ in this approach, and not back, in order to find the external field scattered by the obstacle.

Author (revised)

N93-12366*# National Aeronautics and Space Administration. Lewis Research Center, Cleveland, OH.

DAMPING AND SCATTERING OF ELECTROMAGNETIC WAVES BY SMALL FERRITE SPHERES SUSPENDED IN AN INSULATOR

GERALD W. ENGLERT Aug. 1992 12 p (Contract RTOP 505-62-52) (NASA-TM-105837; E-6363-1; NAS 1.15:105837) Avail: CASI HC A03/MF A01

The intentional degradation of electromagnetic waves by their penetration into a media comprised of somewhat sparsely distributed energy absorbing ferrite spheres suspended in an electrical insulator is investigated. Results are presented in terms of generalized parameters involving wave length and sphere size, sphere resistivity, permeability, and spacing; their influence on dissipation of wave power by eddy currents, magnetic hysteresis, and scattering is shown. Author

N93-12481*# National Aeronautics and Space Administration. Lewis Research Center, Cleveland, OH.

DATA DISTRIBUTION SATELLITE

GRADY H. STEVENS Feb. 1992 17 p Presented at the International Space Year Conference on Earth and Space Science Information Systems, Pasadena, CA, 10-13 Feb. 1992; sponsored by California Inst. of Tech. Previously announced in IAA as A92-48224

(Contract RTOP 144-50-50) (NASA-TM-105778; E-7205; NAS 1.15:105778) Avail: CASI HC A03/MF A01

The Data Distribution Satellite (DDS), operating in conjunction with the planned space network, the National Research and Education Network and its commercial derivatives, would play a key role in networking the emerging supercomputing facilities, national archives, academic, industrial, and government institutions. Centrally located over the United States in geostationary orbit, DDS would carry sophisticated on-board switching and make use of advanced antennas to provide an array of special services. Institutions needing continuous high data rate service would be networked together by use of a microwave switching matrix and

electronically steered hopping beams. Simultaneously, DDS would use other beams and on board processing to interconnect other institutions with lesser, low rate, intermittent needs. Dedicated links to White Sands and other facilities would enable direct access to space payloads and sensor data. Intersatellite links to a second generation ATDRS, called Advanced Space Data Acquisition and Communications System (ASDACS), would eliminate one satellite hop and enhance controllability of experimental payloads by reducing path delay. Similarly, direct access would be available to the supercomputing facilities and national data archives. Economies with DDS would be derived from its ability to switch high rate facilities amongst users needed. At the same time, having a CONUS view, DDS would interconnect with any institution regardless of how remote. Whether one needed high rate service or low rate service would be immaterial. With the capability to assign resources on demand, DDS will need only carry a portion of the resources needed if dedicated facilities were used. Efficiently switching resources to users as needed, DDS would become a very feasible spacecraft, even though it would tie together the space network, the terrestrial network, remote sites, 1000's of small users, and those few who need very large data links intermittently. Author

N93-20257*# National Aeronautics and Space Administration. Lewis Research Center, Cleveland, OH.

COMPRESSING SUBBANDED IMAGE DATA WITH LEMPEL-ZIV-BASED CODERS

DANIEL GLOVER and S. C. KWATRA (Toledo Univ., OH.) Feb. 1993 22 p Proposed for presentation at the Data Compression Conference, Snowbird, UT, 30 Mar. - 1 Apr. 1993; sponsored by the IEEE

(Contract RTOP 144-10-10) (NASA-TM-105998; E-7600; NAS 1.15:105998) Avail: CASI HC A03/MF A01

A method of improving the compression of image data using Lempel-Ziv-based coding is presented. Image data is first processed with a simple transform, such as the Walsh Hadamard Transform, to produce subbands. The subbanded data can be rounded to eight bits or it can be quantized for higher compression at the cost of some reduction in the quality of the reconstructed image. The data is then run-length coded to take advantage of the large runs of zeros produced by quantization. Compression results are presented and contrasted with a subband compression method using quantization followed by run-length coding and Huffman coding. The Lempel-Ziv-based coding in conjunction with run-length coding produces the best compression results at the same reconstruction quality (compared with the Huffman-based coding) on the image data used. Author

N93-20260*# National Aeronautics and Space Administration. Lewis Research Center, Cleveland, OH.

MODAL RING METHOD FOR THE SCATTERING OF ELECTROMAGNETIC WAVES

KENNETH J. BAUMEISTER and KEVIN L. KREIDER (Akron Univ., OH.) Oct. 1993 4 p Proposed for presentation at the 9th Company Conference on the Computation of Electromagnetic Fields, Miami, FL, 31 Oct. - 4 Nov. 1993; sponsored by IEEE (Contract RTOP 505-62-52)

(NASA-TM-105966; E-7489; NAS 1.15:105966) Avail: CASI HC A01/MF A01

The modal ring method for electromagnetic scattering from perfectly electric conducting (PEC) symmetrical bodies is presented. The scattering body is represented by a line of finite elements (triangular) on its outer surface. The infinite computational region surrounding the body is represented analytically by an eigenfunction expansion. The modal ring method effectively reduces the two dimensional scattering problem to a one-dimensional problem similar to the method of moments. The modal element method is capable of handling very high frequency scattering because it has a highly banded solution matrix. Author

N93-22483*# National Aeronautics and Space Administration. Lewis Research Center, Cleveland, OH.

REAL-TIME TRANSMISSION OF DIGITAL VIDEO USING VARIABLE-LENGTH CODING

THOMAS P. BIZON, MARY JO SHALKHAUSER, and WAYNE A. WHYTE, JR. Mar. 1993 17 p Presented at the Data Compression Conference (DCC '93), Snowbird, UT, 30 Mar. - 1 Apr. 1993; sponsored by the IEEE

(Contract RTOP 144-10-10)

(NASA-TM-106092; E-7730; NAS 1.15:106092) Avail: CASI HC A03/MF A01

Huffman coding is a variable-length lossless compression technique where data with a high probability of occurrence is represented with short codewords, while 'not-so-likely' data is assigned longer codewords. Compression is achieved when the high-probability levels occur so frequently that their benefit outweighs any penalty paid when a less likely input occurs. One instance where Huffman coding is extremely effective occurs when data is highly predictable and differential coding can be applied (as with a digital video signal). For that reason, it is desirable to apply this compression technique to digital video transmission; however, special care must be taken in order to implement a communication protocol utilizing Huffman coding. This paper addresses several of the issues relating to the real-time transmission of Huffman-coded digital video over a constant-rate serial channel. Topics discussed include data rate conversion (from variable to a fixed rate), efficient data buffering, channel coding, recovery from communication errors, decoder synchronization, and decoder architectures. A description of the hardware developed to execute Huffman coding and serial transmission is also included. Although this paper focuses on matters relating to Huffman-coded digital video, the techniques discussed can easily be generalized for a variety of applications which require transmission of variable-length data. Author (revised)

N93-26476*# National Aeronautics and Space Administration. Lewis Research Center, Cleveland, OH.

ALLOCATIONS BY THE 1992 WORLD ADMINISTRATIVE RADIO CONFERENCE

ANN O. HEYWARD In JPL, Proceedings of the 16th NASA Propagation Experimenters Meeting (NAPEX 16) and the Advanced Communications Technology Satellite (ACTS) Propagation Studies Miniworkshop p 123-128 1 Aug. 1992

Avail: CASI HC A02/MF A03

An overview of the 1992 World Administrative Radio Conference is presented with viewgraphs. Allocations of radio frequency spectrum are addressed. Mobile satellite service, broadcast satellite service, and uplink power control beacons are also addressed.

CASI

N93-26481*# National Aeronautics and Space Administration. Lewis Research Center, Cleveland, OH.

OLYMPUS/ACTS SCINTILLATION EXPERIMENT AT THE LEWIS RESEARCH CENTER

NOULIE THEOFYLAKTOS In JPL, Proceedings of the 16th NASA Propagation Experimenters Meeting (NAPEX 16) and the Advanced Communications Technology Satellite (ACTS) Propagation Studies Miniworkshop p 171-181 1 Aug. 1992

Avail: CASI HC A03/MF A03

Details of the OLYMPUS/ACTS scintillation experiment at the Lewis Research Center are presented in viewgraph form. Temporal frequency spectra of log-amplitude fluctuations are given. CASI

N93-26903*# National Aeronautics and Space Administration. Lewis Research Center, Cleveland, OH.

SATELLITES AND THE BISDN: AN OVERVIEW OF NASA R/D

E. A. BOBINSKY and W. D. IVANCIC Nov. 1992 10 p Presented at the ISDN/Broadband 1992 Information Gatekeepers, Inc., Reston, VA, 16-20 Nov. 1992

(Contract RTOP 144-10-10)

(NASA-TM-106108; E-7757; NAS 1.15:106108) Avail: CASI HC A02/MF A01

NASA is currently the only U.S. government agency developing

advanced technology on behalf of the commercial communications satellite industry. The Agency's commercial communications program includes several activities which are either directly or indirectly related to the potential use of satellites within a broadband integrated services digital network (BISDN). Lewis Research Center's Space Electronics Division is actively pursuing a number of thrusts aimed at the integration of satellites into the BISDN through the development of high-risk and proof-of-concept technology. Author

N93-31856*# National Aeronautics and Space Administration. Lewis Research Center, Cleveland, OH.

COMBINATORIAL PULSE POSITION MODULATION FOR POWER-EFFICIENT FREE-SPACE LASER COMMUNICATIONS

JAMES M. BUDINGER, M. VANDERAAR (Sverdrup Technology, Inc., Brook Park, OH.), P. WAGNER (Sverdrup Technology, Inc., Brook Park, OH.), and STEVEN BIBYK (Ohio State Univ., Columbus.) Jan. 1993 14 p Presented at the Society of Photo-Optical Instrumentation Engineers Conference, Los Angeles, CA, 16-23 1993; sponsored by the International Society for Optical Engineering

(Contract RTOP 506-72-21)

(NASA-TM-106241; E-7961; NAS 1.15:106241) Avail: CASI HC A03/MF A01

A new modulation technique called combinatorial pulse position modulation (CPPM) is presented as a power-efficient alternative to quaternary pulse position modulation (QPPM) for direct-detection, free-space laser communications. The special case of 16C4PPM is compared to QPPM in terms of data throughput and bit error rate (BER) performance for similar laser power and pulse duty cycle requirements. The increased throughput from CPPM enables the use of forward error corrective (FEC) encoding for a net decrease in the amount of laser power required for a given data throughput compared to uncoded QPPM. A specific, practical case of coded CPPM is shown to reduce the amount of power required to transmit and receive a given data sequence by at least 4.7 dB. Hardware techniques for maximum likelihood detection and symbol timing recovery are presented. Author (revised)

N93-70235*# National Aeronautics and Space Administration. Lewis Research Center, Cleveland, OH.

ACTS SYSTEM HANDBOOK, REVISION CHANGE INDEX

PETER A. LOWRY Mar. 1989 23 p

(NASA-TM-107982; NAS 1.15:107982) CASI HC A03/MF A01

The topics covered include the following: an acts system overview; spacecraft and ground terminal hardware and network control software; baseband processor mode of operation; and microwave switch matrix mode of operation. Author

ELECTRONICS AND ELECTRICAL ENGINEERING

Includes test equipment and maintainability; components, e.g., tunnel diodes and transistors; microminiaturization; and integrated circuitry.

A93-17063* National Aeronautics and Space Administration. Lewis Research Center, Cleveland, OH.

BUFFER LAYERS FOR HIGH-TC THIN FILMS ON SAPPHIRE

X. D. WU, S. R. FOLTYN, R. E. MUENCHHAUSEN, D. W. COOKE (Los Alamos National Lab., NM), A. PIQUE (Neocera, Inc., College Park, MD), D. KALOKITIS, V. PENDRICK, and E. BELOHOUBEK (David Sarnoff Research Center, Princeton, NJ) Journal of Superconductivity (ISSN 0896-1107) vol. 5, no. 4 Aug. 1992 p. 353-359. Research supported by DOE refs

(Contract NAS3-25929)

Copyright

Buffer layers of various oxides including CeO₂ and yttrium-stabilized zirconia (YSZ) have been deposited on R-plane

sapphire. The orientation and crystallinity of the layers were optimized to promote epitaxial growth of $\text{YBa}_2\text{Cu}_3\text{O}_{7-\delta}$ (YBCO) thin films. An ion beam channeling minimum yield of about 3 percent was obtained in the CeO_2 layer on sapphire, indicating excellent crystallinity of the buffer layer. Among the buffer materials used, CeO_2 was found to be the best one for YBCO thin films on R-plane sapphire. High T_c and J_c were obtained in YBCO thin films on sapphire with buffer layers. Surface resistances of the YBCO films were about 4 m Ω at 77 K and 25 GHz. Author

A93-17610* National Aeronautics and Space Administration. Lewis Research Center, Cleveland, OH.

INTERMODULATION IN THE OSCILLATORY MAGNETORESISTANCE OF A TWO-DIMENSIONAL ELECTRON GAS

S. E. SCHACHAM, E. J. HAUGLAND, and S. A. ALTEROVITZ (NASA, Lewis Research Center, Cleveland, OH) Physical Review B - Condensed Matter, 3rd Series (ISSN 0163-1829) vol. 45, no. 23 June 15, 1992 p. 13,417-13,422. Previously announced in STAR as N92-32975 Research supported by National Research Council refs Copyright

The oscillatory magnetoresistance wave form of a 2-D electron gas shows multiple structures when two subbands are populated. In addition to high-field oscillations at a frequency equal to the sum of the two frequencies corresponding to the concentrations of the subbands, and to a superposition at intermediate fields, we observed oscillations at the difference frequency at low fields and higher temperatures. The field range at which the frequency difference is observed increases with increasing temperature. The crossover from superposition to frequency difference is accompanied by a beat. Similar beats, whose field location shows identical temperature dependence, can be observed in data obtained by other groups on different structures. The various components of the wave form can be attributed to different phase relations between the diagonal and off-diagonal elements of the conductivity tensor. It is shown how the intermodulation term, when inserted into the extended oscillatory equation, can give rise to all three structures. Author

A93-20016* National Aeronautics and Space Administration. Lewis Research Center, Cleveland, OH.

NOVEL COPLANAR WAVEGUIDE TO SLOTLINE TRANSITION ON HIGH RESISTIVITY SILICON

R. N. SIMONS, S. R. TAUB, and P. G. YOUNG (NASA, Lewis Research Center, Cleveland, OH) Electronics Letters (ISSN 0013-5194) vol. 28, no. 24 Nov. 19, 1992 p. 2209, 2210. refs Copyright

Two novel coplanar waveguide (CPW) to slotline transitions have been fabricated and tested on high resistivity silicon. The first transition uses an air bridge to couple RF power from the CPW line to the slotline and has the entire circuit on the top side of the wafer. In the second transition, the grounded CPW line and the slotline are on opposite sides of the wafer and are coupled electromagnetically. The measured average intersection loss and return loss per transition are better than 1.5 and 10 dB, respectively, with a bandwidth greater than 30 percent at C-band frequencies. Author

A93-23454* National Aeronautics and Space Administration. Lewis Research Center, Cleveland, OH.

AN ANALYSIS OF THE FREQUENCY LIMITATIONS OF AN $\text{Al}(\text{x})\text{Ga}(1-\text{x})\text{As/GaAs}$ OPTICAL MODULATOR

M. TABIB-AZAR, P. C. CLASPY (Case Western Reserve Univ., Cleveland, OH), C. CHOREY, and K. B. BHASIN (NASA, Lewis Research Center, Cleveland, OH) Microwave and Optical Technology Letters (ISSN 0895-2477) vol. 6, no. 1 Jan. 1993 p. 18-22. refs Copyright

An analysis is made of the frequency response of an $\text{Al}(\text{x})\text{Ga}(1-\text{x})\text{As/GaAs}$ optical modulator operating at a wavelength of 0.83 micron and utilizing the linear-optic effect in a Mach-Zehnder

configuration. It is shown that, in semiconductor modulators, electroabsorption should be taken into account in optimizing the frequency response of the device. It is also shown that, by incorporating an insulator (a semiconductor with a large band gap) between the metallic electrode and the channel, the capacitance of the electroabsorptive modulator can be kept low at a reasonable value under the worst conditions. V.L.

A93-24367* National Aeronautics and Space Administration. Lewis Research Center, Cleveland, OH.

THE STRUCTURAL AND ELECTRICAL PROPERTIES OF LOW-RESISTANCE NI CONTACTS TO INP

NAVID S. FATEMI (Sverdrup Technology, Inc.; NASA, Lewis Research Center, Cleveland, OH) and VICTOR G. WEIZER (NASA, Lewis Research Center, Cleveland, OH) Journal of Applied Physics (ISSN 0021-8979) vol. 73, no. 1 Jan. 1, 1993 p. 289-295. refs

(Contract NAS3-25266)

Copyright

We have investigated the electrical and metallurgical behavior of the Ni-InP contact system. Specific contact resistivity (R_c) values in the low $10 \exp -7 \Omega\text{-sq cm}$ range are achieved with Ni-only contacts on n-InP by sintering at 400 C for several minutes. The postsinter contact metallization consists of three layers, arranged in the sequence: InP/Ni3P/Ni2P/In. Extended sintering (40 min) at 400 C brings about a rise in R_c to the $10 \exp -4 \Omega\text{-sq cm}$ range. After extended sintering, the contact metallization is found to consist of only two layers, arranged in the sequence: InP/Ni2P/In. Based on the correlation between low R_c and the presence of Ni3P at the metal-InP interface, it is suggested that the presence of Ni3P is the cause of the low R_c values. We show that the sintering schedule used to achieve low values of R_c is accompanied by substantial metal-InP interdiffusion that results in severe device degradation. Author

A93-25776* National Aeronautics and Space Administration. Lewis Research Center, Cleveland, OH.

MONOLITHIC MICROWAVE INTEGRATED CIRCUITS FOR SENSORS, RADAR, AND COMMUNICATIONS SYSTEMS; PROCEEDINGS OF THE MEETING, ORLANDO, FL, APR. 2-4, 1991

REGIS F. LEONARD, ED. and KUL B. BHASIN, ED. (NASA, Lewis Research Center, Cleveland, OH) Bellingham, WA Society of Photo-Optical Instrumentation Engineers (SPIE Proceedings. Vol. 1475) 1991 360 p.

(SPIE-1475; ISBN 0-8194-0584-1) Copyright

Consideration is given to MMICs for airborne phased arrays, monolithic GaAs integrated circuit millimeter wave imaging sensors, accurate design of multiport low-noise MMICs up to 20 GHz, an ultralinear low-noise amplifier technology for space communications, variable-gain MMIC module for space applications, a high-efficiency dual-band power amplifier for radar applications, a high-density circuit approach for low-cost MMIC circuits, coplanar SIMMWIC circuits, recent advances in monolithic phased arrays, and system-level integrated circuit development for phased-array antenna applications. Consideration is also given to performance enhancement in future communications satellites with MMIC technology insertion, application of Ka-band MMIC technology for an Orbiter/ACTS communications experiment, a space-based millimeter wave debris tracking radar, low-noise high-yield octave-band feedback amplifiers to 20 GHz, quasi-optical MESFET VCOs, and a high-dynamic-range mixer using novel balun structure. (For individual items see A93-25777 to A93-25814) O.G.

A93-25786* National Aeronautics and Space Administration. Lewis Research Center, Cleveland, OH.

A HIGH EFFICIENCY KA-BAND MONOLITHIC PSEUDOMORPHIC HEMT AMPLIFIER

PAUL SAUNIER, HUA Q. TSERNG, and Y. C. KAO (Texas Instruments Central Research Labs., Dallas) In Monolithic microwave integrated circuits for sensors, radar, and communications systems; Proceedings of the Meeting, Orlando, FL, Apr. 2-4, 1991 Bellingham, WA Society of Photo-Optical

33 ELECTRONICS AND ELECTRICAL ENGINEERING

Instrumentation Engineers 1991 p. 86-90. refs
(Contract NAS3-24239)
Copyright

A monolithic three-stage Ka-band amplifier has been designed and fabricated on a doped channel heterostructure. Devices with gate length of 0.2 micron and gate width of 50, 100, and 250 micron were cascaded. The gate and drain bias networks were also integrated. The small signal gain is 31 dB and the amplifier is capable of an output power of 190 mW with 23 dB gain and 30.2 percent power added efficiency at 31 GHz. This is a record efficiency for a multistage MMIC at this frequency. Author

A93-25796* National Aeronautics and Space Administration. Lewis Research Center, Cleveland, OH.

MILLIMETER-WAVE PSEUDOMORPHIC HEMT MMIC PHASED ARRAY COMPONENTS FOR SPACE COMMUNICATIONS

G. L. LAN, C. K. PAO, C. S. WU, G. MANDOLIA, M. HU, S. YUAN (Hughes Aircraft Co., Microwave Products Div., Torrance, CA), and REGIS LEONARD (NASA, Lewis Research Center, Cleveland, OH) *In* Monolithic microwave integrated circuits for sensors, radar, and communications systems; Proceedings of the Meeting, Orlando, FL, Apr. 2-4, 1991 Bellingham, WA Society of Photo-Optical Instrumentation Engineers 1991 p. 184-192. refs

Copyright

Recent advances in pseudomorphic HEMT MMIC (PMHEMT/MMIC) technology have made it the preferred candidate for high performance millimeter-wave components for phased array applications. This paper describes the development of PMHEMT/MMIC components at Ka-band and V-band. Specifically, the following PMHEMT/MMIC components will be described: power amplifiers at Ka-band; power amplifiers at V-band; and four-bit phase shifters at V-band. For the Ka-band amplifier, 125 mW output power with 5.5 dB gain and 21 percent power added efficiency at 2 dB compression point has been achieved. For the V-band amplifier, 112 mW output power with 6 dB gain and 26 percent power added efficiency has been achieved. And, for the V-band phase shifter, four-bit (45 deg steps) phase shifters with less than 8 dB insertion loss from 61 GHz to 63 GHz will be described. Author

A93-25798 National Aeronautics and Space Administration. Lewis Research Center, Cleveland, OH.

SYSTEM-LEVEL INTEGRATED CIRCUIT (SLIC) DEVELOPMENT FOR PHASED ARRAY ANTENNA APPLICATIONS

K. A. SHALKHAUSER and C. A. RAQUET (NASA, Lewis Research Center, Cleveland, OH) *In* Monolithic microwave integrated circuits for sensors, radar, and communications systems; Proceedings of the Meeting, Orlando, FL, Apr. 2-4, 1991 Bellingham, WA Society of Photo-Optical Instrumentation Engineers 1991 p. 204-209. Previously announced in STAR as N91-23354 (Contract RTOP 650-60-20)

Copyright

A microwave/millimeter wave system-level integrated circuit (SLIC) being developed for use in phased array antenna applications is described. The program goal is to design, fabricate, test, and deliver an advanced integrated circuit that merges radio frequency (RF) monolithic microwave integrated circuit (MMIC) technologies with digital, photonic, and analog circuitry that provide control, support, and interface functions. As a whole, the SLIC will offer improvements in RF device performance, uniformity, and stability while enabling accurate, rapid, repeatable control of the RF signal. Furthermore, the SLIC program addresses issues relating to insertion of solid state devices into antenna systems, such as the reduction in number of bias, control, and signal lines. Program goals, approach, and status are discussed. Author

A93-25800* National Aeronautics and Space Administration. Lewis Research Center, Cleveland, OH.

MIXED APPLICATION MMIC TECHNOLOGIES - PROGRESS IN COMBINING RF, DIGITAL AND PHOTONIC CIRCUITS

S. SWIRHUN, M. BENDETT, V. SOKOLOV, P. BAUHAHN, C.

SULLIVAN, R. MACTAGGART, S. MUKHERJEE, M. HIBBS-BRENNER, and J. MONDAL (Honeywell Systems and Research Center, Bloomington, MN) *In* Monolithic microwave integrated circuits for sensors, radar, and communications systems; Proceedings of the Meeting, Orlando, FL, Apr. 2-4, 1991 Bellingham, WA Society of Photo-Optical Instrumentation Engineers 1991 p. 223-230. Research supported by NASA, U.S. Navy, DARPA, and Honeywell, Inc. refs

Copyright

Approaches for future 'mixed application' monolithic integrated circuits (ICs) employing optical receive/transmit, RF amplification and modulation and digital control functions are discussed. We focus on compatibility of the photonic component fabrication with conventional RF and digital IC technologies. Recent progress at Honeywell in integrating several parts of the desired RF/digital/photonic circuit integration suite required for construction of a future millimeter-wave optically-controlled phased-array element are illustrated. Author

A93-25806 National Aeronautics and Space Administration. Lewis Research Center, Cleveland, OH.

GaAs MONOLITHIC R.F. MODULES FOR SARSAT DISTRESS BEACONS

MICHAEL A. CAULEY (NASA, Lewis Research Center, Cleveland, OH) *In* Monolithic microwave integrated circuits for sensors, radar, and communications systems; Proceedings of the Meeting, Orlando, FL, Apr. 2-4, 1991 Bellingham, WA Society of Photo-Optical Instrumentation Engineers 1991 p. 275-279. Previously announced in STAR as N91-21184 refs (Contract RTOP 342-02-00)

Copyright

Monolithic GaAs UHF components for use in SARSAT Emergency Distress beacons are under development by Microwave Monolithics, Inc., Simi Valley, CA. The components include a bi-phase modulator, driver amplifier, and a 5 watt power amplifier. Author

A93-25808* National Aeronautics and Space Administration. Lewis Research Center, Cleveland, OH.

PHASE SHIFTER TECHNOLOGY ASSESSMENT - PROSPECTS AND APPLICATIONS

VLADIMIR SOKOLOV (Honeywell Systems and Research Center, Bloomington, MN) *In* Monolithic microwave integrated circuits for sensors, radar, and communications systems; Proceedings of the Meeting, Orlando, FL, Apr. 2-4, 1991 Bellingham, WA Society of Photo-Optical Instrumentation Engineers 1991 p. 288-302. Research supported by NASA refs

Copyright

Capabilities and limitations of MMIC phase shifter technology at microwave and millimeter wave frequencies are reviewed. MMIC-based phase arrays make it possible to integrate active elements at the array face, i.e., to incorporate transmit power amplifiers and/or low noise amplifiers at each antenna element. Active elements make it possible to increase power efficiency and reliability and provide graceful degradation. Monolithic integration of the various transmit/receive functions including phase shifting is considered to be feasible through at least the lower millimeter-wave frequency range (about 30-100 GHz). MMIC integration also allows more flexibility in array design including those that are intended for airborne conformal applications. O.G.

A93-25892 National Aeronautics and Space Administration. Lewis Research Center, Cleveland, OH.

ELECTROMECHANICAL SYSTEMS WITH TRANSIENT HIGH POWER RESPONSE OPERATING FROM A RESONANT AC LINK

LINDA M. BURROWS and IRVING G. HANSEN (NASA, Lewis Research Center, Cleveland, OH) *In* IECEC '92; Proceedings of the 27th Intersociety Energy Conversion Engineering Conference, San Diego, CA, Aug. 3-7, 1992. Vol. 1 Warrendale, PA Society of Automotive Engineers, Inc. 1992 p. 1.257-1.260. Previously announced in STAR as N92-28985 refs

(Contract RTOP 906-11-03)

Copyright

The combination of an inherently robust asynchronous (induction) electrical machine with the rapid control of energy provided by a high frequency resonant ac link enables the efficient management of higher power levels with greater versatility. This could have a variety of applications from launch vehicles to all-electric automobiles. These types of systems utilize a machine which is operated by independent control of both the voltage and frequency. This is made possible by using an indirect field-oriented control method which allows instantaneous torque control all four operating quadrants. Incorporating the ac link allows the converter in these systems to switch at the zero crossing of every half cycle of the ac waveform. This zero loss switching of the link allows rapid energy variations to be achieved without the usual frequency proportional switching loss. Several field-oriented control systems were developed under contract to NASA. Author

A93-25894 National Aeronautics and Space Administration. Lewis Research Center, Cleveland, OH.

NEUTRON, GAMMA RAY, AND TEMPERATURE EFFECTS ON THE ELECTRICAL CHARACTERISTICS OF THYRISTORS

A. J. FRASCA (Wittenberg Univ., Springfield, OH) and G. E. SCHWARZE (NASA, Lewis Research Center, Cleveland, OH) / In IECEC '92; Proceedings of the 27th Intersociety Energy Conversion Engineering Conference, San Diego, CA, Aug. 3-7, 1992. Vol. 1 Warrendale, PA Society of Automotive Engineers, Inc. 1992 p. 1.267-1.273. Previously announced in STAR as N92-28432 refs

(Contract RTOP 590-13-31)

Copyright

Experimental data showing the effects of neutrons, gamma rays, and temperature on the electrical and switching characteristics of phase-control and inverter-type SCR's are presented. The special test fixture built for mounting, heating, and instrumenting the test devices is described. Four SCR's were neutron irradiated at 300 K and four at 365 K for fluences up to 3.2×10^{13} pn/sq. cm, and eight were gamma irradiated at 300 K only for gamma doses up to 5.1 Mrads. The electrical measurements were made during irradiation and the switching measurements were made only before and after irradiation. Radiation induced crystal defects, resulting primarily from fast neutrons, caused the reduction of minority carrier lifetime through the generation of R-G centers. The reduction in lifetime caused increases in the on-state voltage drop and in the reverse and forward leakage currents, and decreases in the turn-off time. Author

A93-25895 National Aeronautics and Space Administration. Lewis Research Center, Cleveland, OH.

COMPARISON OF HIGH TEMPERATURE, HIGH FREQUENCY CORE LOSS AND DYNAMIC B-H LOOPS OF A 2V-49FE-49CO AND A GRAIN ORIENTED 3SI-FE ALLOY

W. R. WIESERMAN (Pittsburgh Univ., Johnstown, PA), G. E. SCHWARZE (NASA, Lewis Research Center, Cleveland, OH), and J. M. NIEDRA (Sverdrup Technology, Inc., Cleveland, OH) / In IECEC '92; Proceedings of the 27th Intersociety Energy Conversion Engineering Conference, San Diego, CA, Aug. 3-7, 1992. Vol. 1 Warrendale, PA Society of Automotive Engineers, Inc. 1992 p. 1.275-1.282. Previously announced in STAR as N92-30397 refs

(Contract RTOP 590-13-31)

Copyright

The design of power magnetic components such as transformers, inductors, motors, and generators, requires specific knowledge about the magnetic and electrical characteristics of the magnetic materials used in these components. Limited experimental data exists that characterizes the performance of soft magnetic materials for the combined conditions of high temperature and high frequency over a wide flux density range. An experimental investigation of a 2V-49-Fe-49Co (Supremendur) and a grain oriented 3 Si-Fe (Magnesil) alloy was conducted over the temperature range of 23 to 300 C and frequency range of 0.1 to 10 kHz. The effects of temperature, frequency, and maximum

flux density on the core loss and dynamic B-H loops for sinusoidal voltage excitation conditions are examined for each of these materials. A comparison of the core loss of these two materials is also made over the temperature and frequency range investigated. Author

A93-25896* National Aeronautics and Space Administration. Lewis Research Center, Cleveland, OH.

EVALUATION OF THE BENEFITS OF HIGH TEMPERATURE ELECTRONICS FOR LUNAR POWER SYSTEMS

EDGAR H. FAY (Sverdrup Technology, Inc., Brook Park, OH) / In IECEC '92; Proceedings of the 27th Intersociety Energy Conversion Engineering Conference, San Diego, CA, Aug. 3-7, 1992. Vol. 1 Warrendale, PA Society of Automotive Engineers, Inc. 1992 p. 1.283-1.288. refs

(Contract NAS3-25266)

Copyright

A comparative evaluation is conducted of several approaches to the cooling of a lunar power system's power electronics, in view of the 400 K temperature of the 354-hour lunar day and lunar dust accumulation, which can contaminate power components and radiator surfaces. It is noted that, by raising the power electronics' baseplate temperature to 480 K, no thermal control system is required; the surface of the baseplate acts as its own, waste-heat-rejecting radiator, but the baseplate must be kept clean of lunar dust contamination. O.C.

A93-25919* National Aeronautics and Space Administration. Lewis Research Center, Cleveland, OH.

NASA REQUIREMENTS AND APPLICATIONS ENVIRONMENTS FOR ELECTRICAL POWER WIRING

MARK W. STAVNES and AHMAD N. HAMMOND (Sverdrup Technology, Inc., Brook Park, OH) / In IECEC '92; Proceedings of the 27th Intersociety Energy Conversion Engineering Conference, San Diego, CA, Aug. 3-7, 1992. Vol. 1 Warrendale, PA Society of Automotive Engineers, Inc. 1992 p. 1.461-1.468. refs

(Contract NAS3-25266)

Copyright

While a large data base for electrical arc track-resistant wire insulation exists for aircraft electrical power systems, comparable spacecraft-pertinent data are in limited supply. Existing insulation systems have been found to arc-track at potentials as low as 28 V dc. An account is presently given of the electrical, thermal, mechanical, and operational requirements for specification and testing of candidate wiring systems for spacecraft applications. O.C.

A93-26076 National Aeronautics and Space Administration. Lewis Research Center, Cleveland, OH.

M-H CHARACTERISTICS AND DEMAGNETIZATION RESISTANCE OF SAMARIUM-COBALT PERMANENT MAGNETS TO 300 C

J. M. NIEDRA (Sverdrup Technology, Inc., Brook Park, OH) / In IECEC '92; Proceedings of the 27th Intersociety Energy Conversion Engineering Conference, San Diego, CA, Aug. 3-7, 1992. Vol. 5 Warrendale, PA Society of Automotive Engineers, Inc. 1992 p. 5.303-5.308. Previously announced in STAR as N92-28723 refs

(Contract NAS3-25266; RTOP 590-13-11)

Copyright

The influence of temperature on the M-H demagnetization characteristics of permanent magnets is important information for the full utilization of the capabilities of samarium-cobalt magnets at high temperatures in demagnetization-resistant permanent magnet devices. In high temperature space power converters, such as free-piston Stirling engine driven linear alternators, magnet demagnetization can occur as long-term consequence of thermal agitation of domains and of metallurgical change, and also as an immediate consequence of too large an applied field. Investigated here is the short-term demagnetization resistance to applied fields derived from basic M-H data. These quasistatic demagnetization data were obtained for commercial, high-intrinsic-coercivity,

33 ELECTRONICS AND ELECTRICAL ENGINEERING

Sm2Co17-type magnets from 5 sources, in the temperature range 23 to 300 C. An electromagnet driven, electronic hysteresigraph was used to test the 1-cm cubic samples. The observed variation of the 2nd quadrant M-H characteristics was a typical rapid loss of M-coercivity and a relatively lesser loss of remanence with increasing temperature. Author

A93-26100* National Aeronautics and Space Administration. Lewis Research Center, Cleveland, OH.
OPERATION OF HIGH POWER CONVERTERS IN PARALLEL
D. K. DECKER and L. Y. INOUE (TRW Space and Technology Group, Redondo Beach, CA) In IECEC '92; Proceedings of the 27th Intersociety Energy Conversion Engineering Conference, San Diego, CA, Aug. 3-7, 1992. Vol. 6 Warrendale, PA Society of Automotive Engineers, Inc. 1992 p. 6.49-6.53.
(Contract NAS3-25093)
Copyright

Three different unequal power sharing approaches for parallel operation of converters - droop, master-slave, and proportional adjustment - are discussed. The approaches have been incorporated in the breadboard dc-dc converter units used in the space station power management and distribution dc test bed at the Lewis Research Center, where the system operation has been verified. C.A.B.

A93-26106 National Aeronautics and Space Administration. Lewis Research Center, Cleveland, OH.
LOAD CONVERTER INTERACTIONS WITH THE SECONDARY SYSTEM IN THE SPACE STATION FREEDOM POWER MANAGEMENT AND DISTRIBUTION DC TEST BED
RAMON C. LEBRON (NASA, Lewis Research Center, Cleveland, OH) In IECEC '92; Proceedings of the 27th Intersociety Energy Conversion Engineering Conference, San Diego, CA, Aug. 3-7, 1992. Vol. 6 Warrendale, PA Society of Automotive Engineers, Inc. 1992 p. 6.87-6.92. Previously announced in STAR as N92-34219 refs
(Contract RTOP 474-42-10)
Copyright

The NASA LeRC in Cleveland, Ohio, is responsible for the design, development, and assembly of the Space Station Freedom (SSF) Electrical Power System (EPS). In order to identify and understand system level issues during the SSF program design and development phases, a system Power Management and Distribution (PMAD) dc test bed was assembled. Some of the objectives of this test bed facility are the evaluation of, system efficiency, power quality, system stability, and system protection and reconfiguration schemes. In order to provide a realistic operating scenario, dc Load Converter Units are used in the PMAD dc test bed to characterize the user interface with the power system. These units are dc to dc converters that provide the final system regulation before power is delivered to the load. This final regulation is required on the actual space station because the majority of user loads will require voltage levels different from the secondary bus voltage. This paper describes the testing of load converters in an end to end system environment (from solar array to loads) where their interactions and compatibility with other system components are considered. Some of the system effects of interest that are presented include load converters transient behavior interactions with protective current limiting switchgear, load converters ripple effects, and the effects of load converter constant power behavior with protective features such as foldback. Author

A93-26107 National Aeronautics and Space Administration. Lewis Research Center, Cleveland, OH.
STABILITY TESTING AND ANALYSIS OF A PMAD DC TEST BED FOR THE SPACE STATION FREEDOM
ROBERT M. BUTTON (NASA, Lewis Research Center, Cleveland, OH) and ANDREW S. BRUSH (Sverdrup Technology, Inc., Brook Park, OH) In IECEC '92; Proceedings of the 27th Intersociety Energy Conversion Engineering Conference, San Diego, CA, Aug. 3-7, 1992. Vol. 6 Warrendale, PA Society of Automotive Engineers, Inc. 1992 p. 6.93-6.98. Previously announced in

STAR as N92-31282 refs
(Contract RTOP 474-42-10)
Copyright

The Power Management and Distribution (PMAD) dc Test Bed at the NASA Lewis Research Center is introduced. Its usefulness to the Space Station Freedom Electrical Power (EPS) development and design are discussed in context of verifying system stability. Stability criteria developed by Middlebrook and Cuk are discussed as they apply to constant power dc to dc converters exhibiting negative input impedance at low frequencies. The utility-type Secondary Subsystem is presented and each component is described. The instrumentation used to measure input and output impedance under load is defined. Test results obtained from input and output impedance measurements of test bed components are presented. It is shown that the PMAD dc Test Bed Secondary Subsystem meets the Middlebrook stability criterion for certain loading conditions. Author

A93-26108 National Aeronautics and Space Administration. Lewis Research Center, Cleveland, OH.
EMTP BASED STABILITY ANALYSIS OF SPACE STATION ELECTRIC POWER SYSTEM IN A TEST BED ENVIRONMENT
NARAYAN V. DRAVID (NASA, Lewis Research Center, Cleveland, OH), THOMAS J. KACPURA (Sverdrup Technology, Inc., Brook Park, OH), and ANDREW M. O'CONNOR (Analytical Engineering Corp., North Olmsted, OH) In IECEC '92; Proceedings of the 27th Intersociety Energy Conversion Engineering Conference, San Diego, CA, Aug. 3-7, 1992. Vol. 6 Warrendale, PA Society of Automotive Engineers, Inc. 1992 p. 6.99-6.104. Previously announced in STAR as N93-15503 refs
(Contract RTOP 474-42-10)
Copyright

The Space Station Freedom Electric Power System (EPS) will convert solar energy into electric energy and distribute the same using an 'all dc', Power Management and Distribution (PMAD) System. Power conditioning devices (dc to dc converters) are needed to interconnect parts of this system operating at different nominal voltage levels. Operation of such devices could generate under damped oscillations (instability) under certain conditions. Criteria for instability are examined and verified for a single device. Suggested extension of the criteria to a system operation is examined by using the EMTP model of the PMAD dc test bed. Wherever possible, data from the test bed is compared with the modeling results. Author

A93-27243* National Aeronautics and Space Administration. Lewis Research Center, Cleveland, OH.
SUPERCONDUCTIVITY APPLICATIONS FOR INFRARED AND MICROWAVE DEVICES II; PROCEEDINGS OF THE MEETING, ORLANDO, FL, APR. 4, 5, 1991
VERNON O. HEINEN, ED. and KUL B. BHASIN, ED. (NASA, Lewis Research Center, Cleveland, OH) Bellingham, WA Society of Photo-Optical Instrumentation Engineers (SPIE Proceedings. Vol. 1477) 1991 250 p.
(SPIE-1477; ISBN 0-8194-0586-8) Copyright

Topics discussed include thin-film technology, microwave transmission lines and resonators, microwave devices and circuits, infrared detectors and bolometers, and superconducting junctions. Papers are presented on possible enhancement in bolometric response using free-standing film of YBa2Cu3O(x), aging and surface instability in high-Tc superconductors, epitaxial Ti2Ba2CaCu2O8 thin films on LaAlO3 and their microwave device properties, the performance of stripline resonators using sputtered YBCO films, and a coplanar waveguide microwave filter of YBa2Cu3O7. Attention is also given to the performance characteristics of Y-Ba-Cu-O microwave superconducting detectors, high-Tc bolometer developments for planetary missions, infrared detectors from YBaCuO thin films, high-temperature superconductor junction technology, and submillimeter receiver components using superconducting tunnel junctions. (For individual items see A93-27244 to A93-27248) I.S.

A93-27244 National Aeronautics and Space Administration. Lewis Research Center, Cleveland, OH.

DESIGN ASPECTS AND COMPARISON BETWEEN HIGH TC SUPERCONDUCTING COPLANAR WAVEGUIDE AND MICROSTRIP LINE

K. S. KONG (Texas Univ., Austin), K. B. BHASIN (NASA, Lewis Research Center, Cleveland, OH), and T. ITOH (California Univ., Los Angeles) *In* Superconductivity applications for infrared and microwave devices II; Proceedings of the Meeting, Orlando, FL, Apr. 4, 5, 1991 Bellingham, WA Society of Photo-Optical Instrumentation Engineers 1991 p. 57-65. Previously announced in STAR as N91-27445 refs

(Contract RTOP 506-59-4C; NCC3-192; N00014-89-J-1006)

Copyright

The high T sub c superconducting microstrip line and coplanar waveguide are compared in terms of the loss characteristics and the design aspects. The quality factor Q values for each structure are compared in respect to the same characteristic impedance with the comparable dimensions of the center conductor of the coplanar waveguide and the strip of the microstrip line. Also, the advantages and disadvantages for each structure are discussed in respect to passive microwave circuit applications. Author

A93-27245 National Aeronautics and Space Administration. Lewis Research Center, Cleveland, OH.

COMPARATIVE STUDY OF BOLOMETRIC AND NON-BOLOMETRIC SWITCHING ELEMENTS FOR MICROWAVE PHASE SHIFTERS

MASSOOD TABIB-AZAR (Case Western Reserve Univ., Cleveland, OH), KUL B. BHASIN, and ROBERT R. ROMANOFKY (NASA, Lewis Research Center, Cleveland, OH) *In* Superconductivity applications for infrared and microwave devices II; Proceedings of the Meeting, Orlando, FL, Apr. 4, 5, 1991 Bellingham, WA Society of Photo-Optical Instrumentation Engineers 1991 p. 85-94. Previously announced in STAR as N91-25320 Research supported by Reliance Electric Co. refs

(Contract RTOP 506-44-21; NCC3-203)

Copyright

The performance of semiconductor and high critical temperature superconductor switches is compared as they are used in delay-line-type microwave and millimeter-wave phase shifters. Such factors as their ratios of the off-to-on resistances, parasitic reactances, power consumption, speed, input-to-output isolation, ease of fabrication, and physical dimensions are compared. Owing to their almost infinite off-to-on resistance ratio and excellent input-to-output isolation, bolometric superconducting switches appear to be quite suitable for use in microwave phase shifters; their only drawbacks are their speed and size. The SUPERFET, a novel device whose operation is based on the electric field effect in high critical temperature ceramic superconductors is also discussed. Preliminary results indicate that the SUPERFET is fast and that it can be scaled; therefore, it can be fabricated with dimensions comparable to semiconductor field-effect transistors. Author

A93-32771* National Aeronautics and Space Administration. Lewis Research Center, Cleveland, OH.

MEASUREMENT OF THE TEMPERATURE COEFFICIENT OF RATIO TRANSFORMERS

MATTHEW E. BRIGGS, ROBERT W. GAMMON, and J. N. SHAUMEYER (Maryland Univ., College Park) Review of Scientific Instruments (ISSN 0034-6748) vol. 64, no. 3 March 1993 p. 756-759. refs

(Contract NAS3-25370)

Copyright

We have measured the temperature coefficient of the output of several ratio transformers at ratios near 0.500,000 using an ac bridge and a dual-phase, lock-in amplifier. The two orthogonal output components were each resolved to ± 1 ppb of the bridge drive signal. The results for three commercial ratio transformers between 20 and 50 C range from 0.5 to 100 ppb/K for the signal component in phase with the bridge drive, and from 4 to 300 ppb/K for the quadrature component. Author

A93-35649* National Aeronautics and Space Administration. Lewis Research Center, Cleveland, OH.

EFFECT OF A DIELECTRIC OVERLAY ON A LINEARLY TAPERED SLOT ANTENNA EXCITED BY A COPLANAR WAVEGUIDE

RAINEE N. SIMONS, RICHARD Q. LEE, THOMAS D. PERL (NASA, Lewis Research Center, Cleveland, OH), and JOHN SILVESTRO (Clemson Univ., SC) Microwave and Optical Technology Letters (ISSN 0895-2477) vol. 6, no. 4 March 20, 1993 p. 225-228. refs

Copyright

The effect of a dielectric overlay on a linearly tapered slot antenna (LTSA) is studied. The LTSA under study has very wide bandwidth and excellent radiation patterns. A dielectric overlay improves the patterns and directivity of the antenna by increasing the electrical length and effective aperture of the antenna. A dielectric overlay can also be used to reduce the physical length of the antenna without compromising the pattern quality. AIAA

A93-36514* National Aeronautics and Space Administration. Lewis Research Center, Cleveland, OH.

COPLANAR WAVEGUIDE RADIAL LINE STUB

R. N. SIMONS and S. R. TAUB (NASA, Lewis Research Center, Cleveland, OH) Electronics Letters (ISSN 0013-5194) vol. 29, no. 4 Feb. 18, 1993 p. 412-414. refs

Copyright

A coplanar waveguide radial line stub resonator is experimentally characterized with respect to stub radius, sectoral angle, substrate thickness and relative dielectric constant. A simple closed-form design equation, which predicts the resonance radius of the stub, is presented. Author

A93-36994* National Aeronautics and Space Administration. Lewis Research Center, Cleveland, OH.

INPUT IMPEDANCE OF COAXIALLY FED RECTANGULAR MICROSTRIP ANTENNA ON ELECTRICALLY THICK SUBSTRATE

WEI CHEN, KAI-FONG LEE (Toledo Univ., OH), and R. Q. LEE (NASA, Lewis Research Center, Cleveland, OH) Microwave and Optical Technology Letters (ISSN 0895-2477) vol. 6, no. 6 May 1993 p. 387-390. Research supported by Ohio Supercomputing Center refs

Copyright

A full-wave spectral domain analysis has been used to obtain input-impedance results for a probe-fed rectangular-patch antenna, modeling the source as a magnetic-current frill. Multiple modes are used in the probe surface current to account for axial and azimuthal variations. It is established that maximum resistance is dependent on the substrate loss tangent. The axial variation of the probe current must be taken into account for substrate thicknesses greater than about 0.02 wavelengths. AIAA

A93-37409* National Aeronautics and Space Administration. Lewis Research Center, Cleveland, OH.

HIGH FREQUENCY PERFORMANCE OF

SI(1-X)GE(X)/SI(1-Y)GE(Y)/SI(1-X)GE(X) HBTs

D. ROSENFELD and S. A. ALTEROVITZ (NASA, Lewis Research Center, Cleveland, OH) Electronics Letters (ISSN 0013-5194) vol. 29, no. 3 Feb. 4, 1993 p. 260, 261. refs

Copyright

The results of a theoretical study of the performance of high speed SiGe HBTs is presented. The study includes a group of SiGe HBTs in which the Ge concentration in the base is 20 percent higher than that in the emitter and collector (i.e., $y = x + 0.2$). It is shown that the composition dependences of $f(T)$ and the $f(\max)$ are nonmonotonic. As the Ge composition in the emitter and collector layers is increased, $f(T)$ and $f(\max)$ first decrease, then remain constant and finally increase to attain their highest values. Author (revised)

A93-37413* National Aeronautics and Space Administration. Lewis Research Center, Cleveland, OH.

APPLICATION OF HIGH-QUALITY SiO₂ GROWN BY MULTIPOLAR ECR SOURCE TO SI/SiGe MISFET

K. T. SUNG, W. Q. LI, S. H. LI, S. W. PANG, and P. K. BHATTACHARYA (Michigan Univ., Ann Arbor) Electronics Letters (ISSN 0013-5194) vol. 29, no. 3 Feb. 4, 1993 p. 277, 278. refs

(Contract NAS3-24239)

Copyright

A 5 nm-thick SiO₂ gate was grown on an Si(p+)/Si(0.8)Ge(0.2) modulation-doped heterostructure at 26 C with an oxygen plasma generated by a multipolar electron cyclotron resonance source. The ultrathin oxide has breakdown field above 12 MV/cm and fixed charge density about 3×10^{10} exp 10/sq cm. Leakage current as low as 1/micro-A was obtained with the gate biased at 4 V. The MISFET with 0.25 x 25 sq m gate shows maximum drain current of 41.6 mA/mm and peak transconductance of 21 mS/mm. Author (revised)

A93-37421* National Aeronautics and Space Administration. Lewis Research Center, Cleveland, OH.

HIGH-EFFICIENCY HIGH-GAIN MONOLITHIC HETEROSTRUCTURE FET AMPLIFIER AT 31 GHZ

H. Q. TSERNG, P. SAUNIER, and Y.-C. KAO (Texas Instruments Central Research Labs., Dallas) Electronics Letters (ISSN 0013-5194) vol. 29, no. 3 Feb. 4, 1993 p. 304-306. refs

(Contract NAS3-24239)

Copyright

A three-stage heterostructure FET monolithic amplifier has achieved a power-added efficiency of 36 percent with 200 mW output and 18 dB gain at 31 GHz. At a higher drain voltage, the output power increases to 280 mW (with 17.5 dB gain and 31 percent PAE) at a power density of 0.7 W/mm. The MMIC chip measures 2.63 x 1.35 sq mm and requires only a single drain bias and a single gate bias. Author (revised)

A93-37570* National Aeronautics and Space Administration. Lewis Research Center, Cleveland, OH.

A 1.6-KW, 110-KHZ DC-DC CONVERTER OPTIMIZED FOR IGBT'S

KEMING CHEN (REM Technologies, Inc., Schenectady, NY) and THOMAS A. STUART (Toledo Univ., OH) IEEE Transactions on Power Electronics (ISSN 0885-8993) vol. 8, no. 1 Jan. 1993 p. 18-25. refs

(Contract NAG3-959; NAG3-1102)

Copyright

A full bridge dc-dc converter using a zero-current and zero-voltage switching technique is described. This circuit utilizes the characteristics of the IGBT to achieve power and frequency combinations that are much higher than previously reported for this device. Experimental results are included for a 1.6-kW, 110-kHz converter with 95 percent efficiency. Author

A93-37574* National Aeronautics and Space Administration. Lewis Research Center, Cleveland, OH.

A 10-GHZ AMPLIFIER USING AN EPITAXIAL LIFT-OFF PSEUDOMORPHIC HEMT DEVICE

PAUL G. YOUNG (Toledo Univ., OH), ROBERT R. ROMANOFKY, SAMUEL A. ALTEROVITZ, RAFAEL A. MENA (NASA, Lewis Research Center, Cleveland, OH), and EDWYN D. SMITH (Toledo Univ., OH) IEEE Microwave and Guided Wave Letters (ISSN 1051-8207) vol. 3, no. 4 April 1993 p. 107-109. refs

(Contract NAG3-1226)

Copyright

A process to integrate epitaxial lift-off devices and microstrip circuits has been demonstrated using a pseudomorphic HEMT on an alumina substrate. The circuit was a 10 GHz amplifier with the interconnection between the device and the microstrip circuit being made with photolithographically patterned metal. The measured and modeled response correlated extremely well with a maximum gain of 6.8 dB and a return loss of -14 dB at 10.4 GHz. Author

A93-38994* National Aeronautics and Space Administration. Lewis Research Center, Cleveland, OH.

GREATLY IMPROVED 3C-SiC P-N JUNCTION DIODES GROWN BY CHEMICAL VAPOR DEPOSITION

PHILIP G. NEUDECK, DAVID J. LARKIN (NASA, Lewis Research Center, Cleveland, OH), JONATHAN E. STARR (Ohio Aerospace Inst., Brook Park), J. A. POWELL (NASA, Lewis Research Center, Cleveland, OH), CARL S. SALUPO (Calspan Corp., Middleburg Heights, OH), and LAWRENCE G. MATUS (NASA, Lewis Research Center, Cleveland, OH) IEEE Electron Device Letters (ISSN 0741-3106) vol. 14, no. 3 March 1993 p. 136-139. refs

Copyright

This paper reports the fabrication and initial electrical characterization of greatly improved 3C-SiC (beta-SiC) p-n junction diodes. These diodes, which were grown on commercially available 6H-SiC substrates by chemical vapor deposition, demonstrate rectification to -200 V at room temperature, representing a fourfold improvement in reported 3C-SiC diode blocking voltage. The reverse leakage currents and saturation current densities measured on these diodes also show significant improvement compared to previously reported 3C-SiC p-n junction diodes. When placed under sufficient forward bias, the diodes emit significantly bright green-yellow light. These results should lead to substantial advancements in 3C-SiC transistor performance. Author (revised)

A93-39348* National Aeronautics and Space Administration. Lewis Research Center, Cleveland, OH.

EXTRA HIGH SPEED MODIFIED LUNDELL ALTERNATOR PARAMETERS AND OPEN/SHORT-CIRCUIT CHARACTERISTICS FROM GLOBAL 3D-FE MAGNETIC FIELD SOLUTIONS

R. WANG and N. A. DEMERDASH (Clarkson Univ., Potsdam, NY) IEEE Transactions on Energy Conversion (ISSN 0885-8969) vol. 7, no. 2 June 1992 p. 330-338; Discussion, p. 339; Authors' Closure, IEEE, Winter Meeting, New York, Feb. 3-7, 1991 refs

(Contract NAG3-818)

Copyright

The combined magnetic vector potential - magnetic scalar potential method of computation of 3D magnetic fields by finite elements, introduced in a companion paper, is used for global 3D field analysis and machine performance computations under open-circuit and short-circuit conditions for an example 14.3 kVA modified Lundell alternator, whose magnetic field is of intrinsic 3D nature. The computed voltages and currents under these machine test conditions were verified and found to be in very good agreement with corresponding test data. Results of use of this modelling and computation method in the study of a design alteration example, in which the stator stack length of the example alternator is stretched in order to increase voltage and volt-ampere rating, are given here. These results demonstrate the inadequacy of conventional 2D-based design concepts and the imperative of use of this type of 3D magnetic field modelling in the design and investigation of such machines. Author

A93-39349* National Aeronautics and Space Administration. Lewis Research Center, Cleveland, OH.

COMPUTATION OF LOAD PERFORMANCE AND OTHER PARAMETERS OF EXTRA HIGH SPEED MODIFIED LUNDELL ALTERNATORS FROM 3D-FE MAGNETIC FIELD SOLUTIONS

R. WANG and N. A. DEMERDASH (Clarkson Univ., Potsdam, NY) IEEE Transactions on Energy Conversion (ISSN 0885-8969) vol. 7, no. 2 June 1992 p. 342-350; Discussion, p. 351; Authors' Closure, IEEE, Winter Meeting, New York, Feb. 3-7, 1991 refs

(Contract NAG3-818)

Copyright

The combined magnetic vector potential - magnetic scalar potential method of computation of 3D magnetic fields by finite elements, introduced in a companion paper, in combination with state modeling in the abc-frame of reference, are used for global 3D magnetic field analysis and machine performance computation under rated load and overload condition in an example 14.3 kVA modified Lundell alternator. The results vividly demonstrate the

3D nature of the magnetic field in such machines, and show how this model can be used as an excellent tool for computation of flux density distributions, armature current and voltage waveform profiles and harmonic contents, as well as computation of torque profiles and ripples. Use of the model in gaining insight into locations of regions in the magnetic circuit with heavy degrees of saturation is demonstrated. Experimental results which correlate well with the simulations of the load case are given. Author

A93-39350* National Aeronautics and Space Administration. Lewis Research Center, Cleveland, OH.

THREE DIMENSIONAL MAGNETIC FIELDS IN EXTRA HIGH SPEED MODIFIED LUNDELL ALTERNATORS COMPUTED BY A COMBINED VECTOR-SCALAR MAGNETIC POTENTIAL FINITE ELEMENT METHOD

N. A. DEMERDASH, R. WANG (Clarkson Univ., Potsdam, NY), and R. SECUNDE (NASA, Lewis Research Center, Cleveland, OH) IEEE Transactions on Energy Conversion (ISSN 0885-8969) vol. 7, no. 2 June 1992 p. 353-362; Discussion, p. 362-364; Authors' Closure IEEE, Winter Meeting, New York, Feb. 3-7, 1991 refs (Contract NAG3-818) Copyright

A 3D finite element (FE) approach was developed and implemented for computation of global magnetic fields in a 14.3 kVA modified Lundell alternator. The essence of the new method is the combined use of magnetic vector and scalar potential formulations in 3D FEs. This approach makes it practical, using state of the art supercomputer resources, to globally analyze magnetic fields and operating performances of rotating machines which have truly 3D magnetic flux patterns. The 3D FE-computed fields and machine inductances as well as various machine performance simulations of the 14.3 kVA machine are presented in this paper and its two companion papers. Author (revised)

A93-39351* National Aeronautics and Space Administration. Lewis Research Center, Cleveland, OH.

LOW RESISTANCE SILVER CONTACTS TO INDIUM PHOSPHIDE - ELECTRICAL AND METALLURGICAL CONSIDERATIONS

VICTOR G. WEIZER (NASA, Lewis Research Center, Cleveland, OH) and NAVID S. FATEMI (Sverdrup Technology, Inc., Cleveland, OH) Journal of Applied Physics (ISSN 0021-8979) vol. 73, no. 5 March 1, 1993 p. 2353-2359. refs (Contract NAS3-25266) Copyright

The electrical and metallurgical behavior of the Ag-InP contact system has been investigated. Specific contact resistivity (R_c) values in the low $10 \exp -6$ Ohm sq cm range are readily achieved on n-InP (Si: $1.7 \times 10 \exp 18/\text{cu cm}$) after sintering at 400 C for several minutes. The low R_c values, however, are shown to be accompanied by dissolution of InP into the metallization, resulting in device degradation. An analysis of the sinter-induced metallurgical interactions shows this system to be similar to the well-characterized Au-InP system, albeit with fundamental differences. The similarities include the dissociative diffusion of In, the reaction-suppressing effect of SiO₂ capping, and especially, the formation of a phosphide layer at the metal-InP interface. The low post-sinter R_c values in the Ag-InP system may be due to the presence of a Ag₂P layer at the metal-InP interface; low values of R_c can be achieved without incurring device degrading metallurgical interactions by introducing a thin Ag₂P layer between the InP and the current carrying metallization. Author (revised)

A93-39719* National Aeronautics and Space Administration. Lewis Research Center, Cleveland, OH.

ON THE EFFECTS OF GRID ILL-CODITIONING IN THREE DIMENSIONAL FINITE ELEMENT VECTOR POTENTIAL MAGNETOSTATIC FIELD COMPUTATIONS

R. WANG and N. A. DEMERDASH (Clarkson Univ., Potsdam, NY) IEEE Transactions on Magnetics (ISSN 0018-9464) vol. 26, no. 5 Sept. 1990 p. 2190-2192. refs

(Contract NAG3-818)

Copyright

The effects of finite element grid geometries and associated ill-conditioning were studied in single medium and multi-media (air-iron) three dimensional magnetostatic field computation problems. The sensitivities of these 3D field computations to finite element grid geometries were investigated. It was found that in single medium applications the unconstrained magnetic vector potential curl-curl formulation in conjunction with first order finite elements produce global results which are almost totally insensitive to grid geometries. However, it was found that in multi-media (air-iron) applications first order finite element results are sensitive to grid geometries and consequent elemental shape ill-conditioning. These sensitivities were almost totally eliminated by means of the use of second order finite elements in the field computation algorithms. Practical examples are given in this paper to demonstrate these aspects mentioned above. Author

A93-39720* National Aeronautics and Space Administration. Lewis Research Center, Cleveland, OH.

THEORETICAL AND NUMERICAL DIFFICULTIES IN 3-D VECTOR POTENTIAL METHODS IN FINITE ELEMENT MAGNETOSTATIC COMPUTATIONS

N. A. DEMERDASH and R. WANG (Clarkson Univ., Potsdam, NY) IEEE Transactions on Magnetics (ISSN 0018-9464) vol. 26, no. 5 Sept. 1990 p. 1656-1658. refs (Contract NAG3-818) Copyright

This paper describes the results of application of three well known 3D magnetic vector potential (MVP) based finite element formulations for computation of magnetostatic fields in electrical devices. The three methods were identically applied to three practical examples, the first of which contains only one medium (free space), while the second and third examples contained a mix of free space and iron. The first of these methods is based on the unconstrained curl-curl of the MVP, while the second and third methods are predicated upon constraining the divergence of the MVP 10 zero (Coulomb's Gauge). It was found that the two latter methods cease to give useful and meaningful results when the global solution region contains a mix of media of high and low permeabilities. Furthermore, it was found that their results do not achieve the intended zero constraint on the divergence of the MVP. Author

A93-42550* National Aeronautics and Space Administration. Lewis Research Center, Cleveland, OH.

SIMPLE, EXTREMELY LOW RESISTANCE CONTACT SYSTEM TO N-INP THAT DOES NOT EXHIBIT METAL-SEMICONDUCTOR INTERMIXING DURING SINTERING

VICTOR G. WEIZER (NASA, Lewis Research Center, Cleveland, OH) and NAVID S. FATEMI (Sverdrup Technology, Inc., Brook Park, OH) Applied Physics Letters (ISSN 0003-6951) vol. 62, no. 21 May 24, 1993 p. 2731-2733. refs (Contract NAS3-25266) Copyright

Contact formation to InP is plagued by the violent metal-semiconductor intermixing that takes place during the contact sintering process. We have discovered a truly unique contact system, involving Au and Ge, which is easily fabricated, which exhibits extremely low values of contact resistivity, and in which there is virtually no metal-semiconductor interdiffusion, even after extended sintering. We present a description of this contact system and suggest possible mechanisms to explain the observed behavior. Author

A93-44763 National Aeronautics and Space Administration. Lewis Research Center, Cleveland, OH.

PERFORMANCE OF TLCABACUO 30 GHZ 64 ELEMENT ANTENNA ARRAY

L. L. LEWIS, G. KOEPF (Ball Aerospace Systems Group, Communications Systems Div., Broomfield, CO), K. B. BHASIN (NASA, Lewis Research Center, Cleveland, OH), and M. A. RICHARD (Case Western Reserve Univ., Cleveland, OH) IEEE

Transactions on Applied Superconductivity (ISSN 1051-8223) vol. 3, no. 1, pt. 4 March 1993 p. 2844-2847. 1992 Applied Superconductivity Conference, Chicago, IL, Aug. 23-28, 1992, Proceedings. Pt. 3. A93-44612 18-33 Research supported by NASA refs
Copyright

A 64-element, 30-GHz microstrip antenna array with corporate feed network was designed and built on a 0.254-mm (10-mil) thick lanthanum aluminate substrate. One antenna pattern was fabricated from gold film, and a second pattern used TiCaBaCuO high-temperature superconductor. Both antennas used gold ground planes deposited on the reverse side of the substrate. Gain and radiation patterns were measured for both antennas at room temperature and at cryogenic temperatures. Observations agree well with simple models for loss and microwave beam width, with a gain on boresight of 20.3 dB and beam width of 15 deg for the superconducting antenna. The antenna loss is only 1.9 dB.

Author

A93-44965* National Aeronautics and Space Administration. Lewis Research Center, Cleveland, OH.

PROGRESS IN SILICON CARBIDE SEMICONDUCTOR TECHNOLOGY

J. A. POWELL (NASA, Lewis Research Center, Cleveland, OH), P. G. NEUDECK (Ohio Aerospace Inst., Brook Park), L. G. MATUS (NASA, Lewis Research Center, Cleveland, OH), and J. B. PETIT (Sverdrup Technology, Inc., Brook Park, OH) In Wide band-gap semiconductors Pittsburgh, PA Materials Research Society 1992 p. 495-505. refs

Copyright

Silicon carbide semiconductor technology has been advancing rapidly over the last several years. Advances have been made in boule growth, thin film growth, and device fabrication. This paper will review reasons for the renewed interest in SiC, and will review recent developments in both crystal growth and device fabrication.

Author

A93-47127* National Aeronautics and Space Administration. Lewis Research Center, Cleveland, OH.

DIRECT OPTICAL INJECTION LOCKING OF MONOLITHICALLY INTEGRATED IN(0.53)GA(0.47)AS/IN(0.52)AL(0.48)AS MODFET OSCILLATORS

D. YANG, P. K. BHATTACHARYA, and T. BROCK (Michigan Univ., Ann Arbor) Electronics Letters (ISSN 0013-5194) vol. 29, no. 11 May 27, 1993 p. 944, 945. Research supported by DARPA refs
(Contract NAG3-988; F30602-92-C-0087)

Copyright

The authors have fabricated monolithically integrated In(0.53)Ga(0.47)As/In(0.52)Al(0.48)As 0.25-micron gate MODFET oscillators. The results of direct optical subharmonic injection locking of these oscillator circuits at 10.159 and 19.033 GHz are presented.

Author (revised)

A93-49382* National Aeronautics and Space Administration. Lewis Research Center, Cleveland, OH.

ELLIPSOMETRIC CHARACTERIZATION OF IN(0.52)AL(0.48)AS AND OF MODULATION DOPED FIELD EFFECT TRANSISTOR STRUCTURES ON INP SUBSTRATES

S. A. ALTEROVITZ (NASA, Lewis Research Center, Cleveland, OH), R. M. SIEG (Cleveland State Univ., OH), J. PAMULAPATI, and P. K. BHATTACHARYA (Michigan Univ., Ann Arbor) Applied Physics Letters (ISSN 0003-6951) vol. 62, no. 12 March 22, 1993 p. 1411-1413. refs

Copyright

The dielectric function of a thick layer of In(0.52)Al(0.48)As lattice matched to InP was measured by variable angle spectroscopic ellipsometry in the range 1.9-4.1 eV. The In(0.52)Al(0.48)As was protected from oxidation using a thin In(0.53)Ga(0.47)As cap that was mathematically removed for the dielectric function estimate. The In(0.52)Al(0.48)As dielectric function was then verified by ellipsometric measurements of other

In(0.53)Ga(0.47)As/In(0.52)Al(0.48)As structures, including (MODFET), and is shown to provide accurate structure layer thicknesses.
Author (revised)

A93-49553* National Aeronautics and Space Administration. Lewis Research Center, Cleveland, OH.

A HIGH-EFFICIENCY 59- TO 64-GHZ TWT FOR INTERSATELLITE COMMUNICATIONS

JEFFREY D. WILSON, PETER RAMINS, DALE A. FORCE (NASA, Lewis Research Center, Cleveland, OH), HELEN C. LIMBURG, and IVO TAMMARU (Hughes Aircraft Co., Torrance, CA) In 1991 International Electron Devices Meeting, Washington, Dec. 8-11, 1991, Proceedings New York Institute of Electrical and Electronics Engineers, Inc. 1991 p. 21.2.1-21.2.4. refs
Copyright

The design of a 75-W, 59- to 64-GHz TWT with a predicted overall efficiency in excess of 40 percent is described. This intersatellite communications TWT, designated Model 961HA, employs a coupled-cavity slow-wave structure with a two-step velocity taper and an isotropic graphite multistage depressed collector (MDC). Because the RF efficiency of this TWT is less than 8 percent, an MDC design providing a very high collector efficiency was necessary to achieve the overall efficiency goal of 40 percent.

Author (revised)

A93-50646* National Aeronautics and Space Administration. Lewis Research Center, Cleveland, OH.

A 10 KW DC-DC CONVERTER USING IGBTs WITH ACTIVE SNUBBERS

BRIAN J. MASSERANT, JEFFREY L. SHRIVER, and THOMAS A. STUART (Toledo Univ., OH) IEEE Transactions on Aerospace and Electronic Systems (ISSN 0018-9251) vol. 29, no. 3 July 1993 p. 857-865. IEEE, Power Electronics Specialists' Conference, Seattle, WA, June 20-24, 1993 refs
(Contract NAG3-1102; F33615-90-C-2088)

Copyright

This full bridge dc-dc converter employs zero voltage switching (ZVS) on one leg and zero current switching (ZCS) on the other. This technique produces exceptionally low IGBT switching losses through the use of an active snubber that recycles energy back to the source. Experimental results are presented for a 10 kW, 20 kHz converter.

A93-54442* National Aeronautics and Space Administration. Lewis Research Center, Cleveland, OH.

THE EFFECTS OF STRAIN ON THE MICROWAVE PERFORMANCE OF SiGe HBTs

D. ROSENFELD and S. A. ALTEROVITZ (NASA, Lewis Research Center, Cleveland, OH) Microwave and Optical Technology Letters (ISSN 0895-2477) vol. 6, no. 12 Sept. 20, 1993 p. 689-692. refs

Copyright

Theoretical study results are presented for the effects of strain on the cutoff frequencies of SiGe heterojunction bipolar transistors. The positive role played by the strain on the base resistance and transit time is shown to have a further effect on high-frequency performance.

AIAA

A93-54619* National Aeronautics and Space Administration. Lewis Research Center, Cleveland, OH.

A 10 GHZ Y-BA-CU-O/GAAS HYBRID OSCILLATOR PROXIMITY COUPLED TO A CIRCULAR MICROSTRIP PATCH ANTENNA

NORMAN J. ROHRER (Ohio State Univ., Columbus), M. A. RICHARD (Case Western Reserve Univ., Cleveland, OH), GEORGE J. VALCO (Ohio State Univ., Columbus), and KUL B. BHASIN (NASA, Lewis Research Center, Cleveland, OH) IEEE Transactions on Applied Superconductivity (ISSN 1051-8223) vol. 3, no. 1 March 1993 p. 23-27. refs
(Contract NCC3-197)

Copyright

A 10 GHz hybrid YBCO/GaAs microwave oscillator proximity coupled to a circular microstrip antenna has been designed.

fabricated, and characterized. The oscillator was a reflection mode type using a GaAs MESFET as the active element. The feedline, transmission lines, RF chokes, and bias lines were all fabricated from YBCO superconducting thin films on a 1 cm x 1 cm lanthanum aluminate substrate. The output feedline of the oscillator was wire bonded to a superconducting feedline on a second 1 cm x 1 cm lanthanum aluminate substrate, which was in turn proximity coupled to a circular microstrip patch antenna. Antenna patterns from this active patch antenna and the performance of the oscillator measured at 77 K are reported. The oscillator had a maximum output power of 11.5 dBm at 77 K, which corresponded to an efficiency of 10 percent. In addition, the efficiency of the microstrip patch antenna together with its high temperature superconducting feedline was measured from 85 K to 30 K and was found to be 71 percent at 77 K, increasing to a maximum of 87.4 percent at 30 K.

Author (revised)

A93-55324* National Aeronautics and Space Administration. Lewis Research Center, Cleveland, OH.

DIFFUSION LENGTH VARIATION AND PROTON DAMAGE COEFFICIENTS FOR INP/IN(X)GA(1-X)AS/GAAS SOLAR CELLS

R. K. JAIN, I. WEINBERG, and D. J. FLOOD (NASA, Lewis Research Center, Cleveland, OH) *Journal of Applied Physics* (ISSN 0021-8979) vol. 74, no. 4 Aug. 15, 1993 p. 2948-2950. Research supported by National Research Council and NASA refs

Copyright

Indium phosphide solar cells are more radiation resistant than gallium arsenide and silicon solar cells, and their growth by heteroepitaxy offers additional advantages leading to the development of lighter, mechanically strong and cost-effective cells. Changes in heteroepitaxial InP cell efficiency under 0.5 and 3 MeV proton irradiations are explained by the variation in the minority-carrier diffusion length. The base diffusion length versus proton fluence is calculated by simulating the cell performance. The diffusion length damage coefficient $K(L)$ is plotted as a function of proton fluence.

Author (revised)

A93-56292* National Aeronautics and Space Administration. Lewis Research Center, Cleveland, OH.

DEMONSTRATION OF Y1Ba2Cu3O(7-DELTA) AND COMPLEMENTARY METAL-OXIDE-SEMICONDUCTOR DEVICE FABRICATION ON THE SAME SAPPHIRE SUBSTRATE

M. J. BURNS (Conductus, Inc., Sunnyvale, CA), P. R. DE LA HOUSSEY, S. D. RUSSELL, G. A. GARCIA, S. R. CLAYTON (U.S. Navy, Naval Command, Control and Ocean Surveillance Center, San Diego, CA), W. S. RUBY, and L. P. LEE (Conductus, Inc., Sunnyvale, CA) *Applied Physics Letters* (ISSN 0003-6951) vol. 63, no. 9 Aug. 30, 1993 p. 1282-1284. Research supported by NASA and U.S. Navy refs

Copyright

We report the first fabrication of active semiconductor and high-temperature superconducting devices on the same substrate. Test structures of complementary MOS transistors were fabricated on the same sapphire substrate as test structures of Y1Ba2Cu3O(7-delta) flux-flow transistors, and separately, Y1Ba2Cu3O(7-delta) superconducting quantum interference devices utilizing both biepitaxial and step-edge Josephson junctions. Both semiconductor and superconductor devices were operated at 77 K. The cofabrication of devices using these disparate yet complementary electronic technologies on the same substrate opens the door for the fabrication of true semiconductive/superconductive hybrid integrated circuits capable of exploiting the best features of each of these technologies.

Author (revised)

N93-12301*# National Aeronautics and Space Administration. Lewis Research Center, Cleveland, OH.

PARAMETERIZATION OF SOLAR CELLS

J. APPELBAUM, A. CHAIT, and D. THOMPSON Oct. 1992 23 p

(Contract RTOP 506-41-11)

(NASA-TM-105885; E-7188; NAS 1.15:105885) Avail: CASI HC A03/MF A01

The aggregation (sorting) of the individual solar cells into an array is commonly based on a single operating point on the current-voltage (I-V) characteristic curve. An alternative approach for cell performance prediction and cell screening is provided by modeling the cell using an equivalent electrical circuit, in which the parameters involved are related to the physical phenomena in the device. These analytical models may be represented by a double exponential I-V characteristic with seven parameters, by a double exponential model with five parameters, or by a single exponential equation with four or five parameters. In this article we address issues concerning methodologies for the determination of solar cell parameters based on measured data points of the I-V characteristic, and introduce a procedure for screening of solar cells for arrays. We show that common curve fitting techniques, e.g., least squares, may produce many combinations of parameter values while maintaining a good fit between the fitted and measured I-V characteristics of the cell. Therefore, techniques relying on curve fitting criteria alone cannot be directly used for cell parameterization. We propose a consistent procedure which takes into account the entire set of parameter values for a batch of cells. This procedure is based on a definition of a mean cell representing the batch, and takes into account the relative contribution of each parameter to the overall goodness of fit. The procedure is demonstrated on a batch of 50 silicon cells for Space Station Freedom.

Author

N93-13184*# National Aeronautics and Space Administration. Lewis Research Center, Cleveland, OH.

BATTERY SELECTION FOR SPACE EXPERIMENTS

DAVID R. FRANCISCO /in NASA. Goddard Space Flight Center, The 1992 Shuttle Small Payloads Symposium p 267-276 Oct. 1992

Avail: CASI HC A02/MF A03

This paper will delineate the criteria required for the selection of batteries as a power source for space experiments. Four basic types of batteries will be explored, lead acid, silver zinc, alkaline manganese and nickel cadmium. A detailed description of the lead acid and silver zinc cells while a brief exploration of the alkaline manganese and nickel cadmium will be given. The factors involved in battery selection such as packaging, energy density, discharge voltage regulation, and cost will be thoroughly examined. The pros and cons of each battery type will be explored. Actual laboratory test data acquired for the lead acid and silver zinc cell will be discussed. This data will include discharging under various temperature conditions, after three months of storage and with different types of loads. A description of the required maintenance for each type of battery will be investigated. The lifetime and number of charge/discharge cycles will be discussed.

Author

N93-13286*# National Aeronautics and Space Administration. Lewis Research Center, Cleveland, OH.

ANOMALOUS TWTA OUTPUT POWER SPIKES AND THEIR EFFECT ON A DIGITAL SATELLITE COMMUNICATIONS SYSTEM

BRIAN D. MAY, ROBERT J. KERCZEWSKI, and JAMES S. SVOBODA (Sverdrup Technology, Inc., Brook Park, OH.) Oct. 1992 14 p

(Contract NAS3-25266; RTOP 679-40-00)

(NASA-TM-105875; E-6558; NAS 1.15:105875) Avail: CASI HC A03/MF A01

Several 30 GHz, 60 W traveling wave tube amplifiers (TWTA) were manufactured for the NASA Lewis Research Center's High Burst Rate Link Evaluation Terminal Project. An unusual operating problem characterized by anomalous nonperiodic output power spikes, common to all of the TWTAs proved during testing to significantly affect the performance of a digitally-modulated data transmission test system. Modifications made to the TWTAs significantly curtailed the problem and allowed acceptable system performance to be obtained. This paper presents a discussion of the TWTA output power spike problem, possible causes of the

problem, and the solutions implemented by the manufacturer which improved the TWTa performance to an acceptable level. The results of the testing done at NASA Lewis on the TWTAs both before and after the improvement made by Hughes are presented, and the effects of the output power spikes on the performance of the test system are discussed. Author

N93-15503*# National Aeronautics and Space Administration. Lewis Research Center, Cleveland, OH.

EMTP BASED STABILITY ANALYSIS OF SPACE STATION ELECTRIC POWER SYSTEM IN A TEST BED ENVIRONMENT

NARAYAN V. DRAVID, THOMAS J. KACPURA (Sverdrup Technology, Inc., Brook Park, OH.), and ANDREW M. OCONNOR (Analytical Engineering Corp., North Olmsted, OH.) Aug. 1992 9 p Presented at the 27th Intersociety Energy Conversion Engineering Conference, San Diego, CA, 3-7 Aug. 1992; cosponsored by ANS, SAE, ACS, AIAA, ASME, and IEEE (Contract RTOP 474-42-10) (NASA-TM-105845; E-7288; NAS 1.15:105845) Avail: CASI HC A02/MF A01

The Space Station Freedom Electric Power System (EPS) will convert solar energy into electric energy and distribute the same using an 'all dc', Power Management and Distribution (PMAD) System. Power conditioning devices (dc to dc converters) are needed to interconnect parts of this system operating at different nominal voltage levels. Operation of such devices could generate under damped oscillations (instability) under certain conditions. Criteria for instability are examined and verified for a single device. Suggested extension of the criteria to a system operation is examined by using the EMTP model of the PMAD DC test bed. Wherever possible, data from the test bed is compared with the modeling results. Author

N93-15531*# National Aeronautics and Space Administration. Lewis Research Center, Cleveland, OH.

USER'S GUIDE FOR A LARGE SIGNAL COMPUTER MODEL OF THE HELICAL TRAVELING WAVE TUBE

RAYMOND W. PALMER Washington Dec. 1992 27 p (Contract RTOP 506-72-00) (NASA-TP-3251; E-6804; NAS 1.60:3251) Avail: CASI HC A03/MF A01

The use is described of a successful large-signal, two-dimensional (axisymmetric), deformable disk computer model of the helical traveling wave tube amplifier, an extensively revised and operationally simplified version. We also discuss program input and output and the auxiliary files necessary for operation. Included is a sample problem and its input data and output results. Interested parties may now obtain from the author the FORTRAN source code, auxiliary files, and sample input data on a standard floppy diskette, the contents of which are described herein. Author

N93-16616*# National Aeronautics and Space Administration. Lewis Research Center, Cleveland, OH.

A PROTOTYPE AUTOMATIC PHASE COMPENSATION MODULE

JOHN D. TERRY Dec. 1992 10 p (Contract RTOP 307-51-00) (NASA-TM-105930; E-7441; NAS 1.15:105930) Avail: CASI HC A02/MF A01

The growing demands for high gain and accurate satellite communication systems will necessitate the utilization of large reflector systems. One area of concern of reflector based satellite communication is large scale surface deformations due to thermal effects. These distortions, when present, can degrade the performance of the reflector system appreciable. This performance degradation is manifested by a decrease in peak gain, and increase in sidelobe level, and pointing errors. It is essential to compensate for these distortion effects and to maintain the required system performance in the operating space environment. For this reason the development of a technique to offset the degradation effects is highly desirable. Currently, most research is direct at developing better material for the reflector. These materials have a lower coefficient of linear expansion thereby reducing the surface errors.

Alternatively, one can minimize the distortion effects of these large scale errors by adaptive phased array compensation. Adaptive phased array techniques have been studied extensively at NASA and elsewhere. Presented in this paper is a prototype automatic phase compensation module designed and built at NASA Lewis Research Center which is the first stage of development for an adaptive array compensation module. Author

N93-16713*# National Aeronautics and Space Administration. Lewis Research Center, Cleveland, OH.

INTERIM REPORT ON THE ANALYSIS OF THE MICROWAVE POWER MODULE

PETER RAMINS, RAYMOND W. PALMER, DALE A. FORCE, BEN T. EBIHARA, ROBERT P. GRUBER, and JAMES A. DAYTON, JR. May 1992 14 p (Contract RTOP 506-72-00) (NASA-TM-106012; E-7384; NAS 1.15:106012) Avail: CASI HC A03/MF A01

The results of a traveling wave tube multistage depressed collector (TWT-MDC) design study in support of the DARPA/DoD Microwave Power Module (MPM) Program are described. The study stressed the MDC as a key element in obtaining the required high overall efficiencies in the MPM application. The results showed that an efficient MDC, utilizing conventional design and fabrication techniques can be designed for the first generation MPM TWT, which permits a package one wavelength thick (.66 in. at 18 GHz). The overall TWT efficiency goal of 40 percent for electronic countermeasure (ECM) applications appears to be readily achievable. However, the 50 percent goal for radar applications presents a considerable challenge. Author

N93-20259*# National Aeronautics and Space Administration. Lewis Research Center, Cleveland, OH.

FULL WAVE CHARACTERIZATION OF MICROSTRIP OPEN END DISCONTINUITIES PATTERNED ON ANISOTROPIC SUBSTRATES USING POTENTIAL THEORY

S. S. TONCICH, R. E. COLLIN (Case Western Reserve Univ., Cleveland, OH.), and K. B. BHASIN Feb. 1993 6 p Proposed for presentation at the Electrical and Electronics Engineers, MTT-S International Microwave Symposium, Atlanta, GA, 12-18 Jun. 1993; sponsored by the IEEE Microwave Theory and Techniques Society (Contract RTOP 506-72-1B) (NASA-TM-106037; E-7608; NAS 1.15:106037) Avail: CASI HC A02/MF A01

A technique for a full wave characterization of microstrip open end discontinuities fabricated on uniaxial anisotropic substrates using potential theory is presented. The substrate to be analyzed is enclosed in a cutoff waveguide, with the anisotropic axis aligned perpendicular to the air-dielectric interface. A full description of the sources on the microstrip line is included with edge conditions built in. Extension to other discontinuities is discussed. Author

N93-23394*# National Aeronautics and Space Administration. Lewis Research Center, Cleveland, OH.

SIMULATION OF TUNNELADDER TRAVELING-WAVE TUBE COLD-TEST CHARACTERISTICS: IMPLEMENTATION OF THE THREE-DIMENSIONAL, ELECTROMAGNETIC CIRCUIT ANALYSIS CODE MICRO-SOS

CAROL L. KORY (Ohio Aerospace Inst., Brook Park.) and JEFFREY D. WILSON Mar. 1993 16 p (Contract RTOP 506-44-2B) (NASA-TP-3294; E-7008; NAS 1.60:3294) Avail: CASI HC A03/MF A01

The three-dimensional, electromagnetic circuit analysis code, Micro-SOS, can be used to reduce expensive time-consuming experimental 'cold-testing' of traveling-wave tube (TWT) circuits. The frequency-phase dispersion characteristics and beam interaction impedance of a Tunneladder traveling-wave tube slow-wave structure were simulated using the code. When reasonable dimensional adjustments are made, computer results agree closely with experimental data. Modifications to the circuit

geometry that would make the TunneLadder TWT easier to fabricate for higher frequency operation are explored.

Author (revised)

N93-24746*# National Aeronautics and Space Administration. Lewis Research Center, Cleveland, OH.

RADIATION AND TEMPERATURE EFFECTS ON ELECTRONIC COMPONENTS INVESTIGATED UNDER THE CSTI HIGH CAPACITY POWER PROJECT

GENE E. SCHWARZE, JANIS M. NIEDRA (Sverdrup Technology, Inc., Brook Park, OH.), ALBERT J. FRASCA (Wittenberg Univ., Springfield, OH.), and WILLIAM R. WIESERMAN (Pittsburgh Univ., Johnstown, PA.) Jan. 1993 15 p Presented at the 10th Symposium on Space Nuclear Power and Propulsion, Albuquerque, NM, 10-14 Jan. 1993; sponsored by New Mexico Univ. (Contract RTOP 467-01-21)

(NASA-TM-106096; E-7737; NAS 1.15:106096) Avail: CASI HC A03/MF A01

The effects of nuclear radiation and high temperature environments must be fully known and understood for the electronic components and materials used in both the Power Conditioning and Control subsystem and the reactor Instrumentation and Control subsystem of future high capacity nuclear space power systems. This knowledge is required by the designer of these subsystems in order to develop highly reliable, long-life power systems for future NASA missions. A review and summary of the experimental results obtained for the electronic components and materials investigated under the power management element of the Civilian Space Technology Initiative (CSTI) high capacity power project are presented: (1) neutron, gamma ray, and temperature effects on power semiconductor switches; (2) temperature and frequency effects on soft magnetic materials; and (3) temperature effects on rare earth permanent magnets.

Author (revised)

N93-24889*# National Aeronautics and Space Administration. Lewis Research Center, Cleveland, OH.

A SYSTEM TO MEASURE LIGHTNING-INDUCED TRANSIENTS ON SPACECRAFT UMBILICAL LINES

JEFFREY C. BROWN, NOEL B. SARGENT, and CARL J. WENZLER *In* FAA, The 1992 International Aerospace and Ground Conference on Lightning and Static Electricity: Addendum 8 p Nov. 1992

Avail: CASI HC A02/MF A03

Spacecraft electrical systems are potentially vulnerable during ground operations to damage from lightning-induced transients coupled onto umbilical cables. Limited data are available to compare spacecraft design protection levels with actual transient magnitudes. A system has been designed to accurately measure these transients and verify that spacecraft protection levels have not been exceeded. This paper describes the design and operation of the system and its installation at Launch Complex 36 on the Cape Canaveral Air Force Station (CCAFS).

Author

N93-27002*# National Aeronautics and Space Administration. Lewis Research Center, Cleveland, OH.

DIFFUSION LENGTH VARIATION IN 0.5- AND 3-MEV-PROTON-IRRADIATED, HETEROEPITAXIAL INDIUM PHOSPHIDE SOLAR CELLS

RAJ K. JAIN (National Academy of Sciences - National Research Council, Washington, DC.), IRVING WEINBERG, and DENNIS J. FLOOD Apr. 1993 7 p Presented at the Fifth International Conference on Indium Phosphide and Related Materials, Paris, France, 18-22 Apr. 1993; cosponsored by IEEE Lasers and Electro-Optics Society and IEEE Electron Devices Society (Contract RTOP 506-41-11)

(NASA-TM-106147; E-7792; NAS 1.15:106147) Avail: CASI HC A02/MF A01

Indium phosphide (InP) solar cells are more radiation resistant than gallium arsenide (GaAs) and silicon (Si) solar cells, and their growth by heteroepitaxy offers additional advantages leading to the development of light weight, mechanically strong, and cost-effective cells. Changes in heteroepitaxial InP cell efficiency under 0.5- and 3-MeV proton irradiations have been explained by

the variation in the minority-carrier diffusion length. The base diffusion length versus proton fluence was calculated by simulating the cell performance. The diffusion length damage coefficient, $K(\text{sub } L)$, was also plotted as a function of proton fluence.

Author (revised)

N93-27265*# National Aeronautics and Space Administration. Lewis Research Center, Cleveland, OH.

MICROWAVE CHARACTERIZATION OF SLOTLINE ON HIGH RESISTIVITY SILICON FOR ANTENNA FEED NETWORK

RAINEE N. SIMONS (Sverdrup Technology, Inc., Brook Park, OH.), SUSAN R. TAUB, RICHARD Q. LEE, and PAUL G. YOUNG (Toledo Univ., OH.) Mar. 1993 9 p Proposed for presentation at the 1992 IEEE AP-S International Symposium and URSI Radio Science Meeting, Ann Arbor, MI, 27 Jun. - 2 Jul. 1993; sponsored by IEEE and USNC Commissions A,B,D, and F (Contract RTOP 506-44-2C)

(NASA-TM-106058; E-7659; NAS 1.15:106058) Avail: CASI HC A02/MF A01

Conventional silicon wafers have low resistivity and consequently unacceptably high value of dielectric attenuation constant. Microwave circuits for phased array antenna systems fabricated on these wafers therefore have low efficiency. By choosing a silicon substrate with sufficiently high resistivity it is possible to make the dielectric attenuation constant of the interconnecting microwave transmission lines approach those of GaAs or InP. In order for this to be possible, the transmission lines must be characterized. In this presentation, the effective dielectric constant (epsilon sub eff) and attenuation constant (alpha) of a slotline on high resistivity (5000 to 10 000 ohm-cm) silicon wafer will be discussed. The epsilon sub eff and alpha are determined from the measured resonant frequencies and the corresponding insertion loss of a slotline ring resonator. The results for slotline will be compared with microstrip line and coplanar waveguide.

Author (revised)

N93-27804*# National Aeronautics and Space Administration. Lewis Research Center, Cleveland, OH.

ELECTRICAL POWER SYSTEM WP-04

DONALD L. NORED *In* NASA, Washington, Technology for Space Station Evolution. Volume 4: Power Systems/Propulsion/Robotics p 5-61 1990

Avail: CASI HC A04/MF A04; 1 functional color page

Viewgraphs on Space Station Freedom Electrical Power System (EPS) WP-40 are presented. Topics covered include: key EPS technical requirements; photovoltaic power module systems; solar array assembly; blanket containment box and box positioning subassemblies; solar cell; bypass diode assembly; Kapton with atomic oxygen resistant coating; sequential shunt unit; gimbal assembly; energy storage subsystem; thermal control subsystem; direct current switching unit; integrated equipment assembly; PV cargo element; PMAD system; and PMC and AC architecture.

CASI

N93-27810*# National Aeronautics and Space Administration. Lewis Research Center, Cleveland, OH.

GROWING THE SPACE STATION'S ELECTRICAL POWER PLANT

GALE R. SUNDBERG *In* NASA, Washington, Technology for Space Station Evolution. Volume 4: Power Systems/Propulsion/Robotics p 139-150 1990

Avail: CASI HC A03/MF A04; 1 functional color page

For over a decade NASA LeRC has been defining, demonstrating, and evaluating power electronic components and multi-kilowatt, multiply redundant, electrical power systems as part of OAST charter. Whether one considers aircraft (commercial transport/military), Space Station Freedom, growth station, launch vehicles, or the new Human Exploration Initiative, the conclusions remain the same: high frequency AC power distribution and control is superior to all other approaches for achieving a fast, smart, safe, versatile, and growable electrical power system that will meet a wide range of mission options. To meet the cost and operability goals of future aerospace missions that require significantly higher

33 ELECTRONICS AND ELECTRICAL ENGINEERING

electrical power and longer durations, we must learn to integrate multiple technologies in ways that enhance overall system synergisms. The way NASA is doing business in space electric power is challenged and some approaches for evolving large space vehicles and platforms in well constructed steps to provide safe, ground testable, growable, smart systems that provide simple, replicative logic structures, which enable hardware and software verification, validation, and implementation are proposed. Viewgraphs are included. Author (revised)

N93-28610* National Aeronautics and Space Administration. Lewis Research Center, Cleveland, OH.

DEVELOPMENT OF Si(1-x)Ge(x) TECHNOLOGY FOR MICROWAVE SENSING APPLICATIONS

RAFAEL A. MENA, SUSAN R. TAUB, SAMUEL A. ALTEROVITZ, PAUL E. YOUNG (Toledo Univ., OH.), RAINEE N. SIMONS (Sverdrup Technology, Inc., Brook Park, OH.), and DAVID ROSENFELD May 1993 13 p
(Contract RTOP 505-44-2C)
(NASA-TM-106157; E-7843; NAS 1.15:106157) Avail: CASI HC A03/MF A01

The progress for the first year of the work done under the Director's Discretionary Fund (DDF) research project entitled, 'Development of Si(1-x)Ge(x) Technology for Microwave Sensing Applications.' This project includes basic material characterization studies of silicon-germanium (SiGe), device processing on both silicon (Si) and SiGe substrates, and microwave characterization of transmission lines on silicon substrates. The material characterization studies consisted of ellipsometric and magneto-transport measurements and theoretical calculations of the SiGe band-structure. The device fabrication efforts consisted of establishing SiGe device processing capabilities in the Lewis cleanroom. The characterization of microwave transmission lines included studying the losses of various coplanar transmission lines and the development of transitions on silicon. Each part of the project is discussed individually and the findings for each part are presented. Future directions are also discussed. Author (revised)

34

FLUID MECHANICS AND HEAT TRANSFER

Includes boundary layers; hydrodynamics; fluidics; mass transfer; and ablation cooling.

A93-10653* National Aeronautics and Space Administration. Lewis Research Center, Cleveland, OH.

REFRACTIVE INDEX EFFECTS ON RADIATIVE BEHAVIOR OF A HEATED ABSORBING-EMITTING LAYER

C. M. SPUCKLER and R. SIEGEL (NASA, Lewis Research Center, Cleveland, OH) Journal of Thermophysics and Heat Transfer (ISSN 0887-8722) vol. 6, no. 4 Oct.-Dec. 1992 p. 596-604. refs
Copyright

Temperature distributions and other heat transfer characteristics are analyzed for a heated plane layer of semitransparent material with refractive index not less than 1. The analysis includes heat conduction, emission, and absorption within the layer. The layer has diffuse interfaces; examples are a frosted quartz window used to diffuse incident radiation in high temperature surroundings, or a ceramic layer with small scattering used in high-temperature applications. Each side of the layer is heated by radiation and convection, and interface reflections are included. When the index of refraction is larger than unity, there are total internal reflections of some of the energy within the layer. This has a substantial effect on distributing energy across the layer, and considerably alters the temperature distribution from when the refractive index is unity. Results are given for a gray layer and for a two-band spectral variation of the absorption coefficient.

Radiant energy leaving the surface was examined to determine when it could be used to measure surface temperature accurately. Author

A93-10671* National Aeronautics and Space Administration. Lewis Research Center, Cleveland, OH.

EFFECT OF FREE SURFACE SHAPE ON COMBINED THERMOCAPILLARY AND NATURAL CONVECTION

YASUHIRO KAMOTANI (Case Western Reserve Univ., Cleveland, OH) and JONATHAN PLATT (NASA, Lewis Research Center, Cleveland, OH) Journal of Thermophysics and Heat Transfer (ISSN 0887-8722) vol. 6, no. 4 Oct.-Dec. 1992 p. 721-726. refs
(Contract NAG3-570)
Copyright

Combined thermocapillary and natural convection in an open square cavity with differentially-heated side walls is studied numerically as well as experimentally. The test fluid is silicone oil with Prandtl number of 105. The shape of fluid-free surface is made either flat or curved to study its effect on the flow. A finite difference scheme to deal with a curved free surface is developed. The experimental results shown agree with the numerical results. With the curved-free surface, the flow and local heat transfer rate are reduced in the corner regions, and a sharp peak in heat transfer rate at the top edge of the cold wall disappears. Author

A93-10839* National Aeronautics and Space Administration. Lewis Research Center, Cleveland, OH.

THERMAL OSCILLATIONS IN MATERIALS PROCESSING

SIMON OSTRACH and YASUHIRO KAMOTANI (Case Western Reserve Univ., Cleveland, OH) In Heat and mass transfer in materials processing New York Hemisphere Publishing Corp. 1992 p. 383-409. Research supported by Battelle refs
(Contract NSF MEA-84-01883; NAG3-570)
Copyright

The use of thermosolutal and thermocapillary convection in materials processing is experimentally investigated. The flow patterns, unsteady mass transfer, and unsteady temperature variations seen in thermosolutal convection in enclosures are examined. An extensive research program to understand the role of thermocapillary convection in crystal growth for a variety of configurations is reviewed. C.D.

A93-13789* National Aeronautics and Space Administration. Lewis Research Center, Cleveland, OH.

GRAPHITE FIBER/COPPER MATRIX COMPOSITES FOR SPACE POWER HEAT PIPE FIN APPLICATIONS

DAVID L. MCDANIELS, KARL W. BAKER (NASA, Lewis Research Center, Cleveland, OH), and DAVID L. ELLIS (Case Western Reserve Univ., Cleveland, OH) In Space nuclear power systems; Proceedings of the 8th Symposium, Albuquerque, NM, Jan. 6-10, 1991. Pt. 1 New York American Institute of Physics 1991 p. 313-319. refs
Copyright

High specific thermal conductivity (thermal conductivity divided by density) is a major design criterion for minimizing system mass for space power systems. For nuclear source power systems, graphite fiber reinforced copper matrix (Gr/Cu) composites offer good potential as a radiator fin material operating at service temperatures above 500 K. Specific thermal conductivity in the longitudinal direction is better than beryllium and almost twice that of copper. The high specific thermal conductivity of Gr/Cu offers the potential of reducing radiator mass by as much as 30 percent. Gr/Cu composites also offer the designer a range of available properties for various missions and applications. The properties of Gr/Cu are highly anisotropic. Longitudinal elastic modulus is comparable to beryllium and about three times that of copper. Thermal expansion in the longitudinal direction is near zero, while it exceeds that of copper in the transverse direction. Author

A93-13843* National Aeronautics and Space Administration. Lewis Research Center, Cleveland, OH.

SP-100 HIGH-TEMPERATURE ADVANCED RADIATOR DEVELOPMENT

RICHARD D. ROVANG, MARIBETH E. HUNT (Rockwell International Corp., Rocketdyne Div., Canoga Park, CA), RAY B. DIRLING, JR. (Science Applications International Corp., Santa Ana, CA), and ROBERT A. HOLZL (Delta G Corp., Sun Valley, CA) / *In* Space nuclear power systems; Proceedings of the 8th Symposium, Albuquerque, NM, Jan. 6-10, 1991. Pt. 2 New York American Institute of Physics 1991 p. 702-707. (Contract NAS3-25209)

Copyright

The development of an advanced radiator concept design meeting SP-100 thermoelectric requirements is reported. Carbon-carbon heat pipes are used to produce this lightweight, high-performance radiator. Two feasibility problems had to be solved to enable the design: the production of a carbon-carbon heat pipe tube with integral fins, and the development of a coating that protects the carbon-carbon substrate from 875-K potassium working fluid. Carbon-carbon tubes with integral fins were successfully produced using a T-300 fiber, an angle interlocking weave architecture, and pitch densification. A barrier coating to protect the inside diameter of these tubes which employed the CVD of niobium over a thin rhenium interlayer was developed. The rhenium interlayer proved to be critical to the success of this coating technique by providing a gradation in the coefficient of thermal expansion, carrying a portion of the induced stress load, improving coating adhesion, and providing a partial carbon diffusion barrier.

P.D.

A93-13844* National Aeronautics and Space Administration. Lewis Research Center, Cleveland, OH.

ADVANCED RADIATOR CONCEPTS FEASIBILITY DEMONSTRATION

HYOP S. RHEE, LESTER BEGG, JOSEPH R. WETCH (Space Power, Inc., San Jose, CA), and ALBERT J. JUHASZ (NASA, Lewis Research Center, Cleveland, OH) / *In* Space nuclear power systems; Proceedings of the 8th Symposium, Albuquerque, NM, Jan. 6-10, 1991. Pt. 2 New York American Institute of Physics 1991 p. 708-713. refs (Contract NAS3-25208)

Copyright

An innovative pumped loop concept for 600 K space power system radiators is under development utilizing direct contact heat transfer, which facilitates repeated startup/shutdown of the power system without complex and time-consuming coolant thawing during power startup. The melting/freezing process of Li in a NaK flow was studied experimentally to demonstrate the Li/NaK radiator feasibility during startup (thawing) and shutdown (cold-trapping). Results of the vapor grown carbon fiber/composite thermal conductivity measurements are also presented.

Author

A93-13867* National Aeronautics and Space Administration. Lewis Research Center, Cleveland, OH.

HEAT-PIPE TRANSIENT MODEL FOR SPACE APPLICATIONS

JEAN-MICHEL TOURNIER, MOHAMED S. EL-GENK (New Mexico Univ., Albuquerque), and ALBERT J. JUHASZ (NASA, Lewis Research Center, Cleveland, OH) / *In* Space nuclear power systems; Proceedings of the 8th Symposium, Albuquerque, NM, Jan. 6-10, 1991. Pt. 2 New York American Institute of Physics 1991 p. 857-868. refs (Contract NAG3-941)

Copyright

A two-dimensional model is developed for simulating heat pipes transient performance following changes in the input/rejection power or in the evaporator/condenser temperatures. The model employs the complete form of governing equations and momentum and energy jump conditions at the liquid-vapor interface. Although the model is capable of handling both cylindrical and rectangular geometries, the results reported are for a circular heat pipe with liquid lithium as the working fluid. The model incorporates a variety of other working fluids, such as water, ammonia, potassium, sodium

and mercury, and offers combinations of isothermal, isoflux, convective and radiative heating/cooling conditions in the evaporator and condenser regions of the heat pipe. Results presented are for lithium heat pipes with exponential heating of the evaporator and isothermal cooling of the condenser. Author

A93-13869 National Aeronautics and Space Administration. Lewis Research Center, Cleveland, OH.

CONSTRUCTION AND TESTING OF CERAMIC FABRIC HEAT PIPE WITH WATER WORKING FLUID

ZENEN I. ANTONIAK, BRENT J. WEBB, JAMES M. BATES, and MATTHEW F. COOPER (Battelle Pacific Northwest Labs., Richland, WA) / *In* Space nuclear power systems; Proceedings of the 8th Symposium, Albuquerque, NM, Jan. 6-10, 1991. Pt. 2 New York American Institute of Physics 1991 p. 875-879. Previously announced in STAR as N91-18799 Research supported by DOE, NASA, and USAF refs

Copyright

A prototype ceramic fabric/titanium water heat pipe has been constructed and tested; it transported 25 to 80 W of power at 423 K. Component development and testing is continuing with the aim of providing an improved prototype, with a 38 micron stainless steel liner covered by a biaxially-braided Nextel (trademark) sleeve that is approximately 300 microns thick. This fabric has been tested to 800 K, and its emittance is about 0.5 at that temperature. Advanced versions of the water heat pipe will probably require a coating over the ceramic fabric in order to increase this emittance to the 0.8 to 0.9 range.

Author

A93-13916* National Aeronautics and Space Administration. Lewis Research Center, Cleveland, OH.

MECHANISMS OF VOIDS FORMATION DURING COOLDOWN AND FREEZING OF LITHIUM IN SP-100 TYPE SYSTEMS

JAE Y. YANG and MOHAMED S. EL-GENK (New Mexico Univ., Albuquerque) / *In* Space nuclear power systems; Proceedings of the 8th Symposium, Albuquerque, NM, Jan. 6-10, 1991. Pt. 3 New York American Institute of Physics 1991 p. 1244-1254. refs (Contract NAG3-1045)

Copyright

The mechanisms of void formation during the cooldown and freezing of lithium coolant within the primary loop of SP-100 type systems are investigated. These mechanisms are: (a) homogeneous nucleation, (b) heterogeneous nucleation, (c) normal segregation of helium gas dissolved in liquid lithium, and (d) shrinkage of lithium during freezing. To evaluate the void formation potential due to segregation, a numerical scheme that couples the freezing and mass diffusion processes in both the solid and liquid regions is developed. The results indicated that the formation of He bubbles is unlikely by either homogeneous or heterogeneous nucleation during the cooldown process. However, homogeneous nucleation of He bubbles following the segregation of dissolved He in liquid Lithium ahead of the solid-liquid interface is likely to occur. Results also show that total volume of He void is insignificant when compared to that of shrinkage voids.

Author

A93-13951* National Aeronautics and Space Administration. Lewis Research Center, Cleveland, OH.

EFFECT OF SURFACE TENSION ON THE ONSET OF CONVECTION IN A DOUBLE-DIFFUSIVE LAYER

C. F. CHEN and T. F. SU (Arizona Univ., Tucson) / *Physics of Fluids A* (ISSN 0899-8213) vol. 4, no. 11 Nov. 1992 p. 2360-2367. refs

(Contract NAG3-1268)

Copyright

The effect of surface tension on the stability of a double-diffusive layer is considered using linear stability analysis. The surface tension is assumed to vary linearly with temperature and solute concentration. The eigenvalue problem is solved by the Galerkin method. Results show that the predicted stability boundary based on Marangoni effects alone is completely altered in the presence of buoyancy effects induced by low gravity levels (about $10 \exp -5$ g). At reduced gravity levels, salt-finger instability may onset in the overstable mode due to the stabilizing effect of surface tension.

34 FLUID MECHANICS AND HEAT TRANSFER

Fluid properties in terms of the Prandtl and the Lewis numbers have a profound effect on the stability conditions; opposite stability characteristics are found in salt solutions and in molten metals.

Author

A93-14551* National Aeronautics and Space Administration. Lewis Research Center, Cleveland, OH.

RIPPLE - A NEW MODEL FOR INCOMPRESSIBLE FLOWS WITH FREE SURFACES

D. B. KOTHE and R. C. MJOLSNES (Los Alamos National Lab., NM) AIAA Journal (ISSN 0001-1452) vol. 30, no. 11 Nov. 1992 p. 2694-2700. Previously cited in issue 22, p. 3881, Accession no. A91-52433 AIAA, NASA, and OAI, Conference on Advanced SEI Technologies, Cleveland, OH, Sept. 4-6, 1991, AIAA Paper 91-3548 refs
(Contract W-7405-ENG-36; NASA ORDER C-32008-K)
Copyright

A93-14762* National Aeronautics and Space Administration. Lewis Research Center, Cleveland, OH.

ON THE STRUCTURE OF CELLULAR SOLUTIONS IN RAYLEIGH-BENARD-MARANGONI FLOWS IN SMALL-ASPECT-RATIO CONTAINERS

HENK A. DIJKSTRA (Cornell Univ., Ithaca, NY) Journal of Fluid Mechanics (ISSN 0022-1120) vol. 243 Oct. 1992 p. 73-102. Research supported by U.S. Army refs
(Contract NAG3-801)
Copyright

Multiple steady flow patterns occur in surface-tension/buoyancy-driven convection in a liquid layer heated from below (Rayleigh-Benard-Marangoni flows). Techniques of numerical bifurcation theory are used to study the multiplicity and stability of two-dimensional steady flow patterns (rolls) in rectangular small-aspect-ratio containers as the aspect ratio is varied. For pure Marangoni flows at moderate Biot and Prandtl number, the transitions occurring when paths of codimension 1 singularities intersect determine to a large extent the multiplicity of stable patterns. These transitions also lead, for example, to Hopf bifurcations and stable periodic flows for a small range in aspect ratio. The influence of the type of lateral walls on the multiplicity of steady states is considered. 'No-slip' lateral walls lead to hysteresis effects and typically restrict the number of stable flow patterns (with respect to 'slippery' sidewalls) through the occurrence of saddle node bifurcations. In this way 'no-slip' sidewalls induce a selection of certain patterns, which typically have the largest Nusselt number, through secondary bifurcation.

Author

A93-14771* National Aeronautics and Space Administration. Lewis Research Center, Cleveland, OH.

SOME ASPECTS OF BIFURCATION STRUCTURE OF LAMINAR FLOW IN CURVED DUCTS

HSIAO C. KAO (NASA, Lewis Research Center, Cleveland, OH) Journal of Fluid Mechanics (ISSN 0022-1120) vol. 243 Oct. 1992 p. 519-539. refs
Copyright

A bifurcation study is made of laminar flow in curved ducts. The problem is formulated in a curvilinear coordinate system, and the governing equations, after orthogonal mapping is applied, are solved numerically by an iterative finite-difference method. Many computer runs were made with various duct cross-sections ranging from a circle to a square, to learn the transition of bifurcation structure with this change in cross-section and to reconcile the differences between them. In addition, a simpler technique is proposed to generate symmetric four-cell solutions in a circular pipe and a means is put forward to stabilize four-vortex structures in a complete cross-section.

Author

A93-15063* National Aeronautics and Space Administration. Lewis Research Center, Cleveland, OH.

CALCULATION OF A CIRCULAR JET IN CROSSFLOW WITH A MULTIPLE-TIME-SCALE TURBULENCE MODEL

S.-W. KIM and T. J. BENSON (NASA, Lewis Research Center,

Cleveland, OH) International Journal of Heat and Mass Transfer (ISSN 0017-9310) vol. 35, no. 10 Oct. 1992 p. 2357-2365. Previously announced in STAR as N91-30476 refs
Copyright

Numerical calculation of a three dimensional turbulent flow of a jet in a crossflow using a multiple time scale turbulence model is presented. The turbulence in the forward region of the jet is in a stronger inequilibrium state than that in the wake region of the jet, while the turbulence level in the wake region is higher than that in the front region. The calculated flow and the concentration fields are in very good agreement with the measured data, and it indicated that the turbulent transport of mass, concentration, and momentum is strongly governed by the inequilibrium turbulence. The capability of the multiple time scale turbulence model to resolve the inequilibrium turbulence field is also discussed.

Author

A93-15067* National Aeronautics and Space Administration. Lewis Research Center, Cleveland, OH.

FINITE DIFFERENCE SOLUTION FOR TRANSIENT RADIATIVE COOLING OF A CONDUCTING SEMITRANSSPARENT SQUARE REGION

R. SIEGEL and F. B. MOLLS (NASA, Lewis Research Center, Cleveland, OH) International Journal of Heat and Mass Transfer (ISSN 0017-9310) vol. 35, no. 10 Oct. 1992 p. 2579-2592. refs
Copyright

Transient solutions were obtained for a square region of heat conducting semitransparent material cooling by thermal radiation. The region is in a vacuum environment, so energy is dissipated only by radiation from within the medium leaving through its boundaries. The effect of heat conduction during the transient is to partially equalize the internal temperature distribution. As the optical thickness of the region is increased, the temperature gradients increase near the boundaries and corners, unless heat conduction is large. The solution procedure must provide accurate temperature distributions in these regions to prevent error in the calculated radiation losses. Two-dimensional numerical Gaussian integration is used to obtain the local radiative source term. A finite difference procedure with variable space and time increments is used to solve the transient energy equation. Variable spacing was used to concentrate grid points in regions with large temperature gradients.

Author

A93-16663* National Aeronautics and Space Administration. Lewis Research Center, Cleveland, OH.

NON-PARALLEL EFFECTS IN THE INSTABILITY OF LONG'S VORTEX

M. R. FOSTER (Ohio Aerospace Inst., Brook Park; Ohio State Univ., Columbus) and DAVID JACQMIN (Ohio Aerospace Inst., Brook Park; NASA, Lewis Research Center, Cleveland) Journal of Fluid Mechanics (ISSN 0022-1120) vol. 244 Nov. 1992 p. 289-306. Research supported by Ohio Aerospace Inst refs
Copyright

Asymptotic results obtained by Foster and Smith (1989) for inviscid instability modes of the Type-II Long's vortex is extended to account for the effects of finite Reynolds number. It is shown that the nonparallelism of the flow is more important than the viscous terms in determining the finite-Re behavior due to the radial velocity scales with $Re \exp -1$. A critical layer of the three-layer structure of the parallel-flow instability modes is considerably modified by radial velocity. It is found that for azimuthal wavenumber n greater than 1, the nonparallelism stabilizes the unstable inertial modes, leading to determination of neutral curves. For n less than -1, the nonparallel effects always destabilize the vortex to these helical modes.

O.G.

A93-17258* National Aeronautics and Space Administration. Lewis Research Center, Cleveland, OH.

NONLINEAR EVOLUTION OF MODES IN A COMPRESSIBLE BOUNDARY LAYER

J. S. B. GAJJAR (Exeter Univ., United Kingdom) In Boundary layer transition and control; Proceedings of the Conference, Univ. of Cambridge, United Kingdom, Apr. 8-12, 1991 London Royal

Aeronautical Society 1991 p. 12.1-12.10. Research supported by NASA refs
(Contract SERC-GR/E/7072/6)
Copyright

The nonlinear stability of an oblique mode propagating in a 2D compressible boundary layer is considered under the long wave-length approximation. The growth rate of the wave is assumed to be small so that the ideas of nonlinear critical layers can be applied. It is shown that the spatial/temporal evolution of the mode is governed by a pair of coupled unsteady nonlinear equations for the disturbance vorticity and density. Expressions for the linear growth rate shows clearly the effects of wall heating and cooling, and in particular how heating destabilizes the boundary layer for these long wavelength inviscid modes at $O(1)$ Mach numbers. The numerical solution of the nonlinear problem is discussed and some results are presented.

Author

A93-17416 National Aeronautics and Space Administration. Lewis Research Center, Cleveland, OH.

WEAKLY NONLINEAR MODELS FOR TURBULENT MIXING IN A PLANE MIXING LAYER

WILLIAM W. LIOU (NASA, Lewis Research Center, Cleveland, OH) and PHILIP J. MORRIS (Pennsylvania State Univ., University Park) Physics of Fluids A (ISSN 0899-8213) vol. 4, no. 12 Dec. 1992 p. 2798-2808. refs
(Contract NAG1-657)
Copyright

New closure models for turbulent free shear flows are presented in this paper. They are based on a weakly nonlinear theory with a description of the dominant large-scale structures as instability waves. Two models are presented that describe the evolution of the free shear flows in terms of the time-averaged mean flow and the dominant large-scale turbulent structure. The local characteristics of the large-scale motions are described using linear theory. Their amplitude is determined from an energy integral analysis. The models have been applied to the study of an incompressible mixing layer. For both models, predictions of the mean flow developed are made. In the second model, predictions of the time-dependent motion of the large-scale structures in the mixing layer are made. The predictions show good agreement with experimental observations.

Author

A93-17522* National Aeronautics and Space Administration. Lewis Research Center, Cleveland, OH.

THERMAL RADIATION HEAT TRANSFER (3RD REVISED AND ENLARGED EDITION)

ROBERT SIEGEL (NASA, Lewis Research Center, Cleveland, OH) and JOHN R. HOWELL (Texas Univ., Austin) Washington Hemisphere Publishing Corp. 1992 1090 p. refs
(ISBN 0-89116-271-2) Copyright

This book first reviews the overall aspects and background information related to thermal radiation heat transfer and incorporates new general information, advances in analytical and computational techniques, and new reference material. Coverage focuses on radiation from opaque surfaces, radiation interchange between various types of surfaces enclosing a vacuum or transparent medium, and radiation including the effects of partially transmitting media, such as combustion gases, soot, or windows. Boundary conditions and multiple layers are discussed with information on radiation in materials with nonunity refractive indices.

R.E.P.

A93-18556* National Aeronautics and Space Administration. Lewis Research Center, Cleveland, OH.

HEAT TRANSFER WITH VERY HIGH FREE-STREAM TURBULENCE. I - EXPERIMENTAL DATA. II - ANALYSIS OF RESULTS

P. K. MACIEJEWSKI (Pittsburgh Univ., PA) and R. J. MOFFAT (Stanford Univ., CA) ASME, Transactions, Journal of Heat Transfer (ISSN 0022-1481) vol. 114, no. 4 Nov. 1992 p. 827-839. refs

(Contract NAG3-522)
Copyright

Boundary layer heat transfer with very high freestream turbulence is investigated. The problem is studied experimentally by placing a constant-temperature heat transfer surface at various locations in the margin of a turbulent free jet and measuring both the surface heat transfer rate and the turbulence in the freestream. Freestream turbulent fluctuations 20 to 60 percent relative to the mean velocity augment heat transfer 1.8 to 4 times that which would be predicted locally using accepted correlations for turbulent boundary layers at the same Reynolds number. The correlations of Simonich and Bradshaw (1989), Pedisius et al. (1983), and Blair (1983) each fail to describe the present data. For flows over flat surfaces in air with very high freestream turbulence, greater than 0.2, u' -prime determines h . A new heat transfer parameter, St' -prime, characterizes turbulent boundary layer heat transfer with freestream turbulence on the domain 0-0.65 to within ± 15 percent for high Reynolds number flows with uniform thermal boundary conditions.

C.A.B.

A93-18564* National Aeronautics and Space Administration. Lewis Research Center, Cleveland, OH.

CLOSED-FORM ANALYTICAL SOLUTIONS OF HIGH-TEMPERATURE HEAT PIPE STARTUP AND FROZEN STARTUP LIMITATION

Y. CAO and A. FAGHRI (Wright State Univ., Dayton, OH) ASME, Transactions, Journal of Heat Transfer (ISSN 0022-1481) vol. 114, no. 4 Nov. 1992 p. 1028-1035. ASME, National Heat Transfer Conference, San Diego, CA, Aug. 9-12, 1992 Research supported by NASA refs
(Contract F33615-89-C-2820)
Copyright

Previous numerical and experimental studies indicate that the high-temperature heat pipe startup process is characterized by a moving hot zone with relatively sharp fronts. Based on the above observation, a flat-front model for an approximate analytical solution is proposed. A closed-form solution related to the temperature distribution in the hot zone and the hot zone length as a function of time are obtained. The analytical results agree well with the corresponding experimental data, and provide a quick prediction method for the heat pipe startup performance. Finally, a heat pipe limitation related to the frozen startup process is identified, and an explicit criterion for the high-temperature heat pipe startup is derived. The frozen startup limit identified in this paper provides a fundamental guidance for high-temperature heat pipe design.

Author

A93-18751* National Aeronautics and Space Administration. Lewis Research Center, Cleveland, OH.

MULTIGRID ACCELERATION AND TURBULENCE MODELS FOR COMPUTATIONS OF 3D TURBULENT JETS IN CROSSFLOW

A. O. DEMUREN (Old Dominion Univ., Norfolk, VA) International Journal of Heat and Mass Transfer (ISSN 0017-9310) vol. 35, no. 11 Nov. 1992 p. 2783-2794. refs
(Contract NASA ORDER C-99066-G)
Copyright

A multigrid method is presented for the calculation of three-dimensional turbulent jets in crossflow. Turbulence closure is achieved with either the standard k -epsilon model or a Reynolds stress model (RSM). Multigrid acceleration enables convergence rates which are far superior to that for a single grid method to be obtained with both turbulence models. With the k -epsilon model the rate approaches that for laminar flow, but with RSM it is somewhat slower. The increased stiffness of the system of equation in the latter may be responsible. Computed results with both turbulence models are compared to experimental data for a pair of opposed jets in crossflow. Both models yield reasonable agreement for the mean flow velocity, but RSM yields better predictions of the Reynolds stresses.

Author

34 FLUID MECHANICS AND HEAT TRANSFER

A93-18752* National Aeronautics and Space Administration. Lewis Research Center, Cleveland, OH.

HEAT TRANSFER PERFORMANCE COMPARISONS OF FIVE DIFFERENT RECTANGULAR CHANNELS WITH PARALLEL ANGLED RIBS

J. S. PARK, J. C. HAN, Y. HUANG, S. OU (Texas A & M Univ., College Station), and R. J. BOYLE (NASA, Lewis Research Center, Cleveland, OH) International Journal of Heat and Mass Transfer (ISSN 0017-9310) vol. 35, no. 11 Nov. 1992 p. 2891-2903. refs

(Contract NAG3-311; NAS3-24227)

Copyright

This paper systematically presents the results of heat transfer and friction factor data measured in five short rectangular channels with turbulence promoters. The project investigated the combined effects of the channel aspect ratio, rib angle-of-attack, and flow Reynolds number on heat transfer and pressure drop in rectangular channels with two opposite ribbed walls. The channel aspect ratio (width-to-height, W/H , ribs on side W) varied from $1/4$ to $1/2$, to 1 , 2 , and 4 , while the corresponding rib angles-of-attack α were 90° , 60° , 45° , and 30° , respectively. The Reynolds number range was $10,000$ - $60,000$. The results suggest that the narrow aspect ratio channels (W/H less than 1) give much better heat transfer performance than the wide aspect ratio channels (W/H greater than 1). For the square channel ($W/H = 1$), the $60^\circ/45^\circ$ deg angled ribs provide the best heat transfer performance. For the narrow aspect ratio channel ($W/H = 1/4$ or $1/2$), the $45^\circ/60^\circ$ deg angled ribs are recommended, while the $30^\circ/45^\circ$ deg angled ribs are better for wide aspect ratio channels ($W/H = 4$ or 2). Author

A93-19416 National Aeronautics and Space Administration. Lewis Research Center, Cleveland, OH.

HEAT TRANSFER IN ROTATING SERPENTINE PASSAGES WITH TRIPS SKEWED TO THE FLOW

B. V. JOHNSON, J. H. WAGNER (United Technologies Research Center, East Hartford, CT), G. D. STEUBER (Pratt & Whitney Group, East Hartford, CT), and F. C. YEH (NASA, Lewis Research Center, Cleveland, OH) Jun. 1992 11 p. ASME, International Gas Turbine and Aeroengine Congress and Exposition, 37th, Cologne, Germany, June 1-4, 1992 Previously announced in STAR as N92-20235 Research supported by United Technologies Corp. refs

(Contract NAS3-23691; RTOP 505-62-52)

(ASME PAPER 92-GT-191)

Experiments were conducted to determine the effects of buoyancy and Coriolis forces on heat transfer in turbine blade internal coolant passages. The experiments were conducted with a large scale, multi-pass heat transfer model with both radially inward and outward flow. An analysis of the governing flow equations showed that four parameters influence the heat transfer in rotating passages: coolant-to-wall temperature, rotation number, Reynolds number, and radius-to-passage hydraulic diameter ratio. Results were correlated and compared to previous results from similar stationary and rotating models with smooth walls and with trip strips normal to the flow direction. It was concluded that (1) both Coriolis and buoyancy must be considered in turbine blade cooling designs with trip strips, (2) the effects of rotation are markedly different depending upon the flow direction, and (3) the heat transfer with skewed trip strips is less sensitive to buoyancy than the heat transfer models with either smooth or normal trips. Therefore, skewed trip strips rather than normal trip strips are recommended and geometry-specific tests are required for accurate design. Author

A93-19419* National Aeronautics and Space Administration. Lewis Research Center, Cleveland, OH.

TIME-AVERAGED HEAT TRANSFER AND PRESSURE MEASUREMENTS AND COMPARISON WITH PREDICTION FOR A TWO-STAGE TURBINE

M. G. DUNN, J. KIM (Calspan-UB Research Center, Buffalo, NY), K. C. CIVINSKAS (U.S. Army, Propulsion Directorate; NASA, Lewis Research Center, Cleveland, OH), and R. J. BOYLE (NASA, Lewis

Research Center, Cleveland, OH) Jun. 1992 13 p. ASME, International Gas Turbine and Aeroengine Congress and Exposition, 37th, Cologne, Germany, June 1-4, 1992 refs

(Contract NAG3-581)

(ASME PAPER 92-GT-194)

Time-averaged Stanton number and surface-pressure distributions are reported for the first-stage vane row and the first-stage blade row of the Rocketdyne Space Shuttle Main Engine two-stage fuel-side turbine. These measurements were made at 10 percent, 50 percent, and 90 percent span on both the pressure and suction surfaces of the component. Stanton-number distributions are also reported for the second-stage vane at 50 percent span. A shock tube is used as a short-duration source of heated and pressurized air to which the turbine is subjected. Platinum thin-film gages are used to obtain the heat-flux measurements and miniature silicone-diaphragm pressure transducers are used to obtain the surface pressure measurements. The first-stage vane Stanton number distributions are compared with predictions obtained using a quasi-3D Navier-Stokes solution and a version of STAN5. This same N-S technique was also used to obtain predictions for the first blade and the second vane. Author

A93-19421* National Aeronautics and Space Administration. Lewis Research Center, Cleveland, OH.

WAKE-INDUCED UNSTEADY STAGNATION-REGION HEAT-TRANSFER MEASUREMENTS

P. J. MAGARI and L. E. LAGRAFF (Syracuse Univ., NY) Jun. 1992 8 p. ASME, International Gas Turbine and Aeroengine Congress and Exposition, 37th, Cologne, Germany, June 1-4, 1992 refs

(Contract NAG3-621)

(ASME PAPER 92-GT-196)

Results of an experimental investigation of wake-induced unsteady heat transfer in the stagnation region of a cylinder are presented. A quasi-steady representation of the stator/rotor interaction in a gas turbine using two stationary cylinders in crossflow is created. Time-averaged and time-resolved heat-transfer results are obtained over a wide range of Reynolds numbers at two Mach numbers: one incompressible and one transonic. The augmentation of the heat transfer in the stagnation region due to wake unsteadiness is documented by comparison with isolated cylinder tests. The time-averaged heat-transfer rate at the stagnation line, expressed in terms of the Frossling number, is found to reach a maximum independent of the Reynolds number. The power spectra and cross correlation of the heat-transfer signals in the stagnation region reveal the importance of large vortical structures shed from the upstream wake generator. C.A.B.

A93-19821* National Aeronautics and Space Administration. Lewis Research Center, Cleveland, OH.

FLOW EFFECTS IN A VERTICAL CVD REACTOR

G. W. YOUNG, S. I. HARIHARAN, and R. CARNAHAN (Akron Univ., OH) SIAM Journal on Applied Mathematics (ISSN 0036-1399) vol. 52, no. 6 Dec. 1992 p. 1509-1532. refs

(Contract NCC3-104; NSF DMS-89-57534; NSF DMS-89-21189)

Copyright

A model is presented to simulate the non-Boussinesq flow in a vertical, two-dimensional, chemical vapor deposition reactor under atmospheric pressure. Temperature-dependent conductivity, mass diffusivity, viscosity models, and reactive species mass transfer to the substrate are incorporated. In the limits of small Mach number and small aspect ratio, asymptotic expressions for the flow, temperature, and species fields are developed. Soret diffusion effects are also investigated. Analytical solutions predict an inverse relationship between temperature field and concentration field due to Soret effects. This finding is consistent with numerical simulations, assisting in the understanding of the complex interactions amongst the flow, thermal, and species fields in a chemically reacting system. Author

A93-20141* National Aeronautics and Space Administration. Lewis Research Center, Cleveland, OH.

TWO-, THREE-, AND FOUR-POSTER JETS IN CROSS FLOW
THOMAS J. VUKITS, JOHN P. SULLIVAN, and S. N. B. MURTHY (Purdue Univ., West Lafayette, IN) Jan. 1993 13 p. AIAA, Aerospace Sciences Meeting and Exhibit, 31st, Reno, NV, Jan. 11-14, 1993 refs

(Contract NAG3-943)
(AIAA PAPER 93-0023) Copyright

In connection with the problems of the ingestion of hot exhaust gases in engines of V/STOL and STOVL aircraft in ground effect, a series of studies have been undertaken. Ground impinging, two- and three-poster jets operating in the presence of cross flow were studied. The current paper is divided into two parts. The first part is a comparison of the low speed, two-, three-, and four-poster jet cases, with respect to the flowfield in the region of interaction between the forward and the jet flows. These include cases with mass balanced inlet suction. An analysis of the inlet entry plane of the low speed two- and three-poster jet cases is also given. In the second part, high speed results for a two jet configuration without inlet suction are given. The results are based on quantitative, marker concentration distributions obtained by digitizing video images.

Author

A93-21049* National Aeronautics and Space Administration. Lewis Research Center, Cleveland, OH.

FULLY COUPLED RESONANT-TRIAD INTERACTION IN AN ADVERSE-PRESSURE-GRADIENT BOUNDARY LAYER
M. E. GOLDSTEIN (NASA, Lewis Research Center, Cleveland, OH) and SANG S. LEE (Sverdrup Technology, Inc., Lewis Research Center Group, Cleveland, OH) Journal of Fluid Mechanics (ISSN 0022-1120) vol. 245 Dec. 1992 p. 523-551. refs

The nonlinear resonant-triad interaction, proposed by Raetz (1959), Craik (1971), and others for a Blasius boundary layer, is analyzed here for an adverse-pressure-gradient boundary layer. We assume that the adverse pressure gradient is in some sense weak and, therefore, that the instability growth rate is small. This ensures that there is a well-defined critical layer located somewhere within the flow and that the nonlinear interaction is effectively confined to that layer. The initial interaction is of the parametric resonance type, even when the modal amplitudes are all of the same order. This means that the oblique instability waves exhibit faster than exponential growth and that the growth rate of the two-dimensional mode remains linear. However, the interaction and the resulting growth rates become fully coupled, once oblique-mode amplitudes become sufficiently large, but the coupling terms are now quartic, rather than quadratic as in the Craik (1971) analysis. More importantly, however, new nonlinear interactions, which were not present in the Craik-type analyses, now come into play. These interactions eventually have a dominant effect on the instability wave development.

Author

A93-21060* National Aeronautics and Space Administration. Lewis Research Center, Cleveland, OH.

ON STREAMWISE VORTICES IN HIGH REYNOLDS NUMBER SUPERSONIC AXISYMMETRIC JETS
S. A. ARNETTE, M. SAMIMY, and G. S. ELLIOTT (Ohio State Univ., Columbus) Physics of Fluids A (ISSN 0899-8213) vol. 5, no. 1 Jan. 1993 p. 187-202. Research supported by NSF and Ohio Aerospace Inst. refs

(Contract NAG3-764)
Copyright

Streamwise vortices previously observed in underexpanded jets were studied using pitot pressure measurements and flow visualizations. A simple model was developed that gives reasonable agreement with the pressure measurements. A convergent nozzle and a convergent-divergent nozzle of design Mach number 1.5 were employed to generate jet flows of equivalent Mach numbers up to 2.5. By operating the nozzles fully expanded, overexpanded, and underexpanded, insight into both the occurrence and the cause of formation of the vortices was gained.

L.M.

A93-21652* National Aeronautics and Space Administration. Lewis Research Center, Cleveland, OH.

INFLUENCE OF AMBIENT AIR PRESSURE ON EFFERVESCENT ATOMIZATION
S. K. CHEN, A. H. LEFEBVRE (Purdue Univ., West Lafayette, IN), and J. ROLLBUHLER (NASA, Lewis Research Center, Cleveland, OH) Journal of Propulsion and Power (ISSN 0748-4658) vol. 9, no. 1 Jan.-Feb. 1993 p. 10-15. AIAA, Aerospace Sciences Meeting and Exhibit, 30th, Reno, NV, Jan. 6-9, 1992 refs

(AIAA PAPER 92-0460) Copyright

The influence of ambient air pressure on the drop-size distributions produced in effervescent atomization is examined in this article. Also investigated are the effects on spray characteristics of variations in air/liquid mass ratio, liquid-injection pressure, and atomizer discharge-orifice diameter at different levels of ambient air pressure. It is found that continuous increase in air pressure above the normal atmospheric value causes the mean drop-size to first increase up to a maximum value and then decline. An explanation for this characteristic is provided in terms of the various contributing factors to the overall atomization process. It is also observed that changes in atomizer geometry and operating conditions have little effect on the distribution of drop-sizes in the spray.

Author

A93-21689* National Aeronautics and Space Administration. Lewis Research Center, Cleveland, OH.

LAMINAR/TURBULENT OSCILLATING FLOW IN CIRCULAR PIPES
KYUNG H. AHN (NASA, Lewis Research Center, Cleveland, OH) and MOUNIR B. IBRAHIM (Cleveland State Univ., OH) International Journal of Heat and Fluid Flow (ISSN 0142-727X) vol. 13, no. 4 Dec. 1992 p. 340-346. refs

Copyright

A two-dimensional oscillating flow analysis was conducted simulating the gas flow inside Stirling engine heat exchangers. Both laminar and turbulent oscillating pipe flow were investigated numerically for $Re(max) = 1920$ ($Va = 80$), $10,800$ ($Va = 272$), $19,300$ ($Va = 272$), and $60,800$ ($Va = 126$). The results are compared with experimental results of previous investigators. Predictions of the flow regime are also checked by comparing velocity amplitudes and phase difference with those from laminar theory and quasi-steady profile. A high Reynolds number k-epsilon turbulence model was used for turbulent oscillating pipe flow. Finally, the performance of the k-epsilon model was evaluated to explore the applicability of quasi-steady turbulent models to unsteady oscillating flow analysis.

Author

A93-21712* National Aeronautics and Space Administration. Lewis Research Center, Cleveland, OH.

THE TURBULENT THERMAL BOUNDARY LAYER WITH AN ABRUPT CHANGE FROM A ROUGH TO A SMOOTH WALL
ROBERT P. TAYLOR, J. K. TAYLOR (Mississippi State Univ., Mississippi State), M. H. HOSNI (Kansas State Univ., Manhattan), and HUGH W. COLEMAN (Alabama Univ., Huntsville) International Journal of Heat and Mass Transfer (ISSN 0017-9310) vol. 36, no. 1 Jan. 1993 p. 141-146. refs

(Contract NAG3-1116)

Copyright

The work reported here was motivated by concern over the use of smooth heat flux gages for heat transfer measurements on the otherwise rough turbine blades. Stanton number distributions and boundary layer profiles of mean temperature, mean velocity, and turbulence intensity are reported for a surface with a step change from a rough to a smooth surface. In most cases, the Stanton number immediately downstream of the change in roughness drops below the all-smooth-wall data at the same x-Reynolds number. The alignment of the smooth surface between the bases and crests of the roughness elements is shown to have only a weak effect on the Stanton number distribution. It is concluded that the use of smooth heat flux gages on otherwise rough surfaces can cause large errors. It is recommended that heat transfer data collected in this manner be used with caution.

Author

A93-21715* National Aeronautics and Space Administration. Lewis Research Center, Cleveland, OH.

A STUDY OF CIRCUMFERENTIALLY-HEATED AND BLOCK-HEATED HEAT PIPES. I - EXPERIMENTAL ANALYSIS AND GENERALIZED ANALYTICAL PREDICTION OF CAPILLARY LIMITS. II - THREE-DIMENSIONAL NUMERICAL MODELING AS A CONJUGATE PROBLEM

JOSEPH SCHMALHOFER and AMIR FAGHRI (Wright State Univ., Dayton, OH) International Journal of Heat and Mass Transfer (ISSN 0017-9310) vol. 36, no. 1 Jan. 1993 p. 201-226.

Research supported by NASA refs

(Contract F33615-89-C-2820)

Copyright

The wall and centerline vapor temperatures and heat output are determined experimentally for a low-temperature copper-water heat pipe under uniform circumferential heating and block heating. The time required to reach a vapor temperature of 60 C from an initial ambient temperature of 21 C is determined for both modes of heating. The experimental capillary limit of the heat pipe is compared to the generalized capillary limits for block-heated pipes over a range of vapor temperatures. A three-dimensional numerical model is then developed for determining the temperature, pressure, and velocity distributions in the entire domain of a circumferentially heated and a block-heated pipe. The problem is formulated as a conjugate problem, without the assumption of a uniform vapor temperature. The predictions of the model are found to be in good agreement with the experimental data. V.L.

A93-21717* National Aeronautics and Space Administration. Lewis Research Center, Cleveland, OH.

DISCUSSION OF 'COMPARISON OF TURBULENCE MODELS FOR THE NATURAL CONVECTION BOUNDARY LAYER ALONG A HEATED VERTICAL PLATE'

JOSEPH A. C. HUMPHREY (California Univ., Berkeley) and WAI M. TO (Sverdrup Technology, Inc.; NASA, Lewis Research Center, Cleveland, OH) International Journal of Heat and Mass Transfer (ISSN 0017-9310) vol. 36, no. 1 Jan. 1993 p. 245, 246; Authors' Reply, p. 246, 247. refs

Copyright

The paper presents a critical comment on the work of Henkes and Hoogendoorn. In particular, it is argued that the model of To and Humphrey (TH) (1986) has been implemented incorrectly, rendering invalid the conclusion that the TH model considerably deviates from the other models evaluated. In their response to the criticism, the authors present arguments in support of the correctness of their implementation of the TH model and of the validity of the conclusions reached in their work. V.L.

A93-21725* National Aeronautics and Space Administration. Lewis Research Center, Cleveland, OH.

THE EIGENVALUE SPECTRUM OF THE RAYLEIGH EQUATION FOR A PLANE SHEAR LAYER

WILLIAM W.-W. LIU (NASA, Lewis Research Center, Cleveland, OH) and PHILIP J. MORRIS (Pennsylvania State Univ., University Park) International Journal for Numerical Methods in Fluids (ISSN 0271-2091) vol. 15, no. 12 Dec. 30, 1992 p. 1407-1415. refs

Copyright

The eigenvalue spectrum of the Rayleigh equation is examined using three different solution techniques. In particular, a simple second-order finite difference scheme and two spectral methods, the Chebyshev tau and Chebyshev collocation methods, are used to discretize the equation. All of the approximation methods are shown to be capable of predicting the discrete spectrum as well as the continuous spectrum associated with the critical point singularity for the Rayleigh equation. The global eigenvalue methods considered here provide an efficient way of obtaining either an approximation to the complete eigenvalue spectrum or initial guesses for a local shooting procedure for the discrete part of the spectrum. V.L.

A93-22258* National Aeronautics and Space Administration. Lewis Research Center, Cleveland, OH.

THE DEVELOPMENT OF A TURBULENT JUNCTION VORTEX SYSTEM

F. J. PIERCE (Virginia Polytechnic Inst. and State Univ., Blacksburg) and J. SHIN (NASA, Lewis Research Center, Cleveland, OH) ASME, Transactions, Journal of Fluids Engineering (ISSN 0098-2202) vol. 114, no. 4 Dec. 1992 p. 559-565. refs

Copyright

The growth and development of a horseshoe vortex system in an incompressible, three-dimensional turbulent junction flow were investigated experimentally. A streamlined cylinder mounted with its axis normal to a flat surface was used to generate the junction vortex flow. The flow environment was characterized by a body Reynolds number of 183,000, based on the leading edge diameter of the streamlined cylinder. The study included surface flow visualizations, surface pressure measurements, and mean flow measurements of total pressure, static pressure, and velocity distributions in three planes around the base of the streamlined cylinder, and in two planes in the wake flow. Some characterizations of vortex properties based on the measured mean cross-flow velocity components are presented. The results show the presence of a single large, dominant vortex, with strong evidence of a very small corner vortex in the junction between the cylinder and the flat surface. The center of the dominant vortex drifts away from both the body and the flat surface as the flow develops along and downstream of the body. The growth and development of the core of the large, dominant vortex are documented. Author

A93-22509*# National Aeronautics and Space Administration. Lewis Research Center, Cleveland, OH.

EVALUATION AND APPLICATION OF THE BALDWIN-LOMAX TURBULENCE MODEL IN TWO-DIMENSIONAL, UNSTEADY, COMPRESSIBLE BOUNDARY LAYERS WITH AND WITHOUT SEPARATION IN ENGINE INLETS

BARBARA SAKOWSKI, DOUGLAS DARLING (NASA, Lewis Research Center, Cleveland, OH), ROBERT L. ROACH (Georgia Inst. of Technology, Atlanta), and ALLAN VAN DE WALL (Case Western Reserve Univ., Cleveland, OH) Jul. 1992 10 p. AIAA, SAE, ASME, and ASEE, Joint Propulsion Conference and Exhibit, 28th, Nashville, TN, July 6-8, 1992 Previously announced in STAR as N93-10087 refs

(AIAA PAPER 92-3676) Copyright

The Baldwin-Lomax model is used in many CFD codes because it is quick and easy to implement. In this paper, we discuss implementing the Baldwin-Lomax turbulence model for both steady and unsteady compressible flows. In addition, these flows may be either separated or attached. In order to apply this turbulence model to flows which may be subjected to these conditions, certain modifications should be made to the original Baldwin-Lomax model. We discuss these modifications and determine whether the Baldwin-Lomax model is a viable turbulence model that produces reasonably accurate results for high speed flows that can be found in engine inlets. Author

A93-22622*# National Aeronautics and Space Administration. Lewis Research Center, Cleveland, OH.

A SIMPLIFIED REYNOLDS STRESS MODEL FOR UNSTEADY TURBULENT BOUNDARY LAYERS

SIXIN FAN and BUDUGUR LAKSHMINARAYANA (Pennsylvania State Univ., University Park) Jan. 1993 13 p. AIAA, Aerospace Sciences Meeting and Exhibit, 31st, Reno, NV, Jan. 11-14, 1993 refs

(Contract NAG3-1168)

(AIAA PAPER 93-0204) Copyright

A simplified Reynolds stress model has been developed for the prediction of unsteady turbulent boundary layers. By assuming that the net transport of Reynolds stresses is locally proportional to the net transport of the turbulent kinetic energy, the time dependent full Reynolds stress model is reduced to a set of ordinary differential equations. These equations contain only time derivatives and can be readily integrated in a time dependent boundary layer or Navier-Stokes code. The turbulent kinetic energy and dissipation

rate needed for the model are obtained by solving the k-epsilon equations. This simplified Reynolds stress turbulence model (SRSM) does not use the eddy viscosity assumption, which may not be valid for unsteady turbulent flows. The anisotropy of both the steady and the unsteady turbulent normal stresses can be captured by the SRSM model. Through proper damping of the shear stresses, the present model can be used in the near wall region of turbulent boundary layers. This model has been validated against data for steady and unsteady turbulent boundary layers, including periodic turbulent boundary layers subjected to a mean adverse pressure gradient. For the cases tested, the predicted unsteady velocity and turbulent stress components agree well with the experimental data. Comparison between the predictions from the SRSM model and a k-epsilon model is also presented.

Author

A93-22662* # National Aeronautics and Space Administration. Lewis Research Center, Cleveland, OH.

AN INTERFACE CONFIGURATION EXPERIMENT ON USML-1
PAUL CONCUS (California Univ., Berkeley), ROBERT FINN (Stanford Univ., CA), and MARK WEISLOGEL (NASA, Lewis Research Center, Cleveland, OH) Jan. 1993 7 p. AIAA, Aerospace Sciences Meeting and Exhibit, 31st, Reno, NV, Jan. 11-14, 1993 refs

(Contract NAG3-1143; NSF DMS-89-02831; DE-AC03-76SF-00098)

(AIAA PAPER 93-0253) Copyright

Experiments were carried out for 'exotic' rotationally symmetric containers aboard the first NASA United States Microgravity Laboratory Space Shuttle flight (USML-1). The containers have the property that they admit an entire continuum of distinct equilibrium rotationally-symmetric capillary free-surfaces for a given liquid volume and contact angle. It was found, after the containers were filled in orbit, that an initial equilibrium interface from the symmetric continuum reoriented, when perturbed, to a stable interface that was not rotationally symmetric, as predicted by the mathematical theory.

Author

A93-22664* # National Aeronautics and Space Administration. Lewis Research Center, Cleveland, OH.

FLOW-INFLUENCED STABILIZATION OF LIQUID COLUMNS IN A DYNAMIC PLATEAU CHAMBER

B. J. LOWRY and P. H. STEEN (Cornell Univ., Ithaca, NY) Jan. 1993 6 p. AIAA, Aerospace Sciences Meeting and Exhibit, 31st, Reno, NV, Jan. 11-14, 1993 Research supported by NSERC refs

(Contract NAG3-801)

(AIAA PAPER 93-0255) Copyright

An apparatus designed to imbed a liquid column or bridge in an axial flow is described. The bridge liquid is density matched to the water in the external flow to simulate low gravity (about 0.001 earth G). The influence of flow on shape is the focus. Results show that flow modifies static shapes in a way that can be accounted for by static theory even for moderate deviations from cylindrical shape, at least for low flow rates.

Author

A93-22666* # National Aeronautics and Space Administration. Lewis Research Center, Cleveland, OH.

TIME-DEPENDENT THERMOCAPILLARY CONVECTION IN A CARTESIAN CAVITY - NUMERICAL RESULTS FOR A MODERATE PRANDTL NUMBER FLUID

L. J. PELTIER and S. BIRINGEN (Colorado Univ., Boulder) Jan. 1993 17 p. AIAA, Aerospace Sciences Meeting and Exhibit, 31st, Reno, NV, Jan. 11-14, 1993 refs

(Contract NAG3-1094)

(AIAA PAPER 93-0259) Copyright

The present numerical simulation explores a thermal-convective mechanism for oscillatory thermocapillary convection in a shallow Cartesian cavity for a Prandtl number 6.78 fluid. The computer program developed for this simulation integrates the two-dimensional, time-dependent Navier-Stokes equations and the energy equation by a time-accurate method on a stretched, staggered mesh. Flat free surfaces are assumed. The instability is

shown to depend upon temporal coupling between large scale thermal structures within the flow field and the temperature sensitive free surface. A primary result of this study is the development of a stability diagram presenting the critical Marangoni number separating steady from the time-dependent flow states as a function of aspect ratio for the range of values between 2.3 and 3.8. Within this range, a minimum critical aspect ratio near 2.3 and a minimum critical Marangoni number near 20,000 are predicted below which steady convection is found.

Author

A93-22681* # National Aeronautics and Space Administration. Lewis Research Center, Cleveland, OH.

INFLUENCE OF HEAT TRANSFER RATES ON PRESSURIZATION OF LIQUID/SLUSH HYDROGEN PROPELLANT TANKS

G. P. SASMAL, J. I. HOCHSTEIN (Memphis State Univ., TN), and T. L. HARDY (NASA, Lewis Research Center, Cleveland, OH) Jan. 1993 8 p. AIAA, Aerospace Sciences Meeting and Exhibit, 31st, Reno, NV, Jan. 11-14, 1993 refs (AIAA PAPER 93-0278) Copyright

A multi-dimensional computational model of the pressurization process in liquid/slush hydrogen tank is developed and used to study the influence of heat flux rates at the ullage boundaries on the process. The new model computes these rates and performs an energy balance for the tank wall whereas previous multi-dimensional models required a priori specification of the boundary heat flux rates. Analyses of both liquid hydrogen and slush hydrogen pressurization were performed to expose differences between the two processes. Graphical displays are presented to establish the dependence of pressurization time, pressurant mass required, and other parameters of interest on ullage boundary heat flux rates and pressurant mass flow rate. Detailed velocity fields and temperature distributions are presented for selected cases to further illuminate the details of the pressurization process. It is demonstrated that ullage boundary heat flux rates do significantly effect the pressurization process and that minimizing heat loss from the ullage and maximizing pressurant flow rate minimizes the mass of pressurant gas required to pressurize the tank. It is further demonstrated that proper dimensionless scaling of pressure and time permit all the pressure histories examined during this study to be displayed as a single curve.

Author

A93-22686* # National Aeronautics and Space Administration. Lewis Research Center, Cleveland, OH.

VAPORIZATION HEAT TRANSFER OF DIELECTRIC LIQUIDS ON A WICK-COVERED SURFACE

C. B. GU, L. C. CHOW (Kentucky Univ., Lexington), and K. BAKER (NASA, Lewis Research Center, Cleveland, OH) Jan. 1993 6 p. AIAA, Aerospace Sciences Meeting and Exhibit, 31st, Reno, NV, Jan. 11-14, 1993 refs

(Contract NAG3-1251)

(AIAA PAPER 93-0283) Copyright

Vaporization heat transfer characteristics were measured for the dielectric liquid FC-72 on a horizontal heated surface covered with wire screen wicks with the mesh number for the screens varying from 24 to 100. In such a situation the liquid level can be either higher or lower than the heated surface. When the liquid level was above the heated surface (shallow pool boiling), the height of the liquid level above the surface, h , was varied from 0 to 10 mm. When the liquid level was below the heated surface (evaporation through capillary pumping), the distance from the liquid level to the edge of the surface, L , was adjusted from 0 to 15 mm. Experimental data revealed that the critical heat flux (CHF) decreases as the mesh number is increased from 24 to 100 for both vaporation and shallow pool boiling, showing that the vapor-escaping limit is more important than the capillary limit in flat plate heat pipe application.

Author

A93-23307* # National Aeronautics and Space Administration. Lewis Research Center, Cleveland, OH.

THE EFFECTS OF BUOYANCY ON THE CRITICAL HEAT FLUX IN FORCED CONVECTION

MATTHEW J. BRUSSTAR and HERMAN MERTE, JR. (Michigan Univ., Ann Arbor) Jan. 1993 7 p. AIAA, Aerospace Sciences Meeting and Exhibit, 31st, Reno, NV, Jan. 11-14, 1993 refs (Contract NAG3-589) (AIAA PAPER 93-0575) Copyright

The critical heat flux (CHF) in forced convection over a flat surface at relatively low flow velocities has been found, not unexpectedly, to depend upon the orientation of the buoyancy. The CHF for R-113 was measured at various heating surface orientations for test section Reynolds numbers ranging between 3000 and 6500. In this flow range, the buoyancy force acting on the vapor generally dominates over the flow inertia, yet the inertia would still be substantial were gravity to be reduced. In the experiments of this study, the CHF is determined for heating surface orientations ranging from 0 deg to 360 deg, for flow velocities between 4 cm/s and 35 cm/s, and for subcoolings between 2.8 C and 22.2 C. The results presented here demonstrate the strong influence of buoyancy at low flow velocities, which diminishes as the flow velocity and subcooling are increased. Author

A93-23390* # National Aeronautics and Space Administration. Lewis Research Center, Cleveland, OH.

EFFECTS OF FREE-STREAM TURBULENCE ON BOUNDARY-LAYER TRANSITION

TH. HERBERT (Ohio State Univ., Columbus), G. K. STUCKERT, and V. ESFAHANIAN (DynaFlow, Inc., Columbus, OH) Jan. 1993 16 p. AIAA, Aerospace Sciences Meeting and Exhibit, 31st, Reno, NV, Jan. 11-14, 1993 refs (Contract AF-AFOSR-91-0262; N00014-90-J-1520; NAS3-26602) (AIAA PAPER 93-0488) Copyright

Traditional methods for the prediction of the transition location rest either on lump parameters like the momentum thickness or on N factors obtained from the approximate linear stability characteristics of the flow. These methods account for the effects of the disturbance environment by empirical correlation with observed transition locations. We have developed a highly efficient and accurate approach to stability analysis and transition simulation based on parabolized stability equations (PSE). Here we present a first application of this approach to realistic problems of practical interest. We study the effects of the turbulence level on transition and heat transfer in flows over flat plates, curved plates, and the stator blade of a gas-turbine model. We discuss the formulation of an input model for the PSE analysis in the light of the present knowledge of receptivity mechanisms. The input model is used to compute transition locations for various configurations and flow conditions. The results compare favorably with experimental data. Author

A93-23944* # National Aeronautics and Space Administration. Lewis Research Center, Cleveland, OH.

LAGRANGIAN SOLUTION OF SUPERSONIC REAL GAS FLOWS

CHING-YUEN LOH and MENG-SING LIOU (NASA, Lewis Research Center, Cleveland, OH) Journal of Computational Physics (ISSN 0021-9991) vol. 104, no. 1 Jan. 1993 p. 150-161. refs Copyright

The present extension of a Lagrangian approach of the Riemann solution procedure, which was originally proposed for perfect gases, to real gases, is nontrivial and requires the development of an exact real-gas Riemann solver for the Lagrangian form of the conservation laws. Calculations including complex wave interactions of various types were conducted to test the accuracy and robustness of the approach. Attention is given to the case of 2D oblique waves' capture, where a slip line is clearly in evidence; the real gas effect is demonstrated in the case of a generic engine nozzle. O.C.

A93-24226* # National Aeronautics and Space Administration. Lewis Research Center, Cleveland, OH.

AN EXPERIMENTAL INVESTIGATION OF S-DUCT FLOW CONTROL USING ARRAYS OF LOW-PROFILE VORTEX GENERATORS

B. A. REICHERT and B. J. WENDT (NASA, Lewis Research Center,

Cleveland, OH) Jan. 1993 13 p. AIAA, Aerospace Sciences Meeting and Exhibit, 31st, Reno, NV, Jan. 11-14, 1993 refs (AIAA PAPER 93-0018) Copyright

An experimental investigation was undertaken to measure the effect of various configurations of low-profile vortex generator arrays on the flow in a diffusing S-duct. Three parameters that characterize the vortex generator array were systematically varied to determine their effect: (1) the vortex generator height, (2) the streamwise location of the vortex generator array, and (3) the vortex generator spacing. Each array of vortex generators tested improved total pressure recovery. The configuration employing the largest vortex generators was the most effective in reducing total pressure distortion but did not produce the greatest total pressure recovery. No configuration of vortex generators completely eliminated the flow separation that naturally occurs in the S-duct; however the extent of the separated flow region was reduced. Author

A93-24227* # National Aeronautics and Space Administration. Lewis Research Center, Cleveland, OH.

CRITICAL ASSESSMENT OF REYNOLDS STRESS TURBULENCE MODELS USING HOMOGENEOUS FLOWS

AAMIR SHABBIR and TSAN-HSING SHIH (NASA, Lewis Research Center, Cleveland, OH) Jan. 1993 13 p. AIAA, Aerospace Sciences Meeting and Exhibit, 31st, Reno, NV, Jan. 11-14, 1993 refs (AIAA PAPER 93-0082) Copyright

In modeling the rapid part of the pressure correlation term in the Reynolds stress transport equations, extensive use has been made of its exact properties. These, for example, have been employed in obtaining the widely used LRR model. Some recent proposals have dropped one of these properties to obtain new models. We demonstrate, by computing some simple homogeneous flows, that doing so does not lead to any significant improvements over the LRR model and it is not the right direction in improving the performance of existing models. Author

A93-24228* # National Aeronautics and Space Administration. Lewis Research Center, Cleveland, OH.

A MULTISCALE TURBULENCE MODEL FOR INCOMPRESSIBLE FLOW

B. S. DUNCAN (Sverdrup Technology, Inc.; NASA, Lewis Research Center, Cleveland, OH), W. W. LIU, and T. H. SHIH (NASA, Lewis Research Center, Cleveland, OH) Jan. 1993 13 p. AIAA, Aerospace Sciences Meeting and Exhibit, 31st, Reno, NV, Jan. 11-14, 1993 refs (AIAA PAPER 93-0086) Copyright

A multiple-scale eddy viscosity model is described in this paper. This model splits the energy spectrum into a high wave number regime and a low wave number regime. Dividing the energy spectrum into multiple regimes simplistically emulates the cascade of energy through the turbulence spectrum. The constraints on the model coefficients are determined by examining decaying turbulence and homogeneous turbulence. A direct link between the partitioned energies and the energy transfer process is established through the coefficients. This new model has been calibrated and tested for boundary-free turbulent shear flows. Calculations of mean and turbulent properties show good agreement with experimental data for two mixing layers, a plane jet and a round jet. Author

A93-24229* # National Aeronautics and Space Administration. Lewis Research Center, Cleveland, OH.

PDF APPROACH FOR COMPRESSIBLE TURBULENT REACTING FLOWS

A. T. HSU, Y.-L. P. TSAI, and M. S. RAJU (Sverdrup Technology Inc., Brook Park; NASA, Lewis Research Center, Cleveland, OH) Jan. 1993 16 p. AIAA, Aerospace Sciences Meeting and Exhibit, 31st, Reno, NV, Jan. 11-14, 1993 refs (Contract NAS3-25266) (AIAA PAPER 93-0087) Copyright

The objective of the present work is to develop a probability density function (pdf) turbulence model for compressible reacting

flows for use with a CFD flow solver. The probability density function of the species mass fraction and enthalpy are obtained by solving a pdf evolution equation using a Monte Carlo scheme. The pdf solution procedure is coupled with a compressible CFD flow solver which provides the velocity and pressure fields. A modeled pdf equation for compressible flows, capable of capturing shock waves and suitable to the present coupling scheme, is proposed and tested. Convergence of the combined finite-volume Monte Carlo solution procedure is discussed, and an averaging procedure is developed to provide smooth Monte-Carlo solutions to ensure convergence. Two supersonic diffusion flames are studied using the proposed pdf model and the results are compared with experimental data; marked improvements over CFD solutions without pdf are observed. Preliminary applications of pdf to 3D flows are also reported.

Author

A93-24230* # National Aeronautics and Space Administration, Lewis Research Center, Cleveland, OH.

A COUPLED MULTI-BLOCK SOLUTION PROCEDURE FOR SPRAY COMBUSTION IN COMPLEX GEOMETRIES

KUO-HUEY CHEN (Toledo Univ.; NASA, Lewis Research Center, Cleveland, OH) and JIAN-SHUN SHUEN (Sverdrup Technology, Inc.; NASA, Lewis Research Center, Cleveland, OH) Jan. 1993 28 p. AIAA, Aerospace Sciences Meeting and Exhibit, 31st, Reno, NV, Jan. 11-14, 1993 refs (AIAA PAPER 93-0108) Copyright

Turbulent spray-combusting flow in complex geometries is presently treated by a coupled implicit procedure that employs finite-rate chemistry and real gas properties for combustion, as well as the stochastic separated model for spray and a multiblock treatment for complex geometries. Illustrative numerical tests conducted encompass a steady-state nonreacting backward-facing step flow, a premixed single-phase combustion flow, and spray combustion flow in a gas turbine combustor.

O.C.

A93-24232* # National Aeronautics and Space Administration, Lewis Research Center, Cleveland, OH.

DIRECT CALCULATIONS OF WAVES IN FLUID FLOWS USING A HIGH-ORDER COMPACT DIFFERENCE SCHEME

SHENG-TAO YU (Sverdrup Technology, Inc., Brook Park, OH), LENNART S. HULTGREN, and NAN-SUEY LIU (NASA, Lewis Research Center, Cleveland, OH) Jan. 1993 26 p. AIAA, Aerospace Sciences Meeting and Exhibit, 31st, Reno, NV, Jan. 11-14, 1993 refs (Contract NAS3-25266)

(AIAA PAPER 93-0148) Copyright

The solution of the unsteady Euler equations by a sixth-order compact difference scheme combined with a fourth-order Runge-Kutta method is investigated. Closed-form expressions for the amplification factors and their corresponding dispersion correlations are obtained by Fourier analysis of the fully discretized, two-dimensional Euler equations, and the numerical dissipation, dispersion, and anisotropic effects are assessed. It is found that the CFL limit for stable calculations is about 0.8. For a CFL number equal to 0.6, the smallest wavelength which is resolved without numerical damping is about 6 to 8 grid nodes. For phase speeds corresponding to acoustic waves, the corresponding time period is resolved by about 200 to 300 time steps. Three numerical examples of waves in compressible flow are included.

Author

A93-24235* # National Aeronautics and Space Administration, Lewis Research Center, Cleveland, OH.

ENO-OSHER SCHEMES FOR EULER EQUATIONS

JACOBUS J. VAN DER VEGT (NASA, Lewis Research Center, Cleveland, OH; Stanford Univ., CA) Jan. 1993 12 p. AIAA, Aerospace Sciences Meeting and Exhibit, 31st, Reno, NV, Jan. 11-14, 1993 refs

(AIAA PAPER 93-0335) Copyright

The combination of the Osher approximate Riemann solver for the Euler equations and various ENO schemes is discussed for one-dimensional flow. The three basic approaches, viz., the ENO scheme using primitive variable reconstruction, either with the Cauchy-Kowalewski procedure for time integration or the TVD

Runge-Kutta scheme, and the flux-ENO method are tested on different shock tube cases. The ENO-Osher scheme using the Cauchy-Kowalewski procedure for time integration is found to be the most accurate and robust compared with the other methods and is also computationally efficient. The tests showed that the ENO schemes perform reasonably well, but have problems in cases where two discontinuities are close together. In that case there are not enough points in the smooth part of the flow to create a nonoscillatory interpolation.

Author

A93-24236* # National Aeronautics and Space Administration, Lewis Research Center, Cleveland, OH.

A LEAST-SQUARES FINITE ELEMENT METHOD FOR 3D INCOMPRESSIBLE NAVIER-STOKES EQUATIONS

BO-NAN JIANG (NASA, Lewis Research Center, Cleveland, OH), T. L. LIN (Livermore Software Technology Corp., CA), LIN-JUN HOU, and LOUIS A. POVINELLI (NASA, Lewis Research Center, Cleveland, OH) Jan. 1993 11 p. AIAA, Aerospace Sciences Meeting and Exhibit, 31st, Reno, NV, Jan. 11-14, 1993 refs (AIAA PAPER 93-0338)

The least-squares finite element method (LSFEM) based on the velocity-pressure-vorticity formulation is applied to three-dimensional steady incompressible Navier-Stokes problems. This method can accommodate equal-order interpolations, and results in symmetric, positive definite algebraic system. An additional compatibility equation, i.e., the divergence of vorticity vector should be zero, is included to make the first-order system elliptic. The Newton's method is employed to linearize the partial differential equations, the LSFEM is used to obtain discretized equations, and the system of algebraic equations is solved using the Jacobi preconditioned conjugate gradient method which avoids formation of either element or global matrices (matrix-free) to achieve high efficiency. The flow in a half of 3D cubic cavity is calculated at $Re = 100, 400$, and $1,000$ with $50 \times 52 \times 25$ trilinear elements. The Taylor-Gortler-like vortices are observed at $Re = 1,000$.

Author

A93-24237* # National Aeronautics and Space Administration, Lewis Research Center, Cleveland, OH.

NONLINEAR INTERACTION OF FREQUENCY-DETUNED MODES IN BOUNDARY LAYERS

REDA R. MANKBADI (NASA, Lewis Research Center, Cleveland, OH) Jan. 1993 8 p. AIAA, Aerospace Sciences Meeting and Exhibit, 31st, Reno, NV, Jan. 11-14, 1993 refs (AIAA PAPER 93-0347) Copyright

The present critical-layer asymptotic analysis for the nonlinear interaction of frequency-detuned modes in boundary-layer transition indicates that the interaction between a plane mode at the fundamental frequency and a pair of symmetrical oblique waves at the near-subharmonic frequency amplifies another pair of symmetrical oblique waves at the 'mirror frequency'. This type of interaction is stronger in the frequency-detuned case than the resonant triad case, and leads to a sharp drop in the oblique waves' peak with small detuning.

O.C.

A93-24241* # National Aeronautics and Space Administration, Lewis Research Center, Cleveland, OH.

NATURAL AND THERMOCAPILLARY CONVECTION IN MULTIPLE LIQUID LAYERS

A. PRAKASH, J. N. KOSTER (Colorado Univ., Boulder), and MYRON HILL (NASA, Lewis Research Center, Cleveland, OH) Jan. 1993 9 p. AIAA, Aerospace Sciences Meeting and Exhibit, 31st, Reno, NV, Jan. 11-14, 1993 refs (Contract NAG3-1094)

(AIAA PAPER 93-0469) Copyright

A numerical and experimental investigation is conducted of the fluid dynamics of immiscible liquid layers, as encountered in the liquid encapsulation of electronic melts. Attention is given to the convective flow in multiple liquid layers that are driven by temperature gradients that are either parallel or perpendicular to the liquid/liquid interfaces. The experimental and theoretical results obtained are noted not to be in agreement for differential side-heating of a three-layer system.

O.C.

A93-24401* National Aeronautics and Space Administration. Lewis Research Center, Cleveland, OH.

THREE-DIMENSIONAL BOUNDARY-LAYER INSTABILITY AND SEPARATION INDUCED BY SMALL-AMPLITUDE STREAMWISE VORTICITY IN THE UPSTREAM FLOW

M. E. GOLDSTEIN (NASA, Lewis Research Center, Cleveland, OH) and S. J. LEIB (Sverdrup Technology, Inc.; NASA, Lewis Research Center, Cleveland, OH) Journal of Fluid Mechanics (ISSN 0022-1120) vol. 246 Jan. 1993 p. 21-41. refs Copyright

We consider the effects of a small-amplitude, steady, streamwise vorticity field on the flow over an infinitely thin flat plate in an otherwise uniform stream. We show how the initially linear perturbation, ultimately leads to a small-amplitude but nonlinear cross flow far downstream from the leading edge. This motion is imposed on the boundary-layer flow and eventually causes the boundary layer to separate. The streamwise velocity profiles within the boundary layer become inflexional in localized spanwise regions just upstream of the separation point. The flow in these regions is therefore susceptible to rapidly growing inviscid instabilities. Author

A93-24766* National Aeronautics and Space Administration. Lewis Research Center, Cleveland, OH.

NUMERICAL SIMULATIONS OF A HIGH MACH NUMBER JET FLOW

M. E. HAYDER, ELI TURKEL, and REDA R. MANKBADI (NASA, Lewis Research Center, Cleveland, OH) Jan. 1993 16 p. AIAA, Aerospace Sciences Meeting and Exhibit, 31st, Reno, NV, Jan. 11-14, 1993 refs (AIAA PAPER 93-0653) Copyright

The present 2D simulations of plane and axisymmetric jets, which are relevant to current efforts to suppress the jet exhaust noise of prospective high-speed civil transports, were conducted by solving full Navier-Stokes equations by means of a high-order finite-difference scheme. The results obtained, which were able to generate the correct mode shape after an adjustment region of about 10 diameters, are in good agreement with linear-theory predictions of the growth of instability waves. O.C.

A93-24792* National Aeronautics and Space Administration. Lewis Research Center, Cleveland, OH.

EFFECT OF VAPORIZATION ON CRYOGENIC SPRAY DROPSIZE MEASUREMENT

ROBERT D. INGEBO (NASA, Lewis Research Center, Cleveland, OH) Jan. 1993 9 p. AIAA, Aerospace Sciences Meeting and Exhibit, 31st, Reno, NV, Jan. 11-14, 1993 Previously announced in STAR as N93-13410 refs (AIAA PAPER 93-0692) Copyright

The fluid mechanics of multi-phase flow breakup of liquid nitrogen, LN₂, jets injected into sonic velocity nitrogen gasflow, was experimentally investigated. A scattered-light scanning instrument was used to measure the characteristic droplet size, $D_{(sub\ v.5)}$, of LN₂ sprays and to determine the effect of droplet vaporization on experimental droplet size measurements. Under sonic gas-velocity conditions, liquid-jet breakup occurred in the regime of aerodynamic stripping. As a result, the following correlation of volume-median drop diameter, $D_{(sub\ v.5)}$, with atomizing gas flowrate, $W_{(sub\ g)}$, was derived for two-fluid atomizers: $(D_{(sub\ v.5)})^{(exp\ -1)} = k_{(sub\ c)} (W_{(sub\ g)})^{(sup\ n)}$, where proportionally constant $k_{(sub\ c)}$ and exponent n are functions of droplet vaporization rate. Partially vaporized sprays were investigated and it was found that $n = 1.11$, which is considerably less than the value of 1.33 that is predicted by atomization theory. This was attributed to the evaporative loss of very small droplets. As a result, the following expression was obtained experimentally: $(D_{(sub\ v.5e)})^{(exp\ -1)} = 301 (W_{(sub\ g)})^{(sub\ 1.11)}$. Values of $D_{(sub\ v.5)}$, that existed prior to partial vaporization of the LN₂ sprays, were calculated and the following expression was derived for originally unvaporized LN₂ sprays: $(D_{(sub\ v.5)})^{(exp\ -1)} = 285 (W_{(sub\ g)})^{(sub\ 1.33)}$. This expression agrees well with atomization theory that predicts $n = 1.33$, for liquid jet breakup in high-velocity gasflow. Author

A93-24817* National Aeronautics and Space Administration. Lewis Research Center, Cleveland, OH.

DSMC AND CONTINUUM ANALYSES OF LOW-DENSITY NOZZLE FLOW

CHAN-HONG CHUNG, SUK C. KIM, ROBERT M. STUBBS (NASA, Lewis Research Center, Cleveland, OH), and KENNETH J. DE WITT (Toledo Univ., OH) Jan. 1993 13 p. AIAA, Aerospace Sciences Meeting and Exhibit, 31st, Reno, NV, Jan. 11-14, 1993 refs (Contract NCC3-171; NAS3-25266) (AIAA PAPER 93-0727)

Two different approaches, the direct-simulation Monte Carlo (DSMC) method based on molecular gas dynamics and a finite-volume approximation of the Navier-Stokes equations, which are based on continuum gas dynamics, are employed in the analysis of a low-density gas flow in a small converging-diverging nozzle. The fluid experiences various kinds of flow regimes including continuum, slip, transition, and free-molecular. Results from the two numerical methods are compared with Rothe's experimental data, in which density and rotational temperature variations along the centerline and at various locations inside a low density nozzle were measured by the electron-beam fluorescence technique. The continuum approach showed good agreement with the experimental data as far as density is concerned. The results from the DSMC method showed good agreement with the experimental data both in the density and the rotational temperature. It is also shown that the simulation parameters, such as the gas/surface interaction model, the energy exchange model between rotational and translational modes, and the viscosity temperature exponent, have substantial effects on the results of the DSMC method. Author

A93-24859* National Aeronautics and Space Administration. Lewis Research Center, Cleveland, OH.

USE OF SURFACE HEAT TRANSFER MEASUREMENTS AS A FLOW SEPARATION DIAGNOSTIC IN A TWO-DIMENSIONAL REFLECTED OBLIQUE SHOCK/TURBULENT BOUNDARY LAYER INTERACTION

A. R. PORRO and W. R. HINGST (NASA, Lewis Research Center, Cleveland, OH) Jan. 1993 17 p. AIAA, Aerospace Sciences Meeting and Exhibit, 31st, Reno, NV, Jan. 11-14, 1993 Previously announced in STAR as N93-15355 refs (AIAA PAPER 93-0775) Copyright

The feasibility of using streamwise surface heat transfer measurements to detect the presence of flow separation in a two-dimensional reflected oblique shock/turbulent boundary layer interaction is reported. Surface heat transfer and static pressure data are presented for attached and separated flows for a free stream nominal Mach number range of 2.5 to 3.5 and shock generator angles of 2 to 8 degrees. The static pressure data do show the characteristic triple inflection point distribution for the strongly separated flow cases. The corresponding surface heat transfer data show unique trends that correlate well with the static pressure determination of the extent of the separated flow region. For the incipient or weakly separated flow cases, the static pressure data do not exhibit the characteristic triple inflection point distribution. However, the same trends in the heat transfer data that are seen for the strongly separated flow cases are evident for the weakly separated flows. Hence, the heat transfer data can be used to determine the extent of weakly separated flows when the surface static pressure distributions often can not. Author

A93-24942* National Aeronautics and Space Administration. Lewis Research Center, Cleveland, OH.

PRECONDITIONED CONJUGATE GRADIENT METHODS FOR LOW SPEED FLOW CALCULATIONS

KUMUD AJMANI (NASA, Lewis Research Center, Cleveland, OH), WING-FAI NG (Virginia Polytechnic Inst. and State Univ., Blacksburg), and MENG-SING LIU (NASA, Lewis Research Center, Cleveland, OH) Jan. 1993 12 p. AIAA, Aerospace Sciences Meeting and Exhibit, 31st, Reno, NV, Jan. 11-14, 1993 Previously announced in STAR as N93-14885 refs (Contract RTOP 505-62-21) (AIAA PAPER 93-0881) Copyright

An investigation is conducted into the viability of using a generalized Conjugate Gradient-like method as an iterative solver to obtain steady-state solutions of very low-speed fluid flow problems. Low-speed flow at Mach 0.1 over a backward-facing step is chosen as a representative test problem. The unsteady form of the two dimensional, compressible Navier-Stokes equations are integrated in time using discrete time-steps. The Navier-Stokes equations are cast in an implicit, upwind finite-volume, flux split formulation. The new iterative solver is used to solve a linear system of equations at each step of the time-integration. Preconditioning techniques are used with the new solver to enhance the stability and the convergence rate of the solver and are found to be critical to the overall success of the solver. A study of various preconditioners reveals that a preconditioner based on the lower-upper (L-U)-successive symmetric over-relaxation iterative scheme is more efficient than a preconditioner based on incomplete L-U factorizations of the iteration matrix. The performance of the new preconditioned solver is compared with a conventional line Gauss-Seidel relaxation (LGSR) solver. Overall speed-up factors of 28 (in terms of global time-steps required to converge to a steady-state solution) and 20 (in terms of total CPU time on one processor of a CRAY-YMP) are found in favor of the new preconditioned solver, when compared with the LGSR solver.

Author

A93-24949* National Aeronautics and Space Administration. Lewis Research Center, Cleveland, OH.

APPLICATION OF AN UNSTRUCTURED GRID FLOW SOLVER TO PLANES, TRAINS AND AUTOMOBILES

GREGORY S. SPRAGLE, WAYNE A. SMITH, and YORAM YADLIN (Fluent, Inc., Lebanon, NH) Jan. 1993 11 p. AIAA, Aerospace Sciences Meeting and Exhibit, 31st, Reno, NV, Jan. 11-14, 1993 Research supported by Ford Motor Co. refs (Contract NAS3-25785)

(AIAA PAPER 93-0889) Copyright

Rampant, an unstructured flow solver developed at Fluent Inc., is used to compute three-dimensional, viscous, turbulent, compressible flow fields within complex solution domains. Rampant is an explicit, finite-volume flow solver capable of computing flow fields using either triangular (2d) or tetrahedral (3d) unstructured grids. Local time stepping, implicit residual smoothing, and multigrid techniques are used to accelerate the convergence of the explicit scheme. The paper describes the Rampant flow solver and presents flow field solutions about a plane, train, and automobile.

Author

A93-24965* National Aeronautics and Space Administration. Lewis Research Center, Cleveland, OH.

NARROW BAND NOISE AS A MODEL OF TIME-DEPENDENT ACCELERATIONS - STUDY OF THE STABILITY OF A FLUID SURFACE IN A MICROGRAVITY ENVIRONMENT

JAUME CASADEMUNT, WENBIN ZHANG, JORGE VINALS (Florida State Univ., Tallahassee), and ROBERT F. SEKERKA (Carnegie Mellon Univ., Pittsburgh, PA) Jan. 1993 9 p. AIAA, Aerospace Sciences Meeting and Exhibit, 31st, Reno, NV, Jan. 11-14, 1993 Research supported by Florida State Univ. refs (Contract NAG3-1284; DE-FC05-85ER-25000)

(AIAA PAPER 93-0911) Copyright

We introduce a stochastic model to analyze in quantitative detail the effect of the high frequency components of the residual accelerations onboard spacecraft (often called g-jitter) on fluid motion. The residual acceleration field is modeled as a narrow band noise characterized by three independent parameters: its intensity G squared, a dominant frequency Ω , and a characteristic spectral width $\tau \exp -1$. The white noise limit corresponds to $\Omega \tau$ goes to 0, with G squared τ finite, and the limit of a periodic g-jitter (or deterministic limit) can be recovered for $\Omega \tau$ goes to infinity, G squared finite. The analysis of the response of a fluid surface subjected to a fluctuating gravitational field leads to the stochastic Mathieu equation driven by both additive and multiplicative noise. We discuss the stability of the solutions of this equation in the two limits of white noise

and deterministic forcing, and in the general case of narrow band noise. The results are then applied to typical microgravity conditions.

Author

A93-24968* National Aeronautics and Space Administration. Lewis Research Center, Cleveland, OH.

SCALING ANALYSIS OF GAS-LIQUID TWO-PHASE FLOW PATTERN IN MICROGRAVITY

JINHO LEE (NASA, Lewis Research Center, Cleveland, OH) Jan. 1993 14 p. AIAA, Aerospace Sciences Meeting and Exhibit, 31st, Reno, NV, Jan. 11-14, 1993 refs (AIAA PAPER 93-0914) Copyright

A scaling analysis of gas-liquid two-phase flow pattern in microgravity, based on the dominant physical mechanism, was carried out with the goal of predicting the gas-liquid two-phase flow regime in a pipe under conditions of microgravity. The results demonstrated the effect of inlet geometry on the flow regime transition. A comparison of the predictions with existing experimental data showed good agreement.

I.S.

A93-24982* National Aeronautics and Space Administration. Lewis Research Center, Cleveland, OH.

A STUDY OF COMPRESSIBLE MIXING LAYERS USING FILTERED RAYLEIGH SCATTERING

GREGORY S. ELLIOTT, MO SAMIMY, and STEPHEN A. ARNETTE (Ohio State Univ., Columbus) Jan. 1992 11 p. AIAA, Aerospace Sciences Meeting and Exhibit, 30th, Reno, NV, Jan. 6-9, 1992 refs

(Contract NAG3-764; NSF CTS-90-06879; N00014-90-J-1730)

(AIAA PAPER 92-0175) Copyright

High Reynolds number compressible planar free shear layers were studied using a planar laser visualization technique. Two convective Mach numbers, $M(c) = 0.51$ and 0.86 , were studied in the developing and fully developed regions. The structures in the $M(c) = 0.51$ case were characterized by 2D core and roller regions, similar to subsonic shear layers. Also for the $M(c) = 0.51$ case, plan views in the developing region showed the existence of streamwise streaks, possibly indicating the presence of organized streamwise vorticity. The $M(c) = 0.86$ flow was much less organized than the lower convective Mach number case and highly three dimensional.

Author

A93-25978* National Aeronautics and Space Administration. Lewis Research Center, Cleveland, OH.

FABRICATION OF CARBON-CARBON HEAT PIPES FOR SPACE NUCLEAR POWER APPLICATIONS

RICHARD D. ROVANG, THOMAS R. PALAMIDES, and MARIBETH E. HUNT (Rockwell International Corp., Canoga Park, CA) In IECEC '92; Proceedings of the 27th Intersociety Energy Conversion Engineering Conference, San Diego, CA, Aug. 3-7, 1992. Vol. 2 Warrendale, PA Society of Automotive Engineers, Inc. 1992 p. 2.319-2.322. refs

(Contract NAS3-25209)

Copyright

Significant advancements have been made in the development of lightweight, high performance, carbon-carbon heat pipes for space nuclear power applications. The subject program has progressed through the concept definition and feasibility analysis stages to the current test article component fabrication and assembly phase. This concept utilizes a carbon-carbon tube with integrally woven fins as the primary structural element and radiative surface, Nb-1Zr liners to contain a potassium working fluid, and welded end caps and fill tubes. Various tests have been performed in the development of suitable liner bonding techniques and in the assessment of material stability.

Author

A93-25985* National Aeronautics and Space Administration. Lewis Research Center, Cleveland, OH.

DESIGN OF A CAVITY HEAT PIPE RECEIVER EXPERIMENT

MICHAEL G. SCHNEIDER, MARK H. BREGGE, and WILLIAM J. GREENLEE (Sundstrand Aerospace, Rockford, IL) In IECEC '92; Proceedings of the 27th Intersociety Energy Conversion Engineering Conference, San Diego, CA, Aug. 3-7, 1992. Vol. 2

34 FLUID MECHANICS AND HEAT TRANSFER

Warrendale, PA Society of Automotive Engineers, Inc. 1992
p. 2.369-2.375. refs
(Contract NAS3-25554)
Copyright

A cavity heat pipe experiment has been designed to test the critical issues involved with incorporating thermal energy storage canisters into a heat pipe. The experiment is a replication of the operation of a heat receiver for a Brayton solar dynamic power cycle. The heat receiver is composed of a cylindrical receptor surface and an annular heat pipe with thermal energy storage canisters and gaseous working fluid heat exchanger tubes surrounding it. Hardware for the cavity heat pipe experiment will consist of a sector of the heat pipe, complete with gas tube and thermal energy storage canisters. Thermal cycling tests will be performed on the heat pipe sector to simulate the normal energy charge/discharge cycle of the receiver in a spacecraft application. Author

A93-26087 National Aeronautics and Space Administration. Lewis Research Center, Cleveland, OH.

OVERVIEW OF NASA SUPPORTED STIRLING THERMODYNAMIC LOSS RESEARCH

ROY C. TEW and STEVEN M. GENG (NASA, Lewis Research Center, Cleveland, OH) In IECEC '92; Proceedings of the 27th Intersociety Energy Conversion Engineering Conference, San Diego, CA, Aug. 3-7, 1992. Vol. 5 Warrendale, PA Society of Automotive Engineers, Inc. 1992 p. 5.489-5.494. Previously announced in STAR as N92-27034 refs
(Contract RTOP 590-13-11)
Copyright

NASA is funding research to characterize Stirling machine thermodynamic losses. NASA's primary goal is to improve Stirling design codes to support engine development for space and terrestrial power. However, much of the fundamental data is applicable to Stirling cooling and heat pump applications. The research results are reviewed. Much was learned about oscillating flow hydrodynamics, including laminar/turbulent transition, and tabulated data was documented for further analysis. Now, with a better understanding of the oscillating flow field, it is time to begin measuring the effects of oscillating flow and oscillating pressure level on heat transfer in heat exchanger flow passages and in cylinders. Author

A93-26088* National Aeronautics and Space Administration. Lewis Research Center, Cleveland, OH.

TRANSITION OF OSCILLATORY FLOW IN TUBES - AN EMPIRICAL MODEL FOR APPLICATION TO STIRLING ENGINES

T. W. SIMON (Minnesota Univ., Minneapolis), M. IBRAHIM, M. KANNAPAREDDY (Cleveland State Univ., OH), T. JOHNSON (Minnesota Univ., Minneapolis), and G. FRIEDMAN In IECEC '92; Proceedings of the 27th Intersociety Energy Conversion Engineering Conference, San Diego, CA, Aug. 3-7, 1992. Vol. 5 Warrendale, PA Society of Automotive Engineers, Inc. 1992 p. 5.495-5.502. Research sponsored by NASA refs
Copyright

Attention is given to an empirical model for transition to turbulence in oscillatory flows in straight tubes. Designed after a correlation for transition of a boundary layer on a flat plate, the model yields the laminar flow momentum thickness Reynolds number that must be met before transition to turbulence will occur. The transition point is located by comparing this to the actual momentum thickness Reynolds number. A scheme is proposed for estimating the momentum thickness Reynolds number in terms of the position within the cycle, the maximum value of the diameter Reynolds within the cycle, $Re(max)$, and the dimensionless frequency, Valensi number. Results from an experimental study of oscillatory flow in a tube are employed to develop the model. When the flow is determined to be turbulent, it is proposed that a fully-developed, steady flow friction coefficient be applied. When the flow is laminar, the assumption of fully developed flow cannot be made; thus, a method is suggested for estimating the friction factor. P.D.

A93-26089 National Aeronautics and Space Administration. Lewis Research Center, Cleveland, OH.

HEAT TRANSFER IN OSCILLATING FLOWS WITH SUDDEN CHANGE IN CROSS SECTION

MOUNIR IBRAHIM, WAQAR HASHIM (Cleveland State Univ., OH), ROY C. TEW, and JAMES E. DUDENHOEFER (NASA, Lewis Research Center, Cleveland, OH) In IECEC '92; Proceedings of the 27th Intersociety Energy Conversion Engineering Conference, San Diego, CA, Aug. 3-7, 1992. Vol. 5 Warrendale, PA Society of Automotive Engineers, Inc. 1992 p. 5.503-5.508. Previously announced in STAR as N92-26654 refs
(Contract RTOP 590-13-11)
Copyright

Oscillating fluid flow (zero mean) with heat transfer, between two parallel plates with a sudden change in cross section, was examined computationally. Over 30 different cases were examined; these cases cover wide ranges of $Re_{sub\ max}$ (187.5 to 30,000), Va (1 to 350), expansion ratio (1:2, 1:4, 1:8, and 1:12) and $A_{sub\ r}$ (0.68 to 4). Three different geometric cases were considered (asymmetric expansion and/or contraction, symmetric expansion/contraction, and symmetric blunt body). The heat transfer cases were based on constant wall temperature at higher (heating) or lower (cooling) value than the inflow fluid temperature. As a result of the oscillating flow, the fluid undergoes sudden expansion in one half of the cycle and sudden contraction in the other half. Instantaneous friction factors and heat transfer coefficients, for some ranges of $Re_{sub\ max}$ and Va , deviated substantially from those predicted with steady state correlations. Author

A93-26090* National Aeronautics and Space Administration. Lewis Research Center, Cleveland, OH.

M.I.T. STIRLING-CYCLE HEAT TRANSFER APPARATUS

JOSEPH L. SMITH, JR., JOHN H. LIENHARD, ALEXANDER K. TZIRANIS, and YUNG HO (MIT, Cambridge, MA) In IECEC '92; Proceedings of the 27th Intersociety Energy Conversion Engineering Conference, San Diego, CA, Aug. 3-7, 1992. Vol. 5 Warrendale, PA Society of Automotive Engineers, Inc. 1992 p. 5.509-5.516. Research supported by Martin Marietta Energy Systems, Oak Ridge National Lab., and DOE refs
(Contract NAG3-1076)
Copyright

The design and construction of a two-cylinder apparatus to measure heat transfer under conditions of oscillating pressure and oscillating flow such as found in Stirling-cycle machines are described. The apparatus consists of two large single-stage air compressors joined by a rigid drive shaft between the two crank shafts, and is powered by a 25-hp variable speed DC motor. The apparatus is capable of measuring heat transfer while velocity and pressure change over the range of dimensionless parameters normally found in Stirling cycle machines. It allows each parameter to be varied independently and easily. Instrumentation for the apparatus is adequate for measurement of pressure, time, gas and wall temperature, wall heat flux, and gas velocity. It yields preliminary data which show that the apparatus and data acquisition are operating satisfactorily and produce reasonable results. P.D.

A93-26091* National Aeronautics and Space Administration. Lewis Research Center, Cleveland, OH.

VISUALIZATION OF ENTRY FLOW SEPARATION FOR OSCILLATING FLOW IN TUBES

SONGGANG QIU and TERENCE W. SIMON (Minnesota Univ., Minneapolis) In IECEC '92; Proceedings of the 27th Intersociety Energy Conversion Engineering Conference, San Diego, CA, Aug. 3-7, 1992. Vol. 5 Warrendale, PA Society of Automotive Engineers, Inc. 1992 p. 5.517-5.521. refs
(Contract NAG3-598)
Copyright

Neutrally buoyant helium-filled soap bubbles with laser illumination are used to document entry flow separation for oscillating flow in tubes. For a symmetric entry case, the size of the separation zone appears to mildly depend on Reynolds number in the acceleration phase, but is roughly Reynolds number

independent in the deceleration phase. For the asymmetric entry case, the separation zone was larger and appeared to grow somewhat during the deceleration phase. The separation zones for both entry geometry cases remain relatively small throughout the cycle. This is different from what would be observed in all-laminar, oscillator flows and is probably due to the high turbulence of the flow, particularly during the deceleration phase of the cycle. P.D.

A93-26186* National Aeronautics and Space Administration. Lewis Research Center, Cleveland, OH.
STATISTICAL ANALYSIS OF THE EFFECTS OF HELICITY IN INHOMOGENEOUS TURBULENCE
 NOBUMITSU YOKOI and AKIRA YOSHIZAWA (Tokyo Univ., Japan) *Physics of Fluids A* (ISSN 0899-8213) vol. 5, no. 2 Feb. 1993 p. 464-477. Research supported by NASA refs Copyright

Effects of helicity in three-dimensional incompressible inhomogeneous turbulence are examined with the aid of a two-scale direct-interaction approximation (DIA). The turbulent helicity gives a measure of the reflectional asymmetry in a turbulent flow and its inhomogeneity contributes to the sustainment of large-scale vorticity field in a three-dimensional mean flow. The importance of helicity effects is discussed in the context of flows in a rotating system and swirling flows in a pipe. A three-equation model with the turbulent helicity incorporated is proposed using the theoretical results. The validity of the model is confirmed quantitatively through the application to a decaying swirling flow in a pipe. Author

A93-27900* National Aeronautics and Space Administration. Lewis Research Center, Cleveland, OH.
DOUBLE-DIFFUSIVE FINGERING CONVECTION IN A POROUS MEDIUM
 FALIN CHEN (National Taiwan Univ., Taipei) and C. F. CHEN (Arizona Univ., Tucson) *International Journal of Heat and Mass Transfer* (ISSN 0017-9310) vol. 36, no. 3 Feb. 1993 p. 793-807. refs
 (Contract NSF MSM-87-02732; NAG3-723) Copyright

The characteristics of nonlinear two-dimensional horizontally periodic double-diffusive fingering convection in a saturated porous medium is investigated, using the Darcy equation including Brinkman and Forchheimer terms for the momentum equation. To solve the equations and the corresponding initial and boundary conditions, a Galerkin method is applied in the horizontal direction, and a hybrid finite difference method is used in the vertical direction. The developed computer code was used to compute the thermal convection case, and the results were found to be in good agreement with existing results. I.S.

A93-30125* National Aeronautics and Space Administration. Lewis Research Center, Cleveland, OH.
REFRACTIVE INDEX EFFECTS ON RADIATION IN AN ABSORBING, EMITTING, AND SCATTERING LAMINATED LAYER

R. SIEGEL and C. M. SPUCKLER (NASA, Lewis Research Center, Cleveland, OH) *ASME, Transactions, Journal of Heat Transfer* (ISSN 0022-1481) vol. 115, no. 1 Feb. 1993 p. 194-200. refs Copyright

A simple set of equations is derived for predicting temperature radiative energy flow in a two-region semitransparent laminated layer in the limit of zero heat conduction. The composite is heated on its two sides by unequal amounts of incident radiation. The two layers of the composite have different refractive indices, and each material absorbs, emits, and isotropically scatters radiation. The interfaces are diffuse, and all interface reflections are included. To illustrate the thermal behavior that is readily calculated from the equations, typical results are given for various optical thicknesses and refractive indices of the layers. Internal reflections have a substantial effect on the temperature distribution and radiative heat flow. Author

A93-30127* National Aeronautics and Space Administration. Lewis Research Center, Cleveland, OH.

SIMULATION OF THE EARLY STARTUP PERIOD OF HIGH-TEMPERATURE HEAT PIPES FROM THE FROZEN STATE BY A RAREFIED VAPOR SELF-DIFFUSION MODEL
 Y. CAO and A. FAGHRI (Wright State Univ., Dayton, OH) *ASME, Transactions, Journal of Heat Transfer* (ISSN 0022-1481) vol. 115, no. 1 Feb. 1993 p. 239-246. *ASME, National Heat Transfer Conference*, San Diego, CA, Aug. 9-12, 1992 Research supported by NASA refs
 (Contract F33615-89-C-2820) Copyright

The heat pipe startup process is described physically and is divided into five periods for convenience of analysis. The literature survey revealed that none of the previous attempts to simulate the heat pipe startup process numerically were successful, since the rarefied vapor flow in the heat pipe was not considered. Therefore, a rarefied vapor self-diffusion model is proposed, and the early startup periods, in which the rarefied vapor flow is dominant within the heat pipe, are first simulated numerically. The numerical results show that large vapor density gradients existed along the heat pipe length, and the vapor flow reaches supersonic velocities when the density is extremely low. The numerical results are compared with the experimental data of the early startup period with good agreement. Author

A93-30128* National Aeronautics and Space Administration. Lewis Research Center, Cleveland, OH.

A NUMERICAL ANALYSIS OF HIGH-TEMPERATURE HEAT PIPE STARTUP FROM THE FROZEN STATE
 Y. CAO and A. FAGHRI (Wright State Univ., Dayton, OH) *ASME, Transactions, Journal of Heat Transfer* (ISSN 0022-1481) vol. 115, no. 1 Feb. 1993 p. 247-254. *ASME, National Heat Transfer Conference*, San Diego, CA, Aug. 9-12, 1992 Research supported by NASA refs
 (Contract F33615-89-C-2820) Copyright

Continuum and rarefied vapor flows co-exist along the heat pipe length for most of the startup period. A two-region model is proposed in which the vapor flow in the continuum region is modeled by the compressible Navier-Stokes equations, and the vapor flow in the rarefied region is simulated by a self-diffusion model. The two vapor regions are linked with appropriate boundary conditions, and heat pipe wall, wick, and vapor flow are solved as a conjugate problem. The numerical solutions for the entire heat pipe startup process from the frozen state are compared with the corresponding experimental data with good agreement. Author

A93-30129* National Aeronautics and Space Administration. Lewis Research Center, Cleveland, OH.

RELATIONS FOR LOCAL RADIATIVE HEAT TRANSFER BETWEEN RECTANGULAR BOUNDARIES OF AN ABSORBING-EMITTING MEDIUM

R. SIEGEL (NASA, Lewis Research Center, Cleveland, OH) *ASME, Transactions, Journal of Heat Transfer* (ISSN 0022-1481) vol. 115, no. 1 Feb. 1993 p. 272-276. refs Copyright

An analytical solution was obtained by Siegel (1991, 1992) for local boundary heat fluxes by a radiating medium at uniform temperature in a 2D rectangular region. It is shown here that, after local fluxes from the medium to the walls have been evaluated, it is very easy to compute local fluxes arriving from the adjacent and opposite walls. This extends the previous analysis and provides convenient relations to include radiation from a black boundary, each side of the rectangle being at a different uniform temperature. The final expressions are helpful in performing spectral calculations that must be made for many spectral bands. C.D.

A93-30130* National Aeronautics and Space Administration. Lewis Research Center, Cleveland, OH.

MOLECULAR DYNAMICS OF INTERFACE RUPTURE

JOEL KOPLIK (City College, New York) and JAYANTH R. BANAVAR (Pennsylvania State Univ., University Park) *Physics*

of Fluids A (ISSN 0899-8213) vol. 5, no. 3 March 1993 p. 521-536. refs
(Contract NAG3-1167; NSF CTS-89-12443)
Copyright

Several situations have been studied in which a fluid-vapor or fluid-fluid interface ruptures, using molecular dynamics simulations of 3000 to 20,000 Lennard-Jones molecules in three dimensions. The cases studied are the Rayleigh instability of a liquid thread, the burst of a liquid drop immersed in a second liquid undergoing shear, and the rupture of a liquid sheet in an extensional flow. The late stages of the rupture process involve the gradual withdrawal of molecules from a thinning neck, or the appearance and growth of holes in a sheet. In all cases, it is found that despite the small size of the systems studied, tens of angstroms, the dynamics is in at least qualitative accord with the behavior expected from continuum calculations, and in some cases the agreement is to within tens of percent. Remarkably, this agreement occurs even though the Eulerian velocity and stress fields are essentially unmeasurable - dominated by thermal noise. The limitations and prospects for such molecular simulation techniques are assessed. Author

A93-30134* National Aeronautics and Space Administration. Lewis Research Center, Cleveland, OH.
THE DEVELOPMENT OF A MIXING LAYER UNDER THE ACTION OF WEAK STREAMWISE VORTICES
M. E. GOLDSTEIN and JOSEPH MATHEW (NASA, Lewis Research Center, Cleveland, OH) Physics of Fluids A (ISSN 0899-8213) vol. 5, no. 3 March 1993 p. 600-607. refs
Copyright

The action of weak, streamwise vortices on a plane, incompressible, steady mixing layer is examined in the large Reynolds number limit. The outer, inviscid region is bounded by a vortex sheet to which the viscous region is confined. It is shown that the local linear analysis becomes invalid at streamwise distances $O(\epsilon \sup -1)$, where ϵ much less than 1 is the crossflow amplitude, and a new nonlinear analysis is constructed for this region. Numerical solutions of the nonlinear problem show that the vortex sheet undergoes an $O(1)$ change in position and that the solution is ultimately terminated by a breakdown in the numerical procedure. The corresponding viscous layer shows downstream thickening, but appears to remain well behaved up to the terminal location. Author

A93-30144* National Aeronautics and Space Administration. Lewis Research Center, Cleveland, OH.
ABSOLUTE AND CONVECTIVE INSTABILITY OF A VISCOUS LIQUID JET SURROUNDED BY A VISCOUS GAS IN A VERTICAL PIPE
S. P. LIN and Z. W. LIAN (Clarkson Univ., Potsdam, NY) Physics of Fluids A (ISSN 0899-8213) vol. 5, no. 3 March 1993 p. 771-773. refs
(Contract DAAL03-89-K-0179; NSF MSM-88-17372; NAG3-1402)
Copyright

The absolute and convective instability of a viscous liquid jet emanating into a viscous gas in a vertical pipe is analyzed in a parameter space spanned by the Reynolds number, the Froude number, the Weber number, the viscosity ratio, the density ratio, and the diameter ratio. The numerical results of the analysis are used to demonstrate that reduction in gravity tends to enhance the Rayleigh mode of convective instability which leads to the breakup of a liquid jet into drops of diameters comparable with the jet diameter. On the contrary, the Taylor mode of convective instability that leads to atomization is retarded at reduced gravity. The Rayleigh mode becomes absolutely unstable when the Reynolds number exceeds a critical value for a given set of the rest of the relevant parameters. The domain of absolute instability is significantly enlarged when the effect of gas viscosity is not neglected. Author

A93-30840 National Aeronautics and Space Administration. Lewis Research Center, Cleveland, OH.
CRITICAL COMPARISON OF SECOND-ORDER CLOSURES WITH DIRECT NUMERICAL SIMULATIONS OF HOMOGENEOUS TURBULENCE
TSAN-HSING SHIH (NASA, Lewis Research Center, Cleveland, OH) and JOHN L. LUMLEY (Cornell Univ., Ithaca, NY) AIAA Journal (ISSN 0001-1452) vol. 31, no. 4 April 1993 p. 663-670. Previously announced in STAR as N92-15357 Research supported by USAF refs
(Contract NASA ORDER C-99066-G; RTOP 505-62-21)
Copyright

Recently, several models have been proposed for closing the second-moment equations, in which the velocity-pressure gradient tensor and the dissipation rate tensor are two of the most important terms. In the literature, these correlation tensors are usually decomposed into a so-called rapid term and a return-to-isotropy term. Models of these terms have been used in global flow calculations together with other modeled terms. However, their individual behaviors in different flows have not been fully examined because they are unmeasurable in the laboratory. Recently, the development of direct numerical simulation (DNS) of turbulence has given us the possibility to do this kind of study. With direct numerical simulation, we may use the solution to calculate exactly the values of these correlation terms and then directly compare them with the values from their modeled formulations. In this paper, we make direct comparisons of five representative rapid models and eight return-to-isotropy models using the DNS data of 45 homogeneous flows, which were done by Rogers et al. (1986) and Lee and Reynolds (1985). The purpose of these direct comparisons is to explore the performance of these models in different flows and identify the ones that give the best performance. The paper also describes the modeling procedure, model constraints, and the various evaluated models. The detailed results of the direct comparisons are discussed, and a few concluding remarks on turbulence models are given. Author

A93-30856* National Aeronautics and Space Administration. Lewis Research Center, Cleveland, OH.
NONITERATIVE IMPLICIT METHOD FOR TRACKING PARTICLES IN MIXED LAGRANGIAN-EULERIAN FORMULATIONS
T. I.-P. SHIH and A. DASGUPTA (Carnegie Mellon Univ., Pittsburgh, PA) AIAA Journal (ISSN 0001-1452) vol. 31, no. 4 April 1993 p. 782-784. refs
(Contract NAG3-997)
Copyright

The existing implicit methods for the current initial value problems (IVPs) concerning particle-laden flows are complicated and iterative in nature. This paper presents a noniterative implicit method which can be used with pressure-based as well as with density-based algorithms. The method is illustrated by analyzing a dilute dispersion of noninteracting solid particles in an isothermal flow in a passage bounded by one straight wall and one wavy wall, in which all particles are spherical and have a finite velocity relative to the continuum phase at the inflow boundary. I.S.

A93-31438* National Aeronautics and Space Administration. Lewis Research Center, Cleveland, OH.
REFRACTIVE INDEX AND SCATTERING EFFECTS ON RADIATIVE BEHAVIOR OF A SEMITRANSSPARENT LAYER
C. M. SPUCKLER and R. SIEGEL (NASA, Lewis Research Center, Cleveland, OH) Journal of Thermophysics and Heat Transfer (ISSN 0887-8722) vol. 7, no. 2 Apr.-June 1993 p. 302-310. refs
Copyright

Heat transfer characteristics are analyzed for a plane layer of semitransparent material with refractive index not less than 1. Energy transfer in the material is by conduction, emission, absorption, and isotropic scattering. Each side of the layer is heated by radiation and convection. For a refractive index larger than unity, there is internal reflection of some of the energy within the layer. This, coupled with scattering, has a substantial effect on

distributing energy across the layer and altering the temperature distribution from when the refractive index is unity. The effect of scattering is examined by comparisons with results from an earlier paper for an absorbing layer. Results are given for a gray medium with a scattering albedo up to 0.999, and for a two-band spectral variation of the albedo with one band having low absorption. Radiant energy leaving the surface as a result of emission and scattering was examined to determine if it could be used to accurately indicate the surface temperature. Author

A93-32617* National Aeronautics and Space Administration. Lewis Research Center, Cleveland, OH.

EXPERIMENTS ON THE STABILITY OF A LIQUID BRIDGE IN AN AXIAL ELECTRIC FIELD

SUBRAMANIAN SANKARAN and D. A. SAVILLE (Princeton Univ., NJ) *Physics of Fluids A* (ISSN 0899-8213) vol. 5, no. 4 April 1993 p. 1081-1083. refs (Contract NAG3-259) Copyright

The behavior of a neutrally buoyant liquid bridge was studied in the presence of axial electric fields. Silicone oil and a castor-oil-eugenol mixture were used to form cylinders with slenderness ratios larger than π with strong, axial, dc electric fields. Below a certain field strength, a smooth transition to an axisymmetric, vase-like shape occurred. Circulation patterns were observed in these bridges. At lower field strengths, the bridge shape was more deformed and, at a well-defined field, pinch-off occurred. With ac fields, the field strength required to stabilize the bridge was higher and the collapse of the cylinder was much sharper. Upon interchanging the fluids, a steady axial field was found to destabilize cylinders with slenderness ratios less than 3. This behavior is consistent with that anticipated if the fluids behave as leaky dielectrics but not if they act as perfect dielectrics. Author

A93-32622* National Aeronautics and Space Administration. Lewis Research Center, Cleveland, OH.

NON-OSCILLATORY AND NON-DIFFUSIVE SOLUTION OF CONVECTION PROBLEMS BY THE ITERATIVELY REWEIGHTED LEAST-SQUARES FINITE ELEMENT METHOD

BO-NAN JIANG (NASA, Lewis Research Center, Cleveland, OH) *Journal of Computational Physics* (ISSN 0021-9991) vol. 105, no. 1 March 1993 p. 108-121. refs Copyright

A comparative description is presented for the least-squares FEM (LSFEM) for 2D steady-state pure convection problems. In addition to exhibiting better control of the streamline derivative than the streamline upwinding Petrov-Galerkin method, numerical convergence rates are obtained which show the LSFEM to be virtually optimal. The LSFEM is used as a framework for an iteratively reweighted LSFEM yielding nonoscillatory and nondiffusive solutions for problems with contact discontinuities; this method is shown to convect contact discontinuities without error when using triangular and bilinear elements. AIAA

A93-32627 National Aeronautics and Space Administration. Lewis Research Center, Cleveland, OH.

THE APPLICATION OF PRECONDITIONING IN VISCOUS FLOWS

Y.-H. CHOI (Sverdrup Technology, Inc.; NASA, Lewis Research Center, Cleveland, OH) and C. L. MERKLE (Pennsylvania State Univ., University Park) *Journal of Computational Physics* (ISSN 0021-9991) vol. 105, no. 2 April 1993 p. 207-223. refs (Contract NAS3-25266; NAGW-1356) Copyright

The present time-derivative preconditioning algorithm is effective in flow conditions ranging from inviscid to very diffusive flows, as well as low subsonic to supersonic flow velocities. By means of a preconditioning matrix that (1) introduces well-conditioned eigenvalues and (2) avoids nonphysical time reversals for viscous flows, a mechanism is obtained which controls the inviscid and viscous time-step parameters at very diffusive flows. These capabilities are demonstrated for a variety of sample problems;

convergence rates of solutions that are indistinguishable from those obtained without preconditioning are shown to be accelerated by as much as two orders of magnitude. AIAA

A93-32711* National Aeronautics and Space Administration. Lewis Research Center, Cleveland, OH.

STRUCTURE AND DEVELOPMENT OF STREAMWISE VORTEX ARRAYS EMBEDDED IN A TURBULENT BOUNDARY LAYER

BRUCE J. WENDT, ISAAC GREBER (Case Western Reserve Univ., Cleveland, OH), and WARREN R. HINGST (NASA, Lewis Research Center, Cleveland, OH) *AIAA Journal* (ISSN 0001-1452) vol. 31, no. 2 Feb. 1993 p. 319-325. AIAA, Aerospace Sciences Meeting and Exhibit, 30th, Reno, NV, Jan. 6-9, 1992, AIAA Paper 92-0551. Previously cited in issue 10, p. 1555, Accession no. A92-28204 refs (Contract NAG3-520) Copyright

A93-32724* National Aeronautics and Space Administration. Lewis Research Center, Cleveland, OH.

COMPUTATION OF UNSTEADY SUPERSONIC QUASI-ONE-DIMENSIONAL VISCOUS-INVISCID INTERACTING INTERNAL FLOWFIELDS

TIMOTHY W. SWAFFORD (Mississippi State Univ., Mississippi State) *AIAA Journal* (ISSN 0001-1452) vol. 31, no. 2 Feb. 1993 p. 404-408. refs (Contract NAG3-1170) Copyright

The present steady and unsteady quasi-1D internal supersonic flowfield calculations employs a novel viscous-inviscid interaction technique directly coupling and simultaneously solving the inviscid and viscous equations. The coupled system is numerically solved using a two-stage Runge-Kutta scheme with first-order one-sided spatial differencing. Simple supersonic internal flow test cases are computed to demonstrate the capabilities of the computational procedure. AIAA

A93-34326* National Aeronautics and Space Administration. Lewis Research Center, Cleveland, OH.

THE L SUB 1 FINITE ELEMENT METHOD FOR PURE CONVECTION PROBLEMS

BO-NAN JIANG (Computational Physics System, Ann Arbor, MI) *In Numerical methods in laminar and turbulent flow; Proceedings of the 7th International Conference, Stanford Univ., CA, July 15-19, 1991. Vol. 7, pt. 1 Swansea, United Kingdom Pineridge Press 1991 p. 502-511. Previously announced in STAR as N91-24817 Research supported by NASA refs Copyright*

The least squares (L sub 2) finite element method is introduced for 2-D steady state pure convection problems with smooth solutions. It is proven that the L sub 2 method has the same stability estimate as the original equation, i.e., the L sub 2 method has better control of the streamline derivative. Numerical convergence rates are given to show that the L sub 2 method is almost optimal. This L sub 2 method was then used as a framework to develop an iteratively reweighted L sub 2 finite element method to obtain a least absolute residual (L sub 1) solution for problems with discontinuous solutions. This L sub 1 finite element method produces a nonoscillatory, nondiffusive and highly accurate numerical solution that has a sharp discontinuity in one element on both coarse and fine meshes. A robust reweighting strategy was also devised to obtain the L sub 1 solution in a few iterations. A number of examples solved by using triangle and bilinear elements are presented. Author

A93-34366* National Aeronautics and Space Administration. Lewis Research Center, Cleveland, OH.

CALCULATIONS OF SEPARATED 3-D FLOWS WITH A PRESSURE-STAGGERED NAVIER-STOKES EQUATIONS SOLVER

S.-W. KIM (NASA, Lewis Research Center, Cleveland, OH) *In Numerical methods in laminar and turbulent flow; Proceedings of the 7th International Conference, Stanford Univ., CA, July 15-19,*

34 FLUID MECHANICS AND HEAT TRANSFER

1991. Vol. 7, pt. 2 Swansea, United Kingdom Pineridge Press
1991 p. 1454-1464. Previously announced in STAR as
N91-19367 refs
Copyright

A Navier-Stokes equations solver based on a pressure correction method with a pressure-staggered mesh and calculations of separated three-dimensional flows are presented. It is shown that the velocity pressure decoupling, which occurs when various pressure correction algorithms are used for pressure-staggered meshes, is caused by the ill-conditioned discrete pressure correction equation. The use of a partial differential equation for the incremental pressure eliminates the velocity pressure decoupling mechanism by itself and yields accurate numerical results. Example flows considered are a three-dimensional lid driven cavity flow and a laminar flow through a 90 degree bend square duct. For the lid driven cavity flow, the present numerical results compare more favorably with the measured data than those obtained using a formally third order accurate quadratic upwind interpolation scheme. For the curved duct flow, the present numerical method yields a grid independent solution with a very small number of grid points. The calculated velocity profiles are in good agreement with the measured data. Author (revised)

A93-34371* National Aeronautics and Space Administration.
Lewis Research Center, Cleveland, OH.

AN EFFICIENT AND ROBUST ALGORITHM FOR TWO DIMENSIONAL TIME DEPENDENT INCOMPRESSIBLE NAVIER-STOKES EQUATIONS - HIGH REYNOLDS NUMBER FLOWS

JOHN W. GOODRICH (NASA, Lewis Research Center, Cleveland, OH) /n Numerical methods in laminar and turbulent flow; Proceedings of the 7th International Conference, Stanford Univ., CA, July 15-19, 1991. Vol. 7, pt. 2 Swansea, United Kingdom Pineridge Press 1991 p. 1612-1622. Previously announced in STAR as N92-11320 refs
Copyright

An algorithm is presented for unsteady two-dimensional incompressible Navier-Stokes calculations. This algorithm is based on the fourth order partial differential equation for incompressible fluid flow which uses the streamfunction as the only dependent variable. The algorithm is second order accurate in both time and space. It uses a multigrid solver at each time step. It is extremely efficient with respect to the use of both CPU time and physical memory. It is extremely robust with respect to Reynolds number. Author

A93-34409* National Aeronautics and Space Administration.
Lewis Research Center, Cleveland, OH.

MULTIPLE LARGE-SCALE COHERENT MODE INTERACTIONS IN A DEVELOPING ROUND JET

SANG S. LEE and J. T. C. LIU (Brown Univ., Providence, RI) Journal of Fluid Mechanics (ISSN 0022-1120) vol. 248 March 1993 p. 383-401. Research supported by DARPA refs
(Contract NSF MSM-83-20307; NAG3-1016)
Copyright

The integral energy method has been used to study the nonlinear interactions of the large-scale coherent structure in a spatially developing round jet. The streamwise development of a jet is obtained in terms of the mean flow shear-layer momentum thickness, the wave-mode kinetic energy and the wave-mode phase angle. With the energy method, a system of partial differential equations is reduced to a system of ordinary differential equations. The nonlinear differential equations are solved with initial conditions which are given at the nozzle exit. It is shown that the initial wave-mode energy densities as well as the initial phase angles play a significant role in the streamwise evolution of the large-scale coherent wave modes and the mean flow. Author

A93-34414* National Aeronautics and Space Administration.
Lewis Research Center, Cleveland, OH.

A NOTE ON THE DISTORTION OF A FLAT-PLATE BOUNDARY LAYER BY FREE-STREAM VORTICITY NORMAL TO THE PLATE

M. E. GOLDSTEIN (NASA, Lewis Research Center, Cleveland, OH) and S. J. LEIB (Sverdrup Technology, Inc., Cleveland, OH) Journal of Fluid Mechanics (ISSN 0022-1120) vol. 248 March 1993 p. 531-541. refs
Copyright

The purpose of this note is to construct a local solution that eliminates a residual velocity discontinuity in the inviscid portion of a solution obtained in a recent paper by Goldstein, Leib and Cowley (1992). This result is of importance because it shows that the solution obtained in that paper is entirely non-singular outside the viscous wall boundary layer and that any singularity in the problem will have to arise in the usual way through a breakdown in the viscous boundary layer. Author

A93-35481* National Aeronautics and Space Administration.
Lewis Research Center, Cleveland, OH.

GALLERY OF FLUID MOTION

HELEN L. REED (Arizona State Univ., Tempe) Physics of Fluids A (ISSN 0899-8213) vol. 4, no. 9 Sept. 1992 p. 1869-1881. Research supported by DFG and USAF refs
(Contract NSERC-OGP-41747; NSF DMR-89-01869; NSF CTS-91-15005; NAG3-1268)
Copyright

Winning photographs from the ninth Annual Fluid Mechanics Photo Contest held by the Division of Fluid Dynamics of the American Physical Society in November 1991 are displayed. Pictures are presented of vortex flows, a periodic axisymmetric vortex breakdown in a cylinder with a rotating end wall, impacting water drops, a vortex structure behind a disk started from rest, dynamic stall, blue waves, isotherms in turbulent Rayleigh-Benard convection, a square jet, 'vapor lines' emanating from water droplets, viscosity effects on the directional solidification of NH₄Cl solution in a Hele-Shaw cell, and stationary cross-flow vortices. AIAA

A93-35482* National Aeronautics and Space Administration.
Lewis Research Center, Cleveland, OH.

THE COUPLING OF INTERFACIAL INSTABILITIES AND THE STABILIZATION OF TWO-LAYER ANNULAR FLOWS

HENK A. DIJKSTRA (Utrecht Univ., Netherlands) Physics of Fluids A (ISSN 0899-8213) vol. 4, no. 9 Sept. 1992 p. 1915-1928. refs
(Contract NAG3-801)
Copyright

In this paper the stability of annular pressure-driven parallel flows of two liquids sandwiching a free cylindrical interface is considered. For small to moderate Reynolds numbers, the interface is susceptible to capillary and interfacial wave instabilities, the latter instability caused by a jump in viscosity at the interface. It is shown that favorable velocity profiles in both liquids may stabilize capillary breakup of the interface and suppress the axisymmetric interfacial wave instability. A long-wave analysis leads to the physical mechanism responsible for stabilization of capillary breakup. This physical mechanism is a generalization of that by which capillary breakup is stabilized by interfacial shear in an annular film of a single liquid. Stabilization of intermediate wavelengths is studied with a mechanical energy analysis, which leads to a description of the energetic processes at work. Author

A93-35492 National Aeronautics and Space Administration. Lewis Research Center, Cleveland, OH.

REACTION ZONE STRUCTURE FOR STRONG, WEAK OVERDRIVEN, AND WEAK UNDERDRIVEN OBLIQUE DETONATIONS

JOSEPH M. POWERS and KEITH A. GONTHIER (Notre Dame Univ., IN; NASA, Lewis Research Center, Cleveland, OH) Physics of Fluids A (ISSN 0899-8213) vol. 4, no. 9 Sept. 1992 p. 2082-2089. AIAA, Aerospace Sciences Meeting and Exhibit, 30th, Reno, NV, Jan. 6-9, 1992 Research sponsored by NASA refs
Copyright

A simple dynamic systems analysis is used to give examples of strong, weak overdriven, and weak underdriven oblique

detonations. Steady oblique detonations consisting of a straight lead shock attached to a solid wedge followed by a resolved reaction zone structure are admitted as solutions to the reactive Euler equations. This is demonstrated for a fluid that is taken to be an inviscid, calorically perfect ideal gas that undergoes a two-step irreversible reaction with the first step exothermic and the second step endothermic. This model admits solutions for a continuum of shock wave angles for two classes of solutions identified by a Rankine-Hugoniot analysis: strong and weak overdriven waves. The other class, weak underdriven, is admitted for eigenvalue shock-wave angles. Chapman-Jouguet waves, however, are not admitted. These results contrast those for a corresponding onestep model that, for detonations with a straight lead shock, only admits strong, weak overdriven, and Chapman-Jouguet solutions. Author

A93-35608* National Aeronautics and Space Administration. Lewis Research Center, Cleveland, OH.

FLUID FLOW OF A ROW OF JETS IN CROSSFLOW - A NUMERICAL STUDY

S.-W. KIM and T. J. BENSON (NASA, Lewis Research Center, Cleveland, OH) *AIAA Journal* (ISSN 0001-1452) vol. 31, no. 5 May 1993 p. 806-811. *AIAA, Aerospace Sciences Meeting and Exhibit*, 30th, Reno, NV, Jan. 6-9, 1992, *AIAA Paper* 92-0534. Previously cited in issue 10, p. 1607, Accession no. A92-28198 refs
Copyright

A93-35624* National Aeronautics and Space Administration. Lewis Research Center, Cleveland, OH.

SIMULATION OF THREE-DIMENSIONAL LIQUID SLOSHING FLOWS USING A STRONGLY IMPLICIT CALCULATION PROCEDURE

KUO-HUEY CHEN (NASA, Lewis Research Center, Cleveland, OH) and RICHARD H. PLETCHER (Iowa State Univ. of Science and Technology, Ames) *AIAA Journal* (ISSN 0001-1452) vol. 31, no. 5 May 1993 p. 901-910. *AIAA, Fluid Dynamics, Plasma Dynamics and Lasers Conference*, 22nd, Honolulu, HI, June 24-26, 1991, *AIAA Paper* 91-1661. Previously cited in issue 17, p. 2939, Accession no. A91-42549 refs
(Contract AF-AFOSR-89-0403)
Copyright

A93-36575* National Aeronautics and Space Administration. Lewis Research Center, Cleveland, OH.

CONVECTIVE EFFECTS DURING THE PHYSICAL VAPOR TRANSPORT PROCESS. I - THERMAL CONVECTION

WALTER M. B. DUVAL (NASA, Lewis Research Center, Cleveland, OH) *Journal of Materials Processing & Manufacturing Science* (ISSN 1061-0656) vol. 1 July 1992 p. 83-104. refs
Copyright

The effects of convection on diffusive-convective physical vapor transport process are examined computationally. We analyze conditions ranging from typical laboratory conditions to conditions achievable only in a low gravity environment. This corresponds to thermal Rayleigh numbers $Ra(T)$ ranging from 1.80 to 1.92×10^6 . Our results indicate that the effect of the sublimation and condensation fluxes at the boundaries is to increase the threshold of instability. For typical ground based conditions time dependent oscillatory convection can occur. This results in nonuniform temperature and concentration gradients at the crystal interface. Spectral analysis of the flow field shows regions of both periodic and quasi-periodic states. Low gravity conditions can effectively reduce convective effects, thus resulting in uniform temperature and concentration gradients at the interface, a desirable condition for crystal growth. Author (revised)

A93-37046* National Aeronautics and Space Administration. Lewis Research Center, Cleveland, OH.

MODELING OF LINEAR ISENTROPIC FLOW SYSTEMS

ATHAN D. SARANTOPOULOS and TOM T. HARTLEY (Akrón Univ., OH) *In IEEE International Conference on Systems Engineering*, Dayton, OH, Aug. 1-3, 1991, *Proceedings* New York Institute

of Electrical and Electronics Engineers, Inc. 1991 p. 442-445. Previously announced in STAR as N92-22495 refs
(Contract NAG3-904)
Copyright

A modeling approach for linear isentropic flow systems based on the quasi-one-dimensional Euler equations of non-viscous, compressible flow are presented. Such systems are representative of certain high speed propulsion systems. Accurate models useful in control system studies are developed. A supersonic inlet is considered, and the resulting set of partial differential equations with boundary conditions is solved for a linear transfer matrix using Laplace transforms. Author

A93-37936* National Aeronautics and Space Administration. Lewis Research Center, Cleveland, OH.

EXPERIMENTAL STUDY OF TWO INTERACTING DROPS IN AN IMMISCIBLE FLUID

XIAO GUANG ZHANG, ROBERT H. DAVIS, and MARK F. RUTH (Colorado Univ., Boulder) *Journal of Fluid Mechanics* (ISSN 0022-1120) vol. 249 April 1993 p. 227-239. refs
(Contract NSF CTS-89-14236; NAG3-993; NAG3-1277)
Copyright

Experiments were performed in order to elucidate the effects of hydrodynamic interactions between two drops on their gravity-induced relative motion. The relative trajectories of two drops, their relative velocities, and the travel time for them to flow around each other were measured for different initial horizontal separations. Two size ratios and two viscosity ratios were investigated. Hydrodynamic interactions significantly reduce the relative velocity of two nearby drops and cause them to flow around each other with curved trajectories, resulting in a longer duration of the close encounter, compared with that for two non-interacting drops. These effects increase with decreasing drop separation, decreasing size ratio, and increasing viscosity ratio. Experimental results are in good agreement with theoretical predictions, except when the drops become sufficiently close that interface deformation occurs. Author

A93-38589* National Aeronautics and Space Administration. Lewis Research Center, Cleveland, OH.

STABLE AND LOW DIFFUSIVE HYBRID UPWIND SPLITTING METHODS

FREDERIC COQUEL (ONERA, Chatillon, France) and MENG-SING LIOU (NASA, Lewis Research Center, Cleveland, OH) *ONERA, TP no. 1992-113* 1992 9 p. *European Computational Fluid Dynamics Conference*, 1st, Brussels, Belgium, Sept. 7-11, 1992. Research supported by DRET refs
(ONERA, TP NO. 1992-113)

A new concept for upwinding is introduced, named the hybrid upwind splitting (HUS), which is achieved by combining the basically distinct flux vector splitting (FVS) and the flux difference splitting (FDS) approaches. The HUS approach yields upwind methods which share the robustness of the FVS schemes in the capture of nonlinear waves and the accuracy of some of the FDS schemes. Numerical illustrations are presented proving the relevance of the HUS methods for viscous calculations. AIAA

A93-41708* National Aeronautics and Space Administration. Lewis Research Center, Cleveland, OH.

THERMOCAPILLARY BUBBLE MIGRATION - AN OSEEN-LIKE ANALYSIS OF THE ENERGY EQUATION

R. BALASUBRAMANIAM and L. H. DILL (NASA, Lewis Research Center, Cleveland, OH) *In Microgravity fluid mechanics; Proceedings of the IUTAM Symposium*, Bremen, Germany, Sept. 2-6, 1991. Berlin and New York Springer-Verlag 1992 p. 307-314. refs
Copyright

The thermocapillary migration of a bubble in a liquid possessing a temperature gradient is analyzed in the limit of large Reynolds and Marangoni numbers. Crespo and Manuel (1983) performed an analysis in this limit wherein energy conduction is completely neglected and obtained the bubble migration velocity using energy dissipation arguments. In the present analysis, performed in a

coordinate system moving with the bubble, the velocity field in the convection term in the energy equation is approximated in an Oseen-like manner by replacing it with the velocity field far away from the bubble (i.e., the migration velocity of the bubble). Conduction is retained to satisfy the zero conductive heat flux boundary condition on the bubble surface. An approximate solution has been obtained for the Oseen-like energy equation. The bubble velocity obtained using energy dissipation considerations is in agreement with the result of Crespo and Manuel. The solution shows the thermal boundary layer and wake structure in the vicinity of the bubble. The Oseen-like analysis, however, has inherent limitations, as the flow penetrates the bubble surface. These issues are discussed and the result are compared to those in the literature. Author (revised)

A93-41710* National Aeronautics and Space Administration. Lewis Research Center, Cleveland, OH.

SURFACE TENSION EFFECTS ON THE ONSET OF DOUBLE-DIFFUSIVE CONVECTION

C. F. CHEN (Arizona Univ., Tucson) In Microgravity fluid mechanics; Proceedings of the IUTAM Symposium, Bremen, Germany, Sept. 2-6, 1991 Berlin and New York Springer-Verlag 1992 p. 325-333. refs (Contract NSF MSM-87-02732; NAG3-1268) Copyright

Experiments have been carried out to determine the critical thermal Rayleigh number for onset of convection in a horizontal layer of density-stratified fluid with a free surface when heated from below. Three different aqueous solutions were used: salt, glycerol, and acetic acid. The rates of change in surface tension with concentration for these three solutions are positive, nearly zero, and negative, respectively. Compared to the rigid-rigid boundaries, the critical thermal Rayleigh number was found to be larger by 11.2 percent for the salt solution and smaller by 10.0 percent for the glycerol solution. With the acetic acid solution, however, the effect of the free surface was found to be negligible. Author

A93-41909* National Aeronautics and Space Administration. Lewis Research Center, Cleveland, OH.

NEW TIME SCALE BASED K-EPSILON MODEL FOR NEAR-WALL TURBULENCE

Z. YANG and T. H. SHIH (NASA, Lewis Research Center, Cleveland, OH) AIAA Journal (ISSN 0001-1452) vol. 31, no. 7 July 1993 p. 1191-1198. Previously announced in STAR as N92-32868 refs Copyright

A k-epsilon model is proposed for wall bonded turbulent flows. In this model, the eddy viscosity is characterized by a turbulent velocity scale and a turbulent time scale. The time scale is bounded from below by the Kolmogorov time scale. The dissipation equation is reformulated using this time scale and no singularity exists at the wall. The damping function used in the eddy viscosity is chosen to be a function of $R(\text{sub } y) = (k(\text{sup } 1/2)y)/\nu$ instead of $y(+)$. Hence, the model could be used for flows with separation. The model constants used are the same as in the high Reynolds number standard k-epsilon model. Thus, the proposed model will be also suitable for flows far from the wall. Turbulent channel flows at different Reynolds numbers and turbulent boundary layer flows with and without pressure gradient are calculated. Results show that the model predictions are in good agreement with direct numerical simulation and experimental data. Author

A93-42424* National Aeronautics and Space Administration. Lewis Research Center, Cleveland, OH.

CONVECTIVE EFFECTS DURING THE PHYSICAL VAPOR TRANSPORT PROCESS. II - THERMOSOLUTAL CONVECTION

WALTER M. B. DUVAL (NASA, Lewis Research Center, Cleveland, OH) Journal of Materials Processing & Manufacturing Science (ISSN 1061-0656) vol. 1 Jan. 1993 p. 295-313. refs Copyright

The effect of an inert gas on the diffusive-convective physical vapor transport process is investigated for the case when the

temperature gradient is stabilizing, and the concentration gradient destabilizing, for a wide parametric range. When an inert gas is present, the thermal and solutal convection oppose each other. The solutal field is destabilizing while the thermal field and the advective-diffusive flux stabilize the flow field. When the pressure of the inert component is increased, the stabilizing effect of the advective-diffusive flux is decreased; thus, convection becomes more vigorous. The nonlinear dynamics of the flow field here show a transition from quasi-periodic to chaotic state. When both stabilizing mechanisms are present, the flow field shows a transition to a steady state. Toward steady state, growth and amalgamation of rolls occur, which result in an overturning motion. This leads to a superposed flow consisting of one roll and a unidirectional flow. However, when the pressure is increased, the advective-diffusive stability mechanism is decreased, and oscillations of the flow field occur. The low gravity environment is effective at eliminating oscillatory behavior of the flow field and results in uniform temperature and concentration gradients. Author (revised)

A93-43695* National Aeronautics and Space Administration. Lewis Research Center, Cleveland, OH.

HEAT TRANSFER FROM RADIATIVELY HEATED MATERIAL IN A LOW REYNOLDS NUMBER MICROGRAVITY ENVIRONMENT

H. YAMASHITA, H. R. BAUM, G. KUSHIDA, K. NAKABE, and T. KASHIWAGI (NIST, Building and Fire Research Lab., Gaithersburg, MD) ASME, Transactions, Journal of Heat Transfer (ISSN 0022-1481) vol. 115, no. 2 May 1993 p. 418-425. refs (Contract NASA ORDER C-32000-R) Copyright

A mathematical model of the transient three-dimensional heat transfer between a slowly moving ambient gas stream and a thermally thick or thin flat surface heated by external radiation in a microgravity environment is presented. The problem is motivated in part by fire safety issues in spacecraft. The gas phase is represented by variable property convection-diffusion energy and mass conservation equations valid at low Reynolds numbers. The absence of gravity and low Reynolds number together permit the flow to be represented by a self-consistent velocity potential determined by the ambient velocity and the thermal expansion in the gas. The solid exchanges energy with the gas by conduction/convection and with the surroundings by surface absorption and re-emission of radiation. Heat conduction in the solid is assumed to be one dimensional at each point on the surface as a consequence of the limited times (of order of 10 seconds) of interest in these simulations. Despite the apparent simplicity of the model, the results show a complex thermally induced flow near the heated surface. The thermal exchange between the gas and solid produces an outward source-like flow upstream of the center of the irradiated area and a sink-like flow downstream. The responses of the temperature fields and the associated flows to changes in the intensity of the external radiation and the ambient velocity are discussed. Author

A93-44223* National Aeronautics and Space Administration. Lewis Research Center, Cleveland, OH.

A STUDY OF THE EFFECTS OF MACROSEGREGATION AND BUOYANCY-DRIVEN FLOW IN BINARY MIXTURE SOLIDIFICATION

S. K. SINHA (Delhi Inst. of Technology, India), T. SUNDARARAJAN (Indian Inst. of Technology, Kanpur, India), and V. K. GARG (NASA, Lewis Research Center, Cleveland, OH) International Journal of Heat and Mass Transfer (ISSN 0017-9310) vol. 36, no. 9 June 1993 p. 2349-2358. refs Copyright

A generalized anisotropic porous medium approach is developed for modelling the flow, heat and mass transport processes during binary mixture solidification. Transient predictions are obtained using FEM, coupled with an implicit time-marching scheme, for solidification inside a two-dimensional rectangular enclosure. A parametric study focusing attention on the effects of solutal buoyancy and thermal buoyancy is presented. It is observed that three parameters, namely the thermal Rayleigh number, the solutal

Rayleigh number, and the relative density change parameter, significantly alter the flow fields in the liquid and the mushy regions. Depending upon the nature of these flow fields, the solute enrichment caused by macrosegregation may occur in the top or the bottom region of the enclosure. Author (revised)

A93-44245* National Aeronautics and Space Administration. Lewis Research Center, Cleveland, OH.

A COUPLED IMPLICIT METHOD FOR CHEMICAL NON-EQUILIBRIUM FLOWS AT ALL SPEEDS

JIAN-SHUN SHUEN (Sverdrup Technology, Inc.; NASA, Lewis Research Center, Cleveland, OH), KUO-HUEY CHEN (Toledo Univ.; NASA, Lewis Research Center, Cleveland, OH), and YUNHO CHOI (Sverdrup Technology, Inc.; NASA, Lewis Research Center, Cleveland, OH) *Journal of Computational Physics* (ISSN 0021-9991) vol. 106, no. 2 June 1993 p. 306-318. refs Copyright

The present time-accurate coupled-solution procedure addresses the chemical nonequilibrium Navier-Stokes equations over a wide Mach-number range uses, in conjunction with the strong conservation form of the governing equations, five unknown primitive variables. The numerical tests undertaken address steady convergent-divergent nozzle flows with air dissociation/recombination, dump combustor flows with n-pentane/air chemistry, and unsteady nonreacting cavity flows.

AIAA

A93-44813* National Aeronautics and Space Administration. Lewis Research Center, Cleveland, OH.

THE STRUCTURE OF A THREE-DIMENSIONAL TURBULENT BOUNDARY LAYER

A. T. DEGANI (Lehigh Univ., Bethlehem, PA), F. T. SMITH (Univ. College, London, United Kingdom), and J. D. A. WALKER (Lehigh Univ., Bethlehem, PA) *Journal of Fluid Mechanics* (ISSN 0022-1120) vol. 250 May 1993 p. 43-68. refs (Contract NAG3-771; AF-AFOSR-89-0487) Copyright

The three-dimensional turbulent boundary layer is shown to have a self-consistent two-layer asymptotic structure in the limit of large Reynolds number. In a streamline coordinate system, the streamwise velocity distribution is similar to that in two-dimensional flows, having a defect-function form in the outer layer which is adjusted to zero at the wall through an inner wall layer. An asymptotic expansion accurate to two orders is required for the cross-stream velocity which is shown to exhibit a logarithmic form in the overlap region. The inner wall-layer flow is collateral to leading order but the influence of the pressure gradient, at large but finite Reynolds numbers, is not negligible and can cause substantial skewing of the velocity profile near the wall. Conditions under which the boundary layer achieves self-similarity and the governing set of ordinary differential equations for the outer layer are derived. The calculated solution of these equations is matched asymptotically to an inner wall-layer solution and the composite profiles so formed describe the flow throughout the entire boundary layer. The effects of Reynolds number and cross-stream pressure gradient on the crossstream velocity profile are discussed and it is shown that the location of the maximum cross-stream velocity is within the overlap region. Author

A93-45038*# National Aeronautics and Space Administration. Lewis Research Center, Cleveland, OH.

SEGMENTED MULTIGRID DOMAIN DECOMPOSITION SOLUTIONS FOR THREE DIMENSIONAL VISCOUS RECIRCULATING FLOWS

KUMAR SRINIVASAN and STANLEY G. RUBIN (Cincinnati Univ., OH) *In AIAA Computational Fluid Dynamics Conference, 11th, Orlando, FL, July 6-9, 1993, Technical Papers. Pt. 1* Washington American Institute of Aeronautics and Astronautics 1993 p. 516-529. refs (Contract NAG3-97)

(AIAA PAPER 93-3344) Copyright

A segmented multigrid domain decomposition strategy is combined with a pressure-based form of flux-vector discretization

for 3D incompressible and compressible viscous flow applications. A pressure-based form of flux-vector splitting is applied to the Navier-Stokes (NS) equations, which are represented by an implicit lowest-order reduced NS system and a purely diffusive higher-order deferred corrector. A trapezoidal or boxlike form of discretization insures that all mass conservation properties are satisfied at interfacial and outflow boundaries, even for this primitive-variable nonstaggered grid computation. Improvements in gridding strategy are presented by allowing for disjoint subdomains that provide optimal resolution of disparate flow features. AIAA

A93-45054# National Aeronautics and Space Administration. Lewis Research Center, Cleveland, OH.

MULTIGRID TIME-ACCURATE INTEGRATION OF NAVIER-STOKES EQUATIONS

ANDREA ARNONE (Florence Univ., Italy), MENG-SING LIOU, and LOUIS A. POVINELLI (NASA, Lewis Research Center, Cleveland, OH) *In AIAA Computational Fluid Dynamics Conference, 11th, Orlando, FL, July 6-9, 1993, Technical Papers. Pt. 2* Washington American Institute of Aeronautics and Astronautics 1993 p. 694-702. Research supported by ICOMP and NASA refs (AIAA PAPER 93-3361)

Efficient acceleration techniques typical of explicit steady-state solvers are extended to time-accurate calculations. Stability restrictions are greatly reduced by means of a fully implicit time discretization. A four-stage Runge-Kutta scheme with local time stepping, residual smoothing, and multigriding is used instead of traditional time-expensive factorizations. Some applications to natural and forced unsteady viscous flows show the capability of the procedure. Author

A93-45061*# National Aeronautics and Space Administration. Lewis Research Center, Cleveland, OH.

ON SOLVING THE COMPRESSIBLE NAVIER-STOKES EQUATIONS FOR UNSTEADY FLOWS AT VERY LOW MACH NUMBERS

R. H. PLETCHER (Iowa State Univ. of Science and Technology, Ames; NASA, Lewis Research Center, Cleveland, OH) and K.-H. CHEN (NASA, Lewis Research Center, Cleveland, OH) *In AIAA Computational Fluid Dynamics Conference, 11th, Orlando, FL, July 6-9, 1993, Technical Papers. Pt. 2* Washington American Institute of Aeronautics and Astronautics 1993 p. 765-775. refs (Contract NCC3-233)

(AIAA PAPER 93-3368) Copyright

The properties of a preconditioned, coupled, strongly implicit finite-difference scheme for solving the compressible Navier-Stokes equations in primitive variables are investigated for two unsteady flows at low speeds, namely the impulsively started driven cavity and the startup of pipe flow. For the shear-driven cavity flow, the computational effort was observed to be nearly independent of Mach number, especially at the low end of the range considered. This Mach number independence was also observed for steady pipe flow calculations; however, rather different conclusions were drawn for the unsteady calculations. In the pressure-driven pipe startup problem, the compressibility of the fluid began to significantly influence the physics of the flow development at quite low Mach numbers. The present scheme was observed to produce the expected characteristics of completely incompressible flow when the Mach number was set at very low values. Good agreement with incompressible results available in the literature was observed. Author

A93-45734* National Aeronautics and Space Administration. Lewis Research Center, Cleveland, OH.

VORTICITY DYNAMICS OF INVISCID SHEAR LAYERS

JEFFREY W. YOKOTA (Sverdrup Technology, Inc., Brook Park, OH) *AIAA Journal* (ISSN 0001-1452) vol. 31, no. 8 Aug. 1993 p. 1430-1439. AIAA, Aerospace Sciences Meeting and Exhibit, 30th, Reno, NV, Jan. 6-9, 1992, AIAA Paper 92-0420. Previously cited in issue 09, p. 1413, Accession no. A92-26270 refs

(Contract NAS3-25266)

Copyright

34 FLUID MECHANICS AND HEAT TRANSFER

A93-45963 National Aeronautics and Space Administration. Langley Research Center, Hampton, VA.

ADAPTIVE METHODS IN COMPUTATIONAL FLUID DYNAMICS
J. T. ODEN (Texas Univ., Austin) *In* Finite elements in fluids. Vol. 8 Washington Hemisphere Publishing Corp. 1992 p. 3-30. Research supported by U.S. Navy and NASA refs (Contract NAS1-18746)
Copyright

A review is conducted of the basic components of adaptive methods applicable to very complex problems in fluid dynamics. Attention is given to ways of changing the structure of an approximation to reduce error, techniques for estimating the evolution of error in a CFD calculation, and the range of algorithms that are currently available for mesh-changing functions. Available numerical results which demonstrate the viability of these approaches are discussed. AIAA

A93-45974* National Aeronautics and Space Administration. Lewis Research Center, Cleveland, OH.

DIRECT NUMERICAL SIMULATIONS OF A REACTING TURBULENT MIXING LAYER BY A PSEUDOSPECTRAL-SPECTRAL ELEMENT METHOD
PATRICK A. MCMURTRY (Utah Univ., Salt Lake City) and PEYMAN GIVI (New York State Univ., Buffalo) *In* Finite elements in fluids. Vol. 8 Washington Hemisphere Publishing Corp. 1992 p. 355-378. Research supported by Advanced Combustion Engineering Research Center refs (Contract F49620-85-C-0067; NAG3-1011; NSF CTS-90-12832)
Copyright

An account is given of the implementation of the spectral-element technique for simulating a chemically reacting, spatially developing turbulent mixing layer. Attention is given to experimental and numerical studies that have investigated the development, evolution, and mixing characteristics of shear flows. A mathematical formulation is presented of the physical configuration of the spatially developing reacting mixing layer, in conjunction with a detailed representation of the spectral-element method's application to the numerical simulation of mixing layers. Results from 2D and 3D calculations of chemically reacting mixing layers are given. AIAA

A93-45975* National Aeronautics and Space Administration. Lewis Research Center, Cleveland, OH.

THERMOSOLUTAL CONVECTION DURING DENDRITIC SOLIDIFICATION OF A BINARY ALLOY
JUAN C. HEINRICH and SERGIO FELICELLI (Arizona Univ., Tucson) *In* Finite elements in fluids. Vol. 8 Washington Hemisphere Publishing Corp. 1992 p. 381-400. Research supported by Atomic Energy Commission of Argentina refs (Contract NAG3-723)
Copyright

The FEM model of Heinrich (1988) is presently extended to the case of dendritic vertical solidification under steady-state conditions. An analysis is conducted of the nonlinear governing equations for linear stability, and FEM calculations are performed in cases where instability has been predicted for Pb-Sn melt systems; the results obtained show that the model is more stable than the plane front liquid-solid model, and shows similar, finger-like convection when unstable. It is found that convection in the 'mush' zone is confined to the top of that region; convective motion is driven by convection in the bulk fluid, in the absence of natural convection. AIAA

A93-46407* National Aeronautics and Space Administration. Lewis Research Center, Cleveland, OH.

LOW-TO-HIGH ALTITUDE PREDICTIONS OF THREE-DIMENSIONAL ABLATIVE RE-ENTRY FLOWFIELDS
BILAL A. BHUTTA and CLARK H. LEWIS (VRA, Inc., Blacksburg, VA) *Journal of Spacecraft and Rockets* (ISSN 0022-4650) vol. 30, no. 4 July-Aug. 1993 p. 395-403. AIAA, Aerospace Sciences Meeting and Exhibit, 30th, Reno, NV, Jan. 6-9, 1992, AIAA Paper 92-0366. Previously cited in issue 09, p. 1412.

Accession no. A92-26227 refs
(Contract NAS3-25450)
Copyright

A93-46485* National Aeronautics and Space Administration. Lewis Research Center, Cleveland, OH.

RADIATION HEAT TRANSFER CALCULATIONS USING A CONTROL-ANGLE, CONTROL-VOLUME-BASED DISCRETE ORDINATES METHOD
JOHN C. CHAI (Minnesota Univ., Minneapolis), HAEOK S. LEE (NASA, Lewis Research Center, Cleveland, OH), and SUHAS V. PATANKAR (Minnesota Univ., Minneapolis) Jul. 1993 9 p. AIAA, Thermophysics Conference, 28th, Orlando, FL, July 6-9, 1993 Research supported by Minnesota Supercomputer Inst. refs
(Contract NCC3-238)
(AIAA PAPER 93-2731) Copyright

A control-angle, control-volume-based discrete ordinates method (CA - CV DOM) is presented in this paper. A detailed formulation of the discretization equation is presented in two-dimensional Cartesian coordinate system. The procedure can be extended to curvilinear coordinate system with minor modifications. The step and modified-exponential schemes are used in this study. Present results converged to the grid independent solutions quickly and compared favorably against other published results for six test problems.

A93-46572* National Aeronautics and Space Administration. Lewis Research Center, Cleveland, OH.

VAPORIZATION HEAT TRANSFER OF DIELECTRIC LIQUIDS ON ENHANCED SURFACES COVERED WITH SCREEN WICKS
C. B. GU, L. C. CHOW, M. R. PAIS (Kentucky Univ., Lexington), and K. BAKER (NASA, Lewis Research Center, Cleveland, OH) Jul. 1993 6 p. AIAA, Thermophysics Conference, 28th, Orlando, FL, July 6-9, 1993 refs
(Contract NAG3-1251)
(AIAA PAPER 93-2835) Copyright

Experiments were conducted to investigate the vaporization heat transfer characteristics for the dielectric liquid FC-72 on several wicking surfaces which may be used in flat-plate heat pipes. The wicking materials studied included microstructure enhanced surfaces and coarse surfaces covered with screen meshes. Experimental data for q versus ΔT curves and critical heat fluxes were obtained for the two different operating conditions of a heat pipe, evaporation, and shallow pool boiling. When the liquid level was above the heated surface, the height of the liquid level above the surface was varied from 0 to 10 mm. When the liquid level was below the heated surface, the distance from the liquid level to the edge of the surface was adjusted from 0 to 15 mm. Experimental results revealed that for shallow pool boiling when the heated surface was covered with a wire screen mesh, the heat transfer coefficient increased at lower heat fluxes but the critical heat flux (CHF) decreased for all the surfaces tested. In the case of evaporation, both CHF and the heat transfer coefficient increased as the microstructure surfaces were covered with screen meshes. Author (revised)

A93-46714* National Aeronautics and Space Administration. Lewis Research Center, Cleveland, OH.

THERMOCAPILLARY MIGRATION OF A SMALL CHAIN OF BUBBLES
HUAILIANG WEI and R. S. SUBRAMANIAN (Clarkson Univ., Potsdam, NY) *Physics of Fluids A* (ISSN 0899-8213) vol. 5, no. 7 July 1993 p. 1583-1595. refs
(Contract NAG3-1122)
Copyright

The quasistatic thermocapillary migration of a chain of two or three spherical bubbles in an unbounded fluid possessing a uniform temperature gradient is investigated in the limit of vanishing Reynolds and Peclet numbers. The line of bubble centers is permitted to be either parallel or perpendicular to the direction of the undisturbed temperature gradient. The governing equations are solved by a truncated-series, boundary-collocation technique.

Results are presented which demonstrate the impact of the presence of other bubbles on a test bubble. In the three-bubble case, a simple pairwise-additive approximation is constructed from the reflections solution, and found to perform well except when the bubbles are close to each other. Also, features of the flow topology in the fluid are explored. Separated reverse flow wakes are found in the axisymmetric problem, and other interesting structures are noted for the case in which the line of centers is perpendicular to the applied temperature gradient. The observed flow structure is shown to be the result of superposition of simpler basic flows.

A93-46716* National Aeronautics and Space Administration. Lewis Research Center, Cleveland, OH.

COLLECTIVE EFFECTS OF TEMPERATURE GRADIENTS AND GRAVITY ON DROPLET COALESCENCE

XIAOGUANG ZHANG, HUA WANG, and ROBERT H. DAVIS (Colorado Univ., Boulder) *Physics of Fluids A* (ISSN 0899-8213) vol. 5, no. 7 July 1993 p. 1602-1613. refs (Contract NSF CTS-89-14236; NAG3-993; NAG3-1277; NAG3-1389) Copyright

The interaction and coalescence of small spherical drops in dilute, homogeneous dispersions are considered theoretically under conditions, where drop motion results from gravity settling and thermocapillary migration acting simultaneously. A trajectory analysis is used to predict pairwise collision rates, and population dynamics equations are solved to predict the time evolution of the droplet size distribution. The rate of droplet collisions and growth may be reduced dramatically by antiparallel alignment of the gravitational and thermocapillary velocities. For such antiparallel alignment with the gravitational relative velocity exceeding the thermocapillary relative velocity for two widely separated drops, there is a 'collision-forbidden region' in parameter space. This occurs because the gravitational relative velocity decays more rapidly with decreasing separation distance between the drops than does the thermocapillary relative velocity, and so the resultant relative velocity along the line-of-centers from these two sources combined becomes zero at a finite separation and the drops are unable to collide. As a result, small drops which initially collide and coalesce due to thermocapillary motion will only grow until they reach a critical size for which the oppositely directed gravitational motion balances the thermocapillary motion.

A93-46797* National Aeronautics and Space Administration. Lewis Research Center, Cleveland, OH.

LINEAR INSTABILITY OF CURVED FREE SHEAR LAYERS

WILLIAM W. LIU (NASA, Lewis Research Center, Cleveland, OH) Jul. 1993 12 p. AIAA, Shear Flow Conference, Orlando, FL, July 6-9, 1993 refs (AIAA PAPER 93-3252) Copyright

The linear inviscid hydrodynamic stability of slightly curved free mixing layers is studied in this paper. The disturbance equation is solved numerically using a shooting technique. Two mean velocity profiles that represent stably and unstably curved free mixing layers are considered. Results are shown for cases of five curvature Richardson numbers. The stability characteristics of the shear layer are found to vary significantly with the introduction of the curvature effects. The results also indicate that, in a manner similar to the Goertler vortices observed in a boundary layer along a concave wall, instability modes of spatially developing streamwise vortex pairs may appear in unstable curved mixing layers.

A93-48132* National Aeronautics and Space Administration. Lewis Research Center, Cleveland, OH.

HIGH RESOLUTION NUMERICAL SIMULATION OF THE LINEARIZED EULER EQUATIONS IN CONSERVATION LAW FORM

KIDAMBI SREENIVAS, DAVID L. WHITFIELD (NSF, Engineering Research Center for Computational Field Simulation, Mississippi State, MS), and DENNIS L. HUFF (NASA, Lewis Research Center, Cleveland, OH) Jul. 1993 11 p. AIAA, Fluid Dynamics

Conference, 24th, Orlando, FL, July 6-9, 1993 refs (Contract NAG3-767)

(AIAA PAPER 93-2934) Copyright

A linearized Euler solver based on a high resolution numerical scheme is presented. The approach is to linearize the flux vector as opposed to carrying through the complete linearization analysis with the dependent variable vector written as a sum of the mean and the perturbed flow. This allows the linearized equations to be maintained in conservation law form. The linearized equations are used to compute unsteady flows in turbomachinery blade rows arising due to blade vibrations. Numerical solutions are compared to theoretical results (where available) and to numerical solutions of the nonlinear Euler equations.

A93-48146* National Aeronautics and Space Administration. Lewis Research Center, Cleveland, OH.

INTAKE FLOW MODELING IN A FOUR STROKE DIESEL USING KIVA3

R. P. HESSEL and C. J. RUTLAND (Wisconsin Univ., Madison) Jul. 1993 9 p. AIAA, Fluid Dynamics Conference, 24th, Orlando, FL, July 6-9, 1993 Research supported by Caterpillar, Inc., Cray Research, Inc., and Univ. of Wisconsin refs (Contract NAG3-1087; DAAL03-86-K-0174) (AIAA PAPER 93-2952) Copyright

Intake flow for a dual intake valved diesel engine is modeled using moving valves and realistic geometries. The objectives are to obtain accurate initial conditions for combustion calculations and to provide a tool for studying intake processes. Global simulation parameters are compared with experimental results and show good agreement. The intake process shows a 30 percent difference in mass flows and average swirl in opposite directions across the two intake valves. The effect of the intake process on the flow field at the end of compression is examined. Modeling the intake flow results in swirl and turbulence characteristics that are quite different from those obtained by conventional methods in which compression stroke initial conditions are assumed.

Author (revised)

A93-48231* National Aeronautics and Space Administration. Lewis Research Center, Cleveland, OH.

HIGHER-ORDER ACCURATE OSHER SCHEMES WITH APPLICATION TO COMPRESSIBLE BOUNDARY LAYER STABILITY

J. J. W. VAN DER VEGT (NASA, Lewis Research Center, Brook Park, OH) Jul. 1993 15 p. AIAA, Fluid Dynamics Conference, 24th, Orlando, FL, July 6-9, 1993 refs (AIAA PAPER 93-3051) Copyright

Two fourth order accurate Osher schemes are presented which maintain higher order accuracy on nonuniform grids. They use either a conservative finite difference or finite volume discretization. Both methods are successfully used for direct numerical simulations of flat plate boundary layer instability at different Mach numbers. Results of growth rates of Tollmien-Schlichting waves compare well with direct simulations of incompressible flow and for compressible flow with results obtained by solving the parabolic stability equations.

A93-48249* National Aeronautics and Space Administration. Lewis Research Center, Cleveland, OH.

HIGH ORDER ACCURATE SOLUTIONS OF VISCOUS PROBLEMS

M. E. HAYDER (NASA, Lewis Research Center, Cleveland, OH) and ELI TURKEL (NASA, Lewis Research Center, Cleveland, OH; Tel Aviv Univ., Israel) Jul. 1993 12 p. AIAA, Fluid Dynamics Conference, 24th, Orlando, FL, July 6-9, 1993 refs (AIAA PAPER 93-3074) Copyright

We consider a fourth order extension to MacCormack's scheme. The original extension was fourth order only for the inviscid terms but was second order for the viscous terms. We show how to modify the viscous terms so that the scheme is uniformly fourth order in the spatial derivatives. Applications are given to some boundary layer flows. In addition, for applications to shear flows the effect of the outflow boundary conditions are very important.

We compare the accuracy of several of these different boundary conditions for both boundary layer and shear flows. Stretching at the outflow usually increases the oscillations in the numerical solution but the addition of a filtered sponge layer (with or without stretching) reduces such oscillations. The oscillations are generated by insufficient resolution of the shear layer. When the shear layer is sufficiently resolved then oscillations are not generated and there is less of a need for a nonreflecting boundary condition.

A93-49241 National Aeronautics and Space Administration. Lewis Research Center, Cleveland, OH.

STREAMWISE COMPUTATION OF THREE-DIMENSIONAL FLOWS USING TWO STREAM FUNCTIONS

M. S. GREYWALL (Wichita State Univ., KS) ASME, Transactions, Journal of Fluids Engineering (ISSN 0098-2202) vol. 115, no. 2 June 1993 p. 233-238. Research supported by NASA refs Copyright

An approach to compute 3D flows using two stream functions is presented. The independent variables used are χ , a spatial coordinate, and η and ϵ , values of stream functions along two sets of suitably chosen intersecting stream surfaces. The dependent variables used are the streamwise velocity, and two functions that describe the stream surfaces. Since the value of a stream function is constant along the solid boundaries, this choice of variables makes it easy to satisfy the boundary conditions. To illustrate the approach, computations of incompressible potential flow through a circular-to-rectangular transition duct are also presented. Author (revised)

A93-49662* National Aeronautics and Space Administration. Lewis Research Center, Cleveland, OH.

ATOMIZATION AND VAPORIZATION CHARACTERISTICS OF AIRBLAST FUEL INJECTION INSIDE A VENTURI TUBE

H. SUN, T.-H. CHUE, M.-C. LAI (Wayne State Univ., Detroit, MI), and R. R. TACINA (NASA, Lewis Research Center, Cleveland, OH) Jun. 1993 17 p. AIAA, SAE, ASME, and ASEE, Joint Propulsion Conference and Exhibit, 29th, Monterey, CA, June 28-30, 1993 refs (Contract NAG3-1140; NSF RII-88-05070; DAAL03-92-G-0168) (AIAA PAPER 93-1766) Copyright

This paper describes the experimental and numerical characterization of the capillary fuel injection, atomization, dispersion, and vaporization of liquid fuel in a coflowing air stream inside a single venturi tube. The experimental techniques used are all laser-based. Phase Doppler analyzer was used to characterize the atomization and vaporization process. Planar laser-induced fluorescence visualizations give good qualitative picture of the fuel droplet and vapor distribution. Limited quantitative capabilities of the technique are also demonstrated. A modified version of the KIVA-II was used to simulate the entire spray process, including breakup and vaporization. The advantage of venturi nozzle is demonstrated in terms of better atomization, more uniform F/A distribution, and less pressure drop. Multidimensional spray calculations can be used as a design tool only if care is taken for the proper breakup model, and wall impingement process. Author (revised)

A93-49669* National Aeronautics and Space Administration. Lewis Research Center, Cleveland, OH.

CFD VALIDATION OF SUBSONIC TURBULENT PLANAR SHEAR LAYERS

H. T. LAI and M. S. RAJU (Sverdrup Technology, Inc., Brook Park, OH) Jun. 1993 16 p. AIAA, SAE, ASME, and ASEE, Joint Propulsion Conference and Exhibit, 29th, Monterey, CA, June 28-30, 1993 refs (Contract NAS3-24105; NAS3-25266) (AIAA PAPER 93-1773)

The primary objective of the present study is to assess the limitations and capabilities of RPLUS in predicting the entrainment, mixing, and burning characteristics of a high subsonic planar shear layer; these computations are performed in conjunction with an experiment being conducted at NASA Lewis Research Center. Turbulence is modeled by a two-equation k - ϵ closure modified

for compressibility effects. Combustion is modeled by two different models: one in which a finite-rate laminar chemistry model is used for H_2 - O_2 oxidation, and the other based on a composition joint pdf approach to account for the turbulence-chemistry interaction effects. Between upwind and centered differencing schemes, minimal differences are observed for the flow properties of a nonreacting shear layer case studied. In comparison with experimental data, computed growth rates are underpredicted in both reacting and nonreacting cases of a shear layer, but more severely for the reacting flows. However, the qualitative agreement between computation and experiment is reasonably good for the other observable characteristics, and indicative of potential for further improvements. Author (revised)

A93-49715* National Aeronautics and Space Administration. Marshall Space Flight Center, Huntsville, AL.

CFD ANALYSES OF COOLANT CHANNEL FLOWFIELDS

J. A. YAGLEY, J. FENG, and CHARLES L. MERKLE (Pennsylvania State Univ., University Park) Jun. 1993 14 p. AIAA, SAE, ASME, and ASEE, Joint Propulsion Conference and Exhibit, 29th, Monterey, CA, June 28-30, 1993 refs (Contract NAS8-38861; NSF EEC-91-16806) (AIAA PAPER 93-1830) Copyright

The flowfield characteristics in a rocket engine coolant channels are analyzed by means of a numerical model. The channels are characterized by large length to diameter ratios, high Reynolds numbers, and asymmetrical heating. At representative flow conditions, the channel length is approximately twice the hydraulic entrance length so fully developed conditions are reached. The supercritical hydrogen coolant introduces strong property variations that have a major influence on the developing flow and the resulting heat transfer. Comparisons of constant and variable property solutions show substantial differences. The density variation accelerates the fluid in the channels increasing the pressure drop without an accompanying increase in heat flux. Analyses of the inlet configuration suggest that side entry from a manifold can affect the development of the velocity profile because of vortices generated as the flow enters the channel.

A93-49783* National Aeronautics and Space Administration. Lewis Research Center, Cleveland, OH.

NUMERICAL STUDY OF SHOCK-INDUCED COMBUSTION IN METHANE-AIR MIXTURES

SHAYE YUNGSTER and MARTIN J. RABINOWITZ (NASA, Lewis Research Center, Cleveland, OH) Jun. 1993 14 p. AIAA, SAE, ASME, and ASEE, Joint Propulsion Conference and Exhibit, 29th, Monterey, CA, June 28-30, 1993 refs (AIAA PAPER 93-1917) Copyright

The shock-induced combustion of methane-air mixtures in hypersonic flows is investigated using a new reaction mechanism consisting of 19 reacting species and 52 elementary reactions. This reduced model is derived from a full kinetic mechanism via the Detailed Reduction technique. Zero-dimensional computations of several shock-tube experiments are presented first. The reaction mechanism is then combined with a fully implicit Navier-Stokes CFD code to conduct numerical simulations of two-dimensional and axisymmetric shock-induced combustion experiments of stoichiometric methane-air mixtures at a Mach number of $M = 6.61$. Applications to the ram accelerator concept are also presented.

A93-49816* National Aeronautics and Space Administration. Lewis Research Center, Cleveland, OH.

MIXING AND TRANSIENT INTERFACE CONDENSATION OF A LIQUID HYDROGEN TANK

C. S. LIN (Analex Corp., Brook Park, OH), M. M. HASAN, and T. W. NYLAND (NASA, Lewis Research Center, Cleveland, OH) Jun. 1993 17 p. AIAA, SAE, ASME, and ASEE, Joint Propulsion Conference and Exhibit, 29th, Monterey, CA, June 28-30, 1993 Previously announced in STAR as N93-28252 refs (AIAA PAPER 93-1968) Copyright

Experiments were conducted to investigate the effect of axial jet-induced mixing on the pressure reduction of a thermally stratified

liquid hydrogen tank. The tank was nearly cylindrical, having a volume of about 0.144 cu m with 0.559 m in diameter and 0.711 m length. A mixer/pump unit, which had a jet nozzle outlet of 0.0221 m in diameter was located 0.178 m from the tank bottom and was installed inside the tank to generate the axial jet mixing and tank fluid circulation. Mixing tests began with the tank pressures at which the thermal stratification results in 4.9-6.2 K liquid subcooling. The mixing time and transient vapor condensation rate at the liquid-vapor interface are determined. Two mixing time correlations, based on the thermal equilibrium and pressure equilibrium, are developed and expressed as functions of system and buoyancy parameters. The limited liquid hydrogen data of the present study shows that the modified steady state condensation rate correlation may be used to predict the transient condensation rate in a mixing process if the instantaneous values of jet sub cooling and turbulence intensity at the interface are employed.

Author (revised)

A93-49872*# National Aeronautics and Space Administration. Lewis Research Center, Cleveland, OH.

EXPERIMENTAL INVESTIGATION OF CROSSFLOW JET MIXING IN A RECTANGULAR DUCT

D. S. LISCINSKY, B. TRUE (United Technologies Research Center, East Hartford, CT), and J. D. HOLDEMAN (NASA, Lewis Research Center, Cleveland, OH) Jun. 1993 12 p. AIAA, SAE, ASME, and ASEE, Joint Propulsion Conference and Exhibit, 29th, Monterey, CA, June 28-30, 1993 Previously announced in STAR as N93-27026 refs

(Contract NAS3-25954)

(AIAA PAPER 93-2037) Copyright

An experimental investigation of the mixing of nonreacting opposed rows of jets injected normal to a confined rectangular crossflow has been conducted. Planar Mie-scattering was used to measure the time-average concentration distribution of the jet fluid in planes perpendicular to the duct axis. The mixing effectiveness of round orifice injectors was measured as a function of orifice spacing and orifice diameter. Mixing effectiveness was determined using a spatial unmixedness parameter based on the variance of mean jet concentration distributions. Optimum mixing was obtained when the spacing-to-duct height ratio was inversely proportional to the square root of the jet-to-mainstream momentum-flux ratio. For opposed rows of round holes with centerlines inline, mixing was similar for blockages up to 75 percent. Lower levels of unmixedness were obtained as a function of downstream location when axial injection length was minimized. Mixing may be enhanced if orifice centerlines of opposed rows are staggered, but note that blockage must be less than 50 percent for this configuration.

A93-49877*# National Aeronautics and Space Administration. Lewis Research Center, Cleveland, OH.

CFD MIXING ANALYSIS OF AXIALLY OPPOSED ROWS OF JETS INJECTED INTO CONFINED CROSSFLOW

D. B. BAIN, C. E. SMITH (CFD Research Corp., Huntsville, AL), and J. D. HOLDEMAN (NASA, Lewis Research Center, Cleveland, OH) Jun. 1993 28 p. AIAA, SAE, ASME, and ASEE, Joint Propulsion Conference and Exhibit, 29th, Monterey, CA, June 28-30, 1993 Previously announced in STAR as N93-27128 refs

(Contract NAS3-25967)

(AIAA PAPER 93-2044) Copyright

A CFD parametric study was performed to analyze axially opposed rows of jets mixing with crossflow in a rectangular duct. An isothermal analysis was conducted to determine the influence of lateral geometric arrangement on mixing for the cases of: (1) inline (jets' centerlines aligned with each other on top and bottom walls), and (2) staggered (jets' centerlines offset with each other on top and bottom walls) configurations. For a jet-to-mainstream mass flow ratio (MR) of 2.0, design parameters were systematically varied for jet-to-mainstream momentum-flux ratios (J) between 16 and 64 and orifice spacing-to-duct height ratios (S/H) between 0.125 and 1.5. Comparisons were made between geometries optimized for S/H at a specified J. Inline configurations had a unique spacing for best mixing at a specified J. In contrast, staggered configurations had two 'good mixing' spacings for each

J, one corresponding to optimum inline spacing and the other corresponding to optimum nonimpinging jet spacing. Increasing J resulted in better mixing characteristics if each configuration was optimized with respect to orifice spacing. Mixing performance was shown to be similar to results from previous dilution jet mixing investigations (MR less than 0.5).

Author (revised)

A93-49901*# National Aeronautics and Space Administration. Lewis Research Center, Cleveland, OH.

COMPUTATIONS OF SPRAY, FUEL-AIR MIXING, AND COMBUSTION IN A LEAN-PREMIKED-PREVAPOORIZED COMBUSTOR

A. DASGUPTA, Z. LI, T. I.-P. SHIH (Carnegie Mellon Univ., Pittsburgh, PA), K. KUNDU (NASA, Lewis Research Center, Cleveland, OH), and J. M. DEUR (Sverdrup Technology, Inc., Brook Park, OH) Jun. 1993 13 p. AIAA, SAE, ASME, and ASEE, Joint Propulsion Conference and Exhibit, 29th, Monterey, CA, June 28-30, 1993 refs

(Contract NAG3-1009)

(AIAA PAPER 93-2069) Copyright

A code was developed for computing the multidimensional flow, spray, combustion, and pollutant formation inside gas turbine combustors. The code developed is based on a Lagrangian-Eulerian formulation and utilizes an implicit finite-volume method. The focus of this paper is on the spray part of the code (both formulation and algorithm), and a number of issues related to the computation of sprays and fuel-air mixing in a lean-premixed-prevaporized combustor. The issues addressed include: (1) how grid spacings affect the diffusion of evaporated fuel, and (2) how spurious modes can arise through modelling of the spray in the Lagrangian computations. An upwind interpolation scheme is proposed to account for some effects of grid spacing on the artificial diffusion of the evaporated fuel. Also, some guidelines are presented to minimize errors associated with the spurious modes.

A93-49910*# National Aeronautics and Space Administration. Lewis Research Center, Cleveland, OH.

FINITE ELEMENT CALCULATIONS OF TRANSONIC FLUTTER IN CASCADES

CHINGTENG HSIAO and ODDVAR O. BENDIKSEN (California Univ., Los Angeles) Jun. 1993 15 p. AIAA, SAE, ASME, and ASEE, Joint Propulsion Conference and Exhibit, 29th, Monterey, CA, June 28-30, 1993 refs

(Contract NAS3-26064)

(AIAA PAPER 93-2083) Copyright

Aeroelastic stability and response of turbomachinery cascades operating in the transonic regime are explored using a new computational approach. The two-dimensional unsteady Euler equations are used to model the transonic cascade flows, and the cascade blades are modeled as thin plates. To minimize the discretization incompatibility, both the fluid and the solid domains are discretized using finite element procedures. The fluid and the structural models are coupled at the element level by introducing a channel theory, which is analogous to a strip theory in the classical sense. The system of space-discretized equations is marched forward in time using an explicit four-stage Runge-Kutta scheme. Results of free vibration analyses of typical blades are presented and compared to published finite element and Rayleigh-Ritz results. Aeroelastic stability and response characteristics of several transonic cascades are investigated using the new quasi-3D model. These results demonstrate the present 3D finite element blade model is capable of capturing aeroelastic instabilities involving higher modes, including (plate-type) camber bending modes.

A93-50005*# National Aeronautics and Space Administration. Lewis Research Center, Cleveland, OH.

EFFECTS OF DETAILED DROPLET HEATING MODELS ON TURBULENT SPRAYS VAPORIZATION BEHAVIOR

M. A. MAWID (NASA, Lewis Research Center, Cleveland, OH) Jun. 1993 20 p. AIAA, SAE, ASME, and ASEE, Joint Propulsion Conference and Exhibit, 29th, Monterey, CA, June 28-30, 1993

refs

(AIAA PAPER 93-2193) Copyright

The effects of three different droplet heating models on the vaporization history and internal structure of turbulent liquid fuel sprays were investigated. The models considered were the infinite-diffusion, diffusion-limit, and effective-conductivity models. A numerical solution for the models was developed and implemented in the KIVA-II computer code. Low temperature and relatively high temperature numerical studies were conducted. The low temperature computations were compared with existing experimental data. The comparisons showed that while the infinite-diffusion and diffusion-limit models respectively overpredicted and underpredicted the fuel vapor peak concentration and distribution in the combustor, the effective-conductivity model gave results that were in better agreement with measurements. A limited study for the high temperature case was performed due to lack of experimental data and predictions using the three models were compared with each other.

A93-50050*# National Aeronautics and Space Administration. Lewis Research Center, Cleveland, OH.

HIGH REYNOLDS NUMBER AND TURBULENCE EFFECTS ON AERODYNAMICS AND HEAT TRANSFER IN A TURBINE CASCADE

FREDERICK C. YEH, STEVEN A. HIPPENSTEELE, and G. J. VANFOSSSEN (NASA, Lewis Research Center, Cleveland, OH) Jun. 1993 16 p. AIAA, SAE, ASME, and ASEE, Joint Propulsion Conference and Exhibit, 29th, Monterey, CA, June 28-30, 1993 Previously announced in STAR as N93-29157 refs (AIAA PAPER 93-2252) Copyright

Experimental data on pressure distribution and heat transfer on a turbine airfoil were obtained over a range of Reynolds numbers from 0.75 to 7.5 million and a range of turbulence intensities from 1.8 to about 15 percent. Fundamental heat transfer and pressure distribution data are obtained over a wide range of high Reynolds numbers and to extend the heat transfer data base to include the range of Reynolds numbers encountered in the SSME turbopump turbines. The results obtained indicated that Reynolds number and turbulence intensity have a large effect on both the transition from laminar to turbulent flow and the resulting heat transfer. For a given turbulence intensity, heat transfer for all Reynolds numbers at the leading edge can be correlated with the Frossling number developed for lower Reynolds numbers. For a given turbulence intensity, heat transfer for the airfoil surfaces downstream of the leading edge can be approximately correlated with a dimensionless parameter. Comparison of the experimental results were also made with a numerical solution from a 2D Navier-Stokes code.

Author (revised)

A93-50111*# National Aeronautics and Space Administration. Lewis Research Center, Cleveland, OH.

ATOMIZING-GAS TEMPERATURE EFFECT ON CRYOGENIC SPRAY DROPSIZE

ROBERT D. INGEBO (NASA, Lewis Research Center, Cleveland, OH) Jun. 1993 11 p. AIAA, SAE, ASME, and ASEE, Joint Propulsion Conference and Exhibit, 29th, Monterey, CA, June 28-30, 1993 Previously announced in STAR as N93-25191 refs (AIAA PAPER 93-2333) Copyright

Correlating expressions for two-phase flow breakup of liquid nitrogen, LN₂, jets in sonic velocity nitrogen gasflows were obtained for an atomizing-gas temperature range of 111 to 442 K. The correlations were based on characteristic droplet measurements obtained with a scattered-light scanner. The effect of droplet vaporization on the measurements of the volume-median droplet size was calculated by using previously determined heat and momentum transfer expressions for droplets evaporating in high-velocity gasflow. Finally, the droplet size of the originally unvaporized spray was calculated, normalized with respect to jet diameter and correlated with atomizing-gas flowrate and temperature.

A93-50148*# National Aeronautics and Space Administration. Lewis Research Center, Cleveland, OH.

DEVELOPMENT OF AN EXPLICIT MULTIBLOCK/MULTIGRID FLOW SOLVER FOR VISCOUS FLOWS IN COMPLEX GEOMETRIES

E. STEINTHORSSON (Inst. for Computational Mechanics in Propulsion; NASA, Lewis Research Center, Cleveland, OH), M.-S. LIOU, and L. A. POVINELLI (NASA, Lewis Research Center, Cleveland, OH) Jun. 1993 16 p. AIAA, SAE, ASME, and ASEE, Joint Propulsion Conference and Exhibit, 29th, Monterey, CA, June 28-30, 1993 refs (AIAA PAPER 93-2380) Copyright

A new computer program is being developed for doing accurate simulations of compressible viscous flows in complex geometries. The code employs the full compressible Navier-Stokes equations. The eddy viscosity model of Baldwin and Lomax is used to model the effects of turbulence on the flow. A cell centered finite volume discretization is used for all terms in the governing equations. The Advection Upwind Splitting Method (AUSM) is used to compute the inviscid fluxes, while central differencing is used for the diffusive fluxes. A four-stage Runge-Kutta time integration scheme is used to march solutions to steady state, while convergence is enhanced by a multigrid scheme, local time-stepping and implicit residual smoothing. To enable simulations of flows in complex geometries, the code uses composite structured grid systems where all grid lines are continuous at block boundaries (multiblock grids). Example results are shown a flow in a linear cascade, a flow around a circular pin extending between the main walls in a high aspect-ratio channel, and a flow of air in a radial turbine coolant passage.

A93-50149*# National Aeronautics and Space Administration. Lewis Research Center, Cleveland, OH.

COMPARISON OF REACTING AND NON-REACTING SHEAR LAYERS AT A HIGH SUBSONIC MACH NUMBER

C. T. CHANG, C. J. MAREK (NASA, Lewis Research Center, Cleveland, OH), C. WEY (Sverdrup Technology, Inc., Brook Park, OH), R. A. JONES (Rensselaer Polytechnic Inst., Troy, NY), and M. J. SMITH (Purdue Univ., West Lafayette, IN) Jun. 1993 12 p. AIAA, SAE, ASME, and ASEE, Joint Propulsion Conference and Exhibit, 29th, Monterey, CA, June 28-30, 1993 Previously announced in STAR as N93-27610 refs (AIAA PAPER 93-2381) Copyright

The flow field in a hydrogen-fueled planar reacting shear layer was measured with an LDV system and is compared with a similar air to air case without combustion. Measurements were made with a speed ratio of 0.34 with the highspeed stream at Mach 0.71. They show that the shear layer with reaction grows faster than one without, and both cases are within the range of data scatter presented by the established database. The coupling between the streamwise and the cross-stream turbulence components inside the shear layer is slow, and reaction only increased it slightly. However, a more organized pattern of the Reynolds stress is present in the reacting shear layer, possibly as a result of larger scale structure formation in the layer associated with heat release.

A93-50167*# National Aeronautics and Space Administration. Lewis Research Center, Cleveland, OH.

GRAVITY SENSITIVITY OF A RESISTOJET WATER VAPORIZER

W. E. MORREN (NASA, Lewis Research Center, Cleveland, OH) Jun. 1993 23 p. AIAA, SAE, ASME, and ASEE, Joint Propulsion Conference and Exhibit, 29th, Monterey, CA, June 28-30, 1993 Previously announced in STAR as N93-29194 refs (AIAA PAPER 93-2402) Copyright

A laboratory model of a water vaporizer for resistojet applications was designed, fabricated, and steady and transient characteristics were measured. Vaporizer operation was not impacted by rotation about a horizontal axis normal to its own. The vaporizer was operated under low and high accelerations aboard a jet aircraft for periods up to 25 s at flow rates ranging from 159(10)(exp -6) to 230(10)(exp -6) kg/s. Slight changes in inlet and outlet pressures and some heat exchanger temperatures

were observed during the low-gravity tests. However, the results of these tests indicated probable compatibility of the vaporizer design tested with a low-gravity environment.

A93-50168*# National Aeronautics and Space Administration. Lewis Research Center, Cleveland, OH.

PRELIMINARY ENDURANCE TESTS OF WATER VAPORIZERS FOR RESISTOJET APPLICATIONS

W. E. MORREN and GREGORY S. MACRAE (NASA, Lewis Research Center, Cleveland, OH) Jun. 1993 26 p. AIAA, SAE, ASME, and ASEE, Joint Propulsion Conference and Exhibit, 29th, Monterey, CA, June 28-30, 1993 Previously announced in STAR as N93-28694 refs

(AIAA PAPER 93-2403) Copyright

Three water vaporizers designed for resistojets applications were built and tested for periods up to 500 h and 250 thermal cycles. Two of the vaporizers were not sensitive to orientation with respect to gravity, an indication of likely compatibility with low-gravity environments. Some temperatures and pressures in the third were impacted by orientation, although operation was always stable. The pressure drop across the sand-filled version increased by 147 percent in 38 h and 19 thermal cycles. Bonding of the sand granules in the downstream end of the heat exchanger was the suspected cause of failure of this vaporizer. Pressure drops across the two sintered stainless steel-filled versions were more gradual. One, with a pore size of 60 microns, showed an 80 percent increase in 500 h and 250 thermal cycles and another, with a 10 microns poresize, showed a 29 percent increase in 350 h and 175 thermal cycles. Testing of the latter metal-filled vaporizer was ongoing as of this writing. Oxidation of the porous metal packing materials in these vaporizers, with subsequent deposition of oxide particles within the pores, was believed to have caused the observed increases in pressure drops.

A93-50181*# National Aeronautics and Space Administration. Lewis Research Center, Cleveland, OH.

LOW-G FLUID MIXING - FURTHER RESULTS FROM THE TANK PRESSURE CONTROL EXPERIMENT

M. D. BENTZ (Boeing Defense & Space Group, Seattle, WA), R. H. KNOLL, M. M. HASAN (NASA, Lewis Research Center, Cleveland, OH), and C. S. LIN (Analex Corp., Cleveland, OH) Jun. 1993 7 p. AIAA, SAE, ASME, and ASEE, Joint Propulsion Conference and Exhibit, 29th, Monterey, CA, June 28-30, 1993 refs

(AIAA PAPER 93-2423) Copyright

The Tank Pressure Control Experiment (TPCE) made its first space flight on STS-43 in 1991. Its objective was to test the effectiveness of low-energy axial jet mixing at controlling pressures in low gravity. The experiment used refrigerant 113 at near-saturation conditions, at an 83 percent fill level, to simulate the fluid dynamics and thermodynamics of cryogenic fluids in future space applications. Results from this flight were reported previously. TPCE was again flown in space on STS-52 in 1992, this time primarily to study boiling and related thermal phenomena which will be reported elsewhere. However additional mixing and pressure control data were obtained from the reflight that supplement the data from the first flight.

Author (revised)

A93-50254*# National Aeronautics and Space Administration. Lewis Research Center, Cleveland, OH.

THREE-DIMENSIONAL NUMERICAL SIMULATION OF GRADUAL OPENING IN A WAVE ROTOR PASSAGE

LOUIS M. LAROSILIERE (Ohio Aerospace Inst., Brook Park) Jun. 1993 32 p. AIAA, SAE, ASME, and ASEE, Joint Propulsion Conference and Exhibit, 29th, Monterey, CA, June 28-30, 1993 Previously announced in STAR as N93-29072 Research sponsored by NASA refs

(AIAA PAPER 93-2526) Copyright

The evolution of the contact interface and the propagation of compression waves inside a single wave rotor passage gradually opening to and traversing an inlet port is studied numerically using an inviscid formulation of the governing equations. Insights into the response of the interface and kinematics of the flow field to

various opening times are given. Since the opening time is inversely proportional to the rotational speed of the rotor, the effects of passage rotation such as centripetal and Coriolis accelerations are intrinsically coupled to the gradual opening process. Certain three-dimensional features associated with the gradual opening process as a result of centripetal and Coriolis accelerations are illustrated. For the range of opening times or rotational speeds considered, a portion of the interface behaves like a vortex sheet that can degenerate into a complex interfacial structure. The vortices produced along the interface can serve as a stirring mechanism to promote local mixing. Coriolis and centripetal accelerations can introduce three dimensional effects such as interfacial distortions in meridional planes and spanwise migration of fluid elements.

A93-50255*# National Aeronautics and Space Administration. Lewis Research Center, Cleveland, OH.

ANALYSIS OF UNSTEADY WAVE PROCESSES IN A ROTATING CHANNEL

LOUIS M. LAROSILIERE (Ohio Aerospace Inst., Brook Park) and M. MAWID (Illinois Univ., Chicago) Jun. 1993 21 p. AIAA, SAE, ASME, and ASEE, Joint Propulsion Conference and Exhibit, 29th, Monterey, CA, June 28-30, 1993 Previously announced in STAR as N93-28617 Research sponsored by NASA refs

(AIAA PAPER 93-2527) Copyright

The impact of passage rotation on the gas dynamic wave processes is analyzed through a numerical simulation of ideal shock-tube flow in a closed rotating-channel. Initial conditions are prescribed by assuming homentropic solid-body rotation. Relevant parameters of the problem such as wheel Mach number, hub-to-tip radius ratio, length-to-tip radius ratio, diaphragm temperature ratio, and diaphragm pressure ratio are varied. The results suggest possible criteria for assessing the consequences of passage rotation on the wave processes, and they may therefore be applicable to pressure-exchange wave rotors. It is shown that for a fixed geometry and initial conditions, the contact interface acquires a distorted three-dimensional time-dependent orientation at non-zero wheel Mach numbers. At a fixed wheel Mach number, the level of distortion depends primarily on the density ratio across the interface as well as the hub-to-tip radius ratio. Rarefaction fronts, shocks, and contact interfaces are observed to propagate faster with increasing wheel Mach number.

A93-50280*# National Aeronautics and Space Administration. Lewis Research Center, Cleveland, OH.

CHIMERA GRIDS IN THE SIMULATION OF THREE-DIMENSIONAL FLOWFIELDS IN TURBINE-BLADE-COOLANT PASSAGES

M. A. STEPHENS, M. J. RIMLINGER, T. I.-P. SHIH (Carnegie Mellon Univ., Pittsburgh, PA), and K. C. CIVINSKAS (NASA, Lewis Research Center, Cleveland, OH) Jun. 1993 14 p. AIAA, SAE, ASME, and ASEE, Joint Propulsion Conference and Exhibit, 29th, Monterey, CA, June 28-30, 1993 refs

(Contract NAG3-929)

(AIAA PAPER 93-2559)

When computing flows inside geometrically complex turbine-blade coolant passages, the structure of the grid system used can affect significantly the overall time and cost required to obtain solutions. This paper addresses this issue while evaluating and developing computational tools for the design and analysis of coolant-passages, and is divided into two parts. In the first part, the various types of structured and unstructured grids are compared in relation to their ability to provide solutions in a timely and cost-effective manner. This comparison shows that the overlapping structured grids, known as Chimera grids, can rival and in some instances exceed the cost-effectiveness of unstructured grids in terms of both the man hours needed to generate grids and the amount of computer memory and CPU time needed to obtain solutions. In the second part, a computational tool utilizing Chimera grids was used to compute the flow and heat transfer in two different turbine-blade coolant passages that contain baffles and numerous pin fins. These computations showed the versatility and flexibility offered by Chimera grids.

Author (revised)

A93-50536* National Aeronautics and Space Administration. Lewis Research Center, Cleveland, OH.

COLLAPSE OF THE SOAP-FILM BRIDGE - QUASISTATIC DESCRIPTION

STEVEN A. CRYER (Dow Elanco, Midland, MI) and PAUL H. STEEN (Cornell Univ., Ithaca, NY) *Journal of Colloid and Interface Science* (ISSN 0021-9797) vol. 154, no. 1 Nov. 1992 p. 276-288. refs

(Contract NAG3-801)

Copyright

Observations of the collapse of a soap-film bridge from a connected to a disconnected state are recorded. The equilibrium framework for this nonequilibrium event is classical. Experiments confirm predictions of stable and unstable equilibria. A quasistatic description is introduced for the dynamic states to extend the static theory. It is found to adequately describe the collapse trajectory while the bridge is still connected. Author (revised)

A93-51183* National Aeronautics and Space Administration. Lewis Research Center, Cleveland, OH.

CENTRAL DIFFERENCE TVD SCHEMES FOR TIME DEPENDENT AND STEADY STATE PROBLEMS

P. JORGENSEN (NASA, Lewis Research Center, Cleveland, OH) and E. TURKEL (Tel Aviv Univ., Israel; NASA, Lewis Research Center, Cleveland, OH) *Journal of Computational Physics* (ISSN 0021-9991) vol. 107, no. 2 Aug. 1993 p. 297-308. refs

Copyright

A Runge-Kutta formula in time is presently used to advance schemes in which central differences are used to solve the time-dependent Euler equations; a second difference is added near shocks as an artificial viscosity to reduce the given scheme to a first-order upwind one at shocks. A matrix-valued dissipation is introduced and compared with the scalar viscosity; a connection is shown between this artificial viscosity and flux limiters. The use of various flux limiters for this central difference scheme is compared. AIAA

A93-52008* National Aeronautics and Space Administration. Lewis Research Center, Cleveland, OH.

ACCURACY OF LEAST-SQUARES METHODS FOR THE NAVIER-STOKES EQUATIONS

PAVEL B. BOCHEV and MAX D. GUNZBURGER (Virginia Polytechnic Inst. and State Univ., Blacksburg) *Computers & Fluids* (ISSN 0045-7930) vol. 22, no. 4-5 July-Sept. 1993 p. 549-563. Research supported by NASA refs

(Contract AF-AFOSR-90-0179)

Copyright

Recently there has been substantial interest in least-squares finite element methods for velocity-vorticity-pressure formulations of the incompressible Navier-Stokes equations. The main cause for this interest is the fact that algorithms for the resulting discrete equations can be devised which require the solution of only symmetric, positive definite systems of algebraic equations. On the other hand, it is well-documented that methods using the vorticity as a primary variable often yield very poor approximations. Thus, here we study the accuracy of these methods through a series of computational experiments, and also comment on theoretical error estimates. It is found, despite the failure of standard methods for deriving error estimates, that computational evidence suggests that these methods are, at the least, nearly optimally accurate. Thus, in addition to the desirable matrix properties yielded by least-squares methods, one also obtains accurate approximations.

A93-52310* National Aeronautics and Space Administration. Lewis Research Center, Cleveland, OH.

DYNAMICS AND CONTROL OF COHERENT STRUCTURE IN TURBULENT JETS

REDA R. MANKBADI (NASA, Lewis Research Center, Cleveland, OH) *Applied Mechanics Reviews* (ISSN 0003-6900) vol. 45, no. 6 June 1992 p. 219-248. refs

Copyright

Current understanding of coherent structure dynamics in

incompressible turbulent jets as explained by the nonlinear stability theory is reviewed, focusing on nonswirling turbulent jets. Topics addressed include hydrodynamic stability theory and coherent structures; dynamics of energy transfers among different scales of motion; nonlinear development of amplitude; development of single-frequency coherent mode; fundamental-subharmonic interaction and vortex pairing; and reversal of Reynolds stresses. Attention is also given to the effect of initial phase-difference angle between fundamental and subharmonic, conditions for resonance interaction, modulation of spreading rate by controlling coherent structure, turbulence enhancement or suppression due to excitation, 3D effects, jet noise, and swirling jets. AIAA

A93-52515* National Aeronautics and Space Administration. Lewis Research Center, Cleveland, OH.

THERMOCAPILLARY CONVECTION IN TWO IMMISCIBLE LIQUID LAYERS WITH FREE SURFACE

TAKAO DOI (NASDA, Tokyo, Japan) and JEAN N. KOSTER (Colorado Univ., Boulder) *Physics of Fluids A* (ISSN 0899-8213) vol. 5, no. 8 Aug. 1993 p. 1914-1927. refs

(Contract NAG3-1094)

Copyright

Thermocapillary convection is studied in two immiscible liquid layers with one free surface, one liquid/liquid interface, and differential heating applied parallel to the interfaces. An analytical solution is introduced for infinite horizontal layers. The defining parameter for the flow pattern is λ , the ratio of the temperature coefficient of the interfacial tension to that of the surface tension. Four different flow patterns exist under zero gravity conditions. 'Halt' conditions which halt the fluid motion in the lower encapsulated liquid layer have been found. A numerical experiment is carried out to study effects of vertical end walls on the double layer convection in a 2D cavity. The halt condition obtained from the analytical study is found to be valid in the limit of small Reynolds numbers. The flow in the encapsulated liquid layer can be suppressed substantially. Author (revised)

A93-52751* National Aeronautics and Space Administration. Lewis Research Center, Cleveland, OH.

PROGRESS TOWARDS UNDERSTANDING AND PREDICTING HEAT TRANSFER IN THE TURBINE GAS PATH

ROBERT J. SIMONEAU and FREDERICK F. SIMON (NASA, Lewis Research Center, Cleveland, OH) *International Journal of Heat and Fluid Flow* (ISSN 0142-727X) vol. 14, no. 2 June 1993 p. 106-128. refs

Copyright

A new era is dawning in the ability to predict convection heat transfer in the turbine gas path. We feel that the technical community now has the capability to mount a major assault on this problem, which has eluded significant progress for a long time. In this paper we hope to make a case for this bold statement by reviewing the state of the art in three major and related areas, which we believe are indispensable to the understanding and accurate prediction of turbine gas path heat transfer: configuration-specific experiments, fundamental physics and model development, and code development. We begin our review with the configuration-specific experiments, whose data have provided the big picture and guided both the fundamental modeling research and the code development. Following that, we examine key modeling efforts and comment on what will be needed to incorporate them into the codes. In this region we concentrate on bypass transition, 3D endwalls, and film cooling. We then review progress and directions in the development of computer codes to predict turbine gas path heat transfer. Finally, we cite examples and make observations on the more recent efforts to do all this work in a simultaneous, interactive, and more synergistic manner. We conclude with an assessment of progress, suggestions for how to use the current state of the art, and recommendations for the future. Author (revised)

A93-53585* National Aeronautics and Space Administration. Lewis Research Center, Cleveland, OH.

MEASUREMENTS AND COMPUTATIONAL ANALYSIS OF HEAT TRANSFER AND FLOW IN A SIMULATED TURBINE BLADE INTERNAL COOLING PASSAGE

LOUIS M. RUSSELL (NASA, Lewis Research Center, Cleveland, OH), DOUGLAS R. THURMAN (U.S. Army, Vehicle Propulsion Directorate; NASA, Lewis Research Center, Cleveland, OH), PATRICIA S. SIMONYI (Sverdrup Technology, Inc., Lewis Research Center Group, Brook Park, OH), STEVEN A. HIPPENSTEELE, and PHILIP E. POINSATTE (NASA, Lewis Research Center, Cleveland, OH) Jun. 1993 28 p. AIAA, SAE, ASME, and ASEE, Joint Propulsion Conference and Exhibit, 29th, Monterey, CA, June 28-30, 1993 Previously announced in STAR as N93-31647 refs (AIAA PAPER 93-1797) Copyright

Visual and quantitative information was obtained on heat transfer and flow in a branched-duct test section that had several significant features of an internal cooling passage of a turbine blade. The objective of this study was to generate a set of experimental data that could be used to validate computer codes for internal cooling systems. Surface heat transfer coefficients and entrance flow conditions were measured at entrance Reynolds numbers of 45,000, 335,000, and 726,000. The heat transfer data were obtained using an Inconel heater sheet attached to the surface and coated with liquid crystals. Visual and quantitative flow field results using particle image velocimetry were also obtained for a plane at mid channel height for a Reynolds number of 45,000. The flow was seeded with polystyrene particles and illuminated by a laser light sheet. Computational results were determined for the same configurations and at matching Reynolds numbers; these surface heat transfer coefficients and flow velocities were computed with a commercially available code. The experimental and computational results were compared. Although some general trends did agree, there were inconsistencies in the temperature patterns as well as in the numerical results. These inconsistencies strongly suggest the need for further computational studies on complicated geometries such as the one studied.

A93-53586* National Aeronautics and Space Administration. Lewis Research Center, Cleveland, OH.

A CRITICAL COMPARISON OF SEVERAL LOW REYNOLDS NUMBER K-EPSILON TURBULENCE MODELS FOR FLOW OVER A BACKWARD-FACING STEP

CHRISTOPHER J. STEFFEN, JR. (NASA, Lewis Research Center, Cleveland, OH) Jun. 1993 14 p. AIAA, SAE, ASME, and ASEE, Joint Propulsion Conference and Exhibit, 29th, Monterey, CA, June 28-30, 1993 Previously announced in STAR as N93-32200 refs (AIAA PAPER 93-1927) Copyright

Turbulent backward-facing step flow was examined using four low turbulent Reynolds number k-epsilon models and one standard high Reynolds number technique. A tunnel configuration of 1:9 (step height: exit tunnel height) was used. The models tested include: the original Jones and Launder; Chien; Launder and Sharma; and the recent Shih and Lumley formulation. The experimental reference of Driver and Seegmiller was used to make detailed comparisons between reattachment length, velocity, pressure, turbulent kinetic energy, Reynolds shear stress, and skin friction predictions. The results indicated that the use of a wall function for the standard k-epsilon technique did not reduce the calculation accuracy for this separated flow when compared to the low turbulent Reynolds number techniques.

A93-54053* National Aeronautics and Space Administration. Lewis Research Center, Cleveland, OH.

FLUID DYNAMICS AND CONVECTIVE HEAT TRANSFER IN IMPINGING JETS THROUGH IMPLEMENTATION OF A HIGH RESOLUTION LIQUID CRYSTAL TECHNIQUE

K. KIM, B. WIEDNER, and C. CAMCI (Pennsylvania State Univ., University Park) In ISABE - International Symposium on Air Breathing Engines, 11th, Tokyo, Japan, Sept. 20-24, 1993, Proceedings. Vol. 2 Washington American Institute of Aeronautics

and Astronautics 1993 p. 792-803. refs (Contract NAG3-989; NSF CTS-89-06452) (ISABE 93-7077) Copyright

A combined convective heat transfer and fluid dynamics investigation in a turbulent round jet impinging on a flat surface is presented. The experimental study uses a high resolution liquid crystal technique for the determination of the convective heat transfer coefficients on the impingement plate. The heat transfer experiments are performed using a transient heat transfer method. The mean flow and the character of turbulent flow in the free jet is presented through five hole probe and hot wire measurements, respectively. The flow field character of the region near the impingement plate plays an important role in the amount of convective heat transfer. Detailed surveys obtained from five hole probe and hot wire measurements are provided. An extensive validation of the liquid crystal based heat transfer method against a conventional technique is also presented. After a complete documentation of the mean and turbulent flow field, the convective heat transfer coefficient distributions on the impingement plate are presented. The near wall of the impingement plate and the free jet region is treated separately. The current heat transfer distributions are compared to other studies available from the literature. The present paper contains complete sets of information on the three dimensional mean flow, turbulent velocity fluctuations, and convective heat transfer to the plate. The experiments also prove that the present nonintrusive heat transfer method is highly effective in obtaining high resolution heat transfer maps with a heat transfer coefficient uncertainty of 5.7 percent.

Author (revised)

A93-54454* National Aeronautics and Space Administration. Lewis Research Center, Cleveland, OH.

EFFECT OF RADIATION ON CONVECTION IN A TOP-HEATED ENCLOSURE

H. C. DE GROH, III and M. KASSEMI (NASA, Lewis Research Center, Cleveland, OH) Journal of Thermophysics and Heat Transfer (ISSN 0887-8722) vol. 7, no. 4 Oct.-Dec. 1993 p. 561-568. AIAA, Aerospace Sciences Meeting and Exhibit, 30th, Reno, NV, Jan. 6-9, 1992, AIAA Paper 92-0691. Previously cited in issue 10, p. 1602, Accession no. A92-27058 refs Copyright

A93-54463* National Aeronautics and Space Administration. Lewis Research Center, Cleveland, OH.

VARIABLE REFRACTIVE INDEX EFFECTS ON RADIATION IN SEMITRANSSPARENT SCATTERING MULTILAYERED REGIONS

R. SIEGEL and C. M. SPUCKLER (NASA, Lewis Research Center, Cleveland, OH) Journal of Thermophysics and Heat Transfer (ISSN 0887-8722) vol. 7, no. 4 Oct.-Dec. 1993 p. 624-630. refs

Copyright

A simple set of equations is derived for predicting the temperature distribution and radiative energy flow in a semitransparent layer consisting of an arbitrary number of laminated sublayers that absorb, emit, and scatter radiation. Each sublayer can have a different refractive index and optical thickness. The plane composite region is heated on each exterior side by a different amount of incident radiation. The results are for the limiting case where heat conduction within the layers is very small relative to radiative transfer, and is neglected. The interfaces are assumed diffuse, and all interface reflections are included in the analysis. The thermal behavior is readily calculated from the analytical expressions that are obtained. By using many sublayers, expressions provide the temperature distribution and heat flow for a diffusing medium with a continually varying refractive index, including internal reflection effects caused by refractive index gradients. Temperature and heat flux results are given to show the effect of variations in refractive index and optical thickness through the multilayer laminate.

A93-54483* National Aeronautics and Space Administration. Lewis Research Center, Cleveland, OH.

INTERNAL STRUCTURE OF SHOCK WAVES IN DISPARATE MASS MIXTURES

CHAN-HONG CHUNG (NASA, Lewis Research Center, Cleveland, OH), KENNETH J. DE WITT, DUEN-REN JENG (Toledo Univ., OH), and PAUL F. PENKO (NASA, Lewis Research Center, Cleveland, OH) *Journal of Thermophysics and Heat Transfer* (ISSN 0887-8722) vol. 7, no. 4 Oct.-Dec. 1993 p. 742-744. Abridged. AIAA, Aerospace Sciences Meeting and Exhibit, 30th, Reno, NV, Jan. 6-9, 1992, AIAA Paper 92-0496. Previously cited in issue 10, p. 1607, Accession no. A92-28195 refs (Contract NCC3-171)

A93-55136* National Aeronautics and Space Administration. Lewis Research Center, Cleveland, OH.

A HYDRODYNAMIC MODEL OF THE OSCILLATING SCREEN VISCOMETER

A. M. J. DAVIS (Alabama Univ., Tuscaloosa) *Physics of Fluids A* (ISSN 0899-8213) vol. 5, no. 9 Sept. 1993 p. 2095-2103. refs (Contract NASA ORDER C-32008-A) Copyright

The viscometer consists of an oscillating screen immersed in a fluid and free to rotate about an axis in its plane. The viscosity can be determined from the measured ratio of the periodic driving force to the screen motion when an adequate hydrodynamical model of the immersed oscillator is available. The screen is formed by a square mesh of thin wire whose dimensions invite comparison with asymptotic results for narrow hollow bodies translating in Stokes flow. These indicate that the closed hole structure of the grid plays an important role in determining its motion. It is shown that this role diminishes as the frequency increases. The computed results, obtained from a system of linear equations, are consistent with experimental values over the appropriate range of frequency.

A93-55358* National Aeronautics and Space Administration. Lewis Research Center, Cleveland, OH.

STABILITY OF A FLUID SURFACE IN A MICROGRAVITY ENVIRONMENT

JAUME CASEDEMUNT, WENBIN ZHANG, JORGE VINALS (Florida State Univ., Tallahassee), and ROBERT F. SEKERKA (Carnegie Mellon Univ., Pittsburgh, PA) *AIAA Journal* (ISSN 0001-1452) vol. 31, no. 11 Nov. 1993 p. 2027-2032. AIAA, Aerospace Sciences Meeting and Exhibit, 31st, Reno, NV, Jan. 11-14, 1993, AIAA Paper 93-0911. Previously cited in issue 08, p. 1375, Accession no. A93-24965 refs (Contract NAG3-1284; DE-FC05-85ER-25000) Copyright

A93-55460 National Aeronautics and Space Administration. Lewis Research Center, Cleveland, OH.

NONGRAY GAS ANALYSES FOR REFLECTING WALLS UTILIZING A FLUX TECHNIQUE

J. A. MENART (Minnesota Univ., Minneapolis) and HAEOK S. LEE (NASA, Lewis Research Center, Cleveland, OH) *ASME, Transactions, Journal of Heat Transfer* (ISSN 0022-1481) vol. 115, no. 3 Aug. 1993 p. 645-652. Research supported by Minnesota Supercomputer Inst. refs (Contract NSF CTS-84-51076; NGT-50830) Copyright

A flux formulation for a planar slab of molecular gas radiation bounded by diffuse reflecting walls is developed. While this formulation is limited to the planar geometry, it is useful for studying approximations necessary in modeling nongray radiative heat transfer. The governing equations are derived by considering the history of multiple reflections between the walls. Accurate solutions are obtained by explicitly accounting for a finite number of reflections and approximating the spectral effects of the remaining reflections. Four approximate methods are presented and compared using a single absorption band of H₂O. All four methods reduce to an identical zeroth-order formulation, which accounts for all reflections approximately but does handle nonreflected

radiation correctly. A single absorption band of CO₂ is also considered using the best-behaved approximation for higher orders. A zeroth-order formulation is sufficient to predict the radiative transfer accurately for many cases considered. For highly reflecting walls, higher order solutions are necessary for better accuracy. Including all the important bands of H₂O, the radiative source distributions are also obtained for two different temperature and concentration profiles. Author (revised)

A93-55461* National Aeronautics and Space Administration. Lewis Research Center, Cleveland, OH.

DROPLET VAPORIZATION IN A HIGH-PRESSURE GAS

J. P. HARTFIELD and P. V. FARRELL (Wisconsin Univ., Madison) *ASME, Transactions, Journal of Heat Transfer* (ISSN 0022-1481) vol. 115, no. 3 Aug. 1993 p. 699-706. ASME, Winter Annual Meeting, Atlanta, GA, Dec. 1-6, 1991 refs (Contract NAG3-718) Copyright

Results of an experimental study of the vaporization of single R-113 and n-heptane droplets are presented. Gas temperature is found to have a strong effect on drop vaporization, while gas pressure has a weaker effect. A comparison of data from experiments in near-zero gravity with those conducted in normal gravity shows that the vaporization rate and droplet lifetime are affected depending on the liquid involved. In the case of R-113, the removal of the gravity field in free-fall experiments resulted in an increase of droplet lifetime of about 30 percent, whereas in the case of n-heptane, a much less pronounced effect was observed. AIAA

A93-55473* National Aeronautics and Space Administration. Lewis Research Center, Cleveland, OH.

A NUMERICAL MODEL INCLUDING PID CONTROL OF A MULTIZONE CRYSTAL GROWTH FURNACE

CHARLES H. PANZARELLA and MOHAMMAD KASSEMI (NASA, Lewis Research Center, Cleveland, OH) *In Micro/macro scale phenomena in solidification* New York American Society of Mechanical Engineers 1992 p. 127-139. refs Copyright

This paper presents a 2D axisymmetric combined conduction and radiation model of a multizone crystal growth furnace. The model is based on a programmable multizone furnace (PMZF) designed and built at NASA Lewis Research Center for growing high quality semiconductor crystals. A novel feature of this model is a control algorithm which automatically adjusts the power in any number of independently controlled heaters to establish the desired crystal temperatures in the furnace model. The control algorithm eliminates the need for numerous trial and error runs previously required to obtain the same results. The finite element code, FIDAP, used to develop the furnace model, was modified to directly incorporate the control algorithm. This algorithm, which presently uses PID control, and the associated heat transfer model are briefly discussed. Together, they have been used to predict the heater power distributions for a variety of furnace configurations and desired temperature profiles. Examples are included to demonstrate the effectiveness of the PID controlled model in establishing isothermal, Bridgman, and other complicated temperature profiles in the sample. Finally, an example is given to show how the algorithm can be used to change the desired profile with time according to a prescribed temperature-time evolution.

N93-10039* National Aeronautics and Space Administration. Lewis Research Center, Cleveland, OH.

A SURVEY OF INSTABILITIES WITHIN CENTRIFUGAL PUMPS AND CONCEPTS FOR IMPROVING THE FLOW RANGE OF PUMPS IN ROCKET ENGINES

JOSEPH P. VERES *In JHU, The 1992 JANNAF Propulsion Meeting, Volume 1* p. 615-629 Feb. 1992 Previously announced as N92-18280 Avail: CPIA, 10630 Little Patuxent Pkwy., Suite 202, Columbia, MD, 21044-3200 HC

Design features and concepts that have primary influence on the stable operating flow range of propellant-feed centrifugal

turbopumps in a rocket engine are discussed. One of the throttling limitations of a pump-fed rocket engine is the stable operating range of the pump. Several varieties of pump hydraulic instabilities are mentioned. Some pump design criteria are summarized and a qualitative correlation of key parameters to pump stall and surge are referenced. Some of the design criteria were taken from the literature on high pressure ratio centrifugal compressors. Therefore, these have yet to be validated for extending the stable operating flow range of high-head pumps. Casing treatment devices, dynamic fluid-damping plenums, backflow-stabilizing vanes, and flow-reinjection techniques are summarized. A planned program was undertaken at LeRC to validate these concepts. Technologies developed by this program will be available for the design of turbopumps for advanced space rocket engines for use by NASA in future space missions where throttling is essential. Author

N93-10061* National Aeronautics and Space Administration. Lewis Research Center, Cleveland, OH.

RADIAL TURBINE COOLING

RICHARD J. ROELKE /in VKI, Radial Turbines 38 p 1992
Copyright Avail: CASI HC A03/MF A04

The technology of high temperature cooled radial turbines is reviewed. Aerodynamic performance considerations are described. Heat transfer and structural analysis are addressed, and in doing so the following topics are covered: cooling considerations, hot side convection, coolant side convection, and rotor mechanical analysis. Cooled rotor concepts and fabrication are described, and the following are covered in this context: internally cooled rotor, hot isostatic pressure bonded rotor, laminated rotor, split blade rotor, and the NASA radial turbine program. ESA

N93-10087* National Aeronautics and Space Administration. Lewis Research Center, Cleveland, OH.

EVALUATION AND APPLICATION OF THE BALDWIN-LOMAX TURBULENCE MODEL IN TWO-DIMENSIONAL, UNSTEADY, COMPRESSIBLE BOUNDARY LAYERS WITH AND WITHOUT SEPARATION IN ENGINE INLETS

BARBARA SAKOWSKI, DOUGLAS DARLING, ROBERT L. ROACH (Georgia Inst. of Tech., Atlanta.), and ALLAN VANDEWALL (Case Western Reserve Univ., Cleveland, OH.) 1992 11 p Presented at the 28th Joint Propulsion Conference and Exhibit, Nashville, TN, 6-8 Jul. 1992; cosponsored by AIAA, SAE, ASME, and ASEE (Contract RTOP 505-62-20) (NASA-TM-105810; E-7241; NAS 1.15:105810) Avail: CASI HC A03/MF A01

There is a practical need to model high speed flows that exist in jet engine inlets. The boundary layers that form in these inlets may be turbulent or laminar and either separated or attached. Also, unsteady supersonic inlets may be subject to frequent changes in operating conditions. Some changes in the operating conditions of the inlets may include varying the inlet geometry, bleeds and bypasses, and rotating or translating the centerbody. In addition, the inlet may be either started or unstarted. Therefore, a CFD code, used to model these inlets, may have to run for several different cases. Also, since the flow conditions through an unsteady inlet may be continually fluctuating, the CFD code which models these flows may have to be run over many time steps. Therefore, it would be beneficial that the code run quickly. Many turbulence models, however, are cumbersome to implement and require a lot of computer time to run, since they add to the number of differential equations to be solved to model a flow. The Baldwin-Lomax turbulence model is a popular model. It is an algebraic, eddy viscosity model. The Baldwin-Lomax model is used in many CFD codes because it is quick and easy to implement. In this paper, we will discuss implementing the Baldwin-Lomax turbulence model for both steady and unsteady compressible flows. In addition, these flows may be either separated or attached. In order to apply this turbulence model to flows which may be subjected to these conditions, certain modifications should be made to the original Baldwin-Lomax model. We will discuss these modifications and determine whether the Baldwin-Lomax model is a viable turbulence model that produces reasonably accurate

results for high speed flows that can be found in engine inlets.

Author

N93-10454* National Aeronautics and Space Administration. Lewis Research Center, Cleveland, OH.

A NEW ENERGY TRANSFER MODEL FOR TURBULENT FREE SHEAR FLOW

WILLIAM W.-W. LIU Sep. 1992 13 p
(Contract NASA ORDER C-99066-G; RTOP 505-62-21) (NASA-TM-105854; ICOMP-92-16; CMOTT-92-09; E-7310; NAS 1.15:105854) Avail: CASI HC A03/MF A01

A new model for the energy transfer mechanism in the large-scale turbulent kinetic energy equation is proposed. An estimate of the characteristic length scale of the energy containing large structures is obtained from the wavelength associated with the structures predicted by a weakly nonlinear analysis for turbulent free shear flows. With the inclusion of the proposed energy transfer model, the weakly nonlinear wave models for the turbulent large-scale structures are self-contained and are likely to be independent flow geometries. The model is tested against a plane mixing layer. Reasonably good agreement is achieved. Finally, it is shown by using the Liapunov function method, the balance between the production and the drainage of the kinetic energy of the turbulent large-scale structures is asymptotically stable as their amplitude saturates. The saturation of the wave amplitude provides an alternative indicator for flow self-similarity. Author

N93-10548* National Aeronautics and Space Administration. Lewis Research Center, Cleveland, OH.

A LEAST-SQUARES FINITE ELEMENT METHOD FOR INCOMPRESSIBLE NAVIER-STOKES PROBLEM

BONAN JIANG (Cleveland State Univ., OH.) and LOUIS A. POVINELLI /in Carleton Univ., Proceedings of the Twelfth Canadian Congress of Applied Mechanics, Volumes 1 and 2 p 602-603 May 1989

Copyright Avail: Issuing Activity (Canadian Society for Mechanical Engineering, 2050 Mansfield St., Suite 700, Montreal, Quebec H3A 1Z7 Canada)

Most finite element schemes for solving the Navier-Stokes equations can be categorized into the Galerkin mixed method and the penalty method. The mixed method leads to a saddle-point problem. In order to guarantee the existence of a solution, the combination of velocity and pressure interpolations requires satisfaction of the Ladyzhenskaya Babuska Brezzi (LBB) consistency condition which precludes the use of equal order interpolations and many seemingly natural pairs of velocity and pressure elements. In a previous paper a least-squares finite element method based on the first order velocity-pressure-vorticity formulation for the Stokes problem was proposed. This method leads to a minimization problem. The choice of combination of elements is thus not subject to the LBB condition. The numerical experiments exhibit the optimal rate of convergence for all variables with equal order interpolations. A theoretical error analysis supports the numerical results. In this paper the least-squares finite element method is extended to solving the incompressible Navier-Stokes problem. Author (CISTI)

N93-10735* National Aeronautics and Space Administration. Lewis Research Center, Cleveland, OH.

NAVIER-STOKES TURBINE HEAT TRANSFER PREDICTIONS USING TWO-EQUATION TURBULENCE

ALI A. AMERI and ANDREA ARNONE Aug. 1992 12 p
Presented at the 28th Joint Propulsion Conference and Exhibit, Nashville, TN, 6-8 Jul. 1992; sponsored by AIAA, SAE, ASME, and ASEE (Contract NASA ORDER C-99066-G; RTOP 505-62-52) (NASA-TM-105817; ICOMP-92-14; E-7248; NAS 1.15:105817) Avail: CASI HC A03/MF A01

Navier-Stokes calculations were carried out in order to predict the heat transfer rates on turbine blades. The calculations were performed using TRAF2D which is a two-dimensional, explicit, finite volume mass-averaged Navier-Stokes solver. Turbulence was modeled using q-omega and k-epsilon two-equation models and

the Baldwin-Lomax algebraic model. The model equations along with the flow equations were solved explicitly on a non-periodic C grid. Implicit residual smoothing (IRS) or a combination of multigrid technique and IRS was applied to enhance convergence rates. Calculations were performed to predict the Stanton number distributions on the first stage vane and blade row as well as the second stage vane row of the Rocketdyne Space Shuttle Main Engine (SSME) high pressure fuel turbine. The comparison with the experimental results, although generally favorable, serves to highlight the weaknesses of the turbulence models and the possible areas of improving these models for use in turbomachinery heat transfer calculations. Author

N93-10981* National Aeronautics and Space Administration. Lewis Research Center, Cleveland, OH.

SMALL EXPERIMENTS FOR THE MATURATION OF ORBITAL CRYOGENIC TRANSFER TECHNOLOGIES

DAVID J. CHATO and WILLIAM J. TAYLOR Sep. 1992 11 p
Presented at the 1992 World Space Congress, Washington, DC, 28 Aug. - 5 Sep. 1992; sponsored by the International Astronautical Federation
(Contract RTOP 506-42-73)
(NASA-TM-105849; E-7295; NAS 1.15:105849) Avail: CASI HC A03/MF A01

The no-vent method is a promising approach to handling the problems of low-g venting during propellant transfer. A receiver tank is first cooled to remove thermal energy from the tank wall and the resultant vapor vented overboard. The nozzles mix the incoming liquid and residual vapor in the tank maintaining a thermodynamic state which allows the tank to fill with liquid without venting. Ground based testing at NASA Lewis Research Center (LeRC) has demonstrated the no-vent fill process and attempted to bound its low-gravity performance. But, low-gravity testing is required to validate the method. As an alternative to using a dedicated spacecraft for validation, several small scale experiments to study no-vent fill in low-g were formulated. Cost goals quickly limited the search to two possibilities: a secondary payload on the space shuttle, or a small scale sounding rocket experiment. The key issues of small scale experimentation are discussed, and a conceptual design of a sounding rocket experiment with liquid hydrogen for studying the fill process is presented. Author

N93-11529* National Aeronautics and Space Administration. Lewis Research Center, Cleveland, OH.

DIRECT NUMERICAL SIMULATION OF INSTABILITIES IN PARALLEL FLOW WITH SPHERICAL ROUGHNESS ELEMENTS

R. G. DEANNA Aug. 1992 36 p
(Contract DA PROJ. 1L1-61102-AH-45; RTOP 505-62-OK)
(NASA-TM-105847; E-7291; NAS 1.15:105847;
AVSCOM-TR-92-C-023; AD-A259365) Avail: CASI HC A03/MF A01

Results from a direct numerical simulation of laminar flow over a flat surface with spherical roughness elements using a spectral-element method are given. The numerical simulation approximates roughness as a cellular pattern of identical spheres protruding from a smooth wall. Periodic boundary conditions on the domain's horizontal faces simulate an infinite array of roughness elements extending in the streamwise and spanwise directions, which implies the parallel-flow assumption, and results in a closed domain. A body force, designed to yield the horizontal Blasius velocity in the absence of roughness, sustains the flow. Instabilities above a critical Reynolds number reveal negligible oscillations in the recirculation regions behind each sphere and in the free stream, high-amplitude oscillations in the layer directly above the spheres, and a mean profile with an inflection point near the sphere's crest. The inflection point yields an unstable layer above the roughness (where $U''(y)$ is less than 0) and a stable region within the roughness (where $U''(y)$ is greater than 0). Evidently, the instability begins when the low-momentum or wake region behind an element, being the region most affected by disturbances (purely numerical in this case), goes unstable and moves. In compressible flow with periodic boundaries, this motion sends disturbances to all regions of the

domain. In the unstable layer just above the inflection point, the disturbances grow while being carried downstream with a propagation speed equal to the local mean velocity; they do not grow amid the low energy region near the roughness patch. The most amplified disturbance eventually arrives at the next roughness element downstream, perturbing its wake and inducing a global response at a frequency governed by the streamwise spacing between spheres and the mean velocity of the most amplified layer. Author

N93-13220* National Aeronautics and Space Administration. Lewis Research Center, Cleveland, OH.

AGARD WG13 AERODYNAMICS OF HIGH SPEED AIR INTAKES: ASSESSMENT OF CFD RESULTS

N. C. BISSINGER (Messerschmitt-Boelkow-Blohm G.m.b.H., Munich, Germany), T. J. BENSON, and R. G. BRADLEY, JR. (General Dynamics Corp., Fort Worth, TX.) In AGARD, Aerodynamic Engine/Airframe Integration for High Performance Aircraft and Missiles 24 p Sep. 1992
Copyright Avail: CASI HC A03/MF A04

A brief review of the work accomplished by the numerical subgroup of AGARD Working Group 13 on the aerodynamics of high speed air intakes is presented. This work comprised the selection of test cases for which experimental data were available. The test cases were chosen to range in complexity from normal-shock/boundary-layer interaction to full forebody-inlet combinations. Computations for these test cases were solicited from a large number of organizations and individual researchers within the NATO countries. The computation methods reached from Euler solvers (with and without boundary layer corrections) to full Reynolds averaged Navier-Stokes codes. The group compared these results with the test data available for each test case. A short overview of the CFD methods employed, a description of the test cases selected, and some of the comparisons between CFD solutions and test data are presented. The conclusions and recommendations drawn from this assessment are given. Author

N93-13385* National Aeronautics and Space Administration. Lewis Research Center, Cleveland, OH.

THE FOURTH ANNUAL THERMAL AND FLUIDS ANALYSIS WORKSHOP

1992 276 p Workshop held in Cleveland, OH, 17-21 Aug. 1992
(NASA-CP-10106; E-7346; NAS 1.55:10106) Avail: CASI HC A13/MF A03

The Fourth Annual Thermal and Fluids Analysis Workshop was held from August 17-21, 1992, at NASA Lewis Research Center. The workshop consisted of classes, vendor demonstrations, and paper sessions. The classes and vendor demonstrations provided participants with the information on widely used tools for thermal and fluids analysis. The paper sessions provided a forum for the exchange of information and ideas among thermal and fluids analysts. Paper topics included advances and uses of established thermal and fluids computer codes (such as SINDA and TRASYS) as well as unique modeling techniques and applications.

N93-13395* National Aeronautics and Space Administration. Lewis Research Center, Cleveland, OH.

A COMPRESSIBLE BOUNDARY LAYER ALGORITHM FOR USE WITH SINDA '85

BARBARA SAKOWSKI, DOUGLAS DARLING, and ALLAN VANDEWALL (Case Western Reserve Univ., Cleveland, OH.) In its The Fourth Annual Thermal and Fluids Analysis Workshop p 117-130 1992
Avail: CASI HC A03/MF A03

It is useful to interface a high-speed-flow solution and SINDA to analyze the thermal behavior of systems that include both conduction and high speed flows. When interfacing a high-speed-flow solution to SINDA, it may be necessary to include the viscous effects in the energy equations. Boundary layer effects of interest include heat transfer coefficients (including convection and viscous dissipation) and friction coefficients. To meet this need, a fast, uncoupled, compressible, two-dimensional, boundary layer

algorithm was developed that can model flows with and without separation. This algorithm was used as a subroutine with SINDA. Given the core flow properties and the wall heat flux from SINDA, the boundary layer algorithm returns a wall temperature to SINDA and boundary layer algorithm are iterated until they predict the same wall temperature. Author

N93-13396* National Aeronautics and Space Administration. Lewis Research Center, Cleveland, OH.

THE PROTEUS NAVIER-STOKES CODE

CHARLES E. TOWNE, TRONG T. BUI, RICHARD H. CAVICCHI, JULIANNE M. CONLEY, FRANK B. MOLLS, and JOHN R. SCHWAB *In its* The Fourth Annual Thermal and Fluids Analysis Workshop p 131-154 1992

Avail: CASI HC A03/MF A03

An effort is currently underway at NASA Lewis to develop two- and three-dimensional Navier-Stokes codes, called Proteus, for aerospace propulsion applications. The emphasis in the development of Proteus is not algorithm development or research on numerical methods, but rather the development of the code itself. The objective is to develop codes that are user-oriented, easily-modified, and well-documented. Well-proven, state-of-the-art solution algorithms are being used. Code readability, documentation (both internal and external), and validation are being emphasized. This paper is a status report on the Proteus development effort. The analysis and solution procedure are described briefly, and the various features in the code are summarized. The results from some of the validation cases that have been run are presented for both the two- and three-dimensional codes. Author

N93-13400* National Aeronautics and Space Administration. Lewis Research Center, Cleveland, OH.

ONE-DIMENSIONAL TRANSIENT FINITE DIFFERENCE MODEL OF AN OPERATIONAL SALINITY GRADIENT SOLAR POND

MICHAEL C. HICKS and PETER GOLDING (Texas Univ., El Paso.) *In its* The Fourth Annual Thermal and Fluids Analysis Workshop p 207-219 1992

Avail: CASI HC A03/MF A03

This paper describes the modeling approach used to simulate the transient behavior of a salinity gradient solar pond. A system of finite difference equations are used to generate the time dependent temperature and salinity profiles within the pond. The stability of the pond, as determined by the capacity of the resulting salinity profile to suppress thermal convection within the primary gradient region of the pond, is continually monitored and when necessary adjustments are made to the thickness of the gradient zone. Results of the model are then compared to measurements taken during two representative seasonal periods at the University of Texas at El Paso's (UTEP's) research solar pond. Author

N93-13403* National Aeronautics and Space Administration. Lewis Research Center, Cleveland, OH.

A SINDA '85 NODAL HEAT TRANSFER RATE CALCULATION USER SUBROUTINE

DERRICK J. CHESTON *In its* The Fourth Annual Thermal and Fluids Analysis Workshop p 271-281 1992

Avail: CASI HC A03/MF A03

This paper describes a subroutine, GETQ, which was developed to compute the heat transfer rates through all conductors attached to a node within a SINDA '85 thermal submodel. The subroutine was written for version 2.3 of SINDA '85. Upon calling GETQ, the user supplies the submodel name and node number which the heat transfer rate computation is desired. The returned heat transfer rate values are broken down into linear, nonlinear, source and combined heat loads. Author

N93-14150* National Aeronautics and Space Administration. Lewis Research Center, Cleveland, OH.

CURRENT STATUS OF LIQUID SHEET RADIATOR RESEARCH

DONALD L. CHUBB, FREDERICK D. CALFO, and MATTHEW S. MCMASTER (Toledo Univ., OH.) 1993 15 p Proposed for presentation at the First International Conference on Aerospace Heat Exchanger Technology, Palo Alto, CA, 15-17 Feb. 1993;

sponsored by AIAA and ASME

(Contract RTOP 506-41-11)

(NASA-TM-105764; E-7181; NAS 1.15:105764) Avail: CASI HC A03/MF A01

Initial research on the external flow, low mass liquid sheet radiator (LSR), has been concentrated on understanding its fluid mechanics. The surface tension forces acting at the edges of the sheet produce a triangular planform for the radiating surface of width, W, and length, L. It has been experimentally verified that $(\exp L)/W$ agrees with the theoretical result, $L/W = (We/8)\exp 1/2$, where We is the Weber number. Instability can cause holes to form in regions of large curvature such as where the edge cylinders join the sheet of thickness, tau. The W/tau limit that will cause hole formation with subsequent destruction of the sheet has yet to be reached experimentally. Although experimental measurements of sheet emissivity have not yet been performed because of limited program scope, calculations of the emissivity and sheet lifetime is determined by evaporation losses were made for two silicon based oils; Dow Corning 705 and Me(sub 2). Emissivities greater than 0.75 are calculated for tau greater than or equal to 200 microns for both oils. Lifetimes for Me(sub 2) are much longer than lifetimes for 705. Therefore, Me(sub 2) is the more attractive working fluid for higher temperatures (T greater than or equal to 400 K). Author

N93-14758* National Aeronautics and Space Administration. Lewis Research Center, Cleveland, OH.

SUPERSONIC BOUNDARY-LAYER FLOW TURBULENCE MODELING

CHI-RONG WANG Mar. 1993 12 p Proposed for presentation at the International Conference on Near-Wall Turbulence Flows, Tempe, AZ, 15-18 Mar. 1993

(Contract RTOP 505-62-52)

(NASA-TM-105893; E-7360; NAS 1.15:105893) Avail: CASI HC A03/MF A01

Baldwin-Lomax and kappa-epsilon turbulence models were modified for use in Navier-Stokes numerical computations of Mach 2.9 supersonic turbulent boundary layer flows along compression ramps. The computational results of Reynolds shear stress profiles were compared with experimental data. The Baldwin-Lomax model was modified to account for the Reynolds shear stress amplification within the flow field. A hybrid kappa-epsilon model with viscous sublayer turbulence treatment was constructed to predict the Reynolds shear stress profiles within the entire flow field. These modified turbulence models were effective for the computations of the surface pressure and the skin friction factor variations along an 8 deg ramp surface. The hybrid kappa-epsilon model could improve the predictions of the Reynolds shear stress profile and the skin friction factor near the corner of a 16 deg ramp. Author

N93-14829* National Aeronautics and Space Administration. Lewis Research Center, Cleveland, OH.

SECOND ORDER CLOSURE MODELING OF TURBULENT BUOYANT WALL PLUMES

GANG ZHU (Wayne State Univ., Detroit, MI.), MING-CHIA LAI (Wayne State Univ., Detroit, MI.), and TSAN-HSING SHIH Dec. 1992 14 p

(Contract RTOP 505-62-21)

(NASA-TM-105956; E-7476; NAS 1.15:105956; ICOMP-92-23; CMOTT-92-11) Avail: CASI HC A03/MF A01

Non-intrusive measurements of scalar and momentum transport in turbulent wall plumes, using a combined technique of laser Doppler anemometry and laser-induced fluorescence, has shown some interesting features not present in the free jet or plumes. First, buoyancy-generation of turbulence is shown to be important throughout the flow field. Combined with low-Reynolds-number turbulence and near-wall effect, this may raise the anisotropic turbulence structure beyond the prediction of eddy-viscosity models. Second, the transverse scalar fluxes do not correspond only to the mean scalar gradients, as would be expected from gradient-diffusion modeling. Third, higher-order velocity-scalar correlations which describe turbulent transport phenomena could not be predicted using simple turbulence models. A second-order

closure simulation of turbulent adiabatic wall plumes, taking into account the recent progress in scalar transport, near-wall effect and buoyancy, is reported in the current study to compare with the non-intrusive measurements. In spite of the small velocity scale of the wall plumes, the results showed that low-Reynolds-number correction is not critically important to predict the adiabatic cases tested and cannot be applied beyond the maximum velocity location. The mean and turbulent velocity profiles are very closely predicted by the second-order closure models, but the scalar field is less satisfactory, with the scalar fluctuation level underpredicted. Strong intermittency of the low-Reynolds-number flow field is suspected of these discrepancies. The trends in second- and third-order velocity-scalar correlations, which describe turbulent transport phenomena, are also predicted in general, with the cross-streamwise correlations better than the streamwise one. Buoyancy terms modeling the pressure-correlation are shown to improve the prediction slightly. The effects of equilibrium time-scale ratio and boundary condition are also discussed. Author

N93-14885* National Aeronautics and Space Administration. Lewis Research Center, Cleveland, OH.

PRECONDITIONED CONJUGATE-GRADIENT METHODS FOR LOW-SPEED FLOW CALCULATIONS

KUMUD AJMANI, WING-FAI NG (Virginia Polytechnic Inst. and State Univ., Blacksburg.), and MENG-SING LIOU Jan. 1993 13 p Presented at the 31st Aerospace Sciences Meeting and Exhibit, Reno, NV, 11-14 Jan. 1993

(Contract RTOP 505-62-21)

(NASA-TM-105929; E-7438; NAS 1.15:105929) Avail: CASI HC A03/MF A01

An investigation is conducted into the viability of using a generalized Conjugate Gradient-like method as an iterative solver to obtain steady-state solutions of very low-speed fluid flow problems. Low-speed flow at Mach 0.1 over a backward-facing step is chosen as a representative test problem. The unsteady form of the two dimensional, compressible Navier-Stokes equations is integrated in time using discrete time-steps. The Navier-Stokes equations are cast in an implicit, upwind finite-volume, flux split formulation. The new iterative solver is used to solve a linear system of equations at each step of the time-integration. Preconditioning techniques are used with the new solver to enhance the stability and convergence rate of the solver and are found to be critical to the overall success of the solver. A study of various preconditioners reveals that a preconditioner based on the Lower-Upper Successive Symmetric Over-Relaxation iterative scheme is more efficient than a preconditioner based on Incomplete L-U factorizations of the iteration matrix. The performance of the new preconditioned solver is compared with a conventional Line Gauss-Seidel Relaxation (LGSR) solver. Overall speed-up factors of 28 (in terms of global time-steps required to converge to a steady-state solution) and 20 (in terms of total CPU time on one processor of a CRAY-YMP) are found in favor of the new preconditioned solver, when compared with the LGSR solver.

Author

N93-14914* National Aeronautics and Space Administration. Lewis Research Center, Cleveland, OH.

NUMERICAL STUDY OF MIXING OF TWO FLUIDS UNDER LOW GRAVITY

WALTER M. B. DUVAL Oct. 1992 45 p

(Contract RTOP 674-21-05)

(NASA-TM-105865; E-7326; NAS 1.15:105865) Avail: CASI HC A03/MF A01

The mixing characteristics of two fluids inside a cavity due to buoyancy driven flow fields for low gravity conditions is investigated via numerical experiments. The buoyancy driven flow, depending on the parametric region, stretches and deforms the material interface into a wave morphological pattern. The morphological pattern affects the resulting stratification thickness of the mixed region. Three basic mixing regimes occur: convective, diffusive, and chaotic. In the convective regime, an overturning motion occurs which gives rise to a stable wave formation. This wave oscillates and its decay leads to a stable stratification. Whereas, in the

diffusive regime, the length of the interface remains constant while mixing occurs. This limiting behavior is very important to materials processing in space, and it admits a closed form solution corresponding to vanishing convective terms which agrees with computational results. Finally, in the chaotic regime, the material interface continuously stretches and folds on itself similar to a horseshoe map. The length of stretch of the interface increases exponentially. Internal wavebreaking occurs for this case. This wavebreaking generates local turbulence, and provides an effective mechanism for mixing. Author

N93-15355* National Aeronautics and Space Administration. Lewis Research Center, Cleveland, OH.

USE OF SURFACE HEAT TRANSFER MEASUREMENTS AS A FLOW SEPARATION DIAGNOSTIC IN A TWO DIMENSIONAL REFLECTED OBLIQUE SHOCK/TURBULENT BOUNDARY LAYER INTERACTION

A. ROBERT PORRO and WARREN R. HINGST Jan. 1993 18 p Presented at the 31st Aerospace Sciences Meeting and Exhibit, Reno, NV, 11-14 Jan. 1993; sponsored by AIAA (Contract RTOP 505-62-52)

(NASA-TM-105981; E-7505; NAS 1.15:105981; AIAA PAPER 93-0775) Avail: CASI HC A03/MF A01

The feasibility of using streamwise surface heat transfer measurements to detect the presence of flow separation in a two-dimensional reflected oblique shock/turbulent boundary layer interaction is reported. Surface heat transfer and static pressure data are presented for attached and separated flows for a free stream nominal Mach number range of 2.5 to 3.5 and shock generator angles of 2 to 8 degrees. The static pressure data do show the characteristic triple inflection point distribution for the strongly separated flow cases. The corresponding surface heat transfer data show unique trends that correlate well with the static pressure determination of the extent of the separated flow region. For the incipient or weakly separated flow cases, the static pressure data do not exhibit the characteristic triple inflection point distribution. However, the same trends in the heat transfer data that are seen for the strongly separated flow cases are evident for the weakly separated flows. Hence, the heat transfer data can be used to determine the extent of weakly separated flows when the surface static pressure distributions often can not. Author

N93-15499* National Aeronautics and Space Administration. Lewis Research Center, Cleveland, OH.

ON THE NONLINEAR THREE DIMENSIONAL INSTABILITY OF STOKES LAYERS AND OTHER SHEAR LAYERS TO PAIRS OF OBLIQUE WAVES

XUESONG WU (Imperial Coll. of Science and Technology, London, England), SANG SOO LEE (Sverdrup Technology, Inc., Brook Park, OH.), and STEPHEN J. COWLEY (Cambridge Univ., England) Dec. 1992 51 p

(Contract RTOP 505-62-21)

(NASA-TM-105918; E-7410; ICOMP-92-20; NAS 1.15:105918)

Avail: CASI HC A04/MF A01

The nonlinear evolution of a pair of initially oblique waves in a high Reynolds Number Stokes layer is studied. Attention is focused on times when disturbances of amplitude epsilon have $O(\epsilon \exp(1/3)R)$ growth rates, where R is the Reynolds number. The development of a pair of oblique waves is then controlled by nonlinear critical-layer effects. Viscous effects are included by studying the distinguished scaling $\epsilon = O(R \exp(-1))$. This leads to a complicated modification of the kernel function in the integro-differential amplitude equation. When viscosity is not too large, solutions to the amplitude equation develop a finite-time singularity, indicating that an explosive growth can be introduced by nonlinear effects; we suggest that such explosive growth can lead to the bursts observed in experiments. Increasing the importance of viscosity generally delays the occurrence of the finite-time singularity, and sufficiently large viscosity may lead to the disturbance decaying exponentially. For the special case when the streamwise and spanwise wavenumbers are equal, the solution can evolve into a periodic oscillation. A link between the unsteady

critical-layer approach to high-Reynolds-number flow instability, and the wave vortex approach is identified. Author

N93-15585*# National Aeronautics and Space Administration. Lewis Research Center, Cleveland, OH.

TURBULENT FLUID MOTION IV-AVERAGES, REYNOLDS DECOMPOSITION, AND THE CLOSURE PROBLEM

ROBERT G. DEISSLER Sep. 1992 67 p

(Contract RTOP 505-90-53)

(NASA-TM-105822; E-7253; NAS 1.15:105822) Avail: CASI HC A04/MF A01

Ensemble, time, and space averages as applied to turbulent quantities are discussed, and pertinent properties of the averages are obtained. Those properties, together with Reynolds decomposition, are used to derive the averaged equations of motion and the one- and two-point moment or correlation equations. The terms in the various equations are interpreted. The closure problem of the averaged equations is discussed, and possible closure schemes are considered. Those schemes usually require an input of supplemental information unless the averaged equations are closed by calculating their terms by a numerical solution of the original unaveraged equations. The law of the wall for velocities and temperatures, the velocity- and temperature-defect laws, and the logarithmic laws for velocities and temperatures are derived. Various notions of randomness and their relation to turbulence are considered in light of ergodic theory. Author

N93-15792*# National Aeronautics and Space Administration. Lewis Research Center, Cleveland, OH.

CENTER FOR MODELING OF TURBULENCE AND TRANSITION (CMOTT): RESEARCH BRIEFS, 1992 Progress Reports, May 1991 - May 1992

WILLIAM W. LIOU, ed. and comp. Sep. 1992 190 p

(Contract RTOP 505-62-21)

(NASA-TM-105834; E-7274; NAS 1.15:105834; ICOMP-92-12; CMOTT-92-08) Avail: CASI HC A09/MF A02

The progress is reported of the Center for Modeling of Turbulence and Transition (CMOTT). The main objective of the CMOTT is to develop, validate and implement the turbulence and transition models for practical engineering flows. The flows of interest are three-dimensional, incompressible and compressible flows with chemical reaction. The research covers two-equation (e.g., k- ϵ) and algebraic Reynolds-stress models, second moment closure models, probability density function (pdf) models, Renormalization Group Theory (RNG), Large Eddy Simulation (LES) and Direct Numerical Simulation (DNS).

N93-15795*# National Aeronautics and Space Administration. Lewis Research Center, Cleveland, OH.

MODELING OF TURBULENCE AND TRANSITION

TSAN-HSING SHIH *In its Center for Modeling of Turbulence and Transition (CMOTT): Research Briefs, 1992 p 33-49 Sep. 1992*

Avail: CASI HC A03/MF A02

The first objective is to evaluate current two-equation and second order closure turbulence models using available direct numerical simulations and experiments, and to identify the models which represent the state of the art in turbulence modeling. The second objective is to study the near-wall behavior of turbulence, and to develop reliable models for an engineering calculation of turbulence and transition. The third objective is to develop a two-scale model for compressible turbulence. Author

N93-15796*# National Aeronautics and Space Administration. Lewis Research Center, Cleveland, OH.

TURBULENCE MODELING AND EXPERIMENTS

AAMIR SHABBIR *In its Center for Modeling of Turbulence and Transition (CMOTT): Research Briefs, 1992 p 51-66 Sep. 1992* Avail: CASI HC A03/MF A02

The best way of verifying turbulence is to do a direct comparison between the various terms and their models. The success of this approach depends upon the availability of the data for the exact correlations (both experimental and DNS). The other approach

involves numerically solving the differential equations and then comparing the results with the data. The results of such a computation will depend upon the accuracy of all the modeled terms and constants. Because of this it is sometimes difficult to find the cause of a poor performance by a model. However, such a calculation is still meaningful in other ways as it shows how a complete Reynolds stress model performs. Thirteen homogeneous flows are numerically computed using the second order closure models. We concentrate only on those models which use a linear (or quasi-linear) model for the rapid term. This, therefore, includes the Launder, Reece and Rodi (LRR) model; the isotropization of production (IP) model; and the Speziale, Sarkar, and Gatski (SSG) model. Which of the three models performs better is examined along with what are their weaknesses, if any. The other work reported deal with the experimental balances of the second moment equations for a buoyant plume. Despite the tremendous amount of activity toward the second order closure modeling of turbulence, very little experimental information is available about the budgets of the second moment equations. Part of the problem stems from our inability to measure the pressure correlations. However, if everything else appearing in these equations is known from the experiment, pressure correlations can be obtained as the closing terms. This is the closest we can come to in obtaining these terms from experiment, and despite the measurement errors which might be present in such balances, the resulting information will be extremely useful for the turbulence modelers. The purpose of this part of the work was to provide such balances of the Reynolds stress and heat flux equations for the buoyant plume. Author

N93-15797*# National Aeronautics and Space Administration. Lewis Research Center, Cleveland, OH.

MODELING OF TURBULENT SHEAR FLOWS

WILLIAM W. LIOU *In its Center for Modeling of Turbulence and Transition (CMOTT): Research Briefs, 1992 p 67-81 Sep. 1992* Avail: CASI HC A03/MF A02

The current progress is documented in the research and development of modeling techniques for turbulent shear flows. These include a two-scale model for compressible turbulent flows and a new energy transfer model. The former represents the status of the efforts to identify compressibility effects in turbulence. The energy transfer model refines a weakly nonlinear wave model developed earlier, which models directly the turbulent large structures. The objective of these activities is to develop second-order closures for compressible turbulent flows. Author

N93-15798*# National Aeronautics and Space Administration. Lewis Research Center, Cleveland, OH.

MODELING OF NEAR WALL TURBULENCE AND MODELING OF BYPASS TRANSITION

Z. YANG *In its Center for Modeling of Turbulence and Transition (CMOTT): Research Briefs, 1992 p 83-94 Sep. 1992*

Avail: CASI HC A03/MF A02

The objectives for this project are as follows: (1) Modeling of the near wall turbulence: We aim to develop a second order closure for the near wall turbulence. As a first step of this project, we try to develop a kappa-epsilon model for near wall turbulence. We require the resulting model to be able to handle both near wall turbulence and turbulent flows away from the wall, computationally robust, and applicable for complex flow situations, flow with separation, for example, and (2) Modeling of the bypass transition: We aim to develop a bypass transition model which contains the effect of intermittency. Thus, the model can be used for both the transitional boundary layers and the turbulent boundary layers. We require the resulting model to give a good prediction of momentum and heat transfer within the transitional boundary and a good prediction of the effect of freestream turbulence on transitional boundary layers. Author

N93-15799*# National Aeronautics and Space Administration. Lewis Research Center, Cleveland, OH.

TWO EQUATION MODELLING AND THE PSEUDO COMPRESSIBILITY TECHNIQUE

C. J. STEFFEN, JR. *In its Center for Modeling of Turbulence*

34 FLUID MECHANICS AND HEAT TRANSFER

and Transition (CMOTT): Research Briefs, 1992 p 95-100 Sep. 1992

Avail: CASI HC A02/MF A02

The primary objective of the Center for Modelling of Turbulence and Transition (CMOTT) is to further the understanding of turbulence theory for engineering applications. One important foundation is the establishment of a data base encompassing the multitude of existing models as well as newly proposed ideas. The research effort described is a precursor to an extended survey of two equation turbulence models in the presence of a separated shear layer. Recently, several authors have examined the performance of two equation models in the context of the backward facing step flow. Conflicting results, however, demand that further attention is necessary to properly understand the behavior and limitations of this popular technique, especially the low Reynolds number formulations. The objective is to validate an incompressible Navier Stokes code for use as a numerical test-bed. In turn, this code will be used for analyzing the performance of several two equation models. Author

N93-15801* # National Aeronautics and Space Administration. Lewis Research Center, Cleveland, OH.

BYPASS TRANSITION IN COMPRESSIBLE BOUNDARY LAYERS

J. J. VANDERVEGT *In its* Center for Modeling of Turbulence and Transition (CMOTT): Research Briefs, 1992 p 115-125 Sep. 1992

Avail: CASI HC A03/MF A02

Transition to turbulence in aerospace applications usually occurs in a strongly disturbed environment. For instance, the effects of free-stream turbulence, roughness and obstacles in the boundary layer strongly influence transition. Proper understanding of the mechanisms leading to transition is crucial in the design of aircraft wings and gas turbine blades, because lift, drag and heat transfer strongly depend on the state of the boundary layer, laminar or turbulent. Unfortunately, most of the transition research, both theoretical and experimental, has focused on natural transition. Many practical flows, however, defy any theoretical analysis and are extremely difficult to measure. Morkovin introduced in his review paper the concept of bypass transition as those forms of transition which bypass the known mechanisms of linear and non-linear transition theories and are currently not understood by experiments. In an effort to better understand the mechanisms leading to transition in a disturbed environment, experiments are conducted studying simpler cases, viz. the effects of free stream turbulence on transition on a flat plate. It turns out that these experiments are very difficult to conduct, because generation of free stream turbulence with sufficiently high fluctuation levels and reasonable homogeneity is non trivial. For a discussion see Morkovin. Serious problems also appear due to the fact that at high Reynolds numbers the boundary layers are very thin, especially in the nose region of the plate where the transition occurs, which makes the use of very small probes necessary. The effects of free-stream turbulence on transition are the subject of this research and are especially important in a gas turbine environment, where turbulence intensities are measured between 5 and 20 percent, Wang et al. Due to the fact that the Reynolds number for turbine blades is considerably lower than for aircraft wings, generally a larger portion of the blade will be in a laminar transitional state. The effects of large free stream turbulence in compressible boundary layers at Mach numbers are examined both in the subsonic and transonic regime using direct numerical simulations. The flow is computed over a flat plate and curved surface. while many applications operate in the transonic regime. Due the nature of their numerical scheme, a non-conservation formulation of the Navier-Stokes equations, it is a non-trivial extension to compute flow fields in the transonic regime. This project aims at better understanding the effects of large free-stream turbulence in compressible boundary layers at mach number both in the subsonic and transonic regime using direct numerical simulations. The present project aims at computing the flow over a flat plate and curved surface. This research will provide data which can be used to clarify mechanisms leading to transition in an environment with high free stream turbulence. This

information is useful for the development of turbulence models, which are of great importance for CFD applications, and are currently unreliable for more complex flows, such as transitional flows. Author

N93-16612* # National Aeronautics and Space Administration. Lewis Research Center, Cleveland, OH.

PHYSICAL VAPOR TRANSPORT OF MERCUROS CHLORIDE UNDER A NONLINEAR THERMAL PROFILE

CHRISTOPHE MENNETRIER, WALTER M. B. DUVAL, and NARSINGH B. SINGH (Westinghouse Science and Technology Center, Pittsburgh, PA.) Nov. 1992 18 p (Contract RTOP 674-21-05)

(NASA-TM-105920; E-7413; NAS 1.15:105920) Avail: CASI HC A03/MF A01

Our study investigates numerically the flow field characteristics during the growth of mercurous chloride (Hg_2Cl_2) crystals in a rectangular ampoule under terrestrial and microgravity conditions for a nonlinear thermal gradient. With a residual gas lighter than the nutrient, the solutal Grashof number is dominant. We observe that in tilted configurations, when solutal convection is dominant, the maximum transport rate occurs at approximately 40 percent. For the vertical configurations, we were able to obtain solutions only for the cases either below the critical Rayleigh numbers or the stabilized configurations. The total mass flux decreases exponentially with an increase of pressure of residual gas, but it increases following a power law with the temperature difference driving the transport. The nonlinear thermal gradient appears to destabilize the flow field when thermal convection is dominant for both vertical top-heated and bottom-heated configurations. However, when the solutal Grashof number is dominant, the density gradient resulting from the solutal gradient appears to stabilize the flow for the bottom-heated configuration. The flow field for the top-heated configuration is destabilized for high Grashof numbers. The microgravity environment provides a means for lowering convection. For gravity levels of $10(\exp -3) g(0)$ or less, the Stefan wind drives the flow, and no recirculating cell is predicted. Author

N93-16703* # National Aeronautics and Space Administration. Lewis Research Center, Cleveland, OH.

CRITICAL ASSESSMENT OF REYNOLDS STRESS TURBULENCE MODELS USING HOMOGENEOUS FLOWS

AAMIR SHABBIR and TSAN-HSING SHIH Dec. 1992 31 p Presented at the 31st Aerospace Sciences Meeting, Reno, NV, 11-14 Jan. 1993; sponsored by AIAA (Contract RTOP 505-62-21)

(NASA-TM-105954; ICOMP-92-24; E-7474; NAS 1.15:105954; CMOTT-92-12) Avail: CASI HC A03/MF A01

In modeling the rapid part of the pressure correlation term in the Reynolds stress transport equations, extensive use has been made of its exact properties which were first suggested by Rotta. These, for example, have been employed in obtaining the widely used Launder, Reece and Rodi (LRR) model. Some recent proposals have dropped one of these properties to obtain new models. We demonstrate, by computing some simple homogeneous flows, that doing so does not lead to any significant improvements over the LRR model and it is not the right direction in improving the performance of existing models. The reason for this, in our opinion, is that violation of one of the exact properties can not bring in any new physics into the model. We compute thirteen homogeneous flows using LRR (with a recalibrated rapid term constant), IP and SSG models. The flows computed include the flow through axisymmetric contraction; axisymmetric expansion; distortion by plane strain; and homogeneous shear flows with and without rotation. Results show that for most general representation for a model linear in the anisotropic tensor, performs either better or as good as the other two models of the same level. Author

N93-19969* # National Aeronautics and Space Administration. Lewis Research Center, Cleveland, OH.

THREE-DIMENSIONAL NAVIER-STOKES HEAT TRANSFER PREDICTIONS FOR TURBINE BLADE ROWS

ROBERT J. BOYLE and PAUL W. GIEL (Sverdrup Technology, Inc., Brook Park, OH.) Jul. 1992 16 p Presented at the 28th Joint Propulsion Conference and Exhibit, Nashville, TN, 6-8 Jul. 1992; sponsored by the AIAA, SAE, ASME, and ASEE Previously announced in IAA as A92-54003

(Contract RTOP 505-62-52)

(NASA-TM-105800; E-7230; NAS 1.15:105800; AIAA PAPER 92-3068) Avail: CASI HC A03/MF A01

Results are shown for a three-dimensional Navier-Stokes analysis of both the flow and the surface heat transfer for turbine applications. Heat transfer comparisons are made with the experimental shock-tunnel data of Dunn and Kim, and with the data of Blair for the rotor of the large scale rotating turbine. The analysis was done using the steady-state, three-dimensional, thin-layer Navier-Stokes code developed by Chima, which uses a multistage Runge-Kutta scheme with implicit residual smoothing. An algebraic mixing length turbulence model is used to calculate turbulent eddy viscosity. The variation in heat transfer due to variations in grid parameters is examined. The effects of rotation, tip clearance, and inlet boundary layer thickness variation on the predicted blade and endwall heat transfer are examined. Author

N93-20057*# National Aeronautics and Space Administration. Lewis Research Center, Cleveland, OH.

NUMERICAL SIMULATION OF A HIGH MACH NUMBER JET FLOW

M. EHTESHAM HAYDER, ELI TURKEL, and REDA R. MANKBADI Jan. 1993 17 p Presented at the 31st Aerospace Sciences Meeting and Exhibit, Reno, NV, 11-14 Jan. 1993; sponsored by AIAA

(Contract RTOP 505-62-21)

(NASA-TM-105985; E-7509; NAS 1.15:105985; AIAA PAPER 93-0653; ICOMP-92-26) Avail: CASI HC A03/MF A01

The recent efforts to develop accurate numerical schemes for transition and turbulent flows are motivated, among other factors, by the need for accurate prediction of flow noise. The success of developing high speed civil transport plane (HSCT) is contingent upon our understanding and suppression of the jet exhaust noise. The radiated sound can be directly obtained by solving the full (time-dependent) compressible Navier-Stokes equations. However, this requires computational storage that is beyond currently available machines. This difficulty can be overcome by limiting the solution domain to the near field where the jet is nonlinear and then use acoustic analogy (e.g., Lighthill) to relate the far-field noise to the near-field sources. The later requires obtaining the time-dependent flow field. The other difficulty in aeroacoustics computations is that at high Reynolds numbers the turbulent flow has a large range of scales. Direct numerical simulations (DNS) cannot obtain all the scales of motion at high Reynolds number of technological interest. However, it is believed that the large scale structure is more efficient than the small-scale structure in radiating noise. Thus, one can model the small scales and calculate the acoustically active scales. The large scale structure in the noise-producing initial region of the jet can be viewed as a wavelike nature, the net radiated sound is the net cancellation after integration over space. As such, aeroacoustics computations are highly sensitive to errors in computing the sound sources. It is therefore essential to use a high-order numerical scheme to predict the flow field. The present paper presents the first step in an ongoing effort to predict jet noise. The emphasis here is in accurate prediction of the unsteady flow field. We solve the full time-dependent Navier-Stokes equations by a high order finite difference method. Time accurate spatial simulations of both plane and axisymmetric jet are presented. Jet Mach numbers of 1.5 and 2.1 are considered. Reynolds number in the simulations was about a million. Our numerical model is based on the 2-4 scheme by Gottlieb & Turkel. Bayliss et al. applied the 2-4 scheme in boundary layer computations. This scheme was also used by Ragab and Sheen to study the nonlinear development of supersonic instability waves in a mixing layer. In this study, we present two dimensional direct simulation results for both plane and axisymmetric jets. These results are compared with linear theory

predictions. These computations were made for near nozzle exit region and velocity in spanwise/azimuthal direction was assumed to be zero.

Author

N93-21198*# National Aeronautics and Space Administration. Lewis Research Center, Cleveland, OH.

ON THE STRUCTURE OF GASEOUS CONFINED LAMINAR DIFFUSION FLAMES: NUMERICAL INVESTIGATION

M. A. MAWID, D. L. BULZAN, and S. K. AGGARWAL (Illinois Univ., Chicago.) Feb. 1993 25 p

(Contract RTOP 505-62-21)

(NASA-TM-106039; E-7613; NAS 1.15:106039; ICOMP-93-3)

Avail: CASI HC A03/MF A01

The structure and characteristics of gaseous confined laminar diffusion flames are investigated by numerically solving the time-dependent two-dimensional axisymmetric conservation equations. The numerical model accounts for the important chemical and physical processes involved, including axial diffusion, viscous effects, radial convection, and finite-rate chemistry. The numerical results clearly show that the flame has a finite thickness and leakage of fuel vapor into the flame zone is possible. The effect of heat release is found to induce some radial flow. Predicted flame shape and dimensions are compared to the classical Burke-Schumann flame. The numerically calculated flame is observed to be about 15 percent taller and 5 percent narrower than that of the Burke-Schumann solution under the same conditions.

Author

N93-22596*# National Aeronautics and Space Administration. Lewis Research Center, Cleveland, OH.

STRUCTURE OF CONFINED LAMINAR SPRAY DIFFUSION FLAMES: NUMERICAL INVESTIGATION

M. A. MAWID, D. L. BULZAN, and S. K. AGGARWAL (Illinois Univ., Chicago.) Feb. 1993 29 p

(Contract RTOP 505-62-21)

(NASA-TM-106038; ICOMP-93-2; E-7193; NAS 1.15:106038)

Avail: CASI HC A03/MF A01

The structure of confined laminar spray diffusion flames is investigated numerically by solving the gas-phase conservation equations for mass species, continuity, momentum, and energy and the liquid-phase equations for droplet position, velocity, size, and temperature. A one-step global reaction scheme along with six equilibrium reactions are employed to model the flame chemistry. Monodisperse as well as polydisperse sprays are considered. The numerical results demonstrate that liquid spray flames substantially differ from gaseous flames in their structure, i.e., temperature, concentration, and velocity fields, shape, and dimensions under the same conditions. Spray flames are predicted to be taller and narrower than their counterpart gaseous ones and their shapes are almost cylindrical. This is in agreement with experimental observations. The numerical computations also show that the use of the equilibrium reactions with the one-step reaction scheme decreases the flame temperature compared to the one-step reaction scheme without the equilibrium reactions and more importantly increases the surface area of the flame zone due to a phenomenon termed 'equilibrium broadening.' The spray flames also possess a finite thickness with minimal overlap of the fuel and oxygen species. A case for which a fuel-mixture consisting of 20 to 80 percent gas-liquid by mass is introduced into the combustor is also investigated and compared with predictions using only gaseous or liquid fuel.

Author (revised)

N93-23059*# National Aeronautics and Space Administration. Lewis Research Center, Cleveland, OH.

SUMMARY OF EXPERIMENTAL HEAT-TRANSFER RESULTS FROM THE TURBINE HOT SECTION FACILITY

HERBERT J. GLADDEN and FREDRICK C. YEH Apr. 1993 216 p

(Contract RTOP 505-62-52)

(NASA-TP-3250; E-6615; NAS 1.60:3250) Avail: CASI HC A10/MF A03

Experimental data from the turbine Hot Section Facility are presented and discussed. These data include full-coverage

film-cooled airfoil results as well as special instrumentation results obtained at simulated real engine conditions. Local measurements of airfoil wall temperature, airfoil gas-path static-pressure distribution, and local heat-transfer coefficient distributions are presented and discussed. In addition, measured gas and coolant temperatures and pressures are presented. These data are also compared with analyses from Euler and boundary-layer codes.

Author

N93-23404* # National Aeronautics and Space Administration. Lewis Research Center, Cleveland, OH.

TRANSIENT LIQUID-CRYSTAL TECHNIQUE USED TO PRODUCE HIGH-RESOLUTION CONVECTIVE HEAT-TRANSFER-COEFFICIENT MAPS

STEVEN A. HIPPENSTEELE and PHILIP E. POINSATTE Aug. 1993 11 p Proposed for presentation at the 1993 National Heat Transfer Conference, Atlanta, GA, 8-11 Aug. 1993; sponsored by ASME

(Contract RTOP 505-62-52)

(NASA-TM-106083; E-7702; NAS 1.15:106083) Avail: CASI HC A03/MF A01

In this transient technique the preheated isothermal model wall simulates the classic one-dimensional, semi-infinite wall heat transfer conduction problem. By knowing the temperature of the air flowing through the model, the initial temperature of the model wall, and the surface cooling rate measured at any location with time (using the fast-response liquid-crystal patterns recorded on video tape), the heat transfer coefficient can be calculated for the color isothermal pattern produced. Although the test was run transiently, the heat transfer coefficients are for the steady-state case. The upstream thermal boundary condition was considered to be isothermal. This transient liquid-crystal heat-transfer technique was used in a transient air tunnel in which a square-inlet, 3-to-1 exit transition duct was placed. The duct was preheated prior to allowing room temperature air to be suddenly drawn through it. The resulting isothermal contours on the duct surfaces were revealed using a surface coating of thermochromic liquid crystals that display distinctive colors at particular temperatures. A video record was made of the temperature and time data for all points on the duct surfaces during each test. The duct surfaces were uniformly heated using two heating systems: the first was an automatic temperature-controlled heater blanket completely surrounding the test duct like an oven, and the second was an internal hot-air loop through the inside of the test duct. The hot-air loop path was confined inside the test duct by insulated heat dams located at the inlet and exit ends of the test duct. A recirculating fan moved hot air into the duct inlet, through the duct, out of the duct exit, through the oven, and back to the duct inlet. The temperature nonuniformity of the test duct model wall was held very small. Test results are reported for two inlet Reynolds numbers of 200,000 and 1,150,000 (based on the square-inlet hydraulic diameter) and two free-stream turbulence intensities of about 1 percent, which is typical of wind tunnels, and up to 20 percent (using a grid), which is typical of real engine conditions.

Author (revised)

N93-23736* # National Aeronautics and Space Administration. Lewis Research Center, Cleveland, OH.

A MULTIPLE-SCALE MODEL FOR COMPRESSIBLE TURBULENT FLOWS

WILLIAM W. LIOU and TSAN-HSING SHIH Mar. 1993 23 p (Contract NCC3-233; RTOP 505-90-5K) (NASA-TM-106072; ICOMP-93-07; CMOTT-93-02; E-7679; NAS 1.15:106072) Avail: CASI HC A03/MF A01

A multiple-scale model for compressible turbulent flows is proposed. It is assumed that turbulent eddy shocklets are formed primarily by the 'collisions' of large energetic eddies. The extra straining of the large eddy, due to their interactions with shocklets, enhances the energy cascade to smaller eddies. Model transport equations are developed for the turbulent kinetic energies and the energy transfer rates of the different scale. The turbulent eddy viscosity is determined by the total turbulent kinetic energy and the rate of energy transfer from the large scale to the small scale,

which is different from the energy dissipation rate. The model coefficients in the modeled turbulent transport equations depend on the ratio of the turbulent kinetic energy of the large scale to that of the small scale, which renders the model more adaptive to the characteristics of individual flow. The model is tested against compressible free shear layers. The results agree satisfactorily with measurements.

Author (revised)

N93-23744* # National Aeronautics and Space Administration. Lewis Research Center, Cleveland, OH.

SPRAY COMBUSTION EXPERIMENTS AND NUMERICAL PREDICTIONS

EDWARD J. MULARZ, DANIEL L. BULZAN, and KUO-HUEY CHEN (Toledo Univ., OH.) 1993 23 p Proposed for presentation at the AGARD Symposium on Fuels and Combustion Technology for Advanced Gas Turbine Engines, Rome, Italy, Spring 1993; sponsored by the Advisory Group for Aerospace Research and Development Original contains color illustrations (Contract DA PROJ. 1L1-61102-AH-45)

(NASA-TM-106069; E-7647; NAS 1.15:106069; ARL-MR-69; AD-A267594) Avail: CASI HC A03/MF A01; 2 functional color pages

The next generation of commercial aircraft will include turbofan engines with performance significantly better than those in the current fleet. Control of particulate and gaseous emissions will also be an integral part of the engine design criteria. These performance and emission requirements present a technical challenge for the combustor: control of the fuel and air mixing and control of the local stoichiometry will have to be maintained much more rigorously than with combustors in current production. A better understanding of the flow physics of liquid fuel spray combustion is necessary. This paper describes recent experiments on spray combustion where detailed measurements of the spray characteristics were made, including local drop-size distributions and velocities. Also, an advanced combustor CFD code has been under development and predictions from this code are compared with experimental results. Studies such as these will provide information to the advanced combustor designer on fuel spray quality and mixing effectiveness. Validation of new fast, robust, and efficient CFD codes will also enable the combustor designer to use them as additional design tools for optimization of combustor concepts for the next generation of aircraft engines.

Author

N93-24759* # National Aeronautics and Space Administration. Lewis Research Center, Cleveland, OH.

A THREE-DIMENSIONAL ALGEBRAIC GRID GENERATION SCHEME FOR GAS TURBINE COMBUSTORS WITH INCLINED SLOTS Final Report

S. L. YANG, M. C. CLINE (Los Alamos National Lab., NM.), R. CHEN, and Y. L. CHANG Mar. 1993 25 p

(Contract NAG3-1109; RTOP 537-02-20)

(NASA-CR-191095; E-7674; NAS 1.26:191095) Avail: CASI HC A03/MF A01

A 3D algebraic grid generation scheme is presented for generating the grid points inside gas turbine combustors with inclined slots. The scheme is based on the 2D transfinite interpolation method. Since the scheme is a 2D approach, it is very efficient and can easily be extended to gas turbine combustors with either dilution hole or slot configurations. To demonstrate the feasibility and the usefulness of the technique, a numerical study of the quick-quench/lean-combustion (QQ/LC) zones of a staged turbine combustor is given. Preliminary results illustrate some of the major features of the flow and temperature fields in the QQ/LC zones. Formation of co- and counter-rotating bulk flow and shape temperature fields can be observed clearly, and the resulting patterns are consistent with experimental observations typical of the confined slanted jet-in-cross flow. Numerical solutions show the method to be an efficient and reliable tool for generating computational grids for analyzing gas turbine combustors with slanted slots.

Author

N93-25175*# National Aeronautics and Space Administration. Lewis Research Center, Cleveland, OH.

NONLINEAR EVOLUTION OF THE FIRST MODE SUPERSONIC OBLIQUE WAVES IN COMPRESSIBLE BOUNDARY LAYERS.

PART 1: HEATED/COOLED WALLS

J. S. B. GAJJAR (Manchester Univ., England.) Mar. 1993 32 p (Contract NCC3-233; RTOP 505-62-21)

(NASA-TM-106087; ICOMP-93-08; E-7718; NAS 1.15:106087)

Avail: CASI HC A03/MF A01

The nonlinear stability of an oblique mode propagating in a two-dimensional compressible boundary layer is considered under the long wave-length approximation. The growth rate of the wave is assumed to be small so that the concept of unsteady nonlinear critical layers can be used. It is shown that the spatial/temporal evolution of the mode is governed by a pair of coupled unsteady nonlinear equations for the disturbance vorticity and density. Expressions for the linear growth rate show clearly the effects of wall heating and cooling and in particular how heating destabilizes the boundary layer for these long wavelength inviscid modes at $O(1)$ Mach numbers. A generalized expression for the linear growth rate is obtained and is shown to compare very well for a range of frequencies and wave-angles at moderate Mach numbers with full numerical solutions of the linear stability problem. The numerical solution of the nonlinear unsteady critical layer problem using a novel method based on Fourier decomposition and Chebychev collocation is discussed and some results are presented.

Author (revised)

N93-26203*# National Aeronautics and Space Administration. Lewis Research Center, Cleveland, OH.

AN EXTENDED LAGRANGIAN METHOD

MENG-SING LIOU May 1992 28 p

(Contract RTOP 505-62-52)

(NASA-TM-106129; E-7798; NAS 1.15:106129) Avail: CASI HC A03/MF A01

A unique formulation of describing fluid motion is presented. The method, referred to as 'extended Lagrangian method', is interesting from both theoretical and numerical points of view. The formulation offers accuracy in numerical solution by avoiding numerical diffusion resulting from mixing of fluxes in the Eulerian description. Meanwhile, it also avoids the inaccuracy incurred due to geometry and variable interpolations used by the previous Lagrangian methods. Unlike the Lagrangian method previously imposed which is valid only for supersonic flows, the present method is general and capable of treating subsonic flows as well as supersonic flows. The method proposed in this paper is robust and stable. It automatically adapts to flow features without resorting to clustering, thereby maintaining rather uniform grid spacing throughout and large time step. Moreover, the method is shown to resolve multi-dimensional discontinuities with a high level of accuracy, similar to that found in one-dimensional problems.

Author

N93-26554*# National Aeronautics and Space Administration. Lewis Research Center, Cleveland, OH.

INCOMPRESSIBLE SPECTRAL-ELEMENT METHOD: DERIVATION OF EQUATIONS

RUSSELL G. DEANNA Apr. 1993 88 p

(Contract DA PROJ. 1L1-61102-AH-45; RTOP 505-62-0K)

(NASA-TM-106109; E-7758; NAS 1.15:106109;

AVSCOM-TR-92-C-022; AD-A266374) Avail: CASI HC A05/MF A01

A fractional-step splitting scheme breaks the full Navier-Stokes equations into explicit and implicit portions amenable to the calculus of variations. Beginning with the functional forms of the Poisson and Helmholtz equations, we substitute finite expansion series for the dependent variables and derive the matrix equations for the unknown expansion coefficients. This method employs a new splitting scheme which differs from conventional three-step (nonlinear, pressure, viscous) schemes. The nonlinear step appears in the conventional, explicit manner, the difference occurs in the pressure step. Instead of solving for the pressure gradient using the nonlinear velocity, we add the viscous portion of the

Navier-Stokes equation from the previous time step to the velocity before solving for the pressure gradient. By combining this 'predicted' pressure gradient with the nonlinear velocity in an explicit term, and the Crank-Nicholson method for the viscous terms, we develop a Helmholtz equation for the final velocity.

Author (revised)

N93-26929*# National Aeronautics and Space Administration. Lewis Research Center, Cleveland, OH.

NTR PLUME MODELING

D. BYERS, C.-H. CHUNG, and ROBERT M. STUBBS *In its* Nuclear Propulsion Technical Interchange Meeting, Volume 1 p 453-460 1993

Avail: CASI HC A02/MF A04

Viewgraphs on nuclear thermal propulsion are presented. Topics covered include computational fluid dynamics (CFD) for plume analysis; molecular fluid dynamics; molecular CFD characteristics; direct-simulation Monte-Carlo (DSMC) method; integration of DSMC and Navier-Stokes computations; and density profiles. CASI

N93-26930*# National Aeronautics and Space Administration. Lewis Research Center, Cleveland, OH.

COMPUTATIONAL FLUID DYNAMICS FOR NUCLEAR THERMAL PROPULSION

ROBERT M. STUBBS and SUK C. KIM *In its* Nuclear Propulsion Technical Interchange Meeting, Volume 1 p 461-469 1993

Avail: CASI HC A02/MF A04

Viewgraphs on computational fluid dynamics (CFD) for nuclear thermal propulsion are presented. Topics covered include: hydrogen mass fraction as a function of chamber temperature; specific enthalpy of hydrogen and mole fraction of hydrogen as a function of chamber pressure; and specific impulse as a function of chamber pressure. Wall configurations of several nozzles are shown.

CASI

N93-27010*# National Aeronautics and Space Administration. Lewis Research Center, Cleveland, OH.

REMARKS ON TURBULENT CONSTITUTIVE RELATIONS

TSAN-HSING SHIH and JOHN L. LUMLEY (Cornell Univ., Ithaca, NY.) May 1993 12 p

(Contract NCC3-233; RTOP 505-90-5X)

(NASA-TM-106116; E-7770; NAS 1.15:106116; ICOMP-93-12;

CMOTT-93-6) Avail: CASI HC A03/MF A01

The paper demonstrates that the concept of turbulent constitutive relations can be used to construct general models for various turbulent correlations. Some of the Generalized Cayley-Hamilton formulas for relating tensor products of higher extension to tensor products of lower extension are introduced. The combination of dimensional analysis and invariant theory can lead to 'turbulent constitutive relations' (or general turbulence models) for, in principle, any turbulent correlations. As examples, the constitutive relations for Reynolds stresses and scalar fluxes are derived. The results are consistent with ones from Renormalization Group (RNG) theory and two-scale Direct-Interaction Approximation (DIA) method, but with a more general form.

Author (revised)

N93-27020*# National Aeronautics and Space Administration. Lewis Research Center, Cleveland, OH.

INCREASED HEAT TRANSFER TO ELLIPTICAL LEADING EDGES DUE TO SPANWISE VARIATIONS IN THE FREESTREAM MOMENTUM: NUMERICAL AND EXPERIMENTAL RESULTS

D. L. RIGBY (Sverdrup Technology, Inc., Brook Park, OH.) and G. J. VANFOSSEN Jul. 1992 13 p Presented at the 28th Joint Propulsion Conference and Exhibit, Nashville, TN, 6-8 Jul. 1992; sponsored by AIAA, SAE, ASME, and ASEE

(Contract RTOP 505-62-52)

(NASA-TM-106150; E-7835; NAS 1.15:106150; AIAA PAPER

92-3070) Avail: CASI HC A03/MF A01

A study of the effect of spanwise variation in momentum on leading edge heat transfer is discussed. Numerical and experimental results are presented for both a circular leading edge

and a 3:1 elliptical leading edge. Reynolds numbers in the range of 10,000 to 240,000 based on leading edge diameter are investigated. The surface of the body is held at a constant uniform temperature. Numerical and experimental results with and without spanwise variations are presented. Direct comparison of the two-dimensional results, that is, with no spanwise variations, to the analytical results of Frossling is very good. The numerical calculation, which uses the PARC3D code, solves the three-dimensional Navier-Stokes equations, assuming steady laminar flow on the leading edge region. Experimentally, increases in the spanwise-averaged heat transfer coefficient as high as 50 percent above the two-dimensional value were observed. Numerically, the heat transfer coefficient was seen to increase by as much as 25 percent. In general, under the same flow conditions, the circular leading edge produced a higher heat transfer rate than the elliptical leading edge. As a percentage of the respective two-dimensional values, the circular and elliptical leading edges showed similar sensitivity to spanwise variations in momentum. By equating the root mean square of the amplitude of the spanwise variation in momentum to the turbulence intensity, a qualitative comparison between the present work and turbulent results was possible. It is shown that increases in leading edge heat transfer due to spanwise variations in freestream momentum are comparable to those due to freestream turbulence. Author

N93-27091* # National Aeronautics and Space Administration. Lewis Research Center, Cleveland, OH.

POSITIVITY-PRESERVING NUMERICAL SCHEMES FOR MULTIDIMENSIONAL ADVECTION

B. P. LEONARD, M. K. MACVEAN (Meteorological Office, Bracknell, England.), and A. P. LOCK (Meteorological Office, Bracknell, England.) Mar. 1993 63 p
(Contract NCC3-233; RTOP 505-90-5K)
(NASA-TM-106055; ICOMP-93-05; E-7656; NAS 1.15:106055)
Avail: CASI HC A04/MF A01

This report describes the construction of an explicit, single time-step, conservative, finite-volume method for multidimensional advective flow, based on a uniformly third-order polynomial interpolation algorithm (UTOPIA). Particular attention is paid to the problem of flow-to-grid angle-dependent, anisotropic distortion typical of one-dimensional schemes used component-wise. The third-order multidimensional scheme automatically includes certain cross-difference terms that guarantee good isotropy (and stability). However, above first-order, polynomial-based advection schemes do not preserve positivity (the multidimensional analogue of monotonicity). For this reason, a multidimensional generalization of the first author's universal flux-limiter is sought. This is a very challenging problem. A simple flux-limiter can be found; but this introduces strong anisotropic distortion. A more sophisticated technique, limiting part of the flux and then restoring the isotropy-maintaining cross-terms afterwards, gives more satisfactory results. Test cases are confined to two dimensions; three-dimensional extensions are briefly discussed. Author

N93-27132* # National Aeronautics and Space Administration. Lewis Research Center, Cleveland, OH.

BRUSH SEAL LOW SURFACE SPEED HARD-RUB CHARACTERISTICS

ROBERT C. HENDRICKS, JULIE A. CARLILE, and ANITA D. LIANG Jun. 1993 14 p Presented at the 29th AIAA Joint Propulsion Conference and Exhibit, Monterey, CA, 28-30 Jun. 1993; sponsored by AIAA, SAE, ASME, and ASEE
(Contract RTOP 584-03-11)
(NASA-TM-106169; E-7868; NAS 1.15:106169; AIAA PAPER 93-2534) Avail: CASI HC A03/MF A01

The bristles of a 38.1-mm (1.5-in.) diameter brush seal were flexed by a tapered, 40-tooth rotor operating at 2600 rpm that provided sharp leading-edge impact of the bristles with hard rubbing of the rotor lands. Three separate tests were run with the same brush accumulating over 1.3×10^9 flexure cycles while deteriorating 0.2 mm (0.008 in.) radially. In each, the test bristle incursion depth varied from 0.130 to 0.025 mm (0.005 to 0.001 in.) or less (start to stop), and in the third test the rotor was set

0.25 mm (0.010 in.) eccentric. Runout varied from 0.025 to 0.076 mm (0.001 to 0.003 in.) radially. The bristles wore but did not pull out, fracture, or fragment. Bristle and rotor wear debris were deposited as very fine, nearly amorphous, highly porous materials at the rotor groove leading edges and within the rotor grooves. The land leading edges showed irregular wear and the beginning of a convergent groove that exhibited sharp, detailed wear at the land trailing edges. Surface grooving, burnishing, 'whipping,' and hot spots and streaks were found. With a smooth-plug rotor, post-test leakage increased 30 percent over pretest leakage.

Author (revised)

N93-27155* # National Aeronautics and Space Administration. Lewis Research Center, Cleveland, OH.

COMPARING THE RESULTS OF AN ANALYTICAL MODEL OF THE NO-VENT FILL PROCESS WITH NO-VENT FILL TEST RESULTS FOR A 4.96 CUBIC METERS (175 CUBIC FEET) TANK

WILLIAM J. TAYLOR and DAVID J. CHATO Feb. 1993 24 p
Presented at the 28th Joint Propulsion Conference and Exhibit, Nashville, TN, 6-8 Jul. 1992; sponsored by AIAA, SAE, ASME, and ASEE Previously announced in IAA as A92-54007
(Contract RTOP 506-48-00)
(NASA-TM-106018; E-7575; NAS 1.15:106018) Avail: CASI HC A03/MF A01

The NASA Lewis Research Center (NASA/LeRC) have been investigating a no-vent fill method for refilling cryogenic storage tanks in low gravity. Analytical modeling based on analyzing the heat transfer of a droplet has successfully represented the process in 0.034 m and 0.142 cubic m commercial dewars using liquid nitrogen and hydrogen. Recently a large tank (4.96 cubic m) was tested with hydrogen. This lightweight tank is representative of spacecraft construction. This paper presents efforts to model the large tank test data. The droplet heat transfer model is found to over predict the tank pressure level when compared to the large tank data. A new model based on equilibrium thermodynamics has been formulated. This new model is compared to the published large scale tank's test results as well as some additional test runs with the same equipment. The results are shown to match the test results within the measurement uncertainty of the test data except for the initial transient wall cooldown where it is conservative (i.e., overpredicts the initial pressure spike found in this time frame).

Author (revised)

N93-27161* # National Aeronautics and Space Administration. Lewis Research Center, Cleveland, OH.

CALCULATIONS OF TURBULENT SEPARATED FLOWS

J. ZHU and T. H. SHIH Aug. 1993 20 p Presented at the Second United States National Congress on Computational Mechanics, Washington, DC, 16-18 Aug. 1993; sponsored by The United States Association for Computational Mechanics
(Contract RTOP 505-90-5K)
(NASA-TM-106154; E-7838; NAS 1.15:106154; ICOMP-93-13; CMOTT-93-5) Avail: CASI HC A03/MF A01

A numerical study of incompressible turbulent separated flows is carried out by using two-equation turbulence models of the K-epsilon type. On the basis of realizability analysis, a new formulation of the eddy-viscosity is proposed which ensures the positiveness of turbulent normal stresses - a realizability condition that most existing two-equation turbulence models are unable to satisfy. The present model is applied to calculate two backward-facing step flows. Calculations with the standard K-epsilon model and a recently developed RNG-based K-epsilon model are also made for comparison. The calculations are performed with a finite-volume method. A second-order accurate differencing scheme and sufficiently fine grids are used to ensure the numerical accuracy of solutions. The calculated results are compared with the experimental data for both mean and turbulent quantities. The comparison shows that the present model performs quite well for separated flows.

Author (revised)

N93-27438*# National Aeronautics and Space Administration. Lewis Research Center, Cleveland, OH.

NUMERICAL MODELING OF RUNBACK WATER ON ICE PROTECTED AIRCRAFT SURFACES

KAMEL M. AL-KHALIL (National Academy of Sciences - National Research Council, Washington, DC.), THEO G. KEITH, JR. (Toledo Univ., OH.), and KENNETH J. DEWITT (Toledo Univ., OH.) *In* California State Univ., The Fifth Symposium on Numerical and Physical Aspects of Aerodynamic Flows 12 p 1992
 Avail: CASI HC A03/MF A04

A numerical simulation for 'running wet' aircraft anti-icing systems is developed. The model includes breakup of the water film, which exists in regions of direct impingement, into individual rivulets. The wetness factor distribution resulting from the film breakup and the rivulet configuration on the surface are predicted in the numerical solution procedure. The solid wall is modeled as a multilayer structure and the anti-icing system used is of the thermal type utilizing hot air and/or electrical heating elements embedded with the layers. Details of the calculation procedure and the methods used are presented. Author

N93-28252*# National Aeronautics and Space Administration. Lewis Research Center, Cleveland, OH.

MIXING AND TRANSIENT INTERFACE CONDENSATION OF A LIQUID HYDROGEN TANK

C. S. LIN (Analex Corp., Brook Park, OH.), M. M. HASAN, and T. W. NYLAND Jun. 1993 18 p Proposed for presentation at the 29th Joint Propulsion Conference and Exhibit, Monterey, CA, 28-30 Jun. 1993; sponsored by AIAA, SAE, ASME, and ASEE (Contract RTOP 506-42-73)
 (NASA-TM-106201; E-7910; NAS 1.15:106201; AIAA PAPER 93-1968) Avail: CASI HC A03/MF A01

Experiments were conducted to investigate the effect of axial jet-induced mixing on the pressure reduction of a thermally stratified liquid hydrogen tank. The tank was nearly cylindrical, having a volume of about 0.144 cu m with 0.559 m in diameter and 0.711 m long. A mixer/pump unit, which had a jet nozzle outlet of 0.0221 m in diameter was located 0.178 m from the tank bottom and was installed inside the tank to generate the axial jet mixing and tank fluid circulation. The liquid fill and jet flow rate ranged from 42 to 85 percent (by volume) and 0.409 to 2.43 cu m/hr, respectively. Mixing tests began with the tank pressure ranging from 187.5 to 238.5 kPa at which the thermal stratification results in 4.9 to 6.2 K liquid sub cooling. The mixing time and transient vapor condensation rate at the liquid-vapor interface are determined. Two mixing time correlations, based on the thermal equilibrium and pressure equilibrium, are developed. Both mixing time correlations are expressed as functions of system and buoyancy parameters and compared well with other experimental data. The steady state condensation rate correlation of Sonin et al. based on steam-water data is modified and expressed as a function of jet subcooling. The limited liquid hydrogen data of the present study shows that the modified steady state condensation rate correlation may be used to predict the transient condensation rate in a mixing process if the instantaneous values of jet sub cooling and turbulence intensity at the interface are employed. Author (revised)

N93-28626*# National Aeronautics and Space Administration. Lewis Research Center, Cleveland, OH.

A NEW FLUX CONSERVING NEWTON'S METHOD SCHEME FOR THE TWO-DIMENSIONAL, STEADY NAVIER-STOKES EQUATIONS

JAMES R. SCOTT and SIN-CHUNG CHANG Jun. 1993 47 p Sponsored by NASA, Washington
 (Contract RTOP 505-62-52)
 (NASA-TM-106160; E-7895; NAS 1.15:106160) Avail: CASI HC A03/MF A01

A new numerical method is developed for the solution of the two-dimensional, steady Navier-Stokes equations. The method that is presented differs in significant ways from the established numerical methods for solving the Navier-Stokes equations. The major differences are described. First, the focus of the present

method is on satisfying flux conservation in an integral formulation, rather than on simulating conservation laws in their differential form. Second, the present approach provides a unified treatment of the dependent variables and their unknown derivatives. All are treated as unknowns together to be solved for through simulating local and global flux conservation. Third, fluxes are balanced at cell interfaces without the use of interpolation or flux limiters. Fourth, flux conservation is achieved through the use of discrete regions known as conservation elements and solution elements. These elements are not the same as the standard control volumes used in the finite volume method. Fifth, the discrete approximation obtained on each solution element is a functional solution of both the integral and differential form of the Navier-Stokes equations. Finally, the method that is presented is a highly localized approach in which the coupling to nearby cells is only in one direction for each spatial coordinate, and involves only the immediately adjacent cells. A general third-order formulation for the steady, compressible Navier-Stokes equations is presented, and then a Newton's method scheme is developed for the solution of incompressible, low Reynolds number channel flow. It is shown that the Jacobian matrix is nearly block diagonal if the nonlinear system of discrete equations is arranged approximately and a proper pivoting strategy is used. Numerical results are presented for Reynolds numbers of 100, 1000, and 2000. Finally, it is shown that the present scheme can resolve the developing channel flow boundary layer using as few as six to ten cells per channel width, depending on the Reynolds number. Author (revised)

N93-28627*# National Aeronautics and Space Administration. Lewis Research Center, Cleveland, OH.

PRELIMINARY EXPERIMENTAL RESULTS FOR A CRYOGENIC BRUSH SEAL CONFIGURATION

J. A. CARLILE, R. C. HENDRICKS, R. I. HIBBS (Rockwell International Corp., Canoga Park, CA.), S. E. MCVEY (Rockwell International Corp., Canoga Park, CA.), and J. K. SCHARRER (Rockwell International Corp., Canoga Park, CA.) Jun. 1993 13 p Presented at the 29th AIAA Joint Propulsion Conference and Exhibit, Monterey, CA, 28-30 Jun. 1993; cosponsored by AIAA, SAE, ASME, and ASEE
 (Contract RTOP 584-03-11)
 (NASA-TM-106236; E-7952; NAS 1.15:106236; AIAA PAPER 93-2535) Avail: CASI HC A03/MF A01

Preliminary fluid nitrogen flow data are reported for a five-brush, ceramic-coated-rub-runner brush seal system, where the brushes and the rub runner were placed at each end of a centrally pressurized multifunction tester ('back-to-back' set of brushes) and tested at rotor speeds of 0, 10, 18, and 22.5 krpm. After testing, both the brushes and the ceramic-coated rub runner appeared pristine. The coating withstood both the thermomechanical and dynamic loadings with minor wear track scarring. The bristle tips showed some indication of material shearing (smearing) wear. The Ergun porous flow equation was applied to the brush seal data. The Ergun relation, which required heuristic information to characterize the coefficients, fit the gaseous data but was in poor agreement with the fluid results. The brush seal exit conditions were two phase. Two-phase, choked-flow design charts were applied but required one data point at each rotor speed to define the $(C_{sub} f)A \times \text{Constant}$ flow and area coefficients. Reasonable agreement between prediction and data was found, as expected, but such methods are not to be construed as two-phase-flow brush seal analyses. Author (revised)

N93-28947*# National Aeronautics and Space Administration. Lewis Research Center, Cleveland, OH.

THE DEVELOPMENT OF A MIXING LAYER UNDER THE ACTION OF WEAK STREAMWISE VORTICES

MARVIN E. GOLDSTEIN and JOSEPH MATHEW Mar. 1993 36 p
 (Contract NCC3-233; RTOP 505-62-21)
 (NASA-TM-106089; E-7724; NAS 1.15:106089; ICOMP-93-9)
 Avail: CASI HC A03/MF A01

The action of weak, streamwise vortices on a plane, incompressible, steady mixing layer is examined in the large

Reynolds-number limit. The outer, inviscid region is bounded by a vortex sheet to which the viscous region is confined. It is shown that the local linear analysis becomes invalid at streamwise distances $O(\epsilon \ln \epsilon)$, where ϵ is much less than 1 is the cross flow amplitude, and a new nonlinear analysis is constructed for this region. Numerical solutions of the nonlinear problem show that the vortex sheet undergoes an $O(1)$ change in position and that the solution is ultimately terminated by the appearance of a singularity. The corresponding viscous layer shows downstream thickening, but appears to remain well behaved up to the singular location. Author (revised)

N93-29075* # National Aeronautics and Space Administration. Lewis Research Center, Cleveland, OH.

APPLICATION OF RAY TRACING IN RADIATION HEAT TRANSFER

JOSEPH F. BAUMEISTER Aug. 1993 52 p Presented at the Computer Applications Symposium, Los Angeles, CA, 12 Mar. 1993, and the Thermal and Fluids Analysis Workshop, Cleveland, OH, 16-20 Aug. 1993; cosponsored by ASME and LMU (NASA-TM-106206; E-7915; NAS 1.15:106206) Avail: CASI HC A04/MF A01

This collection of presentation figures displays the capabilities of ray tracing for radiation propagation calculations as compared to an analytical approach. The goal is to introduce the terminology and solution process used in ray tracing, and provide insight into radiation heat transfer principles and analysis tools. A thermal analysis working environment is introduced that solves demanding radiation heat transfer problems based on ray tracing. This information may serve as a reference for designing and building ones own analysis environment. Author

N93-29157* # National Aeronautics and Space Administration. Lewis Research Center, Cleveland, OH.

HIGH REYNOLDS NUMBER AND TURBULENCE EFFECTS ON AERODYNAMICS AND HEAT TRANSFER IN A TURBINE CASCADE

FREDERICK C. YEH, STEVEN A. HIPPENSTEELE, G. JAMES VANFOSSEN, PHILIP E. POINSATTE, and ALI AMERI (Kansas Univ. Center for Research, Inc., Lawrence.) Jun. 1993 17 p Presented at the 29th Joint Propulsion Conference and Exhibit, Monterey, CA, 28-30 Jun. 1993; cosponsored by AIAA, SAE, ASME, and ASEE

(Contract RTOP 505-62-52) (NASA-TM-106187; E-7791; NAS 1.15:106187; AIAA PAPER 93-2252) Avail: CASI HC A03/MF A01

Experimental data on pressure distribution and heat transfer on a turbine airfoil were obtained over a range of Reynolds numbers from 0.75 to 7.5×10^6 and a range of turbulence intensities from 1.8 to about 15 percent. The purpose of this study was to obtain fundamental heat transfer and pressure distribution data over a wide range of high Reynolds numbers and to extend the heat transfer data base to include the range of Reynolds numbers encountered in the Space Shuttle main engine (SSME) turbopump turbines. Specifically, the study aimed to determine (1) the effect of Reynolds number on heat transfer, (2) the effect of upstream turbulence on heat transfer and pressure distribution, and (3) the relationship between heat transfer at high Reynolds numbers and the current data base. The results of this study indicated that Reynolds number and turbulence intensity have a large effect on both the transition from laminar to turbulent flow and the resulting heat transfer. For a given turbulence intensity, heat transfer for all Reynolds numbers at the leading edge can be correlated with the Frossling number developed for lower Reynolds numbers. For a given turbulence intensity, heat transfer for the airfoil surfaces downstream of the leading edge can be approximately correlated with a dimensionless parameter. Comparison of the experimental results were also made with a numerical solution from a two-dimensional Navier-Stokes code. Author (revised)

N93-29161* # National Aeronautics and Space Administration. Lewis Research Center, Cleveland, OH.

A NUMERICAL STUDY OF CONFINED TURBULENT JETS

J. ZHU and T.-H. SHIH Jun. 1993 27 p Prepared for the Winter Annual Meeting, New Orleans, LA, 28 Nov. - 3 Dec. 1993; sponsored by ASME (Contract RTOP 505-90-5K) (NASA-TM-106197; E-7906; NAS 1.26:106197; ICOMP-93-18; CMOTT-93-07) Avail: CASI HC A03/MF A01

A numerical investigation is reported of turbulent incompressible jets confined in two ducts, one cylindrical and the other conical with a 5 degree divergence. In each case, three Craya-Curtet numbers are considered which correspond, respectively, to flow situations with no moderate and strong recirculation. Turbulence closure is achieved by using the k-epsilon model and a recently proposed realizable Reynolds stress algebraic equation model that relates the Reynolds stresses explicitly to the quadratic terms of the mean velocity gradients and ensures the positiveness of each component of the turbulent kinetic energy. Calculations are carried out with a finite-volume procedure using boundary-fitted curvilinear coordinates. A second-order accurate, bounded convection scheme and sufficiently fine grids are used to prevent the solutions from being contaminated by numerical diffusion. The calculated results are compared extensively with the available experimental data. It is shown that the numerical methods presented are capable of capturing the essential flow features observed in the experiments and that the realizable Reynolds stress algebraic equation model performs much better than the k-epsilon model for this class of flows of great practical importance. Author (revised)

N93-29208* # National Aeronautics and Space Administration. Lewis Research Center, Cleveland, OH. Inst. for Computational Mechanics in Propulsion.

ACCURACY OF LEAST-SQUARES METHODS FOR THE NAVIER-STOKES EQUATIONS

PAVEL B. BOCHEV (Virginia Polytechnic Inst. and State Univ., Blacksburg.) and MAX D. GUNZBURGER Jun. 1993 22 p (Contract NCC3-233; RTOP 505-90-5K) (NASA-TM-106209; E-7919; ICOMP-93-19; NAS 1.15:106209) Avail: CASI HC A03/MF A01

Recently there has been substantial interest in least-squares finite element methods for velocity-vorticity-pressure formulations of the incompressible Navier-Stokes equations. The main cause for this interest is the fact that algorithms for the resulting discrete equations can be devised which require the solution of only symmetric, positive definite systems of algebraic equations. On the other hand, it is well-documented that methods using the vorticity as a primary variable often yield very poor approximations. Thus, here we study the accuracy of these methods through a series of computational experiments, and also comment on theoretical error estimates. It is found, despite the failure of standard methods for deriving error estimates, that computational evidence suggests that these methods are, at the least, nearly optimally accurate. Thus, in addition to the desirable matrix properties yielded by least-squares methods, one also obtains accurate approximations. Author (revised)

N93-31147* # National Aeronautics and Space Administration. Lewis Research Center, Cleveland, OH.

NUMERICAL SIMULATIONS OF THREE-DIMENSIONAL LAMINAR FLOW OVER A BACKWARD FACING STEP; FLOW NEAR SIDE WALLS

ERLENDUR STEINTHORSSON, MENG-SING LIOU, LOUIS A. POVINELLI, and ANDREA ARNONE Jul. 1993 10 p Presented at the 1993 ASME Fluids Engineering Division Summer Meeting Symposium on Separated Flows, Washington, DC, 20-24 Jun. 1993; sponsored by ASME (Contract NCC3-233; RTOP 505-90-5K) (NASA-TM-106248; ICOMP-93-21; E-7970; NAS 1.15:106248) Avail: CASI HC A02/MF A01

This paper reports the results of numerical simulations of steady, laminar flow over a backward-facing step. The governing equations used in the simulations are the full 'compressible' Navier-Stokes equations, solutions to which were computed by using a cell-centered, finite volume discretization. The convection terms of the governing equations were discretized by using the Advection

Upwind Splitting Method (AUSM), whereas the diffusion terms were discretized using central differencing formulas. The validity and accuracy of the numerical solutions were verified by comparing the results to existing experimental data for flow at identical Reynolds numbers in the same back step geometry. The paper focuses attention on the details of the flow field near the side wall of the geometry.

Author

N93-31647*# National Aeronautics and Space Administration. Lewis Research Center, Cleveland, OH.

MEASUREMENTS AND COMPUTATIONAL ANALYSIS OF HEAT TRANSFER AND FLOW IN A SIMULATED TURBINE BLADE INTERNAL COOLING PASSAGE

LOUIS M. RUSSELL, DOUGLAS R. THURMAN (Army Research Lab., Cleveland, OH.), PATRICIA S. SIMONYI (Sverdrup Technology, Inc., Brook Park, OH.), STEVEN A. HIPPENSTEELE, and PHILIP E. POINSATTE Jun. 1993 24 p Presented at the 29th Joint Propulsion Conference and Exhibit, Monterey, CA, 28-30 Jun. 1993; sponsored by AIAA, SAE, ASME, and ASEE Original contains color illustrations (Contract RTOP 505-62-52) (NASA-TM-106189; E-7894; NAS 1.15:106189; AIAA PAPER 93-1797; ARL-MR-91) Avail: CASI HC A03/MF A01; 5 functional color pages

Visual and quantitative information was obtained on heat transfer and flow in a branched-duct test section that had several significant features of an internal cooling passage of a turbine blade. The objective of this study was to generate a set of experimental data that could be used to validate computer codes for internal cooling systems. Surface heat transfer coefficients and entrance flow conditions were measured at entrance Reynolds numbers of 45,000, 335,000, and 726,000. The heat transfer data were obtained using an Inconel heater sheet attached to the surface and coated with liquid crystals. Visual and quantitative flow field results using particle image velocimetry were also obtained for a plane at mid channel height for a Reynolds number of 45,000. The flow was seeded with polystyrene particles and illuminated by a laser light sheet. Computational results were determined for the same configurations and at matching Reynolds numbers; these surface heat transfer coefficients and flow velocities were computed with a commercially available code. The experimental and computational results were compared. Although some general trends did agree, there were inconsistencies in the temperature patterns as well as in the numerical results. These inconsistencies strongly suggest the need for further computational studies on complicated geometries such as the one studied.

Author

N93-31860*# National Aeronautics and Space Administration. Lewis Research Center, Cleveland, OH.

HYPERSONIC ENGINE COMPONENT EXPERIMENTS IN HIGH HEAT FLUX, SUPERSONIC FLOW ENVIRONMENT

HERBERT J. GLADDEN and MATTHEW E. MELIS Jul. 1993 21 p Presented at the International Symposium on Optical Applied Science and Engineering, San Diego, CA, 11-16 Jul. 1993; sponsored by SPOIE (Contract RTOP 505-62-52) (NASA-TM-106273; E-8002; NAS 1.15:106273) Avail: CASI HC A03/MF A01

A major concern in advancing the state-of-the-art technologies for hypersonic vehicles is the development of an aeropropulsion system capable of withstanding the sustained high thermal loads expected during hypersonic flight. Even though progress has been made in the computational understanding of fluid dynamics and the physics/chemistry of high speed flight, there is also a need for experimental facilities capable of providing a high heat flux environment for testing component concepts and verifying/calibrating these analyses. A hydrogen/oxygen rocket engine heat source was developed at the NASA Lewis Research Center as one element in a series of facilities at national laboratories designed to fulfill this need. This 'Hot Gas Facility' is capable of providing heat fluxes up to 450 w/sq cm on flat surfaces and up to 5,000 w/sq cm at the leading edge stagnation point of a strut in a supersonic flow stream. Gas temperatures up to 3050

K can also be attained. Two recent experimental programs conducted in this facility are discussed. The objective of the first experiment is to evaluate the erosion and oxidation characteristics of a coating on a cowl leading edge (or strut leading edge) in a supersonic, high heat flux environment. Macrophotographic data from a coated leading edge model show progressive degradation over several thermal cycles at aerothermal conditions representative of high Mach number flight. The objective of the second experiment is to assess the capability of cooling a porous surface exposed to a high temperature, high velocity flow environment and to provide a heat transfer data base for a design procedure. Experimental results from transpiration cooled surfaces in a supersonic flow environment are presented.

Author (revised)

N93-32199*# National Aeronautics and Space Administration. Lewis Research Center, Cleveland, OH.

A RAPID-DISTORTION-THEORY TURBULENCE MODEL FOR DEVELOPED UNSTEADY WALL-BOUNDED FLOW

G. J. BRERETON (Michigan Univ., Ann Arbor.) and R. R. MANKBADI Jul. 1993 20 p (Contract NCC3-233; RTOP 505-90-5K) (NASA-TM-106249; ICOMP-93-22; E-7971; NAS 1.15:106249) Avail: CASI HC A03/MF A01

A new approach to turbulence modeling in unsteady developed flows has recently been introduced, based on results of rapid distortion theory. The approach involves closing the k-epsilon equations for the organized unsteady component of the flow by modeling local unsteadiness as a rapid distortion of the local structure of the parent turbulent flow, in terms of an effective strain parameter $\alpha(\text{sub eff})$. In this paper, the phase-conditioned equations of motion are developed to accommodate a new unsteady dissipation model and local effects of the slow-relaxation time scale of the parent flow. The model equations are tested against measurements of the response of a fully-developed turbulent pipe flow to the superposition of sinusoidal streamwise oscillation. Good agreement is found between measurements and predictions over a wide range of frequencies of unsteadiness, indicating that this approach may be particularly well suited to modeling of unsteady turbulent flows which are perturbations about a well characterized mean.

Author (revised)

N93-32370*# National Aeronautics and Space Administration. Lewis Research Center, Cleveland, OH.

A P-VERSION FINITE ELEMENT METHOD FOR STEADY INCOMPRESSIBLE FLUID FLOW AND CONVECTIVE HEAT TRANSFER

DANIEL L. WINTERSCHEIDT Jul. 1993 27 p (Contract NCC3-233; RTOP 505-90-5K) (NASA-TM-106260; ICOMP-93-23; E-7985; NAS 1.15:106260) Avail: CASI HC A03/MF A01

A new p-version finite element formulation for steady, incompressible fluid flow and convective heat transfer problems is presented. The steady-state residual equations are obtained by considering a limiting case of the least-squares formulation for the transient problem. The method circumvents the Babuska-Brezzi condition, permitting the use of equal-order interpolation for velocity and pressure, without requiring the use of arbitrary parameters. Numerical results are presented to demonstrate the accuracy and generality of the method.

Author

N93-70575*# National Aeronautics and Space Administration. Lewis Research Center, Cleveland, OH.

2ND NASA CFD VALIDATION WORKSHOP

1990 320 p Workshop held in Cleveland, OH, 10-12 Jul. 1990 (NASA-TM-107972; NAS 1.15:107972) Avail: CASI HC A14/MF A03

The purpose of the workshop was to review NASA's progress in CFD validation since the first workshop (held at Ames in 1987) and to affirm the future direction of the NASA CFD validation program. The first session consisted of overviews of CFD validation research at each of the three OMET research centers and at Marshall Space Flight Center. The second session consisted of

34 FLUID MECHANICS AND HEAT TRANSFER

in-depth technical presentations of the best examples of CFD validation work at each center (including Marshall). On the second day the workshop divided into three working groups to discuss CFD validation progress and needs in the subsonic, high-speed, and hypersonic speed ranges. The emphasis of the working groups was on propulsion.

N93-70579*# National Aeronautics and Space Administration. Lewis Research Center, Cleveland, OH.

SUMMARY OF NASA. LEWIS RESEARCH CENTER VALIDATION EFFORTS

RAYMOND E. GAUGLER *In its 2nd NASA CFD Validation Workshop p 100-125 1990*
Avail: CASI HC A03/MF A03

NASA Lewis Research Center personnel presented a summary of LeRC validation experiments. The subjects discussed included: iced wing, linear transonic cascade, transition duct aerodynamics, transition duct heat transfer, low speed centrifugal compressor, turbomachinery blade row interactions, and three dimensional fluid mechanics. P.N.F.

N93-70582*# National Aeronautics and Space Administration. Lewis Research Center, Cleveland, OH.

NASA. LEWIS RESEARCH CENTER/IFMD INLET DUCT AND NOZZLE HIGH SPEED VALIDATION EXPERIMENTS

WARREN HINGST *In its 2nd NASA CFD Validation Workshop p 197-231 1990*

Avail: CASI HC A03/MF A03

Personnel from NASA Lewis Research Center spoke on the subject of inlet duct and nozzle high speed validation experiments to include crossing shocks and boundary layer interaction, unsteady shock/boundary layer interactions, and vortex generators. Attention was also paid to the subjects of high speed mixing and transition ducts. Specific application was made to the NASP hypermixing concepts. P.N.F.

N93-70583*# National Aeronautics and Space Administration. Lewis Research Center, Cleveland, OH.

NASA LOW SPEED CENTRIFUGAL COMPRESSOR

MICHAEL D. HATHAWAY *In its 2nd NASA CFD Validation Workshop p 232-256 1990*

Avail: CASI HC A03/MF A03

The flow characteristics of a low speed centrifugal compressor were examined at NASA Lewis Research Center to improve understanding of the flow in centrifugal compressors, to provide models of various flow phenomena, and to acquire benchmark data for three dimensional viscous flow code validation. The paper describes the objectives, test facilities' instrumentation, and experiment preliminary comparisons. P.N.F.

35

INSTRUMENTATION AND PHOTOGRAPHY

Includes remote sensors; measuring instruments and gages; detectors; cameras and photographic supplies; and holography.

A93-13977* National Aeronautics and Space Administration. Lewis Research Center, Cleveland, OH.

A NEW HUE CAPTURING TECHNIQUE FOR THE QUANTITATIVE INTERPRETATION OF LIQUID CRYSTAL IMAGES USED IN CONVECTIVE HEAT TRANSFER STUDIES

C. CAMCI, K. KIM (Pennsylvania State Univ., University Park), and S. A. HIPPENSTEELE (NASA, Lewis Research Center, Cleveland, OH) *ASME, Transactions, Journal of Turbomachinery (ISSN 0889-504X) vol. 114, no. 4 Oct. 1992 p. 765-775. ASME, International Gas Turbine and Aeroengine Congress and Exposition, 36th, Orlando, FL, June 3-6, 1991, ASME Paper 91-GT-122 refs*

Copyright

A new image processing based color capturing technique for the quantitative interpretation of liquid crystal images used in convective heat transfer studies is presented. This method is highly applicable to the surfaces exposed to convective heating in gas turbine engines. It is shown that, in the single-crystal mode, many of the colors appearing on the heat transfer surface correlate strongly with the local temperature. A very accurate quantitative approach using an experimentally determined linear hue vs temperature relation is found to be possible. The new hue-capturing process is discussed in terms of the strength of the light source illuminating the heat transfer surface, the effect of the orientation of the illuminating source with respect to the surface, crystal layer uniformity, and the repeatability of the process. The present method is more advantageous than the multiple filter method because of its ability to generate many isotherms simultaneously from a single-crystal image at a high resolution in a very time-efficient manner. P.D.

A93-16419* National Aeronautics and Space Administration. Lewis Research Center, Cleveland, OH.

FABRICATION OF THIN FILM HEAT FLUX SENSORS

HERBERT WILL (NASA, Lewis Research Center, Cleveland, OH) *In Annual Health Monitoring Conference for Space Propulsion Systems, 3rd, Cincinnati, OH, Nov. 13, 14, 1991, Proceedings Cincinnati, OH University of Cincinnati 1991 p. 356-365. refs*

Copyright

Thin-film heat-flux sensors have been constructed in the form of arrays of thermocouples on upper and lower surfaces of an insulating layer, so that flux values are proportional to the temperature difference across the upper and lower surface of the insulation material. The sensor thermocouples are connected in thermopile arrangement, and the structure is patterned with photolithographic techniques. Both chromel-alumel and Pt-Pt/Rh thermocouples have been devised; the later produced 28 microvolts when exposed to the radiation of a 1000 C furnace. O.C.

A93-16421* National Aeronautics and Space Administration. Lewis Research Center, Cleveland, OH.

PALLADIUM-CHROMIUM STATIC STRAIN GAGE FOR HIGH TEMPERATURE PROPULSION SYSTEMS

JIH-FEN LEI (Sverdrup Technology, Inc.; NASA, Lewis Research Center, Cleveland, OH) *In Annual Health Monitoring Conference for Space Propulsion Systems, 3rd, Cincinnati, OH, Nov. 13, 14, 1991, Proceedings Cincinnati, OH University of Cincinnati 1991 p. 391-400. refs*

Copyright

The present electrical strain gage for high temperature static strain measurements is in its fine-wire and thin-film forms designed to be temperature-compensated on any substrate material. The gage element is of Pd-Cr alloy, while the compensator is of Pt. Because the thermally-induced apparent strain of this compensated wire strain gage is sufficiently small, with good reproducibility between thermal cycles to 800 C, output figures can be corrected within a reasonable margin of error. O.C.

A93-20454* National Aeronautics and Space Administration. Lewis Research Center, Cleveland, OH.

DESIGN OF AN AUTOMATED IMAGING SYSTEM FOR USE IN A SPACE EXPERIMENT

WILLIAM G. HARTZ, NORA G. BOZZOLO, CATHERINE C. LEWIS, and CHRISTOPHER J. PESTAK (Analex Corp., Cleveland, OH) *In CAN-AM Eastern '90; Proceedings of the 1st Canadian-American Eastern Regional Conference on Applications of Optical Engineering, Rochester, NY, Oct. 4, 5, 1990 Bellingham, WA Society of Photo-Optical Instrumentation Engineers 1991 p. 52-60.*

(Contract NAS3-24564)

Copyright

An experiment, occurring in an orbiting platform, examines the mass transfer across gas-liquid and liquid-liquid interfaces. It employs an imaging system with real time image analysis. The design includes optical design, imager selection and integration,

positioner control, image recording, software development for processing and interfaces to telemetry. It addresses the constraints of weight, volume, and electric power associated with placing the experiment in the Space Shuttle cargo bay. Challenging elements of the design are: imaging and recording of a 200-micron-diameter bubble with a resolution of 2 microns to serve a primary source of data; varying frame rates from 500 per second to 1 frame per second, depending on the experiment phase; and providing three-dimensional information to determine the shape of the bubble. Author

A93-20751* National Aeronautics and Space Administration. Lewis Research Center, Cleveland, OH.

APPLICATION OF NEURAL NETWORKS TO PREDICTION OF ADVANCED COMPOSITE STRUCTURES MECHANICAL RESPONSE AND BEHAVIOR

K. J. CLOS (NASA, Lewis Research Center; Ohio Aerospace Inst., Cleveland), A. VARY, L. BERKE, and H. E. KAUTZ (NASA, Lewis Research Center, Cleveland, OH) *Computing Systems in Engineering* (ISSN 0956-0521) vol. 3, no. 1-4 1992 p. 539-544. High-performance computing for flight vehicles; Proceedings of the Symposium, Washington, Dec. 7-9, 1992. A93-20701 06-61 refs Copyright

Two types of neural networks were used to evaluate acousto-ultrasonic (AU) data for material characterization and mechanical response prediction. The neural networks included a simple feedforward network (backpropagation) and a radial basis functions network. Comparisons of results in terms of accuracy and training time are given. Acousto-ultrasonic (AU) measurements were performed on a series of tensile specimens composed of eight laminated layers of continuous, SiC fiber reinforced Ti-15-3 matrix. The frequency spectrum was dominated by frequencies of longitudinal wave resonance through the thickness of the specimen at the sending transducer. The magnitude of the frequency spectrum of the AU signal was used for calculating a stress-wave factor based on integrating the spectral distribution function and used for comparison with neural networks results. Author

A93-20945* National Aeronautics and Space Administration. Lewis Research Center, Cleveland, OH.

HIERARCHICAL IMAGE CODING WITH DIAMOND-SHAPED SUB-BANDS

XIAOHUI LI, JIE WANG, PETER BAUER, and KEN SAUER (Notre Dame Univ., IN) *In Visual communications and image processing '92; Proceedings of the Meeting, Boston, MA, Nov. 18-20, 1992* Bellingham, WA Society of Photo-Optical Instrumentation Engineers 1992 p. 42-48. refs (Contract NAG3-1186) Copyright

We present a sub-band image coding/decoding system using a diamond-shaped pyramid frequency decomposition to more closely match visual sensitivities than conventional rectangular bands. Filter banks are composed of simple, low order IIR components. The coder is especially designed to function in a multiple resolution reconstruction setting, in situations such as variable capacity channels or receivers, where images must be reconstructed without the entire pyramid of sub-bands. We use a nonlinear interpolation technique for lost subbands to compensate for loss of aliasing cancellation. Author

A93-22309*# National Aeronautics and Space Administration. Lewis Research Center, Cleveland, OH.

NOVEL THIN-FILM HEAT FLUX SENSORS

HEMANSHU BHATT, MARY ZELLER, and HERBERT WILL (NASA, Lewis Research Center, Cleveland, OH) Dec. 1992 9 p. AIAA, International Aerospace Planes Conference, 4th, Orlando, FL, Dec. 1-4, 1992 refs (AIAA PAPER 92-5035) Copyright

A new and simpler design for thin-film heat flux sensors for utilization in high heat flux environments is presented. The design of these sensors consists of a planar differential thermopile made up of a number of thermocouple pairs arranged in a circular array,

two different thermal resistance layers deposited on the inside and outside junctions of the thermopile and a high emissivity coating. This design has shown good potential for measuring heat fluxes in severe environments of aerospace propulsion systems. R.E.P.

A93-22313*# National Aeronautics and Space Administration. Lewis Research Center, Cleveland, OH.

HIGH TEMPERATURE STATIC STRAIN MEASUREMENT WITH AN ELECTRICAL RESISTANCE STRAIN GAGE

JIH-FEN LEI (Sverdrup Technology, Inc.; NASA, Lewis Research Center, Cleveland, OH) Dec. 1992 9 p. AIAA, International Aerospace Planes Conference, 4th, Orlando, FL, Dec. 1-4, 1992 refs (AIAA PAPER 92-5039) Copyright

An electrical resistance strain gage that can supply accurate static strain measurement for NASP application is being developed both in thin film and fine wire forms. This gage is designed to compensate for temperature effects on substrate materials with a wide range of thermal expansion coefficients. Some experimental results of the wire gage tested on one of the NASP structure materials, i.e., titanium matrix composites, are presented. R.E.P.

A93-22314*# National Aeronautics and Space Administration. Lewis Research Center, Cleveland, OH.

STRAIN SENSING TECHNOLOGY FOR HIGH TEMPERATURE APPLICATIONS

W. D. WILLIAMS (NASA, Lewis Research Center, Cleveland, OH) Dec. 1992 12 p. AIAA, International Aerospace Planes Conference, 4th, Orlando, FL, Dec. 1-4, 1992 refs (AIAA PAPER 92-5040) Copyright

This review paper discusses the status of strain sensing technology for high temperature applications. Technologies covered are those supported by NASA such as required for applications in hypersonic vehicles and engines, advanced subsonic engines, as well as material and structure development. The applications may be at temperatures of 540 C (1000 F) to temperatures in excess of 1400 C (2500 F). The most promising technologies at present are the resistance strain gage and remote sensing schemes. Resistance strain gages discussed include the BCL gage, the LaRC compensated gage, and the PdCr gage. Remote sensing schemes such as laser based speckle strain measurement, phase-shifting interferometry and X-ray extensometry will be discussed. Present status and limitations of these technologies are presented. Author

A93-23259*# National Aeronautics and Space Administration. Lewis Research Center, Cleveland, OH.

MOLECULAR FILTER-BASED DIAGNOSTICS IN HIGH SPEED FLOWS

GREGORY S. ELLIOTT, MO SAMIMY, and STEPHEN A. ARNETTE (Ohio State Univ., Columbus) Jan. 1993 18 p. AIAA, Aerospace Sciences Meeting and Exhibit, 31st, Reno, NV, Jan. 11-14, 1993 refs

(Contract NAG3-764; AF-AFOSR-91-0412) (AIAA PAPER 93-0512) Copyright

The use of iodine molecular filters in nonintrusive planar velocimetry methods is examined. Detailed absorption profiles are obtained to highlight the effects that determine the profile shape. It is shown that pressure broadening induced by the presence of a nonabsorbing vapor can be utilized to significantly change the slopes bounding the absorbing region while remaining in the optically-thick regime. R.E.P.

A93-23260*# National Aeronautics and Space Administration. Lewis Research Center, Cleveland, OH.

AIR-MASS FLUX MEASUREMENT SYSTEM USING DOPPLER-SHIFTED FILTERED RAYLEIGH SCATTERING

JOHN A. SHIRLEY and MICHAEL WINTER (United Technologies Research Center, East Hartford, CT) Jan. 1993 10 p. AIAA, Aerospace Sciences Meeting and Exhibit, 31st, Reno, NV, Jan. 11-14, 1993 Research supported by NASA refs (AIAA PAPER 93-0513) Copyright

35 INSTRUMENTATION AND PHOTOGRAPHY

An optical system has been investigated to measure mass flux distributions in the inlet of a high speed air-breathing propulsion system. Rayleigh scattered light from air is proportional to the number density of molecules and hence can be used to ascertain the gas density in a calibrated system. Velocity field measurements are achieved by spectrally filtering the elastically-scattered Doppler-shifted light with an absorbing molecular filter. A novel anamorphic optical collection system is used which allows optical rays from different scattering angles, that have different Doppler shifts, to be recorded separately. This is shown to obviate the need to tune the laser through the absorption to determine velocities, while retaining the ability to make spatially-resolved measurements along a line. By properly selecting the laser tuning and filter parameters, simultaneous density measurements can be made. These properties are discussed in the paper and experiments demonstrating the velocimetry capability are described. Author

A93-23776* National Aeronautics and Space Administration. Lewis Research Center, Cleveland, OH.
LASER ANEMOMETRY - ADVANCES AND APPLICATIONS 1991; PROCEEDINGS OF THE 4TH INTERNATIONAL CONFERENCE, CLEVELAND, OH, AUG. 5-9, 1991. VOLS. 1 & 2
ALEXANDER DYBBS, ED. (Case Western Reserve Univ., Cleveland, OH) and BAHMAN GHORASHI, ED. (Cleveland State Univ., OH) New York American Society of Mechanical Engineers 1991 p. Vol. 1, 409 p.; vol. 2, 453 p. (ISBN 0-7918-0654-5) Copyright

The papers presented in this volume provide an overview of the latest advances in laser anemometry and optical flow diagnostics. Topics discussed include turbulence, jets, and chaos; novel optical techniques for velocity measurements; chemical reactions and combustor flows; and LDA/CFD interface. Attention is also given to particle image velocimetry, high speed flows and aerodynamic flows, internal flows, particle sizing, optics and signal processing, two-phase flows, and general fluid mechanics applications. (For individual items see A93-23777 to A93-23837) V.L.

A93-23783* National Aeronautics and Space Administration. Lewis Research Center, Cleveland, OH.
FIBER OPTIC LASER DOPPLER ANEMOMETRY IN SWIRLING JETS
R. TAGHAVI (Sverdrup Technology, Inc., Brook Park, OH) and E. J. RICE (NASA, Lewis Research Center, Cleveland, OH) /In Laser anemometry - Advances and applications 1991; Proceedings of the 4th International Conference, Cleveland, OH, Aug. 5-9, 1991. Vol. 1 New York American Society of Mechanical Engineers 1991 p. 77-82. refs Copyright

Time-averaged and fluctuating quantities are measured in a free turbulent swirling jet. Data from a two-component laser Doppler anemometry (LDA) are compared to the measurements via hot-wire and 5-hole pitot probes. To acquire the proper seeding density near the axis of a swirling jet for LDA measurements proved difficult. This is due to an imbalance of the centrifugal force and radial pressure gradient, which throws the seeding material off the axis. Despite this problem, close agreement between various measurement techniques is obtained. Author

A93-23788 National Aeronautics and Space Administration. Lewis Research Center, Cleveland, OH.
DEVELOPMENT OF A RAYLEIGH SCATTERING SYSTEM FOR TEMPERATURE MEASUREMENTS IN COMBUSTOR FLOWS
M. V. OTUGEN (Polytechnic Univ., Farmingdale, NY), R. G. SEASHOLTZ (NASA, Lewis Research Center, Cleveland, OH), and K. D. ANNEN (Aerodyne Research, Inc., Billerica, MA) /In Laser anemometry - Advances and applications 1991; Proceedings of the 4th International Conference, Cleveland, OH, Aug. 5-9, 1991. Vol. 1 New York American Society of Mechanical Engineers 1991 p. 115-120. Research supported by Case Western Reserve Univ. and NASA refs Copyright

A dual line laser induced Rayleigh scattering system has been

developed to be used in high temperature gas flows such as in combustors, and preliminary tests have been performed in a hot air jet. The qualification measurements included the collection and analysis of Rayleigh signal for time-resolved gas temperature over the two lines of a copper-vapor laser. The dual line signal collection technique is a feature to be used in detecting and discriminating the surface scattered laser light in the Rayleigh signal. Optical fibers are used to transmit the laser beam to the optical probe bench and to carry the collected signal from the bench to the housing of the signal sensors. Incident laser intensity at the probe volume is measured for both lines at each pulse of the laser. This information is used to normalize the signal. Good agreement has been obtained between the two line Rayleigh scattering and thermocouple results in the particle free co-flowing air jet.

Author

A93-23799* National Aeronautics and Space Administration. Lewis Research Center, Cleveland, OH.
PARTICLE IMAGE VELOCIMETRY FOR THE SURFACE TENSION DRIVEN CONVECTION EXPERIMENT USING A PARTICLE DISPLACEMENT TRACKING TECHNIQUE
MARK P. WERNET and ALEXANDER D. PLINE (NASA, Lewis Research Center, Cleveland, OH) /In Laser anemometry - Advances and applications 1991; Proceedings of the 4th International Conference, Cleveland, OH, Aug. 5-9, 1991. Vol. 1 New York American Society of Mechanical Engineers 1991 p. 315-325. Previously announced in STAR as N91-25382 refs Copyright

The Surface Tension Driven Convection Experiment (STDCE) is a Space Transportation System flight experiment to study both transient and steady thermocapillary fluid flows aboard the USML-1 Spacelab mission planned for 1992. One of the components of data collected during the experiment is a video record of the flow field. This qualitative data is then quantified using an all electronic, two-dimensional particle image velocimetry technique called particle displacement tracking (PDT) which uses a simple space domain particle tracking algorithm. The PDT system is successful in producing velocity vector fields from the raw video data. Application of the PDT technique to a sample data set yielded 1606 vectors in 30 seconds of processing time. A bottom viewing optical arrangement is used to image the illuminated plane, which causes keystone distortion in the final recorded image. A coordinate transformation was incorporated into the system software to correct this viewing angle distortion. PDT processing produced 1.8 percent false identifications, due to random particle locations. A highly successful routine for removing the false identifications was also incorporated, reducing the number of false identifications to 0.2 percent. Author

A93-23800* National Aeronautics and Space Administration. Lewis Research Center, Cleveland, OH.
PARTICLE DISPLACEMENT TRACKING APPLIED TO AIR FLOWS
MARK P. WERNET (NASA, Lewis Research Center, Cleveland, OH) /In Laser anemometry - Advances and applications 1991; Proceedings of the 4th International Conference, Cleveland, OH, Aug. 5-9, 1991. Vol. 1 New York American Society of Mechanical Engineers 1991 p. 327-335. Previously announced in STAR as N91-25387 refs Copyright

Electronic Particle Image Velocimetric (PIV) techniques offer many advantages over conventional photographic PIV methods such as fast turn around times and simplified data reduction. A new all electronic PIV technique was developed which can measure high speed gas velocities. The Particle Displacement Tracking (PDT) technique employs a single CW laser, small seed particles (1 micron), and a single intensified, gated CCD array frame camera to provide a simple and fast method of obtaining two-dimensional velocity vector maps with unambiguous direction determination. Use of a single CCD camera eliminates registration difficulties encountered when multiple cameras are used to obtain velocity magnitude and direction information. An 80386 PC equipped with a large memory buffer frame-grabber board provides all of the

data acquisition and data reduction operations. No array processors of other numerical processing hardware are required. Full video resolution (640 x 480 pixel) is maintained in the acquired images, providing high resolution video frames of the recorded particle images. The time between data acquisition to display of the velocity vector map is less than 40 sec. The new electronic PDT technique is demonstrated on an air nozzle flow with velocities less than 150 m/s.

Author

A93-23801* National Aeronautics and Space Administration. Lewis Research Center, Cleveland, OH.

YOUNG'S FRINGE PARTICLE IMAGE VELOCIMETRY IN THE PRESENCE OF RANDOM PARTICLE MOTIONS

R. RUBINSTEIN and P. S. GREENBERG (NASA, Lewis Research Center, Cleveland, OH) *In* Laser anemometry - Advances and applications 1991; Proceedings of the 4th International Conference, Cleveland, OH, Aug. 5-9, 1991. Vol. 1 New York American Society of Mechanical Engineers 1991 p. 337-340. refs

Copyright

In the Young's fringe approach to particle image velocimetry, random particle motions cause loss of fringe visibility by decorrelating the coherent interexposure particle separations responsible for fringe formation. Since the visibility reduction is determined by the random motion through a Fourier transform relation analogous to the Van Cittert Zernike Theorem, it has been proposed that the random motion can be characterized statistically by analyzing fringe visibility distributions in the transform plane. This paper assesses the accuracy of such measurements. In particular, the effects of finite particle population and of correlated random motion are evaluated. The theory applies to diffusive motion, turbulence, and to random motion caused by mean velocity inhomogeneities.

Author

A93-23814* National Aeronautics and Space Administration. Lewis Research Center, Cleveland, OH.

HIGH-SPEED LASER ANEMOMETRY BASED ON SPECTRALLY RESOLVED RAYLEIGH SCATTERING

R. G. SEASHOLTZ (NASA, Lewis Research Center, Cleveland, OH) *In* Laser anemometry - Advances and applications 1991; Proceedings of the 4th International Conference, Cleveland, OH, Aug. 5-9, 1991. Vol. 2 New York American Society of Mechanical Engineers 1991 p. 465-471. refs

Copyright

Laser anemometry in unseeded flows based on the measurement of the spectrum of Rayleigh scattered laser light is reviewed. The use of molecular scattering avoids the well-known problems (particle lag, biasing effects, seed generation, seed injection) of seeded flows. The fundamental limits on velocity measurement accuracy are determined using maximum likelihood methods. Measurement of the Rayleigh spectrum with scanning Fabry-Perot interferometers is analyzed and accuracy limits are established for both single pass and multi-pass configurations. Multi-pass configurations have much higher selectivity and are needed for measurements where there is a large amount of excess noise caused by stray laser light. It is shown that Rayleigh scattering is particularly useful for supersonic and hypersonic flows. The results of the analysis are compared with measurements obtained with a Rayleigh scattering diagnostic developed for study of the exhaust plume of a small hydrogen-oxygen rocket, where the velocities are in the range 1000 to 5000 m/sec.

Author

A93-23830* National Aeronautics and Space Administration. Lewis Research Center, Cleveland, OH.

SIGNAL PROCESSING CONSIDERATIONS FOR LOW SIGNAL TO NOISE RATIO LASER DOPPLER AND PHASE DOPPLER SIGNALS

K. M. IBRAHIM, G. D. WERTHEIMER, and WILLIAM D. BACHALO (Aerometrics, Inc., Sunnyvale, CA) *In* Laser anemometry - Advances and applications 1991; Proceedings of the 4th International Conference, Cleveland, OH, Aug. 5-9, 1991. Vol. 2 New York American Society of Mechanical Engineers 1991 p. 685-692. Research supported by U.S. Navy refs

(Contract NAS3-25622)

Copyright

The relative performance of current methods used for estimating the phase and the frequency in LDV and phase Doppler applications in low signal to noise ratio conditions is analyzed. These methods include the Fourier analysis and the correlation techniques. Three methods that use the correlation function for frequency and phase estimations are evaluated in terms of accuracy and speed of processing. These methods include: (1) the frequency estimation using zero crossings counting of the auto-correlation function, (2) the Blackman-Tukey method, and (3) the Autoregressive method (AR). The relative performance of these methods is evaluated and compared with the Fourier analysis method which provides the optimum performance in terms of the Maximum Likelihood (ML) criteria.

Author

A93-24024 National Aeronautics and Space Administration. Lewis Research Center, Cleveland, OH.

THREE-DIMENSIONAL COMPUTED TOMOGRAPHY FROM INTERFEROMETRIC MEASUREMENTS WITHIN A NARROW CONE OF VIEWS

ARTHUR J. DECKER (NASA, Lewis Research Center, Cleveland, OH) and STEVEN H. IZEN (Case Western Reserve Univ., Cleveland, OH) *Applied Optics* (ISSN 0003-6935) vol. 31, no. 36 Dec. 20, 1992 p. 7696-7706. Previously announced in STAR as N91-19404 Research supported by NASA and American Society of Electrical Engineers refs

(Contract NAG3-832)

Copyright

A theory to determine the properties of a fluid from measurements of its projections was developed and tested. Viewing cones as small as 10 degrees were evaluated, with the only assumption being that the property was space limited. The results of applying the theory to numerical and actual interferograms of a spherical discontinuity of refractive index are presented. The theory was developed to test the practicality and limits of using three dimensional computer tomography in internal fluid dynamics.

Author

A93-25552*# National Aeronautics and Space Administration. Lewis Research Center, Cleveland, OH.

PULSED LASER RAYLEIGH SCATTERING DIAGNOSTIC FOR HYDROGEN/OXYGEN ROCKET EXIT PLANE FLOWFIELD VELOCIMETRY

FRANK J. ZUPANC (NASA, Lewis Research Center, Cleveland, OH) Jan. 1993 10 p. AIAA, Aerospace Sciences Meeting and Exhibit, 31st, Reno, NV, Jan. 11-14, 1993 refs (AIAA PAPER 93-0805) Copyright

A Doppler-resolved, pulsed laser Rayleigh scattering diagnostic has been developed to obtain local flowfield velocity measurements at the exit plane of a low thrust hydrogen/oxygen rocket engine operating in a high-altitude test facility. Fiber optic signal collection was employed to obtain the forescatter and backscatter Doppler shifts necessary to resolve the axial and radial velocity components. A radial profile was obtained by traversing the collection probes along the beam path at the nozzle exit. The results are compared with theoretical predictions from a full Navier-Stokes model (RK/RPLUS). Significant discrepancies between the measured and predicted axial velocity profiles are observed, in terms of both magnitude and character. Radial velocity measurements exhibit excellent agreement with predictions near the centerline but show some departure off-axis. The discrepancies between theory and experiment are potentially the result of enhanced mixing between the core and fuel-film region beyond that predicted, and/or flow stratification between the hydrogen and oxygen injected into the central core region.

Author

A93-26967* National Aeronautics and Space Administration. Lewis Research Center, Cleveland, OH.

TEMPORAL AVERAGING OF PHASE MEASUREMENTS IN THE PRESENCE OF SPURIOUS PHASE DRIFT - APPLICATION TO PHASE-STEPPED REAL-TIME HOLOGRAPHIC INTERFEROMETRY

B. OVRYN (Sverdrup Technology, Inc., Brook Park; NASA, Lewis Research Center, Cleveland, OH) and E. M. HAACKE (Case Western Reserve Univ., Cleveland, OH) *Applied Optics* (ISSN 0003-6935) vol. 32, no. 2 Jan. 10, 1993 p. 147-154. refs
Copyright

A technique that compensates for low spatial frequency spurious phase changes during an interference experiment is developed; it permits temporal averaging of multiple-phase measurements, made before and after object displacement. The method is tested with phase-stepped real-time holographic interferometry applied to cantilever bending of a piezoelectric bimorph ceramic. Results indicate that temporal averaging of the corrected data significantly reduces the white noise in a phase measurement without incurring systematic errors or sacrificing spatial resolution. White noise is reduced from 3 deg to less than 1 deg using these methods.
Author

A93-28580 National Aeronautics and Space Administration. Lewis Research Center, Cleveland, OH.

X-RAY-BASED DISPLACEMENT MEASUREMENT FOR HOSTILE ENVIRONMENTS

H. A. CANISTRARO, E. H. JORDAN, and D. M. PEASE (Connecticut Univ., Storrs) *Experimental Mechanics* (ISSN 0014-4851) vol. 32, no. 4 Dec. 1992 p. 289-295. Previously announced in STAR as N92-23155 refs
(Contract NAG3-1004; RTOP 505-90-01)
Copyright

A new method on noncontacting, high temperature extensometry based on the focus and scanning of X-rays is currently under development and shows great promise of overcoming limitations associated with available techniques. The chief advantage is the ability to make undisturbed measurements through stratified or flowing gases, smoke, and flame. The system is based on the ability to focus and scan low energy, hard X-rays such as those emanating from copper or molybdenum sources. The X-rays are focused into a narrow and intense line image which can be scanned onto targets that fluoresce secondary X-ray radiation. The final goal of the system is the ability to conduct macroscopic strain measurements in hostile environments by utilizing two or more fluorescing targets. Current work is limited to displacement measurement of a single target with a resolution of 1.25 micro-m and a target temperature of 1200 C, directly through an open flame. The main advantage of the technique lies in the penetrating nature of X-rays which are not affected by the presence of refracting gas layers, smoke, flame, or intense thermal radiation, all of which could render conventional extensometry methods inoperative or greatly compromise their performance.
Author

A93-32918* National Aeronautics and Space Administration. Lewis Research Center, Cleveland, OH.

OPTICAL FIBER SENSOR FOR TEMPERATURE MEASUREMENT FROM 600 TO 1900 C IN GAS TURBINE ENGINES

G. W. TREGAY, P. R. CALABRESE, P. L. KAPLIN, and M. J. FINNEY (Conax Buffalo Corp., NY) *In Specialty fiber optic systems for mobile platforms; Proceedings of the Meeting, Boston, MA, Sept. 5, 1991 Bellingham, WA Society of Photo-Optical Instrumentation Engineers 1991 p. 38-47. refs*
(Contract NAS3-15451)
Copyright

A temperature sensor system has been fabricated specifically for the harsh environment encountered in temperature measurement on gas turbine engines. Four components comprised the system: a thermally emissive source, a high temperature lightguide, a flexible optical cable and an electro-optic signal processor. The emissive source was located inside a sapphire rod so that the sapphire serves as both a lightguide and as a protective shroud. As the probe was heated, the thermal radiation from the emissive source increased with increasing temperature. The flexible optical cable was constructed with 200 micron core fiber and ruggedized for turbine engine applications. The electro-optic signal processor used the ratio of intensity in two wavelength intervals to determine a digital value of the temperature.

The probe tip was operated above 1900 C in a low velocity propane flame and above 1500 C at Mach .37. Probe housings, optical cables, and signal processors were constructed and environmentally tested for the temperature and vibration experienced by turbine engine sensors. This technology was used to build an optical exhaust gas sensor for a General Electric Aircraft Engines F404 turbine. The four optical probes and optical cable were a functional replacement for four thermocouple probes. The system was ground tested for 50 hours with an excess of 1000 thermal cycles. This optical temperature sensor system measured gas temperature up to the operational limit of the turbine engine.
Author

A93-33169* National Aeronautics and Space Administration. Lewis Research Center, Cleveland, OH.

APPLIED HIGH-SPEED IMAGING FOR THE ICING RESEARCH PROGRAM AT NASA LEWIS RESEARCH CENTER

HOWARD SLATER (NASA, Lewis Research Center, Cleveland, OH), JAY OWENS (Cortez III Services Corp., Brook Park, OH), and JAIWON SHIN (NASA, Lewis Research Center, Cleveland, OH) *In Ultrahigh- and high-speed photography, videography, and photonics '91; Proceedings of the Meeting, San Diego, CA, July 24-26, 1991 Bellingham, WA Society of Photo-Optical Instrumentation Engineers 1992 p. 174-189. Previously announced in STAR as N91-26490 refs*
(Contract NAS3-24816)
Copyright

The Icing Research Tunnel at NASA Lewis Research Center provides scientists a scaled, controlled environment to simulate natural icing events. The closed-loop, low speed, refrigerated wind tunnel offers the experimental capability to test for icing certification requirements, analytical model validation and calibration techniques, cloud physics instrumentation refinement, advanced ice protection systems, and rotorcraft icing methodology development. The test procedures for these objectives all require a high degree of visual documentation, both in real-time data acquisition and post-test image processing. Information is provided to scientific, technical, and industrial imaging specialists as well as to research personnel about the high-speed and conventional imaging systems will be on the recent ice protection technology program. Various imaging examples for some of the tests are presented. Additional imaging examples are available from the NASA Lewis Research Center's Photographic and Printing Branch.
Author

A93-35575* National Aeronautics and Space Administration. Lewis Research Center, Cleveland, OH.

AN AUTOMATED THERMOCOUPLE CALIBRATION SYSTEM

MARK D. BETHEA and BRUCE N. ROSENTHAL (NASA, Lewis Research Center, Cleveland, OH) *IEEE Transactions on Instrumentation and Measurement* (ISSN 0018-9456) vol. 41, no. 5 Oct. 1992 p. 702-706. refs
Copyright

An Automated Thermocouple Calibration System (ATCS) was developed for the unattended calibration of type K thermocouples. This system operates from room temperature to 650 C and has been used for calibration of thermocouples in an eight-zone furnace system which may employ as many as 60 thermocouples simultaneously. It is highly efficient, allowing for the calibration of large numbers of thermocouples in significantly less time than required for manual calibrations. The system consists of a personal computer, a data acquisition/control unit, and a laboratory calibration furnace. The calibration furnace is a microprocessor-controlled multipurpose temperature calibrator with an accuracy of ± 0.7 C. The accuracy of the calibration furnace is traceable to the National Institute of Standards and Technology (NIST). The computer software is menu-based to give the user flexibility and ease of use. The user needs no programming experience to operate the systems. This system was specifically developed for use in the Microgravity Materials Science Laboratory (MMSL) at the NASA LeRC.
Author (revised)

A93-37051* National Aeronautics and Space Administration. Lewis Research Center, Cleveland, OH.

COHERENT FIBER OPTIC SENSOR FOR EARLY DETECTION OF CATARACTOGENESIS IN A HUMAN EYE LENS

HARBANS S. DHADWAL (New York State Univ., Stony Brook), RAFAT R. ANSARI (NASA, Lewis Research Center, Cleveland, OH), and MICHAEL A. DELLAVECCHIA (Wills Eye Hospital, Philadelphia, PA) Optical Engineering (ISSN 0091-3286) vol. 32, no. 2 Feb. 1993 p. 233-238. refs

Copyright

A lensless backscatter fiber optic probe is used to measure the size distribution of protein molecules inside an excised, but intact, human eye lens. The fiber optic probe, about 5 mm in diameter, can be positioned arbitrarily close to the anterior surface of the eye; it is a trans-receiver, which delivers a Gaussian laser beam into a small region inside the lens and provides a coherent detection of the laser light scattered by the protein molecules in the backward direction. Protein sizes determined from the fast and slow diffusion coefficients show good correlation with the age of the lens and cataractogenesis.

Author

A93-37862* National Aeronautics and Space Administration. Lewis Research Center, Cleveland, OH.

MINIATURE HIGH TEMPERATURE PLUG-TYPE HEAT FLUX GAUGES

CURT H. LIEBERT (NASA, Lewis Research Center, Cleveland, OH) In International Instrumentation Symposium, 38th, Las Vegas, NV, Apr. 26-30, 1992, Proceedings Research Triangle Park, NC Instrument Society of America 1992 p. 263-271. refs

Copyright

The objective is to describe continuing efforts to develop methods for measuring surface heat flux, gauge active surface temperature, and heat transfer coefficient quantities. The methodology involves inventing a procedure for fabricating improved plug-type heat flux gauges and also for formulating inverse heat conduction models and calculation procedures. These models and procedures are required for making indirect measurements of these quantities from direct temperature measurements at gauge interior locations. Measurements of these quantities were made in a turbine blade thermal cycling tester (TBT) located at MSFC. The TBT partially simulates the turbopump turbine environment in the Space Shuttle Main Engine. After the TBT test, experiments were performed in an arc lamp to analyze gauge quality.

Author

A93-37864* National Aeronautics and Space Administration. Lewis Research Center, Cleveland, OH.

USING SILICON DIODES FOR DETECTING THE LIQUID-VAPOR INTERFACE IN HYDROGEN

PAULA J. DEMPSEY and RICHARD H. FABIK (NASA, Lewis Research Center, Cleveland, OH) In International Instrumentation Symposium, 38th, Las Vegas, NV, Apr. 26-30, 1992, Proceedings Research Triangle Park, NC Instrument Society of America 1992 p. 287-299. Previously announced in STAR as N92-18456 refs

Copyright

Tests were performed using commercially available silicon diode temperature sensors to detect the location of the liquid-vapor interface in hydrogen during ground test programs. Results show that by increasing the current into the sensor, silicon diodes can be used as liquid level point sensors. After cycling the sensors from liquid to vapor several times, it was found that with a 30 mA (milliamps) input current, the sensors respond within 2 seconds by measuring a large voltage difference when transitioning from liquid to vapor across the interface. Nearly instantaneous response resulted during a transition from vapor to liquid. Detailed here are test procedures, experimental results, and guidelines for applying this information to other test facilities.

Author

A93-39347* National Aeronautics and Space Administration. Lewis Research Center, Cleveland, OH.

CAPACITANCE-TYPE BLADE-TIP CLEARANCE MEASUREMENT SYSTEM USING A DUAL AMPLIFIER WITH RAMP/DC INPUTS AND INTEGRATION

GARIMELLA R. SARMA (Analytical Services & Materials, Inc., Hampton, VA) and JOHN P. BARRANGER (NASA, Lewis Research Center, Cleveland, OH) IEEE Transactions on Instrumentation and Measurement (ISSN 0018-9456) vol. 41, no. 5 Oct. 1992 p. 674-678. refs

Copyright

The analysis and prototype results of a dual-amplifier circuit for measuring blade-tip clearance in turbine engines are presented. The capacitance between the blade tip and mounted capacitance electrode within a guard ring of a probe forms one of the feedback elements of an operational amplifier (op amp). The differential equation governing the circuit taking into consideration the nonideal features of the op amp was formulated and solved for two types of inputs (ramp and dc) that are of interest for the application. Under certain time-dependent constraints, it is shown that (1) with a ramp input the circuit has an output voltage proportional to the static tip clearance capacitance, and (2) with a dc input, the output is proportional to the derivative of the clearance capacitance, and subsequent integration recovers the dynamic capacitance. The technique accommodates long cable lengths and environmentally induced changes in cable and probe parameters. System implementation for both static and dynamic measurements having the same high sensitivity is also presented.

Author

A93-40580* National Aeronautics and Space Administration. Lewis Research Center, Cleveland, OH.

THIN FILM DIAMOND MICROSTRUCTURE APPLICATIONS

T. ROPPEL, C. ELLIS, R. RAMESHAM (Auburn Univ., AL), D. JAWORSKE (NASA, Lewis Research Center, Cleveland, OH), M. E. BAGINSKI, and S. Y. LEE (Auburn Univ., AL) In Applications of diamond films and related materials; Proceedings of the 1st International Conference, Auburn, AL, Aug. 17-22, 1991 Amsterdam Elsevier 1991 p. 311-318. refs

Copyright

Selective deposition and abrasion, as well as etching in atomic oxygen or reduced-pressure air, have been used to prepare patterned polycrystalline diamond films which, on further processing by anisotropic Si etching, yield the microstructures of such devices as flow sensors and accelerometers. Both types of sensor have been experimentally tested in the respective functions of hot-wire anemometer and both single- and double-hinged accelerometer.

AIAA

A93-40677* National Aeronautics and Space Administration. Lewis Research Center, Cleveland, OH.

MEASUREMENT OF FREQUENCY RESPONSE IN SHORT THERMOCOUPLE WIRES

L. J. FORNEY, E. L. MEEKS, J. MA (Georgia Inst. of Technology, Atlanta), and G. C. FRALICK (NASA, Lewis Research Center, Cleveland, OH) Review of Scientific Instruments (ISSN 0034-6748) vol. 64, no. 5 May 1993 p. 1280-1286. Previously announced in STAR as N92-11339 Research sponsored by USAF refs

(Contract NCC3-135)

Copyright

Experimental measurements are made for the steady-state frequency response of a supported thermocouple wire. In particular, the effects of axial heat conduction are demonstrated for both a supported one material wire (type K) and a two material wire (type T) with unequal material properties across the junction. The data for the amplitude ratio and phase angle are correlated to within 10 percent with the theoretical predictions of Fralick and Forney (1991). This is accomplished by choosing a natural frequency ω_n for the wire data to correlate the first order response at large gas temperature frequencies. It is found that a large bead size, however, will increase the amplitude ratio at low frequencies but decrease the natural frequency of the wire.

The phase angle data are also distorted for imperfect junctions.
 Author

A93-40683* National Aeronautics and Space Administration. Lewis Research Center, Cleveland, OH.

DESIGN OF A CONSTANT TENSION THERMOCOUPLE RAKE SUITABLE FOR FLAME STUDIES

SANDEEP AHUJA and DAVID L. MILLER (Drexel Univ., Philadelphia, PA) Review of Scientific Instruments (ISSN 0034-6748) vol. 64, no. 5 May 1993 p. 1358, 1359. refs (Contract NAG3-1117) Copyright

An improved, spring-loaded thermocouple rake, suitable for studying flame structure, has been designed. This design keeps the thermocouple under tension thereby ensuring that the thermocouple does not droop due to the thermal expansion of the sensing wire when inserted in the flame. The present design allows the usage of thermocouple wire as small as 0.0508 mm and relative ease in changing thermocouple wire.
 Author

A93-41356* National Aeronautics and Space Administration. Lewis Research Center, Cleveland, OH.

DEVELOPMENT OF A HYDROGEN GAS SENSOR USING MICROFABRICATION TECHNOLOGY

CHUNG-CHIUN LIU, QINGHAI WU, MATTHEW STUCZYNSKI (Case Western Reserve Univ., Cleveland, OH), and GEORGE C. MADZSAR (NASA, Lewis Research Center, Cleveland, OH) Jul. 1992 5 p. SAE, International Conference on Environmental Systems, 22nd, Seattle, WA, July 13-16, 1992 Research supported by Edison Sensor Technology Center refs (Contract NAG3-1149) (SAE PAPER 921176) Copyright

Microfabrication and micromachining technologies are used to produce a hydrogen gas sensor based on a palladium-silver film. The sensor uses a heater that is fabricated by diffusing p-type borones into the substrate, forming a resistance heater. A diode for temperature measurement is produced using p-type boron and n-type phosphor diffused into the substrate. A thickness of the palladium-silver film is approximately 300 arcsec. The hydrogen gas sensor employs the proven palladium-silver diode structure and is surrounded by a phosphor doped resistance heater which can be heated up to a temperature of 250 C. Experimental results show that the sensor is capable of operating over a wide range of hydrogen concentration levels between 0-95 percent without any hysteresis effects.
 AIAA

A93-43689* National Aeronautics and Space Administration. Lewis Research Center, Cleveland, OH.

EVALUATION OF A HUE CAPTURING BASED TRANSIENT LIQUID CRYSTAL METHOD FOR HIGH-RESOLUTION MAPPING OF CONVECTIVE HEAT TRANSFER ON CURVED SURFACES

C. CAMCI, K. KIM (Pennsylvania State Univ., University Park), S. A. HIPPENSTEELE, and P. E. POINSATTE (NASA, Lewis Research Center, Cleveland, OH) ASME, Transactions, Journal of Heat Transfer (ISSN 0022-1481) vol. 115, no. 2 May 1993 p. 311-318. ASME, Winter Annual Meeting, 112th, Atlanta, GA, Dec. 1-6, 1991 refs Copyright

Accurate determination of convective heat transfer coefficients on complex curved surfaces is essential in the aerothermal design and analysis of propulsion system components. The heat transfer surfaces are geometrically very complex in most of the propulsion applications. This study focuses on the evaluation of a hue capturing technique for the heat transfer interpretation of liquid crystal images from a complex curved heat transfer surface. Impulsively starting heat transfer experiments in a square to rectangular transition duct are reported. The present technique is different from existing steady-state hue capturing studies. A real-time hue conversion process on a complex curved surface is adopted for a transient heat transfer technique with high spatial resolution. The study also focuses on the use of encapsulated liquid crystals with narrow color band in contrast to previous

steady-state hue based techniques using wide band liquid crystals. Using a narrow band crystal improves the accuracy of the heat transfer technique. Estimated uncertainty for the heat transfer coefficient from the technique is about 5.9 percent. A complete heat transfer map of the bottom surface was possible using only seven liquid crystal image frames out of the 97 available frames during the transient experiment. Significant variations of heat transfer coefficients are quantitatively visualized on the curved surfaces of the transition duct.
 Author

A93-44190* National Aeronautics and Space Administration. Lewis Research Center, Cleveland, OH.

TEMPORAL AVERAGING IN A TURBULENT ENVIRONMENT - COMPENSATION FOR PHASE DRIFTS IN PHASE SHIFTING INTERFEROMETRY

B. OVRYN and E. M. HAACKE (Case Western Reserve Univ., Cleveland, OH) In Laser interferometry IV: Computer-aided interferometry; Proceedings of the Meeting, San Diego, CA, July 22-24, 1991 Bellingham, WA Society of Photo-Optical Instrumentation Engineers 1992 p. 221-230. Research supported by NASA refs Copyright

In an effort to improve the signal to noise in an interference experiment, we have developed a method to remove systematic phase drift between data sets acquired over long time intervals. Using this technique, it is possible to average repeatedly acquired phase measurements and improve the phase estimate without sacrificing spatial resolution. Results from tests using real-time phase stepping holographic interferometry applied to cantilever bending of a piezoelectric bimorph indicate that white noise has been reduced from 3 to less than 1 deg ($\lambda/360$) by averaging 36 phase compensated data sets before object bending and 36 data sets after bending.
 Author (revised)

A93-44514* National Aeronautics and Space Administration. Lewis Research Center, Cleveland, OH.

NEW TECHNIQUE FOR OIL BACKSTREAMING CONTAMINATION MEASUREMENTS

S. A. ALTEROVITZ, H. J. SPEIER (NASA, Lewis Research Center, Cleveland, OH), R. M. SIEG, M. N. DROTOS (Cleveland State Univ.; NASA, Lewis Research Center, OH), and J. E. DUNNING (Michigan State Univ., East Lansing; NASA, Lewis Research Center, Cleveland, OH) Journal of Vacuum Science and Technology A (ISSN 0734-2101) vol. 10, no. 4 July-Aug. 1992 p. 2099-2104. refs Copyright

The backstreaming contamination in the Space Power Facility, Ohio, was measured using small size clean silicon wafers as contamination sensors placed at all measurement sites. Two ellipsometric models were developed to measure the oil film with the contamination film refractive index of DC 705: a continuous, homogeneous film and islands of oil with the islands varying in coverage fraction and height. The island model improved the ellipsometric analysis quality parameter by up to two orders of magnitude. The continuous film model overestimated the oil volume by about 50 percent.
 AIAA

A93-49457 National Aeronautics and Space Administration. Washington, DC.

MICROMACHINED SILICON CANTILEVER BEAM ACCELEROMETER INCORPORATING AN INTEGRATED OPTICAL WAVEGUIDE

KEVIN E. BURCHAM, GREGORY N. DE BRABANDER, and JOSEPH T. BOYD (Cincinnati Univ., OH) In Integrated optics and microstructures; Proceedings of the Meeting, Boston, MA, Sept. 8, 9, 1992 Bellingham, WA Society of Photo-Optical Instrumentation Engineers 1993 p. 12-18. refs (Contract NAGW-1407; NAG3-852) Copyright

A micromachined cantilever beam accelerometer is described in which beam deflection is determined optically. A diving board structure is anisotropically etched into a silicon wafer. This diving board structure is patterned from the wafer backside so as to

leave a small gap between the tip of the diving board and the opposite fixed edge on the front side of the wafer. In order to sense a realistic range of accelerations, a foot mass incorporated onto the end of the beam is found to provide design flexibility. A silicon nitride optical waveguide is then deposited by low pressure chemical vapor deposition (LPCVD) onto the sample. Beam deflection is measured by the decrease of light coupled across the gap between the waveguide sections. In order to investigate sensor response and simulate deflection of the beam, we utilized a separate beam and waveguide section which could be displaced from one another in a precisely controlled manner. Measurements were performed on samples with gaps of 4.0, 6.0, and 8.0 micron and the variation of the fraction of light coupled across the gap as a function of displacement and gap spacing was found to agree with overlap integral calculations.

A93-49458 National Aeronautics and Space Administration, Washington, DC.

CHARACTERIZATION OF Si₃N₄/SiO₂ OPTICAL CHANNEL WAVEGUIDES BY PHOTON SCANNING TUNNELING MICROSCOPY

YAN WANG, MONA H. CHUDGAR, HOWARD E. JACKSON, JEFFREY S. MILLER, GREGORY N. DE BRABANDER, and JOSEPH T. BOYD (Cincinnati Univ., OH) *In* Integrated optics and microstructures; Proceedings of the Meeting, Boston, MA, Sept. 8, 9, 1992 Bellingham, WA Society of Photo-Optical Instrumentation Engineers 1993 p. 66-69. Research supported by U.S. Army refs (Contract NAGW-1407; NAG3-852) Copyright

Photon scanning tunneling microscopy (PSTM) is used to characterize Si₃N₄/SiO₂ optical channel waveguides being used for integrated optical-micromechanical sensors. PSTM utilizes an optical fiber tapered to a fine point which is piezoelectrically positioned to measure the decay of the evanescent field intensity associated with the waveguide propagating mode. Evanescent field decays are recorded for both ridge channel waveguides and planar waveguide regions. Values for the local effective refractive index are calculated from the data for both polarizations and compared to model calculations.

A93-49459* National Aeronautics and Space Administration, Lewis Research Center, Cleveland, OH.

FOURIER TRANSFORM SPECTROMETRY FOR FIBER-OPTIC SENSOR SYSTEMS

GLENN BEHEIM, MARGARET L. TUMA, JORGE L. SOTOMAYOR (NASA, Lewis Research Center, Cleveland, OH), and JOSEPH M. FLATICO (John Carroll Univ., Cleveland, OH) *In* Integrated optics and microstructures; Proceedings of the Meeting, Boston, MA, Sept. 8, 9, 1992 Bellingham, WA Society of Photo-Optical Instrumentation Engineers 1993 p. 127-136. refs Copyright

An integrated-optic Mach-Zehnder interferometer is used as a Fourier transform spectrometer to analyze the input and output spectra of a temperature-sensing thin-film etalon. This type of spectrometer has an advantage over conventional grating spectrometers because it is better suited for use with time-division-multiplexed sensor networks. In addition, this spectrometer has the potential for low cost due to its use of a component that could be manufactured in large quantities for the optical communications industry.

A93-49469* National Aeronautics and Space Administration, Lewis Research Center, Cleveland, OH.

RF MODULATED FIBER OPTIC SENSING SYSTEMS AND THEIR APPLICATIONS

G. ADAMOVSKY (NASA, Lewis Research Center, Cleveland, OH) and J. G. EUSTACE (John Carroll Univ., University Heights, OH) *In* Specialty fiber optic systems for mobile platforms and plastic optical fibers; Proceedings of the Meeting, Boston, MA, Sept. 9-11, 1992 Bellingham, WA Society of Photo-Optical Instrumentation Engineers 1993 p. 134-139. Previously announced in STAR

as N92-33896 refs
(Contract NAG3-984)
Copyright

A fiber optic sensing system with an intensity sensor and a Radio Frequency (RF) modulated source was shown to have sensitivity and resolution much higher than a comparable system employing low modulating frequencies or DC mode of operation. Also the RF modulation with an appropriate configuration of the sensing system provides compensation for the unwanted intensity losses. The basic principles and applications of a fiber optic sensing system employing an RF modulated source are described. In addition the paper discusses various configurations of the system itself, its components, and modulation and detection schemes. Experimental data are also presented.

A93-49906*# National Aeronautics and Space Administration, Lewis Research Center, Cleveland, OH.

ADVANCED INSTRUMENTATION FOR NEXT-GENERATION AEROSPACE PROPULSION CONTROL SYSTEMS

S. BARKHOUDARIAN, G. S. CROSS (Rockwell International Corp., Rocketdyne Div., Canoga Park, CA), and CARL F. LORENZO (NASA, Lewis Research Center, Cleveland, OH) Jun. 1993 13 p. AIAA, SAE, ASME, and ASEE, Joint Propulsion Conference and Exhibit, 29th, Monterey, CA, June 28-30, 1993 refs (AIAA PAPER 93-2079) Copyright

New control concepts for the next generation of advanced air-breathing and rocket engines and hypersonic combined-cycle propulsion systems are analyzed. The analysis provides a database on the instrumentation technologies for advanced control systems and cross matches the available technologies for each type of engine to the control needs and applications of the other two types of engines. Measurement technologies that are considered to be ready for implementation include optical surface temperature sensors, an isotope wear detector, a brushless torque meter, a fiberoptic deflectometer, an optical absorption leak detector, the nonintrusive speed sensor, and an ultrasonic transducer. It is concluded that all 30 advanced instrumentation technologies considered can be recommended for further development to meet need of the next generation of jet-, rocket-, and hypersonic-engine control systems. AIAA

A93-50085# National Aeronautics and Space Administration, Lewis Research Center, Cleveland, OH.

TIME-SEQUENCED AND SPECTRALLY FILTERED RAYLEIGH IMAGING OF SHOCK WAVE AND BOUNDARY LAYER STRUCTURE FOR INLET CHARACTERIZATION

JOSEPH FORKEY, SANDRINE COGNE, ALEXANDER SMITS, SEYMOUR BOGDONOFF, WALTER R. LEMPET, and RICHARD B. MILES (Princeton Univ., NJ) Jun. 1993 8 p. AIAA, SAE, ASME, and ASEE, Joint Propulsion Conference and Exhibit, 29th, Monterey, CA, June 28-30, 1993 Research supported by USAF and NASA refs (AIAA PAPER 93-2300) Copyright

Multiple pulsed Rayleigh imaging and filtered Rayleigh scattering are used to generate images of a complex boundary layer structure, shock wave/boundary layer interactions, and crossing shock waves. Time-sequenced Rayleigh images taken with a visible, double-pulsed laser system show the evolution of boundary layer structure of the internal flow in a generic cross-shock inlet. The images taken in the inlet give insight into 3D effects caused by the inlet geometry and may be used for modeling the complex flows. AIAA

A93-50144*# National Aeronautics and Space Administration, Lewis Research Center, Cleveland, OH.

THE DEVELOPMENT OF HYDROGEN SENSOR TECHNOLOGY FOR AEROSPACE APPLICATIONS

GARY W. HUNTER, PHILIP G. NEUDECK, G. D. JEFFERSON, G. C. MADZSAR (NASA, Lewis Research Center, Cleveland, OH), C. C. LIU, and Q. H. WU (Case Western Reserve Univ., Cleveland, OH) Jun. 1993 11 p. AIAA, SAE, ASME, and ASEE, Joint Propulsion Conference and Exhibit, 29th, Monterey, CA, June 28-30,

35 INSTRUMENTATION AND PHOTOGRAPHY

1993 refs

(AIAA PAPER 93-2375) Copyright

The motivation and present status of each of the major components of the NASA Lewis Research Center hydrogen sensor program. The testing facility used to test the sensors and the proposed expansion of this facility are discussed. The Schottky diode prototype sensors, the use of SiC as a semiconductor for a hydrogen sensor, and the present characterization of PdCr are addressed. Future directions for the program are examined. It is concluded that results thus far are encouraging and that further development work is necessary. AIAA

A93-51239* National Aeronautics and Space Administration. Lewis Research Center, Cleveland, OH.

CALIBRATION OF THE FORWARD-SCATTERING SPECTROMETER PROBE - MODELING SCATTERING FROM A MULTIMODE LASER BEAM

EDWARD A. HOVENAC (Sverdrup Technology, Inc.; NASA, Lewis Research Center, Cleveland, OH) and JAMES A. LOCK (Cleveland State Univ., OH) *Journal of Atmospheric and Oceanic Technology* (ISSN 0739-0572) vol. 10, no. 4 Aug. 1993 p. 518-525. refs Copyright

Scattering calculations using a detailed model of the multimode laser beam in the forward-scattering spectrometer probe (FSSP) were carried out using a recently developed extension to Mie scattering theory. From this model, new calibration curves for the FSSP were calculated. The difference between the old calibration curves and the new ones is small for droplet diameters less than 10 microns, but the difference increases to approximately 10 percent at diameters of 50 microns. When using glass beads to calibrate the FSSP, calibration errors can be minimized by using glass beads of many different diameters, over the entire range of the FSSP. If the FSSP is calibrated using one-diameter glass beads, then the new formalism is necessary to extrapolate the calibration over the entire range. Author (revised)

A93-53104* National Aeronautics and Space Administration. Lewis Research Center, Cleveland, OH.

FIBER-OPTIC THERMOMETER USING FOURIER TRANSFORM SPECTROSCOPY

GLENN BEHEIM, JORGE L. SOTOMAYOR (NASA, Lewis Research Center, Cleveland, OH), JOSEPH M. FLATICO (John Carroll Univ., Cleveland, OH), and MASSOOD T. AZAR (Case Western Reserve Univ., Cleveland, OH) *In Fiber optic and laser sensors IX; Proceedings of the Meeting, Boston, MA, Sept. 3-5, 1991 Bellingham, WA Society of Photo-Optical Instrumentation Engineers* 1991 p. 64-71. refs Copyright

An integrated-optic Mach-Zender interferometer is used as a Fourier transform spectrometer to analyze the input and output spectra of a temperature-sensing thin-film etalon. This configuration provides a high degree of immunity to the effects of changes in the source spectrum, and it readily permits the interrogation of a number of different sensors using a single spectrometer. In addition, this system has a potentially low cost because it uses optical communications hardware that may in the future be manufactured in large quantities. Author (revised)

A93-53109* National Aeronautics and Space Administration. Lewis Research Center, Cleveland, OH.

MULTIPLE FIBEROPTIC PROBE FOR SEVERAL SENSING APPLICATIONS

HARBANS S. DHADWAL (New York State Univ., Stony Brook) and RAFAT R. ANSARI (New York State Univ., Stony Brook; NASA, Lewis Research Center, Cleveland, OH) *In Fiber optic and laser sensors IX; Proceedings of the Meeting, Boston, MA, Sept. 3-5, 1991 Bellingham, WA Society of Photo-Optical Instrumentation Engineers* 1991 p. 262-272. refs (Contract NCC3-172) Copyright

A multiple fiber-optic particle sizing probe which uses a linear array of 11 optical fibers positioned in the focal plane of a graded index microlens is presented. The probe, a compact optical

spectrum analyzer, provides simultaneous filtering of the angular spectrum of an extended quasi-monochromatic source. Active and passive configurations provide accurate measurements of the particle size distributions. The multiple fiber-optic probe together with processing electronics is a particle sizing sensor which yields the size distribution within 1-2 min. AIAA

A93-53110* National Aeronautics and Space Administration. Lewis Research Center, Cleveland, OH.

FIBEROPTIC SENSING TECHNIQUE EMPLOYING RF MODULATED INTERFEROMETRY

JOHN G. EUSTACE, GREGORY A. COGHLAN, CHRISTIAN M. YORKA, EDWARD F. CAROME (John Carroll Univ., Cleveland, OH), and GRIGORY ADAMOVSKY (NASA, Lewis Research Center, Cleveland, OH) *In Fiber optic and laser sensors IX; Proceedings of the Meeting, Boston, MA, Sept. 3-5, 1991 Bellingham, WA Society of Photo-Optical Instrumentation Engineers* 1991 p. 320-327. refs

(Contract NAG3-984)

Copyright

A detection technique for intensity type fiberoptic sensors is described. It employs a multimode fiber interferometer, with the sensor in one arm, excited by an LED modulated at RF frequencies $f(o)$ and $2f(o)$. Sensor induced changes in intensity result in corresponding changes in the ratio of the detected $f(o)$ and $2f(o)$ signals, thus eliminating various common mode effects. Results obtained with a displacement sensor and preliminary results from a pressure sensor illustrate the capabilities of this technique. Author (revised)

A93-54363 National Aeronautics and Space Administration. Lewis Research Center, Cleveland, OH.

TECHNIQUES FOR IMPROVING THE ACCURACY OF CRYOGENIC TEMPERATURE MEASUREMENT IN GROUND TEST PROGRAMS

PAULA J. DEMPSEY and RICHARD H. FABIK (NASA, Lewis Research Center, Cleveland, OH) *In International Instrumentation Symposium, 39th, Albuquerque, NM, May 2-6, 1993, Proceedings Research Triangle Park, NC Instrument Society of America* 1993 p. 213-226. Previously announced in STAR as N93-22484 refs

(Contract RTOP 593-21-00)

Copyright

The performance of a sensor is often evaluated by determining to what degree of accuracy a measurement can be made using this sensor. The absolute accuracy of a sensor is an important parameter considered when choosing the type of sensor to use in research experiments. Tests were performed to improve the accuracy of cryogenic temperature measurements by calibration of the temperature sensors when installed in their experimental operating environment. The calibration information was then used to correct for temperature sensor measurement errors by adjusting the data acquisition system software. This paper describes a method to improve the accuracy of cryogenic temperature measurements using corrections in the data acquisition system software such that the uncertainty of an individual temperature sensor is improved from plus or minus 0.90 deg R to plus or minus 0.20 deg R over a specified range.

A93-54398 National Aeronautics and Space Administration. Lewis Research Center, Cleveland, OH.

ICING RESEARCH TUNNEL ROTATING BAR CALIBRATION MEASUREMENT SYSTEM

THERESA L. GIBSON (NASA, Lewis Research Center, Cleveland, OH) and JOHN M. DEARMON (Sverdrup Technology, Inc., Brook Park, OH) *In International Instrumentation Symposium, 39th, Albuquerque, NM, May 2-6, 1993, Proceedings Research Triangle Park, NC Instrument Society of America* 1993 p. 889-902. Previously announced in STAR as N93-22598 refs

(Contract RTOP 505-68-84)

Copyright

In order to measure icing patterns across a test section of the Icing Research Tunnel, an automated rotating bar measurement

system was developed at the NASA Lewis Research Center. In comparison with the previously used manual measurement system, this system provides a number of improvements: increased accuracy and repeatability, increased number of data points, reduced tunnel operating time, and improved documentation. The automated system uses a linear variable differential transformer (LVDT) to measure ice accretion. This instrument is driven along the bar by means of an intelligent stepper motor which also controls data recording. This paper describes the rotating bar calibration measurement system.

A93-55368* National Aeronautics and Space Administration. Lewis Research Center, Cleveland, OH.

GAS TEMPERATURE MEASUREMENTS USING THE DUAL-LINE DETECTION RAYLEIGH SCATTERING TECHNIQUE

M. V. OTUGEN (Polytechnic Univ., Brooklyn, NY), KURT D. ANNEN (Aerodyne Research, Inc., Billerica, MA), and RICHARD G. SEASHOLTZ (NASA, Lewis Research Center, Cleveland, OH) AIAA Journal (ISSN 0001-1452) vol. 31, no. 11 Nov. 1993 p. 2098-2103. Previously announced in STAR as N93-13668 refs (Contract NAS3-24613; NAG3-1301)

Copyright

A new laser-induced Rayleigh scattering method is presented for the improved temperature diagnostics of gas flows. In the present technique, the two lines of a copper vapor laser are used to obtain the time and space resolved temperature. A single set of optics is used to form the optical probe and to collect the signal simultaneously from both the 510 nm and the 578 nm lines. The dual-line detection allows for the determination and removal of surface-scattered laser light from a Rayleigh signal thereby improving the applicability of Rayleigh scattering to near wall flows with a high degree of glare. An optical system using the dual-line detection technique is built, calibrated and tested in a hot air jet under various levels of background contamination. The results indicate that highly accurate temperature measurements are possible even when the laser-line background intensity, captured by the collecting optics, is five times that of the Rayleigh signal.

N93-13307*# National Aeronautics and Space Administration. Lewis Research Center, Cleveland, OH.

EXPERIMENTAL TESTING OF FOUR CORRECTION ALGORITHMS FOR THE FORWARD SCATTERING SPECTROMETER PROBE

EDWARD A. HOVENAC (Sverdrup Technology, Inc., Brook Park, OH.), JOHN R. OLDENBURG, and JAMES A. LOCK (Cleveland State Univ., OH.) Oct. 1992 31 p Sponsored in part by FAA (Contract RTOP 505-62-50) (NASA-TM-105906; E-7374; NAS 1.15:105906; DOT/FAA/CT-TN92/29) Avail: CASI HC A03/MF A01

Three number density correction algorithms and one size distribution correction algorithm for the Forward Scattering Spectrometer Probe (FSSP) were compared with data taken by the Phase Doppler Particle Analyzer (PDPA) and an optical number density measuring instrument (NDMI). Of the three number density correction algorithms, the one that compared best to the PDPA and NDMI data was the algorithm developed by Baumgardner, Strapp, and Dye (1985). The algorithm that corrects sizing errors in the FSSP that was developed by Lock and Hovenac (1989) was shown to be within 25 percent of the Phase Doppler measurements at number densities as high as 3000/cc. Author

N93-13410*# National Aeronautics and Space Administration. Lewis Research Center, Cleveland, OH.

EFFECT OF VAPORIZATION ON CRYOGENIC SPRAY DROPSIZE MEASUREMENT

ROBERT D. INGEBRO Oct. 1992 10 p Proposed for presentation at the 31st Aerospace Sciences Meeting and Exhibit, Reno, NV, 11-14 Jan. 1993; sponsored by AIAA (Contract RTOP 505-62-21-00) (NASA-TM-105909; E-7387; NAS 1.15:105909; AIAA PAPER 93-0692) Copyright Avail: CASI HC A02/MF A01

The fluid mechanics of multi-phase flow breakup of liquid nitrogen, LN2, jets injected into sonic velocity nitrogen gasflow, was experimentally investigated. A scattered-light scanning instrument was used to measure the characteristic droplet size, $D_{(sub\ v.5)}$, of LN2 sprays and to determine the effect of droplet vaporization on experimental droplet size measurements. Under sonic gas-velocity conditions, liquid-jet breakup occurred in the regime of aerodynamic stripping. As a result, the following correlation of volume-median drop diameter, $D_{(sub\ v.5)}$, with atomizing gas flowrate, $W_{(sub\ g)}$, was derived for two-fluid atomizers; with atomizing gas flowrate, $W_{(sub\ g)}$, was derived for two-fluid atomizers; $D_{(sub\ v.5)}(exp -1) = k_{(sub\ c)}(W_{(sub\ g)})^{(sup\ n)}$, where proportionally constant $k_{(sub\ c)}$ and exponent n are functions of droplet vaporization rate. Partially vaporized sprays were investigated and it was found that $n = 1.11$, which is considerably less than the value of 1.33 that is predicted by atomization theory. This was attributed to the evaporative loss of very small droplets. As a result, the following expression was obtained experimentally: $D_{(sub\ v.5)}(exp -1) = 301(W_{(sub\ g)})^{(sup\ 1.11)}$. Values of $D_{(sub\ v.5)}$, that existed prior to partial vaporization of the LN2 sprays, were calculated and the following expression was derived for originally unvaporized LN2 sprays: $D_{(sub\ v.5)}(exp -1) = 285(W_{(sub\ g)})^{(sup\ 1.33)}$. This expression agrees well with atomization theory that predicts $n = 1.33$, for liquid jet breakup in high-velocity gasflow. Author

N93-13666*# National Aeronautics and Space Administration. Lewis Research Center, Cleveland, OH.

THIN FILM THERMOCOUPLES FOR HIGH TEMPERATURE MEASUREMENT ON CERAMIC MATERIALS

RAYMOND HOLANDA /in NASA. Langley Research Center, The 1992 NASA Langley Measurement Technology Conference: Measurement Technology for Aerospace Applications in High-Temperature Environments p 81-96 Sep. 1992 Avail: CASI HC A03/MF A04

Thin film thermocouples have been developed for use on metal parts in jet engines to 1000 C. However, advanced propulsion systems are being developed that will use ceramic materials and reach higher temperatures. The purpose of this work is to develop thin film thermocouples for use on ceramic materials. The thin film thermocouples are Pt13Rh/Pt fabricated by the sputtering process. Lead wires are attached using the parallel-gap welding process. The ceramic materials are silicon nitride, silicon carbide, aluminum oxide, and mullite. Both steady state and thermal cycling furnace tests were performed in the temperature range to 1500 C. High-heating-rate tests were performed in an arc lamp heat-flux-calibration facility. The fabrication of the thin film thermocouples is described. The thin film thermocouple output was compared to a reference wire thermocouple. Drift of the thin film thermocouples was determined, and causes of drift are discussed. The results of high-heating-rate tests up to 2500 C/sec are presented. The stability of the ceramic materials is examined. It is concluded that Pt13Rh/Pt thin film thermocouples are capable of meeting lifetime goals of 50 hours or more up to temperatures of 1500 C depending on the stability of the particular ceramic substrate. Author

N93-13667*# National Aeronautics and Space Administration. Lewis Research Center, Cleveland, OH.

FABRICATION OF THIN FILM HEAT FLUX SENSORS

HERBERT A. WILL /in NASA. Langley Research Center, The 1992 NASA Langley Measurement Technology Conference: Measurement Technology for Aerospace Applications in High-Temperature Environments p 97-106 Sep. 1992 Avail: CASI HC A02/MF A04

Prototype thin film heat flux sensors have been constructed and tested. The sensors can be applied to propulsion system materials and components. The sensors can provide steady state and fast transient heat flux information. Fabrication of the sensor does not require any matching of the mounting surface. Heat flux is proportional to the temperature difference across the upper and lower surfaces of an insulation material. The sensor consists of an array of thermocouples on the upper and lower surfaces of

a thin insulating layer. The thermocouples for the sensor are connected in a thermopile arrangement. A 100 thermocouple pair heat flux sensor has been fabricated on silicon wafers. The sensor produced an output voltage of 200-400 microvolts when exposed to a hot air heat gun. A 20 element thermocouple pair heat flux sensor has been fabricated on aluminum oxide sheet. Thermocouples are Pt-Pt/Rh with silicon dioxide as the insulating material. This sensor produced an output of 28 microvolts when exposed to the radiation of a furnace operating at 1000 C. Work is also underway to put this type of heat flux sensor on metal surfaces. Author

N93-13668*# National Aeronautics and Space Administration. Lewis Research Center, Cleveland, OH.

GAS TEMPERATURE MEASUREMENTS USING THE DUAL-LINE DETECTION RAYLEIGH SCATTERING TECHNIQUE

M. VOLKAN OTUGEN (Polytechnic Univ., Brooklyn, NY.), RICHARD G. SEASHOLTZ, and KURT D. ANNEN (Aerodyne Research, Inc., Billerica, MA.) In NASA. Langley Research Center, The 1992 NASA Langley Measurement Technology Conference: Measurement Technology for Aerospace Applications in High-Temperature Environments p 107-126 Sep. 1992 (Contract NAG3-1301)

Avail: CASI HC A03/MF A04

A new laser-induced Rayleigh scattering method is presented for the improved temperature diagnostics of gas flows. In the present technique, the two lines of a copper vapor laser are used to obtain the time and space resolved temperature. A single set of optics is used to form the optical probe and to collect the signal simultaneously from both the 510 nm and the 578 nm lines. The dual-line detection allows for the determination and removal of surface-scattered laser light from a Rayleigh signal thereby improving the applicability of Rayleigh scattering to near wall flows with a high degree of glare. An optical system using the dual-line detection technique is built, calibrated and tested in a hot air jet under various levels of background contamination. The results indicate that highly accurate temperature measurements are possible even when the laser-line background intensity, captured by the collecting optics, is five times that of the Rayleigh signal. Author

N93-13683*# National Aeronautics and Space Administration. Lewis Research Center, Cleveland, OH.

VISUALIZATION OF HYDROGEN INJECTION IN A SCRAMJET ENGINE BY SIMULTANEOUS PLIF IMAGING AND LASER HOLOGRAPHIC IMAGING

ROBERT C. ANDERSON, RICHARD E. TRUCCO (General Applied Science Labs., Inc., Ronkonkoma, NY.), L. F. RUBIN (Rockwell International Corp., Canoga Park, CA.), and D. M. SWAIN (Rockwell International Corp., Canoga Park, CA.) In NASA. Langley Research Center, The 1992 NASA Langley Measurement Technology Conference: Measurement Technology for Aerospace Applications in High-Temperature Environments p 339-354 Sep. 1992

Avail: CASI HC A03/MF A04

Flowfield characterization has been accomplished for several fuel injector configurations using simultaneous planar laser induced fluorescence (PLIF) and laser holographic imaging (LHI). The experiments were carried out in the GASL-NASA HYPULSE real gas expansion tube facility, a pulsed facility with steady test times of about 350 microsec. The tests were done at simulated Mach numbers 13.5 and 17. The focus of this paper is on the measurement technologies used and their application in a research facility. The HYPULSE facility, the models used for the experiments, and the setup for the LHI and PLIF measurements are described. Measurement challenges and solutions are discussed. Results are presented for experiments with several fuel injector configurations and several equivalence ratios. Author

N93-13684*# National Aeronautics and Space Administration. Lewis Research Center, Cleveland, OH.

GAS TEMPERATURE AND DENSITY MEASUREMENTS BASED ON SPECTRALLY RESOLVED RAYLEIGH-BRILLOUIN SCATTERING

RICHARD G. SEASHOLTZ and JAMES A. LOCK (Cleveland State Univ., OH.) In NASA. Langley Research Center, The 1992 NASA Langley Measurement Technology Conference: Measurement Technology for Aerospace Applications in High-Temperature Environments p 355-374 Sep. 1992

Avail: CASI HC A03/MF A04

The use of molecular Rayleigh scattering for measurements of gas density and temperature is evaluated. The technique used is based on the measurement of the spectrum of the scattered light, where both temperature and density are determined from the spectral shape. Planar imaging of Rayleigh scattering from air using a laser light sheet is evaluated for ambient conditions. The Cramer-Rao lower bounds for the shot-noise limited density and temperature measurement uncertainties are calculated for an ideal optical spectrum analyzer and for a planar mirror Fabry-Perot interferometer used in a static, imaging mode. With this technique, a single image of the Rayleigh scattered light can be analyzed to obtain density (or pressure) and temperature. Experimental results are presented for planar measurements taken in a heated air stream. Author

N93-17060*# National Aeronautics and Space Administration. Lewis Research Center, Cleveland, OH.

MULTIWAVELENGTH PYROMETER FOR GRAY AND NON-GRAY SURFACES IN THE PRESENCE OF INTERFERING RADIATION Patent Application

DANIEL NG, inventor (to NASA) 14 Dec. 1992 26 p (NASA-CASE-LEW-15250-1; NAS 1.71:LEW-15250-1;

US-PATENT-APPL-SN-991403) Avail: CASI HC A03/MF A01

A method and apparatus for detecting the temperature of gray and non-gray bodies in the presence of interfering radiation are presented. A gray body has a constant emissivity less than 1 and a non-gray body has an emissivity which varies with wavelength. The emissivity and reflectivity of the surface is determined over a range of wavelengths. Spectra are also measured of the extraneous interference radiation source and the surface of the object to be measured in the presence of the extraneous interference radiation source. An auxiliary radiation source is used to determine the reflectivity of the surface and also the emissivity. The measured spectrum of the surfaces in the presence of the extraneous interference radiation source is set equal to the emissivity of the surface multiplied by a Planck function containing a temperature term T plus the surface reflectivity multiplied by the spectrum of the extraneous interference radiation source. The equation is then solved for T to determine the temperature of the surface. NASA

N93-17777*# National Aeronautics and Space Administration. Lewis Research Center, Cleveland, OH.

A SURVEY AND ANALYSIS OF COMMERCIALLY AVAILABLE HYDROGEN SENSORS

GARY W. HUNTER Nov. 1992 23 p

(Contract RTOP 590-21-11)

(NASA-TM-105878; E-7198; NAS 1.26:105878) Avail: CASI HC A03/MF A01

The performance requirements for hydrogen detection in aerospace applications often exceed those of more traditional applications. In order to ascertain the applicability of existing hydrogen sensors to aerospace applications, a survey was conducted of commercially available point-contact hydrogen sensors, and their operation was analyzed. The operation of the majority of commercial hydrogen sensors falls into four main categories: catalytic combustion, electrochemical, semiconducting oxide sensors, and thermal conductivity detectors. The physical mechanism involved in hydrogen detection for each main category is discussed in detail. From an understanding of the detection mechanism, each category of sensor is evaluated for use in a variety of space and propulsion environments. In order to meet

the needs of aerospace applications, the development of point-contact hydrogen sensors that are based on concepts beyond those used in commercial sensors is necessary. Author

N93-19651*# National Aeronautics and Space Administration. Lewis Research Center, Cleveland, OH.

2D VELOCITY AND TEMPERATURE MEASUREMENTS IN HIGH SPEED FLOWS BASED ON SPECTRALLY RESOLVED RAYLEIGH SCATTERING

RICHARD G. SEASHOLTZ 1992 12 p Presented at the Advanced Research Workshop: New Trends in Instrumentation for Hypersonic Research, Le Fauga-Mauzac, France, 27 Apr. - 1 May 1992; sponsored by NATO (Contract RTOP 505-62-50) (NASA-TM-105784; E-7214; NAS 1.15:105784) Avail: CASI HC A03/MF A01

The use of molecular Rayleigh scattering for measurements of gas velocity and temperature is evaluated. Molecular scattering avoids problems associated with the seeding required by conventional laser anemometry and particle image velocimetry. The technique considered herein is based on the measurement of the spectrum of the scattered light. Planar imaging of Rayleigh scattering using a laser light sheet is evaluated for conditions at 30 km altitude (typical hypersonic flow conditions). The Cramer-Rao lower bounds for velocity and temperature measurement uncertainties are calculated for an ideal optical spectrum analyzer and for a planar mirror Fabry-Perot interferometer used in a static, imaging mode. With this technique, a single image of the Rayleigh scattered light from clean flows can be analyzed to obtain temperature and one component of velocity. Experimental results are presented for planar velocity measurements in a Mach 1.3 air jet. Author

N93-22484*# National Aeronautics and Space Administration. Lewis Research Center, Cleveland, OH.

TECHNIQUES FOR IMPROVING THE ACCURACY OF CRYOGENIC TEMPERATURE MEASUREMENT IN GROUND TEST PROGRAMS

PAULA J. DEMPSEY and RICHARD H. FABIK May 1993 16 p Prepared for presentation at the 39th Aerospace Industries/Test Measurement Symposium, Albuquerque, NM, 3-6 May 1993; sponsored by the Instrument Society of America (Contract RTOP 593-21-00) (NASA-TM-105996; E-7536; NAS 1.15:105996) Avail: CASI HC A03/MF A01

The performance of a sensor is often evaluated by determining to what degree of accuracy a measurement can be made using this sensor. The absolute accuracy of a sensor is an important parameter considered when choosing the type of sensor to use in research experiments. Tests were performed to improve the accuracy of cryogenic temperature measurements by calibration of the temperature sensors when installed in their experimental operating environment. The calibration information was then used to correct for temperature sensor measurement errors by adjusting the data acquisition system software. This paper describes a method to improve the accuracy of cryogenic temperature measurements using corrections in the data acquisition system software such that the uncertainty of an individual temperature sensor is improved from plus or minus 0.90 deg R to plus or minus 0.20 deg R over a specified range. Author (revised)

N93-22598*# National Aeronautics and Space Administration. Lewis Research Center, Cleveland, OH.

ICING RESEARCH TUNNEL ROTATING BAR CALIBRATION MEASUREMENT SYSTEM

THERESA L. GIBSON and JOHN M. DEARMON (Sverdrup Technology, Inc., Brook Park, OH.) Mar. 1993 16 p Prepared for presentation at the 39th Aerospace Industries/Test Measurement Symposium, Albuquerque, NM, 3-6 May 1993; sponsored by the Instrument Society of America (Contract RTOP 505-62-84) (NASA-TM-106010; E-7539; NAS 1.15:106010) Avail: CASI HC A03/MF A01

In order to measure icing patterns across a test section of the Icing Research Tunnel, an automated rotating bar measurement system was developed at the NASA Lewis Research Center. In comparison with the previously used manual measurement system, this system provides a number of improvements: increased accuracy and repeatability, increased number of data points, reduced tunnel operating time, and improved documentation. The automated system uses a linear variable differential transformer (LVDT) to measure ice accretion. This instrument is driven along the bar by means of an intelligent stepper motor which also controls data recording. This paper describes the rotating bar calibration measurement system. Author

N93-22994*# National Aeronautics and Space Administration. Lewis Research Center, Cleveland, OH.

OTV BEARING DEFLECTION INVESTIGATION

B. L. REIMER (Aerojet-General Corp., Sacramento, CA.), R. T. DIEPENBROCK (Aerojet-General Corp., Sacramento, CA.), and M. G. MILLIS Apr. 1993 18 p Sponsored by NASA. Lewis Research Center (Contract F04611-86-C-0010; RTOP 593-12-11) (NASA-TM-106085; E-7714; NAS 1.15:106085) Avail: CASI HC A03/MF A01

The primary goal of the Bearing Deflectometer Investigation was to gain experience in the use of fiber optic displacement probe technology for bearing health monitoring in a liquid hydrogen turbo pump. The work specified in this Task Order was conducted in conjunction with Air Force Rocket Propulsion Laboratory Contract F04611-86-C-0010. APD conducted the analysis and design coordination to provide a displacement probe design compatible with the XLR-134 liquid hydrogen turbo pump assembly (TPA). Specifications and requirements of the bearing deflectometer were established working with Mechanical Technology Instruments, Inc. (MTI). The TPA design accommodated positioning of the probe to measure outer race cyclic deflections of the pump inlet bearing. The fiber optic sensor was installed as required in the TPA and sensor output was recorded during the TPA testing. Data review indicated that no bearing deflection signature could be differentiated from the inherent system noise. Alternate sensor installations were not investigated, but might yield different results. Author

N93-24737*# National Aeronautics and Space Administration. Lewis Research Center, Cleveland, OH.

ICE THICKNESS MEASUREMENT SYSTEM FOR THE ICING RESEARCH TUNNEL CALIBRATION

THERESA L. GIBSON and JOHN M. DEARMON (Sverdrup Technology, Inc., Brook Park, OH.) Jun. 1993 8 p Proposed for presentation at the 1993 SWE National Convention and Student Conference, Chicago, IL, 21-27 Jun. 1993; sponsored by the Society of Women Engineers (Contract RTOP 505-62-84) (NASA-TM-106095; E-7735; NAS 1.15:106095) Avail: CASI HC A02/MF A01

To measure icing patterns across a test section of the Icing Research Tunnel, an automated rotating bar measurement system was developed at NASA LeRC. In comparison with the previously used manual measurement system, this system provides a number of improvements: increased accuracy and repeatability, increased number of data points, reduced tunnel operating time, and improved documentation. The automated system uses a linear variable differential transformer (LVDT) to measure ice accretion. This instrument is driven along the bar by means of an intelligent stepper motor which also controls data recording. This paper describes the rotating bar calibration measurement system. Author (revised)

N93-25173*# National Aeronautics and Space Administration. Lewis Research Center, Cleveland, OH.

DEVELOPMENT OF THIN FILM THERMOCOUPLES ON CERAMIC MATERIALS FOR ADVANCED PROPULSION SYSTEM APPLICATIONS

RAYMOND HOLANDA Feb. 1993 16 p Presented at the Conference for Preparation for Temperature: Its Measurement and

Control in Science and Industry, Toronto, Ontario, 28 Apr. - 2 May 1992; sponsored by AIP, ISA, NIST, and NRC
(Contract RTOP 510-01-50)
(NASA-TM-106017; E-7574; NAS 1.15:106017) Avail: CASI HC A03/MF A01

Thin film thermocouples were developed for use on metal parts in jet engines to 1000 C. However, advanced propulsion systems are being developed that will use ceramic materials and reach higher temperatures. The purpose is to develop thin film thermocouples for use on ceramic materials. The new thin film thermocouples are Pt13Rh/Pt fabricated by the sputtering process. Lead wires are attached using the parallel-gap welding process. The ceramic materials tested are silicon nitride, silicon carbide, aluminum oxide, and mullite. Both steady state and thermal cycling furnace tests were performed in the temperature range to 1500 C. High-heating-rate tests were performed in an arc lamp heat-flux-calibration facility. The fabrication of the thin film thermocouples is described. The thin film thermocouple output was compared to a reference wire thermocouple. Drift of the thin film thermocouples was determined, and causes of drift are discussed. The results of high heating rate tests up to 2500 C/sec are presented. The stability of the ceramic materials is examined. It is concluded that Pt13Rh/Pt thin film thermocouples are capable of meeting lifetime goals of 50 hr or more up to temperatures of 1500 C depending on the stability of the particular ceramic substrate. Author (revised)

N93-25191* National Aeronautics and Space Administration. Lewis Research Center, Cleveland, OH.

ATOMIZING-GAS TEMPERATURE EFFECT ON CRYOGENIC SPRAY DROPSIZE

ROBERT D. INGEBO Jun. 1993 12 p Prepared for presentation at the 29th Joint Propulsion Conference and Exhibit, Monterey, CA, 28-30 Jun. 1993; sponsored by AIAA, SAE, ASME, and ASSEE

(Contract RTOP 505-62-52)
(NASA-TM-106106; E-7754; NAS 1.15:106106) Avail: CASI HC A03/MF A01

Correlating expressions for two-phase flow breakup of liquid nitrogen, LN₂, jets in sonic velocity nitrogen gasflows were obtained for an atomizing-gas temperature range of 111 to 442 K. The correlations were based on characteristic droplet measurements obtained with a scattered-light scanner. The effect of droplet vaporization on the measurements of the volume-median droplet size was calculated by using previously determined heat and momentum transfer expressions for droplets evaporating in high-velocity gasflow. Finally, the droplet size of the originally unvaporized spray was calculated, normalized with respect to jet diameter and correlated with atomizing-gas flowrate and temperature. Author

N93-26906* National Aeronautics and Space Administration. Lewis Research Center, Cleveland, OH.

NEURAL NETWORKS FOR CALIBRATION TOMOGRAPHY

ARTHUR DECKER Jun. 1993 10 p Proposed for presentation at the 1993 International Symposium on Optics, Imaging, and Instrumentation, San Diego, CA, 11-16 Jul. 1993; sponsored by Society of Photo-Optical Instrumentation Engineering
(Contract RTOP 505-62-50)

(NASA-TM-106352; E-7857; NAS 1.15:106352) Avail: CASI HC A02/MF A01

Artificial neural networks are suitable for performing pattern-to-pattern calibrations. These calibrations are potentially useful for facilities operations in aeronautics, the control of optical alignment, and the like. Computed tomography is compared with neural net calibration tomography for estimating density from its x-ray transform. X-ray transforms are measured, for example, in diffuse-illumination, holographic interferometry of fluids. Computed tomography and neural net calibration tomography are shown to have comparable performance for a 10 degree viewing cone and 29 interferograms within that cone. The system of tomography discussed is proposed as a relevant test of neural networks and other parallel processors intended for using flow visualization data. Author (revised)

N93-27001* National Aeronautics and Space Administration. Lewis Research Center, Cleveland, OH.

CALIBRATION OF A SHOCK WAVE POSITION SENSOR USING ARTIFICIAL NEURAL NETWORKS

ARTHUR J. DECKER and KENNETH E. WEILAND May 1993 20 p

(Contract RTOP 505-62-50)
(NASA-TM-106138; E-7819; NAS 1.15:106138) Avail: CASI HC A03/MF A01

This report discusses the calibration of a shock wave position sensor. The position sensor works by using artificial neural networks to map cropped CCD frames of the shadows of the shock wave into the value of the shock wave position. This project was done as a tutorial demonstration of method and feasibility. It used a laboratory shadowgraph, nozzle, and commercial neural network package. The results were quite good, indicating that artificial neural networks can be used efficiently to automate the semi-quantitative applications of flow visualization. Author (revised)

N93-27021* National Aeronautics and Space Administration. Lewis Research Center, Cleveland, OH.

THE DEVELOPMENT OF HYDROGEN SENSOR TECHNOLOGY AT NASA LEWIS RESEARCH CENTER

GARY W. HUNTER, PHILIP G. NEUDECK, G. D. JEFFERSON, G. C. MADZSAR, C. C. LIU (Case Western Reserve Univ., Cleveland, OH.), and Q. H. WU (Case Western Reserve Univ., Cleveland, OH.) May 1993 20 p Presented at the Fourth Annual Space System Health Management Technology Conference, Cincinnati, OH, 17-18 Nov. 1992; sponsored by AIAA
(Contract RTOP 590-21-11)

(NASA-TM-106141; E-7773; NAS 1.15:106141) Avail: CASI HC A03/MF A01

The detection of hydrogen leaks in aerospace applications, especially those involving hydrogen fuel propulsion systems, is of extreme importance for reasons of reliability, safety, and economy. Motivated by leaks occurring in liquid hydrogen lines supplying the main engine of the Space Shuttle, NASA Lewis has initiated a program to develop point-contact hydrogen sensors which address the needs of aerospace applications. Several different approaches are being explored. They include the fabrication of PdAg Schottky diode structures, the characterization of PdCr as a hydrogen sensitive alloy, and the use of SiC as a semiconductor for hydrogen sensors. This paper discusses the motivation behind and present status of each of the major components of the NASA LeRC hydrogen sensor program. Author

N93-27027* National Aeronautics and Space Administration. Lewis Research Center, Cleveland, OH.

FUZZY LOGIC PARTICLE TRACKING VELOCIMETRY

MARK P. WERNET Jun. 1993 10 p Proposed for presentation at the Optical Diagnostics in Fluid and Thermal Flow, San Diego, CA, 11-16 Jul. 1993; sponsored by Society of Photo-Optical Instrumentation Engineers

(Contract RTOP 505-62-50)
(NASA-TM-106194; E-7900; NAS 1.15:106194) Avail: CASI HC A02/MF A01

Fuzzy logic has proven to be a simple and robust method for process control. Instead of requiring a complex model of the system, a user defined rule base is used to control the process. In this paper the principles of fuzzy logic control are applied to Particle Tracking Velocimetry (PTV). Two frames of digitally recorded, single exposure particle imagery are used as input. The fuzzy processor uses the local particle displacement information to determine the correct particle tracks. Fuzzy PTV is an improvement over traditional PTV techniques which typically require a sequence (greater than 2) of image frames for accurately tracking particles. The fuzzy processor executes in software on a PC without the use of specialized array or fuzzy logic processors. A pair of sample input images with roughly 300 particle images each, results in more than 200 velocity vectors in under 8 seconds of processing time. Author (revised)

N93-28053*# National Aeronautics and Space Administration.
Lewis Research Center, Cleveland, OH.

**STATUS OF THE FIBER OPTIC CONTROL SYSTEM
INTEGRATION (FOCSI) PROGRAM**

ROBERT J. BAUMBICK May 1993 17 p

(Contract RTOP 505-62-50)

(NASA-TM-106151; E-7832; NAS 1.15:106151) Avail: CASI HC
A03/MF A01

This report presents a discussion of the progress made in the NASA/NAVY Fiber Optic Control System Integration (FOCSI) program. This program will culminate in open-loop flight tests of passive optical sensors and associated electro-optics on an F-18 aircraft. Currently, the program is in the final stages of hardware fabrication and environmental testing of the passive optical sensors and electro-optics. This program is a foundation for future Fly-by-Light (FBL) programs. The term Fly-by-Light is used to describe the utilization of passive optical sensors and fiber optic data links for monitoring and control of aircraft in which sensor and actuation signals are transmitted optically. The benefits of this technology for advanced aircraft include the following: improved reliability and reduced certification cost due to greater immunity to EME (electromagnetic effects); reduced harness volume and weight; elimination of short circuits and sparking in wiring due to insulation deterioration; lower maintenance costs (fewer components); greater flexibility in data bus protocol and architecture; absence of ground loops; and higher operating temperatures for electrically passive optical sensors.

Author (revised)

N93-31298*# National Aeronautics and Space Administration.
Lewis Research Center, Cleveland, OH.

**HIGH TEMPERATURE, OXIDATION RESISTANT NOBLE
METAL-AL ALLOY THERMOCOUPLE Patent Application**

JAMES L. SMIALEK, inventor (to NASA) and MICHAEL GEDWILL,
inventor (to NASA) 6 Jul. 1993 22 p

(NASA-CASE-LEW-15515-1; NAS 1.71:LEW-15515-1;

US-PATENT-APPL-SN-086584) Avail: CASI HC A03/MF A01

A thermocouple having an electropositive leg formed of a noble metal-Al alloy and an electronegative leg electrically joined at respective ends thereof to form a thermocouple junction. The thermocouple provides for accurate and reproducible measurement of high temperatures (600 - 1300 C) in inert, oxidizing, or reducing environments, gases, or vacuum. Furthermore, the thermocouple circumvents the need for expensive, strategic precious metals such as rhodium as a constituent component. Selective oxidation of rhodium is also thereby precluded.

NASA

N93-31553*# National Aeronautics and Space Administration.
Lewis Research Center, Cleveland, OH.

**PROGRESS IN THE MEASUREMENT OF SSME TURBINE
HEAT FLUX WITH PLUG-TYPE SENSORS**

CURT H. LIEBERT *In its* Structural Integrity and Durability of
Reusable Space Propulsion Systems p 3-7 May 1991

Avail: CASI HC A01/MF A03

Data reduction was completed for tests of plug-type heat flux sensors (gauges) in a turbine blade thermal cycling tester (TBT) that is located at NASA/Marshall Space Flight Center, and a typical gauge is illustrated. This is the first time that heat flux has been measured in a Space Shuttle Main Engine (SSME) Turbopump Turbine environment. The development of the concept for the gauge was performed in a heat flux measurement facility at Lewis. In this facility, transient and steady state absorbed surface heat flux information was obtained from transient temperature measurements taken at points within the gauge. A schematic of the TBT is presented, and plots of the absorbed surface heat flux measured on the three blades tested in the TBT are presented. High quality heat flux values were measured on all three blades. The experiments demonstrated that reliable and durable gauges can be repeatedly fabricated into the airfoils. The experiment heat flux data are being used for verification of SSME analytical stress, boundary layer, and heat transfer design models. Other experimental results and future plans are also presented.

Derived from text

N93-31554*# National Aeronautics and Space Administration.
Lewis Research Center, Cleveland, OH.

**THIN FILM HEAT FLUX SENSOR FOR SPACE SHUTTLE MAIN
ENGINE TURBINE ENVIRONMENT**

HERBERT WILL *In its* Structural Integrity and Durability of
Reusable Space Propulsion Systems p 9-13 May 1991

Avail: CASI HC A01/MF A03

The Space Shuttle Main Engine (SSME) turbine environment stresses engine components to their design limits and beyond. The extremely high temperatures and rapid temperature cycling can easily cause parts to fail if they are not properly designed. Thin film heat flux sensors can provide heat loading information with almost no disturbance of gas flows or of the blade. These sensors can provide steady state and transient heat flux information. A thin film heat flux sensor is described which makes it easier to measure small temperature differences across very thin insulating layers.

Derived from text

N93-31555*# National Aeronautics and Space Administration.
Lewis Research Center, Cleveland, OH.

**THIN FILM THERMOCOUPLES FOR HIGH TEMPERATURE
TURBINE APPLICATION**

LISA C. MARTIN *In its* Structural Integrity and Durability of
Reusable Space Propulsion Systems p 15-20 May 1991

Avail: CASI HC A02/MF A03

The objective is to develop thin film thermocouples (TFTC) for Space Shuttle Main Engine (SSME) components such as the high pressure fuel turbopump (HPFTP) blades and to test TFTC survivability and durability in the SSME environment. The purpose for developing TFTC's for SSME components is to obtain blade temperatures for computational models developed for fluid mechanics and structures. The TFTC must be able to withstand the presence of high temperature, high pressure hydrogen as well as a severe thermal transient due to a cryogenic to combustion temperature change. The TFTC's will eventually be installed and tested on SSME propulsion system components in the SSME test bed engine. The TFTC's were successfully fabricated on flat coupons of MAR-M 246 (Hf+), which is the superalloy material used for HPFTP turbine blades. The TFTC's fabricated on flat coupons survived thermal shock cycling as well as testing in a heat flux measurement facility which provided a rapid thermal transient. The same fabrication procedure was used to deposit TFTC's on HPFTP first stage rotor blades. Other results from the experiments are presented, and future testing plans are discussed.

Derived from text

36

LASERS AND MASERS

Includes parametric amplifiers.

N93-18091*# National Aeronautics and Space Administration.
Lewis Research Center, Cleveland, OH.

**A FUZZY LOGIC BASED CONTROLLER FOR THE
AUTOMATED ALIGNMENT OF A LASER-BEAM-SMOOTHING
SPATIAL FILTER**

M. J. KRASOWSKI and D. E. DICKENS (Dayton Univ., OH.) Dec.
1992 17 p

(Contract RTOP 590-21-11)

(NASA-TM-105994; E-7526; NAS 1.15:105994) Avail: CASI HC
A03/MF A01

A fuzzy logic based controller for a laser-beam-smoothing spatial filter is described. It is demonstrated that a human operator's alignment actions can easily be described by a system of fuzzy rules of inference. The final configuration uses inexpensive, off-the-shelf hardware and allows for a compact, readily implemented embedded control system.

Author

N93-22197* National Aeronautics and Space Administration. Lewis Research Center, Cleveland, OH.

THREE-DIMENSIONAL LASER WINDOW FORMATION FOR INDUSTRIAL APPLICATION

VINCENT G. VERHOFF and DAVID KOWALSKI /in NASA, Washington, Technology 2002: The Third National Technology Transfer Conference and Exposition, Volume 2 p 454-459 Feb. 1993

Avail: CASI HC A04/MF A04

The NASA Lewis Research Center has developed and implemented a unique process for forming flawless three-dimensional, compound-curvature laser windows to extreme accuracies. These windows represent an integral component of specialized nonintrusive laser data acquisition systems that are used in a variety of compressor and turbine research testing facilities. These windows are molded to the flow surface profile of turbine and compressor casings and are required to withstand extremely high pressures and temperatures. This method of glass formation could also be used to form compound-curvature mirrors that would require little polishing and for a variety of industrial applications, including research view ports for testing devices and view ports for factory machines with compound-curvature casings. Currently, sodium-alumino-silicate glass is recommended for three-dimensional laser windows because of its high strength due to chemical strengthening and its optical clarity. This paper discusses the main aspects of three-dimensional laser window formation. It focuses on the unique methodology and the peculiarities that are associated with the formation of these windows.

Author

N93-22198* National Aeronautics and Space Administration. Lewis Research Center, Cleveland, OH.

HIGH PERFORMANCE SAPPHIRE WINDOWS

STEPHEN C. BATES (Advanced Fuel Research, Inc., East Hartford, CT.) and LARRY LIU /in NASA, Washington, Technology 2002: The Third National Technology Transfer Conference and Exposition, Volume 2 p 460-469 Feb. 1993

Avail: CASI HC A02/MF A04

High-quality, wide-aperture optical access is usually required for the advanced laser diagnostics that can now make a wide variety of non-intrusive measurements of combustion processes. Specially processed and mounted sapphire windows are proposed to provide this optical access to extreme environment. Through surface treatments and proper thermal stress design, single crystal sapphire can be a mechanically equivalent replacement for high strength steel. A prototype sapphire window and mounting system have been developed in a successful NASA SBIR Phase 1 project. A large and reliable increase in sapphire design strength (as much as 10x) has been achieved, and the initial specifications necessary for these gains have been defined. Failure testing of small windows has conclusively demonstrated the increased sapphire strength, indicating that a nearly flawless surface polish is the primary cause of strengthening, while an unusual mounting arrangement also significantly contributes to a larger effective strength. Phase 2 work will complete specification and demonstration of these windows, and will fabricate a set for use at NASA. The enhanced capabilities of these high performance sapphire windows will lead to many diagnostic capabilities not previously possible, as well as new applications for sapphire.

Author

N93-31556* National Aeronautics and Space Administration. Lewis Research Center, Cleveland, OH.

RAYLEIGH-BRILLOUIN SCATTERING FOR HIGH-PRESSURE GAS TEMPERATURE MEASUREMENTS

RICHARD G. SEASHOLTZ /in its Structural Integrity and Durability of Reusable Space Propulsion Systems p 21-27 May 1991

Avail: CASI HC A02/MF A03

An experiment was set up to evaluate the feasibility of using Rayleigh-Brillouin scattering as a diagnostic technique for measuring gas temperature in high pressure environments, such as the Space Shuttle Main Engine (SSME) Preburner. A high pressure furnace is used as the scattering chamber. Either nitrogen or hydrogen may be used. An argon ion laser beam is focused

into the furnace. Light backscattering from the gas in the furnace is collected and analyzed with a 5-pass scanning Fabry-Perot interferometer and photon counting electronics. The multi-pass configuration provides the high frequency selectively needed to measure the Brillouin peaks in the presence of large amounts of spuriously scattered light at the laser frequency. Preliminary measurements were made at room temperature in nitrogen at pressures up to 2000 psia. The free spectral range of the interferometer and frequency separation of the Brillouin peaks are determined from measured spectra. Temperature measurements are then obtained using the simple continuum theory with low frequency values of specific heat ratio and shear viscosity. The measured temperatures are within 10 percent of the true value.

Derived from text

37

MECHANICAL ENGINEERING

Includes auxiliary systems (nonpower); machine elements and processes; and mechanical equipment.

A93-11332* National Aeronautics and Space Administration. Lewis Research Center, Cleveland, OH.

ON THE MELT INFILTRATION OF COPPER COATED SILICON CARBIDE WITH AN ALUMINIUM ALLOY

R. ASTHANA (Cleveland State Univ.; NASA, Lewis Research Center, OH) and P. K. ROHATGI (Wisconsin Univ., Milwaukee) Composites Manufacturing (ISSN 0956-7143) vol. 3, no. 2 1992 p. 119-123. Research supported by EPRI, U.S. Navy, Wisconsin Applied Research Grant, and DIN Program of the State of Wisconsin refs

Copyright

Pressure-assisted infiltration of porous compacts of Cu coated and uncoated single crystals of platelet shaped alpha (hexagonal) SiC was used to study infiltration dynamics and particulate wettability with a 2014 Al alloy. The infiltration lengths were measured for a range of experimental variables which included infiltration pressure, infiltration time, and SiC size. A threshold pressure P_{th} for flow initiation through compacts was identified from an analysis of infiltration data; P_{th} decreased while penetration lengths increased with increasing SiC size (more fundamentally, due to changes in interparticle pore size) and with increasing infiltration times. Cu coated SiC led to lower P_{th} and 60-80 percent larger penetration lengths compared to uncoated SiC under identical processing conditions.

Author

A93-14521* National Aeronautics and Space Administration. Lewis Research Center, Cleveland, OH.

MAXIMUM LIFE SPUR GEAR DESIGN

M. SAVAGE, B. J. MACKULIN (Akron Univ., OH), H. H. COE, and J. J. COY (NASA, Lewis Research Center, Cleveland, OH) Journal of Propulsion and Power (ISSN 0748-4658) vol. 8, no. 6 Nov.-Dec. 1992 p. 1273-1281. Previously cited in issue 17, p. 2960, Accession no. A91-41682 AIAA, SAE, ASME, and ASEE, Joint Propulsion Conference, 27th, Sacramento, CA, June 24-26, 1991, AIAA Paper 91-2021 refs

Copyright

A93-14651 National Aeronautics and Space Administration. Lewis Research Center, Cleveland, OH.

DEVELOPMENT OF ADVANCED SEALS FOR SPACE PROPULSION TURBOMACHINERY

ROBERT C. HENDRICKS, ANITA D. LIANG (NASA, Lewis Research Center, Cleveland, OH), DARA W. CHILDS (Texas A & M Univ., College Station), and MARGARET P. PROCTOR (NASA, Lewis Research Center, Cleveland, OH) Apr. 1992 14 p. SAE, Aerospace Atlantic Conference, Dayton, OH, Apr. 7-10, 1992 Previously announced in STAR as N92-24957 refs

(Contract RTOP 590-21-11)

(SAE PAPER 921028) Copyright

Current activities in seals for space propulsion turbomachinery that NASA sponsors are surveyed. The overall objective is to provide the designer and researcher with the concepts and data to control seal dynamics and leakage. Included in the program are low-leakage seals, such as the brush seal, the 'ceramic rope' seal, low-leakage seals for liquid oxygen turbopumps, face seals for two phase flow, and swirl brakes for stability. Two major efforts are summarized: a seal dynamics in rotating machinery, and an effort in seal code development. Author

A93-15681* National Aeronautics and Space Administration. Lewis Research Center, Cleveland, OH.

FRICTION-FACTOR CHARACTERISTICS FOR NARROW CHANNELS WITH HONEYCOMB SURFACES

T. W. HA, G. L. MORRISON, and D. W. CHILDS (Texas A & M Univ., College Station) ASME, Transactions, Journal of Tribology (ISSN 0742-4787) vol. 114, no. 4 Oct. 1992 p. 714-721. ASME and STLE, Joint Tribology Conference, Saint Louis, MO, Oct. 13-16, 1991 refs

(Contract NAG3-181)

(ASME PAPER 91-TRIB-21) Copyright

The experimental determination of friction-factors for the flow of air in a narrow channel lined with various honeycomb geometries has been carried out. Test results show that, generally, the friction-factor is nearly constant or slightly decreases as the Reynolds number increases, a characteristic common to turbulent flow in pipes. However, in some test geometries this trend is remarkably different. The friction factor dramatically drops and then rises as the Reynolds number increases. This phenomenon can be characterized as a 'friction-factor jump'. Further investigations of the acoustic spectrum and friction-factor measurements for a broad range of Reynolds numbers indicate that the 'friction-factor jump' phenomenon is accompanied by an onset of a normal mode resonance excited coherent flow fluctuation structure, which occurs at Reynolds number of the order of 10,000. The purpose of this paper is to explain the friction-factor-jump phenomenon and friction-factor characteristics. Author

A93-15682* National Aeronautics and Space Administration. Lewis Research Center, Cleveland, OH.

FRICTION-FACTOR DATA FOR FLAT-PLATE TESTS OF SMOOTH AND HONEYCOMB SURFACES

T. W. HA and DARA W. CHILDS (Texas A & M Univ., College Station) ASME, Transactions, Journal of Tribology (ISSN 0742-4787) vol. 114, no. 4 Oct. 1992 p. 722-729; Discussion, p. 729, 730. Previously announced in STAR as N89-23876 ASME and STLE, Joint Tribology Conference, Saint Louis, MO, Oct. 13-16, 1991 refs

(Contract NAG3-181)

(ASME PAPER 91-TRIB-20) Copyright

Friction factors for honeycomb surfaces were measured with a flat plate tester. The flat plate test apparatus was described and a method was discussed for determining the friction factor experimentally. The friction factor model was developed for the flat plate test based on the Fanno Line Flow. The comparisons of the friction factor were plotted for smooth surfaces and six-honeycomb surfaces with three-clearances, 6.9 bar to 17.9 bar range of inlet pressures, and 5,000 to 100,000 range of the Reynolds number. The optimum geometries for the maximum friction factor were found as a function of cell width to cell depth and cell width to clearance ratios. Author

A93-15685* National Aeronautics and Space Administration. Lewis Research Center, Cleveland, OH.

STIFFNESS OF MAGNETIC BEARINGS SUBJECTED TO COMBINED STATIC AND DYNAMIC LOADS

D. K. RAO (Mechanical Technology, Inc., Latham, NY), G. V. BROWN (NASA, Lewis Research Center, Cleveland, OH), P. LEWIS, and J. HURLEY (Mechanical Technology, Inc., Latham, NY) ASME, Transactions, Journal of Tribology (ISSN 0742-4787) vol. 114, no. 4 Oct. 1992 p. 785-789. ASME

and STLE, Joint Tribology Conference, Saint Louis, MO, Oct. 13-16, 1991 refs

(ASME PAPER 91-TRIB-27) Copyright

This paper investigates the stiffness of a magnetic bearing that is subjected to the combined action of static and dynamic loads. Since their sum cannot exceed the saturation load, a large static load will imply that the bearing can carry only a small dynamic load. This smaller dynamic load together with the practical vibration amplitude define a practical upper bound to the dynamic stiffness. This paper also presents approximate design formulas and curves for this stiffness capacity as a function of the ratio of dynamic and static loads. In addition, it indicates that vibrations larger than a certain gap fraction can destabilize the magnetic bearing. This gap fraction, called the critical gap fraction, depends on the dynamic and static load ratio. For example, if the dynamic load is half of the static load, the use of more than 25 percent of gap can destabilize the bearing. Author

A93-15686* National Aeronautics and Space Administration. Lewis Research Center, Cleveland, OH.

DETERMINATION OF FORCES IN A MAGNETIC BEARING ACTUATOR - NUMERICAL COMPUTATION WITH COMPARISON TO EXPERIMENT

J. D. KNIGHT, Z. XIA, E. MCCAUL, and H. HACKER, JR. (Duke Univ., Durham, NC) ASME, Transactions, Journal of Tribology (ISSN 0742-4787) vol. 114, no. 4 Oct. 1992 p. 796-801. refs

(Contract NAG3-968)

Copyright

Calculations of the forces exerted on a journal by a magnetic bearing actuator are presented, along with comparisons to experimentally measured forces. The calculations are based on two-dimensional solutions for the flux distribution in the metal parts and free space, using finite but constant permeability in the metals. Above a relative permeability of 10,000 the effects of changes in permeability are negligible, but below 10,000 decreases in permeability cause significant decreases in the force. The calculated forces are shown to depend on the metal permeability more strongly when the journal is displaced from its centered position. The predicted forces in the principal attractive direction are in good agreement with experiment when a relatively low value of permeability is chosen. The forces measured normal to the axis of symmetry when the journal is displaced from that axis, however, are significantly higher than predicted by theory, even with a value of relative permeability larger than 5000. These results indicate a need for further work including nonlinear permeability distributions. Author

A93-15702* National Aeronautics and Space Administration. Lewis Research Center, Cleveland, OH.

TECHNICAL NOTE - PLASMA-SPRAYED CERAMIC THERMAL BARRIER COATINGS FOR SMOOTH INTERMETALLIC ALLOYS

R. A. MILLER and J. DOYCHAK (NASA, Lewis Research Center, Cleveland, OH) Journal of Thermal Spray Technology (ISSN 1059-9630) vol. 1, no. 3 Sept. 1992 p. 211-213. refs

Copyright

A new approach for plasma spray deposition of ceramic thermal barrier coatings directly to smooth substrates is described. Ceramic thermal barrier coatings were directly applied to substrates that had been coated with low-pressure plasma sprayed NiCrAlY bond coats and then centerless ground to simulate a smooth oxidation-resistant substrate. As the high-temperature oxidation behavior of NiAl+Zr is superior to that of MCrAlY alloy, the bond coat is not required for oxidation resistance. O.G.

A93-19494* National Aeronautics and Space Administration. Lewis Research Center, Cleveland, OH.

BRUSH SEAL LEAKAGE PERFORMANCE WITH GASEOUS WORKING FLUIDS AT STATIC AND LOW ROTOR SPEED CONDITIONS

JULIE A. CARLILE, ROBERT C. HENDRICKS, and DENNIS A. YODER (NASA, Lewis Research Center, Cleveland, OH) Jun.

1992 7 p. ASME, International Gas Turbine and Aeroengine Congress and Exposition, 37th, Cologne, Germany, June 1-4, 1992 Previously announced in STAR as N92-16265 refs (ASME PAPER 92-GT-304)

The leakage performance of a brush seal with gaseous working fluids at static and low rotor speed conditions was studied. The leakage results included for air, helium, and carbon dioxide at several bristle/rotor interferences. Also, the effects of packing a lubricant into the bristles and also of reversing the pressure drop across the seal were studied. Results were compared to that of an annular seal at similar operating conditions. In order to generalize the results, they were correlated using corresponding state theory. The brush seal tested had a bore diameter of 3.792 cm (1.4930 in.), a fence height of 0.0635 cm (0.025 in.), and 1800 bristles/cm circumference (4500 bristles/in. circumference). Various bristle/rotor radial interferences were achieved by using a tapered rotor. The brush seal reduced the leakage in comparison to the annular seal, up to 9.5 times. Reversing the pressure drop across the brush seal produced leakage rates approximately the same as that of the annular seal. Addition of a lubricant reduced the leakage by 2.5 times. The air and carbon dioxide data were successfully correlated using corresponding state theory. However, the helium data followed a different curve than the air and carbon dioxide data. Author

A93-22440* National Aeronautics and Space Administration. Lewis Research Center, Cleveland, OH.
DYNAMIC ANALYSIS OF FLEXIBLE GEAR TRAINS/TRANSMISSIONS - AN AUTOMATED APPROACH
F. M. L. AMIROUCHE, N. H. SHAREEF, and M. XIE (Illinois Univ., Chicago) ASME, Transactions, Journal of Applied Mechanics (ISSN 0021-8936) vol. 59, no. 4 Dec. 1992 p. 976-982. Research supported by U.S. Army refs (Contract NAG3-1092)
Copyright

In this paper an automated algorithmic method is presented for the dynamic analysis of geared trains/transmissions. These are treated as a system of interconnected flexible bodies. The procedure developed explains the switching of constraints with time as a result of the change in the contacting areas at the gear teeth. The elastic behavior of the system is studied through the employment of three-dimensional isoparametric elements having six degrees-of-freedom at each node. The contact between the bodies is assumed at the various nodes, which could be either a line or a plane. The kinematical expressions, together with the equations of motion using Kane's method, strain energy concepts, are presented in a matrix form suitable for computer implementation. The constraint Jacobian matrices are generated automatically based on the contact information between the bodies. The concepts of the relative velocity at the contacting points at the tooth pairs and the subsequent use of the transmission ratios in the analysis is presented. Author

A93-23512* National Aeronautics and Space Administration. Lewis Research Center, Cleveland, OH.
TIME-VARIANT ANALYSIS OF ROTORCRAFT SYSTEMS DYNAMICS - AN EXPLOITATION OF VECTOR PROCESSORS
F. M. L. AMIROUCHE, M. XIE, and N. H. SHAREEF (Illinois Univ., Chicago) Journal of Guidance, Control, and Dynamics (ISSN 0731-5090) vol. 16, no. 1 Jan.-Feb. 1993 p. 96-103. refs (Contract NAG3-1092)
Copyright

In this paper a generalized algorithmic procedure is presented for handling constraints in mechanical transmissions. The latter are treated as multibody systems of interconnected rigid/flexible bodies. The constraint Jacobian matrices are generated automatically and suitably updated in time, depending on the geometrical and kinematical constraint conditions describing the interconnection between shafts or gears. The type of constraints are classified based on the interconnection of the bodies by assuming that one or more points of contact exist between them. The effects due to elastic deformation of the flexible bodies are included by allowing each body element to undergo small

deformations. The procedure is based on recursively formulated Kane's dynamical equations of motion and the finite element method, including the concept of geometrical stiffening effects. The method is implemented on an IBM-3090-600j vector processor with pipe-lining capabilities. A significant increase in the speed of execution is achieved by vectorizing the developed code in computationally intensive areas. An example consisting of two meshing disks rotating at high angular velocity is presented. Applications are intended for the study of the dynamic behavior of helicopter transmissions. Author

A93-26051* National Aeronautics and Space Administration. Lewis Research Center, Cleveland, OH.
HFAST - A HARMONIC ANALYSIS PROGRAM FOR STIRLING CYCLES
S. C. HUANG (Mechanical Technology, Inc., Latham, NY) In IECEC '92; Proceedings of the 27th Intersociety Energy Conversion Engineering Conference, San Diego, CA, Aug. 3-7, 1992. Vol. 5 Warrendale, PA Society of Automotive Engineers, Inc. 1992 p. 5.47-5.52. refs (Contract NAS3-25330)
Copyright

HFAST is a general-purpose third-order harmonic analysis and design program for predicting the cyclic-steady state thermodynamic performance of Stirling cycles. It represents the state-of-the-art results of years of research efforts at Mechanical Technology Inc. (MTI) in the development of Stirling cycle machines. The code has been extensively used at MTI to support the development of both free-piston and kinematic Stirling cycle machines. Lately, HFAST has undergone many major improvements, both in the analysis method and in the user's interface. This paper presents a brief description of the current analysis method used in HFAST. Author

A93-26052 National Aeronautics and Space Administration. Lewis Research Center, Cleveland, OH.
COMPARISON OF GLIMPS AND HFAST STIRLING ENGINE CODE PREDICTIONS WITH EXPERIMENTAL DATA
STEVEN M. GENG and ROY C. TEW (NASA, Lewis Research Center, Cleveland, OH) In IECEC '92; Proceedings of the 27th Intersociety Energy Conversion Engineering Conference, San Diego, CA, Aug. 3-7, 1992. Vol. 5 Warrendale, PA Society of Automotive Engineers, Inc. 1992 p. 5.53-5.58. Previously announced in STAR as N92-25395 refs (Contract RTOP 590-13-11)
Copyright

Predictions from GLIMPS and HFAST design codes are compared with experimental data for the RE-1000 and SPRE free piston Stirling engines. Engine performance and available power loss predictions are compared. Differences exist between GLIMPS and HFAST loss predictions. Both codes require engine specific calibration to bring predictions and experimental data into agreement. Author

A93-26069* National Aeronautics and Space Administration. Lewis Research Center, Cleveland, OH.
STIRLING ENGINE - APPROACH FOR LONG-TERM DURABILITY ASSESSMENT
MICHAEL T. TONG (Sverdrup Technology, Inc., Brook Park, OH), PAUL A. BARTOLOTTA, GARY R. HALFORD, and ALAN D. FREED (NASA, Lewis Research Center, Cleveland, OH) In IECEC '92; Proceedings of the 27th Intersociety Energy Conversion Engineering Conference, San Diego, CA, Aug. 3-7, 1992. Vol. 5 Warrendale, PA Society of Automotive Engineers, Inc. 1992 p. 5.209-5.214. refs
Copyright

The approach employed by NASA Lewis for the long-term durability assessment of the Stirling engine hot-section components is summarized. The approach consists of: preliminary structural assessment; development of a viscoplastic constitutive model to accurately determine material behavior under high-temperature thermomechanical loads; an experimental program to characterize material constants for the viscoplastic constitutive model;

finite-element thermal analysis and structural analysis using a viscoplastic constitutive model to obtain stress/strain/temperature at the critical location of the hot-section components for life assessment; and development of a life prediction model applicable for long-term durability assessment at high temperatures. The approach should aid in the provision of long-term structural durability and reliability of Stirling engines. P.D.

A93-26079 National Aeronautics and Space Administration. Lewis Research Center, Cleveland, OH.

MAGNETIC BEARINGS FOR FREE-PISTON STIRLING ENGINES

P. W. CURWEN (Mechanical Technology, Inc., Latham, NY), D. P. FLEMING (NASA, Lewis Research Center, Cleveland, OH), D. K. RAO, and D. S. WILSON (Mechanical Technology, Inc., Latham, NY) *In* IECEC '92; Proceedings of the 27th Intersociety Energy Conversion Engineering Conference, San Diego, CA, Aug. 3-7, 1992. Vol. 5 Warrendale, PA Society of Automotive Engineers, Inc. 1992 p. 5.381-5.386. Previously announced in STAR as N92-30734 refs

(Contract NAS3-26061; RTOP 590-13-11)

Copyright

The feasibility and efficiency of applying magnetic bearings to free-piston Stirling-cycle power conversion machinery currently being developed for long-term space missions are assessed. The study was performed for a 50-kWe Reference Stirling Space Power Converter (RSSPC) which currently uses hydrostatic gas bearings to support the reciprocating displacer and power piston assemblies. Active magnetic bearings of the attractive electromagnetic type are feasible for the RSSPC power piston. Magnetic support of the displacer assembly would require unacceptable changes to the design of the current RSSPC. However, magnetic suspension of both displacer and power piston is feasible for a relative-displacer version of the RSSPC. Magnetic suspension of the RSSPC power piston can potentially increase overall efficiency by 0.5 to 1 percent (0.1 to 0.3 efficiency points). Magnetic bearings will also overcome several operational concerns associated with hydrostatic gas bearing systems. These advantages, however, are accompanied by a 5 percent increase in specific mass of the RSSPC. Author

A93-26080* National Aeronautics and Space Administration. Lewis Research Center, Cleveland, OH.

TRANSIENT LIQUID PHASE DIFFUSION BONDING OF UDIMET 720 FOR STIRLING POWER CONVERTER APPLICATIONS

DONALD L. MITTENDORF and WILLIAM G. BAGGENSTOSS (Allied-Signal Aerospace Co., Tempe, AZ) *In* IECEC '92; Proceedings of the 27th Intersociety Energy Conversion Engineering Conference, San Diego, CA, Aug. 3-7, 1992. Vol. 5 Warrendale, PA Society of Automotive Engineers, Inc. 1992 p. 5.393-5.397. Research supported by NASA refs

Copyright

Udimet 720 has been selected for use on Stirling power converters for space applications. Because Udimet 720 is generally considered susceptible to strain age cracking if traditional fusion welding is used, other joining methods are being considered. A process for transient liquid phase diffusion bonding of Udimet 720 has been theoretically developed in an effort to eliminate the strain age crack concern. This development has taken into account such variables as final grain size, joint homogenization, joint efficiency related to bonding aid material, bonding aid material application method, and thermal cycle. Author

A93-26081* National Aeronautics and Space Administration. Lewis Research Center, Cleveland, OH.

PULSED SINGLE-BLOW REGENERATOR TESTING

J. C. OLDSOHN, T. R. KNOWLES (Energy Science Labs., Inc., San Diego, CA), and J. RAUCH (Sverdrup Technology, Inc., Brook Park, OH) *In* IECEC '92; Proceedings of the 27th Intersociety Energy Conversion Engineering Conference, San Diego, CA, Aug. 3-7, 1992. Vol. 5 Warrendale, PA Society of Automotive Engineers, Inc. 1992 p. 5.399-5.403. refs

(Contract NAS3-26249)

Copyright

A pulsed single-blow method has been developed for testing of Stirling regenerator materials performance. The method uses a tubular flow arrangement with a steady gas flow passing through a regenerator matrix sample that packs the flow channel for a short distance. A wire grid heater spanning the gas flow channel is used to heat a plug of gas by approximately 2 K for approximately 350 ms. Foil thermocouples monitor the gas temperature entering and leaving the sample. Data analysis based on a 1D incompressible-flow thermal model allows the extraction of Stanton number. A figure of merit involving heat transfer and pressure drop is used to present results for steel screens and steel felt. The observations show a lower figure of merit for the materials tested than is expected based on correlations obtained by other methods. Author

A93-27308* National Aeronautics and Space Administration. Lewis Research Center, Cleveland, OH.

CALCULATION OF STIFFNESS AND DAMPING COEFFICIENTS FOR ELASTICALLY SUPPORTED GAS FOIL BEARINGS

J.-P. PENG and M. CARPINO (Pennsylvania State Univ., University Park) ASME, Transactions, Journal of Tribology (ISSN 0742-4787) vol. 115, no. 1 Jan. 1993 p. 20-27. ASME and STLE, Joint Tribology Conference, San Diego, CA, Oct. 18-21, 1992 refs

(Contract NAG3-1052)

Copyright

The stiffness and damping coefficients of an elastically supported gas foil bearing are calculated. A perfect gas is used as the lubricant, and its behavior is described by the Reynolds equation. The structural model consists only of an elastic foundation. The fluid equations and the structural equations are coupled. A perturbation method is used to obtain the linearized dynamic coefficient equations. A finite difference formulation has been developed to solve for the four stiffness and the four damping coefficients. The effect of the bearing compliance on the dynamic coefficients is discussed in this paper. Author

A93-27324* National Aeronautics and Space Administration. Lewis Research Center, Cleveland, OH.

HYBRID ACTIVE VIBRATION CONTROL OF ROTORBEARING SYSTEMS USING PIEZOELECTRIC ACTUATORS

A. B. PALAZZOLO, S. JAGANNATHAN (Texas A & M Univ., College Station), A. F. KASCAK (U.S. Army, Cleveland, OH), G. T. MONTAGUE (Sverdrup Technology, Inc., Cleveland, OH), and L. J. KIRALY (NASA, Lewis Research Center, Cleveland, OH) ASME, Transactions, Journal of Vibration and Acoustics (ISSN 0739-3717) vol. 115, no. 1 Jan. 1993 p. 111-119. Research supported by Texas A & M Turbomachinery Research Consortium and U.S. Army refs

Copyright

The vibrations of a flexible rotor are controlled using piezoelectric actuators. The controller includes active analog components and a hybrid interface with a digital computer. The computer utilizes a grid search algorithm to select feedback gains that minimize a vibration norm at a specific operating speed. These gains are then downloaded as active stillnesses and dampings with a linear fit throughout the operating speed range to obtain a very effective vibration control. Author

A93-31982* National Aeronautics and Space Administration. Lewis Research Center, Cleveland, OH.

MODAL SIMULATION OF GEAR BOX VIBRATION WITH EXPERIMENTAL CORRELATION

F. K. CHOY, Y. F. RUAN (Akron Univ., OH), J. J. ZAKRAJSEK, and F. B. OSWALD (NASA, Lewis Research Center, Cleveland, OH) Journal of Propulsion and Power (ISSN 0748-4658) vol. 9, no. 2 Mar.-Apr. 1993 p. 301-306. AIAA, SAE, ASME, and ASEE, Joint Propulsion Conference and Exhibit, 28th, Nashville, TN, July 6-8, 1992, AIAA Paper 92-3494. Previously cited in issue 23, p. 4157, Accession no. A92-54036 refs

Copyright

A93-33916* National Aeronautics and Space Administration. Lewis Research Center, Cleveland, OH.

A HOT DYNAMIC SEAL RIG FOR MEASURING HYPERSONIC ENGINE SEAL DURABILITY AND FLOW PERFORMANCE

JEFFREY H. MILLER (Sverdrup Technology, Inc., Brook Park, OH), BRUCE M. STEINETZ (NASA, Lewis Research Center, Cleveland, OH), PAUL J. SIROCKY (Sverdrup Technology, Inc., Brook Park, OH), and LAWRENCE A. KREN (Case Western Reserve Univ., Cleveland, OH) *In* AIAA/ASME/ASCE/AHS/ASC Structures, Structural Dynamics, and Materials Conference, 34th and AIAA/ASME Adaptive Structures Forum, La Jolla, CA, Apr. 19-22, 1993, Technical Papers. Pt. 1 Washington American Institute of Aeronautics and Astronautics 1993 p. 445-453. refs (AIAA PAPER 93-1346) Copyright

A test fixture for measuring the dynamic performance of candidate high-temperature engine seal concepts has been installed at NASA Lewis Research Center. The test fixture has been designed to evaluate seal concepts under development for advanced hypersonic engines, such as those being considered for the National Aerospace Plane (NASP). The fixture can measure dynamic seal leakage performance from room temperature up to 840 C (1550 F) and air pressure differentials up to 690 kPa (100 psi). Performance of the seals can be measured while sealing against flat or distorted walls. In the fixture two seals are preloaded against the sides of a 30 cm (1 ft) long saber that slides transverse to the axis of the seals, simulating the scrubbing motion anticipated in these engines. This report covers the capabilities of this test fixture along with preliminary data showing the dependence of seal leakage performance on high temperature cycling. Author

A93-34157# National Aeronautics and Space Administration. Lewis Research Center, Cleveland, OH.

DYNAMICS OF ROTATING MULTICOMPONENT TURBOMACHINERY SYSTEMS

CHARLES LAWRENCE (NASA, Lewis Research Center, Cleveland, OH) *In* AIAA/ASME/ASCE/AHS/ASC Structures, Structural Dynamics, and Materials Conference, 34th and AIAA/ASME Adaptive Structures Forum, La Jolla, CA, Apr. 19-22, 1993, Technical Papers. Pt. 5 Washington American Institute of Aeronautics and Astronautics 1993 p. 2836-2847. Previously announced in STAR as N93-18426 refs (Contract RTOP 505-63-53) (AIAA PAPER 93-1629) Copyright

The ultimate objective of turbomachinery vibration analysis is to predict both the overall, as well as component dynamic response. To accomplish this objective requires complete engine structural models, including multistages of bladed disk assemblies, flexible rotor shafts and bearings, and engine support structures and casings. In the present approach each component is analyzed as a separate structure and boundary information is exchanged at the inter-component connections. The advantage of this tactic is that even though readily available detailed component models are utilized, accurate and comprehensive system response information may be obtained. Sample problems, which include a fixed base rotating blade and a blade on a flexible rotor, are presented.

Author

A93-34241* National Aeronautics and Space Administration. Lewis Research Center, Cleveland, OH.

VIBRATION LOCALIZATION IN MONO- AND BI-COUPLED BLADED DISKS - A TRANSFER MATRIX APPROACH

GISLI OTTARSSON and CHRISTOPHE PIERRE (Michigan Univ., Ann Arbor) *In* AIAA/ASME/ASCE/AHS/ASC Structures, Structural Dynamics, and Materials Conference, 34th and AIAA/ASME Adaptive Structures Forum, La Jolla, CA, Apr. 19-22, 1993, Technical Papers. Pt. 6 Washington American Institute of Aeronautics and Astronautics 1993 p. 3683-3697. refs (Contract NAG3-1163) (AIAA PAPER 93-1492) Copyright

A transfer matrix approach to the analysis of the dynamics of mistuned bladed disks is presented. The study focuses on mono-coupled systems, in which each blade is coupled to its two neighboring blades, and bi-coupled systems, where each blade is

coupled to its four nearest neighbors. Transfer matrices yield the free dynamics, both the characteristic free wave and the normal modes - in closed form for the tuned assemblies. Mistuned assemblies are represented by random transfer matrices and an examination of the effect of mistuning on harmonic wave propagation yields the localization factor - the average rate of spatial wave amplitude decay per blade - in the mono-coupled assembly. Based on a comparison of the wave propagation characteristics of the mono- and bi-coupled assemblies, important conclusions are drawn about the effect of the additional coupling coordinate on the sensitivity to mistuning and the strength of mode localization predicted by a mono-coupled analysis. Author

A93-34493* National Aeronautics and Space Administration. Lewis Research Center, Cleveland, OH.

DEVELOPMENT OF BRAIDED ROPE SEALS FOR HYPERSONIC ENGINE APPLICATIONS - FLOW MODELING

RAJAKKANNU MUTHARASAN (Drexel Univ., Philadelphia, PA), BRUCE M. STEINETZ (NASA, Lewis Research Center, Cleveland, OH), XIAOMING TAO, GUANG-WU DU, and FRANK KO (Drexel Univ., Philadelphia, PA) *Journal of Propulsion and Power* (ISSN 0748-4658) vol. 9, no. 3 May-June 1993 p. 456-461. AIAA, SAE, ASME, and ASEE, Joint Propulsion Conference, 27th, Sacramento, CA, June 24-26, 1991, AIAA Paper 91-2495. Previously cited in issue 17, p. 2960, Accession no. A91-41800 refs

(Contract NAG3-1059) Copyright

A93-35546* National Aeronautics and Space Administration. Lewis Research Center, Cleveland, OH.

THE DETRIMENTAL EFFECT OF FRICTION ON SPACE MICROGRAVITY ROBOTICS

WYATT S. NEWMAN, GREGORY D. GLOSSER (Case Western Reserve Univ., Cleveland, OH), JEFFREY H. MILLER, and DOUGLAS ROHN (NASA, Lewis Research Center, Cleveland, OH) *In* 1992 IEEE International Conference on Robotics and Automation, 8th, Nice, France, May 12-14, 1992, Proceedings. Vol. 2 Los Alamitos, CA IEEE Computer Society Press 1992 p. 1436-1441. refs Copyright

The authors present an analysis of why control systems are ineffective in compensating for acceleration disturbances due to Coulomb friction. Linear arguments indicate that the effects of Coulomb friction on a body are most difficult to reject when the control actuator is separated from the body of compliance. The linear arguments were illustrated in a nonlinear simulation of optimal linear tracking control in the presence of nonlinear friction. The results of endpoint acceleration measurements for four robot designs are presented and are compared with simulation and to equivalent measurements on a human. It is concluded that Coulomb friction in common bearings and transmission induces unacceptable levels of endpoint acceleration, that these accelerations cannot be adequately attenuated by control, and that robots for microgravity work will require special design considerations for inherently low friction. Author

A93-36588* National Aeronautics and Space Administration. Lewis Research Center, Cleveland, OH.

MODAL ANALYSIS OF MULTISTAGE GEAR SYSTEMS COUPLED WITH GEARBOX VIBRATIONS

F. K. CHOY, Y. F. RUAN, Y. K. TU (Akron Univ., OH), J. J. ZAKRAJSEK, and D. P. TOWNSEND (NASA, Lewis Research Center, Cleveland, OH) *ASME, Transactions, Journal of Solar Energy Engineering* (ISSN 0199-6231) vol. 114 Sept. 1992 p. 486-497. Previously announced in STAR as N91-23513 refs Copyright

An analytical procedure to simulate vibrations in gear transmission systems is presented. This procedure couples the dynamics of the rotor-bearing gear system with the vibration in the gear box structure. The model synthesis method is used in solving the overall dynamics of the system, and a variable time-stepping integration scheme is used in evaluating the global

transient vibration of the system. Locally each gear stage is modeled as a multimass rotor-bearing system using a discrete model. The modal characteristics are calculated using the matrix-transfer technique. The gearbox structure is represented by a finite element models, and modal parameters are solved by using NASTRAN. The rotor-gear stages are coupled through nonlinear compliance in the gear mesh while the gearbox structure is coupled through the bearing supports of the rotor system. Transient and steady state vibrations of the coupled system are examined in both time and frequency domains. A typical three-gear system is used as an example for demonstration of the developed procedure. Author

A93-40050* National Aeronautics and Space Administration. Lewis Research Center, Cleveland, OH.

SIMULTANEOUS PRESSURE MEASUREMENT AND HIGH-SPEED PHOTOGRAPHY STUDY OF CAVITATION IN A DYNAMICALLY LOADED JOURNAL BEARING

D. C. SUN (New York State Univ., Binghamton), D. E. BREWE (U.S. Army, Propulsion Directorate; NASA, Lewis Research Center, Cleveland, OH), and P. B. ABEL (NASA, Lewis Research Center, Cleveland, OH) ASME, Transactions, Journal of Tribology (ISSN 0742-4787) vol. 115 Jan. 1993 p. 88-95. refs Copyright

Cavitation of the oil film in a dynamically loaded journal bearing was studied using high-speed photography and pressure measurement simultaneously. Comparison of the visual and pressure data provided considerable insight into the occurrence and non-occurrence of cavitation. It was found that (1), cavitation typically occurred in the form of one bubble with the pressure in the cavitation bubble close to the absolute zero; and (2), for cavitation-producing operating conditions, cavitation did not always occur; with the oil film then supporting a tensile stress. Author

A93-48594* National Aeronautics and Space Administration. Lewis Research Center, Cleveland, OH.

ACTIVELY CONTROLLED SUPERCONDUCTING BEARINGS

YEHA M. EYSSA and X. HUANG (Wisconsin Univ., Madison) In Advances in cryogenic engineering. Vol. 37A - Proceedings of the 1991 Cryogenic Engineering Conference, Univ. of Alabama, Huntsville, June 11-14, 1991 New York Plenum Press 1991 p. 511-517. refs (Contract NAG3-1041) Copyright

Actively controlled conventional radial bearing using copper winding and soft magnetic material can provide only up to 200 N/sq cm of pressure. Large cryogenic pumps for space applications operating at 30,000 rpm and high rpm machines may require larger magnetic pressure. We show that using superconducting winding in the rotor and the stator of a magnetic bearing system increases the pressure by an order of magnitude. The paper addresses winding configuration, stability, ac losses, and power requirement for the superconducting winding. Author (revised)

A93-49244* National Aeronautics and Space Administration. Lewis Research Center, Cleveland, OH.

EFFECT OF FLUID COMPRESSIBILITY ON JOURNAL BEARING PERFORMANCE

FLORIN DIMOFTE (NASA, Lewis Research Center, Cleveland, OH) STLE Tribology Transactions (ISSN 0569-8197) vol. 36, no. 3 July 1993 p. 341-350. ASME and STLE, Tribology Conference, San Diego, CA, Oct. 19-21, 1992 Research sponsored by National Research Council refs Copyright

An analysis was undertaken to determine the effect of fluid film compressibility on the performance of fluid film bearings. A new version of the Reynolds equation was developed, using a polytropic expansion, for both steady-state and dynamic conditions. Polytropic exponents from 1 (isothermal) to 1000 (approaching an incompressible liquid) were evaluated for two bearing numbers, selected from a range of practical interest for cryogenic application, and without cavitation. Bearing loads were insensitive to fluid compressibility for low bearing numbers, as was expected. The

effect of compressibility on attitude angle was significant, even when the bearing number was low. A small amount of fluid compressibility was enough to obtain stable running conditions. Incompressible liquid lacked stability at all conditions. Fluid compressibility can be used to control the bearing dynamic coefficients, thereby influencing the dynamic behavior of the rotor-bearing system.

A93-49841*# National Aeronautics and Space Administration. Lewis Research Center, Cleveland, OH.

DEVELOPMENT OF HYPERSONIC ENGINE SEALS - FLOW EFFECTS OF PRELOAD AND ENGINE PRESSURES

ZHONG CAI, RAJAKKANNU MUTHARASAN, FRANK K. KO (Drexel Univ., Philadelphia, PA), and BRUCE M. STEINETZ (NASA, Lewis Research Center, Cleveland, OH) Jun. 1993 11 p. AIAA, SAE, ASME, and ASEE, Joint Propulsion Conference and Exhibit, 29th, Monterey, CA, June 28-30, 1993 refs (AIAA PAPER 93-1998) Copyright

A new type of engine seal is being developed to meet the needs of advanced hypersonic engines. A seal braided of emerging high temperature ceramic fibers comprised of a sheath-core construction has been selected for study based on its low leakage rates. Flexible, low-leakage, high-temperature seals are required to seal the movable engine panels of advanced ramjet-scrumjet engines either preventing potentially dangerous leakage into backside engine cavities or limiting the purge coolant flow rates through the seals. To predict the leakage through these flexible, porous seal structures as a function of preload and engine pressures, new analytical flow models are required. An empirical leakage resistance/preload model is proposed to characterize the observed decrease in leakage with increasing preload. Empirically determined compression modulus and preload factor are used to correlate experimental leakage data for a wide range of seal architectures. Good agreement between measured and predicted values are observed over a range of engine pressures and seal preload.

A93-49965*# National Aeronautics and Space Administration. Lewis Research Center, Cleveland, OH.

EFFECT OF EXTENDED TOOTH CONTACT ON THE MODELING OF SPUR GEAR TRANSMISSIONS

HSIANG H. LIN, JIFENG WANG (Memphis State Univ., TN), FRED B. OSWALD, and JOHN J. COY (NASA, Lewis Research Center, Cleveland, OH) Jun. 1993 11 p. AIAA, SAE, ASME, and ASEE, Joint Propulsion Conference and Exhibit, 29th, Monterey, CA, June 28-30, 1993 Previously announced in STAR as N93-28411 refs (AIAA PAPER 93-2148) Copyright

In some gear dynamic models, the effect of tooth flexibility is ignored when the model determines which pairs of teeth are in contact. Deflection of loaded teeth is not introduced until the equations of motion are solved. This means the zone of tooth contact and average tooth meshing stiffness are underestimated and the individual tooth load is overstated, especially for heavily-loaded gears. The static transmission error and dynamic load of heavily-loaded, low-contact-ratio spur gears is compared with this effect both neglected and included. Neglecting the effect yields an underestimate of resonance speeds and an overestimate of the dynamic load.

A93-49966*# National Aeronautics and Space Administration. Lewis Research Center, Cleveland, OH.

LOW-NOISE, HIGH-STRENGTH, SPIRAL-BEVEL GEARS FOR HELICOPTER TRANSMISSIONS

DAVID G. LEWICKI, ROBERT F. HANDSCHUH (U.S. Army, Research Lab.; NASA, Lewis Research Center, Cleveland, OH), ZACHARY S. HENRY (Bell Helicopter Textron, Inc., Fort Worth, TX), and FAYDOR L. LITVIN (Illinois Univ., Chicago) Jun. 1993 14 p. AIAA, SAE, ASME, and ASEE, Joint Propulsion Conference and Exhibit, 29th, Monterey, CA, June 28-30, 1993 Previously announced in STAR as N93-23019 refs (AIAA PAPER 93-2149)

Improvements in spiral-bevel gear design were investigated to

support the Army/NASA Advanced Rotorcraft Transmission program. Program objectives were to reduce weight by 25 percent, reduce noise by 10 dB, and increase life to 5000 hr mean-time-between-removal. To help meet these goals, advanced-design spiral-bevel gears were tested in an OH-58D helicopter transmission using the NASA 500-hp Helicopter Transmission Test Stand. Three different gear designs tested included: (1) the current design of the OH-58D transmission except gear material X-53 instead of AISI 9310; (2) a higher-strength design the same as the current but with a full fillet radius to reduce gear tooth bending stress (and thus, weight); and (3) a lower-noise design the same as the high-strength but with modified tooth geometry to reduce transmission error and noise. Noise, vibration, and tooth strain tests were performed and significant gear stress and noise reductions were achieved.

A93-49967* # National Aeronautics and Space Administration. Lewis Research Center, Cleveland, OH.

VIBRATION AND NOISE ANALYSIS OF A GEAR TRANSMISSION SYSTEM

F. K. CHOY, W. QIAN (Akron Univ., OH), J. J. ZAKRAJSEK, and F. B. OSWALD (NASA, Lewis Research Center, Cleveland, OH) Jun. 1993 16 p. AIAA, SAE, ASME, and ASEE, Joint Propulsion Conference and Exhibit, 29th, Monterey, CA, June 28-30, 1993 Previously announced in STAR as N93-27641 refs (AIAA PAPER 93-2150) Copyright

This paper presents a comprehensive procedure to predict both the vibration and noise generated by a gear transmission system under normal operating conditions. The gearbox vibrations were obtained from both numerical simulation and experimental studies using a gear noise test rig. In addition, the noise generated by the gearbox vibrations was recorded during the experimental testing. A numerical method was used to develop linear relationships between the gearbox vibration and the generated noise. The hypercoherence function is introduced to correlate the nonlinear relationship between the fundamental noise frequency and its harmonics. A numerical procedure was developed using both the linear and nonlinear relationships generated from the experimental data to predict noise resulting from the gearbox vibrations. The application of this methodology is demonstrated by comparing the numerical and experimental results from the gear noise test rig.

A93-50080* # National Aeronautics and Space Administration. Lewis Research Center, Cleveland, OH.

DYNAMIC ANALYSIS OF SPUR GEARS USING COMPUTER PROGRAM DANST

FRED B. OSWALD (NASA, Lewis Research Center, Cleveland, OH), HSIANG H. LIN, CHUEN-HUEI LIU (Memphis State Univ., TN), and MARK J. VALCO (U.S. Army, Research Lab.; NASA, Lewis Research Center, Cleveland, OH) Jun. 1993 13 p. AIAA, SAE, ASME, and ASEE, Joint Propulsion Conference and Exhibit, 29th, Monterey, CA, June 28-30, 1993 Previously announced in STAR as N93-28050 refs (AIAA PAPER 93-2295) Copyright

DANST is a computer program for static and dynamic analysis of spur gear systems. The program can be used for parametric studies to predict the effect on dynamic load and tooth bending stress of spur gears due to operating speed, torque, stiffness, damping, inertia, and tooth profile. DANST performs geometric modeling and dynamic analysis for low- or high-contact-ratio spur gears. DANST can simulate gear systems with contact ratio ranging from one to three. It was designed to be easy to use, and it is extensively documented by comments in the source code. This report describes the installation and use of DANST. It covers input data requirements and presents examples. The report also compares DANST predictions for gear tooth loads and bending stress to experimental and finite element results.

A93-50081* # National Aeronautics and Space Administration. Lewis Research Center, Cleveland, OH.

CONTACT STRESS ANALYSIS OF SPIRAL BEVEL GEARS USING NONLINEAR FINITE ELEMENT STATIC ANALYSIS

G. D. BIBEL (North Dakota Univ., Grand Forks), A. KUMAR, S. REDDY (Akron Univ., OH), and ROBERT F. HANDSCHUH (U.S. Army, Research Lab.; NASA, Lewis Research Center, Cleveland, OH) Jun. 1993 11 p. AIAA, SAE, ASME, and ASEE, Joint Propulsion Conference and Exhibit, 29th, Monterey, CA, June 28-30, 1993 Previously announced in STAR as N93-27037 refs (AIAA PAPER 93-2296) Copyright

A procedure is presented for performing three-dimensional stress analysis of spiral bevel gears in mesh using the finite element method. The procedure involves generating a finite element model by solving equations that identify tooth surface coordinates. Coordinate transformations are used to orientate the gear and pinion for gear meshing. Contact boundary conditions are simulated with gap elements. A solution technique for correct orientation of the gap elements is given. Example models and results are presented.

A93-50082* # National Aeronautics and Space Administration. Lewis Research Center, Cleveland, OH.

GENERATION OF HELICAL GEARS WITH NEW SURFACES TOPOLOGY BY APPLICATION OF CNC MACHINES

F. L. LITVIN, N. X. CHEN, C. L. HSIAO (Illinois Univ., Chicago), and ROBERT F. HANDSCHUH (U.S. Army, Research Lab.; NASA, Lewis Research Center, Cleveland, OH) Jun. 1993 5 p. AIAA, SAE, ASME, and ASEE, Joint Propulsion Conference and Exhibit, 29th, Monterey, CA, June 28-30, 1993 Previously announced in STAR as N93-27687 refs (AIAA PAPER 93-2297) Copyright

Analysis of helical involute gears by tooth contact analysis shows that such gears are very sensitive to angular misalignment that leads to edge contact and the potential for high vibration. A new topology of tooth surfaces of helical gears that enables a favorable bearing contact and a reduced level of vibration is described. Methods for grinding of the helical gears with the new topology are proposed. A TCA (tooth contact analysis) program for simulation of meshing and contact of helical gears with the new topology has been developed. Numerical examples that illustrate the proposed ideas are discussed.

A93-50083* # National Aeronautics and Space Administration. Lewis Research Center, Cleveland, OH.

EVALUATION OF A VIBRATION DIAGNOSTIC SYSTEM FOR THE DETECTION OF SPUR GEAR PITTING FAILURES

DENNIS P. TOWNSEND and JAMES J. ZAKRAJSEK (NASA, Lewis Research Center, Cleveland, OH) Jun. 1993 10 p. AIAA, SAE, ASME, and ASEE, Joint Propulsion Conference and Exhibit, 29th, Monterey, CA, June 28-30, 1993 Previously announced in STAR as N93-25672 refs (AIAA PAPER 93-2298) Copyright

A vibration diagnostic system was used to detect spur gear surface pitting fatigue in a closed-loop spur gear fatigue test rig. The diagnostic system, comprising a personal computer with an analog-to-digital conversion board, a diagnostic system unit, and software, uses time-synchronous averaging of the vibration signal to produce a vibration image of each tooth on any gear in a transmission. Several parameters were analyzed including gear pair stress wave and raw baseband vibration, kurtosis, peak ratios, and others. The system provides limits for the various parameters and gives a warning when the limits are exceeded. Several spur gear tests were conducted with this system and vibration data analyzed at 5-min. intervals. The results presented herein show that the system is fairly effective at detecting spur gear tooth surface fatigue pitting failures.

A93-50084* # National Aeronautics and Space Administration. Lewis Research Center, Cleveland, OH.

ENGINEERING SCIENCE RESEARCH ISSUES IN HIGH POWER DENSITY TRANSMISSION DYNAMICS FOR AEROSPACE APPLICATIONS

RAJENDRA SINGH and DONALD R. HOUSER (Ohio State Univ., Columbus) Jun. 1993 12 p. AIAA, SAE, ASME, and ASEE, Joint Propulsion Conference and Exhibit, 29th, Monterey, CA, June 28-30, 1993 Research supported by Gear Dynamics and Gear

Noise Research Lab. Industrial Consortium refs
(Contract DAAL03-92-G-0120; NAG3-773)
(AIAA PAPER 93-2299) Copyright

This paper discusses analytical and experimental approaches that will be needed to understand dynamic, vibro-acoustic and design characteristics of high power density rotorcraft transmissions. Complexities associated with mathematical modeling of such systems will be discussed. An overview of research work planned during the next several years will be presented, with emphasis on engineering science issues such as gear contact mechanics, multi-mesh drive dynamics, parameter uncertainties, vibration transmission through bearings, and vibro-acoustic characteristics of geared rotor systems and housing-mount structures. A few examples of work in progress are cited.

A93-50261* National Aeronautics and Space Administration. Lewis Research Center, Cleveland, OH.

BRUSH SEAL LOW SURFACE SPEED HARD-RUB CHARACTERISTICS

ROBERT C. HENDRICKS, JULIE A. CARLILE, and ANITA D. LIANG (NASA, Lewis Research Center, Cleveland, OH) Jun. 1993 13 p. AIAA, SAE, ASME, and ASEE, Joint Propulsion Conference and Exhibit, 29th, Monterey, CA, June 28-30, 1993 Previously announced in STAR as N93-27132 refs (AIAA PAPER 93-2534) Copyright

The bristles of a 38.1-mm (1.5-in.) diameter brush seal were flexed by a tapered, 40-tooth rotor operating at 2600 rpm that provided sharp leading-edge impact of the bristles with hard rubbing of the rotor lands. Three separate tests were run with the same brush accumulating over 1.3×10^9 flexure cycles while deteriorating 0.2 mm (0.008 in.) radially. In each, the test bristle incursion depth varied from 0.130 to 0.025 mm (0.005 to 0.001 in.) or less (start to stop), and in the third test the rotor was set 0.25 mm (0.010 in.) eccentric. Runout varied from 0.025 to 0.076 mm (0.001 to 0.003 in.) radially. The bristles wore but did not pull out, fracture, or fragment. Bristle and rotor wear debris were deposited as very fine, nearly amorphous, highly porous materials at the rotor groove leading edges and within the rotor grooves. The land leading edges showed irregular wear and the beginning of a convergent groove that exhibited sharp, detailed wear at the land trailing edges. Surface grooving, burnishing, 'whipping,' and hot spots and streaks were found. With a smooth-plug rotor, post-test leakage increased 30 percent over pretest leakage.

A93-50262* National Aeronautics and Space Administration. Lewis Research Center, Cleveland, OH.

PRELIMINARY EXPERIMENTAL RESULTS FOR A CRYOGENIC BRUSH SEAL CONFIGURATION

J. A. CARLILE, R. C. HENDRICKS (NASA, Lewis Research Center, Cleveland, OH), R. I. HIBBS, S. E. MCVEY, and J. K. SCHARRER (Rockwell International Corp., Rocketdyne Div., Canoga Park, CA) Jun. 1993 12 p. AIAA, SAE, ASME, and ASEE, Joint Propulsion Conference and Exhibit, 29th, Monterey, CA, June 28-30, 1993 Previously announced in STAR as N93-28627 refs (AIAA PAPER 93-2535) Copyright

Preliminary fluid nitrogen flow data are reported for a five-brush, ceramic-coated-rub-runner brush seal system, where the brushes and the rub runner were placed at each end of a centrally pressurized multifunction tester ('back-to-back' set of brushes) and tested at rotor speeds of 0, 10, 18, and 22.5 krpm. After testing, both the brushes and the ceramic-coated rub runner appeared pristine. The coating withstood both the thermomechanical and dynamic loadings with minor wear track scarring. The bristle tips showed some indication of material shearing (smearing) wear. The Ergun (1952) porous flow equation was applied to the brush seal data. The Ergun relation fit the gaseous data but was in poor agreement with the fluid results. The brush seal exit conditions were two phase. Two-phase, choked-flow design charts were applied but required one data point at each rotor speed to define the flow and area coefficients. Reasonable agreement between prediction and data was found, but such methods are not to be construed as two-phase-flow brush seal analyses.

Author (revised)

A93-52607 National Aeronautics and Space Administration. Lewis Research Center, Cleveland, OH.

EFFECT OF OUT-OF-ROUNDNESS ON THE PERFORMANCE OF A DIESEL ENGINE CONNECTING-ROD BEARING

D. VIJAYARAGHAVAN (NASA, Lewis Research Center, Cleveland, OH), D. E. BREWE (U.S. Army, Aviation Systems Command; NASA, Lewis Research Center, Cleveland, OH), and T. G. KEITH, JR. (Toledo Univ., OH) ASME, Transactions, Journal of Tribology (ISSN 0742-4787) vol. 115, no. 3 July 1993 p. 538-543. ASME and STLE, Tribology Conference, Saint Louis, MO, Oct. 17-19, 1991. Previously announced in STAR as N92-31536 refs (Contract RTOP 505-63-5A) Copyright

In this paper, the dynamic performance of the Ruston and Hornsby VEB diesel engine connecting-rod bearing with circular and out-of-round profiles is analyzed. The effect of cavitation is considered by using a cavitation algorithm, which mimics JFO boundary conditions. The effect of mass inertia is accounted for by solving coupled nonlinear equations of motion. The journal profiles considered are circular, elliptical, semi-elliptical, and three lobe epicycloid. The predicted journal trajectory and other performance parameters for one complete load cycle are presented for all of the out-of-round profiles and are also compared with the predictions for the circular bearing.

A93-53389* National Aeronautics and Space Administration. Lewis Research Center, Cleveland, OH.

PERFORMANCE AND PROPERTIES OF ATOMIC OXYGEN PROTECTIVE COATINGS FOR POLYMERIC MATERIALS

BRUCE A. BANKS (NASA, Lewis Research Center, Cleveland, OH) and CYNTHIA LAMOREAUX (Cleveland State Univ., OH) In International SAMPE Technical Conference, 24th and International SAMPE Metals and Metals Processing Conference, 3rd, Toronto, Canada, Oct. 20-22, 1992, Proceedings. Vol. 24 Covina, CA Society for the Advancement of Material and Process Engineering 1992 p. T165-T173. refs Copyright

Such large LEO spacecraft as the Space Station Freedom will encounter high atomic oxygen fluences which entail the use of protective coatings for their polymeric structural materials. Such coatings have demonstrated polymer mass losses due to oxidation that are much smaller than those of unprotected materials. Attention is here given to protective and/or electrically conductive coatings of SiO(x), Ge, and indium-tin oxide which have been exposed to atomic oxygen in order to ascertain mass loss, electrical conductivity, and optical property dependence on atomic oxygen exposure.

AIAA

A93-53590* National Aeronautics and Space Administration. Lewis Research Center, Cleveland, OH.

LUBRICATION OF AN 85-MM BALL BEARING WITH RP-1

HAROLD E. ADDY, JR. (NASA, Lewis Research Center, Cleveland, OH) and FREDRICK T. SCHULLER (Sverdrup Technology, Inc., Cleveland, OH) Jun. 1993 10 p. AIAA, SAE, ASME, and ASEE, Joint Propulsion Conference and Exhibit, 29th, Monterey, CA, June 28-30, 1993 Previously announced in STAR as N93-31670 refs (AIAA PAPER 93-2538) Copyright

A parametric experimental investigation of an 85 millimeter bore angular contact ball bearing running in RP-1 fuel was performed at speeds of 10,000 to 24,000 rpm. Thrust loads were varied from 4450 to 17,800 Newtons (1000 to 4000 lbs.). Radial loads were varied from 1335 to 13,350 Newtons (300 to 3000 lbs.). RP-1 lubrication for the bearing was provided through a stationary jet ring located adjacent to the test bearing outer ring. Increases in both the thrust and radial loads resulted in increased bearing temperature, while increases in shaft speed resulted in much more dramatic increases in bearing temperature. These trends are typical for ball bearings operating under these types of conditions. Results are given for outer ring temperatures of the test bearing at the various test conditions employed. In addition, the heat energy removed from the bearing by the RP-1 was determined by measuring the increase in temperature as the RP-1

passed through the bearing. Results showed that the amount of heat energy removed by the RP-1 increased with both shaft speed and RP-1 flow rate to the bearing.

A93-54659* National Aeronautics and Space Administration. Lewis Research Center, Cleveland, OH.

FLOW VISUALIZATION IN A SINGLE SIMULATED BRUSH SEAL

M. J. BRAUN, V. A. CANACCI, M. KAZMIERCHAK (Akron Univ., OH), and R. C. HENDRICKS (NASA, Lewis Research Center, Cleveland, OH) / In Rotating machinery - Dynamics; Proceedings of the 3rd International Symposium on Transport Phenomena and Dynamics of Rotating Machinery (ISROMAC-3), Honolulu, HI, Apr. 1-4, 1990 Bristol, PA Hemisphere Publishing Corp. 1992 p. 161-175. refs

Copyright

A method to visualize and characterize the complex flow fields in brush seals is presented. A configuration characteristic of the brush seal confined in a two-dimensional tunnel with water as the working fluid was studied. Visualization of the flow field revealed regions that are characteristically jetting, vortical, and crossflow and exist upstream, downstream or within the seal. Such flows are engendered by variations in fiber void that are spatial and temporal and affect changes in seal leakage and stability. While the effects of interface motion and cylindrical configuration have not been considered herein, it is believed that the observed flow fields characterize flow phenomenology in brush seals.

N93-10966*# National Aeronautics and Space Administration. Lewis Research Center, Cleveland, OH.

EXPERIMENTAL VALIDATION OF BOUNDARY ELEMENT METHODS FOR NOISE PREDICTION

A. F. SEYBERT (Kentucky Univ., Lexington.) and FRED B. OSWALD Jul. 1992 8 p Presented at the Inter-Noise 1992, Toronto, Ontario, 20-22 Jul. 1992; sponsored by the International Inst. of Noise Control Engineering (Contract DA PROJ. 1L1-62211-A-47-A; RTOP 505-63-36) (NASA-TM-105729; E-7132; NAS 1.15:105729; AVSCOM-TR-92-C-013) Avail: CASI HC A02/MF A01

Experimental validation of methods to predict radiated noise is presented. A combined finite element and boundary element model was used to predict the vibration and noise of a rectangular box excited by a mechanical shaker. The predicted noise was compared to sound power measured by the acoustic intensity method. Inaccuracies in the finite element model shifted the resonance frequencies by about 5 percent. The predicted and measured sound power levels agree within about 2.5 dB. In a second experiment, measured vibration data was used with a boundary element model to predict noise radiation from the top of an operating gearbox. The predicted and measured sound power for the gearbox agree within about 3 dB. Author

N93-10982*# National Aeronautics and Space Administration. Lewis Research Center, Cleveland, OH.

MAXIMUM LIFE SPIRAL BEVEL REDUCTION DESIGN

M. SAVAGE (Akron Univ., OH.), M. G. PRASANNA (Akron Univ., OH.), and H. H. COE Jul. 1992 17 p Presented at the 28th Joint Propulsion Conference and Exhibit, Huntsville, TN, 6-8 Jul. 1992; sponsored by AIAA, SAE, ASME, and ASEE Previously announced in IAA as A92-49030 (Contract DA PROJ. 1L1-62211-A-47-A; RTOP 505-63-36) (NASA-TM-105790; E-7220; NAS 1.15:105790; AVSCOM-TR-92-C-004; AD-A259242) Avail: CASI HC A03/MF A01

Optimization is applied to the design of a spiral bevel gear reduction for maximum life at a given size. A modified feasible directions search algorithm permits a wide variety of inequality constraints and exact design requirements to be met with low sensitivity to initial values. Gear tooth bending strength and minimum contact ratio under load are included in the active constraints. The optimal design of the spiral bevel gear reduction includes the selection of bearing and shaft proportions in addition to gear mesh parameters. System life is maximized subject to a

fixed back-cone distance of the spiral bevel gear set for a specified speed ratio, shaft angle, input torque, and power. Significant parameters in the design are: the spiral angle, the pressure angle, the numbers of teeth on the pinion and gear, and the location and size of the four support bearings. Interpolated polynomials expand the discrete bearing properties and proportions into continuous variables for gradient optimization. After finding the continuous optimum, a designer can analyze near optimal designs for comparison and selection. Design examples show the influence of the bearing lives on the gear parameters in the optimal configurations. For a fixed back-cone distance, optimal designs with larger shaft angles have larger service lives. Author

N93-12203*# National Aeronautics and Space Administration. Lewis Research Center, Cleveland, OH.

AUTOMATIC SYSTEM FOR INSTALLATION AND REPLACEMENT OF SPACE STATION COMPONENTS Patent Application

ANDREW L. GORDAN, inventor (to NASA) and JAMES L. DOLCE, inventor (to NASA) 28 May 1992 19 p (NASA-CASE-LEW-14906-1; NAS 1.71:LEW-14906-1; US-PATENT-APPL-SN-889572) Avail: CASI HC A03/MF A01

Service equipment for use in hostile environments is presented. The equipment includes a detachable service unit secured to a stationary service unit. The detachable service unit includes a housing with an exterior plate, a power control interface for connection to an exterior power source, locating pins located in said exterior plate, an electrical connector in the exterior plate electrically coupled to said power control interface, and a pair of clamping receptacles formed in the exterior plate and located on adjacent opposite edges of the exterior plate. The stationary unit includes an electrical connector for connection to the electrical connector of the detachable service unit, a clamping apparatus for clamping and unclamping the detachable service unit from the stationary unit, a base clamp assembly for mounting the clamping apparatus onto the stationary unit, and locating pin holes for receiving the locating pins and aligning the detachable service unit onto the stationary unit. The detachable service unit have mating scalloped faces which aid in alignment and provide a mechanism for heat dissipation. NASA

N93-12736*# National Aeronautics and Space Administration. Lewis Research Center, Cleveland, OH.

SPLIT TORQUE TRANSMISSION LOAD SHARING

T. L. KRANTZ, M. RASHIDI (Cleveland State Univ., OH.), and J. G. KISH (Sikorsky Aircraft, Stratford, CT.) Oct. 1992 25 p Presented at the Gearbox Configurations of the 1990's, Solihull, England, 28 Oct. 1992; sponsored by the Institute of Mechanical Engineers (Contract DA PROJ. 1L1-62211-A-47-A; RTOP 505-63-36) (NASA-TM-105884; E-7350; NAS 1.15:105884; AVSCOM-TR-92-C-030; AD-A259931) Avail: CASI HC A03/MF A01

Split torque transmissions are attractive alternatives to conventional planetary designs for helicopter transmissions. The split torque designs can offer lighter weight and fewer parts but have not been used extensively for lack of experience, especially with obtaining proper load sharing. Two split torque designs that use different load sharing methods have been studied. Precise indexing and alignment of the geartrain to produce acceptable load sharing has been demonstrated. An elastomeric torque splitter that has large torsional compliance and damping produces even better load sharing while reducing dynamic transmission error and noise. However, the elastomeric torque splitter as now configured is not capable over the full range of operating conditions of a fielded system. A thrust balancing load sharing device was evaluated. Friction forces that oppose the motion of the balance mechanism are significant. A static analysis suggests increasing the helix angle of the input pinion of the thrust balancing design. Also, dynamic analysis of this design predicts good load sharing and significant torsional response to accumulative pitch errors of the gears. Author

N93-14478*# National Aeronautics and Space Administration. Lewis Research Center, Cleveland, OH.

**DEVELOPMENT OF BRAIDED ROPE SEALS FOR
HYPERSONIC ENGINE APPLICATIONS: FLOW MODELING**

RAJAKKANNU MUTHARASAN (Drexel Univ., Philadelphia, PA.), BRUCE M. STEINETZ, XIAOMING TAO (Drexel Univ., Philadelphia, PA.), GUANG-WU DU (Drexel Univ., Philadelphia, PA.), and FRANK KO (Drexel Univ., Philadelphia, PA.) Dec. 1992 22 p Submitted for publication

(Contract RTOP 505-63-5B)

(NASA-TM-105942; E-6166-1; NAS 1.15:105942) Avail: CASI HC A03/MF A01

A new type of engine seal is being developed to meet the needs of advanced hypersonic engines. A seal braided of emerging high temperature ceramic fibers comprised of a sheath-core construction was selected for study based on its low leakage rates. Flexible, low-leakage, high temperature seals are required to seal the movable engine panels of advanced ramjet-scamjet engines either preventing potentially dangerous leakage into backside engine cavities or limiting the purge coolant flow rates through the seals. To predict the leakage through these flexible, porous seal structures new analytical flow models are required. Two such models based on the Kozeny-Carman equations are developed herein and are compared to experimental leakage measurements for simulated pressure and seal gap conditions. The models developed allow prediction of the gas leakage rate as a function of fiber diameter, fiber packing density, gas properties, and pressure drop across the seal. The first model treats the seal as a homogeneous fiber bed. The second model divides the seal into two homogeneous fiber beds identified as the core and the sheath of the seal. Flow resistances of each of the main seal elements are combined to determine the total flow resistance. Comparisons between measured leakage rates and model predictions for seal structures covering a wide range of braid architectures show good agreement. Within the experimental range, the second model provides a prediction within 6 to 13 percent of the flow for many of the cases examined. Areas where future model refinements are required are identified. Author

N93-18321*# National Aeronautics and Space Administration. Lewis Research Center, Cleveland, OH.

**BRUSH SEAL BRISTLE FLEXURE AND HARD-RUB
CHARACTERISTICS**

ROBERT C. HENDRICKS, JULIE A. CARLILE, and ANITA D. LIANG Aug. 1992 23 p Presented at the Seals Workshop, Cleveland, OH, 5-6 Aug. 1992

(Contract RTOP 590-21-11)

(NASA-TM-105864; E-7281; NAS 1.15:105864) Avail: CASI HC A03/MF A01

The bristles of a 38.1-mm (1.5-in) diameter brush seal were flexed by a tapered, 40-tooth rotor operating at 2600 rpm that provided sharp leading-edge impact of the bristles with hard rubbing of the rotor lands. Three separate tests were run with the same brush accumulating over 1.3×10^9 flexure cycles while deteriorating 0.2 mm (0.008 in) radially. In each, the test bristle incursion depth varied from 0.130 to 0.025 mm (0.005 to 0.001 in) or less (start to stop), and in the third test the rotor was set 0.25 mm (0.010 in) eccentric. Runout varied from 0.025 to 0.076 mm (0.001 to 0.003 in) radially. The bristles wore but did not pull out, fracture, or fragment. Bristle and rotor wear debris were deposited as very fine, nearly amorphous, highly porous materials at the rotor groove leading edges and within the rotor grooves. The land leading edges showed irregular wear and the beginning of a convergent groove that exhibited sharp, detailed wear at the land trailing edges. Surface grooving, burnishing, 'whipping,' and hot spots and streaks were found. With a smooth-plug rotor post-test leakage increased 30 percent over pretest leakage. Author

N93-18380*# National Aeronautics and Space Administration. Lewis Research Center, Cleveland, OH.

**INTEGRITY TESTING OF BRUSH SEAL IN SHROUD RING OF
T-700 ENGINE**

ROBERT C. HENDRICKS, THOMAS A. GRIFFIN, GEORGE B. BOBULA, ROBERT C. BILL, and HAROLD W. HOWE (Technetics, Inc., DeLand, FL.) Aug. 1992 25 p Presented at the Seals Workshop, Cleveland, OH, 5-6 Aug. 1992

(Contract RTOP 590-21-11)

(NASA-TM-105863; E-7282; NAS 1.15:105863) Avail: CASI HC A03/MF A01

A split-ring brush seal was fabricated, installed between two labyrinth-honeycomb shroud seals, and tested in the fourth-stage turbine of a T-700 engine. The annealed Haynes 25 bristles rubbed directly against the nonconditioned, irregular Rene 80 turbine blade shroud surface. A total of 30 hr of cyclic and steady-state data were taken with surface speeds to 335 m/s (1100 ft/s) and shroud temperatures to 620 C (1150 F). Wear appeared to be rapid initially, with an orange flash of hot brush fragments during the first engine startup, to minimal after 10 hr of operation. The brush survived the testing but experienced some bristle pullouts and severe bristle wear; some turbine interface wear and possible material transfer was noted. Future design concerns center on tribological behavior at the interface with or without lubricants. Author

N93-19027*# National Aeronautics and Space Administration. Lewis Research Center, Cleveland, OH.

**HIGH-TEMPERATURE, BELLOWS HYBRID SEAL Patent
Application**

B. M. STEINETZ, inventor (to NASA) and P. J. SIROCKY, inventor (to NASA) (Sverdrup Technology, Inc., Brook Park, OH.) 22 Jan. 1993 15 p

(NASA-CASE-LEW-15570-1; NAS 1.71:LEW-15570-1;

US-PATENT-APPL-SN-007874) Avail: CASI HC A03/MF A01

A high-temperature hybrid seal is constructed of multiple elements to meet the many demands placed on the seal. The primary elements are: a central high-temperature bellows, a braided ceramic sheath covering the bellows, an outer abrasion resistant sheath covering the ceramic sheath, and a structurally-sound seal-end termination. NASA

N93-22826*# National Aeronautics and Space Administration. Lewis Research Center, Cleveland, OH.

**EVALUATION OF AN OIL-DEBRIS MONITORING DEVICE FOR
USE IN HELICOPTER TRANSMISSIONS**

DAVID G. LEWICKI, DONALD M. BLANCHETTE (National Defence Headquarters, Ottawa, Ontario.), and GILLES BIRON (Quality Engineering Test Establishment, Hull, Quebec.) Aug. 1992 19 p

(Contract DA PROJ. 1L1-62211-A-47-A; RTOP 505-63-36)

(NASA-TM-105830; E-7265; NAS 1.15:105830;

AVSCOM-TR-92-C-007; AD-A262479) Avail: CASI HC A03/MF A01

Experimental tests were performed on an OH-58A helicopter main-rotor transmission to evaluate an oil-debris monitoring device (ODMD). The tests were performed in the NASA 500-hp Helicopter Transmission Test Stand. Five endurance tests were run as part of a U.S. Navy/NASA/Army advanced lubricants program. The tests were run at 100 percent design speed, 117-percent design torque, and 121 C (250 F) oil inlet temperature. Each test lasted between 29 and 122 hr. The oils that were used conformed to MIL-L-23699 and DOD-L-85734 specifications. One test produced a massive sun-gear fatigue failure; another test produced a small spall on one sun-gear tooth; and a third test produced a catastrophic planet-bearing cage failure. The ODMD results were compared with oil spectroscopy results. The capability of the ODMD to detect transmission component failures was not demonstrated. Two of the five tests produced large amounts of debris. For these two tests, two separate ODMD sensors failed, possibly because of prolonged exposure to relatively high oil temperatures. One test produced a small amount of debris and was not detected by the ODMD or by oil spectroscopy. In general, the ODMD results matched the oil spectroscopy results. The ODMD results were extremely sensitive to oil temperature and flow rate. Author

N93-23019*# National Aeronautics and Space Administration. Lewis Research Center, Cleveland, OH.

LOW-NOISE, HIGH-STRENGTH, SPIRAL-BEVEL GEARS FOR HELICOPTER TRANSMISSIONS

DAVID G. LEWICKI, ROBERT F. HANDSCHUH, ZACHARY S. HENRY (Bell Helicopter Co., Fort Worth, TX.), and FAYDOR L. LITVIN (Chicago Univ., IL.) Jun. 1993 15 p Proposed for presentation at the 29th Joint Propulsion Conference and Exhibit, Monterey, CA, 28-30 Jun. 1993; sponsored by AIAA, SAE, ASME, and ASEE

(Contract DA PROJ. 1L1-62211-A-47-A; RTOP 505-62-10) (NASA-TM-106080; E-7698; NAS 1.15:106080; AIAA PAPER 93-2149; ARL-MR-71; AD-A263116) Avail: CASI HC A03/MF A01

Improvements in spiral-bevel gear design were investigated to support the Army/NASA Advanced Rotorcraft Transmission program. Program objectives were to reduce weight by 25 percent, reduce noise by 10 dB, and increase life to 5000 hr mean-time-between-removal. To help meet these goals, advanced-design spiral-bevel gears were tested in an OH-58D helicopter transmission using the NASA 500-hp Helicopter Transmission Test Stand. Three different gear designs tested included: (1) the current design of the OH-58D transmission except gear material X-53 instead of AISI 9310; (2) a higher-strength design the same as the current but with a full fillet radius to reduce gear tooth bending stress (and thus, weight); and (3) a lower-noise design the same as the high-strength but with modified tooth geometry to reduce transmission error and noise. Noise, vibration, and tooth strain tests were performed and significant gear stress and noise reductions were achieved. Author

N93-23741*# National Aeronautics and Space Administration. Lewis Research Center, Cleveland, OH.

PATTERN CLASSIFIER FOR HEALTH MONITORING OF HELICOPTER GEARBOXES

HSINYUNG CHIN (Massachusetts Univ., Amherst.), KOUROSH DANAI (Massachusetts Univ., Amherst.), and DAVID G. LEWICKI Apr. 1993 15 p Proposed for presentation at the 47th Meeting of the Mechanical Failures Prevention Group, Virginia Beach, VA, 13-15 Apr. 1993; sponsored by ONR

(Contract RTOP 505-62-10; DA PROJ. 1L1-62211-A-47-A) (NASA-TM-106099; E-7741; NAS 1.15:106099; AVSCOM-TR-92-C-033; AD-A263112) Avail: CASI HC A03/MF A01

The application of a newly developed diagnostic method to a helicopter gearbox is demonstrated. This method is a pattern classifier which uses a multi-valued influence matrix (MVIM) as its diagnostic model. The method benefits from a fast learning algorithm, based on error feedback, that enables it to estimate gearbox health from a small set of measurement-fault data. The MVIM method can also assess the diagnosability of the system and variability of the fault signatures as the basis to improve fault signatures. This method was tested on vibration signals reflecting various faults in an OH-58A main rotor transmission gearbox. The vibration signals were then digitized and processed by a vibration signal analyzer to enhance and extract various features of the vibration data. The parameters obtained from this analyzer were utilized to train and test the performance of the MVIM method in both detection and diagnosis. The results indicate that the MVIM method provided excellent detection results when the full range of faults effects on the measurements were included in training, and it had a correct diagnostic rate of 95 percent when the faults were included in training. Author

N93-24751*# National Aeronautics and Space Administration. Lewis Research Center, Cleveland, OH.

GLOBAL DYNAMIC MODELING OF A TRANSMISSION SYSTEM Final Report

F. K. CHOY (Akron Univ., OH.) and W. QIAN (Akron Univ., OH.) Apr. 1993 163 p

(Contract NAG3-900; RTOP 505-62-10) (NASA-CR-191117; E-7731; NAS 1.26:191117; ARL-CR-11; AD-A264968) Avail: CASI HC A08/MF A02

The work performed on global dynamic simulation and noise correlation of gear transmission systems at the University of Akron is outlined. The objective is to develop a comprehensive procedure to simulate the dynamics of the gear transmission system coupled with the effects of gear box vibrations. The developed numerical model is benchmarked with results from experimental tests at NASA Lewis Research Center. The modal synthesis approach is used to develop the global transient vibration analysis procedure used in the model. Modal dynamic characteristics of the rotor-gear-bearing system are calculated by the matrix transfer method while those of the gear box are evaluated by the finite element method (NASTRAN). A three-dimensional, axial-lateral coupled bearing model is used to couple the rotor vibrations with the gear box motion. The vibrations between the individual rotor systems are coupled through the nonlinear gear mesh interactions. The global equations of motion are solved in modal coordinates and the transient vibration of the system is evaluated by a variable time-stepping integration scheme. The relationship between housing vibration and resulting noise of the gear transmission system is generated by linear transfer functions using experimental data. A nonlinear relationship of the noise components to the fundamental mesh frequency is developed using the hypercoherence function. The numerically simulated vibrations and predicted noise of the gear transmission system are compared with the experimental results from the gear noise test rig at NASA Lewis Research Center. Results of the comparison indicate that the global dynamic model developed can accurately simulate the dynamics of a gear transmission system. Author (revised)

N93-25672*# National Aeronautics and Space Administration. Lewis Research Center, Cleveland, OH.

EVALUATION OF A VIBRATION DIAGNOSTIC SYSTEM FOR THE DETECTION OF SPUR GEAR PITTING FAILURES

DENNIS P. TOWNSEND and JAMES J. ZAKRAJSEK Jun. 1993 11 p Proposed for presentation at the 29th Joint Propulsion Conference and Exhibit, Monterey, CA, 28-30 Jun. 1993; sponsored by the AIAA, SAE, ASME, and ASEE

(Contract DA PROJ. 1L1-62211-A-47-A; RTOP 505-62-10) (NASA-TM-106103; E-7752; NAS 1.15:106103; AIAA PAPER 93-2298; ARL-TR-11; AD-A266724) Avail: CASI HC A03/MF A01

A vibration diagnostic system was used to detect spur gear surface pitting fatigue in a closed-loop spur gear fatigue test rig. The diagnostic system, comprising a personal computer with an analog-to-digital conversion board, a diagnostic system unit, and software, uses time-synchronous averaging of the vibration signal to produce a vibration image of each tooth on any gear in a transmission. Several parameters were analyzed including gear pair stress wave and raw baseband vibration, kurtosis, peak ratios, and others. The system provides limits for the various parameters and gives a warning when the limits are exceeded. Several spur gear tests were conducted with this system and vibration data analyzed at 5-min. intervals. The results presented herein show that the system is fairly effective at detecting spur gear tooth surface fatigue pitting failures. Author

N93-27037*# National Aeronautics and Space Administration. Lewis Research Center, Cleveland, OH.

CONTACT STRESS ANALYSIS OF SPIRAL BEVEL GEARS USING NONLINEAR FINITE ELEMENT STATIC ANALYSIS

G. D. BIBEL (North Dakota Univ., Grand Forks.), A. KUMAR (Akron Univ., OH.), S. REDDY (Akron Univ., OH.), and R. HANDSCHUH (Army Research Lab., Cleveland, OH.) May 1993 12 p Presented at the 29th Joint Propulsion Conference and Exhibit, Monterey, CA, 28-30 Jun. 1993; cosponsored by AIAA, SAE, ASME, and ASEE Prepared in cooperation with Army Research Lab., Adelphi, MD

(Contract RTOP 505-62-10; DA PROJ. 1L1-62211-A-47-A) (NASA-TM-106176; E-7876; NAS 1.15:106176; ARL-TR-158; AIAA PAPER 93-2296; AD-A266723) Avail: CASI HC A03/MF A01

A procedure is presented for performing three-dimensional stress analysis of spiral bevel gears in mesh using the finite element method. The procedure involves generating a finite element model

by solving equations that identify tooth surface coordinates. Coordinate transformations are used to orientate the gear and pinion for gear meshing. Contact boundary conditions are simulated with gap elements. A solution technique for correct orientation of the gap elements is given. Example models and results are presented.

Author

N93-27069*# National Aeronautics and Space Administration. Lewis Research Center, Cleveland, OH.

FAULT DETECTION OF HELICOPTER GEARBOXES USING THE MULTI-VALUED INFLUENCE MATRIX METHOD

HSINYUNG CHIN (Massachusetts Univ., Amherst.), KOUROSH DANAI (Massachusetts Univ., Amherst.), and DAVID G. LEWICKI Apr. 1993 32 p

(Contract DA PROJ. 1L1-62211-A-47-A; RTOP 505-63-36)

(NASA-TM-106100; E-7742; NAS 1.15:106100;

AVSCOM-TR-92-C-015) Avail: CASI HC A03/MF A01

In this paper we investigate the effectiveness of a pattern classifying fault detection system that is designed to cope with the variability of fault signatures inherent in helicopter gearboxes. For detection, the measurements are monitored on-line and flagged upon the detection of abnormalities, so that they can be attributed to a faulty or normal case. As such, the detection system is composed of two components, a quantization matrix to flag the measurements, and a multi-valued influence matrix (MVIM) that represents the behavior of measurements during normal operation and at fault instances. Both the quantization matrix and influence matrix are tuned during a training session so as to minimize the error in detection. To demonstrate the effectiveness of this detection system, it was applied to vibration measurements collected from a helicopter gearbox during normal operation and at various fault instances. The results indicate that the MVIM method provides excellent results when the full range of faults effects on the measurements are included in the training set.

Author

N93-27074*# National Aeronautics and Space Administration. Lewis Research Center, Cleveland, OH.

AN ANALYSIS OF GEAR FAULT DETECTION METHODS AS APPLIED TO PITTING FATIGUE FAILURE DATA

J. J. ZAKRAJSEK, D. P. TOWNSEND, and H. J. DECKER Jan. 1993 12 p Presented at the 47th Mechanical Failure Prevention Group, Virginia Beach, VA, 13-15 Apr. 1993 Prepared in cooperation with Army Aviation Systems Command, Cleveland, OH

(Contract RTOP 505-62-10)

(NASA-TM-105950; E-7470; NAS 1.15:105950;

AVSCOM-TR-92-C-035) Avail: CASI HC A03/MF A01

The application of gear fault prediction techniques to experimental data is examined. A single mesh spur gear fatigue rig was used to produce naturally occurring faults on a number of test gear sets. Gear tooth surface pitting was the primary failure mode for a majority of the test runs. The damage ranged from moderate pitting on two teeth in one test to spalling on several teeth in another test. Previously published failure prediction techniques were applied to the data as it was acquired to provide a means of monitoring the test and stopping it when a failure was suspected. A newly developed technique along with variations of published methods were also applied to the experimental data. The published methods experienced some success in detecting initial pitting before it progressed to affect the overall root-mean-square (RMS) vibration level. The new technique robustly detected the damage on all of the tests and, in most cases, continued to react to the damage as it spread and increased in severity. Since no single method was able to consistently predict the damage first on all the runs, it was concluded that the best approach to reliably detect pitting damage is to use a combination of detection methods.

Author (revised)

N93-27133*# National Aeronautics and Space Administration. Lewis Research Center, Cleveland, OH.

FACE-GEAR DRIVES: DESIGN, ANALYSIS, AND TESTING FOR HELICOPTER TRANSMISSION APPLICATIONS

F. L. LITVIN (Illinois Univ., Chicago.), J.-C. WANG (Illinois Univ., Chicago.), R. B. BOSSLER, JR. (Lucas Western, Inc., City of Industry, CA.), Y.-J. D. CHEN (McDonnell-Douglas Helicopter Co., Mesa, AZ.), G. HEATH (McDonnell-Douglas Helicopter Co., Mesa, AZ.), and D. G. LEWICKI Oct. 1992 16 p Presented at the AGMA 1992 Fall Technical Meeting, Baltimore, MD, 26-28 Oct. 1992; sponsored by American Gear Manufacturers Association (Contract DA PROJ. 1L1-62211-A-47-A; RTOP 505-63-36)

(NASA-TM-106101; E-7743; NAS 1.15:106101;

AVSCOM-TR-92-C-009; AD-A266538) Avail: CASI HC A03/MF A01

The use of face-gears in helicopter transmissions was explored. A light-weight, split-torque transmission design utilizing face-gears is described. Face-gear design and geometry were investigated. Topics included tooth generation, limiting inner and outer radii, tooth contact analysis, contact ratio, gear eccentricity, grinding, and structural stiffness. Design charts were developed to determine minimum and maximum face-gear inner and outer radii. An analytical study showed that the face-gear drive is relatively insensitive to gear misalignment with respect to transmission errors, but the tooth contact is affected by misalignment. A method of localizing the bearing contact to permit operation with misalignment was explored. Two new methods for grinding of the face-gear tooth surfaces were also investigated. The proper choice of shaft stiffness enabled good load sharing in the split-torque transmission design. Face-gear experimental studies were also conducted. These tests demonstrated the feasibility of face-gears in high-speed, high-load applications such as helicopter transmissions.

Author

N93-27641*# National Aeronautics and Space Administration. Lewis Research Center, Cleveland, OH.

VIBRATION AND NOISE ANALYSIS OF A GEAR TRANSMISSION SYSTEM

F. K. CHOY (Akron Univ., OH.), W. QIAN (Akron Univ., OH.), J. J. ZAKRAJSEK, and F. B. OSWALD Jun. 1993 17 p Presented at the 28th Joint Propulsion Conference and Exhibit, Monterey, CA, 28-30 Jun. 1993; sponsored by AIAA, SAE, ASME, and ASEE

(Contract RTOP 505-62-10)

(NASA-TM-106162; E-7859; NAS 1.15:106162; AIAA PAPER

93-2150; ARL-MR-77) Avail: CASI HC A03/MF A01

This paper presents a comprehensive procedure to predict both the vibration and noise generated by a gear transmission system under normal operating conditions. The gearbox vibrations were obtained from both numerical simulation and experimental studies using a gear noise test rig. In addition, the noise generated by the gearbox vibrations was recorded during the experimental testing. A numerical method was used to develop linear relationships between the gearbox vibration and the generated noise. The hypercoherence function is introduced to correlate the nonlinear relationship between the fundamental noise frequency and its harmonics. A numerical procedure was developed using both the linear and nonlinear relationships generated from the experimental data to predict noise resulting from the gearbox vibrations. The application of this methodology is demonstrated by comparing the numerical and experimental results from the gear noise test rig.

Author (revised)

N93-27687*# National Aeronautics and Space Administration. Lewis Research Center, Cleveland, OH.

GENERATION OF HELICAL GEARS WITH NEW SURFACES, TOPOLOGY BY APPLICATION OF CNC MACHINES

F. L. LITVIN (Illinois Univ., Chicago.), N. X. CHEN (Illinois Univ., Chicago.), C. L. HSIAO (Illinois Univ., Chicago.), and R. F. HANDSCHUH (Army Research Lab., Cleveland, OH.) May 1993 6 p

Presented at the 29th Joint Propulsion Conference and Exhibit, Monterey, CA, 28-30 Jun. 1993; cosponsored by AIAA, SAE, ASME, ASEE Prepared in cooperation with Army Research Lab., Adelphi, MD

(Contract RTOP 505-62-10; DA PROJ. 1L1-62211-A-47-A)

(NASA-TM-106175; E-7875; NAS 1.15:106175; ARL-TR-9; AIAA PAPER 93-2297; AD-A266233) Avail: CASI HC A02/MF A01

Analysis of helical involute gears by tooth contact analysis shows that such gears are very sensitive to angular misalignment that leads to edge contact and the potential for high vibration. A new topology of tooth surfaces of helical gears that enables a favorable bearing contact and a reduced level of vibration is described. Methods for grinding of the helical gears with the new topology are proposed. A TCA (tooth contact analysis) program for simulation of meshing and contact of helical gears with the new topology has been developed. Numerical examples that illustrate the proposed ideas are discussed. Author

N93-28050* National Aeronautics and Space Administration. Lewis Research Center, Cleveland, OH.

DYNAMIC ANALYSIS OF SPUR GEARS USING COMPUTER PROGRAM DANST

FRED B. OSWALD, HSIANG HSI LIN (Memphis State Univ., TN.), CHUEN-HUEI LIOU (Memphis State Univ., TN.), and MARK J. VALCO Jun. 1993 14 p Proposed for presentation at the 29th Joint Propulsion Conference and Exhibit, Monterey, CA, 28-30 Jun. 1993; sponsored by AIAA, SAE, ASME, and ASEE (Contract DA PROJ. 1L1-62211-A-47-A; RTOP 505-62-10) (NASA-TM-106211; E-7921; NAS 1.15:106211; ARL-TR-171; AIAA PAPER 93-2295) Avail: CASI HC A03/MF A01

DANST is a computer program for static and dynamic analysis of spur gear systems. The program can be used for parametric studies to predict the effect on dynamic load and tooth bending stress of spur gears due to operating speed, torque, stiffness, damping, inertia, and tooth profile. DANST performs geometric modeling and dynamic analysis for low- or high-contact-ratio spur gears. DANST can simulate gear systems with contact ratio ranging from one to three. It was designed to be easy to use, and it is extensively documented by comments in the source code. This report describes the installation and use of DANST. It covers input data requirements and presents examples. The report also compares DANST predictions for gear tooth loads and bending stress to experimental and finite element results.

Author (revised)

N93-28127* National Aeronautics and Space Administration. Lewis Research Center, Cleveland, OH.

AN APPARATUS FOR GRIPPING TEST SPECIMENS Patent Application

REBECCA MACKAY, inventor (to NASA) and MICHAEL V. NATHAL, inventor (to NASA) 2 Apr. 1993 14 p (NASA-CASE-LEW-15345-2; NAS 1.71:LEW-15345-2; US-PATENT-APPL-SN-039735) Avail: CASI HC A03/MF A01

A pair of solid-teeth wedges are employed in an improved gripping system. These wedges fit inside a pair of plates having an angled cavity to accommodate them. As stress is applied to the specimen, the wedges are urged toward the specimen by the angled cavity to increase the gripping force. NASA

N93-28411* National Aeronautics and Space Administration. Lewis Research Center, Cleveland, OH.

EFFECT OF EXTENDED TOOTH CONTACT ON THE MODELING OF SPUR GEAR TRANSMISSIONS

FRED B. OSWALD, JOHN J. COY, HSIANG HSI LIN (Memphis State Univ., TN.), and JIFENG WANG (Memphis State Univ., TN.) May 1993 12 p Presented at the 29th Joint Propulsion Conference and Exhibit, Monterey, CA, 28-30 Jun. 1993; sponsored by AIAA, SAE, ASME, and ASEE Prepared in cooperation with Army Research Lab., Cleveland, OH (Contract DA PROJ. 1L1-62211-A-47-A; RTOP 505-62-10) (NASA-TM-106174; E-7874; NAS 1.15:106174; ARL-TR-159; AIAA PAPER 93-2148) Avail: CASI HC A03/MF A01

In some gear dynamic models, the effect of tooth flexibility is ignored when the model determines which pairs of teeth are in contact. Deflection of loaded teeth is not introduced until the equations of motion are solved. This means the zone of tooth contact and average tooth meshing stiffness are underestimated and the individual tooth load is overstated, especially for heavily-loaded gears. The static transmission error and dynamic load of heavily-loaded, low-contact-ratio spur gears is compared

with this effect both neglected and included. Neglecting the effect yields an underestimate of resonance speeds and an overestimate of the dynamic load. Author (revised)

N93-31314* National Aeronautics and Space Administration. Lewis Research Center, Cleveland, OH.

SERVICE EQUIPMENT FOR USE IN HOSTILE ENVIRONMENTS Patent Application

JAMES L. DOLCE, inventor (to NASA) and ANDREW L. GORDON, inventor (to NASA) (Analytical Engineering Corp., North Olmsted, OH.) 26 Jul. 1993 20 p (NASA-CASE-LEW-14906-2; NAS 1.71:LEW-14906-2; US-PATENT-APPL-SN-104951) Avail: CASI HC A03/MF A01

Service equipment for use in hostile environments includes a detachable service unit secured to a stationary service unit. The detachable service unit includes a housing with an exterior plate, a power control interface for connection to an exterior power source, locating pins located in said exterior plate, an electrical connector in the exterior plate electrically coupled to said power control interface, and a pair of clamping receptacles formed in the exterior plate and located on adjacent opposite edges of the exterior plate. The stationary unit includes an electrical connector for connection to the electrical connector of the detachable service unit, a clamping apparatus for clamping and unclamping the detachable service unit from the stationary unit, a base clamp assembly for mounting the clamping apparatus onto the stationary unit, and locating pin holes for receiving the locating pins and aligning the detachable service unit onto the stationary unit. The detachable service unit and stationary unit have mating scalloped faces which aid in alignment and provide a mechanism for heat dissipation. NASA

N93-31584* National Aeronautics and Space Administration. Lewis Research Center, Cleveland, OH.

THREE-DIMENSIONAL ANALYSIS OF THE PRATT AND WHITNEY ALTERNATE DESIGN SSME FUEL TURBINE

K. R. KIRTLEY (Sverdrup Technology, Inc., Brook Park, OH.), T. A. BEACH (Sverdrup Technology, Inc., Brook Park, OH.), and J. J. ADAMCZYK *In its Structural Integrity and Durability of Reusable Space Propulsion Systems* p 255-262 May 1991 Avail: CASI HC A02/MF A03

The three dimensional viscous time-mean flow in the Pratt and Whitney alternate design space shuttle main engine fuel turbine is simulated using the average passage Navier-Stokes equations. The migration of secondary flows generated by upstream blade rows and their effect on the performance of downstream blade rows is studied. The present simulation confirms that the flow in this two stage turbine is highly three dimensional and dominated by the tip leakage flow. The tip leakage vortex generated by the first blade persists through the second blade and adversely affects its performance. The greatest mixing of the inlet total temperature distortion occurs in the second vane and is due to the large leakage vortex generated by the upstream rotor. It is assumed that the predominant spanwise mixing mechanism in this low aspect ratio turbine is the radial transport due to the deterministically unsteady vortical flow generated by upstream blade rows. A by-product of the analysis is accurate pressure and heat loads for all blade rows under the influence of neighboring blade rows. These aero loads are useful for advanced structural analysis of the vanes and blades. Derived from text

N93-31586* National Aeronautics and Space Administration. Lewis Research Center, Cleveland, OH.

LOCALIZATION OF AEROELASTIC MODES IN MISTUNED HIGH-ENERGY TURBINES

TODD E. SMITH (Sverdrup Technology, Inc., Brook Park, OH.), CHRISTOPHE PIERRE (Michigan Univ., Ann Arbor.), and DURBHA V. MURTHY (Toledo Univ., OH.) *In its Structural Integrity and Durability of Reusable Space Propulsion Systems* p 273-280 May 1991

Avail: CASI HC A02/MF A03

The effects of blade mistuning on the aerodynamic characteristics of a class of bladed-disk assemblies, namely high

energy turbines, are discussed. The specific rotor analyzed is the first stage of turbine blades of the oxidizer turbopump in the Space Shuttle Main Engine. The common occurrence of fatigue cracks for these turbine blades indicates the possibility of high dynamic loading. Since mistuning under conditions of weak interblade coupling has been shown to increase blade response amplitudes drastically for simple structural models of blade assemblies, it provides a plausible explanation for the occurrence of cracks. The focus here is on the effects of frequency mistuning on the aeroelastic stability of the assembly and on the aeroelastic mode shapes. Derived from text

N93-31846* National Aeronautics and Space Administration. Lewis Research Center, Cleveland, OH.

EFFICIENT FAULT DIAGNOSIS OF HELICOPTER GEARBOXES
H. CHIN (Massachusetts Univ., Amherst.), K. DANAI (Massachusetts Univ., Amherst.), and D. G. LEWICKI Jul. 1993 6 p Proposed for presentation at the 12th World Congress International Federation of Automatic Control, Sydney, Australia 19-23 Jul. 1993

(Contract DA PROJ. 1L1-62211-A-47-A; RTOP 505-62-10)
(NASA-TM-106253; E-7975; NAS 1.15:106253;
AVSCOM-TR-92-C-034) Avail: CASI HC A02/MF A01

Application of a diagnostic system to a helicopter gearbox is presented. The diagnostic system is a nonparametric pattern classifier that uses a multi-valued influence matrix (MVIM) as its diagnostic model and benefits from a fast learning algorithm that enables it to estimate its diagnostic model from a small number of measurement-fault data. To test this diagnostic system, vibration measurements were collected from a helicopter gearbox test stand during accelerated fatigue tests and at various fault instances. The diagnostic results indicate that the MVIM system can accurately detect and diagnose various gearbox faults so long as they are included in training. Author (revised)

38

QUALITY ASSURANCE AND RELIABILITY

Includes product sampling procedures and techniques; and quality control.

A93-19486* National Aeronautics and Space Administration. Lewis Research Center, Cleveland, OH.

RELIABILITY ANALYSIS OF STRUCTURAL CERAMIC COMPONENTS USING A THREE-PARAMETER WEIBULL DISTRIBUTION

STEPHEN F. DUFFY, LYNN M. POWERS (NASA, Lewis Research Center; Cleveland State Univ., OH), and ALOIS STARLINGER (NASA, Lewis Research Center, Cleveland, OH) Jun. 1992 9 p. ASME, International Gas Turbine and Aeroengine Congress and Exposition, 37th, Cologne, Germany, June 1-4, 1992 Previously announced in STAR as N92-17060 refs (ASME PAPER 92-GT-296)

Described here are nonlinear regression estimators for the three-parameter Weibull distribution. Issues relating to the bias and invariance associated with these estimators are examined numerically using Monte Carlo simulation methods. The estimators were used to extract parameters from sintered silicon nitride failure data. A reliability analysis was performed on a turbopump blade utilizing the three-parameter Weibull distribution and the estimates from the sintered silicon nitride data. Author

A93-21898* National Aeronautics and Space Administration. Lewis Research Center, Cleveland, OH.

DETECTING LAMB WAVES WITH BROADBAND ACOUSTO-ULTRASONIC SIGNALS IN COMPOSITE STRUCTURES

HAROLD E. KAUTZ (NASA, Lewis Research Center, Cleveland,

OH) Research in Nondestructive Evaluation (ISSN 0934-9847) vol. 4, no. 3 1992 p. 151-164. refs
Copyright

Lamb waves can be produced and detected in ceramic matrix composites (CMC) and metal matrix composites (MMC) plates using the acousto-ultrasonic configuration employing broadband transducers. Experimental dispersion curves of lowest symmetric and lowest antisymmetric modes behave in a manner analogous to the graphite/polymer theoretical curves. In this study a basis has been established for analyzing Lamb wave velocities for characterizing composite plates. Lamb wave dispersion curves and group velocities were correlated with variations in axial stiffness and shear stiffness in MMC and CMC. For CMCs, interfacial shear strength was also correlated with the first antisymmetric Lamb mode. Author

A93-37009* National Aeronautics and Space Administration. Lewis Research Center, Cleveland, OH.

APPLICATION OF NEURAL NETWORKS IN THE ACOUSTO-ULTRASONIC EVALUATION OF METAL-MATRIX COMPOSITE SPECIMENS

KRZYSZTOF J. CIOS (Toledo Univ.; NASA, Lewis Research Center, Cleveland; Ohio Aerospace Inst., Brook Park), ROBERT E. TJIA (Toledo Univ., OH), ALEX VARY, and HAROLD E. KAUTZ (NASA, Lewis Research Center, Cleveland, OH) In IJCNN - International Joint Conference on Neural Networks, Baltimore, MD, June 7-11, 1992, Proceedings. Vol. 2 New York Institute of Electrical and Electronics Engineers, Inc. 1992 p. II-993 to II-998. refs
Copyright

Acousto-ultrasonics (AU) is a nondestructive evaluation (NDE) technique that was devised for the testing of various types of composite materials. A study has been done to determine how effectively the AU technique may be applied to metal-matrix composites (MMCs). The authors use the results and data obtained from that study and apply neural networks to them, particularly in the assessment of mechanical property variations of a specimen from AU measurements. It is assumed that there is no information concerning the important features of the AU signal which relate to the mechanical properties of the specimen. Minimally processed AU measurements are used while relying on the network's ability to extract the significant features of the signal. Author

N93-10963* National Aeronautics and Space Administration. Lewis Research Center, Cleveland, OH.

NONDESTRUCTIVE EVALUATION OF CERAMIC AND METAL MATRIX COMPOSITES FOR NASA'S HITEMP AND ENABLING PROPULSION MATERIALS PROGRAMS

EDWARD R. GENERAZIO Aug. 1992 27 p Presented at the 16th Annual Conference on Composites, Materials, and Structures, Cocoa Beach, FL, 12-15 Jan. 1992
(Contract RTOP 510-01-50)
(NASA-TM-105807; E-7238; NAS 1.15:105807) Avail: CASI HC A03/MF A01

In a preliminary study, ultrasonic, x-ray opaque, and fluorescent dye penetrant techniques were used to evaluate and characterize ceramic and metal matrix composites. Techniques are highlighted for identifying porosity, fiber alignment, fiber uniformity, matrix cracks, fiber fractures, unbonds or disbonds between laminae, and fiber-to-matrix bond variations. The nondestructive evaluations (NDE) were performed during processing and after thermomechanical testing. Specific examples are given for Si₃N₄/SiC (SCS-6 fiber), FeCrAlY/Al₂O₃ fibers, Ti-15-3/SiC (SCS-6 fiber) materials, and Si₃N₄/SiC (SCS-6 fiber) actively cooled panel components. Results of this study indicate that the choice of the NDE tools to be used can be optimized to yield a faithful and accurate evaluation of advanced composites. Author

N93-18422* National Aeronautics and Space Administration. Lewis Research Center, Cleveland, OH.

SELF-GROWING NEURAL NETWORK ARCHITECTURE USING CRISP AND FUZZY ENTROPY

KRZYSZTOF J. CIOS 24 Apr. 1992 17 p Presented at the International Conference on Aerospace Sensing, Orlando, FL,

38 QUALITY ASSURANCE AND RELIABILITY

20-24 Apr. 1992; sponsored by the Society of Photo-Optical Instrumentation Engineers
(Contract RTOP 510-01-50)
(NASA-TM-105677; E-7052; NAS 1.15:105677) Avail: CASI HC A03/MF A01

The paper briefly describes the self-growing neural network algorithm, CID2, which makes decision trees equivalent to hidden layers of a neural network. The algorithm generates a feedforward architecture using crisp and fuzzy entropy measures. The results of a real-life recognition problem of distinguishing defects in a glass ribbon and of a benchmark problem of differentiating two spirals are shown and discussed. Author

N93-27025*# National Aeronautics and Space Administration. Lewis Research Center, Cleveland, OH.

RENEW V3.2 USER'S MANUAL, MAINTENANCE ESTIMATION SIMULATION FOR SPACE STATION FREEDOM PROGRAM

BRUCE L. BREM Apr. 1993 47 p
(NASA-TM-106006; E-7763; NAS 1.15:106006) Avail: CASI HC A03/MF A01

RENEW is a maintenance event estimation simulation program developed in support of the Space Station Freedom Program (SSFP). This simulation uses reliability and maintainability (R&M) and logistics data to estimate both average and time dependent maintenance demands. The simulation uses Monte Carlo techniques to generate failure and repair times as a function of the R&M and logistics parameters. The estimates are generated for a single type of orbital replacement unit (ORU). The simulation has been in use by the SSFP Work Package 4 prime contractor, Rocketdyne, since January 1991. The RENEW simulation gives closer estimates of performance since it uses a time dependent approach and depicts more factors affecting ORU failure and repair than steady state average calculations. RENEW gives both average and time dependent demand values. Graphs of failures over the mission period and yearly failure occurrences are generated. The averages demand rate for the ORU over the mission period is also calculated. While RENEW displays the results in graphs, the results are also available in a data file for further use by spreadsheets or other programs. The process of using RENEW starts with keyboard entry of the R&M and operational data. Once entered, the data may be saved in a data file for later retrieval. The parameters may be viewed and changed after entry using RENEW. The simulation program runs the number of Monte Carlo simulations requested by the operator. Plots and tables of the results can be viewed on the screen or sent to a printer. The results of the simulation are saved along with the input data. Help screens are provided with each menu and data entry screen. Author

N93-27080*# National Aeronautics and Space Administration. Lewis Research Center, Cleveland, OH.

DETERMINATION OF PLATE WAVE VELOCITIES AND DIFFUSE FIELD DECAY RATES WITH BROAD-BAND ACOUSTO-ULTRASONIC SIGNALS

HAROLD E. KAUTZ Jun. 1993 11 p Presented at the Second International Conference on Acousto-Ultrasonics, Atlanta, GA, 24-25 Jun. 1993; sponsored by American Society for Nondestructive Testing
(Contract RTOP 510-01-50)
(NASA-TM-106158; E-7844; NAS 1.15:106158) Avail: CASI HC A03/MF A01

Lowest symmetric and lowest antisymmetric plate wave modes were excited and identified in broad-band acousto-ultrasonic (AU) signals collected from various high temperature composite materials. Group velocities have been determined for these nearly nondispersive modes. An algorithm has been developed and applied to determine phase velocities and hence dispersion curves for the frequency ranges of the broad-band pulses. It is demonstrated that these data are sensitive to changes in the various stiffness moduli of the materials, in agreement by analogy, with the theoretical and experimental results of Tang and Henneke on fiber reinforced polymers. Diffuse field decay rates have been determined in the same specimen geometries and AU configuration

as for the plate wave measurements. These decay rates are of value in assessing degradation such as matrix cracking in ceramic matrix composites. In addition, we verify that diffuse field decay rates respond to fiber/matrix interfacial shear strength and density in ceramic matrix composites. This work shows that velocity/stiffness and decay rate measurements can be obtained in the same set of AU experiments for characterizing materials and in specimens with geometries useful for mechanical measurements. Author

N93-29073*# National Aeronautics and Space Administration. Lewis Research Center, Cleveland, OH.

ACOUSTO-ULTRASONIC ANALYSIS OF FAILURE IN CERAMIC MATRIX COMPOSITE TENSILE SPECIMENS

HAROLD E. KAUTZ and ABHISAK CHULYA (Cleveland State Univ., OH.) Jun. 1993 10 p Presented at the Second International Conference on Acousto-Ultrasonics, Atlanta, GA, 24-25 Jun. 1993; sponsored by American Society for Nondestructive Testing, Inc. (Contract RTOP 510-01-50)
(NASA-TM-106219; E-7930; NAS 1.15:106219) Avail: CASI HC A02/MF A01

Three types of acousto-ultrasonic (AU) measurements, stress-wave factor (SWF), lowest antisymmetric plate mode group velocity (VS), and lowest symmetric plate mode group velocity (VL), were performed on specimens before and after tensile failure. Three different Nicalon fiber architectures with ceramic matrices were tested. These composites were categorized as 1D (unidirectional fiber orientation) SiC/CAS glass ceramic, and 2D and 3D woven SiC/SiC ceramic matrix materials. SWF was found to be degraded after tensile failure in all three material categories. VS was found to be degraded only in the 1D SiC/CAS. VL was difficult to determine on the irregular specimen surfaces but appeared unchanged on all failed specimens. 3D woven specimens with heat-treatment at high temperature exhibited degradation only in SWF. Author

N93-31572*# National Aeronautics and Space Administration. Lewis Research Center, Cleveland, OH.

MAPPING METHODS FOR COMPUTATIONALLY EFFICIENT AND ACCURATE STRUCTURAL RELIABILITY

MICHAEL C. SHIAO (Sverdrup Technology, Inc., Brook Park, OH.) and CHRISTOS C. CHAMIS *In its Structural Integrity and Durability of Reusable Space Propulsion Systems* p 145-158 May 1991
Avail: CASI HC A03/MF A03

The influence of mesh coarseness in the structural reliability is evaluated. The objectives are to describe the alternatives and to demonstrate their effectiveness. The results show that special mapping methods can be developed by using: (1) deterministic structural responses from a fine (convergent) finite element mesh; (2) probabilistic distributions of structural responses from a coarse finite element mesh; (3) the relationship between the probabilistic structural responses from the coarse and fine finite element meshes; and (4) probabilistic mapping. The structural responses from different finite element meshes are highly correlated. Derived from text

N93-31574*# National Aeronautics and Space Administration. Lewis Research Center, Cleveland, OH.

OVERVIEW OF THE FATIGUE/FRACTURE/LIFE PREDICTION WORKING GROUP PROGRAM AT THE LEWIS RESEARCH CENTER Abstract Only

MICHAEL A. MCGAW *In its Structural Integrity and Durability of Reusable Space Propulsion Systems* p 169-170 May 1991
Avail: CASI HC A01/MF A03

The objective is to develop and verify constitutive and life prediction models for materials typically used in hot gas path components of reusable space propulsion systems over the range of relevant operative environments. The efforts were concentrated on the development of crack initiation life prediction methods and on the development of cyclic crack propagation and fracture life prediction methods. Derived from text

N93-70212* National Aeronautics and Space Administration. Lewis Research Center, Cleveland, OH.

THE FIFTH ANNUAL NASA/CONTRACTORS CONFERENCE ON QUALITY AND PRODUCTIVITY. QUALITY: A COMMITMENT TO THE FUTURE Summary Report

Feb. 1989 83 p Conference held in Cleveland, OH, 12-13 Oct. 1988

(NASA-TM-107829; NAS 1.15:197829; PB92-160688) Avail: CASI HC A05/MF A01

The report is a summary of the 5th NASA/Contractors Conference on Quality and Productivity. The theme was 'Quality - A Commitment to the Future'. The summary report highlights the key points: commitment to quality, strategic and long-range planning, quality commitment, risk management, teaming, quality measurement, creating a quality environment, contract incentives, software quality and reliability.

Author

39

STRUCTURAL MECHANICS

Includes structural element design and weight analysis; fatigue; and thermal stress.

A93-12046* National Aeronautics and Space Administration. Lewis Research Center, Cleveland, OH.

THERMO-ELASTOVISCOPLASTIC SNAPTROUGH BEHAVIOR OF CYLINDRICAL PANELS

Y. SONG (Georgia Inst. of Technology, Atlanta) and G. J. SIMITSES (Cincinnati Univ., OH) Computers & Structures (ISSN 0045-7949) vol. 44, no. 6 Sept. 3, 1992 p. 1255-1261. refs (Contract NAG3-534) Copyright

The thermo-elastoviscoplastic snapthrough behavior of simply supported cylindrical panels is investigated. The analysis is based on nonlinear kinematic relations and nonlinear rate-dependent unified constitutive equations which include both Bodner-Partom's and Walker's material models. A finite element approach is employed to predict the inelastic buckling behavior. Numerical examples are given to demonstrate the effects of several parameters which include the temperature, thickness and flatness of the panel. Comparisons of buckling responses between Bodner-Partom's model and Walker's model are given. The creep buckling behavior, as an example of time-dependent inelastic deformation, is also presented.

Author

A93-12119* National Aeronautics and Space Administration. Lewis Research Center, Cleveland, OH.

SINGLE-PARAMETER CHARACTERIZATION OF DISCRETE-DISLOCATION PILEUP TIPFIELD AND ITS APPLICATION TO PHYSICALLY BASED MICRO-MECHANICS

H. W. LIU (Syracuse Univ., NY) and Q. GAO (Southwest Jiaotong Univ., Chengdu, China) In Morris E. Fine Symposium, TMS Fall Meeting, Detroit, MI, Oct. 8-11, 1990, Proceedings Warrendale, PA Minerals, Metals & Materials Society 1991 p. 375-381. refs

(Contract NAG3-837)

Copyright

The equivalence between continuous dislocation pileups and cracks is reviewed. The force on the leading dislocation is defined and a general method of calculation of the force is proposed. The equivalence relations are given. Based on the analysis by Eshelby, Frank, and Nabarro and the numerical calculations by Chou and Li and Armstrong et al, it will be shown that the force, F , on the locked leading dislocation of a discrete pileup is capable of characterizing uniquely the stress, strain, and displacement fields at the tip of the pileup, including the positions of the discrete mobile dislocations behind the leading dislocation. Conversely, the positions of the mobile dislocations can be used to measure F . If the propagation of micro-slips and the initiation of micro-fractures

at the tip of a pileup are controlled by resolved shear stress and normal cleavage stress respectively, the resolved shear stress intensity coefficient, $ReSIC$, and the resolved cleavage stress intensity coefficient, $ReCIC$, must be constant.

Author

A93-12160* National Aeronautics and Space Administration. Lewis Research Center, Cleveland, OH.

PROBABILISTIC EVALUATION OF UNCERTAINTIES AND RISKS IN AEROSPACE COMPONENTS

A. R. SHAH, M. C. SHIAO, V. K. NAGPAL (Sverdrup Technology, Inc., Brook Park, OH), and C. C. CHAMIS (NASA, Lewis Research Center, Cleveland, OH) In Computational nonlinear mechanics in aerospace engineering Washington American Institute of Aeronautics and Astronautics, Inc. 1992 p. 365-415. refs Copyright

A methodology is presented for the computational simulation of primitive variable uncertainties, and attention is given to the simulation of specific aerospace components. Specific examples treated encompass a probabilistic material behavior model, as well as static, dynamic, and fatigue/damage analyses of a turbine blade in a mistuned bladed rotor in the SSME turbopumps. An account is given of the use of the NESSES probabilistic FEM analysis CFD code.

O.C.

A93-13823* National Aeronautics and Space Administration. Lewis Research Center, Cleveland, OH.

HIGH TEMPERATURE VISCOPLASTIC RATCHETTING - MATERIAL RESPONSE OR MODELING ARTIFACT

ALAN D. FREED (NASA, Lewis Research Center, Cleveland, OH) In Space nuclear power systems; Proceedings of the 8th Symposium, Albuquerque, NM, Jan. 6-10, 1991. Pt. 2 New York American Institute of Physics 1991 p. 575-580. refs Copyright

Some of the basic issues of ratchetting behavior that are being addressed by the viscoplastic modeling community are discussed. Some of the shortcomings of existing viscoplastic models are examined in the light of the difficulty involved in using established viscoplastic modeling techniques to predict ratchetting accurately.

C.A.B.

A93-14446* National Aeronautics and Space Administration. Lewis Research Center, Cleveland, OH.

SHAPE REANALYSIS AND SENSITIVITIES UTILIZING PRECONDITIONED ITERATIVE BOUNDARY SOLVERS

K. GURU PRASAD and J. H. KANE (Clarkson Univ., Potsdam, NY) Structural Optimization (ISSN 0934-4373) vol. 4, no. 3-4 Oct. 1992 p. 224-235. refs (Contract NAG3-1089; NSF DDM-89-96171) Copyright

The computational advantages associated with the utilization of preconditioned iterative equation solvers are quantified for the reanalysis of perturbed shapes using continuum structural boundary element analysis (BEA). Both single- and multi-zone three-dimensional problems are examined. Significant reductions in computer time are obtained by making use of previously computed solution vectors and preconditioners in subsequent analyses. The effectiveness of this technique is demonstrated for the computation of shape response sensitivities required in shape optimization. Computer times and accuracies achieved using the preconditioned iterative solvers are compared with those obtained via direct solvers and implicit differentiation of the boundary integral equations. It is concluded that this approach employing preconditioned iterative equation solvers in reanalysis and sensitivity analysis can be competitive with if not superior to those involving direct solvers.

Author

A93-16005* National Aeronautics and Space Administration. Lewis Research Center, Cleveland, OH.

LIMIT PRESSURE OF A CIRCUMFERENTIALLY REINFORCED SIC/TI RING

D. N. ROBINSON and M. S. PASTOR (Akron Univ., OH) Composites Engineering (ISSN 0961-9526) vol. 2, no. 4 May 1992 p. 229-238. Previously announced in STAR as

N92-11387 refs
(Contract NAG3-379)
Copyright

Limit loads under plane stress and plane strain are found for a circumferentially reinforced elastoplastic ring subjected to interior pressure. These are used as bounds on an estimate of the failure pressure of a SiC/Ti test rig that is being fabricated and tested. The ring is to serve as a benchmark against which deformation and failure analysis methods can be assessed. An anisotropic perfect plasticity idealization of the SiC/Ti ring material is made and used in the limit load calculations. An estimate of the failure pressure of the NASA/PW benchmark test ring is given. Author

A93-16203* National Aeronautics and Space Administration. Lewis Research Center, Cleveland, OH.

PROBABILISTIC STRUCTURAL ANALYSIS OF ADAPTIVE/SMART/INTELLIGENT SPACE STRUCTURES

SHANTARAM S. PAI and CHRISTOS C. CHAMIS (NASA, Lewis Research Center, Cleveland, OH) *Journal of Intelligent Material Systems and Structures* (ISSN 1045-389X) vol. 3, no. 4 Oct. 1992 p. 600-616. Previously announced in STAR as N92-22267 refs
Copyright

A three-bay, space, cantilever truss is probabilistically evaluated for adaptive/smart/intelligent behavior. For each behavior, the scatter (ranges) in buckling loads, vibration frequencies, and member axial forces are probabilistically determined. Sensitivities associated with uncertainties in the structure, material and load variables that describe the truss are determined for different probabilities. The relative magnitude for these sensitivities are used to identify significant truss variables that control/classify its behavior to respond as an adaptive/smart/intelligent structure. Results show that the probabilistic buckling loads and vibration frequencies increase for each truss classification, with a substantial increase for intelligent trusses. Similarly, the probabilistic member axial forces reduce for adaptive and intelligent trusses and increase for smart trusses. Author

A93-16406* National Aeronautics and Space Administration. Lewis Research Center, Cleveland, OH.

AN ADVANCED METHOD FOR TRACKING THE EVOLUTION OF FATIGUE DAMAGE IN REUSABLE SPACE PROPULSION SYSTEMS

K. R. RAJAGOPAL, G. ORIENT, J. F. NEWELL (Rockwell International Corp., Canoga Park, CA), and M. MCGAW (NASA, Lewis Research Center, Cleveland, OH) *In Annual Health Monitoring Conference for Space Propulsion Systems*, 3rd, Cincinnati, OH, Nov. 13, 14, 1991, Proceedings Cincinnati, OH University of Cincinnati 1991 p. 111-127. refs
Copyright

NASA-Lewis is actively involved in the general effort to research, develop, test, and evaluate advanced theoretical, analytical, experimental, and probabilistic analysis concepts required for life prediction of liquid rocket engines at the subcomponent, component, and engine system levels. The models developed are oriented toward use in advanced health monitoring systems of space propulsion systems. It is planned to demonstrate the methodology considering a representative set of three components such as a main injector element, a combustion chamber liner, and a turbopump blade. This paper describes the initial development and application of this method to a specific location in the main injector element of the SSME. Further enhancements and various elements of the framework will be completed as the work proceeds in subsequent years. Author

A93-16552* National Aeronautics and Space Administration. Lewis Research Center, Cleveland, OH.

STRUCTURAL DURABILITY OF A COMPOSITE PRESSURE VESSEL

LEVON MINNETYAN (Clarkson Univ., Potsdam, NY), CHRISTOS C. CHAMIS, and PAPPU L. N. MURTHY (NASA, Lewis Research Center, Cleveland, OH) *Journal of Reinforced Plastics and Composites* (ISSN 0731-6844) vol. 11, no. 11 Nov. 1992 p.

1251-1269. refs
(Contract NAG3-1101)
Copyright

The effect of local ply fiber fracture on the load-carrying capability and structural behavior of a composite cylindrical shell under internal pressure is investigated, using the CODSTRAN computer code to simulate the composite structural degradation under loading. Results show that an initial outer-surface defect in the vessel begins to grow at a relatively low pressure but exhibits localized gradual damage growth prior to structural fracture and that an initial inner-surface defect shows an overall damage progression and fracture behavior closely similar to that of the outer surface defect. An initial defect located near the mid-thickness of the shell requires a higher pressure to cause damage initiation, but, once the damage initiation pressure is reached, a sudden structural fracture stage is entered by rapid damage propagation at a slightly higher pressure. I.S.

A93-17246 National Aeronautics and Space Administration. Lewis Research Center, Cleveland, OH.

IMPROVED ACCURACY FOR FINITE ELEMENT STRUCTURAL ANALYSIS VIA AN INTEGRATED FORCE METHOD

S. N. PATNAIK (Ohio Aerospace Inst., Brook Park), D. A. HOPKINS, R. A. AIELLO, and L. BERKE (NASA, Lewis Research Center, Cleveland, OH) *Computers & Structures* (ISSN 0045-7949) vol. 45, no. 3 Oct. 17, 1992 p. 521-542. Previously announced in STAR as N92-22227 refs
(Contract RTOP 505-63-5B)
Copyright

A comparative study was carried out to determine the accuracy of finite element analyses based on the stiffness method, a mixed method, and the new integrated force and dual integrated force methods. The numerical results were obtained with the following software: MSC/NASTRAN and ASKA for the stiffness method; an MHOST implementation method for the mixed method; and GIFT for the integrated force methods. The results indicate that on an overall basis, the stiffness and mixed methods present some limitations. The stiffness method generally requires a large number of elements in the model to achieve acceptable accuracy. The MHOST method tends to achieve a higher degree of accuracy for course models than does the stiffness method implemented by MSC/NASTRAN and ASKA. The two integrated force methods, which bestow simultaneous emphasis on stress equilibrium and strain compatibility, yield accurate solutions with fewer elements in a model. The full potential of these new integrated force methods remains largely unexploited, and they hold the promise of spawning new finite element structural analysis tools. Author

A93-19540* National Aeronautics and Space Administration. Lewis Research Center, Cleveland, OH.

CERAMIC COMPONENT RELIABILITY WITH THE RESTRUCTURED NASA/CARES COMPUTER PROGRAM

LYNN M. POWERS (NASA, Lewis Research Center; Cleveland State Univ., OH), ALOIS STARLINGER, and JOHN P. GYEKENYESI (NASA, Lewis Research Center, Cleveland, OH) Jun. 1992 6 p. ASME, International Gas Turbine and Aeroengine Congress and Exposition, 37th, Cologne, Germany, June 1-4, 1992 Previously announced in STAR as N93-11004 refs
(ASME PAPER 92-GT-383)

The Ceramics Analysis and Reliability Evaluation of Structures (CARES) integrated design program on statistical fast fracture reliability and monolithic ceramic components is enhanced to include the use of a neutral data base, two-dimensional modeling, and variable problem size. The data base allows for the efficient transfer of element stresses, temperatures, and volumes/areas from the finite element output to the reliability analysis program. Elements are divided to insure a direct correspondence between the subelements and the Gaussian integration points. Two-dimensional modeling is accomplished by assessing the volume flaw reliability with shell elements. To demonstrate the improvements in the algorithm, example problems are selected from a round-robin conducted by WELFEP (WEakest Link failure probability prediction by Finite Element Postprocessors). Author

A93-20363*# National Aeronautics and Space Administration. Lewis Research Center, Cleveland, OH.

PROBABILISTIC STRUCTURAL ANALYSIS OF SPACE TRUSS STRUCTURES FOR NONUNIFORM THERMAL ENVIRONMENTAL EFFECTS

SHANTARAM S. PAI (NASA, Lewis Research Center, Cleveland, OH) /in AIAA/USAF/NASA/OAI Symposium on Multidisciplinary Analysis and Optimization, 4th, Cleveland, OH, Sept. 21-23, 1992, Technical Papers. Pt. 2 Washington American Institute of Aeronautics and Astronautics 1992 p. 659-667. refs (AIAA PAPER 92-4769) Copyright

A three-bay, space, cantilever truss is probabilistically evaluated to quantify the range of uncertainties of vibration frequencies and truss free end vertical displacements due to nonuniform thermal loads, applied loads and moments (mechanical loads), and combination of both. The truss members are assumed to be made from (1) aluminum tubes or (2) high modulus graphite-fiber/intermediate modulus epoxy-matrix composite tubes. Cumulative distribution function results show that certain combination of thermal loads with mechanical loads reduce the probabilistic vibration frequencies and increase the magnitude of the truss free end vertical displacements for the aluminum truss. However, for the composite truss, the thermal effects on the probabilistic vibration frequencies are not as substantial as that for an aluminum truss. This can be attributed to the large differences in the values of coefficient of thermal expansion. Finally, the sensitivities associated with the uncertainties in the structural, material and load variables (primitive variables) are investigated. Results indicate that vibration frequencies and truss free end vertical displacements are sensitive to the uncertainties in spatial (geometry) variables as well as member modulus. Author

A93-20397# National Aeronautics and Space Administration. Lewis Research Center, Cleveland, OH.

SINGULARITIES IN OPTIMAL STRUCTURAL DESIGN

S. N. PATNAIK (Ohio Aerospace Inst., Brook Park), J. D. GUPTILL, and L. BERKE (NASA, Lewis Research Center, Cleveland, OH) /in AIAA/USAF/NASA/OAI Symposium on Multidisciplinary Analysis and Optimization, 4th, Cleveland, OH, Sept. 21-23, 1992, Technical Papers. Pt. 2 Washington American Institute of Aeronautics and Astronautics 1992 p. 982-990. Previously announced in STAR as N92-23527 refs (Contract RTOP 307-50-00) (AIAA PAPER 92-4818)

Singularity conditions that arise during structural optimization can seriously degrade the performance of the optimizer. The singularities are intrinsic to the formulation of the structural optimization problem and are not associated with the method of analysis. Certain conditions that give rise to singularities have been identified in earlier papers, encompassing the entire structure. Further examination revealed more complex sets of conditions in which singularities occur. Some of these singularities are local in nature, being associated with only a segment of the structure. Moreover, the likelihood that one of these local singularities may arise during an optimization procedure can be much greater than that of the global singularity identified earlier. Examples are provided of these additional forms of singularities. A framework is also given in which these singularities can be recognized. In particular, the singularities can be identified by examination of the stress displacement relations along with the compatibility conditions and/or the displacement stress relations derived in the integrated force method of structural analysis. Author

A93-20398*# National Aeronautics and Space Administration. Lewis Research Center, Cleveland, OH.

ANALYSIS AND OPTIMAL DESIGN OF THICK COMPOSITE STRUCTURES WITH PASSIVE DAMPING CONSIDERATIONS

D. A. SARAVANOS (Ohio Aerospace Inst., Brook Park; NASA, Lewis Research Center, Cleveland) /in AIAA/USAF/NASA/OAI Symposium on Multidisciplinary Analysis and Optimization, 4th, Cleveland, OH, Sept. 21-23, 1992, Technical Papers. Pt. 2 Washington American Institute of Aeronautics and Astronautics

1992 p. 991-998. refs

(AIAA PAPER 92-4819) Copyright

A design methodology to tailor thick composite plates for optimal static and damping performance is presented. The method is based on discrete layer composite mechanics, hence, is suitable for thick composite laminates. The design criteria include static deflections, frequency and damping constraints. Evaluations on cross-ply simply-supported plates illustrate the advantages of the methodology. Comparisons with design methods based on the classical laminate theory show significant deviations in the resultant optimal designs at higher thicknesses. Author

A93-22426* National Aeronautics and Space Administration. Lewis Research Center, Cleveland, OH.

BOUNDARY FORMULATIONS FOR THREE-DIMENSIONAL CONTINUUM STRUCTURAL SHAPE SENSITIVITY ANALYSIS

J. H. KANE, G. ZHAO, H. WANG, and K. GURU PRASAD (Clarkson Univ., Potsdam, NY) ASME, Transactions, Journal of Applied Mechanics (ISSN 0021-8936) vol. 59, no. 4 Dec. 1992 p. 827-834. refs (Contract NAG3-1089; NSF DDM-89-96171) Copyright

The direct, singular, boundary element analysis formulation is shown to provide a basis for a computationally efficient and accurate shape design sensitivity analysis approach for the structural response of three-dimensional solid objects. The theoretical formulation for surface displacement and traction component sensitivities, and all components of the stress tensor is presented along with a formulation for the recovery of displacement and stress components in the interior of the object under consideration. Discussion of computational issues related to the overall efficiency of these formulations is given, along with numerical results to demonstrate the accuracy and efficiency of this approach. Author

A93-24303 National Aeronautics and Space Administration. Langley Research Center, Hampton, VA.

MEMBRANE TRIANGLES WITH CORNER DRILLING FREEDOMS. I - THE EFF ELEMENT

KEN ALVIN, HORACIO M. DE LA FUENTE, BJORN HAUGEN, and CARLOS A. FELIPPA (Colorado Univ., Boulder) Finite Elements in Analysis and Design (ISSN 0168-874X) vol. 12, no. 3-4 Dec. 1992 p. 163-187. refs (Contract NAG1-756; NAG3-934; NSF ASC-87-17773) Copyright

The formulation of 3-node 9-DOF membrane elements with normal-to-element-plane rotations (drilling freedoms) is examined in the context of parametrized variational principles. In particular, attention is given to the application of the extended free formulation (EFF) to the construction of a triangular membrane element with drilling freedoms that initially has complete quadratic polynomial expansions in each displacement component. The main advantage of the EFF over the free formulation triangle is that an explicit form is obtained for the higher-order stiffness. V.L.

A93-24304 National Aeronautics and Space Administration. Langley Research Center, Hampton, VA.

MEMBRANE TRIANGLES WITH CORNER DRILLING FREEDOMS. II - THE ANDES ELEMENT

CARLOS A. FELIPPA and CARMELO MILITELLO (Colorado Univ., Boulder) Finite Elements in Analysis and Design (ISSN 0168-874X) vol. 12, no. 3-4 Dec. 1992 p. 189-201. refs (Contract NAG1-756; NAG3-934; NSF ASC-87-17773) Copyright

This is the second article in a three-part series on the construction of 3-node, 9-dof membrane elements with normal-to-its-plane rotational freedoms (the so-called drilling freedoms) using parametrized variational principles. In this part, one such element is derived within the context of the assumed natural deviatoric strain (ANDES) formulation. The higher-order strains are obtained by constructing three parallel-to-sides pure-bending modes from which natural strains are obtained at the corner points and interpolated over the element. To attain

rank sufficiency, an additional higher-order 'torsional' mode, corresponding to equal hierarchical rotations at each corner with all other motions precluded, is incorporated. The resulting formulation has five free parameters. When these parameters are optimized against pure bending by energy balance methods, the resulting element is found to coalesce with the optimal EFF element derived in Part I. Numerical integration as a strain filtering device is found to play a key role in this achievement. Author

A93-24305 National Aeronautics and Space Administration. Langley Research Center, Hampton, VA.

MEMBRANE TRIANGLES WITH CORNER DRILLING FREEDOMS. III - IMPLEMENTATION AND PERFORMANCE EVALUATION

CARLOS A. FELIPPA and SCOTT ALEXANDER (Colorado Univ., Boulder) Finite Elements in Analysis and Design (ISSN 0168-874X) vol. 12, no. 3-4 Dec. 1992 p. 203-239. refs (Contract NAG1-756; NAG3-934; NSF ASC-87-17773) Copyright

This paper completes a three-part series on the formulation of 3-node, 9-dof membrane triangles with corner drilling freedoms based on parametrized variational principles. The first four sections cover element implementation details including determination of optimal parameters and treatment of distributed loads. Then three elements of this type, labeled ALL, FF and EFF-ANDES, are tested on standard plane stress problems. ALL represents numerically integrated versions of Allman's 1988 triangle; FF is based on the free formulation triangle presented by Bergan and Felippa in 1985; and EFF-ANDES represent two different formulations of the optimal triangle derived in Parts I and II. The numerical studies indicate that the ALL, FF and EFF-ANDES elements are comparable in accuracy for elements of unitary aspect ratios. The ALL elements are found to stiffen rapidly in inplane bending for high aspect ratios, whereas the FF and EFF elements maintain accuracy. The EFF and ANDES implementations have a moderate edge in formation speed over the FF. Author

A93-25228* National Aeronautics and Space Administration. Lewis Research Center, Cleveland, OH.

DESIGN CONSIDERATIONS FOR A SPACE SHUTTLE MAIN ENGINE TURBINE BLADE MADE OF SINGLE CRYSTAL MATERIAL

A. ABDUL-AZIZ, R. AUGUST, and V. NAGPAL (Sverdrup Technology, Inc.; NASA, Lewis Research Center, Cleveland, OH) Computers & Structures (ISSN 0045-7949) vol. 46, no. 2 Jan. 17, 1993 p. 249-259. refs Copyright

Nonlinear finite-element structural analyses were performed on the first stage high-pressure fuel turbopump blade of the Space Shuttle Main Engine. The analyses examined the structural response and the dynamic characteristics at typical operating conditions. Single crystal material PWA-1480 was considered for the analyses. Structural response and the blade natural frequencies with respect to the crystal orientation were investigated. The analyses were conducted based on typical test stand engine cycle. Influence of combined thermal, aerodynamic, and centrifugal loadings was considered. Results obtained showed that the single crystal secondary orientation effects on the maximum principal stresses are not highly significant. Author

A93-26776 National Aeronautics and Space Administration. Lewis Research Center, Cleveland, OH.

FINITE ELEMENT IMPLEMENTATION OF STATE VARIABLE-BASED VISCOPLASTICITY MODELS

T. Y. P. CHANG, A. F. SALEEB, and I. ISKOVITZ (Akron Univ., OH) Computers & Structures (ISSN 0045-7949) vol. 46, no. 1 Jan. 3, 1993 p. 33-45. Previously announced in STAR as N91-32523 refs (Contract NAG3-901; RTOP 510-01-50) Copyright

The implementation of state variable-based viscoplasticity models is made in a general purpose finite element code for structural applications of metals deformed at elevated

temperatures. Two constitutive models, Walker's and Robinson's models, are studied in conjunction with two implicit integration methods: the trapezoidal rule with Newton-Raphson iterations and an asymptotic integration algorithm. A comparison is made between the two integration methods, and the latter method appears to be computationally more appealing in terms of numerical accuracy and CPU time. However, in order to make the asymptotic algorithm robust, it is necessary to include a self adaptive scheme with subincremental step control and error checking of the Jacobian matrix at the integration points. Three examples are given to illustrate the numerical aspects of the integration methods tested. Author

A93-30042* National Aeronautics and Space Administration. Lewis Research Center, Cleveland, OH.

THE ISOLATION LIMITS OF STOCHASTIC VIBRATION

C. R. KNOPSE and P. E. ALLAIRE (Virginia Univ., Charlottesville) Journal of Sound and Vibration (ISSN 0022-460X) vol. 160, no. 2 Jan. 15, 1993 p. 205-223. Research supported by NASA refs Copyright

The vibration isolation problem is formulated as a 1D kinematic problem. The geometry of the stochastic wall trajectories arising from the stroke constraint is defined in terms of their significant extrema. An optimal control solution for the minimum acceleration return path determines a lower bound on platform mean square acceleration. This bound is expressed in terms of the probability density function on the significant maxima and the conditional fourth moment of the first passage time inverse. The first of these is found analytically while the second is found using a Monte Carlo simulation. The rms acceleration lower bound as a function of available space is then determined through numerical quadrature. C.D.

A93-31295* National Aeronautics and Space Administration. Lewis Research Center, Cleveland, OH.

MICROMECHANICAL STUDIES OF COMPOSITES BY BEM

P. K. BANERJEE, D. P. HENRY, JR., and G. F. DARGUSH (New York State Univ., Amherst) In Enhancing analysis techniques for composite materials; Proceedings of the Symposium, ASME Winter Annual Meeting, Atlanta, GA, Dec. 1-6, 1991 New York American Society of Mechanical Engineers 1991 p. 221-228. refs (Contract NAG3-888) Copyright

Over the last five years BEM has been developed into a very effective tool for micromechanical studies of composites. The analyses developed range from static elastic analysis, steady state heat transfer, steady state and transient thermoelastic analysis, periodic and transient dynamic analysis. Currently some of these analyses are being extended to nonlinear micromechanical analyses involving viscoplasticity, elastoplasticity, combined plasticity fracture and creep. The paper describes some of the results for elastic analysis, heat transfer and thermoelastic analyses. Author

A93-31339* National Aeronautics and Space Administration. Lewis Research Center, Cleveland, OH.

EVOLUTION OF CREEP-FATIGUE LIFE PREDICTION MODELS

GARY R. HALFORD (NASA, Lewis Research Center, Cleveland, OH) In Creep-fatigue interaction at high temperature; Proceedings of the Symposium, 112th ASME Winter Annual Meeting, Atlanta, GA, Dec. 1-6, 1991 New York American Society of Mechanical Engineers 1991 p. 43-57. refs Copyright

The evolution of high-temperature, creep-fatigue, life-prediction methods used for cyclic crack initiation is traced from inception in the late 1940s. The methods reviewed are material models as opposed to structural life prediction models. Material life models are used by both structural durability analysts and by material scientists. The latter use micromechanistic models as guidance to improve a material's crack initiation resistance. Nearly one hundred approaches and their variations have been proposed to date. This

proliferation poses a problem in deciding which method is most appropriate for a given application. Approaches have been identified as being combinations of fourteen different classifications. This review is intended to aid both developers and users of high-temperature fatigue life prediction methods by providing a background from which choices can be made. Author

A93-32410* National Aeronautics and Space Administration. Lewis Research Center, Cleveland, OH.

PROGRAMMING PROBABILISTIC STRUCTURAL ANALYSIS FOR PARALLEL PROCESSING COMPUTERS

ROBERT H. SUES, HEH-CHYUN CHEN (Applied Research Associates, Inc., Raleigh, NC), CHRISTOS C. CHAMIS, and PAPU L. N. MURTHY (NASA, Lewis Research Center, Cleveland, OH) AIAA Journal (ISSN 0001-1452) vol. 30, no. 12 Dec. 1992 p. 2871, 2872. Abridged. AIAA/ASME/ASCE/AHS/ASC Structures, Structural Dynamics, and Materials Conference, 32nd, Baltimore, MD, Apr. 8-10, 1991, Technical Papers. Pt. 2, p. 1243-1253. Previously cited in issue 12, p. 1993, Accession no. A91-31957 refs
(Contract NAS3-25824)
Copyright

A93-32415* National Aeronautics and Space Administration. Lewis Research Center, Cleveland, OH.

EFFECTS OF INTERPLY DAMPING LAYERS ON THE DYNAMIC CHARACTERISTICS OF COMPOSITE PLATES

D. A. SARAVALOS and J. M. PEREIRA (NASA, Lewis Research Center, Cleveland, OH) AIAA Journal (ISSN 0001-1452) vol. 30, no. 12 Dec. 1992 p. 2906-2913. AIAA/ASME/ASCE/AHS/ASC Structures, Structural Dynamics, and Materials Conference, 32nd, Baltimore, MD, Apr. 8-10, 1991, Technical Papers. Pt. 3, p. 2363-2370. Previously cited in issue 12, p. 1999, Accession no. A91-32064 refs
Copyright

A93-32459* National Aeronautics and Space Administration. Lewis Research Center, Cleveland, OH.

INTEGRATED FORCE METHOD - COMPATIBILITY CONDITIONS OF STRUCTURAL MECHANICS FOR FINITE ELEMENT ANALYSIS

SURYA N. PATNAIK, LASZLO BERKE (NASA, Lewis Research Center, Cleveland, OH), and RICHARD H. GALLAGHER (Clarkson Univ., Potsdam, NY) In Mechanics of composites at elevated and cryogenic temperatures; Proceedings of the Symposium, ASME Applied Mechanics Conference, Columbus, OH, June 16-19, 1991 New York American Society of Mechanical Engineers 1991 p. 91-118. refs
Copyright

The equilibrium equations and the compatibility conditions are fundamental to the analyses of structures. However, anyone who undertakes even a cursory generic study of the compatibility conditions can discover, with little effort, that historically this facet of structural mechanics had not been adequately researched by the profession. Now the compatibility conditions (CC's) have been researched and are understood to a great extent. For finite element discretizations, the CC's are banded and can be divided into three distinct categories: (1) the interface CC's, (2) the cluster or field CC's, and (3) the external CC's. The generation of CC's requires the separating of a local region, then writing the deformation displacement relation (ddr) for the region, and finally, the eliminating of the displacements from the ddr. The procedure to generate all three types of CC's is presented and illustrated through examples of finite element models. The uniqueness of the CC's thus generated is shown. The utilization of CC's has resulted in the novel integrated force method (IFM). The solution that is obtained by the IFM converges with a significantly fewer number of elements, compared to the stiffness and the hybrid methods. Author

A93-32462* National Aeronautics and Space Administration. Lewis Research Center, Cleveland, OH.

COMPUTATIONAL MICROMECHANICS OF WOVEN COMPOSITES

DALE A. HOPKINS (NASA, Lewis Research Center, Cleveland, OH), SUNIL SAIGAL, and XIAOGANG ZENG (Carnegie Mellon Univ., Pittsburgh, PA) In Mechanics of composites at elevated and cryogenic temperatures; Proceedings of the Symposium, ASME Applied Mechanics Conference, Columbus, OH, June 16-19, 1991 New York American Society of Mechanical Engineers 1991 p. 145-155. refs
Copyright

The bounds on the equivalent elastic material properties of a composite are presently addressed by a unified energy approach which is valid for both unidirectional and 2D and 3D woven composites. The unit cell considered is assumed to consist, first, of the actual composite arrangement of the fibers and matrix material, and then, of an equivalent pseudohomogeneous material. Equating the strain energies due to the two arrangements yields an estimate of the upper bound for the material equivalent properties; successive increases in the order of displacement field that is assumed in the composite arrangement will successively produce improved upper bound estimates. AIAA

A93-32465* National Aeronautics and Space Administration. Lewis Research Center, Cleveland, OH.

PROBABILISTIC MICROMECHANICS FOR METAL MATRIX COMPOSITES

S. P. ENGELSTAD, J. N. REDDY (Virginia Polytechnic Inst. and State Univ., Blacksburg), and DALE A. HOPKINS (NASA, Lewis Research Center, Cleveland, OH) In Mechanics of composites at elevated and cryogenic temperatures; Proceedings of the Symposium, ASME Applied Mechanics Conference, Columbus, OH, June 16-19, 1991 New York American Society of Mechanical Engineers 1991 p. 181-193. refs
(Contract NAG3-933)
Copyright

A probabilistic micromechanics-based nonlinear analysis procedure is developed to predict and quantify the variability in the properties of high temperature metal matrix composites. Monte Carlo simulation is used to model the probabilistic distributions of the constituent level properties including fiber, matrix, and interphase properties, volume and void ratios, strengths, fiber misalignment, and nonlinear empirical parameters. The procedure predicts the resultant ply properties and quantifies their statistical scatter. Graphite copper and Silicon Carbide Titanium Aluminumide (SCS-6 Ti15) unidirectional plies are considered to demonstrate the predictive capabilities. The procedure is believed to have a high potential for use in material characterization and selection to precede and assist in experimental studies of new high temperature metal matrix composites. Author

A93-32469* National Aeronautics and Space Administration. Lewis Research Center, Cleveland, OH.

THERMALLY-DRIVEN MICROFRACTURE IN HIGH TEMPERATURE METAL MATRIX COMPOSITES

SUBODH K. MITAL and CHRISTOS C. CHAMIS (NASA, Lewis Research Center, Cleveland, OH) In Mechanics of composites at elevated and cryogenic temperatures; Proceedings of the Symposium, ASME Applied Mechanics Conference, Columbus, OH, June 16-19, 1991 New York American Society of Mechanical Engineers 1991 p. 251-256. Previously announced in STAR as N92-15136 refs
Copyright

Microfracture (fiber/matrix fracture, interphase debonding and interply delamination) in high temperature metal matrix composites (HTMMC), subjected to thermal loading, is computationally simulated. Both unidirectional and crossply SiC/Ti15 composites are evaluated for microfracture driven by thermal loads, using multicell finite element models. Results indicate that under thermal loads alone, microfracture propagation is not as sensitive as it is under mechanical loads. Author

A93-32717* National Aeronautics and Space Administration. Lewis Research Center, Cleveland, OH.

PROBABILISTIC NONLINEAR FINITE ELEMENT ANALYSIS OF COMPOSITE STRUCTURES

S. P. ENGELSTAD and J. N. REDDY (Virginia Polytechnic Inst. and State Univ., Blacksburg) *AIAA Journal* (ISSN 0001-1452) vol. 31, no. 2 Feb. 1993 p. 362-369. refs
(Contract NAG3-933) Copyright

A probabilistic finite element analysis procedure for laminated composite shells is developed. A total Lagrangian finite element formulation, employing a degenerated three-dimensional laminated composite shell element with the full Green-Lagrange strains and first-order shear deformable kinematics, is used. The first-order second-moment technique for probabilistic finite element analysis of random fields is employed, and results are presented in the form of mean and variance of the structural response. Reliability calculations are made by using the first-order reliability method combined with sensitivity derivatives from the finite element analysis. Both ply-level and micromechanics-level random variables are incorporated, the latter by means of the Aboudi micromechanics model. Two sample problems are solved to verify the accuracy of the procedures developed and to quantify the variability of certain material type/structure combinations. In general, the procedure is quite effective in determining the response statistics and reliability for linear and geometric nonlinear behavior of laminated composite shells. Author

A93-33898* # National Aeronautics and Space Administration. Lewis Research Center, Cleveland, OH.

BEHAVIOR OF SPINNING LAMINATED COMPOSITE PLATES WITH INITIAL TWIST-EXPERIMENTAL VIBRATIONS, STRAIN, AND DEFLECTION RESULTS

A. J. LAPID, J. B. KOSMATKA (California Univ., La Jolla), and O. MEHMED (NASA, Lewis Research Center, Cleveland, OH) *In AIAA/ASME/ASCE/AHS/ASC Structures, Structural Dynamics, and Materials Conference, 34th and AIAA/ASME Adaptive Structures Forum, La Jolla, CA, Apr. 19-22, 1993, Technical Papers. Pt. 1* Washington American Institute of Aeronautics and Astronautics 1993 p. 255-265. refs
(AIAA PAPER 93-1325) Copyright

The experimental behavior of spinning, pre-twisted laminated composite plates was investigated. The purpose of these experiments was to establish an experimental database consisting of strain, deflections, and natural frequencies as a function of rotational velocity. Six different plate sets were tested, that included three different stacking sequences (two symmetric, one asymmetric), two different initial twist levels (0 deg, 30 deg), and two different initial twist axis locations (midchord, quarter-chord). The plates were spin tested at four different combinations of pitch and sweep. It was observed that the location of the pretwist axis and the level of pretwist greatly affects the strain and deflections of the spinning plate, while only the pretwist level affects the measured natural frequencies. Author (revised)

A93-33915* # National Aeronautics and Space Administration. Lewis Research Center, Cleveland, OH.

DAMAGE PROGRESSION IN STIFFENED COMPOSITE PANELS

LEVON MINNETYAN, JAMES M. RIVERS (Clarkson Univ., Potsdam, NY), CHRISTOS C. CHAMIS, and PAPPU L. N. MURTHY (NASA, Lewis Research Center, Cleveland, OH) *In AIAA/ASME/ASCE/AHS/ASC Structures, Structural Dynamics, and Materials Conference, 34th and AIAA/ASME Adaptive Structures Forum, La Jolla, CA, Apr. 19-22, 1993, Technical Papers. Pt. 1* Washington American Institute of Aeronautics and Astronautics 1993 p. 436-444. refs
(Contract NAG3-1101) (AIAA PAPER 93-1345) Copyright

The design of composite structures requires an evaluation of their safety and durability under service loads and possible overload conditions. This paper presents a computational tool that has been developed to examine the response of stiffened composite panels via the simulation of damage initiation, growth, accumulation, progression, and propagation to structural fracture or co*lapse. The structural durability of a composite panel with a discontinuous stiffener is investigated under compressive loading induced by the gradual displacement of an end support. Results indicate damage

initiation and progression to have significant effects on structural behavior under loading. Utilization of an integrated computer code for structural durability assessment is demonstrated. Author

A93-33941* # National Aeronautics and Space Administration. Lewis Research Center, Cleveland, OH.

CONFIDENCE BOUNDS ON STRUCTURAL RELIABILITY

S. R. MEHTA, T. A. CRUSE, and S. MAHADEVAN (Vanderbilt Univ., Nashville, TN) *In AIAA/ASME/ASCE/AHS/ASC Structures, Structural Dynamics, and Materials Conference, 34th and AIAA/ASME Adaptive Structures Forum, La Jolla, CA, Apr. 19-22, 1993, Technical Papers. Pt. 2* Washington American Institute of Aeronautics and Astronautics 1993 p. 693-700. refs
(Contract NAS3-24389) (AIAA PAPER 93-1377) Copyright

Different approaches for quantifying physical, statistical, and model uncertainties associated with the distribution parameters which are aimed at determining structural reliability are described. Confidence intervals on the distribution parameters of the input random variables are estimated using four algorithms to evaluate uncertainty of the response. Design intervals are evaluated using either Monte Carlo simulation or an iterative approach. A first order approach can be used to compute a first approximation of the design interval, but its accuracy is not satisfactory. The regression approach which combines the iterative approach with Monte Carlo simulation is capable of providing good results if the performance function can be accurately represented using regression analysis. It is concluded that the design interval-based approach seems to be quite general and takes into account distribution and model uncertainties. AIAA

A93-33942* # National Aeronautics and Space Administration. Lewis Research Center, Cleveland, OH.

GLOBAL/LOCAL METHODS FOR PROBABILISTIC STRUCTURAL ANALYSIS

H. R. MILLWATER and Y.-T. WU (Southwest Research Inst., San Antonio, TX) *In AIAA/ASME/ASCE/AHS/ASC Structures, Structural Dynamics, and Materials Conference, 34th and AIAA/ASME Adaptive Structures Forum, La Jolla, CA, Apr. 19-22, 1993, Technical Papers. Pt. 2* Washington American Institute of Aeronautics and Astronautics 1993 p. 701-706. refs
(Contract NAS3-24389) (AIAA PAPER 93-1378) Copyright

A probabilistic global/local method is proposed to reduce the computational requirements of probabilistic structural analysis. A coarser global model is used for most of the computations with a local more refined model used only at key probabilistic conditions. The global model is used to establish the cumulative distribution function (cdf) and the Most Probable Point (MPP). The local model then uses the predicted MPP to adjust the cdf value. The global/local method is used within the advanced mean value probabilistic algorithm. The local model can be more refined with respect to the global model in terms of finer mesh, smaller time step, tighter tolerances, etc. and can be used with linear or nonlinear models. The basis for this approach is described in terms of the correlation between the global and local models which can be estimated from the global and local MPPs. A numerical example is presented using the NESSUS probabilistic structural analysis program with the finite element method used for the structural modeling. The results clearly indicate a significant computer savings with minimal loss in accuracy. Author

A93-33943* # National Aeronautics and Space Administration. Lewis Research Center, Cleveland, OH.

STRUCTURAL SYSTEM RELIABILITY UNDER MULTIPLE FAILURE MODES

S. MAHADEVAN (Vanderbilt Univ., Nashville, TN) and C. C. CHAMIS (NASA, Lewis Research Center, Cleveland, OH) *In AIAA/ASME/ASCE/AHS/ASC Structures, Structural Dynamics, and Materials Conference, 34th and AIAA/ASME Adaptive Structures Forum, La Jolla, CA, Apr. 19-22, 1993, Technical Papers. Pt. 2* Washington American Institute of Aeronautics and

Astronautics 1993 p. 707-713. refs
(Contract NAS3-24389)
(AIAA PAPER 93-1379) Copyright

This paper describes a computational method for system reliability estimation of propulsion structures. The failure domain of the entire structural system is computed through the union of failure regions for various critical system failure modes. The effect of non-critical progressive damage is incorporated through structural reanalysis, resulting in the construction of several linear segments to approximately cover the system failure domain. An adaptive damage imposition scheme is outlined for the sake of computational efficiency. The proposed method is used to construct the system survival cdf (cumulative distribution function) of a two-rotor system.

Author

A93-33972* National Aeronautics and Space Administration. Lewis Research Center, Cleveland, OH.
RELIABILITY BASED STRUCTURAL OPTIMIZATION - A SIMPLIFIED SAFETY INDEX APPROACH

MAHIDHAR V. REDDY, RAMANA V. GRANDHI (Wright State Univ., Dayton, OH), and DALE A. HOPKINS (NASA, Lewis Research Center, Cleveland, OH) In AIAA/ASME/ASCE/AHS/ASC Structures, Structural Dynamics, and Materials Conference, 34th and AIAA/ASME Adaptive Structures Forum, La Jolla, CA, Apr. 19-22, 1993, Technical Papers. Pt. 2 Washington American Institute of Aeronautics and Astronautics 1993 p. 990-999. refs

(AIAA PAPER 93-1418) Copyright

A probabilistic optimal design methodology for complex structures modelled with finite element methods is presented. The main emphasis is on developing probabilistic analysis tools suitable for optimization. An advanced second-moment method is employed to evaluate the failure probability of the performance function. The safety indices are interpolated using the information at mean and most probable failure point. The minimum weight design with an improved safety index limit is achieved by using the extended interior penalty method of optimization. Numerical examples covering beam and plate structures are presented to illustrate the design approach. The results obtained by using the proposed approach are compared with those obtained by using the existing probabilistic optimization techniques.

Author

A93-33990* National Aeronautics and Space Administration. Lewis Research Center, Cleveland, OH.

PROBABILISTIC ASSESSMENT OF COMPOSITE STRUCTURES
MICHAEL C. SHIAO, GALIB H. ABUMERI (Sverdrup Technology, Inc., Brook Park, OH), and CHRISTOS C. CHAMIS (NASA, Lewis Research Center, Cleveland, OH) In AIAA/ASME/ASCE/AHS/ASC Structures, Structural Dynamics, and Materials Conference, 34th and AIAA/ASME Adaptive Structures Forum, La Jolla, CA, Apr. 19-22, 1993, Technical Papers. Pt. 2 Washington American Institute of Aeronautics and Astronautics 1993 p. 1174-1186. refs

(AIAA PAPER 93-1441) Copyright

A general purpose methodology for integrated probabilistic assessment of composite structures is demonstrated using aircraft fuselage type structures with rectangular cutouts. The computational simulation took into account buckling loads, vibration frequencies, global displacements, and local stresses. The procedure was embedded into the computer code IPACS (Integrated Probabilistic Assessment of Composite Structures) that calculates the simulated scatter, the sensitivity of the composite structural behavior to all the primitive variables that affect the structural behavior. The probabilistic assessment for the composite structure with rectangular cutouts indicates that the uncertainty in the longitudinal ply stress is mainly due to uncertainty in the laminate thickness.

AIAA

A93-34033* National Aeronautics and Space Administration. Lewis Research Center, Cleveland, OH.

FORCED RESPONSE OF MISTUNED BLADED DISK ASSEMBLIES

BRIAN C. WATSON, MANOHAR P. KAMAT (Georgia Inst. of

Technology, Atlanta), and DURBHA V. MURTHY (Toledo Univ., OH) In AIAA/ASME/ASCE/AHS/ASC Structures, Structural Dynamics, and Materials Conference, 34th and AIAA/ASME Adaptive Structures Forum, La Jolla, CA, Apr. 19-22, 1993, Technical Papers. Pt. 3 Washington American Institute of Aeronautics and Astronautics 1993 p. 1597-1606. refs

(Contract NGT-50981)

(AIAA PAPER 93-1491) Copyright

A complete analytic model of mistuned bladed disk assemblies, designed to simulate the dynamical behavior of these systems, is analyzed. The model incorporates a generalized method for describing the mistuning of the assembly through the introduction of specific mistuning modes. The model is used to develop a computational bladed disk assembly model for a series of parametric studies. Results are presented demonstrating that the response amplitudes of bladed disk assemblies depend both on the excitation mode and on the mistune mode.

AIAA

A93-34035* National Aeronautics and Space Administration. Lewis Research Center, Cleveland, OH.

PROGRESSIVE MATRIX CRACKING IN OFF-AXIS PLIES OF A GENERAL SYMMETRIC LAMINATE

DAVID J. THOMAS and ROBERT C. WETHERHOLD (New York State Univ., Buffalo) In AIAA/ASME/ASCE/AHS/ASC Structures, Structural Dynamics, and Materials Conference, 34th and AIAA/ASME Adaptive Structures Forum, La Jolla, CA, Apr. 19-22, 1993, Technical Papers. Pt. 3 Washington American Institute of Aeronautics and Astronautics 1993 p. 1613-1623. refs

(Contract NAG3-862)

(AIAA PAPER 93-1494) Copyright

A generalized shear-lag model is derived to determine the average through-the-thickness stress state present in a layer undergoing transverse matrix cracking, by extending the method of Lee and Daniels (1991) to a general symmetric multilayered system. The model is capable of considering cracking in layers of arbitrary orientation, states of general in-plane applied loading, and laminates with a general symmetric stacking sequence. The model is included in a computer program designed for probabilistic laminate analysis, and the results are compared to those determined with the ply drop-off technique.

AIAA

A93-34037* National Aeronautics and Space Administration. Lewis Research Center, Cleveland, OH.

LIFETIME RELIABILITY EVALUATION OF STRUCTURAL CERAMIC PARTS WITH THE CARES/LIFE COMPUTER PROGRAM

NOEL N. NEMETH (NASA, Lewis Research Center, Cleveland, OH), LYNN M. POWERS (Cleveland State Univ., OH), LESLEY A. JANOSIK, and JOHN P. GYEKENYESI (NASA, Lewis Research Center, Cleveland, OH) In AIAA/ASME/ASCE/AHS/ASC Structures, Structural Dynamics, and Materials Conference, 34th and AIAA/ASME Adaptive Structures Forum, La Jolla, CA, Apr. 19-22, 1993, Technical Papers. Pt. 3 Washington American Institute of Aeronautics and Astronautics 1993 p. 1634-1646. refs

(AIAA PAPER 93-1497) Copyright

The computer program CARES/LIFE calculates the time-dependent reliability of monolithic ceramic components subjected to thermomechanical and/or proof test loading. This program is an extension of the CARES (Ceramics Analysis and Reliability Evaluation of Structures) computer program. CARES/LIFE accounts for the phenomenon of subcritical crack growth (SCG) by utilizing the power law, Paris law, or Walker equation. The two-parameter Weibull cumulative distribution function is used to characterize the variation in component strength. The effects of multiaxial stresses are modeled using either the principle of independent action (PIA), Weibull's normal stress averaging method (NSA), or Batdorf's theory. Inert strength and fatigue parameters are estimated from rupture strength data of naturally flawed specimens loaded in static, dynamic, or cyclic fatigue. Two example problems demonstrating cyclic fatigue parameter estimation and component reliability analysis with proof testing are included.

Author

A93-34038*# National Aeronautics and Space Administration. Lewis Research Center, Cleveland, OH.

A NUMERICAL ROUND ROBIN FOR THE RELIABILITY PREDICTION OF STRUCTURAL CERAMICS

LYNN M. POWERS (Cleveland State Univ., OH) and LESLEY A. JANOSIK (NASA, Lewis Research Center, Cleveland, OH) *In* AIAA/ASME/ASCE/AHS/ASC Structures, Structural Dynamics, and Materials Conference, 34th and AIAA/ASME Adaptive Structures Forum, La Jolla, CA, Apr. 19-22, 1993, Technical Papers. Pt. 3 Washington American Institute of Aeronautics and Astronautics 1993 p. 1647-1658. refs (AIAA PAPER 93-1498) Copyright

A round robin has been conducted on integrated fast fracture design programs for brittle materials. An informal working group (WELFEP-WEakest Link failure probability prediction by Finite Element Postprocessors) was formed to discuss and evaluate the implementation of the programs examined in the study. Results from the study have provided insight on the differences between the various programs examined. Conclusions from the study have shown that when brittle materials are used in design, analysis must understand how to apply the concepts presented herein to failure probability analysis. Author

A93-34151*# National Aeronautics and Space Administration. Lewis Research Center, Cleveland, OH.

PROBABILISTIC ASSESSMENT OF ADAPTIVE SPACE TRUSS CONFIGURATIONS FOR THERMAL BUCKLING RESISTANCE

SHANTARAM S. PAI (NASA, Lewis Research Center, Cleveland, OH) *In* AIAA/ASME/ASCE/AHS/ASC Structures, Structural Dynamics, and Materials Conference, 34th and AIAA/ASME Adaptive Structures Forum, La Jolla, CA, Apr. 19-22, 1993, Technical Papers. Pt. 5 Washington American Institute of Aeronautics and Astronautics 1993 p. 2778-2790. refs (AIAA PAPER 93-1622) Copyright

A three-bay, cantilever truss of a type typically used in space structures, is probabilistically evaluated to configure adaptive/smart/intelligent behavior for resisting thermal buckling. This buckling is due to nonuniform thermal loads and a combination of these loads with applied loads and moments (mechanical loads). For each behavior the scatter (ranges) in buckling loads and member axial forces are probabilistically determined. Sensitivities associated with uncertainties in the structural and material variables that describe the truss, as well as scatter in mechanical and thermal loads, are determined for different probabilities. The relative magnitude of these sensitivities are used to identify significant truss variables that control/classify the truss behavior and cause it to respond as an adaptive/smart/ intelligent structure. Results show that the probabilistic buckling loads increase for adaptive and intelligent truss classifications, with a substantial increase for intelligent trusses. Similarly, the probabilistic member axial forces decrease for each truss classification. Author

A93-34155*# National Aeronautics and Space Administration. Lewis Research Center, Cleveland, OH.

COMPUTATIONAL METHODS FOR EFFICIENT STRUCTURAL RELIABILITY AND RELIABILITY SENSITIVITY ANALYSIS

Y.-T. WU (Southwest Research Inst., San Antonio, TX) *In* AIAA/ASME/ASCE/AHS/ASC Structures, Structural Dynamics, and Materials Conference, 34th and AIAA/ASME Adaptive Structures Forum, La Jolla, CA, Apr. 19-22, 1993, Technical Papers. Pt. 5 Washington American Institute of Aeronautics and Astronautics 1993 p. 2817-2826. refs (Contract NAS3-24389) (AIAA PAPER 93-1626) Copyright

This paper presents recent developments in efficient structural reliability analysis methods. The paper proposes an efficient, adaptive importance sampling (AIS) method that can be used to compute reliability and reliability sensitivities. The AIS approach uses a sampling density that is proportional to the joint PDF of the random variables. Starting from an initial approximate failure domain, sampling proceeds adaptively and incrementally with the goal of reaching a sampling domain that is slightly greater than the failure domain to minimize over-sampling in the safe region.

Several reliability sensitivity coefficients are proposed that can be computed directly and easily from the above AIS-based failure points. These probability sensitivities can be used for identifying key random variables and for adjusting design to achieve reliability-based objectives. The proposed AIS methodology is demonstrated using a turbine blade reliability analysis problem. Author

A93-34191*# National Aeronautics and Space Administration. Lewis Research Center, Cleveland, OH.

PROBABILISTICALLY CONFIGURED ADAPTIVE COMPOSITE STRUCTURES

MICHAEL C. SHIAO (Sverdrup Technology, Inc., Brook Park, OH) and CHRISTOS C. CHAMIS (NASA, Lewis Research Center, Cleveland, OH) *In* AIAA/ASME/ASCE/AHS/ASC Structures, Structural Dynamics, and Materials Conference, 34th and AIAA/ASME Adaptive Structures Forum, La Jolla, CA, Apr. 19-22, 1993, Technical Papers. Pt. 6 Washington American Institute of Aeronautics and Astronautics 1993 p. 3198-3208. refs (AIAA PAPER 93-1679) Copyright

A composite wing with spars, bulkheads and built-in sensor/control devices is probabilistically configured with a methodology for the probabilistic assessment of smart composite structures. Structural responses such as changes in angle of attack, vertical displacements and stresses in the non-control and control plies are probabilistically assessed to quantify their respective scatter ranges. Sensitivity factors are evaluated to identify those parameters that have the greatest influence on a specific structural response. Results show that smart composite structures can be configured to control distortions and ply stresses, and to have specified scatter ranges in the frequencies, buckling loads in the presence of defects to satisfy specified design requirements. Author

A93-34938* National Aeronautics and Space Administration. Lewis Research Center, Cleveland, OH.

SINGULARITY IN STRUCTURAL OPTIMIZATION

S. N. PATNAIK (Ohio Aerospace Inst., Brook Park), J. D. GUPTILL, and L. BERKE (NASA, Lewis Research Center, Cleveland, OH) *International Journal for Numerical Methods in Engineering* (ISSN 0029-5981) vol. 36, no. 6 March 30, 1993 p. 931-944. refs Copyright

The conditions under which global and local singularities may arise in structural optimization are examined. Examples of these singularities are presented, and a framework is given within which the singularities can be recognized. It is shown, in particular, that singularities can be identified through the analysis of stress-displacement relations together with compatibility conditions or the displacement-stress relations derived by the integrated force method of structural analysis. Methods of eliminating the effects of singularities are suggested and illustrated numerically. AIAA

A93-38849 National Aeronautics and Space Administration. Lewis Research Center, Cleveland, OH.

AXIAL-TORSIONAL FATIGUE - A STUDY OF TUBULAR SPECIMEN THICKNESS EFFECTS

PETER J. BONACUSE (U.S. Army, Research Lab.; NASA, Lewis Research Center, Cleveland, OH) and SREERAMESH KALLURI (Sverdrup Technology, Inc., Brook Park, OH) *Journal of Testing and Evaluation* (ISSN 0090-3973) vol. 21, no. 3 May 1993 p. 160-167. Previously announced in STAR as N91-14632 refs (Contract RTOP 505-63-1B) Copyright

Experiments were carried out at room temperature on AISI type 316 stainless steel to determine the effect of wall thickness on the cyclic deformation behavior and fatigue life of thin-wall tubular axial-torsional fatigue specimens. The experimental variables examined included the depth of the surface work-hardened layer produced in specimen machining, and the effects of strain range and axial-torsional strain phasing. Tubular fatigue specimens had wall thicknesses of 1.5, 2.0, and 2.5 mm. One as-fabricated specimen from each wall thickness was sectioned for microstructural examination and microhardness

measurement. A specimen of each wall thickness was tested in axial-torsional fatigue experiments for each of the three conditions: high strain range in-phase, low strain range in-phase, and low strain range out-of-phase. The machining-induced work-hardened zone, as a percentage of the gage section material, was found to have a minimal effect on both deformation behavior and fatigue life. Out-of-phase fatigue tests displayed shorter fatigue lives and more cyclic hardening than in-phase tests. Author (revised)

A93-43347* National Aeronautics and Space Administration. Lewis Research Center, Cleveland, OH.

ANALYSIS OF THE ANISOTROPIC VISCOPLASTIC-DAMAGE RESPONSE OF COMPOSITE LAMINATES - CONTINUUM BASIS AND COMPUTATIONAL ALGORITHMS

A. F. SALEEB and T. E. WILT (Akron Univ., OH) International Journal for Numerical Methods in Engineering (ISSN 0029-5981) vol. 36, no. 10 May 30, 1993 p. 1629-1660. refs (Contract NAG3-901) Copyright

The mathematical structure underlying the rate equations of a recently-developed constitutive model for the coupled viscoplastic-damage response of anisotropic composites is critically examined. In this regard, a number of tensor projection operators have been identified, and their properties were exploited to enable the development of a general computational framework for their numerical implementation using the Euler fully-implicit integration method. In particular, this facilitated (i) the derivation of explicit expressions of the (consistent) material tangent stiffnesses that are valid for both three-dimensional as well as subspace (e.g. plane stress) formulations, (ii) the implications of the symmetry or unsymmetry properties of these tangent operators from a thermodynamic standpoint, and (iii) the development of an effective time-step control strategy to ensure accuracy and convergence of the solution. In addition, the special limiting case of inviscid elastoplasticity is treated. The results of several numerical simulations are given to demonstrate the effectiveness of the schemes developed. Author

A93-43651* National Aeronautics and Space Administration. Lewis Research Center, Cleveland, OH.

RATCHETTING BEHAVIOR IN VISCOPLASTICITY - A TECHNICAL NOTE

ALAN D. FREED (NASA, Lewis Research Center, Cleveland, OH) and KEVIN P. WALKER (Engineering Science Software, Inc., Smithfield, RI) European Journal of Mechanics, A/Solids (ISSN 0997-7538) vol. 12, no. 2 1993 p. 191-196. refs (Contract DE-AC02-88ER-13895) Copyright

Viscoplastic models that use the Armstrong and Frederick (1966) kinematic hardening relationship are known to generally overpredict the observed accumulation of ratchet strains. The reason for this behavior is a consequence of the mathematics used to describe Hooke's law and the evolution equations for plastic strain and back stress. Conditions for ratchetting exist whenever there is a cycle-averaged mean stress present over a cyclic loading path. Two types of controlled loading paths are often studied: cyclic relaxation is the ratchet mechanism associated with displacement (strain) control, while cyclic creep is the ratchet mechanism associated with load (stress) control. Overcoming the possible adverse trends in predicted ratchetting behavior is a difficult task, and how one ought to go about doing this is not yet completely clear. We therefore choose to discuss the mathematical cause of ratchetting and how it has been dealt with to date, but make no attempt to correct this flaw. Author (revised)

A93-44440* National Aeronautics and Space Administration. Lewis Research Center, Cleveland, OH.

VARIATION OF THE ENERGY RELEASE RATE AS A CRACK APPROACHES AND PASSES THROUGH AN ELASTIC INCLUSION

RONGSHUN LI and A. CHUDNOVSKY (Illinois Univ., Chicago) International Journal of Fracture (ISSN 0376-9429) vol. 59, no. 4 Feb. 15, 1993 p. R69-R74. Research supported by USAF

refs

(Contract NAG3-1034)

Copyright

The variation of the energy release rate (ERP) at the tip of a crack penetrating an elastic inclusion is analyzed using an approach involving modeling the random array of microcracks or other defects by an elastic inclusion with effective elastic properties. Computations are carried out using a finite element procedure. The eight-noded isoparametric serendipity element with the shift of the midpoint to the quarter-point is used to simulate the singularity at the crack tip, and the crack growth is accommodated by implementing a mesh regeneration technique. The ERP values were calculated for various crack tip positions which simulate the process of the crack approaching and penetrating the inclusion. AIAA

A93-45429* National Aeronautics and Space Administration. Lewis Research Center, Cleveland, OH.

TOPOLOGY AND LAYOUT OPTIMIZATION OF DISCRETE AND CONTINUUM STRUCTURES

MARTIN P. BENDSOE (Technical Univ. of Denmark, Lyngby) and NOBORU KIKUCHI (Michigan Univ., Ann Arbor) In Structural optimization: Status and promise Washington American Institute of Aeronautics and Astronautics, Inc. 1993 p. 517-547. Research supported by STVF refs (Contract N00014-88-K-0637; NAG3-1160; PHS-G2-R01-AR-34399-04) Copyright

The basic features of the ground structure method for truss structure and continuum problems are described. Problems with a large number of potential structural elements are considered using the compliance of the structure as the objective function. The design problem is the minimization of compliance for a given structural weight, and the design variables for truss problems are the cross-sectional areas of the individual truss members, while for continuum problems they are the variable densities of material in each of the elements of the FEM discretization. It is shown how homogenization theory can be applied to provide a relation between material density and the effective material properties of a periodic medium with a known microstructure of material and voids. AIAA

A93-45430* National Aeronautics and Space Administration. Lewis Research Center, Cleveland, OH.

STOCHASTIC SEARCH IN STRUCTURAL OPTIMIZATION - GENETIC ALGORITHMS AND SIMULATED ANNEALING

PRABHAT HAJELA (Rensselaer Polytechnic Inst., Troy, NY) In Structural optimization: Status and promise Washington American Institute of Aeronautics and Astronautics, Inc. 1993 p. 611-635. refs (Contract DAAL03-88-K-0013; NAG3-1196) Copyright

An account is given of illustrative applications of genetic algorithms and simulated annealing methods in structural optimization. The advantages of such stochastic search methods over traditional mathematical programming strategies are emphasized; it is noted that these methods offer a significantly higher probability of locating the global optimum in a multimodal design space. Both genetic-search and simulated annealing can be effectively used in problems with a mix of continuous, discrete, and integer design variables. AIAA

A93-45743* National Aeronautics and Space Administration. Lewis Research Center, Cleveland, OH.

ANALYSIS OF PASSIVE DAMPING IN THICK COMPOSITE STRUCTURES

D. A. SARAVANOS (Ohio Aerospace Inst., Brook Park) AIAA Journal (ISSN 0001-1452) vol. 31, no. 8 Aug. 1993 p. 1503-1510. refs (Contract NCC3-2084) Copyright

Computational mechanics for the prediction of damping and other dynamic characteristics in composite structures of general

thicknesses and laminations are presented. Discrete layer damping mechanics that account for the representation of interlaminar shear effects in the material are summarized. Finite element based structural mechanics for the analysis of damping are described, and a specialty finite element is developed. Applications illustrate the quality of the discrete layer damping mechanics in predicting the damped dynamic characteristics of composite structures with thicker sections and/or laminate configurations that induce interlaminar shear. The results also illustrate and quantify the significance of interlaminar shear damping in such composite structures.

A93-46768* National Aeronautics and Space Administration. Lewis Research Center, Cleveland, OH.

ANALYTICAL STRESS INTENSITY SOLUTION FOR THE STABLE POISSON LOADED SPECIMEN

LOUIS J. GHOSN (Sverdrup Technology, Inc., Lewis Research Center Group, Brook Park, OH), ANTHONY M. CALOMINO (NASA, Lewis Research Center, Cleveland, OH), and DAVID N. BREWER (U.S. Army, Research Lab.; NASA, Lewis Research Center, Cleveland, OH) *International Journal of Fracture* (ISSN 0376-9429) vol. 60, no. 3 April 1, 1993 p. 209-220. refs

Copyright

An analytical calibration of the Stable Poisson Loaded (SPL) specimen is presented. The specimen configuration is similar to the ASTM E-561 compact-tension specimen with displacement controlled wedge loading used for R-curve determination. The crack mouth opening displacements (CMODs) are produced by the diametral expansion of an axially compressed cylindrical pin located in the wake of a machined notch. Due to the unusual loading configuration, a three-dimensional finite element analysis was performed with gap elements simulating the contact between the pin and specimen. In this report, stress intensity factors, CMODs, and crack displacement profiles, are reported for different crack lengths and different contacting conditions. It was concluded that the computed stress intensity factor decreases sharply with increasing crack length thus making the SPL specimen configuration attractive for fracture testing of brittle, high modulus materials.

A93-49028* National Aeronautics and Space Administration. Lewis Research Center, Cleveland, OH.

BOUNDARY FORMULATIONS FOR SENSITIVITY ANALYSIS WITHOUT MATRIX DERIVATIVES

J. H. KANE and K. GURU PRASAD (Clarkson Univ., Potsdam, NY) *AIAA Journal* (ISSN 0001-1452) vol. 31, no. 9 Sept. 1993 p. 1731-1734. refs

(Contract NAG3-1089; NSF DDM-90-19852)

Copyright

A new hybrid approach to continuum structural shape sensitivity analysis employing boundary element analysis (BEA) is presented. The approach uses iterative reanalysis to obviate the need to factor perturbed matrices in the determination of surface displacement and traction sensitivities via a univariate perturbation/finite difference (UPFD) step. The UPFD approach makes it possible to immediately reuse existing subroutines for computation of BEA matrix coefficients in the design sensitivity analysis process. The reanalysis technique computes economical response of univariately perturbed models without factoring perturbed matrices. The approach provides substantial computational economy without the burden of a large-scale reprogramming effort. AIAA

A93-53394* National Aeronautics and Space Administration. Lewis Research Center, Cleveland, OH.

DESIGN FOR PROGRESSIVE FRACTURE IN COMPOSITE SHELL STRUCTURES

LEVON MINNETYAN (Clarkson Univ., Potsdam, NY) and PAPPU L. N. MURTHY (NASA, Lewis Research Center, Cleveland, OH) *In International SAMPE Technical Conference, 24th and International SAMPE Metals and Metals Processing Conference, 3rd, Toronto, Canada, Oct. 20-22, 1992, Proceedings. Vol. 24 Covina, CA Society for the Advancement of Material and Process*

Engineering 1992 p. T227-T240. refs

(Contract NAG3-1101)

Copyright

The load carrying capability and structural behavior of composite shell structures and stiffened curved panels are investigated to provide accurate early design loads. An integrated computer code is utilized for the computational simulation of composite structural degradation under practical loading for realistic design. Damage initiation, growth, accumulation, and propagation to structural fracture are included in the simulation. Progressive fracture investigations providing design insight for several classes of composite shells are presented. Results demonstrate the significance of local defects, interfacial regions, and stress concentrations on the structural durability of composite shells.

A93-53395* National Aeronautics and Space Administration. Lewis Research Center, Cleveland, OH.

DESIGN FOR CYCLIC LOADING ENDURANCE OF COMPOSITES

MICHAEL C. SHIAO (Sverdrup Technology, Inc., Brook Park, OH) and PAPPU L. N. MURTHY (NASA, Lewis Research Center, Cleveland, OH) *In International SAMPE Technical Conference, 24th and International SAMPE Metals and Metals Processing Conference, 3rd, Toronto, Canada, Oct. 20-22, 1992, Proceedings. Vol. 24 Covina, CA Society for the Advancement of Material and Process Engineering* 1992 p. T241-T255. refs

Copyright

The present paper describes the application of the computer code IPACS (Integrated Probabilistic Assessment of Composite Structures) to air craft wing type structures. The code performs a complete probabilistic structural analysis for composites taking into account the uncertainties in geometry, boundary conditions, material properties, laminate lay-ups and loads. Results of the analysis are presented in terms of cumulative distribution functions (CDF) and probability density function (PDF) of life of a wing type composite structure under different hygrothermal environments subjected to random pressure. The sensitivity of fatigue life to a number of critical structural/material variables is also computed from the analysis.

A93-53396* National Aeronautics and Space Administration. Lewis Research Center, Cleveland, OH.

DESIGN FOR INADVERTENT DAMAGE IN COMPOSITE LAMINATES

SURENDRA N. SINGHAL (Sverdrup Technology, Inc., Brook Park, OH) and CHRISTOS C. CHAMIS (NASA, Lewis Research Center, Cleveland, OH) *In International SAMPE Technical Conference, 24th and International SAMPE Metals and Metals Processing Conference, 3rd, Toronto, Canada, Oct. 20-22, 1992, Proceedings. Vol. 24 Covina, CA Society for the Advancement of Material and Process Engineering* 1992 p. T256-T269. refs

Copyright

Simplified predictive methods and models to computationally simulate durability and damage in polymer matrix composite materials/structures are described. The models include (1) progressive fracture, (2) progressively damaged structural behavior, (3) progressive fracture in aggressive environments, (4) stress concentrations, and (5) impact resistance. Several examples are included to illustrate applications of the models and to identify significant parameters and sensitivities. Comparisons with limited experimental data are made.

A93-53418* National Aeronautics and Space Administration. Lewis Research Center, Cleveland, OH.

EFFECT OF SERVICE ENVIRONMENTS ON ADHESIVELY BONDED JOINTS IN COMPOSITE STRUCTURES

S. N. SINGHAL (Sverdrup Technology, Inc., Brook Park, OH), C. C. CHAMIS, and P. L. N. MURTHY (NASA, Lewis Research Center, Cleveland, OH) *In International SAMPE Technical Conference, 24th and International SAMPE Metals and Metals Processing Conference, 3rd, Toronto, Canada, Oct. 20-22, 1992, Proceedings. Vol. 24 Covina, CA Society for the Advancement of Material*

and Process Engineering 1992 p. T536-T550. refs
Copyright

The models employed in the present computational methods for evaluating severe service-environment effects on adhesively bonded joints in composites are based on composite analyses and structural mechanics, encompassing nonlinear environmental degradation. The methods are demonstrated for the case of a butt joint with a single doubler, subjected to the environmental effects as well as static and cyclic loads. The highest joint strength is noted to be required in the case of cyclic loads and hygrothermal service environments; margins of safety for adhesive material stresses decline rapidly in such cases. AIAA

A93-53438* National Aeronautics and Space Administration. Lewis Research Center, Cleveland, OH.

ENVIRONMENTAL EFFECTS ON LONG TERM BEHAVIOR OF COMPOSITE LAMINATES

S. N. SINGHAL (Sverdrup Technology, Inc., Brook Park, OH) and C. C. CHAMIS (NASA, Lewis Research Center, Cleveland, OH) *In* International SAMPE Technical Conference, 24th and International SAMPE Metals and Metals Processing Conference, 3rd, Toronto, Canada, Oct. 20-22, 1992, Proceedings. Vol. 24 Covina, CA Society for the Advancement of Material and Process Engineering 1992 p. T852-T866. refs
Copyright

Model equations are presented for approximate methods simulating the long-term behavior of composite materials and structures in hot/humid service environments. These equations allow laminate property upgradings with time, and can account for the effects of service environments on creep response. These methodologies are illustrated for various individual and coupled temperature/moisture, longitudinal/transverse, and composite material type cases. Creep deformation is noted to rise dramatically for cases of matrix-borne, but not of fiber-borne, loading in hot, humid environments; the coupled influence of temperature and moisture is greater than a mere combination of their individual influences. AIAA

A93-53468* National Aeronautics and Space Administration. Lewis Research Center, Cleveland, OH.

THE CHEMISTRY OF SAUDI ARABIAN SAND - A DEPOSITION PROBLEM ON HELICOPTER TURBINE AIRFOILS

JAMES L. SMIALEK, FRANCES A. ARCHER, and RALPH G. GARLICK (NASA, Lewis Research Center, Cleveland, OH) *In* International SAMPE Technical Conference, 24th and International SAMPE Metals and Metals Processing Conference, 3rd, Toronto, Canada, Oct. 20-22, 1992, Proceedings. Vol. 3 Covina, CA Society for the Advancement of Material and Process Engineering 1992 p. M63-M77. refs
Copyright

Operations in the Persian Gulf have exposed military helicopter turbines to excessive amounts of ingested sand. Fine particles, less than 10 microns, are able to bypass the particle separators and enter the cooling and combustion systems. The initial sand chemistry varies by location, but is made up of a calcium aluminum silicate glass, SiO₂ low quartz, (Ca,Mg)CO₃ dolomite, CaCO₃ calcite, and occasionally NaCl rock salt. The sand reacts in the hot combustion gases and deposits onto the turbine vanes as CaSO₄, glass, and various crystalline silicates. Deposits up to 5 mm thick have been collected. Although cooling hole plugging is a considerable problem, excessive corrosion is not commonly observed due to the high melting point of CaSO₄.

A93-54508* National Aeronautics and Space Administration. Lewis Research Center, Cleveland, OH.

LAYOUT OPTIMIZATION USING THE HOMOGENIZATION METHOD

KATSUYUKI SUZUKI (Tokyo Univ., Japan) and NOBORU KIKUCHI (Michigan Univ., Ann Arbor) *In* Optimization of large structural systems; Proceedings of the NATO/DFG Advanced Study Institute, Berchtesgaden, Germany, Sept. 23-Oct. 4, 1991. Vol. 1 Dordrecht, Netherlands Kluwer Academic Publishers 1993 p. 157-175.

Research supported by Ford Foundation refs
(Contract NSF DDM-89-17430; NIH-AR-34399; NAG3-1160)
Copyright

A generalized layout problem involving sizing, shape, and topology optimization is solved by using the homogenization method for three-dimensional linearly elastic shell structures in order to seek a possibility of establishment of an integrated design system of automotive car bodies, as an extension of the previous work by Bendsoe and Kikuchi. A formulation of a three-dimensional homogenized shell, a solution algorithm, and several examples of computing the optimum layout are presented in this first part of the two articles.

A93-54509* National Aeronautics and Space Administration. Lewis Research Center, Cleveland, OH.

APPLICATIONS TO CAR BODIES - GENERALIZED LAYOUT DESIGN OF THREE-DIMENSIONAL SHELLS

JUNICHI FUKUSHIMA (Toyota Technical Center USA, Inc., Southfield, MI), KATSUYUKI SUZUKI (Tokyo Univ., Japan), and NOBORU KIKUCHI (Michigan Univ., Ann Arbor) *In* Optimization of large structural systems; Proceedings of the NATO/DFG Advanced Study Institute, Berchtesgaden, Germany, Sept. 23-Oct. 4, 1991. Vol. 1 Dordrecht, Netherlands Kluwer Academic Publishers 1993 p. 177-191. Research supported by Ford Foundation refs
(Contract NSF DDM-89-17430; NIH-AR-34399; NAG3-1160)
Copyright

We shall describe applications of the homogenization method, formulated in Part 1, to design layout of car bodies represented by three-dimensional shell structures based on a multi-loading optimization.

A93-55382* National Aeronautics and Space Administration. Lewis Research Center, Cleveland, OH.

RELIABILITY ANALYSIS OF LAMINATED CERAMIC MATRIX COMPOSITES USING SHELL SUBELEMENT TECHNIQUES

A. STARLINGER (NASA, Lewis Research Center, Cleveland, OH), D. J. THOMAS (New York State Univ., Buffalo), S. F. DUFFY (Cleveland State Univ., OH), and J. P. GYKENYESI (NASA, Lewis Research Center, Cleveland, OH) AIAA Journal (ISSN 0001-1452) vol. 31, no. 11 Nov. 1993 p. 2181-2183. AIAA/ASME/ASCE/AHS/ASC Structures, Structural Dynamics and Materials Conference, 33rd, Dallas, TX, Apr. 13-15, 1992, Technical Papers. Pt. 1, p. 444-453. Previously cited in issue 13, p. 2203, Accession no. A92-34322 refs
Copyright

A93-56412* National Aeronautics and Space Administration. Lewis Research Center, Cleveland, OH.

ELASTIC INTERACTIONS OF A FATIGUE CRACK WITH A MICRO-DEFECT BY THE MIXED BOUNDARY INTEGRAL EQUATION METHOD

YUAN J. LUA (Applied Research Associates, Inc., Raleigh, NC), WING K. LIU, and TED BELYTSCHKO (Northwestern Univ., Evanston, IL) International Journal for Numerical Methods in Engineering (ISSN 0029-5981) vol. 36, no. 16 Aug. 30, 1993 p. 2743-2759. Research supported by FAA refs
(Contract NAG3-822; W-7405-ENG-82)
Copyright

In this paper, the mixed boundary integral equation method is developed to study the elastic interactions of a fatigue crack and a micro-defect such as a void, a rigid inclusion or a transformation inclusion. The method of pseudo-tractions is employed to study the effect of a transformation inclusion. An enriched element which incorporates the mixed-mode stress intensity factors is applied to characterize the singularity at a moving crack tip. In order to evaluate the accuracy of the numerical procedure, the analysis of a crack emanating from a circular hole in a finite plate is performed and the results are compared with the available numerical solution. The effects of various micro-defects on the crack path and fatigue life are investigated. The results agree with the experimental observations.

N93-10453*# National Aeronautics and Space Administration. Lewis Research Center, Cleveland, OH.

CALCULATION OF STRESS INTENSITY FACTORS IN AN ISOTROPIC MULTICRACKED PLATE: PART 2: SYMBOLIC/NUMERIC IMPLEMENTATION

S. M. ARNOLD, W. K. BINIENDA (Akron Univ., OH.), H. Q. TAN (Akron Univ., OH.), and M. H. XU (Akron Univ., OH.) Sep. 1992 44 p

(Contract RTOP 510-01-50)

(NASA-TM-105823; E-7254; NAS 1.15:105823) Avail: CASI HC A03/MF A01

Analytical derivations of stress intensity factors (SIF's) of a multicroaked plate can be complex and tedious. Recent advances, however, in intelligent application of symbolic computation can overcome these difficulties and provide the means to rigorously and efficiently analyze this class of problems. Here, the symbolic algorithm required to implement the methodology described in Part 1 is presented. The special problem-oriented symbolic functions to derive the fundamental kernels are described, and the associated automatically generated FORTRAN subroutines are given. As a result, a symbolic/FORTRAN package named SYMFRAC, capable of providing accurate SIF's at each crack tip, was developed and validated. Simple illustrative examples using SYMFRAC show the potential of the present approach for predicting the macrocrack propagation path due to existing microcracks in the vicinity of a macrocrack tip, when the influence of the microcrack's location, orientation, size, and interaction are taken into account. Author

N93-10455*# National Aeronautics and Space Administration. Lewis Research Center, Cleveland, OH.

CALCULATION OF STRESS INTENSITY FACTORS IN AN ISOTROPIC MULTICRACKED PLATE. PART 1: THEORETICAL DEVELOPMENT

W. K. BINIENDA (Akron Univ., OH.), S. M. ARNOLD, and H. Q. TAN (Akron Univ., OH.) Sep. 1992 21 p

(Contract RTOP 510-01-50)

(NASA-TM-105766; E-7183; NAS 1.15:105766) Avail: CASI HC A03/MF A01

An essential part of describing the damage state and predicting the damage growth in a multicroaked plate is the accurate calculation of stress intensity factors (SIF's). Here, a methodology and rigorous solution formulation for SIF's of a multicroaked plate, with fully interacting cracks, subjected to a far-field arbitrary stress state is presented. The fundamental perturbation problem is derived, and the steps needed to formulate the system of singular integral equations whose solution gives rise to the evaluation of the SIF's are identified. This analytical derivation and numerical solution are obtained by using intelligent application of symbolic computations and automatic FORTRAN generation capabilities (described in the second part of this paper). As a result, a symbolic/FORTRAN package, named SYMFRAC, that is capable of providing accurate SIF's at each crack tip was developed and validated. Author

N93-10777*# National Aeronautics and Space Administration. Lewis Research Center, Cleveland, OH.

UNIFIED VISCOPLASTIC BEHAVIOR OF METAL MATRIX COMPOSITES

S. M. ARNOLD, D. N. ROBINSON (Akron Univ., OH.), and P. A. BARTOLOTTA Nov. 1992 11 p Presented at the American Society of Mechanical Engineers Winter Annual Meeting, Anaheim, CA, 8-13 Nov. 1992; sponsored by ASME

(Contract NAG3-379; RTOP 510-01-50)

(NASA-TM-105819; E-7250; NAS 1.15:105819) Avail: CASI HC A03/MF A01

The need for unified constitutive models was recognized more than a decade ago in the results of phenomenological tests on monolithic metals that exhibited strong creep-plasticity interaction. Recently, metallic alloys have been combined to form high-temperature ductile/ductile composite materials, raising the natural question of whether these metallic composites exhibit the same phenomenological features as their monolithic constituents. This question is addressed in the context of a limited, yet definite

(to illustrate creep/plasticity interaction) set of experimental data on the model metal matrix composite (MMC) system W/Kanthal. Furthermore, it is demonstrated that a unified viscoplastic representation, extended for unidirectional composites and correlated to W/Kanthal, can accurately predict the observed longitudinal composite creep/plasticity interaction response and strain rate dependency. Finally, the predicted influence of fiber orientation on the creep response of W/Kanthal is illustrated.

Author

N93-10967*# National Aeronautics and Space Administration. Lewis Research Center, Cleveland, OH.

A CREEP CAVITY GROWTH MODEL FOR CREEP-FATIGUE LIFE PREDICTION OF A UNIDIRECTIONAL W/CU COMPOSITE

YOUNG-SUK KIM (Research Inst. of Industrial Science and Technology, Pohang, Republic of Korea), MICHAEL J. VERRILLI, and GARY R. HALFORD May 1992 19 p Presented at the Second Symposium on Advances in Fatigue Lifetime Predictive Techniques, Pittsburgh, PA, 4-5 May 1992; sponsored by the American Society for Testing and Materials

(Contract RTOP 510-01-50)

(NASA-TM-105780; E-7207; NAS 1.15:105780) Avail: CASI HC A03/MF A01

A microstructural model was developed to predict creep-fatigue life in a (O)(sub 4), 9 volume percent tungsten fiber-reinforced copper matrix composite at the temperature of 833 K. The mechanism of failure of the composite is assumed to be governed by the growth of quasi-equilibrium cavities in the copper matrix of the composite, based on the microscopically observed failure mechanisms. The methodology uses a cavity growth model developed for prediction of creep fracture. Instantaneous values of strain rate and stress in the copper matrix during fatigue cycles were calculated and incorporated in the model to predict cyclic life. The stress in the copper matrix was determined by use of a simple two-bar model for the fiber and matrix during cyclic loading. The model successfully predicted the composite creep-fatigue life under tension-tension cyclic loading through the use of this instantaneous matrix stress level. Inclusion of additional mechanisms such as cavity nucleation, grain boundary sliding, and the effect of fibers on matrix-stress level would result in more generalized predictions of creep-fatigue life. Author

N93-11004*# National Aeronautics and Space Administration. Lewis Research Center, Cleveland, OH.

CERAMIC COMPONENT RELIABILITY WITH THE RESTRUCTURED NASA/CARES COMPUTER PROGRAM

LYNN M. POWERS, ALOIS STARLINGER, and JOHN P. GYEKENYESI Sep. 1992 22 p Presented at the 37th International Gas Turbine and Aeroengine Congress, Cologne, Germany, 1-4 Jun. 1992; sponsored by ASME

(Contract RTOP 505-63-5B)

(NASA-TM-105856; E-6797; NAS 1.15:105856) Avail: CASI HC A03/MF A01

The Ceramics Analysis and Reliability Evaluation of Structures (CARES) integrated design program on statistical fast fracture reliability and monolithic ceramic components is enhanced to include the use of a neutral data base, two-dimensional modeling, and variable problem size. The data base allows for the efficient transfer of element stresses, temperatures, and volumes/areas from the finite element output to the reliability analysis program. Elements are divided to insure a direct correspondence between the subelements and the Gaussian integration points. Two-dimensional modeling is accomplished by assessing the volume flaw reliability with shell elements. To demonstrate the improvements in the algorithm, example problems are selected from a round-robin conducted by WELFEP (WEakest Link failure probability prediction by Finite Element Postprocessors). Author

N93-11403*# National Aeronautics and Space Administration. Lewis Research Center, Cleveland, OH.

APPLICATION OF ARTIFICIAL NEURAL NETWORKS IN NONLINEAR ANALYSIS OF TRUSSES

J. ALAM (Youngstown State Univ., OH.) and L. BERKE Nov. 1991 37 p
(Contract RTOP 307-50-00)
(NASA-TM-105319; E-6676; NAS 1.15:105319) Avail: CASI HC A03/MF A01

A method is developed to incorporate neural network model based upon the Backpropagation algorithm for material response into nonlinear elastic truss analysis using the initial stiffness method. Different network configurations are developed to assess the accuracy of neural network modeling of nonlinear material response. In addition to this, a scheme based upon linear interpolation for material data, is also implemented for comparison purposes. It is found that neural network approach can yield very accurate results if used with care. For the type of problems under consideration, it offers a viable alternative to other material modeling methods. Author

N93-11624* National Aeronautics and Space Administration. Lewis Research Center, Cleveland, OH.

DESIGN OF A HIGH-TEMPERATURE EXPERIMENT FOR EVALUATING ADVANCED STRUCTURAL MATERIALS

THEODORE T. MOCKLER, MARIO CASTRO-CEDEÑO, HERBERT J. GLADDEN, and ALBERT KAUFMAN (Analex Corp., Brook Park, OH.) Aug. 1992 35 p Original contains color illustrations
(Contract RTOP 510-01-50)

(NASA-TM-105833; E-6287; NAS 1.15:105833) Avail: CASI HC A03/MF A01; 16 functional color pages

This report describes the design of an experiment for evaluating monolithic and composite material specimens in a high-temperature environment and subject to big thermal gradients. The material specimens will be exposed to aerothermal loads that correspond to thermally similar engine operating conditions. Materials evaluated in this study were monolithic nickel alloys and silicon carbide. In addition, composites such as tungsten/copper were evaluated. A facility to provide the test environment has been assembled in the Engine Research Building at the Lewis Research Center. The test section of the facility will permit both regular and Schlieren photography, thermal imaging, and laser Doppler anemometry. The test environment will be products of hydrogen-air combustion at temperatures from about 1200 F to as high as 4000 F. The test chamber pressure will vary up to 60 psia, and the free-stream flow velocity can reach Mach 0.9. The data collected will be used to validate thermal and stress analysis models of the specimen. This process of modeling, testing, and validation is expected to yield enhancements to existing analysis tools and techniques.

Author

N93-12277* National Aeronautics and Space Administration. Lewis Research Center, Cleveland, OH.

STOCHASTIC SENSITIVITY MEASURE FOR MISTUNED HIGH-PERFORMANCE TURBINES

DURBHA V. MURTHY (Toledo Univ., OH.) and CHRISTOPHE PIERRE (Michigan Univ., Ann Arbor.) Aug. 1992 21 p Presented at the Fourth International Symposium on Transport Phenomena and Dynamics of Rotating Machinery, Honolulu, HI, 5-9 Apr. 1992
(Contract NAG3-742; NAG3-1163; RTOP 505-62-21)

(NASA-TM-105821; ICOMP-92-13; E-7252; NAS 1.15:105821) Avail: CASI HC A03/MF A01

A stochastic measure of sensitivity is developed in order to predict the effects of small random blade mistuning on the dynamic aeroelastic response of turbomachinery blade assemblies. This sensitivity measure is based solely on the nominal system design (i.e., on tuned system information), which makes it extremely easy and inexpensive to calculate. The measure has the potential to become a valuable design tool that will enable designers to evaluate mistuning effects at a preliminary design stage and thus assess the need for a full mistuned rotor analysis. The predictive capability of the sensitivity measure is illustrated by examining the effects of mistuning on the aeroelastic modes of the first stage of the oxidizer turbopump in the Space Shuttle Main Engine. Results from a full analysis mistuned systems confirm that the simple stochastic sensitivity measure predicts consistently the drastic

changes due to misturning and the localization of aeroelastic vibration to a few blades. Author

N93-12735* National Aeronautics and Space Administration. Lewis Research Center, Cleveland, OH.

PROBABILISTIC EVALUATION OF FUSELAGE-TYPE COMPOSITE STRUCTURES

MICHAEL C. SHIAO (Sverdrup Technology, Inc., Brook Park, OH.) and CHRISTOS C. CHAMIS Nov. 1991 20 p Presented at the Ninth DOD/NASA/FAA Conference on Fibrous Composites, Reno, NV, 3-7 Nov. 1991

(Contract RTOP 553-13-00)

(NASA-TM-105881; E-7348; NAS 1.15:105881) Avail: CASI HC A03/MF A01

A methodology is developed to computationally simulate the uncertain behavior of composite structures. Uncertain behavior is the consequence of the random variation (scatter) of the primitive (independent random) variables at the constituent, ply, laminate and structural levels. This methodology is implemented in the IPACS (Integrated Probabilistic Assessment of Composite Structures) computer code. A fuselage-type composite structure is analyzed to demonstrate the code's capability. The probability distribution functions of structural responses are computed. Sensitivity of a given structural response to each primitive variable is also determined from the analyses. Author

N93-12738* National Aeronautics and Space Administration. Lewis Research Center, Cleveland, OH.

NUMERICAL CALIBRATION OF THE STABLE POISSON LOADED SPECIMEN

LOUIS J. GHOSN (Sverdrup Technology, Inc., Brook Park, OH.), ANTHONY M. CALOMINO, and DAVE N. BREWER (Army Aviation Systems Command, Cleveland, OH.) Oct. 1992 15 p

(Contract RTOP 505-63-5B)

(NASA-TM-105609; E-7335; NAS 1.15:105609) Avail: CASI HC A03/MF A01

An analytical calibration of the Stable Poisson Loaded (SPL) specimen is presented. The specimen configuration is similar to the ASTM E-561 compact-tension specimen with displacement controlled wedge loading used for R-Curve determination. The crack mouth opening displacements (CMOD's) are produced by the diametral expansion of an axially compressed cylindrical pin located in the wake of a machined notch. Due to the unusual loading configuration, a three-dimensional finite element analysis was performed with gap elements simulating the contact between the pin and specimen. In this report, stress intensity factors, CMOD's, and crack displacement profiles are reported for different crack lengths and different contacting conditions. It was concluded that the computed stress intensity factor decreases sharply with increasing crack length, thus making the SPL specimen configuration attractive for fracture testing of brittle, high modulus materials. Author

N93-12739* National Aeronautics and Space Administration. Lewis Research Center, Cleveland, OH.

ON BILINEARITY OF MANSON-COFFIN LOW-CYCLE-FATIGUE RELATIONSHIP

V. M. RADHAKRISHNAN (Indian Inst. of Tech., Madras.) Oct. 1992 14 p

(Contract RTOP 553-13-00)

(NASA-TM-105840; E-7283; NAS 1.15:105840) Avail: CASI HC A03/MF A01

Some alloy systems, such as aluminum-lithium alloys and dual-phase steels, have been found to show a bilinear Manson-Coffin low-cycle-fatigue relationship. This paper shows that such bilinear behavior is related to the cyclic stress-strain curve. A bilinear cyclic stress-strain curve is a likely indication of a bilinear Manson-Coffin relationship. It is shown that materials other than aluminum-lithium alloys and dual-phase steels also may exhibit bilinear Manson-Coffin behavior. Implications for design are discussed. Author

N93-13153*# National Aeronautics and Space Administration. Lewis Research Center, Cleveland, OH.

IN-PHASE AND OUT-OF-PHASE AXIAL-TORSIONAL FATIGUE BEHAVIOR OF HAYNES 188 AT 760 C

SREERAMESH KALLURI and PETER J. BONACUSE Oct. 1991 22 p Presented at the Symposium on Multiaxial Fatigue, San Diego, CA, 14-15 Oct. 1991; sponsored by the American Society for Testing and Materials

(Contract DA PROJ. 1L1-61102-AH-45; RTOP 553-13-00)

(NASA-TM-105765; E-7182; NAS 1.15:105765;

AVSCOM-TR-91-C-046) Avail: CASI HC A03/MF A01

Isothermal, in-phase and out-of-phase axial-torsional fatigue experiments have been conducted at 760 C on uniform gage section, thin-walled tubular specimens of a wrought cobalt-base superalloy, Haynes 188. Test-control and data acquisition were accomplished with a minicomputer. Fatigue lives of the in- and out-of-phase axial-torsional fatigue tests have been estimated with four different multiaxial fatigue life prediction models that were developed primarily for predicting axial-torsional fatigue lives at room temperature. The models investigated were: (1) the von Mises equivalent strain range; (2) the Modified Multiaxiality Factor Approach; (3) the Modified Smith-Watson-Topper Parameter; and (4) the critical shear plane method of Fatemi, Socie, and Kurath. In general, life predictions by the von Mises equivalent strain range model were within a factor of 2 for a majority of the tests and the predictions by the Modified Multiaxiality Factor Approach were within a factor of 2, while predictions of the Modified Smith-Watson-Topper Parameter and of the critical shear plane method of Fatemi, Socie, and Kurath were unconservative and conservative, respectively, by up to factors of 4. In some of the specimens tested under combined axial-torsional loading conditions, fatigue cracks initiated near extensometer indentations. Two design modifications have been proposed to the thin-walled tubular specimen to overcome this problem. Author

N93-13157*# National Aeronautics and Space Administration. Lewis Research Center, Cleveland, OH.

STRUCTURAL OPTIMIZATION OF THIN SHELLS USING FINITE ELEMENT METHOD

PASCAL K. GOTSIS Oct. 1992 26 p

(Contract RTOP 510-01-0A)

(NASA-TM-105903; E-7139; NAS 1.15:105903) Avail: CASI HC A03/MF A01

The objective of the present work was the structural optimization of thin shell structures that are subjected to stress and displacement constraints. In order to accomplish this, the structural optimization computer program DESAP1 was modified and improved. In the static analysis part of the DESAP1 computer program the torsional spring elements, which are used to analyze thin, shallow shell structures, were eliminated by modifying the membrane stiffness matrix of the triangular elements in the local coordinate system and adding a fictitious rotational stiffness matrix. This simplified the DESAP1 program input, improved the accuracy of the analysis, and saved computation time. In the optimization part of the DESAP1 program the stress ratio formula, which redesigns the thickness of each finite element of the structure, was solved by an analytical method. This scheme replaced the iterative solution that was previously used in the DESAP1 program, thus increasing the accuracy and speed of the design. The modified program was used to design a thin, cylindrical shell structure with optimum weight, and the results are reported in this paper. Author

N93-13260*# National Aeronautics and Space Administration. Lewis Research Center, Cleveland, OH.

ANALYSIS OF LARGE QUASISTATIC DEFORMATIONS OF INELASTIC SOLIDS BY A NEW STRESS BASED FINITE ELEMENT METHOD Ph.D. Thesis Final Report

KENNETH W. REED Sep. 1992 253 p

(Contract NAG3-38; RTOP 590-21-11)

(NASA-CR-189235; NAS 1.26:189235) Avail: CASI HC A12/MF A03

A new hybrid stress finite element algorithm suitable for analyses

of large quasistatic deformation of inelastic solids is presented. Principal variables in the formulation are the nominal stress rate and spin. The finite element equations which result are discrete versions of the equations of compatibility and angular momentum balance. Consistent reformulation of the constitutive equation and accurate and stable time integration of the stress are discussed at length. Examples which bring out the feasibility and performance of the algorithm conclude the work. Author

N93-15343*# National Aeronautics and Space Administration. Lewis Research Center, Cleveland, OH.

ROOT DAMAGE ANALYSIS OF AIRCRAFT ENGINE BLADE SUBJECT TO ICE IMPACT

E. S. REDDY (Sverdrup Technology, Inc., Brook Park, OH.), G. H. ABUMERI (Sverdrup Technology, Inc., Brook Park, OH.), C. C. CHAMIS, and P. L. N. MURTHY Aug. 1992 16 p

(Contract RTOP 505-62-0K)

(NASA-TM-105779; E-7206; NAS 1.15:105779) Avail: CASI HC A03/MF A01

The blade root response due to ice impact on an engine blade is simulated using the NASA in-house code BLASIM. The ice piece is modeled as an equivalent spherical object impacting on the leading edge of the blade and has the velocity opposite to that of the aircraft with direction parallel to the engine axis. The effect of ice impact is considered to be an impulse load on the blade with its amplitude computed based on the momentum transfer principle. The blade response due to the impact is carried out by modal superposition using the first three modes. The maximum dynamic stresses at the blade root are computed at the quarter cycle of the first natural frequency. A combined stress failure function based on modified distortion energy is used to study the spanwise bending damage response at the blade root. That damage function reaches maximum value for very low ice speeds and increases steeply with increases in engine speed. Author

N93-15369*# National Aeronautics and Space Administration. Lewis Research Center, Cleveland, OH.

CLOSED FORM EXPRESSIONS FOR CRACK MOUTH DISPLACEMENTS AND STRESS INTENSITY FACTORS FOR CHEVRON NOTCHED SHORT BAR AND SHORT ROD SPECIMENS BASED ON EXPERIMENTAL COMPLIANCE MEASUREMENTS

R. T. BUBSEY, T. W. ORANGE, W. S. PIERCE, and J. L. SHANNON, JR. Oct. 1992 32 p

(Contract RTOP 505-63-5B)

(NASA-TM-83796; E-2293; NAS 1.15:83796) Avail: CASI HC A03/MF A01

A set of equations are presented describing certain fracture mechanics parameters for chevron notch bar and rod specimens. They are developed by fitting compliance calibration data reported earlier. The equations present the various parameters in their most useful forms. The data encompass the entire range of the specimen geometries most commonly used. Their use will facilitate the testing and analysis of brittle metals, ceramics, and glasses. Author

N93-15788*# National Aeronautics and Space Administration. Lewis Research Center, Cleveland, OH.

COMPUTER PROGRAMS TO CHARACTERIZE ALLOYS AND PREDICT CYCLIC LIFE USING THE TOTAL STRAIN VERSION OF STRAINRANGE PARTITIONING: TUTORIAL AND USERS MANUAL, VERSION 1.0

JAMES F. SALTSMAN Washington Dec. 1992 31 p

(Contract RTOP 590-21-11)

(NASA-TM-4425; E-6906; NAS 1.15:4425) Avail: CASI HC A03/MF A01

This manual presents computer programs for characterizing and predicting fatigue and creep-fatigue resistance of metallic materials in the high-temperature, long-life regime for isothermal and nonisothermal fatigue. The programs use the total strain version of Strainrange Partitioning (TS-SRP). An extensive database has also been developed in a parallel effort. This database is probably the largest source of high-temperature, creep-fatigue test data available in the public domain and can be used with other life

prediction methods as well. This users manual, software, and database are all in the public domain and are available through COSMIC (382 East Broad Street, Athens, GA 30602; (404) 542-3265, FAX (404) 542-4807). Two disks accompany this manual. The first disk contains the source code, executable files, and sample output from these programs. The second disk contains the creep-fatigue data in a format compatible with these programs.

Author

N93-17996*# National Aeronautics and Space Administration. Lewis Research Center, Cleveland, OH.

EXPERIMENTAL INVESTIGATION OF CYCLIC THERMOMECHANICAL DEFORMATION IN TORSION

JOHN R. ELLIS, MICHAEL G. CASTELLI (Sverdrup Technology, Inc., Brook Park, OH.), and CHARLES E. BAKIS (Pennsylvania State Univ., University Park.) Nov. 1992 29 p
(Contract RTOP 510-01-50)

(NASA-TM-105938; E-7455; NAS 1.15:105938) Avail: CASI HC A03/MF A01

An investigation of thermomechanical testing and deformation behavior of tubular specimens under torsional loading is described. Experimental issues concerning test accuracy and control specific to thermomechanical loadings under a torsional regime are discussed. A series of shear strain-controlled tests involving the nickel-base superalloy Hastelloy X were performed with various temperature excursions and compared to similar thermomechanical uniaxial tests. The concept and use of second invariants of the deviatoric stress and strain tensors as a means of comparing uniaxial and torsional specimens is also briefly presented and discussed in light of previous thermomechanical tests conducted under uniaxial conditions.

Author

N93-18426*# National Aeronautics and Space Administration. Lewis Research Center, Cleveland, OH.

DYNAMICS OF ROTATING MULTI-COMPONENT TURBOMACHINERY SYSTEMS

CHARLES LAWRENCE Jan. 1993 14 p Presented at the 34th Structures, Structural Dynamics, Materials Conference, La Jolla, CA, 19-21 Apr. 1993; sponsored by AIAA
(Contract RTOP 505-63-53)

(NASA-TM-105997; E-7537; NAS 1.15:105997) Avail: CASI HC A03/MF A01

The ultimate objective of turbomachinery vibration analysis is to predict both the overall, as well as component dynamic response. To accomplish this objective requires complete engine structural models, including multistages of bladed disk assemblies, flexible rotor shafts and bearings, and engine support structures and casings. In the present approach each component is analyzed as a separate structure and boundary information is exchanged at the inter-component connections. The advantage of this tactic is that even though readily available detailed component models are utilized, accurate and comprehensive system response information may be obtained. Sample problems, which include a fixed base rotating blade and a blade on a flexible rotor, are presented.

Author

N93-18875*# National Aeronautics and Space Administration. Lewis Research Center, Cleveland, OH.

STRUCTURAL DYNAMIC TESTING OF COMPOSITE PROPFAN BLADES FOR A CRUISE MISSILE WIND TUNNEL MODEL

STEPHEN D. ELGIN and THOMAS J. SUTLIFF Feb. 1993 19 p

(Contract RTOP 535-03-0B)

(NASA-TM-105272; E-6663; NAS 1.15:105272) Avail: CASI HC A03/MF A01

The Naval Weapons Center at China Lake, California is currently evaluating a counter rotating propfan system as a means of propulsion for the next generation of cruise missiles. The details and results of a structural dynamic test program are presented for scale model graphite-epoxy composite propfan blades. These blades are intended for use on a cruise missile wind tunnel model. Both dynamic characteristics and strain operating limits of the

blades are presented. Complications associated with high strain level fatigue testing methods are also discussed.

Author

N93-18876*# National Aeronautics and Space Administration. Lewis Research Center, Cleveland, OH.

INVERSE KINEMATICS PROBLEM IN ROBOTICS USING NEURAL NETWORKS

BENJAMIN B. CHOI and CHARLES LAWRENCE Oct. 1992 24 p

(Contract RTOP 506-43-41)

(NASA-TM-105869; E-7333; NAS 1.15:105869) Avail: CASI HC A03/MF A01

In this paper, Multilayer Feedforward Networks are applied to the robot inverse kinematic problem. The networks are trained with endeffector position and joint angles. After training, performance is measured by having the network generate joint angles for arbitrary endeffector trajectories. A 3-degree-of-freedom (DOF) spatial manipulator is used for the study. It is found that neural networks provide a simple and effective way to both model the manipulator inverse kinematics and circumvent the problems associated with algorithmic solution methods.

Author

N93-20368*# National Aeronautics and Space Administration. Lewis Research Center, Cleveland, OH.

STRUCTURAL DYNAMICS BRANCH RESEARCH AND ACCOMPLISHMENTS TO FY 1992

CHARLES LAWRENCE Dec. 1992 39 p

(Contract RTOP 505-63-513)

(NASA-TM-105824; E-7237; NAS 1.15:105824) Avail: CASI HC A03/MF A01

This publication contains a collection of fiscal year 1992 research highlights from the Structural Dynamics Branch at NASA LeRC. Highlights from the branch's major work areas--Aeroelasticity, Vibration Control, Dynamic Systems, and Computational Structural Methods are included in the report as well as a listing of the fiscal year 1992 branch publications.

Author

N93-21831*# National Aeronautics and Space Administration. Lewis Research Center, Cleveland, OH.

APPLICATION OF ARTIFICIAL NEURAL NETWORKS TO THE DESIGN OPTIMIZATION OF AEROSPACE STRUCTURAL COMPONENTS

LASZLO BERKE, SURYA N. PATNAIK (Ohio Aerospace Inst., Brook Park.), and PAPPU L. N. MURTHY Mar. 1993 13 p
(Contract RTOP 505-63-5B)

(NASA-TM-4389; E-6994-1; NAS 1.15:4389) Avail: CASI HC A03/MF A01

The application of artificial neural networks to capture structural design expertise is demonstrated. The principal advantage of a trained neural network is that it requires trivial computational effort to produce an acceptable new design. For the class of problems addressed, the development of a conventional expert system would be extremely difficult. In the present effort, a structural optimization code with multiple nonlinear programming algorithms and an artificial neural network code NETS were used. A set of optimum designs for a ring and two aircraft wings for static and dynamic constraints were generated by using the optimization codes. The optimum design data were processed to obtain input and output pairs, which were used to develop a trained artificial neural network with the code NETS. Optimum designs for new design conditions were predicted by using the trained network. Neural net prediction of optimum designs was found to be satisfactory for most of the output design parameters. However, results from the present study indicate that caution must be exercised to ensure that all design variables are within selected error bounds.

Author

N93-23015*# National Aeronautics and Space Administration. Lewis Research Center, Cleveland, OH.

STRUCTURAL ANALYSIS OF HIGH-RPM COMPOSITE PROPFAN BLADES FOR A CRUISE MISSILE WIND TUNNEL MODEL

DAVID A. CAREK Mar. 1993 22 p Original contains color

illustrations

(Contract RTOP 535-03-0B)
(NASA-TM-105267; E-7340; NAS 1.15:105267) Avail: CASI HC
A03/MF A01; 1 functional color page

Analyses were performed on a high-speed composite blade set for the Department of Defense Propfan Missile Interactions Project. The final design iteration, which resulted in the CM2D-2 blade design, is described in this report. Mode shapes, integral order excitation, and stress margins were examined. In addition, geometric corrections were performed to compensate for blade deflection under operating conditions with respect to the aerodynamic design shape. Author

N93-23044*# National Aeronautics and Space Administration. Lewis Research Center, Cleveland, OH.

IMPLEMENTATION OF THE BLOCK-KRYLOV BOUNDARY FLEXIBILITY METHOD OF COMPONENT SYNTHESIS

KELLY S. CARNEY, AYMAN A. ABDALLAH (Analex Corp., Brook Park, OH.), and ARTHUR A. HUCKLEBRIDGE (Case Western Reserve Univ., Cleveland, OH.) May 1993 22 p Proposed for presentation at the 1993 MSC World User's Conference, Washington, DC, 24-28 May 1993; sponsored by the MacNeal-Schwendler Corp.
(NASA-TM-106065; E-7671; NAS 1.15:106065) Avail: CASI HC
A03/MF A01

A method of dynamic substructuring is presented which utilizes a set of static Ritz vectors as a replacement for normal eigenvectors in component mode synthesis. This set of Ritz vectors is generated in a recurrence relationship, which has the form of a block-Krylov subspace. The initial seed to the recurrence algorithm is based on the boundary flexibility vectors of the component. This algorithm is not load-dependent, is applicable to both fixed and free-interface boundary components, and results in a general component model appropriate for any type of dynamic analysis. This methodology was implemented in the MSC/NASTRAN normal modes solution sequence using DMAP. The accuracy is found to be comparable to that of component synthesis based upon normal modes. The block-Krylov recurrence algorithm is a series of static solutions and so requires significantly less computation than solving the normal eigenspace problem. Author (revised)

N93-23406*# National Aeronautics and Space Administration. Lewis Research Center, Cleveland, OH.

FATIGUE CRITERION TO SYSTEM DESIGN, LIFE AND RELIABILITY: A PRIMER

ERWIN V. ZARETSKY Oct. 1992 18 p Workshop on Computational Methods for Failure Analysis and Life Prediction held in Hampton, VA, 14-15 Oct. 1992
(Contract RTOP 505-63-5B)
(NASA-TM-106022; E-7736; NAS 1.15:106022) Avail: CASI HC
A03/MF A01

A method for estimating a component's design survivability by incorporating finite element analysis and probabilistic material properties was developed. The method evaluates design parameters through direct comparisons of component survivability expressed in terms of Weibull parameters. The analysis was applied to a rotating disk with mounting bolt holes. The highest probability of failure occurred at, or near, the maximum shear stress region of the bolt holes. Distribution of material failure as a function of Weibull slope affects the probability of survival. Where Weibull parameters are unknown for a rotating disk, it may be permissible to assume Weibull parameters, as well as the stress-life exponent, in order to determine the qualitative effect of disk speed on the probability of survival. Author

N93-23739*# National Aeronautics and Space Administration. Lewis Research Center, Cleveland, OH.

SOLVING MODAL EQUATIONS OF MOTION WITH INITIAL CONDITIONS USING MSC/NASTRAN DMAP. PART 1: IMPLEMENTING EXACT MODE SUPERPOSITION

AYMAN A. ABDALLAH (Analex Corp., Brook Park, OH.), ALAN R. BARNETT (Analex Corp., Brook Park, OH.), OMAR M. IBRAHIM (Analex Corp., Brook Park, OH.), and RICHARD T. MANELLA May 1993 14 p Presented at the 1993 MSC/NASTRAN World Users' Conference, Arlington, VA, May 1993; sponsored by the MacNeal-Schwendler Corp.
(NASA-TM-106063; E-7669; NAS 1.15:106063) Avail: CASI HC
A03/MF A01

Within the MSC/NASTRAN DMAP (Direct Matrix Abstraction Program) module TRD1, solving physical (coupled) or modal (uncoupled) transient equations of motion is performed using the Newmark-Beta or mode superposition algorithms, respectively. For equations of motion with initial conditions, only the Newmark-Beta integration routine has been available in MSC/NASTRAN solution sequences for solving physical systems and in custom DMAP sequences or alters for solving modal systems. In some cases, one difficulty with using the Newmark-Beta method is that the process of selecting suitable integration time steps for obtaining acceptable results is lengthy. In addition, when very small step sizes are required, a large amount of time can be spent integrating the equations of motion. For certain aerospace applications, a significant time savings can be realized when the equations of motion are solved using an exact integration routine instead of the Newmark-Beta numerical algorithm. In order to solve modal equations of motion with initial conditions and take advantage of efficiencies gained when using uncoupled solution algorithms (like that within TRD1), an exact mode superposition method using MSC/NASTRAN DMAP has been developed and successfully implemented as an enhancement to an existing coupled loads methodology at the NASA Lewis Research Center. Author

N93-23740*# National Aeronautics and Space Administration. Lewis Research Center, Cleveland, OH.

SOLVING MODAL EQUATIONS OF MOTION WITH INITIAL CONDITIONS USING MSC/NASTRAN DMAP. PART 2: COUPLED VERSUS UNCOUPLED INTEGRATION

ALAN R. BARNETT (Analex Corp., Brook Park, OH.), OMAR M. IBRAHIM (Analex Corp., Brook Park, OH.), AYMAN A. ABDALLAH (Analex Corp., Brook Park, OH.), and TIMOTHY L. SULLIVAN May 1993 12 p Presented at the 1993 MSC World Users' Conference, Arlington, VA, May 1993; sponsored by the MacNeal-Schwendler Corp.
(NASA-TM-106064; E-7670; NAS 1.15:106064) Avail: CASI HC
A03/MF A01

By utilizing MSC/NASTRAN DMAP (Direct Matrix Abstraction Program) in an existing NASA Lewis Research Center coupled loads methodology, solving modal equations of motion with initial conditions is possible using either coupled (Newmark-Beta) or uncoupled (exact mode superposition) integration available within module TRD1. Both the coupled and newly developed exact mode superposition methods have been used to perform transient analyses of various space systems. However, experience has shown that in most cases, significant time savings are realized when the equations of motion are integrated using the uncoupled solver instead of the coupled solver. Through the results of a real-world engineering analysis, advantages of using the exact mode superposition methodology are illustrated. Author

N93-23745*# National Aeronautics and Space Administration. Lewis Research Center, Cleveland, OH.

MAPPING METHODS FOR COMPUTATIONALLY EFFICIENT AND ACCURATE STRUCTURAL RELIABILITY

MICHAEL C. SHIAO (Sverdrup Technology, Inc., Brook Park, OH.) and CHRISTOS C. CHAMIS Oct. 1992 23 p Proposed for presentation at the 33rd Structures, Structural Dynamics and Materials Conference, Dallas, TX, 13-15 Apr. 1992 Previously announced in IAA as A92-34321
(Contract RTOP 553-13-00)
(NASA-TM-105892; E-7359; NAS 1.15:105892) Avail: CASI HC
A03/MF A01

Mapping methods are developed to improve the accuracy and efficiency of probabilistic structural analyses with coarse finite element meshes. The mapping methods consist of the following: (1) deterministic structural analyses with fine (convergent) finite element meshes; (2) probabilistic structural analyses with coarse finite element meshes; (3) the relationship between the probabilistic

structural responses from the coarse and fine finite element meshes; and (4) a probabilistic mapping. The results show that the scatter in the probabilistic structural responses and structural reliability can be efficiently predicted using a coarse finite element model and proper mapping methods with good accuracy. Therefore, large structures can be efficiently analyzed probabilistically using finite element methods.

Author (revised)

N93-23746* # National Aeronautics and Space Administration. Lewis Research Center, Cleveland, OH.

COMPUTATIONAL SIMULATION FOR CONCURRENT ENGINEERING OF AEROSPACE PROPULSION SYSTEMS

C. C. CHAMIS and S. N. SINGHAL (Sverdrup Technology, Inc., Brook Park, OH.) Feb. 1993 23 p Presented at the 1992 AIAA Aerospace Design Conference, Irvine, CA, 3-6 Feb. 1992 Previously announced in IAA as A92-33285

(Contract RTOP 323-57-40)

(NASA-TM-106029; E-7592; NAS 1.15:106029) Avail: CASI HC A03/MF A01

Results are summarized for an investigation to assess the infrastructure available and the technology readiness in order to develop computational simulation methods/software for concurrent engineering. These results demonstrate that development of computational simulation methods for concurrent engineering is timely. Extensive infrastructure, in terms of multi-discipline simulation, component-specific simulation, system simulators, fabrication process simulation, and simulation of uncertainties—fundamental to develop such methods, is available. An approach is recommended which can be used to develop computational simulation methods for concurrent engineering of propulsion systems and systems in general. Benefits and issues needing early attention in the development are outlined.

Author (revised)

N93-24909* # National Aeronautics and Space Administration. Lewis Research Center, Cleveland, OH.

EVALUATION OF MARC FOR THE ANALYSIS OF ROTATING COMPOSITE BLADES

KAREN F. BARTOS and MICHAEL A. ERNST Washington Mar. 1993 27 p

(Contract RTOP 535-03-10)

(NASA-TM-4423; E-7163; NAS 1.15:4423) Avail: CASI HC A03/MF A01

The suitability of the MARC code for the analysis of rotating composite blades was evaluated using a four-task process. A nonlinear displacement analysis and subsequent eigenvalue analysis were performed on a rotating spring mass system to ensure that displacement-dependent centrifugal forces were accounted for in the eigenvalue analysis. Normal modes analyses were conducted on isotropic plates with various degrees of twist to evaluate MARC's ability to handle blade twist. Normal modes analyses were conducted on flat composite plates to validate the newly developed coupled COBSTRAN-MARC methodology. Finally, normal modes analyses were conducted on four composite propfan blades that were designed, analyzed, and fabricated at NASA Lewis Research Center. Results were compared with experimental data. The research documented herein presents MARC as a viable tool for the analysis of rotating composite blades.

Author

N93-24913* # National Aeronautics and Space Administration. Lewis Research Center, Cleveland, OH.

HIGH TEMPERATURE COMPOSITE ANALYZER (HITCAN) THEORETICAL MANUAL, VERSION 1.0

J. J. LACKNEY (Sverdrup Technology, Inc., Brook Park, OH.), P. L. N. MURTHY, and P. K. GOTSIS Apr. 1993 58 p

(Contract NAS3-25266; RTOP 505-63-5B)

(NASA-TM-106001; E-7544; NAS 1.15:106001) Avail: CASI HC A04/MF A01

This manual outlines some of the theoretical aspects embedded in the computer code, HITCAN (High Temperature Composite Analyzer). HITCAN is a general purpose computer program for predicting nonlinear global structural and local stress-strain response of arbitrarily oriented, multilayered high temperature metal

matrix composite structures. This code combines composite mechanics and laminate theory with an internal data base of the constituents (matrix, fiber and interface) material properties. The thermal and mechanical properties of the constituents are considered to be nonlinearly dependent on several parameters including temperature, stress and stress rate. The computational procedure for the analysis of the composite structure uses the finite element method. HITCAN consists of three modules: COBSTRAN, METCAN and MHOST. COBSTRAN generates the geometry (pre-processor) and defines the layout of the different plies. METCAN computes the material behavior of the composite and of the constituents. Finally, MHOST is a finite element program based on the mixed iterative solution technique. MHOST has a library for 2D and 3D isoparametric elements. HITCAN is written in FORTRAN 77 computer language and has been configured and executed on the NASA Lewis Research Center CRAY XMP and YMP computers.

Author

N93-25070* # National Aeronautics and Space Administration. Lewis Research Center, Cleveland, OH.

HIGH TEMPERATURE COMPOSITE ANALYZER (HITCAN) USER'S MANUAL, VERSION 1.0

J. J. LACKNEY (Sverdrup Technology, Inc., Brook Park, OH.), S. N. SINGHAL (Sverdrup Technology, Inc., Brook Park, OH.), P. L. N. MURTHY, and P. GOTSIS Apr. 1993 180 p

(Contract RTOP 505-63-5B)

(NASA-TM-106002; E-7545; NAS 1.15:106002) Avail: CASI HC A09/MF A02

This manual describes 'how-to-use' the computer code, HITCAN (High Temperature Composite Analyzer). HITCAN is a general purpose computer program for predicting nonlinear global structural and local stress-strain response of arbitrarily oriented, multilayered high temperature metal matrix composite structures. This code combines composite mechanics and laminate theory with an internal data base for material properties of the constituents (matrix, fiber and interphase). The thermo-mechanical properties of the constituents are considered to be nonlinearly dependent on several parameters including temperature, stress and stress rate. The computation procedure for the analysis of the composite structures uses the finite element method. HITCAN is written in FORTRAN 77 computer language and at present has been configured and executed on the NASA Lewis Research Center CRAY XMP and YMP computers. This manual describes HITCAN's capabilities and limitations followed by input/execution/output descriptions and example problems. The input is described in detail including (1) geometry modeling, (2) types of finite elements, (3) types of analysis, (4) material data, (5) types of loading, (6) boundary conditions, (7) output control, (8) program options, and (9) data bank.

Author

N93-26202* # National Aeronautics and Space Administration. Lewis Research Center, Cleveland, OH.

FABRICATION OF COMPOSITE PROPFAN BLADES FOR A CRUISE MISSILE WIND TUNNEL MODEL

E. BRIAN FITE Apr. 1993 30 p

(Contract RTOP 535-03-10)

(NASA-TM-105270; E-7327; NAS 1.15:105270) Avail: CASI HC A03/MF A01

This report outlines the procedures that were employed in fabricating prototype graphite-epoxy composite prop fan blades. These blades were used in wind tunnel tests that investigated prop fan propulsion system interactions with a missile airframe in order to study the feasibility of an advanced-technology-propfan-propelled missile. Major phases of the blade fabrication presented include machining of the master blade, mold fabrication, ply cutting and assembly, blade curing, and quality assurance. Specifically, four separate designs were fabricated, 18 blades of each geometry, using the same fabrication technique for each design.

Author

N93-26550*# National Aeronautics and Space Administration. Lewis Research Center, Cleveland, OH.

THE INFLUENCE OF PRIMARY AND SECONDARY ORIENTATIONS ON THE ELASTIC RESPONSE OF A NICKEL-BASE SINGLE-CRYSTAL SUPERALLOY

ALI ABDUL-AZIZ (Sverdrup Technology, Inc., Brook Park, OH.), SREERAMESH KALLURI (Sverdrup Technology, Inc., Brook Park, OH.), and MICHAEL A. MCGAW Apr. 1993 13 p Presented at the 38th ASME International Gas Turbine and Aeroengine Congress and Exposition, Cincinnati, OH, 24-27 May 1993; sponsored by ASME
(Contract RTOP 553-13-00)
(NASA-TM-106125; E-7801; NAS 1.15:106125) Avail: CASI HC A03/MF A01

The influence of primary orientation on the elastic response of a (001)-oriented nickel-base single-crystal superalloy, PWA 1480, was investigated under mechanical, thermal, and combined thermal and mechanical loading conditions using finite element techniques. Elastic stress analyses were performed using the MARC finite element code on a square plate of PWA 1480 material. Primary orientation of the single crystal superalloy was varied in increments of 2 deg, from 0 to 10 deg, from the (001) direction. Two secondary orientations (0 and 45 deg) were considered, with respect to the global coordinate system, as the primary orientation angle was varied. The stresses developed within the single crystal plate were determined for each loading condition. In this paper, the influence of the angular offset between the primary crystal orientation and the loading direction on the elastic stress response of the PWA 1480 plate is presented for different loading conditions. The influence of primary orientation angle, when constrained between the bounds considered, was not found to be as significant as the influence of the secondary orientation angle, which is not typically controlled. Author (revised)

N93-26999*# National Aeronautics and Space Administration. Lewis Research Center, Cleveland, OH.

STRUCTURAL TAILORING OF AIRCRAFT ENGINE BLADE SUBJECT TO ICE IMPACT CONSTRAINTS

E. S. REDDY (Sverdrup Technology, Inc., Brook Park, OH.), G. H. ABUMERI (Sverdrup Technology, Inc., Brook Park, OH.), P. L. N. MURTHY, and C. C. CHAMIS Apr. 1993 22 p Presented at the Fourth AIAA/Air Force/OAI Symposium on Multidisciplinary Analysis, Cleveland, OH, 21-23 Sep. 1992; sponsored by AIAA, USAF, and OAI
(Contract RTOP 505-62-0K)
(NASA-TM-106033; E-7599; NAS 1.15:106033) Avail: CASI HC A03/MF A01

Results are presented for the minimum weight design of SR2 unswept blade made of (titanium/graphite-epoxy/titanium) sub s fiber composite. The blade which is rotating at high RPM is subject to ice impact. The root chord length, blade thicknesses at five stations, and graphite-epoxy ply orientation are chosen as design variables. Design constraints are placed on the behavior variables: local leading edge strain and root damage parameter (combined stress failure criteria) as a function due to ice impact, maximum spanwise centrifugal stress at the root of the deformed blade due to local damage, first three natural frequencies, and resonance margin after impact. The method of feasible directions is employed to solve the inequality constrained minimization problem. The effect of ice speed and the ice impact location on the final design are discussed. Author

N93-27009*# National Aeronautics and Space Administration. Lewis Research Center, Cleveland, OH.

CONSIDERATIONS CONCERNING FATIGUE LIFE OF METAL MATRIX COMPOSITES

V. M. RADHAKRISHNAN (Indian Inst. of Tech., Madras.) and PAUL A. BARTOLOTTA May 1993 11 p Sponsored in part by NAS-NRC
(Contract RTOP 510-01-50)
(NASA-TM-106144; E-7823; NAS 1.15:106144) Avail: CASI HC A03/MF A01

Since metal matrix composites (MMC) are composed from two

very distinct materials each having their own physical and mechanical properties, it is feasible that the fatigue resistance depends on the strength of the weaker constituent. Based on this assumption, isothermal fatigue lives of several MMC's were analyzed utilizing a fatigue life diagram approach. For each MMC, the fatigue life diagram was quantified using the mechanical properties of its constituents. The fatigue life regions controlled by fiber fracture and matrix were also quantitatively defined. Author (revised)

N93-27030*# National Aeronautics and Space Administration. Lewis Research Center, Cleveland, OH.

COMPOSITE MICROMECHANICAL MODELING USING THE BOUNDARY ELEMENT METHOD

ROBERT K. GOLDBERG and DALE A. HOPKINS Apr. 1993 15 p Presented at the American Society for Composites Seventh Technical Conference on Composite Materials, University Park, PA, 13-15 Oct. 1992; sponsored by the American Society for Composites
(Contract RTOP 510-01-50)
(NASA-TM-106127; E-7796; NAS 1.15:106127) Avail: CASI HC A03/MF A01

The use of the boundary element method for analyzing composite micromechanical behavior is demonstrated. Stress-strain, heat conduction, and thermal expansion analyses are conducted using the boundary element computer code BEST-CMS, and the results obtained are compared to experimental observations, analytical calculations, and finite element analyses. For each of the analysis types, the boundary element results agree reasonably well with the results from the other methodologies, with explainable discrepancies. Overall, the boundary element method shows promise in providing an alternative method to analyze composite micromechanical behavior. Author (revised)

N93-27088*# National Aeronautics and Space Administration. Lewis Research Center, Cleveland, OH.

A TRANSFER MATRIX APPROACH TO VIBRATION LOCALIZATION IN MISTUNED BLADE ASSEMBLIES

GISLI OTTARSON (Michigan Univ., Ann Arbor.) and CHRITOPHE PIERRE (Michigan Univ., Ann Arbor.) May 1993 39 p
(Contract NCC3-233; RTOP 505-62-21)
(NASA-TM-106112; E-7764; NAS 1.15:106112; ICOMP-93-10)
Avail: CASI HC A03/MF A01

A study of mode localization in mistuned bladed disks is performed using transfer matrices. The transfer matrix approach yields the free response of a general, mono-coupled, perfectly cyclic assembly in closed form. A mistuned structure is represented by random transfer matrices, and the expansion of these matrices in terms of the small mistuning parameter leads to the definition of a measure of sensitivity to mistuning. An approximation of the localization factor, the spatially averaged rate of exponential attenuation per blade-disk sector, is obtained through perturbation techniques in the limits of high and low sensitivity. The methodology is applied to a common model of a bladed disk and the results verified by Monte Carlo simulations. The easily calculated sensitivity measure may prove to be a valuable design tool due to its system-independent quantification of mistuning effects such as mode localization. Author (revised)

N93-28633*# National Aeronautics and Space Administration. Lewis Research Center, Cleveland, OH.

PROBABILISTIC SIMULATION OF MULTI-SCALE COMPOSITE BEHAVIOR

D. G. LIAW (Sverdrup Technology, Inc., Brook Park, OH.), M. C. SHIAO (Sverdrup Technology, Inc., Brook Park, OH.), S. N. SINGHAL (Sverdrup Technology, Inc., Brook Park, OH.), and CHRISTOS C. CHAMIS Jun. 1993 14 p Presented at the 6th Japan-US Conference on Composite Materials, Orlando, FL, 22-25 Jun. 1992
(Contract RTOP 510-02-12)
(NASA-TM-106196; E-7904; NAS 1.15:106196) Avail: CASI HC A03/MF A01

A methodology is developed to computationally assess the

probabilistic composite material properties at all composite scale levels due to the uncertainties in the constituent (fiber and matrix) properties and in the fabrication process variables. The methodology is computationally efficient for simulating the probability distributions of material properties. The sensitivity of the probabilistic composite material property to each random variable is determined. This information can be used to reduce undesirable uncertainties in material properties at the macro scale of the composite by reducing the uncertainties in the most influential random variables at the micro scale. This methodology was implemented into the computer code PICAN (Probabilistic Integrated Composite ANalyzer). The accuracy and efficiency of this methodology are demonstrated by simulating the uncertainties in the material properties of a typical laminate and comparing the results with the Monte Carlo simulation method. The experimental data of composite material properties at all scales fall within the scatters predicted by PICAN. Author

N93-29196*# National Aeronautics and Space Administration. Lewis Research Center, Cleveland, OH.

BOUNDS ON INTERNAL STATE VARIABLES IN VISCOPLASTICITY

ALAN D. FREED Jun. 1993 6 p Prepared for Plasticity 1993, Baltimore, MD, 19-23 Jul. 1993; sponsored by Univ. of Maryland (Contract RTOP 505-63-5A) (NASA-TM-106215; E-7924; NAS 1.15:106215) Avail: CASI HC A02/MF A01

A typical viscoplastic model will introduce up to three types of internal state variables in order to properly describe transient material behavior; they are as follows: the back stress, the yield stress, and the drag strength. Different models employ different combinations of these internal variables--their selection and description of evolution being largely dependent on application and material selection. Under steady-state conditions, the internal variables cease to evolve and therefore become related to the external variables (stress and temperature) through simple functional relationships. A physically motivated hypothesis is presented that links the kinetic equation of viscoplasticity with that of creep under steady-state conditions. From this hypothesis one determines how the internal variables relate to one another at steady state, but most importantly, one obtains bounds on the magnitudes of stress and back stress, and on the yield stress and drag strength. Author (NASDA)

N93-31193*# National Aeronautics and Space Administration. Lewis Research Center, Cleveland, OH.

BLASIM: A COMPUTATIONAL TOOL TO ASSESS ICE IMPACT DAMAGE ON ENGINE BLADES

E. S. REDDY (Sverdrup Technology, Inc., Brook Park, OH.), G. H. ABUMERI (Sverdrup Technology, Inc., Brook Park, OH.), and C. C. CHAMIS Apr. 1993 24 p Presented at the 34th Structures, Structural Dynamics and Materials Conference, La Jolla, CA, 19-22 Apr. 1993; sponsored by AIAA, ASME, ASCE, AHS, and ASC (Contract RTOP 509-10-11) (NASA-TM-106225; E-7944; NAS 1.15:106225) Avail: CASI HC A03/MF A01

A portable computer called BLASIM was developed at NASA LeRC to assess ice impact damage on aircraft engine blades. In addition to ice impact analyses, the code also contains static, dynamic, resonance margin, and supersonic flutter analysis capabilities. Solid, hollow, superhybrid, and composite blades are supported. An optional preprocessor (input generator) was also developed to interactively generate input for BLASIM. The blade geometry can be defined using a series of airfoils at discrete input stations or by a finite element grid. The code employs a coarse, fixed finite element mesh containing triangular plate finite elements to minimize program execution time. Ice piece is modeled using an equivalent spherical objective that has a high velocity opposite that of the aircraft and parallel to the engine axis. For local impact damage assessment, the impact load is considered as a distributed force acting over a region around the impact point. The average radial strain of the finite elements along the leading edge is used as a measure of the local damage. To estimate

damage at the blade root, the impact is treated as an impulse and a combined stress failure criteria is employed. Parametric studies of local and root ice impact damage, and post-impact dynamics are discussed for solid and composite blades.

Author (revised)

N93-31558*# National Aeronautics and Space Administration. Lewis Research Center, Cleveland, OH.

PROGRESS IN SPECKLE-SHIFT STRAIN MEASUREMENT

CHRISTIAN T. LANT (Sverdrup Technology, Inc., Brook Park, OH.), JOHN P. BARRANGER, LAWRENCE G. OBERLE, and LAWRENCE C. GREER, III In its Structural Integrity and Durability of Reusable Space Propulsion Systems p 39-44 May 1991 Avail: CASI HC A02/MF A03

The Instrumentation and Control Technology Division of the Lewis Research Center has been developing an in-house capability to make one dimensional and two dimensional optical strain measurements on high temperature test specimens. The measurements are based on a two-beam speckle-shift technique. The development of composite materials for use in high temperature applications is generating interest in using the speckle-shift technique to measure strains on small diameter fibers and wires of various compositions. The results of preliminary speckle correlation tests on wire and fiber specimens are covered, and the advanced system currently under development is described. Derived from text

N93-31562*# National Aeronautics and Space Administration. Lewis Research Center, Cleveland, OH.

STRUCTURAL DYNAMICS: PROBABILISTIC STRUCTURAL ANALYSIS METHODS. PROGRAM OVERVIEW

CHRISTOS C. CHAMIS and DALE A. HOPKINS In its Structural Integrity and Durability of Reusable Space Propulsion Systems p 65-70 May 1991 Avail: CASI HC A02/MF A03

A brief description is provided of the fundamental aspects of a quantification process. Progress since the last structural durability conference in 1989 is summarized. The methodology to date and that to be developed during the life of the program is presented. The uncertain factors are presented. The approach is outlined that is required to achieve component and/or system certification in the shortest possible time for affordable reliability risk. Two new elements appear in a block diagram: (1) uncertainties in human factor, and (2) uncertainties in the computer code. Research to quantify the uncertainties in the human factor was initiated and is discussed. Derived from text

N93-31575*# National Aeronautics and Space Administration. Lewis Research Center, Cleveland, OH.

CUMULATIVE FATIGUE DAMAGE BEHAVIOR OF MAR M-247

MICHAEL A. MCGAW, GARY R. HALFORD, and SREERAMESH KALLURI (Sverdrup Technology, Inc., Brook Park, OH.) In its Structural Integrity and Durability of Reusable Space Propulsion Systems p 173-177 May 1991 Avail: CASI HC A01/MF A03

The objective was to examine the room temperature fatigue and nonlinear cumulative fatigue damage behavior of the cast nickel-based superalloy, MAR M-247. The fatigue test matrix consisted of single-level, fully reversed fatigue experiments. Two series of tests were performed: one of the two baseline fatigue LCF (Low-Cycle Fatigue) life levels was used in the first loading block, and the HCF (High-Cycle Fatigue) baseline loading level was used in the second block in each series. For each series, duplicate tests were performed at each applied LCF life fraction. Derived from text

ENERGY PRODUCTION AND CONVERSION

Includes specific energy conversion systems, e.g., fuel cells; global sources of energy; geophysical conversion; and windpower.

A93-13826* National Aeronautics and Space Administration. Lewis Research Center, Cleveland, OH.

FREE-PISTON STIRLING ENGINE SYSTEM CONSIDERATIONS FOR VARIOUS SPACE POWER APPLICATIONS

GEORGE R. DOCHAT and MANMOHAN DHAR (Mechanical Technology, Inc., Latham, NY) *In* Space nuclear power systems; Proceedings of the 8th Symposium, Albuquerque, NM, Jan. 6-10, 1991. Pt. 2 New York American Institute of Physics 1991 p. 598a-604a. Research supported by NASA refs Copyright

Free-Piston Stirling Engines (FPSE) have the potential to provide high reliability, long life, and efficient operation. Therefore, they are excellent candidates for the dynamic power conversion module of a space-based, power-generating system. FPSE can be coupled with many potential heat sources (radioisotope, solar, or nuclear reactor), various heat input systems (pumped loop, heat pipe), heat rejection (pumped loop or heat pipe), and various power management and distribution systems (ac, dc, high or low voltage, and fixed or variable load). This paper reviews potential space missions that can be met using free-piston Stirling engines and discusses options of various system integration approaches. This paper briefly outlines the program and recent progress. Author

A93-25867* National Aeronautics and Space Administration. Lewis Research Center, Cleveland, OH.

LONG LIFE REGENERATIVE FUEL CELL TECHNOLOGY DEVELOPMENT PLAN

FRANKLIN D. LITTMAN (Rockwell International Corp., Canoga Park, CA), ROBERT L. CATALDO (NASA, Lewis Research Center, Cleveland, OH), JAMES F. MCELROY (United Technologies Corp., Windsor Locks, CT), and JAY K. STEDMAN *In* IECEC '92; Proceedings of the 27th Intersociety Energy Conversion Engineering Conference, San Diego, CA, Aug. 3-7, 1992. Vol. 1 Warrendale, PA Society of Automotive Engineers, Inc. 1992 p. 1.95-1.100. refs (Contract NAS3-25808) Copyright

This paper summarizes a technology roadmap for completing advanced development of a Proton Exchange Membrane (PEM) Regenerative Fuel Cell (RFC) to meet long life (20,000 hrs at 50 percent duty cycle) mobile or portable power system applications on the surface of the moon and Mars. Development of two different sized RFC power system modules is included in this plan (3 and 7.5 kWe). A conservative approach was taken which includes the development of a Ground Engineering System, Qualification Unit, and Flight Unit. This paper includes a concept description, technology assessment, development issues, development tasks, and development schedule. Author

A93-25868* National Aeronautics and Space Administration. Lewis Research Center, Cleveland, OH.

REGENERATIVE FUEL CELLS

LARRY L. SWETTE, NANCY D. KACKLEY, and ANTHONY B. LACONTI (Giner, Inc., Waltham, MA) *In* IECEC '92; Proceedings of the 27th Intersociety Energy Conversion Engineering Conference, San Diego, CA, Aug. 3-7, 1992. Vol. 1 Warrendale, PA Society of Automotive Engineers, Inc. 1992 p. 1.101-1.106. refs (Contract NAS3-24635) Copyright

A development status evaluation is presented for moderate-temperature, single-unit, regenerative fuel cells using either alkaline or solid polymer proton-exchange membrane (PEM) electrolytes. Attention is given to the results thus far obtained for

Pt, Ir, Rh, and Na(x)Pt₃O₄ catalysts. Alkaline electrolyte tests have been performed on a half-cell basis with a floating-electrode cell; PEM testing has been with complete fuel cells, using Nafion 117. O.C.

A93-25886 National Aeronautics and Space Administration. Lewis Research Center, Cleveland, OH.

VALIDATION TEST OF ADVANCED TECHNOLOGY FOR IPV NICKEL-HYDROGEN FLIGHT CELLS - UPDATE

JOHN J. SMITHRICK (NASA, Lewis Research Center, Cleveland, OH) and STEPHEN W. HALL (U.S. Navy, Naval Weapons Support Center, Crane, IN) *In* IECEC '92; Proceedings of the 27th Intersociety Energy Conversion Engineering Conference, San Diego, CA, Aug. 3-7, 1992. Vol. 1 Warrendale, PA Society of Automotive Engineers, Inc. 1992 p. 1.215-1.225. Previously announced in STAR as N92-27878 refs (Contract RTOP 506-41-21) Copyright

Individual pressure vessel (IPV) nickel-hydrogen technology was advanced at NASA Lewis and under Lewis contracts with the intention of improving cycle life and performance. One advancement was to use 26 percent potassium hydroxide (KOH) electrolyte to improve cycle life. Another advancement was to modify the state-of-the-art cell design to eliminate identified failure modes. The modified design is referred to as the advanced design. A breakthrough in the LEO cycle life of IPV nickel-hydrogen cells has been previously reported. The cycle life of boiler plate cells containing 26 percent KOH electrolyte was about 40,000 LEO cycles compared to 3,500 cycles for cells containing 31 percent KOH. The boiler plate test results are in the process of being validated using flight hardware and real time LEO testing. The primary function of the advanced cell is to store and deliver energy for long-term, LEO spacecraft missions. The new features of this design are: (1) use of 26 percent rather than 31 percent KOH electrolyte; (2) use of a patented catalyzed wall wick; (3) use of serrated-edge separators to facilitate gaseous oxygen and hydrogen flow within the cell, while still maintaining physical contact with the wall wick for electrolyte management; and (4) use of a floating rather than a fixed stack (state-of-the-art) to accommodate nickel electrode expansion due to charge/discharge cycling. The significant improvements resulting from these innovations are: extended cycle life; enhanced thermal, electrolyte, and oxygen management; and accommodation of nickel electrode expansion. Author

A93-25899* National Aeronautics and Space Administration. Lewis Research Center, Cleveland, OH.

INDIUM PHOSPHIDE SOLAR CELLS FOR LASER POWER BEAMING APPLICATIONS

RAJ K. JAIN (NASA, Lewis Research Center, Cleveland, OH) and GEOFFREY A. LANDIS (Sverdrup Technology, Inc., Brook Park, OH) *In* IECEC '92; Proceedings of the 27th Intersociety Energy Conversion Engineering Conference, San Diego, CA, Aug. 3-7, 1992. Vol. 1 Warrendale, PA Society of Automotive Engineers, Inc. 1992 p. 1.303-1.307. refs (Contract NAS3-25266) Copyright

Lasers can be used to transmit power to photovoltaic cells. Solar cell efficiencies are enhanced significantly under monochromatic light, and therefore a laser beam of proper wavelength could be a very effective source of illumination for a solar array operating at very high efficiencies. This work reviews the modeling studies made on indium phosphide solar cells for such an application. These cells are known to be very radiation resistant and have a potential for high efficiency. Effects of cell series resistance, laser intensity, and temperature on cell performance have been discussed. Author

A93-25916 National Aeronautics and Space Administration. Lewis Research Center, Cleveland, OH.

DESIGN AND OPTIMIZATION OF A SELF-DEPLOYING SINGLE AXIS TRACKING PV ARRAY

ANTHONY J. COLOZZA (Sverdrup Technology, Inc., Brook Park,

OH) *In* IECEC '92; Proceedings of the 27th Intersociety Energy Conversion Engineering Conference, San Diego, CA, Aug. 3-7, 1992. Vol. 1 Warrendale, PA Society of Automotive Engineers, Inc. 1992 p. 1.433-1.438. Previously announced in STAR as N92-20671 refs
(Contract NAS3-25266; RTOP 591-14-11)
Copyright

This study was performed in order to design a tracking photovoltaic (PV) array and optimize the design for maximum specific power. The design considerations were minimal deployment time, high reliability, and small stowage volume. The array design was self-deployable, from a compact stowage configuration, using a passive pressurized gas deployment mechanism. The array structural components consist of a combination of beams, columns, and cables used to deploy and orient a flexible PV blanket. Each structural component of the design was analyzed to determine the size necessary to withstand the various forces to which it would be subjected. An optimization was performed to determine the array dimensions and blanket geometry which produce the maximum specific power. The optimization was performed for both lunar and Martian environments with 4 types of PV blankets (silicon, GaAs/Ge, GaAs CLEFT, and amorphous Silicon). For the lunar environment, the amorphous silicon array produced the highest specific power, whereas, for Mars the GaAs CLEFT array produced the highest specific power. A comparison was made to a fixed PV tent array of similar design. The tracking array produced a higher specific power with all types of the PV blankets examined except amorphous silicon at both locations. Author

A93-25947* National Aeronautics and Space Administration. Lewis Research Center, Cleveland, OH.

MODIFIED NASA STANDARD NICKEL-CADMIUM CELL DESIGNS

MICHELLE A. MANZO (NASA, Lewis Research Center, Cleveland, OH) *In* IECEC '92; Proceedings of the 27th Intersociety Energy Conversion Engineering Conference, San Diego, CA, Aug. 3-7, 1992. Vol. 2 Warrendale, PA Society of Automotive Engineers, Inc. 1992 p. 2.105-2.110.
Copyright

The experimental design, parameters, and testing of a modified NASA standard nickel-cadmium cell are discussed. Modifications regarding positive plate loading levels and nickel attack levels, loading levels for the negative plates, interelectrode spacing, and the positive electrode impregnation process are addressed. C.D.

A93-25948* National Aeronautics and Space Administration. Lewis Research Center, Cleveland, OH.

75 AH AND 10 BOILERPLATE NICKEL-HYDROGEN BATTERY DESIGNS AND TEST RESULTS

M. E. DAMAN (Space Systems/Loral, Palo Alto, CA), MICHELLE A. MANZO (NASA, Lewis Research Center, Cleveland, OH), R. CHANG, and E. CRUZ (Space Systems/Loral, Palo Alto, CA) *In* IECEC '92; Proceedings of the 27th Intersociety Energy Conversion Engineering Conference, San Diego, CA, Aug. 3-7, 1992. Vol. 2 Warrendale, PA Society of Automotive Engineers, Inc. 1992 p. 2.111-2.114. refs
Copyright

The results of initial characterization testing of 75 Ah actively cooled bipolar battery designs and 10 boilerplate nickel-hydrogen battery designs are presented. The results demonstrate the extended cycle life capability of the Ah batteries and the high capacity utilizations at various discharge rates of the nickel-hydrogen batteries. C.D.

A93-25974* National Aeronautics and Space Administration. Lewis Research Center, Cleveland, OH.

AN ANALYSIS OF POWER BEAMING FOR THE MOON AND MARS

MARK W. STAVNES (Sverdrup Technology, Inc., Brook Park, OH) *In* IECEC '92; Proceedings of the 27th Intersociety Energy Conversion Engineering Conference, San Diego, CA, Aug. 3-7, 1992. Vol. 2 Warrendale, PA Society of Automotive Engineers,

Inc. 1992 p. 2.293-2.298. refs
(Contract NAS3-25266)
Copyright

A system analysis is presented of orbiting and microwave and laser systems providing power to operations on the surfaces of the moon and Mars. Results are presented for a single stationary surface site, multiple stationary surface sites, and rover vehicles. C.D.

A93-25995* National Aeronautics and Space Administration. Lewis Research Center, Cleveland, OH.

DYNAMIC ISOTOPE POWER SYSTEM DESIGN CONSIDERATIONS FOR HUMAN EXPLORATION OF THE MOON AND MARS

D. J. BENTS, B. I. MCKISSOCK, C. D. RODRIGUEZ (NASA, Lewis Research Center, Cleveland, OH), J. C. HANLON, and P. C. SCHMITZ (Sverdrup Technology, Inc., Brook Park, OH) *In* IECEC '92; Proceedings of the 27th Intersociety Energy Conversion Engineering Conference, San Diego, CA, Aug. 3-7, 1992. Vol. 2 Warrendale, PA Society of Automotive Engineers, Inc. 1992 p. 2.439-2.444. refs
Copyright

Dynamic Isotope Power System (DIPS) alternatives for the surface mission elements associated with a lunar base and subsequent manned Mars expedition were investigated, emphasizing the issue of how the mission environment affects system design. It was found that radiation shielding for human-rated applications has a greater impact on DIPS than any other factor. C.D.

A93-26024* National Aeronautics and Space Administration. Lewis Research Center, Cleveland, OH.

PEM FUEL CELL STACK HEAT AND MASS MANAGEMENT

NICHOLAS E. VANDERBORGH, MICHAEL C. KIMBLE, JAMES R. HUFF, and JAMES C. HEDSTROM (Los Alamos National Lab., NM) *In* IECEC '92; Proceedings of the 27th Intersociety Energy Conversion Engineering Conference, San Diego, CA, Aug. 3-7, 1992. Vol. 3 Warrendale, PA Society of Automotive Engineers, Inc. 1992 p. 3.407-3.411. Research supported by NASA refs
Copyright

PEM stacks are under evaluation as candidates for future space power technology. Results of long-term operation on a set of contemporary stacks fitted with different proton exchange membrane materials are given. Data on water balances show effects of membrane materials on stack performance. Author

A93-26043 National Aeronautics and Space Administration. Lewis Research Center, Cleveland, OH.

EXPERIMENTAL DETERMINATION OF IN SITU UTILIZATION OF LUNAR REGOLITH FOR THERMAL ENERGY STORAGE

SCOTT W. RICHTER (Sverdrup Technology, Inc., Brook Park, OH) *In* IECEC '92; Proceedings of the 27th Intersociety Energy Conversion Engineering Conference, San Diego, CA, Aug. 3-7, 1992. Vol. 4 Warrendale, PA Society of Automotive Engineers, Inc. 1992 p. 4.183-4.188. Previously announced in STAR as N93-16617 refs
(Contract NAS3-25266; RTOP 506-41-31)
Copyright

A Lunar Thermal Energy from Regolith (LUTHER) experiment has been designed and fabricated at the NASA Lewis Research Center to determine the feasibility of using lunar soil as thermal energy storage media. The experimental apparatus includes an alumina ceramic canister which contains simulated lunar regolith, a heater, nine heat shields, a heat transfer cold jacket, and 19 type-B platinum rhodium thermocouples. The simulated lunar regolith is a basalt that closely resembles the lunar basalt returned to earth by the Apollo missions. The experiment will test the effects of vacuum, particle size, and density on the thermophysical properties of the regolith, which include melt temperature, specific heat thermal conductivity, and latent heat of storage. Two separate tests, using two different heaters, will be performed to study the effect of heating the system using radiative and conductive heat

44 ENERGY PRODUCTION AND CONVERSION

transfer. A finite differencing SINDA model was developed at NASA Lewis Research Center to predict the performance of the LUTHER experiment. The code will predict the effects of vacuum, particle size, and density has on the heat transfer to the simulated regolith. Author

A93-26071* National Aeronautics and Space Administration. Lewis Research Center, Cleveland, OH.

UPDATE ON THE ADVANCED STIRLING CONVERSION SYSTEM PROJECT FOR 25 KW DISH STIRLING APPLICATIONS

RICHARD K. SHALTENS, JEFFREY G. SCHREIBER, and WAYNE A. WONG (NASA, Lewis Research Center, Cleveland, OH) / In IECEC '92; Proceedings of the 27th Intersociety Energy Conversion Engineering Conference, San Diego, CA, Aug. 3-7, 1992. Vol. 5 Warrendale, PA Society of Automotive Engineers, Inc. 1992 p. 5.229-5.235. refs
Copyright

Technology development for Stirling convertors directed toward a dynamic power source for space applications is examined. The free-piston Stirling engine has the potential for both solar and nuclear space power applications. Two parallel design directions feature a solar receiver/liquid metal heat transport system, and a free-piston Stirling convertor which incorporates a linear alternator to directly provide the electrical output of about 25 kW to a utility grid. The Cummins Engine Company (CEC) free-piston Stirling convertor incorporates a linear alternator along with hydrodynamic gas bearings to provide noncontacting, wear-free support to the pistons. The Stirling Technology Company design incorporates linear alternator technology with flexures that provide noncontacting support while also supplying much of the spring stiffness needed to obtain proper resonance. P.D.

A93-26072* National Aeronautics and Space Administration. Lewis Research Center, Cleveland, OH.

ASSESSMENT OF 25 KW FREE-PISTON STIRLING TECHNOLOGY ALTERNATIVES FOR SOLAR APPLICATIONS

RAYMOND M. ERBEZNIK, MAURICE A. WHITE, L. B. PENSWICK, RONALD E. NEELY, DARREN C. RITTER (Stirling Technology Co., Richland, WA), and DAVID A. WALLACE (Westinghouse Hanford Co., Richland, WA) / In IECEC '92; Proceedings of the 27th Intersociety Energy Conversion Engineering Conference, San Diego, CA, Aug. 3-7, 1992. Vol. 5 Warrendale, PA Society of Automotive Engineers, Inc. 1992 p. 5.237-5.242. Research supported by DOE (Contract DEN3-377)
Copyright

The final design, construction, and testing of a 25-kW free-piston advanced Stirling conversion system (ASCS) are examined. The final design of the free-piston hydraulic ASCS consists of five subsystems: heat transport subsystem (solar receiver and pool boiler), free-piston hydraulic Stirling engine, hydraulic subsystem, cooling subsystem, and electrical and control subsystem. Advantages and disadvantages are identified for each technology alternative. Technology alternatives considered are gas bearings vs flexure bearings, stationary magnet linear alternator vs moving magnetic linear alternator, and seven different control options. Component designs are generated using available in-house procedures to meet the requirements of the free-piston Stirling convertor configurations. P.D.

A93-26073* National Aeronautics and Space Administration. Lewis Research Center, Cleveland, OH.

OVERVIEW OF THE NASA LEWIS COMPONENT TECHNOLOGY PROGRAM FOR STIRLING POWER CONVERTERS

LANNY G. THIEME and DIANE M. SWEC (NASA, Lewis Research Center, Cleveland, OH) / In IECEC '92; Proceedings of the 27th Intersociety Energy Conversion Engineering Conference, San Diego, CA, Aug. 3-7, 1992. Vol. 5 Warrendale, PA Society of Automotive Engineers, Inc. 1992 p. 5.283-5.288. refs
Copyright

This paper presents an update on the NASA Lewis Stirling

component technology program. The component technology program has been organized as part of the NASA Lewis effort to develop Stirling converter technology for space power applications. The Stirling space power program is part of the High Capacity Power element of the NASA Civil Space Technology Initiative. Lewis is also providing technical management of a DOE-funded project to develop Stirling converter systems for distributed dish solar terrestrial power applications. The Lewis component technology program is coordinated with the primary contract efforts of these projects but is aimed at longer term issues, advanced technologies, and independent assessments. Topics to be discussed include bearings, linear alternators, controls and load interaction, materials/life assessment, and heat exchangers. Author

A93-26078* National Aeronautics and Space Administration. Lewis Research Center, Cleveland, OH.

DYNAMIC ANALYSIS OF FREE-PISTON STIRLING ENGINE/LINEAR ALTERNATOR-LOAD SYSTEM - EXPERIMENTALLY VALIDATED

M. D. KANKAM (NASA, Lewis Research Center, Cleveland, OH), JEFFREY S. RAUCH (Sverdrup Technology, Inc., Brook Park, OH), and WALTER SANTIAGO (NASA, Lewis Research Center, Cleveland, OH) / In IECEC '92; Proceedings of the 27th Intersociety Energy Conversion Engineering Conference, San Diego, CA, Aug. 3-7, 1992. Vol. 5 Warrendale, PA Society of Automotive Engineers, Inc. 1992 p. 5.315-5.323. refs
Copyright

This paper discusses the effects of a variations in system parameters on the dynamic behavior of a Free-Piston Stirling Engine/Linear Alternator (FPSE/LA)-load system. The mathematical formulations incorporates both the mechanical and thermodynamic properties of the FPSE, as well as the electrical equations of the connected load. State-space technique in the frequency domain is applied to the resulting system of equations to facilitate the evaluation of parametric impacts on the system dynamic stability. Also included is a discussion on the system transient stability as affected by sudden changes in some key operating conditions. Some representative results are correlated with experimental data to verify the model and analytic formulation accuracies. Guidelines are given for ranges of the system parameters which will ensure an overall stable operation. Author

A93-34246* National Aeronautics and Space Administration. Lewis Research Center, Cleveland, OH.

I-BIEM CALCULATIONS OF THE FREQUENCY DISPERSION AND AC CURRENT DISTRIBUTION AT DISK AND RING-DISK ELECTRODES

BORIS D. CAHAN (Case Western Reserve Univ., Cleveland, OH) / In Modeling of batteries and fuel cells; Proceedings of the Symposium, Phoenix, AZ, Oct. 13-19, 1991 Pennington, NJ Electrochemical Society, Inc. 1991 p. 324-350. Previously announced in STAR as N91-32559 Research supported by NASA and Ohio Aerospace Inst refs
Copyright

The Iterative Boundary Integral Equation Method (I-BIEM) has been applied to the problem of frequency dispersion at a disk electrode in a finite geometry. The I-BIEM permits the direct evaluation of the AC potential (a complex variable) using complex boundary conditions. The point spacing was made highly nonuniform, to give extremely high resolution in those regions where the variables change most rapidly, i.e., in the vicinity of the edge of the disk. Results are analyzed with respect to IR correction, equipotential surfaces, and reference electrode placement. The current distribution is also examined for a ring-disk configuration, with the ring and the disk at the same AC potential. It is shown that the apparent impedance of the disk is inductive at higher frequencies. The results are compared to analytic calculations from the literature, and usually agree to better than 0.001 percent. Author

A93-51574* National Aeronautics and Space Administration. Lewis Research Center, Cleveland, OH.

LIGHTWEIGHT NICKEL ELECTRODES FOR NICKEL/HYDROGEN CELLS

HONG S. LIM and GABRIELA R. ZELTER (Hughes Aircraft Co., Industrial Electronics Group, Torrance, CA) *Journal of Power Sources* (ISSN 0378-7753) vol. 45, no. 2 June 1993 p. 195-207. refs

(Contract NAS3-22238)

Copyright

Thick nickel electrodes with lightweight substrate material have been prepared and tested in Ni/H₂ boilerplate cells containing 26 percent KOH electrolyte. Lightweight substrates used were either 85 or 90 percent in porosity and either 0.8 or 2 mm in thickness, respectively, compared with 80 to 82 percent porosity and 0.75 to 0.8 mm thickness of the state-of-the-art sintered plaque substrate. All of these thick electrodes had substantially improved theoretical (or chemical) capacity over that of state-of-the-art sintered nickel plaque electrodes. However, utilization of the active material was low (65 to 80 percent) compared with that of the state-of-the-art electrodes (approximately 90 percent) in 26 percent KOH. Due to this low utilization, the electrodes using 85 percent porous substrates did not show any advantage over the state-of-the-art ones. The electrodes using a 90 percent porous substrate, however, showed 17 percent higher usable specific capacity (about 0.13 Ah/g in 26 percent KOH) than that of the state-of-the-art nickel electrodes despite the low utilization. These electrodes achieved up to 4860 cycles at 40 percent depth-of-discharge with neither capacity loss nor any significant changes of rate capability and charging efficiency with cycling. Author (revised)

N93-14004*# National Aeronautics and Space Administration. Lewis Research Center, Cleveland, OH.

ADVANCED PHOTOVOLTAIC POWER SYSTEM TECHNOLOGY FOR LUNAR BASE APPLICATIONS

DAVID J. BRINKER and DENNIS J. FLOOD *In* NASA. Johnson Space Center, The Second Conference on Lunar Bases and Space Activities of the 21st Century, Volume 2 p 593-596 Sep. 1992 Previously announced as N88-26402

Avail: CASI HC A01/MF A03

The development of an advanced photovoltaic power system that would have application for a manned lunar base is currently planned under the Surface Power element of Pathfinder. Significant mass savings over state-of-the-art photovoltaic/battery systems are possible with the use of advanced lightweight solar arrays coupled with regenerative fuel cell storage. The solar blanket, using either ultrathin GaAs or amorphous silicon solar cells, would be integrated with a reduced-g structure. Regenerative fuel cells with high-pressure gas storage in filament-wound tanks are planned for energy storage. An advanced PV/RFC power system is a leading candidate for a manned lunar base as it offers a tremendous weight advantage over state-of-the-art photovoltaic/battery systems and is comparable in mass to other advanced power generation technologies. Author

N93-15523*# National Aeronautics and Space Administration. Lewis Research Center, Cleveland, OH.

POWER REQUIREMENTS FOR THE FIRST LUNAR OUTPOST (FLO)

ROBERT L. CATALDO and JOHN M. BOZEK Jan. 1993 11 p Presented at the Tenth Symposium on Space Power and Propulsion, Albuquerque, NM, 10-14 Jan. 1993; sponsored by New Mexico University

(Contract RTOP 590-49-00)

(NASA-TM-105925; E-7427; NAS 1.15:105925) Avail: CASI HC A03/MF A01

NASA's Exploration Program Office is currently developing a preliminary reference mission description that lays the framework from which the nation can return to the Moon by the end of the decade. The First Lunar Outpost is the initial phase of establishing a permanent presence on the Moon and the next step of sending humans to Mars. Many systems required for missions to Mars will be verified on the Moon, while still accomplishing valuable lunar

science and in-situ resource utilization (ISRU). Some of FLO's major accomplishments will be long duration habitation, extended surface roving (both piloted and teleoperated) and a suite of science experiments, including lunar resources extraction. Of equal challenge will be to provide long life, reliable power sources to meet the needs of a lunar mission. Author

N93-16907*# National Aeronautics and Space Administration. Lewis Research Center, Cleveland, OH.

TECHNOLOGIES

HENRY W. BRANDHORST, JR. *In* NASA. Johnson Space Center, Space Resources. Volume 2: Energy, Power, and Transport p 12-32 1992

Avail: CASI HC A03/MF A02; SOD HC; 4 functional color pages

Energy technologies to meet the power requirements of future space missions are reviewed. Photovoltaic, solar dynamic, and solar thermal technologies are discussed along with techniques for energy storage and power management and distribution. Author

N93-20261*# National Aeronautics and Space Administration. Lewis Research Center, Cleveland, OH.

FLUX CONCENTRATIONS ON SOLAR DYNAMIC COMPONENTS DUE TO MISPOINTING

DANIEL S. RYLICKI Nov. 1992 21 p Original contains color illustrations

(Contract RTOP 474-12-10)

(NASA-TM-105756; E-7168; NAS 1.15:105756) Avail: CASI HC A03/MF A01; 8 functional color pages

Mispointing of the solar dynamic (SD) concentrator designed for use on Space Station Freedom (SSF) causes the optical axis of the concentrator to be nonparallel to the incoming rays from the Sun. This causes solar flux not to be focused into the aperture hole of the receiver and may position the flux on other SSF components. A Rocketdyne analysis has determined the thermal impact of off-axis radiation due to mispointing on elements of the SD module and photovoltaic (PV) arrays. The conclusion was that flux distributions on some of the radiator components, the two-axis gimbal rings, the truss, and the PV arrays could present problems. The OFFSET computer code was used at Lewis Research Center to further investigate these flux distributions incident on components. The Lewis study included distributions for a greater range of mispoint angles than the Rocketdyne study. Author

N93-20493*# National Aeronautics and Space Administration. Lewis Research Center, Cleveland, OH.

LEWIS RESEARCH CENTER BATTERY OVERVIEW

PATRICIA O'DONNELL *In* NASA. Marshall Space Flight Center, The 1992 NASA Aerospace Battery Workshop p 53-85 Feb. 1993

Avail: CASI HC A03/MF A06

The topics covered are presented in viewgraph form and include the following: the Advanced Communications Technology Satellite; the Space Station Freedom (SSF) photovoltaic power module division; Ni/H₂ battery and cell design; individual pressure vessel (IPV) nickel-hydrogen cell testing SSF support; the LeRC Electrochemical Technology Branch; improved design IPV nickel-hydrogen cells; advanced technology for IPV nickel-hydrogen flight cells; a lightweight nickel-hydrogen cell; bipolar nickel-hydrogen battery development and technology; aerospace nickel-metal hydride cells; the NASA Sodium-Sulfur Cell Technology Flight Experiment; and the lithium-carbon dioxide battery thermodynamic model. CASI

N93-23018*# National Aeronautics and Space Administration. Lewis Research Center, Cleveland, OH.

CHANGES IN IMPEDANCE OF NI/CD CELLS WITH VOLTAGE AND CYCLE LIFE

MARGARET A. REID Jul. 1992 12 p Presented at the Second International Symposium on Electrochemical Impedance Spectroscopy, Santa Barbara, CA, 12-17 Jul. 1992; sponsored by the Pennsylvania State Univ.

44 ENERGY PRODUCTION AND CONVERSION

(Contract RTOP 323-57-48)

(NASA-TM-106105; E-7688; NAS 1.15:106105) Avail: CASI HC A03/MF A01

Impedances of aerospace design Super Ni/Cd cells are being measured as functions of voltage and number of cycles. The cells have been cycled over 4400 cycles to date. Analysis of the impedance data has been made using a number of equivalent circuits. The model giving the best fit over the whole range of voltage has a parallel circuit of a kinetic resistance and a constant phase element in series with the ohmic resistance. The values for the circuit elements have been treated as empirical parameters, and no attempt has been made as yet to correlate them with physical and chemical changes in the electrode. No significant changes have been seen as yet with the exception of a decrease in kinetic resistance at low states of charge in the first 500 cycles.

Author

N93-25136* National Aeronautics and Space Administration. Lewis Research Center, Cleveland, OH.

TEST RESULTS OF A STIRLING ENGINE UTILIZING HEAT EXCHANGER MODULES WITH AN INTEGRAL HEAT PIPE

ROBERT C. SKUPINSKI (Sverdrup Technology, Inc., Brook Park, OH.), LEONARD K. TOWER (Sverdrup Technology, Inc., Brook Park, OH.), FRANK J. MADI (Sverdrup Technology, Inc., Brook Park, OH.), and KEVIN D. BRUSK Apr. 1993 13 p (Contract RTOP 590-13-11)

(NASA-TM-105883; E-7681; NAS 1.15:105883) Avail: CASI HC A03/MF A01

The Heat Pipe Stirling Engine (HP-1000), a free-piston Stirling engine incorporating three heat exchanger modules, each having a sodium filled heat pipe, has been tested at the NASA-Lewis Research Center as part of the Civil Space Technology Initiative (CSTI). The heat exchanger modules were designed to reduce the number of potential flow leak paths in the heat exchanger assembly and incorporate a heat pipe as the link between the heat source and the engine. An existing RE-1000 free-piston Stirling engine was modified to operate using the heat exchanger modules. This paper describes heat exchanger module and engine performance during baseline testing. Condenser temperature profiles, brake power, and efficiency are presented and discussed.

Author

N93-27806* National Aeronautics and Space Administration. Lewis Research Center, Cleveland, OH.

ADVANCED SOLAR DYNAMIC TECHNOLOGY PROGRAM

JAMES CALOGERAS In NASA, Washington, Technology for Space Station Evolution. Volume 4: Power Systems/Propulsion/Robotics p 83-115 1990

Avail: CASI HC A03/MF A04; 1 functional color page

Viewgraphs and discussion on Advanced Solar Dynamic Technology Program are presented. Topics covered include: advanced solar dynamic technology program; advanced concentrators; advanced heat receivers; power conversion systems; dished all metal honeycomb sandwich panels; Stirling cavity heat pipe receiver; Brayton solar receiver; and thermal energy storage technology.

CASI

N93-28717* National Aeronautics and Space Administration. Lewis Research Center, Cleveland, OH.

THE PHOTOVOLTAIC ARRAY SPACE POWER PLUS DIAGNOSTICS (PASP PLUS) FLIGHT EXPERIMENT

MICHAEL F. PISZCZOR, HENRY B. CURTIS, DONALD A. GUIDICE (Phillips Lab., Hanscom AFB, MA.), and PAUL S. SEVERANCE (Phillips Lab., Hanscom AFB, MA.) In NASA, Washington, NASA/DOD Flight Experiments Technical Interchange Meeting Proceedings 34 p 1992

Avail: CASI HC A03/MF A10

An overview of the Photovoltaic Array Space Power Plus Diagnostics (PASP Plus) flight experiment is presented in outline and graphic form. The goal of the experiment is to test a variety of photovoltaic cell and array technologies under various space environmental conditions. Experiment objectives, flight hardware,

experiment control and diagnostic instrumentation, and illuminated thermal vacuum testing are addressed.

CASI

N93-28720* National Aeronautics and Space Administration. Lewis Research Center, Cleveland, OH.

THERMAL ENERGY STORAGE FLIGHT EXPERIMENT IN MICROGRAVITY

DAVID NAMKOONG In NASA, Washington, NASA/DOD Flight Experiments Technical Interchange Meeting Proceedings 12 p 1992

Avail: CASI HC A03/MF A10

The Thermal Energy Storage Flight Experiment was designed to characterize void shape and location in LiF-based phase change materials in different energy storage configurations representative of advanced solar dynamic systems. Experiment goals and payload design are described in outline and graphic form.

CASI

N93-28974* National Aeronautics and Space Administration. Lewis Research Center, Cleveland, OH.

ALKALI METAL CARBON DIOXIDE ELECTROCHEMICAL SYSTEM FOR ENERGY STORAGE AND/OR CONVERSION OF CARBON DIOXIDE TO OXYGEN Patent

NORMAN H. HAGEDORN, inventor (to NASA) 25 May 1993 7 p Filed 26 Sep. 1991 Supersedes N92-10222 (30 - 1, p 42)

(NASA-CASE-LEW-14973-1; US-PATENT-5,213,908; US-PATENT-APPL-SN-766593; US-PATENT-CLASS-429-16; US-PATENT-CLASS-429-27; US-PATENT-CLASS-429-29; US-PATENT-CLASS-429-30; US-PATENT-CLASS-429-46; US-PATENT-CLASS-429-103; INT-PATENT-CLASS-H01M-8/14)

Avail: US Patent and Trademark Office

An alkali metal, such as lithium, is the anodic reactant; carbon dioxide or a mixture of carbon dioxide and carbon monoxide is the cathodic reactant; and carbonate of the alkali metal is the electrolyte in an electrochemical cell for the storage and delivery of electrical energy. Additionally, alkali metal-carbon dioxide battery systems include a plurality of such electrochemical cells. Gold is a preferred catalyst for reducing the carbon dioxide at the cathode. The fuel cell of the invention produces electrochemical energy through the use of an anodic reactant which is extremely energetic and light, and a cathodic reactant which can be extracted from its environment and therefore exacts no transportation penalty. The invention is, therefore, especially useful in extraterrestrial environments.

Official Gazette of the U.S. Patent and Trademark Office

N93-29686* National Aeronautics and Space Administration. Lewis Research Center, Cleveland, OH.

THE EFFECT OF THE LOW EARTH ORBIT ENVIRONMENT ON SPACE SOLAR CELLS: RESULTS OF THE ADVANCED PHOTOVOLTAIC EXPERIMENT (S0014)

DAVID J. BRINKER, JOHN R. HICKEY (Eppley Lab., Inc., Newport, RI.), and DAVID A. SCHEIMAN (Sverdrup Technology, Inc., Brook Park, OH.) In NASA, Langley Research Center, LDEF: 69 Months in Space. Part 4: Second Post-Retrieval Symposium p 1291-1302 Apr. 1993

Avail: CASI HC A03/MF A03; 2 functional color pages

The results of post-flight performance testing of the solar cells flown on the Advanced Photovoltaic Experiment are reported. Comparison of post-flight current-voltage characteristics with similar pre-flight data revealed little or no change in solar cell conversion efficiency, confirming the reliability and endurance of space photovoltaic cells. This finding is in agreement with the lack of significant physical changes in the solar cells despite nearly six years in the low Earth orbit environment.

Author

N93-32201* National Aeronautics and Space Administration. Lewis Research Center, Cleveland, OH.

NON-DESTRUCTIVE, ULTRA-LOW RESISTANCE, THERMALLY STABLE CONTACTS FOR USE ON SHALLOW JUNCTION INP SOLAR CELLS

V. G. WEIZER, N. S. FATEMI (Sverdrup Technology, Inc., Arnold AFS, TN.), and A. L. KORENYI-BOTH (Calspan Corp., Cleveland, OH.) May 1993 6 p Presented at the 23rd IEEE Photovoltaic

Specialists Conference, Louisville, KY, 10-14 May 1993; sponsored by IEEE

(Contract RTOP 506-41-11)

(NASA-TM-106228; E-7946; NAS 1.15:106228) Avail: CASI HC A02/MF A01

Contact formation to InP is plagued by violent metal-semiconductor intermixing that takes place during the contact sintering process. Because of this the InP solar cell cannot be sintered after contact deposition. This results in cell contact resistances that are orders of magnitude higher than those that could be achieved if sintering could be performed in a non-destructive manner. We report here on a truly unique contact system involving Au and Ge, which is easily fabricated, which exhibits extremely low values of contact resistivity, and in which there is virtually no metal-semiconductor interdiffusion, even after extended sintering. We present a description of this contact system and suggest possible mechanisms to explain the observed behavior.

Author (revised)

45

ENVIRONMENT POLLUTION

Includes atmospheric, noise, thermal, and water pollution.

N93-27012* National Aeronautics and Space Administration. Lewis Research Center, Cleveland, OH.

NITRIC OXIDE FORMATION IN A LEAN, PREMIXED-PREVAPOORIZED JET A/AIR FLAME TUBE: AN EXPERIMENTAL AND ANALYTICAL STUDY

CHI-MING LEE, JEAN BIANCO (Ohio Aerospace Inst., Brook Park.), JOHN M. DEUR (Sverdrup Technology, Inc., Brook Park, OH.), and BAHMAN GHORASHI (Cleveland State Univ., OH.) Nov. 1992 15 p

(Contract RTOP 537-01-11)

(NASA-TM-105722; E-7121; NAS 1.15:105722) Avail: CASI HC A03/MF A01

An experimental and analytical study was performed on a lean, premixed-prevaporized Jet A/air flame tube. The NO(x) emissions were measured in a flame tube apparatus at inlet temperatures ranging from 755 to 866 K (900 to 1100 F), pressures from 10 to 15 atm, and equivalence ratios from 0.37 to 0.62. The data were then used in regressing an equation to predict the NO(x) production levels in combustors of similar design. Through an evaluation of parameters it was found that NO(x) is dependent on adiabatic flame temperature and combustion residence time, yet independent of pressure and inlet air temperature for the range of conditions studied. This equation was then applied to experimental data that were obtained from the literature, and a good correlation was achieved.

Author

46

GEOPHYSICS

Includes aeronomy; upper and lower atmosphere studies; ionospheric and magnetospheric physics; and geomagnetism.

A93-16347 National Aeronautics and Space Administration. Lewis Research Center, Cleveland, OH.

INTERFERENCE PATTERNS IN THE SPACELAB 2 PLASMA WAVE DATA - OBLIQUE ELECTROSTATIC WAVES GENERATED BY THE ELECTRON BEAM

WEI FENG, DONALD A. GURNETT, and IVER H. CAIRNS (Iowa Univ., Iowa City) Journal of Geophysical Research (ISSN 0148-0227) vol. 97, no. A11 Nov. 1, 1992 p. 17,005-17,018. refs

(Contract NAG3-449; NGL-16-001-043; NAGW-1539; NAGW-2040; NAS8-32807)

Copyright

During the Spacelab 2 mission the University of Iowa's Plasma Diagnostics Package (PDP) explored the plasma environment around the shuttle. Wideband spectrograms of plasma waves were obtained from the PDP at frequencies of 0-30 kHz and at distances up to 400 m from the shuttle. Strong low-frequency (below 10 kHz) electric field noise was observed in the wideband data during two periods in which an electron beam was ejected from the shuttle. This noise shows clear evidence of interference patterns caused by the finite (3.89 m) antenna length. The low-frequency noise was the most dominant type of noise produced by the ejected electron beam. Analysis of antenna interference patterns generated by these waves permits a determination of the wavelength, the direction of propagation, and the location of the source region. The observed waves have a linear dispersion relation very similar to that of ion acoustic waves. The waves are believed to be oblique ion acoustic or high-order ion cyclotron waves generated by a current of ambient electrons returning to the shuttle in response to the ejected electron beam.

Author

52

AEROSPACE MEDICINE

Includes physiological factors; biological effects of radiation; and effects of weightlessness on man and animals.

N93-22188* National Aeronautics and Space Administration. Lewis Research Center, Cleveland, OH.

OPTIMAL DESIGN OF COMPOSITE HIP IMPLANTS USING NASA TECHNOLOGY

T. A. BLAKE (Case Western Reserve Univ., Cleveland, OH.), D. A. SARAVANOS, D. T. DAVY (Case Western Reserve Univ., Cleveland, OH.), S. A. WATERS (Case Western Reserve Univ., Cleveland, OH.), and D. A. HOPKINS /in NASA, Washington, Technology 2002: The Third National Technology Transfer Conference and Exposition, Volume 2 p 377-386 Feb. 1993 (Contract NAG3-1027)

Avail: CASI HC A02/MF A04

Using an adaptation of NASA software, we have investigated the use of numerical optimization techniques for the shape and material optimization of fiber composite hip implants. The original NASA inhouse codes, were originally developed for the optimization of aerospace structures. The adapted code, which was called OPORIM, couples numerical optimization algorithms with finite element analysis and composite laminate theory to perform design optimization using both shape and material design variables. The external and internal geometry of the implant and the surrounding bone is described with quintic spline curves. This geometric representation is then used to create an equivalent 2-D finite element model of the structure. Using laminate theory and the 3-D geometric information, equivalent stiffnesses are generated for each element of the 2-D finite element model, so that the 3-D stiffness of the structure can be approximated. The geometric information to construct the model of the femur was obtained from a CT scan. A variety of test cases were examined, incorporating several implant constructions and design variable sets. Typically the code was able to produce optimized shape and/or material parameters which substantially reduced stress concentrations in the bone adjacent of the implant. The results indicate that this technology can provide meaningful insight into the design of fiber composite hip implants.

Author

N93-25593* National Aeronautics and Space Administration. Lewis Research Center, Cleveland, OH.

A FIBER OPTIC PROBE FOR THE DETECTION OF CATARACTS

RAFAT R. ANSARI and HARBANS S. DHADWAL (State Univ. of

54 MAN/SYSTEM TECHNOLOGY AND LIFE SUPPORT

New York, Stony Brook.) In NASA, Washington, Technology 2002: The Third National Technology Transfer Conference and Exposition, Volume 1 p 308-316 Feb. 1993
Avail: CASI HC A02/MF A04

A compact fiber optic probe developed for on-orbit science experiments was used to detect the onset of cataracts, a capability that could eliminate physicians' guesswork and result in new drugs to 'dissolve' or slow down the cataract formation before surgery is necessary. The probe is based upon dynamic light scattering (DLS) principles. It has no moving parts, no apertures, and requires no optical alignment. It is flexible and easy to use. Results are presented for excised but intact human eye lenses. In a clinical setting, the device can be easily incorporated into a slit-lamp apparatus (ophthalmoscope) for complete eye diagnostics. In this set-up, the integrated fiber optic probe, the size of a pencil, delivers a low power cone of laser light into the eye of a patient and guides the light which is backscattered by the protein molecules of the lens through a receiving optical fiber to a photo detector. The non-invasive DLS measurements provide rapid determination of protein crystalline size and its size distribution in the eye lens.

Author (revised)

54

MAN/SYSTEM TECHNOLOGY AND LIFE SUPPORT

Includes human engineering; biotechnology; and space suits and protective clothing.

N93-31573*# National Aeronautics and Space Administration. Lewis Research Center, Cleveland, OH.

PROBABILISTIC SIMULATION OF THE HUMAN FACTOR IN STRUCTURAL RELIABILITY

ASHWIN R. SHAH (Sverdrup Technology, Inc., Brook Park, OH.) and CHRISTOS C. CHAMIS In *its* Structural Integrity and Durability of Reusable Space Propulsion Systems p 159-168 May 1991
Avail: CASI HC A02/MF A03

Many structural failures have occasionally been attributed to human factors in engineering design, analyses maintenance, and fabrication processes. Every facet of the engineering process is heavily governed by human factors and the degree of uncertainty associated with them. Factors such as societal, physical, professional, psychological, and many others introduce uncertainties that significantly influence the reliability of human performance. Quantifying human factors and associated uncertainties in structural reliability require: (1) identification of the fundamental factors that influence human performance, and (2) models to describe the interaction of these factors. An approach is being developed to quantify the uncertainties associated with the human performance. This approach consists of a multi factor model in conjunction with direct Monte-Carlo simulation.

Derived from text

59

MATHEMATICAL AND COMPUTER SCIENCES (GENERAL)

A93-25084 National Aeronautics and Space Administration. Langley Research Center, Hampton, VA.

NASA CST AIDS U.S. INDUSTRY

JERRY M. HOUSNER (NASA, Langley Research Center, Hampton, VA) and LARRY D. PINSON (NASA, Lewis Research Center,

Cleveland, OH) Aerospace America (ISSN 0740-722X) vol. 31, no. 2 Feb. 1993 p. 20-25.

Copyright

The effect of NASA's computational structures Technology (CST) research on aerospace vehicle design and operation is discussed. The application of this research to proposed version of a high-speed civil transport, to composite structures in aerospace, to the study of crack growth, and to resolving field problems is addressed.

C.D.

N93-26946*# National Aeronautics and Space Administration. Lewis Research Center, Cleveland, OH.

EXPLICIT ROBUST SCHEMES FOR IMPLEMENTATION OF A CLASS OF PRINCIPAL VALUE-BASED CONSTITUTIVE MODELS: SYMBOLIC AND NUMERIC IMPLEMENTATION

S. M. ARNOLD, A. F. SALEEB (Akron Univ., OH.), H. Q. TAN (Akron Univ., OH.), and Y. ZHANG (Akron Univ., OH.) May 1993 55 p

(Contract RTOP 510-01-50)

(NASA-TM-106124; E-7788; NAS 1.15:106124) Avail: CASI HC A04/MF A01

The issue of developing effective and robust schemes to implement a class of the Ogden-type hyperelastic constitutive models is addressed. To this end, special purpose functions (running under MACSYMA) are developed for the symbolic derivation, evaluation, and automatic FORTRAN code generation of explicit expressions for the corresponding stress function and material tangent stiffness tensors. These explicit forms are valid over the entire deformation range, since the singularities resulting from repeated principal-stretch values have been theoretically removed. The required computational algorithms are outlined, and the resulting FORTRAN computer code is presented.

Author

N93-26947*# National Aeronautics and Space Administration. Lewis Research Center, Cleveland, OH.

EXPLICIT ROBUST SCHEMES FOR IMPLEMENTATION OF GENERAL PRINCIPAL VALUE-BASED CONSTITUTIVE MODELS

S. M. ARNOLD, A. F. SALEEB (Akron Univ., OH.), H. Q. TAN (Akron Univ., OH.), and Y. ZHANG (Akron Univ., OH.) Apr. 1993 29 p

(Contract RTOP 510-01-50)

(NASA-TM-106123; E-7787; NAS 1.15:106123) Avail: CASI HC A03/MF A01

The issue of developing effective and robust schemes to implement general hyperelastic constitutive models is addressed. To this end, special purpose functions are used to symbolically derive, evaluate, and automatically generate the associated FORTRAN code for the explicit forms of the corresponding stress function and material tangent stiffness tensors. These explicit forms are valid for the entire deformation range. The analytical form of these explicit expressions is given here for the case in which the strain-energy potential is taken as a nonseparable polynomial function of the principle stretches.

Derived from text

61

COMPUTER PROGRAMMING AND SOFTWARE

Includes computer programs, routines, and algorithms, and specific applications, e.g., CAD/CAM.

A93-20380*# National Aeronautics and Space Administration. Lewis Research Center, Cleveland, OH.

SOFTWARE ISSUES IN THREE DIMENSIONAL CONTINUUM SHAPE OPTIMIZATION EMPLOYING BOUNDARY FORMULATIONS

JAMES H. KANE (Clarkson Univ., Potsdam, NY) In AIAA/USAF/NASA/OAI Symposium on Multidisciplinary Analysis and Optimization, 4th, Cleveland, OH, Sept. 21-23, 1992, Technical

Papers. Pt. 2 Washington American Institute of Aeronautics and Astronautics 1992 p. 844-852. refs
(Contract NAG3-1089; NSF DDM-90-19852)
(AIAA PAPER 92-4792) Copyright

The paper addresses the issue of how individual computational techniques for the accurate and economical calculation of information required for large-scale 3D continuum structural shape optimization via boundary element analysis (BEA) formulations can be prudently selected and incorporated in large-scale BEA programs, employing either direct or iterative equation solvers. A series of techniques that allows for the incorporation of economical shape design sensitivity analysis capability with a minimal amount of software development is described. The use of reanalysis is shown to be the key ingredient associated with each of these techniques. It is concluded that, from a software engineering perspective, capabilities that facilitate 3D shape optimization can be implemented in BEA programs with only modest investments in program development. P.D.

A93-22604*# National Aeronautics and Space Administration. Lewis Research Center, Cleveland, OH.

LEWICE DROPLET TRAJECTORY CALCULATIONS ON A PARALLEL COMPUTER

STEVEN C. CARUSO (Nielsen Engineering & Research, Inc., Mountain View, CA) Jan. 1993 12 p. AIAA, Aerospace Sciences Meeting and Exhibit, 31st, Reno, NV, Jan. 11-14, 1993 refs

(Contract NAS3-26321)

(AIAA PAPER 93-0172) Copyright

A parallel computer implementation (128 processors) of LEWICE, a NASA Lewis code used to predict the time-dependent ice accretion process for two-dimensional aerodynamic bodies of simple geometries, is described. Two-dimensional parallel droplet trajectory calculations are performed to demonstrate the potential benefits of applying parallel processing to ice accretion analysis. Parallel performance is evaluated as a function of the number of trajectories and the number of processors. For comparison, similar trajectory calculations are performed on single-processor Cray computers, and the best parallel results are found to be 33 and 23 times faster, respectively, than those of the Cray XMP and YMP. V.L.

A93-23699# National Aeronautics and Space Administration. Lewis Research Center, Cleveland, OH.

A GRAPHICAL USER-INTERFACE FOR PROPULSION SYSTEM ANALYSIS

BRIAN P. CURLETT (NASA, Lewis Research Center, Cleveland, OH) and KATHLEEN RYALL (Harvard Univ., Cambridge, MA) Jan. 1993 14 p. AIAA, Aerospace Sciences Meeting and Exhibit, 31st, Reno, NV, Jan. 11-14, 1993 Previously announced in STAR as N92-33894 refs

(Contract RTOP 505-69-50)

(AIAA PAPER 93-0223) Copyright

NASA LeRC uses a series of computer codes to calculate installed propulsion system performance and weight. The need to evaluate more advanced engine concepts with a greater degree of accuracy has resulted in an increase in complexity of this analysis system. Therefore, a graphical user interface was developed to allow the analyst to more quickly and easily apply these codes. The development of this interface and the rationale for the approach taken are described. The interface consists of a method of pictorially representing and editing the propulsion system configuration, forms for entering numerical data, on-line help and documentation, post processing of data, and a menu system to control execution. Author

A93-24487*# National Aeronautics and Space Administration. Lewis Research Center, Cleveland, OH.

LV SOFTWARE SUPPORT FOR SUPERSONIC FLOW ANALYSIS

W. A. BELL (Georgia Inst. of Technology, Atlanta) and J. LEPICOVSKY (Sverdrup Technology, Inc., Brook Park, OH) Jul. 1992 11 p. AIAA, Aerospace Ground Testing Conference,

17th, Nashville, TN, July 6-8, 1992 refs

(Contract NAG3-1215)

(AIAA PAPER 92-3900)

The software for configuring an LV counter processor system has been developed using structured design. The LV system includes up to three counter processors and a rotary encoder. The software for configuring and testing the LV system has been developed, tested, and included in an overall software package for data acquisition, analysis, and reduction. Error handling routines respond to both operator and instrument errors which often arise in the course of measuring complex, high-speed flows. The use of networking capabilities greatly facilitates the software development process by allowing software development and testing from a remote site. In addition, high-speed transfers allow graphics files or commands to provide viewing of the data from a remote site. Further advances in data analysis require corresponding advances in procedures for statistical and time series analysis of nonuniformly sampled data. Author

A93-24781*# National Aeronautics and Space Administration. Lewis Research Center, Cleveland, OH.

UNSTRUCTURED 3D DELAUNAY MESH GENERATION APPLIED TO PLANES, TRAINS AND AUTOMOBILES

KENNETH R. BLAKE and GREGORY S. SPRAGLE (Fluent, Inc., Lebanon, NH) Jan. 1993 16 p. AIAA, Aerospace Sciences Meeting and Exhibit, 31st, Reno, NV, Jan. 11-14, 1993 refs
(Contract NAS3-25785)

(AIAA PAPER 93-0673) Copyright

Technical issues associated with domain-tessellation production, including initial boundary node triangulation and volume mesh refinement, are presented for the 'TGrid' 3D Delaunay unstructured grid generation program. The approach employed is noted to be capable of preserving predefined triangular surface facets in the final tessellation. The capabilities of the approach are demonstrated by generating grids about an entire fighter aircraft configuration, a train, and a wind tunnel model of an automobile. O.C.

A93-25527*# National Aeronautics and Space Administration. Lewis Research Center, Cleveland, OH.

BGRID1 - INTERACTIVE THREE-DIMENSIONAL TURBOMACHINERY GRID GENERATION SYSTEM WITH APPLICATIONS

J. M. SHOEMAKER (Sverdrup Technology, Inc., Brook Park, OH) and CHUNILL HAH (NASA, Lewis Research Center, Cleveland, OH) Jan. 1993 12 p. AIAA, Aerospace Sciences Meeting and Exhibit, 31st, Reno, NV, Jan. 11-14, 1993 refs
(AIAA PAPER 93-0430)

An interactive, graphics-based grid generation system for 3D turbomachinery geometries has been developed. The system consists of separate modules for geometry modeling and grid generation. The grid generation method generates a series of 2D grids in the blade-to-blade passage to build up the 3D grid. A Poisson equation with forcing functions selected to control orthogonality and spacing on all boundaries is solved to generate the grid. Interactive definition of Bezier curves and surfaces as internal boundaries is used to improve control of grid quality. A multi-block data structure simplifies the creation of structured H-grids about complex turbomachinery geometries. The multi-block strategy facilitates the creation of a grid in the tip flow region, which is an important contributor to losses within the passage. The grid generation system is applied to several complex geometries including a simple radial impeller, a conventional turbine rotor, the SSME LOX turbine rotor with and without a tip flow grid, a multi-passage inducer-impeller, and a tip-flow cascade. In addition, a calculation of the tip-flow cascade flow field is shown. Author

A93-31009*# National Aeronautics and Space Administration. Lewis Research Center, Cleveland, OH.

DUKSUP - A HIGH THRUST TRAJECTORY OPTIMIZATION CODE

LESLIE R. BALKANYI and O. F. SPURLOCK (NASA, Lewis

Research Center, Cleveland, OH) Feb. 1993 6 p. AIAA, AHS, and ASEE, Aerospace Design Conference, Irvine, CA, Feb. 16-19, 1993
(AIAA PAPER 93-1127) Copyright

Designing missions on expendable launch vehicles (ELV's) includes determining launch vehicle performance capabilities and trajectory characteristics over the range of mission requirements for suitable launch periods. This analysis depends on mathematically modeling both the launch vehicle and the mission requirements. Generally the result is a mathematical model that is described by an objective function to be optimized subject to an assortment of algebraic and dynamic constraints. About 30 years ago, engineers at Lewis Research Center (LeRC) undertook the task of creating a software code to solve 3D versions of such problems and based it on the Calculus of Variations/Optimal Control Theory. One of these codes, DUKSUP, has been in use at LeRC for nearly 25 years, during which time it has played an important role in a large number of studies and actual missions. Currently it is being used by about 12 analysts in the Center's Advanced Space Analysis Office (ASAO) to do mission design, feasibility studies, corroboration of contractor data and planning studies for the Space Exploration Initiative (SEI). Today, it is one of the few ELV mission analysis production codes based on variational methods. With future ELV missions in mind, ASAO is presently creating a new code to upgrade DUKSUP's capabilities.

Author

A93-31341* National Aeronautics and Space Administration. Lewis Research Center, Cleveland, OH.

A HIGH TEMPERATURE FATIGUE LIFE PREDICTION COMPUTER CODE BASED ON THE TOTAL STRAIN VERSION OF STRAINRANGE PARTITIONING (SRP)

MICHAEL A. MCGAW and JAMES F. SALTSMAN (NASA, Lewis Research Center, Cleveland, OH) *In* Creep-fatigue interaction at high temperature; Proceedings of the Symposium, 112th ASME Winter Annual Meeting, Atlanta, GA, Dec. 1-6, 1991 New York American Society of Mechanical Engineers 1991 p. 65-80. refs

Copyright

A recently developed high-temperature fatigue life prediction computer code is presented, based on the Total Strain version of Strainrange Partitioning (TS-SRP). Included in this code are procedures for characterizing the creep-fatigue durability behavior of an alloy according to TS-SRP guidelines and predicting cyclic life for complex cycle types for both isothermal and thermomechanical conditions. A reasonably extensive materials properties database is included with the code.

Author

A93-45009*# National Aeronautics and Space Administration. Lewis Research Center, Cleveland, OH.

A PARALLEL DYNAMIC LOAD BALANCING ALGORITHM FOR 3-D ADAPTIVE UNSTRUCTURED GRIDS

A. VIDWANS, Y. KALLINDERIS (Texas Univ., Austin), and V. VENKATKRISHNAN (Computer Sciences Corp.; NASA, Ames Research Center, Moffett Field, CA) *In* AIAA Computational Fluid Dynamics Conference, 11th, Orlando, FL, July 6-9, 1993, Technical Papers. Pt. 1 Washington American Institute of Aeronautics and Astronautics 1993 p. 176-194. Research supported by DARPA refs

(Contract NSF ASC-91-11540)

(AIAA PAPER 93-3131) Copyright

Adaptive local grid refinement and coarsening results in unequal distribution of workload among the processors of a parallel system. A novel method for balancing the load in cases of dynamically changing tetrahedral grids is developed. The approach employs local exchange of cells among processors in order to redistribute the load equally. An important part of the load balancing algorithm is the method employed by a processor to determine which cells within its subdomain are to be exchanged. Two such methods are presented and compared. The strategy for load balancing is based on the Divide-and-Conquer approach which leads to an efficient parallel algorithm. This method is implemented on a distributed-memory MIMD system.

Author

A93-54704* National Aeronautics and Space Administration. Lewis Research Center, Cleveland, OH.

COMPUTATIONAL SIMULATION OF HOT COMPOSITE STRUCTURES

C. C. CHAMIS, P. L. N. MURTHY, and S. N. SINGHAL (NASA, Lewis Research Center, Cleveland, OH) *In* Composite material technology - 1991; Proceedings of the Symposium, 14th Annual Energy-sources Technology Conference and Exhibition, Houston, TX, Jan. 20-23, 1991 New York American Society of Mechanical Engineers 1991 p. 273-283. Previously announced in STAR as N91-19230 refs

Copyright

Three different computer codes developed in-house are described for application to hot composite structures. These codes include capabilities for: (1) laminate behavior (METCAN); (2) thermal/structural analysis of hot structures made from high temperature metal matrix composites (HITCAN); and (3) laminate tailoring (MMLT). Results for select sample cases are described to demonstrate the versatility as well as the application of these codes to specific situations. The sample case results show that METCAN can be used to simulate cyclic life in high temperature metal matrix composites; HITCAN can be used to evaluate the structural performance of curved panels as well as respective sensitivities of various nonlinearities, and MMLT can be used to tailor the fabrication process in order to reduce residual stresses in the matrix upon cool-down.

N93-11928*# National Aeronautics and Space Administration. Lewis Research Center, Cleveland, OH.

AN EMBEDDED RULE-BASED DIAGNOSTIC EXPERT SYSTEM IN ADA

ROBERT E. JONES and EUGENE M. LIBERMAN (Sverdrup Technology, Inc., Brook Park, OH.) *In* NASA. Lyndon B. Johnson Space Center, Fifth Annual Workshop on Space Operations Applications and Research (SOAR 1991), Volume 1 p 45-51 Jan. 1992

Avail: CASI HC A02/MF A04

Ada is becoming an increasingly popular programming language for large Government-funded software projects. Ada with its portability, transportability, and maintainability lends itself well to today's complex programming environment. In addition, expert systems have also assumed a growing role in providing human-like reasoning capability expertise for computer systems. The integration is discussed of expert system technology with Ada programming language, especially a rule-based expert system using an ART-Ada (Automated Reasoning Tool for Ada) system shell. NASA Lewis was chosen as a beta test site for ART-Ada. The test was conducted by implementing the existing Autonomous Power EXpert System (APEX), a Lisp-based power expert system, in ART-Ada. Three components, the rule-based expert systems, a graphics user interface, and communications software make up SMART-Ada (Systems fault Management with ART-Ada). The rules were written in the ART-Ada development environment and converted to Ada source code. The graphics interface was developed with the Transportable Application Environment (TAE) Plus, which generates Ada source code to control graphics images. SMART-Ada communicates with a remote host to obtain either simulated or real data. The Ada source code generated with ART-Ada, TAE Plus, and communications code was incorporated into an Ada expert system that reads the data from a power distribution test bed, applies the rule to determine a fault, if one exists, and graphically displays it on the screen. The main objective, to conduct a beta test on the ART-Ada rule-based expert system shell, was achieved. The system is operational. New Ada tools will assist in future successful projects. ART-Ada is one such tool and is a viable alternative to the straight Ada code when an application requires a rule-based or knowledge-based approach.

Author

COMPUTER SYSTEMS

Includes computer networks and special application computer systems.

N93-12022*# National Aeronautics and Space Administration. Lewis Research Center, Cleveland, OH.

COMPUTER AIDED DESIGN AND MANUFACTURING OF COMPOSITE PROPPAN BLADES FOR A CRUISE MISSILE WIND TUNNEL MODEL

SCOTT A. THORP and KEVIN M. DOWNEY (Sverdrup Technology, Inc., Brook Park, OH.) Sep. 1992 66 p
(Contract RTOP 535-03-0B)
(NASA-TM-105269; E-6497; NAS 1.15:105269) Avail: CASI HC A04/MF A01

One of the propulsion concepts being investigated for future cruise missiles is advanced unducted propfans. To support the evaluation of this technology applied to the cruise missile, a joint DOD and NASA test project was conducted to design and then test the characteristics of the propfans on a 0.55-scale, cruise missile model in a NASA wind tunnel. The configuration selected for study is a counterrotating rearward swept propfan. The forward blade row, having six blades, rotates in a counterclockwise direction, and the aft blade row, having six blades, rotates in a clockwise direction, as viewed from aft of the test model. Figures show the overall cruise missile and propfan blade configurations. The objective of this test was to evaluate propfan performance and suitability as a viable propulsion option for next generation of cruise missiles. This paper details the concurrent computer aided design, engineering, and manufacturing of the carbon fiber/epoxy propfan blades as the NASA Lewis Research Center. Author

N93-16613*# National Aeronautics and Space Administration. Lewis Research Center, Cleveland, OH.

USER'S MANUAL FOR INTERACTIVE DATA DISPLAY SYSTEM (IDDS)

JAMES D. STEGEMAN Nov. 1992 43 p Original contains color illustrations
(Contract RTOP 505-62-52)
(NASA-TM-105572; E-6897; NAS 1.15:105572) Avail: CASI HC A03/MF A01; 5 functional color pages

A computer graphics package for the visualization of three-dimensional flow in turbomachinery has been developed and tested. This graphics package, called IDDS (Interactive Data Display System), is able to 'unwrap' the volumetric data cone associated with a centrifugal compressor and display the results in an easy to understand two-dimensional manner. IDDS will provide the majority of the visualization and analysis capability for the ICE (Integrated CFD and Experiment) system. This document is intended to serve as a user's manual for IDDS in a stand-alone mode. Currently, IDDS is capable of plotting two- or three-dimensional simulation data, but work is under way to expand IDDS so that experimental data can be accepted, plotted, and compared with a simulation dataset of the actual hardware being tested. Author

N93-27024*# National Aeronautics and Space Administration. Lewis Research Center, Cleveland, OH.

DYNAMIC GAS TEMPERATURE MEASUREMENTS USING A PERSONAL COMPUTER FOR DATA ACQUISITION AND REDUCTION

GUSTAVE C. FRALICK, LAWRENCE G. OBERLE, and LAWRENCE C. GREER, III Apr. 1993 33 p
(Contract RTOP 505-62-50)
(NASA-TM-106119; E-7777; NAS 1.15:106119) Avail: CASI HC A03/MF A01

This report describes a dynamic gas temperature measurement system. It has frequency response to 1000 Hz, and can be used to measure temperatures in hot, high pressure, high velocity flows. A personal computer is used for collecting and processing data, which results in a much shorter wait for results than previously. The data collection process and the user interface are described in detail. The changes made in transporting the software from a mainframe to a personal computer are described in appendices, as is the overall theory of operation. Author

A93-23327*# National Aeronautics and Space Administration. Lewis Research Center, Cleveland, OH.

A QUALITATIVE APPROACH TO SYSTEMIC DIAGNOSIS OF THE SSME

TIMOTHY W. BICKMORE (Aerojet, Propulsion Div., Sacramento, CA) and WILLIAM A. MAUL (Sverdrup Technology, Inc., Brook Park, OH) Jan. 1993 9 p. AIAA, Aerospace Sciences Meeting and Exhibit, 31st, Reno, NV, Jan. 11-14, 1993
(Contract NAS3-25266; NAS3-25883)
(AIAA PAPER 93-0405) Copyright

A generic software architecture has been developed for posttest diagnostics of rocket engines, and is presently being applied to the posttest analysis of the SSME. This investigation deals with the Systems Section module of the architecture, which is presently under development. Overviews of the manual SSME systems analysis process and the overall SSME diagnostic system architecture are presented. R.E.P.

A93-34039*# National Aeronautics and Space Administration. Lewis Research Center, Cleveland, OH.

PARALLEL COMPUTING FOR PROBABILISTIC FATIGUE ANALYSIS

ROBERT H. SUES, YUAN J. LUA, and MARK D. SMITH (Applied Research Associates, Inc., Raleigh, NC) /n
AIAA/ASME/ASCE/AHS/ASC Structures, Structural Dynamics, and Materials Conference, 34th and AIAA/ASME Adaptive Structures Forum, La Jolla, CA, Apr. 19-22, 1993, Technical Papers. Pt. 3 Washington American Institute of Aeronautics and Astronautics 1993 p. 1659-1669. refs
(Contract NAS3-26576)
(AIAA PAPER 93-1499) Copyright

This paper presents the results of Phase I research to investigate the most effective parallel processing software strategies and hardware configurations for probabilistic structural analysis. We investigate the efficiency of both shared and distributed-memory architectures via a probabilistic fatigue life analysis problem. We also present a parallel programming approach, the virtual shared-memory paradigm, that is applicable across both types of hardware. Using this approach, problems can be solved on a variety of parallel configurations, including networks of single or multiprocessor workstations. We conclude that it is possible to effectively parallelize probabilistic fatigue analysis codes; however, special strategies will be needed to achieve large-scale parallelism to keep large number of processors busy and to treat problems with the large memory requirements encountered in practice. We also conclude that distributed-memory architecture is preferable to shared-memory for achieving large scale parallelism; however, in the future, the currently emerging hybrid-memory architectures will likely be optimal. Author

N93-11005*# National Aeronautics and Space Administration. Lewis Research Center, Cleveland, OH.

DESCRIPTION OF THE SSF PMAD DC TESTBED CONTROL SYSTEM DATA ACQUISITION FUNCTION

ANASTACIO N. BAEZ, MICHAEL MACKIN, and THEODORE WRIGHT Aug. 1992 8 p Presented at the 27th Intersociety Energy Conversion Engineering Conference, San Diego, CA, 3-7 Aug. 1992; sponsored by ANS, SAE, ACS, AIAA, ASME, and IEEE
(Contract RTOP 474-42-10)
(NASA-TM-105843; E-7286; NAS 1.15:105843) Avail: CASI HC A02/MF A01

The NASA LERC in Cleveland, Ohio has completed the development and integration of a Power Management and

Distribution (PMAD) DC Testbed. This testbed is a reduced scale representation of the end to end, sources to loads, Space Station Freedom Electrical Power System (SSF EPS). This unique facility is being used to demonstrate DC power generation and distribution, power management and control, and system operation techniques considered to be prime candidates for the Space Station Freedom. A key capability of the testbed is its ability to be configured to address system level issues in support of critical SSF program design milestones. Electrical power system control and operation issues like source control, source regulation, system fault protection, end-to-end system stability, health monitoring, resource allocation, and resource management are being evaluated in the testbed. The SSF EPS control functional allocation between on-board computers and ground based systems is evolving. Initially, ground based systems will perform the bulk of power system control and operation. The EPS control system is required to continuously monitor and determine the current state of the power system. The DC Testbed Control System consists of standard controllers arranged in a hierarchical and distributed architecture. These controllers provide all the monitoring and control functions for the DC Testbed Electrical Power System. Higher level controllers include the Power Management Controller, Load Management Controller, Operator Interface System, and a network of computer systems that perform some of the SSF Ground based Control Center Operation. The lower level controllers include Main Bus Switch Controllers and Photovoltaic Controllers. Power system status information is periodically provided to the higher level controllers to perform system control and operation. The data acquisition function of the control system is distributed among the various levels of the hierarchy. Data requirements are dictated by the control system algorithms being implemented at each level. A functional description of the various levels of the testbed control system architecture, the data acquisition function, and the status of its implementation is presented. Author

N93-12410* # National Aeronautics and Space Administration. Lewis Research Center, Cleveland, OH.
ISDN AT NASA LEWIS RESEARCH CENTER
 CATHERINE MURPHY BAKES (Kent State Univ., OH.), FREDRIC GOLDBERG, and STEVEN W. EUBANKS Oct. 1992 38 p
 (NASA-TM-105911; E-7388; NAS 1.15:105911) Avail: CASI HC A03/MF A01

An expository investigation of the potential impact of the Integrated Services Digital Network (ISDN) at NASA Lewis Research Center is described. To properly frame the subject, the paper contains a detailed survey of the components of Narrowband ISDN. The principles and objectives are presented as decreed by the Consultative Committee for International Telephone and Telegraph (CCITT). The various channel types are delineated and their associated service combinations are described. The subscriber-access network functions are explained pictorially via the ISDN reference configuration. A section on switching techniques is presented to enable the reader to understand the emergence of the concept of fast packet switching. This new technology is designed to operate over the high bandwidth, low error rate transmission media that characterizes the LeRC environment. A brief introduction to the next generation of networks is covered with sections on Broadband ISDM (B-ISDN), Asynchronous Transfer Mode (ATM), and Synchronous Optical Networks (SONET). Applications at LeRC are presented, first in terms of targets of opportunity, then in light of compatibility constraints. In-place pilot projects and testing are described that demonstrate actual usage at LeRC. Author

N93-13154* # National Aeronautics and Space Administration. Lewis Research Center, Cleveland, OH.
TURBOMACHINERY CFD ON PARALLEL COMPUTERS
 RICHARD A. BLECH, EDWARD J. MILNER, ANGELA QUEALY (Sverdrup Technology, Inc., Brook Park, OH.), and SCOTT E. TOWNSEND (Sverdrup Technology, Inc., Brook Park, OH.) Nov. 1992 22 p Proposed for presentation at the Symposium on High-Performance Computing for Flight Vehicles, Washington, DC, 7-9 Dec. 1992

(Contract RTOP 505-62-52)
 (NASA-TM-105932; E-7443; NAS 1.15:105932) Avail: CASI HC A03/MF A01

The role of multistage turbomachinery simulation in the development of propulsion system models is discussed. Particularly, the need for simulations with higher fidelity and faster turnaround time is highlighted. It is shown how such fast simulations can be used in engineering-oriented environments. The use of parallel processing to achieve the required turnaround times is discussed. Current work by several researchers in this area is summarized. Parallel turbomachinery CFD research at the NASA Lewis Research Center is then highlighted. These efforts are focused on implementing the average-passage turbomachinery model on MIMD, distributed memory parallel computers. Performance results are given for inviscid, single blade row and viscous, multistage applications on several parallel computers, including networked workstations. Author

N93-27040* # National Aeronautics and Space Administration. Lewis Research Center, Cleveland, OH.
PARALLEL SOLUTION OF HIGH-ORDER NUMERICAL SCHEMES FOR SOLVING INCOMPRESSIBLE FLOWS
 EDWARD J. MILNER, AVI LIN (Pennsylvania Univ., Philadelphia.), MAY-FUN LIQU, and RICHARD A. BLECH Washington Apr. 1993 14 p Original contains color illustrations
 (Contract NASA ORDER C-99066-G; RTOP 505-62-52)
 (NASA-TM-4451; E-7345; NAS 1.15:4451) Avail: CASI HC A03/MF A01; 1 functional color page

A new parallel numerical scheme for solving incompressible steady-state flows is presented. The algorithm uses a finite-difference approach to solving the Navier-Stokes equations. The algorithms are scalable and expandable. They may be used with only two processors or with as many processors as are available. The code is general and expandable. Any size grid may be used. Four processors of the NASA LeRC Hypercluster were used to solve for steady-state flow in a driven square cavity. The Hypercluster was configured in a distributed-memory, hypercube-like architecture. By using a 50-by-50 finite-difference solution grid, an efficiency of 74 percent (a speedup of 2.96) was obtained. Author (revised)

N93-28628* # National Aeronautics and Space Administration. Lewis Research Center, Cleveland, OH.
A MULTIARCHITECTURE PARALLEL-PROCESSING DEVELOPMENT ENVIRONMENT
 SCOTT TOWNSEND (Sverdrup Technology, Inc., Brook Park, OH.), RICHARD BLECH, and GARY COLE Apr. 1993 8 p Presented at the Seventh International Parallel Processing Symposium, Newport Beach, CA, 13-16 Apr. 1993; sponsored by IEEE Computer Society
 (Contract NAS3-25266; RTOP 505-62-52)
 (NASA-TM-106180; E-7744; NAS 1.15:106180) Avail: CASI HC A02/MF A01

A description is given of the hardware and software of a multiprocessor test bed - the second generation Hypercluster system. The Hypercluster architecture consists of a standard hypercube distributed-memory topology, with multiprocessor shared-memory nodes. By using standard, off-the-shelf hardware, the system can be upgraded to use rapidly improving computer technology. The Hypercluster's multiarchitecture nature makes it suitable for researching parallel algorithms in computational field simulation applications (e.g., computational fluid dynamics). The dedicated test-bed environment of the Hypercluster and its custom-built software allows experiments with various parallel-processing concepts such as message passing algorithms, debugging tools, and computational 'steering'. Such research would be difficult, if not impossible, to achieve on shared, commercial systems. Author (revised)

CYBERNETICS

Includes feedback and control theory, artificial intelligence, robotics and expert systems.

A93-10575* National Aeronautics and Space Administration. Lewis Research Center, Cleveland, OH.

SELF-TUNING MULTIVARIABLE POLE PLACEMENT CONTROL OF A MULTIZONE CRYSTAL GROWTH FURNACE

C. BATUR, R. B. SHARPLESS (Akron Univ., OH), W. M. B. DUVAL, and B. N. ROSENTHAL (NASA, Lewis Research Center, Cleveland, OH) *International Journal of Adaptive Control and Signal Processing* (ISSN 0890-6327) vol. 6, no. 2 March 1992 p. 127-138. refs

Copyright

This paper presents the design and implementation of a multivariable self-tuning temperature controller for the control of lead bromide crystal growth. The crystal grows inside a multizone transparent furnace. There are eight interacting heating zones shaping the axial temperature distribution inside the furnace. A multi-input, multi-output furnace model is identified on-line by a recursive least squares estimation algorithm. A multivariable pole placement controller based on this model is derived and implemented. Comparison between single-input, single-output and multi-input, multi-output self-tuning controllers demonstrates that the zone-to-zone interactions can be minimized better by a multi-input, multi-output controller design. This directly affects the quality of crystal growth.

Author

A93-20388 National Aeronautics and Space Administration. Lewis Research Center, Cleveland, OH.

NEURAL NETWORKS IN STRUCTURAL ANALYSIS AND DESIGN - AN OVERVIEW

P. HAJELA (Rensselaer Polytechnic Inst., Troy, NY) and L. BERKE (NASA, Lewis Research Center, Cleveland, OH) *In AIAA/USAF/NASA/OAI Symposium on Multidisciplinary Analysis and Optimization*, 4th, Cleveland, OH, Sept. 21-23, 1992, Technical Papers. Pt. 2 Washington American Institute of Aeronautics and Astronautics 1992 p. 902-914. refs

(Contract NAG3-1196; NAG1-1269)

(AIAA PAPER 92-4805) Copyright

The present paper provides an overview of the state-of-the-art in the application of neural networks in problems of structural analysis and design, including a survey of published applications in structural engineering. Such applications have included, among others, the use of neural networks in modeling nonlinear analysis of structures, as a rapid reanalysis capability in optimal design, and in developing problem parameter sensitivity of optimal solutions for use in multilevel decomposition based design. While most of the applications reported in the literature have been restricted to the use of the multilayer perceptron architecture and minor variations thereof, other network architectures have also been successfully explored, including the ART network, the counterpropagation network and the Hopfield-Tank model.

Author

A93-20389*# National Aeronautics and Space Administration. Lewis Research Center, Cleveland, OH.

NEURAL NETWORKS FOR STRUCTURAL DESIGN - AN INTEGRATED SYSTEM IMPLEMENTATION

LASZLO BERKE (NASA, Lewis Research Center, Cleveland, OH), WASSIM HAFEZ, and YOH-HAN PAO (Case Western Reserve Univ.; AI WARE, Inc., Cleveland, OH) *In AIAA/USAF/NASA/OAI Symposium on Multidisciplinary Analysis and Optimization*, 4th, Cleveland, OH, Sept. 21-23, 1992, Technical Papers. Pt. 2 Washington American Institute of Aeronautics and Astronautics 1992 p. 915-923. refs

(AIAA PAPER 92-4806) Copyright

The development of powerful automated procedures to aid the

creative designer is becoming increasingly critical for complex design tasks. In the work described here Artificial Neural Nets are applied to acquire structural analysis and optimization domain expertise. Based on initial instructions from the user an automated procedure generates random instances of structural analysis and/or optimization 'experiences' that cover a desired domain. It extracts training patterns from the created instances, constructs and trains an appropriate network architecture and checks the accuracy of net predictions. The final product is a trained neural net that can estimate analysis and/or optimization results instantaneously.

Author

A93-22967* National Aeronautics and Space Administration. Lewis Research Center, Cleveland, OH.

DAMAGE-MITIGATING CONTROL OF AEROSPACE SYSTEMS FOR HIGH PERFORMANCE AND EXTENDED LIFE

ASOK RAY, MIN-KUANG WU, MARC CARPINO (Pennsylvania State Univ., University Park), CARL F. LORENZO, and WALTER C. MERRILL (NASA, Lewis Research Center, Cleveland, OH) *In 1992 American Control Conference*, 11th, Chicago, IL, June 24-26, 1992, Proceedings. Vol. 4 Piscataway, NJ Institute of Electrical and Electronics Engineers 1992 p. 3052-3056. refs

(Contract NAG3-1240)

Copyright

The concept of damage-mitigating control is to minimize fatigue (as well as creep and corrosion) damage of critical components of mechanical structures while simultaneously maximizing the system dynamic performance. Given a dynamic model of the plant and the specifications for performance and stability robustness, the task is to synthesize a control law that would meet the system requirements and, at the same time, satisfy the constraints that are imposed by the material and structural properties of the critical components. The authors present the concept of damage-mitigating control systems design with the following objectives: (1) to achieve high performance with a prolonged life span; and (2) to systematically update the controller as the new technology of advanced materials evolves. The major challenge is to extract the information from the material properties and then utilize this information in a mathematical form so that it can be directly applied to robust control synthesis for mechanical systems. The basic concept of damage-mitigating control is illustrated using a relatively simplified model of a space shuttle main engine.

I.E.

A93-25986* National Aeronautics and Space Administration. Lewis Research Center, Cleveland, OH.

FAULT-TOLERANT ADAPTIVE CONTROL FOR LOAD-FOLLOWING IN STATIC SPACE NUCLEAR POWER SYSTEMS

ALEXANDER G. PARLOS, FETIYE O. ONBASIOGLU, KENNETH L. PEDDICORD (Texas A & M Univ., College Station), and JOHN D. METZGER (Grumman Corp., Bethpage, NY) *In IECEC '92: Proceedings of the 27th Intersociety Energy Conversion Engineering Conference*, San Diego, CA, Aug. 3-7, 1992. Vol. 2 Warrendale, PA Society of Automotive Engineers, Inc. 1992 p. 2.377-2.382. Research supported by SDIO refs

(Contract NAG3-1235)

Copyright

The possible use of a dual-loop model-based adaptive control system for load following in static space nuclear power systems is investigated. The proposed approach has thus far been applied only to a thermoelectric space nuclear power system but is equally applicable to other static space nuclear power systems such as thermionic systems.

C.D.

A93-26650* National Aeronautics and Space Administration. Lewis Research Center, Cleveland, OH.

SELF-GROWING NEURAL NETWORK ARCHITECTURE USING CRISP AND FUZZY ENTROPY

KRZYSZTOF J. CIOS (NASA, Lewis Research Center; Ohio Aerospace Inst., Cleveland) *In Science of artificial neural networks: Proceedings of the Meeting*, Orlando, FL, Apr. 21-24, 1992 Bellingham, WA Society of Photo-Optical Instrumentation Engineers (SPIE Proceedings. Vol. 1710, pt. 2) 1992 p.

838-851. refs
(Contract NSF DDM-90-15333)
Copyright

The paper briefly describes the self-growing neural network algorithm, CID3, which makes decision trees equivalent to hidden layers of a neural network. The algorithm generates a feedforward architecture using crisp and fuzzy entropy measures. The results for a real-life recognition problem of distinguishing defects in a glass ribbon, and for a benchmark problem of telling two spirals apart are shown and discussed. Author

A93-28200* National Aeronautics and Space Administration. Lewis Research Center, Cleveland, OH.

2-D NONLINEAR IIR-FILTERS FOR IMAGE PROCESSING - AN EXPLORATORY ANALYSIS

P. H. BAUER and M. SARTORI (Notre Dame Univ., IN) /In IEEE, International Symposium on Circuits and Systems, Singapore, June 11-14, 1991, Proceedings New York Institute of Electrical and Electronics Engineers 1991 p. 416-419. refs
(Contract NAG3-1186)

Copyright

A new nonlinear IIR filter structure is introduced and its deterministic properties are analyzed. It is shown to be better suited for image processing applications than its linear shift-invariant counterpart. The new structure is obtained from causality inversion of a 2D quarterplane causal linear filter with respect to the two directions of propagation. It is demonstrated, that by using this design, a nonlinear 2D lowpass filter can be constructed, which is capable of effectively suppressing Gaussian or impulse noise without destroying important image information. Author

A93-29338* National Aeronautics and Space Administration. Lewis Research Center, Cleveland, OH.

DYNAMIC MODELING AND CONTROL OF MULTIBODY MECHANICAL SYSTEMS WHICH ARE STRUCTURALLY FLEXIBLE

R. D. QUINN and J.-L. CHEN (Case Western Reserve Univ., Cleveland, OH) /In Dynamics and control of large structures; Proceedings of the 8th VPI&SU Symposium, Blacksburg, VA, May 6-8, 1991 Blacksburg, VA Virginia Polytechnic Institute and State University 1992 p. 119-131. refs
(Contract NAG3-1099)

This paper concerns the dynamic modeling and control of multibody, open-chained, structurally flexible, mechanical systems where the bodies are connected by revolute joints. The equations of motion are formulated based on a matrix form of Lagrange's equations for inertial quasi-coordinates. Each body is treated as a substructure of the system. For the purposes of simulation and control, the equations of motion are separated into two sets of equations using a perturbation approach: one to describe large rigid-body motions of the articulated system and the other to describe small linear motions of the bodies about the large motions. A biologically natural control strategy is used for vibration suppression and tracking the prescribed motion. Author

A93-30492* National Aeronautics and Space Administration. Lewis Research Center, Cleveland, OH.

A NOTE ON DECENTRALIZED INTEGRAL CONTROLLABILITY

O. D. I. NWOKAH, A. E. FRAZHO (Purdue Univ., West Lafayette, IN), and D. K. LE (NASA, Lewis Research Center, Cleveland, OH) International Journal of Control (ISSN 0020-7179) vol. 57, no. 2 Feb. 1993 p. 485-494. refs
(Contract NSF MSS-90-19531)

Copyright

A concept of decentralized integral controllability (DIC) defined on a given gain space Φ is clarified and related to the original definition given by Morari and Zafirou (1989). This leads to a simple proof of the existence of DIC on Φ from which existence conditions for DIC can be routinely deduced in the sense of Morari and Zafirou. Author

A93-34036* National Aeronautics and Space Administration. Lewis Research Center, Cleveland, OH.

PROBABILISTIC SIMULATION OF THE HUMAN FACTOR IN STRUCTURAL RELIABILITY

C. C. CHAMIS (NASA, Lewis Research Center, Cleveland, OH) /In AIAA/ASME/ASCE/AHS/ASC Structures, Structural Dynamics, and Materials Conference, 34th and AIAA/ASME Adaptive Structures Forum, La Jolla, CA, Apr. 19-22, 1993, Technical Papers. Pt. 3 Washington American Institute of Aeronautics and Astronautics 1993 p. 1624-1633. refs
(AIAA PAPER 93-1495) Copyright

A formal approach is described in an attempt to computationally simulate the probable ranges of uncertainties of the human factor in structural probabilistic assessments. A multi-factor interaction equation (MFIE) model has been adopted for this purpose. Human factors such as marital status, professional status, home life, job satisfaction, work load and health, are considered to demonstrate the concept. Parametric studies in conjunction with judgment are used to select reasonable values for the participating factors (primitive variables). Suitability of the MFIE in the subsequently probabilistic sensitivity studies are performed to assess the validity of the whole approach. Results obtained show that the uncertainties for no error range from five to thirty percent for the most optimistic case. Author

A93-34582* National Aeronautics and Space Administration. Lewis Research Center, Cleveland, OH.

A 3-D NONLINEAR RECURSIVE DIGITAL FILTER FOR VIDEO IMAGE PROCESSING

P. H. BAUER and W. QIAN (Notre Dame Univ., IN) /In IEEE Pacific Rim Conference on Communications, Computers and Signal Processing, Victoria, Canada, May 9, 10, 1991, Proceedings New York Institute of Electrical and Electronics Engineers 1991 p. 494-497. refs
(Contract NAG3-1186)

Copyright

This paper introduces a recursive 3-D nonlinear digital filter, which is capable of performing noise suppression without degrading important image information such as edges in space or time. It also has the property of unnoticeable bandwidth reduction immediately after a scene change, which makes the filter an attractive preprocessor to many interframe compression algorithms. The filter consists of a nonlinear 2-D spatial subfilter and a 1-D temporal filter. In order to achieve the required computational speed and increase the flexibility of the filter, all of the linear shift-variant filter modules are of the IIR type. Author

A93-37039 National Aeronautics and Space Administration. Lewis Research Center, Cleveland, OH.

FUZZY EXPERT SYSTEMS VS. NEURAL NETWORKS - TRUCK BACKER-UPPER CONTROL REVISITED

P. A. RAMAMOORTHY and SONG HUANG (Cincinnati Univ., OH) /In IEEE International Conference on Systems Engineering, Dayton, OH, Aug. 1-3, 1991, Proceedings New York Institute of Electrical and Electronics Engineers, Inc. 1991 p. 221-224. Research supported by NASA refs
(Contract NAG3-960; N00014-89-J-1633)

Copyright

It is pointed out that by merging the advantages of fuzzy expert systems and neural networks one can arrive at a more powerful yet more flexible system for inferring and learning. The advantages of fuzzy expert systems are their ability to provide nonlinear mapping through the membership functions and fuzzy rules, and the ability to deal with fuzzy information and incomplete and/or imprecise data. The merger of these two concepts is explained using the truck backer-upper control problem. Novel network architectures obtained by merging these two concepts and simulation results for the truck backer-upper problem using the architecture are shown. Author

A93-53653* National Aeronautics and Space Administration. Lewis Research Center, Cleveland, OH.

DIGITAL CONTROL ALGORITHMS FOR MICROGRAVITY ISOLATION SYSTEMS

A. SINHA and Y.-P. WANG (Pennsylvania State Univ., University Park) ASME, Transactions, Journal of Vibration and Acoustics (ISSN 0739-3717) vol. 115, no. 3 July 1993 p. 256-263. refs

(Contract NAG3-949)

Copyright

New digital control algorithms have been developed to achieve the desired transmissibility function for a microgravity isolation system. Two approaches have been presented for the controller design in the context of a single degree of freedom system for which an attractive electromagnet is used as the actuator. The relative displacement and the absolute acceleration of the mass have been used as feedback signals. The results from numerical studies are presented. It has been found that the resulting transmissibility is quite close to the desired function. Also, the maximum coil currents required by new algorithms are smaller than the maximum current demanded by the previously proposed lead/lag method.

A93-54533* National Aeronautics and Space Administration. Lewis Research Center, Cleveland, OH.

APPLICATION OF NEURAL NETS IN STRUCTURAL OPTIMIZATION

LASZLO BERKE (NASA, Lewis Research Center, Cleveland, OH) and PRABHAT HAJELA (Rensselaer Polytechnic Inst., Troy, NY) /In Optimization of large structural systems; Proceedings of the NATO/DFG Advanced Study Institute, Berchtesgaden, Germany, Sept. 23-Oct. 4, 1991. Vol. 2 Dordrecht, Netherlands Kluwer Academic Publishers 1993 p. 731-745. refs

Copyright

The biological motivation for Artificial Neural Net developments is briefly discussed, and the most popular paradigm, the feedforward supervised learning net with error back propagation training algorithm, is introduced. Possible approaches for utilization in structural optimization is illustrated through simple examples. Other currently ongoing developments for application in structural mechanics are also mentioned.

A93-54534* National Aeronautics and Space Administration. Lewis Research Center, Cleveland, OH.

SELF-ORGANIZATION IN NEURAL NETWORKS - APPLICATIONS IN STRUCTURAL OPTIMIZATION

PRABHAT HAJELA, B. FU (Rensselaer Polytechnic Inst., Troy, NY), and LASZLO BERKE (NASA, Lewis Research Center, Cleveland, OH) /In Optimization of large structural systems; Proceedings of the NATO/DFG Advanced Study Institute, Berchtesgaden, Germany, Sept. 23-Oct. 4, 1991. Vol. 2 Dordrecht, Netherlands Kluwer Academic Publishers 1993 p. 747-765. refs

(Contract NAG3-1196)

Copyright

The present paper discusses the applicability of ART (Adaptive Resonance Theory) networks, and the Hopfield and Elastic networks, in problems of structural analysis and design. A characteristic of these network architectures is the ability to classify patterns presented as inputs into specific categories. The categories may themselves represent distinct procedural solution strategies. The paper shows how this property can be adapted in the structural analysis and design problem. A second application is the use of Hopfield and Elastic networks in optimization problems. Of particular interest are problems characterized by the presence of discrete and integer design variables. The parallel computing architecture that is typical of neural networks is shown to be effective in such problems. Results of preliminary implementations in structural design problems are also included in the paper.

N93-11940*# National Aeronautics and Space Administration. Lewis Research Center, Cleveland, OH.

SPACE COMMUNICATION ARTIFICIAL INTELLIGENCE FOR LINK EVALUATION TERMINAL (SCAILET)

ANOOOSH K. SHAHIDI (Sverdrup Technology, Inc., Brook Park, OH.), RICHARD F. SCHLEGELMILCH (Akron Univ., OH.), EDWARD J. PETRIK, and JERRY L. WALTERS /In NASA. Lyndon B. Johnson Space Center, Fifth Annual Workshop on Space Operations Applications and Research (SOAR 1991), Volume 1 p 130-132 Jan. 1992

Avail: CASI HC A01/MF A04

A software application to assist end-users of the high burst rate (HBR) link evaluation terminal (LET) for satellite communications is being developed. The HBR LET system developed at NASA Lewis Research Center is an element of the Advanced Communications Technology Satellite (ACTS) Project. The HBR LET is divided into seven major subsystems, each with its own expert. Programming scripts, test procedures defined by design engineers, set up the HBR LET system. These programming scripts are cryptic, hard to maintain and require a steep learning curve. These scripts were developed by the system engineers who will not be available for the end-users of the system. To increase end-user productivity a friendly interface needs to be added to the system. One possible solution is to provide the user with adequate documentation to perform the needed tasks. With the complexity of this system the vast amount of documentation needed would be overwhelming and the information would be hard to retrieve. With limited resources, maintenance is another reason for not using this form of documentation. An advanced form of interaction is being explored using current computer techniques. This application, which incorporates a combination of multimedia and artificial intelligence (AI) techniques to provided end-users with an intelligent interface to the HBR LET system, is comprised of an intelligent assistant, intelligent tutoring, and hypermedia documentation. The intelligent assistant and tutoring systems address the critical programming needs of the end-user. Author

N93-18671*# National Aeronautics and Space Administration. Lewis Research Center, Cleveland, OH. Sverdrup Technology Inc.

SCHEDULING LESSONS LEARNED FROM THE AUTONOMOUS POWER SYSTEM

MARK J. RINGER /In NASA. Ames Research Center, Working Notes from the 1992 AAAI Spring Symposium on Practical Approaches to Scheduling and Planning p 52-56 May 1992

Avail: CASI HC A01/MF A02

The Autonomous Power System (APS) project at NASA LeRC is designed to demonstrate the applications of integrated intelligent diagnosis, control, and scheduling techniques to space power distribution systems. The project consists of three elements: the Autonomous Power Expert System (APEX) for Fault Diagnosis, Isolation, and Recovery (FDIR); the Autonomous Intelligent Power Scheduler (AIPS) to efficiently assign activities start times and resources; and power hardware (Brassboard) to emulate a space-based power system. The AIPS scheduler was tested within the APS system. This scheduler is able to efficiently assign available power to the requesting activities and share this information with other software agents within the APS system in order to implement the generated schedule. The AIPS scheduler is also able to cooperatively recover from fault situations by rescheduling the affected loads on the Brassboard in conjunction with the APEX FDIR system. AIPS served as a learning tool and an initial scheduling testbed for the integration of FDIR and automated scheduling systems. Many lessons were learned from the AIPS scheduler and are now being integrated into a new scheduler called SCRAP (Scheduler for Continuous Resource Allocation and Planning). This paper will service three purposes: an overview of the AIPS implementation, lessons learned from the AIPS scheduler, and a brief section on how these lessons are being applied to the new SCRAP scheduler. Author

N93-19018*# National Aeronautics and Space Administration. Lewis Research Center, Cleveland, OH. Dept. of Mechanical Engineering.

REAL-TIME DIAGNOSTICS FOR A REUSABLE ROCKET ENGINE

T. H. GUO, W. MERRILL, and A. DUYAR (Florida Atlantic Univ., Boca Raton.) Aug. 1992 14 p
(Contract RTOP 582-01-41)
(NASA-TM-105792; E-7222; NAS 1.15:105792) Avail: CASI HC A03/MF A01

A hierarchical, decentralized diagnostic system is proposed for the Real-Time Diagnostic System component of the Intelligent Control System (ICS) for reusable rocket engines. The proposed diagnostic system has three layers of information processing: condition monitoring, fault mode detection, and expert system diagnostics. The condition monitoring layer is the first level of signal processing. Here, important features of the sensor data are extracted. These processed data are then used by the higher level fault mode detection layer to do preliminary diagnosis on potential faults at the component level. Because of the closely coupled nature of the rocket engine propulsion system components, it is expected that a given engine condition may trigger more than one fault mode detector. Expert knowledge is needed to resolve the conflicting reports from the various failure mode detectors. This is the function of the diagnostic expert layer. Here, the heuristic nature of this decision process makes it desirable to use an expert system approach. Implementation of the real-time diagnostic system described above requires a wide spectrum of information processing capability. Generally, in the condition monitoring layer, fast data processing is often needed for feature extraction and signal conditioning. This is usually followed by some detection logic to determine the selected faults on the component level. Three different techniques are used to attack different fault detection problems in the NASA LeRC ICS testbed simulation. The first technique employed is the neural network application for real-time sensor validation which includes failure detection, isolation, and accommodation. The second approach demonstrated is the model-based fault diagnosis system using on-line parameter identification. Besides these model based diagnostic schemes, there are still many failure modes which need to be diagnosed by the heuristic expert knowledge. The heuristic expert knowledge is implemented using a real-time expert system tool called G2 by Gensym Corp. Finally, the distributed diagnostic system requires another level of intelligence to oversee the fault mode reports generated by component fault detectors. The decision making at this level can best be done using a rule-based expert system. This level of expert knowledge is also implemented using G2.

Author

N93-22185*# National Aeronautics and Space Administration. Lewis Research Center, Cleveland, OH.

AN ARTIFICIAL INTELLIGENCE-BASED STRUCTURAL HEALTH MONITORING SYSTEM FOR AGING AIRCRAFT

JOSEPH E. GRADY, STANLEY S. TANG (Structural Integrity Associates, Inc., San Jose, CA.), and K. L. CHEN (Structural Integrity Associates, Inc., San Jose, CA.) In NASA, Washington, Technology 2002: The Third National Technology Transfer Conference and Exposition, Volume 2 p 343-351 Feb. 1993
Avail: CASI HC A02/MF A04

To reduce operating expenses, airlines are now using the existing fleets of commercial aircraft well beyond their originally anticipated service lives. The repair and maintenance of these 'aging aircraft' has therefore become a critical safety issue, both to the airlines and the Federal Aviation Administration. This paper presents the results of an innovative research program to develop a structural monitoring system that will be used to evaluate the integrity of in-service aerospace structural components. Currently in the final phase of its development, this monitoring system will indicate when repair or maintenance of a damaged structural component is necessary.

Author

N93-28051*# National Aeronautics and Space Administration. Lewis Research Center, Cleveland, OH.

A MODIFIED APPROACH TO CONTROLLER PARTITIONING
SANJAY GARG and ROBERT J. VEILLETTE (Akron Univ., OH.)
May 1993 25 p
(Contract RTOP 505-62-50)
(NASA-TM-106167; E-7861; NAS 1.15:106167) Avail: CASI HC A03/MF A01

The idea of computing a decentralized control law for the integrated flight/propulsion control of an aircraft by partitioning a given centralized controller is investigated. An existing controller partitioning methodology is described, and a modified approach is proposed with the objective of simplifying the associated controller approximation problem. Under the existing approach, the decentralized control structure is a variable in the partitioning process; by contrast, the modified approach assumes that the structure is fixed a priori. Hence, the centralized controller design may take the decentralized control structure into account. Specifically, the centralized controller may be designed to include all the same inputs and outputs as the decentralized controller; then, the two controllers may be compared directly, simplifying the partitioning process considerably. Following the modified approach, a centralized controller is designed for an example aircraft mode. The design includes all the inputs and outputs to be used in a specified decentralized control structure. However, it is shown that the resulting centralized controller is not well suited for approximation by a decentralized controller of the given structure. The results indicate that it is not practical in general to cast the controller partitioning problem as a direct controller approximation problem.

Author (revised)

N93-31557*# National Aeronautics and Space Administration. Lewis Research Center, Cleveland, OH.

NEURAL NETS FOR ALIGNING OPTICAL COMPONENTS IN HARSH ENVIRONMENTS: BEAM SMOOTHING SPATIAL FILTER AS AN EXAMPLE

ARTHUR J. DECKER and MICHAEL J. KRASOWSKI In its Structural Integrity and Durability of Reusable Space Propulsion Systems p 29-38 May 1991
Avail: CASI HC A02/MF A03

The goal is to develop an approach to automating the alignment and adjustment of optical measurement, visualization, inspection, and control systems. Classical controls, expert systems, and neural networks are three approaches to automating the alignment of an optical system. Neural networks were chosen for this project and the judgements that led to this decision are presented. Neural networks were used to automate the alignment of the ubiquitous laser-beam-smoothing spatial filter. The results and future plans of the project are presented.

Derived from text

NUMERICAL ANALYSIS

Includes iteration, difference equations, and numerical approximation.

A93-24231*# National Aeronautics and Space Administration. Lewis Research Center, Cleveland, OH.

AN EVALUATION OF THREE SPATIAL DIFFERENCING SCHEMES FOR THE DISCRETE ORDINATES METHOD IN PARTICIPATING MEDIA

JOHN C. CHAI (Minnesota Univ., Minneapolis), HAEOK S. LEE (NASA, Lewis Research Center, Cleveland, OH), and SUHAS V. PATANKAR (Minnesota Univ., Minneapolis) Jan. 1993 10 p.
AIAA, Aerospace Sciences Meeting and Exhibit, 31st, Reno, NV, Jan. 11-14, 1993 Research supported by Univ. of Minnesota refs
(Contract NCC3-238)
(AIAA PAPER 93-0140) Copyright

Three popular spatial differencing schemes for the discrete ordinates method are examined for two-dimensional Cartesian coordinates system. These are a positive, the step, and the diamond schemes. Contrary to the common belief that negative intensities will not occur when fine spatial discretization is used with the diamond scheme, under certain conditions, the diamond scheme will produce negative intensities irrespective of the number of control volumes employed. The positive scheme can produce physically unrealistic trends. The diamond and positive schemes are also capable of producing physically unrealistic overshoots. In absorbing-emitting or absorbing-emitting-scattering media, grid refinement can result in negative intensities when the diamond or positive scheme is used.

Author

A93-33899* National Aeronautics and Space Administration. Lewis Research Center, Cleveland, OH.

TRANSITION ELEMENTS BASED ON TRANSFINITE INTERPOLATION

ONUR R. ODABAS (Ohio State Univ., Columbus) and NESRIN SARIGUL-KLIJN (California Univ., Davis) *In* AIAA/ASME/ASCE/AHS/ASC Structures, Structural Dynamics, and Materials Conference, 34th and AIAA/ASME Adaptive Structures Forum, La Jolla, CA, Apr. 19-22, 1993, Technical Papers. Pt. 1 Washington American Institute of Aeronautics and Astronautics 1993 p. 266-272. refs (Contract NAG3-790)

(AIAA PAPER 93-1326) Copyright

In this study the transfinite interpolation methodology, a 'blending-function' method in particular, is utilized for the formulation of transition elements. The method offers a formal way of meeting continuity requirements in a transition element. Element shape functions are derived by blending the continuity requirements of individual boundary segments. The blending directions are naturally orthogonal in rectangular domains therefore interpolation of the boundaries over rectangular 2D and 3D elements can be performed with minimal effort. In triangular domains, however, the choice of blending directions and interpolants is not straightforward. For that reason, two interpolation techniques are proposed for blending of the boundaries of triangular domains. A series of transition elements of various classes compatible with elements of different orders and dimensions is developed and the full potential of the transfinite interpolation, as it applies to element formulation, is explored.

Author

A93-34034* National Aeronautics and Space Administration. Lewis Research Center, Cleveland, OH.

BINARY TREE EIGEN SOLVER IN FINITE ELEMENT ANALYSIS

F. A. AKL (Louisiana Tech Univ., Ruston), D. C. JANETZKE, and L. J. KIRALY (NASA, Lewis Research Center, Cleveland, OH) *In* AIAA/ASME/ASCE/AHS/ASC Structures, Structural Dynamics, and Materials Conference, 34th and AIAA/ASME Adaptive Structures Forum, La Jolla, CA, Apr. 19-22, 1993, Technical Papers. Pt. 3 Washington American Institute of Aeronautics and Astronautics 1993 p. 1607-1612. refs (AIAA PAPER 93-1493) Copyright

This paper presents a transputer-based binary tree eigensolver for the solution of the generalized eigenproblem in linear elastic finite element analysis. The algorithm is based on the method of recursive doubling, which parallel implementation of a number of associative operations on an arbitrary set having N elements is of the order of $O(\log 2N)$, compared to $(N-1)$ steps if implemented sequentially. The hardware used in the implementation of the binary tree consists of 32 transputers. The algorithm is written in OCCAM which is a high-level language developed with the transputers to address parallel programming constructs and to provide the communications between processors. The algorithm can be replicated to match the size of the binary tree transputer network. Parallel and sequential finite element analysis programs have been developed to solve for the set of the least-order eigenpairs using the modified subspace method. The speed-up obtained for a typical analysis problem indicates close agreement with the theoretical prediction given by the method of recursive doubling.

Author

A93-34166* National Aeronautics and Space Administration. Lewis Research Center, Cleveland, OH.

FINITE ELEMENT PROCEDURES FOR COUPLED LINEAR ANALYSIS OF HEAT TRANSFER, FLUID AND SOLID MECHANICS

EDHI SUTJAHJO (Sverdrup Technology, Inc., Brook Park, OH) and CHRISTOS C. CHAMIS (NASA, Lewis Research Center, Cleveland, OH) *In* AIAA/ASME/ASCE/AHS/ASC Structures, Structural Dynamics, and Materials Conference, 34th and AIAA/ASME Adaptive Structures Forum, La Jolla, CA, Apr. 19-22, 1993, Technical Papers. Pt. 5 Washington American Institute of Aeronautics and Astronautics 1993 p. 2919-2933. refs (AIAA PAPER 93-1639) Copyright

Coupled finite element formulations for fluid mechanics, heat transfer, and solid mechanics are derived from the conservation laws for energy, mass, and momentum. To model the physics of interactions among the participating disciplines, the linearized equations are coupled by combining domain and boundary coupling procedures. Iterative numerical solution strategy is presented to solve the equations, with the partitioning of temporal discretization implemented.

Author

A93-45074* National Aeronautics and Space Administration. Lewis Research Center, Cleveland, OH.

AN ASSESSMENT OF SPECTRAL NONOSCILLATORY SCHEMES

AMBADY SURESH (Sverdrup Technology, Inc.; NASA, Lewis Research Center, Cleveland, OH) *In* AIAA Computational Fluid Dynamics Conference, 11th, Orlando, FL, July 6-9, 1993, Technical Papers. Pt. 2 Washington American Institute of Aeronautics and Astronautics 1993 p. 917-928. refs (Contract NAS3-25266)

(AIAA PAPER 93-3383) Copyright

A new spectral nonoscillatory interpolation scheme is proposed that achieves spectral accuracy in smooth regions and is nonoscillatory on piecewise discontinuous data. The essential idea behind the scheme is to increase the order of an ENO scheme in proportion to the number of points, wherever possible. Numerical experiments with the new scheme on interpolation, 1D advection, and 1D gas dynamics confirm the high resolution features of the scheme. Comparisons with the results of earlier spectral nonoscillatory schemes show that the new scheme is competitive both in efficiency and accuracy.

Author

A93-45080* National Aeronautics and Space Administration. Lewis Research Center, Cleveland, OH.

GRID ADAPTATION USING CHIMERA COMPOSITE OVERLAPPING MESHES

KAI-HSIUNG KAO, MENG-SING LIOU (NASA, Lewis Research Center, Cleveland, OH), and CHUEN-YEN CHOW (Colorado Univ., Boulder) *In* AIAA Computational Fluid Dynamics Conference, 11th, Orlando, FL, July 6-9, 1993, Technical Papers. Pt. 2 Washington American Institute of Aeronautics and Astronautics 1993 p. 990-1001. Previously announced in STAR as N93-27065 refs

(Contract NCC3-168; NCC3-233; RTOP 505-90-5X) (AIAA PAPER 93-3389)

The objective of this paper is to perform grid adaptation using composite over-lapping meshes in regions of large gradient to capture the salient features accurately during computation. The Chimera grid scheme, a multiple oversight mesh technique, is used in combination with a Navier-Stokes solver. The numerical solution is first converged to a steady state based on an initial coarse mesh. Solution-adaptive enhancement is then performed by using a secondary fine grid system which oversets on top of the base grid in the high-gradient region, but without requiring the mesh boundaries to join in any special way. Communications through boundary interfaces between those separated grids are carried out using tri-linear interpolation. Applications to the Euler equations for shock reflections and to a shock wave/boundary layer interaction problem are tested. With the present method, the salient features are well resolved.

Author

A93-45967 National Aeronautics and Space Administration. Lewis Research Center, Cleveland, OH.

ALGEBRAIC GRID GENERATION WITH CONTROL POINTS

PETER R. EISEMAN (Columbia Univ., New York), YUNG K. CHOO (NASA, Lewis Research Center, Cleveland, OH), and ROBERT E. SMITH (NASA, Langley Research Center, Hampton, VA) /n Finite elements in fluids. Vol. 8 Washington Hemisphere Publishing Corp. 1992 p. 97-116. refs

Copyright

The control-point form (CPF) formulation is an algebraically defined class of coordinate transformations by means of which the interior form of the coordinates can be manipulated in the local fashion, and any boundary can be either specified or manipulated in a similar manner. Currently, the most intense activity involving CPF is with such graphic interactive codes as TurboI and TurboT, for which detailed illustrative examples are given; these have furnished experience on whose basis future interactive strategies can be developed.

AIAA

A93-54198* National Aeronautics and Space Administration. Lewis Research Center, Cleveland, OH.

SYMMETRIC GALERKIN BOUNDARY FORMULATIONS EMPLOYING CURVED ELEMENTS

J. H. KANE and C. BALAKRISHNA (Clarkson Univ., Potsdam, NY) International Journal for Numerical Methods in Engineering (ISSN 0029-5981) vol. 36, no. 13 July 15, 1993 p. 2157-2187. refs

(Contract NAG3-1089; NSF DDM-90-19852)

Copyright

Accounts of the symmetric Galerkin approach to boundary element analysis (BEA) have recently been published. This paper attempts to add to the understanding of this method by addressing a series of fundamental issues associated with its potential computational efficiency. A new symmetric Galerkin theoretical formulation for both the (harmonic) heat conduction and the (biharmonic) elasticity problem that employs regularized singular and hypersingular boundary integral equations (BIEs) is presented. The novel use of regularized BIEs in the Galerkin context is shown to allow straightforward incorporation of curved, isoparametric elements. A symmetric reusable intrinsic sample point (RISP) numerical integration algorithm is shown to produce a Galerkin (i.e., double) integration strategy that is competitive with its counterpart (i.e., singular) integration procedure in the collocation BEA approach when the time saved in the symmetric equation solution phase is also taken into account. This new formulation is shown to be capable of employing hypersingular BIEs while obviating the requirement of C^1 continuity, a fact that allows the employment of the popular continuous element technology. The behavior of the symmetric Galerkin BEA method with regard to both direct and iterative equation solution operations is also addressed. A series of example problems are presented to quantify the performance of this symmetric approach, relative to the more conventional unsymmetric BEA, in terms of both accuracy and efficiency. It is concluded that appropriate implementations of the symmetric Galerkin approach to BEA indeed have the potential to be competitive with, if not superior to, collocation-based BEA, for large-scale problems.

N93-11254* National Aeronautics and Space Administration. Lewis Research Center, Cleveland, OH.

ON AN ORIGIN OF NUMERICAL DIFFUSION: VIOLATION OF INVARIANCE UNDER SPACE-TIME INVERSION

SIN-CHUNG CHANG Jul. 1992 14 p Presented at the 23rd Modeling and Simulation Conference, Pittsburgh, PA, 30 Apr. - 1 May 1992

(Contract RTOP 505-62-52)

(NASA-TM-105776; E-7066; NAS 1.15:105776) Avail: CASI HC A03/MF A01

The invariant properties of the convection equation $du/dt + adu/dx = 0$ (where d is the partial differential operator) with respect to spatial reflection, time reversal, and space-time inversion are studied. Generally, a finite-difference analog of this equation may possess some or none of these properties. It is shown that, under

certain conditions, the von Neumann amplification factor of an analog satisfies a special relation for each invariant property this analog possesses. Particularly, an analog is neutrally stable and thus free of numerical diffusion if it possesses the invariant property related to space-time inversion. It is also explained why generally (1) an upwind scheme possesses neither the invariant property related to spatial reflection nor that related to space-time inversion, and (2) an explicit scheme possesses neither the invariant property related to time reversal nor that related to space-time inversion. Extension to the viscous case and a remarkable connection between the current work and a new numerical framework for solving conservation laws are also discussed.

Author

N93-11531* National Aeronautics and Space Administration. Lewis Research Center, Cleveland, OH.

COMPARISON OF TRUNCATION ERROR OF FINITE-DIFFERENCE AND FINITE-VOLUME FORMULATIONS OF CONVECTION TERMS

B. P. LEONARD (Akron Univ., OH.) Sep. 1992 15 p (Contract NCC3-233; RTOP 505-62-21)

(NASA-TM-105861; ICOMP-92-19; E-7321; NAS 1.15:105861)

Avail: CASI HC A03/MF A01

Judging by errors in the computational-fluid-dynamics literature in recent years, it is not generally well understood that (above first-order) there are significant differences in spatial truncation error between formulations of convection involving a finite-difference approximation of the first derivative, on the one hand, and a finite-volume model of flux differences across a control-volume cell, on the other. The difference between the two formulations involves a second-order truncation-error term (proportional to the third-derivative of the convected variable). Hence, for example, a third (or higher) order finite-difference approximation for the first-derivative convection term is only second-order accurate when written in conservative control-volume form as a finite-volume formulation, and vice versa.

Author

N93-15341* National Aeronautics and Space Administration. Lewis Research Center, Cleveland, OH.

ENO-OSHER SCHEMES FOR EULER EQUATIONS

JACOBUS J. VANDERVEGT (Stanford Univ., CA.) Nov. 1992 13 p Presented at the 31st Aerospace Science Meeting and Exhibit, Reno, NV, 11-14 Jan. 1993; sponsored by AIAA (Contract NASA ORDER C-99066-G; RTOP 505-62-21) (NASA-TM-105928; E-7435; NAS 1.15:105928; ICOMP-92-21; CMOTT-92-10; AIAA PAPER 92-0335) Avail: CASI HC A03/MF A01

The combination of the Osher approximate Riemann solver for the Euler equations and various ENO schemes is discussed for one-dimensional flow. The three basic approaches, viz. the ENO scheme using primitive variable reconstruction, either with Cauchy-Kowalewski procedure for time integration or the TVD Runge-Kutta scheme, and the flux-ENO method are tested on different shock tube cases. The shock tube cases were chosen to present a serious challenge to the ENO schemes in order to test their ability to capture flow discontinuities, such as shocks. Also the effect of the ordering of the eigen values, viz. natural or reversed ordering, in the Osher scheme is investigated. The ENO schemes are tested up to fifth order accuracy in space and time. The ENO-Osher scheme using the Cauchy-Kowalewski procedure for time integration is found to be the most accurate and robust compared with the other methods and is also computationally efficient. The tests showed that the ENO schemes perform reasonably well, but have problems in cases where two discontinuities are close together. In that case there are not enough points in the smooth part of the flow to create a non-oscillatory interpolation.

Author

N93-22664* National Aeronautics and Space Administration. Lewis Research Center, Cleveland, OH.

A TIME-ACCURATE HIGH-RESOLUTION TVD SCHEME FOR SOLVING THE NAVIER-STOKES EQUATIONS

HYUN DAE KIM and NAN-SUEY LIU Dec. 1992 26 p Original contains color illustrations

(Contract RTOP 505-62-52)

(NASA-TM-106056; E-7466; NAS 1.15:106056) Avail: CASI HC A03/MF A01; 4 functional color pages

A total variation diminishing (TVD) scheme has been developed and incorporated into an existing time-accurate high-resolution Navier-Stokes code. The accuracy and the robustness of the resulting solution procedure have been assessed by performing many calculations in four different areas: shock tube flows, regular shock reflection, supersonic boundary layer, and shock boundary layer interactions. These numerical results compare well with corresponding exact solutions or experimental data.

Author (revised)

N93-22825*# National Aeronautics and Space Administration. Lewis Research Center, Cleveland, OH.

LARGE-SCALE COMPUTATION OF INCOMPRESSIBLE VISCOUS FLOW BY LEAST-SQUARES FINITE ELEMENT METHOD

BO-NAN JIANG, T. L. LIN (Livermore Software Technology Corp., CA.), and LOUIS A. POVINELLI Mar. 1993 22 p

(Contract NCC3-233; RTOP 505-62-21)
(NASA-TM-105904; E-7667; NAS 1.15:105904; ICOMP-93-06)
Avail: CASI HC A03/MF A01

The least-squares finite element method (LSFEM) based on the velocity-pressure-vorticity formulation is applied to large-scale/three-dimensional steady incompressible Navier-Stokes problems. This method can accommodate equal-order interpolations and results in symmetric, positive definite algebraic system which can be solved effectively by simple iterative methods. The first-order velocity-Bernoulli function-vorticity formulation for incompressible viscous flows is also tested. For three-dimensional cases, an additional compatibility equation, i.e., the divergence of the vorticity vector should be zero, is included to make the first-order system elliptic. The simple substitution of the Newton's method is employed to linearize the partial differential equations, the LSFEM is used to obtain discretized equations, and the system of algebraic equations is solved using the Jacobi preconditioned conjugate gradient method which avoids formation of either element or global matrices (matrix-free) to achieve high efficiency. To show the validity of this scheme for large-scale computation, we give numerical results for 2D driven cavity problem at $Re = 10000$ with 408×400 bilinear elements. The flow in a 3D cavity is calculated at $Re = 100, 400$, and $1,000$ with $50 \times 50 \times 50$ trilinear elements. The Taylor-Goertler-like vortices are observed for $Re = 1,000$.

Author

N93-26560*# National Aeronautics and Space Administration. Lewis Research Center, Cleveland, OH.

A BRIEF DESCRIPTION OF A NEW NUMERICAL FRAMEWORK FOR SOLVING CONSERVATION LAWS: THE METHOD OF SPACE-TIME CONSERVATION ELEMENT AND SOLUTION ELEMENT

SIN-CHUNG CHANG and WAI-MING TO (Sverdrup Technology, Inc., Brook Park, OH.) Jul. 1992 17 p Presented at the 13th International Conference on Numerical Methods in Fluid Dynamics, Rome, Italy, 6-10 Jul. 1992

(Contract RTOP 505-62-52)
(NASA-TM-105757; E-7169; NAS 1.26:105757) Avail: CASI HC A03/MF A01

A new numerical method for solving conservation laws is being developed. It differs substantially from the well established methods, i.e., finite difference, finite volume, finite element, and spectral methods, in both concept and methodology. It is much simpler than a typical high resolution method. No flux limiter or any technique related to characteristics is involved. No artificial viscosity or smoothing is introduced, and no moving mesh is used. Yet this method is capable of generating highly accurate shock tube solutions. The slight numerical overshoot and/or oscillations generated can be removed if a simple averaging formula initially used is replaced by a weighted formula. This modification has little effect on other parts of the solution. Because of its simplicity, generalization of this new method for multi-dimensional problems is straightforward.

Derived from text

N93-27061*# National Aeronautics and Space Administration. Lewis Research Center, Cleveland, OH.

INSTITUTE FOR COMPUTATIONAL MECHANICS IN PROPULSION (ICOMP) Annual Report No. 7, 1992

CHARLES E. FEILER, comp. May 1993 56 p

(Contract NCC3-233; RTOP 509-90-5K)
(NASA-TM-106155; ICOMP-93-01; E-7839; NAS 1.15:106155)
Avail: CASI HC A04/MF A01

The Institute for Computational Mechanics in Propulsion (ICOMP) was established at the NASA Lewis Research Center in Cleveland, Ohio to develop techniques to improve problem-solving capabilities in all aspects of computational mechanics related to propulsion. The activities at ICOMP during 1992 are described.

Author

N93-27065*# National Aeronautics and Space Administration. Lewis Research Center, Cleveland, OH.

GRID ADAPTION USING CHIMERA COMPOSITE OVERLAPPING MESHES

KAI-HSIUNG KAO, MENG-SING LIOU, and CHUEN-YEN CHOW (Colorado Univ., Boulder.) May 1993 34 p Proposed for presentation at the 11th AIAA Computational Fluid Dynamics Conference, Orlando, FL, 6-9 Jul. 1993

(Contract NCC3-233; RTOP 505-90-5X)
(NASA-TM-106163; ICOMP-93-16; E-7855; NAS 1.15:106163; AIAA PAPER 93-3389) Avail: CASI HC A03/MF A01

The objective of this paper is to perform grid adaptation using composite overlapping meshes in regions of large gradient to capture the salient features accurately during computation. The Chimera grid scheme, a multiple overset mesh technique, is used in combination with a Navier-Stokes solver. The numerical solution is first converged to a steady state based on an initial coarse mesh. Solution-adaptive enhancement is then performed by using a secondary fine grid system which oversets on top of the base grid in the high-gradient region, but without requiring the mesh boundaries to join in any special way. Communications through boundary interfaces between those separated grids are carried out using tri-linear interpolation. Applications to the Euler equations for shock reflections and to a shock wave/boundary layer interaction problem are tested. With the present method, the salient features are well resolved.

Author (revised)

N93-27068*# National Aeronautics and Space Administration. Lewis Research Center, Cleveland, OH.

ON THE ACCURATE LONG-TIME SOLUTION OF THE WAVE EQUATION IN EXTERIOR DOMAINS: ASYMPTOTIC EXPANSIONS AND CORRECTED BOUNDARY CONDITIONS

THOMAS HAGSTROM (New Mexico Univ., Albuquerque.), S. I. HARIHARAN (Akron Univ., OH.), and R. C. MACCAMY (Carnegie-Mellon Univ., Pittsburgh, PA.) Apr. 1993 45 p

(Contract NCC3-233; RTOP 505-90-54)
(NASA-TM-106117; ICOMP-93-4; E-7772; NAS 1.15:106117)
Avail: CASI HC A03/MF A01

We consider the solution of scattering problems for the wave equation using approximate boundary conditions at artificial boundaries. These conditions are explicitly viewed as approximations to an exact boundary condition satisfied by the solution on the unbounded domain. We study the short and long term behavior of the error. It is provided that, in two space dimensions, no local in time, constant coefficient boundary operator can lead to accurate results uniformly in time for the class of problems we consider. A variable coefficient operator is developed which attains better accuracy (uniformly in time) than is possible with constant coefficient approximations. The theory is illustrated by numerical examples. We also analyze the proposed boundary conditions using energy methods, leading to asymptotically correct error bounds.

Author

N93-31847*# National Aeronautics and Space Administration. Lewis Research Center, Cleveland, OH.

DESKTOP CHAOTIC SYSTEMS: INTUITION AND VISUALIZATION

MICHELLE M. BRIGHT, KEVIN J. MELCHER, HELEN K. GAMMAR

(Akron Univ., OH.), and TOM T. HARTLEY (Akron Univ., OH.)
 Jul. 1993 14 p Presented at the SPIE International Symposium
 on Chaos/Nonlinear Dynamics, San Diego, CA, 11-16 Jul. 1993;
 sponsored by the Society of Photo-Optical Instrumentation
 Engineers
 (Contract RTOP 505-62-50)
 (NASA-TM-106258; E-7983; NAS 1.15:106258) Avail: CASI HC
 A03/MF A01

This paper presents a dynamic study of the Wildwood Pendulum,
 a commercially available desktop system which exhibits a strange
 attractor. The purpose of studying this chaotic pendulum is twofold:
 to gain insight in the paradigmatic approach of modeling, simulating,
 and determining chaos in nonlinear systems; and to provide a
 desktop model of chaos as a visual tool. For this study, the
 nonlinear behavior of this chaotic pendulum is modeled, a computer
 simulation is performed, and an experimental performance is
 measured. An assessment of the pendulum in the phase plane
 shows the strange attractor. Through the use of a box-assisted
 correlation dimension methodology, the attractor dimension is
 determined for both the model and the experimental pendulum
 systems. Correlation dimension results indicate that the pendulum
 and the model are chaotic and their fractal dimensions are
 similar. Author

N93-32200* National Aeronautics and Space Administration.
 Lewis Research Center, Cleveland, OH.

A CRITICAL COMPARISON OF SEVERAL LOW REYNOLDS NUMBER K-EPSILON TURBULENCE MODELS FOR FLOW OVER A BACKWARD FACING STEP

C. J. STEFFEN, JR. Jun. 1993 15 p Presented at the AIAA
 29th Joint Propulsion Conference and Exhibit, Monterey, CA, 28-30
 Jun. 1993; sponsored by AIAA, SAE, ASME, and ASEE
 (Contract NCC3-233; RTOP 505-90-5K)
 (NASA-TM-106173; AIAA PAPER 93-1927; CMOTT-93-9; E-7873;
 NAS 1.15:106173) Avail: CASI HC A03/MF A01

Turbulent backward-facing step flow was examined using four
 low turbulent Reynolds number k-epsilon models and one standard
 high Reynolds number technique. A tunnel configuration of 1:9
 (step height: exit tunnel height) was used. The models tested
 include: the original Jones and Launder; Chien; Launder and
 Sharma; and the recent Shih and Lumley formulation. The
 experimental reference of Driver and Seegmiller was used to make
 detailed comparisons between reattachment length, velocity,
 pressure, turbulent kinetic energy, Reynolds shear stress, and skin
 friction predictions. The results indicated that the use of a wall
 function for the standard k-epsilon technique did not reduce the
 calculation accuracy for this separated flow when compared to
 the low turbulent Reynolds number techniques. Author (revised)

65

STATISTICS AND PROBABILITY

Includes data sampling and smoothing; Monte Carlo method; and
 stochastic processes.

N93-27124* National Aeronautics and Space Administration.
 Lewis Research Center, Cleveland, OH.

BASIC STATISTICAL ANALYSES OF CANDIDATE NICKEL-HYDROGEN CELLS FOR THE SPACE STATION FREEDOM

THOMAS M. MALONEY (Sverdrup Technology, Inc., Brook Park,
 OH.) and DAVID T. FRATE May 1993 76 p
 (NASA-TM-106111; E-7762; NAS 1.15:106111) Avail: CASI HC
 A05/MF A01

Nickel-Hydrogen (Ni/H₂) secondary batteries will be
 implemented as a power source for the Space Station Freedom
 as well as for other NASA missions. Consequently, characterization
 tests of Ni/H₂ cells from Eagle-Picher, Whittaker-Yardney, and
 Hughes were completed at the NASA Lewis Research Center.

Watt-hour efficiencies of each Ni/H₂ cell were measured for
 regulated charge and discharge cycles as a function of temperature,
 charge rate, discharge rate, and state of charge. Temperatures
 ranged from -5 C to 30 C, charge rates ranged from C/10 to 1C,
 discharge rates ranged from C/10 to 2C, and states of charge
 ranged from 20 percent to 100 percent. Results from regression
 analyses and analyses of mean watt-hour efficiencies demonstrated
 that overall performance was best at temperatures between 10 C
 and 20 C while the discharge rate correlated most strongly with
 watt-hour efficiency. In general, the cell with back-to-back electrode
 arrangement, single stack, 26 percent KOH, and serrated zircar
 separator and the cell with a recirculating electrode arrangement,
 unit stack, 31 percent KOH, zircar separators performed best.
 Author (revised)

66

SYSTEMS ANALYSIS

Includes mathematical modeling; network analysis; and operations
 research.

A93-20312* National Aeronautics and Space Administration.
 Lewis Research Center, Cleveland, OH.

NUMERICAL OPTIMIZATION OF COMPOSITE HIP ENDOPROSTHESES UNDER DIFFERENT LOADING CONDITIONS

T. A. BLAKE, D. T. DAVY (Case Western Reserve Univ., Cleveland,
 OH), D. A. SARAVANOS, and D. A. HOPKINS (NASA, Lewis
 Research Center, Cleveland, OH) In AIAA/USAF/NASA/OAI
 Symposium on Multidisciplinary Analysis and Optimization, 4th,
 Cleveland, OH, Sept. 21-23, 1992, Technical Papers. Pt. 1
 Washington American Institute of Aeronautics and Astronautics
 1992 p. 119-129. refs
 (AIAA PAPER 92-4703) Copyright

The optimization of composite hip implants was investigated.
 Emphasis was placed on the effect of shape and material tailoring
 of the implant to improve the implant-bone interaction. A variety
 of loading conditions were investigated to better understand the
 relationship between loading and optimization outcome.
 Comparisons of the initial and optimal models with more complex
 3D finite element models were performed. The results indicate
 that design improvements made using this method result in similar
 improvements in the 3D models. Although the optimization
 outcomes were significantly affected by the choice of loading
 conditions, certain trends were observed that were independent
 of the applied loading. Author

A93-20318* National Aeronautics and Space Administration.
 Lewis Research Center, Cleveland, OH.

MULTIDISCIPLINARY PROPULSION SIMULATION USING NPSS

RUSSELL W. CLAUS, AUSTIN L. EVANS, and GREGORY J.
 FOLLEN (NASA, Lewis Research Center, Cleveland, OH) In
 AIAA/USAF/NASA/OAI Symposium on Multidisciplinary Analysis
 and Optimization, 4th, Cleveland, OH, Sept. 21-23, 1992, Technical
 Papers. Pt. 1 Washington American Institute of Aeronautics
 and Astronautics 1992 p. 191-196. refs
 (AIAA PAPER 92-4709) Copyright

The current status of the Numerical Propulsion System
 Simulation (NPSS) program, a cooperative effort of NASA, industry,
 and universities to reduce the cost and time of advanced technology
 propulsion system development, is reviewed. The technologies
 required for this program include (1) interdisciplinary analysis to
 couple the relevant disciplines, such as aerodynamics, structures,
 heat transfer, combustion, acoustics, controls, and materials; (2)
 integrated systems analysis; (3) a high-performance computing
 platform, including massively parallel processing; and (4) a
 simulation environment providing a user-friendly interface. Several

research efforts to develop these technologies are discussed. V.L.

A93-49930*# National Aeronautics and Space Administration. Lewis Research Center, Cleveland, OH.

STRUCTURED SYSTEM ENGINEERING METHODOLOGIES USED TO DEVELOP A NUCLEAR THERMAL PROPULSION ENGINE

R. CORBAN (NASA, Lewis Research Center, Cleveland, OH) and R. WAGNER (Analytical Engineering Corp., North Olmsted, OH) Jun. 1993 7 p. AIAA, SAE, ASME, and ASEE, Joint Propulsion Conference and Exhibit, 29th, Monterey, CA, June 28-30, 1993 refs

(AIAA PAPER 93-2109)

To facilitate the development of a space nuclear thermal propulsion engine for manned flights to Mars, requirements must be established early in the technology development cycle. The long lead times for the acquisition of the engine system and nuclear test facilities demands that the engine system size, performance and safety goals be defined at the earliest possible time. These systems are highly complex and require a large multidisciplinary systems engineering team to develop and track requirements, and to ensure that the as-built system reflects the intent of the mission. A methodology has been devised which uses sophisticated computer tools to effectively develop and interpret functional requirements, and furnish these to the specification level for implementation.

Author (revised)

N93-22559*# National Aeronautics and Space Administration. Lewis Research Center, Cleveland, OH.

DYNAMIC ANALYSIS OF FREE-PISTON STIRLING ENGINE/LINEAR ALTERNATOR-LOAD SYSTEM-EXPERIMENTALLY VALIDATED

M. DAVID KANKAM, JEFFREY S. RAUCH (Sverdrup Technology, Inc., Brook Park, OH.), and WALTER SANTIAGO Aug. 1992 11 p. Presented at the 27th Intersociety Energy Conversion Engineering Conference, San Diego, CA, 3-7 Aug. 1992; sponsored by ANS, SAE, ASC, AIAA, IEEE, and AICHE

(Contract RTOP 590-13-11)

(NASA-TM-106034; E-7017; NAS 1.15:106034) Avail: CASI HC A03/MF A01

This paper discusses the effects of variations in system parameters on the dynamic behavior of the Free-Piston Stirling Engine/Linear Alternator (FPSE/LA)-load system. The mathematical formulations incorporate both the mechanical and thermodynamic properties of the FPSE, as well as the electrical equations of the connected load. A state-space technique in the frequency domain is applied to the resulting system of equations to facilitate the evaluation of parametric impacts on the system dynamic stability. Also included is a discussion on the system transient stability as affected by sudden changes in some key operating conditions. Some representative results are correlated with experimental data to verify the model and analytic formulation accuracies. Guidelines are given for ranges of the system parameters which will ensure an overall stable operation. Author

N93-23016*# National Aeronautics and Space Administration. Lewis Research Center, Cleveland, OH.

MODELLING A SINGLE PHASE VOLTAGE CONTROLLED RECTIFIER USING LAPLACE TRANSFORMS

L. ALAN KRAFT (Valparaiso Univ., IN.) and M. DAVID KANKAM Sep. 1992 8 p. Presented at the 5th International Conference on Harmonics in Power Systems, Atlanta, GA, 22-25 Sep. 1992; sponsored by IEEE

(Contract RTOP 506-41-41)

(NASA-TM-106005; E-7552; NAS 1.15:106005) Avail: CASI HC A02/MF A01

The development of a 20 kHz, AC power system by NASA for large space projects has spurred a need to develop models for the equipment which will be used on these single phase systems. To date, models for the AC source (i.e., inverters) have been developed. It is the intent of this paper to develop a method to model the single phase voltage controlled rectifiers which will be

attached to the AC power grid as an interface for connected loads. A modified version of EPRI's HARMFLO program is used as the shell for these models. The results obtained from the model developed in this paper are quite adequate for the analysis of problems such as voltage resonance. The unique technique presented in this paper uses the Laplace transforms to determine the harmonic content of the load current of the rectifier rather than a curve fitting technique. Laplace transforms yield the coefficient of the differential equations which model the line current to the rectifier directly.

Author

N93-31145*# National Aeronautics and Space Administration. Lewis Research Center, Cleveland, OH.

MINIMIZE SYSTEM COST BY CHOOSING OPTIMAL SUBSYSTEM RELIABILITY AND REDUNDANCY

RONALD C. SUICH (California State Univ., Fullerton.) and RICHARD L. PATTERSON Jan. 1993 7 p. Presented at the Reliability and Maintainability Symposium, Atlanta, GA, 25-28 Jan. 1993

(Contract RTOP 506-41-41)

(NASA-TM-106251; E-7973; NAS 1.15:106251) Avail: CASI HC A02/MF A01

The basic question which we address in this paper is how to choose among competing subsystems. This paper utilizes both reliabilities and costs to find the subsystems with the lowest overall expected cost. The paper begins by reviewing some of the concepts of expected value. We then address the problem of choosing among several competing subsystems. These concepts are then applied to k-out-of-n: G subsystems. We illustrate the use of the authors' basic program in viewing a range of possible solutions for several different examples. We then discuss the implications of various solutions in these examples.

Author

70

PHYSICS (GENERAL)

A93-32222* National Aeronautics and Space Administration. Lewis Research Center, Cleveland, OH.

NDE OF THE UNIVERSE - NEW WAYS TO LOOK AT OLD FACTS

ALEX VARY (NASA, Lewis Research Center, Cleveland, OH) Materials Evaluation (ISSN 0025-5327) vol. 51, no. 3 March 1993 p. 380-387. refs

Copyright

The paper investigates the relation between cosmology and NDE, emphasizing the need for new approaches and models imposed by new space-age materials. These are frontier materials with tailored microstructures and specially designed properties, such as the ceramic and intermetallic matrix composites for very high temperature power and propulsion systems. These materials require new NDE approaches, which are discussed in this paper.

AIAA

71

ACOUSTICS

Includes sound generation, transmission, and attenuation.

A93-19169* National Aeronautics and Space Administration. Lewis Research Center, Cleveland, OH.

AN ASYMPTOTIC THEORY OF SUPERSONIC PROPELLER NOISE

EDMANE ENVIA (Sverdrup Technology, Inc., Brook Park; NASA,

Lewis Research Center, Cleveland, OH) *In* DGLR/AIAA Aeroacoustics Conference, 14th, Aachen, Germany, May 11-14, 1992, Proceedings. Vol. 1 Bonn Deutsche Gesellschaft fuer Luft- und Raumfahrt 1992 p. 374-382. refs
(Contract NAS3-25266)

A theory for predicting the noise field of a propeller with a realistic blade geometry is presented. The theory, which utilizes a large blade count approximation, provides an efficient formula for predicting the radiation of sound from all three sources of propeller noise. Comparisons with full numerical integration indicate that the noise levels predicted by this formula are quite accurate. Calculations based on this method also show that the radiation from the Lighthill quadrupole source is rather substantial when compared with thickness and loading noise for high speed propellers. A preliminary application of the theory to the problem of the sensitivity of the peak noise levels generated by a supersonic propeller to the variations in its tip helical Mach number has produced a trend that is in qualitative agreement with the experimental observations. Author

A93-19181* National Aeronautics and Space Administration. Lewis Research Center, Cleveland, OH.

INFLUENCE OF AIRFOIL THICKNESS ON SOUND GENERATED BY HIGH-FREQUENCY GUST INTERACTIONS

C. T. TSAI and E. J. KERSCHEN (Arizona Univ., Tucson) *In* DGLR/AIAA Aeroacoustics Conference, 14th, Aachen, Germany, May 11-14, 1992, Proceedings. Vol. 1 Bonn Deutsche Gesellschaft fuer Luft- und Raumfahrt 1992 p. 486-495. refs
(Contract NAG3-357)

The sound radiated by interaction of a short wavelength gust with a symmetric thin airfoil is analyzed. The theory is based on a linearization of the Euler equations about the subsonic mean flow past the airfoil. The sound generation mechanism is found to be concentrated in a local region surrounding the parabolic nose of the airfoil; the size of this local region scales on the gust wavelength. At low Mach numbers, moderate values of airfoil thickness decrease the sound power, while at higher Mach numbers the sound power tends to increase with airfoil thickness. Airfoil thickness produces dramatic changes in the far field directivity. Both the sound power and the directivity are strong functions of the gust orientation. Author

A93-19205* National Aeronautics and Space Administration. Lewis Research Center, Cleveland, OH.

SUPERSONIC JET NOISE REDUCTION BY COAXIAL RECTANGULAR NOZZLES

K. K. AHUJA, J. P. MANES, and K. C. MASSEY (Georgia Inst. of Technology, Atlanta) *In* DGLR/AIAA Aeroacoustics Conference, 14th, Aachen, Germany, May 11-14, 1992, Proceedings. Vol. 2 Bonn Deutsche Gesellschaft fuer Luft- und Raumfahrt 1992 p. 752-760. refs
(Contract NAG3-1066)

A physical understanding of noise reduction mechanisms in supersonic, single, and coaxial rectangular jets is quantified and obtained, with emphasis on shock noise reduction. For all conditions, corresponding acoustic measurements for an equivalent round jet are also obtained so that the noise characteristics of the two types of jets can be compared directly to quantify the noise reductions. Comparisons are thus provided for a single rectangular nozzle vs a single equivalent round nozzle, and a coaxial rectangular nozzle vs an equivalent round nozzle. It is shown that different operating conditions and nozzle arrangements for the same thrust, total exit area, and mass flow rate can produce different noise levels. With at least one stream operated supersonically, the coaxial rectangular nozzle operated in the inverted-velocity profile is always quieter than in the normal velocity profile mode for the same thrust, exit area, and mass flow rate. In general, the coaxial rectangular nozzle is shown to be quieter than an equivalent circular nozzle only for those conditions for which both nozzles are operated supersonically. C.A.B.

A93-19804* National Aeronautics and Space Administration. Lewis Research Center, Cleveland, OH.

ACCURACY CONSIDERATIONS IN THE COMPUTATIONAL ANALYSIS OF JET NOISE

JAMES N. SCOTT (Ohio State Univ., Columbus) Jan. 1993 14 p. AIAA, Aerospace Sciences Meeting and Exhibit, 31st, Reno, NV, Jan. 11-14, 1993 refs
(Contract NAG3-1058)
(AIAA PAPER 93-0146) Copyright

The application of computational fluid dynamics methods to the analysis of problems in aerodynamic noise has resulted in the extension and adaptation of conventional CFD to the discipline now referred to as computational aeroacoustics (CAA). In the analysis of jet noise accurate resolution of a wide range of spatial and temporal scales in the flow field is essential if the acoustic far field is to be predicted. The numerical simulation of unsteady jet flow has been successfully demonstrated and many flow features have been computed with reasonable accuracy. Grid refinement and increased solution time are discussed as means of improving accuracy of Navier-Stokes solutions of unsteady jet flow. In addition various properties of different numerical procedures which influence accuracy are examined with particular emphasis on dispersion and dissipation characteristics. These properties are investigated by using selected schemes to solve model problems for the propagation of a shock wave and a sinusoidal disturbance. The results are compared for the different schemes. Author

A93-20134* National Aeronautics and Space Administration. Lewis Research Center, Cleveland, OH.

MANIPULATION OF UPSTREAM ROTOR LEADING EDGE VORTEX AND ITS EFFECTS ON COUNTER ROTATING PROPELLER NOISE

BECKY SQUIRES (North Carolina State Univ., Raleigh) Jan. 1993 11 p. AIAA, Aerospace Sciences Meeting and Exhibit, 31st, Reno, NV, Jan. 11-14, 1993 refs
(Contract NAG3-855)
(AIAA PAPER 93-0012) Copyright

The leading edge vortex of a counter rotating propeller (CRP) model was altered by using shrouds and by turning the upstream rotors to a forward sweep configuration. Performance, flow, and acoustic data were used to determine the effect of vortex impingement on the noise signature of the CRP system. Forward sweep was found to eliminate the leading edge vortex of the upstream blades. Removal of the vortex had little effect on the tone noise at the forward and rear blade passing frequencies (BPF's) but significantly altered both the sound pressure level and directivity of the interaction tone which occurs at the sum of the two BPF's. A separate manipulation of the leading edge vortex performed by installing shrouds of various inlet length on the CRP verified that diverting the vortex path increases the noise level of the interaction tone. An unexpected link has been established between the interaction tone and the leading edge vortex-blade interaction phenomenon. Author

A93-23241# National Aeronautics and Space Administration. Lewis Research Center, Cleveland, OH.

PROPAGATION OF HIGH FREQUENCY JET NOISE USING GEOMETRIC ACOUSTICS

A. KHAVARAN (Sverdrup Technology, Inc., Brook Park, OH) and E. A. KREJSA (NASA, Lewis Research Center, Cleveland, OH) Jan. 1993 17 p. AIAA, Aerospace Sciences Meeting and Exhibit, 31st, Reno, NV, Jan. 11-14, 1993 Previously announced in STAR as N93-15575 refs
(Contract RTOP 537-02-23)
(AIAA PAPER 93-0147) Copyright

Spherical directivity of noise radiated from a convecting quadrupole source embedded in an arbitrary spreading jet is obtained by ray-tracing methods of geometrical acoustics. The six propagation equations are solved in their general form in a rectangular coordinate system. The noise directivity in the far field is calculated by applying an iteration scheme that finds the required radiation angles at the source resulting in propagation through a given observer point. Factors influencing the zone of silence are

investigated. The caustics of geometrical acoustics and the exact locations where it forms is demonstrated by studying the variation in ray tube area obtained from transport equation. For a ring source convecting along the center-axis of an axisymmetric jet, the polar directivity of the radiated noise is obtained by an integration with respect to azimuthal directivity of compact quadrupole sources distributed on the ring. The Doppler factor is shown to vary slightly from point to point on the ring. Finally the scaling of the directivity pattern with power -3 of Doppler factor is investigated and compared with experimental data. Author

A93-23535* National Aeronautics and Space Administration. Lewis Research Center, Cleveland, OH.

ACOUSTIC RADIATION FROM A THIN AIRFOIL IN NONUNIFORM SUBSONIC FLOWS

H. M. ATASSI, M. DUSEY, and C. M. DAVIS (Notre Dame Univ., IN) AIAA Journal (ISSN 0001-1452) vol. 31, no. 1 Jan. 1993 p. 12-19. Previously cited in issue 02, p. 226, Accession no. A91-12426 AIAA, Aeroacoustics Conference, 13th, Tallahassee, FL, Oct. 22-24, 1990, AIAA Paper 90-3910 refs (Contract NAG3-732) Copyright

A93-24783*# National Aeronautics and Space Administration. Lewis Research Center, Cleveland, OH.

ACOUSTIC MODE MEASUREMENTS IN THE INLET OF A MODEL TURBOFAN USING A CONTINUOUSLY ROTATING RAKE

LAURENCE J. HEIDELBERG (NASA, Lewis Research Center, Cleveland, OH) and DAVID G. HALL (Sverdrup Technology, Inc., Brook Park, OH) Jan. 1993 31 p. AIAA, Aerospace Sciences Meeting and Exhibit, 31st, Reno, NV, Jan. 11-14, 1993 Previously announced in STAR as N93-16705 refs (AIAA PAPER 93-0598) Copyright

Comprehensive measurements of the spinning acoustic mode structure in the inlet of the Advanced Ducted Propeller (ADP) have been completed. These measurements were taken using a unique and previously untried method which was first proposed by T.G. Sofrin. A continuously rotating microphone system was employed. The ADP model was designed and built by Pratt & Whitney and tested in the NASA Lewis 9- by 15-foot Anechoic Wind Tunnel. Three inlet configurations were tested with cut-on and cutoff stator vane sets. The cutoff stator was designed to suppress all modes at the blade passing frequency. Rotating rake measurements indicate that several extraneous circumferential modes were active. The mode orders suggest that their source was an interaction between the rotor and small interruptions in the casing tip treatment. The cut-on stator produced the expected circumferential modes plus higher levels of the unexpected modes seen with the cutoff stator. Author

A93-24821*# National Aeronautics and Space Administration. Lewis Research Center, Cleveland, OH.

MEASURED ACOUSTIC CHARACTERISTICS OF DUCTED SUPERSONIC JETS AT DIFFERENT MODEL SCALES

R. R. JONES, III (Sverdrup Technology, Inc., Arnold AFB, TN), K. K. AHUJA (Georgia Inst. of Technology, Atlanta), CHRISTOPHER K. W. TAM (Florida State Univ., Tallahassee), and M. ABDELWAHAB (NASA, Lewis Research Center, Cleveland, OH) Jan. 1993 12 p. AIAA, Aerospace Sciences Meeting and Exhibit, 31st, Reno, NV, Jan. 11-14, 1993 refs (AIAA PAPER 93-0731)

A large-scale (about a 25x enlargement) model of the Georgia Tech Research Institute (GTRI) hardware was installed and tested in the Propulsion Systems Laboratory of the NASA Lewis Research Center. Acoustic measurements made in these two facilities are compared and the similarity in acoustic behavior over the scale range under consideration is highlighted. The study provide the acoustic data over a relatively large-scale range which may be used to demonstrate the validity of scaling methods employed in the investigation of this phenomena. O.G.

A93-24825*# National Aeronautics and Space Administration. Lewis Research Center, Cleveland, OH.

COMPUTATION OF SUPERSONIC JET NOISE UNDER IMPERFECTLY EXPANDED CONDITIONS

CHAN M. KIM, EUGENE A. KREJSA (NASA, Lewis Research Center, Cleveland, OH), and ABBAS KHAVARAN (Sverdrup Technology, Inc., Brook Park; NASA, Lewis Research Center, Cleveland, OH) Jan. 1993 10 p. AIAA, Aerospace Sciences Meeting and Exhibit, 31st, Reno, NV, Jan. 11-14, 1993 Previously announced in STAR as N93-15430 refs (AIAA PAPER 93-0735) Copyright

The turbulent mixing noise of supersonic jet under imperfectly expanded conditions is calculated for convergent and convergent-divergent (CD) axisymmetric nozzle geometries. The noise prediction incorporates CFD solution of Navier-Stokes equations. The effect of grid resolution on shock structure computation is demonstrated. Mixing noise spectra predicted from fine and coarse grid solutions exhibit little sensitivity to the grid resolution. A proper grid resolution, however, results in a significant improvement in shock capturing capability and helps predictions agree favorably with experimental data. Good agreement between predicted noise spectra and data shows that the CFD-incorporated noise prediction scheme, which was demonstrated for shock-free conditions, works as well for shock-containing flow conditions. Author

A93-25538*# National Aeronautics and Space Administration. Lewis Research Center, Cleveland, OH.

THE STRUCTURE OF SUPERSONIC JET FLOW AND ITS RADIATED SOUND

REDA R. MANKBADI, M. E. HAYDER, and LOUIS A. POVINELLI (NASA, Lewis Research Center, Cleveland, OH) Jan. 1993 20 p. AIAA, Aerospace Sciences Meeting and Exhibit, 31st, Reno, NV, Jan. 11-14, 1993 refs (AIAA PAPER 93-0549) Copyright

Large-eddy simulation of a supersonic jet is presented with emphasis on capturing the unsteady features of the flow pertinent to sound emission. A high-accuracy numerical scheme is used to solve the filtered, unsteady, compressible Navier-Stokes equations while modelling the subgrid-scale turbulence. For random inflow disturbance, the wave-like feature of the large-scale structure is demonstrated. The large-scale structure was then enhanced by imposing harmonic disturbances to the inflow. The limitation of using the full Navier-Stokes equation to calculate the far-field sound is discussed. Application of Lighthill's acoustic analogy is given with the objective of highlighting the difficulties that arise from the non-compactness of the source term. Author

A93-28609* National Aeronautics and Space Administration. Lewis Research Center, Cleveland, OH.

CRUISE NOISE OF AN ADVANCED PROPELLER WITH SWIRL RECOVERY VANES

JAMES H. DITTMAR (NASA, Lewis Research Center, Cleveland, OH) and DAVID G. HALL (Sverdrup Technology, Inc., Brook Park, OH) Journal of Aircraft (ISSN 0021-8669) vol. 30, no. 2 Mar.-Apr. 1993 p. 221-226. Previously cited in issue 02, p. 228, Accession no. A91-12448 AIAA, Aeroacoustics Conference, 13th, Tallahassee, FL, Oct. 22-24, 1990, AIAA Paper 90-3932 refs Copyright

A93-29420 National Aeronautics and Space Administration. Lewis Research Center, Cleveland, OH.

ACOUSTICAL ANALYSIS OF GEAR HOUSING VIBRATION

A. F. SEYBERT, T. W. WU, X. F. WU (Kentucky Univ., Lexington), and FRED B. OSWALD (NASA, Lewis Research Center, Cleveland, OH) In AHS and Royal Aeronautical Society, Technical Specialists' Meeting on Rotorcraft Acoustics/Fluid Dynamics, Philadelphia, PA, Oct. 15-17, 1991, Proceedings Alexandria, VA American Helicopter Society 1991 8 p. Previously announced in STAR as N91-25411 refs (Contract RTOP 505-63-51) Copyright

The modal and acoustical analysis of the NASA gear-noise rig

is described. Experimental modal analysis techniques were used to determine the modes of vibration of the transmission housing. The resulting modal data were then used in a boundary element method (BEM) analysis to calculate the sound pressure and sound intensity on the surface of the housing as well as the radiation efficiency of each mode. The radiation efficiencies of the transmission housing modes are compared with theoretical results for finite, baffled plates. A method that uses the measured mode shapes and the BEM to predict the effect of simple structural changes on the sound radiation efficiency of the modes of vibration is also described. Author

A93-29428* National Aeronautics and Space Administration. Lewis Research Center, Cleveland, OH.

ACTIVE CONTROL OF HELICOPTER TRANSMISSION NOISE

R. H. SPENCER (Boeing Helicopters, Philadelphia, PA), M. J. BURKE, and G. W. TYE (Noise Cancellation Technologies, Inc., Linthicum, MD) *In* AHS and Royal Aeronautical Society, Technical Specialists' Meeting on Rotorcraft Acoustics/Fluid Dynamics, Philadelphia, PA, Oct. 15-17, 1991, Proceedings Alexandria, VA American Helicopter Society 1991 13 p. Research supported by U.S. Army refs (Contract NAS3-25421) Copyright

An account is given of an effort to reduce helicopter transmission noise by 10 dB, using active methods, as part of the NASA-Lewis/U.S. Army Propulsion Directorate Advanced Rotorcraft Transmission technology integration and demonstration program. The transmission used as a test stand is that of the CH-47C forward rotor. Attention is presently given to the active control system's actuators, sensors, and control algorithms. O.C.

A93-51180* National Aeronautics and Space Administration. Lewis Research Center, Cleveland, OH.

DISPERSION-RELATION-PRESERVING FINITE DIFFERENCE SCHEMES FOR COMPUTATIONAL ACOUSTICS

CHRISTOPHER K. W. TAM and JAY C. WEBB (Florida State Univ., Tallahassee) *Journal of Computational Physics* (ISSN 0021-9991) vol. 107, no. 2 Aug. 1993 p. 262-281. refs (Contract NAG3-1267; N00014-89-J-1836) Copyright

Time-marching dispersion-relation-preserving (DRP) schemes can be constructed by optimizing the finite difference approximations of the space and time derivatives in wave number and frequency space. A set of radiation and outflow boundary conditions compatible with the DRP schemes is constructed, and a sequence of numerical simulations is conducted to test the effectiveness of the DRP schemes and the radiation and outflow boundary conditions. Close agreement with the exact solutions is obtained. AIAA

A93-53657 National Aeronautics and Space Administration. Lewis Research Center, Cleveland, OH.

MODAL ELEMENT METHOD FOR SCATTERING AND ABSORBING OF SOUND BY TWO-DIMENSIONAL BODIES

K. J. BAUMEISTER (NASA, Lewis Research Center, Cleveland, OH) and K. L. KREIDER (Akron Univ., OH) *ASME, Transactions, Journal of Vibration and Acoustics* (ISSN 0739-3717) vol. 115, no. 3 July 1993 p. 314-323. ASME, Winter Annual Meeting, Anaheim, CA, Nov. 8-13, 1992. Previously announced in STAR as N92-28984 refs (Contract RTOP 505-62-52) Copyright

The modal element method for acoustic scattering from a 2-D body is presented. The body may be acoustically soft (absorbing) or hard (reflecting). The infinite computational region is divided into two subdomains - the bounded finite element domain, which is characterized by complicated geometry and/or variable material properties, and the surrounding unbounded homogeneous domain. The acoustic pressure field is represented approximately in the finite element domain by a finite element solution, and is represented analytically by an eigenfunction expansion in the homogeneous domain. The two solutions are coupled by the

continuity of pressure and velocity across the interface between the two subdomains. Also, for hard bodies, a compact modal ring grid system is introduced for which computing requirements are drastically reduced. Analysis for 2-D scattering from solid and coated (acoustically treated) bodies is presented, and several simple numerical examples are discussed. In addition, criteria are presented for determining the number of modes to accurately resolve the scattered pressure field from a solid cylinder as a function of the frequency of the incoming wave and the radius of the cylinder.

A93-55861* National Aeronautics and Space Administration. Lewis Research Center, Cleveland, OH.

COMPARISON OF RADIATED NOISE FROM SHROUDED AND UNSHROUDED PROPELLERS

WALTER EVERSMA (Missouri-Rolla Univ., Rolla) *In* International Congress on Recent Developments in Air- and Structure-Borne Sound and Vibration, 2nd, Auburn Univ., AL, Mar. 4-6, 1992, Proceedings. Vol. 1 Auburn, AL Auburn University 1992 p. 121-128. Research supported by NASA refs Copyright

The ducted propeller in a free field is modeled using the finite element method. The generation, propagation, and radiation of sound from a ducted fan is described by the convected wave equation with volumetric body forces. Body forces are used to introduce the blade loading for rotating blades and stationary exit guide vanes. For an axisymmetric nacelle or shroud, the problem is formulated in cylindrical coordinates. For a specified angular harmonic, the angular coordinate is eliminated, resulting in a two-dimensional representation. A finite element discretization based on nine-node quadratic isoparametric elements is used. AIAA

N93-11370*# National Aeronautics and Space Administration. Lewis Research Center, Cleveland, OH.

A CONCEPT FOR A COUNTERROTATING FAN WITH REDUCED TONE NOISE

JAMES H. DITTMAR Aug. 1992 11 p (Contract RTOP 535-03-10) (NASA-TM-105736; E-7138; NAS 1.15:105736) Avail: CASI HC A03/MF A01

As subsonic jet engine designs incorporate higher bypass ratios to reduce jet noise and increase engine cycle efficiency, the fan noise becomes a significant part of the perceived total noise. The conventional method of reducing fan tone noise is to design a low tip-speed device. An alternative approach of using a counterrotating fan with a high number of rotor blades is investigated in this report. The source of noise at the blade passing frequency of this device is the rotor-only mechanism, which is cut off for a subsonic tip speed rotor. The interaction noise occurs at twice the blade passing frequency, which, for this fan, was shifted high enough in frequency to be above the perceived noise rating range. The result was a counterrotating fan which had more potential for tone noise reduction than does the conventional fan. A potential broadband noise reduction was also indicated. Author

N93-15430*# National Aeronautics and Space Administration. Lewis Research Center, Cleveland, OH.

COMPUTATION OF SUPERSONIC JET NOISE UNDER IMPERFECTLY EXPANDED CONDITIONS

CHAN M. KIM, EUGENE A. KREJSA, and ABBAS KHAVARAN (Sverdrup Technology, Inc., Brook Park, OH.) Jan. 1993 11 p Presented at the 31st Aerospace Sciences Meeting and Exhibit, Reno, NV, 11-14 Jan. 1993; Sponsored by AIAA (Contract RTOP 537-02-23) (NASA-TM-105961; E-7481; NAS 1.15:105961; AIAA PAPER 93-0735) Avail: CASI HC A03/MF A01

The turbulent mixing noise of supersonic jet under imperfectly expanded conditions is calculated for convergent and convergent-divergent (CD) axisymmetric nozzle geometries. The noise prediction incorporates CFD solution of Navier-Stokes equations. The effect of grid resolution on shock structure

computation is demonstrated. Mixing noise spectra predicted from fine and coarse grid solutions exhibit little sensitivity to the grid resolution. A proper grid resolution, however, results in a significant improvement in shock capturing capability and helps predictions agree favorably with experimental data. Good agreement between predicted noise spectra and data shows that the CFD-incorporated noise prediction scheme, which was demonstrated for shock-free conditions, works as well for shock-containing flow conditions.

Author

N93-15575*# National Aeronautics and Space Administration. Lewis Research Center, Cleveland, OH.

PROPAGATION OF HIGH FREQUENCY JET NOISE USING GEOMETRIC ACOUSTICS

A. KHAVARAN (Sverdrup Technology, Inc., Brook Park, OH.) and E. A. KREJSA Jan. 1993 18 p Presented at the 31st Aerospace Sciences Meeting and Exhibit, Reno, NV, 11-14 Jan. 1993; sponsored by AIAA

(Contract RTOP 537-02-23)

(NASA-TM-106013; E-7471; NAS 1.15:106013; AIAA PAPER 93-0147) Avail: CASI HC A03/MF A01

Spherical directivity of noise radiated from a convecting quadrupole source embedded in an arbitrary spreading jet is obtained by ray-tracing methods of geometrical acoustics. The six propagation equations are solved in their general form in a rectangular coordinate system. The noise directivity in the far field is calculated by applying an iteration scheme that finds the required radiation angles at the source resulting in propagation through a given observer point. Factors influencing the zone of silence are investigated. The caustics of geometrical acoustics and the exact locations where it forms is demonstrated by studying the variation in ray tube area obtained from transport equation. For a ring source convecting along the center-axis of an axisymmetric jet, the polar directivity of the radiated noise is obtained by an integration with respect to azimuthal directivity of compact quadrupole sources distributed on the ring. The Doppler factor is shown to vary slightly from point to point on the ring. Finally the scaling of the directivity pattern with power -3 of Doppler factor is investigated and compared with experimental data.

Author

N93-17051*# National Aeronautics and Space Administration. Lewis Research Center, Cleveland, OH.

CONSECUTIVE PLATE ACOUSTIC SUPPRESSOR APPARATUS AND METHODS Patent Application

JOSEPH DOYCHAK, inventor (to NASA) and TONY PARROTT, inventor (to NASA) 16 Oct. 1992 20 p (NASA-CASE-LEW-15430-1; NAS 1.71:LEW-15430-1; US-PATENT-APPL-SN-961943) Avail: CASI HC A03/MF A01

An apparatus and method for suppressing acoustic noise utilizes consecutive plates, closely spaced to each other so as to exploit dissipation associated with sound propagation in narrow channels to optimize the acoustic resistance at a liner surface. The closely spaced plates can be utilized as high temperature structural materials for jet engines by constructing the plates from composite materials. Geometries of the plates, such as plate depth, shape, thickness, inter-plate spacing, arrangement, etc., can be selected to achieve bulk material-like behavior.

NASA

N93-26551*# National Aeronautics and Space Administration. Lewis Research Center, Cleveland, OH.

A LARGE HEMI-ANECHOIC ENCLOSURE FOR COMMUNITY-COMPATIBLE AEROACOUSTIC TESTING OF AIRCRAFT PROPULSION SYSTEMS

BETH A. COOPER Apr. 1993 15 p Presented at Noise-Con'93, Williamsburg, VA, 2-5 May 1993; sponsored by Noise-Con (Contract RTOP 537-02-22)

(NASA-TM-106015; E-7572-1; NAS 1.15:106015) Avail: CASI HC A03/MF A01

A large hemianechoic (absorptive walls and acoustically hard floor) noise control enclosure was erected around a complex of test stands at the NASA Lewis Research Center in Cleveland, Ohio. This new state-of-the-art Aeroacoustic Propulsion Laboratory (APL) provides an all-weather, semi secure test environment while

limiting noise to acceptable levels in surrounding residential neighborhoods. The 39.6-m- (130-ft-) diameter geodesic dome houses the new nozzle aeroacoustic test rig (NATR), an ejector-powered Mach 0.3 free jet facility for acoustic testing of supersonic aircraft exhaust nozzles and turbomachinery. A multiaxis, force-measuring, powered lift facility (PLF) stand for testing short takeoff vertical-landing (STOVL) vehicles is also located in the dome. The design of the Aeroacoustic Propulsion Laboratory efficiently accommodates the research functions of two separate test rigs, one of which (NATR) requires a specialized environment for taking acoustic measurements. An absorptive fiberglass wedge treatment on the interior surface of the dome provides a hemianechoic environment for obtaining the accurate acoustic measurements required to meet research program goals. The APL is the first known geodesic dome structure to incorporate transmission-loss properties as well as interior absorption in a free-standing, community-compatible, hemianechoic test facility.

Author

N93-27058*# National Aeronautics and Space Administration. Lewis Research Center, Cleveland, OH.

IN-FLIGHT NEAR- AND FAR-FIELD ACOUSTIC DATA MEASURED ON THE PROPPAN TEST ASSESSMENT (PTA) TESTBED AND WITH AN ADJACENT AIRCRAFT

RICHARD P. WOODWARD and IRVIN J. LOEFFLER Apr. 1993 161 p

(Contract RTOP 535-03-10)

(NASA-TM-103719; E-6402; NAS 1.15:103719) Avail: CASI HC A08/MF A02

Flight tests to define the far-field tone source at cruise conditions were completed on the full-scale SR-7L advanced turboprop that was installed on the left wing of a Gulfstream 2 aircraft. This program, designated Propfan Test Assessment (PTA), involved aeroacoustic testing of the propeller over a range of test conditions. These measurements defined source levels for input into long-distance propagation models to predict en route noise. In-flight data were taken for seven test cases. Near-field acoustic data were taken on the Gulfstream fuselage and on a microphone boom that was mounted on the Gulfstream wing outboard of the propeller. Far-field acoustic data were taken by an acoustically instrumented Learjet that flew in formation with the Gulfstream. These flight tests were flown from El Paso, Texas, and from the NASA Lewis Research Center. A comprehensive listing of the aeroacoustic results from these flight tests which may be used for future analysis are presented.

Author

N93-28953*# National Aeronautics and Space Administration. Lewis Research Center, Cleveland, OH.

JET MIXER NOISE SUPPRESSOR USING ACOUSTIC FEEDBACK Patent Application

EDWARD J. RICE, inventor (to NASA) 14 Apr. 1993 20 p (NASA-CASE-LEW-15170-1; NAS 1.71:LEW-15170-1; US-PATENT-APPL-SN-046256) Avail: CASI HC A03/MF A01

The present invention generally relates to providing an improved jet mixer noise suppressor for high speed jets that rapidly mixes high speed air flow with a lower speed air flow, and more particularly, relates to an improved jet mixer noise suppressor that uses feedback of acoustic waves produced by the interaction of shear flow instability waves with an obstacle downstream of the jet nozzle.

NASA

ATOMIC AND MOLECULAR PHYSICS

Includes atomic structure, electron properties, and molecular spectra.

A93-24142* National Aeronautics and Space Administration. Lewis Research Center, Cleveland, OH.

ROTATIONAL LEVEL-DEPENDENT COLLISIONAL BROADENING AND LINE SHIFT OF THE A2SIGMA(+)-X2PI (1,0) BAND OF OH IN HYDROGEN-AIR COMBUSTION GASES
W. J. KESSLER, M. G. ALLEN, and S. J. DAVIS (Physical Sciences, Inc., Andover, MA) *Journal of Quantitative Spectroscopy & Radiative Transfer* (ISSN 0022-4073) vol. 49, no. 2 Feb. 1993 p. 107-117. refs
(Contract NAS3-26254)

Copyright

Measurements of the collisional broadening and line shift of the (1,0) band of the A2Sigma(+)-X2Pi system of OH are reported in atmospheric pressure hydrogen-air combustion gases. The measurements were made using a single-mode, narrow linewidth, frequency-doubled ring dye laser operating near 283 nm. The OH was generated in the combustion gases of a flat flame H2-air burner. Collisional broadening parameters for equilibrium mixtures of H2, O2, H2O, and N2 were obtained spanning a range of fuel/air equivalence ratios from 0.6 to 1.6 and temperatures from 1500 to 2050 K. Measurements were obtained spanning rotational quantum numbers from 4.5 to 16.5. The collision induced frequency shift was determined to be 0.1 that of the collisional broadening.

Author

A93-44989* National Aeronautics and Space Administration. Lewis Research Center, Cleveland, OH.

GLOBAL EXPRESSION FOR REPRESENTING COHESIVE-ENERGY CURVES. II

HERBERT SCHLOSSER (Cleveland State Univ., OH) and JOHN FERRANTE (NASA, Lewis Research Center, Cleveland, OH) *Physical Review B - Condensed Matter, 3rd Series* (ISSN 0163-1829) vol. 47, no. 2 Jan. 1, 1993 p. 1073-1076. refs
Copyright

Schlosser et al. (1991) showed that the R dependence of the cohesive energy of partially ionic solids may be characterized by a two-term energy relationship consisting of a Coulomb term arising from the charge transfer, ΔZ , and a scaled universal energy function, $E^*(a^*)$, which accounts for the partially covalent character of the bond and for repulsion between the atomic cores for small R; a^* is a scaled length. In the paper by Schlosser et al., the normalized cohesive-energy curves of NaCl-structure alkali-halide crystals were generated with this expression. In this paper we generate the cohesive-energy curves of several families of partially ionic solids with different crystal structures and differing degrees of ionicity. These include the CsCl-structure Cs halides, and the Ti and Ag halides, which have weaker ionic bonding than the alkali halides, and which have the CsCl and NaCl structures, respectively. The cohesive-energy-curve parameters are then used to generate theoretical isothermal compression curves for the Li, Na, K, Cs, and Ag halides. We find good agreement with the available experimental compression data.

Author (revised)

A93-45398* National Aeronautics and Space Administration. Lewis Research Center, Cleveland, OH.

ABSORPTION COEFFICIENTS FOR WATER VAPOR AT 193 NM FROM 300 TO 1073 K

W. J. KESSLER, K. L. CARLETON, and W. J. MARINELLI (Physical Sciences, Inc., Andover, MA) *Journal of Quantitative Spectroscopy and Radiative Transfer* (ISSN 0022-4073) vol. 50, no. 1 July 1993 p. 39-46. refs
(Contract NAS3-26058)

Copyright

Measurements of the water absorption coefficient at 193 nm

from 300 to 1073 K are reported. The measurements were made using broadband VUV radiation and a monochromator-based detection system. The water vapor was generated by a saturator and metered into a flowing, 99 cm absorption cell via a water vapor mass flow meter. The 193 nm absorption coefficient measurements are compared to room temperature and high temperature shock tube measurements with good agreement. The absorption can be parameterized by a nu3 vibrational mode reaction coordinate and the thermal population of the nu3 mode.

Author (revised)

N93-19026*# National Aeronautics and Space Administration. Lewis Research Center, Cleveland, OH.

METHOD AND APPARATUS FOR PRODUCING A THERMAL ATOMIC OXYGEN BEAM Patent Application

B. A. BANKS, inventor (to NASA) and S. K. RUTLEDGE, inventor (to NASA) 25 Jan. 1993 11 p
(NASA-CASE-LEW-15614-1; NAS 1.71:LEW-15614-1; US-PATENT-APPL-SN-008026) Avail: CASI HC A03/MF A01

Atomic oxygen atoms are routed to a material through a sufficiently tortuous path so that vacuum ultraviolet radiation is obstructed from arriving at the surface of the material. However, the material surface continues to be exposed to the atomic oxygen.

NASA

N93-20814*# National Aeronautics and Space Administration. Lewis Research Center, Cleveland, OH.

RECOMMENDED PRACTICES FOR IN-SPACE AND GROUND LABORATORY. ATOMIC OXYGEN EXPOSURE AND ANALYSIS

BRUCE BANKS, STEVE KOONTZ, MATT MCCARGO, GARY PIPPIN, and SHARON RUTLEDGE *In Canadian Space Agency, Protection of Materials and Surface Finishes from the Low Earth Orbit Space Environment* 27 p 1992
Avail: Canadian Space Agency, P.O. Box 7275, Ottawa, ON, Canada K1L 8E3, HC

A detailed guide to testing materials for atomic oxygen durability in earth orbit environments is presented. The steps covered include sample preparation, including masking of the sample, dehydration, weighing, and handling; effective fluence prediction, including the use of witness samples (notably Kapton); plasma facility and operational considerations, involving such matters as avoidance of silicone contamination, the use of continuous versus incremental ashing, and temperature of operation; and erosion yield measurement, with calculation methods and protective coating performance indices provided.

Author (CISTI)

NUCLEAR AND HIGH-ENERGY PHYSICS

Includes elementary and nuclear particles; and reactor theory.

N93-16531*# National Aeronautics and Space Administration. Lewis Research Center, Cleveland, OH.

SYSTEM MODEL DEVELOPMENT FOR NUCLEAR THERMAL PROPULSION

NELSON A. HANNAN (Argonne National Lab., IL.), BRIAN A. WORLEY (Oak Ridge National Lab., TN.), JAMES T. WALTON, KEN R. PERKINS (Brookhaven National Lab., Upton, NY.), JOHN J. BUSKA (Los Alamos National Lab., NM.), and DEAN DOBRANICH (Sandia National Labs., Albuquerque, NM.) 1992 11 p Presented at the 43d Congress of the International Astronautical Federation, Washington, DC, 28 Aug. - 5 Sep. 1992 (Contract DE-AC05-84OR-21400)
(NASA-TM-108157; NAS 1.15:108157; DE92-041262; CONF-9208154-1) Avail: CASI HC A03/MF A01

A critical enabling technology in the evolutionary development of nuclear thermal propulsion (NTP) is the ability to predict the system performance under a variety of operating conditions. This is crucial for mission analysis and for control subsystem testing

as well as for the modeling of various failure modes. Performance must be accurately predicted during steady-state and transient operation, including startup, shutdown and post operation cooling. The development and application of verified and validated system models has the potential to reduce the design, testing, cost and time required for the technology to reach flight-ready status. Since October 1991, the US Department of Energy (DOE), Department of Defense (DOD) and NASA have initiated critical technology development efforts for NTP systems to be used on Space Exploration Initiative (SEI) missions to the Moon and Mars. This paper presents the strategy and progress of an interagency NASA/DOE/DOD team for NTP system modeling. DOE

A93-17343* National Aeronautics and Space Administration. Lewis Research Center, Cleveland, OH.

SYSTEM MODEL DEVELOPMENT FOR NUCLEAR THERMAL PROPULSION

JAMES T. WALTON, NELSON A. HANNAN (Argonne National Lab., IL.), KEN R. PERKINS (Brookhaven National Lab., Upton, NY.), JOHN J. BUKSA (Los Alamos National Lab., NM.), BRIAN A. WORLEY (Oak Ridge National Lab., TN.), and DEAN DOBRANICH (Sandia National Labs., Albuquerque, NM.) 1992 12 p. Presented at the World Space Congress, Washington, DC, 28 Aug. - 5 Sep. 1992 (Contract DE-AC04-76DP-00789) (NASA-TM-108215; NAS 1.15:108215; DE92-000754; SAND-92-1820C; IAF-92-0568; CONF-920879-2) Avail: CASI HC A03/MF A01

A critical enabling technology in the evolutionary development of nuclear thermal propulsion (NTP) is the ability to predict the system performance under a variety of operating conditions. Since October 1991, DOE, DOD, and NASA have initiated critical technology development efforts for NTP systems to be used on Space Exploration Initiative (SEI) missions to the Moon and Mars. This paper presents the strategy and progress of an interagency NASA/DOE/DOD team for NTP system modeling. It is the intent of the interagency team to develop several levels of computer programs to simulate various NTP systems. An interagency team was formed for this task to use the best capabilities available and to assure appropriate peer review. The vision and strategy of the interagency team for developing NTP system models are discussed. A review of the progress on the level 1 interagency model is also presented. DOE

74

OPTICS

Includes light phenomena; and optical devices.

A93-25736* National Aeronautics and Space Administration. Lewis Research Center, Cleveland, OH.

FIBER OPTIC LINK FOR MILLIMETER WAVE COMMUNICATION SATELLITES

D. M. POLIFKO, S. A. MALONE, A. S. DARYOUSH (Drexel Univ., Philadelphia, PA), and R. KUNATH (NASA, Lewis Research Center, Cleveland, OH) /n Optical technology for microwave applications V; Proceedings of the Meeting, Orlando, FL, Apr. 3-5, 1991 Bellingham, WA Society of Photo-Optical Instrumentation Engineers 1991 p. 91-99. refs Copyright

An electrically and optically optimized 18.5 to 19.0 GHz short-haul fiber optic (F.O.) link is presented. A theoretical link analysis of gain, system noise contributions, linearity, and dynamic range is shown as well as the corresponding measurements. Results indicate that by employing reactive matching and on-fiber lensing techniques, performance of high-speed F.O. links are still limited by high relative intensity noise levels and the limited frequency response of the laser. Alternative architectures are

suggested to counteract these limiting problems of current high speed links. Author

A93-49989* National Aeronautics and Space Administration. Lewis Research Center, Cleveland, OH.

COMPOUND CURVATURE LASER WINDOW DEVELOPMENT

VINCENT G. VERHOFF (NASA, Lewis Research Center, Cleveland, OH) Jun. 1993 8 p. AIAA, SAE, ASME, and ASEE, Joint Propulsion Conference and Exhibit, 29th, Monterey, CA, June 28-30, 1993 refs

(AIAA PAPER 93-2177) Copyright

The NASA Lewis Research Center has developed and implemented a unique process for forming flawless compound curvature laser windows. These windows represent a major part of specialized, nonintrusive laser data acquisition systems used in a variety of compressor and turbine research test facilities. This report summarizes the main aspects of compound curvature laser window development. It is an overview of the methodology and the peculiarities associated with the formulation of these windows. Included in this discussion is new information regarding procedures for compound curvature laser window development.

A93-52071* National Aeronautics and Space Administration. Lewis Research Center, Cleveland, OH.

COMPACT COLOR SCHLIEREN OPTICAL SYSTEM

DONALD R. BUCHELE (ADF, Inc., Cleveland, OH) and DEVON W. GRIFFIN (Sverdrup Technology, Inc., Cleveland, OH) Applied Optics (ISSN 0003-6935) vol. 32, no. 22 Aug. 1, 1993 p. 4218-4222. refs

(Contract NAS3-25767; NAS3-25266)

Copyright

A compact optical system for use with rainbow schlieren deflectometry is described. Both halves of the optical system consist of well-corrected telescopes whose refractive elements are all from manufacturer's stock catalogs, with the reflective primary being a spherical surface. As a result, the system is relatively easy to construct and meets the requirement of long focal length for quantitative rainbow schlieren measurements.

A93-52412* National Aeronautics and Space Administration. Lewis Research Center, Cleveland, OH.

MICROEMULSION CHARACTERIZATION BY THE USE OF A NONINVASIVE BACKSCATTER FIBER OPTIC PROBE

RAFAT R. ANSARI (NASA, Lewis Research Center, Case Western Reserve Univ., Cleveland, OH), HARBANS S. DHADWAL (New York State Univ., Stony Brook), H. M. CHEUNG (Akron Univ., OH), and WILLIAM V. MEYER (NASA, Lewis Research Center, Case Western Reserve Univ., Cleveland, OH) Applied Optics (ISSN 0003-6935) vol. 32, no. 21 July 20, 1993 p. 3822-3827. refs

(Contract NCC3-241; NAG3-906)

Copyright

This paper demonstrates the utility of a noninvasive backscatter fiber optic probe for dynamic light-scattering characterization of a microemulsion comprising sodium dodecyl sulfate/1-butanol/brine/heptane. The fiber probe, comprising two optical fibers precisely positioned in a stainless steel body, is a miniaturized and efficient self-beating dynamic light-scattering system. Accuracy of particle size estimation is better than ± 2 percent.

Author (revised)

A93-52414* National Aeronautics and Space Administration. Lewis Research Center, Cleveland, OH.

STATISTICAL FITTING ACCURACY IN PHOTON CORRELATION SPECTROSCOPY

J. N. SHAUMEYER, MATTHEW E. BRIGGS, and ROBERT W. GAMMON (Maryland Univ., College Park) Applied Optics (ISSN 0003-6935) vol. 32, no. 21 July 20, 1993 p. 3871-3879. refs

(Contract NAS3-25370)

Copyright

Continuing our experimental investigation of the fitting accuracy associated with photon correlation spectroscopy, we collect 150

correlograms of light scattered at 90 deg from a thermostated sample of 91-nm-diameter, polystyrene latex spheres in water. The correlograms are taken with two correlators: one with linearly spaced channels and one with geometrically spaced channels. Decay rates are extracted from the single-exponential correlograms with both nonlinear least-squares fits and second-order cumulant fits. We make several statistical comparisons between the two fitting techniques and verify an earlier result that there is no sample-time dependence in the decay rate errors. We find, however, that the two fitting techniques give decay rates that differ by 1 percent. Author (revised)

A93-52415* National Aeronautics and Space Administration. Lewis Research Center, Cleveland, OH.

INTEGRATED FIBER OPTIC PROBE FOR DYNAMIC LIGHT SCATTERING

HARBANS S. DHADWAL, ROMEL R. KHAN, and KWANG SUH (New York State Univ., Stony Brook) Applied Optics (ISSN 0003-6935) vol. 32, no. 21 July 20, 1993 p. 3901-3904. refs

(Contract NCC3-241)

Copyright

An integrated fiber optic probe, comprising a monomode optical fiber fusion spliced to a short length of a graded-index multimode fiber, is fabricated for use as a coherent receiver in dynamic light scattering. The multimode fiber is cleaved to provide a gradient-index fiber lens with a focal length of 125 microns and an f-number close to unity. An integrated fiber receiver is used to measure the intensity-intensity autocorrelation data from a 0.05 percent by weight concentration of an aqueous suspension of polystyrene latex spheres. Analysis of 100 independent data sets indicates that the particle size can be recovered with an accuracy of ± 1 percent. Author (revised)

A93-55687* National Aeronautics and Space Administration. Lewis Research Center, Cleveland, OH.

VECTOR FORMULATION FOR INTERFEROGRAM SURFACE FITTING

DAVID J. FISCHER, JOHN T. O'BRYAN, ROBERT LOPEZ, and H. P. STAHL (Rose-Hulman Inst. of Technology, Terre Haute, IN) Applied Optics (ISSN 0003-6935) vol. 32, no. 25 Sept. 1, 1993 p. 4738-4743. refs

(Contract NAG3-1300)

Copyright

Interferometry is an optical testing technique that quantifies the optical path difference (OPD) between a reference wave front and a test wave front based on the interference of light. Fringes are formed when the OPD is an integral multiple of the illuminating wavelength. The resultant two-dimensional pattern is called an interferogram. The function of any interferogram analysis program is to extract this OPD and to produce a representation of the test wave front (or surface). This is accomplished through a three-step process of sampling, ordering, and fitting. We develop a generalized linear-algebra vector-notation model of the interferogram sampling and fitting process.

N93-11058* National Aeronautics and Space Administration. Lewis Research Center, Cleveland, OH.

PHASE-STEPPING FIBER-OPTIC PROJECTED FRINGE SYSTEM FOR SURFACE TOPOGRAPHY MEASUREMENTS
Patent

CAROLYN R. MERCER, Inventor (to NASA) and GLENN BEHEIM, inventor (to NASA) 8 Sep. 1992 6 p. Filed 13 May 1991 (NASA-CASE-LEW-14996-1; US-PATENT-5,146,293; US-PATENT-APPL-SN-703435; US-PATENT-CLASS-356-356; US-PATENT-CLASS-356-360; US-PATENT-CLASS-356-376; US-PATENT-CLASS-382-26; US-PATENT-CLASS-364-575; INT-PATENT-CLASS-G01B-11/02) Avail: US Patent and Trademark Office

A projected fringe interferometer for measuring the topography of an object is presented. The interferometer periodically steps the phase angle between a pair of light beams emanating from a common source. The steps are $\pi/2$ radians (90 deg) apart, and

at each step a video image of the fringes is recorded and stored. Photodetectors measure either the phase and theta of the beams or $2(\theta)$. Either of the measures can be used to control one of the light beams so that the 90 deg theta is accurately maintained. A camera, a computer, a phase controller, and a phase modulator established closed-loop control of theta. Measuring the phase map of a flat surface establishes a calibration reference.

Official Gazette of the U.S. Patent and Trademark Office

N93-29693*# National Aeronautics and Space Administration. Lewis Research Center, Cleveland, OH.

STUDIES OF EFFECTS ON OPTICAL COMPONENTS AND SENSORS: LDEF EXPERIMENTS AO-147 (ERB COMPONENTS) AND S-0014 (APEX)

JOHN R. HICKEY (Eppler Lab., Inc., Newport, RI.), DAVID J. BRINKER, and PHILIP JENKINS (Sverdrup Technology, Inc., Brook Park, OH.) In NASA. Langley Research Center, LDEF: 69 Months in Space. Part 4: Second Post-Retrieval Symposium p 1375-1388 Apr. 1993

(Contract NAS1-15350; NAS3-25958)

Avail: CASI HC A03/MF A03; 2 functional color pages

Some additional results of testing of optical filters and window materials and thermopile sensors of the two experiments are included. The Advanced Photovoltaic Experiment (APEX) interference filters exhibited much greater degradation in space than the ERB filters. The adhesion of the Indium washers to the APEX interference filters is reported. Author (revised)

75

PLASMA PHYSICS

Includes magnetohydrodynamics and plasma fusion.

A93-49618* National Aeronautics and Space Administration. Lewis Research Center, Cleveland, OH.

ANALYSIS AND DESIGN OF AN ULTRAHIGH TEMPERATURE HYDROGEN-FUELED MHD GENERATOR

JEFFREY P. MODER, LEIK N. MYRABO, and DEBORAH A. KAMINSKI (Rensselaer Polytechnic Inst., Troy, NY) Journal of Propulsion and Power (ISSN 0748-4658) vol. 9, no. 5 Sept.-Oct. 1993 p. 739-748. refs

(Contract NAG3-916)

Copyright

A coupled gas dynamics/radiative heat transfer analysis of partially ionized hydrogen, in local thermodynamic equilibrium, flowing through an ultrahigh temperature (10,000-20,000 K) magnetohydrodynamic (MHD) generator is performed. Gas dynamics are modeled by a set of quasi-one-dimensional, nonlinear differential equations which account for friction, convective and radiative heat transfer, and the interaction between the ionized gas and applied magnetic field. Radiative heat transfer is modeled using nongray, absorbing-emitting 2D and 3D P-1 approximations which permit an arbitrary variation of the spectral absorption coefficient with frequency. Gas dynamics and radiative heat transfer are coupled through the energy equation and through the temperature- and density-dependent absorption coefficient. The resulting nonlinear elliptic problem is solved by iterative methods. Design of such MHD generators as onboard, open-cycle, electric power supplies for a particular advanced airbreathing propulsion concept produced an efficient and compact 128-MWe generator characterized by an extraction ratio of 35.5 percent, a power density of 10,500 MWe/cu m, and a specific (extracted) energy of 324 MJ/kg of hydrogen. The maximum wall heat flux and total wall heat load were 453 MW/sq m and 62 MW, respectively.

Author (revised)

N93-18635* National Aeronautics and Space Administration.
Lewis Research Center, Cleveland, OH.

SECOND MAGNETOPLASMA DYNAMIC THRUSTER WORKSHOP

1992 167 p Workshop held in Cleveland, OH, 19 May 1992
(Contract RTOP 506-42-31)
(NASA-CP-10109; E-7369; NAS 1.55:10109) Avail: CASI HC
A08/MF A02

The meeting focused on progress made in establishing performance and lifetime expectations of magnetoplasmadynamic (MPD) thrusters as functions of power, propellant, and design; models for the plasma flow and electrode components; viability and transportability of quasi-steady thruster testing; engineering requirements for high power, long life thrusters; and facilities and their requirements for performance and life testing.

76

SOLID-STATE PHYSICS

Includes superconductivity.

A93-11475* National Aeronautics and Space Administration.
Lewis Research Center, Cleveland, OH.

LARGE-AREA YBa₂Cu₃O₇(δ) THIN FILMS ON SAPPHIRE FOR MICROWAVE APPLICATIONS

B. F. COLE, G.-C. LIANG, N. NEWMAN, K. CHAR, G. ZAHARCHUK (Conductus, Inc., Sunnyvale, CA), and J. S. MARTENS (Sandia National Labs., Albuquerque, NM) Applied Physics Letters (ISSN 0003-6951) vol. 61, no. 14 Oct. 5, 1992 p. 1727-1729. Research supported by NASA refs Copyright

We have deposited YBa₂Cu₃O₇(δ) (YBCO) films with low microwave surface resistance (Rs) on 5-cm-diam, oxide-buffered sapphire substrates by planar magnetron sputtering. MgO buffer layers are used on M-plane (1 0 -1 0) sapphire, and R-plane (1 -1 0 2) sapphire is buffered by CeO₂. Rs values of 450-620 microhms at 77 K and 10 GHz were measured across an entire 5-cm diam YBCO film on M-plane sapphire. For YBCO on R-plane sapphire, Rs values at 77 K and 10 GHz were 950 microhms for a 5-cm-diam wafer and 700 microhms for 1 x 1 sq cm samples. Author

A93-13880* National Aeronautics and Space Administration.
Lewis Research Center, Cleveland, OH.

SILICON CARBIDE, A SEMICONDUCTOR FOR SPACE POWER ELECTRONICS

J. A. POWELL and LAWRENCE G. MATUS (NASA, Lewis Research Center, Cleveland, OH) In Space nuclear power systems; Proceedings of the 8th Symposium, Albuquerque, NM, Jan. 6-10, 1991. Pt. 3 New York American Institute of Physics 1991 p. 954-959. Previously announced in STAR as N91-14850 refs Copyright

After many years of promise as a high temperature semiconductor, silicon carbide (SiC) is finally emerging as a useful electronic material. Recent significant progress that has led to this emergence has been in the area of crystal growth and device fabrication technology. High quality of single-crystal SiC wafers, up to 25 mm in diameter, can now be produced routinely from boules grown by a high temperature (2700 K) sublimation process. Device fabrication processes, including chemical vapor deposition (CVD), in situ doping during CVD, reactive ion etching, oxidation, metallization, etc. have been used to fabricate p-n junction diodes and MOSFETs. The diode was operated to 870 K and the MOSFET to 770 K. Author

A93-17176* National Aeronautics and Space Administration.
Lewis Research Center, Cleveland, OH.

CARRIER REMOVAL AND DEFECT BEHAVIOR IN P-TYPE INP

I. WEINBERG, C. K. SWARTZ (NASA, Lewis Research Center, Cleveland, OH), and P. J. DREVINSKY (USAF, Phillips Lab.,

Hanscom AFB, MA) Journal of Applied Physics (ISSN 0021-8979) vol. 72, no. 11 Dec. 1, 1992 p. 5509-5511. refs Copyright

A simple expression, obtained from the rate equation for defect production, was used to relate carrier removal to defect production and hole trapping rates in p-type InP after irradiation by 1-MeV electrons. Specific contributions to carrier removal from defect levels H3, H4, and H5 were determined from combined deep-level transient spectroscopy (DLTS) and measured carrier concentrations. An additional contribution was attributed to one or more defects not observed by the present DLTS measurements. The high trapping rate observed for H5 suggests that this defect, if present in relatively high concentration, could be dominant in p-type InP. Author

A93-17513* National Aeronautics and Space Administration.
Lewis Research Center, Cleveland, OH.

EFFECT OF STRAIN AND STRESS ON THE RELATIVE DIMENSIONS OF THE 'HARD' AND 'SOFT' REGIONS IN CREPT NaCl SINGLE CRYSTALS

S. V. RAJ and ALAN D. FREED (NASA, Lewis Research Center, Cleveland, OH) Scripta Metallurgica et Materialia (ISSN 0956-716X) vol. 27, no. 12 Dec. 15, 1992 p. 1741-1746. Research supported by IBM Corp refs Copyright

It is shown that the $L \exp h$ and $L \exp s$ ratio, where these are respectively the average dimensions of the hard and soft regions as a function of stress and strain in crept NaCl single crystals, significantly influences the steady-state creep and power-law breakdown in these crystals. This is suggested to be due to a change in the internal stresses of the material. The present observations also indicate that steady-state creep is more likely to be influenced by the degree of refinement in the cell boundaries within the subgrains than by the formation of equiaxed subgrains under power-law conditions. O.C.

A93-18740* National Aeronautics and Space Administration.
Lewis Research Center, Cleveland, OH.

METHOD FOR CALCULATING ALLOY ENERGETICS

GUILLERMO BOZZOLO (Analex Corp., Brook Park, OH), JOHN FERRANTE (NASA, Lewis Research Center, Cleveland, OH), and JOHN R. SMITH (GM Research Labs., Warren, MI) Physical Review B - Condensed Matter, 3rd Series (ISSN 0163-1829) vol. 45, no. 1 Jan. 1, 1992 p. 493-496. refs Copyright

A semiempirical method for the computation of alloy energies is introduced. It is based on the equivalent-crystal theory of defect-formation energies in elemental solids. The method is both simple and accurate. Heats of formation as a function of composition are computed for some binary alloys of Cu, Ni, Al, Ag, Pd, Pt, and Au using the heats of solution in the dilute limit as experimental input. The separation of heats into strain and chemical components helps in understanding the energetics. In addition, lattice-parameter contractions seen in solid solutions of Ag and Au are accurately predicted. Good agreement with experiment is obtained in all cases. Author

A93-19740* National Aeronautics and Space Administration.
Lewis Research Center, Cleveland, OH.

PREDICTION OF DISLOCATION GENERATION DURING BRIDGMAN GROWTH OF GaAs CRYSTALS

C. T. TSAI (Florida Atlantic Univ., Boca Raton), M. W. YAO (Ohio Aerospace Inst., Brook Park), and ARNON CHAIT (NASA, Lewis Research Center, Cleveland, OH) Journal of Crystal Growth (ISSN 0022-0248) vol. 125, no. 1-2 Nov. 1992 p. 69-80. refs

(Contract NAG3-1314)

Copyright

Dislocation densities are generated in GaAs single crystals due to the excessive thermal stresses induced by temperature variations during growth. A viscoplastic material model for GaAs, which takes into account the movement and multiplication of dislocations in the plastic deformation, is developed according to Haasen's theory.

The dislocation density is expressed as an internal state variable in this dynamic viscoplastic model. The deformation process is a nonlinear function of stress, strain rate, dislocation density and temperature. The dislocation density in the GaAs crystal during vertical Bridgman growth is calculated using a nonlinear finite element model. The dislocation multiplication in GaAs crystals for several temperature fields obtained from thermal modeling of both the GTE GaAs experimental data and artificially designed data are investigated. Author

A93-20643* National Aeronautics and Space Administration. Lewis Research Center, Cleveland, OH.

SINGLE LIQUID SOURCE PLASMA-ENHANCED METALORGANIC CHEMICAL VAPOR DEPOSITION OF HIGH-QUALITY YBa₂Cu₃O_{7-x} THIN FILMS

JIMING ZHANG, ROBIN A. GARDINER, PETER S. KIRLIN, ROBERT W. BOERSTLER, and JOHN STEINBECK (Advanced Technology Materials, Inc., Danbury, CT) Applied Physics Letters (ISSN 0003-6951) vol. 61, no. 24 Dec. 14, 1992 p. 2884-2886. Previously announced in STAR as N93-13100 Research supported by DARPA and U.S. Navy refs (Contract NAS3-25932)

Copyright

High quality YBa₂Cu₃O_{7-x} films were grown in-situ on LaAlO₃ (100) by a novel single liquid source plasma-enhanced metalorganic chemical vapor deposition process. The metalorganic complexes M(thd) (sub n), (thd = 2,2,6,6-tetramethyl-3,5-heptanedionate; M = Y, Ba, Cu) were dissolved in an organic solution and injected into a vaporizer immediately upstream of the reactor inlet. The single liquid source technique dramatically simplifies current CVD processing and can significantly improve the process reproducibility. X-ray diffraction measurements indicated that single phase, highly c-axis oriented YBa₂Cu₃O_{7-x} was formed in-situ at substrate temperature 680 C. The as-deposited films exhibited a mirror-like surface, had transition temperature T(sub cO) approximately equal to 89 K, Delta T(sub c) less than 1 K, and Jc (77 K) = 10(exp 6) A/sq cm. Author

A93-26198* National Aeronautics and Space Administration. Lewis Research Center, Cleveland, OH.

GIANT SUPPRESSION OF FLUX-FLOW RESISTIVITY IN HEAVY-ION IRRADIATED TL₂Ba₂Ca₂Cu₃O₁₀ FILMS - INFLUENCE OF LINEAR DEFECTS ON VORTEX TRANSPORT

R. C. BUDHANI, M. SUENAGA (Brookhaven National Lab., Upton, NY), and S. H. LIU (Nebraska Univ., Lincoln) Physical Review Letters (ISSN 0031-9007) vol. 69, no. 26 Dec. 28, 1992 p. 3816-3819. refs

(Contract DE-AC02-76CH-00016; NAG3-886)

Copyright

A large shift of the onset of flux-flow resistivity and the irreversibility line H(irr)(T) to higher temperatures is observed in TL₂Ba₂Ca₂Cu₃O₁₀ films containing linear defects created by Ag(+21) ion irradiation. The H(irr)(T), which has a characteristic L shape in highly anisotropic TI and Bi based cuprates, becomes more like that of YBa₂Cu₃O₇ in the presence of these defects. The Jc at 77 K also shows a large increase as a result of flux localization at the defects. The transport data indicate that in the H-T plane above H(irr)(T) of the unirradiated material, an ensemble of unoccupied defects is required for effective pinning of each flux line in the system. Author

A93-26930* National Aeronautics and Space Administration. Lewis Research Center, Cleveland, OH.

ENHANCEMENT OF PHOTOLUMINESCENCE INTENSITY OF GAAS WITH CUBIC GAS CHEMICAL VAPOR DEPOSITED USING A STRUCTURALLY DESIGNED SINGLE-SOURCE PRECURSOR

ANDREW N. MACINNES, MICHAEL B. POWER, ANDREW R. BARRON (Harvard Univ., Cambridge, MA), PHILLIP P. JENKINS, and ALOYSIUS F. HEPP (NASA, Lewis Research Center, Cleveland, OH) Applied Physics Letters (ISSN 0003-6951) vol. 62, no. 7 Feb. 15, 1993 p. 711-713. Research supported by

Aluminum Research Board, Inc refs

Copyright

A two order-of-magnitude enhancement of photoluminescence intensity relative to untreated GaAs has been observed for GaAs surfaces coated with chemical vapor-deposited GaS. The increase in photoluminescence intensity can be viewed as an effective reduction in surface recombination velocity and/or band bending. The gallium cluster /-(t-Bu)GaS/4 was used as a single-source precursor for the deposition of GaS thin films. The cubane core of the structurally characterized precursor is retained in the deposited film producing a cubic phase. Furthermore, a near-epitaxial growth is observed for the GaS passivating layer. Films were characterized by transmission electron microscopy, X-ray powder diffraction, and X-ray photoelectron and Rutherford backscattering spectroscopies. Author

A93-32132* National Aeronautics and Space Administration. Lewis Research Center, Cleveland, OH.

INTERFACE DEPENDENCE OF BAND OFFSETS IN LATTICE-MATCHED ISOVALENT HETEROJUNCTIONS

WALTER R. L. LAMBRECHT and BENJAMIN SEGALL (Case Western Reserve Univ., Cleveland, OH) Physical Review B - Condensed Matter, 3rd Series (ISSN 0163-1829) vol. 41, no. 12 April 15, 1990 p. 8353-8358. Research supported by DARPA refs

(Contract N00013-86-K-0773; NAG3-954; NSF PHY-87-0036P)

Copyright

Using a previously developed self-consistent dipole theory, we find that the interface dependence of band offsets for lattice-matched isovalent heterojunction is generally small. Specifically, we find the difference between the (001) and (110) band offsets for the common-anion heterojunctions AlP/GaP, AlAs/GaAs, AlSb/GaSb, and CdTe/HgTe to be, at most, 0.02 eV. An investigation of the various details in the calculations leads to an error estimate of +/-0.03 eV; the differences are therefore insignificant. For the noncommon-anion systems, the difference between two different bonding configurations of the (001) interface is noted. Although the differences between the various interfaces are found to be slightly larger than for the common-anion cases, the only significant difference is found to occur between the In-Sb and Ga-As (001) interfaces, where it is 0.1 eV. In this case, the (110) band offset lies midway between the two. Author

A93-34655* National Aeronautics and Space Administration. Lewis Research Center, Cleveland, OH.

ELLIPSOMETRIC STUDY OF Si(0.5)Ge(0.5)/SI STRAINED-LAYER SUPERLATTICES

R. M. SIEG (Cleveland State Univ.; NASA, Lewis Research Center, OH), S. A. ALTEROVITZ (NASA, Lewis Research Center, Cleveland, OH), E. T. CROKE, and M. J. HARRELL (Hughes Research Labs., Malibu, CA) Applied Physics Letters (ISSN 0003-6951) vol. 62, no. 14 April 5, 1993 p. 1626-1628. refs

Copyright

We present an ellipsometric study of two Si(0.5)Ge(0.5)/Si strained-layer superlattices grown by MBE at low temperature (500 C), and compare our results with X-ray diffraction (XRD) estimates. Excellent agreement is obtained between target values, XRD, and ellipsometry when one of two available Si(x)Ge(1-x) databases is used. We show that ellipsometry can be used to nondestructively determine the number of superlattice periods, layer thicknesses, Si(x)Ge(1-x) composition, and oxide thickness without resorting to additional sources of information. We also note that we do not observe any strain effect on the E1 critical point. Author (revised)

A93-35198* National Aeronautics and Space Administration. Lewis Research Center, Cleveland, OH.

ROOM-TEMPERATURE DETERMINATION OF TWO-DIMENSIONAL ELECTRON GAS CONCENTRATION AND MOBILITY IN HETEROSTRUCTURES

S. E. SCHACHAM, R. A. MENA, E. J. HAUGLAND, and S. A. ALTEROVITZ (NASA, Lewis Research Center, Cleveland, OH)

Applied Physics Letters (ISSN 0003-6951) vol. 62, no. 11 March 15, 1993 p. 1283-1285. refs
Copyright

A technique for determination of room-temperature two-dimensional electron gas (2DEG) concentration and mobility in heterostructures is presented. Using simultaneous fits of the longitudinal and transverse voltages as a function of applied magnetic field, we were able to separate the parameters associated with the 2DEG from those of the parallel layer. Comparison with the Shubnikov-de Haas data derived from measurements at liquid helium temperatures proves that the analysis of the room-temperature data provides an excellent estimate of the 2DEG concentration. In addition we were able to obtain for the first time the room-temperature mobility of the 2DEG, an important parameter to device application. Both results are significantly different from those derived from conventional Hall analysis. Author

A93-35697* National Aeronautics and Space Administration. Lewis Research Center, Cleveland, OH.

ELLIPSOMETRIC STUDY OF METAL-ORGANIC CHEMICALLY VAPOR DEPOSITED III-V SEMICONDUCTOR STRUCTURES
SAMUEL A. ALTEROVITZ (NASA, Lewis Research Center, Cleveland, OH), PATRICIA A. SEKULA-MOISE (Spire Corp., Bedford, MA), ROBERT M. SIEG, MARK N. DROTOS, and NANCY A. BOGNER (Cleveland State Univ., OH) Thin Solid Films (ISSN 0040-6090) vol. 220 1992 p. 241-246. refs
Copyright

An ellipsometric study of MOCVD-grown layers of AlGaAs and InGaAs in thick films and strained layer complex structures is presented. It is concluded that the ternary composition of thick nonstrained layers can be accurately determined to within experimental errors using numerical algorithms. In the case of complex structures, thickness of all layers and the alloy composition of nonstrained layers can be determined simultaneously, provided that the correlations between parameters is no higher than 0.9. AIAA

A93-39362* National Aeronautics and Space Administration. Lewis Research Center, Cleveland, OH.

ELLIPSOMETRIC STUDY OF AMBIENT-PRODUCED OVERLAYER GROWTH RATE ON YBA₂Cu₃O_{7-x} FILMS
ROBERT M. SIEG (Cleveland State Univ., OH), SAMUEL A. ALTEROVITZ, and JOSEPH D. WARNER (NASA, Lewis Research Center, Cleveland, OH) Journal of Applied Physics (ISSN 0021-8979) vol. 73, no. 9 May 1, 1993 p. 4357-4361. refs
Copyright

An ellipsometric study of ambient-reaction-produced BaCO₃ overlayer growth on laser-ablated YBCO is presented as a function of time. The effects of the anisotropy of YBCO on the ellipsometric data inversion process are discussed, and it is concluded that with certain restrictions on the data acquisition method, the anisotropic substrate can be adequately modeled by its isotropic pseudodielectric function for the purpose of overlayer thickness estimation. It is found that after an initial period of rapid growth attributed to the chemical reaction of the exposed surface bonds, the BaCO₃ overlayer growth is linear at 1-2 Å per day. This slow growth rate is attributed to the complexity of the BaCO₃-forming reaction, together with the need for ambient reactants to diffuse through the overlayer. Author (revised)

A93-39854* National Aeronautics and Space Administration. Lewis Research Center, Cleveland, OH.

ATOMIC PROBE MICROSCOPY OF 3C SiC FILMS GROWN ON 6H SiC SUBSTRATES
A. J. STECKL, M. D. ROTH (Cincinnati Univ., OH), J. A. POWELL, and D. J. LARKIN (NASA, Lewis Research Center, Cleveland, OH) Applied Physics Letters (ISSN 0003-6951) vol. 62, no. 20 May 17, 1993 p. 2545-2547. Research supported by Ohio Edison Materials Technology Center refs
Copyright

The surface of 3C SiC films grown on 6H SiC substrates has been studied by atomic probe microscopy in air. Atomic-scale images of the 3C SiC surface have been obtained by STM which

confirm the 111 line type orientation of the cubic 3C layer grown on the 0001 plane type surface of the hexagonal 6H substrate. The nearest-neighbor atomic spacing for the 3C layer has been measured to be 3.29 ± 0.2 Å, which is within 7 percent of the bulk value. Shallow terraces in the 3C layer have been observed by STM to separate regions of very smooth growth in the vicinity of the 3C nucleation point from considerably rougher 3C surface regions. These terraces are oriented at right angles to the growth direction. Atomic force microscopy has been used to study etch pits present on the 6H substrate due to high temperature HCl cleaning prior to CVD growth of the 3C layer. The etch pits have hexagonal symmetry and vary in depth from 50 nm to 1 micron.

Author (revised)

A93-40049 National Aeronautics and Space Administration. Lewis Research Center, Cleveland, OH.

PHOTOLUMINESCENCE INTENSITY ENHANCEMENT OF GaAs BY VAPOR-DEPOSITED GAS - A RATIONAL APPROACH TO SURFACE PASSIVATION

PHILLIP P. JENKINS (Sverdrup Technology, Inc., Brook Park, OH), ALOYSIUS F. HEPP (NASA, Lewis Research Center, Cleveland, OH), MICHAEL B. POWER (NASA, Lewis Research Center, Cleveland, OH; Harvard Univ., Cambridge, MA), ANDREW N. MACINNES (Harvard Univ., Cambridge; Gallia, Inc., Weston, MA), and ANDREW R. BARRON (Harvard Univ., Cambridge, MA) In Chemical perspectives of microelectronic materials III Pittsburgh, PA Materials Research Society (MRS Symposium Proceedings, Vol. 282) 1993 p. 111-116. Research supported by National Research Council, NASA, and Aluminum Research Board, Inc refs

Copyright

A two order-of-magnitude enhancement of photoluminescence intensity relative to untreated GaAs has been observed for GaAs surfaces coated with chemical vapor-deposited GaS. The increase in photoluminescence intensity can be viewed as an effective reduction in surface recombination velocity and/or band bending. The gallium cluster (/t-Bu/GaS)₄ was used as a single-source precursor for the deposition of GaS thin films. The cubane core of the structurally-characterized precursor is retained in the deposited film producing a cubic phase. Furthermore, a near-epitaxial growth is observed for the GaS passivating layer. Films were characterized by transmission electron microscopy, X-ray powder diffraction, and X-ray photoelectron and Rutherford backscattering spectroscopies. Author

A93-40271* National Aeronautics and Space Administration. Lewis Research Center, Cleveland, OH.

COMPOSITION DEPENDENCE OF SUPERCONDUCTIVITY IN YBa₂(Cu_{3-x}Al_x)O_{7-y}

N. P. BANSAL (NASA, Lewis Research Center, Cleveland, OH) Journal of Materials Science (ISSN 0022-2461) vol. 28, no. 9 May 1, 1993 p. 2433-2437. Previously announced in STAR as N92-24715 refs

Copyright

Eleven different compositions in the system YBa₂(Cu_{3-x}Al_x)O_{7-y} (x = 0 to 0.3) have been synthesized and characterized by electrical resistivity measurements, powder X-ray diffraction, and scanning electron microscopy. The superconducting transition temperature T_{sub c} (onset) was almost unaffected by the presence of alumina due to its limited solubility in YBa₂Cu₃O_{7-x}. However, T_{sub c} (R = 0) gradually decreased, and the resistive tails became longer with increasing Al₂O₃ concentration. This was probably due to formation of BaAl₂O₄ and other impurity phases from chemical decomposition of the superconducting phase by reaction with Al₂O₃. Author

A93-40564* National Aeronautics and Space Administration. Lewis Research Center, Cleveland, OH.

HIGH QUALITY FLAME DEPOSITED DIAMOND FILMS FOR INFRARED OPTICAL WINDOWS

Y. TZENG and R. PHILLIPS (Auburn Univ., AL) In Applications of diamond films and related materials; Proceedings of the 1st International Conference, Auburn, AL, Aug. 17-22, 1991

Amsterdam Elsevier 1991 p. 189-196. Research supported by the U.S. Navy, Alabama Research Inst., and NASA refs
Copyright

The IR absorption in polycrystalline diamond films deposited in oxygen-acetylene flames is characterized using FTIR. The one-phonon absorption coefficient in the region from 7 to 12 microns that is related to extrinsic defects in the diamond films shows a strong dependence on the flame conditions as well as the substrate temperature. A high degree of diamond crystalline perfection, as judged from the undetectable one-phonon absorption, is achieved under the optimized deposition conditions for our flame setup. This is further supported by the sharp Raman peak at 1332/cm as well as the high purity in crystal orientation according to the X-ray diffraction pattern measured for the high quality diamond films. Author (revised)

A93-43587* National Aeronautics and Space Administration. Lewis Research Center, Cleveland, OH.

DIRECT OBSERVATION OF POROUS SiC FORMED BY ANODIZATION IN HF

JOSEPH S. SHOR (Kulite Semiconductor Products, Inc., Leonia, NJ), ILANA GRIMBERG, BEN-ZION WEISS (Technion - Israel Inst. of Technology, Haifa), and ANTHONY D. KURTZ (Kulite Semiconductor Products, Inc., Leonia, NJ) Applied Physics Letters (ISSN 0003-6951) vol. 62, no. 22 May 31, 1993 p. 2836-2838. Research supported by NASA refs
Copyright

A process for forming porous SiC from single-crystal SiC wafers has been demonstrated. Porous SiC can be fabricated by anodizing n-type 6H-SiC in HF under UV illumination. TEM reveals pores of sizes 10-30 nm with interpore spacings ranging from roughly 5 to 150 nm. This is the first reported direct observation of porous SiC formation. Author (revised)

A93-44568* National Aeronautics and Space Administration. Lewis Research Center, Cleveland, OH.

LOW TEMPERATURE PHASE FORMATION OF TL-BASED SUPERCONDUCTING THIN FILMS IN REDUCED OXYGEN ATMOSPHERE

C. Y. WU, F. FOONG, S. H. LIOU (Nebraska Univ., Lincoln), and J. C. HO (Wichita State Univ., KS) IEEE Transactions on Applied Superconductivity (ISSN 1051-8223) vol. 3, no. 1, pt. 3 March 1993 p. 1205-1207. 1992 Applied Superconductivity Conference, Chicago, IL, Aug. 23-28, 1992, Proceedings. Pt. 2. A93-44558 18-33 refs
(Contract NAG3-886)
Copyright

Tl-Ba-Cu-O superconducting thin films were prepared by magnetron sputtering with postannealing in a reduced oxygen atmosphere. Single-phase $\text{Ti}_2\text{Ba}_2\text{Ca}_2\text{Cu}_3\text{O}(x)$ can form on the MgO substrate at 800 C under $\text{P}(\text{O}_2)$ about 0.1 atm. However the phase formation temperature can be affected by the starting composition of the film. $\text{Ti}_1\text{Ba}_2\text{Ca}_2\text{Cu}_3\text{O}(x)$ phase can be formed by simply lowering the Ti_2O pressure. The thermal stability of $\text{Ti}_1\text{Ba}_2\text{Ca}_2\text{Cu}_3\text{O}(x)$ phase was studied by resistivity measurements at high temperatures. Author

A93-44607* National Aeronautics and Space Administration. Lewis Research Center, Cleveland, OH.

PROCESSING, ELECTRICAL AND MICROWAVE PROPERTIES OF SPUTTERED TL-CA-BA-CU-O SUPERCONDUCTING THIN FILMS

G. SUBRAMANYAM, V. J. KAPOOR (Cincinnati Univ., OH), C. M. CHOREY (Sverdrup Technology, Inc., Cleveland, OH), and K. B. BHASIN (NASA, Lewis Research Center, Cleveland, OH) IEEE Transactions on Applied Superconductivity (ISSN 1051-8223) vol. 3, no. 1, pt. 3 March 1993 p. 1749-1752. 1992 Applied Superconductivity Conference, Chicago, IL, Aug. 23-28, 1992, Proceedings. Pt. 2. A93-44558 18-33 Research supported by NASA refs
Copyright

A reproducible fabrication process has been established for TiCaBaCuO thin films on LaAlO_3 substrates by RF magnetron

sputtering and post-deposition processing methods. Electrical transport properties of the thin films were measured on patterned four-probe test devices. Microwave properties of the films were obtained from unloaded Q measurements of all-superconducting ring resonators. This paper describes the processing, electrical and microwave properties of $\text{Ti}_2\text{Ca}_1\text{Ba}_2\text{Cu}_2\text{O}(x)$ 2122-plane phase thin films. Author

A93-44822* National Aeronautics and Space Administration. Lewis Research Center, Cleveland, OH.

ALUMINUM ACCEPTOR FOUR PARTICLE BOUND EXCITON COMPLEX IN 4H, 6H, AND 3C SiC

L. L. CLEMEN, R. P. DEVATY, M. F. MACMILLAN, M. YOGANATHAN, W. J. CHOYKE (Pittsburgh Univ., PA), D. J. LARKIN, J. A. POWELL (NASA, Lewis Research Center, Cleveland, OH), J. A. EDMOND, and H. S. KONG (Cree Research, Inc., Durham, NC) Applied Physics Letters (ISSN 0003-6951) vol. 62, no. 23 June 7, 1993 p. 2953-2955. Research supported by U.S. Navy and DARPA refs
Copyright

Evidence is presented for a four particle acceptor complex in 3C, 6H, and 4H SiC, obtained in low-temperature photoluminescence and cathodoluminescence experiments. The new lines were observed in p-type films lightly doped with aluminum, of 6H, 4H, and 3C SiC grown on the silicon (0001) face of 6H SiC under special conditions. The lines increase in intensity as more aluminum is added during growth. The multiplicity of observed lines is consistent with symmetry-based models similar to those which have been proposed to describe 4A centers in p-type zincblende semiconductors. AIAA

A93-46188* National Aeronautics and Space Administration. Lewis Research Center, Cleveland, OH.

SPECTROSCOPIC ELLIPSOMETRY STUDIES OF HF TREATED Si (100) SURFACES

HUADE YAO, JOHN A. WOOLLAM (Nebraska Univ., Lincoln), and SAMUEL A. ALTEROVITZ (NASA, Lewis Research Center, Cleveland, OH) Applied Physics Letters (ISSN 0003-6951) vol. 62, no. 25 June 21, 1993 p. 3324-3326. refs
(Contract NAG3-154)
Copyright

Both ex situ and in situ spectroscopic ellipsometry (SE) measurements were employed to investigate the effect of HF cleaning on Si surfaces. The hydrogen-terminated (H-terminated) Si surface was modeled as an equivalent dielectric layer, and monitored in real time by SE measurements. The SE analyses indicate that, after a 20-sec 9:1 HF dip without rinse, the Si (100) surface was passivated by the hydrogen termination and remained chemically stable. Roughness of the HF-etched bare Si (100) surface was observed, in an ultrahigh vacuum chamber (UHV), and analyzed by the in situ SE. Evidence for desorption of the H-terminated Si surface layer, after being heated to about 550 C in the UHV chamber, is presented and discussed. This is the first use of an ex situ and in situ real-time, nondestructive technique capable of showing state of passivation, the rate of reoxidation, and the surface roughness of the H-terminated Si surfaces. Author (revised)

A93-46729* National Aeronautics and Space Administration. Lewis Research Center, Cleveland, OH.

NUMERICAL MODEL FOR DENDRITIC SOLIDIFICATION OF BINARY ALLOYS

S. D. FELICELLI, J. C. HEINRICH, and D. R. POIRIER (Arizona Univ., Tucson) Numerical Heat Transfer, Part B: Fundamentals (ISSN 1040-7790) vol. 23, no. 4 June 1993 p. 461-481. Research supported by Cray Research, Inc., San Diego Supercomputer Center, and Atomic Energy Commission of Argentina refs
(Contract NAG3-1060)
Copyright

A finite element model capable of simulating solidification of binary alloys and the formation of freckles is presented. It uses a single system of equations to deal with the all-liquid region, the

dendritic region, and the all-solid region. The dendritic region is treated as an anisotropic porous medium. The algorithm uses the bilinear isoparametric element, with a penalty function approximation and a Petrov-Galerkin formulation. Numerical simulations are shown in which an $\text{NH}_4\text{Cl-H}_2\text{O}$ mixture and a Pb-Sn alloy melt are cooled. The solidification process is followed in time. Instabilities in the process can be clearly observed and the final compositions obtained.

Author (revised)

A93-50787* National Aeronautics and Space Administration. Lewis Research Center, Cleveland, OH.

MINORITY CARRIER DIFFUSION LENGTH AND EDGE SURFACE-RECOMBINATION VELOCITY IN INP

ROSHANAK HAKIMZADEH (Sverdrup Technology, Inc., Brook Park; Case Western Reserve Univ., Cleveland, OH) and SHEILA G. BAILEY (NASA, Lewis Research Center, Cleveland, OH) *Journal of Applied Physics* (ISSN 0021-8979) vol. 74, no. 2 July 15, 1993 p. 1118-1123. refs

Copyright

A scanning electron microscope was used to obtain the electron-beam-induced current (EBIC) profiles in InP specimens containing a Schottky barrier perpendicular to the scanned (edge) surface. An independent technique was used to measure the edge surface-recombination velocity. These values were used in a fit of the experimental EBIC data with a theoretical expression for normalized EBIC (Donolato, 1982) to obtain the electron (minority carrier) diffusion length.

Author (revised)

A93-51917* National Aeronautics and Space Administration. Lewis Research Center, Cleveland, OH.

CLOSED-AMPOULE DIFFUSION OF SULFUR INTO CD-DOPED INP SUBSTRATES - DEPENDENCE OF S PROFILES ON DIFFUSION TEMPERATURE AND TIME

MIRCEA FAUR, MARIA FAUR (Cleveland State Univ., OH), FRANK HONECY (NASA, Lewis Research Center, Cleveland, OH), CHANDRA GORADIA, MANJU GORADIA (Cleveland State Univ., OH), DOUGLAS JAYNE (Case Western Reserve Univ., Cleveland, OH), and RALPH CLARK (Cleveland State Univ., OH) *Journal of Vacuum Science and Technology B* (ISSN 0734-211X) vol. 10, no. 4 July-Aug. 1992 p. 1277-1284. refs

(Contract NAG3-2696)

Copyright

In order to optimize the fabrication of $n(+)-p$ InP solar cells made by closed-ampoule diffusion of sulfur into p-InP: Cd substrates, we have investigated the influence of diffusion conditions on sulfur diffusion profiles. We show that S diffusion in InP is dominated by the P vacancy mechanism and is not characterized by a complementary error function as expected for an infinite source diffusion. The S diffusion mechanism in p-InP is qualitatively explained by examining the depth profiles of S, P, and In in the emitter layer and by taking into account the presence and composition of different compounds found to form in the In-P-S-O-Cd system as a result of diffusion.

Author (revised)

A93-52600* National Aeronautics and Space Administration. Lewis Research Center, Cleveland, OH.

EXTENSION OF A NEW SEMIEMPIRICAL METHOD (BFS) AND THE STUDY OF GROUND STATE PROPERTIES OF BINARY ALLOYS

GUILLERMO BOZZOLO (Analex Corp., Brook Park, OH) and JOHN FERRANTE (NASA, Lewis Research Center, Cleveland, OH) *In Materials theory and modelling Pittsburgh, PA Materials Research Society (MRS Symposia Proceedings. Vol. 291)* 1993 p. 389-394. refs

Copyright

We extend the method of Bozzolo, Ferrante and Smith (BFS) for the study of alloy energetics to include a description of the local environment in specific ordered structures. The concept of bond-diagrams is introduced and applied to fcc binary compounds. A simple example of the parameterization of the bond-diagrams is done with reference to available first-principles calculations of Ni-Pt ordered alloys.

A93-52708* National Aeronautics and Space Administration. Lewis Research Center, Cleveland, OH.

ELECTRONIC PASSIVATION OF N- AND P-TYPE GAAS USING CHEMICAL VAPOR DEPOSITED GAS

MASSOOD TABIB-AZAR, SOON KANG (Case Western Reserve Univ., Cleveland, OH), ANDREW N. MACINNES (Gallia, Inc., Weston, MA), MICHAEL B. POWER, ANDREW R. BARRON (Harvard Univ., Cambridge, MA), PHILLIP P. JENKINS, and ALOYSIUS F. HEPP (NASA, Lewis Research Center, Cleveland, OH) *Applied Physics Letters* (ISSN 0003-6951) vol. 63, no. 5 Aug. 2, 1993 p. 625-627. Research supported by NSF, NASA, and National Research Council refs

Copyright

We report on the electronic passivation of n- and p-type GaAs using CVD cubic GaS. Au/GaS/GaAs-fabricated metal-insulator-semiconductor (MIS) structures exhibit classical high-frequency capacitor vs voltage (C-V) behavior with well-defined accumulation and inversion regions. Using high- and low-frequency C-V, the interface trap densities of about $10 \times 10^{11}/\text{eV per sq cm}$ on both n- and p-type GaAs are determined. The electronic condition of GaS/GaAs interface did not show any deterioration after a six week time period.

Author (revised)

A93-53693* National Aeronautics and Space Administration. Lewis Research Center, Cleveland, OH.

DIMINISHING SIGN ANOMALY AND SCALING BEHAVIOR OF THE MIXED-STATE HALL RESISTIVITY IN $\text{TL}_2\text{Ba}_2\text{Ca}_2\text{Cu}_3\text{O}_{10}$ FILMS CONTAINING COLUMNAR DEFECTS

R. C. BUDHANI (Brookhaven National Lab., Upton, NY), S. H. LIOU (Nebraska Univ., Lincoln), and Z. X. CAI (Brookhaven National Lab., Upton, NY) *Physical Review Letters* (ISSN 0031-9007) vol. 71, no. 4 July 26, 1993 p. 621-624. refs

(Contract DE-AC02-76CH-00016; NAG3-886)

Copyright

The issues of sign reversal of the Hall voltage and scaling between longitudinal (ρ_{xx}) and Hall (ρ_{xy}) resistivities are studied in $\text{TL}_2\text{Ba}_2\text{Ca}_2\text{Cu}_3\text{O}_{10}$ films in which the vortex dynamics is drastically changed by flux pinning at heavy-ion-irradiation-induced linear defects. While the sign anomaly diminishes with increasing defect concentration, the power law ρ_{xy} is approximately equal to $\rho_{xx} \exp \beta$, $\beta = 1.85 \pm 0.1$, holds even after irradiation. This result shows that the scaling is a universal feature of the mixed state in this system. The sign anomaly, on the other hand, is not consistent with a model that invokes pinning-induced backflow in the vortex core as the mechanism for this effect.

Author (revised)

A93-54844* National Aeronautics and Space Administration. Lewis Research Center, Cleveland, OH.

ROOM TEMPERATURE SYNTHESIS OF COPPER INDIUM DISELENIDE IN NON-AQUEOUS SOLUTION USING AN ORGANOINDIUM REAGENT

ALOYSIUS F. HEPP, MARIA T. ANDRAS, SHEILA G. BAILEY (NASA, Lewis Research Center, Cleveland, OH), and STAN A. DURAJ (Cleveland State Univ., OH) *Advanced Materials for Optics and Electronics* (ISSN 1057-9257) vol. 1 1992 p. 99-103. Research supported by National Research Council refs

(Contract NCC3-162)

A novel two-phase synthesis of CuInSe_2 at 25 C from Cu_2Se and Cp_3In in 4-methylpyridine has been discovered. Characterization of the material produced shows it to be platelet-shaped crystallites with an average particle size of 10 microns, less than 2 percent C and H, with a small amount of unidentified crystalline impurity. The results demonstrate that it is possible to produce from solution a material that is ordinarily synthesized in bulk or films at much higher temperatures or using extraneous reagents and/or electrons. The use of a solid-state reagent as a starting material which is converted to another solid-state compound by an organometallic reagent has tremendous potential to produce precursors for a wide range of solid-state

materials of interest to the electronics, defense, and aerospace communities. AIAA

A93-55601* National Aeronautics and Space Administration. Lewis Research Center, Cleveland, OH.

THERMAL OXIDATION OF SINGLE-CRYSTAL SILICON CARBIDE - KINETIC, ELECTRICAL, AND CHEMICAL STUDIES
J. B. PETIT (Sverdrup Technology, Inc., Brook Park, OH), P. G. NEUDECK (Ohio Aerospace Inst., Brook Park), L. G. MATUS, and J. A. POWELL (NASA, Lewis Research Center, Cleveland, OH)
In Amorphous and crystalline silicon carbide IV Berlin Springer-Verlag (Springer Proceedings in Physics. Vol. 71) 1992 p. 190-196. refs
Copyright

This paper presents kinetic data from oxidation studies of the polar faces for 3C and 6H SiC in wet and dry oxidizing ambients. Values for the linear and parabolic rate constants were obtained, as well as preliminary results for the activation energies of the rate constants. Examples are presented describing how thermal oxidation can be used to map polytypes and characterize defects in epitaxial layers grown on low tilt angle 6H SiC substrates. Interface widths were measured using Auger electron spectroscopy (AES) with Ar ion beam depth profiling and variable angle spectroscopic ellipsometry (VASE) with effective medium approximation (EMA) models. Preliminary electrical measurements of MOS capacitors are also presented.

A93-55602* National Aeronautics and Space Administration. Lewis Research Center, Cleveland, OH.

GROWTH AND CHARACTERIZATION OF 3C-SiC AND 6H-SiC FILMS ON 6H-SiC WAFERS
J. A. POWELL (NASA, Lewis Research Center, Cleveland, OH), J. B. PETIT (Sverdrup Technology, Inc., Brook Park, OH), L. G. MATUS (NASA, Lewis Research Center, Cleveland, OH), and S. E. LEMPNER (Cleveland State Univ., OH) *In* Amorphous and crystalline silicon carbide III Berlin Springer-Verlag (Springer Proceedings in Physics. Vol. 56) 1992 p. 313-321. refs
Copyright

Single crystal SiC films were grown by CVD on vicinal (0001) SiC wafers cut from boules produced by the modified sublimation method. Wafers with tilt angles less than 0.5 deg yielded 3C-SiC; tilt angles of 3 to 4 deg resulted in 6H-SiC films. The surface morphology of these films, up to 24 microns thick, were investigated as a function of growth parameters such as the Si/C ratio in the input gases and the presence of dopant materials such as nitrogen and trimethylaluminum. Author (revised)

N93-12325*# National Aeronautics and Space Administration. Lewis Research Center, Cleveland, OH.

CONDUCTOR-BACKED COPLANAR WAVEGUIDE RESONATORS OF Y-Ba-Cu-O AND TL-Ba-Ca-Cu-O ON LAALO3

F. A. MIRANDA, K. B. BHASIN, M. A. STAN (Kent State Univ., OH.), K. S. KONG (TRW, Inc., Redondo Beach, CA.), and T. ITOH (California Univ., Los Angeles.) Oct. 1992 6 p Presented at the 1992 Applied Superconductivity Conference, Chicago, IL, 23-28 Aug. 1992; sponsored by IEEE
(Contract RTOP 506-72-1B)
(NASA-TM-105890; E-7356; NAS 1.15:105890) Avail: CASI HC A02/MF A01

Conductor-backed coplanar waveguide (CBCPW) resonators operating at 10.8 GHz have been fabricated from Ti-Ba-Ca-O (TBCCO) and Y-Ba-Cu-O (YBCO) thin films on LaAlO₃. The resonators consist of a coplanar waveguide (CPW) patterned on the superconducting film side of the LaAlO₃ substrate with a gold ground plane coated on the opposite side. These resonators were tested in the temperature range from 14 to 106 K. At 77 K, the best of our TBCCO and YBCO resonators have an unloaded quality factor (Q₀) 7 and 4 times, respectively, larger than that of a similar all-gold resonator. In this study, the Q₀'s of the TBCCO resonators were larger than those of their YBCO counterparts throughout the aforementioned temperature range. Author

N93-17413*# National Aeronautics and Space Administration. Lewis Research Center, Cleveland, OH.

PROCESS FOR THE CONTROLLED GROWTH OF SINGLE-CRYSTAL FILMS OF SILICON CARBIDE POLYTYPES ON SILICON CARBIDE WAFERS Patent Application
DAVID J. LARKIN, inventor (to NASA) and J. ANTHONY POWELL, inventor (to NASA) 9 Nov. 1992 23 p
(NASA-CASE-LEW-15222-3; NAS 1.71:LEW-15222-3; US-PATENT-APPL-SN-973505) Avail: CASI HC A03/MF A01

A method for the controlled growth of single-crystal semiconductor-device-quality films of SiC polytypes on vicinal (0001) SiC wafers with low tilt angles is presented. Both homoepitaxial and heteroepitaxial SiC films can be produced on the same wafer. In particular, 3C-SiC and 6H-SiC films can be produced within selected areas of the same 6H-SiC wafer. NASA

N93-26928*# National Aeronautics and Space Administration. Lewis Research Center, Cleveland, OH.

SILICON CARBIDE SEMICONDUCTOR TECHNOLOGY FOR HIGH TEMPERATURE AND RADIATION ENVIRONMENTS
LAWRENCE G. MATUS *In its* Nuclear Propulsion Technical Interchange Meeting, Volume 1 p 445-452 1993
Avail: CASI HC A02/MF A04

Viewgraphs on silicon carbide semiconductor technology and its potential for enabling electronic devices to function in high temperature and high radiation environments are presented. Topics covered include silicon carbide; sublimation growth of 6H-SiC boules; SiC chemical vapor deposition reaction system; 6H silicon carbide p-n junction diode; silicon carbide MOSFET; and silicon carbide JFET radiation response. CASI

77

THERMODYNAMICS AND STATISTICAL PHYSICS

Includes quantum mechanics; theoretical physics; and Bose and Fermi statistics.

A93-19838* National Aeronautics and Space Administration. Lewis Research Center, Cleveland, OH.

THE SUSCEPTIBILITY CRITICAL EXPONENT FOR A NONAQUEOUS IONIC BINARY MIXTURE NEAR A CONSOLUTE POINT

KAI C. ZHANG, MATTHEW E. BRIGGS, ROBERT W. GAMMON (Maryland Univ., College Park), and J. M. H. LEVELT SENGERS (NIST, Chemical Science and Technology Lab., Gaithersburg, MD) Journal of Chemical Physics (ISSN 0021-9606) vol. 97, no. 11 Dec. 1, 1992 p. 8692-8697. refs
(Contract NAS3-25370)
Copyright

We report turbidity measurements of a nonaqueous ionic solution of triethyl n-hexylammonium triethyl n-hexylboride in diphenyl ether. A classical susceptibility critical exponent $\gamma = 1.01 \pm 0.01$ is obtained over the reduced temperature range t between values of 0.1 and 0.0001. The best fits of the sample transmission had a standard deviation of 0.39 percent over this range. Ising and spherical model critical exponents are firmly excluded. The correlation length amplitude ξ_0 from fitting is 1.0 ± 0.2 nm which is much larger than values found in neutral fluids and some aqueous binary mixtures. Author

A93-21695* National Aeronautics and Space Administration. Lewis Research Center, Cleveland, OH.

COARSENING FOLLOWING A MORPHOLOGICAL INSTABILITY IN THE ONE-SIDED MODEL

JORGE VINALS (Florida State Univ., Tallahassee) and DAVID JASNOW (Pittsburgh Univ., PA) Physical Review A (ISSN 1050-2947) vol. 46, no. 12 Dec. 15, 1992 p. 7777-7782. refs

(Contract NSF DMR-89-14621; NAG3-1284;
DE-FC05-85ER-25000)
Copyright

We study the coarsening of the interfacial pattern separating two coexisting phases after the pattern becomes morphologically unstable. Shortly after the instability, the scale of the structure is given by the most unstable wave number in the linear regime. At later times, nonlinear interactions cause the structure to coarsen. Coarsening is studied by monitoring the time dependence of the two-dimensional power spectrum of the pattern, especially for wave vectors transverse to the direction of growth. Characteristic length scales of the pattern obtained from moments of the power spectrum are asymptotically linear in time. Furthermore, the power spectrum is seen to satisfy a scaling relation, in agreement with previous studies. A normal-velocity autocorrelation function is calculated and found to decay substantially over length scales that are of the order of the scale of the pattern. The issue of spatial anisotropy in the correlation functions is also discussed.

Author

A93-28624* National Aeronautics and Space Administration.
Lewis Research Center, Cleveland, OH.

APPLICATION OF RADIATIVE IMAGE TRANSFER THEORY TO THE ASSESSMENT OF THE OVERALL OTF AND CONTRAST DEGRADATION OF AN IMAGE IN AN INHOMOGENEOUS TURBULENT AND TURBID ATMOSPHERE

ROBERT M. MANNING (NASA, Lewis Research Center, Cleveland, OH) *In* Characterization, propagation, and simulation of sources and backgrounds II; Proceedings of the Meeting, Orlando, FL, Apr. 20-22, 1992 Bellingham, WA Society of Photo-Optical Instrumentation Engineers 1992 p. 205-214. refs
Copyright

A perturbation-theoretic approximation of the radiative transfer equation which neglects photon dispersion is used as a modeling basis for the propagation of the image of a self-luminous target through a turbulent atmosphere which also possesses inhomogeneously distributed turbidity along the propagation path. A contrast ratio is then introduced which provides an indicator of the relative contribution of the unscattered or coherent image component to that of the scattered or incoherent image component. Analytical expressions are then derived for the contrast ratio from the approximate form of the radiative transfer equation in the case of an inhomogeneously dispersed Joss thunderstorm rain distribution in the presence of turbulence. The case is clearly demonstrated for the need to consider a measure of the points of demarcation at which the dominant roles of the scattering processes due to turbidity and turbulence are exchanged. Such a measure can provide a performance parameter for the application of adaptive optics methods that are specific to the particular dominant scattering mechanism given the prevailing target size, total propagation length and overall propagation parameters.

Author

A93-30124* National Aeronautics and Space Administration.
Lewis Research Center, Cleveland, OH.

DISCRETE ORDINATES SOLUTIONS OF NONGRAY RADIATIVE TRANSFER WITH DIFFUSELY REFLECTING WALLS

J. A. MENART (Minnesota Univ., Minneapolis), HAEOK S. LEE (NASA, Lewis Research Center, Cleveland, OH), and TAE-KUK KIM (Chung-Ang Univ., Seoul, Republic of Korea) ASME, Transactions, Journal of Heat Transfer (ISSN 0022-1481) vol. 115, no. 1 Feb. 1993 p. 184-193. ASME, National Heat Transfer Conference, Minneapolis, MN, July 28-31, 1991 Research supported by Univ. of Minnesota refs
(Contract NSF CTS-84-51076)
Copyright

Nongray gas radiation in a plane parallel slab bounded by gray, diffusely reflecting walls is studied using the discrete ordinates method. The spectral equation of transfer is averaged over a narrow wavenumber interval preserving the spectral correlation effect. The governing equations are derived by considering the history of multiple reflections between two reflecting walls. A closure approximation is applied so that only a finite number of reflections

have to be explicitly included. The closure solutions express the physics of the problem to a very high degree and show relatively little error. Numerical solutions are obtained by applying a statistical narrow-band model for gas properties and a discrete ordinates code. The net radiative wall heat fluxes and the radiative source distributions are obtained for different temperature profiles. A zeroth-degree formulation, where no wall reflection is handled explicitly, is sufficient to predict the radiative transfer accurately for most cases considered, when compared with increasingly accurate solutions based on explicitly tracing a larger number of wall reflections without any closure approximation applied.

Author

A93-31427* National Aeronautics and Space Administration.
Lewis Research Center, Cleveland, OH.

DISCRETE ORDINATES SOLUTIONS FOR RADIATIVELY PARTICIPATING MEDIA IN A CYLINDRICAL ENCLOSURE

SLAH JENDOUBI (Minnesota Univ., Minneapolis), HAEOK S. LEE (NASA, Lewis Research Center, Cleveland, OH), and RAE-KUK KIM (Chung-Ang Univ., Seoul, Republic of Korea) Journal of Thermophysics and Heat Transfer (ISSN 0887-8722) vol. 7, no. 2 Apr.-June 1993 p. 213-219. Previously cited in issue 10, p. 1689, Accession no. A92-28185 AIAA, Aerospace Sciences Meeting and Exhibit, 30th, Reno, NV, Jan. 6-9, 1992, AIAA Paper 92-0123 Research supported by Minnesota Supercomputer Inst. refs

(Contract NSF CBT-84-51076)

Copyright

A93-46505*# National Aeronautics and Space Administration.
Lewis Research Center, Cleveland, OH.

THERMOPHYSICAL PROPERTIES OF GAS PHASE URANIUM TETRAFLUORIDE

YOICHI WATANABE and SAMIM ANGHAE (Florida Univ., Gainesville) Jul. 1993 9 p. AIAA, Thermophysics Conference, 28th, Orlando, FL, July 6-9, 1993 Research supported by SDIO refs

(Contract NAS3-26314)

(AIAA PAPER 93-2758) Copyright

Thermophysical data of gaseous uranium tetrafluoride (UF₄) are theoretically obtained by taking into account dissociation of molecules at high temperatures (2000-6000 K). Determined quantities include specific heat, optical opacity, diffusion coefficient, viscosity, and thermal conductivity. A computer program is developed for the calculation.

A93-46569*# National Aeronautics and Space Administration.
Lewis Research Center, Cleveland, OH.

MODELING VOID GROWTH AND MOVEMENT WITH PHASE CHANGE IN THERMAL ENERGY STORAGE CANISTERS

DOUGLAS DARLING, DAVID NAMKOONG, and J. R. L. SKARDA (NASA, Lewis Research Center, Cleveland, OH) Jul. 1993 11 p. AIAA, Thermophysics Conference, 28th, Orlando, FL, July 6-9, 1993 refs

(AIAA PAPER 93-2832) Copyright

A scheme was developed to model the thermal hydrodynamic behavior of thermal energy storage salts. The model included buoyancy, surface tension, viscosity, phases change with density difference, and void growth and movement. The energy, momentum, and continuity equations were solved using a finite volume formulation. The momentum equation was divided into two pieces. The void growth and void movement are modeled between the two pieces of the momentum equations. Results showed this scheme was able to predict the behavior of thermal energy storage salts.

N93-12967*# National Aeronautics and Space Administration.
Lewis Research Center, Cleveland, OH.

COMPUTER PROGRAM FOR CALCULATING AND FITTING THERMODYNAMIC FUNCTIONS

BONNIE J. MCBRIDE and SANFORD GORDON (Gordon, Sanford, Cleveland, OH) Nov. 1992 91 p Sponsored in cooperation with Sverdrup Technology, Inc., Brook Park, OH

(Contract NAS3-25266; RTOP 505-62-52)
(NASA-RP-1271; E-5894; NAS 1.61:1271) Avail: CASI HC
A05/MF A01

A computer program is described which (1) calculates thermodynamic functions (heat capacity, enthalpy, entropy, and free energy) for several optional forms of the partition function, (2) fits these functions to empirical equations by means of a least-squares fit, and (3) calculates, as a function of temperature, heats of formation and equilibrium constants. The program provides several methods for calculating ideal gas properties. For monatomic gases, three methods are given which differ in the technique used for truncating the partition function. For diatomic and polyatomic molecules, five methods are given which differ in the corrections to the rigid-rotator harmonic-oscillator approximation. A method for estimating thermodynamic functions for some species is also given. Author

N93-19977*# National Aeronautics and Space Administration. Lewis Research Center, Cleveland, OH.

THERMODYNAMIC DATA FOR FIFTY REFERENCE ELEMENTS
BONNIE J. MCBRIDE, SANFORD GORDON (Gordon, Sanford, Cleveland, OH), and MARTIN A. RENO (Heidelberg Coll., Tiffin, OH.) Washington Jan. 1993 240 p
(Contract RTOP 505-62-52)
(NASA-TP-3287; E-6874; NAS 1.60:3287) Avail: CASI HC
A11/MF A03

This report is a compilation of thermodynamic functions of 50 elements in their standard reference state. The functions are $C_p(\text{sup } 0)$, $H(\text{sup } 0)(T) - H(\text{sup } 0)(0)$, $S(\text{sup } 0)(T)$, and $-G(\text{sup } 0)(T) - H(\text{sup } 0)(0)$ for the elements Ag, Al, Ar, B, Ba, Be, Br₂, C, Ca, Cd, Cl₂, Co, Cr, Cs, Cu, F₂, Fe, Ge, H₂, He, Hg, I₂, K, Kr, Li, Mg, Mn, Mo, N₂, Na, Nb, Ne, Ni, O₂, P, Pb, Rb, S, Si, Sn, Sr, Ta, Th, Ti, U, V, W, Xe, Zn, and Zr. Deuterium D₂ and electron gas $e(\text{sup } -)$ are also included. The data are tabulated as functions of temperature as well as given in the form of least-squares coefficients for two functional forms for $C_p(\text{sup } 0)$ with integration constants for enthalpy and entropy. One functional form for $C_p(\text{sup } 0)$ is a fourth-order polynomial and the other has two additional terms, one with $T(\text{exp } -1)$ and the other with $T(\text{exp } -2)$. The gases Ar, D₂, $e(\text{sup } -)$, H₂, He, Kr, N₂, Ne, O₂, and Xe are tabulated for temperatures from 100 to 20,000 K. The remaining gases Cl₂ and F₂ are tabulated from 100 to 6000 K and 1000 to 6000 K. The second functional form for $C_p(\text{sup } 0)$ has an additional interval from 6000 to 20,000 K for the gases tabulated to 20,000 K. The fits are constrained so that the match at the common temperature endpoints. The temperature ranges for the condensed species vary with range of the data, phase changes, and shapes of the $C_p(\text{sup } 0)$ curves. Author (revised)

81

ADMINISTRATION AND MANAGEMENT

Includes management planning and research.

N93-26205*# National Aeronautics and Space Administration. Lewis Research Center, Cleveland, OH.

DESIGN AND IMPLEMENTATION OF A PILOT ORIENTATION PROGRAM FOR NEW NASA ENGINEERING EMPLOYEES
RONALD E. GRAHAM, RANDALL B. FURNAS, and MARIA BABULA May 1993 14 p
(NASA-TM-105907; E-7687; NAS 1.15:105907) Avail: CASI HC
A03/MF A01

This paper describes the design and field testing of an orientation program for new employees of NASA Lewis Research Center's Engineering Directorate. A group of new employees designed the program using a series of TQM analysis techniques. The program objectives were: provide consistent treatment for new employees; assist management and clerical staff with their responsibility for orientation; introduce the employee to as many

facets of the organization as possible; allow the employee to feel like a member of the organization as early as possible; maximize the use of existing services; and use up-to-date information. The major aspects of the program included: training of management and clerical staff; lab tours and briefings describing the organization; shepherding, using senior employees as shepherds; a handbook of information about the center and the directorate; a package of information about northeast Ohio; and social activities involving the new employees and shepherds. The program was tested on a pilot group of six new employees over a four month period and was considered to be highly successful by both the employees and management. Aspects of the program have subsequently been adopted for center-wide use. Author

N93-71876*# National Aeronautics and Space Administration. Lewis Research Center, Cleveland, OH.

LOW THRUST PROPULSION

D. BYERS In NASA, Washington, SSTAC/ARTS Review of the Draft Integrated Technology Plan (ITP). Volume 2: Propulsion Systems 18 p 1991
(PR3) Avail: CASI HC A03/MF A03

The topics presented are covered in viewgraph form. The objective is to provide technologies for a broad range of future space systems, such as: planetary and earth-orbital spacecrafts; space station and tended large space systems; and earth-to-orbit and orbit transfer vehicles. CASI

N93-71878*# National Aeronautics and Space Administration. Lewis Research Center, Cleveland, OH.

SPACE R/T BASE: PROPULSION (HIGH THRUST CHEMICAL)

S. GORLAND In NASA, Washington, SSTAC/ARTS Review of the Draft Integrated Technology Plan (ITP). Volume 2: Propulsion Systems 13 p 1991
(PR5) Avail: CASI HC A03/MF A03

The topics presented are covered in viewgraph form. The programmatic objective is to provide a technology base and maintain an institutional capability for continued advances in the development of advanced space propulsion systems to support launch, upper stage, orbit transfer and ascent/descent engines. The technical objectives are to study: (1) validated design and analytical codes for cryogenic turbopump bearings and seals; (2) design methodologies and diagnostic capabilities for combustion stability; and (3) reduced operations cost, increase life, safety, higher energy density propellants, and in-situ engine concepts. CASI

N93-71879*# National Aeronautics and Space Administration. Lewis Research Center, Cleveland, OH.

CRYOGENIC FLUID MANAGEMENT (BASE R/T): CRYOGENIC FLUID SYSTEMS, CRYOGENIC ORBITAL NITROGEN EXPERIMENT (CONE), CRYOGENIC ORBITAL HYDROGEN EXPERIMENT (COHE). (TRANSPORTATION FOCUSED TECHNOLOGY)

PAT SYMONS In NASA, Washington, SSTAC/ARTS Review of the Draft Integrated Technology Plan (ITP). Volume 2: Propulsion Systems 24 p 1991
(PR6) Avail: CASI HC A03/MF A03

The topics presented are covered in viewgraph form. The concluded remarks are: (1) advanced cryogenic fluid systems technology is enhancing or enabling to all known transportation scenarios for space exploration; (2) an integrated/coordinated program involving LeRC/MSFC has been formulated to address all known CFM needs - new needs should they develop, can be accommodated within available skills/facilities; (3) all required/experienced personnel and facilities are finally in place - data from initial ground-based experiments is being collected and analyzed - small scale STS experiments are nearing flight - program is beginning to yield significant results; (4) future proposed funding to primarily come from two sources; and (5) cryogenic fluid experimentation is essential to provide required technology and assure implementation in future NASA missions. CASI

N93-71885*# National Aeronautics and Space Administration. Lewis Research Center, Cleveland, OH.

FOCUSED TECHNOLOGY: NUCLEAR PROPULSION

THOMAS J. MILLER /in NASA, Washington, SSTAC/ARTS Review of the Draft Integrated Technology Plan (ITP). Volume 2: Propulsion Systems 40 p 1991

(PR12) Avail: CASI HC A03/MF A03

The topics presented are covered in viewgraph form and include: nuclear thermal propulsion (NTP), which challenges (1) high temperature fuel and materials, (2) hot hydrogen environment, (3) test facilities, (4) safety, (5) environmental impact compliance, and (6) concept development, and nuclear electric propulsion (NEP), which challenges (1) long operational lifetime, (2) high temperature reactors, turbines, and radiators, (3) high fuel burn-up reactor fuels, and designs, (4) efficient, high temperature power conditioning, (5) high efficiency, and long life thrusters, (6) safety, (7) environmental impact compliance, and (8) concept development.

CASI

82

DOCUMENTATION AND INFORMATION SCIENCE

Includes information management; information storage and retrieval technology; technical writing; graphic arts; and micrography.

N93-14796*# National Aeronautics and Space Administration. Lewis Research Center, Cleveland, OH.

BIBLIOGRAPHY OF LEWIS RESEARCH CENTER TECHNICAL PUBLICATIONS ANNOUNCED IN 1991

Oct. 1992 401 p

(NASA-TM-105595; E-6928; NAS 1.15:105595) Avail: CASI HC A18/MF A04

This compilation of abstracts describes and indexes the technical reporting that resulted from the scientific engineering work performed and managed by the Lewis Research Center in 1991. All the publications were announced in the 1991 issues of STAR (Scientific and Technical Aerospace Reports) and/or IAA (International Aerospace Abstracts). Included are research reports, journal articles, conference presentations, patents and patent applications, and theses.

Author

N93-23002*# National Aeronautics and Space Administration. Lewis Research Center, Cleveland, OH.

TECHNICAL REPORT WRITING

CAROL A. VIDOLI 1992 28 p

(NASA-TM-105419; E-6832; NAS 1.15:105419) Avail: CASI HC A03/MF A01

This manual covers the fundamentals of organizing, writing, and reviewing NASA technical reports. It was written to improve the writing skills of LeRC technical authors and the overall quality of their reports.

Author

N93-25922*# National Aeronautics and Space Administration. Lewis Research Center, Cleveland, OH.

SUBBAND CODING FOR IMAGE DATA ARCHIVING

DANIEL GLOVER and S. C. KWATRA (Toledo Univ., OH.) /in NASA. Goddard Space Flight Center, The Space and Earth Science Data Compression Workshop p 3-16 1993

Avail: CASI HC A03/MF A02

The use of subband coding on image data is discussed. An overview of subband coding is given. Advantages of subbanding for browsing and progressive resolution are presented. Implementations for lossless and lossy coding are discussed. Algorithm considerations and simple implementations of subband systems are given.

Author

N93-28130*# National Aeronautics and Space Administration. Lewis Research Center, Cleveland, OH.

PICTURE DATA COMPRESSION CODER USING SUBBAND/TRANSFORM CODING WITH A

LEMPEL-ZIV-BASED CODER Patent Application

DANIEL R. GLOVER, inventor (to NASA) 11 Mar. 1993 18 p

(NASA-CASE-LEW-15700-1; NAS 1.71:LEW-15700-1;

US-PATENT-APPL-SN-029520) Avail: CASI HC A03/MF A01

The present invention is a subband/transform coding system. The invention produces a digitally encoded signal which is a transformed version of an analog signal such as a video signal. The digitally encoded signal maintains the integrity of the original signal but allows transmission at low data rates. The transformed data is organized into frequency subbands with the lowest frequency subband being a low resolution version of the original signal. Once the data is transformed into subbands, it is coded with statistical coders. The statistical coder used in this invention is a Lempel-Ziv-based coder.

NASA

83

ECONOMICS AND COST ANALYSIS

Includes cost effectiveness studies.

A93-44996# National Aeronautics and Space Administration, Washington, DC.

THE NASA COMPUTATIONAL FLUID DYNAMICS (CFD) PROGRAM - BUILDING TECHNOLOGY TO SOLVE FUTURE CHALLENGES

PAMELA F. RICHARDSON (NASA, Washington), DOUGLAS L. DWOYER (NASA, Langley Research Center, Hampton, VA), PAUL KUTLER (NASA, Ames Research Center, Moffett Field, CA), and LOUIS A. POVINELLI (NASA, Lewis Research Center, Cleveland, OH) /in AIAA Computational Fluid Dynamics Conference, 11th, Orlando, FL, July 6-9, 1993, Technical Papers. Pt. 1 Washington American Institute of Aeronautics and Astronautics 1993 p. 16-20.

(AIAA PAPER 93-3292) Copyright

This paper presents the NASA Computational Fluid Dynamics program in terms of a strategic vision and goals as well as NASA's financial commitment and personnel levels. The paper also identifies the CFD program customers and the support to those customers. In addition, the paper discusses technical emphasis and direction of the program and some recent achievements. NASA's Ames, Langley, and Lewis Research Centers are the research hubs of the CFD program while the NASA Headquarters Office of Aeronautics represents and advocates the program.

Author

85

URBAN TECHNOLOGY AND TRANSPORTATION

Includes applications of space technology to urban problems; technology transfer; technology assessment; and surface and mass transportation.

A93-26012* National Aeronautics and Space Administration. Lewis Research Center, Cleveland, OH.

ELECTRIC AND HYBRID ELECTRIC VEHICLE STUDY UTILIZING A TIME-STEPPING SIMULATION

JEFFREY G. SCHREIBER, RICHARD K. SHALTENS (NASA, Lewis Research Center, Cleveland, OH), and DONALD G. BEREMAND (Sverdrup Technology, Inc., Cleveland, OH) /in IECEC '92; Proceedings of the 27th Intersociety Energy Conversion Engineering Conference, San Diego, CA, Aug. 3-7, 1992. Vol. 3

Warrendale, PA Society of Automotive Engineers, Inc. 1992
p. 3.159-3.165. refs
Copyright

The applicability of NASA's advanced power technologies to electric and hybrid vehicles was assessed using a time-stepping computer simulation to model electric and hybrid vehicles operating over the Federal Urban Driving Schedule (FUDS). Both the energy and power demands of the FUDS were taken into account and vehicle economy, range, and performance were addressed simultaneously. Results indicate that a hybrid electric vehicle (HEV) configured with a flywheel buffer energy storage device and a free-piston Stirling convertor fulfills the emissions, fuel economy, range, and performance requirements that would make it acceptable to the consumer. It is noted that an assessment to determine which of the candidate technologies are suited for the HEV application has yet to be made. A proper assessment should take into account the fuel economy and range, along with the driveability and total emissions produced. O.G.

90

ASTROPHYSICS

Includes cosmology; celestial mechanics; space plasmas; and interstellar and interplanetary gases and dust.

A93-10615 National Aeronautics and Space Administration. Lewis Research Center, Cleveland, OH.

N-POINT CORRELATION FUNCTIONS IN THE CFA AND SSRS REDSHIFT DISTRIBUTION OF GALAXIES

ENRIQUE GAZTANAGA (NASA/Fermilab Astrophysics Center, Batavia, IL) *Astrophysical Journal*, Part 2 - Letters (ISSN 0004-637X) vol. 398, no. 1 Oct. 10, 1992 p. L17-L20. Research supported by DOE and Fulbright/MEC refs (Contract NAGW-2381)
Copyright

Using counts in cells, we estimate the volume-average N-point galaxy correlation functions for $N = 2, 3$, and 4, in redshift samples of the CfA and SSRS catalogs. Volume-limited samples of different sizes are used to study the uncertainties at different scales, the shot noise, and the problem with the boundaries. The hierarchical constants S_3 and S_4 agree well in all samples in CfA and SSRS, with average $S_3 = 194 \pm 0.07$ and $S_4 = 4.56 \pm 0.53$. We compare these results with estimates obtained from angular catalogs and recent analysis over IRAS samples. The amplitudes S_j seem larger in real space than in redshift space, although the values from the angular analysis correspond to smaller scales, where we might expect larger nonperturbative effects. It is also found that S_3 and S_4 are smaller for IRAS than for optical galaxies. This, together with the fact that IRAS galaxies have smaller amplitude for the above correlation functions, indicates that the density fluctuations of IRAS galaxies cannot be simply proportional to the density fluctuations of optical galaxies, i.e., biasing has to be nonlinear between them. Author

A93-11451 National Aeronautics and Space Administration. Lewis Research Center, Cleveland, OH.

GRAVITATIONAL WAVES FROM FIRST-ORDER COSMOLOGICAL PHASE TRANSITIONS

ARTHUR KOSOWSKY, MICHAEL S. TURNER, and RICHARD WATKINS (NASA/Fermilab Astrophysics Center, Batavia; Chicago Univ., IL) *Physical Review Letters* (ISSN 0031-9007) vol. 69, no. 14 Oct. 5, 1992 p. 2026-2029. Research supported by DOE and NSF refs (Contract NAGW-2381)
Copyright

A first-order cosmological phase transition that proceeds through the nucleation and collision of true-vacuum bubbles is a potent source of gravitational radiation. Possibilities for such include first-order inflation, grand-unified-theory-symmetry breaking, and

electroweak-symmetry breaking. We have calculated gravity-wave production from the collision of two scalar-field vacuum bubbles, and, using an approximation based upon these results, from the collision of 20 to 30 vacuum bubbles. We present estimates of the relic background of gravitational waves produced by a first-order phase transition. Author

A93-11876 National Aeronautics and Space Administration. Lewis Research Center, Cleveland, OH.

DARK MATTER, LONG-RANGE FORCES, AND LARGE-SCALE STRUCTURE

BEN-AMI GRADWOHL and JOSHUA A. FRIEMAN (NASA/Fermilab Astrophysics Center, Batavia, IL) *Astrophysical Journal*, Part 1 (ISSN 0004-637X) vol. 398, no. 2 Oct. 20, 1992 p. 407-424. Research supported by DOE refs (Contract NAGW-2381)
Copyright

If the dark matter in galaxies and clusters is nonbaryonic, it can interact with additional long-range fields that are invisible to experimental tests of the equivalence principle. We discuss the astrophysical and cosmological implications of a long-range force coupled only to the dark matter and find rather tight constraints on its strength. If the force is repulsive (attractive), the masses of galaxy groups and clusters (and the mean density of the universe inferred from them) have been systematically underestimated (overestimated). We explore the consequent effects on the two-point correlation function, large-scale velocity flows, and microwave background anisotropies, for models with initial scale-invariant adiabatic perturbations and cold dark matter. Author

A93-16303 National Aeronautics and Space Administration. Lewis Research Center, Cleveland, OH.

COSMIC STRING WITH A LIGHT MASSIVE NEUTRINO

ANDREAS ALBRECHT and ALBERT STEBBINS (NASA/Fermilab Astrophysics Center, Batavia, IL) *Physical Review Letters* (ISSN 0031-9007) vol. 69, no. 18 Nov. 2, 1992 p. 2615-2618. Research supported by DOE refs (Contract NAGW-2381)
Copyright

We have estimated the power spectra of density fluctuations produced by cosmic strings with neutrino hot dark matter (HDM). Normalizing at 8/h Mpc, we find that the spectrum has more power on small scales than HDM + inflation, less than cold dark matter (CDM) + inflation, and significantly less the CDM + strings. With HDM, large wakes give significant contribution to the power on the galaxy scale and may give rise to large sheets of galaxies. Author

A93-17638 National Aeronautics and Space Administration. Lewis Research Center, Cleveland, OH.

THE INFLATION SECTOR OF EXTENDED INFLATION

EDWARD W. KOLB (NASA/Fermilab Astrophysics Center, Batavia; Chicago Univ., IL) *In Primordial nucleosynthesis and evolution of early universe; Proceedings of the International Conference, Tokyo, Japan, Sept. 4-8, 1990* Dordrecht, Netherlands Kluwer Academic Publishers 1991 p. 153-165. Research supported by DOE refs (Contract NAGW-1340)
Copyright

In extended inflation, the inflationary era is brought to a close by the process of percolation of true vacuum bubbles produced in a first-order phase transition. This paper discusses several effects that might obtain if the universe undergoes an inflationary first-order phase transition. Author

A93-17645 National Aeronautics and Space Administration. Lewis Research Center, Cleveland, OH.

LATE-TIME COSMOLOGICAL PHASE TRANSITIONS

DAVID N. SCHRAMM (Chicago Univ.; NASA/Fermilab Astrophysics Center, Batavia, IL) *In Primordial nucleosynthesis and evolution of early universe; Proceedings of the International Conference, Tokyo, Japan, Sept. 4-8, 1990* Dordrecht, Netherlands Kluwer

Academic Publishers 1991 p. 225-242. Previously announced in STAR as N91-18918 Research supported by DOE refs (Contract NAGW-1321; NAGW-1340; NSF AST-88-22595) Copyright

It is shown that the potential galaxy formation and large scale structure problems of objects existing at high redshifts (Z approx. greater than 5), structures existing on scales of 100 M pc as well as velocity flows on such scales, and minimal microwave anisotropies ($(\Delta T)/T$) (approx. less than $10(\exp -5)$) can be solved if the seeds needed to generate structure form in a vacuum phase transition after decoupling. It is argued that the basic physics of such a phase transition is no more exotic than that utilized in the more traditional GUT scale phase transitions, and that, just as in the GUT case, significant random Gaussian fluctuations and/or topological defects can form. Scale lengths of approx. 100 M pc for large scale structure as well as approx. 1 M pc for galaxy formation occur naturally. Possible support for new physics that might be associated with such a late-time transition comes from the preliminary results of the SAGE solar neutrino experiment, implying neutrino flavor mixing with values similar to those required for a late-time transition. It is also noted that a see-saw model for the neutrino masses might also imply a tau neutrino mass that is an ideal hot dark matter candidate. However, in general either hot or cold dark matter can be consistent with a late-time transition.

Author

A93-17646 National Aeronautics and Space Administration. Lewis Research Center, Cleveland, OH.

STOCHASTIC INFLATION LATTICE SIMULATIONS - ULTRA-LARGE SCALE STRUCTURE OF THE UNIVERSE

D. S. SALOPEK (NASA/Fermilab Astrophysics Center, Batavia, IL) *In* Primordial nucleosynthesis and evolution of early universe; Proceedings of the International Conference, Tokyo, Japan, Sept. 4-8, 1990 Dordrecht, Netherlands Kluwer Academic Publishers 1991 p. 253-264. Research supported by DOE refs (Contract NAGW-1340) Copyright

Non-Gaussian fluctuations for structure formation may arise in inflation from the nonlinear interaction of long wavelength gravitational and scalar fields. Long wavelength fields have spatial gradients, a ($\exp -1$), small compared to the Hubble radius, and they are described in terms of classical random fields that are fed by short wavelength quantum noise. Lattice Langevin calculations are given for a toy model with a scalar field interacting with an exponential potential where one can obtain exact analytic solutions of the Fokker-Planck equation. For single scalar field models that are consistent with current microwave background fluctuations, the fluctuations are Gaussian. However, for scales much larger than our observable Universe, one expects large metric fluctuations that are non-Gaussian. This example illuminates non-Gaussian models involving multiple scalar fields which are consistent with current microwave background limits.

Author

A93-17651* National Aeronautics and Space Administration. Lewis Research Center, Cleveland, OH.

THE BEST-FIT UNIVERSE

MICHAEL S. TURNER (NASA/Fermilab Astrophysics Center, Batavia; Chicago Univ., IL) *In* Primordial nucleosynthesis and evolution of early universe; Proceedings of the International Conference, Tokyo, Japan, Sept. 4-8, 1990 Dordrecht, Netherlands Kluwer Academic Publishers 1991 p. 337-350. Previously announced in STAR as N91-16966 Research supported by DOE refs Copyright

Inflation provides very strong motivation for a flat Universe, Harrison-Zel'dovich (constant-curvature) perturbations, and cold dark matter. However, there are a number of cosmological observations that conflict with the predictions of the simplest such model: one with zero cosmological constant. They include the age of the Universe, dynamical determinations of Ω , galaxy-number counts, and the apparent abundance of large-scale structure in the Universe. While the discrepancies are not yet serious enough to rule out the simplest and most well motivated

model, the current data point to a best-fit model with the following parameters: $\Omega_{\text{sub B}}$ approximately equal to 0.03, $\Omega_{\text{sub CDM}}$ approximately equal to 0.17, $\Omega_{\text{sub Lambda}}$ approximately equal to 0.8, and $H(\text{sub } 0)$ approximately equal to 70 km/(sec x Mpc) which improves significantly the concordance with observations. While there is no good reason to expect such a value for the cosmological constant, there is no physical principle that would rule out such.

Author

A93-21508 National Aeronautics and Space Administration. Lewis Research Center, Cleveland, OH.

THE GRAVITATIONAL WAVE CONTRIBUTION TO COSMIC MICROWAVE BACKGROUND ANISOTROPIES AND THE AMPLITUDE OF MASS FLUCTUATIONS FROM COBE RESULTS

FRANCESCO LUCCHINI, SABINO MATARRESE (Padova, Univ., Padua, Italy), and SILVIA MOLLERACH (NASA/Fermilab Astrophysics Center, Batavia, IL) *Astrophysical Journal*, Part 2 - Letters (ISSN 0004-637X) vol. 401, no. 2 Dec. 20, 1992 p. L49-L52. Research supported by MURST, Fondazione Angelo della Riccia, and DOE refs (Contract NAGW-2381) Copyright

A stochastic background of primordial gravitational waves may substantially contribute, via the Sachs-Wolfe effect, to the large-scale cosmic microwave background (CMB) anisotropies recently detected by COBE. This implies a bias in any resulting determination of the primordial amplitude of density fluctuations. We consider the constraints imposed on n is less than 1 ('tilted') power-law fluctuation spectra, taking into account the contribution from both scalar and tensor waves, as predicted by power-law inflation. The gravitational wave contribution to CMB anisotropies generally reduces the required rms level of mass fluctuation, thereby increasing the linear bias parameter, even in models where the spectral index is close to the Harrison-Zel'dovich value $n = 1$. This 'gravitational wave bias' helps to reconcile the predictions of CDM models with observations on pairwise galaxy velocity dispersion on small scales.

Author

A93-23607 National Aeronautics and Space Administration. Lewis Research Center, Cleveland, OH.

THE FIRST THREE MINUTES - 1990 VERSION

DAVID N. SCHRAMM (Chicago, Univ.; NASA/Fermilab Astrophysics Center, Batavia, IL) *In* After the first three minutes; Proceedings of the 1st Astrophysics Workshop, Univ. of Maryland, College Park, Oct. 15-17, 1990 New York American Institute of Physics 1991 p. 12-40. Research supported by DOE refs (Contract NSF AST-88-22595; NAGW-1321; NAGW-1340) Copyright

The present state of understanding of what occurred in the universe's first three minutes is reviewed. Emphasis is on the events that lead to potentially observable consequences and that are model-independent or at least generic to broad classes of models. Inflation, phase transitions, dark matter, and nucleosynthesis are summarized.

C.D.

A93-23650 National Aeronautics and Space Administration. Lewis Research Center, Cleveland, OH.

PHASE SPACE DISTRIBUTION OF HALO PARTICLES AND DETECTION OF WIMPS

DONGSU RYU (NASA/Fermilab Astrophysics Center, Batavia, IL; Princeton Univ. Observatory, NJ) and ARMANDO PEREZ (NASA/Fermilab Astrophysics Center, Batavia, IL; Valencia Univ., Spain) *In* After the first three minutes; Proceedings of the 1st Astrophysics Workshop, Univ. of Maryland, College Park, Oct. 15-17, 1990 New York American Institute of Physics 1991 p. 463-466. Research supported by DOE refs (Contract NAGW-1340) Copyright

We calculate the velocity distribution of halo particles using realistic models for the density profiles of the Galactic disk, spheroid, and halo components. We get the resulting velocity

distribution, which is different from the Maxwellian distribution of isothermal halo. We investigate the consequences concerning the time averaged count rate and the amplitude of the annual modulation in WIMPS detection experiments. Compared to the previous estimate based on the Maxwellian distribution, the time averaged count rate is up to 40 percent larger. On the other hand, the amplitude of the annual modulation is up to a factor of two larger. Author

A93-23990 National Aeronautics and Space Administration. Lewis Research Center, Cleveland, OH.

LARGE- AND SMALL-SCALE CONSTRAINTS ON POWER SPECTRA IN $\Omega = 1$ UNIVERSES

JAMES M. GELB (NASA/Fermilab Astrophysics Center, Batavia, IL), BEN-AMI GRADWOHL (NASA/Fermilab Astrophysics Center, Batavia, IL; California Univ., Los Angeles), and JOSHUA A. FRIEMAN (NASA/Fermilab Astrophysics Center, Batavia, IL) *Astrophysical Journal*, Part 2 - Letters (ISSN 0004-637X) vol. 403, no. 1 Jan. 20, 1993 p. L5-L8. refs (Contract NAGW-2381; NSF AST-90-01762; DE-FG03-91ER-40662)

Copyright

The CDM model of structure formation, normalized on large scales, leads to excessive pairwise velocity dispersions on small scales. In an attempt to circumvent this problem, we study three scenarios (all with $\Omega = 1$) with more large-scale and less small-scale power than the standard CDM model: (1) cold dark matter with significantly reduced small-scale power (inspired by models with an admixture of cold and hot dark matter); (2) cold dark matter with a non-scale-invariant power spectrum; and (3) cold dark matter with coupling of dark matter to a long-range vector field. When normalized to COBE on large scales, such models do lead to reduced velocities on small scales and they produce fewer halos compared with CDM. However, models with sufficiently low small-scale velocities apparently fail to produce an adequate number of halos. Author

A93-24627 National Aeronautics and Space Administration. Lewis Research Center, Cleveland, OH.

PROBING THE STATISTICS OF PRIMORDIAL FLUCTUATIONS AND THEIR EVOLUTION

ENRIQUE GAZTANAGA and JUN'ICHI YOKOYAMA (NASA/Fermilab Astrophysics Center, Batavia, IL) *Astrophysical Journal*, Part 1 (ISSN 0004-637X) vol. 403, no. 2 Feb. 1, 1993 p. 450-465. Research supported by DOE, Ministerio de Educacion y Ciencia of Spain, and Japan Society for the Promotion of Science refs (Contract NAGW-2381)

Copyright

The statistical distribution of fluctuations on various scales is analyzed in terms of the counts in cells of smoothed density fields, using volume-limited samples of galaxy redshift catalogs. It is shown that the distribution on large scales, with volume average of the two-point correlation function of the smoothed field less than about 0.05, is consistent with Gaussian. Statistics are shown to agree remarkably well with the negative binomial distribution, which has hierarchical correlations and a Gaussian behavior at large scales. If these observed properties correspond to the matter distribution, they suggest that our universe started with Gaussian fluctuations and evolved keeping hierarchical form. Author

A93-26263 National Aeronautics and Space Administration. Lewis Research Center, Cleveland, OH.

INFLATION AT THE ELECTROWEAK SCALE

LLOYD KNOX (Chicago Univ., IL) and MICHAEL S. TURNER (Chicago Univ.; NASA/Fermilab Astrophysics Center, Batavia, IL) *Physical Review Letters* (ISSN 0031-9007) vol. 70, no. 4 Jan. 25, 1993 p. 371-374. Research supported by DOE refs (Contract NAGW-2381)

Copyright

We present a model for slow-rollover inflation where the vacuum energy that drives inflation is of the order of $G(F) \exp -2$; unlike most models, the conversion of vacuum energy to radiation

('reheating') is moderately efficient. The scalar field responsible for inflation is a standard-model singlet, develops a vacuum expectation value of $4 \times 10 \exp 6 \text{ GeV}$, has a mass of about 1 GeV, and can play a role in electroweak phenomena. We also discuss models where the energy scale of inflation is somewhat larger, but still well below the unification scale. Author

A93-33513 National Aeronautics and Space Administration. Lewis Research Center, Cleveland, OH.

PRIMORDIAL NUCLEOSYNTHESIS AND THE ABUNDANCES OF BERYLLIUM AND BORON

DAVID THOMAS (Chicago Univ., IL), DAVID N. SCHRAMM (Chicago Univ.; NASA/Fermilab Astrophysics Center, Batavia, IL), KEITH A. OLIVE (Minnesota Univ., Minneapolis), and BRIAN D. FIELDS (Chicago Univ., IL) *Astrophysical Journal*, Part 1 (ISSN 0004-637X) vol. 406, no. 2 April 1, 1993 p. 569-579. refs (Contract DE-AC02-83ER-40105; NAGW-2381)

Copyright

The recently attained ability to make measurements of Be and B as well as to put constraints on Li-6 abundances in metal-poor stars has led to a detailed reexamination of big bang nucleosynthesis in the A is greater than about 6 regime. The nuclear reaction network has been significantly expanded, with many new rates added. It is demonstrated that although a number of A is greater than 7 reaction rates are poorly determined, even with extreme values chosen, the standard homogeneous model is unable to produce significant yields above $A = 7$, and the (Li-7)/(Li-6) ratio always exceeds 500. We also preliminarily explore inhomogeneous models, such as those inspired by a first-order quark-hadron phase transition, where regions with high neutron/proton ratios can allow some leakage up to A is greater than 7. However, models that fit the A is not greater than 7 abundances still seem to have difficulty in obtaining significant A is greater than 7 yields. Author

A93-34776 National Aeronautics and Space Administration. Lewis Research Center, Cleveland, OH.

CHEMICAL AND LUMINOSITY EVOLUTION, AND COUNTS OF GALAXIES IN A MERGER MODEL

P. COLIN (Chicago Univ.; NASA/Fermilab Astrophysics Center, Batavia, IL; Univ. Nacional Autonoma de Mexico, Coyoacan) and D. N. SCHRAMM (Chicago Univ.; NASA/Fermilab Astrophysics Center, Batavia, IL) *Astrophysical Journal*, Part 1 (ISSN 0004-637X) vol. 407, no. 2 April 20, 1993 p. 510-518. Research supported by Univ. Nacional Autonoma de Mexico refs

(Contract NSF AST-90-22629; NAGW-1321;

DE-FG02-91ER-40606)

Copyright

A merger model is applied to the chemical and luminosity evolution of galaxies. Two aspects are focused on. The first is the problem of abundance ratios as a function of metallicity. The second is related to the luminosity evolution of galaxies. In relation to the former, we calculate the evolution of several chemical elements exploring a broad space of possible star formation rates, including those derived using phenomenological arguments from a multiple merger galaxy formation scenario. We are able to reproduce the observed plateau in the ratio of the abundances of oxygen to iron versus metallicity as a direct consequence of one of the merging SFR used; we have utilized a standard Type II supernovae nucleosynthesis scenario coupled with a reasonable binary model for Type Ia supernovae and its consequent nucleosynthetic yields. Following the consequent luminosity effects in a straightforward way enables the estimation of the evolution of bolometric luminosity. We have used our recently developed code for photometric evolution of galaxies to make a preliminary computation of the number-magnitude relationship, assuming a standard picture of galaxy evolution, in the B and K bands. Author (revised)

A93-35444 National Aeronautics and Space Administration. Lewis Research Center, Cleveland, OH.

MICROWAVE ANISOTROPIES IN THE LIGHT OF THE DATA FROM THE COBE SATELLITE

SCOTT DODELSON (NASA/Fermilab Astrophysics Center, Batavia, IL) and JAY M. JUBAS (MIT, Cambridge, MA) *Physical Review Letters* (ISSN 0031-9007) vol. 70, no. 15 April 12, 1993 p. 2224-2227. Research supported by DOE and Sloan Foundation refs

(Contract NAGW-2381; NSF PHY-92-96020)

Copyright

The recent measurement of anisotropies in the cosmic microwave background by the Cosmic Background Explorer (COBE) satellite and the recent South Pole experiment offer an excellent opportunity to probe cosmological theories. We test a class of theories in which the universe today is flat and matter dominated, and primordial perturbations are adiabatic parameterized by an index n . In this class of theories the predicted signal in the South Pole experiment depends on n , the Hubble constant, and the baryon density. For $n = 1$ a large region of this parameter space is ruled out, but there is still a window open which satisfies constraints from COBE, the South Pole experiment, and big bang nucleosynthesis.

Author (revised)

A93-35579 National Aeronautics and Space Administration. Lewis Research Center, Cleveland, OH.

KURTOSIS, SKEWNESS, AND NON-GAUSSIAN COSMOLOGICAL DENSITY PERTURBATIONS

XIAOCHUN LUO and DAVID N. SCHRAMM (Chicago Univ.; NASA/Fermilab Astrophysics Center, Batavia, IL) *Astrophysical Journal*, Part 1 (ISSN 0004-637X) vol. 408, no. 1 May 1, 1993 p. 33-42. Research supported by DOE refs

(Contract NSF AST-90-22629; NAGW-1321; NAGW-2381)

Copyright

Cosmological topological defects as well as some nonstandard inflation models can give rise to non-Gaussian density perturbations. Skewness and kurtosis are the third and fourth moments that measure the deviation of a distribution from a Gaussian. Measurement of these moments for the cosmological density field and for the microwave background temperature anisotropy can provide a test of the Gaussian nature of the primordial fluctuation spectrum. In the case of the density field, the importance of measuring the kurtosis is stressed since it will be preserved through the weakly nonlinear gravitational evolution epoch. Current constraints on skewness and kurtosis of primeval perturbations are obtained from the observed density contrast on small scales and from recent COBE observations of temperature anisotropies on large scales. It is also shown how, in principle, future microwave anisotropy experiments might be able to reveal the initial skewness and kurtosis. It is shown that present data argue that if the initial spectrum is adiabatic, then it is probably Gaussian, but non-Gaussian isocurvature fluctuations are still allowed, and these are what topological defects provide.

Author (revised)

A93-38672 National Aeronautics and Space Administration. Lewis Research Center, Cleveland, OH.

EXTENSION OF THE PARKER BOUND ON THE FLUX OF MAGNETIC MONOPOLES

FRED C. ADAMS, MARCO FATUZZO, KATHERINE FREESE, GREGORY TARLE, RICHARD WATKINS (Michigan Univ., Ann Arbor), and MICHAEL S. TURNER (Chicago Univ.; NASA/Fermilab Astrophysics Center, Batavia, IL) *Physical Review Letters* (ISSN 0031-9007) vol. 70, no. 17 April 26, 1993 p. 2511-2514. refs

(Contract DE-AC02-76ER-01112; NAGW-2802; NSF

PHY-92-96020; NAGW-2381)

Copyright

The Parker bound on the flux of magnetic monopoles is extended and strengthened. A new limit on the survival and growth of a small galactic seed field is obtained which rules out the possibility that monopoles much lighter than $10 \exp 17$ GeV/sq c can provide the closure density of the universe.

AIAA

A93-44385* National Aeronautics and Space Administration. Lewis Research Center, Cleveland, OH.

DARK MATTER AND THE EQUIVALENCE PRINCIPLE

JOSHUA A. FRIEMAN (NASA/Fermilab Astrophysics Center, Batavia, IL) and BEN-AMI GRADWOHL (California Univ., Los Angeles) *Science* (ISSN 0036-8075) vol. 260, no. 5113 June 4, 1993 p. 1441, 1442. refs

Copyright

A survey is presented of the current understanding of dark matter invoked by astrophysical theory and cosmology. Einstein's equivalence principle asserts that local measurements cannot distinguish a system at rest in a gravitational field from one that is in uniform acceleration in empty space. Recent test-methods for the equivalence principle are presently discussed as bases for testing of dark matter scenarios involving the long-range forces between either baryonic or nonbaryonic dark matter and ordinary matter.

AIAA

A93-46201 National Aeronautics and Space Administration. Lewis Research Center, Cleveland, OH.

CLUMPY COLD DARK MATTER

JOSEPH SILK (California Univ., Berkeley) and ALBERT STEBBINS (NASA/Fermilab Astrophysics Center, Batavia, IL) *Astrophysical Journal* - Part 1 (ISSN 0004-637X) vol. 411, no. 2 July 10, 1993 p. 439-449. Research supported by DOE refs

(Contract NAGW-2381)

Copyright

A study is conducted of cold dark matter (CDM) models in which clumpiness will inhere, using cosmic strings and textures suited to galaxy formation. CDM clumps of 10 million solar mass/cu pc density are generated at about $z(\text{eq})$ redshift, with a sizable fraction surviving. Observable implications encompass dark matter cores in globular clusters and in galactic nuclei. Results from terrestrial dark matter detection experiments may be affected by clumpiness in the Galactic halo.

AIAA

A93-50480 National Aeronautics and Space Administration. Lewis Research Center, Cleveland, OH.

OBSERVING THE INFLATION POTENTIAL

EDMUND J. COPELAND (Sussex Univ., Brighton, United Kingdom), EDWARD W. KOLB (NASA/Fermilab Astrophysics Center, Batavia; Chicago Univ., IL), ANDREW R. LIDDLE (Sussex Univ., Brighton, United Kingdom), and JAMES E. LIDSEY (NASA/Fermilab Astrophysics Center, Batavia, IL) *Physical Review Letters* (ISSN 0031-9007) vol. 71, no. 2 July 12, 1993 p. 219-222. Research supported by SERC and DOE refs

(Contract NAGW-2381)

Copyright

We show how observations of the density perturbation (scalar) spectrum and the gravitational wave (tensor) spectrum allow a reconstruction of the potential responsible for cosmological inflation. A complete functional reconstruction or a perturbative approximation about a single scale are possible; the suitability of each approach depends on the data available. Consistency equations between the scalar and tensor spectra are derived, which provide a powerful signal of inflation.

A93-50680 National Aeronautics and Space Administration. Lewis Research Center, Cleveland, OH.

THE THREE-POINT CORRELATION FUNCTION IN AN ENSEMBLE OF THREE-DIMENSIONAL SIMULATIONS

J. N. FRY (NASA/Fermilab Astrophysics Center, Batavia, IL; Florida Univ., Gainesville), A. L. MELOTT (Cambridge Univ. Inst. of Astronomy, United Kingdom; Kansas Univ., Lawrence), and S. F. SHANDARIN *Astrophysical Journal*, Part 1 (ISSN 0004-637X) vol. 412, no. 2 Aug. 1, 1993 p. 504-512. Research supported by DOE refs

(Contract NAGW-2381; NAGW-2923; NSF AST-90-21414)

Copyright

We evaluate the three-point function in Fourier space for an ensemble of three-dimensional 128 exp 3 numerical simulations with initial power spectra characterized by spectral index $n = +1, 0, -1, -2, -3$, with no high-frequency cutoff and with cutoff

$k(c) = 16$ or $k(c) = 4$. To remove dependences on scale and on time, we present results as the reduced amplitude Q in the hierarchical model as a function of the dimensionless variable $kd(\text{rms})$, where $d(\text{rms})$ is the mean square displacement of a particle from its initial position. For scale-free initial conditions, there is no evolution in Q . For initial conditions with a cutoff, Q evolves until the scale of the cutoff is in the nonlinear regime; the results afterwards are no different from those with no initial cutoff. The transition from quasi-linear to nonlinear regimes is followed. In the quasi-linear regime, our results agree well with gravitational perturbation theory predictions, including a marked dependence on the shape of the configuration. In the nonlinear regime, the value of Q for scale-invariant initial conditions is remarkably independent of evolution epoch, of scale, and of configuration shape, and depends on spectral index roughly as $Q = 3/(3 + n)$. Author (revised)

A93-51704* National Aeronautics and Space Administration. Lewis Research Center, Cleveland, OH.

FIRST-ORDER INFLATION

MICHAEL S. TURNER (NASA/Fermilab Astrophysics Center, Batavia, IL) /n The infrared and submillimetre sky after COBE; Proceedings of the NATO Advanced Study Institute, Les Houches, France, Mar. 20-30, 1991 Dordrecht, Netherlands Kluwer Academic Publishers 1992 p. 35-74. refs

Copyright

I discuss the most recent model of inflation. In first-order inflation the inflationary epoch is associated with a first-order phase transition, with the most likely candidate being GUT symmetry breaking. The transition from the false-vacuum inflationary phase to the true-vacuum radiation-dominated phase proceeds through the nucleation and percolation of true-vacuum bubbles. The first successful and simplest model of first-order inflation, extended inflation, is discussed in some detail: evolution of the cosmic-scale factor, reheating, density perturbations, and the production of gravitational waves both from quantum fluctuations and bubble collisions. Particular attention is paid to the most critical issue in any model of first-order inflation: the requirements on the nucleation rate to ensure a graceful transition from the inflationary phase to the radiation-dominated phase. Author (revised)

A93-55051 National Aeronautics and Space Administration. Lewis Research Center, Cleveland, OH.

BIASING AND HIERARCHICAL STATISTICS IN LARGE-SCALE STRUCTURE

J. N. FRY (NASA/Fermilab Astrophysics Center, Batavia, IL; Florida Univ., Gainesville) and ENRIQUE GAZTANAGA (NASA/Fermilab Astrophysics Center, Batavia, IL; Oxford Univ., United Kingdom) Astrophysical Journal, Part 1 (ISSN 0004-637X) vol. 413, no. 2 Aug. 20, 1993 p. 447-452. Research supported by DOE refs (Contract NAGW-2381)

Copyright

In this paper we consider the consequences for galaxy formation of an arbitrary, effectively local biasing transformation of a hierarchical underlying matter distribution. We show that a general form of such a transformation preserves the hierarchical properties and the shape of the dispersion in the limit of small fluctuations, i.e., on large scales, although the values of the hierarchical amplitudes may change arbitrarily. We present expressions for the induced hierarchical amplitudes $S(g, i)$ of the galaxy distribution in terms of the matter amplitudes $S(j)$ and biasing parameters for $j = 3-7$. For higher order correlations, j greater than 2, restricting to a linear bias is not a consistent approximation even at very large scales. To draw any conclusions from the galaxy distribution about matter correlations of order j , properties of biasing must be specified completely to order $j - 1$. Author (revised)

A93-55061* National Aeronautics and Space Administration. Lewis Research Center, Cleveland, OH.

THE BORON-TO-BERYLLIUM RATIO IN HALO STARS - A SIGNATURE OF COSMIC-RAY NUCLEOSYNTHESIS IN THE EARLY GALAXY

T. P. WALKER, G. STEIGMAN (Ohio State Univ., Columbus), D. N. SCHRAMM (Chicago Univ.; NASA/Fermilab Astrophysics Center, Batavia, IL), K. A. OLIVE (Minnesota Univ., Minneapolis), and B. FIELDS (Chicago Univ.; NASA/Fermilab Astrophysics Center, Batavia, IL) Astrophysical Journal, Part 1 (ISSN 0004-637X) vol. 413, no. 2 Aug. 20, 1993 p. 562-570. Research supported by DOE and NSF refs

Copyright

We discuss Galactic cosmic-ray (GCR) spallation production of Li, Be, and B in the early Galaxy with particular attention to the uncertainties in the predictions of this model. The observed correlation between the Be abundance and the metallicity in metal-poor Population II stars requires that Be was synthesized in the early Galaxy. We show that the observations and such Population II GCR synthesis of Be are quantitatively consistent with the big bang nucleosynthesis production of Li-7. We find that there is a nearly model independent lower bound to B/Be of about 7 for GCR synthesis. Recent measurements of B/Be about 10 in HD 140283 are in excellent agreement with the predictions of Population II GCR nucleosynthesis. Measurements of the boron abundance in additional metal-poor halo stars is a key diagnostic of the GCR spallation mechanism. We also show that Population II GCR synthesis can produce amounts of Li-6 which may be observed in the hottest halo stars. Author (revised)

A93-55212 National Aeronautics and Space Administration. Lewis Research Center, Cleveland, OH.

TESTING FOR THE GAUSSIAN NATURE OF COSMOLOGICAL DENSITY PERTURBATIONS THROUGH THE THREE-POINT TEMPERATURE CORRELATION FUNCTION

XIAOCHUN LUO and DAVID N. SCHRAMM (Chicago Univ.; NASA/Fermilab Astrophysics Center, Batavia, IL) Physical Review Letters (ISSN 0031-9007) vol. 71, no. 8 Aug. 23, 1993 p. 1124-1127. Research supported by DOE refs (Contract NSF AST-90-22629; NAGW-1321; NAGW-2381)

Copyright

One of the crucial aspects of density perturbations that are produced by the standard inflation scenario is that they are Gaussian where seeds produced by topological defects tend to be non-Gaussian. The three-point correlation function of the temperature anisotropy of the cosmic microwave background radiation (CBR) provides a sensitive test of this aspect of the primordial density field. In this paper, this function is calculated in the general context of various allowed non-Gaussian models. It is shown that the Cosmic Background Explorer and the forthcoming South Pole and balloon CBR anisotropy data may be able to provide a crucial test of the Gaussian nature of the perturbations.

A93-56494 National Aeronautics and Space Administration. Lewis Research Center, Cleveland, OH.

POPULATION II LI-6 AS A PROBE OF NUCLEOSYNTHESIS AND STELLAR STRUCTURE AND EVOLUTION

GARY STEIGMAN (Ohio State Univ., Columbus), BRIAN D. FIELDS (Chicago Univ., IL), KEITH A. OLIVE (Minnesota Univ., Minneapolis), DAVID N. SCHRAMM (Chicago Univ.; NASA/Fermilab Astrophysics Center, Batavia, IL), and TERRY P. WALKER (Ohio State Univ., Columbus) Astrophysical Journal, Part 2 - Letters (ISSN 0004-637X) vol. 415, no. 1 Sept. 20, 1993 p. L35-L38. Research supported by DOE, NASA, and NSF refs

Copyright

We discuss the importance of Population II Li-6 as a diagnostic for models of primordial nucleosynthesis, cosmic-ray nucleosyntheses in the early Galaxy, and the structure and evolution of metal-poor solar-type stars. The observation of Li-6 in the subdwarf HD 84937 is shown to be consistent with the existing Population II LiBeB data within the context of a simple three-component model: (1) standard big bang nucleosynthesis, (2) Population II cosmic-ray nucleosynthesis, (3) standard (nonrotating) stellar LiBeB depletion. If this interpretation is correct, we predict a potentially detectable boron abundance for this star: about 2×10^{-12} . Subsequent Population II LiBeB observations, and in particular further observations of Population II Li-6, are

shown to be crucial to our understanding of the primordial and early galactic creation and destruction mechanisms for light elements.
Author (revised)

91

LUNAR AND PLANETARY EXPLORATION

Includes planetology; and manned and unmanned flights.

A93-13699 National Aeronautics and Space Administration. Lewis Research Center, Cleveland, OH.

PHOTOVOLTAIC ARRAYS FOR MARTIAN SURFACE POWER
JOSEPH APPELBAUM and GEOFFREY A. LANDIS (NASA, Lewis Research Center, Cleveland, OH) Aug. 1992 22 p. IAF, International Astronautical Congress, 43rd, Washington, Aug. 28-Sept. 5, 1992 Previously announced in STAR as N92-33899 refs

(Contract NAGW-2022; NAS3-25266; RTOP 506-41-11)
(IAF PAPER 92-0591) Copyright

Missions to Mars will require electric power. A leading candidate for providing power is solar power produced by photovoltaic arrays. To design such a power system, detailed information on solar-radiation availability on the Martian surface is necessary. The variation of the solar radiation on the Martian surface is governed by three factors: (1) variation in Mars-sun distance; (2) variation on solar zenith angle due to Martian season and time of day; and (3) dust in the Martian atmosphere. A major concern is the dust storms, which occur on both local and global scales. However, there is still appreciable diffuse sunlight available even at high opacity, so that solar array operation is still possible. Typical results for tracking solar collectors are also shown and compared to the fixed collectors. During the Northern Hemisphere spring and summer the isolation is relatively high, 2-5 kW-hr/sq m-day due to the low optical depth of the Martian atmosphere. These seasons, totalling a full terrestrial year, are the likely ones during which manned mission will be carried out. Author

N93-26392*# National Aeronautics and Space Administration. Lewis Research Center, Cleveland, OH.

ELECTRICAL AND CHEMICAL INTERACTIONS AT MARS WORKSHOP. PART 2: APPENDIX

1992 120 p Workshop held in Cleveland, OH, 19-20 Nov. 1991

(Contract RTOP 506-41-41)
(NASA-CP-10093-PT-2; E-7016-2-PT-2; NAS 1.55:10093-PT-2)
Avail: CASI HC A06/MF A02

The objectives of the workshop were the following: (1) to identify issues related to electrical and chemical interactions between systems and their local environments at Mars; and (2) to recommend means of addressing those issues, including the dispatch of robotic spacecraft to Mars to acquire necessary information. Presentations about Mars' surface and orbital environments, Space Exploration Initiative (SEI) systems, environmental interactions, modeling and analysis, and plans for exploration are presented in viewgraph form.

N93-26395*# National Aeronautics and Space Administration. Lewis Research Center, Cleveland, OH.

REPRESENTATIVE SYSTEMS FOR SPACE EXPLORATION

SCOTT R. GRAHAM *In its* Electrical and Chemical Interactions at Mars Workshop. Part 2: Appendix p 55-68 1992

Avail: CASI HC A03/MF A02

The topics are presented in viewgraph form and include the following: an overview of the synthesis report; specific architecture 4 implementations; and specific power systems/environment issues. Derived from text

N93-26396*# National Aeronautics and Space Administration. Lewis Research Center, Cleveland, OH.

SPACE ENVIRONMENTAL INTERACTIONS FOR THE SPACE EXPLORATION INITIATIVE

DALE C. FERGUSON *In its* Electrical and Chemical Interactions at Mars Workshop. Part 2: Appendix p 69-85 1992

Avail: CASI HC A03/MF A02

The topics are presented in viewgraph form and include the following: atomic oxygen attack; arcing and discharges; micrometeoroids and debris; state-of-the-art computer tools; current collection and snapover; effluents-neutral and ionized; and winds, dust, and contamination. Derived from text

N93-28819*# National Aeronautics and Space Administration. Lewis Research Center, Cleveland, OH.

VENUS INTERIOR STRUCTURE MISSION (VISM):

ESTABLISHING A SEISMIC NETWORK ON VENUS Abstract Only

E. R. STOFAN (Jet Propulsion Lab., California Inst. of Tech., Pasadena.), R. S. SAUNDERS (Jet Propulsion Lab., California Inst. of Tech., Pasadena.), D. SENSKE (Jet Propulsion Lab., California Inst. of Tech., Pasadena.), K. NOCK (Jet Propulsion Lab., California Inst. of Tech., Pasadena.), D. TRALLI (Jet Propulsion Lab., California Inst. of Tech., Pasadena.), P. LUNDGREN (Jet Propulsion Lab., California Inst. of Tech., Pasadena.), S. SMREKAR (Jet Propulsion Lab., California Inst. of Tech., Pasadena.), B. BANERDT (Jet Propulsion Lab., California Inst. of Tech., Pasadena.), W. KAISER (Jet Propulsion Lab., California Inst. of Tech., Pasadena.), J. DUDENHOEFER (Mechanical Technology, Inc., Latham, NY.) et al. *In* Lunar and Planetary Inst., Workshop on Advanced Technologies for Planetary Instruments, Part 1 p 23-24 1993

Avail: CASI HC A01/MF A01

Magellan radar data show the surface of Venus to contain a wide range of geologic features (large volcanoes, extensive rift valleys, etc.). Although networks of interconnecting zones of deformation are identified, a system of spreading ridges and subduction zones like those that dominate the tectonic style of the Earth do not appear to be present. In addition, the absence of a mantle low-viscosity zone suggests a strong link between mantle dynamics and the surface. As a natural follow-on to the Magellan mission, establishing a network of seismometers on Venus will provide detailed quantitative information on the large scale interior structure of the planet. When analyzed in conjunction with image, gravity, and topography information, these data will aid in constraining mechanisms that drive surface deformation. Author (revised)

92

SOLAR PHYSICS

Includes solar activity, solar flares, solar radiation and sunspots.

A93-10357 National Aeronautics and Space Administration. Lewis Research Center, Cleveland, OH.

IMPLICATIONS OF NEW GALLEX RESULTS FOR THE MIKHEYEV-SMIRNOV-WOLFENSTEIN SOLUTION OF THE SOLAR NEUTRINO PROBLEM

JAMES M. GELB (NASA/Fermilab Astrophysics Center, Batavia, IL), WAIKWOK KWONG, and S. P. ROSEN (Texas Univ., Arlington) *Physical Review Letters* (ISSN 0031-9007) vol. 69, no. 13 Sept. 28, 1992 p. 1864-1866. refs

(Contract DE-FG05-92ER-40691; NAGW-2381)

Copyright

We compare the implications for Be-7 and pp neutrinos of the two Mikheyev-Smirnov-Wolfenstein fits to the new GALLEX solar neutrino measurements. Small-mixing-angle solutions tend to suppress the former as electron neutrinos, but not the latter, and large-angle solutions tend to reduce both by about a factor of

93 SPACE RADIATION

two. The consequences for BOREXINO and similar solar neutrino-electron scattering experiments are discussed. Author

93

SPACE RADIATION

Includes cosmic radiation; and inner and outer earth's radiation belts.

A93-10355 National Aeronautics and Space Administration. Lewis Research Center, Cleveland, OH.

COSMIC MICROWAVE BACKGROUND PROBES MODELS OF INFLATION

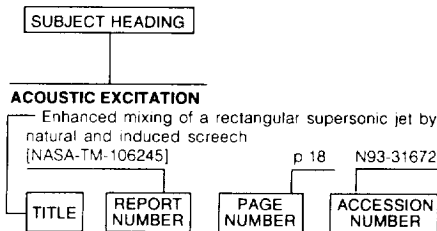
RICHARD L. DAVIS (Pennsylvania Univ., Philadelphia), HARDY M. HODGES (Harvard-Smithsonian Center for Astrophysics, Cambridge, MA), GEORGE F. SMOOT (Lawrence Berkeley Lab., Berkeley, CA), PAUL J. STEINHARDT (Pennsylvania Univ., Philadelphia), and MICHAEL S. TURNER (Chicago Univ.; NASA/Fermilab Astrophysics Center, Batavia, IL) Physical Review Letters (ISSN 0031-9007) vol. 69, no. 13 Sept. 28, 1992 p. 1856-1859. refs

(Contract DE-EY-76-C-02-3071; DE-AC03-76SF-00098; NSF PHY-89-04035; NAGW-2381; NAGW-931)

Copyright

Inflation creates both scalar (density) and tensor (gravity wave) metric perturbations. We find that the tensor-mode contribution to the cosmic microwave background anisotropy on large-angular scales can only exceed that of the scalar mode in models where the spectrum of perturbations deviates significantly from scale invariance. If the tensor mode dominates at large-angular scales, then the value of $\Delta T/T$ predicted on 1 deg is less than if the scalar mode dominates, and, for cold-dark-matter models, bias factors greater than 1 can be made consistent with Cosmic Background Explorer (COBE) DMR results. Author

Typical Subject Index Listing



The subject heading is a key to the subject content of the document. Titles, report numbers, and accession numbers of pertinent documents are provided under each subject heading. When the title is insufficiently descriptive of the document content, a title extension is added, separated from the title by three hyphens. The report number helps to indicate the type of document cited (e.g., NASA report, NASA translation, NASA contractor report). The accession number is the number by which the document abstracts are arranged in this journal and by which the document is sold or requested. The page number helps you locate the citation in the abstract section. The titles, with title extensions if present, are arranged under each subject heading in ascending accession number order. The subject headings have been selected from the latest revision of the *NASA Thesaurus*.

A

ABLATION

Low-to-high altitude predictions of three-dimensional ablative re-entry flowfields p 182 A93-46407

ABRASION

Effects of dust accumulation and removal on radiator surfaces on Mars p 123 A93-13937

Thin film diamond microstructure applications p 209 A93-40580

Degradation of radiator performance on Mars due to dust p 59 N93-15616

ABRASION RESISTANCE

Optical and scratch resistant properties of diamondlike carbon films deposited with single and dual ion beams [NASA-TM-105943] p 95 N93-22586

Optical and scratch resistant properties of diamondlike carbon films deposited with single and dual ion beams p 137 N93-25564

ABSORBERS (MATERIALS)

Modal element method for scattering and absorbing of sound by two-dimensional bodies p 274 A93-53657

ABSORPTION

Optical and scratch resistant properties of diamondlike carbon films deposited with single and dual ion beams p 137 N93-25564

ABSORPTION SPECTRA

Rotational level-dependent collisional broadening and line shift of the A2Sigma(+) - X2Pi(1,0) band of OH in hydrogen-air combustion gases p 276 A93-24142

ABSORPTIVITY

Absorption coefficients for water vapor at 193 nm from 300 to 1073 K p 276 A93-45398

ABSTRACTS

Bibliography on propulsion airframe integration technologies for high-speed civil transport applications, 1980-1991 [NASA-TM-105602] p 1 N93-26136

ABUNDANCE

Primordial nucleosynthesis and the abundances of beryllium and boron p 290 A93-33513

AC GENERATORS

Extra high speed modified Lundell alternator parameters and open/short-circuit characteristics from global 3D-FE magnetic field solutions p 156 A93-39348

Computation of load performance and other parameters of extra high speed modified Lundell alternators from 3D-FE magnetic field solutions p 156 A93-39349

Three dimensional magnetic fields in extra high speed modified Lundell alternators computed by a combined vector-scalar magnetic potential finite element method p 157 A93-39350

Dynamic analysis of Free-Piston Stirling Engine/Linear Alternator-load system-experimentally validated [NASA-TM-106034] p 271 N93-22559

Modelling a single phase voltage controlled rectifier using Laplace transforms [NASA-TM-106005] p 271 N93-23016

ACCELERATED LIFE TESTS

Brush seal bristle flexure and hard-rub characteristics [NASA-TM-105864] p 227 N93-18321

Efficient fault diagnosis of helicopter gearboxes [NASA-TM-106253] p 231 N93-31846

ACCELERATION (PHYSICS)

Narrow band noise as a model of time-dependent accelerations - Study of the stability of a fluid surface in a microgravity environment [AIAA PAPER 93-0911] p 173 A93-24965

Stability of a fluid surface in a microgravity environment p 190 A93-55358

ACCELERATORS

Low-frequency vibration environment for five Shuttle missions [NASA-TM-106059] p 63 N93-28554

ACCELEROMETERS

Review of the Shuttle vibration environment [AIAA PAPER 93-0832] p 51 A93-24902

Low gravity environment on-board Columbia during STS-40 [AIAA PAPER 93-0833] p 142 A93-24903

Micromachined silicon cantilever beam accelerometer incorporating an integrated optical waveguide p 210 A93-49457

Proposed ground-based control of accelerometer on Space Station Freedom p 63 A93-54401

Proposed ground-based control of accelerometer on Space Station Freedom [NASA-TM-105960] p 63 N93-23738

ACCEPTOR MATERIALS

Aluminum acceptor four particle bound exciton complex in 4H, 6H, and 3C SiC p 282 A93-44822

ACCESS CONTROL

Data distribution satellite [NASA-TM-105778] p 149 N93-12481

ACCIDENT PREVENTION

Application of composite materials to impact-insensitive munitions p 97 A93-11459

ACETYLENE

High quality flame deposited diamond films for infrared optical windows p 281 A93-40564

ACOUSTIC ATTENUATION

Consecutive plate acoustic suppressor apparatus and methods [NASA-CASE-LEW-15430-1] p 275 N93-17051

ACOUSTIC DUCTS

Measured acoustic characteristics of ducted supersonic jets at different model scales [AIAA PAPER 93-0731] p 273 A93-24821

ACOUSTIC EMISSION

The effect of ion-plated silver and sliding friction on tensile stress-induced cracking in aluminum oxide p 132 A93-27917

ACOUSTIC EXCITATION

Enhanced mixing of a rectangular supersonic jet by natural and induced screech [NASA-TM-106245] p 18 N93-31672

ACOUSTIC MEASUREMENT

Acoustic mode measurements in the inlet of a model turbofan using a continuously rotating rake - Data collection/analysis techniques [AIAA PAPER 93-0599] p 24 A93-23324

Acoustic mode measurements in the inlet of a model turbofan using a continuously rotating rake [AIAA PAPER 93-0598] p 273 A93-24783

Acoustic mode measurements in the inlet of a model turbofan using a continuously rotating rake: Data collection/analysis techniques [NASA-TM-105936] p 33 N93-15403

Acoustic mode measurements in the inlet of a model turbofan using a continuously rotating rake [NASA-TM-105989] p 34 N93-16705

Rotating rake design for unique measurement of fan-generated spinning acoustic modes [NASA-TM-105946] p 36 N93-26161

Acousto-Ultrasonic analysis of failure in ceramic matrix composite tensile specimens [NASA-TM-106219] p 232 N93-29073

ACOUSTIC PROPERTIES

Takeoff/approach noise for a model counterrotation propeller with a forward-swept upstream rotor [AIAA PAPER 93-0596] p 24 A93-24782

Acoustic mode measurements in the inlet of a model turbofan using a continuously rotating rake [AIAA PAPER 93-0598] p 273 A93-24783

Measured acoustic characteristics of ducted supersonic jets at different model scales [AIAA PAPER 93-0731] p 273 A93-24821

Acoustical evaluation of the NASA Lewis 9 by 15 foot low speed wind tunnel [NASA-TP-3274] p 42 N93-12016

Acoustic mode measurements in the inlet of a model turbofan using a continuously rotating rake [NASA-TM-105989] p 34 N93-16705

Takeoff/approach noise for a model counterrotation propeller with a forward-swept upstream rotor [NASA-TM-105979] p 34 N93-16715

Rotating rake design for unique measurement of fan-generated spinning acoustic modes [NASA-TM-105946] p 36 N93-26161

ACOUSTIC SCATTERING

Modal element method for scattering and absorbing of sound by two-dimensional bodies p 274 A93-53657

ACOUSTIC SIMULATION

The structure of supersonic jet flow and its radiated sound [AIAA PAPER 93-0549] p 273 A93-25538

ACOUSTIC VELOCITY

Atomizing-gas temperature effect on cryogenic spray droplets [AIAA PAPER 93-2333] p 186 A93-50111

Atomizing-gas temperature effect on cryogenic spray droplets [NASA-TM-106106] p 216 N93-25191

ACOUSTICS

Dispersion relation-preserving finite difference schemes for computational acoustics p 274 A93-51180

ACTINIDE SERIES

Chronopotentiometry of refractory metals, actinides and oxyanions in molten salts: A review [NASA-TM-105862] p 120 N93-11545

ACTIVATION ENERGY

Comments on 'Kinetic Study on the Hexacelsian-Celsian Phase Transformation' [NASA-TM-105917] p 136 N93-14886

ACTIVE CONTROL

Prediction of active control of subsonic centrifugal compressor rotating stall [AIAA PAPER 93-0153] p 4 A93-22591

Vibration isolation technology - An executive summary of systems development and demonstration ... for proposed microgravity experiments aboard STS and Space Station Freedom [AIAA PAPER 93-0834] p 55 A93-24904

Evaluation of passive and active vibration control mechanisms in a microgravity environment [AIAA PAPER 93-0838] p 55 A93-24905

Hybrid active vibration control of rotorbearing systems using piezoelectric actuators p 221 A93-27324

ACTS

- Active control of helicopter transmission noise
p 274 A93-29428
- The isolation limits of stochastic vibration
p 236 A93-30042
- Actively controlled superconducting bearings
p 223 A93-48594
- Vibration isolation technology: An executive summary of systems development and demonstration
[NASA-TM-105937] p 1 N93-15573
- Analytical and experimental studies of a short compact subsonic diffuser for a two-dimensional supersonic inlet
[NASA-TP-3247] p 17 N93-24118
- ACTS**
- Advanced Communications Technology Satellite (ACTS)
p 52 A93-24456
- Anomalous TWTA output power spikes and their effect on a digital satellite communications system
[NASA-TM-105875] p 159 N93-13286
- Lewis Research Center battery overview
p 255 N93-20493
- Analysis of MMIC arrays for use in the ACTS Aero Experiment
[NASA-TM-106073] p 53 N93-22589
- OLYMPUS/ACTS scintillation experiment at the Lewis Research Center
p 150 N93-26481
- System overview on electromagnetic compensation for reflector antenna surface distortion
[NASA-TM-106217] p 53 N93-29195
- ACTS system handbook, revision change index
[NASA-TM-107982] p 150 N93-70235
- ACTUATORS**
- Determination of forces in a magnetic bearing actuator - Numerical computation with comparison to experiment
p 219 A93-15686
- An electromechanical actuation system for an expendable launch vehicle
p 50 A93-25891
- Electromechanical systems with transient high power response operating from a resonant ac link
p 152 A93-25892
- Pyrotechnically actuated systems database and applications catalog
p 141 N93-20136
- ADA (PROGRAMMING LANGUAGE)**
- An embedded rule-based diagnostic expert system in Ada
p 260 N93-11928
- ADAPTIVE CONTROL**
- Probabilistic structural analysis of adaptive/smart/intelligent space structures
p 234 A93-16203
- Fault-tolerant adaptive control for load-following in static space nuclear power systems
p 263 A93-25986
- A prototype automatic phase compensation module
[NASA-TM-105930] p 160 N93-16616
- ADHESION**
- Tribological studies of amorphous hydrogenated carbon films in a vacuum, spacelike environment
p 134 A93-40630
- Tribological evaluation and analysis of coating materials
p 135 A93-52896
- ADHESIVE BONDING**
- Effect of service environments on adhesively bonded joints in composite structures
p 242 A93-53418
- ADVECTION**
- An assessment of spectral nonoscillatory schemes
[AIAA PAPER 93-3383] p 267 A93-45074
- Positivity-preserving numerical schemes for multidimensional advection
[NASA-TM-106055] p 200 N93-27091
- AEROACOUSTICS**
- Dispersion-relation-preserving schemes for computational aeroacoustics
p 2 A93-19151
- Influence of airfoil thickness on sound generated by high-frequency gust interactions
p 272 A93-19181
- Supersonic jet noise reduction by coaxial rectangular nozzles
p 272 A93-19205
- Forward rotor vortex effects on counter rotating propeller noise
p 2 A93-19221
- Accuracy considerations in the computational analysis of jet noise
[AIAA PAPER 93-0146] p 272 A93-19804
- Takeoff/approach noise for a model counterrotation propeller with a forward-swept upstream rotor
[AIAA PAPER 93-0596] p 24 A93-24782
- The structure of supersonic jet flow and its radiated sound
[AIAA PAPER 93-0549] p 273 A93-25538
- Takeoff/approach noise for a model counterrotation propeller with a forward-swept upstream rotor
[NASA-TM-105979] p 34 N93-16715
- Numerical simulation of a high Mach number jet flow
[NASA-TM-105985] p 197 N93-20057
- Rotating rake design for unique measurement of fan-generated spinning acoustic modes
[NASA-TM-105946] p 36 N93-26161

- A large hemi-anechoic enclosure for community-compatible aeroacoustic testing of aircraft propulsion systems
[NASA-TM-106015] p 275 N93-26551
- In-flight near- and far-field acoustic data measured on the Proplan Test Assessment (PTA) testbed and with an adjacent aircraft
[NASA-TM-103719] p 275 N93-27058
- AEROBRAKING**
- Nuclear concepts/propulsion
p 85 N93-22093
- AERODYNAMIC CHARACTERISTICS**
- Propulsion and aerodynamic analysis of the Beta II two-stage-to-orbit vehicle
[AIAA PAPER 92-4245] p 50 A93-13332
- Concurrent processing adaptation of aeroelastic analysis of propfans
p 23 A93-14624
- Effects of icing on the aerodynamic performance of high lift airfoils
[AIAA PAPER 93-0026] p 4 A93-20144
- Aerodynamic effects of deicing and anti-icing fluids
p 19 A93-31929
- Comparative wind tunnel tests at high Reynolds numbers of NACA 64 621 airfoils with two aileron configurations
p 9 A93-46823
- Experimental evaluation of a cooled radial-inflow turbine
[AIAA PAPER 93-1795] p 27 A93-49685
- Unsteady aerodynamic flow phenomena in a transonic compressor stage
[AIAA PAPER 93-1868] p 12 A93-49743
- Integrated CFD modeling of gas turbine combustors
[AIAA PAPER 93-2196] p 28 A93-50008
- High Reynolds number and turbulence effects on aerodynamics and heat transfer in a turbine cascade
[AIAA PAPER 93-2252] p 186 A93-50050
- An experimental investigation of the flow in a diffusing S-duct
[NASA-TM-105809] p 32 N93-12077
- AGARD WG13 aerodynamics of high speed air intakes: Assessment of CFD results
p 192 N93-13220
- Selected OAST/OSSA space experiment activities in support of Space Station Freedom
p 60 N93-22636
- Experimental evaluation of a cooled radial-inflow turbine
[NASA-TM-106230] p 38 N93-28697
- High Reynolds number and turbulence effects on aerodynamics and heat transfer in a turbine cascade
[NASA-TM-106187] p 202 N93-29157
- Three-dimensional flow calculations inside SSME GGGT first stage blade rows
p 93 N93-31585
- Localization of aeroelastic modes in mistuned high-energy turbine
p 230 N93-31586
- AERODYNAMIC COEFFICIENTS**
- Experimental and computational ice shapes and resulting drag increase for a NACA 0012 airfoil
p 17 N93-27440
- AERODYNAMIC CONFIGURATIONS**
- Design and test of a small two stage counter-rotating turbine for rocket engine application
[AIAA PAPER 93-2136] p 74 A93-49954
- AERODYNAMIC DRAG**
- An improved far field drag calculation method for nonlinear CFD codes
[AIAA PAPER 93-3417] p 10 A93-47213
- Experimental and computational ice shapes and resulting drag increase for a NACA 0012 airfoil
p 17 N93-27440
- AERODYNAMIC HEAT TRANSFER**
- Increased heat transfer to elliptical leading edges due to spanwise variations in the freestream momentum: Numerical and experimental results
[NASA-TM-106150] p 199 N93-27020
- AERODYNAMIC LOADS**
- Aerolloads and secondary flows in a transonic mixed flow turbine stage
[ASME PAPER 92-GT-72] p 2 A93-19322
- Linearized Euler predictions of unsteady aerodynamic loads in cascades
p 7 A93-29318
- An iterative multidisciplinary analysis for rotor blade shape determination
[AIAA PAPER 93-2085] p 28 A93-49912
- Design of a high-temperature experiment for evaluating advanced structural materials
[NASA-TM-105833] p 245 N93-11624
- Overview of aerothermodynamic loads definition study
p 93 N93-31583
- Three-dimensional analysis of the Pratt and Whitney alternate design SSME fuel turbine
p 230 N93-31584
- 2nd NASA CFD Validation Workshop --- Author
[NASA-TM-107972] p 203 N93-70575
- AERODYNAMIC NOISE**
- Accuracy considerations in the computational analysis of jet noise
[AIAA PAPER 93-0146] p 272 A93-19804
- Effect of tabs on the flow and noise field of an axisymmetric jet
p 25 A93-30833

- A concept for a counterrotating fan with reduced tone noise
[NASA-TM-105736] p 274 N93-11370
- AERODYNAMIC STABILITY**
- An efficient procedure for cascade aeroelastic stability determination using nonlinear, time-marching aerodynamic solvers
[AIAA PAPER 93-1631] p 25 A93-34159
- AERODYNAMIC STALLING**
- Estimation of unsteady lift on a pitching airfoil from wake velocity surveys
[AIAA PAPER 93-0437] p 5 A93-23351
- Estimation of unsteady lift on a pitching airfoil from wake velocity surveys
[NASA-TM-105947] p 15 N93-14791
- AERODYNAMICS**
- Aerodynamic inverse design and analysis for a full engine
[ISABE 93-7086] p 14 A93-54062
- The engine design engine. A clustered computer platform for the aerodynamic inverse design and analysis of a full engine
[NASA-TM-105838] p 15 N93-11223
- AEROELASTICITY**
- Concurrent processing adaptation of aeroelastic analysis of propfans
p 23 A93-14624
- APPLE - An aeroelastic analysis system for turbomachines and propfans
[AIAA PAPER 92-4712] p 23 A93-20320
- Semi-empirical model for prediction of unsteady forces on an airfoil with application to flutter
p 7 A93-31494
- An efficient procedure for cascade aeroelastic stability determination using nonlinear, time-marching aerodynamic solvers
[AIAA PAPER 93-1631] p 25 A93-34159
- Unsteady aerodynamics and flutter of propfans using a three-dimensional Full-Potential Solver
[AIAA PAPER 93-1633] p 25 A93-34161
- Efficient hybrid scheme for the analysis of counter-rotating propellers
p 7 A93-34483
- Aeroelastic dynamics of mistuned blade assemblies with closely spaced blade modes
[AIAA PAPER 93-1628] p 26 A93-37446
- An iterative multidisciplinary analysis for rotor blade shape determination
[AIAA PAPER 93-2085] p 28 A93-49912
- Unsteady aerodynamics and flutter based on the potential equation
[AIAA PAPER 93-2086] p 13 A93-49913
- Optimization of blade arrangement in a randomly mistuned cascade using simulated annealing
[AIAA PAPER 93-2254] p 28 A93-50052
- Stochastic sensitivity measure for mistuned high-performance turbines
[NASA-TM-105821] p 245 N93-12277
- Structural dynamics branch research and accomplishments to FY 1992
[NASA-TM-105824] p 247 N93-20368
- A transfer matrix approach to vibration localization in mistuned blade assemblies
[NASA-TM-106112] p 250 N93-27088
- Localization of aeroelastic modes in mistuned high-energy turbines
p 230 N93-31586
- AERONAUTICS**
- The 1992 Research/Technology report
[NASA-TM-105924] p 1 N93-20902
- AEROSPACE ENGINEERING**
- NASA CST aids U.S. industry --- computational structures technology
p 258 A93-25084
- Probabilistic assessment of composite structures
[AIAA PAPER 93-1441] p 239 A93-33990
- Bibliography of Lewis Research Center Technical Publications announced in 1991
[NASA-TM-105595] p 287 N93-14796
- The 1992 Research/Technology report
[NASA-TM-105924] p 1 N93-20902
- Selected OAST/OSSA space experiment activities in support of Space Station Freedom
p 60 N93-22636
- Solving modal equations of motion with initial conditions using MSC/NASTRAN DMAP. Part 1: Implementing exact mode superposition
[NASA-TM-106063] p 248 N93-23739
- Solving modal equations of motion with initial conditions using MSC/NASTRAN DMAP. Part 2: Coupled versus uncoupled integration
[NASA-TM-106064] p 248 N93-23740
- Power management and distribution technology
p 90 N93-26978
- Radiator technology
p 90 N93-26979
- The development of hydrogen sensor technology at NASA Lewis Research Center
[NASA-TM-106141] p 216 N93-27021
- Four giants of the Lewis Research Center
[NASA-TM-83642] p 1 N93-72738

AEROSPACE ENVIRONMENTS

- Interactions between spacecraft and their environments
[AIAA PAPER 93-0705] p 55 A93-24801
- The detrimental effect of friction on space microgravity robotics
p 222 A93-35546
- The development of hydrogen sensor technology for aerospace applications
[AIAA PAPER 93-2375] p 211 A93-50144
- Electrical and Chemical Interactions at Mars Workshop, Part 2: Appendix
[NASA-CP-10093-PT-2] p 293 N93-26392
- Space environmental interactions for the space exploration initiative
p 293 N93-26396
- Low-frequency vibration environment for five Shuttle missions
[NASA-TM-106059] p 63 N93-28554

AEROSPACE INDUSTRY

- NASA CST aids U.S. industry ... computational structures technology
p 258 A93-25084

AEROSPACE PLANES

- The design and evolution of the Beta two-stage-to-orbit horizontal takeoff and landing launch system
[AIAA PAPER 92-5080] p 50 A93-22350

AEROSPACE SAFETY

- Overview of NASA's microgravity combustion science and fire safety program
p 145 N93-20180
- Soot formation and radiation in turbulent jet diffusion flames under normal and reduced gravity conditions
p 121 N93-20192
- Fire safety practices in the Shuttle and the Space Station Freedom
p 59 N93-20204
- Combustion of solid fuel in very low speed oxygen streams
p 122 N93-20207
- Contributions of microgravity test results to the design of spacecraft fire safety systems
[NASA-TM-106093] p 60 N93-24755
- Nuclear safety policy working group recommendations on nuclear propulsion safety for the space exploration initiative
[NASA-TM-105705] p 88 N93-26200
- The development of hydrogen sensor technology at NASA Lewis Research Center
[NASA-TM-106141] p 216 N93-27021
- Focused technology: Nuclear propulsion
[PR12] p 287 N93-71885

AEROSPACE SCIENCES

- Bibliography of Lewis Research Center Technical Publications announced in 1991
[NASA-TM-105595] p 287 N93-14796

AEROSPACE SYSTEMS

- Space reactor/Stirling cycle systems for high power lunar applications
p 46 A93-13822
- Integrated health monitoring and controls for rocket engines
[SAE PAPER 921031] p 66 A93-14654
- Intercalated graphite fiber composites as EMI shields in aerospace structures
p 104 A93-41573
- Application of artificial neural networks to the design optimization of aerospace structural components
[NASA-TM-4389] p 247 N93-21831
- Overview of the fatigue/fracture/life prediction working group program at the Lewis Research Center
p 232 N93-31574
- Low thrust propulsion
[PR3] p 286 N93-71876

AEROSPACE VEHICLES

- Contributions of microgravity test results to the design of spacecraft fire safety systems
[NASA-TM-106093] p 60 N93-24755
- Structural dynamics: Probabilistic structural analysis methods. Program overview
p 251 N93-31562

AEROTHERMODYNAMICS

- Design of a high-temperature experiment for evaluating advanced structural materials
[NASA-TM-105833] p 245 N93-11624
- Aerothermodynamic flow phenomena of the airframe-integrated supersonic combustion ramjet
[NASA-TM-4376] p 82 N93-15528
- Increased heat transfer to elliptical leading edges due to spanwise variations in the freestream momentum. Numerical and experimental results
[NASA-TM-106150] p 199 N93-27020
- Overview of aerothermodynamic loads definition study
p 93 N93-31583

AGENA ROCKET VEHICLES

- Development and flight history of the SERT II spacecraft
p 71 A93-38976

AGING (MATERIALS)

- Isothermal aging effects on PMR-15 resin
p 131 A93-24508
- Transverse flexural tests as a tool for assessing damage to PMR-15 composites from isothermal aging in air at elevated temperatures
p 100 A93-24514

- Transverse flexural tests as a tool for assessing damage to PMR-15 composites from isothermal aging in air at elevated temperatures
[NASA-TM-105848] p 107 N93-12737

AGING (METALLURGY)

- Transformation to Ni5Al3 in a 63.0 at. pct Ni-Al alloy
p 124 A93-25108

AILERONS

- Comparative wind tunnel tests at high Reynolds numbers of NACA 64 621 airfoils with two aileron configurations
p 9 A93-46823

AIR

- Brush seal leakage performance with gaseous working fluids at static and low rotor speed conditions
[ASME PAPER 92-GT-304] p 219 A93-19494
- Development and use of hydrogen-air torches in an altitude facility
[AIAA PAPER 93-2176] p 42 A93-49988
- Thermomechanical fatigue behavior of SiC/Ti-24Al-11Nb in air and argon environments
[NASA-TM-105723] p 106 N93-11399
- Development and use of hydrogen-air torches in an altitude facility
[NASA-TM-106047] p 43 N93-26214

AIR BREATHING ENGINES

- A new hue capturing technique for the quantitative interpretation of liquid crystal images used in convective heat transfer studies
p 204 A93-13977
- Air-mass flux measurement system using Doppler-shifted filtered Rayleigh scattering
[AIAA PAPER 93-0513] p 205 A93-23260
- CFD for hypersonic propulsion
p 8 A93-42585
- Screening studies of advanced control concepts for airbreathing engines
[AIAA PAPER 92-3320] p 26 A93-49329
- The QED engine spectrum - Fusion-electric propulsion for air-breathing to interstellar flight
[AIAA PAPER 93-2006] p 73 A93-49845
- Screening studies of advanced control concepts for airbreathing engines
[NASA-TM-106042] p 36 N93-25079
- The design and evolution of the beta two-stage-to-orbit horizontal takeoff and landing launch system
[NASA-TM-106118] p 51 N93-27018

AIR COOLING

- Experimental evaluation of a cooled radial-inflow turbine
[AIAA PAPER 93-1795] p 27 A93-49685
- Measurements and computational analysis of heat transfer and flow in a simulated turbine blade internal cooling passage
[AIAA PAPER 93-1797] p 189 A93-53585
- Experimental evaluation of a cooled radial-inflow turbine
[NASA-TM-106230] p 38 N93-28697
- Measurements and computational analysis of heat transfer and flow in a simulated turbine blade internal cooling passage
[NASA-TM-106189] p 203 N93-31647

AIR FLOW

- Friction-factor characteristics for narrow channels with honeycomb surfaces
[ASME PAPER 91-TRIB-21] p 219 A93-15681
- Friction-factor data for flat-plate tests of smooth and honeycomb surfaces
[ASME PAPER 91-TRIB-20] p 219 A93-15682
- Particle displacement tracking applied to air flows
p 206 A93-23800

- Experimental and numerical investigation of supersonic turbulent flow in an annular duct
[AIAA PAPER 93-3123] p 11 A93-48291

- 3-D viscous flow CFD analysis of the propeller effect on an advanced ducted propeller subsonic inlet
[AIAA PAPER 93-1847] p 12 A93-49728

- Jet mixer noise suppressor using acoustic feedback
[NASA-CASE-LEW-15170-1] p 275 N93-28953

- The 3-D viscous flow CFD analysis of the propeller effect on an advanced ducted propeller subsonic inlet
[NASA-TM-106240] p 38 N93-29162

AIR INTAKES

- Intake flow modeling in a four stroke diesel using KIVA3
[AIAA PAPER 93-2952] p 183 A93-48146
- AGARD WG13 aerodynamics of high speed air intakes: Assessment of CFD results
p 192 N93-13220

AIR JETS

- Optimization of circular orifice jets mixing into a heated crossflow in a cylindrical duct
[AIAA PAPER 93-0249] p 24 A93-23246

- Optimization of circular orifice jets mixing into a heated cross flow in a cylindrical duct
[NASA-TM-105984] p 33 N93-15359

- Fuel injector: Air swirl characterization aerothermal modeling, phase 2, volume 1
[NASA-CR-189193-VOL-1] p 35 N93-24754

AIR LAUNCHING

- The design and evolution of the Beta two-stage-to-orbit horizontal takeoff and landing launch system
[AIAA PAPER 92-5080] p 50 A93-22350
- The design and evolution of the beta two-stage-to-orbit horizontal takeoff and landing launch system
[NASA-TM-106118] p 51 N93-27018

AIRCRAFT CONSTRUCTION MATERIALS

- Quantification of uncertainties in composites
[AIAA PAPER 93-1440] p 102 A93-33989
- Overview of NASA's advanced high temperature engine materials technology program
p 94 A93-53453
- Material requirements for the High Speed Civil Transport
[ISABE 93-7067] p 31 A93-54043
- Nondestructive evaluation of ceramic and metal matrix composites for NASA's HITEMP and enabling propulsion materials programs
[NASA-TM-105807] p 231 N93-10963
- Structural tailoring of aircraft engine blade subject to ice impact constraints
[NASA-TM-106033] p 250 N93-26999

AIRCRAFT CONTROL

- Design and evaluation of a robust dynamic neurocontroller for a multivariable aircraft control problem
p 40 A93-37004
- Neurocontrol design and analysis for a multivariable aircraft control problem
p 40 A93-41894
- Analysis of fault-tolerant neurocontrol architectures
[NASA-TM-105898] p 41 N93-12305
- Propulsion system performance resulting from an integrated flight/propulsion control design
[NASA-TM-105874] p 34 N93-15525
- Controller partitioning for integrated flight/propulsion control implementation
[NASA-TM-105804] p 41 N93-21197
- Robustness enhancement of neurocontroller and state estimator
[NASA-TM-106028] p 42 N93-26907
- Status of the Fiber Optic Control System Integration (FOCSI) program
[NASA-TM-106151] p 217 N93-28053

AIRCRAFT DESIGN

- The new challenge of computational aerospace
p 2 A93-14169
- Concurrent optimization of airframe and engine design parameters
[AIAA PAPER 92-4713] p 20 A93-20281
- Structural Tailoring/Analysis for Hypersonic Components - A computational simulation
[AIAA PAPER 92-4722] p 20 A93-20324
- Design of a hypersonic waverider-derived airplane
[AIAA PAPER 93-0401] p 55 A93-21108
- Screening studies of advanced control concepts for airbreathing engines
[AIAA PAPER 92-3320] p 26 A93-49329
- Concurrent optimization of airframe and engine design parameters
[NASA-TM-105908] p 32 N93-12402
- AGARD WG13 aerodynamics of high speed air intakes: Assessment of CFD results
p 192 N93-13220
- Application of artificial neural networks to the design optimization of aerospace structural components
[NASA-TM-4389] p 247 N93-21831
- Screening studies of advanced control concepts for airbreathing engines
[NASA-TM-106042] p 36 N93-25079

AIRCRAFT ENGINES

- Coupled multi-disciplinary simulation of composite engine structures in propulsion environment
[ASME PAPER 92-GT-6] p 23 A93-19279
- Multidisciplinary propulsion simulation using NPSS
[AIAA PAPER 92-4709] p 270 A93-20318
- Structural tailoring of aircraft engine blade subject to ice impact constraints
[AIAA PAPER 92-4710] p 23 A93-20319
- APPLE - An aeroelastic analysis system for turbomachines and propfans
[AIAA PAPER 92-4712] p 23 A93-20320
- Aeroelastic dynamics of mistuned blade assemblies with closely spaced blade modes
[AIAA PAPER 93-1628] p 26 A93-37446
- Screening studies of advanced control concepts for airbreathing engines
[AIAA PAPER 92-3320] p 26 A93-49329
- Flight testing of a fiber optic temperature sensor
p 22 A93-49476
- A review of chemically reactive turbulent flow mixing mechanisms and a new design for a low NO(x) combustor
p 27 A93-49508
- Propulsion technology challenges for turn-of-the-century commercial aircraft
[ISABE 93-7003] p 31 A93-53980
- Emission characteristics of a model gas turbine combustor at practical conditions
[ISABE 93-7023] p 31 A93-53999

AIRCRAFT ICING

- Nondestructive evaluation of ceramic and metal matrix composites for NASA's HITEMP and enabling propulsion materials programs
[NASA-TM-105807] p 231 N93-10963
- Overview of high performance aircraft propulsion research
[NASA-TM-105839] p 32 N93-11530
- Screening studies of advanced control concepts for airbreathing engines
[NASA-TM-106042] p 36 N93-25079
- A large hemi-anechoic enclosure for community-compatible aeroacoustic testing of aircraft propulsion systems
[NASA-TM-106015] p 275 N93-26551
- Structural tailoring of aircraft engine blade subject to ice impact constraints
[NASA-TM-106033] p 250 N93-26999
- Blasim: A computational tool to assess ice impact damage on engine blades
[NASA-TM-106225] p 251 N93-31193
- Propulsion technology challenges for turn-of-the-century commercial aircraft
[NASA-TM-106192] p 39 N93-32351
- AIRCRAFT ICING**
- Effects of icing on the aerodynamic performance of high lift airfoils
[AIAA PAPER 93-0026] p 4 A93-20144
- Structural tailoring of aircraft engine blade subject to ice impact constraints
[AIAA PAPER 92-4710] p 23 A93-20319
- Results of Low Power Deicer tests on a swept inlet component in the NASA Lewis Icing Research Tunnel
[AIAA PAPER 93-0032] p 20 A93-22551
- CFD zonal modeling of leading-edge ice effects for a complete aircraft
[AIAA PAPER 93-0167] p 5 A93-22601
- Modeling and strain gauging of eddy current repulsion deicing systems
[AIAA PAPER 93-0296] p 20 A93-22696
- LDV flowfield measurements on a straight and swept wing with a simulated ice accretion
[AIAA PAPER 93-0300] p 5 A93-23001
- Close-up analysis of aircraft ice accretion
[AIAA PAPER 93-0029] p 18 A93-23239
- Surface roughness due to residual ice in the use of low power deicing systems
[AIAA PAPER 93-0031] p 5 A93-23240
- Numerical modeling of anti-icing systems and comparison to test results on a NACA 0012 airfoil
[AIAA PAPER 93-0170] p 21 A93-23242
- Advancements in the LEWICE Ice Accretion Model
[AIAA PAPER 93-0171] p 18 A93-23243
- Ice accretion and performance degradation calculations with LEWICE/NS
[AIAA PAPER 93-0173] p 18 A93-23244
- Ice accretion prediction for a typical commercial transport aircraft
[AIAA PAPER 93-0174] p 19 A93-23245
- An overview of shed ice impact studies in the NASA Lewis Icing Research Tunnel
[AIAA PAPER 93-0301] p 5 A93-23247
- Aircraft icing problems - After 50 years
[AIAA PAPER 93-0392] p 19 A93-24239
- Results of low power deicer tests on a swept inlet component in the NASA Lewis icing research tunnel
[NASA-TM-105968] p 15 N93-14911
- Surface roughness due to residual ice in the use of low power deicing systems
[NASA-TM-105971] p 16 N93-15338
- Numerical modeling of anti-icing systems and comparison to test results on a NASA 0012 airfoil
[NASA-TM-105975] p 19 N93-15345
- Ice accretion and performance degradation calculations with LEWICE/NS
[NASA-TM-105972] p 19 N93-15354
- Close-up analysis of aircraft ice accretion
[NASA-TM-105952] p 19 N93-15360
- An overview of shed ice impact in the NASA Lewis Icing Research Tunnel
[NASA-TM-105969] p 16 N93-15404
- Ice accretion prediction for a typical commercial transport aircraft
[NASA-TM-105976] p 20 N93-15522
- AIRCRAFT INDUSTRY**
- Propulsion technology challenges for turn-of-the-century commercial aircraft
[ISABE 93-7003] p 31 A93-53980
- Propulsion technology challenges for turn-of-the-century commercial aircraft
[NASA-TM-106192] p 39 N93-32351
- AIRCRAFT MAINTENANCE**
- An artificial intelligence-based structural health monitoring system for aging aircraft p 266 N93-22185

AIRCRAFT MODELS

- Fabrication of composite propfan blades for a cruise missile wind tunnel model
[NASA-TM-105270] p 249 N93-26202

AIRCRAFT NOISE

- Takeoff/approach noise for a model counterrotation propeller with a forward-swept upstream rotor
[ISABE 93-7064] p 24 A93-24782
- Active control of helicopter transmission noise
[NASA-TM-105270] p 274 A93-29428
- Engine technology challenges for a 21st Century High-Speed Civil Transport
[ISABE 93-7064] p 31 A93-54040
- Experimental investigation of an ejector-powered free-jet facility
[NASA-TM-105868] p 16 N93-16704
- Takeoff/approach noise for a model counterrotation propeller with a forward-swept upstream rotor
[NASA-TM-105979] p 34 N93-16715
- Rotating rake design for unique measurement of fan-generated spinning acoustic modes
[NASA-TM-105946] p 36 N93-26161
- Engine technology challenges for a 21st Century High-Speed Civil Transport
[NASA-TM-106216] p 39 N93-31671

AIRCRAFT PARTS

- LEWICE droplet trajectory calculations on a parallel computer
[AIAA PAPER 93-0172] p 259 A93-22604

AIRCRAFT PERFORMANCE

- Concurrent optimization of airframe and engine design parameters
[AIAA PAPER 92-4713] p 20 A93-20281
- Antiwindup analysis and design approaches for MIMO systems
[AIAA PAPER 93-3811] p 30 A93-51403
- Concurrent optimization of airframe and engine design parameters
[NASA-TM-105908] p 32 N93-12402
- Experimental performance of a ventral nozzle with pitch and yaw vectoring capability for SSTOVL aircraft
[NASA-TM-106054] p 36 N93-25129

AIRCRAFT SAFETY

- Aerodynamic effects of deicing and anti-icing fluids
[NASA-TM-105977] p 19 A93-31929
- An artificial intelligence-based structural health monitoring system for aging aircraft p 266 N93-22185

AIRCRAFT STABILITY

- Icing effects on aircraft stability and control determined from flight data - Preliminary results
[AIAA PAPER 93-0398] p 40 A93-23073
- Antiwindup analysis and design approaches for MIMO systems
[AIAA PAPER 93-3811] p 30 A93-51403
- Icing effects on aircraft stability and control determined from flight data: Preliminary results
[NASA-TM-105977] p 41 N93-14831

AIRCRAFT STRUCTURES

- Probabilistically configured adaptive composite structures
[AIAA PAPER 93-1679] p 240 A93-34191
- Probabilistic evaluation of fuselage-type composite structures
[NASA-TM-105881] p 245 N93-12735
- Probabilistic assessment of composite structures
[NASA-TM-106024] p 110 N93-27092
- Numerical modeling of runback water on ice protected aircraft surfaces
[NASA-TM-105947] p 201 N93-27438

AIRCRAFT WAKES

- Estimation of unsteady lift on a pitching airfoil from wake velocity surveys
[AIAA PAPER 93-0437] p 5 A93-23351
- Estimation of unsteady lift on a pitching airfoil from wake velocity surveys
[NASA-TM-105947] p 15 N93-14791

AIRFOIL OSCILLATIONS

- Estimation of unsteady lift on a pitching airfoil from wake velocity surveys
[AIAA PAPER 93-0437] p 5 A93-23351
- Unsteady transonic two-dimensional Euler solutions using finite elements
[NASA-TM-105947] p 8 A93-39412
- Forcing function modeling for flow induced vibration
[ISABE 93-7027] p 31 A93-54003
- Estimation of unsteady lift on a pitching airfoil from wake velocity surveys
[NASA-TM-105947] p 15 N93-14791

AIRFOIL PROFILES

- Forcing function effects on unsteady aerodynamic gust response. II - Low solidity airfoil row response
[ASME PAPER 92-GT-175] p 3 A93-19401
- Comparative wind tunnel tests at high Reynolds numbers of NACA 64 621 airfoils with two aileron configurations
[NASA-TM-106055] p 9 A93-46823

AIRFOILS

- Numerical solutions for unsteady subsonic vortical flows around loaded cascades
[ASME PAPER 92-GT-173] p 3 A93-19399
- Effects of icing on the aerodynamic performance of high lift airfoils
[AIAA PAPER 93-0026] p 4 A93-20144
- Numerical modeling of anti-icing systems and comparison to test results on a NACA 0012 airfoil
[AIAA PAPER 93-0170] p 21 A93-23242
- Estimation of unsteady lift on a pitching airfoil from wake velocity surveys
[AIAA PAPER 93-0437] p 5 A93-23351
- Semi-empirical model for prediction of unsteady forces on an airfoil with application to flutter
[NASA-TM-105975] p 7 A93-31494
- Results of a low power ice protection system test and a new method of imaging data analysis
[NASA-TM-105829] p 21 A93-35932
- Dynamic analysis of a pre-and-post ice impacted blade
[NASA-TM-105829] p 144 N93-12197
- Estimation of unsteady lift on a pitching airfoil from wake velocity surveys
[NASA-TM-105947] p 15 N93-14791
- Numerical modeling of anti-icing systems and comparison to test results on a NACA 0012 airfoil
[NASA-TM-105975] p 19 N93-15345
- Experimental and computational ice shapes and resulting drag increase for a NACA 0012 airfoil
[NASA-TM-105947] p 17 N93-27440

AIRFRAMES

- Concurrent optimization of airframe and engine design parameters
[AIAA PAPER 92-4713] p 20 A93-20281
- Icing effects on aircraft stability and control determined from flight data - Preliminary results
[AIAA PAPER 93-0398] p 40 A93-23073
- An overview of shed ice impact studies in the NASA Lewis Icing Research Tunnel
[AIAA PAPER 93-0301] p 5 A93-23247
- CFD for hypersonic propulsion
[NASA-TM-105908] p 8 A93-42585
- Concurrent optimization of airframe and engine design parameters
[NASA-TM-105908] p 32 N93-12402
- Icing effects on aircraft stability and control determined from flight data: Preliminary results
[NASA-TM-105977] p 41 N93-14831
- An overview of shed ice impact in the NASA Lewis Icing Research Tunnel
[NASA-TM-105969] p 16 N93-15404

AIRLINE OPERATIONS

- An artificial intelligence-based structural health monitoring system for aging aircraft p 266 N93-22185

ALCOHOLS

- Computational predictions of flame spread over alcohol pools
[AIAA PAPER 93-0825] p 115 A93-24895

ALGEBRA

- A three-dimensional algebraic grid generation scheme for gas turbine combustors with inclined slots
[NASA-CR-191095] p 198 N93-24759

ALGORITHMS

- Finite element implementation of state variable-based viscoplasticity models
[NASA-TM-105906] p 236 A93-26776
- An efficient and robust algorithm for two dimensional time dependent incompressible Navier-Stokes equations - High Reynolds number flows
[NASA-TM-105906] p 178 A93-34371
- A parallel dynamic load balancing algorithm for 3-D adaptive unstructured grids
[AIAA PAPER 93-3313] p 260 A93-45009
- Adaptive methods in computational fluid dynamics
[NASA-TM-105906] p 182 A93-45963
- A parameter optimization approach to controller partitioning for integrated flight/propulsion control application
[NASA-TM-105906] p 41 A93-54268
- Experimental testing of four correction algorithms for the forward scattering spectrometer probe
[NASA-TM-105906] p 213 N93-13307
- A compressible boundary layer algorithm for use with SINDA '85
[NASA-TM-105906] p 192 N93-13395
- Solving modal equations of motion with initial conditions using MSC/NASTRAN DMAP. Part 1: Implementing exact mode superposition
[NASA-TM-106063] p 248 N93-23739
- Subband coding for image data archiving
[NASA-TM-105906] p 287 N93-25922
- Explicit robust schemes for implementation of a class of principal value-based constitutive models: Symbolic and numeric implementation
[NASA-TM-106124] p 258 N93-26946
- Parallel solution of high-order numerical schemes for solving incompressible flows
[NASA-TM-4451] p 262 N93-27040
- Positivity-preserving numerical schemes for multidimensional advection
[NASA-TM-106055] p 200 N93-27091

ALIGNMENT

- A fuzzy logic based controller for the automated alignment of a laser-beam-smoothing spatial filter [NASA-TM-105994] p 217 N93-18091
- Neural nets for aligning optical components in harsh environments: Beam smoothing spatial filter as an example p 266 N93-31557

ALKALI METAL COMPOUNDS

- Global expression for representing cohesive-energy curves. II p 276 A93-44989

ALKALI METALS

- Ion exchange polymers and method for making [NASA-CASE-LEW-15576-1] p 139 N93-31316

ALKALINE BATTERIES

- Validation test of advanced technology for IPV nickel-hydrogen flight cells - Update p 252 A93-25886
- Battery selection for space experiments p 159 N93-13184
- Battery selection for Space Shuttle experiments [NASA-TM-106142] p 61 N93-27038

ALKALINE EARTH METALS

- Ion exchange polymers and method for making [NASA-CASE-LEW-15576-1] p 139 N93-31316

ALKANES

- Computational/experimental basis for conducting alkane droplet combustion experiments on space-based-platforms p 117 A93-41711

ALKYL COMPOUNDS

- Substituted 1,1,1-triaryl 2,2,2-trifluoroethanes and processes for their synthesis [NASA-CASE-LEW-14345-7] p 95 N93-17412

ALLOYING

- The kinetics of composite particle formation during mechanical alloying p 125 A93-29534
- High temperature creep and oxidation resistant chromium silicide matrix alloy containing molybdenum [NASA-CASE-LEW-15697-1] p 130 N93-29172

ALLOYS

- Computer programs to characterize alloys and predict cyclic life using the total strain version of strainrange partitioning: Tutorial and users manual, version 1.0 [NASA-TM-4425] p 246 N93-15788

ALTERNATING CURRENT

- Electromechanical systems with transient high power response operating from a resonant ac link p 152 A93-25892
- I-BIEM calculations of the frequency dispersion and ac current distribution at disk and ring-disk electrodes p 254 A93-34246
- Modelling a single phase voltage controlled rectifier using Laplace transforms [NASA-TM-106005] p 271 N93-23016
- Growing the Space Station's electrical power plant p 161 N93-27810

ALUMINIDES

- Elevated temperature compressive properties of reaction milled NiAl-AlN and Zr-doped NiAl-AlN composites p 97 A93-11422
- Influence of grain size on the creep behavior of HfC-dispersed NiAl p 123 A93-17674
- Effect of oxidation on the mechanical properties of a NbAl₃ alloy at intermediate temperatures p 124 A93-20667
- Chromium and reactive element modified aluminide diffusion coatings on superalloys - Environmental testing p 126 A93-37899
- Creep deformation of B2 aluminides p 126 A93-44887
- Containerless automated processing of intermetallic compounds and composites p 144 A93-52183
- Chemical stability of titanium diboride reinforcement in nickel aluminide matrices p 105 A93-52473
- Predicting the oxidative lifetime of beta NiAl-Zr alloys p 127 A93-53939
- Thermomechanical fatigue behavior of SiC/Ti-24Al-11Nb in air and argon environments [NASA-TM-105723] p 106 N93-11399

ALUMINUM

- Initial study of void formation during aluminum solidification in reduced gravity p 142 A93-12013
- Low earth simulation and materials characterization p 44 A93-32293
- Some aspects of secondary atomization of aluminum/hydrocarbon slurry propellants p 140 A93-34478
- Aluminum acceptor four particle bound exciton complex in 4H, 6H, and 3C SiC p 282 A93-44822
- Technology for gelled liquid cryogenic propellants - Metallized hydrogen/aluminum [AIAA PAPER 93-1878] p 140 A93-49752
- ALUMINUM ALLOYS**
- On the melt infiltration of copper coated silicon carbide with an aluminum alloy p 218 A93-11332
- Room temperature cyclic deformation behavior of cast and extruded NiAl p 122 A93-12130

- Observations on infiltration of silicon carbide compacts with an aluminum alloy p 97 A93-12356
- The effect of microalloying additions on the tensile properties of polycrystalline NiAl p 123 A93-17516
- Ignition and combustion of aluminum/magnesium alloy particles in O₂ at high pressures p 113 A93-22030
- Transformation to Ni₅Al₃ in a 63.0 at. pct Ni-Al alloy p 124 A93-25108
- Grain boundary resistance to fatigue crack growth p 125 A93-29570
- Transverse ductility of metal matrix composites p 101 A93-31355
- Ductility of a continuous fiber reinforced aluminum matrix composite p 102 A93-32471
- Viscoplasticity with creep and plasticity bounds p 125 A93-32925
- Diffusional transport and predicting oxidative failure during cyclic oxidation of beta-NiAl alloys p 126 A93-50370
- Thermodynamics of iron-aluminum alloys at 1573 K p 127 A93-52879
- Fabrication and properties of functionally graded NiAl/Al₂O₃ composites p 105 A93-54116
- Review of the physical and mechanical properties and potential applications of the B2 compound NiAl: Unabridged version of a paper published in International materials review [NASA-TM-105598] p 127 N93-11635
- High temperature, oxidation resistant noble metal-Al alloy thermocouple [NASA-CASE-LEW-15515-1] p 217 N93-31298
- ALUMINUM ARSENIDES**
- Direct optical injection locking of monolithically integrated In(0.53)Ga(0.47)As/In(0.52)Al(0.48)As MODFET oscillators p 158 A93-47127
- ALUMINUM COATINGS**
- The effects of simulated low Earth orbit environments on spacecraft thermal control coatings [NASA-TM-106146] p 61 N93-27019
- ALUMINUM COMPOUNDS**
- SIMS studies of oxide growth on beta-NiAl p 127 A93-53469
- ALUMINUM GALLIUM ARSENIDES**
- Intermodulation in the oscillatory magnetoresistance of a two-dimensional electron gas p 151 A93-17610
- An analysis of the frequency limitations of an Al(x)Ga(1-x)As/GaAs optical modulator p 151 A93-23454
- ALUMINUM GRAPHITE COMPOSITES**
- Thermal emittance enhancement of graphite-aluminum and graphite-copper composite radiator surfaces for space power applications p 105 A93-53455
- ALUMINUM NITRIDES**
- Elevated temperature compressive properties of reaction milled NiAl-AlN and Zr-doped NiAl-AlN composites p 97 A93-11422
- CVD of SiC and AlN using cyclic organometallic precursors p 117 A93-39525
- ALUMINUM OXIDES**
- Effects of precracking methods on the fracture properties of alumina p 131 A93-16645
- Fracture toughness of advanced ceramics at room temperature p 131 A93-20842
- The effect of ion-plated silver and sliding friction on tensile stress-induced cracking in aluminum oxide p 132 A93-27917
- Sliding wear of self-mated Al₂O₃-SiC whisker-reinforced composites at 23-1200 C p 101 A93-29948
- Ductility of a continuous fiber reinforced aluminum matrix composite p 102 A93-32471
- Effect of thermal cycling on interface bonding requirements in Al₂O₃ fiber-reinforced superalloy composites p 103 A93-35882
- Composition dependence of superconductivity in YBa₂(Cu(3-x)Al(x))O(y) p 281 A93-40271
- X-ray photoelectron spectroscopy study of the stability of Fomblin Z25 on the native oxide of aluminum p 134 A93-44883
- Effect of environment on fracture toughness of 96 wt pct alumina p 134 A93-44955
- An analysis of the wear behavior of SiC whisker-reinforced alumina from 25 to 1200 C p 104 A93-49253
- SIMS studies of oxide growth on beta-NiAl p 127 A93-53469
- Fabrication and properties of functionally graded NiAl/Al₂O₃ composites p 105 A93-54116
- Silicon carbide fiber reinforced strontium aluminosilicate glass-ceramic matrix composite [NASA-CASE-LEW-15263-1] p 106 N93-11543
- Tensile creep behavior of polycrystalline alumina fibers [NASA-TM-106269] p 138 N93-30938
- Stress-rupture behavior of small diameter polycrystalline alumina fibers [NASA-TM-106256] p 139 N93-32382

ALUMINUM SILICATES

- Kinetics of hexacelsian-to-celsian phase transformation in SrAl₂Si₂O₈ p 134 A93-40293
- Kinetics of hexacelsian to celsian phase transformation in SrAl₂Si₂O₈ [NASA-TM-105913] p 136 N93-16372
- Fiber-reinforced monoclinic celsian matrix composite material [NASA-CASE-LEW-15269-1] p 108 N93-20040
- ALUMINUM-LITHIUM ALLOYS**
- On bilinearity of Manson-Coffin low-cycle-fatigue relationship [NASA-TM-105840] p 245 N93-12739

AMORPHOUS MATERIALS

- Comparison of high frequency, high temperature core loss and B-H loop characteristics of an 80 Ni-Fe crystalline alloy and two iron-based amorphous alloys p 123 A93-13882
- Tribological studies of amorphous hydrogenated carbon films in a vacuum, spacelike environment p 134 A93-40630
- Friction and wear of plasma-deposited amorphous hydrogenated films on silicon nitride p 135 A93-52181
- Optical and scratch resistant properties of diamondlike carbon films deposited with single and dual ion beams [NASA-TM-105943] p 95 N93-22586
- Optical and scratch resistant properties of diamondlike carbon films deposited with single and dual ion beams p 137 N93-25564

AMPLIFIER DESIGN

- A 10-GHz amplifier using an epitaxial lift-off pseudomorphic HEMT device p 156 A93-37574

AMPLIFIERS

- Capacitance-type blade-tip clearance measurement system using a dual amplifier with ramp/dc inputs and integration p 209 A93-39347

ANALOG CIRCUITS

- Analysis of fault-tolerant neurocontrol architectures [NASA-TM-105898] p 41 N93-12305

ANALOG TO DIGITAL CONVERTERS

- Evaluation of a vibration diagnostic system for the detection of spur gear pitting failures [AIAA PAPER 93-2298] p 224 A93-50083
- Evaluation of a vibration diagnostic system for the detection of spur gear pitting failures [NASA-TM-106103] p 228 N93-25672

ANECHOIC CHAMBERS

- A large hemi-anechoic enclosure for community-compatible aeroacoustic testing of aircraft propulsion systems [NASA-TM-106015] p 275 N93-26551

ANELASTICITY

- Thermo-elastoviscoplastic snapthrough behavior of cylindrical panels p 233 A93-12046

ANGLE OF ATTACK

- Icing effects on aircraft stability and control determined from flight data - Preliminary results [AIAA PAPER 93-0398] p 40 A93-23073
- Effect of a rotating propeller on the separation angle of attack [AIAA PAPER 93-0017] p 6 A93-24978
- Installed F/A-18 inlet flow calculations at 60 deg angle-of-attack and 10 deg side slip [AIAA PAPER 93-1806] p 12 A93-49695
- Icing effects on aircraft stability and control determined from flight data: Preliminary results [NASA-TM-105977] p 41 N93-14831
- Effect of a rotating propeller on the separation angle of attack and distortion in ducted propeller inlets [NASA-TM-105935] p 16 N93-16625

ANHYDRIDES

- Substituted 1,1,1-triaryl 2,2,2-trifluoroethanes and processes for their synthesis [NASA-CASE-LEW-14345-7] p 95 N93-17412

ANIONS

- Chronopotentiometry of refractory metals, actinides and oxyanions in molten salts: A review [NASA-TM-105862] p 120 N93-11545

ANISOTROPIC MEDIA

- Discrete ordinates solutions for radiatively participating media in a cylindrical enclosure p 285 A93-31427
- Full wave characterization of microstrip open end discontinuities patterned on anisotropic substrates using potential theory [NASA-TM-106037] p 160 N93-20259

ANISOTROPY

- The gravitational wave contribution to cosmic microwave background anisotropies and the amplitude of mass fluctuations from COBE results p 289 A93-21508
- Microwave anisotropies in the light of the data from the COBE satellite p 291 A93-35444

ANNEALING

- Processing and microstructure of Nb-1 percent Zr-0.1 percent C alloy sheet [NASA-TM-105921] p 128 N93-15524

ANNULAR DUCTS

ANNULAR DUCTS

- Experimental and numerical investigation of supersonic turbulent flow in an annular duct [AIAA PAPER 93-3123] p 11 A93-48291
- ANNULAR FLOW**
 - Three-dimensional unstructured grid Euler method applied to turbine blades [AIAA PAPER 93-0196] p 6 A93-24233
 - The coupling of interfacial instabilities and the stabilization of two-layer annular flows p 178 A93-35482
 - A numerical investigation of supersonic strut/endwall interactions in annular flow with varying strut thickness [AIAA PAPER 93-2927] p 10 A93-48128
 - Experimental and numerical investigation of supersonic turbulent flow in an annular duct [AIAA PAPER 93-3123] p 11 A93-48291
 - Investigation of a strut/endwall interaction in supersonic annular flow [AIAA PAPER 93-1925] p 12 A93-49791
 - Computation of the flow field in an annular gas turbine combustor [AIAA PAPER 93-2074] p 28 A93-49903
- ANODES**
 - Effects of anode material on arcjet performance p 79 N93-10044
 - Effects of anode material on arcjet performance [NASA-TM-105799] p 79 N93-10197
 - 100-kW class applied-field MPD thruster component wear [NASA-TM-106023] p 85 N93-22482
 - Alkali metal carbon dioxide electrochemical system for energy storage and/or conversion of carbon dioxide to oxygen [NASA-CASE-LEW-14973-1] p 256 N93-28974
- ANODIZING**
 - Direct observation of porous SiC formed by anodization in HF p 282 A93-43587
- ANTENNA ARRAYS**
 - System-level integrated circuit (SLIC) development for phased array antenna applications p 152 A93-25798
 - Phase shifter technology assessment - Prospects and applications p 152 A93-25808
 - Multiple-access phased array antenna simulator for a digital beam-forming system investigation p 148 A93-26237
 - Directivity versus element spacing for a scanning array p 148 A93-36991
 - Performance of TiCaBaCuO 30 GHz 64 element antenna array p 157 A93-44763
 - A prototype automatic phase compensation module [NASA-TM-105930] p 160 N93-16616
 - Microwave characterization of slotline on high resistivity silicon for antenna feed network [NASA-TM-106058] p 161 N93-27265
- ANTENNA DESIGN**
 - Multiple-access phased array antenna simulator for a digital beam-forming system investigation p 148 A93-26237
 - Analysis of reflector antenna system including frequency selective surfaces p 52 A93-32820
 - Performance of TiCaBaCuO 30 GHz 64 element antenna array p 157 A93-44763
 - Microwave characterization of slotline on high resistivity silicon for antenna feed network [NASA-TM-106058] p 161 N93-27265
 - System overview on electromagnetic compensation for reflector antenna surface distortion [NASA-TM-106217] p 53 N93-29195
- ANTENNA FEEDS**
 - Input impedance of coaxially fed rectangular microstrip antenna on electrically thick substrate p 155 A93-36994
 - Microwave characterization of slotline on high resistivity silicon for antenna feed network [NASA-TM-106058] p 161 N93-27265
- ANTENNA RADIATION PATTERNS**
 - Analysis of reflector antenna system including frequency selective surfaces p 52 A93-32820
 - System overview on electromagnetic compensation for reflector antenna surface distortion [NASA-TM-106217] p 53 N93-29195
- ANTIFRICTION BEARINGS**
 - The detrimental effect of friction on space microgravity robotics p 222 A93-35546
- ANTICING ADDITIVES**
 - Aerodynamic effects of deicing and anti-icing fluids p 19 A93-31929
- APERTURES**
 - A fiber optic probe for the detection of cataracts p 257 N93-25593
- APPLICATIONS PROGRAMS (COMPUTERS)**
 - Qualitative model-based diagnostics for rocket systems [AIAA PAPER 93-1779] p 72 A93-49674

- Computational simulation of hot composite structures p 260 A93-54704
- An interactive preprocessor for the NASA engine performance program [NASA-TM-105786] p 32 N93-10983
- An embedded rule-based diagnostic expert system in Ada p 260 N93-11928
- Space Communication Artificial Intelligence for Link Evaluation Terminal (SCAILET) p 265 N93-11940
- Computer program for calculating and fitting thermodynamic functions p 285 N93-12967
- [NASA-RP-1271] p 192 N93-13395
- A compressible boundary layer algorithm for use with SINDA '85 p 193 N93-13403
- A SINDA '85 nodal heat transfer rate calculation user subroutine p 160 N93-15531
- User's guide for a large signal computer model of the helical traveling wave tube [NASA-TP-3251] p 160 N93-15531
- A critical analysis of the accuracy of several numerical techniques for combustion kinetic rate equations [NASA-TP-3315] p 34 N93-16941
- Second generation integrated composite analyzer (ICAN) computer code p 108 N93-18139
- [NASA-TP-3290] p 84 N93-19106
- Program ELM: A tool for rapid thermal-hydraulic analysis of solid-core nuclear rocket fuel elements [NASA-TM-105867] p 84 N93-19106
- Explicit robust schemes for implementation of a class of principal value-based constitutive models: Symbolic and numeric implementation [NASA-TM-106124] p 258 N93-26946
- Explicit robust schemes for implementation of general principal value-based constitutive models [NASA-TM-106123] p 258 N93-26947
- Overview of NASA/DOE/DOD interagency modeling team and activities p 89 N93-26952
- NEP systems model p 91 N93-26987
- Probabilistic assessment of composite structures [NASA-TM-106024] p 110 N93-27092
- Qualitative model-based diagnostics for rocket systems [NASA-TM-106234] p 51 N93-28052
- APPROACH**
 - Takeoff/approach noise for a model counterrotation propeller with a forward-swept upstream rotor [AIAA PAPER 93-0596] p 24 A93-24782
 - Takeoff/approach noise for a model counterrotation propeller with a forward-swept upstream rotor [NASA-TM-105979] p 34 N93-16715
- APPROACH CONTROL**
 - Controller partitioning for integrated flight/propulsion control implementation [NASA-TM-105804] p 41 N93-21197
- APPROXIMATION**
 - An integral equation solution for multistage turbomachinery design calculations [NASA-TM-105970] p 33 N93-15521
- AQUEOUS SOLUTIONS**
 - Surface tension effects on the onset of double-diffusive convection p 180 A93-41710
- ARC CHAMBERS**
 - Investigation of a subsonic-arc-attachment thruster using segmented anodes [AIAA PAPER 93-1899] p 73 A93-49769
- ARC JET ENGINES**
 - A comparison of arcjet plume properties to model predictions [AIAA PAPER 93-0820] p 67 A93-24891
 - Extended life and performance test of a low-power arcjet p 70 A93-32554
 - Simulating a 1-kW arcjet thruster using a nonlinear active load p 48 A93-34482
 - The effects of 1 kW class arcjet thruster plumes on spacecraft charging and spacecraft thermal control materials p 57 A93-35050
 - Performance of a low-power subsonic-arc-attachment arcjet thruster [AIAA PAPER 93-1898] p 72 A93-49768
 - Investigation of a subsonic-arc-attachment thruster using segmented anodes [AIAA PAPER 93-1899] p 73 A93-49769
 - Recent testing of 30 KW hydrogen arcjet thrusters [AIAA PAPER 93-1902] p 73 A93-49772
 - Low power arcjet system spacecraft impacts [AIAA PAPER 93-2392] p 76 A93-50157
 - A soft-start circuit for arcjet ignition [AIAA PAPER 93-2396] p 76 A93-50161
 - EOTV propellant tank pressure control and liquid dynamics [AIAA PAPER 93-2399] p 77 A93-50164
 - Monte Carlo and experimental studies of nozzle flow in a low-power hydrogen arcjet [AIAA PAPER 93-2529] p 77 A93-50257
 - Plume characteristics of an arcjet thruster [AIAA PAPER 93-2530] p 77 A93-50258

- 10 kW power electronics for hydrogen arcjets p 79 N93-10033
- Effects of anode material on arcjet performance p 79 N93-10044
- Effects of anode material on arcjet performance [NASA-TM-105799] p 79 N93-10197
- The 10 kW power electronics for hydrogen arcjets [NASA-TM-105614] p 81 N93-12484
- Development of arcjet and ion propulsion for spacecraft stationkeeping [NASA-TM-106102] p 85 N93-23747
- ARC SPRAYING**
 - Tensile strain-rate sensitivity of tungsten/niobium composites at 1300 to 1600 K p 97 A93-14840
- ARCHITECTURE (COMPUTERS)**
 - Parallel computing for probabilistic fatigue analysis [AIAA PAPER 93-1499] p 261 A93-34039
 - Analysis of fault-tolerant neurocontrol architectures [NASA-TM-105898] p 41 N93-12305
 - Self-growing neural network architecture using crisp and fuzzy entropy [NASA-TM-105677] p 231 N93-18422
 - A multiarchitecture parallel-processing development environment [NASA-TM-106180] p 262 N93-28628
- ARGON**
 - Thermomechanical fatigue behavior of SiC/Ti-24Al-11Nb in air and argon environments [NASA-TM-105723] p 106 N93-11399
 - Nuclear electric propulsion options for piloted Mars missions p 90 N93-26985
- ARMOR**
 - Optimization of armored spherical tanks for storage on the lunar surface p 47 A93-25866
- ARRAYS**
 - Space transfer with ground-based laser/electric propulsion [NASA-TM-106060] p 84 N93-20615
- ARTIFICIAL INTELLIGENCE**
 - Space Communication Artificial Intelligence for Link Evaluation Terminal (SCAILET) p 265 N93-11940
 - Real-time diagnostics for a reusable rocket engine [NASA-TM-105792] p 266 N93-19018
- ARTIFICIAL SATELLITES**
 - COLD-SAT dynamic model [NASA-TM-105185] p 59 N93-19988
- ASTRONAUTS**
 - Space Nuclear Thermal Propulsion Test Facilities Subpanel [NASA-TM-105708] p 87 N93-25105
- ASTRONOMICAL MODELS**
 - Stochastic inflation lattice simulations - Ultra-large scale structure of the universe p 289 A93-17646
 - The best-fit universe --- cosmological models p 289 A93-17651
 - Chemical and luminosity evolution, and counts of galaxies in a merger model p 290 A93-34776
- ASYMPTOTIC METHODS**
 - Asymptotic analysis with reduced chemistry for the burning of n-heptane droplets p 113 A93-13323
 - An asymptotic theory of supersonic propeller noise p 271 A93-19169
 - Flow effects in a vertical CVD reactor p 166 A93-19821
 - Nonlinear interaction of frequency-detuned modes in boundary layers [AIAA PAPER 93-0347] p 171 A93-24237
 - Finite element implementation of state variable-based viscoplasticity models p 236 A93-26776
- ASYMPTOTIC SERIES**
 - On the accurate long-time solution of the wave equation in exterior domains: Asymptotic expansions and corrected boundary conditions [NASA-TM-106117] p 269 N93-27068
- ATMOSPHERIC CHEMISTRY**
 - Lunar and Martian environmental interactions with nuclear power system radiators [NASA-TM-105747] p 80 N93-10965
 - Electrical and Chemical Interactions at Mars Workshop. Part 2: Appendix [NASA-CP-10093-PT-2] p 293 N93-26392
- ATMOSPHERIC PRESSURE**
 - A kinetic and equilibrium analysis of silicon carbide chemical vapor deposition on monofilaments [NASA-TM-106137] p 96 N93-27003
- ATMOSPHERIC TURBULENCE**
 - Application of radiative image transfer theory to the assessment of the overall OTF and contrast degradation of an image in an inhomogeneous turbulent and turbid atmosphere p 285 A93-28624
- ATOMIC BEAMS**
 - Method and apparatus for producing a thermal atomic oxygen beam [NASA-CASE-LEW-15614-1] p 276 N93-19026

ATOMIZERS

Velocity and drop size measurements in a swirl-stabilized, combustor spray
[NASA-TM-106130] p 37 N93-27130

ATOMIZING

Influence of ambient air pressure on effervescent atomization
[AIAA PAPER 92-0460] p 167 A93-21652
Some aspects of secondary atomization of aluminum/hydrocarbon slurry propellants
p 140 A93-34478

Atomization and vaporization characteristics of airblast fuel injection inside a venturi tube
[AIAA PAPER 93-1766] p 184 A93-49662
Atomizing-gas temperature effect on cryogenic spray droplet size
[AIAA PAPER 93-2333] p 186 A93-50111
Laser-induced fluorescence detection strategies for sodium atoms and compounds in high-pressure combustors
p 119 A93-52423
Fuel injector: Air swirl characterization aerothermal modeling, phase 2, volume 1
[NASA-CR-189193-VOL-1] p 35 N93-24754
Atomizing-gas temperature effect on cryogenic spray droplet size
[NASA-TM-106106] p 216 N93-25191

AUGER SPECTROSCOPY

Auger electron spectroscopy study of oxidation of a PdCr alloy used for high-temperature sensors
[NASA-TM-106212] p 129 N93-23418

AUTOMATIC CONTROL

Lessons learned from the Autonomous Power System
p 68 A93-25879
Description of the SSF PMAD dc testbed control system data acquisition function
p 47 A93-26103
Description of the SSF PMAD DC testbed control system data acquisition function
[NASA-TM-105843] p 261 N93-11005
Ice thickness measurement system for the icing research tunnel calibration
[NASA-TM-106095] p 215 N93-24737
Neural nets for aligning optical components in harsh environments: Beam smoothing spatial filter as an example
p 266 N93-31557

AUTOMATION

Design of an automated imaging system for use in a space experiment
p 204 A93-20454

AUTONOMY

Scheduling lessons learned from the Autonomous Power System
p 265 N93-18671

AUXILIARY POWER SOURCES

Comparison of all-electric secondary power systems for civil transport
p 24 A93-25997
Comparison of all-electric secondary power systems for civil subsonic transports
[NASA-TM-105852] p 32 N93-10456

AUXILIARY PROPULSION

Low-Isp derated ion thruster operation
[AIAA PAPER 92-3203] p 64 A93-13696

AVERAGE

Turbulent fluid motion IV-averages, Reynolds decomposition, and the closure problem
[NASA-TM-105822] p 195 N93-15585

AVIATION METEOROLOGY

Two and three-dimensional prediffuser combustor studies with air-water mixture
[AIAA PAPER 93-0240] p 113 A93-22652

AXIAL FLOW

Flow-influenced stabilization of liquid columns in a dynamic plateau chamber
[AIAA PAPER 93-0255] p 169 A93-22664

AXIAL FLOW TURBINES

Three-dimensional flow field in a turbine nozzle passage
[AIAA PAPER 93-2556] p 13 A93-50278

AXIAL LOADS

Analytical stress intensity solution for the Stable Poisson Loaded specimen
p 242 A93-46768
Environmental effects on long term behavior of composite laminates
p 243 A93-53438
Lubrication of an 85-mm ball bearing with RP-1
[AIAA PAPER 93-2538] p 225 A93-53590
In-phase and out-of-phase axial-torsional fatigue behavior of Haynes 188 at 760 C
[NASA-TM-105765] p 246 N93-13153
Lubrication of an 85-mm ball bearing with RP-1
[NASA-TM-106254] p 51 N93-31670

AXIAL STRAIN

Axial-torsional fatigue - A study of tubular specimen thickness effects
p 240 A93-38849

AXISYMMETRIC FLOW

On streamwise vortices in high Reynolds number supersonic axisymmetric jets
p 167 A93-21060
Critical assessment of Reynolds stress turbulence models using homogeneous flows
[AIAA PAPER 93-0082] p 170 A93-24227

Effect of tabs on the flow and noise field of an axisymmetric jet
p 25 A93-30833
Performance comparison of axisymmetric and three-dimensional hydrogen film coolant injection in a 110N hydrogen/oxygen rocket
[NASA-TM-105967] p 83 N93-16714
Numerical simulation of a high Mach number jet flow
[NASA-TM-105985] p 197 N93-20057

B**BACKGROUND RADIATION**

Cosmic microwave background probes models of inflation
p 294 A93-10355

BACKSCATTERING

Microemulsion characterization by the use of a noninvasive backscatter fiber optic probe
p 277 A93-52412
A fiber optic probe for the detection of cataracts
p 257 N93-25593

BACKWARD FACING STEPS

A coupled multi-block solution procedure for spray combustion in complex geometries
[AIAA PAPER 93-0108] p 171 A93-24230
Preconditioned Conjugate Gradient methods for low speed flow calculations
[AIAA PAPER 93-0881] p 172 A93-24942
A critical comparison of several low Reynolds number k-epsilon turbulence models for flow over a backward-facing step
[AIAA PAPER 93-1927] p 189 A93-53586
Preconditioned conjugate-gradient methods for low-speed flow calculations
[NASA-TM-105929] p 194 A93-14885
A realizable Reynolds stress algebraic equation model
[NASA-TM-105993] p 16 N93-16596
Calculations of turbulent separated flows
[NASA-TM-106154] p 200 N93-27161
Numerical simulations of three-dimensional laminar flow over a backward facing step; flow near side walls
[NASA-TM-106248] p 202 N93-31147
A critical comparison of several low Reynolds number k-epsilon turbulence models for flow over a backward facing step
[NASA-TM-106173] p 270 N93-32200

BALL BEARINGS

Lubrication of an 85-mm ball bearing with RP-1
[AIAA PAPER 93-2538] p 225 A93-53590
Lubrication of an 85-mm ball bearing with RP-1
[NASA-TM-106254] p 51 N93-31670

BAND STRUCTURE OF SOLIDS

Interface dependence of band offsets in lattice-matched isovalent heterojunctions
p 280 A93-32132

BARIUM COMPOUNDS

Fiber-reinforced monoclinic cerium matrix composite material
[NASA-CASE-LEW-15269-1] p 108 N93-20040

BARIUM OXIDES

Composition dependence of superconductivity in YBa₂(Cu_{1-x}Al_x)O_{7-y}
p 281 A93-40271

BASALT

Experimental determination of in situ utilization of lunar regolith for thermal energy storage
p 253 A93-26043

BEACONS

GaAs monolithic R.F. modules for SARSAT distress beacons
p 152 A93-25806

BEAM INJECTION

Interference patterns in the Spacelab 2 plasma wave data - Oblique electrostatic waves generated by the electron beam
p 257 A93-16347

BEAMS (SUPPORTS)

A new pre-loaded beam geometric stiffness matrix with full rigid body capabilities
p 54 A93-12145
Evaluation of passive and active vibration control mechanisms in a microgravity environment
[AIAA PAPER 93-0838] p 55 A93-24905
Analysis of precracking parameters for ceramic single-edge-precracked-beam specimens
p 133 A93-38887

Analysis of precracking parameters and fracture toughness for ceramic single-edge-precracked-beam specimens
[NASA-TM-105568] p 135 N93-10962
The effect of contact stresses in four-point bend testing of graphite/epoxy and graphite/PMR-15 composite beams
[NASA-TM-105891] p 107 N93-12076

BEARINGS

Evaluation of a vibration diagnostic system for the detection of spur gear pitting failures
[AIAA PAPER 93-2298] p 224 A93-50083
Effect of out-of-roundness on the performance of a diesel engine connecting-rod bearing
p 225 A93-52607

Maximum life spiral bevel reduction design
[NASA-TM-105790] p 226 N93-10982
Summary of the NASA Lewis component technology program for Stirling power converters
[NASA-TM-105640] p 82 N93-15526
Evaluation of an oil-debris monitoring device for use in helicopter transmissions
[NASA-TM-105830] p 227 N93-22826
Evaluation of a vibration diagnostic system for the detection of spur gear pitting failures
[NASA-TM-106103] p 228 N93-25672

BELLOWS

High-temperature, bellows hybrid seal
[NASA-CASE-LEW-15570-1] p 227 N93-19027

BEND TESTS

Transverse flexural tests as a tool for assessing damage to PMR-15 composites from isothermal aging in air at elevated temperatures
p 100 A93-24514
Nondestructive evaluation of a ceramic matrix composite material
p 102 A93-33016
Elevated-temperature fracture resistances of monolithic and composite ceramics using chevron-notched bend tests
p 133 A93-38888
The effect of contact stresses in four-point bend testing of graphite/epoxy and graphite/PMR-15 composite beams
[NASA-TM-105891] p 107 N93-12076
Transverse flexural tests as a tool for assessing damage to PMR-15 composites from isothermal aging in air at elevated temperatures
[NASA-TM-105848] p 107 N93-12737

BENDING

Effects of thermal and mechanical fatigue on the flexural strength of G40-600/PMR-15 cross-ply laminates
[NASA-TM-106016] p 108 N93-20317
Fuzzy sets predict flexural strength and density of silicon nitride ceramics
[NASA-TM-106049] p 110 N93-27270

BENDING FATIGUE

Low-noise, high-strength, spiral-bevel gears for helicopter transmissions
[AIAA PAPER 93-2149] p 223 A93-49966
Dynamic analysis of spur gears using computer program DANST
[AIAA PAPER 93-2295] p 224 A93-50080
Effects of thermal and mechanical fatigue on the flexural strength of G40-600/PMR-15 cross-ply laminates
[NASA-TM-106016] p 108 N93-20317
Low-noise, high-strength, spiral-bevel gears for helicopter transmissions
[NASA-TM-106080] p 228 N93-23019
NDE of PWA 1480 single crystal turbine blade material
[NASA-TM-106140] p 38 N93-27640
Dynamic analysis of spur gears using computer program DANST
[NASA-TM-106211] p 230 N93-28050

BENZENE

Benzonorbornadiene end caps for PMR resins
p 94 A93-35700

BERYLLIUM

Primordial nucleosynthesis and the abundances of beryllium and boron
p 290 A93-33513
The boron-to-beryllium ratio in halo stars - A signature of cosmic-ray nucleosynthesis in the early Galaxy
p 292 A93-55061

BERYLLIUM ISOTOPES

Implications of new GALEX results for the Mikhayev-Smirnov-Wolfenstein solution of the solar neutrino problem
p 293 A93-10357

BIBLIOGRAPHIES

Bibliography of Lewis Research Center Technical Publications announced in 1991
[NASA-TM-105595] p 287 N93-14796
Bibliography on propulsion airframe integration technologies for high-speed civil transport applications, 1980-1991
[NASA-TM-105602] p 1 N93-26136

BIG BANG COSMOLOGY

The first three minutes - 1990 version --- of early universe after Big Bang
p 289 A93-23607
Inflation at the electroweak scale
p 290 A93-26263
Primordial nucleosynthesis and the abundances of beryllium and boron
p 290 A93-33513
Microwave anisotropies in the light of the data from the COBE satellite
p 291 A93-35444

BINARY ALLOYS

Heats of formation of bcc binary alloys
p 123 A93-17609
Method for calculating alloy energetics
p 279 A93-18740
Determination of parameters of a method for predicting alloy properties
p 126 A93-39796
Thermosolutal convection during dendritic solidification of a binary alloy
p 182 A93-45975

BINARY DATA

- Numerical model for dendritic solidification of binary alloys p 282 A93-46729
 Extension of a new semiempirical method (BFS) and the study of ground state properties of binary alloys p 283 A93-52600
 Determination of parameters of a new method for predicting alloy properties [NASA-TM-105895] p 127 N93-11609
- BINARY DATA**
 An alternative model for estimating liquid diffusion coefficients requiring no viscosity data [NASA-TM-106079] p 96 N93-23014
- BINARY MIXTURES**
 The susceptibility critical exponent for a nonaqueous ionic binary mixture near a consolute point p 284 A93-19838
 The kinetics of composite particle formation during mechanical alloying p 125 A93-29534
 A study of the effects of macrosegregation and buoyancy-driven flow in binary mixture solidification p 180 A93-44223
- BINARY SYSTEMS (MATERIALS)**
 Simple, extremely low resistance contact system to n-InP that does not exhibit metal-semiconductor intermixing during sintering p 157 A93-42550
- BINDERS (MATERIALS)**
 Guanidine based vehicle/binders for use with oxides, metals, and ceramics [NASA-CASE-LEW-15314-2] p 138 N93-28423
- BIOGRAPHY**
 Four giants of the Lewis Research Center [NASA-TM-83642] p 1 N93-72738
- BIOINSTRUMENTATION**
 Coherent fiber optic sensor for early detection of cataractogenesis in a human eye lens p 209 A93-37051
- BIPOLAR TRANSISTORS**
 High frequency performance of $\text{Si}(1-x)\text{Ge}(x)/\text{Si}(1-y)\text{Ge}(y)/\text{Si}(1-x)\text{Ge}(x)$ HBTs p 155 A93-37409
 A 10 kW dc-dc converter using IGBTs with active snubbers --- Insulated Gate Bipolar Transistor p 158 A93-50646
 The effects of strain on the microwave performance of SiGe HBTs p 158 A93-54442
- BIT ERROR RATE**
 SITE project. Phase 1: Continuous data bit-error-rate testing [NASA-TP-3279] p 58 N93-11001
 Optical communications and a comparison of optical technologies for a high data rate return link from Mars [NASA-TP-3180] p 52 N93-18854
 Combinatorial pulse position modulation for power-efficient free-space laser communications [NASA-TM-106241] p 150 N93-31856
- BLADE TIPS**
 Experimental investigation of counter-rotating propfan flutter at cruise conditions [AIAA PAPER 93-1632] p 25 A93-34160
 Capacitance-type blade-tip clearance measurement system using a dual amplifier with ramp/dc inputs and integration p 209 A93-39347
 A concept for a counterrotating fan with reduced tone noise [NASA-TM-105736] p 274 N93-11370
 Study of the capacitance technique for measuring high-temperature blade tip clearance on ceramic rotors [NASA-TM-105978] p 35 N93-23013
- BLADE-VORTEX INTERACTION**
 Forward rotor vortex effects on counter rotating propeller noise p 2 A93-19221
 Manipulation of upstream rotor leading edge vortex and its effects on counter rotating propeller noise [AIAA PAPER 93-0012] p 272 A93-20134
- BLADES**
 Structural dynamic testing of composite propfan blades for a cruise missile wind tunnel model [NASA-TM-105272] p 247 N93-18875
- BLUNT BODIES**
 Flowfield dynamics in blunt fin-induced shock wave/turbulent boundary layer interactions [AIAA PAPER 93-3133] p 11 A93-48298
- BODY CENTERED CUBIC LATTICES**
 Heats of formation of bcc binary alloys p 123 A93-17609
 Determination of parameters of a method for predicting alloy properties p 126 A93-39796
 Diffusional transport and predicting oxidative failure during cyclic oxidation of beta-NiAl alloys p 126 A93-50370
 Multilayer relaxation and surface energies of fcc and bcc metals using equivalent crystal theory p 119 A93-52872
 Determination of parameters of a new method for predicting alloy properties [NASA-TM-105895] p 127 N93-11609

BOILING

- Electrical design of Space Shuttle payload G-534: The pool boiling experiment [NASA-TM-106143] p 62 N93-27260

BONDING

- Transient liquid phase diffusion bonding of Udimet 720 for Stirling power converter applications p 221 A93-26080
 Comments on 'Kinetic Study on the Hexacelsian-Celsian Phase Transformation' [NASA-TM-105917] p 136 N93-14886

BOOSTER ROCKET ENGINES

- Combustion-wave ignition for rocket engines p 78 N93-10016

BOOSTER ROCKETS

- Propulsion and aerodynamic analysis of the Beta II two-stage-to-orbit vehicle [AIAA PAPER 92-4245] p 50 A93-13332

BORON

- Primordial nucleosynthesis and the abundances of beryllium and boron p 290 A93-33513

BOROSILICATE GLASS

- Nondestructive evaluation of a ceramic matrix composite material p 102 A93-33016
 Ceramic fiber reinforced glass-ceramic matrix composite [NASA-CASE-LEW-15262-1] p 109 N93-26100

BOULES

- Silicon carbide semiconductor technology for high temperature and radiation environments p 284 N93-26928

BOUNDARIES

- Implementation of the block-Krylov boundary flexibility method of component synthesis [NASA-TM-106065] p 248 N93-23044

BOUNDARY CONDITIONS

- Nonreflecting boundary conditions for linearized unsteady aerodynamic calculations [AIAA PAPER 93-0882] p 7 A93-25553
 The application of preconditioning in viscous flows p 177 A93-32627
 High order accurate solutions of viscous problems [AIAA PAPER 93-3074] p 183 A93-48249
 On the accurate long-time solution of the wave equation in exterior domains: Asymptotic expansions and corrected boundary conditions [NASA-TM-106117] p 269 N93-27068

BOUNDARY ELEMENT METHOD

- Shape reanalysis and sensitivities utilizing preconditioned iterative boundary solvers p 233 A93-14446
 Software issues in three dimensional continuum shape optimization employing boundary formulations [AIAA PAPER 92-4792] p 258 A93-20380
 Boundary formulations for three-dimensional continuum structural shape sensitivity analysis p 235 A93-22426
 Acoustical analysis of gear housing vibration p 273 A93-29420
 Micromechanical studies of composites by BEM p 236 A93-31295
 Boundary formulations for sensitivity analysis without matrix derivatives p 242 A93-49028
 Symmetric Galerkin boundary formulations employing curved elements p 268 A93-54198
 Experimental validation of boundary element methods for noise prediction [NASA-TM-105729] p 226 N93-10966
 Composite micromechanical modeling using the boundary element method [NASA-TM-106127] p 250 N93-27030

BOUNDARY INTEGRAL METHOD

- BIEM calculations of the frequency dispersion and ac current distribution at disk and ring-disk electrodes p 254 A93-34246
 Elastic interactions of a fatigue crack with a micro-defect by the mixed boundary integral equation method p 243 A93-56412

- Software issues in three dimensional continuum shape optimization employing boundary formulations [AIAA PAPER 92-4792] p 258 A93-20380

- Boundary formulations for three-dimensional continuum structural shape sensitivity analysis p 235 A93-22426

- Acoustical analysis of gear housing vibration p 273 A93-29420

- Micromechanical studies of composites by BEM p 236 A93-31295

- Boundary formulations for sensitivity analysis without matrix derivatives p 242 A93-49028

- Symmetric Galerkin boundary formulations employing curved elements p 268 A93-54198

- Experimental validation of boundary element methods for noise prediction [NASA-TM-105729] p 226 N93-10966

- Composite micromechanical modeling using the boundary element method [NASA-TM-106127] p 250 N93-27030

- BIEM calculations of the frequency dispersion and ac current distribution at disk and ring-disk electrodes p 254 A93-34246

- Elastic interactions of a fatigue crack with a micro-defect by the mixed boundary integral equation method p 243 A93-56412

BOUNDARY LAYER CONTROL

- Bypass transition in compressible boundary layers p 196 N93-15801
 Analytical and experimental studies of a short compact subsonic diffuser for a two-dimensional supersonic inlet [NASA-TP-3247] p 17 N93-24118

BOUNDARY LAYER FLOW

- Use of surface heat transfer measurements as a flow separation diagnostic in a two-dimensional reflected oblique shock/turbulent boundary layer interaction [AIAA PAPER 93-0775] p 172 A93-24859
 A note on the distortion of a flat-plate boundary layer by free-stream vorticity normal to the plate p 178 A93-34414
 High order accurate solutions of viscous problems [AIAA PAPER 93-3074] p 183 A93-48249
 A time-accurate high-resolution TVD scheme for solving the Navier-Stokes equations p 13 A93-52006

- Supersonic boundary-layer flow turbulence modeling [NASA-TM-105893] p 193 N93-14758

- Use of surface heat transfer measurements as a flow separation diagnostic in a two dimensional reflected oblique shock/turbulent boundary layer interaction [NASA-TM-105981] p 194 N93-15355

- A time-accurate high-resolution TVD scheme for solving the Navier-Stokes equations [NASA-TM-106056] p 268 N93-22664

- Surface and flow field measurements in a symmetric crossing shock wave/turbulent boundary-layer interaction [NASA-TM-106086] p 17 N93-24911

- NASA, Lewis Research Center/IFMD inlet duct and nozzle high speed validation experiments p 204 N93-70582

- Three-dimensional boundary-layer instability and separation induced by small-amplitude streamwise vorticity in the upstream flow p 172 A93-24401

- Use of surface heat transfer measurements as a flow separation diagnostic in a two dimensional reflected oblique shock/turbulent boundary layer interaction [AIAA PAPER 93-0775] p 172 A93-24859

- 3-D viscous flow CFD analysis of the propeller effect on an advanced ducted propeller subsonic inlet [AIAA PAPER 93-1847] p 12 A93-49728

- Use of surface heat transfer measurements as a flow separation diagnostic in a two dimensional reflected oblique shock/turbulent boundary layer interaction [NASA-TM-105981] p 194 N93-15355

- Analytical and experimental studies of a short compact subsonic diffuser for a two-dimensional supersonic inlet [NASA-TP-3247] p 17 N93-24118

- The 3-D viscous flow CFD analysis of the propeller effect on an advanced ducted propeller subsonic inlet [NASA-TM-106240] p 38 N93-29162

- Nonlinear evolution of modes in a compressible boundary layer p 164 A93-17258

- Fully coupled resonant-triad interaction in an adverse-pressure-gradient boundary layer p 167 A93-21049

- Three-dimensional boundary-layer instability and separation induced by small-amplitude streamwise vorticity in the upstream flow p 172 A93-24401

- Linear instability of curved free shear layers [AIAA PAPER 93-3252] p 183 A93-46797

- Higher-order accurate Osher schemes with application to compressible boundary layer stability [AIAA PAPER 93-3051] p 183 A93-48231

- Fully coupled resonant-triad interaction in an adverse-pressure-gradient boundary layer p 167 A93-21049

- Effects of free-stream turbulence on boundary-layer transition [AIAA PAPER 93-0488] p 170 A93-23390

- Nonlinear interaction of frequency-detuned modes in boundary layers [AIAA PAPER 93-0347] p 171 A93-24237

- Modeling of near wall turbulence and modeling of bypass transition p 195 N93-15798

- NASA, Lewis Research Center/IFMD inlet duct and nozzle high speed validation experiments p 204 N93-70582

- Nonlinear interaction of frequency-detuned modes in boundary layers [AIAA PAPER 93-0347] p 171 A93-24237

- AGARD WG13 aerodynamics of high speed air intakes: Assessment of CFD results p 192 N93-13220

- Double-diffusive fingering convection in a porous medium p 175 A93-27900

- Some aspects of bifurcation structure of laminar flow in curved ducts p 164 A93-14771

- Comparison of dynamic isotope power systems for distributed planetary surface applications p 46 A93-13825

- Optimization of closed Brayton cycles for space power generation p 68 A93-25859

- BIPS Turboalternator-Compressor characteristics and application to the NASA Solar Dynamic Ground Demonstration Program p 69 A93-25965

- Evolving SP-100 powerplants via electric propulsion to GEO and lunar orbit p 70 A93-34492

- Closed Brayton Cycle power system with a high temperature pellet bed reactor heat source for NEP applications [NASA-TM-105933] p 82 N93-14482

- The 20 kWe NEP system studies p 90 N93-26971

- BRIDGMAN METHOD**
Prediction of dislocation generation during Bridgman growth of GaAs crystals p 279 A93-19740
- BRILLOUIN EFFECT**
Rayleigh-Brillouin scattering for high-pressure gas temperature measurements p 218 N93-31556
- BRITTLE MATERIALS**
Model of brittle matrix composite toughening based on discrete fiber reinforcement p 104 A93-40888
Numerical calibration of the stable poisson loaded specimen
[NASA-TM-105609] p 245 N93-12738
- BROADBAND**
Satellites and the BSDN: An overview of NASA R/D [NASA-TM-106108] p 150 N93-26903
Determination of plate wave velocities and diffuse field decay rates with broad-band acousto-ultrasonic signals [NASA-TM-106158] p 232 N93-27080
- BROADCASTING**
Direct Broadcast Satellite: Radio Program [NASA-TM-105910] p 52 N93-11430
Utilizing a TDRS satellite for direct broadcast satellite-radio propagation experiments and demonstrations [NASA-TM-106172] p 53 N93-27064
- BROMINE**
Properties of hybrid CVD/PAN graphite fibers and their bromine intercalation compounds p 98 A93-17675
- BROMINE COMPOUNDS**
Properties of hybrid CVD/PAN graphite fibers and their bromine intercalation compounds p 98 A93-17675
- BRUSH SEALS**
Development of advanced seals for space propulsion turbomachinery [SAE PAPER 921028] p 218 A93-14651
Brush seal leakage performance with gaseous working fluids at static and low rotor speed conditions [ASME PAPER 92-GT-304] p 219 A93-19494
Brush seal low surface speed hard-rub characteristics [AIAA PAPER 93-2534] p 225 A93-50261
Preliminary experimental results for a cryogenic brush seal configuration [AIAA PAPER 93-2535] p 225 A93-50262
Flow visualization in a single simulated brush seal p 226 A93-54659
Brush seal bristle flexure and hard-rub characteristics [NASA-TM-105864] p 227 N93-18321
Integrity testing of brush seal in shroud ring of T-700 engine [NASA-TM-105863] p 227 N93-18380
Brush seal low surface speed hard-rub characteristics [NASA-TM-106169] p 200 N93-27132
Preliminary experimental results for a cryogenic brush seal configuration [NASA-TM-106236] p 201 N93-28627
- BRUSHES**
Integrity testing of brush seal in shroud ring of T-700 engine [NASA-TM-105863] p 227 N93-18380
- BUBBLES**
Gravitational waves from first-order cosmological phase transitions p 288 A93-11451
Nucleate pool boiling in the long duration low gravity environment of the space shuttle [AIAA PAPER 93-0465] p 142 A93-23371
Thermocapillary bubble migration - An Oseen-like analysis of the energy equation p 179 A93-41708
Nucleate pool boiling in the long duration low gravity environment of the Space Shuttle [NASA-TM-105973] p 144 N93-15420
- BUCKLING**
Probabilistic assessment of adaptive space truss configurations for thermal buckling resistance [AIAA PAPER 93-1622] p 240 A93-34151
- BUOYANCY**
Effect of free surface shape on combined thermocapillary and natural convection p 162 A93-10671
Heat transfer in rotating serpentine passages with trips skewed to the flow [ASME PAPER 92-GT-191] p 166 A93-19416
The effects of buoyancy on the critical heat flux in forced convection [AIAA PAPER 93-0575] p 169 A93-23307
Computational predictions of flame spread over alcohol pools [AIAA PAPER 93-0825] p 115 A93-24895
Numerical computation of low-speed concurrent flow flame spread in mixed buoyant and forced flow [AIAA PAPER 93-0827] p 115 A93-24897
A study of the effects of macrosegregation and buoyancy-driven flow in binary mixture solidification p 180 A93-44223
Second order closure modeling of turbulent buoyant wall plumes [NASA-TM-105956] p 193 N93-14829
- Numerical study of mixing of two fluids under low gravity [NASA-TM-105865] p 194 N93-14914
Experiments on a round turbulent buoyant plume [NASA-TM-105955] p 141 N93-16384
Effects of buoyancy on laminar, transitional, and turbulent gas jet diffusion flames p 121 N93-20189
Flame spread across liquid pools p 122 N93-20209
Heat transfer in rotating serpentine passages with selected model orientation for smooth or skewed trip walls [NASA-TM-106126] p 147 N93-25177
- BURNERS**
The multi-heat addition turbine engine [AIAA PAPER 92-4272] p 22 A93-13334
- BURNING RATE**
Experiments on the effect of initial diameter in spherically symmetric droplet combustion of sooting fuels [AIAA PAPER 93-0130] p 139 A93-22577
Computational/experimental basis for conducting alkane droplet combustion experiments on space-based-platforms p 117 A93-41711
Effects of detailed droplet heating models on turbulent sprays vaporization behavior [AIAA PAPER 93-2193] p 185 A93-50005
Premixed flame propagation in an optically thick gas p 119 A93-55381
Calculations of combustion response profiles and oscillations [NASA-TM-106135] p 87 N93-25236
Smoldering combustion in microgravity: USML-1 glovebox experiment No. 6 [NASA-TM-105012] p 146 N93-70290
- C**
- CABLES**
A system to measure lightning-induced transients on spacecraft umbilical lines p 161 N93-24889
- CADMIUM**
Closed-ampoule diffusion of sulfur into Cd-doped InP substrates - Dependence of S profiles on diffusion temperature and time p 283 A93-51917
- CALCIUM FLUORIDES**
Mechanical properties of Haynes Alloy 188 after exposure to LiF-22CaF₂, air, and vacuum at 1093 K for periods up to 10,000 hours p 126 A93-36586
- CALCULUS OF VARIATIONS**
Incompressible spectral-element method: Derivation of equations [NASA-TM-106109] p 199 N93-26554
- CALIBRATING**
Novel thin-film heat flux sensors [AIAA PAPER 92-5035] p 205 A93-22309
Applied high-speed imaging for the icing research program at NASA Lewis Research Center p 208 A93-33169
An Automated Thermocouple Calibration System p 208 A93-35575
Analytical stress intensity solution for the Stable Poisson Loaded specimen p 242 A93-46768
Icing Research Tunnel rotating bar calibration measurement system p 212 A93-54398
Numerical calibration of the stable poisson loaded specimen [NASA-TM-105609] p 245 N93-12738
Icing research tunnel rotating bar calibration measurement system [NASA-TM-106010] p 215 N93-22598
Ice thickness measurement system for the icing research tunnel calibration [NASA-TM-106095] p 215 N93-24737
Neural networks for calibration tomography [NASA-TM-106352] p 216 N93-26906
Calibration of a shock wave position sensor using artificial neural networks [NASA-TM-106138] p 216 N93-27001
- CANTILEVER BEAMS**
Micromachined silicon cantilever beam accelerometer incorporating an integrated optical waveguide p 210 A93-49457
- CANTILEVER MEMBERS**
Probabilistic assessment of adaptive space truss configurations for thermal buckling resistance [AIAA PAPER 93-1622] p 240 A93-34151
- CAPACITANCE**
Capacitance-type blade-tip clearance measurement system using a dual amplifier with ramp/dc inputs and integration p 209 A93-39347
Study of the capacitance technique for measuring high-temperature blade tip clearance on ceramic rotors [NASA-TM-105978] p 35 N93-23013
- CAPACITANCE-VOLTAGE CHARACTERISTICS**
Lightweight nickel electrodes for nickel/hydrogen cells p 255 A93-51574
- CAPE KENNEDY LAUNCH COMPLEX**
A system to measure lightning-induced transients on spacecraft umbilical lines p 161 N93-24889
- CAPILLARY FLOW**
A study of circumferentially-heated and block-heated heat pipes. I - Experimental analysis and generalized analytical prediction of capillary limits. II - Three-dimensional numerical modeling as a conjugate problem p 168 A93-21715
Time-dependent thermocapillary convection in a Cartesian cavity - Numerical results for a moderate Prandtl number fluid [AIAA PAPER 93-0259] p 169 A93-22666
Particle image velocimetry for the Surface Tension Driven Convection Experiment using a particle displacement tracking technique p 206 A93-23799
Computational predictions of flame spread over alcohol pools [AIAA PAPER 93-0825] p 115 A93-24895
Ground-based PIV and numerical flow visualization results from the Surface Tension Driven Convection Experiment p 143 A93-33075
On accurate determination of contact angle p 143 A93-41678
Thermocapillary bubble migration - An Oseen-like analysis of the energy equation p 179 A93-41708
Thermocapillary migration of a small chain of bubbles p 182 A93-46714
Collective effects of temperature gradients and gravity on droplet coalescence p 183 A93-46716
Atomization and vaporization characteristics of airblast fuel injection inside a venturi tube [AIAA PAPER 93-1766] p 184 A93-49662
- CARBIDES**
Thermal stability of the microstructure of an aged Nb-Zr-C alloy p 122 A93-13776
- CARBON**
Greatly improved 3C-SiC p-n junction diodes grown by chemical vapor deposition p 156 A93-38994
Tribological studies of amorphous hydrogenated carbon films in a vacuum, spacelike environment p 134 A93-40630
Chemical reactions in the processing of MoSi₂ + carbon compacts p 119 A93-53733
Studies on the reactive melt infiltration of silicon and silicon-molybdenum alloys in porous carbon [NASA-TM-105860] p 136 N93-12398
Optical and scratch resistant properties of diamondlike carbon films deposited with single and dual ion beams [NASA-TM-105943] p 95 N93-22586
Optical and scratch resistant properties of diamondlike carbon films deposited with single and dual ion beams p 137 N93-25564
- CARBON COMPOUNDS**
The microstructural evolution, crystallography, and thermal processing of ultrahigh carbon Fe-1.85 pct C melt-spun ribbon p 125 A93-32934
- CARBON DIOXIDE**
Brush seal leakage performance with gaseous working fluids at static and low rotor speed conditions [ASME PAPER 92-GT-304] p 219 A93-19494
Lunar and Martian environmental interactions with nuclear power system radiators [NASA-TM-105747] p 80 N93-10965
Alkali metal carbon dioxide electrochemical system for energy storage and/or conversion of carbon dioxide to oxygen [NASA-CASE-LEW-14973-1] p 256 N93-28974
- CARBON FIBER REINFORCED PLASTICS**
Intercalated graphite fiber composites as EMI shields in aerospace structures p 104 A93-41573
- CARBON FIBERS**
Void control in the crystallization of lithium fluoride p 97 A93-13760
Graphite fiber/copper matrix composites for space power heat pipe fin applications p 162 A93-13789
Properties of hybrid CVD/PAN graphite fibers and their bromine intercalation compounds p 98 A93-17675
Thermal conductivity and thermal expansion of graphite fiber-reinforced copper matrix composites p 100 A93-25104
Heat transfer device [NASA-CASE-LEW-14162-4] p 108 N93-20568
Fiber shape effects on metal matrix composite behavior [NASA-TM-106067] p 109 N93-26704
Apparatus for intercalating large quantities of fibrous structures [NASA-CASE-LEW-15077-2] p 111 N93-29609
Method for producing hybrid graphite composite [NASA-CASE-LEW-15241-2] p 112 N93-31296
- CARBON-CARBON COMPOSITES**
SP-100 high-temperature advanced radiator development p 163 A93-13843
Fabrication of carbon-carbon heat pipes for space nuclear power applications p 173 A93-25978

CARGO SPACECRAFT

- Method for producing hybrid graphite composite
[NASA-CASE-LEW-15241-2] p 112 N93-31296
- CARGO SPACECRAFT**
The 100-500 kWe NEP systems p 90 N93-26984
- CARRIER MOBILITY**
Room-temperature determination of two-dimensional electron gas concentration and mobility in heterostructures p 280 A93-35198
- CARRIER TRANSPORT (SOLID STATE)**
Carrier removal and defect behavior in p-type InP p 279 A93-17176
Diffusion length variation in 0.5- and 3-MeV proton-irradiated, heteroepitaxial indium phosphide solar cells p 161 N93-27002
[NASA-TM-106147]
- CASCADE FLOW**
Numerical solutions for unsteady subsonic vortical flows around loaded cascades p 3 A93-19399
[ASME PAPER 92-GT-173]
Forcing function effects on unsteady aerodynamic gust response. II - Low solidity airfoil row response p 3 A93-19401
[ASME PAPER 92-GT-175]
An algebraic turbulence model for three-dimensional viscous flows p 4 A93-22552
[AIAA PAPER 93-0083]
High accuracy computation of fluid-structure interaction in transonic cascades p 6 A93-23387
[AIAA PAPER 93-0485]
Three-dimensional unstructured grid Euler method applied to turbine blades p 6 A93-24233
[AIAA PAPER 93-0196]
Multigrid calculation of three-dimensional viscous cascade flows p 8 A93-42889
Averaging techniques for steady and unsteady calculations of a transonic fan stage p 11 A93-48241
[AIAA PAPER 93-3065]
Blade row interaction effects on flutter and forced response p 28 A93-49911
[AIAA PAPER 93-2084]
Chimera grids in the simulation of three-dimensional flowfields in turbine-blade-coolant passages p 187 A93-50280
[AIAA PAPER 93-2559]
Forcing function modeling for flow induced vibration [ISABE 93-7027] p 31 A93-54003
Analysis of high Reynolds number inviscid/viscid interactions in cascades p 15 A93-55351
An algebraic turbulence model for three-dimensional viscous flows p 1 N93-14102
[NASA-TM-105931]
- CASING**
Numerical simulation of compressor endwall and casing treatment flow phenomena p 4 A93-19490
[ASME PAPER 92-GT-300]
- CAST ALLOYS**
Room temperature cyclic deformation behavior of cast and extruded NiAl p 122 A93-12130
On the drag of model dendrite fragments at low Reynolds number p 128 N93-19974
[NASA-TM-105916]
- CASTING**
Observations on infiltration of silicon carbide compacts with an aluminum alloy p 97 A93-12356
Silicon carbide fiber reinforced strontium aluminosilicate glass-ceramic matrix composite p 106 N93-11543
[NASA-CASE-LEW-15263-1]
- CATALOGS (PUBLICATIONS)**
Pyrotechnically actuated systems database and applications catalog p 141 N93-20136
- CATALYSIS**
Validation test of advanced technology for IPV nickel-hydrogen flight cells - Update p 252 A93-25886
Catalytic ignition model in monolithic reactor with in-depth reaction p 119 A93-51641
- CATALYSTS**
Atomic oxygen protective coating with resistance to undercutting at defect sites p 137 N93-20566
[NASA-CASE-LEW-15306-1]
Method for retarding oxidation of an organic substrate p 138 N93-28425
[NASA-CASE-LEW-15306-2]
- CATALYTIC ACTIVITY**
A survey and analysis of commercially available hydrogen sensors p 214 N93-17777
[NASA-TM-105878]
- CATARACTS**
Coherent fiber optic sensor for early detection of cataractogenesis in a human eye lens p 209 A93-37051
A fiber optic probe for the detection of cataracts p 257 N93-25593
- CATHODES**
100-kW class applied-field MPD thruster component wear p 85 N93-22482
[NASA-TM-106023]

- Alkali metal carbon dioxide electrochemical system for energy storage and/or conversion of carbon dioxide to oxygen p 256 N93-28974
[NASA-CASE-LEW-14973-1]
- CAVITATION FLOW**
Simultaneous pressure measurement and high-speed photography study of cavitation in a dynamically loaded journal bearing p 223 A93-40050
Thermocapillary migration of a small chain of bubbles p 182 A93-46714
Effect of out-of-roundness on the performance of a diesel engine connecting-rod bearing p 225 A93-52607
- CAVITIES**
Calculations of separated 3-D flows with a pressure-staggered Navier-Stokes equations solver p 177 A93-34366
A reciprocity formulation for the EM scattering by an obstacle within a large open cavity p 149 A93-52237
A creep cavity growth model for creep-fatigue life prediction of a unidirectional W/Cu composite p 244 N93-10967
[NASA-TM-105780]
Jet Engine hot parts IR Analysis Procedure (J-EIRP) p 21 N93-22588
[NASA-TM-105914]
- CAVITY FLOW**
Effect of free surface shape on combined thermocapillary and natural convection p 162 A93-10671
Time-dependent thermocapillary convection in a Cartesian cavity - Numerical results for a moderate Prandtl number fluid p 169 A93-22666
[AIAA PAPER 93-0259]
Driven cavity simulation of turbomachine blade flows with vortex control p 6 A93-24238
[AIAA PAPER 93-0390]
On solving the compressible Navier-Stokes equations for unsteady flows at very low Mach numbers p 181 A93-45061
[AIAA PAPER 93-3368]
Parallel solution of high-order numerical schemes for solving incompressible flows p 262 N93-27040
[NASA-TM-4451]
- CENTER OF GRAVITY**
Experimental performance of a ventral nozzle with pitch and yaw vectoring capability for SSTOVL aircraft p 36 N93-25129
[NASA-TM-106054]
- CENTRAL PROCESSING UNITS**
Concurrent processing adaptation of aeroelastic analysis of propfans p 23 A93-14624
- CENTRIFUGAL COMPRESSORS**
Experimental and computational investigation of the NASA Low-Speed Centrifugal Compressor flow field p 4 A93-19436
[ASME PAPER 92-GT-213]
Prediction of active control of subsonic centrifugal compressor rotating stall p 4 A93-22591
[AIAA PAPER 93-0153]
A model for the selective amplification of spatially coherent waves in a centrifugal compressor on the verge of rotating stall p 13 A93-50039
[AIAA PAPER 93-2236]
A survey of instabilities within centrifugal pumps and concepts for improving the flow range of pumps in rocket engines p 190 N93-10039
Summary of NASA, Lewis Research Center validation efforts p 204 N93-70579
NASA low speed centrifugal compressor p 204 N93-70583
- CENTRIFUGAL FORCE**
Three-dimensional numerical simulation of gradual opening in a wave rotor passage p 187 A93-50254
[AIAA PAPER 93-2526]
- CENTRIFUGAL PUMPS**
A survey of instabilities within centrifugal pumps and concepts for improving the flow range of pumps in rocket engines p 190 N93-10039
- CERAMIC COATINGS**
Technical note - Plasma-sprayed ceramic thermal barrier coatings for smooth intermetallic alloys p 219 A93-15702
Plasma sprayed ceramic thermal barrier coating for NiAl-based intermetallic alloys p 130 N93-31294
[NASA-CASE-LEW-15535-1]
- CERAMIC FIBERS**
Prediction of chemical vapor deposition rates on monofilaments and its implications for fiber properties p 113 A93-17198
Fatigue-environment interactions in a SiC/Ti-15-3 composite p 100 A93-26275
Creep and stress relaxation modeling of polycrystalline ceramic fibers p 132 A93-31354
Transverse ductility of metal matrix composites p 101 A93-31355
Relative sliding durability of two candidate high-temperature oxide fiber seal materials p 132 A93-31983
Microchemical analysis of the SCS-6 silicon carbide fiber p 135 A93-53734

- Relative sliding durability of candidate high temperature fiber seal materials p 95 N93-10978
[NASA-TM-105806]
Fiber-reinforced monoclinic celsian matrix composite material p 108 N93-20040
[NASA-CASE-LEW-15269-1]
Sliding durability of candidate seal fiber materials in hydrogen from 25 to 900 C p 95 N93-22590
[NASA-TM-105939]
Ceramic fiber reinforced glass-ceramic matrix composite p 109 N93-26100
[NASA-CASE-LEW-15262-1]
- CERAMIC MATRIX COMPOSITES**
Ceramic matrix composite applications in advanced liquid fuel rocket engine turbomachinery p 99 A93-19502
[ASME PAPER 92-GT-316]
Ceramic matrix composites for rocket engine turbine applications p 99 A93-19547
[ASME PAPER 92-GT-394]
Detecting Lamb waves with broadband acousto-ultrasonic signals in composite structures p 231 A93-21898
Corrosion of silicon-based ceramics in combustion environments p 131 A93-22984
Effect of HIPing on the effective thermal conductivity/diffusivity and the interfacial thermal conductance of uniaxial SiC fibre-reinforced RBSN p 100 A93-26674
Creep and stress relaxation modeling of polycrystalline ceramic fibers p 132 A93-31354
NDE of the universe - New ways to look at old facts p 271 A93-32222
Mechanics of interfaces in fiber reinforced SiC/RBSN ceramic matrix composites --- reaction bonded silicon nitride p 102 A93-32466
Nondestructive evaluation of a ceramic matrix composite material p 102 A93-33016
A generic model for creep rupture lifetime estimation on fibrous ceramic composites p 103 A93-38895
Tensile creep and creep-recovery behavior of a SiC-fiber-Si3N4-matrix composite p 104 A93-40290
An analysis of the wear behavior of SiC whisker-reinforced alumina from 25 to 1200 C p 104 A93-49253
Ultrasonic assessment of interfacial oxidation damage in ceramic matrix composites p 105 A93-52919
Approaches to polymer-derived CMC matrices p 105 A93-53446
Material requirements for the High Speed Civil Transport p 31 A93-54043
[ISABE 93-7067]
Reliability analysis of laminated ceramic matrix composites using shell subelement techniques p 243 A93-55382
Aerospace applications --- of refractory ceramic materials p 135 A93-55472
Nondestructive evaluation of ceramic and metal matrix composites for NASA's HITEMP and enabling propulsion materials programs p 231 N93-10963
[NASA-TM-105807]
Silicon carbide fiber reinforced strontium aluminosilicate glass-ceramic matrix composite p 106 N93-11543
[NASA-CASE-LEW-15263-1]
Fiber-reinforced monoclinic celsian matrix composite material p 108 N93-20040
[NASA-CASE-LEW-15269-1]
Determination of plate wave velocities and diffuse field decay rates with broad-band acousto-ultrasonic signals p 232 N93-27080
[NASA-TM-106158]
Ceramic matrix composites properties/microstresses with complete and partial interphase bond p 111 N93-29071
[NASA-TM-106136]
Acousto-Ultrasonic analysis of failure in ceramic matrix composite tensile specimens p 232 N93-29073
[NASA-TM-106219]
SiC fiber-reinforced Celsian glass-ceramic matrix composite p 112 N93-31293
[NASA-CASE-LEW-15264-1]
Method of producing a ceramic fiber-reinforced glass-ceramic matrix composite p 112 N93-31299
[NASA-CASE-LEW-15264-2]
- CERAMICS**
Effect of hydrogen on the strength and microstructure of selected ceramics p 130 A93-13613
Construction and testing of ceramic fabric heat pipe with water working fluid p 163 A93-13869
Development of advanced seals for space propulsion turbomachinery p 218 A93-14651
[SAE PAPER 921028]
Reliability analysis of structural ceramic components using a three-parameter Weibull distribution p 231 A93-19486
[ASME PAPER 92-GT-296]
Ceramic component reliability with the restructured NASA/CARES computer program p 234 A93-19540
[ASME PAPER 92-GT-383]

- Fracture toughness of advanced ceramics at room temperature p 131 A93-20842
- Refractive index and scattering effects on radiative behavior of a semitransparent layer p 176 A93-31438
- Lifetime reliability evaluation of structural ceramic parts with the CARES/LIFE computer program [AIAA PAPER 93-1497] p 239 A93-34037
- A numerical round robin for the reliability prediction of structural ceramics [AIAA PAPER 93-1498] p 240 A93-34038
- Analysis of precracking parameters for ceramic single-edge-precracked-beam specimens p 133 A93-38887
- Elevated-temperature fracture resistances of monolithic and composite ceramics using chevron-notched bend tests p 133 A93-38888
- CVD of silicon carbide on structural fibers - Microstructure and composition p 117 A93-39521
- Overview of NASA's advanced high temperature engine materials technology program p 94 A93-53453
- Reliability analysis of laminated ceramic matrix composites using shell subelement techniques p 243 A93-55382
- Aerospace applications ... of refractory ceramic materials p 135 A93-55472
- Analysis of precracking parameters and fracture toughness for ceramic single-edge-precracked-beam specimens [NASA-TM-105568] p 135 A93-10962
- Ceramic component reliability with the restructured NASA/CARES computer program [NASA-TM-105856] p 244 A93-11004
- Thin film thermocouples for high temperature measurement on ceramic materials p 213 A93-13666
- Method of applying a thermal barrier coating system to a substrate [NASA-CASE-LEW-15020-2] p 107 A93-14706
- Study of the capacitance technique for measuring high-temperature blade tip clearance on ceramic rotors [NASA-TM-105978] p 35 A93-23013
- Development of thin film thermocouples on ceramic materials for advanced propulsion system applications [NASA-TM-106017] p 215 A93-25173
- Vickers indentation hardness of stoichiometric and reduced single crystal TiO₂ (rutile) from 25 to 800 C [NASA-TM-105959] p 96 A93-26204
- Determination of plate wave velocities and diffuse field decay rates with broad-band acousto-ultrasonic signals [NASA-TM-106158] p 232 A93-27080
- Radial basis function network learns ceramic processing and predicts related strength and density [NASA-TM-106048] p 110 A93-27129
- Fuzzy sets predict flexural strength and density of silicon nitride ceramics [NASA-TM-106049] p 110 A93-27270
- Guandine based vehicle/binders for use with oxides, metals, and ceramics [NASA-CASE-LEW-15314-2] p 138 A93-28423
- Soft computing in design and manufacturing of advanced materials [NASA-TM-106032] p 111 A93-28624
- CERIUM OXIDES**
- Buffer layers for high-Tc thin films on sapphire p 150 A93-17063
- CHANNEL FLOW**
- Friction-factor characteristics for narrow channels with honeycomb surfaces [ASME PAPER 91-TRIB-21] p 219 A93-15681
- Heat transfer performance comparisons of five different rectangular channels with parallel angled ribs p 166 A93-18752
- Heat transfer in oscillating flows with sudden change in cross section p 174 A93-26089
- New time scale based k-epsilon model for near-wall turbulence p 180 A93-41909
- CFD analyses of coolant channel flowfields [AIAA PAPER 93-1830] p 184 A93-49715
- Analysis of unsteady wave processes in a rotating channel [AIAA PAPER 93-2527] p 187 A93-50255
- Thermal stratification potential in rocket engine coolant channels p 78 A93-10019
- Program ELM: A tool for rapid thermal-hydraulic analysis of solid-core nuclear rocket fuel elements [NASA-TM-105867] p 84 A93-19106
- A new flux conserving Newton's method scheme for the two-dimensional, steady Navier-Stokes equations [NASA-TM-106160] p 201 A93-28626
- CHAOS**
- Desktop chaotic systems: Intuition and visualization [NASA-TM-106258] p 269 A93-31847
- CHARGE EFFICIENCY**
- Lightweight nickel electrodes for nickel/hydrogen cells p 255 A93-51574
- CHARGED PARTICLES**
- Transfer Orbit Plasma Interaction Experiment (TROPIX) p 45 A93-28734
- CHEMICAL ANALYSIS**
- Thermal stability of the microstructure of an aged Nb-Zr-C alloy p 122 A93-13776
- CHEMICAL COMPOSITION**
- Glass formation, properties and structure of soda-yttria-silica glasses p 131 A93-20464
- CVD of silicon carbide on structural fibers - Microstructure and composition p 117 A93-39521
- The chemistry of Saudi Arabian sand - A deposition problem on helicopter turbine airfoils p 243 A93-53468
- Microchemical analysis of the SCS-6 silicon carbide fiber p 135 A93-53734
- The effect of processing and compositional changes on the tribology of PM212 in air [NASA-TM-105945] p 95 A93-15576
- Spectroscopic wear detector [NASA-CASE-LEW-15200-1] p 83 A93-18856
- Determination of the oxidative stability of perfluoropolyalkyl ethers and correlation with chemical structure [NASA-TM-106223] p 139 A93-32367
- CHEMICAL ELEMENTS**
- Thermodynamic data for fifty reference elements [NASA-TP-3287] p 286 A93-19977
- CHEMICAL ENERGY**
- Determination of parameters of a method for predicting alloy properties p 126 A93-39796
- Determination of parameters of a new method for predicting alloy properties [NASA-TM-105895] p 127 A93-11609
- CHEMICAL EQUILIBRIUM**
- A kinetic and equilibrium analysis of silicon carbide chemical vapor deposition on monofilaments [NASA-TM-106137] p 96 A93-27003
- CHEMICAL EVOLUTION**
- Chemical and luminosity evolution, and counts of galaxies in a merger model p 290 A93-34776
- CHEMICAL PROPERTIES**
- Electrical and Chemical Interactions at Mars Workshop. Part 2: Appendix [NASA-CP-10093-PT-2] p 293 A93-26392
- CHEMICAL PROPULSION**
- Prediction of engine and near-field plume reacting flows in low-thrust chemical rockets [AIAA PAPER 93-0237] p 66 A93-22649
- Atomic hydrogen propellants - Historical perspectives and future possibilities [AIAA PAPER 93-0244] p 140 A93-24234
- Atomic hydrogen propellants: Historical perspectives and future possibilities [NASA-TM-106053] p 84 A93-20614
- Space chemical propulsion test facilities at NASA Lewis Research Center [NASA-TM-106050] p 85 A93-23405
- CHEMICAL REACTIONS**
- Simplified jet fuel reaction mechanism for lean burn combustion application [AIAA PAPER 93-0021] p 113 A93-23238
- Interactions between spacecraft and their environments [AIAA PAPER 93-0705] p 55 A93-24801
- Ellipsometric study of ambient-produced overlayer growth rate on YBa₂Cu₃O_{7-x} films p 281 A93-39362
- Thermodynamics of Si-C-O system p 133 A93-39584
- Simplified jet-A kinetic mechanism for combustor application [NASA-TM-105940] p 120 A93-15504
- Center for Modeling of Turbulence and Transition (CMOTT): Research Briefs, 1992 [NASA-TM-105834] p 195 A93-15792
- LSENS, a general chemical kinetics and sensitivity analysis code for gas-phase reactions: User's guide [NASA-TM-105851] p 121 A93-16614
- Substituted 1,1,1-triaryl 2,2,2-trifluoroethanes and processes for their synthesis [NASA-CASE-LEW-14345-7] p 95 A93-17412
- Electrical and Chemical Interactions at Mars Workshop. Part 2: Appendix [NASA-CP-10093-PT-2] p 293 A93-26392
- CHEMICAL REACTORS**
- Flow effects in a vertical CVD reactor p 166 A93-19821
- Computer modeling of a hot filament diamond deposition reactor p 94 A93-40618
- CHIPS (ELECTRONICS)**
- Analysis of fault-tolerant neurocontrol architectures [NASA-TM-105898] p 41 A93-12305
- CHLORIDES**
- Physical vapor transport of mercurous chloride under a nonlinear thermal profile [NASA-TM-105920] p 196 A93-16612
- CHOKED FLOW**
- Preliminary experimental results for a cryogenic brush seal configuration [AIAA PAPER 93-2535] p 225 A93-50262
- Preliminary experimental results for a cryogenic brush seal configuration [NASA-TM-106236] p 201 A93-28627
- CHROMIUM**
- Thermal stability of the microstructure of an aged Nb-Zr-C alloy p 122 A93-13776
- The kinetics of composite particle formation during mechanical alloying p 125 A93-29534
- CHROMIUM ALLOYS**
- Palladium-chromium static strain gage for high temperature propulsion systems p 204 A93-16421
- Reaction layer formation at the graphite/copper-chromium alloy interface p 100 A93-25105
- Auger electron spectroscopy study of oxidation of a PdCr alloy used for high-temperature sensors [NASA-TM-106212] p 129 A93-23418
- High temperature creep and oxidation resistant chromium silicide matrix alloy containing molybdenum [NASA-CASE-LEW-15697-1] p 130 A93-29172
- CHROMIUM CARBIDES**
- The effect of processing and compositional changes on the tribology of PM212 in air [NASA-TM-105945] p 95 A93-15576
- Properties of extruded PS-212 type self-lubricating materials p 138 A93-25565
- CIRCUIT DIAGRAMS**
- Design aspects and comparison between high Tc superconducting coplanar waveguide and microstrip line p 155 A93-27244
- CIVIL AVIATION**
- The NASA Computational Fluid Dynamics (CFD) program - Building technology to solve future challenges [AIAA PAPER 93-3292] p 287 A93-44996
- Overview of NASA's advanced high temperature engine materials technology program p 94 A93-53453
- Propulsion technology challenges for turn-of-the-century commercial aircraft [ISABE 93-7003] p 31 A93-53980
- Engine technology challenges for a 21st Century High-Speed Civil Transport [ISABE 93-7064] p 31 A93-54040
- Material requirements for the High Speed Civil Transport [ISABE 93-7067] p 31 A93-54043
- An artificial intelligence-based structural health monitoring system for aging aircraft p 266 A93-22185
- Bibliography on propulsion airframe integration technologies for high-speed civil transport applications, 1980-1991 [NASA-TM-105602] p 1 A93-26136
- Engine technology challenges for a 21st Century High-Speed Civil Transport [NASA-TM-106216] p 39 A93-31671
- Propulsion technology challenges for turn-of-the-century commercial aircraft [NASA-TM-106192] p 39 A93-32351
- CLAMPS**
- Automatic system for installation and replacement of Space Station components [NASA-CASE-LEW-14906-1] p 226 A93-12203
- An apparatus for gripping test specimens [NASA-CASE-LEW-15345-2] p 230 A93-28127
- Service equipment for use in hostile environments [NASA-CASE-LEW-14906-2] p 230 A93-31314
- CLASSIFIERS**
- Pattern classifier for health monitoring of helicopter gearboxes [NASA-TM-106099] p 228 A93-23741
- CLEARANCES**
- Capacitance-type blade-tip clearance measurement system using a dual amplifier with ramp/dc inputs and integration p 209 A93-39347
- Study of the capacitance technique for measuring high-temperature blade tip clearance on ceramic rotors [NASA-TM-105978] p 35 A93-23013
- CLOSED CYCLES**
- Closed Brayton Cycle power system with a high temperature pellet bed reactor heat source for NEP applications [NASA-TM-105933] p 82 A93-14482
- CLOSURE LAW**
- Turbulent fluid motion IV-averages, Reynolds decomposition, and the closure problem [NASA-TM-105822] p 195 A93-15585

CLOSURES

CLOSURES

Critical comparison of second-order closures with direct numerical simulations of homogeneous turbulence p 176 A93-30840

CLUMPS

Clumpy cold dark matter p 291 A93-46201

CMOS

Demonstration of Y1Ba2Cu3O(7-delta) and complementary metal-oxide-semiconductor device fabrication on the same sapphire substrate p 159 A93-56292

COALESCING

Collective effects of temperature gradients and gravity on droplet coalescence p 183 A93-46716

COARSENESS

Coarsening following a morphological instability in the one-sided model p 284 A93-21695

COATING

Chemical vapor deposition modeling for high temperature materials p 116 A93-39503
Oxidation resistant overlay coatings for low expansion substrates p 138 A93-31300
[NASA-CASE-LEW-15154-2]

COATINGS

The effect of ion-plated silver and sliding friction on tensile stress induced cracking in aluminum oxide p 132 A93-27917

Enhanced plasma current collection from weakly conducting solar array blankets p 62 A93-27081
[NASA-TM-106168]

COAXIAL CABLES

Input impedance of coaxially fed rectangular microstrip antenna on electrically thick substrate p 155 A93-36994

COAXIAL NOZZLES

Supersonic jet noise reduction by coaxial rectangular nozzles p 272 A93-19205

COBALT ALLOYS

In-phase and out-of-phase axial-torsional fatigue behavior of Haynes 188 at 760 C p 246 A93-13153
[NASA-TM-105765]
A statistical analysis of elevated temperature gravimetric cyclic oxidation data of 36 Ni- and Co-base superalloys based on an oxidation attack parameter p 128 A93-18069
[NASA-TM-105934]

CODERS

Picture data compression coder using subband/transform coding with a Lempel-Ziv-based coder p 287 A93-28130
[NASA-CASE-LEW-15700-1]

CODING

Compressing subbanded image data with Lempel-Ziv-based coders p 149 A93-20257
[NASA-TM-105998]
Subband coding for image data archiving p 287 A93-25922

Picture data compression coder using subband/transform coding with a Lempel-Ziv-based coder p 287 A93-28130
[NASA-CASE-LEW-15700-1]

COEFFICIENT OF FRICTION

Tribological evaluation and analysis of coating materials p 135 A93-52896

COEFFICIENTS

Thermodynamic data for fifty reference elements p 286 A93-19977
[NASA-TP-3287]

COHESION

Global expression for representing cohesive-energy curves II p 276 A93-44989

COLD FLOW TESTS

Measured acoustic characteristics of ducted supersonic jets at different model scales p 273 A93-24821
[AIAA PAPER 93-0731]
A full-scale STOVL ejector experiment p 35 A93-22480
[NASA-TM-106019]

COLD ROLLING

Processing and microstructure of Nb-1 percent Zr-0.1 percent C alloy sheet p 128 A93-15524
[NASA-TM-105921]

COLLIMATION

Multiple-access phased array antenna simulator for a digital beam-forming system investigation p 148 A93-26237

COLLIMATORS

Compact color schlieren optical system p 277 A93-52071

COLOR PHOTOGRAPHY

Compact color schlieren optical system p 277 A93-52071

COLUMBIA (ORBITER)

Low gravity environment on-board Columbia during STS-40 p 142 A93-24903
[AIAA PAPER 93-0833]

COMBUSTIBLE FLOW

PdI prediction of supersonic hydrogen flames p 114 A93-23358
[AIAA PAPER 93-0448]

Numerical study of shock-induced combustion in methane-air mixtures p 184 A93-49783
[AIAA PAPER 93-1917]

Nonintrusive, multipoint velocity measurements in high-pressure combustion flows p 118 A93-49867
[AIAA PAPER 93-2032]

Comparison of reacting and non-reacting shear layers at a high subsonic Mach number p 186 A93-50149
[AIAA PAPER 93-2381]

Comparison of reacting and non-reacting shear layers at a high subsonic Mach number p 38 A93-27610
[NASA-TM-106198]

COMBUSTION

The Second International Microgravity Combustion Workshop p 145 A93-20178
[NASA-CP-10113]

Overview of NASA's microgravity combustion science and fire safety program p 145 A93-20180

Capabilities and constraints of typical space flight hardware p 145 A93-20183

Capabilities and constraints of combustion diagnostics in microgravity p 145 A93-20185

Effects of buoyancy on laminar, transitional, and turbulent gas jet diffusion flames p 121 A93-20189

Soot formation and radiation in turbulent jet diffusion flames under normal and reduced gravity conditions p 121 A93-20192

Visualization and imaging methods for flames in microgravity p 121 A93-20193

Selected microgravity combustion diagnostic techniques p 121 A93-20194

Fire safety practices in the Shuttle and the Space Station Freedom p 59 A93-20204

Opposed-flow flame spreading in reduced gravity p 121 A93-20206

Combustion of solid fuel in very low speed oxygen streams p 122 A93-20207

Combustion of interacting droplet arrays in a microgravity environment p 122 A93-20217

COMBUSTION CHAMBERS

Numerical simulation of a low-emission gas turbine combustor using KIVA-II p 22 A93-14077

Hydrocarbon-fuel/copper combustion chamber liner compatibility, corrosion prevention, and refurbishment p 139 A93-14510

Two and three-dimensional prediffuser combustor studies with air-water mixture p 113 A93-22652
[AIAA PAPER 93-0240]

Simplified jet fuel reaction mechanism for lean burn combustion application p 113 A93-23238
[AIAA PAPER 93-0021]

A numerical study of mixing in supersonic combustors with hypermixing injectors p 25 A93-27801
[AIAA PAPER 93-0215]

A review of chemically reactive turbulent flow mixing mechanisms and a new design for a low NO(x) combustor p 27 A93-49508

Mixing in the dome region of a staged gas turbine combustor p 27 A93-49612

An efficient liner cooling scheme for advanced small gas turbine combustors p 27 A93-49660
[AIAA PAPER 93-1763]

Experimental investigation of crossflow jet mixing in a rectangular duct p 185 A93-49872
[AIAA PAPER 93-2037]

An analytical study of dilution jet mixing in a cylindrical duct p 27 A93-49876
[AIAA PAPER 93-2043]

Integrated CFD modeling of gas turbine combustors p 28 A93-50008
[AIAA PAPER 93-2196]

A simplified reaction mechanism for calculation of emissions in hydrocarbon (Jet-A) combustion p 118 A93-50116
[AIAA PAPER 93-2341]

Emission characteristics of a model gas turbine combustor at practical conditions p 31 A93-53999
[ISABE 93-7023]

Hot fire test results of subscale tubular combustion chambers p 79 A93-10020

Hot fire fatigue testing results for the compliant combustion chamber p 79 A93-10038

Hot fire fatigue testing results for the compliant combustion chamber p 80 A93-10743
[NASA-TP-3223]

Test program to provide validation data for the Rocket Combustor Interactive Design (ROCCID) code p 120 A93-11450

Hot fire test results of subscale tubular combustion chambers p 81 A93-11614
[NASA-TP-3222]

Simplified jet-A kinetic mechanism for combustor application p 120 A93-15504
[NASA-TM-105940]

Performance and heat transfer characteristics of a carbon monoxide/oxygen rocket engine p 84 A93-18878
[NASA-TM-105897]

Fuel injector: Air swirl characterization aerothermal modeling, phase 2, volume 1 p 35 A93-24754
[NASA-CR-189193-VOL-1]

A three-dimensional algebraic grid generation scheme for gas turbine combustors with inclined slots p 198 A93-24759
[NASA-CR-191095]

Nitric oxide formation in a lean, premixed-prevaporized jet A/air flame tube: An experimental and analytical study p 257 A93-27012
[NASA-TM-105722]

Experimental investigation of crossflow jet mixing in a rectangular duct p 36 A93-27026
[NASA-TM-106152]

An analytical study of dilution jet mixing in a cylindrical duct p 37 A93-27160
[NASA-TM-106181]

COMBUSTION CHEMISTRY

Premixed flame propagation in combustible particle cloud mixtures p 115 A93-24808
[AIAA PAPER 93-0713]

Soot agglomeration in isolated, free droplet combustion p 115 A93-24893
[AIAA PAPER 93-0823]

Asymptotic analysis for the burning of n-heptane droplets using a four-step reduced mechanism p 117 A93-41952

A thermal NO(x) prediction model - Scalar computation module for CFD codes with fluid and kinetic effects p 119 A93-50147
[AIAA PAPER 93-2378]

Catalytic ignition model in monolithic reactor with in-depth reaction p 119 A93-51641

Laser-induced fluorescence detection strategies for sodium atoms and compounds in high-pressure combustors p 119 A93-52423

LENS, a general chemical kinetics and sensitivity analysis code for gas-phase reactions: User's guide p 121 A93-16614
[NASA-TM-105851]

COMBUSTION CONTROL

Velocity and drop size measurements in a swirl-stabilized, combustor spray p 37 A93-27130
[NASA-TM-106130]

COMBUSTION EFFICIENCY

Development and use of hydrogen-air torches in an altitude facility p 42 A93-49988
[AIAA PAPER 93-2176]

Development and use of hydrogen-air torches in an altitude facility p 43 A93-26214
[NASA-TM-106047]

COMBUSTION PHYSICS

Supercritical droplet combustion and related transport phenomena p 115 A93-24885
[AIAA PAPER 93-0812]

Laser-induced fluorescence measurements of nitric oxide in laminar C2H6/O2/N2 flames at high pressure p 116 A93-28253

Intensified array camera imaging of solid surface combustion aboard the NASA Learjet p 143 A93-30858

Some aspects of secondary atomization of aluminum/hydrocarbon slurry propellants p 140 A93-34478

Computational/experimental basis for conducting alkane droplet combustion experiments on space-based-platforms p 117 A93-41711

Computations of spray, fuel-air mixing, and combustion in a lean-premixed-prevaporized combustor p 185 A93-49901
[AIAA PAPER 93-2069]

Secondary atomization in the combustion of electrostatic sprays p 118 A93-50110
[AIAA PAPER 93-2332]

Overview of NASA's microgravity combustion science and fire safety program p 145 A93-20180

Visualization and imaging methods for flames in microgravity p 121 A93-20193

Calculations of combustion response profiles and oscillations p 87 A93-25236
[NASA-TM-106135]

Velocity and drop size measurements in a swirl-stabilized, combustor spray p 37 A93-27130
[NASA-TM-106130]

2nd NASA CFD Validation Workshop --- Author p 203 A93-70575
[NASA-TM-107972]

COMBUSTION PRODUCTS

Corrosion of silicon-based ceramics in combustion environments p 131 A93-22984

Rotational level-dependent collisional broadening and line shift of the A2Sigma(+) - X2Pi (1,0) band of OH in hydrogen-air combustion gases p 276 A93-24142

Soot agglomeration in isolated, free droplet combustion p 115 A93-24893
[AIAA PAPER 93-0823]

COMBUSTION STABILITY

Numerical computation of low-speed concurrent flow flame spread in mixed buoyant and forced flow p 115 A93-24897
[AIAA PAPER 93-0827]

- Test program to provide validation data for the Rocket Combustor Interactive Design (ROCCID) code p 120 N93-11450
- Calculations of combustion response profiles and oscillations [NASA-TM-106135] p 87 N93-25236
- COMBUSTION TEMPERATURE**
- Experimental observations of the effect of gravity changes on smoldering combustion [AIAA PAPER 93-0829] p 116 A93-24899
- A laboratory model of a hydrogen/oxygen engine for combustion and nozzle studies [AIAA PAPER 93-1825] p 48 A93-49711
- Initial results from the NASA Lewis wave rotor experiment [AIAA PAPER 93-2521] p 30 A93-53589
- Initial results from the NASA-Lewis wave rotor experiment [NASA-TM-106148] p 39 N93-32368
- COMMERCIAL AIRCRAFT**
- Effects of turbine cooling assumptions on performance and sizing of high-speed civil transport [AIAA PAPER 92-4217] p 22 A93-13383
- Ice accretion prediction for a typical commercial transport aircraft [AIAA PAPER 93-0174] p 19 A93-23245
- Comparison of all-electric secondary power systems for civil transport p 24 A93-25997
- Propulsion technology challenges for turn-of-the-century commercial aircraft [ISABE 93-7003] p 31 A93-53980
- Comparison of all-electric secondary power systems for civil subsonic transports [NASA-TM-105852] p 32 N93-10456
- Ice accretion prediction for a typical commercial transport aircraft [NASA-TM-105976] p 20 N93-15522
- An artificial intelligence-based structural health monitoring system for aging aircraft p 266 N93-22185
- Propulsion technology challenges for turn-of-the-century commercial aircraft [NASA-TM-106192] p 39 N93-32351
- COMMERCIAL SPACECRAFT**
- Direct Broadcast Satellite: Radio Program [NASA-TM-105910] p 52 N93-11430
- COMMUNICATION NETWORKS**
- The performance evaluation of a new neural network based traffic management scheme for a satellite communication network p 147 A93-10929
- High data rate applications of ACTS technology p 52 A93-17329
- Space Communication Artificial Intelligence for Link Evaluation Terminal (SCAILET) p 265 N93-11940
- ISDN at NASA Lewis Research Center [NASA-TM-105911] p 262 N93-12410
- COMMUNICATION SATELLITES**
- High data rate applications of ACTS technology p 52 A93-17329
- Direct Broadcast Satellite: Radio Program [NASA-TM-105910] p 52 N93-11430
- Fault-tolerant onboard digital information switching and routing for communications satellites [NASA-TM-4471] p 53 N93-26895
- Satellites and the BISDN: An overview of NASA R/D [NASA-TM-106108] p 150 N93-26903
- ACTS system handbook, revision change index [NASA-TM-107982] p 150 N93-70235
- COMPONENT RELIABILITY**
- Ceramic component reliability with the restructured NASA/CARES computer program [ASME PAPER 92-GT-383] p 234 A93-19540
- Ceramic component reliability with the restructured NASA/CARES computer program [NASA-TM-105856] p 244 N93-11004
- Life extending control: An interdisciplinary engineering thrust p 93 N93-31581
- COMPOSITE MATERIALS**
- Application of composite materials to impact-insensitive munitions p 97 A93-11459
- Refractive index effects on radiation in an absorbing, emitting, and scattering laminated layer p 175 A93-30125
- Progressive matrix cracking in off-axis plies of a general symmetric laminate [AIAA PAPER 93-1494] p 239 A93-34035
- Elevated-temperature fracture resistances of monolithic and composite ceramics using chevron-notched bend tests p 133 A93-38888
- Environmental effects on long term behavior of composite laminates p 243 A93-53438
- Design of a high-temperature experiment for evaluating advanced structural materials [NASA-TM-105833] p 245 N93-11624
- The effect of processing and compositional changes on the tribology of PM212 in air [NASA-TM-105945] p 95 N93-15576
- Heat transfer device [NASA-CASE-LEW-14162-4] p 108 N93-20568
- Properties of extruded PS-212 type self-lubricating materials p 138 N93-25565
- Composite micromechanical modeling using the boundary element method [NASA-TM-106127] p 250 N93-27030
- Probabilistic sizing of laminates with uncertainties [NASA-TM-106145] p 110 N93-27082
- Semiconductor cooling apparatus [NASA-CASE-LEW-14162-3] p 111 N93-29614
- Oxidation resistant overlay coatings for low expansion substrates [NASA-CASE-LEW-15154-2] p 138 N93-31300
- Stress-rupture behavior of small diameter polycrystalline alumina fibers [NASA-TM-106256] p 139 N93-32382
- COMPOSITE STRUCTURES**
- Probabilistic structural analysis of adaptive/smart/intelligent space structures p 234 A93-16203
- Structural durability of a composite pressure vessel p 234 A93-16552
- Coupled multi-disciplinary simulation of composite engine structures in propulsion environment [ASME PAPER 92-GT-6] p 23 A93-19279
- Analysis and optimal design of thick composite structures with passive damping considerations [AIAA PAPER 92-4819] p 235 A93-20398
- Application of neural networks to prediction of advanced composite structures mechanical response and behavior p 205 A93-20751
- Detecting Lamb waves with broadband acousto-ultrasonic signals in composite structures p 231 A93-21898
- Effects of interply damping layers on the dynamic characteristics of composite plates p 237 A93-32415
- Damage progression in stiffened composite panels [AIAA PAPER 93-1345] p 238 A93-33915
- Probabilistic assessment of composite structures [AIAA PAPER 93-1441] p 239 A93-33990
- Probabilistic simulation of stress concentration in composite laminates [AIAA PAPER 93-1442] p 103 A93-33991
- Global/local finite element analysis for textile composites [AIAA PAPER 93-1506] p 103 A93-34045
- Probabilistically configured adaptive composite structures [AIAA PAPER 93-1679] p 240 A93-34191
- Analysis of the anisotropic viscoplastic-damage response of composite laminates - Continuum basis and computational algorithms p 241 A93-43347
- Analysis of passive damping in thick composite structures p 241 A93-45743
- Design for progressive fracture in composite shell structures p 242 A93-53394
- Design for cyclic loading endurance of composites p 242 A93-53395
- Effect of service environments on adhesively bonded joints in composite structures p 242 A93-53418
- Computational simulation of hot composite structures p 260 A93-54704
- Computer aided design and manufacturing of composite propfan blades for a cruise missile wind tunnel model [NASA-TM-105269] p 261 N93-12022
- The effect of contact stresses in four-point bend testing of graphite/epoxy and graphite/PMR-15 composite beams [NASA-TM-105891] p 107 N93-12076
- Thermostructural tailoring of fiber composite structures [NASA-TM-105882] p 107 N93-12078
- Probabilistic evaluation of fuselage-type composite structures [NASA-TM-105881] p 245 N93-12735
- Progress toward a tungsten alloy wire/high temperature alloy composite turbine blade [NASA-TM-105901] p 128 N93-15586
- Progressive delamination in polymer matrix composite laminates: A new approach p 108 N93-21515
- Structural analysis of high-rpm composite propfan blades for a cruise missile wind tunnel model [NASA-TM-105267] p 247 N93-23015
- Solar concentrators for advanced solar-dynamic power systems in space [NASA-CR-187148] p 85 N93-23017
- High Temperature Composite Analyzer (HITCAN) theoretical manual, version 1.0 [NASA-TM-106001] p 249 N93-24913
- High temperature composite analyzer (HITCAN) user's manual, version 1.0 [NASA-TM-106002] p 249 N93-25070
- Graphite/epoxy composite laminates with co-cured interlaminar damping layers p 109 N93-25587
- Dynamic characteristics of specialty composite structures with embedded damping layers [NASA-TM-106165] p 110 N93-26705
- Probabilistic sizing of laminates with uncertainties [NASA-TM-106145] p 110 N93-27082
- Probabilistic composite analysis p 112 N93-30868
- COMPOUNDING**
- Elevated temperature compressive properties of reaction milled NiAl-AlN and Zr-doped NiAl-AlN composites p 97 A93-11422
- COMPRESSIBLE BOUNDARY LAYER**
- Evaluation and application of the Baldwin-Lomax turbulence model in two-dimensional, unsteady, compressible boundary layers with and without separation in engine inlets [AIAA PAPER 92-3676] p 2 A93-14118
- Nonlinear evolution of modes in a compressible boundary layer p 164 A93-17258
- Evaluation and application of the Baldwin-Lomax turbulence model in two-dimensional, unsteady, compressible boundary layers with and without separation in engine inlets [AIAA PAPER 92-3676] p 168 A93-22509
- Higher-order accurate Osher schemes with application to compressible boundary layer stability [AIAA PAPER 93-3051] p 183 A93-48231
- Evaluation and application of the Baldwin-Lomax turbulence model in two-dimensional, unsteady, compressible boundary layers with and without separation in engine inlets [NASA-TM-105810] p 191 N93-10087
- A compressible boundary layer algorithm for use with SINDA '85 p 192 N93-13395
- Two equation modelling and the pseudo compressibility technique p 195 N93-15799
- Bypass transition in compressible boundary layers p 196 N93-15801
- Nonlinear evolution of the first mode supersonic oblique waves in compressible boundary layers. Part 1: Heated/cooled walls [NASA-TM-106087] p 199 N93-25175
- COMPRESSIBLE FLOW**
- PDF approach for compressible turbulent reacting flows [AIAA PAPER 93-0087] p 170 A93-24229
- A study of compressible mixing layers using filtered Rayleigh scattering [AIAA PAPER 92-0175] p 173 A93-24982
- The application of preconditioning in viscous flows p 177 A93-32627
- Modeling of linear isentropic flow systems p 179 A93-37046
- On solving the compressible Navier-Stokes equations for unsteady flows at very low Mach numbers [AIAA PAPER 93-3368] p 181 A93-45061
- Navier-Stokes analysis of three-dimensional S-ducts p 9 A93-45146
- Analysis of unsteady wave processes in a rotating channel [AIAA PAPER 93-2527] p 187 A93-50255
- An experimental investigation of the flow in a diffusing S-duct [NASA-TM-105809] p 32 N93-12077
- An integral equation solution for multistage turbomachinery design calculations [NASA-TM-105970] p 33 N93-15521
- A multiple-scale model for compressible turbulent flows [NASA-TM-106072] p 198 N93-23736
- COMPRESSION LOADS**
- Analytical stress intensity solution for the Stable Poisson Loaded specimen p 242 A93-46768
- COMPRESSION WAVES**
- Three-dimensional numerical simulation of gradual opening in a wave rotor passage [AIAA PAPER 93-2526] p 187 A93-50254
- COMPRESSIVE STRENGTH**
- Elevated temperature compressive properties of reaction milled NiAl-AlN and Zr-doped NiAl-AlN composites p 97 A93-11422
- COMPRESSOR BLADES**
- Numerical simulation of compressor endwall and casing treatment flow phenomena [ASME PAPER 92-GT-300] p 4 A93-19490
- Forced response of mistuned bladed disk assemblies [AIAA PAPER 93-1491] p 239 A93-34033
- COMPRESSOR ROTORS**
- Mathematical relationship between two sets of laser anemometer measurements for resolving the total velocity vector [NASA-TM-105986] p 35 N93-22599
- COMPRESSORS**
- Three-dimensional laser window formation for industrial application p 218 N93-22197

COMPUTATION

Calculation of stress intensity factors in an isotropic multitracked plate: Part 2: Symbolic/numeric implementation

[NASA-TM-105823] p 244 A93-10453

COMPUTATIONAL ASTROPHYSICS

First-order inflation --- in cosmology

p 292 A93-51704

COMPUTATIONAL CHEMISTRY

A simplified reaction mechanism for calculation of emissions in hydrocarbon (Jet-A) combustion

[AIAA PAPER 93-2341] p 118 A93-50116

A critical analysis of the accuracy of several numerical techniques for combustion kinetic rate equations

[NASA-TP-3315] p 34 A93-16941

COMPUTATIONAL FLUID DYNAMICS

The new challenge of computational aerocience

p 2 A93-14169

Study on vortex flow control of inlet distortion

p 2 A93-14520

RIPPLE - A new model for incompressible flows with free surfaces

p 164 A93-14551

Non-parallel effects in the instability of Long's vortex

p 164 A93-16663

Multigrid acceleration and turbulence models for computations of 3D turbulent jets in crossflow

p 165 A93-18751

Experimental and computational investigation of the NASA Low-Speed Centrifugal Compressor flow field

[ASME PAPER 92-GT-213] p 4 A93-19436

Numerical simulation of compressor endwall and casing treatment flow phenomena

[ASME PAPER 92-GT-300] p 4 A93-19490

Accuracy considerations in the computational analysis of jet noise

[AIAA PAPER 93-0146] p 272 A93-19804

The eigenvalue spectrum of the Rayleigh equation for a plane shear layer

p 168 A93-21725

An algebraic turbulence model for three-dimensional viscous flows

[AIAA PAPER 93-0083] p 4 A93-22552

CFD zonal modeling of leading-edge ice effects for a complete aircraft

[AIAA PAPER 93-0167] p 5 A93-22601

Time-dependent thermocapillary convection in a Cartesian cavity - Numerical results for a moderate Prandtl number fluid

[AIAA PAPER 93-0259] p 169 A93-22666

An improved numerical model for wave rotor design and analysis

[AIAA PAPER 93-0482] p 24 A93-23384

PDF approach for compressible turbulent reacting flows

[AIAA PAPER 93-0087] p 170 A93-24229

Direct calculations of waves in fluid flows using a high-order compact difference scheme

[AIAA PAPER 93-0148] p 171 A93-24232

ENO-Osher schemes for Euler equations

[AIAA PAPER 93-0335] p 171 A93-24235

Driven cavity simulation of turbomachine blade flows with vortex control

[AIAA PAPER 93-0390] p 6 A93-24238

Three-dimensional Navier-Stokes calculations using solution-adapted grids

[AIAA PAPER 93-0431] p 6 A93-24240

Three-dimensional boundary-layer instability and separation induced by small-amplitude streamwise vorticity in the upstream flow

[AIAA PAPER 93-0653] p 172 A93-24766

Numerical simulation of a high Mach number jet flow

[AIAA PAPER 93-0827] p 115 A93-24897

Preconditioned Conjugate Gradient methods for low speed flow calculations

[AIAA PAPER 93-0881] p 172 A93-24942

Application of an unstructured grid flow solver to planes, trains and automobiles

[AIAA PAPER 93-0889] p 173 A93-24949

Computing 3-D steady supersonic flow via a new Lagrangian approach

[AIAA PAPER 93-0891] p 6 A93-24951

Bgrid - Interactive three-dimensional turbomachinery grid generation system with applications

[AIAA PAPER 93-0430] p 259 A93-25527

The structure of supersonic jet flow and its radiated sound

[AIAA PAPER 93-0549] p 273 A93-25538

Nonreflecting boundary conditions for linearized unsteady aerodynamic calculations

[AIAA PAPER 93-0882] p 7 A93-25553

Statistical analysis of the effects of helicity in inhomogeneous turbulence

p 175 A93-26186

A numerical study of mixing in supersonic combustors with hypermixing injectors

[AIAA PAPER 93-0215] p 25 A93-27801

Computation of unsteady supersonic quasi-one-dimensional viscous-inviscid interacting internal flowfields

p 177 A93-32724

Study on vortex generator flow control for the management of inlet distortion

p 7 A93-34488

Computational study of advanced exhaust system transition ducts with experimental validation

p 7 A93-34490

The coupling of interfacial instabilities and the stabilization of two-layer annular flows

p 178 A93-35482

PNS predictions for supersonic/hypersonic flows over finned missile configurations

[AIAA PAPER 92-2695] p 7 A93-37374

Stable and low diffusive hybrid upwind splitting methods

[ONERA, TP NO. 1992-113] p 179 A93-38589

Characteristics of three-dimensional turbulent jets in crossflow

p 8 A93-38695

New time scale based k-epsilon model for near-wall turbulence

p 180 A93-41909

CFD for hypersonic propulsion

p 8 A93-42585

Multigrid calculation of three-dimensional viscous cascade flows

p 8 A93-42889

A coupled implicit method for chemical non-equilibrium flows at all speeds

p 181 A93-44245

The structure of a three-dimensional turbulent boundary layer

p 181 A93-44813

The NASA Computational Fluid Dynamics (CFD) program - Building technology to solve future challenges

[AIAA PAPER 93-3292] p 287 A93-44996

Field by field hybrid upwind splitting methods

[AIAA PAPER 93-3302] p 8 A93-45000

An extended Lagrangian method

[AIAA PAPER 93-3305] p 8 A93-45003

A parallel dynamic load balancing algorithm for 3-D adaptive unstructured grids

[AIAA PAPER 93-3313] p 260 A93-45009

Two-dimensional CFD modeling of wave rotor flow dynamics

[AIAA PAPER 93-3318] p 9 A93-45014

An accuracy assessment of Cartesian-mesh approaches for the Euler equations

[AIAA PAPER 93-3335] p 9 A93-45029

Segmented multigrid domain decomposition solutions for three dimensional viscous recirculating flows

[AIAA PAPER 93-3344] p 181 A93-45038

Grid adaptation using Chimera composite overlapping meshes

[AIAA PAPER 93-3389] p 267 A93-45080

Navier-Stokes analysis of three-dimensional S-ducts

p 9 A93-45146

Adaptive methods in computational fluid dynamics

p 182 A93-45963

Direct numerical simulations of a reacting turbulent mixing layer by a pseudospectral-spectral element method

p 182 A93-45974

Low-to-high altitude predictions of three-dimensional ablative re-entry flowfields

p 182 A93-46407

Adaptive computations of flow around a delta wing with vortex breakdown

[AIAA PAPER 93-3400] p 10 A93-47202

An improved far field drag calculation method for nonlinear CFD codes

[AIAA PAPER 93-3417] p 10 A93-47213

High resolution numerical simulation of the linearized Euler equations in conservation law form

[AIAA PAPER 93-2934] p 183 A93-48132

Some practical turbulence modeling options for Reynolds-averaged full Navier-Stokes calculations of three-dimensional flows

[AIAA PAPER 93-2964] p 10 A93-48158

Streamwise computation of three-dimensional flows using two stream functions

p 184 A93-49241

CFD validation of subsonic turbulent planar shear layers

[AIAA PAPER 93-1773] p 184 A93-49669

CFD analyses of coolant channel flowfields

[AIAA PAPER 93-1830] p 184 A93-49715

Calculation of scramjet inlet with thick boundary-layer ingestion

[AIAA PAPER 93-1836] p 12 A93-49720

3-D viscous flow CFD analysis of the propeller effect on an advanced ducted propeller subsonic inlet

[AIAA PAPER 93-1847] p 12 A93-49728

Numerical study of shock-induced combustion in methane-air mixtures

[AIAA PAPER 93-1917] p 184 A93-49783

CFD mixing analysis of axially opposed rows of jets injected into confined crossflow

[AIAA PAPER 93-2044] p 185 A93-49877

Computation of the flow field in an annular gas turbine combustor

[AIAA PAPER 93-2074] p 28 A93-49903

An iterative multidisciplinary analysis for rotor blade shape determination

[AIAA PAPER 93-2085] p 28 A93-49912

Integrated CFD modeling of gas turbine combustors

[AIAA PAPER 93-2196] p 28 A93-50008

A simplified reaction mechanism for calculation of emissions in hydrocarbon (Jet-A) combustion

[AIAA PAPER 93-2341] p 118 A93-50116

A thermal NO(x) prediction model - Scalar computation module for CFD codes with fluid and kinetic effects

[AIAA PAPER 93-2378] p 119 A93-50147

Development of an explicit multiblock/multigrid flow solver for viscous flows in complex geometries

[AIAA PAPER 93-2380] p 186 A93-50148

Low-g fluid mixing - Further results from the Tank Pressure Control Experiment

[AIAA PAPER 93-2423] p 187 A93-50181

A comparison between numerically modelled and experimentally measured loss mechanisms in wave rotors

[AIAA PAPER 93-2522] p 30 A93-50252

Analysis of unsteady wave processes in a rotating channel

[AIAA PAPER 93-2527] p 187 A93-50255

Assessment of three numerical methods for the computation of a low-density plume flow

[AIAA PAPER 93-2528] p 77 A93-50256

Navier-Stokes analysis of radial turbine rotor performance

[AIAA PAPER 93-2555] p 30 A93-50277

Central difference TVD schemes for time dependent and steady state problems

p 188 A93-51183

A time-accurate high-resolution TVD scheme for solving the Navier-Stokes equations

p 13 A93-52006

Dynamics and control of coherent structure in turbulent jets

p 188 A93-52310

Progress towards understanding and predicting heat transfer in the turbine gas path

p 188 A93-52751

Low-Reynolds-number k-epsilon model for unsteady turbulent boundary-layer flows

p 14 A93-53208

Aerodynamic inverse design and analysis for a full engine

[ISABE 93-7086] p 14 A93-54062

A hydrodynamic model of the oscillating screen viscometer

p 190 A93-55136

A least-squares finite element method for incompressible Navier-Stokes problem

p 191 A93-10548

Overview of high performance aircraft propulsion research

[NASA-TM-105839] p 32 A93-11530

Comparison of truncation error of finite-difference and finite-volume formulations of convection terms

[NASA-TM-105861] p 268 A93-11531

An improved numerical model for wave rotor design and analysis

[NASA-TM-105915] p 33 A93-12418

Turbomachinery CFD on parallel computers

[NASA-TM-105932] p 262 A93-13154

AGARD WG13 aerodynamics of high speed air intakes: Assessment of CFD results

p 192 A93-13220

The Fourth Annual Thermal and Fluids Analysis Workshop

[NASA-CP-10106] p 192 A93-13385

The Proteus Navier-Stokes code

p 193 A93-13396

An algebraic turbulence model for three-dimensional viscous flows

[NASA-TM-105931] p 1 A93-14102

Supersonic boundary-layer flow turbulence modeling

[NASA-TM-105893] p 193 A93-14758

Preconditioned conjugate-gradient methods for low-speed flow calculations

[NASA-TM-105929] p 194 A93-14885

Critical assessment of Reynolds stress turbulence models using homogeneous flows

[NASA-TM-105954] p 196 A93-16703

A time-accurate high-resolution TVD scheme for solving the Navier-Stokes equations

[NASA-TM-106056] p 268 A93-22664

A multiple-scale model for compressible turbulent flows

[NASA-TM-106072] p 198 A93-23736

Spray combustion experiments and numerical predictions

[NASA-TM-106069] p 198 A93-23744

An extended Lagrangian method

[NASA-TM-106129] p 199 A93-26203

Incompressible spectral-element method: Derivation of equations

[NASA-TM-106109] p 199 A93-26554

A brief description of a new numerical framework for solving conservation laws: The method of space-time conservation element and solution element

[NASA-TM-105757] p 269 A93-26560

NTR plume modeling

p 199 A93-26929

- Computational fluid dynamics for nuclear thermal propulsion p 199 N93-26930
- Remarks on turbulent constitutive relations [NASA-TM-106116] p 199 N93-27010
- Institute for Computational Mechanics in Propulsion (ICOMP) p 269 N93-27061
- Grid adaption using Chimera composite overlapping meshes [NASA-TM-106163] p 269 N93-27065
- Positivity-preserving numerical schemes for multidimensional advection [NASA-TM-106055] p 200 N93-27091
- CFD mixing analysis of axially opposed rows of jets injected into confined crossflow [NASA-TM-106179] p 37 N93-27128
- Calculations of turbulent separated flows [NASA-TM-106154] p 200 N93-27161
- A new flux conserving Newton's method scheme for the two-dimensional, steady Navier-Stokes equations [NASA-TM-106160] p 201 N93-28626
- The development of a mixing layer under the action of weak streamwise vortices [NASA-TM-106089] p 201 N93-28947
- The 3-D viscous flow CFD analysis of the propeller effect on an advanced ducted propeller subsonic inlet [NASA-TM-106240] p 38 N93-29162
- Accuracy of least-squares methods for the Navier-Stokes equations [NASA-TM-106209] p 202 N93-29208
- Navier-Stokes analysis of three-dimensional flow and heat transfer inside turbine blade rows p 39 N93-29963
- Numerical simulations of three-dimensional laminar flow over a backward facing step; flow near side walls [NASA-TM-106248] p 202 N93-31147
- Three-dimensional flow calculations inside SSME GGT first stage blade rows p 93 N93-31585
- 2nd NASA CFD Validation Workshop --- Author [NASA-TM-107972] p 203 N93-70575
- Summary of NASA Lewis Research Center validation efforts p 204 N93-70579
- NASA Lewis Research Center/IFMD inlet duct and nozzle high speed validation experiments p 204 N93-70582
- NASA low speed centrifugal compressor p 204 N93-70583
- COMPUTATIONAL GEOMETRY**
- On the effects of grid ill-conditioning in three dimensional finite element vector potential magnetostatic field computations p 157 A93-39719
- COMPUTATIONAL GRIDS**
- Multigrid acceleration and turbulence models for computations of 3D turbulent jets in crossflow p 165 A93-18751
- An evaluation of three spatial differencing schemes for the discrete ordinates method in participating media [AIAA PAPER 93-0140] p 266 A93-24231
- Three-dimensional unstructured grid Euler method applied to turbine blades [AIAA PAPER 93-0196] p 6 A93-24233
- Three-dimensional Navier-Stokes calculations using solution-adapted grids [AIAA PAPER 93-0431] p 6 A93-24240
- Unstructured 3D Delaunay mesh generation applied to planes, trains and automobiles [AIAA PAPER 93-0673] p 259 A93-24781
- Transition elements based on transfinite interpolation [AIAA PAPER 93-1326] p 267 A93-33899
- Global/local methods for probabilistic structural analysis [AIAA PAPER 93-1378] p 238 A93-33942
- Calculations of separated 3-D flows with a pressure-staggered Navier-Stokes equations solver p 177 A93-34366
- On the effects of grid ill-conditioning in three dimensional finite element vector potential magnetostatic field computations p 157 A93-39719
- Field by field hybrid upwind splitting methods [AIAA PAPER 93-3302] p 8 A93-45000
- A parallel dynamic load balancing algorithm for 3-D adaptive unstructured grids [AIAA PAPER 93-3313] p 260 A93-45009
- An accuracy assessment of Cartesian-mesh approaches for the Euler equations [AIAA PAPER 93-3335] p 9 A93-45029
- Grid adaptation using Chimera composite overlapping meshes [AIAA PAPER 93-3389] p 267 A93-45080
- A new flux splitting scheme p 9 A93-47189
- Adaptive computations of flow around a delta wing with vortex breakdown [AIAA PAPER 93-3400] p 10 A93-47202
- Higher-order accurate Osher schemes with application to compressible boundary layer stability [AIAA PAPER 93-3051] p 183 A93-48231
- A three-dimensional algebraic grid generation scheme for gas turbine combustors with inclined slots [NASA-CR-191095] p 198 N93-24759
- An extended Lagrangian method [NASA-TM-106129] p 199 N93-26203
- Grid adaption using Chimera composite overlapping meshes [NASA-TM-106163] p 269 N93-27065
- Blasim: A computational tool to assess ice impact damage on engine blades [NASA-TM-106225] p 251 N93-31193
- Mapping methods for computationally efficient and accurate structural reliability p 232 N93-31572
- COMPUTER AIDED DESIGN**
- The new challenge of computational aerocience p 2 A93-14169
- Maximum life spur gear design p 218 A93-14521
- Neural networks for structural design - An integrated system implementation [AIAA PAPER 92-4806] p 263 A93-20389
- Boundary formulations for three-dimensional continuum structural shape sensitivity analysis p 235 A93-22426
- LV software support for supersonic flow analysis [AIAA PAPER 92-3900] p 259 A93-24487
- NASA CST aids U.S. industry --- computational structures technology p 258 A93-25084
- Computer modeling of a hot filament diamond deposition reactor p 94 A93-40618
- Derated ion thruster development status [AIAA PAPER 93-2225] p 75 A93-50031
- Generation of helical gears with new surfaces topology by application of CNC machines [AIAA PAPER 93-2297] p 224 A93-50082
- Aerodynamic inverse design and analysis for a full engine [ISABE 93-7086] p 14 A93-54062
- A parameter optimization approach to controller partitioning for integrated flight/propulsion control application p 41 A93-54268
- An interactive preprocessor for the NASA engine performance program [NASA-TM-105786] p 32 N93-10983
- The engine design engine. A clustered computer platform for the aerodynamic inverse design and analysis of a full engine [NASA-TM-105838] p 15 N93-11223
- Test program to provide validation data for the Rocket Combustor Interactive Design (ROCCID) code p 120 N93-11450
- Computer aided design and manufacturing of composite propfan blades for a cruise missile wind tunnel model [NASA-TM-105269] p 261 N93-12022
- Thermostructural tailoring of fiber composite structures [NASA-TM-105882] p 107 N93-12078
- Structural optimization of thin shells using finite element method [NASA-TM-105903] p 246 N93-13157
- Application of artificial neural networks to the design optimization of aerospace structural components [NASA-TM-4389] p 247 N93-21831
- Overview of NASA/DOE/DOD interagency modeling team and activities p 89 N93-26952
- Radial basis function network learns ceramic processing and predicts related strength and density [NASA-TM-106048] p 110 N93-27129
- Generation of helical gears with new surfaces, topology by application of CNC machines [NASA-TM-106175] p 229 N93-27687
- Structural dynamics: Probabilistic structural analysis methods. Program overview p 251 N93-31562
- COMPUTER AIDED MANUFACTURING**
- Computer aided design and manufacturing of composite propfan blades for a cruise missile wind tunnel model [NASA-TM-105269] p 261 N93-12022
- Soft computing in design and manufacturing of advanced materials [NASA-TM-106032] p 111 N93-28624
- COMPUTER AIDED TOMOGRAPHY**
- Three-dimensional computed tomography from interferometric measurements within a narrow cone of views p 207 A93-24024
- Neural networks for calibration tomography [NASA-TM-106352] p 216 N93-26906
- COMPUTER GRAPHICS**
- A graphical user-interface for propulsion system analysis [AIAA PAPER 93-0223] p 259 A93-23699
- Bgrdi - Interactive three-dimensional turbomachinery grid generation system with applications [AIAA PAPER 93-0430] p 259 A93-25527
- User's manual for Interactive Data Display System (IDDS) [NASA-TM-105572] p 261 N93-16613
- Dynamic gas temperature measurements using a personal computer for data acquisition and reduction [NASA-TM-106119] p 261 N93-27024
- RENEW v3.2 user's manual, maintenance estimation simulation for Space Station Freedom Program [NASA-TM-106006] p 232 N93-27025
- COMPUTER PROGRAMMING**
- Software issues in three dimensional continuum shape optimization employing boundary formulations [AIAA PAPER 92-4792] p 258 A93-20380
- Programming probabilistic structural analysis for parallel processing computers p 237 A93-32410
- A SINDA '85 nodal heat transfer rate calculation user subroutine p 193 N93-13403
- COMPUTER PROGRAMS**
- Improved accuracy for finite element structural analysis via an integrated force method p 234 A93-17246
- Ceramic component reliability with the restructured NASA/CARES computer program [ASME PAPER 92-GT-383] p 234 A93-19540
- Numerical modeling of anti-icing systems and comparison to test results on a NACA 0012 airfoil [AIAA PAPER 93-0170] p 21 A93-23242
- Advancements in the LEWICE Ice Accretion Model [AIAA PAPER 93-0171] p 18 A93-23243
- Ice accretion and performance degradation calculations with LEWICE/NS [AIAA PAPER 93-0173] p 18 A93-23244
- Ice accretion prediction for a typical commercial transport aircraft [AIAA PAPER 93-0174] p 19 A93-23245
- A qualitative approach to systemic diagnosis of the SSME [AIAA PAPER 93-0405] p 261 A93-23327
- Energy loss analysis of an integrated space power distribution system p 68 A93-25958
- Overview of NASA supported Stirling thermodynamic loss research p 174 A93-26087
- Computational characterization of high temperature composites via METCAN p 102 A93-32461
- Transition elements based on transfinite interpolation [AIAA PAPER 93-1326] p 267 A93-33899
- Lifetime reliability evaluation of structural ceramic parts with the CARES/LIFE computer program [AIAA PAPER 93-1497] p 239 A93-34037
- BLASIM - A computational tool to assess ice impact damage on engine blades [AIAA PAPER 93-1638] p 26 A93-34165
- Dynamic analysis of spur gears using computer program DANST [AIAA PAPER 93-2295] p 224 A93-50080
- An RL10A-3-3A rocket engine model using the Rocket Engine Transient Simulator (ROCETS) software [AIAA PAPER 93-2357] p 75 A93-50129
- Design for cyclic loading endurance of composites p 242 A93-53395
- Maximum life spiral bevel reduction design [NASA-TM-105790] p 226 N93-10982
- Ceramic component reliability with the restructured NASA/CARES computer program [NASA-TM-105856] p 244 A93-11004
- The engine design engine. A clustered computer platform for the aerodynamic inverse design and analysis of a full engine [NASA-TM-105838] p 15 N93-11223
- Dynamic analysis of a pre-and-post ice impacted blade [NASA-TM-105829] p 144 N93-12197
- Probabilistic evaluation of fuselage-type composite structures [NASA-TM-105881] p 245 N93-12735
- The Fourth Annual Thermal and Fluids Analysis Workshop [NASA-CP-10106] p 192 N93-13385
- The Proteus Navier-Stokes code p 193 N93-13396
- Energy loss analysis of an integrated space power distribution system [NASA-TM-105772] p 141 N93-14834
- Root damage analysis of aircraft engine blade subject to ice impact [NASA-TM-105779] p 246 N93-15343
- Numerical modeling of anti-icing systems and comparison to test results on a NACA 0012 airfoil [NASA-TM-105975] p 19 N93-15345
- Ice accretion and performance degradation calculations with LEWICE/NS [NASA-TM-105972] p 19 N93-15354
- Development of NASA/DOE NTP system performance models [NASA-TM-105982] p 82 N93-15428
- Ice accretion prediction for a typical commercial transport aircraft [NASA-TM-105976] p 20 N93-15522
- Computer programs to characterize alloys and predict cyclic life using the total strain version of strainrange partitioning: Tutorial and users manual, version 1.0 [NASA-TM-4425] p 246 N93-15788

- LENS, a general chemical kinetics and sensitivity analysis code for gas-phase reactions: User's guide
[NASA-TM-105851] p 121 N93-16614
- System model development for nuclear thermal propulsion
[NASA-TM-108215] p 277 N93-17343
- Experimentation in the low-density plume of a simulated electrothermal thruster for computer code validation
[NASA-CR-191112] p 87 N93-24758
- Evaluation of MARC for the analysis of rotating composite blades
[NASA-TM-4423] p 249 N93-24909
- High Temperature Composite Analyzer (HITCAN) theoretical manual, version 1.0
[NASA-TM-106001] p 249 N93-24913
- High temperature composite analyzer (HITCAN) user's manual, version 1.0
[NASA-TM-106002] p 249 N93-25070
- METAL matrix composite Analyzer (METCAN): Theoretical manual
[NASA-TM-106025] p 109 N93-26552
- Probabilistic sizing of laminates with uncertainties
[NASA-TM-106145] p 110 N93-27082
- Dynamic analysis of spur gears using computer program DANST
[NASA-TM-106211] p 230 N93-28050
- Ceramic matrix composites properties/microstresses with complete and partial interphase bond
[NASA-TM-106136] p 111 N93-29071
- ACTS system handbook, revision change index
[NASA-TM-107982] p 150 N93-70235
- COMPUTER SYSTEMS DESIGN**
A multiarchitecture parallel-processing development environment
[NASA-TM-106180] p 262 N93-28628
- COMPUTER SYSTEMS PROGRAMS**
A multiarchitecture parallel-processing development environment
[NASA-TM-106180] p 262 N93-28628
- COMPUTER TECHNIQUES**
Particle displacement tracking applied to air flows
p 206 N93-23800
- A high temperature fatigue life prediction computer code based on the Total Strain Version of Strainrange Partitioning (SRP)
p 260 N93-31341
- Dynamic gas temperature measurements using a personal computer for data acquisition and reduction
[NASA-TM-106119] p 261 N93-27024
- Ceramic matrix composites properties/microstresses with complete and partial interphase bond
[NASA-TM-106136] p 111 N93-29071
- COMPUTER VISION**
A fuzzy logic based controller for the automated alignment of a laser-beam-smoothing spatial filter
[NASA-TM-105994] p 217 N93-18091
- COMPUTERIZED SIMULATION**
Dynamic analysis of a pre-and-post ice impacted blade
[AIAA PAPER 92-4273] p 22 N93-13333
- Numerical simulation of a low-emission gas turbine combustor using KIVA-II
p 22 N93-14077
- RIPPLE - A new model for incompressible flows with free surfaces
p 164 N93-14551
- Three-dimensional finite element simulation of intermingled-fiber hybrid composite behavior
p 98 N93-15729
- Coupled multi-disciplinary simulation of composite engine structures in propulsion environment
[ASME PAPER 92-GT-6] p 23 N93-19279
- CFD zonal modeling of leading-edge ice effects for a complete aircraft
[AIAA PAPER 93-0167] p 5 N93-22601
- Simplified jet fuel reaction mechanism for lean burn combustion application
[AIAA PAPER 93-0021] p 113 N93-23238
- Plasma sheath effects on ion collection by a pinhole
[AIAA PAPER 93-0567] p 55 N93-24243
- Numerical simulations of a high Mach number jet flow
[AIAA PAPER 93-0653] p 172 N93-24766
- DSMC and continuum analyses of low-density nozzle flow
[AIAA PAPER 93-0727] p 172 N93-24817
- NASA CST aids U.S. industry ... computational structures technology
p 258 N93-25084
- Electric and hybrid electric vehicle study utilizing a time-stepping simulation
p 287 N93-26012
- Critical comparison of second-order closures with direct numerical simulations of homogeneous turbulence
p 176 N93-30840
- Probabilistic simulation of stress concentration in composite laminates
[AIAA PAPER 93-1442] p 103 N93-33991
- Probabilistic simulation of the human factor in structural reliability
[AIAA PAPER 93-1495] p 264 N93-34036

- Modeling of linear isentropic flow systems
p 179 N93-37046
- Vorticity dynamics of inviscid shear layers
p 181 N93-45734
- The promising chemical kinetics for the simulation of propane-air combustion with KIVA-II code
[AIAA PAPER 93-2189] p 118 N93-50001
- Generation of helical gears with new surfaces topology by application of CNC machines
[AIAA PAPER 93-2297] p 224 N93-50082
- Three-dimensional numerical simulation of gradual opening in a wave rotor passage
[AIAA PAPER 93-2526] p 187 N93-50254
- Nonlinear dynamic simulation of single- and multi-spool core engines
[AIAA PAPER 93-2580] p 30 N93-50294
- Design for progressive fracture in composite shell structures
p 242 N93-53394
- Design for inadvertent damage in composite laminates
p 242 N93-53396
- Internal structure of shock waves in disparate mass mixtures
p 190 N93-54483
- Probabilistic evaluation of fuselage-type composite structures
[NASA-TM-105881] p 245 N93-12735
- Turbomachinery CFD on parallel computers
[NASA-TM-105932] p 262 N93-13154
- A SINDA '85 nodal heat transfer rate calculation user subroutine
p 193 N93-13403
- Simplified jet-A kinetic mechanism for combustor application
[NASA-TM-105940] p 120 N93-15504
- User's guide for a large signal computer model of the helical traveling wave tube
[NASA-TP-3251] p 160 N93-15531
- System model development for nuclear thermal propulsion
[NASA-TM-108157] p 276 N93-16531
- User's manual for Interactive Data Display System (IIDS)
[NASA-TM-105572] p 261 N93-16613
- System model development for nuclear thermal propulsion
[NASA-TM-108215] p 277 N93-17343
- COLD-SAT dynamic model
[NASA-TM-105185] p 59 N93-19988
- Progressive delamination in polymer matrix composite laminates: A new approach
p 108 N93-21515
- Simulation of TunnelLadder traveling-wave tube cold-test characteristics: Implementation of the three-dimensional, electromagnetic circuit analysis code micro-SOS
[NASA-TP-3294] p 160 N93-23394
- Computational simulation for concurrent engineering of aerospace propulsion systems
[NASA-TM-106029] p 249 N93-23746
- Nuclear Engine System Simulation (NESS): Version 2.0: Program user's guide
[NASA-CR-191081] p 85 N93-23875
- Nuclear Engine System Simulation (NESS): Volume 1: Program user's guide
[NASA-CR-191080] p 86 N93-23876
- Plasma sheath effects on ion collection by a pinhole
[NASA-TM-106098] p 60 N93-25090
- Gas turbine system simulation: An object-oriented approach
[NASA-TM-106044] p 36 N93-25673
- Overview of NASA/DOE/DOD interagency modeling team and activities
p 89 N93-26952
- Rocket engine numerical simulator
p 89 N93-26962
- RENEW v3.2 user's manual, maintenance estimation simulation for Space Station Freedom Program
[NASA-TM-106006] p 232 N93-27025
- A transfer matrix approach to vibration localization in mistuned blade assemblies
[NASA-TM-106112] p 250 N93-27088
- Numerical modeling of runback water on ice protected aircraft surfaces
p 201 N93-27438
- Generation of helical gears with new surfaces, topology by application of CNC machines
[NASA-TM-106175] p 229 N93-27687
- Probabilistic simulation of multi-scale composite behavior
[NASA-TM-106196] p 250 N93-28633
- Ceramic matrix composites properties/microstresses with complete and partial interphase bond
[NASA-TM-106136] p 111 N93-29071
- Probabilistic composite analysis
p 112 N93-30868
- Desktop chaotic systems: Intuition and visualization
[NASA-TM-106258] p 269 N93-31847
- CONCENTRATION (COMPOSITION)**
Composition dependence of superconductivity in YBa₂Cu_{3-x}Al_x(O_y)
p 281 N93-40271
- CONCENTRATORS**
Flux concentrations on solar dynamic components due to mispointing
[NASA-TM-105756] p 255 N93-20261

CONCURRENT PROCESSING

- Concurrent processing adaptation of aeroelastic analysis of propfans
p 23 N93-14624

CONDUCTING FLUIDS

- Computational/experimental basis for conducting alkane droplet combustion experiments on space-based-platforms
p 117 N93-41711

CONDUCTIVE HEAT TRANSFER

- Refractive index effects on radiative behavior of a heated absorbing-emitting layer
p 162 N93-10653
- Measurement of frequency response in short thermocouple wires
p 209 N93-40677
- Efficient finite element method for aircraft deicing problems
p 21 N93-52443
- A SINDA '85 nodal heat transfer rate calculation user subroutine
p 193 N93-13403
- Transient liquid-crystal technique used to produce high-resolution convective heat-transfer-coefficient maps
[NASA-TM-106083] p 198 N93-23404

CONFERENCES

- Space nuclear power systems; Proceedings of the 8th Symposium, Albuquerque, NM, Jan. 6-10, 1991, Pts. 1-3
[ISBN 0-88318-838-4] p 64 N93-13751
- Space nuclear power systems 1989; Proceedings of the 6th Symposium, Albuquerque, NM, Jan. 8-12, 1989. Vols. 1 & 2 ... Book
p 66 N93-20752
- [ISBN 0-89464-030-5]
- Laser anemometry - Advances and applications 1991; Proceedings of the 4th International Conference, Cleveland, OH, Aug. 5-9, 1991. Vols. 1 & 2
[ISBN 0-7918-0654-5] p 206 N93-23776
- Monolithic microwave integrated circuits for sensors, radar, and communications systems; Proceedings of the Meeting, Orlando, FL, Apr. 2-4, 1991
[SPIE-1475] p 151 N93-25776
- Superconductivity applications for infrared and microwave devices II; Proceedings of the Meeting, Orlando, FL, Apr. 4, 5, 1991
[SPIE-1477] p 154 N93-27243
- Nuclear Propulsion Technical Interchange Meeting, volume 1
[NASA-CP-10116-VOL-1] p 89 N93-26908
- Nuclear Propulsion Technical Interchange Meeting, volume 2
[NASA-CP-10116-VOL-2] p 89 N93-26951
- Structural Integrity and Durability of Reusable Space Propulsion Systems
[NASA-CP-10064] p 93 N93-31552

CONFINEMENT

- Structure of confined laminar spray diffusion flames: Numerical investigation
[NASA-TM-106038] p 197 N93-22596
- A numerical study of confined turbulent jets
[NASA-TM-106197] p 202 N93-29161

CONFORMAL MAPPING

- Mapping methods for computationally efficient and accurate structural reliability
[NASA-TM-105892] p 248 N93-23745

CONICAL NOZZLES

- Assessment of three numerical methods for the computation of a low-density plume flow
[AIAA PAPER 93-2528] p 77 N93-50256
- Experimentation in the low-density plume of a simulated electrothermal thruster for computer code validation
[NASA-CR-191112] p 87 N93-24758

CONJUGATE GRADIENT METHOD

- Large-scale computation of incompressible viscous flow by least-squares finite element method
[NASA-TM-105904] p 269 N93-22825

CONJUGATES

- Preconditioned Conjugate Gradient methods for low speed flow calculations
[AIAA PAPER 93-0881] p 172 N93-24942
- Preconditioned conjugate-gradient methods for low-speed flow calculations
[NASA-TM-105929] p 194 N93-14885

CONSERVATION EQUATIONS

- A critical analysis of the accuracy of several numerical techniques for combustion kinetic rate equations
[NASA-TP-3315] p 34 N93-16941
- On the structure of gaseous confined laminar diffusion flames: Numerical investigation
[NASA-TM-106039] p 197 N93-21198

CONSERVATION LAWS

- High resolution numerical simulation of the linearized Euler equations in conservation law form
[AIAA PAPER 93-2934] p 183 N93-48132
- On an origin of numerical diffusion: Violation of invariance under space-time inversion
[NASA-TM-105776] p 268 N93-11254
- A brief description of a new numerical framework for solving conservation laws: The method of space-time conservation element and solution element
[NASA-TM-105757] p 269 N93-26560

- A new flux conserving Newton's method scheme for the two-dimensional, steady Navier-Stokes equations [NASA-TM-106160] p 201 N93-28626
- CONSTITUTIVE EQUATIONS**
- Critical experiments of the self-consistent model for polycrystalline Hastelloy-X p 124 A93-21958
- A constitutive model for the high temperature inelastic response of nickel base superalloys p 124 A93-21959
- Stirling engine - Approach for long-term durability assessment p 220 A93-26069
- Analysis of the anisotropic viscoplastic-damage response of composite laminates - Continuum basis and computational algorithms p 241 A93-43347
- Analysis of large quasistatic deformations of inelastic solids by a new stress based finite element method [NASA-CR-189235] p 246 N93-13260
- Explicit robust schemes for implementation of a class of principal value-based constitutive models: Symbolic and numeric implementation [NASA-TM-106124] p 258 N93-26946
- Explicit robust schemes for implementation of general principal value-based constitutive models [NASA-TM-106123] p 258 N93-26947
- CONSTRUCTORS**
- Effects of anode material on arcjet performance p 79 N93-10044
- Effects of anode material on arcjet performance [NASA-TM-105799] p 79 N93-10197
- CONSTRUCTION MATERIALS**
- Lifetime reliability evaluation of structural ceramic parts with the CARES/LIFE computer program [AIAA PAPER 93-1497] p 239 A93-34037
- A numerical round robin for the reliability prediction of structural ceramics [AIAA PAPER 93-1498] p 240 A93-34038
- CONTACT LOADS**
- Effect of extended tooth contact on the modeling of spur gear transmissions [AIAA PAPER 93-2148] p 223 A93-49965
- Contact stress analysis of spiral bevel gears using nonlinear finite element static analysis [AIAA PAPER 93-2296] p 224 A93-50081
- The effect of contact stresses in four-point bend testing of graphite/epoxy and graphite/PMR-15 composite beams [NASA-TM-105891] p 107 N93-12076
- Contact stress analysis of spiral bevel gears using nonlinear finite element static analysis [NASA-TM-106176] p 228 N93-27037
- Effect of extended tooth contact on the modeling of spur gear transmissions [NASA-TM-106174] p 230 N93-28411
- CONTACT RESISTANCE**
- Low resistance silver contacts to indium phosphide - Electrical and metallurgical considerations p 157 A93-39351
- Simple, extremely low resistance contact system to n-InP that does not exhibit metal-semiconductor intermixing during sintering p 157 A93-42550
- Non-destructive, ultra-low resistance, thermally stable contacts for use on shallow junction InP solar cells [NASA-TM-106228] p 256 N93-32201
- CONTACTORS**
- Plasma contactor technology for Space Station Freedom [AIAA PAPER 93-2228] p 57 A93-50034
- CONTINUOUS RADIATION**
- A high-efficiency 59- to 64-GHz TWT for intersatellite communications p 158 A93-49553
- SITE project. Phase 1: Continuous data bit-error-rate testing [NASA-TP-3279] p 58 N93-11001
- CONTINUOUS WAVE LASERS**
- Particle displacement tracking applied to air flows p 206 A93-23800
- CONTINUUM MECHANICS**
- Software issues in three dimensional continuum shape optimization employing boundary formulations [AIAA PAPER 92-4792] p 258 A93-20380
- CONTINUUM MODELING**
- Analysis of the anisotropic viscoplastic-damage response of composite laminates - Continuum basis and computational algorithms p 241 A93-43347
- Boundary formulations for sensitivity analysis without matrix derivatives p 242 A93-49028
- CONTINUUMS**
- Topology and layout optimization of discrete and continuum structures p 241 A93-45429
- CONTRAROTATING PROPELLERS**
- Forward rotor vortex effects on counter rotating propeller noise p 2 A93-19221
- Takeoff/approach noise for a model counterrotation propeller with a forward-swept upstream rotor [AIAA PAPER 93-0596] p 24 A93-24782
- Takeoff/approach noise for a model counterrotation propeller with a forward-swept upstream rotor [NASA-TM-105979] p 34 N93-16715
- CONTROL EQUIPMENT**
- An electromechanical actuation system for an expendable launch vehicle p 50 A93-25891
- Electrical design of payload G-534: The Pool Boiling Experiment p 144 N93-13170
- Electrical design of Space Shuttle payload G-534: The pool boiling experiment [NASA-TM-106143] p 62 N93-27260
- CONTROL SIMULATION**
- Evaluation of passive and active vibration control mechanisms in a microgravity environment [AIAA PAPER 93-0838] p 55 A93-24905
- Identification of propulsion systems [NASA-TM-106007] p 35 N93-20109
- CONTROL STABILITY**
- A note on decentralized integral controllability p 264 A93-30492
- Design and evaluation of a robust dynamic neurocontroller for a multivariable aircraft control problem p 40 A93-37004
- CONTROL SYSTEMS DESIGN**
- Control-structure interaction study for the Space Station solar dynamic power module p 54 A93-13132
- Optimal control study for the Space Station Solar Dynamic power module p 54 A93-13133
- Analysis of airflow and engine control interactions and integrated flight/propulsion control p 40 A93-14596
- Damage-mitigating control of aerospace systems for high performance and extended life p 263 A93-22967
- Electromechanical systems with transient high power response operating from a resonant ac link p 152 A93-25892
- A free-piston Stirling engine/linear alternator controls and load interaction test facility p 146 A93-26077
- Description of the SSF PMAD dc testbed control system data acquisition function p 47 A93-26103
- Power system monitoring and source control of the Space Station Freedom dc-power system testbed p 69 A93-26109
- Robust integrated flight/propulsion control design for a STOVU aircraft using H-infinity control design techniques p 40 A93-26432
- Dynamic modeling and control of multibody mechanical systems which are structurally flexible p 264 A93-29338
- Review of the FOCSI (Fiber Optic Control System Integration) program --- applications in aircraft flight control p 21 A93-32916
- Design and evaluation of a robust dynamic neurocontroller for a multivariable aircraft control problem p 40 A93-37004
- Fuzzy expert systems vs. neural networks - Truck backer-upper control revisited p 264 A93-37039
- Screening studies of advanced control concepts for airbreathing engines [AIAA PAPER 92-3320] p 26 A93-49329
- Advanced instrumentation for next-generation aerospace propulsion control systems [AIAA PAPER 93-2079] p 211 A93-49906
- Cryogenic propellant thermal control system design considerations, analyses, and concepts applied to a Mars human exploration mission [AIAA PAPER 93-2353] p 75 A93-50126
- Application of controller partitioning optimization procedure to integrated flight/propulsion control design for a STOVU aircraft [AIAA PAPER 93-3766] p 40 A93-51361
- Integrated flight/propulsion control - Subsystem specifications for performance [AIAA PAPER 93-3808] p 41 A93-51400
- Antiwindup analysis and design approaches for MIMO systems [AIAA PAPER 93-3811] p 30 A93-51403
- Digital control algorithms for microgravity isolation systems p 265 A93-53653
- A parameter optimization approach to controller partitioning for integrated flight/propulsion control application p 41 A93-54268
- System model development for nuclear thermal propulsion [NASA-TM-105761] p 80 N93-10457
- Power system monitoring and source control of the Space Station Freedom DC power system testbed [NASA-TM-105841] p 80 N93-10734
- Description of the SSF PMAD DC testbed control system data acquisition function [NASA-TM-105843] p 261 N93-11005
- A fuzzy logic based controller for the automated alignment of a laser-beam-smoothing spatial filter [NASA-TM-105994] p 217 N93-18091
- Controller partitioning for integrated flight/propulsion control implementation [NASA-TM-105804] p 41 N93-21197
- Stability testing and analysis of a PMAD dc test bed for the Space Station Freedom p 154 A93-26107
- Design and evaluation of a robust dynamic neurocontroller for a multivariable aircraft control problem p 40 A93-37004
- A parameter optimization approach to controller partitioning for integrated flight/propulsion control application p 41 A93-54268
- Phase-stepping fiber-optic projected fringe system for surface topography measurements [NASA-CASE-LEW-14996-1] p 278 N93-11058
- Propulsion system performance resulting from an integrated flight/propulsion control design [NASA-TM-105874] p 34 N93-15525
- A fuzzy logic based controller for the automated alignment of a laser-beam-smoothing spatial filter [NASA-TM-105994] p 217 N93-18091
- Controller partitioning for integrated flight/propulsion control implementation [NASA-TM-105804] p 41 N93-21197
- A modified approach to controller partitioning [NASA-TM-106167] p 266 N93-28051
- CONVECTION**
- Particle image velocimetry for the Surface Tension Driven Convection Experiment using a particle displacement tracking technique p 206 A93-23799
- Absolute and convective instability of a viscous liquid jet surrounded by a viscous gas in a vertical pipe p 176 A93-30144
- Ground-based PIV and numerical flow visualization results from the Surface Tension Driven Convection Experiment p 143 A93-33075
- The L sub 1 finite element method for pure convection problems p 177 A93-34326
- A new flux splitting scheme p 9 A93-47189
- Physical vapor transport of mercurous chloride under a nonlinear thermal profile [NASA-TM-105920] p 196 N93-16612
- CONVECTION-DIFFUSION EQUATION**
- Double-diffusive fingering convection in a porous medium p 175 A93-27900
- Non-oscillatory and non-diffusive solution of convection problems by the iteratively reweighted least-squares finite element method p 177 A93-32622
- Convective effects during the physical vapor transport process. I - Thermal convection p 179 A93-36575
- On an origin of numerical diffusion: Violation of invariance under space-time inversion [NASA-TM-105776] p 268 N93-11254
- CONVECTIVE FLOW**
- Natural and thermocapillary convection in multiple liquid layers [AIAA PAPER 93-0469] p 171 A93-24241
- Surface tension effects on the onset of double-diffusive convection p 180 A93-41710
- Convective effects during the physical vapor transport process. II - Thermosolutal convection p 180 A93-42424
- Droplet vaporization in a high-pressure gas p 190 A93-55461
- A numerical study of confined turbulent jets [NASA-TM-106197] p 202 N93-29161
- CONVECTIVE HEAT TRANSFER**
- A new hue capturing technique for the quantitative interpretation of liquid crystal images used in convective heat transfer studies p 204 A93-13977
- Refractive index and scattering effects on radiative behavior of a semitransparent layer p 176 A93-31438
- Evaluation of a hue capturing based transient liquid crystal method for high-resolution mapping of convective heat transfer on curved surfaces p 210 A93-43689
- Progress towards understanding and predicting heat transfer in the turbine gas path p 188 A93-52751
- Fluid dynamics and convective heat transfer in impinging jets through implementation of a high resolution liquid crystal technique [ISABE 93-7077] p 189 A93-54053

- A p-version finite element method for steady incompressible fluid flow and convective heat transfer [NASA-TM-106260] p 203 N93-32370
- CONVERGENT-DIVERGENT NOZZLES**
- Computation of supersonic jet noise under imperfectly expanded conditions [AIAA PAPER 93-0735] p 273 A93-24825
- Computation of supersonic jet noise under imperfectly expanded conditions [NASA-TM-105961] p 274 N93-15430
- Nuclear thermal rocket nozzle testing and evaluation program [NASA-TM-105962] p 83 N93-15571
- CONVOLUTION INTEGRALS**
- Modifying real convolutional codes for protecting digital filtering systems p 148 A93-38221
- COOLANTS**
- Mechanisms of voids formation during cooldown and freezing of lithium in SP-100 type systems p 163 A93-13916
- Performance comparison of axisymmetric and three-dimensional hydrogen film coolant injection in a 110N hydrogen/oxygen rocket [NASA-TM-105967] p 83 N93-16714
- COOLING**
- Effects of turbine cooling assumptions on performance and sizing of high-speed civil transport [AIAA PAPER 92-4217] p 22 A93-13383
- Finite difference solution for transient radiative cooling of a conducting semitransparent square region p 164 A93-15067
- Tank chilldown analysis and verification with a flightweight, 175 cu ft tank under normal gravity with liquid hydrogen p 140 N93-10045
- Radial turbine cooling p 191 N93-10061
- Radial turbine cooling [NASA-TM-105658] p 15 N93-13292
- Semiconductor cooling apparatus [NASA-CASE-LEW-14162-3] p 111 N93-29614
- COOLING FINNS**
- Graphite fiber/copper matrix composites for space power heat pipe lin applications p 162 A93-13789
- COOLING SYSTEMS**
- Heat transfer in rotating serpentine passages with trips skewed to the flow [ASME PAPER 92-GT-191] p 166 A93-19416
- An efficient liner cooling scheme for advanced small gas turbine combustors [AIAA PAPER 93-1763] p 27 A93-49660
- Reliability assessment of thrust chamber cooling concepts using probabilistic analysis techniques [AIAA PAPER 93-2163] p 75 A93-49978
- Measurements and computational analysis of heat transfer and flow in a simulated turbine blade internal cooling passage p 189 A93-53585
- [AIAA PAPER 93-1797] p 189 A93-53585
- Program ELM: A tool for rapid thermal-hydraulic analysis of solid-core nuclear rocket fuel elements [NASA-TM-105867] p 84 N93-19106
- Measurements and computational analysis of heat transfer and flow in a simulated turbine blade internal cooling passage [NASA-TM-106189] p 203 N93-31647
- COORDINATE TRANSFORMATIONS**
- Algebraic grid generation with control points p 268 A93-45967
- COPLANARITY**
- Effect of a dielectric overlay on a linearly tapered slot antenna excited by a coplanar waveguide p 155 A93-35649
- Coplanar waveguide radial line stub p 155 A93-36514
- COPPER**
- On the melt infiltration of copper coated silicon carbide with an aluminum alloy p 218 A93-11332
- Graphite fiber/copper matrix composites for space power heat pipe lin applications p 162 A93-13789
- Thermal conductivity and thermal expansion of graphite fiber-reinforced copper matrix composites p 100 A93-25104
- The kinetics of composite particle formation during mechanical alloying p 125 A93-29534
- A model for predicting high-temperature fatigue failure of a W/Cu composite p 112 N93-31579
- COPPER ALLOYS**
- Reaction layer formation at the graphite/copper-chromium alloy interface p 100 A93-25105
- COPPER OXIDES**
- Performance of TiCaBaCuO 30 GHz 64 element antenna array p 157 A93-44763
- COPPER SELENIDES**
- Room temperature synthesis of copper indium diselenide in non-aqueous solution using an organoindium reagent p 283 A93-54844

- CORES**
- Nonlinear dynamic simulation of single- and multi-spool core engines [AIAA PAPER 93-2580] p 30 A93-50294
- CORIOLIS EFFECT**
- Heat transfer in rotating serpentine passages with trips skewed to the flow [ASME PAPER 92-GT-191] p 166 A93-19416
- Three-dimensional numerical simulation of gradual opening in a wave rotor passage [AIAA PAPER 93-2526] p 187 A93-50254
- Heat transfer in rotating serpentine passages with selected model orientation for smooth or skewed trip walls [NASA-TM-106126] p 147 N93-25177
- CORRECTION**
- Calculations of separated 3-D flows with a pressure-staggered Navier-Stokes equations solver p 177 A93-34366
- CORRELATION**
- N-point correlation functions in the CfA and SSRS redshift distribution of galaxies p 288 A93-10615
- Atomizing-gas temperature effect on cryogenic spray dropsize [AIAA PAPER 93-2333] p 186 A93-50111
- Statistical fitting accuracy in photon correlation spectroscopy p 277 A93-52414
- Atomizing-gas temperature effect on cryogenic spray dropsize [NASA-TM-106106] p 216 N93-25191
- CORROSION**
- A statistical analysis of elevated temperature gravimetric cyclic oxidation data of 36 Ni- and Co-base superalloys based on an oxidation attack parameter [NASA-TM-105934] p 128 N93-18069
- CORROSION PREVENTION**
- Hydrocarbon-fuel/copper combustion chamber liner compatibility, corrosion prevention, and refurbishment p 139 A93-14510
- CORROSION RESISTANCE**
- Corrosion of silicon-based ceramics in combustion environments p 131 A93-22984
- CORROSION TESTS**
- The chemistry of Saudi Arabian sand - A deposition problem on helicopter turbine airfoils p 243 A93-53468
- COSMIC BACKGROUND EXPLORER SATELLITE**
- Cosmic microwave background probes models of inflation p 294 A93-10355
- The gravitational wave contribution to cosmic microwave background anisotropies and the amplitude of mass fluctuations from COBE results p 289 A93-21508
- Microwave anisotropies in the light of the data from the COBE satellite p 291 A93-35444
- COSMIC DUST**
- Space environmental interactions for the space exploration initiative p 293 N93-26396
- COSMIC RAYS**
- NDE of the universe - New ways to look at old facts p 271 A93-32222
- COSMOLOGY**
- Gravitational waves from first-order cosmological phase transitions p 288 A93-11451
- Dark matter, long-range forces, and large-scale structure p 288 A93-11876
- Cosmic string with a light massive neutrino p 288 A93-16303
- The inflation sector of extended inflation p 288 A93-17638
- Late-time cosmological phase transitions p 288 A93-17645
- Stochastic inflation lattice simulations - Ultra-large scale structure of the universe p 289 A93-17646
- The best-fit universe --- cosmological models p 289 A93-17651
- The gravitational wave contribution to cosmic microwave background anisotropies and the amplitude of mass fluctuations from COBE results p 289 A93-21508
- Large- and small-scale constraints on power spectra in Omega 1 universes p 290 A93-23990
- Kurtosis, skewness, and non-Gaussian cosmological density perturbations p 291 A93-35579
- Dark matter and the equivalence principle p 291 A93-44385
- Clumpy cold dark matter p 291 A93-46201
- Observing the inflation potential --- in models of cosmological inflation p 291 A93-50480
- First-order inflation --- in cosmology p 292 A93-51704
- Testing for the Gaussian nature of cosmological density perturbations through the three-point temperature correlation function p 292 A93-55212
- COST ANALYSIS**
- The NASA Electric Propulsion Program [AIAA PAPER 93-1935] p 73 A93-49797

- Minimize system cost by choosing optimal subsystem reliability and redundancy [NASA-TM-106251] p 271 N93-31145
- COST EFFECTIVENESS**
- Key issues in space nuclear power challenges for the future p 65 A93-13905
- COST REDUCTION**
- Key issues in space nuclear power challenges for the future p 65 A93-13905
- Evolving SP-100 powerplants via electric propulsion to GEO and lunar orbit p 70 A93-34492
- Small Stirling dynamic isotope power system for robotic space missions [NASA-TM-105785] p 92 N93-28686
- COSTS**
- Battery selection for Space Shuttle experiments [NASA-TM-106142] p 61 N93-27038
- COUNTER ROTATION**
- Manipulation of upstream rotor leading edge vortex and its effects on counter rotating propeller noise [AIAA PAPER 93-0012] p 272 A93-20134
- Takeoff/approach noise for a model counterrotation propeller with a forward-swept upstream rotor [AIAA PAPER 93-0596] p 24 A93-24782
- Experimental investigation of counter-rotating propfan flutter at cruise conditions [AIAA PAPER 93-1632] p 25 A93-34160
- Efficient hybrid scheme for the analysis of counter-rotating propellers p 7 A93-34483
- A concept for a counterrotating fan with reduced tone noise [NASA-TM-105736] p 274 N93-11370
- Takeoff/approach noise for a model counterrotation propeller with a forward-swept upstream rotor [NASA-TM-105979] p 34 N93-16715
- COUNTERS**
- Compressing subbanded image data with Lempel-Ziv-based coders [NASA-TM-105998] p 149 N93-20257
- COUPLED MODES**
- The coupling of interfacial instabilities and the stabilization of two-layer annular flows p 178 A93-35482
- COUPLES**
- Modal analysis of multistage gear systems coupled with gearbox vibrations p 222 A93-36588
- CRACK GEOMETRY**
- Evaluation of the fracture toughness of Nb-40Al-8Cr-1W-1Y-0.05B intermetallic material by indentation techniques p 124 A93-24066
- Progressive matrix cracking in off-axis plies of a general symmetric laminate [AIAA PAPER 93-1494] p 239 A93-34035
- Analysis of precracking parameters for ceramic single-edge-precracked-beam specimens p 133 A93-38887
- Analytical stress intensity solution for the Stable Poisson Loaded specimen p 242 A93-46768
- Elastic interactions of a fatigue crack with a micro-defect by the mixed boundary integral equation method p 243 A93-56412
- Analysis of precracking parameters and fracture toughness for ceramic single-edge-precracked-beam specimens [NASA-TM-105568] p 135 N93-10962
- CRACK INITIATION**
- The effect of ion-plated silver and sliding friction on tensile stress-induced cracking in aluminum oxide p 132 A93-27917
- Evolution of creep-fatigue life prediction models p 236 A93-31339
- Progressive delamination in polymer matrix composite laminates: A new approach p 108 N93-21515
- CRACK OPENING DISPLACEMENT**
- Analytical stress intensity solution for the Stable Poisson Loaded specimen p 242 A93-46768
- Numerical calibration of the stable poisson loaded specimen [NASA-TM-105609] p 245 N93-12738
- Closed form expressions for crack mouth displacements and stress intensity factors for chevron notched short bar and short rod specimens based on experimental compliance measurements [NASA-TM-83796] p 246 N93-15369
- CRACK PROPAGATION**
- Transient liquid phase diffusion bonding of Udimet 720 for Stirling power converter applications p 221 A93-26080
- Interaction of cracks between two adjacent indents in glass p 132 A93-27115
- Grain boundary resistance to fatigue crack growth p 125 A93-29570
- Elevated-temperature fracture resistances of monolithic and composite ceramics using chevron-notched bend tests p 133 A93-38888

SUBJECT INDEX

Variation of the energy release rate as a crack approaches and passes through an elastic inclusion p 241 A93-44440

Subcritical crack growth in soda-lime glass in combined mode I and mode II loading p 134 A93-52151

Design for progressive fracture in composite shell structures p 242 A93-53394

Design for inadvertent damage in composite laminates p 242 A93-53396

Calculation of stress intensity factors in an isotropic multicracked plate: Part 2: Symbolic/numeric implementation [NASA-TM-105823] p 244 A93-10453

Numerical calibration of the stable poisson loaded specimen [NASA-TM-105609] p 245 A93-12738

Low cycle fatigue behavior of polycrystalline NiAl at 300 and 1000 K [NASA-TM-105987] p 129 A93-26898

CRAACK TIPS

Single-parameter characterization of discrete-dislocation pileup tipfield and its application to physically based micro-mechanics p 233 A93-12119

Calculation of stress intensity factors in an isotropic multicracked plate: Part 2: Symbolic/numeric implementation [NASA-TM-105823] p 244 A93-10453

Calculation of stress intensity factors in an isotropic multicracked plate. Part 1: Theoretical development [NASA-TM-105766] p 244 A93-10455

Closed form expressions for crack mouth displacements and stress intensity factors for chevron notched short bar and short rod specimens based on experimental compliance measurements [NASA-TM-83796] p 246 A93-15369

CRAACKING (FRACTURING)

Effects of precracking methods on the fracture properties of alumina p 131 A93-16645

Residual strain gradient determination in metal matrix composites by synchrotron X-ray energy dispersive diffraction p 103 A93-39580

Thermomechanical fatigue behavior of SiC/Ti-24Al-11Nb in air and argon environments [NASA-TM-105723] p 106 A93-11399

The effect of contact stresses in four-point bend testing of graphite/epoxy and graphite/PMR-15 composite beams [NASA-TM-105891] p 107 A93-12076

An overview of elevated temperature damage mechanisms and fatigue behavior of a unidirectional SCS-6/Ti-15-3 composite [NASA-TM-106131] p 109 A93-26702

CRAACKS

The effect of ion-plated silver and sliding friction on tensile stress-induced cracking in aluminum oxide p 132 A93-27917

Analysis of precracking parameters for ceramic single-edge-precracked-beam specimens p 133 A93-38887

Analysis of precracking parameters and fracture toughness for ceramic single-edge-precracked-beam specimens [NASA-TM-105568] p 135 A93-10962

Nondestructive evaluation of ceramic and metal matrix composites for NASA's HITEMP and enabling propulsion materials programs [NASA-TM-105807] p 231 A93-10963

External stress-corrosion cracking of a 1.22-m-diameter type 316 stainless steel air valve [NASA-TP-3190] p 129 A93-26201

NDE of PWA 1480 single crystal turbine blade material [NASA-TM-106140] p 38 A93-27640

CREEP ANALYSIS

Stirling engine - Approach for long-term durability assessment p 220 A93-26069

CREEP BUCKLING

Thermo-elastoviscoplastic snapthrough behavior of cylindrical panels p 233 A93-12046

CREEP PROPERTIES

Influence of grain size on the creep behavior of HfC-dispersed NiAl p 123 A93-17674

Creep behavior of tungsten fiber reinforced niobium metal matrix composites p 99 A93-20758

Evolution of creep-fatigue life prediction models p 236 A93-31339

Creep and stress relaxation modeling of polycrystalline ceramic fibers p 132 A93-31354

Tensile creep and creep-recovery behavior of a SiC-fiber-Si3N4-matrix composite p 104 A93-40290

Unified viscoplastic behavior of metal matrix composites [NASA-TM-105819] p 244 A93-10777

A creep cavity growth model for creep-fatigue life prediction of a unidirectional W/Cu composite [NASA-TM-105780] p 244 A93-10967

Bounds on internal state variables in viscoplasticity [NASA-TM-106215] p 251 A93-29196

CREEP RUPTURE STRENGTH

The role of the interface in refractory metal alloy composites p 97 A93-13777

Properties of pure nickel after long term exposures to LiOH and vacuum at 775 K p 123 A93-18075

Creep-rupture strength of a Ni-base superalloy at 1400 K p 124 A93-20556

Creep behavior of tungsten fiber reinforced niobium metal matrix composites p 99 A93-20758

Preliminary evaluation of tensile and stress-rupture behavior of W + 24 at. pct Re + 0.4 at. pct HfC wire p 125 A93-25119

A generic model for creep rupture lifetime estimation on fibrous ceramic composites p 103 A93-38895

Stress-rupture behavior of small diameter polycrystalline alumina fibers [NASA-TM-106256] p 139 A93-32382

CREEP STRENGTH

Thermal stability of the microstructure of an aged Nb-Zr-C alloy p 122 A93-13776

The effect of microalloying additions on the tensile properties of polycrystalline NiAl p 123 A93-17516

Creep behavior of tungsten fiber reinforced niobium metal matrix composites p 99 A93-20758

Creep deformation of B2 aluminides p 126 A93-44887

Environmental effects on long term behavior of composite laminates p 243 A93-53438

Computer programs to characterize alloys and predict cyclic life using the total strain version of strainrange partitioning: Tutorial and users manual, version 1.0 [NASA-TM-4425] p 246 A93-15788

High temperature creep and oxidation resistant chromium silicide matrix alloy containing molybdenum [NASA-CASE-LEW-15697-1] p 130 A93-29172

Tensile creep behavior of polycrystalline alumina fibers [NASA-TM-106269] p 138 A93-30938

CREEP TESTS

Effect of strain and stress on the relative dimensions of the 'hard' and 'soft' regions in crept NaCl single crystals p 279 A93-17513

Tensile creep behavior of polycrystalline alumina fibers [NASA-TM-106269] p 138 A93-30938

CRITERIA

Fatigue criterion to system design, life and reliability: A primer [NASA-TM-106022] p 248 A93-23406

CRITICAL LOADING

The effect of ion-plated silver and sliding friction on tensile stress-induced cracking in aluminum oxide p 132 A93-27917

Damage progression in stiffened composite panels [AIAA PAPER 93-1345] p 238 A93-33915

CRITICAL TEMPERATURE

The susceptibility critical exponent for a nonaqueous ionic binary mixture near a consolute point p 284 A93-19838

CROSS CORRELATION

Progress in speckle-shift strain measurement p 251 A93-31558

CROSS COUPLING

Analysis of airframe and engine control interactions and integrated flight/propulsion control p 40 A93-14596

CROSS FLOW

Calculation of a circular jet in crossflow with a multiple-time-scale turbulence model p 164 A93-15063

Multigrid acceleration and turbulence models for computations of 3D turbulent jets in crossflow p 165 A93-18751

Two-, three-, and four-poster jets in cross flow [AIAA PAPER 93-0023] p 167 A93-20141

Optimization of circular orifice jets mixing into a heated crossflow in a cylindrical duct [AIAA PAPER 93-0249] p 24 A93-23246

Structure and development of streamwise vortex arrays embedded in a turbulent boundary layer p 177 A93-32711

Fluid flow of a row of jets in crossflow - A numerical study p 179 A93-35608

Characteristics of three-dimensional turbulent jets in crossflow p 8 A93-38695

The structure of a three-dimensional turbulent boundary layer p 181 A93-44813

Experimental investigation of crossflow jet mixing in a rectangular duct [AIAA PAPER 93-2037] p 185 A93-49872

CFD mixing analysis of axially opposed rows of jets injected into confined crossflow [AIAA PAPER 93-2044] p 185 A93-49877

Mixing of multiple jets with a confined subsonic crossflow p 15 A93-54324

CRYOGENIC ROCKET PROPELLANTS

Optimization of circular orifice jets mixing into a heated cross flow in a cylindrical duct [NASA-TM-105984] p 33 A93-15359

Experimental investigation of crossflow jet mixing in a rectangular duct [NASA-TM-106152] p 36 A93-27026

CFD mixing analysis of axially opposed rows of jets injected into confined crossflow [NASA-TM-106179] p 37 A93-27128

CROSSLINKING

Ion exchange polymers and method for making [NASA-CASE-LEW-15576-1] p 139 A93-31316

CRUISE MISSILES

Computer aided design and manufacturing of composite propfan blades for a cruise missile wind tunnel model [NASA-TM-105269] p 261 A93-12022

Structural analysis of high-rpm composite propfan blades for a cruise missile wind tunnel model [NASA-TM-105267] p 247 A93-23015

Fabrication of composite propfan blades for a cruise missile wind tunnel model [NASA-TM-105270] p 249 A93-26202

CRUISING FLIGHT

Cruise noise of an advanced propeller with swirl recovery vanes p 273 A93-28609

CRYOGENIC EQUIPMENT

Effect of fluid compressibility on journal bearing performance p 223 A93-49244

Preliminary experimental results for a cryogenic brush seal configuration [AIAA PAPER 93-2535] p 225 A93-50262

Comparing the results of an analytical model of the no-vent fill process with no-vent fill test results for a 4.96 cubic meters (175 cubic feet) tank [NASA-TM-106018] p 200 A93-27155

Preliminary experimental results for a cryogenic brush seal configuration [NASA-TM-106236] p 201 A93-28627

CRYOGENIC FLUID STORAGE

The CONE program - An overview ... Cryogenic Orbital Nitrogen Experiment p 146 A93-48637

Autogenous pressurization of cryogenic vessels using submerged vapor injection p 71 A93-48648

Tank chilldown analysis and verification with a lightweight, 175 cu ft tank under normal gravity with liquid hydrogen p 140 A93-10045

COLD-SAT dynamic model [NASA-TM-105185] p 59 A93-19988

Comparing the results of an analytical model of the no-vent fill process with no-vent fill test results for a 4.96 cubic meters (175 cubic feet) tank [NASA-TM-106018] p 200 A93-27155

Orbital storage and supply of subcritical liquid nitrogen p 62 A93-27801

Tank Pressure Control Experiment/Thermal Phenomena (TPCE/TP) p 92 A93-28713

CRYOGENIC FLUIDS

Effect of vaporization on cryogenic spray droplets measurement [AIAA PAPER 93-0692] p 172 A93-24792

Supercritical droplet combustion and related transport phenomena [AIAA PAPER 93-0812] p 115 A93-24885

Technology for gelled liquid cryogenic propellants - Metallized hydrogen/aluminum [AIAA PAPER 93-1878] p 140 A93-49752

Tank chilldown analysis and verification with a lightweight, 175 cu ft tank under normal gravity with liquid hydrogen p 140 A93-10045

Effect of vaporization on cryogenic spray droplets measurement [NASA-TM-105909] p 213 A93-13410

Selected OAST/OSSA space experiment activities in support of Space Station Freedom p 60 A93-22636

Tank Pressure Control Experiment/Thermal Phenomena (TPCE/TP) p 92 A93-28713

Cryogenic fluid management (base R/T): Cryogenic fluid systems, Cryogenic Orbital Nitrogen Experiment (CONE), Cryogenic Orbital Hydrogen Experiment (COHE), (Transportation focused technology) [PR6] p 286 A93-71879

CRYOGENIC ROCKET PROPELLANTS

Small experiments for the maturation of orbital cryogenic transfer technologies [IAF PAPER 92-0777] p 64 A93-13698

Hydrocarbon-fuel/copper combustion chamber liner compatibility, corrosion prevention, and refurbishment p 139 A93-14510

Technology for gelled liquid cryogenic propellants - Metallized hydrogen/aluminum [AIAA PAPER 93-1878] p 140 A93-49752

Ground testing for the no-vent fill of cryogenic tanks - Results of tests for a 71 cubic foot tank [AIAA PAPER 93-1967] p 73 A93-49815

Design of an Advanced Expander Test Bed [AIAA PAPER 93-2133] p 48 A93-49952

CRYOGENIC STORAGE

- Cryogenic propellant thermal control system design considerations, analyses, and concepts applied to a Mars human exploration mission
[AIAA PAPER 93-2353] p 75 A93-50126
- Small experiments for the maturation of orbital cryogenic transfer technologies
[NASA-TM-105849] p 192 N93-10981
- CRYOGENIC STORAGE**
Optimization of armored spherical tanks for storage on the lunar surface p 47 A93-25866
- CRYOGENIC TEMPERATURE**
Elevated temperature compressive properties of reaction milled NiAl-AIN and Zr-doped NiAl-AIN composites p 97 A93-11422
- Actively controlled superconducting bearings p 223 A93-48594
- Techniques for improving the accuracy of cryogenic temperature measurement in ground test programs p 212 A93-54363
- Techniques for improving the accuracy of cryogenic temperature measurement in ground test programs
[NASA-TM-105996] p 215 N93-22484
- CRYOGENICS**
Comparing the results of an analytical model of the no-vent fill process with no-vent fill test results for a 4.96 cubic meters (175 cubic feet) tank
[NASA-TM-106018] p 200 N93-27155
- Cryogenic fluid management (base R/T): Cryogenic fluid systems, Cryogenic Orbital Nitrogen Experiment (CONE), Cryogenic Orbital Hydrogen Experiment (COHE). (Transportation focused technology)
[PR6] p 286 N93-71879
- CRYSTAL DEFECTS**
Initial study of void formation during aluminum solidification in reduced gravity p 142 A93-12013
- Void control in the crystallization of lithium fluoride p 97 A93-13760
- Carrier removal and defect behavior in p-type InP p 279 A93-17176
- Heats of formation of bcc binary alloys p 123 A93-17609
- Method for calculating alloy energetics p 279 A93-18740
- Diminishing sign anomaly and scaling behavior of the mixed-state Hall resistivity in $\text{Ti}_2\text{Ba}_2\text{Ca}_2\text{Cu}_3\text{O}_{10}$ films containing columnar defects p 283 A93-53693
- Low cycle fatigue behavior of polycrystalline NiAl at 300 and 1000 K
[NASA-TM-105987] p 129 N93-26898
- CRYSTAL DISLOCATIONS**
Single-parameter characterization of discrete-dislocation pileup tipfield and its application to physically based micro-mechanics p 233 A93-12119
- Prediction of dislocation generation during Bridgman growth of GaAs crystals p 279 A93-19740
- CRYSTAL GROWTH**
Self-tuning multivariable pole placement control of a multizone crystal growth furnace p 263 A93-10575
- Thermal oscillations in materials processing p 162 A93-10839
- Silicon carbide, a semiconductor for space power electronics p 279 A93-13880
- Prediction of dislocation generation during Bridgman growth of GaAs crystals p 279 A93-19740
- Flow-influenced stabilization of liquid columns in a dynamic plateau chamber
[AIAA PAPER 93-0255] p 169 A93-22664
- IDGE - A test of dendritic growth theory using space flight
[AIAA PAPER 93-0260] p 143 A93-25515
- Ellipsometric study of metal-organic chemically vapor deposited III-V semiconductor structures p 281 A93-35697
- Convective effects during the physical vapor transport process. I - Thermal convection p 179 A93-36575
- Atomic probe microscopy of 3C SiC films grown on 6H SiC substrates p 281 A93-39854
- Convective effects during the physical vapor transport process. II - Thermosolutal convection p 180 A93-42424
- Progress in silicon carbide semiconductor technology p 158 A93-44965
- Scientific basis for the Isothermal Dendritic Growth Experiment - A USMP-2 space flight experiment p 143 A93-50455
- A numerical model including PID control of a multizone crystal growth furnace p 190 A93-55473
- Growth and characterization of 3C-SiC and 6H-SiC films on 6H-SiC wafers p 284 A93-55602
- Physical vapor transport of mercurous chloride under a nonlinear thermal profile
[NASA-TM-105920] p 196 N93-16612
- Process for the controlled growth of single-crystal films of silicon carbide polytypes on silicon carbide wafers
[NASA-CASE-LEW-15222-3] p 284 N93-17413

Secondary orientation effects in a single crystal superalloy under mechanical and thermal loads p 130 N93-31578

CRYSTAL LATTICES

Multilayer relaxation and surface energies of fcc and bcc metals using equivalent crystal theory p 119 A93-52872

CRYSTAL STRUCTURE

Heats of formation of bcc binary alloys p 123 A93-17609

Ellipsometric study of metal-organic chemically vapor deposited III-V semiconductor structures p 281 A93-35697

Determination of parameters of a method for predicting alloy properties p 126 A93-39796

Solid lubricants p 135 A93-55471

Determination of parameters of a new method for predicting alloy properties
[NASA-TM-105895] p 127 N93-11609

Processing and microstructure of Nb-1 percent Zr-0.1 percent C alloy sheet
[NASA-TM-105921] p 128 N93-15524

The influence of primary and secondary orientations on the elastic response of a nickel-base single-crystal superalloy
[NASA-TM-106125] p 250 N93-26550

Secondary orientation effects in a single crystal superalloy under mechanical and thermal loads p 130 N93-31578

CRYSTALLINITY

Single liquid source plasma-enhanced metalorganic chemical vapor deposition of high-quality $\text{YBa}_2\text{Cu}_3\text{O}_{7-x}$ thin films p 280 A93-20643

CRYSTALLIZATION

Void control in the crystallization of lithium fluoride p 97 A93-13760

Thermosolutal convection during dendritic solidification of a binary alloy p 182 A93-45975

Comments on 'Kinetic Study on the Hexacelsian-Celsian Phase Transformation'
[NASA-TM-105917] p 136 N93-14886

CRYSTALLOGRAPHY

The viscoplastic behavior of Hastelloy-X single crystal p 125 A93-27486

The microstructural evolution, crystallography, and thermal processing of ultrahigh carbon Fe-1.85 pct C melt-spun ribbon p 125 A93-32934

Vickers indentation hardness of stoichiometric and reduced single crystal TiO_2 (rutile) from 25 to 800 C
[NASA-TM-105959] p 96 N93-26204

CUMULATIVE DAMAGE

Structural durability of a composite pressure vessel p 234 A93-16552

Damage progression in stiffened composite panels
[AIAA PAPER 93-1345] p 238 A93-33915

Structural system reliability under multiple failure modes
[AIAA PAPER 93-1379] p 238 A93-33943

Evolution of damage and plasticity in titanium-based, fiber-reinforced composites p 104 A93-48498

Cumulative fatigue damage behavior of MAR M-247 p 251 N93-31575

CURING

Computational simulation of surface waviness in graphite/epoxy woven composites due to initial curing p 98 A93-15822

Lower temperature curing thermoset polyimides utilizing a substituted norbornene endcap p 134 A93-44526

CURRENT DISTRIBUTION
I-BIEM calculations of the frequency dispersion and ac current distribution at disk and ring-disk electrodes p 254 A93-34246

CURVED PANELS

Thermo-elastoviscoplastic snapthrough behavior of cylindrical panels p 233 A93-12046

CYCLIC LOADS

Room temperature cyclic deformation behavior of cast and extruded NiAl p 122 A93-12130

High temperature viscoplastic ratchetting - Material response or modeling artifact p 233 A93-13823

Ratchetting behavior in viscoplasticity - A technical note p 241 A93-43651

Design for cyclic loading endurance of composites p 242 A93-53395

Effect of service environments on adhesively bonded joints in composite structures p 242 A93-53418

On bilinearity of Manson-Coffin low-cycle-fatigue relationship
[NASA-TM-105840] p 245 N93-12739

Structural dynamics: Probabilistic structural analysis methods. Program overview p 251 N93-31562

CYCLOTRON RESONANCE
Application of high-quality SiO_2 grown by multipolar ECR source to Si/SiGe MISFET p 156 A93-37413

Low Earth orbital atomic oxygen environmental simulation facility for space materials evaluation
[NASA-TM-106128] p 96 N93-27266

CYLINDRICAL BODIES

Mixing and transient interface condensation of a liquid hydrogen tank
[AIAA PAPER 93-1968] p 184 A93-49816

Mixing and transient interface condensation of a liquid hydrogen tank
[NASA-TM-106201] p 201 N93-28252

A numerical study of confined turbulent jets
[NASA-TM-106197] p 202 N93-29161

CYLINDRICAL COORDINATES

Discrete ordinates solutions for radiatively participating media in a cylindrical enclosure p 285 A93-31427

CYLINDRICAL SHELLS

Structural durability of a composite pressure vessel p 234 A93-16552

Finite element calculations of transonic flutter in cascades
[AIAA PAPER 93-2083] p 185 A93-49910

Structural optimization of thin shells using finite element method
[NASA-TM-105903] p 246 N93-13157

D

DAMAGE

Damage-mitigating control of space propulsion systems for high performance and extended life
[AIAA PAPER 93-2080] p 74 A93-49907

DAMAGE ASSESSMENT

An advanced method for tracking the evolution of fatigue damage in reusable space propulsion systems p 234 A93-16406

Transverse flexural tests as a tool for assessing damage to PMR-15 composites from isothermal aging in air at elevated temperatures p 100 A93-24514

Forced response of mistuned bladed disk assemblies
[AIAA PAPER 93-1491] p 239 A93-34033

BLASIM - A computational tool to assess ice impact damage on engine blades
[AIAA PAPER 93-1638] p 26 A93-34165

Analysis of the anisotropic viscoplastic-damage response of composite laminates - Continuum basis and computational algorithms p 241 A93-43347

Transverse flexural tests as a tool for assessing damage to PMR-15 composites from isothermal aging in air at elevated temperatures p 107 N93-12737

Progressive delamination in polymer matrix composite laminates: A new approach p 108 N93-21515

An overview of elevated temperature damage mechanisms and fatigue behavior of a unidirectional SCS-6/Ti-15-3 composite p 109 N93-26702

[NASA-TM-106131] p 109 N93-26702

Life extending control: An interdisciplinary engineering thrust p 93 N93-31581

DAMPING

Damping of thermal acoustic oscillations in hydrogen systems p 146 A93-48589

ICAN/DAMP-integrated composite analyzer with damping analysis capabilities: User's manual
[NASA-TP-3292] p 106 N93-12015

Damping and scattering of electromagnetic waves by small ferrite spheres suspended in an insulator
[NASA-TM-105837] p 149 N93-12366

DARK MATTER

Cosmic microwave background probes models of inflation p 294 A93-10355

Dark matter, long-range forces, and large-scale structure p 288 A93-11876

Cosmic string with a light massive neutrino p 288 A93-16303

The best-fit universe --- cosmological models p 289 A93-17651

The first three minutes - 1990 version --- of early universe after Big Bang p 289 A93-23607

Large- and small-scale constraints on power spectra in Omega - 1 universes p 290 A93-23990

Microwave anisotropies in the light of the data from the COBE satellite p 291 A93-35444

Dark matter and the equivalence principle p 291 A93-44385

Clumpy cold dark matter p 291 A93-46201

DATA ACQUISITION

A free-piston Stirling engine/linear alternator controls and load interaction test facility p 146 A93-26077

Description of the SSF PMAD dc testbed control system data acquisition function p 47 A93-26103

Compound curvature laser window development
[AIAA PAPER 93-2177] p 277 A93-49989

Icing Research Tunnel rotating bar calibration measurement system p 212 A93-54398

Description of the SSF PMAD DC testbed control system data acquisition function
[NASA-TM-105843] p 261 N93-11005

Icing research tunnel rotating bar calibration measurement system
[NASA-TM-106010] p 215 N93-22598

Ice thickness measurement system for the icing research tunnel calibration
[NASA-TM-106095] p 215 N93-24737

A system to measure lightning-induced transients on spacecraft umbilical lines
p 161 N93-24889

Dynamic gas temperature measurements using a personal computer for data acquisition and reduction
[NASA-TM-106119] p 261 N93-27024

DATA BASES

Computer programs to characterize alloys and predict cyclic life using the total strain version of strainrange partitioning: Tutorial and users manual, version 1.0
[NASA-TM-4425] p 246 N93-15788

Pyrotechnically actuated systems database and applications catalog
p 141 N93-20136

Bibliography on propulsion airframe integration technologies for high-speed civil transport applications, 1980-1991
[NASA-TM-105602] p 1 N93-26136

DATA COMPRESSION

An all digital implementation of a modified Hamming net for video compression with prediction and quantization circuits
p 148 A93-37038

Compressing subbanded image data with Lempel-Ziv-based coders
[NASA-TM-105998] p 149 N93-20257

Real-time transmission of digital video using variable-length coding
[NASA-TM-106092] p 150 N93-22483

Picture data compression coder using subband/transform coding with a Lempel-Ziv-based coder
[NASA-CASE-LEW-15700-1] p 287 N93-28130

DATA LINKS

Fiber optic link for millimeter wave communication satellites
p 277 A93-25736

Multiple-access phased array antenna simulator for a digital beam-forming system investigation
p 148 A93-26237

Space Communication Artificial Intelligence for Link Evaluation Terminal (SCAILET)
p 265 N93-11940

Data distribution satellite
[NASA-TM-105778] p 149 N93-12481

Optical communications and a comparison of optical technologies for a high data rate return link from Mars
[NASA-TP-3180] p 52 N93-18854

Analysis of MMIC arrays for use in the ACTS Aero Experiment
[NASA-TM-106073] p 53 N93-22589

Status of the Fiber Optic Control System Integration (FOCSI) program
[NASA-TM-106151] p 217 N93-28053

DATA MANAGEMENT

Description of the PMAD systems test bed facility and data system
p 47 A93-26102

DATA PROCESSING

Second generation integrated composite analyzer (ICAN) computer code
[NASA-TP-3290] p 108 N93-18139

Subband coding for image data archiving
p 287 N93-25922

DATA RECORDING

Ice thickness measurement system for the icing research tunnel calibration
[NASA-TM-106095] p 215 N93-24737

DATA REDUCTION

Dynamic gas temperature measurements using a personal computer for data acquisition and reduction
[NASA-TM-106119] p 261 N93-27024

DATA RETRIEVAL

RENEW v3.2 user's manual, maintenance estimation simulation for Space Station Freedom Program
[NASA-TM-106006] p 232 N93-27025

DATA SIMULATION

Chimera grids in the simulation of three-dimensional flowfields in turbine-blade-coolant passages
[AIAA PAPER 93-2559] p 187 A93-50280

DATA STRUCTURES

Adaptive methods in computational fluid dynamics
p 182 A93-45963

DATA SYSTEMS

Subband coding for image data archiving
p 287 N93-25922

DATA TRANSMISSION

Anomalous TWTA output power spikes and their effect on a digital satellite communications system
[NASA-TM-105875] p 159 N93-13286

DC GENERATORS

Overview and evolution of the LeRC PMAD DC test bed
p 47 A93-26099

DEBRIS

Evaluation of an oil-debris monitoring device for use in helicopter transmissions
[NASA-TM-105830] p 227 N93-22826

DECAY RATES

Determination of plate wave velocities and diffuse field decay rates with broad-band acousto-ultrasonic signals
[NASA-TM-106158] p 232 N93-27080

DECOMPOSITION

Interfacial chemistry of a perfluoropolyether lubricant studied by X-ray photoelectron spectroscopy and temperature desorption spectroscopy
p 133 A93-38473

Composition dependence of superconductivity in YBa₂(Cu(3-x)Al(x))O(y)
p 281 A93-40271

Interfacial chemistry of a perfluoropolyether lubricant studied by XPS and TDS
[NASA-TM-106014] p 137 N93-22560

DEFECTS

Nondestructive evaluation of ceramic and metal matrix composites for NASA's HITEMP and enabling propulsion materials programs
[NASA-TM-105807] p 231 N93-10963

NDE of PWA 1480 single crystal turbine blade material
[NASA-TM-106140] p 38 N93-27640

DEFLECTION

Behavior of spinning laminated composite plates with initial twist-experimental vibrations, strain, and deflection results
[AIAA PAPER 93-1325] p 238 A93-33898

OTV bearing deflection investigation
[NASA-TM-106085] p 215 N93-22994

DEFORMATION

High-temperature deformation and microstructural analysis for silicon nitride-scandium(III) oxide
p 131 A93-20468

Finite element implementation of state variable-based viscoplasticity models
p 236 A93-26776

Deformation and failure mechanisms in metal matrix composites
p 102 A93-31359

Axial-torsional fatigue - A study of tubular specimen thickness effects
p 240 A93-38849

Environmental effects on long term behavior of composite laminates
p 243 A93-53438

Analysis of large quasistatic deformations of inelastic solids by a new stress based finite element method
[NASA-CR-189235] p 246 N93-13260

Experimental investigation of cyclic thermomechanical deformation in torsion
[NASA-TM-105938] p 247 N93-17996

DEGRADATION

Tensile strain-rate sensitivity of tungsten/nibium composites at 1300 to 1600 K
p 97 A93-14840

Isothermal aging effects on PMR-15 resin
p 131 A93-24508

Progressive delamination in polymer matrix composite laminates: A new approach
p 108 N93-21515

DEGREES OF FREEDOM

Membrane triangles with corner drilling freedoms. I - The EFF element
p 235 A93-24303

Membrane triangles with corner drilling freedoms. II - The ANDES element
p 235 A93-24304

Membrane triangles with corner drilling freedoms. III - Implementation and performance evaluation
p 236 A93-24305

DEICERS

Results of Low Power Deicer tests on a swept inlet component in the NASA Lewis Icing Research Tunnel
[AIAA PAPER 93-0032] p 20 A93-22551

Modeling and strain gauging of eddy current repulsion deicing systems
[AIAA PAPER 93-0296] p 20 A93-22696

Surface roughness due to residual ice in the use of low power deicing systems
[AIAA PAPER 93-0031] p 5 A93-23240

Numerical modeling of anti-icing systems and comparison to test results on a NACA 0012 airfoil
[AIAA PAPER 93-0170] p 21 A93-23242

Results of a low power ice protection system test and a new method of imaging data analysis
p 21 A93-35932

Efficient finite element method for aircraft deicing problems
p 21 A93-52443

Results of low power deicer tests on a swept inlet component in the NASA Lewis icing research tunnel
[NASA-TM-105968] p 15 N93-14911

Surface roughness due to residual ice in the use of low power deicing systems
[NASA-TM-105971] p 16 N93-15338

Numerical modeling of anti-icing systems and comparison to test results on a NASA 0012 airfoil
[NASA-TM-105975] p 19 N93-15345

DEICING

Results of Low Power Deicer tests on a swept inlet component in the NASA Lewis Icing Research Tunnel
[AIAA PAPER 93-0032] p 20 A93-22551

Aerodynamic effects of deicing and anti-icing fluids
p 19 A93-31929

Results of a low power ice protection system test and a new method of imaging data analysis
p 21 A93-35932

Efficient finite element method for aircraft deicing problems
p 21 A93-52443

Results of low power deicer tests on a swept inlet component in the NASA Lewis icing research tunnel
[NASA-TM-105968] p 15 N93-14911

DELAMINATING

Thermally-driven microfracture in high temperature metal matrix composites
p 237 A93-32469

Progressive matrix cracking in off-axis plies of a general symmetric laminate
[AIAA PAPER 93-1494] p 239 A93-34035

Fracture toughness testing of polymer matrix composites
[NASA-TP-3199] p 107 N93-12302

Progressive delamination in polymer matrix composite laminates: A new approach
p 108 N93-21515

DELTA WINGS

Adaptive computations of flow around a delta wing with vortex breakdown
[AIAA PAPER 93-3400] p 10 A93-47202

DEMAGNETIZATION

M-H characteristics and demagnetization resistance of samarium-cobalt permanent magnets to 300 C
p 153 A93-26076

DENDRITIC CRYSTALS

Thermosolutal convection during cellular arrayed growth of Pb-Sn alloys
[AIAA PAPER 93-0262] p 142 A93-22668

IDGE - A test of dendritic growth theory using space flight
[AIAA PAPER 93-0260] p 143 A93-25515

Melt infiltration of silicon carbide compacts. II - Evaluation of solidification microstructures
p 101 A93-28283

Thermosolutal convection during dendritic solidification of a binary alloy
p 182 A93-45975

Numerical model for dendritic solidification of binary alloys
p 282 A93-46729

Scientific basis for the Isothermal Dendritic Growth Experiment - A USMP-2 space flight experiment
p 143 A93-50455

On the drag of model dendrite fragments at low Reynolds number
[NASA-TM-105916] p 128 N93-19974

DENSIFICATION

Properties of extruded PS-212 type self-lubricating materials
p 138 N93-25565

DENSIMETERS

Experimental testing of four correction algorithms for the forward scattering spectrometer probe
[NASA-TM-105906] p 213 N93-13307

DENSITY (MASS/VOLUME)

Testing for the Gaussian nature of cosmological density perturbations through the three-point temperature correlation function
p 292 A93-55212

DENSITY DISTRIBUTION

Kurtosis, skewness, and non-Gaussian cosmological density perturbations
p 291 A93-35579

DENSITY MEASUREMENT

Gas temperature and density measurements based on spectrally resolved Rayleigh-Brillouin scattering
p 214 N93-13684

Characterization and durability testing of plasma-sprayed zirconia-yttria and hafnia-yttria thermal barrier coatings. Part 1: Effect of spray parameters on the performance of several lots of partially stabilized zirconia-yttria powder
[NASA-TP-3295] p 128 N93-22556

DEPLOYMENT

Design of deployable-truss masts for Space Station
[AIAA PAPER 93-0975] p 56 A93-30899

DEPOSITION

Optical and scratch resistant properties of diamondlike carbon films deposited with single and dual ion beams
p 137 N93-25564

Non-destructive, ultra-low resistance, thermally stable contacts for use on shallow junction InP solar cells
[NASA-TM-106228] p 256 N93-32201

DESIGN ANALYSIS

Stirling engine - Available tools for long-life assessment ... for space propulsion
p 65 A93-13824

Comparison of dynamic isotope power systems for distributed planetary surface applications
p 46 A93-13825

Shape reanalysis and sensitivities utilizing preconditioned iterative boundary solvers
p 233 A93-14446

- Maximum life spur gear design p 218 A93-14521
Design of an automated imaging system for use in a space experiment p 204 A93-20454
An improved numerical model for wave rotor design and analysis p 24 A93-23384
[AIAA PAPER 93-0482] p 24 A93-23384
75 Ah and 10 boilerplate nickel-hydrogen battery designs and test results p 253 A93-25948
Design of a cavity heat pipe receiver experiment p 173 A93-25985
Analysis and design of an ultrahigh temperature hydrogen-fueled MHD generator p 278 A93-49618
Design of an Advanced Expander Test Bed [AIAA PAPER 93-2133] p 48 A93-49952
Reliability assessment of thrust chamber cooling concepts using probabilistic analysis techniques [AIAA PAPER 93-2163] p 75 A93-49978
Validation test of 125 Ah advanced design IPV nickel-hydrogen flight cells p 78 A93-50822
Reliability analysis of laminated ceramic matrix composites using shell subelement techniques p 243 A93-55382
Maximum life spiral bevel reduction design [NASA-TM-105790] p 226 A93-10982
An improved numerical model for wave rotor design and analysis [NASA-TM-105915] p 33 A93-12418
Validation test of 125 Ah advanced design IPV nickel-hydrogen flight cells [NASA-TM-105912] p 81 A93-14079
Identification of propulsion systems [NASA-TM-106007] p 35 A93-20109
Application of artificial neural networks to the design optimization of aerospace structural components [NASA-TM-4389] p 247 A93-21831
Optimal design of composite hip implants using NASA technology p 257 A93-22188
Nuclear Engine System Simulation (NESS): Volume 1: Program user's guide [NASA-CR-191080] p 86 A93-23876
Radiator technology p 90 A93-26979
NEP systems model p 91 A93-26987
- DESIGN TO COST**
A comparison of nuclear thermal rocket development cost and schedule for piloted missions to Mars [AIAA PAPER 93-2263] p 44 A93-50057
- DESTRUCTIVE TESTS**
Hot fire test results of subscale tubular combustion chambers p 79 A93-10020
- DETECTION**
Using silicon diodes for detecting the liquid-vapor interface in hydrogen p 209 A93-37864
An analysis of gear fault detection methods as applied to pitting fatigue failure data [NASA-TM-105950] p 229 A93-27074
- DETONABLE GAS MIXTURES**
Effects of particulate radiation on premixed gas flames [AIAA PAPER 93-0711] p 114 A93-24806
Numerical study of shock-induced combustion in methane-air mixtures [AIAA PAPER 93-1917] p 184 A93-49783
- DETONATION**
Application of composite materials to impact-insensitive munitions p 97 A93-11459
- DETONATION WAVES**
Reaction zone structure for strong, weak overdriven, and weak underdriven oblique detonations p 178 A93-35492
- DIAGNOSIS**
Qualitative model-based diagnostics for rocket systems [AIAA PAPER 93-1779] p 72 A93-49674
Real-time diagnostics for a reusable rocket engine [NASA-TM-105792] p 266 A93-19018
Capabilities and constraints of combustion diagnostics in microgravity p 145 A93-20185
Selected microgravity combustion diagnostic techniques p 121 A93-20194
Flame spread across liquid pools p 122 A93-20209
High performance sapphire windows p 218 A93-22198
A fiber optic probe for the detection of cataracts p 257 A93-25593
Qualitative model-based diagnostics for rocket systems [NASA-TM-106234] p 51 A93-28052
- DIAMINES**
Substituted 1,1,1-triaryl 2,2,2-trifluoroethanes and processes for their synthesis [NASA-CASE-LEW-14345-7] p 95 A93-17412
- DIAMOND FILMS**
High quality flame deposited diamond films for infrared optical windows p 281 A93-40564
Thin film diamond microstructure applications p 209 A93-40580
- Computer modeling of a hot filament diamond deposition reactor p 94 A93-40618
Tribological evaluation and analysis of coating materials p 135 A93-52896
Friction and wear of plasma-deposited diamond films [NASA-TM-105926] p 136 A93-19035
- DIAMONDS**
Optical and scratch resistant properties of diamondlike carbon films deposited with single and dual ion beams p 137 A93-25564
- DIATOMIC MOLECULES**
Computer program for calculating and fitting thermodynamic functions [NASA-RP-1271] p 285 A93-12967
- DIELECTRIC PROPERTIES**
Experiments on the stability of a liquid bridge in an axial electric field p 177 A93-32617
- DIELECTRICS**
Vaporization heat transfer of dielectric liquids on a wick-covered surface [AIAA PAPER 93-0283] p 169 A93-22686
Effect of a dielectric overlay on a linearly tapered slot antenna excited by a coplanar waveguide p 155 A93-35649
Vaporization heat transfer of dielectric liquids on enhanced surfaces covered with screen wicks [AIAA PAPER 93-2835] p 182 A93-46572
- DIESEL ENGINES**
Intake flow modeling in a four stroke diesel using KIVA3 [AIAA PAPER 93-2952] p 183 A93-48146
Effect of out-of-roundness on the performance of a diesel engine connecting-rod bearing p 225 A93-52607
- DIFFERENCE EQUATIONS**
Direct calculations of waves in fluid flows using a high-order compact difference scheme [AIAA PAPER 93-0148] p 171 A93-24232
Central difference TVD schemes for time dependent and steady state problems p 188 A93-51183
- DIFFERENTIAL EQUATIONS**
Eno-Osher schemes for Euler equations [NASA-TM-105928] p 268 A93-15341
Turbulence modeling and experiments p 195 A93-15796
A critical analysis of the accuracy of several numerical techniques for combustion kinetic rate equations [NASA-TP-3315] p 34 A93-16941
- DIFFERENTIAL PULSE CODE MODULATION**
An all digital implementation of a modified Hamming net for video compression with prediction and quantization circuits p 148 A93-37038
- DIFFRACTION PATTERNS**
Temporal averaging in a turbulent environment - Compensation for phase drifts in phase shifting interferometry p 210 A93-44190
Vector formulation for interferogram surface fitting p 278 A93-55687
- DIFFUSE RADIATION**
Photovoltaic arrays for Martian surface power [IAF PAPER 92-0591] p 293 A93-13699
- DIFFUSION**
Reaction layer formation at the graphite/copper-chromium alloy interface p 100 A93-25105
Closed-amplitude diffusion of sulfur into Cd-doped InP substrates - Dependence of S profiles on diffusion temperature and time p 283 A93-51917
- DIFFUSION COEFFICIENT**
An alternative model for estimating liquid diffusion coefficients requiring no viscosity data [NASA-TM-106079] p 96 A93-23014
- DIFFUSION FLAMES**
Multigrid methods for numerical simulation of laminar diffusion flames [AIAA PAPER 93-0236] p 113 A93-22648
PDF approach for compressible turbulent reacting flows [AIAA PAPER 93-0087] p 170 A93-24229
Comparison of numerical model results with diffusion flames in microgravity [AIAA PAPER 93-0707] p 114 A93-24803
Structure of soot-containing laminar jet diffusion flames [AIAA PAPER 93-0708] p 114 A93-24804
Effects of gravity on the transition to turbulence of gas jet diffusion flames [AIAA PAPER 93-0710] p 114 A93-24805
Downward diffusion flame spread and extinction in variable gravitational fields - Lunar and Martian simulations [AIAA PAPER 93-0828] p 115 A93-24898
Asymptotic analysis for the burning of n-heptane droplets using a four-step reduced mechanism p 117 A93-41952
- Secondary atomization in the combustion of electrostatic sprays [AIAA PAPER 93-2332] p 118 A93-50110
Effects of buoyancy on laminar, transitional, and turbulent gas jet diffusion flames p 121 A93-20189
Soot formation and radiation in turbulent jet diffusion flames under normal and reduced gravity conditions p 121 A93-20192
Selected microgravity combustion diagnostic techniques p 121 A93-20194
On the structure of gaseous confined laminar diffusion flames: Numerical investigation [NASA-TM-106039] p 197 A93-21198
Structure of confined laminar spray diffusion flames: Numerical investigation [NASA-TM-106038] p 197 A93-22596
- DIFFUSION LENGTH**
Diffusion length variation in 0.5- and 3-MeV-proton-irradiated, heteroepitaxial indium phosphide solar cells [NASA-TM-106147] p 161 A93-27002
- DIFFUSION PUMPS**
New technique for oil backstreaming contamination measurements p 210 A93-44514
- DIFFUSION THEORY**
Diffusional transport and predicting oxidative failure during cyclic oxidation of beta-NiAl alloys p 126 A93-50370
On an origin of numerical diffusion: Violation of invariance under space-time inversion [NASA-TM-105776] p 268 A93-11254
- DIFFUSION WELDING**
Summary of the NASA Lewis component technology program for Stirling power converters [NASA-TM-105640] p 82 A93-15526
- DIFFUSIVITY**
An alternative model for estimating liquid diffusion coefficients requiring no viscosity data [NASA-TM-106079] p 96 A93-23014
- DIGITAL ELECTRONICS**
Mixed application MMIC technologies - Progress in combining RF, digital and photonic circuits p 152 A93-25800
- DIGITAL FILTERS**
2-D nonlinear IIR-filters for image processing - An exploratory analysis p 264 A93-28200
A 3-D nonlinear recursive digital filter for video image processing p 264 A93-34582
Modifying real convolutional codes for protecting digital filtering systems p 148 A93-38221
- DIGITAL SIMULATION**
Structural Tailoring/Analysis for Hypersonic Components - A computational simulation [AIAA PAPER 92-4722] p 20 A93-20324
Computational methods for efficient structural reliability and reliability sensitivity analysis [AIAA PAPER 93-1626] p 240 A93-34155
High resolution numerical simulation of the linearized Euler equations in conservation law form [AIAA PAPER 93-2934] p 183 A93-48132
Numerical simulation of a shock wave/turbulent boundary layer interaction in a duct [AIAA PAPER 93-3127] p 11 A93-48293
Modeling of turbulence and transition p 195 A93-15795
- DIGITAL SYSTEMS**
A free-piston Stirling engine/linear alternator controls and load interaction test facility p 146 A93-26077
ISDN at NASA Lewis Research Center [NASA-TM-105911] p 262 A93-12410
Satellites and the BISDN: An overview of NASA R/D [NASA-TM-106108] p 150 A93-26903
- DIGITAL TECHNIQUES**
A new hue capturing technique for the quantitative interpretation of liquid crystal images used in convective heat transfer studies p 204 A93-13977
An all digital implementation of a modified Hamming net for video compression with prediction and quantization circuits p 148 A93-37038
- DIGITAL TELEVISION**
Real-time transmission of digital video using variable-length coding [NASA-TM-106092] p 150 A93-22483
- DILUTION**
An analytical study of dilution jet mixing in a cylindrical duct [AIAA PAPER 93-2043] p 27 A93-49876
An analytical study of dilution jet mixing in a cylindrical duct [NASA-TM-106181] p 37 A93-27160
- DIMENSIONAL MEASUREMENT**
Progress in speckle-shift strain measurement p 251 A93-31558
- DIODES**
Using silicon diodes for detecting the liquid-vapor interface in hydrogen p 209 A93-37864

- DIRECT BROADCAST SATELLITES**
 Direct Broadcast Satellite: Radio Program
 [NASA-TM-105910] p 52 N93-11430
- DIRECTIONAL SOLIDIFICATION (CRYSTALS)**
 Initial study of void formation during aluminum solidification in reduced gravity p 142 A93-12013
 Effect of surface tension on the onset of convection in a double-diffusive layer p 163 A93-13951
 Coarsening following a morphological instability in the one-sided model p 284 A93-21695
 Thermosolutal convection during cellular arrayed growth of Pb-Sn alloys
 [AIAA PAPER 93-0262] p 142 A93-22668
 Effect of tensile mean stress on fatigue behavior of single-crystal and directionally solidified superalloys p 125 A93-33011
 Containerless automated processing of intermetallic compounds and composites p 144 A93-52183
- DIRECTIVITY**
 Directivity versus element spacing for a scanning array p 148 A93-36991
- DISCONTINUITY**
 The L sub 1 finite element method for pure convection problems p 177 A93-34326
 Full wave characterization of microstrip open end discontinuities patterned on anisotropic substrates using potential theory
 [NASA-TM-106037] p 160 N93-20259
- DISPLACEMENT**
 Modeling and strain gauging of eddy current repulsion deicing systems
 [AIAA PAPER 93-0296] p 20 A93-22696
 OTV bearing deflection investigation
 [NASA-TM-106085] p 215 N93-22994
- DISPLACEMENT MEASUREMENT**
 X-ray-based displacement measurement for hostile environments p 208 A93-28580
- DISPLAY DEVICES**
 Application of ray tracing in radiation heat transfer
 [NASA-TM-106206] p 202 N93-29075
- DISSIPATION**
 New time scale based k-epsilon model for near-wall turbulence p 180 A93-41909
 Consecutive plate acoustic suppressor apparatus and methods
 [NASA-CASE-LEW-15430-1] p 275 N93-17051
 A rapid-distortion-theory turbulence model for developed unsteady wall-bounded flow
 [NASA-TM-106249] p 203 N93-32199
- DISTORTION**
 Study on vortex flow control of inlet distortion p 2 A93-14520
 A rapid-distortion-theory turbulence model for developed unsteady wall-bounded flow
 [NASA-TM-106249] p 203 N93-32199
- DISTRIBUTED PARAMETER SYSTEMS**
 Confidence bounds on structural reliability
 [AIAA PAPER 93-1377] p 238 A93-33941
- DISTRIBUTION FUNCTIONS**
 Global/local methods for probabilistic structural analysis
 [AIAA PAPER 93-1378] p 238 A93-33942
- DOCUMENTATION**
 Bibliography of Lewis Research Center Technical Publications announced in 1991
 [NASA-TM-105595] p 287 N93-14796
- DOMES (STRUCTURAL FORMS)**
 Mixing in the dome region of a staged gas turbine combustor p 27 A93-49612
- DOPED CRYSTALS**
 Elevated temperature compressive properties of reaction milled NiAl-AIN and Zr-doped NiAl-AIN composites p 97 A93-11422
 Intermodulation in the oscillatory magnetoresistance of a two-dimensional electron gas p 151 A93-17610
 High-temperature deformation and microstructural analysis for silicon nitride-scandium(III) oxide p 131 A93-20468
 Room-temperature determination of two-dimensional electron gas concentration and mobility in heterostructures p 280 A93-35198
 Closed-ampoule diffusion of sulfur into Cd-doped InP substrates - Dependence of S profiles on diffusion temperature and time p 283 A93-51917
 Texturing of InP surfaces for device applications
 [NASA-TM-106061] p 129 N93-28618
- DOPPLER EFFECT**
 Liquid water content measurements using the Phase Doppler Particle Analyzer in the NASA Lewis Icing Research Tunnel
 [AIAA PAPER 93-0298] p 42 A93-23698
 Nonintrusive, multipoint velocity measurements in high-pressure combustion flows
 [AIAA PAPER 93-2032] p 118 A93-49867
- DOSIMETERS**
 Determination of atomic oxygen fluence using spectrophotometric analysis of infrared transparent witness coupons for long duration exposure tests
 [NASA-TM-106021] p 96 N93-22605
- DRAG**
 On the drag of model dendrite fragments at low Reynolds number
 [NASA-TM-105916] p 128 N93-19974
 Bounds on internal state variables in viscoplasticity
 [NASA-TM-106215] p 251 N93-29196
- DRAG COEFFICIENTS**
 An improved far field drag calculation method for nonlinear CFD codes
 [AIAA PAPER 93-3417] p 10 A93-47213
- DRIFT (INSTRUMENTATION)**
 Thin film thermocouples for high temperature measurement on ceramic materials p 213 N93-13666
- DROP SIZE**
 Experiments on the effect of initial diameter in spherically symmetric droplet combustion of sooting fuels
 [AIAA PAPER 93-0130] p 139 A93-22577
 LEWICE droplet trajectory calculations on a parallel computer
 [AIAA PAPER 93-0172] p 259 A93-22604
 Effect of vaporization on cryogenic spray droplet size measurement
 [AIAA PAPER 93-0692] p 172 A93-24792
 Experimental study of two interacting drops in an immiscible fluid p 179 A93-37936
 Secondary atomization in the combustion of electrostatic sprays
 [AIAA PAPER 93-2332] p 118 A93-50110
 Calibration of the forward-scattering spectrometer probe - Modeling scattering from a multimode laser beam p 212 A93-51239
 Droplet vaporization in a high-pressure gas p 190 A93-55461
 Coaxial injector spray characterization using water/air as simulants p 120 N93-11452
 Effect of vaporization on cryogenic spray droplet size measurement
 [NASA-TM-105909] p 213 N93-13410
 Structure of confined laminar spray diffusion flames: Numerical investigation
 [NASA-TM-106038] p 197 N93-22596
 Velocity and drop size measurements in a swirl-stabilized, combustor spray
 [NASA-TM-106130] p 37 N93-27130
- DROP TOWERS**
 Finite element calculations of transonic flutter in cascades
 [AIAA PAPER 93-2083] p 185 A93-49910
 Capabilities and constraints of NASA's ground-based reduced gravity facilities p 49 N93-20184
 Capabilities and constraints of combustion diagnostics in microgravity p 145 N93-20185
 Opposed-flow flame spreading in reduced gravity p 121 N93-20206
 Contributions of microgravity test results to the design of spacecraft fire safety systems
 [NASA-TM-106093] p 60 N93-24755
- DROPS (LIQUIDS)**
 Supercritical droplet combustion and related transport phenomena
 [AIAA PAPER 93-0812] p 115 A93-24885
 Soot agglomeration in isolated, free droplet combustion
 [AIAA PAPER 93-0823] p 115 A93-24893
 Computational/experimental basis for conducting alkane droplet combustion experiments on space-based-platforms p 117 A93-41711
 Collective effects of temperature gradients and gravity on droplet coalescence p 183 A93-46716
 Effects of detailed droplet heating models on turbulent sprays vaporization behavior
 [AIAA PAPER 93-2193] p 185 A93-50005
 Atomizing-gas temperature effect on cryogenic spray droplet size
 [AIAA PAPER 93-2333] p 186 A93-50111
 Experimental testing of four correction algorithms for the forward scattering spectrometer probe
 [NASA-TM-105906] p 213 N93-13307
 Combustion of interacting droplet arrays in a microgravity environment p 122 N93-20217
 Atomizing-gas temperature effect on cryogenic spray droplet size
 [NASA-TM-106106] p 216 N93-25191
- DUCT GEOMETRY**
 Some aspects of bifurcation structure of laminar flow in curved ducts p 164 A93-14771
 An experimental investigation of S-duct flow control using arrays of low-profile vortex generators
 [AIAA PAPER 93-0018] p 170 A93-24226
- Computational study of advanced exhaust system transition ducts with experimental validation p 7 A93-34490
- DUCTED FAN ENGINES**
 Acoustic mode measurements in the inlet of a model turbofan using a continuously rotating rake
 [AIAA PAPER 93-0598] p 273 A93-24783
 Acoustic mode measurements in the inlet of a model turbofan using a continuously rotating rake
 [NASA-TM-105989] p 34 N93-16705
- DUCTED FANS**
 Comparison of radiated noise from shrouded and unshrouded propellers p 274 A93-55861
- DUCTED FLOW**
 Study on vortex flow control of inlet distortion p 2 A93-14520
 Optimization of circular orifice jets mixing into a heated crossflow in a cylindrical duct
 [AIAA PAPER 93-0249] p 24 A93-23246
 An experimental investigation of S-duct flow control using arrays of low-profile vortex generators
 [AIAA PAPER 93-0018] p 170 A93-24226
 Navier-Stokes analysis of three-dimensional S-ducts p 9 A93-45146
 A three-dimensional pressure flux-split RNS application to sub/supersonic flow in inlets and ducts
 [AIAA PAPER 93-3063] p 11 A93-48239
 Experimental and numerical investigation of supersonic turbulent flow in an annular duct
 [AIAA PAPER 93-3123] p 11 A93-48291
 Numerical simulation of a shock wave/turbulent boundary layer interaction in a duct
 [AIAA PAPER 93-3127] p 11 A93-48293
 Investigation of a strut/endwall interaction in supersonic annular flow
 [AIAA PAPER 93-1925] p 12 A93-49791
 Experimental investigation of crossflow jet mixing in a rectangular duct
 [AIAA PAPER 93-2037] p 185 A93-49872
 CFD mixing analysis of axially opposed rows of jets injected into confined crossflow
 [AIAA PAPER 93-2044] p 185 A93-49877
 A comparative study of Full Navier-Stokes and Reduced Navier-Stokes analyses for separating flows within a diffusing inlet S-duct
 [AIAA PAPER 93-2154] p 13 A93-49970
 An experimental investigation of the flow in a diffusing S-duct
 [NASA-TM-105809] p 32 N93-12077
 Optimization of circular orifice jets mixing into a heated cross flow in a cylindrical duct
 [NASA-TM-105984] p 33 N93-15359
 An experimental investigation of S-duct flow control using arrays of low-profile vortex generators
 [NASA-TM-106030] p 17 N93-19968
 Transient liquid-crystal technique used to produce high-resolution convective heat-transfer-coefficient maps
 [NASA-TM-106083] p 198 N93-23404
 Experimental investigation of crossflow jet mixing in a rectangular duct
 [NASA-TM-106152] p 36 N93-27026
 CFD mixing analysis of axially opposed rows of jets injected into confined crossflow
 [NASA-TM-106179] p 37 N93-27128
 A numerical study of confined turbulent jets
 [NASA-TM-106197] p 202 N93-29161
 Summary of NASA Lewis Research Center validation efforts p 204 N93-70579
- DUCTILITY**
 Transverse ductility of metal matrix composites p 101 A93-31355
 Ductility of a continuous fiber reinforced aluminum matrix composite p 102 A93-32471
 Progress toward a tungsten alloy wire/high temperature alloy composite turbine blade
 [NASA-TM-105901] p 128 N93-15586
- DUCTS**
 Study on vortex flow control of inlet distortion p 2 A93-14520
 Calculations of separated 3-D flows with a pressure-staggered Navier-Stokes equations solver p 177 A93-34366
 An experimental investigation of S-duct flow control using arrays of low-profile vortex generators
 [NASA-TM-106030] p 17 N93-19968
- DURABILITY**
 Structural durability of a composite pressure vessel p 234 A93-16552
 Relative sliding durability of two candidate high-temperature oxide fiber seal materials p 132 A93-31983
 Durability testing of the AJ10-221 490 N high performance (321 sec lps) engine
 [AIAA PAPER 93-2130] p 74 A93-49949

DUST

- Relative sliding durability of candidate high temperature fiber seal materials
[NASA-TM-105806] p 95 N93-10978
- Issues/considerations and performance prediction of LEO protective coatings p 137 N93-20813
- Sliding durability of candidate seal fiber materials in hydrogen from 25 to 900 C
[NASA-TM-105939] p 95 N93-22590
- Low Earth orbital atomic oxygen environmental simulation facility for space materials evaluation
[NASA-TM-106128] p 96 N93-27266

DUST

- Effects of dust accumulation and removal on radiator surfaces on Mars p 123 A93-13937

DUST STORMS

- Photovoltaic arrays for Martian surface power
[IAF PAPER 92-0591] p 293 A93-13699
- Lunar and Martian environmental interactions with nuclear power system radiators
[NASA-TM-105747] p 80 N93-10965
- Degradation of radiator performance on Mars due to dust p 59 N93-15616

DYNAMIC CHARACTERISTICS

- Dynamic analysis of a pre-and-post ice impacted blade
[AIAA PAPER 92-4273] p 22 A93-13333
- Nonlinear dynamic simulation of single- and multi-spool core engines
[AIAA PAPER 93-2580] p 30 A93-50294
- Global dynamic modeling of a transmission system
[NASA-CR-191117] p 228 N93-24751
- Dynamic characteristics of specialty composite structures with embedded damping layers
[NASA-TM-106165] p 110 N93-26705

DYNAMIC CONTROL

- Space Station Freedom beta gimbal control via sensitivity models
[NASA-TM-106000] p 60 N93-22551

DYNAMIC LOADS

- Stiffness of magnetic bearings subjected to combined static and dynamic loads
[ASME PAPER 91-TRIB-27] p 219 A93-15685
- The application of structural reliability techniques to plume impingement loading of the Space Station Freedom Photovoltaic Array
[AIAA PAPER 93-1338] p 56 A93-33908
- A parallel dynamic load balancing algorithm for 3-D adaptive unstructured grids
[AIAA PAPER 93-3313] p 260 A93-45009
- Effect of extended tooth contact on the modeling of spur gear transmissions
[AIAA PAPER 93-2148] p 223 A93-49965
- Dynamic analysis of spur gears using computer program DANST
[AIAA PAPER 93-2295] p 224 A93-50080
- Root damage analysis of aircraft engine blade subject to ice impact
[NASA-TM-105779] p 246 N93-15343
- The application of structural reliability techniques to plume impingement loading of the Space Station Freedom Photovoltaic Array
[NASA-TM-105949] p 59 N93-17988
- Dynamic analysis of Free-Piston Stirling Engine/Linear Alternator-load system experimentally validated
[NASA-TM-106034] p 271 N93-22559
- Dynamic analysis of spur gears using computer program DANST
[NASA-TM-106211] p 230 N93-28050
- Effect of extended tooth contact on the modeling of spur gear transmissions
[NASA-TM-106174] p 230 N93-28411
- Localization of aeroelastic modes in mistuned high-energy turbines p 230 N93-31586

DYNAMIC MODELS

- Dynamic modeling and control of multibody mechanical systems which are structurally flexible
p 264 A93-29338
- Modal simulation of gear box vibration with experimental correlation p 221 A93-31982
- Reaction zone structure for strong, weak overdriven, and weak underdriven oblique detonations
p 178 A93-35492
- Identification of the open loop dynamics of the T700 turboshaft engine p 26 A93-35934
- Effect of extended tooth contact on the modeling of spur gear transmissions
[AIAA PAPER 93-2148] p 223 A93-49965
- COLD-SAT dynamic model
[NASA-TM-105185] p 59 N93-19988
- Effect of extended tooth contact on the modeling of spur gear transmissions
[NASA-TM-106174] p 230 N93-28411

DYNAMIC PRESSURE

- User manual for NASA Lewis 10 by 10 foot supersonic wind tunnel
[NASA-TM-105626] p 42 N93-15498

DYNAMIC RESPONSE

- Semi-empirical model for prediction of unsteady forces on an airfoil with application to flutter p 7 A93-31494
- The application of structural reliability techniques to plume impingement loading of the Space Station Freedom Photovoltaic Array
[AIAA PAPER 93-1338] p 56 A93-33908
- Dynamics of rotating multicomponent turbomachinery systems
[AIAA PAPER 93-1629] p 222 A93-34157
- Stochastic sensitivity measure for mistuned high-performance turbines
[NASA-TM-105821] p 245 N93-12277
- The application of structural reliability techniques to plume impingement loading of the Space Station Freedom Photovoltaic Array
[NASA-TM-105949] p 59 N93-17988
- Dynamics of rotating multi-component turbomachinery systems
[NASA-TM-105997] p 247 N93-18426

DYNAMIC STABILITY

- Dynamic analysis of Free-Piston Stirling Engine/Linear Alternator-load system experimentally validated
[NASA-TM-106034] p 271 N93-22559

DYNAMIC STRUCTURAL ANALYSIS

- Modal test/analysis correlation of Space Station structures using nonlinear sensitivity
[AIAA PAPER 92-4731] p 55 A93-20330
- Probabilistic structural analysis of space truss structures for nonuniform thermal environmental effects
[AIAA PAPER 92-4769] p 235 A93-20363
- Design considerations for a Space Shuttle Main Engine turbine blade made of single crystal material
p 236 A93-25228
- Semi-empirical model for prediction of unsteady forces on an airfoil with application to flutter p 7 A93-31494
- Effects of interply damping layers on the dynamic characteristics of composite plates p 237 A93-32415
- Dynamics of rotating multicomponent turbomachinery systems
[AIAA PAPER 93-1629] p 222 A93-34157
- Unsteady aerodynamics and flutter of propfans using a three-dimensional Full-Potential Solver
[AIAA PAPER 93-1633] p 25 A93-34161
- On the static stability of forward swept propfans
[AIAA PAPER 93-1634] p 26 A93-34162
- Unsteady aerodynamics and flutter based on the potential equation
[AIAA PAPER 93-2086] p 13 A93-49913
- Vibration and noise analysis of a gear transmission system
[AIAA PAPER 93-2150] p 224 A93-49967
- Self-organization in neural networks - Applications in structural optimization p 265 A93-54534
- Dynamics of rotating multi-component turbomachinery systems
[NASA-TM-105997] p 247 N93-18426
- Structural dynamic testing of composite propfan blades for a cruise missile wind tunnel model
[NASA-TM-105272] p 247 N93-18875
- Structural dynamics branch research and accomplishments to FY 1992
[NASA-TM-105824] p 247 N93-20368
- Implementation of the block-Krylov boundary flexibility method of component synthesis
[NASA-TM-106065] p 248 N93-23044
- Dynamic characteristics of specialty composite structures with embedded damping layers
[NASA-TM-106165] p 110 N93-26705
- A transfer matrix approach to vibration localization in mistuned blade assemblies
[NASA-TM-106112] p 250 N93-27088
- Vibration and noise analysis of a gear transmission system
[NASA-TM-106162] p 229 N93-27641
- Structural Integrity and Durability of Reusable Space Propulsion Systems
[NASA-CP-10064] p 93 N93-31552
- Structural dynamics: Probabilistic structural analysis methods. Program overview p 251 N93-31562
- DYNAMIC TESTS**
- Structural dynamic testing of composite propfan blades for a cruise missile wind tunnel model
[NASA-TM-105272] p 247 N93-18875
- DYNAMICAL SYSTEMS**
- Dynamic modeling and control of multibody mechanical systems which are structurally flexible
p 264 A93-29338

E

EARTH MAGNETOSPHERE

- Transfer Orbit Plasma Interaction Experiment
(TROPIX) p 45 N93-28734

EARTH ORBITAL ENVIRONMENTS

- Small experiments for the maturation of orbital cryogenic transfer technologies
[IAF PAPER 92-0777] p 64 A93-13698
- On-orbit characterization of electric propulsion on LEO satellites p 67 A93-25303
- Indium phosphide solar cells for laser power beaming applications p 252 A93-25899
- Low earth simulation and materials characterization
p 44 A93-32293
- Space Station Freedom structure floating potential and the probability of arcing p 57 A93-39265
- Performance and properties of atomic oxygen protective coatings for polymeric materials p 225 A93-53389
- LDEF yaw and pitch angle estimates p 58 N93-12772
- Low Earth orbit atomic oxygen simulation for durability evaluation of solar reflector surfaces p 58 N93-15594
- Simulation of the synergistic low Earth orbit effects of vacuum thermal cycling, vacuum UV radiation, and atomic oxygen p 58 N93-15595
- The use of plasma ashers and Monte Carlo modeling for the projection of atomic oxygen durability of protected polymers in low Earth orbit p 58 N93-15596
- Leveling coatings for reducing the atomic oxygen defect density in protected graphite fiber epoxy composites
p 59 N93-15597
- Issues/considerations and performance prediction of LEO protective coatings p 137 N93-20813
- Recommended practices for in-space and ground laboratory. Atomic oxygen exposure and analysis
p 276 N93-20814
- Plasma current collection of Z-93 thermal control paint as measured in the Lewis Research Center's plasma interaction facility
[NASA-TM-106132] p 61 N93-26215
- The effects of simulated low Earth orbit environments on spacecraft thermal control coatings
[NASA-TM-106146] p 61 N93-27019
- Low Earth orbital atomic oxygen environmental simulation facility for space materials evaluation
[NASA-TM-106128] p 96 N93-27266
- Monte Carlo modeling of atomic oxygen attack of polymers with protective coatings on LDEF
p 138 N93-28282
- Solar Array Module Plasma Interaction Experiment (SAMPIE) p 62 N93-28716
- The Photovoltaic Array Space Power Plus diagnostics (PASP Plus) flight experiment p 256 N93-28717
- The effect of the low Earth orbit environment on space solar cells: Results of the Advanced Photovoltaic Experiment (S0014) p 256 N93-29686
- EARTH TERMINALS**
- Analysis of MMIC arrays for use in the ACTS Aero Experiment
[NASA-TM-106073] p 53 N93-22589
- EARTH-MARS TRAJECTORIES**
- The QED engine spectrum - Fusion-electric propulsion for air-breathing to interstellar flight
[AIAA PAPER 93-2006] p 73 A93-49845
- ECONOMIC FACTORS**
- Engine technology challenges for a 21st Century High-Speed Civil Transport
[ISABE 93-7064] p 31 A93-54040
- Engine technology challenges for a 21st Century High-Speed Civil Transport
[NASA-TM-106216] p 39 N93-31671
- EDDY CURRENTS**
- Modeling and strain gauging of eddy current repulsion deicing systems
[AIAA PAPER 93-0296] p 20 A93-22696
- EDDY VISCOSITY**
- A multiple-scale turbulence model for incompressible flow
[AIAA PAPER 93-0086] p 170 A93-24228
- New time scale based k-epsilon model for near-wall turbulence p 180 A93-41909
- Second order closure modeling of turbulent buoyant wall plumes
[NASA-TM-105956] p 193 N93-14829
- A multiple-scale model for compressible turbulent flows
[NASA-TM-106072] p 198 N93-23736
- EDUCATION**
- Design and implementation of a pilot orientation program for new NASA engineering employees
[NASA-TM-105907] p 286 N93-26205
- Efficient fault diagnosis of helicopter gearboxes
[NASA-TM-106253] p 231 N93-31846
- EFFERVESCENCE**
- Influence of ambient air pressure on effervescent atomization
[AIAA PAPER 92-0460] p 167 A93-21652
- EIGENVALUES**
- The eigenvalue spectrum of the Rayleigh equation for a plane shear layer p 168 A93-21725

- An efficient procedure for cascade aeroelastic stability determination using nonlinear, time-marching aerodynamic solvers
[AIAA PAPER 93-1631] p 25 A93-34159
- EIGENVECTORS**
Modal ring method for the scattering of electromagnetic waves
[NASA-TM-105966] p 149 N93-20260
Implementation of the block-Krylov boundary flexibility method of component synthesis
[NASA-TM-106065] p 248 N93-23044
- EJECTORS**
Initial development of the two-dimensional ejector shear layer - Experimental results
[AIAA PAPER 93-2440] p 29 A93-50192
Comparison of the initial development of shear layers in two-dimensional and axisymmetric ejector configurations
[AIAA PAPER 93-2441] p 29 A93-50193
Experimental investigation of an ejector-powered free-jet facility
[NASA-TM-105868] p 16 N93-16704
A full-scale STOVL ejector experiment
[NASA-TM-106019] p 35 N93-22480
- ELASTIC BODIES**
Calculation of stiffness and damping coefficients for elastically supported gas foil bearings
p 221 A93-27308
Variation of the energy release rate as a crack approaches and passes through an elastic inclusion
p 241 A93-44440
Analysis of large quasistatic deformations of inelastic solids by a new stress based finite element method
[NASA-CR-189235] p 246 N93-13260
- ELASTIC DEFORMATION**
Room temperature cyclic deformation behavior of cast and extruded NiAl
p 122 A93-12130
Dynamic analysis of flexible gear trains/transmissions - An automated approach
p 220 A93-22440
Effect of extended tooth contact on the modeling of spur gear transmissions
[AIAA PAPER 93-2148] p 223 A93-49965
Effect of extended tooth contact on the modeling of spur gear transmissions
[NASA-TM-106174] p 230 N93-28411
- ELASTIC PROPERTIES**
Ultrasonic and micromechanical study of damage and elastic properties of SiC/RBSN ceramic composites --- Reaction Bonded Silicon Nitride
p 99 A93-19624
Computational micromechanics of woven composites
p 237 A93-32462
Hot fire fatigue testing results for the compliant combustion chamber
p 79 N93-10038
Calculation of stress intensity factors in an isotropic multiaxial plate. Part 1: Theoretical development
[NASA-TM-105766] p 244 N93-10455
Hot fire fatigue testing results for the compliant combustion chamber
[NASA-TP-3223] p 80 N93-10743
The influence of primary and secondary orientations on the elastic response of a nickel-base single-crystal superalloy
[NASA-TM-106125] p 250 N93-26550
Explicit robust schemes for implementation of a class of principal value-based constitutive models: Symbolic and numeric implementation
[NASA-TM-106124] p 258 N93-26946
Explicit robust schemes for implementation of general principal value-based constitutive models
[NASA-TM-106123] p 258 N93-26947
Secondary orientation effects in a single crystal superalloy under mechanical and thermal loads
p 130 N93-31578
- ELASTIC SHELLS**
Layout optimization using the homogenization method
p 243 A93-54508
- ELASTODYNAMICS**
Micromechanical studies of composites by BEM
p 236 A93-31295
- ELASTOPLASTICITY**
Limit pressure of a circumferentially reinforced SiC/Ti ring
p 233 A93-16005
Analysis of large quasistatic deformations of inelastic solids by a new stress based finite element method
[NASA-CR-189235] p 246 N93-13260
- ELECTRIC ARCS**
NASA requirements and applications environments for electrical power wiring
p 153 A93-25919
Arcing rates for High Voltage Solar Arrays - Theory, experiment, and predictions
p 70 A93-32567
Space Station Freedom structure floating potential and the probability of arcing
p 57 A93-39265
Space environmental interactions for the space exploration initiative
p 293 N93-26396

ELECTRIC BATTERIES

- Electric and hybrid electric vehicle study utilizing a time-stepping simulation
p 287 A93-26012
Electrical design of payload G-534: The Pool Boiling Experiment
p 144 N93-13170
Lewis Research Center battery overview
p 255 N93-20493

ELECTRIC BRIDGES

- Experiments on the stability of a liquid bridge in an axial electric field
p 177 A93-32617
A 1.6-kW, 110-kHz dc-dc converter optimized for IGBT's
p 156 A93-37570
A 10 kW dc-dc converter using IGBTs with active snubbers --- Insulated Gate Bipolar Transistor
p 158 A93-50646

ELECTRIC CONDUCTORS

- Modal ring method for the scattering of electromagnetic waves
[NASA-TM-105966] p 149 N93-20260
Apparatus for intercalating large quantities of fibrous structures
[NASA-CASE-LEW-15077-2] p 111 N93-29609

ELECTRIC CONNECTORS

- Service equipment for use in hostile environments
[NASA-CASE-LEW-14906-2] p 230 N93-31314

ELECTRIC CONTACTS

- The structural and electrical properties of low-resistance Ni contacts to InP
p 151 A93-24367
Low resistance silver contacts to indium phosphide - Electrical and metallurgical considerations
p 157 A93-39351

ELECTRIC DISCHARGES

- The QED engine spectrum - Fusion-electric propulsion for air-breathing to interstellar flight
[AIAA PAPER 93-2006] p 73 A93-49845
Electrical and Chemical Interactions at Mars Workshop. Part 2: Appendix
[NASA-CP-10093-PT-2] p 293 N93-26392
Space environmental interactions for the space exploration initiative
p 293 N93-26396

ELECTRIC ENERGY STORAGE

- Electrical power system WP-04
p 161 N93-27804
Alkali metal carbon dioxide electrochemical system for energy storage and/or conversion of carbon dioxide to oxygen
[NASA-CASE-LEW-14973-1] p 256 N93-28974

ELECTRIC FIELDS

- Experiments on the stability of a liquid bridge in an axial electric field
p 177 A93-32617
Secondary atomization in the combustion of electrostatic sprays
[AIAA PAPER 93-2332] p 118 A93-50110

ELECTRIC GENERATORS

- Optimization of closed Brayton cycles for space power generation
p 68 A93-25859
Comparison of all-electric secondary power systems for civil transport
p 24 A93-25997
Comparison of all-electric secondary power systems for civil subsonic transports
[NASA-TM-105852] p 32 N93-10456

ELECTRIC MOTOR VEHICLES

- Electromechanical systems with transient high power response operating from a resonant ac link
p 152 A93-25892
Electric and hybrid electric vehicle study utilizing a time-stepping simulation
p 287 A93-26012

ELECTRIC POTENTIAL

- Energy loss analysis of an integrated space power distribution system
p 68 A93-25958
Plasma contactor technology for Space Station Freedom
[AIAA PAPER 93-2228] p 57 A93-50034
Effects of anode material on arcjet performance
p 79 N93-10044
Effects of anode material on arcjet performance
[NASA-TM-105799] p 79 N93-10197
Energy loss analysis of an integrated space power distribution system
[NASA-TM-105772] p 141 N93-14834
Changes in impedance of Ni/Cd cells with voltage and cycle life
[NASA-TM-106105] p 255 N93-23018

ELECTRIC POWER

- Power system technology discipline
p 62 N93-27862

ELECTRIC POWER SUPPLIES

- Design and emplacement of an integrated lunar power system - Issues and concerns
p 46 A93-13908
Comparison of all-electric secondary power systems for civil transport
p 24 A93-25997
PEM fuel cell stack heat and mass management
p 253 A93-26024
Electrical characterization of a Space Station Freedom alpha utility transfer assembly
p 56 A93-26101
Analysis and design of an ultrahigh temperature hydrogen-fueled MHD generator
p 278 A93-49618

- Simplified power processing for inert gas ion thrusters
[AIAA PAPER 93-2397] p 76 A93-50162
Comparison of all-electric secondary power systems for civil subsonic transports
[NASA-TM-105852] p 32 N93-10456
Electrical design of payload G-534: The Pool Boiling Experiment
p 144 N93-13170
Advanced photovoltaic power system technology for lunar base applications
p 255 N93-14004
Modelling a single phase voltage controlled rectifier using Laplace transforms
[NASA-TM-106005] p 271 N93-23016

ELECTRIC POWER TRANSMISSION

- A study of electric power transmission lines for use on the lunar surface
p 46 A93-13901

ELECTRIC PROPULSION

- On-orbit characterization of electric propulsion on LEO satellites
p 67 A93-25303
Development and flight history of the SERT II spacecraft
p 71 A93-38976
Measurement and analysis of a small nozzle plume in vacuum
p 71 A93-42895
The NASA Electric Propulsion Program
[AIAA PAPER 93-1935] p 73 A93-49797
The QED engine spectrum - Fusion-electric propulsion for air-breathing to interstellar flight
[AIAA PAPER 93-2006] p 73 A93-49845
Preliminary investigation of high power microwave plasmas for electrothermal thruster use
[AIAA PAPER 93-2106] p 74 A93-49928
Plasma contactor technology for Space Station Freedom
[AIAA PAPER 93-2228] p 57 A93-50034
EOTV propellant tank pressure control and liquid dynamics
[AIAA PAPER 93-2399] p 77 A93-50164
BMDO electric space-propulsion program
[AIAA PAPER 93-1934] p 78 A93-50322
Electric propulsion - An evolutionary technology
p 78 A93-56168
Preliminary characterization of a water vaporizer for resistojet applications
[NASA-TM-105877] p 80 N93-11402
Ion thruster development at NASA Lewis Research Center
[NASA-TM-105983] p 82 N93-15429
Space transfer with ground-based laser/electric propulsion
[NASA-TM-106060] p 84 N93-20615
100-kW class applied-field MPD thruster component wear
[NASA-TM-106023] p 85 N93-22482
Measurement and analysis of a small nozzle plume in vacuum
[NASA-TM-106066] p 88 N93-26561
Preliminary investigation of high power microwave plasmas for electrothermal thruster use
[NASA-TM-106207] p 92 N93-29158
- ELECTRIC ROCKET ENGINES**
100-kW class applied-field MPD thruster component wear
[NASA-TM-106023] p 85 N93-22482
NEP technology: FY 1992 milestones (NASA LeRC)
p 90 N93-26977

ELECTRIC SWITCHES

- Neutron, gamma ray, and temperature effects on the electrical characteristics of thyristors
p 153 A93-25894
A 10 kW dc-dc converter using IGBTs with active snubbers --- Insulated Gate Bipolar Transistor
p 158 A93-50646

ELECTRIC WIRE

- Measurement of frequency response in short thermocouple wires
p 209 A93-40677

ELECTRICAL FAULTS

- Electrical and Chemical Interactions at Mars Workshop. Part 2: Appendix
[NASA-CP-10093-PT-2] p 293 N93-26392

ELECTRICAL IMPEDANCE

- Hydrodynamic behavior and electrochemical impedance of the Hanging Meniscus Rotating Disk (HMRD) electrode. I - Meniscus shape under rotation. II - I-BIEM calculations of frequency dispersion and minimization
p 116 A93-34247
Input impedance of coaxially fed rectangular microstrip antenna on electrically thick substrate
p 155 A93-36994
Changes in impedance of Ni/Cd cells with voltage and cycle life
[NASA-TM-106105] p 255 N93-23018

ELECTRICAL INSULATION

- Damping and scattering of electromagnetic waves by small ferrite spheres suspended in an insulator
[NASA-TM-105837] p 149 N93-12366

ELECTRICAL MEASUREMENT

A system to measure lightning-induced transients on spacecraft umbilical lines p 161 N93-24889

ELECTRICAL PROPERTIES

Neutron, gamma ray, and temperature effects on the electrical characteristics of thyristors p 153 A93-25894

Greatly improved 3C-SiC p-n junction diodes grown by chemical vapor deposition p 156 A93-38994

Processing, electrical and microwave properties of sputtered Ti-Ca-Ba-Cu-O superconducting thin films p 282 A93-44607

Electrical and Chemical Interactions at Mars Workshop. Part 2: Appendix [NASA-CP-10093-PT-2] p 293 N93-26392

ELECTRICAL RESISTANCE

Comparative study of bolometric and non-bolometric switching elements for microwave phase shifters p 155 A93-27245

ELECTRICAL RESISTIVITY

Novel coplanar waveguide to slotline transition on high resistivity silicon p 151 A93-20016

High temperature static strain measurement with an electrical resistance strain gage [AIAA PAPER 92-5039] p 205 A93-22313

Composition dependence of superconductivity in YBa₂(Cu_{3-x}Al(x))O_y p 281 A93-40271

Diminishing sign anomaly and scaling behavior of the mixed-state Hall resistivity in Ti₂Ba₂Ca₂Cu₃O₁₀ films containing columnar defects p 283 A93-53693

Method for producing hybrid graphite composite [NASA-CASE-LEW-15241-2] p 112 N93-31296

Non-destructive, ultra-low resistance, thermally stable contacts for use on shallow junction InP solar cells [NASA-TM-106228] p 256 N93-32201

ELECTRO-OPTICS

Status of the Fiber Optic Control System Integration (FOCSI) program [NASA-TM-106151] p 217 N93-28053

ELECTROCHEMICAL CELLS

Lewis Research Center battery overview p 255 N93-20493

Alkali metal carbon dioxide electrochemical system for energy storage and/or conversion of carbon dioxide to oxygen [NASA-CASE-LEW-14973-1] p 256 N93-28974

ELECTROCHEMISTRY

A survey and analysis of commercially available hydrogen sensors [NASA-TM-105878] p 214 N93-17777

ELECTRODE MATERIALS

Pressure dependence of the oxygen reduction reaction at the platinum microelectrode/naion interface - Electrode kinetics and mass transport p 112 A93-11450

Lightweight nickel electrodes for nickel/hydrogen cells p 255 A93-51574

ELECTRODEPOSITION

Chronopotentiometry of refractory metals, actinides and oxanions in molten salts: A review [NASA-TM-105862] p 120 N93-11545

ELECTRODES

I-BIEM calculations of the frequency dispersion and ac current distribution at disk and ring-disk electrodes p 254 A93-34246

Hydrodynamic behavior and electrochemical impedance of the Hanging Meniscus Rotating Disk (HM-RD) electrode. I - Meniscus shape under rotation. II - I-BIEM calculations of frequency dispersion and minimization p 116 A93-34247

ELECTROMAGNETIC COUPLING

Novel coplanar waveguide to slotline transition on high resistivity silicon p 151 A93-20016

ELECTROMAGNETIC FIELDS

A reciprocity formulation for the EM scattering by an obstacle within a large open cavity p 149 A93-52237

ELECTROMAGNETIC INTERFERENCE

Intercalated graphite fiber composites as EMI shields in aerospace structures p 104 A93-41573

Multiwavelength pyrometer for gray and non-gray surfaces in the presence of interfering radiation [NASA-CASE-LEW-15250-1] p 214 N93-17060

ELECTROMAGNETIC PROPULSION

Electromagnetic powered vehicles (EMPV) for Mars exploration p 47 A93-20761

Electromagnetic propulsion for spacecraft [AIAA PAPER 93-1086] p 69 A93-30975

ELECTROMAGNETIC PULSES

EMTP based stability analysis of Space Station Electric Power System in a test bed environment p 154 A93-26108

EMTP based stability analysis of space station electric power system in a test bed environment [NASA-TM-105845] p 160 N93-15503

ELECTROMAGNETIC RADIATION

Modal ring method for the scattering of electromagnetic waves [NASA-TM-105966] p 149 N93-20260

ELECTROMAGNETIC SCATTERING

A reciprocity formulation for the EM scattering by an obstacle within a large open cavity p 149 A93-52237

Damping and scattering of electromagnetic waves by small ferrite spheres suspended in an insulator [NASA-TM-105837] p 149 N93-12366

Modal ring method for the scattering of electromagnetic waves [NASA-TM-105966] p 149 N93-20260

ELECTROMAGNETIC SHIELDING

Intercalated graphite fiber composites as EMI shields in aerospace structures p 104 A93-41573

ELECTROMAGNETS

M-H characteristics and demagnetization resistance of samarium-cobalt permanent magnets to 300 C p 153 A93-26076

ELECTROMECHANICAL DEVICES

An electromechanical actuation system for an expendable launch vehicle p 50 A93-25891

Electromechanical systems with transient high power response operating from a resonant ac link p 152 A93-25892

ELECTROMECHANICS

An electromechanical actuation system for an expendable launch vehicle p 50 A93-25891

ELECTROMETERS

Acceptance testing of the prototype electrometer for the SAMPIE flight experiment [NASA-TM-105880] p 57 N93-10841

ELECTRON BEAMS

Interference patterns in the Spacelab 2 plasma wave data - Oblique electrostatic waves generated by the electron beam p 257 A93-16347

ELECTRON CYCLOTRON HEATING

Low earth simulation and materials characterization p 44 A93-32293

ELECTRON ENERGY

Reaction layer formation at the graphite/copper-chromium alloy interface p 100 A93-25105

ELECTRON GAS

Intermodulation in the oscillatory magnetoresistance of a two-dimensional electron gas p 151 A93-17610

Room-temperature determination of two-dimensional electron gas concentration and mobility in heterostructures p 280 A93-35198

ELECTRON IRRADIATION

Carrier removal and defect behavior in p-type InP p 279 A93-17176

ELECTRON SCATTERING

Implications of new GALLEX results for the Mikheyev-Smirnov-Wolfenstein solution of the solar neutrino problem p 293 A93-10357

ELECTRON SPECTROSCOPY

Auger electron spectroscopy study of oxidation of a PdCr alloy used for high-temperature sensors [NASA-TM-106212] p 129 N93-23418

ELECTRONIC EQUIPMENT

Electrical and Chemical Interactions at Mars Workshop. Part 2: Appendix [NASA-CP-10093-PT-2] p 293 N93-26392

Electrical design of Space Shuttle payload G-534: The pool boiling experiment [NASA-TM-106143] p 62 N93-27260

Service equipment for use in hostile environments [NASA-CASE-LEW-14906-2] p 230 N93-31314

ELECTROSTATIC WAVES

Electrodynamic interactions between a space station and the ionospheric plasma environment p 56 A93-29156

ELECTROTHERMAL ENGINES

Low power arcjet system spacecraft impacts [AIAA PAPER 93-2392] p 76 A93-50157

ELLIPSONETRY

Ellipsometric study of Si(0.5)Ge(0.5)/Si strained-layer superlattices p 280 A93-34655

Ellipsometric study of metal-organic chemically vapor deposited III-V semiconductor structures p 281 A93-35697

Spectroscopic ellipsometry studies of HF treated Si(100) surfaces p 282 A93-46188

Ellipsometric characterization of In(0.52)Al(0.48)As and of modulation doped field effect transistor structures on InP substrates p 158 A93-49382

ELLIPTICAL ORBITS

Minimum-fuel, power-limited transfers between coplanar elliptical orbits p 45 A93-31532

EMISSION

Current status of liquid sheet radiator research [NASA-TM-105764] p 193 N93-14150

Multiwavelength pyrometer for gray and non-gray surfaces in the presence of interfering radiation [NASA-CASE-LEW-15250-1] p 214 N93-17060

EMULSIONS

Microemulsion characterization by the use of a noninvasive backscatter fiber optic probe p 277 A93-52412

ENCAPSULATING

Natural and thermocapillary convection in multiple liquid layers [AIAA PAPER 93-0469] p 171 A93-24241

END-TO-END DATA SYSTEMS

Description of the SSF PMAD dc testbed control system data acquisition function p 47 A93-26103

Description of the SSF PMAD DC testbed control system data acquisition function [NASA-TM-105843] p 261 N93-11005

ENERGETIC PARTICLES

Implications of new GALLEX results for the Mikheyev-Smirnov-Wolfenstein solution of the solar neutrino problem p 293 A93-10357

ENERGY ABSORPTION FILMS

Novel thin-film heat flux sensors [AIAA PAPER 92-5035] p 205 A93-22309

ENERGY BUDGETS

PEM fuel cell stack heat and mass management p 253 A93-26024

ENERGY CONVERSION

Magnetic bearings for free-piston Stirling engines p 221 A93-26079

ENERGY CONVERSION EFFICIENCY

Parameterization of solar cells [NASA-TM-105885] p 159 N93-12301

Test results of a Stirling engine utilizing heat exchanger modules with an integral heat pipe [NASA-TM-105883] p 256 N93-25136

The effect of the low Earth orbit environment on space solar cells: Results of the Advanced Photovoltaic Experiment (S0014) p 256 N93-29686

ENERGY DISSIPATION

Flame balls - Past, present and future [AIAA PAPER 93-0712] p 114 A93-24807

Energy loss analysis of an integrated space power distribution system p 68 A93-25958

Energy loss analysis of an integrated space power distribution system [NASA-TM-105772] p 141 N93-14834

ENERGY GAPS (SOLID STATE)

Application of high-quality SiO₂ grown by multipolar ECR source to Si/SiGe MISFET p 156 A93-37413

ENERGY REQUIREMENTS

Design of small Stirling dynamic isotope power system for robotic space missions [NASA-TM-105919] p 141 N93-12085

ENERGY SPECTRA

A multiple-scale turbulence model for incompressible flow [AIAA PAPER 93-0086] p 170 A93-24228

ENERGY STORAGE

Validation test of advanced technology for IPV nickel-hydrogen flight cells - Update p 252 A93-25886

Design of a cavity heat pipe receiver experiment p 173 A93-25985

PEM fuel cell stack heat and mass management p 253 A93-26024

Lightweight nickel electrodes for nickel/hydrogen cells p 255 A93-51574

Advanced photovoltaic power system technology for lunar base applications p 255 N93-14004

Power system technology discipline p 62 N93-27862

ENERGY TECHNOLOGY

Electrical characterization of a Space Station Freedom alpha utility transfer assembly p 56 A93-26101

Technologies --- space power sources p 255 N93-16907

ENERGY TRANSFER

A new energy transfer model for turbulent free shear flow [NASA-TM-105854] p 191 N93-10454

Multi-heat addition turbine engine [NASA-CASE-LEW-15094-1] p 35 N93-22034

ENGINE AIRFRAME INTEGRATION

Analysis of airframe and engine control interactions and integrated flight/propulsion control p 40 A93-14596

Concurrent optimization of airframe and engine design parameters [AIAA PAPER 92-4713] p 20 A93-20281

A comparative study of multivariable robustness analysis methods as applied to integrated flight and propulsion control [AIAA PAPER 93-3809] p 21 A93-51401

Concurrent optimization of airframe and engine design parameters [NASA-TM-105908] p 32 N93-12402

Aerothermodynamic flow phenomena of the
airframe-integrated supersonic combustion ramjet
[NASA-TM-4376] p 82 N93-15528

ENGINE ANALYZERS

Nonlinear dynamic simulation of single- and multi-spool
core engines
[AIAA PAPER 93-2580] p 30 A93-50294

A three-dimensional algebraic grid generation scheme
for gas turbine combustors with inclined slots
[NASA-CR-191095] p 198 N93-24759

ENGINE CONTROL

Integrated health monitoring and controls for rocket
engines
[SAE PAPER 921031] p 66 A93-14654

Screening studies of advanced control concepts for
airbreathing engines
[AIAA PAPER 92-3320] p 26 A93-49329

Advanced instrumentation for next-generation
aerospace propulsion control systems
[AIAA PAPER 93-2079] p 211 A93-49906

Screening studies of advanced control concepts for
airbreathing engines
[NASA-TM-106042] p 36 N93-25079

A modified approach to controller partitioning
[NASA-TM-106167] p 266 N93-28051

ENGINE COOLANTS

CFD analyses of coolant channel flowfields
[AIAA PAPER 93-1830] p 184 A93-49715

Chimera grids in the simulation of three-dimensional
flowfields in turbine-blade-coolant passages
[AIAA PAPER 93-2559] p 187 A93-50280

Thermal stratification potential in rocket engine coolant
channels p 78 N93-10019

ENGINE DESIGN

Effects of turbine cooling assumptions on performance
and sizing of high-speed civil transport
[AIAA PAPER 92-4217] p 22 A93-13383

An efficient constraint to account for mistuning effects
in the optimal design of engine rotors
[AIAA PAPER 92-4711] p 23 A93-20280

Concurrent optimization of airframe and engine design
parameters
[AIAA PAPER 92-4713] p 20 A93-20281

Structural tailoring of aircraft engine blade subject to
ice impact constraints
[AIAA PAPER 92-4710] p 23 A93-20319

APPLE - An aeroelastic analysis system for
turbomachines and propfans
[AIAA PAPER 92-4712] p 23 A93-20320

A graphical user-interface for propulsion system
analysis
[AIAA PAPER 93-0223] p 259 A93-23699

Design considerations for a Space Shuttle Main Engine
turbine blade made of single crystal material
p 236 A93-25228

An efficient liner cooling scheme for advanced small
gas turbine combustors
[AIAA PAPER 93-1763] p 27 A93-49660

Experimental evaluation of a cooled radial-inflow
turbine
[AIAA PAPER 93-1795] p 27 A93-49685

Reliability studies of Integrated Modular Engine system
designs
[AIAA PAPER 93-1886] p 72 A93-49759

Analytic methods for design of wave cycles for wave
rotor core engines
[AIAA PAPER 93-2523] p 30 A93-50253

Propulsion technology challenges for turn-of-the-century
commercial aircraft
[ISABE 93-7003] p 31 A93-53980

Aerodynamic inverse design and analysis for a full
engine
[ISABE 93-7086] p 14 A93-54062

An interactive preprocessor for the NASA engine
performance program
[NASA-TM-105786] p 32 N93-10983

The engine design engine. A clustered computer
platform for the aerodynamic inverse design and analysis
of a full engine
[NASA-TM-105838] p 15 N93-11223

A concept for a counterrotating fan with reduced tone
noise
[NASA-TM-105736] p 274 N93-11370

Design of small Stirling dynamic isotope power system
for robotic space missions
[NASA-TM-105919] p 141 N93-12085

Concurrent optimization of airframe and engine design
parameters
[NASA-TM-105908] p 32 N93-12402

Second Magnetoplasma-dynamic Thruster Workshop
[NASA-CP-10109] p 279 N93-18635

Spray combustion experiments and numerical
predictions
[NASA-TM-106069] p 198 N93-23744

Nuclear Engine System Simulation (NESS). Volume 1:
Program user's guide
[NASA-CR-191080] p 86 N93-23876

Overview of NASA/DOE/DOD interagency modeling
team and activities p 89 N93-26952

Reliability studies of integrated modular engine system
designs
[NASA-TM-106178] p 91 N93-27022

Small Stirling dynamic isotope power system for robotic
space missions
[NASA-TM-105785] p 92 N93-28686

Experimental evaluation of a cooled radial-inflow
turbine
[NASA-TM-106230] p 38 N93-28697

Propulsion technology challenges for turn-of-the-century
commercial aircraft
[NASA-TM-106192] p 39 N93-32351

ENGINE FAILURE

Implementation of a model based fault detection and
diagnosis technique for actuation faults of the SSME
p 47 A93-16413

Implementation of a model based fault detection and
diagnosis for actuation faults of the Space Shuttle main
engine
[NASA-TM-105781] p 49 N93-11401

ENGINE INLETS

Evaluation and application of the Baldwin-Lomax
turbulence model in two-dimensional, unsteady,
compressible boundary layers with and without separation
in engine inlets
[AIAA PAPER 92-3676] p 2 A93-14118

Evaluation and application of the Baldwin-Lomax
turbulence model in two-dimensional, unsteady,
compressible boundary layers with and without separation
in engine inlets
[AIAA PAPER 92-3676] p 168 A93-22509

Results of Low Power Deicer tests on a swept inlet
component in the NASA Lewis Icing Research Tunnel
[AIAA PAPER 93-0032] p 20 A93-22551

Acoustic mode measurements in the inlet of a model
turbofan using a continuously rotating rake
[AIAA PAPER 93-0598] p 273 A93-24783

Study on vortex generator flow control for the
management of inlet distortion p 7 A93-34488

A lag model for turbulent boundary layers developing
over rough bleed surfaces
[AIAA PAPER 93-2988] p 10 A93-48181

3-D viscous flow CFD analysis of the propeller effect
on an advanced ducted propeller subsonic inlet
[AIAA PAPER 93-1847] p 12 A93-49728

Evaluation and application of the Baldwin-Lomax
turbulence model in two-dimensional, unsteady,
compressible boundary layers with and without separation
in engine inlets
[NASA-TM-105810] p 191 N93-10087

Results of low power deicer tests on a swept inlet
component in the NASA Lewis icing research tunnel
[NASA-TM-105968] p 15 N93-14911

Acoustic mode measurements in the inlet of a model
turbofan using a continuously rotating rake
[NASA-TM-105989] p 34 N93-16705

Analytical and experimental studies of a short compact
subsonic diffuser for a two-dimensional supersonic inlet
[NASA-TP-3247] p 17 N93-24118

The 3-D viscous flow CFD analysis of the propeller effect
on an advanced ducted propeller subsonic inlet
[NASA-TM-106240] p 38 N93-29162

ENGINE MONITORING INSTRUMENTS

Implementation of a model based fault detection and
diagnosis technique for actuation faults of the SSME
p 47 A93-16413

An SSME High Pressure Oxidizer Turbopump diagnostic
system using G2 real-time expert system
p 66 A93-16415

Fabrication of thin film heat flux sensors
p 204 A93-16419

Palladium-chromium static strain gage for high
temperature propulsion systems p 204 A93-16421

Air-mass flux measurement system using
Doppler-shifted filtered Rayleigh scattering
[AIAA PAPER 93-0513] p 205 A93-23260

Advanced instrumentation for next-generation
aerospace propulsion control systems
[AIAA PAPER 93-2079] p 211 A93-49906

Implementation of a model based fault detection and
diagnosis for actuation faults of the Space Shuttle main
engine
[NASA-TM-105781] p 49 N93-11401

ENGINE NOISE

Acoustic mode measurements in the inlet of a model
turbofan using a continuously rotating rake
[AIAA PAPER 93-0598] p 273 A93-24783

A concept for a counterrotating fan with reduced tone
noise
[NASA-TM-105736] p 274 N93-11370

Experimental investigation of an ejector-powered free-jet
facility
[NASA-TM-105868] p 16 N93-16704

Acoustic mode measurements in the inlet of a model
turbofan using a continuously rotating rake
[NASA-TM-105989] p 34 N93-16705

ENGINE PARTS

Stirling engine - Available tools for long-life assessment
... for space propulsion p 65 A93-13824

Coupled multi-disciplinary simulation of composite
engine structures in propulsion environment
[ASME PAPER 92-GT-6] p 23 A93-19279

Results of Low Power Deicer tests on a swept inlet
component in the NASA Lewis Icing Research Tunnel
[AIAA PAPER 93-0032] p 20 A93-22551

Overview of the NASA Lewis component technology
program for Stirling power converters
p 254 A93-26073

Results of low power deicer tests on a swept inlet
component in the NASA Lewis icing research tunnel
[NASA-TM-105968] p 15 N93-14911

Integrity testing of brush seal in shroud ring of T-700
engine
[NASA-TM-105863] p 227 N93-18380

Jet Engine hot parts IR Analysis Procedure (J-EIRP)
[NASA-TM-105914] p 21 N93-22588

Study of the capacitance technique for measuring
high-temperature blade tip clearance on ceramic rotors
[NASA-TM-105978] p 35 N93-23013

ENGINE TESTING LABORATORIES

A large hemi-anechoic enclosure for
community-compatible aeroacoustic testing of aircraft
propulsion systems
[NASA-TM-106015] p 275 N93-26551

ENGINE TESTS

Low-ISP derated ion thruster operation
[AIAA PAPER 92-3203] p 64 A93-13696

Comparison of GLIMPS and HFASST Stirling engine code
predictions with experimental data p 220 A93-26052

Extended life and performance test of a low-power
arcjet p 70 A93-32554

Design of an Advanced Expander Test Bed
[AIAA PAPER 93-2133] p 48 A93-49952

Design of an oxygen turbopump for use in an Advanced
Expander Test Bed engine
[AIAA PAPER 93-2137] p 48 A93-49955

Development and use of hydrogen-air torches in an
altitude facility
[AIAA PAPER 93-2176] p 42 A93-49988

In-stream measurements of combustion during Mach 5
to 7 tests of the Hypersonic Research Engine (HRE)
[AIAA PAPER 93-2324] p 28 A93-50104

Test program to provide validation data for the Rocket
Combustor Interactive Design (ROCCID) code
p 120 N93-11450

Design of a high-temperature experiment for evaluating
advanced structural materials
[NASA-TM-105833] p 245 N93-11624

Test results of a Stirling engine utilizing heat exchanger
modules with an integral heat pipe
[NASA-TM-105883] p 256 N93-25136

External stress-corrosion cracking of a 1.22-m-diameter
type 316 stainless steel air valve
[NASA-TP-3190] p 129 N93-26201

Development and use of hydrogen-air torches in an
altitude facility
[NASA-TM-106047] p 43 N93-26214

A large hemi-anechoic enclosure for
community-compatible aeroacoustic testing of aircraft
propulsion systems
[NASA-TM-106015] p 275 N93-26551

Facilities p 49 N93-26963

Plum Brook facilities p 49 N93-26964

NEP facilities (LeRC) p 49 N93-26965

Hypersonic engine component experiments in high heat
flux, supersonic flow environment
[NASA-TM-106273] p 203 N93-31860

ENGINEERING MANAGEMENT

Computational simulation for concurrent engineering of
aerospace propulsion systems
[NASA-TM-106029] p 249 N93-23746

ENTHALPY

Thermodynamic data for fifty reference elements
[NASA-TP-3287] p 286 N93-19977

Computational fluid dynamics for nuclear thermal
propulsion p 199 N93-26930

ENTROPY

Self-growing neural network architecture using crisp and
fuzzy entropy p 263 A93-26650

Thermodynamic data for fifty reference elements
[NASA-TP-3287] p 286 N93-19977

ENTROPY (STATISTICS)

Self-growing neural network architecture using crisp and
fuzzy entropy
[NASA-TM-105677] p 231 N93-18422

ENVIRONMENT EFFECTS

- Simulation of the synergistic low Earth orbit effects of vacuum thermal cycling, vacuum UV radiation, and atomic oxygen p 58 N93-15595
- Characteristics of hypervelocity impact craters on LDEF experiment S1003 and implications of small particle impacts on reflective surfaces p 62 N93-29363
- ENVIRONMENTAL SIMULATION**
- Low Earth orbit atomic oxygen simulation for durability evaluation of solar reflector surfaces p 58 N93-15594
- Simulation of the synergistic low Earth orbit effects of vacuum thermal cycling, vacuum UV radiation, and atomic oxygen p 58 N93-15595
- The use of plasma ashers and Monte Carlo modeling for the projection of atomic oxygen durability of protected polymers in low Earth orbit p 58 N93-15596
- Low Earth orbital atomic oxygen environmental simulation facility for space materials evaluation [NASA-TM-106128] p 96 N93-27266
- ENVIRONMENTAL MONITORING**
- Lewis safety manual [NASA-TM-104438] p 147 N93-70966
- ENVIRONMENTAL TESTS**
- Effect of oxidation on the mechanical properties of a NbAl₃ alloy at intermediate temperatures p 124 A93-20667
- Fatigue-environment interactions in a SiC/Ti-15-3 composite p 100 A93-26275
- Effect of environment on fracture toughness of 96 wt pct alumina p 134 A93-44955
- Design for inadvertent damage in composite laminates p 242 A93-53396
- Effect of service environments on adhesively bonded joints in composite structures p 242 A93-53418
- Environmental effects on long term behavior of composite laminates p 243 A93-53438
- Thermomechanical fatigue behavior of SiC/Ti-24Al-11Nb in air and argon environments [NASA-TM-105723] p 106 N93-11399
- Issues/considerations and performance prediction of LEO protective coatings p 137 N93-20813
- Recommended practices for in-space and ground laboratory. Atomic oxygen exposure and analysis p 276 N93-20814
- Plasma current collection of Z-93 thermal control paint as measured in the Lewis Research Center's plasma interaction facility [NASA-TM-106132] p 61 N93-26215
- The effects of simulated low Earth orbit environments on spacecraft thermal control coatings [NASA-TM-106146] p 61 N93-27019
- Low Earth orbital atomic oxygen environmental simulation facility for space materials evaluation [NASA-TM-106128] p 96 N93-27266
- Focused technology: Nuclear propulsion [PR12] p 287 N93-71885
- EPITAXY**
- A 10-GHz amplifier using an epitaxial lift-off pseudomorphic HEMT device p 156 A93-37574
- Diffusion length variation in 0.5- and 3-MeV proton-irradiated, heteroepitaxial indium phosphide solar cells [NASA-TM-106147] p 161 N93-27002
- EPOXY MATRIX COMPOSITES**
- Computer aided design and manufacturing of composite propan blades for a cruise missile wind tunnel model [NASA-TM-105269] p 261 N93-12022
- Leveling coatings for reducing the atomic oxygen defect density in protected graphite fiber epoxy composites [NASA-TM-105732] p 136 N93-15344
- Leveling coatings for reducing the atomic oxygen defect density in protected graphite fiber epoxy composites p 59 N93-15597
- EQUATIONS OF MOTION**
- Modal simulation of gear box vibration with experimental correlation p 221 A93-31982
- Turbulent fluid motion IV-averages, Reynolds decomposition, and the closure problem [NASA-TM-105822] p 195 N93-15585
- Solving modal equations of motion with initial conditions using MSC/NASTRAN DMAP. Part 1: Implementing exact mode superposition [NASA-TM-106063] p 248 N93-23739
- Solving modal equations of motion with initial conditions using MSC/NASTRAN DMAP. Part 2: Coupled versus uncoupled integration [NASA-TM-106064] p 248 N93-23740
- A rapid-distortion-theory turbulence model for developed unsteady wall-bounded flow [NASA-TM-106249] p 203 N93-32199
- EQUILIBRIUM EQUATIONS**
- Integrated force method - Compatibility conditions of structural mechanics for finite element analysis p 237 A93-32459

EQUILIBRIUM FLOW

- Collapse of the soap-film bridge - Quasistatic description p 188 A93-50536
- EQUIVALENCE**
- Dark matter and the equivalence principle p 291 A93-44385
- EQUIVALENT CIRCUITS**
- Parameterization of solar cells [NASA-TM-105885] p 159 N93-12301
- EROSION**
- Erosion rate diagnostics in ion thrusters using laser-induced fluorescence p 70 A93-34481
- The chemistry of Saudi Arabian sand - A deposition problem on helicopter turbine airfoils p 243 A93-53468
- 100-kW class applied-field MPD thruster component wear [NASA-TM-106023] p 85 N93-22482
- ERROR ANALYSIS**
- Implementation of a model based fault detection and diagnosis technique for actuation faults of the SSME p 47 A93-16413
- Reliability assessment of thrust chamber cooling concepts using probabilistic analysis techniques [AIAA PAPER 93-2163] p 75 A93-49978
- Accuracy of least-squares methods for the Navier-Stokes equations p 188 A93-52008
- Implementation of a model based fault detection and diagnosis for actuation faults of the Space Shuttle main engine [NASA-TM-105781] p 49 N93-11401
- A critical analysis of the accuracy of several numerical techniques for combustion kinetic rate equations [NASA-TP-3315] p 34 N93-16941
- Thermoviscoplastic analysis of fibrous periodic composites using triangular subvolumes [NASA-TM-106076] p 111 N93-29074
- Efficient fault diagnosis of helicopter gearboxes [NASA-TM-106253] p 231 N93-31846
- ERROR DETECTION CODES**
- Modifying real convolutional codes for protecting digital filtering systems p 148 A93-38221
- ESSENTIALLY NON-OSCILLATORY SCHEMES**
- An assessment of spectral nonoscillatory schemes [AIAA PAPER 93-3383] p 267 A93-45074
- Eno-Osher schemes for Euler equations [NASA-TM-105928] p 268 N93-15341
- ESTIMATING**
- An alternative model for estimating liquid diffusion coefficients requiring no viscosity data [NASA-TM-106079] p 96 N93-23014
- ETCHING**
- Thin film diamond microstructure applications p 209 A93-40580
- Texturing of InP surfaces for device applications [NASA-TM-106061] p 129 N93-28618
- ETHERS**
- X-ray photoelectron spectroscopy study of the stability of Fomblin Z25 on the native oxide of aluminum p 134 A93-44883
- Determination of the thermal stability of perfluoropolyalkyl ethers by tensimetry [NASA-TM-106081] p 137 N93-25093
- Determination of the oxidative stability of perfluoropolyalkyl ethers and correlation with chemical structure [NASA-TM-106223] p 139 N93-32367
- EULER EQUATIONS OF MOTION**
- Dispersion-relation-preserving schemes for computational aeroacoustics p 2 A93-19151
- Direct calculations of waves in fluid flows using a high-order compact difference scheme [AIAA PAPER 93-0148] p 171 A93-24232
- Three-dimensional unstructured grid Euler method applied to turbine blades [AIAA PAPER 93-0196] p 6 A93-24233
- ENO-Osher schemes for Euler equations [AIAA PAPER 93-0335] p 171 A93-24235
- Linearized Euler predictions of unsteady aerodynamic loads in cascades p 7 A93-29318
- Unsteady blade pressures on a propan at takeoff - Euler analysis and flight data p 26 A93-37389
- Unsteady transonic two-dimensional Euler solutions using finite elements p 8 A93-39412
- An accuracy assessment of Cartesian-mesh approaches for the Euler equations [AIAA PAPER 93-3335] p 9 A93-45029
- Grid adaptation using Chimera composite overlapping meshes [AIAA PAPER 93-3389] p 267 A93-45080
- A new flux splitting scheme p 9 A93-47189
- High resolution numerical simulation of the linearized Euler equations in conservation law form [AIAA PAPER 93-2934] p 183 A93-48132
- Dispersion-relation-preserving finite difference schemes for computational acoustics p 274 A93-51180

- Central difference TVD schemes for time dependent and steady state problems p 188 A93-51183
- Eno-Osher schemes for Euler equations [NASA-TM-105928] p 268 N93-15341
- A brief description of a new numerical framework for solving conservation laws: The method of space-time conservation element and solution element [NASA-TM-105757] p 269 N93-26560
- Grid adaption using Chimera composite overlapping meshes [NASA-TM-106163] p 269 N93-27065
- EULER-LAGRANGE EQUATION**
- Computing 3-D steady supersonic flow via a new Lagrangian approach [AIAA PAPER 93-0891] p 6 A93-24951
- Noniterative implicit method for tracking particles in mixed Lagrangian-Eulerian formulations p 176 A93-30856
- EUTECTICS**
- Tribological and microstructural comparison of HIPped PM212 and PM212/Au self-lubricating composites p 93 A93-13505
- The effect of porosity and gamma-gamma' eutectic content on the low cycle fatigue behavior of hydrogen-charged PWA-1480 p 130 N93-31576
- EVOLUTION (DEVELOPMENT)**
- The first three minutes - 1990 version --- of early universe after Big Bang p 289 A93-23607
- Probing the statistics of primordial fluctuations and their evolution p 290 A93-24627
- Vorticity dynamics of inviscid shear layers p 181 A93-45734
- EXCITONS**
- Aluminum acceptor four particle bound exciton complex in 4H, 6H, and 3C SiC p 282 A93-44822
- EXHAUST EMISSION**
- An analytical study of dilution jet mixing in a cylindrical duct [AIAA PAPER 93-2043] p 27 A93-49876
- CFD mixing analysis of axially opposed rows of jets injected into confined crossflow [AIAA PAPER 93-2044] p 185 A93-49877
- Emission characteristics of a model gas turbine combustor at practical conditions [ISABE 93-7023] p 31 A93-53999
- CFD mixing analysis of axially opposed rows of jets injected into confined crossflow [NASA-TM-106179] p 37 N93-27128
- An analytical study of dilution jet mixing in a cylindrical duct [NASA-TM-106181] p 37 N93-27160
- EXHAUST FLOW SIMULATION**
- Measurement and analysis of a small nozzle plume in vacuum p 71 A93-42895
- Effects of flow-path variations on internal reversing flow in a tailpipe offtake configuration for ASTOVL aircraft [AIAA PAPER 93-2438] p 29 A93-50190
- Measurement and analysis of a small nozzle plume in vacuum [NASA-TM-106066] p 88 N93-26561
- Effects of flow-path variations on internal reversing flow in a tailpipe offtake configuration for ASTOVL aircraft [NASA-TM-106149] p 38 N93-29065
- EXHAUST GASES**
- Laser Rayleigh and Raman diagnostics for small hydrogen/oxygen rockets [NASA-TM-105999] p 83 N93-17995
- EXHAUST NOZZLES**
- In-stream measurements of combustion during Mach 5 to 7 tests of the Hypersonic Research Engine (HRE) [AIAA PAPER 93-2324] p 28 A93-50104
- Performance characteristics of a variable-area vane nozzle for vectoring an ASTOVL exhaust jet up to 45 deg [AIAA PAPER 93-2437] p 29 A93-50189
- Effects of flow-path variations on internal reversing flow in a tailpipe offtake configuration for ASTOVL aircraft [AIAA PAPER 93-2438] p 29 A93-50190
- Supersonic investigation of two dimensional hypersonic exhaust nozzles [NASA-TM-105687] p 33 N93-15342
- Experimental investigation of an ejector-powered free-jet facility [NASA-TM-105868] p 16 N93-16704
- Performance characteristics of a variable-area vane nozzle for vectoring an ASTOVL exhaust jet up to 45 deg [NASA-TM-106114] p 37 N93-27131
- Effects of flow-path variations on internal reversing flow in a tailpipe offtake configuration for ASTOVL aircraft [NASA-TM-106149] p 38 N93-29065
- EXHAUST SYSTEMS**
- Computational study of advanced exhaust system transition ducts with experimental validation p 7 A93-34490

- Development and use of hydrogen-air torches in an altitude facility
[AIAA PAPER 93-2176] p 42 A93-49988
- Effects of flow-path variations on internal reversing flow in a tailpipe offtake configuration for ASTOVL aircraft
[AIAA PAPER 93-2438] p 29 A93-50190
- Development and use of hydrogen-air torches in an altitude facility
[NASA-TM-106047] p 43 N93-26214
- Effects of flow-path variations on internal reversing flow in a tailpipe offtake configuration for ASTOVL aircraft
[NASA-TM-106149] p 38 N93-29065
- EXPENDABLE STAGES (SPACECRAFT)**
- An electromechanical actuation system for an expendable launch vehicle p 50 A93-25891
- EXPERIMENT DESIGN**
- Small experiments for the maturation of orbital cryogenic transfer technologies
[IAF PAPER 92-0777] p 64 A93-13698
- Modified NASA standard nickel-cadmium cell designs p 253 A93-25947
- An approach to studying the reliability of microgravity experiments
[AIAA PAPER 93-1024] p 44 A93-30937
- Capabilities and constraints of typical space flight hardware p 145 N93-20183
- Laser ignition application in a space experiment
[NASA-TM-106133] p 145 N93-25337
- EXPERT SYSTEMS**
- An SSME High Pressure Oxidizer Turbopump diagnostic system using G2 real-time expert system p 66 A93-16415
- Lessons learned from the Autonomous Power System p 68 A93-25879
- Fuzzy expert systems vs. neural networks - Truck backer-upper control revisited p 264 A93-37039
- An embedded rule-based diagnostic expert system in Ada p 260 N93-11928
- Scheduling lessons learned from the Autonomous Power System p 265 N93-18671
- Real-time diagnostics for a reusable rocket engine
[NASA-TM-105792] p 266 N93-19018
- Application of artificial neural networks to the design optimization of aerospace structural components
[NASA-TM-4389] p 247 N93-21831
- EXPLOSIVE DEVICES**
- Pyrotechnically actuated systems database and applications catalog p 141 N93-20136
- EXPOSURE**
- Isothermal aging effects on PMR-15 resin p 131 A93-24508
- EXPULSION**
- Pressurization and expulsion of a flightweight liquid hydrogen tank
[AIAA PAPER 93-1966] p 73 A93-49814
- EXTENSOMETERS**
- Strain sensing technology for high temperature applications
[AIAA PAPER 92-5040] p 205 A93-22314
- EXTINGUISHING**
- Asymptotic analysis for the burning of n-heptane droplets using a four-step reduced mechanism p 117 A93-41952
- EXTRATERRESTRIAL RESOURCES**
- Representative systems for space exploration p 293 N93-26395
- EXTREMELY HIGH FREQUENCIES**
- A high efficiency Ka-band monolithic pseudomorphic HEMT amplifier p 151 A93-25786
- EXTRUDING**
- Room temperature cyclic deformation behavior of cast and extruded NiAl p 122 A93-12130
- Properties of extruded PS-212 type self-lubricating materials p 138 N93-25565
- EYE (ANATOMY)**
- A fiber optic probe for the detection of cataracts p 257 N93-25593
- F**
- F-18 AIRCRAFT**
- Installed F/A-18 inlet flow calculations at 60 deg angle-of-attack and 10 deg side slip
[AIAA PAPER 93-1806] p 12 A93-49695
- Status of the Fiber Optic Control System Integration (FOCSI) program
[NASA-TM-106151] p 217 N93-28053
- FABRICATION**
- Fabrication of thin film heat flux sensors p 204 A93-16419
- Combined micromechanical and fabrication process optimization for metal-matrix composites p 99 A93-18990
- System-level integrated circuit (SLIC) development for phased array antenna applications p 152 A93-25798
- Photovoltaic Array Space Power flight experiment plus diagnostics (PASP+) modules p 68 A93-25898
- Transient liquid phase diffusion bonding of Udimet 720 for Stirling power converter applications p 221 A93-26080
- Design and fabrication of a hydrogen/oxygen thrust chamber assembly
[AIAA PAPER 93-2132] p 74 A93-49951
- Fabrication and properties of functionally graded NiAl/Al₂O₃ composites p 105 A93-54116
- Room temperature synthesis of copper indium diselenide in non-aqueous solution using an organoindium reagent p 283 A93-54844
- Demonstration of Y1Ba2Cu3O(7-delta) and complementary metal-oxide-semiconductor device fabrication on the same sapphire substrate p 159 A93-56292
- Effects of anode material on arcjet performance
[NASA-TM-105799] p 79 N93-10197
- Silicon carbide fiber reinforced strontium aluminosilicate glass-ceramic matrix composite
[NASA-CASE-LEW-15263-1] p 106 N93-11543
- Fabrication of thin film heat flux sensors p 213 N93-13667
- Fiber-reinforced monoclinic celsian matrix composite material
[NASA-CASE-LEW-15269-1] p 108 N93-20040
- Solar concentrators for advanced solar-dynamic power systems in space
[NASA-CR-187148] p 85 N93-23017
- Computational simulation for concurrent engineering of aerospace propulsion systems
[NASA-TM-106029] p 249 N93-23746
- Fabrication of composite propfan blades for a cruise missile wind tunnel model
[NASA-TM-105270] p 249 N93-26202
- The development of hydrogen sensor technology at NASA Lewis Research Center
[NASA-TM-106141] p 216 N93-27021
- FABRICS**
- Construction and testing of ceramic fabric heat pipe with water working fluid p 163 A93-13869
- FABRY-PEROT SPECTROMETERS**
- A plume spectroscopy system for flight applications
[AIAA PAPER 93-2511] p 63 A93-50242
- FACE CENTERED CUBIC LATTICES**
- Multilayer relaxation and surface energies of fcc and bcc metals using equivalent crystal theory p 119 A93-52873
- Heat of segregation of single substitutional impurities p 119 A93-52873
- FAILURE**
- Fatigue criterion to system design, life and reliability: A primer
[NASA-TM-106022] p 248 N93-23406
- FAILURE ANALYSIS**
- Implementation of a model based fault detection and diagnosis technique for actuation faults of the SSME p 47 A93-16413
- Ceramic component reliability with the restructured NASA/CARES computer program
[ASME PAPER 92-GT-383] p 234 A93-19540
- Microfracture in high temperature metal matrix crossply laminates p 101 A93-31356
- Deformation and failure mechanisms in metal matrix composites p 102 A93-31359
- Mechanics of interfaces in fiber reinforced SiC/RBSN ceramic matrix composites --- reaction bonded silicon nitride p 102 A93-32466
- Probabilistic simulation of the human factor in structural reliability
[AIAA PAPER 93-1495] p 264 A93-34036
- A numerical round robin for the reliability prediction of structural ceramics
[AIAA PAPER 93-1498] p 240 A93-34038
- Computational methods for efficient structural reliability and reliability sensitivity analysis
[AIAA PAPER 93-1626] p 240 A93-34155
- Modifying real convolutional codes for protecting digital filtering systems p 148 A93-38221
- Reliability studies of Integrated Modular Engine system designs
[AIAA PAPER 93-1886] p 72 A93-49759
- Reliability assessment of thrust chamber cooling concepts using probabilistic analysis techniques
[AIAA PAPER 93-2163] p 75 A93-49978
- Evaluation of a vibration diagnostic system for the detection of spur gear pitting failures
[AIAA PAPER 93-2298] p 224 A93-50083
- Diffusional transport and predicting oxidative failure during cyclic oxidation of beta-NiAl alloys p 126 A93-50370
- Hot fire test results of subscale tubular combustion chambers p 79 N93-10020
- Ceramic component reliability with the restructured NASA/CARES computer program
[NASA-TM-105856] p 244 N93-11004
- Implementation of a model based fault detection and diagnosis for actuation faults of the Space Shuttle main engine
[NASA-TM-105781] p 49 N93-11401
- Second generation integrated composite analyzer (ICAN) computer code
[NASA-TP-3290] p 108 N93-18139
- Evaluation of an oil-debris monitoring device for use in helicopter transmissions
[NASA-TM-105830] p 227 N93-22826
- Pattern classifier for health monitoring of helicopter gearboxes
[NASA-TM-106099] p 228 N93-23741
- Evaluation of a vibration diagnostic system for the detection of spur gear pitting failures
[NASA-TM-106103] p 228 N93-25672
- External stress-corrosion cracking of a 1.22-m-diameter type 316 stainless steel air valve
[NASA-TP-3190] p 129 N93-26201
- Structural tailoring of aircraft engine blade subject to ice impact constraints
[NASA-TM-106033] p 250 N93-26999
- Reliability studies of integrated modular engine system designs
[NASA-TM-106178] p 91 N93-27022
- RENEW v3.2 user's manual, maintenance estimation simulation for Space Station Freedom Program
[NASA-TM-106006] p 232 N93-27025
- Fault detection of helicopter gearboxes using the multi-valued influence matrix method
[NASA-TM-106100] p 229 N93-27069
- An analysis of gear fault detection methods as applied to pitting fatigue failure data
[NASA-TM-105950] p 229 N93-27074
- Probabilistic sizing of laminates with uncertainties
[NASA-TM-106145] p 110 N93-27082
- Acousto-Ultrasonic analysis of failure in ceramic matrix composite tensile specimens
[NASA-TM-106219] p 232 N93-29073
- Cumulative fatigue damage behavior of MAR M-247 p 251 N93-31575
- FAILURE MODES**
- Structural system reliability under multiple failure modes
[AIAA PAPER 93-1379] p 238 A93-33943
- Progressive matrix cracking in off-axis plies of a general symmetric laminate
[AIAA PAPER 93-1494] p 239 A93-34035
- Reliability studies of Integrated Modular Engine system designs
[AIAA PAPER 93-1886] p 72 A93-49759
- Subcritical crack growth in soda-lime glass in combined mode I and mode II loading p 134 A93-52151
- System model development for nuclear thermal propulsion
[NASA-TM-105761] p 80 N93-10457
- Real-time diagnostics for a reusable rocket engine
[NASA-TM-105792] p 266 N93-19018
- Reliability studies of integrated modular engine system designs
[NASA-TM-106178] p 91 N93-27022
- An analysis of gear fault detection methods as applied to pitting fatigue failure data
[NASA-TM-105950] p 229 N93-27074
- FAIRINGS**
- Close-up analysis of aircraft ice accretion
[AIAA PAPER 93-0029] p 18 A93-23239
- Close-up analysis of aircraft ice accretion
[NASA-TM-105952] p 19 N93-15360
- FAN BLADES**
- Coupled multi-disciplinary simulation of composite engine structures in propulsion environment
[ASME PAPER 92-GT-6] p 23 A93-19279
- A concept for a counterrotating fan with reduced tone noise
[NASA-TM-105736] p 274 N93-11370
- Structural analysis of high-rpm composite propfan blades for a cruise missile wind tunnel model
[NASA-TM-105267] p 247 N93-23015
- Blasim: A computational tool to assess ice impact damage on engine blades
[NASA-TM-106225] p 251 N93-31193
- FAR FIELDS**
- Analysis of reflector antenna system including frequency selective surfaces p 52 A93-32820
- An improved far field drag calculation method for nonlinear CFD codes
[AIAA PAPER 93-3417] p 10 A93-47213
- FAR ULTRAVIOLET RADIATION**
- Method and apparatus for producing a thermal atomic oxygen beam
[NASA-CASE-LEW-15614-1] p 276 N93-19026

FAST NEUTRONS

FAST NEUTRONS

Neutron, gamma ray, and temperature effects on the electrical characteristics of thyristors p 153 A93-25894

FAST NUCLEAR REACTORS

Multimegawatt potassium Rankine power for nuclear electric power p 65 A93-13797

FATIGUE (MATERIALS)

An advanced method for tracking the evolution of fatigue damage in reusable space propulsion systems p 234 A93-16406
Elastic interactions of a fatigue crack with a micro-defect by the mixed boundary integral equation method p 243 A93-56412

Computer programs to characterize alloys and predict cyclic life using the total strain version of strainrange partitioning: Tutorial and users manual, version 1.0 [NASA-TM-4425] p 246 A93-15788
Considerations concerning fatigue life of metal matrix composites [NASA-TM-106144] p 250 A93-27009

FATIGUE LIFE

Damage-mitigating control of aerospace systems for high performance and extended life p 263 A93-22967
Grain boundary resistance to fatigue crack growth p 125 A93-29570
Evolution of creep-fatigue life prediction models p 236 A93-31339

A high temperature fatigue life prediction computer code based on the Total Strain Version of Strainrange Partitioning (SRP) p 260 A93-31341
Fatigue life prediction of an intermetallic matrix composite at elevated temperatures p 101 A93-31358

Forced response of mistuned bladed disk assemblies [AIAA PAPER 93-1491] p 239 A93-34033
Parallel computing for probabilistic fatigue analysis [AIAA PAPER 93-1499] p 261 A93-34039
Axial-torsional fatigue - A study of tubular specimen thickness effects p 240 A93-38849

Damage-mitigating control of space propulsion systems for high performance and extended life [AIAA PAPER 93-2080] p 74 A93-49907
Reliability assessment of thrust chamber cooling concepts using probabilistic analysis techniques p 75 A93-49978
Design for cyclic loading endurance of composites p 242 A93-53395

Hot fire test results of subscale tubular combustion chambers p 79 A93-10020
Hot fire fatigue testing results for the compliant combustion chamber p 79 A93-10038
Hot fire fatigue testing results for the compliant combustion chamber [NASA-TP-3223] p 80 A93-10743

Thermomechanical fatigue behavior of SiC/Ti-24Al-11Nb in air and argon environments [NASA-TM-105723] p 106 A93-11399
Hot fire test results of subscale tubular combustion chambers [NASA-TP-3222] p 81 A93-11614

On bilinearity of Manson-Coffin low-cycle-fatigue relationship [NASA-TM-105840] p 245 A93-12739
In-phase and out-of-phase axial-torsional fatigue behavior of Haynes 188 at 760 C [NASA-TM-105765] p 246 A93-13153

Computer programs to characterize alloys and predict cyclic life using the total strain version of strainrange partitioning: Tutorial and users manual, version 1.0 [NASA-TM-4425] p 246 A93-15788

An overview of elevated temperature damage mechanisms and fatigue behavior of a unidirectional SCS-6/Ti-15-3 composite p 109 A93-26702
Low cycle fatigue behavior of polycrystalline NiAl at 300 and 1000 K [NASA-TM-105987] p 129 A93-26898

Considerations concerning fatigue life of metal matrix composites [NASA-TM-106144] p 250 A93-27009
Overview of the fatigue/fracture/life prediction working group program at the Lewis Research Center p 232 A93-31574

Cumulative fatigue damage behavior of MAR M-247 p 251 A93-31575
The effect of porosity and gamma-gamma' eutectic content on the low cycle fatigue behavior of hydrogen-charged PWA-1480 p 130 A93-31576

A model for predicting high-temperature fatigue failure of a W/Cu composite p 112 A93-31579

FATIGUE TESTS

Effects of precracking methods on the fracture properties of alumina p 131 A93-16645

Effect of tensile mean stress on fatigue behavior of single-crystal and directionally solidified superalloys p 125 A93-33011

Axial-torsional fatigue - A study of tubular specimen thickness effects p 240 A93-38849

Evaluation of a vibration diagnostic system for the detection of spur gear pitting failures [AIAA PAPER 93-2298] p 224 A93-50083
Brush seal low surface speed hard-rub characteristics [AIAA PAPER 93-2534] p 225 A93-50261

Thermomechanical fatigue behavior of SiC/Ti-24Al-11Nb in air and argon environments [NASA-TM-105723] p 106 A93-11399
On bilinearity of Manson-Coffin low-cycle-fatigue relationship [NASA-TM-105840] p 245 A93-12739

Evaluation of a vibration diagnostic system for the detection of spur gear pitting failures [NASA-TM-106103] p 228 A93-25672
Low cycle fatigue behavior of polycrystalline NiAl at 300 and 1000 K [NASA-TM-105987] p 129 A93-26898

Brush seal low surface speed hard-rub characteristics [NASA-TM-106169] p 200 A93-27132
Cumulative fatigue damage behavior of MAR M-247 p 251 A93-31575
Efficient fault diagnosis of helicopter gearboxes [NASA-TM-106253] p 231 A93-31846

Efficient fault diagnosis of helicopter gearboxes [NASA-TM-106253] p 231 A93-31846

FAULT DETECTION

Implementation of a model based fault detection and diagnosis technique for actuation faults of the SSME p 47 A93-16413

Implementation of a model based fault detection and diagnosis for actuation faults of the Space Shuttle main engine [NASA-TM-105781] p 49 A93-11401

Fault detection of helicopter gearboxes using the multi-valued influence matrix method [NASA-TM-106100] p 229 A93-27069
An analysis of gear fault detection methods as applied to pitting fatigue failure data [NASA-TM-105950] p 229 A93-27074

FAULT TOLERANCE

Fault-tolerant adaptive control for load-following in static space nuclear power systems p 263 A93-25986
Modifying real convolutional codes for protecting digital filtering systems p 148 A93-38221

Fluid design studies of integrated modular engine system [AIAA PAPER 93-1887] p 72 A93-49760
Predicted performance of an Integrated Modular Engine system [AIAA PAPER 93-1888] p 72 A93-49761

Analysis of fault-tolerant neurocontrol architectures [NASA-TM-105898] p 41 A93-12305
Fault-tolerant onboard digital information switching and routing for communications satellites [NASA-TM-4471] p 53 A93-26895

FAULT TREES

Reliability studies of Integrated Modular Engine system designs [AIAA PAPER 93-1886] p 72 A93-49759

Reliability studies of integrated modular engine system designs [NASA-TM-106178] p 91 A93-27022

FAULTS

Qualitative model-based diagnostics for rocket systems [NASA-TM-106234] p 51 A93-28052

FEEDBACK CONTROL

Analysis of airframe and engine control interactions and integrated flight/propulsion control p 40 A93-14596
Integrated health monitoring and controls for rocket engines [SAE PAPER 921031] p 66 A93-14654

A note on decentralized integral controllability p 264 A93-30492
Review of the FOCSI (Fiber Optic Control System Integration) program --- applications in aircraft flight control p 21 A93-32916

Applied high-speed imaging for the icing research program at NASA Lewis Research Center p 208 A93-33169
Digital control algorithms for microgravity isolation systems p 265 A93-53653

A parameter optimization approach to controller partitioning for integrated flight/propulsion control application p 41 A93-54268
Phase-stepping fiber-optic projected fringe system for surface topography measurements [NASA-CASE-LEW-14996-1] p 278 A93-11058

Propulsion system performance resulting from an integrated flight/propulsion control design [NASA-TM-105874] p 34 A93-15525

Controller partitioning for integrated flight/propulsion control implementation [NASA-TM-105804] p 41 A93-21197

Space Station Freedom beta gimbal control via sensitivity models [NASA-TM-106000] p 60 A93-22551
A neural network-based estimator for the mixture ratio of the Space Shuttle Main Engine [NASA-TM-106070] p 87 A93-25089

FEEDFORWARD CONTROL

Self-growing neural network architecture using crisp and fuzzy entropy p 263 A93-26650
Identification of the open loop dynamics of the T700 turboshaft engine p 26 A93-35934

Application of artificial neural networks in nonlinear analysis of trusses [NASA-TM-105319] p 244 A93-11403
Inverse kinematics problem in robotics using neural networks [NASA-TM-105869] p 247 A93-18876

FELDSPARS

Kinetics of hexacelsian-to-celsian phase transformation in SrAl2Si2O8 p 134 A93-40293
Kinetics of hexacelsian to celsian phase transformation in SrAl2Si2O8 [NASA-TM-105913] p 136 A93-16372

FEMUR

Optimal design of composite hip implants using NASA technology p 257 A93-22188

FERRITES

Damping and scattering of electromagnetic waves by small ferrite spheres suspended in an insulator [NASA-TM-105837] p 149 A93-12366

FIBER COMPOSITES

Graphite fiber/copper matrix composites for space power heat pipe fin applications p 162 A93-13789
Tensile strain-rate sensitivity of tungsten/nickel composites at 1300 to 1600 K p 97 A93-14840
Three-dimensional finite element simulation of intermingled-fiber hybrid composite behavior p 98 A93-15729

Computational simulation of surface waviness in graphite/epoxy woven composites due to initial curing p 98 A93-15822

Prediction of chemical vapor deposition rates on monofilaments and its implications for fiber properties p 113 A93-17198

Ceramic matrix composite applications in advanced liquid fuel rocket engine turbomachinery [ASME PAPER 92-GT-316] p 99 A93-19502

Ceramic matrix composites for rocket engine turbine applications [ASME PAPER 92-GT-394] p 99 A93-19547

Numerical optimization of composite hip endoprostheses under different loading conditions [AIAA PAPER 92-4703] p 270 A93-20312

Structural tailoring of aircraft engine blade subject to ice impact constraints [AIAA PAPER 92-4710] p 23 A93-20319

Application of neural networks to prediction of advanced composite structures mechanical response and behavior p 205 A93-20751

Creep behavior of tungsten fiber reinforced niobium metal matrix composites p 99 A93-20758

Transverse flexural tests as a tool for assessing damage to PMR-15 composites from isothermal aging in air at elevated temperatures p 100 A93-24514

Thermal conductivity and thermal expansion of graphite fiber-reinforced copper matrix composites p 100 A93-25104

Melt infiltration of silicon carbide compacts II - Evaluation of solidification microstructures p 101 A93-28283

Micromechanical studies of composites by BEM p 236 A93-31295

Transverse ductility of metal matrix composites p 101 A93-31355

Computational characterization of high temperature composites via METCAN p 102 A93-32461

Probabilistic micromechanics for metal matrix composites p 237 A93-32465

Mechanics of interfaces in fiber reinforced SiC/RBSN ceramic matrix composites --- reaction bonded silicon nitride p 102 A93-32466

Ductility of a continuous fiber reinforced aluminum matrix composite p 102 A93-32471

Nondestructive evaluation of a ceramic matrix composite material p 102 A93-33016

Quantification of uncertainties in composites [AIAA PAPER 93-1440] p 102 A93-33989

Probabilistic assessment of composite structures [AIAA PAPER 93-1441] p 239 A93-33990
Effect of thermal cycling on interface bonding requirements in Al2O3 fiber-reinforced superalloy composites p 103 A93-35882

- A generic model for creep rupture lifetime estimation on fibrous ceramic composites p 103 A93-38895
- Residual strain gradient determination in metal matrix composites by synchrotron X-ray energy dispersive diffraction p 103 A93-39580
- Model of brittle matrix composite toughening based on discrete fiber reinforcement p 104 A93-40888
- The effect of multiple compliant layers at the fiber-matrix interface on residual thermal stresses in metal matrix composites p 104 A93-42085
- Evolution of damage and plasticity in titanium-based, fiber-reinforced composites p 104 A93-48498
- Ultrasonic assessment of interfacial oxidation damage in ceramic matrix composites p 105 A93-52919
- The effect of fiber microstructure on evolution of residual stresses in silicon carbide/titanium aluminide composites p 106 A93-54771
- Aerospace applications --- of refractory ceramic materials p 135 A93-55472
- Interfacial and capillary phenomena in solidification processing of metal-matrix composites p 106 A93-56351
- A creep cavity growth model for creep-fatigue life prediction of a unidirectional W/Cu composite [NASA-TM-105780] p 244 A93-10967
- Thermomechanical fatigue behavior of SiC/Ti-24Al-11Nb in air and argon environments [NASA-TM-105723] p 106 N93-11399
- Silicon carbide fiber reinforced strontium aluminosilicate glass-ceramic matrix composite [NASA-CASE-LEW-15263-1] p 106 N93-11543
- Computer aided design and manufacturing of composite propan blades for a cruise missile wind tunnel model [NASA-TM-105269] p 261 N93-12022
- Thermostructural tailoring of fiber composite structures [NASA-TM-105882] p 107 N93-12078
- Fracture toughness testing of polymer matrix composites [NASA-TP-3199] p 107 N93-12302
- Transverse flexural tests as a tool for assessing damage to PMR-15 composites from isothermal aging in air at elevated temperatures [NASA-TM-105848] p 107 N93-12737
- Leveling coatings for reducing the atomic oxygen defect density in protected graphite fiber epoxy composites [NASA-TM-105732] p 136 N93-15344
- Second generation integrated composite analyzer (ICAN) computer code [NASA-TP-3290] p 108 N93-18139
- Fiber-reinforced monoclinic celsian matrix composite material [NASA-CASE-LEW-15269-1] p 108 N93-20040
- Effects of thermal and mechanical fatigue on the flexural strength of G40-600/PMR-15 cross-ply laminates [NASA-TM-106016] p 108 N93-20317
- Optimal design of composite hip implants using NASA technology p 257 N93-22188
- High Temperature Composite Analyzer (HITCAN) theoretical manual, version 1.0 [NASA-TM-106001] p 249 N93-24913
- High temperature composite analyzer (HITCAN) user's manual, version 1.0 [NASA-TM-106002] p 249 N93-25070
- MetAl matrix composite ANalyzer (METCAN): Theoretical manual [NASA-TM-106025] p 109 N93-26552
- Fiber shape effects on metal matrix composite behavior [NASA-TM-106067] p 109 N93-26704
- Structural tailoring of aircraft engine blade subject to ice impact constraints [NASA-TM-106033] p 250 N93-26999
- Determination of plate wave velocities and diffuse field decay rates with broad-band acousto-ultrasonic signals [NASA-TM-106158] p 232 N93-27080
- Probabilistic simulation of multi-scale composite behavior [NASA-TM-106196] p 250 N93-28633
- Ceramic matrix composites properties/microstresses with complete and partial interphase bond [NASA-TM-106136] p 111 N93-29071
- Thermoviscoplastic analysis of fibrous periodic composites using triangular subvolumes [NASA-TM-106076] p 111 N93-29074
- Tensile creep behavior of polycrystalline alumina fibers [NASA-TM-106269] p 138 N93-30938
- SiC fiber-reinforced Celsian glass-ceramic matrix composite [NASA-CASE-LEW-15264-1] p 112 N93-31293
- Method of producing a ceramic fiber-reinforced glass-ceramic matrix composite [NASA-CASE-LEW-15264-2] p 112 N93-31299
- FIBER OPTICS**
- Fiber optic laser Doppler anemometry in swirling jets p 206 A93-23783
- Fiber optic link for millimeter wave communication satellites p 277 A93-25736
- Review of the FOCSI (Fiber Optic Control System Integration) program --- applications in aircraft flight control p 21 A93-32916
- Optical fiber sensor for temperature measurement from 600 to 1900 C in gas turbine engines p 208 A93-32918
- Coherent fiber optic sensor for early detection of cataractogenesis in a human eye lens p 209 A93-37051
- Direct optical injection locking of monolithically integrated In(0.53)Ga(0.47)As/In(0.52)Al(0.48)As MODFET oscillators p 158 A93-47127
- Fourier transform spectrometry for fiber-optic sensor systems p 211 A93-49459
- RF modulated fiber optic sensing systems and their applications p 211 A93-49469
- Flight testing of a fiber optic temperature sensor p 22 A93-49476
- Microemulsion characterization by the use of a noninvasive backscatter fiber optic probe p 277 A93-52412
- Integrated fiber optic probe for dynamic light scattering p 278 A93-52415
- Fiber-optic thermometer using Fourier transform spectroscopy p 212 A93-53104
- Multiple fiberoptic probe for several sensing applications p 212 A93-53109
- Fiberoptic sensing technique employing RF modulated interferometry p 212 A93-53110
- Phase-stepping fiber-optic projected fringe system for surface topography measurements [NASA-CASE-LEW-14996-1] p 278 N93-11058
- OTV bearing deflection investigation [NASA-TM-106085] p 215 N93-22994
- A fiber optic probe for the detection of cataracts p 257 N93-25593
- Status of the Fiber Optic Control System Integration (FOCSI) program [NASA-TM-106151] p 217 N93-28053
- FIBER ORIENTATION**
- Acousto-Ultrasonic analysis of failure in ceramic matrix composite tensile specimens [NASA-TM-106219] p 232 N93-29073
- FIBER STRENGTH**
- Relative sliding durability of two candidate high-temperature oxide fiber seal materials p 132 A93-31983
- Effect of high temperature annealing on the microstructure of SCS-6 SiC fibers p 133 A93-39513
- Relative sliding durability of candidate high temperature fiber seal materials [NASA-TM-105806] p 95 N93-10978
- FIBERS**
- Development of braided rope seals for hypersonic engine applications - Flow modeling p 222 A93-34493
- FIELD EFFECT TRANSISTORS**
- Silicon carbide, a semiconductor for space power electronics p 279 A93-13880
- High-efficiency high-gain monolithic heterostructure FET amplifier at 31 GHz p 156 A93-37421
- The 10 kW power electronics for hydrogen arcjets [NASA-TM-105614] p 81 N93-12484
- FIGHTER AIRCRAFT**
- Computational study of advanced exhaust system transition ducts with experimental validation p 7 A93-34490
- Screening studies of advanced control concepts for airbreathing engines [AIAA PAPER 92-3320] p 26 A93-49329
- A parameter optimization approach to controller partitioning for integrated flight/propulsion control application p 41 A93-54268
- Overview of high performance aircraft propulsion research [NASA-TM-105839] p 32 N93-11530
- Screening studies of advanced control concepts for airbreathing engines [NASA-TM-106042] p 36 N93-25079
- FILM COOLING**
- Numerical study of nozzle wall cooling for nuclear thermal rockets [AIAA PAPER 93-2498] p 77 A93-50232
- Performance comparison of axisymmetric and three-dimensional hydrogen film coolant injection in a 110N hydrogen/oxygen rocket [NASA-TM-105967] p 83 N93-16714
- Small hydrogen/oxygen rocket flowfield behavior from heat flux measurements [NASA-TM-106233] p 91 N93-28619
- FILTERS**
- Molecular filter-based diagnostics in high speed flows [AIAA PAPER 93-0512] p 205 A93-23259
- FINITE DIFFERENCE THEORY**
- Some aspects of bifurcation structure of laminar flow in curved ducts p 164 A93-14771
- Finite difference solution for transient radiative cooling of a conducting semitransparent square region p 164 A93-15067
- Numerical simulations of a high Mach number jet flow [AIAA PAPER 93-0653] p 172 A93-24766
- On solving the compressible Navier-Stokes equations for unsteady flows at very low Mach numbers [AIAA PAPER 93-3368] p 181 A93-45061
- Radiation heat transfer calculations using a control-angle, control-volume-based discrete ordinates method [AIAA PAPER 93-2731] p 182 A93-46485
- Dispersion-relation-preserving finite difference schemes for computational acoustics p 274 A93-51180
- A time-accurate high-resolution TVD scheme for solving the Navier-Stokes equations p 13 A93-52006
- On an origin of numerical diffusion: Violation of invariance under space-time inversion [NASA-TM-105776] p 268 N93-11254
- Comparison of truncation error of finite-difference and finite-volume formulations of convection terms [NASA-TM-105861] p 268 N93-11531
- One-dimensional transient finite difference model of an operational salinity gradient solar pond p 193 N93-13400
- Numerical simulation of a high Mach number jet flow [NASA-TM-105985] p 197 N93-20057
- A time-accurate high-resolution TVD scheme for solving the Navier-Stokes equations [NASA-TM-106056] p 268 N93-22664
- FINITE ELEMENT METHOD**
- Three-dimensional finite element simulation of intermingled-fiber hybrid composite behavior p 98 A93-15729
- Fiber shape effects on metal matrix composite behavior p 98 A93-15752
- Computational simulation of surface waviness in graphite/epoxy woven composites due to initial curing p 98 A93-15822
- Improved accuracy for finite element structural analysis via an integrated force method p 234 A93-17246
- Modal test/analysis correlation of Space Station structures using nonlinear sensitivity [AIAA PAPER 92-4731] p 55 A93-20330
- High accuracy computation of fluid-structure interaction in transonic cascades [AIAA PAPER 93-0485] p 6 A93-23387
- A least-squares finite element method for 3D incompressible Navier-Stokes equations [AIAA PAPER 93-0338] p 171 A93-24236
- Membrane triangles with corner drilling freedoms. I - The EFF element p 235 A93-24303
- Membrane triangles with corner drilling freedoms. II - The ANDES element p 235 A93-24304
- Membrane triangles with corner drilling freedoms. III - Implementation and performance evaluation p 236 A93-24305
- Design considerations for a Space Shuttle Main Engine turbine blade made of single crystal material p 236 A93-25228
- Finite element implementation of state variable-based viscoplasticity models p 236 A93-26776
- Microfracture in high temperature metal matrix crossply laminates p 101 A93-31356
- Integrated force method - Compatibility conditions of structural mechanics for finite element analysis p 237 A93-32459
- Non-oscillatory and non-diffusive solution of convection problems by the iteratively reweighted least-squares finite element method p 177 A93-32622
- Probabilistic nonlinear finite element analysis of composite structures p 237 A93-32717
- Transition elements based on transfinite interpolation [AIAA PAPER 93-1326] p 267 A93-33899
- Binary tree eigen solver in finite element analysis [AIAA PAPER 93-1493] p 267 A93-34034
- Global/local finite element analysis for textile composites [AIAA PAPER 93-1506] p 103 A93-34045
- Finite element procedures for coupled linear analysis of heat transfer, fluid and solid mechanics [AIAA PAPER 93-1639] p 267 A93-34166
- The L sub 1 finite element method for pure convection problems p 177 A93-34326
- Modal analysis of multistage gear systems coupled with gearbox vibrations p 222 A93-36588
- Extra high speed modified Lundell alternator parameters and open/short-circuit characteristics from global 3D-FE magnetic field solutions p 156 A93-39348
- Computation of load performance and other parameters of extra high speed modified Lundell alternators from 3D-FE magnetic field solutions p 156 A93-39349

FINITE VOLUME METHOD

- Three dimensional magnetic fields in extra high speed modified Lundell alternators computed by a combined vector-scalar magnetic potential finite element method p 157 A93-39350
- Unsteady transonic two-dimensional Euler solutions using finite elements p 8 A93-39412
- On the effects of grid ill-conditioning in three dimensional finite element vector potential magnetostatic field computations p 157 A93-39719
- Theoretical and numerical difficulties in 3-D vector potential methods in finite element magnetostatic computations p 157 A93-39720
- Analysis of passive damping in thick composite structures p 241 A93-45743
- Contact stress analysis of spiral bevel gears using nonlinear finite element static analysis [AIAA PAPER 93-2296] p 224 A93-50081
- Accuracy of least-squares methods for the Navier-Stokes equations p 188 A93-52008
- Efficient finite element method for aircraft deicing problems p 21 A93-52443
- Modal element method for scattering and absorbing of sound by two-dimensional bodies p 274 A93-53657
- Comparison of radiated noise from shrouded and unshrouded propellers p 274 A93-55861
- A least-squares finite element method for incompressible Navier-Stokes problem p 191 A93-10548
- Experimental validation of boundary element methods for noise prediction [NASA-TM-105729] p 226 A93-10966
- Numerical calibration of the stable poisson loaded specimen [NASA-TM-105609] p 245 A93-12738
- Structural optimization of thin shells using finite element method [NASA-TM-105903] p 246 A93-13157
- Analysis of large quasistatic deformations of inelastic solids by a new stress based finite element method [NASA-CR-189235] p 246 A93-13260
- Modal ring method for the scattering of electromagnetic waves [NASA-TM-105966] p 149 A93-20260
- Progressive delamination in polymer matrix composite laminates: A new approach p 108 A93-21515
- Optimal design of composite hip implants using NASA technology p 257 A93-22188
- Large-scale computation of incompressible viscous flow by least-squares finite element method [NASA-TM-105904] p 269 A93-22825
- Study of the capacitance technique for measuring high-temperature blade tip clearance on ceramic rotors [NASA-TM-105978] p 35 A93-23013
- Mapping methods for computationally efficient and accurate structural reliability [NASA-TM-105892] p 248 A93-23745
- Evaluation of MARC for the analysis of rotating composite blades [NASA-TM-4423] p 249 A93-24909
- High Temperature Composite Analyzer (HITCAN) theoretical manual, version 1.0 [NASA-TM-106001] p 249 A93-24913
- High temperature composite analyzer (HITCAN) user's manual, version 1.0 p 249 A93-25070
- [NASA-TM-106002] p 249 A93-25070
- Stress distribution in composite flatwise tension test specimens [NASA-TM-106074] p 108 A93-25071
- The influence of primary and secondary orientations on the elastic response of a nickel-base single-crystal superalloy [NASA-TM-106125] p 250 A93-26550
- Contact stress analysis of spiral bevel gears using nonlinear finite element static analysis [NASA-TM-106176] p 228 A93-27037
- Small hydrogen/oxygen rocket flowfield behavior from heat flux measurements [NASA-TM-106233] p 91 A93-28619
- Accuracy of least-squares methods for the Navier-Stokes equations [NASA-TM-106209] p 202 A93-29208
- Blasim: A computational tool to assess ice impact damage on engine blades [NASA-TM-106225] p 251 A93-31193
- Mapping methods for computationally efficient and accurate structural reliability p 232 A93-31572
- A p-version finite element method for steady incompressible fluid flow and convective heat transfer [NASA-TM-106260] p 203 A93-32370
- FINITE VOLUME METHOD**
- High accuracy computation of fluid-structure interaction in transonic cascades [AIAA PAPER 93-0485] p 6 A93-23387
- Application of an unstructured grid flow solver to planes, trains and automobiles [AIAA PAPER 93-0889] p 173 A93-24949

- A numerical study of mixing in supersonic combustors with hypermixing injectors [AIAA PAPER 93-0215] p 25 A93-27801
- Comparison of truncation error of finite-difference and finite-volume formulations of convection terms [NASA-TM-105861] p 268 A93-11531
- Positivity-preserving numerical schemes for multidimensional advection [NASA-TM-106055] p 200 A93-27091
- FINS**
- Flowfield dynamics in blunt fin-induced shock wave/turbulent boundary layer interactions [AIAA PAPER 93-3133] p 11 A93-48298
- FIR FILTERS**
- Modifying real convolutional codes for protecting digital filtering systems p 148 A93-38221
- FIRE EXTINGUISHERS**
- Fire safety practices in the Shuttle and the Space Station Freedom p 59 A93-20204
- FIRE PREVENTION**
- Downward diffusion flame spread and extinction in variable gravitational fields - Lunar and Martian simulations [AIAA PAPER 93-0828] p 115 A93-24898
- Contributions of microgravity test results to the design of spacecraft fire-safety systems [AIAA PAPER 93-1152] p 56 A93-31028
- Overview of NASA's microgravity combustion science and fire safety program p 145 A93-20180
- Fire safety practices in the Shuttle and the Space Station Freedom p 59 A93-20204
- Contributions of microgravity test results to the design of spacecraft fire safety systems [NASA-TM-106093] p 60 A93-24755
- FIRES**
- Effects of buoyancy on laminar, transitional, and turbulent gas jet diffusion flames p 121 A93-20189
- Opposed-flow flame spreading in reduced gravity p 121 A93-20206
- Combustion of solid fuel in very low speed oxygen streams p 122 A93-20207
- Smoldering combustion in microgravity. USML-1 glovebox experiment No. 6 [NASA-TM-105012] p 146 A93-70290
- FISSION PRODUCTS**
- Analysis of plume backflow around a nozzle lip in a nuclear rocket [AIAA PAPER 93-2497] p 77 A93-50231
- FLAME PLATING**
- High quality flame deposited diamond films for infrared optical windows p 281 A93-40564
- FLAME PROBES**
- Design of a constant tension thermocouple rake suitable for flame studies p 210 A93-40683
- FLAME PROPAGATION**
- Premixed flame propagation in combustible particle cloud mixtures [AIAA PAPER 93-0713] p 115 A93-24808
- Computational predictions of flame spread over alcohol pools [AIAA PAPER 93-0825] p 115 A93-24895
- Numerical computation of low-speed concurrent flow flame spread in mixed buoyant and forced flow [AIAA PAPER 93-0827] p 115 A93-24897
- Downward diffusion flame spread and extinction in variable gravitational fields - Lunar and Martian simulations [AIAA PAPER 93-0828] p 115 A93-24898
- Intensified array camera imaging of solid surface combustion aboard the NASA Learjet p 143 A93-30858
- A comparison of numerical and analytical solution of the creeping flame spread over thermally thin material p 117 A93-41954
- Mechanisms of microgravity flame spread over a thin solid fuel - Oxygen and opposed flow effects p 140 A93-50368
- Premixed flame propagation in an optically thick gas p 119 A93-55381
- Combustion-wave ignition for rocket engines p 78 A93-10016
- Opposed-flow flame spreading in reduced gravity p 121 A93-20206
- Flame spread across liquid pools p 122 A93-20209
- Contributions of microgravity test results to the design of spacecraft fire safety systems [NASA-TM-106093] p 60 A93-24755
- Nitric oxide formation in a lean, premixed-prevaporized jet A/air flame tube: An experimental and analytical study [NASA-TM-105722] p 257 A93-27012
- FLAME RETARDANTS**
- Contributions of microgravity test results to the design of spacecraft fire-safety systems [AIAA PAPER 93-1152] p 56 A93-31028

FLAME STABILITY

- Flame balls - Past, present and future [AIAA PAPER 93-0712] p 114 A93-24807
- Analytical and numerical modeling of flame-balls in hydrogen-air mixtures p 118 A93-46009

FLAME TEMPERATURE

- Design of a constant tension thermocouple rake suitable for flame studies p 210 A93-40683
- A comparison of numerical and analytical solution of the creeping flame spread over thermally thin material p 117 A93-41954
- Structure of confined laminar spray diffusion flames: Numerical investigation [NASA-TM-106038] p 197 A93-22596
- Nitric oxide formation in a lean, premixed-prevaporized jet A/air flame tube: An experimental and analytical study [NASA-TM-105722] p 257 A93-27012

FLAMES

- Laser-induced fluorescence measurements of nitric oxide in laminar C₂H₆/O₂/N₂ flames at high pressure p 116 A93-28253
- Effects of buoyancy on laminar, transitional, and turbulent gas jet diffusion flames p 121 A93-20189
- Soot formation and radiation in turbulent jet diffusion flames under normal and reduced gravity conditions p 121 A93-20192
- Visualization and imaging methods for flames in microgravity p 121 A93-20193
- Selected microgravity combustion diagnostic techniques p 121 A93-20194
- Fire safety practices in the Shuttle and the Space Station Freedom p 59 A93-20204
- Opposed-flow flame spreading in reduced gravity p 121 A93-20206
- Combustion of solid fuel in very low speed oxygen streams p 122 A93-20207
- Flame spread across liquid pools p 122 A93-20209
- Contributions of microgravity test results to the design of spacecraft fire safety systems [NASA-TM-106093] p 60 A93-24755

FLAMMABILITY

- Contributions of microgravity test results to the design of spacecraft fire safety systems [NASA-TM-106093] p 60 A93-24755
- Smoldering combustion in microgravity. USML-1 glovebox experiment No. 6 [NASA-TM-105012] p 146 A93-70290

FLAT PLATES

- Discussion of 'Comparison of turbulence models for the natural convection boundary layer along a heated vertical plate' p 168 A93-21717
- A note on the distortion of a flat-plate boundary layer by free-stream vorticity normal to the plate p 178 A93-34414

FLAT SURFACES

- Direct numerical simulation of instabilities in parallel flow with spherical roughness elements [NASA-TM-105847] p 192 A93-11529

FLEXIBILITY

- Implementation of the block-Krylov boundary flexibility method of component synthesis [NASA-TM-106065] p 248 A93-23044

FLEXIBLE BODIES

- Dynamic analysis of flexible gear trains/transmissions - An automated approach p 220 A93-22440
- Time-variant analysis of rotorcraft systems dynamics - An exploitation of vector processors p 220 A93-23512

- Dynamic modeling and control of multibody mechanical systems which are structurally flexible p 264 A93-29338

- Analysis of passive damping in thick composite structures p 241 A93-45743

FLEXING

- Transverse flexural tests as a tool for assessing damage to PMR-15 composites from isothermal aging in air at elevated temperatures p 100 A93-24514

- Transverse flexural tests as a tool for assessing damage to PMR-15 composites from isothermal aging in air at elevated temperatures [NASA-TM-105848] p 107 A93-12737

- Fuzzy sets predict flexural strength and density of silicon nitride ceramics [NASA-TM-106049] p 110 A93-27270

FLIGHT CHARACTERISTICS

- A modified approach to controller partitioning [NASA-TM-106167] p 266 A93-28051

FLIGHT CONTROL

- Robust integrated flight/propulsion control design for a STOLV aircraft using H-infinity control design techniques p 40 A93-26432

- Review of the FOCSI (Fiber Optic Control System Integration) program --- applications in aircraft flight control p 21 A93-32916

- Design and evaluation of a robust dynamic neurocontroller for a multivariable aircraft control problem p 40 A93-37004
- Application of controller partitioning optimization procedure to integrated flight/propulsion control design for a STOVL aircraft p 40 A93-51361
- [AIAA PAPER 93-3766] p 40 A93-51361
- Integrated flight/propulsion control - Subsystem specifications for performance p 41 A93-51400
- [AIAA PAPER 93-3808] p 41 A93-51400
- A comparative study of multivariable robustness analysis methods as applied to integrated flight and propulsion control p 21 A93-51401
- [AIAA PAPER 93-3809] p 21 A93-51401
- Antiwindup analysis and design approaches for MIMO systems p 30 A93-51403
- [AIAA PAPER 93-3811] p 30 A93-51403
- A parameter optimization approach to controller partitioning for integrated flight/propulsion control application p 41 A93-54268
- [AIAA PAPER 93-3809] p 41 A93-54268
- Controller partitioning for integrated flight/propulsion control implementation p 41 N93-21197
- [NASA-TM-105804] p 41 N93-21197
- FLIGHT ENVELOPES**
- Icing effects on aircraft stability and control determined from flight data - Preliminary results p 40 A93-23073
- [AIAA PAPER 93-0398] p 40 A93-23073
- Icing effects on aircraft stability and control determined from flight data - Preliminary results p 41 N93-14831
- [NASA-TM-105977] p 41 N93-14831
- FLIGHT HAZARDS**
- Two and three-dimensional prediffuser combustor studies with air-water mixture p 113 A93-22652
- [AIAA PAPER 93-0240] p 113 A93-22652
- FLIGHT OPTIMIZATION**
- Application of controller partitioning optimization procedure to integrated flight/propulsion control design for a STOVL aircraft p 40 A93-51361
- [AIAA PAPER 93-3766] p 40 A93-51361
- FLIGHT SAFETY**
- Aircraft icing problems - After 50 years p 19 A93-24239
- [AIAA PAPER 93-0392] p 19 A93-24239
- FLIGHT TESTS**
- Icing effects on aircraft stability and control determined from flight data - Preliminary results p 40 A93-23073
- [AIAA PAPER 93-0398] p 40 A93-23073
- Liquid water content measurements using the Phase Doppler Particle Analyzer in the NASA Lewis Icing Research Tunnel p 42 A93-23698
- [AIAA PAPER 93-0298] p 42 A93-23698
- Flight testing of a fiber optic temperature sensor p 22 A93-49476
- [AIAA PAPER 93-0298] p 22 A93-49476
- Icing effects on aircraft stability and control determined from flight data: Preliminary results p 41 N93-14831
- [NASA-TM-105977] p 41 N93-14831
- Summary and recommendations on nuclear electric propulsion technology for the space exploration initiative p 86 N93-24744
- [NASA-TM-105707] p 86 N93-24744
- Status of the Fiber Optic Control System Integration (FOCSI) program p 217 N93-28053
- [NASA-TM-106151] p 217 N93-28053
- FLIGHT ZONES**
- Thermal oscillations in materials processing p 162 A93-10839
- [AIAA PAPER 93-0488] p 162 A93-10839
- On the shear stabilization of capillary break-up of finite liquid bridges p 143 A93-32069
- [AIAA PAPER 93-0488] p 143 A93-32069
- FLOW CHARACTERISTICS**
- Stirling engine - Available tools for long-life assessment --- for space propulsion p 65 A93-13824
- [AIAA PAPER 93-13824] p 65 A93-13824
- Some aspects of bifurcation structure of laminar flow in curved ducts p 164 A93-14771
- [AIAA PAPER 93-14771] p 164 A93-14771
- The development of a turbulent junction vortex system p 168 A93-22258
- [AIAA PAPER 93-22258] p 168 A93-22258
- Effects of free-stream turbulence on boundary-layer transition p 170 A93-23390
- [AIAA PAPER 93-0488] p 170 A93-23390
- Multiple large-scale coherent mode interactions in a developing round jet p 178 A93-34409
- [AIAA PAPER 93-34409] p 178 A93-34409
- An investigation of shock wave turbulent boundary layer interaction with bleed through slanted slots p 11 A93-48184
- [AIAA PAPER 93-2992] p 11 A93-48184
- CFD analyses of coolant channel flowfields p 184 A93-49715
- [AIAA PAPER 93-1830] p 184 A93-49715
- Effects of flow-path variations on internal reversing flow in a tailpipe offtake configuration for ASTOVL aircraft p 29 A93-50190
- [AIAA PAPER 93-2438] p 29 A93-50190
- Flow visualization in a single simulated brush seal p 226 A93-54659
- [AIAA PAPER 93-54659] p 226 A93-54659
- Effects of flow-path variations on internal reversing flow in a tailpipe offtake configuration for ASTOVL aircraft p 38 N93-29065
- [NASA-TM-106149] p 38 N93-29065
- NASA Lewis Research Center/IFMD inlet duct and nozzle high speed validation experiments p 204 N93-70582
- [AIAA PAPER 93-204] p 204 N93-70582
- NASA low speed centrifugal compressor p 204 N93-70583
- [AIAA PAPER 93-204] p 204 N93-70583
- FLOW DISTORTION**
- A note on the distortion of a flat-plate boundary layer by free-stream vorticity normal to the plate p 178 A93-34414
- [AIAA PAPER 93-34414] p 178 A93-34414
- FLOW DISTORTION**
- Study on vortex flow control of inlet distortion p 2 A93-14520
- [AIAA PAPER 93-14520] p 2 A93-14520
- Calculation of a circular jet in crossflow with a multiple-time-scale turbulence model p 164 A93-15063
- [AIAA PAPER 93-15063] p 164 A93-15063
- Experimental and computational investigation of the NASA Low-Speed Centrifugal Compressor flow field p 4 A93-19436
- [ASME PAPER 92-GT-213] p 4 A93-19436
- LDV flowfield measurements on a straight and swept wing with a simulated ice accretion p 5 A93-23001
- [AIAA PAPER 93-0300] p 5 A93-23001
- Ice accretion and performance degradation calculations with LEWICE/NS p 18 A93-23244
- [AIAA PAPER 93-0173] p 18 A93-23244
- Estimation of unsteady lift on a pitching airfoil from wake velocity surveys p 5 A93-23351
- [AIAA PAPER 93-0437] p 5 A93-23351
- An experimental investigation of S-duct flow control using arrays of low-profile vortex generators p 170 A93-24226
- [AIAA PAPER 93-0018] p 170 A93-24226
- Navier-Stokes calculations for the unsteady flowfield of turbomachinery p 6 A93-24786
- [AIAA PAPER 93-0676] p 6 A93-24786
- Use of surface heat transfer measurements as a flow separation diagnostic in a two-dimensional reflected oblique shock/turbulent boundary layer interaction p 172 A93-24859
- [AIAA PAPER 93-0775] p 172 A93-24859
- Application of an unstructured grid flow solver to planes, trains and automobiles p 173 A93-24949
- [AIAA PAPER 93-0889] p 173 A93-24949
- Overview of NASA supported Stirling thermodynamic loss research p 174 A93-26087
- [AIAA PAPER 93-0889] p 174 A93-26087
- Effect of tabs on the flow and noise field of an axisymmetric jet p 25 A93-30833
- [AIAA PAPER 93-0889] p 25 A93-30833
- Critical comparison of second-order closures with direct numerical simulations of homogeneous turbulence p 176 A93-30840
- [AIAA PAPER 93-0889] p 176 A93-30840
- Computation of unsteady supersonic quasi-one-dimensional viscous-inviscid interacting internal flowfields p 177 A93-32724
- [AIAA PAPER 93-0889] p 177 A93-32724
- Ground-based PIV and numerical flow visualization results from the Surface Tension Driven Convection Experiment p 143 A93-33075
- [AIAA PAPER 93-0889] p 143 A93-33075
- Fluid flow of a row of jets in crossflow - A numerical study p 179 A93-35608
- [AIAA PAPER 93-0889] p 179 A93-35608
- PNS predictions for supersonic/hypersonic flows over finned missile configurations p 7 A93-37374
- [AIAA PAPER 92-2695] p 7 A93-37374
- Hypersonic stability and transition p 8 A93-42579
- [AIAA PAPER 93-0889] p 8 A93-42579
- CFD for hypersonic propulsion p 8 A93-42585
- [AIAA PAPER 93-0889] p 8 A93-42585
- Vorticity dynamics of inviscid shear layers p 181 A93-45734
- [AIAA PAPER 93-0889] p 181 A93-45734
- Low-to-high altitude predictions of three-dimensional ablative re-entry flowfields p 182 A93-46407
- [AIAA PAPER 93-0889] p 182 A93-46407
- Streamwise computation of three-dimensional flows using two stream functions p 184 A93-49241
- [AIAA PAPER 93-0889] p 184 A93-49241
- Calculation of scramjet inlet with thick boundary-layer ingestion p 12 A93-49720
- [AIAA PAPER 93-1836] p 12 A93-49720
- Unsteady aerodynamic flow phenomena in a transonic compressor stage p 12 A93-49743
- [AIAA PAPER 93-1868] p 12 A93-49743
- Computation of the flow field in an annular gas turbine combustor p 28 A93-49903
- [AIAA PAPER 93-2074] p 28 A93-49903
- Time-sequenced and spectrally filtered Rayleigh imaging of shock wave and boundary layer structure for inlet characterization p 211 A93-50085
- [AIAA PAPER 93-2300] p 211 A93-50085
- Comparison of reacting and non-reacting shear layers at a high subsonic Mach number p 186 A93-50149
- [AIAA PAPER 93-2381] p 186 A93-50149
- Three-dimensional numerical simulation of gradual opening in a wave rotor passage p 187 A93-50254
- [AIAA PAPER 93-2526] p 187 A93-50254
- Navier-Stokes analysis of radial turbine rotor performance p 30 A93-50277
- [AIAA PAPER 93-2555] p 30 A93-50277
- Chimera grids in the simulation of three-dimensional flowfields in turbine-blade-coolant passages p 187 A93-50280
- [AIAA PAPER 93-2559] p 187 A93-50280
- Measurements and computational analysis of heat transfer and flow in a simulated turbine blade internal cooling passage p 189 A93-53585
- [AIAA PAPER 93-1797] p 189 A93-53585
- Laser velocimeter measurements of the flow field generated by a forward-swept propfan during flutter p 14 A93-53591
- [AIAA PAPER 93-2919] p 14 A93-53591
- Direct numerical simulation of instabilities in parallel flow with spherical roughness elements p 192 N93-11529
- [NASA-TM-105847] p 192 N93-11529
- Supersonic boundary-layer flow turbulence modeling [NASA-TM-105893] p 193 N93-14758
- Estimation of unsteady lift on a pitching airfoil from wake velocity surveys p 15 N93-14791
- [NASA-TM-105947] p 15 N93-14791
- Ice accretion and performance degradation calculations with LEWICE/NS p 19 N93-15354
- [NASA-TM-105972] p 19 N93-15354
- Use of surface heat transfer measurements as a flow separation diagnostic in a two dimensional reflected oblique shock/turbulent boundary layer interaction p 194 N93-15355
- [NASA-TM-105981] p 194 N93-15355
- An integral equation solution for multistage turbomachinery design calculations p 33 N93-15521
- [NASA-TM-105970] p 33 N93-15521
- Turbulence modeling and experiments p 195 N93-15796
- [NASA-TM-105970] p 195 N93-15796
- Modeling of turbulent shear flows p 195 N93-15797
- Two equation modelling and the pseudo compressibility technique p 195 N93-15799
- [NASA-TM-105970] p 195 N93-15799
- Physical vapor transport of mercurous chloride under a nonlinear thermal profile p 196 N93-16612
- [NASA-TM-105920] p 196 N93-16612
- Mathematical relationship between two sets of laser anemometer measurements for resolving the total velocity vector p 35 N93-22599
- [NASA-TM-105986] p 35 N93-22599
- A three-dimensional algebraic grid generation scheme for gas turbine combustors with inclined slots p 198 N93-24759
- [NASA-CR-191095] p 198 N93-24759
- Surface and flow field measurements in a symmetric crossing shock wave/turbulent boundary-layer interaction p 17 N93-24911
- [NASA-TM-106086] p 17 N93-24911
- Measurement and analysis of a small nozzle plume in vacuum p 88 N93-26561
- [NASA-TM-106066] p 88 N93-26561
- Comparison of reacting and non-reacting shear layers at a high subsonic Mach number p 38 N93-27610
- [NASA-TM-106198] p 38 N93-27610
- Small hydrogen/oxygen rocket flowfield behavior from heat flux measurements p 91 N93-28619
- [NASA-TM-106233] p 91 N93-28619
- Measurements and computational analysis of heat transfer and flow in a simulated turbine blade internal cooling passage p 203 N93-31647
- [NASA-TM-106189] p 203 N93-31647
- FLOW EQUATIONS**
- Modeling of linear isentropic flow systems p 179 A93-37046
- [AIAA PAPER 93-3074] p 179 A93-37046
- High order accurate solutions of viscous problems p 183 A93-48249
- [AIAA PAPER 93-3074] p 183 A93-48249
- Preliminary experimental results for a cryogenic brush seal configuration p 225 A93-50262
- [AIAA PAPER 93-2535] p 225 A93-50262
- Navier-Stokes turbine heat transfer predictions using two-equation turbulence p 191 N93-10735
- [NASA-TM-105817] p 191 N93-10735
- An integral equation solution for multistage turbomachinery design calculations p 33 N93-15521
- [NASA-TM-105970] p 33 N93-15521
- Preliminary experimental results for a cryogenic brush seal configuration p 201 N93-28627
- [NASA-TM-106236] p 201 N93-28627
- FLOW GEOMETRY**
- A coupled multi-block solution procedure for spray combustion in complex geometries p 171 A93-24230
- [AIAA PAPER 93-0108] p 171 A93-24230
- Multiple large-scale coherent mode interactions in a developing round jet p 178 A93-34409
- [AIAA PAPER 93-34409] p 178 A93-34409
- An accuracy assessment of Cartesian-mesh approaches for the Euler equations p 9 A93-45029
- [AIAA PAPER 93-3335] p 9 A93-45029
- Linear instability of curved free shear layers p 183 A93-46797
- [AIAA PAPER 93-3252] p 183 A93-46797
- Intake flow modeling in a four stroke diesel using KIVA3 p 183 A93-48146
- [AIAA PAPER 93-2952] p 183 A93-48146
- Internal structure of shock waves in disparate mass mixtures p 190 A93-54483
- [AIAA PAPER 93-2952] p 190 A93-54483
- A new energy transfer model for turbulent free shear flow p 191 N93-10454
- [NASA-TM-105854] p 191 N93-10454
- 2nd NASA CFD Validation Workshop --- Author p 203 N93-70575
- [NASA-TM-107972] p 203 N93-70575
- FLOW MEASUREMENT**
- High-speed laser anemometry based on spectrally resolved Rayleigh scattering p 207 A93-23814
- [AIAA PAPER 93-23814] p 207 A93-23814
- Measurement and analysis of a small nozzle plume in vacuum p 71 A93-42895
- [AIAA PAPER 93-3335] p 71 A93-42895
- Gas temperature and density measurements based on spectrally resolved Rayleigh-Brillouin scattering p 214 N93-13684
- [NASA-TM-105999] p 214 N93-13684
- Laser Rayleigh and Raman diagnostics for small hydrogen/oxygen rockets p 83 N93-17995
- [NASA-TM-105999] p 83 N93-17995

- Surface and flow field measurements in a symmetric crossing shock wave/turbulent boundary-layer interaction
[NASA-TM-106086] p 17 N93-24911
- Pulsed laser Rayleigh scattering diagnostic for hydrogen/oxygen rocket exit plane flowfield velocimetry
[NASA-TM-106213] p 88 N93-26149
- Fuzzy logic particle tracking velocimetry
[NASA-TM-106194] p 216 N93-27027
- Turbulence measurement in a reacting and non-reacting shear layer at a high subsonic Mach number
[NASA-TM-106186] p 18 N93-31839
- 2nd NASA CFD Validation Workshop --- Author
[NASA-TM-107972] p 203 N93-70575
- Summary of NASA Lewis Research Center validation efforts
p 204 N93-70579
- NASA low speed centrifugal compressor
p 204 N93-70583
- FLOW STABILITY**
- Non-parallel effects in the instability of Long's vortex
p 164 A93-16663
- Stability of fully developed rotating stall
[ASME PAPER 92-GT-57] p 23 A93-19307
- Flow-influenced stabilization of liquid columns in a dynamic plateau chamber
[AIAA PAPER 93-0255] p 169 A93-22664
- Effects of free-stream turbulence on boundary-layer transition
[AIAA PAPER 93-0488] p 170 A93-23390
- Preconditioned Conjugate Gradient methods for low speed flow calculations
[AIAA PAPER 93-0881] p 172 A93-24942
- On the shear stabilization of capillary break-up of finite liquid bridges
p 143 A93-32069
- The coupling of interfacial instabilities and the stabilization of two-layer annular flows
p 178 A93-35482
- Convective effects during the physical vapor transport process. II - Thermosolutal convection
p 180 A93-42424
- Hypersonic stability and transition
p 8 A93-42579
- Flow instability in particle-bed nuclear reactors
[AIAA PAPER 93-1758] p 71 A93-49657
- A model for the selective amplification of spatially coherent waves in a centrifugal compressor on the verge of rotating stall
[AIAA PAPER 93-2236] p 13 A93-50039
- Preconditioned conjugate-gradient methods for low-speed flow calculations
[NASA-TM-105929] p 194 A93-14885
- On the nonlinear three dimensional instability of Stokes layers and other shear layers to pairs of oblique waves
[NASA-TM-105918] p 194 A93-15499
- Positivity-preserving numerical schemes for multidimensional advection
[NASA-TM-106055] p 200 N93-27091
- FLOW THEORY**
- 2nd NASA CFD Validation Workshop --- Author
[NASA-TM-107972] p 203 N93-70575
- Summary of NASA Lewis Research Center validation efforts
p 204 N93-70579
- FLOW VELOCITY**
- Forcing function effects on unsteady aerodynamic gust response. I - Forcing functions
[ASME PAPER 92-GT-174] p 3 A93-19400
- Flow-influenced stabilization of liquid columns in a dynamic plateau chamber
[AIAA PAPER 93-0255] p 169 A93-22664
- The effects of buoyancy on the critical heat flux in forced convection
[AIAA PAPER 93-0575] p 169 A93-23307
- Effect of a rotating propeller on the separation angle of attack
[AIAA PAPER 93-0017] p 6 A93-24978
- The structure of a three-dimensional turbulent boundary layer
p 181 A93-44813
- Performance of a low-power subsonic-arc-attachment arcjet thruster
[AIAA PAPER 93-1898] p 72 A93-49768
- Mixing and transient interface condensation of a liquid hydrogen tank
[AIAA PAPER 93-1968] p 184 A93-49816
- Nonintrusive, multipoint velocity measurements in high-pressure combustion flows
[AIAA PAPER 93-2032] p 118 A93-49867
- Gravity sensitivity of a resistojet water vaporizer
[AIAA PAPER 93-2402] p 186 A93-50167
- Three-dimensional flow field in a turbine nozzle passage
[AIAA PAPER 93-2556] p 13 A93-50278
- Development of braided rope seals for hypersonic engine applications. Flow modeling
[NASA-TM-105942] p 227 N93-14478
- Experiments on a round turbulent buoyant plume
[NASA-TM-105955] p 141 N93-16384
- Effect of a rotating propeller on the separation angle of attack and distortion in ducted propeller inlets
[NASA-TM-105935] p 16 N93-16625
- Fuzzy logic particle tracking velocimetry
[NASA-TM-106194] p 216 N93-27027
- Mixing and transient interface condensation of a liquid hydrogen tank
[NASA-TM-106201] p 201 N93-28252
- Gravity sensitivity of a resistojet water vaporizer
[NASA-TM-106220] p 92 N93-29194
- FLOW VISUALIZATION**
- Fully coupled resonant-triad interaction in an adverse-pressure-gradient boundary layer
p 167 A93-21049
- On streamwise vortices in high Reynolds number supersonic axisymmetric jets
p 167 A93-21060
- A study of compressible mixing layers using filtered Rayleigh scattering
[AIAA PAPER 92-0175] p 173 A93-24982
- Visualization of entry flow separation for oscillating flow in tubes
p 174 A93-26091
- Gallery of fluid motion
p 178 A93-35481
- Time-sequenced and spectrally filtered Rayleigh imaging of shock wave and boundary layer structure for inlet characterization
[AIAA PAPER 93-2300] p 211 A93-50085
- Unsteady wing surface pressures in the wake of a propeller
p 14 A93-52436
- Flow visualization in a single simulated brush seal
p 226 A93-54659
- Visualization of hydrogen injection in a scramjet engine by simultaneous PLIF imaging and laser holographic imaging
p 214 A93-13683
- Visualization and imaging methods for flames in microgravity
p 121 N93-20193
- Neural networks for calibration tomography
[NASA-TM-106352] p 216 N93-26906
- Calibration of a shock wave position sensor using artificial neural networks
[NASA-TM-106138] p 216 N93-27001
- FLOWMETERS**
- A new hue capturing technique for the quantitative interpretation of liquid crystal images used in convective heat transfer studies
p 204 A93-13977
- FLUENCE**
- Determination of atomic oxygen fluence using spectrophotometric analysis of infrared transparent witness coupons for long duration exposure tests
[NASA-TM-106021] p 96 N93-22605
- FLUID DYNAMICS**
- Calculation of a circular jet in crossflow with a multiple-time-scale turbulence model
p 164 A93-15063
- An interface configuration experiment on USML-1
[AIAA PAPER 93-0253] p 169 A93-22662
- Three-dimensional computed tomography from interferometric measurements within a narrow cone of views
p 207 A93-24024
- Critical comparison of second-order closures with direct numerical simulations of homogeneous turbulence
p 176 A93-30840
- An efficient procedure for cascade aeroelastic stability determination using nonlinear, time-marching aerodynamic solvers
[AIAA PAPER 93-1631] p 25 A93-34159
- An efficient and robust algorithm for two dimensional time dependent incompressible Navier-Stokes equations - High Reynolds number flows
p 178 A93-34371
- Fluid dynamics and convective heat transfer in impinging jets through implementation of a high resolution liquid crystal technique
[ISABE 93-7077] p 189 A93-54053
- Selected OAST/OSSA space experiment activities in support of Space Station Freedom
p 60 N93-22636
- Conceptual design for the Space Station Freedom fluid physics/dynamics facility
[NASA-TM-103663] p 61 N93-26209
- FLUID FILLED SHELLS**
- On the structure of cellular solutions in Rayleigh-Benard-Marangoni flows in small-aspect-ratio containers
p 164 A93-14762
- FLUID FILMS**
- Simultaneous pressure measurement and high-speed photography study of cavitation in a dynamically loaded journal bearing
p 223 A93-40050
- New technique for oil backstreaming contamination measurements
p 210 A93-44514
- Effect of fluid compressibility on journal bearing performance
p 223 A93-49244
- Collapse of the soap-film bridge - Quasistatic description
p 188 A93-50536
- FLUID FLOW**
- Preconditioned Conjugate Gradient methods for low speed flow calculations
[AIAA PAPER 93-0881] p 172 A93-24942
- Critical comparison of second-order closures with direct numerical simulations of homogeneous turbulence
p 176 A93-30840
- Ground-based PIV and numerical flow visualization results from the Surface Tension Driven Convection Experiment
p 143 A93-33075
- An efficient and robust algorithm for two dimensional time dependent incompressible Navier-Stokes equations - High Reynolds number flows
p 178 A93-34371
- Development of braided rope seals for hypersonic engine applications - Flow modeling
p 222 A93-34493
- Development of braided rope seals for hypersonic engine applications. Flow modeling
[NASA-TM-105942] p 227 N93-14478
- Preconditioned conjugate-gradient methods for low-speed flow calculations
[NASA-TM-105929] p 194 A93-14885
- FLUID INJECTION**
- Performance comparison of axisymmetric and three-dimensional hydrogen film coolant injection in a 110N hydrogen/oxygen rocket
[NASA-TM-105967] p 83 N93-16714
- FLUID JETS**
- Mixing and transient interface condensation of a liquid hydrogen tank
[AIAA PAPER 93-1968] p 184 A93-49816
- Experimental investigation of crossflow jet mixing in a rectangular duct
[AIAA PAPER 93-2037] p 185 A93-49872
- Experimental investigation of crossflow jet mixing in a rectangular duct
[NASA-TM-106152] p 36 N93-27026
- Mixing and transient interface condensation of a liquid hydrogen tank
[NASA-TM-106201] p 201 N93-28252
- FLUID MANAGEMENT**
- Tank chilldown analysis and verification with a flightweight, 175 cu ft tank under normal gravity with liquid hydrogen
p 140 N93-10045
- COLD-SAT dynamic model
[NASA-TM-105185] p 59 N93-19988
- Orbital storage and supply of subcritical liquid nitrogen
p 62 N93-27801
- Fluid management system technology discipline
p 62 N93-27861
- Cryogenic fluid management (base R/T): Cryogenic fluid systems, Cryogenic Orbital Nitrogen Experiment (CONE), Cryogenic Orbital Hydrogen Experiment (COHE), (Transportation focused technology)
[PR6] p 286 N93-71879
- FLUID MECHANICS**
- A review of design concepts for the Advanced Fluids Module (AFM) project
[AIAA PAPER 93-0258] p 43 A93-23700
- Finite element procedures for coupled linear analysis of heat transfer, fluid and solid mechanics
[AIAA PAPER 93-1639] p 267 A93-34166
- Computer modeling of a hot filament diamond deposition reactor
p 94 A93-40618
- Current status of liquid sheet radiator research
[NASA-TM-105764] p 193 N93-14150
- Summary of NASA Lewis Research Center validation efforts
p 204 N93-70579
- FLUOROPOLYMERS**
- Interfacial chemistry of a perfluoropolyether lubricant studied by X-ray photoelectron spectroscopy and temperature desorption spectroscopy
p 133 A93-38473
- Interfacial chemistry of a perfluoropolyether lubricant studied by XPS and TDS
[NASA-TM-106014] p 137 N93-22560
- Determination of the thermal stability of perfluoropolyalkyl ethers by tensimetry
[NASA-TM-106081] p 137 N93-25093
- FLUTTER**
- Unsteady aerodynamics and flutter of propfans using a three-dimensional Full-Potential Solver
[AIAA PAPER 93-1633] p 25 A93-34161
- Unsteady aerodynamics and flutter based on the potential equation
[AIAA PAPER 93-2086] p 13 A93-49913
- Laser velocimeter measurements of the flow field generated by a forward-swept propfan during flutter
[AIAA PAPER 93-2919] p 14 A93-53591
- FLUTTER ANALYSIS**
- Semi-empirical model for prediction of unsteady forces on an airfoil with application to flutter
p 7 A93-31494
- Blade row interaction effects on flutter and forced response
[AIAA PAPER 93-2084] p 28 A93-49911
- FLUX (RATE)**
- A new flux conserving Newton's method scheme for the two-dimensional, steady Navier-Stokes equations
[NASA-TM-106160] p 201 N93-28626

FLUX DENSITY

- Battery selection for space experiments p 159 A93-13184
- Battery selection for Space Shuttle experiments [NASA-TM-106142] p 61 N93-27038

FLUX PINNING

- Giant suppression of flux-flow resistivity in heavy-ion irradiated $\text{Ti2Ba2Ca2Cu3O}_{10}$ films - Influence of linear defects on vortex transport p 280 A93-26198

FLUX VECTOR SPLITTING

- Segmented multigrid domain decomposition procedure for incompressible viscous flows p 99 A93-19123
- Stable and low diffusive hybrid upwind splitting methods [ONERA, TP NO. 1992-113] p 179 A93-38589
- Field by field hybrid upwind splitting methods [AIAA PAPER 93-3302] p 8 A93-45000
- A new flux splitting scheme p 9 A93-47189
- A three-dimensional pressure flux-split RNS application to sub/supersonic flow in inlets and ducts [AIAA PAPER 93-3063] p 11 A93-48239
- An extended Lagrangian method [NASA-TM-106129] p 199 N93-26203

FLYWHEELS

- Electric and hybrid electric vehicle study utilizing a time-stepping simulation p 287 A93-26012

FOILS

- Calculation of stiffness and damping coefficients for elastically supported gas foil bearings p 221 A93-27308

FORCE DISTRIBUTION

- Determination of forces in a magnetic bearing actuator - Numerical computation with comparison to experiment p 219 A93-15686
- Integrated force method - Compatibility conditions of structural mechanics for finite element analysis p 237 A93-32459

FORCED CONVECTION

- The effects of buoyancy on the critical heat flux in forced convection [AIAA PAPER 93-0575] p 169 A93-23307
- Numerical computation of low-speed concurrent flow flame spread in mixed buoyant and forced flow [AIAA PAPER 93-0827] p 115 A93-24897

FORECASTING

- Key issues in space nuclear power challenges for the future p 65 A93-13905

FORWARD SCATTERING

- Calibration of the forward-scattering spectrometer probe - Modeling scattering from a multimode laser beam p 212 A93-51239
- Experimental testing of four correction algorithms for the forward scattering spectrometer probe [NASA-TM-105906] p 213 N93-13307

FOSSIL FUELS

- Electric and hybrid electric vehicle study utilizing a time-stepping simulation p 287 A93-26012

FOURIER TRANSFORMATION

- The three-point correlation function in an ensemble of three-dimensional simulations ... in gravitational perturbation theory p 291 A93-50680
- Fiber-optic thermometer using Fourier transform spectroscopy p 212 A93-53104

FRACTALS

- Desktop chaotic systems: Intuition and visualization [NASA-TM-106258] p 269 N93-31847

FRACTURE MECHANICS

- Interaction of cracks between two adjacent indents in glass p 132 A93-27115
- Deformation and failure mechanisms in metal matrix composites p 102 A93-31359
- Thermally-driven microfracture in high temperature metal matrix composites p 237 A93-32469
- A numerical round robin for the reliability prediction of structural ceramics [AIAA PAPER 93-1498] p 240 A93-34038
- Model of brittle matrix composite toughening based on discrete fiber reinforcement p 104 A93-40888
- Variation of the energy release rate as a crack approaches and passes through an elastic inclusion p 241 A93-44440
- Effect of environment on fracture toughness of 96 wt pct alumina p 134 A93-44955
- Subcritical crack growth in soda-lime glass in combined mode I and mode II loading p 134 A93-52151
- Elastic interactions of a fatigue crack with a micro-defect by the mixed boundary integral equation method p 243 A93-56412
- Calculation of stress intensity factors in an isotropic multiracked plate: Part 2: Symbolic/numeric implementation [NASA-TM-105823] p 244 N93-10453
- Calculation of stress intensity factors in an isotropic multiracked plate: Part 1: Theoretical development [NASA-TM-105766] p 244 N93-10455

- Closed form expressions for crack mouth displacements and stress intensity factors for chevron notched short bar and short rod specimens based on experimental compliance measurements [NASA-TM-83796] p 246 N93-15369
- Overview of the fatigue/fracture/life prediction working group program at the Lewis Research Center p 232 N93-31574

- Stress-rupture behavior of small diameter polycrystalline alumina fibers [NASA-TM-106256] p 139 N93-32382

FRACTURE STRENGTH

- Indentation flaw formation and strength response of silicon nitride ceramics at low indentation loads p 130 A93-15994
- Effects of precracking methods on the fracture properties of alumina p 131 A93-16645
- Fracture toughness testing of polymer matrix composites p 99 A93-18709
- Fracture toughness of advanced ceramics at room temperature p 131 A93-20842
- Evaluation of the fracture toughness of Nb-40Al-8Cr-1W-1Y-0.05B intermetallic material by indentation techniques p 124 A93-24066
- Analysis of precracking parameters for ceramic single-edge-precracked-beam specimens p 133 A93-38887
- Elevated-temperature fracture resistances of monolithic and composite ceramics using chevron-notched bend tests p 133 A93-38888
- Effect of environment on fracture toughness of 96 wt pct alumina p 134 A93-44955
- Analysis of precracking parameters and fracture toughness for ceramic single-edge-precracked-beam specimens [NASA-TM-105568] p 135 N93-10962
- Fracture toughness testing of polymer matrix composites [NASA-TP-3199] p 107 N93-12302
- Numerical calibration of the stable poisson loaded specimen [NASA-TM-105609] p 245 N93-12738
- Effects of thermal and mechanical fatigue on the flexural strength of G40-600/PMR-15 cross-ply laminates [NASA-TM-106016] p 108 N93-20317
- Progressive delamination in polymer matrix composite laminates: A new approach p 108 N93-21515
- Considerations concerning fatigue life of metal matrix composites [NASA-TM-106144] p 250 N93-27009
- Fuzzy sets predict flexural strength and density of silicon nitride ceramics [NASA-TM-106049] p 110 N93-27270

FRACTURES (MATERIALS)

- Microfracture in high temperature metal matrix crossply laminates p 101 A93-31356
- Thermally-driven microfracture in high temperature metal matrix composites p 237 A93-32469
- Nondestructive evaluation of ceramic and metal matrix composites for NASA's HITEMP and enabling propulsion materials programs [NASA-TM-105807] p 231 N93-10963

FRACTURING

- Ceramic component reliability with the restructured NASA/CARES computer program [ASME PAPER 92-GT-383] p 234 A93-19540
- Thermally-driven microfracture in high temperature metal matrix composites p 237 A93-32469
- A creep cavity growth model for creep-fatigue life prediction of a unidirectional W/Cu composite [NASA-TM-105780] p 244 N93-10967
- Ceramic component reliability with the restructured NASA/CARES computer program [NASA-TM-105856] p 244 N93-11004

FREE BOUNDARIES

- RIPPLE - A new model for incompressible flows with free surfaces p 164 A93-14551
- Surface tension effects on the onset of double-diffusive convection p 180 A93-41710

FREE CONVECTION

- Effect of free surface shape on combined thermocapillary and natural convection p 162 A93-10671
- Discussion of 'Comparison of turbulence models for the natural convection boundary layer along a heated vertical plate' p 168 A93-21717
- Time-dependent thermocapillary convection in a Cartesian cavity - Numerical results for a moderate Prandtl number fluid [AIAA PAPER 93-0259] p 169 A93-22666
- Thermosolutal convection during cellular arrayed growth of Pb-Sn alloys [AIAA PAPER 93-0262] p 142 A93-22668
- Double-diffusive fingering convection in a porous medium p 175 A93-27900

- Convective effects during the physical vapor transport process. I - Thermal convection p 179 A93-36575
- Effect of radiation on convection in a top-heated enclosure p 189 A93-54454
- One-dimensional transient finite difference model of an operational salinity gradient solar pond p 193 N93-13400

FREE FALL

- Capabilities and constraints of NASA's ground-based reduced gravity facilities p 49 N93-20184

FREE FLOW

- Heat transfer with very high free-stream turbulence. I - Experimental data. II - Analysis of results p 165 A93-18556
- Thermocapillary migration of a small chain of bubbles p 182 A93-46714
- Bypass transition in compressible boundary layers p 196 N93-15801
- Transient liquid-crystal technique used to produce high-resolution convective heat-transfer-coefficient maps [NASA-TM-106083] p 198 N93-23404
- Increased heat transfer to elliptical leading edges due to spanwise variations in the freestream momentum: Numerical and experimental results [NASA-TM-106150] p 199 N93-27020

FREE JETS

- Streamwise vorticity generation and mixing enhancement in free jets by 'delta-tabs' [AIAA PAPER 93-3253] p 14 A93-53592
- Second order closure modeling of turbulent buoyant wall plumes [NASA-TM-105956] p 193 N93-14829
- Experimental investigation of an ejector-powered free-jet facility [NASA-TM-105868] p 16 N93-16704
- Streamwise vorticity generation and mixing enhancement in free jets by delta-tabs [NASA-TM-106235] p 17 N93-31648

FREE RADICALS

- Atomic hydrogen propellants - Historical perspectives and future possibilities [AIAA PAPER 93-0244] p 140 A93-24234

FREE VIBRATION

- Dynamic analysis of a pre-and-post ice impacted blade [NASA-TM-105829] p 144 N93-12197

FREE-PISTON ENGINES

- Free-piston Stirling Engine system considerations for various space power applications p 252 A93-13826
- HFAST - A harmonic analysis program for Stirling cycles p 220 A93-26051
- Comparison of GLIMPS and HFAST Stirling engine code predictions with experimental data p 220 A93-26052
- Assessment of 25 kW free-piston Stirling technology alternatives for solar applications p 254 A93-26072
- Dynamic analysis of free-piston Stirling engine/linear alternator-load system - Experimentally validated p 254 A93-26078
- Magnetic bearings for free-piston Stirling engines p 221 A93-26079

- Small Stirling dynamic isotope power system for robotic space missions [NASA-TM-105785] p 92 N93-28686

FREQUENCIES

- Vibration and noise analysis of a gear transmission system [AIAA PAPER 93-2150] p 224 A93-49967
- Vibration and noise analysis of a gear transmission system [NASA-TM-106162] p 229 N93-27641

FREQUENCY DISTRIBUTION

- System overview on electromagnetic compensation for reflector antenna surface distortion [NASA-TM-106217] p 53 N93-29195

FREQUENCY DIVISION MULTIPLE ACCESS

- Efficient demultiplexing algorithm for noncontiguous carriers p 148 A93-32561

FREQUENCY MEASUREMENT

- Measurement of frequency response in short thermocouple wires p 209 A93-40677

FREQUENCY MODULATION

- RF modulated fiber optic sensing systems and their applications p 211 A93-49469
- Fiber-optic sensing technique employing RF modulated interferometry p 212 A93-53110

FREQUENCY RESPONSE

- An analysis of the frequency limitations of an $\text{Al(x)Ga(1-x)As/GaAs}$ optical modulator p 151 A93-23454
- Measurement of frequency response in short thermocouple wires p 209 A93-40677

FREQUENCY SHIFT

- Rotational level-dependent collisional broadening and line shift of the $\text{A}^2\Sigma^+_{g,1}(1,0)$ band of OH in hydrogen-air combustion gases p 276 A93-24142

FRICION

FRICION

- Tribological and mechanical comparison of sintered and HIPped PM212 - High temperature self-lubricating composites p 94 A93-13506
An analysis of the wear behavior of SiC whisker-reinforced alumina from 25 to 1200 C p 104 A93-49253
Friction and wear of plasma-deposited amorphous hydrogenated films on silicon nitride p 135 A93-52181

FRICION FACTOR

- Friction-factor characteristics for narrow channels with honeycomb surfaces [ASME PAPER 91-TRIB-21] p 219 A93-15681
Friction-factor data for flat-plate tests of smooth and honeycomb surfaces [ASME PAPER 91-TRIB-20] p 219 A93-15682
Space Station Freedom beta gimbal control via sensitivity models p 60 N93-22551 [NASA-TM-106000]
Tribological characteristics of perfluoropolyether liquid lubricants under sliding conditions in high vacuum [NASA-TM-106257] p 139 N93-32352

FRICION MEASUREMENT

- A vacuum (10 exp -9 torr) friction apparatus for determining friction and endurance life of MoS(x) films p 146 A93-49245

FRICION REDUCTION

- The detrimental effect of friction on space microgravity robotics p 222 A93-35546

FUEL CELLS

- Pressure dependence of the oxygen reduction reaction at the platinum microelectrode/nation interface - Electrode kinetics and mass transport p 112 A93-11450
PEM fuel cell stack heat and mass management p 253 A93-26024

FUEL COMBUSTION

- Experiments on the effect of initial diameter in spherically symmetric droplet combustion of sooting fuels [AIAA PAPER 93-0130] p 139 A93-22577
Premixed flame propagation in combustible particle cloud mixtures [AIAA PAPER 93-0713] p 115 A93-24808
Spray combustion experiments and numerical predictions [NASA-TM-106069] p 198 N93-23744
Nitric oxide formation in a lean, premixed-prevaporized jet A/air flame tube: An experimental and analytical study [NASA-TM-105722] p 257 N93-27012

FUEL CONSUMPTION

- The multi-heat addition turbine engine [AIAA PAPER 92-4272] p 22 A93-13334

FUEL CONTROL

- A neural network-based estimator for the mixture ratio of the Space Shuttle Main Engine [NASA-TM-106070] p 87 N93-25089

FUEL FLOW

- US/CIS integrated NTRF [AIAA PAPER 93-2367] p 76 A93-50138
Visualization of hydrogen injection in a scramjet engine by simultaneous PLIF imaging and laser holographic imaging p 214 N93-13683
Propulsion system performance resulting from an integrated flight/propulsion control design [NASA-TM-105874] p 34 N93-15525
Combustion of solid fuel in very low speed oxygen streams p 122 N93-20207

FUEL INJECTION

- Influence of ambient air pressure on effervescent atomization [AIAA PAPER 92-0460] p 167 A93-21652
A numerical study of mixing in supersonic combustors with hypermixing injectors [AIAA PAPER 93-0215] p 25 A93-27801
Atomization and vaporization characteristics of airblast fuel injection inside a venturi tube [AIAA PAPER 93-1766] p 184 A93-49662
Performance of a low-power subsonic-arc-attachment arcjet thruster [AIAA PAPER 93-1898] p 72 A93-49768
Coaxial injector spray characterization using water/air as simulants p 120 N93-11452
Visualization of hydrogen injection in a scramjet engine by simultaneous PLIF imaging and laser holographic imaging p 214 N93-13683
Fuel injector: Air swirl characterization aerothermal modeling, phase 2, volume 1 [NASA-CR-189193-VOL-1] p 35 N93-24754

FUEL PUMPS

- Design and test of a small two stage counter-rotating turbine for rocket engine application [AIAA PAPER 93-2136] p 74 A93-49954
Three-dimensional analysis of the Pratt and Whitney alternate design SSME fuel turbine p 230 N93-31584

FUEL SPRAYS

- Influence of ambient air pressure on effervescent atomization [AIAA PAPER 92-0460] p 167 A93-21652
Effect of vaporization on cryogenic spray droplet measurement [AIAA PAPER 93-0692] p 172 A93-24792
Soot agglomeration in isolated, free droplet combustion [AIAA PAPER 93-0823] p 115 A93-24893
Computations of spray, fuel-air mixing, and combustion in a lean-premixed-prevaporized combustor [AIAA PAPER 93-2069] p 185 A93-49901
Effects of detailed droplet heating models on turbulent sprays vaporization behavior [AIAA PAPER 93-2193] p 185 A93-50005
Secondary atomization in the combustion of electrostatic sprays [AIAA PAPER 93-2332] p 118 A93-50110
Atomizing-gas temperature effect on cryogenic spray droplet [AIAA PAPER 93-2333] p 186 A93-50111
Effect of vaporization on cryogenic spray droplet measurement [NASA-TM-105909] p 213 N93-13410
Atomizing-gas temperature effect on cryogenic spray droplet [NASA-TM-106106] p 216 N93-25191

FUEL SYSTEMS

- The development of hydrogen sensor technology at NASA Lewis Research Center [NASA-TM-106141] p 216 N93-27021

FUEL TANK PRESSURIZATION

- Influence of heat transfer rates on pressurization of liquid/slush hydrogen propellant tanks [AIAA PAPER 93-0278] p 169 A93-22681
Pressurization and expulsion of a lightweight liquid hydrogen tank [AIAA PAPER 93-1966] p 73 A93-49814

FUEL TANKS

- EOTV propellant tank pressure control and liquid dynamics [AIAA PAPER 93-2399] p 77 A93-50164

FUEL-AIR RATIO

- Simplified jet fuel reaction mechanism for lean burn combustion application [AIAA PAPER 93-0021] p 113 A93-23238
Structure of soot-containing laminar jet diffusion flames [AIAA PAPER 93-0708] p 114 A93-24804
Effects of particulate radiation on premixed gas flames [AIAA PAPER 93-0711] p 114 A93-24806
Flame balls - Past, present and future [AIAA PAPER 93-0712] p 114 A93-24807
Numerical study of shock-induced combustion in methane-air mixtures [AIAA PAPER 93-1917] p 184 A93-49783
Computations of spray, fuel-air mixing, and combustion in a lean-premixed-prevaporized combustor [AIAA PAPER 93-2069] p 185 A93-49901
The promising chemical kinetics for the simulation of propane-air combustion with KIVA-II code [AIAA PAPER 93-2189] p 118 A93-50001
Simplified jet-A kinetic mechanism for combustor application [NASA-TM-105940] p 120 N93-15504

FULL SCALE TESTS

- A full-scale STOVJ ejector experiment [NASA-TM-106019] p 35 N93-22480

FUNCTIONAL DESIGN SPECIFICATIONS

- Integrated flight/propulsion control - Subsystem specifications for performance [AIAA PAPER 93-3808] p 41 A93-51400

FUNCTIONALLY GRADIENT MATERIALS

- Fabrication and properties of functionally graded NiAl/Al₂O₃ composites p 105 A93-54116

FURNACES

- Self-tuning multivariable pole placement control of a multizone crystal growth furnace p 263 A93-10575
Numerical model for the Programmable Multizone Furnace (PMZF) [AIAA PAPER 93-0471] p 142 A93-24242
A numerical model including PID control of a multizone crystal growth furnace p 190 A93-55473
A multi-zone muffle furnace design [NASA-TM-106153] p 145 N93-27011

FUSELAGES

- Probabilistic evaluation of fuselage-type composite structures [NASA-TM-105881] p 245 N93-12735

FUZZY SETS

- Fuzzy sets predict flexural strength and density of silicon nitride ceramics [NASA-TM-106049] p 110 N93-27270

- Soft computing in design and manufacturing of advanced materials [NASA-TM-106032] p 111 N93-28624

FUZZY SYSTEMS

- Self-growing neural network architecture using crisp and fuzzy entropy p 263 A93-26650
Fuzzy expert systems vs. neural networks - Truck backer-upper control revisited p 264 A93-37039
A fuzzy logic based controller for the automated alignment of a laser-beam-smoothing spatial filter [NASA-TM-105994] p 217 N93-18091
Self-growing neural network architecture using crisp and fuzzy entropy p 231 N93-18422
Fuzzy logic particle tracking velocimetry [NASA-TM-106194] p 216 N93-27027

G

GALACTIC CLUSTERS

- N-point correlation functions in the CfA and SSRS redshift distribution of galaxies p 288 A93-10615
Probing the statistics of primordial fluctuations and their evolution p 290 A93-24627

GALACTIC EVOLUTION

- Late-time cosmological phase transitions p 288 A93-17645
The best-fit universe --- cosmological models p 289 A93-17651
Chemical and luminosity evolution, and counts of galaxies in a merger model p 290 A93-34776
Extension of the Parker bound on the flux of magnetic monopoles p 291 A93-38672
Clumpy cold dark matter p 291 A93-46201
Biasing and hierarchical statistics in large-scale structure p 292 A93-55051
The boron-to-beryllium ratio in halo stars - A signature of cosmic-ray nucleosynthesis in the early Galaxy p 292 A93-55061

GALACTIC HALOS

- Phase space distribution of halo particles and detection of WIMPS --- weakly interacting massive particles p 289 A93-23650

GALACTIC STRUCTURE

- Biasing and hierarchical statistics in large-scale structure p 292 A93-55051

GALERKIN METHOD

- Non-oscillatory and non-diffusive solution of convection problems by the iteratively reweighted least-squares finite element method p 177 A93-32622
Symmetric Galerkin boundary formulations employing curved elements p 268 A93-54198

GALLIUM ARSENIDES

- Intermodulation in the oscillatory magnetoresistance of a two-dimensional electron gas p 151 A93-17610
Prediction of dislocation generation during Bridgman growth of GaAs crystals p 279 A93-19740
GaAs monolithic R.F. modules for SARSAT distress beacons p 152 A93-25806
Enhancement of photoluminescence intensity of GaAs with cubic GaS chemical vapor deposited using a structurally designed single-source precursor p 280 A93-26930
Electronic passivation of n- and p-type GaAs using chemical vapor deposited GaS p 283 A93-52708
Diffusion length variation and proton damage coefficients for InP/In(x)Ga(1-x)As/GaAs solar cells p 159 A93-55324

- Microwave characterization of slotline on high resistivity silicon for antenna feed network [NASA-TM-106058] p 161 N93-27265

GALLIUM COMPOUNDS

- Photoluminescence intensity enhancement of GaAs by vapor-deposited GaS - A rational approach to surface passivation p 281 A93-40049

GAMMA RAYS

- Neutron, gamma ray, and temperature effects on the electrical characteristics of thyristors p 153 A93-25894

GAS ATOMIZATION

- Secondary atomization in the combustion of electrostatic sprays [AIAA PAPER 93-2332] p 118 A93-50110
Atomizing-gas temperature effect on cryogenic spray droplet [AIAA PAPER 93-2333] p 186 A93-50111
Atomizing-gas temperature effect on cryogenic spray droplet [NASA-TM-106106] p 216 N93-25191

GAS BEARINGS

- Magnetic bearings for free-piston Stirling engines p 221 A93-26079

- GAS DENSITY**
 DSMC and continuum analyses of low-density nozzle flow
 [AIAA PAPER 93-0727] p 172 A93-24817
 Gas temperature and density measurements based on spectrally resolved Rayleigh-Brillouin scattering p 214 N93-13684
- GAS DETECTORS**
 Development of a hydrogen gas sensor using microfabrication technology
 [SAE PAPER 921176] p 210 A93-41356
 The development of hydrogen sensor technology for aerospace applications
 [AIAA PAPER 93-2375] p 211 A93-50144
 A survey and analysis of commercially available hydrogen sensors
 [NASA-TM-105878] p 214 N93-17777
 The development of hydrogen sensor technology at NASA Lewis Research Center
 [NASA-TM-106141] p 216 N93-27021
- GAS DISCHARGE TUBES**
 Preliminary investigation of high power microwave plasmas for electrothermal thruster use
 [AIAA PAPER 93-2106] p 74 A93-49928
 Preliminary investigation of high power microwave plasmas for electrothermal thruster use
 [NASA-TM-106207] p 92 N93-29158
- GAS DYNAMICS**
 Three-dimensional numerical simulation of gradual opening in a wave rotor passage
 [AIAA PAPER 93-2526] p 187 A93-50254
 Analysis of unsteady wave processes in a rotating channel
 [AIAA PAPER 93-2527] p 187 A93-50255
 Dynamic gas temperature measurements using a personal computer for data acquisition and reduction
 [NASA-TM-106119] p 261 N93-27024
- GAS FLOW**
 An improved numerical model for wave rotor design and analysis
 [AIAA PAPER 93-0482] p 24 A93-23384
 Development of a Rayleigh scattering system for temperature measurements in combustor flows
 p 206 A93-23788
 Lagrangian solution of supersonic real gas flows
 p 170 A93-23944
 DSMC and continuum analyses of low-density nozzle flow
 [AIAA PAPER 93-0727] p 172 A93-24817
 Calculations of low Reynolds number rocket nozzles
 [AIAA PAPER 93-0888] p 67 A93-24948
 Absolute and convective instability of a viscous liquid jet surrounded by a viscous gas in a vertical pipe
 p 176 A93-30144
 Convective effects during the physical vapor transport process. II - Thermosolutal convection
 p 180 A93-42424
 Preliminary investigation of high power microwave plasmas for electrothermal thruster use
 [AIAA PAPER 93-2106] p 74 A93-49928
 Premixed flame propagation in an optically thick gas
 p 119 A93-55381
 An improved numerical model for wave rotor design and analysis
 [NASA-TM-105915] p 33 N93-12418
 2D velocity and temperature measurements in high speed flows based on spectrally resolved Rayleigh scattering
 [NASA-TM-105784] p 215 N93-19651
 NTR plume modeling
 p 199 N93-26929
 Preliminary investigation of high power microwave plasmas for electrothermal thruster use
 [NASA-TM-106207] p 92 N93-29158
- GAS GENERATORS**
 An improved numerical model for wave rotor design and analysis
 [AIAA PAPER 93-0482] p 24 A93-23384
 An improved numerical model for wave rotor design and analysis
 [NASA-TM-105915] p 33 N93-12418
- GAS INJECTION**
 Autogenous pressurization of cryogenic vessels using submerged vapor injection
 p 71 A93-48648
- GAS JETS**
 Effect of vaporization on cryogenic spray droplet size measurement
 [AIAA PAPER 93-0692] p 172 A93-24792
 Effects of gravity on the transition to turbulence of gas jet diffusion flames
 [AIAA PAPER 93-0710] p 114 A93-24805
 Atomizing-gas temperature effect on cryogenic spray droplet size
 [AIAA PAPER 93-2333] p 186 A93-50111
 Effect of vaporization on cryogenic spray droplet size measurement
 [NASA-TM-105909] p 213 N93-13410
- Selected microgravity combustion diagnostic techniques p 121 N93-20194
 Atomizing-gas temperature effect on cryogenic spray droplet size
 [NASA-TM-106106] p 216 N93-25191
- GAS MIXTURES**
 Premixed flame propagation in combustible particle cloud mixtures
 [AIAA PAPER 93-0713] p 115 A93-24808
 Analytical and numerical modeling of flame-balls in hydrogen-air mixtures
 p 118 A93-46009
 Development and use of hydrogen-air torches in an altitude facility
 [AIAA PAPER 93-2176] p 42 A93-49988
 Internal structure of shock waves in disparate mass mixtures
 p 190 A93-54483
 Development and use of hydrogen-air torches in an altitude facility
 [NASA-TM-106047] p 43 N93-26214
- GAS PRESSURE**
 Influence of ambient air pressure on effervescent atomization
 [AIAA PAPER 92-0460] p 167 A93-21652
 Low temperature phase formation of Ti-based superconducting thin films in reduced oxygen atmosphere
 p 282 A93-44568
 Droplet vaporization in a high-pressure gas
 p 190 A93-55461
 Rayleigh-Brillouin scattering for high-pressure gas temperature measurements
 p 218 N93-31556
- GAS TEMPERATURE**
 A study of circumferentially-heated and block-heated heat pipes. I - Experimental analysis and generalized analytical prediction of capillary limits. II - Three-dimensional numerical modeling as a conjugate problem
 p 168 A93-21715
 Development of a Rayleigh scattering system for temperature measurements in combustor flows
 p 206 A93-23788
 Flight testing of a fiber optic temperature sensor
 p 22 A93-49476
 Secondary atomization in the combustion of electrostatic sprays
 [AIAA PAPER 93-2332] p 118 A93-50110
 Gas temperature measurements using the dual-line detection Rayleigh scattering technique
 p 213 A93-55368
 Nongray gas analyses for reflecting walls utilizing a flux technique
 p 190 A93-55460
 Gas temperature measurements using the dual-line detection Rayleigh scattering technique
 p 214 N93-13668
 Gas temperature and density measurements based on spectrally resolved Rayleigh-Brillouin scattering
 p 214 N93-13684
 2D velocity and temperature measurements in high speed flows based on spectrally resolved Rayleigh scattering
 [NASA-TM-105784] p 215 N93-19651
 A full-scale STOVL ejector experiment
 [NASA-TM-106019] p 35 N93-22480
 Dynamic gas temperature measurements using a personal computer for data acquisition and reduction
 [NASA-TM-106119] p 261 N93-27024
 Rayleigh-Brillouin scattering for high-pressure gas temperature measurements
 p 218 N93-31556
- GAS TRANSPORT**
 Convective effects during the physical vapor transport process. I - Thermal convection
 p 179 A93-36575
- GAS TURBINE ENGINES**
 Stirling engine - Available tools for long-life assessment
 --- for space propulsion
 p 65 A93-13824
 Heat transfer in rotating serpentine passages with trips skewed to the flow
 [ASME PAPER 92-GT-191] p 166 A93-19416
 Ceramic matrix composites for rocket engine turbine applications
 [ASME PAPER 92-GT-394] p 99 A93-19547
 An efficient constraint to account for mistuning effects in the optimal design of engine rotors
 [AIAA PAPER 92-4711] p 23 A93-20280
 APPLE - An aeroelastic analysis system for turbomachines and propfans
 [AIAA PAPER 92-4712] p 23 A93-20320
 Two and three-dimensional prediffuser combustor studies with air-water mixture
 [AIAA PAPER 93-0240] p 113 A93-22652
 An improved numerical model for wave rotor design and analysis
 [AIAA PAPER 93-0482] p 24 A93-23384
 A graphical user-interface for propulsion system analysis
 [AIAA PAPER 93-0223] p 259 A93-23699
 Driven cavity simulation of turbomachine blade flows with vortex control
 [AIAA PAPER 93-0390] p 6 A93-24238
- Screening studies of advanced control concepts for airbreathing engines
 [AIAA PAPER 92-3320] p 26 A93-49329
 Mixing in the dome region of a staged gas turbine combustor
 p 27 A93-49612
 An efficient liner cooling scheme for advanced small gas turbine combustors
 [AIAA PAPER 93-1763] p 27 A93-49660
 An analytical study of dilution jet mixing in a cylindrical duct
 [AIAA PAPER 93-2043] p 27 A93-49876
 Computations of spray, fuel-air mixing, and combustion in a lean-premixed-prevaporized combustor
 [AIAA PAPER 93-2069] p 185 A93-49901
 Computation of the flow field in an annular gas turbine combustor
 [AIAA PAPER 93-2074] p 28 A93-49903
 Integrated CFD modeling of gas turbine combustors
 [AIAA PAPER 93-2196] p 28 A93-50008
 Effects of flow-path variations on internal reversing flow in a tailpipe offtake configuration for ASTOVL aircraft
 [AIAA PAPER 93-2438] p 29 A93-50190
 Nonlinear dynamic simulation of single- and multi-spool core engines
 [AIAA PAPER 93-2580] p 30 A93-50294
 Progress towards understanding and predicting heat transfer in the turbine gas path
 p 188 A93-52751
 Propulsion technology challenges for turn-of-the-century commercial aircraft
 [ISABE 93-7003] p 31 A93-53980
 Emission characteristics of a model gas turbine combustor at practical conditions
 [ISABE 93-7023] p 31 A93-53999
 Mixing of multiple jets with a confined subsonic crossflow
 p 15 A93-54324
 An interactive preprocessor for the NASA engine performance program
 [NASA-TM-105786] p 32 N93-10983
 An improved numerical model for wave rotor design and analysis
 [NASA-TM-105915] p 33 N93-12418
 Bypass transition in compressible boundary layers
 p 196 N93-15801
 Summary of experimental heat-transfer results from the turbine hot section facility
 [NASA-TP-3250] p 197 N93-23059
 Spray combustion experiments and numerical predictions
 [NASA-TM-106069] p 198 N93-23744
 A three-dimensional algebraic grid generation scheme for gas turbine combustors with inclined slots
 [NASA-CR-191095] p 198 N93-24759
 Screening studies of advanced control concepts for airbreathing engines
 [NASA-TM-106042] p 36 N93-25079
 Gas turbine system simulation: An object-oriented approach
 [NASA-TM-106044] p 36 N93-25673
 Nitric oxide formation in a lean, premixed-prevaporized jet A/air flame tube: An experimental and analytical study
 [NASA-TM-105722] p 257 N93-27012
 An analytical study of dilution jet mixing in a cylindrical duct
 [NASA-TM-106181] p 37 N93-27160
 Effects of flow-path variations on internal reversing flow in a tailpipe offtake configuration for ASTOVL aircraft
 [NASA-TM-106149] p 38 N93-29065
 Propulsion technology challenges for turn-of-the-century commercial aircraft
 [NASA-TM-106192] p 39 N93-32351
- GAS TURBINES**
 Experimental investigation of crossflow jet mixing in a rectangular duct
 [AIAA PAPER 93-2037] p 185 A93-49872
 Closed Brayton Cycle power system with a high temperature pellet bed reactor heat source for NEP applications
 [NASA-TM-105933] p 82 N93-14482
 Multi-heat addition turbine engine
 [NASA-CASE-LEW-15094-1] p 35 N93-22034
 Experimental investigation of crossflow jet mixing in a rectangular duct
 [NASA-TM-106152] p 36 N93-27026
- GAS-SOLID INTERACTIONS**
 Heat transfer from radiatively heated material in a low Reynolds number microgravity environment
 p 180 A93-43695
- GAS-SOLID INTERFACES**
 Onset conditions for gas phase reaction and nucleation in the CVD of transition metal oxides
 p 116 A93-39508
- GASEOUS DIFFUSION**
 Simulation of the early startup period of high-temperature heat pipes from the frozen state by a rarefied vapor self-diffusion model
 p 175 A93-30127

GASEOUS FUELS

On the structure of gaseous confined laminar diffusion flames: Numerical investigation
[NASA-TM-106039] p 197 N93-21198

GASEOUS FUELS

Premixed flame propagation in combustible particle cloud mixtures
[AIAA PAPER 93-0713] p 115 A93-24808
Thermophysical properties of gas phase uranium tetrafluoride
[AIAA PAPER 93-2758] p 285 A93-46505
Design of an oxygen turbopump for use in an Advanced Expander Test Bed engine
[AIAA PAPER 93-2137] p 48 A93-49955

GASEOUS ROCKET PROPELLANTS

A new facility for advanced rocket propulsion research
[AIAA PAPER 93-1859] p 48 A93-49737
Combustion-wave ignition for rocket engines
p 78 N93-10016
A new facility for advanced rocket propulsion research
[NASA-TM-106193] p 49 N93-28696

GATES (CIRCUITS)

A 10 kW dc-dc converter using IGBTs with active snubbers --- Insulated Gate Bipolar Transistor
p 158 A93-50646

GEAR TEETH

Effect of extended tooth contact on the modeling of spur gear transmissions
[AIAA PAPER 93-2148] p 223 A93-49965
Low-noise, high-strength, spiral-bevel gears for helicopter transmissions
[AIAA PAPER 93-2149] p 223 A93-49966
Dynamic analysis of spur gears using computer program DANST
[AIAA PAPER 93-2295] p 224 A93-50080
Contact stress analysis of spiral bevel gears using nonlinear finite element static analysis
[AIAA PAPER 93-2296] p 224 A93-50081
Generation of helical gears with new surfaces topology by application of CNC machines
[AIAA PAPER 93-2297] p 224 A93-50082
Evaluation of a vibration diagnostic system for the detection of spur gear pitting failures
[AIAA PAPER 93-2298] p 224 A93-50083
Maximum life spiral bevel reduction design
[NASA-TM-105790] p 226 N93-10982
Low-noise, high-strength, spiral-bevel gears for helicopter transmissions
[NASA-TM-106080] p 228 N93-23019
Evaluation of a vibration diagnostic system for the detection of spur gear pitting failures
[NASA-TM-106103] p 228 N93-25672
Contact stress analysis of spiral bevel gears using nonlinear finite element static analysis
[NASA-TM-106176] p 228 N93-27037
An analysis of gear fault detection methods as applied to pitting fatigue failure data
[NASA-TM-105950] p 229 N93-27074
Face-gear drives: Design, analysis, and testing for helicopter transmission applications
[NASA-TM-106101] p 229 N93-27133
Generation of helical gears with new surfaces, topology by application of CNC machines
[NASA-TM-106175] p 229 N93-27687
Dynamic analysis of spur gears using computer program DANST
[NASA-TM-106211] p 230 N93-28050
Effect of extended tooth contact on the modeling of spur gear transmissions
[NASA-TM-106174] p 230 N93-28411

GEARS

Maximum life spur gear design p 218 A93-14521
Dynamic analysis of flexible gear trains/transmissions - An automated approach p 220 A93-22440
Acoustical analysis of gear housing vibration p 273 A93-29420
Modal simulation of gear box vibration with experimental correlation p 221 A93-31982
Modal analysis of multistage gear systems coupled with gearbox vibrations p 222 A93-36588
Low-noise, high-strength, spiral-bevel gears for helicopter transmissions
[AIAA PAPER 93-2149] p 223 A93-49966
Vibration and noise analysis of a gear transmission system
[AIAA PAPER 93-2150] p 224 A93-49967
Dynamic analysis of spur gears using computer program DANST
[AIAA PAPER 93-2295] p 224 A93-50080
Generation of helical gears with new surfaces topology by application of CNC machines
[AIAA PAPER 93-2297] p 224 A93-50082
Experimental validation of boundary element methods for noise prediction
[NASA-TM-105729] p 226 N93-10966
Maximum life spiral bevel reduction design
[NASA-TM-105790] p 226 N93-10982

Evaluation of an oil-debris monitoring device for use in helicopter transmissions
[NASA-TM-105830] p 227 N93-22826
Low-noise, high-strength, spiral-bevel gears for helicopter transmissions
[NASA-TM-106080] p 228 N93-23019
Pattern classifier for health monitoring of helicopter gearboxes
[NASA-TM-106099] p 228 N93-23741
Global dynamic modeling of a transmission system
[NASA-CR-191117] p 228 N93-24751
Fault detection of helicopter gearboxes using the multi-valued influence matrix method
[NASA-TM-106100] p 229 N93-27069
Vibration and noise analysis of a gear transmission system
[NASA-TM-106162] p 229 N93-27641
Generation of helical gears with new surfaces, topology by application of CNC machines
[NASA-TM-106175] p 229 N93-27687
Dynamic analysis of spur gears using computer program DANST
[NASA-TM-106211] p 230 N93-28050
Efficient fault diagnosis of helicopter gearboxes
[NASA-TM-106253] p 231 N93-31846

GELLED ROCKET PROPELLANTS

Some aspects of secondary atomization of aluminum/hydrocarbon slurry propellants
p 140 A93-34478
Technology for gelled liquid cryogenic propellants - Metalized hydrogen/aluminum
[AIAA PAPER 93-1878] p 140 A93-49752

GENETIC ALGORITHMS

Stochastic search in structural optimization - Genetic algorithms and simulated annealing p 241 A93-45430

GEOMETRICAL ACOUSTICS

Propagation of high frequency jet noise using geometric acoustics
[AIAA PAPER 93-0147] p 272 A93-23241
Propagation of high frequency jet noise using geometric acoustics
[NASA-TM-106013] p 275 N93-15575

GEOSYNCHRONOUS ORBITS

Data distribution satellite
[NASA-TM-105778] p 149 N93-12481

GERMANIDES

Ellipsometric study of Si(0.5)Ge(0.5)/Si strained-layer superlattices p 280 A93-34655
Application of high-quality SiO₂ grown by multipolar ECR source to Si/SiGe MISFET p 156 A93-37413

GERMANIUM COMPOUNDS

High frequency performance of Si(1-x)Ge(x)/Si(1-y)Ge(y)/Si(1-x)Ge(x) HBTs
p 155 A93-37409
Development of Si(1-x)Ge(x) technology for microwave sensing applications
[NASA-TM-106157] p 162 N93-28610

GET AWAY SPECIALS (STS)

Electrical design of Space Shuttle payload G-534: The pool boiling experiment
[NASA-TM-106143] p 62 N93-27260

GIMBALS

Space Station Freedom beta gimbal control via sensitivity models
[NASA-TM-106000] p 60 N93-22551

GLASS

Glass formation, properties and structure of soda-yttria-silica glasses p 131 A93-20464
Interaction of cracks between two adjacent indents in glass p 132 A93-27115
Kinetics of hexacelsian-to-celsian phase transformation in SrAl₂Si₂O₈ p 134 A93-40293
Subcritical crack growth in soda-lime glass in combined mode I and mode II loading p 134 A93-52151
Kinetics of hexacelsian to celsian phase transformation in SrAl₂Si₂O₈
[NASA-TM-105913] p 136 N93-16372
SiC fiber-reinforced Celsian glass-ceramic matrix composite
[NASA-CASE-LEW-15264-1] p 112 N93-31293
Method of producing a ceramic fiber-reinforced glass-ceramic matrix composite
[NASA-CASE-LEW-15264-2] p 112 N93-31299

GLASS FIBERS

Fiber-reinforced monoclinic celsian matrix composite material
[NASA-CASE-LEW-15269-1] p 108 N93-20040
Ceramic fiber reinforced glass-ceramic matrix composite
[NASA-CASE-LEW-15262-1] p 109 N93-26100

GLAZES

Results of a low power ice protection system test and a new method of imaging data analysis
p 21 A93-35932

GOLD

Tribological and microstructural comparison of HIPped PM212 and PM212/Au self-lubricating composites
p 93 A93-13505

GOODNESS OF FIT

Statistical fitting accuracy in photon correlation spectroscopy p 277 A93-52414

GRADIENT INDEX OPTICS

Multiple fiberoptic probe for several sensing applications p 212 A93-53109

GRADIENTS

One-dimensional transient finite difference model of an operational salinity gradient solar pond
p 193 N93-13400

GRAIN BOUNDARIES

Thermal stability of the microstructure of an aged Nb-Zr-C alloy p 122 A93-13776
High-temperature deformation and microstructural analysis for silicon nitride-scandium(III) oxide
p 131 A93-20468
Grain boundary resistance to fatigue crack growth
p 125 A93-29570

GRAIN SIZE

Influence of grain size on the creep behavior of HfC-dispersed NiAl p 123 A93-17674
Effect of high temperature annealing on the microstructure of SCS-6 SiC fibers p 133 A93-39513
Tensile creep behavior of polycrystalline alumina fibers
[NASA-TM-106269] p 138 N93-30938

GRAND UNIFIED THEORY

Extension of the Parker bound on the flux of magnetic monopoles p 291 A93-38672

GRAPHICAL USER INTERFACE

A graphical user-interface for propulsion system analysis
[AIAA PAPER 93-0223] p 259 A93-23699

GRAPHITE

Properties of hybrid CVD/PAN graphite fibers and their bromine intercalation compounds p 98 A93-17675
Thermal conductivity and thermal expansion of graphite fiber-reinforced copper matrix composites
p 100 A93-25104
Reaction layer formation at the graphite/copper-chromium alloy interface
p 100 A93-25105
Solid lubricants p 135 A93-55471
Heat transfer device
[NASA-CASE-LEW-14162-4] p 108 N93-20568
Apparatus for intercalating large quantities of fibrous structures
[NASA-CASE-LEW-15077-2] p 111 N93-29609

GRAPHITE-EPOXY COMPOSITES

Computational simulation of surface waviness in graphite/epoxy woven composites due to initial curing
p 98 A93-15822
Effects of interply damping layers on the dynamic characteristics of composite plates p 237 A93-32415
Probabilistic nonlinear finite element analysis of composite structures p 237 A93-32717
Intercalated graphite fiber composites as EMI shields in aerospace structures p 104 A93-41573
Probabilistic micromechanics and macromechanics of polymer matrix composites p 105 A93-54705
The effect of contact stresses in four-point bend testing of graphite/epoxy and graphite/PMR-15 composite beams
[NASA-TM-105891] p 107 N93-12076
Leveling coatings for reducing the atomic oxygen defect density in protected graphite fiber epoxy composites
[NASA-TM-105732] p 136 N93-15344
Leveling coatings for reducing the atomic oxygen defect density in protected graphite fiber epoxy composites
p 59 N93-15597
Structural dynamic testing of composite propfan blades for a cruise missile wind tunnel model
[NASA-TM-105272] p 247 N93-18875
Stress distribution in composite flatwise tension test specimens
[NASA-TM-106074] p 108 N93-25071
Graphite/epoxy composite laminates with co-cured interlaminar damping layers p 109 N93-25587
Fabrication of composite propfan blades for a cruise missile wind tunnel model
[NASA-TM-105270] p 249 N93-26202
Structural tailoring of aircraft engine blade subject to ice impact constraints
[NASA-TM-106033] p 250 N93-26999

GRAPHITE-POLYIMIDE COMPOSITES

Transverse flexural tests as a tool for assessing damage to PMR-15 composites from isothermal aging in air at elevated temperatures p 100 A93-24514
The effect of contact stresses in four-point bend testing of graphite/epoxy and graphite/PMR-15 composite beams
[NASA-TM-105891] p 107 N93-12076

- Transverse flexural tests as a tool for assessing damage to PMR-15 composites from isothermal aging in air at elevated temperatures
[NASA-TM-105848] p 107 N93-12737
- Effects of thermal and mechanical fatigue on the flexural strength of G40-600/PMR-15 cross-ply laminates
[NASA-TM-106016] p 108 N93-20317
- GRAPHITIZATION**
Method for producing hybrid graphite composite
[NASA-CASE-LEW-15241-2] p 112 N93-31296
- GRAVITATION**
Gravity sensitivity of a resistojet water vaporizer
[AIAA PAPER 93-2402] p 186 A93-50167
- Capabilities and constraints of typical space flight hardware
p 145 N93-20183
- Capabilities and constraints of NASA's ground-based reduced gravity facilities
p 49 N93-20184
- Flame spread across liquid pools
p 122 N93-20209
- Combustion of interacting droplet arrays in a microgravity environment
p 122 N93-20217
- Gravity sensitivity of a resistojet water vaporizer
[NASA-TM-106220] p 92 N93-29194
- GRAVITATION THEORY**
The three-point correlation function in an ensemble of three-dimensional simulations --- in gravitational perturbation theory
p 291 A93-50680
- GRAVITATIONAL EFFECTS**
Nucleate pool boiling in the long duration low gravity environment of the space shuttle
[AIAA PAPER 93-0465] p 142 A93-23371
- Comparison of numerical model results with diffusion flames in microgravity
[AIAA PAPER 93-0707] p 114 A93-24803
- Effects of gravity on the transition to turbulence of gas jet diffusion flames
[AIAA PAPER 93-0710] p 114 A93-24805
- Experimental observations of the effect of gravity changes on smoldering combustion
[AIAA PAPER 93-0829] p 116 A93-24899
- Vibration isolation technology - An executive summary of systems development and demonstration --- for proposed microgravity experiments aboard STS and Space Station Freedom
[AIAA PAPER 93-0834] p 55 A93-24904
- Experimental study of two interacting drops in an immiscible fluid
p 179 A93-37936
- On accurate determination of contact angle
p 143 A93-41678
- Collective effects of temperature gradients and gravity on droplet coalescence
p 183 A93-46716
- Gravity sensitivity of a resistojet water vaporizer
[AIAA PAPER 93-2402] p 186 A93-50167
- Nucleate pool boiling in the long duration low gravity environment of the Space Shuttle
[NASA-TM-105973] p 144 N93-15420
- Vibration isolation technology: An executive summary of systems development and demonstration
[NASA-TM-105937] p 1 N93-15573
- Effects of buoyancy on laminar, transitional, and turbulent gas jet diffusion flames
p 121 N93-20189
- Opposed-flow flame spreading in reduced gravity
p 121 N93-20206
- Flame spread across liquid pools
p 122 N93-20209
- Contributions of microgravity test results to the design of spacecraft fire safety systems
[NASA-TM-106093] p 60 N93-24755
- Low-frequency vibration environment for five Shuttle missions
[NASA-TM-106059] p 63 N93-28554
- Gravity sensitivity of a resistojet water vaporizer
[NASA-TM-106220] p 92 N93-29194
- Smoldering combustion in microgravity. USML-1 glovebox experiment No. 6
[NASA-TM-105012] p 146 N93-70290
- GRAVITATIONAL FIELDS**
Stochastic inflation lattice simulations - Ultra-large scale structure of the universe
p 289 A93-17646
- Dark matter and the equivalence principle
p 291 A93-44385
- GRAVITATIONAL WAVES**
Gravitational waves from first-order cosmological phase transitions
p 288 A93-11451
- The gravitational wave contribution to cosmic microwave background anisotropies and the amplitude of mass fluctuations from COBE results
p 289 A93-21508
- Observing the inflation potential --- in models of cosmological inflation
p 291 A93-50480
- GRAVITY WAVES**
Cosmic microwave background probes models of inflation
p 294 A93-10355
- GRID GENERATION (MATHEMATICS)**
Ice accretion and performance degradation calculations with LEWICE/NS
[AIAA PAPER 93-0173] p 18 A93-23244
- Unstructured 3D Delaunay mesh generation applied to planes, trains and automobiles
[AIAA PAPER 93-0673] p 259 A93-24781
- Bgrid - Interactive three-dimensional turbomachinery grid generation system with applications
[AIAA PAPER 93-0430] p 259 A93-25527
- Linearized Euler predictions of unsteady aerodynamic loads in cascades
p 7 A93-29318
- Grid adaptation using Chimera composite overlapping meshes
[AIAA PAPER 93-3389] p 267 A93-45080
- Algebraic grid generation with control points
p 268 A93-45967
- Ice accretion and performance degradation calculations with LEWICE/NS
[NASA-TM-105972] p 19 N93-15354
- Mapping methods for computationally efficient and accurate structural reliability
[NASA-TM-105892] p 248 N93-23745
- A three-dimensional algebraic grid generation scheme for gas turbine combustors with inclined slots
[NASA-CR-191095] p 198 N93-24759
- An extended Lagrangian method
[NASA-TM-106129] p 199 N93-26203
- Grid adaptation using Chimera composite overlapping meshes
[NASA-TM-106163] p 269 N93-27065
- GROUND BASED CONTROL**
Proposed ground-based control of accelerometer on Space Station Freedom
p 63 A93-54401
- Proposed ground-based control of accelerometer on Space Station Freedom
[NASA-TM-105960] p 63 N93-23738
- GROUND EFFECT (AERODYNAMICS)**
Two-, three-, and four-poster jets in cross flow
[AIAA PAPER 93-0023] p 167 A93-20141
- GROUND OPERATIONAL SUPPORT SYSTEM**
A system to measure lightning-induced transients on spacecraft umbilical lines
p 161 N93-24889
- GROUND STATE**
Extension of a new semiempirical method (BFS) and the study of ground state properties of binary alloys
p 283 A93-52600
- GROUND TESTS**
The ground testing of a 2 kW solar dynamic space power system
p 68 A93-25918
- A function approximation approach to anomaly detection in propulsion system test data
[AIAA PAPER 93-1776] p 71 A93-49671
- Ground testing for the no-vent fill of cryogenic tanks - Results of tests for a 71 cubic foot tank
[AIAA PAPER 93-1967] p 73 A93-49815
- Design of an Advanced Expander Test Bed
[AIAA PAPER 93-2133] p 48 A93-49952
- Plasma chamber testing of APSA coupons for the SAMPIE flight experiment
[NASA-TM-106084] p 60 N93-23742
- GROUND WIND**
Effects of dust accumulation and removal on radiator surfaces on Mars
p 123 A93-13937
- GUANIDINES**
Guandine based vehicle/binders for use with oxides, metals, and ceramics
[NASA-CASE-LEW-15314-2] p 138 N93-28423
- GUIDE VANES**
Comparison of radiated noise from shrouded and unshrouded propellers
p 274 A93-55861
- GUST LOADS**
Influence of airfoil thickness on sound generated by high-frequency gust interactions
p 272 A93-19181
- Forcing function effects on unsteady aerodynamic gust response. I - Forcing functions
[ASME PAPER 92-GT-174] p 3 A93-19400
- Forcing function effects on unsteady aerodynamic gust response. II - Low solidity airfoil row response
[ASME PAPER 92-GT-175] p 3 A93-19401
- Forcing function modeling for flow induced vibration
[ISABE 93-7027] p 31 A93-54003
- H**
- H-INFINITY CONTROL**
Robust integrated flight/propulsion control design for a STOVL aircraft using H-infinity control design techniques
p 40 A93-26432
- HAFNIUM CARBIDES**
Influence of grain size on the creep behavior of HfC-dispersed NiAl
p 123 A93-17674
- Preliminary evaluation of tensile and stress-rupture behavior of W + 24 at. pct Re + 0.4 at. pct HfC wire
p 125 A93-25119
- HALL EFFECT**
Diminishing sign anomaly and scaling behavior of the mixed-state Hall resistivity in Ti2Ba2Ca2Cu3O10 films containing columnar defects
p 283 A93-53693
- HARDENING (MATERIALS)**
Ratchetting behavior in viscoplasticity - A technical note
p 241 A93-43651
- HARMONIC ANALYSIS**
HFAST - A harmonic analysis program for Stirling cycles
p 220 A93-26051
- HASTELLOY (TRADEMARK)**
Critical experiments of the self-consistent model for polycrystalline Hastelloy-X
p 124 A93-21958
- The viscoplastic behavior of Hastelloy-X single crystal
p 125 A93-27486
- Experimental investigation of cyclic thermomechanical deformation in torsion
[NASA-TM-105938] p 247 N93-17996
- HEAT ENGINES**
The multi-heat addition turbine engine
[AIAA PAPER 92-4272] p 22 A93-13334
- HEAT EXCHANGERS**
Pulsed single-blow regenerator testing
p 221 A93-26081
- Preliminary endurance tests of water vaporizers for resistojet applications
[AIAA PAPER 93-2403] p 187 A93-50168
- Preliminary characterization of a water vaporizer for resistojet applications
[NASA-TM-105877] p 80 N93-11402
- Summary of the NASA Lewis component technology program for Stirling power converters
[NASA-TM-105640] p 82 N93-15526
- Test results of a Stirling engine utilizing heat exchanger modules with an integral heat pipe
[NASA-TM-105883] p 256 N93-25136
- Preliminary endurance tests of water vaporizers for resistojet applications
[NASA-TM-106222] p 92 N93-28694
- HEAT FLUX**
Fabrication of thin film heat flux sensors
p 204 A93-16419
- The turbulent thermal boundary layer with an abrupt change from a rough to a smooth wall
p 167 A93-21712
- Novel thin-film heat flux sensors
[AIAA PAPER 92-5035] p 205 A93-22309
- Influence of heat transfer rates on pressurization of liquid/slush hydrogen propellant tanks
[AIAA PAPER 93-0278] p 169 A93-22681
- The effects of buoyancy on the critical heat flux in forced convection
[AIAA PAPER 93-0575] p 169 A93-23307
- M.I.T. Stirling-cycle heat transfer apparatus
p 174 A93-26090
- Relations for local radiative heat transfer between rectangular boundaries of an absorbing-emitting medium
p 175 A93-30129
- Miniature high temperature plug-type heat flux gauges
p 209 A93-37862
- Progress towards understanding and predicting heat transfer in the turbine gas path
p 188 A93-52751
- Fabrication of thin film heat flux sensors
p 213 N93-13667
- Small hydrogen/oxygen rocket flowfield behavior from heat flux measurements
[NASA-TM-106233] p 91 N93-28619
- Progress in the measurement of SSME turbine heat flux with plug-type sensors
p 217 N93-31553
- Thin film heat flux sensor for Space Shuttle Main Engine turbine environment
p 217 N93-31554
- Thin film thermocouples for high temperature turbine application
p 217 N93-31555
- Hypersonic engine component experiments in high heat flux, supersonic flow environment
[NASA-TM-106273] p 203 N93-31860
- Non-contact heat flux measurement using a transparent sensor
[NASA-TM-106252] p 142 N93-32330
- HEAT MEASUREMENT**
Wake-induced unsteady stagnation-region heat-transfer measurements
[ASME PAPER 92-GT-196] p 166 A93-19421
- Miniature high temperature plug-type heat flux gauges
p 209 A93-37862
- Progress in the measurement of SSME turbine heat flux with plug-type sensors
p 217 N93-31553
- Thin film heat flux sensor for Space Shuttle Main Engine turbine environment
p 217 N93-31554
- Thin film thermocouples for high temperature turbine application
p 217 N93-31555
- HEAT OF COMBUSTION**
Performance and heat transfer characteristics of a carbon monoxide/oxygen rocket engine
[NASA-TM-105897] p 84 N93-18878
- HEAT OF FORMATION**
Heats of formation of bcc binary alloys
p 123 A93-17609
- Method for calculating alloy energetics
p 279 A93-18740

HEAT PIPES

Determination of parameters of a method for predicting alloy properties p 126 A93-39796
 Determination of parameters of a new method for predicting alloy properties [NASA-TM-105895] p 127 N93-11609

HEAT PIPES

SP-100 high-temperature advanced radiator development p 163 A93-13843
 Heat-pipe transient model for space applications p 163 A93-13867
 Construction and testing of ceramic fabric heat pipe with water working fluid p 163 A93-13869
 Closed-form analytical solutions of high-temperature heat pipe startup and frozen startup limitation p 165 A93-18564

A study of circumferentially-heated and block-heated heat pipes. I - Experimental analysis and generalized analytical prediction of capillary limits. II - Three-dimensional numerical modeling as a conjugate problem p 168 A93-21715
 Fabrication of carbon-carbon heat pipes for space nuclear power applications p 173 A93-25978
 Design of a cavity heat pipe receiver experiment p 173 A93-25985

Simulation of the early startup period of high-temperature heat pipes from the frozen state by a rarefied vapor self-diffusion model p 175 A93-30127

A numerical analysis of high-temperature heat pipe startup from the frozen state p 175 A93-30128
 Vaporization heat transfer of dielectric liquids on enhanced surfaces covered with screen wicks [AIAA PAPER 93-2835] p 182 A93-46572

Summary of the NASA Lewis component technology program for Stirling power converters p 82 N93-15526 [NASA-TM-105640]
 Test results of a Stirling engine utilizing heat exchanger modules with an integral heat pipe p 256 N93-25136 [NASA-TM-105883]
 Radiator technology p 90 N93-26979

HEAT RADIATORS

Effects of dust accumulation and removal on radiator surfaces on Mars p 123 A93-13937
 On protection of Freedom's solar dynamic radiator from the orbital debris environment. II - Further testing and analyses p 70 A93-36589
 Thermal emittance enhancement of graphite-aluminum and graphite-copper composite radiator surfaces for space power applications p 105 A93-53455

HEAT RESISTANT ALLOYS

Creep-rupture strength of a Ni-base superalloy at 1400 K p 124 A93-20556
 A constitutive model for the high temperature inelastic response of nickel base superalloys p 124 A93-21959
 Design considerations for a Space Shuttle Main Engine turbine blade made of single crystal material p 236 A93-25228

Effect of tensile mean stress on fatigue behavior of single-crystal and directionally solidified superalloys p 125 A93-33011

Effect of thermal cycling on interface bonding requirements in Al₂O₃ fiber-reinforced superalloy composites p 103 A93-35882

Chromium and reactive element modified aluminide diffusion coatings on superalloys - Environmental testing p 126 A93-37899

Material requirements for the High Speed Civil Transport p 31 A93-54043 [ISABE 93-7067]

In-phase and out-of-phase axial-torsional fatigue behavior of Haynes 188 at 760 C p 246 N93-13153 [NASA-TM-105765]

Experimental investigation of cyclic thermomechanical deformation in torsion p 247 N93-17996 [NASA-TM-105938]

A statistical analysis of elevated temperature gravimetric cyclic oxidation data of 36 Ni- and Co-base superalloys based on an oxidation attack parameter p 128 N93-18069 [NASA-TM-105934]

High-temperature, bellows hybrid seal p 227 N93-19027 [NASA-CASE-LEW-15570-1]

Study of the capacitance technique for measuring high-temperature blade tip clearance on ceramic rotors [NASA-TM-105978] p 35 N93-23013

The influence of primary and secondary orientations on the elastic response of a nickel-base single-crystal superalloy p 250 N93-26550 [NASA-TM-106125]

High temperature creep and oxidation resistant chromium silicide matrix alloy containing molybdenum [NASA-CASE-LEW-15697-1] p 130 N93-29172

Oxidation resistant overlay coatings for low expansion substrates p 138 N93-31300 [NASA-CASE-LEW-15154-2]

Cumulative fatigue damage behavior of MAR M-247 p 251 N93-31575

The effect of porosity and gamma-gamma' eutectic content on the low cycle fatigue behavior of hydrogen-charged PWA-1480 p 130 N93-31576
 Secondary orientation effects in a single crystal superalloy under mechanical and thermal loads p 130 N93-31578

HEAT SINKS

Vaporization heat transfer of dielectric liquids on enhanced surfaces covered with screen wicks [AIAA PAPER 93-2835] p 182 A93-46572
 Semiconductor cooling apparatus [NASA-CASE-LEW-14162-3] p 111 N93-29614

HEAT SOURCES

Comparison of dynamic isotope power systems for distributed planetary surface applications p 46 A93-13825

Design of small Stirling dynamic isotope power system for robotic space missions p 141 N93-12085 [NASA-TM-105919]

Closed Brayton Cycle power system with a high temperature pellet bed reactor heat source for NEP applications p 82 N93-14482 [NASA-TM-105933]

HEAT STORAGE

Void control in the crystallization of lithium fluoride p 97 A93-13760
 An Isotope-Powered Thermal Storage unit for space applications p 65 A93-13877

Properties of pure nickel after long term exposures to LiOH and vacuum at 775 K p 123 A93-18075

Experimental determination of in situ utilization of lunar regolith for thermal energy storage p 253 A93-26043
 Modeling void growth and movement with phase change in thermal energy storage canisters p 285 A93-46569 [AIAA PAPER 93-2832]

Advanced solar dynamic technology program p 256 N93-27806

Thermal energy storage flight experiment in microgravity p 256 N93-28720

HEAT TRANSFER

Advanced radiator concepts feasibility demonstration --- for space power system p 163 A93-13844

Heat transfer performance comparisons of five different rectangular channels with parallel angled ribs p 166 A93-18752

Heat transfer in rotating serpentine passages with trips skewed to the flow p 166 A93-19416 [ASME PAPER 92-GT-191]

Time-averaged heat transfer and pressure measurements and comparison with prediction for a two-stage turbine p 166 A93-19419 [ASME PAPER 92-GT-194]

Wake-induced unsteady stagnation-region heat-transfer measurements p 166 A93-19421 [ASME PAPER 92-GT-196]

A study of circumferentially-heated and block-heated heat pipes. I - Experimental analysis and generalized analytical prediction of capillary limits. II - Three-dimensional numerical modeling as a conjugate problem p 168 A93-21715

An algebraic turbulence model for three-dimensional viscous flows p 4 A93-22552 [AIAA PAPER 93-0083]

Vaporization heat transfer of dielectric liquids on a wick-covered surface p 169 A93-22686 [AIAA PAPER 93-0283]

Close-up analysis of aircraft ice accretion [AIAA PAPER 93-0029] p 18 A93-23239

Use of surface heat transfer measurements as a flow separation diagnostic in a two-dimensional reflected oblique shock/turbulent boundary layer interaction p 172 A93-24859 [AIAA PAPER 93-0775]

Finite element procedures for coupled linear analysis of heat transfer, fluid and solid mechanics p 267 A93-34166 [AIAA PAPER 93-1639]

Heat transfer from radiatively heated material in a low Reynolds number microgravity environment p 180 A93-43695

Effects of detailed droplet heating models on turbulent sprays vaporization behavior p 185 A93-50005 [AIAA PAPER 93-2193]

High Reynolds number and turbulence effects on aerodynamics and heat transfer in a turbine cascade [AIAA PAPER 93-2252] p 186 A93-50050

Chimera grids in the simulation of three-dimensional flowfields in turbine-blade-coolant passages p 187 A93-50280 [AIAA PAPER 93-2559]

Measurements and computational analysis of heat transfer and flow in a simulated turbine blade internal cooling passage p 189 A93-53585 [AIAA PAPER 93-1797]

Radiation and phase change of lithium fluoride in an annulus p 144 A93-54460

Thermal stratification potential in rocket engine coolant channels p 78 N93-10019

Radial turbine cooling p 191 N93-10061

Navier-Stokes turbine heat transfer predictions using two-equation turbulence p 191 N93-10735 [NASA-TM-105817]

Electrical design of payload G-534: The Pool Boiling Experiment p 144 N93-13170

An algebraic turbulence model for three-dimensional viscous flows p 1 N93-14102 [NASA-TM-105931]

Use of surface heat transfer measurements as a flow separation diagnostic in a two dimensional reflected oblique shock/turbulent boundary layer interaction p 194 N93-15355 [NASA-TM-105981]

Close-up analysis of aircraft ice accretion p 19 N93-15360 [NASA-TM-105952]

Performance and heat transfer characteristics of a carbon monoxide/oxygen rocket engine p 84 N93-18878 [NASA-TM-105897]

Three-dimensional Navier-Stokes heat transfer predictions for turbine blade rows p 196 N93-19969 [NASA-TM-105800]

Heat transfer device p 108 N93-20568 [NASA-CASE-LEW-14162-4]

Multi-heat addition turbine engine p 35 N93-22034 [NASA-CASE-LEW-15094-1]

Summary of experimental heat-transfer results from the turbine hot section facility p 197 N93-23059 [NASA-TP-3250]

Heat transfer in rotating serpentine passages with selected model orientation for smooth or skewed trip walls p 147 N93-25177 [NASA-TM-106126]

Increased heat transfer to elliptical leading edges due to spanwise variations in the freestream momentum: Numerical and experimental results p 199 N93-27020 [NASA-TM-106150]

Small hydrogen/oxygen rocket flowfield behavior from heat flux measurements p 91 N93-28619 [NASA-TM-106233]

High Reynolds number and turbulence effects on aerodynamics and heat transfer in a turbine cascade [NASA-TM-106187] p 202 N93-29157

Semiconductor cooling apparatus p 111 N93-29614 [NASA-CASE-LEW-14162-3]

Navier-Stokes analysis of three-dimensional flow and heat transfer inside turbine blade rows p 39 N93-29963

Overview of aerothermodynamic loads definition study p 93 N93-31583

Measurements and computational analysis of heat transfer and flow in a simulated turbine blade internal cooling passage p 203 N93-31647 [NASA-TM-106189]

Summary of NASA Lewis Research Center validation efforts p 204 N93-70579

HEAT TRANSFER COEFFICIENTS

Heat transfer in rotating serpentine passages with trips skewed to the flow p 166 A93-19416 [ASME PAPER 92-GT-191]

Advancements in the LEWICE Ice Accretion Model [AIAA PAPER 93-0171] p 18 A93-23243

Heat transfer in oscillating flows with sudden change in cross section p 174 A93-26089

Miniature high temperature plug-type heat flux gauges p 209 A93-37862

Evaluation of a hue capturing based transient liquid crystal method for high-resolution mapping of convective heat transfer on curved surfaces p 210 A93-43689

Measurements and computational analysis of heat transfer and flow in a simulated turbine blade internal cooling passage p 189 A93-53585 [AIAA PAPER 93-1797]

Program ELM: A tool for rapid thermal-hydraulic analysis of solid-core nuclear rocket fuel elements p 84 N93-19106 [NASA-TM-105867]

Summary of experimental heat-transfer results from the turbine hot section facility p 197 N93-23059 [NASA-TP-3250]

Transient liquid-crystal technique used to produce high-resolution convective heat-transfer-coefficient maps [NASA-TM-106083] p 198 N93-23404

Measurements and computational analysis of heat transfer and flow in a simulated turbine blade internal cooling passage p 203 N93-31647 [NASA-TM-106189]

HEAT TRANSMISSION

Numerical model for the Programmable Multirole Furnace (PMZF) p 142 A93-24242 [AIAA PAPER 93-0471]

Preliminary investigation of high power microwave plasmas for electrothermal thruster use p 74 A93-49928 [AIAA PAPER 93-2106]

Preliminary investigation of high power microwave plasmas for electrothermal thruster use p 92 N93-29158 [NASA-TM-106207]

Overview of aerothermodynamic loads definition study p 93 N93-31583

HEATING

Numerical modeling of runback water on ice protected aircraft surfaces p 201 N93-27438

HELICAL FLOW

Statistical analysis of the effects of helicity in inhomogeneous turbulence p 175 A93-26186

HELICOPTER DESIGN

Active control of helicopter transmission noise p 274 A93-29428

Split torque transmission load sharing [NASA-TM-105884] p 226 N93-12736

Face-gear drives: Design, analysis, and testing for helicopter transmission applications [NASA-TM-106101] p 229 N93-27133

HELICOPTER ENGINES

Identification of the open loop dynamics of the T700 turboshaft engine p 26 A93-35934

Analytic methods for design of wave cycles for wave rotor core engines [AIAA PAPER 93-2523] p 30 A93-50253

The chemistry of Saudi Arabian sand - A deposition problem on helicopter turbine airfoils p 243 A93-53468

Integrity testing of brush seal in shroud ring of T-700 engine [NASA-TM-105863] p 227 N93-18380

HELICOPTER PROPELLER DRIVE

Modal simulation of gear box vibration with experimental correlation p 221 A93-31982

Low-noise, high-strength, spiral-bevel gears for helicopter transmissions [AIAA PAPER 93-2149] p 223 A93-49966

Split torque transmission load sharing [NASA-TM-105884] p 226 N93-12736

Evaluation of an oil-debris monitoring device for use in helicopter transmissions [NASA-TM-105830] p 227 N93-22826

Low-noise, high-strength, spiral-bevel gears for helicopter transmissions [NASA-TM-106080] p 228 N93-23019

Fault detection of helicopter gearboxes using the multi-valued influence matrix method [NASA-TM-106100] p 229 N93-27069

Face-gear drives: Design, analysis, and testing for helicopter transmission applications [NASA-TM-106101] p 229 N93-27133

HELICOPTERS

Efficient fault diagnosis of helicopter gearboxes [NASA-TM-106253] p 231 N93-31846

HELIUM

Brush seal leakage performance with gaseous working fluids at static and low rotor speed conditions [ASME PAPER 92-GT-304] p 219 A93-19494

Closed Brayton Cycle power system with a high temperature pellet bed reactor heat source for NEP applications [NASA-TM-105933] p 82 N93-14482

HEPTANES

Asymptotic analysis with reduced chemistry for the burning of n-heptane droplets p 113 A93-13323

Asymptotic analysis for the burning of n-heptane droplets using a four-step reduced mechanism p 117 A93-41952

HETERODYNING

Optical communications and a comparison of optical technologies for a high data rate return link from Mars [NASA-TP-3180] p 52 N93-18854

HETEROJUNCTION DEVICES

Interface dependence of band offsets in lattice-matched isovalent heterojunctions p 280 A93-32132

High frequency performance of Si(1-x)Ge(x)/Si(1-y)Ge(y)/Si(1-x)Ge(x) HBTs p 155 A93-37409

Application of high-quality SiO₂ grown by multipolar ECR source to Si/SiGe MISFET p 156 A93-37413

High-efficiency high-gain monolithic heterostructure FET amplifier at 31 GHz p 156 A93-37421

The effects of strain on the microwave performance of SiGe HBTs p 158 A93-54442

HETEROJUNCTIONS

Intermodulation in the oscillatory magnetoresistance of a two-dimensional electron gas p 151 A93-17610

HEURISTIC METHODS

Real-time diagnostics for a reusable rocket engine [NASA-TM-105792] p 266 N93-19018

HIGH ALTITUDE TESTS

Pulsed laser Rayleigh scattering diagnostic for hydrogen/oxygen rocket exit plane flowfield velocimetry [AIAA PAPER 93-0805] p 207 A93-25552

HIGH ELECTRON MOBILITY TRANSISTORS

A high efficiency Ka-band monolithic pseudomorphic HEMT amplifier p 151 A93-25786

Millimeter-wave pseudomorphic HEMT MMIC phased array components for space communications p 152 A93-25796

A 10-GHz amplifier using an epitaxial lift-off pseudomorphic HEMT device p 156 A93-37574

Development of Si(1-x)Ge(x) technology for microwave sensing applications [NASA-TM-106157] p 162 N93-28610

HIGH ENERGY FUELS

Atomic hydrogen propellants - Historical perspectives and future possibilities [AIAA PAPER 93-0244] p 140 A93-24234

HIGH FREQUENCIES

Comparison of high temperature, high frequency core loss and dynamic B-H loops of a 2V-49Fe-49Co and a grain oriented 3Si-Fe alloy p 153 A93-25895

HIGH PRESSURE

Laser-induced fluorescence measurements of nitric oxide in laminar C₂H₆/O₂/N₂ flames at high pressure p 116 A93-28253

HIGH RESOLUTION

Evaluation of a hue capturing based transient liquid crystal method for high-resolution mapping of convective heat transfer on curved surfaces p 210 A93-43689

Fluid dynamics and convective heat transfer in impinging jets through implementation of a high resolution liquid crystal technique [ISABE 93-7077] p 189 A93-54053

HIGH REYNOLDS NUMBER

On streamwise vortices in high Reynolds number supersonic axisymmetric jets p 167 A93-21060

Thermocapillary bubble migration - An Oseen-like analysis of the energy equation p 179 A93-41708

The structure of a three-dimensional turbulent boundary layer p 181 A93-44813

Comparative wind tunnel tests at high Reynolds numbers of NACA 64 621 airfoils with two aileron configurations p 9 A93-46823

CFD analyses of coolant channel flowfields [AIAA PAPER 93-1830] p 184 A93-49715

High Reynolds number and turbulence effects on aerodynamics and heat transfer in a turbine cascade [AIAA PAPER 93-2252] p 186 A93-50050

Analysis of high Reynolds number inviscid/vicid interactions in cascades p 15 A93-55351

On the nonlinear three dimensional instability of Stokes layers and other shear layers to pairs of oblique waves [NASA-TM-105918] p 194 N93-15499

A realizable Reynolds stress algebraic equation model [NASA-TM-105993] p 16 N93-16596

The development of a mixing layer under the action of weak streamwise vortices [NASA-TM-106089] p 201 N93-28947

High Reynolds number and turbulence effects on aerodynamics and heat transfer in a turbine cascade [NASA-TM-106187] p 202 N93-29157

HIGH SPEED

Applied high-speed imaging for the icing research program at NASA Lewis Research Center p 208 A93-33169

Modeling of linear isentropic flow systems p 179 A93-37046

A compressible boundary layer algorithm for use with SINDA '85 p 192 N93-13395

Analytical and experimental studies of a short compact subsonic diffuser for a two-dimensional supersonic inlet [NASA-TP-3247] p 17 N93-24118

HIGH TEMPERATURE

Tribological and mechanical comparison of sintered and HIPped PM212 - High temperature self-lubricating composites p 94 A93-13506

Tailored metal matrix laminates for high-temperature performance p 98 A93-15753

High-temperature deformation and microstructural analysis for silicon nitride-scandium(III) oxide p 131 A93-20468

High temperature static strain measurement with an electrical resistance strain gage [AIAA PAPER 92-5039] p 205 A93-22313

Comparison of high temperature, high frequency core loss and dynamic B-H loops of a 2V-49Fe-49Co and a grain oriented 3Si-Fe alloy p 153 A93-25895

M-H characteristics and demagnetization resistance of samarium-cobalt permanent magnets to 300 C p 153 A93-26076

Microfracture in high temperature metal matrix crossply laminates p 101 A93-31356

Thermally-driven microfracture in high temperature metal matrix composites p 237 A93-32469

Miniature high temperature plug-type heat flux gauges p 209 A93-37862

Three-dimensional laser window formation for industrial application p 218 N93-22197

Study of the capacitance technique for measuring high-temperature blade tip clearance on ceramic rotors [NASA-TM-105978] p 35 N93-23013

High temperature creep and oxidation resistant chromium silicide matrix alloy containing molybdenum [NASA-CASE-LEW-15697-1] p 130 N93-29172

Progress in speckle-shift strain measurement p 251 N93-31558

Focused technology: Nuclear propulsion [PR12] p 287 N93-71885

HIGH TEMPERATURE AIR

Mechanical properties of Haynes Alloy 188 after exposure to LiF-22CaF₂ air, and vacuum at 1093 K for periods up to 10,000 hours p 126 A93-36586

Numerical modeling of runback water on ice protected aircraft surfaces p 201 N93-27438

HIGH TEMPERATURE ENVIRONMENTS

Palladium-chromium static strain gage for high temperature propulsion systems p 204 A93-16421

Overview of NASA's advanced high temperature engine materials technology program p 94 A93-53453

Gas temperature measurements using the dual-line detection Rayleigh scattering technique p 213 A93-55368

Design of a high-temperature experiment for evaluating advanced structural materials [NASA-TM-105833] p 245 N93-11624

Thin film thermocouples for high temperature measurement on ceramic materials p 213 N93-13666

Fabrication of thin film heat flux sensors p 213 N93-13667

Gas temperature measurements using the dual-line detection Rayleigh scattering technique p 214 N93-13668

Sliding durability of candidate seal fiber materials in hydrogen from 25 to 900 C p 95 N93-22590

Auger electron spectroscopy study of oxidation of a PdCr alloy used for high-temperature sensors [NASA-TM-106212] p 129 N93-23418

Radiation and temperature effects on electronic components investigated under the CSTI high capacity power project [NASA-TM-106096] p 161 N93-24746

Silicon carbide semiconductor technology for high temperature and radiation environments p 284 N93-26928

Power management and distribution technology p 90 N93-26978

A model for predicting high-temperature fatigue failure of a W/Cu composite p 112 N93-31579

HIGH TEMPERATURE GAS COOLED REACTORS

Closed Brayton Cycle power system with a high temperature pellet bed reactor heat source for NEP applications [NASA-TM-105933] p 82 N93-14482

HIGH TEMPERATURE GASES

Corrosion of silicon-based ceramics in combustion environments p 131 A93-22984

Nonintrusive, multipoint velocity measurements in high-pressure combustion flows [AIAA PAPER 93-2032] p 118 A93-49867

Plume characteristics of an arcjet thruster [AIAA PAPER 93-2530] p 77 A93-50258

Droplet vaporization in a high-pressure gas p 190 A93-55461

Spectroscopic wear detector [NASA-CASE-LEW-15200-1] p 83 N93-18856

HIGH TEMPERATURE NUCLEAR REACTORS

Ultra-high temperature vapor-core reactor - Magnetohydrodynamic system for space nuclear electric power p 66 A93-21663

HIGH TEMPERATURE SUPERCONDUCTORS

Large-area YBa₂Cu₃O_{7-δ} thin films on sapphire for microwave applications p 279 A93-11475

Giant suppression of flux-flow resistivity in heavy-ion irradiated Ti₂Ba₂Ca₂Cu₃O₁₀ films - Influence of linear defects on vortex transport p 280 A93-26198

Design aspects and comparison between high T_c superconducting coplanar waveguide and microstrip line p 155 A93-27244

Processing, electrical and microwave properties of sputtered Ti-Ca-Ba-Cu-O superconducting thin films p 282 A93-44607

Performance of TiCaBaCuO 30 GHz 64 element antenna array p 157 A93-44763

Diminishing sign anomaly and scaling behavior of the mixed-state Hall resistivity in Ti₂Ba₂Ca₂Cu₃O₁₀ films containing columnar defects p 283 A93-53693

HIGH TEMPERATURE TESTS

Properties of pure nickel after long term exposures to LiOH and vacuum at 775 K p 123 A93-18075

Creep-rupture strength of a Ni-base superalloy at 1400 K p 124 A93-20556

A constitutive model for the high temperature inelastic response of nickel base superalloys p 124 A93-21959

Strain sensing technology for high temperature applications [AIAA PAPER 92-5040] p 205 A93-22314

Reaction layer formation at the graphite/copper-chromium alloy interface p 100 A93-25105

- The viscoplastic behavior of Hastelloy-X single crystal p 125 A93-27486
- X-ray-based displacement measurement for hostile environments p 208 A93-28580
- Measurement of the temperature coefficient of ratio transformers p 155 A93-32771
- Optical fiber sensor for temperature measurement from 600 to 1900 C in gas turbine engines p 208 A93-32918
- A hot dynamic seal rig for measuring hypersonic engine seal durability and flow performance [AIAA PAPER 93-1346] p 222 A93-33916
- Creep deformation of B2 aluminides p 126 A93-44887
- Stress relaxation of low pressure plasma-sprayed NiCrAlY alloys p 127 A93-52870
- Relative sliding durability of candidate high temperature fiber seal materials p 95 N93-10978
- Development of thin film thermocouples on ceramic materials for advanced propulsion system applications [NASA-TM-106017] p 215 N93-25173
- An overview of elevated temperature damage mechanisms and fatigue behavior of a unidirectional SCS-6/Ti-15-3 composite [NASA-TM-106131] p 109 N93-26702
- Hypersonic engine component experiments in high heat flux, supersonic flow environment [NASA-TM-106273] p 203 N93-31860
- HIGH THRUST**
- Optimal impulsive intercept with low-thrust rendezvous return p 45 A93-34521
- Space R/T base: Propulsion (high thrust chemical) [PRS] p 286 N93-71878
- HIGH VOLTAGES**
- The interaction of high voltage systems with the environments of the moon and Mars [AIAA PAPER 93-0704] p 67 A93-24800
- The interaction of high voltage systems with the environments of the Moon and Mars [NASA-TM-106107] p 61 N93-26148
- HOLES (MECHANICS)**
- Fatigue criterion to system design, life and reliability: A primer [NASA-TM-106022] p 248 N93-23406
- HOLLOW CATHODES**
- Plasma contactor technology for Space Station Freedom [AIAA PAPER 93-2228] p 57 A93-50034
- HOLOGRAPHIC INTERFEROMETRY**
- Temporal averaging of phase measurements in the presence of spurious phase drift - Application to phase-stepped real-time holographic interferometry p 207 A93-26967
- Temporal averaging in a turbulent environment - Compensation for phase drifts in phase shifting interferometry p 210 A93-44190
- HOLOGRAPHY**
- Three-dimensional computed tomography from interferometric measurements within a narrow cone of views p 207 A93-24024
- Visualization of hydrogen injection in a scramjet engine by simultaneous PLIF imaging and laser holographic imaging p 214 N93-13683
- HOMODYNE RECEPTION**
- Optical communications and a comparison of optical technologies for a high data rate return link from Mars [NASA-TP-3180] p 52 N93-18854
- HOMOGENEOUS TURBULENCE**
- Critical assessment of Reynolds stress turbulence models using homogeneous flows [AIAA PAPER 93-0082] p 170 A93-24227
- A multiple-scale turbulence model for incompressible flow [AIAA PAPER 93-0086] p 170 A93-24228
- Statistical analysis of the effects of helicity in inhomogeneous turbulence p 175 A93-26186
- Critical comparison of second-order closures with direct numerical simulations of homogeneous turbulence p 176 A93-30840
- Turbulence modeling and experiments p 195 N93-15796
- HONEYCOMB STRUCTURES**
- Friction-factor characteristics for narrow channels with honeycomb surfaces [ASME PAPER 91-TRIB-21] p 219 A93-15681
- Friction-factor data for flat-plate tests of smooth and honeycomb surfaces [ASME PAPER 91-TRIB-20] p 219 A93-15682
- Integrity testing of brush seal in shroud ring of T-700 engine [NASA-TM-105863] p 227 N93-18380
- Solar concentrators for advanced solar-dynamic power systems in space [NASA-CR-187148] p 85 N93-23017
- HORIZONTAL SPACECRAFT LANDING**
- The design and evolution of the beta two-stage-to-orbit horizontal takeoff and landing launch system [NASA-TM-106118] p 51 N93-27018
- HORSESHOE VORTICES**
- The development of a turbulent junction vortex system p 168 A93-22258
- HOT CORROSION**
- Diffusional transport and predicting oxidative failure during cyclic oxidation of beta-NiAl alloys p 126 A93-50370
- HOT ISOSTATIC PRESSING**
- Effect of HIPing on the effective thermal conductivity/diffusivity and the interfacial thermal conductance of uniaxial SiC fibre-reinforced RBSN p 100 A93-26674
- HOT PRESSING**
- Silicon carbide fiber reinforced strontium aluminosilicate glass-ceramic matrix composite [NASA-CASE-LEW-15263-1] p 106 N93-11543
- HOUSINGS**
- Acoustical analysis of gear housing vibration p 273 A93-29420
- HUBBLE CONSTANT**
- Microwave anisotropies in the light of the data from the COBE satellite p 291 A93-35444
- HUMAN FACTORS ENGINEERING**
- Probabilistic simulation of the human factor in structural reliability [AIAA PAPER 93-1495] p 264 A93-34036
- Probabilistic simulation of the human factor in structural reliability p 258 N93-31573
- HUMAN PERFORMANCE**
- Probabilistic simulation of the human factor in structural reliability p 258 N93-31573
- HUMAN-COMPUTER INTERFACE**
- A graphical user-interface for propulsion system analysis [AIAA PAPER 93-0223] p 259 A93-23699
- An embedded rule-based diagnostic expert system in Ada p 260 N93-11928
- Space Communication Artificial Intelligence for Link Evaluation Terminal (SCAILET) p 265 N93-11940
- HYBRID COMPOSITES**
- Three-dimensional finite element simulation of intermingled-fiber hybrid composite behavior p 98 A93-15729
- Method for producing hybrid graphite composite [NASA-CASE-LEW-15241-2] p 112 N93-31296
- HYDRAULIC EQUIPMENT**
- Life extending control: An interdisciplinary engineering thrust p 93 N93-31581
- HYDROCARBON COMBUSTION**
- Asymptotic analysis with reduced chemistry for the burning of n-heptane droplets p 113 A93-13323
- Asymptotic analysis for the burning of n-heptane droplets using a four-step reduced mechanism p 117 A93-41952
- The promising chemical kinetics for the simulation of propane-air combustion with KIVA-II code [AIAA PAPER 93-2189] p 118 A93-50001
- HYDROCARBON FUELS**
- Hydrocarbon-fuel/copper combustion chamber liner compatibility, corrosion prevention, and refurbishment p 139 A93-14510
- Structure of soot-containing laminar jet diffusion flames [AIAA PAPER 93-0708] p 114 A93-24804
- A simplified reaction mechanism for calculation of emissions in hydrocarbon (Jet-A) combustion [AIAA PAPER 93-2341] p 118 A93-50116
- HYDRODYNAMIC EQUATIONS**
- Experimental study of two interacting drops in an immiscible fluid p 179 A93-37936
- HYDRODYNAMICS**
- Modeling void growth and movement with phase change in thermal energy storage canisters [AIAA PAPER 93-2832] p 285 A93-46569
- Effect of radiation on convection in a top-heated enclosure p 189 A93-54454
- A hydrodynamic model of the oscillating screen viscometer p 190 A93-55136
- HYDROFLUORIC ACID**
- Direct observation of porous SiC formed by anodization in HF p 282 A93-43587
- HYDROGEN**
- Effect of hydrogen on the strength and microstructure of selected ceramics p 130 A93-13613
- Analytical and numerical modeling of flame-balls in hydrogen-air mixtures p 118 A93-46009
- Technology for gelled liquid cryogenic propellants - Metallized hydrogen/aluminum [AIAA PAPER 93-1878] p 140 A93-49752
- Development and use of hydrogen-air torches in an altitude facility [AIAA PAPER 93-2176] p 42 A93-49988
- 10 kW power electronics for hydrogen arcjets p 79 N93-10033
- The 10 kW power electronics for hydrogen arcjets [NASA-TM-105614] p 81 N93-12484
- Performance comparison of axisymmetric and three-dimensional hydrogen film coolant injection in a 110N hydrogen/oxygen rocket [NASA-TM-105967] p 83 N93-16714
- A survey and analysis of commercially available hydrogen sensors [NASA-TM-105878] p 214 N93-17777
- Atomic hydrogen propellants: Historical perspectives and future possibilities [NASA-TM-106053] p 84 N93-20614
- Sliding durability of candidate seal fiber materials in hydrogen from 25 to 900 C [NASA-TM-105939] p 95 N93-22590
- Development and use of hydrogen-air torches in an altitude facility [NASA-TM-106047] p 43 N93-26214
- The effect of porosity and gamma-gamma' eutectic content on the low cycle fatigue behavior of hydrogen-charged PWA-1480 p 130 N93-31576
- HYDROGEN ATOMS**
- Atomic hydrogen propellants - Historical perspectives and future possibilities [AIAA PAPER 93-0244] p 140 A93-24234
- Atomic hydrogen propellants: Historical perspectives and future possibilities [NASA-TM-106053] p 84 N93-20614
- HYDROGEN ENGINES**
- Recent testing of 30 KW hydrogen arcjet thrusters [AIAA PAPER 93-1902] p 73 A93-49772
- Monte Carlo and experimental studies of nozzle flow in a low-power hydrogen arcjet [AIAA PAPER 93-2529] p 77 A93-50257
- HYDROGEN FUELS**
- Pd prediction of supersonic hydrogen flames [AIAA PAPER 93-0448] p 114 A93-23358
- Flame balls - Past, present and future [AIAA PAPER 93-0712] p 114 A93-24807
- Analysis and design of an ultrahigh temperature hydrogen-fueled MHD generator p 278 A93-49618
- The development of hydrogen sensor technology for aerospace applications [AIAA PAPER 93-2375] p 211 A93-50144
- Visualization of hydrogen injection in a scramjet engine by simultaneous PLIF imaging and laser holographic imaging p 214 N93-13683
- The development of hydrogen sensor technology at NASA Lewis Research Center [NASA-TM-106141] p 216 N93-27021
- HYDROGEN OXYGEN ENGINES**
- Hydrocarbon-fuel/copper combustion chamber liner compatibility, corrosion prevention, and refurbishment p 139 A93-14510
- Ceramic matrix composites for rocket engine turbine applications [ASME PAPER 92-GT-394] p 99 A93-19547
- Pulsed laser Rayleigh scattering diagnostic for hydrogen/oxygen rocket exit plane flowfield velocimetry [AIAA PAPER 93-0805] p 207 A93-25552
- Development of a hydrogen gas sensor using microfabrication technology [SAE PAPER 92-1176] p 210 A93-41356
- A laboratory model of a hydrogen/oxygen engine for combustion and nozzle studies [AIAA PAPER 93-1825] p 48 A93-49711
- Prospects for utilization of air liquefaction and enrichment system (ALES) propulsion in fully reusable launch vehicles [AIAA PAPER 93-2025] p 74 A93-49861
- Design and fabrication of a hydrogen/oxygen thrust chamber assembly [AIAA PAPER 93-2132] p 74 A93-49951
- An RL10A-3-3A rocket engine model using the Rocket Engine Transient Simulator (ROCETS) software [AIAA PAPER 93-2357] p 75 A93-50129
- Combustion-wave ignition for rocket engines p 78 N93-10016
- Hot fire test results of subscale tubular combustion chambers p 79 N93-10020
- Hot fire test results of subscale tubular combustion chambers [NASA-TP-3222] p 81 N93-11614
- Performance comparison of axisymmetric and three-dimensional hydrogen film coolant injection in a 110N hydrogen/oxygen rocket [NASA-TM-105967] p 83 N93-16714
- Laser Rayleigh and Raman diagnostics for small hydrogen/oxygen rockets [NASA-TM-105999] p 83 N93-17995
- Pulsed laser Rayleigh scattering diagnostic for hydrogen/oxygen rocket exit plane flowfield velocimetry [NASA-TM-106213] p 88 N93-26149

- The design and evolution of the beta two-stage-to-orbit horizontal takeoff and landing launch system
[NASA-TM-106118] p 51 N93-27018
- Small hydrogen/oxygen rocket flowfield behavior from heat flux measurements
[NASA-TM-106233] p 91 N93-28619
- Hypersonic engine component experiments in high heat flux, supersonic flow environment
[NASA-TM-106273] p 203 N93-31860
- HYDROGENATION**
Tribological studies of amorphous hydrogenated carbon films in a vacuum, spacelike environment
p 134 A93-40630
- HYDROSTATIC PRESSURE**
Flame spread across liquid pools p 122 N93-20209
- HYDROTHERMAL STRESS ANALYSIS**
Second generation integrated composite analyzer (ICAN) computer code
[NASA-TP-3290] p 108 N93-18139
- HYPERCUBE MULTIPROCESSORS**
A multiarchitecture parallel-processing development environment
[NASA-TM-106180] p 262 N93-28628
- HYPERSONIC AIRCRAFT**
Structural Tailoring/Analysis for Hypersonic Components - A computational simulation
[AIAA PAPER 92-4722] p 20 A93-20324
- HYPERSONIC COMBUSTION**
In-stream measurements of combustion during Mach 5 to 7 tests of the Hypersonic Research Engine (HRE)
[AIAA PAPER 93-2324] p 28 A93-50104
- HYPERSONIC FLIGHT**
Reaction zone structure for strong, weak overdriven, and weak underdriven oblique detonations
p 178 A93-35492
- CFD for hypersonic propulsion p 8 A93-42585
- Hypersonic engine component experiments in high heat flux, supersonic flow environment
[NASA-TM-106273] p 203 N93-31860
- HYPERSONIC FLOW**
High-speed laser anemometry based on spectrally resolved Rayleigh scattering p 207 A93-23814
- A hot dynamic seal rig for measuring hypersonic engine seal durability and flow performance
[AIAA PAPER 93-1346] p 222 A93-33916
- PNS predictions for supersonic/hypersonic flows over finned missile configurations
[AIAA PAPER 92-2695] p 7 A93-37374
- Calculation of scramjet inlet with thick boundary-layer ingestion
[AIAA PAPER 93-1836] p 12 A93-49720
- HYPERSONIC NOZZLES**
Supersonic investigation of two dimensional hypersonic exhaust nozzles
[NASA-TM-105687] p 33 N93-15342
- HYPERSONIC REENTRY**
Low-to-high altitude predictions of three-dimensional ablative re-entry flowfields p 182 A93-46407
- HYPERSONIC SPEED**
Supersonic investigation of two dimensional hypersonic exhaust nozzles
[NASA-TM-105687] p 33 N93-15342
- HYPERSONIC VEHICLES**
Design of a hypersonic waverider-derived airplane
[AIAA PAPER 93-0401] p 55 A93-21108
- Development of braided rope seals for hypersonic engine applications - Flow modeling p 222 A93-34493
- Hypersonic stability and transition p 8 A93-42579
- Advanced instrumentation for next-generation aerospace propulsion control systems
[AIAA PAPER 93-2079] p 211 A93-49906
- Development of braided rope seals for hypersonic engine applications: Flow modeling
[NASA-TM-105942] p 227 N93-14478
- The design and evolution of the beta two-stage-to-orbit horizontal takeoff and landing launch system
[NASA-TM-106118] p 51 N93-27018
- HYPERSONIC WIND TUNNELS**
In-stream measurements of combustion during Mach 5 to 7 tests of the Hypersonic Research Engine (HRE)
[AIAA PAPER 93-2324] p 28 A93-50104
- HYPERSONICS**
CFD for hypersonic propulsion p 8 A93-42585
- HYPERVELOCITY IMPACT**
On protection of Freedom's solar dynamic radiator from the orbital debris environment. I - Preliminary analysis and testing p 70 A93-36197
- On protection of Freedom's solar dynamic radiator from the orbital debris environment. II - Further testing and analyses p 70 A93-36589
- Characteristics of hypervelocity impact craters on LDEF experiment S1003 and implications of small particle impacts on reflective surfaces p 62 N93-29363
- HYSTERESIS**
Comparison of high frequency, high temperature core loss and B-H loop characteristics of an 80 Ni-Fe crystalline alloy and two iron-based amorphous alloys
p 123 A93-13882
- ICE**
Dynamic analysis of a pre-and-post ice impacted blade
[NASA-TM-105829] p 144 N93-12197
- Root damage analysis of aircraft engine blade subject to ice impact
[NASA-TM-105779] p 246 N93-15343
- Ice thickness measurement system for the icing research tunnel calibration
[NASA-TM-106095] p 215 N93-24737
- Structural tailoring of aircraft engine blade subject to ice impact constraints
[NASA-TM-106033] p 250 N93-26999
- Experimental and computational ice shapes and resulting drag increase for a NACA 0012 airfoil
p 17 N93-27440
- Blasim: A computational tool to assess ice impact damage on engine blades
[NASA-TM-106225] p 251 N93-31193
- ICE CLOUDS**
Liquid water content measurements using the Phase Doppler Particle Analyzer in the NASA Lewis Icing Research Tunnel
[AIAA PAPER 93-0298] p 42 A93-23698
- ICE FORMATION**
LEWICE droplet trajectory calculations on a parallel computer
[AIAA PAPER 93-0172] p 259 A93-22604
- Icing effects on aircraft stability and control determined from flight data - Preliminary results
[AIAA PAPER 93-0396] p 40 A93-23073
- Close-up analysis of aircraft ice accretion
[AIAA PAPER 93-0029] p 18 A93-23239
- Advancements in the LEWICE Ice Accretion Model
[AIAA PAPER 93-0171] p 18 A93-23243
- Ice accretion and performance degradation calculations with LEWICE/NS
[AIAA PAPER 93-0173] p 18 A93-23244
- Ice accretion prediction for a typical commercial transport aircraft
[AIAA PAPER 93-0174] p 19 A93-23245
- An overview of shed ice impact studies in the NASA Lewis Icing Research Tunnel
[AIAA PAPER 93-0301] p 5 A93-23247
- Applied high-speed imaging for the icing research program at NASA Lewis Research Center
p 208 A93-33169
- BLASIM - A computational tool to assess ice impact damage on engine blades
[AIAA PAPER 93-1638] p 26 A93-34165
- Results of a low power ice protection system test and a new method of imaging data analysis
p 21 A93-35932
- Icing Research Tunnel rotating bar calibration measurement system p 212 A93-54398
- Icing effects on aircraft stability and control determined from flight data: Preliminary results
[NASA-TM-105977] p 41 N93-14831
- Ice accretion and performance degradation calculations with LEWICE/NS
[NASA-TM-105972] p 19 N93-15354
- Close-up analysis of aircraft ice accretion
[NASA-TM-105952] p 19 N93-15360
- An overview of shed ice impact in the NASA Lewis Icing Research Tunnel
[NASA-TM-105969] p 16 N93-15404
- Ice accretion prediction for a typical commercial transport aircraft
[NASA-TM-105976] p 20 N93-15522
- Icing research tunnel rotating bar calibration measurement system
[NASA-TM-106010] p 215 N93-22598
- Ice thickness measurement system for the icing research tunnel calibration
[NASA-TM-106095] p 215 N93-24737
- Experimental and computational ice shapes and resulting drag increase for a NACA 0012 airfoil
p 17 N93-27440
- ICE PREVENTION**
Results of Low Power Deicer tests on a swept inlet component in the NASA Lewis Icing Research Tunnel
[AIAA PAPER 93-0032] p 20 A93-22551
- Surface roughness due to residual ice in the use of low power deicing systems
[AIAA PAPER 93-0031] p 5 A93-23240
- Numerical modeling of anti-icing systems and comparison to test results on a NACA 0012 airfoil
[AIAA PAPER 93-0170] p 21 A93-23242
- Results of a low power ice protection system test and a new method of imaging data analysis
p 21 A93-35932
- Results of low power deicer tests on a swept inlet component in the NASA Lewis icing research tunnel
[NASA-TM-105968] p 15 N93-14911
- Surface roughness due to residual ice in the use of low power deicing systems
[NASA-TM-105971] p 16 N93-15338
- Numerical modeling of anti-icing systems and comparison to test results on a NACA 0012 airfoil
[NASA-TM-105975] p 19 N93-15345
- Numerical modeling of runback water on ice protected aircraft surfaces p 201 N93-27438
- IDEAL GAS**
An improved numerical model for wave rotor design and analysis
[AIAA PAPER 93-0482] p 24 A93-23384
- An improved numerical model for wave rotor design and analysis
[NASA-TM-105915] p 33 N93-12418
- IGNITION**
Development and use of hydrogen-air torches in an altitude facility
[AIAA PAPER 93-2176] p 42 A93-49988
- A soft-start circuit for arcjet ignition
[AIAA PAPER 93-2396] p 76 A93-50161
- Catalytic ignition model in monolithic reactor with in-depth reaction p 119 A93-51641
- Combustion-wave ignition for rocket engines
p 78 N93-10016
- Development and use of hydrogen-air torches in an altitude facility
[NASA-TM-106047] p 43 N93-26214
- IGNITION LIMITS**
Analytical and numerical modeling of flame-balls in hydrogen-air mixtures p 118 A93-46009
- Smoldering combustion in microgravity. USML-1 glovebox experiment No. 6
[NASA-TM-105012] p 146 N93-70290
- IGNITION SYSTEMS**
Laser ignition application in a space experiment
[NASA-TM-106133] p 145 N93-25337
- IMAGE ANALYSIS**
Evaluation of a vibration diagnostic system for the detection of spur gear pitting failures
[AIAA PAPER 93-2298] p 224 A93-50083
- Evaluation of a vibration diagnostic system for the detection of spur gear pitting failures
[NASA-TM-106103] p 228 N93-25672
- IMAGE CONTRAST**
Application of radiative image transfer theory to the assessment of the overall OTF and contrast degradation of an image in an inhomogeneous turbulent and turbid atmosphere p 285 A93-28624
- IMAGE FILTERS**
2-D nonlinear IIR-filters for image processing - An exploratory analysis p 264 A93-28200
- IMAGE PROCESSING**
2-D nonlinear IIR-filters for image processing - An exploratory analysis p 264 A93-28200
- Application of radiative image transfer theory to the assessment of the overall OTF and contrast degradation of an image in an inhomogeneous turbulent and turbid atmosphere p 285 A93-28624
- Applied high-speed imaging for the icing research program at NASA Lewis Research Center
p 208 A93-33169
- A 3-D nonlinear recursive digital filter for video image processing p 264 A93-34582
- Results of a low power ice protection system test and a new method of imaging data analysis
p 21 A93-35932
- Evaluation of a hue capturing based transient liquid crystal method for high-resolution mapping of convective heat transfer on curved surfaces p 210 A93-43689
- Calibration of a shock wave position sensor using artificial neural networks
[NASA-TM-106136] p 216 N93-27001
- IMAGE RECONSTRUCTION**
Compressing subbanded image data with Lempel-Ziv-based coders
[NASA-TM-105998] p 149 N93-20257
- IMAGE RESOLUTION**
Hierarchical image coding with diamond-shaped sub-bands p 205 A93-20945
- IMAGES**
Picture data compression coder using subband/transform coding with a Lempel-Ziv-based coder
[NASA-CASE-LEW-15700-1] p 287 N93-28130

IMAGING SPECTROMETERS

IMAGING SPECTROMETERS

- Calibration of the forward-scattering spectrometer probe
- Modeling scattering from a multimode laser beam

IMAGING TECHNIQUES

- A new hue capturing technique for the quantitative interpretation of liquid crystal images used in convective heat transfer studies
- Design of an automated imaging system for use in a space experiment
- Particle image velocimetry for the Surface Tension Driven Convection Experiment using a particle displacement tracking technique
- Particle displacement tracking applied to air flows
- Young's fringe particle image velocimetry in the presence of random particle motions
- Applied high-speed imaging for the icing research program at NASA Lewis Research Center
- Results of a low power ice protection system test and a new method of imaging data analysis
- Visualization of hydrogen injection in a scramjet engine by simultaneous PLIF imaging and laser holographic imaging
- 2D velocity and temperature measurements in high speed flows based on spectrally resolved Rayleigh scattering
- Visualization and imaging methods for flames in microgravity
- IMPACT DAMAGE**
 - Dynamic analysis of a pre-and-post ice impacted blade
 - BLASIM - A computational tool to assess ice impact damage on engine blades
 - Dynamic analysis of a pre-and-post ice impacted blade
 - Structural tailoring of aircraft engine blade subject to ice impact constraints
 - Blasim: A computational tool to assess ice impact damage on engine blades
- IMPACT LOADS**
 - Blasim: A computational tool to assess ice impact damage on engine blades
- IMPACT RESISTANCE**
 - Application of composite materials to impact-insensitive munitions
 - Global/local finite element analysis for textile composites
 - Design for inadvertent damage in composite laminates
- IMPACT TESTS**
 - An overview of shed ice impact studies in the NASA Lewis Icing Research Tunnel
 - On protection of Freedom's solar dynamic radiator from the orbital debris environment. I - Preliminary analysis and testing
 - An overview of shed ice impact in the NASA Lewis Icing Research Tunnel
- IMPEDANCE MATCHING**
 - Design aspects and comparison between high T_c superconducting coplanar waveguide and microstrip line
- IMPEDANCE MEASUREMENT**
 - Stability testing and analysis of a PMAD dc test bed for the Space Station Freedom
- IMPELLERS**
 - Bgrid - Interactive three-dimensional turbomachinery grid generation system with applications
- IMPLANTATION**
 - Optimal design of composite hip implants using NASA technology
- IMPURITIES**
 - Composition dependence of superconductivity in YBa₂(Cu_{3-x}Al_x)O_{7-y}
 - Heat of segregation of single substitutional impurities
- IN-FLIGHT MONITORING**
 - An SSME High Pressure Oxidizer Turbopump diagnostic system using G2 real-time expert system

- Characterization of in-flight performance of ion propulsion systems
- INCLUSIONS**
 - Variation of the energy release rate as a crack approaches and passes through an elastic inclusion
- INCOMPRESSIBLE FLOW**
 - RIPPLE - A new model for incompressible flows with free surfaces
 - Weakly nonlinear models for turbulent mixing in a plane mixing layer
 - Segmented multigrid domain decomposition procedure for incompressible viscous flows
 - The development of a turbulent junction vortex system
 - A multiple-scale turbulence model for incompressible flow
 - A least-squares finite element method for 3D incompressible Navier-Stokes equations
 - The development of a mixing layer under the action of weak streamwise vortices
 - Semi-empirical model for prediction of unsteady forces on an airfoil with application to flutter
 - An efficient and robust algorithm for two dimensional time dependent incompressible Navier-Stokes equations
 - High Reynolds number flows
 - New time scale based k-epsilon model for near-wall turbulence
 - Accuracy of least-squares methods for the Navier-Stokes equations
 - A least-squares finite element method for incompressible Navier-Stokes problem
 - Direct numerical simulation of instabilities in parallel flow with spherical roughness elements
 - Large-scale computation of incompressible viscous flow by least-squares finite element method
 - Incompressible spectral-element method: Derivation of equations
 - Parallel solution of high-order numerical schemes for solving incompressible flows
 - Accuracy of least-squares methods for the Navier-Stokes equations
 - A p-version finite element method for steady incompressible fluid flow and convective heat transfer
- INCOMPRESSIBLE FLUIDS**
 - An efficient and robust algorithm for two dimensional time dependent incompressible Navier-Stokes equations
 - High Reynolds number flows
 - A p-version finite element method for steady incompressible fluid flow and convective heat transfer
- INDENTATION**
 - Indentation flaw formation and strength response of silicon nitride ceramics at low indentation loads
 - Fracture toughness of advanced ceramics at room temperature
 - Evaluation of the fracture toughness of Nb-40Al-8Cr-1W-1Y-0.05B intermetallic material by indentation techniques
 - Vickers indentation hardness of stoichiometric and reduced single crystal TiO₂ (rutile) from 25 to 800 C
- INDEPENDENT VARIABLES**
 - Probabilistic assessment of composite structures
- INDEXES (DOCUMENTATION)**
 - Bibliography of Lewis Research Center Technical Publications announced in 1991
- INDIUM ARSENIDES**
 - Ellipsometric characterization of In(0.52)Al(0.48)As and of modulation doped field effect transistor structures on InP substrates
- INDIUM COMPOUNDS**
 - Room temperature synthesis of copper indium diselenide in non-aqueous solution using an organoindium reagent
- INDIUM GALLIUM ARSENIDES**
 - Direct optical injection locking of monolithically integrated In(0.53)Ga(0.47)As/In(0.52)Al(0.48)As MODFET oscillators
 - Diffusion length variation and proton damage coefficients for InP/In(x)Ga(1-x)As/GaAs solar cells

INDIUM PHOSPHIDES

- Carrier removal and defect behavior in p-type InP
- The structural and electrical properties of low-resistance Ni contacts to InP
- Indium phosphide solar cells for laser power beaming applications
- Low resistance silver contacts to indium phosphide - Electrical and metallurgical considerations
- Simple, extremely low resistance contact system to n-InP that does not exhibit metal-semiconductor intermixing during sintering
- Ellipsometric characterization of In(0.52)Al(0.48)As and of modulation doped field effect transistor structures on InP substrates
- Minority carrier diffusion length and edge surface-recombination velocity in InP
- Closed-ampoule diffusion of sulfur into Cd-doped InP substrates - Dependence of S profiles on diffusion temperature and time
- Diffusion length variation and proton damage coefficients for InP/In(x)Ga(1-x)As/GaAs solar cells
- Diffusion length variation in 0.5- and 3-MeV-proton-irradiated, heteroepitaxial indium phosphide solar cells
- Texturing of InP surfaces for device applications
- Non-destructive, ultra-low resistance, thermally stable contacts for use on shallow junction InP solar cells
- INDIUM SULFIDES**
 - Metal-organic chemical vapour deposition of polycrystalline tetragonal indium sulphide (InS) thin films
- INDUCTANCE**
 - Extra high speed modified Lundell alternator parameters and open/short-circuit characteristics from global 3D-FE magnetic field solutions
 - Computation of load performance and other parameters of extra high speed modified Lundell alternators from 3D-FE magnetic field solutions
- INDUCTION MOTORS**
 - Electromechanical systems with transient high power response operating from a resonant ac link
- INDUCTORS**
 - Comparison of high temperature, high frequency core loss and dynamic B-H loops of a 2V-49Fe-49Co and a grain oriented 3Si-Fe alloy
- INDUSTRIAL PLANTS**
 - Three-dimensional laser window formation for industrial application
- INDUSTRIAL SAFETY**
 - Lewis safety manual
- INELASTIC STRESS**
 - A constitutive model for the high temperature inelastic response of nickel base superalloys
- INERTIA**
 - Vibration isolation technology - An executive summary of systems development and demonstration --- for proposed microgravity experiments aboard STS and Space Station Freedom
 - Vibration isolation technology: An executive summary of systems development and demonstration
- INFILTRATION**
 - On the melt infiltration of copper coated silicon carbide with an aluminium alloy
 - Observations on infiltration of silicon carbide compacts with an aluminium alloy
 - Melt infiltration of silicon carbide compacts. I - Study of infiltration dynamics
 - Melt infiltration of silicon carbide compacts. II - Evaluation of solidification microstructures
 - Studies on the reactive melt infiltration of silicon and silicon-molybdenum alloys in porous carbon
- INFLATING**
 - The inflation sector of extended inflation
 - Stochastic inflation lattice simulations - Ultra-large scale structure of the universe
 - First-order inflation --- in cosmology
- INFORMATION FLOW**
 - Fault-tolerant onboard digital information switching and routing for communications satellites

- INFORMATION SYSTEMS**
Data distribution satellite
[NASA-TM-105778] p 149 N93-12481
- INFRARED ABSORPTION**
High quality flame deposited diamond films for infrared optical windows p 281 A93-40564
- INFRARED DETECTORS**
Superconductivity applications for infrared and microwave devices II; Proceedings of the Meeting, Orlando, FL, Apr. 4, 5, 1991
[SPIE-1477] p 154 A93-27243
- INFRARED RADIATION**
Jet Engine hot parts IR Analysis Procedure (J-EIRP)
[NASA-TM-105914] p 21 N93-22588
- INFRARED SPECTROMETERS**
Fiber-optic thermometer using Fourier transform spectroscopy p 212 A93-53104
- INFRARED SPECTROSCOPY**
Determination of atomic oxygen fluence using spectrophotometric analysis of infrared transparent witness coupons for long duration exposure tests
[NASA-TM-106021] p 96 N93-22605
- INFRARED WINDOWS**
High quality flame deposited diamond films for infrared optical windows p 281 A93-40564
- INGESTION (ENGINES)**
Two and three-dimensional prediffuser combustor studies with air-water mixture
[AIAA PAPER 93-0240] p 113 A93-22652
- INJECTION LOCKING**
Direct optical injection locking of monolithically integrated $\text{In}(0.53)\text{Ga}(0.47)\text{As}/\text{In}(0.52)\text{Al}(0.48)\text{As}$ MODFET oscillators p 158 A93-47127
- INJECTORS**
A numerical study of mixing in supersonic combustors with hypermixing injectors
[AIAA PAPER 93-0215] p 25 A93-27801
Coaxial injector spray characterization using water/air as simulants p 120 N93-11452
- INLET AIRFRAME CONFIGURATIONS**
A comparative study of Full Navier-Stokes and Reduced Navier-Stokes analyses for separating flows within a diffusing inlet S-duct
[AIAA PAPER 93-2154] p 13 A93-49970
- INLET FLOW**
Effect of a rotating propeller on the separation angle of attack
[AIAA PAPER 93-0017] p 6 A93-24978
Visualization of entry flow separation for oscillating flow in tubes p 174 A93-26091
Intake flow modeling in a four stroke diesel using KIVA3
[AIAA PAPER 93-2952] p 183 A93-48146
Installed F/A-18 inlet flow calculations at 60 deg angle-of-attack and 10 deg side slip
[AIAA PAPER 93-1806] p 12 A93-49695
Calculation of scramjet inlet with thick boundary-layer ingestion
[AIAA PAPER 93-1836] p 12 A93-49720
3-D viscous flow CFD analysis of the propeller effect on an advanced ducted propeller subsonic inlet
[AIAA PAPER 93-1847] p 12 A93-49728
A comparative study of Full Navier-Stokes and Reduced Navier-Stokes analyses for separating flows within a diffusing inlet S-duct
[AIAA PAPER 93-2154] p 13 A93-49970
Time-sequenced and spectrally filtered Rayleigh imaging of shock wave and boundary layer structure for inlet characterization
[AIAA PAPER 93-2300] p 211 A93-50085
An experimental investigation of the flow in a diffusing S-duct
[NASA-TM-105809] p 32 N93-12077
Effect of a rotating propeller on the separation angle of attack and distortion in ducted propeller inlets
[NASA-TM-105935] p 16 N93-16625
The 3-D viscous flow CFD analysis of the propeller effect on an advanced ducted propeller subsonic inlet
[NASA-TM-106240] p 38 N93-29162
Three-dimensional flow calculations inside SSME GGGT first stage blade rows p 93 N93-31585
- INLET PRESSURE**
Friction-factor data for flat-plate tests of smooth and honeycomb surfaces
[ASME PAPER 91-TRIB-20] p 219 A93-15682
- INLET TEMPERATURE**
Initial results from the NASA Lewis wave rotor experiment
[AIAA PAPER 93-2521] p 30 A93-53589
Nitric oxide formation in a lean, premixed-prevaporized jet A/air flame tube: An experimental and analytical study
[NASA-TM-105722] p 257 N93-27012
Initial results from the NASA-Lewis wave rotor experiment
[NASA-TM-106148] p 39 N93-32368
- INORGANIC SULFIDES**
Enhancement of photoluminescence intensity of GaAs with cubic GaS chemical vapor deposited using a structurally designed single-source precursor p 280 A93-26930
- INSTALLING**
Automatic system for installation and replacement of Space Station components
[NASA-CASE-LEW-14906-1] p 226 N93-12203
- INSTRUMENT COMPENSATION**
Advanced Communications Technology Satellite (ACTS) p 52 A93-24456
- INSTRUMENT ERRORS**
Techniques for improving the accuracy of cryogenic temperature measurement in ground test programs p 212 A93-54363
Techniques for improving the accuracy of cryogenic temperature measurement in ground test programs
[NASA-TM-105996] p 215 N93-22484
- INSULATORS**
Damping and scattering of electromagnetic waves by small ferrite spheres suspended in an insulator
[NASA-TM-105837] p 149 N93-12366
- INTAKE SYSTEMS**
Study on vortex flow control of inlet distortion p 2 A93-14520
- INTEGRAL EQUATIONS**
Elastic interactions of a fatigue crack with a micro-defect by the mixed boundary integral equation method p 243 A93-56412
An integral equation solution for multistage turbomachinery design calculations
[NASA-TM-105970] p 33 N93-15521
- INTEGRATED CIRCUITS**
Monolithic microwave integrated circuits for sensors, radar, and communications systems; Proceedings of the Meeting, Orlando, FL, Apr. 2-4, 1991
[SPIE-1475] p 151 A93-25776
A high efficiency Ka-band monolithic pseudomorphic HEMT amplifier p 151 A93-25786
Millimeter-wave pseudomorphic HEMT MMIC phased array components for space communications p 152 A93-25796
System-level integrated circuit (SLIC) development for phased array antenna applications p 152 A93-25798
Mixed application MMIC technologies - Progress in combining RF, digital and photonic circuits p 152 A93-25800
Phase shifter technology assessment - Prospects and applications p 152 A93-25808
Direct optical injection locking of monolithically integrated $\text{In}(0.53)\text{Ga}(0.47)\text{As}/\text{In}(0.52)\text{Al}(0.48)\text{As}$ MODFET oscillators p 158 A93-47127
Analysis of MMIC arrays for use in the ACTS Aero Experiment
[NASA-TM-106073] p 53 N93-22589
- INTEGRATED OPTICS**
Micromachined silicon cantilever beam accelerometer incorporating an integrated optical waveguide p 210 A93-49457
Characterization of $\text{Si}_3\text{N}_4/\text{SiO}_2$ optical channel waveguides by photon scanning tunneling microscopy p 211 A93-49458
Fourier transform spectrometry for fiber-optic sensor systems p 211 A93-49459
Integrated fiber optic probe for dynamic light scattering p 278 A93-52415
Fiber-optic thermometer using Fourier transform spectroscopy p 212 A93-53104
- INTERACTING GALAXIES**
Chemical and luminosity evolution, and counts of galaxies in a merger model p 290 A93-34776
- INTERACTIONAL AERODYNAMICS**
A parametric study of bleed in shock boundary layer interactions
[AIAA PAPER 93-0294] p 5 A93-22694
High accuracy computation of fluid-structure interaction in transonic cascades
[AIAA PAPER 93-0485] p 6 A93-23387
Multiple large-scale coherent mode interactions in a developing round jet p 178 A93-34409
A numerical investigation of supersonic strut/endpoint interactions in annular flow with varying strut thickness
[AIAA PAPER 93-2927] p 10 A93-48128
An investigation of shock wave turbulent boundary layer interaction with bleed through slanted slots
[AIAA PAPER 93-2992] p 11 A93-48184
Numerical simulation of a shock wave/turbulent boundary layer interaction in a duct
[AIAA PAPER 93-3127] p 11 A93-48293
Flowfield dynamics in blunt fin-induced shock wave/turbulent boundary layer interactions
[AIAA PAPER 93-3133] p 11 A93-48298
Investigation of a strut/endpoint interaction in supersonic annular flow
[AIAA PAPER 93-1925] p 12 A93-49791
- Comparison of radiated noise from shrouded and unshrouded propellers p 274 A93-55861
AGARD WG13 aerodynamics of high speed air intakes: Assessment of CFD results p 192 N93-13220
2nd NASA CFD Validation Workshop --- Author
[NASA-TM-107972] p 203 N93-70575
- INTERACTIONS**
Experimental study of two interacting drops in an immiscible fluid p 179 A93-37936
- INTERACTIVE CONTROL**
Proposed ground-based control of accelerometer on Space Station Freedom p 63 A93-54401
An interactive preprocessor for the NASA engine performance program
[NASA-TM-105786] p 32 N93-10983
Proposed ground-based control of accelerometer on Space Station Freedom
[NASA-TM-105960] p 63 N93-23738
- INTERCALATION**
Properties of hybrid CVD/PAN graphite fibers and their bromine intercalation compounds p 98 A93-17675
Apparatus for intercalating large quantities of fibrous structures
[NASA-CASE-LEW-15077-2] p 111 N93-29609
- INTERFACE STABILITY**
The coupling of interfacial instabilities and the stabilization of two-layer annular flows p 178 A93-35482
Residual strain gradient determination in metal matrix composites by synchrotron X-ray energy dispersive diffraction p 103 A93-39580
Interfacial and capillary phenomena in solidification processing of metal-matrix composites p 106 A93-56351
- INTERFACES**
Reaction layer formation at the graphite/copper-chromium alloy interface p 100 A93-25105
- INTERFACIAL TENSION**
Effect of surface tension on the onset of convection in a double-diffusive layer p 163 A93-13951
RIPPLE - A new model for incompressible flows with free surfaces p 164 A93-14551
On the structure of cellular solutions in Rayleigh-Benard-Marangoni flows in small-aspect-ratio containers p 164 A93-14762
Particle image velocimetry for the Surface Tension Driven Convection Experiment using a particle displacement tracking technique p 206 A93-23799
Ground-based PIV and numerical flow visualization results from the Surface Tension Driven Convection Experiment p 143 A93-33075
Surface tension effects on the onset of double-diffusive convection p 180 A93-41710
Collapse of the soap-film bridge - Quasistatic description p 188 A93-50536
- INTERFEROMETERS**
Phase-stepping fiber-optic projected fringe system for surface topography measurements
[NASA-CASE-LEW-14996-1] p 278 N93-11058
- INTERFEROMETRY**
Three-dimensional computed tomography from interferometric measurements within a narrow cone of views p 207 A93-24024
Fiberoptic sensing technique employing RF modulated interferometry p 212 A93-53110
Vector formulation for interferogram surface fitting p 278 A93-55687
Calibration of a shock wave position sensor using artificial neural networks
[NASA-TM-106138] p 216 N93-27001
- INTERLAMINAR STRESS**
Fracture toughness testing of polymer matrix composites p 99 A93-18709
Effects of interply damping layers on the dynamic characteristics of composite plates p 237 A93-32415
- INTERMETALLICS**
Technical note - Plasma-sprayed ceramic thermal barrier coatings for smooth intermetallic alloys p 219 A93-15702
Effect of oxidation on the mechanical properties of a NbAl₃ alloy at intermediate temperatures p 124 A93-20667
Evaluation of the fracture toughness of Nb-40Al-8Cr-1W-1Y-0.05B intermetallic material by indentation techniques p 124 A93-24066
Containerless automated processing of intermetallic compounds and composites p 144 A93-52183
Chemical stability of titanium diboride reinforcement in nickel aluminide matrices p 105 A93-52473
Overview of NASA's advanced high temperature engine materials technology program p 94 A93-53453
SIMS studies of oxide growth on beta-NiAl p 127 A93-53469

INTERMODULATION

- Material requirements for the High Speed Civil Transport
[ISABE 93-7067] p 31 A93-54043
- Interfacial shear strength of cast and directionally solidified AlAl-sapphire fiber composites p 106 A93-55685

INTERMODULATION

- Intermodulation in the oscillatory magnetoresistance of a two-dimensional electron gas p 151 A93-17610

INTERNAL COMBUSTION ENGINES

- Intake flow modeling in a four stroke diesel using KIVA3
[AIAA PAPER 93-2952] p 183 A93-48146

INTERNAL FRICTION

- The detrimental effect of friction on space microgravity robotics p 222 A93-35546

INTERNATIONAL COOPERATION

- U.S./CIS eye joint nuclear rocket venture p 71 A93-49334

INTERPLANETARY FLIGHT

- Establishing the infrastructure - An integrated Space Transportation System p 50 A93-12072
- Robotic planetary mission benefits from nuclear electric propulsion p 43 A93-25854

INTERPOLATION

- Calculations of separated 3-D flows with a pressure-staggered Navier-Stokes equations solver p 177 A93-34366
- Algebraic grid generation with control points p 268 A93-45967

INTERSTELLAR MAGNETIC FIELDS

- Extension of the Parker bound on the flux of magnetic monopoles p 291 A93-38672

INTERSTELLAR RADIATION

- Cosmic microwave background probes models of inflation p 294 A93-10355

INTERSTELLAR SPACECRAFT

- The QED engine spectrum - Fusion-electric propulsion for air-breathing to interstellar flight
[AIAA PAPER 93-2006] p 73 A93-49845

INVARIANCE

- On an origin of numerical diffusion: Violation of invariance under space-time inversion
[NASA-TM-105776] p 268 A93-11254

INVENTIONS

- Picture data compression coder using subband/transform coding with a Lempel-Ziv-based coder
[NASA-CASE-LEW-15700-1] p 287 A93-28130

INVERSE KINEMATICS

- Inverse kinematics problem in robotics using neural networks
[NASA-TM-105869] p 247 A93-18876

INVERSIONS

- On an origin of numerical diffusion: Violation of invariance under space-time inversion
[NASA-TM-105776] p 268 A93-11254

INVERTERS

- Modelling a single phase voltage controlled rectifier using Laplace transforms
[NASA-TM-106005] p 271 A93-23016

INVISCID FLOW

- Aerodynamic design of turbomachinery blading in three-dimensional flow - An application to radial inflow turbines
[ASME PAPER 92-GT-74] p 3 A93-19324
- Computation of unsteady supersonic quasi-one-dimensional viscous-inviscid interacting internal flowfields p 177 A93-32724
- A note on the distortion of a flat-plate boundary layer by free-stream vorticity normal to the plate p 178 A93-34414
- Efficient hybrid scheme for the analysis of counter-rotating propellers p 7 A93-34483
- Modeling of linear isentropic flow systems p 179 A93-37046
- Stable and low diffusive hybrid upwind splitting methods
[ONERA, TP NO. 1992-113] p 179 A93-38589
- Vorticity dynamics of inviscid shear layers p 181 A93-45734
- Linear instability of curved free shear layers
[AIAA PAPER 93-3252] p 183 A93-46797
- Three-dimensional numerical simulation of gradual opening in a wave rotor passage
[AIAA PAPER 93-2526] p 187 A93-50254
- Analysis of high Reynolds number inviscid/viscid interactions in cascades p 15 A93-55351
- An integral equation solution for multistage turbomachinery design calculations
[NASA-TM-105970] p 33 A93-15521
- Nonlinear evolution of the first mode supersonic oblique waves in compressible boundary layers Part 1: Heated/cooled walls
[NASA-TM-106087] p 199 A93-25175

ION BEAMS

- Optical and scratch resistant properties of diamondlike carbon films deposited with single and dual ion beams p 137 A93-25564
- Characteristics of hypervelocity impact craters on LDEF experiment S1003 and implications of small particle impacts on reflective surfaces p 62 A93-29363

ION CURRENTS

- Plasma sheath effects on ion collection by a pinhole
[AIAA PAPER 93-0567] p 55 A93-24243
- Plasma sheath effects on ion collection by a pinhole
[NASA-TM-106098] p 60 A93-25090

ION ENGINES

- Erosion rate diagnostics in ion thrusters using laser-induced fluorescence p 70 A93-34481
- The 100-500 kWe NEP systems p 90 A93-26984
- Thruster models for NEP system analysis p 91 A93-26988

ION EXCHANGE MEMBRANE ELECTROLYTES

- Pressure dependence of the oxygen reduction reaction at the platinum microelectrode/nation interface - Electrode kinetics and mass transport p 112 A93-11450
- PEM fuel cell stack heat and mass management p 253 A93-26024

ION EXCHANGING

- Ion exchange polymers and method for making
[NASA-CASE-LEW-15576-1] p 139 A93-31316

ION PROPULSION

- Low-Isp derated ion thruster operation
[AIAA PAPER 92-3203] p 64 A93-13696
- Development and flight history of the SERT II spacecraft p 71 A93-38976
- Characterization of in-flight performance of ion propulsion systems
[AIAA PAPER 93-2217] p 75 A93-50023
- Derated ion thruster development status
[AIAA PAPER 93-2225] p 75 A93-50031
- Simplified power processing for inert gas ion thrusters
[AIAA PAPER 93-2397] p 76 A93-50162
- Ion thruster development at NASA Lewis Research Center p 82 A93-15429
- [NASA-TM-105983] p 82 A93-15429
- Development of arcjet and ion propulsion for spacecraft stationkeeping
[NASA-TM-106102] p 85 A93-23747
- Nuclear electric propulsion for planetary science missions: NASA technology program planning
[NASA-TM-106139] p 88 A93-26210
- NEP technology: FY 1992 milestones (NASA LeRC) p 90 A93-26977
- The 100-500 kWe NEP systems p 90 A93-26984
- Nuclear electric propulsion options for piloted Mars missions p 90 A93-26985
- IONIC CRYSTALS
- Global expression for representing cohesive-energy curves II p 276 A93-44989
- IONOSPHERIC ELECTRON DENSITY
- Interference patterns in the Spacelab 2 plasma wave data - Oblique electrostatic waves generated by the electron beam p 257 A93-16347

IRON ALLOYS

- Comparison of high frequency, high temperature core loss and B-H loop characteristics of an 80 Ni-Fe crystalline alloy and two iron-based amorphous alloys p 123 A93-13882
- The microstructural evolution, crystallography, and thermal processing of ultrahigh carbon Fe-1.85 pct C melt-spun ribbon p 125 A93-32934
- Thermodynamics of iron-aluminum alloys at 1573 K p 127 A93-52879

ISENTROPIC PROCESSES

- Modeling of linear isentropic flow systems p 179 A93-37046

ISOTHERMAL FLOW

- Noniterative implicit method for tracking particles in mixed Lagrangian-Eulerian formulations p 176 A93-30856

ISOTHERMAL PROCESSES

- Isothermal aging effects on PMR-15 resin p 131 A93-24508
- Transverse flexural tests as a tool for assessing damage to PMR-15 composites from isothermal aging in air at elevated temperatures p 100 A93-24514
- Scientific basis for the Isothermal Dendritic Growth Experiment - A USMP-2 space flight experiment p 143 A93-50455
- Transverse flexural tests as a tool for assessing damage to PMR-15 composites from isothermal aging in air at elevated temperatures
[NASA-TM-105848] p 107 A93-12737

ISOTOPES

- Dynamic Isotope Power System design considerations for human exploration of the moon and Mars p 253 A93-25995

ISOTROPY

- Calculation of stress intensity factors in an isotropic multiaxial cracked plate: Part 2: Symbolic/numeric implementation p 244 A93-10453
- [NASA-TM-105823] p 244 A93-10453
- Calculation of stress intensity factors in an isotropic multiaxial cracked plate: Part 1: Theoretical development
[NASA-TM-105766] p 244 A93-10455

ITERATION

- Shape reanalysis and sensitivities utilizing preconditioned iterative boundary solvers p 233 A93-14446

- Propagation of high frequency jet noise using geometric acoustics p 272 A93-23241
- [AIAA PAPER 93-0147] p 272 A93-23241
- Propagation of high frequency jet noise using geometric acoustics p 275 A93-15575
- [NASA-TM-106013] p 275 A93-15575

ITERATIVE SOLUTION

- Non-oscillatory and non-diffusive solution of convection problems by the iteratively reweighted least-squares finite element method p 177 A93-32622

- I-BIEM calculations of the frequency dispersion and ac current distribution at disk and ring-disk electrodes p 254 A93-34246

- An iterative multidisciplinary analysis for rotor blade shape determination p 28 A93-49912
- [AIAA PAPER 93-2085] p 28 A93-49912
- Large-scale computation of incompressible viscous flow by least-squares finite element method
[NASA-TM-105904] p 269 A93-22825

J

JACOBI MATRIX METHOD

- Dynamic analysis of flexible gear trains/transmissions - An automated approach p 220 A93-22440
- Time-variant analysis of rotorcraft systems dynamics - An exploitation of vector processors p 220 A93-23512

JET AIRCRAFT NOISE

- Propagation of high frequency jet noise using geometric acoustics p 272 A93-23241
- [AIAA PAPER 93-0147] p 272 A93-23241
- Acoustic mode measurements in the inlet of a model turbofan using a continuously rotating rake
[AIAA PAPER 93-0598] p 273 A93-24783
- Computation of supersonic jet noise under imperfectly expanded conditions p 273 A93-24825
- [AIAA PAPER 93-0735] p 273 A93-24825
- A concept for a counterrotating fan with reduced tone noise
[NASA-TM-105736] p 274 A93-11370
- Computation of supersonic jet noise under imperfectly expanded conditions
[NASA-TM-105961] p 274 A93-15430
- Propagation of high frequency jet noise using geometric acoustics p 275 A93-15575
- [NASA-TM-106013] p 275 A93-15575
- Acoustic mode measurements in the inlet of a model turbofan using a continuously rotating rake
[NASA-TM-105989] p 34 A93-16705
- Numerical simulation of a high Mach number jet flow
[NASA-TM-105985] p 197 A93-20057
- Jet mixer noise suppressor using acoustic feedback
[NASA-CASE-LEW-15170-1] p 275 A93-28953

JET ENGINE FUELS

- Simplified jet fuel reaction mechanism for lean burn combustion application
[AIAA PAPER 93-0021] p 113 A93-23238
- Simplified jet-A kinetic mechanism for combustor application
[NASA-TM-105940] p 120 A93-15504

JET ENGINES

- Evaluation and application of the Baldwin-Lomax turbulence model in two-dimensional, unsteady, compressible boundary layers with and without separation in engine inlets
[AIAA PAPER 92-3676] p 2 A93-14118
- Study on vortex flow control of inlet distortion p 2 A93-14520
- Evaluation and application of the Baldwin-Lomax turbulence model in two-dimensional, unsteady, compressible boundary layers with and without separation in engine inlets
[AIAA PAPER 92-3676] p 168 A93-22509
- Identification of the open loop dynamics of the T700 turboshaft engine p 26 A93-35934
- Initial results from the NASA Lewis wave rotor experiment
[AIAA PAPER 93-2521] p 30 A93-53589

- Evaluation and application of the Baldwin-Lomax turbulence model in two-dimensional, unsteady, compressible boundary layers with and without separation in engine inlets
[NASA-TM-105810] p 191 N93-10087
- A concept for a counterrotating fan with reduced tone noise
[NASA-TM-105736] p 274 N93-11370
- Jet Engine hot parts IR Analysis Procedure (J-EIRP)
[NASA-TM-105914] p 21 N93-22588
- External stress-corrosion cracking of a 1.22-m-diameter type 316 stainless steel air valve
[NASA-TP-3190] p 129 N93-26201
- Initial results from the NASA-Lewis wave rotor experiment
[NASA-TM-106148] p 39 N93-32368
- ### JET FLOW
- Accuracy considerations in the computational analysis of jet noise
[AIAA PAPER 93-0146] p 272 A93-19804
- Two-, three-, and four-poster jets in cross flow
[AIAA PAPER 93-0023] p 167 A93-20141
- Fiber optic laser Doppler anemometry in swirling jets
p 206 A93-23783
- Numerical simulations of a high Mach number jet flow
[AIAA PAPER 93-0653] p 172 A93-24766
- Structure of soot-containing laminar jet diffusion flames
[AIAA PAPER 93-0708] p 114 A93-24804
- Effect of tabs on the flow and noise field of an axisymmetric jet
p 25 A93-30833
- Multiple large-scale coherent mode interactions in a developing round jet
p 178 A93-34409
- Fluid flow of a row of jets in crossflow - A numerical study
p 179 A93-35608
- Mixing and transient interface condensation of a liquid hydrogen tank
[AIAA PAPER 93-1968] p 184 A93-49816
- Mixing of multiple jets with a confined subsonic crossflow
p 15 A93-54324
- Experiments on a round turbulent buoyant plume
[NASA-TM-105955] p 141 N93-16384
- Numerical simulation of a high Mach number jet flow
[NASA-TM-105985] p 197 N93-20057
- Selected microgravity combustion diagnostic techniques
p 121 N93-20194
- Mixing and transient interface condensation of a liquid hydrogen tank
[NASA-TM-106201] p 201 N93-28252
- A numerical study of confined turbulent jets
[NASA-TM-106197] p 202 N93-29161
- ### JET IMPINGEMENT
- The application of structural reliability techniques to plume impingement loading of the Space Station Freedom Photovoltaic Array
[AIAA PAPER 93-1338] p 56 A93-33908
- Fluid dynamics and convective heat transfer in impinging jets through implementation of a high resolution liquid crystal technique
[ISABE 93-7077] p 189 A93-54053
- The application of structural reliability techniques to plume impingement loading of the Space Station Freedom Photovoltaic Array
[NASA-TM-105949] p 59 N93-17988
- ### JET MIXING FLOW
- Optimization of circular orifice jets mixing into a heated crossflow in a cylindrical duct
[AIAA PAPER 93-0249] p 24 A93-23246
- A numerical study of mixing in supersonic combustors with hypermixing injectors
[AIAA PAPER 93-0215] p 25 A93-27801
- Mixing and transient interface condensation of a liquid hydrogen tank
[AIAA PAPER 93-1968] p 184 A93-49816
- Experimental investigation of crossflow jet mixing in a rectangular duct
[AIAA PAPER 93-2037] p 185 A93-49872
- An analytical study of dilution jet mixing in a cylindrical duct
[AIAA PAPER 93-2043] p 27 A93-49876
- CFD mixing analysis of axially opposed rows of jets injected into confined crossflow
[AIAA PAPER 93-2044] p 185 A93-49877
- Low-g fluid mixing - Further results from the Tank Pressure Control Experiment
[AIAA PAPER 93-2423] p 187 A93-50181
- Comparison of the initial development of shear layers in two-dimensional and axisymmetric ejector configurations
[AIAA PAPER 93-2441] p 29 A93-50193
- Streamwise vorticity generation and mixing enhancement in free jets by 'delta-tabs'
[AIAA PAPER 93-3253] p 14 A93-53592
- Optimization of circular orifice jets mixing into a heated cross flow in a cylindrical duct
[NASA-TM-105984] p 33 N93-15359
- Experimental investigation of crossflow jet mixing in a rectangular duct
[NASA-TM-106152] p 36 N93-27026
- CFD mixing analysis of axially opposed rows of jets injected into confined crossflow
[NASA-TM-106179] p 37 N93-27128
- An analytical study of dilution jet mixing in a cylindrical duct
[NASA-TM-106181] p 37 N93-27160
- Mixing and transient interface condensation of a liquid hydrogen tank
[NASA-TM-106201] p 201 N93-28252
- Streamwise vorticity generation and mixing enhancement in free jets by delta-tabs
[NASA-TM-106235] p 17 N93-31648
- Enhanced mixing of a rectangular supersonic jet by natural and induced screech
[NASA-TM-106245] p 18 N93-31672
- ### JET PROPULSION
- Engine technology challenges for a 21st Century High-Speed Civil Transport
[ISABE 93-7064] p 31 A93-54040
- Engine technology challenges for a 21st Century High-Speed Civil Transport
[NASA-TM-106216] p 39 N93-31671
- ### JOINTS (ANATOMY)
- Numerical optimization of composite hip endoprostheses under different loading conditions
[AIAA PAPER 92-4703] p 270 A93-20312
- ### JOINTS (JUNCTIONS)
- Ceramic matrix composites properties/microstresses with complete and partial interphase bond
[NASA-TM-106136] p 111 N93-29071
- ### JOURNAL BEARINGS
- Stiffness of magnetic bearings subjected to combined static and dynamic loads
[ASME PAPER 91-TRIB-27] p 219 A93-15685
- Determination of forces in a magnetic bearing actuator - Numerical computation with comparison to experiment
p 219 A93-15686
- Calculation of stiffness and damping coefficients for elastically supported gas foil bearings
p 221 A93-27308
- Simultaneous pressure measurement and high-speed photography study of cavitation in a dynamically loaded journal bearing
p 223 A93-40050
- Effect of fluid compressibility on journal bearing performance
p 223 A93-49244
- ### JUDGMENTS
- Jet Engine hot parts IR Analysis Procedure (J-EIRP)
[NASA-TM-105914] p 21 N93-22588
- ## K
- ### K-EPSILON TURBULENCE MODEL
- Multigrid acceleration and turbulence models for computations of 3D turbulent jets in crossflow
p 165 A93-18751
- A simplified Reynolds stress model for unsteady turbulent boundary layers
[AIAA PAPER 93-0204] p 168 A93-22622
- New time scale based k-epsilon model for near-wall turbulence
p 180 A93-41909
- Some practical turbulence modeling options for Reynolds-averaged full Navier-Stokes calculations of three-dimensional flows
[AIAA PAPER 93-2964] p 10 A93-48158
- CFD validation of subsonic turbulent planar shear layers
[AIAA PAPER 93-1773] p 184 A93-49669
- A thermal NO(x) prediction model - Scalar computation module for CFD codes with fluid and kinetic effects
[AIAA PAPER 93-2378] p 119 A93-50147
- Low-Reynolds-number k-epsilon model for unsteady turbulent boundary-layer flows
p 14 A93-53208
- A critical comparison of several low Reynolds number k-epsilon turbulence models for flow over a backward-facing step
[AIAA PAPER 93-1927] p 189 A93-53586
- Navier-Stokes turbine heat transfer predictions using two-equation turbulence
[NASA-TM-105817] p 191 N93-10735
- Supersonic boundary-layer flow turbulence modeling
[NASA-TM-105893] p 193 N93-14758
- A realizable Reynolds stress algebraic equation model
[NASA-TM-105993] p 16 N93-16596
- Fuel injector: Air swirl characterization aerothermal modeling, phase 2, volume 1
[NASA-CR-189193-VOL-1] p 35 N93-24754
- Calculations of turbulent separated flows
[NASA-TM-106154] p 200 N93-27161
- A numerical study of confined turbulent jets
[NASA-TM-106197] p 202 N93-29161
- A rapid-distortion-theory turbulence model for developed unsteady wall-bounded flow
[NASA-TM-106249] p 203 N93-32199
- A critical comparison of several low Reynolds number k-epsilon turbulence models for flow over a backward facing step
[NASA-TM-106173] p 270 N93-32200
- ### KALMAN FILTERS
- On-line implementation of nonlinear parameter estimation for the Space Shuttle main engine
[NASA-TM-106097] p 88 N93-26211
- ### KAPTON (TRADEMARK)
- Plasma chamber testing of APSA coupons for the SAMPIE flight experiment
[AIAA PAPER 93-0568] p 67 A93-24244
- Performance and properties of atomic oxygen protective coatings for polymeric materials
p 225 A93-53389
- The evolution of procurement and assurance methods used to proof an advanced space material
p 94 A93-53392
- Plasma chamber testing of APSA coupons for the SAMPIE flight experiment
[NASA-TM-106084] p 60 N93-23742
- Enhanced plasma current collection from weakly conducting solar array blankets
[NASA-TM-106168] p 62 N93-27081
- ### KERNEL FUNCTIONS
- On the nonlinear three dimensional instability of Stokes layers and other shear layers to pairs of oblique waves
[NASA-TM-105918] p 194 N93-15499
- ### KINEMATIC EQUATIONS
- Dynamic analysis of flexible gear trains/transmissions - An automated approach
p 220 A93-22440
- ### KINEMATICS
- Vorticity dynamics of inviscid shear layers
p 181 A93-45734
- ### KINETIC ENERGY
- A new energy transfer model for turbulent free shear flow
[NASA-TM-105854] p 191 N93-10454
- A multiple-scale model for compressible turbulent flows
[NASA-TM-106072] p 198 N93-23736
- ### KINETIC EQUATIONS
- Bounds on internal state variables in viscoplasticity
[NASA-TM-106215] p 251 N93-29196
- ### KNOWLEDGE BASES (ARTIFICIAL INTELLIGENCE)
- An embedded rule-based diagnostic expert system in Ada
p 260 N93-11928
- ### KNUDSEN GAGES
- Thermodynamics of iron-aluminum alloys at 1573 K
p 127 A93-52879
- ### KRYPTON
- The 100-500 kWe NEP systems
p 90 N93-26984
- ### KURTOSIS
- Kurtosis, skewness, and non-Gaussian cosmological density perturbations
p 291 A93-35579
- Evaluation of a vibration diagnostic system for the detection of spur gear pitting failures
[AIAA PAPER 93-2298] p 224 A93-50083
- Evaluation of a vibration diagnostic system for the detection of spur gear pitting failures
[NASA-TM-106103] p 228 N93-25672
- ## L
- ### LAGRANGE MULTIPLIERS
- Lagrangian solution of supersonic real gas flows
p 170 A93-23944
- ### LAGRANGIAN FUNCTION
- An extended Lagrangian method
[AIAA PAPER 93-3305] p 8 A93-45003
- An extended Lagrangian method
[NASA-TM-106129] p 199 N93-26203
- ### LAMB WAVES
- Detecting Lamb waves with broadband acousto-ultrasonic signals in composite structures
p 231 A93-21898
- ### LAMINAR FLOW
- Some aspects of bifurcation structure of laminar flow in curved ducts
p 164 A93-14771
- Laminar/turbulent oscillating flow in circular pipes
p 167 A93-21689
- Multigrid methods for numerical simulation of laminar diffusion flames
[AIAA PAPER 93-0236] p 113 A93-22648
- Structure of soot-containing laminar jet diffusion flames
[AIAA PAPER 93-0708] p 114 A93-24804
- Overview of NASA supported Stirling thermodynamic loss research
p 174 A93-26087
- Heat transfer in oscillating flows with sudden change in cross section
p 174 A93-26089

- Laser-induced fluorescence measurements of nitric oxide in laminar C₂H₆/O₂/N₂ flames at high pressure p 116 A93-28253
- High Reynolds number and turbulence effects on aerodynamics and heat transfer in a turbine cascade [AIAA PAPER 93-2252] p 186 A93-50050
- Direct numerical simulation of instabilities in parallel flow with spherical roughness elements [NASA-TM-105847] p 192 N93-11529
- Effects of buoyancy on laminar, transitional, and turbulent gas jet diffusion flames p 121 N93-20189
- Soot formation and radiation in turbulent jet diffusion flames under normal and reduced gravity conditions p 121 N93-20192
- On the structure of gaseous confined laminar diffusion flames: Numerical investigation [NASA-TM-106039] p 197 N93-21198
- Structure of confined laminar spray diffusion flames: Numerical investigation [NASA-TM-106038] p 197 N93-22596
- Increased heat transfer to elliptical leading edges due to spanwise variations in the freestream momentum: Numerical and experimental results [NASA-TM-106150] p 199 N93-27020
- High Reynolds number and turbulence effects on aerodynamics and heat transfer in a turbine cascade [NASA-TM-106187] p 202 N93-29157
- Numerical simulations of three-dimensional laminar flow over a backward facing step; flow near side walls [NASA-TM-106248] p 202 N93-31147
- LAMINAR HEAT TRANSFER**
- Heat transfer in oscillating flows with sudden change in cross section p 174 A93-26089
- LAMINATES**
- Tailored metal matrix laminates for high-temperature performance p 98 A93-15753
- Analysis and optimal design of thick composite structures with passive damping considerations [AIAA PAPER 92-4819] p 235 A93-20398
- Refractive index effects on radiation in an absorbing, emitting, and scattering laminated layer p 175 A93-30125
- Microfracture in high temperature metal matrix crossply laminates p 101 A93-31356
- Deformation and failure mechanisms in metal matrix composites p 102 A93-31359
- Probabilistic nonlinear finite element analysis of composite structures p 237 A93-32717
- Behavior of spinning laminated composite plates with initial twist-experimental vibrations, strain, and deflection results [AIAA PAPER 93-1325] p 238 A93-33898
- Probabilistic simulation of stress concentration in composite laminates [AIAA PAPER 93-1442] p 103 A93-33991
- Analysis of passive damping in thick composite structures p 241 A93-45743
- Effect of service environments on adhesively bonded joints in composite structures p 242 A93-53418
- Environmental effects on long term behavior of composite laminates p 243 A93-53438
- Variable refractive index effects on radiation in semitransparent scattering multilayered regions p 189 A93-54463
- Probabilistic micromechanics and macromechanics of polymer matrix composites p 105 A93-54705
- Reliability analysis of laminated ceramic matrix composites using shell subelement techniques p 243 A93-55382
- ICAN/DAMP-integrated composite analyzer with damping analysis capabilities: User's manual [NASA-TP-3292] p 106 N93-12015
- Fracture toughness testing of polymer matrix composites [NASA-TP-3199] p 107 N93-12302
- Probabilistic evaluation of fuselage-type composite structures [NASA-TM-105881] p 245 N93-12735
- Second generation integrated composite analyzer (ICAN) computer code [NASA-TP-3290] p 108 N93-18139
- Effects of thermal and mechanical fatigue on the flexural strength of G40-600/PMR-15 cross-ply laminates [NASA-TM-106016] p 108 N93-20317
- Progressive delamination in polymer matrix composite laminates: A new approach p 108 N93-21515
- Optimal design of composite hip implants using NASA technology p 257 N93-22188
- High Temperature Composite Analyzer (HITCAN) theoretical manual, version 1.0 [NASA-TM-106001] p 249 N93-24913
- High temperature composite analyzer (HITCAN) user's manual, version 1.0 [NASA-TM-106002] p 249 N93-25070
- Stress distribution in composite flatwise tension test specimens [NASA-TM-106074] p 108 N93-25071
- Graphite/epoxy composite laminates with co-cured interlaminar damping layers p 109 N93-25587
- Dynamic characteristics of specialty composite structures with embedded damping layers [NASA-TM-106165] p 110 N93-26705
- Structural tailoring of aircraft engine blade subject to ice impact constraints [NASA-TM-106033] p 250 N93-26999
- Probabilistic sizing of laminates with uncertainties [NASA-TM-106145] p 110 N93-27082
- Probabilistic assessment of composite structures [NASA-TM-106024] p 110 N93-27092
- Metal Matrix Laminate Tailoring (MMLT) code: User's manual [NASA-TM-106052] p 111 N93-28681
- Ceramic matrix composites properties/microstresses with complete and partial interphase bond [NASA-TM-106136] p 111 N93-29071
- LAND MOBILE SATELLITE SERVICE**
- Performance evaluation of land mobile satellite system under fading and interference using multiple TCM by Monte-Carlo simulation p 147 A93-10958
- LAPLACE TRANSFORMATION**
- Modelling a single phase voltage controlled rectifier using Laplace transforms [NASA-TM-106005] p 271 N93-23016
- LARGE SPACE STRUCTURES**
- Grounding of space structures p 54 A93-12144
- Probabilistic structural analysis of adaptive/smart/intelligent space structures p 234 A93-16203
- Probabilistic structural analysis of space truss structures for nonuniform thermal environmental effects [AIAA PAPER 92-4769] p 235 A93-20363
- Evaluation of passive and active vibration control mechanisms in a microgravity environment [AIAA PAPER 93-0838] p 55 A93-24905
- Probabilistic assessment of adaptive space truss configurations for thermal buckling resistance [AIAA PAPER 93-1622] p 240 A93-34151
- Space Station Freedom structure floating potential and the probability of arcing p 57 A93-39265
- Control/structure interactions of Space Station solar dynamic modules p 57 A93-41878
- LASER ABLATION**
- Ellipsometric study of ambient-produced overlayer growth rate on YBaCu₃O(7-x) films p 281 A93-39362
- LASER ANEMOMETERS**
- Experimental and computational investigation of the NASA Low-Speed Centrifugal Compressor flow field [ASME PAPER 92-GT-213] p 4 A93-19436
- Laser anemometry - Advances and applications 1991; Proceedings of the 4th International Conference, Cleveland, OH, Aug. 5-9, 1991. Vols. 1 & 2 [ISBN 0-7918-0654-5] p 206 A93-23776
- High-speed laser anemometry based on spectrally resolved Rayleigh scattering p 207 A93-23814
- Mathematical relationship between two sets of laser anemometer measurements for resolving the total velocity vector [NASA-TM-105986] p 35 N93-22599
- LASER APPLICATIONS**
- Strain sensing technology for high temperature applications [AIAA PAPER 92-5040] p 205 A93-22314
- Liquid water content measurements using the Phase Doppler Particle Analyzer in the NASA Lewis Icing Research Tunnel [AIAA PAPER 93-0298] p 42 A93-23698
- Particle displacement tracking applied to air flows p 206 A93-23800
- Gas temperature measurements using the dual-line detection Rayleigh scattering technique p 213 A93-55368
- Gas temperature measurements using the dual-line detection Rayleigh scattering technique p 214 N93-13668
- Laser ignition application in a space experiment [NASA-TM-106133] p 145 N93-25337
- Rayleigh-Brillouin scattering for high-pressure gas temperature measurements p 218 N93-31556
- LASER BEAMS**
- Photovoltaic receivers for laser beamed power in space p 66 A93-21664
- Calibration of the forward-scattering spectrometer probe - Modeling scattering from a multimode laser beam p 212 A93-51239
- A fuzzy logic based controller for the automated alignment of a laser-beam-smoothing spatial filter [NASA-TM-105994] p 217 N93-18091
- LASER DOPPLER VELOCIMETERS**
- LDV flowfield measurements on a straight and swept wing with a simulated ice accretion [AIAA PAPER 93-0300] p 5 A93-23001
- Fiber optic laser Doppler anemometry in swirling jets p 206 A93-23783
- Signal processing considerations for low signal to noise ratio laser Doppler and phase Doppler signals p 207 A93-23830
- LV software support for supersonic flow analysis [AIAA PAPER 92-3900] p 259 A93-24487
- Pulsed laser Rayleigh scattering diagnostic for hydrogen/oxygen rocket exit plane flowfield velocimetry [AIAA PAPER 93-0805] p 207 A93-25552
- Three-dimensional flow field in a turbine nozzle passage [AIAA PAPER 93-2556] p 13 A93-50278
- Pulsed laser Rayleigh scattering diagnostic for hydrogen/oxygen rocket exit plane flowfield velocimetry [NASA-TM-106213] p 88 N93-26149
- LASER INDUCED FLUORESCENCE**
- Laser-induced fluorescence measurements of nitric oxide in laminar C₂H₆/O₂/N₂ flames at high pressure p 116 A93-28253
- Erosion rate diagnostics in ion thrusters using laser-induced fluorescence p 70 A93-34481
- Laser-induced fluorescence detection strategies for sodium atoms and compounds in high-pressure combustors p 119 A93-52423
- Visualization of hydrogen injection in a scramjet engine by simultaneous PLIF imaging and laser holographic imaging p 214 N93-13683
- Second order closure modeling of turbulent buoyant wall plumes [NASA-TM-105956] p 193 N93-14829
- LASER POWER BEAMING**
- Photovoltaic receivers for laser beamed power in space p 66 A93-21664
- Indium phosphide solar cells for laser power beaming applications p 252 A93-25899
- An analysis of power beaming for the moon and Mars p 253 A93-25974
- Space transfer with ground-based laser/electric propulsion [NASA-TM-106060] p 84 N93-20615
- LASER WINDOWS**
- Compound curvature laser window development [AIAA PAPER 93-2177] p 277 A93-49989
- Three-dimensional laser window formation for industrial application p 218 N93-22197
- LATTICE PARAMETERS**
- Thermal stability of the microstructure of an aged Nb-Zr-C alloy p 122 A93-13776
- LATTICES (MATHEMATICS)**
- Stochastic inflation lattice simulations - Ultra-large scale structure of the universe p 289 A93-17646
- LAUNCH VEHICLES**
- Integrated health monitoring and controls for rocket engines [SAE PAPER 921031] p 66 A93-14654
- An electromechanical actuation system for an expendable launch vehicle p 50 A93-25891
- Atomic hydrogen propellants: Historical perspectives and future possibilities [NASA-TM-106053] p 84 N93-20614
- Space propulsion p 84 N93-22092
- LAUNCHING BASES**
- A system to measure lightning-induced transients on spacecraft umbilical lines p 161 N93-24889
- LAY-UP**
- Probabilistic micromechanics and macromechanics of polymer matrix composites p 105 A93-54705
- LAYOUTS**
- Layout optimization using the homogenization method p 243 A93-54508
- Applications to car bodies - Generalized layout design of three-dimensional shells p 243 A93-54509
- LEAD ACID BATTERIES**
- Battery selection for space experiments p 159 N93-13184
- Battery selection for Space Shuttle experiments [NASA-TM-106142] p 61 N93-27038
- LEAD ALLOYS**
- Thermosolubil convection during cellular arrayed growth of Pb-Sn alloys [AIAA PAPER 93-0262] p 142 A93-22668
- LEADING EDGES**
- Influence of airfoil thickness on sound generated by high-frequency gust interactions p 272 A93-19181
- CFD zonal modeling of leading-edge ice effects for a complete aircraft [AIAA PAPER 93-0167] p 5 A93-22601
- Brush seal low surface speed hard-rub characteristics [AIAA PAPER 93-2534] p 225 A93-50261
- Unsteady wing surface pressures in the wake of a propeller p 14 A93-52436

- Root damage analysis of aircraft engine blade subject to ice impact
[NASA-TM-105779] p 246 N93-15343
- Structural tailoring of aircraft engine blade subject to ice impact constraints
[NASA-TM-106033] p 250 N93-26999
- Increased heat transfer to elliptical leading edges due to spanwise variations in the freestream momentum: Numerical and experimental results
[NASA-TM-106150] p 199 N93-27020
- Brush seal low surface speed hard-rub characteristics
[NASA-TM-106169] p 200 N93-27132
- LEAKAGE**
- Development of advanced seals for space propulsion turbomachinery
[SAE PAPER 921028] p 218 A93-14651
- Brush seal leakage performance with gaseous working fluids at static and low rotor speed conditions
[ASME PAPER 92-GT-304] p 219 A93-19494
- Development of braided rope seals for hypersonic engine applications - Flow modeling p 222 A93-34493
- Development of hypersonic engine seals - Flow effects of preload and engine pressures
[AIAA PAPER 93-1998] p 223 A93-49841
- Brush seal low surface speed hard-rub characteristics
[AIAA PAPER 93-2534] p 225 A93-50261
- Flow visualization in a single simulated brush seal
p 226 A93-54659
- Brush seal bristle flexure and hard-rub characteristics
[NASA-TM-105864] p 227 N93-18321
- The development of hydrogen sensor technology at NASA Lewis Research Center
[NASA-TM-106141] p 216 N93-27021
- Brush seal low surface speed hard-rub characteristics
[NASA-TM-106169] p 200 N93-27132
- LEAR JET AIRCRAFT**
- Microgravity research on the NASA Lewis Learjet test facility
[AIAA PAPER 93-0573] p 43 A93-24245
- LEAST SQUARES METHOD**
- A least-squares finite element method for 3D incompressible Navier-Stokes equations
[AIAA PAPER 93-0338] p 171 A93-24236
- Non-oscillatory and non-diffusive solution of convection problems by the iteratively reweighted least-squares finite element method
p 177 A93-32622
- The L sub 1 finite element method for pure convection problems
p 177 A93-34326
- Accuracy of least-squares methods for the Navier-Stokes equations
p 188 A93-52008
- A least-squares finite element method for incompressible Navier-Stokes problem
p 191 N93-10548
- Computer program for calculating and fitting thermodynamic functions
[NASA-RP-1271] p 285 N93-12967
- Large-scale computation of incompressible viscous flow by least-squares finite element method
[NASA-TM-105904] p 269 N93-22825
- LENSES**
- A fiber optic probe for the detection of cataracts
p 257 N93-25593
- LEVELING**
- Leveling coatings for reducing the atomic oxygen defect density in protected graphite fiber epoxy composites
[NASA-TM-105732] p 136 N93-15344
- LIFE (DURABILITY)**
- Low-lsp derated ion thruster operation
[AIAA PAPER 92-3203] p 64 A93-13696
- Stirling engine - Available tools for long-life assessment --- for space propulsion
p 65 A93-13824
- Maximum life spur gear design
p 218 A93-14521
- Validation test of advanced technology for IPV nickel-hydrogen flight cells - Update
p 252 A93-25886
- Stirling engine - Approach for long-term durability assessment
p 220 A93-26069
- A hot dynamic seal rig for measuring hypersonic engine seal durability and flow performance
[AIAA PAPER 93-1346] p 222 A93-33916
- Lifetime reliability evaluation of structural ceramic parts with the CARES/LIFE computer program
[AIAA PAPER 93-1497] p 239 A93-34037
- Computational simulation of hot composite structures
p 260 A93-54704
- A creep cavity growth model for creep-fatigue life prediction of a unidirectional W/Cu composite
[NASA-TM-105780] p 244 N93-10967
- Life extending control: An interdisciplinary engineering thrust
p 93 N93-31581
- LIFE CYCLE COSTS**
- U.S./CIS eye joint nuclear rocket venture
p 71 A93-49334
- LIFT**
- Estimation of unsteady lift on a pitching airfoil from wake velocity surveys
[AIAA PAPER 93-0437] p 5 A93-23351
- Estimation of unsteady lift on a pitching airfoil from wake velocity surveys
[NASA-TM-105947] p 15 N93-14791
- LIFT DEVICES**
- Effects of icing on the aerodynamic performance of high lift airfoils
[AIAA PAPER 93-0026] p 4 A93-20144
- LIGHT BEAMS**
- A fiber optic probe for the detection of cataracts
p 257 N93-25593
- LIGHT MODULATION**
- An analysis of the frequency limitations of an Al(x)Ga(1-x)As/GaAs optical modulator
p 151 A93-23454
- Fiber optic sensing technique employing RF modulated interferometry
p 212 A93-53110
- LIGHT SCATTERING**
- Refractive index and scattering effects on radiative behavior of a semitransparent layer
p 176 A93-31438
- Coherent fiber optic sensor for early detection of cataractogenesis in a human eye lens
p 209 A93-37051
- Calibration of the forward-scattering spectrometer probe - Modeling scattering from a multimode laser beam
p 212 A93-51239
- Microemulsion characterization by the use of a noninvasive backscatter fiber optic probe
p 277 A93-52412
- Statistical fitting accuracy in photon correlation spectroscopy
p 277 A93-52414
- Integrated fiber optic probe for dynamic light scattering
p 278 A93-52415
- Laser Rayleigh and Raman diagnostics for small hydrogen/oxygen rockets
[NASA-TM-105999] p 83 N93-17995
- A fiber optic probe for the detection of cataracts
p 257 N93-25593
- Pulsed laser Rayleigh scattering diagnostic for hydrogen/oxygen rocket exit plane flowfield velocimetry
[NASA-TM-106213] p 88 N93-26149
- Rayleigh-Brillouin scattering for high-pressure gas temperature measurements
p 218 N93-31556
- LIGHTHILL METHOD**
- An asymptotic theory of supersonic propeller noise
p 271 A93-19169
- LIGHTNING**
- A system to measure lightning-induced transients on spacecraft umbilical lines
p 161 N93-24889
- LINE CURRENT**
- Modelling a single phase voltage controlled rectifier using Laplace transforms
[NASA-TM-106005] p 271 N93-23016
- LINE SPECTRA**
- Rotational level-dependent collisional broadening and line shift of the A2Sigma(+)-X2Pi(1,0) band of OH in hydrogen-air combustion gases
p 276 A93-24142
- LINEAR ALTERNATORS**
- M-H characteristics and demagnetization resistance of samarium-cobalt permanent magnets to 300 C
p 153 A93-26076
- Dynamic analysis of free-piston Stirling engine/linear alternator-load system - Experimentally validated
p 254 A93-26078
- LINEAR ARRAYS**
- Multiple fiberoptic probe for several sensing applications
p 212 A93-53109
- LINEAR SYSTEMS**
- Modeling of linear isentropic flow systems
p 179 A93-37046
- Calculation of stress intensity factors in an isotropic multiracked plate. Part 1: Theoretical development
[NASA-TM-105766] p 244 N93-10455
- LININGS**
- Consecutive plate acoustic suppressor apparatus and methods
[NASA-CASE-LEW-15430-1] p 275 N93-17051
- LIQUID ATOMIZATION**
- Coaxial injector spray characterization using water/air as simulants
p 120 N93-11452
- LIQUID COOLING**
- Mechanisms of voids formation during cooldown and freezing of lithium in SP-100 type systems
p 163 A93-13916
- LIQUID CRYSTALS**
- A new hue capturing technique for the quantitative interpretation of liquid crystal images used in convective heat transfer studies
p 204 A93-13977
- Evaluation of a hue capturing based transient liquid crystal method for high-resolution mapping of convective heat transfer on curved surfaces
p 210 A93-43689
- Fluid dynamics and convective heat transfer in impinging jets through implementation of a high resolution liquid crystal technique
[ISABE 93-7077] p 189 A93-54053
- Transient liquid-crystal technique used to produce high-resolution convective heat-transfer-coefficient maps
[NASA-TM-106083] p 198 N93-23404
- LIQUID FLOW**
- Absolute and convective instability of a viscous liquid jet surrounded by a viscous gas in a vertical pipe
p 176 A93-30144
- Mixing and transient interface condensation of a liquid hydrogen tank
[AIAA PAPER 93-1968] p 184 A93-49816
- Thermocapillary convection in two immiscible liquid layers with free surface
p 188 A93-52515
- Current status of liquid sheet radiator research
[NASA-TM-105764] p 193 N93-14150
- Mixing and transient interface condensation of a liquid hydrogen tank
[NASA-TM-106201] p 201 N93-28252
- LIQUID FUELS**
- Supercritical droplet combustion and related transport phenomena
[AIAA PAPER 93-0812] p 115 A93-24885
- Flame spread across liquid pools
p 122 N93-20209
- Spray combustion experiments and numerical predictions
[NASA-TM-106069] p 198 N93-23744
- LIQUID HYDROGEN**
- Damping of thermal acoustic oscillations in hydrogen systems
p 146 A93-48589
- Autogenous pressurization of cryogenic vessels using submerged vapor injection
p 71 A93-48648
- Pressurization and expulsion of a lightweight liquid hydrogen tank
[AIAA PAPER 93-1966] p 73 A93-49814
- Mixing and transient interface condensation of a liquid hydrogen tank
[AIAA PAPER 93-1968] p 184 A93-49816
- EOTV propellant tank pressure control and liquid dynamics
[AIAA PAPER 93-2399] p 77 A93-50164
- Tank chilldown analysis and verification with a lightweight, 175 cu ft tank under normal gravity with liquid hydrogen
p 140 N93-10045
- Space propulsion
The development of hydrogen sensor technology at NASA Lewis Research Center
[NASA-TM-106141] p 216 N93-27021
- Comparing the results of an analytical model of the no-vent fill process with no-vent fill test results for a 4.96 cubic meters (175 cubic feet) tank
[NASA-TM-106018] p 200 N93-27155
- Mixing and transient interface condensation of a liquid hydrogen tank
[NASA-TM-106201] p 201 N93-28252
- LIQUID INJECTION**
- Single liquid source plasma-enhanced metalorganic chemical vapor deposition of high-quality YBa2Cu3O(7-x) thin films
p 280 A93-20643
- LIQUID METAL COOLED REACTORS**
- Advanced radiator concepts feasibility demonstration --- for space power system
p 163 A93-13844
- LIQUID METALS**
- Melt infiltration of silicon carbide compacts. I - Study of infiltration dynamics
p 101 A93-27494
- LIQUID NITROGEN**
- Effect of vaporization on cryogenic spray droplets measurement
[AIAA PAPER 93-0692] p 172 A93-24792
- Atomizing-gas temperature effect on cryogenic spray droplets
[AIAA PAPER 93-2333] p 186 A93-50111
- Effect of vaporization on cryogenic spray droplets measurement
[NASA-TM-105909] p 213 N93-13410
- Atomizing-gas temperature effect on cryogenic spray droplets
[NASA-TM-106106] p 216 N93-25191
- Comparing the results of an analytical model of the no-vent fill process with no-vent fill test results for a 4.96 cubic meters (175 cubic feet) tank
[NASA-TM-106018] p 200 N93-27155
- Orbital storage and supply of subcritical liquid nitrogen
p 62 N93-27801
- LIQUID OXYGEN**
- Design of an oxygen turbopump for use in an Advanced Expander Test Bed engine
[AIAA PAPER 93-2137] p 48 A93-49955
- LIQUID PHASES**
- Transient liquid phase diffusion bonding of Udimet 720 for Stirling power converter applications
p 221 A93-26080
- Vaporization heat transfer of dielectric liquids on enhanced surfaces covered with screen wicks
[AIAA PAPER 93-2835] p 182 A93-46572
- Tank chilldown analysis and verification with a lightweight, 175 cu ft tank under normal gravity with liquid hydrogen
p 140 N93-10045

LIQUID PROPELLANT ROCKET ENGINES

LIQUID PROPELLANT ROCKET ENGINES

- Ceramic matrix composite applications in advanced liquid fuel rocket engine turbomachinery [ASME PAPER 92-GT-316] p 99 A93-19502
- A function approximation approach to anomaly detection in propulsion system test data p 71 A93-49671
- [AIAA PAPER 93-1776] p 71 A93-49671
- A laboratory model of a hydrogen/oxygen engine for combustion and nozzle studies p 48 A93-49711
- [AIAA PAPER 93-1825] p 48 A93-49711
- Prospects for utilization of air liquefaction and enrichment system (ALES) propulsion in fully reusable launch vehicles p 74 A93-49861
- [AIAA PAPER 93-2025] p 74 A93-49861
- Durability testing of the AJ10-221 490 N high performance (321 sec isp) engine p 74 A93-49949
- [AIAA PAPER 93-2130] p 74 A93-49949
- Design and fabrication of a hydrogen/oxygen thrust chamber assembly p 74 A93-49951
- [AIAA PAPER 93-2132] p 74 A93-49951
- An RL10A-3-3A rocket engine model using the Rocket Engine Transient Simulator (ROCETS) software p 75 A93-50129
- [AIAA PAPER 93-2357] p 75 A93-50129
- Coaxial injector spray characterization using water/air as simulants p 120 N93-11452
- A neural network-based estimator for the mixture ratio of the Space Shuttle Main Engine p 87 N93-25089
- [NASA-TM-106070] p 87 N93-25089
- Rocket engine numerical simulator p 89 N93-26962
- [NASA-TM-106070] p 89 N93-26962
- LIQUID ROCKET PROPELLANTS**
- A new facility for advanced rocket propulsion research [AIAA PAPER 93-1859] p 48 A93-49737
- Low thrust chemical rocket technology p 83 N93-15572
- [NASA-TM-105927] p 83 N93-15572
- Comparing the results of an analytical model of the no-vent fill process with no-vent fill test results for a 4.96 cubic meters (175 cubic feet) tank p 200 N93-27155
- [NASA-TM-106018] p 200 N93-27155
- A new facility for advanced rocket propulsion research [NASA-TM-106193] p 49 N93-28696
- [NASA-TM-106193] p 49 N93-28696
- LIQUID SLOSHING**
- Simulation of three-dimensional liquid sloshing flows using a strongly implicit calculation procedure p 179 A93-35624
- [NASA-TM-106274] p 179 A93-35624
- LIQUID SURFACES**
- Flow-influenced stabilization of liquid columns in a dynamic plateau chamber p 169 A93-22664
- [AIAA PAPER 93-0255] p 169 A93-22664
- Vaporization heat transfer of dielectric liquids on a wick-covered surface p 169 A93-22686
- [AIAA PAPER 93-0283] p 169 A93-22686
- On the shear stabilization of capillary break-up of finite liquid bridges p 143 A93-32069
- Collapse of the soap-film bridge - Quasistatic description p 188 A93-50536
- [NASA-TM-106074] p 188 A93-50536
- LIQUID-GAS MIXTURES**
- Prediction of gas-liquid two-phase flow regime in microgravity p 145 N93-30939
- [NASA-TM-106274] p 145 N93-30939
- LIQUID-LIQUID INTERFACES**
- The susceptibility critical exponent for a nonaqueous ionic binary mixture near a consolute point p 284 A93-19838
- [NASA-TM-106074] p 284 A93-19838
- Experiments on the stability of a liquid bridge in an axial electric field p 177 A93-32617
- Experimental study of two interacting drops in an immiscible fluid p 179 A93-37936
- Thermocapillary convection in two immiscible liquid layers with free surface p 168 A93-52515
- [NASA-TM-106074] p 168 A93-52515
- LIQUID-SOLID INTERFACES**
- High accuracy computation of fluid-structure interaction in transonic cascades p 6 A93-23387
- [AIAA PAPER 93-0485] p 6 A93-23387
- Thermosolutal convection during dendritic solidification of a binary alloy p 182 A93-45975
- Numerical model for dendritic solidification of binary alloys p 282 A93-46729
- [NASA-TM-106074] p 282 A93-46729
- LIQUID-VAPOR INTERFACES**
- An interface configuration experiment on USML-1 [AIAA PAPER 93-0253] p 169 A93-22662
- [AIAA PAPER 93-0253] p 169 A93-22662
- Narrow band noise as a model of time-dependent accelerations - Study of the stability of a fluid surface in a microgravity environment p 173 A93-24965
- [AIAA PAPER 93-0911] p 173 A93-24965
- Scaling analysis of gas-liquid two-phase flow pattern in microgravity p 173 A93-24968
- [AIAA PAPER 93-0914] p 173 A93-24968
- Molecular dynamics of interface rupture p 175 A93-30130
- Using silicon diodes for detecting the liquid-vapor interface in hydrogen p 209 A93-37864
- Mixing and transient interface condensation of a liquid hydrogen tank p 184 A93-49816
- [AIAA PAPER 93-1968] p 184 A93-49816
- Stability of a fluid surface in a microgravity environment p 190 A93-55358
- [NASA-TM-106211] p 190 A93-55358

- Mixing and transient interface condensation of a liquid hydrogen tank p 201 N93-28252
- [NASA-TM-106201] p 201 N93-28252
- LIQUIDS**
- Experiments on the stability of a liquid bridge in an axial electric field p 177 A93-32617
- [NASA-TM-106201] p 177 A93-32617
- LITHIUM**
- Mechanisms of voids formation during cooldown and freezing of lithium in SP-100 type systems p 163 A93-13916
- Alkali metal carbon dioxide electrochemical system for energy storage and/or conversion of carbon dioxide to oxygen p 256 N93-28974
- [NASA-CASE-LEW-14973-1] p 256 N93-28974
- LITHIUM COOLED REACTOR EXPERIMENT**
- Multimegawatt potassium Rankine power for nuclear electric power p 65 A93-13797
- [NASA-TM-106201] p 65 A93-13797
- LITHIUM FLUORIDES**
- Void control in the crystallization of lithium fluoride p 97 A93-13760
- Mechanical properties of Haynes Alloy 188 after exposure to LiF-22CaF₂ air, and vacuum at 1093 K for periods up to 10,000 hours p 126 A93-36586
- Modeling void growth and movement with phase change in thermal energy storage canisters p 285 A93-46569
- [AIAA PAPER 93-2832] p 285 A93-46569
- Radiation and phase change of lithium fluoride in an annulus p 144 A93-54460
- [NASA-TM-106201] p 144 A93-54460
- LITHIUM HYDRIDES**
- Shielding analysis for a manned Mars rover powered by an SP-100 type reactor p 45 A93-13793
- [NASA-TM-106201] p 45 A93-13793
- LITHIUM HYDROXIDES**
- Properties of pure nickel after long term exposures to LiOH and vacuum at 775 K p 123 A93-18075
- [NASA-TM-106201] p 123 A93-18075
- LITHIUM ISOTOPES**
- Population II Li-6 as a probe of nucleosynthesis and stellar structure and evolution p 292 A93-56494
- [NASA-TM-106201] p 292 A93-56494
- LOAD CARRYING CAPACITY**
- Tailored metal matrix laminates for high-temperature performance p 98 A93-15753
- [NASA-TM-106201] p 98 A93-15753
- LOAD DISTRIBUTION (FORCES)**
- Limit pressure of a circumferentially reinforced SiC/Ti ring p 233 A93-16005
- Subcritical crack growth in soda-lime glass in combined mode I and mode II loading p 134 A93-52151
- Design for progressive fracture in composite shell structures p 242 A93-53394
- Split torque transmission load sharing p 226 N93-12736
- [NASA-TM-105884] p 226 N93-12736
- LOAD TESTS**
- A free-piston Stirling engine/linear alternator controls and load interaction test facility p 146 A93-26077
- Fracture toughness testing of polymer matrix composites p 107 N93-12302
- [NASA-TP-3199] p 107 N93-12302
- On bilinearity of Manson-Coffin low-cycle-fatigue relationship p 245 N93-12739
- [NASA-TM-105840] p 245 N93-12739
- Experimental investigation of cyclic thermomechanical deformation in torsion p 247 N93-17996
- [NASA-TM-105938] p 247 N93-17996
- Dynamic analysis of Free-Piston Stirling Engine/Linear Alternator-load system experimentally validated p 271 N93-22559
- [NASA-TM-106034] p 271 N93-22559
- Stress distribution in composite flatwise tension test specimens p 108 N93-25071
- [NASA-TM-106074] p 108 N93-25071
- LOADING RATE**
- Applications to car bodies - Generalized layout design of three-dimensional shells p 243 A93-54509
- [NASA-TM-106201] p 243 A93-54509
- LOADS (FORCES)**
- Numerical optimization of composite hip endoprostheses under different loading conditions p 270 A93-20312
- [AIAA PAPER 92-4703] p 270 A93-20312
- Energy loss analysis of an integrated space power distribution system p 68 A93-25958
- A free-piston Stirling engine/linear alternator controls and load interaction test facility p 146 A93-26077
- Power system monitoring and source control of the Space Station Freedom dc-power system testbed p 69 A93-26109
- Thermally-driven microfracture in high temperature metal matrix composites p 237 A93-32469
- Dynamic analysis of spur gears using computer program DANST p 224 A93-50080
- [AIAA PAPER 93-2295] p 224 A93-50080
- Power system monitoring and source control of the Space Station Freedom DC power system testbed p 80 N93-10734
- [NASA-TM-105841] p 80 N93-10734
- Energy loss analysis of an integrated space power distribution system p 141 N93-14834
- [NASA-TM-105772] p 141 N93-14834
- Dynamic analysis of spur gears using computer program DANST p 230 N93-28050
- [NASA-TM-106211] p 230 N93-28050

LOCAL AREA NETWORKS

- The engine design engine. A clustered computer platform for the aerodynamic inverse design and analysis of a full engine p 15 N93-11223
- [NASA-TM-105838] p 15 N93-11223

LONG DURATION EXPOSURE FACILITY

- The evolution of procurement and assurance methods used to proof an advanced space material p 94 A93-53392
- LDEF yaw and pitch angle estimates p 58 N93-12772
- Monte Carlo modeling of atomic oxygen attack of polymers with protective coatings on LDEF p 138 N93-28282
- Characteristics of hypervelocity impact craters on LDEF experiment S1003 and implications of small particle impacts on reflective surfaces p 62 N93-29363
- Studies of effects on optical components and sensors: LDEF experiments AO-147 (ERB components) and S-0014 (APEX) p 278 N93-29693

LONG TERM EFFECTS

- Nucleate pool boiling in the long duration low gravity environment of the space shuttle p 142 A93-23371
- [AIAA PAPER 93-0465] p 142 A93-23371
- Nucleate pool boiling in the long duration low gravity environment of the Space Shuttle p 144 N93-15420
- [NASA-TM-105973] p 144 N93-15420

LOSSES

- Overview of NASA supported Stirling thermodynamic loss research p 174 A93-26087
- Initial results from the NASA Lewis wave rotor experiment p 30 A93-53589
- [AIAA PAPER 93-2521] p 30 A93-53589
- Initial results from the NASA-Lewis wave rotor experiment p 39 N93-32368
- [NASA-TM-106148] p 39 N93-32368

LOW DENSITY FLOW

- Assessment of three numerical methods for the computation of a low-density plume flow p 77 A93-50256
- [AIAA PAPER 93-2528] p 77 A93-50256

LOW FREQUENCIES

- Stability testing and analysis of a PMAD dc test bed for the Space Station Freedom p 154 A93-26107
- RF modulated fiber optic sensing systems and their applications p 211 A93-49469

LOW NOISE

- Low-noise, high-strength, spiral-bevel gears for helicopter transmissions p 223 A93-49966
- [AIAA PAPER 93-2149] p 223 A93-49966
- Low-noise, high-strength, spiral-bevel gears for helicopter transmissions p 228 N93-23019
- [NASA-TM-106080] p 228 N93-23019

LOW PASS FILTERS

- 2-D nonlinear IIR-filters for image processing - An exploratory analysis p 264 A93-28200

LOW RESISTANCE

- Low resistance silver contacts to indium phosphide - Electrical and metallurgical considerations p 157 A93-39351

LOW REYNOLDS NUMBER

- Calculations of low Reynolds number rocket nozzles [AIAA PAPER 93-0888] p 67 A93-24948
- Heat transfer from radiatively heated material in a low Reynolds number microgravity environment p 180 A93-43695
- Calculation of scramjet inlet with thick boundary-layer ingestion p 12 A93-49720
- [AIAA PAPER 93-1836] p 12 A93-49720
- Low-Reynolds-number k-epsilon model for unsteady turbulent boundary-layer flows p 14 A93-53208
- A critical comparison of several low Reynolds number k-epsilon turbulence models for flow over a backward-facing step p 189 A93-53586
- [AIAA PAPER 93-1927] p 189 A93-53586
- On the drag of model dendrite fragments at low Reynolds number p 128 N93-19974
- [NASA-TM-105916] p 128 N93-19974
- A new flux conserving Newton's method scheme for the two-dimensional, steady Navier-Stokes equations p 201 N93-28626
- [NASA-TM-106160] p 201 N93-28626
- A critical comparison of several low Reynolds number k-epsilon turbulence models for flow over a backward facing step p 270 N93-32200
- [NASA-TM-106173] p 270 N93-32200
- LOW SPEED**
- Preconditioned Conjugate Gradient methods for low speed flow calculations p 172 A93-24942
- [AIAA PAPER 93-0881] p 172 A93-24942
- Preconditioned conjugate-gradient methods for low-speed flow calculations p 194 N93-14885
- [NASA-TM-105929] p 194 N93-14885
- Combustion of solid fuel in very low speed oxygen streams p 122 N93-20207

LOW SPEED WIND TUNNELS

Applied high-speed imaging for the icing research program at NASA Lewis Research Center
p 208 A93-33169

Acoustical evaluation of the NASA Lewis 9 by 15 foot low speed wind tunnel
[NASA-TP-3274] p 42 N93-12016

LOW THRUST

Prediction of engine and near-field plume reacting flows in low-thrust chemical rockets
[AIAA PAPER 93-0237] p 66 A93-22649

Optimal impulsive intercept with low-thrust rendezvous return
p 45 A93-34521

Monte Carlo and experimental studies of nozzle flow in a low-power hydrogen arcjet
[AIAA PAPER 93-2529] p 77 A93-50257

Low thrust chemical rocket technology
[NASA-TM-105927] p 83 N93-15572

LOW THRUST PROPULSION

A laboratory model of a hydrogen/oxygen engine for combustion and nozzle studies
[AIAA PAPER 93-1825] p 48 A93-49711

The NASA Electric Propulsion Program
[AIAA PAPER 93-1935] p 73 A93-49797

Low power arcjet system spacecraft impacts
[AIAA PAPER 93-2392] p 76 A93-50157

EOTV propellant tank pressure control and liquid dynamics
[AIAA PAPER 93-2399] p 77 A93-50164

Low thrust propulsion
[PR3] p 286 N93-71876

LUBRICANT TESTS

Lubrication of an 85-mm ball bearing with RP-1
[AIAA PAPER 93-2538] p 225 A93-53590

Lubrication of an 85-mm ball bearing with RP-1
[NASA-TM-106254] p 51 N93-31670

LUBRICANTS

Interfacial chemistry of a perfluoropolyether lubricant studied by X-ray photoelectron spectroscopy and temperature desorption spectroscopy
p 133 A93-38473

X-ray photoelectron spectroscopy study of the stability of Fomblin Z25 on the native oxide of aluminum
p 134 A93-44883

Interfacial chemistry of a perfluoropolyether lubricant studied by XPS and TDS
[NASA-TM-106014] p 137 N93-22560

Tribological characteristics of perfluoropolyether liquid lubricants under sliding conditions in high vacuum
[NASA-TM-106257] p 139 N93-32352

LUBRICATING OILS

Simultaneous pressure measurement and high-speed photography study of cavitation in a dynamically loaded journal bearing
p 223 A93-40050

New technique for oil backstreaming contamination measurements
p 210 A93-44514

Tribological characteristics of perfluoropolyether liquid lubricants under sliding conditions in high vacuum
[NASA-TM-106257] p 139 N93-32352

LUBRICATION

Tribological and mechanical comparison of sintered and HIPped PM212 - High temperature self-lubricating composites
p 94 A93-13506

Lubrication of an 85-mm ball bearing with RP-1
[AIAA PAPER 93-2538] p 225 A93-53590

Vickers indentation hardness of stoichiometric and reduced single crystal TiO₂ (rutile) from 25 to 800 C
[NASA-TM-105959] p 96 N93-26204

Lubrication of an 85-mm ball bearing with RP-1
[NASA-TM-106254] p 51 N93-31670

LUBRICATION SYSTEMS

Evaluation of an oil-debris monitoring device for use in helicopter transmissions
[NASA-TM-105830] p 227 N93-22826

LUMINOSITY

Chemical and luminosity evolution, and counts of galaxies in a merger model
p 290 A93-34776

LUNAR BASED EQUIPMENT

Optimization of armored spherical tanks for storage on the lunar surface
p 47 A93-25866

Evaluation of the benefits of high temperature electronics for lunar power systems
p 153 A93-25896

Design and optimization of a self-deploying single axis tracking PV array
p 252 A93-25916

LUNAR BASES

Space reactor/Stirling cycle systems for high power lunar applications
p 46 A93-13822

Lunar in-core thermionic nuclear reactor power system conceptual design
p 46 A93-13836

A study of electric power transmission lines for use on the lunar surface
p 46 A93-13901

Design and emplacement of an integrated lunar power system - Issues and concerns
p 46 A93-13908

Evaluation of the benefits of high temperature electronics for lunar power systems
p 153 A93-25896

Lunar and Martian environmental interactions with nuclear power system radiators
[NASA-TM-105747] p 80 N93-10965

Advanced photovoltaic power system technology for lunar base applications
p 255 N93-14004

Power requirements for the first lunar outpost (FLO)
[NASA-TM-105925] p 255 N93-15523

Space Nuclear Thermal Propulsion Test Facilities Subpanel
[NASA-TM-105708] p 87 N93-25105

An evolution strategy for lunar nuclear surface power
p 91 N93-27963

LUNAR ENVIRONMENT

The interaction of high voltage systems with the environments of the moon and Mars
[AIAA PAPER 93-0704] p 67 A93-24800

Dynamic Isotope Power System design considerations for human exploration of the moon and Mars
p 253 A93-25995

Lunar and Martian environmental interactions with nuclear power system radiators
[NASA-TM-105747] p 80 N93-10965

The interaction of high voltage systems with the environments of the Moon and Mars
[NASA-TM-106107] p 61 N93-26148

LUNAR EXPLORATION

Nuclear thermal propulsion transportation systems for lunar/Mars exploration
[NASA-TM-105870] p 81 N93-12363

System model development for nuclear thermal propulsion
[NASA-TM-108215] p 277 N93-17343

LUNAR FLIGHT

Lunar mission design using Nuclear Thermal Rockets
p 65 A93-13767

LUNAR LANDING

Space Nuclear Thermal Propulsion Test Facilities Subpanel
[NASA-TM-105708] p 87 N93-25105

LUNAR ROCKS

Experimental determination of in situ utilization of lunar regolith for thermal energy storage
p 253 A93-26043

LUNAR SURFACE

An analysis of power beaming for the moon and Mars
p 253 A93-25974

An evolution strategy for lunar nuclear surface power
p 91 N93-27963

M**MACH NUMBER**

Numerical simulations of a high Mach number jet flow
[AIAA PAPER 93-0653] p 172 A93-24766

A coupled implicit method for chemical non-equilibrium flows at all speeds
p 181 A93-44245

Flowfield dynamics in blunt fin-induced shock wave/turbulent boundary layer interactions
[AIAA PAPER 93-3133] p 111 A93-48298

Prospects for utilization of air liquefaction and enrichment system (ALES) propulsion in fully reusable launch vehicles
[AIAA PAPER 93-2025] p 74 A93-49861

In-stream measurements of combustion during Mach 5 to 7 tests of the Hypersonic Research Engine (HRE)
[AIAA PAPER 93-2324] p 28 A93-50104

Effects of flow-path variations on internal reversing flow in a tailpipe offtake configuration for ASTOVL aircraft
[AIAA PAPER 93-2438] p 29 A93-50190

User manual for NASA Lewis 10 by 10 foot supersonic wind tunnel
[NASA-TM-105626] p 42 N93-15498

Effects of flow-path variations on internal reversing flow in a tailpipe offtake configuration for ASTOVL aircraft
[NASA-TM-106149] p 38 N93-29065

MACH-ZEHNDER INTERFEROMETERS

Fourier transform spectrometry for fiber-optic sensor systems
p 211 A93-49459

Fiber-optic thermometer using Fourier transform spectroscopy
p 212 A93-53104

MACHINE LEARNING

Neural networks in structural analysis and design - An overview
[AIAA PAPER 92-4805] p 263 A93-20388

Self-growing neural network architecture using crisp and fuzzy entropy
p 263 A93-26650

Application of neural nets in structural optimization
p 265 A93-54533

MACROMOLECULES

Benzonorbornadiene end caps for PMR resins
p 94 A93-35700

MAGNESIUM ALLOYS

Ignition and combustion of aluminum/magnesium alloy particles in O₂ at high pressures
p 113 A93-22030

MAGNETIC BEARINGS

Stiffness of magnetic bearings subjected to combined static and dynamic loads
[ASME PAPER 91-TRIB-27] p 219 A93-15685

Determination of forces in a magnetic bearing actuator - Numerical computation with comparison to experiment
p 219 A93-15686

Magnetic bearings for free-piston Stirling engines
p 221 A93-26079

Hybrid active vibration control of rotorbearing systems using piezoelectric actuators
p 221 A93-27324

Actively controlled superconducting bearings
p 223 A93-48594

MAGNETIC CORES

Comparison of high frequency, high temperature core loss and B-H loop characteristics of an 80 Ni-Fe crystalline alloy and two iron-based amorphous alloys
p 123 A93-13882

Comparison of high temperature, high frequency core loss and dynamic B-H loops of a 2V-49Fe-49Co and a grain oriented 3Si-Fe alloy
p 153 A93-25895

MAGNETIC EFFECTS

Preliminary investigation of high power microwave plasmas for electrothermal thruster use
[AIAA PAPER 93-2106] p 74 A93-49928

Preliminary investigation of high power microwave plasmas for electrothermal thruster use
[NASA-TM-106207] p 92 N93-29158

MAGNETIC FIELD CONFIGURATIONS

Room-temperature determination of two-dimensional electron gas concentration and mobility in heterostructures
p 280 A93-35198

Extra high speed modified Lundell alternator parameters and open/short-circuit characteristics from global 3D-FE magnetic field solutions
p 156 A93-39348

Computation of load performance and other parameters of extra high speed modified Lundell alternators from 3D-FE magnetic field solutions
p 156 A93-39349

Three dimensional magnetic fields in extra high speed modified Lundell alternators computed by a combined vector-scalar magnetic potential finite element method
p 157 A93-39350

MAGNETIC FLUX

Determination of forces in a magnetic bearing actuator - Numerical computation with comparison to experiment
p 219 A93-15686

MAGNETIC MATERIALS

Comparison of high frequency, high temperature core loss and B-H loop characteristics of an 80 Ni-Fe crystalline alloy and two iron-based amorphous alloys
p 123 A93-13882

Comparison of high temperature, high frequency core loss and dynamic B-H loops of a 2V-49Fe-49Co and a grain oriented 3Si-Fe alloy
p 153 A93-25895

MAGNETIC MEASUREMENT

Determination of forces in a magnetic bearing actuator - Numerical computation with comparison to experiment
p 219 A93-15686

MAGNETIC MONOPOLES

Extension of the Parker bound on the flux of magnetic monopoles
p 291 A93-38672

MAGNETIC PROPERTIES

Damping and scattering of electromagnetic waves by small ferrite spheres suspended in an insulator
[NASA-TM-105837] p 149 N93-12366

MAGNETIC SUSPENSION

Vibration isolation technology - An executive summary of systems development and demonstration --- for proposed microgravity experiments aboard STS and Space Station Freedom
[AIAA PAPER 93-0834] p 55 A93-24904

Magnetic bearings for free-piston Stirling engines
p 221 A93-26079

Vibration isolation technology: An executive summary of systems development and demonstration
[NASA-TM-105937] p 1 N93-15573

MAGNETOHYDRODYNAMIC FLOW

A comparison of arcjet plume properties to model predictions
[AIAA PAPER 93-0820] p 67 A93-24891

Electrodynamic interactions between a space station and the ionospheric plasma environment
p 56 A93-29156

Second Magnetoplasmadynamic Thruster Workshop
[NASA-CP-10109] p 279 N93-18635

MAGNETOHYDRODYNAMIC GENERATORS

Analysis and design of an ultrahigh temperature hydrogen-fueled MHD generator
p 278 A93-49618

MAGNETOPLASMA DYNAMICS

Low power pulsed MPD thruster system analysis and applications
[AIAA PAPER 93-2391] p 76 A93-50156

Second Magnetoplasmadynamic Thruster Workshop
[NASA-CP-10109] p 279 N93-18635

NEP technology: FY 1992 milestones (NASA LeRC)
p 90 N93-26977

- Thruster models for NEP system analysis p 91 N93-26988
- MAGNETORESISTIVITY**
Intermodulation in the oscillatory magnetoresistance of a two-dimensional electron gas p 151 A93-17610
- MAGNETOSTATIC FIELDS**
Three dimensional magnetic fields in extra high speed modified Lundell alternators computed by a combined vector-scalar magnetic potential finite element method p 157 A93-39350
On the effects of grid ill-conditioning in three dimensional finite element vector potential magnetostatic field computations p 157 A93-39719
Theoretical and numerical difficulties in 3-D vector potential methods in finite element magnetostatic computations p 157 A93-39720
- MAGNETRON SPUTTERING**
Low temperature phase formation of Ti-based superconducting thin films in reduced oxygen atmosphere p 282 A93-44568
Processing, electrical and microwave properties of sputtered Ti-Ca-Ba-Cu-O superconducting thin films p 282 A93-44607
- MAINTENANCE**
An interactive preprocessor for the NASA engine performance program [NASA-TM-105786] p 32 N93-10983
- MANAGEMENT METHODS**
NTP comparison process p 89 N93-26926
RENEW v3.2 user's manual, maintenance estimation simulation for Space Station Freedom Program [NASA-TM-106006] p 232 N93-27025
- MANAGEMENT PLANNING**
The Fifth Annual NASA/Contractors Conference on Quality and Productivity. Quality: A Commitment to the Future [NASA-TM-107829] p 233 N93-70212
- MANAGEMENT SYSTEMS**
Power management and distribution technology p 90 N93-26978
Fluid management system technology discipline p 62 N93-27861
- MANEUVERABILITY**
Overview of high performance aircraft propulsion research [NASA-TM-105839] p 32 N93-11530
- MANIFOLDS**
Fluid design studies of integrated modular engine system [AIAA PAPER 93-1887] p 72 A93-49760
- MANNED MARS MISSIONS**
Establishing the infrastructure - An integrated Space Transportation System p 50 A93-12072
Planning for the Space Exploration Initiative - The nuclear propulsion option p 43 A93-13752
Lunar mission design using Nuclear Thermal Rockets p 65 A93-13767
Estimates of power requirements for a Manned Mars Rover powered by a nuclear reactor p 45 A93-13783
Shielding analysis for a manned Mars rover powered by an SP-100 type reactor p 45 A93-13793
Metalized propellants for the human exploration of Mars p 66 A93-14509
Electromagnetic powered vehicles (EMPV) for Mars exploration p 47 A93-20761
Dynamic Isotope Power System design considerations for human exploration of the moon and Mars p 253 A93-25995
A comparison of nuclear thermal rocket development cost and schedule for piloted missions to Mars [AIAA PAPER 93-2263] p 44 A93-50057
Progress report on nuclear propulsion for space exploration and science [AIAA PAPER 93-2352] p 44 A93-50125
Cryogenic propellant thermal control system design considerations, analyses, and concepts applied to a Mars human exploration mission [AIAA PAPER 93-2353] p 75 A93-50126
NASA's progress in nuclear electric propulsion technology [AIAA PAPER 93-1936] p 78 A93-53587
Lunar and Martian environmental interactions with nuclear power system radiators [NASA-TM-105747] p 80 N93-10965
Space Nuclear Thermal Propulsion Test Facilities Subpanel [NASA-TM-105708] p 87 N93-25105
Power management and distribution technology p 90 N93-26978
Radiator technology p 90 N93-26979
Nuclear electric propulsion options for piloted Mars missions p 90 N93-26985
NASA's progress in nuclear electric propulsion technology [NASA-TM-106272] p 93 N93-31858
- MANNED SPACE FLIGHT**
Space vehicle design and operation for efficient use of Nuclear Thermal Propulsion [AIAA PAPER 93-1946] p 44 A93-49804
- MANUALS**
An interactive preprocessor for the NASA engine performance program [NASA-TM-105786] p 32 N93-10983
User manual for NASA Lewis 10 by 10 foot supersonic wind tunnel [NASA-TM-105626] p 42 N93-15498
Technical report writing [NASA-TM-105419] p 287 N93-23002
NASA Lewis 8- by 6-foot supersonic wind tunnel user manual [NASA-TM-105771] p 43 N93-25080
- MANUFACTURING**
Containerless automated processing of intermetallic compounds and composites p 144 A93-52183
- MARANGONI CONVECTION**
Effect of surface tension on the onset of convection in a double-diffusive layer p 163 A93-13951
On the structure of cellular solutions in Rayleigh-Benard-Marangoni flows in small-aspect-ratio containers p 164 A93-14762
Thermocapillary bubble migration - An Oseen-like analysis of the energy equation p 179 A93-41708
Finite element calculations of transonic flutter in cascades [AIAA PAPER 93-2083] p 185 A93-49910
Thermocapillary convection in two immiscible liquid layers with free surface p 188 A93-52515
- MARS (PLANET)**
Effects of dust accumulation and removal on radiator surfaces on Mars p 123 A93-13937
Nuclear thermal propulsion transportation systems for lunar/Mars exploration [NASA-TM-105870] p 81 N93-12363
Electrical and Chemical Interactions at Mars Workshop. Part 2: Appendix [NASA-CP-10093-PT-2] p 293 N93-26392
Representative systems for space exploration p 293 N93-26395
- MARS ATMOSPHERE**
Photovoltaic arrays for Martian surface power [IAF PAPER 92-0591] p 293 A93-13699
Electrical and Chemical Interactions at Mars Workshop. Part 2: Appendix [NASA-CP-10093-PT-2] p 293 N93-26392
- MARS ENVIRONMENT**
The interaction of high voltage systems with the environments of the moon and Mars [AIAA PAPER 93-0704] p 67 A93-24800
Lunar and Martian environmental interactions with nuclear power system radiators [NASA-TM-105747] p 80 N93-10965
Degradation of radiator performance on Mars due to dust p 59 N93-15616
The interaction of high voltage systems with the environments of the Moon and Mars [NASA-TM-106107] p 61 N93-26148
Electrical and Chemical Interactions at Mars Workshop. Part 2: Appendix [NASA-CP-10093-PT-2] p 293 N93-26392
- MARS LANDING**
Power requirements for the first lunar outpost (FLO) [NASA-TM-105925] p 255 N93-15523
Space Nuclear Thermal Propulsion Test Facilities Subpanel [NASA-TM-105708] p 87 N93-25105
- MARS OBSERVER**
Monte Carlo analysis of the Titan III/Transfer Orbit Stage guidance system for the Mars Observer mission [AIAA PAPER 93-3889] p 50 A93-51473
- MARS SAMPLE RETURN MISSIONS**
Benefits of in situ propellant utilization for a Mars sample return mission [AIAA PAPER 93-2244] p 140 A93-50046
Benefits of in situ propellant utilization for a Mars sample return mission [NASA-TM-106243] p 141 N93-28695
- MARS SURFACE**
Photovoltaic arrays for Martian surface power [IAF PAPER 92-0591] p 293 A93-13699
Effects of dust accumulation and removal on radiator surfaces on Mars p 123 A93-13937
An analysis of power beaming for the moon and Mars p 253 A93-25974
Degradation of radiator performance on Mars due to dust p 59 N93-15616
Electrical and Chemical Interactions at Mars Workshop. Part 2: Appendix [NASA-CP-10093-PT-2] p 293 N93-26392
- MASS DISTRIBUTION**
Biasing and hierarchical statistics in large-scale structure p 292 A93-55051
- MASS FLOW**
Air-mass flux measurement system using Doppler-shifted filtered Rayleigh scattering [AIAA PAPER 93-0513] p 205 A93-23260
A comparison of numerical and analytical solution of the creeping flame spread over thermally thin material p 117 A93-41954
CFD mixing analysis of axially opposed rows of jets injected into confined crossflow [AIAA PAPER 93-2044] p 185 A93-49877
A comparison between numerically modelled and experimentally measured loss mechanisms in wave rotors [AIAA PAPER 93-2522] p 30 A93-50252
CFD mixing analysis of axially opposed rows of jets injected into confined crossflow [NASA-TM-106179] p 37 N93-27128
- MASS FLOW RATE**
A soft-start circuit for arcjet ignition [AIAA PAPER 93-2396] p 76 A93-50161
- MASS SPECTROSCOPY**
Thermodynamics of iron-aluminum alloys at 1573 K p 127 A93-52879
- MASS TRANSFER**
Pressure dependence of the oxygen reduction reaction at the platinum microelectrode/nafion interface - Electrode kinetics and mass transport p 112 A93-11450
Autogenous pressurization of cryogenic vessels using submerged vapor injection p 71 A93-48648
- MATHEMATICAL MODELS**
Stirling engine - Available tools for long-life assessment --- for space propulsion p 65 A93-13824
Probabilistic structural analysis of adaptive/smart/intelligent space structures p 234 A93-16203
Implementation of a model based fault detection and diagnosis technique for actuation faults of the SSME p 47 A93-16413
Improved accuracy for finite element structural analysis via an integrated force method p 234 A93-17246
Coupled multi-disciplinary simulation of composite engine structures in propulsion environment [ASME PAPER 92-GT-6] p 23 A93-19279
Coarsening following a morphological instability in the one-sided model p 284 A93-21695
Influence of heat transfer rates on pressurization of liquid/slush hydrogen propellant tanks [AIAA PAPER 93-0278] p 169 A93-22681
Numerical modeling of anti-icing systems and comparison to test results on a NACA 0012 airfoil [AIAA PAPER 93-0170] p 21 A93-23242
Ice accretion prediction for a typical commercial transport aircraft [AIAA PAPER 93-0174] p 19 A93-23245
An improved numerical model for wave rotor design and analysis [AIAA PAPER 93-0482] p 24 A93-23384
Numerical model for the Programmable Multirole Furnace (PMZF) [AIAA PAPER 93-0471] p 142 A93-24242
Comparison of numerical model results with diffusion flames in microgravity [AIAA PAPER 93-0707] p 114 A93-24803
Comparison of GLIMPS and HFAST Stirling engine code predictions with experimental data p 220 A93-26052
Simulation of the early startup period of high-temperature heat pipes from the frozen state by a rarefied vapor self-diffusion model p 175 A93-30127
A numerical analysis of high-temperature heat pipe startup from the frozen state p 175 A93-30128
Microfracture in high temperature metal matrix crossply laminates p 101 A93-31356
Evaluation of the Munich Method for modeling rocket engine performance p 70 A93-31968
Modal simulation of gear box vibration with experimental correlation p 221 A93-31982
Applied high-speed imaging for the icing research program at NASA Lewis Research Center p 208 A93-33169
Modal analysis of multistage gear systems coupled with gearbox vibrations p 222 A93-36588
Modeling of linear isentropic flow systems p 179 A93-37046
A comparison of numerical and analytical solution of the creeping flame spread over thermally thin material p 117 A93-41954
Heat transfer from radiatively heated material in a low Reynolds number microgravity environment p 180 A93-43695
Algebraic grid generation with control points p 268 A93-45967
A new flux splitting scheme p 9 A93-47189
An analytical study of dilution jet mixing in a cylindrical duct [AIAA PAPER 93-2043] p 27 A93-49876

Effect of extended tooth contact on the modeling of spur gear transmissions p 223 A93-49965
[AIAA PAPER 93-2148]
Contact stress analysis of spiral bevel gears using nonlinear finite element static analysis p 224 A93-50081
[AIAA PAPER 93-2296]
Effect of out-of-roundness on the performance of a diesel engine connecting-rod bearing p 225 A93-52607
A numerical model including PID control of a multizone crystal growth furnace p 190 A93-55473
Unified viscoplastic behavior of metal matrix composites p 244 N93-10777
[NASA-TM-105819]
A creep cavity growth model for creep-fatigue life prediction of a unidirectional W/Cu composite p 244 N93-10967
[NASA-TM-105780]
Implementation of a model based fault detection and diagnosis for actuation faults of the Space Shuttle main engine p 49 N93-11401
[NASA-TM-105781]
Application of artificial neural networks in nonlinear analysis of trusses p 244 N93-11403
[NASA-TM-105319]
An improved numerical model for wave rotor design and analysis p 33 N93-12418
[NASA-TM-105915]
Development of braided rope seals for hypersonic engine applications: Flow modeling p 227 N93-14478
[NASA-TM-105942]
Numerical modeling of anti-icing systems and comparison to test results on a NASA 0012 airfoil p 19 N93-15345
[NASA-TM-105975]
Ice accretion prediction for a typical commercial transport aircraft p 20 N93-15522
[NASA-TM-105976]
The use of plasma ashers and Monte Carlo modeling for the projection of atomic oxygen durability of protected polymers in low Earth orbit p 58 N93-15596
Modeling of turbulent shear flows p 195 N93-15797
Two equation modelling and the pseudo compressibility technique p 195 N93-15799
System model development for nuclear thermal propulsion p 277 N93-17343
[NASA-TM-108215]
Flame spread across liquid pools p 122 N93-20209
On the structure of gaseous confined laminar diffusion flames: Numerical investigation p 197 N93-21196
[NASA-TM-106039]
Optimal design of composite hip implants using NASA technology p 257 N93-22188
Global dynamic modeling of a transmission system p 228 N93-24751
[NASA-CR-191117]
METAL matrix composite Analyzer (METCAN): Theoretical manual p 109 N93-26552
[NASA-TM-106025]
Fiber shape effects on metal matrix composite behavior p 109 N93-26704
[NASA-TM-106067]
Nuclear thermal propulsion technology overview p 89 N93-26927
NTR plume modeling p 199 N93-26929
Explicit robust schemes for implementation of a class of principal value-based constitutive models: Symbolic and numeric implementation p 258 N93-26946
[NASA-TM-106124]
Explicit robust schemes for implementation of general principal value-based constitutive models p 258 N93-26947
[NASA-TM-106123]
Overview of NASA/DOE/DOD interagency modeling team and activities p 89 N93-26952
Composite micromechanical modeling using the boundary element method p 250 N93-27030
[NASA-TM-106127]
Contact stress analysis of spiral bevel gears using nonlinear finite element static analysis p 228 N93-27037
[NASA-TM-106176]
Comparing the results of an analytical model of the no-vent fill process with no-vent fill test results for a 4.96 cubic meters (175 cubic feet) tank p 200 N93-27155
[NASA-TM-106018]
An analytical study of dilution jet mixing in a cylindrical duct p 37 N93-27160
[NASA-TM-106181]
Numerical modeling of runback water on ice protected aircraft surfaces p 201 N93-27438
Effect of extended tooth contact on the modeling of spur gear transmissions p 230 N93-28411
[NASA-TM-106174]
A numerical study of confined turbulent jets p 202 N93-29161
[NASA-TM-106197]
Overview of the fatigue/fracture/life prediction working group program at the Lewis Research Center p 232 N93-31574
A model for predicting high-temperature fatigue failure of a W/Cu composite p 112 N93-31579

MATRICES (MATHEMATICS)

Boundary formulations for sensitivity analysis without matrix derivatives p 242 A93-49028
A transfer matrix approach to vibration localization in mistuned blade assemblies p 250 N93-27088
[NASA-TM-106112]
MATRIX MATERIALS
Progressive matrix cracking in off-axis plies of a general symmetric laminate p 239 A93-34035
[AIAA PAPER 93-1494]
Kinetics of hexacelsian-to-celsian phase transformation in SrAl₂Si₂O₈ p 134 A93-40293
Model of brittle matrix composite toughening based on discrete fiber reinforcement p 104 A93-40888
Approaches to polymer-derived CMC matrices p 105 A93-53446
Probabilistic micromechanics and macromechanics of polymer matrix composites p 105 A93-54705
ICAN/DAMP-integrated composite analyzer with damping analysis capabilities: User's manual p 106 N93-12015
[NASA-TP-3292]
Kinetics of hexacelsian to celsian phase transformation in SrAl₂Si₂O₈ p 136 N93-16372
[NASA-TM-105913]
Probabilistic simulation of multi-scale composite behavior p 250 N93-28633
[NASA-TM-106196]
Acousto-Ultrasonic analysis of failure in ceramic matrix composite tensile specimens p 232 N93-29073
[NASA-TM-106219]
MATRIX METHODS
Solving modal equations of motion with initial conditions using MSC/NASTRAN DMAP. Part 1: Implementing exact mode superposition p 248 N93-23739
[NASA-TM-106063]
Solving modal equations of motion with initial conditions using MSC/NASTRAN DMAP. Part 2: Coupled versus uncoupled integration p 248 N93-23740
[NASA-TM-106064]
A transfer matrix approach to vibration localization in mistuned blade assemblies p 250 N93-27088
[NASA-TM-106112]
MEASURE AND INTEGRATION
Improved accuracy for finite element structural analysis via an integrated force method p 234 A93-17246
MEASURING INSTRUMENTS
X-ray-based displacement measurement for hostile environments p 208 A93-28580
Miniature high temperature plug-type heat flux gauges p 209 A93-37862
A system to measure lightning-induced transients on spacecraft umbilical lines p 161 N93-24889
Progress in the measurement of SSME turbine heat flux with plug-type sensors p 217 N93-31553
Thin film heat flux sensor for Space Shuttle Main Engine turbine environment p 217 N93-31554
Thin film thermocouples for high temperature turbine application p 217 N93-31555
MECHANICAL DEVICES
An apparatus for gripping test specimens p 230 N93-28127
[NASA-CASE-LEW-15345-2]
Service equipment for use in hostile environments p 230 N93-31314
[NASA-CASE-LEW-14906-2]
MECHANICAL MEASUREMENT
Determination of plate wave velocities and diffuse field decay rates with broad-band acousto-ultrasonic signals p 232 N93-27080
[NASA-TM-106158]
MECHANICAL PROPERTIES
Stirling engine - Available tools for long-life assessment --- for space propulsion p 65 A93-13824
Effect of oxidation on the mechanical properties of a NbAl₃ alloy at intermediate temperatures p 124 A93-20667
Critical experiments of the self-consistent model for polycrystalline Hastelloy-X p 124 A93-21958
A constitutive model for the high temperature inelastic response of nickel base superalloys p 124 A93-21959
Transverse flexural tests as a tool for assessing damage to PMR-15 composites from isothermal aging in air at elevated temperatures p 100 A93-24514
Grain boundary resistance to fatigue crack growth p 125 A93-29570
Quantification of uncertainties in composites p 102 A93-33989
[AIAA PAPER 93-1440]
Mechanical properties of Haynes Alloy 188 after exposure to LiF-22CaF₂, air, and vacuum at 1093 K for periods up to 10,000 hours p 126 A93-36586
Aerospace applications --- of refractory ceramic materials p 135 A93-55472
Review of the physical and mechanical properties and potential applications of the B2 compound NiAl: Unabridged version of a paper published in International materials review p 127 N93-11635
[NASA-TM-105598]

Transverse flexural tests as a tool for assessing damage to PMR-15 composites from isothermal aging in air at elevated temperatures p 107 N93-12737
[NASA-TM-105848]
High Temperature Composite Analyzer (HITCAN) theoretical manual, version 1.0 p 249 N93-24913
[NASA-TM-106001]
Considerations concerning fatigue life of metal matrix composites p 250 N93-27009
[NASA-TM-106144]
Soft computing in design and manufacturing of advanced materials p 111 N93-28624
[NASA-TM-106032]
Probabilistic simulation of multi-scale composite behavior p 250 N93-28633
[NASA-TM-106196]
MELT SPINNING
The microstructural evolution, crystallography, and thermal processing of ultrahigh carbon Fe-1.85 pct C melt-spun ribbon p 125 A93-32934
MELTS (CRYSTAL GROWTH)
On the shear stabilization of capillary break-up of finite liquid bridges p 143 A93-32069
Thermocapillary convection in two immiscible liquid layers with free surface p 188 A93-52515
Studies on the reactive melt infiltration of silicon and silicon-molybdenum alloys in porous carbon p 136 N93-12398
[NASA-TM-105860]
On the drag of model dendrite fragments at low Reynolds number p 128 N93-19974
[NASA-TM-105916]
MEMBRANES
Membrane triangles with corner drilling freedoms. I - The EFF element p 235 A93-24303
Membrane triangles with corner drilling freedoms. II - The ANDES element p 235 A93-24304
Membrane triangles with corner drilling freedoms. III - Implementation and performance evaluation p 236 A93-24305
MEMORY (COMPUTERS)
Concurrent processing adaptation of aeroelastic analysis of propfans p 23 A93-14624
Parallel computing for probabilistic fatigue analysis [AIAA PAPER 93-1499] p 261 A93-34039
MENISCI
Hydrodynamic behavior and electrochemical impedance of the Hanging Meniscus Rotating Disk (HMRD) electrode. I - Meniscus shape under rotation. II - I-BIEM calculations of frequency dispersion and minimization p 116 A93-34247
MERCURY COMPOUNDS
Physical vapor transport of mercurous chloride under a nonlinear thermal profile p 196 N93-16612
[NASA-TM-105920]
METAL BONDING
Stress relaxation of low pressure plasma-sprayed NiCrAlY alloys p 127 A93-52870
METAL COATINGS
On the melt infiltration of copper coated silicon carbide with an aluminum alloy p 218 A93-11332
Chronopotentiometry of refractory metals, actinides and oxyanions in molten salts: A review p 120 N93-11545
[NASA-TM-105862]
Issues/considerations and performance prediction of LEO protective coatings p 137 N93-20813
METAL COMBUSTION
Ignition and combustion of aluminum/magnesium alloy particles in O₂ at high pressures p 113 A93-22030
METAL CRYSTALS
Method for calculating alloy energetics p 279 A93-18740
The viscoplastic behavior of Hastelloy-X single crystal p 125 A93-27486
METAL FATIGUE
A high temperature fatigue life prediction computer code based on the Total Strain Version of Strainrange Partitioning (SRP) p 260 A93-31341
Fatigue life prediction of an intermetallic matrix composite at elevated temperatures p 101 A93-31358
Effect of tensile mean stress on fatigue behavior of single-crystal and directionally solidified superalloys p 125 A93-33011
On bilinearity of Manson-Coffin low-cycle-fatigue relationship p 245 N93-12739
[NASA-TM-105840]
In-phase and out-of-phase axial-torsional fatigue behavior of Haynes 188 at 760 C p 246 N93-13153
[NASA-TM-105765]
METAL FIBERS
The role of the interface in refractory metal alloy composites p 97 A93-13777
A model for predicting high-temperature fatigue failure of a W/Cu composite p 112 N93-31579

METAL FILMS

- The effect of ion-plated silver and sliding friction on tensile stress-induced cracking in aluminum oxide p 132 A93-27917
- Low earth simulation and materials characterization p 44 A93-32293
- Development of a hydrogen gas sensor using microfabrication technology [SAE PAPER 921176] p 210 A93-41356

METAL HALIDES

- Global expression for representing cohesive-energy curves. II p 276 A93-44989

METAL IONS

- Ion exchange polymers and method for making [NASA-CASE-LEW-15576-1] p 139 A93-31316

METAL MATRIX COMPOSITES

- On the melt infiltration of copper coated silicon carbide with an aluminum alloy p 218 A93-11332
- Elevated temperature compressive properties of reaction milled NiAl-AlN and Zr-doped NiAl-AlN composites p 97 A93-11422
- Observations on infiltration of silicon carbide compacts with an aluminum alloy p 97 A93-12356
- The role of the interface in refractory metal alloy composites p 97 A93-13777
- Graphite fiber/copper matrix composites for space power heat pipe fin applications p 162 A93-13789
- Fiber shape effects on metal matrix composite behavior p 98 A93-15752
- Tailored metal matrix laminates for high-temperature performance p 98 A93-15753
- Limit pressure of a circumferentially reinforced SiC/Ti ring p 233 A93-16005
- Combined micromechanical and fabrication process optimization for metal-matrix composites p 99 A93-18990
- Creep behavior of tungsten fiber reinforced niobium metal matrix composites p 99 A93-20758
- Detecting Lamb waves with broadband acousto-ultrasonic signals in composite structures p 231 A93-21898
- Thermal conductivity and thermal expansion of graphite fiber-reinforced copper matrix composites p 100 A93-25104
- Fatigue-environment interactions in a SiC/Ti-15-3 composite p 100 A93-26275
- Melt infiltration of silicon carbide compacts. I - Study of infiltration dynamics p 101 A93-27494
- Melt infiltration of silicon carbide compacts. II - Evaluation of solidification microstructures p 101 A93-28283
- Transverse ductility of metal matrix composites p 101 A93-31355
- Microfracture in high temperature metal matrix crossply laminates p 101 A93-31356
- Fatigue life prediction of an intermetallic matrix composite at elevated temperatures p 101 A93-31358
- Deformation and failure mechanisms in metal matrix composites p 102 A93-31359
- NDE of the universe - New ways to look at old facts p 271 A93-32222
- Computational characterization of high temperature composites via METCAN p 102 A93-32461
- Probabilistic micromechanics for metal matrix composites p 237 A93-32465
- Thermally-driven microfracture in high temperature metal matrix composites p 237 A93-32469
- Ductility of a continuous fiber reinforced aluminum matrix composite p 102 A93-32471
- Effect of thermal cycling on interface bonding requirements in Al₂O₃ fiber-reinforced superalloy composites p 103 A93-35882
- Application of neural networks in the acousto-ultrasonic evaluation of metal-matrix composite specimens p 231 A93-37009
- Residual strain gradient determination in metal matrix composites by synchrotron X-ray energy dispersive diffraction p 103 A93-39580
- The effect of multiple compliant layers at the fiber-matrix interface on residual thermal stresses in metal matrix composites p 104 A93-42085
- Evolution of damage and plasticity in titanium-based, fiber-reinforced composites p 104 A93-48498
- Containerless automated processing of intermetallic compounds and composites p 144 A93-52183
- Chemical stability of titanium diboride reinforcement in nickel aluminide matrices p 105 A93-52473
- Thermal emittance enhancement of graphite-aluminum and graphite-copper composite radiator surfaces for space power applications p 105 A93-53455
- Computational simulation of hot composite structures p 260 A93-54704
- The effect of fiber microstructure on evolution of residual stresses in silicon carbide/titanium aluminide composites p 106 A93-54771

- Interfacial shear strength of cast and directionally solidified NiAl-sapphire fiber composites p 106 A93-55685

- Interfacial and capillary phenomena in solidification processing of metal-matrix composites p 106 A93-56351

- Unified viscoplastic behavior of metal matrix composites [NASA-TM-105819] p 244 A93-10777

- Nondestructive evaluation of ceramic and metal matrix composites for NASA's HITEMP and enabling propulsion materials programs [NASA-TM-105807] p 231 A93-10963

- A creep cavity growth model for creep-fatigue life prediction of a unidirectional W/Cu composite [NASA-TM-105780] p 244 A93-10967

- Thermomechanical fatigue behavior of SiC/Ti-24Al-11Nb in air and argon environments [NASA-TM-105723] p 106 A93-11399

- High Temperature Composite Analyzer (HITCAN) theoretical manual, version 1.0 [NASA-TM-106001] p 249 A93-24913

- High temperature composite analyzer (HITCAN) user's manual, version 1.0 [NASA-TM-106002] p 249 A93-25070

- METAL matrix composite ANalyzer (METCAN): Theoretical manual [NASA-TM-106025] p 109 A93-26552

- An overview of elevated temperature damage mechanisms and fatigue behavior of a unidirectional SCS-6/Ti-15-3 composite [NASA-TM-106131] p 109 A93-26702

- Fiber shape effects on metal matrix composite behavior [NASA-TM-106067] p 109 A93-26704

- Considerations concerning fatigue life of metal matrix composites [NASA-TM-106144] p 250 A93-27009

- Determination of plate wave velocities and diffuse field decay rates with broad-band acousto-ultrasonic signals [NASA-TM-106158] p 232 A93-27080

- Metal Matrix Laminate Tailoring (MMLT) code: User's manual [NASA-TM-106052] p 111 A93-28681

- Thermoviscoplastic analysis of fibrous periodic composites using triangular subvolumes [NASA-TM-106076] p 111 A93-29074

- A model for predicting high-temperature fatigue failure of a W/Cu composite p 112 A93-31579

METAL OXIDES

- Onset conditions for gas phase reaction and nucleation in the CVD of transition metal oxides p 116 A93-39508

METAL PARTICLES

- The kinetics of composite particle formation during mechanical alloying p 125 A93-29534

METAL POWDER

- Ignition and combustion of aluminum/magnesium alloy particles in O₂ at high pressures p 113 A93-22030

METAL PROPELLANTS

- Metallized propellants for the human exploration of Mars p 66 A93-14509

- Ignition and combustion of aluminum/magnesium alloy particles in O₂ at high pressures p 113 A93-22030

METAL SHEETS

- Processing and microstructure of Nb-1 percent Zr-0.1 percent C alloy sheet [NASA-TM-105921] p 128 A93-15524

METAL SURFACES

- Interfacial chemistry of a perfluoropolyether lubricant studied by X-ray photoelectron spectroscopy and temperature desorption spectroscopy p 133 A93-38473

- Multilayer relaxation and surface energies of fcc and bcc metals using equivalent crystal theory p 119 A93-52872

- Interfacial chemistry of a perfluoropolyether lubricant studied by XPS and TDS [NASA-TM-106014] p 137 A93-22560

METALLICITY

- The boron-to-beryllium ratio in halo stars - A signature of cosmic-ray nucleosynthesis in the early Galaxy p 292 A93-55061

- Population II Li-6 as a probe of nucleosynthesis and stellar structure and evolution p 292 A93-56494

METALLIZING

- Technology for gelled liquid cryogenic propellants - Metallized hydrogen/aluminum [AIAA PAPER 93-1878] p 140 A93-49752

METALLOGRAPHY

- Thermal stability of the microstructure of an aged Nb-Zr-C alloy p 122 A93-13776

- External stress-corrosion cracking of a 1.22-m-diameter type 316 stainless steel air valve [NASA-TP-3190] p 129 A93-26201

METALORGANIC CHEMICAL VAPOR DEPOSITION

- Single liquid source plasma-enhanced metalorganic chemical vapor deposition of high-quality YBa₂Cu₃O_{7-x} thin films p 280 A93-20643

- Ellipsometric study of metal-organic chemically vapor deposited III-V semiconductor structures p 281 A93-35697

- Metal-organic chemical vapour deposition of polycrystalline tetragonal indium sulphide (InS) thin films p 116 A93-36584

- CVD of SiC and AlN using cyclic organometallic precursors p 117 A93-39525

METALS

- Finite element implementation of state variable-based viscoplasticity models p 236 A93-26776

- Guanidine based vehicle/binders for use with oxides, metals, and ceramics [NASA-CASE-LEW-15314-2] p 138 A93-28423

METEORITE CRATERS

- Characteristics of hypervelocity impact craters on LDEF experiment S1003 and implications of small particle impacts on reflective surfaces p 62 A93-29363

METEOROID CONCENTRATION

- Characteristics of hypervelocity impact craters on LDEF experiment S1003 and implications of small particle impacts on reflective surfaces p 62 A93-29363

METEOROID PROTECTION

- Optimization of armored spherical tanks for storage on the lunar surface p 47 A93-25866

- On protection of Freedom's solar dynamic radiator from the orbital debris environment. I - Preliminary analysis and testing p 70 A93-36197

METHANATION

- Benefits of in situ propellant utilization for a Mars sample return mission [AIAA PAPER 93-2244] p 140 A93-50046

- Benefits of in situ propellant utilization for a Mars sample return mission [NASA-TM-106243] p 141 A93-28695

METHANE

- Comparison of numerical model results with diffusion flames in microgravity [AIAA PAPER 93-0707] p 114 A93-24803

- Effects of particulate radiation on premixed gas flames [AIAA PAPER 93-0711] p 114 A93-24806

- Numerical study of shock-induced combustion in methane-air mixtures [AIAA PAPER 93-1917] p 184 A93-49783

METHOD OF MOMENTS

- Spectral-domain moment-method analysis of coplanar microstrip parasitic subarrays p 148 A93-35016

MICROANALYSIS

- Microchemical analysis of the SCS-6 silicon carbide fiber p 135 A93-53734

MICROCRACKS

- Microfracture in high temperature metal matrix crossply laminates p 101 A93-31356

- Thermally-driven microfracture in high temperature metal matrix composites p 237 A93-32469

- Calculation of stress intensity factors in an isotropic multicracked plate. Part 2: Symbolic/numeric implementation [NASA-TM-105823] p 244 A93-10453

- Calculation of stress intensity factors in an isotropic multicracked plate. Part 1: Theoretical development [NASA-TM-105766] p 244 A93-10455

MICROGRAVITY

- Initial study of void formation during aluminum solidification in reduced gravity p 142 A93-12013

- Effect of surface tension on the onset of convection in a double-diffusive layer p 163 A93-13951

- An interface configuration experiment on USML-1 [AIAA PAPER 93-0253] p 169 A93-22662

- Nucleate pool boiling in the long duration low gravity environment of the space shuttle [AIAA PAPER 93-0465] p 142 A93-23371

- Natural and thermocapillary convection in multiple liquid layers [AIAA PAPER 93-0469] p 171 A93-24241

- Numerical model for the Programmable Multitrole Furnace (PMZF) [AIAA PAPER 93-0471] p 142 A93-24242

- Microgravity research on the NASA Lewis Learjet test facility [AIAA PAPER 93-0573] p 43 A93-24245

- Comparison of numerical model results with diffusion flames in microgravity [AIAA PAPER 93-0707] p 114 A93-24803

- Effects of gravity on the transition to turbulence of gas jet diffusion flames [AIAA PAPER 93-0710] p 114 A93-24805

- Flame balls - Past, present and future [AIAA PAPER 93-0712] p 114 A93-24807

- Downward diffusion flame spread and extinction in variable gravitational fields - Lunar and Martian simulations
[AIAA PAPER 93-0828] p 115 A93-24898
- Low gravity environment on-board Columbia during STS-40
[AIAA PAPER 93-0833] p 142 A93-24903
- Evaluation of passive and active vibration control mechanisms in a microgravity environment
[AIAA PAPER 93-0838] p 55 A93-24905
- Narrow band noise as a model of time-dependent accelerations - Study of the stability of a fluid surface in a microgravity environment
[AIAA PAPER 93-0911] p 173 A93-24965
- Scaling analysis of gas-liquid two-phase flow pattern in microgravity
[AIAA PAPER 93-0914] p 173 A93-24968
- IDGE - A test of dendritic growth theory using space flight
[AIAA PAPER 93-0260] p 143 A93-25515
- Intensified array camera imaging of solid surface combustion aboard the NASA Learjet
p 143 A93-30858
- Contributions of microgravity test results to the design of spacecraft fire-safety systems
[AIAA PAPER 93-1152] p 56 A93-31028
- Ground-based PIV and numerical flow visualization results from the Surface Tension Driven Convection Experiment
p 143 A93-33075
- The detrimental effect of friction on space microgravity robotics
p 222 A93-35546
- Convective effects during the physical vapor transport process. I - Thermal convection
p 179 A93-36575
- On accurate determination of contact angle
p 143 A93-41678
- Surface tension effects on the onset of double-diffusive convection
p 180 A93-41710
- Heat transfer from radiatively heated material in a low Reynolds number microgravity environment
p 180 A93-43695
- Thermocapillary migration of a small chain of bubbles
p 182 A93-46714
- The CONE program - An overview --- Cryogenic Orbital Nitrogen Experiment
p 146 A93-48637
- Autogenous pressurization of cryogenic vessels using submerged vapor injection
p 71 A93-48648
- Gravity sensitivity of a resistojel water vaporizer
[AIAA PAPER 93-2402] p 186 A93-50167
- Preliminary endurance tests of water vaporizers for resistojel applications
[AIAA PAPER 93-2403] p 187 A93-50168
- Low-g fluid mixing - Further results from the Tank Pressure Control Experiment
[AIAA PAPER 93-2423] p 187 A93-50181
- Mechanisms of microgravity flame spread over a thin solid fuel - Oxygen and opposed flow effects
p 140 A93-50368
- Scientific basis for the Isothermal Dendritic Growth Experiment - A USMP-2 space flight experiment
p 143 A93-50455
- Digital control algorithms for microgravity isolation systems
p 265 A93-53653
- Proposed ground-based control of accelerometer on Space Station Freedom
p 63 A93-54401
- Radiation and phase change of lithium fluoride in an annulus
p 144 A93-54460
- Stability of a fluid surface in a microgravity environment
p 190 A93-55358
- Premixed flame propagation in an optically thick gas
p 119 A93-55381
- Tank chilldown analysis and verification with a flightweight, 175 cu ft tank under normal gravity with liquid hydrogen
p 140 A93-10045
- Small experiments for the maturation of orbital cryogenic transfer technologies
[NASA-TM-105849] p 192 A93-10981
- Numerical study of mixing of two fluids under low gravity
[NASA-TM-105865] p 194 A93-14914
- Nucleate pool boiling in the long duration low gravity environment of the Space Shuttle
[NASA-TM-105973] p 144 A93-15420
- The Second International Microgravity Combustion Workshop
[NASA-CP-10113] p 145 A93-20178
- Overview of NASA's microgravity combustion science and fire safety program
p 145 A93-20180
- Capabilities and constraints of typical space flight hardware
p 145 A93-20183
- Capabilities and constraints of NASA's ground-based reduced gravity facilities
p 49 A93-20184
- Capabilities and constraints of combustion diagnostics in microgravity
p 145 A93-20185
- Soot formation and radiation in turbulent jet diffusion flames under normal and reduced gravity conditions
p 121 A93-20192
- Visualization and imaging methods for flames in microgravity
p 121 A93-20193
- Selected microgravity combustion diagnostic techniques
p 121 A93-20194
- Fire safety practices in the Shuttle and the Space Station Freedom
p 59 A93-20204
- Opposed-flow flame spreading in reduced gravity
p 121 A93-20206
- Combustion of solid fuel in very low speed oxygen streams
p 122 A93-20207
- Flame spread across liquid pools
p 122 A93-20209
- Combustion of interacting droplet arrays in a microgravity environment
p 122 A93-20217
- Proposed ground-based control of accelerometer on Space Station Freedom
[NASA-TM-105960] p 63 A93-23738
- Contributions of microgravity test results to the design of spacecraft fire safety systems
[NASA-TM-106093] p 60 A93-24755
- Conceptual design for the Space Station Freedom fluid physics/dynamics facility
[NASA-TM-103663] p 61 A93-26209
- A multi-zone muffle furnace design
[NASA-TM-106153] p 145 A93-27011
- Comparing the results of an analytical model of the no-vent fill process with no-vent fill test results for a 4.96 cubic meters (175 cubic feet) tank
[NASA-TM-106018] p 200 A93-27155
- Preliminary endurance tests of water vaporizers for resistojel applications
[NASA-TM-106222] p 92 A93-28694
- Tank Pressure Control Experiment/Thermal Phenomena (TPCE/TP)
p 92 A93-28713
- Thermal energy storage flight experiment in microgravity
p 256 A93-28720
- Gravity sensitivity of a resistojel water vaporizer
[NASA-TM-106220] p 92 A93-29194
- Prediction of gas-liquid two-phase flow regime in microgravity
[NASA-TM-106274] p 145 A93-30939
- Smoldering combustion in microgravity. USML-1 glovebox experiment No. 6
[NASA-TM-105012] p 146 A93-70290
- MICROGRAVITY APPLICATIONS**
- Proposed ground-based control of accelerometer on Space Station Freedom
p 63 A93-54401
- The Second International Microgravity Combustion Workshop
[NASA-CP-10113] p 145 A93-20178
- Proposed ground-based control of accelerometer on Space Station Freedom
[NASA-TM-105960] p 63 A93-23738
- Laser ignition application in a space experiment
[NASA-TM-106133] p 145 A93-25337
- A multi-zone muffle furnace design
[NASA-TM-106153] p 145 A93-27011
- Low-frequency vibration environment for five Shuttle missions
[NASA-TM-106059] p 63 A93-28554
- MICROHARDNESS**
- Vickers indentation hardness of stoichiometric and reduced single crystal TiO₂ (rutile) from 25 to 800 C
[NASA-TM-105959] p 96 A93-26204
- MICROMECHANICS**
- Single-parameter characterization of discrete-dislocation pileup tipfield and its application to physically based micro-mechanics
p 233 A93-12119
- Combined micromechanical and fabrication process optimization for metal-matrix composites
p 99 A93-18990
- Ultrasonic and micromechanical study of damage and elastic properties of SiC/RBSN ceramic composites --- Reaction Bonded Silicon Nitride
p 99 A93-19624
- Micromechanical studies of composites by BEM
p 236 A93-31295
- Computational micromechanics of woven composites
p 237 A93-32462
- Probabilistic micromechanics for metal matrix composites
p 237 A93-32465
- Micromachined silicon cantilever beam accelerometer incorporating an integrated optical waveguide
p 210 A93-49457
- Characterization of Si₃N₄/SiO₂ optical channel waveguides by photon scanning tunneling microscopy
p 211 A93-49458
- Probabilistic micromechanics and macromechanics of polymer matrix composites
p 105 A93-54705
- ICAN/DAMP-integrated composite analyzer with damping analysis capabilities: User's manual
[NASA-TP-3292] p 106 A93-12015
- Second generation integrated composite analyzer (ICAN) computer code
[NASA-TP-3290] p 108 A93-18139
- High Temperature Composite Analyzer (HITCAN) theoretical manual, version 1.0
[NASA-TM-106001] p 249 A93-24913
- METal matrix composite ANalyzer (METCAN): Theoretical manual
[NASA-TM-106025] p 109 A93-26552
- Composite micromechanical modeling using the boundary element method
[NASA-TM-106127] p 250 A93-27030
- Probabilistic sizing of laminates with uncertainties
[NASA-TM-106145] p 110 A93-27082
- MICROMETEOROIDS**
- Interactions between spacecraft and their environments
[AIAA PAPER 93-0705] p 55 A93-24801
- On protection of Freedom's solar dynamic radiator from the orbital debris environment. I - Preliminary analysis and testing
p 70 A93-36197
- Characteristics of hypervelocity impact craters on LDEF experiment S1003 and implications of small particle impacts on reflective surfaces
p 62 A93-29363
- MICROPHONES**
- Acoustic mode measurements in the inlet of a model turbofan using a continuously rotating rake - Data collection/analysis techniques
[AIAA PAPER 93-0599] p 24 A93-23324
- Acoustic mode measurements in the inlet of a model turbofan using a continuously rotating rake
[AIAA PAPER 93-0598] p 273 A93-24783
- Acoustic mode measurements in the inlet of a model turbofan using a continuously rotating rake: Data collection/analysis techniques
[NASA-TM-105936] p 33 A93-15403
- Acoustic mode measurements in the inlet of a model turbofan using a continuously rotating rake
[NASA-TM-105989] p 34 A93-16705
- MICROSTRIP ANTENNAS**
- Spectral-domain moment-method analysis of coplanar microstrip parasitic subarrays
p 148 A93-35016
- Input impedance of coaxially fed rectangular microstrip antenna on electrically thick substrate
p 155 A93-36994
- Performance of TiCaBaCuO 30 GHz 64 element antenna array
p 157 A93-44763
- A 10 GHz Y-Ba-Cu-O/GaAs hybrid oscillator proximity coupled to a circular microstrip patch antenna
p 158 A93-54619
- MICROSTRIP DEVICES**
- A 10-GHz amplifier using an epitaxial lift-off pseudomorphic HEMT device
p 156 A93-37574
- Full wave characterization of microstrip open end discontinuities patterned on anisotropic substrates using potential theory
[NASA-TM-106037] p 160 A93-20259
- MICROSTRIP TRANSMISSION LINES**
- Design aspects and comparison between high T_c superconducting coplanar waveguide and microstrip line
p 155 A93-27244
- Comparative study of bolometric and non-bolometric switching elements for microwave phase shifters
p 155 A93-27245
- A 10 GHz Y-Ba-Cu-O/GaAs hybrid oscillator proximity coupled to a circular microstrip patch antenna
p 158 A93-54619
- Microwave characterization of slotline on high resistivity silicon for antenna feed network
[NASA-TM-106058] p 161 A93-27265
- MICROSTRUCTURE**
- Tribological and microstructural comparison of HiPPed PM212 and PM212/Au self-lubricating composites
p 93 A93-13505
- Effect of hydrogen on the strength and microstructure of selected ceramics
p 130 A93-13613
- Thermal stability of the microstructure of an aged Nb-Zr-C alloy
p 122 A93-13776
- High-temperature deformation and microstructural analysis for silicon nitride-scandium(III) oxide
p 131 A93-20468
- Sliding wear of self-mated Al₂O₃-SiC whisker-reinforced composites at 23-1200 C
p 101 A93-29948
- The microstructural evolution, crystallography, and thermal processing of ultrahigh carbon Fe-1.85 pct C melt-spun ribbon
p 125 A93-32934
- Effect of high temperature annealing on the microstructure of SCS-6 SiC fibers
p 133 A93-39513
- CVD of silicon carbide on structural fibers - Microstructure and composition
p 117 A93-39521
- Thin film diamond microstructure applications
p 209 A93-40580
- A creep cavity growth model for creep-fatigue life prediction of a unidirectional W/Cu composite
[NASA-TM-105780] p 244 A93-10967
- Review of the physical and mechanical properties and potential applications of the B2 compound NiAl: Unabridged version of a paper published in International materials review
[NASA-TM-105598] p 127 A93-11635

MICROWAVE AMPLIFIERS

- Processing and microstructure of Nb-1 percent Zr-0.1 percent C alloy sheet
[NASA-TM-105921] p 128 N93-15524
- Properties of extruded PS-212 type self-lubricating materials p 138 N93-25565
- External stress-corrosion cracking of a 1.22-m-diameter type 316 stainless steel air valve
[NASA-TP-3190] p 129 N93-26201

MICROWAVE AMPLIFIERS

- High-efficiency high-gain monolithic heterostructure FET amplifier at 31 GHz p 156 A93-37421
- Anomalous TWTA output power spikes and their effect on a digital satellite communications system
[NASA-TM-105875] p 159 N93-13286

MICROWAVE ANTENNAS

- Multiple-access phased array antenna simulator for a digital beam-forming system investigation p 148 A93-26237
- Analysis of MMIC arrays for use in the ACTS Aero Experiment
[NASA-TM-106073] p 53 N93-22589

MICROWAVE CIRCUITS

- Monolithic microwave integrated circuits for sensors, radar, and communications systems; Proceedings of the Meeting, Orlando, FL, Apr. 2-4, 1991 p 151 A93-25776
- [SPIE-1475]
- A high efficiency Ka-band monolithic pseudomorphic HEMT amplifier p 151 A93-25786
- Millimeter-wave pseudomorphic HEMT MMIC phased array components for space communications p 152 A93-25796
- System-level integrated circuit (SLIC) development for phased array antenna applications p 152 A93-25798
- Mixed application MMIC technologies - Progress in combining RF, digital and photonic circuits p 152 A93-25800
- Phase shifter technology assessment - Prospects and applications p 152 A93-25808
- Design aspects and comparison between high Tc superconducting coplanar waveguide and microstrip line p 155 A93-27244
- Comparative study of bolometric and non-bolometric switching elements for microwave phase shifters p 155 A93-27245

- A 10-GHz amplifier using an epitaxial lift-off pseudomorphic HEMT device p 156 A93-37574
- Analysis of MMIC arrays for use in the ACTS Aero Experiment
[NASA-TM-106073] p 53 N93-22589
- Simulation of Tunnel Ladder traveling-wave tube cold-test characteristics; Implementation of the three-dimensional, electromagnetic circuit analysis code micro-SOS
[NASA-TP-3294] p 160 N93-23394
- Microwave characterization of slotline on high resistivity silicon for antenna feed network
[NASA-TM-106058] p 161 N93-27265

MICROWAVE EMISSION

- Full wave characterization of microstrip open end discontinuities patterned on anisotropic substrates using potential theory
[NASA-TM-106037] p 160 N93-20259

MICROWAVE EQUIPMENT

- Large-area YBa₂Cu₃O₇(δ) thin films on sapphire for microwave applications p 279 A93-11475
- Superconductivity applications for infrared and microwave devices II; Proceedings of the Meeting, Orlando, FL, Apr. 4, 5, 1991 p 154 A93-27243
- [SPIE-1477]
- The effects of strain on the microwave performance of SiGe HBTs p 158 A93-54442
- SITE project. Phase 1. Continuous data bit-error-rate testing
[NASA-TP-3279] p 58 N93-11001
- Interim report on the analysis of the microwave power module
[NASA-TM-106012] p 160 N93-16713

MICROWAVE OSCILLATORS

- A 10 GHz Y-Ba-Cu-O/GaAs hybrid oscillator proximity coupled to a circular microstrip patch antenna p 158 A93-54619

MICROWAVE POWER BEAMING

- Electromagnetic powered vehicles (EMPV) for Mars exploration p 47 A93-20761
- An analysis of power beaming for the moon and Mars p 253 A93-25974

MICROWAVE RESONANCE

- Coplanar waveguide radial line stub p 155 A93-36514
- Processing, electrical and microwave properties of sputtered Ti-Ca-Ba-Cu-O superconducting thin films p 282 A93-44607

MICROWAVE SENSORS

- Monolithic microwave integrated circuits for sensors, radar, and communications systems; Proceedings of the Meeting, Orlando, FL, Apr. 2-4, 1991 p 151 A93-25776
- [SPIE-1475]

MICROWAVE SPECTRA

- Cosmic microwave background probes models of inflation p 294 A93-10355

MICROWAVE SWITCHING

- Comparative study of bolometric and non-bolometric switching elements for microwave phase shifters p 155 A93-27245

- Data distribution satellite
[NASA-TM-105778] p 149 N93-12481

MICROWAVE TRANSMISSION

- Microwave characterization of slotline on high resistivity silicon for antenna feed network p 161 N93-27265
- [NASA-TM-106058]
- Development of Si(1-x)Ge(x) technology for microwave sensing applications p 162 N93-28610
- [NASA-TM-106157]

MICROWAVES

- The gravitational wave contribution to cosmic microwave background anisotropies and the amplitude of mass fluctuations from COBE results p 289 A93-21508
- GaAs monolithic R.F. modules for SRSAT distress beacons p 152 A93-25806
- Microwave anisotropies in the light of the data from the COBE satellite p 291 A93-35444
- Preliminary investigation of high power microwave plasmas for electrothermal thruster use p 74 A93-49928
- [AIAA PAPER 93-2106]
- The effects of strain on the microwave performance of SiGe HBTs p 158 A93-54442
- Microwave characterization of slotline on high resistivity silicon for antenna feed network p 161 N93-27265
- [NASA-TM-106058]
- Preliminary investigation of high power microwave plasmas for electrothermal thruster use p 92 N93-29158
- [NASA-TM-106207]

MIE SCATTERING

- Molecular filter-based diagnostics in high speed flows
[AIAA PAPER 93-0512] p 205 A93-23259

MILITARY AIRCRAFT

- The NASA Computational Fluid Dynamics (CFD) program - Building technology to solve future challenges
[AIAA PAPER 93-3292] p 287 A93-44996

MILKY WAY GALAXY

- Phase space distribution of halo particles and detection of WIMPS --- weakly interacting massive particles p 289 A93-23650

MILLIMETER WAVES

- Fiber optic link for millimeter wave communication satellites p 277 A93-25736
- Millimeter-wave pseudomorphic HEMT MMIC phased array components for space communications p 152 A93-25796
- Phase shifter technology assessment - Prospects and applications p 152 A93-25808

MILLING (MACHINING)

- The kinetics of composite particle formation during mechanical alloying p 125 A93-29534

MIMO (COMPUTERS)

- LEWICE droplet trajectory calculations on a parallel computer
[AIAA PAPER 93-0172] p 259 A93-22604

MIMO (CONTROL SYSTEMS)

- Self-tuning multivariable pole placement control of a multizone crystal growth furnace p 263 A93-10575
- Antwindup analysis and design approaches for MIMO systems
[AIAA PAPER 93-3811] p 30 A93-51403

MINIATURIZATION

- Miniature high temperature plug-type heat flux gauges p 209 A93-37862

MINORITY CARRIERS

- Minority carrier diffusion length and edge surface-recombination velocity in InP p 283 A93-50787
- Diffusion length variation in 0.5- and 3-MeV-proton-irradiated, heteroepitaxial indium phosphide solar cells p 161 N93-27002
- [NASA-TM-106147]

MIRRORS

- Solar concentrators for advanced solar-dynamic power systems in space p 85 N93-23017
- [NASA-CR-187148]

MISALIGNMENT

- Flux concentrations on solar dynamic components due to mispointing
[NASA-TM-105756] p 255 N93-20261

MISSILE CONFIGURATIONS

- PNS predictions for supersonic/hypersonic flows over finned missile configurations p 7 A93-37374
- [AIAA PAPER 92-2695]
- Structural analysis of high-rpm composite propfan blades for a cruise missile wind tunnel model p 247 N93-23015
- [NASA-TM-105267]
- Fabrication of composite propfan blades for a cruise missile wind tunnel model p 249 N93-26202
- [NASA-TM-105270]

MISSION PLANNING

- Establishing the infrastructure - An integrated Space Transportation System p 50 A93-12072
- A comparison of Nuclear Thermal Propulsion concepts - Results of a workshop p 65 A93-13850
- Robotic planetary mission benefits from nuclear electric propulsion p 43 A93-25854
- DUKSUP - A high thrust trajectory optimization code
[AIAA PAPER 93-1127] p 259 A93-31009
- Evolving SP-100 powerplants via electric propulsion to GEO and lunar orbit p 70 A93-34492
- A comparison of nuclear thermal rocket development cost and schedule for piloted missions to Mars
[AIAA PAPER 93-2263] p 44 A93-50057
- Progress report on nuclear propulsion for space exploration and science p 44 A93-50125
- [AIAA PAPER 93-2352]
- Summary and recommendations on nuclear electric propulsion technology for the space exploration initiative
[NASA-TM-105707] p 86 N93-24744
- Nuclear safety policy working group recommendations on nuclear propulsion safety for the space exploration initiative p 88 N93-26200
- [NASA-TM-105705]
- Representative systems for space exploration p 293 N93-26395

Nuclear electric propulsion systems overview

- The 20 kWe NEP system studies p 49 N93-26970
- The 20 kWe NEP flight system p 90 N93-26971
- The 20 kWe NEP flight system p 90 N93-26983

MISTUNING (TURBOMACHINERY)

- An efficient constraint to account for mistuning effects in the optimal design of engine rotors p 23 A93-20280
- [AIAA PAPER 92-4711]
- Vibration localization in mono- and bi-coupled bladed disks - A transfer matrix approach p 222 A93-34241
- [AIAA PAPER 93-1492]
- Aeroelastic dynamics of mistuned blade assemblies with closely spaced blade modes p 26 A93-37446
- [AIAA PAPER 93-1628]
- Optimization of blade arrangement in a randomly mistuned cascade using simulated annealing
[AIAA PAPER 93-2254] p 28 A93-50052

MIXED OXIDES

- Giant suppression of flux-flow resistivity in heavy-ion irradiated Ti₂Ba₂Ca₂Cu₃O₁₀ films - Influence of linear defects on vortex transport p 280 A93-26198
- Low temperature phase formation of Ti-based superconducting thin films in reduced oxygen atmosphere p 282 A93-44568
- Diminishing sign anomaly and scaling behavior of the mixed-state Hall resistivity in Ti₂Ba₂Ca₂Cu₃O₁₀ films containing columnar defects p 283 A93-53693

MIXING

- Numerical study of mixing of two fluids under low gravity
[NASA-TM-105865] p 194 N93-14914
- Tank Pressure Control Experiment/Thermal Phenomena (TPCE/TP) p 92 N93-28713

MIXING LAYERS (FLUIDS)

- Weakly nonlinear models for turbulent mixing in a plane mixing layer p 165 A93-17416
- A multiple-scale turbulence model for incompressible flow p 170 A93-24228
- [AIAA PAPER 93-0086]
- A study of compressible mixing layers using filtered Rayleigh scattering
[AIAA PAPER 92-0175] p 173 A93-24982
- The development of a mixing layer under the action of weak streamwise vortices p 176 A93-30134
- Noniterative implicit method for tracking particles in mixed Lagrangian-Eulerian formulations p 176 A93-30856
- Direct numerical simulations of a reacting turbulent mixing layer by a pseudospectral-spectral element method p 182 A93-45974
- Linear instability of curved free shear layers
[AIAA PAPER 93-3252] p 183 A93-46797
- Streamwise vorticity generation and mixing enhancement in free jets by 'delta-tabs'
[AIAA PAPER 93-3253] p 14 A93-53592
- A new energy transfer model for turbulent free shear flow
[NASA-TM-105854] p 191 N93-10454
- The development of a mixing layer under the action of weak streamwise vortices p 201 N93-28947
- [NASA-TM-106089]
- Jet mixer noise suppressor using acoustic feedback
[NASA-CASE-LEW-15170-1] p 275 N93-28953
- Streamwise vorticity generation and mixing enhancement in free jets by delta-tabs
[NASA-TM-106235] p 17 N93-31648
- Turbulence measurement in a reacting and non-reacting shear layer at a high subsonic Mach number
[NASA-TM-106186] p 18 N93-31839

MIXING LENGTH FLOW THEORY

Mixing of multiple jets with a confined subsonic crossflow p 15 A93-54324

MOBILE COMMUNICATION SYSTEMS

Performance evaluation of land mobile satellite system under fading and interference using multiple TCM by Monte-Carlo simulation p 147 A93-10958
Direct Broadcast Satellite: Radio Program [NASA-TM-105910] p 52 N93-11430
Allocations by the 1992 World Administrative Radio Conference p 150 N93-26476

MODAL RESPONSE

A new pre-loaded beam geometric stiffness matrix with full rigid body capabilities p 54 A93-12145
An efficient constraint to account for mistuning effects in the optimal design of engine rotors [AIAA PAPER 92-4711] p 23 A93-20280
Aeroelastic dynamics of mistuned blade assemblies with closely spaced blade modes [AIAA PAPER 93-1628] p 26 A93-37446
Solving modal equations of motion with initial conditions using MSC/NASTRAN DMAP. Part 1: Implementing exact mode superposition [NASA-TM-106063] p 248 N93-23739
Solving modal equations of motion with initial conditions using MSC/NASTRAN DMAP. Part 2: Coupled versus uncoupled integration [NASA-TM-106064] p 248 N93-23740
Global dynamic modeling of a transmission system [NASA-CR-191117] p 228 N93-24751

MODFETS

Intermodulation in the oscillatory magnetoresistance of a two-dimensional electron gas p 151 A93-17610
Direct optical injection locking of monolithically integrated In(0.53)Ga(0.47)As/In(0.52)Al(0.48)As MODFET oscillators p 158 A93-47127
Ellipsometric characterization of In(0.52)Al(0.48)As and of modulation doped field effect transistor structures on InP substrates p 158 A93-49382

MODULARITY

Reliability studies of Integrated Modular Engine system designs [AIAA PAPER 93-1886] p 72 A93-49759
Reliability studies of integrated modular engine system designs [NASA-TM-106178] p 91 N93-27022

MODULATION DOPING

Ellipsometric characterization of In(0.52)Al(0.48)As and of modulation doped field effect transistor structures on InP substrates p 158 A93-49382

MODULATORS

GaAs monolithic R.F. modules for SAR/SAT distress beacons p 152 A93-25806

MODULES

Test results of a Stirling engine utilizing heat exchanger modules with an integral heat pipe [NASA-TM-105883] p 256 N93-25136

MODULUS OF ELASTICITY

The effect of multiple compliant layers at the fiber-matrix interface on residual thermal stresses in metal matrix composites p 104 A93-42085

MOISTURE CONTENT

Liquid water content measurements using the Phase Doppler Particle Analyzer in the NASA Lewis Icing Research Tunnel [AIAA PAPER 93-0298] p 42 A93-23698

MOLECULAR ABSORPTION

Development of a hydrogen gas sensor using microfabrication technology [SAE PAPER 92-1176] p 210 A93-41356

MOLECULAR COLLISIONS

Rotational level-dependent collisional broadening and line shift of the A2Sigma(+)-X2Pi(1,0) band of OH in hydrogen-air combustion gases p 276 A93-24142

MOLECULAR DIFFUSION

An alternative model for estimating liquid diffusion coefficients requiring no viscosity data [NASA-TM-106079] p 96 N93-23014

MOLECULAR DYNAMICS

Molecular dynamics of interface rupture p 175 A93-30130

MOLECULAR EXCITATION

Absorption coefficients for water vapor at 193 nm from 300 to 1073 K p 276 A93-45398

MOLECULAR GASES

DSMC and continuum analyses of low-density nozzle flow [AIAA PAPER 93-0727] p 172 A93-24817
Nongray gas analyses for reflecting walls utilizing a flux technique p 190 A93-55460

MOLECULAR INTERACTIONS

Analysis of plume backflow around a nozzle lip in a nuclear rocket [AIAA PAPER 93-2497] p 77 A93-50231

MOLECULAR PHYSICS

Molecular dynamics of interface rupture p 175 A93-30130

MOLTEN SALTS

Void control in the crystallization of lithium fluoride p 97 A93-13760
Properties of pure nickel after long term exposures to LiOH and vacuum at 775 K p 123 A93-18075
Chronopotentiometry of refractory metals, actinides and oxyanions in molten salts: A review [NASA-TM-105862] p 120 N93-11545

MOLYBDENUM ALLOYS

Studies on the reactive melt infiltration of silicon and silicon-molybdenum alloys in porous carbon [NASA-TM-105860] p 136 N93-12398
High temperature creep and oxidation resistant chromium silicide matrix alloy containing molybdenum [NASA-CASE-LEW-15697-1] p 130 N93-29172

MOLYBDENUM COMPOUNDS

Chemical reactions in the processing of MoSi2 + carbon compacts p 119 A93-53733

MOLYBDENUM DISULFIDES

Solid lubricants p 135 A93-55471

MOLYBDENUM SULFIDES

A vacuum (10 exp -9 torr) friction apparatus for determining friction and endurance life of MoS(x) films p 146 A93-49245

MOMENTUM

Optimization of circular orifice jets mixing into a heated crossflow in a cylindrical duct [AIAA PAPER 93-0249] p 24 A93-23246
Optimization of circular orifice jets mixing into a heated cross flow in a cylindrical duct [NASA-TM-105984] p 33 N93-15359
Increased heat transfer to elliptical leading edges due to spanwise variations in the freestream momentum: Numerical and experimental results [NASA-TM-106150] p 199 N93-27020

MOMENTUM TRANSFER

Second order closure modeling of turbulent buoyant wall plumes [NASA-TM-105956] p 193 N93-14829
Root damage analysis of aircraft engine blade subject to ice impact [NASA-TM-105779] p 246 N93-15343

MONATOMIC GASES

Computer program for calculating and fitting thermodynamic functions [NASA-RP-1271] p 285 N93-12967
Atomic hydrogen propellants: Historical perspectives and future possibilities [NASA-TM-106053] p 84 N93-20614

MONITORS

Integrated health monitoring and controls for rocket engines [SAE PAPER 92-1031] p 66 A93-14654
An artificial intelligence-based structural health monitoring system for aging aircraft p 266 N93-22185
Evaluation of an oil-debris monitoring device for use in helicopter transmissions [NASA-TM-105830] p 227 N93-22826
Pattern classifier for health monitoring of helicopter gearboxes [NASA-TM-106099] p 228 N93-23741

MONOMERS

Lower temperature curing thermoset polyimides utilizing a substituted norbornene endcap p 134 A93-44526

MONOTONE FUNCTIONS

Positivity-preserving numerical schemes for multidimensional advection [NASA-TM-106055] p 200 N93-27091

MONTE CARLO METHOD

Performance evaluation of land mobile satellite system under fading and interference using multiple TCM by Monte-Carlo simulation p 147 A93-10958
PDF approach for compressible turbulent reacting flows [AIAA PAPER 93-0087] p 170 A93-24229
DSMC and continuum analyses of low-density nozzle flow [AIAA PAPER 93-0727] p 172 A93-24817
The application of structural reliability techniques to plume impingement loading of the Space Station Freedom Photovoltaic Array [AIAA PAPER 93-1338] p 56 A93-33908
Reliability assessment of thrust chamber cooling concepts using probabilistic analysis techniques [AIAA PAPER 93-2163] p 75 A93-49978
Monte Carlo analysis of the Titan III/Transfer Orbit Stage guidance system for the Mars Observer mission [AIAA PAPER 93-3889] p 50 A93-51473
Internal structure of shock waves in disparate mass mixtures p 190 A93-54483
The use of plasma asher and Monte Carlo modeling for the projection of atomic oxygen durability of protected polymers in low Earth orbit p 58 N93-15596

The application of structural reliability techniques to plume impingement loading of the Space Station Freedom Photovoltaic Array [NASA-TM-105949] p 59 N93-17988
RENEW v3.2 user's manual, maintenance estimation simulation for Space Station Freedom Program [NASA-TM-106006] p 232 N93-27025
A transfer matrix approach to vibration localization in mistuned blade assemblies [NASA-TM-106112] p 250 N93-27088
Monte Carlo modeling of atomic oxygen attack of polymers with protective coatings on LDEF p 138 N93-28282

MORPHOLOGY

Coarsening following a morphological instability in the one-sided model p 284 A93-21695

MOUNTING

High performance sapphire windows p 218 N93-22198

MULLITES

Sliding durability of candidate seal fiber materials in hydrogen from 25 to 900 C [NASA-TM-105939] p 95 N93-22590

MULTIBEAM ANTENNAS

Advanced Communications Technology Satellite (ACTS) p 52 A93-24456

MULTIGRID METHODS

Segmented multigrid domain decomposition procedure for incompressible viscous flows p 99 A93-19123
Multigrid methods for numerical simulation of laminar diffusion flames [AIAA PAPER 93-0236] p 113 A93-22648
Application of an unstructured grid flow solver to planes, trains and automobiles [AIAA PAPER 93-0889] p 173 A93-24949
Characteristics of three-dimensional turbulent jets in crossflow p 8 A93-38695
Multigrid calculation of three-dimensional viscous cascade flows p 8 A93-42889
Segmented multigrid domain decomposition solutions for three dimensional viscous recirculating flows [AIAA PAPER 93-3344] p 181 A93-45038
Multigrid time-accurate integration of Navier-Stokes equations [AIAA PAPER 93-3361] p 181 A93-45054
Development of an explicit multiblock/multigrid flow solver for viscous flows in complex geometries [AIAA PAPER 93-2380] p 186 A93-50148

MULTIPHASE FLOW

Aeroloids and secondary flows in a transonic mixed flow turbine stage [ASME PAPER 92-GT-72] p 2 A93-19322
Optimization of circular orifice jets mixing into a heated crossflow in a cylindrical duct [AIAA PAPER 93-0249] p 24 A93-23246
Effect of vaporization on cryogenic spray droplet size measurement [AIAA PAPER 93-0692] p 172 A93-24792
Effect of vaporization on cryogenic spray droplet size measurement [NASA-TM-105909] p 213 N93-13410
Optimization of circular orifice jets mixing into a heated cross flow in a cylindrical duct [NASA-TM-105984] p 33 N93-15359

MULTIPLE ACCESS

GSFC conceptual design study for an inter-satellite Optical Multiple Access communication system p 52 A93-18966
Multiple-access phased array antenna simulator for a digital beam-forming system investigation p 148 A93-26237

MULTIPROCESSING (COMPUTERS)

LEWICE droplet trajectory calculations on a parallel computer [AIAA PAPER 93-0172] p 259 A93-22604
A multiarchitecture parallel-processing development environment [NASA-TM-106180] p 262 N93-28628

MULTISTAGE ROCKET VEHICLES

Propulsion and aerodynamic analysis of the Beta II two-stage-to-orbit vehicle [AIAA PAPER 92-4245] p 50 A93-13332
The design and evolution of the beta two-stage-to-orbit horizontal takeoff and landing launch system [NASA-TM-106118] p 51 N93-27018

MULTIVARIABLE CONTROL

A note on decentralized integral controllability p 264 A93-30492
Design and evaluation of a robust dynamic neurocontroller for a multivariable aircraft control problem p 40 A93-37004

N

N-TYPE SEMICONDUCTORS

Simple, extremely low resistance contact system to n-InP that does not exhibit metal-semiconductor intermixing during sintering p 157 A93-42550
 Direct observation of porous SiC formed by anodization in HF p 282 A93-43587
 Electronic passivation of n- and p-type GaAs using chemical vapor deposited GaS p 283 A93-52708

NASA PROGRAMS

NASA CST aids U.S. industry - computational structures technology p 258 A93-25084
 The NASA CSTI High Capacity Power Project p 69 A93-26105
 The NASA Computational Fluid Dynamics (CFD) program - Building technology to solve future challenges [AIAA PAPER 93-3292] p 287 A93-44996
 Propulsion technology challenges for turn-of-the-century commercial aircraft [ISABE 93-7003] p 31 A93-53980
 The NASA CSTI high capacity power project [NASA-TM-105813] p 48 A93-11398
 ISDN at NASA Lewis Research Center [NASA-TM-105911] p 262 A93-12410
 Bibliography of Lewis Research Center Technical Publications announced in 1991 [NASA-TM-105595] p 287 A93-14796
 Structural dynamics branch research and accomplishments to FY 1992 [NASA-TM-105824] p 247 A93-20368
 Technical report writing [NASA-TM-105419] p 287 A93-23002
 Design and implementation of a pilot orientation program for new NASA engineering employees [NASA-TM-105907] p 286 A93-26205
 Systems overview p 89 A93-26915
 Plum Brook facilities p 49 A93-26964
 NEP facilities (LeRC) p 49 A93-26965
 Propulsion technology challenges for turn-of-the-century commercial aircraft [NASA-TM-106192] p 39 A93-32351
 Four giants of the Lewis Research Center [NASA-TM-83642] p 1 A93-72738

NASA SPACE PROGRAMS

Nuclear propulsion technology development - A joint NASA/Department of Energy project p 64 A93-12074
 Nuclear Propulsion Project Workshop summary p 64 A93-13765
 Advanced Communications Technology Satellite (ACTS) p 52 A93-24456
 Advances in NASA's Nuclear Thermal Propulsion Technology project [AIAA PAPER 93-2258] p 75 A93-50056
 Venus Interior Structure Mission (VISM): Establishing a seismic network on Venus p 293 A93-28819

NASTRAN

Computational simulation of surface waviness in graphite/epoxy woven composites due to initial curing p 98 A93-15822
 Modal analysis of multistage gear systems coupled with gearbox vibrations p 222 A93-36588
 Solving modal equations of motion with initial conditions using MSC/NASTRAN DMAP. Part 1: Implementing exact mode superposition [NASA-TM-106063] p 248 A93-23739
 Solving modal equations of motion with initial conditions using MSC/NASTRAN DMAP. Part 2: Coupled versus uncoupled integration [NASA-TM-106064] p 248 A93-23740

NATIONAL AEROSPACE PLANE PROGRAM

High temperature static strain measurement with an electrical resistance strain gage [AIAA PAPER 92-5039] p 205 A93-22313

NAVIER-STOKES EQUATION

Segmented multigrid domain decomposition procedure for incompressible viscous flows p 99 A93-19123
 An algebraic turbulence model for three-dimensional viscous flows [AIAA PAPER 93-0083] p 4 A93-22552
 A simplified Reynolds stress model for unsteady turbulent boundary layers [AIAA PAPER 93-0204] p 168 A93-22622
 A parametric study of bleed in shock boundary layer interactions [AIAA PAPER 93-0294] p 5 A93-22694
 Ice accretion and performance degradation calculations with LEWICE/NS [AIAA PAPER 93-0173] p 18 A93-23244
 A least-squares finite element method for 3D incompressible Navier-Stokes equations [AIAA PAPER 93-0338] p 171 A93-24236
 Three-dimensional Navier-Stokes calculations using solution-adapted grids [AIAA PAPER 93-0431] p 6 A93-24240

Navier-Stokes calculations for the unsteady flowfield of turbomachinery [AIAA PAPER 93-0676] p 6 A93-24786
 Calculations of low Reynolds number rocket nozzles [AIAA PAPER 93-0888] p 67 A93-24948
 The structure of supersonic jet flow and its radiated sound [AIAA PAPER 93-0549] p 273 A93-25538
 A numerical study of mixing in supersonic combustors with hypermixing injectors [AIAA PAPER 93-0215] p 25 A93-27801
 Calculations of separated 3-D flows with a pressure-staggered Navier-Stokes equations solver p 177 A93-34366
 An efficient and robust algorithm for two dimensional time dependent incompressible Navier-Stokes equations - High Reynolds number flows p 178 A93-34371
 Study on vortex generator flow control for the management of inlet distortion p 7 A93-34488
 Computational study of advanced exhaust system transition ducts with experimental validation p 7 A93-34490
 Stable and low diffusive hybrid upwind splitting methods [ONERA, TP NO. 1992-113] p 179 A93-38589
 A coupled implicit method for chemical non-equilibrium flows at all speeds p 181 A93-44245
 Two-dimensional CFD modeling of wave rotor flow dynamics [AIAA PAPER 93-3318] p 9 A93-45014
 Segmented multigrid domain decomposition solutions for three dimensional viscous recirculating flows [AIAA PAPER 93-3344] p 181 A93-45038
 Multigrid time-accurate integration of Navier-Stokes equations [AIAA PAPER 93-3361] p 181 A93-45054
 On solving the compressible Navier-Stokes equations for unsteady flows at very low Mach numbers [AIAA PAPER 93-3368] p 181 A93-45061
 Grid adaptation using Chimera composite overlapping meshes [AIAA PAPER 93-3389] p 267 A93-45080
 Navier-Stokes analysis of three-dimensional S-ducts p 9 A93-45146
 A new flux splitting scheme p 9 A93-47189
 Some practical turbulence modeling options for Reynolds-averaged full Navier-Stokes calculations of three-dimensional flows [AIAA PAPER 93-2964] p 10 A93-48158
 3-D viscous flow CFD analysis of the propeller effect on an advanced ducted propeller subsonic inlet [AIAA PAPER 93-1847] p 12 A93-49728
 A comparative study of Full Navier-Stokes and Reduced Navier-Stokes analyses for separating flows within a diffusing inlet S-duct [AIAA PAPER 93-2154] p 13 A93-49970
 High Reynolds number and turbulence effects on aerodynamics and heat transfer in a turbine cascade [AIAA PAPER 93-2252] p 186 A93-50050
 Assessment of three numerical methods for the computation of a low-density plume flow [AIAA PAPER 93-2528] p 77 A93-50256
 Navier-Stokes analysis of radial turbine rotor performance [AIAA PAPER 93-2555] p 30 A93-50277
 A time-accurate high-resolution TVD scheme for solving the Navier-Stokes equations p 13 A93-52006
 Accuracy of least-squares methods for the Navier-Stokes equations p 188 A93-52008
 Three-dimensional flow analysis inside turbomachinery stages with steady and unsteady Navier-Stokes method [ISABE 93-7095] p 14 A93-54071
 A least-squares finite element method for incompressible Navier-Stokes problem p 191 A93-10548
 Navier-Stokes turbine heat transfer predictions using two-equation turbulence [NASA-TM-105817] p 191 A93-10735
 The Proteus Navier-Stokes code p 193 A93-13396
 An algebraic turbulence model for three-dimensional viscous flows [NASA-TM-105931] p 1 A93-14102
 Supersonic boundary-layer flow turbulence modeling [NASA-TM-105893] p 193 A93-14758
 Ice accretion and performance degradation calculations with LEWICE/NS [NASA-TM-105972] p 19 A93-15354
 Low thrust chemical rocket technology [NASA-TM-105927] p 83 A93-15572
 Two equation modeling and the pseudo compressibility technique p 195 A93-15799
 Three-dimensional Navier-Stokes heat transfer predictions for turbine blade rows [NASA-TM-105800] p 196 A93-19969
 Numerical simulation of a high Mach number jet flow [NASA-TM-105985] p 197 A93-20057

A time-accurate high-resolution TVD scheme for solving the Navier-Stokes equations [NASA-TM-106056] p 268 A93-22664
 Large-scale computation of incompressible viscous flow by least-squares finite element method [NASA-TM-105904] p 268 A93-22825
 Incompressible spectral-element method: Derivation of equations [NASA-TM-106109] p 199 A93-26554
 Increased heat transfer to elliptical leading edges due to spanwise variations in the freestream momentum: Numerical and experimental results [NASA-TM-106150] p 199 A93-27020
 Grid adaption using Chimera composite overlapping meshes [NASA-TM-106163] p 269 A93-27065
 A new flux conserving Newton's method scheme for the two-dimensional, steady Navier-Stokes equations [NASA-TM-106160] p 201 A93-28626
 High Reynolds number and turbulence effects on aerodynamics and heat transfer in a turbine cascade [NASA-TM-106187] p 202 A93-29157
 The 3-D viscous flow CFD analysis of the propeller effect on an advanced ducted propeller subsonic inlet [NASA-TM-106240] p 38 A93-29162
 Accuracy of least-squares methods for the Navier-Stokes equations [NASA-TM-106209] p 202 A93-29208
 Navier-Stokes analysis of three-dimensional flow and heat transfer inside turbine blade rows p 39 A93-29963
 Numerical simulations of three-dimensional laminar flow over a backward facing step; flow near side walls [NASA-TM-106248] p 202 A93-31147

NEAR FIELDS

Prediction of engine and near-field plume reacting flows in low-thrust chemical rockets [AIAA PAPER 93-0237] p 66 A93-22649

NETWORK ANALYSIS

Data distribution satellite [NASA-TM-105778] p 149 A93-12481

NETWORK CONTROL

Neurocontrol design and analysis for a multivariable aircraft control problem p 40 A93-41894
 Application of artificial neural networks in nonlinear analysis of trusses [NASA-TM-105319] p 244 A93-11403
 Neural nets for aligning optical components in harsh environments: Beam smoothing spatial filter as an example p 266 A93-31557
 ACTS system handbook, revision change index [NASA-TM-107982] p 150 A93-70235

NETWORK SYNTHESIS

Modified NASA standard nickel-cadmium cell designs p 253 A93-25947
 75 Ah and 10 boilerplate nickel-hydrogen battery designs and test results p 253 A93-25948
 A 10-GHz amplifier using an epitaxial lift-off pseudomorphic HEMT device p 156 A93-37574

NEUMANN PROBLEM

On an origin of numerical diffusion: Violation of invariance under space-time inversion [NASA-TM-105776] p 268 A93-11254

NEURAL NETS

The performance evaluation of a new neural network based traffic management scheme for a satellite communication network p 147 A93-10929
 Neural networks in structural analysis and design - An overview [AIAA PAPER 92-4805] p 263 A93-20388
 Neural networks for structural design - An integrated system implementation [AIAA PAPER 92-4806] p 263 A93-20389
 Application of neural networks to prediction of advanced composite structures mechanical response and behavior p 205 A93-20751
 Self-growing neural network architecture using crisp and fuzzy entropy p 263 A93-26650
 Design and evaluation of a robust dynamic neurocontroller for a multivariable aircraft control problem p 40 A93-37004
 Application of neural networks in the acousto-ultrasonic evaluation of metal-matrix composite specimens p 231 A93-37009
 Fuzzy expert systems vs. neural networks - Truck backer-upper control revisited p 264 A93-37039
 Neurocontrol design and analysis for a multivariable aircraft control problem p 40 A93-41894
 A function approximation approach to anomaly detection in propulsion system test data [AIAA PAPER 93-1776] p 71 A93-49671
 Application of neural nets in structural optimization p 265 A93-54533
 Self-organization in neural networks - Applications in structural optimization p 265 A93-54534

- Application of artificial neural networks in nonlinear analysis of trusses
[NASA-TM-105319] p 244 N93-11403
- Analysis of fault-tolerant neurocontrol architectures
[NASA-TM-105898] p 41 N93-12305
- Self-growing neural network architecture using crisp and fuzzy entropy
[NASA-TM-105677] p 231 N93-18422
- Inverse kinematics problem in robotics using neural networks
[NASA-TM-105869] p 247 N93-18876
- Real-time diagnostics for a reusable rocket engine
[NASA-TM-105792] p 266 N93-19018
- Application of artificial neural networks to the design optimization of aerospace structural components
[NASA-TM-4389] p 247 N93-21831
- A neural network-based estimator for the mixture ratio of the Space Shuttle Main Engine
[NASA-TM-106070] p 87 N93-25089
- Neural networks for calibration tomography
[NASA-TM-106352] p 216 N93-26906
- Robustness enhancement of neurocontroller and state estimator
[NASA-TM-106028] p 42 N93-26907
- Calibration of a shock wave position sensor using artificial neural networks
[NASA-TM-106138] p 216 N93-27001
- Radial basis function network learns ceramic processing and predicts related strength and density
[NASA-TM-106048] p 110 N93-27129
- Fuzzy sets predict flexural strength and density of silicon nitride ceramics
[NASA-TM-106049] p 110 N93-27270
- Soft computing in design and manufacturing of advanced materials
[NASA-TM-106012] p 111 N93-28624
- Neural nets for aligning optical components in harsh environments: Beam smoothing spatial filter as an example
[NASA-TM-106125] p 266 N93-31557
- NEUTRINOS**
- Cosmic string with a light massive neutrino
p 288 A93-16303
- NICKEL**
- The structural and electrical properties of low-resistance Ni contacts to InP
p 151 A93-24367
- NICKEL ALLOYS**
- Room temperature cyclic deformation behavior of cast and extruded NiAl
p 122 A93-12130
- Comparison of high frequency, high temperature core loss and B-H loop characteristics of an 80 Ni-Fe crystalline alloy and two iron-based amorphous alloys
p 123 A93-13882
- The effect of microalloying additions on the tensile properties of polycrystalline NiAl
p 123 A93-17516
- Influence of grain size on the creep behavior of HfC-dispersed NiAl
p 123 A93-17674
- Properties of pure nickel after long term exposures to LiOH and vacuum at 775 K
p 123 A93-18075
- Creep-rupture strength of a Ni-base superalloy at 1400 K
p 124 A93-20556
- A constitutive model for the high temperature inelastic response of nickel base superalloys
p 124 A93-21959
- Transformation to Ni₅Al₃ in a 63.0 at. pct Ni-Al alloy
p 124 A93-25108
- Effect of tensile mean stress on fatigue behavior of single-crystal and directionally solidified superalloys
p 125 A93-33011
- Creep deformation of B2 aluminides
p 126 A93-44887
- Diffusional transport and predicting oxidative failure during cyclic oxidation of beta-NiAl alloys
p 126 A93-50370
- Chemical stability of titanium diboride reinforcement in nickel aluminide matrices
p 105 A93-52473
- Stress relaxation of low pressure plasma-sprayed NiCrAlY alloys
p 127 A93-52870
- Predicting the oxidative lifetime of beta NiAl-Zr alloys
p 127 A93-53939
- Fabrication and properties of functionally graded NiAl/Al₂O₃ composites
p 105 A93-54116
- Review of the physical and mechanical properties and potential applications of the B2 compound NiAl: Unabridged version of a paper published in International materials review
[NASA-TM-105598] p 127 N93-11635
- Experimental investigation of cyclic thermomechanical deformation in torsion
[NASA-TM-105938] p 247 N93-17996
- A statistical analysis of elevated temperature gravimetric cyclic oxidation data of 36 Ni- and Co-base superalloys based on an oxidation attack parameter
[NASA-TM-105934] p 128 N93-18069
- The influence of primary and secondary orientations on the elastic response of a nickel-base single-crystal superalloy
[NASA-TM-106125] p 250 N93-26550
- Cumulative fatigue damage behavior of MAR M-247
p 251 N93-31575
- The effect of porosity and gamma-gamma' eutectic content on the low cycle fatigue behavior of hydrogen-charged PWA-1480
p 130 N93-31576
- Secondary orientation effects in a single crystal superalloy under mechanical and thermal loads
p 130 N93-31578
- NICKEL CADMIUM BATTERIES**
- Modified NASA standard nickel-cadmium cell designs
p 253 A93-25947
- Battery selection for space experiments
p 159 N93-13184
- Changes in impedance of Ni/Cd cells with voltage and cycle life
[NASA-TM-106105] p 255 N93-23018
- Battery selection for Space Shuttle experiments
[NASA-TM-106142] p 61 N93-27038
- NICKEL COMPOUNDS**
- Elevated temperature compressive properties of reaction milled NiAl-AIN and Zr-doped NiAl-AIN composites
p 97 A93-11422
- SIMS studies of oxide growth on beta-NiAl
p 127 A93-53469
- NICKEL HYDROGEN BATTERIES**
- Validation test of advanced technology for IPV nickel-hydrogen flight cells - Update
p 252 A93-25886
- 75 Ah and 10 boilerplate nickel-hydrogen battery designs and test results
p 253 A93-25948
- Validation test of 125 Ah advanced design IPV nickel-hydrogen flight cells
p 78 A93-50822
- Lightweight nickel electrodes for nickel/hydrogen cells
p 255 A93-51574
- Validation test of 125 Ah advanced design IPV nickel-hydrogen flight cells
[NASA-TM-105912] p 81 N93-14079
- Lewis Research Center battery overview
p 255 N93-20493
- Basic statistical analyses of candidate nickel-hydrogen cells for the Space Station Freedom
[NASA-TM-106111] p 270 N93-27124
- NIOBIUM**
- Thermal stability of the microstructure of an aged Nb-Zr-C alloy
p 122 A93-13776
- Tensile strain-rate sensitivity of tungsten/niobium composites at 1300 to 1600 K
p 97 A93-14840
- The kinetics of composite particle formation during mechanical alloying
p 125 A93-29534
- NIOBIUM ALLOYS**
- Effect of oxidation on the mechanical properties of a NbAl₃ alloy at intermediate temperatures
p 124 A93-20667
- Creep behavior of tungsten fiber reinforced niobium metal matrix composites
p 99 A93-20758
- Processing and microstructure of Nb-1 percent Zr-0.1 percent C alloy sheet
[NASA-TM-105921] p 128 N93-15524
- NIOBIUM CARBIDES**
- Processing and microstructure of Nb-1 percent Zr-0.1 percent C alloy sheet
[NASA-TM-105921] p 128 N93-15524
- NIOBIUM COMPOUNDS**
- Evaluation of the fracture toughness of Nb-40Al-8Cr-1W-1Y-0.05B intermetallic material by indentation techniques
p 124 A93-24066
- NITRIC OXIDE**
- Laser-induced fluorescence measurements of nitric oxide in laminar C₂H₆/O₂/N₂ flames at high pressure
p 116 A93-28253
- Nitric oxide formation in a lean, premixed-prevaporized jet A/air flame tube: An experimental and analytical study
[NASA-TM-105722] p 257 N93-27012
- NITROGEN**
- Preliminary experimental results for a cryogenic brush seal configuration
[AIAA PAPER 93-2535] p 225 A93-50262
- Preliminary experimental results for a cryogenic brush seal configuration
[NASA-TM-106236] p 201 N93-28627
- NITROGEN OXIDES**
- A review of chemically reactive turbulent flow mixing mechanisms and a new design for a low NO(x) combustor
p 27 A93-49508
- A thermal NO(x) prediction model - Scalar computation module for CFD codes with fluid and kinetic effects
[AIAA PAPER 93-2378] p 119 A93-50147
- NOISE (SOUND)**
- Vibration and noise analysis of a gear transmission system
[AIAA PAPER 93-2150] p 224 A93-49967
- Vibration and noise analysis of a gear transmission system
[NASA-TM-106162] p 229 N93-27641
- NOISE INTENSITY**
- Fiber optic link for millimeter wave communication satellites
p 277 A93-25736
- NOISE PREDICTION**
- Computation of supersonic jet noise under imperfectly expanded conditions
[AIAA PAPER 93-0735] p 273 A93-24825
- Experimental validation of boundary element methods for noise prediction
[NASA-TM-105729] p 226 N93-10966
- Computation of supersonic jet noise under imperfectly expanded conditions
[NASA-TM-105961] p 274 N93-15430
- NOISE PREDICTION (AIRCRAFT)**
- Acoustical analysis of gear housing vibration
p 273 A93-29420
- NOISE PROPAGATION**
- Propagation of high frequency jet noise using geometric acoustics
[AIAA PAPER 93-0147] p 272 A93-23241
- Comparison of radiated noise from shrouded and unshrouded propellers
p 274 A93-55861
- Propagation of high frequency jet noise using geometric acoustics
[NASA-TM-106013] p 275 N93-15575
- Rotating rake design for unique measurement of fan-generated spinning acoustic modes
[NASA-TM-105946] p 36 N93-26161
- NOISE REDUCTION**
- Supersonic jet noise reduction by coaxial rectangular nozzles
p 272 A93-19205
- 2-D nonlinear IIR-filters for image processing - An exploratory analysis
p 264 A93-28200
- Engineering science research issues in high power density transmission dynamics for aerospace applications - rotorcraft geared rotors
[AIAA PAPER 93-2299] p 224 A93-50084
- A concept for a counterrotating fan with reduced tone noise
[NASA-TM-105736] p 274 N93-11370
- Consecutive plate acoustic suppressor apparatus and methods
[NASA-CASE-LEW-15430-1] p 275 N93-17051
- Graphite/epoxy composite laminates with co-cured interlaminar damping layers
p 109 N93-25587
- Rotating rake design for unique measurement of fan-generated spinning acoustic modes
[NASA-TM-105946] p 36 N93-26161
- A large hemi-anechoic enclosure for community-compatible aeroacoustic testing of aircraft propulsion systems
[NASA-TM-106015] p 275 N93-26551
- Jet mixer noise suppressor using acoustic feedback
[NASA-CASE-LEW-15170-1] p 275 N93-28953
- NOISE SPECTRA**
- Narrow band noise as a model of time-dependent accelerations - Study of the stability of a fluid surface in a microgravity environment
[AIAA PAPER 93-0911] p 173 A93-24965
- Stability of a fluid surface in a microgravity environment
p 190 A93-55358
- NONAQUEOUS ELECTROLYTES**
- The susceptibility critical exponent for a nonaqueous ionic binary mixture near a consolute point
p 284 A93-19838
- NONDESTRUCTIVE TESTS**
- Application of neural networks to prediction of advanced composite structures mechanical response and behavior
p 205 A93-20751
- NDE of the universe - New ways to look at old facts
p 271 A93-32222
- Nondestructive evaluation of a ceramic matrix composite material
p 102 A93-33016
- Application of neural networks in the acousto-ultrasonic evaluation of metal-matrix composite specimens
p 231 A93-37009
- Spectroscopic ellipsometry studies of HF treated Si(100) surfaces
p 282 A93-46188
- Compound curvature laser window development
[AIAA PAPER 93-2177] p 277 A93-49989
- Ultrasonic assessment of interfacial oxidation damage in ceramic matrix composites
p 105 A93-52919
- Nondestructive evaluation of ceramic and metal matrix composites for NASA's HITEMP and enabling propulsion materials programs
[NASA-TM-105807] p 231 N93-10963
- Spectroscopic wear detector
[NASA-CASE-LEW-15200-1] p 83 N93-18856
- Determination of plate wave velocities and diffuse field decay rates with broad-band acousto-ultrasonic signals
[NASA-TM-106156] p 232 N93-27080
- NDE of PWA 1480 single crystal turbine blade material
[NASA-TM-106140] p 38 N93-27640

NONEQUILIBRIUM FLOW

- Acousto-Ultrasonic analysis of failure in ceramic matrix composite tensile specimens [NASA-TM-106219] p 232 N93-29073
- NON-EQUILIBRIUM FLOW**
 - A coupled implicit method for chemical non-equilibrium flows at all speeds p 181 A93-44245
 - Monte Carlo and experimental studies of nozzle flow in a low-power hydrogen arcjet [AIAA PAPER 93-2529] p 77 A93-50257
- NONFLAMMABLE MATERIALS**
 - Experimental observations of the effect of gravity changes on smoldering combustion [AIAA PAPER 93-0829] p 116 A93-24899
- NONGRAY GAS**
 - Discrete ordinates solutions of nongray radiative transfer with diffusely reflecting walls p 285 A93-30124
 - Nongray gas analyses for reflecting walls utilizing a flux technique p 190 A93-55460
- NONINTRUSIVE MEASUREMENT**
 - Microemulsion characterization by the use of a noninvasive backscatter fiber optic probe p 277 A93-52412
 - High performance sapphire windows p 218 N93-22198
- NONLINEAR EQUATIONS**
 - Nonlinear evolution of the first mode supersonic oblique waves in compressible boundary layers. Part 1: Heated/cooled walls [NASA-TM-106087] p 199 N93-25175
- NONLINEAR EVOLUTION EQUATIONS**
 - Nonlinear evolution of modes in a compressible boundary layer p 164 A93-17258
- NONLINEAR FILTERS**
 - 2-D nonlinear IIR-filters for image processing - An exploratory analysis p 264 A93-28200
- NONLINEAR PROGRAMMING**
 - Application of artificial neural networks to the design optimization of aerospace structural components [NASA-TM-4389] p 247 N93-21831
- NONLINEAR SYSTEMS**
 - An improved far field drag calculation method for nonlinear CFD codes [AIAA PAPER 93-3417] p 10 A93-47213
 - Application of artificial neural networks in nonlinear analysis of trusses [NASA-TM-105319] p 244 N93-11403
 - On-line implementation of nonlinear parameter estimation for the Space Shuttle main engine [NASA-TM-106097] p 88 N93-26211
 - Thermoviscoplastic analysis of fibrous periodic composites using triangular subvolumes [NASA-TM-106076] p 111 N93-29074
 - Desktop chaotic systems: Intuition and visualization [NASA-TM-106258] p 269 N93-31847
- NONLINEARITY**
 - Vibration and noise analysis of a gear transmission system [AIAA PAPER 93-2150] p 224 A93-49967
 - A new energy transfer model for turbulent free shear flow [NASA-TM-105854] p 191 N93-10454
 - Nonlinear evolution of the first mode supersonic oblique waves in compressible boundary layers. Part 1: Heated/cooled walls [NASA-TM-106087] p 199 N93-25175
 - Vibration and noise analysis of a gear transmission system [NASA-TM-106162] p 229 N93-27641
- NONUNIFORM FLOW**
 - Acoustic radiation from a thin airfoil in nonuniform subsonic flows p 273 A93-23535
- NORMAL SHOCK WAVES**
 - AGARD WG13 aerodynamics of high speed air intakes: Assessment of CFD results p 192 N93-13220
- NOTCH TESTS**
 - Closed form expressions for crack mouth displacements and stress intensity factors for chevron notched short bar and short rod specimens based on experimental compliance measurements [NASA-TM-83796] p 246 N93-15369
- NOZZLE DESIGN**
 - Supersonic jet noise reduction by coaxial rectangular nozzles p 272 A93-19205
 - Performance characteristics of a variable-area vane nozzle for vectoring an ASTOVL exhaust jet up to 45 deg [AIAA PAPER 93-2437] p 29 A93-50189
 - Performance characteristics of a variable-area vane nozzle for vectoring an ASTOVL exhaust jet up to 45 deg [NASA-TM-106114] p 37 N93-27131
- NOZZLE FLOW**
 - DSMC and continuum analyses of low-density nozzle flow [AIAA PAPER 93-0727] p 172 A93-24817

- Multiple large-scale coherent mode interactions in a developing round jet p 178 A93-34409
- Flip-flop jet nozzle extended to supersonic flows p 8 A93-39409
- CFD for hypersonic propulsion p 8 A93-42585
- A coupled implicit method for chemical non-equilibrium flows at all speeds p 181 A93-44245
- A laboratory model of a hydrogen/oxygen engine for combustion and nozzle studies [AIAA PAPER 93-1825] p 48 A93-49711
- Investigation of a subsonic-arc-attachment thruster using segmented anodes [AIAA PAPER 93-1899] p 73 A93-49769
- Performance characteristics of a variable-area vane nozzle for vectoring an ASTOVL exhaust jet up to 45 deg [AIAA PAPER 93-2437] p 29 A93-50189
- Effects of flow-path variations on internal reversing flow in a tailpipe offtake configuration for ASTOVL aircraft [AIAA PAPER 93-2438] p 29 A93-50190
- Analysis of plume backflow around a nozzle lip in a nuclear rocket [AIAA PAPER 93-2497] p 77 A93-50231
- Assessment of three numerical methods for the computation of a low-density plume flow [AIAA PAPER 93-2528] p 77 A93-50256
- Monte Carlo and experimental studies of nozzle flow in a low-power hydrogen arcjet [AIAA PAPER 93-2529] p 77 A93-50257
- Three-dimensional flow field in a turbine nozzle passage [AIAA PAPER 93-2556] p 13 A93-50278
- Experimentation in the low-density plume of a simulated electrothermal thruster for computer code validation [NASA-CR-191112] p 87 N93-24758
- Measurement and analysis of a small nozzle plume in vacuum [NASA-TM-106066] p 88 N93-26561
- Performance characteristics of a variable-area vane nozzle for vectoring an ASTOVL exhaust jet up to 45 deg [NASA-TM-106114] p 37 N93-27131
- Effects of flow-path variations on internal reversing flow in a tailpipe offtake configuration for ASTOVL aircraft [NASA-TM-106149] p 38 N93-29065
- NOZZLE GEOMETRY**
 - Supersonic jet noise reduction by coaxial rectangular nozzles p 272 A93-19205
 - Computation of supersonic jet noise under imperfectly expanded conditions [AIAA PAPER 93-0735] p 273 A93-24825
 - Calculations of low Reynolds number rocket nozzles [AIAA PAPER 93-0888] p 67 A93-24948
 - Flip-flop jet nozzle extended to supersonic flows p 8 A93-39409
 - Investigation of a subsonic-arc-attachment thruster using segmented anodes [AIAA PAPER 93-1899] p 73 A93-49769
 - Supersonic investigation of two dimensional hypersonic exhaust nozzles [NASA-TM-105687] p 33 N93-15342
 - Computation of supersonic jet noise under imperfectly expanded conditions [NASA-TM-105961] p 274 N93-15430
 - Enhanced mixing of a rectangular supersonic jet by natural and induced screech [NASA-TM-106245] p 18 N93-31672
- NOZZLE INSERTS**
 - Streamwise vorticity generation and mixing enhancement in free jets by 'delta-labs' [AIAA PAPER 93-3253] p 14 A93-53592
 - Streamwise vorticity generation and mixing enhancement in free jets by delta-labs [NASA-TM-106235] p 17 N93-31648
- NRX REACTORS**
 - Program ELM: A tool for rapid thermal-hydraulic analysis of solid-core nuclear rocket fuel elements [NASA-TM-105867] p 84 N93-19106
- NUCLEAR ASTROPHYSICS**
 - Cosmic string with a light massive neutrino p 288 A93-16303
 - The first three minutes - 1990 version --- of early universe after Big Bang p 289 A93-23607
 - Primordial nucleosynthesis and the abundances of beryllium and boron p 290 A93-33513
- NUCLEAR ELECTRIC POWER GENERATION**
 - Estimates of power requirements for a Manned Mars Rover powered by a nuclear reactor p 45 A93-13783
- NUCLEAR ELECTRIC PROPULSION**
 - Multimegawatt potassium Rankine power for nuclear electric power p 65 A93-13797
 - Robotic planetary mission benefits from nuclear electric propulsion p 43 A93-25854
 - Design of structures for Nuclear Electric Propulsion vehicles [AIAA PAPER 93-1393] p 57 A93-33955

- Evolving SP-100 powerplants via electric propulsion to GEO and lunar orbit p 70 A93-34492
- Progress report on nuclear propulsion for space exploration and science [AIAA PAPER 93-2352] p 44 A93-50125
- NASA's progress in nuclear electric propulsion technology [AIAA PAPER 93-1936] p 78 A93-53587
- Electric propulsion - An evolutionary technology p 78 A93-56168
- Nuclear concepts/propulsion p 85 N93-22093
- Nuclear thermal propulsion technology: Results of an interagency panel in FY 1991 [NASA-TM-105711] p 86 N93-24740
- Summary and recommendations on nuclear electric propulsion technology for the space exploration initiative [NASA-TM-105707] p 86 N93-24744
- Space Nuclear Thermal Propulsion Test Facilities Subpanel [NASA-TM-105708] p 87 N93-25105
- Nuclear safety policy working group recommendations on nuclear propulsion safety for the space exploration initiative [NASA-TM-105705] p 88 N93-26200
- Nuclear electric propulsion for planetary science missions: NASA technology program planning [NASA-TM-106139] p 88 N93-26210
- Nuclear Propulsion Technical Interchange Meeting, volume 1 [NASA-CP-10116-VOL-1] p 89 N93-26908
- Focused technology: Nuclear propulsion p 89 N93-26912
- Nuclear Propulsion Technical Interchange Meeting, volume 2 [NASA-CP-10116-VOL-2] p 89 N93-26951
- Plum Brook facilities p 49 N93-26964
- NEP facilities (LeRC) p 49 N93-26965
- Nuclear electric propulsion systems overview p 49 N93-26970
- The 20 kWe NEP system studies p 90 N93-26971
- NEP technology: FY 1992 milestones (NASA LeRC) p 90 N93-26977
- Power management and distribution technology p 90 N93-26978
- Radiator technology p 90 N93-26979
- The 20 kWe NEP flight system p 90 N93-26983
- The 100-500 kWe NEP systems p 90 N93-26984
- Nuclear electric propulsion options for piloted Mars missions p 90 N93-26985
- NEP systems model p 90 N93-26986
- NEP systems model p 91 N93-26987
- Thruster models for NEP system analysis p 91 N93-26988
- NASA's progress in nuclear electric propulsion technology [NASA-TM-106272] p 93 N93-31858
- Focused technology: Nuclear propulsion [PR12] p 287 N93-71885
- NUCLEAR ENERGY**
 - Space nuclear power systems 1989; Proceedings of the 6th Symposium, Albuquerque, NM, Jan 8-12, 1989. Vols. 1 & 2 --- Book [ISBN 0-89464-030-5] p 66 A93-20752
- NUCLEAR ENGINE FOR ROCKET VEHICLES**
 - Lunar mission design using Nuclear Thermal Rockets p 65 A93-13767
 - Nuclear thermal propulsion transportation systems for lunar/Mars exploration [NASA-TM-105870] p 81 N93-12363
 - Program ELM: A tool for rapid thermal-hydraulic analysis of solid-core nuclear rocket fuel elements [NASA-TM-105867] p 84 N93-19106
 - Nuclear Engine System Simulation (NESS): Version 2.0: Program user's guide [NASA-CR-191081] p 85 N93-23875
 - Nuclear Engine System Simulation (NESS): Volume 1: Program user's guide [NASA-CR-191080] p 86 N93-23876
- NUCLEAR FUEL ELEMENTS**
 - Flow instability in particle-bed nuclear reactors [AIAA PAPER 93-1758] p 71 A93-49657
 - US/CIS integrated NTR [AIAA PAPER 93-2367] p 76 A93-50138
- NUCLEAR FUELS**
 - Advances in NASA's Nuclear Thermal Propulsion Technology project [AIAA PAPER 93-2258] p 75 A93-50056
 - A comparison of nuclear thermal rocket development cost and schedule for piloted missions to Mars [AIAA PAPER 93-2263] p 44 A93-50057
 - Program ELM: A tool for rapid thermal-hydraulic analysis of solid-core nuclear rocket fuel elements [NASA-TM-105867] p 84 N93-19106
 - Focused technology: Nuclear propulsion [PR12] p 287 N93-71885

NUCLEAR FUSION

- Primordial nucleosynthesis and the abundances of beryllium and boron p 290 A93-33513
 The boron-to-beryllium ratio in halo stars - A signature of cosmic-ray nucleosynthesis in the early Galaxy p 292 A93-55061
 Population II Li-6 as a probe of nucleosynthesis and stellar structure and evolution p 292 A93-56494

NUCLEAR POWER REACTORS

- Lunar in-core thermionic nuclear reactor power system conceptual design p 46 A93-13836
 Key issues in space nuclear power challenges for the future p 65 A93-13905

NUCLEAR PROPULSION

- Nuclear propulsion technology development - A joint NASA/Department of Energy project p 64 A93-12074
 Space nuclear power systems, Proceedings of the 8th Symposium, Albuquerque, NM, Jan. 6-10, 1991, Pts. 1-3 [ISBN 0-88318-838-4] p 64 A93-13751
 Planning for the Space Exploration Initiative - The nuclear propulsion option p 43 A93-13752
 Nuclear Propulsion Project Workshop summary p 64 A93-13765
 Lunar mission design using Nuclear Thermal Rockets p 65 A93-13767
 A comparison of Nuclear Thermal Propulsion concepts - Results of a workshop p 65 A93-13850
 Flow instability in particle-bed nuclear reactors [AIAA PAPER 93-1758] p 71 A93-49657
 Structured system engineering methodologies used to develop a nuclear thermal propulsion engine [AIAA PAPER 93-2109] p 271 A93-49930
 Advances in NASA's Nuclear Thermal Propulsion Technology project [AIAA PAPER 93-2258] p 75 A93-50056
 System model development for nuclear thermal propulsion [NASA-TM-105761] p 80 A93-10457
 Nuclear thermal propulsion transportation systems for lunar/Mars exploration [NASA-TM-105870] p 81 A93-12363
 Development of NASA/DOE NTP system performance models [NASA-TM-105982] p 82 A93-15428
 Nuclear thermal rocket nozzle testing and evaluation program [NASA-TM-105962] p 83 A93-15571
 System model development for nuclear thermal propulsion [NASA-TM-108157] p 276 A93-16531
 System model development for nuclear thermal propulsion [NASA-TM-108215] p 277 A93-17343
 Nuclear Engine System Simulation (NESS), Version 2.0: Program user's guide [NASA-CR-191081] p 85 A93-23875
 Nuclear Engine System Simulation (NESS), Volume 1: Program user's guide [NASA-CR-191080] p 86 A93-23876
 Radiation and temperature effects on electronic components investigated under the CSTI high capacity power project [NASA-TM-106096] p 161 A93-24746
 Space exploration initiative candidate nuclear propulsion test facilities [NASA-TM-105710] p 86 A93-24753
 Nuclear safety policy working group recommendations on nuclear propulsion safety for the space exploration initiative [NASA-TM-105705] p 88 A93-26200
 Nuclear Propulsion Technical Interchange Meeting, volume 1 [NASA-CP-10116-VOL-1] p 89 A93-26908
 Focused technology: Nuclear propulsion p 89 A93-26912
 Systems overview p 89 A93-26915
 NTP comparison process p 89 A93-26926
 Nuclear thermal propulsion technology overview p 89 A93-26927
 NTR plume modeling p 199 A93-26929
 Computational fluid dynamics for nuclear thermal propulsion p 199 A93-26930
 Nuclear Propulsion Technical Interchange Meeting, volume 2 [NASA-CP-10116-VOL-2] p 89 A93-26951
 Overview of NASA/DOE/DOD interagency modeling team and activities p 89 A93-26952
 Rocket engine numerical simulator p 89 A93-26962
 Facilities p 49 A93-26963
 Nuclear electric propulsion systems overview p 49 A93-26970

NUCLEAR RADIATION

- Radiation and temperature effects on electronic components investigated under the CSTI high capacity power project [NASA-TM-106096] p 161 A93-24746

NUCLEAR REACTORS

- Space reactor/Stirling cycle systems for high power lunar applications p 46 A93-13822
 Nuclear Propulsion Technical Interchange Meeting, volume 2 [NASA-CP-10116-VOL-2] p 89 A93-26951
 Nuclear electric propulsion systems overview p 49 A93-26970

NUCLEAR ROCKET ENGINES

- Lunar mission design using Nuclear Thermal Rockets p 65 A93-13767
 U.S./CIS eye joint nuclear rocket venture p 71 A93-49334
 Space vehicle design and operation for efficient use of Nuclear Thermal Propulsion [AIAA PAPER 93-1946] p 44 A93-49804
 A comparison of nuclear thermal rocket development cost and schedule for piloted missions to Mars [AIAA PAPER 93-2263] p 44 A93-50057
 US/CIS integrated NTR [AIAA PAPER 93-2367] p 76 A93-50138
 Analysis of plume backflow around a nozzle lip in a nuclear rocket [AIAA PAPER 93-2497] p 77 A93-50231
 Numerical study of nozzle wall cooling for nuclear thermal rockets [AIAA PAPER 93-2498] p 77 A93-50232
 Nuclear thermal propulsion transportation systems for lunar/Mars exploration [NASA-TM-105870] p 81 A93-12363
 System model development for nuclear thermal propulsion [NASA-TM-108157] p 276 A93-16531
 Nuclear Propulsion Technical Interchange Meeting, volume 1 [NASA-CP-10116-VOL-1] p 89 A93-26908
 Systems overview p 89 A93-26915
 Nuclear Propulsion Technical Interchange Meeting, volume 2 [NASA-CP-10116-VOL-2] p 89 A93-26951
 Rocket engine numerical simulator p 89 A93-26962
 Facilities p 49 A93-26963
 Plum Brook facilities p 49 A93-26964
 NEP facilities (LeRC) p 49 A93-26965

NUCLEATE BOILING

- Nucleate pool boiling in the long duration low gravity environment of the space shuttle [AIAA PAPER 93-0465] p 142 A93-23371
 Electrical design of payload G-534: The Pool Boiling Experiment p 144 A93-13170
 Nucleate pool boiling in the long duration low gravity environment of the Space Shuttle [NASA-TM-105973] p 144 A93-15420
 Tank Pressure Control Experiment/Thermal Phenomena (TPCE/TP) p 92 A93-28713

NUMERICAL ANALYSIS

- Spray combustion experiments and numerical predictions [NASA-TM-106069] p 198 A93-23744
 Parallel solution of high-order numerical schemes for solving incompressible flows [NASA-TM-4451] p 262 A93-27040

NUMERICAL CONTROL

- Radiation heat transfer calculations using a control-angle, control-volume-based discrete ordinates method [AIAA PAPER 93-2731] p 182 A93-46485
 Digital control algorithms for microgravity isolation systems p 265 A93-53653

NUMERICAL FLOW VISUALIZATION

- Ground-based PIV and numerical flow visualization results from the Surface Tension Driven Convection Experiment p 143 A93-33075
 Fluid flow of a row of jets in crossflow - A numerical study p 179 A93-35608
 Simulation of three-dimensional liquid sloshing flows using a strongly implicit calculation procedure p 179 A93-35624
 Direct numerical simulation of instabilities in parallel flow with spherical roughness elements [NASA-TM-105847] p 192 A93-11529
 User's manual for Interactive Data Display System (IDDS) [NASA-TM-105572] p 261 A93-16613

NUMERICAL INTEGRATION

- Finite element implementation of state variable-based viscoplasticity models p 236 A93-26776
 Computational micromechanics of woven composites p 237 A93-32462
 Analysis of the anisotropic viscoplastic-damage response of composite laminates - Continuum basis and computational algorithms p 241 A93-43347

NUMERICAL STABILITY

- The L sub 1 finite element method for pure convection problems p 177 A93-34326

OBJECT-ORIENTED PROGRAMMING

- Gas turbine system simulation: An object-oriented approach [NASA-TM-106044] p 36 A93-25673

OBLIQUE SHOCK WAVES

- A parametric study of bleed in shock boundary layer interactions [AIAA PAPER 93-0294] p 5 A93-22694
 Reaction zone structure for strong, weak overdriven, and weak underdriven oblique detonations p 178 A93-35492
 An investigation of shock wave turbulent boundary layer interaction with bleed through slanted slots [AIAA PAPER 93-2992] p 11 A93-48184
 Numerical simulation of a shock wave/turbulent boundary layer interaction in a duct [AIAA PAPER 93-3127] p 11 A93-48293
 Nonlinear evolution of the first mode supersonic oblique waves in compressible boundary layers. Part 1: Heated/cooled walls [NASA-TM-106087] p 199 A93-25175

OH-58 HELICOPTER

- Low-noise, high-strength, spiral-bevel gears for helicopter transmissions [AIAA PAPER 93-2149] p 223 A93-49966
 Low-noise, high-strength, spiral-bevel gears for helicopter transmissions [NASA-TM-106080] p 228 A93-23019
 Pattern classifier for health monitoring of helicopter gearboxes [NASA-TM-106099] p 228 A93-23741

OILS

- Evaluation of an oil-debris monitoring device for use in helicopter transmissions [NASA-TM-105830] p 227 A93-22826

ON-LINE SYSTEMS

- On-line implementation of nonlinear parameter estimation for the Space Shuttle main engine [NASA-TM-106097] p 88 A93-26211

ONBOARD DATA PROCESSING

- Data distribution satellite [NASA-TM-105778] p 149 A93-12481

ONE DIMENSIONAL FLOW

- ENO-Osher schemes for Euler equations [AIAA PAPER 93-0335] p 171 A93-24235

OPEN CIRCUIT VOLTAGE

- Extra high speed modified Lundell alternator parameters and open/short-circuit characteristics from global 3D-FE magnetic field solutions p 156 A93-39348

OPERATING COSTS

- Comparison of all-electric secondary power systems for civil transport p 24 A93-25997
 Comparison of all-electric secondary power systems for civil subsonic transports [NASA-TM-105852] p 32 A93-10456

OPERATING TEMPERATURE

- The multi-heat addition turbine engine [AIAA PAPER 92-4272] p 22 A93-13334
 Lubrication of an 85-mm ball bearing with RP-1 [AIAA PAPER 93-2538] p 225 A93-53590
 Study of the capacitance technique for measuring high-temperature blade tip clearance on ceramic rotors [NASA-TM-105978] p 35 A93-23013
 Lubrication of an 85-mm ball bearing with RP-1 [NASA-TM-106254] p 51 A93-31670

OPTICAL COMMUNICATION

- GSFC conceptual design study for an inter-satellite Optical Multiple Access communication system p 52 A93-18966
 Optical communications and a comparison of optical technologies for a high data rate return link from Mars [NASA-TP-3180] p 52 A93-18854
 Combinatorial pulse position modulation for power-efficient free-space laser communications [NASA-TM-106241] p 150 A93-31856

OPTICAL EQUIPMENT

- Studies of effects on optical components and sensors: LDEF experiments AO-147 (ERB components) and S-0014 (APEX) p 278 A93-29693

OPTICAL FIBERS

- Fiber optic link for millimeter wave communication satellites p 277 A93-25736
 Optical fiber sensor for temperature measurement from 600 to 1900 C in gas turbine engines p 208 A93-32918
 RF modulated fiber optic sensing systems and their applications p 211 A93-49469
 A fiber optic probe for the detection of cataracts p 257 A93-25593

OPTICAL FILTERS

- Hierarchical image coding with diamond-shaped sub-bands p 205 A93-20945

OPTICAL MATERIALS

- Studies of effects on optical components and sensors: LDEF experiments AO-147 (ERB components) and S-0014 (APEX) p 278 N93-29693
- Neural nets for aligning optical components in harsh environments: Beam smoothing spatial filter as an example p 266 N93-31557
- OPTICAL MATERIALS**
- Optical and scratch resistant properties of diamondlike carbon films deposited with single and dual ion beams p 137 N93-25564
- Studies of effects on optical components and sensors: LDEF experiments AO-147 (ERB components) and S-0014 (APEX) p 278 N93-29693
- OPTICAL MEASUREMENT**
- Gas temperature measurements using the dual-line detection Rayleigh scattering technique p 213 A93-55368
- Gas temperature measurements using the dual-line detection Rayleigh scattering technique p 214 N93-13668
- Neural nets for aligning optical components in harsh environments: Beam smoothing spatial filter as an example p 266 N93-31557
- Progress in speckle-shift strain measurement p 251 N93-31558
- OPTICAL MEASURING INSTRUMENTS**
- Development of a Rayleigh scattering system for temperature measurements in combustor flows p 206 A93-23788
- Review of the FOCSI (Fiber Optic Control System Integration) program --- applications in aircraft flight control p 21 A93-32916
- Optical fiber sensor for temperature measurement from 600 to 1900 C in gas turbine engines p 208 A93-32918
- Coherent fiber optic sensor for early detection of cataractogenesis in a human eye lens p 209 A93-37051
- Multiple fiberoptic probe for several sensing applications p 212 A93-53109
- OTV bearing deflection investigation [NASA-TM-106085] p 215 N93-22994
- Status of the Fiber Optic Control System Integration (FOCSI) program [NASA-TM-106151] p 217 N93-28053
- OPTICAL PATHS**
- Vector formulation for interferogram surface fitting p 278 A93-55687
- OPTICAL PROPERTIES**
- Radiation and phase change of lithium fluoride in an annulus p 144 A93-54460
- Optical and scratch resistant properties of diamondlike carbon films deposited with single and dual ion beams [NASA-TM-105943] p 95 N93-22586
- Optical and scratch resistant properties of diamondlike carbon films deposited with single and dual ion beams p 137 N93-25564
- The effects of simulated low Earth orbit environments on spacecraft thermal control coatings [NASA-TM-106146] p 61 N93-27019
- OPTICAL PYROMETERS**
- Gas temperature measurements using the dual-line detection Rayleigh scattering technique p 213 A93-55368
- Gas temperature measurements using the dual-line detection Rayleigh scattering technique p 214 N93-13668
- Multiwavelength pyrometer for gray and non-gray surfaces in the presence of interfering radiation [NASA-CASE-LEW-15250-1] p 214 N93-17060
- OPTICAL THICKNESS**
- Photovoltaic arrays for Martian surface power [IAF PAPER 92-0591] p 293 A93-13699
- An evaluation of three spatial differencing schemes for the discrete ordinates method in participating media [AIAA PAPER 93-0140] p 266 A93-24231
- Discrete ordinates solutions for radiatively participating media in a cylindrical enclosure p 285 A93-31427
- Variable refractive index effects on radiation in semitransparent scattering multilayered regions p 189 A93-54463
- OPTICAL WAVEGUIDES**
- Micromachined silicon cantilever beam accelerometer incorporating an integrated optical waveguide p 210 A93-49457
- Characterization of Si₃N₄/SiO₂ optical channel waveguides by photon scanning tunneling microscopy p 211 A93-49458
- OPTIMAL CONTROL**
- Optimal control study for the Space Station Solar Dynamic power module p 54 A93-13133
- Control-structure interaction p 54 A93-14687
- DUK SUP - A high thrust trajectory optimization code [AIAA PAPER 93-1127] p 259 A93-31009
- Neurocontrol design and analysis for a multivariable aircraft control problem p 40 A93-41894

- Damage-mitigating control of space propulsion systems for high performance and extended life [AIAA PAPER 93-2080] p 74 A93-49907
- OPTIMIZATION**
- Maximum life spur gear design p 218 A93-14521
- Combined micromechanical and fabrication process optimization for metal-matrix composites p 99 A93-18990
- Numerical optimization of composite hip endoprostheses under different loading conditions [AIAA PAPER 92-4703] p 270 A93-20312
- Multidisciplinary propulsion simulation using NPSS [AIAA PAPER 92-4709] p 270 A93-20318
- Structural Tailoring/Analysis for Hypersonic Components - A computational simulation [AIAA PAPER 92-4722] p 20 A93-20324
- Software issues in three dimensional continuum shape optimization employing boundary formulations [AIAA PAPER 92-4792] p 258 A93-20380
- Singularities in optimal structural design [AIAA PAPER 92-4818] p 235 A93-20397
- Analysis and optimal design of thick composite structures with passive damping considerations [AIAA PAPER 92-4819] p 235 A93-20398
- Optimization of closed Brayton cycles for space power generation p 68 A93-25859
- Reliability based structural optimization - A simplified safety index approach [AIAA PAPER 93-1418] p 239 A93-33972
- Singularity in structural optimization p 240 A93-34938
- A 1.6-kW, 110-kHz dc-dc converter optimized for IGBT's p 156 A93-37570
- Topology and layout optimization of discrete and continuum structures p 241 A93-45429
- Stochastic search in structural optimization - Genetic algorithms and simulated annealing p 241 A93-45430
- Adaptive methods in computational fluid dynamics p 182 A93-45963
- Optimization of blade arrangement in a randomly mistuned cascade using simulated annealing [AIAA PAPER 93-2254] p 28 A93-50052
- Layout optimization using the homogenization method p 243 A93-54508
- Applications to car bodies - Generalized layout design of three-dimensional shells p 243 A93-54509
- Self-organization in neural networks - Applications in structural optimization p 265 A93-54534
- Maximum life spiral bevel reduction design [NASA-TM-105790] p 226 N93-10982
- OPTOELECTRONIC DEVICES**
- An analysis of the frequency limitations of an Al(x)Ga(1-x)As/GaAs optical modulator p 151 A93-23454
- ORBIT CALCULATION**
- Minimum-fuel, power-limited transfers between coplanar elliptical orbits p 45 A93-31532
- ORBIT TRANSFER VEHICLES**
- Low power pulsed MPD thruster system analysis and applications [AIAA PAPER 93-2391] p 76 A93-50156
- Space transfer with ground-based laser/electric propulsion [NASA-TM-106060] p 84 A93-20615
- OTV bearing deflection investigation [NASA-TM-106085] p 215 N93-22994
- Representative systems for space exploration p 293 N93-26395
- Low thrust propulsion [PR3] p 286 N93-71876
- ORBITAL RENDEZVOUS**
- Optimal impulsive intercept with low-thrust rendezvous return p 45 A93-34521
- ORBITAL SERVICING**
- Ground testing for the no-vent fill of cryogenic tanks - Results of tests for a 71 cubic foot tank [AIAA PAPER 93-1967] p 73 A93-49815
- Small experiments for the maturation of orbital cryogenic transfer technologies [NASA-TM-105849] p 192 N93-10981
- Automatic system for installation and replacement of Space Station components [NASA-CASE-LEW-14906-1] p 226 N93-12203
- ORBITAL SPACE TESTS**
- Recommended practices for in-space and ground laboratory. Atomic oxygen exposure and analysis p 276 N93-20814
- ORDNANCE**
- Application of composite materials to impact-insensitive munitions p 97 A93-11459
- ORGANIC COMPOUNDS**
- Scientific basis for the Isothermal Dendritic Growth Experiment - A USMP-2 space flight experiment p 143 A93-50455

- Guanidine based vehicle/binders for use with oxides, metals, and ceramics [NASA-CASE-LEW-15314-2] p 138 N93-28423
- Method for retarding oxidation of an organic substrate [NASA-CASE-LEW-15306-2] p 138 N93-28425
- ORGANOMETALLIC COMPOUNDS**
- CVD of SiC and AlN using cyclic organometallic precursors p 117 A93-39525
- ORIFICE FLOW**
- An analytical study of dilution jet mixing in a cylindrical duct [AIAA PAPER 93-2043] p 27 A93-49876
- An analytical study of dilution jet mixing in a cylindrical duct [NASA-TM-106181] p 37 N93-27160
- ORTHOPEDICS**
- Numerical optimization of composite hip endoprostheses under different loading conditions [AIAA PAPER 92-4703] p 270 A93-20312
- ORTHOTROPIC PLATES**
- Behavior of spinning laminated composite plates with initial twist-experimental vibrations, strain, and deflection results [AIAA PAPER 93-1325] p 238 A93-33898
- OSCILLATING FLOW**
- Laminar/turbulent oscillating flow in circular pipes p 167 A93-21689
- Overview of NASA supported Stirling thermodynamic loss research p 174 A93-26087
- Transition of oscillatory flow in tubes - An empirical model for application to Stirling engines p 174 A93-26088
- Heat transfer in oscillating flows with sudden change in cross section p 174 A93-26089
- M.I.T. Stirling-cycle heat transfer apparatus p 174 A93-26090
- Visualization of entry flow separation for oscillating flow in tubes p 174 A93-26091
- Flip-flop jet nozzle extended to supersonic flows p 8 A93-39409
- OSCILLATIONS**
- Intermodulation in the oscillatory magnetoresistance of a two-dimensional electron gas p 151 A93-17610
- OSCILLATORS**
- Direct optical injection locking of monolithically integrated In(0.53)Ga(0.47)As/In(0.52)Al(0.48)As MODFET oscillators p 158 A93-47127
- OSEEN APPROXIMATION**
- Thermocapillary bubble migration - An Oseen-like analysis of the energy equation p 179 A93-41708
- OXIDATION**
- Asymptotic analysis with reduced chemistry for the burning of n-heptane droplets p 113 A93-13323
- Ultrasonic assessment of interfacial oxidation damage in ceramic matrix composites p 105 A93-52919
- Thermal oxidation of single-crystal silicon carbide - Kinetic, electrical, and chemical studies p 284 A93-55601
- A statistical analysis of elevated temperature gravimetric cyclic oxidation data of 36 Ni- and Co-base superalloys based on an oxidation attack parameter [NASA-TM-105934] p 128 N93-18069
- Auger electron spectroscopy study of oxidation of a PdCr alloy used for high-temperature sensors [NASA-TM-106212] p 129 N93-23418
- Determination of the oxidative stability of perfluoropolyalkyl ethers and correlation with chemical structure [NASA-TM-106223] p 139 N93-32367
- OXIDATION RESISTANCE**
- Role of Si₂N₂O in the passive oxidation of chemically-vapor-deposited Si₃N₄ p 131 A93-16520
- Effect of oxidation on the mechanical properties of a NbAl₃ alloy at intermediate temperatures p 124 A93-20667
- Transverse flexural tests as a tool for assessing damage to PMR-15 composites from isothermal aging in air at elevated temperatures p 100 A93-24514
- Predicting the oxidative lifetime of beta NiAl-Zr alloys p 127 A93-53939
- Transverse flexural tests as a tool for assessing damage to PMR-15 composites from isothermal aging in air at elevated temperatures [NASA-TM-105848] p 107 N93-12737
- A statistical analysis of elevated temperature gravimetric cyclic oxidation data of 36 Ni- and Co-base superalloys based on an oxidation attack parameter [NASA-TM-105934] p 128 N93-18069
- Oxidation resistant overlay coatings for low expansion substrates [NASA-CASE-LEW-15154-1] p 137 N93-19332
- Atomic oxygen protective coating with resistance to undercutting at defect sites [NASA-CASE-LEW-15306-1] p 137 N93-20566
- Method for retarding oxidation of an organic substrate [NASA-CASE-LEW-15306-2] p 138 N93-28425

- High temperature creep and oxidation resistant chromium silicide matrix alloy containing molybdenum [NASA-CASE-LEW-15697-1] p 130 N93-29172
- High temperature, oxidation resistant noble metal-Al alloy thermocouple [NASA-CASE-LEW-15515-1] p 217 N93-31298
- Oxidation resistant overlay coatings for low expansion substrates [NASA-CASE-LEW-15154-2] p 138 N93-31300
- OXIDATION-REDUCTION REACTIONS**
- Mechanism of incipient oxidation of bulk chemical vapor deposited Si₃N₄ p 132 A93-32299
- Chronopotentiometry of refractory metals, actinides and oxyanions in molten salts: A review [NASA-TM-105862] p 120 N93-11545
- OXIDE FILMS**
- Buffer layers for high-T_c thin films on sapphire p 150 A93-17063
- Mechanism of incipient oxidation of bulk chemical vapor deposited Si₃N₄ p 132 A93-32299
- Chromium and reactive element modified aluminate diffusion coatings on superalloys - Environmental testing p 126 A93-37899
- Chronopotentiometry of refractory metals, actinides and oxyanions in molten salts: A review [NASA-TM-105862] p 120 N93-11545
- A survey and analysis of commercially available hydrogen sensors [NASA-TM-105878] p 214 N93-17777
- OXIDES**
- Guandine based vehicle/binders for use with oxides, metals, and ceramics [NASA-CASE-LEW-15314-2] p 138 N93-28423
- OXYGEN**
- Mechanisms of microgravity flame spread over a thin solid fuel - Oxygen and opposed flow effects p 140 A93-50368
- Combustion of solid fuel in very low speed oxygen streams p 122 N93-20207
- OXYGEN ATOMS**
- Plasma chamber testing of APSA coupons for the SAMPIE flight experiment [AIAA PAPER 93-0568] p 67 A93-24244
- Performance and properties of atomic oxygen protective coatings for polymeric materials p 225 A93-53389
- LDEF yaw and pitch angle estimates p 58 N93-12772
- Leveling coatings for reducing the atomic oxygen defect density in protected graphite fiber epoxy composites [NASA-TM-105732] p 136 N93-15344
- Low Earth orbit atomic oxygen simulation for durability evaluation of solar reflector surfaces p 58 N93-15594
- Simulation of the synergistic low Earth orbit effects of vacuum thermal cycling, vacuum UV radiation, and atomic oxygen p 58 N93-15595
- The use of plasma ashers and Monte Carlo modeling for the projection of atomic oxygen durability of protected polymers in low Earth orbit p 58 N93-15596
- Method and apparatus for producing a thermal atomic oxygen beam [NASA-CASE-LEW-15614-1] p 276 N93-19026
- Atomic oxygen protective coating with resistance to undercutting at defect sites [NASA-CASE-LEW-15306-1] p 137 N93-20566
- Determination of atomic oxygen fluence using spectrophotometric analysis of infrared transparent witness coupons for long duration exposure tests [NASA-TM-106021] p 96 N93-22605
- Space environmental interactions for the space exploration initiative p 293 N93-26396
- Low Earth orbital atomic oxygen environmental simulation facility for space materials evaluation [NASA-TM-106128] p 96 N93-27266
- Monte Carlo modeling of atomic oxygen attack of polymers with protective coatings on LDEF p 138 N93-28282
- Method for retarding oxidation of an organic substrate [NASA-CASE-LEW-15306-2] p 138 N93-28425
- OXYGEN PLASMA**
- Low earth simulation and materials characterization p 44 A93-32293
- The evolution of procurement and assurance methods used to proof an advanced space material p 94 A93-53392
- Leveling coatings for reducing the atomic oxygen defect density in protected graphite fiber epoxy composites [NASA-TM-105732] p 136 N93-15344
- Leveling coatings for reducing the atomic oxygen defect density in protected graphite fiber epoxy composites p 59 N93-15597
- OXYGEN PRODUCTION**
- Benefits of in situ propellant utilization for a Mars sample return mission [AIAA PAPER 93-2244] p 140 A93-50046
- Benefits of in situ propellant utilization for a Mars sample return mission [NASA-TM-106243] p 141 N93-28695
- Alkali metal carbon dioxide electrochemical system for energy storage and/or conversion of carbon dioxide to oxygen [NASA-CASE-LEW-14973-1] p 256 N93-28974
- OXYGEN-HYDROCARBON ROCKET ENGINES**
- Test program to provide validation data for the Rocket Combustor Interactive Design (ROCCID) code p 120 N93-11450
- OXYNITRIDES**
- Role of Si₂N₂O in the passive oxidation of chemically-vapor-deposited Si₃N₄ p 131 A93-16520
- Mechanism of incipient oxidation of bulk chemical vapor deposited Si₃N₄ p 132 A93-32299
- OZONE DEPLETION**
- Engine technology challenges for a 21st Century High-Speed Civil Transport [ISABE 93-7064] p 31 A93-54040
- Engine technology challenges for a 21st Century High-Speed Civil Transport [NASA-TM-106216] p 39 N93-31671
- P**
- P-N JUNCTIONS**
- Silicon carbide, a semiconductor for space power electronics p 279 A93-13880
- Greatly improved 3C-SiC p-n junction diodes grown by chemical vapor deposition p 156 A93-38994
- P-TYPE SEMICONDUCTORS**
- Carrier removal and defect behavior in p-type InP p 279 A93-17176
- Aluminum acceptor four particle bound exciton complex in 4H, 6H, and 3C SiC p 282 A93-44822
- Electronic passivation of n- and p-type GaAs using chemical vapor deposited GaS p 283 A93-52708
- PACKAGING**
- Battery selection for space experiments p 159 N93-13184
- Battery selection for Space Shuttle experiments [NASA-TM-106142] p 61 N93-27038
- PACKET SWITCHING**
- Fault-tolerant onboard digital information switching and routing for communications satellites [NASA-TM-4471] p 53 N93-26895
- PACKING DENSITY**
- Development of braided rope seals for hypersonic engine applications: Flow modeling [NASA-TM-105942] p 227 N93-14478
- PAINTS**
- Plasma current collection of Z-93 thermal control paint as measured in the Lewis Research Center's plasma interaction facility [NASA-TM-106132] p 61 N93-26215
- PALLADIUM**
- Auger electron spectroscopy study of oxidation of a PdCr alloy used for high-temperature sensors [NASA-TM-106212] p 129 N93-23418
- PALLADIUM ALLOYS**
- Palladium-chromium static strain gage for high temperature propulsion systems p 204 A93-16421
- Development of a hydrogen gas sensor using microfabrication technology [SAE PAPER 921176] p 210 A93-41356
- PANEL METHOD (FLUID DYNAMICS)**
- Analytical and experimental studies of a short compact subsonic diffuser for a two-dimensional supersonic inlet [NASA-TP-3247] p 17 N93-24118
- PANELS**
- Progressive delamination in polymer matrix composite laminates: A new approach p 108 N93-21515
- PAPER (MATERIAL)**
- Intensified array camera imaging of solid surface combustion aboard the NASA Learjet p 143 A93-30858
- PARALLEL FLOW**
- The coupling of interfacial instabilities and the stabilization of two-layer annular flows p 178 A93-35482
- Performance characteristics of a variable-area vane nozzle for vectoring an ASTOVL exhaust jet up to 45 deg [AIAA PAPER 93-2437] p 29 A93-50189
- Direct numerical simulation of instabilities in parallel flow with spherical roughness elements [NASA-TM-105847] p 192 N93-11529
- Performance characteristics of a variable-area vane nozzle for vectoring an ASTOVL exhaust jet up to 45 deg [NASA-TM-106114] p 37 N93-27131
- PARALLEL PLATES**
- Heat transfer in oscillating flows with sudden change in cross section p 174 A93-26089
- Consecutive plate acoustic suppressor apparatus and methods [NASA-CASE-LEW-15430-1] p 275 N93-17051
- PARALLEL PROCESSING (COMPUTERS)**
- The new challenge of computational aerospace p 2 A93-14169
- LEWICE droplet trajectory calculations on a parallel computer [AIAA PAPER 93-0172] p 259 A93-22604
- Programming probabilistic structural analysis for parallel processing computers p 237 A93-32410
- Binary tree eigen solver in finite element analysis [AIAA PAPER 93-1493] p 267 A93-34034
- Parallel computing for probabilistic fatigue analysis [AIAA PAPER 93-1499] p 261 A93-34039
- A parallel dynamic load balancing algorithm for 3-D adaptive unstructured grids [AIAA PAPER 93-3313] p 260 A93-45009
- The engine design engine. A clustered computer platform for the aerodynamic inverse design and analysis of a full engine [NASA-TM-105838] p 15 N93-11223
- Analysis of fault-tolerant neurocontrol architectures [NASA-TM-105898] p 41 N93-12305
- Turbomachinery CFD on parallel computers [NASA-TM-105932] p 262 N93-13154
- Neural networks for calibration tomography [NASA-TM-106352] p 216 N93-26906
- Parallel solution of high-order numerical schemes for solving incompressible flows [NASA-TM-4451] p 262 N93-27040
- A multichitecture parallel-processing development environment [NASA-TM-106180] p 262 N93-28628
- PARALLEL PROGRAMMING**
- Binary tree eigen solver in finite element analysis [AIAA PAPER 93-1493] p 267 A93-34034
- PARAMETER IDENTIFICATION**
- Icing effects on aircraft stability and control determined from flight data - Preliminary results [AIAA PAPER 93-0398] p 40 A93-23073
- Icing effects on aircraft stability and control determined from flight data: Preliminary results [NASA-TM-105977] p 41 N93-14831
- PARAMETERIZATION**
- Parameterization of solar cells [NASA-TM-105885] p 159 N93-12301
- PARTIAL DIFFERENTIAL EQUATIONS**
- An efficient and robust algorithm for two dimensional time dependent incompressible Navier-Stokes equations - High Reynolds number flows p 178 A93-34371
- Modeling of linear isentropic flow systems p 179 A93-37046
- PARTICLE DENSITY (CONCENTRATION)**
- Experimental testing of four correction algorithms for the forward scattering spectrometer probe [NASA-TM-105906] p 213 N93-13307
- PARTICLE LADEN JETS**
- Noniterative implicit method for tracking particles in mixed Lagrangian-Eulerian formulations p 176 A93-30856
- PARTICLE MASS**
- Phase space distribution of halo particles and detection of WIMPS --- weakly interacting massive particles p 289 A93-23650
- PARTICLE MOTION**
- Particle displacement tracking applied to air flows p 206 A93-23800
- Young's fringe particle image velocimetry in the presence of random particle motions p 207 A93-23801
- PARTICLE SIZE DISTRIBUTION**
- Effects of particulate radiation on premixed gas flames [AIAA PAPER 93-0711] p 114 A93-24806
- Multiple fiberoptic probe for several sensing applications p 212 A93-53109
- Experimental testing of four correction algorithms for the forward scattering spectrometer probe [NASA-TM-105906] p 213 N93-13307
- PARTICLE TRAJECTORIES**
- LEWICE droplet trajectory calculations on a parallel computer [AIAA PAPER 93-0172] p 259 A93-22604
- Particle image velocimetry for the Surface Tension Driven Convection Experiment using a particle displacement tracking technique p 206 A93-23799
- Particle displacement tracking applied to air flows p 206 A93-23800
- Plasma sheath effects on ion collection by a pinhole [AIAA PAPER 93-0567] p 55 A93-24243
- Plasma sheath effects on ion collection by a pinhole [NASA-TM-106098] p 60 N93-25090

PARTITIONS (MATHEMATICS)

Application of controller partitioning optimization procedure to integrated flight/propulsion control design for a STOVL aircraft
[AIAA PAPER 93-3766] p 40 A93-51361

PASSIVE SATELLITES

A prototype automatic phase compensation module
[NASA-TM-105930] p 160 N93-16616

PASSIVITY

Photoluminescence intensity enhancement of GaAs by vapor-deposited GaS - A rational approach to surface passivation p 281 A93-40049
Electronic passivation of n- and p-type GaAs using chemical vapor deposited GaS p 283 A93-52708

PATIENTS

A fiber optic probe for the detection of cataracts p 257 N93-25593

PATTERN RECOGNITION

Application of artificial neural networks in nonlinear analysis of trusses p 244 N93-11403
[NASA-TM-105319]
Real-time diagnostics for a reusable rocket engine [NASA-TM-105792] p 266 N93-19018
Efficient fault diagnosis of helicopter gearboxes [NASA-TM-106253] p 231 N93-31846

PAYLOAD DELIVERY (STS)

Propulsion and aerodynamic analysis of the Beta II two-stage-to-orbit vehicle p 50 A93-13332
[AIAA PAPER 92-4245]

PEBBLE BED REACTORS

Flow instability in particle-bed nuclear reactors [AIAA PAPER 93-1758] p 71 A93-49657

PELLETS

Closed Brayton Cycle power system with a high temperature pellet bed reactor heat source for NEP applications p 82 N93-14482
[NASA-TM-105933]

PENDULUMS

Desktop chaotic systems: Intuition and visualization [NASA-TM-106258] p 269 N93-31847

PENETRANTS

NDE of PWA 1480 single crystal turbine blade material [NASA-TM-106140] p 38 N93-27640

PENETRATION

On protection of Freedom's solar dynamic radiator from the orbital debris environment. II - Further testing and analyses p 70 A93-36589

PERFLUORO COMPOUNDS

Interfacial chemistry of a perfluoropolyether lubricant studied by X-ray photoelectron spectroscopy and temperature desorption spectroscopy p 133 A93-38473

X-ray photoelectron spectroscopy study of the stability of Fomblin Z25 on the native oxide of aluminum p 134 A93-44883

Interfacial chemistry of a perfluoropolyether lubricant studied by XPS and TDS p 137 N93-22560

Determination of the thermal stability of perfluoropolyalkyl ethers by tensimetry [NASA-TM-106081] p 137 N93-25093

Tribological characteristics of perfluoropolyether liquid lubricants under sliding conditions in high vacuum [NASA-TM-106257] p 139 N93-32352

PERFORATED PLATES

Forcing function effects on unsteady aerodynamic gust response. I - Forcing functions p 3 A93-19400
[ASME PAPER 92-GT-174]

Forcing function effects on unsteady aerodynamic gust response. II - Low solidity airfoil row response [ASME PAPER 92-GT-175] p 3 A93-19401

PERFORMANCE PREDICTION

Performance evaluation of land mobile satellite system under fading and interference using multiple TCM by Monte-Carlo simulation p 147 A93-10958

Prediction of chemical vapor deposition rates on monofilaments and its implications for fiber properties p 113 A93-17198

Time-averaged heat transfer and pressure measurements and comparison with prediction for a two-stage turbine p 166 A93-19419

Prediction of dislocation generation during Bridgman growth of GaAs crystals p 279 A93-19740

Prediction of active control of subsonic centrifugal compressor rotating stall [AIAA PAPER 93-0153] p 4 A93-22591

Pdf prediction of supersonic hydrogen flames [AIAA PAPER 93-0448] p 114 A93-23358

A comparison of arcjet plume properties to model predictions [AIAA PAPER 93-0820] p 67 A93-24891

BIPS Turboalternator-Compressor characteristics and application to the NASA Solar Dynamic Ground Demonstration Program p 69 A93-25965

HFAST - A harmonic analysis program for Stirling cycles p 220 A93-26051

Comparison of GLIMPS and HFAST Stirling engine code predictions with experimental data p 220 A93-26052

Evaluation of the Munich Method for modeling rocket engine performance p 70 A93-31968

A numerical round robin for the reliability prediction of structural ceramics [AIAA PAPER 93-1498] p 240 A93-34038

Integrated flight/propulsion control - Subsystem specifications for performance [AIAA PAPER 93-3808] p 41 A93-51400

Effect of out-of-roundness on the performance of a diesel engine connecting-rod bearing p 225 A93-52607

An interactive preprocessor for the NASA engine performance program [NASA-TM-105786] p 32 N93-10983

Parameterization of solar cells [NASA-TM-105885] p 159 N93-12301

Development of NASA/DOE NTP system performance models [NASA-TM-105982] p 82 N93-15428

Interim report on the analysis of the microwave power module [NASA-TM-106012] p 160 N93-16713

System model development for nuclear thermal propulsion [NASA-TM-108215] p 277 N93-17343

On-line implementation of nonlinear parameter estimation for the Space Shuttle main engine [NASA-TM-106097] p 88 N93-26211

Solar array electrical performance assessment for Space Station Freedom [NASA-TM-106161] p 91 N93-27039

Validation test of advanced technology for IPV nickel-hydrogen flight cells - Update p 252 A93-25886

Free-piston Stirling component test power converter test results and potential Stirling applications p 68 A93-25964

Comparison of GLIMPS and HFAST Stirling engine code predictions with experimental data p 220 A93-26052

Overview and evolution of the LeRC PMAD DC test bed p 47 A93-26099

Load converter interactions with the secondary system in the Space Station Freedom power management and distribution dc test bed p 154 A93-26106

Solar array electrical performance assessment for Space Station Freedom [AIAA PAPER 93-1052] p 69 A93-30956

Durability testing of the AJ10-221 490 N high performance (321 sec lps) engine [AIAA PAPER 93-2130] p 74 A93-49949

Performance characteristics of a variable-area vane nozzle for vectoring an ASTOVL exhaust jet up to 45 deg [AIAA PAPER 93-2437] p 29 A93-50189

A plume spectroscopy system for flight applications [AIAA PAPER 93-2511] p 63 A93-50242

Validation test of 125 Ah advanced design IPV nickel-hydrogen flight cells p 78 A93-50822

Acceptance testing of the prototype electrometer for the SAMPIE flight experiment [NASA-TM-105880] p 57 N93-10841

Validation test of 125 Ah advanced design IPV nickel-hydrogen flight cells [NASA-TM-105912] p 81 N93-14079

Test results of a Stirling engine utilizing heat exchanger modules with an integral heat pipe [NASA-TM-105883] p 256 N93-25136

Solar array electrical performance assessment for Space Station Freedom [NASA-TM-106161] p 91 N93-27039

Performance characteristics of a variable-area vane nozzle for vectoring an ASTOVL exhaust jet up to 45 deg [NASA-TM-106114] p 37 N93-27131

M-H characteristics and demagnetization resistance of samarium-cobalt permanent magnets to 300 C p 153 A93-26076

Development of braided rope seals for hypersonic engine applications: Flow modeling [NASA-TM-105942] p 227 N93-14478

Evaluation of a vibration diagnostic system for the detection of spur gear pitting failures [AIAA PAPER 93-2298] p 224 A93-50083

Evaluation of a vibration diagnostic system for the detection of spur gear pitting failures [NASA-TM-106103] p 228 N93-25672

Dynamic gas temperature measurements using a personal computer for data acquisition and reduction [NASA-TM-106119] p 261 N93-27024

PERMEABILITY

PERMANENT MAGNETS

PERMEABILITY

PERMANENT MAGNETS

PERMEABILITY

PERMANENT MAGNETS

PERMEABILITY

PERMANENT MAGNETS

PERMEABILITY

PERMANENT MAGNETS

PERMEABILITY

PERMANENT MAGNETS

PERMEABILITY

PERMANENT MAGNETS

PERMEABILITY

PERSONNEL

Four giants of the Lewis Research Center [NASA-TM-83642] p 1 N93-72738

PERSONNEL DEVELOPMENT

Design and implementation of a pilot orientation program for new NASA engineering employees [NASA-TM-105907] p 286 N93-26205

PERTURBATION

Testing for the Gaussian nature of cosmological density perturbations through the three-point temperature correlation function p 292 A93-55212

PERTURBATION THEORY

The best-fit universe --- cosmological models p 289 A93-17651

Observing the inflation potential --- in models of cosmological inflation p 291 A93-50480

The three-point correlation function in an ensemble of three-dimensional simulations --- in gravitational perturbation theory p 291 A93-50680

PHASE CHANGE MATERIALS

An Isotope-Powered Thermal Storage unit for space applications p 65 A93-13877

Modeling void growth and movement with phase change in thermal energy storage canisters [AIAA PAPER 93-2832] p 285 A93-46569

Radiation and phase change of lithium fluoride in an annulus p 144 A93-54460

Thermal energy storage flight experiment in microgravity p 256 N93-28720

PHASE DEVIATION

Temporal averaging of phase measurements in the presence of spurious phase drift - Application to phase-stepped real-time holographic interferometry p 207 A93-26967

PHASE MODULATION

Optical communications and a comparison of optical technologies for a high data rate return link from Mars [NASA-TP-3180] p 52 N93-18854

PHASE SEPARATION (MATERIALS)

Heat of segregation of single substitutional impurities p 119 A93-52873

PHASE SHIFT

Strain sensing technology for high temperature applications [AIAA PAPER 92-5040] p 205 A93-22314

Temporal averaging in a turbulent environment - Compensation for phase drifts in phase shifting interferometry p 210 A93-44190

Phase-stepping fiber-optic projected fringe system for surface topography measurements [NASA-CASE-LEW-14996-1] p 278 N93-11058

Phase shifter technology assessment - Prospects and applications p 152 A93-25808

Comparative study of bolometric and non-bolometric switching elements for microwave phase shifters p 155 A93-27245

Analysis of MMIC arrays for use in the ACTS Aero Experiment [NASA-TM-106073] p 53 N93-22589

PHASE STABILITY (MATERIALS)

Effect of surface tension on the onset of convection in a double-diffusive layer p 163 A93-13951

PHASE TRANSFORMATIONS

Gravitational waves from first-order cosmological phase transitions p 288 A93-11451

Late-time cosmological phase transitions p 288 A93-17645

Transformation to Ni₅Al₃ in a 63.0 at. pct Ni-Al alloy p 124 A93-25108

Kinetics of hexacelsian-to-celsian phase transformation in SrAl₂Si₂O₈ p 134 A93-40293

Efficient finite element method for aircraft deicing problems p 21 A93-52443

Comments on 'Kinetic Study on the Hexacelsian-Celsian Phase Transformation' [NASA-TM-105917] p 136 N93-14886

Kinetics of hexacelsian to celsian phase transformation in SrAl₂Si₂O₈ [NASA-TM-105913] p 136 N93-16372

PHASED ARRAYS

Millimeter-wave pseudomorphic HEMT MMIC phased array components for space communications p 152 A93-25796

System-level integrated circuit (SLIC) development for phased array antenna applications p 152 A93-25798

Multiple-access phased array antenna simulator for a digital beam-forming system investigation p 148 A93-26237

A prototype automatic phase compensation module [NASA-TM-105930] p 160 N93-16616

Microwave characterization of slotline on high resistivity silicon for antenna feed network [NASA-TM-106058] p 161 N93-27265

- PHOTODISSOCIATION**
Absorption coefficients for water vapor at 193 nm from 300 to 1073 K p 276 A93-45398
- PHOTOELECTRON SPECTROSCOPY**
Interfacial chemistry of a perfluoropolyether lubricant studied by X-ray photoelectron spectroscopy and temperature desorption spectroscopy p 133 A93-38473
X-ray photoelectron spectroscopy study of the stability of Fomblin Z25 on the native oxide of aluminum p 134 A93-44883
Interfacial chemistry of a perfluoropolyether lubricant studied by XPS and TDS [NASA-TM-106014] p 137 N93-22560
- PHOTOGRAPHS**
Capabilities and constraints of combustion diagnostics in microgravity p 145 N93-20185
- PHOTOLUMINESCENCE**
Enhancement of photoluminescence intensity of GaAs with cubic GaS chemical vapor deposited using a structurally designed single-source precursor p 280 A93-26930
Photoluminescence intensity enhancement of GaAs by vapor-deposited GaS - A rational approach to surface passivation p 281 A93-40049
- PHOTOMETERS**
Phase-stepping fiber-optic projected fringe system for surface topography measurements [NASA-CASE-LEW-14996-1] p 278 N93-11058
- PHOTONICS**
Mixed application MMIC technologies - Progress in combining RF, digital and photonic circuits p 152 A93-25800
- PHOTOVOLTAIC CELLS**
Photovoltaic arrays for Martian surface power [IAF PAPER 92-0591] p 293 A93-13699
Photovoltaic Array Space Power flight experiment plus diagnostics (PASP+) modules p 68 A93-25898
Thermal control system for Space Station Freedom photovoltaic power module [SAE PAPER 921110] p 57 A93-41305
Lewis Research Center battery overview p 255 N93-20493
Space transfer with ground-based laser/electric propulsion [NASA-TM-106060] p 84 N93-20615
Solar array electrical performance assessment for Space Station Freedom [NASA-TM-106161] p 91 N93-27039
The Photovoltaic Array Space Power Plus diagnostics (PASP Plus) flight experiment p 256 N93-28717
- PIEZOELECTRIC TRANSDUCERS**
Hybrid active vibration control of rotorbearing systems using piezoelectric actuators p 221 A93-27324
- PILOT TRAINING**
Aircraft icing problems - After 50 years [AIAA PAPER 93-0392] p 19 A93-24239
- PINHOLES**
Plasma sheath effects on ion collection by a pinhole [AIAA PAPER 93-0567] p 55 A93-24243
Plasma sheath effects on ion collection by a pinhole [NASA-TM-106098] p 60 N93-25090
- PIPE FLOW**
Laminar/turbulent oscillating flow in circular pipes p 167 A93-21689
Transition of oscillatory flow in tubes - An empirical model for application to Stirling engines p 174 A93-26088
Visualization of entry flow separation for oscillating flow in tubes p 174 A93-26091
A comparison between numerically modelled and experimentally measured loss mechanisms in wave rotors [AIAA PAPER 93-2522] p 30 A93-50252
Prediction of gas-liquid two-phase flow regime in microgravity [NASA-TM-106274] p 145 N93-30939
A rapid-distortion-theory turbulence model for developed unsteady wall-bounded flow [NASA-TM-106249] p 203 N93-32199
- PIPES (TUBES)**
Scaling analysis of gas-liquid two-phase flow pattern in microgravity [AIAA PAPER 93-0914] p 173 A93-24968
Absolute and convective instability of a viscous liquid jet surrounded by a viscous gas in a vertical pipe p 176 A93-30144
Axial-torsional fatigue - A study of tubular specimen thickness effects p 240 A93-38849
- PISTON ENGINES**
A free-piston Stirling engine/linear alternator controls and load interaction test facility p 146 A93-26077
Design of small Stirling dynamic isotope power system for robotic space missions [NASA-TM-105919] p 141 N93-12085
- Dynamic analysis of Free-Piston Stirling Engine/Linear Alternator-load system-experimentally validated [NASA-TM-106034] p 271 N93-22559
Small Stirling dynamic isotope power system for robotic space missions [NASA-TM-105785] p 92 N93-28686
- PITCH (INCLINATION)**
LDEF yaw and pitch angle estimates p 58 N93-12772
- PITCHING MOMENTS**
Estimation of unsteady lift on a pitching airfoil from wake velocity surveys [AIAA PAPER 93-0437] p 5 A93-23351
Estimation of unsteady lift on a pitching airfoil from wake velocity surveys [NASA-TM-105947] p 15 N93-14791
- PITOT TUBES**
Measurement and analysis of a small nozzle plume in vacuum p 71 A93-42895
- PITTING**
Evaluation of a vibration diagnostic system for the detection of spur gear pitting failures [AIAA PAPER 93-2298] p 224 A93-50083
Evaluation of a vibration diagnostic system for the detection of spur gear pitting failures [NASA-TM-106103] p 228 N93-25672
An analysis of gear fault detection methods as applied to pitting fatigue failure data [NASA-TM-105950] p 229 N93-27074
- PLANAR STRUCTURES**
Conductor-backed coplanar waveguide resonators of Y-Ba-Cu-O and Ti-Ba-Ca-Cu-O on LaAlO₃ [NASA-TM-105890] p 284 N93-12325
- PLANE STRAIN**
Limit pressure of a circumferentially reinforced SiC/Ti ring p 233 A93-16005
- PLANE STRESS**
Limit pressure of a circumferentially reinforced SiC/Ti ring p 233 A93-16005
- PLANE WAVES**
Nonlinear interaction of frequency-detuned modes in boundary layers [AIAA PAPER 93-0347] p 171 A93-24237
- PLANETARY ENVIRONMENTS**
Environmental interactions and the SP-100 power system [NASA-TM-105866] p 84 N93-18877
- PLANETARY MANTLES**
Venus Interior Structure Mission (VISM): Establishing a seismic network on Venus p 293 N93-28819
- PLANETARY STRUCTURE**
Venus Interior Structure Mission (VISM): Establishing a seismic network on Venus p 293 N93-28819
- PLANETARY SURFACES**
Comparison of dynamic isotope power systems for distributed planetary surface applications p 46 A93-13825
- PLASMA CLOUDS**
Arcing rates for High Voltage Solar Arrays - Theory, experiment, and predictions p 70 A93-32567
- PLASMA CURRENTS**
Plasma chamber testing of APSA coupons for the SAMPIE flight experiment [AIAA PAPER 93-0568] p 67 A93-24244
Acceptance testing of the prototype electrometer for the SAMPIE flight experiment [NASA-TM-105880] p 57 N93-10841
Plasma chamber testing of APSA coupons for the SAMPIE flight experiment [NASA-TM-106084] p 60 N93-23742
Plasma current collection of Z-93 thermal control paint as measured in the Lewis Research Center's plasma interaction facility [NASA-TM-106132] p 61 N93-26215
Enhanced plasma current collection from weakly conducting solar array blankets [NASA-TM-106168] p 62 N93-27081
- PLASMA ELECTRODES**
Second Magnetoplasmadynamic Thruster Workshop [NASA-CP-10109] p 279 N93-18635
- PLASMA ENGINES**
Second Magnetoplasmadynamic Thruster Workshop [NASA-CP-10109] p 279 N93-18635
- PLASMA INTERACTION EXPERIMENT**
Acceptance testing of the prototype electrometer for the SAMPIE flight experiment [NASA-TM-105880] p 57 N93-10841
The use of plasma ashers and Monte Carlo modeling for the projection of atomic oxygen durability of protected polymers in low Earth orbit p 58 N93-15596
Transfer Orbit Plasma Interaction Experiment (TROPIX) p 45 N93-28734
- PLASMA INTERACTIONS**
Plasma chamber testing of APSA coupons for the SAMPIE flight experiment [AIAA PAPER 93-0568] p 67 A93-24244
- Interactions between spacecraft and their environments [AIAA PAPER 93-0705] p 55 A93-24801
Electrodynamic interactions between a space station and the ionospheric plasma environment p 56 A93-29156
Solar array module plasma interactions experiment (SAMPIE) - Science and technology objectives p 71 A93-46418
Leveling coatings for reducing the atomic oxygen defect density in protected graphite fiber epoxy composites p 59 N93-15597
Environmental interactions and the SP-100 power system [NASA-TM-105866] p 84 N93-18877
Plasma chamber testing of APSA coupons for the SAMPIE flight experiment [NASA-TM-106084] p 60 N93-23742
The interaction of high voltage systems with the environments of the Moon and Mars [NASA-TM-106107] p 61 N93-26148
Plasma current collection of Z-93 thermal control paint as measured in the Lewis Research Center's plasma interaction facility [NASA-TM-106132] p 61 N93-26215
Transfer Orbit Plasma Interaction Experiment (TROPIX) p 45 N93-28734
- PLASMA JETS**
Single liquid source plasma-enhanced metalorganic chemical vapor deposition of high-quality YBa₂Cu₃O_{7-x} thin films p 280 A93-20643
A comparison of arcjet plume properties to model predictions [AIAA PAPER 93-0820] p 67 A93-24891
Preliminary investigation of high power microwave plasmas for electrothermal thruster use [AIAA PAPER 93-2106] p 74 A93-49928
Preliminary investigation of high power microwave plasmas for electrothermal thruster use [NASA-TM-106207] p 92 N93-29158
- PLASMA LAYERS**
Plasma sprayed ceramic thermal barrier coating for NiAl-based intermetallic alloys [NASA-CASE-LEW-15535-1] p 130 N93-31294
- PLASMA PHYSICS**
Second Magnetoplasmadynamic Thruster Workshop [NASA-CP-10109] p 279 N93-18635
- PLASMA PROPULSION**
Ultrahigh temperature vapor-core reactor - Magnetohydrodynamic system for space nuclear electric power p 66 A93-21663
Electromagnetic propulsion for spacecraft [AIAA PAPER 93-1086] p 69 A93-30975
Development and flight history of the SERT II spacecraft p 71 A93-38976
Plasma contactor technology for Space Station Freedom [AIAA PAPER 93-2228] p 57 A93-50034
Low power pulsed MPD thruster system analysis and applications [AIAA PAPER 93-2391] p 76 A93-50156
BMDO electric space-propulsion program [AIAA PAPER 93-1934] p 78 A93-50322
Second Magnetoplasmadynamic Thruster Workshop [NASA-CP-10109] p 279 N93-18635
NEP technology: FY 1992 milestones (NASA LeRC) p 90 N93-26977
- PLASMA RADIATION**
Method and apparatus for producing a thermal atomic oxygen beam [NASA-CASE-LEW-15614-1] p 276 N93-19026
- PLASMA SHEATHS**
Plasma sheath effects on ion collection by a pinhole [AIAA PAPER 93-0567] p 55 A93-24243
Plasma sheath effects on ion collection by a pinhole [NASA-TM-106098] p 60 N93-25090
Enhanced plasma current collection from weakly conducting solar array blankets [NASA-TM-106168] p 62 N93-27081
- PLASMA SPRAYING**
Technical note - Plasma-sprayed ceramic thermal barrier coatings for smooth intermetallic alloys p 219 A93-15702
Friction and wear of plasma-deposited amorphous hydrogenated films on silicon nitride p 135 A93-52181
Stress relaxation of low pressure plasma-sprayed NiCrAlY alloys p 127 A93-52870
Tribological evaluation and analysis of coating materials p 135 A93-52896
Characterization and durability testing of plasma-sprayed zirconia-yttria and hafnia-yttria thermal barrier coatings. Part 1: Effect of spray parameters on the performance of several lots of partially stabilized zirconia-yttria powder [NASA-TP-3295] p 128 N93-22556

PLASMA WAVES

- Plasma sprayed ceramic thermal barrier coating for NiAl-based intermetallic alloys p 130 N93-31294
[NASA-CASE-LEW-15535-1]

PLASMA WAVES

- Interference patterns in the Spacelab 2 plasma wave data - Oblique electrostatic waves generated by the electron beam p 257 A93-16347

PLASMAS (PHYSICS)

- Environmental interactions and the SP-100 power system p 84 N93-18877
[NASA-TM-105866]

PLASTIC DEFORMATION

- Grain boundary resistance to fatigue crack growth p 125 A93-29570
Viscoplasticity with creep and plasticity bounds p 125 A93-32925
Ratchetting behavior in viscoplasticity - A technical note p 241 A93-43651
Evolution of damage and plasticity in titanium-based, fiber-reinforced composites p 104 A93-48498
On bilinearity of Manson-Coffin low-cycle-fatigue relationship p 245 N93-12739
[NASA-TM-105840]

PLASTIC PROPERTIES

- Unified viscoplastic behavior of metal matrix composites p 244 N93-10777
[NASA-TM-105819]

PLATES (STRUCTURAL MEMBERS)

- Calculation of stress intensity factors in an isotropic multiaxial plate. Part 2: Symbolic/numeric implementation p 244 N93-10453
[NASA-TM-105823]
Calculation of stress intensity factors in an isotropic multiaxial plate. Part 1: Theoretical development p 244 N93-10455
[NASA-TM-105766]

PLATINUM

- Pressure dependence of the oxygen reduction reaction at the platinum microelectrode/nafion interface - Electrode kinetics and mass transport p 112 A93-11450

PLUG NOZZLES

- Reliability assessment of thrust chamber cooling concepts using probabilistic analysis techniques p 75 A93-49978
[AIAA PAPER 93-2163]
Nuclear thermal rocket nozzle testing and evaluation program p 83 N93-15571
[NASA-TM-105962]

PLUMES

- A comparison of arcjet plume properties to model predictions p 67 A93-24891
[AIAA PAPER 93-0820]
The application of structural reliability techniques to plume impingement loading of the Space Station Freedom Photovoltaic Array p 56 A93-33908
[AIAA PAPER 93-1338]
Measurement and analysis of a small nozzle plume in vacuum p 71 A93-42895
Low power arcjet system spacecraft impacts p 76 A93-50157
[AIAA PAPER 93-2392]
Assessment of three numerical methods for the computation of a low-density plume flow p 77 A93-50256
[AIAA PAPER 93-2528]
Second order closure modeling of turbulent buoyant wall plumes p 193 N93-14829
[NASA-TM-105956]
Low thrust chemical rocket technology p 83 N93-15572
[NASA-TM-105927]
Turbulence modeling and experiments p 195 N93-15796
Experiments on a round turbulent buoyant plume p 141 N93-16384
[NASA-TM-105955]
The application of structural reliability techniques to plume impingement loading of the Space Station Freedom Photovoltaic Array p 59 N93-17988
[NASA-TM-105949]
Laser Rayleigh and Raman diagnostics for small hydrogen/oxygen rockets p 83 N93-17995
[NASA-TM-105999]
Experimentation in the low-density plume of a simulated electrothermal thruster for computer code validation p 87 N93-24758
[NASA-CR-191112]
Measurement and analysis of a small nozzle plume in vacuum p 88 N93-26561
[NASA-TM-106066]
NTR plume modeling p 199 N93-26929

PLY ORIENTATION

- Tailored metal matrix laminates for high-temperature performance p 98 A93-15753
Progressive matrix cracking in off-axis plies of a general symmetric laminate p 239 A93-34035
[AIAA PAPER 93-1494]
Structural tailoring of aircraft engine blade subject to ice impact constraints p 250 N93-26999
[NASA-TM-106033]

POINTING CONTROL SYSTEMS

- Optimal control study for the Space Station Solar Dynamic power module p 54 A93-13133

- Control-structure interaction p 54 A93-14687
Control/structure interactions of Space Station solar dynamic modules p 57 A93-41878
Space Station Freedom beta gimbal control via sensitivity models p 60 N93-22551
[NASA-TM-106000]

POLICIES

- Lewis safety manual p 147 N93-70966
[NASA-TM-104438]

POLYCRYSTALS

- The effect of microalloying additions on the tensile properties of polycrystalline NiAl p 123 A93-17516
Critical experiments of the self-consistent model for polycrystalline Hastelloy-X p 124 A93-21958
Creep and stress relaxation modeling of polycrystalline ceramic fibers p 132 A93-31354
Metal-organic chemical vapour deposition of polycrystalline tetragonal indium sulphide (InS) thin films p 116 A93-36584
Thin film diamond microstructure applications p 209 A93-40580
Low cycle fatigue behavior of polycrystalline NiAl at 300 and 1000 K p 129 N93-26898
[NASA-TM-105987]
Tensile creep behavior of polycrystalline alumina fibers p 138 N93-30938
[NASA-TM-106269]

POLYIMIDE RESINS

- Isothermal aging effects on PMR-15 resin p 131 A93-24508
Lower temperature curing thermoset polyimides utilizing a substituted norbornene endcap p 134 A93-44526

POLYIMIDES

- Benzonorbornadiene end caps for PMR resins p 94 A93-35700

POLYMER CHEMISTRY

- Ion exchange polymers and method for making p 139 N93-31316
[NASA-CASE-LEW-15576-1]

POLYMER MATRIX COMPOSITES

- Computational simulation of surface waviness in graphite/epoxy woven composites due to initial curing p 98 A93-15822
Fracture toughness testing of polymer matrix composites p 99 A93-18709
Design for inadvertent damage in composite laminates p 242 A93-53396
Approaches to polymer-derived CMC matrices p 105 A93-53446
Overview of NASA's advanced high temperature engine materials technology program p 94 A93-53453
Probabilistic micromechanics and macromechanics of polymer matrix composites p 105 A93-54705
ICAN/DAMP-integrated composite analyzer with damping analysis capabilities: User's manual p 106 N93-12015
[NASA-TP-3292]
Fracture toughness testing of polymer matrix composites p 107 N93-12302
[NASA-TP-3199]
Progressive delamination in polymer matrix composite laminates: A new approach p 108 N93-21515
Dynamic characteristics of specialty composite structures with embedded damping layers p 110 N93-26705
[NASA-TM-106165]
Probabilistic simulation of multi-scale composite behavior p 250 N93-28633
[NASA-TM-106196]

POLYMERIC FILMS

- Monte Carlo modeling of atomic oxygen attack of polymers with protective coatings on LDEF p 138 N93-28282

POLYMERIZATION

- Lower temperature curing thermoset polyimides utilizing a substituted norbornene endcap p 134 A93-44526

POLYMERS

- Performance and properties of atomic oxygen protective coatings for polymeric materials p 225 A93-53389
Solid lubricants p 135 A93-55471
Atomic oxygen protective coating with resistance to undercutting at defect sites p 137 N93-20566
[NASA-CASE-LEW-15306-1]
Ion exchange polymers and method for making p 139 N93-31316
[NASA-CASE-LEW-15576-1]

POLYNOMIALS

- Vector formulation for interferogram surface fitting p 278 A93-55687

POLYTETRAFLUOROETHYLENE

- Determination of the oxidative stability of perfluoropolyalkyl ethers and correlation with chemical structure p 139 N93-32367
[NASA-TM-106223]

POLYURETHANE FOAM

- Experimental observations of the effect of gravity changes on smoldering combustion p 116 A93-24899
[AIAA PAPER 93-0829]

POLYVINYL ALCOHOL

- Ion exchange polymers and method for making p 139 N93-31316
[NASA-CASE-LEW-15576-1]

POROSITY

- Nondestructive evaluation of ceramic and metal matrix composites for NASA's HITEMP and enabling propulsion materials programs p 231 N93-10963
[NASA-TM-105807]
The effect of porosity and gamma-gamma' eutectic content on the low cycle fatigue behavior of hydrogen-charged PWA-1480 p 130 N93-31576

POROUS BOUNDARY LAYER CONTROL

- A lag model for turbulent boundary layers developing over rough bleed surfaces p 10 A93-48181
[AIAA PAPER 93-2988]

POROUS MATERIALS

- Double-diffusive lingering convection in a porous medium p 175 A93-27900
Development of braided rope seals for hypersonic engine applications - Flow modeling p 222 A93-34493
Direct observation of porous SiC formed by anodization in HF p 282 A93-43587
Studies on the reactive melt infiltration of silicon and silicon-molybdenum alloys in porous carbon p 136 N93-12398
[NASA-TM-105860]
Development of braided rope seals for hypersonic engine applications: Flow modeling p 227 N93-14478
[NASA-TM-105942]

PORTABLE EQUIPMENT

- Direct Broadcast Satellite: Radio Program p 52 N93-11430
[NASA-TM-105910]

POSITION (LOCATION)

- A transfer matrix approach to vibration localization in mistuned blade assemblies p 250 N93-27088
[NASA-TM-106112]

POSTFLIGHT ANALYSIS

- A qualitative approach to systemic diagnosis of the SSME p 261 A93-23327
[AIAA PAPER 93-0405]
The effect of the low Earth orbit environment on space solar cells: Results of the Advanced Photovoltaic Experiment (S0014) p 256 N93-29686

POTASSIUM

- Multimegawatt potassium Rankine power for nuclear electric power p 65 A93-13797
Nuclear electric propulsion options for piloted Mars missions p 90 N93-26985

POTASSIUM HYDROXIDES

- Lightweight nickel electrodes for nickel/hydrogen cells p 255 A93-51574

POTENTIAL THEORY

- Full wave characterization of microstrip open end discontinuities patterned on anisotropic substrates using potential theory p 160 N93-20259
[NASA-TM-106037]

POTENTIOMETRIC ANALYSIS

- Chronopotentiometry of refractory metals, actinides and oxyanions in molten salts: A review p 120 N93-11545
[NASA-TM-105862]

POWDER (PARTICLES)

- Chemical reactions in the processing of MoSi₂ + carbon compacts p 119 A93-53733
Characterization and durability testing of plasma-sprayed zirconia-yttria and hafnia-yttria thermal barrier coatings. Part 1: Effect of spray parameters on the performance of several lots of partially stabilized zirconia-yttria powder p 128 N93-22556
[NASA-TP-3295]
Ceramic fiber reinforced glass-ceramic matrix composite p 109 N93-26100
[NASA-CASE-LEW-15262-1]

POWDER METALLURGY

- Tribological and microstructural comparison of HIPped PM212 and PM212/Au self-lubricating composites p 93 A93-13505
Chromium and reactive element modified aluminide diffusion coatings on superalloys - Environmental testing p 126 A93-37899
The effect of processing and compositional changes on the tribology of PM212 in air p 95 N93-15576
[NASA-TM-105945]
Properties of extruded PS-212 type self-lubricating materials p 138 N93-25565

POWER AMPLIFIERS

- A high efficiency Ka-band monolithic pseudomorphic HEMT amplifier p 151 A93-25786
GaAs monolithic R.F. modules for SARSA distress beacons p 152 A93-25806
High-efficiency high-gain monolithic heterostructure FET amplifier at 31 GHz p 156 A93-37421

POWER CONDITIONING

- Load converter interactions with the secondary system in the Space Station Freedom power management and distribution dc test bed p 154 A93-26106
Stability testing and analysis of a PMAD dc test bed for the Space Station Freedom p 154 A93-26107

- EMTP based stability analysis of Space Station Electric Power System in a test bed environment
p 154 A93-26108
- Ion thruster development at NASA Lewis Research Center
[NASA-TM-105983] p 82 N93-15429
- EMTP based stability analysis of space station electric power system in a test bed environment
[NASA-TM-105845] p 160 N93-15503
- Power requirements for the first lunar outpost (FLO)
[NASA-TM-105925] p 255 N93-15523
- POWER CONVERTERS**
- Free-piston Stirling component test power converter test results and potential Stirling applications
p 68 A93-25964
- M-H characteristics and demagnetization resistance of samarium-cobalt permanent magnets to 300 C
p 153 A93-26076
- Magnetic bearings for free-piston Stirling engines
p 221 A93-26079
- Load converter interactions with the secondary system in the Space Station Freedom power management and distribution dc test bed
p 154 A93-26106
- Stability testing and analysis of a PMAD dc test bed for the Space Station Freedom
p 154 A93-26107
- Summary of the NASA Lewis component technology program for Stirling power converters
[NASA-TM-105640] p 82 N93-15526
- POWER EFFICIENCY**
- A high efficiency Ka-band monolithic pseudomorphic HEMT amplifier
p 151 A93-25786
- Electromagnetic propulsion for spacecraft
[AIAA PAPER 93-1086] p 69 A93-30975
- Preliminary investigation of high power microwave plasmas for electrothermal thruster use
[AIAA PAPER 93-2106] p 74 A93-49928
- 10 kW power electronics for hydrogen arcjets
p 79 N93-10033
- The 10 kW power electronics for hydrogen arcjets
[NASA-TM-105614] p 81 N93-12484
- Preliminary investigation of high power microwave plasmas for electrothermal thruster use
[NASA-TM-106207] p 92 N93-29158
- Combinatorial pulse position modulation for power-efficient free-space laser communications
[NASA-TM-106241] p 150 N93-31856
- POWER SPECTRA**
- Coarsening following a morphological instability in the one-sided model
p 284 A93-21695
- Large- and small-scale constraints on power spectra in $\Omega = 1$ universes
p 290 A93-23990
- The three-point correlation function in an ensemble of three-dimensional simulations ... in gravitational perturbation theory
p 291 A93-50680
- POWER SUPPLIES**
- Power requirements for the first lunar outpost (FLO)
[NASA-TM-105925] p 255 N93-15523
- POWER TRANSMISSION**
- Lessons learned from the Autonomous Power System
p 68 A93-25879
- POWERED LIFT AIRCRAFT**
- Effects of flow-path variations on internal reversing flow in a tailpipe offtake configuration for ASTOVL aircraft
[AIAA PAPER 93-2438] p 29 A93-50190
- A full-scale STOVL ejector experiment
[NASA-TM-106019] p 35 N93-22480
- Experimental performance of a ventral nozzle with pitch and yaw vectoring capability for SSTOVL aircraft
[NASA-TM-106054] p 36 N93-25129
- Effects of flow-path variations on internal reversing flow in a tailpipe offtake configuration for ASTOVL aircraft
[NASA-TM-106149] p 38 N93-29065
- PRANDTL NUMBER**
- Time-dependent thermocapillary convection in a Cartesian cavity - Numerical results for a moderate Prandtl number fluid
[AIAA PAPER 93-0259] p 169 A93-22666
- PREDATORS**
- Overview of aerothermodynamic loads definition study
p 93 N93-31583
- PRECONDITIONING**
- Preconditioned Conjugate Gradient methods for low speed flow calculations
[AIAA PAPER 93-0881] p 172 A93-24942
- The application of preconditioning in viscous flows
p 177 A93-32627
- Preconditioned conjugate-gradient methods for low-speed flow calculations
[NASA-TM-105929] p 194 N93-14885
- PREDICTION ANALYSIS TECHNIQUES**
- Stirling engine - Available tools for long-life assessment ... for space propulsion
p 65 A93-13824
- The effect of ion-plated silver and sliding friction on tensile stress-induced cracking in aluminum oxide
p 132 A93-27917
- Reliability assessment of thrust chamber cooling concepts using probabilistic analysis techniques
[AIAA PAPER 93-2163] p 75 A93-49978
- Navier-Stokes turbine heat transfer predictions using two-equation turbulence
[NASA-TM-105817] p 191 N93-10735
- Computer programs to characterize alloys and predict cyclic life using the total strain version of strainrange partitioning. Tutorial and users manual, version 1.0
[NASA-TM-4425] p 246 N93-15788
- Three-dimensional Navier-Stokes heat transfer predictions for turbine blade rows
[NASA-TM-105800] p 196 N93-19969
- An alternative model for estimating liquid diffusion coefficients requiring no viscosity data
[NASA-TM-106079] p 96 N93-23014
- Considerations concerning fatigue life of metal matrix composites
[NASA-TM-106144] p 250 N93-27009
- An analysis of gear fault detection methods as applied to pitting fatigue failure data
[NASA-TM-105950] p 229 N93-27074
- Fuzzy sets predict flexural strength and density of silicon nitride ceramics
[NASA-TM-106049] p 110 N93-27270
- Overview of the fatigue/fracture/life prediction working group program at the Lewis Research Center
p 232 N93-31574
- A model for predicting high-temperature fatigue failure of a W/Cu composite
p 112 N93-31579
- Life extending control: An interdisciplinary engineering thrust
p 93 N93-31581
- PREDICTIONS**
- Evolution of creep-fatigue life prediction models
p 236 A93-31339
- A high temperature fatigue life prediction computer code based on the Total Strain Version of Strainrange Partitioning (SRP)
p 260 A93-31341
- Spray combustion experiments and numerical predictions
[NASA-TM-106069] p 198 N93-23744
- PREFORMS**
- Observations on infiltration of silicon carbide compacts with an aluminum alloy
p 97 A93-12356
- Studies on the reactive melt infiltration of silicon and silicon-molybdenum alloys in porous carbon
[NASA-TM-105860] p 136 N93-12398
- PREMIXED FLAMES**
- Pdf prediction of supersonic hydrogen flames
[AIAA PAPER 93-0448] p 114 A93-23358
- A coupled multi-block solution procedure for spray combustion in complex geometries
[AIAA PAPER 93-0108] p 171 A93-24230
- Effects of particulate radiation on premixed gas flames
[AIAA PAPER 93-0711] p 114 A93-24806
- Flame balls - Past, present and future
[AIAA PAPER 93-0712] p 114 A93-24807
- Premixed flame propagation in combustible particle cloud mixtures
[AIAA PAPER 93-0713] p 115 A93-24808
- Analytical and numerical modeling of flame-balls in hydrogen-air mixtures
p 118 A93-46009
- Computations of spray, fuel-air mixing, and combustion in a lean-premixed-prevaporized combustor
[AIAA PAPER 93-2069] p 185 A93-49901
- Premixed flame propagation in an optically thick gas
p 119 A93-55381
- PREPREGS**
- Graphite/epoxy composite laminates with co-cured interlaminar damping layers
p 109 N93-25587
- PREPROCESSING**
- An interactive preprocessor for the NASA engine performance program
[NASA-TM-105786] p 32 N93-10983
- PRESSURE CHAMBERS**
- Rayleigh-Brillouin scattering for high-pressure gas temperature measurements
p 218 N93-31556
- PRESSURE DEPENDENCE**
- Pressure dependence of the oxygen reduction reaction at the platinum microelectrode/nafion interface - Electrode kinetics and mass transport
p 112 A93-11450
- PRESSURE DISTRIBUTION**
- M.I.T. Stirling-cycle heat transfer apparatus
p 174 A93-26090
- High Reynolds number and turbulence effects on aerodynamics and heat transfer in a turbine cascade
[AIAA PAPER 93-2252] p 186 A93-50050
- Surface and flow field measurements in a symmetric crossing shock wave/turbulent boundary-layer interaction
[NASA-TM-106086] p 17 N93-24911
- High Reynolds number and turbulence effects on aerodynamics and heat transfer in a turbine cascade
[NASA-TM-106187] p 202 N93-29157
- PRESSURE EFFECTS**
- Computational simulation of surface waviness in graphite/epoxy woven composites due to initial curing
p 98 A93-15822
- PRESSURE GRADIENTS**
- New time scale based k-epsilon model for near-wall turbulence
p 180 A93-41909
- Hypersonic stability and transition
p 8 A93-42579
- A lag model for turbulent boundary layers developing over rough bleed surfaces
[AIAA PAPER 93-2988] p 10 A93-48181
- PRESSURE MEASUREMENT**
- Time-averaged heat transfer and pressure measurements and comparison with prediction for a two-stage turbine
[ASME PAPER 92-GT-194] p 166 A93-19419
- Measurement and analysis of a small nozzle plume in vacuum
p 71 A93-42895
- Comparative wind tunnel tests at high Reynolds numbers of NACA 64 621 airfoils with two aileron configurations
p 9 A93-46823
- In-stream measurements of combustion during Mach 5 to 7 tests of the Hypersonic Research Engine (HRE)
[AIAA PAPER 93-2324] p 28 A93-50104
- EOTV propellant tank pressure control and liquid dynamics
[AIAA PAPER 93-2399] p 77 A93-50164
- Three-dimensional flow field in a turbine nozzle passage
[AIAA PAPER 93-2556] p 13 A93-50278
- Unsteady wing surface pressures in the wake of a propeller
p 14 A93-52436
- Surface and flow field measurements in a symmetric crossing shock wave/turbulent boundary-layer interaction
[NASA-TM-106086] p 17 N93-24911
- Measurement and analysis of a small nozzle plume in vacuum
[NASA-TM-106066] p 88 N93-26561
- PRESSURE OSCILLATIONS**
- Calculations of combustion response profiles and oscillations
[NASA-TM-106135] p 87 N93-25236
- PRESSURE RATIO**
- Averaging techniques for steady and unsteady calculations of a transonic fan stage
[AIAA PAPER 93-3065] p 11 A93-48241
- Supersonic investigation of two dimensional hypersonic exhaust nozzles
[NASA-TM-105687] p 33 N93-15342
- Experimental performance of a ventral nozzle with pitch and yaw vectoring capability for SSTOVL aircraft
[NASA-TM-106054] p 36 N93-25129
- PRESSURE RECOVERY**
- An experimental investigation of S-duct flow control using arrays of low-profile vortex generators
[NASA-TM-106030] p 17 N93-19968
- PRESSURE REDUCTION**
- Mixing and transient interface condensation of a liquid hydrogen tank
[AIAA PAPER 93-1968] p 184 A93-49816
- Low-g fluid mixing - Further results from the Tank Pressure Control Experiment
[AIAA PAPER 93-2423] p 187 A93-50181
- An experimental investigation of S-duct flow control using arrays of low-profile vortex generators
[NASA-TM-106030] p 17 N93-19968
- Mixing and transient interface condensation of a liquid hydrogen tank
[NASA-TM-106201] p 201 N93-28252
- PRESSURE REGULATORS**
- Tank Pressure Control Experiment/Thermal Phenomena (TPCE/TP)
p 92 N93-28713
- PRESSURE SENSORS**
- Fiberoptic sensing technique employing RF modulated interferometry
p 212 A93-53110
- PRESSURE VESSELS**
- Structural durability of a composite pressure vessel
p 234 A93-16552
- Validation test of advanced technology for IPV nickel-hydrogen flight cells - Update
p 252 A93-25886
- Validation test of 125 Ah advanced design IPV nickel-hydrogen flight cells
p 78 A93-50822
- Validation test of 125 Ah advanced design IPV nickel-hydrogen flight cells
[NASA-TM-105912] p 81 N93-14079
- Lewis Research Center battery overview
p 255 N93-20493
- PRESSURIZING**
- Autogenous pressurization of cryogenic vessels using submerged vapor injection
p 71 A93-48648
- PRESTRESSING**
- A new pre-loaded beam geometric stiffness matrix with full rigid body capabilities
p 54 A93-12145
- Effects of precracking methods on the fracture properties of alumina
p 131 A93-16645

PROBABILITY DENSITY FUNCTIONS

- Pdf prediction of supersonic hydrogen flames
[AIAA PAPER 93-0448] p 114 A93-23358
- PDF approach for compressible turbulent reacting flows
[AIAA PAPER 93-0087] p 170 A93-24229
- Design for cyclic loading endurance of composites
[NASA-TM-106145] p 242 A93-53395
- Probabilistic sizing of laminates with uncertainties
[NASA-TM-106145] p 110 N93-27082

PROBABILITY DISTRIBUTION FUNCTIONS

- Probabilistic evaluation of fuselage-type composite structures
[NASA-TM-105881] p 245 N93-12735

PROBABILITY THEORY

- Probabilistic evaluation of uncertainties and risks in aerospace components p 233 A93-12160
- Programming probabilistic structural analysis for parallel processing computers p 237 A93-32410
- Probabilistic micromechanics for metal matrix composites p 237 A93-32465
- Global/local methods for probabilistic structural analysis
[AIAA PAPER 93-1378] p 238 A93-33942
- Structural system reliability under multiple failure modes
[AIAA PAPER 93-1379] p 238 A93-33943
- Quantification of uncertainties in composites
[AIAA PAPER 93-1440] p 102 A93-33989
- Probabilistic assessment of composite structures
[AIAA PAPER 93-1441] p 239 A93-33990
- Probabilistic simulation of stress concentration in composite laminates
[AIAA PAPER 93-1442] p 103 A93-33991
- Probabilistic simulation of the human factor in structural reliability
[AIAA PAPER 93-1495] p 264 A93-34036
- Parallel computing for probabilistic fatigue analysis
[AIAA PAPER 93-1499] p 261 A93-34039
- Probabilistically configured adaptive composite structures
[AIAA PAPER 93-1679] p 240 A93-34191
- Reliability assessment of thrust chamber cooling concepts using probabilistic analysis techniques
[AIAA PAPER 93-2163] p 75 A93-49978
- Probabilistic micromechanics and macromechanics of polymer matrix composites p 105 A93-54705
- Mapping methods for computationally efficient and accurate structural reliability
[NASA-TM-105892] p 248 N93-23745
- Probabilistic simulation of multi-scale composite behavior
[NASA-TM-106196] p 250 N93-28633
- Probabilistic composite analysis p 112 N93-30868
- Structural dynamics. Probabilistic structural analysis methods. Program overview p 251 N93-31562
- Mapping methods for computationally efficient and accurate structural reliability p 232 N93-31572
- Probabilistic simulation of the human factor in structural reliability p 258 N93-31573

PROBLEM SOLVING

- Self-growing neural network architecture using crisp and fuzzy entropy p 263 A93-26650

PROCESS CONTROL (INDUSTRY)

- Containerless automated processing of intermetallic compounds and composites p 144 A93-52183

PRODUCTIVITY

- The Fifth Annual NASA/Contractors Conference on Quality and Productivity. Quality: A Commitment to the Future
[NASA-TM-107829] p 233 N93-70212

PROJECT MANAGEMENT

- Nuclear thermal propulsion technology. Results of an interagency panel in FY 1991
[NASA-TM-105711] p 86 N93-24740
- Systems overview p 89 N93-26915
- The Fifth Annual NASA/Contractors Conference on Quality and Productivity. Quality: A Commitment to the Future
[NASA-TM-107829] p 233 N93-70212

PROJECT PLANNING

- Nuclear Propulsion Project Workshop summary p 64 A93-13765
- Nuclear thermal propulsion technology. Results of an interagency panel in FY 1991
[NASA-TM-105711] p 86 N93-24740
- Nuclear electric propulsion for planetary science missions. NASA technology program planning
[NASA-TM-106139] p 88 N93-26210

PROP-FAN TECHNOLOGY

- APPLE - An aeroelastic analysis system for turbomachines and propfans
[AIAA PAPER 92-4712] p 23 A93-20320
- Navier-Stokes calculations for the unsteady flowfield of turbomachinery
[AIAA PAPER 93-0676] p 6 A93-24786

- Experimental investigation of counter-rotating propfan flutter at cruise conditions
[AIAA PAPER 93-1632] p 25 A93-34160

- Unsteady aerodynamics and flutter of propfans using a three-dimensional Full-Potential Solver
[AIAA PAPER 93-1633] p 25 A93-34161

- On the static stability of forward swept propfans
[AIAA PAPER 93-1634] p 26 A93-34162
- Unsteady blade pressures on a propfan at takeoff - Euler analysis and flight data p 26 A93-37389
- Unsteady aerodynamics and flutter based on the potential equation
[AIAA PAPER 93-2086] p 13 A93-49913

- Computer aided design and manufacturing of composite propfan blades for a cruise missile wind tunnel model
[NASA-TM-105269] p 261 N93-12022

- Structural dynamic testing of composite propfan blades for a cruise missile wind tunnel model
[NASA-TM-105272] p 247 N93-18875

- Structural analysis of high-rpm composite propfan blades for a cruise missile wind tunnel model
[NASA-TM-105267] p 247 N93-23015

- Evaluation of MARC for the analysis of rotating composite blades
[NASA-TM-4423] p 249 N93-24909
- Fabrication of composite propfan blades for a cruise missile wind tunnel model
[NASA-TM-105270] p 249 N93-26202

- In-flight near- and far-field acoustic data measured on the Propfan Test Assessment (PTA) testbed and with an adjacent aircraft
[NASA-TM-103719] p 275 N93-27058

- Acoustic mode measurements in the inlet of a model turbofan using a continuously rotating rake
[AIAA PAPER 93-0598] p 273 A93-24783

- Acoustic mode measurements in the inlet of a model turbofan using a continuously rotating rake
[NASA-TM-105989] p 34 N93-16705

- The promising chemical kinetics for the simulation of propane-air combustion with KIVA-II code
[AIAA PAPER 93-2189] p 118 A93-50001

- Combustion-wave ignition for rocket engines
[AIAA PAPER 93-2244] p 140 A93-50046

- Performance and heat transfer characteristics of a carbon monoxide/oxygen rocket engine
[NASA-TM-105897] p 84 N93-18878

- Benefits of in situ propellant utilization for a Mars sample return mission
[AIAA PAPER 93-2244] p 140 A93-50046

- Benefits of in situ propellant utilization for a Mars sample return mission
[NASA-TM-106243] p 141 N93-28695

- Coaxial injector spray characterization using water/air as simulants p 120 N93-11452

- Influence of heat transfer rates on pressurization of liquid/slush hydrogen propellant tanks
[AIAA PAPER 93-0278] p 169 A93-22681

- Low-g fluid mixing - Further results from the Tank Pressure Control Experiment
[AIAA PAPER 93-2423] p 187 A93-50181

- Small experiments for the maturation of orbital cryogenic transfer technologies
[IAF PAPER 92-0777] p 64 A93-13698

- Ground testing for the no-vent fill of cryogenic tanks - Results of tests for a 71 cubic foot tank
[AIAA PAPER 93-1967] p 73 A93-49815

- Small experiments for the maturation of orbital cryogenic transfer technologies
[NASA-TM-105849] p 192 N93-10981

- Comparing the results of an analytical model of the no-vent fill process with no-vent fill test results for a 4.96 cubic meters (175 cubic feet) tank
[NASA-TM-106018] p 200 N93-27155

- Cruise noise of an advanced propeller with swirl recovery vanes p 273 A93-28609

- BLASIM - A computational tool to assess ice impact damage on engine blades
[AIAA PAPER 93-1638] p 26 A93-34165

- Root damage analysis of aircraft engine blade subject to ice impact
[NASA-TM-105779] p 246 N93-15343

- Evaluation of MARC for the analysis of rotating composite blades
[NASA-TM-4423] p 249 N93-24909

- Efficient hybrid scheme for the analysis of counter-rotating propellers p 7 A93-34483

PROPELLER FANS

- Concurrent processing adaptation of aeroelastic analysis of propfans p 23 A93-14624
- Unsteady blade pressures on a propfan at takeoff - Euler analysis and flight data p 26 A93-37389

- Laser velocimeter measurements of the flow field generated by a forward-swept propfan during flutter
[AIAA PAPER 93-2919] p 14 A93-53591

- Computer aided design and manufacturing of composite propfan blades for a cruise missile wind tunnel model
[NASA-TM-105269] p 261 N93-12022

- Structural dynamic testing of composite propfan blades for a cruise missile wind tunnel model
[NASA-TM-105272] p 247 N93-18875

- Structural analysis of high-rpm composite propfan blades for a cruise missile wind tunnel model
[NASA-TM-105267] p 247 N93-23015

- Evaluation of MARC for the analysis of rotating composite blades
[NASA-TM-4423] p 249 N93-24909
- Fabrication of composite propfan blades for a cruise missile wind tunnel model
[NASA-TM-105270] p 249 N93-26202

- In-flight near- and far-field acoustic data measured on the Propfan Test Assessment (PTA) testbed and with an adjacent aircraft
[NASA-TM-103719] p 275 N93-27058

- An asymptotic theory of supersonic propeller noise p 271 A93-19169

- Forward rotor vortex effects on counter rotating propeller noise p 2 A93-19221
- Manipulation of upstream rotor leading edge vortex and its effects on counter rotating propeller noise
[AIAA PAPER 93-0012] p 272 A93-20134

- Cruise noise of an advanced propeller with swirl recovery vanes p 273 A93-28609
- In-flight near- and far-field acoustic data measured on the Propfan Test Assessment (PTA) testbed and with an adjacent aircraft
[NASA-TM-103719] p 275 N93-27058

- Unsteady wing surface pressures in the wake of a propeller p 14 A93-52436

- Control-structure interaction study for the Space Station solar dynamic power module p 54 A93-13132

- Control-structure interaction p 54 A93-14687
- Numerical model for the Programmable Multirole Furnace (PMZF)
[AIAA PAPER 93-0471] p 142 A93-24242

- A numerical model including PID control of a multizone crystal growth furnace p 190 A93-55473

- Integrated flight/propulsion control - Subsystem specifications for performance
[AIAA PAPER 93-3808] p 41 A93-51400

- A comparative study of multivariable robustness analysis methods as applied to integrated flight and propulsion control
[AIAA PAPER 93-3809] p 21 A93-51401

- A parameter optimization approach to controller partitioning for integrated flight/propulsion control application
[AIAA PAPER 93-3809] p 21 A93-51401

- The new challenge of computational aeroscience p 2 A93-14169

- Metallized propellants for the human exploration of Mars p 66 A93-14509

- Integrated health monitoring and controls for rocket engines
[SAE PAPER 921031] p 66 A93-14654

- A graphical user-interface for propulsion system analysis
[AIAA PAPER 93-0223] p 259 A93-23699

- CFD for hypersonic propulsion p 8 A93-42585

- Reliability studies of Integrated Modular Engine system designs
[AIAA PAPER 93-1886] p 72 A93-49759

- Prospects for utilization of air liquefaction and enrichment system (ALES) propulsion in fully reusable launch vehicles
[AIAA PAPER 93-2025] p 74 A93-49861

- Structured system engineering methodologies used to develop a nuclear thermal propulsion engine
[AIAA PAPER 93-2109] p 271 A93-49930

- NASA's progress in nuclear electric propulsion technology
[AIAA PAPER 93-1936] p 78 A93-53587

- Electric propulsion - An evolutionary technology p 78 A93-56168

- 10 kW power electronics for hydrogen arcjets
p 79 N93-10033
- Preliminary characterization of a water vaporizer for
resistojet applications
[NASA-TM-105877] p 80 N93-11402
- Overview of high performance aircraft propulsion
research
[NASA-TM-105839] p 32 N93-11530
- Nuclear thermal propulsion transportation systems for
lunar/Mars exploration
[NASA-TM-105870] p 81 N93-12363
- The 10 kW power electronics for hydrogen arcjets
[NASA-TM-105614] p 81 N93-12484
- Development of NASA/DOE NTP system performance
models
[NASA-TM-105982] p 82 N93-15428
- Nuclear thermal rocket nozzle testing and evaluation
program
[NASA-TM-105962] p 83 N93-15571
- Identification of propulsion systems
[NASA-TM-106007] p 35 N93-20109
- Space propulsion p 84 N93-22092
- Nuclear concepts/propulsion p 85 N93-22093
- Computational simulation for concurrent engineering of
aerospace propulsion systems
[NASA-TM-106029] p 249 N93-23746
- Nuclear thermal propulsion technology: Results of an
interagency panel in FY 1991
[NASA-TM-105711] p 86 N93-24740
- Nuclear Propulsion Technical Interchange Meeting,
volume 2
[NASA-CP-10116-VOL-2] p 89 N93-26951
- Nuclear electric propulsion systems overview
p 49 N93-26970
- The 20 kWe NEP system studies p 90 N93-26971
- The 20 kWe NEP flight system p 90 N93-26983
- NEP systems model p 91 N93-26987
- The development of hydrogen sensor technology at
NASA Lewis Research Center
[NASA-TM-106141] p 216 N93-27021
- Reliability studies of integrated modular engine system
designs
[NASA-TM-106178] p 91 N93-27022
- NASA's progress in nuclear electric propulsion
technology
[NASA-TM-106272] p 93 N93-31858
- Space R/T base: Propulsion (high thrust chemical)
[PR5] p 286 N93-71878
- PROPULSION SYSTEM PERFORMANCE**
- Integrated health monitoring and controls for rocket
engines
[SAE PAPER 921031] p 66 A93-14654
- Concurrent optimization of airframe and engine design
parameters
[AIAA PAPER 92-4713] p 20 A93-20281
- Multidisciplinary propulsion simulation using NPSS
[AIAA PAPER 92-4709] p 270 A93-20318
- Structural Tailoring/Analysis for Hypersonic
Components - A computational simulation
[AIAA PAPER 92-4722] p 20 A93-20324
- A graphical user-interface for propulsion system
analysis
[AIAA PAPER 93-0223] p 259 A93-23699
- Atomic hydrogen propellants - Historical perspectives
and future possibilities
[AIAA PAPER 93-0244] p 140 A93-24234
- Electromagnetic propulsion for spacecraft
[AIAA PAPER 93-1086] p 69 A93-30975
- Modeling of linear isentropic flow systems
p 179 A93-37046
- CFD for hypersonic propulsion p 8 A93-42585
- Screening studies of advanced control concepts for
airbreathing engines
[AIAA PAPER 92-3320] p 26 A93-49329
- A function approximation approach to anomaly detection
in propulsion system test data
[AIAA PAPER 93-1776] p 71 A93-49671
- Predicted performance of an Integrated Modular Engine
system
[AIAA PAPER 93-1888] p 72 A93-49761
- Performance of a low-power subsonic-arc-attachment
arcjet thruster
[AIAA PAPER 93-1898] p 72 A93-49768
- Recent testing of 30 KW hydrogen arcjet thrusters
[AIAA PAPER 93-1902] p 73 A93-49772
- The NASA Electric Propulsion Program
[AIAA PAPER 93-1935] p 73 A93-49797
- Advanced instrumentation for next-generation
aerospace propulsion control systems
[AIAA PAPER 93-2079] p 211 A93-49906
- Damage-mitigating control of space propulsion systems
for high performance and extended life
[AIAA PAPER 93-2080] p 74 A93-49907
- Durability testing of the AJ10-221 490 N high
performance (321 sec lsp) engine
[AIAA PAPER 93-2130] p 74 A93-49949
- Development and use of hydrogen-air torches in an
altitude facility
[AIAA PAPER 93-2176] p 42 A93-49988
- Characterization of in-flight performance of ion
propulsion systems
[AIAA PAPER 93-2217] p 75 A93-50023
- Advances in NASA's Nuclear Thermal Propulsion
Technology project
[AIAA PAPER 93-2258] p 75 A93-50056
- An RL10A-3-3A rocket engine model using the Rocket
Engine Transient Simulator (ROCETS) software
[AIAA PAPER 93-2357] p 75 A93-50129
- BMDO electric space-propulsion program
[AIAA PAPER 93-1934] p 78 A93-50322
- Hot fire test results of subscale tubular combustion
chambers p 79 N93-10020
- 10 kW power electronics for hydrogen arcjets
p 79 N93-10033
- An interactive preprocessor for the NASA engine
performance program
[NASA-TM-105786] p 32 N93-10983
- Preliminary characterization of a water vaporizer for
resistojet applications
[NASA-TM-105877] p 80 N93-11402
- Overview of high performance aircraft propulsion
research
[NASA-TM-105839] p 32 N93-11530
- Hot fire test results of subscale tubular combustion
chambers
[NASA-TP-3222] p 81 N93-11614
- Nuclear thermal propulsion transportation systems for
lunar/Mars exploration
[NASA-TM-105870] p 81 N93-12363
- Concurrent optimization of airframe and engine design
parameters
[NASA-TM-105908] p 32 N93-12402
- The 10 kW power electronics for hydrogen arcjets
[NASA-TM-105614] p 81 N93-12484
- Development of NASA/DOE NTP system performance
models
[NASA-TM-105982] p 82 N93-15428
- Ion thruster development at NASA Lewis Research
Center
[NASA-TM-105983] p 82 N93-15429
- Propulsion system performance resulting from an
integrated flight/propulsion control design
[NASA-TM-105874] p 34 N93-15525
- Nuclear thermal rocket nozzle testing and evaluation
program
[NASA-TM-105962] p 83 N93-15571
- System model development for nuclear thermal
propulsion
[NASA-TM-108157] p 276 N93-16531
- Performance comparison of axisymmetric and
three-dimensional hydrogen film coolant injection in a 110N
hydrogen/oxygen rocket
[NASA-TM-105967] p 83 N93-16714
- System model development for nuclear thermal
propulsion
[NASA-TM-108215] p 277 N93-17343
- Identification of propulsion systems
[NASA-TM-106007] p 35 N93-20109
- Nuclear concepts/propulsion p 85 N93-22093
- Computational simulation for concurrent engineering of
aerospace propulsion systems
[NASA-TM-106029] p 249 N93-23746
- Nuclear thermal propulsion technology: Results of an
interagency panel in FY 1991
[NASA-TM-105711] p 86 N93-24740
- Screening studies of advanced control concepts for
airbreathing engines
[NASA-TM-106042] p 36 N93-25079
- Test results of a Stirling engine utilizing heat exchanger
modules with an integral heat pipe
[NASA-TM-105883] p 256 N93-25136
- On-line implementation of nonlinear parameter
estimation for the Space Shuttle main engine
[NASA-TM-106097] p 88 N93-26211
- Development and use of hydrogen-air torches in an
altitude facility
[NASA-TM-106047] p 43 N93-26214
- Nuclear Propulsion Technical Interchange Meeting,
volume 2
[NASA-CP-10116-VOL-2] p 89 N93-26951
- Overview of NASA/DOE/DOD interagency modeling
team and activities p 89 N93-26952
- Nuclear electric propulsion systems overview
p 49 N93-26970
- The 20 kWe NEP flight system p 90 N93-26983
- NEP systems model p 91 N93-26987
- Thruster models for NEP system analysis
p 91 N93-26988
- The development of hydrogen sensor technology at
NASA Lewis Research Center
[NASA-TM-106141] p 216 N93-27021
- A modified approach to controller partitioning
[NASA-TM-106167] p 266 N93-28051
- Space R/T base: Propulsion (high thrust chemical)
[PR5] p 286 N93-71878
- PROPYL COMPOUNDS**
- Computational predictions of flame spread over alcohol
pools
[AIAA PAPER 93-0825] p 115 A93-24895
- PROTECTION**
- Power system monitoring and source control of the
Space Station Freedom dc-power system testbed
p 69 A93-26109
- On protection of Freedom's solar dynamic radiator from
the orbital debris environment. II - Further testing and
analyses p 70 A93-36589
- Power system monitoring and source control of the
Space Station Freedom DC power system testbed
[NASA-TM-105841] p 80 N93-10734
- PROTECTIVE COATINGS**
- Low earth simulation and materials characterization
p 44 A93-32293
- Chromium and reactive element modified aluminate
diffusion coatings on superalloys - Environmental testing
p 126 A93-37899
- Performance and properties of atomic oxygen protective
coatings for polymeric materials p 225 A93-53389
- The evolution of procurement and assurance methods
used to proof an advanced space material
p 94 A93-53392
- Solid lubricants p 135 A93-55471
- Leveling coatings for reducing the atomic oxygen defect
density in protected graphite fiber epoxy composites
[NASA-TM-105732] p 136 N93-15344
- Leveling coatings for reducing the atomic oxygen defect
density in protected graphite fiber epoxy composites
p 59 N93-15597
- Oxidation resistant overlay coatings for low expansion
substrates
[NASA-CASE-LEW-15154-1] p 137 N93-19332
- Atomic oxygen protective coating with resistance to
undercutting at defect sites
[NASA-CASE-LEW-15306-1] p 137 N93-20566
- Issues/considerations and performance prediction of
LEO protective coatings p 137 N93-20813
- The effects of simulated low Earth orbit environments
on spacecraft thermal control coatings
[NASA-TM-106146] p 61 N93-27019
- Monte Carlo modeling of atomic oxygen attack of
polymers with protective coatings on LDEF
p 138 N93-28282
- Characteristics of hypervelocity impact craters on LDEF
experiment S1003 and implications of small particle
impacts on reflective surfaces p 62 N93-29363
- Plasma sprayed ceramic thermal barrier coating for
NiAl-based intermetallic alloys
[NASA-CASE-LEW-15535-1] p 130 N93-31294
- Oxidation resistant overlay coatings for low expansion
substrates
[NASA-CASE-LEW-15154-2] p 138 N93-31300
- PROTOCOL (COMPUTERS)**
- The engine design engine. A clustered computer
platform for the aerodynamic inverse design and analysis
of a full engine
[NASA-TM-105838] p 15 N93-11223
- PROTON IRRADIATION**
- Diffusion length variation and proton damage
coefficients for InP/In(x)Ga(1-x)As/GaAs solar cells
p 159 A93-55324
- Diffusion length variation in 0.5- and
3-MeV-proton-irradiated, heteroepitaxial indium phosphide
solar cells
[NASA-TM-106147] p 161 N93-27002
- PUBLIC HEALTH**
- Lewis safety manual
[NASA-TM-104438] p 147 N93-70966
- PULSE DURATION MODULATION**
- The 10 kW power electronics for hydrogen arcjets
[NASA-TM-105614] p 81 N93-12484
- PULSE POSITION MODULATION**
- Combinatorial pulse position modulation for
power-efficient free-space laser communications
[NASA-TM-106241] p 150 N93-31856
- PUMP SEALS**
- An SSME High Pressure Oxidizer Turbopump diagnostic
system using G2 real-time expert system
p 66 A93-16415
- PUMPS**
- Actively controlled superconducting bearings
p 223 A93-48594
- PYROLYSIS**
- Numerical computation of low-speed concurrent flow
flame spread in mixed buoyant and forced flow
[AIAA PAPER 93-0827] p 115 A93-24897
- PYROLYTIC GRAPHITE**
- Semiconductor cooling apparatus
[NASA-CASE-LEW-14162-3] p 111 N93-29614

PYROTECHNICS

PYROTECHNICS

Pyrotechnically actuated systems database and applications catalog p 141 N93-20136

Q

QUADRATURE PHASE SHIFT KEYING

Performance evaluation of land mobile satellite system under fading and interference using multiple TCM by Monte-Carlo simulation p 147 A93-10958

QUANTITATIVE ANALYSIS

Determination of the oxidative stability of perfluoropolyalkyl ethers and correlation with chemical structure [NASA-TM-106223] p 139 N93-32367

R

RADAR TRACKING

Monolithic microwave integrated circuits for sensors, radar, and communications systems; Proceedings of the Meeting, Orlando, FL, Apr. 2-4, 1991 [SPIE-1475] p 151 A93-25776

RADIAL FLOW

Aerodynamic design of turbomachinery blading in three-dimensional flow - An application to radial inflow turbines [ASME PAPER 92-GT-74] p 3 A93-19324
Radial turbine cooling p 191 N93-10061

RADIANT HEATING

Refractive index effects on radiative behavior of a heated absorbing-emitting layer p 162 A93-10653

RADIATION ABSORPTION

Refractive index effects on radiative behavior of a heated absorbing-emitting layer p 162 A93-10653

RADIATION DAMAGE

Neutron, gamma ray, and temperature effects on the electrical characteristics of thyristors p 153 A93-25894

RADIATION DETECTORS

Multiwavelength pyrometer for gray and non-gray surfaces in the presence of interfering radiation [NASA-CASE-LEW-15250-1] p 214 N93-17060

RADIATION EFFECTS

Interactions between spacecraft and their environments [AIAA PAPER 93-0705] p 55 A93-24801
Effects of particulate radiation on premixed gas flames [AIAA PAPER 93-0711] p 114 A93-24806
Neutron, gamma ray, and temperature effects on the electrical characteristics of thyristors p 153 A93-25894

Effect of radiation on convection in a top-heated enclosure p 189 A93-54454

Radiation and phase change of lithium fluoride in an annulus p 144 A93-54460

Radiation and temperature effects on electronic components investigated under the CSTI high capacity power project [NASA-TM-106096] p 161 N93-24746

Silicon carbide semiconductor technology for high temperature and radiation environments p 284 N93-26928

Transfer Orbit Plasma Interaction Experiment (TROPIX) p 45 N93-28734

Studies of effects on optical components and sensors: LDEF experiments AO-147 (ERB components) and S-0014 (APEX) p 278 N93-29693

RADIATION PROTECTION

Nuclear safety policy working group recommendations on nuclear propulsion safety for the space exploration initiative [NASA-TM-105705] p 88 N93-26200

RADIATION PYROMETERS

Multiwavelength pyrometer for gray and non-gray surfaces in the presence of interfering radiation [NASA-CASE-LEW-15250-1] p 214 N93-17060

RADIATION SHIELDING

Shielding analysis for a manned Mars rover powered by an SP-100 type reactor p 45 A93-13793
Dynamic Isotope Power System design considerations for human exploration of the moon and Mars p 253 A93-25995

RADIATION SOURCES

Propagation of high frequency jet noise using geometric acoustics [AIAA PAPER 93-0147] p 272 A93-23241

Propagation of high frequency jet noise using geometric acoustics [NASA-TM-106013] p 275 N93-15575

RADIATION TOLERANCE

Diffusion length variation and proton damage coefficients for InP/In(x)Ga(1-x)As/GaAs solar cells p 159 A93-55324

RADIATIVE HEAT TRANSFER

Refractive index effects on radiative behavior of a heated absorbing-emitting layer p 162 A93-10653

Finite difference solution for transient radiative cooling of a conducting semitransparent square region p 164 A93-15067

Thermal radiation heat transfer (3rd revised and enlarged edition) --- Book [ISBN 0-89116-271-2] p 165 A93-17522

An evaluation of three spatial differencing schemes for the discrete ordinates method in participating media [AIAA PAPER 93-0140] p 266 A93-24231

Discrete ordinates solutions of nongray radiative transfer with diffusely reflecting walls p 285 A93-30124

Refractive index effects on radiation in an absorbing, emitting, and scattering laminated layer p 175 A93-30125

Relations for local radiative heat transfer between rectangular boundaries of an absorbing-emitting medium p 175 A93-30129

Refractive index and scattering effects on radiative behavior of a semitransparent layer p 176 A93-31438

Heat transfer from radiatively heated material in a low Reynolds number microgravity environment p 180 A93-43695

Radiation heat transfer calculations using a control-angle, control-volume-based discrete ordinates method [AIAA PAPER 93-2731] p 182 A93-46485

Analysis and design of an ultrahigh temperature hydrogen-fueled MHD generator p 278 A93-49618

Effect of radiation on convection in a top-heated enclosure p 189 A93-54454

Variable refractive index effects on radiation in semitransparent scattering multilayered regions p 189 A93-54463

Nongray gas analyses for reflecting walls utilizing a flux technique p 190 A93-55460

Soot formation and radiation in turbulent jet diffusion flames under normal and reduced gravity conditions p 121 N93-20192

Jet Engine hot parts IR Analysis Procedure (J-EIRP) [NASA-TM-105914] p 21 N93-22588

Application of ray tracing in radiation heat transfer [NASA-TM-106206] p 202 N93-29075

RADIATIVE TRANSFER

Thermal radiation heat transfer (3rd revised and enlarged edition) --- Book [ISBN 0-89116-271-2] p 165 A93-17522

Application of radiative image transfer theory to the assessment of the overall OTF and contrast degradation of an image in an inhomogeneous turbulent and turbid atmosphere p 285 A93-28624

Discrete ordinates solutions for radiatively participating media in a cylindrical enclosure p 285 A93-31427

RADIATORS

Degradation of radiator performance on Mars due to dust p 59 N93-15616

RADIO COMMUNICATION

Allocations by the 1992 World Administrative Radio Conference p 150 N93-26476

RADIO FREQUENCIES

System-level integrated circuit (SLIC) development for phased array antenna applications p 152 A93-25798

Mixed application MMIC technologies - Progress in combining RF, digital and photonic circuits p 152 A93-25800

GaAs monolithic R.F. modules for SARSAAT distress beacons p 152 A93-25806

RF modulated fiber optic sensing systems and their applications p 211 A93-49469

Fiberoptic sensing technique employing RF modulated interferometry p 212 A93-53110

Allocations by the 1992 World Administrative Radio Conference p 150 N93-26476

RADIO RECEIVERS

Direct Broadcast Satellite: Radio Program [NASA-TM-105910] p 52 N93-11430

RADIO TRANSMISSION

Utilizing a TDRS satellite for direct broadcast satellite-radio propagation experiments and demonstrations [NASA-TM-106172] p 53 N93-27064

RADIOISOTOPE BATTERIES

Versatile dynamic isotope power systems for the exploration of space p 46 A93-13819

An Isotope-Powered Thermal Storage unit for space applications p 65 A93-13877

RADOME MATERIALS

Fiber-reinforced monoclinic celsian matrix composite material [NASA-CASE-LEW-15269-1] p 108 N93-20040

RAMAN SPECTRA

Low thrust chemical rocket technology [NASA-TM-105927] p 83 N93-15572

Laser Rayleigh and Raman diagnostics for small hydrogen/oxygen rockets [NASA-TM-105999] p 83 N93-17995

RAMJET ENGINES

The design and evolution of the beta two-stage-to-orbit horizontal takeoff and landing launch system [NASA-TM-106118] p 51 N93-27018

RANDOM PROCESSES

Stochastic inflation lattice simulations - Ultra-large scale structure of the universe p 289 A93-17646

RANDOM VARIABLES

Confidence bounds on structural reliability [AIAA PAPER 93-1377] p 238 A93-33941

Probabilistic assessment of composite structures [NASA-TM-106024] p 110 N93-27092

RANKINE CYCLE

Multimegawatt potassium Rankine power for nuclear electric power p 65 A93-13797

Nuclear electric propulsion options for piloted Mars missions p 90 N93-26985

RAPID QUENCHING (METALLURGY)

Influence of grain size on the creep behavior of HfC-dispersed NiAl p 123 A93-17674

The microstructural evolution, crystallography, and thermal processing of ultrahigh carbon Fe-1.85 pct C melt-spun ribbon p 125 A93-32934

RARE GASES

Simplified power processing for inert gas ion thrusters [AIAA PAPER 93-2397] p 76 A93-50162

RATES (PER TIME)

Optical communications and a comparison of optical technologies for a high data rate return link from Mars [NASA-TP-3180] p 52 N93-18854

RAY TRACING

Propagation of high frequency jet noise using geometric acoustics [AIAA PAPER 93-0147] p 272 A93-23241

Propagation of high frequency jet noise using geometric acoustics [NASA-TM-106013] p 275 N93-15575

Application of ray tracing in radiation heat transfer [NASA-TM-106206] p 202 N93-29075

RAYLEIGH EQUATIONS

The eigenvalue spectrum of the Rayleigh equation for a plane shear layer p 168 A93-21725

RAYLEIGH NUMBER

Convective effects during the physical vapor transport process. I - Thermal convection p 179 A93-36575

Surface tension effects on the onset of double-diffusive convection p 180 A93-41710

RAYLEIGH SCATTERING

Air-mass flux measurement system using Doppler-shifted filtered Rayleigh scattering [AIAA PAPER 93-0513] p 205 A93-23260

Development of a Rayleigh scattering system for temperature measurements in combustor flows p 206 A93-23788

High-speed laser anemometry based on spectrally resolved Rayleigh scattering p 207 A93-23814

A study of compressible mixing layers using filtered Rayleigh scattering [AIAA PAPER 92-0175] p 173 A93-24982

Pulsed laser Rayleigh scattering diagnostic for hydrogen/oxygen rocket exit plane flowfield velocimetry [AIAA PAPER 93-0805] p 207 A93-25552

Gas temperature measurements using the dual-line detection Rayleigh scattering technique p 213 A93-55368

Gas temperature measurements using the dual-line detection Rayleigh scattering technique p 214 N93-13668

Gas temperature and density measurements based on spectrally resolved Rayleigh-Brillouin scattering p 214 N93-13684

Laser Rayleigh and Raman diagnostics for small hydrogen/oxygen rockets [NASA-TM-105999] p 83 N93-17995

2D velocity and temperature measurements in high speed flows based on spectrally resolved Rayleigh scattering [NASA-TM-105784] p 215 N93-19651

Pulsed laser Rayleigh scattering diagnostic for hydrogen/oxygen rocket exit plane flowfield velocimetry [NASA-TM-106213] p 88 N93-26149

Rayleigh-Brillouin scattering for high-pressure gas temperature measurements p 218 N93-31556

RAYLEIGH-BENARD CONVECTION

On the structure of cellular solutions in Rayleigh-Benard-Marangoni flows in small-aspect-ratio containers p 164 A93-14762

Thermosolutal convection during dendritic solidification of a binary alloy p 182 A93-45975

REACTING FLOW

Numerical simulation of a low-emission gas turbine combustor using KIVA-II p 22 A93-14077

- Flow effects in a vertical CVD reactor
p 166 A93-19821
- Multigrid methods for numerical simulation of laminar diffusion flames
[AIAA PAPER 93-0236] p 113 A93-22648
- Prediction of engine and near-field plume reacting flows in low-thrust chemical rockets
[AIAA PAPER 93-0237] p 66 A93-22649
- PDF approach for compressible turbulent reacting flows
[AIAA PAPER 93-0087] p 170 A93-24229
- A coupled implicit method for chemical non-equilibrium flows at all speeds
p 181 A93-44245
- Direct numerical simulations of a reacting turbulent mixing layer by a pseudospectral-spectral element method
p 182 A93-45974
- A review of chemically reactive turbulent flow mixing mechanisms and a new design for a low NO(x) combustor
p 27 A93-49508
- CFD validation of subsonic turbulent planar shear layers
[AIAA PAPER 93-1773] p 184 A93-49669
- A simplified reaction mechanism for calculation of emissions in hydrocarbon (Jet-A) combustion
[AIAA PAPER 93-2341] p 118 A93-50116
- Comparison of reacting and non-reacting shear layers at a high subsonic Mach number
[AIAA PAPER 93-2381] p 186 A93-50149
- Performance comparison of axisymmetric and three-dimensional hydrogen film coolant injection in a 110N hydrogen/oxygen rocket
[NASA-TM-105967] p 83 N93-16714
- Comparison of reacting and non-reacting shear layers at a high subsonic Mach number
[NASA-TM-106198] p 38 N93-27610
- Turbulence measurement in a reacting and non-reacting shear layer at a high subsonic Mach number
[NASA-TM-106186] p 18 N93-31839
- REACTION BONDING**
- Ultrasonic and micromechanical study of damage and elastic properties of SiC/RBSN ceramic composites ---
Reaction Bonded Silicon Nitride p 99 A93-19624
- Reaction layer formation at the graphite/copper-chromium alloy interface
p 100 A93-25105
- REACTION KINETICS**
- Pressure dependence of the oxygen reduction reaction at the platinum microelectrode/nafion interface - Electrode kinetics and mass transport
p 112 A93-11450
- Asymptotic analysis with reduced chemistry for the burning of n-heptane droplets
p 113 A93-13323
- Simplified jet fuel reaction mechanism for lean burn combustion application
[AIAA PAPER 93-0021] p 113 A93-23238
- Chemical vapor deposition modeling for high temperature materials
p 116 A93-39503
- Onset conditions for gas phase reaction and nucleation in the CVD of transition metal oxides
p 116 A93-39508
- Kinetics of hexacelsian-to-celsian phase transformation in SrAl₂Si₂O₈
p 134 A93-40293
- The promising chemical kinetics for the simulation of propane-air combustion with KIVA-II code
[AIAA PAPER 93-2189] p 118 A93-50001
- Chemical reactions in the processing of MoSi₂ - carbon compacts
p 119 A93-53733
- Thermal oxidation of single-crystal silicon carbide - Kinetic, electrical, and chemical studies
p 284 A93-55601
- Comments on 'Kinetic Study on the Hexacelsian-Celsian Phase Transformation'
[NASA-TM-105917] p 136 N93-14886
- Simplified jet-A kinetic mechanism for combustor application
[NASA-TM-105940] p 120 N93-15504
- Kinetics of hexacelsian to celsian phase transformation in SrAl₂Si₂O₈
[NASA-TM-105913] p 136 N93-16372
- LSENS, a general chemical kinetics and sensitivity analysis code for gas-phase reactions: User's guide
[AIAA PAPER 105851] p 121 N93-16614
- A critical analysis of the accuracy of several numerical techniques for combustion kinetic rate equations
[NASA-TP-3315] p 34 N93-16941
- A kinetic and equilibrium analysis of silicon carbide chemical vapor deposition on monofilaments
[NASA-TM-106137] p 96 N93-27003
- REACTIVITY**
- Studies on the reactive melt infiltration of silicon and silicon-molybdenum alloys in porous carbon
[NASA-TM-105860] p 136 N93-12398
- REACTOR CORES**
- A comparison of Nuclear Thermal Propulsion concepts - Results of a workshop
US/CIS integrated NTRC
[AIAA PAPER 93-2367] p 76 A93-50138
- REACTOR DESIGN**
- Lunar in-core thermionic nuclear reactor power system conceptual design
p 46 A93-13836
- Advanced radiator concepts feasibility demonstration --- for space power system
p 163 A93-13844
- A comparison of Nuclear Thermal Propulsion concepts - Results of a workshop
p 65 A93-13850
- Ultrahigh temperature vapor-core reactor - Magnetohydrodynamic system for space nuclear electric power
p 66 A93-21663
- 100-kWe lunar/Mars surface power utilizing the SP-100 reactor with dynamic conversion
p 67 A93-25856
- U.S./CIS eye joint nuclear rocket venture
p 71 A93-49334
- A comparison of nuclear thermal rocket development cost and schedule for piloted missions to Mars
[AIAA PAPER 93-2263] p 44 A93-50057
- Nuclear Engine System Simulation (NESS): Volume 1: Program user's guide
[NASA-CR-191080] p 86 N93-23876
- REACTOR MATERIALS**
- The role of the interface in refractory metal alloy composites
p 97 A93-13777
- SP-100 high-temperature advanced radiator development
p 163 A93-13843
- REACTOR SAFETY**
- Space nuclear power systems 1989; Proceedings of the 6th Symposium, Albuquerque, NM, Jan. 8-12, 1989. Vols. 1 & 2 --- Book
[ISBN 0-89464-030-5] p 66 A93-20752
- REAL GASES**
- Lagrangian solution of supersonic real gas flows
p 170 A93-23944
- REAL TIME OPERATION**
- Implementation of a model based fault detection and diagnosis technique for actuation faults of the SSME
p 47 A93-16413
- An SSME High Pressure Oxidizer Turbopump diagnostic system using G2 real-time expert system
p 66 A93-16415
- High data rate applications of ACTS technology
p 52 A93-17329
- Temporal averaging of phase measurements in the presence of spurious phase drift - Application to phase-stepped real-time holographic interferometry
p 207 A93-26967
- An all digital implementation of a modified Hamming net for video compression with prediction and quantization circuits
p 148 A93-37038
- Implementation of a model based fault detection and diagnosis for actuation faults of the Space Shuttle main engine
[NASA-TM-105781] p 49 N93-11401
- Real-time diagnostics for a reusable rocket engine
[NASA-TM-105792] p 266 N93-19018
- Real-time transmission of digital video using variable-length coding
[NASA-TM-106092] p 150 N93-22483
- RECEIVERS**
- Photovoltaic receivers for laser beamed power in space
p 66 A93-21664
- Design of a cavity heat pipe receiver experiment
p 173 A93-25985
- Optical communications and a comparison of optical technologies for a high data rate return link from Mars
[NASA-TP-3180] p 52 N93-18854
- RECIPROCITY THEOREM**
- A reciprocity formulation for the EM scattering by an obstacle within a large open cavity
p 149 A93-52237
- RECIRCULATIVE FLUID FLOW**
- Flow effects in a vertical CVD reactor
p 166 A93-19821
- Segmented multigrid domain decomposition solutions for three dimensional viscous recirculating flows
[AIAA PAPER 93-3344] p 181 A93-45038
- RECOMBINATION REACTIONS**
- Minority carrier diffusion length and edge surface-recombination velocity in InP
p 283 A93-50787
- RECTANGLES**
- Relations for local radiative heat transfer between rectangular boundaries of an absorbing-emitting medium
p 175 A93-30129
- RECTANGULAR PANELS**
- Damage progression in stiffened composite panels
[AIAA PAPER 93-1345] p 238 A93-33915
- RECTANGULAR PLATES**
- Analysis of passive damping in thick composite structures
p 241 A93-45743
- RECTIFIERS**
- Modelling a single phase voltage controlled rectifier using Laplace transforms
[NASA-TM-106005] p 271 N93-23016
- RED SHIFT**
- N-point correlation functions in the CIA and SSRS redshift distribution of galaxies
p 288 A93-10615
- Clumpy cold dark matter p 291 A93-46201
- REDUCED ORDER FILTERS**
- A three-dimensional pressure flux-split RNS application to sub/supersonic flow in inlets and ducts
[AIAA PAPER 93-3063] p 11 A93-48239
- REDUCTION (CHEMISTRY)**
- Pressure dependence of the oxygen reduction reaction at the platinum microelectrode/nafion interface - Electrode kinetics and mass transport
p 112 A93-11450
- Asymptotic analysis with reduced chemistry for the burning of n-heptane droplets
p 113 A93-13323
- REDUNDANCY**
- Minimize system cost by choosing optimal subsystem reliability and redundancy
[NASA-TM-106251] p 271 N93-31145
- REFILLING**
- Comparing the results of an analytical model of the no-vent fill process with no-vent fill test results for a 4.96 cubic meters (175 cubic feet) tank
[NASA-TM-106018] p 200 N93-27155
- REFLECTANCE**
- Multiwavelength pyrometer for gray and non-gray surfaces in the presence of interfering radiation
[NASA-CASE-LEW-15250-1] p 214 N93-17060
- Texturing of InP surfaces for device applications
[NASA-TM-106061] p 129 N93-28618
- REFLECTED WAVES**
- Nongray gas analyses for reflecting walls utilizing a flux technique
p 190 A93-55460
- REFLECTION**
- Modal element method for scattering and absorbing of sound by two-dimensional bodies
p 274 A93-53657
- REFLECTOR ANTENNAS**
- Analysis of reflector antenna system including frequency selective surfaces
p 52 A93-32820
- System overview on electromagnetic compensation for reflector antenna surface distortion
[NASA-TM-106217] p 53 N93-29195
- REFLECTORS**
- A prototype automatic phase compensation module
[NASA-TM-105930] p 160 N93-16616
- REFRACTIVITY**
- Refractive index effects on radiative behavior of a heated absorbing-emitting layer
p 162 A93-10653
- Three-dimensional computed tomography from interferometric measurements within a narrow cone of views
p 207 A93-24024
- Refractive index effects on radiation in an absorbing, emitting, and scattering laminated layer
p 175 A93-30125
- Refractive index and scattering effects on radiative behavior of a semitransparent layer
p 176 A93-31438
- Variable refractive index effects on radiation in semitransparent scattering multilayered regions
p 189 A93-54463
- Optical and scratch resistant properties of diamondlike carbon films deposited with single and dual ion beams
p 137 N93-25564
- REFRACTORY COATINGS**
- Chronopotentiometry of refractory metals, actinides and oxyanions in molten salts: A review
[NASA-TM-105862] p 120 N93-11545
- REFRACTORY MATERIALS**
- High temperature viscoplastic ratchetting - Material response or modeling artifact
p 233 A93-13823
- Chemical vapor deposition modeling for high temperature materials
p 116 A93-39503
- Aerospace applications --- of refractory ceramic materials
p 135 A93-55472
- Development of thin film thermocouples on ceramic materials for advanced propulsion system applications
[NASA-TM-106017] p 215 N93-25173
- Properties of extruded PS-212 type self-lubricating materials
p 138 N93-25565
- Determination of plate wave velocities and diffuse field decay rates with broad-band acousto-ultrasonic signals
[NASA-TM-106158] p 232 N93-27080
- Radial basis function network learns ceramic processing and predicts related strength and density
[NASA-TM-106048] p 110 N93-27129
- Soft computing in design and manufacturing of advanced materials
[NASA-TM-106032] p 111 N93-28624
- SiC fiber-reinforced Celsian glass-ceramic matrix composite
[NASA-CASE-LEW-15264-1] p 112 N93-31293
- Method of producing a ceramic fiber-reinforced glass-ceramic matrix composite
[NASA-CASE-LEW-15264-2] p 112 N93-31299
- REFRACTORY METAL ALLOYS**
- The role of the interface in refractory metal alloy composites
p 97 A93-13777
- REFRACTORY METALS**
- Chronopotentiometry of refractory metals, actinides and oxyanions in molten salts: A review
[NASA-TM-105862] p 120 N93-11545

REFUELING

REFUELING

- Ground testing for the no-vent fill of cryogenic tanks -
Results of tests for a 71 cubic foot tank
[AIAA PAPER 93-1967] p 73 A93-49815
Small experiments for the maturation of orbital cryogenic
transfer technologies
[NASA-TM-105849] p 192 N93-10981

REGENERATIVE COOLING

- Numerical study of nozzle wall cooling for nuclear
thermal rockets
[AIAA PAPER 93-2498] p 77 A93-50232

REGENERATIVE FUEL CELLS

- Estimates of power requirements for a Manned Mars
Rover powered by a nuclear reactor p 45 A93-13783
Optimization of armored spherical tanks for storage on
the lunar surface p 47 A93-25866
Long life Regenerative Fuel Cell technology
development plan p 252 A93-25867
Regenerative fuel cells p 252 A93-25868
Advanced photovoltaic power system technology for
lunar base applications p 255 N93-14004

REGENERATORS

- Pulsed single-blow regenerator testing
p 221 A93-26081

REGOLITH

- Experimental determination of in situ utilization of lunar
regolith for thermal energy storage p 253 A93-26043

REGRESSION ANALYSIS

- A statistical analysis of elevated temperature gravimetric
cyclic oxidation data of 36 Ni- and Co-base superalloys
based on an oxidation attack parameter
[NASA-TM-105934] p 128 N93-18069
Basic statistical analyses of candidate nickel-hydrogen
cells for the Space Station Freedom
[NASA-TM-106111] p 270 N93-27124

REINFORCED PLATES

- Effects of interply damping layers on the dynamic
characteristics of composite plates p 237 A93-32415

REINFORCING FIBERS

- Fiber shape effects on metal matrix composite
behavior p 98 A93-15752
Effect of high temperature annealing on the
microstructure of SCS-6 SiC fibers p 133 A93-39513
CVD of silicon carbide on structural fibers -
Microstructure and composition p 117 A93-39521
Tensile creep and creep-recovery behavior of a
SiC-fiber-Si3N4-matrix composite p 104 A93-40290
Interfacial shear strength of cast and directionally
solidified NiAl-sapphire fiber composites p 106 A93-55685
Development of braided rope seals for hypersonic
engine applications: Flow modeling
[NASA-TM-105942] p 227 N93-14478
SiC fiber-reinforced Celsian glass-ceramic matrix
composite
[NASA-CASE-LEW-15264-1] p 112 N93-31293
Method of producing a ceramic fiber-reinforced
glass-ceramic matrix composite
[NASA-CASE-LEW-15264-2] p 112 N93-31299
Progress in speckle-shift strain measurement
p 251 N93-31558
Stress-rupture behavior of small diameter polycrystalline
alumina fibers
[NASA-TM-106256] p 139 N93-32382

RELATIVITY

- Phase space distribution of halo particles and detection
of WIMPS --- weakly interacting massive particles
p 289 A93-23650

RELAXATION (MECHANICS)

- Multilayer relaxation and surface energies of fcc and
bcc metals using equivalent crystal theory
p 119 A93-52872

RELAY SATELLITES

- GSFC conceptual design study for an inter-satellite
Optical Multiple Access communication system
p 52 A93-18966
Multiple-access phased array antenna simulator for a
digital beam-forming system investigation
p 148 A93-26237

RELIABILITY

- On protection of Freedom's solar dynamic radiator from
the orbital debris environment II - Further testing and
analyses p 70 A93-36589
Fatigue criterion to system design, life and reliability: A
primer
[NASA-TM-106022] p 248 N93-23406

RELIABILITY ANALYSIS

- Reliability analysis of structural ceramic components
using a three-parameter Weibull distribution
[ASME PAPER 92-GT-296] p 231 A93-19486
Ceramic component reliability with the restructured
NASA/CARES computer program
[ASME PAPER 92-GT-383] p 234 A93-19540
An approach to studying the reliability of microgravity
experiments
[AIAA PAPER 93-1024] p 44 A93-30937

- Extended life and performance test of a low-power
arcjet p 70 A93-32554

- Computational methods for efficient structural reliability
and reliability sensitivity analysis
[AIAA PAPER 93-1626] p 240 A93-34155

- Reliability studies of Integrated Modular Engine system
designs
[AIAA PAPER 93-1886] p 72 A93-49759

- Reliability assessment of thrust chamber cooling
concepts using probabilistic analysis techniques
[AIAA PAPER 93-2163] p 75 A93-49978

- Reliability analysis of laminated ceramic matrix
composites using shell subelement techniques
p 243 A93-55382

- Ceramic component reliability with the restructured
NASA/CARES computer program
[NASA-TM-105856] p 244 N93-11004

- Reliability studies of integrated modular engine system
designs
[NASA-TM-106178] p 91 N93-27022

- Probabilistic sizing of laminates with uncertainties
[NASA-TM-106145] p 110 N93-27082

- Minimize system cost by choosing optimal subsystem
reliability and redundancy
[NASA-TM-106251] p 271 N93-31145

RELIABILITY ENGINEERING

- Ceramic component reliability with the restructured
NASA/CARES computer program
[ASME PAPER 92-GT-383] p 234 A93-19540
Fluid design studies of integrated modular engine
system
[AIAA PAPER 93-1887] p 72 A93-49760
Ceramic component reliability with the restructured
NASA/CARES computer program
[NASA-TM-105856] p 244 N93-11004
Life extending control: An interdisciplinary engineering
trust p 93 N93-31581

RELIC RADIATION

- The gravitational wave contribution to cosmic microwave
background anisotropies and the amplitude of mass
fluctuations from COBE results p 289 A93-21508

REMOTE SENSING

- Strain sensing technology for high temperature
applications
[AIAA PAPER 92-5040] p 205 A93-22314
X-ray-based displacement measurement for hostile
environments p 208 A93-28580

REMOTE SENSORS

- Non-contact heat flux measurement using a transparent
sensor
[NASA-TM-106252] p 142 N93-32330

RENORMALIZATION GROUP METHODS

- Remarks on turbulent constitutive relations
[NASA-TM-106116] p 199 N93-27010

REQUIREMENTS

- Design and test of a small two stage counter-rotating
turbine for rocket engine application
[AIAA PAPER 93-2136] p 74 A93-49954

RESEARCH AIRCRAFT

- Icing effects on aircraft stability and control determined
from flight data - Preliminary results
[AIAA PAPER 93-0398] p 40 A93-23073
Icing effects on aircraft stability and control determined
from flight data: Preliminary results
[NASA-TM-105977] p 41 N93-14831

RESEARCH AND DEVELOPMENT

- The NASA CSTI High Capacity Power Project
p 69 A93-26105
The NASA CSTI high capacity power project
[NASA-TM-105813] p 48 N93-11398
Current status of liquid sheet radiator research
[NASA-TM-105764] p 193 N93-14150
The 1992 Research/Technology report
[NASA-TM-105924] p 1 N93-20902
Satellites and the BISON: An overview of NASA R/D
[NASA-TM-106108] p 150 N93-26903

RESEARCH FACILITIES

- Structural dynamics branch research and
accomplishments to FY 1992
[NASA-TM-105824] p 247 N93-20368
Space exploration initiative candidate nuclear propulsion
test facilities
[NASA-TM-105710] p 86 N93-24753
Facilities
Plum Brook facilities p 49 N93-26963
NEP facilities (LeRC) p 49 N93-26964
Hypersonic engine component experiments in high heat
flux, supersonic flow environment
[NASA-TM-106273] p 203 N93-31860
Four giants of the Lewis Research Center
[NASA-TM-83642] p 1 N93-72738

RESEARCH PROJECTS

- The 1992 Research/Technology report
[NASA-TM-105924] p 1 N93-20902
NASA low speed centrifugal compressor
p 204 N93-70583

RESIDUAL STRESS

- Tensile strain-rate sensitivity of tungsten/niobium
composites at 1300 to 1600 K p 97 A93-14840
Tailored metal matrix laminates for high-temperature
performance p 98 A93-15753
Combined micromechanical and fabrication process
optimization for metal-matrix composites p 99 A93-18990
Effect of thermal cycling on interface bonding
requirements in Al2O3 fiber-reinforced superalloy
composites p 103 A93-35882
Elevated-temperature fracture resistances of monolithic
and composite ceramics using chevron-notched bend
tests p 133 A93-38888
Residual strain gradient determination in metal matrix
composites by synchrotron X-ray energy dispersive
diffraction p 103 A93-39580
The effect of multiple compliant layers at the fiber-matrix
interface on residual thermal stresses in metal matrix
composites p 104 A93-42085
Computational simulation of hot composite structures
p 260 A93-54704
The effect of fiber microstructure on evolution of residual
stresses in silicon carbide/titanium aluminate composites
p 106 A93-54771

RESIN MATRIX COMPOSITES

- Approaches to polymer-derived CMC matrices
p 105 A93-53446

RESISTANCE HEATING

- Efficient finite element method for aircraft deicing
problems p 21 A93-52443

RESISTOJET ENGINES

- Calculations of low Reynolds number rocket nozzles
[AIAA PAPER 93-0888] p 67 A93-24948
Gravity sensitivity of a resistojets water vaporizer
[AIAA PAPER 93-2402] p 186 A93-50167
Preliminary endurance tests of water vaporizers for
resistojet applications
[AIAA PAPER 93-2403] p 187 A93-50168
Preliminary characterization of a water vaporizer for
resistojet applications
[NASA-TM-105877] p 80 N93-11402
Experimentation in the low-density plume of a simulated
electrothermal thruster for computer code validation
[NASA-CR-191112] p 87 N93-24758
Preliminary endurance tests of water vaporizers for
resistojet applications
[NASA-TM-106222] p 92 N93-28694
Gravity sensitivity of a resistojets water vaporizer
[NASA-TM-106220] p 92 N93-29194

RESOLUTION

- Mathematical relationship between two sets of laser
anemometer measurements for resolving the total velocity
vector
[NASA-TM-105986] p 35 N93-22599

RESONANT FREQUENCIES

- Dynamic analysis of a pre-and-post ice impacted
blade
[AIAA PAPER 92-4273] p 22 A93-13333
Fully coupled resonant-triad interaction in an
adverse-pressure-gradient boundary layer
p 167 A93-21049

- Measurement of frequency response in short
thermocouple wires p 209 A93-40677
Experimental validation of boundary element methods
for noise prediction
[NASA-TM-105729] p 226 N93-10966

- Dynamic analysis of a pre-and-post ice impacted
blade
[NASA-TM-105829] p 144 N93-12197

RESONANT VIBRATION

- A new pre-loaded beam geometric stiffness matrix with
full rigid body capabilities p 54 A93-12145

RESONATORS

- Coplanar waveguide radial line stub
p 155 A93-36514
Conductor-backed coplanar waveguide resonators of
Y-Ba-Cu-O and Ti-Ba-Ca-Cu-O on LaAlO3
[NASA-TM-105890] p 284 N93-12325

RESOURCE ALLOCATION

- Scheduling lessons learned from the Autonomous Power
System p 265 N93-18671

REUSABLE LAUNCH VEHICLES

- Prospects for utilization of air liquefaction and
enrichment system (ALES) propulsion in fully reusable
launch vehicles
[AIAA PAPER 93-2025] p 74 A93-49861
The design and evolution of the beta two-stage-to-orbit
horizontal takeoff and landing launch system
[NASA-TM-106118] p 51 N93-27018

REUSABLE ROCKET ENGINES

- An advanced method for tracking the evolution of fatigue
damage in reusable space propulsion systems
p 234 A93-16406

- Ceramic matrix composites for rocket engine turbine applications
[ASME PAPER 92-GT-394] p 99 A93-19547
- Damage-mitigating control of space propulsion systems for high performance and extended life
[AIAA PAPER 93-2080] p 74 A93-49907
- Real-time diagnostics for a reusable rocket engine
[NASA-TM-105792] p 266 N93-19018
- Overview of the fatigue/fracture/life prediction working group program at the Lewis Research Center
p 232 N93-31574
- REVERSED FLOW**
Effects of flow-path variations on internal reversing flow in a tailpipe offtake configuration for ASTOVL aircraft
[AIAA PAPER 93-2438] p 29 A93-50190
- Effects of flow-path variations on internal reversing flow in a tailpipe offtake configuration for ASTOVL aircraft
[NASA-TM-106149] p 38 N93-29065
- REYNOLDS EQUATION**
Calculation of stiffness and damping coefficients for elastically supported gas foil bearings
p 221 A93-27308
- Some practical turbulence modeling options for Reynolds-averaged full Navier-Stokes calculations of three-dimensional flows
[AIAA PAPER 93-2964] p 10 A93-48158
- REYNOLDS NUMBER**
New time scale based k-epsilon model for near-wall turbulence
p 180 A93-41909
- Direct numerical simulation of instabilities in parallel flow with spherical roughness elements
[NASA-TM-105847] p 192 N93-11529
- User manual for NASA Lewis 10 by 10 foot supersonic wind tunnel
[NASA-TM-105626] p 42 N93-15498
- REYNOLDS STRESS**
A simplified Reynolds stress model for unsteady turbulent boundary layers
[AIAA PAPER 93-0204] p 168 A93-22622
- Critical assessment of Reynolds stress turbulence models using homogeneous flows
[AIAA PAPER 93-0082] p 170 A93-24227
- A critical comparison of several low Reynolds number k-epsilon turbulence models for flow over a backward-facing step
[AIAA PAPER 93-1927] p 189 A93-53586
- Center for Modeling of Turbulence and Transition (CMOTT): Research Briefs, 1992
[NASA-TM-105834] p 195 N93-15792
- Turbulence modeling and experiments
p 195 N93-15796
- A realizable Reynolds stress algebraic equation model
[NASA-TM-105993] p 16 N93-16596
- Critical assessment of Reynolds stress turbulence models using homogeneous flows
[NASA-TM-105954] p 196 N93-16703
- A critical comparison of several low Reynolds number k-epsilon turbulence models for flow over a backward facing step
[NASA-TM-106173] p 270 N93-32200
- RHENIUM**
Low thrust chemical rocket technology
[NASA-TM-105927] p 83 N93-15572
- RHENIUM ALLOYS**
Preliminary evaluation of tensile and stress-rupture behavior of W + 24 at. pct Re + 0.4 at. pct HfC wire
p 125 A93-25119
- RIBBONS**
The microstructural evolution, crystallography, and thermal processing of ultrahigh carbon Fe-1.85 pct C melt-spun ribbon
p 125 A93-32934
- RIBS (SUPPORTS)**
Heat transfer performance comparisons of five different rectangular channels with parallel angled ribs
p 166 A93-18752
- RICCATI EQUATION**
Optimal control study for the Space Station Solar Dynamic power module
p 54 A93-13133
- RIGID STRUCTURES**
A new pre-loaded beam geometric stiffness matrix with full rigid body capabilities
p 54 A93-12145
- COLD-SAT dynamic model
[NASA-TM-105185] p 59 N93-19988
- RING STRUCTURES**
I-BIEM calculations of the frequency dispersion and ac current distribution at disk and ring-disk electrodes
p 254 A93-34246
- Application of artificial neural networks to the design optimization of aerospace structural components
[NASA-TM-4389] p 247 N93-21831
- RISK**
Probabilistic evaluation of uncertainties and risks in aerospace components
p 233 A93-12160
- RL-10-A-3 ENGINE**
An RL10A-3-3A rocket engine model using the Rocket Engine Transient Simulator (ROCETS) software
[AIAA PAPER 93-2357] p 75 A93-50129
- ROBOT DYNAMICS**
The detrimental effect of friction on space microgravity robotics
p 222 A93-35546
- Inverse kinematics problem in robotics using neural networks
[NASA-TM-105869] p 247 N93-18876
- ROBOTICS**
Inverse kinematics problem in robotics using neural networks
[NASA-TM-105869] p 247 N93-18876
- Small Stirling dynamic isotope power system for robotic space missions
[NASA-TM-105785] p 92 N93-28686
- ROBUSTNESS (MATHEMATICS)**
Robust integrated flight/propulsion control design for a STOVL aircraft using H-infinity control design techniques
p 40 A93-26432
- Design and evaluation of a robust dynamic neurocontroller for a multivariable aircraft control problem
p 40 A93-37004
- Field by field hybrid upwind splitting methods
[AIAA PAPER 93-3302] p 8 A93-45000
- Integrated flight/propulsion control - Subsystem specifications for performance
[AIAA PAPER 93-3808] p 41 A93-51400
- A comparative study of multivariable robustness analysis methods as applied to integrated flight and propulsion control
[AIAA PAPER 93-3809] p 21 A93-51401
- Robustness enhancement of neurocontroller and state estimator
[NASA-TM-106028] p 42 N93-26907
- Explicit robust schemes for implementation of general principal value-based constitutive models
[NASA-TM-106123] p 258 N93-26947
- ROCKET ENGINE CASES**
Application of composite materials to impact-insensitive munitions
p 97 A93-11459
- ROCKET ENGINE CONTROL**
A neural network-based estimator for the mixture ratio of the Space Shuttle Main Engine
[NASA-TM-106070] p 87 N93-25089
- ROCKET ENGINE DESIGN**
Reliability studies of Integrated Modular Engine system designs
[AIAA PAPER 93-1886] p 72 A93-49759
- Fluid design studies of integrated modular engine system
[AIAA PAPER 93-1887] p 72 A93-49760
- Predicted performance of an Integrated Modular Engine system
[AIAA PAPER 93-1888] p 72 A93-49761
- Performance of a low-power subsonic-arc-attachment arcjet thruster
[AIAA PAPER 93-1898] p 72 A93-49768
- Investigation of a subsonic-arc-attachment thruster using segmented anodes
[AIAA PAPER 93-1899] p 73 A93-49769
- Recent testing of 30 KW hydrogen arcjet thrusters
[AIAA PAPER 93-1902] p 73 A93-49772
- Structured system engineering methodologies used to develop a nuclear thermal propulsion engine
[AIAA PAPER 93-2109] p 271 A93-49930
- Design and fabrication of a hydrogen/oxygen thrust chamber assembly
[AIAA PAPER 93-2132] p 74 A93-49951
- Design and test of a small two stage counter-rotating turbine for rocket engine application
[AIAA PAPER 93-2136] p 74 A93-49954
- A comparison of nuclear thermal rocket development cost and schedule for piloted missions to Mars
[AIAA PAPER 93-2263] p 44 A93-50057
- An RL10A-3-3A rocket engine model using the Rocket Engine Transient Simulator (ROCETS) software
[AIAA PAPER 93-2357] p 75 A93-50129
- BMDO electric space-propulsion program
[AIAA PAPER 93-1934] p 78 A93-50322
- A survey of instabilities within centrifugal pumps and concepts for improving the flow range of pumps in rocket engines
p 190 N93-10039
- Test program to provide validation data for the Rocket Combustor Interactive Design (ROCCID) code
p 120 N93-11450
- Second Magnetoplasmodynamic Thruster Workshop
[NASA-CP-10109] p 279 N93-18635
- Nuclear thermal propulsion technology: Results of an interagency panel in FY 1991
[NASA-TM-105711] p 86 N93-24740
- Rocket engine numerical simulator
p 89 N93-26962
- Reliability studies of integrated modular engine system designs
[NASA-TM-106178] p 91 N93-27022
- ROCKET ENGINES**
Integrated health monitoring and controls for rocket engines
[SAE PAPER 921031] p 66 A93-14654
- Evaluation of the Munich Method for modeling rocket engine performance
p 70 A93-31968
- Qualitative model-based diagnostics for rocket systems
[AIAA PAPER 93-1779] p 72 A93-49674
- CFD analyses of coolant channel flowfields
[AIAA PAPER 93-1830] p 184 A93-49715
- A new facility for advanced rocket propulsion research
[AIAA PAPER 93-1859] p 48 A93-49737
- Advanced instrumentation for next-generation aerospace propulsion control systems
[AIAA PAPER 93-2079] p 211 A93-49906
- Development and use of hydrogen-air torches in an altitude facility
[AIAA PAPER 93-2176] p 42 A93-49988
- Thermal stratification potential in rocket engine coolant channels
p 78 N93-10019
- A survey of instabilities within centrifugal pumps and concepts for improving the flow range of pumps in rocket engines
p 190 N93-10039
- Performance and heat transfer characteristics of a carbon monoxide/oxygen rocket engine
[NASA-TM-105897] p 84 N93-18878
- Development and use of hydrogen-air torches in an altitude facility
[NASA-TM-106047] p 43 N93-26214
- Qualitative model-based diagnostics for rocket systems
[NASA-TM-106234] p 51 N93-28052
- A new facility for advanced rocket propulsion research
[NASA-TM-106193] p 49 N93-28696
- ROCKET EXHAUST**
The application of structural reliability techniques to plume impingement loading of the Space Station Freedom Photovoltaic Array
[AIAA PAPER 93-1338] p 56 A93-33908
- Analysis of plume backflow around a nozzle lip in a nuclear rocket
[AIAA PAPER 93-2497] p 77 A93-50231
- A plume spectroscopy system for flight applications
[AIAA PAPER 93-2511] p 63 A93-50242
- Plume characteristics of an arcjet thruster
[AIAA PAPER 93-2530] p 77 A93-50258
- The application of structural reliability techniques to plume impingement loading of the Space Station Freedom Photovoltaic Array
[NASA-TM-105949] p 59 N93-17988
- Laser Rayleigh and Raman diagnostics for small hydrogen/oxygen rockets
[NASA-TM-105999] p 83 N93-17995
- Pulsed laser Rayleigh scattering diagnostic for hydrogen/oxygen rocket exit plane flowfield velocimetry
[NASA-TM-106213] p 88 N93-26149
- ROCKET LININGS**
Hot fire test results of subscale tubular combustion chambers
p 79 N93-10020
- Hot fire test results of subscale tubular combustion chambers
[NASA-TP-3222] p 81 N93-11614
- ROCKET NOZZLES**
Calculations of low Reynolds number rocket nozzles
[AIAA PAPER 93-0888] p 67 A93-24948
- Numerical study of nozzle wall cooling for nuclear thermal rockets
[AIAA PAPER 93-2498] p 77 A93-50232
- Nuclear thermal propulsion technology overview
p 89 N93-26927
- ROCKET OXIDIZERS**
A neural network-based estimator for the mixture ratio of the Space Shuttle Main Engine
[NASA-TM-106070] p 87 N93-25089
- ROCKET PROPELLANTS**
Benefits of in situ propellant utilization for a Mars sample return mission
[AIAA PAPER 93-2244] p 140 A93-50046
- Atomic hydrogen propellants: Historical perspectives and future possibilities
[NASA-TM-106053] p 84 N93-20614
- Benefits of in situ propellant utilization for a Mars sample return mission
[NASA-TM-106243] p 141 N93-28695
- ROCKET TEST FACILITIES**
Design of an Advanced Expander Test Bed
[AIAA PAPER 93-2133] p 48 A93-49952
- Space chemical propulsion test facilities at NASA Lewis Research Center
[NASA-TM-106050] p 85 N93-23405
- RODS**
Effect of out-of-roundness on the performance of a diesel engine connecting-rod bearing
p 225 A93-52607

ROTARY WING AIRCRAFT

Closed form expressions for crack mouth displacements and stress intensity factors for chevron notched short bar and short rod specimens based on experimental compliance measurements
[NASA-TM-83796] p 246 N93-15369

ROTARY WING AIRCRAFT

An overview of shed ice impact studies in the NASA Lewis Icing Research Tunnel
[AIAA PAPER 93-0301] p 5 A93-23247
Time-variant analysis of rotorcraft systems dynamics - An exploitation of vector processors p 220 A93-23512

Engineering science research issues in high power density transmission dynamics for aerospace applications --- rotorcraft geared rotors
[AIAA PAPER 93-2299] p 224 A93-50084

An overview of shed ice impact in the NASA Lewis Icing Research Tunnel
[NASA-TM-105969] p 16 N93-15404

ROTATING DISKS

Forced response of mistuned bladed disk assemblies
[AIAA PAPER 93-1491] p 239 A93-34033
I-BIEM calculations of the frequency dispersion and ac current distribution at disk and ring-disk electrodes p 254 A93-34246

Hydrodynamic behavior and electrochemical impedance of the Hanging Meniscus Rotating Disk (HMRD) electrode. I - Meniscus shape under rotation. II - I-BIEM calculations of frequency dispersion and minimization p 116 A93-34247

Fatigue criterion to system design, life and reliability: A primer
[NASA-TM-106022] p 248 N93-23406

ROTATING FLUIDS

Analysis of unsteady wave processes in a rotating channel
[AIAA PAPER 93-2527] p 187 A93-50255

Heat transfer in rotating serpentine passages with selected model orientation for smooth or skewed trip walls
[NASA-TM-106126] p 147 N93-25177

ROTATING STALLS

Stability of fully developed rotating stall
[ASME PAPER 92-GT-57] p 23 A93-19307

Prediction of active control of subsonic centrifugal compressor rotating stall
[AIAA PAPER 93-0153] p 4 A93-22591

A model for the selective amplification of spatially coherent waves in a centrifugal compressor on the verge of rotating stall
[AIAA PAPER 93-2236] p 13 A93-50039

ROTATION

Acoustic mode measurements in the inlet of a model turbofan using a continuously rotating rake - Data collection/analysis techniques p 24 A93-23324
[AIAA PAPER 93-0599]

Acoustic mode measurements in the inlet of a model turbofan using a continuously rotating rake: Data collection/analysis techniques
[NASA-TM-105936] p 33 N93-15403

Rotating rake design for unique measurement of fan-generated spinning acoustic modes
[NASA-TM-105946] p 36 N93-26161

ROTOR AERODYNAMICS

Aerodynamic design of turbomachinery blading in three-dimensional flow - An application to radial inflow turbines p 3 A93-19324
[ASME PAPER 92-GT-74]

Analytic methods for design of wave cycles for wave rotor core engines p 30 A93-50253
[AIAA PAPER 93-2523]

Laser velocimeter measurements of the flow field generated by a forward-swept propfan during flutter
[AIAA PAPER 93-2919] p 14 A93-53591

Radial turbine cooling p 191 N93-10061
Localization of aeroelastic modes in mistuned high-energy turbines p 230 N93-31586

ROTOR BLADES

Dynamic analysis of a pre-and-post ice impacted blade
[AIAA PAPER 92-4273] p 22 A93-13333

Structural tailoring of aircraft engine blade subject to ice impact constraints p 23 A93-20319
[AIAA PAPER 92-4710]

An iterative multidisciplinary analysis for rotor blade shape determination p 28 A93-49912
[AIAA PAPER 93-2085]

A comparison between numerically modelled and experimentally measured loss mechanisms in wave rotors p 30 A93-50252
[AIAA PAPER 93-2522]

Radial turbine cooling p 15 N93-13292
[NASA-TM-105658]

ROTOR BLADES (TURBOMACHINERY)

Aerodynamic design of turbomachinery blading in three-dimensional flow - An application to radial inflow turbines p 3 A93-19324
[ASME PAPER 92-GT-74]

Heat transfer in rotating serpentine passages with trips skewed to the flow p 166 A93-19416
[ASME PAPER 92-GT-191]

Linearized Euler predictions of unsteady aerodynamic loads in cascades p 7 A93-29318
Dynamics of rotating multicomponent turbomachinery systems p 222 A93-34157
[AIAA PAPER 93-1629]

Dynamics of rotating multi-component turbomachinery systems p 247 N93-18426
[NASA-TM-105997]

ROTOR BODY INTERACTIONS

Forcing function effects on unsteady aerodynamic gust response. I - Forcing functions p 3 A93-19400
[ASME PAPER 92-GT-174]

ROTOR DYNAMICS

Bgrid - Interactive three-dimensional turbomachinery grid generation system with applications p 259 A93-25527
[AIAA PAPER 93-0430]

Hybrid active vibration control of rotorbearing systems using piezoelectric actuators p 221 A93-27324
Dynamics of rotating multicomponent turbomachinery systems p 222 A93-34157
[AIAA PAPER 93-1629]

Vibration localization in mono- and bi-coupled bladed disks - A transfer matrix approach p 222 A93-34241
[AIAA PAPER 93-1492]

Two-dimensional CFD modeling of wave rotor flow dynamics p 9 A93-45014
[AIAA PAPER 93-3318]

Design of an oxygen turbopump for use in an Advanced Expander Test Bed engine p 48 A93-49955
[AIAA PAPER 93-2137]

Dynamics of rotating multi-component turbomachinery systems p 247 N93-18426
[NASA-TM-105997]

ROTOR SPEED

Brush seal leakage performance with gaseous working fluids at static and low rotor speed conditions p 219 A93-19494
[ASME PAPER 92-GT-304]

ROTORORS

An improved numerical model for wave rotor design and analysis p 24 A93-23364
[AIAA PAPER 93-0482]

Modal analysis of multistage gear systems coupled with gearbox vibrations p 222 A93-36588
Experimental evaluation of a cooled radial-inflow turbine p 27 A93-49685
[AIAA PAPER 93-1795]

Three-dimensional numerical simulation of gradual opening in a wave rotor passage p 187 A93-50254
[AIAA PAPER 93-2526]

Brush seal low surface speed hard-rub characteristics p 225 A93-50261
[AIAA PAPER 93-2534]

Initial results from the NASA Lewis wave rotor experiment p 30 A93-53589
[AIAA PAPER 93-2521]

Stochastic sensitivity measure for mistuned high-performance turbines p 245 N93-12277
[NASA-TM-105821]

An improved numerical model for wave rotor design and analysis p 33 N93-12418
[NASA-TM-105915]

Brush seal bristle flexure and hard-rub characteristics p 227 N93-18321
[NASA-TM-105864]

Study of the capacitance technique for measuring high-temperature blade tip clearance on ceramic rotors p 35 N93-23013
[NASA-TM-105978]

Brush seal low surface speed hard-rub characteristics p 200 N93-27132
[NASA-TM-106169]

Experimental evaluation of a cooled radial-inflow turbine p 38 N93-28697
[NASA-TM-106230]

Initial results from the NASA-Lewis wave rotor experiment p 39 N93-32368
[NASA-TM-106148]

ROVING VEHICLES

Estimates of power requirements for a Manned Mars Rover powered by a nuclear reactor p 45 A93-13783
Shielding analysis for a manned Mars rover powered by an SP-100 type reactor p 45 A93-13793

Electromagnetic powered vehicles (EMPV) for Mars exploration p 47 A93-20761
[NASA-TM-106148]

RP-1 ROCKET PROPELLANTS

Some aspects of secondary atomization of aluminum/hydrocarbon slurry propellants p 140 A93-34478
[NASA-TM-106254]

Lubrication of an 85-mm ball bearing with RP-1 p 225 A93-53590
[AIAA PAPER 93-2538]

Lubrication of an 85-mm ball bearing with RP-1 p 51 N93-31670
[NASA-TM-106254]

RUNGE-KUTTA METHOD

Direct calculations of waves in fluid flows using a high-order compact difference scheme p 171 A93-24232
[AIAA PAPER 93-0148]

Eno-Osher schemes for Euler equations p 268 N93-15341
[NASA-TM-105928]

RUTILE

Vickers indentation hardness of stoichiometric and reduced single crystal TiO₂ (rutile) from 25 to 800 C p 96 N93-26204
[NASA-TM-105959]

S

S WAVES

Jet mixer noise suppressor using acoustic feedback [NASA-CASE-LEW-15170-1] p 275 N93-28953

SAFETY DEVICES

A system to measure lightning-induced transients on spacecraft umbilical lines p 161 N93-24889

SAFETY FACTORS

Contributions of microgravity test results to the design of spacecraft fire-safety systems p 56 A93-31028
[AIAA PAPER 93-1152]

Reliability based structural optimization - A simplified safety index approach p 239 A93-33972
[AIAA PAPER 93-1418]

SAFETY MANAGEMENT

Lewis safety manual p 147 N93-70966
[NASA-TM-104438]

SALINITY

One-dimensional transient finite difference model of an operational salinity gradient solar pond p 193 N93-13400

SANDS

The chemistry of Saudi Arabian sand - A deposition problem on helicopter turbine airfoils p 243 A93-53468

SANDWICH STRUCTURES

Solar concentrators for advanced solar-dynamic power systems in space p 85 N93-23017
[NASA-CR-187148]

SAPPHIRE

Large-area YBa₂Cu₃O₇(δ) thin films on sapphire for microwave applications p 279 A93-11475
Buffer layers for high-T_c thin films on sapphire p 150 A93-17063

Interfacial shear strength of cast and directionally solidified NiAl-sapphire fiber composites p 106 A93-55685

Demonstration of YBa₂Cu₃O₇(δ) and complementary metal-oxide-semiconductor device fabrication on the same sapphire substrate p 159 A93-56292

High performance sapphire windows p 218 N93-22198

SARSAT

GaAs monolithic R.F. modules for SARSAT distress beacons p 152 A93-25806

SATELLITE ANTENNAS

A prototype automatic phase compensation module [NASA-TM-105930] p 160 N93-16616

SATELLITE ATTITUDE CONTROL

COLD-SAT dynamic model p 59 N93-19988
[NASA-TM-105185]

SATELLITE COMMUNICATION

The performance evaluation of a new neural network based traffic management scheme for a satellite communication network p 147 A93-10929

GSFC conceptual design study for an inter-satellite Optical Multiple Access communication system p 52 A93-18966

Efficient demultiplexing algorithm for noncontiguous carriers p 148 A93-32561

A high-efficiency 59- to 64-GHz TWT for intersatellite communications p 158 A93-49553

SITE project. Phase 1: Continuous data bit-error-rate testing [NASA-TP-3279] p 58 N93-11001

Space Communication Artificial Intelligence for Link Evaluation Terminal (SCAILET) p 265 N93-11940

Anomalous TWTA output power spikes and their effect on a digital satellite communications system p 159 N93-13286
[NASA-TM-105875]

A prototype automatic phase compensation module [NASA-TM-105930] p 160 N93-16616

Allocations by the 1992 World Administrative Radio Conference p 150 N93-26476

Satellites and the BISDN: An overview of NASA R/D [NASA-TM-106108] p 150 N93-26903

Utilizing a TDRS satellite for direct broadcast satellite-radio propagation experiments and demonstrations [NASA-TM-106172] p 53 N93-27064

SATELLITE NETWORKS

- The performance evaluation of a new neural network based traffic management scheme for a satellite communication network p 147 A93-10929
- A high-efficiency 59- to 64-GHz TWT for intersatellite communications p 158 A93-49553
- ISDN at NASA Lewis Research Center [NASA-TM-105911] p 262 N93-12410

SATELLITE ORIENTATION

- LDEF yaw and pitch angle estimates p 58 N93-12772

SATELLITE POWER TRANSMISSION

- An analysis of power beaming for the moon and Mars p 253 A93-25974

SATELLITE TEMPERATURE

- The effects of simulated low Earth orbit environments on spacecraft thermal control coatings [NASA-TM-106146] p 61 N93-27019

SATELLITE TRANSMISSION

- OLYMPUS/ACTS scintillation experiment at the Lewis Research Center p 150 N93-26481
- Utilizing a TDRS satellite for direct broadcast satellite-radio propagation experiments and demonstrations [NASA-TM-106172] p 53 N93-27064

SAUDI ARABIA

- The chemistry of Saudi Arabian sand - A deposition problem on helicopter turbine airfoils p 243 A93-53468

SCALARS

- Stochastic inflation lattice simulations - Ultra-large scale structure of the universe p 289 A93-17646

SCALE MODELS

- Measured acoustic characteristics of ducted supersonic jets at different model scales [AIAA PAPER 93-0731] p 273 A93-24821

SCALING LAWS

- Scaling analysis of gas-liquid two-phase flow pattern in microgravity [AIAA PAPER 93-0914] p 173 A93-24968

SCANNING TUNNELING MICROSCOPY

- Characterization of Si₃N₄/SiO₂ optical channel waveguides by photon scanning tunneling microscopy p 211 A93-49458

SCATTERING

- Discrete ordinates solutions for radiatively participating media in a cylindrical enclosure p 285 A93-31427

SCHEDULES

- Scheduling lessons learned from the Autonomous Power System p 265 N93-18671

SCHEDULING

- Scheduling lessons learned from the Autonomous Power System p 265 N93-18671

SCHLIEREN PHOTOGRAPHY

- Compact color schlieren optical system p 277 A93-52071

SCHOTTKY DIODES

- Development of a hydrogen gas sensor using microfabrication technology [SAE PAPER 921176] p 210 A93-41356
- The development of hydrogen sensor technology for aerospace applications [AIAA PAPER 93-2375] p 211 A93-50144
- The development of hydrogen sensor technology at NASA Lewis Research Center [NASA-TM-106141] p 216 N93-27021

SCINTILLATION

- OLYMPUS/ACTS scintillation experiment at the Lewis Research Center p 150 N93-26481

SEALING

- Friction-factor data for flat-plate tests of smooth and honeycomb surfaces [ASME PAPER 91-TRIB-20] p 219 A93-15682
- Method of applying a thermal barrier coating system to a substrate [NASA-CASE-LEW-15020-2] p 107 N93-14706

SEALS (STOPPERS)

- Relative sliding durability of two candidate high-temperature oxide fiber seal materials p 132 A93-31983
- A hot dynamic seal rig for measuring hypersonic engine seal durability and flow performance [AIAA PAPER 93-1346] p 222 A93-33916
- Development of braided rope seals for hypersonic engine applications - Flow modeling p 222 A93-34493
- Development of hypersonic engine seals - Flow effects of preload and engine pressures [AIAA PAPER 93-1998] p 223 A93-49841
- Relative sliding durability of candidate high temperature fiber seal materials [NASA-TM-105806] p 95 N93-10978
- Development of braided rope seals for hypersonic engine applications: Flow modeling [NASA-TM-105942] p 227 N93-14478
- High-temperature, bellows hybrid seal [NASA-CASE-LEW-15570-1] p 227 N93-19027

- Sliding durability of candidate seal fiber materials in hydrogen from 25 to 900 C [NASA-TM-105939] p 95 N93-22590

SECONDARY FLOW

- Aeroloids and secondary flows in a transonic mixed flow turbine stage [ASME PAPER 92-GT-72] p 2 A93-19322
- Study on vortex generator flow control for the management of inlet distortion p 7 A93-34488
- Initial development of the two-dimensional ejector shear layer - Experimental results [AIAA PAPER 93-2440] p 29 A93-50192

SECONDARY ION MASS SPECTROMETRY

- SIMS studies of oxide growth on beta-NiAl p 127 A93-53469

SEISMOGRAPHS

- Venus Interior Structure Mission (VISM): Establishing a seismic network on Venus p 293 N93-28819

SEISMOLOGY

- Venus Interior Structure Mission (VISM): Establishing a seismic network on Venus p 293 N93-28819

SELECTIVE SURFACES

- Analysis of reflector antenna system including frequency selective surfaces p 52 A93-32820

SELF ADAPTIVE CONTROL SYSTEMS

- Self-tuning multivariable pole placement control of a multizone crystal growth furnace p 263 A93-10575

SELF CONSISTENT FIELDS

- Critical experiments of the self-consistent model for polycrystalline Hastelloy-X p 124 A93-21958

SELF ERECTING DEVICES

- Design and optimization of a self-deploying single axis tracking PV array p 252 A93-25916

SELF EXCITATION

- Enhanced mixing of a rectangular supersonic jet by natural and induced screech [NASA-TM-106245] p 18 N93-31672

SELF LUBRICATING MATERIALS

- Properties of extruded PS-212 type self-lubricating materials p 138 N93-25565

SELF LUBRICATION

- The effect of processing and compositional changes on the tribology of PM212 in air [NASA-TM-105945] p 95 N93-15576

SELF ORGANIZING SYSTEMS

- Neural networks in structural analysis and design - An overview [AIAA PAPER 92-4805] p 263 A93-20388
- Self-organization in neural networks - Applications in structural optimization p 265 A93-54534

SEMICONDUCTING FILMS

- Enhancement of photoluminescence intensity of GaAs with cubic GaS chemical vapor deposited using a structurally designed single-source precursor p 280 A93-26930
- Ellipsometric study of metal-organic chemically vapor deposited III-V semiconductor structures p 281 A93-35697
- Metal-organic chemical vapour deposition of polycrystalline tetragonal indium sulphide (InS) thin films p 116 A93-36584
- Atomic probe microscopy of 3C SiC films grown on 6H SiC substrates p 281 A93-39854
- Progress in silicon carbide semiconductor technology p 158 A93-44965
- Process for the controlled growth of single-crystal films of silicon carbide polytypes on silicon carbide wafers [NASA-CASE-LEW-15222-3] p 284 N93-17413

SEMICONDUCTOR DEVICES

- Neutron, gamma ray, and temperature effects on the electrical characteristics of thyristors p 153 A93-25894
- Interface dependence of band offsets in lattice-matched isovalent heterojunctions p 280 A93-32132
- The development of hydrogen sensor technology for aerospace applications [AIAA PAPER 93-2375] p 211 A93-50144
- Process for the controlled growth of single-crystal films of silicon carbide polytypes on silicon carbide wafers [NASA-CASE-LEW-15222-3] p 284 N93-17413
- A survey and analysis of commercially available hydrogen sensors [NASA-TM-105878] p 214 N93-17777
- Semiconductor cooling apparatus [NASA-CASE-LEW-14162-3] p 111 N93-29614

SEMICONDUCTOR LASERS

- Space transfer with ground-based laser/electric propulsion [NASA-TM-106060] p 84 N93-20615

SEMICONDUCTORS (MATERIALS)

- Silicon carbide, a semiconductor for space power electronics p 279 A93-13880
- Ellipsometric study of metal-organic chemically vapor deposited III-V semiconductor structures p 281 A93-35697

- Progress in silicon carbide semiconductor technology p 158 A93-44965

- Room temperature synthesis of copper indium diselenide in non-aqueous solution using an organoindium reagent p 283 A93-54844
- Electrical design of payload G-534: The Pool Boiling Experiment p 144 N93-13170
- Radiation and temperature effects on electronic components investigated under the CSTI high capacity power project [NASA-TM-106096] p 161 N93-24746
- Silicon carbide semiconductor technology for high temperature and radiation environments p 284 N93-26928

SENSITIVITY

- Computational methods for efficient structural reliability and reliability sensitivity analysis [AIAA PAPER 93-1626] p 240 A93-34155

SENSORS

- The development of hydrogen sensor technology at NASA Lewis Research Center p 216 N93-27021
- Thin film heat flux sensor for Space Shuttle Main Engine turbine environment p 217 N93-31554

SEPARATED FLOW

- An experimental investigation of S-duct flow control using arrays of low-profile vortex generators [AIAA PAPER 93-0018] p 170 A93-24226
- Use of surface heat transfer measurements as a flow separation diagnostic in a two-dimensional reflected oblique shock/turbulent boundary layer interaction [AIAA PAPER 93-0775] p 172 A93-24859
- Effect of a rotating propeller on the separation angle of attack [AIAA PAPER 93-0017] p 6 A93-24978
- Calculations of separated 3-D flows with a pressure-staggered Navier-Stokes equations solver p 177 A93-34366
- 3-D viscous flow CFD analysis of the propeller effect on an advanced ducted propeller subsonic inlet [AIAA PAPER 93-1847] p 12 A93-49728
- A comparative study of Full Navier-Stokes and Reduced Navier-Stokes analyses for separating flows within a diffusing inlet S-duct [AIAA PAPER 93-2154] p 13 A93-49970
- A critical comparison of several low Reynolds number k-epsilon turbulence models for flow over a backward-facing step [AIAA PAPER 93-1927] p 189 A93-53586
- Use of surface heat transfer measurements as a flow separation diagnostic in a two dimensional reflected oblique shock/turbulent boundary layer interaction [NASA-TM-105981] p 194 N93-15355
- A realizable Reynolds stress algebraic equation model [NASA-TM-105993] p 16 N93-16596
- Effect of a rotating propeller on the separation angle of attack and distortion in ducted propeller inlets [NASA-TM-105935] p 16 N93-16625
- Analytical and experimental studies of a short compact subsonic diffuser for a two-dimensional supersonic inlet [NASA-TP-3247] p 17 N93-24118
- Surface and flow field measurements in a symmetric crossing shock wave/turbulent boundary-layer interaction [NASA-TM-106086] p 17 N93-24911
- Calculations of turbulent separated flows [NASA-TM-106154] p 200 N93-27161
- The 3-D viscous flow CFD analysis of the propeller effect on an advanced ducted propeller subsonic inlet [NASA-TM-106240] p 38 N93-29162
- A critical comparison of several low Reynolds number k-epsilon turbulence models for flow over a backward facing step [NASA-TM-106173] p 270 N93-32200

SERT 2 SPACECRAFT

- Development and flight history of the SERT II spacecraft p 71 A93-38976

SERVICE LIFE

- An advanced method for tracking the evolution of fatigue damage in reusable space propulsion systems p 234 A93-16406
- Damage-mitigating control of aerospace systems for high performance and extended life p 263 A93-22967
- Long life Regenerative Fuel Cell technology development plan p 252 A93-25867
- A vacuum (10 exp -9 torr) friction apparatus for determining friction and endurance life of MoS(x) films p 146 A93-49245
- Derailed ion thruster development status [AIAA PAPER 93-2225] p 75 A93-50031
- Maximum life spiral bevel reduction design [NASA-TM-105790] p 226 N93-10982
- 100-kW class applied-field MPD thruster component wear [NASA-TM-106023] p 85 N93-22482

- Structural Integrity and Durability of Reusable Space Propulsion Systems
[NASA-CP-10064] p 93 N93-31552
- SHAFTS (MACHINE ELEMENTS)**
Maximum life spiral bevel reduction design
[NASA-TM-105790] p 226 N93-10982
- SHAPE CONTROL**
Grounding of space structures p 54 A93-12144
Boundary formulations for three-dimensional continuum structural shape sensitivity analysis p 235 A93-22426
- SHAPE FUNCTIONS**
Transition elements based on transfinite interpolation [AIAA PAPER 93-1326] p 267 A93-33899
Boundary formulations for sensitivity analysis without matrix derivatives p 242 A93-49028
- SHAPES**
Shape reanalysis and sensitivities utilizing preconditioned iterative boundary solvers p 233 A93-14446
Fiber shape effects on metal matrix composite behavior p 98 A93-15752
Hydrodynamic behavior and electrochemical impedance of the Hanging Meniscus Rotating Disk (HMRD) electrode. I - Meniscus shape under rotation. II - I-BIEM calculations of frequency dispersion and minimization p 116 A93-34247
An iterative multidisciplinary analysis for rotor blade shape determination [AIAA PAPER 93-2085] p 28 A93-49912
Optimal design of composite hip implants using NASA technology p 257 N93-22188
Fiber shape effects on metal matrix composite behavior [NASA-TM-106067] p 109 N93-26704
Experimental and computational ice shapes and resulting drag increase for a NACA 0012 airfoil p 17 N93-27440
- SHEAR FLOW**
Weakly nonlinear models for turbulent mixing in a plane mixing layer p 165 A93-17416
A new energy transfer model for turbulent free shear flow [NASA-TM-105854] p 191 N93-10454
Modeling of turbulent shear flows p 195 N93-15797
- SHEAR LAYERS**
The eigenvalue spectrum of the Rayleigh equation for a plane shear layer p 168 A93-21725
A study of compressible mixing layers using filtered Rayleigh scattering [AIAA PAPER 92-0175] p 173 A93-24982
Vorticity dynamics of inviscid shear layers p 181 A93-45734
Linear instability of curved free shear layers [AIAA PAPER 93-3252] p 183 A93-46797
CFD validation of subsonic turbulent planar shear layers [AIAA PAPER 93-1773] p 184 A93-49669
Comparison of reacting and non-reacting shear layers at a high subsonic Mach number [AIAA PAPER 93-2381] p 186 A93-50149
Initial development of the two-dimensional ejector shear layer - Experimental results [AIAA PAPER 93-2440] p 29 A93-50192
Comparison of the initial development of shear layers in two-dimensional and axisymmetric ejector configurations [AIAA PAPER 93-2441] p 29 A93-50193
On the nonlinear three dimensional instability of Stokes layers and other shear layers to pairs of oblique waves [NASA-TM-105918] p 194 N93-15499
Two equation modelling and the pseudo compressibility technique p 195 N93-15799
Comparison of reacting and non-reacting shear layers at a high subsonic Mach number [NASA-TM-106198] p 38 N93-27610
The development of a mixing layer under the action of weak streamwise vortices [NASA-TM-106089] p 201 N93-28947
Enhanced mixing of a rectangular supersonic jet by natural and induced screech [NASA-TM-106245] p 18 N93-31672
Turbulence measurement in a reacting and non-reacting shear layer at a high subsonic Mach number [NASA-TM-106186] p 18 N93-31839
- SHEAR STRAIN**
Experimental investigation of cyclic thermomechanical deformation in torsion [NASA-TM-105938] p 247 N93-17996
- SHEAR STRENGTH**
Transverse flexural tests as a tool for assessing damage to PMR-15 composites from isothermal aging in air at elevated temperatures p 100 A93-24514
Interfacial shear strength of cast and directionally solidified NiAl-sapphire fiber composites p 106 A93-55685
- Transverse flexural tests as a tool for assessing damage to PMR-15 composites from isothermal aging in air at elevated temperatures [NASA-TM-105848] p 107 N93-12737
Determination of plate wave velocities and diffuse field decay rates with broad-band acousto-ultrasonic signals [NASA-TM-106158] p 232 N93-27080
- SHEAR STRESS**
On the shear stabilization of capillary break-up of finite liquid bridges p 143 A93-32069
Effect of service environments on adhesively bonded joints in composite structures p 242 A93-53418
A critical comparison of several low Reynolds number k-epsilon turbulence models for flow over a backward-facing step [AIAA PAPER 93-1927] p 189 A93-53586
Fatigue criterion to system design, life and reliability: A primer [NASA-TM-106022] p 248 N93-23406
A critical comparison of several low Reynolds number k-epsilon turbulence models for flow over a backward facing step [NASA-TM-106173] p 270 N93-32200
- SHEARING**
Preliminary experimental results for a cryogenic brush seal configuration [AIAA PAPER 93-2535] p 225 A93-50262
Preliminary experimental results for a cryogenic brush seal configuration [NASA-TM-106236] p 201 N93-28627
- SHEATHS**
High-temperature, bellows hybrid seal [NASA-CASE-LEW-15570-1] p 227 N93-19027
- SHEETS**
Current status of liquid sheet radiator research [NASA-TM-105764] p 193 N93-14150
- SHELLS (STRUCTURAL FORMS)**
Probabilistic nonlinear finite element analysis of composite structures p 237 A93-32717
Design for progressive fracture in composite shell structures p 242 A93-53394
Applications to car bodies - Generalized layout design of three-dimensional shells p 243 A93-54509
- SHIELDING**
On protection of Freedom's solar dynamic radiator from the orbital debris environment. I - Preliminary analysis and testing p 70 A93-36197
- SHOCK LAYERS**
AGARD WG13 aerodynamics of high speed air intakes: Assessment of CFD results p 192 N93-13220
- SHOCK TUBES**
Visualization of hydrogen injection in a scramjet engine by simultaneous PLIF imaging and laser holographic imaging p 214 N93-13683
Eno-Osher schemes for Euler equations [NASA-TM-105928] p 268 N93-15341
- SHOCK WAVE INTERACTION**
A parametric study of bleed in shock boundary layer interactions [AIAA PAPER 93-0294] p 5 A93-22694
Two-dimensional CFD modeling of wave rotor flow dynamics [AIAA PAPER 93-3318] p 9 A93-45014
An investigation of shock wave turbulent boundary layer interaction with bleed through slanted slots [AIAA PAPER 93-2992] p 11 A93-48184
Numerical simulation of a shock wave/turbulent boundary layer interaction in a duct [AIAA PAPER 93-3127] p 11 A93-48293
Flowfield dynamics in blunt fin-induced shock wave/turbulent boundary layer interactions [AIAA PAPER 93-3133] p 11 A93-48298
Numerical study of shock-induced combustion in methane-air mixtures [AIAA PAPER 93-1917] p 184 A93-49783
Time-sequenced and spectrally filtered Rayleigh imaging of shock wave and boundary layer structure for inlet characterization [AIAA PAPER 93-2300] p 211 A93-50085
A time-accurate high-resolution TVD scheme for solving the Navier-Stokes equations p 13 A93-52006
AGARD WG13 aerodynamics of high speed air intakes: Assessment of CFD results p 192 N93-13220
A time-accurate high-resolution TVD scheme for solving the Navier-Stokes equations [NASA-TM-106056] p 268 N93-22664
- SHOCK WAVE PROFILES**
Analytic methods for design of wave cycles for wave rotor core engines [AIAA PAPER 93-2523] p 30 A93-50253
- SHOCK WAVE PROPAGATION**
Reaction zone structure for strong, weak overdriven, and weak underdriven oblique detonations p 178 A93-35492
- Surface and flow field measurements in a symmetric crossing shock wave/turbulent boundary-layer interaction [NASA-TM-106086] p 17 N93-24911
- SHOCK WAVES**
Use of surface heat transfer measurements as a flow separation diagnostic in a two-dimensional reflected oblique shock/turbulent boundary layer interaction [AIAA PAPER 93-0775] p 172 A93-24859
Analysis of unsteady wave processes in a rotating channel [AIAA PAPER 93-2527] p 187 A93-50255
A time-accurate high-resolution TVD scheme for solving the Navier-Stokes equations p 13 A93-52006
Internal structure of shock waves in disparate mass mixtures p 190 A93-54483
Use of surface heat transfer measurements as a flow separation diagnostic in a two dimensional reflected oblique shock/turbulent boundary layer interaction [NASA-TM-105981] p 194 N93-15355
A time-accurate high-resolution TVD scheme for solving the Navier-Stokes equations [NASA-TM-106056] p 268 N93-22664
Calibration of a shock wave position sensor using artificial neural networks [NASA-TM-106138] p 216 N93-27001
NASA, Lewis Research Center/IFMD inlet duct and nozzle high speed validation experiments p 204 N93-70582
- SHORT CIRCUIT CURRENTS**
Extra high speed modified Lundell alternator parameters and open/short-circuit characteristics from global 3D-FE magnetic field solutions p 156 A93-39348
- SHROUDED PROPELLERS**
Forward rotor vortex effects on counter rotating propeller noise p 2 A93-19221
Acoustic mode measurements in the inlet of a model turbofan using a continuously rotating rake - Data collection/analysis techniques [AIAA PAPER 93-0599] p 244 A93-23324
Acoustic mode measurements in the inlet of a model turbofan using a continuously rotating rake [AIAA PAPER 93-0598] p 273 A93-24783
Effect of a rotating propeller on the separation angle of attack [AIAA PAPER 93-0017] p 6 A93-24978
3-D viscous flow CFD analysis of the propeller effect on an advanced ducted propeller subsonic inlet [AIAA PAPER 93-1847] p 12 A93-49728
Comparison of radiated noise from shrouded and unshrouded propellers p 274 A93-55861
Acoustic mode measurements in the inlet of a model turbofan using a continuously rotating rake: Data collection/analysis techniques [NASA-TM-105936] p 33 N93-15403
Effect of a rotating propeller on the separation angle of attack and distortion in ducted propeller inlets [NASA-TM-105935] p 16 N93-16625
Acoustic mode measurements in the inlet of a model turbofan using a continuously rotating rake [NASA-TM-105989] p 34 N93-16705
Rotating rake design for unique measurement of fan-generated spinning acoustic modes [NASA-TM-105946] p 36 N93-26161
The 3-D viscous flow CFD analysis of the propeller effect on an advanced ducted propeller subsonic inlet [NASA-TM-106240] p 38 N93-29162
- SHROUDS**
Integrity testing of brush seal in shroud ring of T-700 engine [NASA-TM-105863] p 227 N93-18380
- SIDESLIP**
Installed F/A-18 inlet flow calculations at 60 deg angle-of-attack and 10 deg side slip [AIAA PAPER 93-1806] p 12 A93-49695
- SIGNAL ANALYZERS**
Pattern classifier for health monitoring of helicopter gearboxes [NASA-TM-106099] p 228 N93-23741
- SIGNAL ENCODING**
Hierarchical image coding with diamond-shaped sub-bands p 205 A93-20945
Real-time transmission of digital video using variable-length coding [NASA-TM-106092] p 150 N93-22483
- SIGNAL PROCESSING**
Signal processing considerations for low signal to noise ratio laser Doppler and phase Doppler signals p 207 A93-23830
Real-time diagnostics for a reusable rocket engine [NASA-TM-105792] p 266 N93-19018
- SIGNAL RECEPTION**
Utilizing a TDRS satellite for direct broadcast satellite-radio propagation experiments and demonstrations [NASA-TM-106172] p 53 N93-27064

SIGNAL TO NOISE RATIOS

Signal processing considerations for low signal to noise ratio laser Doppler and phase Doppler signals

p 207 A93-23830

Optical communications and a comparison of optical technologies for a high data rate return link from Mars [NASA-TP-3180]

p 52 N93-18854

SIGNAL TRANSMISSION

Real-time transmission of digital video using variable-length coding [NASA-TM-106092]

p 150 N93-22483

SIGNATURE ANALYSIS

Pattern classifier for health monitoring of helicopter gearboxes [NASA-TM-106099]

p 228 N93-23741

SILICATES

Glass formation, properties and structure of soda-yttria-silica glasses

p 131 A93-20464

SILICIDES

Chemical reactions in the processing of MoSi₂ + carbon compacts

p 119 A93-53733

High temperature creep and oxidation resistant chromium silicide matrix alloy containing molybdenum [NASA-CASE-LEW-15697-1]

p 130 N93-29172

SILICON

Intermodulation in the oscillatory magnetoresistance of a two-dimensional electron gas

p 151 A93-17610

Novel coplanar waveguide to slotline transition on high resistivity silicon

p 151 A93-20016

Using silicon diodes for detecting the liquid-vapor interface in hydrogen

p 209 A93-37864

Spectroscopic ellipsometry studies of HF treated Si(100) surfaces

p 282 A93-46188

Microwave characterization of slotline on high resistivity silicon for antenna feed network [NASA-TM-106058]

p 161 N93-27265

SILICON ALLOYS

Studies on the reactive melt infiltration of silicon and silicon-molybdenum alloys in porous carbon [NASA-TM-105860]

p 136 N93-12398

SILICON CARBIDES

On the melt infiltration of copper coated silicon carbide with an aluminum alloy

p 218 A93-11332

Observations on infiltration of silicon carbide compacts with an aluminum alloy

p 97 A93-12356

Silicon carbide, a semiconductor for space power electronics

p 279 A93-13880

Prediction of chemical vapor deposition rates on monofilaments and its implications for fiber properties

p 113 A93-17198

Ultrasonic and micromechanical study of damage and elastic properties of SiC/RBSN ceramic composites ...

Reaction Bonded Silicon Nitride

p 99 A93-19624

Single liquid source plasma-enhanced metalorganic chemical vapor deposition of high-quality YBa₂Cu₃O_{7-x} thin films

p 280 A93-20643

Corrosion of silicon-based ceramics in combustion environments

p 131 A93-22984

Fatigue-environment interactions in a SiC/Ti-15-3 composite

p 100 A93-26275

Effect of HIPing on the effective thermal conductivity/diffusivity and the interfacial thermal conductance of uniaxial SiC fibre-reinforced RBSN

p 100 A93-26674

Melt infiltration of silicon carbide compacts. I - Study of infiltration dynamics

p 101 A93-27494

Melt infiltration of silicon carbide compacts. II - Evaluation of solidification microstructures

p 101 A93-28283

Sliding wear of self-mated Al₂O₃-SiC whisker-reinforced composites at 23-1200 C

p 101 A93-29948

Mechanics of interfaces in fiber reinforced SiC/RBSN ceramic matrix composites ... reaction bonded silicon nitride

p 102 A93-32466

Greatly improved 3C-SiC p-n junction diodes grown by chemical vapor deposition

p 156 A93-38994

Effect of high temperature annealing on the microstructure of SCS-6 SiC fibers

p 133 A93-39513

CVD of silicon carbide on structural fibers - Microstructure and composition

p 117 A93-39521

CVD of SiC and AlN using cyclic organometallic precursors

p 117 A93-39525

Thermodynamics of Si-C-O system

p 133 A93-39584

Atomic probe microscopy of 3C SiC films grown on 6H SiC substrates

p 281 A93-39854

Tensile creep and creep-recovery behavior of a SiC-fiber-Si₃N₄-matrix composite

p 104 A93-40290

Direct observation of porous SiC formed by anodization in HF

p 282 A93-43587

Aluminum acceptor four particle bound exciton complex in 4H, 6H, and 3C SiC

p 282 A93-44822

Progress in silicon carbide semiconductor technology

p 158 A93-44965

An analysis of the wear behavior of SiC whisker-reinforced alumina from 25 to 1200 C

p 104 A93-49253

Microchemical analysis of the SCS-6 silicon carbide fiber

p 135 A93-53734

The effect of fiber microstructure on evolution of residual stresses in silicon carbide/titanium aluminate composites

p 106 A93-54771

Thermal oxidation of single-crystal silicon carbide - Kinetic, electrical, and chemical studies

p 264 A93-55601

Growth and characterization of 3C-SiC and 6H-SiC films on 6H-SiC wafers

p 284 A93-55602

Thermomechanical fatigue behavior of SiC/Ti-24Al-11Nb in air and argon environments

p 106 N93-11399

Silicon carbide fiber reinforced strontium aluminosilicate glass-ceramic matrix composite

p 106 N93-11543

Process for the controlled growth of single-crystal films of silicon carbide polytypes on silicon carbide wafers

p 284 N93-17413

Silicon carbide semiconductor technology for high temperature and radiation environments

p 284 N93-26928

A kinetic and equilibrium analysis of silicon carbide chemical vapor deposition on monofilaments

p 96 N93-27003

SiC fiber-reinforced Celsian glass-ceramic matrix composite

p 112 N93-31293

Method of producing a ceramic fiber-reinforced glass-ceramic matrix composite

p 112 N93-31299

SILICON COMPOUNDS

Ellipsometric study of Si(0.5)Ge(0.5)/Si strained-layer superlattices

p 280 A93-34655

High frequency performance of Si(1-x)Ge(x)/Si(1-y)Ge(y)/Si(1-x)Ge(x) HBTs

p 155 A93-37409

Application of high-quality SiO₂ grown by multipolar ECR source to Si/SiGe MISFET

p 156 A93-37413

Development of Si(1-x)Ge(x) technology for microwave sensing applications

p 162 N93-28610

SILICON CONTROLLED RECTIFIERS

Neutron, gamma ray, and temperature effects on the electrical characteristics of thyristors

p 153 A93-25894

SILICON DIOXIDE

Application of high-quality SiO₂ grown by multipolar ECR source to Si/SiGe MISFET

p 156 A93-37413

SILICON JUNCTIONS

Micromachined silicon cantilever beam accelerometer incorporating an integrated optical waveguide

p 210 A93-49457

SILICON NITRIDES

Indentation flaw formation and strength response of silicon nitride ceramics at low indentation loads

p 130 A93-15994

Role of Si₂N₂O in the passive oxidation of chemically-vapor-deposited Si₃N₄

p 131 A93-16520

Reliability analysis of structural ceramic components using a three-parameter Weibull distribution

p 231 A93-19486

Ultrasonic and micromechanical study of damage and elastic properties of SiC/RBSN ceramic composites ...

Reaction Bonded Silicon Nitride

p 99 A93-19624

Fracture toughness of advanced ceramics at room temperature

p 131 A93-20842

Corrosion of silicon-based ceramics in combustion environments

p 131 A93-22984

Mechanism of incipient oxidation of bulk chemical vapor deposited Si₃N₄

p 132 A93-32299

Mechanics of interfaces in fiber reinforced SiC/RBSN ceramic matrix composites ... reaction bonded silicon nitride

p 102 A93-32466

Characterization of Si₃N₄/SiO₂ optical channel waveguides by photon scanning tunneling microscopy

p 211 A93-49458

Friction and wear of plasma-deposited amorphous hydrogenated films on silicon nitride

p 135 A93-52181

Tribological evaluation and analysis of coating materials

p 135 A93-52896

Fuzzy sets predict flexural strength and density of silicon nitride ceramics

p 110 N93-27270

SILICON OXIDES

Thermodynamics of Si-C-O system

p 133 A93-39584

Characterization of Si₃N₄/SiO₂ optical channel waveguides by photon scanning tunneling microscopy

p 211 A93-49458

SILVER

The effect of ion-plated silver and sliding friction on tensile stress-induced cracking in aluminum oxide

p 132 A93-27917

Low resistance silver contacts to indium phosphide - Electrical and metallurgical considerations

p 157 A93-39351

SILVER ALLOYS

Development of a hydrogen gas sensor using microfabrication technology [SAE PAPER 921176]

p 210 A93-41356

SILVER ZINC BATTERIES

Battery selection for space experiments

p 159 N93-13184

Battery selection for Space Shuttle experiments [NASA-TM-106142]

p 61 N93-27038

SIMULATED ANNEALING

Stochastic search in structural optimization - Genetic algorithms and simulated annealing

p 241 A93-45430

Optimization of blade arrangement in a randomly mistuned cascade using simulated annealing [AIAA PAPER 93-2254]

p 28 A93-50052

SIMULATION

Computational simulation of surface waviness in graphite/epoxy woven composites due to initial curing

p 98 A93-15822

Modal simulation of gear box vibration with experimental correlation

p 221 A93-31982

SIMULATORS

Multiple-access phased array antenna simulator for a digital beam-forming system investigation

p 148 A93-26237

Rocket engine numerical simulator

p 89 N93-26962

SINGLE CHANNEL PER CARRIER TRANSMISSION

Efficient demultiplexing algorithm for noncontiguous carriers

p 148 A93-32561

SINGLE CRYSTALS

Thermal oscillations in materials processing [NASA-TM-106142]

p 162 A93-10839

Effect of strain and stress on the relative dimensions of the 'hard' and 'soft' regions in crept NaCl single crystals

p 279 A93-17513

Prediction of dislocation generation during Bridgman growth of GaAs crystals

p 279 A93-19740

The viscoplastic behavior of Hastelloy-X single crystal

p 125 A93-27486

Melt infiltration of silicon carbide compacts. I - Study of infiltration dynamics

p 101 A93-27494

Effect of tensile mean stress on fatigue behavior of single-crystal and directionally solidified superalloys

p 125 A93-33011

Direct observation of porous SiC formed by anodization in HF

p 282 A93-43587

SIMS studies of oxide growth on beta-NiAl

p 127 A93-53469

Thermal oxidation of single-crystal silicon carbide - Kinetic, electrical, and chemical studies

p 284 A93-55601

Growth and characterization of 3C-SiC and 6H-SiC films on 6H-SiC wafers

p 284 A93-55602

Process for the controlled growth of single-crystal films of silicon carbide polytypes on silicon carbide wafers

p 284 A93-17413

High performance sapphire windows

p 218 N93-22198

Vickers indentation hardness of stoichiometric and reduced single crystal TiO₂ (rutile) from 25 to 800 C

p 282 A93-43587

NDE of PWA 1480 single crystal turbine blade material [NASA-TM-106140]

p 303 N93-27640

The effect of porosity and gamma-gamma' eutectic content on the low cycle fatigue behavior of hydrogen-charged PWA-1480

p 130 N93-31576

Secondary orientation effects in a single crystal superalloy under mechanical and thermal loads

p 130 N93-31578

SINGLE STAGE TO ORBIT VEHICLES

The QED engine spectrum - Fusion-electric propulsion for air-breathing to interstellar flight [AIAA PAPER 93-2006]

p 73 A93-49845

Prospects for utilization of air liquefaction and enrichment system (ALES) propulsion in fully reusable launch vehicles

p 74 A93-49861

SINGULARITY (MATHEMATICS)

Singularities in optimal structural design [AIAA PAPER 92-4818]

p 235 A93-20397

Singularity in structural optimization

p 240 A93-34938

Explicit robust schemes for implementation of a class of principal value-based constitutive models. Symbolic and numeric implementation

p 258 N93-26946

SINTERING

SINTERING

Tribological and mechanical comparison of sintered and HIPped PM212 - High temperature self-lubricating composites p 94 A93-13506

Reliability analysis of structural ceramic components using a three-parameter Weibull distribution p 231 A93-19486 [ASME PAPER 92-GT-296]

Simple, extremely low resistance contact system to n-InP that does not exhibit metal-semiconductor intermixing during sintering p 157 A93-42550

Fuzzy sets predict flexural strength and density of silicon nitride ceramics p 110 N93-27270 [NASA-TM-106049]

Non-destructive, ultra-low resistance, thermally stable contacts for use on shallow junction InP solar cells [NASA-TM-106228] p 256 N93-32201

SIZE DETERMINATION

Calibration of the forward-scattering spectrometer probe - Modeling scattering from a multimode laser beam p 212 A93-51239

SKEWNESS

Kurtosis, skewness, and non-Gaussian cosmological density perturbations p 291 A93-35579

SKIN FRICTION

Low-Reynolds-number k-epsilon model for unsteady turbulent boundary-layer flows p 14 A93-53208

SLIDING

Sliding wear of self-mated Al₂O₃-SiC whisker-reinforced composites at 23-1200 C p 101 A93-29948

An analysis of the wear behavior of SiC whisker reinforced alumina from 25 to 1200 C p 104 A93-49253

SLIDING FRICTION

Tribological and microstructural comparison of HIPped PM212 and PM212/Au self-lubricating composites p 93 A93-13505

The effect of ion-plated silver and sliding friction on tensile stress-induced cracking in aluminum oxide p 132 A93-27917

Relative sliding durability of two candidate high-temperature oxide fiber seal materials p 132 A93-31983

A vacuum (10 exp -9 torr) friction apparatus for determining friction and endurance life of MoSi(x) films p 146 A93-49245

Relative sliding durability of candidate high temperature fiber seal materials [NASA-TM-105806] p 95 N93-10978

Friction and wear of plasma-deposited diamond films [NASA-TM-105926] p 136 N93-19035

Sliding durability of candidate seal fiber materials in hydrogen from 25 to 900 C p 95 N93-22590 [NASA-TM-105939]

Tribological characteristics of perfluoropolyether liquid lubricants under sliding conditions in high vacuum [NASA-TM-106257] p 139 N93-32352

SLOT ANTENNAS

Effect of a dielectric overlay on a linearly tapered slot antenna excited by a coplanar waveguide p 155 A93-35649

Microwave characterization of slotline on high resistivity silicon for antenna feed network [NASA-TM-106058] p 161 N93-27265

SLOTS

Analytical and experimental studies of a short compact subsonic diffuser for a two-dimensional supersonic inlet [NASA-TP-3247] p 17 N93-24118

A three-dimensional algebraic grid generation scheme for gas turbine combustors with inclined slots [NASA-CR-191095] p 198 N93-24759

SLURRY PROPELLANTS

Some aspects of secondary atomization of aluminum/hydrocarbon slurry propellants p 140 A93-34478

SLUSH HYDROGEN

Damping of thermal acoustic oscillations in hydrogen systems p 146 A93-48589

SMART STRUCTURES

Probabilistic structural analysis of adaptive/smart/intelligent space structures p 234 A93-16203

Probabilistic assessment of adaptive space truss configurations for thermal buckling resistance [AIAA PAPER 93-1622] p 240 A93-34151

Probabilistically configured adaptive composite structures [AIAA PAPER 93-1679] p 240 A93-34191

Growing the Space Station's electrical power plant p 161 N93-27810

SMOKE DETECTORS

Contributions of microgravity test results to the design of spacecraft fire safety systems [NASA-TM-106093] p 60 N93-24755

SODIUM

Laser-induced fluorescence detection strategies for sodium atoms and compounds in high-pressure combustors p 119 A93-52423

SODIUM CHLORIDES

Effect of strain and stress on the relative dimensions of the 'hard' and 'soft' regions in crept NaCl single crystals p 279 A93-17513

SODIUM COMPOUNDS

Laser-induced fluorescence detection strategies for sodium atoms and compounds in high-pressure combustors p 119 A93-52423

SODIUM PEROXIDES

Glass formation, properties and structure of soda-yttria-silica glasses p 131 A93-20464

SODIUM SULFUR BATTERIES

Lewis Research Center battery overview p 255 N93-20493

SOFTWARE ENGINEERING

LV software support for supersonic flow analysis [AIAA PAPER 92-3900] p 259 A93-24487

SOFTWARE TOOLS

An embedded rule-based diagnostic expert system in Ada p 260 N93-11928

SOLAR ARRAYS

Grounding of space structures p 54 A93-12144

Photovoltaic arrays for Martian surface power [IAF PAPER 92-0591] p 293 A93-13699

Photovoltaic receivers for laser beamed power in space p 66 A93-21664

Plasma chamber testing of APSA coupons for the SAMPIE flight experiment [AIAA PAPER 93-0568] p 67 A93-24244

Photovoltaic Array Space Power flight experiment plus diagnostics (PASP+) modules p 68 A93-25898

Design and optimization of a self-deploying single axis tracking PV array p 252 A93-25916

Electrical characterization of a Space Station Freedom alpha utility transfer assembly p 56 A93-26101

Design of deployable-truss masts for Space Station [AIAA PAPER 93-0975] p 56 A93-30899

Solar array electrical performance assessment for Space Station Freedom [AIAA PAPER 93-1052] p 69 A93-30956

Arcing rates for High Voltage Solar Arrays - Theory, experiment, and predictions p 70 A93-32567

The application of structural reliability techniques to plume impingement loading of the Space Station Freedom Photovoltaic Array p 56 A93-33908

[AIAA PAPER 93-1338] Thermal control system for Space Station Freedom photovoltaic power module p 57 A93-41305

[SAE PAPER 92-1110] Solar array module plasma interactions experiment (SAMPIE) - Science and technology objectives p 71 A93-46418

The evolution of procurement and assurance methods used to proof an advanced space material p 94 A93-53392

Room temperature synthesis of copper indium diselenide in non-aqueous solution using an organoindium reagent p 283 A93-54844

Acceptance testing of the prototype electrometer for the SAMPIE flight experiment [NASA-TM-105880] p 57 N93-10841

Parameterization of solar cells [NASA-TM-105885] p 159 N93-12301

Advanced photovoltaic power system technology for lunar base applications p 255 N93-14004

The use of plasma ashers and Monte Carlo modeling for the projection of atomic oxygen durability of protected polymers in low Earth orbit p 58 N93-15596

The application of structural reliability techniques to plume impingement loading of the Space Station Freedom Photovoltaic Array p 59 N93-17988

[NASA-TM-105949] Space Station Freedom beta gimbal control via sensitivity models p 60 N93-22551

[NASA-TM-106000] Plasma chamber testing of APSA coupons for the SAMPIE flight experiment p 60 N93-23742

[NASA-TM-106084] Solar array electrical performance assessment for Space Station Freedom [NASA-TM-106161] p 91 N93-27039

Enhanced plasma current collection from weakly conducting solar array blankets p 62 N93-27081

[NASA-TM-106168] Electrical power system WP-04 p 161 N93-27804

Solar Array Module Plasma Interaction Experiment (SAMPIE) p 62 N93-28716

The Photovoltaic Array Space Power Plus diagnostics (PASP Plus) flight experiment p 256 N93-28717

SOLAR BLANKETS Design and optimization of a self-deploying single axis tracking PV array p 252 A93-25916

Advanced photovoltaic power system technology for lunar base applications p 255 N93-14004

SOLAR CELLS

Estimates of power requirements for a Manned Mars Rover powered by a nuclear reactor p 45 A93-13783

Indium phosphide solar cells for laser power beaming applications p 252 A93-25899

Closed-ampoule diffusion of sulfur into Cd-doped InP substrates - Dependence of S profiles on diffusion temperature and time p 283 A93-51917

Diffusion length variation and proton damage coefficients for InP/In(x)Ga(1-x)As/GaAs solar cells p 159 A93-55324

Parameterization of solar cells [NASA-TM-105885] p 159 N93-12301

Advanced photovoltaic power system technology for lunar base applications p 255 N93-14004

Plasma chamber testing of APSA coupons for the SAMPIE flight experiment p 60 N93-23742

Diffusion length variation in 0.5- and 3-MeV-proton-irradiated, heteroepitaxial indium phosphide solar cells p 161 N93-27002

[NASA-TM-106147] Enhanced plasma current collection from weakly conducting solar array blankets p 62 N93-27081

[NASA-TM-106168] Low Earth orbital atomic oxygen environmental simulation facility for space materials evaluation [NASA-TM-106128] p 96 N93-27266

Texturing of InP surfaces for device applications [NASA-TM-106061] p 129 N93-28618

The Photovoltaic Array Space Power Plus diagnostics (PASP Plus) flight experiment p 256 N93-28717

The effect of the low Earth orbit environment on space solar cells: Results of the Advanced Photovoltaic Experiment (S0014) p 256 N93-29686

Non-destructive, ultra-low resistance, thermally stable contacts for use on shallow junction InP solar cells [NASA-TM-106228] p 256 N93-32201

SOLAR COLLECTORS Photovoltaic arrays for Martian surface power [IAF PAPER 92-0591] p 293 A93-13699

Solar concentrators for advanced solar-dynamic power systems in space p 85 N93-23017

[NASA-CR-187148] Advanced solar dynamic technology program p 256 N93-27806

SOLAR DYNAMIC POWER SYSTEMS Control-structure interaction study for the Space Station solar dynamic power module p 54 A93-13132

Optimal control study for the Space Station Solar Dynamic power module p 54 A93-13133

Control-structure interaction p 54 A93-14687

Properties of pure nickel after long term exposures to LiOH and vacuum at 775 K p 123 A93-18075

The ground testing of a 2 kW solar dynamic space power system p 68 A93-25918

BIPS Turboalternator-Compressor characteristics and application to the NASA Solar Dynamic Ground Demonstration Program p 69 A93-25965

Design of a cavity heat pipe receiver experiment p 173 A93-25985

Experimental determination of in situ utilization of lunar regolith for thermal energy storage p 253 A93-26043

Update on the advanced Stirling conversion system project for 25 kW dish Stirling applications p 254 A93-26071

Assessment of 25 kW free-piston Stirling technology alternatives for solar applications p 254 A93-26072

On protection of Freedom's solar dynamic radiator from the orbital debris environment I - Preliminary analysis and testing p 70 A93-36197

Control/structure interactions of Space Station solar dynamic modules p 57 A93-41878

Solar concentrators for advanced solar-dynamic power systems in space p 85 N93-23017

[NASA-CR-187148] Advanced solar dynamic technology program p 256 N93-27806

Thermal energy storage flight experiment in microgravity p 256 N93-28720

SOLAR ELECTRIC PROPULSION Low power pulsed MPD thruster system analysis and applications [AIAA PAPER 93-2391] p 76 A93-50156

10 kW power electronics for hydrogen arcjets p 79 N93-10033

The 10 kW power electronics for hydrogen arcjets [NASA-TM-105614] p 81 N93-12484

SOLAR ENERGY EMTF based stability analysis of Space Station Electric Power System in a test bed environment p 154 A93-26108

- Space transportation alternatives for large space programs - The International Space University summer session - 1992
[AIAA PAPER 93-2278] p 44 A93-53588
- EMTP based stability analysis of space station electric power system in a test bed environment
[NASA-TM-105845] p 160 N93-15503
- SOLAR ENERGY CONVERSION**
Update on the advanced Stirling conversion system project for 25 kW dish Stirling applications
p 254 A93-26071
- Overview of the NASA Lewis component technology program for Stirling power converters
p 254 A93-26073
- Technologies --- space power sources
p 255 N93-16907
- SOLAR FLUX**
Lunar and Martian environmental interactions with nuclear power system radiators
[NASA-TM-105747] p 80 N93-10965
- Flux concentrations on solar dynamic components due to mispointing
[NASA-TM-105756] p 255 N93-20261
- SOLAR GENERATORS**
Design and optimization of a self-deploying single axis tracking PV array
p 252 A93-25916
- Energy loss analysis of an integrated space power distribution system
p 68 A93-25958
- Energy loss analysis of an integrated space power distribution system
[NASA-TM-105772] p 141 N93-14834
- Low Earth orbital atomic oxygen environmental simulation facility for space materials evaluation
[NASA-TM-106128] p 96 N93-27266
- SOLAR NEUTRINOS**
Implications of new GALLEX results for the Mikheyev-Smirnov-Wolfenstein solution of the solar neutrino problem
p 293 A93-10357
- Late-time cosmological phase transitions
p 288 A93-17645
- SOLAR PONDS (HEAT STORAGE)**
One-dimensional transient finite difference model of an operational salinity gradient solar pond
p 193 N93-13400
- SOLAR RADIATION**
Photovoltaic arrays for Martian surface power
[IAF PAPER 92-0591] p 293 A93-13699
- SOLAR REFLECTORS**
Low Earth orbit atomic oxygen simulation for durability evaluation of solar reflector surfaces
p 58 N93-15594
- SOLAR SPECTRA**
The effect of the low Earth orbit environment on space solar cells: Results of the Advanced Photovoltaic Experiment (S0014)
p 256 N93-29686
- SOLID LUBRICANTS**
Tribological studies of amorphous hydrogenated carbon films in a vacuum, spacelike environment
p 134 A93-40630
- A vacuum (10 exp -9 torr) friction apparatus for determining friction and endurance life of MoS(x) films
p 146 A93-49245
- Solid lubricants
p 135 A93-55471
- The effect of processing and compositional changes on the tribology of PM212 in air
[NASA-TM-105945] p 95 N93-15576
- Properties of extruded PS-212 type self-lubricating materials
p 138 N93-25565
- Vickers indentation hardness of stoichiometric and reduced single crystal TiO2 (rutile) from 25 to 800 C
[NASA-TM-105959] p 96 N93-26204
- SOLID MECHANICS**
Improved accuracy for finite element structural analysis via an integrated force method
p 234 A93-17246
- Finite element procedures for coupled linear analysis of heat transfer, fluid and solid mechanics
[AIAA PAPER 93-1639] p 267 A93-34166
- Institute for Computational Mechanics in Propulsion (ICOMP)
[NASA-TM-106155] p 269 N93-27061
- SOLID PHASES**
Kinetics of hexacelsian-to-celsian phase transformation in SrAl2Si2O8
p 134 A93-40293
- Kinetics of hexacelsian to celsian phase transformation in SrAl2Si2O8
[NASA-TM-105913] p 136 N93-16372
- SOLID PROPELLANT COMBUSTION**
Downward diffusion flame spread and extinction in variable gravitational fields - Lunar and Martian simulations
[AIAA PAPER 93-0828] p 115 A93-24898
- Mechanisms of microgravity flame spread over a thin solid fuel - Oxygen and opposed flow effects
p 140 A93-50368
- SOLID PROPELLANT IGNITION**
Ignition and combustion of aluminum/magnesium alloy particles in O2 at high pressures
p 113 A93-22030
- SOLID SURFACES**
Intensified array camera imaging of solid surface combustion aboard the NASA Learjet
p 143 A93-30858
- SOLID-SOLID INTERFACES**
The role of the interface in refractory metal alloy composites
p 97 A93-13777
- Effect of HIPing on the effective thermal conductivity/diffusivity and the interfacial thermal conductance of uniaxial SiC fibre-reinforced RBSN
p 100 A93-26674
- Interface dependence of band offsets in lattice-matched isovalent heterojunctions
p 280 A93-32132
- Photoluminescence intensity enhancement of GaAs by vapor-deposited GaS - A rational approach to surface passivation
p 281 A93-40049
- The effect of multiple compliant layers at the fiber-matrix interface on residual thermal stresses in metal matrix composites
p 104 A93-42085
- Heat of segregation of single substitutional impurities
p 119 A93-52873
- Interfacial shear strength of cast and directionally solidified NiAl-sapphire fiber composites
p 106 A93-55685
- SOLIDIFICATION**
A study of the effects of macrosegregation and buoyancy-driven flow in binary mixture solidification
p 180 A93-44223
- Numerical model for dendritic solidification of binary alloys
p 282 A93-46729
- Interfacial and capillary phenomena in solidification processing of metal-matrix composites
p 106 A93-56351
- On the drag of model dendrite fragments at low Reynolds number
[NASA-TM-105916] p 128 N93-19974
- SOLIDS**
Analysis of large quasistatic deformations of inelastic solids by a new stress based finite element method
[NASA-CR-189235] p 246 N93-13260
- SOLUBILITY**
Natural and thermocapillary convection in multiple liquid layers
[AIAA PAPER 93-0469] p 171 A93-24241
- Composition dependence of superconductivity in YBa2(Cu(3-x)Al(x))O(y)
p 281 A93-40271
- SOLUTES**
Thermosolutal convection during cellular arrayed growth of Pb-Sn alloys
[AIAA PAPER 93-0262] p 142 A93-22668
- An alternative model for estimating liquid diffusion coefficients requiring no viscosity data
[NASA-TM-106079] p 96 N93-23014
- SOLVENTS**
An alternative model for estimating liquid diffusion coefficients requiring no viscosity data
[NASA-TM-106079] p 96 N93-23014
- SOOT**
Experiments on the effect of initial diameter in spherically symmetric droplet combustion of sooting fuels
[AIAA PAPER 93-0130] p 139 A93-22577
- Structure of soot-containing laminar jet diffusion flames
[AIAA PAPER 93-0708] p 114 A93-24804
- Soot agglomeration in isolated, free droplet combustion
[AIAA PAPER 93-0823] p 115 A93-24893
- Soot formation and radiation in turbulent jet diffusion flames under normal and reduced gravity conditions
p 121 N93-20192
- Selected microgravity combustion diagnostic techniques
p 121 N93-20194
- SOUND INTENSITY**
The structure of supersonic jet flow and its radiated sound
[AIAA PAPER 93-0549] p 273 A93-25538
- SOUND PRESSURE**
Acoustic mode measurements in the inlet of a model turbofan using a continuously rotating rake - Data collection/analysis techniques
[AIAA PAPER 93-0599] p 24 A93-23324
- Takeoff/approach noise for a model counterrotation propeller with a forward-swept upstream rotor
[AIAA PAPER 93-0596] p 24 A93-24782
- Modal element method for scattering and absorbing of sound by two-dimensional bodies
p 274 A93-53657
- Acoustic mode measurements in the inlet of a model turbofan using a continuously rotating rake: Data collection/analysis techniques
[NASA-TM-105936] p 33 N93-15403
- Takeoff/approach noise for a model counterrotation propeller with a forward-swept upstream rotor
[NASA-TM-105979] p 34 N93-16715
- SOUND PROPAGATION**
Consecutive plate acoustic suppressor apparatus and methods
[NASA-CASE-LEW-15430-1] p 275 N93-17051
- SOUND WAVES**
Influence of airfoil thickness on sound generated by high-frequency gust interactions
p 272 A93-19181
- Acoustic radiation from a thin airfoil in nonuniform subsonic flows
p 273 A93-23535
- Direct calculations of waves in fluid flows using a high-order compact difference scheme
[AIAA PAPER 93-0148] p 171 A93-24232
- Damping of thermal acoustic oscillations in hydrogen systems
p 146 A93-48589
- Blade row interaction effects on flutter and forced response
[AIAA PAPER 93-2084] p 28 A93-49911
- Dispersion-relation-preserving finite difference schemes for computational acoustics
p 274 A93-51180
- Jet mixer noise suppressor using acoustic feedback
[NASA-CASE-LEW-15170-1] p 275 N93-28953
- SPACE BASES**
Space R/T base: Propulsion (high thrust chemical)
[PR5] p 286 N93-71878
- SPACE COMMERCIALIZATION**
Key issues in space nuclear power challenges for the future
p 65 A93-13905
- SPACE COMMUNICATION**
Monolithic microwave integrated circuits for sensors, radar, and communications systems; Proceedings of the Meeting, Orlando, FL, Apr 2-4, 1991
[SPIE-1475] p 151 A93-25776
- Millimeter-wave pseudomorphic HEMT MMIC phased array components for space communications
p 152 A93-25796
- System overview on electromagnetic compensation for reflector antenna surface distortion
[NASA-TM-106217] p 53 N93-29195
- SPACE DEBRIS**
Interactions between spacecraft and their environments
[AIAA PAPER 93-0705] p 55 A93-24801
- On protection of Freedom's solar dynamic radiator from the orbital debris environment. I - Preliminary analysis and testing
p 70 A93-36197
- On protection of Freedom's solar dynamic radiator from the orbital debris environment. II - Further testing and analyses
p 70 A93-36589
- Space environmental interactions for the space exploration initiative
p 293 N93-26396
- Characteristics of hypervelocity impact craters on LDEF experiment S1003 and implications of small particle impacts on reflective surfaces
p 62 N93-29363
- SPACE DENSITY**
Kurtosis, skewness, and non-Gaussian cosmological density perturbations
p 291 A93-35579
- Observing the inflation potential --- in models of cosmological inflation
p 291 A93-50480
- SPACE ELECTRIC ROCKET TESTS**
Development and flight history of the SERT II spacecraft
p 71 A93-38976
- SPACE ENVIRONMENT SIMULATION**
Measurement and analysis of a small nozzle plume in vacuum
p 71 A93-42895
- New technique for oil backstreaming contamination measurements
p 210 A93-44514
- Recommended practices for in-space and ground laboratory Atomic oxygen exposure and analysis
p 276 N93-20814
- Determination of atomic oxygen fluence using spectrophotometric analysis of infrared transparent witness coupons for long duration exposure tests
[NASA-TM-106021] p 96 N93-22605
- SPACE ERECTABLE STRUCTURES**
Design of structures for Nuclear Electric Propulsion vehicles
[AIAA PAPER 93-1393] p 57 A93-33955
- SPACE EXPLORATION**
Establishing the infrastructure - An integrated Space Transportation System
p 50 A93-12072
- Planning for the Space Exploration Initiative - The nuclear propulsion option
p 43 A93-13752
- Nuclear Propulsion Project Workshop summary
p 64 A93-13765
- The interaction of high voltage systems with the environments of the moon and Mars
[AIAA PAPER 93-0704] p 67 A93-24800
- Evolving SP-100 powerplants via electric propulsion to GEO and lunar orbit
p 70 A93-34492
- Space vehicle design and operation for efficient use of Nuclear Thermal Propulsion
[AIAA PAPER 93-1946] p 44 A93-49804
- System model development for nuclear thermal propulsion
[NASA-TM-105761] p 80 N93-10457

SPACE FLIGHT

Nuclear thermal propulsion transportation systems for lunar/Mars exploration p 81 N93-12363
[NASA-TM-105870]

System model development for nuclear thermal propulsion p 277 N93-17343
[NASA-TM-108215]

Nuclear concepts/propulsion p 85 N93-22093

Summary and recommendations on nuclear electric propulsion technology for the space exploration initiative p 86 N93-24744
[NASA-TM-105707]

Space Nuclear Thermal Propulsion Test Facilities Subpanel p 87 N93-25105
[NASA-TM-105708]

Nuclear safety policy working group recommendations on nuclear propulsion safety for the space exploration initiative p 88 N93-26200
[NASA-TM-105705]

Electrical and Chemical Interactions at Mars Workshop. Part 2: Appendix p 293 N93-26392
[NASA-CP-10093-PT-2]

Representative systems for space exploration p 293 N93-26395

Space environmental interactions for the space exploration initiative p 293 N93-26396

Nuclear electric propulsion systems overview p 49 N93-26970

The 20 kWe NEP flight system p 90 N93-26983

SPACE FLIGHT

The 1992 Research/Technology report p 1 N93-20902
[NASA-TM-105924]

SPACE LOGISTICS

RENEW v3.2 user's manual, maintenance estimation simulation for Space Station Freedom Program p 232 N93-27025
[NASA-TM-106006]

SPACE MAINTENANCE

Automatic system for installation and replacement of Space Station components p 226 N93-12203
[NASA-CASE-LEW-14906-1]

SPACE MISSIONS

Design of small Stirling dynamic isotope power system for robotic space missions p 141 N93-12085
[NASA-TM-105919]

Nuclear safety policy working group recommendations on nuclear propulsion safety for the space exploration initiative p 88 N93-26200
[NASA-TM-105705]

Representative systems for space exploration p 293 N93-26395

Nuclear electric propulsion systems overview p 49 N93-26970

The 20 kWe NEP system studies p 90 N93-26971

Small Stirling dynamic isotope power system for robotic space missions p 92 N93-28686
[NASA-TM-105785]

Venus Interior Structure Mission (VISM): Establishing a seismic network on Venus p 293 N93-28819

SPACE PLASMAS

Electrodynamic interactions between a space station and the ionospheric plasma environment p 56 A93-29156

Plasma chamber testing of APSA coupons for the SAMPIE flight experiment p 60 N93-23742
[NASA-TM-106084]

SPACE PLATFORMS

Vibration isolation technology - An executive summary of systems development and demonstration ... for proposed microgravity experiments aboard STS and Space Station Freedom p 55 A93-24904
[AIAA PAPER 93-0834]

Computational/experimental basis for conducting alkane droplet combustion experiments on space-based-platforms p 117 A93-41711

Vibration isolation technology: An executive summary of systems development and demonstration p 1 N93-15573
[NASA-TM-105937]

SPACE POWER REACTORS

Space nuclear power systems; Proceedings of the 8th Symposium, Albuquerque, NM, Jan. 6-10, 1991. Pts. 1-3 [ISBN 0-88318-838-4] p 64 A93-13751

The role of the interface in refractory metal alloy composites p 97 A93-13777

Estimates of power requirements for a Manned Mars Rover powered by a nuclear reactor p 45 A93-13783

Graphite fiber/copper matrix composites for space power heat pipe fin applications p 162 A93-13789

Shielding analysis for a manned Mars rover powered by an SP-100 type reactor p 45 A93-13793

Multimegawatt potassium Rankine power for nuclear electric power p 65 A93-13797

Space reactor/Stirling cycle systems for high power lunar applications p 46 A93-13822

SP-100 high-temperature advanced radiator development p 163 A93-13843

Advanced radiator concepts feasibility demonstration ... for space power system p 163 A93-13844

Heat-pipe transient model for space applications p 163 A93-13867

Comparison of high frequency, high temperature core loss and B-H loop characteristics of an 80 Ni-Fe crystalline alloy and two iron-based amorphous alloys p 123 A93-13882

Mechanisms of voids formation during cooldown and freezing of lithium in SP-100 type systems p 163 A93-13916

Space nuclear power systems 1989; Proceedings of the 6th Symposium, Albuquerque, NM, Jan. 8-12, 1989. Vols. 1 & 2 --- Book p 66 A93-20752
[ISBN 0-89464-030-5]

Ultrahigh temperature vapor-core reactor - Magnetohydrodynamic system for space nuclear electric power p 66 A93-21663

100-kWe lunar/Mars surface power utilizing the SP-100 reactor with dynamic conversion p 67 A93-25856

Fabrication of carbon-carbon heat pipes for space nuclear power applications p 173 A93-25978

Fault-tolerant adaptive control for load-following in static space nuclear power systems p 263 A93-25986

The NASA CSTI High Capacity Power Project p 69 A93-26105

Design of structures for Nuclear Electric Propulsion vehicles p 57 A93-33955
[AIAA PAPER 93-1393]

Evolving SP-100 powerplants via electric propulsion to GEO and lunar orbit p 70 A93-34492

Lunar and Martian environmental interactions with nuclear power system radiators p 80 N93-10965
[NASA-TM-105747]

The NASA CSTI high capacity power project p 48 N93-11398
[NASA-TM-105813]

Closed Brayton Cycle power system with a high temperature pellet bed reactor heat source for NEP applications p 82 N93-14482
[NASA-TM-105933]

System model development for nuclear thermal propulsion p 277 N93-17343
[NASA-TM-108215]

Environmental interactions and the SP-100 power system p 84 N93-18877
[NASA-TM-105866]

Nuclear electric propulsion for planetary science missions: NASA technology program planning p 88 N93-26210
[NASA-TM-106139]

Representative systems for space exploration p 293 N93-26395

Nuclear Propulsion Technical Interchange Meeting, volume 2 p 89 N93-26951
[NASA-CP-10116-VOL-2]

The 20 kWe NEP system studies p 90 N93-26971

The 100-500 kWe NEP systems p 90 N93-26984

Nuclear electric propulsion options for piloted Mars missions p 90 N93-26985

An evolution strategy for lunar nuclear surface power p 91 N93-27963

SPACE PROCESSING

Thermal oscillations in materials processing p 162 A93-10839

Initial study of void formation during aluminum solidification in reduced gravity p 142 A93-12013

Flow-influenced stabilization of liquid columns in a dynamic plateau chamber p 169 A93-22664
[AIAA PAPER 93-0255]

Natural and thermocapillary convection in multiple liquid layers p 171 A93-24241
[AIAA PAPER 93-0469]

IDGE - A test of dendritic growth theory using space flight p 143 A93-25515
[AIAA PAPER 93-0260]

Numerical study of mixing of two fluids under low gravity p 194 N93-14914
[NASA-TM-105865]

A multi-zone muffle furnace design p 145 N93-27011
[NASA-TM-106153]

SPACE PROGRAMS

Space transportation alternatives for large space programs - The International Space University summer session - 1992 p 44 A93-53588
[AIAA PAPER 93-2278]

SPACE SHUTTLE MAIN ENGINE

Probabilistic evaluation of uncertainties and risks in aerospace components p 233 A93-12160

Integrated health monitoring and controls for rocket engines p 66 A93-14654
[SAE PAPER 921031]

Implementation of a model based fault detection and diagnosis technique for actuation faults of the SSME p 47 A93-16413

An SSME High Pressure Oxidizer Turbopump diagnostic system using G2 real-time expert system p 66 A93-16415

A qualitative approach to systemic diagnosis of the SSME p 261 A93-23327
[AIAA PAPER 93-0405]

Design considerations for a Space Shuttle Main Engine turbine blade made of single crystal material p 236 A93-25228

Structural system reliability under multiple failure modes p 238 A93-33943
[AIAA PAPER 93-1379]

Miniature high temperature plug-type heat flux gauges p 209 A93-37862

A function approximation approach to anomaly detection in propulsion system test data p 71 A93-49671
[AIAA PAPER 93-1776]

High Reynolds number and turbulence effects on aerodynamics and heat transfer in a turbine cascade p 186 A93-50050
[AIAA PAPER 93-2252]

The development of hydrogen sensor technology for aerospace applications p 211 A93-50144
[AIAA PAPER 93-2375]

Implementation of a model based fault detection and diagnosis for actuation faults of the Space Shuttle main engine p 49 N93-11401
[NASA-TM-105781]

A neural network-based estimator for the mixture ratio of the Space Shuttle Main Engine p 87 N93-25089
[NASA-TM-106070]

Calculations of combustion response profiles and oscillations p 87 N93-25236
[NASA-TM-106135]

On-line implementation of nonlinear parameter estimation for the Space Shuttle main engine p 88 N93-26211
[NASA-TM-106097]

The design and evolution of the beta two-stage-to-orbit horizontal takeoff and landing launch system p 51 N93-27018
[NASA-TM-106118]

High Reynolds number and turbulence effects on aerodynamics and heat transfer in a turbine cascade p 202 N93-29157
[NASA-TM-106187]

Structural Integrity and Durability of Reusable Space Propulsion Systems p 93 N93-31552
[NASA-CP-10064]

Progress in the measurement of SSME turbine heat flux with plug-type sensors p 217 N93-31553

Thin film heat flux sensor for Space Shuttle Main Engine turbine environment p 217 N93-31554

Thin film thermocouples for high temperature turbine application p 217 N93-31555

Overview of aerothermodynamic loads definition study p 93 N93-31583

Three-dimensional analysis of the Pratt and Whitney alternate design SSME fuel turbine p 230 N93-31584

Three-dimensional flow calculations inside SSME GGGT first stage blade rows p 93 N93-31585

Localization of aeroelastic modes in mistuned high-energy turbines p 230 N93-31586

SPACE SHUTTLE MISSIONS

Low-frequency vibration environment for five Shuttle missions p 63 N93-28554
[NASA-TM-106059]

SPACE SHUTTLE PAYLOADS

A review of design concepts for the Advanced Fluids Module (AFM) project p 43 A93-23700
[AIAA PAPER 93-0258]

Review of the Shuttle vibration environment p 51 A93-24902
[AIAA PAPER 93-0832]

Low gravity environment on-board Columbia during STS-40 p 142 A93-24903
[AIAA PAPER 93-0833]

An approach to studying the reliability of microgravity experiments p 44 A93-30937
[AIAA PAPER 93-1024]

Solar array module plasma interactions experiment (SAMPIE) - Science and technology objectives p 71 A93-46418

Electrical design of Space Shuttle payload G-534. The pool boiling experiment p 62 N93-27260
[NASA-TM-106143]

SPACE SHUTTLES

Titan III feasibility for HL-20 prototype missions p 50 A93-53747

Capabilities and constraints of typical space flight hardware p 145 N93-20183

Fire safety practices in the Shuttle and the Space Station Freedom p 59 N93-20204

Battery selection for Space Shuttle experiments p 61 N93-27038
[NASA-TM-106142]

SPACE STATION FREEDOM

Control-structure interaction study for the Space Station solar dynamic power module p 54 A93-13132

Optimal control study for the Space Station Solar Dynamic power module p 54 A93-13133

A review of design concepts for the Advanced Fluids Module (AFM) project p 43 A93-23700
[AIAA PAPER 93-0258]

- The ground testing of a 2 kWe solar dynamic space power system p 68 A93-25918
- BIPS Turboalternator-Compressor characteristics and application to the NASA Solar Dynamic Ground Demonstration Program p 69 A93-25965
- Overview and evolution of the LeRC PMAD DC test bed p 47 A93-26099
- Operation of high power converters in parallel p 154 A93-26100
- Electrical characterization of a Space Station Freedom alpha utility transfer assembly p 56 A93-26101
- Description of the PMAD systems test bed facility and data system p 47 A93-26102
- Description of the SSF PMAD dc testbed control system data acquisition function p 47 A93-26103
- Load converter interactions with the secondary system in the Space Station Freedom power management and distribution dc test bed p 154 A93-26106
- Stability testing and analysis of a PMAD dc test bed for the Space Station Freedom p 154 A93-26107
- Power system monitoring and source control of the Space Station Freedom dc-power system testbed p 69 A93-26109
- Design of deployable-truss masts for Space Station [AIAA PAPER 93-0975] p 56 A93-30899
- The application of structural reliability techniques to plume impingement loading of the Space Station Freedom Photovoltaic Array [AIAA PAPER 93-1338] p 56 A93-33908
- Space Station Freedom structure floating potential and the probability of arcing p 57 A93-39265
- Thermal control system for Space Station Freedom photovoltaic power module [SAE PAPER 921110] p 57 A93-41305
- Control/structure interactions of Space Station solar dynamic modules p 57 A93-41878
- The CONE program - An overview --- Cryogenic Orbital Nitrogen Experiment p 146 A93-48637
- Plasma contactor technology for Space Station Freedom [AIAA PAPER 93-2228] p 57 A93-50034
- The evolution of procurement and assurance methods used to proof an advanced space material p 94 A93-53392
- Proposed ground-based control of accelerometer on Space Station Freedom p 63 A93-54401
- Electric propulsion - An evolutionary technology p 78 A93-56168
- Power system monitoring and source control of the Space Station Freedom DC power system testbed [NASA-TM-105841] p 80 A93-10734
- Description of the SSF PMAD DC testbed control system data acquisition function [NASA-TM-105843] p 261 A93-11005
- The application of structural reliability techniques to plume impingement loading of the Space Station Freedom Photovoltaic Array [NASA-TM-105949] p 59 A93-17988
- Overview of NASA's microgravity combustion science and fire safety program p 145 A93-20180
- Fire safety practices in the Shuttle and the Space Station Freedom p 59 A93-20204
- Flux concentrations on solar dynamic components due to mispointing [NASA-TM-105756] p 255 A93-20261
- Lewis Research Center battery overview p 255 A93-20493
- The 1992 Research/Technology report [NASA-TM-105924] p 1 A93-20902
- Space Station Freedom beta gimbal control via sensitivity models [NASA-TM-106000] p 60 A93-22551
- Selected OAST/OSSA space experiment activities in support of Space Station Freedom p 60 A93-22636
- Proposed ground-based control of accelerometer on Space Station Freedom [NASA-TM-105960] p 63 A93-23738
- Space Nuclear Thermal Propulsion Test Facilities Subpanel [NASA-TM-105708] p 87 A93-25105
- Conceptual design for the Space Station Freedom fluid physics/dynamics facility [NASA-TM-103663] p 61 A93-26209
- Plasma current collection of Z-93 thermal control paint as measured in the Lewis Research Center's plasma interaction facility [NASA-TM-106132] p 61 A93-26215
- The effects of simulated low Earth orbit environments on spacecraft thermal control coatings [NASA-TM-106146] p 61 A93-27019
- RENEW v3.2 user's manual, maintenance estimation simulation for Space Station Freedom Program [NASA-TM-106006] p 232 A93-27025
- Solar array electrical performance assessment for Space Station Freedom [NASA-TM-106161] p 91 A93-27039
- Basic statistical analyses of candidate nickel-hydrogen cells for the Space Station Freedom [NASA-TM-106111] p 270 A93-27124
- Low Earth orbital atomic oxygen environmental simulation facility for space materials evaluation [NASA-TM-106128] p 96 A93-27266
- Electrical power system WP-04 p 161 A93-27804
- Advanced solar dynamic technology program p 256 A93-27806
- Fluid management system technology discipline p 62 A93-27861
- Power system technology discipline p 62 A93-27862
- SPACE STATION POWER SUPPLIES**
- Control-structure interaction p 54 A93-14687
- The ground testing of a 2 kWe solar dynamic space power system p 68 A93-25918
- Overview and evolution of the LeRC PMAD DC test bed p 47 A93-26099
- Operation of high power converters in parallel p 154 A93-26100
- Electrical characterization of a Space Station Freedom alpha utility transfer assembly p 56 A93-26101
- Description of the PMAD systems test bed facility and data system p 47 A93-26102
- Description of the SSF PMAD dc testbed control system data acquisition function p 47 A93-26103
- Load converter interactions with the secondary system in the Space Station Freedom power management and distribution dc test bed p 154 A93-26106
- Stability testing and analysis of a PMAD dc test bed for the Space Station Freedom p 154 A93-26107
- EMTP based stability analysis of Space Station Electric Power System in a test bed environment p 154 A93-26108
- Power system monitoring and source control of the Space Station Freedom dc-power system testbed p 69 A93-26109
- Solar array electrical performance assessment for Space Station Freedom [AIAA PAPER 93-1052] p 69 A93-30956
- Thermal control system for Space Station Freedom photovoltaic power module [SAE PAPER 921110] p 57 A93-41305
- Power system monitoring and source control of the Space Station Freedom DC power system testbed [NASA-TM-105841] p 80 A93-10734
- Description of the SSF PMAD DC testbed control system data acquisition function [NASA-TM-105843] p 261 A93-11005
- EMTP based stability analysis of space station electric power system in a test bed environment [NASA-TM-105845] p 160 A93-15503
- Technologies --- space power sources p 255 A93-16907
- Lewis Research Center battery overview p 255 A93-20493
- Solar array electrical performance assessment for Space Station Freedom [NASA-TM-106161] p 91 A93-27039
- Electrical power system WP-04 p 161 A93-27804
- Advanced solar dynamic technology program p 256 A93-27806
- Growing the Space Station's electrical power plant p 161 A93-27810
- Power system technology discipline p 62 A93-27862
- SPACE STATION STRUCTURES**
- Control-structure interaction study for the Space Station solar dynamic power module p 54 A93-13132
- Modal test/analysis correlation of Space Station structures using nonlinear sensitivity [AIAA PAPER 92-4731] p 55 A93-20330
- The application of structural reliability techniques to plume impingement loading of the Space Station Freedom Photovoltaic Array [AIAA PAPER 93-1338] p 56 A93-33908
- Control/structure interactions of Space Station solar dynamic modules p 57 A93-41878
- The application of structural reliability techniques to plume impingement loading of the Space Station Freedom Photovoltaic Array [NASA-TM-105949] p 59 A93-17988
- Growing the Space Station's electrical power plant p 161 A93-27810
- SPACE STATIONS**
- Electrodynamic interactions between a space station and the ionospheric plasma environment p 56 A93-29156
- On protection of Freedom's solar dynamic radiator from the orbital debris environment II - Further testing and analyses p 70 A93-36589
- Control/structure interactions of Space Station solar dynamic modules p 57 A93-41878
- Preliminary characterization of a water vaporizer for resistojet applications [NASA-TM-105877] p 80 A93-11402
- Automatic system for installation and replacement of Space Station components [NASA-CASE-LEW-14906-1] p 226 A93-12203
- Conceptual design for the Space Station Freedom fluid physics/dynamics facility [NASA-TM-103663] p 61 A93-26209
- Low thrust propulsion [PR3] p 286 A93-71876
- SPACE TRANSPORTATION**
- Establishing the infrastructure - An integrated Space Transportation System p 50 A93-12072
- Progress report on nuclear propulsion for space exploration and science [AIAA PAPER 93-2352] p 44 A93-50125
- Space transportation alternatives for large space programs - The International Space University summer session - 1992 [AIAA PAPER 93-2278] p 44 A93-53588
- Cryogenic fluid management (base R/T): Cryogenic fluid systems, Cryogenic Orbital Nitrogen Experiment (CONE), Cryogenic Orbital Hydrogen Experiment (COHE). (Transportation focused technology) [PR6] p 286 A93-71879
- SPACE TRANSPORTATION SYSTEM**
- The CONE program - An overview --- Cryogenic Orbital Nitrogen Experiment p 146 A93-48637
- Space vehicle design and operation for efficient use of Nuclear Thermal Propulsion [AIAA PAPER 93-1946] p 44 A93-49804
- Low-g fluid mixing - Further results from the Tank Pressure Control Experiment [AIAA PAPER 93-2423] p 187 A93-50181
- Nuclear thermal propulsion transportation systems for lunar/Mars exploration [NASA-TM-105870] p 81 A93-12363
- Electrical design of Space Shuttle payload G-534: The pool boiling experiment [NASA-TM-106143] p 62 A93-27260
- Cryogenic fluid management (base R/T): Cryogenic fluid systems, Cryogenic Orbital Nitrogen Experiment (CONE), Cryogenic Orbital Hydrogen Experiment (COHE). (Transportation focused technology) [PR6] p 286 A93-71879
- SPACE TRANSPORTATION SYSTEM FLIGHTS**
- Ground-based PIV and numerical flow visualization results from the Surface Tension Driven Convection Experiment p 143 A93-33075
- Electrical design of Space Shuttle payload G-534: The pool boiling experiment [NASA-TM-106143] p 62 A93-27260
- SPACE-TIME FUNCTIONS**
- On an origin of numerical diffusion: Violation of invariance under space-time inversion [NASA-TM-105776] p 268 A93-11254
- SPACEBORNE EXPERIMENTS**
- An interface configuration experiment on USML-1 [AIAA PAPER 93-0253] p 169 A93-22662
- A review of design concepts for the Advanced Fluids Module (AFM) project [AIAA PAPER 93-0258] p 43 A93-23700
- Review of the Shuttle vibration environment [AIAA PAPER 93-0832] p 51 A93-24902
- Low gravity environment on-board Columbia during STS-40 [AIAA PAPER 93-0833] p 142 A93-24903
- Photovoltaic Array Space Power flight experiment plus diagnostics (PASP+) modules p 68 A93-25898
- An approach to studying the reliability of microgravity experiments [AIAA PAPER 93-1024] p 44 A93-30937
- Solar array module plasma interactions experiment (SAMPIE) - Science and technology objectives p 71 A93-46418
- Scientific basis for the Isothermal Dendritic Growth Experiment - A USMP-2 space flight experiment p 143 A93-50455
- Proposed ground-based control of accelerometer on Space Station Freedom p 63 A93-54401
- Acceptance testing of the prototype electrometer for the SAMPIE flight experiment [NASA-TM-105880] p 57 A93-10841
- Small experiments for the maturation of orbital cryogenic transfer technologies [NASA-TM-105849] p 192 A93-10981
- LDEF yaw and pitch angle estimates p 58 A93-12772
- Capabilities and constraints of typical space flight hardware p 145 A93-20183
- Selected OAST/OSSA space experiment activities in support of Space Station Freedom p 60 A93-22636
- Proposed ground-based control of accelerometer on Space Station Freedom [NASA-TM-105960] p 63 A93-23738

SPACECRAFT ANTENNAS

- Laser ignition application in a space experiment
[NASA-TM-106133] p 145 N93-25337
- Conceptual design for the Space Station Freedom fluid physics/dynamics facility
[NASA-TM-103663] p 61 N93-26209
- A multi-zone muffle furnace design
[NASA-TM-106153] p 145 N93-27011
- Battery selection for Space Shuttle experiments
[NASA-TM-106142] p 61 N93-27038
- Electrical design of Space Shuttle payload G-534. The pool boiling experiment
[NASA-TM-106143] p 62 N93-27260
- Tank Pressure Control Experiment/Thermal Phenomena (TPCE/TP)
p 92 N93-28713
- Solar Array Module Plasma Interaction Experiment (SAMPIE)
p 62 N93-28716
- The Photovoltaic Array Space Power Plus diagnostics (PASP Plus) flight experiment
p 256 N93-28717
- Thermal energy storage flight experiment in microgravity
p 256 N93-28720

SPACECRAFT ANTENNAS

- System overview on electromagnetic compensation for reflector antenna surface distortion
[NASA-TM-106217] p 53 N93-29195

SPACECRAFT CHARGING

- Plasma sheath effects on ion collection by a pinhole
[AIAA PAPER 93-0567] p 55 A93-24243
- Interactions between spacecraft and their environments
[AIAA PAPER 93-0705] p 55 A93-24801
- Electrodynamic interactions between a space station and the ionospheric plasma environment
p 56 A93-29156
- The effects of 1 kW class arcjet thruster plumes on spacecraft charging and spacecraft thermal control materials
p 57 A93-35050
- Low power arcjet system spacecraft impacts
[AIAA PAPER 93-2392] p 76 A93-50157
- Plasma sheath effects on ion collection by a pinhole
[NASA-TM-106098] p 60 N93-25090
- Space environmental interactions for the space exploration initiative
p 293 N93-26396
- Enhanced plasma current collection from weakly conducting solar array blankets
[NASA-TM-106168] p 62 N93-27081
- Solar Array Module Plasma Interaction Experiment (SAMPIE)
p 62 N93-28716

SPACECRAFT COMPONENTS

- ACTS system handbook, revision change index
[NASA-TM-107982] p 150 N93-70235

SPACECRAFT CONFIGURATIONS

- The design and evolution of the Beta two-stage-to-orbit horizontal takeoff and landing launch system
[AIAA PAPER 92-5080] p 50 A93-22350

SPACECRAFT CONSTRUCTION MATERIALS

- High temperature static strain measurement with an electrical resistance strain gage
[AIAA PAPER 92-5039] p 205 A93-22313
- Aerospace applications ... of refractory ceramic materials
p 135 A93-55472
- Low Earth orbit atomic oxygen simulation for durability evaluation of solar reflector surfaces
p 58 N93-15594
- Simulation of the synergistic low Earth orbit effects of vacuum thermal cycling, vacuum UV radiation, and atomic oxygen
p 58 N93-15595
- Recommended practices for in-space and ground laboratory. Atomic oxygen exposure and analysis
p 276 N93-20814
- Plasma current collection of Z-93 thermal control paint as measured in the Lewis Research Center's plasma interaction facility
[NASA-TM-106132] p 61 N93-26215
- The effects of simulated low Earth orbit environments on spacecraft thermal control coatings
[NASA-TM-106146] p 61 N93-27019
- Low Earth orbital atomic oxygen environmental simulation facility for space materials evaluation
[NASA-TM-106128] p 96 N93-27266

SPACECRAFT CONTAMINATION

- New technique for oil backstreaming contamination measurements
p 210 A93-44514
- Space environmental interactions for the space exploration initiative
p 293 N93-26396
- The effects of simulated low Earth orbit environments on spacecraft thermal control coatings
[NASA-TM-106146] p 61 N93-27019

SPACECRAFT CONTROL

- Grounding of space structures
p 54 A93-12144
- Damage-mitigating control of aerospace systems for high performance and extended life
p 263 A93-22967
- Monte Carlo analysis of the Titan III/Transfer Orbit Stage guidance system for the Mars Observer mission
[AIAA PAPER 93-3889] p 50 A93-51473
- Space Station Freedom beta gimbal control via sensitivity models
[NASA-TM-106000] p 60 N93-22551

SPACECRAFT DESIGN

- The design and evolution of the Beta two-stage-to-orbit horizontal takeoff and landing launch system
[AIAA PAPER 92-5080] p 50 A93-22350
- Design of deployable-truss masts for Space Station
[AIAA PAPER 93-0975] p 56 A93-30899
- Contributions of microgravity test results to the design of spacecraft fire-safety systems
[AIAA PAPER 93-1152] p 56 A93-31028
- Space Station Freedom structure floating potential and the probability of arcing
p 57 A93-39265
- Space vehicle design and operation for efficient use of Nuclear Thermal Propulsion
[AIAA PAPER 93-1946] p 44 A93-49804
- Application of artificial neural networks to the design optimization of aerospace structural components
[NASA-TM-4389] p 247 N93-21831
- A system to measure lightning-induced transients on spacecraft umbilical lines
p 161 N93-24889
- Overview of NASA/DOE/DOD interagency modeling team and activities
p 89 N93-26952
- The 20 kW NEP system studies
p 90 N93-26971
- ACTS system handbook, revision change index
[NASA-TM-107982] p 150 N93-70235

SPACECRAFT DOCKING

- The application of structural reliability techniques to plume impingement loading of the Space Station Freedom Photovoltaic Array
[AIAA PAPER 93-1338] p 56 A93-33908
- The application of structural reliability techniques to plume impingement loading of the Space Station Freedom Photovoltaic Array
[NASA-TM-105949] p 59 N93-17988

SPACECRAFT ELECTRONIC EQUIPMENT

- NASA requirements and applications environments for electrical power wiring
p 153 A93-25919
- A system to measure lightning-induced transients on spacecraft umbilical lines
p 161 N93-24889

SPACECRAFT ENVIRONMENTS

- Review of the Shuttle vibration environment
[AIAA PAPER 93-0832] p 51 A93-24902
- Low gravity environment on-board Columbia during STS-40
[AIAA PAPER 93-0833] p 142 A93-24903
- The effects of simulated low Earth orbit environments on spacecraft thermal control coatings
[NASA-TM-106146] p 61 N93-27019

SPACECRAFT INSTRUMENTS

- Design of an automated imaging system for use in a space experiment
p 204 A93-20454

SPACECRAFT LAUNCHING

- Key issues in space nuclear power challenges for the future
p 65 A93-13905
- Benefits of in situ propellant utilization for a Mars sample return mission
[AIAA PAPER 93-2244] p 140 A93-50046
- Titan III feasibility for HL-20 prototype missions
p 50 A93-53747
- The design and evolution of the beta two-stage-to-orbit horizontal takeoff and landing launch system
[NASA-TM-106118] p 51 N93-27018
- Benefits of in situ propellant utilization for a Mars sample return mission
[NASA-TM-106243] p 141 N93-28695

SPACECRAFT MAINTENANCE

- RENEW v3.2 user's manual, maintenance estimation simulation for Space Station Freedom Program
[NASA-TM-106006] p 232 N93-27025

SPACECRAFT MODELS

- COLD-SAT dynamic model
[NASA-TM-105185] p 59 N93-19988
- Space Station Freedom beta gimbal control via sensitivity models
[NASA-TM-106000] p 60 N93-22551

SPACECRAFT MODULES

- Conceptual design for the Space Station Freedom fluid physics/dynamics facility
[NASA-TM-103663] p 61 N93-26209

SPACECRAFT PERFORMANCE

- Damage-mitigating control of aerospace systems for high performance and extended life
p 263 A93-22967

SPACECRAFT POWER SUPPLIES

- Versatile dynamic isotope power systems for the exploration of space
p 46 A93-13819
- Comparison of dynamic isotope power systems for distributed planetary surface applications
p 46 A93-13825
- Free-piston Stirling Engine system considerations for various space power applications
p 252 A93-13826
- An Isotope-Powered Thermal Storage unit for space applications
p 65 A93-13877
- Silicon carbide, a semiconductor for space power electronics
p 279 A93-13880
- Key issues in space nuclear power challenges for the future
p 65 A93-13905

The interaction of high voltage systems with the environments of the moon and Mars

- [AIAA PAPER 93-0704] p 67 A93-24800
- 100-kWe lunar/Mars surface power utilizing the SP-100 reactor with dynamic conversion
p 67 A93-25856
- Optimization of closed Brayton cycles for space power generation
p 68 A93-25859
- Long life Regenerative Fuel Cell technology development plan
p 252 A93-25867
- Lessons learned from the Autonomous Power System
p 68 A93-25879
- Validation test of advanced technology for IPV nickel-hydrogen flight cells - Update
p 252 A93-25886
- Evaluation of the benefits of high temperature electronics for lunar power systems
p 153 A93-25896
- Photovoltaic Array Space Power flight experiment plus diagnostics (PASP +) modules
p 68 A93-25898
- NASA requirements and applications environments for electrical power wiring
p 153 A93-25919
- Modified NASA standard nickel-cadmium cell designs
p 253 A93-25947
- 75 Ah and 10 boilerplate nickel-hydrogen battery designs and test results
p 253 A93-25948
- Energy loss analysis of an integrated space power distribution system
p 68 A93-25958
- Free-piston Stirling component test power converter test results and potential Stirling applications
p 68 A93-25964
- Dynamic Isotope Power System design considerations for human exploration of the moon and Mars
p 253 A93-25995
- Overview of the NASA Lewis component technology program for Stirling power converters
p 254 A93-26073
- Magnetic bearings for free-piston Stirling engines
p 221 A93-26079
- Overview and evolution of the LeRC PMAD DC test bed
p 47 A93-26099
- The NASA CSTI High Capacity Power Project
p 69 A93-26105
- Solar array module plasma interactions experiment (SAMPIE) - Science and technology objectives
p 71 A93-46418
- Low power arcjet system spacecraft impacts
[AIAA PAPER 93-2392] p 76 A93-50157
- Thermal emittance enhancement of graphite-aluminum and graphite-copper composite radiator surfaces for space power applications
p 105 A93-53455
- Space transportation alternatives for large space programs - The International Space University summer session - 1992
[AIAA PAPER 93-2278] p 44 A93-53588
- The NASA CSTI high capacity power project
p 48 N93-11398
- [NASA-TM-105813] Design of small Stirling dynamic isotope power system for robotic space missions
p 141 N93-12085
- [NASA-TM-105919] Energy loss analysis of an integrated space power distribution system
p 141 N93-14834
- [NASA-TM-105772] Technologies ... space power sources
p 255 N93-16907
- Scheduling lessons learned from the Autonomous Power System
p 265 N93-18671
- Lewis Research Center battery overview
p 255 N93-20493
- Modelling a single phase voltage controlled rectifier using Laplace transforms
[NASA-TM-106005] p 271 N93-23016
- Solar concentrators for advanced solar-dynamic power systems in space
p 85 N93-23017
- Plasma chamber testing of APSA coupons for the SAMPIE flight experiment
[NASA-TM-106084] p 60 N93-23742
- Radiation and temperature effects on electronic components investigated under the CSTI high capacity power project
[NASA-TM-106096] p 161 N93-24746
- The interaction of high voltage systems with the environments of the Moon and Mars
[NASA-TM-106107] p 61 N93-26148
- NEP systems model
p 90 N93-26986
- Enhanced plasma current collection from weakly conducting solar array blankets
[NASA-TM-106168] p 62 N93-27081
- Basic statistical analyses of candidate nickel-hydrogen cells for the Space Station Freedom
[NASA-TM-106111] p 270 N93-27124
- Low Earth orbital atomic oxygen environmental simulation facility for space materials evaluation
[NASA-TM-106128] p 96 N93-27266
- Solar Array Module Plasma Interaction Experiment (SAMPIE)
p 62 N93-28716
- The Photovoltaic Array Space Power Plus diagnostics (PASP Plus) flight experiment
p 256 N93-28717

SPACECRAFT PROPULSION

- Development of advanced seals for space propulsion turbomachinery
 - [SAE PAPER 921028] p 218 A93-14651
- On-orbit characterization of electric propulsion on LEO satellites
 - p 67 A93-25303
- Extended life and performance test of a low-power arcjet
 - p 70 A93-32554
- Arcing rates for High Voltage Solar Arrays - Theory, experiment, and predictions
 - p 70 A93-32567
- Development and flight history of the SERT II spacecraft
 - p 71 A93-38976
- A new facility for advanced rocket propulsion research
 - [AIAA PAPER 93-1859] p 48 A93-49737
- Predicted performance of an Integrated Modular Engine system
 - [AIAA PAPER 93-1888] p 72 A93-49761
- The NASA Electric Propulsion Program
 - [AIAA PAPER 93-1935] p 73 A93-49797
- Characterization of in-flight performance of ion propulsion systems
 - [AIAA PAPER 93-2217] p 75 A93-50023
- Monte Carlo and experimental studies of nozzle flow in a low-power hydrogen arcjet
 - [AIAA PAPER 93-2529] p 77 A93-50257
- NASA's progress in nuclear electric propulsion technology
 - [AIAA PAPER 93-1936] p 78 A93-53587
- System model development for nuclear thermal propulsion
 - [NASA-TM-105761] p 80 N93-10457
- Preliminary characterization of a water vaporizer for resistojets applications
 - [NASA-TM-105877] p 80 N93-11402
- Nuclear thermal propulsion transportation systems for lunar/Mars exploration
 - [NASA-TM-105870] p 81 N93-12363
- The 10 kW power electronics for hydrogen arcjets
 - [NASA-TM-105614] p 81 N93-12484
- The Proteus Navier-Stokes code
 - p 193 N93-13396
- Low thrust chemical rocket technology
 - [NASA-TM-105927] p 83 N93-15572
- Second Magnetoplasmadynamic Thruster Workshop
 - [NASA-CP-10109] p 279 N93-18635
- Atomic hydrogen propellants: Historical perspectives and future possibilities
 - [NASA-TM-106053] p 84 N93-20614
- Space transfer with ground-based laser/electric propulsion
 - [NASA-TM-106060] p 84 N93-20615
- Space propulsion
 - p 84 N93-22092
- Development of arcjet and ion propulsion for spacecraft stationkeeping
 - [NASA-TM-106102] p 85 N93-23747
- Summary and recommendations on nuclear electric propulsion technology for the space exploration initiative
 - [NASA-TM-105707] p 86 N93-24744
- Space exploration initiative candidate nuclear propulsion test facilities
 - [NASA-TM-105710] p 86 N93-24753
- Nuclear electric propulsion for planetary science missions: NASA technology program planning
 - [NASA-TM-106139] p 88 N93-26210
- Nuclear Propulsion Technical Interchange Meeting, volume 1
 - [NASA-CP-10116-VOL-1] p 89 N93-26908
- Focused technology: Nuclear propulsion
 - p 89 N93-26912
- Systems overview
 - p 89 N93-26915
- Nuclear Propulsion Technical Interchange Meeting, volume 2
 - [NASA-CP-10116-VOL-2] p 89 N93-26951
- Overview of NASA/DOE/DOD interagency modeling team and activities
 - p 89 N93-26952
- Rocket engine numerical simulator
 - p 89 N93-26962
- Facilities
 - p 49 N93-26963
- Plum Brook facilities
 - p 49 N93-26964
- Nuclear electric propulsion systems overview
 - p 49 N93-26970
- NEP technology: FY 1992 milestones (NASA LeRC)
 - p 90 N93-26977
- Power management and distribution technology
 - p 90 N93-26978
- Radiator technology
 - p 90 N93-26979
- The 20 kWe NEP flight system
 - p 90 N93-26983
- NEP systems model
 - p 90 N93-26986
- Institute for Computational Mechanics in Propulsion (ICOMP)
 - [NASA-TM-106155] p 269 N93-27061
- Orbital storage and supply of subcritical liquid nitrogen
 - p 62 N93-27801
- A new facility for advanced rocket propulsion research
 - [NASA-TM-106193] p 49 N93-28696
- Structural Integrity and Durability of Reusable Space Propulsion Systems
 - [NASA-CP-10064] p 93 N93-31552

Overview of the fatigue/fracture/life prediction working group program at the Lewis Research Center

- p 232 N93-31574
- NASA's progress in nuclear electric propulsion technology
 - [NASA-TM-106272] p 93 N93-31858
- Space R/T base: Propulsion (high thrust chemical)
 - [PR5] p 286 N93-36178
- Focused technology: Nuclear propulsion
 - [PR12] p 287 N93-71885
- SPACECRAFT RADIATORS**
 - SP-100 high-temperature advanced radiator development
 - p 163 A93-13843
 - Advanced radiator concepts feasibility demonstration --- for space power system
 - p 163 A93-13844
 - On protection of Freedom's solar dynamic radiator from the orbital debris environment. I - Preliminary analysis and testing
 - p 70 A93-36197
 - Thermophysical properties of gas phase uranium tetrafluoride
 - [AIAA PAPER 93-2758] p 285 A93-46505
 - Current status of liquid sheet radiator research
 - [NASA-TM-105764] p 193 N93-14150
 - The 100-500 kWe NEP systems
 - p 90 N93-26984
- SPACECRAFT RELIABILITY**
 - RENEW v3.2 user's manual, maintenance estimation simulation for Space Station Freedom Program
 - [NASA-TM-106006] p 232 N93-27025
- SPACECRAFT SHIELDING**
 - Method for retarding oxidation of an organic substrate
 - [NASA-CASE-LEW-15306-2] p 138 N93-28425
- SPACECRAFT STABILITY**
 - Control-structure interaction study for the Space Station solar dynamic power module
 - p 54 A93-13132
- SPACECRAFT STRUCTURES**
 - Probabilistic structural analysis of adaptive/smart/intelligent space structures
 - p 234 A93-16203
 - Performance and properties of atomic oxygen protective coatings for polymeric materials
 - p 225 A93-53389
 - Digital control algorithms for microgravity isolation systems
 - p 265 A93-53653
- SPACECRAFT TRACKING**
 - Control-structure interaction
 - p 54 A93-14687
- SPACELAB**
 - Interference patterns in the Spacelab 2 plasma wave data - Oblique electrostatic waves generated by the electron beam
 - p 257 A93-16347
 - Ground-based PIV and numerical flow visualization results from the Surface Tension Driven Convection Experiment
 - p 143 A93-33075
 - Overview of NASA's microgravity combustion science and fire safety program
 - p 145 N93-20180
 - Electrical design of Space Shuttle payload G-534: The pool boiling experiment
 - [NASA-TM-106143] p 62 N93-27260
- SPACING**
 - An experimental investigation of S-duct flow control using arrays of low-profile vortex generators
 - [NASA-TM-106030] p 17 N93-19968
- SPATIAL FILTERING**
 - Temporal averaging of phase measurements in the presence of spurious phase drift - Application to phase-stepped real-time holographic interferometry
 - p 207 A93-26967
 - A fuzzy logic based controller for the automated alignment of a laser-beam-smoothing spatial filter
 - [NASA-TM-105994] p 217 N93-18091
 - Neural nets for aligning optical components in harsh environments: Beam smoothing spatial filter as an example
 - p 266 N93-31557
- SPECIFIC IMPULSE**
 - Electromagnetic propulsion for spacecraft
 - [AIAA PAPER 93-1086] p 69 A93-30975
 - Performance of a low-power subsonic-arc-attachment arcjet thruster
 - [AIAA PAPER 93-1898] p 72 A93-49768
 - Durability testing of the AJ10-221 490 N high performance (321 sec isp) engine
 - [AIAA PAPER 93-2130] p 74 A93-49949
 - Cryogenic propellant thermal control system design considerations, analyses, and concepts applied to a Mars human exploration mission
 - [AIAA PAPER 93-2353] p 75 A93-50126
 - 10 kW power electronics for hydrogen arcjets
 - p 79 N93-10033
 - Development of arcjet and ion propulsion for spacecraft stationkeeping
 - [NASA-TM-106102] p 85 N93-23747
 - Computational fluid dynamics for nuclear thermal propulsion
 - p 199 N93-26930
- SPECIFICATIONS**
 - Solar array electrical performance assessment for Space Station Freedom
 - [AIAA PAPER 93-1052] p 69 A93-30956

SPECIMEN GEOMETRY

- Fracture toughness testing of polymer matrix composites
 - [NASA-TP-3199] p 107 N93-12302

SPECIMENS

- Numerical calibration of the stable poisson loaded specimen
 - [NASA-TM-105609] p 245 N93-12738

SPECKLE PATTERNS

- Progress in speckle-shift strain measurement
 - p 251 N93-31558

SPECTRA

- OLYMPUS/ACTS scintillation experiment at the Lewis Research Center
 - p 150 N93-26481

SPECTRAL CORRELATION

- The three-point correlation function in an ensemble of three-dimensional simulations --- in gravitational perturbation theory
 - p 291 A93-50680

SPECTRAL LINE WIDTH

- Rotational level-dependent collisional broadening and line shift of the A2Sigma(+) - X2Pi(1,0) band of OH in hydrogen-air combustion gases
 - p 276 A93-24142

SPECTRAL METHODS

- The eigenvalue spectrum of the Rayleigh equation for a plane shear layer
 - p 168 A93-21725
- Spectral-domain moment-method analysis of coplanar microstrip parasitic subarrays
 - p 148 A93-35016
- An assessment of spectral nonoscillatory schemes
 - [AIAA PAPER 93-3383] p 267 A93-45074
- Incompressible spectral-element method: Derivation of equations
 - [NASA-TM-106109] p 199 N93-26554

SPECTRAL RESOLUTION

- High-speed laser anemometry based on spectrally resolved Rayleigh scattering
 - p 207 A93-23814

SPECTRAL SIGNATURES

- A plume spectroscopy system for flight applications
 - [AIAA PAPER 93-2511] p 63 A93-50242

SPECTROMETERS

- Experimental testing of four correction algorithms for the forward scattering spectrometer probe
 - [NASA-TM-105906] p 213 N93-13307

SPECTROPHOTOMETRY

- Determination of atomic oxygen fluence using spectrophotometric analysis of infrared transparent witness coupons for long duration exposure tests
 - [NASA-TM-106021] p 96 N93-22605

SPECTROSCOPIC ANALYSIS

- Spectroscopic wear detector
 - [NASA-CASE-LEW-15200-1] p 83 N93-18856

SPECTROSCOPY

- Statistical fitting accuracy in photon correlation spectroscopy
 - p 277 A93-52414

SPECTRUM ANALYSIS

- Spectroscopic ellipsometry studies of HF treated Si(100) surfaces
 - p 282 A93-46188
- Fourier transform spectrometry for fiber-optic sensor systems
 - p 211 A93-49459

SPHERES

- Damping and scattering of electromagnetic waves by small ferrite spheres suspended in an insulator
 - [NASA-TM-105837] p 149 N93-12366

SPHERICAL TANKS

- Optimization of armored spherical tanks for storage on the lunar surface
 - p 47 A93-25866

SPIN DYNAMICS

- Behavior of spinning laminated composite plates with initial twist-experimental vibrations, strain, and deflection results
 - [AIAA PAPER 93-1325] p 238 A93-33898

SPIRALS

- Maximum life spiral bevel reduction design
 - [NASA-TM-105790] p 226 N93-10982

SPLINES

- Optimal design of composite hip implants using NASA technology
 - p 257 N93-22188

SPLITTING

- A new flux splitting scheme
 - p 9 A93-47189

SPRAYED COATINGS

- Plasma sprayed ceramic thermal barrier coating for NiAl-based intermetallic alloys
 - [NASA-CASE-LEW-15535-1] p 130 N93-31294

SPRAYERS

- Coaxial injector spray characterization using water/air as simulants
 - p 120 N93-11452
- Combustion of interacting droplet arrays in a microgravity environment
 - p 122 N93-20217
- Structure of confined laminar spray diffusion flames: Numerical investigation
 - [NASA-TM-106038] p 197 N93-22596
- Spray combustion experiments and numerical predictions
 - [NASA-TM-106069] p 198 N93-23744
- Fuel injector: Air swirl characterization aerothermal modeling, phase 2, volume 1
 - [NASA-CR-189193-VOL-1] p 35 N93-24754

SPRAYING

- Velocity and drop size measurements in a swirl-stabilized, combustor spray
[NASA-TM-106130] p 37 N93-27130
- SPRAYING**
A coupled multi-block solution procedure for spray combustion in complex geometries
[AIAA PAPER 93-0108] p 171 A93-24230
- SPREADING**
Opposed-flow flame spreading in reduced gravity
p 121 N93-20206
- STABILITY**
Determination of the oxidative stability of perfluoropolyalkyl ethers and correlation with chemical structure
[NASA-TM-106223] p 139 N93-32367
- STABILITY TESTS**
Overview and evolution of the LeRC PMAD DC test bed
p 47 A93-26099
- STAGNATION POINT**
Wake-induced unsteady stagnation-region heat-transfer measurements
[ASME PAPER 92-GT-196] p 166 A93-19421
- STAGNATION PRESSURE**
Initial results from the NASA Lewis wave rotor experiment
[AIAA PAPER 93-2521] p 30 A93-53589
Experimentation in the low-density plume of a simulated electrothermal thruster for computer code validation
[NASA-CR-191112] p 87 N93-24758
Initial results from the NASA-Lewis wave rotor experiment
[NASA-TM-106148] p 39 N93-32368
- STAGNATION TEMPERATURE**
Experimentation in the low-density plume of a simulated electrothermal thruster for computer code validation
[NASA-CR-191112] p 87 N93-24758
- STAINLESS STEELS**
Axial-torsional fatigue - A study of tubular specimen thickness effects
p 240 A93-38849
External stress-corrosion cracking of a 1.22-m-diameter type 316 stainless steel air valve
[NASA-TP-3190] p 129 N93-26201
- STANTON NUMBER**
Time-averaged heat transfer and pressure measurements and comparison with prediction for a two-stage turbine
[ASME PAPER 92-GT-194] p 166 A93-19419
- STAR DISTRIBUTION**
Biasing and hierarchical statistics in large-scale structure
p 292 A93-55051
- STAR FORMATION**
Late-time cosmological phase transitions
p 288 A93-17645
- STARTERS**
A soft-start circuit for arcjet ignition
[AIAA PAPER 93-2396] p 76 A93-50161
- STARTING**
Closed-form analytical solutions of high-temperature heat pipe startup and frozen startup limitation
p 165 A93-18564
Simulation of the early startup period of high-temperature heat pipes from the frozen state by a rarefied vapor self-diffusion model
p 175 A93-30127
A numerical analysis of high-temperature heat pipe startup from the frozen state
p 175 A93-30128
- STATE ESTIMATION**
Power system monitoring and source control of the Space Station Freedom dc-power system testbed
p 69 A93-26109
Power system monitoring and source control of the Space Station Freedom DC power system testbed
[NASA-TM-105841] p 80 N93-10734
- STATIC CHARACTERISTICS**
On the static stability of forward swept proptans
[AIAA PAPER 93-1634] p 26 A93-34162
- STATIC LOADS**
Stiffness of magnetic bearings subjected to combined static and dynamic loads
[ASME PAPER 91-TRIB-27] p 219 A93-15685
Fault-tolerant adaptive control for load-following in static space nuclear power systems
p 263 A93-25986
Effect of service environments on adhesively bonded joints in composite structures
p 242 A93-53418
- STATIC PRESSURE**
An experimental investigation of S-duct flow control using arrays of low-profile vortex generators
[NASA-TM-106030] p 17 N93-19968
Surface and flow field measurements in a symmetric crossing shock wave/turbulent boundary-layer interaction
[NASA-TM-106086] p 17 N93-24911
- STATIC STABILITY**
On the static stability of forward swept proptans
[AIAA PAPER 93-1634] p 26 A93-34162

STATIONKEEPING

- Electric propulsion - An evolutionary technology
p 78 A93-56168
Development of arcjet and ion propulsion for spacecraft stationkeeping
[NASA-TM-106102] p 85 N93-23747

STATISTICAL ANALYSIS

- Probing the statistics of primordial fluctuations and their evolution
p 290 A93-24627
Statistical analysis of the effects of helicity in inhomogeneous turbulence
p 175 A93-26186
Statistical fitting accuracy in photon correlation spectroscopy
p 277 A93-52414
On-line implementation of nonlinear parameter estimation for the Space Shuttle main engine
[NASA-TM-106097] p 88 N93-26211

STATOR BLADES

- Forcing function effects on unsteady aerodynamic gust response. II - Low solidity airfoil row response
[ASME PAPER 92-GT-175] p 3 A93-19401

STEADY FLOW

- On the structure of cellular solutions in Rayleigh-Benard-Marangoni flows in small-aspect-ratio containers
p 164 A93-14762
Computing 3-D steady supersonic flow via a new Lagrangian approach
[AIAA PAPER 93-0891] p 6 A93-24951
The development of a mixing layer under the action of weak streamwise vortices
p 176 A93-30134
Averaging techniques for steady and unsteady calculations of a transonic fan stage
[AIAA PAPER 93-3065] p 11 A93-48241
Three-dimensional flow analysis inside turbomachinery stages with steady and unsteady Navier-Stokes method
[ISABE 93-7095] p 14 A93-54071
An integral equation solution for multistage turbomachinery design calculations
[NASA-TM-105970] p 33 N93-15521
Increased heat transfer to elliptical leading edges due to spanwise variations in the freestream momentum: Numerical and experimental results
[NASA-TM-106150] p 199 N93-27020
Numerical simulations of three-dimensional laminar flow over a backward facing step; flow near side walls
[NASA-TM-106248] p 202 N93-31147
A p-version finite element method for steady incompressible fluid flow and convective heat transfer
[NASA-TM-106260] p 203 N93-32370

STEADY STATE

- Preconditioned Conjugate Gradient methods for low speed flow calculations
[AIAA PAPER 93-0881] p 172 A93-24942
Measurement of frequency response in short thermocouple wires
p 209 A93-40677
Central difference TVD schemes for time dependent and steady state problems
p 188 A93-51183
System model development for nuclear thermal propulsion
p 80 N93-10457
[NASA-TM-105761] p 80 N93-10457
Preconditioned conjugate-gradient methods for low-speed flow calculations
[NASA-TM-105929] p 194 N93-14885
Parallel solution of high-order numerical schemes for solving incompressible flows
[NASA-TM-4451] p 262 N93-27040

STEADY STATE CREEP

- Viscoplasticity with creep and plasticity bounds
p 125 A93-32925
Creep deformation of B2 aluminides
p 126 A93-44887

STEELS

- On bilinearity of Manson-Coffin low-cycle-fatigue relationship
[NASA-TM-105840] p 245 N93-12739
Tribological characteristics of perfluoropolyether liquid lubricants under sliding conditions in high vacuum
[NASA-TM-106257] p 139 N93-32352

STELLAR COMPOSITION

- The boron-to-beryllium ratio in halo stars - A signature of cosmic-ray nucleosynthesis in the early Galaxy
p 292 A93-55061

STELLAR EVOLUTION

- Population II Li-6 as a probe of nucleosynthesis and stellar structure and evolution
p 292 A93-56494

STELLAR STRUCTURE

- Population II Li-6 as a probe of nucleosynthesis and stellar structure and evolution
p 292 A93-56494

STELLITE (TRADEMARK)

- Mechanical properties of Haynes Alloy 188 after exposure to LiF-22CaF₂ air, and vacuum at 1093 K for periods up to 10,000 hours
p 126 A93-36586

STIFFENING

- Grounding of space structures
p 54 A93-12144
Damage progression in stiffened composite panels
[AIAA PAPER 93-1345] p 238 A93-33915

STIFFNESS

- Stiffness of magnetic bearings subjected to combined static and dynamic loads
[ASME PAPER 91-TRIB-27] p 219 A93-15685
Calculation of stiffness and damping coefficients for elastically supported gas foil bearings
p 221 A93-27308

STIFFNESS MATRIX

- A new pre-loaded beam geometric stiffness matrix with full rigid body capabilities
p 54 A93-12145
Application of artificial neural networks in nonlinear analysis of trusses
[NASA-TM-105319] p 244 N93-11403

STIRLING CYCLE

- Space reactor/Stirling cycle systems for high power lunar applications
p 46 A93-13822
High temperature viscoplastic ratchetting - Material response or modeling artifact
p 233 A93-13823
Comparison of dynamic isotope power systems for distributed planetary surface applications
p 46 A93-13825
Free-piston Stirling Engine system considerations for various space power applications
p 252 A93-13826
Electric and hybrid electric vehicle study utilizing a time-stepping simulation
p 287 A93-26012
HFAST - A harmonic analysis program for Stirling cycles
p 220 A93-26051
A free-piston Stirling engine/linear alternator controls and load interaction test facility
p 146 A93-26077
Pulsed single-blow regenerator testing
p 221 A93-26081

- Overview of NASA supported Stirling thermodynamic loss research
p 174 A93-26087
M.I.T. Stirling-cycle heat transfer apparatus
p 174 A93-26090

- Dynamic analysis of Free-Piston Stirling Engine/Linear Alternator-load system-experimentally validated
[NASA-TM-106034] p 271 N93-22559
Small Stirling dynamic isotope power system for robotic space missions
[NASA-TM-105785] p 92 N93-28686

STIRLING ENGINES

- Stirling engine - Available tools for long-life assessment ... for space propulsion
p 65 A93-13824
Free-piston Stirling component test power converter test results and potential Stirling applications
p 68 A93-25964
Comparison of GLIMPS and HFAST Stirling engine code predictions with experimental data
p 220 A93-26052
Stirling engine - Approach for long-term durability assessment
p 220 A93-26069
Update on the advanced Stirling conversion system project for 25 kW dish Stirling applications
p 254 A93-26071
Assessment of 25 kW free-piston Stirling technology alternatives for solar applications
p 254 A93-26072
Overview of the NASA Lewis component technology program for Stirling power converters
p 254 A93-26073

- M-H characteristics and demagnetization resistance of samarium-cobalt permanent magnets to 300 C
p 153 A93-26076

- Dynamic analysis of free-piston Stirling engine/linear alternator-load system - Experimentally validated
p 254 A93-26078

- Magnetic bearings for free-piston Stirling engines
p 221 A93-26079

- Transient liquid phase diffusion bonding of Udimet 720 for Stirling power converter applications
p 221 A93-26080

- Transition of oscillatory flow in tubes - An empirical model for application to Stirling engines
p 174 A93-26088
M.I.T. Stirling-cycle heat transfer apparatus
p 174 A93-26090

- Visualization of entry flow separation for oscillating flow in tubes
p 174 A93-26091

- Design of small Stirling dynamic isotope power system for robotic space missions
[NASA-TM-105919] p 141 N93-12085

- Summary of the NASA Lewis component technology program for Stirling power converters
[NASA-TM-105640] p 82 N93-15526

- Test results of a Stirling engine utilizing heat exchanger modules with an integral heat pipe
[NASA-TM-105883] p 256 N93-25136

- Small Stirling dynamic isotope power system for robotic space missions
[NASA-TM-105785] p 92 N93-28686

STOCHASTIC PROCESSES

- A coupled multi-block solution procedure for spray combustion in complex geometries
[AIAA PAPER 93-0108] p 171 A93-24230
The isolation limits of stochastic vibration
p 236 A93-30042

- Stochastic sensitivity measure for mistuned high-performance turbines
[NASA-TM-105821] p 245 N93-12277
- Fuel injector: Air swirl characterization aerothermal modeling, phase 2, volume 1
[NASA-CR-189193-VOL-1] p 35 N93-24754
- STOICHIOMETRY**
- Natural and thermocapillary convection in multiple liquid layers
[AIAA PAPER 93-0469] p 171 A93-24241
- Vickers indentation hardness of stoichiometric and reduced single crystal TiO₂ (rutile) from 25 to 800 C
[NASA-TM-105959] p 96 N93-26204
- STOKES FLOW**
- A hydrodynamic model of the oscillating screen viscometer
p 190 A93-55136
- On the nonlinear three dimensional instability of Stokes layers and other shear layers to pairs of oblique waves
[NASA-TM-105918] p 194 N93-15499
- STORABLE PROPELLANTS**
- Low thrust chemical rocket technology
[NASA-TM-105927] p 83 N93-15572
- STORAGE BATTERIES**
- Basic statistical analyses of candidate nickel-hydrogen cells for the Space Station Freedom
[NASA-TM-106111] p 270 N93-27124
- STORAGE TANKS**
- Optimization of armored spherical tanks for storage on the lunar surface
p 47 A93-25866
- Pressurization and expulsion of a lightweight liquid hydrogen tank
[AIAA PAPER 93-1966] p 73 A93-49814
- Tank chilldown analysis and verification with a lightweight, 175 cu ft tank under normal gravity with liquid hydrogen
p 140 N93-10045
- Comparing the results of an analytical model of the no-vent fill process with no-vent fill test results for a 4.96 cubic meters (175 cubic feet) tank
[NASA-TM-106018] p 200 N93-27155
- STOVL AIRCRAFT**
- Robust integrated flight/propulsion control design for a STOVL aircraft using H-infinity control design techniques
p 40 A93-26432
- Application of controller partitioning optimization procedure to integrated flight/propulsion control design for a STOVL aircraft
p 40 A93-51361
- Overview of high performance aircraft propulsion research
[NASA-TM-105839] p 32 N93-11530
- Propulsion system performance resulting from an integrated flight/propulsion control design
[NASA-TM-105874] p 34 N93-15525
- Controller partitioning for integrated flight/propulsion control implementation
[NASA-TM-105804] p 41 N93-21197
- STRAIN DISTRIBUTION**
- High temperature viscoplastic ratchetting - Material response or modeling artifact
p 233 A93-13823
- Thermoviscoplastic analysis of fibrous periodic composites using triangular subvolumes
[NASA-TM-106076] p 111 N93-29074
- STRAIN ENERGY METHODS**
- Method for calculating alloy energetics
p 279 A93-18740
- STRAIN ENERGY RELEASE RATE**
- Variation of the energy release rate as a crack approaches and passes through an elastic inclusion
p 241 A93-44440
- STRAIN GAGES**
- Palladium-chromium static strain gage for high temperature propulsion systems
p 204 A93-16421
- High temperature static strain measurement with an electrical resistance strain gage
[AIAA PAPER 92-5039] p 205 A93-22313
- Strain sensing technology for high temperature applications
[AIAA PAPER 92-5040] p 205 A93-22314
- Auger electron spectroscopy study of oxidation of a PdCr alloy used for high-temperature sensors
[NASA-TM-106212] p 129 N93-23418
- STRAIN MEASUREMENT**
- High temperature static strain measurement with an electrical resistance strain gage
[AIAA PAPER 92-5039] p 205 A93-22313
- Modeling and strain gauging of eddy current repulsion deicing systems
[AIAA PAPER 93-0296] p 20 A93-22696
- Behavior of spinning laminated composite plates with initial twist-experimental vibrations, strain, and deflection results
[AIAA PAPER 93-1325] p 238 A93-33898
- Residual strain gradient determination in metal matrix composites by synchrotron X-ray energy dispersive diffraction
p 103 A93-39580
- Progress in speckle-shift strain measurement
p 251 N93-31558
- STRAIN RATE**
- Effect of strain and stress on the relative dimensions of the 'hard' and 'soft' regions in crept NaCl single crystals
p 279 A93-17513
- On bilinearity of Manson-Coffin low-cycle-fatigue relationship
[NASA-TM-105840] p 245 N93-12739
- STRATIFICATION**
- Thermal stratification potential in rocket engine coolant channels
p 78 N93-10019
- Numerical study of mixing of two fluids under low gravity
[NASA-TM-105865] p 194 N93-14914
- STRATIFIED FLOW**
- Thermal stratification potential in rocket engine coolant channels
p 78 N93-10019
- STREAK PHOTOGRAPHY**
- Ground-based PIV and numerical flow visualization results from the Surface Tension Driven Convection Experiment
p 143 A93-33075
- Effects of flow-path variations on internal reversing flow in a tailpipe offtake configuration for ASTOVL aircraft
[AIAA PAPER 93-2438] p 29 A93-50190
- Effects of flow-path variations on internal reversing flow in a tailpipe offtake configuration for ASTOVL aircraft
[NASA-TM-106149] p 38 N93-29065
- STREAM FUNCTIONS (FLUIDS)**
- Structure and development of streamwise vortex arrays embedded in a turbulent boundary layer
p 177 A93-32711
- Streamwise computation of three-dimensional flows using two stream functions
p 184 A93-49241
- STREAMS**
- Combustion of solid fuel in very low speed oxygen streams
p 122 N93-20207
- STRESS ANALYSIS**
- Effect of strain and stress on the relative dimensions of the 'hard' and 'soft' regions in crept NaCl single crystals
p 279 A93-17513
- Probabilistic assessment of composite structures
[AIAA PAPER 93-1441] p 239 A93-33990
- Global/local finite element analysis for textile composites
[AIAA PAPER 93-1506] p 103 A93-34045
- Singularity in structural optimization
p 240 A93-34938
- An analysis of the wear behavior of SiC whisker-reinforced alumina from 25 to 1200 C
p 104 A93-49253
- Contact stress analysis of spiral bevel gears using nonlinear finite element static analysis
[AIAA PAPER 93-2296] p 224 A93-50081
- The effects of strain on the microwave performance of SiGe HBTs
p 158 A93-54442
- The effect of contact stresses in four-point bend testing of graphite/epoxy and graphite/PMR-15 composite beams
[NASA-TM-105891] p 107 N93-12076
- Numerical calibration of the stable poisson loaded specimen
[NASA-TM-105609] p 245 N93-12738
- Turbulence modeling and experiments
p 195 N93-15796
- A realizable Reynolds stress algebraic equation model
[NASA-TM-105993] p 16 N93-16596
- External stress-corrosion cracking of a 1.22-m-diameter type 316 stainless steel air valve
[NASA-TP-3190] p 129 N93-26201
- The influence of primary and secondary orientations on the elastic response of a nickel-base single-crystal superalloy
[NASA-TM-106125] p 250 N93-26550
- Contact stress analysis of spiral bevel gears using nonlinear finite element static analysis
[NASA-TM-106176] p 228 N93-27037
- Ceramic matrix composites properties/microstresses with complete and partial interphase bond
[NASA-TM-106136] p 111 N93-29071
- A numerical study of confined turbulent jets
[NASA-TM-106197] p 202 N93-29161
- STRESS CONCENTRATION**
- Probabilistic simulation of stress concentration in composite laminates
[AIAA PAPER 93-1442] p 103 A93-33991
- Design for inadvertent damage in composite laminates
p 242 A93-53396
- Probabilistic assessment of composite structures
[NASA-TM-106024] p 110 N93-27092
- STRESS CORROSION CRACKING**
- External stress-corrosion cracking of a 1.22-m-diameter type 316 stainless steel air valve
[NASA-TP-3190] p 129 N93-26201
- STRESS DISTRIBUTION**
- Singularities in optimal structural design
[AIAA PAPER 92-4818] p 235 A93-20397
- Boundary formulations for three-dimensional continuum structural shape sensitivity analysis
p 235 A93-22426
- Analysis of precracking parameters for ceramic single-edge-precracked-beam specimens
p 133 A93-38887
- The effect of fiber microstructure on evolution of residual stresses in silicon carbide/titanium aluminide composites
p 106 A93-54771
- Reliability analysis of laminated ceramic matrix composites using shell subelement techniques
p 243 A93-55382
- Analysis of precracking parameters and fracture toughness for ceramic single-edge-precracked-beam specimens
[NASA-TM-105568] p 135 N93-10962
- Stress distribution in composite flatwise tension test specimens
[NASA-TM-106074] p 108 N93-25071
- Thermoviscoplastic analysis of fibrous periodic composites using triangular subvolumes
[NASA-TM-106076] p 111 N93-29074
- STRESS FUNCTIONS**
- Root damage analysis of aircraft engine blade subject to ice impact
[NASA-TM-105779] p 246 N93-15343
- Explicit robust schemes for implementation of general principal value-based constitutive models
[NASA-TM-106123] p 258 N93-26947
- STRESS INTENSITY FACTORS**
- Single-parameter characterization of discrete-dislocation pileup tipfield and its application to physically based micro-mechanics
p 233 A93-12119
- Analysis of precracking parameters for ceramic single-edge-precracked-beam specimens
p 133 A93-38887
- Analytical stress intensity solution for the Stable Poisson Loaded specimen
p 242 A93-46768
- Calculation of stress intensity factors in an isotropic multiaxial plate: Part 2: Symbolic/numeric implementation
[NASA-TM-105823] p 244 N93-10453
- Calculation of stress intensity factors in an isotropic multiaxial plate: Part 1: Theoretical development
[NASA-TM-105766] p 244 N93-10455
- Analysis of precracking parameters and fracture toughness for ceramic single-edge-precracked-beam specimens
[NASA-TM-105568] p 135 N93-10962
- Numerical calibration of the stable poisson loaded specimen
[NASA-TM-105609] p 245 N93-12738
- Closed form expressions for crack mouth displacements and stress intensity factors for chevron notched short bar and short rod specimens based on experimental compliance measurements
[NASA-TM-83796] p 246 N93-15369
- Progressive delamination in polymer matrix composite laminates: A new approach
p 108 N93-21515
- STRESS RELAXATION**
- Creep and stress relaxation modeling of polycrystalline ceramic fibers
p 132 A93-31354
- Stress relaxation of low pressure plasma-sprayed NiCrAlY alloys
p 127 A93-52870
- STRESS-STRAIN DIAGRAMS**
- Viscoplasticity with creep and plasticity bounds
p 125 A93-32925
- STRESS-STRAIN RELATIONSHIPS**
- Stirling engine - Available tools for long-life assessment --- for space propulsion
p 65 A93-13824
- Limit pressure of a circumferentially reinforced SiC/Ti ring
p 233 A93-16005
- Improved accuracy for finite element structural analysis via an integrated force method
p 234 A93-17246
- Ratchetting behavior in viscoplasticity - A technical note
p 241 A93-43651
- On bilinearity of Manson-Coffin low-cycle-fatigue relationship
[NASA-TM-105840] p 245 N93-12739
- Thermoviscoplastic analysis of fibrous periodic composites using triangular subvolumes
[NASA-TM-106076] p 111 N93-29074
- STRIATION**
- Ratchetting behavior in viscoplasticity - A technical note
p 241 A93-43651
- STRING THEORY**
- Cosmic string with a light massive neutrino
p 288 A93-16303
- Clumpy cold dark matter
p 291 A93-46201
- STRONTIUM COMPOUNDS**
- Kinetics of hexacelsian-to-celsian phase transformation in SrAl₂Si₂O₈
p 134 A93-40293

- Kinetics of hexacelsian to celsian phase transformation in $\text{SrAl}_2\text{Si}_2\text{O}_8$
[NASA-TM-105913] p 136 N93-16372
- STRONTIUM OXIDES**
Silicon carbide fiber reinforced strontium aluminosilicate glass-ceramic matrix composite
[NASA-CASE-LEW-15263-1] p 106 N93-11543
- STRUCTURAL ANALYSIS**
Computational simulation of surface waviness in graphite/epoxy woven composites due to initial curing p 98 A93-15822
Probabilistic structural analysis of adaptive/smart/intelligent space structures p 234 A93-16203
Structural durability of a composite pressure vessel p 234 A93-16552
Improved accuracy for finite element structural analysis via an integrated force method p 234 A93-17246
Coupled multi-disciplinary simulation of composite engine structures in propulsion environment [ASME PAPER 92-GT-6] p 23 A93-19279
Structural Tailoring/Analysis for Hypersonic Components - A computational simulation [AIAA PAPER 92-4722] p 20 A93-20324
Neural networks in structural analysis and design - An overview p 263 A93-20388
Singularities in optimal structural design [AIAA PAPER 92-4818] p 235 A93-20397
Acoustical analysis of gear housing vibration p 273 A93-29420
Programming probabilistic structural analysis for parallel processing computers p 237 A93-32410
Integrated force method - Compatibility conditions of structural mechanics for finite element analysis p 237 A93-32459
Probabilistic nonlinear finite element analysis of composite structures p 237 A93-32717
Global/local methods for probabilistic structural analysis [AIAA PAPER 93-1378] p 238 A93-33942
Parallel computing for probabilistic fatigue analysis [AIAA PAPER 93-1499] p 261 A93-34039
Probabilistically configured adaptive composite structures [AIAA PAPER 93-1679] p 240 A93-34191
Singularity in structural optimization p 240 A93-34938
Variation of the energy release rate as a crack approaches and passes through an elastic inclusion p 241 A93-44440
Boundary formulations for sensitivity analysis without matrix derivatives p 242 A93-49028
Reliability assessment of thrust chamber cooling concepts using probabilistic analysis techniques [AIAA PAPER 93-2163] p 75 A93-49978
Computational simulation of hot composite structures p 260 A93-54704
Elastic interactions of a fatigue crack with a micro-defect by the mixed boundary integral equation method p 243 A93-56412
Radial turbine cooling p 191 N93-10061
Application of artificial neural networks in nonlinear analysis of trusses [NASA-TM-105319] p 244 N93-11403
Thermostructural tailoring of fiber composite structures [NASA-TM-105882] p 107 N93-12078
Probabilistic evaluation of fuselage-type composite structures [NASA-TM-105881] p 245 N93-12735
Second generation integrated composite analyzer (ICAN) computer code [NASA-TP-3290] p 108 N93-18139
Structural analysis of high-rpm composite propfan blades for a cruise missile wind tunnel model [NASA-TM-105267] p 247 N93-23015
Mapping methods for computationally efficient and accurate structural reliability [NASA-TM-105892] p 248 N93-23745
Evaluation of MARC for the analysis of rotating composite blades [NASA-TM-4423] p 249 N93-24909
High temperature composite analyzer (HITCAN) user's manual, version 1.0 [NASA-TM-106002] p 249 N93-25070
Probabilistic sizing of laminates with uncertainties [NASA-TM-106145] p 110 N93-27082
Probabilistic assessment of composite structures [NASA-TM-106024] p 110 N93-27092
Face-gear drives: Design, analysis, and testing for helicopter transmission applications [NASA-TM-106101] p 229 N93-27133
Metal Matrix Laminate Tailoring (MMLT) code: User's manual [NASA-TM-106052] p 111 N93-28681
Probabilistic composite analysis p 112 N93-30868

- Mapping methods for computationally efficient and accurate structural reliability p 232 N93-31572
- STRUCTURAL DESIGN**
Grounding of space structures p 54 A93-12144
Probabilistic evaluation of uncertainties and risks in aerospace components p 233 A93-12160
Shape reanalysis and sensitivities utilizing preconditioned iterative boundary solvers p 233 A93-14446
Reliability analysis of structural ceramic components using a three-parameter Weibull distribution [ASME PAPER 92-GT-296] p 231 A93-19486
Neural networks in structural analysis and design - An overview p 263 A93-20388
Neural networks for structural design - An integrated system implementation [AIAA PAPER 92-4806] p 263 A93-20389
Singularities in optimal structural design [AIAA PAPER 92-4818] p 235 A93-20397
Analysis and optimal design of thick composite structures with passive damping considerations [AIAA PAPER 92-4819] p 235 A93-20398
NASA CST aids U.S. industry --- computational structures technology p 258 A93-25084
Design and optimization of a self-deploying single axis tracking PV array p 252 A93-25916
Fabrication of carbon-carbon heat pipes for space nuclear power applications p 173 A93-25978
Finite element implementation of state variable-based viscoplasticity models p 236 A93-26776
Design of structures for Nuclear Electric Propulsion vehicles [AIAA PAPER 93-1393] p 57 A93-33955
Probabilistic simulation of the human factor in structural reliability [AIAA PAPER 93-1495] p 264 A93-34036
Probabilistically configured adaptive composite structures [AIAA PAPER 93-1679] p 240 A93-34191
Topology and layout optimization of discrete and continuum structures p 241 A93-45429
Stochastic search in structural optimization - Genetic algorithms and simulated annealing p 241 A93-45430
Application of neural nets in structural optimization p 265 A93-54533
Self-organization in neural networks - Applications in structural optimization p 265 A93-54534
Structural optimization of thin shells using finite element method [NASA-TM-105903] p 246 N93-13157
Application of artificial neural networks to the design optimization of aerospace structural components [NASA-TM-4389] p 247 N93-21831
Structural tailoring of aircraft engine blade subject to ice impact constraints [NASA-TM-106033] p 250 N93-26999
- STRUCTURAL DESIGN CRITERIA**
Boundary formulations for three-dimensional continuum structural shape sensitivity analysis p 235 A93-22426
Damage progression in stiffened composite panels [AIAA PAPER 93-1345] p 238 A93-33915
Confidence bounds on structural reliability [AIAA PAPER 93-1377] p 238 A93-33941
Reliability based structural optimization - A simplified safety index approach [AIAA PAPER 93-1418] p 239 A93-33972
- STRUCTURAL FAILURE**
Structural system reliability under multiple failure modes [AIAA PAPER 93-1379] p 238 A93-33943
Reliability assessment of thrust chamber cooling concepts using probabilistic analysis techniques [AIAA PAPER 93-2163] p 75 A93-49978
Probabilistic composite analysis p 112 N93-30868
- STRUCTURAL MEMBERS**
Probabilistic evaluation of uncertainties and risks in aerospace components p 233 A93-12160
Lifetime reliability evaluation of structural ceramic parts with the CARES/LIFE computer program [AIAA PAPER 93-1497] p 239 A93-34037
- STRUCTURAL PROPERTIES (GEOLOGY)**
Venus Interior Structure Mission (VISM): Establishing a seismic network on Venus p 293 N93-28819
- STRUCTURAL RELIABILITY**
Probabilistic structural analysis of adaptive/smart/intelligent space structures p 234 A93-16203
The application of structural reliability techniques to plume impingement loading of the Space Station Freedom Photovoltaic Array [AIAA PAPER 93-1338] p 56 A93-33908
Confidence bounds on structural reliability [AIAA PAPER 93-1377] p 238 A93-33941

- Structural system reliability under multiple failure modes [AIAA PAPER 93-1379] p 238 A93-33943
Reliability based structural optimization - A simplified safety index approach [AIAA PAPER 93-1418] p 239 A93-33972
Probabilistic simulation of the human factor in structural reliability [AIAA PAPER 93-1495] p 264 A93-34036
Lifetime reliability evaluation of structural ceramic parts with the CARES/LIFE computer program [AIAA PAPER 93-1497] p 239 A93-34037
A numerical round robin for the reliability prediction of structural ceramics [AIAA PAPER 93-1498] p 240 A93-34038
Computational methods for efficient structural reliability and reliability sensitivity analysis [AIAA PAPER 93-1626] p 240 A93-34155
The application of structural reliability techniques to plume impingement loading of the Space Station Freedom Photovoltaic Array [NASA-TM-105949] p 59 N93-17988
Mapping methods for computationally efficient and accurate structural reliability [NASA-TM-105892] p 248 N93-23745
Probabilistic sizing of laminates with uncertainties [NASA-TM-106145] p 110 N93-27082
Structural Integrity and Durability of Reusable Space Propulsion Systems [NASA-CP-10064] p 93 N93-31552
Mapping methods for computationally efficient and accurate structural reliability p 232 N93-31572
Probabilistic simulation of the human factor in structural reliability p 258 N93-31573
- STRUCTURAL STABILITY**
Numerical calibration of the stable poisson loaded specimen [NASA-TM-105609] p 245 N93-12738
- STRUCTURAL VIBRATION**
An efficient constraint to account for mistuning effects in the optimal design of engine rotors [AIAA PAPER 92-4711] p 23 A93-20280
Modal test/analysis correlation of Space Station structures using nonlinear sensitivity [AIAA PAPER 92-4731] p 55 A93-20330
Probabilistic structural analysis of space truss structures for nonuniform thermal environmental effects [AIAA PAPER 92-4769] p 235 A93-20363
Review of the Shuttle vibration environment [AIAA PAPER 93-0832] p 51 A93-24902
Narrow band noise as a model of time-dependent accelerations - Study of the stability of a fluid surface in a microgravity environment [AIAA PAPER 93-0911] p 173 A93-24965
Probabilistic assessment of composite structures [AIAA PAPER 93-1441] p 239 A93-33990
Vibration localization in mono- and bi-coupled bladed disks - A transfer matrix approach [AIAA PAPER 93-1492] p 222 A93-34241
Forcing function modeling for flow induced vibration [ISABE 93-7027] p 31 A93-54003
Stability of a fluid surface in a microgravity environment p 190 A93-55358
Pattern classifier for health monitoring of helicopter gearboxes [NASA-TM-106099] p 228 N93-23741
Global dynamic modeling of a transmission system [NASA-CR-191117] p 228 N93-24751
A transfer matrix approach to vibration localization in mistuned blade assemblies [NASA-TM-106112] p 250 N93-27088
- STRUCTURAL WEIGHT**
Pressurization and expulsion of a lightweight liquid hydrogen tank [AIAA PAPER 93-1966] p 73 A93-49814
- STRUTS**
A numerical investigation of supersonic strut/ndwall interactions in annular flow with varying strut thickness [AIAA PAPER 93-2927] p 10 A93-48128
Investigation of a strut/ndwall interaction in supersonic annular flow [AIAA PAPER 93-1925] p 12 A93-49791
- SUBROUTINES**
A SINDA '85 nodal heat transfer rate calculation user subroutine p 193 N93-13403
- SUBSONIC FLOW**
Influence of airfoil thickness on sound generated by high-frequency gust interactions p 272 A93-19181
Numerical solutions for unsteady subsonic vortical flows around loaded cascades [ASME PAPER 92-GT-173] p 3 A93-19399
Prediction of active control of subsonic centrifugal compressor rotating stall [AIAA PAPER 93-0153] p 4 A93-22591
Acoustic radiation from a thin airfoil in nonuniform subsonic flows p 273 A93-23535

Unsteady aerodynamics and flutter of propfans using a three-dimensional Full-Potential Solver [AIAA PAPER 93-1633] p 25 A93-34161

An extended Lagrangian method [AIAA PAPER 93-3305] p 8 A93-45003

A three-dimensional pressure flux-split RNS application to sub/supersonic flow in inlets and ducts [AIAA PAPER 93-3063] p 11 A93-48239

CFD validation of subsonic turbulent planar shear layers [AIAA PAPER 93-1773] p 184 A93-49669

3-D viscous flow CFD analysis of the propeller effect on an advanced ducted propeller subsonic inlet [AIAA PAPER 93-1847] p 12 A93-49728

Unsteady aerodynamics and flutter based on the potential equation [AIAA PAPER 93-2086] p 13 A93-49913

Comparison of reacting and non-reacting shear layers at a high subsonic Mach number [AIAA PAPER 93-2381] p 186 A93-50149

Mixing of multiple jets with a confined subsonic crossflow [AIAA PAPER 93-54324] p 15 A93-54324

An experimental investigation of the flow in a diffusing S-duct [NASA-TM-105809] p 32 N93-12077

An extended Lagrangian method [NASA-TM-106129] p 199 N93-26203

Comparison of reacting and non-reacting shear layers at a high subsonic Mach number [NASA-TM-106198] p 38 N93-27610

The 3-D viscous flow CFD analysis of the propeller effect on an advanced ducted propeller subsonic inlet [NASA-TM-106240] p 38 N93-29162

SUBSONIC SPEED

Acoustic mode measurements in the inlet of a model turbofan using a continuously rotating rake - Data collection/analysis techniques [AIAA PAPER 93-0599] p 24 A93-23324

Preconditioned Conjugate Gradient methods for low speed flow calculations [AIAA PAPER 93-0881] p 172 A93-24942

Effect of a rotating propeller on the separation angle of attack [AIAA PAPER 93-0017] p 6 A93-24978

A concept for a counterrotating fan with reduced tone noise [NASA-TM-105736] p 274 N93-11370

Preconditioned conjugate-gradient methods for low-speed flow calculations [NASA-TM-105929] p 194 N93-14885

Acoustic mode measurements in the inlet of a model turbofan using a continuously rotating rake: Data collection/analysis techniques [NASA-TM-105936] p 33 N93-15403

Effect of a rotating propeller on the separation angle of attack and distortion in ducted propeller inlets [NASA-TM-105935] p 16 N93-16625

SUBSONIC WIND TUNNELS

Experimental investigation of an ejector-powered free-jet facility [NASA-TM-105868] p 16 N93-16704

SUBSTRATES

Input impedance of coaxially fed rectangular microstrip antenna on electrically thick substrate p 155 A93-36994

Method of applying a thermal barrier coating system to a substrate [NASA-CASE-LEW-15020-2] p 107 N93-14706

Oxidation resistant overlay coatings for low expansion substrates [NASA-CASE-LEW-15154-1] p 137 N93-19332

SUCTION

Hypersonic stability and transition p 8 A93-42579

SULFUR

Closed-ampoule diffusion of sulfur into Cd-doped InP substrates - Dependence of S profiles on diffusion temperature and time p 283 A93-51917

SUPERCOMPUTERS

The engine design engine. A clustered computer platform for the aerodynamic inverse design and analysis of a full engine [NASA-TM-105838] p 15 N93-11223

SUPERCONDUCTING FILMS

Buffer layers for high-Tc thin films on sapphire p 150 A93-17063

Giant suppression of flux-flow resistivity in heavy-ion irradiated Ti2Ba2Ca2Cu3O10 films - Influence of linear defects on vortex transport p 280 A93-26198

Low temperature phase formation of Ti-based superconducting thin films in reduced oxygen atmosphere p 282 A93-44568

Processing, electrical and microwave properties of sputtered Ti-Ca-Ba-Cu-O superconducting thin films p 282 A93-44607

Conductor-backed coplanar waveguide resonators of Y-Ba-Cu-O and Ti-Ba-Ca-Cu-O on LaAlO3 [NASA-TM-105890] p 284 N93-12325

SUPERCONDUCTING MAGNETS

Actively controlled superconducting bearings p 223 A93-48594

Preliminary investigation of high power microwave plasmas for electrothermal thruster use [AIAA PAPER 93-2106] p 74 A93-49928

Preliminary investigation of high power microwave plasmas for electrothermal thruster use [NASA-TM-106207] p 92 N93-29158

SUPERCONDUCTIVITY

Superconductivity applications for infrared and microwave devices II, Proceedings of the Meeting, Orlando, FL, Apr. 4, 5, 1991 p 154 A93-27243

[SPIE-1477] p 154 A93-27243

Composition dependence of superconductivity in YBa2Cu3-xAlxO(y) p 281 A93-40271

SUPERCOOLING

IDGE - A test of dendritic growth theory using space flight [AIAA PAPER 93-0260] p 143 A93-25515

SUPERCritical FLUIDS

Supercritical droplet combustion and related transport phenomena [AIAA PAPER 93-0812] p 115 A93-24885

SUPERHEATING

Tank Pressure Control Experiment/Thermal Phenomena (TPCE/TP) p 92 N93-28713

SUPERLATTICES

Ellipsometric study of Si(0.5)Ge(0.5)/Si strained-layer superlattices p 280 A93-34655

SUPERSONIC AIRCRAFT

Overview of high performance aircraft propulsion research [NASA-TM-105839] p 32 N93-11530

Experimental performance of a ventral nozzle with pitch and yaw vectoring capability for SSTOVL aircraft [NASA-TM-106054] p 36 N93-25129

SUPERSONIC BOUNDARY LAYERS

A time-accurate high-resolution TVD scheme for solving the Navier-Stokes equations p 13 A93-52006

A time-accurate high-resolution TVD scheme for solving the Navier-Stokes equations [NASA-TM-106056] p 268 N93-22664

SUPERSONIC COMBUSTION

Pdf prediction of supersonic hydrogen flames [AIAA PAPER 93-0448] p 114 A93-23358

Nonintrusive, multipoint velocity measurements in high-pressure combustion flows [AIAA PAPER 93-2032] p 118 A93-49867

Aerothermodynamic flow phenomena of the airframe-integrated supersonic combustion ramjet [NASA-TM-4376] p 82 N93-15528

SUPERSONIC COMBUSTION RAMJET ENGINES

A numerical study of mixing in supersonic combustors with hypermixing injectors [AIAA PAPER 93-0215] p 25 A93-27801

Calculation of scramjet inlet with thick boundary-layer ingestion [AIAA PAPER 93-1836] p 12 A93-49720

Development of hypersonic engine seals - Flow effects of preload and engine pressures [AIAA PAPER 93-1998] p 223 A93-49841

Visualization of hydrogen injection in a scramjet engine by simultaneous PLIF imaging and laser holographic imaging p 214 N93-13683

Aerothermodynamic flow phenomena of the airframe-integrated supersonic combustion ramjet [NASA-TM-4376] p 82 N93-15528

SUPERSONIC COMMERCIAL AIR TRANSPORT

Engine technology challenges for a 21st Century High-Speed Civil Transport [ISABE 93-7064] p 31 A93-54040

Engine technology challenges for a 21st Century High-Speed Civil Transport [NASA-TM-106216] p 39 N93-31671

SUPERSONIC FLIGHT

Overview of high performance aircraft propulsion research [NASA-TM-105839] p 32 N93-11530

SUPERSONIC FLOW

An asymptotic theory of supersonic propeller noise p 271 A93-19169

Molecular filter-based diagnostics in high speed flows [AIAA PAPER 93-0512] p 205 A93-23259

Lagrangian solution of supersonic real gas flows p 170 A93-23944

LV software support for supersonic flow analysis [AIAA PAPER 92-3900] p 259 A93-24487

Computing 3-D steady supersonic flow via a new Lagrangian approach [AIAA PAPER 93-0891] p 6 A93-24951

A numerical study of mixing in supersonic combustors with hypermixing injectors [AIAA PAPER 93-0215] p 25 A93-27801

Computation of unsteady supersonic quasi-one-dimensional viscous-inviscid interacting internal flowfields p 177 A93-32724

An extended Lagrangian method [AIAA PAPER 93-3305] p 8 A93-45003

An accuracy assessment of Cartesian-mesh approaches for the Euler equations [AIAA PAPER 93-3335] p 9 A93-45029

A numerical investigation of supersonic strut/endwall interactions in annular flow with varying strut thickness [AIAA PAPER 93-2927] p 10 A93-48128

A three-dimensional pressure flux-split RNS application to sub/supersonic flow in inlets and ducts [AIAA PAPER 93-3063] p 11 A93-48239

Experimental and numerical investigation of supersonic turbulent flow in an annular duct [AIAA PAPER 93-3123] p 11 A93-48291

Investigation of a strut/endwall interaction in supersonic annular flow [AIAA PAPER 93-1925] p 12 A93-49791

Plume characteristics of an arcjet thruster [AIAA PAPER 93-2530] p 77 A93-50258

Supersonic boundary-layer flow turbulence modeling [NASA-TM-105893] p 193 N93-14758

Surface and flow field measurements in a symmetric crossing shock wave/turbulent boundary-layer interaction [NASA-TM-106086] p 17 N93-24911

Nonlinear evolution of the first mode supersonic oblique waves in compressible boundary layers. Part 1: Heated/cooled walls [NASA-TM-106087] p 199 N93-25175

An extended Lagrangian method [NASA-TM-106129] p 199 N93-26203

Hypersonic engine component experiments in high heat flux, supersonic flow environment [NASA-TM-106273] p 203 N93-31860

SUPERSONIC INLETS

Evaluation and application of the Baldwin-Lomax turbulence model in two-dimensional, unsteady, compressible boundary layers with and without separation in engine inlets [AIAA PAPER 92-3676] p 2 A93-14118

Evaluation and application of the Baldwin-Lomax turbulence model in two-dimensional, unsteady, compressible boundary layers with and without separation in engine inlets [AIAA PAPER 92-3676] p 168 A93-22509

Modeling of linear isentropic flow systems p 179 A93-37046

Evaluation and application of the Baldwin-Lomax turbulence model in two-dimensional, unsteady, compressible boundary layers with and without separation in engine inlets [NASA-TM-105810] p 191 N93-10087

Analytical and experimental studies of a short compact subsonic diffuser for a two-dimensional supersonic inlet [NASA-TP-3247] p 17 N93-24118

SUPERSONIC JET FLOW

Supersonic jet noise reduction by coaxial rectangular nozzles p 272 A93-19205

On streamwise vortices in high Reynolds number supersonic axisymmetric jets p 167 A93-21060

Measured acoustic characteristics of ducted supersonic jets at different model scales [AIAA PAPER 93-0731] p 273 A93-24821

Computation of supersonic jet noise under imperfectly expanded conditions [AIAA PAPER 93-0735] p 273 A93-24825

The structure of supersonic jet flow and its radiated sound [AIAA PAPER 93-0549] p 273 A93-25538

Flip-flop jet nozzle extended to supersonic flows p 8 A93-39409

Streamwise vorticity generation and mixing enhancement in free jets by 'delta-tabs' [AIAA PAPER 93-3253] p 14 A93-53592

Computation of supersonic jet noise under imperfectly expanded conditions [NASA-TM-105961] p 274 N93-15430

Streamwise vorticity generation and mixing enhancement in free jets by delta-tabs [NASA-TM-106235] p 17 N93-31648

Enhanced mixing of a rectangular supersonic jet by natural and induced screech [NASA-TM-106245] p 18 N93-31672

SUPERSONIC SPEED

Effects of turbine cooling assumptions on performance and sizing of high-speed civil transport [AIAA PAPER 92-4217] p 22 A93-13383

SUPERSONIC TRANSPORTS

- Screening studies of advanced control concepts for airbreathing engines
[AIAA PAPER 92-3320] p 26 A93-49329
- Material requirements for the High Speed Civil Transport
[ISABE 93-7067] p 31 A93-54043
- Screening studies of advanced control concepts for airbreathing engines
[NASA-TM-106042] p 36 N93-25079
- Bibliography on propulsion airframe integration technologies for high-speed civil transport applications, 1980-1991
[NASA-TM-105602] p 1 N93-26136

SUPERSONIC WIND TUNNELS

- User manual for NASA Lewis 10 by 10 foot supersonic wind tunnel
[NASA-TM-105626] p 42 N93-15498
- NASA Lewis 8- by 6-foot supersonic wind tunnel user manual
[NASA-TM-105771] p 43 N93-25080

SURFACE COOLING

- Transient liquid-crystal technique used to produce high-resolution convective heat-transfer-coefficient maps
[NASA-TM-106083] p 198 N93-23404

SURFACE DEFECTS

- Leveling coatings for reducing the atomic oxygen defect density in protected graphite fiber epoxy composites
p 59 N93-15597

SURFACE DIFFUSION

- Effect of surface tension on the onset of convection in a double-diffusive layer
p 163 A93-13951

SURFACE DISTORTION

- System overview on electromagnetic compensation for reflector antenna surface distortion
[NASA-TM-106217] p 53 N93-29195

SURFACE GEOMETRY

- Effect of free surface shape on combined thermocapillary and natural convection
p 162 A93-10671
- Evaluation of a hue capturing based transient liquid crystal method for high-resolution mapping of convective heat transfer on curved surfaces
p 210 A93-43689

SURFACE LAYERS

- Atomic probe microscopy of 3C SiC films grown on 6H SiC substrates
p 281 A93-39854

SURFACE PROPERTIES

- Friction-factor data for flat-plate tests of smooth and honeycomb surfaces
[ASME PAPER 91-TRIB-20] p 219 A93-15682

SURFACE REACTIONS

- Prediction of chemical vapor deposition rates on monofilaments and its implications for fiber properties
p 113 A93-17198
- Interfacial chemistry of a perfluoropolyether lubricant studied by X-ray photoelectron spectroscopy and temperature desorption spectroscopy
p 133 A93-38473
- Ellipsometric study of ambient-produced overlayer growth rate on YBa₂Cu₃O_{7-x} films
p 281 A93-39362

- Heat of segregation of single substitutional impurities
p 119 A93-52873

- Interfacial chemistry of a perfluoropolyether lubricant studied by XPS and TDS
[NASA-TM-106014] p 137 N93-22560
- A kinetic and equilibrium analysis of silicon carbide chemical vapor deposition on monofilaments
[NASA-TM-106137] p 96 N93-27003

SURFACE ROUGHNESS

- The turbulent thermal boundary layer with an abrupt change from a rough to a smooth wall
p 167 A93-21712
- Close-up analysis of aircraft ice accretion
[AIAA PAPER 93-0029] p 18 A93-23239
- Surface roughness due to residual ice in the use of low power deicing systems
[AIAA PAPER 93-0031] p 5 A93-23240
- A lag model for turbulent boundary layers developing over rough bleed surfaces
[AIAA PAPER 93-2988] p 10 A93-48181
- Direct numerical simulation of instabilities in parallel flow with spherical roughness elements
[NASA-TM-105847] p 192 N93-11529
- Surface roughness due to residual ice in the use of low power deicing systems
[NASA-TM-105971] p 16 N93-15338
- Close-up analysis of aircraft ice accretion
[NASA-TM-105952] p 19 N93-15360
- Friction and wear of plasma-deposited diamond films
[NASA-TM-105926] p 136 N93-19035

SURFACE ROUGHNESS EFFECTS

- Leveling coatings for reducing the atomic oxygen defect density in protected graphite fiber epoxy composites
p 59 N93-15597

SURFACE STABILITY

- Narrow band noise as a model of time-dependent accelerations - Study of the stability of a fluid surface in a microgravity environment
[AIAA PAPER 93-0911] p 173 A93-24965
- Collapse of the soap-film bridge - Quasistatic description
p 188 A93-50536
- Stability of a fluid surface in a microgravity environment
p 190 A93-55358

SURFACE TREATMENT

- Refractive index effects on radiative behavior of a heated absorbing-emitting layer
p 162 A93-10653
- Miniature high temperature plug-type heat flux gauges
p 209 A93-37862
- Multiwavelength pyrometer for gray and non-gray surfaces in the presence of interfering radiation
[NASA-CASE-LEW-15250-1] p 214 N93-17060

SURFACE TREATMENT

- High performance sapphire windows
p 218 N93-22198

SURGES

- EMTP based stability analysis of Space Station Electric Power System in a test bed environment
p 154 A93-26108
- EMTP based stability analysis of space station electric power system in a test bed environment
[NASA-TM-105845] p 160 N93-15503
- A system to measure lightning-induced transients on spacecraft umbilical lines
p 161 N93-24889

SURVEYS

- A survey and analysis of commercially available hydrogen sensors
[NASA-TM-105878] p 214 N93-17777

SWEEP EFFECT

- On the static stability of forward swept propanes
[AIAA PAPER 93-1634] p 26 A93-34162

SWEEP WINGS

- LDV flowfield measurements on a straight and swept wing with a simulated ice accretion
[AIAA PAPER 93-0300] p 5 A93-23001

SWIRLING

- Fiber optic laser Doppler anemometry in swirling jets
p 206 A93-23783
- Cruise noise of an advanced propeller with swirl recovery vanes
p 273 A93-28609

SWITCHES

- Radiation and temperature effects on electronic components investigated under the CSTI high capacity power project
[NASA-TM-106096] p 161 N93-24746

SWITCHING CIRCUITS

- Comparative study of bolometric and non-bolometric switching elements for microwave phase shifters
p 155 A93-27245
- A 1.6-kW, 110-kHz dc-dc converter optimized for IGBT's
p 156 A93-37570

SYMBOLIC PROGRAMMING

- Calculation of stress intensity factors in an isotropic multiaxial cracked plate: Part 2: Symbolic/numeric implementation
[NASA-TM-105823] p 244 N93-10453

SYNCHRONOUS SATELLITES

- Electromagnetic powered vehicles (EMPV) for Mars exploration
p 47 A93-20761

SYNTHESIS (CHEMISTRY)

- Substituted 1,1,1-triaryl 2,2,2-trifluoroethanes and processes for their synthesis
[NASA-CASE-LEW-14345-7] p 95 N93-17412
- Ion exchange polymers and method for making
[NASA-CASE-LEW-15576-1] p 139 N93-31316

SYNTHETIC RESINS

- Benzonorborene end caps for PMR resins
p 94 A93-35700

SYSTEM IDENTIFICATION

- Identification of the open loop dynamics of the T700 turboshaft engine
p 26 A93-35934
- Identification of propulsion systems
[NASA-TM-106007] p 35 N93-20109

SYSTEMS ANALYSIS

- A qualitative approach to systemic diagnosis of the SSME
[AIAA PAPER 93-0405] p 261 A93-23327
- A graphical user-interface for propulsion system analysis
[AIAA PAPER 93-0223] p 259 A93-23699
- Structured system engineering methodologies used to develop a nuclear thermal propulsion engine
[AIAA PAPER 93-2109] p 271 A93-49930
- A comparative study of multivariable robustness analysis methods as applied to integrated flight and propulsion control
[AIAA PAPER 93-3809] p 21 A93-51401
- NTP comparison process
p 89 N93-26926
- NEP systems model
p 90 N93-26986
- NEP systems model
p 91 N93-26987

- Thruster models for NEP system analysis

p 91 N93-26988

SYSTEMS ENGINEERING

- Design and emplacement of an integrated lunar power system - Issues and concerns
p 46 A93-13908
- A qualitative approach to systemic diagnosis of the SSME
[AIAA PAPER 93-0405] p 261 A93-23327
- 100-kWe lunar/Mars surface power utilizing the SP-100 reactor with dynamic conversion
p 67 A93-25856
- Long life Regenerative Fuel Cell technology development plan
p 252 A93-25867
- Regenerative fuel cells
p 252 A93-25868
- Overview of the NASA Lewis component technology program for Stirling power converters
p 254 A93-26073
- Solar array electrical performance assessment for Space Station Freedom
[AIAA PAPER 93-1052] p 69 A93-30956
- Structured system engineering methodologies used to develop a nuclear thermal propulsion engine
[AIAA PAPER 93-2109] p 271 A93-49930
- System model development for nuclear thermal propulsion
[NASA-TM-105761] p 80 N93-10457
- NTP comparison process
p 89 N93-26926
- Minimize system cost by choosing optimal subsystem reliability and redundancy
[NASA-TM-106251] p 271 N93-31145

SYSTEMS INTEGRATION

- Neural networks for structural design - An integrated system implementation
[AIAA PAPER 92-4806] p 263 A93-20389
- Predicted performance of an Integrated Modular Engine system
[AIAA PAPER 93-1888] p 72 A93-49761
- US/CIS integrated NTR
[AIAA PAPER 93-2367] p 76 A93-50138
- Application of controller partitioning optimization procedure to integrated flight/propulsion control design for a STOV aircraft
[AIAA PAPER 93-3766] p 40 A93-51361
- Integrated flight/propulsion control - Subsystem specifications for performance
[AIAA PAPER 93-3808] p 41 A93-51400
- SITE project. Phase 1: Continuous data bit-error-rate testing
[NASA-TP-3279] p 58 N93-11001
- Bibliography on propulsion airframe integration technologies for high-speed civil transport applications, 1980-1991
[NASA-TM-105602] p 1 N93-26136
- Radiator technology
p 90 N93-26979
- Status of the Fiber Optic Control System Integration (FOCSI) program
[NASA-TM-106151] p 217 N93-28053

SYSTEMS MANAGEMENT

- Description of the SSF PMAD dc testbed control system data acquisition function
p 47 A93-26103
- Power system monitoring and source control of the Space Station Freedom dc-power system testbed
p 69 A93-26109
- Power system monitoring and source control of the Space Station Freedom DC power system testbed
[NASA-TM-105841] p 80 N93-10734
- Description of the SSF PMAD DC testbed control system data acquisition function
[NASA-TM-105843] p 261 N93-11005

SYSTEMS SIMULATION

- Multidisciplinary propulsion simulation using NPSS
[AIAA PAPER 92-4709] p 270 A93-20318
- Simulating a 1-kW arcjet thruster using a nonlinear active load
p 48 A93-34482
- Computational simulation for concurrent engineering of aerospace propulsion systems
[NASA-TM-106029] p 249 N93-23746
- NEP systems model
p 90 N93-26986

SYSTEMS STABILITY

- Probabilistic evaluation of uncertainties and risks in aerospace components
p 233 A93-12160
- Analysis of airframe and engine control interactions and integrated flight/propulsion control
p 40 A93-14596
- Coarsening following a morphological instability in the one-sided model
p 284 A93-21695
- Stability testing and analysis of a PMAD dc test bed for the Space Station Freedom
p 154 A93-26107
- A survey of instabilities within centrifugal pumps and concepts for improving the flow range of pumps in rocket engines
p 190 N93-10039

T

TABS (CONTROL SURFACES)

- Streamwise vorticity generation and mixing enhancement in free jets by 'delta-tabs' [AIAA PAPER 93-3253] p 14 A93-53592
- Streamwise vorticity generation and mixing enhancement in free jets by delta-tabs [NASA-TM-106235] p 17 N93-31648

TAKEOFF

- Takeoff/approach noise for a model counterrotation propeller with a forward-swept upstream rotor [AIAA PAPER 93-0596] p 24 A93-24782
- Unsteady blade pressures on a propfan at takeoff - Euler analysis and flight data p 26 A93-37389
- Effects of flow-path variations on internal reversing flow in a tailpipe offtake configuration for ASTOVL aircraft [AIAA PAPER 93-2438] p 29 A93-50190
- Takeoff/approach noise for a model counterrotation propeller with a forward-swept upstream rotor [NASA-TM-105979] p 34 N93-16715
- Effects of flow-path variations on internal reversing flow in a tailpipe offtake configuration for ASTOVL aircraft [NASA-TM-106149] p 38 N93-29065

TAYLOR INSTABILITY

- Numerical study of mixing of two fluids under low gravity [NASA-TM-105865] p 194 N93-14914

TAYLOR SERIES

- Comparison of truncation error of finite-difference and finite-volume formulations of convection terms [NASA-TM-105861] p 268 N93-11531

TDR SATELLITES

- Utilizing a TDRS satellite for direct broadcast satellite-radio propagation experiments and demonstrations [NASA-TM-106172] p 53 N93-27064

TECHNICAL WRITING

- Technical report writing [NASA-TM-105419] p 287 N93-23002

TECHNOLOGICAL FORECASTING

- The NASA Computational Fluid Dynamics (CFD) program - Building technology to solve future challenges [AIAA PAPER 93-3292] p 287 A93-44996
- Advances in NASA's Nuclear Thermal Propulsion Technology project [AIAA PAPER 93-2258] p 75 A93-50056
- Progress report on nuclear propulsion for space exploration and science [AIAA PAPER 93-2352] p 44 A93-50125

TECHNOLOGY ASSESSMENT

- Phase shifter technology assessment - Prospects and applications p 152 A93-25808
- Propulsion technology challenges for turn-of-the-century commercial aircraft [ISABE 93-7003] p 31 A93-53980
- Computational simulation for concurrent engineering of aerospace propulsion systems [NASA-TM-106029] p 249 N93-23746
- Nuclear thermal propulsion technology overview p 89 N93-26927
- In-flight near- and far-field acoustic data measured on the Propfan Test Assessment (PTA) testbed and with an adjacent aircraft [NASA-TM-103719] p 275 N93-27058
- Propulsion technology challenges for turn-of-the-century commercial aircraft [NASA-TM-106192] p 39 N93-32351

TECHNOLOGY TRANSFER

- U.S./CIS eye joint nuclear rocket venture p 71 A93-49334

TECHNOLOGY UTILIZATION

- Selected OAST/OSSA space experiment activities in support of Space Station Freedom p 60 N93-22636
- Development of Si(1-x)Ge(x) technology for microwave sensing applications [NASA-TM-106157] p 162 N93-28610

TELEBOTANICS

- Robotic planetary mission benefits from nuclear electric propulsion p 43 A93-25854

TELESCOPES

- Compact color schlieren optical system p 277 A93-52071

TEMPERATURE CONTROL

- Self-tuning multivariable pole placement control of a multizone crystal growth furnace p 263 A93-10575
- Closed-form analytical solutions of high-temperature heat pipe startup and frozen startup limitation p 165 A93-18564
- Numerical model for the Programmable Multirole Furnace (PMZF) [AIAA PAPER 93-0471] p 142 A93-24242
- Evaluation of the benefits of high temperature electronics for lunar power systems p 153 A93-25896

Thermal control system for Space Station Freedom photovoltaic power module p 57 A93-41305

Cryogenic propellant thermal control system design considerations, analyses, and concepts applied to a Mars human exploration mission [AIAA PAPER 93-2353] p 75 A93-50126

Plasma current collection of Z-93 thermal control paint as measured in the Lewis Research Center's plasma interaction facility [NASA-TM-106132] p 61 N93-26215

The effects of simulated low Earth orbit environments on spacecraft thermal control coatings [NASA-TM-106146] p 61 N93-27019

Electrical power system WP-04 p 161 N93-27804

TEMPERATURE DEPENDENCE

Relative sliding durability of two candidate high-temperature oxide fiber seal materials p 132 A93-31983

TEMPERATURE DISTRIBUTION

Refractive index effects on radiation in an absorbing, emitting, and scattering laminated layer p 175 A93-30125

Variable refractive index effects on radiation in semitransparent scattering multilayered regions p 189 A93-54463

Testing for the Gaussian nature of cosmological density perturbations through the three-point temperature correlation function p 292 A93-55212

Reliability analysis of laminated ceramic matrix composites using shell subelement techniques p 243 A93-55382

Thermal stratification potential in rocket engine coolant channels p 78 N93-10019

Review of the physical and mechanical properties and potential applications of the B2 compound NiAl: Unabridged version of a paper published in International materials review [NASA-TM-105598] p 127 N93-11635

Structure of confined laminar spray diffusion flames: Numerical investigation [NASA-TM-106038] p 197 N93-22596

Summary of experimental heat-transfer results from the turbine hot section facility [NASA-TP-3250] p 197 N93-23059

TEMPERATURE EFFECTS

Computational simulation of surface waviness in graphite/epoxy woven composites due to initial curing p 98 A93-15822

Probabilistic structural analysis of space truss structures for nonuniform thermal environmental effects [AIAA PAPER 92-4769] p 235 A93-20363

High-temperature deformation and microstructural analysis for silicon nitride-scandium(III) oxide p 131 A93-20468

Isothermal aging effects on PMR-15 resin p 131 A93-24508

Thermal conductivity and thermal expansion of graphite fiber-reinforced copper matrix composites p 100 A93-25104

Neutron, gamma ray, and temperature effects on the electrical characteristics of thyristors p 153 A93-25894

Comparison of high temperature, high frequency core loss and dynamic B-H loops of a 2V-49Fe-49Co and a grain oriented 3Si-Fe alloy p 153 A93-25895

Stirling engine - Approach for long-term durability assessment p 220 A93-26069

M-H characteristics and demagnetization resistance of samarium-cobalt permanent magnets to 300 C p 153 A93-26076

Thermally-driven microfracture in high temperature metal matrix composites p 237 A93-32469

Measurement of the temperature coefficient of ratio transformers p 155 A93-32771

Elevated-temperature fracture resistances of monolithic and composite ceramics using chevron-notched bend tests p 133 A93-38888

CVD of silicon carbide on structural fibers - Microstructure and composition p 117 A93-39521

Measurement of frequency response in short thermocouple wires p 209 A93-40677

Damping of thermal acoustic oscillations in hydrogen systems p 146 A93-48589

Atomizing-gas temperature effect on cryogenic spray droplets [AIAA PAPER 93-2333] p 186 A93-50111

Computational simulation of hot composite structures p 260 A93-54704

Design of a high-temperature experiment for evaluating advanced structural materials [NASA-TM-105833] p 245 N93-11624

TEMPERATURE MEASURING INSTRUMENTS

Review of the physical and mechanical properties and potential applications of the B2 compound NiAl: Unabridged version of a paper published in International materials review [NASA-TM-105598] p 127 N93-11635

Flux concentrations on solar dynamic components due to mispointing [NASA-TM-105756] p 255 N93-20261

Study of the capacitance technique for measuring high-temperature blade tip clearance on ceramic rotors [NASA-TM-105978] p 35 N93-23013

Radiation and temperature effects on electronic components investigated under the CSTI high capacity power project [NASA-TM-106096] p 161 N93-24746

Atomizing-gas temperature effect on cryogenic spray droplets [NASA-TM-106106] p 216 N93-25191

System overview on electromagnetic compensation for reflector antenna surface distortion [NASA-TM-106217] p 53 N93-29195

TEMPERATURE GRADIENTS

Thermosolutal convection during cellular arrayed growth of Pb-Sn alloys [AIAA PAPER 93-0262] p 142 A93-22668

Thermocapillary bubble migration - An Oseen-like analysis of the energy equation p 179 A93-41708

Thermocapillary migration of a small chain of bubbles p 182 A93-46714

Collective effects of temperature gradients and gravity on droplet coalescence p 183 A93-46716

Design of a high-temperature experiment for evaluating advanced structural materials [NASA-TM-105833] p 245 N93-11624

Physical vapor transport of mercurous chloride under a nonlinear thermal profile [NASA-TM-105920] p 196 N93-16612

A multi-zone muffle furnace design [NASA-TM-106153] p 145 N93-27011

TEMPERATURE MEASUREMENT

Novel thin-film heat flux sensors [AIAA PAPER 92-5035] p 205 A93-22309

Development of a Rayleigh scattering system for temperature measurements in combustor flows p 206 A93-23788

Miniature high temperature plug-type heat flux gauges p 209 A93-37862

Techniques for improving the accuracy of cryogenic temperature measurement in ground test programs p 212 A93-54363

Gas temperature measurements using the dual-line detection Rayleigh scattering technique p 213 A93-55368

Thin film thermocouples for high temperature measurement on ceramic materials p 213 N93-13666

Fabrication of thin film heat flux sensors p 213 N93-13667

Gas temperature measurements using the dual-line detection Rayleigh scattering technique p 214 N93-13668

Gas temperature and density measurements based on spectrally resolved Rayleigh-Brillouin scattering p 214 N93-13684

Multiwavelength pyrometer for gray and non-gray surfaces in the presence of interfering radiation [NASA-CASE-LEW-15250-1] p 214 N93-17060

Laser Rayleigh and Raman diagnostics for small hydrogen/oxygen rockets [NASA-TM-105999] p 83 N93-17995

2D velocity and temperature measurements in high speed flows based on spectrally resolved Rayleigh scattering [NASA-TM-105784] p 215 N93-19651

Techniques for improving the accuracy of cryogenic temperature measurement in ground test programs [NASA-TM-105996] p 215 N93-22484

Summary of experimental heat-transfer results from the turbine hot section facility [NASA-TP-3250] p 197 N93-23059

Dynamic gas temperature measurements using a personal computer for data acquisition and reduction [NASA-TM-106119] p 261 N93-27024

High temperature, oxidation resistant noble metal-Al alloy thermocouple [NASA-CASE-LEW-15515-1] p 217 N93-31298

Rayleigh-Brillouin scattering for high-pressure gas temperature measurements p 218 N93-31556

Non-contact heat flux measurement using a transparent sensor [NASA-TM-106252] p 142 N93-32330

TEMPERATURE MEASURING INSTRUMENTS

Fourier transform spectrometry for fiber-optic sensor systems p 211 A93-49459

Flight testing of a fiber optic temperature sensor p 22 A93-49476

TEMPERATURE PROBES

Fabrication of thin film heat flux sensors
p 213 N93-13667

TEMPERATURE PROFILES

A study of circumferentially-heated and block-heated heat pipes. I - Experimental analysis and generalized analytical prediction of capillary limits. II - Three-dimensional numerical modeling as a conjugate problem
p 168 A93-21715
Design of a constant tension thermocouple rake suitable for flame studies
p 210 A93-40683

TEMPERATURE SENSORS

Fabrication of thin film heat flux sensors
p 204 A93-16419
Optical fiber sensor for temperature measurement from 600 to 1900 C in gas turbine engines
p 208 A93-32918
Using silicon diodes for detecting the liquid-vapor interface in hydrogen
p 209 A93-37864
Fiber-optic thermometer using Fourier transform spectroscopy
p 212 A93-53104
Techniques for improving the accuracy of cryogenic temperature measurement in ground test programs
p 212 A93-54363
Techniques for improving the accuracy of cryogenic temperature measurement in ground test programs
[NASA-TM-105996]
p 215 N93-22484

TEMPORAL RESOLUTION

Multigrid time-accurate integration of Navier-Stokes equations
[AIAA PAPER 93-3361]
p 181 A93-45054

TENSILE CREEP

Tensile creep and creep-recovery behavior of a SiC-fiber-Si3N4-matrix composite
p 104 A93-40290
Tensile creep behavior of polycrystalline alumina fibers
[NASA-TM-106269]
p 138 N93-30938

TENSILE PROPERTIES

Tensile strain-rate sensitivity of tungsten/niobium composites at 1300 to 1600 K
p 97 A93-14840
The effect of microalloying additions on the tensile properties of polycrystalline NiAl
p 123 A93-17516
Preliminary evaluation of tensile and stress-rupture behavior of W + 24 at pct Re + 0.4 at pct HfC wire
p 125 A93-25119

TENSILE STRENGTH

Properties of pure nickel after long term exposures to LiOH and vacuum at 775 K
p 123 A93-18075
Relative sliding durability of candidate high temperature fiber seal materials
[NASA-TM-105806]
p 95 N93-10978

TENSILE STRESS

Effect of tensile mean stress on fatigue behavior of single-crystal and directionally solidified superalloys
p 125 A93-33011
Simultaneous pressure measurement and high-speed photography study of cavitation in a dynamically loaded journal bearing
p 223 A93-40050

TENSILE TESTS

The role of the interface in refractory metal alloy composites
p 97 A93-13777
Mechanics of interfaces in fiber reinforced SiC/RBSN ceramic matrix composites --- reaction bonded silicon nitride
p 102 A93-32466
Nondestructive evaluation of a ceramic matrix composite material
p 102 A93-33016
Progress toward a tungsten alloy wire/high temperature alloy composite turbine blade
[NASA-TM-105901]
p 128 N93-15586
Stress distribution in composite flatwise tension test specimens
[NASA-TM-106074]
p 108 N93-25071
Acousto-Ultrasonic analysis of failure in ceramic matrix composite tensile specimens
[NASA-TM-106219]
p 232 N93-29073

TENSORS

Critical comparison of second-order closures with direct numerical simulations of homogeneous turbulence
p 176 A93-30840

TERMINAL GUIDANCE

ACTS system handbook, revision change index
[NASA-TM-107982]
p 150 N93-70235

TERMINOLOGY

Application of ray tracing in radiation heat transfer
[NASA-TM-106206]
p 202 N93-29075

TEST CHAMBERS

Acoustical evaluation of the NASA Lewis 9 by 15 foot low speed wind tunnel
[NASA-TP-3274]
p 42 N93-12016
Ice thickness measurement system for the icing research tunnel calibration
[NASA-TM-106095]
p 215 N93-24737

TEST EQUIPMENT

Evaluation of a vibration diagnostic system for the detection of spur gear pitting failures
[AIAA PAPER 93-2298]
p 224 A93-50083

Evaluation of a vibration diagnostic system for the detection of spur gear pitting failures
[NASA-TM-106103]
p 228 N93-25672
An apparatus for gripping test specimens
[NASA-CASE-LEW-15345-2]
p 230 N93-28127

TEST FACILITIES

A free-piston Stirling engine/linear alternator controls and load interaction test facility
p 146 A93-26077
Simulating a 1-kW arcjet thruster using a nonlinear active load
p 48 A93-34482
Using silicon diodes for detecting the liquid-vapor interface in hydrogen
p 209 A93-37864
A new facility for advanced rocket propulsion research
[AIAA PAPER 93-1859]
p 48 A93-49737
Experimental investigation of an ejector-powered free-jet facility
[NASA-TM-105868]
p 16 N93-16704
Nuclear thermal propulsion technology: Results of an interagency panel in FY 1991
[NASA-TM-105711]
p 86 N93-24740
Space exploration initiative candidate nuclear propulsion test facilities
[NASA-TM-105710]
p 86 N93-24753
Space Nuclear Thermal Propulsion Test Facilities Subpanel
[NASA-TM-105708]
p 87 N93-25105
Conceptual design for the Space Station Freedom fluid physics/dynamics facility
[NASA-TM-103663]
p 61 N93-26209
Nuclear Propulsion Technical Interchange Meeting, volume 2
[NASA-CP-10116-VOL-2]
p 89 N93-26951
Facilities
p 49 N93-26963
Plum Brook facilities
p 49 N93-26964
NEP facilities (LeRC)
p 49 N93-26965
A new facility for advanced rocket propulsion research
[NASA-TM-106193]
p 49 N93-28696
Summary of NASA, Lewis Research Center validation efforts
p 204 N93-70579
NASA low speed centrifugal compressor
p 204 N93-70583
Focused technology: Nuclear propulsion
[PR12]
p 287 N93-71885

TEST FIRING

Qualitative model-based diagnostics for rocket systems
[AIAA PAPER 93-1779]
p 72 A93-49674
Durability testing of the AJ10-221 490 N high performance (321 sec lsp) engine
[AIAA PAPER 93-2130]
p 74 A93-49949
Hot fire test results of subscale tubular combustion chambers
p 79 N93-10020
Hot fire test results of subscale tubular combustion chambers
[NASA-TP-3222]
p 81 N93-11614
Qualitative model-based diagnostics for rocket systems
[NASA-TM-106234]
p 51 N93-28052

TEST STANDS

Plasma chamber testing of APSA coupons for the SAMPE flight experiment
[AIAA PAPER 93-0568]
p 67 A93-24244
Microgravity research on the NASA Lewis Learjet test facility
[AIAA PAPER 93-0573]
p 43 A93-24245
Overview and evolution of the LeRC PMAD DC test bed
p 47 A93-26099
Description of the PMAD systems test bed facility and data system
p 47 A93-26102
EMTP based stability analysis of Space Station Electric Power System in a test bed environment
p 154 A93-26108
Design and fabrication of a hydrogen/oxygen thrust chamber assembly
[AIAA PAPER 93-2132]
p 74 A93-49951
Design of an oxygen turbopump for use in an Advanced Expander Test Bed engine
[AIAA PAPER 93-2137]
p 48 A93-49955
EMTP based stability analysis of space station electric power system in a test bed environment
[NASA-TM-105845]
p 160 N93-15503
Evaluation of an oil-debris monitoring device for use in helicopter transmissions
[NASA-TM-105830]
p 227 N93-22826
A large hemi-anechoic enclosure for community-compatible aeroacoustic testing of aircraft propulsion systems
[NASA-TM-106015]
p 275 N93-26551
Fault-tolerant onboard digital information switching and routing for communications satellites
[NASA-TM-4471]
p 53 N93-26895

TESTING TIME

System model development for nuclear thermal propulsion
[NASA-TM-105761]
p 80 N93-10457

TEXTILES

Global/local finite element analysis for textile composites
[AIAA PAPER 93-1506]
p 103 A93-34045

THALLIUM COMPOUNDS

Low temperature phase formation of Ti-based superconducting thin films in reduced oxygen atmosphere
p 282 A93-44568
Processing, electrical and microwave properties of sputtered Ti-Ca-Ba-Cu-O superconducting thin films
p 282 A93-44607
Performance of TiCaBaCuO 30 GHz 64 element antenna array
p 157 A93-44763
Diminishing sign anomaly and scaling behavior of the mixed-state Hall resistivity in Ti2Ba2Ca2Cu3O10 films containing columnar defects
p 283 A93-53693

THERMAL ANALYSIS

Cryogenic propellant thermal control system design considerations, analyses, and concepts applied to a Mars human exploration mission
[AIAA PAPER 93-2353]
p 75 A93-50126
Computational simulation of hot composite structures
p 260 A93-54704
Tank chardown analysis and verification with a lightweight, 175 cu ft tank under normal gravity with liquid hydrogen
p 140 N93-10045
Thermostructural tailoring of fiber composite structures
[NASA-TM-105882]
p 107 N93-12078
The Fourth Annual Thermal and Fluids Analysis Workshop
[NASA-CP-10106]
p 192 N93-13385
Application of ray tracing in radiation heat transfer
[NASA-TM-106206]
p 202 N93-29075
Determination of the oxidative stability of perfluoropolyalkyl ethers and correlation with chemical structure
[NASA-TM-106223]
p 139 N93-32367

THERMAL BOUNDARY LAYER

The turbulent thermal boundary layer with an abrupt change from a rough to a smooth wall
p 167 A93-21712
Discussion of 'Comparison of turbulence models for the natural convection boundary layer along a heated vertical plate'
p 168 A93-21717

THERMAL CONDUCTIVITY

Graphite fiber/copper matrix composites for space power heat pipe fin applications
p 162 A93-13789
Thermal conductivity and thermal expansion of graphite fiber-reinforced copper matrix composites
p 100 A93-25104
Effect of HIPing on the effective thermal conductivity/diffusivity and the interfacial thermal conductance of uniaxial SiC fibre-reinforced RBSN
p 100 A93-26674
A survey and analysis of commercially available hydrogen sensors
[NASA-TM-105878]
p 214 N93-17777
Heat transfer device
[NASA-CASE-LEW-14162-4]
p 108 N93-20568
Semiconductor cooling apparatus
[NASA-CASE-LEW-14162-3]
p 111 N93-29614

THERMAL CONTROL COATINGS

Technical note: Plasma-sprayed ceramic thermal barrier coatings for smooth intermetallic alloys
p 219 A93-15702
Stress relaxation of low pressure plasma-sprayed NiCrAlY alloys
p 127 A93-52870
Method of applying a thermal barrier coating system to a substrate
[NASA-CASE-LEW-15020-2]
p 107 N93-14706
Oxidation resistant overlay coatings for low expansion substrates
[NASA-CASE-LEW-15154-1]
p 137 N93-19332
Characterization and durability testing of plasma-sprayed zirconia-yttria and hafnia-yttria thermal barrier coatings. Part 1: Effect of spray parameters on the performance of several lots of partially stabilized zirconia-yttria powder
[NASA-TP-3295]
p 128 N93-22556
Plasma sprayed ceramic thermal barrier coating for NiAl-based intermetallic alloys
[NASA-CASE-LEW-15535-1]
p 130 N93-31294

THERMAL CYCLING TESTS

Ductility of a continuous fiber reinforced aluminum matrix composite
p 102 A93-32471
Effect of thermal cycling on interface bonding requirements in Al2O3 fiber-reinforced superalloy composites
p 103 A93-35882
Hot fire fatigue testing results for the compliant combustion chamber
p 79 N93-10038
Hot fire fatigue testing results for the compliant combustion chamber
[NASA-TP-3223]
p 80 N93-10743
Thin film thermocouples for high temperature measurement on ceramic materials
p 213 N93-13666

- Simulation of the synergistic low Earth orbit effects of vacuum thermal cycling, vacuum UV radiation, and atomic oxygen p 58 N93-15595
- Effects of thermal and mechanical fatigue on the flexural strength of G40-600/PMR-15 cross-ply laminates [NASA-TM-106016] p 108 N93-20317
- Development of thin film thermocouples on ceramic materials for advanced propulsion system applications [NASA-TM-106017] p 215 N93-25173
- Progress in the measurement of SSME turbine heat flux with plug-type sensors p 217 N93-31553
- THERMAL DECOMPOSITION**
- Determination of the thermal stability of perfluoropolyalkyl ethers by tensimetry [NASA-TM-106081] p 137 N93-25093
- THERMAL DEGRADATION**
- A statistical analysis of elevated temperature gravimetric cyclic oxidation data of 36 Ni- and Co-base superalloys based on an oxidation attack parameter [NASA-TM-105934] p 128 N93-18069
- THERMAL DIFFUSIVITY**
- Effect of HIPing on the effective thermal conductivity/diffusivity and the interfacial thermal conductance of uniaxial SiC fibre-reinforced RBSN p 100 A93-26674
- Characterization and durability testing of plasma-sprayed zirconia-yttria and hafnia-yttria thermal barrier coatings. Part 1: Effect of spray parameters on the performance of several lots of partially stabilized zirconia-yttria powder [NASA-TP-3295] p 128 N93-22556
- THERMAL EMISSION**
- Thermal emittance enhancement of graphite-aluminum and graphite-copper composite radiator surfaces for space power applications p 105 A93-53455
- THERMAL ENERGY**
- Design of a cavity heat pipe receiver experiment p 173 A93-25985
- Experimental determination of in situ utilization of lunar regolith for thermal energy storage p 253 A93-26043
- Magnetic bearings for free-piston Stirling engines p 221 A93-26079
- US/CIS integrated NTRE [AIAA PAPER 93-2367] p 76 A93-50138
- THERMAL EXPANSION**
- Thermal conductivity and thermal expansion of graphite fiber-reinforced copper matrix composites p 100 A93-25104
- Computational characterization of high temperature composites via METCAN p 102 A93-32461
- Hot fire fatigue testing results for the compliant combustion chamber p 79 N93-10038
- Hot fire fatigue testing results for the compliant combustion chamber [NASA-TP-3223] p 80 N93-10743
- Oxidation resistant overlay coatings for low expansion substrates [NASA-CASE-LEW-15154-1] p 137 N93-19332
- THERMAL FATIGUE**
- Fatigue-environment interactions in a SiC/Ti-15-3 composite p 100 A93-26275
- Fatigue life prediction of an intermetallic matrix composite at elevated temperatures p 101 A93-31358
- Hot fire fatigue testing results for the compliant combustion chamber p 79 N93-10038
- Hot fire fatigue testing results for the compliant combustion chamber [NASA-TP-3223] p 80 N93-10743
- A creep cavity growth model for creep-fatigue life prediction of a unidirectional W/Cu composite [NASA-TM-105780] p 244 N93-10967
- Thermomechanical fatigue behavior of SiC/Ti-24Al-11Nb in air and argon environments [NASA-TM-105723] p 106 N93-11399
- Effects of thermal and mechanical fatigue on the flexural strength of G40-600/PMR-15 cross-ply laminates [NASA-TM-106016] p 108 N93-20317
- Cumulative fatigue damage behavior of MAR M-247 p 251 N93-31575
- Secondary orientation effects in a single crystal superalloy under mechanical and thermal loads p 130 N93-31578
- THERMAL MAPPING**
- Evaluation of a hue capturing based transient liquid crystal method for high-resolution mapping of convective heat transfer on curved surfaces p 210 A93-43689
- THERMAL PROTECTION**
- The effects of 1 kW class arcjet thruster plumes on spacecraft charging and spacecraft thermal control materials p 57 A93-35050
- The effects of simulated low Earth orbit environments on spacecraft thermal control coatings [NASA-TM-106146] p 61 N93-27019
- THERMAL RADIATION**
- Thermal radiation heat transfer (3rd revised and enlarged edition) --- Book p 165 A93-17522
- [ISBN 0-89116-271-2]
- A SINDA '85 nodal heat transfer rate calculation user subroutine p 193 N93-13403
- Jet Engine hot parts IR Analysis Procedure (J-EIRP) [NASA-TM-105914] p 21 N93-22588
- THERMAL REACTORS**
- Program ELM: A tool for rapid thermal-hydraulic analysis of solid-core nuclear rocket fuel elements [NASA-TM-105867] p 84 N93-19106
- THERMAL RESISTANCE**
- Fabrication of carbon-carbon heat pipes for space nuclear power applications p 173 A93-25978
- Probabilistic micromechanics for metal matrix composites p 237 A93-32465
- THERMAL STABILITY**
- Thermal stability of the microstructure of an aged Nb-Zr-C alloy p 122 A93-13776
- Transverse flexural tests as a tool for assessing damage to PMR-15 composites from isothermal aging in air at elevated temperatures p 100 A93-24514
- Computational characterization of high temperature composites via METCAN p 102 A93-32461
- Low temperature phase formation of Ti-based superconducting thin films in reduced oxygen atmosphere p 282 A93-44568
- Transverse flexural tests as a tool for assessing damage to PMR-15 composites from isothermal aging in air at elevated temperatures [NASA-TM-105848] p 107 N93-12737
- Determination of the thermal stability of perfluoropolyalkyl ethers by tensimetry [NASA-TM-106081] p 137 N93-25093
- Non-destructive, ultra-low resistance, thermally stable contacts for use on shallow junction InP solar cells [NASA-TM-106228] p 256 N93-32201
- THERMAL STRESSES**
- Probabilistic structural analysis of space truss structures for nonuniform thermal environmental effects [AIAA PAPER 92-4769] p 235 A93-20363
- Thermally-driven microfracture in high temperature metal matrix composites p 237 A93-32469
- Probabilistic assessment of adaptive space truss configurations for thermal buckling resistance [AIAA PAPER 93-1622] p 240 A93-34151
- The effect of multiple compliant layers at the fiber-matrix interface on residual thermal stresses in metal matrix composites p 104 A93-42085
- Creep deformation of B2 aluminides p 126 A93-44887
- Flow instability in particle-bed nuclear reactors [AIAA PAPER 93-1758] p 71 A93-49657
- Effects of anode material on arcjet performance p 79 N93-10044
- Effects of anode material on arcjet performance [NASA-TM-105799] p 79 N93-10197
- Design of a high-temperature experiment for evaluating advanced structural materials [NASA-TM-105833] p 245 N93-11624
- Experimental investigation of cyclic thermomechanical deformation in torsion [NASA-TM-105938] p 247 N93-17996
- High performance sapphire windows p 218 N93-22198
- THERMIONIC CONVERTERS**
- Thermophysical properties of gas phase uranium tetrafluoride [AIAA PAPER 93-2758] p 285 A93-46505
- THERMIONIC EMISSION**
- Lunar in-core thermionic nuclear reactor power system conceptual design p 46 A93-13836
- THERMIONIC POWER GENERATION**
- An evolution strategy for lunar nuclear surface power p 91 N93-27963
- THERMOCHEMISTRY**
- Benzonorbomadiene end caps for PMR resins p 94 A93-35700
- Chemical vapor deposition modeling for high temperature materials p 116 A93-39503
- Thermal oxidation of single-crystal silicon carbide - Kinetic, electrical, and chemical studies p 284 A93-55601
- THERMOCOUPLE PYROMETERS**
- Non-contact heat flux measurement using a transparent sensor [NASA-TM-106252] p 142 N93-32330
- THERMOCOUPLES**
- An Automated Thermocouple Calibration System p 208 A93-35575
- Measurement of frequency response in short thermocouple wires p 209 A93-40677
- Design of a constant tension thermocouple rake suitable for flame studies p 210 A93-40683
- Thin film thermocouples for high temperature measurement on ceramic materials p 213 N93-13666
- Fabrication of thin film heat flux sensors p 213 N93-13667
- Development of thin film thermocouples on ceramic materials for advanced propulsion system applications [NASA-TM-106017] p 215 N93-25173
- Dynamic gas temperature measurements using a personal computer for data acquisition and reduction [NASA-TM-106119] p 261 N93-27024
- High temperature, oxidation resistant noble metal-Al alloy thermocouple [NASA-CASE-LEW-15515-1] p 217 N93-31298
- Thin film thermocouples for high temperature turbine application p 217 N93-31555
- THERMODYNAMIC EFFICIENCY**
- HFAST - A harmonic analysis program for Stirling cycles p 220 A93-26051
- THERMODYNAMIC PROPERTIES**
- Thermodynamics of Si-C-O system p 133 A93-39584
- THERMODYNAMICS**
- Tailored metal matrix laminates for high-temperature performance p 98 A93-15753
- Overview of NASA supported Stirling thermodynamic loss research p 174 A93-26087
- Thermodynamics of iron-aluminum alloys at 1573 K p 127 A93-52879
- Computer program for calculating and fitting thermodynamic functions [NASA-RP-1271] p 285 N93-12967
- Thermodynamic data for fifty reference elements [NASA-TP-3287] p 286 N93-19977
- Stress-rupture behavior of small diameter polycrystalline alumina fibers [NASA-TM-106256] p 139 N93-32382
- THERMOELASTICITY**
- Thermo-elastoviscoplastic snapthrough behavior of cylindrical panels p 233 A93-12046
- THERMOELECTRIC GENERATORS**
- Versatile dynamic isotope power systems for the exploration of space p 46 A93-13819
- Comparison of dynamic isotope power systems for distributed planetary surface applications p 46 A93-13825
- An Isotope-Powered Thermal Storage unit for space applications p 65 A93-13877
- An evolution strategy for lunar nuclear surface power p 91 N93-27963
- THERMOELECTRIC POWER GENERATION**
- The NASA CSTI High Capacity Power Project p 69 A93-26105
- The NASA CSTI high capacity power project [NASA-TM-105813] p 48 N93-11398
- THERMOELECTRICITY**
- An evolution strategy for lunar nuclear surface power p 91 N93-27963
- THERMOPHYSICAL PROPERTIES**
- Thermophysical properties of gas phase uranium tetrafluoride [AIAA PAPER 93-2758] p 285 A93-46505
- THERMOPILES**
- Novel thin-film heat flux sensors [AIAA PAPER 92-5035] p 205 A93-22309
- Fabrication of thin film heat flux sensors p 213 N93-13667
- THERMOSETTING RESINS**
- Lower temperature curing thermoset polyimides utilizing a substituted norbornene endcap p 134 A93-44526
- THICK PLATES**
- Analysis and optimal design of thick composite structures with passive damping considerations [AIAA PAPER 92-4819] p 235 A93-20398
- THICKNESS**
- Ice thickness measurement system for the icing research tunnel calibration [NASA-TM-106095] p 215 N93-24737
- THICKNESS RATIO**
- A numerical investigation of supersonic strut/endwall interactions in annular flow with varying strut thickness [AIAA PAPER 93-2927] p 10 A93-48128
- THIN AIRFOILS**
- Influence of airfoil thickness on sound generated by high-frequency gust interactions p 272 A93-19181
- Acoustic radiation from a thin airfoil in nonuniform subsonic flows p 273 A93-23535
- THIN FILMS**
- Large-area YBa₂Cu₃O₇(δ) thin films on sapphire for microwave applications p 279 A93-11475
- Fabrication of thin film heat flux sensors p 204 A93-16419
- Buffer layers for high-T_c thin films on sapphire p 150 A93-17063
- Single liquid source plasma-enhanced metalorganic chemical vapor deposition of high-quality YBa₂Cu₃O₇(δ) thin films p 280 A93-20643

- Metal-organic chemical vapour deposition of polycrystalline tetragonal indium sulphide (InS) thin films
[NASA-TM-106248] p 116 A93-36584
- Ellipsometric study of ambient-produced overlayer growth rate on YBa₂Cu₃O_{7-x} films
p 281 A93-39362
- Thin film diamond microstructure applications
p 209 A93-40580
- Tribological studies of amorphous hydrogenated carbon films in a vacuum, space-like environment
p 134 A93-40630
- Progress in silicon carbide semiconductor technology
p 158 A93-44965
- Friction and wear of plasma-deposited amorphous hydrogenated films on silicon nitride
p 135 A93-52181
- Effect of out-of-roundness on the performance of a diesel engine connecting-rod bearing
p 225 A93-52607
- Growth and characterization of 3C-SiC and 6H-SiC films on 6H-SiC wafers
p 284 A93-55602
- Conductor-backed coplanar waveguide resonators of Y-Ba-Cu-O and Ti-Ba-Ca-Cu-O on LaAlO₃
[NASA-TM-105890] p 284 A93-12325
- Thin film thermocouples for high temperature measurement on ceramic materials
p 213 A93-13666
- Fabrication of thin film heat flux sensors
p 213 A93-13667
- Optical and scratch resistant properties of diamondlike carbon films deposited with single and dual ion beams
[NASA-TM-105943] p 95 A93-22586
- Development of thin film thermocouples on ceramic materials for advanced propulsion system applications
[NASA-TM-106017] p 215 A93-25173
- Optical and scratch resistant properties of diamondlike carbon films deposited with single and dual ion beams
p 137 A93-25564
- Thin film heat flux sensor for Space Shuttle Main Engine turbine environment
p 217 A93-31554
- Thin film thermocouples for high temperature turbine application
p 217 A93-31555
- THIN WALLED SHELLS**
- Design for progressive fracture in composite shell structures
p 242 A93-53394
- Structural optimization of thin shells using finite element method
[NASA-TM-105903] p 246 A93-13157
- Probabilistic assessment of composite structures
[NASA-TM-106024] p 110 A93-27092
- THREE DIMENSIONAL BODIES**
- Boundary formulations for three-dimensional continuum structural shape sensitivity analysis
p 235 A93-22426
- Navier-Stokes analysis of three-dimensional S-ducts
p 9 A93-45146
- Layout optimization using the homogenization method
p 243 A93-54508
- Applications to car bodies - Generalized layout design of three-dimensional shells
p 243 A93-54509
- THREE DIMENSIONAL BOUNDARY LAYER**
- Three-dimensional boundary-layer instability and separation induced by small-amplitude streamwise vorticity in the upstream flow
p 172 A93-24401
- The structure of a three-dimensional turbulent boundary layer
p 181 A93-44813
- The development of a mixing layer under the action of weak streamwise vortices
[NASA-TM-106089] p 201 A93-28947
- NASA, Lewis Research Center/IFMD inlet duct and nozzle high speed validation experiments
p 204 A93-70582
- THREE DIMENSIONAL COMPOSITES**
- Three-dimensional finite element simulation of intermingled-fiber hybrid composite behavior
p 98 A93-15729
- Fiber shape effects on metal matrix composite behavior
p 98 A93-15752
- Computational micromechanics of woven composites
p 237 A93-32462
- THREE DIMENSIONAL FLOW**
- Calculation of a circular jet in crossflow with a multiple-time-scale turbulence model
p 164 A93-15063
- Multigrid acceleration and turbulence models for computations of 3D turbulent jets in crossflow
p 165 A93-18751
- Aerodynamic design of turbomachinery blading in three-dimensional flow - An application to radial inflow turbines
[ASME PAPER 92-GT-74] p 3 A93-19324
- Three-dimensional flow phenomena in a transonic, high-through-flow, axial-flow compressor stage
[ASME PAPER 92-GT-169] p 3 A93-19395
- Numerical solutions for unsteady subsonic vortical flows around loaded cascades
[ASME PAPER 92-GT-173] p 3 A93-19399

- An algebraic turbulence model for three-dimensional viscous flows
[AIAA PAPER 93-0083] p 4 A93-22552
- Three-dimensional unstructured grid Euler method applied to turbine blades
[AIAA PAPER 93-0196] p 6 A93-24233
- A least-squares finite element method for 3D incompressible Navier-Stokes equations
[AIAA PAPER 93-0338] p 171 A93-24236
- Driven cavity simulation of turbomachine blade flows with vortex control
[AIAA PAPER 93-0390] p 6 A93-24238
- Three-dimensional Navier-Stokes calculations using solution-adapted grids
[AIAA PAPER 93-0431] p 6 A93-24240
- Application of an unstructured grid flow solver to planes, trains and automobiles
[AIAA PAPER 93-0889] p 173 A93-24949
- Computing 3-D steady supersonic flow via a new Lagrangian approach
[AIAA PAPER 93-0891] p 6 A93-24951
- Nonreflecting boundary conditions for linearized unsteady aerodynamic calculations
[AIAA PAPER 93-0882] p 7 A93-25553
- Statistical analysis of the effects of helicity in inhomogeneous turbulence
p 175 A93-26186
- A numerical study of mixing in supersonic combustors with hypermixing injectors
[AIAA PAPER 93-0215] p 25 A93-27801
- Calculations of separated 3-D flows with a pressure-staggered Navier-Stokes equations solver
p 177 A93-34366
- Simulation of three-dimensional liquid sloshing flows using a strongly implicit calculation procedure
p 179 A93-35624
- CFD for hypersonic propulsion
p 8 A93-42585
- Multigrid calculation of three-dimensional viscous cascade flows
p 8 A93-42889
- Segmented multigrid domain decomposition solutions for three dimensional viscous recirculating flows
[AIAA PAPER 93-3344] p 181 A93-45038
- Low-to-high altitude predictions of three-dimensional ablative re-entry flowfields
p 182 A93-46407
- Some practical turbulence modeling options for Reynolds-averaged full Navier-Stokes calculations of three-dimensional flows
[AIAA PAPER 93-2964] p 10 A93-48158
- A three-dimensional pressure flux-split RNS application to sub/supersonic flow in inlets and ducts
[AIAA PAPER 93-3063] p 11 A93-48239
- Streamwise computation of three-dimensional flows using two stream functions
p 184 A93-49241
- 3-D viscous flow CFD analysis of the propeller effect on an advanced ducted propeller subsonic inlet
[AIAA PAPER 93-1847] p 12 A93-49728
- Unsteady aerodynamic flow phenomena in a transonic compressor stage
[AIAA PAPER 93-1868] p 12 A93-49743
- Computation of the flow field in an annular gas turbine combustor
[AIAA PAPER 93-2074] p 28 A93-49903
- A comparative study of Full Navier-Stokes and Reduced Navier-Stokes analyses for separating flows within a diffusing inlet S-duct
[AIAA PAPER 93-2154] p 13 A93-49970
- Three-dimensional flow field in a turbine nozzle passage
[AIAA PAPER 93-2556] p 13 A93-50278
- Progress towards understanding and predicting heat transfer in the turbine gas path
p 188 A93-52751
- Three-dimensional flow analysis inside turbomachinery stages with steady and unsteady Navier-Stokes method
[ISABE 93-7095] p 14 A93-54071
- Mixing of multiple jets with a confined subsonic crossflow
p 15 A93-54324
- An algebraic turbulence model for three-dimensional viscous flows
[NASA-TM-105931] p 1 N93-14102
- Center for Modeling of Turbulence and Transition (CMOTT): Research Briefs, 1992
[NASA-TM-105834] p 195 N93-15792
- User's manual for Interactive Data Display System (IDDS)
[NASA-TM-105572] p 261 N93-16613
- Performance comparison of axisymmetric and three-dimensional hydrogen film coolant injection in a 110N hydrogen/oxygen rocket
[NASA-TM-105967] p 83 N93-16714
- The 3-D viscous flow CFD analysis of the propeller effect on an advanced ducted propeller subsonic inlet
[NASA-TM-106240] p 38 N93-29162
- Navier-Stokes analysis of three-dimensional flow and heat transfer inside turbine blade rows
p 39 N93-29963

- Numerical simulations of three-dimensional laminar flow over a backward facing step; flow near side walls
[NASA-TM-106248] p 202 N93-31147
- Overview of aerothermodynamic loads definition study
p 93 N93-31583
- Three-dimensional analysis of the Pratt and Whitney alternate design SSME fuel turbine
p 230 N93-31584
- Three-dimensional flow calculations inside SSME GGGT first stage blade rows
p 93 N93-31585
- THREE DIMENSIONAL MODELS**
- Coupled multi-disciplinary simulation of composite engine structures in propulsion environment
[ASME PAPER 92-GT-6] p 23 A93-19279
- Experimental and computational investigation of the NASA Low-Speed Centrifugal Compressor flow field
[ASME PAPER 92-GT-213] p 4 A93-19436
- Numerical optimization of composite hip endoprostheses under different loading conditions
[AIAA PAPER 92-4703] p 270 A93-20312
- A study of circumferentially-heated and block-heated heat pipes. I - Experimental analysis and generalized analytical prediction of capillary limits. II - Three-dimensional numerical modeling as a conjugate problem
p 168 A93-21715
- Unstructured 3D Delaunay mesh generation applied to planes, trains and automobiles
[AIAA PAPER 93-0673] p 259 A93-24781
- Modal simulation of gear box vibration with experimental correlation
p 221 A93-31982
- On the effects of grid ill-conditioning in three dimensional finite element vector potential magnetostatic field computations
p 157 A93-39719
- A numerical investigation of supersonic strut/endwall interactions in annular flow with varying strut thickness
[AIAA PAPER 93-2927] p 10 A93-48128
- Integrated CFD modeling of gas turbine combustors
[AIAA PAPER 93-2196] p 28 A93-50008
- Three-dimensional numerical simulation of gradual opening in a wave rotor passage
[AIAA PAPER 93-2526] p 187 A93-50254
- The three-point correlation function in an ensemble of three-dimensional simulations ... in gravitational perturbation theory
p 291 A93-50680
- Three-dimensional Navier-Stokes heat transfer predictions for turbine blade rows
[NASA-TM-105800] p 196 N93-19969
- THROATS**
- Experimentation in the low-density plume of a simulated electrothermal thruster for computer code validation
[NASA-CR-191112] p 87 N93-24758
- THROTTLING**
- A survey of instabilities within centrifugal pumps and concepts for improving the flow range of pumps in rocket engines
p 190 N93-10039
- THRUST**
- The multi-heat addition turbine engine
[AIAA PAPER 92-4272] p 22 A93-13334
- THRUST AUGMENTATION**
- A full-scale STOVL ejector experiment
[NASA-TM-106019] p 35 N93-22480
- THRUST CHAMBERS**
- Hydrocarbon-fuel/copper combustion chamber liner compatibility, corrosion prevention, and refurbishment
p 139 A93-14510
- Design and fabrication of a hydrogen/oxygen thrust chamber assembly
[AIAA PAPER 93-2132] p 74 A93-49951
- Reliability assessment of thrust chamber cooling concepts using probabilistic analysis techniques
[AIAA PAPER 93-2163] p 75 A93-49978
- Hot fire fatigue testing results for the compliant combustion chamber
p 79 N93-10038
- Hot fire fatigue testing results for the compliant combustion chamber
[NASA-TP-3223] p 80 N93-10743
- THRUST LOADS**
- Lubrication of an 85-mm ball bearing with RP-1
[AIAA PAPER 93-2538] p 225 A93-53590
- Lubrication of an 85-mm ball bearing with RP-1
[NASA-TM-106254] p 51 N93-31670
- THRUST MEASUREMENT**
- Characterization of in-flight performance of ion propulsion systems
[AIAA PAPER 93-2217] p 75 A93-50023
- THRUST VECTOR CONTROL**
- An electromechanical actuation system for an expendable launch vehicle
p 50 A93-25891
- THRUSTORS**
- Detailed ion thruster development status
[AIAA PAPER 93-2225] p 75 A93-50031
- Preliminary characterization of a water vaporizer for resistojel applications
[NASA-TM-105877] p 80 N93-11402
- Second Magnetoplasma dynamic Thruster Workshop
[NASA-CP-10109] p 279 N93-18635

THULIUM COMPOUNDS

Giant suppression of flux-flow resistivity in heavy-ion irradiated Ti2Ba2Ca2Cu3O10 films - Influence of linear defects on vortex transport p 280 A93-26198

THYRISTORS

Neutron, gamma ray, and temperature effects on the electrical characteristics of thyristors p 153 A93-25894

TILT ROTOR AIRCRAFT

Active control of helicopter transmission noise p 274 A93-29428

Screening studies of advanced control concepts for airbreathing engines [AIAA PAPER 92-3320] p 26 A93-49329

Screening studies of advanced control concepts for airbreathing engines [NASA-TM-106042] p 36 N93-25079

TIME DEPENDENCE

Central difference TVD schemes for time dependent and steady state problems p 188 A93-51183

TIME DIVISION MULTIPLEXING

Efficient demultiplexing algorithm for noncontiguous carriers p 148 A93-32561

TIME MARCHING

The application of preconditioning in viscous flows p 177 A93-32627

An efficient procedure for cascade aeroelastic stability determination using nonlinear, time-marching aerodynamic solvers [AIAA PAPER 93-1631] p 25 A93-34159

3-D viscous flow CFD analysis of the propeller effect on an advanced ducted propeller subsonic inlet [AIAA PAPER 93-1847] p 12 A93-49728

The 3-D viscous flow CFD analysis of the propeller effect on an advanced ducted propeller subsonic inlet [NASA-TM-106240] p 38 N93-29162

TIN ALLOYS

Thermosolutal convection during cellular arrayed growth of Pb-Sn alloys [AIAA PAPER 93-0262] p 142 A93-22668

TIP SPEED

A concept for a counterrotating fan with reduced tone noise [NASA-TM-105736] p 274 N93-11370

TITAN 3 LAUNCH VEHICLE

Monte Carlo analysis of the Titan III/Transfer Orbit Stage guidance system for the Mars Observer mission [AIAA PAPER 93-3889] p 50 A93-51473

Titan III feasibility for HL-20 prototype missions p 50 A93-53747

TITANIUM

Construction and testing of ceramic fabric heat pipe with water working fluid p 163 A93-13869

TITANIUM ALLOYS

Fatigue-environment interactions in a SiC/Ti-15-3 composite p 100 A93-26275

Transverse ductility of metal matrix composites p 101 A93-31355

Deformation and failure mechanisms in metal matrix composites p 102 A93-31359

Evolution of damage and plasticity in titanium-based, fiber-reinforced composites p 104 A93-48498

The effect of fiber microstructure on evolution of residual stresses in silicon carbide/titanium aluminide composites p 106 A93-54771

Thermomechanical fatigue behavior of SiC/Ti-24Al-11Nb in air and argon environments [NASA-TM-105723] p 106 N93-11399

TITANIUM BORIDES

Chemical stability of titanium diboride reinforcement in nickel aluminide matrices p 105 A93-52473

TITANIUM OXIDES

Vickers indentation hardness of stoichiometric and reduced single crystal TiO_2 (rutile) from 25 to 800 C [NASA-TM-105959] p 96 N93-26204

TOLERANCES (MECHANICS)

An overview of shed ice impact studies in the NASA Lewis Icing Research Tunnel [AIAA PAPER 93-0301] p 5 A93-23247

An overview of shed ice impact in the NASA Lewis Icing Research Tunnel [NASA-TM-105969] p 16 N93-15404

Structural dynamics: Probabilistic structural analysis methods. Program overview p 251 N93-31562

TOLLMIEN-SCHLICHTING WAVES

Fully coupled resonant-triad interaction in an adverse-pressure-gradient boundary layer p 167 A93-21049

Higher-order accurate Osher schemes with application to compressible boundary layer stability [AIAA PAPER 93-3051] p 183 A93-48231

TOPOGRAPHY

Three-dimensional computed tomography from interferometric measurements within a narrow cone of views p 207 A93-24024

TOPOGRAPHY

Phase-stepping fiber-optic projected fringe system for surface topography measurements [NASA-CASE-LEW-14996-1] p 278 N93-11058

TOPOLOGY

Topology and layout optimization of discrete and continuum structures p 241 A93-45429

Layout optimization using the homogenization method p 243 A93-54508

TORCHES

Development and use of hydrogen-air torches in an altitude facility [AIAA PAPER 93-2176] p 42 A93-49968

Development and use of hydrogen-air torches in an altitude facility [NASA-TM-106047] p 43 N93-26214

TORQUE

Split torque transmission load sharing [NASA-TM-105884] p 226 N93-12736

TORSION

In-phase and out-of-phase axial-torsional fatigue behavior of Haynes 188 at 760 C [NASA-TM-105765] p 246 N93-13153

Experimental investigation of cyclic thermomechanical deformation in torsion [NASA-TM-105938] p 247 N93-17996

TOTAL QUALITY MANAGEMENT

Design and implementation of a pilot orientation program for new NASA engineering employees [NASA-TM-105907] p 286 N93-26205

The Fifth Annual NASA/Contractors Conference on Quality and Productivity. Quality: A Commitment to the Future [NASA-TM-107829] p 233 N93-70212

TOUGHNESS

Analysis of precracking parameters for ceramic single-edge-precracked-beam specimens p 133 A93-38887

Analysis of precracking parameters and fracture toughness for ceramic single-edge-precracked-beam specimens [NASA-TM-105568] p 135 N93-10962

Fracture toughness testing of polymer matrix composites [NASA-TP-3199] p 107 N93-12302

TRACKING (POSITION)

Particle image velocimetry for the Surface Tension Driven Convection Experiment using a particle displacement tracking technique p 206 A93-23799

Design and optimization of a self-deploying single axis tracking PV array p 252 A93-25916

Control/structure interactions of Space Station solar dynamic modules p 57 A93-41878

TRAINING DEVICES

Design and implementation of a pilot orientation program for new NASA engineering employees [NASA-TM-105907] p 286 N93-26205

TRAJECTORY OPTIMIZATION

Microgravity research on the NASA Lewis Learjet test facility [AIAA PAPER 93-0573] p 43 A93-24245

DUKSUP - A high thrust trajectory optimization code [AIAA PAPER 93-1127] p 259 A93-31009

Minimum-fuel, power-limited transfers between coplanar elliptical orbits p 45 A93-31532

Optimal impulsive intercept with low-thrust rendezvous return p 45 A93-34521

TRAJECTORY PLANNING

DUKSUP - A high thrust trajectory optimization code [AIAA PAPER 93-1127] p 259 A93-31009

Monte Carlo analysis of the Titan III/Transfer Orbit Stage guidance system for the Mars Observer mission [AIAA PAPER 93-3889] p 50 A93-51473

TRANSFER FUNCTIONS

Self-tuning multivariable pole placement control of a multizone crystal growth furnace p 263 A93-10575

High data rate applications of ACTS technology p 52 A93-17329

Radiation heat transfer calculations using a control-angle, control-volume-based discrete ordinates method [AIAA PAPER 93-2731] p 182 A93-46485

A transfer matrix approach to vibration localization in mistuned blade assemblies [NASA-TM-106112] p 250 N93-27088

TRANSFER ORBITS

Minimum-fuel, power-limited transfers between coplanar elliptical orbits p 45 A93-31532

EOTV propellant tank pressure control and liquid dynamics [AIAA PAPER 93-2399] p 77 A93-50164

Monte Carlo analysis of the Titan III/Transfer Orbit Stage guidance system for the Mars Observer mission [AIAA PAPER 93-3889] p 50 A93-51473

Transfer Orbit Plasma Interaction Experiment (TROPIX) p 45 N93-28734

TRANSFORMERS

Comparison of high temperature, high frequency core loss and dynamic B-H loops of a 2V-49Fe-49Co and a grain oriented 3Si-Fe alloy p 153 A93-25895

Measurement of the temperature coefficient of ratio transformers p 155 A93-32771

TRANSIENT RESPONSE

Heat-pipe transient model for space applications p 163 A93-13867

Electromechanical systems with transient high power response operating from a resonant ac link p 152 A93-25892

A free-piston Stirling engine/linear alternator controls and load interaction test facility p 146 A93-26077

Solving modal equations of motion with initial conditions using MSC/NASTRAN DMAP. Part 1: Implementing exact mode superposition [NASA-TM-106063] p 248 N93-23739

Solving modal equations of motion with initial conditions using MSC/NASTRAN DMAP. Part 2: Coupled versus uncoupled integration [NASA-TM-106064] p 248 N93-23740

TRANSITION FLOW

Effects of gravity on the transition to turbulence of gas jet diffusion flames [AIAA PAPER 93-0710] p 114 A93-24805

Transition of oscillatory flow in tubes - An empirical model for application to Stirling engines p 174 A93-26088

Hypersonic stability and transition p 8 A93-42579

Modeling of turbulence and transition p 195 N93-15795

TRANSITION METALS

Onset conditions for gas phase reaction and nucleation in the CVD of transition metal oxides p 116 A93-39508

TRANSMISSION LINES

A study of electric power transmission lines for use on the lunar surface p 46 A93-13901

A high-efficiency 59- to 64-GHz TWT for intersatellite communications p 158 A93-49553

TRANSMISSION LOSS

Energy loss analysis of an integrated space power distribution system p 68 A93-25958

Design aspects and comparison between high Tc superconducting coplanar waveguide and microstrip line p 155 A93-27244

Energy loss analysis of an integrated space power distribution system [NASA-TM-105772] p 141 N93-14834

TRANSMISSIONS (MACHINE ELEMENTS)

Dynamic analysis of flexible gear trains/transmissions - An automated approach p 220 A93-22440

Time-variant analysis of rotorcraft systems dynamics - An exploitation of vector processors p 220 A93-23512

Acoustical analysis of gear housing vibration p 273 A93-29420

Active control of helicopter transmission noise p 274 A93-29428

Modal simulation of gear box vibration with experimental correlation p 221 A93-31982

Low-noise, high-strength, spiral-bevel gears for helicopter transmissions [AIAA PAPER 93-2149] p 223 A93-49966

Engineering science research issues in high power density transmission dynamics for aerospace applications --- rotorcraft geared rotors [AIAA PAPER 93-2299] p 224 A93-50084

Split torque transmission load sharing [NASA-TM-105884] p 226 N93-12736

Evaluation of an oil-debris monitoring device for use in helicopter transmissions [NASA-TM-105830] p 227 N93-22826

Low-noise, high-strength, spiral-bevel gears for helicopter transmissions [NASA-TM-106080] p 228 N93-23019

Pattern classifier for health monitoring of helicopter gearboxes [NASA-TM-106099] p 228 N93-23741

Global dynamic modeling of a transmission system [NASA-CR-191117] p 228 N93-24751

Fault detection of helicopter gearboxes using the multi-valued influence matrix method [NASA-TM-106100] p 229 N93-27069

Face-gear drives: Design, analysis, and testing for helicopter transmission applications [NASA-TM-106101] p 229 N93-27133

TRANSONIC COMPRESSORS

Unsteady aerodynamic flow phenomena in a transonic compressor stage [AIAA PAPER 93-1868] p 12 A93-49743

TRANSONIC FLOW

Aeroloading and secondary flows in a transonic mixed flow turbine stage [ASME PAPER 92-GT-72] p 2 A93-19322

- Three-dimensional flow phenomena in a transonic, high-through-flow, axial-flow compressor stage
[ASME PAPER 92-GT-169] p 3 A93-19395
- High accuracy computation of fluid-structure interaction in transonic cascades
[AIAA PAPER 93-0485] p 6 A93-23387
- Experimental investigation of counter-rotating propfan flutter at cruise conditions
[AIAA PAPER 93-1632] p 25 A93-34160
- Unsteady transonic two-dimensional Euler solutions using finite elements p 8 A93-39412
- Averaging techniques for steady and unsteady calculations of a transonic fan stage
[AIAA PAPER 93-3065] p 11 A93-48241
- TRANSONIC FLUTTER**
- Experimental investigation of counter-rotating propfan flutter at cruise conditions
[AIAA PAPER 93-1632] p 25 A93-34160
- TRANSONIC WIND TUNNELS**
- NASA Lewis 8- by 6-foot supersonic wind tunnel user manual
[NASA-TM-105771] p 43 N93-25080
- TRANSPARENCE**
- Refractive index and scattering effects on radiative behavior of a semitransparent layer p 176 A93-31438
- Variable refractive index effects on radiation in semitransparent scattering multilayered regions p 189 A93-54463
- TRANSPONDERS**
- SITE project. Phase 1: Continuous data bit-error-rate testing
[NASA-TP-3279] p 58 N93-11001
- TRANSPORT AIRCRAFT**
- Effects of turbine cooling assumptions on performance and sizing of high-speed civil transport
[AIAA PAPER 92-4217] p 22 A93-13383
- Ice accretion prediction for a typical commercial transport aircraft
[AIAA PAPER 93-0174] p 19 A93-23245
- Comparison of all-electric secondary power systems for civil transport p 24 A93-25997
- Propulsion technology challenges for turn-of-the-century commercial aircraft
[ISABE 93-7003] p 31 A93-53980
- Comparison of all-electric secondary power systems for civil subsonic transports
[NASA-TM-105852] p 32 N93-10456
- Ice accretion prediction for a typical commercial transport aircraft
[NASA-TM-105976] p 20 N93-15522
- Propulsion technology challenges for turn-of-the-century commercial aircraft
[NASA-TM-106192] p 39 N93-32351
- TRANSPORT PROPERTIES**
- Critical assessment of Reynolds stress turbulence models using homogeneous flows
[AIAA PAPER 93-0082] p 170 A93-24227
- An evaluation of three spatial differencing schemes for the discrete ordinates method in participating media
[AIAA PAPER 93-0140] p 266 A93-24231
- Supercritical droplet combustion and related transport phenomena
[AIAA PAPER 93-0812] p 115 A93-24885
- Diffusional transport and predicting oxidative failure during cyclic oxidation of beta-NiAl alloys p 126 A93-50370
- TRANSPORT THEORY**
- Convective effects during the physical vapor transport process. II - Thermosolutal convection p 180 A93-42424
- TRANSPUTERS**
- Binary tree eigen solver in finite element analysis
[AIAA PAPER 93-1493] p 267 A93-34034
- TRANSVERSE LOADS**
- Environmental effects on long term behavior of composite laminates p 243 A93-53438
- TRAVELING WAVE TUBES**
- A high-efficiency 59- to 64-GHz TWT for intersatellite communications p 15R A93-49553
- Anomalous TWTA output power spikes and their effect on a digital satellite communications system
[NASA-TM-105875] p 159 N93-13286
- User's guide for a large signal computer model of the helical traveling wave tube
[NASA-TP-3251] p 160 N93-15531
- Interim report on the analysis of the microwave power module
[NASA-TM-106012] p 160 N93-16713
- Simulation of TunnelLadder traveling-wave tube cold-test characteristics. Implementation of the three-dimensional, electromagnetic circuit analysis code micro-SOS
[NASA-TP-3294] p 160 N93-23394
- TREES (MATHEMATICS)**
- Binary tree eigen solver in finite element analysis
[AIAA PAPER 93-1493] p 267 A93-34034

TRELLIS CODING

- Performance evaluation of land mobile satellite system under fading and interference using multiple TCM by Monte-Carlo simulation p 147 A93-10958

TRIANGLES

- Membrane triangles with corner drilling freedoms. I - The EFF element p 235 A93-24303
- Membrane triangles with corner drilling freedoms. II - The ANDES element p 235 A93-24304
- Membrane triangles with corner drilling freedoms. III - Implementation and performance evaluation p 236 A93-24305

TRIBOLOGY

- Tribological and microstructural comparison of HIPped PM212 and PM212/Au self-lubricating composites p 93 A93-13505
- Tribological and mechanical comparison of sintered and HIPped PM212 - High temperature self-lubricating composites p 94 A93-13506
- Interfacial chemistry of a perfluoropolyether lubricant studied by X-ray photoelectron spectroscopy and temperature desorption spectroscopy p 133 A93-38473
- Tribological studies of amorphous hydrogenated carbon films in a vacuum, spacelike environment p 134 A93-40630
- Tribological evaluation and analysis of coating materials p 135 A93-52896
- Solid lubricants p 135 A93-55471
- The effect of processing and compositional changes on the tribology of PM212 in air p 95 N93-15576
- Interfacial chemistry of a perfluoropolyether lubricant studied by XPS and TDS
[NASA-TM-106014] p 137 N93-22560
- Properties of extruded PS-212 type self-lubricating materials p 138 A93-25565
- Tribological characteristics of perfluoropolyether liquid lubricants under sliding conditions in high vacuum
[NASA-TM-106257] p 139 N93-32352

TRUNCATION ERRORS

- Comparison of truncation error of finite-difference and finite-volume formulations of convection terms
[NASA-TM-105861] p 268 N93-11531

TRUSSES

- Probabilistic structural analysis of adaptive/smart/intelligent space structures p 234 A93-16203
- Probabilistic structural analysis of space truss structures for nonuniform thermal environmental effects
[AIAA PAPER 92-4769] p 235 A93-20363
- Design of deployable-truss masts for Space Station
[AIAA PAPER 93-0975] p 56 A93-30899
- Probabilistic assessment of adaptive space truss configurations for thermal buckling resistance
[AIAA PAPER 93-1622] p 240 A93-34151
- Topology and layout optimization of discrete and continuum structures p 241 A93-45429
- Application of neural nets in structural optimization p 265 A93-54533
- Application of artificial neural networks in nonlinear analysis of trusses
[NASA-TM-105319] p 244 N93-11403

TUNGSTEN

- Shielding analysis for a manned Mars rover powered by an SP-100 type reactor p 45 A93-13793
- Effects of anode material on arcjet performance p 79 N93-10044
- A model for predicting high-temperature fatigue failure of a W/Cu composite p 112 N93-31579

TUNGSTEN ALLOYS

- Tensile strain-rate sensitivity of tungsten/nickel composites at 1300 to 1600 K p 97 A93-14840
- Creep behavior of tungsten fiber reinforced nickel metal matrix composites p 99 A93-20758
- Preliminary evaluation of tensile and stress-rupture behavior of W + 24 at. pct Re + 0.4 at. pct HfC wire p 125 A93-25119
- Progress toward a tungsten alloy wire/high temperature alloy composite turbine blade
[NASA-TM-105901] p 128 N93-15586
- TUNGSTEN COMPOUNDS**
- Solid lubricants p 135 A93-55471

TUNING

- Nonlinear interaction of frequency-detuned modes in boundary layers
[AIAA PAPER 93-0347] p 171 A93-24237
- A transfer matrix approach to vibration localization in mistuned blade assemblies
[NASA-TM-106112] p 250 N93-27088
- Localization of aeroelastic modes in mistuned high-energy turbines p 230 N93-31586

TURBIDITY

- The susceptibility critical exponent for a nonequilibrium binary mixture near a consolute point p 284 A93-19838

TURBINE BLADES

- Heat transfer with very high free-stream turbulence. I - Experimental data. II - Analysis of results p 165 A93-18556
- Aeroloads and secondary flows in a transonic mixed flow turbine stage
[ASME PAPER 92-GT-72] p 2 A93-19322
- The turbulent thermal boundary layer with an abrupt change from a rough to a smooth wall p 167 A93-21712
- Three-dimensional unstructured grid Euler method applied to turbine blades
[AIAA PAPER 93-0196] p 6 A93-24233
- Design considerations for a Space Shuttle Main Engine turbine blade made of single crystal material p 236 A93-25228
- Reliability based structural optimization - A simplified safety index approach
[AIAA PAPER 93-1418] p 239 A93-33972
- Forced response of mistuned bladed disk assemblies
[AIAA PAPER 93-1491] p 239 A93-34033
- Computational methods for efficient structural reliability and reliability sensitivity analysis
[AIAA PAPER 93-1626] p 240 A93-34155
- Blade row interaction effects on flutter and forced response
[AIAA PAPER 93-2084] p 28 A93-49911
- Optimization of blade arrangement in a randomly mistuned cascade using simulated annealing
[AIAA PAPER 93-2254] p 28 A93-50052
- Chimera grids in the simulation of three-dimensional flowfields in turbine-blade-coolant passages
[AIAA PAPER 93-2559] p 187 A93-50280
- Measurements and computational analysis of heat transfer and flow in a simulated turbine blade internal cooling passage
[AIAA PAPER 93-1797] p 189 A93-53585
- Forcing function modeling for flow induced vibration
[ISABE 93-7027] p 31 A93-54003
- Navier-Stokes turbine heat transfer predictions using two-equation turbulence
[NASA-TM-105817] p 191 N93-10735
- Stochastic sensitivity measure for mistuned high-performance turbines
[NASA-TM-105821] p 245 N93-12277
- Radial turbine cooling
[NASA-TM-105658] p 15 N93-13292
- Progress toward a tungsten alloy wire/high temperature alloy composite turbine blade
[NASA-TM-105901] p 128 N93-15586
- Bypass transition in compressible boundary layers p 196 N93-15801
- Three-dimensional Navier-Stokes heat transfer predictions for turbine blade rows
[NASA-TM-105800] p 196 N93-19969
- Summary of experimental heat-transfer results from the turbine hot section facility
[NASA-TP-3250] p 197 N93-23059
- Heat transfer in rotating serpentine passages with selected model orientation for smooth or skewed trip walls
[NASA-TM-106126] p 147 N93-25177
- NDE of PWA 1480 single crystal turbine blade material
[NASA-TM-106140] p 38 N93-27640
- Navier-Stokes analysis of three-dimensional flow and heat transfer inside turbine blade rows p 39 N93-29963
- Progress in the measurement of SSME turbine heat flux with plug-type sensors p 217 N93-31553
- Thin film heat flux sensor for Space Shuttle Main Engine turbine environment p 217 N93-31554
- Thin film thermocouples for high temperature turbine application p 217 N93-31555
- Three-dimensional flow calculations inside SSME GGGT first stage blade rows p 93 N93-31585
- Localization of aeroelastic modes in mistuned high-energy turbines p 230 N93-31586
- Measurements and computational analysis of heat transfer and flow in a simulated turbine blade internal cooling passage
[NASA-TM-106189] p 203 N93-31647
- TURBINE ENGINES**
- The multi-heat addition turbine engine
[AIAA PAPER 92-4272] p 22 A93-13334
- Numerical simulation of a low-emission gas turbine combustor using KIVA-II p 22 A93-14077
- Navier-Stokes analysis of radial turbine rotor performance
[AIAA PAPER 93-2555] p 30 A93-50277
- The chemistry of Saudi Arabian sand - A deposition problem on helicopter turbine airfoils p 243 A93-53468
- Integrity testing of brush seal in shroud ring of T-700 engine
[NASA-TM-105863] p 227 N93-18380

- Multi-heat addition turbine engine
[NASA-CASE-LEW-15094-1] p 35 N93-22034
- TURBINE PUMPS**
Development of advanced seals for space propulsion turbomachinery
[SAE PAPER 921028] p 218 A93-14651
An SSME High Pressure Oxidizer Turbopump diagnostic system using G2 real-time expert system
p 66 A93-16415
Reliability analysis of structural ceramic components using a three-parameter Weibull distribution
[ASME PAPER 92-GT-296] p 231 A93-19486
Ceramic matrix composite applications in advanced liquid fuel rocket engine turbomachinery
[ASME PAPER 92-GT-316] p 99 A93-19502
Ceramic matrix composites for rocket engine turbine applications
[ASME PAPER 92-GT-394] p 99 A93-19547
Forced response of mistuned bladed disk assemblies
[AIAA PAPER 93-1491] p 239 A93-34033
Miniature high temperature plug-type heat flux gauges
p 209 A93-37862
Design and test of a small two stage counter-rotating turbine for rocket engine application
[AIAA PAPER 93-2136] p 74 A93-49954
Design of an oxygen turbopump for use in an Advanced Expander Test Bed engine
[AIAA PAPER 93-2137] p 48 A93-49955
High Reynolds number and turbulence effects on aerodynamics and heat transfer in a turbine cascade
[AIAA PAPER 93-2252] p 186 A93-50050
A survey of instabilities within centrifugal pumps and concepts for improving the flow range of pumps in rocket engines
p 190 N93-10039
Stochastic sensitivity measure for mistuned high-performance turbines
[NASA-TM-105821] p 245 N93-12277
OTV bearing deflection investigation
[NASA-TM-106085] p 215 N93-22994
On-line implementation of nonlinear parameter estimation for the Space Shuttle main engine
[NASA-TM-106097] p 88 N93-26211
High Reynolds number and turbulence effects on aerodynamics and heat transfer in a turbine cascade
[NASA-TM-106187] p 202 N93-29157
Structural Integrity and Durability of Reusable Space Propulsion Systems
[NASA-CP-10064] p 93 N93-31552
Progress in the measurement of SSME turbine heat flux with plug-type sensors
p 217 N93-31553
Thin film heat flux sensor for Space Shuttle Main Engine turbine environment
p 217 N93-31554
Thin film thermocouples for high temperature turbine application
p 217 N93-31555
Three-dimensional analysis of the Pratt and Whitney alternate design SSME fuel turbine
p 230 N93-31584
Three-dimensional flow calculations inside SSME GGGT first stage blade rows
p 93 N93-31585
Localization of aeroelastic modes in mistuned high-energy turbines
p 230 N93-31586
- TURBINE WHEELS**
Aerodynamic design of turbomachinery blading in three-dimensional flow - An application to radial inflow turbines
[ASME PAPER 92-GT-74] p 3 A93-19324
- TURBINES**
Effects of turbine cooling assumptions on performance and sizing of high-speed civil transport
[AIAA PAPER 92-4217] p 22 A93-13383
Experimental evaluation of a cooled radial-inflow turbine
[AIAA PAPER 93-1795] p 27 A93-49685
Radial turbine cooling
p 191 N93-10061
Navier-Stokes turbine heat transfer predictions using two-equation turbulence
[NASA-TM-105817] p 191 N93-10735
Radial turbine cooling
[NASA-TM-105658] p 15 N93-13292
Three-dimensional laser window formation for industrial application
p 218 N93-22197
Experimental evaluation of a cooled radial-inflow turbine
[NASA-TM-106230] p 38 N93-28697
- TURBOCOMPRESSORS**
Stability of fully developed rotating stall
[ASME PAPER 92-GT-57] p 23 A93-19307
Three-dimensional flow phenomena in a transonic, high-through-flow, axial-flow compressor stage
[ASME PAPER 92-GT-169] p 3 A93-19395
Numerical simulation of compressor endwall and casing treatment flow phenomena
[ASME PAPER 92-GT-300] p 4 A93-19490

- TURBOFAN AIRCRAFT**
In-flight near- and far-field acoustic data measured on the Propfan Test Assessment (PTA) testbed and with an adjacent aircraft
[NASA-TM-103719] p 275 N93-27058
- TURBOFAN ENGINES**
Nonlinear dynamic simulation of single- and multi-spool core engines
[AIAA PAPER 93-2580] p 30 A93-50294
- TURBOFANS**
Acoustic mode measurements in the inlet of a model turbofan using a continuously rotating rake - Data collection/analysis techniques
[AIAA PAPER 93-0599] p 24 A93-23324
Averaging techniques for steady and unsteady calculations of a transonic fan stage
[AIAA PAPER 93-3065] p 11 A93-48241
Propulsion technology challenges for turn-of-the-century commercial aircraft
[ISABE 93-7003] p 31 A93-53980
Acoustic mode measurements in the inlet of a model turbofan using a continuously rotating rake: Data collection/analysis techniques
[NASA-TM-105936] p 33 N93-15403
Propulsion technology challenges for turn-of-the-century commercial aircraft
[NASA-TM-106192] p 39 N93-32351
- TURBOJET ENGINE CONTROL**
Application of controller partitioning optimization procedure to integrated flight/propulsion control design for a STOVL aircraft
[AIAA PAPER 93-3766] p 40 A93-51361
- TURBOJET ENGINES**
A hot dynamic seal rig for measuring hypersonic engine seal durability and flow performance
[AIAA PAPER 93-1346] p 222 A93-33916
- TURBOMACHINE BLADES**
Driven cavity simulation of turbomachine blade flows with vortex control
[AIAA PAPER 93-0390] p 6 A93-24238
Vibration localization in mono- and bi-coupled bladed disks - A transfer matrix approach
[AIAA PAPER 93-1492] p 222 A93-34241
High resolution numerical simulation of the linearized Euler equations in conservation law form
[AIAA PAPER 93-2934] p 183 A93-48132
- TURBOMACHINERY**
Development of advanced seals for space propulsion turbomachinery
[SAE PAPER 921028] p 218 A93-14651
Ceramic matrix composite applications in advanced liquid fuel rocket engine turbomachinery
[ASME PAPER 92-GT-316] p 99 A93-19502
Navier-Stokes calculations for the unsteady flowfield of turbomachinery
[AIAA PAPER 93-0676] p 6 A93-24786
Bgndi - Interactive three-dimensional turbomachinery grid generation system with applications
[AIAA PAPER 93-0430] p 259 A93-25527
Dynamics of rotating multicomponent turbomachinery systems
[AIAA PAPER 93-1629] p 222 A93-34157
Aerodynamic inverse design and analysis for a full engine
[ISABE 93-7086] p 14 A93-54062
Three-dimensional flow analysis inside turbomachinery stages with steady and unsteady Navier-Stokes method
[ISABE 93-7095] p 14 A93-54071
Analysis of high Reynolds number inviscid/viscid interactions in cascades
p 15 A93-55351
Stochastic sensitivity measure for mistuned high-performance turbines
[NASA-TM-105821] p 245 N93-12277
Turbomachinery CFD on parallel computers
[NASA-TM-105932] p 262 N93-13154
User's manual for Interactive Data Display System (IDDS)
[NASA-TM-105572] p 261 N93-16613
Dynamics of rotating multi-component turbomachinery systems
[NASA-TM-105997] p 247 N93-18426
Study of the capacitance technique for measuring high-temperature blade tip clearance on ceramic rotors
[NASA-TM-105978] p 35 N93-23013
- TURBOPROP AIRCRAFT**
Takeoff/approach noise for a model counterrotation propeller with a forward-swept upstream rotor
[AIAA PAPER 93-0596] p 24 A93-24782
Takeoff/approach noise for a model counterrotation propeller with a forward-swept upstream rotor
[NASA-TM-105979] p 34 N93-16715
- TURBOSHAPTS**
Identification of the open loop dynamics of the T700 turboshaft engine
p 26 A93-35934

- TURBULENCE**
New time scale based k-epsilon model for near-wall turbulence
p 180 A93-41909
Comparison of reacting and non-reacting shear layers at a high subsonic Mach number
[AIAA PAPER 93-2381] p 186 A93-50149
Navier-Stokes turbine heat transfer predictions using two-equation turbulence
[NASA-TM-105817] p 191 N93-10735
Experiments on a round turbulent buoyant plume
[NASA-TM-105955] p 141 N93-16384
Remarks on turbulent constitutive relations
[NASA-TM-106116] p 199 N93-27010
Increased heat transfer to elliptical leading edges due to spanwise variations in the freestream momentum: Numerical and experimental results
[NASA-TM-106150] p 199 N93-27020
Comparison of reacting and non-reacting shear layers at a high subsonic Mach number
[NASA-TM-106198] p 38 N93-27610
A numerical study of confined turbulent jets
[NASA-TM-106197] p 202 N93-29161
- TURBULENCE EFFECTS**
Heat transfer with very high free-stream turbulence. I - Experimental data. II - Analysis of results
p 165 A93-18556
Heat transfer performance comparisons of five different rectangular channels with parallel angled ribs
p 166 A93-18752
High Reynolds number and turbulence effects on aerodynamics and heat transfer in a turbine cascade
[AIAA PAPER 93-2252] p 186 A93-50050
Second order closure modeling of turbulent buoyant wall plumes
[NASA-TM-105956] p 193 N93-14829
Turbulent fluid motion IV-averages, Reynolds decomposition, and the closure problem
[NASA-TM-105822] p 195 N93-15585
Modeling of near wall turbulence and modeling of bypass transition
p 195 N93-15798
Bypass transition in compressible boundary layers
p 196 N93-15801
High Reynolds number and turbulence effects on aerodynamics and heat transfer in a turbine cascade
[NASA-TM-106187] p 202 N93-29157
- TURBULENCE MODELS**
Evaluation and application of the Baldwin-Lomax turbulence model in two-dimensional, unsteady, compressible boundary layers with and without separation in engine inlets
[AIAA PAPER 92-3676] p 2 A93-14118
Calculation of a circular jet in crossflow with a multiple-time-scale turbulence model
p 164 A93-15063
Discussion of 'Comparison of turbulence models for the natural convection boundary layer along a heated vertical plate'
p 168 A93-21717
Evaluation and application of the Baldwin-Lomax turbulence model in two-dimensional, unsteady, compressible boundary layers with and without separation in engine inlets
[AIAA PAPER 92-3676] p 168 A93-22509
An algebraic turbulence model for three-dimensional viscous flows
[AIAA PAPER 93-0083] p 4 A93-22552
Critical assessment of Reynolds stress turbulence models using homogeneous flows
[AIAA PAPER 93-0082] p 170 A93-24227
A multiple-scale turbulence model for incompressible flow
[AIAA PAPER 93-0086] p 170 A93-24228
Unsteady aerodynamic flow phenomena in a transonic compressor stage
[AIAA PAPER 93-1868] p 12 A93-49743
Three-dimensional flow analysis inside turbomachinery stages with steady and unsteady Navier-Stokes method
[ISABE 93-7095] p 14 A93-54071
Evaluation and application of the Baldwin-Lomax turbulence model in two-dimensional, unsteady, compressible boundary layers with and without separation in engine inlets
[NASA-TM-105810] p 191 N93-10087
An algebraic turbulence model for three-dimensional viscous flows
[NASA-TM-105931] p 1 N93-14102
Center for Modeling of Turbulence and Transition (CMOTT): Research Briefs, 1992
[NASA-TM-105834] p 195 N93-15792
Modeling of turbulence and transition
p 195 N93-15795
Turbulence modeling and experiments
p 195 N93-15796
Modeling of turbulent shear flows
p 195 N93-15797
Modeling of near wall turbulence and modeling of bypass transition
p 195 N93-15798

Two equation modelling and the pseudo compressibility technique p 195 N93-15799

Critical assessment of Reynolds stress turbulence models using homogeneous flows [NASA-TM-105954] p 196 N93-16703

A multiple-scale model for compressible turbulent flows [NASA-TM-106072] p 198 N93-23736

Remarks on turbulent constitutive relations [NASA-TM-106116] p 199 N93-27010

Navier-Stokes analysis of three-dimensional flow and heat transfer inside turbine blade rows p 39 N93-29963

Overview of aerothermodynamic loads definition study p 93 N93-31583

TURBULENT BOUNDARY LAYER

Heat transfer with very high free-stream turbulence. I - Experimental data. II - Analysis of results p 165 A93-18556

The turbulent thermal boundary layer with an abrupt change from a rough to a smooth wall p 167 A93-21712

A simplified Reynolds stress model for unsteady turbulent boundary layers [AIAA PAPER 93-0204] p 168 A93-22622

A parametric study of bleed in shock boundary layer interactions [AIAA PAPER 93-0294] p 5 A93-22694

Structure and development of streamwise vortex arrays embedded in a turbulent boundary layer p 177 A93-32711

New time scale based k-epsilon model for near-wall turbulence p 180 A93-41909

The structure of a three-dimensional turbulent boundary layer p 181 A93-44813

A lag model for turbulent boundary layers developing over rough bleed surfaces [AIAA PAPER 93-2988] p 10 A93-48181

An investigation of shock wave turbulent boundary layer interaction with bleed through slanted slots [AIAA PAPER 93-2992] p 11 A93-48184

Numerical simulation of a shock wave/turbulent boundary layer interaction in a duct [AIAA PAPER 93-3127] p 11 A93-48293

Flowfield dynamics in blunt fin-induced shock wave/turbulent boundary layer interactions [AIAA PAPER 93-3133] p 11 A93-48298

CFD validation of subsonic turbulent planar shear layers [AIAA PAPER 93-1773] p 184 A93-49669

Time-sequenced and spectrally filtered Rayleigh imaging of shock wave and boundary layer structure for inlet characterization [AIAA PAPER 93-2300] p 211 A93-50085

Low-Reynolds-number k-epsilon model for unsteady turbulent boundary-layer flows p 14 A93-53208

Supersonic boundary-layer flow turbulence modeling [NASA-TM-105893] p 193 A93-14758

Modeling of near wall turbulence and modeling of bypass transition p 195 N93-15798

Surface and flow field measurements in a symmetric crossing shock wave/turbulent boundary-layer interaction [NASA-TM-106086] p 17 N93-24911

TURBULENT COMBUSTION

A coupled multi-block solution procedure for spray combustion in complex geometries [AIAA PAPER 93-0108] p 171 A93-24230

Intake flow modeling in a four stroke diesel using KIVA3 [AIAA PAPER 93-2952] p 183 A93-48146

A review of chemically reactive turbulent flow mixing mechanisms and a new design for a low NO(x) combustor p 27 A93-49508

CFD validation of subsonic turbulent planar shear layers [AIAA PAPER 93-1773] p 184 A93-49669

A simplified reaction mechanism for calculation of emissions in hydrocarbon (Jet-A) combustion [AIAA PAPER 93-2341] p 118 A93-50116

Turbulence measurement in a reacting and non-reacting shear layer at a high subsonic Mach number [NASA-TM-106186] p 18 N93-31839

TURBULENT DIFFUSION

Effects of detailed droplet heating models on turbulent sprays vaporization behavior [AIAA PAPER 93-2193] p 185 A93-50005

TURBULENT FLOW

Calculation of a circular jet in crossflow with a multiple-time-scale turbulence model p 164 A93-15063

Laminar/turbulent oscillating flow in circular pipes p 167 A93-21689

The development of a turbulent junction vortex system p 168 A93-22258

Effects of free-stream turbulence on boundary-layer transition [AIAA PAPER 93-0488] p 170 A93-23390

PDF approach for compressible turbulent reacting flows [AIAA PAPER 93-0087] p 170 A93-24229

Statistical analysis of the effects of helicity in inhomogeneous turbulence p 175 A93-26186

New time scale based k-epsilon model for near-wall turbulence p 180 A93-41909

Experimental and numerical investigation of supersonic turbulent flow in an annular duct [AIAA PAPER 93-3123] p 11 A93-48291

High Reynolds number and turbulence effects on aerodynamics and heat transfer in a turbine cascade [AIAA PAPER 93-2252] p 186 A93-50050

Development of an explicit multiblock/multigrad flow solver for viscous flows in complex geometries [AIAA PAPER 93-2380] p 186 A93-50148

A critical comparison of several low Reynolds number k-epsilon turbulence models for flow over a backward-facing step [AIAA PAPER 93-1927] p 189 A93-53586

A new energy transfer model for turbulent free shear flow [NASA-TM-105854] p 191 N93-10454

Turbulent fluid motion IV-averages, Reynolds decomposition, and the closure problem [NASA-TM-105822] p 195 N93-15585

Modeling of turbulence and transition p 195 N93-15795

Modeling of turbulent shear flows p 195 N93-15797

Modeling of near wall turbulence and modeling of bypass transition p 195 N93-15798

A realizable Reynolds stress algebraic equation model [NASA-TM-105993] p 16 N93-16596

Critical assessment of Reynolds stress turbulence models using homogeneous flows [NASA-TM-105954] p 196 N93-16703

Program ELM: A tool for rapid thermal-hydraulic analysis of solid-core nuclear rocket fuel elements [NASA-TM-105867] p 84 N93-19106

Effects of buoyancy on laminar, transitional, and turbulent gas jet diffusion flames p 121 N93-20189

A multiple-scale model for compressible turbulent flows [NASA-TM-106072] p 198 N93-23736

Remarks on turbulent constitutive relations [NASA-TM-106116] p 199 N93-27010

Calculations of turbulent separated flows [NASA-TM-106154] p 200 N93-27161

High Reynolds number and turbulence effects on aerodynamics and heat transfer in a turbine cascade [NASA-TM-106187] p 202 N93-29157

A numerical study of confined turbulent jets [NASA-TM-106197] p 202 N93-29161

Turbulence measurement in a reacting and non-reacting shear layer at a high subsonic Mach number [NASA-TM-106186] p 18 N93-31839

A rapid-distortion-theory turbulence model for developed unsteady wall-bounded flow [NASA-TM-106249] p 203 N93-32199

A critical comparison of several low Reynolds number k-epsilon turbulence models for flow over a backward facing step [NASA-TM-106173] p 270 N93-32200

TURBULENT HEAT TRANSFER

Heat transfer with very high free-stream turbulence. I - Experimental data. II - Analysis of results p 165 A93-18556

TURBULENT JETS

Multigrad acceleration and turbulence models for computations of 3D turbulent jets in crossflow p 165 A93-18751

Effects of gravity on the transition to turbulence of gas jet diffusion flames [AIAA PAPER 93-0710] p 114 A93-24805

Fluid flow of a row of jets in crossflow - A numerical study p 179 A93-35608

Characteristics of three-dimensional turbulent jets in crossflow p 8 A93-36695

Dynamics and control of coherent structure in turbulent jets p 188 A93-52310

Experiments on a round turbulent buoyant plume [NASA-TM-105955] p 141 N93-16384

Soot formation and radiation in turbulent jet diffusion flames under normal and reduced gravity conditions p 121 N93-20192

A numerical study of confined turbulent jets [NASA-TM-106197] p 202 N93-29161

TURBULENT MIXING

Weakly nonlinear models for turbulent mixing in a plane mixing layer p 165 A93-17416

Computation of supersonic jet noise under imperfectly expanded conditions [AIAA PAPER 93-0735] p 273 A93-24825

Direct numerical simulations of a reacting turbulent mixing layer by a pseudospectral-spectral element method p 182 A93-45974

A review of chemically reactive turbulent flow mixing mechanisms and a new design for a low NO(x) combustor p 27 A93-49508

Mixing in the dome region of a staged gas turbine combustor p 27 A93-49612

Computation of supersonic jet noise under imperfectly expanded conditions [NASA-TM-105961] p 274 N93-15430

TURBULENT WAKES

Laser velocimeter measurements of the flow field generated by a forward-swept propfan during flutter [AIAA PAPER 93-2919] p 14 A93-53591

TVD SCHEMES

Central difference TVD schemes for time dependent and steady state problems p 188 A93-51183

A time-accurate high-resolution TVD scheme for solving the Navier-Stokes equations p 13 A93-52006

Eno-Osher schemes for Euler equations [NASA-TM-105928] p 268 N93-15341

A time-accurate high-resolution TVD scheme for solving the Navier-Stokes equations [NASA-TM-106056] p 268 N93-22664

TWISTING

Behavior of spinning laminated composite plates with initial twist-experimental vibrations, strain, and deflection results [AIAA PAPER 93-1325] p 238 A93-33898

TWO DIMENSIONAL BOUNDARY LAYER

Evaluation and application of the Baldwin-Lomax turbulence model in two-dimensional, unsteady, compressible boundary layers with and without separation in engine inlets [AIAA PAPER 92-3676] p 2 A93-14118

Evaluation and application of the Baldwin-Lomax turbulence model in two-dimensional, unsteady, compressible boundary layers with and without separation in engine inlets [AIAA PAPER 92-3676] p 168 A93-22509

Evaluation and application of the Baldwin-Lomax turbulence model in two-dimensional, unsteady, compressible boundary layers with and without separation in engine inlets [NASA-TM-105810] p 191 N93-10087

A compressible boundary layer algorithm for use with SINDA '85 p 192 N93-13395

Nonlinear evolution of the first mode supersonic oblique waves in compressible boundary layers. Part 1: Heated/cooled walls [NASA-TM-106087] p 199 N93-25175

TWO DIMENSIONAL FLOW

Unsteady transonic two-dimensional Euler solutions using finite elements p 8 A93-39412

Two-dimensional CFD modeling of wave rotor flow dynamics [AIAA PAPER 93-3318] p 9 A93-45014

Initial development of the two-dimensional ejector shear layer - Experimental results [AIAA PAPER 93-2440] p 29 A93-50192

Comparison of the initial development of shear layers in two-dimensional and axisymmetric ejector configurations [AIAA PAPER 93-2441] p 29 A93-50193

Supersonic investigation of two dimensional hypersonic exhaust nozzles [NASA-TM-105687] p 33 N93-15342

TWO DIMENSIONAL MODELS

Weakly nonlinear models for turbulent mixing in a plane mixing layer p 165 A93-17416

Ceramic component reliability with the restructured NASA/CARES computer program [ASME PAPER 92-GT-383] p 234 A93-19540

Room-temperature determination of two-dimensional electron gas concentration and mobility in heterostructures p 280 A93-35198

A lag model for turbulent boundary layers developing over rough bleed surfaces [AIAA PAPER 93-2988] p 10 A93-48181

Ceramic component reliability with the restructured NASA/CARES computer program [NASA-TM-105856] p 244 N93-11004

TWO FLUID MODELS

Initial development of the two-dimensional ejector shear layer - Experimental results [AIAA PAPER 93-2440] p 29 A93-50192

Comparison of the initial development of shear layers in two-dimensional and axisymmetric ejector configurations [AIAA PAPER 93-2441] p 29 A93-50193

Numerical study of mixing of two fluids under low gravity [NASA-TM-105865] p 194 N93-14914

TWO PHASE FLOW

- Scaling analysis of gas-liquid two-phase flow pattern in microgravity
[AIAA PAPER 93-0914] p 173 A93-24968
- Atomizing-gas temperature effect on cryogenic spray droplet size
[AIAA PAPER 93-2333] p 186 A93-50111
- Preliminary endurance tests of water vaporizers for resistojel applications
[AIAA PAPER 93-2403] p 187 A93-50168
- Atomizing-gas temperature effect on cryogenic spray droplet size
[NASA-TM-106106] p 216 N93-25191
- Preliminary endurance tests of water vaporizers for resistojel applications
[NASA-TM-106222] p 92 N93-28694
- Prediction of gas-liquid two-phase flow regime in microgravity
[NASA-TM-106274] p 145 N93-30939

TWO STAGE TURBINES

- Time-averaged heat transfer and pressure measurements and comparison with prediction for a two-stage turbine
[ASME PAPER 92-GT-194] p 166 A93-19419
- Three-dimensional analysis of the Pratt and Whitney alternate design SSME fuel turbine p 230 N93-31584

U**UDIMET ALLOYS**

- Transient liquid phase diffusion bonding of Udimet 720 for Stirling power converter applications p 221 A93-26080

ULTRAHIGH FREQUENCIES

- GaAs monolithic R.F. modules for SARSAT distress beacons p 152 A93-25806

ULTRASONIC FLAW DETECTION

- Ultrasonic and micromechanical study of damage and elastic properties of SiC/RBSN ceramic composites --- Reaction Bonded Silicon Nitride p 99 A93-19624
- Ultrasonic assessment of interfacial oxidation damage in ceramic matrix composites p 105 A93-52919

ULTRASONIC TESTS

- Application of neural networks to prediction of advanced composite structures mechanical response and behavior p 205 A93-20751
- Application of neural networks in the acousto-ultrasonic evaluation of metal-matrix composite specimens p 231 A93-37009

- Determination of plate wave velocities and diffuse field decay rates with broad-band acousto-ultrasonic signals [NASA-TM-106158] p 232 N93-27080

- Acousto-Ultrasonic analysis of failure in ceramic matrix composite tensile specimens [NASA-TM-106219] p 232 N93-29073

ULTRASONIC WAVE TRANSDUCERS

- Detecting Lamb waves with broadband acousto-ultrasonic signals in composite structures p 231 A93-21898

ULTRASONICS

- Determination of plate wave velocities and diffuse field decay rates with broad-band acousto-ultrasonic signals [NASA-TM-106158] p 232 N93-27080

ULTRAVIOLET ABSORPTION

- Absorption coefficients for water vapor at 193 nm from 300 to 1073 K p 276 A93-45398

ULTRAVIOLET RADIATION

- Simulation of the synergistic low Earth orbit effects of vacuum thermal cycling, vacuum UV radiation, and atomic oxygen p 58 N93-15595

UNIFORM FLOW

- Three-dimensional boundary-layer instability and separation induced by small-amplitude streamwise vorticity in the upstream flow p 172 A93-24401

UNIVERSE

- N-point correlation functions in the CfA and SSRS redshift distribution of galaxies p 288 A93-10615
- Dark matter, long-range forces, and large-scale structure p 288 A93-11876
- The inflation sector of extended inflation p 288 A93-17638
- Stochastic inflation lattice simulations - Ultra-large scale structure of the universe p 289 A93-17646
- The best-fit universe --- cosmological models p 289 A93-17651
- The first three minutes - 1990 version --- of early universe after Big Bang p 289 A93-23607
- Large- and small-scale constraints on power spectra in Omega = 1 universes p 290 A93-23990
- Probing the statistics of primordial fluctuations and their evolution p 290 A93-24627
- Kurtosis, skewness, and non-Gaussian cosmological density perturbations p 291 A93-35579

UNIVERSITIES

- Space transportation alternatives for large space programs - The International Space University summer session - 1992 [AIAA PAPER 93-2278] p 44 A93-53588

UNMANNED SPACECRAFT

- NASA's progress in nuclear electric propulsion technology [AIAA PAPER 93-1936] p 78 A93-53587
- NASA's progress in nuclear electric propulsion technology [NASA-TM-106272] p 93 N93-31858

UNSTEADY AERODYNAMICS

- Concurrent processing adaptation of aeroelastic analysis of propfans p 23 A93-14624
- Numerical solutions for unsteady subsonic vortical flows around loaded cascades [ASME PAPER 92-GT-173] p 3 A93-19399
- Forcing function effects on unsteady aerodynamic gust response. I - Forcing functions [ASME PAPER 92-GT-174] p 3 A93-19400
- Forcing function effects on unsteady aerodynamic gust response. II - Low solidity airfoil row response [ASME PAPER 92-GT-175] p 3 A93-19401
- Estimation of unsteady lift on a pitching airfoil from wake velocity surveys [AIAA PAPER 93-0437] p 5 A93-23351
- Acoustic radiation from a thin airfoil in nonuniform subsonic flows p 273 A93-23535
- Nonreflecting boundary conditions for linearized unsteady aerodynamic calculations [AIAA PAPER 93-0882] p 7 A93-25553
- Linearized Euler predictions of unsteady aerodynamic loads in cascades p 7 A93-29318
- Semi-empirical model for prediction of unsteady forces on an airfoil with application to flutter p 7 A93-31494
- Unsteady aerodynamics and flutter of propfans using a three-dimensional Full-Potential Solver [AIAA PAPER 93-1633] p 25 A93-34161
- Efficient hybrid scheme for the analysis of counter-rotating propellers p 7 A93-34483
- Unsteady transonic two-dimensional Euler solutions using finite elements p 8 A93-39412
- Averaging techniques for steady and unsteady calculations of a transonic fan stage [AIAA PAPER 93-3065] p 11 A93-48241
- Blade row interaction effects on flutter and forced response [AIAA PAPER 93-2084] p 28 A93-49911
- Unsteady aerodynamics and flutter based on the potential equation [AIAA PAPER 93-2086] p 13 A93-49913
- Analytic methods for design of wave cycles for wave rotor core engines [AIAA PAPER 93-2523] p 30 A93-50253
- Forcing function modeling for flow induced vibration [ISABE 93-7027] p 31 A93-54003
- Estimation of unsteady lift on a pitching airfoil from wake velocity surveys [NASA-TM-105947] p 15 N93-14791

UNSTEADY FLOW

- Wake-induced unsteady stagnation-region heat-transfer measurements [ASME PAPER 92-GT-196] p 166 A93-19421
- A simplified Reynolds stress model for unsteady turbulent boundary layers [AIAA PAPER 93-0204] p 168 A93-22622
- Time-dependent thermocapillary convection in a Cartesian cavity - Numerical results for a moderate Prandtl number fluid [AIAA PAPER 93-0259] p 169 A93-22666
- An improved numerical model for wave rotor design and analysis [AIAA PAPER 93-0482] p 24 A93-23384
- Nonlinear interaction of frequency-detuned modes in boundary layers [AIAA PAPER 93-0347] p 171 A93-24237
- Navier-Stokes calculations for the unsteady flowfield of turbomachinery [AIAA PAPER 93-0676] p 6 A93-24786
- Linearized Euler predictions of unsteady aerodynamic loads in cascades p 7 A93-29318
- Computation of unsteady supersonic quasi-one-dimensional viscous-inviscid interacting internal flowfields p 177 A93-32724
- Unsteady blade pressures on a propfan at takeoff - Euler analysis and flight data p 26 A93-37389
- Heat transfer from radiatively heated material in a low Reynolds number microgravity environment p 180 A93-43695
- A coupled implicit method for chemical non-equilibrium flows at all speeds p 181 A93-44245
- Two-dimensional CFD modeling of wave rotor flow dynamics [AIAA PAPER 93-3318] p 9 A93-45014

USER MANUALS (COMPUTER PROGRAMS)

- Multigrid time-accurate integration of Navier-Stokes equations [AIAA PAPER 93-3361] p 181 A93-45054
- On solving the compressible Navier-Stokes equations for unsteady flows at very low Mach numbers [AIAA PAPER 93-3368] p 181 A93-45061
- Vorticity dynamics of inviscid shear layers p 181 A93-45734
- High resolution numerical simulation of the linearized Euler equations in conservation law form [AIAA PAPER 93-2934] p 183 A93-48132
- Unsteady aerodynamic flow phenomena in a transonic compressor stage [AIAA PAPER 93-1868] p 12 A93-49743
- Analysis of unsteady wave processes in a rotating channel [AIAA PAPER 93-2527] p 187 A93-50255
- Low-Reynolds-number k-epsilon model for unsteady turbulent boundary-layer flows p 14 A93-53208
- Three-dimensional flow analysis inside turbomachinery stages with steady and unsteady Navier-Stokes method [ISABE 93-7095] p 14 A93-54071
- An improved numerical model for wave rotor design and analysis [NASA-TM-105915] p 33 N93-12418
- A rapid-distortion-theory turbulence model for developed unsteady wall-bounded flow [NASA-TM-106249] p 203 N93-32199
- UNSWEEP WINGS**
- LDV flowfield measurements on a straight and swept wing with a simulated ice accretion [AIAA PAPER 93-0300] p 5 A93-23001
- UPLINKING**
- Anomalous TWTA output power spikes and their effect on a digital satellite communications system [NASA-TM-105875] p 159 N93-13286
- UPWIND SCHEMES (MATHEMATICS)**
- Stable and low diffusive hybrid upwind splitting methods [ONERA, TP NO. 1992-113] p 179 A93-38589
- Field by field hybrid upwind splitting methods [AIAA PAPER 93-3302] p 8 A93-45000
- An extended Lagrangian method [AIAA PAPER 93-3305] p 8 A93-45003
- URANIUM FLUORIDES**
- Thermophysical properties of gas phase uranium tetrafluoride [AIAA PAPER 93-2758] p 285 A93-46505
- URANIUM PLASMAS**
- Ultrahigh temperature vapor-core reactor - Magnetohydrodynamic system for space nuclear electric power p 66 A93-21663
- USER MANUALS (COMPUTER PROGRAMS)**
- An interactive preprocessor for the NASA engine performance program [NASA-TM-105786] p 32 N93-10983
- ICAN/DAMP-integrated composite analyzer with damping analysis capabilities: User's manual [NASA-TP-3292] p 106 N93-12015
- Computer programs to characterize alloys and predict cyclic life using the total strain version of strainrange partitioning: Tutorial and users manual, version 1.0 [NASA-TM-4425] p 246 N93-15788
- User's manual for Interactive Data Display System (IDDS) [NASA-TM-105572] p 261 N93-16613
- LENS, a general chemical kinetics and sensitivity analysis code for gas-phase reactions: User's guide [NASA-TM-105851] p 121 N93-16614
- Second generation integrated composite analyzer (ICAN) computer code [NASA-TP-3290] p 108 N93-18139
- Nuclear Engine System Simulation (NESS). Version 2.0: Program user's guide [NASA-CR-191081] p 85 N93-23875
- Nuclear Engine System Simulation (NESS). Volume 1: Program user's guide [NASA-CR-191080] p 86 N93-23876
- High temperature composite analyzer (HITCAN) user's manual, version 1.0 [NASA-TM-106002] p 249 N93-25070
- Metal matrix composite Analyzer (METCAN): Theoretical manual [NASA-TM-106025] p 109 N93-26552
- RENEW v3.2 user's manual, maintenance estimation simulation for Space Station Freedom Program [NASA-TM-106006] p 232 N93-27025
- Metal Matrix Laminate Tailoring (MMLT) code: User's manual [NASA-TM-106052] p 111 N93-28681

V

V GROOVES

- Texturing of InP surfaces for device applications
[NASA-TM-106061] p 129 N93-28618

V/STOL AIRCRAFT

- Performance characteristics of a variable-area vane nozzle for vectoring an ASTOVL exhaust jet up to 45 deg
[AIAA PAPER 93-2437] p 29 A93-50189
Effects of flow-path variations on internal reversing flow in a tailpipe offtake configuration for ASTOVL aircraft
[AIAA PAPER 93-2438] p 29 A93-50190
A full-scale STOVL ejector experiment
[NASA-TM-106019] p 35 N93-22480
Experimental performance of a ventral nozzle with pitch and yaw vectoring capability for SSTOVL aircraft
[NASA-TM-106054] p 36 N93-25129
Performance characteristics of a variable-area vane nozzle for vectoring an ASTOVL exhaust jet up to 45 deg
[NASA-TM-106114] p 37 N93-27131
Effects of flow-path variations on internal reversing flow in a tailpipe offtake configuration for ASTOVL aircraft
[NASA-TM-106149] p 38 N93-29065

VACUUM

- Inflation at the electroweak scale p 290 A93-26263

VACUUM EFFECTS

- Experimental determination of in situ utilization of lunar regolith for thermal energy storage p 253 A93-26043
Simulation of the synergistic low Earth orbit effects of vacuum thermal cycling, vacuum UV radiation, and atomic oxygen p 58 N93-15595

VACUUM TESTS

- Mechanical properties of Haynes Alloy 188 after exposure to LiF-22CaF₂, air, and vacuum at 1093 K for periods up to 10,000 hours p 126 A93-36586
Spectroscopic ellipsometry studies of HF treated Si (100) surfaces p 282 A93-46188

VALVES

- External stress-corrosion cracking of a 1.22-m-diameter type 316 stainless steel air valve
[NASA-TP-3190] p 129 N93-26201

VANES

- Cruise noise of an advanced propeller with swirl recovery vanes p 273 A93-28609

VAPOR DEPOSITION

- Silicon carbide, a semiconductor for space power electronics p 279 A93-13880
Role of Si₂N₂O in the passive oxidation of chemically-vapor-deposited Si₃N₄ p 131 A93-16520
Prediction of chemical vapor deposition rates on monofilaments and its implications for fiber properties p 113 A93-17198
Properties of hybrid CVD/PAN graphite fibers and their bromine intercalation compounds p 98 A93-17675
Flow effects in a vertical CVD reactor p 166 A93-19821
Enhancement of photoluminescence intensity of GaAs with cubic GaS chemical vapor deposited using a structurally designed single-source precursor p 280 A93-26930
Mechanism of incipient oxidation of bulk chemical vapor deposited Si₃N₄ p 132 A93-32299
Greatly improved 3C-SiC p-n junction diodes grown by chemical vapor deposition p 156 A93-38994
Chemical vapor deposition modeling for high temperature materials p 116 A93-39503
Onset conditions for gas phase reaction and nucleation in the CVD of transition metal oxides p 116 A93-39508

- CVD of silicon carbide on structural fibers - Microstructure and composition p 117 A93-39521
Atomic probe microscopy of 3C SiC films grown on 6H SiC substrates p 281 A93-39854

- Photoluminescence intensity enhancement of GaAs by vapor-deposited GaS - A rational approach to surface passivation p 281 A93-40049

- Computer modeling of a hot filament diamond deposition reactor p 94 A93-40618

- Electronic passivation of n- and p-type GaAs using chemical vapor deposited GaS p 283 A93-52708
Growth and characterization of 3C-SiC and 6H-SiC films on 6H-SiC wafers p 284 A93-55602

- Friction and wear of plasma-deposited diamond films [NASA-TM-105926] p 136 N93-19035

- A kinetic and equilibrium analysis of silicon carbide chemical vapor deposition on monofilaments [NASA-TM-106137] p 96 N93-27003

- SiC fiber-reinforced Celsian glass-ceramic matrix composite [NASA-CASE-LEW-15264-1] p 112 N93-31293

- Method of producing a ceramic fiber-reinforced glass-ceramic matrix composite [NASA-CASE-LEW-15264-2] p 112 N93-31299

VAPOR PHASES

- LENS, a general chemical kinetics and sensitivity analysis code for gas-phase reactions: User's guide [NASA-TM-105851] p 121 N93-16614
Structure of confined laminar spray diffusion flames: Numerical investigation [NASA-TM-106038] p 197 N93-22596
A kinetic and equilibrium analysis of silicon carbide chemical vapor deposition on monofilaments [NASA-TM-106137] p 96 N93-27003

VAPORIZERS

- Gravity sensitivity of a resistojet water vaporizer [AIAA PAPER 93-2402] p 186 A93-50167
Preliminary endurance tests of water vaporizers for resistojet applications [AIAA PAPER 93-2403] p 187 A93-50168
Preliminary characterization of a water vaporizer for resistojet applications [NASA-TM-105877] p 80 N93-11402
Preliminary endurance tests of water vaporizers for resistojet applications [NASA-TM-106222] p 92 N93-28694
Gravity sensitivity of a resistojet water vaporizer [NASA-TM-106220] p 92 N93-29194

VAPORIZING

- Vaporization heat transfer of dielectric liquids on a wick-covered surface [AIAA PAPER 93-0283] p 169 A93-22686
Effect of vaporization on cryogenic spray droplet measurement [AIAA PAPER 93-0692] p 172 A93-24792
Simulation of the early startup period of high-temperature heat pipes from the frozen state by a rarefied vapor self-diffusion model p 175 A93-30127
A numerical analysis of high-temperature heat pipe startup from the frozen state p 175 A93-30128
A comparison of numerical and analytical solution of the creeping flame spread over thermally thin material p 117 A93-41954

- Vaporization heat transfer of dielectric liquids on enhanced surfaces covered with screen wicks [AIAA PAPER 93-2835] p 182 A93-46572
Atomization and vaporization characteristics of airblast fuel injection inside a venturi tube [AIAA PAPER 93-1766] p 184 A93-49662
Effects of detailed droplet heating models on turbulent sprays vaporization behavior [AIAA PAPER 93-2193] p 185 A93-50005
Atomizing-gas temperature effect on cryogenic spray droplet [AIAA PAPER 93-2333] p 186 A93-50111
Droplet vaporization in a high-pressure gas p 190 A93-55461
Effect of vaporization on cryogenic spray droplet measurement [NASA-TM-105909] p 213 N93-13410
Atomizing-gas temperature effect on cryogenic spray droplet [NASA-TM-106106] p 216 N93-25191

VAPORS

- Physical vapor transport of mercurous chloride under a nonlinear thermal profile [NASA-TM-105920] p 196 N93-16612

VARIABLE CYCLE ENGINES

- Effects of turbine cooling assumptions on performance and sizing of high-speed civil transport [AIAA PAPER 92-4217] p 22 A93-13383

VECTOR PROCESSING (COMPUTERS)

- Time-variant analysis of rotorcraft systems dynamics - An exploitation of vector processors p 220 A93-23512
On the effects of grid ill-conditioning in three dimensional finite element vector potential magnetostatic field computations p 157 A93-39719

VECTOR QUANTIZATION

- An all digital implementation of a modified Hamming net for video compression with prediction and quantization circuits p 148 A93-37038

VECTORS (MATHEMATICS)

- Theoretical and numerical difficulties in 3-D vector potential methods in finite element magnetostatic computations p 157 A93-39720

VELOCITY DISTRIBUTION

- Ground-based PIV and numerical flow visualization results from the Surface Tension Driven Convection Experiment p 143 A93-33075
Calculations of separated 3-D flows with a pressure-staggered Navier-Stokes equations solver p 177 A93-34366
Coaxial injector spray characterization using water/air as simulants p 120 N93-11452
Direct numerical simulation of instabilities in parallel flow with spherical roughness elements [NASA-TM-105847] p 192 N93-11529

- Structure of confined laminar spray diffusion flames: Numerical investigation [NASA-TM-106038] p 197 N93-22596

- Mathematical relationship between two sets of laser anemometer measurements for resolving the total velocity vector [NASA-TM-105986] p 35 N93-22599

VELOCITY MEASUREMENT

- Experimental and computational investigation of the NASA Low-Speed Centrifugal Compressor flow field [ASME PAPER 92-GT-213] p 4 A93-19436
Molecular filter-based diagnostics in high speed flows [AIAA PAPER 93-0512] p 205 A93-23259
Laser anemometry - Advances and applications 1991; Proceedings of the 4th International Conference, Cleveland, OH, Aug 5-9, 1991 Vols. 1 & 2 [ISBN 0-7918-0654-5] p 206 A93-23776
Fiber optic laser Doppler anemometry in swirling jets p 206 A93-23783
Particle image velocimetry for the Surface Tension Driven Convection Experiment using a particle displacement tracking technique p 206 A93-23799
Particle displacement tracking applied to air flows p 206 A93-23800
Young's fringe particle image velocimetry in the presence of random particle motions p 207 A93-23801

- Signal processing considerations for low signal to noise ratio laser Doppler and phase Doppler signals p 207 A93-23830

- Nonintrusive, multipoint velocity measurements in high-pressure combustion flows [AIAA PAPER 93-2032] p 118 A93-49867

- Second order closure modeling of turbulent buoyant wall plumes [NASA-TM-105956] p 193 N93-14829

- 2D velocity and temperature measurements in high speed flows based on spectrally resolved Rayleigh scattering [NASA-TM-105784] p 215 N93-19651

- Mathematical relationship between two sets of laser anemometer measurements for resolving the total velocity vector [NASA-TM-105986] p 35 N93-22599

- Pulsed laser Rayleigh scattering diagnostic for hydrogen/oxygen rocket exit plane flowfield velocimetry [NASA-TM-106213] p 88 N93-26149

- Fuzzy logic particle tracking velocimetry [NASA-TM-106194] p 216 N93-27027

- Velocity and drop size measurements in a swirl-stabilized, combustor spray [NASA-TM-106130] p 37 N93-27130

- Turbulence measurement in a reacting and non-reacting shear layer at a high subsonic Mach number [NASA-TM-106186] p 18 N93-31839

VENTING

- Small experiments for the maturation of orbital cryogenic transfer technologies [NASA-TM-105849] p 192 N93-10981

VENTURI TUBES

- Atomization and vaporization characteristics of airblast fuel injection inside a venturi tube [AIAA PAPER 93-1766] p 184 A93-49662

VENUS (PLANET)

- Venus Interior Structure Mission (VISM): Establishing a seismic network on Venus p 293 N93-28819

VERTICAL LANDING

- Effects of flow-path variations on internal reversing flow in a tailpipe offtake configuration for ASTOVL aircraft [AIAA PAPER 93-2438] p 29 A93-50190
Effects of flow-path variations on internal reversing flow in a tailpipe offtake configuration for ASTOVL aircraft [NASA-TM-106149] p 38 N93-29065

VERY LARGE SCALE INTEGRATION

- Analysis of fault-tolerant neurocontrol architectures [NASA-TM-105898] p 41 N93-12305

VIBRATION

- Modal simulation of gear box vibration with experimental correlation p 221 A93-31982
Dynamics of rotating multicomponent turbomachinery systems [AIAA PAPER 93-1629] p 222 A93-34157
Modal analysis of multistage gear systems coupled with gearbox vibrations p 222 A93-36588
Vibration and noise analysis of a gear transmission system [AIAA PAPER 93-2150] p 224 A93-49967
Evaluation of a vibration diagnostic system for the detection of spur gear pitting failures [AIAA PAPER 93-2298] p 224 A93-50083
Experimental validation of boundary element methods for noise prediction [NASA-TM-105729] p 226 N93-10966
Dynamics of rotating multi-component turbomachinery systems [NASA-TM-105997] p 247 N93-18426

- Evaluation of a vibration diagnostic system for the detection of spur gear pitting failures
[NASA-TM-106103] p 228 N93-25672
- Vibration and noise analysis of a gear transmission system
[NASA-TM-106162] p 229 N93-27641
- VIBRATION DAMPING**
- Analysis and optimal design of thick composite structures with passive damping considerations
[AIAA PAPER 92-4819] p 235 A93-20398
- Evaluation of passive and active vibration control mechanisms in a microgravity environment
[AIAA PAPER 93-0838] p 55 A93-24905
- Calculation of stiffness and damping coefficients for elastically supported gas foil bearings
p 221 A93-27308
- Hybrid active vibration control of rotor-bearing systems using piezoelectric actuators
p 221 A93-27324
- Effects of interply damping layers on the dynamic characteristics of composite plates
p 237 A93-32415
- Analysis of passive damping in thick composite structures
p 241 A93-45743
- Generation of helical gears with new surfaces topology by application of CNC machines
[AIAA PAPER 93-2297] p 224 A93-50082
- Engineering science research issues in high power density transmission dynamics for aerospace applications --- rotorcraft geared rotors
[AIAA PAPER 93-2299] p 224 A93-50084
- Digital control algorithms for microgravity isolation systems
p 265 A93-53653
- Structural dynamics branch research and accomplishments to FY 1992
[NASA-TM-105824] p 247 N93-20368
- Graphite/epoxy composite laminates with co-cured interlaminar damping layers
p 109 N93-25587
- Dynamic characteristics of specialty composite structures with embedded damping layers
[NASA-TM-106165] p 110 N93-26705
- Generation of helical gears with new surfaces, topology by application of CNC machines
[NASA-TM-106175] p 229 N93-27687
- VIBRATION EFFECTS**
- Low-frequency vibration environment for five Shuttle missions
[NASA-TM-106059] p 63 N93-28554
- VIBRATION ISOLATORS**
- Vibration isolation technology - An executive summary of systems development and demonstration --- for proposed microgravity experiments aboard STS and Space Station Freedom
[AIAA PAPER 93-0834] p 55 A93-24904
- Evaluation of passive and active vibration control mechanisms in a microgravity environment
[AIAA PAPER 93-0838] p 55 A93-24905
- The isolation limits of stochastic vibration
p 236 A93-30042
- Vibration isolation technology: An executive summary of systems development and demonstration
[NASA-TM-105937] p 1 N93-15573
- VIBRATION MEASUREMENT**
- Fault detection of helicopter gearboxes using the multi-valued influence matrix method
[NASA-TM-106100] p 229 N93-27069
- Low-frequency vibration environment for five Shuttle missions
[NASA-TM-106059] p 63 N93-28554
- Efficient fault diagnosis of helicopter gearboxes
[NASA-TM-106253] p 231 N93-31846
- VIBRATION METERS**
- Proposed ground-based control of accelerometer on Space Station Freedom
p 63 A93-54401
- Proposed ground-based control of accelerometer on Space Station Freedom
[NASA-TM-105960] p 63 N93-23738
- VIBRATION MODE**
- Dynamic analysis of a pre-and-post ice impacted blade
[AIAA PAPER 92-4273] p 22 A93-13333
- Modal test/analysis correlation of Space Station structures using nonlinear sensitivity
[AIAA PAPER 92-4731] p 55 A93-20330
- Acoustical analysis of gear housing vibration
p 273 A93-29420
- Modal simulation of gear box vibration with experimental correlation
p 221 A93-31982
- Dynamic analysis of a pre-and-post ice impacted blade
[NASA-TM-105829] p 144 N93-12197
- Localization of aeroelastic modes in mistuned high-energy turbines
p 230 N93-31586
- VIBRATION TESTS**
- Behavior of spinning laminated composite plates with initial twist-experimental vibrations, strain, and deflection results
[AIAA PAPER 93-1325] p 238 A93-33898
- Low-noise, high-strength, spiral-bevel gears for helicopter transmissions
[AIAA PAPER 93-2149] p 223 A93-49966
- Derated ion thruster development status
[AIAA PAPER 93-2225] p 75 A93-50031
- Low-noise, high-strength, spiral-bevel gears for helicopter transmissions
[NASA-TM-106080] p 228 N93-23019
- VIDEO COMPRESSION**
- An all digital implementation of a modified Hamming net for video compression with prediction and quantization circuits
p 148 A93-37038
- VIDEO DATA**
- Ground-based PIV and numerical flow visualization results from the Surface Tension Driven Convection Experiment
p 143 A93-33075
- VIDEO SIGNALS**
- An all digital implementation of a modified Hamming net for video compression with prediction and quantization circuits
p 148 A93-37038
- Real-time transmission of digital video using variable-length coding
[NASA-TM-106092] p 150 N93-22483
- Picture data compression coder using subband/transform coding with a Lempel-Ziv-based coder
[NASA-CASE-LEW-15700-1] p 287 N93-28130
- VISCOELASTIC DAMPING**
- Graphite/epoxy composite laminates with co-cured interlaminar damping layers
p 109 N93-25587
- VISCOMETERS**
- A hydrodynamic model of the oscillating screen viscometer
p 190 A93-55136
- VISCOPLASTICITY**
- Thermo-elastoviscoplastic snapthrough behavior of cylindrical panels
p 233 A93-12046
- High temperature viscoplastic ratchetting - Material response or modeling artifact
p 233 A93-13823
- Stirling engine - Approach for long-term durability assessment
p 220 A93-26069
- Finite element implementation of state variable-based viscoplasticity models
p 236 A93-26776
- The viscoplastic behavior of Hastelloy-X single crystal
p 125 A93-27486
- Viscoplasticity with creep and plasticity bounds
p 125 A93-32925
- Analysis of the anisotropic viscoplastic-damage response of composite laminates - Continuum basis and computational algorithms
p 241 A93-43347
- Ratchetting behavior in viscoplasticity - A technical note
p 241 A93-43651
- Unified viscoplastic behavior of metal matrix composites
[NASA-TM-105819] p 244 N93-10777
- Analysis of large quasistatic deformations of inelastic solids by a new stress based finite element method
[NASA-CR-189235] p 246 N93-13260
- Thermoviscoplastic analysis of fibrous periodic composites using triangular subvolumes
[NASA-TM-106076] p 111 N93-29074
- Bounds on internal state variables in viscoplasticity
[NASA-TM-106215] p 251 N93-29196
- VISCOUS FLOW**
- Segmented multigrid domain decomposition procedure for incompressible viscous flows
p 99 A93-19123
- Aeroloids and secondary flows in a transonic mixed flow turbine stage
[ASME PAPER 92-GT-72] p 2 A93-19322
- An algebraic turbulence model for three-dimensional viscous flows
[AIAA PAPER 93-0083] p 4 A93-22552
- Absolute and convective instability of a viscous liquid jet surrounded by a viscous gas in a vertical pipe
p 176 A93-30144
- The application of preconditioning in viscous flows
p 177 A93-32627
- Computation of unsteady supersonic quasi-one-dimensional viscous-inviscid interacting internal flowfields
p 177 A93-32724
- CFD for hypersonic propulsion
p 8 A93-42585
- Multigrid calculation of three-dimensional viscous cascade flows
p 8 A93-42889
- Segmented multigrid domain decomposition solutions for three dimensional viscous recirculating flows
[AIAA PAPER 93-3344] p 181 A93-45038
- High order accurate solutions of viscous problems
[AIAA PAPER 93-3074] p 183 A93-48249
- Streamwise computation of three-dimensional flows using two stream functions
p 184 A93-49241
- 3-D viscous flow CFD analysis of the propeller effect on an advanced ducted propeller subsonic inlet
[AIAA PAPER 93-1847] p 12 A93-49728
- Development of an explicit multiblock/multigrid flow solver for viscous flows in complex geometries
[AIAA PAPER 93-2380] p 186 A93-50148
- A comparison between numerically modelled and experimentally measured loss mechanisms in wave rotors
[AIAA PAPER 93-2522] p 30 A93-50252
- Analysis of high Reynolds number inviscid/viscid interactions in cascades
p 15 A93-55351
- A compressible boundary layer algorithm for use with SINDA '85
p 192 N93-13395
- An algebraic turbulence model for three-dimensional viscous flows
[NASA-TM-105931] p 1 N93-14102
- On the nonlinear three dimensional instability of Stokes layers and other shear layers to pairs of oblique waves
[NASA-TM-105918] p 194 N93-15499
- Large-scale computation of incompressible viscous flow by least-squares finite element method
[NASA-TM-105904] p 269 N93-22825
- The 3-D viscous flow CFD analysis of the propeller effect on an advanced ducted propeller subsonic inlet
[NASA-TM-106240] p 38 N93-29162
- Three-dimensional analysis of the Pratt and Whitney alternate design SSME fuel turbine
p 230 N93-31584
- VISUAL SIGNALS**
- Hierarchical image coding with diamond-shaped sub-bands
p 205 A93-20945
- VOICE OF AMERICA**
- Direct Broadcast Satellite Radio Program
[NASA-TM-105910] p 52 N93-11430
- VOIDS**
- Initial study of void formation during aluminum solidification in reduced gravity
p 142 A93-12013
- Mechanisms of voids formation during cooldown and freezing of lithium in SP-100 type systems
p 163 A93-13916
- Modeling void growth and movement with phase change in thermal energy storage canisters
[AIAA PAPER 93-2832] p 285 A93-46569
- NDE of PWA 1480 single crystal turbine blade material
[NASA-TM-106140] p 38 N93-27640
- VOLTAGE CONVERTERS (DC TO DC)**
- Operation of high power converters in parallel
p 154 A93-26100
- Load converter interactions with the secondary system in the Space Station Freedom power management and distribution dc test bed
p 154 A93-26106
- Stability testing and analysis of a PMAD dc test bed for the Space Station Freedom
p 154 A93-26107
- A 1.6-kW, 110-kHz dc-dc converter optimized for IGBT's
p 156 A93-37570
- A 10 kW dc-dc converter using IGBTs with active snubbers --- Insulated Gate Bipolar Transistor
p 158 A93-50646
- VOLTAGE REGULATORS**
- Battery selection for space experiments
p 159 N93-13184
- VORTEX BREAKDOWN**
- Gallery of fluid motion
p 178 A93-35481
- Adaptive computations of flow around a delta wing with vortex breakdown
[AIAA PAPER 93-3400] p 10 A93-47202
- VORTEX GENERATORS**
- Study on vortex flow control of inlet distortion
p 2 A93-14520
- Wake-induced unsteady stagnation-region heat-transfer measurements
[ASME PAPER 92-GT-196] p 166 A93-19421
- An experimental investigation of S-duct flow control using arrays of low-profile vortex generators
[AIAA PAPER 93-0018] p 170 A93-24226
- Study on vortex generator flow control for the management of inlet distortion
p 7 A93-34488
- Streamwise vorticity generation and mixing enhancement in free jets by 'delta-tabs'
[AIAA PAPER 93-3253] p 14 A93-53592
- An experimental investigation of S-duct flow control using arrays of low-profile vortex generators
[NASA-TM-106030] p 17 N93-19968
- Streamwise vorticity generation and mixing enhancement in free jets by delta-tabs
[NASA-TM-106235] p 17 N93-31648
- VORTEX SHEETS**
- Three-dimensional numerical simulation of gradual opening in a wave rotor passage
[AIAA PAPER 93-2526] p 187 A93-50254
- The development of a mixing layer under the action of weak streamwise vortices
[NASA-TM-106089] p 201 N93-28947
- VORTICES**
- Study on vortex flow control of inlet distortion
p 2 A93-14520
- Non-parallel effects in the instability of Long's vortex
p 164 A93-16663
- Forward rotor vortex effects on counter rotating propeller noise
p 2 A93-19221

- Numerical solutions for unsteady subsonic vortical flows around loaded cascades
[ASME PAPER 92-GT-173] p 3 A93-19399
- On streamwise vortices in high Reynolds number supersonic axisymmetric jets p 167 A93-21060
- Driven cavity simulation of turbomachine blade flows with vortex control
[AIAA PAPER 93-0390] p 6 A93-24238
- Giant suppression of flux-flow resistivity in heavy-ion irradiated Ti2Ba2Ca2Cu3O10 films - Influence of linear defects on vortex transport p 280 A93-26198
- The development of a mixing layer under the action of weak streamwise vortices p 176 A93-30134
- Effects of flow-path variations on internal reversing flow in a tailpipe offtake configuration for ASTOVL aircraft
[AIAA PAPER 93-2438] p 29 A93-50190
- Three-dimensional numerical simulation of gradual opening in a wave rotor passage
[AIAA PAPER 93-2526] p 187 A93-50254
- Streamwise vorticity generation and mixing enhancement in free jets by 'delta-tabs'
[AIAA PAPER 93-3253] p 14 A93-53592
- Large-scale computation of incompressible viscous flow by least-squares finite element method
[NASA-TM-105904] p 269 A93-22825
- Effects of flow-path variations on internal reversing flow in a tailpipe offtake configuration for ASTOVL aircraft
[NASA-TM-106149] p 38 A93-29065
- Streamwise vorticity generation and mixing enhancement in free jets by delta-tabs
[NASA-TM-106235] p 17 A93-31648
- VORTICITY**
- Study on vortex flow control of inlet distortion
p 2 A93-14520
- Three-dimensional boundary-layer instability and separation induced by small-amplitude streamwise vorticity in the upstream flow p 172 A93-24401
- Statistical analysis of the effects of helicity in inhomogeneous turbulence p 175 A93-26186
- Structure and development of streamwise vortex arrays embedded in a turbulent boundary layer p 177 A93-32711
- A note on the distortion of a flat-plate boundary layer by free-stream vorticity normal to the plate p 178 A93-34414
- Characteristics of three-dimensional turbulent jets in crossflow p 8 A93-38695
- Vorticity dynamics of inviscid shear layers p 181 A93-45734
- Large-scale computation of incompressible viscous flow by least-squares finite element method
[NASA-TM-105904] p 269 A93-22825
- Nonlinear evolution of the first mode supersonic oblique waves in compressible boundary layers. Part 1: Heated/cooled walls
[NASA-TM-106087] p 199 A93-25175
- VSAT (NETWORK)**
- System overview on electromagnetic compensation for reflector antenna surface distortion
[NASA-TM-106217] p 53 A93-29195

W

WAFERS

- Silicon carbide, a semiconductor for space power electronics p 279 A93-13880
- Growth and characterization of 3C-SiC and 6H-SiC films on 6H-SiC wafers p 284 A93-55602

WAKES

- Calculation of a circular jet in crossflow with a multiple-time-scale turbulence model p 164 A93-15063

WALL FLOW

- Numerical simulation of compressor endwall and casing treatment flow phenomena
[ASME PAPER 92-GT-300] p 4 A93-19490
- New time scale based k-epsilon model for near-wall turbulence p 180 A93-41909
- Investigation of a strut/endwall interaction in supersonic annular flow
[AIAA PAPER 93-1925] p 12 A93-49791
- Modeling of turbulence and transition p 195 A93-15795
- Modeling of near wall turbulence and modeling of bypass transition p 195 A93-15798
- Numerical simulations of three-dimensional laminar flow over a backward facing step; flow near side walls
[NASA-TM-106248] p 202 A93-31147
- WALL TEMPERATURE**
- Relations for local radiative heat transfer between rectangular boundaries of an absorbing-emitting medium p 175 A93-30129
- Numerical study of nozzle wall cooling for nuclear thermal rockets
[AIAA PAPER 93-2498] p 77 A93-50232

- Nongray gas analyses for reflecting walls utilizing a flux technique p 190 A93-55460
- Thermal stratification potential in rocket engine coolant channels p 78 A93-10019
- Summary of experimental heat-transfer results from the turbine hot section facility
[NASA-TP-3250] p 197 A93-23059
- WALLS**
- Discrete ordinates solutions of nongray radiative transfer with diffusely reflecting walls p 285 A93-30124
- Axial-torsional fatigue - A study of tubular specimen thickness effects p 240 A93-38849
- Initial results from the NASA Lewis wave rotor experiment
[AIAA PAPER 93-2521] p 30 A93-53589
- Second order closure modeling of turbulent buoyant wall plumes
[NASA-TM-105956] p 193 A93-14829
- Nonlinear evolution of the first mode supersonic oblique waves in compressible boundary layers. Part 1: Heated/cooled walls
[NASA-TM-106087] p 199 A93-25175
- Initial results from the NASA Lewis wave rotor experiment
[NASA-TM-106148] p 39 A93-32368
- WATER**
- Construction and testing of ceramic fabric heat pipe with water working fluid p 163 A93-13869
- Preliminary endurance tests of water vaporizers for resistojet applications
[AIAA PAPER 93-2403] p 187 A93-50168
- Preliminary endurance tests of water vaporizers for resistojet applications
[NASA-TM-106222] p 92 A93-28694
- WATER TREATMENT**
- Ion exchange polymers and method for making
[NASA-CASE-LEW-15576-1] p 139 A93-31316
- WATER TUNNEL TESTS**
- Flow visualization in a single simulated brush seal p 226 A93-54659
- WATER VAPOR**
- Absorption coefficients for water vapor at 193 nm from 300 to 1073 K p 276 A93-45398
- Gravity sensitivity of a resistojet water vaporizer
[AIAA PAPER 93-2402] p 186 A93-50167
- Preliminary characterization of a water vaporizer for resistojet applications
[NASA-TM-105877] p 80 A93-11402
- Gravity sensitivity of a resistojet water vaporizer
[NASA-TM-106220] p 92 A93-29194
- WAVE DISPERSION**
- Dispersion-relation-preserving schemes for computational aeroacoustics p 2 A93-19151
- WAVE EQUATIONS**
- On the accurate long-time solution of the wave equation in exterior domains: Asymptotic expansions and corrected boundary conditions
[NASA-TM-106117] p 269 A93-27068
- WAVE FRONT RECONSTRUCTION**
- Vector formulation for interferogram surface fitting p 278 A93-55687
- WAVE INTERACTION**
- Fully coupled resonant-triad interaction in an adverse-pressure-gradient boundary layer p 167 A93-21049
- WAVE PROPAGATION**
- Dispersion-relation-preserving schemes for computational aeroacoustics p 2 A93-19151
- Blade row interaction effects on flutter and forced response
[AIAA PAPER 93-2084] p 28 A93-49911
- A model for the selective amplification of spatially coherent waves in a centrifugal compressor on the verge of rotating stall
[AIAA PAPER 93-2236] p 13 A93-50039
- Three-dimensional numerical simulation of gradual opening in a wave rotor passage
[AIAA PAPER 93-2526] p 187 A93-50254
- WAVE REFLECTION**
- Discrete ordinates solutions of nongray radiative transfer with diffusely reflecting walls p 285 A93-30124
- WAVE SCATTERING**
- On the accurate long-time solution of the wave equation in exterior domains: Asymptotic expansions and corrected boundary conditions
[NASA-TM-106117] p 269 A93-27068
- WAVEGUIDES**
- Novel coplanar waveguide to slotline transition on high resistivity silicon p 151 A93-20016
- Effect of a dielectric overlay on a linearly tapered slot antenna excited by a coplanar waveguide p 155 A93-35649
- Coplanar waveguide radial line stub p 155 A93-36514
- A reciprocity formulation for the EM scattering by an obstacle within a large open cavity p 149 A93-52237

- Conductor-backed coplanar waveguide resonators of Y-Ba-Cu-O and Ti-Ba-Ca-Cu-O on LaAlO3
[NASA-TM-105890] p 284 A93-12325
- WAVERIDERS**
- Design of a hypersonic waverider-derived airplane
[AIAA PAPER 93-0401] p 55 A93-21108
- WEAK ENERGY INTERACTIONS**
- Inflation at the electroweak scale p 290 A93-26263
- WEAK INTERACTIONS (FIELD THEORY)**
- Phase space distribution of halo particles and detection of WIMPS --- weakly interacting massive particles p 289 A93-23650
- WEAR**
- Tribological and mechanical comparison of sintered and HIPped PM212 - High temperature self-lubricating composites p 94 A93-13506
- Sliding wear of self-mated Al2O3-SiC whisker-reinforced composites at 23-1200 C p 101 A93-29948
- Relative sliding durability of two candidate high-temperature oxide fiber seal materials p 132 A93-31983
- A vacuum (10 exp -9 torr) friction apparatus for determining friction and endurance life of MoS(x) films p 146 A93-49245
- An analysis of the wear behavior of SiC whisker-reinforced alumina from 25 to 1200 C p 104 A93-49253
- Preliminary experimental results for a cryogenic brush seal configuration
[AIAA PAPER 93-2535] p 225 A93-50262
- Friction and wear of plasma-deposited amorphous hydrogenated films on silicon nitride p 135 A93-52181
- Spectroscopic wear detector
[NASA-CASE-LEW-15200-1] p 83 A93-18856
- Friction and wear of plasma-deposited diamond films
[NASA-TM-105926] p 136 A93-19035
- 100-kW class applied-field MPD thruster component wear
[NASA-TM-106023] p 85 A93-22482
- Preliminary experimental results for a cryogenic brush seal configuration
[NASA-TM-106236] p 201 A93-28627
- Tribological characteristics of perfluoropolyether liquid lubricants under sliding conditions in high vacuum
[NASA-TM-106257] p 139 A93-32352
- WEAR RESISTANCE**
- Tribological and microstructural comparison of HIPped PM212 and PM212/Au self-lubricating composites p 93 A93-13505
- The effect of processing and compositional changes on the tribology of PM212 in air
[NASA-TM-105945] p 95 A93-15576
- WEAR TESTS**
- Brush seal low surface speed hard-rub characteristics
[AIAA PAPER 93-2534] p 225 A93-50261
- Relative sliding durability of candidate high temperature fiber seal materials
[NASA-TM-105806] p 95 A93-10978
- Brush seal bristle flexure and hard-rub characteristics
[NASA-TM-105864] p 227 A93-18321
- Integrity testing of brush seal in shroud ring of T-700 engine
[NASA-TM-105863] p 227 A93-18380
- Brush seal low surface speed hard-rub characteristics
[NASA-TM-106169] p 200 A93-27132
- WEAVING**
- Computational simulation of surface waviness in graphite/epoxy woven composites due to initial curing p 98 A93-15822
- WEDGES**
- An apparatus for gripping test specimens
[NASA-CASE-LEW-15345-2] p 230 A93-28127
- WEIBULL DENSITY FUNCTIONS**
- Reliability analysis of structural ceramic components using a three-parameter Weibull distribution
[ASME PAPER 92-GT-296] p 231 A93-19486
- Fatigue criterion to system design, life and reliability A primer
[NASA-TM-106022] p 248 A93-23406
- WEIGHT REDUCTION**
- Structural tailoring of aircraft engine blade subject to ice impact constraints
[AIAA PAPER 92-4710] p 23 A93-20319
- WEIGHTLESSNESS**
- On the shear stabilization of capillary break-up of finite liquid bridges p 143 A93-32069
- Conceptual design for the Space Station Freedom fluid physics/dynamics facility
[NASA-TM-103663] p 61 A93-26209
- WEIGHTLESSNESS SIMULATION**
- Finite element calculations of transonic flutter in cascades
[AIAA PAPER 93-2083] p 185 A93-49910

WELDED JOINTS

External stress-corrosion cracking of a 1.22-m-diameter type 316 stainless steel air valve
[NASA-TP-3190] p 129 N93-26201

WHISKER COMPOSITES

Indentation flaw formation and strength response of silicon nitride ceramics at low indentation loads
p 130 A93-15994
Sliding wear of self-mated Al₂O₃-SiC whisker-reinforced composites at 23-1200 C
p 101 A93-29948
An analysis of the wear behavior of SiC whisker-reinforced alumina from 25 to 1200 C
p 104 A93-49253

WIND TUNNEL APPARATUS

Icing Research Tunnel rotating bar calibration measurement system
p 212 A93-54398
Icing research tunnel rotating bar calibration measurement system
[NASA-TM-106010] p 215 N93-22598
NASA Lewis 8- by 6-foot supersonic wind tunnel user manual
[NASA-TM-105771] p 43 N93-25080

WIND TUNNEL MODELS

Forcing function effects on unsteady aerodynamic gust response. I - Forcing functions
[ASME PAPER 92-GT-174] p 3 A93-19400
Forcing function effects on unsteady aerodynamic gust response. II - Low solidity airfoil row response
[ASME PAPER 92-GT-175] p 3 A93-19401
Computer aided design and manufacturing of composite propfan blades for a cruise missile wind tunnel model
[NASA-TM-105269] p 261 N93-12022
Structural dynamic testing of composite propfan blades for a cruise missile wind tunnel model
[NASA-TM-105272] p 247 N93-18875
Structural analysis of high-rpm composite propfan blades for a cruise missile wind tunnel model
[NASA-TM-105267] p 247 N93-23015
Fabrication of composite propfan blades for a cruise missile wind tunnel model
[NASA-TM-105270] p 249 N93-26202

WIND TUNNEL TESTS

Results of Low Power Deicer tests on a swept inlet component in the NASA Lewis Icing Research Tunnel
[AIAA PAPER 93-0032] p 20 A93-22551
LDV flowfield measurements on a straight and swept wing with a simulated ice accretion
[AIAA PAPER 93-0300] p 5 A93-23001
An overview of shed ice impact studies in the NASA Lewis Icing Research Tunnel
[AIAA PAPER 93-0301] p 5 A93-23247
Takeoff/approach noise for a model counterrotation propeller with a forward-swept upstream rotor
[AIAA PAPER 93-0596] p 24 A93-24782
Experimental investigation of counter-rotating propfan flutter at cruise conditions
[AIAA PAPER 93-1632] p 25 A93-34160
Comparative wind tunnel tests at high Reynolds numbers of NACA 64-621 airfoils with two aileron configurations
p 9 A93-46823
Comparison of reacting and non-reacting shear layers at a high subsonic Mach number
[AIAA PAPER 93-2381] p 186 A93-50149
Computer aided design and manufacturing of composite propfan blades for a cruise missile wind tunnel model
[NASA-TM-105269] p 261 N93-12022
Results of low power deicer tests on a swept inlet component in the NASA Lewis icing research tunnel
[NASA-TM-105968] p 15 N93-14911
An overview of shed ice impact in the NASA Lewis Icing Research Tunnel
[NASA-TM-105969] p 16 N93-15404
User manual for NASA Lewis 10 by 10 foot supersonic wind tunnel
[NASA-TM-105626] p 42 N93-15498
Takeoff/approach noise for a model counterrotation propeller with a forward-swept upstream rotor
[NASA-TM-105979] p 34 N93-16715
Structural analysis of high-rpm composite propfan blades for a cruise missile wind tunnel model
[NASA-TM-105267] p 247 N93-23015
Fabrication of composite propfan blades for a cruise missile wind tunnel model
[NASA-TM-105270] p 249 N93-26202
Comparison of reacting and non-reacting shear layers at a high subsonic Mach number
[NASA-TM-106198] p 38 N93-27610

WIND TUNNELS

Close-up analysis of aircraft ice accretion
[AIAA PAPER 93-0029] p 18 A93-23239
Icing Research Tunnel rotating bar calibration measurement system
p 212 A93-54398
Close-up analysis of aircraft ice accretion
[NASA-TM-105952] p 19 N93-15360

Icing research tunnel rotating bar calibration measurement system
[NASA-TM-106010] p 215 N93-22598

WINDOWS (APERTURES)

High performance sapphire windows
p 218 N93-22198

WING FLAPS

Icing effects on aircraft stability and control determined from flight data - Preliminary results
[AIAA PAPER 93-0398] p 40 A93-23073
Icing effects on aircraft stability and control determined from flight data: Preliminary results
[NASA-TM-105977] p 41 N93-14831

WING PROFILES

Effects of free-stream turbulence on boundary-layer transition
[AIAA PAPER 93-0488] p 170 A93-23390

WING SLOTS

An investigation of shock wave turbulent boundary layer interaction with bleed through slanted slots
[AIAA PAPER 93-2392] p 11 A93-48184

WING TIP VORTICES

Unsteady wing surface pressures in the wake of a propeller
p 14 A93-52436

WINGS

Design for cyclic loading endurance of composites
p 242 A93-53395
Application of artificial neural networks to the design optimization of aerospace structural components
[NASA-TM-4389] p 247 N93-21831
Probabilistic assessment of composite structures
[NASA-TM-106024] p 110 N93-27092
WIRE
Preliminary evaluation of tensile and stress-rupture behavior of W + 24 at pct Re + 0.4 at pct HfC wire
p 125 A93-25119
Progress toward a tungsten alloy wire/high temperature alloy composite turbine blade
[NASA-TM-105901] p 128 N93-15586
Auger electron spectroscopy study of oxidation of a PdCr alloy used for high-temperature sensors
[NASA-TM-106212] p 129 N93-23418
Progress in speckle-shift strain measurement
p 251 N93-31558

WIRING

NASA requirements and applications environments for electrical power wiring
p 153 A93-25919

WORK FUNCTIONS

Effects of anode material on arcjet performance
p 79 N93-10044
Effects of anode material on arcjet performance
[NASA-TM-105799] p 79 N93-10197

WORKING FLUIDS

Construction and testing of ceramic fabric heat pipe with water working fluid
p 163 A93-13869
Current status of liquid sheet radiator research
[NASA-TM-105764] p 193 N93-14150
Closed Brayton Cycle power system with a high temperature pellet bed reactor heat source for NEP applications
[NASA-TM-105933] p 82 N93-14482

WOVEN COMPOSITES

Computational micromechanics of woven composites
p 237 A93-32462
Acousto-Ultrasonic analysis of failure in ceramic matrix composite tensile specimens
[NASA-TM-106219] p 232 N93-29073

WROUGHT ALLOYS

In-phase and out-of-phase axial-torsional fatigue behavior of Haynes 188 at 760 C
[NASA-TM-105765] p 246 N93-13153

X**X RAY ANALYSIS**

Thermal stability of the microstructure of an aged Nb-Zr-C alloy
p 122 A93-13776

X RAY APPARATUS

X-ray-based displacement measurement for hostile environments
p 208 A93-28580

X RAY DIFFRACTION

Composition dependence of superconductivity in YBa₂(Cu_{3-x}Al_x)O_y
p 281 A93-40271

X RAY SOURCES

X-ray-based displacement measurement for hostile environments
p 208 A93-28580

X RAY SPECTROSCOPY

Interfacial chemistry of a perfluoropolyether lubricant studied by X-ray photoelectron spectroscopy and temperature desorption spectroscopy
p 133 A93-38473
X-ray photoelectron spectroscopy study of the stability of Fomblin Z25 on the native oxide of aluminum
p 134 A93-44883

Interfacial chemistry of a perfluoropolyether lubricant studied by XPS and TDS
[NASA-TM-106014] p 137 N93-22560

XENON

Low-isp derated ion thruster operation
[AIAA PAPER 92-3203] p 64 A93-13696
Derated ion thruster development status
[AIAA PAPER 93-2225] p 75 A93-50031
Simplified power processing for inert gas ion thrusters
[AIAA PAPER 93-2397] p 76 A93-50162

Y**YAW**

LDEF yaw and pitch angle estimates
p 58 N93-12772

YBCO SUPERCONDUCTORS

Large-area YBa₂Cu₃O₇(δ) thin films on sapphire for microwave applications
p 279 A93-11475
Buffer layers for high-T_c thin films on sapphire
p 150 A93-17063
Single liquid source plasma-enhanced metalorganic chemical vapor deposition of high-quality YBa₂Cu₃O₇(δ) thin films
p 280 A93-20643
Ellipsometric study of ambient-produced overlayer growth rate on YBa₂Cu₃O₇(δ) films
p 281 A93-39362
A 10 GHz Y-Ba-Cu-O/GaAs hybrid oscillator proximity coupled to a circular microstrip patch antenna
p 158 A93-54619
Demonstration of Y₁Ba₂Cu₃O₇(δ) and complementary metal-oxide-semiconductor device fabrication on the same sapphire substrate
p 159 A93-56292
Conductor-backed coplanar waveguide resonators of Y-Ba-Cu-O and Ti-Ba-Cu-Cu-O on LaAlO₃
[NASA-TM-105890] p 284 N93-12325

YIELD STRENGTH

Progress toward a tungsten alloy wire/high temperature alloy composite turbine blade
[NASA-TM-105901] p 128 N93-15586
Fuzzy sets predict flexural strength and density of silicon nitride ceramics
[NASA-TM-106049] p 110 N93-27270
Bounds on internal state variables in viscoplasticity
[NASA-TM-106215] p 251 N93-29196

YTTRIA-STABILIZED ZIRCONIA

Characterization and durability testing of plasma-sprayed zirconia-yttria and hafnia-yttria thermal barrier coatings. Part 1: Effect of spray parameters on the performance of several lots of partially stabilized zirconia-yttria powder
[NASA-TP-3295] p 128 N93-22556

YTTRIUM OXIDES

Glass formation, properties and structure of soda-yttria-silica glasses
p 131 A93-20464

Z**ZIRCONIUM**

Thermal stability of the microstructure of an aged Nb-Zr-C alloy
p 122 A93-13776

ZIRCONIUM ALLOYS

Predicting the oxidative lifetime of beta NiAl-Zr alloys
p 127 A93-53939

ZIRCONIUM CARBIDES

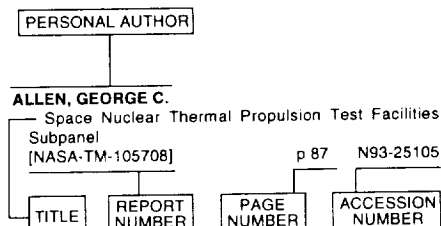
Processing and microstructure of Nb-1 percent Zr-0.1 percent C alloy sheet
[NASA-TM-105921] p 128 N93-15524

ZIRCONIUM OXIDES

Buffer layers for high-T_c thin films on sapphire
p 150 A93-17063
Fracture toughness of advanced ceramics at room temperature
p 131 A93-20842

PERSONAL AUTHOR INDEX

Typical Personal Author Index Listing



Listings in this index are arranged alphabetically by personal author. The title of the document is used to provide a brief description of the subject matter. The report number helps to indicate the type of document (e.g., NASA report, translation, NASA contractor report). The page and accession numbers are located beneath and to the right of the title. Under any one author's name the accession numbers are arranged in sequence.

A

ABBUD-MADRID, ANGEL

Effects of particulate radiation on premixed gas flames
[AIAA PAPER 93-0711] p 114 A93-24806
Premixed flame propagation in an optically thick gas
p 119 A93-55381

ABDALLAH, AYMAN A.

Implementation of the block-Krylov boundary flexibility method of component synthesis
[NASA-TM-106065] p 248 A93-23044
Solving modal equations of motion with initial conditions using MSC/NASTRAN DMAP. Part 1: Implementing exact mode superposition
[NASA-TM-106063] p 248 A93-23739
Solving modal equations of motion with initial conditions using MSC/NASTRAN DMAP. Part 2: Coupled versus uncoupled integration
[NASA-TM-106064] p 248 A93-23740

ABDELWAHAB, M.

Measured acoustic characteristics of ducted supersonic jets at different model scales
[AIAA PAPER 93-0731] p 273 A93-24821

ABDUL-AZIZ, A.

Design considerations for a Space Shuttle Main Engine turbine blade made of single crystal material
p 236 A93-25228

ABDUL-AZIZ, ALI

The influence of primary and secondary orientations on the elastic response of a nickel-base single-crystal superalloy
[NASA-TM-106125] p 250 A93-26550
Secondary orientation effects in a single crystal superalloy under mechanical and thermal loads
p 130 A93-31578

ABEL, P. B.

Simultaneous pressure measurement and high-speed photography study of cavitation in a dynamically loaded journal bearing
p 223 A93-40050

ABEL, PHILLIP B.

A vacuum (10 exp -9 torr) friction apparatus for determining friction and endurance life of MoS(x) films
p 146 A93-49245

ABOUELKHEIR, M.

Nonlinear dynamic simulation of single- and multi-spool core engines
[AIAA PAPER 93-2580] p 30 A93-50294

ABUMERI, G.

Structural Tailoring/Analysis for Hypersonic Components - A computational simulation
[AIAA PAPER 92-4722] p 20 A93-20324

ABUMERI, G. H.

Dynamic analysis of a pre-and-post ice impacted blade
[AIAA PAPER 92-4273] p 22 A93-13333
Structural tailoring of aircraft engine blade subject to ice impact constraints
[AIAA PAPER 92-4710] p 23 A93-20319
BLASIM - A computational tool to assess ice impact damage on engine blades
[AIAA PAPER 93-1638] p 26 A93-34165
Dynamic analysis of a pre-and-post ice impacted blade
[NASA-TM-105829] p 144 A93-12197
Root damage analysis of aircraft engine blade subject to ice impact
[NASA-TM-105779] p 246 A93-15343
Structural tailoring of aircraft engine blade subject to ice impact constraints
[NASA-TM-106033] p 250 A93-26999
Blasim: A computational tool to assess ice impact damage on engine blades
[NASA-TM-106225] p 251 A93-31193

ABUMERI, GALIB H.

Probabilistic assessment of composite structures
[AIAA PAPER 93-1441] p 239 A93-33990

ACOSTA, R. J.

System overview on electromagnetic compensation for reflector antenna surface distortion
[NASA-TM-106217] p 53 A93-29195

ACOSTA, WALDO A.

An efficient liner cooling scheme for advanced small gas turbine combustors
[AIAA PAPER 93-1763] p 27 A93-49660

ACQUAVIVA, THOMAS H.

Thermostructural tailoring of fiber composite structures
[NASA-TM-105882] p 107 A93-12078

ADAMCZYK, J. J.

Numerical simulation of compressor endwall and casing treatment flow phenomena
[ASME PAPER 92-GT-300] p 4 A93-19490
Three-dimensional analysis of the Pratt and Whitney alternate design SSME fuel turbine
p 230 A93-31584

ADAMOVSKY, G.

RF modulated fiber optic sensing systems and their applications
p 211 A93-49469

ADAMOVSKY, GRIGORY

Fiber optic sensing technique employing RF modulated interferometry
p 212 A93-53110

ADAMS, DICK

Aerodynamic effects of deicing and anti-icing fluids
p 19 A93-31929

ADAMS, FRED C.

Extension of the Parker bound on the flux of magnetic monopoles
p 291 A93-38672

ADAMS, NEIL S.

COLD-SAT dynamic model
[NASA-TM-105185] p 59 A93-19988

ADAMS, STEVEN F.

Photovoltaic Array Space Power flight experiment plus diagnostics (PASP+) modules
p 68 A93-25898

ADDY, HAROLD E., JR.

Lubrication of an 85-mm ball bearing with RP-1
[AIAA PAPER 93-2538] p 225 A93-53590
Lubrication of an 85-mm ball bearing with RP-1
[NASA-TM-106254] p 51 A93-31670

ADKINS, KENNETH

An all digital implementation of a modified Hamming net for video compression with prediction and quantization circuits
p 148 A93-37038

ADKINS, VICKI

Description of the PMAD systems test bed facility and data system
p 47 A93-26102

AGGARWAL, S. K.

On the structure of gaseous confined laminar diffusion flames: Numerical investigation
[NASA-TM-106039] p 197 A93-21198
Structure of confined laminar spray diffusion flames: Numerical investigation
[NASA-TM-106038] p 197 A93-22596

AHMADI, G.

Evaluation of passive and active vibration control mechanisms in a microgravity environment
[AIAA PAPER 93-0838] p 55 A93-24905

AHN, KYUNG H.

Laminar/turbulent oscillating flow in circular pipes
p 167 A93-21689

AHN, MYONG K.

Lower temperature curing thermoset polyimides utilizing a substituted norbornene endcap
p 134 A93-44526

AHUJA, K. K.

Supersonic jet noise reduction by coaxial rectangular nozzles
p 272 A93-19205
Measured acoustic characteristics of ducted supersonic jets at different model scales
[AIAA PAPER 93-0731] p 273 A93-24821

AHUJA, SANDEEP

Design of a constant tension thermocouple rake suitable for flame studies
p 210 A93-40683

AIELLO, R. A.

Improved accuracy for finite element structural analysis via an integrated force method
p 234 A93-17246

AIKIN, B. J. M.

The kinetics of composite particle formation during mechanical alloying
p 125 A93-29534

AJMANI, KUMUD

Preconditioned Conjugate Gradient methods for low speed flow calculations
[AIAA PAPER 93-0881] p 172 A93-24942
Preconditioned conjugate-gradient methods for low-speed flow calculations
[NASA-TM-105929] p 194 A93-14885

AKL, F. A.

Binary tree eigen solver in finite element analysis
[AIAA PAPER 93-1493] p 267 A93-34034

AL-KHALIL, KAMEL M.

Numerical modeling of anti-icing systems and comparison to test results on a NACA 0012 airfoil
[AIAA PAPER 93-0170] p 21 A93-23242
Ice accretion and performance degradation calculations with LEWICE/NS
[AIAA PAPER 93-0173] p 18 A93-23244
Numerical modeling of anti-icing systems and comparison to test results on a NACA 0012 airfoil
[NASA-TM-105975] p 19 A93-15345
Ice accretion and performance degradation calculations with LEWICE/NS
[NASA-TM-105972] p 19 A93-15354
Numerical modeling of runback water on ice protected aircraft surfaces
p 201 A93-27438

ALAM, J.

Application of artificial neural networks in nonlinear analysis of trusses
[NASA-TM-105319] p 244 A93-11403

ALBRECHT, ANDREAS

Cosmic string with a light massive neutrino
p 288 A93-16303

ALEXANDER, SCOTT

Membrane triangles with corner drilling freedoms. III - Implementation and performance evaluation
p 236 A93-24305

ALEXOVICH, ROBERT E.

Multiple-access phased array antenna simulator for a digital beam-forming system investigation
p 148 A93-26237

ALLAIRE, P. E.

The isolation limits of stochastic vibration
p 236 A93-30042

ALLEN, GEORGE C.

Space Nuclear Thermal Propulsion Test Facilities Subpanel
[NASA-TM-105708] p 87 A93-25105

- ALLEN, M.**
Nonintrusive, multipoint velocity measurements in high-pressure combustion flows
[AIAA PAPER 93-2032] p 118 A93-49867
- ALLEN, M. G.**
Rotational level-dependent collisional broadening and line shift of the A2Sigma(+) - X2Pi(1,0) band of OH in hydrogen-air combustion gases p 276 A93-24142
- ALSTON, WILLIAM B.**
Substituted 1,1,1-triaryl 2,2,2-trifluoroethanes and processes for their synthesis
[NASA-CASE-LEW-14345-7] p 95 N93-17412
- ALTENBURGER, GENE P.**
Simulating a 1-kW arcjet thruster using a nonlinear active load p 48 A93-34482
- ALTENKIRCH, ROBERT A.**
Opposed-flow flame spreading in reduced gravity p 121 N93-20206
- ALTEROVITZ, S. A.**
Intermodulation in the oscillatory magnetoresistance of a two-dimensional electron gas p 151 A93-17610
Ellipsometric study of Si(0.5)Ge(0.5)/Si strained-layer superlattices p 280 A93-34655
Room-temperature determination of two-dimensional electron gas concentration and mobility in heterostructures p 280 A93-35198
High frequency performance of Si(1-x)Ge(x)/Si(1-y)Ge(y)/Si(1-x)Ge(x) HBTs p 155 A93-37409
New technique for oil backstreaming contamination measurements p 210 A93-44514
Ellipsometric characterization of In(0.52)Al(0.48)As and of modulation doped field effect transistor structures on InP substrates p 158 A93-49382
The effects of strain on the microwave performance of SiGe HBTs p 158 A93-54442
- ALTEROVITZ, SAMUEL A.**
Ellipsometric study of metal-organic chemically vapor deposited III-V semiconductor structures p 281 A93-35697
A 10-GHz amplifier using an epitaxial lift-off pseudomorphic HEMT device p 156 A93-37574
Ellipsometric study of ambient-produced overlayer growth rate on YBa2Cu3O(7-x) films p 281 A93-39362
Spectroscopic ellipsometry studies of HF treated Si(100) surfaces p 282 A93-46188
Development of Si(1-x)Ge(x) technology for microwave sensing applications [NASA-TM-106157] p 162 N93-28610
- ALVIN, KEN**
Membrane triangles with corner drilling freedoms. I - The EFF element p 235 A93-24303
- AMATO, C.**
CVD of SiC and AlN using cyclic organometallic precursors p 117 A93-39525
- AMERI, ALI**
High Reynolds number and turbulence effects on aerodynamics and heat transfer in a turbine cascade [NASA-TM-106187] p 202 N93-29157
- AMERI, ALI A.**
Navier-Stokes turbine heat transfer predictions using two-equation turbulence [NASA-TM-105817] p 191 N93-10735
- AMIROUCHE, F. M. L.**
Dynamic analysis of flexible gear trains/transmissions - An automated approach p 220 A93-22440
Time-variant analysis of rotorcraft systems dynamics - An exploitation of vector processors p 220 A93-23512
- AMUNDSEN, PETER C.**
BIPS Turboalternator-Compressor characteristics and application to the NASA Solar Dynamic Ground Demonstration Program p 69 A93-25965
- ANDERSON, B. H.**
A comparative study of Full Navier-Stokes and Reduced Navier-Stokes analyses for separating flows within a diffusing inlet S-duct [AIAA PAPER 93-2154] p 13 A93-49970
- ANDERSON, BERNHARD H.**
Study on vortex flow control of inlet distortion p 2 A93-14520
Study on vortex generator flow control for the management of inlet distortion p 7 A93-34488
- ANDERSON, DAVID J.**
Bibliography on propulsion airframe integration technologies for high-speed civil transport applications, 1980-1991 [NASA-TM-105602] p 1 N93-26136
- ANDERSON, ROBERT C.**
Visualization of hydrogen injection in a scramjet engine by simultaneous PLIF imaging and laser holographic imaging p 214 N93-13683
- ANDRAS, MARIA T.**
Room temperature synthesis of copper indium diselenide in non-aqueous solution using an organoindium reagent p 283 A93-54844
- ANDRO, MONTY**
Multiple-access phased array antenna simulator for a digital beam-forming system investigation p 148 A93-26237
- ANGEL, PAUL W.**
Glass formation, properties and structure of soda-yttria-silica glasses p 131 A93-20464
- ANGHAIE, SAMIM**
Ultrahigh temperature vapor-core reactor - Magnetohydrodynamic system for space nuclear electric power p 66 A93-21663
Thermophysical properties of gas phase uranium tetrafluoride [AIAA PAPER 93-2758] p 285 A93-46505
- ANGUS, JOHN C.**
Computer modeling of a hot filament diamond deposition reactor p 94 A93-40618
- ANNEN, K. D.**
Development of a Rayleigh scattering system for temperature measurements in combustor flows p 206 A93-23788
- ANNEN, KURT D.**
Gas temperature measurements using the dual-line detection Rayleigh scattering technique p 213 A93-55368
Gas temperature measurements using the dual-line detection Rayleigh scattering technique p 214 N93-13668
- ANSARI, NIRWAN**
The performance evaluation of a new neural network based traffic management scheme for a satellite communication network p 147 A93-10929
- ANSARI, RAFAT R.**
Coherent fiber optic sensor for early detection of cataractogenesis in a human eye lens p 209 A93-37051
Microemulsion characterization by the use of a noninvasive backscatter fiber optic probe p 277 A93-52412
Multiple fiberoptic probe for several sensing applications p 212 A93-53109
A fiber optic probe for the detection of cataracts p 257 N93-25593
- ANTONIAK, ZENEN I.**
Construction and testing of ceramic fabric heat pipe with water working fluid p 163 A93-13869
- ANZIC, J.**
Leveling coatings for reducing the atomic oxygen defect density in protected graphite fiber epoxy composites [NASA-TM-105732] p 136 N93-15344
Leveling coatings for reducing the atomic oxygen defect density in protected graphite fiber epoxy composites p 59 N93-15597
- APPELBAUM, J.**
Parameterization of solar cells [NASA-TM-105885] p 159 N93-12301
- APPELBAUM, JOSEPH**
Photovoltaic arrays for Martian surface power [IAF PAPER 92-0591] p 293 A93-13699
- APPLEBY, A. J.**
Pressure dependence of the oxygen reduction reaction at the platinum microelectrode/nafion interface - Electrode kinetics and mass transport p 112 A93-11450
- ARCHER, FRANCES A.**
The chemistry of Saudi Arabian sand - A deposition problem on helicopter turbine airfoils p 243 A93-53468
- ARIF, HUGH**
The CONE program - An overview p 146 A93-48637
- ARMAND, SASAN**
Modal test/analysis correlation of Space Station structures using nonlinear sensitivity [AIAA PAPER 92-4731] p 55 A93-20330
- ARMENTI, J.**
The effects of 1 kW class arcjet thruster plumes on spacecraft charging and spacecraft thermal control materials p 57 A93-35050
- ARNETTE, S. A.**
On streamwise vortices in high Reynolds number supersonic axisymmetric jets p 167 A93-21060
- ARNETTE, STEPHEN A.**
Molecular filter-based diagnostics in high speed flows [AIAA PAPER 93-0512] p 205 A93-23259
A study of compressible mixing layers using filtered Rayleigh scattering [AIAA PAPER 92-0175] p 173 A93-24982
- ARNOLD, S. M.**
Calculation of stress intensity factors in an isotropic multiaxial plate: Part 2: Symbolic/numeric implementation [NASA-TM-105823] p 244 N93-10453
- Calculation of stress intensity factors in an isotropic multiaxial plate: Part 1: Theoretical development [NASA-TM-105766] p 244 N93-10455
Unified viscoplastic behavior of metal matrix composites [NASA-TM-105819] p 244 N93-10777
Explicit robust schemes for implementation of a class of principal value-based constitutive models: Symbolic and numeric implementation [NASA-TM-106124] p 258 N93-26946
Explicit robust schemes for implementation of general principal value-based constitutive models [NASA-TM-106123] p 258 N93-26947
- ARNONE, A.**
Multigrad calculation of three-dimensional viscous cascade flows p 8 A93-42889
- ARNONE, ANDREA**
Multigrad time-accurate integration of Navier-Stokes equations [AIAA PAPER 93-3361] p 181 A93-45054
Navier-Stokes turbine heat transfer predictions using two-equation turbulence [NASA-TM-105817] p 191 N93-10735
Numerical simulations of three-dimensional laminar flow over a backward facing step; flow near side walls [NASA-TM-106248] p 202 N93-31147
- ARRINGTON, LYNN A.**
A laboratory model of a hydrogen/oxygen engine for combustion and nozzle studies [AIAA PAPER 93-1825] p 48 A93-49711
Performance comparison of axisymmetric and three-dimensional hydrogen film coolant injection in a 110N hydrogen/oxygen rocket [NASA-TM-105967] p 83 N93-16714
- ASTHANA, R.**
On the melt infiltration of copper coated silicon carbide with an aluminum alloy p 218 A93-11332
Observations on infiltration of silicon carbide compacts with an aluminum alloy p 97 A93-12356
Interfacial shear strength of cast and directionally solidified NiAl-sapphire fiber composites p 106 A93-55685
Interfacial and capillary phenomena in solidification processing of metal-matrix composites p 106 A93-56351
- ASTHANA, RAJIV**
Melt infiltration of silicon carbide compacts. I - Study of infiltration dynamics p 101 A93-27494
Melt infiltration of silicon carbide compacts. II - Evaluation of solidification microstructures p 101 A93-28283
- ATASSI, H. M.**
Numerical solutions for unsteady subsonic vortical flows around loaded cascades [ASME PAPER 92-GT-173] p 3 A93-19399
Acoustic radiation from a thin airfoil in nonuniform subsonic flows p 273 A93-23535
- ATHAYALE, M. M.**
Driven cavity simulation of turbomachine blade flows with vortex control [AIAA PAPER 93-0390] p 6 A93-24238
- AUER, BRUCE M.**
The use of plasma ashers and Monte Carlo modeling for the projection of atomic oxygen durability of protected polymers in low Earth orbit p 58 N93-15596
Monte Carlo modeling of atomic oxygen attack of polymers with protective coatings on LOEF p 138 N93-28282
- AUGUST, R.**
Design considerations for a Space Shuttle Main Engine turbine blade made of single crystal material p 236 A93-25228
- AVEDISIAN, C. T.**
Experiments on the effect of initial diameter in spherically symmetric droplet combustion of sooting fuels [AIAA PAPER 93-0130] p 139 A93-22577
- AYDELOTT, JOHN C.**
Orbital storage and supply of subcritical liquid nitrogen p 62 N93-27801
- AYER, T. C.**
Analysis of high Reynolds number inviscid/viscid interactions in cascades p 15 A93-55351
- AYERS, J. D.**
The microstructural evolution, crystallography, and thermal processing of ultrahigh carbon Fe-1.85 pct C melt-spun ribbon p 125 A93-32934
- AZAR, MASSOOD T.**
Fiber-optic thermometer using Fourier transform spectroscopy p 212 A93-53104

B

- BAAKLINI, G. Y.**
Ultrasonic and micromechanical study of damage and elastic properties of SiC/RBSN ceramic composites p 99 A93-19624
Ultrasonic assessment of interfacial oxidation damage in ceramic matrix composites p 105 A93-52919
- BAAKLINI, GEORGE Y.**
Soft computing in design and manufacturing of advanced materials [NASA-TM-106032] p 111 N93-28624
- BAAKLINI, GEORGE Y.**
Radial basis function network learns ceramic processing and predicts related strength and density [NASA-TM-106048] p 110 N93-27129
Fuzzy sets predict flexural strength and density of silicon nitride ceramics [NASA-TM-106049] p 110 N93-27270
- BABULA, MARIA**
Design and implementation of a pilot orientation program for new NASA engineering employees [NASA-TM-105907] p 286 N93-26205
- BACHALO, E. J.**
Liquid water content measurements using the Phase Doppler Particle Analyzer in the NASA Lewis Icing Research Tunnel [AIAA PAPER 93-0298] p 42 A93-23698
- BACHALO, W. D.**
Liquid water content measurements using the Phase Doppler Particle Analyzer in the NASA Lewis Icing Research Tunnel [AIAA PAPER 93-0298] p 42 A93-23698
- BACHALO, WILLIAM D.**
Signal processing considerations for low signal to noise ratio laser Doppler and phase Doppler signals p 207 A93-23830
- BAEZ, ANASTACIO N.**
Description of the SSF PMAD dc testbed control system data acquisition function p 47 A93-26103
Power system monitoring and source control of the Space Station Freedom dc-power system testbed p 69 A93-26109
Power system monitoring and source control of the Space Station Freedom DC power system testbed [NASA-TM-105841] p 80 N93-10734
Description of the SSF PMAD DC testbed control system data acquisition function [NASA-TM-105843] p 261 N93-11005
- BAGGENSTOSS, WILLIAM G.**
Transient liquid phase diffusion bonding of Udimet 720 for Stirling power converter applications p 221 A93-26080
- BAGINSKI, M. E.**
Thin film diamond microstructure applications p 209 A93-40580
- BAHADORI, M. Y.**
Effects of gravity on the transition to turbulence of gas jet diffusion flames [AIAA PAPER 93-0710] p 114 A93-24805
- BAHADORI, M. YOUSEF**
Effects of buoyancy on laminar, transitional, and turbulent gas jet diffusion flames p 121 N93-20189
- BAILEY, F. R.**
The new challenge of computational aeroscience p 2 A93-14169
- BAILEY, SHEILA G.**
Minority carrier diffusion length and edge surface-recombination velocity in InP p 283 A93-50787
Room temperature synthesis of copper indium diselenide in non-aqueous solution using an organoindium reagent p 283 A93-54844
Texturing of InP surfaces for device applications [NASA-TM-106061] p 129 N93-28618
- BAILEY, WILLIAM J.**
The CONE program - An overview p 146 A93-48637
- BAIN, D. B.**
CFD mixing analysis of axially opposed rows of jets injected into confined crossflow [AIAA PAPER 93-2044] p 185 A93-49877
CFD mixing analysis of axially opposed rows of jets injected into confined crossflow [NASA-TM-106179] p 37 N93-27128
- BAKER, K.**
Vaporization heat transfer of dielectric liquids on a wick-covered surface [AIAA PAPER 93-0283] p 169 A93-22686
Vaporization heat transfer of dielectric liquids on enhanced surfaces covered with screen wicks [AIAA PAPER 93-2835] p 182 A93-46572
- BAKER, KARL W.**
Graphite fiber/copper matrix composites for space power heat pipe fin applications p 162 A93-13789
- BAKES, CATHERINE MURPHY**
ISDN at NASA Lewis Research Center [NASA-TM-105911] p 262 N93-12410
- BAKHLE, MILIND A.**
APPLE - An aeroelastic analysis system for turbomachines and propfans [AIAA PAPER 92-4712] p 23 A93-20320
An efficient procedure for cascade aeroelastic stability determination using nonlinear, time-marching aerodynamic solvers [AIAA PAPER 93-1631] p 25 A93-34159
Unsteady aerodynamics and flutter of propfans using a three-dimensional Full-Potential Solver [AIAA PAPER 93-1633] p 25 A93-34161
Unsteady aerodynamics and flutter based on the potential equation [AIAA PAPER 93-2086] p 13 A93-49913
- BAKIS, CHARLES E.**
Experimental investigation of cyclic thermomechanical deformation in torsion [NASA-TM-105938] p 247 N93-17996
- BALAKRISHNA, C.**
Symmetric Galerkin boundary formulations employing curved elements p 268 A93-54198
- BALASUBRAMANIAM, R.**
Thermocapillary bubble migration - An Oseen-like analysis of the energy equation p 179 A93-41708
- BALDWIN, DARRELL**
Space exploration initiative candidate nuclear propulsion test facilities [NASA-TM-105710] p 86 N93-24753
- BALKANYI, LESLIE R.**
DUK SUP - A high thrust trajectory optimization code [AIAA PAPER 93-1127] p 259 A93-31009
- BALL, CALVIN L.**
Propulsion technology challenges for turn-of-the-century commercial aircraft [ISABE 93-7003] p 31 A93-53980
Propulsion technology challenges for turn-of-the-century commercial aircraft [NASA-TM-106192] p 39 N93-32351
- BALOMBIN, JOSEPH L.**
Advanced Communications Technology Satellite (ACTS) p 52 A93-24456
- BANAVAR, JAYANTH R.**
Molecular dynamics of interface rupture p 175 A93-30130
- BANERDT, B.**
Venus Interior Structure Mission (VISM): Establishing a seismic network on Venus p 293 N93-28819
- BANERJEE, P. K.**
Micromechanical studies of composites by BEM p 236 A93-31295
- BANGALORE, A.**
Effects of icing on the aerodynamic performance of high lift airfoils [AIAA PAPER 93-0026] p 4 A93-20144
- BANKS, B. A.**
Method and apparatus for producing a thermal atomic oxygen beam [NASA-CASE-LEW-15614-1] p 276 N93-19026
- BANKS, BRUCE**
Recommended practices for in-space and ground laboratory. Atomic oxygen exposure and analysis p 276 N93-20814
- BANKS, BRUCE A.**
Performance and properties of atomic oxygen protective coatings for polymeric materials p 225 A93-53389
LDEF yaw and pitch angle estimates p 58 N93-12772
Low Earth orbit atomic oxygen simulation for durability evaluation of solar reflector surfaces p 58 N93-15594
The use of plasma ashers and Monte Carlo modeling for the projection of atomic oxygen durability of protected polymers in low Earth orbit p 58 N93-15596
Atomic oxygen protective coating with resistance to undercutting at defect sites [NASA-CASE-LEW-15306-1] p 137 N93-20566
Heat transfer device [NASA-CASE-LEW-14162-4] p 108 N93-20568
Issues/considerations and performance prediction of LEO protective coatings p 137 N93-20813
Optical and scratch resistant properties of diamondlike carbon films deposited with single and dual ion beams [NASA-TM-105943] p 95 N93-22586
Optical and scratch resistant properties of diamondlike carbon films deposited with single and dual ion beams p 137 N93-25564
Low Earth orbital atomic oxygen environmental simulation facility for space materials evaluation [NASA-TM-106128] p 96 N93-27266
Monte Carlo modeling of atomic oxygen attack of polymers with protective coatings on LDEF p 138 N93-28282
Method for retarding oxidation of an organic substrate [NASA-CASE-LEW-15306-2] p 138 N93-28425
- Characteristics of hypervelocity impact craters on LDEF experiment S1003 and implications of small particle impacts on reflective surfaces p 62 N93-29363
Semiconductor cooling apparatus [NASA-CASE-LEW-14162-3] p 111 N93-29614
- BANSAL, N. P.**
Composition dependence of superconductivity in YBa₂(Cu_{3-x})Al_{1(x)}O₇(y) p 281 A93-40271
Fiber-reinforced monoclinic celsian matrix composite material [NASA-CASE-LEW-15269-1] p 108 N93-20040
Method of producing a ceramic fiber-reinforced glass-ceramic matrix composite [NASA-CASE-LEW-15264-2] p 112 N93-31299
- BANSAL, NAROTTAM**
Silicon carbide fiber reinforced strontium aluminosilicate glass-ceramic matrix composite [NASA-CASE-LEW-15263-1] p 106 N93-11543
- BANSAL, NAROTTAM P.**
Kinetics of hexacelsian-to-celsian phase transformation in SrAl₂Si₂O₈ p 134 A93-40293
Chronopotentiometry of refractory metals, actinides and oxyanions in molten salts: A review [NASA-TM-105862] p 120 N93-11545
Comments on 'Kinetic Study on the Hexacelsian-Celsian Phase Transformation' [NASA-TM-105917] p 136 N93-14886
Kinetics of hexacelsian to celsian phase transformation in SrAl₂Si₂O₈ [NASA-TM-105913] p 136 N93-16372
Ceramic fiber reinforced glass-ceramic matrix composite [NASA-CASE-LEW-15262-1] p 109 N93-26100
SiC fiber-reinforced Celsian glass-ceramic matrix composite [NASA-CASE-LEW-15264-1] p 112 N93-31293
- BAR-ON, ISA**
Fracture toughness of advanced ceramics at room temperature p 131 A93-20842
- BARANKIEWICZ, WENDY S.**
A full-scale STOVLE ejector experiment [NASA-TM-106019] p 35 N93-22480
- BARI, ROBERT A.**
Nuclear safety policy working group recommendations on nuclear propulsion safety for the space exploration initiative [NASA-TM-105705] p 88 N93-26200
- BARKHOUDARIAN, S.**
Advanced instrumentation for next-generation aerospace propulsion control systems [AIAA PAPER 93-2079] p 211 A93-49906
- BARNES, PAUL N.**
Friction and wear of plasma-deposited diamond films [NASA-TM-105926] p 136 N93-19035
- BARNETT, ALAN R.**
Solving modal equations of motion with initial conditions using MSC/NASTRAN DMAP. Part 1: Implementing exact mode superposition [NASA-TM-106063] p 248 N93-23739
Solving modal equations of motion with initial conditions using MSC/NASTRAN DMAP. Part 2: Coupled versus uncoupled integration [NASA-TM-106064] p 248 N93-23740
- BARNETT, JOHN W.**
Nuclear Propulsion Project Workshop summary p 64 A93-13765
- BARNETT, M.**
Analysis of high Reynolds number inviscid/viscid interactions in cascades p 15 A93-55351
- BARNETT, MARK**
Low-Reynolds-number k-epsilon model for unsteady turbulent boundary-layer flows p 14 A93-53208
- BARNHART, D.**
On-orbit characterization of electric propulsion on LEO satellites p 67 A93-25303
- BARRANGER, JOHN P.**
Capacitance-type blade-tip clearance measurement system using a dual amplifier with ramp/dc inputs and integration p 209 A93-39347
Study of the capacitance technique for measuring high-temperature blade tip clearance on ceramic rotors [NASA-TM-105978] p 35 N93-23013
Progress in speckle-shift strain measurement p 251 N93-31558
- BARRETT, C. A.**
Diffusional transport and predicting oxidative failure during cyclic oxidation of beta-NiAl alloys p 126 A93-50370
- BARRETT, CHARLES A.**
A statistical analysis of elevated temperature gravimetric cyclic oxidation data of 36 Ni- and Co-base superalloys based on an oxidation attack parameter [NASA-TM-105934] p 128 N93-18069

- BARRON, ANDREW R.**
Enhancement of photoluminescence intensity of GaAs with cubic GaS chemical vapor deposited using a structurally designed single-source precursor p 280 A93-26930
Metal-organic chemical vapour deposition of polycrystalline tetragonal indium sulphide (InS) thin films p 116 A93-36584
Photoluminescence intensity enhancement of GaAs by vapor-deposited GaS - A rational approach to surface passivation p 281 A93-40049
Electronic passivation of n- and p-type GaAs using chemical vapor deposited GaS p 283 A93-52708
- BARTOLOTTA, P. A.**
Fatigue life prediction of an intermetallic matrix composite at elevated temperatures p 101 A93-31358
Unified viscoplastic behavior of metal matrix composites [NASA-TM-105819] p 244 A93-10777
- BARTOLOTTA, PAUL A.**
Stirling engine - Available tools for long-life assessment p 65 A93-13824
Stirling engine - Approach for long-term durability assessment p 220 A93-26069
Thermomechanical fatigue behavior of SiC/Ti-24Al-11Nb in air and argon environments [NASA-TM-105723] p 106 A93-11399
Considerations concerning fatigue life of metal matrix composites [NASA-TM-106144] p 250 A93-27009
- BARTOS, KAREN F.**
Evaluation of MARC for the analysis of rotating composite blades [NASA-TM-4423] p 249 A93-24909
- BATES, JAMES M.**
Construction and testing of ceramic fabric heat pipe with water working fluid p 163 A93-13869
- BATES, STEPHEN C.**
High performance sapphire windows p 218 A93-22198
- BATUR, C.**
Self-tuning multivariable pole placement control of a multizone crystal growth furnace p 263 A93-10575
- BAUER, P. H.**
2-D nonlinear IIR-filters for image processing - An exploratory analysis p 264 A93-28200
A 3-D nonlinear recursive digital filter for video image processing p 264 A93-34582
- BAUER, PETER**
Hierarchical image coding with diamond-shaped sub-bands p 205 A93-20945
- BAUGHER, C. R.**
Low gravity environment on-board Columbia during STS-40 [AIAA PAPER 93-0833] p 142 A93-24903
- BAUGHER, CHARLES R.**
Review of the Shuttle vibration environment [AIAA PAPER 93-0832] p 51 A93-24902
- BAUGHER, GEORGE R.**
Low-frequency vibration environment for five Shuttle missions [NASA-TM-106059] p 63 A93-28554
- BAUHANN, P.**
Mixed application MMIC technologies - Progress in combining RF, digital and photonic circuits p 152 A93-25800
- BAUM, H. R.**
Heat transfer from radiatively heated material in a low Reynolds number microgravity environment p 180 A93-43695
- BAUMBICK, ROBERT**
Review of the FOCSI (Fiber Optic Control System Integration) program p 21 A93-32916
- BAUMBICK, ROBERT J.**
Status of the Fiber Optic Control System Integration (FOCSI) program [NASA-TM-106151] p 217 A93-28053
- BAUMEISTER, ERNIE B.**
Multimegawatt potassium Rankine power for nuclear electric power p 65 A93-13797
- BAUMEISTER, JOSEPH F.**
Jet Engine hot parts IR Analysis Procedure (J-EIRP) [NASA-TM-105914] p 21 A93-22588
Application of ray tracing in radiation heat transfer [NASA-TM-106206] p 202 A93-29075
- BAUMEISTER, K. J.**
Modal element method for scattering and absorbing of sound by two-dimensional bodies p 274 A93-53657
- BAUMEISTER, KENNETH J.**
Modal ring method for the scattering of electromagnetic waves [NASA-TM-105966] p 149 A93-20260
- BEACH, T. A.**
Aeroloads and secondary flows in a transonic mixed flow turbine stage [ASME PAPER 92-GT-72] p 2 A93-19322
Three-dimensional analysis of the Pratt and Whitney alternate design SSME fuel turbine p 230 A93-31584
- BEATTIE, DOUG R.**
Monte Carlo and experimental studies of nozzle flow in a low-power hydrogen arcjet [AIAA PAPER 93-2529] p 77 A93-50257
- BEATTIE, J. R.**
Erosion rate diagnostics in ion thrusters using laser-induced fluorescence p 70 A93-34481
- BEAVER, BRIAN A.**
Titan III feasibility for HL-20 prototype missions p 50 A93-53747
- BECUS, GEORGES A.**
Optimization of blade arrangement in a randomly mistuned cascade using simulated annealing [AIAA PAPER 93-2254] p 28 A93-50052
- BEGG, LESTER**
Advanced radiator concepts feasibility demonstration p 163 A93-13844
- BEHBEHANI, M. K.**
The effect of microalloying additions on the tensile properties of polycrystalline NiAl p 123 A93-17516
- BEHEIM, GLENN**
Fourier transform spectrometry for fiber-optic sensor systems p 211 A93-49459
Fiber-optic thermometer using Fourier transform spectroscopy p 212 A93-53104
Phase-stepping fiber-optic projected fringe system for surface topography measurements [NASA-CASE-LEW-14996-1] p 278 A93-11058
- BEHRENDT, D. R.**
Studies on the reactive melt infiltration of silicon and silicon-molybdenum alloys in porous carbon [NASA-TM-105860] p 136 A93-12398
- BELL, STEPHEN C.**
Monte Carlo analysis of the Titan III/Transfer Orbit Stage guidance system for the Mars Observer mission [AIAA PAPER 93-3889] p 50 A93-51473
- BELL, W. A.**
LV software support for supersonic flow analysis [AIAA PAPER 92-3900] p 259 A93-24487
- BELOHOUBEK, E.**
Buffer layers for high-Tc thin films on sapphire p 150 A93-17063
- BELYTSCHKO, TED**
Elastic interactions of a fatigue crack with a micro-defect by the mixed boundary integral equation method p 243 A93-56412
- BENDETT, M.**
Mixed application MMIC technologies - Progress in combining RF, digital and photonic circuits p 152 A93-25800
- BENDIKSEN, ODDVAR O.**
Unsteady transonic two-dimensional Euler solutions using finite elements p 8 A93-39412
Finite element calculations of transonic flutter in cascades [AIAA PAPER 93-2083] p 185 A93-49910
- BENDSOE, MARTIN P.**
Topology and layout optimization of discrete and continuum structures p 241 A93-45429
- BENJAMIN, M. A.**
Initial development of the two-dimensional ejector shear layer - Experimental results [AIAA PAPER 93-2440] p 29 A93-50192
Comparison of the initial development of shear layers in two-dimensional and axisymmetric ejector configurations [AIAA PAPER 93-2441] p 29 A93-50193
- BENKO, STEPHEN E.**
A laboratory model of a hydrogen/oxygen engine for combustion and nozzle studies [AIAA PAPER 93-1825] p 48 A93-49711
- BENNETT, GARY L.**
Planning for the Space Exploration Initiative - The nuclear propulsion option p 43 A93-13752
The NASA Electric Propulsion Program [AIAA PAPER 93-1935] p 73 A93-49797
Progress report on nuclear propulsion for space exploration and science [AIAA PAPER 93-2352] p 44 A93-50125
- BENSON, SCOTT W.**
Titan III feasibility for HL-20 prototype missions p 50 A93-53747
- BENSON, T. J.**
Calculation of a circular jet in crossflow with a multiple-time-scale turbulence model p 164 A93-15063
Fluid flow of a row of jets in crossflow - A numerical study p 179 A93-35608
AGARD WG13 aerodynamics of high speed air intakes. Assessment of CFD results p 192 A93-13220
- BENTON, MAX**
Design of deployable-truss masts for Space Station [AIAA PAPER 93-0975] p 56 A93-30899
- BENTS, D. J.**
Optimization of armored spherical tanks for storage on the lunar surface p 47 A93-25866
Dynamic Isotope Power System design considerations for human exploration of the moon and Mars p 253 A93-25995
Design of small Stirling dynamic isotope power system for robotic space missions [NASA-TM-105919] p 141 A93-12085
Small Stirling dynamic isotope power system for robotic space missions [NASA-TM-105785] p 92 A93-28686
- BENTS, DAVID J.**
Comparison of dynamic isotope power systems for distributed planetary surface applications p 46 A93-13825
- BENTZ, M. D.**
Nucleate pool boiling in the long duration low gravity environment of the space shuttle p 142 A93-23371
Low-g fluid mixing - Further results from the Tank Pressure Control Experiment [AIAA PAPER 93-2423] p 187 A93-50181
Nucleate pool boiling in the long duration low gravity environment of the Space Shuttle [NASA-TM-105973] p 144 A93-15420
- BEREMAND, DONALD G.**
Electric and hybrid electric vehicle study utilizing a time-stepping simulation p 287 A93-26012
- BERENDT, MARJORIE**
The evolution of procurement and assurance methods used to proof an advanced space material p 94 A93-53392
- BERKE, L.**
Improved accuracy for finite element structural analysis via an integrated force method p 234 A93-17246
Neural networks in structural analysis and design - An overview [AIAA PAPER 92-4805] p 263 A93-20388
Singularities in optimal structural design [AIAA PAPER 92-4818] p 235 A93-20397
Application of neural networks to prediction of advanced composite structures mechanical response and behavior p 205 A93-20751
Singularity in structural optimization p 240 A93-34938
Application of artificial neural networks in nonlinear analysis of trusses [NASA-TM-105319] p 244 A93-11403
- BERKE, LASZLO**
Modal test/analysis correlation of Space Station structures using nonlinear sensitivity [AIAA PAPER 92-4731] p 55 A93-20330
Neural networks for structural design - An integrated system implementation [AIAA PAPER 92-4806] p 263 A93-20389
Integrated force method - Compatibility conditions of structural mechanics for finite element analysis p 237 A93-32459
Application of neural nets in structural optimization p 265 A93-54533
Self-organization in neural networks - Applications in structural optimization p 265 A93-54534
Application of artificial neural networks to the design optimization of aerospace structural components [NASA-TM-4389] p 247 A93-21831
- BERNS, DARREN H.**
Performance of a low-power subsonic-arc-attachment arcjet thruster [AIAA PAPER 93-1898] p 72 A93-49768
Investigation of a subsonic-arc-attachment thruster using segmented anodes [AIAA PAPER 93-1899] p 73 A93-49769
- BERTON, JEFFREY J.**
An interactive preprocessor for the NASA engine performance program [NASA-TM-105786] p 32 A93-10983
- BETHEA, MARK D.**
An Automated Thermocouple Calibration System p 208 A93-35575
- BHASIN, K. B.**
An analysis of the frequency limitations of an Al(x)Ga(1-x)As/GaAs optical modulator p 151 A93-23454
Design aspects and comparison between high Tc superconducting coplanar waveguide and microstrip line p 155 A93-27244
Processing, electrical and microwave properties of sputtered Ti-Ca-Ba-Cu-O superconducting thin films p 282 A93-44607
Performance of TiCaBaCuO 30 GHz 64 element antenna array p 157 A93-44763

- Conductor-backed coplanar waveguide resonators of Y-Ba-Cu-O and Ti-Ba-Ca-Cu-O on LaAlO₃ [NASA-TM-105890] p 284 N93-12325
- Full wave characterization of microstrip open end discontinuities patterned on anisotropic substrates using potential theory [NASA-TM-106037] p 160 N93-20259
- BHASIN, KUL B.**
- Monolithic microwave integrated circuits for sensors, radar, and communications systems; Proceedings of the Meeting, Orlando, FL, Apr. 2-4, 1991 [SPIE-1475] p 151 A93-25776
- Superconductivity applications for infrared and microwave devices II; Proceedings of the Meeting, Orlando, FL, Apr. 4, 5, 1991 [SPIE-1477] p 154 A93-27243
- Comparative study of bolometric and non-bolometric switching elements for microwave phase shifters p 155 A93-27245
- A 10 GHz Y-Ba-Cu-O/GaAs hybrid oscillator proximity coupled to a circular microstrip patch antenna p 158 A93-54619
- BHATT, H.**
- Effect of HIPing on the effective thermal conductivity/diffusivity and the interfacial thermal conductance of uniaxial SiC fibre-reinforced RBSN p 100 A93-26674
- BHATT, HEMANSHU**
- Novel thin-film heat flux sensors [AIAA PAPER 92-5035] p 205 A93-22309
- BHATT, R. T.**
- Effect of HIPing on the effective thermal conductivity/diffusivity and the interfacial thermal conductance of uniaxial SiC fibre-reinforced RBSN p 100 A93-26674
- Effect of high temperature annealing on the microstructure of SCS-6 SiC fibers p 133 A93-39513
- BHATTACHARJEE, SUBRATA**
- A comparison of numerical and analytical solution of the creeping flame spread over thermally thin material p 117 A93-41954
- Opposed-flow flame spreading in reduced gravity p 121 N93-20206
- BHATTACHARYA, P. K.**
- Application of high-quality SiO₂ grown by multipolar ECR source to Si/SiGe MISFET p 156 A93-37413
- Direct optical injection locking of monolithically integrated In(0.53)Ga(0.47)As/In(0.52)Al(0.48)As MODFET oscillators p 158 A93-47127
- Ellipsometric characterization of In(0.52)Al(0.48)As and of modulation doped field effect transistor structures on InP substrates p 158 A93-49382
- BHUTTA, BILAL A.**
- PNS predictions for supersonic/hypersonic flows over finned missile configurations [AIAA PAPER 92-2695] p 7 A93-37374
- Low-to-high altitude predictions of three-dimensional ablative re-entry flowfields p 182 A93-46407
- BIANCO, JEAN**
- Nitric oxide formation in a lean, premixed-prevaporized jet A/air flame tube: An experimental and analytical study [NASA-TM-105722] p 257 N93-27012
- BIANCHI, ROBERT**
- Chromium and reactive element modified aluminate diffusion coatings on superalloys - Environmental testing p 126 A93-37899
- BIBEL, G. D.**
- Contact stress analysis of spiral bevel gears using nonlinear finite element static analysis [AIAA PAPER 93-2296] p 224 A93-50081
- Contact stress analysis of spiral bevel gears using nonlinear finite element static analysis [NASA-TM-106176] p 228 N93-27037
- BIBYK, STEVEN**
- An all digital implementation of a modified Hamming net for video compression with prediction and quantization circuits p 148 A93-37038
- Combinatorial pulse position modulation for power-efficient free-space laser communications [NASA-TM-106241] p 150 N93-31856
- BICKMORE, TIMOTHY W.**
- A qualitative approach to systemic diagnosis of the SSME [AIAA PAPER 93-0405] p 261 A93-23327
- BIDWELL, C. S.**
- Ice accretion prediction for a typical commercial transport aircraft [AIAA PAPER 93-0174] p 19 A93-23245
- Ice accretion prediction for a typical commercial transport aircraft [NASA-TM-105976] p 20 N93-15522
- BIESIADNY, THOMAS J.**
- Overview of high performance aircraft propulsion research [NASA-TM-105839] p 32 N93-11530
- BILL, ROBERT C.**
- Integrity testing of brush seal in shroud ring of T-700 engine [NASA-TM-105863] p 227 N93-18380
- BINDER, MICHAEL**
- Predicted performance of an Integrated Modular Engine system [AIAA PAPER 93-1888] p 72 A93-49761
- An RL10A-3-3A rocket engine model using the Rocket Engine Transient Simulator (ROCETS) software [AIAA PAPER 93-2357] p 75 A93-50129
- BINIENDA, W. K.**
- Calculation of stress intensity factors in an isotropic multicracked plate. Part 2: Symbolic/numeric implementation [NASA-TM-105823] p 244 N93-10453
- Calculation of stress intensity factors in an isotropic multicracked plate. Part 1: Theoretical development [NASA-TM-105766] p 244 N93-10455
- BINIENDA, WIESLAW K.**
- The effect of contact stresses in four-point bend testing of graphite/epoxy and graphite/PMR-15 composite beams [NASA-TM-105891] p 107 N93-12076
- BIRCHENROUGH, ARTHUR**
- Description of the PMAD systems test bed facility and data system p 47 A93-26102
- BIRINGEN, S.**
- Time-dependent thermocapillary convection in a Cartesian cavity - Numerical results for a moderate Prandtl number fluid [AIAA PAPER 93-0259] p 169 A93-22666
- BIRON, GILLES**
- Evaluation of an oil-debris monitoring device for use in helicopter transmissions [NASA-TM-105830] p 227 N93-22826
- BISSINGER, N. C.**
- AGARD WG13 aerodynamics of high speed air intakes: Assessment of CFD results p 192 N93-13220
- BITTKER, DAVID A.**
- LENS, a general chemical kinetics and sensitivity analysis code for gas-phase reactions: User's guide [NASA-TM-105851] p 121 N93-16614
- BIZON, THOMAS P.**
- Real-time transmission of digital video using variable-length coding [NASA-TM-106092] p 150 N93-22483
- BLACK, DAVID R.**
- Residual strain gradient determination in metal matrix composites by synchrotron X-ray energy dispersive diffraction p 103 A93-39580
- BLAKE, KENNETH R.**
- Unstructured 3D Delaunay mesh generation applied to planes, trains and automobiles [AIAA PAPER 93-0673] p 259 A93-24781
- BLAKE, T. A.**
- Numerical optimization of composite hip endoprostheses under different loading conditions [AIAA PAPER 92-4703] p 270 A93-20312
- Optimal design of composite hip implants using NASA technology p 257 N93-22188
- BLANCHARD, R. C.**
- Low gravity environment on-board Columbia during STS-40 [AIAA PAPER 93-0833] p 142 A93-24903
- BLANCHETTE, DONALD M.**
- Evaluation of an oil-debris monitoring device for use in helicopter transmissions [NASA-TM-105830] p 227 N93-22826
- BLECH, RICHARD**
- A multiarchitecture parallel-processing development environment [NASA-TM-106180] p 262 N93-28628
- BLECH, RICHARD A.**
- Turbomachinery CFD on parallel computers [NASA-TM-105932] p 262 N93-13154
- Parallel solution of high-order numerical schemes for solving incompressible flows [NASA-TM-4451] p 262 N93-27040
- BLOOMFIELD, HARVEY**
- Estimates of power requirements for a Manned Mars Rover powered by a nuclear reactor p 45 A93-13783
- BOBINSKY, E. A.**
- Satellites and the BISON: An overview of NASA R/D [NASA-TM-106108] p 150 N93-26903
- BOBULA, GEORGE B.**
- Integrity testing of brush seal in shroud ring of T-700 engine [NASA-TM-105863] p 227 N93-18380
- BOCHEV, PAVEL B.**
- Accuracy of least-squares methods for the Navier-Stokes equations p 188 A93-52008
- Accuracy of least-squares methods for the Navier-Stokes equations [NASA-TM-106209] p 202 N93-29208
- BOERSTLER, ROBERT W.**
- Single liquid source plasma-enhanced metalorganic chemical vapor deposition of high-quality YBa₂Cu₃O_{7-x} thin films p 280 A93-20643
- BOGDANSKI, MICHAEL S.**
- Tribological and microstructural comparison of HIPped PM212 and PM212/Au self-lubricating composites p 93 A93-13505
- Tribological and mechanical comparison of sintered and HIPped PM212 - High temperature self-lubricating composites p 94 A93-13506
- The effect of processing and compositional changes on the tribology of PM212 in air [NASA-TM-105945] p 95 N93-15576
- Optical and scratch resistant properties of diamondlike carbon films deposited with single and dual ion beams [NASA-TM-105943] p 95 N93-22586
- Optical and scratch resistant properties of diamondlike carbon films deposited with single and dual ion beams p 137 N93-25564
- BOGDONOFF, SEYMOUR**
- Time-sequenced and spectrally filtered Rayleigh imaging of shock wave and boundary layer structure for inlet characterization [AIAA PAPER 93-2300] p 211 A93-50085
- BOGNER, NANCY A.**
- Ellipsometric study of metal-organic chemically vapor deposited III-V semiconductor structures p 281 A93-35697
- BOGORAD, A.**
- The effects of 1 kW class arcjet thruster plumes on spacecraft charging and spacecraft thermal control materials p 57 A93-35050
- BOGORAD, A. L.**
- Low power arcjet system spacecraft impacts [AIAA PAPER 93-2392] p 76 A93-50157
- BOLDMAN, D. R.**
- Effect of a rotating propeller on the separation angle of attack [AIAA PAPER 93-0017] p 6 A93-24978
- Effect of a rotating propeller on the separation angle of attack and distortion in ducted propeller inlets [NASA-TM-106240] p 16 N93-16625
- BOLDMAN, DONALD R.**
- 3-D viscous flow CFD analysis of the propeller effect on an advanced ducted propeller subsonic inlet [AIAA PAPER 93-1847] p 12 A93-49728
- The 3-D viscous flow CFD analysis of the propeller effect on an advanced ducted propeller subsonic inlet [NASA-TM-106240] p 38 N93-29162
- BOLLENBACHER, GARY**
- COLD-SAT dynamic model [NASA-TM-105185] p 59 N93-19988
- BONACUSE, PETER J.**
- Axial-torsional fatigue - A study of tubular specimen thickness effects p 240 A93-38849
- In-phase and out-of-phase axial-torsional fatigue behavior of Haynes 188 at 760 C [NASA-TM-105765] p 246 N93-13153
- BOND, THOMAS H.**
- Results of Low Power Deicer tests on a swept inlet component in the NASA Lewis Icing Research Tunnel [AIAA PAPER 93-0032] p 20 A93-22551
- Surface roughness due to residual ice in the use of low power deicing systems [AIAA PAPER 93-0031] p 5 A93-23240
- An overview of shed ice impact studies in the NASA Lewis Icing Research Tunnel [AIAA PAPER 93-0301] p 5 A93-23247
- Results of a low power ice protection system test and a new method of imaging data analysis p 21 A93-35932
- Results of low power deicer tests on a swept inlet component in the NASA Lewis icing research tunnel [NASA-TM-105968] p 15 N93-14911
- Surface roughness due to residual ice in the use of low power deicing systems [NASA-TM-105971] p 16 N93-15338
- An overview of shed ice impact in the NASA Lewis Icing Research Tunnel [NASA-TM-105969] p 16 N93-15404
- Experimental and computational ice shapes and resulting drag increase for a NACA 0012 airfoil p 17 N93-27440
- BOND, W. H.**
- Prospects for utilization of air liquefaction and enrichment system (ALES) propulsion in fully reusable launch vehicles [AIAA PAPER 93-2025] p 74 A93-49861
- BOOK, P. O.**
- Sliding wear of self-mated Al₂O₃-SiC whisker-reinforced composites at 23-1200 C p 101 A93-29948
- BOOK, PATRICIA O.**
- Creep-rupture strength of a Ni-base superalloy at 1400 K p 124 A93-20556

BOOTH, ROY E.

The effects of simulated low Earth orbit environments on spacecraft thermal control coatings
[NASA-TM-106146] p 61 N93-27019

BOROWSKI, STANLEY K.

Lunar mission design using Nuclear Thermal Rockets
p 65 A93-13767

Space vehicle design and operation for efficient use of Nuclear Thermal Propulsion
[AIAA PAPER 93-1946] p 44 A93-49804

A comparison of nuclear thermal rocket development cost and schedule for piloted missions to Mars
[AIAA PAPER 93-2263] p 44 A93-50057

Nuclear thermal propulsion transportation systems for lunar/Mars exploration
[NASA-TM-105870] p 81 N93-12363

BOSCHITSCH, ALEXANDER

High accuracy computation of fluid-structure interaction in transonic cascades
[AIAA PAPER 93-0485] p 6 A93-23387

BOSELA, P. A.

Grounding of space structures p 54 A93-12144

A new pre-loaded beam geometric stiffness matrix with full rigid body capabilities p 54 A93-12145

BOSSLER, R. B., JR.

Face-gear drives: Design, analysis, and testing for helicopter transmission applications
[NASA-TM-106101] p 229 N93-27133

BOWDEN, MARY

Design of deployable-truss masts for Space Station
[AIAA PAPER 93-0975] p 56 A93-30899

BOWLES, KENNETH J.

Isothermal aging effects on PMR-15 resin p 131 A93-24508

Transverse flexural tests as a tool for assessing damage to PMR-15 composites from isothermal aging in air at elevated temperatures p 100 A93-24514

Transverse flexural tests as a tool for assessing damage to PMR-15 composites from isothermal aging in air at elevated temperatures
[NASA-TM-105848] p 107 N93-12737

BOWMAN, C.

The effects of 1 kW class arcjet thruster plumes on spacecraft charging and spacecraft thermal control materials p 57 A93-35050

BOWMAN, RANDY R.

Review of the physical and mechanical properties and potential applications of the B2 compound NiAl. Unabridged version of a paper published in International materials review
[NASA-TM-105598] p 127 N93-11635

BOYD, DARWIN L.

Auger electron spectroscopy study of oxidation of a PdCr alloy used for high-temperature sensors
[NASA-TM-106212] p 129 N93-23418

BOYD, I. D.

Measurement and analysis of a small nozzle plume in vacuum p 71 A93-42895

Measurement and analysis of a small nozzle plume in vacuum
[NASA-TM-106066] p 88 N93-26561

BOYD, IAIN D.

Assessment of three numerical methods for the computation of a low-density plume flow
[AIAA PAPER 93-2528] p 77 A93-50256

Monte Carlo and experimental studies of nozzle flow in a low-power hydrogen arcjet
[AIAA PAPER 93-2529] p 77 A93-50257

BOYD, JOSEPH T.

Micromachined silicon cantilever beam accelerometer incorporating an integrated optical waveguide p 210 A93-49457

Characterization of Si3N4/SiO2 optical channel waveguides by photon scanning tunneling microscopy p 211 A93-49458

BOYER, E. O.

Microgravity research on the NASA Lewis Learjet test facility
[AIAA PAPER 93-0573] p 43 A93-24245

BOYLE, R. J.

Heat transfer performance comparisons of five different rectangular channels with parallel angled ribs p 166 A93-18752

Time-averaged heat transfer and pressure measurements and comparison with prediction for a two-stage turbine
[ASME PAPER 92-GT-194] p 166 A93-19419

An algebraic turbulence model for three-dimensional viscous flows
[AIAA PAPER 93-0083] p 4 A93-22552

An algebraic turbulence model for three-dimensional viscous flows
[NASA-TM-105931] p 1 N93-14102

BOYLE, ROBERT J.

Three-dimensional Navier-Stokes heat transfer predictions for turbine blade rows
[NASA-TM-105800] p 196 N93-19969

BOZEK, JOHN

Space transfer with ground-based laser/electric propulsion
[NASA-TM-106060] p 84 N93-20615

BOZEK, JOHN M.

Power requirements for the first lunar outpost (FLO)
[NASA-TM-105925] p 255 N93-15523

BOZZOLO, GUILLERMO

Heats of formation of bcc binary alloys p 123 A93-17609

Method for calculating alloy energetics p 279 A93-18740

Determination of parameters of a method for predicting alloy properties p 126 A93-39796

Extension of a new semiempirical method (BFS) and the study of ground state properties of binary alloys p 283 A93-52600

Multilayer relaxation and surface energies of fcc and bcc metals using equivalent crystal theory p 119 A93-52872

Heat of segregation of single substitutional impurities p 119 A93-52873

Determination of parameters of a new method for predicting alloy properties
[NASA-TM-105895] p 127 N93-11609

BOZZOLO, NORA G.

Design of an automated imaging system for use in a space experiment p 204 A93-20454

BRABBS, THEODORE A.

Multi-heat addition turbine engine
[NASA-CASE-LEW-15094-1] p 35 N93-22034

BRADLEY, R. G., JR.

AGARD WG13 aerodynamics of high speed air intakes: Assessment of CFD results p 192 N93-13220

BRADY, R. A.

Mixing in the dome region of a staged gas turbine combustor p 27 A93-49612

BRAGG, M. B.

LDV flowfield measurements on a straight and swept wing with a simulated ice accretion
[AIAA PAPER 93-0300] p 5 A93-23001

BRANDHORST, HENRY

Power system technology discipline p 62 N93-27862

BRANDHORST, HENRY W., JR.

Key issues in space nuclear power challenges for the future p 65 A93-13905

Technologies p 255 N93-16907

BRANSTROM, B. R.

Design and test of a small two stage counter-rotating turbine for rocket engine application
[AIAA PAPER 93-2136] p 74 A93-49954

BRAUN, M. J.

Flow visualization in a single simulated brush seal p 226 A93-54659

BREAM, BRUCE L.

RENEW v3.2 user's manual, maintenance estimation simulation for Space Station Freedom Program
[NASA-TM-106006] p 232 N93-27025

BREGE, MARK H.

Design of a cavity heat pipe receiver experiment p 173 A93-25985

BREISACHER, KEVIN J.

Calculations of combustion response profiles and oscillations
[NASA-TM-106135] p 87 N93-25236

BRERETON, G. J.

A rapid-distortion-theory turbulence model for developed unsteady wall-bounded flow
[NASA-TM-106249] p 203 N93-32199

BREUER, KENNETH S.

Close-up analysis of aircraft ice accretion
[AIAA PAPER 93-0029] p 18 A93-23239

Close-up analysis of aircraft ice accretion
[NASA-TM-105952] p 19 N93-15360

BREWE, D. E.

Simultaneous pressure measurement and high-speed photography study of cavitation in a dynamically loaded journal bearing p 223 A93-40050

Effect of out-of-roundness on the performance of a diesel engine connecting-rod bearing p 225 A93-52607

BREWER, DAVE N.

Numerical calibration of the stable poisson loaded specimen
[NASA-TM-105609] p 245 N93-12738

BREWER, DAVID N.

Analytical stress intensity solution for the Stable Poisson Loaded specimen p 242 A93-46768

BRIGGS, MATTHEW E.

The susceptibility critical exponent for a nonaqueous ionic binary mixture near a consolute point p 284 A93-19838

Measurement of the temperature coefficient of ratio transformers p 155 A93-32771

Statistical fitting accuracy in photon correlation spectroscopy p 277 A93-52414

BRIGHT, MICHELLE M.

Desktop chaotic systems: Intuition and visualization
[NASA-TM-106258] p 269 N93-31847

BRINDLEY, W. J.

Stress relaxation of low pressure plasma-sprayed NiCrAlY alloys p 127 A93-52870

Oxidation resistant overlay coatings for low expansion substrates
[NASA-CASE-LEW-15154-1] p 137 N93-19332

Oxidation resistant overlay coatings for low expansion substrates
[NASA-CASE-LEW-15154-2] p 138 N93-31300

BRINKER, DAVID J.

Advanced photovoltaic power system technology for lunar base applications p 255 N93-14004

The effect of the low Earth orbit environment on space solar cells: Results of the Advanced Photovoltaic Experiment (S0014) p 256 N93-29686

Studies of effects on optical components and sensors. LDEF experiments AO-147 (ERB components) and S-0014 (APEX) p 278 N93-29693

BRISCO, HOLLY

Solar array electrical performance assessment for Space Station Freedom
[AIAA PAPER 93-1052] p 69 A93-30956

Solar array electrical performance assessment for Space Station Freedom
[NASA-TM-106161] p 91 N93-27039

BRITTON, RANDALL K.

An overview of shed ice impact studies in the NASA Lewis Icing Research Tunnel
[AIAA PAPER 93-0301] p 5 A93-23247

An overview of shed ice impact in the NASA Lewis Icing Research Tunnel
[NASA-TM-105969] p 16 N93-15404

BROCK, T.

Direct optical injection locking of monolithically integrated In(0.53)Ga(0.47)As/In(0.52)Al(0.48)As MODFET oscillators p 158 A93-47127

BROCKMEYER, JERRY W.

Ceramic matrix composite applications in advanced liquid fuel rocket engine turbomachinery
[ASME PAPER 92-GT-316] p 99 A93-19502

BROPHY, JOHN R.

The NASA Electric Propulsion Program
[AIAA PAPER 93-1935] p 73 A93-49797

BMDQ electric space-propulsion program
[AIAA PAPER 93-1934] p 78 A93-50322

BROWN, G. V.

Stiffness of magnetic bearings subjected to combined static and dynamic loads
[ASME PAPER 91-TRIB-27] p 219 A93-15685

BROWN, H. C.

Fiber shape effects on metal matrix composite behavior p 98 A93-15752

Computational characterization of high temperature composites via METCAN p 102 A93-32461

Fiber shape effects on metal matrix composite behavior
[NASA-TM-106067] p 109 N93-26704

BROWN, JEFFREY C.

A system to measure lightning-induced transients on spacecraft umbilical lines p 161 N93-24889

BRUCKNER, ERIC J.

The effects of simulated low Earth orbit environments on spacecraft thermal control coatings
[NASA-TM-106146] p 61 N93-27019

Low Earth orbital atomic oxygen environmental simulation facility for space materials evaluation
[NASA-TM-106128] p 96 N93-27266

BRUNO, RONALD

GSFC conceptual design study for an inter-satellite Optical Multiple Access communication system p 52 A93-18966

BRUNS, J. E.

Navier-Stokes analysis of three-dimensional S-ducts p 9 A93-45146

BRUSH, ANDREW S.

Stability testing and analysis of a PMAD dc test bed for the Space Station Freedom p 154 A93-26107

BRUSK, KEVIN D.

Test results of a Stirling engine utilizing heat exchanger modules with an integral heat pipe
[NASA-TM-105883] p 256 N93-25136

BRUSNIAK, L.

Flowfield dynamics in blunt fin-induced shock wave/turbulent boundary layer interactions
[AIAA PAPER 93-3133] p 11 A93-48298

BRUSSTAR, MATTHEW J.

The effects of buoyancy on the critical heat flux in forced convection

[AIAA PAPER 93-0575] p 169 A93-23307

BUBSEY, R. T.

Closed form expressions for crack mouth displacements and stress intensity factors for chevron notched short bar and short rod specimens based on experimental compliance measurements

[NASA-TM-83796] p 246 N93-15369

BUCHHELE, DONALD R.

Compact color schlieren optical system

p 277 A93-52071

BUCKLAND, JULIA H.

On-line implementation of nonlinear parameter estimation for the Space Shuttle main engine

[NASA-TM-106097] p 88 N93-26211

BUCKMASTER, J.

Flame balls - Past, present and future

[AIAA PAPER 93-0712] p 114 A93-24807

Analytical and numerical modeling of flame-balls in hydrogen-air mixtures

p 118 A93-46009

BUDHANI, R. C.

Giant suppression of flux-flow resistivity in heavy-ion irradiated Ti2Ba2Ca2Cu3O10 films - Influence of linear defects on vortex transport

p 280 A93-26198

Diminishing sign anomaly and scaling behavior of the mixed-state Hall resistivity in Ti2Ba2Ca2Cu3O10 films containing columnar defects

p 283 A93-53693

BUDINGER, J.

Efficient demultiplexing algorithm for noncontiguous carriers

p 148 A93-32561

BUDINGER, JAMES M.

Combinatorial pulse position modulation for power-efficient free-space laser communications

[NASA-TM-106241] p 150 N93-31856

BUFFUM, DANIEL H.

Blade row interaction effects on flutter and forced response

[AIAA PAPER 93-2084] p 28 A93-49911

BUI, TRONG T.

Some practical turbulence modeling options for Reynolds-averaged full Navier-Stokes calculations of three-dimensional flows

[AIAA PAPER 93-2964] p 10 A93-48158

The Proteus Navier-Stokes code

p 193 N93-13396

BUKSA, JOHN H.

System model development for nuclear thermal propulsion

[NASA-TM-105761] p 80 N93-10457

BUKSA, JOHN J.

System model development for nuclear thermal propulsion

[NASA-TM-108215] p 277 N93-17343

BULMAN, M. J.

US/CIS integrated NTRE

[AIAA PAPER 93-2367] p 76 A93-50138

BULZAN, D. L.

On the structure of gaseous confined laminar diffusion flames: Numerical investigation

[NASA-TM-106039] p 197 N93-21198

Structure of confined laminar spray diffusion flames: Numerical investigation

[NASA-TM-106038] p 197 N93-22596

BULZAN, DANIEL L.

Spray combustion experiments and numerical predictions

[NASA-TM-106069] p 198 N93-23744

Velocity and drop size measurements in a swirl-stabilized, combustor spray

[NASA-TM-106130] p 37 N93-27130

BURCHAM, KEVIN E.

Micromachined silicon cantilever beam accelerometer incorporating an integrated optical waveguide

p 210 A93-49457

BURKHARDT, LEO

The design and evolution of the Beta two-stage-to-orbit horizontal takeoff and landing launch system

[AIAA PAPER 92-5080] p 50 A93-22350

BURKHARDT, LEO A.

The design and evolution of the beta two-stage-to-orbit horizontal takeoff and landing launch system

[NASA-TM-106118] p 51 N93-27018

BURKE, LUKE A.

Lower temperature curing thermoset polyimides utilizing a substituted norbornene endcap

p 134 A93-44526

BURKE, M. J.

Active control of helicopter transmission noise

p 274 A93-29428

BURKHARDT, LEO

Design of a hypersonic waverider-derived airplane

[AIAA PAPER 93-0401] p 55 A93-21108

BURKHOLDER, ROBERT J.

A reciprocity formulation for the EM scattering by an obstacle within a large open cavity

p 149 A93-52237

BURLEY, RICHARD R.

Analytical and experimental studies of a short compact subsonic diffuser for a two-dimensional supersonic inlet

[NASA-TP-3247] p 17 N93-24118

BURNS, M. J.

Demonstration of Y1Ba2Cu3O(7-delta) and complementary metal-oxide-semiconductor device fabrication on the same sapphire substrate

p 159 A93-56292

BURROWS, LINDA M.

An electromechanical actuation system for an expendable launch vehicle

p 50 A93-25891

Electromechanical systems with transient high power response operating from a resonant ac link

p 152 A93-25892

BURTON, RODNEY L.

Ignition and combustion of aluminum/magnesium alloy particles in O2 at high pressures

p 113 A93-22030

BUSKA, JOHN J.

System model development for nuclear thermal propulsion

[NASA-TM-108157] p 276 N93-16531

BUSSARD, ROBERT W.

The QED engine spectrum - Fusion-electric propulsion for air-breathing to interstellar flight

[AIAA PAPER 93-2006] p 73 A93-49845

BUTLER, G. W.

A comparison of arcjet plume properties to model predictions

[AIAA PAPER 93-0820] p 67 A93-24891

BUTTON, ROBERT M.

Stability testing and analysis of a PMAD dc test bed for the Space Station Freedom

p 154 A93-26107

BYERS, D.

NTR plume modeling

Low thrust propulsion

[PR3] p 286 N93-71876

C**CAHAN, BORIS D.**

I-BIEM calculations of the frequency dispersion and ac current distribution at disk and ring-disk electrodes

p 254 A93-34246

Hydrodynamic behavior and electrochemical impedance of the Hanging Meniscus Rotating Disk (HMRD) electrode. I - Meniscus shape under rotation. II - I-BIEM calculations of frequency dispersion and minimization

p 116 A93-34247

CAI, Z. X.

Diminishing sign anomaly and scaling behavior of the mixed-state Hall resistivity in Ti2Ba2Ca2Cu3O10 films containing columnar defects

p 283 A93-53693

CAI, ZHONG

Development of hypersonic engine seals - Flow effects of preload and engine pressures

[AIAA PAPER 93-1998] p 223 A93-49841

CAIRNS, IVER H.

Interference patterns in the Spacelab 2 plasma wave data - Oblique electrostatic waves generated by the electron beam

p 257 A93-16347

CALABRESE, P. R.

Optical fiber sensor for temperature measurement from 600 to 1900 C in gas turbine engines

p 208 A93-32918

Flight testing of a fiber optic temperature sensor

p 22 A93-49476

CALFO, FREDERICK D.

Current status of liquid sheet radiator research

[NASA-TM-105764] p 193 N93-14150

Space chemical propulsion test facilities at NASA Lewis Research Center

[NASA-TM-106050] p 85 N93-23405

CALOGERAS, JAMES

Advanced solar dynamic technology program

p 256 N93-27806

CALOGERAS, JAMES E.

The ground testing of a 2 kW solar dynamic space power system

p 68 A93-25918

CALOMINO, ANTHONY M.

Analytical stress intensity solution for the Stable Poisson Loaded specimen

p 242 A93-46768

Numerical calibration of the stable poisson loaded specimen

[NASA-TM-105609] p 245 N93-12738

CAMCI, C.

A new hue capturing technique for the quantitative interpretation of liquid crystal images used in convective heat transfer studies

p 204 A93-13977

Evaluation of a hue capturing based transient liquid crystal method for high-resolution mapping of convective heat transfer on curved surfaces

p 210 A93-43689

Fluid dynamics and convective heat transfer in impinging jets through implementation of a high resolution liquid crystal technique

[ISABE 93-7077] p 189 A93-54053

CANACCI, V. A.

Flow visualization in a single simulated brush seal

p 226 A93-54659

CANISTRARO, H. A.

X-ray-based displacement measurement for hostile environments

p 208 A93-28580

CAO, Y.

Closed-form analytical solutions of high-temperature heat pipe startup and frozen startup limitation

p 165 A93-18564

Simulation of the early startup period of high-temperature heat pipes from the frozen state by a rarefied vapor self-diffusion model

p 175 A93-30127

A numerical analysis of high-temperature heat pipe startup from the frozen state

p 175 A93-30128

CAPPELLI, M. A.

A comparison of arcjet plume properties to model predictions

[AIAA PAPER 93-0820] p 67 A93-24891

CAPPELLI, MARK A.

Monte Carlo and experimental studies of nozzle flow in a low-power hydrogen arcjet

[AIAA PAPER 93-2529] p 77 A93-50257

Plume characteristics of an arcjet thruster

[AIAA PAPER 93-2530] p 77 A93-50258

CARBONI, JEANNE D.

Supersonic investigation of two dimensional hypersonic exhaust nozzles

[NASA-TM-105687] p 33 N93-15342

CARD, J. M.

Asymptotic analysis with reduced chemistry for the burning of n-heptane droplets

p 113 A93-13323

Asymptotic analysis for the burning of n-heptane droplets using a four-step reduced mechanism

p 117 A93-41952

CAREK, DAVID A.

Structural analysis of high-rpm composite propfan blades for a cruise missile wind tunnel model

[NASA-TM-105267] p 247 N93-23015

CAREK, JERRY

Fluid design studies of integrated modular engine system

[AIAA PAPER 93-1887] p 72 A93-49760

Design of an oxygen turbopump for use in an Advanced Expander Test Bed engine

[AIAA PAPER 93-2137] p 48 A93-49955

CARLETON, K. L.

Absorption coefficients for water vapor at 193 nm from 300 to 1073 K

p 276 A93-45398

CARLILE, J. A.

Preliminary experimental results for a cryogenic brush seal configuration

[AIAA PAPER 93-2535] p 225 A93-50262

Preliminary experimental results for a cryogenic brush seal configuration

[NASA-TM-106236] p 201 N93-28627

CARLILE, JULIE A.

Brush seal leakage performance with gaseous working fluids at static and low rotor speed conditions

[ASME PAPER 92-GT-304] p 219 A93-19494

Brush seal low surface speed hard-rub characteristics

[AIAA PAPER 93-2534] p 225 A93-50261

Brush seal bristle flexure and hard-rub characteristics

[NASA-TM-105864] p 227 N93-18321

Brush seal low surface speed hard-rub characteristics

[NASA-TM-106169] p 200 N93-27132

CARNAHAN, R.

Flow effects in a vertical CVD reactor

p 166 A93-19821

CARNEY, KELLY S.

The application of structural reliability techniques to plume impingement loading of the Space Station Freedom Photovoltaic Array

[AIAA PAPER 93-1338] p 56 A93-33908

The application of structural reliability techniques to plume impingement loading of the Space Station Freedom Photovoltaic Array

[NASA-TM-105949] p 59 N93-17988

Implementation of the block-Krylov boundary flexibility method of component synthesis

[NASA-TM-106065] p 248 N93-23044

CAROME, EDWARD F.

Fiberoptic sensing technique employing RF modulated interferometry

p 212 A93-53110

CARPINO, M.

Calculation of stiffness and damping coefficients for elastically supported gas foil bearings

p 221 A93-27308

CARPINO, MARC

Damage-mitigating control of aerospace systems for high performance and extended life

p 263 A93-22967

CARTER, CAMPBELL D.

Damage-mitigating control of space propulsion systems for high performance and extended life
[AIAA PAPER 93-2080] p 74 A93-49907

CARTER, CAMPBELL D.

Laser-induced fluorescence measurements of nitric oxide in laminar C₂H₆/O₂/N₂ flames at high pressure
p 116 A93-28253

CARUSO, STEVEN C.

LEWICE droplet trajectory calculations on a parallel computer
[AIAA PAPER 93-0172] p 259 A93-22604

CASADEMUNT, JAUME

Narrow band noise as a model of time-dependent accelerations - Study of the stability of a fluid surface in a microgravity environment
[AIAA PAPER 93-0911] p 173 A93-24965
Stability of a fluid surface in a microgravity environment
p 190 A93-55358

CASHMAN, WILLIAM F.

Advanced Communications Technology Satellite (ACTS)
p 52 A93-24456

CASTELLI, MICHAEL G.

Experimental investigation of cyclic thermomechanical deformation in torsion
[NASA-TM-105938] p 247 N93-17996
An overview of elevated temperature damage mechanisms and fatigue behavior of a unidirectional SCS-6/Ti-15-3 composite
[NASA-TM-106131] p 109 N93-26702

CASTILLO, J.

Onset conditions for gas phase reaction and nucleation in the CVD of transition metal oxides
p 116 A93-39508

CASTRO-CEDENO, MARIO

Design of a high-temperature experiment for evaluating advanced structural materials
[NASA-TM-105833] p 245 N93-11624

CATALDO, ROBERT

Estimates of power requirements for a Manned Mars Rover powered by a nuclear reactor
p 45 A93-13783
Versatile dynamic isotope power systems for the exploration of space
p 46 A93-13819
Design and emplacement of an integrated lunar power system - Issues and concerns
p 46 A93-13908

CATALDO, ROBERT L.

Long life Regenerative Fuel Cell technology development plan
p 252 A93-25867
Power requirements for the first lunar outpost (FLO)
[NASA-TM-105925] p 255 N93-15523

CAULEY, MICHAEL A.

GaAs monolithic R.F. modules for SAR/SAT distress beacons
p 152 A93-25806

CAVATORTA, ENRICO

Study on vortex flow control of inlet distortion
p 2 A93-14520

CAVENY, LEONARD H.

BMDO electric space-propulsion program
[AIAA PAPER 93-1934] p 78 A93-50322

CAVICCHI, RICHARD H.

The Proteus Navier-Stokes code
p 193 N93-13396

CHAI, JOHN C.

An evaluation of three spatial differencing schemes for the discrete ordinates method in participating media
[AIAA PAPER 93-0140] p 266 A93-24231
Radiation heat transfer calculations using a control-angle, control-volume-based discrete ordinates method
[AIAA PAPER 93-2731] p 182 A93-46485

CHAIT, A.

Parameterization of solar cells
[NASA-TM-105885] p 159 N93-12301

CHAIT, ARNON

Prediction of dislocation generation during Bridgman growth of GaAs crystals
p 279 A93-19740

CHAMIS, C. C.

Probabilistic evaluation of uncertainties and risks in aerospace components
p 233 A93-12160
Dynamic analysis of a pre-and-post ice impacted blade
[AIAA PAPER 92-4273] p 22 A93-13333
Tailored metal matrix laminates for high-temperature performance
p 98 A93-15753
Combined micromechanical and fabrication process optimization for metal-matrix composites
p 99 A93-18990
Structural tailoring of aircraft engine blade subject to ice impact constraints
[AIAA PAPER 92-4710] p 23 A93-20319
Structural system reliability under multiple failure modes
[AIAA PAPER 93-1379] p 238 A93-33943
Probabilistic simulation of stress concentration in composite laminates
[AIAA PAPER 93-1442] p 103 A93-33991

Probabilistic simulation of the human factor in structural reliability
[AIAA PAPER 93-1495] p 264 A93-34036

BLASIM - A computational tool to assess ice impact damage on engine blades
[AIAA PAPER 93-1638] p 26 A93-34165

Effect of service environments on adhesively bonded joints in composite structures
p 242 A93-53418
Environmental effects on long term behavior of composite laminates
p 243 A93-53438
Computational simulation of hot composite structures
p 260 A93-54704

Probabilistic micromechanics and macromechanics of polymer matrix composites
p 105 A93-54705
Dynamic analysis of a pre-and-post ice impacted blade
[NASA-TM-105829] p 144 N93-12197

Root damage analysis of aircraft engine blade subject to ice impact
[NASA-TM-105779] p 246 N93-15343

Progressive delamination in polymer matrix composite laminates: A new approach
p 108 N93-21515

Computational simulation for concurrent engineering of aerospace propulsion systems
[NASA-TM-106029] p 249 N93-23746

METAL matrix composite ANalyzer (METCAN): Theoretical manual
[NASA-TM-106025] p 109 N93-26552

Fiber shape effects on metal matrix composite behavior
[NASA-TM-106067] p 109 N93-26704

Dynamic characteristics of specialty composite structures with embedded damping layers
[NASA-TM-106165] p 110 N93-26705

Structural tailoring of aircraft engine blade subject to ice impact constraints
[NASA-TM-106033] p 250 N93-26999

Probabilistic sizing of laminates with uncertainties
[NASA-TM-106145] p 110 N93-27082

Probabilistic assessment of composite structures
[NASA-TM-106024] p 110 N93-27092

Probabilistic composite analysis
p 112 N93-30868

Blasim: A computational tool to assess ice impact damage on engine blades
[NASA-TM-106225] p 251 N93-31193

CHAMIS, CHRISTOS C.

Three-dimensional finite element simulation of intermingled-fiber hybrid composite behavior
p 98 A93-15729

Computational simulation of surface waviness in graphite/epoxy woven composites due to initial curing
p 98 A93-15822

Probabilistic structural analysis of adaptive/smart/intelligent space structures
p 234 A93-16203

Structural durability of a composite pressure vessel
p 234 A93-16552

Coupled multi-disciplinary simulation of composite engine structures in propulsion environment
[ASME PAPER 92-GT-6] p 23 A93-19279

Structural Tailoring/Analysis for Hypersonic Components - A computational simulation
[AIAA PAPER 92-4722] p 20 A93-20324

Microfracture in high temperature metal matrix crossply laminates
p 101 A93-31356

Programming probabilistic structural analysis for parallel processing computers
p 237 A93-32410

Computational characterization of high temperature composites via METCAN
p 102 A93-32461

Thermally-driven microfracture in high temperature metal matrix composites
p 237 A93-32469

Damage progression in stiffened composite panels
[AIAA PAPER 93-1345] p 238 A93-33915

Quantification of uncertainties in composites
[AIAA PAPER 93-1440] p 102 A93-33989

Probabilistic assessment of composite structures
[AIAA PAPER 93-1441] p 239 A93-33990

Finite element procedures for coupled linear analysis of heat transfer, fluid and solid mechanics
[AIAA PAPER 93-1639] p 267 A93-34166

Probabilistically configured adaptive composite structures
[AIAA PAPER 93-1679] p 240 A93-34191

Design for inadvertent damage in composite laminates
p 242 A93-53396

Probabilistic evaluation of fuselage-type composite structures
[NASA-TM-105881] p 245 N93-12735

Mapping methods for computationally efficient and accurate structural reliability
[NASA-TM-105892] p 248 N93-23745

Probabilistic simulation of multi-scale composite behavior
[NASA-TM-106196] p 250 N93-28633

Ceramic matrix composites properties/microstresses with complete and partial interphase bond
[NASA-TM-106136] p 111 N93-29071

Structural dynamics: Probabilistic structural analysis methods. Program overview
p 251 N93-31562

Mapping methods for computationally efficient and accurate structural reliability
p 232 N93-31572

Probabilistic simulation of the human factor in structural reliability
p 258 N93-31573

CHANG, C. T.

Comparison of reacting and non-reacting shear layers at a high subsonic Mach number
[AIAA PAPER 93-2381] p 186 A93-50149

Comparison of reacting and non-reacting shear layers at a high subsonic Mach number
[NASA-TM-106198] p 38 N93-27610

Turbulence measurement in a reacting and non-reacting shear layer at a high subsonic Mach number
[NASA-TM-106186] p 18 N93-31839

CHANG, R.

75 Ah and 10 boilerplate nickel-hydrogen battery designs and test results
p 253 A93-25948

CHANG, SIN-CHUNG

On an origin of numerical diffusion: Violation of invariance under space-time inversion
[NASA-TM-105776] p 268 N93-11264

A brief description of a new numerical framework for solving conservation laws: The method of space-time conservation element and solution element
[NASA-TM-105757] p 269 N93-26560

A new flux conserving Newton's method scheme for the two-dimensional, steady Navier-Stokes equations
[NASA-TM-106160] p 201 N93-28626

CHANG, T. Y. P.

Finite element implementation of state variable-based viscoplasticity models
p 236 A93-26776

CHANG, Y. L.

A three-dimensional algebraic grid generation scheme for gas turbine combustors with inclined slots
[NASA-CR-191095] p 198 N93-24759

CHANG, YALE

Application of composite materials to impact-insensitive munitions
p 97 A93-11459

CHAR, K.

Large-area YBa₂Cu₃O(7- δ) thin films on sapphire for microwave applications
p 279 A93-11475

CHATO, DAVID J.

Small experiments for the maturation of orbital cryogenic transfer technologies
[IAF PAPER 92-0777] p 64 A93-13698

Ground testing for the no-vent fill of cryogenic tanks - Results of tests for a 71 cubic foot tank
[AIAA PAPER 93-1967] p 73 A93-49815

Small experiments for the maturation of orbital cryogenic transfer technologies
[NASA-TM-105849] p 192 N93-10981

Comparing the results of an analytical model of the no-vent fill process with no-vent fill test results for a 4.96 cubic meters (175 cubic feet) tank
[NASA-TM-106018] p 200 N93-27155

CHEN, C. F.

Effect of surface tension on the onset of convection in a double-diffusive layer
p 163 A93-13951

Double-diffusive fingering convection in a porous medium
p 175 A93-27900

Surface tension effects on the onset of double-diffusive convection
p 180 A93-41710

CHEN, FALIN

Double-diffusive fingering convection in a porous medium
p 175 A93-27900

CHEN, GUNG

Secondary atomization in the combustion of electrostatic sprays
[AIAA PAPER 93-2332] p 118 A93-50110

CHEN, HEH-CHYUN

Programming probabilistic structural analysis for parallel processing computers
p 237 A93-32410

CHEN, J.-L.

Dynamic modeling and control of multibody mechanical systems which are structurally flexible
p 264 A93-29338

CHEN, JEN P.

Navier-Stokes calculations for the unsteady flowfield of turbomachinery
[AIAA PAPER 93-0676] p 6 A93-24786

CHEN, K. L.

An artificial intelligence-based structural health monitoring system for aging aircraft
p 266 N93-22185

CHEN, K.-H.

On solving the compressible Navier-Stokes equations for unsteady flows at very low Mach numbers
[AIAA PAPER 93-3368] p 181 A93-45061

CHEN, KEMING

A 1.6-kW, 110-kHz dc-dc converter optimized for IGBT's
p 156 A93-37570

- CHEN, KUO-HUEY**
A coupled multi-block solution procedure for spray combustion in complex geometries
[AIAA PAPER 93-0108] p 171 A93-24230
Simulation of three-dimensional liquid sloshing flows using a strongly implicit calculation procedure p 179 A93-35624
A coupled implicit method for chemical non-equilibrium flows at all speeds p 181 A93-44245
Spray combustion experiments and numerical predictions
[NASA-TM-106069] p 198 N93-23744
- CHEN, N. X.**
Generation of helical gears with new surfaces topology by application of CNC machines
[AIAA PAPER 93-2297] p 224 A93-50082
Generation of helical gears with new surfaces, topology by application of CNC machines
[NASA-TM-106175] p 229 N93-27687
- CHEN, QI**
Grain boundary resistance to fatigue crack growth p 125 A93-29570
- CHEN, R.**
Numerical simulation of a low-emission gas turbine combustor using KIVA-II p 22 A93-14077
A three-dimensional algebraic grid generation scheme for gas turbine combustors with inclined slots
[NASA-CR-191095] p 198 N93-24759
- CHEN, S. K.**
Influence of ambient air pressure on effervescent atomization
[AIAA PAPER 92-0460] p 167 A93-21652
- CHEN, WEI**
Spectral-domain moment-method analysis of coplanar microstrip parasitic subarrays p 148 A93-35016
Input impedance of coaxially fed rectangular microstrip antenna on electrically thick substrate p 155 A93-36994
- CHEN, Y.-J. D.**
Face-gear drives: Design, analysis, and testing for helicopter transmission applications
[NASA-TM-106101] p 229 N93-27133
- CHENG, J.**
Control-structure interaction study for the Space Station solar dynamic power module p 54 A93-13132
- CHENG, JOSEPH K.**
Control-structure interaction p 54 A93-14687
- CHEONG, DEOCK-SOO**
High-temperature deformation and microstructural analysis for silicon nitride-scandium(III) oxide p 131 A93-20468
- CHESTON, DERRICK J.**
A SINDA '85 nodal heat transfer rate calculation user subroutine p 193 N93-13403
- CHEUNG, H. M.**
Microemulsion characterization by the use of a noninvasive backscatter fiber optic probe p 277 A93-52412
- CHIARAMONTE, FRANCIS P.**
Initial study of void formation during aluminum solidification in reduced gravity p 142 A93-12013
- CHILDS, D. W.**
Friction-factor characteristics for narrow channels with honeycomb surfaces
[ASME PAPER 91-TRIB-21] p 219 A93-15681
- CHILDS, DARA W.**
Development of advanced seals for space propulsion turbomachinery
[SAE PAPER 921028] p 218 A93-14651
Friction-factor data for flat-plate tests of smooth and honeycomb surfaces
[ASME PAPER 91-TRIB-20] p 219 A93-15682
- CHIMA, R. V.**
An algebraic turbulence model for three-dimensional viscous flows p 4 A93-22552
Averaging techniques for steady and unsteady calculations of a transonic fan stage
[AIAA PAPER 93-3065] p 11 A93-48241
An algebraic turbulence model for three-dimensional viscous flows
[NASA-TM-105931] p 1 N93-14102
- CHIMA, RODRICK V.**
Two-dimensional CFD modeling of wave rotor flow dynamics
[AIAA PAPER 93-3318] p 9 A93-45014
- CHIN, H.**
Efficient fault diagnosis of helicopter gearboxes
[NASA-TM-106253] p 231 N93-31846
- CHIN, HSINYUNG**
Pattern classifier for health monitoring of helicopter gearboxes
[NASA-TM-106099] p 228 N93-23741
Fault detection of helicopter gearboxes using the multi-valued influence matrix method
[NASA-TM-106100] p 229 N93-27069
- CHO, KYU**
Fracture toughness of advanced ceramics at room temperature p 131 A93-20842
- CHO, MENGU**
Arcing rates for High Voltage Solar Arrays - Theory, experiment, and predictions p 70 A93-32567
Space Station Freedom structure floating potential and the probability of arcing p 57 A93-39265
- CHO, SEONG Y.**
Computational/experimental basis for conducting alkane droplet combustion experiments on space-based-platforms p 117 A93-41711
- CHOI, BENJAMIN B.**
Inverse kinematics problem in robotics using neural networks
[NASA-TM-105869] p 247 N93-18876
- CHOI, M. Y.**
Soot agglomeration in isolated, free droplet combustion
[AIAA PAPER 93-0823] p 115 A93-24893
- CHOI, MUN Y.**
Computational/experimental basis for conducting alkane droplet combustion experiments on space-based-platforms p 117 A93-41711
- CHOI, S. R.**
Evaluation of the fracture toughness of Nb-40Al-8Cr-1W-0.05B intermetallic material by indentation techniques p 124 A93-24066
Interaction of cracks between two adjacent indents in glass p 132 A93-27115
- CHOI, SUNG R.**
Indentation flow formation and strength response of silicon nitride ceramics at low indentation loads p 130 A93-15994
Analysis of precracking parameters for ceramic single-edge-precracked-beam specimens p 133 A93-38887
Effect of environment on fracture toughness of 96 wt pct alumina p 134 A93-44955
Analysis of precracking parameters and fracture toughness for ceramic single-edge-precracked-beam specimens
[NASA-TM-105568] p 135 N93-10962
- CHOI, Y.-H.**
The application of preconditioning in viscous flows p 177 A93-32627
- CHOI, YUNHO**
A coupled implicit method for chemical non-equilibrium flows at all speeds p 181 A93-44245
- CHOO, Y. K.**
Three-dimensional Navier-Stokes calculations using solution-adapted grids
[AIAA PAPER 93-0431] p 6 A93-24240
- CHOO, YUNG K.**
Algebraic grid generation with control points p 268 A93-45967
- CHOPRA, M. A.**
Thermosolutal convection during cellular arrayed growth of Pb-Sn alloys
[AIAA PAPER 93-0262] p 142 A93-22668
- CHOREY, C.**
An analysis of the frequency limitations of an $\text{Al}(x)\text{Ga}(1-x)\text{As}/\text{GaAs}$ optical modulator p 151 A93-23454
- CHOREY, C. M.**
Processing, electrical and microwave properties of sputtered Ti-Ca-Ba-Cu-O superconducting thin films p 282 A93-44607
- CHOW, CHUEN-YEN**
Grid adaptation using Chimera composite overlapping meshes
[AIAA PAPER 93-3389] p 267 A93-45080
Grid adaption using Chimera composite overlapping meshes
[NASA-TM-106163] p 269 N93-27065
- CHOW, L. C.**
Vaporization heat transfer of dielectric liquids on a wick-covered surface p 169 A93-22686
[AIAA PAPER 93-0283] p 169 A93-22686
Vaporization heat transfer of dielectric liquids on enhanced surfaces covered with screen wicks
[AIAA PAPER 93-2835] p 182 A93-46572
- CHOY, F. K.**
Modal simulation of gear box vibration with experimental correlation p 221 A93-31982
Modal analysis of multistage gear systems coupled with gearbox vibrations p 222 A93-36588
Vibration and noise analysis of a gear transmission system
[AIAA PAPER 93-2150] p 224 A93-49967
Global dynamic modeling of a transmission system
[NASA-CR-191117] p 228 N93-24751
Vibration and noise analysis of a gear transmission system
[NASA-TM-106162] p 229 N93-27641
- CHOYKE, W. J.**
Aluminum acceptor four particle bound exciton complex in 4H, 6H, and 3C SiC p 282 A93-44822
- CHRISS, R. M.**
Experimental and computational investigation of the NASA Low-Speed Centrifugal Compressor flow field
[ASME PAPER 92-GT-213] p 4 A93-19436
- CHRISTIAN, JOSE L., JR.**
Electromagnetic powered vehicles (EMPV) for Mars exploration p 47 A93-20761
- CHRISTIANSEN, ERIC L.**
On protection of Freedom's solar dynamic radiator from the orbital debris environment. I - Preliminary analysis and testing p 70 A93-36197
On protection of Freedom's solar dynamic radiator from the orbital debris environment. II - Further testing and analyses p 70 A93-36589
- CHU, Y. C.**
Ultrasonic and micromechanical study of damage and elastic properties of SiC/RBSN ceramic composites p 99 A93-19624
Ultrasonic assessment of interfacial oxidation damage in ceramic matrix composites p 105 A93-52919
- CHUANG, TZE-JER**
A generic model for creep rupture lifetime estimation on fibrous ceramic composites p 103 A93-38895
- CHUBB, DONALD L.**
Current status of liquid sheet radiator research
[NASA-TM-105764] p 193 N93-14150
- CHUCKSA, RONALD J.**
Conceptual design for the Space Station Freedom fluid physics/dynamics facility
[NASA-TM-103663] p 61 N93-26209
- CHUDGAR, MONA H.**
Characterization of $\text{Si}_3\text{N}_4/\text{SiO}_2$ optical channel waveguides by photon scanning tunneling microscopy p 211 A93-49458
- CHUDNOVSKY, A.**
Variation of the energy release rate as a crack approaches and passes through an elastic inclusion p 241 A93-44440
- CHUE, T.-H.**
Atomization and vaporization characteristics of airblast fuel injection inside a venturi tube
[AIAA PAPER 93-1766] p 184 A93-49662
- CHULYA, ABHISAK**
Mechanics of interfaces in fiber reinforced SiC/RBSN ceramic matrix composites p 102 A93-32466
Analysis of precracking parameters for ceramic single-edge-precracked-beam specimens p 133 A93-38887
Analysis of precracking parameters and fracture toughness for ceramic single-edge-precracked-beam specimens
[NASA-TM-105568] p 135 N93-10962
Acousto-Ultrasonic analysis of failure in ceramic matrix composite tensile specimens
[NASA-TM-106219] p 232 N93-29073
- CHUN, KUE**
A review of chemically reactive turbulent flow mixing mechanisms and a new design for a low $\text{NO}(x)$ combustor p 27 A93-49508
A thermal $\text{NO}(x)$ prediction model - Scalar computation module for CFD codes with fluid and kinetic effects
[AIAA PAPER 93-2378] p 119 A93-50147
- CHUNG, C.-H.**
NTR plume modeling p 199 N93-26929
- CHUNG, CHAN H.**
Analysis of plume backflow around a nozzle lip in a nuclear rocket p 77 A93-50231
[AIAA PAPER 93-2497] p 77 A93-50231
- CHUNG, CHAN-HONG**
DSMC and continuum analyses of low-density nozzle flow
[AIAA PAPER 93-0727] p 172 A93-24817
Internal structure of shock waves in disparate mass mixtures p 190 A93-54483
- CIOS, K. J.**
Application of neural networks to prediction of advanced composite structures mechanical response and behavior p 205 A93-20751
- CIOS, KRZYSZTOF J.**
Self-growing neural network architecture using crisp and fuzzy entropy p 263 A93-26650
Application of neural networks in the acousto-ultrasonic evaluation of metal-matrix composite specimens p 231 A93-37009
Self-growing neural network architecture using crisp and fuzzy entropy p 231 N93-18422
[NASA-TM-105677] p 231 N93-18422
Radial basis function network learns ceramic processing and predicts related strength and density
[NASA-TM-106048] p 110 N93-27129
Fuzzy sets predict flexural strength and density of silicon nitride ceramics
[NASA-TM-106049] p 110 N93-27270

- Soft computing in design and manufacturing of advanced materials
[NASA-TM-106032] p 111 N93-28624
- CIVINSKAS, K. C.**
Time-averaged heat transfer and pressure measurements and comparison with prediction for a two-stage turbine
[ASME PAPER 92-GT-194] p 166 A93-19419
Chimera grids in the simulation of three-dimensional flowfields in turbine-blade-coolant passages
[AIAA PAPER 93-2559] p 187 A93-50280
- CLARK, IVAN O.**
Comparison of numerical model results with diffusion flames in microgravity
[AIAA PAPER 93-0707] p 114 A93-24803
- CLARK, JOHN S.**
Nuclear propulsion technology development - A joint NASA/Department of Energy project p 64 A93-12074
Nuclear Propulsion Project Workshop summary p 64 A93-13765
A comparison of Nuclear Thermal Propulsion concepts - Results of a workshop p 65 A93-13850
U.S./CIS eye joint nuclear rocket venture p 71 A93-49334
A comparison of nuclear thermal rocket development cost and schedule for piloted missions to Mars
[AIAA PAPER 93-2263] p 44 A93-50057
Nuclear thermal propulsion transportation systems for lunar/Mars exploration
[NASA-TM-105870] p 81 N93-12363
Nuclear thermal propulsion technology: Results of an interagency panel in FY 1991
[NASA-TM-105711] p 86 N93-24740
Space exploration initiative candidate nuclear propulsion test facilities
[NASA-TM-105710] p 86 N93-24753
Space Nuclear Thermal Propulsion Test Facilities Subpanel
[NASA-TM-105708] p 87 N93-25105
- CLARK, RALPH**
Closed-ampoule diffusion of sulfur into Cd-doped InP substrates - Dependence of S profiles on diffusion temperature and time p 283 A93-51917
- CLARK, WILLIAM S.**
Nonreflecting boundary conditions for linearized unsteady aerodynamic calculations
[AIAA PAPER 93-0882] p 7 A93-25553
Linearized Euler predictions of unsteady aerodynamic loads in cascades p 7 A93-29318
- CLARKE, ERNEST**
GSFC conceptual design study for an inter-satellite Optical Multiple Access communication system p 52 A93-18966
- CLASPY, P. C.**
An analysis of the frequency limitations of an Al(x)Ga(1-x)As/GaAs optical modulator p 151 A93-23454
- CLAUS, RUSSELL W.**
Multidisciplinary propulsion simulation using NPSS
[AIAA PAPER 92-4709] p 270 A93-20318
- CLAYTON, S. R.**
Demonstration of Y1Ba2Cu3O(7-delta) and complementary metal-oxide-semiconductor device fabrication on the same sapphire substrate p 159 A93-56292
- CLEAVER, WILLIAM M.**
Metal-organic chemical vapour deposition of polycrystalline tetragonal indium sulphide (InS) thin films p 116 A93-36584
- CLEMEN, L. L.**
Aluminum acceptor four particle bound exciton complex in 4H, 6H, and 3C SiC p 282 A93-44822
- CLINE, M. C.**
Numerical simulation of a low-emission gas turbine combustor using KIVA-II p 22 A93-14077
A three-dimensional algebraic grid generation scheme for gas turbine combustors with inclined slots
[NASA-CR-191095] p 198 N93-24759
- CLINE, MICHAEL C.**
Computation of the flow field in an annular gas turbine combustor
[AIAA PAPER 93-2074] p 28 A93-49903
- COE, H. H.**
Maximum life spur gear design p 218 A93-14521
Maximum life spiral bevel reduction design
[NASA-TM-105790] p 226 N93-10982
- COGHLAN, GREGORY A.**
Fiberoptic sensing technique employing RF modulated interferometry p 212 A93-53110
- COGNE, SANDRINE**
Time-sequenced and spectrally filtered Rayleigh imaging of shock wave and boundary layer structure for inlet characterization
[AIAA PAPER 93-2300] p 211 A93-50085
- COIRIER, WILLIAM J.**
An accuracy assessment of Cartesian-mesh approaches for the Euler equations
[AIAA PAPER 93-3335] p 9 A93-45029
- COLE, B. F.**
Large-area YBa2Cu3O(7-delta) thin films on sapphire for microwave applications p 279 A93-11475
- COLE, GARY**
A multiarchitecture parallel-processing development environment
[NASA-TM-106180] p 262 N93-28628
- COLEMAN, HUGH W.**
The turbulent thermal boundary layer with an abrupt change from a rough to a smooth wall p 167 A93-21712
- COLIN, P.**
Chemical and luminosity evolution, and counts of galaxies in a merger model p 290 A93-34776
- COLLIN, R. E.**
Full wave characterization of microstrip open end discontinuities patterned on anisotropic substrates using potential theory
[NASA-TM-106037] p 160 N93-20259
- COLLINS, J.**
Onset conditions for gas phase reaction and nucleation in the CVD of transition metal oxides p 116 A93-39508
- COLLINS, JOHN T.**
Lunar mission design using Nuclear Thermal Rockets p 65 A93-13767
- COLOZZA, ANTHONY J.**
Design and optimization of a self-deploying single axis tracking PV array p 252 A93-25916
- CONCUS, P.**
On accurate determination of contact angle p 143 A93-41678
- CONCUS, PAUL**
An interface configuration experiment on USML-1
[AIAA PAPER 93-0253] p 169 A93-22662
- CONLEY, JULIANNE M.**
The Proteus Navier-Stokes code p 193 N93-13396
- COOKE, D. W.**
Buffer layers for high-Tc thin films on sapphire p 150 A93-17063
- COOLEY, CHRISTINE B.**
Design of an oxygen turbopump for use in an Advanced Expander Test Bed engine
[AIAA PAPER 93-2137] p 48 A93-49955
- COOLEY, WILLIAM T.**
Photovoltaic Array Space Power flight experiment plus diagnostics (PASP+) modules p 68 A93-25898
- COOPER, BETH A.**
A large hemi-anechoic enclosure for community-compatible aeroacoustic testing of aircraft propulsion systems
[NASA-TM-106015] p 275 N93-26551
- COOPER, MATTHEW F.**
Construction and testing of ceramic fabric heat pipe with water working fluid p 163 A93-13869
- COPELAND, EDMUND J.**
Observing the inflation potential p 291 A93-50480
- COPENHAVER, W. W.**
Unsteady aerodynamic flow phenomena in a transonic compressor stage
[AIAA PAPER 93-1868] p 12 A93-49743
Three-dimensional flow analysis inside turbomachinery stages with steady and unsteady Navier-Stokes method
[ISABE 93-7095] p 14 A93-54071
- COPENHAVER, WILLIAM W.**
Three-dimensional flow phenomena in a transonic, high-through-flow, axial-flow compressor stage
[ASME PAPER 92-GT-169] p 3 A93-19395
- COQUEL, FREDERIC**
Stable and low diffusive hybrid upwind splitting methods
[ONERA, TP NO. 1992-113] p 179 A93-38589
Field by field hybrid upwind splitting methods
[AIAA PAPER 93-3302] p 8 A93-45000
- CORBAN, R.**
Structured system engineering methodologies used to develop a nuclear thermal propulsion engine
[AIAA PAPER 93-2109] p 271 A93-49930
- CORBAN, ROBERT**
Systems overview p 89 N93-26915
NTP comparison process p 89 N93-26926
- COURTNEY, T. H.**
The kinetics of composite particle formation during mechanical alloying p 125 A93-29534
- COWLEY, STEPHEN J.**
On the nonlinear three dimensional instability of Stokes layers and other shear layers to pairs of oblique waves
[NASA-TM-105918] p 194 A93-15499
- COY, J. J.**
Maximum life spur gear design p 218 A93-14521
- COY, JOHN J.**
Effect of extended tooth contact on the modeling of spur gear transmissions
[AIAA PAPER 93-2148] p 223 A93-49965
Effect of extended tooth contact on the modeling of spur gear transmissions
[NASA-TM-106174] p 230 N93-28411
- CROKE, E. T.**
Ellipsometric study of Si(0.5)Ge(0.5)/Si strained-layer superlattices p 280 A93-34655
- CROOK, A. J.**
Numerical simulation of compressor endwall and casing treatment flow phenomena
[ASME PAPER 92-GT-300] p 4 A93-19490
- CROSS, G. S.**
Advanced instrumentation for next-generation aerospace propulsion control systems
[AIAA PAPER 93-2079] p 211 A93-49906
- CRUSE, T. A.**
Confidence bounds on structural reliability
[AIAA PAPER 93-1377] p 238 A93-33941
- CRUZ, E.**
75 Ah and 10 boilerplate nickel-hydrogen battery designs and test results p 253 A93-25948
- CRYER, STEVEN A.**
Collapse of the soap-film bridge - Quasistatic description p 188 A93-50536
- CULL, RONALD C.**
Electromagnetic powered vehicles (EMPV) for Mars exploration p 47 A93-20761
- CULLEY, DENNIS E.**
Laser ignition application in a space experiment
[NASA-TM-106133] p 145 N93-25337
- CULLINGFORD, HATICE S.**
Nuclear safety policy working group recommendations on nuclear propulsion safety for the space exploration initiative
[NASA-TM-105705] p 88 N93-26200
- CULVER, D. W.**
US/CIS integrated NTRE
[AIAA PAPER 93-2367] p 76 A93-50138
- CURLETT, BRIAN P.**
A graphical user-interface for propulsion system analysis
[AIAA PAPER 93-0223] p 259 A93-23699
- CURRAN, F. M.**
Effects of anode material on arcjet performance p 79 N93-10044
- CURRAN, FRANCIS M.**
Extended life and performance test of a low-power arcjet p 70 A93-32554
The NASA Electric Propulsion Program
[AIAA PAPER 93-1935] p 73 A93-49797
BMDO electric space-propulsion program
[AIAA PAPER 93-1934] p 78 A93-50322
Electric propulsion - An evolutionary technology p 78 A93-56168
Development of arcjet and ion propulsion for spacecraft stationkeeping
[NASA-TM-106102] p 85 N93-23747
- CURRAN, FRANK M.**
Effects of anode material on arcjet performance
[NASA-TM-105799] p 79 N93-10197
- CURTIS, HENRY B.**
The Photovoltaic Array Space Power Plus diagnostics (PASP Plus) flight experiment p 256 N93-28717
- CURWEN, P. W.**
Magnetic bearings for free-piston Stirling engines p 221 A93-26079

D

- D'YAKOV, E. K.**
US/CIS integrated NTRE
[AIAA PAPER 93-2367] p 76 A93-50138
- D'YAKOV, EVGENIJ K.**
U.S./CIS eye joint nuclear rocket venture p 71 A93-49334
- DAHL, MILO D.**
Acoustical evaluation of the NASA Lewis 9 by 15 foot low speed wind tunnel
[NASA-TP-3274] p 42 N93-12016
- DAI, XIAOWEN**
Damage-mitigating control of space propulsion systems for high performance and extended life
[AIAA PAPER 93-2080] p 74 A93-49907
- DAMAN, M. E.**
75 Ah and 10 boilerplate nickel-hydrogen battery designs and test results p 253 A93-25948
- DANAI, K.**
Efficient fault diagnosis of helicopter gearboxes
[NASA-TM-106253] p 231 N93-31846

DANAI, KOUROSH

- Pattern classifier for health monitoring of helicopter gearboxes
[NASA-TM-106099] p 228 N93-23741
- Fault detection of helicopter gearboxes using the multi-valued influence matrix method
[NASA-TM-106100] p 229 N93-27069

DARGUSH, G. F.

- Micromechanical studies of composites by BEM
p 236 A93-31295

DARLING, DOUGLAS

- Evaluation and application of the Baldwin-Lomax turbulence model in two-dimensional, unsteady, compressible boundary layers with and without separation in engine inlets
[AIAA PAPER 92-3676] p 2 A93-14118
- Evaluation and application of the Baldwin-Lomax turbulence model in two-dimensional, unsteady, compressible boundary layers with and without separation in engine inlets
[AIAA PAPER 92-3676] p 168 A93-22509
- Modeling void growth and movement with phase change in thermal energy storage canisters
[AIAA PAPER 93-2832] p 285 A93-46569
- Evaluation and application of the Baldwin-Lomax turbulence model in two-dimensional, unsteady, compressible boundary layers with and without separation in engine inlets
[NASA-TM-105810] p 191 N93-10087
- A compressible boundary layer algorithm for use with SINDA '85
p 192 N93-13395

DARYOUSH, A. S.

- Fiber optic link for millimeter wave communication satellites
p 277 A93-25736

DASGUPTA, A.

- Noniterative implicit method for tracking particles in mixed Lagrangian-Eulerian formulations
p 176 A93-30856
- Computations of spray, fuel-air mixing, and combustion in a lean-premixed-prevaporized combustor
[AIAA PAPER 93-2069] p 185 A93-49901

DAVIC, JAMES R.

- Propulsion and aerodynamic analysis of the Beta II two-stage-to-orbit vehicle
[AIAA PAPER 92-4245] p 50 A93-13332

DAVIDIAN, KEN

- Rocket engine numerical simulator p 89 N93-26962

DAVIDIAN, KENNETH O.

- Nuclear thermal rocket nozzle testing and evaluation program
[NASA-TM-105962] p 83 N93-15571

DAVIS, A. M. J.

- A hydrodynamic model of the oscillating screen viscometer
p 190 A93-55136

DAVIS, C. M.

- Acoustic radiation from a thin airfoil in nonuniform subsonic flows
p 273 A93-23535

DAVIS, D. O.

- Surface and flow field measurements in a symmetric crossing shock wave/turbulent boundary-layer interaction
[NASA-TM-106086] p 17 N93-24911

DAVIS, GARY A.

- Unsteady transonic two-dimensional Euler solutions using finite elements
p 8 A93-39412

DAVIS, RICHARD L.

- Cosmic microwave background probes models of inflation
p 294 A93-10355

DAVIS, ROBERT H.

- Experimental study of two interacting drops in an immiscible fluid
p 179 A93-37936
- Collective effects of temperature gradients and gravity on droplet coalescence
p 183 A93-46716

DAVIS, S.

- Nonintrusive, multipoint velocity measurements in high-pressure combustion flows
[AIAA PAPER 93-2032] p 118 A93-49867

DAVIS, S. J.

- Rotational level-dependent collisional broadening and line shift of the A2Sigma(+) - X2Pi (1,0) band of OH in hydrogen-air combustion gases
p 276 A93-24142

DAVY, D. T.

- Numerical optimization of composite hip endoprostheses under different loading conditions
[AIAA PAPER 92-4703] p 270 A93-20312
- Optimal design of composite hip implants using NASA technology
p 257 N93-22188

DAYTON, JAMES A., JR.

- Interim report on the analysis of the microwave power module
[NASA-TM-106012] p 160 N93-16713

DE BRABANDER, GREGORY N.

- Micromachined silicon cantilever beam accelerometer incorporating an integrated optical waveguide
p 210 A93-49457

- Characterization of Si3N4/SiO2 optical channel waveguides by photon scanning tunneling microscopy
p 211 A93-49458

DE GROH, H. C., III

- Effect of radiation on convection in a top-heated enclosure
p 189 A93-54454

DE LA FUENTE, HORACIO M.

- Membrane triangles with corner drilling freedoms. I - The EFF element
p 235 A93-24303

DE LA HOUSSE, P. R.

- Demonstration of Y1Ba2Cu3O(7-delta) and complementary metal-oxide-semiconductor device fabrication on the same sapphire substrate
p 159 A93-56292

DE WITT, KENNETH J.

- Initial study of void formation during aluminum solidification in reduced gravity
p 142 A93-12013
- DSMC and continuum analyses of low-density nozzle flow
[AIAA PAPER 93-0727] p 172 A93-24817
- Analysis of plume backflow around a nozzle lip in a nuclear rocket
[AIAA PAPER 93-2497] p 77 A93-50231
- Efficient finite element method for aircraft deicing problems
p 21 A93-52443
- Internal structure of shock waves in disparate mass mixtures
p 190 A93-54483

DEADMORE, DANIEL L.

- Vickers indentation hardness of stoichiometric and reduced single crystal TiO2 (rutile) from 25 to 800 C
[NASA-TM-105959] p 96 N93-26204

DEANNA, R. G.

- Direct numerical simulation of instabilities in parallel flow with spherical roughness elements
[NASA-TM-105847] p 192 N93-11529

DEANNA, RUSSELL G.

- Incompressible spectral-element method: Derivation of equations
[NASA-TM-106109] p 199 N93-26554

DEARMON, JOHN M.

- Icing Research Tunnel rotating bar calibration measurement system
p 212 A93-54398
- Icing research tunnel rotating bar calibration measurement system
[NASA-TM-106010] p 215 N93-22598
- Ice thickness measurement system for the icing research tunnel calibration
[NASA-TM-106095] p 215 N93-24737

DEBONIS, J. R.

- Navier-Stokes analysis of three-dimensional S-ducts
p 9 A93-45146

DECKER, ARTHUR

- Neural networks for calibration tomography
[NASA-TM-106352] p 216 N93-26906

DECKER, ARTHUR J.

- Three-dimensional computed tomography from interferometric measurements within a narrow cone of views
p 207 A93-24024
- Calibration of a shock wave position sensor using artificial neural networks
[NASA-TM-106138] p 216 N93-27001
- Neural nets for aligning optical components in harsh environments: Beam smoothing spatial filter as an example
p 266 N93-31557

DECKER, D. K.

- Operation of high power converters in parallel
p 154 A93-26100

DECKER, H. J.

- An analysis of gear fault detection methods as applied to pitting fatigue failure data
[NASA-TM-105950] p 229 N93-27074

DEGANI, A. T.

- The structure of a three-dimensional turbulent boundary layer
p 181 A93-44813

DEGROH, H. C., III

- On the drag of model dendrite fragments at low Reynolds number
[NASA-TM-105916] p 128 N93-19974

DEGROH, K. K.

- Leveling coatings for reducing the atomic oxygen defect density in protected graphite fiber epoxy composites
[NASA-TM-105732] p 136 N93-15344

DEGROH, KIM K.

- Low Earth orbit atomic oxygen simulation for durability evaluation of solar reflector surfaces
p 58 N93-15594
- Simulation of the synergistic low Earth orbit effects of vacuum thermal cycling, vacuum UV radiation, and atomic oxygen
p 58 N93-15595
- The use of plasma ashers and Monte Carlo modeling for the projection of atomic oxygen durability of protected polymers in low Earth orbit
p 58 N93-15596
- Leveling coatings for reducing the atomic oxygen defect density in protected graphite fiber epoxy composites
p 59 N93-15597

- Monte Carlo modeling of atomic oxygen attack of polymers with protective coatings on LDEF
p 138 N93-28282

DEGROOT, WILHELMUS A.

- Laser Rayleigh and Raman diagnostics for small hydrogen/oxygen rockets
[NASA-TM-105999] p 83 N93-17995

DESSLER, ROBERT G.

- Turbulent fluid motion IV-averages, Reynolds decomposition, and the closure problem
[NASA-TM-105822] p 195 N93-15585

DELLACORTE, C.

- Sliding wear of self-mated Al2O3-SiC whisker-reinforced composites at 23-1200 C
p 101 A93-29948

DELLACORTE, CHRISTOPHER

- Tribological and microstructural comparison of HIPped PM212 and PM212/Au self-lubricating composites
p 93 A93-13505
- Tribological and mechanical comparison of sintered and HIPped PM212 - High temperature self-lubricating composites
p 94 A93-13506
- Relative sliding durability of two candidate high-temperature oxide fiber seal materials
p 132 A93-31983

- An analysis of the wear behavior of SiC whisker-reinforced alumina from 25 to 1200 C
p 104 A93-49253

- Relative sliding durability of candidate high temperature fiber seal materials
[NASA-TM-105806] p 95 N93-10978

- The effect of processing and compositional changes on the tribology of PM212 in air
[NASA-TM-105945] p 95 N93-15576

- Sliding durability of candidate seal fiber materials in hydrogen from 25 to 900 C
[NASA-TM-105939] p 95 N93-22590

- Vickers indentation hardness of stoichiometric and reduced single crystal TiO2 (rutile) from 25 to 800 C
[NASA-TM-105959] p 96 N93-26204

DELLAVECCHIA, MICHAEL A.

- Coherent fiber optic sensor for early detection of cataractogenesis in a human eye lens
p 209 A93-37051

DELOMBARD, R.

- Low gravity environment on-board Columbia during STS-40
[AIAA PAPER 93-0833] p 142 A93-24903

DELOMBARD, RICHARD

- Review of the Shuttle vibration environment
[AIAA PAPER 93-0832] p 51 A93-24902
- Proposed ground-based control of accelerometer on Space Station Freedom
p 63 A93-54401
- Selected OAST/OSSA space experiment activities in support of Space Station Freedom
p 60 N93-22636
- Proposed ground-based control of accelerometer on Space Station Freedom
[NASA-TM-105960] p 63 N93-23738
- Low-frequency vibration environment for five Shuttle missions
[NASA-TM-106059] p 63 N93-28554

DEMERDASH, N. A.

- Extra high speed modified Lundell alternator parameters and open/short-circuit characteristics from global 3D-FE magnetic field solutions
p 156 A93-39348
- Computation of load performance and other parameters of extra high speed modified Lundell alternators from 3D-FE magnetic field solutions
p 156 A93-39349
- Three dimensional magnetic fields in extra high speed modified Lundell alternators computed by a combined vector-scalar magnetic potential finite element method
p 157 A93-39350

- On the effects of grid ill-conditioning in three dimensional finite element vector potential magnetostatic field computations
p 157 A93-39719

- Theoretical and numerical difficulties in 3-D vector potential methods in finite element magnetostatic computations
p 157 A93-39720

DEMPSEY, PAULA J.

- Using silicon diodes for detecting the liquid-vapor interface in hydrogen
p 209 A93-37864
- Techniques for improving the accuracy of cryogenic temperature measurement in ground test programs
p 212 A93-54363

- Techniques for improving the accuracy of cryogenic temperature measurement in ground test programs
[NASA-TM-105996] p 215 N93-22484

DEMUREN, A. O.

- Multigrid acceleration and turbulence models for computations of 3D turbulent jets in crossflow
p 165 A93-18751

- Characteristics of three-dimensional turbulent jets in crossflow
p 8 A93-38695

DESTRO-SIDIK, K. E.

- Numerical model for the Programmable Multirole Furnace (PMZF)
[AIAA PAPER 93-0471] p 142 A93-24242

DEUR, J. M.

Computations of spray, fuel-air mixing, and combustion in a lean-premixed-prevaporized combustor
[AIAA PAPER 93-2069] p 185 A93-49901
A simplified reaction mechanism for calculation of emissions in hydrocarbon (Jet-A) combustion
[AIAA PAPER 93-2341] p 118 A93-50116

DEUR, JOHN M.

Computation of the flow field in an annular gas turbine combustor
[AIAA PAPER 93-2074] p 28 A93-49903
Nitric oxide formation in a lean, premixed-prevaporized jet A/air flame tube: An experimental and analytical study
[NASA-TM-105722] p 257 N93-27012

DEVATY, R. P.

Aluminum acceptor four particle bound exciton complex in 4H, 6H, and 3C SiC p 282 A93-44822

DEVER, JOYCE A.

Simulation of the synergistic low Earth orbit effects of vacuum thermal cycling, vacuum UV radiation, and atomic oxygen p 58 N93-15595
The effects of simulated low Earth orbit environments on spacecraft thermal control coatings
[NASA-TM-106146] p 61 N93-27019
Low Earth orbital atomic oxygen environmental simulation facility for space materials evaluation
[NASA-TM-106128] p 96 N93-27266

DEVER, THERESE M.

Simulation of the synergistic low Earth orbit effects of vacuum thermal cycling, vacuum UV radiation, and atomic oxygen p 58 N93-15595

DEVINCENT, SANDRA M.

Reaction layer formation at the graphite/copper-chromium alloy interface p 100 A93-25105

DEVRIES, CHRISTOPHER

Characteristics of hypervelocity impact craters on LDEF experiment S1003 and implications of small particle impacts on reflective surfaces p 62 N93-29363

DEWITT, K. J.

Measurement and analysis of a small nozzle plume in vacuum p 71 A93-42895
Measurement and analysis of a small nozzle plume in vacuum
[NASA-TM-106066] p 88 N93-26561

DEWITT, KENNETH J.

Numerical modeling of runback water on ice protected aircraft surfaces p 201 N93-27438

DHADWAL, HARBANS S.

Coherent fiber optic sensor for early detection of cataractogenesis in a human eye lens p 209 A93-37051

Microemulsion characterization by the use of a noninvasive backscatter fiber optic probe p 277 A93-52412

Integrated fiber optic probe for dynamic light scattering p 278 A93-52415

Multiple fiber optic probe for several sensing applications p 212 A93-53109

A fiber optic probe for the detection of cataracts p 257 N93-25593

DHAR, MANMOHAN

Free-piston Stirling Engine system considerations for various space power applications p 252 A93-13826

DIAZ, NILS J.

Ultrahigh temperature vapor-core reactor - Magnetohydrodynamic system for space nuclear electric power p 66 A93-21663

DICARLO, J. A.

Fiber-reinforced monoclinic celsian matrix composite material
[NASA-CASE-LEW-15269-1] p 108 N93-20040

DICARLO, JAMES A.

Creep and stress relaxation modeling of polycrystalline ceramic fibers p 132 A93-31354
Stress-rupture behavior of small diameter polycrystalline alumina fibers
[NASA-TM-106256] p 139 N93-32382

DICICCO, L. D.

Experimental evaluation of a cooled radial-inflow turbine
[AIAA PAPER 93-1795] p 27 A93-49685

DICICCO, L. DANIELLE

Experimental evaluation of a cooled radial-inflow turbine
[NASA-TM-106230] p 38 N93-28697

DICKENS, D. E.

A fuzzy logic based controller for the automated alignment of a laser-beam-smoothing spatial filter
[NASA-TM-105994] p 217 N93-18091

DICKMAN, JOHN ELLIS

Power management and distribution technology p 90 N93-26978

DIEPENBROCK, R. T.

OTV bearing deflection investigation
[NASA-TM-106085] p 215 N93-22994

DIETRICH, DANIEL L.

Combustion of interacting droplet arrays in a microgravity environment p 122 N93-20217

DJIKSTRA, HENK A.

On the structure of cellular solutions in Rayleigh-Benard-Marangoni flows in small-aspect-ratio containers p 164 A93-14762
On the shear stabilization of capillary break-up of finite liquid bridges p 143 A93-32069
The coupling of interfacial instabilities and the stabilization of two-layer annular flows p 178 A93-35482

DILL, L. H.

Thermocapillary bubble migration - An Oseen-like analysis of the energy equation p 179 A93-41708

DIMOFFE, FLORIN

Effect of fluid compressibility on journal bearing performance p 223 A93-49244

DIRLING, RAY B., JR.

SP-100 high-temperature advanced radiator development p 163 A93-13843

DITTMAR, JAMES H.

Cruise noise of an advanced propeller with swirl recovery vanes p 273 A93-28609
A concept for a counterrotating fan with reduced tone noise
[NASA-TM-105736] p 274 N93-11370

DOBRANICH, DEAN

System model development for nuclear thermal propulsion
[NASA-TM-105761] p 80 N93-10457

System model development for nuclear thermal propulsion
[NASA-TM-108157] p 276 N93-16531

System model development for nuclear thermal propulsion
[NASA-TM-108215] p 277 N93-17343

DOCHAT, G. R.

Free-piston Stirling component test power converter test results and potential Stirling applications p 68 A93-25964

DOCHAT, GEORGE R.

Free-piston Stirling Engine system considerations for various space power applications p 252 A93-13826

DODELSON, SCOTT

Microwave anisotropies in the light of the data from the COBE satellite p 291 A93-35444

DOHERTY, MICHAEL P.

NASA's progress in nuclear electric propulsion technology
[AIAA PAPER 93-1936] p 78 A93-53587

Summary and recommendations on nuclear electric propulsion technology for the space exploration initiative
[NASA-TM-105707] p 86 N93-24744

Nuclear electric propulsion for planetary science missions: NASA technology program planning
[NASA-TM-106139] p 88 N93-26210

Nuclear electric propulsion systems overview
[NASA-TM-105913] p 49 N93-26970

NASA's progress in nuclear electric propulsion technology
[NASA-TM-106272] p 93 N93-31858

DOI, TAKAO

Thermocapillary convection in two immiscible liquid layers with free surface p 188 A93-52515

DOLCE, JAMES L.

Automatic system for installation and replacement of Space Station components
[NASA-CASE-LEW-14906-1] p 226 N93-12203

Service equipment for use in hostile environments
[NASA-CASE-LEW-14906-2] p 230 N93-31314

DOLLING, D. S.

Flowfield dynamics in blunt fin-induced shock wave/turbulent boundary layer interactions
[AIAA PAPER 93-3133] p 11 A93-48298

DOMONKOS, MATTHEW

Low power pulsed MPD thruster system analysis and applications
[AIAA PAPER 93-2391] p 76 A93-50156

DONALDSON, K. Y.

Effect of HIPing on the effective thermal conductivity/diffusivity and the interfacial thermal conductance of uniaxial SiC fibre-reinforced RBSN p 100 A93-26674

DOWELL, E. H.

Semi-empirical model for prediction of unsteady forces on an airfoil with application to flutter p 7 A93-31494

DOWELL, EARL H.

An efficient procedure for cascade aeroelastic stability determination using nonlinear, time-marching aerodynamic solvers
[AIAA PAPER 93-1631] p 25 A93-34159

DOWNEY, KEVIN M.

Computer aided design and manufacturing of composite propfan blades for a cruise missile wind tunnel model
[NASA-TM-105269] p 261 N93-12022

DOYCHAK, J.

Technical note - Plasma-sprayed ceramic thermal barrier coatings for smooth intermetallic alloys p 219 A93-15702

Effect of oxidation on the mechanical properties of a NbAl3 alloy at intermediate temperatures p 124 A93-20667

Diffusional transport and predicting oxidative failure during cyclic oxidation of beta-NiAl alloys p 126 A93-50370

SIMS studies of oxide growth on beta-NiAl p 127 A93-53469

Plasma sprayed ceramic thermal barrier coating for NiAl-based intermetallic alloys
[NASA-CASE-LEW-15535-1] p 130 N93-31294

DOYCHAK, JOSEPH

Consecutive plate acoustic suppressor apparatus and methods
[NASA-CASE-LEW-15430-1] p 275 N93-17051

DRAVID, NARAYAN V.

EMTP based stability analysis of Space Station Electric Power System in a test bed environment p 154 A93-26108

EMTP based stability analysis of space station electric power system in a test bed environment
[NASA-TM-105845] p 160 N93-15503

DRENNAN, S. A.

Emission characteristics of a model gas turbine combustor at practical conditions
[ISABE 93-7023] p 31 A93-53999

DRESHFIELD, R. L.

Progress toward a tungsten alloy wire/high temperature alloy composite turbine blade
[NASA-TM-105901] p 128 N93-15586

DRESHFIELD, ROBERT L.

NDE of PWA 1480 single crystal turbine blade material
[NASA-TM-106140] p 38 N93-27640

The effect of porosity and gamma-gamma' eutectic content on the low cycle fatigue behavior of hydrogen-charged PWA-1480 p 130 N93-31576

DREVINSKY, P. J.

Carrier removal and defect behavior in p-type InP p 279 A93-17176

DROTOS, M. N.

New technique for oil backstreaming contamination measurements p 210 A93-44514

DROTOS, MARK N.

Ellipsometric study of metal-organic chemically vapor deposited III-V semiconductor structures p 281 A93-35697

DRUMMOND, CHARLES H., III

Kinetics of hexacelsian-to-celsian phase transformation in SrAl2Si2O8 p 134 A93-40293

Comments on 'Kinetic Study on the Hexacelsian-Celsian Phase Transformation'
[NASA-TM-105917] p 136 N93-14886

Kinetics of hexacelsian to celsian phase transformation in SrAl2Si2O8
[NASA-TM-105913] p 136 N93-16372

DRUMMOND, COLIN K.

Gas turbine system simulation: An object-oriented approach
[NASA-TM-106044] p 36 N93-25673

DRYER, F. L.

Soot agglomeration in isolated, free droplet combustion
[AIAA PAPER 93-0823] p 115 A93-24893

DRYER, FREDERICK L.

Computational/experimental basis for conducting alkane droplet combustion experiments on space-based-platforms p 117 A93-41711

DU, GUANG-WU

Development of braided rope seals for hypersonic engine applications - Flow modeling p 222 A93-34493

Development of braided rope seals for hypersonic engine applications: Flow modeling
[NASA-TM-105942] p 227 N93-14478

DUDENHOEFFER, J.

The NASA CSTI High Capacity Power Project p 69 A93-26105

The NASA CSTI high capacity power project
[NASA-TM-105813] p 48 N93-11398

Venus Interior Structure Mission (VISM): Establishing a seismic network on Venus p 293 N93-28819

DUDENHOEFFER, JAMES E.

Heat transfer in oscillating flows with sudden change in cross section p 174 A93-26089

DUFFLOCQ, M.

Initial development of the two-dimensional ejector shear layer - Experimental results
[AIAA PAPER 93-2440] p 29 A93-50192

E

- Comparison of the initial development of shear layers in two-dimensional and axisymmetric ejector configurations [AIAA PAPER 93-2441] p 29 A93-50193
- DUFFY, S. F.**
Reliability analysis of laminated ceramic matrix composites using shell subelement techniques p 243 A93-55382
- DUFFY, STEPHEN F.**
Reliability analysis of structural ceramic components using a three-parameter Weibull distribution [ASME PAPER 92-GT-296] p 231 A93-19486
- DUGAN, EDWARD T.**
Ultrahigh temperature vapor-core reactor - Magnetohydrodynamic system for space nuclear electric power p 66 A93-21663
- DUKE, JOHN C., JR.**
Nondestructive evaluation of a ceramic matrix composite material p 102 A93-33016
- DUNCAN, B. S.**
A multiple-scale turbulence model for incompressible flow [AIAA PAPER 93-0086] p 170 A93-24228
- DUNCAN, D. B.**
A plume spectroscopy system for flight applications [AIAA PAPER 93-2511] p 63 A93-50242
- DUNN, M. G.**
Time-averaged heat transfer and pressure measurements and comparison with prediction for a two-stage turbine [ASME PAPER 92-GT-194] p 166 A93-19419
- DUNNING, J. E.**
New technique for oil backstreaming contamination measurements p 210 A93-44514
- DURAJ, STAN A.**
Room temperature synthesis of copper indium diselenide in non-aqueous solution using an organoindium reagent p 283 A93-54844
- DURING, W. W.**
Low gravity environment on-board Columbia during STS-40 [AIAA PAPER 93-0833] p 142 A93-24903
- DUSEY, M.**
Acoustic radiation from a thin airfoil in nonuniform subsonic flows p 273 A93-23535
- DUSTIN, MILES O.**
The ground testing of a 2 kWe solar dynamic space power system p 68 A93-25918
- DUVAL, W. M. B.**
Self-tuning multivariable pole placement control of a multizone crystal growth furnace p 263 A93-10575
- DUVAL, WALTER M. B.**
Convective effects during the physical vapor transport process. I - Thermal convection p 179 A93-36575
Convective effects during the physical vapor transport process. II - Thermosolutal convection p 180 A93-42424
Numerical study of mixing of two fluids under low gravity [NASA-TM-105865] p 194 A93-14914
Physical vapor transport of mercurous chloride under a nonlinear thermal profile [NASA-TM-105920] p 196 A93-16612
- DUYAR, A.**
Implementation of a model based fault detection and diagnosis technique for actuation faults of the SSME p 47 A93-16413
Implementation of a model based fault detection and diagnosis for actuation faults of the Space Shuttle main engine [NASA-TM-105781] p 49 A93-11401
Real-time diagnostics for a reusable rocket engine [NASA-TM-105792] p 266 A93-19018
- DUYAR, AHMET**
Identification of the open loop dynamics of the T700 turboshaft engine p 26 A93-35934
Identification of propulsion systems [NASA-TM-106007] p 35 A93-20109
- DWOYER, DOUGLAS L.**
The new challenge of computational aeroscience p 2 A93-14169
The NASA Computational Fluid Dynamics (CFD) program - Building technology to solve future challenges [AIAA PAPER 93-3292] p 287 A93-44996
- DYBBS, ALEXANDER**
Laser anemometry - Advances and applications 1991; Proceedings of the 4th International Conference, Cleveland, OH, Aug. 5-9, 1991. Vols. 1 & 2 [ISBN 0-7918-0654-5] p 206 A93-23776
- DZIEDZIC, WILLIAM M.**
Design of a hypersonic waverider-derived airplane [AIAA PAPER 93-0401] p 55 A93-21108
- EBIHARA, BEN T.**
Interim report on the analysis of the microwave power module [NASA-TM-106012] p 160 A93-16713
- ECKEL, ANDREW J.**
Effect of hydrogen on the strength and microstructure of selected ceramics p 130 A93-13613
Ceramic matrix composites for rocket engine turbine applications [ASME PAPER 92-GT-394] p 99 A93-19547
- EDELMAN, AMY L.**
Titan III feasibility for HL-20 prototype missions p 50 A93-53747
- EDELMAN, RAYMOND B.**
Effects of buoyancy on laminar, transitional, and turbulent gas jet diffusion flames p 121 A93-20189
- EDMOND, J. A.**
Aluminum acceptor four particle bound exciton complex in 4H, 6H, and 3C SiC p 282 A93-44822
- EDWARDS, JONATHAN L.**
Monte Carlo modeling of atomic oxygen attack of polymers with protective coatings on LDEF p 138 A93-28282
- EHRESMAN, C. M.**
Two and three-dimensional predifuser combustor studies with air-water mixture [AIAA PAPER 93-0240] p 113 A93-22652
- EIFLER, P.**
Pdf prediction of supersonic hydrogen flames [AIAA PAPER 93-0448] p 114 A93-23358
- EISEMAN, PETER R.**
Algebraic grid generation with control points p 268 A93-45967
- EL-GENK, MOHAMED S.**
Space nuclear power systems; Proceedings of the 8th Symposium, Albuquerque, NM, Jan. 6-10, 1991. Pts. 1-3 [ISBN 0-88318-838-4] p 64 A93-13751
Estimates of power requirements for a Manned Mars Rover powered by a nuclear reactor p 45 A93-13783
Shielding analysis for a manned Mars rover powered by an SP-100 type reactor p 45 A93-13793
Heat-pipe transient model for space applications p 163 A93-13867
Mechanisms of voids formation during cooldown and freezing of lithium in SP-100 type systems p 163 A93-13916
Space nuclear power systems 1989; Proceedings of the 6th Symposium, Albuquerque, NM, Jan. 8-12, 1989. Vols. 1 & 2 [ISBN 0-89464-030-5] p 66 A93-20752
Closed Brayton Cycle power system with a high temperature pellet bed reactor heat source for NEP applications [NASA-TM-105933] p 82 A93-14482
- ELGIN, STEPHEN D.**
Structural dynamic testing of composite propfan blades for a cruise missile wind tunnel model [NASA-TM-105272] p 247 A93-18875
- ELLIOTT, G. S.**
On streamwise vortices in high Reynolds number supersonic axisymmetric jets p 167 A93-21060
- ELLIOTT, GREGORY S.**
Molecular filter-based diagnostics in high speed flows [AIAA PAPER 93-0512] p 205 A93-23259
A study of compressible mixing layers using filtered Rayleigh scattering [AIAA PAPER 92-0175] p 173 A93-24982
- ELLIS, C.**
Thin film diamond microstructure applications p 209 A93-40580
- ELLIS, DAVID L.**
Graphite fiber/copper matrix composites for space power heat pipe fin applications p 162 A93-13789
Thermal conductivity and thermal expansion of graphite fiber-reinforced copper matrix composites p 100 A93-25104
- ELLIS, J. R.**
Evolution of damage and plasticity in titanium-based, fiber-reinforced composites p 104 A93-48498
- ELLIS, JOHN R.**
Experimental investigation of cyclic thermomechanical deformation in torsion [NASA-TM-105938] p 247 A93-17996
- ELLISON, J.**
Evaluation of passive and active vibration control mechanisms in a microgravity environment [AIAA PAPER 93-0838] p 55 A93-24905
- ENGELSTAD, S. P.**
Probabilistic micromechanics for metal matrix composites p 237 A93-32465
Probabilistic nonlinear finite element analysis of composite structures p 237 A93-32717
- ENGLERT, GERALD W.**
Damping and scattering of electromagnetic waves by small ferrite spheres suspended in an insulator [NASA-TM-105837] p 149 A93-12366
- ENGLISH, ROBERT E.**
Evolving SP-100 powerplants via electric propulsion to GEO and lunar orbit p 70 A93-34492
- ENVIA, EDMANE**
An asymptotic theory of supersonic propeller noise p 271 A93-19169
- ERBEZNIK, RAYMOND M.**
Assessment of 25 kW free-piston Stirling technology alternatives for solar applications p 254 A93-26072
- ERNST, MICHAEL A.**
Evaluation of MARC for the analysis of rotating composite blades [NASA-TM-4423] p 249 A93-24909
- ESFAHANIAN, V.**
Effects of free-stream turbulence on boundary-layer transition [AIAA PAPER 93-0488] p 170 A93-23390
- ESKER, BARBARA S.**
Performance characteristics of a variable-area vane nozzle for vectoring an ASTOVL exhaust jet up to 45 deg [AIAA PAPER 93-2437] p 29 A93-50189
Effects of flow-path variations on internal reversing flow in a tailpipe offtake configuration for ASTOVL aircraft [AIAA PAPER 93-2438] p 29 A93-50190
Experimental performance of a ventral nozzle with pitch and yaw vectoring capability for SSTOVL aircraft [NASA-TM-106054] p 36 A93-25129
Performance characteristics of a variable-area vane nozzle for vectoring an ASTOVL exhaust jet up to 45 deg [NASA-TM-106114] p 37 A93-27131
Effects of flow-path variations on internal reversing flow in a tailpipe offtake configuration for ASTOVL aircraft [NASA-TM-106149] p 38 A93-29065
- EUBANKS, STEVEN W.**
ISDN at NASA Lewis Research Center [NASA-TM-105911] p 262 A93-12410
- EUSTACE, J. G.**
RF modulated fiber optic sensing systems and their applications p 211 A93-49469
- EUSTACE, JOHN G.**
Fiberoptic sensing technique employing RF modulated interferometry p 212 A93-53110
- EVANS, AUSTIN L.**
Multidisciplinary propulsion simulation using NPSS [AIAA PAPER 92-4709] p 270 A93-20318
- EVERSMAN, WALTER**
Comparison of radiated noise from shrouded and unshrouded propellers p 274 A93-55861
- EYSSA, YEHIA M.**
Actively controlled superconducting bearings p 223 A93-48594

F

- FABIK, RICHARD H.**
Using silicon diodes for detecting the liquid-vapor interface in hydrogen p 209 A93-37864
Techniques for improving the accuracy of cryogenic temperature measurement in ground test programs p 212 A93-54363
Techniques for improving the accuracy of cryogenic temperature measurement in ground test programs [NASA-TM-105996] p 215 A93-22484
- FAETH, G. M.**
Structure of soot-containing laminar jet diffusion flames [AIAA PAPER 93-0708] p 114 A93-24804
- FAGHRI, A.**
Closed-form analytical solutions of high-temperature heat pipe startup and frozen startup limitation p 165 A93-18564
Simulation of the early startup period of high-temperature heat pipes from the frozen state by a rarefied vapor self-diffusion model p 175 A93-30127
A numerical analysis of high-temperature heat pipe startup from the frozen state p 175 A93-30128
- FAGHRI, AMIR**
A study of circumferentially-heated and block-heated heat pipes. I - Experimental analysis and generalized analytical prediction of capillary limits. II - Three-dimensional numerical modeling as a conjugate problem p 168 A93-21715
- FAN, SIXIN**
A simplified Reynolds stress model for unsteady turbulent boundary layers [AIAA PAPER 93-0204] p 168 A93-22622
Low-Reynolds-number k-epsilon model for unsteady turbulent boundary-layer flows p 14 A93-53208

- FANG, HO**
Fracture toughness of advanced ceramics at room temperature p 131 A93-20842
- FANG, J.**
Numerical solutions for unsteady subsonic vortical flows around loaded cascades [ASME PAPER 92-GT-173] p 3 A93-19399
- FARMER, S. C.**
Sliding wear of self-mated Al₂O₃-SiC whisker-reinforced composites at 23-1200 C p 101 A93-29948
- FARMER, SERENE C.**
Microchemical analysis of the SCS-6 silicon carbide fiber p 135 A93-53734
- FAROKHI, S.**
Computational study of advanced exhaust system transition ducts with experimental validation p 7 A93-34490
- FARRELL, P. V.**
Droplet vaporization in a high-pressure gas p 190 A93-55461
- FATEMI, N. S.**
Non-destructive, ultra-low resistance, thermally stable contacts for use on shallow junction InP solar cells [NASA-TM-106228] p 256 A93-32201
- FATEMI, NAVID S.**
The structural and electrical properties of low-resistance Ni contacts to InP p 151 A93-24367
Low resistance silver contacts to indium phosphide - Electrical and metallurgical considerations p 157 A93-39351
Simple, extremely low resistance contact system to n-InP that does not exhibit metal-semiconductor intermixing during sintering p 157 A93-42550
Texturing of InP surfaces for device applications [NASA-TM-106061] p 129 A93-28618
- FATUZZO, MARCO**
Extension of the Parker bound on the flux of magnetic monopoles p 291 A93-38672
- FAUR, MARIA**
Closed-ampoule diffusion of sulfur into Cd-doped InP substrates - Dependence of S profiles on diffusion temperature and time p 283 A93-51917
- FAUR, MIRCEA**
Closed-ampoule diffusion of sulfur into Cd-doped InP substrates - Dependence of S profiles on diffusion temperature and time p 283 A93-51917
- FAY, EDGAR H.**
Evaluation of the benefits of high temperature electronics for lunar power systems p 153 A93-25896
- FEILER, CHARLES E.**
Institute for Computational Mechanics in Propulsion (ICOMP) [NASA-TM-106155] p 269 A93-27061
- FELDER, JAMES L.**
Predicted performance of an integrated Modular Engine system [AIAA PAPER 93-1888] p 72 A93-49761
- FELICELLI, S. D.**
Numerical model for dendritic solidification of binary alloys p 282 A93-46729
- FELICELLI, SERGIO**
Thermosolutal convection during dendritic solidification of a binary alloy p 182 A93-45975
- FELIPPA, CARLOS A.**
Membrane triangles with corner drilling freedoms. I - The EFF element p 235 A93-24303
Membrane triangles with corner drilling freedoms. II - The ANDES element p 235 A93-24304
Membrane triangles with corner drilling freedoms. III - Implementation and performance evaluation p 236 A93-24305
- FENG, J.**
CFD analyses of coolant channel flowfields [AIAA PAPER 93-1830] p 184 A93-49715
- FENG, WEI**
Interference patterns in the Spacelab 2 plasma wave data - Oblique electrostatic waves generated by the electron beam p 257 A93-16347
- FERBER, MATTISON K.**
Effects of precracking methods on the fracture properties of alumina p 131 A93-16645
Elevated-temperature fracture resistances of monolithic and composite ceramics using chevron-notched bend tests p 133 A93-38888
- FERGUSON, D.**
The NASA CSTI High Capacity Power Project p 69 A93-26105
The NASA CSTI high capacity power project [NASA-TM-105813] p 48 A93-11398
- FERGUSON, DALE C.**
Interactions between spacecraft and their environments [AIAA PAPER 93-0705] p 55 A93-24801
Solar array module plasma interactions experiment (SAMPIE) - Science and technology objectives p 71 A93-46418
- Environmental interactions and the SP-100 power system [NASA-TM-105866] p 84 A93-18877
Space environmental interactions for the space exploration initiative p 293 A93-26396
Solar Array Module Plasma Interaction Experiment (SAMPIE) p 62 A93-28716
- FERRKUL, PAUL V.**
Numerical computation of low-speed concurrent flow flame spread in mixed buoyant and forced flow [AIAA PAPER 93-0827] p 115 A93-24897
Combustion of solid fuel in very low speed oxygen streams p 122 A93-20207
- FERNANDEZ-PELLO, A. C.**
Experimental observations of the effect of gravity changes on smoldering combustion [AIAA PAPER 93-0829] p 116 A93-24899
- FERRANTE, JOHN**
Heats of formation of bcc binary alloys p 123 A93-17609
Method for calculating alloy energetics p 279 A93-18740
Determination of parameters of a method for predicting alloy properties p 126 A93-39796
Global expression for representing cohesive-energy curves. II p 276 A93-44989
Extension of a new semiempirical method (BFS) and the study of ground state properties of binary alloys p 283 A93-52600
Multilayer relaxation and surface energies of fcc and bcc metals using equivalent crystal theory p 119 A93-52872
Heat of segregation of single substitutional impurities p 119 A93-52873
Determination of parameters of a new method for predicting alloy properties [NASA-TM-105895] p 127 A93-11609
- FERTIS, D. G.**
Grounding of space structures p 54 A93-12144
A new pre-loaded beam geometric stiffness matrix with full rigid body capabilities p 54 A93-12145
- FIELDS, B.**
The boron-to-beryllium ratio in halo stars - A signature of cosmic-ray nucleosynthesis in the early Galaxy p 292 A93-55061
- FIELDS, BRIAN D.**
Primordial nucleosynthesis and the abundances of beryllium and boron p 290 A93-33513
Population II Li-6 as a probe of nucleosynthesis and stellar structure and evolution p 292 A93-56494
- FINKE, A. K.**
Design and test of a small two stage counter-rotating turbine for rocket engine application [AIAA PAPER 93-2136] p 74 A93-49954
- FINN, R.**
On accurate determination of contact angle p 143 A93-41678
- FINN, ROBERT**
An interface configuration experiment on USML-1 [AIAA PAPER 93-0253] p 169 A93-22662
- FINNEY, M. J.**
Optical fiber sensor for temperature measurement from 600 to 1900 C in gas turbine engines p 208 A93-32918
Flight testing of a fiber optic temperature sensor p 22 A93-49476
- FISCHER, DAVID J.**
Vector formulation for interferogram surface fitting p 278 A93-55687
- FITE, E. BRIAN**
Fabrication of composite propan blades for a cruise missile wind tunnel model [NASA-TM-105270] p 249 A93-26202
- FLATICO, JOSEPH M.**
Fourier transform spectrometry for fiber-optic sensor systems p 211 A93-49459
Fiber-optic thermometer using Fourier transform spectroscopy p 212 A93-53104
- FLEETER, SANFORD**
Forcing function effects on unsteady aerodynamic gust response. I - Forcing functions [ASME PAPER 92-GT-174] p 3 A93-19400
Forcing function effects on unsteady aerodynamic gust response. II - Low solidity airfoil row response [ASME PAPER 92-GT-175] p 3 A93-19401
Prediction of active control of subsonic centrifugal compressor rotating stall [AIAA PAPER 93-0153] p 4 A93-22591
A model for the selective amplification of spatially coherent waves in a centrifugal compressor on the verge of rotating stall [AIAA PAPER 93-2236] p 13 A93-50039
Forcing function modeling for flow induced vibration [ISABE 93-7027] p 31 A93-54003
- FLEMIG, D. P.**
Magnetic bearings for free-piston Stirling engines p 221 A93-26079
- FLEMING, MICHAEL L.**
On protection of Freedom's solar dynamic radiator from the orbital debris environment. I - Preliminary analysis and testing p 70 A93-36197
On protection of Freedom's solar dynamic radiator from the orbital debris environment. II - Further testing and analyses p 70 A93-36589
- FLOOD, D. J.**
Diffusion length variation and proton damage coefficients for InP/In(x)Ga(1-x)As/GaAs solar cells p 159 A93-55324
- FLOOD, DENNIS J.**
Advanced photovoltaic power system technology for lunar base applications p 255 A93-14004
Diffusion length variation in 0.5- and 3-MeV-proton-irradiated, heteroepitaxial indium phosphide solar cells [NASA-TM-106147] p 161 A93-27002
- FOERSTER, GEORGE**
Initial study of void formation during aluminum solidification in reduced gravity p 142 A93-12013
- FOLEY, MICHAEL**
Fracture toughness of advanced ceramics at room temperature p 131 A93-20842
- FOLLEN, GREGORY J.**
Multidisciplinary propulsion simulation using NPSS [AIAA PAPER 92-4709] p 270 A93-20318
Gas turbine system simulation: An object-oriented approach [NASA-TM-106044] p 36 A93-25673
- FOLTYN, S. R.**
Buffer layers for high-Tc thin films on sapphire p 150 A93-17063
- FONG, DON**
Description of the PMAD systems test bed facility and data system p 47 A93-26102
- FOONG, F.**
Low temperature phase formation of Ti-based superconducting thin films in reduced oxygen atmosphere p 282 A93-44568
- FORCE, DALE A.**
A high-efficiency 59- to 64-GHz TWT for intersatellite communications p 158 A93-49553
Interim report on the analysis of the microwave power module [NASA-TM-106012] p 160 A93-16713
- FORKAPA, MARK**
Degradation of radiator performance on Mars due to dust p 59 A93-15616
- FORKAPA, MARK J.**
Thermal emittance enhancement of graphite-aluminum and graphite-copper composite radiator surfaces for space power applications p 105 A93-53455
- FORKEY, JOSEPH**
Time-sequenced and spectrally filtered Rayleigh imaging of shock wave and boundary layer structure for inlet characterization [AIAA PAPER 93-2300] p 211 A93-50085
- FORNEY, L. J.**
Measurement of frequency response in short thermocouple wires p 209 A93-40677
- FOSTER, M. R.**
Non-parallel effects in the instability of Long's vortex p 164 A93-16663
- FOX, NEIL**
GSFC conceptual design study for an inter-satellite Optical Multiple Access communication system p 52 A93-18966
- FRALICK, G. C.**
Measurement of frequency response in short thermocouple wires p 209 A93-40677
- FRALICK, GUSTAVE C.**
Dynamic gas temperature measurements using a personal computer for data acquisition and reduction [NASA-TM-106119] p 261 A93-27024
- FRANCISCO, DAVID R.**
Electrical design of payload G-534: The Pool Boiling Experiment p 144 A93-13170
Battery selection for space experiments p 159 A93-13184
Battery selection for Space Shuttle experiments [NASA-TM-106142] p 61 A93-27038
Electrical design of Space Shuttle payload G-534: The pool boiling experiment [NASA-TM-106143] p 62 A93-27260
- FRANCISCUS, LEO C.**
The multi-heat addition turbine engine [AIAA PAPER 92-4272] p 22 A93-13334
Multi-heat addition turbine engine [NASA-CASE-LEW-15094-1] p 35 A93-22034

FRANKENFIELD, BRUCE

Fluid design studies of integrated modular engine system
[AIAA PAPER 93-1887] p 72 A93-49760

FRANKLIN, J. E.

Hydrocarbon-fuel/copper combustion chamber liner compatibility, corrosion prevention, and refurbishment
p 139 A93-14510

FRASCA, A. J.

Neutron, gamma ray, and temperature effects on the electrical characteristics of thyristors
p 153 A93-25894

FRASCA, ALBERT J.

Radiation and temperature effects on electronic components investigated under the CSTI high capacity power project
[NASA-TM-106096] p 161 N93-24746

FRATE, DAVID T.

Basic statistical analyses of candidate nickel-hydrogen cells for the Space Station Freedom
[NASA-TM-106111] p 270 N93-27124

FRAZHO, A. E.

A note on decentralized integral controllability
p 264 A93-30492

FREED, ALAN D.

High temperature viscoplastic ratchetting - Material response or modeling artifact p 233 A93-13823
Effect of strain and stress on the relative dimensions of the 'hard' and 'soft' regions in crept NaCl single crystals p 279 A93-17513
Stirling engine - Approach for long-term durability assessment p 120 A93-26069
Viscoplasticity with creep and plasticity bounds p 125 A93-32925

The effect of multiple compliant layers at the fiber-matrix interface on residual thermal stresses in metal matrix composites p 104 A93-42085
Ratchetting behavior in viscoplasticity - A technical note p 241 A93-43651

The effect of fiber microstructure on evolution of residual stresses in silicon carbide/titanium aluminide composites p 106 A93-54771

Thermoviscoplastic analysis of fibrous periodic composites using triangular subvolumes
[NASA-TM-106076] p 111 N93-29074

Bounds on internal state variables in viscoplasticity
[NASA-TM-106215] p 251 N93-29196

FRESE, KATHERINE

Extension of the Parker bound on the flux of magnetic monopoles p 291 A93-38672

FRIEDMAN, G.

Transition of oscillatory flow in tubes - An empirical model for application to Stirling engines p 174 A93-26088

FRIEDMAN, ROBERT

Contributions of microgravity test results to the design of spacecraft fire-safety systems p 56 A93-31028
[AIAA PAPER 93-1152]
Fire safety practices in the Shuttle and the Space Station Freedom p 59 N93-20204
Contributions of microgravity test results to the design of spacecraft fire safety systems
[NASA-TM-106093] p 60 N93-24755

FRIEMAN, JOSHUA A.

Dark matter, long-range forces, and large-scale structure p 288 A93-11876
Large- and small-scale constraints on power spectra in $\Omega_m = 1$ universes p 290 A93-23990
Dark matter and the equivalence principle p 291 A93-44385

FRONEK, DENNIS

Initial results from the NASA Lewis wave rotor experiment
[AIAA PAPER 93-2521] p 30 A93-53589

Initial results from the NASA-Lewis wave rotor experiment
[NASA-TM-106148] p 39 N93-32368

FRY, J. N.

The three-point correlation function in an ensemble of three-dimensional simulations p 291 A93-50680
Biasing and hierarchical statistics in large-scale structure p 292 A93-55051

FRYE, ROBERT J.

Overview and evolution of the LeRC PMAD DC test bed p 47 A93-26099

FU, B.

Self-organization in neural networks - Applications in structural optimization p 265 A93-54534

FUJIKAWA, G.

Analysis of reflector antenna system including frequency selective surfaces p 52 A93-32820

FUJIKAWA, GENE

SITE project. Phase 1: Continuous data bit-error-rate testing
[NASA-TP-3279] p 58 N93-11001

FUKUSHIMA, JUNICHI

Applications to car bodies - Generalized layout design of three-dimensional shells p 243 A93-54509

FULLER, E. J.

Integrated CFD modeling of gas turbine combustors
[AIAA PAPER 93-2196] p 28 A93-50008

FULTON, CHRISTOPHER

Qualitative model-based diagnostics for rocket systems
[AIAA PAPER 93-1779] p 72 A93-49674

Qualitative model-based diagnostics for rocket systems
[NASA-TM-106234] p 51 N93-28052

FURNAS, RANDALL B.

Design and implementation of a pilot orientation program for new NASA engineering employees
[NASA-TM-105907] p 286 N93-26205

G**GABB, T. P.**

Fatigue-environment interactions in a SiC/Ti-15-3 composite p 100 A93-26275
A model for predicting high-temperature fatigue failure of a W/Cu composite p 112 N93-31579

GABB, TIMOTHY P.

The effect of porosity and gamma-gamma' eutectic content on the low cycle fatigue behavior of hydrogen-charged PWA-1480 p 130 N93-31576

GAETA, C. J.

Erosion rate diagnostics in ion thrusters using laser-induced fluorescence p 70 A93-34481

GAGE, M. L.

Hydrocarbon-fuel/copper combustion chamber liner compatibility, corrosion prevention, and refurbishment
p 139 A93-14510

GAIER, J. R.

Heat transfer device
[NASA-CASE-LEW-14162-4] p 108 N93-20568

GAIER, JAMES R.

Effects of dust accumulation and removal on radiator surfaces on Mars p 123 A93-13937

Properties of hybrid CVD/PAN graphite fibers and their bromine intercalation compounds p 98 A93-17675
Intercalated graphite fiber composites as EMI shields in aerospace structures p 104 A93-41573

Lunar and Martian environmental interactions with nuclear power system radiators
[NASA-TM-105747] p 80 N93-10965

Degradation of radiator performance on Mars due to dust p 59 N93-15616

Apparatus for intercalating large quantities of fibrous structures
[NASA-CASE-LEW-15077-2] p 111 N93-29609

Semiconductor cooling apparatus
[NASA-CASE-LEW-14162-3] p 111 N93-29614

Method for producing hybrid graphite composite
[NASA-CASE-LEW-15241-2] p 112 N93-31296

GAJJAR, J. S. B.

Nonlinear evolution of modes in a compressible boundary layer p 164 A93-17258

Nonlinear evolution of the first mode supersonic oblique waves in compressible boundary layers. Part 1: Heated/cooled walls
[NASA-TM-106087] p 199 N93-25175

GALLAGHER, RICHARD H.

Integrated force method - Compatibility conditions of structural mechanics for finite element analysis
p 237 A93-32459

GALLUP, DONALD R.

Lunar in-core thermionic nuclear reactor power system conceptual design p 46 A93-13836

GAMMON, ROBERT W.

The susceptibility critical exponent for a nonaqueous ionic binary mixture near a consolute point p 284 A93-19838

Measurement of the temperature coefficient of ratio transformers p 155 A93-32771

Statistical fitting accuracy in photon correlation spectroscopy p 277 A93-52414

GAO, Q.

Single-parameter characterization of discrete-dislocation pileup tipfield and its application to physically based micro-mechanics p 233 A93-12119

GARCIA, G. A.

Demonstration of Y1Ba2Cu3O(7-delta) and complementary metal-oxide-semiconductor device fabrication on the same sapphire substrate p 159 A93-56292

GARDINER, ROBIN A.

Single liquid source plasma-enhanced metalorganic chemical vapor deposition of high-quality YBa2Cu3O(7-x) thin films p 280 A93-20643

GARG, S.

Design and evaluation of a robust dynamic neurocontroller for a multivariable aircraft control problem p 40 A93-37004

GARG, SANJAY

Robust integrated flight/propulsion control design for a STOVL aircraft using H-infinity control design techniques p 40 A93-26432

Neurocontrol design and analysis for a multivariable aircraft control problem p 40 A93-41894

Application of controller partitioning optimization procedure to integrated flight/propulsion control design for a STOVL aircraft p 40 A93-51361

A parameter optimization approach to controller partitioning for integrated flight/propulsion control application p 41 A93-54268

Propulsion system performance resulting from an integrated flight/propulsion control design
[NASA-TM-105874] p 34 N93-15525

Controller partitioning for integrated flight/propulsion control implementation
[NASA-TM-105804] p 41 N93-21197

A modified approach to controller partitioning
[NASA-TM-106167] p 266 N93-28051

GARG, V. K.

A study of the effects of macrosegregation and buoyancy-driven flow in binary mixture solidification p 180 A93-44223

GARLICK, RALPH G.

The chemistry of Saudi Arabian sand - A deposition problem on helicopter turbine airfoils p 243 A93-53466

GARSCADDEN, ALAN

Friction and wear of plasma-deposited diamond films
[NASA-TM-105926] p 136 N93-19035

GAUGLER, RAYMOND E.

Overview of aerothermodynamic loads definition study p 93 N93-31583
Summary of NASA, Lewis Research Center validation efforts p 204 N93-70579

GAUSTAD, KRISTA L.

A study of electric power transmission lines for use on the lunar surface p 46 A93-13901

GAYDA, J.

Fatigue-environment interactions in a SiC/Ti-15-3 composite p 100 A93-26275

GAYDA, JOHN

An overview of elevated temperature damage mechanisms and fatigue behavior of a unidirectional SCS-6/Ti-15-3 composite p 109 N93-26702

The effect of porosity and gamma-gamma' eutectic content on the low cycle fatigue behavior of hydrogen-charged PWA-1480 p 130 N93-31576

GAZTANAGA, ENRIQUE

N-point correlation functions in the CIA and SSRS redshift distribution of galaxies p 288 A93-10615

Probing the statistics of primordial fluctuations and their evolution p 290 A93-24627

Biasing and hierarchical statistics in large-scale structure p 292 A93-55051

GEBAUER, LINDA

LDEF yaw and pitch angle estimates p 58 N93-12772

The use of plasma ashers and Monte Carlo modeling for the projection of atomic oxygen durability of protected polymers in low Earth orbit p 58 N93-15596

Monte Carlo modeling of atomic oxygen attack of polymers with protective coatings on LDEF p 138 N93-28282

GEDNEY, RICHARD T.

Advanced Communications Technology Satellite (ACTS) p 52 A93-24456

GEDWILL, MICHAEL

High temperature, oxidation resistant noble metal-Al alloy thermocouple
[NASA-CASE-LEW-15515-1] p 217 N93-31298

GELB, JAMES M.

Implications of new GALLEX results for the Mikheyev-Smirnov-Wolfenstein solution of the solar neutrino problem p 293 A93-10357

Large- and small-scale constraints on power spectra in $\Omega_m = 1$ universes p 290 A93-23990

GENERAZIO, EDWARD R.

Nondestructive evaluation of ceramic and metal matrix composites for NASA's HITEMP and enabling propulsion materials programs
[NASA-TM-105807] p 231 N93-10963

GENG, STEVEN M.

Comparison of GLIMPS and HFAST Stirling engine code predictions with experimental data p 220 A93-26052

Overview of NASA supported Stirling thermodynamic loss research p 174 A93-26087

GEORGE, JEFFREY A.

The 20 kWe NEP system studies p 90 N93-26971

- The 100-500 kWe NEP systems p 90 N93-26984
Nuclear electric propulsion options for piloted Mars missions p 90 N93-26985
NEP systems model p 90 N93-26986
NEP systems model p 91 N93-26987
- GEORGE, WILLIAM K.**
Experiments on a round turbulent buoyant plume [NASA-TM-105955] p 141 N93-16384
- GESSNER, F. B.**
A numerical investigation of supersonic strut/endwall interactions in annular flow with varying strut thickness [AIAA PAPER 93-2927] p 10 A93-48128
Experimental and numerical investigation of supersonic turbulent flow in an annular duct [AIAA PAPER 93-3123] p 11 A93-48291
Investigation of a strut/endwall interaction in supersonic annular flow [AIAA PAPER 93-1925] p 12 A93-49791
- GHORASHI, BAHMAN**
Simplified jet fuel reaction mechanism for lean burn combustion application [AIAA PAPER 93-0021] p 113 A93-23238
Laser anemometry - Advances and applications 1991: Proceedings of the 4th International Conference, Cleveland, OH, Aug 5-9, 1991. Vols. 1 & 2 [ISBN 0-7918-0654-5] p 206 A93-23776
A review of chemically reactive turbulent flow mixing mechanisms and a new design for a low NO(x) combustor p 27 A93-49508
A thermal NO(x) prediction model - Scalar computation module for CFD codes with fluid and kinetic effects [AIAA PAPER 93-2378] p 119 A93-50147
Simplified jet-A kinetic mechanism for combustor application [NASA-TM-105940] p 120 N93-15504
Nitric oxide formation in a lean, premixed-prevaporized jet A/air flame tube: An experimental and analytical study [NASA-TM-105722] p 257 N93-27012
- GHOSH, ASISH**
Elevated-temperature fracture resistances of monolithic and composite ceramics using chevron-notched bend tests p 133 A93-38888
- GHOSH, LOUIS J.**
Analytical stress intensity solution for the Stable Poisson Loaded specimen p 242 A93-46768
Numerical calibration of the stable poisson loaded specimen [NASA-TM-105609] p 245 N93-12738
- GIBB, JAMES**
Study on vortex generator flow control for the management of inlet distortion p 7 A93-34488
- GIBSON, THERESA L.**
Icing Research Tunnel rotating bar calibration measurement system p 212 A93-54398
Icing research tunnel rotating bar calibration measurement system [NASA-TM-106010] p 215 N93-22598
Ice thickness measurement system for the icing research tunnel calibration [NASA-TM-106095] p 215 N93-24737
- GIEL, P. W.**
An algebraic turbulence model for three-dimensional viscous flows [AIAA PAPER 93-0083] p 4 A93-22552
An algebraic turbulence model for three-dimensional viscous flows [NASA-TM-105931] p 1 N93-14102
- GIEL, PAUL W.**
Three-dimensional Navier-Stokes heat transfer predictions for turbine blade rows [NASA-TM-105800] p 196 N93-19969
- GILKEY, SAMUEL**
Engine technology challenges for a 21st Century High-Speed Civil Transport [ISABE 93-7064] p 31 A93-54040
Engine technology challenges for a 21st Century High-Speed Civil Transport [NASA-TM-106216] p 39 N93-31671
- GILLAND, JAMES H.**
Low power pulsed MPD thruster system analysis and applications [AIAA PAPER 93-2391] p 76 A93-50156
- GILLAND, JIM**
The 20 kWe NEP flight system p 90 N93-26983
NEP systems model p 90 N93-26986
Thruster models for NEP system analysis p 91 N93-26988
- GINSBURG, MARC A.**
Monte Carlo analysis of the Titan III/ Transfer Orbit Stage guidance system for the Mars Observer mission [AIAA PAPER 93-3889] p 50 A93-51473
- GINTY, CAROL A.**
Overview of NASA's advanced high temperature engine materials technology program p 94 A93-53453
- Second generation integrated composite analyzer (ICAN) computer code [NASA-TP-3290] p 108 N93-18139
- GIOVANGIOLI, V.**
Analytical and numerical modeling of flame-balls in hydrogen-air mixtures p 118 A93-46009
- GIVI, PEYMAN**
Direct numerical simulations of a reacting turbulent mixing layer by a pseudospectral-spectral element method p 182 A93-45974
- GLADDEN, HERBERT J.**
Design of a high-temperature experiment for evaluating advanced structural materials [NASA-TM-105833] p 245 N93-11624
Summary of experimental heat-transfer results from the turbine hot section facility [NASA-TP-3250] p 197 N93-23059
Hypersonic engine component experiments in high heat flux, supersonic flow environment [NASA-TM-106273] p 203 N93-31860
- GLICKSMAN, M. E.**
IDGE - A test of dendritic growth theory using space flight [AIAA PAPER 93-0260] p 143 A93-25515
Scientific basis for the Isothermal Dendritic Growth Experiment - A USMP-2 space flight experiment p 143 A93-50455
- GLOSSER, GREGORY D.**
The detrimental effect of friction on space microgravity robotics p 222 A93-35546
- GLOVER, DANIEL**
Compressing subbanded image data with Lempel-Ziv-based coders [NASA-TM-105998] p 149 N93-20257
Subband coding for image data archiving p 287 N93-25922
- GLOVER, DANIEL R.**
Picture data compression coder using subband/transform coding with a Lempel-Ziv-based coder [NASA-CASE-LEW-15700-1] p 287 N93-28130
- GOKOGLU, S. A.**
Prediction of chemical vapor deposition rates on monofilaments and its implications for fiber properties p 113 A93-17198
A kinetic and equilibrium analysis of silicon carbide chemical vapor deposition on monofilaments [NASA-TM-106137] p 96 N93-27003
- GOKOGLU, SULEYMAN A.**
Chemical vapor deposition modeling for high temperature materials p 116 A93-39503
CVD of silicon carbide on structural fibers - Microstructure and composition p 117 A93-39521
- GOLDBERG, FREDRIC**
ISDN at NASA Lewis Research Center [NASA-TM-105911] p 262 N93-12410
- GOLDBERG, ROBERT K.**
Composite micromechanical modeling using the boundary element method [NASA-TM-106127] p 250 N93-27030
- GOLDING, PETER**
One-dimensional transient finite difference model of an operational salinity gradient solar pond p 193 N93-13400
- GOLDSBY, J. C.**
Tensile creep behavior of polycrystalline alumina fibers [NASA-TM-106269] p 138 N93-30938
- GOLDSBY, JON C.**
Stress-rupture behavior of small diameter polycrystalline alumina fibers [NASA-TM-106256] p 139 N93-32382
- GOLDSTEIN, M. E.**
Fully coupled resonant-triad interaction in an adverse-pressure-gradient boundary layer p 167 A93-21049
Three-dimensional boundary-layer instability and separation induced by small-amplitude streamwise vorticity in the upstream flow p 172 A93-24401
The development of a mixing layer under the action of weak streamwise vortices p 176 A93-30134
A note on the distortion of a flat-plate boundary layer by free-stream vorticity normal to the plate p 178 A93-34414
- GOLDSTEIN, MARVIN E.**
The development of a mixing layer under the action of weak streamwise vortices [NASA-TM-106089] p 201 N93-28947
- GOMEZ, ALESSANDRO**
Secondary atomization in the combustion of electrostatic sprays [AIAA PAPER 93-2332] p 118 A93-50110
- GONTHIER, KEITH A.**
Reaction zone structure for strong, weak overdriven, and weak underdriven oblique detonations p 178 A93-35492
- GOOD, BRIAN**
Heat of segregation of single substitutional impurities p 119 A93-52873
- GOODRICH, JOHN W.**
An efficient and robust algorithm for two dimensional time dependent incompressible Navier-Stokes equations - High Reynolds number flows p 178 A93-34371
- GORADIA, CHANDRA**
Closed-ampoule diffusion of sulfur into Cd-doped InP substrates - Dependence of S profiles on diffusion temperature and time p 283 A93-51917
- GORADIA, MANJU**
Closed-ampoule diffusion of sulfur into Cd-doped InP substrates - Dependence of S profiles on diffusion temperature and time p 283 A93-51917
- GORDAN, ANDREW L.**
Automatic system for installation and replacement of Space Station components [NASA-CASE-LEW-14906-1] p 226 N93-12203
- GORDON, ANDREW L.**
Service equipment for use in hostile environments [NASA-CASE-LEW-14906-2] p 230 N93-31314
- GORDON, LLOYD B.**
A study of electric power transmission lines for use on the lunar surface p 46 A93-13901
- GORDON, SANFORD**
Computer program for calculating and fitting thermodynamic functions [NASA-RP-1271] p 285 N93-12967
Thermodynamic data for fifty reference elements [NASA-TP-3287] p 286 N93-19977
- GORLA, RAMA S. R.**
The promising chemical kinetics for the simulation of propane-air combustion with KIVA-II code [AIAA PAPER 93-2189] p 118 A93-50001
- GORLAND, S.**
Space R/T base: Propulsion (high thrust chemical) [PR5] p 286 N93-71878
- GOTSIS, P.**
High temperature composite analyzer (HITCAN) user's manual, version 1.0 [NASA-TM-106002] p 249 N93-25070
- GOTSIS, P. K.**
High Temperature Composite Analyzer (HITCAN) theoretical manual, version 1.0 [NASA-TM-106001] p 249 N93-24913
- GOTSIS, PASCAL K.**
Structural optimization of thin shells using finite element method [NASA-TM-105903] p 246 N93-13157
- GOTTI, DANIEL J.**
Initial study of void formation during aluminum solidification in reduced gravity p 142 A93-12013
- GRADWOHL, BEN-AMI**
Dark matter, long-range forces, and large-scale structure p 288 A93-11876
Large- and small-scale constraints on power spectra in Omega = 1 universes p 290 A93-23990
Dark matter and the equivalence principle p 291 A93-44385
- GRADY, JOSEPH E.**
Application of composite materials to impact-insensitive munitions p 97 A93-11459
Fracture toughness testing of polymer matrix composites p 99 A93-18709
Fracture toughness testing of polymer matrix composites [NASA-TP-3199] p 107 N93-12302
An artificial intelligence-based structural health monitoring system for aging aircraft p 266 N93-22185
- GRAHAM, M. J.**
SIMS studies of oxide growth on beta-NiAl p 127 A93-53469
- GRAHAM, ROBERT W.**
Lewis safety manual [NASA-TM-104438] p 147 N93-70966
Four giants of the Lewis Research Center [NASA-TM-83642] p 1 N93-72738
- GRAHAM, RONALD E.**
Space Station Freedom beta gimbal control via sensitivity models [NASA-TM-106000] p 60 N93-22551
Design and implementation of a pilot orientation program for new NASA engineering employees [NASA-TM-105907] p 286 N93-26205
- GRAHAM, SCOTT R.**
Representative systems for space exploration p 293 N93-26395
- GRANDHI, RAMANA V.**
Reliability based structural optimization - A simplified safety index approach [AIAA PAPER 93-1418] p 239 A93-33972
- GRATZ, ROY F.**
Substituted 1,1,1-triaryl 2,2,2-trifluoroethanes and processes for their synthesis [NASA-CASE-LEW-14345-7] p 95 N93-17412

H

- GRAY, HUGH R.**
Overview of NASA's advanced high temperature engine materials technology program p 94 A93-53453
- GRAYSON, GARY D.**
Combustion of solid fuel in very low speed oxygen streams p 122 N93-20207
- GREBER, ISAAC**
Structure and development of streamwise vortex arrays embedded in a turbulent boundary layer p 177 A93-32711
Numerical simulation of a shock wave/turbulent boundary layer interaction in a duct [AIAA PAPER 93-3127] p 11 A93-48293
- GREEN, G. J.**
Soot agglomeration in isolated, free droplet combustion [AIAA PAPER 93-0823] p 115 A93-24893
- GREEN, JAMES M.**
A new facility for advanced rocket propulsion research [AIAA PAPER 93-1859] p 48 A93-49737
A new facility for advanced rocket propulsion research [NASA-TM-106193] p 49 A93-28696
- GREENBERG, P. S.**
Young's fringe particle image velocimetry in the presence of random particle motions p 207 A93-23801
- GREENBERG, PAUL S.**
Capabilities and constraints of combustion diagnostics in microgravity p 145 N93-20185
Soot formation and radiation in turbulent jet diffusion flames under normal and reduced gravity conditions p 121 N93-20192
Selected microgravity combustion diagnostic techniques p 121 N93-20194
- GREENLEE, WILLIAM J.**
Design of a cavity heat pipe receiver experiment p 173 A93-25985
- GREER, LAWRENCE C., III**
Dynamic gas temperature measurements using a personal computer for data acquisition and reduction [NASA-TM-106119] p 261 N93-27024
Progress in speckle-shift strain measurement p 251 N93-31558
- GREGOREK, G. M.**
Comparative wind tunnel tests at high Reynolds numbers of NACA 64 621 airfoils with two aileron configurations p 9 A93-46823
- GREITZER, E. M.**
Numerical simulation of compressor endwall and casing treatment flow phenomena [ASME PAPER 92-GT-300] p 4 A93-19490
- GREYWALL, M. S.**
Streamwise computation of three-dimensional flows using two stream functions p 184 A93-49241
- GRIFFIN, DEVON W.**
Compact color schlieren optical system p 277 A93-52071
Soot formation and radiation in turbulent jet diffusion flames under normal and reduced gravity conditions p 121 N93-20192
Selected microgravity combustion diagnostic techniques p 121 N93-20194
- GRIFFIN, THOMAS A.**
Integrity testing of brush seal in shroud ring of T-700 engine [NASA-TM-105863] p 227 N93-18380
- GRIMBERG, ILANA**
Direct observation of porous SiC formed by anodization in HF p 282 A93-43587
- GROBSTEIN, TONI**
The role of the interface in refractory metal alloy composites p 97 A93-13777
- GROBSTEIN, TONI L.**
Creep behavior of tungsten fiber reinforced niobium metal matrix composites p 99 A93-20758
- GRODSINSKY, C.**
Evaluation of passive and active vibration control mechanisms in a microgravity environment [AIAA PAPER 93-0838] p 55 A93-24905
- GRODSINSKY, C. M.**
Microgravity research on the NASA Lewis Learjet test facility [AIAA PAPER 93-0573] p 43 A93-24245
Vibration isolation technology - An executive summary of systems development and demonstration [AIAA PAPER 93-0834] p 55 A93-24904
- GRODSINSKY, CARLOS M.**
Vibration isolation technology: An executive summary of systems development and demonstration [NASA-TM-105937] p 1 N93-15573
- GROSSKOPF, PAUL P.**
Nondestructive evaluation of a ceramic matrix composite material p 102 A93-33016
- GRUBER, ROBERT P.**
Interim report on the analysis of the microwave power module [NASA-TM-106012] p 160 N93-16713
- GU, C. B.**
Vaporization heat transfer of dielectric liquids on a wick-covered surface [AIAA PAPER 93-0283] p 169 A93-22686
Vaporization heat transfer of dielectric liquids on enhanced surfaces covered with screen wicks [AIAA PAPER 93-2835] p 182 A93-46572
- GU, YOUNG**
Damping of thermal acoustic oscillations in hydrogen systems p 146 A93-48589
- GU, ZHEN**
Identification of the open loop dynamics of the T700 turboshaft engine p 26 A93-35934
- GUIDICE, DONALD A.**
The Photovoltaic Array Space Power Plus diagnostics (PASP Plus) flight experiment p 256 N93-28717
- GUNAWARDENA, S. R.**
Transverse ductility of metal matrix composites p 101 A93-31355
- GUNZBURGER, MAX D.**
Accuracy of least-squares methods for the Navier-Stokes equations p 188 A93-52008
Accuracy of least-squares methods for the Navier-Stokes equations [NASA-TM-106209] p 202 N93-29208
- GUO, T. H.**
Integrated health monitoring and controls for rocket engines [SAE PAPER 921031] p 66 A93-14654
Real-time diagnostics for a reusable rocket engine [NASA-TM-105792] p 266 N93-19018
A neural network-based estimator for the mixture ratio of the Space Shuttle Main Engine [NASA-TM-106070] p 87 N93-25089
- GUO, T.-H.**
Implementation of a model based fault detection and diagnosis technique for actuation faults of the SSME p 47 A93-16413
Implementation of a model based fault detection and diagnosis for actuation faults of the Space Shuttle main engine [NASA-TM-105781] p 49 N93-11401
- GUO, TEN-HUEI**
An SSME High Pressure Oxidizer Turbopump diagnostic system using G2 real-time expert system p 66 A93-16415
Identification of propulsion systems [NASA-TM-106007] p 35 N93-20109
- GUPTA, VINAY K.**
Modal test/analysis correlation of Space Station structures using nonlinear sensitivity [AIAA PAPER 92-4731] p 55 A93-20330
- GUPTILL, J. D.**
Singularities in optimal structural design [AIAA PAPER 92-4818] p 235 A93-20397
Singularity in structural optimization p 240 A93-34938
- GURNETT, DONALD A.**
Interference patterns in the Spacelab 2 plasma wave data - Oblique electrostatic waves generated by the electron beam p 257 A93-16347
- GURU PRASAD, K.**
Shape reanalysis and sensitivities utilizing preconditioned iterative boundary solvers p 233 A93-14446
Boundary formulations for three-dimensional continuum structural shape sensitivity analysis p 235 A93-22426
Boundary formulations for sensitivity analysis without matrix derivatives p 242 A93-49028
- GYEKENYESI, J. P.**
Reliability analysis of laminated ceramic matrix composites using shell subelement techniques p 243 A93-55382
- GYEKENYESI, JOHN P.**
Ceramic component reliability with the restructured NASA/CARES computer program [ASME PAPER 92-GT-383] p 234 A93-19540
Mechanics of interfaces in fiber reinforced SiC/RBSN ceramic matrix composites p 102 A93-32466
Lifetime reliability evaluation of structural ceramic parts with the CARES/LIFE computer program [AIAA PAPER 93-1497] p 239 A93-34037
Ceramic component reliability with the restructured NASA/CARES computer program [NASA-TM-105856] p 244 N93-11004
- HA, T. W.**
Friction-factor characteristics for narrow channels with honeycomb surfaces [ASME PAPER 91-TRIB-21] p 219 A93-15681
Friction-factor data for flat-plate tests of smooth and honeycomb surfaces [ASME PAPER 91-TRIB-20] p 219 A93-15682
- HAAKE, E. M.**
Temporal averaging of phase measurements in the presence of spurious phase drift - Application to phase-stepped real-time holographic interferometry p 207 A93-26967
Temporal averaging in a turbulent environment - Compensation for phase drifts in phase shifting interferometry p 210 A93-44190
- HAAG, THOMAS W.**
Extended life and performance test of a low-power arcjet p 70 A93-32554
Recent testing of 30 KW hydrogen arcjet thrusters [AIAA PAPER 93-1902] p 73 A93-49772
Derated ion thruster development status [AIAA PAPER 93-2225] p 75 A93-50031
Development of arcjet and ion propulsion for spacecraft stationkeeping [NASA-TM-106102] p 85 N93-23747
- HACHA, THOMAS H.**
Thermal control system for Space Station Freedom photovoltaic power module [SAE PAPER 921110] p 57 A93-41305
- HACKER, H., JR.**
Determination of forces in a magnetic bearing actuator - Numerical computation with companion to experiment p 219 A93-15686
- HAFEZ, WASSIM**
Neural networks for structural design - An integrated system implementation [AIAA PAPER 92-4806] p 263 A93-20389
- HAGEDORN, NORMAN H.**
Alkali metal carbon dioxide electrochemical system for energy storage and/or conversion of carbon dioxide to oxygen [NASA-CASE-LEW-14973-1] p 256 N93-28974
- HAGGARD, JOHN B.**
Combustion of interacting droplet arrays in a microgravity environment p 122 N93-20217
- HAGGARD, JOHN B., JR.**
Computational/experimental basis for conducting alkane droplet combustion experiments on space-based-platforms p 117 A93-41711
- HAGSTROM, THOMAS**
On the accurate long-time solution of the wave equation in exterior domains. Asymptotic expansions and corrected boundary conditions [NASA-TM-106117] p 269 N93-27068
- HAH, C.**
Unsteady aerodynamic flow phenomena in a transonic compressor stage [AIAA PAPER 93-1868] p 12 A93-49743
Three-dimensional flow analysis inside turbomachinery stages with steady and unsteady Navier-Stokes method [ISABE 93-7095] p 14 A93-54071
Navier-Stokes analysis of three-dimensional flow and heat transfer inside turbine blade rows p 39 N93-29963
- HAH, CHUNILL**
Three-dimensional flow phenomena in a transonic, high-through-flow, axial-flow compressor stage [ASME PAPER 92-GT-169] p 3 A93-19395
Three-dimensional unstructured grid Euler method applied to turbine blades [AIAA PAPER 93-0196] p 6 A93-24233
Bgndi - Interactive three-dimensional turbomachinery grid generation system with applications [AIAA PAPER 93-0430] p 259 A93-25527
Three-dimensional flow calculations inside SSME GGGT first stage blade rows p 93 N93-31585
- HAHN, R. C.**
IDGE - A test of dendritic growth theory using space flight [AIAA PAPER 93-0260] p 143 A93-25515
Scientific basis for the Isothermal Dendritic Growth Experiment - A USMP-2 space flight experiment p 143 A93-50455
- HAILYE, MICHAEL**
Flip-flop jet nozzle extended to supersonic flows p 8 A93-39409
- HAISSIG, CHRISTINE M.**
Minimum-fuel, power-limited transfers between coplanar elliptical orbits p 45 A93-31532
- HAJELA, P.**
Neural networks in structural analysis and design - An overview [AIAA PAPER 92-4805] p 263 A93-20388

HAJELA, PRABHAT

- Stochastic search in structural optimization - Genetic algorithms and simulated annealing p 241 A93-45430
Application of neural nets in structural optimization p 265 A93-54533
Self-organization in neural networks - Applications in structural optimization p 265 A93-54534

HAKIMZADEH, ROSHANAK

- Minority carrier diffusion length and edge surface-recombination velocity in InP p 283 A93-50787

HALE, JEFFREY S.

- Low earth simulation and materials characterization p 44 A93-32293

HALFORD, GARY R.

- Stirling engine - Available tools for long-life assessment p 65 A93-13824
Stirling engine - Approach for long-term durability assessment p 220 A93-26069
Evolution of creep-fatigue life prediction models p 236 A93-31339
A creep cavity growth model for creep-fatigue life prediction of a unidirectional W/Cu composite [NASA-TM-105780] p 244 A93-10967
Cumulative fatigue damage behavior of MAR M-247 p 251 A93-31575

HALL, DAVID G.

- Acoustic mode measurements in the inlet of a model turbofan using a continuously rotating rake - Data collection/analysis techniques [AIAA PAPER 93-0599] p 24 A93-23324
Takeoff/approach noise for a model counterrotation propeller with a forward-swept upstream rotor [AIAA PAPER 93-0596] p 24 A93-24782
Acoustic mode measurements in the inlet of a model turbofan using a continuously rotating rake [AIAA PAPER 93-0598] p 273 A93-24783
Cruise noise of an advanced propeller with swirl recovery vanes p 273 A93-28609
Acoustic mode measurements in the inlet of a model turbofan using a continuously rotating rake: Data collection/analysis techniques [NASA-TM-105936] p 33 A93-15403
Acoustic mode measurements in the inlet of a model turbofan using a continuously rotating rake [NASA-TM-105989] p 34 A93-16705
Takeoff/approach noise for a model counterrotation propeller with a forward-swept upstream rotor [NASA-TM-105979] p 34 A93-16715

HALL, KENNETH C.

- Nonreflecting boundary conditions for linearized unsteady aerodynamic calculations [AIAA PAPER 93-0882] p 7 A93-25553
Linearized Euler predictions of unsteady aerodynamic loads in cascades p 7 A93-29318

HALL, STEPHEN W.

- Validation test of advanced technology for IPV nickel-hydrogen flight cells - Update p 252 A93-25886
Validation test of 125 Ah advanced design IPV nickel-hydrogen flight cells p 78 A93-50822
Validation test of 125 Ah advanced design IPV nickel-hydrogen flight cells [NASA-TM-105912] p 81 A93-14079

HAMED, A.

- A parametric study of bleed in shock boundary layer interactions [AIAA PAPER 93-0294] p 5 A93-22694
An investigation of shock wave turbulent boundary layer interaction with bleed through slanted slots [AIAA PAPER 93-2992] p 11 A93-48184

HAMLEY, J. A.

- Simplified power processing for inert gas ion thrusters [AIAA PAPER 93-2397] p 76 A93-50162

HAMLEY, JOHN A.

- Plasma contactor technology for Space Station Freedom [AIAA PAPER 93-2228] p 57 A93-50034
A soft-start circuit for arcjet ignition [AIAA PAPER 93-2396] p 76 A93-50161
10 kW power electronics for hydrogen arcjets p 79 A93-10033
The 10 kW power electronics for hydrogen arcjets [NASA-TM-105614] p 81 A93-12484
Ion thruster development at NASA Lewis Research Center [NASA-TM-105983] p 82 A93-15429

HAMMOND, AHMAD N.

- NASA requirements and applications environments for electrical power wiring p 153 A93-25919

HAN, J. C.

- Heat transfer performance comparisons of five different rectangular channels with parallel angled ribs p 166 A93-18752

HANDSCHUH, R.

- Contact stress analysis of spiral bevel gears using nonlinear finite element static analysis [NASA-TM-106176] p 228 A93-27037

HANDSCHUH, R. F.

- Generation of helical gears with new surfaces, topology by application of CNC machines [NASA-TM-106175] p 229 A93-27687

HANDSCHUH, ROBERT F.

- Low-noise, high-strength, spiral-bevel gears for helicopter transmissions [AIAA PAPER 93-2149] p 223 A93-49966
Contact stress analysis of spiral bevel gears using nonlinear finite element static analysis [AIAA PAPER 93-2296] p 224 A93-50081
Generation of helical gears with new surfaces topology by application of CNC machines [AIAA PAPER 93-2297] p 224 A93-50082
Low-noise, high-strength, spiral-bevel gears for helicopter transmissions [NASA-TM-106080] p 228 A93-23019

HANLON, J. C.

- Dynamic Isotope Power System design considerations for human exploration of the moon and Mars p 253 A93-25995

HANLON, JAMES C.

- Comparison of dynamic isotope power systems for distributed planetary surface applications p 46 A93-13825
Optimization of closed Brayton cycles for space power generation p 68 A93-25859

HANN, RAIFORD E.

- Glass formation, properties and structure of soda-yttria-silica glasses p 131 A93-20464

HANNAN, NELSON A.

- System model development for nuclear thermal propulsion [NASA-TM-105761] p 80 A93-10457
System model development for nuclear thermal propulsion [NASA-TM-108157] p 276 A93-16531
System model development for nuclear thermal propulsion [NASA-TM-108215] p 277 A93-17343

HANSEN, IRVING G.

- Electromechanical systems with transient high power response operating from a resonant ac link p 152 A93-25892

HANSMAN, R. J., JR.

- Close-up analysis of aircraft ice accretion [AIAA PAPER 93-0029] p 18 A93-23239

HANSMAN, R. JOHN

- Close-up analysis of aircraft ice accretion [NASA-TM-105952] p 19 A93-15360

HANSON, R. K.

- A comparison of arcjet plume properties to model predictions [AIAA PAPER 93-0820] p 67 A93-24891

HANSON, RONALD K.

- Plume characteristics of an arcjet thruster [AIAA PAPER 93-2530] p 77 A93-50258

HARDY, ALVA C.

- Nuclear safety policy working group recommendations on nuclear propulsion safety for the space exploration initiative [NASA-TM-105705] p 88 A93-26200

HARDY, T. L.

- Influence of heat transfer rates on pressurization of liquid/slush hydrogen propellant tanks [AIAA PAPER 93-0278] p 169 A93-22681

HARDY, TERRY L.

- Reliability studies of Integrated Modular Engine system designs [AIAA PAPER 93-1886] p 72 A93-49759

- Reliability studies of integrated modular engine system designs [NASA-TM-106178] p 91 A93-27022

HARIHARAN, S. I.

- Flow effects in a vertical CVD reactor p 166 A93-19821
On the accurate long-time solution of the wave equation in exterior domains: Asymptotic expansions and corrected boundary conditions [NASA-TM-106117] p 269 A93-27068

HARLOFF, G. J.

- Navier-Stokes analysis of three-dimensional S-ducts p 9 A93-45146
A numerical investigation of supersonic strut/endwall interactions in annular flow with varying strut thickness [AIAA PAPER 93-2927] p 10 A93-48128
Experimental and numerical investigation of supersonic turbulent flow in an annular duct [AIAA PAPER 93-3123] p 11 A93-48291
Investigation of a strut/endwall interaction in supersonic annular flow [AIAA PAPER 93-1925] p 12 A93-49791

HARPER, MICHAEL R.

- Computation of the flow field in an annular gas turbine combustor [AIAA PAPER 93-2074] p 28 A93-49903

HARPER, WILLIAM B., JR.

- BIPS Turboalternator-Compressor characteristics and application to the NASA Solar Dynamic Ground Demonstration Program p 69 A93-25965
Closed Brayton Cycle power system with a high temperature pellet bed reactor heat source for NEP applications [NASA-TM-105933] p 82 A93-14482

HARRELL, M. J.

- Ellipsometric study of Si(0.5)Ge(0.5)/Si strained-layer superlattices p 280 A93-34655

HARTFIELD, J. P.

- Droplet vaporization in a high-pressure gas p 190 A93-55461

HARTLEY, TOM T.

- Modeling of linear isentropic flow systems p 179 A93-37046
Desktop chaotic systems: intuition and visualization [NASA-TM-106258] p 269 A93-31847

HARTY, RICHARD B.

- 100-kWe lunar/Mars surface power utilizing the SP-100 reactor with dynamic conversion p 67 A93-25856

HARTZ, WILLIAM G.

- Design of an automated imaging system for use in a space experiment p 204 A93-20454

HASAN, M. M.

- Nucleate pool boiling in the long duration low gravity environment of the space shuttle [AIAA PAPER 93-0465] p 142 A93-23371
Mixing and transient interface condensation of a liquid hydrogen tank [AIAA PAPER 93-1968] p 184 A93-49816
Low-g fluid mixing - Further results from the Tank Pressure Control Experiment [AIAA PAPER 93-2423] p 187 A93-50181
Nucleate pool boiling in the long duration low gravity environment of the Space Shuttle [NASA-TM-105973] p 144 A93-15420
Mixing and transient interface condensation of a liquid hydrogen tank [NASA-TM-106201] p 201 A93-28252
Tank Pressure Control Experiment/Thermal Phenomena (TPCE/TP) p 92 A93-28713

HASHIM, WAQAR

- Heat transfer in oscillating flows with sudden change in cross section p 174 A93-26089

HASSELMAN, D. P. H.

- Effect of HIPing on the effective thermal conductivity/diffusivity and the interfacial thermal conductance of uniaxial SiC fibre-reinforced RBSN p 100 A93-26674

HASTINGS, D. E.

- Electrodynamical interactions between a space station and the ionospheric plasma environment p 56 A93-29156

HASTINGS, DANIEL E.

- Arcing rates for High Voltage Solar Arrays - Theory, experiment, and predictions p 70 A93-32567
Space Station Freedom structure floating potential and the probability of arcing p 57 A93-39265

HATHAWAY, M. D.

- Experimental and computational investigation of the NASA Low-Speed Centrifugal Compressor flow field [ASME PAPER 92-GT-213] p 4 A93-19436

HATHAWAY, MICHAEL D.

- NASA low speed centrifugal compressor p 204 A93-70583

HAUGEN, BJORN

- Membrane triangles with corner drilling freedoms. I - The EFF element p 235 A93-24303

HAUGLAND, E. J.

- Intermodulation in the oscillatory magnetoresistance of a two-dimensional electron gas p 151 A93-17610
Room-temperature determination of two-dimensional electron gas concentration and mobility in heterostructures p 280 A93-35198

HAUSMANN, CLIFFORD R.

- Rotating rake design for unique measurement of fan-generated spinning acoustic modes [NASA-TM-105946] p 36 A93-26161

HAWTHORNE, W. R.

- Aerodynamic design of turbomachinery blading in three-dimensional flow - An application to radial inflow turbines [ASME PAPER 92-GT-74] p 3 A93-19324

HAYDER, M. E.

- Numerical simulations of a high Mach number jet flow [AIAA PAPER 93-0653] p 172 A93-24766
The structure of supersonic jet flow and its radiated sound [AIAA PAPER 93-0549] p 273 A93-25538

- High order accurate solutions of viscous problems
[AIAA PAPER 93-3074] p 183 A93-48249
- HAYDER, M. EHTESHAM**
Numerical simulation of a high Mach number jet flow
[NASA-TM-105985] p 197 N93-20057
- HAZAN, DIDIER**
Close-up analysis of aircraft ice accretion
[AIAA PAPER 93-0029] p 18 A93-23239
Close-up analysis of aircraft ice accretion
[NASA-TM-105952] p 19 N93-15360
- HEATH, G.**
Face-gear drives: Design, analysis, and testing for helicopter transmission applications
[NASA-TM-106101] p 229 N93-27133
- HEBSUR, M.**
Effect of oxidation on the mechanical properties of a NbAl₃ alloy at intermediate temperatures
p 124 A93-20667
- HEBSUR, M. G.**
Evaluation of the fracture toughness of Nb-40Al-8Cr-1W-1Y-0.05B intermetallic material by indentation techniques
p 124 A93-24066
- HECHT, RALPH J.**
Material requirements for the High Speed Civil Transport
[ISABE 93-7067] p 31 A93-54043
- HEDGEPEETH, JOHN M.**
Design of structures for Nuclear Electric Propulsion vehicles
[AIAA PAPER 93-1393] p 57 A93-33955
- HEGSTROM, JAMES C.**
PEM fuel cell stack heat and mass management
p 253 A93-26024
- HEFETZ, M.**
Ultrasonic and micromechanical study of damage and elastic properties of SiC/RBSN ceramic composites
p 99 A93-19624
- HEGDE, U.**
Effects of gravity on the transition to turbulence of gas jet diffusion flames
[AIAA PAPER 93-0710] p 114 A93-24805
- HEIDELBERG, LAURENCE**
Acoustic mode measurements in the inlet of a model turbofan using a continuously rotating rake - Data collection/analysis techniques
[AIAA PAPER 93-0599] p 24 A93-23324
Acoustic mode measurements in the inlet of a model turbofan using a continuously rotating rake: Data collection/analysis techniques
[NASA-TM-105936] p 33 N93-15403
- HEIDELBERG, LAURENCE J.**
Acoustic mode measurements in the inlet of a model turbofan using a continuously rotating rake
[AIAA PAPER 93-0598] p 273 A93-24783
Acoustic mode measurements in the inlet of a model turbofan using a continuously rotating rake
[NASA-TM-105989] p 34 N93-16705
- HEINEN, VERNON O.**
Superconductivity applications for infrared and microwave devices II. Proceedings of the Meeting, Orlando, FL, Apr. 4, 5, 1991
[SPIE-1477] p 154 A93-27243
- HEINRICH, J. C.**
Numerical model for dendritic solidification of binary alloys
p 282 A93-46729
- HEINRICH, JUAN C.**
Thermosolutal convection during dendritic solidification of a binary alloy
p 182 A93-45975
- HELMICK, LARRY A.**
Determination of the thermal stability of perfluoropolyalkyl ethers by tensimetry
[NASA-TM-106081] p 137 N93-25093
- HELMICK, LARRY S.**
Tribological characteristics of perfluoropolyether liquid lubricants under sliding conditions in high vacuum
[NASA-TM-106257] p 139 N93-32352
Determination of the oxidative stability of perfluoropolyalkyl ethers and correlation with chemical structure
[NASA-TM-106223] p 139 N93-32367
- HELMS, IRA**
Nuclear thermal propulsion technology: Results of an interagency panel in FY 1991
[NASA-TM-105711] p 86 N93-24740
- HENDERSON, GREGORY H.**
Forcing function effects on unsteady aerodynamic gust response. I - Forcing functions
[ASME PAPER 92-GT-174] p 3 A93-19400
Forcing function effects on unsteady aerodynamic gust response. II - Low solidity airfoil row response
[ASME PAPER 92-GT-175] p 3 A93-19401
- HENDERSON, T. L.**
Three-dimensional Navier-Stokes calculations using solution-adapted grids
[AIAA PAPER 93-0431] p 6 A93-24240
- HENDRICKS, R. C.**
Driven cavity simulation of turbomachine blade flows with vortex control
[AIAA PAPER 93-0390] p 6 A93-24238
Preliminary experimental results for a cryogenic brush seal configuration
[AIAA PAPER 93-2535] p 225 A93-50262
Flow visualization in a single simulated brush seal
p 226 A93-54659
Preliminary experimental results for a cryogenic brush seal configuration
[NASA-TM-106236] p 201 N93-28627
- HENDRICKS, ROBERT C.**
Development of advanced seals for space propulsion turbomachinery
[SAE PAPER 92-1028] p 218 A93-14651
Brush seal leakage performance with gaseous working fluids at static and low rotor speed conditions
[ASME PAPER 92-GT-304] p 219 A93-19494
Brush seal low surface speed hard-rub characteristics
[AIAA PAPER 93-2534] p 225 A93-50261
Brush seal bristle flexure and hard-rub characteristics
[NASA-TM-105864] p 227 N93-18321
Integrity testing of brush seal in shroud ring of T-700 engine
[NASA-TM-105863] p 227 N93-18380
Brush seal low surface speed hard-rub characteristics
[NAXA-TM-106169] p 200 N93-27132
- HENRY, D. P., JR.**
Micromechanical studies of composites by BEM
p 236 A93-31295
- HENRY, ZACHARY S.**
Low-noise, high-strength, spiral-bevel gears for helicopter transmissions
[AIAA PAPER 93-2149] p 223 A93-49966
Low-noise, high-strength, spiral-bevel gears for helicopter transmissions
[NASA-TM-106080] p 228 N93-23019
- HEPP, ALOYSIUS F.**
Enhancement of photoluminescence intensity of GaAs with cubic GaS chemical vapor deposited using a structurally designed single-source precursor
p 280 A93-26930
Metal-organic chemical vapour deposition of polycrystalline tetragonal indium sulphide (InS) thin films
p 116 A93-36584
Photoluminescence intensity enhancement of GaAs by vapor-deposited GaS - A rational approach to surface passivation
p 281 A93-40049
Electronic passivation of n- and p-type GaAs using chemical vapor deposited GaS
p 283 A93-52708
Room temperature synthesis of copper indium diselenide in non-aqueous solution using an organoindium reagent
p 283 A93-54844
- HERBACH, B. A.**
IDGE - A test of dendritic growth theory using space flight
[AIAA PAPER 93-0260] p 143 A93-25515
- HERBELL, THOMAS P.**
Effect of hydrogen on the strength and microstructure of selected ceramics
p 130 A93-13613
Ceramic matrix composites for rocket engine turbine applications
[ASME PAPER 92-GT-394] p 99 A93-19547
Aerospace applications
p 135 A93-55472
- HERBERT, TH.**
Effects of free-stream turbulence on boundary-layer transition
[AIAA PAPER 93-0488] p 170 A93-23390
- HERNACKI, THOMAS R.**
Design and fabrication of a hydrogen/oxygen thrust chamber assembly
[AIAA PAPER 93-2132] p 74 A93-49951
- HERR, JOEL L.**
Plasma sheath effects on ion collection by a pinhole
[AIAA PAPER 93-0567] p 55 A93-24243
Plasma sheath effects on ion collection by a pinhole
[NASA-TM-106098] p 60 N93-25090
- HERRERA-FIERRO, PILAR**
Interfacial chemistry of a perfluoropolyether lubricant studied by X-ray photoelectron spectroscopy and temperature desorption spectroscopy
p 133 A93-38473
X-ray photoelectron spectroscopy study of the stability of Fomblin Z25 on the native oxide of aluminum
p 134 A93-44883
- HERRERA-FIERRO, PILAR C.**
Interfacial chemistry of a perfluoropolyether lubricant studied by XPS and TDS
[NASA-TM-106014] p 137 N93-22560
- HESEL, R. P.**
Intake flow modeling in a four stroke diesel using KIVA3
[AIAA PAPER 93-2952] p 183 A93-48146
- HEUER, ARTHUR H.**
Chemical reactions in the processing of MoSi₂ + carbon compacts
p 119 A93-53733
- HEYWARD, ANN O.**
Allocations by the 1992 World Administrative Radio Conference
p 150 N93-26476
- HIBBS-BRENNER, M.**
Mixed application MMIC technologies - Progress in combining RF, digital and photonic circuits
p 152 A93-25800
- HIBBS, R. I.**
Preliminary experimental results for a cryogenic brush seal configuration
[AIAA PAPER 93-2535] p 225 A93-50262
Preliminary experimental results for a cryogenic brush seal configuration
[NASA-TM-106236] p 201 N93-28627
- HICKEY, JOHN R.**
The effect of the low Earth orbit environment on space solar cells: Results of the Advanced Photovoltaic Experiment (S0014)
p 256 N93-29686
Studies of effects on optical components and sensors: LDEF experiments AO-147 (ERB components) and S-0014 (APEX)
p 278 N93-29693
- HICKMAN, MARK**
Transfer Orbit Plasma Interaction Experiment (TROPIX)
p 45 N93-28734
- HICKS, MICHAEL C.**
One-dimensional transient finite difference model of an operational salinity gradient solar pond
p 193 N93-13400
- HILL, GERALD M.**
10 kW power electronics for hydrogen arcjets
p 79 N93-10033
The 10 kW power electronics for hydrogen arcjets
[NASA-TM-105614] p 81 N93-12484
- HILL, MYRON**
Natural and thermocapillary convection in multiple liquid layers
[AIAA PAPER 93-0469] p 171 A93-24241
- HILL, MYRON E.**
A review of design concepts for the Advanced Fluids Module (AFM) project
[AIAA PAPER 93-0258] p 43 A93-23700
- HILLARD, G. B.**
Plasma chamber testing of APSA coupons for the SAMPIE flight experiment
[AIAA PAPER 93-0568] p 67 A93-24244
The interaction of high voltage systems with the environments of the moon and Mars
[AIAA PAPER 93-0704] p 67 A93-24800
Solar array module plasma interactions experiment (SAMPIE) - Science and technology objectives
p 71 A93-46418
- HILLARD, G. BARRY**
Acceptance testing of the prototype electrometer for the SAMPIE flight experiment
[NASA-TM-105880] p 57 N93-10841
Plasma chamber testing of APSA coupons for the SAMPIE flight experiment
[NASA-TM-106084] p 60 N93-23742
The interaction of high voltage systems with the environments of the Moon and Mars
[NASA-TM-106107] p 61 N93-26148
Plasma current collection of Z-93 thermal control paint as measured in the Lewis Research Center's plasma interaction facility
[NASA-TM-106132] p 61 N93-26215
Enhanced plasma current collection from weakly conducting solar array blankets
[NASA-TM-106168] p 62 N93-27081
- HINES, RICHARD**
Engine technology challenges for a 21st Century High-Speed Civil Transport
[ISABE 93-7064] p 31 A93-54040
Engine technology challenges for a 21st Century High-Speed Civil Transport
[NASA-TM-106216] p 39 N93-31671
- HINGST, W. R.**
Use of surface heat transfer measurements as a flow separation diagnostic in a two-dimensional reflected oblique shock/turbulent boundary layer interaction
[AIAA PAPER 93-0775] p 172 A93-24859
Surface and flow field measurements in a symmetric crossing shock wave/turbulent boundary-layer interaction
[NASA-TM-106086] p 17 N93-24911
- HINGST, WARREN**
NASA Lewis Research Center/IFMD inlet duct and nozzle high speed validation experiments
p 204 N93-70582
- HINGST, WARREN R.**
Structure and development of streamwise vortex arrays embedded in a turbulent boundary layer
p 177 A93-32711

- Use of surface heat transfer measurements as a flow separation diagnostic in a two dimensional reflected oblique shock/turbulent boundary layer interaction [NASA-TM-105981] p 194 N93-15355
- HIPPENSTEELE, S. A.**
A new hue capturing technique for the quantitative interpretation of liquid crystal images used in convective heat transfer studies p 204 A93-13977
Evaluation of a hue capturing based transient liquid crystal method for high-resolution mapping of convective heat transfer on curved surfaces p 210 A93-43689
- HIPPENSTEELE, STEVEN A.**
High Reynolds number and turbulence effects on aerodynamics and heat transfer in a turbine cascade [AIAA PAPER 93-2252] p 186 A93-50050
Measurements and computational analysis of heat transfer and flow in a simulated turbine blade internal cooling passage p 189 A93-53585
Transient liquid-crystal technique used to produce high-resolution convective heat-transfer-coefficient maps [NASA-TM-106083] p 198 N93-23404
High Reynolds number and turbulence effects on aerodynamics and heat transfer in a turbine cascade [NASA-TM-106187] p 202 N93-29157
Measurements and computational analysis of heat transfer and flow in a simulated turbine blade internal cooling passage [NASA-TM-106189] p 203 N93-31647
- HO, BARRY PING HSIAO**
Effects of thermal and mechanical fatigue on the flexural strength of G40-600/PMR-15 cross-ply laminates [NASA-TM-106016] p 108 N93-20317
- HO, J. C.**
Low temperature phase formation of Ti-based superconducting thin films in reduced oxygen atmosphere p 282 A93-44568
- HO, YUNG**
M.I.T. Stirling-cycle heat transfer apparatus p 174 A93-26090
- HOCHSTEIN, J. I.**
Influence of heat transfer rates on pressurization of liquid/slush hydrogen propellant tanks [AIAA PAPER 93-0278] p 169 A93-22681
- HODGE, JOHN R.**
Space vehicle design and operation for efficient use of Nuclear Thermal Propulsion [AIAA PAPER 93-1946] p 44 A93-49804
- HODGES, HARDY M.**
Cosmic microwave background probes models of inflation p 294 A93-10355
- HOFFMAN, DAVID J.**
Cryogenic propellant thermal control system design considerations, analyses, and concepts applied to a Mars human exploration mission [AIAA PAPER 93-2353] p 75 A93-50126
- HOLANDA, RAYMOND**
Thin film thermocouples for high temperature measurement on ceramic materials p 213 N93-13666
Development of thin film thermocouples on ceramic materials for advanced propulsion system applications [NASA-TM-106017] p 215 N93-25173
- HOLCOMB, ROBERT S.**
Summary and recommendations on nuclear electric propulsion technology for the space exploration initiative [NASA-TM-105707] p 86 N93-24744
- HOLDEMAN, J. D.**
Optimization of circular orifice jets mixing into a heated crossflow in a cylindrical duct p 24 A93-23246 [AIAA PAPER 93-0249]
Experimental investigation of crossflow jet mixing in a rectangular duct p 185 A93-49872 [AIAA PAPER 93-2037]
An analytical study of dilution jet mixing in a cylindrical duct p 27 A93-49876 [AIAA PAPER 93-2043]
CFD mixing analysis of axially opposed rows of jets injected into confined crossflow p 185 A93-49877 [AIAA PAPER 93-2044]
Optimization of circular orifice jets mixing into a heated cross flow in a cylindrical duct p 33 N93-15359 [NASA-TM-105984]
Experimental investigation of crossflow jet mixing in a rectangular duct p 36 N93-27026 [NASA-TM-106152]
CFD mixing analysis of axially opposed rows of jets injected into confined crossflow p 37 N93-27128 [NASA-TM-106179]
An analytical study of dilution jet mixing in a cylindrical duct p 37 N93-27160 [NASA-TM-106181]
- HOLDEMAN, JAMES D.**
Mixing of multiple jets with a confined subsonic crossflow p 15 A93-54324
- HOLLANSWORTH, JAMES E.**
Direct Broadcast Satellite: Radio Program [NASA-TM-105910] p 52 N93-11430
Utilizing a TDRS satellite for direct broadcast satellite-radio propagation experiments and demonstrations [NASA-TM-106172] p 53 N93-27064
- HOLMES, JOHN W.**
Tensile creep and creep-recovery behavior of a SiC-fiber-Si3N4-matrix composite p 104 A93-40290
- HOLOWECKY, BRIAN R.**
A parameter optimization approach to controller partitioning for integrated flight/propulsion control application p 41 A93-54268
- HOLZL, ROBERT A.**
SP-100 high-temperature advanced radiator development p 163 A93-13843
- HOMER, G. D.**
Hydrocarbon-fuel/copper combustion chamber liner compatibility, corrosion prevention, and refurbishment p 139 A93-14510
- HONECY, FRANK**
Closed-ampoule diffusion of sulfur into Cd-doped InP substrates - Dependence of S profiles on diffusion temperature and time p 283 A93-51917
- HONECY, FRANK S.**
A vacuum (10 exp -9 torr) friction apparatus for determining friction and endurance life of MoS(x) films p 146 A93-49245
- HOOVER, MARK D.**
Space nuclear power systems; Proceedings of the 8th Symposium, Albuquerque, NM, Jan. 6-10, 1991. Pts. 1-3 [ISBN 0-88318-838-4] p 64 A93-13751
Space nuclear power systems 1989; Proceedings of the 6th Symposium, Albuquerque, NM, Jan. 8-12, 1989. Vols. 1 & 2 [ISBN 0-89464-030-5] p 66 A93-20752
- HOPKINS, D. A.**
Improved accuracy for finite element structural analysis via an integrated force method p 234 A93-17246
Numerical optimization of composite hip endoprostheses under different loading conditions [AIAA PAPER 92-4703] p 270 A93-20312
Optimal design of composite hip implants using NASA technology p 257 N93-22188
- HOPKINS, DALE A.**
Structural Tailoring/Analysis for Hypersonic Components - A computational simulation [AIAA PAPER 92-4722] p 20 A93-20324
Computational micromechanics of woven composites p 237 A93-32462
Probabilistic micromechanics for metal matrix composites p 237 A93-32465
Reliability based structural optimization - A simplified safety index approach p 239 A93-33972 [AIAA PAPER 93-1418]
Composite micromechanical modeling using the boundary element method p 250 N93-27030 [NASA-TM-106127]
Structural dynamics: Probabilistic structural analysis methods. Program overview p 251 N93-31562
- HOSNI, M. H.**
The turbulent thermal boundary layer with an abrupt change from a rough to a smooth wall p 167 A93-21712
- HOTES, DEBORAH**
Effects of dust accumulation and removal on radiator surfaces on Mars p 123 A93-13937
- HOU, LIN-JUN**
A least-squares finite element method for 3D incompressible Navier-Stokes equations [AIAA PAPER 93-0338] p 171 A93-24236
- HOUSER, DONALD R.**
Engineering science research issues in high power density transmission dynamics for aerospace applications [AIAA PAPER 93-2299] p 224 A93-50084
- HOUSNER, JERRY M.**
NASA CST aids U.S. industry p 258 A93-25084
- HOVENAC, EDWARD A.**
Calibration of the forward-scattering spectrometer probe - Modeling scattering from a multimode laser beam p 212 A93-51239
Experimental testing of four correction algorithms for the forward scattering spectrometer probe [NASA-TM-105906] p 213 N93-13307
- HOWARD, LAURA S.**
Thermal control system for Space Station Freedom photovoltaic power module [SAE PAPER 921110] p 57 A93-41305
- HOWE, HAROLD W.**
Integrity testing of brush seal in shroud ring of T-700 engine [NASA-TM-105863] p 227 N93-18380
- HOWE, STEVEN**
Nuclear thermal propulsion technology: Results of an interagency panel in FY 1991 [NASA-TM-105711] p 86 N93-24740
- HOWELL, JOHN R.**
Thermal radiation heat transfer (3rd revised and enlarged edition) [ISBN 0-89116-271-2] p 165 A93-17522
- HOYT, W. A.**
A function approximation approach to anomaly detection in propulsion system test data [AIAA PAPER 93-1776] p 71 A93-49671
- HSIAO, C. L.**
Generation of helical gears with new surfaces topology by application of CNC machines [AIAA PAPER 93-2297] p 224 A93-50082
Generation of helical gears with new surfaces, topology by application of CNC machines [NASA-TM-106175] p 229 N93-27687
- HSIAO, CHINGTENG**
Finite element calculations of transonic flutter in cascades [AIAA PAPER 93-2083] p 185 A93-49910
- HSIEH, K. C.**
Supercritical droplet combustion and related transport phenomena [AIAA PAPER 93-0812] p 115 A93-24885
- HSIEH, KWANG-CHUNG**
Ground-based PIV and numerical flow visualization results from the Surface Tension Driven Convection Experiment p 143 A93-33075
- HSU, A. T.**
PDF approach for compressible turbulent reacting flows [AIAA PAPER 93-0087] p 170 A93-24229
- HU, M.**
Millimeter-wave pseudomorphic HEMT MMIC phased array components for space communications p 152 A93-25796
- HUANG, J. R.**
Efficient finite element method for aircraft deicing problems p 21 A93-52443
- HUANG, PAO S.**
Study on vortex flow control of inlet distortion p 2 A93-14520
- HUANG, S. C.**
HFAST - A harmonic analysis program for Stirling cycles p 220 A93-26051
- HUANG, SONG**
Fuzzy expert systems vs. neural networks - Truck backer-upper control revisited p 264 A93-37039
- HUANG, W.**
Three-dimensional Navier-Stokes calculations using solution-adapted grids [AIAA PAPER 93-0431] p 6 A93-24240
- HUANG, X.**
Actively controlled superconducting bearings p 223 A93-48594
- HUANG, Y.**
Heat transfer performance comparisons of five different rectangular channels with parallel angled ribs p 166 A93-18752
- HUBER, F. W.**
Design and test of a small two stage counter-rotating turbine for rocket engine application [AIAA PAPER 93-2136] p 74 A93-49954
- HUBER, GARY T.**
Development and use of hydrogen-air torches in an altitude facility [AIAA PAPER 93-2176] p 42 A93-49988
Development and use of hydrogen-air torches in an altitude facility [NASA-TM-106047] p 43 N93-26214
- HUBER, W. G.**
Establishing the infrastructure - An integrated Space Transportation System p 50 A93-12072
- HUBLER, D.**
The engine design engine - A clustered computer platform for the aerodynamic inverse design and analysis of a full engine [NASA-TM-105838] p 15 N93-11223
- HUCKLEBRIDGE, ARTHUR A.**
Implementation of the block-Krylov boundary flexibility method of component synthesis [NASA-TM-106065] p 248 N93-23044
- HUFF, DENNIS L.**
High resolution numerical simulation of the linearized Euler equations in conservation law form [AIAA PAPER 93-2934] p 183 A93-48132
- HUFF, JAMES R.**
PEM fuel cell stack heat and mass management p 253 A93-26024
- HULL, DAVID R.**
Effect of hydrogen on the strength and microstructure of selected ceramics p 130 A93-13613

HULTGREN, LENNART S.

Direct calculations of waves in fluid flows using a high-order compact difference scheme
[AIAA PAPER 93-0148] p 171 A93-24232

HUMPHREY, JOSEPH A. C.

Discussion of 'Comparison of turbulence models for the natural convection boundary layer along a heated vertical plate'
p 168 A93-21717

HUNT, JAMES L.

Design of a hypersonic waverider-derived airplane
[AIAA PAPER 93-0401] p 55 A93-21108

HUNT, MARIBETH E.

SP-100 high-temperature advanced radiator development p 163 A93-13843
Fabrication of carbon-carbon heat pipes for space nuclear power applications p 173 A93-25978

HUNTER, GARY W.

The development of hydrogen sensor technology for aerospace applications
[AIAA PAPER 93-2375] p 211 A93-50144

A survey and analysis of commercially available hydrogen sensors
[NASA-TM-105878] p 214 A93-17777

The development of hydrogen sensor technology at NASA Lewis Research Center
[NASA-TM-106141] p 216 A93-27021

HURLEY, J.

Stiffness of magnetic bearings subjected to combined static and dynamic loads
[ASME PAPER 91-TRIB-27] p 219 A93-15685

HURWITZ, FRANCES I.

Approaches to polymer-derived CMC matrices
p 105 A93-53446

HWANG, D. P.

Effect of a rotating propeller on the separation angle of attack
[AIAA PAPER 93-0017] p 6 A93-24978

Effect of a rotating propeller on the separation angle of attack and distortion in ducted propeller inlets
[NASA-TM-105935] p 16 A93-16625

HYER, PAUL V.

Comparison of numerical model results with diffusion flames in microgravity
[AIAA PAPER 93-0707] p 114 A93-24803

I**IANCULESCU, G.**

Control-structure interaction study for the Space Station solar dynamic power module p 54 A93-13132
Optimal control study for the Space Station Solar Dynamic power module p 54 A93-13133

IANCULESCU, GEORGE D.

Control-structure interaction p 54 A93-14687

IBRAHIM, K. M.

Signal processing considerations for low signal to noise ratio laser Doppler and phase Doppler signals
p 207 A93-23830

IBRAHIM, M.

Transition of oscillatory flow in tubes - An empirical model for application to Stirling engines p 174 A93-26088

IBRAHIM, MOUNIR

Heat transfer in oscillating flows with sudden change in cross section p 174 A93-26089
3-D viscous flow CFD analysis of the propeller effect on an advanced ducted propeller subsonic inlet
[AIAA PAPER 93-1847] p 12 A93-49728

The 3-D viscous flow CFD analysis of the propeller effect on an advanced ducted propeller subsonic inlet
[NASA-TM-106240] p 38 A93-29162

IBRAHIM, MOUNIR B.

Laminar/turbulent oscillating flow in circular pipes
p 167 A93-21689

IBRAHIM, OMAR M.

Solving modal equations of motion with initial conditions using MSC/NASTRAN DMAP. Part 1: Implementing exact mode superposition
[NASA-TM-106063] p 248 A93-23739
Solving modal equations of motion with initial conditions using MSC/NASTRAN DMAP. Part 2: Coupled versus uncoupled integration
[NASA-TM-106064] p 248 A93-23740

IEK, C.

Effect of a rotating propeller on the separation angle of attack
[AIAA PAPER 93-0017] p 6 A93-24978

Effect of a rotating propeller on the separation angle of attack and distortion in ducted propeller inlets
[NASA-TM-105935] p 16 A93-16625

IEK, CHANTHY

3-D viscous flow CFD analysis of the propeller effect on an advanced ducted propeller subsonic inlet
[AIAA PAPER 93-1847] p 12 A93-49728

Analytical and experimental studies of a short compact subsonic diffuser for a two-dimensional supersonic inlet
[NASA-TP-3247] p 17 A93-24118

The 3-D viscous flow CFD analysis of the propeller effect on an advanced ducted propeller subsonic inlet
[NASA-TM-106240] p 38 A93-29162

IGNACZAK, LOUIS R.

Development and flight history of the SERT II spacecraft p 71 A93-38976

INGEBO, ROBERT D.

Effect of vaporization on cryogenic spray droplet size measurement
[AIAA PAPER 93-0692] p 172 A93-24792

Atomizing-gas temperature effect on cryogenic spray droplet size
[AIAA PAPER 93-2333] p 186 A93-50111

Effect of vaporization on cryogenic spray droplet size measurement
[NASA-TM-105909] p 213 A93-13410

Atomizing-gas temperature effect on cryogenic spray droplet size
[NASA-TM-106106] p 216 A93-25191

INOUE, L. Y.

Operation of high power converters in parallel
p 154 A93-26100

INTERANTE, L. V.

CVD of SiC and AlN using cyclic organometallic precursors p 117 A93-39525

ISKOVITZ, I.

Finite element implementation of state variable-based viscoplasticity models p 236 A93-26776

ITOH, T.

Design aspects and comparison between high Tc superconducting coplanar waveguide and microstrip line
p 155 A93-27244

Conductor-backed coplanar waveguide resonators of Y-Ba-Cu-O and Ti-Ba-Ca-Cu-O on LaAlO₃
[NASA-TM-105890] p 284 A93-12325

IVANCIC, W. D.

Satellites and the BISON: An overview of NASA R/D
[NASA-TM-106108] p 150 A93-26903

IZEN, STEVEN H.

Three-dimensional computed tomography from interferometric measurements within a narrow cone of views
p 207 A93-24024

J**JACKSON, G. S.**

Experiments on the effect of initial diameter in spherically symmetric droplet combustion of sooting fuels
[AIAA PAPER 93-0130] p 139 A93-22577

JACKSON, HOWARD E.

Characterization of Si₃N₄/SiO₂ optical channel waveguides by photon scanning tunneling microscopy
p 211 A93-49458

Friction and wear of plasma-deposited diamond films
[NASA-TM-105926] p 136 A93-19035

JACOBSON, N. S.

Thermodynamics of Si-C-O system
p 133 A93-39584

JACOBSON, NATHAN S.

Corrosion of silicon-based ceramics in combustion environments p 131 A93-22984
Thermodynamics of iron-aluminum alloys at 1573 K
p 127 A93-52879

Chemical reactions in the processing of MoSi₂ + carbon compacts p 119 A93-53733

JACQUIN, DAVID

Non-parallel effects in the instability of Long's vortex
p 164 A93-16663

JAGANNATHAN, S.

Hybrid active vibration control of rotorbearing systems using piezoelectric actuators p 221 A93-27324

JAIN, R. K.

Diffusion length variation and proton damage coefficients for InP/In(x)Ga(1-x)As/GaAs solar cells
p 159 A93-55324

JAIN, RAJ K.

Indium phosphide solar cells for laser power beaming applications p 252 A93-25899
Diffusion length variation in 0.5- and 3-MeV-proton-irradiated, heteroepitaxial indium phosphide solar cells
[NASA-TM-106147] p 161 A93-27002

JAMALI, M. M.

Efficient demultiplexing algorithm for noncontiguous carriers p 148 A93-32561

JAMESON, LORIN W.

The QED engine spectrum - Fusion-electric propulsion for air-breathing to interstellar flight
[AIAA PAPER 93-2006] p 73 A93-49845

JANETZKE, D. C.

Concurrent processing adaptation of aeroelastic analysis of proflans p 23 A93-14624

Binary tree eigen solver in finite element analysis
[AIAA PAPER 93-1493] p 267 A93-34034

JANKOVSKY, AMY

Qualitative model-based diagnostics for rocket systems
[AIAA PAPER 93-1779] p 72 A93-49674

Qualitative model-based diagnostics for rocket systems
[NASA-TM-106234] p 51 A93-28052

JANKOVSKY, ROBERT S.

Hot fire test results of subscale tubular combustion chambers p 79 A93-10020

Hot fire fatigue testing results for the compliant combustion chamber p 79 A93-10038

Hot fire fatigue testing results for the compliant combustion chamber
[NASA-TP-3223] p 80 A93-10743

Hot fire test results of subscale tubular combustion chambers
[NASA-TP-3222] p 81 A93-11614

JANOSIK, LESLEY A.

Lifetime reliability evaluation of structural ceramic parts with the CARES/LIFE computer program
[AIAA PAPER 93-1497] p 239 A93-34037

A numerical round robin for the reliability prediction of structural ceramics
[AIAA PAPER 93-1498] p 240 A93-34038

JANSSON, S.

Transverse ductility of metal matrix composites
p 101 A93-31355

Ductility of a continuous fiber reinforced aluminum matrix composite p 102 A93-32471

JASKOWIAK, MARTHA H.

Guanidine based vehicle/binders for use with oxides, metals, and ceramics
[NASA-CASE-LEW-15314-2] p 138 A93-28423

JASNOW, DAVID

Coarsening following a morphological instability in the one-sided model p 284 A93-21695

JASSOWSKI, D. M.

Durability testing of the AJ10-221 490 N high performance (321 sec lsp) engine
[AIAA PAPER 93-2130] p 74 A93-49949

JAWORSKE, D.

Thin film diamond microstructure applications
p 209 A93-40580

JAWORSKE, D. A.

Leveling coatings for reducing the atomic oxygen defect density in protected graphite fiber epoxy composites
[NASA-TM-105732] p 136 A93-15344

Leveling coatings for reducing the atomic oxygen defect density in protected graphite fiber epoxy composites
p 59 A93-15597

JAWORSKE, DONALD A.

Void control in the crystallization of lithium fluoride
p 97 A93-13760

Determination of atomic oxygen fluence using spectrophotometric analysis of infrared transparent witness coupons for long duration exposure tests
[NASA-TM-106021] p 96 A93-22605

JAYNE, D. T.

Mechanism of incipient oxidation of bulk chemical vapor deposited Si₃N₄ p 132 A93-32299

JAYNE, DOUGLAS

Isothermal aging effects on PMR-15 resin
p 131 A93-24508

Closed-ampoule diffusion of sulfur into Cd-doped InP substrates - Dependence of S profiles on diffusion temperature and time p 283 A93-51917

JEFFERSON, G. D.

The development of hydrogen sensor technology for aerospace applications
[AIAA PAPER 93-2375] p 211 A93-50144

The development of hydrogen sensor technology at NASA Lewis Research Center
[NASA-TM-106141] p 216 A93-27021

JENDOUBI, SLAH

Discrete ordinates solutions for radiatively participating media in a cylindrical enclosure p 285 A93-31427

JENG, DUEN-REN

Internal structure of shock waves in disparate mass mixtures p 190 A93-54483

JENKINS, MICHAEL G.

Effects of precracking methods on the fracture properties of alumina p 131 A93-16645

Elevated-temperature fracture resistances of monolithic and composite ceramics using chevron-notched bend tests p 133 A93-38888

JENKINS, PHILIP

Studies of effects on optical components and sensors: LDEF experiments AO-147 (ERB components) and S-0014 (APEX) p 278 A93-29693

JENKINS, PHILLIP P.

- Enhancement of photoluminescence intensity of GaAs with cubic GaS chemical vapor deposited using a structurally designed single-source precursor p 280 A93-26930
- Photoluminescence intensity enhancement of GaAs by vapor-deposited GaS - A rational approach to surface passivation p 281 A93-40049
- Electronic passivation of n- and p-type GaAs using chemical vapor deposited GaS p 283 A93-52708
- JERACKI, ROBERT J.**
- Takeoff/approach noise for a model counterrotation propeller with a forward-swept upstream rotor [AIAA PAPER 93-0596] p 24 A93-24782
- Takeoff/approach noise for a model counterrotation propeller with a forward-swept upstream rotor [NASA-TM-105979] p 34 A93-16715
- JHA, SUNIL C.**
- Influence of grain size on the creep behavior of HfC-dispersed NiAl p 123 A93-17674
- JIANG, BO-NAN**
- A least-squares finite element method for 3D incompressible Navier-Stokes equations [AIAA PAPER 93-0338] p 171 A93-24236
- Non-oscillatory and non-diffusive solution of convection problems by the iteratively reweighted least-squares finite element method p 177 A93-32622
- The L sub 1 finite element method for pure convection problems p 177 A93-34326
- Large-scale computation of incompressible viscous flow by least-squares finite element method [NASA-TM-105904] p 269 A93-22825
- JIANG, BONAN**
- A least-squares finite element method for incompressible Navier-Stokes problem p 191 A93-10548
- JOBE, J. MARCUS**
- Characterization and durability testing of plasma-sprayed zirconia-yttria and hafnia-yttria thermal barrier coatings. Part 1: Effect of spray parameters on the performance of several lots of partially stabilized zirconia-yttria powder [NASA-TP-3295] p 128 A93-22556
- JOHNS, ALBERT L.**
- Analytical and experimental studies of a short compact subsonic diffuser for a two-dimensional supersonic inlet [NASA-TP-3247] p 17 A93-24118
- JOHNSON, ANDREW M.**
- Material requirements for the High Speed Civil Transport [ISABE 93-7067] p 31 A93-54043
- JOHNSON, B. V.**
- Heat transfer in rotating serpentine passages with trips skewed to the flow [ASME PAPER 92-GT-191] p 166 A93-19416
- Heat transfer in rotating serpentine passages with selected model orientation for smooth or skewed trip walls [NASA-TM-106126] p 147 A93-25177
- JOHNSON, D. R.**
- Containerless automated processing of intermetallic compounds and composites p 144 A93-52183
- JOHNSON, DERECK F.**
- External stress-corrosion cracking of a 1.22-m-diameter type 316 stainless steel air valve [NASA-TP-3190] p 129 A93-26201
- JOHNSON, P. D.**
- Design and test of a small two stage counter-rotating turbine for rocket engine application [AIAA PAPER 93-2136] p 74 A93-49954
- JOHNSON, RICHARD A.**
- Versatile dynamic isotope power systems for the exploration of space p 46 A93-13819
- JOHNSON, T.**
- Transition of oscillatory flow in tubes - An empirical model for application to Stirling engines p 174 A93-26088
- JOHNSTON, J. C.**
- Initial study of void formation during aluminum solidification in reduced gravity p 142 A93-12013
- JOHNSTON, R. T.**
- Unsteady wing surface pressures in the wake of a propeller p 14 A93-52436
- JONES, J. W.**
- Tensile creep and creep-recovery behavior of a SiC-fiber-Si₃N₄-matrix composite p 104 A93-40290
- JONES, R. A.**
- Comparison of reacting and non-reacting shear layers at a high subsonic Mach number [AIAA PAPER 93-2381] p 186 A93-50149
- Comparison of reacting and non-reacting shear layers at a high subsonic Mach number [NASA-TM-106198] p 38 A93-27610
- Turbulence measurement in a reacting and non-reacting shear layer at a high subsonic Mach number [NASA-TM-106186] p 18 A93-31839

JONES, R. R., III

- Measured acoustic characteristics of ducted supersonic jets at different model scales [AIAA PAPER 93-0731] p 273 A93-24821
- JONES, ROBERT E.**
- An embedded rule-based diagnostic expert system in Ada p 260 A93-11928
- JONES, WILLIAM R.**
- X-ray photoelectron spectroscopy study of the stability of Fomblin Z25 on the native oxide of aluminum p 134 A93-44883
- JONES, WILLIAM R., JR.**
- Interfacial chemistry of a perfluoropolyether lubricant studied by X-ray photoelectron spectroscopy and temperature desorption spectroscopy p 133 A93-38473
- Interfacial chemistry of a perfluoropolyether lubricant studied by XPS and TDS [NASA-TM-106014] p 137 A93-22560
- Determination of the thermal stability of perfluoropolyalkyl ethers by tensimetry [NASA-TM-106081] p 137 A93-25093
- Tribological characteristics of perfluoropolyether liquid lubricants under sliding conditions in high vacuum [NASA-TM-106257] p 139 A93-32352
- Determination of the oxidative stability of perfluoropolyalkyl ethers and correlation with chemical structure [NASA-TM-106223] p 139 A93-32367
- JORDAN, E. H.**
- X-ray-based displacement measurement for hostile environments p 208 A93-28580
- JORDAN, ERIC H.**
- Critical experiments of the self-consistent model for polycrystalline Hastelloy-X p 124 A93-21958
- The viscoplastic behavior of Hastelloy-X single crystal p 125 A93-27486
- Thermoviscoplastic analysis of fibrous periodic composites using triangular subvolumes [NASA-TM-106076] p 111 A93-29074
- JORGENSEN, P.**
- Central difference TVD schemes for time dependent and steady state problems p 188 A93-51183
- JOSLIN, S. M.**
- Containerless automated processing of intermetallic compounds and composites p 144 A93-52183
- JUBAS, JAY M.**
- Microwave anisotropies in the light of the data from the COBE satellite p 291 A93-35444
- JUHASZ, A.**
- The NASA CSTI High Capacity Power Project p 69 A93-26105
- The NASA CSTI high capacity power project [NASA-TM-105813] p 48 A93-11398
- JUHASZ, ALBERT J.**
- Advanced radiator concepts feasibility demonstration p 163 A93-13844
- Heat-pipe transient model for space applications p 163 A93-13867
- Closed Brayton Cycle power system with a high temperature pellet bed reactor heat source for NEP applications [NASA-TM-105933] p 82 A93-14482
- Radiator technology p 90 A93-26979
- JURNG, J.**
- Structure of soot-containing laminar jet diffusion flames [AIAA PAPER 93-0708] p 114 A93-24804

K**KABIS, HANEE Z.**

- Design of a hypersonic waverider-derived airplane [AIAA PAPER 93-0401] p 55 A93-21108
- KACKLEY, NANCY D.**
- Regenerative fuel cells p 252 A93-25868
- KACPURA, THOMAS J.**
- EMTP based stability analysis of Space Station Electric Power System in a test bed environment p 154 A93-26108
- EMTP based stability analysis of space station electric power system in a test bed environment [NASA-TM-105845] p 160 A93-15503
- KACZYNSKI, KENNETH J.**
- Thermal stratification potential in rocket engine coolant channels p 78 A93-10019
- Nuclear thermal rocket nozzle testing and evaluation program [NASA-TM-105962] p 83 A93-15571
- KAISER, W.**
- Venus Interior Structure Mission (VISM). Establishing a seismic network on Venus p 293 A93-28819
- KALAMAS, J.**
- Flow instability in particle-bed nuclear reactors [AIAA PAPER 93-1758] p 71 A93-49657

KALLINDERIS, Y.

- A parallel dynamic load balancing algorithm for 3-D adaptive unstructured grids [AIAA PAPER 93-3313] p 260 A93-45009
- KALLURI, SREERAMESH**
- Effect of tensile mean stress on fatigue behavior of single-crystal and directionally solidified superalloys p 125 A93-33011
- Axial-torsional fatigue - A study of tubular specimen thickness effects p 240 A93-38849
- In-phase and out-of-phase axial-torsional fatigue behavior of Haynes 188 at 760 C [NASA-TM-105765] p 246 A93-13153
- The influence of primary and secondary orientations on the elastic response of a nickel-base single-crystal superalloy [NASA-TM-106125] p 250 A93-26550
- Cumulative fatigue damage behavior of MAR M-247 p 251 A93-31575
- Secondary orientation effects in a single crystal superalloy under mechanical and thermal loads p 130 A93-31578
- KALOKITIS, D.**
- Buffer layers for high-Tc thin films on sapphire p 150 A93-17063
- KAMAT, MANOHAR P.**
- Forced response of mistuned bladed disk assemblies [AIAA PAPER 93-1491] p 239 A93-34033
- KAMINSKI, DEBORAH A.**
- Analysis and design of an ultrahigh temperature hydrogen-fueled MHD generator p 278 A93-49618
- KAMOTANI, YASUHIRO**
- Effect of free surface shape on combined thermocapillary and natural convection p 162 A93-10671
- Thermal oscillations in materials processing p 162 A93-10839
- KANE, J. H.**
- Shape reanalysis and sensitivities utilizing preconditioned iterative boundary solvers p 233 A93-14446
- Boundary formulations for three-dimensional continuum structural shape sensitivity analysis p 235 A93-22426
- Boundary formulations for sensitivity analysis without matrix derivatives p 242 A93-49028
- Symmetric Galerkin boundary formulations employing curved elements p 268 A93-54198
- KANE, JAMES H.**
- Software issues in three dimensional continuum shape optimization employing boundary formulations [AIAA PAPER 92-4792] p 258 A93-20380
- KANG, SOON**
- Electronic passivation of n- and p-type GaAs using chemical vapor deposited GaS p 283 A93-52708
- KANKAM, M. D.**
- Energy loss analysis of an integrated space power distribution system p 68 A93-25958
- A free-piston Stirling engine/linear alternator controls and load interaction test facility p 146 A93-26077
- Dynamic analysis of free-piston Stirling engine/linear alternator-load system - Experimentally validated p 254 A93-26078
- KANKAM, M. DAVID**
- Energy loss analysis of an integrated space power distribution system [NASA-TM-105772] p 141 A93-14834
- Dynamic analysis of Free-Piston Stirling Engine/Linear Alternator-load system-experimentally validated [NASA-TM-106034] p 271 A93-22559
- Modeling a single phase voltage controlled rectifier using Laplace transforms [NASA-TM-106005] p 271 A93-23016
- KANNAPAREDDY, M.**
- Transition of oscillatory flow in tubes - An empirical model for application to Stirling engines p 174 A93-26088
- KAU, HSIAO C.**
- Some aspects of bifurcation structure of laminar flow in curved ducts p 164 A93-14771
- KAU, KAI-HSIUNG**
- Grid adaptation using Chimera composite overlapping meshes [AIAA PAPER 93-3389] p 267 A93-45080
- Grid adaption using Chimera composite overlapping meshes [NASA-TM-106163] p 269 A93-27065
- KAU, Y. C.**
- A high efficiency Ka-band monolithic pseudomorphic HEMT amplifier p 151 A93-25786
- KAU, Y.-C.**
- High-efficiency high-gain monolithic heterostructure FET amplifier at 31 GHz p 156 A93-37421
- KAPLIN, P. L.**
- Optical fiber sensor for temperature measurement from 600 to 1900 C in gas turbine engines p 208 A93-32918

- KAPOOR, K.**
A comparative study of Full Navier-Stokes and Reduced Navier-Stokes analyses for separating flows within a diffusing inlet S-duct
[AIAA PAPER 93-2154] p 13 A93-49970
- KAPOOR, V. J.**
Processing, electrical and microwave properties of sputtered Ti-Ca-Ba-Cu-O superconducting thin films
p 282 A93-44607
- KASCAK, A. F.**
Hybrid active vibration control of rotorbearing systems using piezoelectric actuators p 221 A93-27324
- KASHIWAGI, T.**
Heat transfer from radiatively heated material in a low Reynolds number microgravity environment
p 180 A93-43695
- KASSEMI, M.**
Numerical model for the Programmable Multirole Furnace (PMZF)
[AIAA PAPER 93-0471] p 142 A93-24242
Effect of radiation on convection in a top-heated enclosure p 189 A93-54454
- KASSEMI, MOHAMMAD**
A numerical model including PID control of a multizone crystal growth furnace p 190 A93-55473
- KATZAN, CYNTHIA M.**
Lunar and Martian environmental interactions with nuclear power system radiators
[NASA-TM-105747] p 80 N93-10965
- KAUFMAN, ALBERT**
Design of a high-temperature experiment for evaluating advanced structural materials
[NASA-TM-105833] p 245 N93-11624
- KAUL, RICHARD**
An all digital implementation of a modified Hamming net for video compression with prediction and quantization circuits p 148 A93-37038
- KAUTZ, H. E.**
Application of neural networks to prediction of advanced composite structures mechanical response and behavior p 205 A93-20751
- KAUTZ, HAROLD E.**
Detecting Lamb waves with broadband acousto-ultrasonic signals in composite structures p 231 A93-21898
Application of neural networks in the acousto-ultrasonic evaluation of metal-matrix composite specimens p 231 A93-37009
Determination of plate wave velocities and diffuse field decay rates with broadband acousto-ultrasonic signals [NASA-TM-106158] p 232 N93-27080
Acousto-Ultrasonic analysis of failure in ceramic matrix composite tensile specimens p 232 N93-29073
- KAZA, K. R. V.**
Semi-empirical model for prediction of unsteady forces on an airfoil with application to flutter p 7 A93-31494
- KAZAROFF, JOHN M.**
Hot fire test results of subscale tubular combustion chambers p 79 N93-10020
Hot fire fatigue testing results for the compliant combustion chamber p 79 N93-10038
Hot fire fatigue testing results for the compliant combustion chamber p 80 N93-10743
Hot fire test results of subscale tubular combustion chambers p 81 N93-11614
Space propulsion p 84 N93-22092
- KAZMIERCHAK, M.**
Flow visualization in a single simulated brush seal p 226 A93-54659
- KEITH, T. G., JR.**
Effect of out-of-roundness on the performance of a diesel engine connecting-rod bearing p 225 A93-52607
- KEITH, THEO G., JR.**
Unsteady aerodynamics and flutter based on the potential equation [AIAA PAPER 93-2086] p 13 A93-49913
Efficient finite element method for aircraft deicing problems p 21 A93-52443
Numerical modeling of runback water on ice protected aircraft surfaces p 201 N93-27438
- KELLEY, JAMES H.**
Robotic planetary mission benefits from nuclear electric propulsion p 43 A93-25854
- KENNEDY, VANCE O.**
Lower temperature curing thermoset polyimides utilizing a substituted norbornene endcap p 134 A93-44526
- KENNEY, C. S.**
Optimal control study for the Space Station Solar Dynamic power module p 54 A93-13133
- KENNEY, CHARLES S.**
Control-structure interaction p 54 A93-14687
- KERCZEWSKI, ROBERT J.**
Multiple-access phased array antenna simulator for a digital beam-forming system investigation p 148 A93-26237
SITE project. Phase 1: Continuous data bit-error-rate testing [NASA-TP-3279] p 58 N93-11001
Anomalous TWTA output power spikes and their effect on a digital satellite communications system [NASA-TM-105875] p 159 N93-13286
- KERHO, M. F.**
LDV flowfield measurements on a straight and swept wing with a simulated ice accretion [AIAA PAPER 93-0300] p 5 A93-23001
- KERREBROCK, J. L.**
Flow instability in particle-bed nuclear reactors [AIAA PAPER 93-1758] p 71 A93-49657
- KERSCHEN, E. J.**
Influence of airfoil thickness on sound generated by high-frequency gust interactions p 272 A93-19181
- KERSLAKE, WILLIAM R.**
Development and flight history of the SERT II spacecraft p 71 A93-38976
- KESSLER, W.**
Nonintrusive, multipoint velocity measurements in high-pressure combustion flows [AIAA PAPER 93-2032] p 118 A93-49867
- KESSLER, W. J.**
Rotational level-dependent collisional broadening and line shift of the A2Sigma(+)X2Pi(1,0) band of OH in hydrogen-air combustion gases p 276 A93-24142
Absorption coefficients for water vapor at 193 nm from 300 to 1073 K p 276 A93-45398
- KHADKIKAR, P. S.**
Transformation to Ni5Al3 in a 63.0 at. pct Ni-Al alloy p 124 A93-25108
- KHAN, ROMEL R.**
Integrated fiber optic probe for dynamic light scattering p 278 A93-52415
- KHAVARAN, A.**
Propagation of high frequency jet noise using geometric acoustics [AIAA PAPER 93-0147] p 272 A93-23241
Propagation of high frequency jet noise using geometric acoustics [NASA-TM-106013] p 275 N93-15575
- KHAVARAN, ABBAS**
Computation of supersonic jet noise under imperfectly expanded conditions [AIAA PAPER 93-0735] p 273 A93-24825
Computation of supersonic jet noise under imperfectly expanded conditions [NASA-TM-105961] p 274 N93-15430
- KHODADOUST, A.**
LDV flowfield measurements on a straight and swept wing with a simulated ice accretion [AIAA PAPER 93-0300] p 5 A93-23001
- KHOSLA, P. K.**
A three-dimensional pressure flux-split RNS application to sub/supersonic flow in inlets and ducts [AIAA PAPER 93-3063] p 11 A93-48239
- KIKUCHI, NOBORU**
Topology and layout optimization of discrete and continuum structures p 241 A93-45429
Layout optimization using the homogenization method p 243 A93-54508
Applications to car bodies - Generalized layout design of three-dimensional shells p 243 A93-54509
- KIM, CHAN M.**
Computation of supersonic jet noise under imperfectly expanded conditions [AIAA PAPER 93-0735] p 273 A93-24825
Computation of supersonic jet noise under imperfectly expanded conditions [NASA-TM-105961] p 274 N93-15430
- KIM, HYECHUL**
Fault-tolerant onboard digital information switching and routing for communications satellites [NASA-TM-4471] p 53 N93-26895
- KIM, HYUN D.**
A time-accurate high-resolution TVD scheme for solving the Navier-Stokes equations p 13 A93-52006
- KIM, HYUN DAE**
A time-accurate high-resolution TVD scheme for solving the Navier-Stokes equations [NASA-TM-106056] p 268 N93-22664
- KIM, J.**
Time-averaged heat transfer and pressure measurements and comparison with prediction for a two-stage turbine [ASME PAPER 92-GT-194] p 166 A93-19419
- KIM, JUNGHWAN**
Performance evaluation of land mobile satellite system under fading and interference using multiple TCM by Monte-Carlo simulation p 147 A93-10958
- KIM, K.**
A new hue capturing technique for the quantitative interpretation of liquid crystal images used in convective heat transfer studies p 204 A93-13977
Evaluation of a hue capturing based transient liquid crystal method for high-resolution mapping of convective heat transfer on curved surfaces p 210 A93-43689
Fluid dynamics and convective heat transfer in impinging jets through implementation of a high resolution liquid crystal technique [ISABE 93-7077] p 189 A93-54053
- KIM, M.**
Control-structure interaction study for the Space Station solar dynamic power module p 54 A93-13132
- KIM, RAE-KUK**
Discrete ordinates solutions for radiatively participating media in a cylindrical enclosure p 285 A93-31427
- KIM, S. C.**
Calculation of scramjet inlet with thick boundary-layer ingestion [AIAA PAPER 93-1836] p 12 A93-49720
- KIM, S.-W.**
Calculation of a circular jet in crossflow with a multiple-time-scale turbulence model p 164 A93-15063
Calculations of separated 3-D flows with a pressure-staggered Navier-Stokes equations solver p 177 A93-34366
Fluid flow of a row of jets in crossflow - A numerical study p 179 A93-35608
- KIM, SUK C.**
DSMC and continuum analyses of low-density nozzle flow [AIAA PAPER 93-0727] p 172 A93-24817
Calculations of low Reynolds number rocket nozzles [AIAA PAPER 93-0888] p 67 A93-24948
Analysis of plume backflow around a nozzle lip in a nuclear rocket [AIAA PAPER 93-2497] p 77 A93-50231
Numerical study of nozzle wall cooling for nuclear thermal rockets [AIAA PAPER 93-2498] p 77 A93-50232
Computational fluid dynamics for nuclear thermal propulsion p 199 N93-26930
- KIM, TAE-KUK**
Discrete ordinates solutions of nongray radiative transfer with diffusely reflecting walls p 285 A93-30124
- KIM, Y.-S.**
A model for predicting high-temperature fatigue failure of a W/Cu composite p 112 N93-31579
- KIM, YOUNG-SUK**
A creep cavity growth model for creep-fatigue life prediction of a unidirectional W/Cu composite [NASA-TM-105780] p 244 N93-10967
- KIMBLE, MICHAEL C.**
PEM fuel cell stack heat and mass management p 253 A93-26024
- KIMNACH, GREG L.**
Power system monitoring and source control of the Space Station Freedom dc-power system testbed p 69 A93-26109
Power system monitoring and source control of the Space Station Freedom DC power system testbed [NASA-TM-105841] p 80 N93-10734
- KING, D. Q.**
A comparison of arcjet plume properties to model predictions [AIAA PAPER 93-0820] p 67 A93-24891
- KING, ROGER J.**
Simulating a 1-kW arcjet thruster using a nonlinear active load p 48 A93-34482
- KIRALY, L. J.**
Hybrid active vibration control of rotorbearing systems using piezoelectric actuators p 221 A93-27324
Binary tree eigen solver in finite element analysis [AIAA PAPER 93-1493] p 267 A93-34034
- KIRLIN, PETER S.**
Single liquid source plasma-enhanced metalorganic chemical vapor deposition of high-quality YBa2Cu3O(7-x) thin films p 280 A93-20643
- KIRTLEY, K. R.**
Aeroloads and secondary flows in a transonic mixed flow turbine stage [ASME PAPER 92-GT-72] p 2 A93-19322
Three-dimensional analysis of the Pratt and Whitney alternate design SSME fuel turbine p 230 N93-31584
- KISEL, MARTIN**
A multi-zone muffle furnace design [NASA-TM-106153] p 145 A93-27011
- KISH, J. G.**
Split torque transmission load sharing [NASA-TM-105884] p 226 N93-12736
- KLEM, MARK D.**
Test program to provide validation data for the Rocket Combustor Interactive Design (ROCCID) code p 120 N93-11450

- Coaxial injector spray characterization using water/air as simulants p 120 N93-11452
- KLIMA, STANLEY J.**
NDE of PWA 1480 single crystal turbine blade material [NASA-TM-106140] p 38 N93-27640
- KNIGHT, D. A.**
Optimization of armored spherical tanks for storage on the lunar surface p 47 A93-25866
- KNIGHT, J. D.**
Determination of forces in a magnetic bearing actuator - Numerical computation with comparison to experiment p 219 A93-15686
- KNOLL, R. H.**
Nucleate pool boiling in the long duration low gravity environment of the space shuttle [AIAA PAPER 93-0465] p 142 A93-23371
Low-g fluid mixing - Further results from the Tank Pressure Control Experiment [AIAA PAPER 93-2423] p 187 A93-50181
Nucleate pool boiling in the long duration low gravity environment of the Space Shuttle [NASA-TM-105973] p 144 N93-15420
Tank Pressure Control Experiment/Thermal Phenomena (TPCE/TP) p 92 N93-28713
- KNOPSE, C. R.**
The isolation limits of stochastic vibration p 236 A93-30042
- KNOWLES, T. R.**
Pulsed single-blow regenerator testing p 221 A93-26081
- KNOX, LLOYD**
Inflation at the electroweak scale p 290 A93-26263
- KO, FRANK**
Development of braided rope seals for hypersonic engine applications - Flow modeling p 222 A93-34493
Development of braided rope seals for hypersonic engine applications: Flow modeling [NASA-TM-105942] p 227 N93-14478
- KO, FRANK K.**
Development of hypersonic engine seals - Flow effects of preload and engine pressures [AIAA PAPER 93-1998] p 223 A93-49841
- KOEPP, G.**
Performance of TiCaBaCuO₃₀ GHz 64 element antenna array p 157 A93-44763
- KOLB, EDWARD W.**
The inflation sector of extended inflation p 288 A93-17638
Observing the inflation potential p 291 A93-50480
- KOLECKI, JOSEPH C.**
The interaction of high voltage systems with the environments of the moon and Mars [AIAA PAPER 93-0704] p 67 A93-24800
The interaction of high voltage systems with the environments of the Moon and Mars [NASA-TM-106107] p 61 N93-26148
- KOLLMANN, W.**
Pdf prediction of supersonic hydrogen flames [AIAA PAPER 93-0448] p 114 A93-23358
- KONG, H. S.**
Aluminum acceptor four particle bound exciton complex in 4H, 6H, and 3C SiC p 282 A93-44822
- KONG, K. S.**
Design aspects and comparison between high Tc superconducting coplanar waveguide and microstrip line p 155 A93-27244
Conductor-backed coplanar waveguide resonators of Y-Ba-Cu-O and Ti-Ba-Ca-Cu-O on LaAlO₃ [NASA-TM-105890] p 284 N93-12325
- KONNO, KEVIN**
Acoustic mode measurements in the inlet of a model turbofan using a continuously rotating rake - Data collection/analysis techniques [AIAA PAPER 93-0599] p 24 A93-23324
Acoustic mode measurements in the inlet of a model turbofan using a continuously rotating rake: Data collection/analysis techniques [NASA-TM-105936] p 33 N93-15403
- KONNO, KEVIN E.**
Rotating rake design for unique measurement of fan-generated spinning acoustic modes [NASA-TM-105946] p 36 N93-26161
- KOONTZ, STEVE**
Recommended practices for in-space and ground laboratory. Atomic oxygen exposure and analysis p 276 N93-20814
- KOPLIK, JOEL**
Molecular dynamics of interface rupture p 175 A93-30130
- KORENYI-BOTH, A. L.**
Non-destructive, ultra-low resistance, thermally stable contacts for use on shallow junction InP solar cells [NASA-TM-106228] p 256 N93-32201
- KORY, CAROL L.**
Simulation of TunnelLadder traveling-wave tube cold-test characteristics: Implementation of the three-dimensional, electromagnetic circuit analysis code micro-SOS [NASA-TP-3294] p 160 N93-23394
- KOSMATKA, J. B.**
Behavior of spinning laminated composite plates with initial twist-experimental vibrations, strain, and deflection results [AIAA PAPER 93-1325] p 238 A93-33898
- KOSOWSKY, ARTHUR**
Gravitational waves from first-order cosmological phase transitions p 288 A93-11451
- KOSS, M. B.**
IDGE - A test of dendritic growth theory using space flight [AIAA PAPER 93-0260] p 143 A93-25515
Scientific basis for the Isothermal Dendritic Growth Experiment - A USMP-2 space flight experiment p 143 A93-50455
- KOSTER, J. N.**
Natural and thermocapillary convection in multiple liquid layers [AIAA PAPER 93-0469] p 171 A93-24241
- KOSTER, JEAN N.**
Thermocapillary convection in two immiscible liquid layers with free surface p 188 A93-52515
- KOTHE, D. B.**
RIPPLE - A new model for incompressible flows with free surfaces p 164 A93-14551
- KOUDELKA, JOHN M.**
Capabilities and constraints of typical space flight hardware p 145 N93-20183
- KOWALSKI, DAVID**
Three-dimensional laser window formation for industrial application p 218 N93-22197
- KOYLU, U. O.**
Structure of soot-containing laminar jet diffusion flames [AIAA PAPER 93-0708] p 114 A93-24804
- KOZAR, ROBERT**
Plum Brook facilities p 49 N93-26964
- KRAFT, L. ALAN**
Modelling a single phase voltage controlled rectifier using Laplace transforms [NASA-TM-106005] p 271 N93-23016
- KRANTZ, T. L.**
Split torque transmission load sharing [NASA-TM-105884] p 226 N93-12736
- KRASOWSKI, M. J.**
A fuzzy logic based controller for the automated alignment of a laser-beam-smoothing spatial filter [NASA-TM-105994] p 217 N93-18091
- KRASOWSKI, MICHAEL J.**
Neural nets for aligning optical components in harsh environments: Beam smoothing spatial filter as an example p 266 N93-31557
- KREIDER, K. L.**
Modal element method for scattering and absorbing of sound by two-dimensional bodies p 274 A93-53657
- KREIDER, KEVIN L.**
Modal ring method for the scattering of electromagnetic waves [NASA-TM-105966] p 149 N93-20260
- KREJSA, E. A.**
Propagation of high frequency jet noise using geometric acoustics [AIAA PAPER 93-0147] p 272 A93-23241
Propagation of high frequency jet noise using geometric acoustics [NASA-TM-106013] p 275 N93-15575
- KREJSA, EUGENE A.**
Computation of supersonic jet noise under imperfectly expanded conditions [AIAA PAPER 93-0735] p 273 A93-24825
Computation of supersonic jet noise under imperfectly expanded conditions [NASA-TM-105961] p 274 N93-15430
- KREN, LAWRENCE A.**
A hot dynamic seal rig for measuring hypersonic engine seal durability and flow performance [AIAA PAPER 93-1346] p 222 A93-33916
- KRIER, HERMAN**
Ignition and combustion of aluminum/magnesium alloy particles in O₂ at high pressures p 113 A93-22030
- KROEGER, E. W.**
EOTV propellant tank pressure control and liquid dynamics [AIAA PAPER 93-2399] p 77 A93-50164
- KROLIKOWSKI, C. R.**
Numerical model for the Programmable Multirole Furnace (PMZF) [AIAA PAPER 93-0471] p 142 A93-24242
- KROLL, J. T.**
Optimization of circular orifice jets mixing into a heated crossflow in a cylindrical duct p 24 A93-23246 [AIAA PAPER 93-0249]
Optimization of circular orifice jets mixing into a heated cross flow in a cylindrical duct [NASA-TM-105984] p 33 N93-15359
- KRUPAR, MARTIN J.**
Laser velocimeter measurements of the flow field generated by a forward-swept propfan during flutter [AIAA PAPER 93-2919] p 14 A93-53591
- KU, JERRY C.**
Soot formation and radiation in turbulent jet diffusion flames under normal and reduced gravity conditions p 121 N93-20192
- KUCZMARSKI, M.**
Prediction of chemical vapor deposition rates on monofilaments and its implications for fiber properties p 113 A93-17198
- KUCZMARSKI, M. A.**
A kinetic and equilibrium analysis of silicon carbide chemical vapor deposition on monofilaments [NASA-TM-106137] p 96 N93-27003
- KUCZMARSKI, MARIA A.**
Computer modeling of a hot filament diamond deposition reactor p 94 A93-40618
- KUIVINEN, DAVID E.**
External stress-corrosion cracking of a 1.22-m-diameter type 316 stainless steel air valve [NASA-TP-3190] p 129 N93-26201
- KUMAR, A.**
Contact stress analysis of spiral bevel gears using nonlinear finite element static analysis [AIAA PAPER 93-2296] p 224 A93-50081
Contact stress analysis of spiral bevel gears using nonlinear finite element static analysis [NASA-TM-106176] p 228 N93-27037
- KUNATH, R.**
Fiber optic link for millimeter wave communication satellites p 277 A93-25736
- KUNDU, K.**
Computations of spray, fuel-air mixing, and combustion in a lean-premixed-prevaporized combustor [AIAA PAPER 93-2069] p 185 A93-49901
- KUNDU, K. P.**
A simplified reaction mechanism for calculation of emissions in hydrocarbon (Jet-A) combustion [AIAA PAPER 93-2341] p 118 A93-50116
- KUNDU, KRISHNA**
Simplified jet fuel reaction mechanism for lean burn combustion application [AIAA PAPER 93-0021] p 113 A93-23238
Simplified jet-A kinetic mechanism for combustor application [NASA-TM-105940] p 120 N93-15504
- KUNDU, KRISHNA P.**
Computation of the flow field in an annular gas turbine combustor [AIAA PAPER 93-2074] p 28 A93-49903
The promising chemical kinetics for the simulation of propane-air combustion with KIVA-II code [AIAA PAPER 93-2189] p 118 A93-50001
- KUNINAKA, HITOSHI**
Arcing rates for High Voltage Solar Arrays - Theory, experiment, and predictions p 70 A93-32567
- KUNTZ, TODD A.**
Residual strain gradient determination in metal matrix composites by synchrotron X-ray energy dispersive diffraction p 103 A93-39580
- KURKOV, ANATOLE P.**
Experimental investigation of counter-rotating propfan flutter at cruise conditions [AIAA PAPER 93-1632] p 25 A93-34160
- KURTZ, ANTHONY D.**
Direct observation of porous SiC formed by anodization in HF p 282 A93-43587
- KUSHIDA, G.**
Heat transfer from radiatively heated material in a low Reynolds number microgravity environment p 180 A93-43695
- KUSSMAUL, MICHAEL T.**
Optical and scratch resistant properties of diamondlike carbon films deposited with single and dual ion beams [NASA-TM-105943] p 95 N93-22586
Optical and scratch resistant properties of diamondlike carbon films deposited with single and dual ion beams p 137 N93-25564
- KUTLER, PAUL**
The NASA Computational Fluid Dynamics (CFD) program - Building technology to solve future challenges [AIAA PAPER 93-3292] p 287 A93-44996
- KWA, S. C.**
Performance evaluation of land mobile satellite system under fading and interference using multiple TCM by Monte-Carlo simulation p 147 A93-10958

KWATRA, S. C.

- Efficient demultiplexing algorithm for noncontiguous carriers p 148 A93-32561
 Compressing subbanded image data with Lempel-Ziv-based coders [NASA-TM-105998] p 149 N93-20257
 Subband coding for image data archiving p 287 N93-25922

KWON, OH J.

- Three-dimensional unstructured grid Euler method applied to turbine blades [AIAA PAPER 93-0196] p 6 A93-24233

KWONG, WAIK WOK

- Implications of new GALLEX results for the Mikheyev-Smirnov-Wolfenstein solution of the solar neutrino problem p 293 A93-10357

L**LACKNEY, J. J.**

- High Temperature Composite Analyzer (HITCAN) theoretical manual, version 1.0 [NASA-TM-106001] p 249 N93-24913

- High temperature composite analyzer (HITCAN) user's manual, version 1.0 [NASA-TM-106002] p 249 N93-25070

LACONTI, ANTHONY B.

- Regenerative fuel cells p 252 A93-25868

LACOVIC, RAYMOND F.

- Autogenous pressurization of cryogenic vessels using submerged vapor injection p 71 A93-48648

LAGRAFF, L. E.

- Wake-induced unsteady stagnation-region heat-transfer measurements [ASME PAPER 92-GT-196] p 166 A93-19421

LAI, H. T.

- CFD validation of subsonic turbulent planar shear layers [AIAA PAPER 93-1773] p 184 A93-49669
 Calculation of scramjet inlet with thick boundary-layer ingestion [AIAA PAPER 93-1836] p 12 A93-49720

LAI, M.-C.

- Atomization and vaporization characteristics of airblast fuel injection inside a venturi tube [AIAA PAPER 93-1766] p 184 A93-49662

LAI, MING-CHIA

- Second order closure modeling of turbulent buoyant wall plumes [NASA-TM-105956] p 193 N93-14829

LAING, PETER

- Two and three-dimensional prediffuser combustor studies with air-water mixture [AIAA PAPER 93-0240] p 113 A93-22652

LAKE, MAX L.

- Properties of hybrid CVD/PAN graphite fibers and their bromine intercalation compounds p 98 A93-17675

LAKSHMINARAYANA, B.

- Three-dimensional flow field in a turbine nozzle passage [AIAA PAPER 93-2556] p 13 A93-50278

LAKSHMINARAYANA, BUDUGUR

- A simplified Reynolds stress model for unsteady turbulent boundary layers [AIAA PAPER 93-0204] p 168 A93-22622
 Low-Reynolds-number k-epsilon model for unsteady turbulent boundary-layer flows p 14 A93-53208

LAMB, MILTON

- Supersonic investigation of two dimensional hypersonic exhaust nozzles [NASA-TM-105687] p 33 N93-15342

LAMBRECHT, WALTER R. L.

- Interface dependence of band offsets in lattice-matched isovalent heterojunctions p 280 A93-32132

LAMOREAUX, CYNTHIA

- Performance and properties of atomic oxygen protective coatings for polymeric materials p 225 A93-53389

LAN, G. L.

- Millimeter-wave pseudomorphic HEMT MMIC phased array components for space communications p 152 A93-25796

LANDIS, GEOFFREY A.

- Photovoltaic arrays for Martian surface power [IAF PAPER 92-0591] p 293 A93-13699
 Photovoltaic receivers for laser beamed power in space p 66 A93-21664
 Indium phosphide solar cells for laser power beaming applications p 252 A93-25899
 Space transfer with ground-based laser/electric propulsion [NASA-TM-106060] p 84 A93-20615
 Texturing of InP surfaces for device applications [NASA-TM-106061] p 129 N93-28618

LANNUTTI, J. J.

- Fabrication and properties of functionally graded NiAl/Al₂O₃ composites p 105 A93-54116

LANT, CHRISTIAN T.

- Progress in speckle-shift strain measurement p 251 N93-31558

LAPID, A. J.

- Behavior of spinning laminated composite plates with initial twist-experimental vibrations, strain, and deflection results [AIAA PAPER 93-1325] p 238 A93-33898

LARKIN, D. J.

- CVD of SiC and AlN using cyclic organometallic precursors p 117 A93-39525
 Atomic probe microscopy of 3C SiC films grown on 6H SiC substrates p 281 A93-39854
 Aluminum acceptor four particle bound exciton complex in 4H, 6H, and 3C SiC p 282 A93-44822

LARKIN, DAVID J.

- Greatly improved 3C-SiC p-n junction diodes grown by chemical vapor deposition p 156 A93-38994
 Process for the controlled growth of single-crystal films of silicon carbide polytypes on silicon carbide wafers [NASA-CASE-LEW-15222-3] p 284 N93-17413

LARKIN, M.

- Effect of a rotating propeller on the separation angle of attack [AIAA PAPER 93-0017] p 6 A93-24978
 Effect of a rotating propeller on the separation angle of attack and distortion in ducted propeller inlets [NASA-TM-105935] p 16 N93-16625

LAROSILIERE, L. M.

- Navier-Stokes analysis of radial turbine rotor performance [AIAA PAPER 93-2555] p 30 A93-50277

LAROSILIERE, LOUIS M.

- Three-dimensional numerical simulation of gradual opening in a wave rotor passage [AIAA PAPER 93-2526] p 187 A93-50254
 Analysis of unsteady wave processes in a rotating channel [AIAA PAPER 93-2527] p 187 A93-50255

LARSON, C. A.

- Effects of anode material on arcjet performance p 79 N93-10044
 Effects of anode material on arcjet performance [NASA-TM-105799] p 79 N93-10197

LAUB, A. J.

- Optimal control study for the Space Station Solar Dynamic power module p 54 A93-13133

LAUB, ALAN J.

- Control-structure interaction p 54 A93-14687

LAUR, MICHELE

- Forward rotor vortex effects on counter rotating propeller noise p 2 A93-19221

LAURENDEAU, NORMAND M.

- Laser-induced fluorescence measurements of nitric oxide in laminar C₂H₆/O₂/N₂ flames at high pressure p 116 A93-28253

LAVELLE, THOMAS M.

- Concurrent optimization of airframe and engine design parameters [AIAA PAPER 92-4713] p 20 A93-20281
 Concurrent optimization of airframe and engine design parameters [NASA-TM-105908] p 32 N93-12402

LAWLESS, PATRICK B.

- Prediction of active control of subsonic centrifugal compressor rotating stall [AIAA PAPER 93-0153] p 4 A93-22591
 A model for the selective amplification of spatially coherent waves in a centrifugal compressor on the verge of rotating stall [AIAA PAPER 93-2236] p 13 A93-50039

LAWRENCE, CHARLES

- Design of structures for Nuclear Electric Propulsion vehicles [AIAA PAPER 93-1393] p 57 A93-33955
 Dynamics of rotating multicomponent turbomachinery systems [AIAA PAPER 93-1629] p 222 A93-34157
 Dynamics of rotating multi-component turbomachinery systems [NASA-TM-105997] p 247 N93-18426
 Inverse kinematics problem in robotics using neural networks [NASA-TM-105869] p 247 N93-18876
 Structural dynamics branch research and accomplishments to FY 1992 [NASA-TM-105824] p 247 N93-20368

LE, D. K.

- A note on decentralized integral controllability p 264 A93-30492

LEAVITT, LAURENCE D.

- Supersonic investigation of two dimensional hypersonic exhaust nozzles [NASA-TM-105687] p 33 N93-15342

LEBRON, RAMON C.

- Load converter interactions with the secondary system in the Space Station Freedom power management and distribution dc test bed p 154 A93-26106

LECKIE, F. A.

- Transverse ductility of metal matrix composites p 101 A93-31355

LECKIE, FREDERICK A.

- Ductility of a continuous fiber reinforced aluminum matrix composite p 102 A93-32471

LEDNICER, D. A.

- CFD zonal modeling of leading-edge ice effects for a complete aircraft [AIAA PAPER 93-0167] p 5 A93-22601

LEE, CHI-MING

- Simplified jet fuel reaction mechanism for lean burn combustion application [AIAA PAPER 93-0021] p 113 A93-23238
 Simplified jet-A kinetic mechanism for combustor application [NASA-TM-105940] p 120 N93-15504
 Nitric oxide formation in a lean, premixed-prevaporized jet A/air flame tube: An experimental and analytical study [NASA-TM-105722] p 257 N93-27012

LEE, H.-J.

- Fiber shape effects on metal matrix composite behavior p 98 A93-15752
 Fiber shape effects on metal matrix composite behavior [NASA-TM-106067] p 109 N93-26704

LEE, HAEOK S.

- An evaluation of three spatial differencing schemes for the discrete ordinates method in participating media [AIAA PAPER 93-0140] p 266 A93-24231
 Discrete ordinates solutions of nongray radiative transfer with diffusely reflecting walls p 285 A93-30124
 Discrete ordinates solutions for radiatively participating media in a cylindrical enclosure p 285 A93-31427
 Radiation heat transfer calculations using a control-angle, control-volume-based discrete ordinates method [AIAA PAPER 93-2731] p 182 A93-46485
 Nongray gas analyses for reflecting walls utilizing a flux technique p 190 A93-55460

LEE, J.

- A numerical study of mixing in supersonic combustors with hypermixing injectors [AIAA PAPER 93-0215] p 25 A93-27801
 A lag model for turbulent boundary layers developing over rough bleed surfaces [AIAA PAPER 93-2988] p 10 A93-48181

LEE, JAMES H.

- Nuclear safety policy working group recommendations on nuclear propulsion safety for the space exploration initiative [NASA-TM-105705] p 88 N93-26200

LEE, JINHO

- Scaling analysis of gas-liquid two-phase flow pattern in microgravity [AIAA PAPER 93-0914] p 173 A93-24968
 Prediction of gas-liquid two-phase flow regime in microgravity [NASA-TM-106274] p 145 N93-30939

LEE, K. D.

- Three-dimensional Navier-Stokes calculations using solution-adapted grids [AIAA PAPER 93-0431] p 6 A93-24240

LEE, KAI-FONG

- Spectral-domain moment-method analysis of coplanar microstrip parasitic subarrays p 148 A93-35016
 Input impedance of coaxially fed rectangular microstrip antenna on electrically thick substrate p 155 A93-36994

LEE, KANG N.

- Chemical reactions in the processing of MoSi₂ + carbon compacts p 119 A93-53733

LEE, L. P.

- Demonstration of Y1Ba₂Cu₃O₇(δ) and complementary metal-oxide-semiconductor device fabrication on the same sapphire substrate p 159 A93-56292

LEE, R.

- Analysis of MMIC arrays for use in the ACTS Aero Experiment [NASA-TM-106073] p 53 N93-22589

LEE, R. Q.

- Spectral-domain moment-method analysis of coplanar microstrip parasitic subarrays p 148 A93-35016
 Directivity versus element spacing for a scanning array p 148 A93-36991

- Input impedance of coaxially fed rectangular microstrip antenna on electrically thick substrate p 155 A93-36994
- LEE, RICHARD Q.**
Effect of a dielectric overlay on a linearly tapered slot antenna excited by a coplanar waveguide p 155 A93-35649
Microwave characterization of slotline on high resistivity silicon for antenna feed network [NASA-TM-106058] p 161 A93-27265
- LEE, S. W.**
Analysis of reflector antenna system including frequency selective surfaces p 52 A93-32820
- LEE, S. Y.**
Thin film diamond microstructure applications p 209 A93-40580
- LEE, SANG S.**
Fully coupled resonant-triad interaction in an adverse-pressure-gradient boundary layer p 167 A93-21049
Multiple large-scale coherent mode interactions in a developing round jet p 178 A93-34409
- LEE, SANG SOO**
On the nonlinear three dimensional instability of Stokes layers and other shear layers to pairs of oblique waves [NASA-TM-105918] p 194 A93-15499
- LEFEBVRE, A. H.**
Influence of ambient air pressure on effervescent atomization [AIAA PAPER 92-0460] p 167 A93-21652
- LEGNER, H.**
Nonintrusive, multipoint velocity measurements in high-pressure combustion flows [AIAA PAPER 93-2032] p 118 A93-49867
- LEI, JIH-FEN**
Palladium-chromium static strain gage for high temperature propulsion systems p 204 A93-16421
High temperature static strain measurement with an electrical resistance strain gage [AIAA PAPER 92-5039] p 205 A93-22313
- LEIB, S. J.**
Three-dimensional boundary-layer instability and separation induced by small-amplitude streamwise vorticity in the upstream flow p 172 A93-24401
A note on the distortion of a flat-plate boundary layer by free-stream vorticity normal to the plate p 178 A93-34414
- LEISSLER, GEORGE W.**
Characterization and durability testing of plasma-sprayed zirconia-yttria and hafnia-yttria thermal barrier coatings. Part 1. Effect of spray parameters on the performance of several lots of partially stabilized zirconia-yttria powder [NASA-TP-3295] p 128 A93-22556
- LEKAN, JACK**
Capabilities and constraints of NASA's ground-based reduced gravity facilities p 49 A93-20184
- LEMBECK, CATHERINE A.**
Optimal impulsive intercept with low-thrust rendezvous return p 45 A93-34521
- LEMPERT, WALTER R.**
Time-sequenced and spectrally filtered Rayleigh imaging of shock wave and boundary layer structure for inlet characterization [AIAA PAPER 93-2300] p 211 A93-50085
- LEMPNER, S. E.**
Growth and characterization of 3C-SiC and 6H-SiC films on 6H-SiC wafers p 284 A93-55602
- LEONARD, B. P.**
Comparison of truncation error of finite-difference and finite-volume formulations of convection terms [NASA-TM-105861] p 268 A93-11531
Positivity-preserving numerical schemes for multidimensional advection [NASA-TM-106055] p 200 A93-27091
- LEONARD, REGIS**
Millimeter-wave pseudomorphic HEMT MMIC phased array components for space communications p 152 A93-25796
- LEONARD, REGIS F.**
Monolithic microwave integrated circuits for sensors, radar, and communications systems; Proceedings of the Meeting, Orlando, FL, Apr. 2-4, 1991 [SPIE-1475] p 151 A93-25776
- LEONHARDT, TODD A.**
Isothermal aging effects on PMR-15 resin p 131 A93-24508
- LEPICOVSKY, J.**
LV software support for supersonic flow analysis [AIAA PAPER 92-3900] p 259 A93-24487
- LERCH, B. A.**
Room temperature cyclic deformation behavior of cast and extruded NiAl p 122 A93-12130
Fatigue-environment interactions in a SiC/Ti-15-3 composite p 100 A93-26275
- LERCH, BRADLEY A.**
Low cycle fatigue behavior of polycrystalline NiAl at 300 and 1000 K [NASA-TM-105987] p 129 A93-26898
- LEVELT SENGERS, J. M. H.**
The susceptibility critical exponent for a nonaqueous ionic binary mixture near a consolute point p 284 A93-19838
- LEVINE, STANLEY R.**
Aerospace applications p 135 A93-55472
- LEWANDOWSKI, J. J.**
Chemical stability of titanium diboride reinforcement in nickel aluminide matrices p 105 A93-52473
- LEWICKI, D. G.**
Face-gear drives: Design, analysis, and testing for helicopter transmission applications [NASA-TM-106101] p 229 A93-27133
Efficient fault diagnosis of helicopter gearboxes [NASA-TM-106253] p 231 A93-31846
- LEWICKI, DAVID G.**
Low-noise, high-strength, spiral-bevel gears for helicopter transmissions [AIAA PAPER 93-2149] p 223 A93-49966
Evaluation of an oil-debris monitoring device for use in helicopter transmissions [NASA-TM-105830] p 227 A93-22826
Low-noise, high-strength, spiral-bevel gears for helicopter transmissions [NASA-TM-106080] p 228 A93-23019
Pattern classifier for health monitoring of helicopter gearboxes [NASA-TM-106099] p 228 A93-23741
Fault detection of helicopter gearboxes using the multi-valued influence matrix method [NASA-TM-106100] p 229 A93-27069
- LEWIS, CATHERINE C.**
Design of an automated imaging system for use in a space experiment p 204 A93-20454
- LEWIS, CLARK H.**
PNS predictions for supersonic/hypersonic flows over finned missile configurations [AIAA PAPER 92-2695] p 7 A93-37374
Low-to-high altitude predictions of three-dimensional ablative re-entry flowfields p 182 A93-46407
- LEWIS, L. L.**
Performance of TiCaBaCuO₃ 30 GHz 64 element antenna array p 157 A93-44763
- LEWIS, P.**
Stiffness of magnetic bearings subjected to combined static and dynamic loads [ASME PAPER 91-TRIB-27] p 219 A93-15685
- LEZBERG, ERWIN A.**
In-stream measurements of combustion during Mach 5 to 7 tests of the Hypersonic Research Engine (HRE) [AIAA PAPER 93-2324] p 28 A93-50104
- LI, RONGSHUN**
Variation of the energy release rate as a crack approaches and passes through an elastic inclusion p 241 A93-44440
- LI, S. H.**
Application of high-quality SiO₂ grown by multipolar ECR source to Si/SiGe MISFET p 156 A93-37413
- LI, W. Q.**
Application of high-quality SiO₂ grown by multipolar ECR source to Si/SiGe MISFET p 156 A93-37413
- LI, XIAOHUI**
Hierarchical image coding with diamond-shaped sub-bands p 205 A93-20945
- LI, Z.**
Computations of spray, fuel-air mixing, and combustion in a lean-premixed-prevaporized combustor [AIAA PAPER 93-2069] p 185 A93-49901
- LIAN, Z. W.**
Absolute and convective instability of a viscous liquid jet surrounded by a viscous gas in a vertical pipe p 176 A93-30144
- LIANG, ANITA D.**
Development of advanced seals for space propulsion turbomachinery [SAE PAPER 921028] p 218 A93-14651
Brush seal low surface speed hard-rub characteristics [AIAA PAPER 93-2534] p 225 A93-50261
Brush seal bristle flexure and hard-rub characteristics [NASA-TM-105864] p 227 A93-18321
Brush seal low surface speed hard-rub characteristics [NASA-TM-106169] p 200 A93-27132
- LIANG, G.-C.**
Large-area YBa₂Cu₃O₇(δ) thin films on sapphire for microwave applications p 279 A93-11475
- LIANG, D. G.**
Quantification of uncertainties in composites [AIAA PAPER 93-1440] p 102 A93-33989
Probabilistic sizing of laminates with uncertainties [NASA-TM-106145] p 110 A93-27082
- Probabilistic simulation of multi-scale composite behavior [NASA-TM-106196] p 250 A93-28633
- LIANG, L.**
Probabilistic simulation of stress concentration in composite laminates [AIAA PAPER 93-1442] p 103 A93-33991
- LIBERMAN, EUGENE M.**
An embedded rule-based diagnostic expert system in Ada p 260 A93-11928
- LICHT, B. W.**
Numerical model for the Programmable Multirole Furnace (PMZF) [AIAA PAPER 93-0471] p 142 A93-24242
- LICHTIN, D. A.**
The effects of 1 kW class arcjet thruster plumes on spacecraft charging and spacecraft thermal control materials p 57 A93-35050
Low power arcjet system spacecraft impacts [AIAA PAPER 93-2392] p 76 A93-50157
- LIDDLE, ANDREW R.**
Observing the inflation potential p 291 A93-50480
- LIDSEY, JAMES E.**
Observing the inflation potential p 291 A93-50480
- LIEBERT, CURT H.**
Miniature high temperature plug-type heat flux gauges p 209 A93-37862
Progress in the measurement of SSME turbine heat flux with plug-type sensors p 217 A93-31553
- LIEBESKIND, J. G.**
A comparison of arcjet plume properties to model predictions [AIAA PAPER 93-0820] p 67 A93-24891
- LIEBESKIND, JOHN G.**
Plume characteristics of an arcjet thruster [AIAA PAPER 93-2530] p 77 A93-50258
- LIENHARD, JOHN H.**
M.I.T. Stirling-cycle heat transfer apparatus p 174 A93-26090
- LIM, HONG S.**
Lightweight nickel electrodes for nickel/hydrogen cells p 255 A93-51574
- LIMBURG, HELEN C.**
A high-efficiency 59- to 64-GHz TWT for intersatellite communications p 158 A93-49553
- LIN, AVI**
Parallel solution of high-order numerical schemes for solving incompressible flows [NASA-TM-4451] p 262 A93-27040
- LIN, C. S.**
Nucleate pool boiling in the long duration low gravity environment of the space shuttle [AIAA PAPER 93-0465] p 142 A93-23371
Mixing and transient interface condensation of a liquid hydrogen tank [AIAA PAPER 93-1968] p 184 A93-49816
Low-g fluid mixing - Further results from the Tank Pressure Control Experiment [AIAA PAPER 93-2423] p 187 A93-50181
Nucleate pool boiling in the long duration low gravity environment of the Space Shuttle [NASA-TM-105973] p 144 A93-15420
Mixing and transient interface condensation of a liquid hydrogen tank [NASA-TM-106201] p 201 A93-28252
- LIN, HSIANG H.**
Effect of extended tooth contact on the modeling of spur gear transmissions [AIAA PAPER 93-2148] p 223 A93-49965
Dynamic analysis of spur gears using computer program DANST [AIAA PAPER 93-2295] p 224 A93-50080
- LIN, HSIANG HSI**
Dynamic analysis of spur gears using computer program DANST [NASA-TM-106211] p 230 A93-28050
Effect of extended tooth contact on the modeling of spur gear transmissions [NASA-TM-106174] p 230 A93-28411
- LIN, S. P.**
Absolute and convective instability of a viscous liquid jet surrounded by a viscous gas in a vertical pipe p 176 A93-30144
- LIN, T. L.**
A least-squares finite element method for 3D incompressible Navier-Stokes equations [AIAA PAPER 93-0338] p 171 A93-24236
Large-scale computation of incompressible viscous flow by least-squares finite element method [NASA-TM-105904] p 269 A93-22825
- LINNE, DIANE L.**
Performance and heat transfer characteristics of a carbon monoxide/oxygen rocket engine [NASA-TM-105897] p 84 A93-18878

LIU, CHUEN-HUEI

- Dynamic analysis of spur gears using computer program
DANST
[AIAA PAPER 93-2295] p 224 A93-50080
- Dynamic analysis of spur gears using computer program
DANST
[NASA-TM-106211] p 230 N93-28050

LIU, LARRY

- High performance sapphire windows
p 218 N93-22198

LIU, LARRY C.

- Combustion-wave ignition for rocket engines
p 78 N93-10016
- Laser ignition application in a space experiment
[NASA-TM-106133] p 145 N93-25337

LIU, M.-S.

- Computing 3-D steady supersonic flow via a new
Lagrangian approach
[AIAA PAPER 93-0891] p 6 A93-24951
- Multigrd calculation of three-dimensional viscous
cascade flows p 8 A93-42889
- Development of an explicit multiblock/multigrd flow
solver for viscous flows in complex geometries
[AIAA PAPER 93-2380] p 186 A93-50148

LIU, MAY-FUN

- Parallel solution of high-order numerical schemes for
solving incompressible flows
[NASA-TM-4451] p 262 N93-27040

LIU, MENG-SING

- Lagrangian solution of supersonic real gas flows
p 170 A93-23944
- Preconditioned Conjugate Gradient methods for low
speed flow calculations
[AIAA PAPER 93-0881] p 172 A93-24942
- Stable and low diffusive hybrid upwind splitting
methods
[ONERA, TP NO. 1992-113] p 179 A93-38589
- Field by field hybrid upwind splitting methods
[AIAA PAPER 93-3302] p 8 A93-45000
- An extended Lagrangian method
[AIAA PAPER 93-3305] p 8 A93-45003
- Multigrd time-accurate integration of Navier-Stokes
equations
[AIAA PAPER 93-3361] p 181 A93-45054
- Grid adaptation using Chimera composite overlapping
meshes
[AIAA PAPER 93-3389] p 267 A93-45080
- A new flux splitting scheme
p 9 A93-47189
- Preconditioned conjugate-gradient methods for
low-speed flow calculations
[NASA-TM-105929] p 194 N93-14885
- An extended Lagrangian method
[NASA-TM-106129] p 199 N93-26203
- Grid adaption using Chimera composite overlapping
meshes
[NASA-TM-106163] p 269 N93-27065
- Numerical simulations of three-dimensional laminar flow
over a backward facing step; flow near side walls
[NASA-TM-106248] p 202 N93-31147

LIU, S. H.

- Giant suppression of flux-flow resistivity in heavy-ion
irradiated Ti₂Ba₂Ca₂Cu₃O₁₀ films - Influence of linear
defects on vortex transport p 280 A93-26198
- Low temperature phase formation of Ti-based
superconducting thin films in reduced oxygen
atmosphere p 282 A93-44568
- Diminishing sign anomaly and scaling behavior of the
mixed-state Hall resistivity in Ti₂Ba₂Ca₂Cu₃O₁₀ films
containing columnar defects p 283 A93-53693

LIU, W. W.

- A multiple-scale turbulence model for incompressible
flow
[AIAA PAPER 93-0086] p 170 A93-24228

LIU, WILLIAM W.

- Weakly nonlinear models for turbulent mixing in a plane
mixing layer p 165 A93-17416
- Linear instability of curved free shear layers
[AIAA PAPER 93-3252] p 183 A93-46797
- Center for Modeling of Turbulence and Transition
(CMOTT): Research Briefs, 1992
[NASA-TM-105834] p 195 N93-15792
- Modeling of turbulent shear flows p 195 N93-15797
- A multiple-scale model for compressible turbulent
flows
[NASA-TM-106072] p 198 N93-23736

LIU, WILLIAM W.-W.

- The eigenvalue spectrum of the Rayleigh equation for
a plane shear layer p 168 A93-21725
- A new energy transfer model for turbulent free shear
flow
[NASA-TM-105854] p 191 N93-10454

LIPPKE, C.

- Nonlinear dynamic simulation of single- and multi-spool
core engines
[AIAA PAPER 93-2580] p 30 A93-50294

LISANO, MICHAEL E.

- An Isotope-Powered Thermal Storage unit for space
applications p 65 A93-13877

LISCINSKY, D. S.

- Experimental investigation of crossflow jet mixing in a
rectangular duct
[AIAA PAPER 93-2037] p 185 A93-49872
- Experimental investigation of crossflow jet mixing in a
rectangular duct
[NASA-TM-106152] p 36 N93-27026

LITT, JONATHAN S.

- Identification of the open loop dynamics of the T700
turboshaft engine p 26 A93-35934

LITTMAN, FRANKLIN D.

- Long life Regenerative Fuel Cell technology
development plan p 252 A93-25867

LITVIN, F. L.

- Generation of helical gears with new surfaces topology
by application of CNC machines
[AIAA PAPER 93-2297] p 224 A93-50082
- Face-gear drives: Design, analysis, and testing for
helicopter transmission applications
[NASA-TM-106101] p 229 N93-27133
- Generation of helical gears with new surfaces, topology
by application of CNC machines
[NASA-TM-106175] p 229 N93-27687

LITVIN, FAYDOR L.

- Low-noise, high-strength, spiral-bevel gears for
helicopter transmissions
[AIAA PAPER 93-2149] p 223 A93-49966
- Low-noise, high-strength, spiral-bevel gears for
helicopter transmissions
[NASA-TM-106080] p 228 N93-23019

LIU, C.

- Multigrd methods for numerical simulation of laminar
diffusion flames
[AIAA PAPER 93-0236] p 113 A93-22648

LIU, C. C.

- The development of hydrogen sensor technology for
aerospace applications
[AIAA PAPER 93-2375] p 211 A93-50144
- The development of hydrogen sensor technology at
NASA Lewis Research Center
[NASA-TM-106141] p 216 N93-27021

LIU, CHUNG-CHIUN

- Development of a hydrogen gas sensor using
microfabrication technology
[SAE PAPER 92-1176] p 210 A93-41356

LIU, DEQUAN

- The performance evaluation of a new neural network
based traffic management scheme for a satellite
communication network p 147 A93-10929

LIU, H. W.

- Single-parameter characterization of
discrete-dislocation pileup tipfield and its application to
physically based micro-mechanics p 233 A93-12119
- Grain boundary resistance to fatigue crack growth
p 125 A93-29570

LIU, J. T. C.

- Multiple large-scale coherent mode interactions in a
developing round jet p 178 A93-34409

LIU, NAN-SUEY

- Direct calculations of waves in fluid flows using a
high-order compact difference scheme
[AIAA PAPER 93-0148] p 171 A93-24232
- A time-accurate high-resolution TVD scheme for solving
the Navier-Stokes equations p 13 A93-52006
- A time-accurate high-resolution TVD scheme for solving
the Navier-Stokes equations
[NASA-TM-106056] p 268 N93-22664

LIU, WING K.

- Elastic interactions of a fatigue crack with a micro-defect
by the mixed boundary integral equation method
p 243 A93-56412

LIU, Z.

- Multigrd methods for numerical simulation of laminar
diffusion flames
[AIAA PAPER 93-0236] p 113 A93-22648

LIVNEH, MORDECHAI

- Lower temperature curing thermoset polyimides utilizing
a substituted norbornene endcap p 134 A93-44526

LOCCI, I. E.

- Effect of oxidation on the mechanical properties of a
NbAl₃ alloy at intermediate temperatures
p 124 A93-20667
- Transformation to Ni₅Al₃ in a 63.0 at. pct Ni-Al alloy
p 124 A93-25108
- The microstructural evolution, crystallography, and
thermal processing of ultrahigh carbon Fe-1.85 pct C
melt-spun ribbon p 125 A93-32934

LOCK, A. P.

- Positivity-preserving numerical schemes for
multidimensional advection
[NASA-TM-106055] p 200 N93-27091

LOCK, JAMES A.

- Calibration of the forward-scattering spectrometer probe
- Modeling scattering from a multimode laser beam
p 212 A93-51239
- Experimental testing of four correction algorithms for
the forward scattering spectrometer probe
[NASA-TM-105906] p 213 N93-13307
- Gas temperature and density measurements based on
spectrally resolved Rayleigh-Brillouin scattering
p 214 N93-13684

LOEFFLER, IRVIN J.

- In-flight near- and far-field acoustic data measured on
the Propfan Test Assessment (PTA) testbed and with an
adjacent aircraft
[NASA-TM-103719] p 275 N93-27058

LOGSDON, K. A.

- Vibration isolation technology - An executive summary
of systems development and demonstration
[AIAA PAPER 93-0834] p 55 A93-24904

LOGSDON, KIRK A.

- Vibration isolation technology: An executive summary
of systems development and demonstration
[NASA-TM-105937] p 1 N93-15573

LOH, C. Y.

- Computing 3-D steady supersonic flow via a new
Lagrangian approach
[AIAA PAPER 93-0891] p 6 A93-24951

LOH, CHING-YUEN

- Lagrangian solution of supersonic real gas flows
p 170 A93-23944

LONG, MARY JO

- Experimental investigation of an ejector-powered free-jet
facility
[NASA-TM-105868] p 16 N93-16704

LOPEZ, ROBERT

- Vector formulation for interferogram surface fitting
p 278 A93-55687

LORENCE, CHRISTOPHER B.

- Nonreflecting boundary conditions for linearized
unsteady aerodynamic calculations
[AIAA PAPER 93-0882] p 7 A93-25553

LORENZO, CARL F.

- Damage-mitigating control of aerospace systems for
high performance and extended life p 263 A93-22967
- Screening studies of advanced control concepts for
airbreathing engines
[AIAA PAPER 92-3320] p 26 A93-49329
- Advanced instrumentation for next-generation
aerospace propulsion control systems
[AIAA PAPER 93-2079] p 211 A93-49906
- Damage-mitigating control of space propulsion systems
for high performance and extended life
[AIAA PAPER 93-2080] p 74 A93-49907
- Screening studies of advanced control concepts for
airbreathing engines
[NASA-TM-106042] p 36 N93-25079
- Life extending control: An interdisciplinary engineering
thrust p 93 N93-31581

LOTTIG, ROY A.

- Development and use of hydrogen-air torches in an
altitude facility
[AIAA PAPER 93-2176] p 42 A93-49988
- Development and use of hydrogen-air torches in an
altitude facility
[NASA-TM-106047] p 43 N93-26214

LOVELL, T. A.

- A comparative study of multivariable robustness analysis
methods as applied to integrated flight and propulsion
control
[AIAA PAPER 93-3809] p 21 A93-51401

LOWRY, B. J.

- Flow-influenced stabilization of liquid columns in a
dynamic plateau chamber
[AIAA PAPER 93-0255] p 169 A93-22664

LOWRY, PETER A.

- ACTS system handbook, revision change index
[NASA-TM-107982] p 150 N93-70235

LUA, YUAN J.

- Parallel computing for probabilistic fatigue analysis
[AIAA PAPER 93-1499] p 261 A93-34039
- Elastic interactions of a fatigue crack with a micro-defect
by the mixed boundary integral equation method
p 243 A93-56412

LUBOMSKI, J. F.

- Vibration isolation technology - An executive summary
of systems development and demonstration
[AIAA PAPER 93-0834] p 55 A93-24904

LUBOMSKI, JOSEPH F.

- Vibration isolation technology: An executive summary
of systems development and demonstration
[NASA-TM-105937] p 1 N93-15573

LUCCIN, FRANCESCO

- The gravitational wave contribution to cosmic microwave
background anisotropies and the amplitude of mass
fluctuations from COBE results p 289 A93-21508

LUMLEY, JOHN L.

- Critical comparison of second-order closures with direct numerical simulations of homogeneous turbulence
p 176 A93-30840
- A realizable Reynolds stress algebraic equation model
[NASA-TM-105993] p 16 N93-16596
- Remarks on turbulent constitutive relations
[NASA-TM-106116] p 199 N93-27010

LUND, KURT O.

- Radiation and phase change of lithium fluoride in an annulus
p 144 A93-54460

LUNDGREN, P.

- Venus Interior Structure Mission (VISM). Establishing a seismic network on Venus
p 293 N93-28819

LUO, XIAOCHUN

- Kurtosis, skewness, and non-Gaussian cosmological density perturbations
p 291 A93-35579
- Testing for the Gaussian nature of cosmological density perturbations through the three-point temperature correlation function
p 292 A93-55212

LUTON, MICHAEL J.

- Elevated temperature compressive properties of reaction milled NiAl-AlN and Zr-doped NiAl-AlN composites
p 97 A93-11422

LY, J.

- Control-structure interaction study for the Space Station solar dynamic power module
p 54 A93-13132
- Optimal control study for the Space Station Solar Dynamic power module
p 54 A93-13133

LY, JASON H. Q.

- Control-structure interaction
p 54 A93-14687

M**MA, J.**

- Measurement of frequency response in short thermocouple wires
p 209 A93-40677

MACCAMY, R. C.

- On the accurate long-time solution of the wave equation in exterior domains: Asymptotic expansions and corrected boundary conditions
[NASA-TM-106117] p 269 N93-27068

MACIEJEWSKI, P. K.

- Heat transfer with very high free-stream turbulence. I - Experimental data. II - Analysis of results
p 165 A93-18556

MACINNES, ANDREW N.

- Enhancement of photoluminescence intensity of GaAs with cubic GaS chemical vapor deposited using a structurally designed single-source precursor
p 280 A93-26930
- Metal-organic chemical vapour deposition of polycrystalline tetragonal indium sulphide (InS) thin films
p 116 A93-36584
- Photoluminescence intensity enhancement of GaAs by vapor-deposited GaS - A rational approach to surface passivation
p 281 A93-40049
- Electronic passivation of n- and p-type GaAs using chemical vapor deposited GaS
p 283 A93-52708

MAKAY, REBECCA

- An apparatus for gripping test specimens
[NASA-CASE-LEW-15345-2] p 230 N93-28127

MACKIN, MICHAEL

- Description of the SSF PMAD dc testbed control system data acquisition function
p 47 A93-26103
- Description of the SSF PMAD DC testbed control system data acquisition function
[NASA-TM-105843] p 261 N93-11005

MACKULIN, B. J.

- Maximum life spur gear design
p 218 A93-14521

MACMILLAN, M. F.

- Aluminum acceptor four particle bound exciton complex in 4H, 6H, and 3C SiC
p 282 A93-44822

MACRAE, GREGORY S.

- Preliminary endurance tests of water vaporizers for resistojet applications
[AIAA PAPER 93-2403] p 187 A93-50168
- Preliminary endurance tests of water vaporizers for resistojet applications
[NASA-TM-106222] p 92 N93-28694

MACTAGGART, R.

- Mixed application MMIC technologies - Progress in combining RF, digital and photonic circuits
p 152 A93-25800

MACVEAN, M. K.

- Positivity-preserving numerical schemes for multidimensional advection
[NASA-TM-106055] p 200 N93-27091

MADI, FRANK J.

- A free-piston Stirling engine/linear alternator controls and load interaction test facility
p 146 A93-26077
- Test results of a Stirling engine utilizing heat exchanger modules with an integral heat pipe
[NASA-TM-105883] p 256 N93-25136

MADZSAR, G. C.

- The development of hydrogen sensor technology for aerospace applications
[AIAA PAPER 93-2375] p 211 A93-50144
- A plume spectroscopy system for flight applications
[AIAA PAPER 93-2511] p 63 A93-50242
- The development of hydrogen sensor technology at NASA Lewis Research Center
[NASA-TM-106141] p 216 N93-27021

MADZSAR, GEORGE C.

- Development of a hydrogen gas sensor using microfabrication technology
[SAE PAPER 92-1176] p 210 A93-41356
- Spectroscopic wear detector
[NASA-CASE-LEW-15200-1] p 83 N93-18856

MAGARI, P. J.

- Wake-induced unsteady stagnation-region heat-transfer measurements
[ASME PAPER 92-GT-196] p 166 A93-19421

MAHADEVAN, S.

- Confidence bounds on structural reliability
[AIAA PAPER 93-1377] p 238 A93-33941
- Structural system reliability under multiple failure modes
[AIAA PAPER 93-1379] p 238 A93-33943

MAHAJAN, A. J.

- Semi-empirical model for prediction of unsteady forces on an airfoil with application to flutter
p 7 A93-31494

MAHAJAN, APARAJIT J.

- An efficient procedure for cascade aeroelastic stability determination using nonlinear, time-marching aerodynamic solvers
[AIAA PAPER 93-1631] p 25 A93-34159
- An iterative multidisciplinary analysis for rotor blade shape determination
[AIAA PAPER 93-2085] p 28 A93-49912

MAJUMDAR, B. S.

- Deformation and failure mechanisms in metal matrix composites
p 102 A93-31359
- Evolution of damage and plasticity in titanium-based, fiber-reinforced composites
p 104 A93-48498

MAKEL, D. B.

- A plume spectroscopy system for flight applications
[AIAA PAPER 93-2511] p 63 A93-50242

MALONE, S. A.

- Fiber optic link for millimeter wave communication satellites
p 277 A93-25736

MALONEY, THOMAS M.

- Basic statistical analyses of candidate nickel-hydrogen cells for the Space Station Freedom
[NASA-TM-106111] p 270 N93-27124

MALOW, STUART A.

- Chemical reactions in the processing of MoSi₂ + carbon compacts
p 119 A93-53733

MANDOLIA, G.

- Millimeter-wave pseudomorphic HEMT MMIC phased array components for space communications
p 152 A93-25796

MANELLA, RICHARD T.

- Solving modal equations of motion with initial conditions using MSC/NASTRAN DMAP. Part 1: Implementing exact mode superposition
[NASA-TM-106063] p 248 N93-23739

MANES, J. P.

- Supersonic jet noise reduction by coaxial rectangular nozzles
p 272 A93-19205

MANKBADI, R. R.

- A rapid-distortion-theory turbulence model for developed unsteady wall-bounded flow
[NASA-TM-106249] p 203 N93-32199

MANKBADI, REDA R.

- Nonlinear interaction of frequency-detuned modes in boundary layers
[AIAA PAPER 93-0347] p 171 A93-24237

MANUEL, J. A.

- Numerical simulations of a high Mach number jet flow
[AIAA PAPER 93-0653] p 172 A93-24766
- The structure of supersonic jet flow and its radiated sound
[AIAA PAPER 93-0549] p 273 A93-25538

MANUEL, J. A.

- Dynamics and control of coherent structure in turbulent jets
p 188 A93-52310
- Numerical simulation of a high Mach number jet flow
[NASA-TM-105985] p 197 N93-20057

MANNING, ROBERT M.

- Application of radiative image transfer theory to the assessment of the overall OTF and contrast degradation of an image in an inhomogeneous turbulent and turbid atmosphere
p 285 A93-28624

MANTENIEKS, MARIS A.

- 100-kW class applied-field MPD thruster component wear
[NASA-TM-106023] p 85 N93-22482

MANZO, MICHELLE A.

- Modified NASA standard nickel-cadmium cell designs
p 253 A93-25947

- 75 Ah and 10 boilerplate nickel-hydrogen battery designs and test results
p 253 A93-25948

MARABITO, MARK

- Properties of hybrid CVD/PAN graphite fibers and their bromine intercalation compounds
p 98 A93-17675

MARCOPOLO, VINCENT R.

- Antiwindup analysis and design approaches for MIMO systems
[AIAA PAPER 93-3811] p 30 A93-51403

MAREK, C. J.

- Comparison of reacting and non-reacting shear layers at a high subsonic Mach number
[AIAA PAPER 93-2381] p 186 A93-50149
- Comparison of reacting and non-reacting shear layers at a high subsonic Mach number
[NASA-TM-106198] p 38 N93-27610
- Turbulence measurement in a reacting and non-reacting shear layer at a high subsonic Mach number
[NASA-TM-106186] p 18 N93-31839

MARINELLI, W. J.

- Absorption coefficients for water vapor at 193 nm from 300 to 1073 K
p 276 A93-45398

MARSHALL, ALBERT C.

- Nuclear safety policy working group recommendations on nuclear propulsion safety for the space exploration initiative
[NASA-TM-105705] p 88 N93-26200

MARTENS, J. S.

- Large-area YBa₂Cu₃O₇(δ) thin films on sapphire for microwave applications
p 279 A93-11475

MARTIN, CHARLES R.

- Pressure dependence of the oxygen reduction reaction at the platinum microelectrode/nafion interface - Electrode kinetics and mass transport
p 112 A93-11450

MARTIN, GARY L.

- Review of the Shuttle vibration environment
[AIAA PAPER 93-0832] p 51 A93-24902
- Low-frequency vibration environment for five Shuttle missions
[NASA-TM-106059] p 63 N93-28554

MARTIN, LISA C.

- Thin film thermocouples for high temperature turbine application
p 217 N93-31555

MARTINELL, JOHN

- Space Nuclear Thermal Propulsion Test Facilities Subpanel
[NASA-TM-105708] p 87 N93-25105

MARTINEZ-SANCHEZ, M.

- Electrodynamic interactions between a space station and the ionospheric plasma environment
p 56 A93-29156

MASE, G. T.

- Probabilistic micromechanics and macromechanics of polymer matrix composites
p 105 A93-54705

MASON, LEE S.

- Space reactor/Stirling cycle systems for high power lunar applications
p 46 A93-13822
- Lunar in-core thermionic nuclear reactor power system conceptual design
p 46 A93-13836
- 100-kWe lunar/Mars surface power utilizing the SP-100 reactor with dynamic conversion
p 67 A93-25856
- An evolution strategy for lunar nuclear surface power
p 91 N93-27963

MASSERANT, BRIAN J.

- A 10 kW dc-dc converter using IGBTs with active snubbers
p 158 A93-50646

MASSEY, K. C.

- Supersonic jet noise reduction by coaxial rectangular nozzles
p 272 A93-19205

MASUKO, MASABUMI

- Tribological characteristics of perfluoropolyether liquid lubricants under sliding conditions in high vacuum
[NASA-TM-106257] p 139 N93-32352

MATARRESE, SABINO

- The gravitational wave contribution to cosmic microwave background anisotropies and the amplitude of mass fluctuations from COBE results
p 289 A93-21508

MATHEW, JOSEPH

- The development of a mixing layer under the action of weak streamwise vortices
p 176 A93-30134
- The development of a mixing layer under the action of weak streamwise vortices
[NASA-TM-106089] p 201 N93-28947

MATTOSSIAN, J. N.

- Erosion rate diagnostics in ion thrusters using laser-induced fluorescence
p 70 A93-34481

MATTERN, DUANE

- Propulsion system performance resulting from an integrated flight/propulsion control design
[NASA-TM-105874] p 34 N93-15525

MATTHIENSEN, D. H.

- Low gravity environment on-board Columbia during STS-40
[AIAA PAPER 93-0833] p 142 A93-24903

- MATUS, L. G.**
Progress in silicon carbide semiconductor technology
p 158 A93-44965
Thermal oxidation of single-crystal silicon carbide -
Kinetic, electrical, and chemical studies
p 284 A93-55601
Growth and characterization of 3C-SiC and 6H-SiC films
on 6H-SiC wafers
p 284 A93-55602
- MATUS, LAWRENCE G.**
Silicon carbide, a semiconductor for space power
electronics
p 279 A93-13880
Greatly improved 3C-SiC p-n junction diodes grown by
chemical vapor deposition
p 156 A93-38994
Silicon carbide semiconductor technology for high
temperature and radiation environments
p 284 A93-26928
- MAUL, WILLIAM**
Qualitative model-based diagnostics for rocket
systems
[AIAA PAPER 93-1779]
p 72 A93-49674
Qualitative model-based diagnostics for rocket
systems
[NASA-TM-106234]
p 51 A93-28052
- MAUL, WILLIAM A.**
A qualitative approach to systemic diagnosis of the
SSME
[AIAA PAPER 93-0405]
p 261 A93-23327
- MAWID, M.**
Analysis of unsteady wave processes in a rotating
channel
[AIAA PAPER 93-2527]
p 187 A93-50255
- MAWID, M. A.**
Effects of detailed droplet heating models on turbulent
sprays vaporization behavior
[AIAA PAPER 93-2193]
p 185 A93-50005
On the structure of gaseous confined laminar diffusion
flames: Numerical investigation
[NASA-TM-106039]
p 197 A93-21198
Structure of confined laminar spray diffusion flames:
Numerical investigation
[NASA-TM-106038]
p 197 A93-22596
- MAY, BRIAN D.**
Anomalous TWTA output power spikes and their effect
on a digital satellite communications system
[NASA-TM-105875]
p 159 A93-13286
- MAYA, ISAAC**
Ultrahigh temperature vapor-core reactor -
Magnetohydrodynamic system for space nuclear electric
power
p 66 A93-21663
- MAYNARD, WILL**
GSFC conceptual design study for an inter-satellite
Optical Multiple Access communication system
p 52 A93-18966
- MCCARDLE, JACK G.**
Performance characteristics of a variable-area vane
nozzle for vectoring an ASTOVL exhaust jet up to 45
deg
[AIAA PAPER 93-2437]
p 29 A93-50189
Effects of flow-path variations on internal reversing flow
in a tailpipe offtake configuration for ASTOVL aircraft
[AIAA PAPER 93-2438]
p 29 A93-50190
Experimental performance of a ventral nozzle with pitch
and yaw vectoring capability for SSTOVL aircraft
[NASA-TM-106054]
p 36 A93-25129
Performance characteristics of a variable-area vane
nozzle for vectoring an ASTOVL exhaust jet up to 45
deg
[NASA-TM-106114]
p 37 A93-27131
Effects of flow-path variations on internal reversing flow
in a tailpipe offtake configuration for ASTOVL aircraft
[NASA-TM-106149]
p 38 A93-29065
- MCBEATH, GIORGIO**
A review of chemically reactive turbulent flow mixing
mechanisms and a new design for a low NO(x)
combustor
p 27 A93-49508
A thermal NO(x) prediction model - Scalar computation
module for CFD codes with fluid and kinetic effects
[AIAA PAPER 93-2378]
p 119 A93-50147
- MCCBRIDE, BONNIE J.**
Computer program for calculating and fitting
thermodynamic functions
[NASA-RP-1271]
p 285 A93-12967
Thermodynamic data for fifty reference elements
[NASA-TP-3287]
p 286 A93-19977
- MCCARGO, MATT**
Recommended practices for in-space and ground
laboratory. Atomic oxygen exposure and analysis
p 276 A93-20814
- MCCAUGHAN, F. E.**
Stability of fully developed rotating stall
[ASME PAPER 92-GT-57]
p 23 A93-19307
- MCCAUL, E.**
Determination of forces in a magnetic bearing actuator
- Numerical computation with comparison to experiment
p 219 A93-15686
- MCCOLLUM, T.**
Leveling coatings for reducing the atomic oxygen defect
density in protected graphite fiber epoxy composites
[NASA-TM-105732]
p 136 A93-15344
Leveling coatings for reducing the atomic oxygen defect
density in protected graphite fiber epoxy composites
p 59 A93-15597
- MCCORMICK, S.**
Multigrid methods for numerical simulation of laminar
diffusion flames
[AIAA PAPER 93-0236]
p 113 A93-22648
- MCCULLOCH, WILLIAM H.**
Nuclear safety policy working group recommendations
on nuclear propulsion safety for the space exploration
initiative
[NASA-TM-105705]
p 88 A93-26200
- MCDANIELS, DAVID L.**
Graphite fiber/copper matrix composites for space
power heat pipe fin applications
p 162 A93-13789
Thermal conductivity and thermal expansion of graphite
fiber-reinforced copper matrix composites
p 100 A93-25104
- MCDANIEL, PATRICK**
Nuclear thermal propulsion technology: Results of an
interagency panel in FY 1991
[NASA-TM-105711]
p 86 A93-24740
- MCDONELL, V. G.**
Fuel injector. Air swirl characterization aerothermal
modeling, phase 2, volume 1
[NASA-CR-189193-VOL-1]
p 35 A93-24754
- MCELROY, JAMES F.**
Long life Regenerative Fuel Cell technology
development plan
p 252 A93-25867
- MCFARLAND, ERIC R.**
An integral equation solution for multistage
turbomachinery design calculations
[NASA-TM-105970]
p 33 A93-15521
- MCGAW, M.**
An advanced method for tracking the evolution of fatigue
damage in reusable space propulsion systems
p 234 A93-16406
- MCGAW, MICHAEL A.**
A high temperature fatigue life prediction computer code
based on the Total Strain Version of Strainrange
Partitioning (SRP)
p 260 A93-31341
Effect of tensile mean stress on fatigue behavior of
single-crystal and directionally solidified superalloys
p 125 A93-33011
The influence of primary and secondary orientations on
the elastic response of a nickel-base single-crystal
superalloy
[NASA-TM-106125]
p 250 A93-26550
Overview of the fatigue/fracture/life prediction working
group program at the Lewis Research Center
p 232 A93-31574
Cumulative fatigue damage behavior of MAR M-247
p 251 A93-31575
Secondary orientation effects in a single crystal
superalloy under mechanical and thermal loads
p 130 A93-31578
- MCILWAIN, M. C.**
US/CIS integrated NTR
[AIAA PAPER 93-2367]
p 76 A93-50138
- MCILWAIN, MELVIN C.**
U.S./CIS eye joint nuclear rocket venture
p 71 A93-49334
Nuclear thermal propulsion transportation systems for
lunar/Mars exploration
[NASA-TM-105870]
p 81 A93-12363
- MCKISSOCK, B. I.**
Dynamic Isotope Power System design considerations
for human exploration of the moon and Mars
p 253 A93-25995
Design of small Stirling dynamic isotope power system
for robotic space missions
[NASA-TM-105919]
p 141 A93-12085
- MCKISSOCK, BARBARA I.**
Comparison of dynamic isotope power systems for
distributed planetary surface applications
p 46 A93-13825
- MCMANUS, K.**
Nonintrusive, multipoint velocity measurements in
high-pressure combustion flows
[AIAA PAPER 93-2032]
p 118 A93-49867
- MCMASTER, MATTHEW S.**
Current status of liquid sheet radiator research
[NASA-TM-105764]
p 193 A93-14150
- MCMURTRY, PATRICK A.**
Direct numerical simulations of a reacting turbulent
mixing layer by a pseudospectral-spectral element
method
p 182 A93-45974
- MCVEY, S. E.**
Preliminary experimental results for a cryogenic brush
seal configuration
[AIAA PAPER 93-2535]
p 225 A93-50262
- Preliminary experimental results for a cryogenic brush
seal configuration
[NASA-TM-106236]
p 201 A93-28627
- MEADOR, MARY A. B.**
Lower temperature curing thermoset polyimides utilizing
a substituted norbornene endcap
p 134 A93-44526
- MEASE, KENNETH D.**
Minimum-fuel, power-limited transfers between coplanar
elliptical orbits
p 45 A93-31532
- MEERS, E. L.**
Measurement of frequency response in short
thermocouple wires
p 209 A93-40677
- MEHMED, O.**
Behavior of spinning laminated composite plates with
initial twist-experimental vibrations, strain, and deflection
results
[AIAA PAPER 93-1325]
p 238 A93-33898
On the static stability of forward swept propfans
[AIAA PAPER 93-1634]
p 26 A93-34162
- MEHMED, ORAL**
APPLE - An aeroelastic analysis system for
turbomachines and propfans
[AIAA PAPER 92-4712]
p 23 A93-20320
Experimental investigation of counter-rotating propfan
flutter at cruise conditions
[AIAA PAPER 93-1632]
p 25 A93-34160
- MEHROTRA, GOPAL M.**
Thermodynamics of iron-aluminum alloys at 1573 K
p 127 A93-52879
- MEHTA, S. R.**
Confidence bounds on structural reliability
[AIAA PAPER 93-1377]
p 238 A93-33941
- MEISSNER, D. L.**
Measurement and analysis of a small nozzle plume in
vacuum
p 71 A93-42895
Measurement and analysis of a small nozzle plume in
vacuum
[NASA-TM-106066]
p 88 A93-26561
- MEISSNER, DANA L.**
Experimentation in the low-density plume of a simulated
electrothermal thruster for computer code validation
[NASA-CR-191112]
p 87 A93-24758
- MELCHER, KEVIN J.**
Desktop chaotic systems: Intuition and visualization
[NASA-TM-106258]
p 269 A93-31847
- MELIS, MATTHEW E.**
Hypersonic engine component experiments in high heat
flux, supersonic flow environment
[NASA-TM-106273]
p 203 A93-31860
- MELOTT, A. L.**
The three-point correlation function in an ensemble of
three-dimensional simulations
p 291 A93-50680
- MENA, R. A.**
Room-temperature determination of two-dimensional
electron gas concentration and mobility in
heterostructures
p 280 A93-35198
- MENA, RAFAEL A.**
A 10-GHz amplifier using an epitaxial lift-off
pseudomorphic HEMT device
p 156 A93-37574
Development of Si(1-x)Ge(x) technology for microwave
sensing applications
[NASA-TM-106157]
p 162 A93-28610
- MENART, J. A.**
Discrete ordinates solutions of nongray radiative transfer
with diffusely reflecting walls
p 285 A93-30124
Nongray gas analyses for reflecting walls utilizing a flux
technique
p 190 A93-55460
- MENNETRIER, CHRISTOPHE**
Physical vapor transport of mercurous chloride under
a nonlinear thermal profile
[NASA-TM-105920]
p 196 A93-16612
- MERCER, CAROLYN R.**
Phase-stepping fiber-optic projected fringe system for
surface topography measurements
[NASA-CASE-LEW-14996-1]
p 278 A93-11058
- MERKLE, C. L.**
The application of preconditioning in viscous flows
p 177 A93-32627
- MERKLE, CHARLES L.**
Prediction of engine and near-field plume reacting flows
in low-thrust chemical rockets
[AIAA PAPER 93-0237]
p 66 A93-22649
CFD analyses of coolant channel flowfields
[AIAA PAPER 93-1830]
p 184 A93-49715
- MEROLLA, ANTHONY**
Lessons learned from the Autonomous Power System
p 68 A93-25879
- MERRILL, W.**
Implementation of a model based fault detection and
diagnosis technique for actuation faults of the SSME
p 47 A93-16413
Design and evaluation of a robust dynamic
neurocontroller for a multivariable aircraft control
problem
p 40 A93-37004

- Implementation of a model based fault detection and diagnosis for actuation faults of the Space Shuttle main engine
[NASA-TM-105781] p 49 N93-11401
- Analysis of fault-tolerant neurocontrol architectures
[NASA-TM-105898] p 41 N93-12305
- Real-time diagnostics for a reusable rocket engine
[NASA-TM-105792] p 266 N93-19018
- MERRILL, W. C.**
Integrated health monitoring and controls for rocket engines
[SAE PAPER 921031] p 66 A93-14654
- MERRILL, WALTER**
Neurocontrol design and analysis for a multivariable aircraft control problem p 40 A93-41894
- Identification of propulsion systems
[NASA-TM-106007] p 35 N93-20109
- MERRILL, WALTER C.**
Damage-mitigating control of aerospace systems for high performance and extended life p 263 A93-22967
- Screening studies of advanced control concepts for airbreathing engines
[AIAA PAPER 92-3320] p 26 A93-49329
- Screening studies of advanced control concepts for airbreathing engines
[NASA-TM-106042] p 36 N93-25079
- Life extending control. An interdisciplinary engineering thrust p 93 N93-31581
- MERROW, JAMES E.**
Characteristics of hypervelocity impact craters on LDEF experiment S1003 and implications of small particle impacts on reflective surfaces p 62 N93-29363
- MERTE, HERMAN, JR.**
The effects of buoyancy on the critical heat flux in forced convection
[AIAA PAPER 93-0575] p 169 A93-23307
- MESANDER, GEERT A.**
Results of a low power ice protection system test and a new method of imaging data analysis p 21 A93-35932
- MESEROLE, J. S.**
Nucleate pool boiling in the long duration low gravity environment of the space shuttle
[AIAA PAPER 93-0465] p 142 A93-23371
- Nucleate pool boiling in the long duration low gravity environment of the Space Shuttle
[NASA-TM-105973] p 144 N93-15420
- METCALF, KENNETH J.**
Design and emplacement of an integrated lunar power system - Issues and concerns p 46 A93-13908
- METZGER, JOHN D.**
Fault-tolerant adaptive control for load-following in static space nuclear power systems p 263 A93-25986
- METZLER, ALLEN J.**
In-stream measurements of combustion during Mach 5 to 7 tests of the Hypersonic Research Engine (HRE)
[AIAA PAPER 93-2324] p 28 A93-50104
- MEYER, CLAUDIA**
Qualitative model-based diagnostics for rocket systems
[AIAA PAPER 93-1779] p 72 A93-49674
- Qualitative model-based diagnostics for rocket systems
[NASA-TM-106234] p 51 N93-28052
- MEYER, WILLIAM V.**
Microemulsion characterization by the use of a noninvasive backscatter fiber optic probe p 277 A93-52412
- MICHAL, G. M.**
Transformation to Ni₅Al₃ in a 63.0 at. pct Ni-Al alloy p 124 A93-25108
- MICHAL, GARY M.**
Reaction layer formation at the graphite/copper-chromium alloy interface p 100 A93-25105
- MICKLOW, G. J.**
Numerical simulation of a low-emission gas turbine combustor using KIVA-II p 22 A93-14077
- MICKLOW, GERALD J.**
Computation of the flow field in an annular gas turbine combustor
[AIAA PAPER 93-2074] p 28 A93-49903
- MIDEA, ANTHONY C.**
Propulsion and aerodynamic analysis of the Beta II two-stage-to-orbit vehicle
[AIAA PAPER 92-4245] p 50 A93-13332
- MILES, RICHARD B.**
Time-sequenced and spectrally filtered Rayleigh imaging of shock wave and boundary layer structure for inlet characterization
[AIAA PAPER 93-2300] p 211 A93-50085
- MILITELLO, CARMELO**
Membrane triangles with corner drilling freedoms. II - The ANDES element p 235 A93-24304
- MILLER, D. P.**
Fabrication and properties of functionally graded NiAl/Al₂O₃ composites p 105 A93-54116
- MILLER, DAVID L.**
Design of a constant tension thermocouple rake suitable for flame studies p 210 A93-40683
- MILLER, FLETCHER**
Flame spread across liquid pools p 122 N93-20209
- MILLER, JEFFREY H.**
A hot dynamic seal rig for measuring hypersonic engine seal durability and flow performance
[AIAA PAPER 93-1346] p 222 A93-33916
- The detrimental effect of friction on space microgravity robotics p 222 A93-35546
- MILLER, JEFFREY S.**
Characterization of Si₃N₄/SiO₂ optical channel waveguides by photon scanning tunneling microscopy p 211 A93-49458
- MILLER, R. A.**
Technical note - Plasma-sprayed ceramic thermal barrier coatings for smooth intermetallic alloys p 219 A93-15702
- Oxidation resistant overlay coatings for low expansion substrates
[NASA-CASE-LEW-15154-1] p 137 N93-19332
- Plasma sprayed ceramic thermal barrier coating for NiAl-based intermetallic alloys
[NASA-CASE-LEW-15535-1] p 130 N93-31294
- Oxidation resistant overlay coatings for low expansion substrates
[NASA-CASE-LEW-15154-2] p 138 N93-31300
- MILLER, ROBERT A.**
Method of applying a thermal barrier coating system to a substrate
[NASA-CASE-LEW-15020-2] p 107 N93-14706
- Characterization and durability testing of plasma-sprayed zirconia-yttria and hafnia-yttria thermal barrier coatings. Part 1: Effect of spray parameters on the performance of several lots of partially stabilized zirconia-yttria powder
[NASA-TP-3295] p 128 N93-22556
- MILLER, THOMAS J.**
Planning for the Space Exploration Initiative - The nuclear propulsion option p 43 A93-13752
- Nuclear Propulsion Project Workshop summary p 64 A93-13765
- A comparison of nuclear thermal rocket development cost and schedule for piloted missions to Mars
[AIAA PAPER 93-2263] p 44 A93-50057
- Progress report on nuclear propulsion for space exploration and science
[AIAA PAPER 93-2352] p 44 A93-50125
- Nuclear concepts/propulsion p 85 N93-22093
- Focused technology: Nuclear propulsion p 89 N93-26912
- Focused technology: Nuclear propulsion [PR12] p 287 N93-71885
- MILLIS, M. G.**
OTV bearing deflection investigation
[NASA-TM-106085] p 215 N93-22994
- MILLS, JOSEPH C.**
Multimegawatt potassium Rankine power for nuclear electric power p 65 A93-13797
- MILLWATER, H. R.**
Global/local methods for probabilistic structural analysis
[AIAA PAPER 93-1378] p 238 A93-33942
- MILNER, EDWARD J.**
Turbomachinery CFD on parallel computers
[NASA-TM-105932] p 262 N93-13154
- Parallel solution of high-order numerical schemes for solving incompressible flows
[NASA-TM-4451] p 262 N93-27040
- MINNETYAN, L.**
Progressive delamination in polymer matrix composite laminates: A new approach p 108 N93-21515
- MINNETYAN, LEVON**
Structural durability of a composite pressure vessel p 234 A93-16552
- Damage progression in stiffened composite panels
[AIAA PAPER 93-1345] p 238 A93-33915
- Design for progressive fracture in composite shell structures p 242 A93-53394
- MIRANDA, F. A.**
Conductor-backed coplanar waveguide resonators of Y-Ba-Cu-O and Ti-Ba-Ca-Cu-O on LaAlO₃
[NASA-TM-105890] p 284 N93-12325
- MIRTIKH, MICHAEL J.**
Optical and scratch resistant properties of diamondlike carbon films deposited with single and dual ion beams
[NASA-TM-105943] p 95 N93-22586
- Optical and scratch resistant properties of diamondlike carbon films deposited with single and dual ion beams p 137 N93-25564
- Characteristics of hypervelocity impact craters on LDEF experiment S1003 and implications of small particle impacts on reflective surfaces p 62 N93-29363
- MISRA, AJAY K.**
Effect of hydrogen on the strength and microstructure of selected ceramics p 130 A93-13613
- Effect of thermal cycling on interface bonding requirements in Al₂O₃ fiber-reinforced superalloy composites p 103 A93-35882
- MITAL, SUBODH K.**
Three-dimensional finite element simulation of intermingled-fiber hybrid composite behavior p 98 A93-15729
- Microfracture in high temperature metal matrix crossply laminates p 101 A93-31356
- Thermally-driven microfracture in high temperature metal matrix composites p 237 A93-32469
- Ceramic matrix composites properties/microstresses with complete and partial interphase bond
[NASA-TM-106136] p 111 N93-29071
- MITCHELL, D. F.**
SIMS studies of oxide growth on beta-NiAl p 127 A93-53469
- MITCHELL, JOHN C.**
Design of an Advanced Expander Test Bed
[AIAA PAPER 93-2133] p 48 A93-49952
- MITTENDORF, DONALD L.**
Transient liquid phase diffusion bonding of Udimet 720 for Stirling power converter applications p 221 A93-26080
- MIYOSHI, KAZUHISA**
Tribological studies of amorphous hydrogenated carbon films in a vacuum, spacelike environment p 134 A93-40630
- A vacuum (10 exp -9 torr) friction apparatus for determining friction and endurance life of MoS(x) films p 146 A93-49245
- Friction and wear of plasma-deposited amorphous hydrogenated films on silicon nitride p 135 A93-52181
- Tribological evaluation and analysis of coating materials p 135 A93-52896
- Friction and wear of plasma-deposited diamond films
[NASA-TM-105926] p 136 N93-19035
- MIZUKAMI, MASASHI**
Bibliography on propulsion airframe integration technologies for high-speed civil transport applications, 1980-1991
[NASA-TM-105602] p 1 N93-26136
- MJOLSNES, R. C.**
RIPPLE - A new model for incompressible flows with free surfaces p 164 A93-14551
- MOCKLER, THEODORE T.**
Design of a high-temperature experiment for evaluating advanced structural materials
[NASA-TM-105833] p 245 N93-11624
- MOCSARI, JEFFREY C.**
Analytic methods for design of wave cycles for wave rotor core engines
[AIAA PAPER 93-2523] p 30 A93-50253
- MODER, JEFFREY P.**
Analysis and design of an ultrahigh temperature hydrogen-fueled MHD generator p 278 A93-49618
- MODIANO, DAVID L.**
Adaptive computations of flow around a delta wing with vortex breakdown
[AIAA PAPER 93-3400] p 10 A93-47202
- MOFFAT, R. J.**
Heat transfer with very high free-stream turbulence. I - Experimental data. II - Analysis of results p 165 A93-18556
- MOINUDDIN, ALIA**
Properties of hybrid CVD/PAN graphite fibers and their bromine intercalation compounds p 98 A93-17675
- MOLLERACH, SILVIA**
The gravitational wave contribution to cosmic microwave background anisotropies and the amplitude of mass fluctuations from COBE results p 289 A93-21508
- MOLLS, F. B.**
Finite difference solution for transient radiative cooling of a conducting semitransparent square region p 164 A93-15067
- MOLLS, FRANK B.**
The Proteus Navier-Stokes code p 193 N93-13396
- MONDAL, J.**
Mixed application MMIC technologies - Progress in combining RF, digital and photonic circuits p 152 A93-25800
- MONGIA, H. C.**
An analytical study of dilution jet mixing in a cylindrical duct
[AIAA PAPER 93-2043] p 27 A93-49876
- Fuel injector: Air swirl characterization aerothermal modeling, phase 2, volume 1
[NASA-CR-189193-VOL-1] p 35 N93-24754

- An analytical study of dilution jet mixing in a cylindrical duct
[NASA-TM-106181] p 37 N93-27160
- MONGIA, HUKAM C.**
An efficient liner cooling scheme for advanced small gas turbine combustors
[AIAA PAPER 93-1763] p 27 A93-49660
- MONTAGUE, G. T.**
Hybrid active vibration control of rotorbearing systems using piezoelectric actuators p 221 A93-27324
- MOORE, ALLAN S.**
External stress-corrosion cracking of a 1.22-m-diameter type 316 stainless steel air valve
[NASA-TP-3190] p 129 N93-26201
- MOORE, THOMAS J.**
External stress-corrosion cracking of a 1.22-m-diameter type 316 stainless steel air valve
[NASA-TP-3190] p 129 N93-26201
- MORALES, WILFREDO**
An alternative model for estimating liquid diffusion coefficients requiring no viscosity data
[NASA-TM-106079] p 96 N93-23014
- MOREI, MICHAEL R.**
Tailored metal matrix laminates for high-temperature performance p 98 A93-15753
- MOREL, M.**
Combined micromechanical and fabrication process optimization for metal-matrix composites p 99 A93-18990
- MOREL, M. R.**
Metal Matrix Laminate Tailoring (MMLT) code: User's manual
[NASA-TM-106052] p 111 N93-28681
- MORILAK, DANIEL P.**
An approach to studying the reliability of microgravity experiments
[AIAA PAPER 93-1024] p 44 A93-30937
- MORLEY, NICHOLAS J.**
Estimates of power requirements for a Manned Mars Rover powered by a nuclear reactor p 45 A93-13783
Shielding analysis for a manned Mars rover powered by an SP-100 type reactor p 45 A93-13793
- MORREN, SYBIL H.**
A laboratory model of a hydrogen/oxygen engine for combustion and nozzle studies
[AIAA PAPER 93-1825] p 48 A93-49711
- MORREN, W. E.**
Gravity sensitivity of a resistojet water vaporizer
[AIAA PAPER 93-2402] p 186 A93-50167
Preliminary endurance tests of water vaporizers for resistojet applications
[AIAA PAPER 93-2403] p 187 A93-50168
- MORREN, W. EARL**
Preliminary characterization of a water vaporizer for resistojet applications
[NASA-TM-105877] p 80 N93-11402
Preliminary endurance tests of water vaporizers for resistojet applications
[NASA-TM-106222] p 92 N93-28694
Gravity sensitivity of a resistojet water vaporizer
[NASA-TM-106220] p 92 N93-29194
- MORRIS, PHILIP J.**
Weakly nonlinear models for turbulent mixing in a plane mixing layer p 165 A93-17416
The eigenvalue spectrum of the Rayleigh equation for a plane shear layer p 168 A93-21725
- MORRISON, G. L.**
Friction-factor characteristics for narrow channels with honeycomb surfaces
[ASME PAPER 91-TRIB-21] p 219 A93-15681
- MORSCHER, GREGORY N.**
Creep and stress relaxation modeling of polycrystalline ceramic fibers p 132 A93-31354
- MORTAZAVI, S.**
Structure of soot-containing laminar jet diffusion flames
[AIAA PAPER 93-0708] p 114 A93-24804
- MOSES, PAUL L.**
Design of a hypersonic waverider-derived airplane
[AIAA PAPER 93-0401] p 55 A93-21108
- MUELLER, DONN C.**
Some aspects of secondary atomization of aluminum/hydrocarbon slurry propellants p 140 A93-34478
- MUENCHHAUSEN, R. E.**
Buffer layers for high-Tc thin films on sapphire p 150 A93-17063
- MUKHERJEE, S.**
Mixed application MMIC technologies - Progress in combining RF, digital and photonic circuits p 152 A93-25890
- MULARZ, EDWARD J.**
Spray combustion experiments and numerical predictions
[NASA-TM-106069] p 198 N93-23744
- MULHALL, P.**
Nonintrusive, multipoint velocity measurements in high-pressure combustion flows
[AIAA PAPER 93-2032] p 118 A93-49867
- MURMAN, EARLL M.**
Adaptive computations of flow around a delta wing with vortex breakdown
[AIAA PAPER 93-3400] p 10 A93-47202
- MURTHY, D. V.**
Concurrent processing adaptation of aeroelastic analysis of propfans p 23 A93-14624
- MURTHY, DURBHA V.**
An efficient constraint to account for mistuning effects in the optimal design of engine rotors
[AIAA PAPER 92-4711] p 23 A93-20280
Forced response of mistuned bladed disk assemblies
[AIAA PAPER 93-1491] p 239 A93-34033
Aeroelastic dynamics of mistuned blade assemblies with closely spaced blade modes
[AIAA PAPER 93-1628] p 26 A93-37446
Stochastic sensitivity measure for mistuned high-performance turbines
[NASA-TM-105821] p 245 N93-12277
Localization of aeroelastic modes in mistuned high-energy turbines p 230 N93-31586
- MURTHY, P. L. N.**
Dynamic analysis of a pre-and-post ice impacted blade
[AIAA PAPER 92-4273] p 22 A93-13333
Structural tailoring of aircraft engine blade subject to ice impact constraints
[AIAA PAPER 92-4710] p 23 A93-20319
Quantification of uncertainties in composites
[AIAA PAPER 93-1440] p 102 A93-33989
Probabilistic simulation of stress concentration in composite laminates
[AIAA PAPER 93-1442] p 103 A93-33991
Effect of service environments on adhesively bonded joints in composite structures p 242 A93-53418
Computational simulation of hot composite structures p 260 A93-54704
Probabilistic micromechanics and macromechanics of polymer matrix composites p 105 A93-54705
Dynamic analysis of a pre-and-post ice impacted blade
[NASA-TM-105829] p 144 N93-12197
Root damage analysis of aircraft engine blade subject to ice impact
[NASA-TM-105779] p 246 N93-15343
Progressive delamination in polymer matrix composite laminates: A new approach p 108 N93-21515
High Temperature Composite Analyzer (HITCAN) theoretical manual, version 1.0
[NASA-TM-106001] p 249 N93-24913
High temperature composite analyzer (HITCAN) user's manual, version 1.0
[NASA-TM-106002] p 249 N93-25070
Metal matrix composite ANalyzer (METCAN): Theoretical manual
[NASA-TM-106025] p 109 N93-26552
Structural tailoring of aircraft engine blade subject to ice impact constraints p 250 N93-26999
Metal Matrix Laminate Tailoring (MMLT) code: User's manual
[NASA-TM-106052] p 111 N93-28681
Probabilistic composite analysis p 112 N93-30868
- MURTHY, PAPPU L. N.**
Computational simulation of surface waviness in graphite/epoxy woven composites due to initial curing p 98 A93-15822
Structural durability of a composite pressure vessel p 234 A93-16552
Damage progression in stiffened composite panels
[AIAA PAPER 93-1345] p 238 A93-33915
Design for progressive fracture in composite shell structures p 242 A93-53394
Design for cyclic loading endurance of composites p 242 A93-53395
Second generation integrated composite analyzer (ICAN) computer code
[NASA-TP-3290] p 108 N93-18139
Application of artificial neural networks to the design optimization of aerospace structural components
[NASA-TM-4389] p 247 N93-21831
Ceramic matrix composites properties/microstresses with complete and partial interphase bond
[NASA-TM-106136] p 111 N93-29071
- MURTHY, PAPU L. N.**
Programming probabilistic structural analysis for parallel processing computers p 237 A93-32410
- MURTHY, S. N. B.**
Two-, three-, and four-poster jets in cross flow
[AIAA PAPER 93-0023] p 167 A93-20141
- Two and three-dimensional predifuser combustor studies with air-water mixture
[AIAA PAPER 93-0240] p 113 A93-22652
- MUSGRAVE, J.**
Implementation of a model based fault detection and diagnosis technique for actuation faults of the SSME p 47 A93-16413
Implementation of a model based fault detection and diagnosis for actuation faults of the Space Shuttle main engine
[NASA-TM-105781] p 49 N93-11401
A neural network-based estimator for the mixture ratio of the Space Shuttle Main Engine
[NASA-TM-106070] p 87 N93-25089
- MUSGRAVE, J. L.**
Integrated health monitoring and controls for rocket engines
[SAE PAPER 921031] p 66 A93-14654
- MUSGRAVE, JEFFREY L.**
On-line implementation of nonlinear parameter estimation for the Space Shuttle main engine
[NASA-TM-106097] p 88 N93-26211
- MUTHARASAN, RAJAKKANNU**
Development of braided rope seals for hypersonic engine applications - Flow modeling p 222 A93-34493
Development of hypersonic engine seals - Flow effects of preload and engine pressures
[AIAA PAPER 93-1998] p 223 A93-49841
Development of braided rope seals for hypersonic engine applications: Flow modeling
[NASA-TM-105942] p 227 N93-14478
- MYERS, IRA T.**
Electromagnetic powered vehicles (EMPV) for Mars exploration p 47 A93-20761
- MYERS, ROGER M.**
Electromagnetic propulsion for spacecraft
[AIAA PAPER 93-1086] p 69 A93-30975
A laboratory model of a hydrogen/oxygen engine for combustion and nozzle studies
[AIAA PAPER 93-1825] p 48 A93-49711
Low power pulsed MPD thruster system analysis and applications
[AIAA PAPER 93-2391] p 76 A93-50156
Electric propulsion - An evolutionary technology p 78 A93-56168
100-kW class applied-field MPD thruster component wear
[NASA-TM-106023] p 85 N93-22482
- MYRABO, LEIK N.**
Analysis and design of an ultrahigh temperature hydrogen-fueled MHD generator p 278 A93-49618

N

- NAGAMATSU, H. T.**
Calculation of scramjet inlet with thick boundary-layer ingestion
[AIAA PAPER 93-1836] p 12 A93-49720
- NAGEL, ROBERT T.**
Forward rotor vortex effects on counter rotating propeller noise p 2 A93-19221
- NAGPAL, V.**
Design considerations for a Space Shuttle Main Engine turbine blade made of single crystal material p 236 A93-25228
- NAGPAL, V. K.**
Probabilistic evaluation of uncertainties and risks in aerospace components p 233 A93-12160
- NAKABE, K.**
Heat transfer from radiatively heated material in a low Reynolds number microgravity environment p 180 A93-43695
- NALIM, M. R.**
Analytic methods for design of wave cycles for wave rotor core engines
[AIAA PAPER 93-2523] p 30 A93-50253
- NALLASAMY, M.**
Unsteady blade pressures on a propfan at takeoff - Euler analysis and flight data p 26 A93-37389
- NAMKOONG, DAVID**
Modeling void growth and movement with phase change in thermal energy storage canisters
[AIAA PAPER 93-2832] p 285 A93-46569
Thermal energy storage flight experiment in microgravity p 256 N93-28720
- NARAYANAN, G. V.**
Structural Tailoring/Analysis for Hypersonic Components - A computational simulation
[AIAA PAPER 92-4722] p 20 A93-20324
- NASH, STEVEN**
Three-dimensional flow calculations inside SSME GGGT first stage blade rows p 93 N93-31585
- NATHAL, M. V.**
Creep deformation of B2 aluminides p 126 A93-44887

NATHAL, MICHAEL V.

- Creep-rupture strength of a Ni-base superalloy at 1400 K p 124 A93-20556
 Review of the physical and mechanical properties and potential applications of the B2 compound NiAl: Unabridged version of a paper published in International materials review p 127 N93-11635
 [NASA-TM-105598]
 An apparatus for gripping test specimens [NASA-CASE-LEW-15345-2] p 230 N93-28127

NEELY, RONALD E.

- Assessment of 25 kW free-piston Stirling technology alternatives for solar applications p 254 A93-26072

NEIGHBORS, W. K.

- Integrated flight/propulsion control - Subsystem specifications for performance [AIAA PAPER 93-3808] p 41 A93-51400

NELSON, AMY

- Plasma contactor technology for Space Station Freedom [AIAA PAPER 93-2228] p 57 A93-50034

NEMETH, NOEL N.

- Lifetime reliability evaluation of structural ceramic parts with the CARES/LIFE computer program [AIAA PAPER 93-1497] p 239 A93-34037

NERADKA, VINCENT F.

- Application of composite materials to impact-insensitive munitions p 97 A93-11459

NESBITT, J. A.

- Diffusional transport and predicting oxidative failure during cyclic oxidation of beta-NiAl alloys p 126 A93-50370
 Predicting the oxidative lifetime of beta NiAl-Zr alloys p 127 A93-53939

NEUDECK, P. G.

- Progress in silicon carbide semiconductor technology p 158 A93-44965
 Thermal oxidation of single-crystal silicon carbide - Kinetic, electrical, and chemical studies p 284 A93-55601

NEUDECK, PHILIP G.

- Greatly improved 3C-SiC p-n junction diodes grown by chemical vapor deposition p 156 A93-38994
 The development of hydrogen sensor technology for aerospace applications [AIAA PAPER 93-2375] p 211 A93-50144
 The development of hydrogen sensor technology at NASA Lewis Research Center [NASA-TM-106141] p 216 N93-27021

NEUMANN, ERIC S.

- Initial study of void formation during aluminum solidification in reduced gravity p 142 A93-12013
 Capabilities and constraints of NASA's ground-based reduced gravity facilities p 49 N93-20184

NEUPERT, W.

- Low gravity environment on-board Columbia during STS-40 [AIAA PAPER 93-0833] p 142 A93-24903

NEWAZ, G.

- Deformation and failure mechanisms in metal matrix composites p 102 A93-31359

NEWAZ, G. M.

- Evolution of damage and plasticity in titanium-based, fiber-reinforced composites p 104 A93-48498

NEWELL, J. F.

- An advanced method for tracking the evolution of fatigue damage in reusable space propulsion systems p 234 A93-16406

NEWELL, JAMES F.

- Modal test/analysis correlation of Space Station structures using nonlinear sensitivity [AIAA PAPER 92-4731] p 55 A93-20330

NEWMAN, N.

- Large-area YBa₂Cu₃O₇(δ) thin films on sapphire for microwave applications p 279 A93-11475

NEWMAN, WYATT S.

- The detrimental effect of friction on space microgravity robotics p 222 A93-35546

NG, DANIEL

- Multiwavelength pyrometer for gray and non-gray surfaces in the presence of interfering radiation [NASA-CASE-LEW-15250-1] p 214 N93-17060
 Non-contact heat flux measurement using a transparent sensor [NASA-TM-106252] p 142 N93-32330

NG, WING-FAI

- Preconditioned Conjugate Gradient methods for low speed flow calculations [AIAA PAPER 93-0881] p 172 A93-24942
 Preconditioned conjugate-gradient methods for low-speed flow calculations [NASA-TM-105929] p 194 N93-14885

NGUYEN, H. L.

- Numerical simulation of a low-emission gas turbine combustor using KIVA-II p 22 A93-14077

NGUYEN, THONG V.

- Test program to provide validation data for the Rocket Combustor Interactive Design (ROCCID) code p 120 N93-11450

NICHOLS, LESTER D.

- The new challenge of computational aerospace p 2 A93-14169

NIEDERAUER, GEORGE F.

- Nuclear safety policy working group recommendations on nuclear propulsion safety for the space exploration initiative [NASA-TM-105705] p 88 N93-26200

NIEDRA, J. M.

- Comparison of high temperature, high frequency core loss and dynamic B-H loops of a 2V-49Fe-49Co and a grain oriented 3Si-Fe alloy p 153 A93-25895
 M-H characteristics and demagnetization resistance of samarium-cobalt permanent magnets to 300 C p 153 A93-26076

NIEDRA, JANIS M.

- Comparison of high frequency, high temperature core loss and B-H loop characteristics of an 80 Ni-Fe crystalline alloy and two iron-based amorphous alloys p 123 A93-13882

- Radiation and temperature effects on electronic components investigated under the CSTI high capacity power project [NASA-TM-106096] p 161 N93-24746

NIKJOOY, M.

- Fuel injector: Air swirl characterization aerothermal modeling, phase 2, volume 1 [NASA-CR-189193-VOL-1] p 35 N93-24754

NING, X. J.

- Effect of high temperature annealing on the microstructure of SCS-6 SiC fibers p 133 A93-39513

NING, XIAN-JIE

- Microchemical analysis of the SCS-6 silicon carbide fiber p 135 A93-53734

NOCK, K.

- Venus Interior Structure Mission (VISM): Establishing a seismic network on Venus p 293 N93-28819

NOEBE, R. D.

- Room temperature cyclic deformation behavior of cast and extruded NiAl p 122 A93-12130
 The effect of microalloying additions on the tensile properties of polycrystalline NiAl p 123 A93-17516
 Containerless automated processing of intermetallic compounds and composites p 144 A93-52183
 Fabrication and properties of functionally graded NiAl/Al₂O₃ composites p 105 A93-54116
 Interfacial shear strength of cast and directionally solidified NiAl-sapphire fiber composites p 106 A93-55685

NOEBE, RONALD D.

- Review of the physical and mechanical properties and potential applications of the B2 compound NiAl: Unabridged version of a paper published in International materials review [NASA-TM-105598] p 127 N93-11635
 Low cycle fatigue behavior of polycrystalline NiAl at 300 and 1000 K [NASA-TM-105987] p 129 N93-26898

NORED, DONALD L.

- Electrical power system WP-04 p 161 N93-27804

NORRIS, RICK

- The design and evolution of the Beta two-stage-to-orbit horizontal takeoff and landing launch system [AIAA PAPER 92-5080] p 50 A93-22350

NORRIS, RICK B.

- The design and evolution of the beta two-stage-to-orbit horizontal takeoff and landing launch system [NASA-TM-106118] p 51 N93-27018

NOWLIN, BRENT C.

- Experimental evaluation of a cooled radial-inflow turbine [AIAA PAPER 93-1795] p 27 A93-49685

- Experimental evaluation of a cooled radial-inflow turbine [NASA-TM-106230] p 38 N93-28697

NWOKAH, O. D. I.

- A note on decentralized integral controllability p 264 A93-30492

NYLAND, T. W.

- Mixing and transient interface condensation of a liquid hydrogen tank [AIAA PAPER 93-1968] p 184 A93-49816

- Mixing and transient interface condensation of a liquid hydrogen tank [NASA-TM-106201] p 201 N93-28252

O**O'BRYAN, JOHN T.**

- Vector formulation for interferogram surface fitting p 278 A93-55687

O'CONNOR, ANDREW M.

- EMTP based stability analysis of Space Station Electric Power System in a test bed environment p 154 A93-26108

OBERLE, LAWRENCE G.

- Dynamic gas temperature measurements using a personal computer for data acquisition and reduction [NASA-TM-106119] p 261 N93-27024
 Progress in speckle-shift strain measurement p 251 N93-31558

OCONNOR, ANDREW M.

- EMTP based stability analysis of space station electric power system in a test bed environment [NASA-TM-105845] p 160 N93-15503

CONNOR, KENNETH

- Lewis safety manual [NASA-TM-104438] p 147 N93-70966

ODABAS, ONUR R.

- Transition elements based on transfinite interpolation [AIAA PAPER 93-1326] p 267 A93-33899

ODEN, J. T.

- Adaptive methods in computational fluid dynamics p 182 A93-45963

ODONNELL, PATRICIA

- Lewis Research Center battery overview p 255 N93-20493

OECHSLE, V. L.

- An analytical study of dilution jet mixing in a cylindrical duct [AIAA PAPER 93-2043] p 27 A93-49876

- An analytical study of dilution jet mixing in a cylindrical duct [NASA-TM-106181] p 37 N93-27160

OEFFTERING, RICHARD C.

- Conceptual design for the Space Station Freedom fluid physics/dynamics facility [NASA-TM-103663] p 61 N93-26209

OGBUJI, L. U. T.

- Mechanism of incipient oxidation of bulk chemical vapor deposited Si₃N₄ p 132 A93-32299

OGBUJI, LINUS U. J. T.

- Role of Si₂N₂O in the passive oxidation of chemically-vapor-deposited Si₃N₄ p 131 A93-16520

OHLLINGER, WAYNE L.

- Plasma contactor technology for Space Station Freedom [AIAA PAPER 93-2228] p 57 A93-50034

OKIISHI, THEODORE H.

- An experimental investigation of the flow in a diffusing S-duct [NASA-TM-105809] p 32 N93-12077

OLDENBURG, J. R.

- Liquid water content measurements using the Phase Doppler Particle Analyzer in the NASA Lewis Icing Research Tunnel [AIAA PAPER 93-0298] p 42 A93-23698

OLDENBURG, JOHN R.

- Experimental testing of four correction algorithms for the forward scattering spectrometer probe [NASA-TM-105906] p 213 N93-13307

OLDSON, J. C.

- Pulsed single-blow regenerator testing p 221 A93-26081

OLESON, STEVE

- Space transfer with ground-based laser/electric propulsion [NASA-TM-106060] p 84 N93-20615

OLIVE, K. A.

- The boron-to-beryllium ratio in halo stars - A signature of cosmic-ray nucleosynthesis in the early Galaxy p 292 A93-55061

OLIVE, KEITH A.

- Primordial nucleosynthesis and the abundances of beryllium and boron p 290 A93-33513
 Population II Li-6 as a probe of nucleosynthesis and stellar structure and evolution p 292 A93-56494

OLIVER, B. F.

- Containerless automated processing of intermetallic compounds and composites p 144 A93-52183

OLLE, RAYMOND

- Effects of dust accumulation and removal on radiator surfaces on Mars p 123 A93-13937

OLSON, S. L.

- Mechanisms of microgravity flame spread over a thin solid fuel - Oxygen and opposed flow effects p 140 A93-50368

OLSON, SANDRA L.

- Opposed-flow flame spreading in reduced gravity p 121 N93-20206

OMALLEY, TERENCE F.

- Conceptual design for the Space Station Freedom fluid physics/dynamics facility [NASA-TM-103663] p 61 N93-26209

ONBASIOGLU, FETIYE O.

- Fault-tolerant adaptive control for load-following in static space nuclear power systems p 263 A93-25986

- OPILA, E. J.**
Thermodynamics of Si-C-O system p 133 A93-39584
- ORANGE, T. W.**
Closed form expressions for crack mouth displacements and stress intensity factors for chevron notched short bar and short rod specimens based on experimental compliance measurements [NASA-TM-83796] p 246 N93-15369
- ORANGE, THOMAS W.**
NDE of PWA 1480 single crystal turbine blade material [NASA-TM-106140] p 38 N93-27640
- ORIENT, G.**
An advanced method for tracking the evolution of fatigue damage in reusable space propulsion systems p 234 A93-16406
- OSTRACH, SIMON**
Thermal oscillations in materials processing p 162 A93-10839
- OSWALD, F. B.**
Modal simulation of gear box vibration with experimental correlation p 221 A93-31982
Vibration and noise analysis of a gear transmission system [AIAA PAPER 93-2150] p 224 A93-49967
Vibration and noise analysis of a gear transmission system [NASA-TM-106162] p 229 N93-27641
- OSWALD, FRED B.**
Acoustical analysis of gear housing vibration p 273 A93-29420
Effect of extended tooth contact on the modeling of spur gear transmissions [AIAA PAPER 93-2148] p 223 A93-49965
Dynamic analysis of spur gears using computer program DANST [AIAA PAPER 93-2295] p 224 A93-50080
Experimental validation of boundary element methods for noise prediction [NASA-TM-105729] p 226 N93-10966
Dynamic analysis of spur gears using computer program DANST [NASA-TM-106211] p 230 N93-28050
Effect of extended tooth contact on the modeling of spur gear transmissions [NASA-TM-106174] p 230 N93-28411
- OTTARSON, GISLI**
A transfer matrix approach to vibration localization in mistuned blade assemblies [NASA-TM-106112] p 250 N93-27088
- OTTARSSON, GISLI**
An efficient constraint to account for mistuning effects in the optimal design of engine rotors [AIAA PAPER 92-4711] p 23 A93-20280
Vibration localization in mono- and bi-coupled bladed disks - A transfer matrix approach [AIAA PAPER 93-1492] p 222 A93-34241
- OTUGEN, M. V.**
Development of a Rayleigh scattering system for temperature measurements in combustor flows p 206 A93-23788
Gas temperature measurements using the dual-line detection Rayleigh scattering technique p 213 A93-55368
- OTUGEN, M. VOLKAN**
Gas temperature measurements using the dual-line detection Rayleigh scattering technique p 214 N93-13668
- OU, S.**
Heat transfer performance comparisons of five different rectangular channels with parallel angled ribs p 166 A93-18752
- OUZTS, PETER J.**
Screening studies of advanced control concepts for airbreathing engines [AIAA PAPER 92-3320] p 26 A93-49329
Screening studies of advanced control concepts for airbreathing engines [NASA-TM-106042] p 36 N93-25079
- OVRYN, B.**
Temporal averaging of phase measurements in the presence of spurious phase drift - Application to phase-stepped real-time holographic interferometry p 207 A93-26967
Temporal averaging in a turbulent environment - Compensation for phase drifts in phase shifting interferometry p 210 A93-44190
- OWEN, ALBERT K.**
Mathematical relationship between two sets of laser anemometer measurements for resolving the total velocity vector [NASA-TM-105986] p 35 N93-22599
- OWENS, JAY**
Applied high-speed imaging for the icing research program at NASA Lewis Research Center p 208 A93-33169
- OZGUNER, UMUT**
Space Station Freedom beta gimbal control via sensitivity models [NASA-TM-106000] p 60 N93-22551
- P**
- PACK, WILLIAM D.**
In-stream measurements of combustion during Mach 5 to 7 tests of the Hypersonic Research Engine (HRE) [AIAA PAPER 93-2324] p 28 A93-50104
- PAI, SHANTARAM S.**
Probabilistic structural analysis of adaptive/smart/intelligent space structures p 234 A93-16203
Probabilistic structural analysis of space truss structures for nonuniform thermal environmental effects [AIAA PAPER 92-4769] p 235 A93-20363
Probabilistic assessment of adaptive space truss configurations for thermal buckling resistance [AIAA PAPER 93-1622] p 240 A93-34151
- PAIS, M. R.**
Vaporization heat transfer of dielectric liquids on enhanced surfaces covered with screen wicks [AIAA PAPER 93-2835] p 182 A93-46572
- PALAMIDES, THOMAS R.**
Fabrication of carbon-carbon heat pipes for space nuclear power applications p 173 A93-25978
- PALASZEWSKI, BRYAN**
Metalized propellants for the human exploration of Mars p 66 A93-14509
Atomic hydrogen propellants - Historical perspectives and future possibilities [AIAA PAPER 93-0244] p 140 A93-24234
Technology for gelled liquid cryogenic propellants - Metalized hydrogen/aluminum [AIAA PAPER 93-1878] p 140 A93-49752
Space transportation alternatives for large space programs - The International Space University summer session - 1992 [AIAA PAPER 93-2278] p 44 A93-53588
Atomic hydrogen propellants: Historical perspectives and future possibilities [NASA-TM-106053] p 84 N93-20614
- PALAZZOLO, A. B.**
Hybrid active vibration control of rotorbearing systems using piezoelectric actuators p 221 A93-27324
- PALCHESKY, J. W.**
Low power arcjet system spacecraft impacts [AIAA PAPER 93-2392] p 76 A93-50157
- PALMER, RAYMOND W.**
User's guide for a large signal computer model of the helical traveling wave tube [NASA-TP-3251] p 160 N93-15531
Interim report on the analysis of the microwave power module [NASA-TM-106012] p 160 N93-16713
- PAMULAPATI, J.**
Ellipsometric characterization of In(0.52)Al(0.48)As and of modulation doped field effect transistor structures on InP substrates p 158 A93-49382
- PANDA, J.**
Estimation of unsteady lift on a pitching airfoil from wake velocity surveys [AIAA PAPER 93-0437] p 5 A93-23351
Estimation of unsteady lift on a pitching airfoil from wake velocity surveys [NASA-TM-105947] p 15 N93-14791
- PANDEY, P.**
Optimal control study for the Space Station Solar Dynamic power module p 54 A93-13133
- PANG, S. W.**
Application of high-quality SiO₂ grown by multipolar ECR source to Si/SiGe MISFET p 156 A93-37413
- PANIGOT, MICHAEL J.**
Benzonorbornadiene end caps for PMR resins p 94 A93-35700
- PANZARELLA, C. H.**
Numerical model for the Programmable Multirole Furnace (PMZF) [AIAA PAPER 93-0471] p 142 A93-24242
- PANZARELLA, CHARLES H.**
A numerical model including PID control of a multizone crystal growth furnace p 190 A93-55473
- PAO, C. K.**
Millimeter-wave pseudomorphic HEMT MMIC phased array components for space communications p 152 A93-25796
- PAO, YOH-HAN**
Neural networks for structural design - An integrated system implementation [AIAA PAPER 92-4806] p 263 A93-20389
- PAPADOPOULOS, DEMETRIOS S.**
The effect of contact stresses in four-point bend testing of graphite/epoxy and graphite/PMR-15 composite beams [NASA-TM-105891] p 107 N93-12076
- PAPADOPOULOS, P. M.**
Optimal control study for the Space Station Solar Dynamic power module p 54 A93-13133
- PAPADOPOULOS, PHILIP M.**
Control-structure interaction p 54 A93-14687
- PARK, J. S.**
Heat transfer performance comparisons of five different rectangular channels with parallel angled ribs p 166 A93-18752
- PARK, YONG H.**
Tensile creep and creep-recovery behavior of a SiC-fiber-Si₃N₄-matrix composite p 104 A93-40290
- PARKER, T.**
Nonintrusive, multipoint velocity measurements in high-pressure combustion flows [AIAA PAPER 93-2032] p 118 A93-49867
- PARKES, JAMES**
Plasma contactor technology for Space Station Freedom [AIAA PAPER 93-2228] p 57 A93-50034
- PARLOS, ALEXANDER G.**
Fault-tolerant adaptive control for load-following in static space nuclear power systems p 263 A93-25986
- PARROTT, TONY**
Consecutive plate acoustic suppressor apparatus and methods [NASA-CASE-LEW-15430-1] p 275 N93-17051
- PARTHASARATHY, ARVIND**
Pressure dependence of the oxygen reduction reaction at the platinum microelectrode/nafion interface - Electrode kinetics and mass transport p 112 A93-11450
- PASCHAL, WILLIAM A.**
Study on vortex flow control of inlet distortion p 2 A93-14520
- PASKIN, MARC D.**
An efficient liner cooling scheme for advanced small gas turbine combustors [AIAA PAPER 93-1763] p 27 A93-49660
- PASTOR, M. S.**
Limit pressure of a circumferentially reinforced SiC/Ti ring p 233 A93-16005
- PATANKAR, SUHAS V.**
An evaluation of three spatial differencing schemes for the discrete ordinates method in participating media [AIAA PAPER 93-0140] p 266 A93-24231
Radiation heat transfer calculations using a control-angle, control-volume-based discrete ordinates method [AIAA PAPER 93-2731] p 182 A93-46485
- PATHAK, PRABHAKAR H.**
A reciprocity formulation for the EM scattering by an obstacle within a large open cavity p 149 A93-52237
- PATNAIK, S. N.**
Improved accuracy for finite element structural analysis via an integrated force method p 234 A93-17246
Singularity in structural optimization p 240 A93-34938
- PATNAIK, SURYA N.**
Integrated force method - Compatibility conditions of structural mechanics for finite element analysis p 237 A93-32459
Application of artificial neural networks to the design optimization of aerospace structural components [NASA-TM-4389] p 247 N93-21831
- PATNAIK, S. N.**
Singularities in optimal structural design [AIAA PAPER 92-4818] p 235 A93-20397
- PATTERSON, MICHAEL J.**
Low-Isp derated ion thruster operation [AIAA PAPER 92-3203] p 64 A93-13696
Derated ion thruster development status [AIAA PAPER 93-2225] p 75 A93-50031
Plasma contactor technology for Space Station Freedom [AIAA PAPER 93-2228] p 57 A93-50034
Ion thruster development at NASA Lewis Research Center [NASA-TM-105983] p 82 N93-15429
Development of arcjet and ion propulsion for spacecraft stationkeeping [NASA-TM-106102] p 85 N93-23747
- PATTERSON, R.**
The NASA CSTI High Capacity Power Project p 69 A93-26105
The NASA CSTI high capacity power project [NASA-TM-105813] p 48 N93-11398

PATTERSON, RICHARD L.

- PATTERSON, RICHARD L.**
Minimize system cost by choosing optimal subsystem reliability and redundancy
[NASA-TM-106251] p 271 N93-31145
- PATTISON, WILLIAM W.**
Design of an oxygen turbopump for use in an Advanced Expander Test Bed engine
[AIAA PAPER 93-2137] p 48 A93-49955
- PAVLI, AL J.**
Hot fire fatigue testing results for the compliant combustion chamber p 79 N93-10038
- PAVLI, ALBERT J.**
Hot fire test results of subscale tubular combustion chambers p 79 N93-10020
Hot fire fatigue testing results for the compliant combustion chamber p 80 N93-10743
Hot fire test results of subscale tubular combustion chambers p 81 N93-11614
[NASA-TP-3222]
- PAVSHUK, VLADIMIR A.**
U.S./CIS eye joint nuclear rocket venture p 71 A93-49334
- PAXSON, DANIEL E.**
An improved numerical model for wave rotor design and analysis p 24 A93-23384
[AIAA PAPER 93-0482]
A comparison between numerically modelled and experimentally measured loss mechanisms in wave rotors p 30 A93-50252
[AIAA PAPER 93-2522]
An improved numerical model for wave rotor design and analysis p 33 N93-12418
[NASA-TM-105915]
- PAYNTER, G. C.**
A lag model for turbulent boundary layers developing over rough bleed surfaces p 10 A93-48181
[AIAA PAPER 93-2988]
- PEASE, D. M.**
X-ray-based displacement measurement for hostile environments p 208 A93-28580
- PEDDICORD, KENNETH L.**
Fault-tolerant adaptive control for load-following in static space nuclear power systems p 263 A93-25986
- PEECOOK, KEITH M.**
Advances in NASA's Nuclear Thermal Propulsion Technology project p 75 A93-50056
[AIAA PAPER 93-2258]
NASA's progress in nuclear electric propulsion technology p 78 A93-53587
[AIAA PAPER 93-1936]
NASA's progress in nuclear electric propulsion technology p 93 N93-31858
[NASA-TM-106272]
- PEGG, ROBERT J.**
Design of a hypersonic waverider-derived airplane p 55 A93-21108
[AIAA PAPER 93-0401]
- PELACCIO, DENNIS G.**
Nuclear Engine System Simulation (NESS). Version 2.0: Program user's guide p 85 N93-23875
[NASA-CR-191081]
Nuclear Engine System Simulation (NESS). Volume 1: Program user's guide p 86 N93-23876
[NASA-CR-191080]
- PELLACCIO, DENNIS G.**
Nuclear thermal propulsion transportation systems for lunar/Mars exploration p 81 N93-12363
[NASA-TM-105870]
- PELTIER, L. J.**
Time-dependent thermocapillary convection in a Cartesian cavity - Numerical results for a moderate Prandtl number fluid p 169 A93-22666
[AIAA PAPER 93-0259]
- PENCIL, E.**
The effects of 1 kW class arcjet thruster plumes on spacecraft charging and spacecraft thermal control materials p 57 A93-35050
- PENCIL, ERIC J.**
Low power arcjet system spacecraft impacts p 76 A93-50157
[AIAA PAPER 93-2392]
Development of arcjet and ion propulsion for spacecraft stationkeeping p 85 N93-23747
[NASA-TM-106102]
- PENDRICK, V.**
Buffer layers for high-Tc thin films on sapphire p 150 A93-17063
- PENG, J.-P.**
Calculation of stiffness and damping coefficients for elastically supported gas foil bearings p 221 A93-27308
- PENKO, P. F.**
Measurement and analysis of a small nozzle plume in vacuum p 71 A93-42895
Measurement and analysis of a small nozzle plume in vacuum p 88 N93-26561
[NASA-TM-106066]

- PENKO, PAUL F.**
Assessment of three numerical methods for the computation of a low-density plume flow p 77 A93-50256
[AIAA PAPER 93-2528]
Internal structure of shock waves in disparate mass mixtures p 190 A93-54483
- PENSWICK, L. B.**
Assessment of 25 kW free-piston Stirling technology alternatives for solar applications p 254 A93-26072
- PEPPER, STEPHEN V.**
Interfacial chemistry of a perfluoropolyether lubricant studied by X-ray photoelectron spectroscopy and temperature desorption spectroscopy p 133 A93-38473
X-ray photoelectron spectroscopy study of the stability of Fomblin Z25 on the native oxide of aluminum p 134 A93-44883
A vacuum (10 exp -9 torr) friction apparatus for determining friction and endurance life of MoS(x) films p 146 A93-49245
Interfacial chemistry of a perfluoropolyether lubricant studied by XPS and TDS p 137 N93-22560
[NASA-TM-106014]
- PEREIRA, J. M.**
Effects of interply damping layers on the dynamic characteristics of composite plates p 237 A93-32415
- PEREIRA, J. MICHAEL**
Stress distribution in composite flatwise tension test specimens p 108 N93-25071
[NASA-TM-106074]
Graphite/epoxy composite laminates with co-cured interlaminar damping layers p 109 N93-25587
- PEREZ-DAVIS, MARLA E.**
Effects of dust accumulation and removal on radiator surfaces on Mars p 123 A93-13937
Lunar and Martian environmental interactions with nuclear power system radiators p 80 N93-10965
[NASA-TM-105747]
Degradation of radiator performance on Mars due to dust p 59 N93-15616
- PEREZ, ARMANDO**
Phase space distribution of halo particles and detection of WIMPS p 289 A93-23650
- PERKINS, DAVID**
Space Nuclear Thermal Propulsion Test Facilities Subpanel p 87 N93-25105
[NASA-TM-105708]
- PERKINS, KEN R.**
System model development for nuclear thermal propulsion p 80 N93-10457
[NASA-TM-105761]
System model development for nuclear thermal propulsion p 276 N93-16531
[NASA-TM-108157]
System model development for nuclear thermal propulsion p 277 N93-17343
[NASA-TM-108215]
- PERKINS, PORTER J.**
Aircraft icing problems - After 50 years p 19 A93-24239
[AIAA PAPER 93-0392]
- PERL, THOMAS D.**
Multiple-access phased array antenna simulator for a digital beam-forming system investigation p 148 A93-26237
Effect of a dielectric overlay on a linearly tapered slot antenna excited by a coplanar waveguide p 155 A93-35649
- PERRY, WILLIAM D.**
Void control in the crystallization of lithium fluoride p 97 A93-13760
- PESTAK, CHRISTOPHER J.**
Design of an automated imaging system for use in a space experiment p 204 A93-20454
- PETERSEN, T. V.**
A plume spectroscopy system for flight applications p 63 A93-50242
[AIAA PAPER 93-2511]
- PETIT, J. B.**
Progress in silicon carbide semiconductor technology p 158 A93-44965
Thermal oxidation of single-crystal silicon carbide - Kinetic, electrical, and chemical studies p 284 A93-55601
Growth and characterization of 3C-SiC and 6H-SiC films on 6H-SiC wafers p 284 A93-55602
- PETLEY, DENNIS H.**
Design of a hypersonic waverider-derived airplane p 55 A93-21108
[AIAA PAPER 93-0401]
- PETRIK, EDWARD J.**
Space Communication Artificial Intelligence for Link Evaluation Terminal (SCALET) p 265 N93-11940
- PETROSKY, LYMAN**
Nuclear Engine System Simulation (NESS). Version 2.0: Program user's guide p 85 N93-23875
[NASA-CR-191081]

- PETROSKY, LYMAN J.**
Nuclear Engine System Simulation (NESS). Volume 1: Program user's guide p 86 N93-23876
[NASA-CR-191080]
- PEUSSA, JOUKO**
Elevated-temperature fracture resistances of monolithic and composite ceramics using chevron-notched bend tests p 133 A93-38888
- PHAENGSOOK, N.**
Effects of icing on the aerodynamic performance of high lift airfoils p 4 A93-20144
[AIAA PAPER 93-0026]
- PHILIPP, WARREN H.**
Guanidine based vehicle/binders for use with oxides, metals, and ceramics p 138 N93-28423
[NASA-CASE-LEW-15314-2]
Ion exchange polymers and method for making p 139 N93-31316
[NASA-CASE-LEW-15576-1]
- PHILLIPS, R.**
High quality flame deposited diamond films for infrared optical windows p 281 A93-40564
- PHILLIPS, STEPHEN M.**
Antiwindup analysis and design approaches for MIMO systems p 30 A93-51403
[AIAA PAPER 93-3811]
- PIERCE, F. J.**
The development of a turbulent junction vortex system p 168 A93-22258
- PIERCE, W. S.**
Closed form expressions for crack mouth displacements and stress intensity factors for chevron notched short bar and short rod specimens based on experimental compliance measurements p 246 N93-15369
[NASA-TM-83796]
- PIERRE, CHRISTOPHE**
An efficient constraint to account for mistuning effects in the optimal design of engine rotors p 23 A93-20280
[AIAA PAPER 92-4711]
Vibration localization in mono- and bi-coupled bladed disks - A transfer matrix approach p 222 A93-34241
[AIAA PAPER 93-1492]
Aeroelastic dynamics of mistuned blade assemblies with closely spaced blade modes p 26 A93-37446
[AIAA PAPER 93-1628]
Stochastic sensitivity measure for mistuned high-performance turbines p 245 N93-12277
[NASA-TM-105821]
Localization of aeroelastic modes in mistuned high-energy turbines p 230 N93-31586
- PIERRE, CHRISTOPHE**
A transfer matrix approach to vibration localization in mistuned blade assemblies p 250 N93-27088
[NASA-TM-106112]
- PIETRZYK, J. R.**
EOTV propellant tank pressure control and liquid dynamics p 77 A93-50164
[AIAA PAPER 93-2399]
- PINCKNEY, S. Z.**
Design of a hypersonic waverider-derived airplane p 55 A93-21108
[AIAA PAPER 93-0401]
- PINDERA, MAREK-JERZY**
The effect of multiple compliant layers at the fiber-matrix interface on residual thermal stresses in metal matrix composites p 104 A93-42085
The effect of fiber microstructure on evolution of residual stresses in silicon carbide/titanium aluminate composites p 106 A93-54771
- PINERO, L. R.**
Simplified power processing for inert gas ion thrusters p 76 A93-50162
[AIAA PAPER 93-2397]
- PINERO, LUIS R.**
10 kW power electronics for hydrogen arcjets p 79 N93-10033
The 10 kW power electronics for hydrogen arcjets p 81 N93-12484
[NASA-TM-105614]
- PINSON, LARRY D.**
NASA CST aids U.S. industry p 258 A93-25084
- PIPPIN, GARY**
Recommended practices for in-space and ground laboratory. Atomic oxygen exposure and analysis p 276 N93-20814
- PIQUE, A.**
Buffer layers for high-Tc thin films on sapphire p 150 A93-17063
- PIROUZ, P.**
Effect of high temperature annealing on the microstructure of SCS-6 SiC fibers p 133 A93-39513
- PIROUZ, PIROUZ**
Microchemical analysis of the SCS-6 silicon carbide fiber p 135 A93-53734
- PISCHEL, K.**
The engine design engine. A clustered computer platform for the aerodynamic inverse design and analysis of a full engine p 15 N93-11223
[NASA-TM-105838]

- PISZCZOR, MICHAEL F.**
Photovoltaic Array Space Power flight experiment plus diagnostics (PASP+) modules p 68 A93-25898
The Photovoltaic Array Space Power Plus diagnostics (PASP Plus) flight experiment p 256 N93-28717
- PLACHTA, DAVID W.**
Cryogenic propellant thermal control system design considerations, analyses, and concepts applied to a Mars human exploration mission [AIAA PAPER 93-2353] p 75 A93-50126
- PLATT, JONATHAN**
Effect of free surface shape on combined thermocapillary and natural convection p 162 A93-10671
- PLATT, JONATHAN A.**
Prediction of gas-liquid two-phase flow regime in microgravity [NASA-TM-106274] p 145 N93-30939
- PLENCNER, ROBERT M.**
Concurrent optimization of airframe and engine design parameters [AIAA PAPER 92-4713] p 20 A93-20281
An interactive preprocessor for the NASA engine performance program [NASA-TM-105786] p 32 N93-10983
Concurrent optimization of airframe and engine design parameters [NASA-TM-105908] p 32 N93-12402
- PLETCHER, R. H.**
On solving the compressible Navier-Stokes equations for unsteady flows at very low Mach numbers [AIAA PAPER 93-3368] p 181 A93-45061
- PLETCHER, RICHARD H.**
Simulation of three-dimensional liquid sloshing flows using a strongly implicit calculation procedure p 179 A93-35624
- PLINE, ALEXANDER D.**
Particle image velocimetry for the Surface Tension Driven Convection Experiment using a particle displacement tracking technique p 206 A93-23799
Ground-based PIV and numerical flow visualization results from the Surface Tension Driven Convection Experiment p 143 A93-33075
- PODBOY, GARY G.**
Takeoff/approach noise for a model counterrotation propeller with a forward-swept upstream rotor [AIAA PAPER 93-0596] p 24 A93-24782
Laser velocimeter measurements of the flow field generated by a forward-swept propfan during flutter [AIAA PAPER 93-2919] p 14 A93-53591
Takeoff/approach noise for a model counterrotation propeller with a forward-swept upstream rotor [NASA-TM-105979] p 34 N93-16715
- PODLESKI, S. D.**
Installed F/A-18 inlet flow calculations at 60 deg angle-of-attack and 10 deg side slip [AIAA PAPER 93-1806] p 12 A93-49695
- PODOJIL, G.**
Leveling coatings for reducing the atomic oxygen defect density in protected graphite fiber epoxy composites [NASA-TM-105732] p 136 N93-15344
Leveling coatings for reducing the atomic oxygen defect density in protected graphite fiber epoxy composites p 59 N93-15597
- PODOJIL, GREGG M.**
Determination of atomic oxygen fluence using spectrophotometric analysis of infrared transparent witness coupons for long duration exposure tests [NASA-TM-106021] p 96 N93-22605
- POINSATTE, P. E.**
Evaluation of a hue capturing based transient liquid crystal method for high-resolution mapping of convective heat transfer on curved surfaces p 210 A93-43689
- POINSATTE, PHILIP E.**
Measurements and computational analysis of heat transfer and flow in a simulated turbine blade internal cooling passage [AIAA PAPER 93-1797] p 189 A93-53585
Transient liquid-crystal technique used to produce high-resolution convective heat-transfer-coefficient maps [NASA-TM-106083] p 198 N93-23404
High Reynolds number and turbulence effects on aerodynamics and heat transfer in a turbine cascade [NASA-TM-106187] p 202 N93-29157
Measurements and computational analysis of heat transfer and flow in a simulated turbine blade internal cooling passage [NASA-TM-106189] p 203 N93-31647
- POIRIER, D. R.**
Numerical model for dendritic solidification of binary alloys p 282 A93-46729
- POLIFKO, D. M.**
Fiber optic link for millimeter wave communication satellites p 277 A93-25736
- PORDAL, H. S.**
A three-dimensional pressure flux-split RNS application to sub/supersonic flow in inlets and ducts [AIAA PAPER 93-3063] p 11 A93-48239
- PORRO, A. R.**
Use of surface heat transfer measurements as a flow separation diagnostic in a two-dimensional reflected oblique shock/turbulent boundary layer interaction [AIAA PAPER 93-0775] p 172 A93-24859
- PORRO, A. ROBERT**
Use of surface heat transfer measurements as a flow separation diagnostic in a two dimensional reflected oblique shock/turbulent boundary layer interaction [NASA-TM-105981] p 194 N93-15355
- POTAPCZUK, MARK G.**
Numerical modeling of anti-icing systems and comparison to test results on a NACA 0012 airfoil [AIAA PAPER 93-0170] p 21 A93-23242
Ice accretion and performance degradation calculations with LEWICE/NS [AIAA PAPER 93-0173] p 18 A93-23244
Numerical modeling of anti-icing systems and comparison to test results on a NACA 0012 airfoil [NASA-TM-105975] p 19 N93-15345
Ice accretion and performance degradation calculations with LEWICE/NS [NASA-TM-105972] p 19 N93-15354
- POVINELLI, L. A.**
Multigrid calculation of three-dimensional viscous cascade flows p 8 A93-42889
Development of an explicit multiblock/multigrid flow solver for viscous flows in complex geometries [AIAA PAPER 93-2380] p 186 A93-50148
- POVINELLI, LOUIS A.**
A least-squares finite element method for 3D incompressible Navier-Stokes equations [AIAA PAPER 93-0338] p 171 A93-24236
The structure of supersonic jet flow and its radiated sound [AIAA PAPER 93-0549] p 273 A93-25538
CFD for hypersonic propulsion p 8 A93-42585
The NASA Computational Fluid Dynamics (CFD) program - Building technology to solve future challenges [AIAA PAPER 93-3292] p 267 A93-44996
Multigrid time-accurate integration of Navier-Stokes equations [AIAA PAPER 93-3361] p 181 A93-45054
A least-squares finite element method for incompressible Navier-Stokes problem p 191 N93-10548
Large-scale computation of incompressible viscous flow by least-squares finite element method [NASA-TM-105904] p 269 N93-22825
Numerical simulations of three-dimensional laminar flow over a backward facing step; flow near side walls [NASA-TM-106248] p 202 N93-31147
- POWELL, J. A.**
Silicon carbide, a semiconductor for space power electronics p 279 A93-13880
Greatly improved 3C-SiC p-n junction diodes grown by chemical vapor deposition p 156 A93-38994
Atomic probe microscopy of 3C SiC films grown on 6H SiC substrates p 281 A93-39854
Aluminum acceptor four particle bound exciton complex in 4H, 6H, and 3C SiC p 282 A93-44822
Progress in silicon carbide semiconductor technology p 158 A93-44965
Thermal oxidation of single-crystal silicon carbide - Kinetic, electrical, and chemical studies p 284 A93-55601
Growth and characterization of 3C-SiC and 6H-SiC films on 6H-SiC wafers p 284 A93-55602
- POWELL, J. ANTHONY**
Process for the controlled growth of single-crystal films of silicon carbide polytypes on silicon carbide wafers [NASA-CASE-LEW-15222-3] p 284 N93-17413
- POWELL, KENNETH G.**
An accuracy assessment of Cartesian-mesh approaches for the Euler equations [AIAA PAPER 93-3335] p 9 A93-45029
- POWER, JOHN L.**
Preliminary investigation of high power microwave plasmas for electrothermal thruster use [AIAA PAPER 93-2106] p 74 A93-49928
Preliminary investigation of high power microwave plasmas for electrothermal thruster use [NASA-TM-106207] p 92 N93-29158
- POWER, MICHAEL B.**
Enhancement of photoluminescence intensity of GaAs with cubic GaS chemical vapor deposited using a structurally designed single-source precursor p 280 A93-26930
Metal-organic chemical vapour deposition of polycrystalline tetragonal indium sulphide (InS) thin films p 116 A93-36584
- Photoluminescence intensity enhancement of GaAs by vapor-deposited GaS - A rational approach to surface passivation p 281 A93-40049
Electronic passivation of n- and p-type GaAs using chemical vapor deposited GaS p 283 A93-52708
- POWERS, JOSEPH M.**
Reaction zone structure for strong, weak overdriven, and weak underdriven oblique detonations p 178 A93-35492
- POWERS, LYNN M.**
Reliability analysis of structural ceramic components using a three-parameter Weibull distribution [ASME PAPER 92-GT-296] p 231 A93-19486
Ceramic component reliability with the restructured NASA/CARES computer program [ASME PAPER 92-GT-383] p 234 A93-19540
Lifetime reliability evaluation of structural ceramic parts with the CARES/LIFE computer program [AIAA PAPER 93-1497] p 239 A93-34037
A numerical round robin for the reliability prediction of structural ceramics [AIAA PAPER 93-1498] p 240 A93-34038
Ceramic component reliability with the restructured NASA/CARES computer program [NASA-TM-105856] p 244 N93-11004
- PRAKASH, A.**
Natural and thermocapillary convection in multiple liquid layers [AIAA PAPER 93-0469] p 171 A93-24241
- PRASANNA, M. G.**
Maximum life spiral bevel reduction design [NASA-TM-105790] p 226 N93-10982
- PRESCOTT, R.**
SIMS studies of oxide growth on beta-NiAl p 127 A93-53469
- PRIEM, RICHARD J.**
Calculations of combustion response profiles and oscillations [NASA-TM-106135] p 87 N93-25236
- PROCTOR, MARGARET P.**
Development of advanced seals for space propulsion turbomachinery [SAE PAPER 921028] p 218 A93-14651
- PRUSSING, JOHN E.**
Optimal impulsive intercept with low-thrust rendezvous return p 45 A93-34521
- PRZEKAS, A. J.**
Driven cavity simulation of turbomachine blade flows with vortex control [AIAA PAPER 93-0390] p 6 A93-24238
- PUTERBAUGH, S. L.**
Three-dimensional flow analysis inside turbomachinery stages with steady and unsteady Navier-Stokes method [ISABE 93-7095] p 14 A93-54071
- PUTERBAUGH, S. L.**
Unsteady aerodynamic flow phenomena in a transonic compressor stage [AIAA PAPER 93-1868] p 12 A93-49743
- PUTERBAUGH, STEVEN L.**
Three-dimensional flow phenomena in a transonic, high-through-flow, axial-flow compressor stage [ASME PAPER 92-GT-169] p 3 A93-19395
- PUTT, CHARLES W.**
Gas turbine system simulation: An object-oriented approach [NASA-TM-106044] p 36 N93-25673

Q

QAMMAR, HELEN K.

Desktop chaotic systems: Intuition and visualization [NASA-TM-106258] p 269 N93-31847

QIAN, W.

A 3-D nonlinear recursive digital filter for video image processing p 264 A93-34582

Vibration and noise analysis of a gear transmission system [AIAA PAPER 93-2150] p 224 A93-49967

Global dynamic modeling of a transmission system [NASA-CR-191117] p 228 N93-24751

Vibration and noise analysis of a gear transmission system [NASA-TM-106162] p 229 N93-27641

QIU, SONGGANG

Visualization of entry flow separation for oscillating flow in tubes p 174 A93-26091

QUACKENBUSH, TODD

High accuracy computation of fluid-structure interaction in transonic cascades [AIAA PAPER 93-0485] p 6 A93-23387

QUEALY, ANGELA

Turbomachinery CFD on parallel computers [NASA-TM-105932] p 262 N93-13154

QUINN, GEORGE D.

QUINN, GEORGE D.

Fracture toughness of advanced ceramics at room temperature p 131 A93-20842

QUINN, R. D.

Dynamic modeling and control of multibody mechanical systems which are structurally flexible p 264 A93-29338

QUINN, ROGER D.

Control/structure interactions of Space Station solar dynamic modules p 57 A93-41878

QUINN, TODD M.

Lessons learned from the Autonomous Power System p 68 A93-25879

QUINTANA, JORGE A.

Fault-tolerant onboard digital information switching and routing for communications satellites p 53 N93-26895 [NASA-TM-4471]

R

RABINOWITZ, MARTIN J.

Numerical study of shock-induced combustion in methane-air mixtures p 184 A93-49783 [AIAA PAPER 93-1917]

RADHAKRISHNAN, KRISHNAN

A critical analysis of the accuracy of several numerical techniques for combustion kinetic rate equations p 34 N93-16941 [NASA-TP-3315]

RADHAKRISHNAN, KRISHNAN

LENS, a general chemical kinetics and sensitivity analysis code for gas-phase reactions: User's guide p 121 N93-16614 [NASA-TM-105851]

RADHAKRISHNAN, V. M.

On bilinearity of Manson-Coffin low-cycle-fatigue relationship p 245 N93-12739 [NASA-TM-105840]
Considerations concerning fatigue life of metal matrix composites p 250 N93-27009 [NASA-TM-106144]

RADO, LEONARD G.

The evolution of procurement and assurance methods used to proof an advanced space material p 94 A93-53392

RAITANO, PAUL

A new facility for advanced rocket propulsion research p 48 A93-49737 [AIAA PAPER 93-1859]
A new facility for advanced rocket propulsion research p 49 N93-28696 [NASA-TM-106193]

RAJ, S. V.

Effect of strain and stress on the relative dimensions of the 'hard' and 'soft' regions in crept NaCl single crystals p 279 A93-17513
Effect of oxidation on the mechanical properties of a NbAl3 alloy at intermediate temperatures p 124 A93-20667

RAJ, SAI V.

High temperature creep and oxidation resistant chromium silicide matrix alloy containing molybdenum p 130 N93-29172 [NASA-CASE-LEW-15697-1]

RAJAGOPAL, K. R.

An advanced method for tracking the evolution of fatigue damage in reusable space propulsion systems p 234 A93-16406

RAJU, M. S.

PDF approach for compressible turbulent reacting flows p 170 A93-24229 [AIAA PAPER 93-0087]
CFD validation of subsonic turbulent planar shear layers p 184 A93-49669 [AIAA PAPER 93-1773]

RAMAMOORTHY, P. A.

Fuzzy expert systems vs. neural networks - Truck backer-upper control revisited p 264 A93-37039

RAMAN, GANESH

Flip-flop jet nozzle extended to supersonic flows p 8 A93-39409
Enhanced mixing of a rectangular supersonic jet by natural and induced screech p 18 N93-31672 [NASA-TM-106245]

RAMESHAM, R.

Thin film diamond microstructure applications p 209 A93-40580

RAMINS, PETER

A high-efficiency 59- to 64-GHz TWT for intersatellite communications p 158 A93-49553
Interim report on the analysis of the microwave power module p 160 N93-16713 [NASA-TM-106012]

RANAUDO, R. J.

Icing effects on aircraft stability and control determined from flight data - Preliminary results p 40 A93-23073 [AIAA PAPER 93-0398]
Icing effects on aircraft stability and control determined from flight data: Preliminary results p 41 N93-14831 [NASA-TM-105977]

RAO, D. K.

Stiffness of magnetic bearings subjected to combined static and dynamic loads p 219 A93-15685 [ASME PAPER 91-TRIB-27]
Magnetic bearings for free-piston Stirling engines p 221 A93-26079

RAO, PRABHAKARA P.

Monte Carlo analysis of the Titan III/Transfer Orbit Stage guidance system for the Mars Observer mission p 50 A93-51473 [AIAA PAPER 93-3889]

RAPP, DOUGLAS C.

Reliability studies of Integrated Modular Engine system designs p 72 A93-49759 [AIAA PAPER 93-1886]
Reliability assessment of thrust chamber cooling concepts using probabilistic analysis techniques p 75 A93-49978 [AIAA PAPER 93-2163]
Reliability studies of integrated modular engine system designs p 91 N93-27022 [NASA-TM-106178]

RAPP, ROBERT A.

Chromium and reactive element modified aluminide diffusion coatings on superalloys - Environmental testing p 126 A93-37899

RAQUET, C. A.

System-level integrated circuit (SLIC) development for phased array antenna applications p 152 A93-25798

RASHIDI, M.

Split torque transmission load sharing p 226 N93-12736 [NASA-TM-105884]

RATVASKY, T. P.

Icing effects on aircraft stability and control determined from flight data - Preliminary results p 40 A93-23073 [AIAA PAPER 93-0398]
Icing effects on aircraft stability and control determined from flight data: Preliminary results p 41 N93-14831 [NASA-TM-105977]

RAUCH, J.

Pulsed single-blow regenerator testing p 221 A93-26081

RAUCH, JEFFREY S.

A free-piston Stirling engine/linear alternator controls and load interaction test facility p 146 A93-26077
Dynamic analysis of free-piston Stirling engine/linear alternator-load system - Experimentally validated p 254 A93-26078
Dynamic analysis of Free-Piston Stirling Engine/Linear Alternator-load system-experimentally validated p 271 N93-22559 [NASA-TM-106034]

RAWLIN, V. K.

Simplified power processing for inert gas ion thrusters p 76 A93-50162 [AIAA PAPER 93-2397]

RAWLIN, VINCENT K.

Characterization of in-flight performance of ion propulsion systems p 75 A93-50023 [AIAA PAPER 93-2217]
Ion thruster development at NASA Lewis Research Center p 82 N93-15429 [NASA-TM-105983]
Development of arcjet and ion propulsion for spacecraft stationkeeping p 85 N93-23747 [NASA-TM-106102]

RAY, ASOK

Damage-mitigating control of aerospace systems for high performance and extended life p 263 A93-22967
Damage-mitigating control of space propulsion systems for high performance and extended life p 74 A93-49907 [AIAA PAPER 93-2080]

RAY, RANJAN

Influence of grain size on the creep behavior of HIC-dispersed NiAl p 123 A93-17674

REDDY, D. R.

A comparative study of Full Navier-Stokes and Reduced Navier-Stokes analyses for separating flows within a diffusing inlet S-duct p 13 A93-49970 [AIAA PAPER 93-2154]

REDDY, E. S.

Dynamic analysis of a pre-and-post ice impacted blade p 22 A93-13333 [AIAA PAPER 92-4273]
Structural tailoring of aircraft engine blade subject to ice impact constraints p 23 A93-20319 [AIAA PAPER 92-4710]
Structural Tailoring/Analysis for Hypersonic Components - A computational simulation p 20 A93-20324 [AIAA PAPER 92-4722]
BLASIM - A computational tool to assess ice impact damage on engine blades p 26 A93-34165 [AIAA PAPER 93-1638]
Dynamic analysis of a pre-and-post ice impacted blade p 144 N93-12197 [NASA-TM-105829]
Root damage analysis of aircraft engine blade subject to ice impact p 246 N93-15343 [NASA-TM-105779]

PERSONAL AUTHOR INDEX

Structural tailoring of aircraft engine blade subject to ice impact constraints p 250 N93-26999 [NASA-TM-106033]
Blasim: A computational tool to assess ice impact damage on engine blades p 251 N93-31193 [NASA-TM-106225]

REDDY, J. N.

Probabilistic micromechanics for metal matrix composites p 237 A93-32465
Probabilistic nonlinear finite element analysis of composite structures p 237 A93-32717

REDDY, MAHIDHAR V.

Reliability based structural optimization - A simplified safety index approach p 239 A93-33972 [AIAA PAPER 93-1418]

REDDY, S.

Contact stress analysis of spiral bevel gears using nonlinear finite element static analysis p 224 A93-50081 [AIAA PAPER 93-2296]
Contact stress analysis of spiral bevel gears using nonlinear finite element static analysis p 228 N93-27037 [NASA-TM-106176]

REDDY, T. S. R.

APPLE - An aeroelastic analysis system for turbomachines and propfans p 23 A93-20320 [AIAA PAPER 92-4712]
Unsteady aerodynamics and flutter of propfans using a three-dimensional Full-Potential Solver p 25 A93-34161 [AIAA PAPER 93-1633]

REDINBO, G. R.

Modifying real convolutional codes for protecting digital filtering systems p 148 A93-38221

REED, BRIAN D.

A laboratory model of a hydrogen/oxygen engine for combustion and nozzle studies p 48 A93-49711 [AIAA PAPER 93-1825]
Performance comparison of axisymmetric and three-dimensional hydrogen film coolant injection in a 110N hydrogen/oxygen rocket p 83 N93-16714 [NASA-TM-105967]
Small hydrogen/oxygen rocket flowfield behavior from heat flux measurements p 91 N93-28619 [NASA-TM-106233]

REED, HELEN L.

Gallery of fluid motion p 178 A93-35481

REED, KENNETH W.

Analysis of large quasistatic deformations of inelastic solids by a new stress based finite element method p 246 N93-13260 [NASA-CR-189235]

REEDER, M. F.

Effect of tabs on the flow and noise field of an axisymmetric jet p 25 A93-30833

REEHORST, ANDREW

Close-up analysis of aircraft ice accretion p 18 A93-23239 [AIAA PAPER 93-0029]
Close-up analysis of aircraft ice accretion p 19 N93-15360 [NASA-TM-105952]

REICHERT, B. A.

An experimental investigation of S-duct flow control using arrays of low-profile vortex generators p 170 A93-24226 [AIAA PAPER 93-0018]

REICHERT, BRUCE A.

An experimental investigation of the flow in a diffusing S-duct p 32 N93-12077 [NASA-TM-105809]
An experimental investigation of S-duct flow control using arrays of low-profile vortex generators p 17 N93-19968 [NASA-TM-106030]

REID, MARGARET A.

Changes in impedance of Ni/Cd cells with voltage and cycle life p 255 N93-23018 [NASA-TM-106105]

REIMER, B. L.

OTV bearing deflection investigation p 215 N93-22994 [NASA-TM-106085]

REINHARDT, KITT C.

Photovoltaic Array Space Power flight experiment plus diagnostics (PASP+) modules p 68 A93-25898

REINMANN, JOHN J.

Aerodynamic effects of deicing and anti-icing fluids p 19 A93-31929

REISEL, JOHN R.

Laser-induced fluorescence measurements of nitric oxide in laminar C2H6/O2/N2 flames at high pressure p 116 A93-28253

REMP, KERRY

Nuclear safety policy working group recommendations on nuclear propulsion safety for the space exploration initiative p 88 N93-26200 [NASA-TM-105705]

RENO, MARTIN A.

Thermodynamic data for fifty reference elements p 286 N93-19977 [NASA-TP-3287]

RENZ, DAVID D.

Comparison of all-electric secondary power systems for civil transport p 24 A93-25997

- Comparison of all-electric secondary power systems for civil subsonic transports
[NASA-TM-105852] p 32 N93-10456
- RESHOTKO, ELI**
Hypersonic stability and transition p 8 A93-42579
- RESLER, EDWIN L., JR.**
Analytic methods for design of wave cycles for wave rotor core engines
[AIAA PAPER 93-2523] p 30 A93-50253
- REVIERE, R. D.**
Containerless automated processing of intermetallic compounds and composites p 144 A93-52183
- RHATIGAN, JENNIFER L.**
On protection of Freedom's solar dynamic radiator from the orbital debris environment. I - Preliminary analysis and testing p 70 A93-36197
On protection of Freedom's solar dynamic radiator from the orbital debris environment. II - Further testing and analyses p 70 A93-36589
- RHEE, HYOP S.**
Advanced radiator concepts feasibility demonstration p 163 A93-13844
- RHO, E.**
Analysis of MMIC arrays for use in the ACTS Aero Experiment
[NASA-TM-106073] p 53 N93-22589
- RIBEIRO, P. F.**
Energy loss analysis of an integrated space power distribution system p 68 A93-25958
Energy loss analysis of an integrated space power distribution system
[NASA-TM-105772] p 141 N93-14834
- RICE, E. J.**
Fiber optic laser Doppler anemometry in swirling jets p 206 A93-23783
- RICE, EDWARD J.**
Flip-flop jet nozzle extended to supersonic flows p 8 A93-39409
Jet mixer noise suppressor using acoustic feedback
[NASA-CASE-LEW-15170-1] p 275 N93-28953
Enhanced mixing of a rectangular supersonic jet by natural and induced screech
[NASA-TM-106245] p 18 N93-31672
- RICE, JOHN W.**
Nuclear safety policy working group recommendations on nuclear propulsion safety for the space exploration initiative
[NASA-TM-105705] p 88 N93-26200
- RICHARD, M. A.**
Performance of TiCaBaCuO 30 GHz 64 element antenna array p 157 A93-44763
A 10 GHz Y-Ba-Cu-O/GaAs hybrid oscillator proximity coupled to a circular microstrip patch antenna p 158 A93-54619
- RICHARDSON, PAMELA F.**
The NASA Computational Fluid Dynamics (CFD) program - Building technology to solve future challenges
[AIAA PAPER 93-3292] p 287 A93-44996
- RICHTER, SCOTT W.**
Experimental determination of in situ utilization of lunar regolith for thermal energy storage p 253 A93-26043
- RIEKE, W. J.**
Microgravity research on the NASA Lewis Learjet test facility
[AIAA PAPER 93-0573] p 43 A93-24245
- RIEKE, WILLIAM J.**
Aircraft icing problems - After 50 years
[AIAA PAPER 93-0392] p 19 A93-24239
- RIGBY, D. L.**
Increased heat transfer to elliptical leading edges due to spanwise variations in the freestream momentum: Numerical and experimental results
[NASA-TM-106150] p 199 N93-27020
- RIGNEY, J. D.**
Chemical stability of titanium diboride reinforcement in nickel aluminide matrices p 105 A93-52473
- RILEY, BEN R.**
Assessment of three numerical methods for the computation of a low-density plume flow
[AIAA PAPER 93-2528] p 77 A93-50256
- RIMLINGER, M. J.**
Chimera grids in the simulation of three-dimensional flowfields in turbine-blade-coolant passages
[AIAA PAPER 93-2559] p 187 A93-50280
- RINGER, MARK J.**
Lessons learned from the Autonomous Power System p 68 A93-25879
Scheduling lessons learned from the Autonomous Power System p 265 N93-18671
- RISTIC, D.**
Three-dimensional flow field in a turbine nozzle passage
[AIAA PAPER 93-2556] p 13 A93-50278
- RITTER, DARREN C.**
Assessment of 25 kW free-piston Stirling technology alternatives for solar applications p 254 A93-26072
- RITZERT, F. J.**
Progress toward a tungsten alloy wire/high temperature alloy composite turbine blade
[NASA-TM-105901] p 128 N93-15586
- RIVERS, JAMES M.**
Damage progression in stiffened composite panels
[AIAA PAPER 93-1345] p 238 A93-33915
- ROACH, ROBERT L.**
Evaluation and application of the Baldwin-Lomax turbulence model in two-dimensional, unsteady, compressible boundary layers with and without separation in engine inlets
[AIAA PAPER 92-3676] p 2 A93-14118
Evaluation and application of the Baldwin-Lomax turbulence model in two-dimensional, unsteady, compressible boundary layers with and without separation in engine inlets
[AIAA PAPER 92-3676] p 168 A93-22509
Evaluation and application of the Baldwin-Lomax turbulence model in two-dimensional, unsteady, compressible boundary layers with and without separation in engine inlets
[NASA-TM-105810] p 191 N93-10087
- ROAN, V. P.**
Initial development of the two-dimensional ejector shear layer - Experimental results
[AIAA PAPER 93-2440] p 29 A93-50192
Comparison of the initial development of shear layers in two-dimensional and axisymmetric ejector configurations
[AIAA PAPER 93-2441] p 29 A93-50193
- ROBERTS, GARY D.**
The effect of contact stresses in four-point bend testing of graphite/epoxy and graphite/PMR-15 composite beams
[NASA-TM-105891] p 107 N93-12076
Effects of thermal and mechanical fatigue on the flexural strength of G40-600/PMR-15 cross-ply laminates
[NASA-TM-106016] p 108 N93-20317
- ROBERTS, TED A.**
Ignition and combustion of aluminum/magnesium alloy particles in O₂ at high pressures p 113 A93-22030
- ROBIN, JAMES E.**
Design and emplacement of an integrated lunar power system - Issues and concerns p 46 A93-13908
- ROBINSON, D. N.**
Limit pressure of a circumferentially reinforced SiC/Ti ring p 233 A93-16005
Unified viscoplastic behavior of metal matrix composites
[NASA-TM-105819] p 244 N93-10777
- ROCHOW, RICHARD**
US/CIS integrated NTRE
[AIAA PAPER 93-2367] p 76 A93-50138
- ROCK, STEPHEN M.**
Integrated flight/propulsion control - Subsystem specifications for performance
[AIAA PAPER 93-3808] p 41 A93-51400
- ROCKWELL, RICHARD**
Solar concentrators for advanced solar-dynamic power systems in space
[NASA-CR-187148] p 85 N93-23017
- RODRIGUEZ, AGUSTIN M.**
Multilayer relaxation and surface energies of fcc and bcc metals using equivalent crystal theory p 119 A93-52872
- RODRIGUEZ, C. D.**
Dynamic Isotope Power System design considerations for human exploration of the moon and Mars p 253 A93-25995
- RODRIGUEZ, ELVIN**
Simulation of the synergistic low Earth orbit effects of vacuum thermal cycling, vacuum UV radiation, and atomic oxygen p 58 N93-15595
- ROELKE, RICHARD J.**
Radial turbine cooling p 191 N93-10061
Radial turbine cooling
[NASA-TM-105658] p 15 N93-13292
- ROGERS, M. J. B.**
Low gravity environment on-board Columbia during STS-40
[AIAA PAPER 93-0833] p 142 A93-24903
- ROGO, CASS**
Aeroloids and secondary flows in a transonic mixed flow turbine stage
[ASME PAPER 92-GT-72] p 2 A93-19322
- ROHATGI, P. K.**
On the melt infiltration of copper coated silicon carbide with an aluminum alloy p 218 A93-11332
Observations on infiltration of silicon carbide compacts with an aluminum alloy p 97 A93-12356
- ROHATGI, PRADEEP K.**
Melt infiltration of silicon carbide compacts. I - Study of infiltration dynamics p 101 A93-27494
- Melt infiltration of silicon carbide compacts. II - Evaluation of solidification microstructures p 101 A93-28283
- ROHN, DOUGLAS**
The detrimental effect of friction on space microgravity robotics p 222 A93-35546
- ROHRER, NORMAN J.**
A 10 GHz Y-Ba-Cu-O/GaAs hybrid oscillator proximity coupled to a circular microstrip patch antenna p 158 A93-54619
- ROJAS, A.**
Scientific basis for the Isothermal Dendritic Growth Experiment - A USMP-2 space flight experiment p 143 A93-50455
- ROKHLIN, S. I.**
Ultrasonic and micromechanical study of damage and elastic properties of SiC/RBSN ceramic composites p 99 A93-19624
Ultrasonic assessment of interfacial oxidation damage in ceramic matrix composites p 105 A93-52919
- ROLLBUHLER, J.**
Influence of ambient air pressure on effervescent atomization
[AIAA PAPER 92-0460] p 167 A93-21652
- ROMANOFSKY, ROBERT R.**
Comparative study of bolometric and non-bolometric switching elements for microwave phase shifters p 155 A93-27245
A 10-GHz amplifier using an epitaxial lift-off pseudomorphic HEMT device p 156 A93-37574
- RONNEY, P.**
Flame balls - Past, present and future
[AIAA PAPER 93-0712] p 114 A93-24807
- RONNEY, PAUL D.**
Effects of particulate radiation on premixed gas flames
[AIAA PAPER 93-0711] p 114 A93-24806
Premixed flame propagation in an optically thick gas p 119 A93-55381
- ROPPEL, T.**
Thin film diamond microstructure applications p 209 A93-40580
- ROSE, M. F.**
An Isotope-Powered Thermal Storage unit for space applications p 65 A93-13877
- ROSEN, S. P.**
Implications of new GALLEX results for the Mikheyev-Smirnov-Wolfenstein solution of the solar neutrino problem p 293 A93-10357
- ROSENBERG, S. D.**
Hydrocarbon-fuel/copper combustion chamber liner compatibility, corrosion prevention, and refurbishment p 139 A93-14510
Durability testing of the AJ10-221 490 N high performance (321 sec lsp) engine
[AIAA PAPER 93-2130] p 74 A93-49949
- ROSENFELD, D.**
High frequency performance of Si(1-x)Ge(x)/Si(1-y)Ge(y)/Si(1-x)Ge(x) HBTs p 155 A93-37409
The effects of strain on the microwave performance of SiGe HBTs p 158 A93-54442
- ROSENFELD, DAVID**
Development of Si(1-x)Ge(x) technology for microwave sensing applications
[NASA-TM-106157] p 162 N93-28610
- ROSENTHAL, B. N.**
Self-tuning multivariable pole placement control of a multizone crystal growth furnace p 263 A93-10575
- ROSENTHAL, BRUCE N.**
An Automated Thermocouple Calibration System p 208 A93-35575
- ROSNER, D. E.**
Onset conditions for gas phase reaction and nucleation in the CVD of transition metal oxides p 116 A93-39508
- ROSS, H. D.**
Computational predictions of flame spread over alcohol pools
[AIAA PAPER 93-0825] p 115 A93-24895
- ROSS, HOWARD**
Flame spread across liquid pools p 122 N93-20209
- ROSS, HOWARD D.**
Overview of NASA's microgravity combustion science and fire safety program p 145 N93-20180
- ROTH, M. D.**
Atomic probe microscopy of 3C SiC films grown on 6H SiC substrates p 281 A93-39854
- ROTH, MARY E.**
An electromechanical actuation system for an expendable launch vehicle p 50 A93-25891
- ROUGE, C. J.**
Oxidation resistant overlay coatings for low expansion substrates
[NASA-CASE-LEW-15154-1] p 137 N93-19332

- Oxidation resistant overlay coatings for low expansion substrates
[NASA-CASE-LEW-15154-2] p 138 N93-31300
- ROUSSEL, P.**
Low gravity environment on-board Columbia during STS-40
[AIAA PAPER 93-0833] p 142 A93-24903
- ROYANG, RICHARD D.**
Multimegawatt potassium Rankine power for nuclear electric power p 65 A93-13797
SP-100 high-temperature advanced radiator development p 163 A93-13843
Fabrication of carbon-carbon heat pipes for space nuclear power applications p 173 A93-25978
- ROWE, NEIL D.**
A multi-zone muffle furnace design
[NASA-TM-106153] p 145 N93-27011
- ROWEY, R. J.**
Design and test of a small two stage counter-rotating turbine for rocket engine application
[AIAA PAPER 93-2136] p 74 A93-49954
- RUAN, Y. F.**
Modal simulation of gear box vibration with experimental correlation p 221 A93-31982
Modal analysis of multistage gear systems coupled with gearbox vibrations p 222 A93-36588
- RUBIN, L. F.**
Visualization of hydrogen injection in a scramjet engine by simultaneous PLIF imaging and laser holographic imaging p 214 N93-13683
- RUBIN, S. G.**
A three-dimensional pressure flux-split RNS application to sub/supersonic flow in inlets and ducts
[AIAA PAPER 93-3063] p 11 A93-48239
- RUBIN, STANLEY G.**
Segmented multigrid domain decomposition procedure for incompressible viscous flows p 99 A93-19123
Segmented multigrid domain decomposition solutions for three dimensional viscous recirculating flows
[AIAA PAPER 93-3344] p 181 A93-45038
- RUBINSTEIN, ASHER A.**
Model of brittle matrix composite toughening based on discrete fiber reinforcement p 104 A93-40888
- RUBINSTEIN, R.**
Young's fringe particle image velocimetry in the presence of random particle motions p 207 A93-23801
- RUBY, W. S.**
Demonstration of Y1Ba2Cu3O(7-delta) and complementary metal-oxide-semiconductor device fabrication on the same sapphire substrate p 159 A93-56292
- RUDOFF, R. C.**
Liquid water content measurements using the Phase Doppler Particle Analyzer in the NASA Lewis Icing Research Tunnel
[AIAA PAPER 93-0298] p 42 A93-23698
- RUMSEY, C. L.**
Estimation of unsteady lift on a pitching airfoil from wake velocity surveys
[AIAA PAPER 93-0437] p 5 A93-23351
Estimation of unsteady lift on a pitching airfoil from wake velocity surveys
[NASA-TM-105947] p 15 N93-14791
- RUSSELL, LOUIS M.**
Measurements and computational analysis of heat transfer and flow in a simulated turbine blade internal cooling passage
[AIAA PAPER 93-1797] p 189 A93-53585
Measurements and computational analysis of heat transfer and flow in a simulated turbine blade internal cooling passage
[NASA-TM-106189] p 203 N93-31647
- RUSSELL, S. D.**
Demonstration of Y1Ba2Cu3O(7-delta) and complementary metal-oxide-semiconductor device fabrication on the same sapphire substrate p 159 A93-56292
- RUTH, MARK F.**
Experimental study of two interacting drops in an immiscible fluid p 179 A93-37936
- RUTLAND, C. J.**
Intake flow modeling in a four stroke diesel using KIVA3
[AIAA PAPER 93-2952] p 183 A93-48146
- RUTLEDGE, S. K.**
Method and apparatus for producing a thermal atomic oxygen beam
[NASA-CASE-LEW-15614-1] p 276 N93-19026
- RUTLEDGE, SHARON**
Recommended practices for in-space and ground laboratory Atomic oxygen exposure and analysis p 276 N93-20814
- RUTLEDGE, SHARON K.**
Effects of dust accumulation and removal on radiator surfaces on Mars p 123 A93-13937

- Thermal emittance enhancement of graphite-aluminum and graphite-copper composite radiator surfaces for space power applications p 105 A93-53455
The use of plasma ashers and Monte Carlo modeling for the projection of atomic oxygen durability of protected polymers in low Earth orbit p 58 N93-15596
Degradation of radiator performance on Mars due to dust p 59 N93-15616
Atomic oxygen protective coating with resistance to undercutting at defect sites
[NASA-CASE-LEW-15306-1] p 137 N93-20566
The effects of simulated low Earth orbit environments on spacecraft thermal control coatings
[NASA-TM-106146] p 61 N93-27019
Low Earth orbital atomic oxygen environmental simulation facility for space materials evaluation
[NASA-TM-106128] p 96 N93-27266
Method for retarding oxidation of an organic substrate
[NASA-CASE-LEW-15306-2] p 138 N93-28425
Characteristics of hypervelocity impact craters on LDEF experiment S1003 and implications of small particle impacts on reflective surfaces p 62 N93-29363
- RYALL, KATHLEEN**
A graphical user-interface for propulsion system analysis
[AIAA PAPER 93-0223] p 259 A93-23699
- RYLICKI, DANIEL S.**
Flux concentrations on solar dynamic components due to mispointing
[NASA-TM-105756] p 255 N93-20261
- RYU, DONGSU**
Phase space distribution of halo particles and detection of WIMPS p 289 A93-23650

S

- SACKSTEDER, KURT R.**
Downward diffusion flame spread and extinction in variable gravitational fields - Lunar and Martian simulations
[AIAA PAPER 93-0828] p 115 A93-24898
Opposed-flow flame spreading in reduced gravity p 121 N93-20206
Combustion of solid fuel in very low speed oxygen streams p 122 N93-20207
- SAIGAL, SUNIL**
Computational micromechanics of woven composites p 237 A93-32462
- SAIYED, NASEEM H.**
Tank shutdown analysis and verification with a flightweight, 175 cu ft tank under normal gravity with liquid hydrogen p 140 N93-10045
- SAKOWSKI, BARBARA**
Evaluation and application of the Baldwin-Lomax turbulence model in two-dimensional, unsteady, compressible boundary layers with and without separation in engine inlets
[AIAA PAPER 92-3676] p 2 A93-14118
Evaluation and application of the Baldwin-Lomax turbulence model in two-dimensional, unsteady, compressible boundary layers with and without separation in engine inlets
[AIAA PAPER 92-3676] p 168 A93-22509
Evaluation and application of the Baldwin-Lomax turbulence model in two-dimensional, unsteady, compressible boundary layers with and without separation in engine inlets
[NASA-TM-105810] p 191 N93-10087
A compressible boundary layer algorithm for use with SINDA '85 p 192 N93-13395
- SALEEM, A. F.**
Finite element implementation of state variable-based viscoplasticity models p 236 A93-26776
Analysis of the anisotropic viscoplastic-damage response of composite laminates - Continuum basis and computational algorithms p 241 A93-43347
Explicit robust schemes for implementation of a class of principal value-based constitutive models: Symbolic and numeric implementation
[NASA-TM-106124] p 258 N93-26946
Explicit robust schemes for implementation of general principal value-based constitutive models
[NASA-TM-106123] p 258 N93-26947
- SALEM, J. A.**
Evaluation of the fracture toughness of Nb-40Al-8Cr-1W-1Y-0.05B intermetallic material by indentation techniques p 124 A93-24066
Interaction of cracks between two adjacent indents in glass p 132 A93-27115
- SALEM, JONATHAN**
Fracture toughness of advanced ceramics at room temperature p 131 A93-20842
- SALEM, JONATHAN A.**
Indentation flaw formation and strength response of silicon nitride ceramics at low indentation loads p 130 A93-15994
Effects of precracking methods on the fracture properties of alumina p 131 A93-16645
Analysis of precracking parameters for ceramic single-edge-precracked-beam specimens p 133 A93-38887
Elevated-temperature fracture resistances of monolithic and composite ceramics using chevron-notched bend tests p 133 A93-38888
Effect of environment on fracture toughness of 96 wt pct alumina p 134 A93-44955
Analysis of precracking parameters and fracture toughness for ceramic single-edge-precracked-beam specimens
[NASA-TM-105568] p 135 N93-10962
- SALOPEK, D. S.**
Stochastic inflation lattice simulations - Ultra-large scale structure of the universe p 289 A93-17646
- SALTSMAN, JAMES F.**
A high temperature fatigue life prediction computer code based on the Total Strain Version of Strainrange Partitioning (SRP) p 260 A93-31341
Computer programs to characterize alloys and predict cyclic life using the total strain version of strainrange partitioning: Tutorial and users manual, version 1.0
[NASA-TM-4425] p 246 N93-15788
- SALUPO, CARL S.**
Greatly improved 3C-SiC p-n junction diodes grown by chemical vapor deposition p 156 A93-38994
- SAMIMY, M.**
On streamwise vortices in high Reynolds number supersonic axisymmetric jets p 167 A93-21060
Effect of tabs on the flow and noise field of an axisymmetric jet p 25 A93-30833
- SAMIMY, MO**
Molecular filter-based diagnostics in high speed flows
[AIAA PAPER 93-0512] p 205 A93-23259
A study of compressible mixing layers using filtered Rayleigh scattering
[AIAA PAPER 92-0175] p 173 A93-24982
- SAMUELSEN, G. S.**
Optimization of circular orifice jets mixing into a heated crossflow in a cylindrical duct p 24 A93-23246
Mixing in the dome region of a staged gas turbine combustor p 27 A93-49612
Emission characteristics of a model gas turbine combustor at practical conditions
[ISABE 93-7023] p 31 A93-53999
Optimization of circular orifice jets mixing into a heated cross flow in a cylindrical duct p 33 N93-15359
Fuel injector: Air swirl characterization aerothermal modeling, phase 2, volume 1
[NASA-CR-189193-VOL-1] p 35 N93-24754
- SANDERS, WILLIAM A.**
High-temperature deformation and microstructural analysis for silicon nitride-scandium(III) oxide p 131 A93-20468
- SANFELIZ, JOSE G.**
Computational simulation of surface waviness in graphite/epoxy woven composites due to initial curing p 98 A93-15822
ICAN/DAMP-integrated composite analyzer with damping analysis capabilities: User's manual
[NASA-TP-3292] p 106 N93-12015
Second generation integrated composite analyzer (ICAN) computer code
[NASA-TP-3290] p 108 N93-18139
- SANGIOVANNI, J. J.**
Soot agglomeration in isolated, free droplet combustion
[AIAA PAPER 93-0823] p 115 A93-24893
- SANKAR, L. N.**
Effects of icing on the aerodynamic performance of high lift airfoils
[AIAA PAPER 93-0026] p 4 A93-20144
- SANKAR, LAKSHMI N.**
Efficient hybrid scheme for the analysis of counter-rotating propellers p 7 A93-34483
- SANKARAN, SUBRAMANIAN**
Experiments on the stability of a liquid bridge in an axial electric field p 177 A93-32617
- SANKOVIC, J.**
On-orbit characterization of electric propulsion on LEO satellites p 67 A93-25303
- SANKOVIC, JOHN M.**
Performance of a low-power subsonic-arc-attachment arcjet thruster
[AIAA PAPER 93-1898] p 72 A93-49768
Investigation of a subsonic-arc-attachment thruster using segmented anodes
[AIAA PAPER 93-1899] p 73 A93-49769

PERSONAL AUTHOR INDEX

- A soft-start circuit for arcjet ignition
[NASA PAPER 93-2396] p 76 A93-50161
- Effects of anode material on arcjet performance
p 79 N93-10044
- Effects of anode material on arcjet performance
[NASA-TM-105799] p 79 N93-10197
- Development of arcjet and ion propulsion for spacecraft stationkeeping
[NASA-TM-106102] p 85 N93-23747
- SANTIAGO, WALTER**
- A free-piston Stirling engine/linear alternator controls and load interaction test facility p 146 A93-26077
- Dynamic analysis of free-piston Stirling engine/linear alternator-load system - Experimentally validated p 254 A93-26078
- Dynamic analysis of Free-Piston Stirling Engine/Linear Alternator-load system-experimentally validated
[NASA-TM-106034] p 271 N93-22559
- SANZ, J.**
- The engine design engine. A clustered computer platform for the aerodynamic inverse design and analysis of a full engine
[NASA-TM-105838] p 15 N93-11223
- SANZ, JOSE M.**
- Aerodynamic inverse design and analysis for a full engine
[ISABE 93-7086] p 14 A93-54062
- SARANTOPOULOS, ATHAN D.**
- Modeling of linear isentropic flow systems p 179 A93-37046
- SARAVANOS, D. A.**
- Combined micromechanical and fabrication process optimization for metal-matrix composites p 99 A93-18990
- Numerical optimization of composite hip endoprostheses under different loading conditions
[AIAA PAPER 92-4703] p 270 A93-20312
- Analysis and optimal design of thick composite structures with passive damping considerations
[AIAA PAPER 92-4819] p 235 A93-20398
- Effects of interply damping layers on the dynamic characteristics of composite plates p 237 A93-32415
- Analysis of passive damping in thick composite structures p 241 A93-45743
- Optimal design of composite hip implants using NASA technology p 257 N93-22188
- Dynamic characteristics of specialty composite structures with embedded damping layers p 110 N93-26705
- [NASA-TM-106165]
- Metal Matrix Laminate Tailoring (MMLT) code: User's manual
[NASA-TM-106052] p 111 N93-28681
- SARAVANOS, DIMITRIOS A.**
- ICAN/DAMP-integrated composite analyzer with damping analysis capabilities: User's manual
[NASA-TP-3292] p 106 N93-12015
- SARAVANOS, DIMITRIS A.**
- Tailored metal matrix laminates for high-temperature performance p 98 A93-15753
- SARGENT, NOEL B.**
- A system to measure lightning-induced transients on spacecraft umbilical lines p 161 N93-24889
- SARIGUL-KLIJN, NESRIN**
- Transition elements based on transfinite interpolation
[AIAA PAPER 93-1326] p 267 A93-33899
- SARMA, GARIMELLA R.**
- Capacitance-type blade-tip clearance measurement system using a dual amplifier with ramp/dc inputs and integration p 209 A93-39347
- SARMIENTO, C.**
- The effects of 1 kW class arcjet thruster plumes on spacecraft charging and spacecraft thermal control materials p 57 A93-35050
- SARMIENTO, CHARLES J.**
- Investigation of a subsonic-arc-attachment thruster using segmented anodes
[AIAA PAPER 93-1899] p 73 A93-49769
- Low power arcjet system spacecraft impacts
[AIAA PAPER 93-2392] p 76 A93-50157
- SARTORI, M.**
- 2-D nonlinear IIR-filters for image processing - An exploratory analysis p 264 A93-28200
- SARVER-VERHEY, TIMOTHY**
- Plasma contactor technology for Space Station Freedom
[AIAA PAPER 93-2228] p 57 A93-50034
- SARVER-VERHEY, TIMOTHY R.**
- Ion thruster development at NASA Lewis Research Center
[NASA-TM-105983] p 82 N93-15429
- SASMAL, G. P.**
- Influence of heat transfer rates on pressurization of liquid/slush hydrogen propellant tanks
[AIAA PAPER 93-0278] p 169 A93-22681
- SAUER, KEN**
- Hierarchical image coding with diamond-shaped sub-bands p 205 A93-20945
- SAUNDERS, R. S.**
- Venus Interior Structure Mission (VISM): Establishing a seismic network on Venus p 293 N93-28819
- SAUNIER, P.**
- High-efficiency high-gain monolithic heterostructure FET amplifier at 31 GHz p 156 A93-37421
- SAUNIER, PAUL**
- A high efficiency Ka-band monolithic pseudomorphic HEMT amplifier p 151 A93-25786
- SAVAGE, M.**
- Maximum life spur gear design p 218 A93-14521
- Maximum life spiral bevel reduction design
[NASA-TM-105790] p 226 N93-10982
- SAVILLE, D. A.**
- Experiments on the stability of a liquid bridge in an axial electric field p 177 A93-32617
- SAWYER, J. CHARLES, JR.**
- Nuclear safety policy working group recommendations on nuclear propulsion safety for the space exploration initiative
[NASA-TM-105705] p 88 N93-26200
- SCHACHAM, S. E.**
- Intermodulation in the oscillatory magnetoresistance of a two-dimensional electron gas p 151 A93-17610
- Room-temperature determination of two-dimensional electron gas concentration and mobility in heterostructures p 280 A93-35198
- SCHAFFNER, MICHAEL S.**
- Plasma contactor technology for Space Station Freedom
[AIAA PAPER 93-2228] p 57 A93-50034
- SCHARRER, J. K.**
- Preliminary experimental results for a cryogenic brush seal configuration
[AIAA PAPER 93-2535] p 225 A93-50262
- Preliminary experimental results for a cryogenic brush seal configuration
[NASA-TM-106236] p 201 N93-28627
- SCHIEL, CHRISTINE M.**
- Nuclear Engine System Simulation (NESS). Version 2.0: Program user's guide
[NASA-CR-191081] p 85 N93-23875
- Nuclear Engine System Simulation (NESS). Volume 1: Program user's guide
[NASA-CR-191080] p 86 N93-23876
- SCHIEIMAN, DAVID A.**
- The effect of the low Earth orbit environment on space solar cells: Results of the Advanced Photovoltaic Experiment (S0014) p 256 N93-29686
- SCHIERMAN, JOHN D.**
- Analysis of airframe and engine control interactions and integrated flight/propulsion control p 40 A93-14596
- A comparative study of multivariable robustness analysis methods as applied to integrated flight and propulsion control
[AIAA PAPER 93-3809] p 21 A93-51401
- SCHILLER, D. N.**
- Computational predictions of flame spread over alcohol pools
[AIAA PAPER 93-0825] p 115 A93-24895
- SCHILLER, DAVID**
- Flame spread across liquid pools p 122 N93-20209
- SCHLEGELMILCH, RICHARD F.**
- Space Communication Artificial Intelligence for Link Evaluation Terminal (SCAILET) p 265 N93-11940
- SCHLOSSER, HERBERT**
- Global expression for representing cohesive-energy curves. II p 276 A93-44989
- SCHMALHOFFER, JOSEPH**
- A study of circumferentially-heated and block-heated heat pipes. I - Experimental analysis and generalized analytical prediction of capillary limits. II - Three-dimensional numerical modeling as a conjugate problem p 168 A93-21715
- SCHMIDT, DAVID K.**
- Analysis of airframe and engine control interactions and integrated flight/propulsion control p 40 A93-14596
- A comparative study of multivariable robustness analysis methods as applied to integrated flight and propulsion control
[AIAA PAPER 93-3809] p 21 A93-51401
- SCHMIDT, PHILLIP H.**
- Application of controller partitioning optimization procedure to integrated flight/propulsion control design for a STOV aircraft
[AIAA PAPER 93-3766] p 40 A93-51361
- A parameter optimization approach to controller partitioning for integrated flight/propulsion control application p 41 A93-54268
- SCHMITZ, P.**
- The NASA CSTI High Capacity Power Project p 69 A93-26105
- The NASA CSTI high capacity power project
[NASA-TM-105813] p 48 N93-11398
- SCHMITZ, P. C.**
- Dynamic Isotope Power System design considerations for human exploration of the moon and Mars p 253 A93-25995
- Design of small Stirling dynamic isotope power system for robotic space missions
[NASA-TM-105919] p 141 N93-12085
- SCHMITZ, PAUL C.**
- Space reactor/Stirling cycle systems for high power lunar applications p 46 A93-13822
- Comparison of dynamic isotope power systems for distributed planetary surface applications p 46 A93-13825
- Lunar in-core thermionic nuclear reactor power system conceptual design p 46 A93-13836
- SCHNEIDER, MICHAEL G.**
- Design of a cavity heat pipe receiver experiment p 173 A93-25985
- SCHNEIDER, STEVEN J.**
- Low thrust chemical rocket technology
[NASA-TM-105927] p 83 N93-15572
- SCHOBEIRI, T.**
- Nonlinear dynamic simulation of single- and multi-spool core engines
[AIAA PAPER 93-2580] p 30 A93-50294
- SCHOENMAN, L.**
- Durability testing of the AJ10-221 490 N high performance (321 sec lsp) engine
[AIAA PAPER 93-2130] p 74 A93-49949
- SCHOENWALD, DAVID A.**
- Space Station Freedom beta gimbal control via sensitivity models
[NASA-TM-106000] p 60 N93-22551
- SCHRAMM, D. N.**
- Chemical and luminosity evolution, and counts of galaxies in a merger model p 290 A93-34776
- The boron-to-beryllium ratio in halo stars - A signature of cosmic-ray nucleosynthesis in the early Galaxy p 292 A93-55061
- SCHRAMM, DAVID N.**
- Late-time cosmological phase transitions p 288 A93-17645
- The first three minutes - 1990 version p 289 A93-23607
- Primordial nucleosynthesis and the abundances of beryllium and boron p 290 A93-33513
- Kurtosis, skewness, and non-Gaussian cosmological density perturbations p 291 A93-35579
- Testing for the Gaussian nature of cosmological density perturbations through the three-point temperature correlation function p 292 A93-55212
- Population II Li-6 as a probe of nucleosynthesis and stellar structure and evolution p 292 A93-56494
- SCHREIBER, J. G.**
- Design of small Stirling dynamic isotope power system for robotic space missions
[NASA-TM-105919] p 141 N93-12085
- SCHREIBER, JEFFREY G.**
- Electric and hybrid electric vehicle study utilizing a time-stepping simulation p 287 A93-26012
- Update on the advanced Stirling conversion system project for 25 kW dish Stirling applications p 254 A93-26071
- SCHULLER, FREDERICK T.**
- Lubrication of an 85-mm ball bearing with RP-1
[NASA-TM-106254] p 51 N93-31670
- SCHULLER, FREDRICK T.**
- Lubrication of an 85-mm ball bearing with RP-1
[AIAA PAPER 93-2538] p 225 A93-53590
- SCHUSTER, J. R.**
- EOTV propellant tank pressure control and liquid dynamics
[AIAA PAPER 93-2399] p 77 A93-50164
- SCHWAB, JOHN R.**
- The Proteus Navier-Stokes code p 193 N93-13396
- SCHWARZE, G.**
- The NASA CSTI High Capacity Power Project p 69 A93-26105
- The NASA CSTI high capacity power project
[NASA-TM-105813] p 48 N93-11398
- SCHWARZE, G. E.**
- Neutron, gamma ray, and temperature effects on the electrical characteristics of thyristors p 153 A93-25894
- Comparison of high temperature, high frequency core loss and dynamic B-H loops of a 2V-49Fe-49Co and a grain oriented 3Si-Fe alloy p 153 A93-25895
- SCHWARZE, GENE E.**
- Comparison of high frequency, high temperature core loss and B-H loop characteristics of an 80 Ni-Fe crystalline alloy and two iron-based amorphous alloys p 123 A93-13882

- Radiation and temperature effects on electronic components investigated under the CSTI high capacity power project
[NASA-TM-106096] p 161 N93-24746
- SCHWEIGER, P.**
Effect of a rotating propeller on the separation angle of attack
[AIAA PAPER 93-0017] p 6 A93-24978
Effect of a rotating propeller on the separation angle of attack and distortion in ducted propeller inlets
[NASA-TM-105935] p 16 N93-16625
- SCOTT, CURTIS A.**
Stress distribution in composite flatwise tension test specimens
[NASA-TM-106074] p 108 N93-25071
- SCOTT, JAMES N.**
Accuracy considerations in the computational analysis of jet noise
[AIAA PAPER 93-0146] p 272 A93-19804
- SCOTT, JAMES R.**
A new flux conserving Newton's method scheme for the two-dimensional, steady Navier-Stokes equations
[NASA-TM-106160] p 201 N93-28626
- SEASHOLTZ, R. G.**
Development of a Rayleigh scattering system for temperature measurements in combustor flows
p 206 A93-23788
High-speed laser anemometry based on spectrally resolved Rayleigh scattering
p 207 A93-23814
- SEASHOLTZ, RICHARD G.**
Gas temperature measurements using the dual-line detection Rayleigh scattering technique
p 213 A93-55368
Gas temperature measurements using the dual-line detection Rayleigh scattering technique
p 214 N93-13668
Gas temperature and density measurements based on spectrally resolved Rayleigh-Brillouin scattering
p 214 N93-13684
2D velocity and temperature measurements in high speed flows based on spectrally resolved Rayleigh scattering
[NASA-TM-105784] p 215 N93-19651
Rayleigh-Brillouin scattering for high-pressure gas temperature measurements
p 218 N93-31556
- SECUNDE, R.**
Three dimensional magnetic fields in extra high speed modified Lundell alternators computed by a combined vector-scalar magnetic potential finite element method
p 157 A93-39350
- SEFCIK, ROBERT J.**
A comparison of nuclear thermal rocket development cost and schedule for piloted missions to Mars
[AIAA PAPER 93-2263] p 44 A93-50057
- SEGALL, BENJAMIN**
Interface dependence of band offsets in lattice-matched isovalent heterojunctions
p 280 A93-32132
- SEIDEL, JONATHAN A.**
Concurrent optimization of airframe and engine design parameters
[AIAA PAPER 92-4713] p 20 A93-20281
Concurrent optimization of airframe and engine design parameters
[NASA-TM-105908] p 32 N93-12402
- SEKERKA, ROBERT F.**
Narrow band noise as a model of time-dependent accelerations - Study of the stability of a fluid surface in a microgravity environment
[AIAA PAPER 93-0911] p 173 A93-24965
Stability of a fluid surface in a microgravity environment
p 190 A93-55358
- SEKULA-MOISE, PATRICIA A.**
Ellipsometric study of metal-organic chemically vapor deposited III-V semiconductor structures
p 281 A93-35697
- SENICK, PAUL F.**
Effects of turbine cooling assumptions on performance and sizing of high-speed civil transport
[AIAA PAPER 92-4217] p 22 A93-13383
- SENSE, D.**
Venus Interior Structure Mission (VISM). Establishing a seismic network on Venus
p 293 N93-28819
- SESHADRI, K.**
Premixed flame propagation in combustible particle cloud mixtures
[AIAA PAPER 93-0713] p 115 A93-24808
- SEVERANCE, PAUL S.**
The Photovoltaic Array Space Power Plus diagnostics (PASP Plus) flight experiment
p 256 N93-28717
- SEYBERT, A. F.**
Acoustical analysis of gear housing vibration
p 273 A93-29420
Experimental validation of boundary element methods for noise prediction
[NASA-TM-105729] p 226 N93-10966
- SHABBIR, AAMIR**
Critical assessment of Reynolds stress turbulence models using homogeneous flows
[AIAA PAPER 93-0082] p 170 A93-24227
Turbulence modeling and experiments
p 195 N93-15796
Experiments on a round turbulent buoyant plume
[NASA-TM-105955] p 141 N93-16384
Critical assessment of Reynolds stress turbulence models using homogeneous flows
[NASA-TM-105954] p 196 N93-16703
- SHAH, A. R.**
Probabilistic evaluation of uncertainties and risks in aerospace components
p 233 A93-12160
Probabilistic sizing of laminates with uncertainties
[NASA-TM-106145] p 110 N93-27082
- SHAH, ASHWIN R.**
Probabilistic simulation of the human factor in structural reliability
p 258 N93-31573
- SHAH, RAJESH**
Thermosolutal convection during cellular arrayed growth of Pb-Sn alloys
[AIAA PAPER 93-0262] p 142 A93-22668
- SHAHIDI, ANOOSH K.**
Space Communication Artificial Intelligence for Link Evaluation Terminal (SCALET)
p 265 N93-11940
- SHAKER, F. J.**
Grounding of space structures
p 54 A93-12144
A new pre-loaded beam geometric stiffness matrix with full rigid body capabilities
p 54 A93-12145
- SHALKHAUSER, K. A.**
System-level integrated circuit (SLIC) development for phased array antenna applications
p 152 A93-25798
- SHALKHAUSER, MARY JO**
Real-time transmission of digital video using variable-length coding
[NASA-TM-106092] p 150 N93-22483
Fault-tolerant onboard digital information switching and routing for communications satellites
[NASA-TM-14471] p 53 N93-26895
- SHALTENS, RICHARD K.**
Electric and hybrid electric vehicle study utilizing a time-stepping simulation
p 287 A93-26012
Update on the advanced Stirling conversion system project for 25 kW dish Stirling applications
p 254 A93-26071
- SHANDARIN, S. F.**
The three-point correlation function in an ensemble of three-dimensional simulations
p 291 A93-50680
- SHANNON, J. L., JR.**
Closed form expressions for crack mouth displacements and stress intensity factors for chevron notched short bar and short rod specimens based on experimental compliance measurements
[NASA-TM-83796] p 246 N93-15369
- SHANNON, JOHN L., JR.**
Effects of precracking methods on the fracture properties of alumina
p 131 A93-16645
- SHAREEF, N. H.**
Dynamic analysis of flexible gear trains/transmissions - An automated approach
p 220 A93-22440
Time-variant analysis of rotorcraft systems dynamics - An exploitation of vector processors
p 220 A93-23512
- SHARPLESS, R. B.**
Self-tuning multivariate pole placement control of a multizone crystal growth furnace
p 263 A93-10575
- SHAUMEYER, J. N.**
Measurement of the temperature coefficient of ratio transformers
p 155 A93-32771
Statistical fitting accuracy in photon correlation spectroscopy
p 277 A93-52414
- SHAW, ROBERT J.**
Engine technology challenges for a 21st Century High-Speed Civil Transport
[ISABE 93-7064] p 31 A93-54040
Engine technology challenges for a 21st Century High-Speed Civil Transport
[NASA-TM-106216] p 39 N93-31671
- SHETTY, DINESH K.**
Subcritical crack growth in soda-lime glass in combined mode I and mode II loading
p 134 A93-52151
- SHI, SHIXIANG**
Critical experiments of the self-consistent model for polycrystalline Hastelloy-X
p 124 A93-21958
The viscoplastic behavior of Hastelloy-X single crystal
p 125 A93-27486
- SHIAO, M. C.**
Probabilistic evaluation of uncertainties and risks in aerospace components
p 233 A93-12160
Probabilistic simulation of multi-scale composite behavior
[NASA-TM-106196] p 250 N93-28633
- SHIAO, MICHAEL C.**
Probabilistic assessment of composite structures
[AIAA PAPER 93-1441] p 239 A93-33990
- Probabilistically configured adaptive composite structures
[AIAA PAPER 93-1679] p 240 A93-34191
Design for cyclic loading endurance of composites
p 242 A93-53395
Probabilistic evaluation of fuselage-type composite structures
[NASA-TM-105881] p 245 N93-12735
Mapping methods for computationally efficient and accurate structural reliability
[NASA-TM-105892] p 248 N93-23745
Probabilistic assessment of composite structures
[NASA-TM-106024] p 110 N93-27092
Mapping methods for computationally efficient and accurate structural reliability
p 232 N93-31572
- SHIH, S. H.**
A parametric study of bleed in shock boundary layer interactions
[AIAA PAPER 93-0294] p 5 A93-22694
An investigation of shock wave turbulent boundary layer interaction with bleed through slanted slots
[AIAA PAPER 93-2992] p 11 A93-48184
- SHIH, T. H.**
A multiple-scale turbulence model for incompressible flow
[AIAA PAPER 93-0086] p 170 A93-24228
New time scale based k-epsilon model for near-wall turbulence
p 180 A93-41909
Calculations of turbulent separated flows
[NASA-TM-106154] p 200 N93-27161
- SHIH, T. I.-P.**
Noniterative implicit method for tracking particles in mixed Lagrangian-Eulerian formulations
p 176 A93-30856
Computations of spray, fuel-air mixing, and combustion in a lean-premixed-prevaporized combustor
[AIAA PAPER 93-2069] p 185 A93-49901
Chimera grids in the simulation of three-dimensional flowfields in turbine-blade-coolant passages
[AIAA PAPER 93-2559] p 187 A93-50280
- SHIH, T.-H.**
A numerical study of confined turbulent jets
[NASA-TM-106197] p 202 N93-29161
- SHIH, TSAN-HSING**
Critical assessment of Reynolds stress turbulence models using homogeneous flows
[AIAA PAPER 93-0082] p 170 A93-24227
Critical comparison of second-order closures with direct numerical simulations of homogeneous turbulence
p 176 A93-30840
Second order closure modeling of turbulent buoyant wall plumes
[NASA-TM-105956] p 193 N93-14829
Modeling of turbulence and transition
p 195 N93-15795
A realizable Reynolds stress algebraic equation model
[NASA-TM-105993] p 16 N93-16596
Critical assessment of Reynolds stress turbulence models using homogeneous flows
[NASA-TM-105954] p 196 N93-16703
A multiple-scale model for compressible turbulent flows
[NASA-TM-106072] p 198 N93-23736
Remarks on turbulent constitutive relations
[NASA-TM-106116] p 199 N93-27010
- SHIN, J.**
The development of a turbulent junction vortex system
p 168 A93-22258
- SHIN, JAIWON**
Results of Low Power Deicer tests on a swept inlet component in the NASA Lewis Icing Research Tunnel
[AIAA PAPER 93-0032] p 20 A93-22551
Surface roughness due to residual ice in the use of low power deicing systems
[AIAA PAPER 93-0031] p 5 A93-23240
Applied high-speed imaging for the icing research program at NASA Lewis Research Center
p 208 A93-33169
Results of a low power ice protection system test and a new method of imaging data analysis
p 21 A93-35932
Results of low power deicer tests on a swept inlet component in the NASA Lewis icing research tunnel
[NASA-TM-105968] p 15 N93-14911
Surface roughness due to residual ice in the use of low power deicing systems
[NASA-TM-105971] p 16 N93-15338
Experimental and computational ice shapes and resulting drag increase for a NACA 0012 airfoil
p 17 N93-27440
- SHIRLEY, JOHN A.**
Air-mass flux measurement system using Doppler-shifted filtered Rayleigh scattering
[AIAA PAPER 93-0513] p 205 A93-23260

- SHOEMAKER, J. M.**
Bgridi - Interactive three-dimensional turbomachinery grid generation system with applications
[AIAA PAPER 93-0430] p 259 A93-25527
- SHOLES, ELIZABETH H.**
Titan III feasibility for HL-20 prototype missions
p 50 A93-53747
- SHOR, JOSEPH S.**
Direct observation of porous SiC formed by anodization in HF
p 282 A93-43587
- SHRIVER, JEFFREY L.**
A 10 kW dc-dc converter using IGBTs with active snubbers
p 158 A93-50646
- SHUEN, J. S.**
Supercritical droplet combustion and related transport phenomena
[AIAA PAPER 93-0812] p 115 A93-24885
- SHUEN, JIAN-SHUN**
A coupled multi-block solution procedure for spray combustion in complex geometries
[AIAA PAPER 93-0108] p 171 A93-24230
A coupled implicit method for chemical non-equilibrium flows at all speeds
p 181 A93-44245
- SHYNE, RICKY J.**
Supersonic investigation of two dimensional hypersonic exhaust nozzles
[NASA-TM-105687] p 33 N93-15342
- SIEG, R. M.**
Ellipsometric study of Si(0.5)Ge(0.5)/Si strained-layer superlattices
p 280 A93-34655
New technique for oil backstreaming contamination measurements
p 210 A93-44514
Ellipsometric characterization of In(0.52)Al(0.48)As and of modulation doped field effect transistor structures on InP substrates
p 158 A93-49382
- SIEG, ROBERT M.**
Ellipsometric study of metal-organic chemically vapor deposited III-V semiconductor structures
p 281 A93-35697
Ellipsometric study of ambient-produced overlayer growth rate on YBa₂Cu₃O(7-x) films
p 281 A93-39362
- SIEGEL, R.**
Refractive index effects on radiative behavior of a heated absorbing-emitting layer
p 162 A93-10653
Finite difference solution for transient radiative cooling of a conducting semitransparent square region
p 164 A93-15067
Refractive index effects on radiation in an absorbing, emitting, and scattering laminated layer
p 175 A93-30125
Relations for local radiative heat transfer between rectangular boundaries of an absorbing-emitting medium
p 175 A93-30129
Refractive index and scattering effects on radiative behavior of a semitransparent layer
p 176 A93-31438
Variable refractive index effects on radiation in semitransparent scattering multilayered regions
p 189 A93-54463
- SIEGEL, ROBERT**
Thermal radiation heat transfer (3rd revised and enlarged edition)
[ISBN 0-89116-271-2] p 165 A93-17522
- SILK, JOSEPH**
Clumpy cold dark matter
p 291 A93-46201
- SILVESTRO, JOHN**
Effect of a dielectric overlay on a linearly tapered slot antenna excited by a coplanar waveguide
p 155 A93-35649
- SIMITSES, G. J.**
Thermo-elastoviscoplastic snapthrough behavior of cylindrical panels
p 233 A93-12046
- SIMON, FREDERICK F.**
Progress towards understanding and predicting heat transfer in the turbine gas path
p 188 A93-52751
- SIMON, T. W.**
Transition of oscillatory flow in tubes - An empirical model for application to Stirling engines
p 174 A93-26088
- SIMON, TERENCE W.**
Visualization of entry flow separation for oscillating flow in tubes
p 174 A93-26091
- SIMONEAU, ROBERT J.**
Progress towards understanding and predicting heat transfer in the turbine gas path
p 188 A93-52751
- SIMONS, R. N.**
Novel coplanar waveguide to slotline transition on high resistivity silicon
p 151 A93-20016
Coplanar waveguide radial line stub
p 155 A93-36514
- SIMONS, RAINÉE N.**
Effect of a dielectric overlay on a linearly tapered slot antenna excited by a coplanar waveguide
p 155 A93-35649
Microwave characterization of slotline on high resistivity silicon for antenna feed network
[NASA-TM-106058] p 161 N93-27265
- Development of Si(1-x)Ge(x) technology for microwave sensing applications
[NASA-TM-106157] p 162 N93-28610
- SIMONYI, PATRICIA S.**
Measurements and computational analysis of heat transfer and flow in a simulated turbine blade internal cooling passage
[AIAA PAPER 93-1797] p 189 A93-53585
Measurements and computational analysis of heat transfer and flow in a simulated turbine blade internal cooling passage
[NASA-TM-106189] p 203 N93-31647
- SINGH, DILEEP**
Subcritical crack growth in soda-lime glass in combined mode I and mode II loading
p 134 A93-52151
- SINGH, M.**
Studies on the reactive melt infiltration of silicon and silicon-molybdenum alloys in porous carbon
[NASA-TM-105860] p 136 N93-12398
- SINGH, NARSINGH B.**
Physical vapor transport of mercurous chloride under a nonlinear thermal profile
[NASA-TM-105920] p 196 N93-16612
- SINGH, RAJENDRA**
Engineering science research issues in high power density transmission dynamics for aerospace applications
[AIAA PAPER 93-2299] p 224 A93-50084
- SINGHAL, S. N.**
Quantification of uncertainties in composites
[AIAA PAPER 93-1440] p 102 A93-33989
Effect of service environments on adhesively bonded joints in composite structures
p 242 A93-53418
Environmental effects on long term behavior of composite laminates
p 243 A93-53438
Computational simulation of hot composite structures
p 260 A93-54704
Computational simulation for concurrent engineering of aerospace propulsion systems
[NASA-TM-106029] p 249 N93-23746
High temperature composite analyzer (HITCAN) user's manual, version 1.0
[NASA-TM-106002] p 249 N93-25070
Probabilistic simulation of multi-scale composite behavior
[NASA-TM-106196] p 250 N93-28633
- SINGHAL, SURENDRA N.**
Coupled multi-disciplinary simulation of composite engine structures in propulsion environment
[ASME PAPER 92-GT-6] p 23 A93-19279
Design for inadvertent damage in composite laminates
p 242 A93-53396
- SINHA, A.**
Digital control algorithms for microgravity isolation systems
p 265 A93-53653
- SINHA, S. K.**
A study of the effects of macrosegregation and buoyancy-driven flow in binary mixture solidification
p 180 A93-44223
- SIRBAUGH, JAMES R.**
An improved far field drag calculation method for nonlinear CFD codes
[AIAA PAPER 93-3417] p 10 A93-47213
- SIRIGNANO, W. A.**
Computational predictions of flame spread over alcohol pools
[AIAA PAPER 93-0825] p 115 A93-24895
- SIRIGNANO, WILLIAM A.**
Flame spread across liquid pools
p 122 N93-20209
- SIROCKY, P. J.**
High-temperature, bellows hybrid seal
[NASA-CASE-LEW-15570-1] p 227 N93-19027
- SIROCKY, PAUL J.**
A hot dynamic seal rig for measuring hypersonic engine seal durability and flow performance
[AIAA PAPER 93-1346] p 222 A93-33916
- SKARDA, J. R. L.**
Modeling void growth and movement with phase change in thermal energy storage canisters
[AIAA PAPER 93-2832] p 285 A93-46569
- SKUPINSKI, ROBERT C.**
Test results of a Stirling engine utilizing heat exchanger modules with an integral heat pipe
[NASA-TM-105883] p 256 N93-25136
- SLATER, HOWARD**
Applied high-speed imaging for the icing research program at NASA Lewis Research Center
p 208 A93-33169
- SLINEY, H. E.**
Properties of extruded PS-212 type self-lubricating materials
p 138 N93-25565
- SLINEY, HAROLD E.**
Tribological and microstructural comparison of HIPped PM212 and PM212/Au self-lubricating composites
p 93 A93-13505
- Tribological and mechanical comparison of sintered and HIPped PM212 - High temperature self-lubricating composites
p 94 A93-13506
The effect of ion-plated silver and sliding friction on tensile stress-induced cracking in aluminum oxide
p 132 A93-27917
p 135 A93-55471
Solid lubricants
p 135 A93-55471
The effect of processing and compositional changes on the tribology of PM212 in air
[NASA-TM-105945] p 95 N93-15576
- SLOAN, M. L.**
A lag model for turbulent boundary layers developing over rough bleed surfaces
[AIAA PAPER 93-2988] p 10 A93-48181
- SMETANIKOV, VLADIMIR**
U.S./CIS eye joint nuclear rocket venture
p 71 A93-49334
- SMETANNIKOV, V. P.**
US/CIS integrated NTRE
[AIAA PAPER 93-2367] p 76 A93-50138
- SMIALEK, J. L.**
Oxidation resistant overlay coatings for low expansion substrates
[NASA-CASE-LEW-15154-1] p 137 N93-19332
Oxidation resistant overlay coatings for low expansion substrates
[NASA-CASE-LEW-15154-2] p 138 N93-31300
- SMIALEK, JAMES L.**
Chromium and reactive element modified aluminide diffusion coatings on superalloys - Environmental testing
p 126 A93-37899
The chemistry of Saudi Arabian sand - A deposition problem on helicopter turbine airfoils
p 243 A93-53468
High temperature, oxidation resistant noble metal-Al alloy thermocouple
[NASA-CASE-LEW-15515-1] p 217 N93-31298
- SMITH, BRYAN K.**
Solar array electrical performance assessment for Space Station Freedom
[AIAA PAPER 93-1052] p 69 A93-30956
Solar array electrical performance assessment for Space Station Freedom
[NASA-TM-106161] p 91 N93-27039
- SMITH, C. E.**
CFD mixing analysis of axially opposed rows of jets injected into confined crossflow
[AIAA PAPER 93-2044] p 185 A93-49877
Integrated CFD modeling of gas turbine combustors
[AIAA PAPER 93-2196] p 28 A93-50008
CFD mixing analysis of axially opposed rows of jets injected into confined crossflow
[NASA-TM-106179] p 37 N93-27128
- SMITH, C. F.**
Navier-Stokes analysis of three-dimensional S-ducts
p 9 A93-45146
- SMITH, EDWYN D.**
A 10-GHz amplifier using an epitaxial lift-off pseudomorphic HEMT device
p 156 A93-37574
- SMITH, F. T.**
The structure of a three-dimensional turbulent boundary layer
p 181 A93-44813
- SMITH, GREGORY P.**
Laser-induced fluorescence detection strategies for sodium atoms and compounds in high-pressure combustors
p 119 A93-52423
- SMITH, JOHN R.**
Method for calculating alloy energetics
p 279 A93-18740
- SMITH, JOSEPH L., JR.**
M.I.T. Stirling-cycle heat transfer apparatus
p 174 A93-26090
- SMITH, M. J.**
Comparison of reacting and non-reacting shear layers at a high subsonic Mach number
[AIAA PAPER 93-2381] p 186 A93-50149
Comparison of reacting and non-reacting shear layers at a high subsonic Mach number
[NASA-TM-106198] p 38 N93-27610
Turbulence measurement in a reacting and non-reacting shear layer at a high subsonic Mach number
[NASA-TM-106186] p 18 N93-31839
- SMITH, MARK D.**
Parallel computing for probabilistic fatigue analysis
[AIAA PAPER 93-1499] p 261 A93-34039
- SMITH, ROBERT E.**
Algebraic grid generation with control points
p 268 A93-45967
- SMITH, SAMUEL O.**
Modeling and strain gauging of eddy current repulsion deicing systems
[AIAA PAPER 93-0296] p 20 A93-22696
- SMITH, TIMOTHY D.**
Design and fabrication of a hydrogen/oxygen thrust chamber assembly
[AIAA PAPER 93-2132] p 74 A93-49951

SMITH, TODD E.

Localization of aeroelastic modes in mistuned high-energy turbines p 230 N93-31586

SMITH, WAYNE A.

Application of an unstructured grid flow solver to planes, trains and automobiles [AIAA PAPER 93-0889] p 173 A93-24949

SMITHRICK, JOHN J.

Validation test of advanced technology for IPV nickel-hydrogen flight cells - Update p 252 A93-25886
Validation test of 125 Ah advanced design IPV nickel-hydrogen flight cells p 78 A93-50822
Validation test of 125 Ah advanced design IPV nickel-hydrogen flight cells [NASA-TM-105912] p 81 N93-14079

SMITS, ALEXANDER

Time-sequenced and spectrally filtered Rayleigh imaging of shock wave and boundary layer structure for inlet characterization [AIAA PAPER 93-2300] p 211 A93-50085

SMOOKE, M.

Flame balls - Past, present and future [AIAA PAPER 93-0712] p 114 A93-24807
Analytical and numerical modeling of flame-balls in hydrogen-air mixtures p 118 A93-46009

SMOOT, GEORGE F.

Cosmic microwave background probes models of inflation p 294 A93-10355

SMREKAR, S.

Venus Interior Structure Mission (VISM): Establishing a seismic network on Venus p 293 N93-28619

SNYDER, DAVID B.

Plasma sheath effects on ion collection by a pinhole [AIAA PAPER 93-0567] p 55 A93-24243
Plasma sheath effects on ion collection by a pinhole [NASA-TM-106098] p 60 N93-25090

SOEDER, JAMES F.

Overview and evolution of the LeRC PMAD DC test bed p 47 A93-26099

SOEDER, RONALD H.

User manual for NASA Lewis 10 by 10 foot supersonic wind tunnel [NASA-TM-105626] p 42 N93-15498
NASA Lewis 8- by 6-foot supersonic wind tunnel user manual [NASA-TM-105771] p 43 N93-25080

SOHN, PHILIP Y.

Advanced Communications Technology Satellite (ACTS) p 52 A93-24456

SOKOLOV, V.

Mixed application MMIC technologies - Progress in combining RF, digital and photonic circuits p 152 A93-25800

SOKOLOV, VLADIMIR

Phase shifter technology assessment - Prospects and applications p 152 A93-25808

SOLTIS, R. F.

Properties of extruded PS-212 type self-lubricating materials p 138 N93-25565

SONG, Y.

Thermo-elastoviscoplastic snapthrough behavior of cylindrical panels p 233 A93-12046

SONI, NITIN J.

Fault-tolerant onboard digital information switching and routing for communications satellites [NASA-TM-4471] p 53 N93-26895

SONNENFROH, D.

Nonintrusive, multipoint velocity measurements in high-pressure combustion flows [AIAA PAPER 93-2032] p 118 A93-49867

SOTOMAYOR, JORGE L.

Fourier transform spectrometry for fiber-optic sensor systems p 211 A93-49459
Fiber-optic thermometer using Fourier transform spectroscopy p 212 A93-53104

SOTOS, RAYMOND G.

Capabilities and constraints of NASA's ground-based reduced gravity facilities p 49 N93-20184

SOULAS, GEORGE C.

Plasma contactor technology for Space Station Freedom [AIAA PAPER 93-2228] p 57 A93-50034

SOVEY, JAMES S.

Characterization of in-flight performance of ion propulsion systems [AIAA PAPER 93-2217] p 75 A93-50023

Electric propulsion - An evolutionary technology p 78 A93-56168

Ion thruster development at NASA Lewis Research Center [NASA-TM-105983] p 82 N93-15429

Development of arcjet and ion propulsion for spacecraft stationkeeping [NASA-TM-106102] p 85 N93-23747

SOVEY, JIM

NEP technology: FY 1992 milestones (NASA LeRC) p 90 N93-26977

SOWA, W. A.

Optimization of circular orifice jets mixing into a heated crossflow in a cylindrical duct [AIAA PAPER 93-0249] p 24 A93-23246

Mixing in the dome region of a staged gas turbine combustor p 27 A93-49612

Emission characteristics of a model gas turbine combustor at practical conditions [ISABE 93-7023] p 31 A93-53999

Optimization of circular orifice jets mixing into a heated cross flow in a cylindrical duct [NASA-TM-105984] p 33 N93-15359

SPLAVINS, TALIVALDIS

The effect of ion-plated silver and sliding friction on tensile stress-induced cracking in aluminum oxide p 132 A93-27917

A vacuum (10 exp -9 torr) friction apparatus for determining friction and endurance life of MoS(x) films p 146 A93-49245

SPANOS, G.

The microstructural evolution, crystallography, and thermal processing of ultrahigh carbon Fe-1.85 pct C melt-spun ribbon p 125 A93-32934

SPEIER, H. J.

New technique for oil backstreaming contamination measurements p 210 A93-44514

SPENCE, RODNEY L.

Optical communications and a comparison of optical technologies for a high data rate return link from Mars [NASA-TP-3180] p 52 N93-18854

SPENCER, R. H.

Active control of helicopter transmission noise p 274 A93-29428

SPOTH, KEVIN A.

Design of a hypersonic waverider-derived airplane [AIAA PAPER 93-0401] p 55 A93-21108

SPRAGLE, GREGORY S.

Unstructured 3D Delaunay mesh generation applied to planes, trains and automobiles [AIAA PAPER 93-0673] p 259 A93-24781

Application of an unstructured grid flow solver to planes, trains and automobiles [AIAA PAPER 93-0889] p 173 A93-24949

SPROUSE, KENNETH M.

Design and emplacement of an integrated lunar power system - Issues and concerns p 46 A93-13908

SPUCKLER, C. M.

Refractive index effects on radiative behavior of a heated absorbing-emitting layer p 162 A93-10653

Refractive index effects on radiation in an absorbing, emitting, and scattering laminated layer p 175 A93-30125

Refractive index and scattering effects on radiative behavior of a semitransparent layer p 176 A93-31438

Variable refractive index effects on radiation in semitransparent scattering multilayered regions p 189 A93-54463

SPUCKLER, CHARLES M.

Non-contact heat flux measurement using a transparent sensor [NASA-TM-106252] p 142 N93-32330

SPURLOCK, O. F.

DUKSUP - A high thrust trajectory optimization code [AIAA PAPER 93-1127] p 259 A93-31009

SQUIRES, BECKY

Forward rotor vortex effects on counter rotating propeller noise p 2 A93-19221

Manipulation of upstream rotor leading edge vortex and its effects on counter rotating propeller noise [AIAA PAPER 93-0012] p 272 A93-20134

SREENIVAS, KIDAMBI

High resolution numerical simulation of the linearized Euler equations in conservation law form [AIAA PAPER 93-2934] p 183 A93-48132

SRINIVASAN, KUMAR

Segmented multigrid domain decomposition procedure for incompressible viscous flows p 99 A93-19123

Segmented multigrid domain decomposition solutions for three dimensional viscous recirculating flows [AIAA PAPER 93-3344] p 181 A93-45038

SRINIVASAN, SUPRAMANIAM

Pressure dependence of the oxygen reduction reaction at the platinum microelectrode/nafion interface - Electrode kinetics and mass transport p 112 A93-11450

SRIVASTAVA, R.

APPLE - An aeroelastic analysis system for turbomachines and proplans [AIAA PAPER 92-4712] p 23 A93-20320

On the static stability of forward swept proplans [AIAA PAPER 93-1634] p 26 A93-34162

Efficient hybrid scheme for the analysis of counter-rotating propellers p 7 A93-34483

STADNIK, ANDREW G.

Versatile dynamic isotope power systems for the exploration of space p 46 A93-13819

STAHL, H. P.

Vector formulation for interferogram surface fitting p 278 A93-55687

STAN, M. A.

Conductor-backed coplanar waveguide resonators of Y-Ba-Cu-O and Ti-Ba-Ca-Cu-O on LaAlO3 [NASA-TM-105890] p 284 N93-12325

STANCATI, MICHAEL L.

Lunar mission design using Nuclear Thermal Rockets p 65 A93-13767

STANCATI, MIKE L.

Space vehicle design and operation for efficient use of Nuclear Thermal Propulsion [AIAA PAPER 93-1946] p 44 A93-49804

STANLEY, MARLAND

Nuclear thermal propulsion technology: Results of an interagency panel in FY 1991 [NASA-TM-105711] p 86 N93-24740

STARKOVICH, JOHN

Technology for gelled liquid cryogenic propellants - Metallized hydrogen/aluminum [AIAA PAPER 93-1878] p 140 A93-49752

STARLINGER, A.

Reliability analysis of laminated ceramic matrix composites using shell subelement techniques p 243 A93-55382

STARLINGER, ALOIS

Reliability analysis of structural ceramic components using a three-parameter Weibull distribution [ASME PAPER 92-GT-296] p 231 A93-19486

Ceramic component reliability with the restructured NASA/CARES computer program [ASME PAPER 92-GT-383] p 234 A93-19540

Ceramic component reliability with the restructured NASA/CARES computer program [NASA-TM-105856] p 244 N93-11004

STARR, JONATHAN E.

Greatly improved 3C-SiC p-n junction diodes grown by chemical vapor deposition p 156 A93-38994

STAVNES, MARK

Space transfer with ground-based laser/electric propulsion [NASA-TM-106060] p 84 N93-20615

STAVNES, MARK W.

NASA requirements and applications environments for electrical power wiring p 153 A93-25919

An analysis of power beaming for the moon and Mars p 253 A93-25974

STEBBINS, ALBERT

Cosmic string with a light massive neutrino p 288 A93-16303

Clumpy cold dark matter p 291 A93-46201

STECKL, A. J.

Atomic probe microscopy of 3C SiC films grown on 6H SiC substrates p 281 A93-39854

STEDMAN, JAY K.

Long life Regenerative Fuel Cell technology development plan p 252 A93-25867

STEEN, P. H.

Flow-influenced stabilization of liquid columns in a dynamic plateau chamber [AIAA PAPER 93-0255] p 169 A93-22664

STEEN, PAUL H.

Collapse of the soap-film bridge - Quasistatic description p 188 A93-50536

STEFFEN, C. J., JR.

Two equation modeling and the pseudo compressibility technique p 195 N93-15799

A critical comparison of several low Reynolds number k-epsilon turbulence models for flow over a backward facing step [NASA-TM-106173] p 270 N93-32200

STEFFEN, CHRISTOPHER J., JR.

A new flux splitting scheme p 9 A93-47189

A critical comparison of several low Reynolds number k-epsilon turbulence models for flow over a backward-facing step [AIAA PAPER 93-1927] p 189 A93-53586

STEFFES, PAUL

Pyrotechnically actuated systems database and applications catalog p 141 N93-20136

STEFKO, GEORGE L.

An iterative multidisciplinary analysis for rotor blade shape determination [AIAA PAPER 93-2085] p 28 A93-49912

STEGEMAN, JAMES D.

User's manual for Interactive Data Display System (IDS) [NASA-TM-105572] p 261 N93-16613

STEIGMAN, G.

The boron-to-beryllium ratio in halo stars - A signature of cosmic-ray nucleosynthesis in the early Galaxy p 292 A93-55061

STEIGMAN, GARY

Population II Li-6 as a probe of nucleosynthesis and stellar structure and evolution p 292 A93-56494

STEINBECK, JOHN

Single liquid source plasma-enhanced metalorganic chemical vapor deposition of high-quality YBa₂Cu₃O(7-x) thin films p 280 A93-20643

STEINETZ, B. M.

High-temperature, bellows hybrid seal [NASA-CASE-LEW-15570-1] p 227 N93-19027

STEINETZ, BRUCE M.

Relative sliding durability of two candidate high-temperature oxide fiber seal materials p 132 A93-31983

A hot dynamic seal rig for measuring hypersonic engine seal durability and flow performance [AIAA PAPER 93-1346] p 222 A93-33916

Development of braided rope seals for hypersonic engine applications - Flow modeling p 222 A93-34493

Development of hypersonic engine seals - Flow effects of preload and engine pressures [AIAA PAPER 93-1998] p 223 A93-49841

Relative sliding durability of candidate high temperature fiber seal materials [NASA-TM-105806] p 95 N93-10978

Development of braided rope seals for hypersonic engine applications: Flow modeling [NASA-TM-105942] p 227 N93-14478

Sliding durability of candidate seal fiber materials in hydrogen from 25 to 900 C [NASA-TM-105939] p 95 N93-22590

STEINHARDT, PAUL J.

Cosmic microwave background probes models of inflation p 294 A93-10355

STEINTHORSSON, E.

Development of an explicit multiblock/multigrid flow solver for viscous flows in complex geometries [AIAA PAPER 93-2380] p 186 A93-50148

STEINTHORSSON, ERELENDUR

Numerical simulations of three-dimensional laminar flow over a backward facing step; flow near side walls [NASA-TM-106248] p 202 N93-31147

STEPHENS, JOSEPH R.

Material requirements for the High Speed Civil Transport [ISABE 93-7067] p 31 A93-54043

STEPHENS, M. A.

Chimera grids in the simulation of three-dimensional flowfields in turbine-blade-coolant passages [AIAA PAPER 93-2559] p 187 A93-50280

STERN, ALAN L.

Advanced Communications Technology Satellite (ACTS) p 52 A93-24456

STEBER, G. D.

Heat transfer in rotating serpentine passages with trips skewed to the flow [ASME PAPER 92-GT-191] p 166 A93-19416

Heat transfer in rotating serpentine passages with selected model orientation for smooth or skewed trip walls [NASA-TM-106126] p 147 N93-25177

STEVENS, DANIEL R.

Design of a hypersonic waverider-derived airplane [AIAA PAPER 93-0401] p 55 A93-21108

STEVENS, GRADY H.

Performance evaluation of land mobile satellite system under fading and interference using multiple TCM by Monte-Carlo simulation p 147 A93-10958

Data distribution satellite [NASA-TM-105778] p 149 N93-12481

STIDHAM, CURTIS R.

Simulation of the synergistic low Earth orbit effects of vacuum thermal cycling, vacuum UV radiation, and atomic oxygen p 58 N93-15595

The effects of simulated low Earth orbit environments on spacecraft thermal control coatings [NASA-TM-106146] p 61 N93-27019

Low Earth orbital atomic oxygen environmental simulation facility for space materials evaluation [NASA-TM-106128] p 96 N93-27266

STOCHL, R. J.

Pressurization and expulsion of a lightweight liquid hydrogen tank [AIAA PAPER 93-1966] p 73 A93-49814

STOCHL, ROBERT J.

Autogenous pressurization of cryogenic vessels using submerged vapor injection p 71 A93-48648

STOCKER, D. P.

Effects of gravity on the transition to turbulence of gas jet diffusion flames [AIAA PAPER 93-0710] p 114 A93-24805

STOCKER, DENNIS P.

Comparison of numerical model results with diffusion flames in microgravity [AIAA PAPER 93-0707] p 114 A93-24803

Effects of buoyancy on laminar, transitional, and turbulent gas jet diffusion flames p 121 N93-20189

STOFAN, E. R.

Venus Interior Structure Mission (VISM): Establishing a seismic network on Venus p 293 N93-28819

STONE, JAMES R.

Advances in NASA's Nuclear Thermal Propulsion Technology project [AIAA PAPER 93-2258] p 75 A93-50056

NASA's progress in nuclear electric propulsion technology [AIAA PAPER 93-1936] p 78 A93-53587

Nuclear thermal propulsion technology overview p 89 N93-26927

NASA's progress in nuclear electric propulsion technology [NASA-TM-106272] p 93 N93-31858

STOFFER, D. C.

A constitutive model for the high temperature inelastic response of nickel base superalloys p 124 A93-21959

STRASH, D. J.

CFD zonal modeling of leading-edge ice effects for a complete aircraft [AIAA PAPER 93-0167] p 5 A93-22601

STRAZISAR, A. J.

Experimental and computational investigation of the NASA Low-Speed Centrifugal Compressor flow field [ASME PAPER 92-GT-213] p 4 A93-19436

STREET, KENNETH W., JR.

Ion exchange polymers and method for making [NASA-CASE-LEW-15576-1] p 139 N93-31316

STUART, THOMAS A.

A 1.6-kW, 110-kHz dc-dc converter optimized for IGBT's p 156 A93-37570

A 10 kW dc-dc converter using IGBT's with active snubbers p 158 A93-50646

STUBBS, ROBERT M.

DSMC and continuum analyses of low-density nozzle flow [AIAA PAPER 93-0727] p 172 A93-24817

Analysis of plume backflow around a nozzle lip in a nuclear rocket [AIAA PAPER 93-2497] p 77 A93-50231

Numerical study of nozzle wall cooling for nuclear thermal rockets [AIAA PAPER 93-2498] p 77 A93-50232

NTR plume modeling p 199 N93-26929

Computational fluid dynamics for nuclear thermal propulsion p 199 N93-26930

STUCKERT, G. K.

Effects of free-stream turbulence on boundary-layer transition [AIAA PAPER 93-0488] p 170 A93-23390

STUCZYNSKI, MATTHEW

Development of a hydrogen gas sensor using microfabrication technology [SAE PAPER 921176] p 210 A93-41356

STUEBER, THOMAS J.

Simulation of the synergistic low Earth orbit effects of vacuum thermal cycling, vacuum UV radiation, and atomic oxygen p 58 N93-15595

The effects of simulated low Earth orbit environments on spacecraft thermal control coatings [NASA-TM-106146] p 61 N93-27019

Low Earth orbital atomic oxygen environmental simulation facility for space materials evaluation [NASA-TM-106128] p 96 N93-27266

SU, T. F.

Effect of surface tension on the onset of convection in a double-diffusive layer p 163 A93-13951

SUBRAMANIAN, R. S.

Thermocapillary migration of a small chain of bubbles p 182 A93-46714

SUBRAMANYAM, G.

Processing, electrical and microwave properties of sputtered Ti-Ca-Ba-Cu-O superconducting thin films p 282 A93-44607

SUENAGA, M.

Giant suppression of flux-flow resistivity in heavy-ion irradiated Ti₂Ba₂Ca₂Cu₃O₁₀ films - Influence of linear defects on vortex transport p 280 A93-26198

SUES, ROBERT H.

Programming probabilistic structural analysis for parallel processing computers p 237 A93-32410

Parallel computing for probabilistic fatigue analysis [AIAA PAPER 93-1499] p 261 A93-34039

SUH, KWANG

Integrated fiber optic probe for dynamic light scattering p 278 A93-52415

SUICH, RONALD C.

Minimize system cost by choosing optimal subsystem reliability and redundancy [NASA-TM-106251] p 271 N93-31145

SUKENIK, CHAIM N.

Benzonorbornadiene end caps for PMR resins p 94 A93-35700

Lower temperature curing thermoset polyimides utilizing a substituted norbornene endcap p 134 A93-44526

SULLIVAN, C.

Mixed application MMIC technologies - Progress in combining RF, digital and photonic circuits p 152 A93-25800

SULLIVAN, DANIEL J.

Preliminary investigation of high power microwave plasmas for electrothermal thruster use [AIAA PAPER 93-2106] p 74 A93-49928

Preliminary investigation of high power microwave plasmas for electrothermal thruster use [NASA-TM-106207] p 92 N93-29158

SULLIVAN, J. P.

Unsteady wing surface pressures in the wake of a propeller p 14 A93-52436

SULLIVAN, JOHN P.

Two-, three-, and four-poster jets in cross flow [AIAA PAPER 93-0023] p 167 A93-20141

SULLIVAN, TIMOTHY L.

Solving modal equations of motion with initial conditions using MSC/NASTRAN DMAP Part 2: Coupled versus uncoupled integration [NASA-TM-106064] p 248 N93-23740

SUMMA, J. M.

CFD zonal modeling of leading-edge ice effects for a complete aircraft [AIAA PAPER 93-0167] p 5 A93-22601

SUMRALL, J. P.

Establishing the infrastructure - An integrated Space Transportation System p 50 A93-12072

SUN, D. C.

Simultaneous pressure measurement and high-speed photography study of cavitation in a dynamically loaded journal bearing p 223 A93-40050

SUN, H.

Atomization and vaporization characteristics of airblast fuel injection inside a venturi tube [AIAA PAPER 93-1766] p 184 A93-49662

SUN, JUN

Soot formation and radiation in turbulent jet diffusion flames under normal and reduced gravity conditions p 121 N93-20192

SUNDARARAJAN, T.

A study of the effects of macrosegregation and buoyancy-driven flow in binary mixture solidification p 180 A93-44223

SUNDBERG, GALE R.

Growing the Space Station's electrical power plant p 161 N93-27810

SUNDERLAND, P. B.

Structure of soot-containing laminar jet diffusion flames [AIAA PAPER 93-0708] p 114 A93-24804

SUNG, K. T.

Application of high-quality SiO₂ grown by multipolar ECR source to Si/SiGe MISFET p 156 A93-37413

SURESH, AMBADI

An assessment of spectral nonoscillatory schemes [AIAA PAPER 93-3383] p 267 A93-45074

SUTJAHJO, EDHI

Finite element procedures for coupled linear analysis of heat transfer, fluid and solid mechanics [AIAA PAPER 93-1639] p 267 A93-34166

SUTLIFF, THOMAS J.

Structural dynamic testing of composite propfan blades for a cruise missile wind tunnel model [NASA-TM-105272] p 247 N93-18875

SUTTER, JAMES K.

Benzonorbornadiene end caps for PMR resins p 94 A93-35700

Lower temperature curing thermoset polyimides utilizing a substituted norbornene endcap p 134 A93-44526

SUZUKI, KATSUYUKI

Layout optimization using the homogenization method of three-dimensional shells p 243 A93-54508

Applications to car bodies - Generalized layout design of three-dimensional shells p 243 A93-54509

SVOBODA, JAMES S.

Anomalous TWTA output power spikes and their effect on a digital satellite communications system [NASA-TM-105875] p 159 N93-13286

SWAFFORD, TIMOTHY W.

Computation of unsteady supersonic quasi-one-dimensional viscous-inviscid interacting internal flowfields p 177 A93-32724

SWAIN, D. M.

Visualization of hydrogen injection in a scramjet engine by simultaneous PLIF imaging and laser holographic imaging p 214 N93-13683

SWARTWOUT, GREGORY

Three-dimensional flow calculations inside SSME GGGT first stage blade rows p 93 N93-31585

SWARTZ, C. K.

Carner removal and defect behavior in p-type InP p 279 A93-17176

SWEC, DIANE M.

- Overview of the NASA Lewis component technology program for Stirling power converters p 254 A93-26073
- Summary of the NASA Lewis component technology program for Stirling power converters [NASA-TM-105640] p 82 N93-15526

SWETTE, LARRY L.

- Regenerative fuel cells p 252 A93-25868

SWIRHUN, S.

- Mixed application MMIC technologies - Progress in combining RF, digital and photonic circuits p 152 A93-25800

SYMONS, E. PATRICK

- Fluid management system technology discipline p 62 N93-27861

SYMONS, PAT

- Cryogenic fluid management (base R/T): Cryogenic fluid systems, Cryogenic Orbital Nitrogen Experiment (CONE), Cryogenic Orbital Hydrogen Experiment (COHE). (Transportation focused technology) [PR6] p 286 N93-71879

SYNOWICKI, R. A.

- Low earth simulation and materials characterization p 44 A93-32293

SZTANDERA, LESZEK M.

- Fuzzy sets predict flexural strength and density of silicon nitride ceramics [NASA-TM-106049] p 110 N93-27270

T**T'EN, JAMES S.**

- Catalytic ignition model in monolithic reactor with in-depth reaction p 119 A93-51641

TABATA, WILLIAM K.

- Design of an Advanced Expander Test Bed [AIAA PAPER 93-2133] p 48 A93-49952

TABIB-AZAR, M.

- An analysis of the frequency limitations of an Al(x)Ga(1-x)As/GaAs optical modulator p 151 A93-23454

TABIB-AZAR, MASSOOD

- Comparative study of bolometric and non-bolometric switching elements for microwave phase shifters p 155 A93-27245
- Electronic passivation of n- and p-type GaAs using chemical vapor deposited GaS p 283 A93-52708

TACINA, R. R.

- Atomization and vaporization characteristics of airblast fuel injection inside a venturi tube [AIAA PAPER 93-1766] p 184 A93-49662

TAGHAVI, R.

- Fiber optic laser Doppler anemometry in swirling jets p 206 A93-23783
- Computational study of advanced exhaust system transition ducts with experimental validation p 7 A93-34490

TAM, CHRISTOPHER K. W.

- Dispersion-relation-preserving schemes for computational aeroacoustics p 2 A93-19151
- Measured acoustic characteristics of ducted supersonic jets at different model scales [AIAA PAPER 93-0731] p 273 A93-24821
- Dispersion-relation-preserving finite difference schemes for computational acoustics p 274 A93-51180

TAMMARU, IVO

- A high-efficiency 59- to 64-GHz TWT for intersatellite communications p 158 A93-49553

TAN, C. S.

- Aerodynamic design of turbomachinery blading in three-dimensional flow - An application to radial inflow turbines [ASME PAPER 92-GT-74] p 3 A93-19324
- Numerical simulation of compressor endwall and casing treatment flow phenomena [ASME PAPER 92-GT-300] p 4 A93-19490

TAN, H. Q.

- Calculation of stress intensity factors in an isotropic multicroacked plate. Part 2: Symbolic/numeric implementation [NASA-TM-105823] p 244 A93-10453
- Calculation of stress intensity factors in an isotropic multicroacked plate. Part 1: Theoretical development [NASA-TM-105766] p 244 A93-10455
- Explicit robust schemes for implementation of a class of principal value-based constitutive models: Symbolic and numeric implementation [NASA-TM-106124] p 258 A93-26946
- Explicit robust schemes for implementation of general principal value-based constitutive models [NASA-TM-106123] p 258 A93-26947

TANG, STANLEY S.

- An artificial intelligence-based structural health monitoring system for aging aircraft p 266 N93-22185

TAO, XIAOMING

- Development of braided rope seals for hypersonic engine applications - Flow modeling p 222 A93-34493
- Development of braided rope seals for hypersonic engine applications: Flow modeling [NASA-TM-105942] p 227 N93-14478

TARLE, GREGORY

- Extension of the Parker bound on the flux of magnetic monopoles p 291 A93-38672

TAUB, S. R.

- Novel coplanar waveguide to slotline transition on high resistivity silicon p 151 A93-20016
- Coplanar waveguide radial line stub p 155 A93-36514

TAUB, SUSAN R.

- Microwave characterization of slotline on high resistivity silicon for antenna feed network [NASA-TM-106058] p 161 N93-27265
- Development of Si(1-x)Ge(x) technology for microwave sensing applications [NASA-TM-106157] p 162 N93-28610

TAYLOR, J. K.

- The turbulent thermal boundary layer with an abrupt change from a rough to a smooth wall p 167 A93-21712

TAYLOR, JOHN G.

- Supersonic investigation of two dimensional hypersonic exhaust nozzles [NASA-TM-105687] p 33 N93-15342

TAYLOR, ROBERT P.

- The turbulent thermal boundary layer with an abrupt change from a rough to a smooth wall p 167 A93-21712

TAYLOR, WILLIAM J.

- Small experiments for the maturation of orbital cryogenic transfer technologies [IAF PAPER 92-0777] p 64 A93-13698
- Small experiments for the maturation of orbital cryogenic transfer technologies [NASA-TM-105849] p 192 N93-10981
- Comparing the results of an analytical model of the no-vent fill process with no-vent fill test results for a 4.96 cubic meters (175 cubic feet) tank [NASA-TM-106018] p 200 N93-27155

TELESMA, JACK

- External stress-corrosion cracking of a 1.22-m-diameter type 316 stainless steel air valve [NASA-TP-3190] p 129 N93-26201

TEREPKA, FRANCIS M.

- CVD of silicon carbide on structural fibers - Microstructure and composition p 117 A93-39521

TERLEP, JUDITH A.

- Simulation of the synergistic low Earth orbit effects of vacuum thermal cycling, vacuum UV radiation, and atomic oxygen p 58 N93-15595

TERRY, J. D.

- System overview on electromagnetic compensation for reflector antenna surface distortion [NASA-TM-106217] p 53 N93-29195

TERRY, JOHN D.

- A prototype automatic phase compensation module [NASA-TM-105930] p 160 N93-16616

TEW, ROY C.

- Comparison of GLIMPS and HFAST Stirling engine code predictions with experimental data p 220 A93-26052
- Overview of NASA supported Stirling thermodynamic loss research p 174 A93-26087
- Heat transfer in oscillating flows with sudden change in cross section p 174 A93-26089

TEWARI, S. N.

- Thermosolutal convection during cellular arrayed growth of Pb-Sn alloys [AIAA PAPER 93-0262] p 142 A93-22668
- Interfacial shear strength of cast and directionally solidified NiAl-sapphire fiber composites p 106 A93-55685
- Interfacial and capillary phenomena in solidification processing of metal-matrix composites p 106 A93-56351

THAGGARD, MICHAEL

- An approach to studying the reliability of microgravity experiments [AIAA PAPER 93-1024] p 44 A93-30937

THANAWALA, A. A.

- Efficient demultiplexing algorithm for noncontiguous carriers p 148 A93-32561

THEOFLAKTOS, NOULIE

- OLYMPUS/ACTS scintillation experiment at the Lewis Research Center p 150 N93-26481

THIEME, LANNY G.

- Overview of the NASA Lewis component technology program for Stirling power converters p 254 A93-26073
- Summary of the NASA Lewis component technology program for Stirling power converters [NASA-TM-105640] p 82 N93-15526

THOMAS, D. J.

- Reliability analysis of laminated ceramic matrix composites using shell subelement techniques p 243 A93-55382

THOMAS, DAVID

- Primordial nucleosynthesis and the abundances of beryllium and boron p 290 A93-33513

THOMAS, DAVID J.

- Progressive matrix cracking in off-axis plies of a general symmetric laminate [AIAA PAPER 93-1494] p 239 A93-34035

THOMPSON, D.

- Parameterization of solar cells [NASA-TM-105885] p 159 N93-12301

THOMPSON, EDWARD A.

- Optimization of blade arrangement in a randomly mistuned cascade using simulated annealing [AIAA PAPER 93-2254] p 28 A93-50052

THOMPSON, ROBERT L.

- Conceptual design for the Space Station Freedom fluid physics/dynamics facility [NASA-TM-103663] p 61 N93-26209

THORP, SCOTT A.

- Computer aided design and manufacturing of composite propan blades for a cruise missile wind tunnel model [NASA-TM-105269] p 261 N93-12022

THURMAN, DOUGLAS R.

- Measurements and computational analysis of heat transfer and flow in a simulated turbine blade internal cooling passage [AIAA PAPER 93-1797] p 189 A93-53585
- Measurements and computational analysis of heat transfer and flow in a simulated turbine blade internal cooling passage [NASA-TM-106189] p 203 N93-31647

TIEN, JAMES S.

- Numerical computation of low-speed concurrent flow flame spread in mixed buoyant and forced flow [AIAA PAPER 93-0827] p 115 A93-24897
- Downward diffusion flame spread and extinction in variable gravitational fields - Lunar and Martian simulations [AIAA PAPER 93-0828] p 115 A93-24898
- Combustion of solid fuel in very low speed oxygen streams p 122 N93-20207

TIEN, TA-CHING

- Catalytic ignition model in monolithic reactor with in-depth reaction p 119 A93-51641

TIKARE, VEENA

- Effect of environment on fracture toughness of 96 wt pct alumina p 134 A93-44955

TIMMERHAUS, KLAUS D.

- Damping of thermal acoustic oscillations in hydrogen systems p 146 A93-48589

TIRRES, LIZET

- Experimental evaluation of a cooled radial-inflow turbine [AIAA PAPER 93-1795] p 27 A93-49685

- Experimental evaluation of a cooled radial-inflow turbine [NASA-TM-106230] p 38 A93-28697

TITRAN, R.

- The NASA CSTI high capacity power project [NASA-TM-105813] p 48 A93-11398

TITRAN, R. H.

- Tensile strain-rate sensitivity of tungsten/nibium composites at 1300 to 1600 K p 97 A93-14840

TITRAN, ROBERT H.

- Thermal stability of the microstructure of an aged Nb-Zr-C alloy p 122 A93-13776
- Processing and microstructure of Nb-1 percent Zr-0.1 percent C alloy sheet [NASA-TM-105921] p 128 N93-15524

TJIA, ROBERT E.

- Application of neural networks in the acousto-ultrasonic evaluation of metal-matrix composite specimens p 231 A93-37009
- Radial basis function network learns ceramic processing and predicts related strength and density [NASA-TM-106048] p 110 N93-27129

TO, WAI M.

- Discussion of 'Comparison of turbulence models for the natural convection boundary layer along a heated vertical plate' p 168 A93-21717

TO, WAI-MING

- A brief description of a new numerical framework for solving conservation laws: The method of space-time conservation element and solution element [NASA-TM-105757] p 269 N93-26560

TONCICH, S. S.

- Full wave characterization of microstrip open end discontinuities patterned on anisotropic substrates using potential theory [NASA-TM-106037] p 160 N93-20259

- TONG, LI**
Soot formation and radiation in turbulent jet diffusion flames under normal and reduced gravity conditions
p 121 N93-20192
- TONG, MICHAEL T.**
Stirling engine - Approach for long-term durability assessment
p 220 A93-26069
- TORERO, J. L.**
Experimental observations of the effect of gravity changes on smoldering combustion
[AIAA PAPER 93-0829] p 116 A93-24899
- TOURNIER, JEAN-MICHEL**
Heat-pipe transient model for space applications
p 163 A93-13867
- TOWER, LEONARD K.**
Test results of a Stirling engine utilizing heat exchanger modules with an integral heat pipe
[NASA-TM-105883] p 256 N93-25136
- TOWNE, CHARLES E.**
The Proteus Navier-Stokes code
p 193 N93-13396
- TOWNSEND, D. P.**
Modal analysis of multistage gear systems coupled with gearbox vibrations
p 222 A93-36588
An analysis of gear fault detection methods as applied to pitting fatigue failure data
[NASA-TM-105950] p 229 N93-27074
- TOWNSEND, DENNIS P.**
Evaluation of a vibration diagnostic system for the detection of spur gear pitting failures
[AIAA PAPER 93-2298] p 224 A93-50083
Evaluation of a vibration diagnostic system for the detection of spur gear pitting failures
[NASA-TM-106103] p 228 N93-25672
- TOWNSEND, SCOTT**
A multiarchitecture parallel-processing development environment
[NASA-TM-106180] p 262 N93-28628
- TOWNSEND, SCOTT E.**
Turbomachinery CFD on parallel computers
[NASA-TM-105932] p 262 N93-13154
- TRALLI, D.**
Venus Interior Structure Mission (VISM): Establishing a seismic network on Venus
p 293 N93-28819
- TRASE, LARRY**
Description of the PMAD systems test bed facility and data system
p 47 A93-26102
- TREGAY, G. W.**
Optical fiber sensor for temperature measurement from 600 to 1900 C in gas turbine engines
p 208 A93-32918
Flight testing of a fiber optic temperature sensor
p 22 A93-49476
- TROUDET, T.**
Design and evaluation of a robust dynamic neurocontroller for a multivariable aircraft control problem
p 40 A93-37004
Analysis of fault-tolerant neurocontrol architectures
[NASA-TM-105898] p 41 N93-12305
- TROUDET, TERRY**
Neurocontrol design and analysis for a multivariable aircraft control problem
p 40 A93-41894
Robustness enhancement of neurocontroller and state estimator
[NASA-TM-106028] p 42 N93-26907
- TROWBRIDGE, DANIEL A.**
Application of composite materials to impact-insensitive munitions
p 97 A93-11459
- TRUCCO, RICHARD E.**
Visualization of hydrogen injection in a scramjet engine by simultaneous PLIF imaging and laser holographic imaging
p 214 N93-13683
- TRUE, B.**
Experimental investigation of crossflow jet mixing in a rectangular duct
[AIAA PAPER 93-2037] p 185 A93-49872
Experimental investigation of crossflow jet mixing in a rectangular duct
[NASA-TM-106152] p 36 N93-27026
- TSAI, C. T.**
Influence of airfoil thickness on sound generated by high-frequency gust interactions
p 272 A93-19181
Prediction of dislocation generation during Bridgman growth of GaAs crystals
p 279 A93-19740
- TSAI, Y.-L. P.**
PDF approach for compressible turbulent reacting flows
[AIAA PAPER 93-0087] p 170 A93-24229
- TSCHEN, PETER S.**
A review of design concepts for the Advanced Fluids Module (AFM) project
[AIAA PAPER 93-0258] p 43 A93-23700
- TSENG, H. Q.**
High-efficiency high-gain monolithic heterostructure FET amplifier at 31 GHz
- TSENG, HUA Q.**
A high efficiency Ka-band monolithic pseudomorphic HEMT amplifier
p 151 A93-25786
- TU, Y. K.**
Modal analysis of multistage gear systems coupled with gearbox vibrations
p 222 A93-36588
- TUCKER, STEPHEN**
Cryogenic propellant thermal control system design considerations, analyses, and concepts applied to a Mars human exploration mission
[AIAA PAPER 93-2353] p 75 A93-50126
- TUMA, MARGARET L.**
Fourier transform spectrometry for fiber-optic sensor systems
p 211 A93-49459
- TURKEL, E.**
Central difference TVD schemes for time dependent and steady state problems
p 188 A93-51183
- TURKEL, ELI**
Numerical simulations of a high Mach number jet flow
[AIAA PAPER 93-0653] p 172 A93-24766
High order accurate solutions of viscous problems
[AIAA PAPER 93-3074] p 183 A93-48249
Numerical simulation of a high Mach number jet flow
[NASA-TM-105985] p 197 N93-20057
- TURLEY, R. S.**
Erosion rate diagnostics in ion thrusters using laser-induced fluorescence
p 70 A93-34481
- TURNER, MICHAEL S.**
Cosmic microwave background probes models of inflation
p 294 A93-10355
Gravitational waves from first-order cosmological phase transitions
p 288 A93-11451
The best-fit universe
p 289 A93-17651
Inflation at the electroweak scale
p 290 A93-26263
Extension of the Parker bound on the flux of magnetic monopoles
p 291 A93-38672
First-order inflation
p 292 A93-51704
- URNS, STEPHEN R.**
Some aspects of secondary atomization of aluminum/hydrocarbon slurry propellants
p 140 A93-34478
- TWEEDT, D. L.**
Averaging techniques for steady and unsteady calculations of a transonic fan stage
[AIAA PAPER 93-3065] p 11 A93-48241
- TYE, G. W.**
Active control of helicopter transmission noise
p 274 A93-29428
- TZENG, Y.**
High quality flame deposited diamond films for infrared optical windows
p 281 A93-40564
- TZIRANIS, ALEXANDER K.**
M.I.T. Stirling-cycle heat transfer apparatus
p 174 A93-26090

U

- URASEK, DONALD C.**
Space chemical propulsion test facilities at NASA Lewis Research Center
[NASA-TM-106050] p 85 N93-23405
- URBAN, D.**
Experimental observations of the effect of gravity changes on smoldering combustion
[AIAA PAPER 93-0829] p 116 A93-24899
- URBAN, DAVID L.**
Contributions of microgravity test results to the design of spacecraft fire-safety systems
[AIAA PAPER 93-1152] p 56 A93-31028
Contributions of microgravity test results to the design of spacecraft fire safety systems
[NASA-TM-106093] p 60 N93-24755
- UZ, MEHMET**
Thermal stability of the microstructure of an aged Nb-Zr-C alloy
p 122 A93-13776
Processing and microstructure of Nb-1 percent Zr-0.1 percent C alloy sheet
[NASA-TM-105921] p 128 N93-15524

V

- VALCO, GEORGE J.**
A 10 GHz Y-Ba-Cu-O/GaAs hybrid oscillator proximity coupled to a circular microstrip patch antenna
p 158 A93-54619
- VALCO, MARK J.**
Dynamic analysis of spur gears using computer program DANST
[AIAA PAPER 93-2295] p 224 A93-50080
Dynamic analysis of spur gears using computer program DANST
[NASA-TM-106211] p 230 N93-28050
- VAN DE WALL, ALLAN**
Evaluation and application of the Baldwin-Lomax turbulence model in two-dimensional, unsteady, compressible boundary layers with and without separation in engine inlets
[AIAA PAPER 92-3676] p 2 A93-14118
Evaluation and application of the Baldwin-Lomax turbulence model in two-dimensional, unsteady, compressible boundary layers with and without separation in engine inlets
[AIAA PAPER 92-3676] p 168 A93-22509
- VAN DER VEGT, J. J. W.**
Higher-order accurate Osher schemes with application to compressible boundary layer stability
[AIAA PAPER 93-3051] p 183 A93-48231
- VAN DER VEGT, JACOBUS J.**
ENO-Osher schemes for Euler equations
[AIAA PAPER 93-0335] p 171 A93-24235
- VAN DRESAR, N. T.**
Pressurization and expulsion of a lightweight liquid hydrogen tank
[AIAA PAPER 93-1966] p 73 A93-49814
- VAN DRESAR, NEIL T.**
Autogenous pressurization of cryogenic vessels using submerged vapor injection
p 71 A93-48648
- VANDERAAR, M.**
Combinatorial pulse position modulation for power-efficient free-space laser communications
[NASA-TM-106241] p 150 N93-31856
- VANDERAAR, MARK J.**
Performance evaluation of land mobile satellite system under fading and interference using multiple TCM by Monte-Carlo simulation
p 147 A93-10958
- VANDERBORG, NICHOLAS E.**
PEM fuel cell stack heat and mass management
p 253 A93-26024
- VANDERSANDE, J.**
The NASA CSTI High Capacity Power Project
p 69 A93-26105
The NASA CSTI high capacity power project
[NASA-TM-105813] p 48 N93-11398
- VANDERVEGT, J. J.**
Bypass transition in compressible boundary layers
p 196 N93-15801
- VANDERVEGT, JACOBUS J.**
ENO-Osher schemes for Euler equations
[NASA-TM-105928] p 268 N93-15341
- VANDEWALL, ALLAN**
Evaluation and application of the Baldwin-Lomax turbulence model in two-dimensional, unsteady, compressible boundary layers with and without separation in engine inlets
[NASA-TM-105810] p 191 N93-10087
A compressible boundary layer algorithm for use with SINDA '85
p 192 N93-13395
- VANFOSSEN, G. J.**
High Reynolds number and turbulence effects on aerodynamics and heat transfer in a turbine cascade
[AIAA PAPER 93-2252] p 186 A93-50050
Increased heat transfer to elliptical leading edges due to spanwise variations in the freestream momentum: Numerical and experimental results
[NASA-TM-106150] p 199 N93-27020
- VANFOSSEN, G. JAMES**
High Reynolds number and turbulence effects on aerodynamics and heat transfer in a turbine cascade
[NASA-TM-106187] p 202 N93-29157
- VARDE, UDAY**
Benzonorborene end caps for PMR resins
p 94 A93-35700
- VARGAS-ABURTO, CARLOS**
Auger electron spectroscopy study of oxidation of a PdCr alloy used for high-temperature sensors
[NASA-TM-106212] p 129 N93-23418
- VARGAS, MARIO**
Close-up analysis of aircraft ice accretion
[AIAA PAPER 93-0029] p 18 A93-23239
Close-up analysis of aircraft ice accretion
[NASA-TM-105952] p 19 N93-15360
- VARY, A.**
Application of neural networks to prediction of advanced composite structures mechanical response and behavior
p 205 A93-20751
- VARY, ALEX**
NDE of the universe - New ways to look at old facts
p 271 A93-32222
Application of neural networks in the acousto-ultrasonic evaluation of metal-matrix composite specimens
p 231 A93-37009
Radial basis function network learns ceramic processing and predicts related strength and density
[NASA-TM-106048] p 110 N93-27129
Fuzzy sets predict flexural strength and density of silicon nitride ceramics
[NASA-TM-106049] p 110 N93-27270

- Soft computing in design and manufacturing of advanced materials
[NASA-TM-106032] p 111 N93-28624
- VAUGHAN, DAVID F.**
Effects of buoyancy on laminar, transitional, and turbulent gas jet diffusion flames p 121 N93-20189
- VEDULA, K.**
Transformation to Ni₅Al₃ in a 63.0 at pct Ni-Al alloy p 124 A93-25108
- VEILLETTE, ROBERT J.**
A modified approach to controller partitioning
[NASA-TM-106167] p 266 N93-28051
- VEITCH, L. C.**
Prediction of chemical vapor deposition rates on monofilaments and its implications for fiber properties p 113 A93-17198
- VEITCH, LISA C.**
CVD of silicon carbide on structural fibers - Microstructure and composition p 117 A93-39521
Guanidine based vehicle/binders for use with oxides, metals, and ceramics
[NASA-CASE-LEW-15314-2] p 138 N93-28423
- VELAZQUEZ, MATTHEW T.**
Ice accretion and performance degradation calculations with LEWICE/NS
[AIAA PAPER 93-0173] p 18 A93-23244
Ice accretion and performance degradation calculations with LEWICE/NS
[NASA-TM-105972] p 19 N93-15354
- VELOSA, A.**
Scientific basis for the Isothermal Dendritic Growth Experiment - A USMP-2 space flight experiment p 143 A93-50455
- VENKATKRISHNAN, V.**
A parallel dynamic load balancing algorithm for 3-D adaptive unstructured grids
[AIAA PAPER 93-3313] p 260 A93-45009
- VERDON, J. M.**
Analysis of high Reynolds number inviscid/viscid interactions in cascades p 15 A93-55351
- VERES, J. P.**
Design and test of a small two stage counter-rotating turbine for rocket engine application
[AIAA PAPER 93-2136] p 74 A93-49954
- VERES, JOSEPH P.**
A survey of instabilities within centrifugal pumps and concepts for improving the flow range of pumps in rocket engines p 190 N93-10039
- VERHOFF, VINCENT G.**
Compound curvature laser window development
[AIAA PAPER 93-2177] p 277 A93-49989
Three-dimensional laser window formation for industrial application p 218 N93-22197
- VERRILLI, M. J.**
A model for predicting high-temperature fatigue failure of a W/Cu composite p 112 N93-31579
- VERRILLI, MICHAEL J.**
A creep cavity growth model for creep-fatigue life prediction of a unidirectional W/Cu composite
[NASA-TM-105780] p 244 N93-10967
Thermomechanical fatigue behavior of SiC/Ti-24Al-11Nb in air and argon environments
[NASA-TM-105723] p 106 N93-11399
- VETRONE, ROBERT H.**
NEP facilities (LeRC) p 49 N93-26965
- VIDOLI, CAROL A.**
Technical report writing
[NASA-TM-105419] p 287 N93-23002
- VIDWANS, A.**
A parallel dynamic load balancing algorithm for 3-D adaptive unstructured grids
[AIAA PAPER 93-3313] p 260 A93-45009
- VIJAYARAGHAVAN, D.**
Effect of out-of-roundness on the performance of a diesel engine connecting-rod bearing p 225 A93-52607
- VINALS, JORGE**
Coarsening following a morphological instability in the one-sided model p 284 A93-21695
Narrow band noise as a model of time-dependent accelerations - Study of the stability of a fluid surface in a microgravity environment
[AIAA PAPER 93-0911] p 173 A93-24965
Stability of a fluid surface in a microgravity environment p 190 A93-55358
- VINARCIK, E. J.**
Diffusional transport and predicting oxidative failure during cyclic oxidation of beta-NiAl alloys p 126 A93-50370
Predicting the oxidative lifetime of beta NiAl-Zr alloys p 127 A93-53939
- VINH, NGUYEN X.**
Minimum-fuel, power-limited transfers between coplanar elliptical orbits p 45 A93-31532

- VOLD, C. L.**
The microstructural evolution, crystallography, and thermal processing of ultrahigh carbon Fe-1.85 pct C melt-spun ribbon p 125 A93-32934
- VONDEAK, THOMAS**
High data rate applications of ACTS technology p 52 A93-17329
- VUKITS, THOMAS J.**
Two-, three-, and four-poster jets in cross flow
[AIAA PAPER 93-0023] p 167 A93-20141

W

- WADEL, MARY F.**
Benefits of in situ propellant utilization for a Mars sample return mission
[AIAA PAPER 93-2244] p 140 A93-50046
Benefits of in situ propellant utilization for a Mars sample return mission
[NASA-TM-106243] p 141 N93-28695
- WADLEY, HAYDN N. G.**
Residual strain gradient determination in metal matrix composites by synchrotron X-ray energy dispersive diffraction p 103 A93-39580
- WAGNER, J. H.**
Heat transfer in rotating serpentine passages with trips skewed to the flow
[ASME PAPER 92-GT-191] p 166 A93-19416
Heat transfer in rotating serpentine passages with selected model orientation for smooth or skewed trip walls
[NASA-TM-106126] p 147 N93-25177
- WAGNER, P.**
Combinatorial pulse position modulation for power-efficient free-space laser communications
[NASA-TM-106241] p 150 N93-31856
- WAGNER, R.**
Structured system engineering methodologies used to develop a nuclear thermal propulsion engine
[AIAA PAPER 93-2109] p 271 A93-49930
- WALKER, BRUCE K.**
On-line implementation of nonlinear parameter estimation for the Space Shuttle main engine
[NASA-TM-106097] p 88 N93-26211
- WALKER, J. D. A.**
The structure of a three-dimensional turbulent boundary layer p 181 A93-44813
- WALKER, KEVIN P.**
Critical experiments of the self-consistent model for polycrystalline Hastelloy-X p 124 A93-21958
The viscoplastic behavior of Hastelloy-X single crystal p 125 A93-27486
Viscoplasticity with creep and plasticity bounds p 125 A93-32925
Ratchetting behavior in viscoplasticity - A technical note p 241 A93-43651
Thermoviscoplastic analysis of fibrous periodic composites using triangular subvolumes
[NASA-TM-106076] p 111 N93-29074
- WALKER, R. E.**
Test program to provide validation data for the Rocket Combustor Interactive Design (ROCCID) code p 120 N93-11450
- WALKER, T. P.**
The boron-to-beryllium ratio in halo stars - A signature of cosmic-ray nucleosynthesis in the early Galaxy p 292 A93-55061
- WALKER, TERRY P.**
Population II Li-6 as a probe of nucleosynthesis and stellar structure and evolution p 292 A93-56494
- WALLACE, DAVID A.**
Assessment of 25 kW free-piston Stirling technology alternatives for space applications p 254 A93-26072
- WALLACE, JOHN F.**
Effects of thermal and mechanical fatigue on the flexural strength of G40-600/PMR-15 cross-ply laminates
[NASA-TM-106016] p 108 N93-20317
- WALTERS, JERRY L.**
Space Communication Artificial Intelligence for Link Evaluation Terminal (SCALET) p 265 N93-11940
- WALTON, JAMES T.**
System model development for nuclear thermal propulsion
[NASA-TM-105761] p 80 N93-10457
Development of NASA/DOE NTP system performance models
[NASA-TM-105982] p 82 N93-15428
Aerothermodynamic flow phenomena of the airframe-integrated supersonic combustion ramjet
[NASA-TM-4376] p 82 N93-15528
System model development for nuclear thermal propulsion
[NASA-TM-108157] p 276 N93-16531

- System model development for nuclear thermal propulsion
[NASA-TM-108215] p 277 N93-17343
Program ELM: A tool for rapid thermal-hydraulic analysis of solid-core nuclear rocket fuel elements
[NASA-TM-105867] p 84 N93-19106
Overview of NASA/DOE/DOD interagency modeling team and activities p 89 N93-26952
- WALTON, JOANNE C.**
Multiple-access phased array antenna simulator for a digital beam-forming system investigation p 148 A93-26237
- WANG, CHI-RONG**
Supersonic boundary-layer flow turbulence modeling
[NASA-TM-105893] p 193 N93-14758
- WANG, H.**
Boundary formulations for three-dimensional continuum structural shape sensitivity analysis p 235 A93-22426
- WANG, HUA**
Collective effects of temperature gradients and gravity on droplet coalescence p 183 A93-46716
- WANG, J.**
Electrodynamic interactions between a space station and the ionospheric plasma environment p 56 A93-29156
- WANG, J.-C.**
Face-gear drives: Design, analysis, and testing for helicopter transmission applications
[NASA-TM-106101] p 229 N93-27133
- WANG, JIE**
Hierarchical image coding with diamond-shaped sub-bands p 205 A93-20945
- WANG, JIFENG**
Effect of extended tooth contact on the modeling of spur gear transmissions
[AIAA PAPER 93-2148] p 223 A93-49965
Effect of extended tooth contact on the modeling of spur gear transmissions
[NASA-TM-106174] p 230 N93-28411
- WANG, JIONG**
Space Station Freedom structure floating potential and the probability of arcing p 57 A93-39265
- WANG, R.**
Extra high speed modified Lundell alternator parameters and open/short-circuit characteristics from global 3D-FE magnetic field solutions p 156 A93-39348
Computation of load performance and other parameters of extra high speed modified Lundell alternators from 3D-FE magnetic field solutions p 156 A93-39349
Three dimensional magnetic fields in extra high speed modified Lundell alternators computed by a combined vector-scalar magnetic potential finite element method p 157 A93-39350
On the effects of grid ill-conditioning in three dimensional finite element vector potential magnetostatic field computations p 157 A93-39719
Theoretical and numerical difficulties in 3-D vector potential methods in finite element magnetostatic computations p 157 A93-39720
- WANG, Y.-P.**
Digital control algorithms for microgravity isolation systems p 265 A93-53653
- WANG, YAN**
Characterization of Si₃N₄/SiO₂ optical channel waveguides by photon scanning tunneling microscopy p 211 A93-49458
- WARNER, JOSEPH D.**
Ellipsometric study of ambient-produced overlayer growth rate on YBa₂Cu₃O_{7-x} films p 281 A93-39362
- WARREN, JOHN W.**
Space Nuclear Thermal Propulsion Test Facilities Subpanel
[NASA-TM-105708] p 87 N93-25105
- WASHLOCK, PAUL A.**
Computer modeling of a hot filament diamond deposition reactor p 94 A93-40618
- WATANABE, YOICHI**
Thermophysical properties of gas phase uranium tetrafluoride
[AIAA PAPER 93-2758] p 285 A93-46505
- WATERS, JOHN F.**
Benzonorbornadiene end caps for PMR resins p 94 A93-35700
Lower temperature curing thermoset polyimides utilizing a substituted norbornene endcap p 134 A93-44526
- WATERS, S. A.**
Optimal design of composite hip implants using NASA technology p 257 N93-22188
- WATERS, W. J.**
Properties of extruded PS-212 type self-lubricating materials p 138 N93-25565
- WATKINS, RICHARD**
Gravitational waves from first-order cosmological phase transitions p 288 A93-11451

- Extension of the Parker bound on the flux of magnetic monopoles p 291 A93-38672
- WATSON, BRIAN C.**
Forced response of mistuned bladed disk assemblies [AIAA PAPER 93-1491] p 239 A93-34033
- WEBB, BRENT J.**
Construction and testing of ceramic fabric heat pipe with water working fluid p 163 A93-13869
- WEBB, JAY C.**
Dispersion-relation-preserving schemes for computational aeroacoustics p 2 A93-19151
Dispersion-relation-preserving finite difference schemes for computational acoustics p 274 A93-51180
- WEI, HUALIANG**
Thermocapillary migration of a small chain of bubbles p 182 A93-46714
- WEIDMAN, P. D.**
On the drag of model dendrite fragments at low Reynolds number [NASA-TM-105916] p 128 N93-19974
- WEILAND, KAREN J.**
Intensified array camera imaging of solid surface combustion aboard the NASA Learjet p 143 A93-30858
Visualization and imaging methods for flames in microgravity p 121 N93-20193
- WEILAND, KAREN J. R.**
Laser-induced fluorescence detection strategies for sodium atoms and compounds in high-pressure combustors p 119 A93-52423
- WEILAND, KENNETH E.**
Calibration of a shock wave position sensor using artificial neural networks [NASA-TM-106138] p 216 N93-27001
- WEINBERG, I.**
Carrier removal and defect behavior in p-type InP p 279 A93-17176
Diffusion length variation and proton damage coefficients for InP/In(x)Ga(1-x)As/GaAs solar cells p 159 A93-55324
- WEINBERG, IRVING**
Diffusion length variation in 0.5- and 3-MeV-proton-irradiated, heteroepitaxial indium phosphide solar cells [NASA-TM-106147] p 161 N93-27002
- WEISLOGEL, MARK**
An interface configuration experiment on USML-1 [AIAA PAPER 93-0253] p 169 A93-22662
- WEISS, BEN-ZION**
Direct observation of porous SiC formed by anodization in HF p 282 A93-43587
- WEISS, JONATHAN M.**
Prediction of engine and near-field plume reacting flows in low-thrust chemical rockets [AIAA PAPER 93-0237] p 66 A93-22649
- WEIZER, V. G.**
Non-destructive, ultra-low resistance, thermally stable contacts for use on shallow junction InP solar cells [NASA-TM-106228] p 256 N93-32201
- WEIZER, VICTOR G.**
The structural and electrical properties of low-resistance Ni contacts to InP p 151 A93-24367
Low resistance silver contacts to indium phosphide - Electrical and metallurgical considerations p 157 A93-39351
Simple, extremely low resistance contact system to n-InP that does not exhibit metal-semiconductor intermixing during sintering p 157 A93-42550
- WELCH, GERARD E.**
Two-dimensional CFD modeling of wave rotor flow dynamics [AIAA PAPER 93-3318] p 9 A93-45014
- WELLBORN, STEVEN R.**
An experimental investigation of the flow in a diffusing S-duct [NASA-TM-105809] p 32 N93-12077
- WENDT, B. J.**
An experimental investigation of S-duct flow control using arrays of low-profile vortex generators [AIAA PAPER 93-0018] p 170 A93-24226
- WENDT, BRUCE J.**
Structure and development of streamwise vortex arrays embedded in a turbulent boundary layer p 177 A93-32711
An experimental investigation of S-duct flow control using arrays of low-profile vortex generators [NASA-TM-106030] p 17 N93-19968
- WENZLER, CARL J.**
A system to measure lightning-induced transients on spacecraft umbilical lines p 161 N93-24889
- WERNER, MARK P.**
Ground-based PIV and numerical flow visualization results from the Surface Tension Driven Convection Experiment p 143 A93-33075
- WERNET, MARK P.**
Particle image velocimetry for the Surface Tension Driven Convection Experiment using a particle displacement tracking technique p 206 A93-23799
Particle displacement tracking applied to air flows p 206 A93-23800
Fuzzy logic particle tracking velocimetry [NASA-TM-106194] p 216 N93-27027
- WERTHEIMER, G. D.**
Signal processing considerations for low signal to noise ratio laser Doppler and phase Doppler signals p 207 A93-23830
- WETCH, JOSEPH R.**
Advanced radiator concepts feasibility demonstration p 163 A93-13844
- WETHERHOLD, ROBERT C.**
Progressive matrix cracking in off-axis plies of a general symmetric laminate [AIAA PAPER 93-1494] p 239 A93-34035
- WEY, C.**
Comparison of reacting and non-reacting shear layers at a high subsonic Mach number [AIAA PAPER 93-2381] p 186 A93-50149
Comparison of reacting and non-reacting shear layers at a high subsonic Mach number p 38 N93-27610
Turbulence measurement in a reacting and non-reacting shear layer at a high subsonic Mach number [NASA-TM-106166] p 18 N93-31839
- WHEELER, DONALD R.**
A vacuum (10 exp -9 torr) friction apparatus for determining friction and endurance life of MoS(x) films p 146 A93-49245
- WHITCOMB, JOHN**
Global/local finite element analysis for textile composites [AIAA PAPER 93-1506] p 103 A93-34045
- WHITE, MAURICE A.**
Assessment of 25 kW free-piston Stirling technology alternatives for solar applications p 254 A93-26072
- WHITEHEAD, BRUCE A.**
A function approximation approach to anomaly detection in propulsion system test data [AIAA PAPER 93-1776] p 71 A93-49671
- WHITFIELD, DAVID L.**
Navier-Stokes calculations for the unsteady flowfield of turbomachinery [AIAA PAPER 93-0676] p 6 A93-24786
High resolution numerical simulation of the linearized Euler equations in conservation law form [AIAA PAPER 93-2934] p 183 A93-48132
- WHITTENBERGER, J. D.**
Elevated temperature compressive properties of reaction milled NiAl-AIN and Zr-doped NiAl-AIN composites p 97 A93-11422
Influence of grain size on the creep behavior of HfC-dispersed NiAl p 123 A93-17674
Properties of pure nickel after long term exposures to LiOH and vacuum at 775 K p 123 A93-18075
Creep-rupture strength of a Ni-base superalloy at 1400 K p 124 A93-20556
Mechanical properties of Haynes Alloy 188 after exposure to LiF-22CaF2, air, and vacuum at 1093 K for periods up to 10,000 hours p 126 A93-36586
Stress relaxation of low pressure plasma-sprayed NiCrAlY alloys p 127 A93-52870
- WHYTE, WAYNE A., JR.**
Real-time transmission of digital video using variable-length coding [NASA-TM-106092] p 150 N93-22483
- WIEDNER, B.**
Fluid dynamics and convective heat transfer in impinging jets through implementation of a high resolution liquid crystal technique [ISABE 93-7077] p 189 A93-54053
- WIESERMAN, W. R.**
Comparison of high temperature, high frequency core loss and dynamic B-H loops of a 2V-49Fe-49Co and a grain oriented 3Si-Fe alloy p 153 A93-25895
- WIESERMAN, WILLIAM R.**
Comparison of high frequency, high temperature core loss and B-H loop characteristics of an 80 Ni-Fe crystalline alloy and two iron-based amorphous alloys p 123 A93-13882
Radiation and temperature effects on electronic components investigated under the CSTI high capacity power project [NASA-TM-106096] p 161 N93-24746
- WILL, HERBERT**
Fabrication of thin film heat flux sensors p 204 A93-16419
Novel thin-film heat flux sensors [AIAA PAPER 92-5035] p 205 A93-22309
Thin film heat flux sensor for Space Shuttle Main Engine turbine environment p 217 N93-31554
- WILL, HERBERT A.**
Fabrication of thin film heat flux sensors p 213 N93-13667
- WILLIAMS, F. A.**
Asymptotic analysis with reduced chemistry for the burning of n-heptane droplets p 113 A93-13323
- WILLIAMS, GEORGE J., JR.**
Derated ion thruster development status [AIAA PAPER 93-2225] p 75 A93-50031
- WILLIAMS, J. D.**
Erosion rate diagnostics in ion thrusters using laser-induced fluorescence p 70 A93-34481
- WILLIAMS, K. E.**
A numerical investigation of supersonic strut/endwall interactions in annular flow with varying strut thickness [AIAA PAPER 93-2927] p 10 A93-48128
Experimental and numerical investigation of supersonic turbulent flow in an annular duct [AIAA PAPER 93-3123] p 11 A93-48291
Investigation of a strut/endwall interaction in supersonic annular flow [AIAA PAPER 93-1925] p 12 A93-49791
- WILLIAMS, MARC H.**
Unsteady aerodynamics and flutter based on the potential equation [AIAA PAPER 93-2086] p 13 A93-49913
- WILLIAMS, REX**
Versatile dynamic isotope power systems for the exploration of space p 46 A93-13819
- WILLIAMS, W. D.**
Strain sensing technology for high temperature applications [AIAA PAPER 92-5040] p 205 A93-22314
- WILLIAMSON, W. S.**
Erosion rate diagnostics in ion thrusters using laser-induced fluorescence p 70 A93-34481
- WILSON, D. S.**
Magnetic bearings for free-piston Stirling engines p 221 A93-26079
- WILSON, JACK**
An improved numerical model for wave rotor design and analysis [AIAA PAPER 93-0482] p 24 A93-23384
Initial results from the NASA Lewis wave rotor experiment [AIAA PAPER 93-2521] p 30 A93-53589
An improved numerical model for wave rotor design and analysis [NASA-TM-105915] p 33 N93-12418
Initial results from the NASA-Lewis wave rotor experiment [NASA-TM-106148] p 39 N93-32368
- WILSON, JEFFREY D.**
A high-efficiency 59- to 64-GHz TWT for intersatellite communications p 158 A93-49553
Simulation of TunneLadder traveling-wave tube cold-test characteristics: Implementation of the three-dimensional, electromagnetic circuit analysis code micro-SOS [NASA-TP-3294] p 160 N93-23394
- WILT, T. E.**
Analysis of the anisotropic viscoplastic-damage response of composite laminates - Continuum basis and computational algorithms p 241 A93-43347
- WINSA, E.**
Scientific basis for the Isothermal Dendritic Growth Experiment - A USMP-2 space flight experiment p 143 A93-50455
- WINSA, E. A.**
IDGE - A test of dendritic growth theory using space flight [AIAA PAPER 93-0260] p 143 A93-25515
- WINTER, J.**
The NASA CSTI High Capacity Power Project [NASA-TM-105813] p 48 N93-11398
- WINTER, MICHAEL**
Air-mass flux measurement system using Doppler-shifted filtered Rayleigh scattering [AIAA PAPER 93-0513] p 205 A93-23260
- WINTERSCHIEDT, DANIEL L.**
A p-version finite element method for steady incompressible fluid flow and convective heat transfer [NASA-TM-106260] p 203 N93-32370
- WISE, MICHAEL L.**
Laser-induced fluorescence detection strategies for sodium atoms and compounds in high-pressure combustors p 119 A93-52423
- WITHROW, C. A.**
Design of small Stirling dynamic isotope power system for robotic space missions [NASA-TM-105919] p 141 N93-12085
- WITHROW, COLLEEN A.**
Comparison of dynamic isotope power systems for distributed planetary surface applications p 46 A93-13825

WONG, WAYNE A.

Update on the advanced Stirling conversion system project for 25 kW dish Stirling applications p 254 A93-26071

WOO, KYEONGSIK

Global/local finite element analysis for textile composites [AIAA PAPER 93-1506] p 103 A93-34045

WOOD, J. R.

Experimental and computational investigation of the NASA Low-Speed Centrifugal Compressor flow field [ASME PAPER 92-GT-213] p 4 A93-19436

WOODWARD, RICHARD P.

Takeoff/approach noise for a model counterrotation propeller with a forward-swept upstream rotor [AIAA PAPER 93-0596] p 24 A93-24782
Acoustical evaluation of the NASA Lewis 9 by 15 foot low speed wind tunnel [NASA-TP-3274] p 42 N93-12016

Takeoff/approach noise for a model counterrotation propeller with a forward-swept upstream rotor [NASA-TM-105979] p 34 N93-16715
In-flight near- and far-field acoustic data measured on the Proplan Test Assessment (PTA) testbed and with an adjacent aircraft [NASA-TM-103719] p 275 N93-27058

WOOLAM, JOHN A.

Low earth simulation and materials characterization p 44 A93-32293
Spectroscopic ellipsometry studies of HF treated Si (100) surfaces p 282 A93-46188

WORLEY, BRIAN A.

System model development for nuclear thermal propulsion [NASA-TM-105761] p 80 N93-10457
System model development for nuclear thermal propulsion [NASA-TM-108157] p 276 N93-16531
System model development for nuclear thermal propulsion [NASA-TM-108215] p 277 N93-17343

WRIGHT, DAVID L.

Advanced Communications Technology Satellite (ACTS) p 52 A93-24456

WRIGHT, THEODORE

Description of the SSF PMAD dc testbed control system data acquisition function p 47 A93-26103
Description of the SSF PMAD DC testbed control system data acquisition function [NASA-TM-105843] p 261 N93-11005

WRIGHT, WILLIAM B.

Advancements in the LEWICE Ice Accretion Model [AIAA PAPER 93-0171] p 18 A93-23243

WU, C.

Computational study of advanced exhaust system transition ducts with experimental validation p 7 A93-34490

WU, C. S.

Millimeter-wave pseudomorphic HEMT MMIC phased array components for space communications p 152 A93-25796

WU, C. Y.

Low temperature phase formation of Ti-based superconducting thin films in reduced oxygen atmosphere p 282 A93-44568

WU, MIN-KUANG

Damage-mitigating control of aerospace systems for high performance and extended life p 263 A93-22967
Damage-mitigating control of space propulsion systems for high performance and extended life [AIAA PAPER 93-2080] p 74 A93-49907

WU, Q. H.

The development of hydrogen sensor technology for aerospace applications [AIAA PAPER 93-2375] p 211 A93-50144

The development of hydrogen sensor technology at NASA Lewis Research Center [NASA-TM-106141] p 216 N93-27021

WU, QINGHAI

Development of a hydrogen gas sensor using microfabrication technology [SAE PAPER 921176] p 210 A93-41356

WU, RICHARD L. C.

Friction and wear of plasma-deposited diamond films [NASA-TM-105926] p 136 N93-19035

WU, T. W.

Acoustical analysis of gear housing vibration p 273 A93-29420

WU, X. D.

Buffer layers for high-Tc thin films on sapphire p 150 A93-17063

WU, X. F.

Acoustical analysis of gear housing vibration p 273 A93-29420

WU, XUESONG

On the nonlinear three dimensional instability of Stokes layers and other shear layers to pairs of oblique waves [NASA-TM-105918] p 194 N93-15499

WU, Y.-T.

Global/local methods for probabilistic structural analysis [AIAA PAPER 93-1378] p 238 A93-33942
Computational methods for efficient structural reliability and reliability sensitivity analysis [AIAA PAPER 93-1626] p 240 A93-34155

WYSS, M. L.

Averaging techniques for steady and unsteady calculations of a transonic fan stage [AIAA PAPER 93-3065] p 11 A93-48241

X**XIA, Z.**

Determination of forces in a magnetic bearing actuator - Numerical computation with comparison to experiment p 219 A93-15686

XIE, M.

Dynamic analysis of flexible gear trains/transmissions - An automated approach p 220 A93-22440
Time-variant analysis of rotorcraft systems dynamics - An exploitation of vector processors p 220 A93-23512

XU, M. H.

Calculation of stress intensity factors in an isotropic multicroaked plate: Part 2: Symbolic/numeric implementation [NASA-TM-105823] p 244 N93-10453

XUE, HONG X.

Stability of fully developed rotating stall [ASME PAPER 92-GT-57] p 23 A93-19307

Y**YADLIN, YORAM**

Application of an unstructured grid flow solver to planes, trains and automobiles [AIAA PAPER 93-0889] p 173 A93-24949

YAGLEY, J. A.

CFD analyses of coolant channel flowfields [AIAA PAPER 93-1830] p 184 A93-49715

YAMASHITA, H.

Heat transfer from radiatively heated material in a low Reynolds number microgravity environment p 180 A93-43695

YANG, B.

Premixed flame propagation in combustible particle cloud mixtures [AIAA PAPER 93-0713] p 115 A93-24808

YANG, D.

Direct optical injection locking of monolithically integrated In(0.53)Ga(0.47)As/In(0.52)Al(0.48)As MODFET oscillators p 158 A93-47127

YANG, JAE Y.

Mechanisms of voids formation during cooldown and freezing of lithium in SP-100 type systems p 163 A93-13916

YANG, S. L.

Numerical simulation of a low-emission gas turbine combustor using KIVA-II p 22 A93-14077
A three-dimensional algebraic grid generation scheme for gas turbine combustors with inclined slots [NASA-CR-191095] p 198 N93-24759

YANG, VIGOR

Supercritical droplet combustion and related transport phenomena [AIAA PAPER 93-0812] p 115 A93-24885

YANG, WEI-LI

Numerical simulation of a shock wave/turbulent boundary layer interaction in a duct [AIAA PAPER 93-3127] p 11 A93-48293

YANG, Y. L.

Aerodynamic design of turbomachinery blading in three-dimensional flow - An application to radial inflow turbines [ASME PAPER 92-GT-74] p 3 A93-19324

YANG, Z.

New time scale based k-epsilon model for near-wall turbulence p 180 A93-41909
Modeling of near wall turbulence and modeling of bypass transition p 195 N93-15798

YAO, HUADE

Spectroscopic ellipsometry studies of HF treated Si (100) surfaces p 282 A93-46188

YAO, M. W.

Prediction of dislocation generation during Bridgman growth of GaAs crystals p 279 A93-19740

YEH, F. C.

Heat transfer in rotating serpentine passages with trips skewed to the flow [ASME PAPER 92-GT-191] p 166 A93-19416
Heat transfer in rotating serpentine passages with selected model orientation for smooth or skewed trip walls [NASA-TM-106126] p 147 N93-25177

YEH, FREDERICK C.

High Reynolds number and turbulence effects on aerodynamics and heat transfer in a turbine cascade [AIAA PAPER 93-2252] p 186 A93-50050
High Reynolds number and turbulence effects on aerodynamics and heat transfer in a turbine cascade [NASA-TM-106187] p 202 N93-29157

YEH, FREDRICK C.

Summary of experimental heat-transfer results from the turbine hot section facility [NASA-TP-3250] p 197 N93-23059

YEN, CHEN-WAN

Robotic planetary mission benefits from nuclear electric propulsion p 43 A93-25854

YENNI, EDWARD J.

Electrical characterization of a Space Station Freedom alpha utility transfer assembly p 56 A93-26101

YEUN, J. J.

A parametric study of bleed in shock boundary layer interactions [AIAA PAPER 93-0294] p 5 A93-22694
An investigation of shock wave turbulent boundary layer interaction with bleed through slanted slots [AIAA PAPER 93-2992] p 11 A93-48184

YI, A. C.

Prospects for utilization of air liquefaction and enrichment system (ALES) propulsion in fully reusable launch vehicles [AIAA PAPER 93-2025] p 74 A93-49861

YING, S. J.

The promising chemical kinetics for the simulation of propane-air combustion with KIVA-II code [AIAA PAPER 93-2189] p 118 A93-50001

YODER, DENNIS A.

Brush seal leakage performance with gaseous working fluids at static and low rotor speed conditions [ASME PAPER 92-GT-304] p 219 A93-19494

YOGANATHAN, M.

Aluminum acceptor four particle bound exciton complex in 4H, 6H, and 3C SiC p 282 A93-44822

YOKOI, NOBUMITSU

Statistical analysis of the effects of helicity in inhomogeneous turbulence p 175 A93-26186

YOKOTA, JEFFREY W.

Vorticity dynamics of inviscid shear layers p 181 A93-45734

YOKOYAMA, JUN'ICHI

Probing the statistics of primordial fluctuations and their evolution p 290 A93-24627

YORKA, CHRISTIAN M.

Fiberoptic sensing technique employing RF modulated interferometry p 212 A93-53110

YOSHIZAWA, AKIRA

Statistical analysis of the effects of helicity in inhomogeneous turbulence p 175 A93-26186

YOUNG, G. W.

Flow effects in a vertical CVD reactor p 166 A93-19821

YOUNG, P. G.

Novel coplanar waveguide to slotline transition on high resistivity silicon p 151 A93-20016

YOUNG, PAUL E.

Development of Si(1-x)Ge(x) technology for microwave sensing applications [NASA-TM-106157] p 162 N93-28610

YOUNG, PAUL G.

A 10-GHz amplifier using an epitaxial lift-off pseudomorphic HEMT device p 156 A93-37574

Microwave characterization of slotline on high resistivity silicon for antenna feed network [NASA-TM-106058] p 161 N93-27265

YOUNGS, WILEY J.

Lower temperature curing thermoset polyimides utilizing a substituted norbornene endcap p 134 A93-44526

YU, JOHN

Multiple-access phased array antenna simulator for a digital beam-forming system investigation p 148 A93-26237

YU, SHENG-TAO

Direct calculations of waves in fluid flows using a high-order compact difference scheme [AIAA PAPER 93-0148] p 171 A93-24232

YUAN, S.

Millimeter-wave pseudomorphic HEMT MMIC phased array components for space communications p 152 A93-25796

YUN, H. M.

Tensile strain-rate sensitivity of tungsten/nibium composites at 1300 to 1600 K p 97 A93-14840
Preliminary evaluation of tensile and stress-rupture behavior of W + 24 at. pct Re + 0.4 at. pct HfC wire p 125 A93-25119

Tensile creep behavior of polycrystalline alumina fibers [NASA-TM-106269] p 138 N93-30938

YUN, HEE M.

The role of the interface in refractory metal alloy composites p 97 A93-13777

YUN, HEE MANN

Stress-rupture behavior of small diameter polycrystalline alumina fibers [NASA-TM-106256] p 139 N93-32382

YUNGSTER, SHAYE

Numerical study of shock-induced combustion in methane-air mixtures [AIAA PAPER 93-1917] p 184 A93-49783

YUNIS, ISAM S.

The application of structural reliability techniques to plume impingement loading of the Space Station Freedom Photovoltaic Array [AIAA PAPER 93-1338] p 56 A93-33908
Control/structure interactions of Space Station solar dynamic modules p 57 A93-41878
The application of structural reliability techniques to plume impingement loading of the Space Station Freedom Photovoltaic Array [NASA-TM-105949] p 59 N93-17988

Z**ZACCARIA, M.**

Three-dimensional flow field in a turbine nozzle passage [AIAA PAPER 93-2556] p 13 A93-50278

ZAGAR, BERNHARD

Modifying real convolutional codes for protecting digital filtering systems p 148 A93-38221

ZAHAARCHUK, G.

Large-area YBa₂Cu₃O₇(δ) thin films on sapphire for microwave applications p 279 A93-11475

ZAKHEM, R.

On the drag of model dendrite fragments at low Reynolds number [NASA-TM-105916] p 128 N93-19974

ZAKRAJSEK, J. J.

Modal simulation of gear box vibration with experimental correlation p 221 A93-31982
Modal analysis of multistage gear systems coupled with gearbox vibrations p 222 A93-36588
Vibration and noise analysis of a gear transmission system [AIAA PAPER 93-2150] p 224 A93-49967
An analysis of gear fault detection methods as applied to pitting fatigue failure data [NASA-TM-105950] p 229 N93-27074
Vibration and noise analysis of a gear transmission system [NASA-TM-106162] p 229 N93-27641

ZAKRAJSEK, JAMES J.

Evaluation of a vibration diagnostic system for the detection of spur gear pitting failures [AIAA PAPER 93-2298] p 224 A93-50083
Evaluation of a vibration diagnostic system for the detection of spur gear pitting failures [NASA-TM-106103] p 228 N93-25672

ZALLER, MICHELLE M.

Coaxial injector spray characterization using water/air as simulants p 120 N93-11452

ZAMAN, A. J.

System overview on electromagnetic compensation for reflector antenna surface distortion [NASA-TM-106217] p 53 N93-29195

ZAMAN, K. B. M. Q.

Estimation of unsteady lift on a pitching airfoil from wake velocity surveys [AIAA PAPER 93-0437] p 5 A93-23351
Effect of tabs on the flow and noise field of an axisymmetric jet p 25 A93-30833
Streamwise vorticity generation and mixing enhancement in free jets by 'delta-tabs' [AIAA PAPER 93-3253] p 14 A93-53592
Estimation of unsteady lift on a pitching airfoil from wake velocity surveys [NASA-TM-105947] p 15 N93-14791
Streamwise vorticity generation and mixing enhancement in free jets by delta-tabs [NASA-TM-106235] p 17 N93-31648

ZAMAN, Z.

Analysis of MMIC arrays for use in the ACTS Aero Experiment [NASA-TM-106073] p 53 N93-22589

ZARETSKY, ERWIN V.

Fatigue criterion to system design, life and reliability: A primer [NASA-TM-106022] p 248 N93-23406

ZELEZNIK, FRANK J.

Evaluation of the Munich Method for modeling rocket engine performance p 70 A93-31968

ZELLER, MARY

Novel thin-film heat flux sensors [AIAA PAPER 92-5035] p 205 A93-22309

ZELLER, MARY V.

Auger electron spectroscopy study of oxidation of a PdCr alloy used for high-temperature sensors [NASA-TM-106212] p 129 N93-23418

ZELTER, GABRIELA R.

Lightweight nickel electrodes for nickel/hydrogen cells p 255 A93-51574

ZENG, XIAOGANG

Computational micromechanics of woven composites p 237 A93-32462

ZHANG, JIMING

Single liquid source plasma-enhanced metalorganic chemical vapor deposition of high-quality YBa₂Cu₃O_{7-x} thin films p 280 A93-20643

ZHANG, KAI C.

The susceptibility critical exponent for a nonaqueous ionic binary mixture near a consolute point p 284 A93-19838

ZHANG, WENBIN

Narrow band noise as a model of time-dependent accelerations - Study of the stability of a fluid surface in a microgravity environment [AIAA PAPER 93-0911] p 173 A93-24965
Stability of a fluid surface in a microgravity environment p 190 A93-55358

ZHANG, XIAOQUANG

Experimental study of two interacting drops in an immiscible fluid p 179 A93-37936
Collective effects of temperature gradients and gravity on droplet coalescence p 183 A93-46716

ZHANG, Y.

Explicit robust schemes for implementation of a class of principal value-based constitutive models: Symbolic and numeric implementation [NASA-TM-106124] p 258 N93-26946
Explicit robust schemes for implementation of general principal value-based constitutive models [NASA-TM-106123] p 258 N93-26947

ZHAO, G.

Boundary formulations for three-dimensional continuum structural shape sensitivity analysis p 235 A93-22426

ZHOU, L.

Effects of gravity on the transition to turbulence of gas jet diffusion flames [AIAA PAPER 93-0710] p 114 A93-24805

ZHOU, LIMING

Effects of buoyancy on laminar, transitional, and turbulent gas jet diffusion flames p 121 N93-20189

ZHU, GANG

Second order closure modeling of turbulent buoyant wall plumes [NASA-TM-105956] p 193 N93-14829

ZHU, J.

Calculations of turbulent separated flows [NASA-TM-106154] p 200 N93-27161
A numerical study of confined turbulent jets [NASA-TM-106197] p 202 N93-29161

ZHU, JIANG

A realizable Reynolds stress algebraic equation model [NASA-TM-105993] p 16 N93-16596

ZIEMIANSKI, JOSEPH A.

Propulsion technology challenges for turn-of-the-century commercial aircraft [ISABE 93-7003] p 31 A93-53980

Propulsion technology challenges for turn-of-the-century commercial aircraft [NASA-TM-106192] p 39 N93-32351

ZIMMERMAN, M.

Directivity versus element spacing for a scanning array p 148 A93-36991

Analysis of MMIC arrays for use in the ACTS Aero Experiment [NASA-TM-106073] p 53 N93-22589

ZIMMERMAN, M. L.

Analysis of reflector antenna system including frequency selective surfaces p 52 A93-32820

ZOECKLER, JOSEPH G.

A new facility for advanced rocket propulsion research [AIAA PAPER 93-1859] p 48 A93-49737

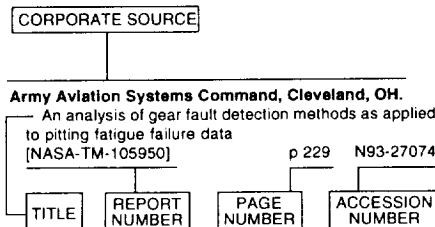
A new facility for advanced rocket propulsion research [NASA-TM-106193] p 49 N93-28696

ZUPANC, FRANK J.

Pulsed laser Rayleigh scattering diagnostic for hydrogen/oxygen rocket exit plane flowfield velocimetry [AIAA PAPER 93-0805] p 207 A93-25552

Laser Rayleigh and Raman diagnostics for small hydrogen/oxygen rockets [NASA-TM-105999] p 83 N93-17995
Pulsed laser Rayleigh scattering diagnostic for hydrogen/oxygen rocket exit plane flowfield velocimetry [NASA-TM-106213] p 88 N93-26149

Typical Corporate Source Index Listing



Listings in this index are arranged alphabetically by corporate source. The title of the document is used to provide a brief description of the subject matter. The page number and the accession number are included in each entry to assist the user in locating the abstract in the abstract section. If applicable, a report number is also included as an aid in identifying the document.

A

- Army Aviation Systems Command, Cleveland, OH.**
An analysis of gear fault detection methods as applied to pitting fatigue failure data [NASA-TM-105950] p 229 N93-27074
- Army Research Lab., Adelphi, MD.**
Contact stress analysis of spiral bevel gears using nonlinear finite element static analysis [NASA-TM-106176] p 228 N93-27037
- Generation of helical gears with new surfaces, topology by application of CNC machines [NASA-TM-106175] p 229 N93-27687
- Army Research Lab., Cleveland, OH.**
Effect of extended tooth contact on the modeling of spur gear transmissions [NASA-TM-106174] p 230 N93-28411

J

- Jet Propulsion Lab., California Inst. of Tech., Pasadena.**
Nuclear Propulsion Project Workshop summary p 64 A93-13765
- Robotic planetary mission benefits from nuclear electric propulsion p 43 A93-25854
- The NASA CSTI High Capacity Power Project p 69 A93-26105
- Electrodynamic interactions between a space station and the ionospheric plasma environment p 56 A93-29156
- The NASA Electric Propulsion Program [AIAA PAPER 93-1935] p 73 A93-49797
- BMDO electric space-propulsion program [AIAA PAPER 93-1934] p 78 A93-50322

N

- National Aeronautics and Space Administration, Washington, DC.**
Cosmic microwave background probes models of inflation p 294 A93-10355
- Implications of new GALLEX results for the Mikheyev-Smirnov-Wolfenstein solution of the solar neutrino problem p 293 A93-10357
- N-point correlation functions in the CIA and SSRS redshift distribution of galaxies p 288 A93-10615
- Gravitational waves from first-order cosmological phase transitions p 288 A93-11451
- Dark matter, long-range forces, and large-scale structure p 288 A93-11876
- Effects of turbine cooling assumptions on performance and sizing of high-speed civil transport [AIAA PAPER 92-4217] p 22 A93-13383
- Tribological and microstructural comparison of HIPped PM212 and PM212/Au self-lubricating composites p 93 A93-13505
- Tribological and mechanical comparison of sintered and HIPped PM212 - High temperature self-lubricating composites p 94 A93-13506
- Effect of hydrogen on the strength and microstructure of selected ceramics p 130 A93-13613
- Low-isp derated ion thruster operation [AIAA PAPER 92-3203] p 64 A93-13696
- Photovoltaic arrays for Martian surface power [IAF PAPER 92-0591] p 293 A93-13699
- Space nuclear power systems; Proceedings of the 8th Symposium, Albuquerque, NM, Jan. 6-10, 1991. Pts. 1-3 [ISBN 0-88318-838-4] p 64 A93-13751
- Planning for the Space Exploration Initiative - The nuclear propulsion option p 43 A93-13752
- Void control in the crystallization of lithium fluoride p 97 A93-13760
- Thermal stability of the microstructure of an aged Nb-Zr-C alloy p 122 A93-13776
- Space reactor/Stirling cycle systems for high power lunar applications p 46 A93-13822
- Stirling engine - Available tools for long-life assessment p 65 A93-13824
- Comparison of dynamic isotope power systems for distributed planetary surface applications p 46 A93-13825
- Key issues in space nuclear power challenges for the future p 65 A93-13905
- Effects of dust accumulation and removal on radiator surfaces on Mars p 123 A93-13937
- Evaluation and application of the Baldwin-Lomax turbulence model in two-dimensional, unsteady, compressible boundary layers with and without separation in engine inlets [AIAA PAPER 92-3676] p 2 A93-14118
- Development of advanced seals for space propulsion turbomachinery [SAE PAPER 921028] p 218 A93-14651
- Integrated health monitoring and controls for rocket engines [SAE PAPER 921031] p 66 A93-14654
- Tensile strain-rate sensitivity of tungsten/nibium composites at 1300 to 1600 K p 97 A93-14840
- Tailored metal matrix laminates for high-temperature performance p 98 A93-15753
- Computational simulation of surface waviness in graphite/epoxy woven composites due to initial curing p 98 A93-15822
- Cosmic string with a light massive neutrino p 288 A93-16303
- Interference patterns in the Spacelab 2 plasma wave data - Oblique electrostatic waves generated by the electron beam p 257 A93-16347
- Role of Si₂N₂O in the passive oxidation of chemically-vapor-deposited Si₃N₄ p 131 A93-16520
- Improved accuracy for finite element structural analysis via an integrated force method p 234 A93-17246
- Heats of formation of bcc binary alloys p 123 A93-17609
- The inflation sector of extended inflation p 288 A93-17638

- Late-time cosmological phase transitions p 288 A93-17645
- Stochastic inflation lattice simulations - Ultra-large scale structure of the universe p 289 A93-17646
- Properties of hybrid CVD/PAN graphite fibers and their bromine intercalation compounds p 98 A93-17675
- Heat transfer in rotating serpentine passages with trips skewed to the flow [ASME PAPER 92-GT-191] p 166 A93-19416
- Concurrent optimization of airframe and engine design parameters [AIAA PAPER 92-4713] p 20 A93-20281
- Modal test/analysis correlation of Space Station structures using nonlinear sensitivity [AIAA PAPER 92-4731] p 55 A93-20330
- Singularities in optimal structural design [AIAA PAPER 92-4818] p 235 A93-20397
- Glass formation, properties and structure of soda-yttria-silica glasses p 131 A93-20464
- Creep behavior of tungsten fiber reinforced niobium metal matrix composites p 99 A93-20758
- The gravitational wave contribution to cosmic microwave background anisotropies and the amplitude of mass fluctuations from COBE results p 289 A93-21508
- Prediction of engine and near-field plume reacting flows in low-thrust chemical rockets [AIAA PAPER 93-0237] p 66 A93-22649
- Simplified jet fuel reaction mechanism for lean burn combustion application [AIAA PAPER 93-0021] p 113 A93-23238
- Close-up analysis of aircraft ice accretion [AIAA PAPER 93-0029] p 18 A93-23239
- Surface roughness due to residual ice in the use of low power deicing systems [AIAA PAPER 93-0031] p 5 A93-23240
- Propagation of high frequency jet noise using geometric acoustics [AIAA PAPER 93-0147] p 272 A93-23241
- Numerical modeling of anti-icing systems and comparison to test results on a NACA 0012 airfoil [AIAA PAPER 93-0170] p 21 A93-23242
- Advancements in the LEWICE Ice Accretion Model [AIAA PAPER 93-0171] p 18 A93-23243
- Ice accretion and performance degradation calculations with LEWICE/NS [AIAA PAPER 93-0173] p 18 A93-23244
- Ice accretion prediction for a typical commercial transport aircraft [AIAA PAPER 93-0174] p 19 A93-23245
- Optimization of circular orifice jets mixing into a heated crossflow in a cylindrical duct [AIAA PAPER 93-0249] p 24 A93-23246
- Acoustic mode measurements in the inlet of a model turbofan using a continuously rotating rake - Data collection/analysis techniques [AIAA PAPER 93-0599] p 24 A93-23324
- Estimation of unsteady lift on a pitching airfoil from wake velocity surveys [AIAA PAPER 93-0437] p 5 A93-23351
- Nucleate pool boiling in the long duration low gravity environment of the space shuttle [AIAA PAPER 93-0465] p 142 A93-23371
- An improved numerical model for wave rotor design and analysis [AIAA PAPER 93-0482] p 24 A93-23384
- The first three minutes - 1990 version p 289 A93-23607
- Phase space distribution of halo particles and detection of WIMPS p 289 A93-23650
- A graphical user-interface for propulsion system analysis [AIAA PAPER 93-0223] p 259 A93-23699
- A review of design concepts for the Advanced Fluids Module (AFM) project [AIAA PAPER 93-0258] p 43 A93-23700
- Development of a Rayleigh scattering system for temperature measurements in combustor flows p 206 A93-23788
- Large- and small-scale constraints on power spectra in Omega - 1 universes p 290 A93-23990

Three-dimensional computed tomography from interferometric measurements within a narrow cone of views p 207 A93-24024

Numerical model for the Programmable Multirole Furnace (PMZF) p 142 A93-24242

Isothermal aging effects on PMR-15 resin p 131 A93-24508

Transverse flexural tests as a tool for assessing damage to PMR-15 composites from isothermal aging in air at elevated temperatures p 100 A93-24514

Probing the statistics of primordial fluctuations and their evolution p 290 A93-24627

Comparison of numerical model results with diffusion flames in microgravity p 114 A93-24803

Review of the Shuttle vibration environment [AIAA PAPER 93-0707] p 51 A93-24902

Low gravity environment on-board Columbia during STS-40 [AIAA PAPER 93-0833] p 142 A93-24903

Vibration isolation technology - An executive summary of systems development and demonstration [AIAA PAPER 93-0834] p 55 A93-24904

Evaluation of passive and active vibration control mechanisms in a microgravity environment [AIAA PAPER 93-0838] p 55 A93-24905

Preconditioned Conjugate Gradient methods for low speed flow calculations [AIAA PAPER 93-0881] p 172 A93-24942

Effect of a rotating propeller on the separation angle of attack [AIAA PAPER 93-0017] p 6 A93-24978

Thermal conductivity and thermal expansion of graphite fiber-reinforced copper matrix composites p 100 A93-25104

Reaction layer formation at the graphite/copper-chromium alloy interface p 100 A93-25105

System-level integrated circuit (SLIC) development for phased array antenna applications p 152 A93-25798

GaAs monolithic R.F. modules for SAR/SAT distress beacons p 152 A93-25806

Robotic planetary mission benefits from nuclear electric propulsion p 43 A93-25854

Optimization of armored spherical tanks for storage on the lunar surface p 47 A93-25866

Validation test of advanced technology for IPV nickel-hydrogen flight cells - Update p 252 A93-25886

An electromechanical actuation system for an expendable launch vehicle p 50 A93-25891

Electromechanical systems with transient high power response operating from a resonant ac link p 152 A93-25892

Neutron, gamma ray, and temperature effects on the electrical characteristics of thyristors p 153 A93-25894

Comparison of high temperature, high frequency core loss and dynamic B-H loops of a 2V-49Fe-49Co and a grain oriented 3Si-Fe alloy p 153 A93-25895

Design and optimization of a self-deploying single axis tracking PV array p 252 A93-25916

Energy loss analysis of an integrated space power distribution system p 68 A93-25958

Comparison of all-electric secondary power systems for civil transport p 24 A93-25997

Experimental determination of in situ utilization of lunar regolith for thermal energy storage p 253 A93-26043

Comparison of GLIMPS and HFAST Stirling engine code predictions with experimental data p 220 A93-26052

M-H characteristics and demagnetization resistance of samarium-cobalt permanent magnets to 300 C p 153 A93-26076

A free-piston Stirling engine/linear alternator controls and load interaction test facility p 146 A93-26077

Magnetic bearings for free-piston Stirling engines p 221 A93-26079

Overview of NASA supported Stirling thermodynamic loss research p 174 A93-26087

Heat transfer in oscillating flows with sudden change in cross section p 174 A93-26089

Overview and evolution of the LeRC PMAD DC test bed p 47 A93-26099

The NASA CSTI High Capacity Power Project p 69 A93-26105

Load converter interactions with the secondary system in the Space Station Freedom power management and distribution dc test bed p 154 A93-26106

Stability testing and analysis of a PMAD dc test bed for the Space Station Freedom p 154 A93-26107

EMTP based stability analysis of Space Station Electric Power System in a test bed environment p 154 A93-26108

Power system monitoring and source control of the Space Station Freedom dc-power system testbed p 69 A93-26109

Multiple-access phased array antenna simulator for a digital beam-forming system investigation p 148 A93-26237

Inflation at the electroweak scale p 290 A93-26263

Finite element implementation of state variable-based viscoplasticity models p 236 A93-26776

Design aspects and comparison between high Tc superconducting coplanar waveguide and microstrip line p 155 A93-27244

Comparative study of bolometric and non-bolometric switching elements for microwave phase shifters p 155 A93-27245

A numerical study of mixing in supersonic combustors with hypermixing injectors [AIAA PAPER 93-0215] p 25 A93-27801

The effect of ion-plated silver and sliding friction on tensile stress-induced cracking in aluminum oxide p 132 A93-27917

X-ray-based displacement measurement for hostile environments p 208 A93-28580

Acoustical analysis of gear housing vibration p 273 A93-29420

Critical comparison of second-order closures with direct numerical simulations of homogeneous turbulence p 176 A93-30840

Microfracture in high temperature metal matrix crossply laminates p 101 A93-31356

Fatigue life prediction of an intermetallic matrix composite at elevated temperatures p 101 A93-31358

The application of preconditioning in viscous flows p 177 A93-32627

Effect of tensile mean stress on fatigue behavior of single-crystal and directionally solidified superalloys p 125 A93-33011

Ground-based PIV and numerical flow visualization results from the Surface Tension Driven Convection Experiment p 143 A93-33075

Primordial nucleosynthesis and the abundances of beryllium and boron p 290 A93-33513

Forced response of mistuned bladed disk assemblies [AIAA PAPER 93-1491] p 239 A93-34033

Dynamics of rotating multicomponent turbomachinery systems [AIAA PAPER 93-1629] p 222 A93-34157

Some aspects of secondary atomization of aluminum/hydrocarbon slurry propellants p 140 A93-34478

Chemical and luminosity evolution, and counts of galaxies in a merger model p 290 A93-34776

Microwave anisotropies in the light of the data from the COBE satellite p 291 A93-35444

Reaction zone structure for strong, weak overdriven, and weak underdriven oblique detonations p 178 A93-35492

Kurtosis, skewness, and non-Gaussian cosmological density perturbations p 291 A93-35579

Benzonorbornadiene end caps for PMR resins p 94 A93-35700

Design and evaluation of a robust dynamic neurocontroller for a multivariable aircraft control problem p 40 A93-37004

Fuzzy expert systems vs. neural networks - Truck backer-upper control revisited p 264 A93-37039

Extension of the Parker bound on the flux of magnetic monopoles p 291 A93-38672

Axial-torsional fatigue - A study of tubular specimen thickness effects p 240 A93-38849

Analysis of precracking parameters for ceramic single-edge-precracked-beam specimens p 133 A93-38887

Chemical vapor deposition modeling for high temperature materials p 116 A93-39503

Onset conditions for gas phase reaction and nucleation in the CVD of transition metal oxides p 116 A93-39508

CVD of silicon carbide on structural fibers - Microstructure and composition p 117 A93-39521

Determination of parameters of a method for predicting alloy properties p 126 A93-39796

Photoluminescence intensity enhancement of GaAs by vapor-deposited GaS - A rational approach to surface passivation p 261 A93-40049

Kinetics of hexacelsian-to-celsian phase transformation in SrAl₂Si₂O₈ p 134 A93-40293

Computational/experimental basis for conducting alkane droplet combustion experiments on space-based-platforms p 117 A93-41711

Performance of TiCaBaCuO₃₀ GHz 64 element antenna array p 157 A93-44763

The NASA Computational Fluid Dynamics (CFD) program - Building technology to solve future challenges [AIAA PAPER 93-3292] p 287 A93-44996

Multigrid time-accurate integration of Navier-Stokes equations [AIAA PAPER 93-3361] p 181 A93-45054

Grid adaptation using Chimera composite overlapping meshes [AIAA PAPER 93-3389] p 267 A93-45080

Clumpy cold dark matter p 291 A93-46201

A new flux splitting scheme p 9 A93-47189

Streamwise computation of three-dimensional flows using two stream functions p 184 A93-49241

Screening studies of advanced control concepts for airbreathing engines p 26 A93-49329

Micromachined silicon cantilever beam accelerometer incorporating an integrated optical waveguide p 210 A93-49457

Characterization of Si₃N₄/SiO₂ optical channel waveguides by photon scanning tunneling microscopy p 211 A93-49458

Investigation of a strut/endwall interaction in supersonic annular flow p 12 A93-49791

The NASA Electric Propulsion Program [AIAA PAPER 93-1935] p 73 A93-49797

Progress report on nuclear propulsion for space exploration and science [AIAA PAPER 93-2352] p 44 A93-50125

Observing the inflation potential p 291 A93-50480

The three-point correlation function in an ensemble of three-dimensional simulations p 291 A93-50680

Validation test of 125 Ah advanced design IPV nickel-hydrogen flight cells p 78 A93-50822

A time-accurate high-resolution TVD scheme for solving the Navier-Stokes equations p 13 A93-52006

Effect of out-of-roundness on the performance of a diesel engine connecting-rod bearing p 225 A93-52607

Approaches to polymer-derived CMC matrices p 105 A93-53446

Space transportation alternatives for large space programs - The International Space University summer session - 1992 [AIAA PAPER 93-2278] p 44 A93-53588

Modal element method for scattering and absorbing of sound by two-dimensional bodies p 274 A93-53657

Propulsion technology challenges for turn-of-the-century commercial aircraft [ISABE 93-7003] p 31 A93-53980

Engine technology challenges for a 21st Century High-Speed Civil Transport [ISABE 93-7064] p 31 A93-54040

A parameter optimization approach to controller partitioning for integrated flight/propulsion control application p 41 A93-54268

Techniques for improving the accuracy of cryogenic temperature measurement in ground test programs p 212 A93-54363

Icing Research Tunnel rotating bar calibration measurement system p 212 A93-54398

Proposed ground-based control of accelerometer on Space Station Freedom p 63 A93-54401

Biasing and hierarchical statistics in large-scale structure p 292 A93-55051

Testing for the Gaussian nature of cosmological density perturbations through the three-point temperature correlation function p 292 A93-55212

Nongray gas analyses for reflecting walls utilizing a flux technique p 190 A93-55460

Solid lubricants p 135 A93-55471

Population II Li-6 as a probe of nucleosynthesis and stellar structure and evolution p 292 A93-56494

National Aeronautics and Space Administration. Ames Research Center, Moffett Field, CA.

The new challenge of computational aerosecure p 2 A93-14169

Unsteady transonic two-dimensional Euler solutions using finite elements p 8 A93-39412

The NASA Computational Fluid Dynamics (CFD) program - Building technology to solve future challenges [AIAA PAPER 93-3292] p 287 A93-44996

National Aeronautics and Space Administration. Goddard Space Flight Center, Greenbelt, MD.

GSFC conceptual design study for an inter-satellite Optical Multiple Access communication system p 52 A93-18966

Low gravity environment on-board Columbia during STS-40 [AIAA PAPER 93-0833] p 142 A93-24903

National Aeronautics and Space Administration. Hugh L. Dryden Flight Research Facility, Edwards, CA.

Flight testing of a fiber optic temperature sensor p 22 A93-49476

National Aeronautics and Space Administration. Lyndon B. Johnson Space Center, Houston, TX.

Pressure dependence of the oxygen reduction reaction at the platinum microelectrode/nafion interface - Electrode kinetics and mass transport p 112 A93-11450

Construction and testing of ceramic fabric heat pipe with water working fluid p 163 A93-13869

Optimal impulsive intercept with low-thrust rendezvous return p 45 A93-34521
 On protection of Freedom's solar dynamic radiator from the orbital debris environment. I - Preliminary analysis and testing p 70 A93-36197
 On protection of Freedom's solar dynamic radiator from the orbital debris environment. II - Further testing and analyses p 70 A93-36589

**National Aeronautics and Space Administration.
 Langley Research Center, Hampton, VA.**

The new challenge of computational aeroscience p 2 A93-14169
 Weakly nonlinear models for turbulent mixing in a plane mixing layer p 165 A93-17416
 Neural networks in structural analysis and design - An overview p 263 A93-20388
 [AIAA PAPER 92-4805] Design of a hypersonic waverider-derived airplane p 55 A93-21108
 [AIAA PAPER 93-0401] Estimation of unsteady lift on a pitching airfoil from wake velocity surveys p 5 A93-23351
 [AIAA PAPER 93-0437] Membrane triangles with corner drilling freedoms. I - The EFF element p 235 A93-24303
 Membrane triangles with corner drilling freedoms. II - The ANDES element p 235 A93-24304
 Membrane triangles with corner drilling freedoms. III - Implementation and performance evaluation p 236 A93-24305
 Comparison of numerical model results with diffusion flames in microgravity p 114 A93-24803
 [AIAA PAPER 93-0707] Low gravity environment on-board Columbia during STS-40 p 142 A93-24903
 [AIAA PAPER 93-0833] NASA CST aids U.S. industry p 258 A93-25084
 Global/local finite element analysis for textile composites p 103 A93-34045
 [AIAA PAPER 93-1506] The NASA Computational Fluid Dynamics (CFD) program - Building technology to solve future challenges p 287 A93-44996
 [AIAA PAPER 93-3292] Adaptive methods in computational fluid dynamics p 182 A93-45963
 Algebraic grid generation with control points p 268 A93-45967
 Time-sequenced and spectrally filtered Rayleigh imaging of shock wave and boundary layer structure for inlet characterization p 211 A93-50085
 [AIAA PAPER 93-2300]

**National Aeronautics and Space Administration.
 Marshall Space Flight Center, Huntsville, AL.**

Establishing the infrastructure - An integrated Space Transportation System p 50 A93-12072
 Interference patterns in the Spacelab 2 plasma wave data - Oblique electrostatic waves generated by the electron beam p 257 A93-16347
 Supercritical droplet combustion and related transport phenomena p 115 A93-24685
 [AIAA PAPER 93-0812] Review of the Shuttle vibration environment p 51 A93-24902
 [AIAA PAPER 93-0832] Low gravity environment on-board Columbia during STS-40 p 142 A93-24903
 [AIAA PAPER 93-0833] CFD analyses of coolant channel flowfields p 184 A93-49715
 [AIAA PAPER 93-1830] Cryogenic propellant thermal control system design considerations, analyses, and concepts applied to a Mars human exploration mission p 75 A93-50126
 [AIAA PAPER 93-2353]

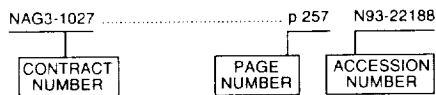
S

Sverdrup Technology, Inc., Brook Park, OH.

The 20 kWe NEP flight system p 90 N93-26983
 NEP systems model p 90 N93-26986
 Thruster models for NEP system analysis p 91 N93-26988

CONTRACT NUMBER INDEX

Typical Contract Number Index Listing



Listings in this index are arranged alphanumerically by contract number. Under each contract number the accession numbers denoting documents that have been produced as a result of research done under the contract are shown. The accession number denotes the number by which the citation is identified in the abstract section. Preceding the accession number is the page number on which the citation may be found.

AF-AFOSR-89-0223 p 116 A93-39508
AF-AFOSR-89-0395A p 10 A93-47202
AF-AFOSR-89-0403 p 179 A93-35624
AF-AFOSR-89-0487 p 181 A93-44813
AF-AFOSR-89-0508 p 105 A93-52473
AF-AFOSR-90-0096 p 99 A93-19123
AF-AFOSR-90-0179 p 188 A93-52008
AF-AFOSR-91-0101 p 5 A93-22694
AF-AFOSR-91-0240 p 54 A93-13133
AF-AFOSR-91-0262 p 54 A93-14687
AF-AFOSR-91-0412 p 170 A93-23390
AF-AFOSR-91-0412 p 205 A93-23259
DA PROJ. 1L1-61102-AH-45 p 192 N93-11529
DA PROJ. 1L1-61102-AH-45 p 246 N93-13153
DA PROJ. 1L1-61102-AH-45 p 35 N93-22599
DA PROJ. 1L1-61102-AH-45 p 198 N93-23744
DA PROJ. 1L1-61102-AH-45 p 199 N93-26554
DA PROJ. 1L1-62211-A-47-A p 226 N93-10966
DA PROJ. 1L1-62211-A-47-A p 226 N93-10982
DA PROJ. 1L1-62211-A-47-A p 226 N93-12736
DA PROJ. 1L1-62211-A-47-A p 227 N93-22826
DA PROJ. 1L1-62211-A-47-A p 228 N93-23019
DA PROJ. 1L1-62211-A-47-A p 228 N93-23741
DA PROJ. 1L1-62211-A-47-A p 228 N93-25672
DA PROJ. 1L1-62211-A-47-A p 228 N93-27037
DA PROJ. 1L1-62211-A-47-A p 229 N93-27069
DA PROJ. 1L1-62211-A-47-A p 229 N93-27133
DA PROJ. 1L1-62211-A-47-A p 229 N93-27687
DA PROJ. 1L1-62211-A-47-A p 230 N93-28050
DA PROJ. 1L1-62211-A-47-A p 230 N93-28411
DA PROJ. 1L1-62211-A-47-A p 231 N93-31846
DAAL03-86-K-0174 p 183 A93-48146
DAAL03-88-K-0013 p 241 A93-45430
DAAL03-89-K-0179 p 176 A93-30144
DAAL03-92-G-0120 p 224 A93-50084
DAAL03-92-G-0168 p 184 A93-49662
DE-AC02-76CH-00016 p 280 A93-26198
DE-AC02-76CH-00016 p 283 A93-53693
DE-AC02-76ER-01112 p 291 A93-38672
DE-AC02-83ER-40105 p 290 A93-33513
DE-AC02-88ER-13895 p 125 A93-27486
DE-AC02-88ER-13895 p 241 A93-43651
DE-AC03-76SF-00098 p 294 A93-10355
DE-AC03-76SF-00098 p 169 A93-22662
DE-AC03-76SF-00098 p 143 A93-41678
DE-AC03-88NE-32129 p 46 A93-13819
DE-AC04-76DP-00789 p 277 N93-17343
DE-AC05-84OR-21400 p 131 A93-20842
DE-AC05-84OR-21400 p 133 A93-38888
DE-AC05-84OR-21400 p 276 N93-16531
DE-AC07-88ID-12749 p 65 A93-13797

DE-AC21-87MC-24012 p 119 A93-52423
DE-AI01-91CR-50306 p 93 A93-13505
DE-AI03-86SF-16310 p 122 A93-13776
DE-AI03-86SF-16310 p 99 A93-20758
DE-AI03-86SF-16310 p 128 N93-15524
DE-AI05-87OR-21749 p 130 A93-15994
DE-AI05-87OR-21749 p 133 A93-38887
DE-AI05-87OR-21749 p 135 N93-10962
DE-EY-76-C-02-3071 p 294 A93-10355
DE-FC05-85ER-25000 p 284 A93-21695
DE-FC05-85ER-25000 p 173 A93-24965
DE-FC05-85ER-25000 p 190 A93-55358
DE-FC05-85ER-25000 p 124 A93-21958
DE-FC05-85ER-25000 p 125 A93-27486
DE-FC05-85ER-25000 p 290 A93-34776
DE-FC05-85ER-25000 p 290 A93-23990
DE-FC05-85ER-25000 p 293 A93-10357
DEN3-377 p 254 A93-26072
DTFA03-83-A-00328 p 113 A93-22652
F04611-86-C-0010 p 215 N93-22994
F08635-90-C-0100 p 31 A93-53999
F30602-92-C-0087 p 158 A93-47127
F30602-92-C-0087 p 165 A93-18564
F33615-89-C-2820 p 168 A93-21715
F33615-89-C-2820 p 175 A93-30127
F33615-89-C-2820 p 175 A93-30128
F33615-90-C-2088 p 158 A93-50646
F49620-85-C-0067 p 182 A93-45974
NAGW-1321 p 288 A93-17645
NAGW-1321 p 289 A93-23607
NAGW-1321 p 290 A93-34776
NAGW-1321 p 291 A93-35579
NAGW-1321 p 292 A93-55212
NAGW-1340 p 288 A93-17638
NAGW-1340 p 288 A93-17645
NAGW-1340 p 289 A93-17646
NAGW-1340 p 289 A93-23607
NAGW-1340 p 289 A93-23650
NAGW-1356 p 66 A93-22649
NAGW-1356 p 177 A93-32627
NAGW-1407 p 140 A93-34478
NAGW-1407 p 210 A93-49457
NAGW-1407 p 211 A93-49458
NAGW-1539 p 257 A93-16347
NAGW-2022 p 293 A93-13699
NAGW-2040 p 257 A93-16347
NAGW-2381 p 294 A93-10355
NAGW-2381 p 293 A93-10357
NAGW-2381 p 288 A93-10615
NAGW-2381 p 288 A93-11451
NAGW-2381 p 288 A93-11876
NAGW-2381 p 288 A93-16303
NAGW-2381 p 289 A93-21508
NAGW-2381 p 290 A93-23990
NAGW-2381 p 290 A93-24627
NAGW-2381 p 290 A93-26263
NAGW-2381 p 290 A93-33513
NAGW-2381 p 291 A93-35444
NAGW-2381 p 291 A93-35579
NAGW-2381 p 291 A93-38672
NAGW-2381 p 291 A93-46201
NAGW-2381 p 291 A93-50480
NAGW-2381 p 291 A93-50680
NAGW-2381 p 292 A93-55051
NAGW-2381 p 292 A93-55212
NAGW-2381 p 291 A93-38672
NAGW-2923 p 291 A93-50680
NAGW-931 p 294 A93-10355
NAG1-1269 p 263 A93-20388
NAG1-1324 p 103 A93-34045
NAG1-657 p 165 A93-17416
NAG1-756 p 235 A93-24303
NAG1-756 p 235 A93-24304
NAG1-756 p 236 A93-24305
NAG3-1004 p 208 A93-28580
NAG3-1009 p 185 A93-49901
NAG3-1011 p 182 A93-45974
NAG3-1016 p 178 A93-34409
NAG3-1018 p 146 A93-48589
NAG3-1020 p 66 A93-22649
NAG3-1023 p 11 A93-48298
NAG3-1027 p 257 N93-22188
NAG3-1034 p 241 A93-44440

NAG3-1040 p 77 A93-50257
NAG3-1041 p 223 A93-48594
NAG3-1044 p 140 A93-34478
NAG3-1045 p 163 A93-13916
NAG3-1046 p 115 A93-24897
NAG3-1046 p 115 A93-24898
NAG3-1052 p 221 A93-27308
NAG3-1055 p 46 A93-13901
NAG3-1058 p 272 A93-19804
NAG3-1059 p 222 A93-34493
NAG3-1060 p 282 A93-46729
NAG3-1066 p 272 A93-19205
NAG3-1068 p 25 A93-34159
NAG3-1068 p 28 A93-49912
NAG3-1076 p 174 A93-26090
NAG3-1081 p 113 A93-13323
NAG3-1082 p 117 A93-41952
NAG3-1087 p 148 A93-37038
NAG3-1087 p 183 A93-48146
NAG3-1089 p 233 A93-14446
NAG3-1089 p 258 A93-20380
NAG3-1089 p 235 A93-22426
NAG3-1089 p 242 A93-49028
NAG3-1089 p 268 A93-54198
NAG3-1089 p 220 A93-22440
NAG3-1089 p 220 A93-23512
NAG3-1092 p 169 A93-22666
NAG3-1092 p 171 A93-24241
NAG3-1092 p 188 A93-52515
NAG3-1099 p 264 A93-29338
NAG3-1099 p 57 A93-41878
NAG3-1101 p 234 A93-16552
NAG3-1101 p 238 A93-33915
NAG3-1102 p 242 A93-53394
NAG3-1102 p 48 A93-34482
NAG3-1106 p 156 A93-37570
NAG3-1106 p 158 A93-50646
NAG3-1109 p 144 A93-54460
NAG3-1109 p 22 A93-14077
NAG3-1110 p 198 N93-24759
NAG3-1110 p 24 A93-23246
NAG3-1113 p 33 N93-15359
NAG3-1113 p 22 A93-14077
NAG3-1117 p 28 A93-49903
NAG3-1116 p 167 A93-21712
NAG3-1117 p 210 A93-40683
NAG3-1122 p 182 A93-46714
NAG3-1124 p 27 A93-49612
NAG3-1134 p 31 A93-53999
NAG3-1137 p 5 A93-23001
NAG3-1137 p 23 A93-20320
NAG3-1140 p 184 A93-49662
NAG3-1143 p 169 A93-22662
NAG3-1143 p 143 A93-41678
NAG3-1146 p 41 A93-54268
NAG3-1149 p 210 A93-41356
NAG3-1160 p 241 A93-45429
NAG3-1163 p 243 A93-54508
NAG3-1163 p 243 A93-54509
NAG3-1163 p 222 A93-34241
NAG3-1163 p 26 A93-37446
NAG3-1166 p 245 N93-12277
NAG3-1167 p 148 A93-38221
NAG3-1167 p 175 A93-30130
NAG3-1168 p 168 A93-22622
NAG3-1170 p 14 A93-53208
NAG3-1170 p 177 A93-32724
NAG3-1173 p 28 A93-50052
NAG3-1177 p 41 A93-51400
NAG3-1177 p 11 A93-48239
NAG3-1179 p 23 A93-19307
NAG3-1184 p 113 A93-22030
NAG3-1186 p 205 A93-20945
NAG3-1186 p 264 A93-28200
NAG3-1186 p 264 A93-34582
NAG3-1187 p 29 A93-50192
NAG3-1187 p 29 A93-50193
NAG3-1192 p 7 A93-25553
NAG3-1192 p 7 A93-29318
NAG3-1196 p 263 A93-20388
NAG3-1196 p 241 A93-45430
NAG3-1196 p 265 A93-54534
NAG3-1198 p 26 A93-35934

NAG3-1213

NAG3-1213 p 5 A93-22694
 NAG3-1215 p 259 A93-24487
 NAG3-1220 p 99 A93-19624
 p 105 A93-52919
 NAG3-1226 p 156 A93-37574
 NAG3-1230 p 23 A93-20320
 NAG3-1232 p 30 A93-51403
 NAG3-1234 p 23 A93-20320
 p 25 A93-34159
 p 25 A93-34161
 p 13 A93-49913
 NAG3-1235 p 263 A93-25986
 NAG3-1240 p 263 A93-22967
 p 74 A93-49907
 NAG3-1242 p 114 A93-24806
 p 119 A93-55381
 p 147 A93-10929
 NAG3-1244 p 114 A93-24804
 NAG3-1245 p 169 A93-22686
 NAG3-1251 p 182 A93-46572
 p 112 A93-11450
 NAG3-1255 p 118 A93-50110
 NAG3-1259 p 2 A93-19151
 NAG3-1267 p 274 A93-51180
 p 163 A93-13951
 NAG3-1268 p 178 A93-35481
 p 180 A93-41710
 p 103 A93-34045
 NAG3-1270 p 179 A93-37936
 NAG3-1277 p 183 A93-46716
 NAG3-1284 p 284 A93-21695
 p 173 A93-24965
 p 190 A93-55358
 NAG3-1297 p 115 A93-24808
 NAG3-1300 p 278 A93-55687
 NAG3-1301 p 213 A93-55368
 p 214 N93-13668
 p 279 A93-19740
 NAG3-1314 p 183 A93-46716
 NAG3-1389 p 176 A93-30144
 NAG3-1402 p 77 A93-50256
 NAG3-1451 p 77 A93-50257
 p 282 A93-46188
 NAG3-154 p 147 A93-10958
 NAG3-157 p 219 A93-15681
 NAG3-181 p 219 A93-15682
 p 177 A93-32617
 NAG3-259 p 283 A93-51917
 NAG3-2696 p 166 A93-18752
 NAG3-311 p 9 A93-46823
 NAG3-330 p 272 A93-19181
 NAG3-357 p 10 A93-48128
 NAG3-376 p 11 A93-48291
 p 12 A93-49791
 NAG3-379 p 233 A93-16005
 p 244 N93-10777
 NAG3-38 p 246 N93-13260
 NAG3-397 p 99 A93-19123
 NAG3-443 p 116 A93-24899
 NAG3-449 p 257 A93-16347
 NAG3-476 p 149 A93-52237
 NAG3-481 p 113 A93-22652
 NAG3-512 p 124 A93-21958
 p 125 A93-27486
 p 177 A93-32711
 NAG3-520 p 165 A93-18556
 NAG3-522 p 233 A93-12046
 NAG3-534 p 162 A93-10671
 NAG3-570 p 162 A93-10839
 p 87 N93-24758
 NAG3-577 p 166 A93-19419
 NAG3-581 p 169 A93-23307
 NAG3-589 p 174 A93-26091
 NAG3-598 p 166 A93-19421
 NAG3-621 p 115 A93-24895
 NAG3-627 p 18 A93-23239
 NAG3-666 p 19 N93-15360
 p 56 A93-29156
 p 57 A93-39265
 NAG3-695 p 190 A93-55461
 p 175 A93-27900
 p 182 A93-45975
 NAG3-718 p 7 A93-31494
 NAG3-723 p 25 A93-34159
 p 11 A93-48293
 NAG3-724 p 7 A93-34483
 NAG3-725 p 3 A93-19399
 NAG3-730 p 273 A93-23535
 NAG3-732 p 245 N93-12277
 p 77 A93-50256
 NAG3-742 p 167 A93-21060
 NAG3-746 p 205 A93-23259
 NAG3-764 p 173 A93-24982
 p 183 A93-48132
 NAG3-767 p 4 A93-20144
 NAG3-768 p 181 A93-44813
 NAG3-771 p 181 A93-44813

NAG3-772 p 3 A93-19324
 NAG3-773 p 224 A93-50084
 NAG3-789 p 134 A93-52151
 NAG3-790 p 267 A93-33899
 NAG3-799 p 148 A93-32561
 NAG3-801 p 164 A93-14762
 p 169 A93-22664
 p 143 A93-32069
 p 178 A93-35482
 p 188 A93-50536
 NAG3-805 p 45 A93-34521
 NAG3-809 p 119 A93-51641
 NAG3-818 p 156 A93-39348
 p 156 A93-39349
 p 157 A93-39350
 p 157 A93-39719
 p 157 A93-39720
 NAG3-822 p 243 A93-56412
 NAG3-832 p 207 A93-24024
 NAG3-836 p 114 A93-23358
 NAG3-837 p 233 A93-12119
 p 125 A93-29570
 NAG3-841 p 7 A93-34490
 NAG3-852 p 210 A93-49457
 p 211 A93-49458
 NAG3-855 p 2 A93-19221
 p 272 A93-20134
 NAG3-862 p 239 A93-34035
 NAG3-869 p 6 A93-24786
 NAG3-876 p 144 A93-52183
 NAG3-884 p 116 A93-39508
 NAG3-886 p 280 A93-26198
 p 282 A93-44568
 p 283 A93-53693
 NAG3-888 p 236 A93-31295
 NAG3-900 p 228 N93-24751
 NAG3-901 p 236 A93-26776
 p 241 A93-43347
 NAG3-904 p 179 A93-37046
 NAG3-906 p 277 A93-52412
 NAG3-915 p 45 A93-31532
 NAG3-916 p 278 A93-49618
 NAG3-929 p 187 A93-50280
 NAG3-933 p 237 A93-32465
 p 237 A93-32717
 NAG3-934 p 235 A93-24303
 p 235 A93-24304
 p 236 A93-24305
 NAG3-941 p 163 A93-13867
 NAG3-943 p 167 A93-20141
 NAG3-949 p 265 A93-53653
 NAG3-954 p 280 A93-32132
 NAG3-959 p 156 A93-37570
 NAG3-95 p 44 A93-32293
 NAG3-960 p 264 A93-37039
 NAG3-967 p 104 A93-40888
 NAG3-968 p 219 A93-15686
 NAG3-97 p 181 A93-45038
 NAG3-984 p 211 A93-49469
 p 212 A93-53110
 NAG3-987 p 139 A93-22577
 NAG3-988 p 158 A93-47127
 NAG3-989 p 189 A93-54053
 NAG3-992 p 45 A93-13783
 p 45 A93-13793
 NAG3-993 p 179 A93-37936
 p 183 A93-46716
 NAG3-997 p 176 A93-30856
 NAG3-998 p 40 A93-14596
 p 21 A93-51401
 p 112 A93-11450
 NASA ORDER C-30050-R p 22 A93-14077
 p 28 A93-49903
 NASA ORDER C-32000-R p 180 A93-43695
 NASA ORDER C-32008-A p 190 A93-55136
 NASA ORDER C-32008-K p 164 A93-14551
 NASA ORDER C-82000-R p 103 A93-38895
 NASA ORDER C-99066-G p 165 A93-18751
 p 176 A93-30840
 p 101 A93-31356
 p 8 A93-38695
 p 191 N93-10454
 p 191 N93-10735
 p 268 N93-15341
 p 16 N93-16596
 p 262 N93-27040
 p 278 N93-29693
 p 182 A93-45963
 p 115 A93-24893
 p 208 A93-32918
 p 255 A93-51574
 p 121 N93-20189
 p 166 A93-19416
 p 121 N93-20206
 p 184 A93-49669
 p 12 A93-49720

NAS3-24227 p 166 A93-18752
 NAS3-24239 p 151 A93-25786
 p 156 A93-37413
 p 156 A93-37421
 NAS3-24350 p 35 N93-24754
 NAS3-24389 p 238 A93-33941
 p 238 A93-33942
 p 238 A93-33943
 p 240 A93-34155
 p 204 A93-20454
 NAS3-24564 p 213 A93-55368
 NAS3-24613 p 252 A93-25868
 NAS3-24635 p 117 A93-41711
 NAS3-24640 p 208 A93-33169
 NAS3-24816 p 146 A93-48637
 NAS3-25063 p 139 A93-14510
 NAS3-25070 p 54 A93-13132
 NAS3-25082 p 54 A93-13133
 p 54 A93-14687
 p 94 A93-53392
 NAS3-25091 p 52 A93-18966
 NAS3-25093 p 154 A93-26100
 NAS3-25208 p 163 A93-13844
 NAS3-25209 p 163 A93-13843
 p 173 A93-25978
 NAS3-25266 p 50 A93-13332
 p 293 A93-13699
 p 271 A93-19169
 p 2 A93-19322
 p 20 A93-20324
 p 66 A93-21664
 p 18 A93-23243
 p 261 A93-23327
 p 170 A93-24229
 p 171 A93-24232
 p 55 A93-24243
 p 151 A93-24367
 p 114 A93-24805
 p 172 A93-24817
 p 67 A93-24948
 p 68 A93-25859
 p 68 A93-25879
 p 153 A93-25896
 p 252 A93-25899
 p 252 A93-25916
 p 153 A93-25919
 p 253 A93-25974
 p 253 A93-26043
 p 153 A93-26076
 p 146 A93-26077
 p 25 A93-27801
 p 177 A93-32627
 p 143 A93-33075
 p 57 A93-33955
 p 26 A93-37389
 p 157 A93-39351
 p 157 A93-42550
 p 267 A93-45074
 p 9 A93-45146
 p 181 A93-45734
 p 10 A93-47213
 p 10 A93-48128
 p 11 A93-48291
 p 184 A93-49669
 p 72 A93-49674
 p 12 A93-49695
 p 12 A93-49720
 p 72 A93-49761
 p 12 A93-49791
 p 75 A93-49978
 p 75 A93-50129
 p 77 A93-50231
 p 77 A93-50232
 p 277 A93-52071
 p 120 N93-11452
 p 285 N93-12967
 p 159 N93-13286
 p 128 N93-22556
 p 249 N93-24913
 p 262 N93-28628
 NAS3-25280 p 85 N93-23017
 NAS3-25330 p 220 A93-26051
 NAS3-25368 p 143 A93-50455
 NAS3-25370 p 284 A93-19838
 p 155 A93-32771
 p 277 A93-52414
 NAS3-25421 p 274 A93-29428
 NAS3-25425 p 15 A93-55351
 NAS3-25450 p 7 A93-37374
 p 182 A93-46407
 p 70 A93-34481
 NAS3-25553 p 173 A93-25985
 NAS3-25554 p 120 N93-11450
 NAS3-25556 p 207 A93-23830
 NAS3-25622 p 63 A93-50242
 NAS3-25624 p 42 A93-23698
 NAS3-25653 p 42 A93-23698

CONTRACT NUMBER INDEX

CONTRACT NUMBER INDEX

RTOP 505-62-52

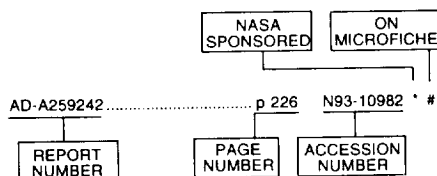
NAS3-25711	p 56	A93-26101	NGL-22-069-640	p 18	A93-23239	RTOP 467-01-21	p 161	N93-24746
NAS3-25767	p 277	A93-52071	NGT-5037	p 116	A93-39508	RTOP 468-02-11	p 91	N93-27022
NAS3-25776	p 147	N93-70966	NGT-50825	p 55	A93-24905	RTOP 474-12-10	p 255	N93-20261
NAS3-25785	p 259	A93-24781	NGT-50830	p 190	A93-55460	RTOP 474-42-10	p 47	A93-26099
	p 173	A93-24949	NGT-50981	p 239	A93-34033		p 154	A93-26106
NAS3-25790	p 103	A93-39580	NIH-AR-34399	p 243	A93-54508		p 154	A93-26107
NAS3-25807	p 50	A93-51473		p 243	A93-54509		p 154	A93-26108
NAS3-25808	p 65	A93-13797	NSERC-OGP-41747	p 178	A93-35481		p 69	A93-26109
	p 46	A93-13908	NSF ASC-87-17773	p 235	A93-24303		p 80	N93-10734
	p 252	A93-25867		p 235	A93-24304		p 261	N93-11005
NAS3-25809	p 65	A93-13767		p 236	A93-24305		p 160	N93-15503
	p 85	N93-23875	NSF ASC-91-11540	p 260	A93-45009	RTOP 474-46-10	p 55	A93-20330
	p 86	N93-23876	NSF AST-88-22595	p 288	A93-17645		p 61	N93-27019
NAS3-25824	p 237	A93-32410		p 289	A93-23607		p 91	N93-27039
NAS3-25883	p 261	A93-23327	NSF AST-90-01762	p 290	A93-23990		p 96	N93-27266
NAS3-25929	p 150	A93-17063	NSF AST-90-21414	p 291	A93-50680	RTOP 505-01-50	p 120	N93-11545
NAS3-25932	p 280	A93-20643	NSF AST-90-22629	p 290	A93-34776	RTOP 505-03-10	p 6	A93-24978
NAS3-25950	p 27	A93-49876		p 291	A93-35579		p 16	N93-16625
NAS3-25954	p 185	A93-49872		p 292	A93-55212		p 38	N93-29162
NAS3-25958	p 278	N93-29693	NSF ATM-80-23699	p 141	N93-16384	RTOP 505-31-42	p 34	N93-16941
NAS3-25960	p 72	A93-49761	NSF CBT-84-51076	p 285	A93-31427	RTOP 505-44-2C	p 162	N93-28610
NAS3-25963	p 10	A93-48181	NSF CTS-84-51076	p 285	A93-30124	RTOP 505-52-62	p 5	A93-23351
NAS3-25967	p 185	A93-49877		p 190	A93-55460		p 15	N93-14791
NAS3-25972	p 77	A93-50164	NSF CTS-89-06452	p 189	A93-54053	RTOP 505-53-1A	p 137	N93-25093
NAS3-25982	p 114	A93-24805	NSF CTS-89-12443	p 175	A93-30130		p 139	N93-32367
	p 121	N93-20189	NSF CTS-89-14236	p 179	A93-37936	RTOP 505-61-52	p 9	A93-47189
NAS3-26053	p 102	A93-31359		p 183	A93-46716	RTOP 505-62-0K	p 192	N93-11529
NAS3-26058	p 276	A93-45398	NSF CTS-89-18527	p 113	A93-13323		p 246	N93-15343
NAS3-26061	p 221	A93-26079	NSF CTS-90-06879	p 173	A93-24982		p 199	N93-26554
NAS3-26064	p 6	A93-23387	NSF CTS-90-12832	p 182	A93-45974		p 250	N93-26999
	p 8	A93-39412	NSF CTS-91-15005	p 178	A93-35481	RTOP 505-62-00	p 131	A93-20464
	p 185	A93-49910	NSF DDM-89-17430	p 243	A93-54508		p 21	N93-22588
NAS3-26249	p 221	A93-26081		p 243	A93-54509	RTOP 505-62-10	p 24	A93-23384
NAS3-26252	p 20	A93-22696	NSF DDM-89-96171	p 233	A93-14446		p 31	A93-53980
NAS3-26254	p 276	A93-24142		p 235	A93-22426		p 33	N93-12418
NAS3-26310	p 5	A93-22601	NSF DDM-90-15333	p 263	A93-26650		p 228	N93-23019
NAS3-26314	p 66	A93-21663	NSF DDM-90-19852	p 258	A93-20380		p 228	N93-23741
	p 285	A93-46505		p 242	A93-49028		p 228	N93-24751
NAS3-26321	p 259	A93-22604		p 268	A93-54198		p 228	N93-25672
NAS3-26328	p 113	A93-22648	NSF DMR-89-01869	p 178	A93-35481		p 228	N93-27037
NAS3-26576	p 261	A93-34039	NSF DMR-89-14621	p 284	A93-21695		p 229	N93-27074
NAS3-26602	p 170	A93-23390	NSF DMS-89-02831	p 169	A93-22662		p 229	N93-27641
NAS3-26616	p 28	A93-50008		p 143	A93-41678		p 229	N93-27687
NAS3-26711	p 73	A93-49845	NSF DMS-89-21189	p 166	A93-19821		p 230	N93-28050
NAS3-39184	p 71	A93-49671	NSF DMS-89-57534	p 166	A93-19821		p 230	N93-28411
NAS5-31170	p 52	A93-18966	NSF ECS-87-18897	p 54	A93-13133		p 231	N93-31846
NAS8-32807	p 257	A93-16347	NSF ECS-92-16386	p 74	A93-49907		p 39	N93-32351
NAS8-38861	p 184	A93-49715	NSF EEC-91-16806	p 184	A93-49715		p 39	N93-32368
NCC2-374	p 8	A93-39412	NSF MEA-84-01883	p 162	A93-10839	RTOP 505-62-20	p 2	A93-14118
NCC3-104	p 166	A93-19821	NSF MIP-90-02664	p 148	A93-38221		p 191	N93-10087
NCC3-124	p 8	A93-42579	NSF MSM-83-16833	p 141	N93-16384	RTOP 505-62-21-00	p 213	N93-13410
NCC3-135	p 209	A93-40677	NSF MSM-83-20307	p 178	A93-34409	RTOP 505-62-21	p 172	A93-24942
NCC3-162	p 283	A93-54844	NSF MSM-87-02732	p 175	A93-27900		p 176	A93-30840
NCC3-168	p 267	A93-45080		p 180	A93-41710		p 191	N93-10454
NCC3-171	p 172	A93-24817	NSF MSM-88-17372	p 176	A93-30144		p 268	N93-11531
	p 77	A93-50231	NSF MSS-90-19531	p 264	A93-30492		p 42	N93-12016
	p 190	A93-54483	NSF PHY-87-0036P	p 280	A93-32132		p 245	N93-12277
NCC3-172	p 212	A93-53109	NSF PHY-89-04035	p 294	A93-10355		p 193	N93-14829
NCC3-192	p 155	A93-27244	NSF PHY-92-96020	p 291	A93-35444		p 194	N93-14885
NCC3-197	p 158	A93-54619		p 291	A93-38672		p 268	N93-15341
NCC3-19	p 123	A93-13937	NSF RII-88-05070	p 184	A93-49662		p 194	N93-15499
NCC3-203	p 155	A93-27245	NSG-3555	p 13	A93-50278		p 195	N93-15792
NCC3-208/4	p 110	N93-26705	N00013-86-K-0773	p 280	A93-32132		p 141	N93-16384
NCC3-2084	p 241	A93-45743	N00014-86-K-0773	p 119	A93-53733		p 16	N93-16596
NCC3-221	p 117	A93-41954	N00014-87-K-0030	p 126	A93-37899		p 121	N93-16614
	p 121	N93-20206	N00014-88-K-0637	p 241	A93-45429		p 196	N93-16703
NCC3-233	p 181	A93-45061	N00014-89-J-1006	p 155	A93-27244		p 197	N93-20057
	p 267	A93-45080	N00014-89-J-1007	p 149	A93-52237		p 197	N93-21198
	p 268	N93-11531	N00014-89-J-1633	p 264	A93-37039		p 197	N93-22596
	p 269	N93-22825	N00014-89-J-1836	p 2	A93-19151		p 269	N93-22825
	p 198	N93-23736		p 274	A93-51180		p 199	N93-25175
	p 199	N93-25175	N00014-90-J-1520	p 170	A93-23390		p 250	N93-27088
	p 199	N93-27010	N00014-90-J-1730	p 173	A93-24982		p 201	N93-28947
	p 269	N93-27061	N00014-90-J-1765	p 126	A93-37899	RTOP 505-62-40	p 25	A93-27801
	p 269	N93-27065	N00014-91-J-1917	p 117	A93-39525	RTOP 505-62-50	p 40	A93-37004
	p 269	N93-27068	N00039-89-C-0001	p 97	A93-11459		p 26	A93-49329
	p 250	N93-27088	PHS-G2-R01-AR-34399-04	p 241	A93-45429		p 41	A93-54268
	p 200	N93-27091	RTOP 106-70-00	p 53	N93-27064		p 41	N93-12305
	p 201	N93-28947	RTOP 141-20-0J	p 95	N93-22586		p 213	N93-13307
	p 202	N93-29208	RTOP 144-10-10	p 149	N93-20257		p 34	N93-15525
	p 202	N93-31147		p 150	N93-22483		p 215	N93-19651
	p 203	N93-32199		p 150	N93-26903		p 41	N93-21197
	p 270	N93-32200	RTOP 144-10-2A	p 52	N93-11430		p 36	N93-25079
	p 203	N93-32370	RTOP 144-50-50	p 149	N93-12481		p 216	N93-26906
NCC3-238	p 266	A93-24231	RTOP 303-50-00	p 142	N93-32330		p 42	N93-26907
	p 182	A93-46485	RTOP 307-50-00	p 235	A93-20397		p 216	N93-27001
NCC3-239	p 114	A93-24805		p 244	N93-11403		p 261	N93-27024
NCC3-241	p 277	A93-52412	RTOP 307-51-00	p 160	N93-16616		p 216	N93-27027
	p 278	A93-52415	RTOP 316-30-19	p 52	N93-18854		p 266	N93-28051
NCC3-287	p 106	A93-55685	RTOP 323-51-60	p 38	N93-27640		p 217	N93-28053
NCC3-73	p 133	A93-39513	RTOP 323-53-62	p 60	N93-24755		p 269	N93-31847
	p 135	A93-53734	RTOP 323-57-4B	p 255	N93-23018	RTOP 505-62-51	p 36	N93-25673
NCC3-94	p 100	A93-25104	RTOP 323-57-40	p 249	N93-23746	RTOP 505-62-52	p 166	A93-19416
	p 100	A93-25105	RTOP 326-81-10	p 46	A93-13825		p 13	A93-52006
NGL-16-001-043	p 257	A93-16347		p 47	A93-25866		p 274	A93-53657
NGL-22-0069-640	p 19	N93-15360	RTOP 342-02-00	p 152	A93-25806		p 191	N93-10735

p 15 N93-11223	p 18 A93-23243	RTOP 506-44-2B	p 160 N93-23394
p 268 N93-11254	p 18 A93-23244	RTOP 506-44-2C	p 161 N93-27265
p 32 N93-12077	p 19 A93-23245	RTOP 506-44-21	p 155 A93-27245
p 149 N93-12366	p 24 A93-23246	RTOP 506-46-11	p 84 N93-20615
p 285 N93-12967	p 41 N93-14831	RTOP 506-48-00	p 200 N93-27155
p 262 N93-13154	p 15 N93-14911	RTOP 506-48-2B	p 62 N93-27081
p 193 N93-14758	p 16 N93-15338	RTOP 506-49-00	p 89 N93-26908
p 194 N93-15355	p 19 N93-15345		p 89 N93-26951
p 33 N93-15521	p 19 N93-15354	RTOP 506-59-4C	p 155 A93-27244
p 261 N93-16613	p 19 N93-15360	RTOP 506-72-00	p 160 N93-15531
p 17 N93-19968	p 20 N93-15522		p 160 N93-16713
p 196 N93-19969	p 32 N93-11530	RTOP 506-72-1B	p 284 N93-12325
p 286 N93-19977	p 35 N93-22480		p 160 N93-20259
p 149 N93-20260	p 36 N93-25129	RTOP 506-72-1C	p 53 N93-22589
p 268 N93-22664	p 37 N93-27131	RTOP 506-72-21	p 53 N93-26895
p 197 N93-23059	p 38 N93-29065		p 150 N93-31856
p 198 N93-23404	p 212 A93-54398	RTOP 509-10-11	p 251 N93-31193
p 35 N93-24754	p 51 N93-27018	RTOP 509-90-5K	p 269 N93-27061
p 17 N93-24911	p 20 A93-20281	RTOP 510-01-0A	p 246 N93-13157
p 147 N93-25177	p 259 A93-23699	RTOP 510-01-01	p 117 A93-39521
p 216 N93-25191	p 32 N93-10983	RTOP 510-01-08	p 98 A93-15753
p 199 N93-26203	p 32 N93-12402	RTOP 510-01-50	p 131 A93-24508
p 269 N93-26560	p 208 A93-28580		p 100 A93-24514
p 199 N93-27020	p 198 N93-23736		p 236 A93-26776
p 262 N93-27040	p 200 N93-27091		p 101 A93-31358
p 37 N93-27130	p 200 N93-27161		p 116 A93-39503
p 38 N93-27610	p 202 N93-29161		p 134 A93-40293
p 201 N93-28626	p 202 N93-29208		p 244 N93-10453
p 262 N93-28628	p 202 N93-31147		p 244 N93-10455
p 202 N93-29157	p 203 N93-32199		p 244 N93-10777
p 203 N93-31647	p 270 N93-32200		p 231 N93-10963
p 17 N93-31648	p 203 N93-32370		p 244 N93-10967
p 18 N93-31672	p 267 A93-45080		p 106 N93-11399
p 18 N93-31839	p 199 N93-27010		p 245 N93-11624
p 203 N93-31860	p 269 N93-27065		p 107 N93-12737
p 17 N93-24118	p 123 A93-17609		p 136 N93-14886
p 42 N93-15498	p 107 N93-12078		p 136 N93-16372
p 215 N93-22598	p 126 A93-39796		p 247 N93-17996
p 215 N93-24737	p 127 N93-11609		p 231 N93-18422
p 43 N93-25080	p 195 N93-15585		p 35 N93-23013
p 129 N93-26201	p 269 N93-27068		p 215 N93-25173
p 43 N93-26214	p 110 N93-27270		p 109 N93-26552
p 133 A93-38887	p 293 A93-13699		p 109 N93-26704
p 94 A93-13506	p 159 N93-12301		p 129 N93-26898
p 95 N93-10978	p 193 N93-14150		p 258 N93-26946
p 95 N93-22590	p 161 N93-27002		p 258 N93-26947
p 96 N93-26204	p 129 N93-28618		p 250 N93-27009
p 240 A93-38849	p 256 N93-32201		p 250 N93-27030
p 107 N93-12302	p 252 A93-25886		p 232 N93-27080
p 108 N93-25071	p 78 A93-50822		p 111 N93-28624
p 135 N93-10962	p 81 N93-14079		p 111 N93-28681
p 110 N93-27129	p 253 A93-26043		p 111 N93-29071
p 226 N93-10966	p 85 N93-23017		p 232 N93-29073
p 226 N93-10982	p 98 A93-17675		p 139 N93-32382
p 226 N93-12736	p 50 A93-25891	RTOP 510-02-12	p 110 N93-26705
p 227 N93-22826	p 68 A93-25958		p 110 N93-27082
p 229 N93-27069	p 80 N93-10965		p 110 N93-27092
p 229 N93-27133	p 141 N93-14834		p 250 N93-28633
p 100 A93-25105	p 136 N93-15344	RTOP 510-06-50	p 109 N93-26702
p 105 A93-53446	p 96 N93-22605	RTOP 510-10-50	p 101 A93-31356
p 93 A93-13505	p 271 N93-23016	RTOP 535-03-0B	p 261 N93-12022
p 132 A93-27917	p 60 N93-25090		p 247 N93-18875
p 225 A93-52607	p 61 N93-26148		p 247 N93-23015
p 135 A93-55471	p 61 N93-26215	RTOP 535-03-01	p 36 N93-26161
p 127 N93-11635	p 293 N93-26392	RTOP 535-03-10	p 24 A93-23324
p 107 N93-12076	p 271 N93-31145		p 274 N93-11370
p 95 N93-15576	p 84 N93-20614		p 33 N93-15403
p 128 N93-18069	p 64 A93-13696		p 34 N93-16705
p 108 N93-20317	p 79 N93-10197		p 34 N93-16715
p 128 N93-22556	p 80 N93-11402		p 249 N93-24909
p 137 N93-22560	p 81 N93-12484		p 249 N93-26202
p 96 N93-23014	p 82 N93-15429		p 275 N93-27058
p 96 N93-27003	p 83 N93-15572	RTOP 535-05-10	p 15 N93-13292
p 111 N93-29074	p 83 N93-16714		p 1 N93-14102
p 251 N93-29196	p 83 N93-17995		p 38 N93-28697
p 139 N93-32352	p 279 N93-18635	RTOP 537-01-11	p 113 A93-23238
p 98 A93-15822	p 85 N93-22482		p 120 N93-15504
p 234 A93-17246	p 85 N93-23747		p 257 N93-27012
p 244 N93-11004	p 87 N93-24758	RTOP 537-01-22	p 22 A93-13383
p 245 N93-12738	p 88 N93-26149	RTOP 537-02-00	p 31 A93-54040
p 227 N93-14478	p 88 N93-26561		p 39 N93-31671
p 246 N93-15369	p 91 N93-28619	RTOP 537-02-20	p 33 N93-15359
p 108 N93-18139	p 92 N93-28694		p 198 N93-24759
p 247 N93-21831	p 92 N93-29158	RTOP 537-02-21	p 36 N93-27026
p 248 N93-23406	p 92 N93-29194		p 37 N93-27128
p 249 N93-24913	p 66 A93-14654		p 37 N93-27160
p 249 N93-25070	p 83 N93-15571	RTOP 537-02-22	p 275 N93-26551
p 247 N93-20368	p 84 N93-18878	RTOP 537-02-23	p 272 A93-23241
p 273 A93-29420	p 35 N93-20109		p 274 N93-15430
p 222 A93-34157	p 141 N93-28695		p 275 N93-15575
p 106 N93-12015	p 49 N93-28696		p 16 N93-16704
p 247 N93-18426	p 192 N93-10981	RTOP 537-04-10	p 1 N93-26136
p 144 N93-12197	p 59 N93-19988	RTOP 537-04-21	p 136 N93-12398
p 18 A93-23239	p 201 N93-28252	RTOP 538-01-10	p 138 N93-30938
p 5 A93-23240	p 136 N93-19035		p 24 A93-25997
p 21 A93-23242	p 247 N93-18876		p 32 N93-10456

RTOP 553-13-00	p 125	A93-33011	RTOP 694-03-08	p 145	N93-25337
	p 245	N93-12735	RTOP 763-01-21	p 33	N93-15342
	p 245	N93-12739	RTOP 763-22-28	p 95	N93-10978
	p 246	N93-13153	RTOP 763-22-51	p 129	N93-23418
	p 248	N93-23745	RTOP 906-11-03	p 152	A93-25892
	p 250	N93-26550	SERC-GR/E/7072/6	p 164	A93-17258
	p 93	N93-31552	W-7405-ENG-36	p 164	A93-14551
RTOP 579-50-00	p 53	N93-29195	W-7405-ENG-82	p 243	A93-56412
RTOP 582-01-11	p 130	A93-13613			
	p 87	N93-25089			
RTOP 582-01-41	p 49	N93-11401			
	p 266	N93-19018			
RTOP 584-03-11	p 85	N93-23405			
	p 88	N93-26211			
	p 200	N93-27132			
	p 51	N93-28052			
	p 201	N93-28627			
	p 51	N93-31670			
RTOP 584-04-21	p 93	N93-31858			
RTOP 586-01-11	p 99	A93-20758			
RTOP 589-01-1B	p 57	N93-10841			
	p 60	N93-23742			
RTOP 589-01-2C	p 144	N93-15420			
RTOP 589-10-2C	p 142	A93-23371			
RTOP 590-13-00	p 69	A93-26105			
	p 48	N93-11398			
RTOP 590-13-11	p 46	A93-13822			
	p 65	A93-13824			
	p 65	A93-13905			
	p 97	A93-14840			
	p 100	A93-25104			
	p 220	A93-26052			
	p 153	A93-26076			
	p 146	A93-26077			
	p 221	A93-26079			
	p 174	A93-26087			
	p 174	A93-26089			
	p 141	N93-12085			
	p 82	N93-14482			
	p 128	N93-15524			
	p 82	N93-15526			
	p 271	N93-22559			
	p 256	N93-25136			
RTOP 590-13-31	p 153	A93-25894			
	p 153	A93-25895			
RTOP 590-13-51	p 84	N93-18877			
RTOP 590-21-11	p 218	A93-14651			
	p 246	N93-13260			
	p 128	N93-15586			
	p 246	N93-15788			
	p 214	N93-17777			
	p 217	N93-18091			
	p 227	N93-18321			
	p 227	N93-18380			
	p 87	N93-25236			
	p 216	N93-27021			
RTOP 590-49-00	p 255	N93-15523			
RTOP 591-14-11	p 252	A93-25916			
RTOP 591-14-41	p 123	A93-13937			
RTOP 593-00-71	p 82	N93-15428			
RTOP 593-12-11	p 215	N93-22994			
RTOP 593-12-21	p 80	N93-10743			
	p 81	N93-11614			
RTOP 593-21-00	p 212	A93-54363			
	p 215	N93-22484			
RTOP 593-71-00	p 80	N93-10457			
	p 81	N93-12363			
	p 84	N93-19106			
	p 85	N93-23875			
	p 86	N93-23876			
	p 86	N93-24740			
	p 86	N93-24753			
	p 87	N93-25105			
	p 88	N93-26200			
RTOP 593-72-00	p 86	N93-24744			
	p 88	N93-26210			
RTOP 596-13-11	p 92	N93-28686			
RTOP 650-60-20	p 152	A93-25798			
RTOP 650-60-23	p 148	A93-26237			
	p 58	N93-11001			
RTOP 674-21-05	p 194	N93-14914			
	p 196	N93-16612			
RTOP 674-22-05	p 145	N93-20178			
RTOP 674-27-05	p 128	N93-19974			
RTOP 679-40-00	p 159	N93-13286			
RTOP 694-03-OH	p 63	A93-54401			
RTOP 694-03-0A	p 145	N93-30939			
RTOP 694-03-0C	p 55	A93-24904			
	p 1	N93-15573			
	p 145	N93-27011			
RTOP 694-03-0H	p 63	N93-23738			
	p 63	N93-28554			
RTOP 694-03-00	p 143	A93-33075			
RTOP 694-03-03	p 61	N93-26209			
	p 61	N93-27038			
	p 62	N93-27260			

REPORT/ACCESSION NUMBER INDEX

Typical Report/Accession Number Index Listing



Listings in this index are arranged alphanumerically by report number. The page number indicates the page on which the citation is located. The accession number denotes the number by which the citation is identified. An asterisk (*) indicates that the item is a NASA report. A pound sign (#) indicates that the item is available on microfiche.

AD-A259242	p 226	N93-10982 * #	AIAA PAPER 92-5080	p 51	N93-27018 * #	AIAA PAPER 93-0549	p 273	A93-25538 * #
AD-A259365	p 192	N93-11529 * #	AIAA PAPER 93-0012	p 272	A93-20134 * #	AIAA PAPER 93-0567	p 55	A93-24243 * #
AD-A259931	p 226	N93-12736 * #	AIAA PAPER 93-0017	p 6	A93-24978 #	AIAA PAPER 93-0568	p 67	A93-24244 * #
AD-A262479	p 227	N93-22826 * #	AIAA PAPER 93-0017	p 16	N93-16625 * #	AIAA PAPER 93-0568	p 60	N93-23742 * #
AD-A263112	p 228	N93-23741 * #	AIAA PAPER 93-0018	p 170	A93-24226 * #	AIAA PAPER 93-0573	p 43	A93-24245 * #
AD-A263116	p 228	N93-23019 * #	AIAA PAPER 93-0021	p 113	A93-23238 #	AIAA PAPER 93-0575	p 169	A93-23307 * #
AD-A264968	p 228	N93-24751 * #	AIAA PAPER 93-0021	p 120	N93-15504 * #	AIAA PAPER 93-0596	p 24	A93-24782 * #
AD-A266233	p 229	N93-27687 * #	AIAA PAPER 93-0023	p 167	A93-20141 * #	AIAA PAPER 93-0596	p 34	N93-16715 * #
AD-A266374	p 199	N93-26554 * #	AIAA PAPER 93-0026	p 4	A93-20144 * #	AIAA PAPER 93-0598	p 273	A93-24783 * #
AD-A266538	p 229	N93-27133 * #	AIAA PAPER 93-0029	p 18	A93-23239 #	AIAA PAPER 93-0598	p 34	N93-16705 * #
AD-A266723	p 228	N93-27037 * #	AIAA PAPER 93-0029	p 19	N93-15360 * #	AIAA PAPER 93-0599	p 24	A93-23324 * #
AD-A266724	p 228	N93-25672 * #	AIAA PAPER 93-0031	p 5	A93-23240 #	AIAA PAPER 93-0599	p 33	N93-15403 * #
AD-A267594	p 198	N93-23744 * #	AIAA PAPER 93-0031	p 16	N93-15338 * #	AIAA PAPER 93-0653	p 172	A93-24766 * #
			AIAA PAPER 93-0032	p 20	A93-22551 * #	AIAA PAPER 93-0653	p 197	N93-20057 * #
			AIAA PAPER 93-0032	p 15	N93-14911 * #	AIAA PAPER 93-0673	p 259	A93-24781 * #
			AIAA PAPER 93-0082	p 170	A93-24227 * #	AIAA PAPER 93-0676	p 6	A93-24786 * #
			AIAA PAPER 93-0083	p 4	A93-22552 * #	AIAA PAPER 93-0692	p 172	A93-24792 * #
			AIAA PAPER 93-0086	p 170	A93-24228 * #	AIAA PAPER 93-0692	p 213	N93-13410 * #
			AIAA PAPER 93-0087	p 170	A93-24229 * #	AIAA PAPER 93-0704	p 67	A93-24800 * #
			AIAA PAPER 93-0108	p 171	A93-24230 * #	AIAA PAPER 93-0704	p 61	N93-26148 * #
			AIAA PAPER 93-0130	p 139	A93-22577 * #	AIAA PAPER 93-0705	p 55	A93-24801 * #
			AIAA PAPER 93-0140	p 266	A93-24231 * #	AIAA PAPER 93-0707	p 114	A93-24803 * #
			AIAA PAPER 93-0146	p 272	A93-19804 * #	AIAA PAPER 93-0708	p 114	A93-24804 * #
			AIAA PAPER 93-0147	p 272	A93-23241 * #	AIAA PAPER 93-0710	p 114	A93-24805 * #
			AIAA PAPER 93-0147	p 275	N93-15575 * #	AIAA PAPER 93-0711	p 114	A93-24806 * #
			AIAA PAPER 93-0148	p 171	A93-24232 * #	AIAA PAPER 93-0712	p 114	A93-24807 * #
			AIAA PAPER 93-0153	p 4	A93-22591 * #	AIAA PAPER 93-0713	p 115	A93-24808 * #
			AIAA PAPER 93-0167	p 5	A93-22601 * #	AIAA PAPER 93-0727	p 172	A93-24817 * #
			AIAA PAPER 93-0170	p 21	A93-23242 * #	AIAA PAPER 93-0731	p 273	A93-24821 * #
			AIAA PAPER 93-0170	p 19	N93-15345 * #	AIAA PAPER 93-0735	p 273	A93-24825 * #
			AIAA PAPER 93-0171	p 18	A93-23243 * #	AIAA PAPER 93-0735	p 274	N93-15430 * #
			AIAA PAPER 93-0172	p 259	A93-22604 * #	AIAA PAPER 93-0775	p 172	A93-24859 * #
			AIAA PAPER 93-0173	p 18	A93-23244 * #	AIAA PAPER 93-0775	p 194	N93-15355 * #
			AIAA PAPER 93-0173	p 19	N93-15354 * #	AIAA PAPER 93-0805	p 207	A93-25552 * #
			AIAA PAPER 93-0174	p 19	A93-23245 * #	AIAA PAPER 93-0805	p 88	N93-26149 * #
			AIAA PAPER 93-0174	p 20	N93-15522 * #	AIAA PAPER 93-0812	p 115	A93-24885 * #
			AIAA PAPER 93-0196	p 6	A93-24233 * #	AIAA PAPER 93-0820	p 67	A93-24891 * #
			AIAA PAPER 93-0204	p 168	A93-22622 * #	AIAA PAPER 93-0823	p 115	A93-24893 * #
			AIAA PAPER 93-0215	p 25	A93-27801 * #	AIAA PAPER 93-0825	p 115	A93-24895 * #
			AIAA PAPER 93-0223	p 259	A93-23699 * #	AIAA PAPER 93-0827	p 115	A93-24897 * #
			AIAA PAPER 93-0236	p 113	A93-22648 * #	AIAA PAPER 93-0828	p 115	A93-24898 * #
			AIAA PAPER 93-0237	p 66	A93-22649 * #	AIAA PAPER 93-0829	p 116	A93-24899 * #
			AIAA PAPER 93-0240	p 113	A93-22652 * #	AIAA PAPER 93-0832	p 51	A93-24902 * #
			AIAA PAPER 93-0244	p 140	A93-24234 * #	AIAA PAPER 93-0833	p 142	A93-24903 * #
			AIAA PAPER 93-0249	p 24	A93-23246 * #	AIAA PAPER 93-0834	p 55	A93-24904 * #
			AIAA PAPER 93-0249	p 33	N93-15359 * #	AIAA PAPER 93-0838	p 55	A93-24905 * #
			AIAA PAPER 93-0253	p 169	A93-22662 * #	AIAA PAPER 93-0881	p 172	A93-24942 * #
			AIAA PAPER 93-0255	p 169	A93-22664 * #	AIAA PAPER 93-0882	p 7	A93-25553 * #
			AIAA PAPER 93-0258	p 43	A93-23700 * #	AIAA PAPER 93-0888	p 67	A93-24948 * #
			AIAA PAPER 93-0259	p 169	A93-22666 * #	AIAA PAPER 93-0889	p 173	A93-24949 * #
			AIAA PAPER 93-0260	p 143	A93-25515 * #	AIAA PAPER 93-0891	p 6	A93-24951 * #
			AIAA PAPER 93-0262	p 142	A93-22668 * #	AIAA PAPER 93-0911	p 173	A93-24965 * #
			AIAA PAPER 93-0278	p 169	A93-22681 * #	AIAA PAPER 93-0914	p 173	A93-24968 * #
			AIAA PAPER 93-0283	p 169	A93-22686 * #	AIAA PAPER 93-0975	p 56	A93-30899 * #
			AIAA PAPER 93-0294	p 5	A93-22694 * #	AIAA PAPER 93-1024	p 44	A93-30937 * #
			AIAA PAPER 93-0296	p 20	A93-22696 * #	AIAA PAPER 93-1052	p 69	A93-30956 * #
			AIAA PAPER 93-0298	p 42	A93-23698 * #	AIAA PAPER 93-1086	p 69	A93-30975 * #
			AIAA PAPER 93-0300	p 5	A93-23001 * #	AIAA PAPER 93-1127	p 259	A93-31009 * #
			AIAA PAPER 93-0301	p 5	A93-23247 * #	AIAA PAPER 93-1152	p 56	A93-31028 * #
			AIAA PAPER 93-0301	p 16	N93-15404 * #	AIAA PAPER 93-1152	p 60	N93-24755 * #
			AIAA PAPER 93-0335	p 171	A93-24235 * #	AIAA PAPER 93-1325	p 238	A93-33898 * #
			AIAA PAPER 93-0338	p 171	A93-24236 * #	AIAA PAPER 93-1326	p 267	A93-33899 * #
			AIAA PAPER 93-0347	p 171	A93-24237 * #	AIAA PAPER 93-1338	p 56	A93-33908 * #
			AIAA PAPER 93-0390	p 6	A93-24238 * #	AIAA PAPER 93-1338	p 59	N93-17988 * #
			AIAA PAPER 93-0392	p 19	A93-24239 * #	AIAA PAPER 93-1345	p 238	A93-33915 * #
			AIAA PAPER 93-0398	p 40	A93-23073 * #	AIAA PAPER 93-1346	p 222	A93-33916 * #
			AIAA PAPER 93-0398	p 41	N93-14831 * #	AIAA PAPER 93-1377	p 238	A93-33941 * #
			AIAA PAPER 93-0401	p 55	A93-21108 * #	AIAA PAPER 93-1378	p 238	A93-33942 * #
			AIAA PAPER 93-0405	p 261	A93-23327 * #	AIAA PAPER 93-1379	p 238	A93-33943 * #
			AIAA PAPER 93-0430	p 259	A93-25527 * #	AIAA PAPER 93-1393	p 57	A93-33955 * #
			AIAA PAPER 93-0431	p 6	A93-24240 * #	AIAA PAPER 93-1418	p 239	A93-33972 * #
			AIAA PAPER 93-0437	p 5	A93-23351 * #	AIAA PAPER 93-1440	p 102	A93-33989 * #
			AIAA PAPER 93-0448	p 114	A93-23358 * #	AIAA PAPER 93-1441	p 239	A93-33990 * #
			AIAA PAPER 93-0465	p 142	A93-23371 * #	AIAA PAPER 93-1442	p 103	A93-33991 * #
			AIAA PAPER 93-0465	p 144	N93-15420 * #	AIAA PAPER 93-1491	p 239	A93-34033 * #
			AIAA PAPER 93-0469	p 171	A93-24241 * #	AIAA PAPER 93-1492	p 222	A93-34241 * #
			AIAA PAPER 93-0471	p 142	A93-24242 * #	AIAA PAPER 93-1493	p 267	A93-34034 * #
			AIAA PAPER 93-0482	p 24	A93-23384 * #	AIAA PAPER 93-1494	p 239	A93-34035 * #
			AIAA PAPER 93-0482	p 33	N93-12418 * #	AIAA PAPER 93-1495	p 264	A93-34036 * #
			AIAA PAPER 93-0485	p 6	A93-23387 * #	AIAA PAPER 93-1497	p 239	A93-34037 * #
			AIAA PAPER 93-0488	p 170	A93-23390 * #	AIAA PAPER 93-1498	p 240	A93-34038 * #
			AIAA PAPER 93-0512	p 205	A93-23259 * #	AIAA PAPER 93-1499	p 261	A93-34039 * #
			AIAA PAPER 93-0513	p 205	A93-23260 * #	AIAA PAPER 93-1506	p 103	A93-34045 * #

AIAA PAPER 93-1622	p 240	A93-34151 * #	AIAA PAPER 93-2236	p 13	A93-50039 * #	AIAA PAPER 93-3318	p 9	A93-45014 * #
AIAA PAPER 93-1626	p 240	A93-34155 * #	AIAA PAPER 93-2244	p 140	A93-50046 * #	AIAA PAPER 93-3335	p 9	A93-45029 * #
AIAA PAPER 93-1628	p 26	A93-37446 * #	AIAA PAPER 93-2244	p 141	N93-28695 * #	AIAA PAPER 93-3344	p 181	A93-45038 * #
AIAA PAPER 93-1629	p 222	A93-34157 * #	AIAA PAPER 93-2252	p 186	A93-50050 * #	AIAA PAPER 93-3361	p 181	A93-45054 * #
AIAA PAPER 93-1631	p 25	A93-34159 * #	AIAA PAPER 93-2252	p 202	N93-29157 * #	AIAA PAPER 93-3368	p 181	A93-45061 * #
AIAA PAPER 93-1632	p 25	A93-34160 * #	AIAA PAPER 93-2254	p 28	A93-50052 * #	AIAA PAPER 93-3383	p 267	A93-45074 * #
AIAA PAPER 93-1633	p 25	A93-34161 * #	AIAA PAPER 93-2258	p 75	A93-50056 * #	AIAA PAPER 93-3389	p 267	A93-45080 * #
AIAA PAPER 93-1634	p 26	A93-34162 * #	AIAA PAPER 93-2263	p 44	A93-50057 * #	AIAA PAPER 93-3389	p 269	N93-27065 * #
AIAA PAPER 93-1638	p 26	A93-34165 * #	AIAA PAPER 93-2278	p 44	A93-53588 * #	AIAA PAPER 93-3400	p 10	A93-47202 * #
AIAA PAPER 93-1639	p 267	A93-34166 * #	AIAA PAPER 93-2295	p 224	A93-50080 * #	AIAA PAPER 93-3417	p 10	A93-47213 * #
AIAA PAPER 93-1679	p 240	A93-34191 * #	AIAA PAPER 93-2295	p 230	N93-28050 * #	AIAA PAPER 93-3766	p 40	A93-51361 * #
AIAA PAPER 93-1758	p 71	A93-49657 * #	AIAA PAPER 93-2296	p 224	A93-50081 * #	AIAA PAPER 93-3808	p 41	A93-51400 * #
AIAA PAPER 93-1763	p 27	A93-49660 * #	AIAA PAPER 93-2296	p 226	N93-27037 * #	AIAA PAPER 93-3809	p 21	A93-51401 * #
AIAA PAPER 93-1766	p 184	A93-49662 * #	AIAA PAPER 93-2297	p 224	A93-50082 * #	AIAA PAPER 93-3811	p 30	A93-51403 * #
AIAA PAPER 93-1773	p 184	A93-49669 * #	AIAA PAPER 93-2297	p 229	N93-27687 * #	AIAA PAPER 93-3889	p 50	A93-51473 * #
AIAA PAPER 93-1776	p 71	A93-49671 * #	AIAA PAPER 93-2298	p 224	A93-50083 * #			
AIAA PAPER 93-1779	p 72	A93-49674 * #	AIAA PAPER 93-2298	p 228	N93-25672 * #	ARL-CR-11	p 228	N93-24751 * #
AIAA PAPER 93-1779	p 51	N93-28052 * #	AIAA PAPER 93-2299	p 224	A93-50084 * #			
AIAA PAPER 93-1795	p 27	A93-49685 * #	AIAA PAPER 93-2300	p 211	A93-50085 * #	ARL-MR-69	p 198	N93-23744 * #
AIAA PAPER 93-1795	p 38	N93-28697 * #	AIAA PAPER 93-2324	p 28	A93-50104 * #	ARL-MR-71	p 228	N93-23019 * #
AIAA PAPER 93-1797	p 189	A93-53585 * #	AIAA PAPER 93-2332	p 118	A93-50110 * #	ARL-MR-77	p 229	N93-27641 * #
AIAA PAPER 93-1797	p 203	N93-31647 * #	AIAA PAPER 93-2333	p 186	A93-50111 * #	ARL-MR-91	p 203	N93-31647 * #
AIAA PAPER 93-1806	p 12	A93-49695 * #	AIAA PAPER 93-2341	p 118	A93-50116 * #			
AIAA PAPER 93-1825	p 48	A93-49711 * #	AIAA PAPER 93-2352	p 44	A93-50125 * #	ARL-TR-11	p 228	N93-25672 * #
AIAA PAPER 93-1830	p 184	A93-49715 * #	AIAA PAPER 93-2353	p 75	A93-50126 * #	ARL-TR-158	p 228	N93-27037 * #
AIAA PAPER 93-1836	p 12	A93-49720 * #	AIAA PAPER 93-2357	p 75	A93-50129 * #	ARL-TR-159	p 230	N93-28411 * #
AIAA PAPER 93-1847	p 12	A93-49728 * #	AIAA PAPER 93-2367	p 76	A93-50138 * #	ARL-TR-171	p 230	N93-28050 * #
AIAA PAPER 93-1847	p 38	N93-29162 * #	AIAA PAPER 93-2375	p 211	A93-50144 * #	ARL-TR-9	p 229	N93-27687 * #
AIAA PAPER 93-1859	p 48	A93-49737 * #	AIAA PAPER 93-2378	p 119	A93-50147 * #			
AIAA PAPER 93-1859	p 49	N93-28696 * #	AIAA PAPER 93-2380	p 186	A93-50148 * #	ASME PAPER 91-TRIB-20	p 219	A93-15682 * #
AIAA PAPER 93-1868	p 12	A93-49743 * #	AIAA PAPER 93-2381	p 186	A93-50149 * #	ASME PAPER 91-TRIB-21	p 219	A93-15681 * #
AIAA PAPER 93-1878	p 140	A93-49752 * #	AIAA PAPER 93-2381	p 38	N93-27610 * #	ASME PAPER 91-TRIB-27	p 219	A93-15685 * #
AIAA PAPER 93-1886	p 72	A93-49759 * #	AIAA PAPER 93-2391	p 76	A93-50156 * #	ASME PAPER 92-GT-169	p 3	A93-19395 * #
AIAA PAPER 93-1886	p 91	N93-27022 * #	AIAA PAPER 93-2392	p 76	A93-50157 * #	ASME PAPER 92-GT-173	p 3	A93-19399 * #
AIAA PAPER 93-1887	p 72	A93-49760 * #	AIAA PAPER 93-2396	p 76	A93-50161 * #	ASME PAPER 92-GT-174	p 3	A93-19400 * #
AIAA PAPER 93-1888	p 72	A93-49761 * #	AIAA PAPER 93-2397	p 76	A93-50162 * #	ASME PAPER 92-GT-175	p 3	A93-19401 * #
AIAA PAPER 93-1898	p 72	A93-49768 * #	AIAA PAPER 93-2399	p 77	A93-50164 * #	ASME PAPER 92-GT-191	p 166	A93-19416 * #
AIAA PAPER 93-1899	p 73	A93-49769 * #	AIAA PAPER 93-2402	p 186	A93-50167 * #	ASME PAPER 92-GT-194	p 166	A93-19419 * #
AIAA PAPER 93-1902	p 73	A93-49772 * #	AIAA PAPER 93-2402	p 92	N93-29194 * #	ASME PAPER 92-GT-196	p 166	A93-19421 * #
AIAA PAPER 93-1917	p 184	A93-49783 * #	AIAA PAPER 93-2403	p 187	A93-50168 * #	ASME PAPER 92-GT-213	p 4	A93-19436 * #
AIAA PAPER 93-1925	p 12	A93-49791 * #	AIAA PAPER 93-2403	p 92	N93-28694 * #	ASME PAPER 92-GT-296	p 231	A93-19486 * #
AIAA PAPER 93-1927	p 189	A93-53586 * #	AIAA PAPER 93-2423	p 187	A93-50181 * #	ASME PAPER 92-GT-300	p 4	A93-19490 * #
AIAA PAPER 93-1927	p 270	N93-32200 * #	AIAA PAPER 93-2437	p 29	A93-50189 * #	ASME PAPER 92-GT-304	p 219	A93-19494 * #
AIAA PAPER 93-1934	p 78	A93-50322 * #	AIAA PAPER 93-2437	p 37	N93-27131 * #	ASME PAPER 92-GT-316	p 99	A93-19502 * #
AIAA PAPER 93-1935	p 73	A93-49797 * #	AIAA PAPER 93-2438	p 29	A93-50190 * #	ASME PAPER 92-GT-383	p 234	A93-19540 * #
AIAA PAPER 93-1936	p 78	A93-53587 * #	AIAA PAPER 93-2438	p 38	N93-29065 * #	ASME PAPER 92-GT-394	p 99	A93-19547 * #
AIAA PAPER 93-1936	p 93	N93-31858 * #	AIAA PAPER 93-2440	p 29	A93-50192 * #	ASME PAPER 92-GT-57	p 23	A93-19307 * #
AIAA PAPER 93-1946	p 44	A93-49804 * #	AIAA PAPER 93-2441	p 29	A93-50193 * #	ASME PAPER 92-GT-6	p 23	A93-19279 * #
AIAA PAPER 93-1966	p 73	A93-49814 * #	AIAA PAPER 93-2497	p 77	A93-50231 * #	ASME PAPER 92-GT-72	p 2	A93-19322 * #
AIAA PAPER 93-1967	p 73	A93-49815 * #	AIAA PAPER 93-2498	p 77	A93-50232 * #	ASME PAPER 92-GT-74	p 3	A93-19324 * #
AIAA PAPER 93-1968	p 184	A93-49816 * #	AIAA PAPER 93-2511	p 63	A93-50242 * #			
AIAA PAPER 93-1968	p 201	N93-28252 * #	AIAA PAPER 93-2521	p 30	A93-53589 * #	AVSCOM-TR-91-C-046	p 246	N93-13153 * #
AIAA PAPER 93-1998	p 223	A93-49841 * #	AIAA PAPER 93-2521	p 39	N93-32368 * #	AVSCOM-TR-92-C-004	p 226	N93-10982 * #
AIAA PAPER 93-2006	p 73	A93-49845 * #	AIAA PAPER 93-2522	p 30	A93-50252 * #	AVSCOM-TR-92-C-007	p 227	N93-22826 * #
AIAA PAPER 93-2025	p 74	A93-49861 * #	AIAA PAPER 93-2523	p 30	A93-50253 * #	AVSCOM-TR-92-C-009	p 229	N93-27133 * #
AIAA PAPER 93-2032	p 118	A93-49867 * #	AIAA PAPER 93-2526	p 187	A93-50254 * #	AVSCOM-TR-92-C-013	p 226	N93-10966 * #
AIAA PAPER 93-2037	p 185	A93-49872 * #	AIAA PAPER 93-2527	p 187	A93-50255 * #	AVSCOM-TR-92-C-015	p 229	N93-27069 * #
AIAA PAPER 93-2037	p 36	N93-27026 * #	AIAA PAPER 93-2528	p 77	A93-50256 * #	AVSCOM-TR-92-C-022	p 199	N93-26554 * #
AIAA PAPER 93-2043	p 27	A93-49876 * #	AIAA PAPER 93-2529	p 77	A93-50257 * #	AVSCOM-TR-92-C-023	p 192	N93-11529 * #
AIAA PAPER 93-2043	p 37	N93-27160 * #	AIAA PAPER 93-2530	p 77	A93-50258 * #	AVSCOM-TR-92-C-030	p 226	N93-12736 * #
AIAA PAPER 93-2044	p 185	A93-49877 * #	AIAA PAPER 93-2534	p 225	A93-50261 * #	AVSCOM-TR-92-C-033	p 228	N93-23741 * #
AIAA PAPER 93-2044	p 37	N93-27128 * #	AIAA PAPER 93-2534	p 200	N93-27132 * #	AVSCOM-TR-92-C-034	p 231	N93-31846 * #
AIAA PAPER 93-2069	p 185	A93-49901 * #	AIAA PAPER 93-2535	p 225	A93-50262 * #	AVSCOM-TR-92-C-035	p 229	N93-27074 * #
AIAA PAPER 93-2074	p 28	A93-49903 * #	AIAA PAPER 93-2535	p 201	N93-28627 * #	AVSCOM-TR-92-C-038	p 35	N93-22599 * #
AIAA PAPER 93-2079	p 211	A93-49906 * #	AIAA PAPER 93-2538	p 225	A93-53590 * #			
AIAA PAPER 93-2080	p 74	A93-49907 * #	AIAA PAPER 93-2538	p 51	N93-31670 * #	CMOTT-92-08	p 195	N93-15792 * #
AIAA PAPER 93-2083	p 185	A93-49910 * #	AIAA PAPER 93-2555	p 30	A93-50277 * #	CMOTT-92-09	p 191	N93-10454 * #
AIAA PAPER 93-2084	p 28	A93-49911 * #	AIAA PAPER 93-2556	p 13	A93-50278 * #	CMOTT-92-10	p 268	N93-15341 * #
AIAA PAPER 93-2085	p 28	A93-49912 * #	AIAA PAPER 93-2559	p 187	A93-50280 * #	CMOTT-92-11	p 193	N93-14829 * #
AIAA PAPER 93-2086	p 13	A93-49913 * #	AIAA PAPER 93-2580	p 30	A93-50294 * #	CMOTT-92-12	p 196	N93-16703 * #
AIAA PAPER 93-2106	p 74	A93-49928 * #	AIAA PAPER 93-2731	p 182	A93-46485 * #	CMOTT-92-13	p 141	N93-16384 * #
AIAA PAPER 93-2106	p 92	N93-29158 * #	AIAA PAPER 93-2758	p 285	A93-46505 * #	CMOTT-92-14	p 16	N93-16596 * #
AIAA PAPER 93-2109	p 271	A93-49930 * #	AIAA PAPER 93-2832	p 285	A93-46569 * #	CMOTT-93-02	p 198	N93-23736 * #
AIAA PAPER 93-2130	p 74	A93-49949 * #	AIAA PAPER 93-2835	p 182	A93-46572 * #	CMOTT-93-07	p 202	N93-29161 * #
AIAA PAPER 93-2132	p 74	A93-49951 * #	AIAA PAPER 93-2919	p 14	A93-53591 * #	CMOTT-93-5	p 200	N93-27161 * #
AIAA PAPER 93-2133	p 48	A93-49952 * #	AIAA PAPER 93-2927	p 10	A93-48128 * #	CMOTT-93-6	p 199	N93-27010 * #
AIAA PAPER 93-2136	p 74	A93-49954 * #	AIAA PAPER 93-2934	p 183	A93-48132 * #	CMOTT-93-9	p 270	N93-32200 * #
AIAA PAPER 93-2137	p 48	A93-49955 * #	AIAA PAPER 93-2952	p 183	A93-48146 * #			
AIAA PAPER 93-2148	p 223	A93-49965 * #	AIAA PAPER 93-2964	p 10	A93-48158 * #	CONF-9208154-1	p 276	N93-16531 * #
AIAA PAPER 93-2148	p 230	N93-28411 * #	AIAA PAPER 93-2988	p 10	A93-48181 * #	CONF-920879-2	p 277	N93-17343 * #
AIAA PAPER 93-2149	p 223	A93-49966 * #	AIAA PAPER 93-2992	p 11	A93-48184 * #			
AIAA PAPER 93-2149	p 228	N93-23019 * #	AIAA PAPER 93-3051	p 183	A93-48231 * #	DE92-000754	p 277	N93-17343 * #
AIAA PAPER 93-2150	p 224	A93-49967 * #	AIAA PAPER 93-3063	p 11	A93-48239 * #	DE92-041262	p 276	N93-16531 * #
AIAA PAPER 93-2150	p 229	N93-27641 * #	AIAA PAPER 93-3065	p 11	A93-48241 * #			
AIAA PAPER 93-2154	p 13	A93-49970 * #	AIAA PAPER 93-3074	p 183	A93-48249 * #	DOT/FAA/CT-TN92/29	p 213	N93-13307 * #
AIAA PAPER 93-2162	p 91	N93-28619 * #	AIAA PAPER 93-3123	p 11	A93-48291 * #			
AIAA PAPER 93-2163	p 75	A93-49978 * #	AIAA PAPER 93-3127	p 11	A93-48293 * #	E-2087	p 1	N93-72738 * #
AIAA PAPER 93-2176	p 42	A93-49988 * #	AIAA PAPER 93-3133	p 11	A93-48298 * #	E-2293	p 246	N93-15369 * #
AIAA PAPER 93-2176	p 43	N93-26214 * #	AIAA PAPER 93-3252	p 183	A93-46797 * #	E-5861	p 34	N93-16941 * #
AIAA PAPER 93-2177	p 277	A93-49989 * #	AIAA PAPER 93-3253	p 14	A93-53592 * #	E-5868	p 61	N93-26209 * #
AIAA PAPER 93-2189	p 118	A93-50001 * #	AIAA PAPER 93-3253	p 17	N93-31648 * #	E-5894	p 285	N93-12967 * #
AIAA PAPER 93-2193	p 185	A93-50005 * #	AIAA PAPER 93-3263	p 18	N93-31672 * #	E-6030	p 52	N93-18854 * #
AIAA PAPER 93-2196	p 28	A93-50008 * #	AIAA PAPER 93-3292	p 287	A93-44996 * #	E-6068	p 93	N93-31552 * #
AIAA PAPER 93-2217	p 75	A93-50023 * #	AIAA PAPER 93-3302	p 8	A93-45000 * #	E-6137	p 42	N93-12016 * #
AIAA PAPER 93-2225	p 75	A93-50031 * #	AIAA PAPER 93-3305	p 8	A93-45003 * #	E-6166-1	p 227	N93-14478 * #
AIAA PAPER 93-2228	p 57	A93-50034 * #	AIAA PAPER 93-3313	p 260	A93-45009 * #	E-6277	p 147	N93-70966 * #

E-6287	p 245	N93-11624 * #	E-7284	p 80	N93-10734 * #	E-7498	p 19	N93-15345 * #
E-6363-1	p 149	N93-12366 * #	E-7286	p 261	N93-11005 * #	E-7499	p 20	N93-15522 * #
E-6372	p 128	N93-18069 * #	E-7288	p 160	N93-15503 * #	E-7500	p 41	N93-14831 * #
E-6402	p 275	N93-27058 * #	E-7291	p 192	N93-11529 * #	E-7502	p 35	N93-23013 * #
E-6455	p 107	N93-12302 * #	E-7293	p 107	N93-12737 * #	E-7505	p 194	N93-15355 * #
E-6483	p 59	N93-19988 * #	E-7295	p 192	N93-10981 * #	E-7506	p 82	N93-15428 * #
E-6497	p 261	N93-12022 * #	E-7299	p 121	N93-16614 * #	E-7507	p 82	N93-15429 * #
E-6513	p 58	N93-11001 * #	E-7300	p 32	N93-10456 * #	E-7508	p 33	N93-15359 * #
E-6558	p 159	N93-13286 * #	E-7309	p 145	N93-20178 * #	E-7509	p 197	N93-20057 * #
E-6615	p 197	N93-23059 * #	E-7310	p 191	N93-10454 * #	E-7511	p 35	N93-22599 * #
E-6663	p 247	N93-18875 * #	E-7320	p 136	N93-12398 * #	E-7521	p 84	N93-18878 * #
E-6676	p 244	N93-11403 * #	E-7321	p 268	N93-11531 * #	E-7525	p 16	N93-16596 * #
E-6751	p 82	N93-15528 * #	E-7322	p 120	N93-11545 * #	E-7526	p 217	N93-18091 * #
E-6797	p 244	N93-11004 * #	E-7326	p 194	N93-14914 * #	E-7536	p 215	N93-22484 * #
E-6804	p 160	N93-15531 * #	E-7327	p 249	N93-26202 * #	E-7537	p 247	N93-18426 * #
E-6810	p 129	N93-26201 * #	E-7328	p 84	N93-18877 * #	E-7538	p 129	N93-23418 * #
E-6831	p 108	N93-18139 * #	E-7330	p 84	N93-19106 * #	E-7539	p 215	N93-22598 * #
E-6832	p 287	N93-23002 * #	E-7331	p 16	N93-16704 * #	E-7540	p 83	N93-17995 * #
E-6849	p 81	N93-11614 * #	E-7332	p 53	N93-26895 * #	E-7543	p 60	N93-22551 * #
E-6850	p 80	N93-10743 * #	E-7333	p 247	N93-18876 * #	E-7544	p 249	N93-24913 * #
E-6873	p 79	N93-10197 * #	E-7334	p 81	N93-12363 * #	E-7545	p 249	N93-25070 * #
E-6874	p 286	N93-19977 * #	E-7335	p 245	N93-12738 * #	E-7552	p 271	N93-23016 * #
E-6889-1	p 137	N93-22560 * #	E-7339	p 34	N93-15525 * #	E-7566	p 129	N93-26898 * #
E-6893	p 135	N93-10962 * #	E-7340	p 247	N93-23015 * #	E-7571	p 95	N93-22586 * #
E-6897	p 261	N93-16613 * #	E-7342	p 80	N93-11402 * #	E-7572-1	p 275	N93-26551 * #
E-6898	p 106	N93-12015 * #	E-7343	p 57	N93-10841 * #	E-7573	p 108	N93-20317 * #
E-6906	p 246	N93-15788 * #	E-7345	p 262	N93-27040 * #	E-7574	p 215	N93-25173 * #
E-6925	p 127	N93-11635 * #	E-7346	p 192	N93-13385 * #	E-7575	p 200	N93-27155 * #
E-692R	p 287	N93-14796 * #	E-7348	p 245	N93-12735 * #	E-7582	p 96	N93-22605 * #
E-6938	p 1	N93-26136 * #	E-7349	p 107	N93-12078 * #	E-7583	p 128	N93-19974 * #
E-6951	p 81	N93-12484 * #	E-7350	p 226	N93-12736 * #	E-7586	p 85	N93-22482 * #
E-6967	p 42	N93-15498 * #	E-7351	p 38	N93-27640 * #	E-7587	p 110	N93-27092 * #
E-6994-1	p 247	N93-21831 * #	E-7355	p 52	N93-11430 * #	E-7588	p 109	N93-26552 * #
E-7008	p 160	N93-23394 * #	E-7356	p 284	N93-12325 * #	E-7590	p 42	N93-26907 * #
E-7016-2-PT-2	p 293	N93-26392 * #	E-7358	p 107	N93-12076 * #	E-7592	p 249	N93-23746 * #
E-7017	p 271	N93-22559 * #	E-7359	p 248	N93-23745 * #	E-7593-VOL-1	p 35	N93-24754 * #
E-7022	p 15	N93-13292 * #	E-7360	p 193	N93-14758 * #	E-7595	p 17	N93-19968 * #
E-7045-1	p 80	N93-10965 * #	E-7361	p 127	N93-11609 * #	E-7597	p 111	N93-28624 * #
E-7052	p 231	N93-18422 * #	E-7368	p 128	N93-15586 * #	E-7599	p 250	N93-26999 * #
E-7055	p 141	N93-14834 * #	E-7369	p 279	N93-18635 * #	E-7600	p 149	N93-20257 * #
E-7066	p 268	N93-11254 * #	E-7374	p 213	N93-13307 * #	E-7605	p 21	N93-22588 * #
E-7067	p 33	N93-15342 * #	E-7382	p 32	N93-12402 * #	E-7608	p 160	N93-20259 * #
E-7070-1	p 82	N93-15526 * #	E-7383	p 88	N93-26561 * #	E-7613	p 197	N93-21198 * #
E-7079	p 145	N93-30939 * #	E-7384	p 160	N93-16713 * #	E-7620	p 36	N93-25079 * #
E-7099	p 86	N93-24740 * #	E-7387	p 213	N93-13410 * #	E-7622	p 86	N93-23876 * #
E-7111	p 17	N93-24118 * #	E-7388	p 262	N93-12410 * #	E-7623	p 85	N93-23875 * #
E-7121	p 257	N93-27012 * #	E-7393	p 81	N93-14079 * #	E-7632	p 36	N93-25673 * #
E-7122	p 106	N93-11399 * #	E-7395	p 141	N93-12085 * #	E-7633	p 43	N93-26214 * #
E-7132	p 226	N93-10966 * #	E-7397	p 136	N93-16372 * #	E-7638-VOL-1	p 89	N93-26908 * #
E-7136	p 136	N93-15344 * #	E-7398	p 33	N93-12418 * #	E-7638-VOL-2	p 89	N93-26951 * #
E-7138	p 274	N93-11370 * #	E-7408	p 136	N93-14886 * #	E-7640	p 85	N93-23405 * #
E-7139	p 246	N93-13157 * #	E-7410	p 194	N93-15499 * #	E-7643	p 38	N93-29065 * #
E-7151	p 128	N93-22556 * #	E-7413	p 196	N93-16612 * #	E-7644	p 111	N93-28681 * #
E-7163	p 249	N93-24909 * #	E-7414	p 128	N93-15524 * #	E-7646	p 84	N93-20614 * #
E-7168	p 255	N93-20261 * #	E-7425	p 1	N93-20902 * #	E-7647	p 198	N93-23744 * #
E-7169	p 269	N93-26560 * #	E-7427	p 255	N93-15523 * #	E-7648	p 36	N93-25129 * #
E-7171	p 35	N93-20109 * #	E-7431	p 136	N93-19035 * #	E-7656	p 200	N93-27091 * #
E-7178	p 80	N93-10457 * #	E-7433-1	p 35	N93-22480 * #	E-7659	p 161	N93-27265 * #
E-7181	p 193	N93-14150 * #	E-7434	p 83	N93-15572 * #	E-7661	p 63	N93-28554 * #
E-7182	p 246	N93-13153 * #	E-7435	p 268	N93-15341 * #	E-7663	p 84	N93-20615 * #
E-7183	p 244	N93-10455 * #	E-7438	p 194	N93-14885 * #	E-7664	p 129	N93-28618 * #
E-7188	p 159	N93-12301 * #	E-7441	p 160	N93-16616 * #	E-7667	p 269	N93-22825 * #
E-7193	p 197	N93-22596 * #	E-7442	p 1	N93-14102 * #	E-7669	p 248	N93-23739 * #
E-7196	p 43	N93-25080 * #	E-7443	p 262	N93-13154 * #	E-7670	p 248	N93-23740 * #
E-7198	p 214	N93-17777 * #	E-7445	p 60	N93-24755 * #	E-7671	p 248	N93-23044 * #
E-7205	p 149	N93-12481 * #	E-7446	p 82	N93-14482 * #	E-7672	p 109	N93-26704 * #
E-7206	p 246	N93-15343 * #	E-7451	p 16	N93-16625 * #	E-7674	p 198	N93-24759 * #
E-7207	p 244	N93-10967 * #	E-7452	p 33	N93-15403 * #	E-7675	p 87	N93-25089 * #
E-7208	p 49	N93-11401 * #	E-7454	p 1	N93-15573 * #	E-7679	p 198	N93-23736 * #
E-7210	p 41	N93-12305 * #	E-7455	p 247	N93-17996 * #	E-7681	p 256	N93-25136 * #
E-7214	p 215	N93-19651 * #	E-7456	p 95	N93-22590 * #	E-7682	p 53	N93-22589 * #
E-7215	p 92	N93-28686 * #	E-7457	p 120	N93-15504 * #	E-7683	p 108	N93-25071 * #
E-7216	p 32	N93-10983 * #	E-7462	p 95	N93-15576 * #	E-7686	p 111	N93-29074 * #
E-7220	p 226	N93-10982 * #	E-7464	p 96	N93-26204 * #	E-7687	p 286	N93-26205 * #
E-7222	p 266	N93-19018 * #	E-7465	p 15	N93-14791 * #	E-7688	p 255	N93-23018 * #
E-7230	p 196	N93-19969 * #	E-7466	p 268	N93-22664 * #	E-7695	p 96	N93-23014 * #
E-7234	p 41	N93-21197 * #	E-7468	p 59	N93-17988 * #	E-7698	p 228	N93-23019 * #
E-7236	p 95	N93-10978 * #	E-7470	p 229	N93-27074 * #	E-7699	p 137	N93-25093 * #
E-7237	p 247	N93-20368 * #	E-7471	p 275	N93-15575 * #	E-7702	p 198	N93-23404 * #
E-7238	p 231	N93-10963 * #	E-7473	p 19	N93-15360 * #	E-7707	p 60	N93-23742 * #
E-7240	p 32	N93-12077 * #	E-7474	p 196	N93-16703 * #	E-7712	p 85	N93-23017 * #
E-7241	p 191	N93-10087 * #	E-7475	p 141	N93-16384 * #	E-7714	p 215	N93-22994 * #
E-7244	p 48	N93-11398 * #	E-7476	p 193	N93-14829 * #	E-7716	p 17	N93-24911 * #
E-7248	p 191	N93-10735 * #	E-7476	p 34	N93-16705 * #	E-7718	p 199	N93-25175 * #
E-7250	p 244	N93-10777 * #	E-7478	p 63	N93-23738 * #	E-7722	p 85	N93-23747 * #
E-7252	p 245	N93-12277 * #	E-7479	p 34	N93-16715 * #	E-7724	p 201	N93-28947 * #
E-7253	p 195	N93-15585 * #	E-7481	p 274	N93-15430 * #	E-7728	p 87	N93-24758 * #
E-7254	p 244	N93-10453 * #	E-7482	p 83	N93-15571 * #	E-7729	p 109	N93-26702 * #
E-7264	p 144	N93-12197 * #	E-7485	p 144	N93-15420 * #	E-7730	p 150	N93-22483 * #
E-7265	p 227	N93-22826 * #	E-7489	p 149	N93-20260 * #	E-7731	p 228	N93-24751 * #
E-7274	p 195	N93-15792 * #	E-7490	p 83	N93-16714 * #	E-7735	p 215	N93-24737 * #
E-7278	p 15	N93-11223 * #	E-7492	p 16	N93-15404 * #	E-7736	p 248	N93-23406 * #
E-7280	p 32	N93-11530 * #	E-7493	p 33	N93-15521 * #	E-7737	p 161	N93-24746 * #
E-7281	p 227	N93-18321 * #	E-7494	p 16	N93-15338 * #	E-7738	p 88	N93-26211 * #
E-7282	p 227	N93-18380 * #	E-7495	p 15	N93-14911 * #	E-7739	p 88	N93-26149 * #
E-7283	p 245	N93-12739 * #	E-7497	p 19	N93-15354 * #	E-7740	p 60	N93-25090 * #

E-7741	p 228	N93-23741 * #	E-7948	p 38	N93-28697 * #	NAS 1.15.105269	p 261	N93-12022 * #
E-7742	p 229	N93-27069 * #	E-7952	p 201	N93-28627 * #	NAS 1.15.105270	p 249	N93-26202 * #
E-7743	p 229	N93-27133 * #	E-7953	p 91	N93-28619 * #	NAS 1.15.105272	p 247	N93-18875 * #
E-7744	p 262	N93-28628 * #	E-7954	p 51	N93-28052 * #	NAS 1.15.105319	p 244	N93-11403 * #
E-7748	p 91	N93-27039 * #	E-7955	p 17	N93-31648 * #	NAS 1.15.105419	p 287	N93-23002 * #
E-7752	p 228	N93-25672 * #	E-7958	p 38	N93-29162 * #	NAS 1.15.105568	p 135	N93-10962 * #
E-7754	p 216	N93-25191 * #	E-7961	p 150	N93-31856 * #	NAS 1.15.105572	p 261	N93-16613 * #
E-7756	p 61	N93-26148 * #	E-7964	p 18	N93-31672 * #	NAS 1.15.105595	p 287	N93-14796 * #
E-7757	p 150	N93-26903 * #	E-7970	p 202	N93-31147 * #	NAS 1.15.105598	p 127	N93-11635 * #
E-7758	p 199	N93-26554 * #	E-7971	p 203	N93-32199 * #	NAS 1.15.105602	p 1	N93-26136 * #
E-7759	p 86	N93-24753 * #	E-7973	p 271	N93-31145 * #	NAS 1.15.105609	p 245	N93-12738 * #
E-7762	p 270	N93-27124 * #	E-7974	p 142	N93-32330 * #	NAS 1.15.105614	p 81	N93-12484 * #
E-7763	p 232	N93-27025 * #	E-7975	p 231	N93-31846 * #	NAS 1.15.105626	p 42	N93-15498 * #
E-7764	p 250	N93-27088 * #	E-7978	p 51	N93-31670 * #	NAS 1.15.105640	p 82	N93-15526 * #
E-7768	p 37	N93-27131 * #	E-7979	p 139	N93-32382 * #	NAS 1.15.105658	p 15	N93-13292 * #
E-7770	p 199	N93-27010 * #	E-7980	p 139	N93-32352 * #	NAS 1.15.105677	p 231	N93-18422 * #
E-7772	p 269	N93-27068 * #	E-7983	p 269	N93-31847 * #	NAS 1.15.105687	p 33	N93-15342 * #
E-7773	p 216	N93-27021 * #	E-7985	p 203	N93-32370 * #	NAS 1.15.105705	p 88	N93-26200 * #
E-7774	p 91	N93-27022 * #	E-7995	p 138	N93-30938 * #	NAS 1.15.105707	p 86	N93-24744 * #
E-7775	p 87	N93-25236 * #	E-8000	p 93	N93-31858 * #	NAS 1.15.105708	p 87	N93-25105 * #
E-7776	p 51	N93-27018 * #	E-8002	p 203	N93-31860 * #	NAS 1.15.105710	p 86	N93-24753 * #
E-7777	p 261	N93-27024 * #				NAS 1.15.105711	p 86	N93-24740 * #
E-7781	p 87	N93-25105 * #	IAF PAPER 92-0591	p 293	A93-13699	NAS 1.15.105722	p 257	N93-27012 * #
E-7782	p 88	N93-26200 * #	IAF PAPER 92-0777	p 64	A93-13698 *	NAS 1.15.105723	p 106	N93-11399 * #
E-7783	p 86	N93-24744 * #				NAS 1.15.105729	p 226	N93-10966 * #
E-7787	p 258	N93-26947 * #	IAF-92-0568	p 277	N93-17343 * #	NAS 1.15.105732	p 136	N93-15344 * #
E-7788	p 258	N93-26946 * #	IAF-92-0607	p 85	N93-23747 * #	NAS 1.15.105736	p 274	N93-11370 * #
E-7791	p 202	N93-29157 * #	IAF-92-0669	p 83	N93-15572 * #	NAS 1.15.105747	p 80	N93-10965 * #
E-7792	p 161	N93-27002 * #				NAS 1.15.105756	p 255	N93-20261 * #
E-7793	p 147	N93-25177 * #	ICOMP-92-12	p 195	N93-15792 * #	NAS 1.15.105761	p 80	N93-10457 * #
E-7794	p 110	N93-27270 * #	ICOMP-92-13	p 245	N93-12277 * #	NAS 1.15.105764	p 193	N93-14150 * #
E-7795	p 110	N93-27129 * #	ICOMP-92-14	p 191	N93-10735 * #	NAS 1.15.105765	p 246	N93-13153 * #
E-7796	p 250	N93-27030 * #	ICOMP-92-16	p 191	N93-10454 * #	NAS 1.15.105766	p 244	N93-10455 * #
E-7797	p 96	N93-27266 * #	ICOMP-92-19	p 268	N93-11531 * #	NAS 1.15.105771	p 43	N93-25080 * #
E-7798	p 199	N93-26203 * #	ICOMP-92-20	p 194	N93-15499 * #	NAS 1.15.105772	p 141	N93-14834 * #
E-7799	p 37	N93-27130 * #	ICOMP-92-21	p 268	N93-15341 * #	NAS 1.15.105776	p 268	N93-11254 * #
E-7801	p 250	N93-26550 * #	ICOMP-92-23	p 193	N93-14829 * #	NAS 1.15.105778	p 149	N93-12481 * #
E-7804	p 61	N93-26215 * #	ICOMP-92-24	p 196	N93-16703 * #	NAS 1.15.105779	p 246	N93-15343 * #
E-7805	p 145	N93-25337 * #	ICOMP-92-25	p 141	N93-16384 * #	NAS 1.15.105780	p 244	N93-10967 * #
E-7814	p 36	N93-26161 * #	ICOMP-92-26	p 197	N93-20057 * #	NAS 1.15.105781	p 49	N93-11401 * #
E-7816	p 111	N93-29071 * #	ICOMP-92-27	p 16	N93-16596 * #	NAS 1.15.105784	p 215	N93-19651 * #
E-7818	p 96	N93-27003 * #	ICOMP-93-01	p 269	N93-27061 * #	NAS 1.15.105785	p 92	N93-28666 * #
E-7819	p 216	N93-27001 * #	ICOMP-93-05	p 200	N93-27091 * #	NAS 1.15.105786	p 32	N93-10983 * #
E-7820	p 88	N93-26210 * #	ICOMP-93-06	p 269	N93-22825 * #	NAS 1.15.105790	p 226	N93-10982 * #
E-7822	p 61	N93-27038 * #	ICOMP-93-07	p 198	N93-23736 * #	NAS 1.15.105792	p 266	N93-19018 * #
E-7823	p 250	N93-27009 * #	ICOMP-93-08	p 199	N93-25175 * #	NAS 1.15.105799	p 79	N93-10197 * #
E-7824	p 62	N93-27260 * #	ICOMP-93-10	p 250	N93-27088 * #	NAS 1.15.105800	p 196	N93-19969 * #
E-7826	p 110	N93-27082 * #	ICOMP-93-12	p 199	N93-27010 * #	NAS 1.15.105804	p 41	N93-22197 * #
E-7829	p 61	N93-27019 * #	ICOMP-93-13	p 200	N93-27161 * #	NAS 1.15.105806	p 95	N93-10978 * #
E-7831	p 39	N93-32368 * #	ICOMP-93-16	p 269	N93-27065 * #	NAS 1.15.105807	p 231	N93-10963 * #
E-7832	p 217	N93-28053 * #	ICOMP-93-18	p 202	N93-29161 * #	NAS 1.15.105809	p 32	N93-12077 * #
E-7834	p 36	N93-27026 * #	ICOMP-93-19	p 202	N93-29208 * #	NAS 1.15.105810	p 191	N93-10087 * #
E-7835	p 199	N93-27020 * #	ICOMP-93-21	p 202	N93-31147 * #	NAS 1.15.105813	p 48	N93-11398 * #
E-7837	p 145	N93-27011 * #	ICOMP-93-22	p 203	N93-32199 * #	NAS 1.15.105817	p 191	N93-10735 * #
E-7838	p 200	N93-27161 * #	ICOMP-93-23	p 203	N93-32370 * #	NAS 1.15.105819	p 244	N93-10777 * #
E-7839	p 269	N93-27061 * #	ICOMP-93-2	p 197	N93-22596 * #	NAS 1.15.105821	p 245	N93-12277 * #
E-7843	p 162	N93-28610 * #	ICOMP-93-3	p 197	N93-21198 * #	NAS 1.15.105822	p 195	N93-15585 * #
E-7844	p 232	N93-27080 * #	ICOMP-93-4	p 269	N93-27068 * #	NAS 1.15.105823	p 244	N93-10453 * #
E-7855	p 269	N93-27065 * #	ICOMP-93-9	p 201	N93-28947 * #	NAS 1.15.105824	p 247	N93-20368 * #
E-7857	p 216	N93-26906 * #				NAS 1.15.105829	p 144	N93-12197 * #
E-7859	p 229	N93-27641 * #	INT-PATENT-CLASS-B01J-19/28	p 111	N93-29609 *	NAS 1.15.105830	p 227	N93-22826 * #
E-7860	p 62	N93-27081 * #	INT-PATENT-CLASS-B05D-1/02	p 107	N93-14706 *	NAS 1.15.105833	p 245	N93-11624 * #
E-7861	p 266	N93-28051 * #	INT-PATENT-CLASS-B05D-3/12	p 107	N93-14706 *	NAS 1.15.105834	p 195	N93-15792 * #
E-7863	p 110	N93-26705 * #				NAS 1.15.105837	p 149	N93-12366 * #
E-7868	p 200	N93-27132 * #	INT-PATENT-CLASS-F02K-3/04	p 35	N93-22034 *	NAS 1.15.105838	p 15	N93-11223 * #
E-7870	p 92	N93-29194 * #	INT-PATENT-CLASS-F02K-3/08	p 35	N93-22034 *	NAS 1.15.105839	p 32	N93-11530 * #
E-7871	p 92	N93-28694 * #				NAS 1.15.105840	p 245	N93-12739 * #
E-7872	p 53	N93-27064 * #	INT-PATENT-CLASS-G01B-11/02	p 278	N93-11058 *	NAS 1.15.105841	p 80	N93-10734 * #
E-7873	p 270	N93-32200 * #	INT-PATENT-CLASS-G01J-3/00	p 83	N93-18856 *	NAS 1.15.105843	p 261	N93-11005 * #
E-7874	p 230	N93-28411 * #	INT-PATENT-CLASS-G01N-21/00	p 83	N93-18856 *	NAS 1.15.105845	p 160	N93-15503 * #
E-7875	p 229	N93-27687 * #				NAS 1.15.105847	p 192	N93-11529 * #
E-7876	p 228	N93-27037 * #	INT-PATENT-CLASS-H01M-8/14	p 256	N93-28974 *	NAS 1.15.105848	p 107	N93-12737 * #
E-7884	p 37	N93-27128 * #	INT-PATENT-CLASS-H05K-7/20	p 111	N93-29614 *	NAS 1.15.105849	p 192	N93-10981 * #
E-7887	p 37	N93-27160 * #				NAS 1.15.105851	p 121	N93-16614 * #
E-7891	p 18	N93-31839 * #	ISABE 93-7003	p 31	A93-53980	NAS 1.15.105852	p 32	N93-10456 * #
E-7894	p 203	N93-31647 * #	ISABE 93-7023	p 31	A93-53999 *	NAS 1.15.105854	p 191	N93-10454 * #
E-7895	p 201	N93-28626 * #	ISABE 93-7027	p 31	A93-54003 *	NAS 1.15.105856	p 244	N93-11004 * #
E-7898	p 39	N93-32351 * #	ISABE 93-7064	p 31	A93-54040 *	NAS 1.15.105860	p 136	N93-12398 * #
E-7899	p 49	N93-28696 * #	ISABE 93-7067	p 31	A93-54043 *	NAS 1.15.105861	p 268	N93-11531 * #
E-7900	p 216	N93-27027 * #	ISABE 93-7077	p 189	A93-54053 *	NAS 1.15.105862	p 120	N93-11545 * #
E-7904	p 250	N93-28633 * #	ISABE 93-7086	p 14	A93-54062 *	NAS 1.15.105863	p 227	N93-18380 * #
E-7905	p 38	N93-27610 * #	ISABE 93-7095	p 14	A93-54071 *	NAS 1.15.105864	p 227	N93-18321 * #
E-7906	p 202	N93-29161 * #				NAS 1.15.105865	p 194	N93-14914 * #
E-7910	p 201	N93-28252 * #	ISBN 0-7918-0654-5	p 206	A93-23776 *	NAS 1.15.105866	p 84	N93-18877 * #
E-7915	p 202	N93-29075 * #	ISBN 0-8194-0584-1	p 151	A93-25776 *	NAS 1.15.105867	p 84	N93-19106 * #
E-7917	p 92	N93-29158 * #	ISBN 0-8194-0586-8	p 154	A93-27243 *	NAS 1.15.105868	p 16	N93-16704 * #
E-7919	p 202	N93-29208 * #	ISBN 0-88318-838-4	p 64	A93-13751	NAS 1.15.105869	p 247	N93-18876 * #
E-7921	p 230	N93-28050 * #	ISBN 0-89116-271-2	p 165	A93-17522 *	NAS 1.15.105870	p 81	N93-12363 * #
E-7924	p 251	N93-29196 * #	ISBN 0-89464-030-5	p 66	A93-20752 *	NAS 1.15.105874	p 34	N93-15525 * #
E-7925	p 39	N93-31671 * #				NAS 1.15.105875	p 159	N93-13286 * #
E-7926	p 141	N93-28695 * #	NAS 1.15.103663	p 61	N93-26209 * #	NAS 1.15.105877	p 80	N93-11402 * #
E-7928	p 53	N93-29195 * #	NAS 1.15.103719	p 275	N93-27058 * #	NAS 1.15.105880	p 57	N93-10841 * #
E-7930	p 232	N93-29073 * #	NAS 1.15.104438	p 147	N93-70966 *	NAS 1.15.105881	p 245	N93-12735 * #
E-7940	p 139	N93-32367 * #	NAS 1.15.105012	p 146	N93-70290 *	NAS 1.15.105882	p 107	N93-12078 * #
E-7944	p 251	N93-31193 * #	NAS 1.15.105185	p 59	N93-19988 *	NAS 1.15.105883	p 256	N93-25136 * #
E-7946	p 256	N93-32201 * #	NAS 1.15.105267	p 247	N93-23015 * #	NAS 1.15.105884	p 226	N93-12736 * #

NAS 1.15:105885	p 159	N93-12301 *	#	NAS 1.15:106015	p 275	N93-26551 *	#	NAS 1.15:106144	p 250	N93-27009 *	#
NAS 1.15:105890	p 284	N93-12325 *	#	NAS 1.15:106016	p 108	N93-20317 *	#	NAS 1.15:106145	p 110	N93-27082 *	#
NAS 1.15:105891	p 107	N93-12076 *	#	NAS 1.15:106017	p 215	N93-25173 *	#	NAS 1.15:106146	p 61	N93-27019 *	#
NAS 1.15:105892	p 248	N93-23745 *	#	NAS 1.15:106018	p 200	N93-27155 *	#	NAS 1.15:106147	p 161	N93-27002 *	#
NAS 1.15:105893	p 193	N93-14758 *	#	NAS 1.15:106019	p 35	N93-22480 *	#	NAS 1.15:106148	p 39	N93-32368 *	#
NAS 1.15:105895	p 127	N93-11609 *	#	NAS 1.15:106021	p 96	N93-22605 *	#	NAS 1.15:106149	p 38	N93-29065 *	#
NAS 1.15:105897	p 84	N93-18878 *	#	NAS 1.15:106022	p 248	N93-23406 *	#	NAS 1.15:106150	p 199	N93-27020 *	#
NAS 1.15:105898	p 41	N93-12305 *	#	NAS 1.15:106023	p 85	N93-22482 *	#	NAS 1.15:106151	p 217	N93-28053 *	#
NAS 1.15:105901	p 128	N93-15586 *	#	NAS 1.15:106024	p 110	N93-27092 *	#	NAS 1.15:106152	p 36	N93-27026 *	#
NAS 1.15:105903	p 246	N93-13157 *	#	NAS 1.15:106025	p 109	N93-26552 *	#	NAS 1.15:106153	p 145	N93-27011 *	#
NAS 1.15:105904	p 269	N93-22825 *	#	NAS 1.15:106028	p 42	N93-26907 *	#	NAS 1.15:106154	p 200	N93-27161 *	#
NAS 1.15:105906	p 213	N93-13307 *	#	NAS 1.15:106029	p 249	N93-23746 *	#	NAS 1.15:106155	p 269	N93-27061 *	#
NAS 1.15:105907	p 286	N93-26205 *	#	NAS 1.15:106030	p 17	N93-19968 *	#	NAS 1.15:106157	p 162	N93-28610 *	#
NAS 1.15:105908	p 32	N93-12402 *	#	NAS 1.15:106032	p 111	N93-28624 *	#	NAS 1.15:106158	p 232	N93-27080 *	#
NAS 1.15:105909	p 213	N93-13410 *	#	NAS 1.15:106033	p 250	N93-26999 *	#	NAS 1.15:106160	p 201	N93-28626 *	#
NAS 1.15:105910	p 52	N93-11430 *	#	NAS 1.15:106034	p 271	N93-22559 *	#	NAS 1.15:106161	p 91	N93-27039 *	#
NAS 1.15:105911	p 262	N93-12410 *	#	NAS 1.15:106037	p 160	N93-20259 *	#	NAS 1.15:106162	p 229	N93-27641 *	#
NAS 1.15:105912	p 81	N93-14079 *	#	NAS 1.15:106038	p 197	N93-22596 *	#	NAS 1.15:106163	p 269	N93-27065 *	#
NAS 1.15:105913	p 136	N93-16372 *	#	NAS 1.15:106039	p 197	N93-21198 *	#	NAS 1.15:106165	p 110	N93-26705 *	#
NAS 1.15:105914	p 21	N93-22588 *	#	NAS 1.15:106042	p 36	N93-25079 *	#	NAS 1.15:106167	p 266	N93-28051 *	#
NAS 1.15:105915	p 33	N93-12418 *	#	NAS 1.15:106044	p 36	N93-25673 *	#	NAS 1.15:106168	p 62	N93-27081 *	#
NAS 1.15:105916	p 128	N93-19974 *	#	NAS 1.15:106047	p 43	N93-26214 *	#	NAS 1.15:106169	p 200	N93-27132 *	#
NAS 1.15:105917	p 136	N93-14886 *	#	NAS 1.15:106048	p 110	N93-27129 *	#	NAS 1.15:106172	p 53	N93-27064 *	#
NAS 1.15:105918	p 194	N93-15499 *	#	NAS 1.15:106049	p 110	N93-27270 *	#	NAS 1.15:106173	p 270	N93-32200 *	#
NAS 1.15:105919	p 141	N93-12085 *	#	NAS 1.15:106050	p 85	N93-23405 *	#	NAS 1.15:106174	p 230	N93-28411 *	#
NAS 1.15:105920	p 196	N93-16612 *	#	NAS 1.15:106052	p 111	N93-28681 *	#	NAS 1.15:106175	p 229	N93-27687 *	#
NAS 1.15:105921	p 128	N93-15524 *	#	NAS 1.15:106053	p 84	N93-20614 *	#	NAS 1.15:106176	p 228	N93-27037 *	#
NAS 1.15:105924	p 1	N93-20902 *	#	NAS 1.15:106054	p 36	N93-25129 *	#	NAS 1.15:106178	p 91	N93-27022 *	#
NAS 1.15:105925	p 255	N93-15523 *	#	NAS 1.15:106055	p 200	N93-27091 *	#	NAS 1.15:106179	p 37	N93-27128 *	#
NAS 1.15:105926	p 136	N93-19035 *	#	NAS 1.15:106056	p 268	N93-22664 *	#	NAS 1.15:106180	p 262	N93-28628 *	#
NAS 1.15:105927	p 83	N93-15572 *	#	NAS 1.15:106058	p 161	N93-27265 *	#	NAS 1.15:106181	p 37	N93-27160 *	#
NAS 1.15:105928	p 268	N93-15341 *	#	NAS 1.15:106059	p 63	N93-28554 *	#	NAS 1.15:106186	p 18	N93-31839 *	#
NAS 1.15:105929	p 194	N93-14885 *	#	NAS 1.15:106060	p 84	N93-20615 *	#	NAS 1.15:106187	p 202	N93-29157 *	#
NAS 1.15:105930	p 160	N93-16616 *	#	NAS 1.15:106061	p 129	N93-28618 *	#	NAS 1.15:106189	p 203	N93-31647 *	#
NAS 1.15:105931	p 1	N93-14102 *	#	NAS 1.15:106063	p 248	N93-23739 *	#	NAS 1.15:106192	p 39	N93-32351 *	#
NAS 1.15:105932	p 262	N93-13154 *	#	NAS 1.15:106064	p 248	N93-23740 *	#	NAS 1.15:106193	p 49	N93-28696 *	#
NAS 1.15:105933	p 82	N93-14482 *	#	NAS 1.15:106065	p 248	N93-23044 *	#	NAS 1.15:106194	p 216	N93-27027 *	#
NAS 1.15:105934	p 128	N93-18069 *	#	NAS 1.15:106067	p 109	N93-26704 *	#	NAS 1.15:106196	p 250	N93-28633 *	#
NAS 1.15:105935	p 16	N93-16625 *	#	NAS 1.15:106069	p 198	N93-23744 *	#	NAS 1.15:106198	p 38	N93-27610 *	#
NAS 1.15:105936	p 33	N93-15403 *	#	NAS 1.15:106070	p 87	N93-25089 *	#	NAS 1.15:106201	p 201	N93-28252 *	#
NAS 1.15:105937	p 1	N93-15573 *	#	NAS 1.15:106072	p 198	N93-23736 *	#	NAS 1.15:106206	p 202	N93-29075 *	#
NAS 1.15:105938	p 247	N93-17996 *	#	NAS 1.15:106073	p 53	N93-22589 *	#	NAS 1.15:106207	p 92	N93-29158 *	#
NAS 1.15:105939	p 95	N93-22590 *	#	NAS 1.15:106074	p 108	N93-25071 *	#	NAS 1.15:106209	p 202	N93-29208 *	#
NAS 1.15:105940	p 120	N93-15504 *	#	NAS 1.15:106076	p 111	N93-29074 *	#	NAS 1.15:106211	p 230	N93-28050 *	#
NAS 1.15:105942	p 227	N93-14478 *	#	NAS 1.15:106079	p 96	N93-23014 *	#	NAS 1.15:106212	p 129	N93-23418 *	#
NAS 1.15:105943	p 95	N93-22586 *	#	NAS 1.15:106080	p 228	N93-23019 *	#	NAS 1.15:106213	p 88	N93-26149 *	#
NAS 1.15:105945	p 95	N93-15576 *	#	NAS 1.15:106081	p 137	N93-25093 *	#	NAS 1.15:106215	p 251	N93-29196 *	#
NAS 1.15:105946	p 36	N93-26161 *	#	NAS 1.15:106083	p 198	N93-23404 *	#	NAS 1.15:106216	p 39	N93-31671 *	#
NAS 1.15:105947	p 15	N93-14791 *	#	NAS 1.15:106084	p 60	N93-23742 *	#	NAS 1.15:106217	p 53	N93-29195 *	#
NAS 1.15:105949	p 59	N93-17988 *	#	NAS 1.15:106085	p 215	N93-22994 *	#	NAS 1.15:106219	p 232	N93-29073 *	#
NAS 1.15:105950	p 229	N93-27074 *	#	NAS 1.15:106086	p 17	N93-24911 *	#	NAS 1.15:106220	p 92	N93-29194 *	#
NAS 1.15:105952	p 19	N93-15360 *	#	NAS 1.15:106087	p 199	N93-25175 *	#	NAS 1.15:106222	p 92	N93-28694 *	#
NAS 1.15:105954	p 196	N93-16703 *	#	NAS 1.15:106089	p 201	N93-28947 *	#	NAS 1.15:106223	p 139	N93-32367 *	#
NAS 1.15:105955	p 141	N93-16384 *	#	NAS 1.15:106092	p 150	N93-22483 *	#	NAS 1.15:106225	p 251	N93-31193 *	#
NAS 1.15:105956	p 193	N93-14829 *	#	NAS 1.15:106093	p 60	N93-24755 *	#	NAS 1.15:106228	p 256	N93-32201 *	#
NAS 1.15:105959	p 96	N93-26204 *	#	NAS 1.15:106095	p 215	N93-24737 *	#	NAS 1.15:106230	p 38	N93-28697 *	#
NAS 1.15:105960	p 63	N93-23738 *	#	NAS 1.15:106096	p 161	N93-24746 *	#	NAS 1.15:106233	p 91	N93-28619 *	#
NAS 1.15:105961	p 274	N93-15430 *	#	NAS 1.15:106097	p 88	N93-26211 *	#	NAS 1.15:106234	p 51	N93-28052 *	#
NAS 1.15:105962	p 83	N93-15571 *	#	NAS 1.15:106098	p 60	N93-25090 *	#	NAS 1.15:106235	p 17	N93-31648 *	#
NAS 1.15:105966	p 149	N93-20260 *	#	NAS 1.15:106099	p 228	N93-23741 *	#	NAS 1.15:106236	p 201	N93-28627 *	#
NAS 1.15:105967	p 83	N93-16714 *	#	NAS 1.15:106100	p 229	N93-27069 *	#	NAS 1.15:106240	p 38	N93-29162 *	#
NAS 1.15:105968	p 15	N93-14911 *	#	NAS 1.15:106101	p 229	N93-27133 *	#	NAS 1.15:106241	p 150	N93-31856 *	#
NAS 1.15:105969	p 16	N93-15404 *	#	NAS 1.15:106102	p 85	N93-23747 *	#	NAS 1.15:106243	p 141	N93-28695 *	#
NAS 1.15:105970	p 33	N93-15521 *	#	NAS 1.15:106103	p 228	N93-25672 *	#	NAS 1.15:106245	p 18	N93-31672 *	#
NAS 1.15:105971	p 16	N93-15338 *	#	NAS 1.15:106105	p 255	N93-23018 *	#	NAS 1.15:106248	p 202	N93-31147 *	#
NAS 1.15:105972	p 19	N93-15354 *	#	NAS 1.15:106106	p 216	N93-25191 *	#	NAS 1.15:106249	p 203	N93-32199 *	#
NAS 1.15:105973	p 144	N93-15420 *	#	NAS 1.15:106107	p 61	N93-26148 *	#	NAS 1.15:106251	p 271	N93-31145 *	#
NAS 1.15:105975	p 19	N93-15345 *	#	NAS 1.15:106108	p 150	N93-26903 *	#	NAS 1.15:106252	p 142	N93-32330 *	#
NAS 1.15:105976	p 20	N93-15522 *	#	NAS 1.15:106109	p 199	N93-26554 *	#	NAS 1.15:106253	p 231	N93-31846 *	#
NAS 1.15:105977	p 41	N93-14831 *	#	NAS 1.15:106111	p 270	N93-27124 *	#	NAS 1.15:106254	p 51	N93-31670 *	#
NAS 1.15:105978	p 35	N93-23013 *	#	NAS 1.15:106112	p 250	N93-27088 *	#	NAS 1.15:106257	p 139	N93-32382 *	#
NAS 1.15:105979	p 34	N93-16715 *	#	NAS 1.15:106114	p 37	N93-27131 *	#	NAS 1.15:106258	p 139	N93-32352 *	#
NAS 1.15:105981	p 194	N93-15355 *	#	NAS 1.15:106116	p 199	N93-27010 *	#	NAS 1.15:106260	p 269	N93-31847 *	#
NAS 1.15:105982	p 82	N93-15428 *	#	NAS 1.15:106117	p 269	N93-27068 *	#	NAS 1.15:106269	p 203	N93-32370 *	#
NAS 1.15:105983	p 82	N93-15429 *	#	NAS 1.15:106118	p 51	N93-27018 *	#	NAS 1.15:106272	p 138	N93-30938 *	#
NAS 1.15:105984	p 33	N93-15359 *	#	NAS 1.15:106119	p 261	N93-27024 *	#	NAS 1.15:106273	p 93	N93-31858 *	#
NAS 1.15:105985	p 197	N93-20057 *	#	NAS 1.15:106123	p 258	N93-26947 *	#	NAS 1.15:106274	p 203	N93-31860 *	#
NAS 1.15:105986	p 35	N93-22599 *	#	NAS 1.15:106125	p 258	N93-26946 *	#	NAS 1.15:106275	p 145	N93-30939 *	#
NAS 1.15:105987	p 129	N93-26898 *	#	NAS 1.15:106126	p 250	N93-26550 *	#	NAS 1.15:106277	p 216	N93-26906 *	#
NAS 1.15:105989	p 34	N93-16705 *	#	NAS 1.15:106127	p 147	N93-25177 *	#	NAS 1.15:106279	p 203	N93-70575 *	#
NAS 1.15:105993	p 16	N93-16596 *	#	NAS 1.15:106128	p 250	N93-27030 *	#	NAS 1.15:106282	p 150	N93-70235 *	#
NAS 1.15:105994	p 217	N93-18091 *	#	NAS 1.15:106129	p 96	N93-27266 *	#	NAS 1.15:106285	p 276	N93-16531 *	#
NAS 1.15:105996	p 215	N93-22484 *	#	NAS 1.15:106130	p 199	N93-26203 *	#	NAS 1.15:106287	p 277	N93-17343 *	#
NAS 1.15:105997	p 247	N93-18426 *	#	NAS 1.15:106131	p 37	N93-27130 *	#	NAS 1.15:106289	p 233	N93-70212 *	#
NAS 1.15:105998	p 149	N93-20257 *	#	NAS 1.15:106132	p 109	N93-26702 *	#	NAS 1.15:106291	p 82	N93-15528 *	#
NAS 1.15:105999	p 83	N93-17995 *	#	NAS 1.15:106133	p 61	N93-26215 *	#	NAS 1.15:106292	p 247	N93-21831 *	#
NAS 1.15:106000	p 60	N93-22551 *	#	NAS 1.15:106135	p 145	N93-25337 *	#	NAS 1.15:106293	p 249	N93-24909 *	#
NAS 1.15:106001	p 249	N93-24913 *	#	NAS 1.15:106136	p 87	N93-25236 *	#	NAS 1.15:106294	p 246	N93-15788 *	#
NAS 1.15:106002	p 249	N93-25070 *	#	NAS 1.15:106137	p 111	N93-29071 *	#	NAS 1.15:106295	p 262	N93-27040 *	#
NAS 1.15:106											

NAS 1.26 187148	p 85	N93-23017 * #	NASA-CP-10106	p 192	N93-13385 * #	NASA-TM-105849	p 192	N93-10981 * #
NAS 1.26 189193-VOL-1	p 35	N93-24754 * #	NASA-CP-10109	p 279	N93-18635 * #	NASA-TM-105851	p 121	N93-16614 * #
NAS 1.26 189235	p 246	N93-13260 * #	NASA-CP-10113	p 145	N93-20178 * #	NASA-TM-105852	p 32	N93-10456 * #
NAS 1.26 191080	p 86	N93-23876 * #	NASA-CP-10116-VOL-1	p 89	N93-26908 * #	NASA-TM-105854	p 191	N93-10454 * #
NAS 1.26 191081	p 85	N93-23875 * #	NASA-CP-10116-VOL-2	p 89	N93-26951 * #	NASA-TM-105856	p 244	N93-11004 * #
NAS 1.26 191095	p 198	N93-24759 * #				NASA-TM-105860	p 136	N93-12398 * #
NAS 1.26 191112	p 87	N93-24758 * #	NASA-CR-187148	p 85	N93-23017 * #	NASA-TM-105861	p 268	N93-11531 * #
NAS 1.26 191117	p 228	N93-24751 * #	NASA-CR-189193-VOL-1	p 35	N93-24754 * #	NASA-TM-105862	p 120	N93-11545 * #
NAS 1.55 10064	p 93	N93-31552 * #	NASA-CR-189235	p 246	N93-13260 * #	NASA-TM-105863	p 227	N93-18380 * #
NAS 1.55 10093-PT-2	p 293	N93-26392 * #	NASA-CR-191080	p 86	N93-23876 * #	NASA-TM-105864	p 227	N93-18321 * #
NAS 1.55 10106	p 192	N93-13385 * #	NASA-CR-191081	p 85	N93-23875 * #	NASA-TM-105865	p 194	N93-14914 * #
NAS 1.55 10109	p 279	N93-18635 * #	NASA-CR-191095	p 198	N93-24759 * #	NASA-TM-105866	p 84	N93-18877 * #
NAS 1.55 10113	p 145	N93-20178 * #	NASA-CR-191112	p 87	N93-24758 * #	NASA-TM-105867	p 84	N93-19106 * #
NAS 1.55 10116-VOL-1	p 89	N93-26908 * #	NASA-CR-191117	p 228	N93-24751 * #	NASA-TM-105868	p 16	N93-16704 * #
NAS 1.55 10116-VOL-2	p 89	N93-26951 * #				NASA-TM-105869	p 247	N93-18876 * #
NAS 1.60 3180	p 52	N93-18854 * #	NASA-RP-1271	p 285	N93-12967 * #	NASA-TM-105870	p 81	N93-12363 * #
NAS 1.60 3190	p 129	N93-26201 * #				NASA-TM-105874	p 34	N93-15525 * #
NAS 1.60 3199	p 107	N93-12302 * #	NASA-TM-103663	p 61	N93-26209 * #	NASA-TM-105875	p 159	N93-13286 * #
NAS 1.60 3222	p 81	N93-11614 * #	NASA-TM-103719	p 275	N93-27058 * #	NASA-TM-105877	p 80	N93-11402 * #
NAS 1.60 3223	p 80	N93-10743 * #	NASA-TM-104438	p 147	N93-70966 * #	NASA-TM-105878	p 214	N93-17777 * #
NAS 1.60 3247	p 17	N93-24118 * #	NASA-TM-105012	p 146	N93-70290 * #	NASA-TM-105880	p 57	N93-10841 * #
NAS 1.60 3250	p 197	N93-23059 * #	NASA-TM-105185	p 59	N93-19988 * #	NASA-TM-105881	p 245	N93-12735 * #
NAS 1.60 3251	p 160	N93-15531 * #	NASA-TM-105267	p 247	N93-23015 * #	NASA-TM-105882	p 107	N93-12078 * #
NAS 1.60 3274	p 42	N93-12016 * #	NASA-TM-105269	p 261	N93-12022 * #	NASA-TM-105883	p 256	N93-25136 * #
NAS 1.60 3279	p 58	N93-11001 * #	NASA-TM-105270	p 249	N93-26202 * #	NASA-TM-105884	p 226	N93-12736 * #
NAS 1.60 3287	p 286	N93-19977 * #	NASA-TM-105272	p 247	N93-18875 * #	NASA-TM-105885	p 159	N93-12301 * #
NAS 1.60 3290	p 108	N93-18139 * #	NASA-TM-105319	p 244	N93-11403 * #	NASA-TM-105890	p 284	N93-12325 * #
NAS 1.60 3292	p 106	N93-12015 * #	NASA-TM-105419	p 287	N93-23002 * #	NASA-TM-105891	p 107	N93-12076 * #
NAS 1.60 3294	p 160	N93-23394 * #	NASA-TM-105568	p 135	N93-10962 * #	NASA-TM-105892	p 248	N93-23745 * #
NAS 1.60 3295	p 128	N93-22556 * #	NASA-TM-105572	p 261	N93-16613 * #	NASA-TM-105893	p 193	N93-14758 * #
NAS 1.60 3315	p 34	N93-16941 * #	NASA-TM-105595	p 287	N93-14796 * #	NASA-TM-105895	p 127	N93-11609 * #
NAS 1.61 1271	p 285	N93-12967 * #	NASA-TM-105598	p 127	N93-11635 * #	NASA-TM-105897	p 84	N93-18878 * #
NAS 1.71 LEW-14162-4	p 108	N93-20568 * #	NASA-TM-105602	p 1	N93-26136 * #	NASA-TM-105898	p 41	N93-12305 * #
NAS 1.71 LEW-14345-7	p 95	N93-17412 * #	NASA-TM-105609	p 245	N93-12738 * #	NASA-TM-105901	p 128	N93-15586 * #
NAS 1.71 LEW-14906-1	p 226	N93-12203 * #	NASA-TM-105614	p 81	N93-12484 * #	NASA-TM-105903	p 246	N93-13157 * #
NAS 1.71 LEW-14906-2	p 230	N93-31314 * #	NASA-TM-105626	p 42	N93-15498 * #	NASA-TM-105904	p 269	N93-22825 * #
NAS 1.71 LEW-15154-1	p 137	N93-19332 * #	NASA-TM-105640	p 82	N93-15526 * #	NASA-TM-105906	p 213	N93-13307 * #
NAS 1.71 LEW-15154-2	p 138	N93-31300 * #	NASA-TM-105658	p 15	N93-13292 * #	NASA-TM-105907	p 286	N93-26205 * #
NAS 1.71 LEW-15170-1	p 275	N93-28953 * #	NASA-TM-105677	p 231	N93-18422 * #	NASA-TM-105908	p 32	N93-12402 * #
NAS 1.71 LEW-15222-3	p 284	N93-17413 * #	NASA-TM-105687	p 33	N93-15342 * #	NASA-TM-105909	p 213	N93-13410 * #
NAS 1.71 LEW-15241-2	p 112	N93-31296 * #	NASA-TM-105705	p 88	N93-26200 * #	NASA-TM-105910	p 52	N93-11430 * #
NAS 1.71 LEW-15250-1	p 214	N93-17060 * #	NASA-TM-105707	p 86	N93-24744 * #	NASA-TM-105911	p 262	N93-12410 * #
NAS 1.71 LEW-15263-1	p 106	N93-11543 * #	NASA-TM-105708	p 87	N93-25105 * #	NASA-TM-105912	p 81	N93-14079 * #
NAS 1.71 LEW-15264-1	p 112	N93-31293 * #	NASA-TM-105710	p 86	N93-24753 * #	NASA-TM-105913	p 136	N93-16372 * #
NAS 1.71 LEW-15264-2	p 112	N93-31299 * #	NASA-TM-105711	p 86	N93-24740 * #	NASA-TM-105914	p 21	N93-22588 * #
NAS 1.71 LEW-15269-1	p 108	N93-20040 * #	NASA-TM-105722	p 257	N93-27012 * #	NASA-TM-105915	p 33	N93-12418 * #
NAS 1.71 LEW-15306-1	p 137	N93-20566 * #	NASA-TM-105723	p 106	N93-11399 * #	NASA-TM-105916	p 128	N93-19974 * #
NAS 1.71 LEW-15306-2	p 138	N93-28425 * #	NASA-TM-105729	p 226	N93-10966 * #	NASA-TM-105917	p 136	N93-14886 * #
NAS 1.71 LEW-15314-2	p 138	N93-28423 * #	NASA-TM-105732	p 136	N93-15344 * #	NASA-TM-105918	p 194	N93-15499 * #
NAS 1.71 LEW-15345-2	p 230	N93-28127 * #	NASA-TM-105736	p 274	N93-11370 * #	NASA-TM-105919	p 141	N93-12085 * #
NAS 1.71 LEW-15430-1	p 275	N93-17051 * #	NASA-TM-105747	p 80	N93-10965 * #	NASA-TM-105920	p 196	N93-16612 * #
NAS 1.71 LEW-15515-1	p 217	N93-31298 * #	NASA-TM-105756	p 255	N93-20261 * #	NASA-TM-105921	p 128	N93-15524 * #
NAS 1.71 LEW-15535-1	p 130	N93-31294 * #	NASA-TM-105757	p 269	N93-26560 * #	NASA-TM-105924	p 1	N93-20902 * #
NAS 1.71 LEW-15570-1	p 227	N93-19027 * #	NASA-TM-105761	p 80	N93-10457 * #	NASA-TM-105925	p 255	N93-15523 * #
NAS 1.71 LEW-15576-1	p 139	N93-31316 * #	NASA-TM-105764	p 193	N93-14150 * #	NASA-TM-105926	p 136	N93-19035 * #
NAS 1.71 LEW-15614-1	p 276	N93-19026 * #	NASA-TM-105765	p 246	N93-13153 * #	NASA-TM-105927	p 83	N93-15572 * #
NAS 1.71 LEW-15697-1	p 130	N93-29172 * #	NASA-TM-105766	p 244	N93-10455 * #	NASA-TM-105928	p 268	N93-15341 * #
NAS 1.71 LEW-15700-1	p 287	N93-28130 * #	NASA-TM-105771	p 43	N93-25080 * #	NASA-TM-105929	p 194	N93-14885 * #
			NASA-TM-105772	p 141	N93-14834 * #	NASA-TM-105930	p 160	N93-16616 * #
NASA-CASE-LEW-14162-3	p 111	N93-29614 * #	NASA-TM-105776	p 268	N93-11254 * #	NASA-TM-105931	p 1	N93-14102 * #
NASA-CASE-LEW-14162-4	p 108	N93-20568 * #	NASA-TM-105778	p 149	N93-12481 * #	NASA-TM-105932	p 262	N93-13154 * #
NASA-CASE-LEW-14345-7	p 95	N93-17412 * #	NASA-TM-105779	p 246	N93-15343 * #	NASA-TM-105933	p 82	N93-14482 * #
NASA-CASE-LEW-14906-1	p 226	N93-12203 * #	NASA-TM-105780	p 244	N93-10967 * #	NASA-TM-105934	p 128	N93-18069 * #
NASA-CASE-LEW-14906-2	p 230	N93-31314 * #	NASA-TM-105781	p 49	N93-11401 * #	NASA-TM-105935	p 16	N93-16625 * #
NASA-CASE-LEW-14973-1	p 256	N93-28974 * #	NASA-TM-105784	p 215	N93-19651 * #	NASA-TM-105936	p 33	N93-15403 * #
NASA-CASE-LEW-14996-1	p 278	N93-11058 * #	NASA-TM-105785	p 92	N93-28666 * #	NASA-TM-105937	p 1	N93-15573 * #
NASA-CASE-LEW-15020-2	p 107	N93-14706 * #	NASA-TM-105786	p 32	N93-10983 * #	NASA-TM-105938	p 247	N93-17996 * #
NASA-CASE-LEW-15077-2	p 111	N93-29609 * #	NASA-TM-105790	p 226	N93-10982 * #	NASA-TM-105939	p 95	N93-22590 * #
NASA-CASE-LEW-15094-1	p 35	N93-22034 * #	NASA-TM-105792	p 266	N93-19018 * #	NASA-TM-105940	p 120	N93-15504 * #
NASA-CASE-LEW-15154-1	p 137	N93-19332 * #	NASA-TM-105799	p 79	N93-10197 * #	NASA-TM-105942	p 227	N93-14478 * #
NASA-CASE-LEW-15154-2	p 138	N93-31300 * #	NASA-TM-105800	p 196	N93-19969 * #	NASA-TM-105943	p 95	N93-22586 * #
NASA-CASE-LEW-15170-1	p 275	N93-28953 * #	NASA-TM-105804	p 41	N93-21197 * #	NASA-TM-105945	p 95	N93-15576 * #
NASA-CASE-LEW-15200-1	p 83	N93-18856 * #	NASA-TM-105806	p 95	N93-10978 * #	NASA-TM-105946	p 36	N93-26161 * #
NASA-CASE-LEW-15222-3	p 284	N93-17413 * #	NASA-TM-105807	p 231	N93-10963 * #	NASA-TM-105947	p 15	N93-14791 * #
NASA-CASE-LEW-15241-2	p 112	N93-31296 * #	NASA-TM-105809	p 32	N93-12077 * #	NASA-TM-105949	p 59	N93-17988 * #
NASA-CASE-LEW-15250-1	p 214	N93-17060 * #	NASA-TM-105810	p 191	N93-10087 * #	NASA-TM-105950	p 229	N93-27074 * #
NASA-CASE-LEW-15262-1	p 109	N93-26100 * #	NASA-TM-105813	p 48	N93-11398 * #	NASA-TM-105952	p 19	N93-15360 * #
NASA-CASE-LEW-15263-1	p 106	N93-11543 * #	NASA-TM-105817	p 191	N93-10735 * #	NASA-TM-105954	p 196	N93-16703 * #
NASA-CASE-LEW-15264-1	p 112	N93-31293 * #	NASA-TM-105819	p 244	N93-10777 * #	NASA-TM-105955	p 141	N93-16384 * #
NASA-CASE-LEW-15264-2	p 112	N93-31299 * #	NASA-TM-105821	p 245	N93-12277 * #	NASA-TM-105956	p 193	N93-14829 * #
NASA-CASE-LEW-15269-1	p 108	N93-20040 * #	NASA-TM-105822	p 195	N93-15585 * #	NASA-TM-105959	p 96	N93-26204 * #
NASA-CASE-LEW-15306-1	p 137	N93-20566 * #	NASA-TM-105823	p 244	N93-10453 * #	NASA-TM-105960	p 63	N93-23738 * #
NASA-CASE-LEW-15306-2	p 138	N93-28425 * #	NASA-TM-105824	p 247	N93-20368 * #	NASA-TM-105961	p 274	N93-15430 * #
NASA-CASE-LEW-15314-2	p 138	N93-28423 * #	NASA-TM-105829	p 144	N93-12197 * #	NASA-TM-105962	p 83	N93-15571 * #
NASA-CASE-LEW-15345-2	p 230	N93-28127 * #	NASA-TM-105830	p 227	N93-28282 * #	NASA-TM-105966	p 149	N93-20260 * #
NASA-CASE-LEW-15430-1	p 275	N93-17051 * #	NASA-TM-105833	p 245	N93-11624 * #	NASA-TM-105967	p 83	N93-16714 * #
NASA-CASE-LEW-15515-1	p 217	N93-31298 * #	NASA-TM-105834	p 195	N93-15792 * #	NASA-TM-105968	p 15	N93-14911 * #
NASA-CASE-LEW-15535-1	p 130	N93-31294 * #	NASA-TM-105837	p 149	N93-12366 * #	NASA-TM-105969	p 16	N93-15404 * #
NASA-CASE-LEW-15570-1	p 227	N93-19027 * #	NASA-TM-105839	p 15	N93-11223 * #	NASA-TM-105970	p 33	N93-15521 * #
NASA-CASE-LEW-15576-1	p 139	N93-31316 * #	NASA-TM-105840	p 32	N93-11530 * #	NASA-TM-105971	p 16	N93-15338 * #
NASA-CASE-LEW-15614-1	p 276	N93-19026 * #	NASA-TM-105841	p 245	N93-12739 * #	NASA-TM-105972	p 19	N93-15354 * #
NASA-CASE-LEW-15697-1	p 130	N93-29172 * #	NASA-TM-105843	p 80	N93-10734 * #	NASA-TM-105973	p 144	N93-15420 * #
NASA-CASE-LEW-15700-1	p 287	N93-28130 * #	NASA-TM-105843	p 261	N93-11005 * #	NASA-TM-105975	p 19	N93-15345 * #
			NASA-TM-105845	p 160	N93-15503 * #	NASA-TM-105976	p 20	N93-15522 * #
NASA-CP-10064	p 93	N93-31552 * #	NASA-TM-105847	p 192	N93-11529 * #	NASA-TM-105977	p 41	N93-14831 * #
NASA-CP-10093-PT-2	p 293	N93-26392 * #	NASA-TM-105848	p 107	N93-12737 * #	NASA-TM-105978	p 35	N93-23013 * #

NASA-TM-105979	p 34	N93-16715 *	#	NASA-TM-106112	p 250	N93-27088 *	#	NASA-TM-106254	p 51	N93-31670 *	#
NASA-TM-105981	p 194	N93-15355 *	#	NASA-TM-106114	p 37	N93-27131 *	#	NASA-TM-106256	p 139	N93-32382 *	#
NASA-TM-105982	p 82	N93-15428 *	#	NASA-TM-106116	p 199	N93-27010 *	#	NASA-TM-106257	p 139	N93-32352 *	#
NASA-TM-105983	p 82	N93-15429 *	#	NASA-TM-106117	p 269	N93-27068 *	#	NASA-TM-106258	p 269	N93-31847 *	#
NASA-TM-105984	p 33	N93-15359 *	#	NASA-TM-106118	p 51	N93-27018 *	#	NASA-TM-106260	p 203	N93-32370 *	#
NASA-TM-105985	p 197	N93-20057 *	#	NASA-TM-106119	p 261	N93-27024 *	#	NASA-TM-106269	p 138	N93-30938 *	#
NASA-TM-105986	p 35	N93-22599 *	#	NASA-TM-106123	p 258	N93-26947 *	#	NASA-TM-106272	p 93	N93-31858 *	#
NASA-TM-105987	p 129	N93-26898 *	#	NASA-TM-106124	p 258	N93-26946 *	#	NASA-TM-106273	p 203	N93-31860 *	#
NASA-TM-105989	p 34	N93-16705 *	#	NASA-TM-106125	p 250	N93-26550 *	#	NASA-TM-106274	p 145	N93-30939 *	#
NASA-TM-105993	p 16	N93-16596 *	#	NASA-TM-106126	p 147	N93-25177 *	#	NASA-TM-106352	p 216	N93-26906 *	#
NASA-TM-105994	p 217	N93-18091 *	#	NASA-TM-106127	p 250	N93-27030 *	#	NASA-TM-107829	p 233	N93-70212 *	#
NASA-TM-105996	p 215	N93-22484 *	#	NASA-TM-106128	p 96	N93-27266 *	#	NASA-TM-107972	p 203	N93-70575 *	#
NASA-TM-105997	p 247	N93-18426 *	#	NASA-TM-106129	p 199	N93-26203 *	#	NASA-TM-107982	p 150	N93-70235 *	#
NASA-TM-105998	p 149	N93-20257 *	#	NASA-TM-106130	p 37	N93-27130 *	#	NASA-TM-108157	p 276	N93-16531 *	#
NASA-TM-105999	p 83	N93-17995 *	#	NASA-TM-106131	p 109	N93-26702 *	#	NASA-TM-108215	p 277	N93-17343 *	#
NASA-TM-106000	p 60	N93-22551 *	#	NASA-TM-106132	p 61	N93-26215 *	#	NASA-TM-4376	p 82	N93-15528 *	#
NASA-TM-106001	p 249	N93-24913 *	#	NASA-TM-106133	p 145	N93-25337 *	#	NASA-TM-4389	p 247	N93-21831 *	#
NASA-TM-106002	p 249	N93-25070 *	#	NASA-TM-106135	p 87	N93-25236 *	#	NASA-TM-4423	p 249	N93-24909 *	#
NASA-TM-106005	p 271	N93-23016 *	#	NASA-TM-106136	p 111	N93-29071 *	#	NASA-TM-4425	p 246	N93-15788 *	#
NASA-TM-106006	p 232	N93-27025 *	#	NASA-TM-106137	p 96	N93-27003 *	#	NASA-TM-4451	p 262	N93-27040 *	#
NASA-TM-106007	p 35	N93-20109 *	#	NASA-TM-106138	p 216	N93-27001 *	#	NASA-TM-4471	p 53	N93-26895 *	#
NASA-TM-106010	p 215	N93-22598 *	#	NASA-TM-106139	p 88	N93-26210 *	#	NASA-TM-83642	p 1	N93-72738 *	#
NASA-TM-106012	p 160	N93-16713 *	#	NASA-TM-106140	p 38	N93-27640 *	#	NASA-TM-83796	p 246	N93-15369 *	#
NASA-TM-106013	p 275	N93-15575 *	#	NASA-TM-106141	p 216	N93-27021 *	#				
NASA-TM-106014	p 137	N93-22560 *	#	NASA-TM-106142	p 61	N93-27038 *	#	NASA-TP-3180	p 52	N93-18854 *	#
NASA-TM-106015	p 275	N93-26551 *	#	NASA-TM-106143	p 62	N93-27260 *	#	NASA-TP-3190	p 129	N93-26201 *	#
NASA-TM-106016	p 108	N93-20317 *	#	NASA-TM-106144	p 250	N93-27009 *	#	NASA-TP-3199	p 107	N93-12302 *	#
NASA-TM-106017	p 215	N93-25173 *	#	NASA-TM-106145	p 110	N93-27082 *	#	NASA-TP-3222	p 81	N93-11614 *	#
NASA-TM-106018	p 200	N93-27155 *	#	NASA-TM-106146	p 61	N93-27019 *	#	NASA-TP-3223	p 80	N93-10743 *	#
NASA-TM-106019	p 35	N93-22480 *	#	NASA-TM-106147	p 161	N93-27002 *	#	NASA-TP-3247	p 17	N93-24118 *	#
NASA-TM-106021	p 96	N93-22605 *	#	NASA-TM-106148	p 39	N93-32368 *	#	NASA-TP-3250	p 197	N93-23059 *	#
NASA-TM-106022	p 248	N93-23406 *	#	NASA-TM-106149	p 38	N93-29065 *	#	NASA-TP-3251	p 160	N93-15531 *	#
NASA-TM-106023	p 85	N93-22482 *	#	NASA-TM-106150	p 199	N93-27020 *	#	NASA-TP-3274	p 42	N93-12016 *	#
NASA-TM-106024	p 110	N93-27092 *	#	NASA-TM-106151	p 217	N93-28053 *	#	NASA-TP-3279	p 58	N93-11001 *	#
NASA-TM-106025	p 109	N93-26552 *	#	NASA-TM-106152	p 36	N93-27026 *	#	NASA-TP-3287	p 286	N93-19977 *	#
NASA-TM-106028	p 42	N93-26907 *	#	NASA-TM-106153	p 145	N93-27011 *	#	NASA-TP-3290	p 108	N93-18139 *	#
NASA-TM-106029	p 249	N93-23746 *	#	NASA-TM-106154	p 200	N93-27161 *	#	NASA-TP-3292	p 106	N93-12015 *	#
NASA-TM-106030	p 17	N93-19968 *	#	NASA-TM-106155	p 269	N93-27061 *	#	NASA-TP-3294	p 160	N93-23394 *	#
NASA-TM-106032	p 111	N93-28624 *	#	NASA-TM-106157	p 162	N93-28610 *	#	NASA-TP-3295	p 128	N93-22556 *	#
NASA-TM-106033	p 250	N93-26999 *	#	NASA-TM-106158	p 232	N93-27080 *	#	NASA-TP-3315	p 34	N93-16941 *	#
NASA-TM-106034	p 271	N93-22559 *	#	NASA-TM-106160	p 201	N93-28626 *	#				
NASA-TM-106037	p 160	N93-20259 *	#	NASA-TM-106161	p 91	N93-27039 *	#	ONERA, TP NO. 1992-113	p 179	A93-38589 *	
NASA-TM-106038	p 197	N93-22596 *	#	NASA-TM-106162	p 229	N93-27641 *	#				
NASA-TM-106039	p 197	N93-21198 *	#	NASA-TM-106163	p 269	N93-27065 *	#	PB92-160688	p 233	N93-70212 *	#
NASA-TM-106042	p 36	N93-25079 *	#	NASA-TM-106165	p 110	N93-26705 *	#				
NASA-TM-106044	p 36	N93-25673 *	#	NASA-TM-106167	p 266	N93-28051 *	#	PR12	p 287	N93-71885 *	#
NASA-TM-106047	p 43	N93-26214 *	#	NASA-TM-106168	p 62	N93-27081 *	#	PR3	p 286	N93-71876 *	#
NASA-TM-106048	p 110	N93-27129 *	#	NASA-TM-106169	p 200	N93-27132 *	#	PR5	p 286	N93-71878 *	#
NASA-TM-106049	p 110	N93-27270 *	#	NASA-TM-106172	p 53	N93-27064 *	#	PR6	p 286	N93-71879 *	#
NASA-TM-106050	p 85	N93-23405 *	#	NASA-TM-106173	p 270	N93-32200 *	#				
NASA-TM-106052	p 111	N93-28681 *	#	NASA-TM-106174	p 230	N93-28411 *	#	SAE PAPER 921028	p 218	A93-14651	
NASA-TM-106053	p 84	N93-20614 *	#	NASA-TM-106175	p 229	N93-27687 *	#	SAE PAPER 921031	p 66	A93-14654	
NASA-TM-106054	p 36	N93-25129 *	#	NASA-TM-106176	p 228	N93-27037 *	#	SAE PAPER 921110	p 57	A93-41305 *	
NASA-TM-106055	p 200	N93-27091 *	#	NASA-TM-106178	p 91	N93-27022 *	#	SAE PAPER 921176	p 210	A93-41356 *	
NASA-TM-106056	p 268	N93-22664 *	#	NASA-TM-106179	p 37	N93-27128 *	#				
NASA-TM-106058	p 161	N93-27265 *	#	NASA-TM-106180	p 262	N93-28628 *	#	SAND-92-1820C	p 277	N93-17343 *	#
NASA-TM-106059	p 63	N93-28554 *	#	NASA-TM-106181	p 37	N93-27160 *	#				
NASA-TM-106060	p 84	N93-20615 *	#	NASA-TM-106186	p 18	N93-31839 *	#	SPIE-1475	p 151	A93-25776 *	
NASA-TM-106061	p 129	N93-28618 *	#	NASA-TM-106187	p 202	N93-29157 *	#	SPIE-1477	p 154	A93-27243 *	
NASA-TM-106063	p 248	N93-23739 *	#	NASA-TM-106189	p 203	N93-31647 *	#				
NASA-TM-106064	p 248	N93-23740 *	#	NASA-TM-106192	p 39	N93-32351 *	#	US-PATENT-APPL-SN-007874	p 227	N93-19027 *	#
NASA-TM-106065	p 248	N93-23044 *	#	NASA-TM-106193	p 49	N93-28696 *	#	US-PATENT-APPL-SN-008026	p 276	N93-19026 *	#
NASA-TM-106066	p 88	N93-26561 *	#	NASA-TM-106194	p 216	N93-27027 *	#	US-PATENT-APPL-SN-017402	p 108	N93-20568 *	#
NASA-TM-106067	p 109	N93-26704 *	#	NASA-TM-106196	p 250	N93-28633 *	#	US-PATENT-APPL-SN-029520	p 287	N93-28130 *	#
NASA-TM-106069	p 198	N93-23744 *	#	NASA-TM-106197	p 202	N93-29161 *	#	US-PATENT-APPL-SN-039735	p 230	N93-28127 *	#
NASA-TM-106070	p 87	N93-25089 *	#	NASA-TM-106198	p 38	N93-27610 *	#	US-PATENT-APPL-SN-046256	p 275	N93-28953 *	#
NASA-TM-106072	p 198	N93-23736 *	#	NASA-TM-106201	p 201	N93-28252 *	#	US-PATENT-APPL-SN-065794	p 138	N93-28425 *	#
NASA-TM-106073	p 53	N93-22589 *	#	NASA-TM-106206	p 202	N93-29075 *	#	US-PATENT-APPL-SN-067184	p 130	N93-29172 *	#
NASA-TM-106074	p 108	N93-25071 *	#	NASA-TM-106207	p 92	N93-29158 *	#	US-PATENT-APPL-SN-081180	p 138	N93-28423 *	#
NASA-TM-106076	p 111	N93-29074 *	#	NASA-TM-106209	p 202	N93-29208 *	#	US-PATENT-APPL-SN-081910	p 139	N93-31316 *	#
NASA-TM-106079	p 96	N93-23014 *	#	NASA-TM-106211	p 230	N93-28050 *	#	US-PATENT-APPL-SN-083246	p 138	N93-31300 *	#
NASA-TM-106080	p 228	N93-23019 *	#	NASA-TM-106212	p 129	N93-23418 *	#	US-PATENT-APPL-SN-084058	p 112	N93-31299 *	#
NASA-TM-106081	p 137	N93-25093 *	#	NASA-TM-106213	p 88	N93-26149 *	#	US-PATENT-APPL-SN-086584	p 217	N93-31298 *	#
NASA-TM-106083	p 198	N93-23404 *	#	NASA-TM-106215	p 251	N93-29196 *	#	US-PATENT-APPL-SN-094732	p 112	N93-31296 *	#
NASA-TM-106084	p 60	N93-23742 *	#	NASA-TM-106216	p 39	N93-31671 *	#	US-PATENT-APPL-SN-104951	p 230	N93-31314 *	#
NASA-TM-106085	p 215	N93-22994 *	#	NASA-TM-106217	p 53	N93-29195 *	#	US-PATENT-APPL-SN-501893	p 111	N93-29614 *	#
NASA-TM-106086	p 17	N93-24911 *	#	NASA-TM-106219	p 232	N93-29073 *	#	US-PATENT-APPL-SN-601957	p 107	N93-14706 *	#
NASA-TM-106087	p 199	N93-25175 *	#	NASA-TM-106220	p 92	N93-29194 *	#	US-PATENT-APPL-SN-608493	p 111	N93-29609 *	#
NASA-TM-106089	p 201	N93-28947 *	#	NASA-TM-106222	p 92	N93-28694 *	#	US-PATENT-APPL-SN-647902	p 35	N93-22034 *	#
NASA-TM-106092	p 150	N93-22483 *	#	NASA-TM-106223	p 139	N93-32367 *	#	US-PATENT-APPL-SN-657238	p 111	N93-29614 *	#
NASA-TM-106093	p 60	N93-24755 *	#	NASA-TM-106225	p 251	N93-31193 *	#	US-PATENT-APPL-SN-703435	p 278	N93-11058 *	#
NASA-TM-106095	p 215	N93-24737 *	#	NASA-TM-106228	p 256	N93-32201 *	#	US-PATENT-APPL-SN-708255	p 107	N93-14706 *	#
NASA-TM-106096	p 161	N93-24746 *	#	NASA-TM-106230	p 38	N93-28697 *	#	US-PATENT-APPL-SN-722446	p 83	N93-18856 *	#
NASA-TM-106097	p 88	N93-26211 *	#	NASA-TM-106233	p 91	N93-28619 *	#	US-PATENT-APPL-SN-735548	p 111	N93-29609 *	#
NASA-TM-106098	p 60	N93-25090 *	#	NASA-TM-106234	p 51	N93-28052 *	#	US-PATENT-APPL-SN-766593	p 256	N93-28974 *	#
NASA-TM-106099	p 228	N93-23741 *	#	NASA-TM-106235	p 17	N93-31648 *	#	US-PATENT-APPL-SN-872262	p 112	N93-31293 *	#
NASA-TM-106100	p 229	N93-27069 *	#	NASA-TM-106236	p 201	N93-28627 *	#	US-PATENT-APPL-SN-880851	p 111	N93-29614 *	#
NASA-TM-106101	p 229	N93-27133 *	#	NASA-TM-106240	p 38	N93-29162 *	#	US-PATENT-APPL-SN-889572	p 226	N93-12203 *	#
NASA-TM-106102	p 85	N93-23747 *	#	NASA-TM-106241	p 150	N93-31856 *	#	US-PATENT-APPL-SN-892054	p 106	N93-11543 *	#
NASA-TM-106103	p 228	N93-25672 *	#	NASA-TM-106243	p 141	N93-28695 *	#	US-PATENT-APPL-SN-892055	p 109	N93-26100 *	#
NASA-TM-106105	p 255	N93-23018 *	#	NASA-TM-106245	p 18	N93-31672 *	#	US-PATENT-APPL-SN-909345	p 137	N93-20566 *	#
NASA-TM-106106	p 216	N93-25191 *	#	NASA-TM-106248	p 202	N93-31147 *	#	US-PATENT-APPL-SN-961943	p 275	N93-17051 *	#
NASA-TM-106107	p 61	N93-26148 *	#	NASA-TM-106249	p 203	N93-32199 *	#	US-PATENT-APPL-SN-970669	p 130	N93-31294 *	#
NASA-TM-106108	p 150	N93-26903 *	#	NASA-TM-106251	p 271	N93-31145 *	#	US-PATENT-APPL-SN-973505	p 284	N93-17413 *	#
NASA-TM-106109	p 199	N93-26554									

US-PATENT-APPL-SN-991403

REPORT/ACCESSION NUMBER INDEX

US-PATENT-APPL-SN-991403	p 214	N93-17060 * #
US-PATENT-APPL-SN-993743	p 137	N93-19332 * #
US-PATENT-CLASS-165-185	p 111	N93-29614 *
US-PATENT-CLASS-174-163	p 111	N93-29614 *
US-PATENT-CLASS-264-58	p 109	N93-26100 *
US-PATENT-CLASS-356-300	p 83	N93-18856 *
US-PATENT-CLASS-356-311	p 83	N93-18856 *
US-PATENT-CLASS-356-356	p 278	N93-11058 *
US-PATENT-CLASS-356-360	p 278	N93-11058 *
US-PATENT-CLASS-356-36	p 83	N93-18856 *
US-PATENT-CLASS-356-376	p 278	N93-11058 *
US-PATENT-CLASS-361-386	p 111	N93-29614 *
US-PATENT-CLASS-364-575	p 278	N93-11058 *
US-PATENT-CLASS-382-26	p 278	N93-11058 *
US-PATENT-CLASS-422-136	p 111	N93-29609 *
US-PATENT-CLASS-422-209	p 111	N93-29609 *
US-PATENT-CLASS-427-367	p 107	N93-14706 *
US-PATENT-CLASS-427-404	p 107	N93-14706 *
US-PATENT-CLASS-427-419 2	p 107	N93-14706 *
US-PATENT-CLASS-427-456	p 107	N93-14706 *
US-PATENT-CLASS-428-428	p 109	N93-26100 *
US-PATENT-CLASS-428-614	p 111	N93-29614 *
US-PATENT-CLASS-428-698	p 109	N93-26100 *
US-PATENT-CLASS-429-103	p 256	N93-28974 *
US-PATENT-CLASS-429-16	p 256	N93-28974 *
US-PATENT-CLASS-429-27	p 256	N93-28974 *
US-PATENT-CLASS-429-29	p 256	N93-28974 *
US-PATENT-CLASS-429-30	p 256	N93-28974 *
US-PATENT-CLASS-429-46	p 256	N93-28974 *
US-PATENT-CLASS-501-32	p 109	N93-26100 *
US-PATENT-CLASS-501-89	p 109	N93-26100 *
US-PATENT-CLASS-501-8	p 109	N93-26100 *
US-PATENT-CLASS-501-95	p 109	N93-26100 *
US-PATENT-CLASS-60-223	p 83	N93-18856 *
US-PATENT-CLASS-60-226 1	p 35	N93-22034 *
US-PATENT-CLASS-60-39.17	p 35	N93-22034 *
US-PATENT-CLASS-73-86	p 83	N93-18856 *
US-PATENT-5,146,293	p 278	N93-11058 *
US-PATENT-5,169,674	p 107	N93-14706 *
US-PATENT-5,184,460	p 35	N93-22034 *
US-PATENT-5,187,542	p 83	N93-18856 *
US-PATENT-5,213,908	p 256	N93-28974 *
US-PATENT-5,214,004	p 109	N93-26100 *
US-PATENT-5,224,030	p 111	N93-29614 *
US-PATENT-5,225,171	p 111	N93-29609 *

REPORT DOCUMENTATION PAGEForm Approved
OMB No. 0704-0188

Public reporting burden for this collection of information is estimated to average 1 hour per response, including the time for reviewing instructions, searching existing data sources, gathering and maintaining the data needed, and completing and reviewing the collection of information. Send comments regarding this burden estimate or any other aspect of this collection of information, including suggestions for reducing this burden, to Washington Headquarters Services, Directorate for Information Operations and Reports, 1215 Jefferson Davis Highway, Suite 1204, Arlington, VA 22202-4302, and to the Office of Management and Budget, Paperwork Reduction Project (0704-0188), Washington, DC 20503.

1. AGENCY USE ONLY (Leave blank)		2. REPORT DATE November 1994	3. REPORT TYPE AND DATES COVERED Technical Memorandum	
4. TITLE AND SUBTITLE Bibliography of Lewis Research Center Technical Publications Announced in 1993			5. FUNDING NUMBERS	
6. AUTHOR(S)				
7. PERFORMING ORGANIZATION NAME(S) AND ADDRESS(ES) National Aeronautics and Space Administration Lewis Research Center Cleveland, Ohio 44135-3191			8. PERFORMING ORGANIZATION REPORT NUMBER E-8984	
9. SPONSORING/MONITORING AGENCY NAME(S) AND ADDRESS(ES) National Aeronautics and Space Administration Washington, D.C. 20546-0001			10. SPONSORING/MONITORING AGENCY REPORT NUMBER NASA TM-106666	
11. SUPPLEMENTARY NOTES Compiled by the Publishing Services Team, Lewis Research Center. Responsible person, Joyce Cieszewski, organization code 1800, (216) 433-5797.				
12a. DISTRIBUTION/AVAILABILITY STATEMENT Unclassified - Unlimited Subject Category 82			12b. DISTRIBUTION CODE	
13. ABSTRACT (Maximum 200 words) This compilation of abstracts describes and indexes the technical reporting that resulted from the scientific and engineering work performed and managed by the Lewis Research Center in 1993. All the publications were announced in the 1993 issues of STAR (Scientific and Technical Aerospace Reports) and/or IAA (International Aerospace Abstracts). Included are research reports, journal articles, conference presentations, patents and patent applications, and theses.				
14. SUBJECT TERMS Bibliographies; Abstracts; Documentation; Indexes (Documentation)			15. NUMBER OF PAGES 470	
			16. PRICE CODE A20	
17. SECURITY CLASSIFICATION OF REPORT Unclassified	18. SECURITY CLASSIFICATION OF THIS PAGE Unclassified	19. SECURITY CLASSIFICATION OF ABSTRACT Unclassified	20. LIMITATION OF ABSTRACT	